

Placido Neri · Jonathan L. Sessler  
Mei-Xiang Wang *Editors*

# Calixarenes and Beyond

 Springer

# Calixarenes and Beyond





Placido Neri • Jonathan L. Sessler  
Mei-Xiang Wang  
Editors

# Calixarenes and Beyond

 Springer

*Editors*

Placido Neri  
Dipartimento di Chimica e Biologia  
“A. Zambelli”  
Università di Salerno  
Fisciano, Salerno, Italy

Jonathan L. Sessler  
Department of Chemistry  
The University of Texas  
Austin, TX, USA

Mei-Xiang Wang  
Department of Chemistry  
Tsinghua University  
Beijing, China

ISBN 978-3-319-31865-3      ISBN 978-3-319-31867-7 (eBook)  
DOI 10.1007/978-3-319-31867-7

Library of Congress Control Number: 2016948862

© Springer International Publishing Switzerland 2016

This work is subject to copyright. All rights are reserved by the Publisher, whether the whole or part of the material is concerned, specifically the rights of translation, reprinting, reuse of illustrations, recitation, broadcasting, reproduction on microfilms or in any other physical way, and transmission or information storage and retrieval, electronic adaptation, computer software, or by similar or dissimilar methodology now known or hereafter developed.

The use of general descriptive names, registered names, trademarks, service marks, etc. in this publication does not imply, even in the absence of a specific statement, that such names are exempt from the relevant protective laws and regulations and therefore free for general use.

The publisher, the authors and the editors are safe to assume that the advice and information in this book are believed to be true and accurate at the date of publication. Neither the publisher nor the authors or the editors give a warranty, express or implied, with respect to the material contained herein or for any errors or omissions that may have been made.

Printed on acid-free paper

This Springer imprint is published by Springer Nature  
The registered company is Springer International Publishing AG Switzerland

# Foreword

In the Spring of 1970 I became, by default, the chairman of the Department of Chemistry at Washington University in St Louis. It was not a happy time to be a chairman; the United States was mired down in a disastrous war in Vietnam, the federal and private support for science was declining, the faculty was dispirited, and the mood of the country was one of anger and despair. It was in this time of national and private discontent that calixarene chemistry was born. Seeking to restore my own faltering research funding I embarked on a quest to build enzyme mimics, focusing on a group of macrocyclic compounds that had come to my attention through an association with the Petrolite Corporation. These were thought at the time to be cyclic tetramers formed by the condensation of formaldehyde and *para*-substituted phenols whose basket-like shape promised to provide interesting mimics for the active site contour of an enzyme. Enthused by this prospect, I sought first to find a simple designation for these compounds to complement the very extended name assigned by *Chemical Abstracts*. Using the word “calix” (from the shape of a Greek vase called a “calix crater”) as the prefix and “arene” (denoting the presence of aryl residues in the cyclic array) as the suffix, the word “calixarene” was coined. This proved to be a felicitous choice which, along with the subsequent demonstration of how to make calixarenes of various sizes in good yields, brought these compounds to the attention of the chemical world and set in motion the creation of what is now called “calixarene chemistry”. The impressive size to which the field has grown is a nice example of the power of an apt name coupled with a readily accessible source of the materials in question. During the almost half century since the scarcely noticed birth of calixarene chemistry, the efforts of hundreds of talented and devoted researchers have spawned several thousand journal articles, many book chapters, a handful of books and 13 international conferences. This great effort has created a sturdy platform that now provides the basis for the next advances that will take us “*beyond* calixarene chemistry” into new

and even more exciting territories. To quote Alfred Lord Tennyson, “All experience is an arch wherethrough gleams that untraveled world whose margin fades forever and forever as I move.”

Seattle, WA, USA  
February 2016

C. David Gutsche

# Preface

The word *calixarene* was coined by C. David Gutsche, and appeared in print in 1974, to define the cup-shaped molecules obtained from the condensation of *p*-substituted phenols with formaldehyde. **Beyond** this early meaning, the term was then extended to define the carbonious macrocyclic skeleton of  $[1_n]$  metacyclophanes independent of their starting materials. In this way, several other macrocycles obtained from different phenolic compounds and different aldehydes came to be included under the calixarene umbrella. In particular, the Högberg macrocycles, obtained from resorcinol and alkylaldehydes, started to be viewed as differently substituted “calixarenes”. These compounds are now referred to as *calixresorcinarenes*, *resorcinarenes*, or *resorcarennes*. Similarly, their analogues derived from pyrogallol are now called *pyrogallolarenes*.

**Beyond** the carbonious skeleton, calixarene-like macrocycles containing sulphur atoms as bridges (*thiacalixarenes*) were also synthesized. They were then quickly followed by others containing oxygens (*oxacalixarenes*), nitrogen (*azacalixarenes*), or other heteroatoms (*heteracalixarenes*). A further addition came with the advent of macrocycles containing more than one bridging atom (*homocalixarenes*, *homooxacalixarenes*, or *homoheteracalixarenes*). **Beyond** the benzenoid rings, several others aromatic and heteroaromatics rings, such as naphthalene, pyrrole, pyridine, etc., were also used to construct macrocycles that bear resemblance to calixarenes giving rise to *calixnaphthalenes*, *calixpyrroles*, *calixpyridines*, etc.

**Beyond** the *meta*-bridging emblematic of calixarenes ( $[1_n]$ metacyclophanes), the community now embraces related macrocycles having different bridging positions. These include systems where *ortho*- and *para*-bridging were also used to construct, respectively, *cyclotrimeratrilenes* ( $[1_3]$ orthocyclophanes) and *pillararenes* ( $[1_n]$ paracyclophanes).

As suggested by the title, *Calixarenes and Beyond* aims to give an update on the chemistry of this ever-growing family of macrocycles, including related compounds **beyond** any strict or rigorous definition. In addition to their ostensibly similar structural features, the *fil-rouge* connecting the macrocycles discussed in

this book is their chemical relationship, particularly as it relates to their complementary supramolecular properties. With the exception of the newer members, the basic chemistry of this family has been thoroughly investigated, leading to solid and well-established preparative procedures and functionalization methods. However, since the turn to the third millennium, there has been a steady shift to go from synthesis and analysis of basic recognition features to an exploitation of their supramolecular properties in an increasing number of applications that span an increasing broad array of fields.

The present multi-author book, *Calixarenes and Beyond*, provides a forum for summarizing the current state-of-the-art in calixarene-related research. Given the present trends, much of the focus is on properties and applications. However, advances in the synthetic chemistry of calixarenes and related systems are also included. This preparative effort has reached a very high level of sophistication targeting more subtle and specific modifications or syntheses that are more difficult than previously considered tenable. The basic molecular recognition studies have moved from the classical cation and anion binding to an exploitation of these features, and those involving neutral substrates, towards the creation of well-defined multi-molecular assemblies. Many of these latter are endowed with very peculiar switching abilities and provide tantalizing glimpses of a future fully populated with interpenetrated architectures and molecular machines. Investigations in the biomedical field have reached an impressive level of precision and efficiency and provide a window into future real-life applications. A wealth of new materials with smart and marvelous properties has emerged with possible technological applications. As editors we have tried to give a complete picture of this scenario. Of course, we recognize that it is impossible to have a comprehensive coverage in a single medium-size volume. Therefore, we apologize in advance knowing full well that, from a combination necessity and our own shortcomings, some topics have been neglected or not appropriately treated.

The 39 chapters of this book are written by highly active, world-renowned authors who hail from dozens of countries. Their expertise and first-hand understanding of the field provides a wealth of perspectives, while giving specific overviews of particular topics that is second to none. Moreover, the authors' passion for the field and their enthusiasm for their own contributions permeates every page of the book. We thus like to think that *Calixarenes and Beyond* will provide a timely summary of the field—one that is both vibrant in its youth and solid in its maturity—while setting forth a full spectrum of opportunities that will take the field of calixarenes *beyond* the limits of our current imagination. Personally, we believe the best is yet to come. This book, we hope, will be the steppingstone to that bright future.

Salerno, Italy  
Austin, TX, USA  
Beijing, China  
February 2016

Placido Neri  
Jonathan L. Sessler  
Mei-Xiang Wang

# Contents

<b>1</b>	<b>Introduction and History</b> . . . . .	1
	David N. Reinhoudt	
<b>2</b>	<b>Chiral Calixarenes and Resorcinarenes</b> . . . . .	13
	Michał Wierzbicki, Hanna Jędrzejewska, and Agnieszka Szumna	
<b>3</b>	<b>Meta Substitution of Calixarenes</b> . . . . .	43
	Ondrej Kundrat and Pavel Lhoták	
<b>4</b>	<b>Preparation of Methylene-Substituted Calixarenes</b> . . . . .	75
	Silvio E. Biali	
<b>5</b>	<b>Calix[5]arene: from Capsules to Polymers</b> . . . . .	95
	Melchiorre F. Parisi, Giuseppe Gattuso, Anna Notti, Ilenia Pisagatti, and Sebastiano Pappalardo	
<b>6</b>	<b>Calix[6]azacryptand-Based Receptors</b> . . . . .	113
	Gaël De Leener, Steven Moerkerke, Roy Lavendomme, Olivia Reinaud, and Ivan Jabin	
<b>7</b>	<b>Large Calixarenes</b> . . . . .	141
	Carmen Talotta, Carmine Gaeta, Annunziata Soriente, Margherita De Rosa, Corrada Geraci, and Placido Neri	
<b>8</b>	<b>Resorc[4]arenes as Preorganized Synthons for Surface Recognition and Host-Guest Chemistry</b> . . . . .	175
	Ilaria D'Acquarica, Francesca Ghirga, Cinzia Ingallina, Deborah Quaglio, Giovanni Zappia, Gloria Uccello-Barretta, Federica Balzano, and Bruno Botta	
<b>9</b>	<b>A Chronology of Cavitands</b> . . . . .	195
	Anthony Wishard and Bruce C. Gibb	
<b>10</b>	<b>Calix[4]arenes and Resorcinarenes Bridged at the Wider Rim</b> . . . . .	235
	Daniel A. Tan and Mauro Mocerino	



<b>11</b>	<b><i>N</i>-Alkyl Ammonium Resorcinarene Salts: A Versatile Family of Calixarene-Related Host Molecules</b> . . . . .	255
	Ngong Kodiah Beyeh and Kari Rissanen	
<b>12</b>	<b>Functionalized Calixpyrroles: Building Blocks for Self-Assembly</b> . . . . .	285
	Gabriela I. Vargas-Zúñiga, Jonathan L. Sessler, and Steffen Bähring	
<b>13</b>	<b>Thiacalixarenes</b> . . . . .	335
	Nobuhiko Iki	
<b>14</b>	<b>Azacalixaromatics</b> . . . . .	363
	De-Xian Wang and Mei-Xiang Wang	
<b>15</b>	<b>Oxacalixarenes</b> . . . . .	399
	Reuben Hudson and Jeffrey L. Katz	
<b>16</b>	<b>Homoheteracalix[<i>n</i>]arenes (X = S, Se, N)</b> . . . . .	421
	Joice Thomas, Aliya S. Gusak, and Wim Dehaen	
<b>17</b>	<b>Functionalization and Properties of Homooxacalixarenes</b> . . . . .	445
	Paula M. Marcos	
<b>18</b>	<b>Triptycene-Derived Calixarenes, Heteracalixarenes and Analogues</b> . . . . .	467
	Chuan-Feng Chen, Han-Xiao Wang, Ying Han, and Ying-Xian Ma	
<b>19</b>	<b>Pillar[<i>n</i>]arenes: Easy-to-Make Pillar-Shaped Macrocyclic Hosts for Supramolecular Chemistry</b> . . . . .	485
	Tomoki Ogoshi and Tada-aki Yamagishi	
<b>20</b>	<b>Function-Directed Supramolecular Assembly Based on Water Soluble Calixarenes</b> . . . . .	511
	Yu Liu, Pei-Yu Li, and Yong Chen	
<b>21</b>	<b>Water-Soluble Cryptophanes: Design and Properties</b> . . . . .	525
	Thierry Brotin, Alexandre Martinez, and Jean-Pierre Dutasta	
<b>22</b>	<b>Calixsugars: Finally Reaching Their Therapeutic Potential?</b> . . . . .	559
	Susan E. Matthews	
<b>23</b>	<b>New Technologies Powered by Protein-Binding Calixarenes</b> . . . . .	601
	Meagan A. Beatty and Fraser Hof	
<b>24</b>	<b>Calix[<i>n</i>]arenes and Nucleic Acids</b> . . . . .	627
	Max Sena Peters and Thomas Schrader	
<b>25</b>	<b>Structural Trends in Calix[4]arene-Supported Cluster Chemistry</b> . . . . .	671
	Marco Coletta, Euan K. Brechin, and Scott J. Dalgarno	

<b>26 Calixarenes as Supramolecular Catalysts Endowed with Esterase and Phosphodiesterase Activity . . . . .</b>	<b>691</b>
Riccardo Salvio, Roberta Cacciapaglia, and Alessandro Casnati	
<b>27 Calixarenes in Organo and Biomimetic Catalysis . . . . .</b>	<b>719</b>
Mustafa Yilmaz and Serkan Sayin	
<b>28 Fluorescent Calixarene Hosts . . . . .</b>	<b>743</b>
Rajesh Kumar, Yujin Jung, and Jong Seung Kim	
<b>29 Calixarene Threading by Viologen-Based Axles . . . . .</b>	<b>761</b>
Arturo Arduini, Guido Orlandini, Andrea Secchi, Alberto Credi, Serena Silvi, and Margherita Venturi	
<b>30 Calixarene Threading via Superweak Anion . . . . .</b>	<b>783</b>
Carmine Gaeta, Carmen Talotta, Margherita De Rosa, Annunziata Soriente, and Placido Neri	
<b>31 Hydrogen Bond Hexameric Capsules: Structures, Host-Guest Interactions, Guest Affinities, and Catalysis . . . . .</b>	<b>811</b>
Yoram Cohen, Sarit Slovak, and Liat Avram	
<b>32 Self-Assembled Dimeric Containers Based on Calix[4]arene, Resorcin[4]arene and Calix[4]pyrrole Scaffolds . . . . .</b>	<b>843</b>
G. Aragay and P. Ballester	
<b>33 Calixarenes and Fullerenes . . . . .</b>	<b>879</b>
Paris E. Georghiou	
<b>34 Calixarene-Encapsulated Nanoparticles: Synthesis, Stabilization, and Self-Assembly . . . . .</b>	<b>921</b>
Alexander Wei	
<b>35 Calixarenes and Nanoparticles . . . . .</b>	<b>941</b>
Francesco Vita, Arturo Arduini, and Andrea Secchi	
<b>36 Calixarenes and Pillarenes on Surfaces . . . . .</b>	<b>965</b>
Li-Li Tan and Ying-Wei Yang	
<b>37 Calixarenes and Resorcinarenes at Interfaces . . . . .</b>	<b>987</b>
Ludovico Tulli and Patrick Shahgaldian	
<b>38 Solid State Features of Calixarenes . . . . .</b>	<b>1011</b>
Kinga Suwinska	
<b>39 Gas Sorption and Storage Properties of Calixarenes . . . . .</b>	<b>1037</b>
Rahul S. Patil, Debasis Banerjee, Jerry L. Atwood, and Praveen K. Thallapally	
<b>Index . . . . .</b>	<b>1057</b>

# Chapter 1

## Introduction and History

David N. Reinhoudt

The ‘lock-and-key’ concept formulated more than a Century ago by Emil Fischer has guided chemists and biologists to understand molecular interactions, enzyme reactivity and material properties. The same concept has inspired synthetic chemists in their design of synthetic receptors and catalysts.

Building blocks for synthetic receptors that have a rigid 3-D structure play an important role in the synthesis of molecular receptors and enzyme models. Inside the confined space of these rigid building blocks the shape and functionality is very precisely defined.

In this book the chemistry of Calixarenes, rigid vase-like molecules, is described. For their widespread use in supramolecular chemistry, two aspects are crucial. First, their large scale synthesis is relatively simple from cheap starting materials. Second, they can be selectively functionalized at different positions which render them attractive starting materials from a synthesis point of view.

The members of the cyclodextrin family (**1**) are the prototype of building blocks that have a molecular cavity and that can be prepared on large, industrial scale. They are reported in the literature for the first time in 1891 by Villiers [1] as crystalline products that are formed by enzymatic degradation of starch. Schardinger [2] identified the cyclic structure and the enzyme that is responsible for the formation of cyclodextrins from starch, but it was only in 1938 that Freudenberg characterized them as cyclic structures of  $\alpha$ -1,4-linked glucose units [3]. In 1965 the first X-ray structure was published of an  $\alpha$ -cyclodextrin salt complex that revealed the rigid molecular cavity [4]. The outer rims of the cyclodextrins are decorated with hydroxyl groups which render them more or less soluble in water (Fig. 1.1).

---

D.N. Reinhoudt (✉)

Department of Inorganic Material Science, MESA+ Institute for Nanotechnology,  
University of Twente, 217, Enschede, The Netherlands  
e-mail: [d.n.reinhoudt@utwente.nl](mailto:d.n.reinhoudt@utwente.nl)

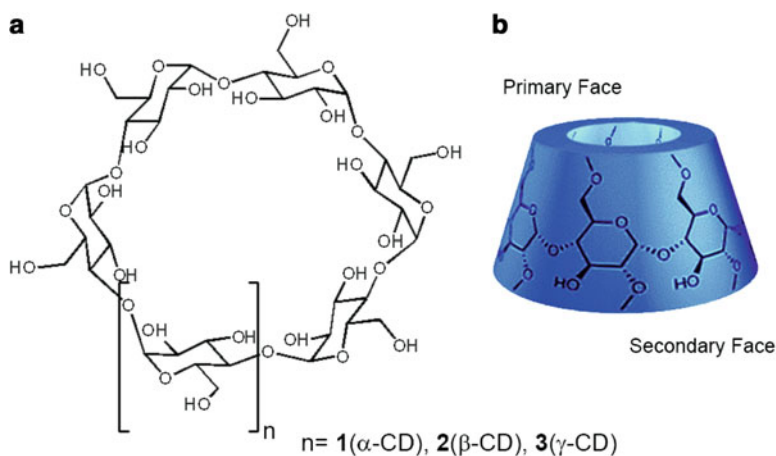


**Fig. 1.1** Structures of cyclodextrins (1)

In the cyclodextrins the rigid non-polar cavity is formed by the carbon atoms of the glucose units with the hydrogen atoms at C(3) and C(5) pointing into the cavity. The cavity volumes of the  $\alpha$ -,  $\beta$ -, and  $\gamma$ -cyclodextrins are 176, 346, and 510 Å<sup>3</sup>, respectively. In these rigid cavities organic guests can be complexed, the driving force being the hydrophobic interaction between host and guest and the liberation of water molecules from the cavity.

A family of *synthetic* molecules that have a rigid, apolar cavity are the Cucurbiturils (2). The history of these condensation products of glycoluril and formaldehyde goes back to 1905 when Behrend and coworkers [5] described that under strongly acidic conditions a product was obtained that was slightly soluble in aqueous acids or bases [6]. Decades later in 1981 Bill Mock and his group reinvestigated this work and isolated and characterized a complex of calcium bisulfate and a cyclic molecule that is composed of 6 glycoluril units linked by 12 methylene bridges [6]. They proposed the name cucurbituril because of the pumpkin (Cucurbitaceae)-like structure. Almost 20 years later Kim and his group in Korea isolated and characterized three other members of the cucurbituril family, CB(5), -(7), and -(8). More recently even higher members of this family have been reported [7] (Fig. 1.2).

There are several similarities between the cyclodextrins and the cucurbiturils. They both come in different ring sizes; they have an apolar cavity and rims lined with polar moieties that render them slightly soluble in aqueous solutions. Second they both have structures with a high degree of symmetry which makes selective functionalization, other than mono or complete, difficult. The most important similarity is that they both can complex organic molecules in their apolar cavity with size- and structure -dependent selectivity. The latter is the main reason that these molecules have become the most important receptors for supramolecular chemistry *in water*, with many practical applications.

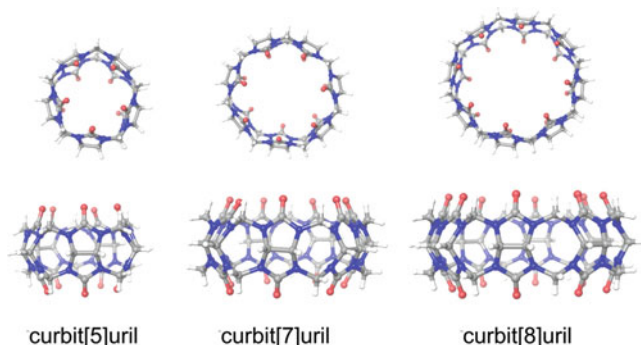


**Fig. 1.2** Structures of cucurbiturils (2)

A similar cyclo-condensation reaction as between glycoluril and formaldehyde that gives rise to the cucurbiturils is the basis of a third class of basket-like molecules. In 1872 Baeyer reported the formation of resinous material from the reaction of formaldehyde and phenol which was the basis for the work of Baekeland's discovery of the first synthetic plastic that had practical application, Bakelite [8].

In 1940 a *cyclic* tetrameric structure was proposed by Niederl and Vogel [9] for the acid-catalyzed reaction products of resorcinol with aldehydes. The structural evidence was based only on molecular weight determinations which pointed to a 4:4 adduct of resorcinol and the aldehyde. It took until 1968 before the X-ray analysis by Erdtman, Högberg, and coworkers definitely proved the structure [10]. These molecules became available in larger quantities by the work of Högberg et al. [10].

Soon after the publication of Niederl and Vogel, it was Zinke in 1944 who isolated from a reaction of a *para*-substituted phenol, viz. *p*-1,1,3,3-tetramethylbutyl phenol and formaldehyde a compound that had a molecular weight of 876 in agreement with a *cyclotetrameric* structure [11]. Not much later Cornforth and his coworkers at the Shell – Laboratories in the UK found that the product reported by Zinke was not a single compound but a mixture of cyclic reaction products [12].

This apparent controversy was resolved by the seminal work of David Gutsche who developed reproducible synthetic procedures for the family of vase-like compounds, which in 1975 he called Calixarenes. David became interested in the chemistry of the Zinke compounds because he was a consultant to the Petrolite Corporation that produced surfactants for the oil industry. One of their products was a linear oligomer obtained from reaction of *p*-*tert*-butylphenol and formaldehyde. Problems in the production process led to a detailed study of the reaction and during the more detailed investigations the Petrolite team rediscovered the crystalline Zinke compound. David's personal interest in these macrocyclic molecules was their possible use as platforms for enzyme mimics, in particular the Aldolase catalysis. Although he never realized such an artificial enzyme, David devoted

most of his academic career to the chemistry of the calixarenes. For a more detailed history of this chemistry the reader is referred to the books published by David Gutsche [8].



*The first time I met David Gutsche was in my laboratory in Twente in the 1980s, when he was making a lecture tour in Europe. I had followed the story of the calixarenes since the early 1970s when my colleague at Shell, Sir John Cornforth, gave me samples of the LBC and HBC products that he had obtained from the condensation of *p*-tert-butylphenol and formaldehyde. David told me about his Petrolite connection and how he became involved. We discussed his ideas on synthetic enzyme mimics of aldolase based on the cone conformer of calix[4]arene and our urease mimic based on uranyl salenophenes. Since that first meeting we have been in close contact. During this period David and Alice moved several times. First from Washington University in St. Louis to TCU in Fort Worth as the Robert A. Welsh Professor of Chemistry, then to the University of Arizona in Tucson, and finally to retire in Seattle. He published many important research papers and several books and book chapters. David is beyond any doubt the godfather of modern Calixarene chemistry who made the major members of the calix family available on large laboratory scale. A condition for the work by many others. In 2002 he received the Izatt Christensen Award in Macrocyclic Chemistry. During the 13th International Conference on Calixarenes, the first David Gutsche Award in Calixarene Chemistry was presented to another pioneer of the field, Rocco Ungaro of the University of Parma.*

The ultimate structure proof came in the case of calix[4]arene from the Parma group of Rocco Ungaro, Andrea Pochini and Giovanni Andreetti [13] (Fig. 1.3).

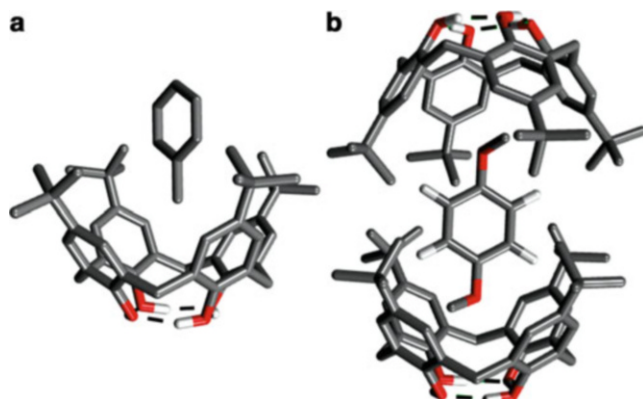


**Fig. 1.3** X-ray crystal structures of the *p*-*tert*-butylcalix[4]arene and (a) toluene 1:1 complex and (b) anisole 2:1 complex (the two statistically equivalent OCH<sub>3</sub> anisole groups are shown)



*Rocco Ungaro was born in the South of Italy, in Anzi. He studied chemistry at the University of Parma where he graduated with Professor Giuseppe Casnati in 1968. He worked with Johannes Smid at the State University of New York in Syracuse (NY) as a post-doctoral research fellow. When he returned to Parma he started in collaboration with Andrea Pochini and Giovanni Andreotti a study on the reactions of the metal templated cyclo-oligomerization of phenols and formaldehyde. In 1979 the Parma group made a seminal contribution to the emerging field of Calixarene Chemistry. The resolution the X-ray structure not only definitely proved the cyclic structure for calixarenes, but also showed the presence of toluene as a guest molecule. My collaboration with Rocco began in 1985 when we were interested in kinetically stable complexes of radioactive Rb<sup>+</sup> ions for the study of renal blood flow. He played a prominent role in establishing the first European network in Supramolecular chemistry.*

Many years before Gutsche found effective synthetic procedures for the various calixarenes, Hayes and Hunter [14] reported a stepwise preparation of calixarenes. This method was many years later investigated in Mainz by Herman Kämmerer and by Volker Böhmer [15]. Their method comprises the tedious synthesis of linear precursors and their subsequent cyclisation.

Now there are a number of classes of molecules that are structurally related to the calixarenes, like the oxa-, aza-, and thiacalixarenes, the chemistry of which is described in Chaps. 13–15.

Calix[ $n$ ]arenes have been synthesized by one-step procedures from  $n = 4$  to 20 in good to very poor yields. From a practical point of view only the synthesis of the smaller members of this family of macrocycles has been optimized. *p*-*tert*-Butylcalix[4]arene can be prepared in bulk quantities according what Gutsche has described as the *Modified Zinke-Cornforth Procedure* [16], by reaction of *p*-*tert*-butylphenol and formaldehyde in the presence of small quantities of NaOH at 110–120 °C. The yield of the cyclic tetramer can be as high as 60%. At higher concentration of base, under the same conditions, the cyclic hexamer becomes the predominant and even the only product in 65% yield. This *p*-*tert*-butylcalix[6]arene can be synthesized in even higher yield (80–85%) from what Gutsche calls the *Modified Petrolite Procedure*. Through a slightly different *Standard Petrolite Procedure* the *p*-*tert*-butylcalix[8]arene can be prepared in 60–65% yield. Two other members of this family ( $n = 5$  and 7) have been prepared in modest yields of 10–20%, the other larger calixarenes up to  $n = 20$  have been isolated and characterized but in low yields.

As already mentioned, the step-wise procedures reported by Haynes and Hunter in 1956, were extensively explored in Mainz by Kämmerer [17] and later by Volker Böhmer [18] (Fig. 1.4). In time these multistep syntheses actually preceded the work of Gutsche but never became of practical importance.

Confusion about the stereochemistry of the calix[4]- and [8]arenes already played a role in the work of Cornforth et al. mentioned above. They attributed the different physical properties of the high and low melting fractions (HBC and LBC, respectively) to different conformers of the cyclic tetramer (a calix[4]arene), because on the basis of their space filling molecular models they believed that the phenolic OH groups could not rotate through the annulus. And this could give rise to four different rotational diastereoisomers (Fig. 1.5).

However, Kämmerer showed later by temperature-dependent <sup>1</sup>H NMR spectroscopy of what was definitely a cyclic tetramer, that the nonequivalent protons of the bridging methylene groups at room temperature, became equivalent at 60 °C. This was first interpreted by Kämmerer in terms of conversion of two of the Cornforth's diastereoisomers but a few years later [19] correctly interpreted as the mirror image conformational interconversion of the cone structure (Fig. 1.5). In 1985 Gutsche et al. [20] proved that the HBC fraction of Cornforth was the cyclic octamer.

Calix[4]arenes can exist in four different conformations, the cone, partial cone, 1,2-, and 1,3-alternate (Fig. 1.5), which differ in thermodynamic stability. With larger substituents at the phenolic oxygens the interconversion of the different conformers is no longer possible, and different stable conformers can be



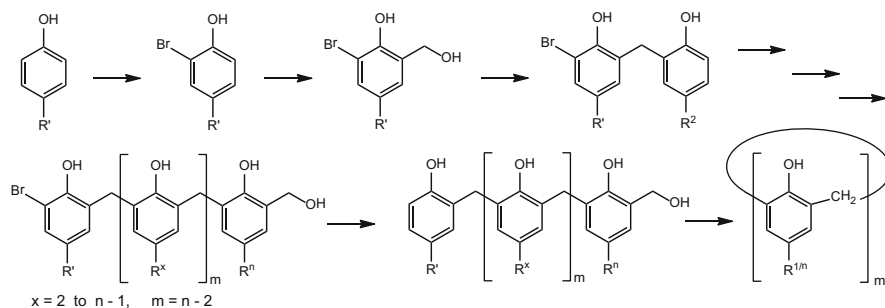
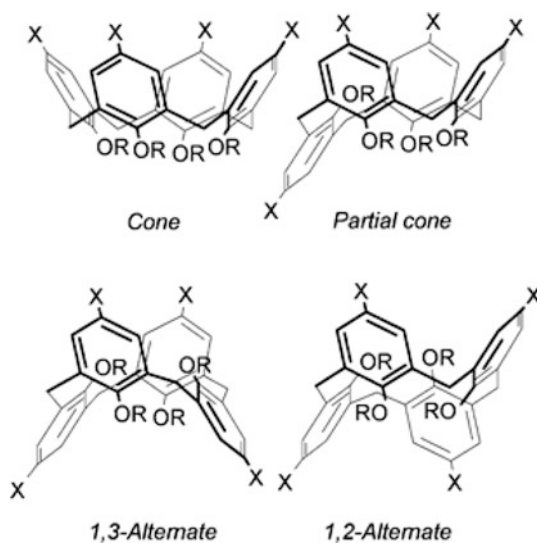


**Fig. 1.4** The Kämmerer-Böhmer stepwise synthesis of Calixarenes

**Fig. 1.5** The four different conformers of Calix[4]arenes



synthesized. The larger calixarenes are more flexible and the energy barriers for interconversion become lower.

The stereochemistry of the related calix[4]resorcinarenes is, for the parent compounds derived from condensation of resorcinols with formaldehyde, similar to the calix[4]arenes. In the NMR spectra the bridging methylene groups show up as an AB quartet at low temperature which coalesces at higher temperatures. When they are obtained from higher aldehydes, the stereochemical outcome of the reaction is much more complex. The conformation of the macrocyclic ring can adopt five extreme conformations, the crown, boat, chair, diamond, and saddle. The

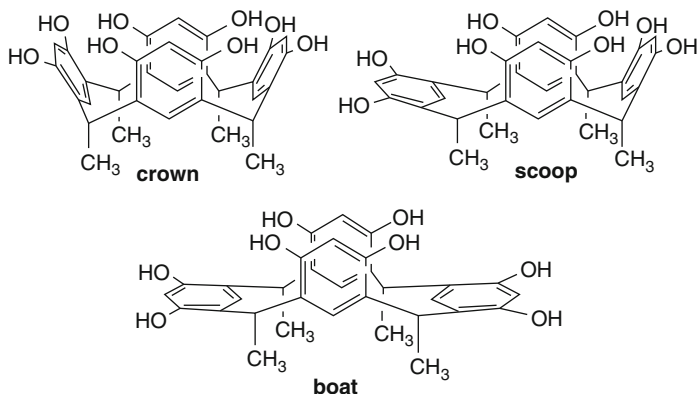
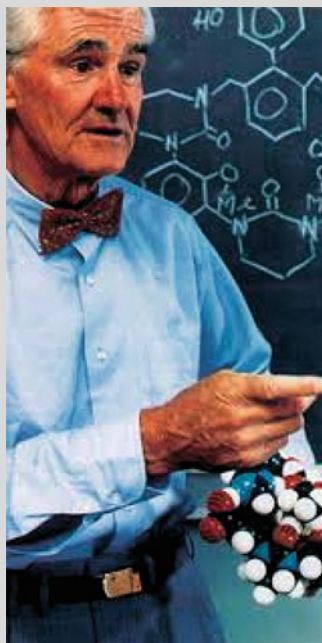


**Fig. 1.6** Representative examples of conformations of calix[4]recorcinarenes

relative configuration of the substituents at the methylene bridges can be ccc, cct, ctt, and tct and the substituents can be axial or equatorial. However, in practice only a few isomers have been isolated [21]. Representative examples are given in Fig. 1.6.

In general an efficient synthesis of the vase-like molecules from simple building blocks results in highly symmetrical molecules with a high degree of functional degeneracy. In order to convert them in useful, selectively functionalized building blocks, their symmetry will have to be broken in a selective way. In this respect the calix[4]arenes are unique because they have been functionalized selectively, mainly by alkylation of the lower rim phenolic hydroxyl groups, or selective dealkylation of the *para*-alkyl groups. This ability to modify the chemistry at both rims render them useful building blocks for incorporation in complex chemical structures. Other calixarenes are more difficult to functionalize, although calix[6]arene has been selectively alkylated in the 1,3,5-positions [22]. Functionalization of calix[4]recorcinarenes starts with the selective electrophilic substitution, like bromination, at the four positions in between the hydroxyl groups [23]. Subsequent bridging with bromochloromethane gives the cavitands, highly rigid molecules that have a crown-like conformation with a  $C_{4v}$  symmetry. This bridging can also be partly to give useful building blocks for further synthesis (vide infra). This chemistry has been extensively developed by Donald Cram for their use in the synthesis of (hemi)carcerands and cavitands. This field is described in detail by Bruce Gibbs in Chap. 9.



*My first meeting with Don Cram was at a conference in Louvain-la Neuve, organized by Leon Ghoseh and Gunther Viehe in the early 1970s. He gave a very inspiring talk, perhaps one of his first on host-guest chemistry. At the diner he played his guitar and sang country and western songs. He accepted to come to visit my labs at Shell and the University of Twente. For me Don became a great source of inspiration and scientific mentor. Many times I visited and lectured at UCLA and at his marvelous home in the canyons we could play with CPK models till late at night. The Nobel Prize in 1987 was not only a personal recognition but was felt also as a recognition for a new field of host-guest chemistry and chemistry beyond the molecule. Cram's contributions are many, but in the framework of this book it is his extensive use of recorcinarenes as the building blocks for molecular containers in which small guestmolecules can be incarcerated.*

As mentioned above rigid vase-like molecules are interesting because of their rigid 3-D structure that defines precisely the space inside the cavity. The cavity of the cone of calix[4]arene is small but it can be enlarged by the covalent combination with other components that deepen or close the cavity. In this ways compartments are formed in which guest species can be confined. The calix–crown ether combinations [24] can complex potassium or cesium ions with remarkable selectivities. Combined with terphenyls, 1,3-dialkylcalix[4]arenes give the calixspherands that can complex alkali cations with very high kinetic stability [25]. Combination of

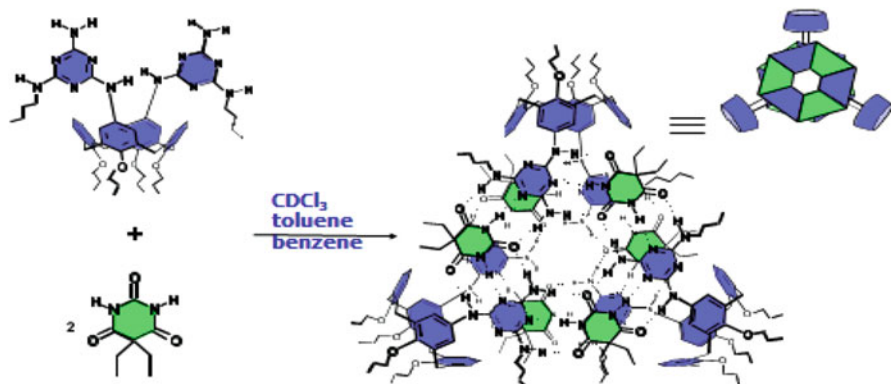


**Fig. 1.7** Assembly of calixarenes and barbiturates via H-bonding

calix[4]arene with the recorcinarenes building block resulted in both the 1:1 and 2:2 product, respectively. The latter is a molecule that has a rigid cavity in which solvent molecules are complexed. In the cavity of the first a solvent molecule is incarcerated during the synthesis [26].

Not only the covalent combination of calixarenes with other building blocks leads to products with precisely defined molecular cavities. Julius Rebek and his group at Scripps were the first to explore the non-covalent assembly of calix[4]arenes to dimeric capsules in which small guest molecules can be complexed [27]. Together with the group of Volker Böhmer they have explored this self-assembly in great detail [28]. This chemistry is described by Aragay and Ballester in Chap. 32.

In another strategy aimed at the self-assembly of calixarenes in noncovalent capsules that can complex larger guests, our group at Twente has used the so-called rosette motif that was originally introduced by George Whitesides. By decorating (poly) calix[4]arenes with melamine residues and addition of complementary barbiturates or cyanurates, large H-bonded assemblies with high kinetic stabilities were formed quantitatively [29] (Fig. 1.7). In the inner space of these assemblies discrete trimers of alizarins could be encapsulated [30]. Hexameric complexes of calix[4]resorcinarenes and their (molecular recognition) properties are dealt with by Cohen et al. in Chap. 31.

Another way to assemble calixarenes into defined capsules that have well-defined intramolecular space, is via ionic interactions [31].

Calixarenes have used for many different purposes that are the subject of several of the following chapters of this book. The original motivation of David Gutsche for developing the calixarene chemistry was their use as a concave platform for aldolase mimics and this idea has also been explored extensively by others. Part of this chemistry is described by Casnati et al. in Chap. 26 and by Yilmaz in Chap. 27.

Application areas where calixarenes have had a large impact are sensing and membrane separation technologies, and materials chemistry.

## References

1. Villiers, A. *Compt. Rend.* **1891**, *112*, 536–238; Szejli, J. *Chem. Rev.* **1998**, *98*, 1743–1753.
2. Schardinger, F. Z. *Untersuch. Nahr. U. Genussm.* **1903**, *6*, 865.
3. Freudenberg, K.; Rapp, W. *Ber. Dtsch. Chem. Ges.* **1936**, *69*, 2041–2045.
4. Hybl, A.; Rundle, R. E.; Williams, D. E. *J. Am. Chem. Soc.* **1965**, *87*, 2779–2788.
5. Behrend, R.; Meyer, E.; Rusche, F. *Liebigs Ann. Chem.* **1905**, *339*, 1–37.
6. Freeman, W. A.; Mock, W. L.; Shi, N.-Y. *J. Am. Chem. Soc.* **1981**, *103*, 7367–7368; Mock, W. L.; Shih, N.-Y. *J. Org. Chem.* **1983**, *48*, 3618–19.
7. Assaf, K. I.; Nau, W. M. *Chem. Soc. Rev.* **2015**, *44*, 394–418.
8. Gutsche, C. D. *Calixarenes: An Introduction*; Royal Society of Chemistry: Cambridge U.K., 2008.
9. Niederl, J. B.; Vogel, H. J. *J. Am. Chem. Soc.* **1940**, *62*, 2512–2514.
10. Erdtman, H.; Högborg, S.; Abrahamsson, S.; Nilsson, B. *Tetrahedron Lett.* **1968**, *14*, 1679–1682.
11. Zinke, A.; Ziegler, E. *Ber. Dtsch. Chem. Ges.* **1944**, *77*, 264–272
12. Cornforth, J. W.; D'Arcy, P.; Nicholls, G. A.; Rees, R. J. W.; Stock, J. A. *Br. J. Pharmacol.*, **1955**, *10*, 73–86.
13. Andreetti, G. D.; Ungaro, R.; Pochini, A. *J. Chem. Soc. Chem. Comm.* **1979**, 1005–1007.
14. Hayes, B. T.; Hunter, R. F. *J. Appl. Chem.*, **1958**, *8*, 743–748. P. Timmerman, W. Verboom, and D. N. Reinhoudt *Tetrahedron* **1996**, *52*, 2663–2704.
15. Vicens, J.; Böhmer, V., in *Calixarenes: a versatile class of macrocyclic compounds in Topics in Inclusion Science*; David, J. E. D., Ed.; Acad. Publ., Kluwer 1990.
16. *Ref 14*, P28.
17. Kämmerer, H.; Happel, G.; Caesar, F. *Makromol. Chem.* **1972**, *162*, 179–197.
18. *Ref 17*, p 39–45.
19. Happel, G.; Mathiasch, B.; Kämmerer, H. *Makromol. Chem.* **1975**, *176*, 3317–3334.
20. Gutsche, C. D.; Gutsche, A. E.; Karaulov, A. I. *J. Inclusion Phenom.* **1985**, *3*, 447–451.
21. Cram, D. J.; Cram, J. M. *Container Molecules and Their Guests*; Royal Society of Chemistry: Cambridge, 1994.
22. Janssen, R. G.; Verboom, W.; Reinhoudt, D. N.; Casnati, A.; Freriks, M.; Pochini, A.; Ugozzoli, F.; Ungaro, R.; M. Nieto, P.; Carramolino, M.; Cuevas, F.; Prados, P.; de Mendoza, J. *Synthesis* **1993**, 380–386.
23. Cram, D. J.; Karch, S.; Kim, H.-E.; Knobler, C. B.; Maverick, E. F.; Ericson, J. L.; Helgeson, R. C. *J. Am. Chem. Soc.* **1988**, *110*, 2229–2237.
24. Ghidini, E.; Ugozzoli, F.; Ungaro, R.; Harkema, S.; A. Abu El-Fadl, Reinhoudt, D. N. *J. Am. Chem. Soc.* **1990**, *112*, 6979–6985.
25. Reinhoudt, D.N.; Dijkstra, P. J.; in'tVeld, P. J. A.; Bugge, K. E.; Harkema, S.; Ungaro, R.; Ghidini, E. *J. Am. Chem. Soc.* **1987**, *109*, 4761–4762.
26. Timmerman, P.; Verboom, W.; van Veggel, F. C. J. M.; van Duynhoven, J. P. M.; Reinhoudt, D. N. *Angew. Chem. Int. Ed. Engl.* **1994**, *33*, 2345–2348; Timmerman, P.; Verboom, W.; F.C.J. M., van Veggel; van Hoorn, W.P. ; Reinhoudt, D. N. *Angew. Chem. Int. Ed. Engl.* **1994**, *33*, 1292–1295.
27. Shimizu, K. D.; Rebek, J. Jr *Proc. Natl. Acad. Sci. U. S. A.* **1995**, *92*, 12403–12407.
28. Mogck, O.; Böhmer, V.; Vogt, W. *Tetrahedron* **1996**, *52*, 8489–8496.
29. Prins, L. J.; Timmerman, P.; Reinhoudt, D. N. *Angew. Chem. Int. Ed. Engl.* **2001**, *40*, 2382–2426.
30. Kerckhoffs, J. M. C. A.; van Leeuwen, F.W.B.; Spek, A. L.; Kooijman, H.; Crego Calama, M.; Reinhoudt, D. N. *Angew. Chem. Int. Ed. Engl.* **2003**, *42*, 5717–5722.
31. Corbilingi, F.; Fiammengo, R.; Timmerman, P.; Crego Calama, M.; Versluis, K. Heck, A. J. R.; Luyten, I.; Reinhoudt, D. N. *J. Am. Chem. Soc.* **2002**, *124*, 6569–6575.

# Chapter 2

## Chiral Calixarenes and Resorcinarenes

Michał Wierzbicki, Hanna Jędrzejewska, and Agnieszka Szumna

### 2.1 Introduction

Differentiation between enantiomers is the immanent feature of biological receptors, most frequently achieved by surrounding of a guest molecule within a well-organized chiral binding site. Calixarenes, the *meta*-substituted cyclophanes (including also resorcinarenes, oxacalixarenes and homocalixarenes), have well-defined, modifiable hydrophobic cavities, that appear to be ideal platforms for the elaboration of artificial receptors. Therefore, the natural consequence of initial studies on host-guest interactions of achiral calixarenes was synthesis and complexation studies of chiral calixarenes. Since the earliest synthesis of chiral calixarene reported by Gutsche in 1979 [1] the field has expanded enormously and evolved in diverse directions. Effective chiral receptors based on calixarenes contributed to a better understanding of biological systems, have found applications in recognition of chiral guests in solution, as chromatography stationary phases, [2, 3] enantioselective membrane carriers [4, 5] and as catalysts [6]. Their potential has also been demonstrated in interactions with biological molecules, [7, 8] protein recognition, [9, 10] formation of gels [11] and antimicrobial activity [12]. A new direction that arose as a result of simultaneous development of nanotechnology and synthetic methodology involves application of chiral calixarenes as building blocks for construction of nanoscale based objects.

The variety of types of chiral calixarenes is exceptionally broad. We will discuss here the main strategies for obtaining chiral calixarenes involving classic approach via attachment of auxiliary/ies with stereogenic centers. We will also focus on

---

M. Wierzbicki • H. Jędrzejewska • A. Szumna (✉)  
Institute of Organic Chemistry, Polish Academy of Sciences, Kasprzaka 44/52, 01-224  
Warsaw, Poland  
e-mail: [michal.wierzbicki@icho.edu.pl](mailto:michal.wierzbicki@icho.edu.pl); [hanna.jedrzejewska@icho.edu.pl](mailto:hanna.jedrzejewska@icho.edu.pl);  
[agnieszka.szumna@icho.edu.pl](mailto:agnieszka.szumna@icho.edu.pl)

unique features of calixarenes that enable formation of chiral structures in a non-classic way – through generation of inherent chirality and supramolecular chirality. Many additional examples of chiral calixarenes, particularly peptidocalixarenes and glycolcalixarenes can be also found in other chapters of this book.

## 2.2 Chiral Substituents

Attachment of chiral substituents to calixarene skeleton is the first, the most straightforward and still the most popular way to construct chiral calixarenes. In 1979 Gutsche reported the synthesis of the first chiral calixarene by attaching camphorosulfonyl group to *p*-*t*Bu-calix[8]arene [1]. Nowadays, attachment of virtually any chiral moiety at the selected position is synthetically feasible. However, some chiral groups, due to their availability and versatility, have been particularly widely exploited, for example amino acid derivatives, peptides, carbohydrates, chiral amines and axially chiral groups.

### 2.2.1 Amino Acid Derivatives and Peptides

Utilization of amino acids and peptides as chiral modifiers of calixarenes has many advantages: amino acids and peptides are biocompatible, they are natural and versatile sources of chirality and their derivatives are easily available. Additionally, amino acids and peptides have rich chemistry of non-covalent interactions (mostly hydrogen bonds, both in their backbones and side chains) and considerable conformational flexibility. Therefore, they can assist in the recognition processes by forming numerous attractive forces and by adaptation of a binding site by an induced-fit mechanism. On the other hand, the same features that constitute the strength of peptidocalixarenes, render such hosts extremely difficult to design. The non-covalent interactions often form intramolecularly and engage potential binding sites precluding effective guest complexation. When the non-covalent interactions form intermolecularly, they may cause non-specific aggregation that considerably reduces solubility. However, when properly designed, peptidocalixarenes form well-defined molecular cavitands and capsules that exhibit interesting complexation properties.

#### 2.2.1.1 Cavitands and Semi-Open Structures

The direct connection of an amino acid or a peptide to a calixarene scaffold at the upper rim requires the presence of an acid or an amino functionality in a calixarene. Such an approach has been widely studied in the group of Ungaro (for review see ref. [13]). For example, calix[4]arene di- or tetracarboxylic acids have been used to

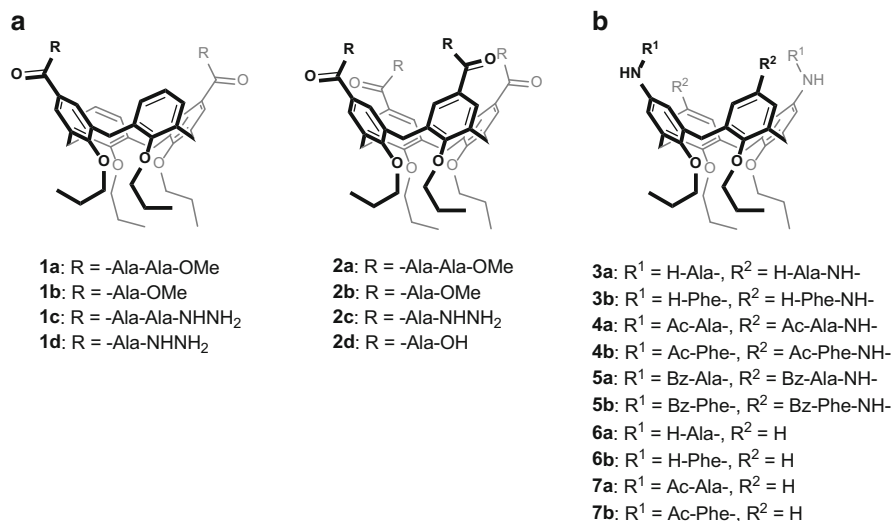


**Fig. 2.1** Peptidocalixarenes: calixarenes modified at upper rims with peptides connected through: (a) the *N*-terminus; (b) the *C*-terminus

connect peptides through their *N*-termini forming *N*-peptidocalixarenes **1a–2d** (Fig. 2.1) [14]. Hydrazides **1c** and **1d** exhibited moderate binding properties towards short peptides, lauric acid and its derivatives and receptor **2b** towards ammonium salts. *C*-Peptidocalixarenes (with peptides connected via *C*-termini), for example **3a–7b**, on the contrary to *N*-peptidocalixarenes, display a pronounced tendency to aggregate and form self-complementary interactions [15]. Such tendency has a profound effect on recognition properties. For example, for the interaction of host **6a** with carboxylate anions a higher  $K_a$  was observed in DMSO (more polar solvent) than in  $CDCl_3$  (less polar solvent) although both are very low. It was attributed to the formation of intramolecular hydrogen bonds in a less polar solvent ( $CDCl_3$ ) that engaged binding sites that consequently hampered guest complexation.

A unique example of a chiral calix[4]arene functionalized at the upper rim with an amino acid is the aminophosphonic acid derivative **8** (Fig. 2.2). Its synthesis using Pudovik-type addition was reported recently by the group of Kalchenko [16]. The synthesis of **8** is a very rare example that utilizes diastereoselective pathways to achieve chiral calixarenes. In most cases chiral groups are simply attached to the macrocyclic ring. Here, the stereogenic centers were introduced on an imine-calixarene scaffold using a chiral auxiliary strategy.

Resorcin[4]arenes, the resorcinol analogs of calix[4]arenes (also called calix[4]resorcinols), were also modified at their upper rims with amino acids or peptides at two possible positions: either at oxygen atoms or at the *ortho* positions. Resorcinarenes substituted with amino acid amides at oxygen atoms have found applications as chiral stationary phases (CSP) in capillary gas chromatography [17]. In particular, exhaustive *O*-alkylation of resorcin[4]arene using L-valine



**Fig. 2.2** Chiral aminophosphonic acid derivative of calix[4]arene

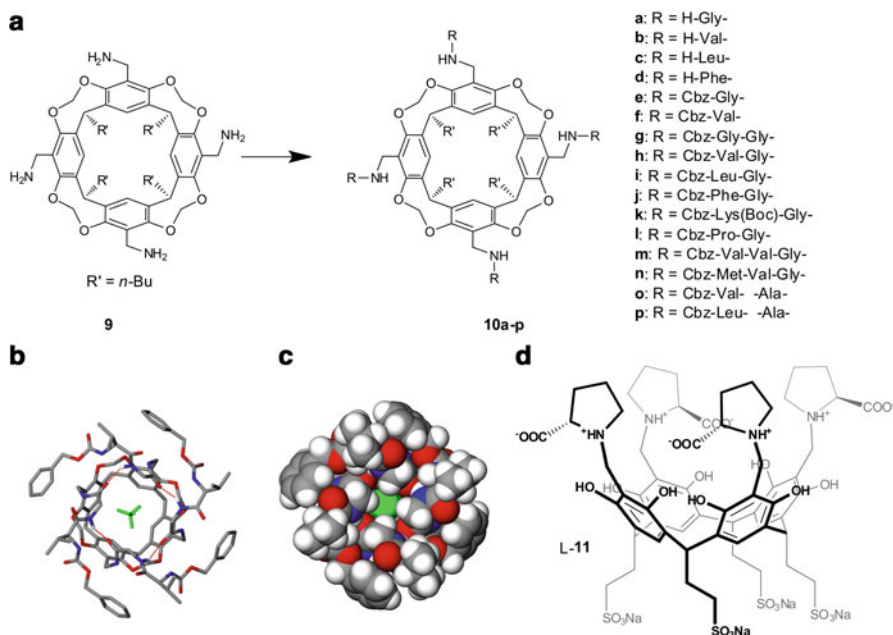
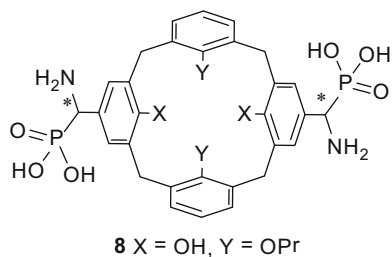


**Fig. 2.3** (a, d) Resorcinarenes with amino acids and peptides attached at the upper rims; (b, c) suggested molecular structure of cavitant **10h** with complexed acetonitrile molecule (Based on NOE and molecular modeling, courtesy of prof. M. Feigl)

derivative and subsequent chemical bonding to a poly(hydro)dimethylsiloxane gave a chiral stationary phase, named Chirasil-Calix, having good thermal and long-term stability. The central *ortho* position of the resorcinol ring has also been used to attach peptides either using their *C*- or *N*-termini (Fig. 2.3). Simple amino acids, like proline [18] and variously substituted hydroxyprolines [19] were attached to resorcin[4]arenes using single step Mannich reaction to obtain water soluble chiral resorcin[4]arenes, for example **L-11**. Such derivatives were successfully used as NMR chiral resolving agents for chiral substrates possessing pyridyl, phenyl, and bicyclic aromatic rings in their structures. Peptidoresorcin[4]arenes **10g-l** were obtained by attachment of peptides through their *C*-termini to

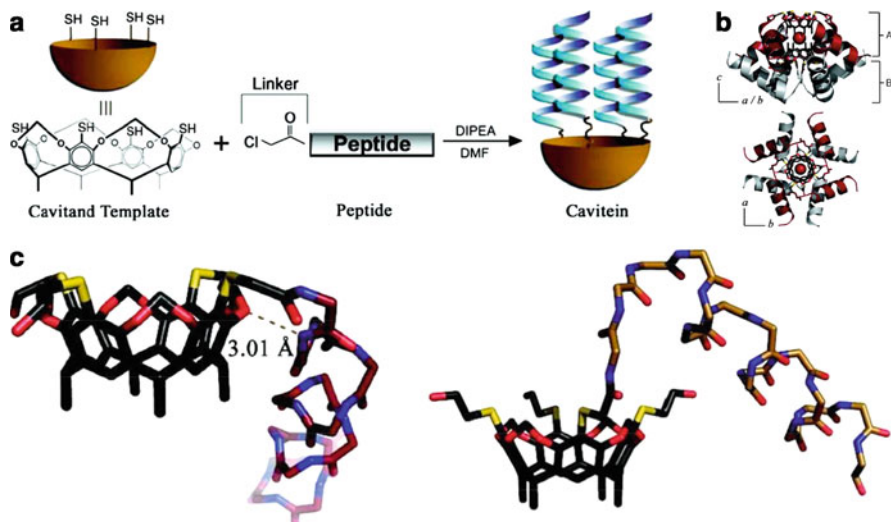


**Fig. 2.4** (a) Design of caviteins – helical bundles of proteins above the cavitand; (b) the X-ray structure of cavitein with helices containing 16 amino acid residues; (c) *side* view showing position of a helix in respect to the cavitand (the remaining three of the helices were removed for clarity) (Reprinted with permission from [22]. Copyright 2009 American Chemical Society)

aminomethylated cavitand **9** using classical peptide chemistry (Fig. 2.3a) [20]. Such derivatives form complexes with acetonitrile molecules which are kinetically stable on the NMR timescale. Based on molecular modeling and NOE experiments, the authors suggest that the cavitands are closed at their upper parts by hydrogen bonds that restrict guest's release (Fig. 2.3b, c). Much longer amino acid sequences (up to 16 amino acid residues) attached to resorcinarenes were tested in the group of Sherman. The authors envisioned such peptidoresorcinarenes as a new family of *de novo* proteins called *caviteins* (from the combination of cavitand + protein, Fig. 2.4) [21]. Resorcin[4]arenes were expected to act as rigid organic scaffolds to organize peptide helical bundles or form  $\beta$ -sheets. However, for structures based on thioether linker and sequences promoting formation of  $\alpha$ -helices such organization was not achieved. X-ray structure of a cavitein containing 16 amino acid residues at each arm shows the peptides wrapping independently downward around the cavitand bowl (Fig. 2.4b) [22].

Another approach to functionalize calixarenes and resorcinarenes with peptides consists in modification of lower rims. Such a modification requires introduction of all potential binding sites within substituents since derivatives do not take advantage of the inclusion properties of the calixarene hydrophobic cavity. Additionally, the lower rim is much more narrow than the upper rim, and, therefore peptides are arranged in close proximity. As a consequence, it is difficult to avoid adverse intramolecular non-covalent interactions. In fact, derivatives **12** and **13** exhibit

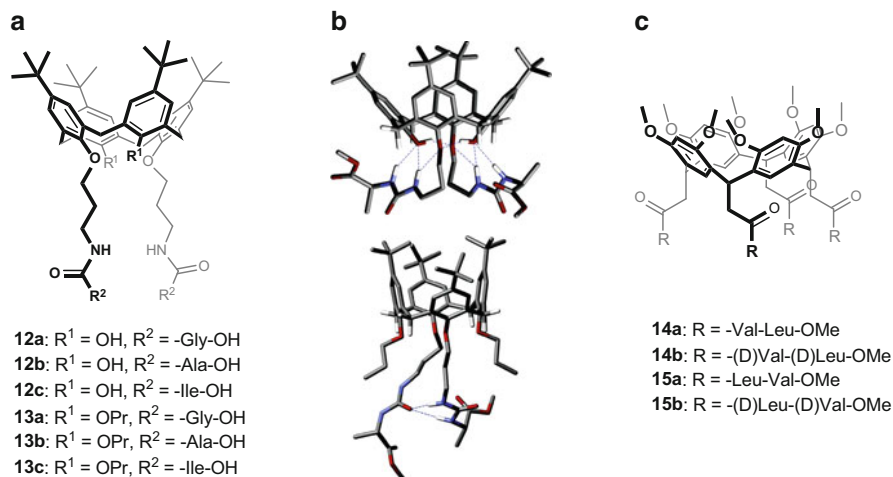


**Fig. 2.5** (a, c) Peptidocalixarenes and peptidoresorcinarenes with peptides connected at the lower rim; (b) lowest energy conformations for **12b** and **13b** (Reprinted with permission from [23]. Copyright 2009 American Chemical Society)

intramolecular hydrogen bonding (Fig. 2.5) [23]. Therefore, **12** and **13** display only weak complexing properties towards anions of *N*-acetylated amino acids in CDCl<sub>3</sub>, and again the  $K_a$  values were higher in a more polar solvent, which is a characteristic feature of breaking of the intramolecular hydrogen bonding system during complexation. Even though the association constants were not high, the host was able to recognize enantiomers of selected *N*-acetylated amino acids (max.  $K_a(D)/K_a(L) = 4.1$  for **13b**). Resorcinarenes functionalized at their lower rim by amino acid derivatives were studied for their enantioselective guest binding both in solution [24] and in the gas phase (Fig. 2.5c) [25, 26]. Octamethyl resorcin[4]arene tetrafunctionalized at the lower rim with valyl-leucine and leucyl-valine methyl esters (**14** and **15** respectively) are capable of recognizing some dipeptides as guests, both in solution and in the gas phase. Association constants of 2030 and 186 M<sup>-1</sup> (CDCl<sub>3</sub>) were found for interaction of **14a** with trifluoroacetates of L-Val-L-LeuOMe and D-Val-D-LeuOMe respectively, indicating a substantial chiral recognition (one order of magnitude).

### 2.2.1.2 Capsules

Many examples of peptidocalixarenes and peptidoresorcinarenes show a natural tendency of peptidic backbones to form arrays of self-complementary hydrogen bonds that is often perceived as a disadvantage in construction of chiral receptors. However, such arrays, when rationally optimized, can be of great significance for formation of supramolecular aggregates of finite or infinite sizes. For example, calix[4]arenes **16-25** with two peptides mounted on the same scaffold using

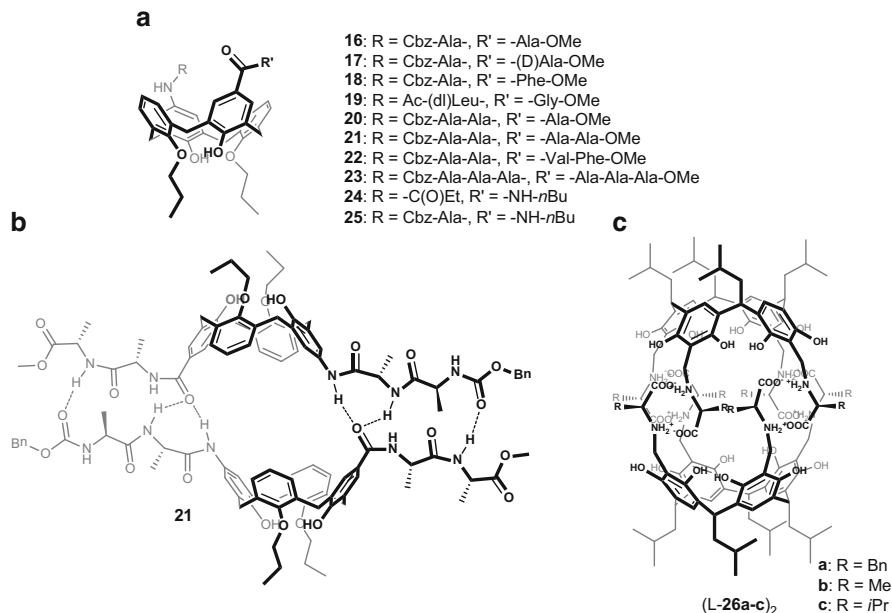


**Fig. 2.6** Examples of peptidocalixarenes forming capsules

respectively *N*-terminus and *C*-terminus are able to dimerize by formation of an antiparallel  $\beta$ -sheet structure (for **21–23**  $K_{\text{dim}} = 70\text{--}950 \text{ M}^{-1}$  in  $\text{CDCl}_3$ , Fig. 2.6b) [27]. Another example is the dimeric capsule (L-26a)<sub>2</sub> that is made of simple amino acids connected using the Mannich reaction to the resorcin[4]arene scaffold [28]. Capsule (L-26a)<sub>2</sub> utilizes self-complementarity of ionic hydrogen bonds between amine and carboxylate groups. Hydrophobic side chains of amino acids (e.g., of alanine or phenylalanine) are positioned at the outer surface of the capsule that renders the capsule hydrophobic. In hydrophobic environment, the ionic hydrogen bonds are strong and therefore the capsule is highly stable. Therefore, L-26a dimerizes quantitatively already in the reaction mixture and is isolated solely as a dimer (L-26a)<sub>2</sub>. Capsular dimers (L-26a)<sub>2</sub> and (L-26b)<sub>2</sub> have two unique features: they are chiral and have all polar groups gathered in their interiors, which makes them very efficient in chiral recognition of small polar molecules [29, 30]. Chirality plays a crucial role in the recognition properties and also in the self-assembly process. For phenylalanine derivatives capsules made of two hemispheres having different chirality, i.e. (L-26a)(D-26a), are considerably more stable than capsules with two hemispheres of the same chirality, i.e. (L-26a)<sub>2</sub>. However, for valine derivatives, due to the close proximity of branched side chains, homochiral capsules (L-26c)<sub>2</sub> are not formed at all, while heterochiral capsules (L-26c)(D-26c) are easily formed [31]. It has far-reaching consequences, requiring a “mutualistic approach” to the synthesis. The hemispheres, L-26c or D-26c, being constituents of the heterochiral capsules, cannot be simply obtained by chemical

synthesis as pure substances (due to formation of many products as a result of subsequent Mannich reactions). However, when both enantiomers are present at the final stages of the reaction, the mixture equilibrates, the side products are eliminated and the heterochiral capsule (L-**26c**)(D-**26c**) is amplified. These results show that even though none of the enantiomeric hemispheres can be obtained separately, it is still possible to obtain a hybrid capsule due to the mutual benefits originating from self-assembly. However, since the initial stages of the reaction are irreversible under the applied conditions, the system requires pre-equilibration of the two enantiomeric hemispheres separately prior to the mixing. Therefore, even though “mutualistic approach” facilitates effective synthesis of hybrid capsules, a full self-sorting process, i.e. amplification of selected capsules from initial mixture of many components, is not possible using the Mannich reaction.

The possibility of chiral self-sorting driven by self-assembly and chirality was further developed by means of dynamic covalent chemistry, i.e. by utilizing of reversible chemical reactions. Tetraformylresorcin[4]arene was used as a macrocyclic scaffold and peptides were attached by the imine formation reaction (Fig. 2.7a) [32]. Depending on the peptide length, either homochiral or heterochiral self-assembled dimeric capsules were formed in a highly regioselective and diastereoselective way (for discussion of inherent chirality of such capsules see page 28). When peptides having different length or different chirality were mixed and used in the reaction with tetraformylresorcin[4]arene, high fidelity self-sorting was observed. Only capsules consisting of peptides of the same length and proper chirality (homochiral for di- and tetrapeptides and heterochiral for mono- and tripeptides) were exclusively formed. These results point at the crucial role of chirality and efficient self-assembly for amplification of chiral peptide capsules and show that a dynamic approach can be effective in formation of even large peptidic capsules (Fig. 2.7c). However, imine linkers were kinetically labile and prone to hydrolysis, which hampered further applications. Therefore, more stable acylhydrazone linkers were also tested [33]. When tetraformylresorcin[4]arene reacted with peptide hydrazides, self-assembled chiral capsules (L-**31a**)<sub>2</sub> – (L-**32b**)<sub>2</sub> were also formed (Fig. 2.7b), which indeed proved to be kinetically more stable. It should be noted that for acylhydrazone capsules the peptides were attached using their C-termini, which results in different binding motifs and different geometries than for the imine capsules with peptides connected using N-termini. However, for acylhydrazone capsules efficient chiral self-sorting was also observed, always preferring, independently of the peptide length, the homochiral arrangement (Fig. 2.7d). The acylhydrazone capsules are able to complex large spherical guests, for example fullerenes. However, the complexation process is hedged by a high kinetic barrier. Therefore, complexation of fullerenes can only be realized at the step of capsule formation (during chemical reaction) or, by pushing fullerenes into capsules by mechanochemical methods. Interestingly, the chiral cavity has a profound effect on the <sup>13</sup>C NMR spectrum of fullerene C<sub>70</sub>. Enantiotopic carbon atoms became diastereotopic in the chiral environment and therefore exhibited different chemical shifts.

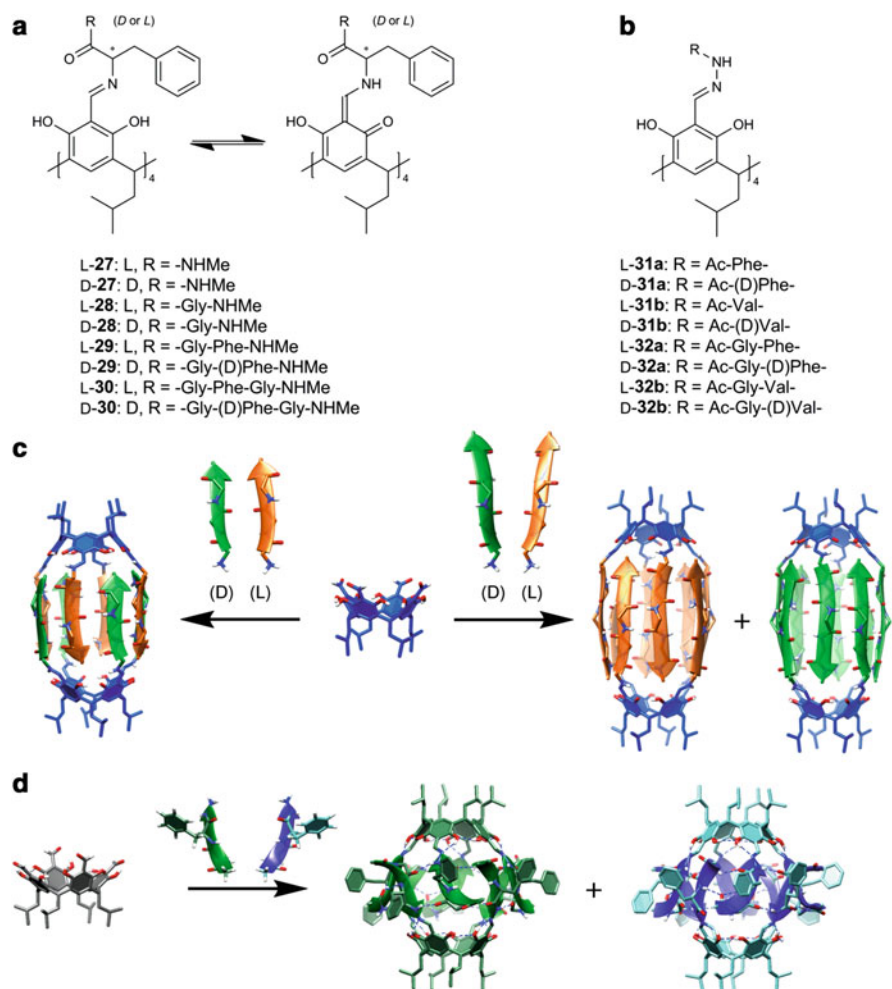


**Fig. 2.7** Resorcinarene-peptide capsules based on (a) imine linkers and (b) acylhydrazones. Formation of self-assembled capsules by chiral self-sorting: (c) imine derivatives **27–30**; (d) acylhydrazone derivatives **31–32**

### 2.2.2 Carbohydrates

Carbohydrates, similarly to peptides, are natural sources of chirality and also offer a wide range of non-covalent interactions. Molecular recognition of carbohydrates by biological receptors mediates a variety of physiologically relevant processes, including recruitment of leucocytes to inflammatory sites, clearance of glycoproteins from the circulatory system, cell interactions in the immune system, as well as adhesion of bacteria or viruses to host cells. It has been shown that multivalency is especially important for carbohydrate–receptor interactions. The glycoside cluster

effect, a special case of multivalency involving carbohydrates, is a powerful tool exploited by Nature to make relatively weak interactions stronger and more specific.

Calixarenes, as multiple-site macrocycles, are ideal scaffolds for the construction of multivalent glycosylated ligands. The class of calixarenes bearing at least one carbohydrate unit appended to their structure has been named as glyco-calixarenes. Currently, there are many examples of glyco-calixarenes starting from relatively simple calixarenes and resorcinarenes modified by mono or polysaccharides at the upper or lower rim up to dendrimer-type of structures (Fig. 2.8, for review see ref. [34, 35]). Although glyco-calixarenes are intrinsically chiral, they have rarely been studied for typical chiral recognition [36]. A vast majority of them was tested for interactions with biological targets which, as a rule, also involve chiral interactions. Most of the biological properties reported for glyco-calixarenes are related to their binding abilities to lectins (carbohydrate-binding proteins). As it was sought, in many cases sugar affinity for lectin is significantly increased for glyco-calixarenes compared to monovalent saccharides. Selective interactions with specific lectins, e. g. *Pseudomonas aeruginosa* Lectin A with **34**, may lead to inhibition of infectious bacterium cell growth [37]. In combination with protein binding, glyco-calixarenes can carry out other tasks, potentially useful in medicine, mainly drug delivery (Fig. 2.9). Examples include the saccharide-selective delivery of fluorescent Calcein to liver cells by **35**, [38] delivery of bisphosphonates by **36** (relevant in osteoporosis and Paget's disease), [39] or anticancer vaccine candidate [40]. The multivalency of glyco-calixarenes can be further increased by their tendency to aggregate due to the simultaneous presence of hydrophilic saccharide units close to the highly hydrophobic calixarene scaffold. When properly loaded with cargo, these aggregates can be exploited as site-specific drug delivery systems, because they are able to interact with lectins [41] or for targeted gene-delivery since they can form clusters around the plasmid DNA (glycoresorcinarene **35**) [42].

### 2.2.3 Amines and Derivatives

Chiral amines have found many applications as reagents for resolving racemic compounds, as ligands in asymmetric synthesis and as drug candidates. Many of them are easily available because they are natural products, for example those originating from the alkaloid family. The main purpose of calixarenes modified with chiral amines and their derivatives (mostly amides and metal complexes) is resolution of chiral acidic species and asymmetric catalysis (Fig. 2.10). For example, calixarenes **37a** and **37b**, bearing optically pure amino alcohol groups at their lower rims, exhibit efficient chiral recognition ability towards  $\alpha$ -hydroxyacids ( $K_a(S)/K_a(R)$  up to 28 for **37a**) [43]. Even higher values for chiral recognition of mandelic acid were obtained for a calixarene bridged at the lower rim with chiral amino alcohol ( $K_a(S)/K_a(R) = 102$ ) [44]. Cinchona alkaloid derivative **38** was used



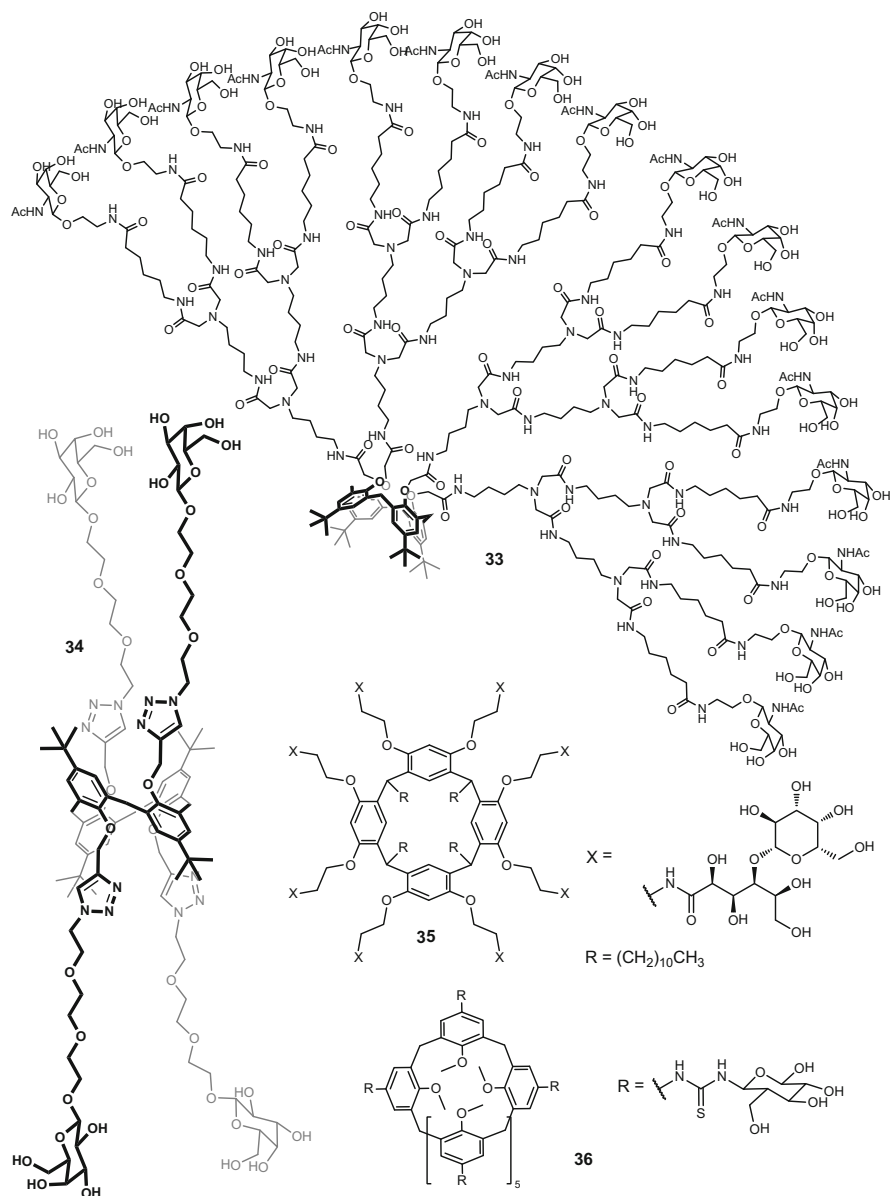


**Fig. 2.8** Examples of glycolcalixarenes

as a chiral phase-transfer catalyst in alkylation of glycine derivatives with benzyl bromide with moderate efficiency (up to 57% *ee*) [45].

Chiral amines were also attached to higher calix[n]arenes ( $n > 4$ ) providing larger and more flexible cavities for complexation. For example, calix[6]arenes



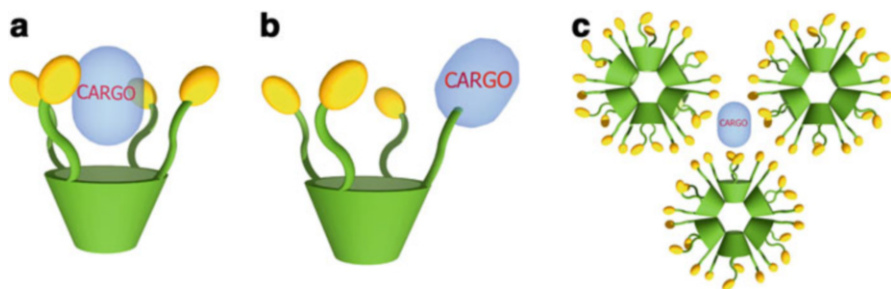


**Fig. 2.9** Different strategies for drug delivery using glycolcalixarene vectors: (a) noncovalent encapsulation in the cavity; (b) covalent attachment and (c) noncovalent encapsulation in a self-assembled cluster

were bridged at their lower rims with chiral cyclic or acyclic amine linkages (**40**) [46]. Complexation of chiral guests lead to the formation of diastereomeric *endo*-complexes at 2:1 ratio for ( $\pm$ )-4-methylimidazolidin-2-one and 6:4 ratio for ( $\pm$ )-propane-1,2-diol [47].

Although amines themselves exhibit catalytic activity, many of them were further transformed into chiral metal complexes (Fig. 2.10). For example, chiral bimetallic cobalt-salen-calixarene **41** was prepared and tested in the hydrolytic kinetic resolution of racemic epoxides [48]. Kinetic studies revealed that the two catalytic units on the upper rim are able to activate the reactants in a cooperative and primarily intramolecular mode. Higher stability was found for the bimetallic catalyst as compared to a monometallic reference complex and high enantioselectivity for kinetic resolution of epoxides was observed. However, the real benefit from applying a calixarene scaffold is difficult to assess since the monomeric catalyst was already similarly effective in the reaction under consideration. Another salen-calixarene **42** with a combined chirality coming from stereogenic centers and inherent chirality of a *meta*-substituted ring and containing monometallic Mn = O active site, was applied in an epoxidation reaction of model alkenes and showed moderate *ee* values (up to 72 %) [49].

Interestingly, interactions between chiral amines and acid components can be transformed into macroscopic properties. For example, chiral amine **39a** (Figs. 2.10 and 2.11) upon interaction with L- or D-tartaric acid self-assembles into nanofibers leading to gel formation [11]. Fibrous assemblies of **39a**-D-tartaric acid are less stable than **39a**-L-tartaric acid due to the unmatched interaction between the chiral centers. To minimize unfavorable interactions they form nano-vesicles. The macroscopic result of this phenomenon was the difference in sol-gel behavior of two diastereomeric salts. This unusual heat-set behavior of **39a**-D-tartaric acid system was explained by lowering unfavorable interactions as the temperature increases that allowed for formation of the nanofibers.

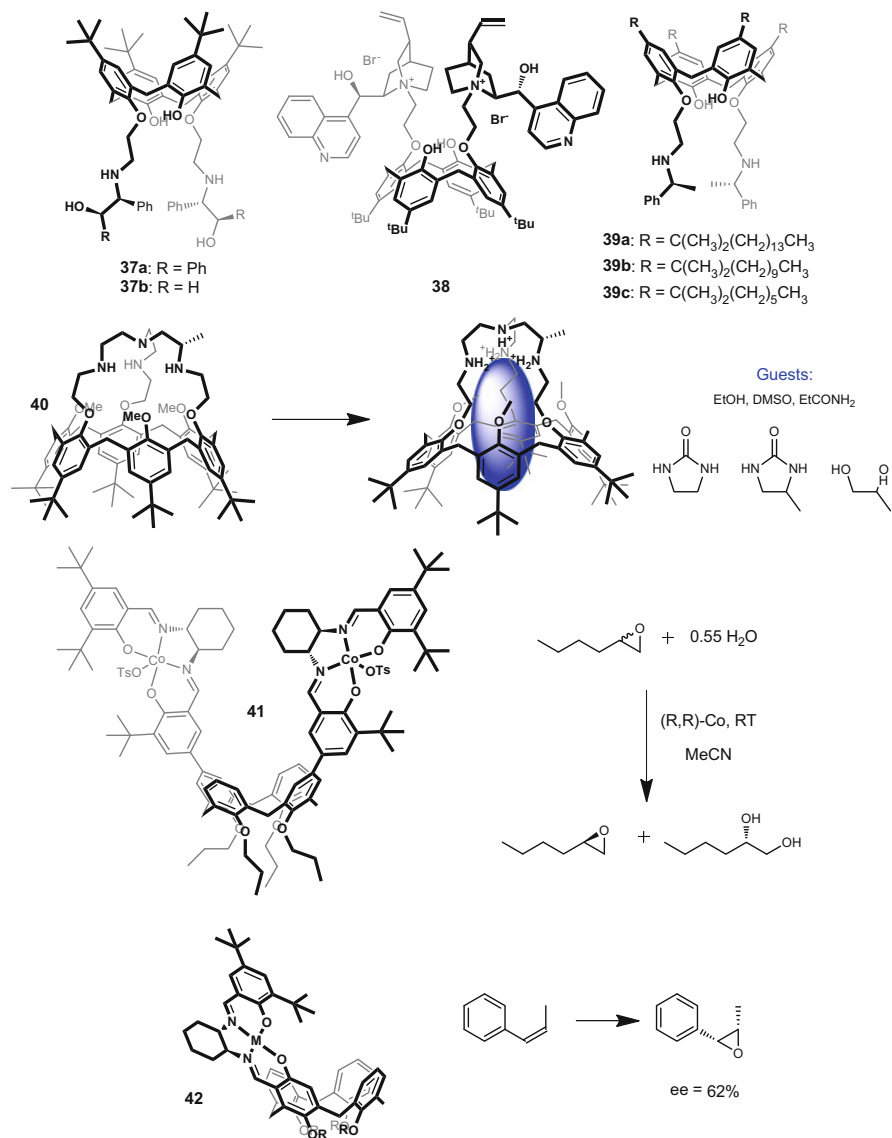
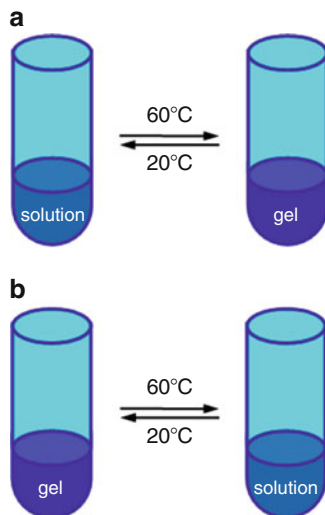


Fig. 2.10 Examples of calixarenes modified with chiral amines and their metal complexes

## 2.2.4 Groups with Axial Chirality

Many axially chiral compounds are “Privileged Chiral Ligands”. It means that it is highly probable that their application will lead to high enantioselectivity and/or activity of the resulting chiral catalysts. It is no wonder that many efforts have been made in order to attach axially chiral substituents, for example easily available

**Fig. 2.11** Formation of heat-set gels for salts of **39a** with: (a) L-tartaric acid and (b) D-tartaric acid



BINOL, to the calixarene scaffold (Fig. 2.12) [50, 51]. Most of the obtained derivatives, like receptor **46**, were tested for chiral recognition [52]. Axially chiral ligands are often transformed into their metal complexes in order to create catalytically active species and new hosts for recognition. For example, chiral calix[5]arenes *R*-**45** and *S*-**45** were transformed into their copper(II) complex and complexation properties towards carbohydrates were explored [51]. Fluorescent titration experiments showed that they selectively recognized D-(+)-gluconic acid  $\delta$ -lactone with the association constant  $K_a(R) = 4.45 \times 10^4 \text{ M}^{-1}$  and  $K_a(S) = 1.81 \times 10^4 \text{ M}^{-1}$  respectively (MeCN–H<sub>2</sub>O 4:1 v/v, pH 7.4). BINOL rhodium complexes of calixarenes **47** were tested as catalysts in asymmetric hydrogenation reactions. Diphosphites **47** exhibited high enantiomeric excess for prochiral olefins, (*ee* up to 94 %) [53] while diphosphites **48** gave up to 98 % *ee* for hydrogenation of methyl acetamidoacrylate [54].

### 2.2.5 Modifications of the Bridges

Bridges between aromatic rings of calixarenes and resorcinarenes are commonly considered chemically inert. Therefore, substitution of the bridges is the least common among modifications due to synthetic difficulties. However, in some cases, the modifications can be introduced prior to the cyclization step, as in **49** (Fig. 2.13) [55, 56]. Another possibility involves using thiacalixarenes. Oxidation of the adjacent sulfide functional groups in an *anti*-relationship leads to an inherently chiral structure **50** [57]. It should be noted however, that inherent chirality in this case is inextricably bound to stereogenic centers at the sulfur atoms.

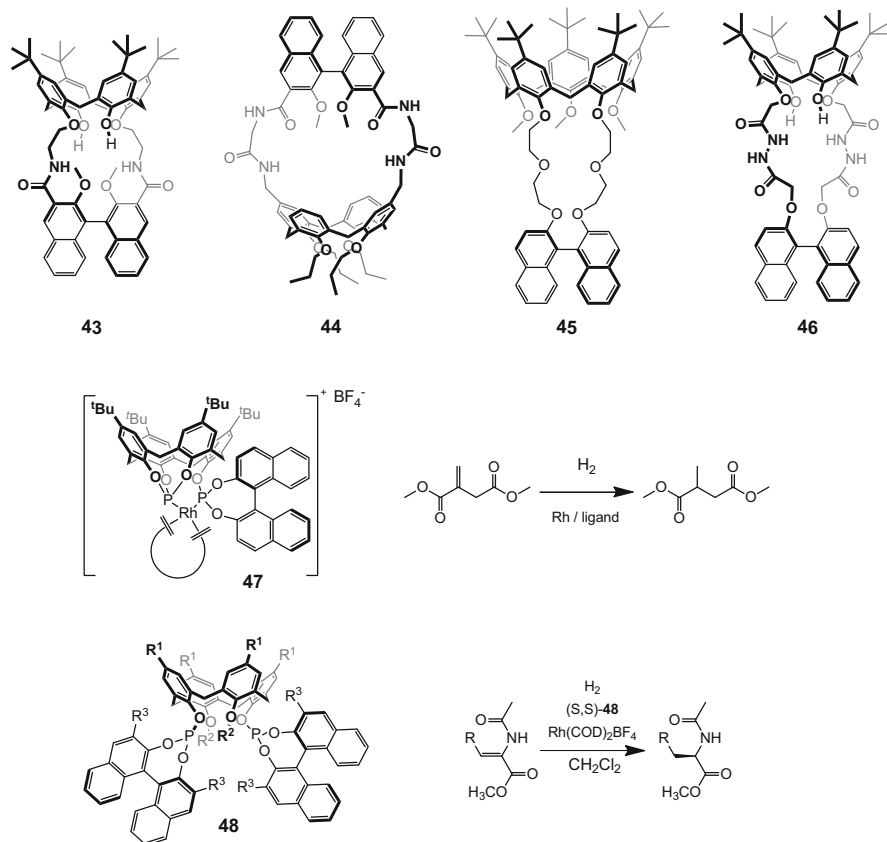
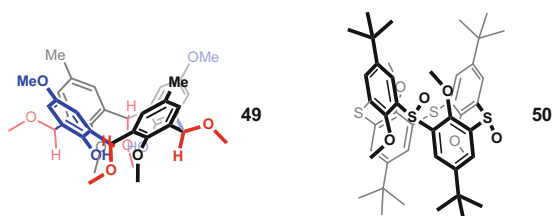


Fig. 2.12 Examples of calixarenes with axially chiral groups

Fig. 2.13 Examples of chiral calixarenes by modifications of the bridges



## 2.3 Inherent Chirality

The unique feature of calixarenes is their concave structure that clearly distinguishes the upper and lower rims. When the inversion of the concave structure is hindered, an asymmetric/dissymmetric substitution pattern leads to the formation of chiral structures (Fig. 2.14). This type of chirality is known as inherent chirality. Calix[4]arenes were the first scaffolds for which the term “inherent chirality” was

**Fig. 2.14** Inherent chirality of calixarenes

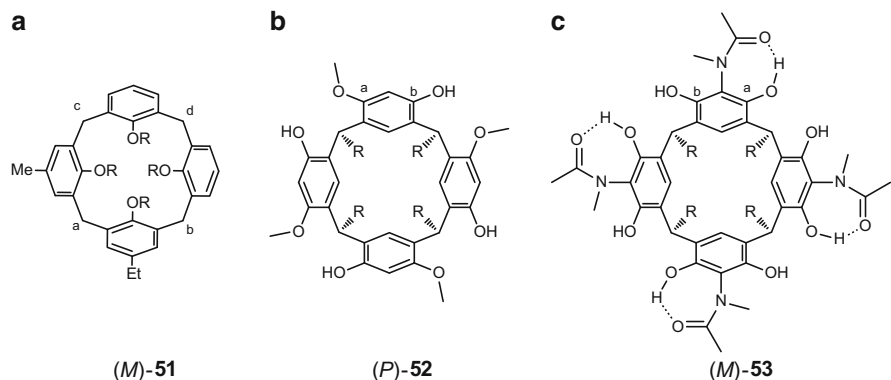
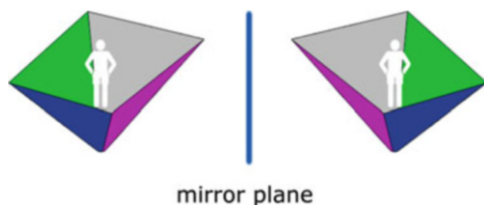


**Fig. 2.15** General rules for stereochemical notation for inherently chiral calixarenes. In all cases R denotes an unspecified substituent

applied [58]. Although during the next decades many other molecular platforms have been applied for the construction of inherently chiral structures, [59] calixarenes still dominate the field – see reviews ref. [59–64].

The first, more general definition of inherent chirality was formulated in 2004 by the group of Mandolini and Schiaffino [65] and later slightly modified by Szumna [59] to be consistent with stereochemical formalism. The definition reads: “*inherent chirality arises from the introduction of a curvature in an ideal planar structure that is devoid of perpendicular symmetry planes in its bidimensional representation*” [59]. Therefore, the resulting 3D molecules have  $C_n$  symmetry. The stereochemical nomenclature of inherently chiral compounds is not always consistent, since the priority rules and reference points cannot be set consistently for all types of compounds. Whenever possible, the accepted description of inherent chirality involves application of (*P*)/(*M*) notation by taking into account the priority of two neighboring aromatic substituents according to Cahn-Ingold-Prelog rules (for examples see compounds 51–53, Fig. 2.15). It should be noted that this notation is not always applicable to some inherently chiral compounds, and, in many cases, a 3D figure is the only unambiguous stereochemical representation.

Calix[4]arenes with unprotected OH groups in the lower rim undergo through-annulus inversion and therefore cannot be inherently chiral. The substitution of OH groups with alkyl chains (of at least *n*-Pr size) blocks the inversion and the resulting

macrocycle can be fixed in one of the four conformations (*cone*, *partial cone*, *1,2-alternate* and *1,3-alternate*). Each of these conformations can produce inherently chiral structures provided proper substitution. Inherent chirality is observed for compounds containing at least three different subunits, i.e. ABCC or ABCD patterns or by introducing directionality. From the synthetic point of view, access to inherently chiral calixarenes is usually not as straightforward as that of calixarenes with chirality based on stereogenic centers. This is due to problems with regioselectivity, control over conformation and optical resolution.

The synthetically simplest route to obtain inherently chiral calixarenes is to introduce two different substituents at the neighboring hydroxyl groups at the lower rim or to generate different spatial positions in order to create an ABCC pattern. Such a modification can be made using the basic calixarene skeleton. For example, in the group of Kalchenko an ABCC pattern was obtained by 1,2-regioselective proximal substitution to obtain inherently chiral **54** that after resolution of diastereoisomers was transformed into enantiomers of **55** (Fig. 2.16) [66]. Differentiation of substitution pattern by spatial positions [67] is exemplified by **59**, [68] containing two identical substituents however at different fixed spatial positions. Modification of two neighboring positions in order to create inherently

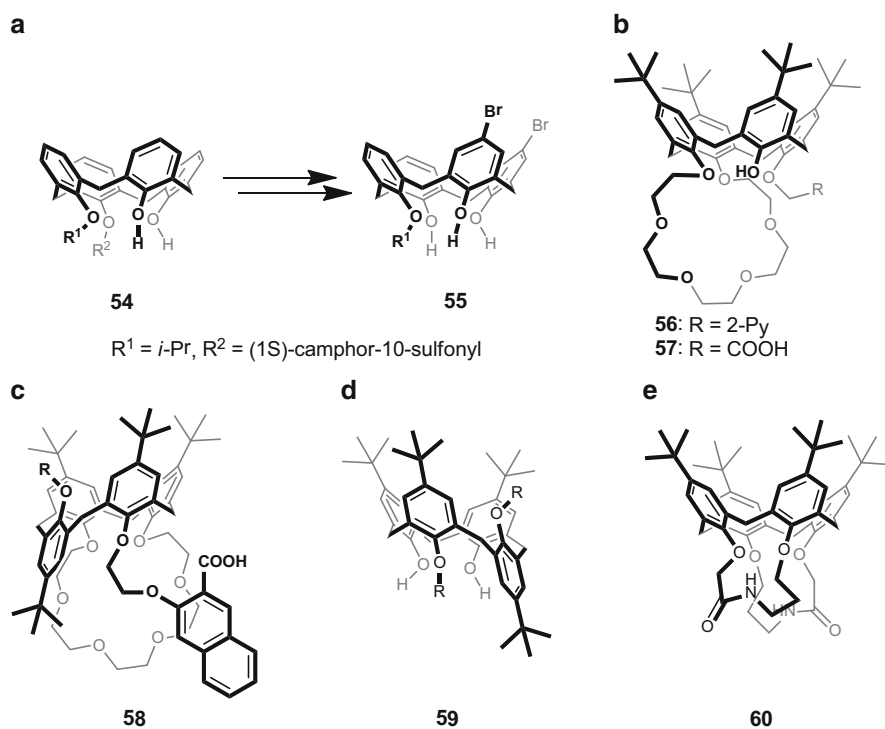
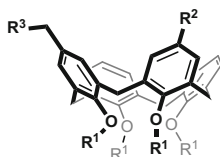


**Fig. 2.16** Inherent chirality of calixarenes introduced by: (a, b) lower rim substitution; (c, d) spacial alignment; (e) directional bridging

**Fig. 2.17** Inherent chirality introduced by upper rim substitution



**61:**  $R^1 = \text{Pr}$ ,  $R^2 = \text{OH}$ ,  $R^3 = \text{NBu}_2$

**62:**  $R^1 = \text{Bn}$ ,  $R^2 = \text{COOH}$ ,  $R^3 = \text{NH}_2$

**63:**  $R^1 = \text{Bn}$ ,  $R^2 = \text{CH}_2\text{OH}$ ,  $R^3 = \text{NH}_2$

chiral calixarenes opens the possibility to form crown ether-type bridges, like in **56**, **57** [69, 70] and **58** (Fig. 2.16). Such derivatives gain a lot of attention due to possible applications in complexation of chiral ammonium ions by means of  $\text{N}^+ \cdots \text{H} \cdots \text{O}$  hydrogen bonding. Indeed, in the group of Pappalardo, derivative **56** was used for recognition of (*R*)- and (*S*)-1-phenyl-ethylammonium picrates. Derivative **58** (partial-cone conformation) forms diastereomeric salts with leucinol with considerably different association constants for enantiomers ( $K_a = 50 \text{ M}^{-1}$  and  $143 \text{ M}^{-1}$  in  $\text{CD}_2\text{Cl}_2$ , *de* 48 %) [71].

Yet another approach for differentiation of substituents at the lower rim involves directional bridging. The bridge can be placed at any position, however, in practice, the most convenient location is the lower rim oxygen atoms (Fig. 2.16e). For example such directional linkages composed of carboxamide [72] or ester [73] moieties were introduced by a cyclization reaction to give inherently chiral calixarene **60** possessing  $C_2$  symmetry.

Modifications of upper rims of calixarenes in order to introduce inherent chirality requires more synthetic steps. However, the effort can pay off since such derivatives can take full advantage of the calixarene bowl. This approach was used by the groups of Shimizu to obtain amino phenol **61**, amino acid **62** and amino alcohol **63** presenting inherent chirality based on upper rim functionalization (Fig. 2.17). Amino phenol **61** is able to recognize enantiomers of mandelic acid through formation of diastereomeric salts (*de* 37.5 %) [74]. Calix[4]arene **61** was also used as a catalyst in asymmetric Michael additions of thiophenols and cyclohexenones [75]. Yields of the reactions were high, but the enantiomeric excesses were low (*ee* up to 16 %). Introduction of an additional aromatic ring at the upper rim of calix[4]arene (in consequence, formation of the macrocycle of ABCD type) resulted in higher enantioselectivity (*ee* up to 31 % for the same Michael addition) [76].

The internal dynamic of a macrocyclic ring of calixarenes can present a substantial challenge for formation of inherently chiral structures. In general, rotation of subunits causes racemization. However, if the rotation is only partial, the resulting structures may retain their chirality. An ingenious example of that type is an inherently chiral tri-*O*-alkylated homooxacalix[3]arene **64** exhibiting pseudo- $C_2$  symmetry (Fig. 2.18) [77]. Although the methoxyl group can pass through the macrocyclic ring (but the two butoxyl groups cannot), the molecule retains its chirality since the resulting structure is identical (Fig. 2.18b). The enantiomers of **64** were separated using chiral HPLC and the resulting hosts gave an impressive *de* of 72 % for complexation of amino acid esters (as picrate salts).

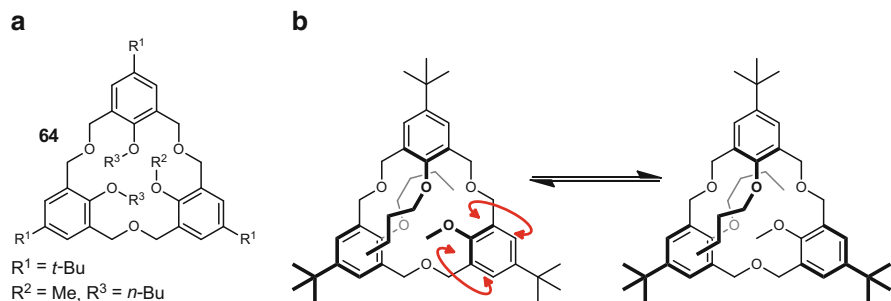


**Fig. 2.18** (a) A dynamic, yet inherently chiral homooxacalix[3]arene, (b) the methoxyl group passing through the macrocyclic ring of **64**, producing superimposable structures

Differentiation of the edges of a phenolic ring also introduces the required directionality to the calixarene structure that results in inherent chirality. Differentiation of only single ring is sufficient to generate an inherently chiral structure. Such an approach can potentially give products with more compact chiral binding sites since they are positioned close to the cavity. However, from the synthetic point of view this approach is toilsome mainly due to regioselectivity problems. Therefore, the number of examples is limited. In the group of Chen and Huang various inherently chiral derivatives were obtained based on *meta*-substitution involving calix[4]quinolone **65**, [78] salphen **66** [79] or proline derivative **67** (Fig. 2.19) [80]. The efficiency of **67**, a calixarene that combines inherent and classical chirality, has been tested in the enantioselective aldol reaction between 4-nitroaldehyde and cyclohexanone [80]. High yields and *ee* values up to 66% were obtained. For the synthesis of **65**, **66** and **67** see Chap. 3.

Resorcin[4]arenes, in contrary to calixarenes, are better candidates for generation of inherent chirality by edge modification at upper rims due the presence of OH groups. For resorcin[4]arenes regioselective substitution of all four rings is usually synthetically easier than modification of only one edge (for calixarenes the opposite is true). In many cases, formation of  $C_4$ -symmetric products is highly preferred due to stabilization of their structures by maximization of a number of intramolecular hydrogen bonds. It should be noted that for resorcinarenes (in contrary to calixarenes) an inherently chiral substitution pattern leads simultaneously to generation of stereogenic centers at the bridging atoms (i.e. formation of classical chiral centers at bridging atoms).

The conceptually simplest  $C_4$ -symmetric inherently chiral resorcinarene **68** (Fig. 2.19) was synthesized by a single step simple condensation of 3-methoxyphenol with aldehydes catalyzed by Lewis acid as a single regioisomer in 80% yield [81] and separated into enantiomers [82, 83]. Recently inherently chiral cyano-substituted resorcin[4]arene **69** was also synthesized [84]. The cyano group, as a versatile synthon in organic chemistry, allowed for its transformation into inherently chiral ketones, aldehydes, amides, and amines [85]. Edge modifications of resorcinarenes can also be realized by means of ring closing. In 1992 it was



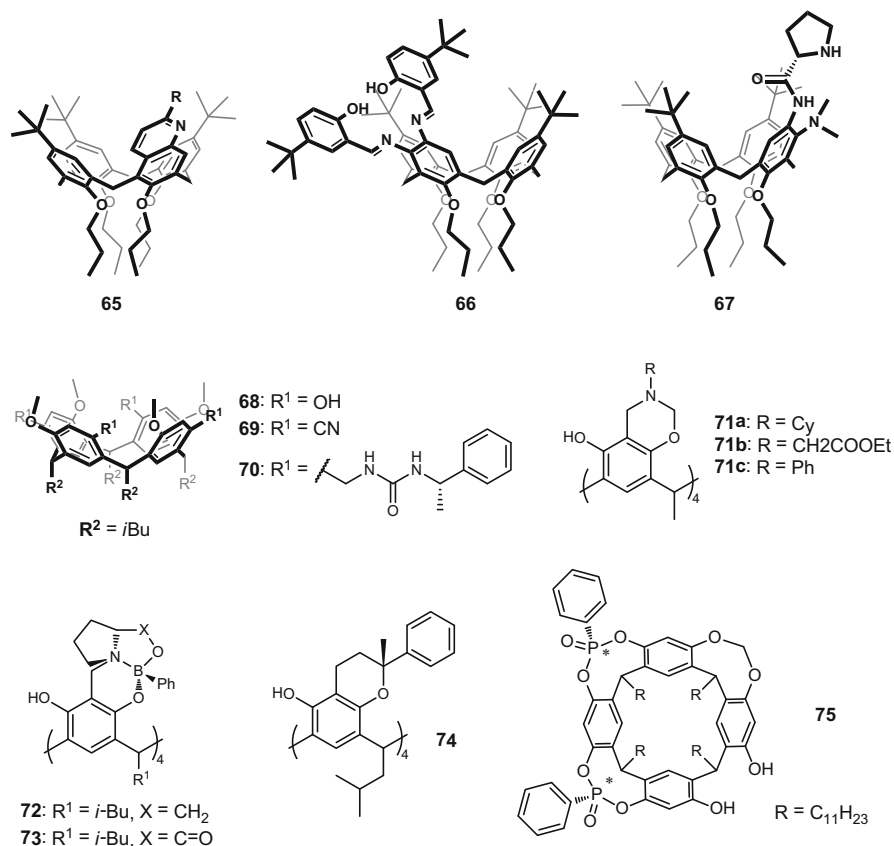


**Fig. 2.19** Inherently chiral calixarenes (including resorcinarenes) obtained by edge substitution

shown that the Mannich reaction of resorcinarene with primary amines and formaldehyde gives tetrabenzoxazines **71** [86, 87]. The  $C_4$ -symmetric isomers, that were formed regioselectively are chiral due to directional closing of the benzoxazine rings [88]. Using chiral amines, diastereoselective syntheses of tetrabenzoxazines were accomplished [89–91] in a kinetically controlled way [92]. Alternative ring closing reactions involve coordination to boron atoms, like for **72** and **73**, [93, 94] and, more recently the Diels-Alder reaction, like for **74** [95]. It is worth noting that in all cases ring closing reactions proceeded with exceptional diastereoselectivity. Inherently chiral resorcin[4]arenes of  $C_1$  symmetry, e. g. **75**, were obtained by the group of Dutasta using differentiation of hydroxyl groups using phosphonate bridges and tested towards complexation of various chiral neurotransmitters [96]. The enantiopure **75** showed considerable diastereoselectivity (*dr* up to 2.5:1 for pseudoephedrine) and complete chemoselectivity (towards ephedrine).

## 2.4 Non-covalent Chirality and Supramolecular Chirality

The chemistry of calixarenes is dominated by the presence of various non-covalent intramolecular and intermolecular interactions that control their structure and properties. Such non-covalent interactions can be exploited as additional parameters to control/induce chirality. For systems with chirality achieved/controlled mainly in a non-covalent way, the terms “non-covalent chirality” and “supramolecular chirality” are used. Although both terms originate from non-covalent interactions the term “non-covalent chirality” is mainly used for systems involving intramolecular interactions, while “supramolecular chirality” consists in dissymmetric arrangement of molecules in a non-covalent multi-molecular assembly (involving intermolecular interactions) [97]. In analogy to differentiation between covalent and non-covalent bonds, the distinction between “classical chirality” and “supramolecular chirality” is often based on thermodynamic parameters. And similarly, the distinction is not always unambiguous. Non-covalent interactions are generally much weaker and kinetically less stable than covalent interactions. Therefore, assemblies with supramolecular chirality are often highly dynamic. However, presence of numerous non-covalent interactions contributes significantly to the overall stability of the system, and the stability can even approach the limits known for covalent species. On the other limit, we find species with very low stability, and, for them, the question remains where the simple diastereomeric interaction ends and the supramolecular chirality starts. All these limits have not been precisely defined yet and currently the use of the terms relies mostly upon generation (or not) of new properties.

Dynamic character of systems with supramolecular chirality presents a significant challenge for both the synthesis and the applications. Separation of enantiomers is, in most cases, not possible. Therefore, the introduction of additional chiral auxiliaries is usually required in order to induce substantial diastereomeric excess of one of the inherently chiral assemblies. One can envision that supramolecular chirality generated this way can greatly support (or hamper) efficiency and selectivity in chiral recognition. However, the main advantage of supramolecular chirality comes from the fact that such chirality is not a fixed parameter anymore, and, therefore it can be modulated by external factors. This way such stimuli-responsive chiral systems can be created.

One of the early examples of resorcin[4]arenes with add-on features due to non-covalent chirality was deep cavitand amide **76** (Fig. 2.20) [98]. Cavitand **76** has “doors” at the upper rim that are controlled by a unidirectional cooperative belt of hydrogen bonds. The “doors” can close clockwise or counterclockwise, and, in the presence of additional chirality centers, one of the directions is preferred (*de* 50 %) [98]. The chiral vessels exhibit preferential binding of enantiomers of various small molecules, e. g. *trans*-cyclohexanediol (60 % *de*). Other resorcin[4]arenes with inherently chiral conformations were reported by Schmidt et al. [99] and the group of Szumna [100, 101]. Amide substituted resorcin[4]arenes like **77**, **78** and **79** exist in inherently chiral kite conformations that are stabilized by an unidirectional

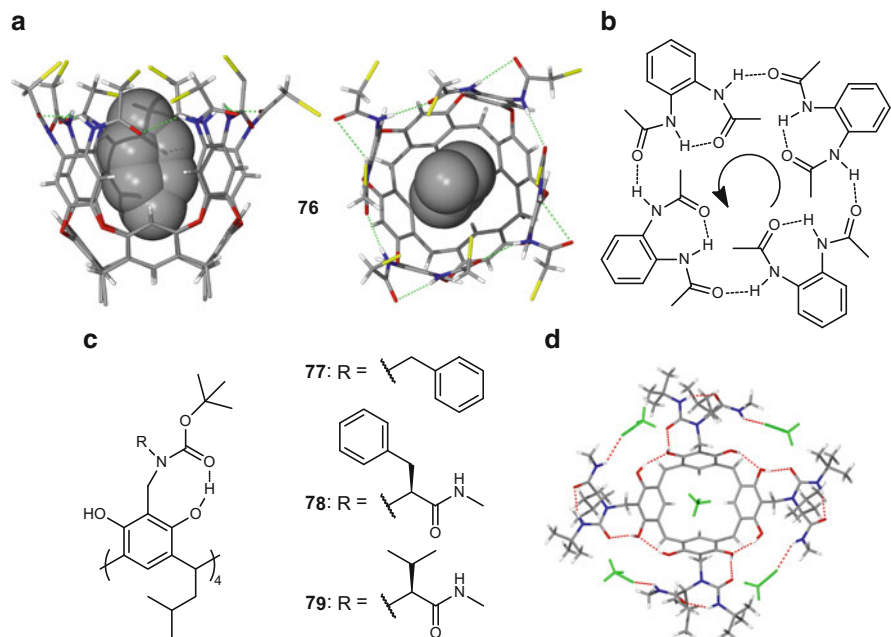


**Fig. 2.20** Cavitanths with a chiral system of hydrogen bonds: (a) X-ray structure, (b) schematic view of the H-bond array in **76** (c) structures of cavitanths **77–79**, (d) crystal structure of **79**

system of eight hydrogen bonds (both in the solid state and in solution). This dynamic system of hydrogen bonding undergoes inversion characterized by a relatively high energy barrier (14.6–18.5 kcal mol<sup>-1</sup>) consistent with simultaneous rupture of all eight hydrogen bonds. This is quite a surprising result, considering that the hydrogen bond system is not strictly cooperative. However, rotation of just one unit creates an unfavorable pattern of the adjacent hydrogen bonds, that is responsible for an apparent cooperativity. An even more stable pattern was obtained for resorcinarenes substituted with amino acid derivatives (for example **78**). In this case, inherently chiral conformations were stabilized by a total of twelve hydrogen bonds. The presence of additional stereogenic centers causes formation of two diastereomeric inherently chiral conformations *M* and *P* in unequal amounts (*de* in the range of 72–95 %).

An interesting example of dynamic chirality was observed for iminoresorcin[4]arenes **81** and **27–30** (Figs. 2.21 and 2.6). Iminoresorcin[4]arenes **81** and **27–30** were obtained by reaction of tetraformylresorcin[4]arene **80** with various amines [32, 102]. It was found that they exist exclusively as keto-enamine tautomers both in solution and in the solid state. The tautomerization proceeds in a highly regioselective manner, i.e. all carbonyl atoms are directed to the same side of the macrocyclic ring, leading to exclusive formation C<sub>4</sub>-symmetric inherently chiral structures, stabilized by hydrogen bonding (Fig. 2.21b). For aliphatic chiral amines **81** two inherently chiral *M* and *P* diastereoisomers were clearly visible in NMR

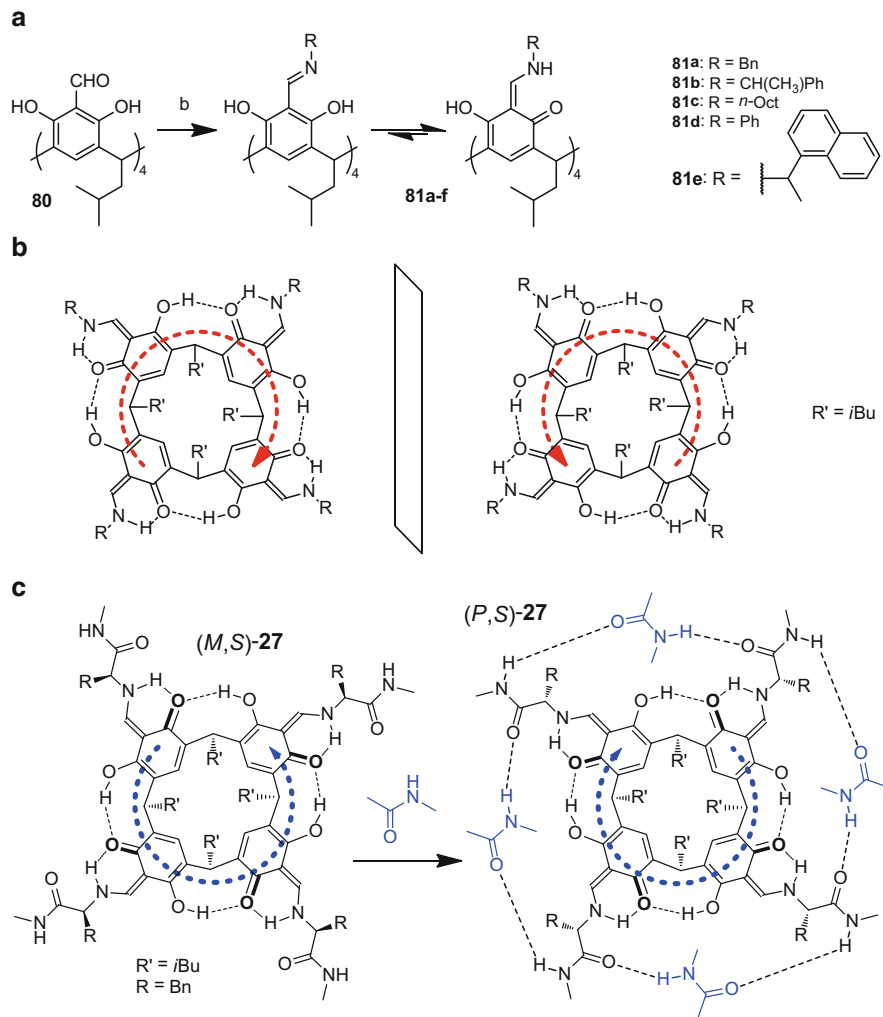


**Fig. 2.21** Dynamic inherent chirality based on tautomeric equilibration

spectra and chemical exchange between them was slow on the NMR timescale [102]. For amino acid derivatives **27–30** presence of only single diastereoisomers was observed, meaning that tautomerization proceeded not only in a highly regioselective but also diastereoselective way (d.e. >95 %) [32]. Such amino acid iminoresorcin[4]arenes have a high propensity towards self-assembly and formation of capsular dimers (discussed in Sect. 2.2.1). For example, L-**27** exists as a concave monomer in a homochiral form, however, upon addition of its enantiomer D-**27**, it self-assembles to form a centrosymmetric capsular dimer (L-**27**)(D-**27**). It was found that inherent chirality is different in the self-assembled dimer than in a non-assembled monomer [103]. The change of inherent chirality proceeds during

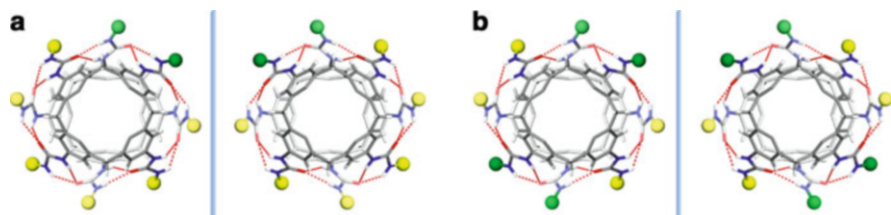


**Fig. 2.22** Supramolecular chirality by dimerization of achiral monomers of: (a) ABBB type; (b) ABAB type

association with either the second enantiomer (to form a capsular dimer) or with the achiral small molecules, for example, *N*-methyl acetamide (to form a cavitand, Fig. 2.21c). It is important to note that change of inherent chirality requires concerted breakage of hydrogen bonding system, rotation around single (or partially single) bonds and isomerization by tautomerization. The whole process is slow on the NMR timescale (EXSY, no exchange detected using mixing time 1.5 s), however it proceeds in the range of few minutes. Thus the diastereoisomers are still dynamic and cannot be isolated, however, the kinetic barrier was substantially increased compared to cavitands based solely on hydrogen bonding. Due to numerous processes involved in maintaining and change of chirality of iminoresorcin[4]arenes **81** and **27–30** it is difficult to classify them to a specific category. The compounds exhibit features of inherent chirality, non-covalent chirality and atropisomerism generated by means of combination of non-covalent interactions and regioselective tautomerization.

Supramolecular chirality involves generation of chirality during the aggregate formation. In the group of Böhmer chirality was generated during formation of non-covalent dimers of calix[4]arenes substituted at their wide rim by four urea residues (Fig. 2.22). The dimeric capsules are held together by a seam of hydrogen bonds between N–H and O in non-polar solvents. Dimerization of achiral tetraurea calix[4]arene monomers leads to formation of chiral structures, provided that monomers are substituted with different A and B groups at phenolic units [104, 105]. The ABBB, AABB and ABAB substitution patterns of monomers produce dimers with supramolecular chirality only due to the mutual arrangement of the two calixarenes (although obviously as racemic mixtures).

Increasing the number of intermolecular non-covalent interactions leads to chiral aggregates having even higher kinetic stability, allowing even for separation of enantiomers (for reviews see ref. [97, 106, 107]). For example, in the group of Reinhoudt a disubstituted melamine calixarene **82** was obtained (Fig. 2.23). Upon addition of barbituric or cyanuric acid, calixarene **82** assembles into a [3+6] rosette-type of structures, by means of 36 hydrogen bonds. The supramolecular chirality comes from highly regioselective self-assembly and antiparallel arrangement of melamine fragments having three different types of HB-donor amine groups. This way the rosette is  $D_3$ -symmetric and chiral. It is worth to note that none of the components is chiral, but the whole assembled system possesses supramolecular chirality. The chiral rosettes are unique examples of non-covalent

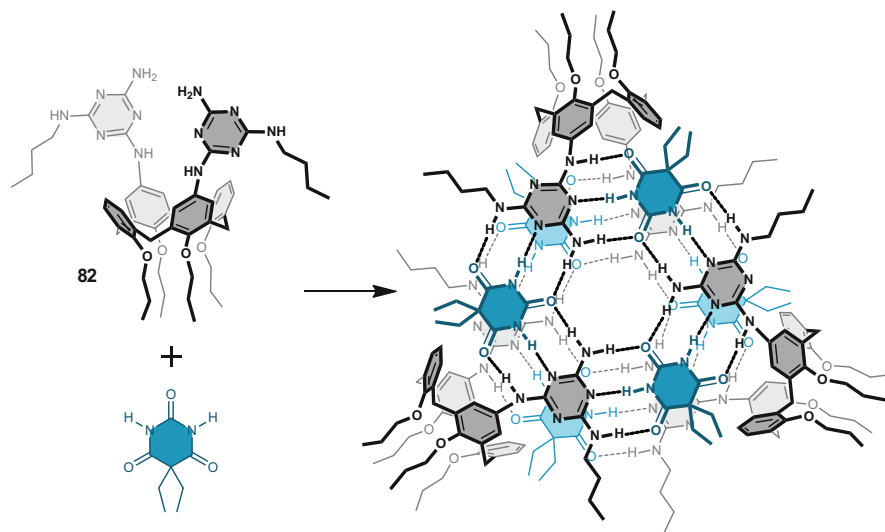


Fig. 2.23 Rosette structure formed of **82** and barbituric acid

assemblies that are kinetically stable enough to be isolated as single enantiomers. Moreover, the synthesis of a given enantiomer can be performed in a stereospecific way. To achieve this, firstly, selective formation of a given (*P*) or (*M*) assembly was achieved by the introduction stereogenic centers either at the calix[4]arene dimelamine or barbituric/cyanuric acid derivative. Diastereomeric excess in both cases was high (de 96 %) [108]. Subsequent exchange of the chiral barbiturate for an achiral cyanurate gave an enantiopure assembly with an *ee* of 96 %. The resulting structure was still optically active, although none of its components were chiral. Generation of single enantiomers was also achieved in a non-covalent way. Additional complexation of chiral acids or diacids by a racemic mixture of amino-substituted double rosette assemblies gave supramolecular chiral assemblies in which the *de* is ca. 90 % [109, 110]. The removal of the diacids led also to the formation of enantiopure assemblies. Chiral memory effect, which is inextricably connected with kinetic stability of the rosettes, was also observed in this case. Interestingly, when racemic mixtures of calix[4]arene dimelamine were used, the resulting rosettes were homochiral (no mixed-chirality rosettes were detected), meaning that assembly leads to effective chiral self-sorting.

## 2.5 Conclusions and Outlook

A review of the literature concerning chiral calixarenes (including resorcinarenes) emphasizes the variety of structures that can be obtained using the macrocyclic scaffold and highlights the diversity of their applications. Since their first discovery

in 1979 enormous progressions have been made in the synthesis and applications of chiral calixarenes. This resulted in the compilation of hundreds of chiral calixarenes. Their recognition properties are also quite well known. Each of the subtopics covered in this chapter already has several specialized reviews. Obviously, there is still space for obtaining interesting results in the field of chiral recognition by chiral calixarenes. However, it needs to be noted that nowadays the area is quite mature. The future outlook for this area brings an impression that researches are now exploring practical aspects of the existing knowledge. They are aiming at transferring molecular recognition events into macroscopic properties that opens the field for new fascinating designs and discoveries. It can be envisioned that new smart materials including supramolecular self-healing gels, chiral nanomaterials and molecular machines may emerge as a result of application of chiral calixarenes.

## References

1. Muthukrishnan, R.; Gutsche, C. D. *J. Org. Chem.* **1979**, *44*, 3962–3964.
2. Meyer, R.; Jira, T. *Curr. Anal. Chem.* **2007**, *3*, 161–170.
3. Krawinkler, K. H.; Maier, N. M.; Sajovic, E.; Lindner, W. *J. Chromatogr. A* **2004**, *1053*, 119–131.
4. Mutihac, L. *Current drug discovery technologies* **2008**, *5*, 98–104.
5. Ganjali, M. R.; Norouzi, P.; Rezapour, M.; Faridbod, F.; Pourjavid, M. R. *Sensors* **2006**, *6*, 1018–1086.
6. Homden, D. M.; Redshaw, C. *Chem. Rev.* **2008**, *108*, 5086–5130.
7. Baldini, L.; Casnati, A.; Sansone, F.; Ungaro, R. *Chem. Soc. Rev.* **2007**, *36*, 254–266.
8. Ludwig, R. *Microchim. Acta* **2005**, *152*, 1–19.
9. Coleman, A. W.; Perret, F.; Moussa, A.; Dupin, M.; Gu, Y.; Perron, H. Calix[n]arenes as protein sensors. In *Creative Chemical Sensor Systems*; Schrader, T. Ed.; Springer: Berlin Heidelberg, **2007**, Topics in Current Chemistry Vol. 277, Part A; pp 31–88.
10. D'Acquarica, I.; Cerreto, A.; Delle Monache, G.; Subrizi, F.; Boffi, A.; Tafi, A.; Forli, S.; Botta, B. *J. Org. Chem.* **2011**, *76*, 4396–4407.
11. Zhou, J. L.; Chen, X. J.; Zheng, Y. S. *Chem. Commun.* **2007**, 5200–5202.
12. a) Hamuro, Y.; Calama, M. C.; Park, H. S.; Hamilton, A. D. *Angew. Chem. Int. Ed.* **1997**, *36*, 2680–2683. b) Brewster, R. E.; Caran, K. L.; Sasine, J. S.; Shuker, S. B. *Curr. Org. Chem.* **2004**, *8*, 867–881. c) Hülsbusch, C. M.; Feigel, M. *J. Incl. Phenom. Macrocycl. Chem.* **2007**, *59*, 53–63. d) Lazzarotto, M.; Sansone, F.; Baldini, L.; Casnati, A.; Cozzini, P.; Ungaro, R. *Eur. J. Org. Chem.* **2001**, 595–602.
13. Casnati, A.; Sansone, F.; Ungaro, R. *Acc. Chem. Res.* **2003**, *36*, 246–254.
14. Sansone, F.; Barbosa, S.; Casnati, A.; Fabbi, M.; Pochini, A.; Ugozzoli, F.; Ungaro, R. *Eur. J. Org. Chem.* **1998**, 897–905.
15. Lazzarotto, M.; Sansone, F.; Baldini, L.; Casnati, A.; Cozzini, P.; Ungaro, R. *Eur. J. Org. Chem.* **2001**, 595–602.
16. Cherenok, S.; Vovk, A.; Muravyova, I.; Shivanyuk, A.; Kukhar, V.; Lipkowski, J.; Kalchenko, V. *Org. Lett.* **2006**, *8*, 549–552.
17. Ruderisch, A.; Pfeiffer, J.; Schurig, V. *Tetrahedron: Asymmetry* **2001**, *12*, 2025–2030.
18. Yanagihara, R.; Tominaga, M.; Aoyama, Y. *J. Org. Chem.* **1994**, *59*, 6865–6867.
19. O'Farrell, C. M.; Chudomel, J. M.; Collins, J. M.; Dignam, C. F.; Wenzel T. *J. Org. Chem.* **2008**, *73*, 2843–2851.

20. Berghaus, C.; Feigel, M. *Eur. J. Org. Chem.* **2003**, 3200–3208.
21. Gibb, B. C.; Mezo, A. R.; Causton, A. S.; Fraser, J. R.; Tsai, F. C. S.; Sherman, J. C. *Tetrahedron* **1995**, *51*, 8719–8732.
22. Freeman, J. O.; Lee, W. C.; Murphy, M. E. P.; Sherman, J. C. *J. Am. Chem. Soc.* **2009**, *131*, 7421–7429.
23. Yakovenko, A. V.; Boyko, V. I.; Kalchenko, V. I.; Baldini, L.; Casnati, A.; Sansone, F.; Ungaro, R. *J. Org. Chem.* **2007**, *72*, 3223–3231.
24. Botta, B.; D’Acquarica, I.; Delle Monache, G.; Subissati, D.; Uccello–Barretta, G.; Mastrini, M.; Nazzi, S.; Speranza, M. *J. Org. Chem.* **2007**, *72*, 9283–9290.
25. Botta, B.; Botta, M.; Filippi, A.; Tafi, A.; Delle Monache, G.; Speranza, M. *J. Am. Chem. Soc.* **2002**, *124*, 7658–7659.
26. Tafi, A.; Botta, B.; Botta, M.; Delle Monache, G.; Filippi, A.; Speranza, M. *Chem. Eur. J.* **2004**, *10*, 4126–4135.
27. Sansone, F.; Barbosa, S.; Casnati, A.; Fabbi, M.; Pochini, A.; Ugozzoli, F.; Ungaro, R. *Eur. J. Org. Chem.* **2008**, 869–886.
28. Kuberski, B.; Szumna, A. *Chem. Commun.* **2009**, 1959–1961.
29. Szumna, A. *Chem. Commun.* **2009**, 4191–4193.
30. Szumna, A. *Chem. Eur. J.* **2009**, *15*, 12381–12388.
31. Wierzbicki, M.; Szumna, A. *Chem. Commun.* **2013**, *49*, 3860–3862.
32. Jędrzejewska, H.; Wierzbicki, M.; Cmoch, P.; Rissanen, K.; Szumna, A. *Angew. Chem. Int. Ed.* **2014**, *53*, 13760–13764.
33. Szymański, M.; Wierzbicki, M.; Gilski, M.; Jędrzejewska, H.; Szytylko, M.; Cmoch, P.; Shkurenko, A.; Jaskolski, M.; Szumna, A. *Chem. Eur. J.* **2016**, *22*, 3148–3155.
34. Sansone, F.; Casnati, A. *Chem. Soc. Rev.* **2013**, *42*, 4623–4639.
35. Aoyama, Y. *Chem. Eur. J.* **2004**, *10*, 588–593.
36. Budka, J.; Tkadlecová, M.; Lhoták, P.; Stibor, I. *Tetrahedron* **2000**, *56*, 1883–1887.
37. Cecioni, S.; Lalor, R.; Blanchard, B.; Praly, J. P.; Imberty, A.; Matthews, S. E.; Vidal, S. *Chem. Eur. J.* **2009**, *15*, 13232–13240.
38. Fujimoto, K.; Miyata, T.; Aoyama, Y. *J. Am. Chem. Soc.* **2000**, *122*, 3558–3559.
39. Torvinen, M.; Kalenius, E.; Sansone, F.; Casnati, A.; Turhanen, P.; Janis, J. *Supramol. Chem.* **2012**, *24*, 228–233.
40. Geraci, C.; Consoli, G. M. L.; Galante, E.; Bousquet, E.; Pappalardo, M.; Spadaro, A. *Bioconjugate Chem.* **2008**, *19*, 751–758.
41. Sansone, F.; Baldini, L.; Casnati, A.; Ungaro, R. *Supramol. Chem.* **2008**, *20*, 161–168.
42. Aoyama, Y.; Kanamori, T.; Nakai, T.; Sasaki, T.; Horiuchi, S.; Sando, S.; Niidome, T. *J. Am. Chem. Soc.* **2003**, *125*, 3455–3457.
43. Zheng, Y. S.; Zhang, C. *Org. Lett.* **2004**, *6*, 1189–1192.
44. Liu, X. X.; Zheng, Y. S. *Tetrahedron Lett.* **2006**, *47*, 6357–6360.
45. Bozkurt, S.; Durmaz, M.; Yilmaz, M.; Sirit, A. *Tetrahedron: Asymmetry* **2008**, *19*, 618–623.
46. Garrier, E.; Le Gac, S.; Jabin, I. *Tetrahedron: Asymmetry* **2005**, *16*, 3767–3771.
47. Darbost, U.; Zeng, X.; Giorgi, M.; Jabin, I. *J. Org. Chem.* **2005**, *70*, 10552–10560.
48. Wezenberg, S. J.; Kleij, A. W. *Adv. Synth. Catal.* **2010**, *352*, 85–91.
49. Amato, M. E.; Ballistreri, F. P.; Pappalardo, A.; Tomaselli, G. A.; Toscano, R. M.; Williams, D. *J. Eur. J. Org. Chem.* **2005**, 3562–3570.
50. Pinkhassik, E.; Stibor, I.; Casnati, A.; Ungaro, R. *J. Org. Chem.* **1997**, *62*, 8654–8659.
51. Li, S. Y.; Zheng, Q. Y.; Chen, C. F.; Huang, Z. T. *Tetrahedron: Asymmetry* **2005**, *16*, 2816–2820.
52. Hu, C.; Huang, X.; Chen, Z.; He, Y. *Chinese J. Chem.* **2009**, *27*, 157–162.
53. Marson, A.; Freixa, Z.; Kamer, P. C. J.; van Leeuwen, P. W. N. M. *Eur. J. Inorg. Chem.* **2007**, 4587–4591.
54. Liua, S.; Sandovalb, C. A. *J. Mol. Catal. A: Chemical* **2010**, *325*, 65–72.
55. Gopalsamuthiram, V.; Huang, R.; Wulff, W. D. *Chem. Commun.* **2010**, *46*, 8213–8215.



56. Gopalsamuthiram, V.; Predeus, A. V.; Huang, R. H.; Wulff, W. D. *J. Am. Chem. Soc.* **2009**, *131*, 18018–18019.
57. Morohashi, N.; Iki, N.; Onodera, T.; Kabuto, C.; Miyano, S. *Tetrahedron Lett.* **2000**, *41*, 5093–5097.
58. Böhmer, V.; Kraft, D.; Tabatabai, M. *J. Incl. Phenom. Mol. Recog. Chem.* **1994**, *19*, 17–39.
59. Szumna, A. *Chem. Soc. Rev.* **2010**, *39*, 4274–4285.
60. Böhmer, V. *Liebigs Ann.–Recl.* **1997**, 2019–2030.
61. Zheng, Y. S.; Luo, J. *J. Incl. Phenom. Macrocycl. Chem.* **2011**, *71*, 35–56.
62. Luo, J.; Zheng, Q.; Chen, C.; Huang, Z. *Prog. Chem.* **2006**, *18*, 897–906.
63. McIlldowie, M. J.; Mocerino, M.; Ogden, M. I. *Supramol. Chem.* **2010**, *22*, 13–39.
64. Li, S. Y.; Xu, Y. W.; Liu, J. M.; Su, C. Y. *Int. J. Mol. Sci.* **2011**; *12*, 429–455.
65. Dalla Cort, A.; Mandolini, L.; Pasquini, C.; Schiaffino, L. *New. J. Chem.* **2004**, *28*, 1198–1199.
66. Boyko, V. I.; Yakovenko, A. V.; Matvieiev, Y. I.; Kalchenko, O. I.; Shishkin, O. V.; Shishkina S. V.; Kalchenko, V. I. *Tetrahedron* **2008**, *64*, 7567–7573.
67. Otsuka, T.; Shinkai, S. *Supramol. Sci.* **1996**, *3*, 189–205.
68. Narumi, F.; Hattori, T.; Morohashi, N.; Matsumura, N.; Yamabuki, W.; Kameyama, H.; Miyano, S. *Org. Biomol. Chem.* **2004**, *2*, 890–898.
69. Arnaud-Neu, F.; Caccamese, S.; Fuangswasdi, S.; Pappalardo, S.; Parisi, M. F.; Petringa, A.; Principato, G. *J. Org. Chem.* **1997**, *62*, 8041–8048.
70. Luo, J.; Zheng, Q. Y.; Chen, C. F.; Huang, Z. T. *Chem. Eur. J.* **2005**, *11*, 5917–5928.
71. Luo, J.; Zheng, Q. Y.; Chen, C. F.; Huang, Z. T. *Tetrahedron* **2005**, *61*, 8517–8528.
72. Bitter, I.; Grun, A.; Toth, G.; Balazs, B.; Horvath, G.; Toke, L. *Tetrahedron* **1998**, *54*, 3857–3866.
73. Lhoták, P.; Dudič, M.; Stibor, I.; Petříčková, H.; Sýkora, J.; Hodačová, J. *Chem. Commun.* **2001**, 731–732.
74. Shirakawa, S.; Moriyama, A.; Shimizu, S. *Org. Lett.* **2007**, *9*, 3117–3120.
75. Shirakawa, S.; Moriyama, A.; Shimizu, S. *Eur. J. Org. Chem.* **2008**, 5957–5964.
76. Shirakawa, S.; Kimura, T.; Murata, S.; Shimizu, S. *J. Org. Chem.* **2009**, *74*, 1288–1296.
77. Araki, K.; Inada, K.; Shinkai, S. *Angew. Chem. Int. Ed. Engl.* **1996**, *35*, 72–74.
78. Miao, R.; Zheng, Q. Y.; Chen, C. F.; Huang, Z. T. *J. Org. Chem.* **2005**, *70*, 7662–7671.
79. Xu, Z. X.; Huang, Z. T.; Chen, C. F. *Tetrahedron Lett.* **2009**, *50*, 5430–5433.
80. Xu, Z. X.; Li, G. K.; Chen, C. F.; Huang, Z. T. *Tetrahedron* **2008**, *64*, 8668–8675, and references therein.
81. McIlldowie, M. J.; Mocerino, M.; Skelton, B. W.; White, A. H. *Org. Lett.* **2000**, *2*, 3869–3871.
82. Klaes, M.; Neumann, B.; Stammner, H. G.; Mattay, J. *Eur. J. Org. Chem.* **2005**, 864–868.
83. Buckley, B. R.; Page, P. C. B.; Chan, Y.; Heaney, H.; Klaes, M.; McIlldowie, M. J.; McKee, V.; Mattay, J.; Mocerino, M.; Moreno, E.; Skelton, B. W.; White, A. H. *Eur. J. Org. Chem.* **2006**, 5135–5151.
84. Wiegmann, S.; Neumann, B.; Stammner, H. G.; Mattay, J. *Eur. J. Org. Chem.* **2012**, 3955–3961.
85. Wiegmann, S.; Fukuhara, G.; Neumann, B.; Stammner, H. G.; Inoue, Y.; Mattay, J. *Eur. J. Org. Chem.* **2013**, 1240–1245.
86. Matsushita, Y.; Matsui, T. *Tetrahedron Lett.* **1993**, *46*, 7433–7436.
87. Schneider, H. J.; Schneider, U. *J. Incl. Phenom. Macrocycl. Chem.* **1994**, *19*, 67–83.
88. Amecke, R.; Böhmer, V.; Paulus, E. F.; Vogt, W. *J. Am. Chem. Soc.* **1995**, *117*, 3286–3287.
89. Iwanek, W.; Mattay, J. *Liebigs Ann. Chem.* **1995**, 1463–1466.
90. Arnecke, R.; Böhmer, V.; Friebe, S.; Gebauer, S.; Krauss, G. J.; Thondorf, I.; Vogt, W. *Tetrahedron Lett.* **1995**, *36*, 6221–6224.
91. El Gihani, M. T.; Heaney, H.; Slawin, A. M. Z. *Tetrahedron Lett.* **1995**, *36*, 4905–4908.
92. Schmidt, C.; Paulus, E. F.; Böhmer, V.; Vogt, W. *New J. Chem.* **2001**, *25*, 374–378, and references therein.

93. Iwanek, W.; Urbaniak, M.; Gawdzik, B.; Schurig, V. *Tetrahedron: Asymmetry* **2003**, *14*, 2787–2792.
94. Iwanek, W.; Frohlich, R.; Schwab, P.; Schurig, V. *Chem. Commun.* **2002**, 2516–2517.
95. Iwanek, W.; Stefańska, K.; Szumna, A.; Wierzbicki, M. *RSC Adv.* **2016**, *6*, 13027–13031.
96. Vachon, J.; Harthong, S.; Jeanneau, E.; Aronica, C.; Vanthuyne, N.; Roussel, C.; Dutasta, J. P. *Org. Biomol. Chem.* **2011**, *9*, 5086–5091.
97. Mateos–Timoneda, M. A. *Chem. Soc. Rev.* **2004**, *33*, 363–372.
98. Shivanyuk, A.; Rissanen, K.; Korner, S. K.; Rudkevich, D. M.; Rebek, J. *Helv. Chim. Acta* **2000**, *83*, 1778–1790, and references therein.
99. Schmidt, C.; Paulus, E. F.; Böhmer, V.; Vogt, W. *New J. Chem.* **2000**, *24*, 123–125.
100. Szumna, A. *Org. Biomol. Chem.* **2007**, *5*, 1358–1368.
101. Kuberski, B.; Pecul, M.; Szumna, A. *Eur. J. Org. Chem.* **2008**, 3069–3078.
102. Grajda, M.; Wierzbicki, M.; Cmoch, P.; Szumna, A. *J. Org. Chem.*, **2013**, *78*, 11597–11601.
103. Jędrzejewska, H.; Kwit, M.; Szumna, A. *Chem Commun.* **2015**, *51*, 13799–13801.
104. Rudzevich, Y.; Rudzevich, V.; Böhmer, V. *Supramol. Chem.* **2010**, *22*, 717–725.
105. Pop, A.; Vysotsky, M. O.; Saadioui, M.; Bohmer, V. *Chem. Commun.* **2003**, 1124–1125.
106. Luo, J.; Zheng, Y. S. *Curr. Org. Chem.* **2012**, *16*, 483–506.
107. Vázquez–Campos, S.; Crego–Calama, M.; Reinhoudt, D. N. *Supramol. Chem.* **2007**, *19*, 95–106.
108. Prins, L. J.; Huskens, J.; de Jong, F.; Timmerman, P.; Reinhoudt, D. N. *Nature* **1999**, *398*, 498–502.
109. Ishi-i, T.; Crego–Calama, M.; Timmerman, P.; Reinhoudt, D. N.; Shinkai, S. *Angew. Chem. Int. Ed.* **2002**, *41*, 1924–1929.
110. Ishi-i, T.; Crego–Calama, M.; Timmerman, P.; Reinhoudt, D. N.; Shinkai, S. *J. Am. Chem. Soc.* **2002**, *124*, 14631–14641.

# Chapter 3

## *Meta* Substitution of Calixarenes

Ondrej Kundrat and Pavel Lhoták

### 3.1 Foreword

One of the main advantages of the chemistry of calixarenes is the fact that they can be, with only few limitations, easily derivatised by numerous functional groups. This feature makes calixarenes very attractive starting point in the design of various receptors and building blocks as we can introduce the required substituents into a basic calixarene skeleton almost at will. Especially calix[4]arene became a frequently exploited molecule in supramolecular chemistry and one can find many regioselective transformations of its basic structure in the literature. The combination of well-established chemistry and a tuneable three-dimensional shape of its molecule (*cone*, *partial cone*, *1,2-alternate*, *1,3-alternate*) makes this compound very attractive in the design of more elaborated systems.

Electrophilic aromatic substitutions represent the most straightforward approach to the derivatisation of the upper rim in the classical calixarene series. Because of the general reactivity of calixarene skeleton, both direct and *ipso*-substitutions provide exclusively the corresponding *para*-substituted (*para* substitution relative to phenolic oxygen groups) compounds. These compounds then serve as valuable intermediates for further chemical transformations, e.g. in the design and synthesis of novel receptors/ligands. While direct *para*-substitution is the most common way of upper rim derivatisation, the *meta* positions of phenolic subunits have been inaccessible by direct reactions until recently. Obviously, whereas the *para* isomers of calixarenes are usually achiral compounds (due to the symmetry of calixarene molecules), the *meta* substitution should lead to inherently chiral systems with many possible applications in the design of chiral receptors. Moreover, the *meta*

---

O. Kundrat • P. Lhoták (✉)

University of Chemistry and Technology, Prague, Technická 5, 166 28 Prague 6, Czech Republic

e-mail: [lhotakp@vscht.cz](mailto:lhotakp@vscht.cz)

substitution still denotes a synthetic challenge thus representing intricately accessible substitution pattern in the chemistry of calixarenes.

Based on the above, this chapter is focused on the synthesis and some selected properties of *meta*-substituted calix[4]arenes known in the state of the art. The review is by no means comprehensive, but rather should be meant as an overview of the most common ways leading to the *meta*-substituted isomers, showing the synthetic strategies and approaches that can address this least accessible position of a basic calix[4]arene skeleton.

## 3.2 Basic Strategies for *Meta*-substituted Calixarenes

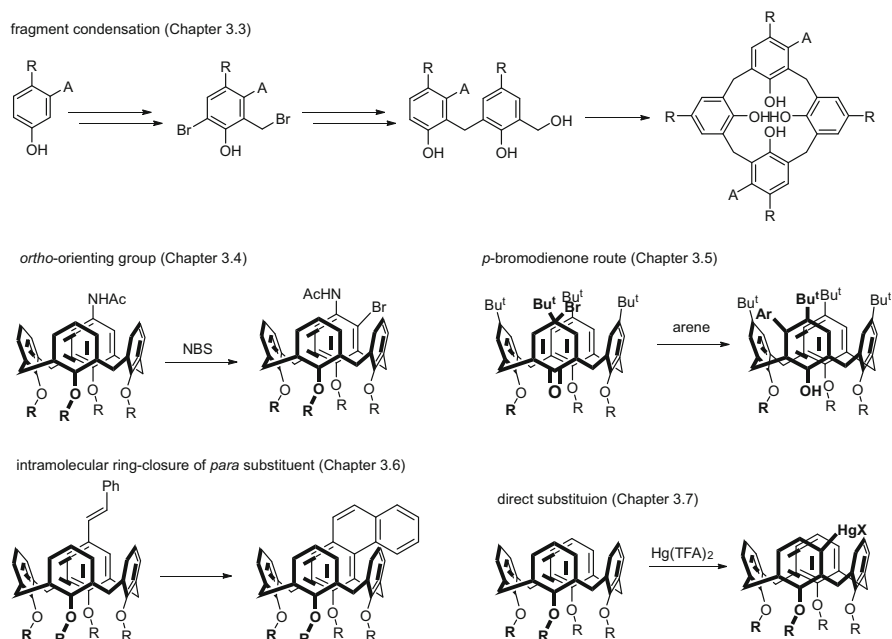
The oldest way providing *meta*-substituted calixarenes is based on the **step-by-step** or **fragment condensation method** (Scheme 3.1). This strategy represents a convergent stepwise synthesis of calixarene skeleton starting from suitable linear building blocks possessing *meta*-substituents within the molecules (see Sect. 3.3). On one hand, the final cyclization can provide *meta*-substituted macrocycles with almost limitless type of substitution. On the other hand, the overall yields of this approach are very low and depending on a particular substitution pattern. Moreover, the condensation reactions work well only with derivatives possessing free phenolic functions. Consequently, this approach leads to lower rim unsubstituted calixarenes.

Another strategy is based on the presence of **specific functional group** introduced previously into the *para* position of calixarene skeleton. This group then governs (***ortho*-orienting effect**) the introduction of new substituent into its *ortho* position thus overall leading to *meta* substituted products (see Sect. 3.4).

A novel strategy – so called “***p*-bromodienone route**” – was reported recently as a conceptually novel approach for the direct introduction of substituents into the *meta* position of calixarenes (see Sect. 3.5). In the key step, the calixarene *p*-bromodienone derivative undergoes a silver-mediated nucleophilic substitution and a subsequent rearomatization with a range of arenes to yield *meta* substituted isomers. Limitations of this approach involve relatively low yields (<30 %) and the formation of *p*-substituted compounds as byproducts, both depending on the reactivity of aromatic substrate.

Another possibility of *meta* substitution is represented by the **intramolecular ring closure reaction** of suitable substituent introduced into the *para*-position. This approach (see Sect. 3.6), so far only rarely used in calixarene chemistry, leads to systems with condensed polycyclic arrangement. As an example we can mention the photochemical condensation of styryl-substituted calixarene to form a compound containing a phenanthrene moiety (Scheme 3.1).

Very recently an unprecedented direct electrophilic substitution of calix[4]arenes leading to *meta*-substitution was described (see Sect. 3.7). Thus, the use of mercury (II) trifluoroacetate as an electrophile provides exclusively *meta*-



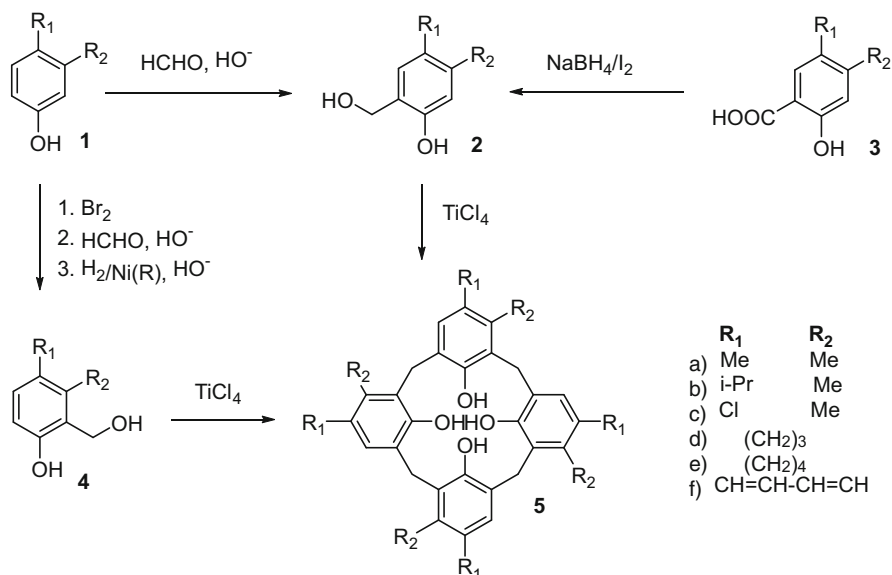
**Scheme 3.1** Strategies for *meta*-substituted calixarenes

organomercury derivatives that can be transformed into various products so far inaccessible in calixarene chemistry.

### 3.3 Fragment Condensation Method

From the synthetic point of view, the simplest case of the fragment condensation method is represented by the condensation of four identical *meta* substituted phenolic units, thus forming inherently chiral calixarenes possessing  $C_4$  symmetry. Theoretically, the reaction of *meta*-substituted phenols of type **1** with formaldehyde could lead directly to final calixarene structures **5**. In reality, this seemingly simple method can lead to a complex mixture of several regioisomers with different directions of *meta*-substituents. To avoid such a complication, the starting phenols **1** were reacted with the stoichiometric amount of formaldehyde in aqueous alkaline solution to give the corresponding 6-hydroxymethyl derivatives **2a-c** (Scheme 3.2) in a reasonable yield (around 50%) [1].

The naphthalene derivative **2f** was obtained by sodium borohydride reduction of the corresponding acid. While a direct reaction of 5,6,7,8-tetrahydro-2-naphthol **1e** with formaldehyde led to 2-hydroxymethyl derivative **4e** in 20% yield, similar hydroxymethylation of 5-indanol **1d** failed. The corresponding compound **4d** was accessible via rather complicated reaction pathway consisting of the bromination



**Scheme 3.2** Fragment condensation method

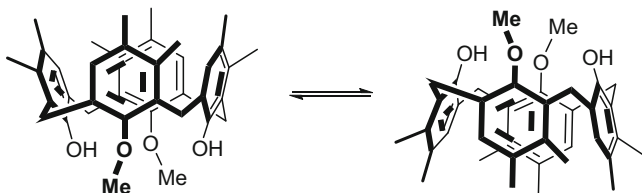
(84 %), subsequent hydroxymethylation (70 %) and final hydrogenolysis of bromine atom (rt, normal pressure, alkaline medium, Raney nickel) in 48 % yield.

The condensation of the monohydroxymethylated precursors **2** or **4** was carried out in dioxane, using  $\text{TiCl}_4$  as a catalyst. The yield of pure **5** varied between 5 % for **5f** to 30 % for **5b**. Although, in principle higher members of the calixarene family could be also formed by this condensation, calix[4]arenes **5** were the only reported cyclic compounds (confirmed by MS) [1].

Calix[4]arenes **5** can be converted to the tetraester derivatives by reaction with ethyl bromoacetate in the presence of  $\text{NaH}$  as a base. Interestingly, while **5a** provided the corresponding *cone* conformation as the sole product (62 % yield), **5b** gave a mixture of the *cone* (34 %) and the *partial cone* (30 %) conformations. This indicates rather unexpected influence of *para*-substituents (methyl versus isopropyl) on the conformational outcome of the alkylation reaction [1, 2].

Calix[4]arene **5a** and its partly and fully methylated ethers were investigated by applying various force fields or the PM3 semiempirical molecular orbital method. By exploration of the conformational space by random conformational searching, the numerous local energy minima were found differing in the torsion angles around the aryl-methylene bonds. By adjustment of selected parameters of the TRIPOS force field, a good agreement with experimental data was found [3].

An interesting application was found for 25,27-dimethoxy derivative of calix[4]arene **5a**, which exists exclusively as a *cone* conformation. This conformation is stable on the NMR time scale up to the highest accessible temperatures (125 °C in  $\text{CDCl}_2-\text{CDCl}_2$ ), in other words, the *cone-cone* interconversion cannot be studied by NMR technique. On the other hand, as the *meta* substituted calixarene in the *cone*



**Scheme 3.3** The *cone-cone* interconversion of 25,27-dimethoxy derivative of **5a**

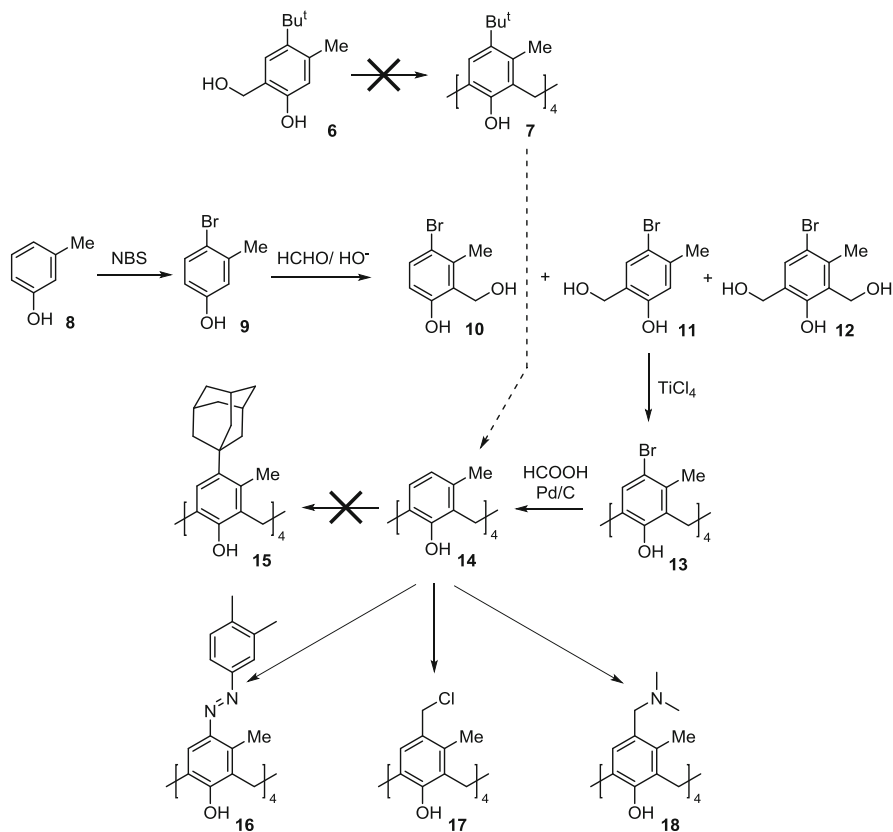
conformation is inherently chiral, the *cone-cone* interconversion represents the racemization process (Scheme 3.3) as the enantiomers are interconverting into each other. Thus, the rate constants of the thermal racemization were measured at various temperatures (from 283 to 323 K), and the resulting values were used for the construction of the corresponding Arrhenius plot. The application of Eyring equation led finally to the activation data ( $\Delta H^\ddagger = 15.6 \text{ kcal mol}^{-1}$ ,  $\Delta S^\ddagger = -25.3 \text{ cal mol}^{-1} \text{ K}^{-1}$ ,  $\Delta G^\ddagger = 23.3 \text{ kcal mol}^{-1}$  at  $T = 303 \text{ K}$ ) [4].

The resolution of racemate, the key prerequisite for the above study, was carried out by HPLC on a chiral stationary phase (Daicel Chiralpak AD). In this context, the resolution of racemates of some *meta* substituted calix[4]arenes on the 40–50 mg scale was reported. The corresponding circular dichroism (CD) spectra were obtained in all cases to confirm the separation [5].

The attempt to synthesize *meta*-methylcalix[4]arene **14** using the well-established procedure with *tert*-butyl protecting group, that can be easily removed, was unsuccessful due to the unexpected problems with the first step. Indeed, the cyclization reactions of **6** (Scheme 3.4) failed to give **7** under both basic and acidic conditions [6].

The alternative way to **14** is outlined in Scheme 3.4. The regioselective bromination of *m*-cresol **8** with NBS in DMF provided 4-bromo-3-methylphenol **9** in high yield (85 %). The key step was the hydroxymethylation of **9** to give isomer **11**. The reaction of **9** with aqueous HCHO and NaOH yielded a mixture of products **10**, **11** and **12** along with the starting material. The desired product **11** (30 %) and a small amount of the regioisomer **10** (5 %) were collected as a one fraction by chromatography. As the purity of **11** was proven critical to the cyclization, it was necessary to remove even trace amounts of **10** by fractional recrystallization from  $\text{CHCl}_3$ . The cyclization of **11** to form *para*-bromo derivative **13** in 25 % yield was accomplished by reaction with  $\text{TiCl}_4$  in a 1,4-dioxane solution. The final step was hydrogenolysis of bromine using Pd-C/formic acid in DMF which provided calixarene **14** in essentially quantitative yield. Despite the *meta*-substitution, the reactivity of **14** is similar to that of unsubstituted parent calix[4]arene as demonstrated by its transformations into the corresponding derivatives **16**, **17** and **18**.

Compound **5a** possessing the  $C_4$  symmetry was reacted with  $\text{WCl}_6$  in benzene to produce the dichlorotungsten complex **rac-19** in 81 % [7]. This complex was then resolved via diastereomeric intermediates. Thus, the reaction of **rac-19** with (*1S,2S*)-*trans*-cyclohexane-1,2-diol gave a diastereomeric mixture of **20** and **21**. Similarly, (*1S,2S*)-1,2-diphenylethane-1,2-diol provided a mixture of **22** and **23** in

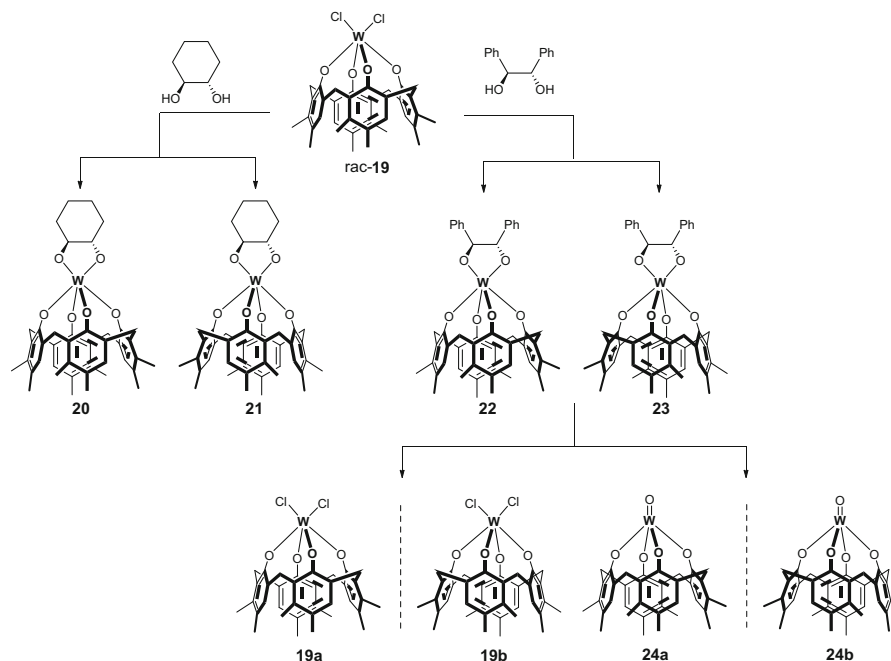


**Scheme 3.4** The alternative way to **14**

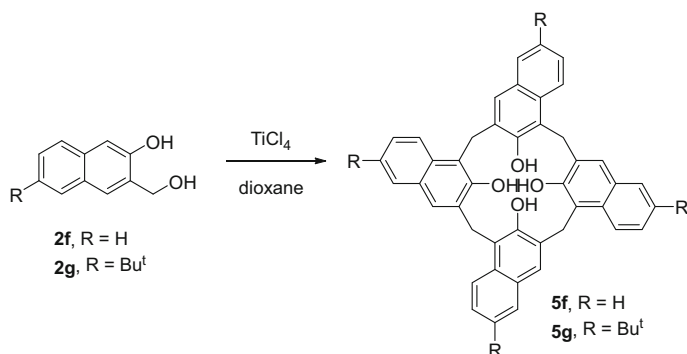
75 % yield, easily separable by flash chromatography. The separated diastereomers were then converted to the respective enantiomers **19a** and **19b** in near quantitative yield when treated with excess AlCl<sub>3</sub> (refluxing CHCl<sub>3</sub>, 3 min). The treatment of **22** and **23** with trimethylsilyl triflate followed by an aqueous workup gave enantiomers **24a** and **24b** (Scheme 3.5).

The self-condensation of 3-hydroxymethyl-2-naphthol **2f** with TiCl<sub>4</sub> gave the corresponding calixarene **5f** in 13 % yield (Scheme 3.6). Interestingly, the same reaction with 6-*tert*-butyl derivative **2g** provided macrocycle **5g** in a reasonable 31 % yield (Scheme 3.6). As found by <sup>1</sup>H NMR, both calixarenes are conformationally flexible at room temperature since the methylene protons appeared as a sharp singlet corresponding probably to the fast *cone*–*cone* interconversion. At lower temperatures, the signal of methylene bridges split into a well-resolved AB quartet indicating the *cone* conformation [8]. The crystallographic analysis of **5f** showed a typical *pinched cone* conformation with an unusual dimeric structure based on the inclusion of one naphthalene subunit into the cavity of the neighbour molecule (Fig. 3.1). The distance between the two coplanar naphthalene moieties





**Scheme 3.5** Tungsten complexes of *meta*-substituted calix[4]arenes

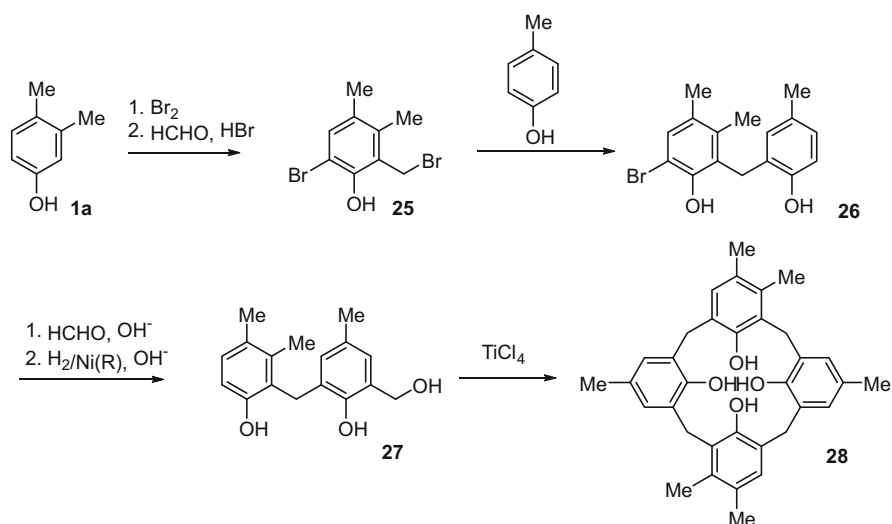
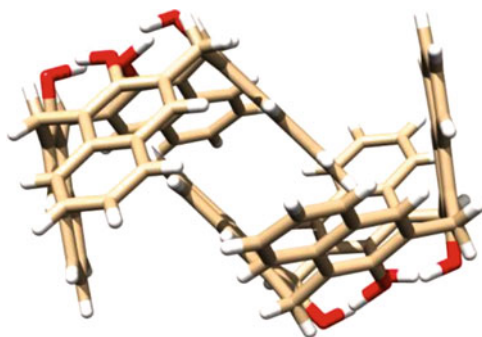


**Scheme 3.6** The self-condensation of 3-hydroxymethyl-2-naphthols

(3.45 Å) corresponds to  $\pi$ - $\pi$  interactions. Regioisomer of **5f** possessing lower  $C_{2v}$  symmetry was also prepared by the cyclocondensation of a key bisnaphthylmethane intermediate with formaldehyde [9].

To exploit the extended calixarene cavity capable of the  $\pi$ - $\pi$  interactions, the complexation ability of **5f**, **5g** towards fullerene  $C_{60}$  was studied using UV/Vis titration experiments in benzene, toluene and  $CS_2$  [10]. The results obtained, especially very high complexation constants in  $CS_2$ , were later revisited. The

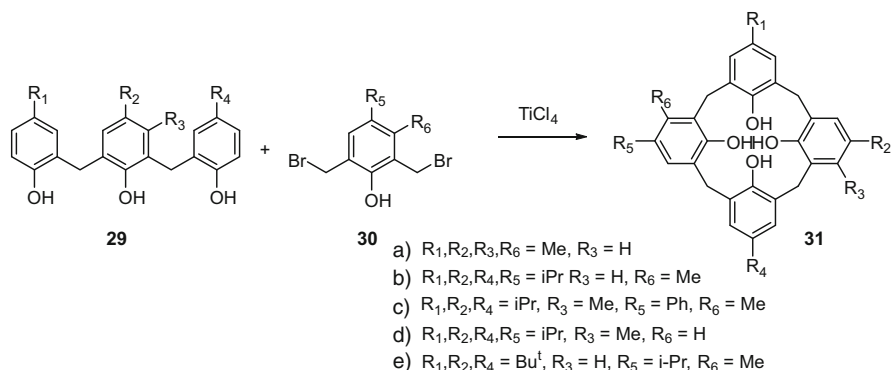
**Fig. 3.1** The X-ray structure of **5f** showing a dimeric motif



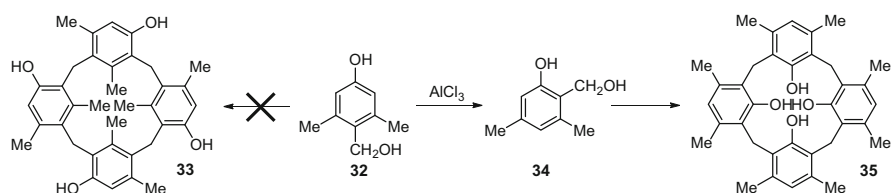
**Scheme 3.7** Pathway leading to derivative **28** possessing a  $C_2$  symmetry

complexation behaviour of calix[4]naphthalenes **5f** and **5g** with  $C_{60}$  in toluene and carbon disulfide was re-examined [11] using the combination of UV/Vis and NMR methods. While **5g** formed a 1:1 complex with  $C_{60}$  in toluene ( $176 \pm 21 \text{ M}^{-1}$  by UV/Vis,  $217 \pm 44 \text{ M}^{-1}$  by NMR), neither UV/Vis nor NMR titrations provided unequivocal evidence for the complexation of  $C_{60}$  in  $CS_2$ .

The synthesis of *meta*-substituted calixarenes with lower symmetry involves usually more steps, and consequently, it represents a synthetic challenge. A reaction pathway leading to derivative **28** possessing the  $C_2$  symmetry is outlined in Scheme 3.7 [1, 2]. Starting 3,4-dimethylphenol **1a** was regioselectively brominated in position 6 (76%), followed by bromomethylation in position 2 (49%) to give derivative **25**. A subsequent condensation with excess of *p*-cresol led to bisphenolic compound **26** (69%), which was hydroxymethylated (72%) and the remaining bromine atom was removed by hydrogenolysis on Raney nickel (85%) to yield



**Scheme 3.8** The cyclocondensation of trinuclear oligomers **29**



**Scheme 3.9** Preparation of octakis *meta*-substituted calixarene **35**

mono(hydroxymethyl) dimer **27**. The final cyclization with  $\text{TiCl}_4$  provided calix[4]arene **28** in acceptable 20 % yield.

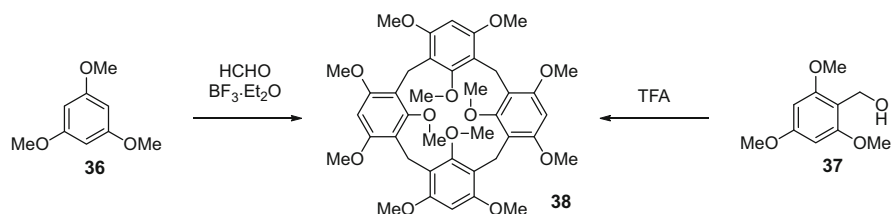
The cyclocondensation of trinuclear oligomers **29** with appropriate 2,6-bis(bromomethyl)phenols **30** (Scheme 3.8) represents another way to products possessing no symmetry elements – calix[4]arenes **31** [12]. The key prerequisite is the application of high dilution conditions leading to products **31a-d** in 10–35 % yield. Similarly, *tert*-butyl derivative **31e** was obtained in 9 % yield, and then alkylated to give the *cone* conformation, which was resolved into pure enantiomers using chiral column - Daicel Chiralpak OP(+) [13].

When a solution of 2,6-dimethyl-4-hydroxybenzyl alcohol **32** in nitrobenzene was treated with 0.5 equiv. of  $\text{AlCl}_3$  at 90 °C, the expected macrocycle **33** was not observed, but isomeric calixarene **35** was isolated as the sole product in 28 % yield [14]. This remarkably simple preparation of octakis *meta*-substituted calixarene **35** probably involves the rearrangement of **32–34** prior to the cyclization (Scheme 3.9). Indeed, when **34** was submitted to the same reaction conditions, **35** was obtained in 50 % yield. Dynamic behaviour of **35** was studied using the combination of NMR study and molecular mechanics calculations. The NMR spectra are in agreement with a species that is conformationally mobile on the NMR time scale at room temperature. The increased flexibility of **35** compared to parent calix[4]arene can be ascribed to the lower energy barrier for inversion due to the steric repulsions

between the methyl groups at neighbouring rings as well as to the presence of weaker intramolecular hydrogen bonds which hold the conformation [15].

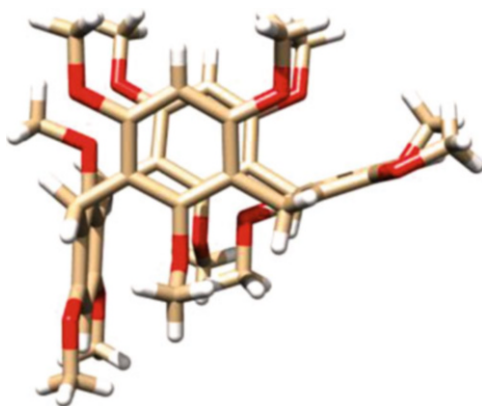
Another very simple preparation of calixarene with all *meta* positions substituted was described recently [16]. The condensation of 1,3,5-trimethoxybenzene **36** with paraformaldehyde in the presence of  $\text{BF}_3 \cdot \text{Et}_2\text{O}$  as a Lewis acid catalyst successfully rendered calix[4]arene **38** in 43 % yield. This condensation is rather exceptional as this is the first example of calixarene formation where alkylated phenol (not free one) was used (Scheme 3.10). As the macrocycle lacks free phenolic functions that usually hold the *cone* conformation via circular hydrogen bonds, the *partial cone* was found to be the preferred conformation in the solid state (Fig. 3.2). As shown by dynamic NMR study, the same conformation is preferred also in solution at low temperature ( $\text{CDCl}_3$ ,  $-40^\circ\text{C}$ ) while at room temperature the system is conformationally mobile. When 2,4,6-trimethoxybenzyl alcohol **37** was treated [17] with TFA (10 % in  $\text{CHCl}_3$ ) for 2 h at room temperature and the resulting solution was diluted with carbon tetrachloride and evaporated, maroon-red crystals of complex **38**·2.5 TFA was isolated in 88 % yield. The colourless, TFA-free calixarene **38** can be obtained by triturating of this complex with acetone (74 %). Alternatively, free **38** can be isolated directly by washing the reaction mixture of alcohol **37** and TFA with aqueous  $\text{K}_2\text{CO}_3$  (89 %).

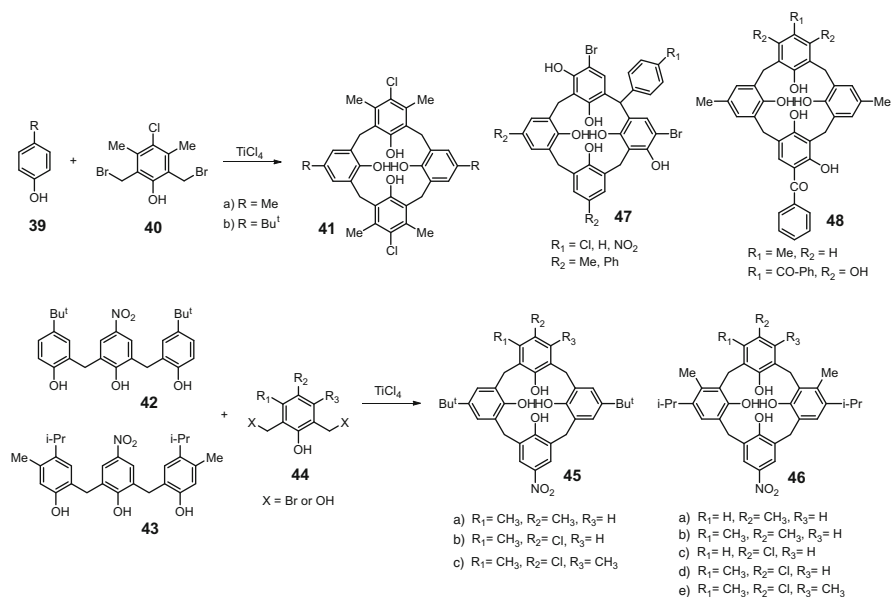
Achiral *meta*-substituted calix[4]arenes **41** with  $C_{2v}$  symmetry were prepared [18] by condensation of phenols **39** with bis(bromomethyl) phenol derivative



**Scheme 3.10** The condensation of 1,3,5-trimethoxybenzene **36**

**Fig. 3.2** The X-ray structure of **38** showing the *partial cone* conformation



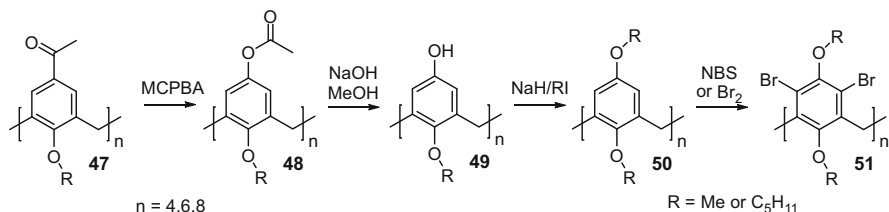


**Scheme 3.11** Fragment condensations

**40** under the catalysis of  $\text{TiCl}_4$ , both compounds were formed only in low yield (8–10%). A similar type of condensation reaction, although in less symmetrical fashion, was carried out to obtain compounds **45** and **46** (Scheme 3.11). Fragment condensations of linear trimers **42** or **43**, containing the *p*-nitrophenol unit in the middle, with the bis(bromomethyl)ated or bis(hydroxymethyl)ated phenol **44** that forms the opposite phenolic unit in the calix[4]arene, were carried out. As expected, the yields of final cyclization step only seldom exceed 10% (e.g. 21% for **46a**), and especially in systems where methyl groups in *meta*-positions come into a close proximity the yields are extremely low (3% for **46b** or **46d**, 0.6% for **46e**) [19]. Similar strategy was used also in the synthesis of **47** (prepared by 2+2 condensation in 10% yield) or for the preparation of **48** (3+1 condensation in 8% yield) [20].

### 3.4 Introduction of *Ortho*-orienting Group into the *Para* Position

Introduction of a strong electron-releasing substituent (*ortho/para* directing) into the *para* position of calixarene skeleton can be used for directing electrophilic substitution into the *meta* position. So far only few examples of this strategy have been published as even the introduction of *ortho/para* directing substituent itself is not a simple task. Thus, the introduction of ether functions into the *para* position of

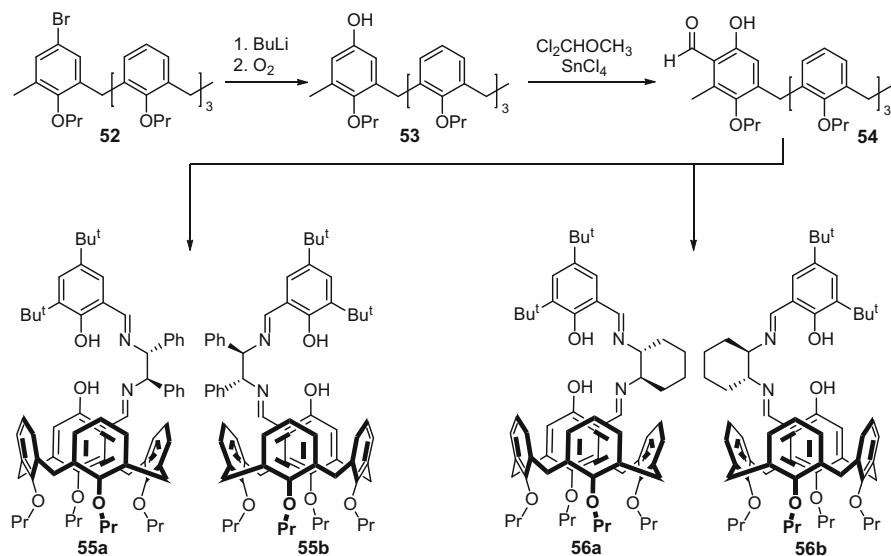


**Scheme 3.12** Introduction of a strong electron-releasing substituent (*ortho/para* directing) into the *para* position

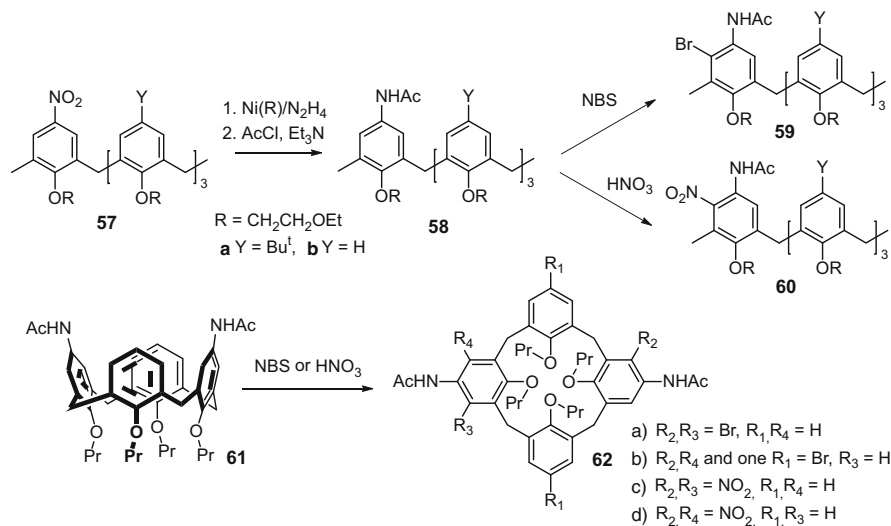
calix[*n*]arenes ( $n = 4, 6, 8$ ) was described [21]. The whole synthesis starts with Friedel–Craft acetylation of alkoxy-calix[*n*]arenes (Scheme 3.12) to yield acetylated compounds **47**, subsequent Baeyer–Villiger reaction under carefully controlled conditions gave acetoxycalixarenes **48**. These intermediates can be hydrolysed to provide *para*-hydroxy derivatives **49** that are finally alkylated to provide derivatives **50**. These electron rich macrocycles were exposed to acetyl chloride under Friedel–Crafts conditions without any evidence of reaction. On the other hand, electrophilic bromination gave the expected perbromo derivatives of calix[4]arene and calix[8]arene **51** ( $n = 4, 8$ ) in acceptable (32–67 %) yields. The reaction of calix[6]arene **50** ( $n = 6$ ) with bromine resulted in a complex mixture of products (containing expected product **51**) which could not be separated [22].

A similar approach was applied in the preparation of novel chiral (salen)  $\text{Mn}^{\text{III}}$  and  $\text{UO}_2$  complexes containing a calix[4]arene unit in the ligand framework (Scheme 3.13) [23]. Starting bromo derivative **52** immobilized in the *cone* conformation was transformed into the corresponding hydroxycalixarene **53**. Gross formylation with dichloromethyl methyl ether/ $\text{SnCl}_4$  led regioselectively to salicyl aldehyde derivative **54** in 75 % yield. This compound was reacted with (*1R,2R*)-1,2-diphenylethylenediamine or (*1R*)-trans-1,2-cyclohexanediamine to provide pairs of diastereomers **55** and **56** that were separated using column chromatography and used for the preparation of chiral metal complexes. The  $\text{Mn}^{\text{III}}$  complexes were applied as catalysts in enantioselective epoxidation of alkenes with  $\text{NaClO}$ .

The starting mono(acetamido)-substituted calix[4]arenes **58** (Scheme 3.14), immobilised in the *cone* conformation, bearing at the *para* positions of the other rings *tert*-butyl groups or hydrogen atoms, were prepared by reduction of the corresponding mononitrocalix[4]arenes **57** with Raney nickel and hydrazine followed by acylation with acetyl chloride in 60–66 % overall yields. The reaction of **58a** with 1.2 equiv. of NBS in butan-2-one for 24 h at room temperature gave monobromocalix[4]arene **59a** in 64 % yield after column chromatography. A similar reaction of **58b**, without *para-tert*-butyl groups at the other aromatic rings, afforded compound **59b** in 58 % (Scheme 3.14) [24]. This indicated that despite possible steric hindrance, bromination did also take place adjacent to the acetamido group and not at the free *para* positions of the phenolic subunits. Similar results were also obtained for nitration reaction where compounds **60a** and **60b** were obtained in excellent yields (98 % and 91 %, respectively). Subsequently, the

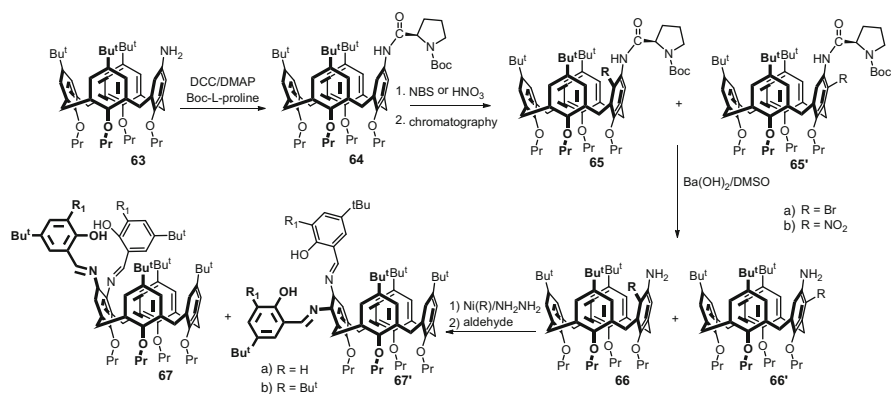


**Scheme 3.13** Preparation of chiral (salen)Mn<sup>III</sup> and UO<sub>2</sub> complexes containing a calix[4]arene unit in the ligand framework



**Scheme 3.14** *Meta*-brominated or nitrated derivatives

behaviour of the bisderivative **61** towards the *meta* substitution was studied. Bromination with 2.4 equiv. of NBS gave a complicated reaction mixture from which two compounds were isolated - the desired dibromo derivative **62a** (10%) and tribromocalix[4]arene **62b** (22%) with an ambiguous position of the third



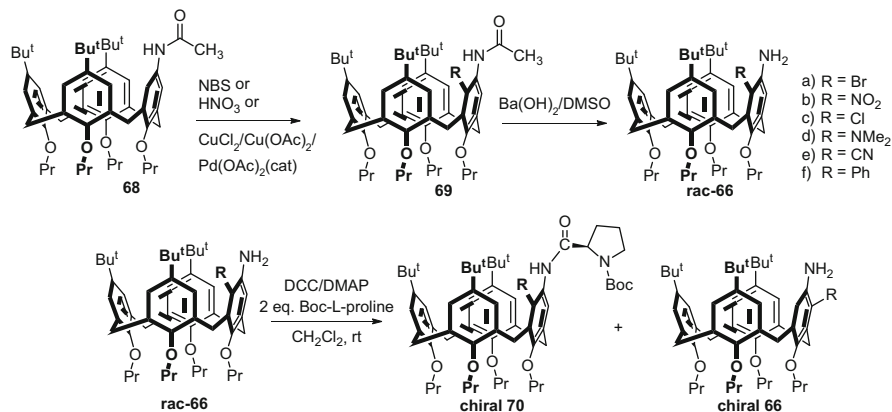
**Scheme 3.15** Resolution of *meta*-brominated or nitrated derivatives

bromine atom (R<sub>1</sub>). Nitration of **61** with 2.7 equiv. of 65% HNO<sub>3</sub> at room temperature gave a mixture of chiral **62c** and achiral **62d** isomers, isolated by column chromatography in 53% and 18% yield, respectively.

Similar strategy was used for the resolution of *meta*-brominated or nitrated derivatives (Scheme 3.15). Starting from aminocalix[4]arene **63**, amide **64** was prepared in 71% yield by the reaction with Boc-L-proline in the presence of DCC and DMAP. Bromination of this compound with an excess of NBS gave the mixture of diastereomers **65a** and **65a'** in 83% total yield, which could be readily separated by preparative TLC. The final hydrolysis of chiral auxiliary group (L-proline) to provide pure enantiomers **66a** (82%) and **66a'** (85%) was carried out with Ba(OH)<sub>2</sub>·8H<sub>2</sub>O in *n*-butanol/DMSO mixture. Moreover, the nitration of **64** with 100% HNO<sub>3</sub> gave the mixture of diastereomers **65b** and **65b'** which were separated by column chromatography, the final deprotection to yield *meta*-nitro compounds **66b** (86%) and **66b'** (88%) was carried out under identical conditions as described for bromo derivative [25]. These enantiomers were reduced using Raney nickel in hydrazine and then reacted with commercially available 3-*tert*-butylsalicylaldehyde or 3,5-di-*tert*-butylsalicylaldehyde to give the salphen ligands **67** and **67'** in good yields [26]. Reactions of **67a** and **67'a** with metal acetates (M(OAc)<sub>2</sub>, M = Ni<sup>2+</sup>, Zn<sup>2+</sup>, Cu<sup>2+</sup>) provided the corresponding chiral salphen complexes in 80–95% yields. On the other hand, the same reactions with **67b** and **67'b** did not lead to expected complexes, probably due to the steric hindrance of additional Bu<sup>t</sup> group. Structures of type **65/65'** bearing L-proline and (CH<sub>3</sub>)<sub>2</sub>N- moieties were used as organocatalysts for enantioselective aldol reactions [27]. The reaction between 4-nitrobenzaldehyde and cyclopentanone at –20 °C gave the *anti*-aldol product up to 94% ee, while the *anti*-aldol product in up to 94:6 dr and 79% ee was obtained when 4-cyanobenzaldehyde was used.

Starting from aminocalix[4]arene **63**, compound **68** was prepared in 65% yield by the reaction with acetyl chloride (Scheme 3.16). Bromination with NBS in butan-2-one gave *meta*-bromo derivative **69a** in 62% yield. Subsequent hydrolysis with Ba(OH)<sub>2</sub> in *n*-butanol/DMSO provided racemic **rac-66a** in 95% yield.

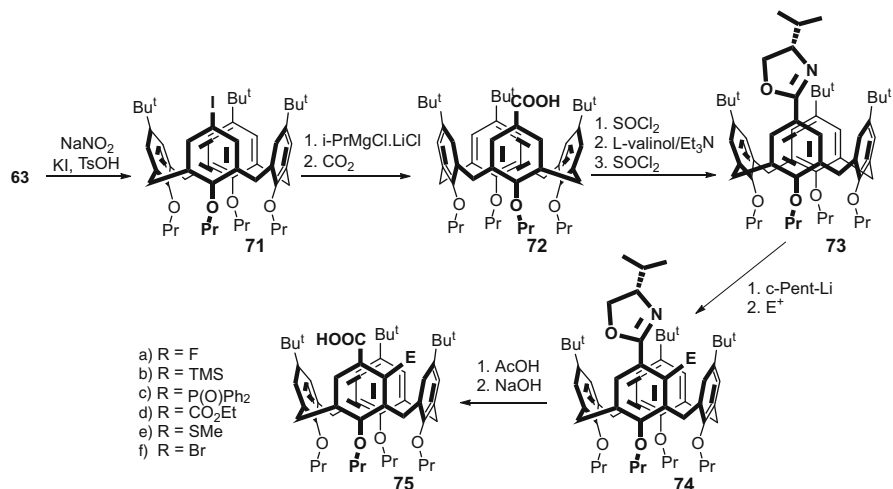




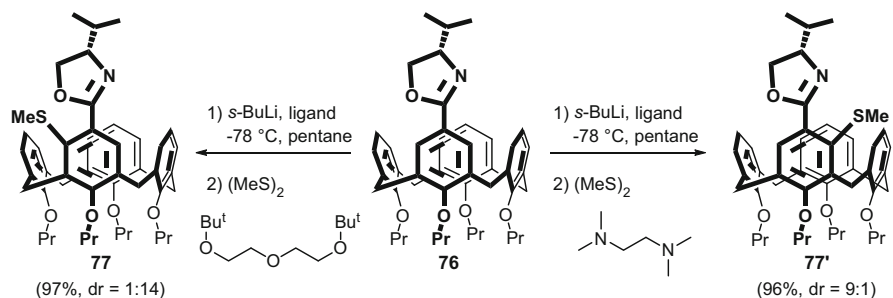
**Scheme 3.16** Kinetic resolution process

Similarly, nitration with HNO<sub>3</sub> (100 %) led to racemic *meta*-nitro compound **69b** in 95 % yield, which was then hydrolyzed to **rac-66b** in 90 % yield (Scheme 3.16) [28]. While the chlorination of **68** with NCS did not work, the corresponding *meta*-chloro product **69c** was obtained by the reaction with CuCl<sub>2</sub> in the presence of Pd(OAc)<sub>2</sub> and Cu(OAc)<sub>2</sub> in 49 % yield. Hydrolysis of **69c** to **rac-66c** was accomplished by *t*-BuONa in *n*-butanol/DMSO in 81 % yield. Reduction of compound **69b** with Raney nickel and hydrazine hydrate in THF, followed by methylation with HCHO/NaBH<sub>3</sub>CN and by final hydrolysis gave *meta*-dimethylamino substituted calix[4]arene **rac-66d**. The key step in the preparation of derivative **rac-66e** was the Pd-catalysed nucleophilic substitution of **69b** with CuCN. Phenyl substituent in **rac-66e** was introduced via Suzuki coupling of **69b** with phenylboronic acid in the presence of Pd(PPh<sub>3</sub>)<sub>4</sub> and Na<sub>2</sub>CO<sub>3</sub>. Previously was shown that 2.0 equiv. of Boc-L-proline could serve as a highly effective chiral acylating reagent for the nonenzymatic kinetic resolution of **rac-66b** to yield chiral **70b** and recovered chiral **66b** (Scheme 3.16) [29]. The kinetic resolution of other racemic aminocalix[4]arenes **rac-66** was studied with Boc-L-proline and Cbz-L-proline. The authors have found that the nature of the *meta*-substituent exhibited profound effect in the control of stereoselectivity of the kinetic resolution process [28].

Recently, a chiral oxazoline as an *ortho*-lithiation directing group was introduced into calix[4]arene to allow the asymmetric functionalization of the upper rim of the calixarene. Starting amino derivative **63** was iodinated via diazotization to give **71** in 79 % yield (Scheme 3.17). Corresponding carboxylic acid **72** (60 %) was then obtained by metallation with *i*-PrMgCl·LiCl and CO<sub>2</sub>. An oxazoline moiety was then introduced using standard conditions with L-valinol to provide **73** in 94 % yield. The best results in *ortho*-lithiation were achieved by cyclopentyllithium (6 eq.) and TMEDA (12 eq.) in Et<sub>2</sub>O at -78 °C, subsequent quenching with electrophile then led to the isolation of the main diastereomers **74a-f** in good yields (62–73 %). To remove the oxazoline chiral auxiliary, a two-step microwave



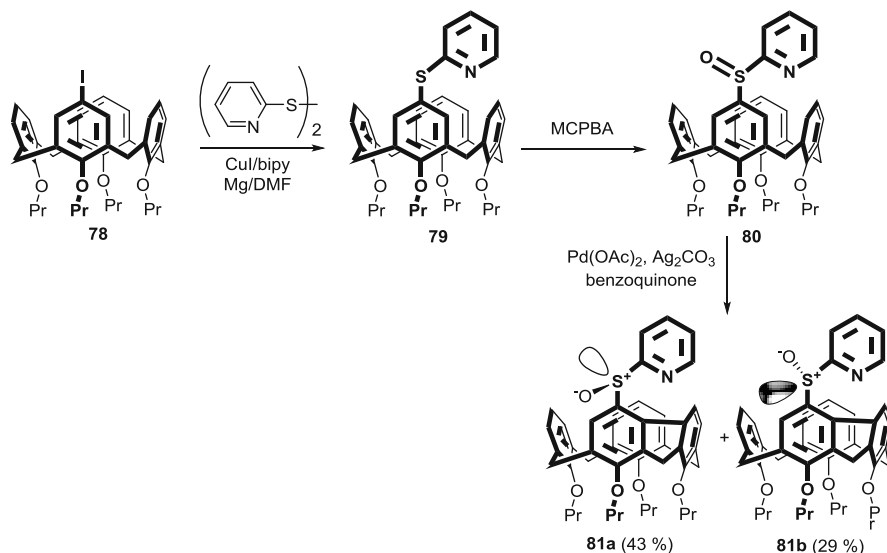
**Scheme 3.17** Chiral oxazoline as an *ortho*-lithiation directing group



**Scheme 3.18** Direction of asymmetric *ortho*-lithiation can be completely reversed by the choice of a suitable achiral ligand

reaction was revealed as the most efficient. Thus, heating the oxazolines **74** in aqueous acetic acid at 170 °C for 1 h followed by heating with ethanolic solution of sodium hydroxide to 140 °C gave the inherently chiral carboxylic acids **75a,c-f** in good yields (TMS derivative **74b** decomposed under reaction conditions) [30].

It was demonstrated that the diastereoselectivity of *ortho*-lithiation depends on a fine balance between ligand and alkyl lithium choice [31]. The optimization of the reaction conditions with starting oxazoline derivative **76** (prepared analogously to compound **73**) led to the conclusion that the direction of asymmetric *ortho*-lithiation, imposed by a chiral oxazoline moiety, can be completely reversed by the choice of a suitable achiral ligand (Scheme 3.18). Thus, the best result was obtained by the combination of *N,N,N',N'*-tetramethylethylenediamine (TMEDA) and *sec*-BuLi in pentane, that led to diastereomer **77'** in 96 % yield and dr = 9:1

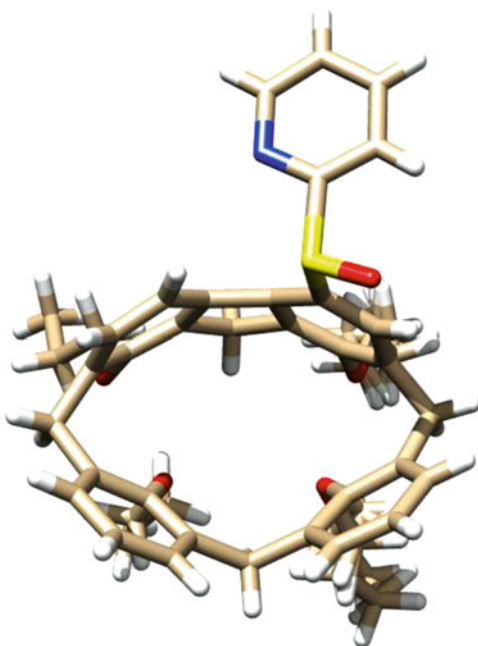


**Scheme 3.19** Synthesis of unprecedented derivatives with intramolecularly bridged *meta* positions of two neighbouring aromatic subunits

(Scheme 3.18). On the other hand, the di-*tert*-butyl ether of diethylene glycol exhibited high preference for the opposite diastereomer, providing **77** in excellent yield (97 %, dr = 1:14) [32]. Inherently chiral bidentate (*S/N*) ligands of type **77**/**77'** (and their *tert*-butyl counterparts) were evaluated for their catalytic ability in the Pd-catalysed Tsuji–Trost allylation reaction. The results proved that these ligands are both efficient and selective. On the other hand, they also suggested that the selectivity was largely due to the chiral oxazoline moiety and not due to the inherent chirality of the calixarene system [33].

The introduction of a 2-pyridylsulphoxide moiety into the upper rim of calix[4]arenes enabled the synthesis of unprecedented derivatives with intramolecularly bridged *meta* positions of two neighbouring aromatic subunits (Scheme 3.19). Starting iodocalix[4]arene **78** in the *cone* conformation was transformed into sulphide **79** (55 %) using the reaction with 2-pyridine disulphide and a CuI/Mg/Bipy catalytic system in DMF. The oxidation to sulphoxide **80** was smoothly accomplished with *meta*-chloroperoxybenzoic acid in chloroform (87 % yield). Sulphoxide **80** was then subjected to the reaction with Pd(OAc)<sub>2</sub> (10 mol%), Ag<sub>2</sub>CO<sub>3</sub> and benzoquinone (oxidants) in a DCE–benzene mixture (attempted arylation with benzene). Instead of the introduction of phenyl ring, the formation of two new compounds **81a** (43 %) and **81b** (29 %) was observed [34]. These diastereomers represent a completely novel type of substitution pattern in calix[4]arene chemistry with very rigid and distorted cavities as documented by X-ray structure of compound **80a** (Fig. 3.3).

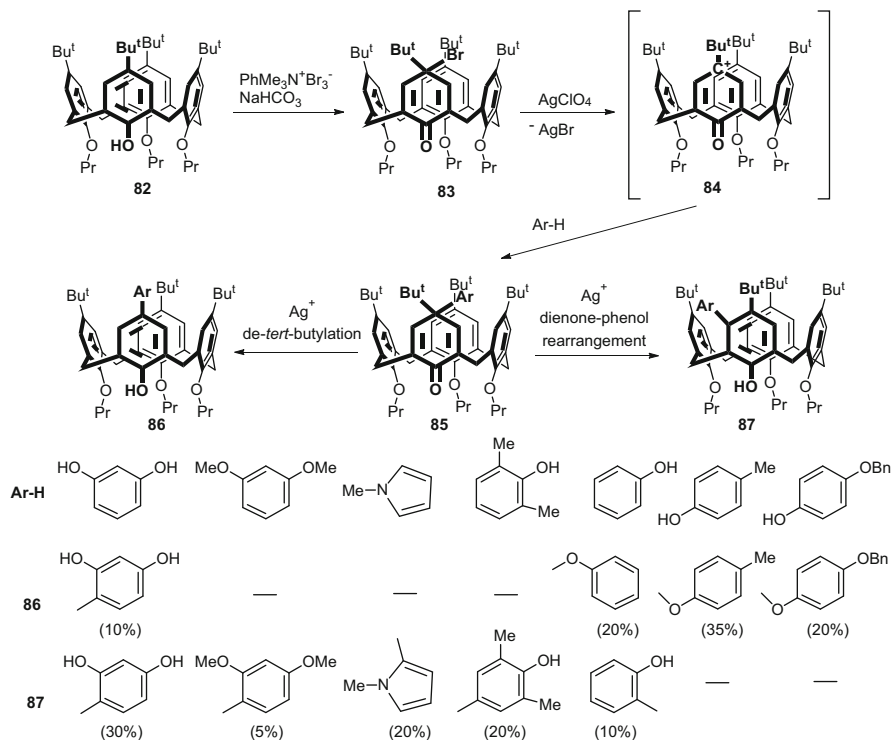
**Fig. 3.3** The X-ray structure of **81a**



### 3.5 Bromodienone Route

This strategy is based on the silver-mediated nucleophilic substitution of calixarene *p*-bromodienone derivatives with selected aromatic substrates. Starting calixarene *p*-bromodienone **83** was easily obtained in 81% yield via the oxidation of tripropoxycalix[4]arene **82** with trimethylphenylammonium tribromide and a saturated solution of NaHCO<sub>3</sub> (Scheme 3.20). In this context, it was found that calixarenes *p*-bromodienones are generally accessible if the reacting phenol rings in the starting calixarene molecule are in non-proximal positions. Alternatively, *p*-bromodienones based on calix[8]arenes were also prepared using Br<sub>2</sub>/AcOH as the brominating agent [35].

Calixarene *p*-bromodienone derivatives were found synthetically useful as they can react with various nucleophiles (e.g. alcohols or acetate) in the presence of AgClO<sub>4</sub> to give the corresponding *para*-substituted (alkoxy or acetoxy) derivatives [36]. Interestingly, if activated aromatic substrates were used for this reaction, an aryloxonium cation **84**, initially formed upon precipitation of AgBr, can react by electrophilic aromatic substitution reaction. Obviously, cation **84** can capture an aromatic nucleophile to give dienone intermediate **85** which then undergoes *de-tert*-butylation and re-aromatization to give *para*-substituted isomers **86**. At the same time, there is one more reaction pathway, namely dienone-phenol rearrangement with 1,2-migration of aryl moiety into the *meta* position, assuming that the aryl group has higher migration capacity compared with *tert*-butyl group [37]. This

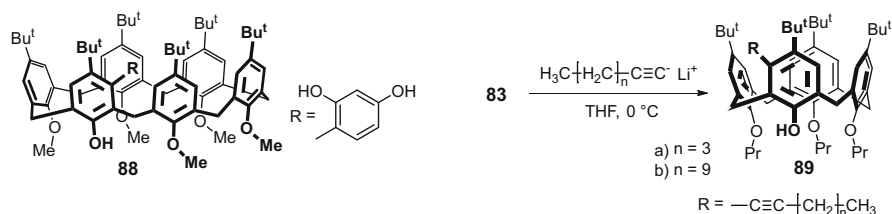
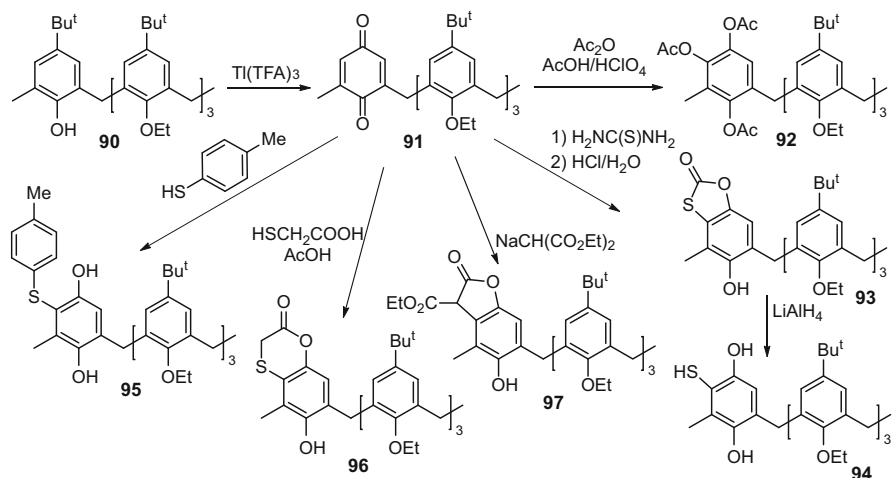


**Scheme 3.20** Calixarene *p*-bromodienone route

mechanism leads to the formation of derivatives **87**, although the yields of *meta*-products are usually low. Moreover, as can be seen in Scheme 3.20, in case of phenols substituted in *para*-position with an alkyl, alkoxy, and hydroxy groups, only C-O coupled products of type **86** (*p*-aryloxy derivatives) were formed. Very recently, the same reaction of the corresponding *p*-bromodienone derivative (prepared from the pentamethoxycalix[6]arene) led to the isolation of calix[6]arene **88** (30% yield) bearing the 2,4-dihydroxyphenyl group in the *meta*-position. This indicates that this strategy is applicable also for bigger calixarene molecules [38].

The analogous reaction of **83** with phloroglucinol (1,3,5-trihydroxybenzene) led to the corresponding isomer of type **87** in 10% yield. The racemic mixture of this compound was resolved by chiral HPLC on Chiralpak ADH stationary phase using propan-2-ol/hexane (2:98) as mobile phase. The absolute configuration of the two separated enantiomers was determined by the comparison of experimentally measured optical rotation dispersion and electronic circular dichroism with DFT calculations of these chiroptical properties [39].

As reported recently [40], the application of carbon nucleophiles such as acetylide ions proceeds entirely via dienone-phenol rearrangement pathway. Thus, a THF solution of the appropriate acetylide was added to a solution of

Scheme 3.21 Derivatives **88** and **89**

Scheme 3.22 Nucleophilic additions to quinones

*p*-bromodienone **83** (Scheme 3.21) in the same solvent. The corresponding *meta*-substituted products **89a** and **89b** were isolated in acceptable yields (48 % and 43 %, respectively) after a column chromatography.

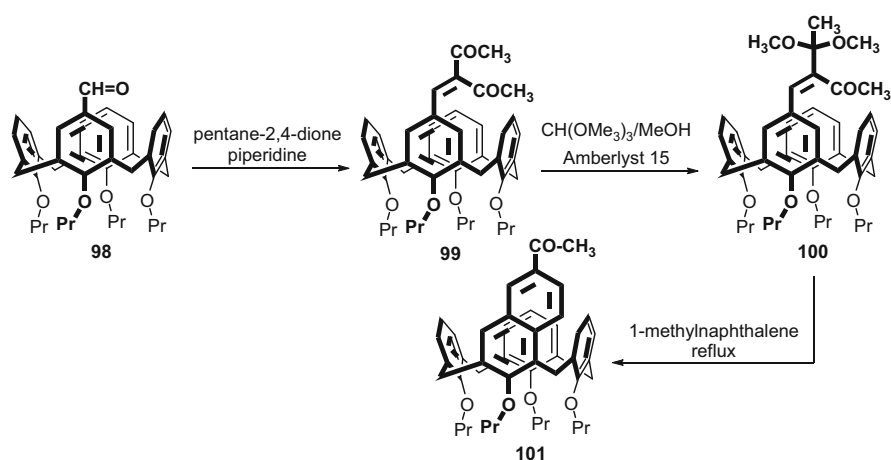
As the nucleophilic additions to quinones often proceed as a 1,4-addition (conjugate addition), the reactivity of calix[4]arene monoquinone was studied to assess the synthetic potential of this method in the preparation of the *meta*-substituted calixarenes (Scheme 3.22). Starting quinone **91** was obtained in 51 % yield by the oxidation of triethoxy derivative **90** with thallium(III) trifluoroacetate [41]. The reaction of **91** with thiourea in HOAc/HCl formed an *S*-arylthiuronium salt which, without isolation, provided the benzoxathiolone **93** in 80 % yield. Subsequent reduction with  $\text{LiAlH}_4$  led to *meta*-thiol **94** in 63 % yield. Similarly, the reaction with thiols gave the corresponding conjugate addition products in high yields. Thus, the reaction of **91** with *p*-thiocresol in HOAc at room temperature afforded **95** in 80 % yield, while thioglycolic acid under heating gave **96** in 81 % yield. The wide range of possibilities of this approach can be further documented by the treatment of **91** with  $\text{Ac}_2\text{O}/\text{HOAc}$  in the presence of  $\text{HClO}_4$  leading to triacetate

**92** in 62 % yield, or by the formation of **97** (67 %) produced by reaction with sodium salt of diethyl malonate [42].

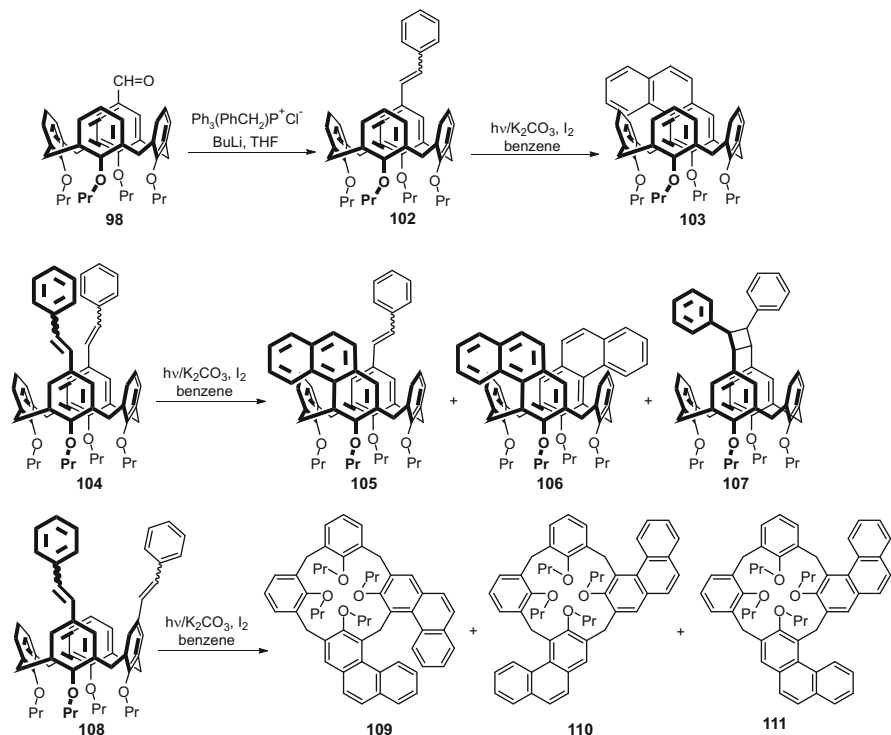
### 3.6 Intramolecular Ring-Closure of *Para* Substituent

Generally, the number of suitable reactions applicable in this strategy is rather limited. Moreover, suitable starting compounds are usually not easily accessible. As a result, this approach has been only rarely used so far. One of the few examples of this approach is depicted in Scheme 3.23. Starting aldehyde **98** (accessible from the corresponding bromo derivative via lithiation and reaction with DMF) was subjected to Knoevenagel condensation with acetylacetone in the presence of piperidine as a catalyst to give **99** in 87 % yield. The acetalization step was carried out by stirring a solution of **99** in a HC(OCH<sub>3</sub>)<sub>3</sub>-MeOH mixture in the presence of Amberlyst-15. This method led selectively to acetal **100** in the *trans* position to the aromatic ring which could be transformed into the naphthalene product by pyrolytic reaction. This final step was accomplished by refluxing **100** in 1-methylnaphthalene solution (ca 240 °C) to give **101** in overall 19 % yield (based on **99**) [43].

A similar approach based on the well-known photochemical oxidative cyclization of stilbenes was reported (Scheme 3.24). Stilbene derivative **102** was obtained in 86 % yield by Wittig reaction from aldehyde **98** as a mixture of stereoisomers (*E*:*Z* = 60:40). The isomers were separable by chromatography, but in fact it was not necessary as the quantum yield of the photo-induced (*E/Z*) isomerization generally is much higher than that of the subsequent electrocyclic ring closure. Subsequent photolysis in benzene (125-W Hg medium-pressure lamp, quartz filter) in the presence of I<sub>2</sub> and K<sub>2</sub>CO<sub>3</sub> gave expected calixphenanthrene **103** in excellent yield



**Scheme 3.23** Intramolecular ring-closure of *para* substituent



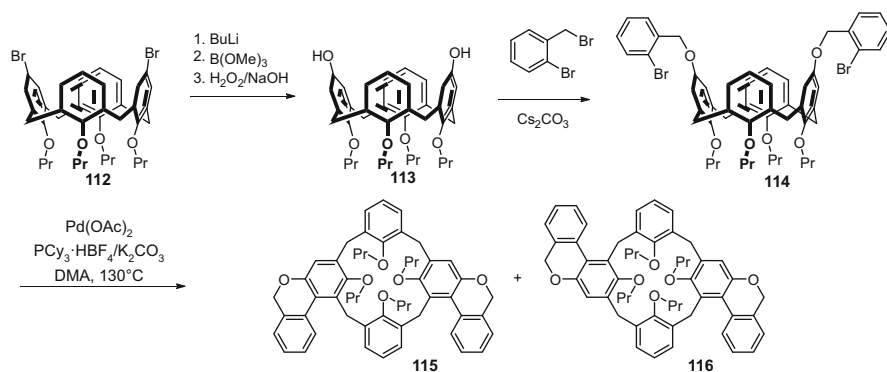
**Scheme 3.24** Photochemical oxidative cyclization of stilbenes

(86 %). The same reaction conditions in the absence of base led to the cleavage of calixarene skeleton [44].

Analogous reaction sequences were used to prepare starting bis(stilbene) derivatives **104** and **108**. The photocyclization of distal compound **104** gave under optimized reaction conditions ( $I_2$ ,  $K_2CO_3$ ) a complex reaction mixture from which expected bis(phenanthrene) **106** was isolated in only 6% yield using HPLC. The main products were represented by monoderivative **105** (25%), and surprisingly, by compound **107** formed in 37% yield by photochemical transannular [2+2] cycloaddition reaction [45]. On the other hand, no such [2+2] cycloaddition product was observed in the case of proximally disubstituted distyrylcalixarene **108**, where a mixture of three theoretically possible diastereomers of calix-bis-phenanthrenes **109–111** was obtained. The individual isomers were separated by HPLC in 27%, 7% and 14% yields, respectively.

An efficient method for intramolecular direct arylation was employed on a doubly functionalized calix[4]arene fixed in the *cone* conformation (Scheme 3.25). Dihydroxycalixarene **113** was obtained from dibromide **112** in 84% yield using lithiation, calixboronate formation and the final oxidative carbon-boron bond cleavage. The hydroxy groups of **113** were reacted with benzyl bromide (Williamson ether synthesis) and  $Cs_2CO_3$  in acetone to produce corresponding





**Scheme 3.25** The intramolecular direct arylation method

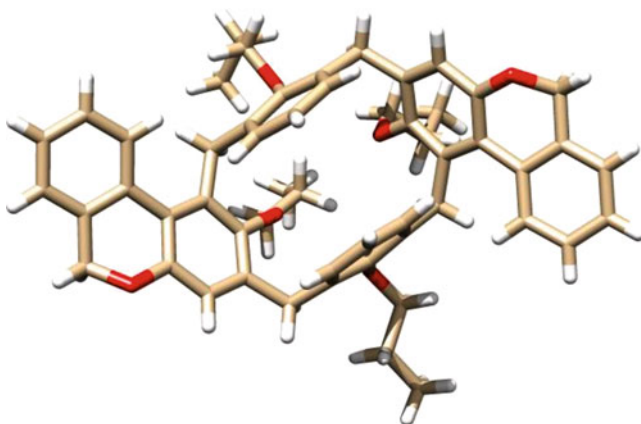
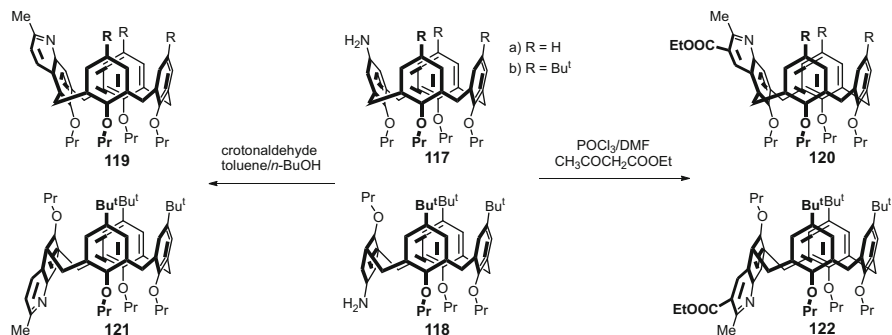


**Fig. 3.4** The X-ray structure of **116** showing the *pinched cone* conformation of this compound

dibenzyl ether **114** in 65 % yield. Subsequent direct Pd-catalyzed arylation afforded a 1:1 mixture (94 % overall yield) of achiral  $C_s$  symmetrical isomer **115** and chiral calix[4]arene **116** possessing  $C_2$  symmetry [46]. The X-ray crystallography of **116** revealed that compound adopts the *pinched cone* conformation with the substituted aromatic units pointing outwards from the cavity (Fig. 3.4).

Two synthetic strategies known from the chemistry of quinoline derivatives were adopted to generate racemic calix[4]quinolines immobilised in the *cone* or in the *partial cone* conformations (Scheme 3.26) [47]. Thus, starting amino derivative **117a** reacted with ethyl acetoacetate and Vilsmeier reagent to provide **120a** in 47 % yield. A similar reaction with de-*tert*-butylated analogue **117b** gave **120b** in lower yield (30 %). The construction of quinoline moiety using crotonaldehyde at reflux in *n*-BuOH/H<sub>2</sub>O led to calix[4]quinoline **119b** in 72 % yield. Hydrolysis of compounds **120a,b** or oxidation of the methyl group in compound **119b** afforded the corresponding carboxylic acids. These compounds were then separated into



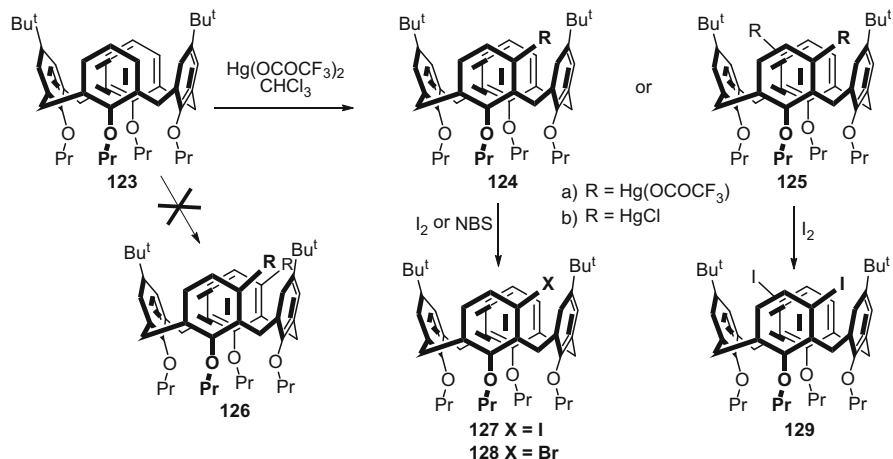
**Scheme 3.26** Two synthetic strategies from the chemistry of quinoline derivatives

enantiomers through the separation of their diastereomers derived from (*S*)-BINOL or (*R*)-phenylglycinol by common column chromatography or preparative TLC. Interestingly, exactly the same chemistry was done with compounds **121** and **122**, which are probably the only representatives of the *meta*-substituted *partial cone* conformations described so far.

### 3.7 Direct *Meta*-substitution

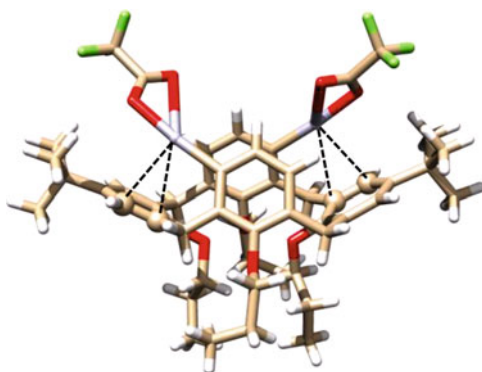
As already mentioned, an electrophilic aromatic substitution is a very straightforward method for the modification of classical calix[*n*]arenes, giving exclusively the *para*-substituted products. Only very recently it was found out that the mercuration of *O*-alkylated calix[4]arenes possesses an unprecedented regioselectivity and the corresponding *meta*-substituted organomercurials can be obtained in good yields. Thus, although the organomercury derivatives are not well-accepted by the chemical community due to their possible toxicity, they offer a direct way to *meta*-substituted calix[4]arenes otherwise inaccessible by common synthetic chemistry.

The reaction of di-*tert*-butylated compound **123** with mercury (II) trifluoroacetate in chloroform led either to monosubstituted compound **124a** or disubstituted derivative **125a** depending on the stoichiometry of reactants (Scheme 3.27) [48]. The X-ray structure of **125a** showed an interesting stabilization of the system (Fig. 3.5) via cation- $\pi$  interactions between mercury atoms and the neighbour aromatic subunits ( $\eta^2$ -complex). As trifluoroacetates **124a** and **125a** could not be purified on silica gel, they were transformed by reaction with aqueous NaCl in acetone into corresponding chloromercurio derivatives **124b** and **125b**, that were finally isolated by column chromatography in 44 % and 42 % yields, respectively. Interestingly, in case of disubstituted products only inherently chiral isomer **125** was isolated, while the formation of “*meso*” compound **126** was not observed at all. To show the synthetic usefulness of organomercurial intermediates, the



**Scheme 3.27** Unprecedented regioselectivity of direct mercuration of calix[4]arenes

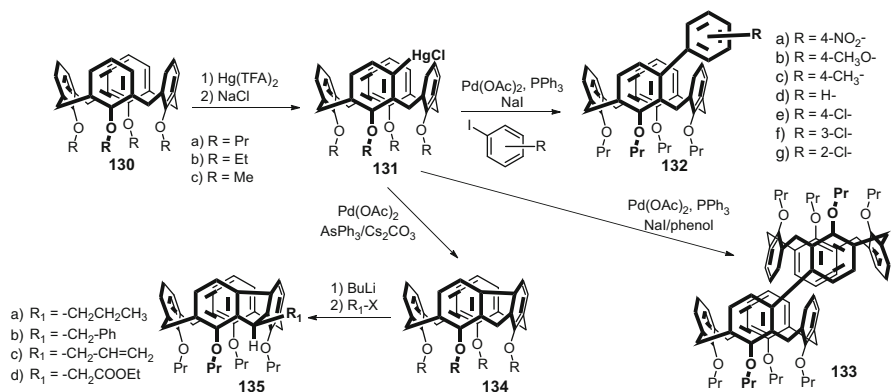
**Fig. 3.5** The X-ray structure of **125a** with Hg-aromatic interactions



chloromercurio compounds **124b** and **125b** were converted into the corresponding halogen derivatives **127–129** by reactions with  $\text{I}_2$  or NBS.

Although the unusual substitution pattern (the presence of two *tert*-butyl groups) in starting compound **123** originally suggested that the substitution could play a role in this uncommon regioselectivity, the same type of regioselectivity in the reaction with unsubstituted calix[4]arenes **130a–c** has excluded this possibility. The quantum chemical calculations indicated that the driving force could be the stabilization of the transition state where the  $\sigma$ -complex in the *meta*-position is stabilized by additional interactions between the mercury cation and neighbour aromatic sub-units (cation- $\pi$ ) while the *para*-substitution cannot exhibit this kind of stabilization because of the wrong mutual position.

The reaction of **130a** with one equiv. of  $\text{Hg}(\text{TFA})_2$  in  $\text{CHCl}_3$  gave smoothly monosubstituted product **131a** in 70% overall yield (Scheme 3.28). The Pd-catalysed arylation ( $\text{Pd}(\text{OAc})_2/\text{PPh}_3/\text{NaI}/\text{Ar-I}$ ) was then used to form



**Scheme 3.28** Unprecedented *meta*-aryl-substituted isomers obtained via organomercurial intermediates

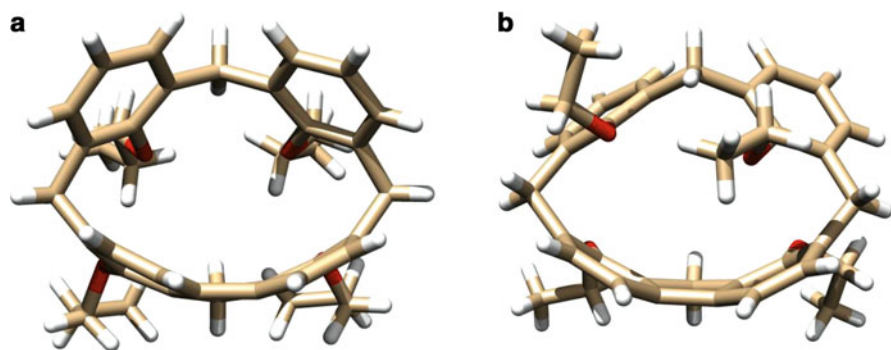
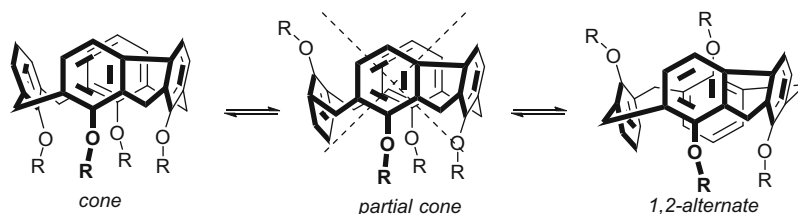


**Fig. 3.6** The X-ray structures of **a** **134a** (*cone* conformation) and **b** **134b'** (*1,2-alternate*)

compounds **132a-f** possessing various substituted aryl moieties in the *meta* position of basic skeleton. The organomercurial intermediates thus allow the formation of *meta*-aryl-substituted isomers representing a unique substitution pattern in calixarene chemistry. Moreover, the formation of dimeric structure **133a** (29 % yield) was achieved when phenol was added as a part of the catalytic mixture [49].

The formation of organomercury intermediate **131a** allows the Pd-catalysed bridging of the two neighbouring aromatic moieties to form compound **134a** possessing additional single bond in the upper rim of the molecule (Scheme 3.28) [50]. The screening of various reaction conditions known for Pd-catalysed cross-coupling reactions revealed Pd(OAc)<sub>2</sub>/AsPh<sub>3</sub>/Cs<sub>2</sub>CO<sub>3</sub> as the best catalytic system leading to **134a** in 64 % yield. The introduction of a short bridge between two neighbouring *meta* positions leads to substantial distortion and high rigidity of the *cone* conformation (Fig. 3.6a). To show the general synthetic applicability of this strategy, a similar reaction pathway starting from conformationally mobile



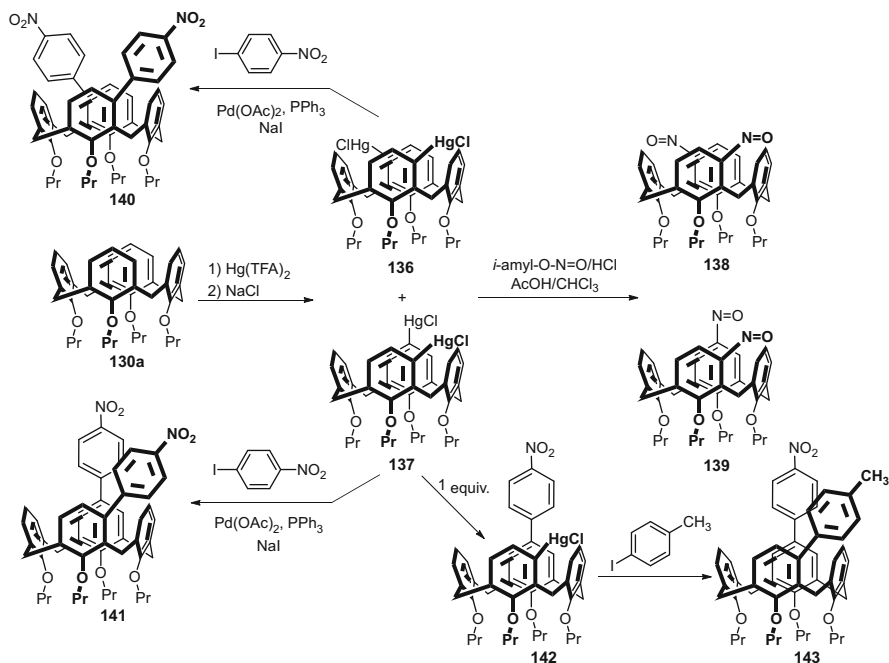
**Scheme 3.29** Conformational mobility of **134c** ( $R = \text{Me}$ )

tetraethoxy- and tetramethoxycalixarenes **130b** and **130c** was carried out. Methoxy derivative **134c** was obtained in 39 % yield (overall from **130c**) thus proving that the above synthetic protocol is suitable even for the non-immobilised derivatives.

The compounds of type **134**, possessing an additional single bond in the upper rim, formally contain a fluorene moiety within their structures. As the acidity of hydrogens in position 9 of fluorene is well-known, deprotonation of **134a** with a strong base and subsequent alkylation of carbanion formed was studied (Scheme 3.28). Although the fluorene part of calixarene molecule in **134a** is far from planarity, the reaction with BuLi worked well and one hydrogen pointing away from the cavity could be regioselectively and stereoselectively substituted to form alkylated derivatives **135a-d** in good yields (**135a**, 89 %; **135b**, 64 %; **135c**, 72 %; **135d**, 46 % yield, respectively) [51].

The  $^1\text{H}$  NMR spectrum of **134c** in  $\text{CD}_2\text{Cl}_2$  showed time-averaged signals indicating the conformational mobility (equilibrium of several conformations under fast exchange conditions) of this compound at room temperature (Scheme 3.29). On the other hand, the spectrum acquired at 203 K confirmed the presence of the two conformations – *cone* and *1,2-alternate* in a 4:1 ratio. In this context, although the *partial cone* conformer should be the logical intermediate in this equilibrium, it was not observed in the mixture. This indicates that the *partial cone* conformation is thermodynamically less stable if compared with other two conformations. Similarly, the Pd-catalysed bridging reaction with ethoxy derivative **130b** (via the formation of **131b**) gave a mixture of the two isolable conformers consisting of the *cone* **134b** (25 % yield) and the *1,2-alternate* **134b'** (15 %) isomers (both yields based on **130b**) [50]. Very unusual shape of the cavity of the *1,2-alternate* conformer **134b'** (5.643 Å for short diagonal, 8.137 Å for long diagonal) reflects a severe distortion of this calix[4]arene due to the single-bond bridge (Fig. 3.6b). Again, the formation of the *partial cone* conformer was not observed.

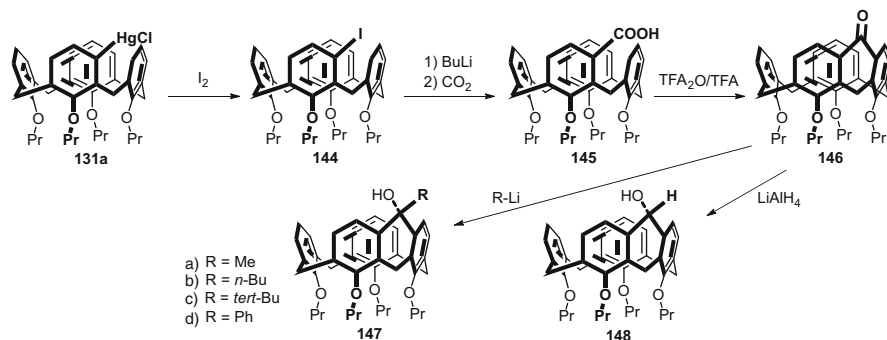
The regioselectivity of the dimercurcation reaction was studied using the *cone* conformer **130a** [52]. If we consider the monomercurcation of individual aromatic rings, theoretically up to 10 different regioisomers could be obtained. Fortunately, the reaction provided a mixture of only two dimercurated products (*meta,meta* **136** and *meta,para* **137**) in approximately a 1:1 ratio (Scheme 3.30). Both regioisomers represent inherently chiral systems with so far inaccessible substitution patterns. The arylation reactions of **136** and **137** using excess of *p*-nitrophenyl iodide and Pd(OAc) $_2$ /PPh $_3$ /NaI catalytic system gave smoothly the corresponding diarylated



**Scheme 3.30** Regioselectivity of the dimercuration reaction

isomers **140** and **141** in about 50 % yields. The same reaction conditions with **137** using only 1 equiv. of *p*-nitrophenyl iodide led to monosubstituted isomer **142** in 40 % yield, thus confirming the higher reactivity of HgCl group in the *para* position. This paved the way to the introduction of two different aryl groups into the *para* and *meta* positions, like in derivative **143**.

The unusual substitution patterns mentioned above were studied for their conformational preferences and dynamic behaviour in solution, as this knowledge could be useful for the future applications of these systems. Using the reaction of isopentyl nitrite and HCl at low temperature (0 °C), the organomercurials **136** and **137** were transformed into the corresponding nitroso derivatives **138** and **139** in essentially quantitative yields [53]. A dynamic study of *meta*, *para* isomer **139** revealed a typical behaviour for a *pinched cone*-*pinched cone* interconversion with time-averaged signals at ambient temperature and the doubling of their numbers under slow exchange conditions (203 K). On the other hand, the  $^1\text{H}$  NMR spectra of *meta*, *meta* isomer **138** remained unchanged throughout the whole temperature interval indicating that this compound adopts only one of the two possible *pinched cone* conformations. This unique conformational behaviour was confirmed by the application of Residual Dipolar Couplings method (RDC). It revealed that the specific *pinched cone* conformation is that with both nitroso groups on the flattened (directing outside from the cavity) aromatic rings. Recently, the corresponding



**Scheme 3.31** Preparation of a novel type of calix[4]arene with two neighbouring aromatic units bridged by a ketone moiety

*meta*, *meta* and *meta*, *para* dinitro derivatives were prepared by the oxidation of nitroso compounds **138** and **139** with *m*-chloroperbenzoic acid and their electrochemical reduction was studied [54].

Organomercury intermediate **131a** in the *cone* conformation was transformed into corresponding iodocalix[4]arene **144** (86 %) which was used for the preparation of compound **145** (96 %) with carboxylic acid functionality in the *meta* position of calixarene skeleton (Scheme 3.31) [55]. This arrangement allowed the preparation of a novel type of calix[4]arene with two neighbouring aromatic units bridged by a ketone moiety. Thus, while the reaction of **145** with POCl<sub>3</sub> did not lead to the expected Friedel-Crafts intramolecular acylation, stirring with a trifluoroacetic anhydride–TFA mixture gave smoothly ketone-bridged calixarene **146** in 95 % yield. The reactivity of the ketone group towards the addition of organolithium compounds was studied. It was found that nucleophiles come from the outside of the cavity thus providing the corresponding hydroxy derivatives **147** in good yields (**147a**, 88 %; **147b**, 48 %; **147c**, 51 %; **147d**; 93 %). The same stereochemistry was achieved by reduction of **146** with LiAlH<sub>4</sub>. Hydroxy derivative **148**, formed in 95 % yield, was found to complex some selected neutral compounds via the cooperative effect of hydrogen bonding (from OH group) and CH – π interactions (from cavity).

### 3.8 Conclusions and Outlook

In this chapter, we have shown several approaches to the synthesis of *meta*-substituted calixarenes, and discussed their advantages and drawbacks. While the step-by-step or fragment condensation methods represent more or less traditional strategies with many synthetic limitations, the introduction of orienting group into the *para* position or, the most recently, a direct substitution via organomercurial intermediates, show a promising potential for future. We would like to stress again

that *meta*-substituted calixarenes mostly possess inherent chirality and now, having quite simple methods for their synthesis, scientific interests could focus on their use as novel receptors for chiral recognition. Last but not least, the novel types of calixarenes with so far unknown substitution patterns, such as upper rim bridged derivatives, are good examples of enormous vitality of calixarene chemistry.

## References

1. Andreetti, G. D.; Böhmer, V.; Jordon, J. G.; Tabatabai, M.; Ugozzoli, F.; Vogt, W.; Wolff, A. *J. Org. Chem.* **1993**, *58*, 4023–4032.
2. Wolff, A.; Böhmer, V.; Vogt, W.; Ugozzoli, F.; Andreetti, G. D. *J. Org. Chem.* **1990**, *55*, 5665–5667.
3. Thondorf, I.; Hillig, G.; Brandt, W.; Brenn, J.; Barth, A.; Böhmer, V. *J. Chem. Soc., Perkin Trans. 2* **1994**, 2259–2267.
4. Kusano, T.; Tabatabai, M.; Okamoto, Y.; Böhmer, V. *J. Am. Chem. Soc.* **1999**, *121*, 3789–3790.
5. Pickard, S. T.; Pirkle, W. H.; Tabatabai, M.; Vogt, W.; Böhmer, V. *Chirality* **1993**, *5*, 310–314.
6. Fu, D.-K.; Xu, B.; Swager, T. M. *J. Org. Chem.* **1996**, *61*, 802–804.
7. Xu, B.; Carroll, P. J.; Swager, T. M. *Angew. Chem., Int. Ed. Engl.* **1996**, *35*, 2094–2097.
8. Georghiou, P. E.; Ashram, M.; Clase, H. J.; Bridson, J. N. *J. Org. Chem.* **1998**, *63*, 1819–1826.
9. Chowdhury, S.; Georghiou, P. E. *J. Org. Chem.* **2002**, *67*, 6808–6811.
10. Georghiou, P. E.; Mizyed, S.; Chowdhury, S. *Tetrahedron Lett.* **1999**, *40*, 611–614.
11. Georghiou, P. E.; Tran, A. H.; Stroud, S. S.; Thompson, D. W. *Tetrahedron* **2006**, *62*, 2036–2044.
12. Casabianca, H.; Royer, J.; Satrallah, A.; Taty-C, A.; Vicens, J. *Tetrahedron Lett.* **1987**, *28*, 6595–6596.
13. (a) Shinkai, S.; Arimura, T.; Kawabata, H.; Murakami, H.; Araki, K.; Iwamoto, K.; Matsuda, T. *J. Chem. Soc., Chem. Commun.* **1990**, 1734–1736; (b) Shinkai, S.; Arimura, T.; Kawabata, H.; Murakami, H.; Iwamoto, K. *J. Chem. Soc., Perkin Trans. 1* **1991**, 2429–2434.
14. Dahan, E.; Biali, S. E. *J. Org. Chem.* **1989**, *54*, 6003–6004.
15. Dahan, E.; Biali, S. E. *J. Org. Chem.* **1991**, *56*, 7269–7274.
16. Ogoshi, T.; Kitajima, K.; Umeda, K.; Hiramitsu, S.; Kanai, S.; Fujinami, S.; Yamagishi, T.-a.; Nakamoto, Y. *Tetrahedron* **2009**, *65*, 10644–10649.
17. Falana, O. M.; Keehn, P. M.; Stevenson, R. *Org. Biomol. Chem.* **2011**, *9*, 8147–8154.
18. Böhmer, V.; Jung, K.; Schoen, M.; Wolff, A. *J. Org. Chem.* **1992**, *57*, 790–792.
19. Backes, M.; Böhmer, V.; Ferguson, G.; Gruttner, C.; Schmidt, C.; Vogt, W.; Ziat, K. *J. Chem. Soc., Perkin Trans. 2* **1997**, 1193–1200.
20. Tabatabai, M.; Vogt, W.; Böhmer, V. *Tetrahedron Lett.* **1990**, *31*, 3295–3298.
21. Mascal, M.; Naven, R. T.; Warmuth, R. *Tetrahedron Lett.* **1995**, *36*, 9361–9364.
22. Mascal, M.; Warmuth, R.; Naven, R. T.; Edwards, R. A.; Hursthouse, M. B.; Hibbs, D. E. *J. Chem. Soc., Perkin Trans. 1* **1999**, 3435–3441.
23. Amato, M. E.; Ballistreri, F. P.; Pappalardo, A.; Tomaselli, G. A.; Toscano, R. M.; Williams, D. J. *Eur. J. Org. Chem.* **2005**, 3562–3570.
24. Verboom, W.; Bodewes, P. J.; van Essen, G.; Timmerman, P.; van Hummel, G. J.; Harkema, S.; Reinhoudt, D. N. *Tetrahedron* **1995**, *51*, 499–512.
25. Xu, Z.-X.; Zhang, C.; Zheng, Q.-Y.; Chen, C.-F.; Huang, Z.-T. *Org. Lett.* **2007**, *9*, 4447–4450.
26. Xu, Z.-X.; Huang, Z.-T.; Chen, C.-F. *Tetrahedron Lett.* **2009**, *50*, 5430–5433.
27. Xu, Z.-X.; Li, G.-K.; Chen, C.-F.; Huang, Z.-T. *Tetrahedron* **2008**, *64*, 8668–8675.
28. Xu, Z. X.; Zhang, C.; Huang, Z. T.; Chen, C. F. *Chin. Sci. Bull.* **2010**, *55*, 2859–2869.
29. Xu, Z.-X.; Zhang, C.; Yang, Y.; Chen, C.-F.; Huang, Z.-T. *Org. Lett.* **2008**, *10*, 477–479.



30. Herbert, S. A.; Arnott, G. E. *Org. Lett.* **2009**, *11*, 4986–4989.
31. Herbert, S. A.; Arnott, G. E. *Org. Lett.* **2010**, *12*, 4600–4603.
32. Herbert, S. A.; Castell, D. C.; Clayden, J.; Arnott, G. E. *Org. Lett.* **2013**, *15*, 3334–3337.
33. Herbert, S. A.; van Laeren, L. J.; Castell, D. C.; Arnott, G. E. *Beilstein J. Org. Chem.* **2014**, *10*, 2751–2755.
34. Holub, J.; Eigner, V.; Vrzal, L.; Dvorakova, H.; Lhotak, P. *Chem. Commun.* **2013**, *49*, 2798–2800.
35. Gaeta, C.; Martino, M.; Neri, P. *Tetrahedron Lett.* **2003**, *44*, 9155–9159.
36. Troisi, F.; Pierro, T.; Gaeta, C.; Neri, P. *Org. Lett.* **2009**, *11*, 697–700.
37. Troisi, F.; Pierro, T.; Gaeta, C.; Carratu, M.; Neri, P. *Tetrahedron Lett.* **2009**, *50*, 4416–4419.
38. De Rosa, M.; Soriente, A.; Concilio, G.; Talotta, C.; Gaeta, C.; Neri, P. *J. Org. Chem.* **2015**, *80*, 7295–7300.
39. Talotta, C.; Gaeta, C.; Troisi, F.; Monaco, G.; Zanasi, R.; Mazzeo, G.; Rosini, C.; Neri, P. *Org. Lett.* **2010**, *12*, 2912–2915.
40. Gaeta, C.; Troisi, F.; Talotta, C.; Pierro, T.; Neri, P. *J. Org. Chem.* **2012**, *77*, 3634–3639.
41. Van Loon, J. D.; Arduini, A.; Coppi, L.; Verboom, W.; Pochini, A.; Ungaro, R.; Harkema, S.; Reinhoudt, D. N. *J. Org. Chem.* **1990**, *55*, 5639–5646.
42. Reddy, P. A.; Gutsche, C. D. *J. Org. Chem.* **1993**, *58*, 3245–3251.
43. Ikeda, A.; Yoshimura, M.; Lhotak, P.; Shinkai, S. *J. Chem. Soc., Perkin Trans. 1* **1996**, 1945–1950.
44. Mastalerz, M.; Hueggenberg, W.; Dyker, G. *Eur. J. Org. Chem.* **2006**, 3977–3987.
45. Hueggenberg, W.; Seper, A.; Oppel, I. M.; Dyker, G. *Eur. J. Org. Chem.* **2010**, 6786–6797.
46. Barton, O. G.; Neumann, B.; Stammler, H. G.; Mattay, J. *Org. Biomol. Chem.* **2008**, *6*, 104–111.
47. Miao, R.; Zheng, Q.-Y.; Chen, C.-F.; Huang, Z.-T. *J. Org. Chem.* **2005**, *70*, 7662–7671.
48. Slavik, P.; Dudic, M.; Flidrova, K.; Sykora, J.; Cisarova, I.; Bohm, S.; Lhotak, P. *Org. Lett.* **2012**, *14*, 3628–3631.
49. Slavik, P.; Flidrova, K.; Dvorakova, H.; Eigner, V.; Lhotak, P. *Org. Biomol. Chem.* **2013**, *11*, 5528–5534.
50. Flidrova, K.; Slavik, P.; Eigner, V.; Dvorakova, H.; Lhotak, P. *Chem. Commun.* **2013**, *49*, 6749–6751.
51. Slavik, P.; Dvorakova, H.; Eigner, V.; Lhotak, P. *Chem. Commun.* **2014**, *50*, 10112–10114.
52. Flidrova, K.; Bohm, S.; Dvorakova, H.; Eigner, V.; Lhotak, P. *Org. Lett.* **2014**, *16*, 138–141.
53. Vrzal, L.; Flidrova, K.; Tobrman, T.; Dvorakova, H.; Lhotak, P. *Chem. Commun.* **2014**, *50*, 7590–7592.
54. Liska, A.; Flidrova, K.; Lhotak, P.; Ludvik, J. *Monatsh. Chem.* **2015**, *146*, 857–862.
55. Slavik, P.; Eigner, V.; Lhotak, P. *Org. Lett.* **2015**, *17*, 2788–2791.

# Chapter 4

## Preparation of Methylene-Substituted Calixarenes

Silvio E. Biali

### 4.1 Introduction

The preparation of calixarene derivatives with single, several, or all methylene bridges substituted is a challenging synthetic task [1]. In contrast to the lower-rim OH groups which can be readily derivatized by acylation and alkylation reactions, the functionalization of the saturated methylene groups requires more elaborated synthetic pathways. From a supramolecular point of view, these functionalized systems are of interest since they may incorporate additional binding sites near the cavity while keeping intact the array of binding groups at the lower-rim positions of the aryl rings. Furthermore, the introduction of substituents at the bridges can be a useful tool for the design of macrocycles with a preorganized (and rigid) cavity of a desired geometry since the substituents may both determine the preferred conformation of the macrocycle, and increase its rigidity.

### 4.2 Configurational Stereoisomerism

In a calixarene derivative with all methylene bridges monosubstituted (i.e., possessing  $\text{Ar}_2\text{CHR}$  subunits) the substituted carbon bridges constitute stereogenic centers. As a result, several configurational isomers are possible. If all substituents at the bridges are identical, the number of configurational isomers roughly increases with the increase of size of the calix[ $n$ ]arene scaffold (and the number of stereocenters present). For example under a timescale of fast ring inversion, 4, 8 and 18 diastereomeric forms are possible for calix[4]-, calix[6]- and calix[8]arene

---

S.E. Biali (✉)

Institute of Chemistry, The Hebrew University of Jerusalem, Jerusalem 91904, Israel  
e-mail: [silvio.biali@mail.huji.ac.il](mailto:silvio.biali@mail.huji.ac.il)

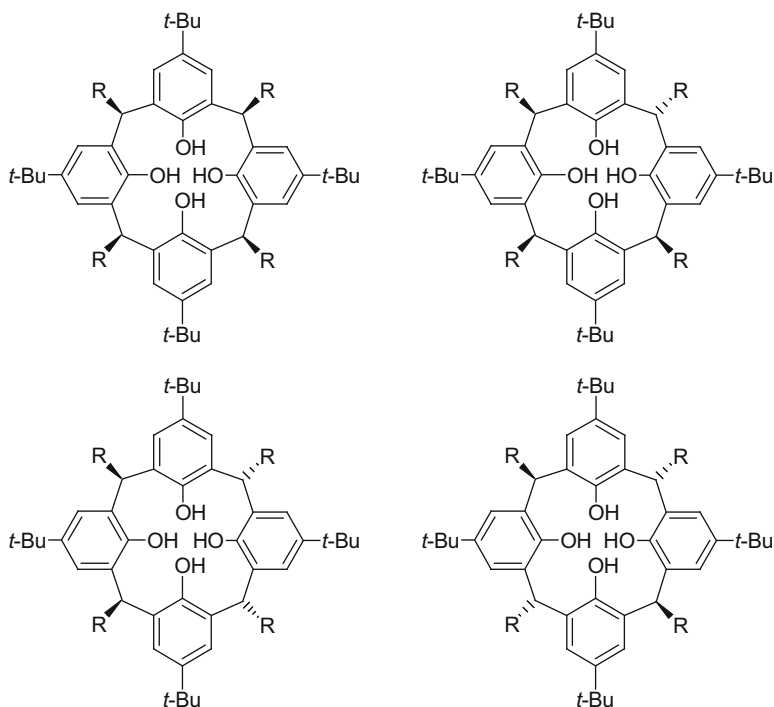


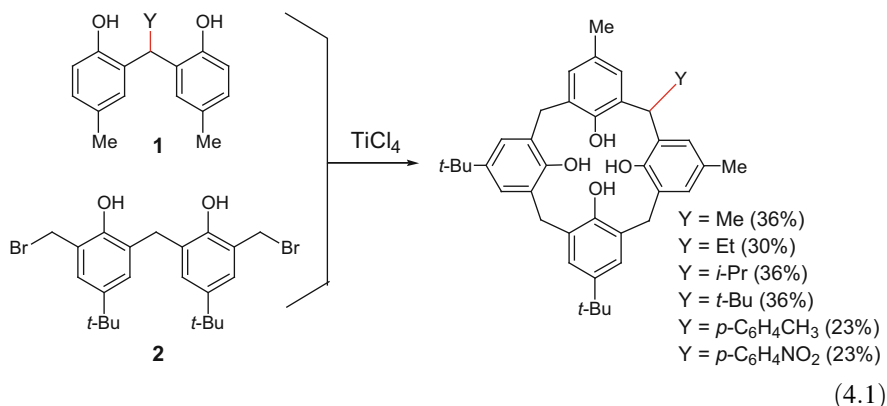
**Fig. 4.1** The four possible configurational isomers of a calix[4]arene possessing four identically monosubstituted methylene bridges

derivatives with all bridges monosubstituted by identical substituents, respectively. The four possible configurational isomers of a calix[4]arene monosubstituted at each bridge are depicted in Fig. 4.1 [2]. Due to the large number of possible stereoisomeric products, the stereoselective preparation of a methylene-functionalized calixarenes with part (or all) bridges monosubstituted represents a substantial synthetic challenge.

### 4.3 Cyclization of Fragments

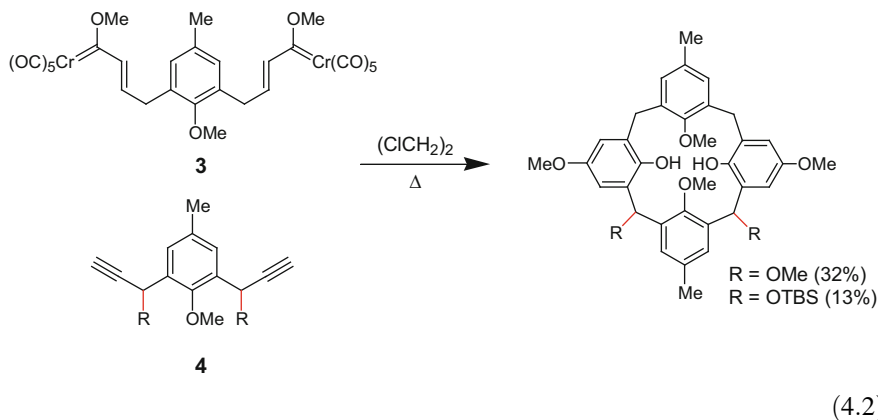
Several synthetic strategies have been utilized for the preparation of methylene-functionalized calixarenes. The first general strategy (the “fragment condensation” method) [3] was introduced by the groups of Böhmer and Sartori and involves the preparation of fragments possessing the desired functional groups (for example, the phenol dimer with a substituted methylene bridge **1** and the bis(bromomethyl) phenol dimer **2**). In the second step these fragments are cyclocondensed to afford the substituted calixarenes (a (2 + 2) condensation). The cyclocondensation step is conducted in the presence of a Lewis acid (e.g.,  $\text{TiCl}_4$ ) and generally involves

Friedel-Crafts alkylations as exemplified in Eq. (4.1). If both fragments possess a monosubstituted methylene, the reaction affords calix[4]arene derivatives with a pair of distal bridges monosubstituted. (3 + 2) fragment condensations yield substituted calix[5]arene derivatives, but with lower yields than the (2 + 2) condensation since calix[8]arene derivatives are obtained as side products [4].



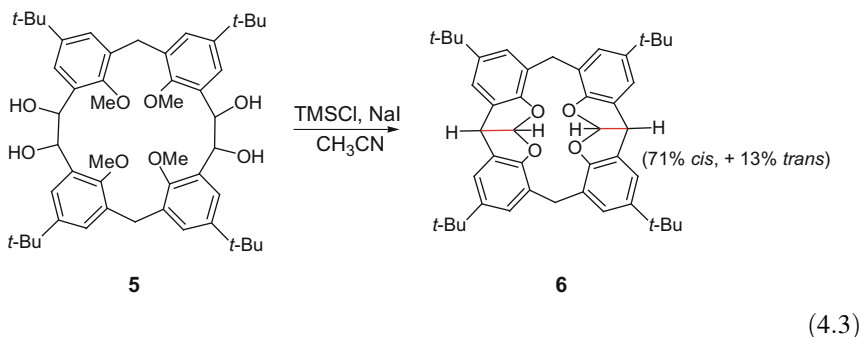
The fragment condensation methodology was also successfully applied by Chen and coworkers for the preparation of calixarenes containing a triptycene moiety (see Chap. 18 in this book) [5].

More recently Wulff and coworkers introduced a method based on the reaction of diynes **4** with bis(carbene) complexes **3** (Eq. 4.2) [6]. In contrast to the “classical” fragment condensation method, two phenol rings are formed during the key cyclization step. Since bonds to the substituted methylenes are not cleaved in the cyclization step, this method allows the preparation of chiral, optically active methylene-substituted calix[4]arenes, starting from the appropriate enantiopure precursors.



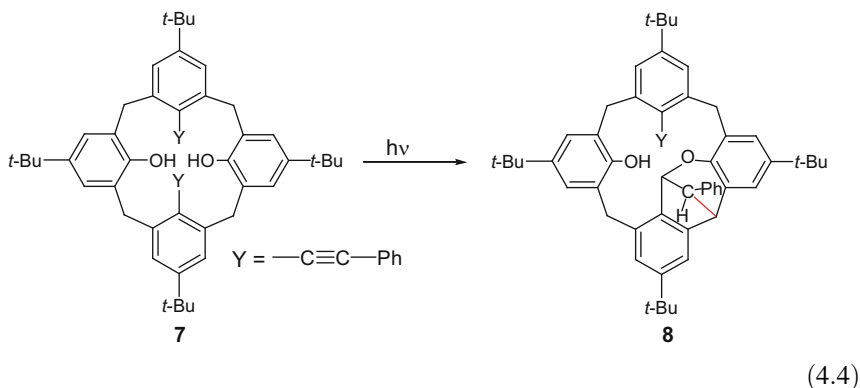
#### 4.4 Ring Contraction

A novel approach for the preparation of the calix[4]arene scaffold involves ring contraction via rearrangement of a macrocycle incorporating pinacol subunits (**5**). By this approach Sawada and coworkers synthesized a calix[4]arene derivative with two distal methylene bridges functionalized (**6**) (Eq. 4.3) [7].

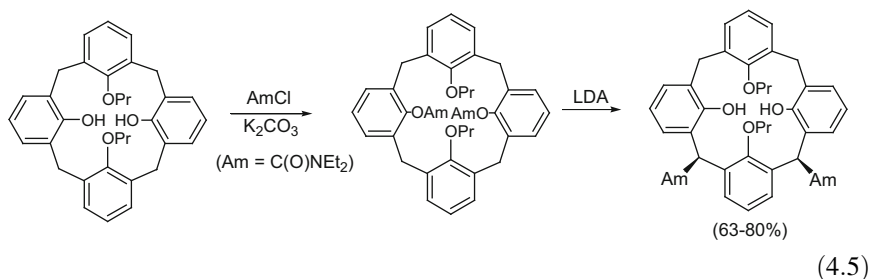


#### 4.5 Direct Modification of the Methylene Groups of a Calix [n]arene Derivative. Modification of One or Two Bridges

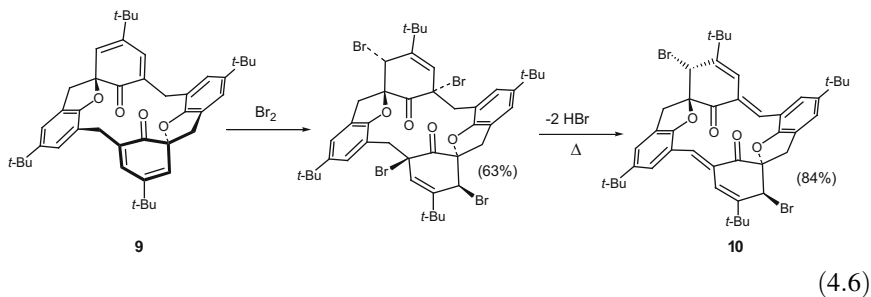
An alternative strategy for the preparation of methylene-functionalized calixarenes involves the direct functionalization of the methylene groups of a calixarene derivative. In contrast to the fragment condensation method, by starting from a preformed macrocycle, this approach avoids the need to optimize the reaction conditions for the cyclization step. Some calixarene derivatives undergo reactions yielding derivatives possessing one or two alkylated bridges with specific substituents. Buccella and Parkin reported that the oxidative addition of a C-H bond in a tungsten complex of the parent calix[4]arene affords an alkyl hydride species where a single methylene group is metalated [8]. Georghiou and coworkers reported that bis(phenylethynyl)calix[4]arene **7** undergoes photochemical cycloisomerization to afford the calixarene derivative **8** where a single methylene bridge is at a bridgehead position of a [3.2.1] bicyclic subunit (Eq. 4.4) [9].



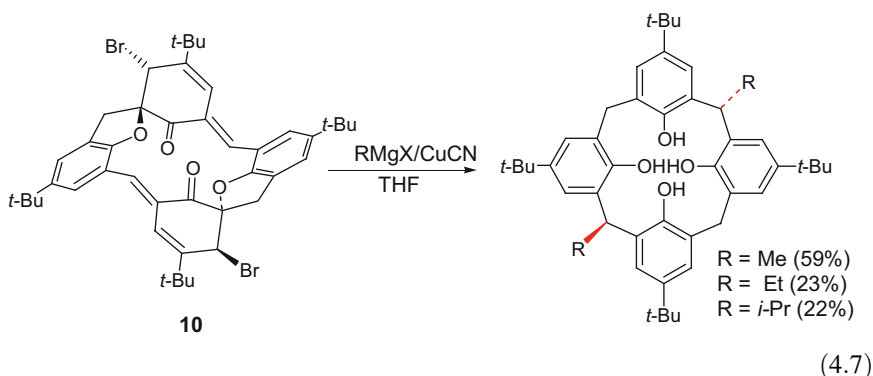
Reinhoudt and Snieckus reported that calixarene bis-O-carbamate derivatives upon treatment with LDA undergo homologous anionic *ortho* Fries rearrangement affording calixarenes with two bridges functionalized by carboxamide groups. Depending on the stereochemistry of the reacting atropisomer, monorearranged or bisrearranged (proximal or distal) products are obtained. In the case of the cone atropisomer, the reaction afforded a derivative with two proximal bridges monosubstituted (diaxial isomer, Eq. 4.5) [10].



An approach allowing the incorporation of a large array of substituents into two distal bridges involves the reaction of the bis(bromospirodiene) derivative **10** with nucleophiles. Bis(spirodiene) **10** was prepared from the *meso* bis(spirodienone) derivative **9** via an addition-elimination sequence (Eq. 4.6) [11a].

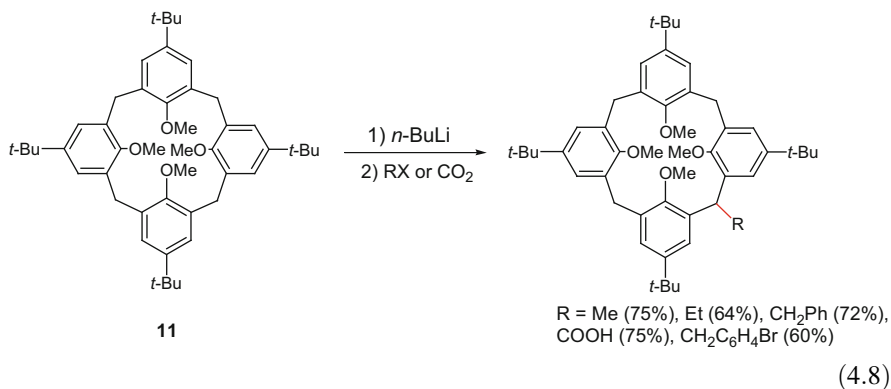


The *meso* bis(bromospirodiene) derivative **10** possesses  $C_i$  symmetry and reacts in stereoselective fashion with nucleophiles affording exclusively the *trans* product. In the case of the reaction with organocopper reagents, the resulting products undergo reduction under the reaction conditions, affording in a one-pot reaction the tetrahydrocalix[4]arene derivatives monosubstituted at two opposite bridges in *trans* fashion (Eq. 4.7) [11].



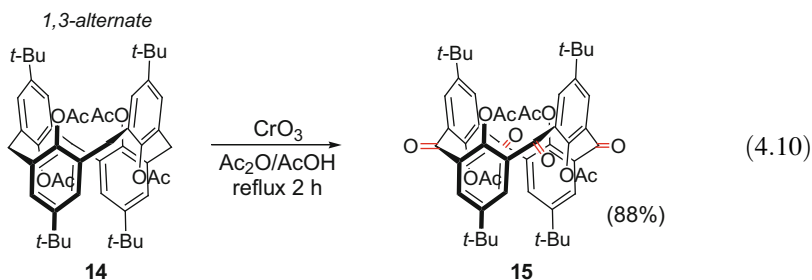
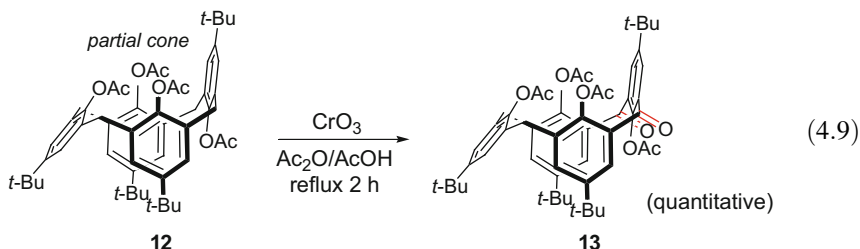
A very useful synthetic approach involving the lithiation of the tetramethylether derivative of *p*-*tert*-butylcalix[4]arene (**11**) followed by reaction with an electrophilic reagent (Eq. 4.8), was introduced by Fantini. This method allows the preparation of calix[4]arenes monosubstituted at a single bridge by a large number of substituents [12–14]. Even in the presence of a large excess of the alkyllithium, only calix[4]arene derivatives substituted at a single bridge are obtained. Metalated cavitands of a derivative with a large alkyl substituent on a bridge have been recently reported by Zhao and Swager [15]. If necessary the method can be repeated twice allowing access to distally disubstituted derivatives [13e]. For calix[6]arenes the lithiation/alkylation method affords, in one synthetic step, derivatives with two opposite bridges monoalkylated [16].

Calix[*n*]arenes with part or all the methylene bridges monosubstituted have been prepared by the ketocalixarene or bromocalixarene routes (see below).



## 4.6 Preparation of Ketocalixarenes

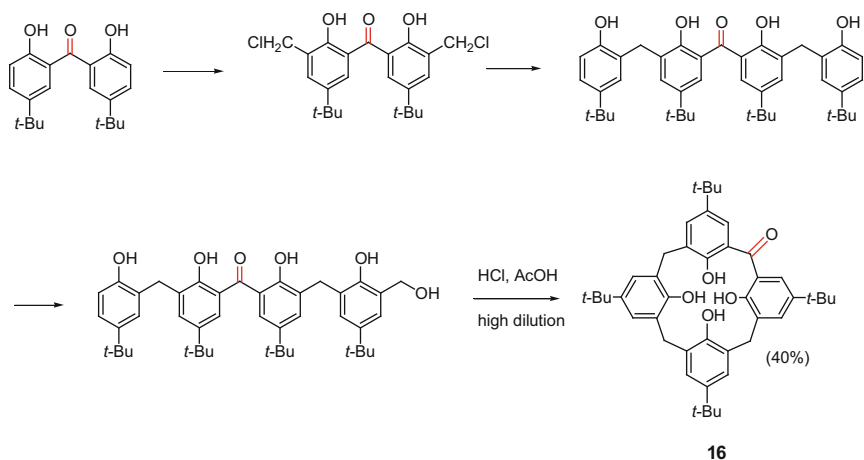
Ketocalix[*n*]arenes are calixarenes derivatives where all or part of the methylene bridges have been replaced by carbonyl groups. As reported in 1990, tetrahydroxy ketocalix[4]arene can be prepared via  $\text{CrO}_3$  oxidation of the methylene groups of *p*-*tert*-butylcalix[4]arene tetraacetate followed by hydrolysis of the product [17]. In the tetraacetate derivative, the different up-down arrangements of the rings (e.g., *partial cone*, *1,3-alternate* and *1,2-alternate*) represent atropisomeric forms that can be separated by fractional crystallization [18] and are stable at room temperature although they mutually isomerize in  $\text{DMSO-}d_6$  at  $150\text{ }^\circ\text{C}$  [19]. The oxidation step is sensitive to the steric arrangements of the rings. Methylene groups located between geminal rings oriented *anti* are oxidized faster than those located between rings oriented *syn* [20]. This differential reactivity allowed the preparation of proximal dioxocalix[4]arene **13** by oxidation of the *partial-cone* atropisomers of *p*-*tert*-butylcalix[4]arene tetraacetate (**12**) (Eq. 4.9). Oxidation of the *1,3-alternate* atropisomer **14**, where all methylene groups are located in between geminal rings oriented *anti*, affords the tetraoxo derivative **15** (Eq. 4.10). Triketocalix[4]arene was recently isolated from the product mixture of the partial oxidation of the *1,3-alternate* atropisomer of *p*-*tert*-butylcalix[4]arene **14** tetraacetate with  $\text{CrO}_3$  [21].



A monooxocalix[4]arene tetraacetate was prepared in low yield by partial oxidation of the mixture of atropisomers of *p*-*tert*-butylcalix[4]arene tetraacetate, [17a] while the parent tetrahydroxy compound **16** was prepared by Sone and

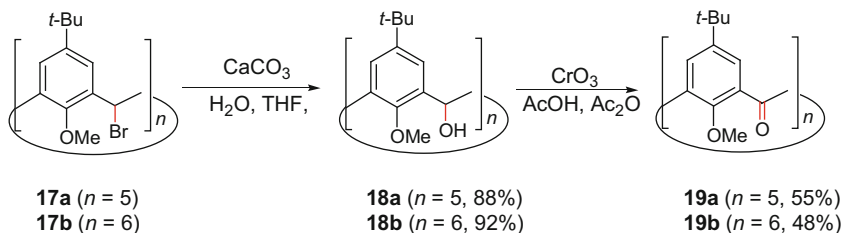


coworkers, via a stepwise route involving cyclization of an acyclic analogue possessing a single carbonyl group (Eq. 4.11) [17c]. The synthetic scheme was also successfully applied for the preparation of the larger calix[5]- and calix[6] arene monooxo derivatives [17c].



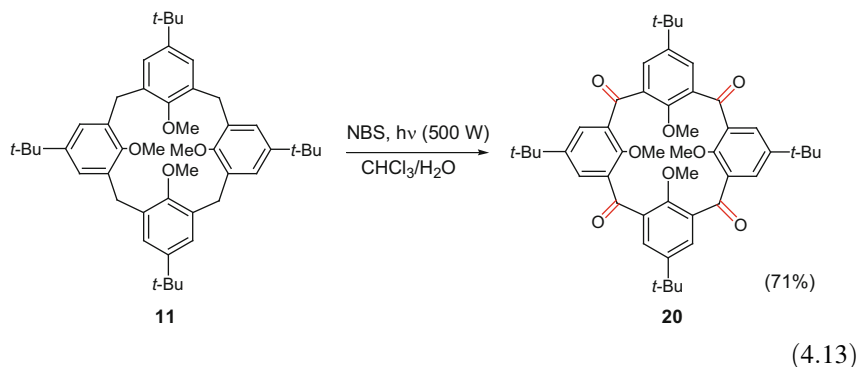
(4.11)

The methyl ethers of large-ring keto[n]calixarenes **19** ( $n = 5, 6$ ) have been prepared from the corresponding bromocalixarenes **17** (see below) via a two-step process involving basic hydrolysis, followed by  $\text{CrO}_3$  oxidation of the respective hydroxymethylene derivatives **18** (Eq. 4.12) [22].

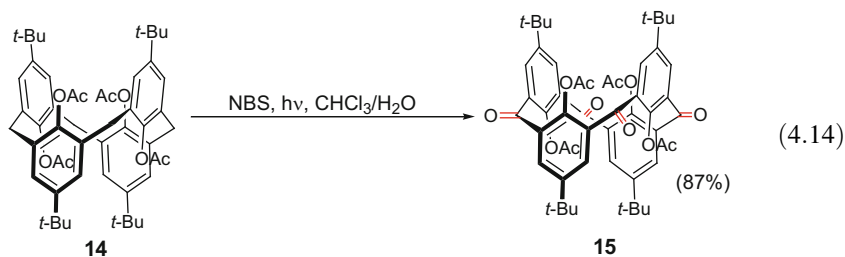


(4.12)

Recently, a shorter synthesis of the tetramethylether of ketocalix[4]arene (**20**) was introduced by Fischer and coworkers. Photochemical bromination (UV irradiation) of calix[4]arene tetramethyl ether **11** with a large excess of NBS and a mixture of  $\text{CHCl}_3$ /water as a solvent afforded **20** in one step (Eq. 4.13) [23].



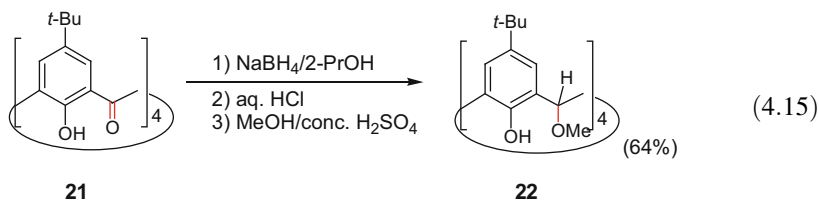
Similar reaction conditions were also applied for the oxidation of the *1,3-alternate* atropisomer of *p*-*tert*-butylcalix[4]arene tetraacetate **14** to afford **15** (Eq. 4.14) [24]. Instead of the UV irradiation described in the preparation of **20**, a simpler irradiation with a spot lamp was used.



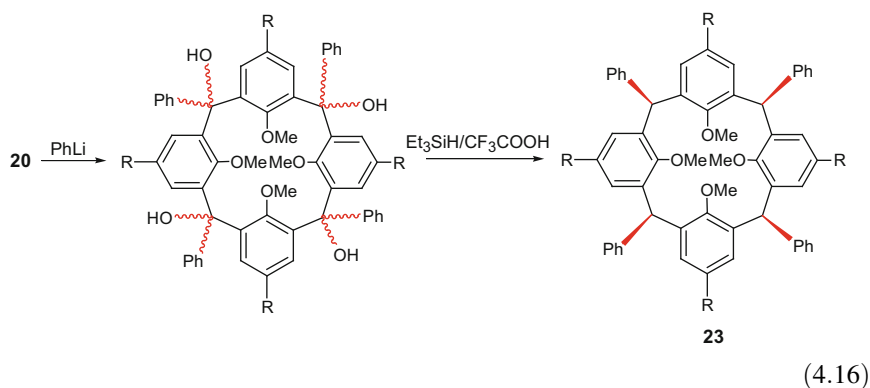
## 4.7 Reaction of Ketocalixarenes with Nucleophiles

In principle the synthetic availability of ketocalixarenes should allow the preparation of a wide array of methylene-substituted calixarene derivatives via nucleophilic reaction to the carbonyl groups [25]. A unique feature of this approach is that systems possessing disubstituted bridges are synthetically accessible.

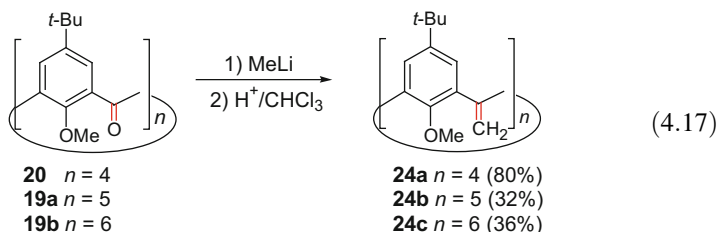
It has been reported that reduction of the carbonyl groups of tetrahydroxyketocalix[4]arene **21** with  $\text{NaBH}_4$  in 2-propanol, followed by heating to reflux the product in  $\text{MeOH}/\text{H}_2\text{SO}_4$ , affords an octahydroxycalix[4]arene [17a]. However, a recent reinvestigation of the reaction indicated that after the work-up reported in the literature, the product of the reaction consist of an isomeric mixture of the tetrahydroxycalix[4]arene derivative **22**, where all bridges are monosubstituted by a methoxy group (Eq. 4.15) [26].



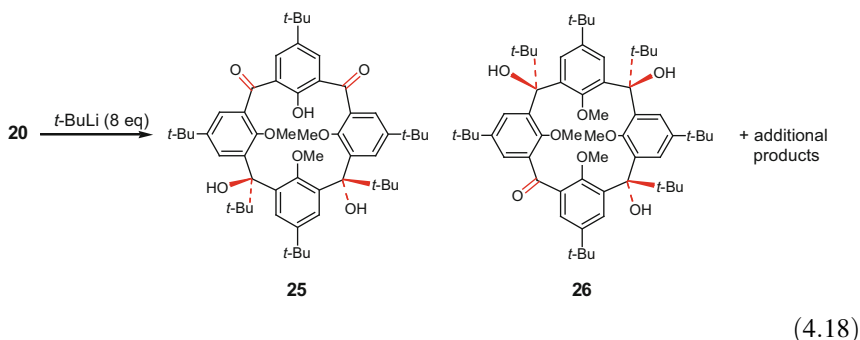
A calix[4]arene derivative with all bridges substituted by phenyl rings (**23**) was synthesized by a two-step sequence involving addition of PhLi to **20** followed by ionic hydrogenation of the product (Eq. 4.16). The addition step proceeds in non-stereoselective fashion, affording a mixture of all possible stereoisomers, but the reduction step yields only the *all-cis* derivative (which is presumably the most stable isomer of the product) [25a].



Addition of MeLi to ketocalix[*n*]arenes (*n* = 4,5,6; protected as methyl ethers) proceeds in non-stereoselective fashion affording mixtures of stereoisomeric products. Multifold acid-catalyzed elimination of water affords the calixradialenes **24**, i.e., calixarenes possessing exocyclic double bonds at the bridges (Eq. 4.17) [21, 22].

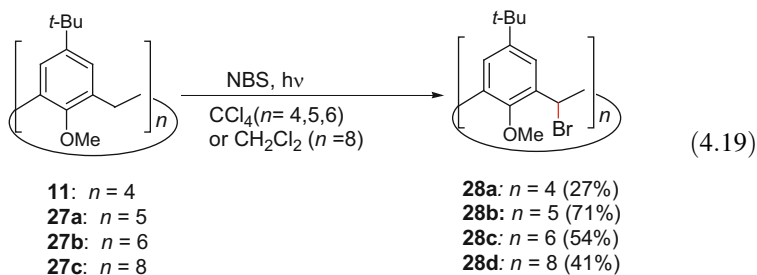


The reaction of the ketocalix[4]arene **20** with excess *t*-BuLi does not afford a tetraaddition product (presumably due to the steric hindrance that would result in the product). From the product mixture, diaddition (**25**) and triaddition (**26**) derivatives were isolated in low yield (Eq. 4.18). A phenolic OH group is present in the diaddition product **25** indicating that, under the reaction conditions, a O-Me bond cleavage took place. Notably, in both compounds the barrier of rotation of *t*-Bu groups at the bridges is substantial, as evidenced by temperature-dependent NMR data [25c].

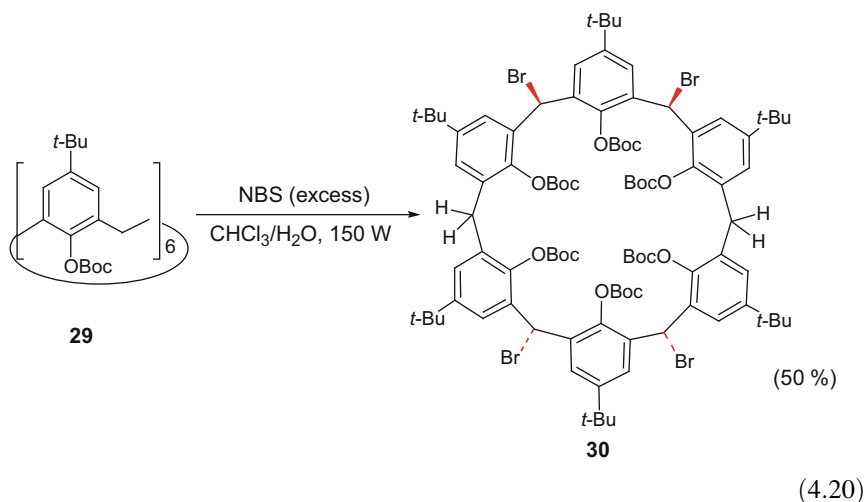


## 4.8 Preparation of Bromocalixarenes

Calix[*n*]arene derivatives with all the methylene bridges monosubstituted by bromine atoms (that will be referred as “bromocalixarenes”) have been prepared via radical or photochemical reaction of the corresponding calix[*n*]arene methyl ethers with NBS in a chlorinated solvent (usually CCl<sub>4</sub>, Eq. 4.19). For **11** [27], **27a** [28], **27b** [29, 30], and the methyl-ether derivative of de-*tert*-butylated calix[4]arene [31], the main product is the *all-cis* isomer, as corroborated by X-ray crystallography. The photochemical bromination of **27c** yields an achiral isomer with bilateral symmetry of the octabromo derivative as the kinetic product, that upon standing in chloroform isomerizes to an equilibrium mixture of isomers [32, 33]. From the equilibrium mixture, a single isomer was isolated via trituration with cold isopropanol [32].



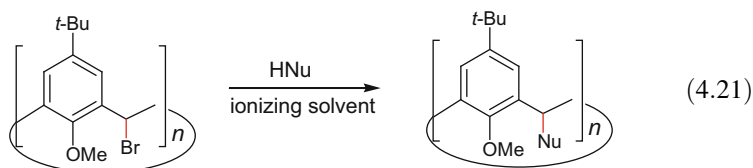
Notably, bromination of the Boc-protected derivative of calix[6]arene **29** [34] with excess NBS under irradiation proceeds only up to the tetrabromo step, affording the 1,2,4,5 *cis-trans-cis* tetrabromo derivative **30** (Eq. 4.20) [35]. The relative inertness of the methylene groups of the tetrabromo derivative to undergo further bromination may be related to the isoclinal disposition of the methylene hydrogens and/or their steric shielding by the bulky neighbouring groups. The Boc-protected tetrabromo derivative **30** could in principle provide an entry into methylene-substituted calixarenes possessing the array of intraannular OH bonds intact (e.g., via substitution of the bromine groups followed by deprotection of the OH groups).



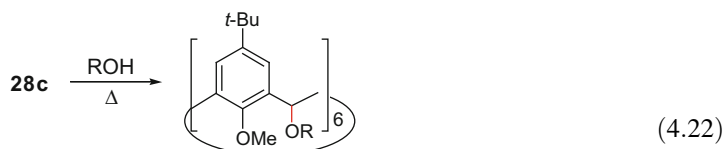
## 4.9 Reaction of Bromocalixarenes with Nucleophiles

Nucleophilic substitution reactions of bromocalixarenes (where the bromine atoms are located at the bridges) enable the incorporation of O-, N-, S-, and even some C-nucleophiles at the bridges. Typical reaction conditions involve heating to reflux a mixture of the bromocalixarene and the nucleophile in an ionizing solvent medium (Eq. 4.21). The reaction is usually performed in the absence of a Lewis acid with the ionizing solvent providing the polar medium necessary for the heterolytic C-Br cleavage and the stabilization of the benzhydrylic-type

carbocation intermediates. In general a precondition for the success of this type of reaction is that HNu (the conjugated acid of the nucleophile Nu<sup>-</sup>) must be a stronger nucleophile than the ionizing solvent (which is present in excess). Fluorinated solvents such as 2,2,2-trifluoroethanol (TFE), 1,1,1,3,3,3-hexafluoroisopropanol (HFIP) and in some cases trifluoroacetic acid (TFA), possessing high ionizing properties but low nucleophilicities, have been successfully applied [27, 28, 30, 32].

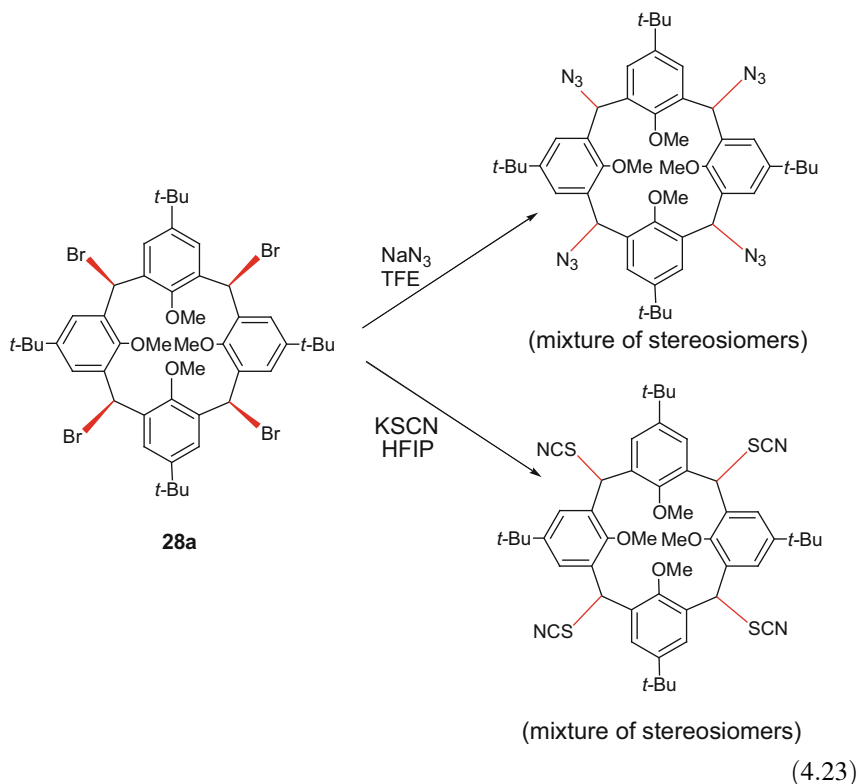


The reaction of bromocalix[4]arene **28a** with alcohols must be conducted in a mixture of the alcohol nucleophile and the ionizing solvent, but for the larger calixarenes the reaction proceeds even in the absence of the additional fluorinated alcohol [30]. Some typical reactions of bromocalix[6]arene **28c** are exemplified in Eq. (4.22). Notably, in most cases the reaction proceeds in stereoselective fashion affording mainly the *all-cis* derivative. The reaction fails for tertiary alcohols while in the reaction with secondary alcohols, a competing reaction was observed yielding reduced bridges. This reaction most likely involves hydride transfer from the secondary alcohol to the benzydrylic carbocation intermediates [30].

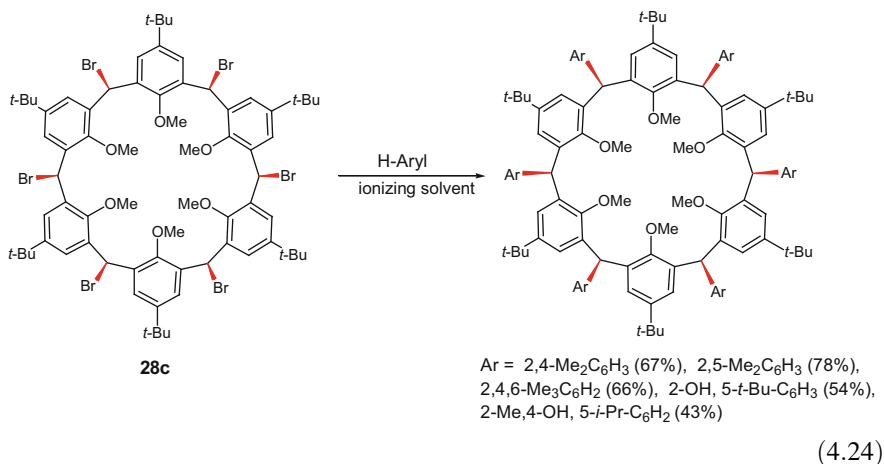


R = Me (43%), Et (37%), *n*-Pr (45%), *i*-Pr (60%),  
*n*-Bu (53%), CH<sub>2</sub>CF<sub>3</sub> (52%), cyclopentyl (37%),  
 cyclohexyl (21%), CH(CF<sub>3</sub>)<sub>2</sub> (21%)

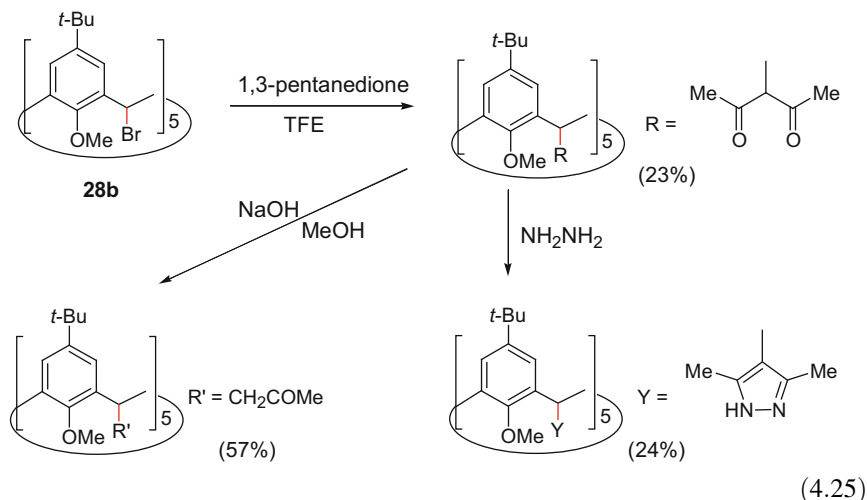
The reaction of bromocalix[4]arene **28a** with highly reactive linear nucleophiles (such as azide ion and thiocyanide) proceeds with poor selectivity affording mixtures of stereoisomers (Eq. 4.23) [27b].



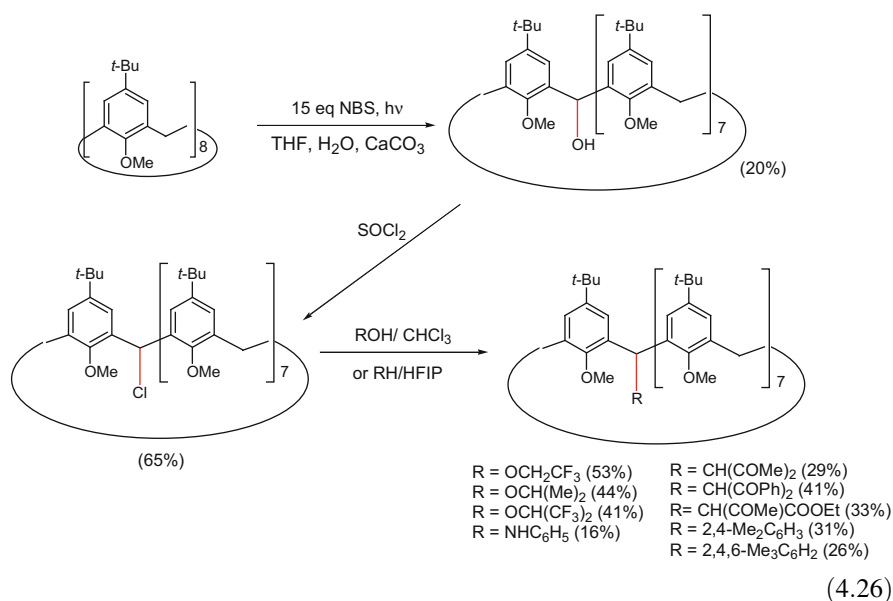
Incorporation of aryl groups at the bridges can be achieved by a solvolytic Friedel-Crafts reaction (in the absence of a Lewis acid) simply by refluxing a mixture of the bromocalixarenes, the aromatic ring and the ionizing solvent (TFE for the electron-rich substrates or hexafluoroisopropanol, Eq. 4.24) [36]. In all case examined, the reaction proceeds in stereoselective fashion affording exclusively the *all-cis* derivative.



Bromocalixarenes **28b** and **28c** react with highly enolizable compounds such as 1,3-pentanedione, affording calixarenes incorporating acetylacetonyl groups at the bridges. These groups can be further modified via reaction with hydrazine or via base catalyzed fragmentation as exemplified in Eq. 4.25 for **28b** [27, 28].



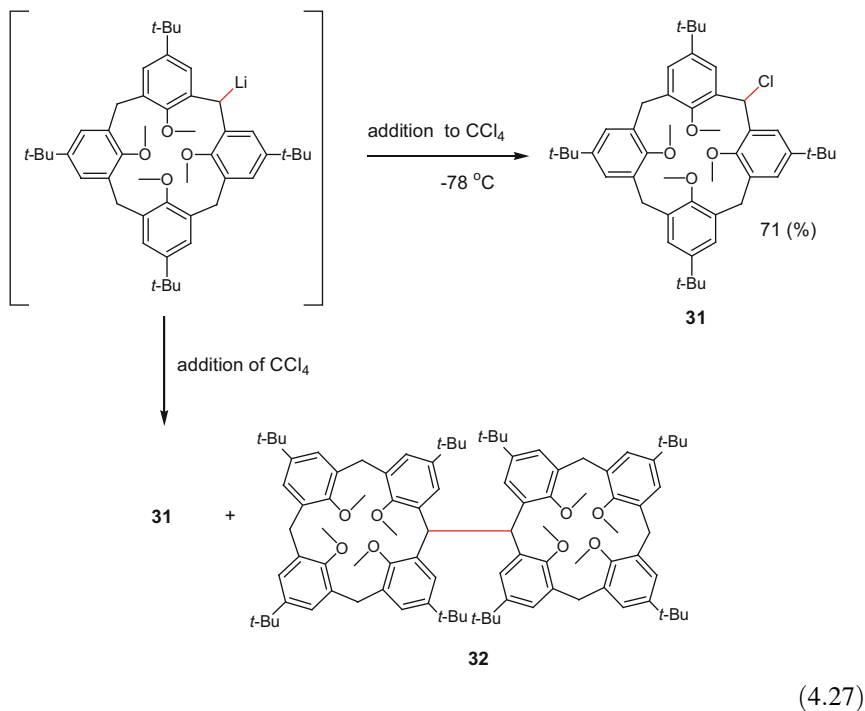
The modification of single methylene group of the methyl ethers of calix[6]- or calix[8]arene has been achieved via photochemical reaction with NBS in a THF/water/ $\text{CaCO}_3$  mixture [37]. The reaction affords a mixture of products and from it the corresponding monohydroxycalixarenes were isolated. The OH group was replaced by chlorine via reaction with  $\text{SOCl}_2$ , and the resulting chloro derivatives reacted under  $\text{S}_{\text{N}}1$  conditions with a wide array of nucleophiles, as exemplified in Eq. 4.26 for a calix[8]arene derivative.



- |                                       |   |
|---------------------------------------|---|
| R = $\text{OCH}_2\text{CF}_3$ (53%)   | R = $\text{CH}(\text{COMe})_2$ (29%)                          |
| R = $\text{OCH}(\text{Me})_2$ (44%)   | R = $\text{CH}(\text{COPh})_2$ (41%)                          |
| R = $\text{OCH}(\text{CF}_3)_2$ (41%) | R = $\text{CH}(\text{COMe})\text{COOEt}$ (33%)                |
| R = $\text{NHC}_6\text{H}_5$ (16%)    | R = 2,4-Me <sub>2</sub> C <sub>6</sub> H <sub>3</sub> (31%)   |
|                                       | R = 2,4,6-Me <sub>3</sub> C <sub>6</sub> H <sub>2</sub> (26%) |



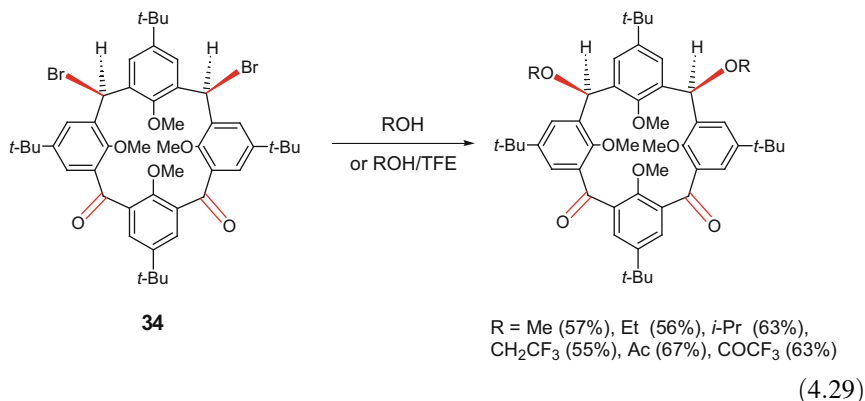
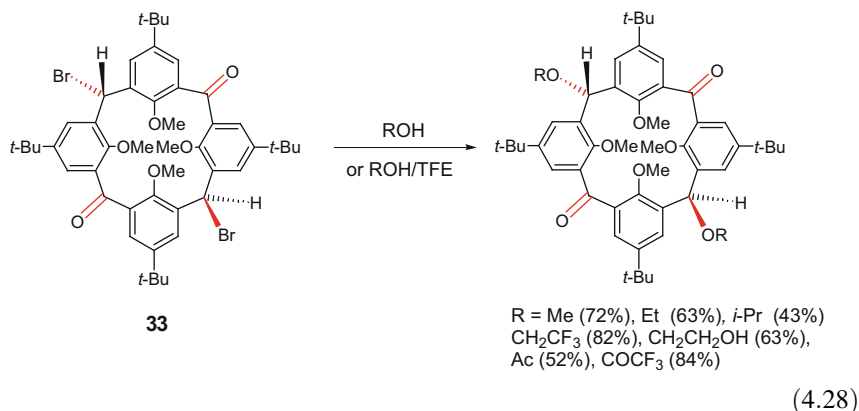
The preparation of a monochloro derivative of the tetramethyl ether of calix[4]arene (**35**) was reported by Fantini and coworkers via lithiation of **11** (reaction with BuLi) followed by addition of the monolithiated derivative to a large excess of CCl<sub>4</sub> (reverse addition). The direct addition of CCl<sub>4</sub> to the lithiated calixarene yielded a mixture of the chlorocalixarene **31** and dicalixarene **32** (Eq. 4.27) [12d]. Fischer and Weber have utilized the monolithiated calixarene derivative as an entry point for the preparation of dicalixarenes interconnected by flexible linkages [38–40].



## 4.10 Calixarenes with Two Types of Modified Bridges

Calix[4]arenes possessing pairs of carbonyl groups and bromomethylene groups located at distal (*trans* isomer, **33**) or proximal (*cis* isomer, **34**) bridges were prepared via photochemical bromination of tetramethoxycalix[4]arene with 6.3 equivalents of NBS followed by hydrolysis of the dibromomethylene groups of the corresponding hexabromocalix[4]arene derivatives [41]. The reaction of both compounds with alcohols and carboxylic acid proceeds in stereoselective fashion (Eqs. 4.28 and 4.29). Under S<sub>N</sub>1 conditions the bromomethylene groups of both compounds also react with a wide range of nucleophiles, providing a synthetic entry

into derivatives possessing both a pair of carbonyls and a pair of monosubstituted bridges.



## References

1. For recent reviews on calixarenes modified at the methylene bridges see: a) Sliwa, W.; Deska, M. *Arkivoc*, **2012**, (i) 173. b) Deska, M.; Dondela, B.; Sliwa, W. *Arkivoc*, **2015**, (i) 29.
2. (a) For a review on the conformational analysis of calix[4]arenes substituted at one or two methylene bridges see: Simaan, S.; Biali, S.E. *J. Phys. Org. Chem.* **2004**, *17*, 752.
3. (a) Tabatabai, M.; Vogt, W.; Böhmer, V. *Tetrahedron. Lett.* **1990**, *31*, 3295. (b) Sartori, G.; Maggi, R.; Bigi, F.; Arduini, A.; Pastorio, A.; Porta, C. *J. Chem. Soc., Perkin Trans. 1*, **1994**, 1657. (c) Biali, S. E.; Böhmer, V.; Cohen, S.; Ferguson, G.; Grüttner, C.; Grynszpan, F.; Paulus, E. F.; Thondorf, I.; Vogt, W. *J. Am. Chem. Soc.* **1996**, *118*, 12938. (d) Bergamaschi, M.; Bigi, F.; Lanfranchi, M.; Maggi, R.; Pastorio, A.; Pellinghelli, M. A.; Peri, F.; Porta, C.; Sartori, G. *Tetrahedron* **1997**, *53*, 13037. (e) For a review on the synthesis of calixarenes via the stepwise and fragment condensation methods see: Böhmer, V. *Liebigs Ann./Recueil* **1997**, 2019.

4. Biali, S. E.; Böhmer, V.; Columbus, I.; Ferguson, G.; Grüttner, C.; Grynszpan, F.; Paulus, E. F.; Thondorf, I. *J. Chem. Soc., Perkin Trans. 2*, **1998**, 2261.
5. (a) Tian, X.-H.; Hao, X.; Liang, T.-L.; Chen, C.-F. *Chem. Commun.* **2009**, 6771. (b) Tian, X.-H.; Chen, C.-F.; *Chem. Eur. J.* **2010**, *16*, 8072. (c) Tian, X.-H.; Chen, C.-F. *Org. Lett.* **2010**, *12*, 524. (d) Chen, C.-F. *Chem. Commun.* **2011**, *47*, 6771. (e) Jiang, Y.; Chen, C.-F. *Eur. J. Org. Chem.* **2011**, 6377.
6. (a) Gopalsamuthiram, V.; Predeus, A. V.; Huang, R. H.; Wulff, W. D. *J. Am. Chem. Soc.*, **2009**, *131*, 18018. (b) Gopalsamuthiram, V.; Huang, R. H.; Wulff, W. D. *Chem. Commun.* **2010**, *46*, 8213.
7. Sawada, T.; Nishiyama, Y.; Tabuchi, W.; Ishikawa, M.; Tsutsumi, E.; Kuwahara, Y.; Shosenji, H. *Org. Lett.* **2006**, *8*, 1995.
8. Buccella, D.; Parkin, G. *J. Am. Chem. Soc.* **2006**, *128*, 16358.
9. Al-Saraierh, H.; Miller, D. O.; Georghiou, P. E. *J. Org. Chem.* **2007**, *72*, 4532.
10. Middel, O.; Greff, Z.; Taylor, N. J.; Verboom, W.; Reinhoudt, D. N.; Snieckus, V. *J. Org. Chem.*, **2000**, *65*, 667.
11. (a) Agbaria, K.; Biali, S. E. *J. Am. Chem. Soc.*, **2001**, *123*, 12495. (b) Simaan, S.; Biali, S. E. *J. Org. Chem.* **2003**, *68*, 3634. (c) Simaan, S.; Biali, S. E. *J. Org. Chem.* **2003**, *68*, 7685. (d) Simaan, S.; Biali, S. E. *J. Org. Chem.* **2004**, *69*, 95. (e) Simaan, S.; Biali, S. E. *Org. Lett.* **2005**, *7*, 1817.
12. (a) Scully, P. A.; Hamilton, T. M.; Bennett, J. L. *Org. Lett.* **2001**, *3*, 2741. (b) Hertel, M. P.; Behrle, A. C.; Williams, S. A.; Schmidt, J. A. R.; Fantini, J. L. *Tetrahedron* **2009**, *65*, 8657. (c) Hardman, M. J.; Thomas, A. M.; Carroll, L. T.; Williams, L. C.; Parkin, S.; Fantini, J. L. *Tetrahedron*, **2011**, *67*, 7027. (d) Carroll, L. T.; Hill, P. A.; Ngo, C. Q.; Klatt, K. P.; Fantini, J. L. *Tetrahedron*, **2013**, *69*, 5002. (e) For the regioselective methylene alkylation of a meta-bridged calix[4]arene see: Slavik, P.; Dvorakova, H.; Eigner, V.; Lhotak, P. *Chem. Commun.* **2014**, *50*, 10112.
13. (a) Gruber, T.; Gruner, M.; Fischer, C.; Seichter, W.; Bombicz, P.; Weber, E. *New J. Chem.* **2010**, *34*, 250. (b) Gruner, M.; Fischer, C.; Gruber, T.; Weber, E. *Supramol. Chem.* **2010**, *22*, 256. (c) Fischer, C.; Lin, G.; Seichter, W.; Weber, E. *Tetrahedron*, **2011**, *76*, 5656. (d) Fischer, C.; Gruber, T.; Seichter, W.; Weber, E. *Org. Biomol. Chem.* **2011**, *9*, 4347. (e) Fischer, C.; Katzsch, F.; Weber, E. *Tetrahedron Lett.* **2013**, *54*, 2874.
14. For recent calculations on the relative stabilities of the conformations of calix[4]arenes monosubstituted at a single methylene bridge see : Park, K.; Son, H.-J.; Choe, J.-I. *J. Ind. Eng. Chem.* **2014**, *20*, 3276.
15. Zhao, Y.; Swager, T. M. *Eur. J. Org. Chem.* **2015**, 4593.
16. Arora, S.; Sharma, S.; Mithu, V. S.; Hee-Lee, C.; Singh, K. *Chem. Commun.* **2015**, *51*, 4227.
17. (a) Görmär, G.; Seiffarth, K.; Schultz, M.; Zimmerman, J.; Flämig, G. *Macromol. Chem.* **1990**, *191*, 81. See also: (b) Ninagawa, A.; Cho, K.; Matsuda, H. *Makromol. Chem.* **1985**, *186*, 1379. (c) Ito, K.; Izawa, S.; Ohba, T.; Ohba, Y.; Sone, T. *Tetrahedron Lett.* **1996**, *37*, 5959. (d) Matsuda, K.; Nakamura, N.; Takahashi, K.; Inoue, K.; Koga, N.; Iwamura, H. *J. Am. Chem. Soc.* **1995**, *117*, 5550.
18. Jaime, C.; de Mendoza, J.; Prados, P.; Nieto, P. M.; Sanchez, C. *J. Org. Chem.* **1991**, *56*, 3372.
19. Akabori, S.; Sannohe, H.; Habata, Y.; Mukoyama, Y.; Ishii, T. *J. J. Chem. Soc., Chem. Commun.* **1996**, 1467.
20. Seri, N.; Thondorf, I.; Biali, S. E. *J. Org. Chem.* **2004**, *69*, 4774.
21. Shalev, O.; Biali, S. E. *J. Org. Chem.* **2014**, *79*, 8584.
22. Poms, D.; Itzhak, N.; Kuno, L.; Biali, S. E. *J. Org. Chem.* **2014**, *79*, 538.
23. (a) Fischer, C.; Lin, G.; Seichter, W.; Weber, E. *Tetrahedron Lett.* **2013**, *54*, 2187. (b) See also: He, C.; Zhang, X.; Huang, R.; Pan, J.; Li, J.; Ling, X.; Xiong, Y.; Zhu, X. *Tetrahedron Lett.* **2014**, *55*, 4458.
24. Itzhak, N.; Biali, S. E. *Eur. J. Org. Chem.* **2015**, 3221.
25. (a) Kuno, L.; Seri, N.; Biali, S. E. *Org. Lett.* **2007**, *9*, 1577. (b) Kuno, L.; Biali, S. E. *J. Org. Chem.*, **2009**, *74*, 48. (c) Kuno, L.; Biali, S. E. *Org. Lett.* **2009**, *11*, 3662.

26. Itzhak, N.; Biali, S. E. *Synthesis* **2015**, *47*, 1678.
27. (a) Columbus, I.; Biali, S. E. *Org. Lett.* **2007**, *9*, 2927. (b) Columbus, I.; Biali, S. E. *J. Org. Chem.* **2008**, *73*, 2598.
28. Kogan, K.; Biali, S. E. *J. Org. Chem.* **2009**, *74*, 7172.
29. Kumar, S. K.; Chawla, H. M.; Varadarajan, R. *Tetrahedron Lett.* **2002**, *43*, 7073.
30. Kogan, K.; Columbus, I.; Biali, S. E. *J. Org. Chem.* **2008**, *73*, 7327.
31. Klenke, B.; Näther, C.; Friedrichsen, W. *Tetrahedron Lett.* **1998**, *39*, 8967.
32. Kogan, K.; Biali, S. E. *J. Org. Chem.*, **2011**, *76*, 7240
33. Poms, D.; Leader, A.; Biali, S. E. *Arkivoc* **2015** (iii) 7.
34. Ménand, M.; Leroy, A.; Marrot, J.; Luhmer, M.; Jabin, I. *Angew. Chem. Int. Ed. Eng.* **2009**, *48*, 5509.
35. Leader, A.; Itzhak, N.; Bogoslavsky, B.; Biali, S. E. *Eur. J. Org. Chem.* **2015**, 6489.
36. Kogan, K.; Itzhak, N.; Biali, S. E. *Supram. Chem.* **2010**, *22*, 704.
37. (a) Itzhak, N.; Biali, S. E. *J. Org. Chem.*, **2010**, *75*, 3437. (b) Itzhak, N.; Kogan, K.; Biali, S. E. *Eur. J. Org. Chem.* **2011**, 6581.
38. Fischer, C.; Weber, E. *J. Incl. Phenom. Macrocycl. Chem.* **2014**, *79*, 151.
39. For a recent example of two calix[4]arene subunits interconnected by a methylene bridge see: Lappchen, T.; Dings, R. P.M.; Rossin, R.; Simon, J. F.; Visser, T. J.; Bakker, M.; Walhe, P.; van Mourik, T.; Donato, K.; van Beijnum, J. R.; Griffioen, A. W.; Lub, J.; Robillard, M. S.; Mayo, K. H.; Grüll, H. *Eur. J. Med. Chem.* **2015**, *89*, 279.
40. For polymetallic clusters of the bicalixarene, see: McLellan, R.; Palacios, M. A.; Beavers, C. M.; Teat, S. J.; Piligkos, S.; Brechin, E. K.; Dalgarno, S. J. *Chem. Eur. J.* **2015**, *21*, 2804.
41. Kuno, L.; Biali, S. E. *J. Org. Chem.* **2011**, *76*, 3664.

# Chapter 5

## Calix[5]arene: from Capsules to Polymers

Melchiorre F. Parisi, Giuseppe Gattuso, Anna Notti, Ilenia Pisagatti,  
and Sebastiano Pappalardo

### 5.1 Introduction

Supramolecular polymers [1] are arrays of monomeric components held together by reversible and highly directional non-covalent bonds. Owing to the dynamic and reversible nature of the non-covalent interactions between monomers, supramolecular polymers, unlike ‘classic’ ones, display some unconventional properties. Stimuli-responsiveness, adaptive behavior and shape memory are some of the appealing features that place these species at the forefront of material sciences research [2]. Multiple hydrogen bonds, metal-ligand coordination, electrostatic interactions,  $\pi$ – $\pi$  stacking, or combinations of these are, by far, the most common intermolecular non-covalent interactions used in supramolecular polymerization. In addition, supramolecular oligomer/polymer formation may also be driven by host-guest interactions as a result of spontaneous processes of iterative association between complementary monomers. This approach to the non-covalent linking of monomers may lead to the assembly of two different types of aggregates that, borrowing the terminology from classical polycondensation polymers, can be described as AA/BB- and AB-type polymers. The former consist of homoditopic complementary monomer pairs, i.e., a two-binding site receptor unit (AA) paired to a bidentate guest molecule (BB), whereas the latter are built from heteroditopic monomers simultaneously embedding a host (A) and a complementary guest (B) moiety on the same molecule. Both types of polymers, however, have similar

---

M.F. Parisi (✉) • G. Gattuso • A. Notti • I. Pisagatti  
Dipartimento di Scienze Chimiche, Biologiche, Farmaceutiche ed Ambientali,  
Università di Messina, viale F. Stagno d’Alcontres 31, 98166 Messina, Italy  
e-mail: [mparisi@unime.it](mailto:mparisi@unime.it)

S. Pappalardo  
Dipartimento di Scienze Chimiche, Università di Catania, viale A. Doria 6,  
Università di Catania, 95125 Catania, Italy

self-assembly behavior, their chain-growth proceeds generally under thermodynamic control, and their number-average degree of polymerization ( $DP$ ) can generally be described (or predicted) by taking into account the Carothers' equation [3]. The host-guest approach to supramolecular polymers offers considerable advantages over other methods, given that choosing among very different host-guest pairs allows for the design of polymeric materials capable of displaying the most diverse properties, including the ability to respond to quite a variety of different chemical or physical external stimuli. Furthermore, the simultaneous use of different host-guest recognition motifs allows easy access to multi-component copolymeric systems whose self-assembly and self-sorting is regulated by orthogonal and hierarchical recognition processes [4].

The chemistry of supramolecular polymers has been extensively reviewed [5]. In the past two decades, general overviews as well as more specific surveys have focused on individual classes of polymers or on the mechanisms and thermodynamics of supramolecular polymerization. The present chapter aims to retrace the genesis and the evolution of that subgroup of supramolecular polymers that share the calix[5]arene skeleton as their common building block. To this end, relevant examples of dimeric capsules and/or encapsulation complexes key to the subsequent design of polycapsular AA/BB-type arrays, as well as discoveries pivotal to an effective self-assembly of AB-type architectures are surveyed in parallel.

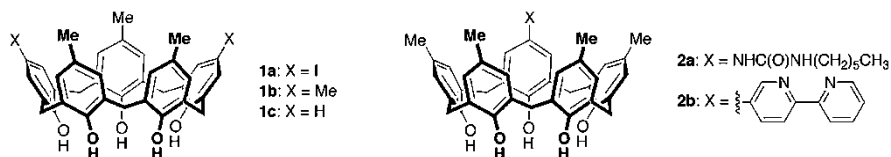
## 5.2 The Calix[5]arene Scaffold

Among the so-called conventional calix[ $n$ ]arenes,  $n = 4-8$ , the odd-numbered members (i.e.,  $n = 5$  and 7) have enjoyed less attention than their even-numbered analogues, most likely as a result of their low-yielding syntheses [6]. Despite this disadvantage, calix[5]arenes have attracted some degree of attention in relation to their potential use as a building block for the construction of more complex supramolecular architectures. Leaving aside those instances where the calix[5]arene framework has just been used as a molecular scaffold to arrange different functional groups in the tri-dimensional space for specific needs, in all the other cases, including capsule and polycapsule formation, calix[5]arene recognition/binding properties directly connected to the macrocyclic cavity preponderantly rest on: (i)  $\pi-\pi$  interactions, (ii) *endo*-cavity hydrogen bonding and (iii) electrostatic attractive forces, when present as *p*-sulfonate derivatives.

### 5.2.1 The Calix[5]arene/Fullerene “AA/BB-type” Motif

The remarkable affinity between calix[5]arenes and fullerenes ( $C_{60}$  and  $C_{70}$ ) was first reported by Fukazawa's group in 1997 [7]. Calix[5]arene derivatives **1a-c** – bearing at their wider rim iodine, methyl or hydrogen substituents – were found to

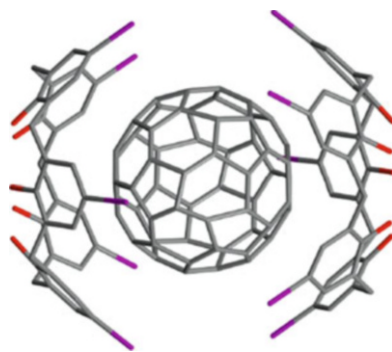
bind  $C_{60}$  with association constants ( $K_a$ ) in the 200–2,000  $M^{-1}$  range in low-polarity solvents such as toluene, benzene, carbon disulfide or *o*-dichlorobenzene. This remarkable result was ascribed to a favorable stereoelectronic matching between the convex surface of  $C_{60}$  and the concave cavity of the receptors that effectively interact with each other through  $\pi$ – $\pi$  interactions and van der Waals contacts. *p*-Benzylcalix[5]arene [8] and *p*-phenylcalix[5]arene [9] were also seen to enjoy similar advantageous host-guest interactions by readily forming, in the presence of  $C_{60}$ , dimeric capsular complexes in the solid state.



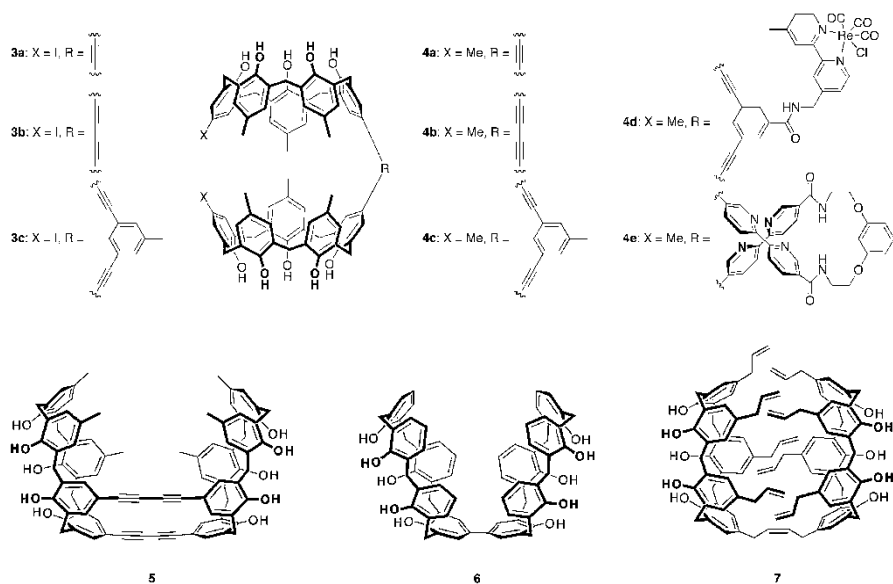
In solution,  $C_{60}$  binds to the three calix[5]arenes **1a–c** with a 1:1 stoichiometry and the same is true in the solid state for **1b–c** [10]. Diiodo derivative **1a** and  $C_{60}$ , on the other hand, afforded purple prism-shaped single crystals that, when subjected to X-ray crystallographic analysis, revealed the formation of a 2:1 host-guest capsular assembly, with up to 144 short ( $<4.0$  Å) contacts observed between the aromatic carbon atoms of **1a** and  $C_{60}$  (Fig. 5.1).

Structural refinement of these host molecules was later pursued by the same group on a double track. In the non-covalent direction, studies were finalized to the design of calix[5]arene pentols fitted, at the wider rim, with a molecular hook capable of facilitating  $C_{60}$  and  $C_{70}$  capsule formation via additional self-assembling interactions between the two sub-units. To this end, ureido **2a** [11] and 2,2'-bipyridyl (bpy) derivative **2b** [12] were endowed with a self-complementary hydrogen-bond donor/acceptor group and a metal-acceptor ( $Ag^+$ ) binding site, respectively.

**Fig. 5.1** Solid-state structure of  $1a \supset C_{60} \subset 1a$ , displaying a pseudo  $D_{5d}$  symmetry as a result of the positional disorder of the two iodine atoms over the *para*-positions of the five phenol rings [7]



In the covalent direction, efforts were focused on the preparation [13] of a number of convergent-cavity bis-calix[5]arenes (**3a–c** and **4a–c**), capable of binding  $C_{60}$  even more efficiently ( $K_a$  up to  $7.6 \times 10^4 \text{ M}^{-1}$  in toluene). Separate from these, not being strictly linked to the development of supramolecular polymers, but still very much related to the bis-calix[5]arene/fullerene host-guest complementarity theme, the following examples deserve to be mentioned: (a) the highly sensitive chemosensor **4d**, incorporating a  $\text{Re}(\text{bpy})(\text{CO})_3\text{Cl}$  moiety as the signaling unit [14]; (b) the bis-calix[5]arene **4e** with a lateral allosteric pocket for metal ( $\text{Cu}^+$ ) binding [15]; and (c) the cage-shaped doubly-linked bis-calixarene **5** (in the *syn* conformation) for the encapsulation of higher fullerenes ( $K_{as}$   $9 \times 10^4$  and  $1.1 \times 10^5 \text{ M}^{-1}$  in the case of  $C_{76}$  and  $C_{78}$ , respectively) [16] reported by Fukazawa and Haino as well as the bridgeless [17] bis-calix[5]arene **6** and the octa-allyl [18] derivative **7** synthesized by Gutsche and coworkers.

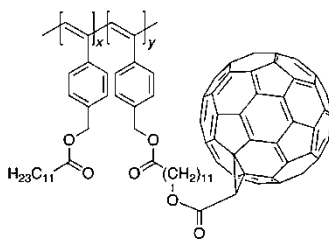
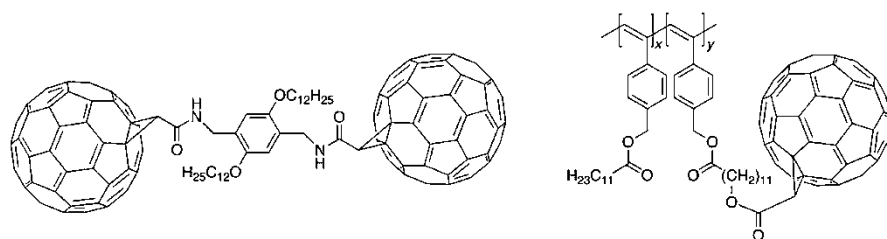
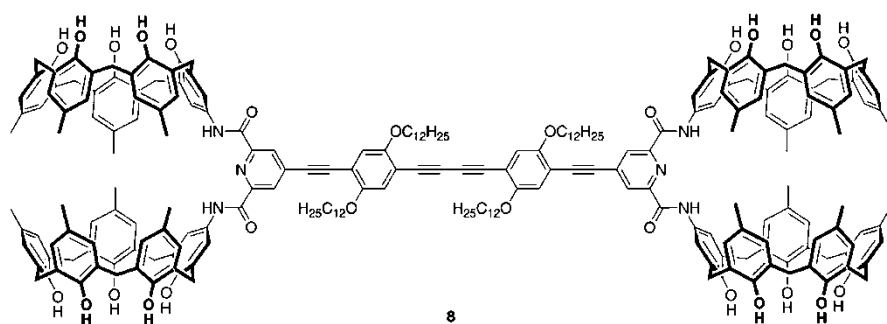


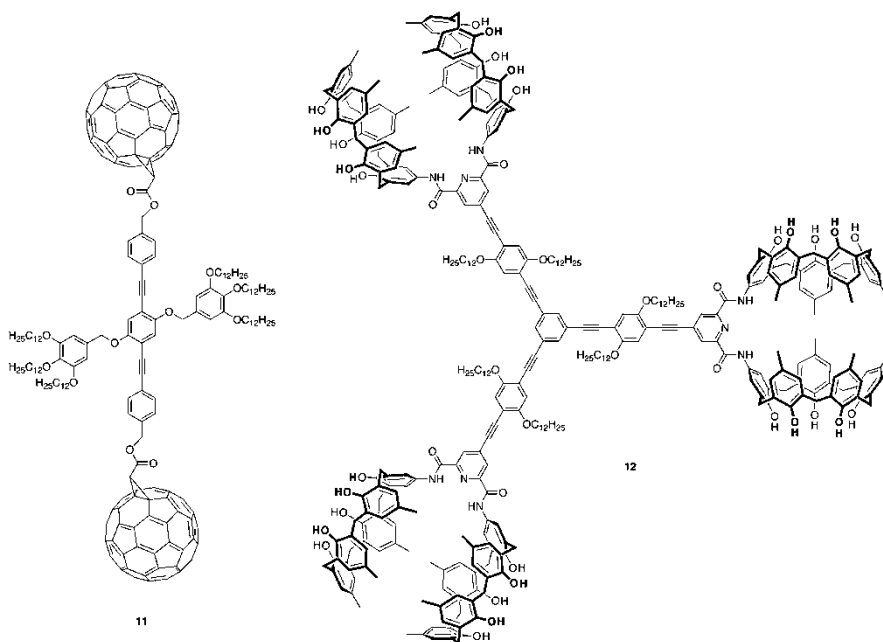
Even though receptors **3** and **4** were found to preferentially bind  $C_{70}$  over  $C_{60}$ , they later became the key building-blocks for the construction of polymeric arrays of the host-guest type, owing to their proclivity to bind concave-surfaced guests. Haino et al. synthesized tetra-calix[5]arene **8** and demonstrated that, in the presence of the complementary dumbbell-shaped bis- $C_{60}$  guest **9**, this ditopic monomer iteratively self-assembles into AA/BB-type supramolecular oligomers [19]. In solution ( $2 \times 10^{-4} \text{ M}$  in  $\text{CDCl}_3$ ) diffusion NMR studies indicated the formation of trimeric species on average but, in the solid state, polymer-like morphologies, resembling spider-web fibers of nano-sized thickness, were detected by SEM (scanning electron microscopy) and AFM



(atomic force microscopy). The same tetra-calixarene **8** was later employed in supramolecular cross-linking experiments in the presence of the C<sub>60</sub>-decorated phenylacetylene polymer **10** [20]. Compound **8** acts in this case as a homoditopic non-covalent cross-linker, encapsulating the C<sub>60</sub> moieties grafted onto adjacent chains of polymer **10**. In toluene, size-exclusion chromatography measurements, carried out upon increasing addition of **8** to **10**, confirmed a progressive increase of the average molecular weight (from 18,000 to 32,000) and the polydispersity index (from 1.38 to 2.81). Field emission scanning electron microscopy of thin films – from cast benzene solutions of **8** and **10** – showed the formation of a widespread fibrous network and AFM revealed the presence of well-oriented fibrils with a uniform diameter.

Other intriguing results were obtained by Haino and coworkers with the combined use of the extended dumbbell-shaped C<sub>60</sub> guest **11** and either homoditopic tetra-calixarene **8** or homotriplic hexa-calix[5]arene **12** host monomers [21]. <sup>1</sup>H NMR DOSY (diffusion-ordered spectroscopy) studies showed that, in the 10 mM range (CDCl<sub>3</sub>), host and guest ditopic monomers **8** and **11** (1:1 equiv.) produced linear supramolecular polymers displaying an estimated average *DP* of 83, whereas the triplic/ditopic pair **12/11** (2:3 equiv.) yielded polymeric networks with a *DP* as high as 151.





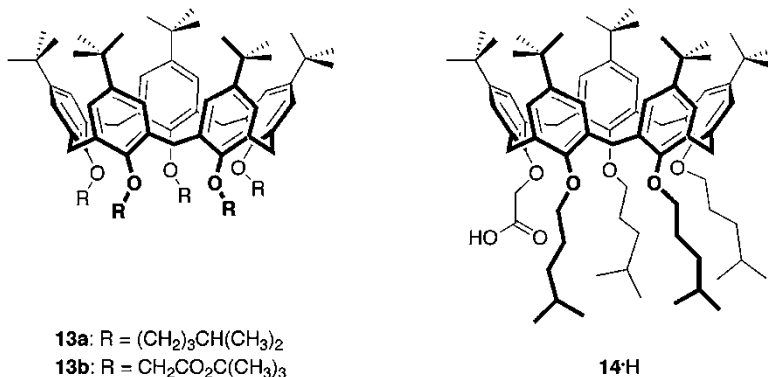
Interesting observations, in support of the formation of polymeric species with different morphologies, came from viscometry studies carried out at variable temperature. Upon raising the concentration or lowering the temperature, the viscosity of the **12/11** mixture was seen to increase more significantly than that of the **8/11** pair, leading the Authors to conclude that – in the semi-diluted regime – the latter forms rigid rod-like aggregates that affect viscosity only to a limited extent, as a result of a progressively hindered molecular rotation. Conversely, in the case of the tritopic/ditopic monomer pair **12/11**, the pronounced viscosity increase noticed in response to higher concentrations (or lower temperatures) was attributed to the formation of tri-dimensional networks, rapidly growing as a result of a supramolecular cross-linking process.

It is worth mentioning that so far no AB-type supramolecular polymers have been built exploiting the calix[5]arene/C<sub>60</sub> recognition motif. A calix[5]arene bearing a C<sub>60</sub>-terminated pendant group at its upper rim has been described, but no evidence of its behavior as a potential monomer was reported [22].

### 5.2.2 The Calix[5]arene/Alkanediyldiammonium Ion “AA/BB-type” Motif

The year after Fukazawa’s report on fullerene recognition [7], S. Pappalardo and coworkers, following up earlier studies on calix[5]arene crown-5 derivatives [23], noticed that *p*-*tert*-butylcalix[5]arenes – locked in a *cone* conformation [24] – act as very selective receptors of linear primary alkylammonium ions [25]. Owing to the

remarkable stereoelectronic matching between these unbranched cations and the  $\pi$ -electron rich cavity of the macrocycle, penta-*O*-alkyl- **13a** and penta-*O*-alkoxycarbonylmethyl-calix[5]arenes **13b**, among many others [26], were shown to selectively bind *n*-butylammonium ions *endo*-cavity, with association constants of up to  $10^6 \text{ M}^{-1}$  ( $\text{CH}_2\text{Cl}_2$ ) and with a selectivity – with respect to isomeric branched alkylammonium ions – of *ca.*  $10^3$  [25a].



Differently from fullerene recognition, which relies entirely on  $\pi$ – $\pi$  interactions, alkylammonium recognition by calix[5]arenes takes advantage of a wider set of weak forces. As shown later by Parisi et al. by single-crystal X-ray studies [27], the binding of these guests within the cavity of *p*-*tert*-butylcalix[5]arenes is secured by an interplay of non-covalent forces including: tripodal hydrogen bonding (of the ammonium moiety to the phenolic oxygen atoms) and CH– $\pi$  interactions, the latter occurring between the  $\alpha$ - and  $\beta$ -methylene hydrogen atoms of the guest alkyl chain and four distinct aromatic rings of the host (Fig. 5.2a). Additional stabilization of these 1:1 host-guest complexes may also be provided, in the case of ionizable carboxylcalix[5]arene **14-H**, by an additional intermolecular ammonium-carboxylate salt bridge [28] (Fig. 5.2b).

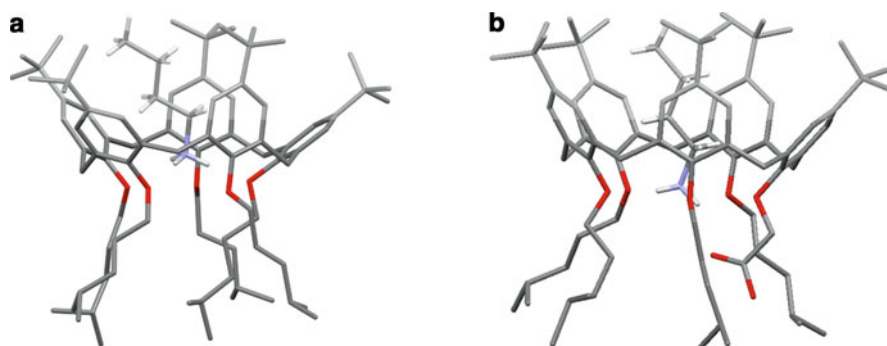
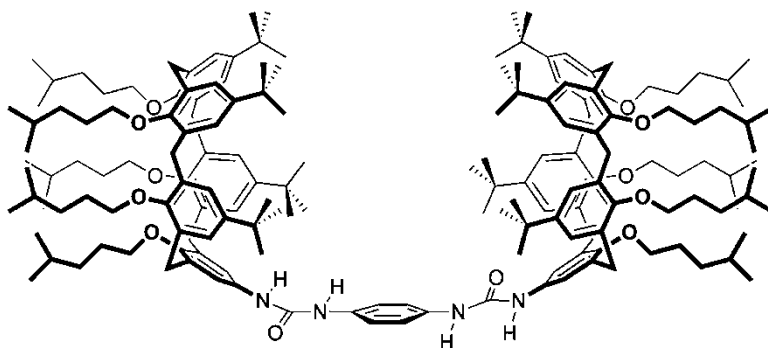


**Fig. 5.2** Solid-state structures of the: (a)  $n\text{-BuNH}_3^+ \subset \mathbf{13a}$  [27a] and (b)  $n\text{-BuNH}_3^+ \subset \mathbf{14-H}$  [28] *endo*-cavity complexes

These findings paved the way for the use of the calix[5]arene-alkylammonium ion recognition motif in the assembly of capsules and supramolecular polymers. Chronologically, the first guest-induced dimeric capsules of this type were detected by Parisi and coworkers upon exposure of derivatives **13** to  $\alpha,\omega$ -alkanediyl diammonium dipicrates of appropriate length ( ${}^+\text{H}_3\text{N}(\text{CH}_2)_n\text{NH}_3^+$ ,  $n = 8, 9, 10, 12$ ) [29]. These mixtures, depending on the host-to-guest ratio used, yielded 1:1 and 2:1 complexes. Based on electrospray ionization mass spectrometry measurements and  ${}^1\text{H}$  NMR titration experiments ( $\text{CDCl}_3/\text{CD}_3\text{OD}$ , 2:1), encapsulation of the 1,10-decanediyl diammonium over the longer 1,12-dodecanediyl diammonium guest was seen to prevail in the case of **13a**. Formation of capsular ion-paired complexes [30] with long-chain diammonium dichloride salts was later reported by S. Pappalardo, Parisi and coworkers with bis-calix[5]arene **15** [31]. This heterotetrotopic receptor was seen to selectively bind  $\text{Cl}^-\text{H}_3\text{N}^+(\text{CH}_2)_{12}\text{NH}_3^+\text{Cl}^-$  very efficiently ( $K_a$   $2.4 \times 10^3 \text{ M}^{-1}$ ) even in a highly competitive solvent mixture ( $\text{CDCl}_3/(\text{CD}_3)_2\text{SO}$ , 3:2) by combining the cooperative action of two converging calix [5]arene cavities in the encapsulation of the dication with the ability of the two ureido moieties to bind the relevant counterions.



15

More recent examples illustrating the efficacy of a proton-transfer-mediated self-assembly process in the context of capsule formation have been reported by Parisi et al. [32]. Overall, molecular encapsulation of a diamine (i.e.,  $\text{H}_2\text{N}(\text{CH}_2)_n\text{NH}_2$ ,  $n = 10, 11$  and  $12$ ) within two molecules of carboxylcalix[5]arene **14-H** was shown to take place as a result of two protonation reactions and a total of 20 non-covalent interactions including, in the case of the 1,11-undecanediyl diammonium ion/carboxylatecalix[5]arene **14**<sup>-</sup> capsule [32a], two endohedral carboxylate-ammonium salt bridges, six hydrogen bonds and eight  $\text{CH}\cdots\pi$  contacts (all of them of the host-to-guest type), as well as four (host-to-host) van der Waals contacts (Fig. 5.3). Calculation of the capsular inner space and the volumes of the guests used, revealed packing coefficients in the 61–69% range, very close, in more than one case, to the ideal 70% value postulated by Mecozzi and Rebek for the formation of capsules in the solid state [33].

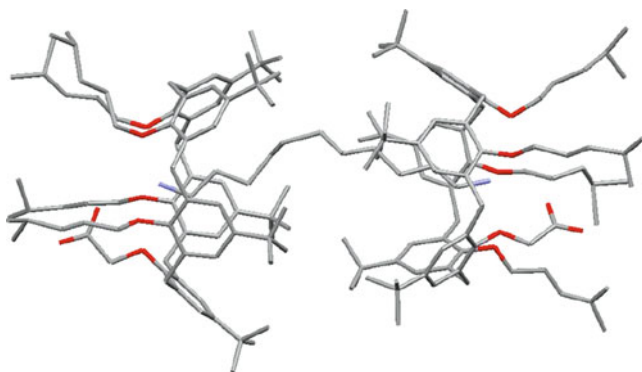


**Fig. 5.3** Solid-state structure of  $14a^- \cdot H_3N^+C_{11}NH_3^+ \cdot 14a^-$

As mentioned earlier, all this information provided the conceptual framework for the development of supramolecular polymers based on homoditopic complementary and heteroditopic self-complementary components. Specifically, it was envisaged that  $A \supset BB \subset A$  dimeric capsular assemblies would become AA/BB-type supramolecular polymers when two calix[5]arene molecules were linked together in a divergent fashion (via their narrow rims) to yield AA host monomers to be used in conjunction with BB guest monomers (i.e.,  $\alpha,\omega$ -alkanediyldiammonium ions of the required length). On the other hand, replacement of a *p-tert*-butylcalix[5]arene lower-rim alkyl group with a long-chained alkylammonium one was conceived as a valuable way of preparing suitable AB-type supramolecular monomer precursors (see next paragraph).

In this context, divergent-cavity bis-calix[5]arenes **16a–c** were synthesized by S. Pappalardo, Parisi et al. using *p*-, *m*- or *o*-xylyl spacers and their self-assembly behavior in the presence of 1,10-decanediyldiammonium dipicrate was analyzed in depth by diffusion NMR techniques and  $^1H$  NMR titration/dilution experiments [34]. These complementary homoditopic bis-calixarene/diammonium systems were found to dynamically respond to concentration and/or molar ratios between the two components, self-assembling at will into four different types of supermolecules, the most interesting being the oligomeric polycapsular assembly designated as type-D in Fig. 5.4. These species were found to grow on average up to an 8-mer in the case of bis-calixarene **16a**, further growth being prevented – according to micro-equilibria studies – by the competitive formation of type-B complexes (i.e., a bis-calixarene complex with both cavities filled by diammonium ions).

Gattuso et al. designed a divergent-cavity heterotetratopic AA-type monomer – bearing two additional anion binding sites – with a topology opposite to that seen for the convergent-cavity derivative **15** [35]. In this case, two calix[5]bis-crown-3 derivatives were joined together via a 1,4-bis-ureidophenylene moiety and the resulting divergent bis-calixarene **17** yielded, in the presence of the complementary 1,8-octanediyldiammonium dichloride, supramolecular oligomers consisting of three bis-calixarene and three diammonium guest molecules. This limited growth, with respect to **16**, likely depended on the methyl (instead of *p-tert*-butyl) substitution at the wider rim and the conformational rigidity imposed by the two crown-3

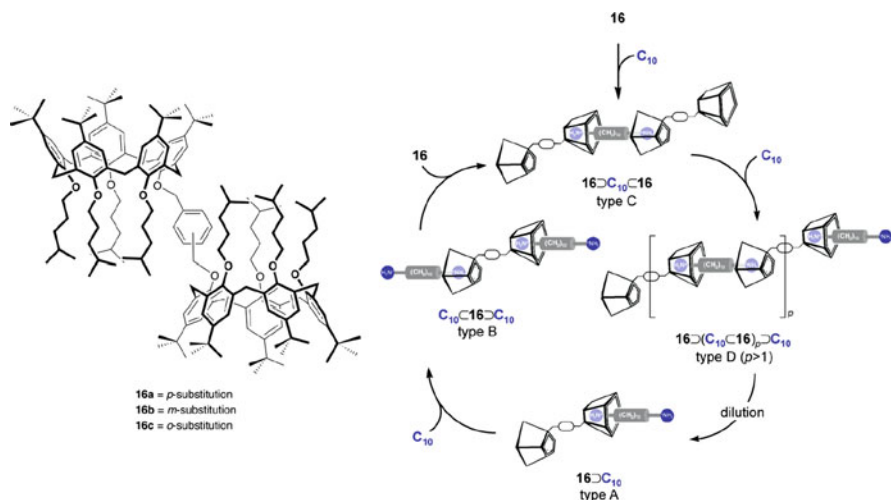
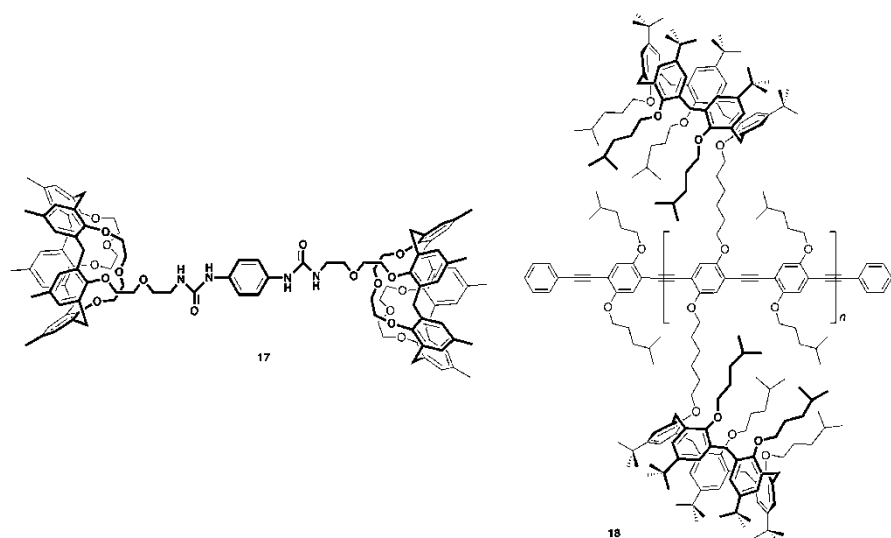


**Fig. 5.4** Cyclic reversible self-assembly dynamics of bis-calix[5]arenes **16** and  $H_3N^+(CH_2)_{10}NH_3^+$  ( $C_{10}$ ) monomers

ether moieties at the narrow rim that negatively counter-balanced the beneficial effect expected from an ion-paired assisted polymerization process.

A. Pappalardo and coworkers focused on the calix[5]arene/diammonium ion recognition motif for the supramolecular cross-linking of calix[5]arene-tethered poly(*p*-phenyleneethynylene) covalent polymers **18** [36]. Treatment of **18** with 0.5 equiv. of 1,10-decanediyl diammonium dipicrate led to the formation of polycapsular polymeric cross-linked networks, whereas presaturation of the calixarene cavities with an excess of same guest molecules led to ‘isolated’ strands of bis-*endo*-cavity arrays. Authors were able to show that the cross-linked material withstood several base/acid ( $Et_3N/TFA$ ) promoted disassembly and reassembly cycles.



### 5.2.3 The Calix[5]arene/Alkylammonium Ion “AB-type” Motif

The unlimited possibilities of functionalization offered by calixarene chemistry led Parisi et al. to prepare aminododecyloxy derivative **19** as the first prototype of a heteroditopic AB-type calix[5]arene monomer precursor [37]. Exposure of **19** to organic or inorganic acids (HCl, HBr, picric acid) triggered an iterative intermolecular *endo*-cavity inclusion process, leading to the formation of supra-molecular oligo/polymers (Fig. 5.5). The efficiency of the self-assembly, and hence the average degree of polymerization, was seen to strongly depend on the nature of the acid used to promote protonation of the amino pendant group. In line with the Hofmeister trend [38], anions forming tight ion pairs with the positively charged monomer were seen to hamper polymer formation, by halting the growth of the chain at a few monomer units. In other words, the counterion was found to effectively compete with the calixarene cavity for the alkylammonium guest moiety progressively attenuating the polymer-monomer association constant [39]. Among the alkylammonium monomers under investigation those formed upon picric acid (PicH) addition polymerized more efficiently (average  $DP = 20$  at 40 mM), forming fibers up to 100 mm long and about 800 nm wide upon evaporation of the solvent.

Gattuso et al. carried out studies on the chain-length regulation of a calix[5]arene-based AB-type polymer structurally related to **19**, by using A- or B-type orthogonal monotopic chain terminators, the latter consisting in either a competitive host or guest molecule such as **13b** or  $n\text{-BuNH}_3^+\text{PF}_6^-$ , respectively [40]. Counterion-dependence of polymer growth was lastly overridden by resorting to ionizable monomers equipped with an ancillary binding site for counterion recognition. Heteropolytopic ureidocalix[5]arene receptors (e.g., **15**, **17** and many others [41]), because of their ion-pair recognition properties [30], were used as model structures. These species had separately been shown to be able to simultaneously recognize and bind both the cation – within the calixarene cavity – and the pertinent counterion – by hydrogen-bond anchorage to the ureido site – of a given salt, ultimately overcoming the adverse ion-pairing effects connected with the recognition of a charged guest by a neutral receptor in low polarity solvents. Aminocalix[5]

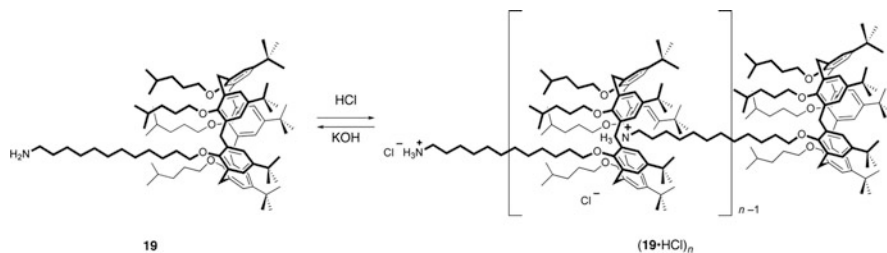
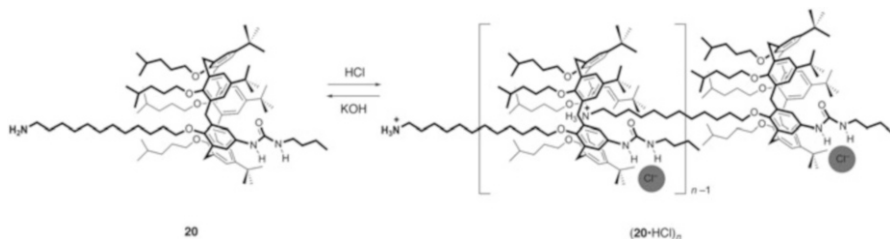


Fig. 5.5 Reversible assembly-disassembly of the AB-type supramolecular polymer  $(\mathbf{19} \cdot \text{HCl})_n$



**Fig. 5.6** Reversible assembly-disassembly of AB-type supramolecular polymers  $(\mathbf{20}\cdot\text{HCl})_n$

arene **19** was therefore fitted by Gattuso et al. with an auxiliary upper-rim *n*-butylureido group, and the resulting monomer precursor **20** was tested for self-assembly upon treatment with a range of different acids [42] (Fig. 5.6). The approach proved to be successful, with an approximate threefold increase in the *DP* value of  $(\mathbf{20}\cdot\text{HCl})_n$  (with respect to  $(\mathbf{19}\cdot\text{HCl})_n$ ), as shown by a combination of  $^1\text{H}$  and diffusion NMR studies. The polymer was found to be stable over a wide temperature range ( $-60$  to  $100$  °C). Additional light scattering investigations showed that this supramolecular polymer assembles according to a rather unusual mechanism, whereby the monomers would first assemble into concentration-independent random-coiled strands, and the resulting oligomers would then form concentration-dependent clusters with radii as large as 150 nm in the semi-dilute regime ( $[\mathbf{20}\cdot\text{HCl}] = 0.1$  g/cm $^3$ ) [43].

Given the evidence that anions docked onto the ancillary ureido binding site contribute to the overall polymerization process, Authors envisaged that protonation of monomer precursor **20** with a chiral acid would be a feasible way to gain access to chiral supramolecular polymers [42]. Accordingly, treatment of **20** with either (*R*)- or (*S*)-mandelic acid induced the assembly of supramolecular polymers with opposite helical chirality, as shown by the induced circular dichroism traces of opposite sign. In addition, such polymeric arrays showed ‘chiral memory’ upon treatment with a stronger acid ( $\text{CF}_3\text{CO}_2\text{H}$ ) and consequent replacement of the backbone-docked counterions (i.e., trifluoroacetate instead of mandelate). In other words, the resulting species retained chirality despite the replacement of the chiral elements responsible for the asymmetry of the initial polymer.

#### 5.2.4 The *p*-Sulfonatocalix[5]arene/Organic Cation Motif

This section deals with a third recognition motif that has mainly been used to assemble calix[4]arene-based supramolecular polymers, but has also generated a couple of examples of calix[5]arene-based polymers. The molecular recognition between *p*-sulfonatocalix[*n*]arenes ( $n=4-8$ ) and positively charged species (organic or inorganic) in aqueous medium heavily relies on Coulombic interactions



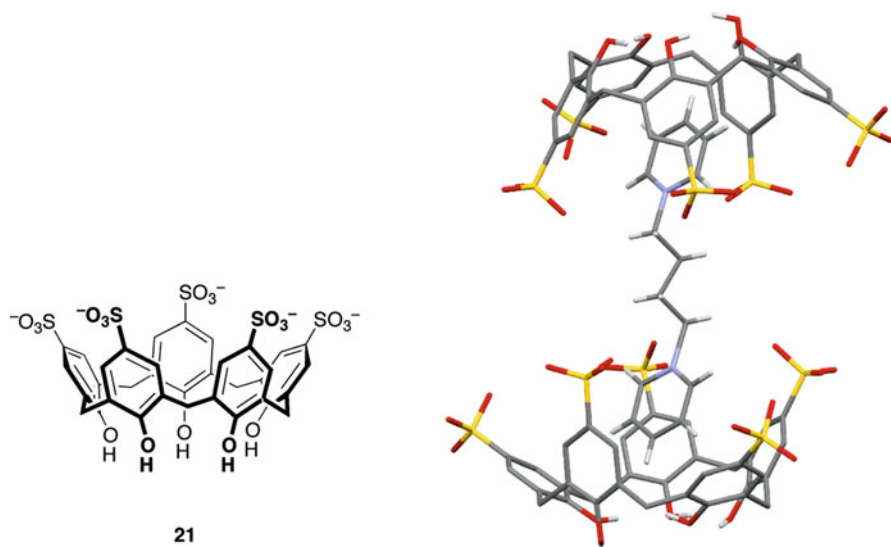


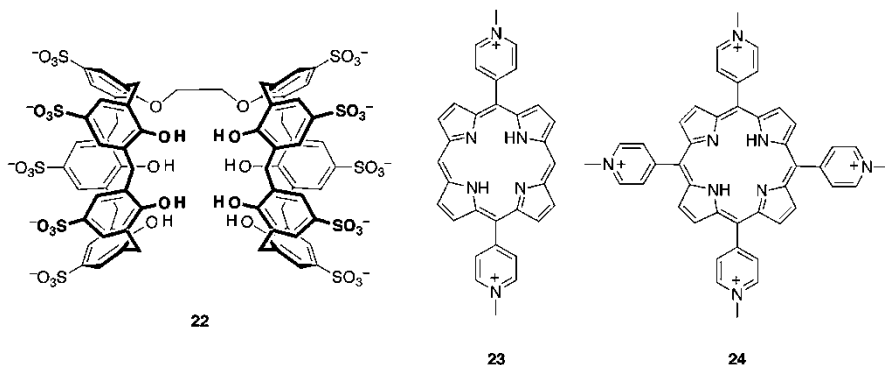
**Fig. 5.7** The solid-state structure of the capsular complex **21**⊃BPDB⊂**21** [47]

and, consequently, is less sensitive to the more stringent stereoelectronic constraints seen in Sects. 2.1, 2.2, and 2.3 for uncharged calixarenes. As a result, a variety of oligo/polymeric architectures with different functions have been obtained, irrespective of the size of the macrocycle used [44].

*p*-Sulfonatocalix[5]arene **21** has been shown to bind, with fairly low selectivity, a number of positively charged guests, ranging from metal to organic cations [45]. Inspiration for the design of suitable complementary homoditopic host and guest monomers adequate for AA/BB-type iterative polymerization came, also in the case of *p*-sulfonatocalix[5]arene **21**, from X-ray studies related to specific tailor-made ditopic guests. These include, among others [46], the dimeric capsules reported by Liu and coworkers [47] using the 1,4-bis-pyridiniumbutane (BPDB) ion (Fig. 5.7).

The host-guest sulfonate/methylpyridinium recognition motif was later used by Liu's group to control the morphology of supramolecular aggregates in water [48]. Divergent-cavity bis-*p*-sulfonatocalix[5]arene **22**, in the presence of complementary dicationic or tetracationic porphyrines **23** and **24**, was seen to assemble into 1D or 2D architectures, respectively. In this case, in consideration of the fact that the negative charges on the calixarene host molecule outnumber the positive ones on the guest, Authors proposed an assembly mode that involves not only a host-guest interaction process but also the contribution of additional porphyrin molecules surrounding the host-guest capsular subunit to ultimately provide charge balance. Structural assignments of the postulated polymeric nanostructures were supported by AFM and SEM data, while fluorescence spectroscopy and

electrochemical measurements showed that calixarenes and porphyrins act as effective electron donor-acceptor pairs.



Liu and coworkers have more recently used *p*-sulfonatocalix[5]arene **21** and homoditopic bis-*p*-sulfonatocalix[5]arene **22** to explore the aggregation behavior of the 1-pyrenemethylaminium (PMA) cation [49]. While PMA on its own – above its critical aggregation concentration – gave fiber-like aggregates in the micrometer range, the assembly mode and consequently the morphology of the aggregates formed upon addition of either **21** or **22** was seen to change dramatically. Calixarene **21** prompted the formation of vesicles with a size distribution of 22–247 nm while bis-calixarene **22**, on the other hand, induced the association of 1D nanorods (in the 200 nm range). Based on the fact that PMA and **21** or **22** may aggregate via electrostatic interactions – between the host sulfonate groups and the guest ammonium moiety – as well as  $\pi$ – $\pi$  stacking interactions – between the aromatic pyrene rings present in the guest – Authors concluded that the different morphologies (i.e., vesicles vs nanorods) relate to the different stoichiometric ratios employed (and hence charge balance) and the different conformational rigidity of the mono- and ditopic host molecules **21** and **22**.

### 5.3 Conclusions and Outlook

In this chapter, we have focused on the contribution made by calix[5]arenes to the field of supramolecular polymers. Similar to other macrocycles such as crown ethers, cyclodextrins, cucurbiturils, pillararenes and the like, calix[5]arene-based oligo/polymer formation relies primarily on host-guest interactions. To date, the three strategies successfully employed for the construction of AA/BB- and/or AB-type polymers include:  $C_{60}$  encapsulation, alkylammonium/ $\alpha,\omega$ -alkanediyldiammonium ion complexation and organic cation recognition. Using these strategies, linear architectures, entangled networks and supramolecular vesicles have so far been generated. There is, however, still a long way to

go to push this class of compounds to the forefront of materials science research. It is our hope that this brief overview will provide food for thought, encouraging future research in these and other directions that will lead to new discoveries in the challenging and exciting field of supramolecular polymerization.

## References

1. *Supramolecular Polymers*; Ciferri, A., Ed.; 2nd ed.; CRC Press: Boca Raton, FL, **2005**.
2. (a) Yan, X.; Wang, F.; Zheng B.; Huang, F. *Chem. Soc. Rev.* **2012**, *41*, 6042–6065; (b) Ma, X.; He, T. *Acc. Chem. Res.* **2014**, *47*, 1971–1981.
3. Elias, H.-G. *An Introduction to Polymer Science*; VCH: Weinheim, 1997.
4. (a) Yang, S. K.; Ambadec A. V.; Weck, M. *Chem. Soc. Rev.* **2011**, *40*, 129–137; (b) Li, S.-H.; Xiao, T.; Lin, C.; Wang, L. *Chem. Soc. Rev.* **2012**, *41*, 5950–5968; (c) Wei, P.; Yan, X.; Huang, F. *Chem. Soc. Rev.* **2015**, *44*, 815–832.
5. For a few selected review articles, see: (a) Martin, R. B. *Chem. Rev.* **1996**, *96*, 3043–3064; (b) Brunsveld, L.; Folmer, B. J. B.; Meijer, E. W.; Sijbesma, R. P. *Chem. Rev.* **2001**, *101*, 4071–4097; (c) De Greef, T. F. A.; Smulders, M. M. J.; Wolfs, M.; Schenning, A. P. H. J.; Sijbesma, R. P.; Meijer E. W. *Chem. Rev.* **2009**, *109*, 5687–5754; (d) Sameni, S.; Jeunesse, C.; Matta, D.; Harrowfield, J. *Chem. Soc. Rev.* **2009**, *38*, 2117–2146; (e) Liu, Y.; Wang, Z.; Zhang, X. *Chem. Soc. Rev.* **2012**, *41*, 5922–5932; (f) Guo, D.-S.; Liu, Y. *Chem. Soc. Rev.* **2012**, *41*, 5907–5921; (g) Rotzler, J.; Mayor, M. *Chem. Soc. Rev.* **2013**, *42*, 44–62; (h) Haino, T. *Polym. J.* **2013**, *45*, 363–383; (i) Haino, T. *Chem. Rec.* **2015**, *15*, 837–853; (j) Yang, L.; Tan, X.; Wang, Z.; Zhang, X. *Chem. Rev.* **2015**, *115*, 7196–7239.
6. (a) Gutsche, C. D. *Calixarenes* in Monographs in Supramolecular Chemistry; Stoddart, J. F. (Ed.); The Royal Society of Chemistry: London, 1989; (b) *Calixarenes. A Versatile Class of Macrocyclic Compounds*. Vicens, J., Bohmer, V. (Eds.); Kluwer Academic Publishers: Dordrecht, 1991; (c) Gutsche, C. D. *Calixarenes Revisited* in Monographs in Supramolecular Chemistry; Stoddart, J. F. (Ed.); The Royal Society of Chemistry: London, 1998; (d) *Calixarenes 2001*, Asfari, Z.; Böhmer, F.; Harrowfield, J.; Vicens, J. (Eds.); Kluwer Academic Publishers, Dordrecht, **2001**.
7. Haino, T.; Yanase M.; Fukazawa, Y. *Angew. Chem. Int. Ed. Engl.* **1997**, *36*, 259–260.
8. Atwood, J. L.; Barbour, L. J.; Nichols, P. J.; Raston, C. L.; Sandoval, C. A. *Chem. – Eur. J.* **1999**, *5*, 990–996.
9. Makha, M.; Hardie, M. J.; Raston, C. L. *Chem. Commun.* **2002**, 1446–1447.
10. Haino, T.; Yanase M.; Fukazawa, Y. *Tetrahedron Lett.* **1997**, *38*, 3739–3742.
11. Yanase M.; Haino, T.; Fukazawa, Y. *Tetrahedron Lett.* **1999**, *40*, 2781–2784.
12. Haino, T.; Araki, H.; Yamanaka, Y.; Fukazawa, Y. *Tetrahedron Lett.* **2001**, *38*, 3739–3742.
13. (a) Haino, T.; Yanase, M.; Fukazawa, Y. *Angew. Chem. Int. Ed. Engl.* **1998**, *37*, 997–998; (b) Haino, T.; Yanase M.; Fukunaga, C.; Fukazawa, Y. *Tetrahedron* **2006**, *62*, 2025–2035.
14. Haino, T.; Araki, H.; Fujiwara, Y.; Tanimoto, Y.; Fukazawa, Y. *Chem. Commun.* **2002**, 2148–2149.
15. Haino, T.; Yamanaka, Y.; Araki, H.; Fukazawa, Y. *Chem. Commun.* **2002**, 402–403.
16. Haino, T.; Fukunaga, C.; Fukazawa, Y. *Org. Lett.* **2006**, *8*, 3545–3548.
17. Wang, J.; Bodige, S. G.; Watson, W. H.; Gutsche, C. D. *J. Org. Chem.* **2000**, *65*, 8260–8263.
18. Wang, J.; Gutsche, C. D. *J. Am. Chem. Soc.* **1998**, *120*, 12226–12231.
19. Haino, T.; Matsumoto, Y.; Fukazawa, Y. *J. Am. Chem. Soc.* **2005**, *127*, 8936–8937.
20. Haino, T.; Hirai, E.; Fujiwara, Y.; Kashiwara, K. *Angew. Chem. Int. Ed.* **2010**, *49*, 7899–7903.
21. Hirao, T.; Masatoshi, M.; Yamago, S.; Haino, T. *Chem. – Eur. J.* **2014**, *20*, 16138–16146.
22. Haino, T.; Yanase M.; Fukazawa, Y. *Tetrahedron Lett.* **2005**, *46*, 1411–1414.
23. Pappalardo, A.; Parisi, M. F. *J. Org. Chem.* **1996**, *61*, 8724–8725.

24. Stewart, D. R.; Krawiec, M.; Kashyap, R. P.; Watson, W. H.; Gutsche, C. D. *J. Am. Chem. Soc.* **1995**, *117*, 586–601.
25. (a) Arnaud-Neu, F.; Fuangswasdi, S.; Notti, A.; Pappalardo, S.; Parisi, M. F. *Angew. Chem. Int. Ed. Engl.* **1998**, *37*, 112–114; (b) Ferguson, G.; Notti, A.; Pappalardo, S.; Parisi, M. F.; Spek, A. L. *Tetrahedron Lett.* **1998**, *39*, 1965–1968.
26. For a more comprehensive account of selectively modified calix[5]arenes see: Notti, A.; Parisi, M. F.; Pappalardo, S. in *Calixarenes 2001*, Asfari, Z.; Böhmer, F.; Harrowfield, J.; Vicens, J. (Eds); Kluwer Academic Publishers, Dordrecht, **2001**, p. 54.
27. (a) Gattuso, G.; Notti, A.; Pappalardo, S.; Parisi, M. F.; Pilati, T.; Resnati, G.; Terraneo, G. *CrystEngComm* **2009**, *11*, 1204–1206; (b) Gattuso, G.; Notti, A.; Pappalardo, S.; Parisi, M. F.; Pilati, T.; Terraneo, G. *CrystEngComm* **2012**, *14*, 2621–2625.
28. Capici, C.; Gattuso, G.; Notti, A.; Parisi, M. F.; Pappalardo, S.; Brancatelli, G.; Geremia, S. *J. Org. Chem.* **2012**, *77*, 9668–9675.
29. Garozzo, D.; Gattuso, G.; Kohnke, F. H.; Malvagna, P.; Notti, A.; Occhipinti, S.; Pappalardo, S.; Parisi, M. F.; Pisagatti, I. *Tetrahedron Lett.* **2002**, *43*, 7663–7667.
30. (a) Beer, P. D.; Gale, P. A. *Angew. Chem. Int. Ed.* **2001**, *40*, 487–516; (b) Kim, S. K.; Sessler, J. L. *Chem. Soc. Rev.* **2010**, *39*, 3784–3809.
31. Garozzo, D.; Gattuso, G.; Notti, A.; Pappalardo, A.; Pappalardo, S.; Parisi, M. F.; Perez, M.; Pisagatti, I. *Angew. Chem. Int. Ed.* **2005**, *44*, 4892–4896.
32. (a) Brancatelli, G.; Gattuso, G.; Geremia, S.; Notti, A.; Pappalardo, S.; Parisi, M. F.; Pisagatti, I. *Org. Lett.* **2014**, *16*, 2354–2357; (b) Brancatelli, G.; Gattuso, G.; Geremia, S.; Manganaro, N.; Notti, A.; Pappalardo, S.; Parisi, M. F.; Pisagatti, I. *CrystEngComm* **2015**, *17*, 7915–7921.
33. Mecozzi, S.; Rebek, J., Jr. *Chem. – Eur. J.* **1998**, *4*, 1016–1022.
34. (a) Garozzo, D.; Gattuso, G.; Kohnke, F. H.; Notti, A.; Pappalardo, S.; Parisi, M. F.; Pisagatti, I.; White, A. J. P.; Williams, D. J. *Org. Lett.* **2003**, *5*, 4025–4028; (b) Gattuso, G.; Notti, A.; Pappalardo, A.; Parisi, M. F.; Pisagatti, I.; Pappalardo, S.; Garozzo, D.; Messina, A.; Cohen, Y.; Slovak, S. *J. Org. Chem.* **2008**, *73*, 7280–7289.
35. Gargiulli, C.; Gattuso, G.; Notti, A.; Pappalardo, S.; Parisi, M. F. *Tetrahedron Lett.* **2011**, *52*, 7116–7120.
36. Pappalardo, A.; Ballistreri, F. P.; Li Destri, G.; Mineo, P. G.; Tomaselli, G. A.; Toscano, R. M.; Trusso Sfrassetto, G. *Macromolecules* **2012**, *45*, 7549–7556.
37. Pappalardo, S.; Villari, V.; Slovak, S.; Cohen, Y.; Gattuso, G.; Notti, A.; Pappalardo, A.; Pisagatti, I.; Parisi, M. F. *Chem. – Eur. J.* **2007**, *13*, 8164–8173.
38. Hofmeister, F. *Arch. Exp. Pathol. Pharmacol.* **1888**, *24*, 247–260.
39. Martin, R. B. *Chem. Rev.* **1996**, *96*, 3043–3064.
40. Gargiulli, C.; Gattuso, G.; Notti, A.; Pappalardo, S.; Parisi, M. F. *Tetrahedron Lett.* **2011**, *52*, 6460–6464.
41. (a) Ballistreri, F. P.; Notti, A.; Pappalardo, S.; Parisi, M. F.; Pisagatti, I. *Org. Lett.* **2003**, *5*, 1071–1074; (b) Gargiulli, C.; Gattuso, G.; Liotta, C.; Notti, A.; Parisi, M. F.; Pisagatti, I.; Pappalardo, S. *J. Org. Chem.* **2009**, *74*, 4350–4353; (c) Capici, C.; De Zorzi, R.; Gargiulli, C.; Gattuso, G.; Geremia, S.; Notti, A.; Pappalardo, S.; Parisi, M. F.; Puntoriero, F. *Tetrahedron* **2010**, *66*, 4987–4993.
42. Capici, C.; Cohen, Y.; D’Urso, A.; Gattuso, G.; Notti, A.; Pappalardo, A.; Pappalardo, S.; Parisi, M. F.; Purrello, R.; Slovak, S.; Villari, V. *Angew. Chem. Int. Ed.* **2011**, *50*, 11956–11961.
43. Villari, V.; Gattuso, G.; Notti, A.; Pappalardo, A.; Micali, N. *J. Phys. Chem. B* **2012**, *116*, 5537–5541.
44. Among many, see: (a) Atwood, J. L.; Barbour, L. J.; Hardie, M. J.; Raston, C. L. *Coord. Chem. Rev.*, **2001**, *222*, 3–32; (b) Perret, F.; Lazar, A. N.; Coleman, A. W. *Chem. Commun.* **2006**, 2425–2438; (c) Guo, D.-S.; Liu, Y. *Acc. Chem. Res.* **2014**, *47*, 1925–1934; (d) Basilio, N.; Francisco, V.; Garcia-Rio, L. *Int. J. Mol. Sci.* **2014**, *14*, 3140–3157, and references therein.
45. Guo, D.-S.; Wang, K.; Liu, Y. *J. Incl. Phenom. Macrocyclic. Chem.* **2008**, *62*, 1–21.

46. (a) Ling, I.; Alias, Y.; Skelton, B. W.; Raston, C. L. *Cryst. Growth Des.* **2012**, *12*, 1564–1570;  
(b) Ling, I.; Boulos, R. A.; Skelton, B. W.; Sobolev, A. N.; Alias, Y.; Raston, C. L. *Cryst. Growth Des.* **2013**, *13*, 2025–2035.
47. Su, X.; Guo, D.-S.; Liu, Y. *CrystEngComm* **2010**, *12*, 947–952.
48. Guo, D.-S.; Chen, K.; Zhang, H.-Q.; Liu, Y. *Chem. Asian J.* **2009**, *4*, 436–445.
49. Wang, K.; Guo, D.-S.; Liu, Y. *Chem. – Eur. J.* **2012**, *18*, 8758–8764.

# Chapter 6

## Calix[6]azacryptand-Based Receptors

Gaël De Leener, Steven Moerkerke, Roy Lavendomme, Olivia Reinaud,  
and Ivan Jabin

### 6.1 Introduction

The design of synthetic receptors that can selectively bind, with a high affinity, charged or neutral species is a major objective in supramolecular chemistry [1]. Indeed, such receptors find many applications in various areas such as catalysis, biomimicry, drug delivery, materials science and biological or environmental analyses [1, 2]. Combining a buried polar site to a hydrophobic pocket is a recurrent strategy encountered in Nature to efficiently and selectively bind ligands [3]. Thus, an appealing approach for the elaboration of artificial receptors consists of associating a cavity-based macrocyclic compound to a polar polyfunctional binding site that can recognize the guest through specific interactions (H-bonding, charge-charge, coordination to a metal center, etc.) [4]. Similarly to natural systems, the cavity may indeed (i) ensure a very high selectivity in terms of size and shape complementarities and/or (ii) drive apolar guests into its hydrophobic inner space when water is the solvent [4]. Among the various cavitands that can be used for the

---

G. De Leener

Laboratoire de Chimie et de Biochimie Pharmacologiques et Toxicologiques (CNRS UMR 8601), Université Paris Descartes, Sorbonne Paris Cité, 45 rue des Saints Pères, 75006 Paris, France

Laboratoire de Chimie Organique, Université libre de Bruxelles (ULB),  
Avenue F. D. Roosevelt 50, CP160/06, 1050 Brussels, Belgium

S. Moerkerke • R. Lavendomme • I. Jabin (✉)

Laboratoire de Chimie Organique, Université libre de Bruxelles (ULB),  
Avenue F. D. Roosevelt 50, CP160/06, 1050 Brussels, Belgium  
e-mail: [ijabin@ulb.ac.be](mailto:ijabin@ulb.ac.be)

O. Reinaud

Laboratoire de Chimie et de Biochimie Pharmacologiques et Toxicologiques (CNRS UMR 8601), Université Paris Descartes, Sorbonne Paris Cité, 45 rue des Saints Pères, 75006 Paris, France

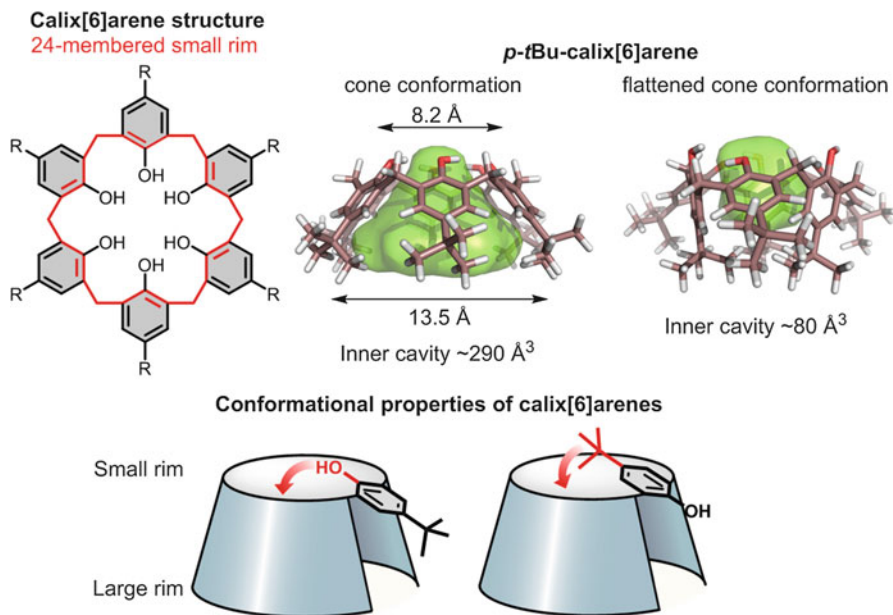


**Fig. 6.1** Calix[6]arene structural features. Distances have been measured on energy minimized structures. Volumes have been calculated with PLATON software after obstructing small and/or large rim holes (Probe radius = 1.2 Å; Grid step = 0.2 Å; Atomic radii: C = 1.70 Å; H = 1.20 Å; O = 1.52 Å) [15]

construction of such bio-inspired receptors, calix[*n*]arenes [5] are particularly attractive because many synthetic methodologies have been developed for their selective modification [5, 6]. However, in comparison with other cavitands (e.g. cyclodextrins [7], cucurbiturils [8] or resorcinarenes [9]), the cavity of calixarenes has been little exploited to date as a binding pocket. Indeed, in the case of calix[4]arenes, on the one hand, their conical cavity is too small to host efficiently organic molecules and, on the other hand, the reduced size of their 16-membered small rim prevents guest *through-the-annulus* threading. This oligomer is thus mostly used as a platform for the preorganization of a binding site outside of the cavity [10]. Higher oligomers (i.e. calix[5,6,8]arenes) have a size adapted for guest *through-the-annulus* threading (small rim  $\geq 20$  atoms) and the inclusion of organic molecules (see Fig. 6.1 for calix[6]arenes) [11]. However, their increased flexibility, due to the easy ring inversion of their phenolic units, constitutes an obstacle for obtaining a host with a well-defined cavity. Different groups have reported that the conformational flexibility of calix[6]arenes can be restricted either by the introduction of covalent bridges between the phenolic units [12], the use of self-assembly processes [13] or the introduction of coordinating groups on the small rim [4, 14] (Fig. 6.2). With these strategies, it is possible to inhibit the ring inversion and constrain the calix[6]arene structure in the open-ended cone conformation, which is ideal for the elaboration of the above mentioned artificial

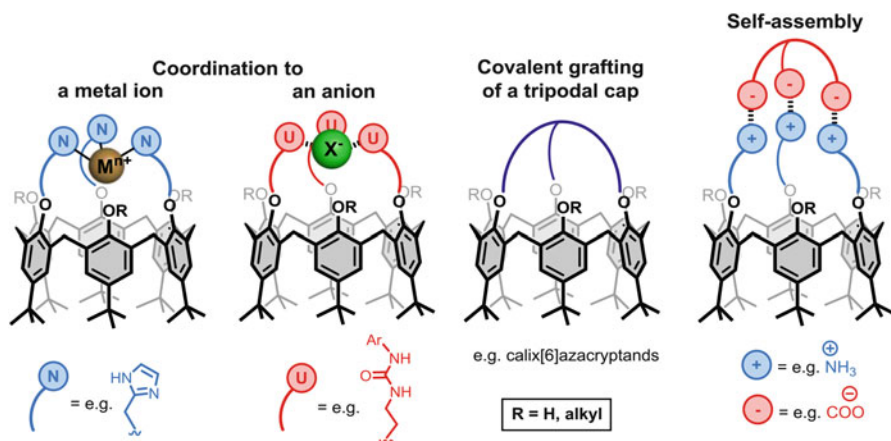


**Fig. 6.2** Different strategies for the rigidification of calix[6]arenes

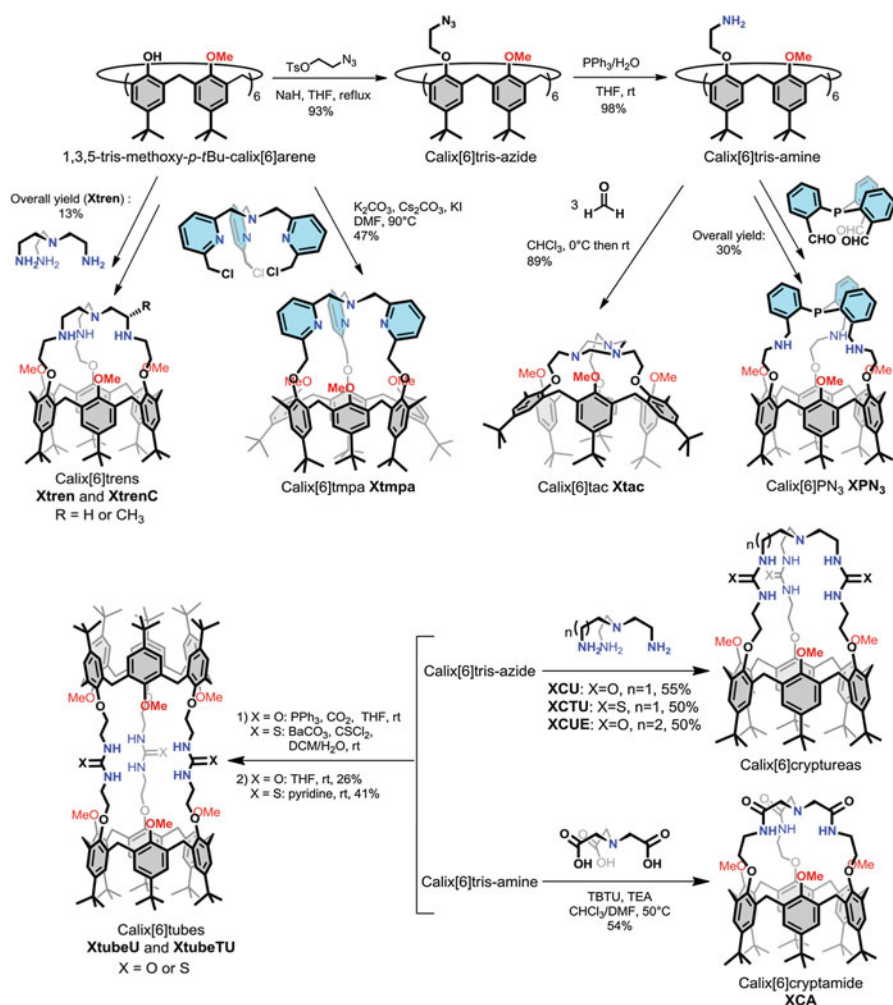
bio-inspired receptors. In this regard, different families of calix[6]arenes bearing a covalent poly-aza cap have been developed. These so-called calix[6]azacryptands present a grid-like nitrogenous cap (i) that closes and rigidifies the conic cavity at the narrow rim, (ii) that can establish multiple and strong interactions (chelate effect) with a given guest and (iii) that can potentially be protonated, allowing an acid-base control of the complexation properties. The present chapter describes the main results that were reported for this class of receptors over the last decade.

## 6.2 Synthesis of the Calix[6]azacryptands

The synthetic approach for the elaboration of the calix[6]azacryptands consists of introducing the tripodal aza unit through a macrocyclization reaction as the key step (Schemes 6.1 and 6.2). All the members of the first generation of calix[6]azacryptands (**Xtren** [16], **XtrenC** [17], **Xtmpa** [18], **Xtac** [19], **XPN<sub>3</sub>** [20], **XCU** [21], **XCUE** [22], **XCTU** [23], **XCA** [24], **XtubeU** [25] and **XtubeTU** [26]) were obtained from the well-known  $C_{3v}$  symmetrical 1,3,5-tris-methoxy-*p*-*t*Bu-calix[6]arene platform. [27] The macrocyclization reactions were achieved either directly with this platform or with the highly versatile calix[6]tris-azide and calix[6]tris-amine building-blocks. In some cases, the macrocyclization reaction required specific conditions (i.e. high dilution and use of a template). Most of the calix[6]azacryptands can be prepared on a gram scale.

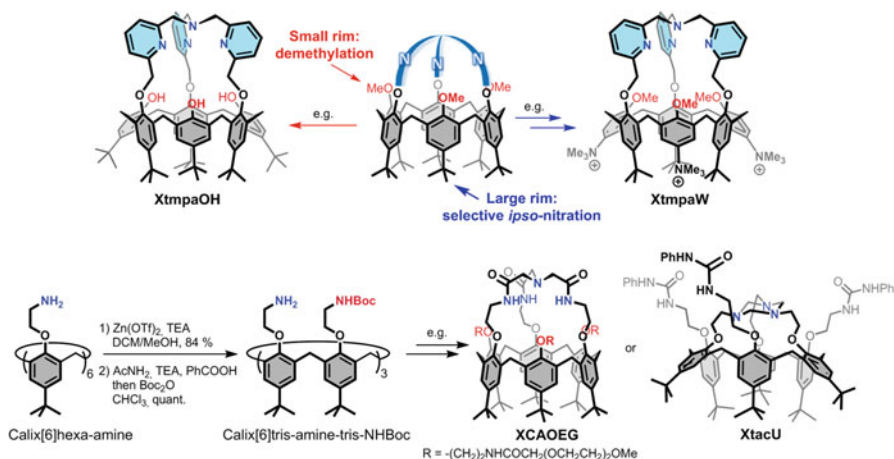
Different strategies for the selective functionalization of the calix[6]azacryptands were developed in order to introduce recognition, sensing or hydrophilic sub-units or for their grafting on surfaces (Scheme 6.2). Post-functionalization of the previously synthesized calix[6]azacryptands was developed





**Scheme 6.1** Synthesis of the calix[6]azacryptands from the 1,3,5-tris-methoxy-*p*-*t*Bu-calix[6]arene platform

either at the small or at the large rim. First, selective demethylation of the methoxy groups by trimethylsilyl iodide (TMSI) was achieved in high yields, leading to phenol groups that can be further functionalized [28]. Interestingly, the reaction is fast and selective only when the calixarene adopts a conformation with the methoxy groups projected outside of the cavity. Therefore, a supramolecular assistance-based strategy that consists of exploiting the host-guest properties of the receptors in order to change their conformation and to permit their selective demethylation was used. Secondly, the large rim can be selectively post-functionalized by *ipso*-nitration of three of the six aromatic units in moderate to high yield [29]. The selectivity is based on the control of the large rim reactivity by the small rim



**Scheme 6.2** Synthesis of functionalized calix[6]azacryptands

substitution pattern. The nitro groups can be further converted for example into hydrophilic trimethylammonium groups, allowing the water-solubilization of the receptor (e.g. **XtmpaW**) [30]. Finally, functionalized calix[6]azacryptands were also prepared by replacing the starting trimethylated platform by a more sophisticated  $C_{3v}$  building-block, i.e. the calix[6]arene-tris-amine-tris-NHBoc (Scheme 6.2). This versatile compound was efficiently obtained in two steps from the calix[6]arene-hexa-amine through the selective protection of three amino arms in alternating positions. This platform can lead in a few steps to different calix[6]azacryptands bearing either additional recognition units (**XtacU**) [31] or hydrophilic oligo(ethylene glycol) units (**XCAOEG**) [32].

### 6.3 Calix[6]azacryptands as Selective Anion Receptors

As stated in several recent reviews [33], the design of efficient receptors for the recognition and sensing of anions is an important challenge [34]. Indeed, anions are ubiquitous in Nature and some are biologically important (chloride, sulfate, etc.) or constitute major pollution hazards (pertechnetate, phosphate, nitrate, etc.). If many calix[4]arene-based anion receptors have been reported [35], surprisingly, only a few examples of such receptors have been described from calix[6]arenes [36].

Calix[6]azacryptands bearing a tris-urea or tris-thiourea cap (i.e. **XCU**, **XCTU** and **XCUE**) revealed to be remarkable neutral receptors for anions notably in terms of selectivity and control of the guest release (Fig. 6.3) [22, 23, 37]. These hosts strongly bind anions in CD<sub>3</sub>CN/CDCl<sub>3</sub> through H-bonding interactions, as shown by the significant <sup>1</sup>H NMR downfield shift of the NH protons of their converging (thio)ureido groups. The recognition proceeds through an induced-fit process that

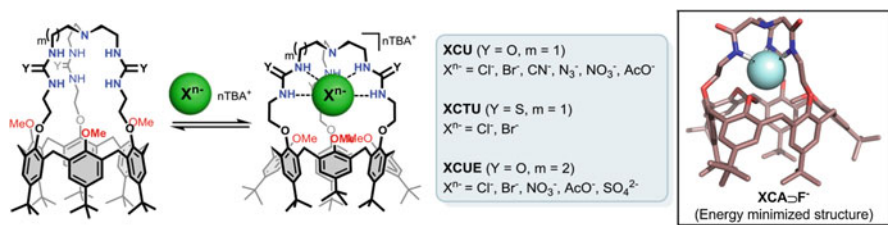


**Fig. 6.3** Complexation of anions by receptors **XCU**, **XCTU**, **XCUE**. *Inset*: energy minimized structure of **XCA-F**. H-bonds are indicated by *dashed lines*

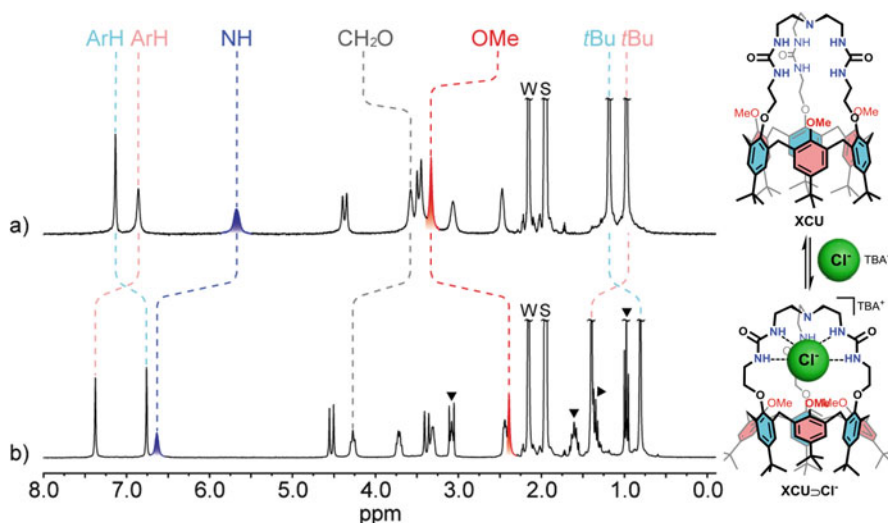


**Fig. 6.4**  $^1H$  NMR spectra ( $CD_3CN$ , 300 MHz, 298 K) of (a) **XCU**; (b) after addition of 1 equiv. of  $TBA^+Cl^-$ .  $\blacktriangledown$ :  $TBA^+$ ; w water, s residual solvent. H-bonds are indicated by *dashed lines*

involves the favorable filling of the cavity by the methoxy groups, a conformational flip of the aromatic units and the spreading of the (thio)ureido arms (Fig. 6.4). Interestingly, a rare case [38] of anion binding that is slow on the NMR time scale at room temperature is observed with the thiourea receptor **XCTU**. The association constants  $K_a$  displayed in Table 6.1 indicate that the binding discrimination is mostly based on the size of the anions. Indeed, with the more rigid receptors **XCU** and **XCTU**, the smallness of the recognition site delimited by the tris-ureido cap and the introverted methoxy groups leads to a high selectivity for the small chloride anion. In contrast, the enlarged binding site of **XCUE** poorly recognizes  $Cl^-$  and displays a stronger affinity for the larger acetate and sulfate anions. The constants obtained with **XCTU** are one order of magnitude higher than those obtained with **XCU**, showing a stronger ability of the thiourea groups for anion binding than the urea groups. This is due to the higher acidity of thiourea groups

**Table 6.1** Association constants  $K_a$  of tris(thio)urea-calix[6]azacryptands toward anions  $X^{n-}$ 

		$K_a$ ( $M^{-1}$ ) <sup>a</sup>		
		XCU	XCTU	XCUE
Anion $X^{n-}$ <sup>b</sup>	Geometry of $X^{n-}$	CD <sub>3</sub> CN/CDCl <sub>3</sub> (8:2)	CD <sub>3</sub> CN/CDCl <sub>3</sub> (8:2)	CD <sub>3</sub> CN/CDCl <sub>3</sub> (7:3)
Cl <sup>-</sup>	Spherical	$1.2 \times 10^{5c}$	$1.4 \times 10^{6c}$	58
Br <sup>-</sup>	Spherical	$9.1 \times 10^{3c,d}$	$1.1 \times 10^{5c,d}$	22
I <sup>-</sup>	Spherical	Not detected	–	–
CN <sup>-</sup>	Linear	$640^{e, f}$	–	–
NO <sub>3</sub> <sup>-</sup>	Trigonal	$98^f$	–	48
AcO <sup>-</sup>	V-shaped	$160^{e, f}$	–	300
SO <sub>4</sub> <sup>2-</sup>	Tetrahedral	nd <sup>g</sup>	–	$1.6 \times 10^4$

These results are likely due to an *exo*-complexation of the anion

<sup>a</sup> $K_a$  determined at 298 K and defined as:  $K_a = [\text{host} \supset X^{n-}] / ([\text{host}] [X^{n-}])$ . Errors estimated  $\pm 10\%$

<sup>b</sup>TBA<sup>+</sup> salts

<sup>c</sup>Determined via Isothermal Titration Calorimetry

<sup>d</sup>Unpublished results

<sup>e</sup>Determined at 243 K

<sup>f</sup>Determined in CD<sub>3</sub>CN

<sup>g</sup>Not determined because a weak complexation and an abnormal looking titration curve were observed

( $pK_a = 21.0$  vs.  $26.9$  in DMSO for thiourea and urea, respectively) [39] and their lower tendency to self-associate [40]. Very interestingly, the binding of Cl<sup>-</sup> is also efficient in a competing environment:  $K_a = 40 M^{-1}$  and  $200 M^{-1}$  respectively with XCU and XCTU at 298 K in a 8:2 mixture of CD<sub>3</sub>OD/CDCl<sub>3</sub> (unpublished results). This remarkable result highlights the fact that neutral receptors can bind anions in protic solvents provided that they possess a highly preorganized H-bonding recognition site isolated from the solvent.

The more rigid triamide host XCA displays a remarkable selectivity for fluoride ( $K_a = ca. 300 M^{-1}$  in chloroform) in comparison to other anions ( $K_a < 25 M^{-1}$  for Cl<sup>-</sup>, AcO<sup>-</sup>, MeSO<sub>3</sub><sup>-</sup> or NO<sub>3</sub><sup>-</sup> in chloroform) [24]. Indeed, as seen with an energy-minimized structure of XCA $\supset$ F<sup>-</sup>, only the fluoride anion can be accommodated within the small binding pocket formed by the three convergent NH amido groups of the cap (Fig. 6.3). All the other anions are recognized outside of the cap through H-bonding interactions with a priori only one amido group, explaining their low affinity for XCA.

While one might have expected a reinforcement of the anion binding with the protonation of the receptors XCU, XCTU, XCUE and XCA, the addition of a stoichiometric amount of a strong acid (e.g. picric acid) leads to a complete release of the anion and the further addition of a base restores cleanly the host-guest complex. This acid-base control of the binding properties is highly reminiscent of allosteric processes encountered in natural systems. Finally, the more flexible XtubeU and XtubeTU are unable to bind efficiently anions in chloroform



1/3/0.1/0.05 relative affinities, respectively, whereas inclusion of  $\text{Me}_4\text{N}^+\text{Pic}^-$  is not detected [42]. By analogy with **Xtac**, the recognition is rationalized by H-bonding, CH- $\pi$  and  $\pi$ -cationic interactions between the binding partners. However, in the case of this more basic host, a competitive mono-protonation of the tren cap is observed upon the addition of primary and secondary ammonium ions. This competitive protonation can be overpassed by the addition of an excess of the corresponding free amine.

Among the different tris-(thio)ureido receptors, only **XCUE** is able to *endo*-complex ammonium ions associated to weakly coordinating anions [22]. The mode of recognition strongly differs from that of the poly-amino calix[6]azacryptands (Fig. 6.5). Indeed, NMR studies clearly indicate that the inclusion of the ammonium ion  $\text{R}^1\text{R}^2\text{NH}_2^+$  (with  $\text{R}^1 = \text{alkyl}$  and  $\text{R}^2 = \text{H}$  or  $\text{alkyl}$ ) into the heart of the cavity proceeds with the concomitant protonation of the bridging tertiary amine of the cap. Actually, the dicationic complexes  $\text{XCUE}\cdot\text{H}^+\supset\text{R}^1\text{R}^2\text{NH}_2^+$  are the only observable host-guest species, showing that prior protonation of the cap is mandatory for the recognition process. These results constitute a unique case of *endo*-complexation of ammonium ions by a cationic receptor. The energy minimized structure of  $\text{XCUE}\cdot\text{H}^+\supset\text{PrNH}_3^+$  shows that the  $\text{NH}^+$  proton is hydrogen bonded with an introverted ureido arm of the cap (Fig. 6.5), the ammonium ion sitting in the cavity and being stabilized through H-bonding interactions with phenoxy oxygen atoms of the calixarene framework. In other words, the  $\text{NH}^+$  proton can be considered as an heterotropic allosteric activator that triggers the binding of the ammonium ions through a rigidification of the tris-ureido cap and, as a consequence, of the whole receptor.

**Heteromultitopic Receptors for Organic Contact Ion-Pairs and Ion-Triads** Heteroditopic receptors capable of binding simultaneously a cation and an anion may find applications in membrane transport, salt extraction and the sensing of charged species [43]. Such ion-pair receptors could offer considerable advantages in terms of affinity or selectivity in comparison to monotopic receptors. In particular, the binding of the two ions in contact presents the advantage of avoiding the highly unfavorable energetic cost that would result from their dissociation. Only a few examples of ion-pair receptors have been reported from calix[6]arenes, the most significant ones being calix[6]arene-based systems that bind separated ion-pairs and that have been used as wheels for rotaxane synthesis and self-assembled materials [44]. More generally, examples of metal-free receptors that can bind ion-pairs [45] or form cascade complexes [46] are extremely rare in the literature.

The ability of the heteroditopic tris-urea and tris-amide-based receptors **XCUC** and **XCA** to recognize an ammonium ion simultaneously to an anion was investigated by NMR spectroscopy in chloroform [24, 37]. In all cases, the complexation of the ammonium ion only proceeds when an anion is simultaneously bound in the H-bonding donor cap (Fig. 6.6). This positive cooperativity is due to the close



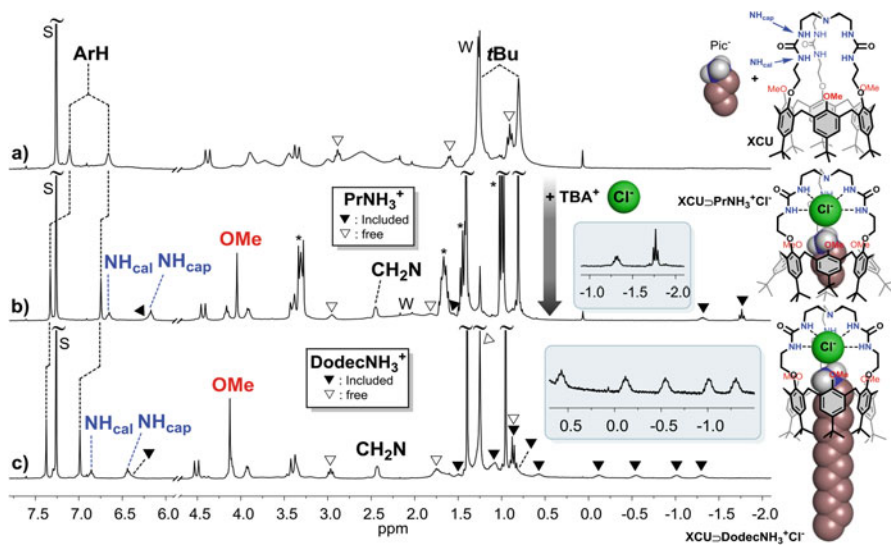


**Fig. 6.6** <sup>1</sup>H NMR spectra (CDCl<sub>3</sub>, 300 MHz, 298 K) of (a) XCU + PrNH<sub>3</sub><sup>+</sup>Pic<sup>-</sup>; (b) after addition of TBA<sup>+</sup>Cl<sup>-</sup>; (c) XCU + dodecNH<sub>3</sub><sup>+</sup>Cl<sup>-</sup>. \*: TBA<sup>+</sup>; w water, s residual solvent. H-bonds are indicated by dashed lines

proximity between the two complexed ions and thus to their strong electrostatic interaction.

In the case of the tris-ureido receptor XCU, ternary complexes with various anions X<sup>-</sup> (X<sup>-</sup> = F<sup>-</sup>, Cl<sup>-</sup> or Br<sup>-</sup>) and linear ammonium ions of various length (e.g. propyl-, hexyl- or dodecylammonium) are obtained (Fig. 6.7). This tris-ureido receptor is also able to bind bulkier quaternary ammonium salts and biologically relevant ammonium salts such as the neurotransmitter acetylcholine chloride or a dopamine hydrochloride derivative. High cumulative binding constants are obtained in chloroform: e.g.  $\beta_2 > 1.6 \times 10^9 \text{ M}^{-2}$  for PrNH<sub>3</sub><sup>+</sup>Cl<sup>-</sup>. Very interestingly, most of the ternary host-guest complexes are stable in a protic environment, for instance the complex with acetylcholine chloride was still visible in a mixture of CD<sub>3</sub>OD/CDCl<sub>3</sub> (4:1). Regarding the selectivity, a lower affinity is observed for the guests possessing an alkyl chain longer than propyl. Indeed, a steric clash occurs with the introverted *t*Bu groups that close the cavity of the host, forcing the calix[6]arene skeleton to adopt an energetically unfavorable straight conformation [14].

In the case of the tris-amido host XCA, the binding of contact ion-pairs exclusively proceeds with F<sup>-</sup> as the anionic partner (Fig. 6.7). This remarkable selectivity is clearly due to the smallness of the binding pocket provided by the convergent NH groups of the tris-amido cap. Interestingly, <sup>1</sup>H and <sup>19</sup>F NMR experiments revealed significant scalar couplings between the fluoride anion of the ternary complexes and the NH amido protons as well as the NH<sub>3</sub><sup>+</sup> of the included propylammonium ion (i.e. <sup>1</sup>HJ scalar couplings across N-H...F<sup>-</sup> hydrogen bonds). Finally, in the case of receptors XCU and XCA, the protonation of the cap of the

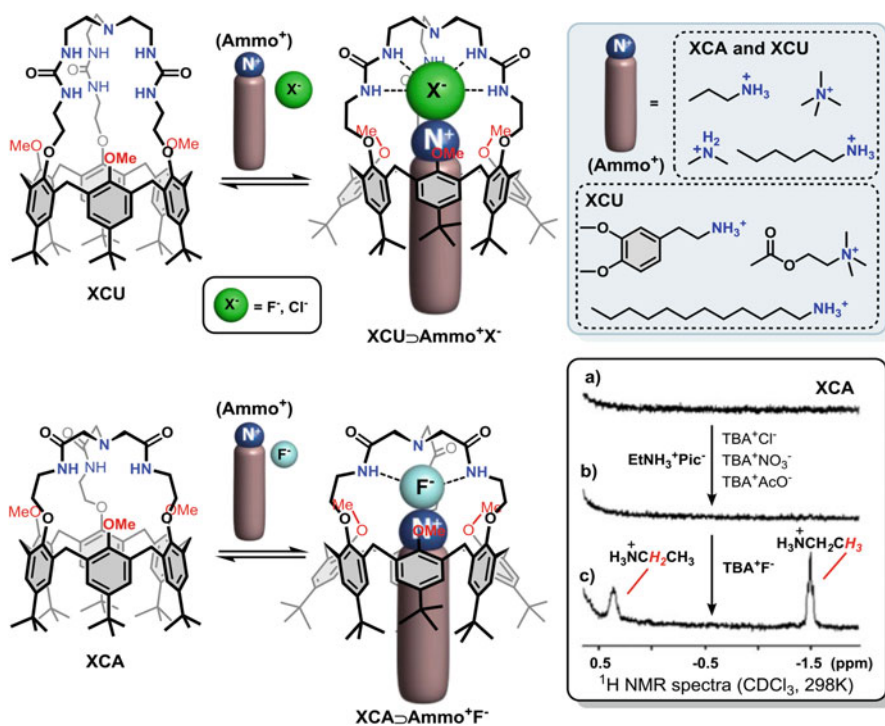


**Fig. 6.7** Host-guest properties of heteroditopic tris-amide and tris-urea-based receptors **XCU** and **XCA** toward organic contact ion-pairs. H-bonds are indicated by *dashed lines*. *Inset*: <sup>1</sup>H NMR spectra (CDCl<sub>3</sub>, 300 MHz, 298 K) of (a) **XCA**; (b) after addition of EtNH<sub>3</sub><sup>+</sup>Pic<sup>-</sup>, TBA<sup>+</sup>Cl<sup>-</sup>, TBA<sup>+</sup>NO<sub>3</sub><sup>-</sup> and TBA<sup>+</sup>AcO<sup>-</sup>; (c) after addition of TBA<sup>+</sup>F<sup>-</sup>

ternary complexes triggers the release of the anion and, as a consequence, of the ammonium ion.

The heterotritopic receptors **XtubeU** and **XtubeTU** are especially efficient for the cooperative binding of organic ion-triplets, i.e. an anion sandwiched between two ammonium ions (Fig. 6.8) [25, 26]. A high selectivity for linear ammonium ions RNH<sub>3</sub><sup>+</sup> (with R = e.g. Et, Pr, Hex or Dodec) associated with doubly charged anions such as sulfate is observed in chloroform and in protic media. For example, only the complex **XtubeU**⊃(PrNH<sub>3</sub><sup>+</sup>)<sub>2</sub>SO<sub>4</sub><sup>2-</sup> is detected upon the addition of 1 equiv. of (PrNH<sub>3</sub><sup>+</sup>)<sub>2</sub>SO<sub>4</sub><sup>2-</sup> and a large excess of TBA<sup>+</sup>Cl<sup>-</sup> (>110 equiv.) to **XtubeU**, showing a remarkable selectivity for the dicharged anion ( $K_{SO42-/Cl-} > 10^4$ ). The efficiency of these receptors is mostly due to the proximity of their three recognition sites that allows the binding of the three ions in contact. The resulting neutral [1+1+2] quaternary complexes represent rare examples of metal-free cascade complexes [46, 47]. The X-ray structure of the quaternary complex **XtubeU**⊃(EtNH<sub>3</sub><sup>+</sup>)<sub>2</sub>SO<sub>4</sub><sup>2-</sup> shows an inner tunnel in which the three ionic species are aligned in contact (distances between the two ammonium ions and the anion: d(N<sup>+</sup>⋯O) = 2.649 and 2.855 Å, Fig. 6.8). The oxygen atoms of the OMe groups direct



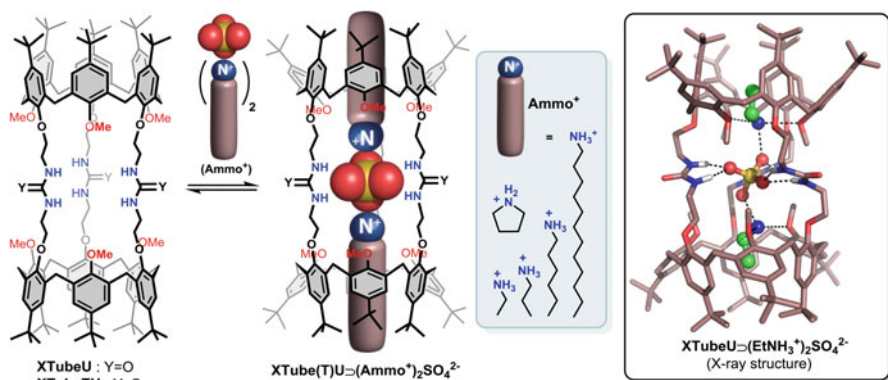


**Fig. 6.8** Host-guest properties of **XtubeU** and **XtubeTU** toward ion-triads. *Inset*: X-ray structure of **XtubeU**⊃(EtNH<sub>3</sub><sup>+</sup>)<sub>2</sub>SO<sub>4</sub><sup>2-</sup>. H-bonds are indicated by *dashed lines*

their lone pair electrons towards the inside of the tube in order to establish H-bonding interactions with the ammonium ions. These latter are further stabilized by H-bonding and ionic interactions with the sandwiched sulfate anion. Interestingly, the ureido linkers wrap around the sulfate anion and adopt a helical shape in order to maximize the number of H-bonding interactions. The <sup>1</sup>H NMR spectra of the quaternary complexes obtained with **XtubeU** and **XtubeTU** show a splitting of the ArH and CH<sub>2</sub> resonances (Fig. 6.9). This is due to the helical arrangement of the (thio)ureido linkers, which also takes place in solution and leads to a pair of D<sub>3</sub>-symmetrical enantiomers that are in conformational equilibrium (coalescence of the signals is observed at high T). In other words, the helicity is efficiently transmitted to the calixarene cavities, providing a chiral environment that is experienced by the guest ammonium ions. In comparison to **XtubeU**, the receptor **XtubeTU** displays enhanced binding properties thanks to the higher acidity of its thioureido groups and their lower ability to self-associate: e.g. **XtubeU** vs **XtubeTU**, K<sub>a</sub> (M<sup>-1</sup>) = 4.0 × 10<sup>3</sup> vs 3.6 × 10<sup>4</sup> for (PrNH<sub>3</sub><sup>+</sup>)<sub>2</sub>SO<sub>4</sub><sup>2-</sup> in CDCl<sub>3</sub>/CD<sub>3</sub>OD (1:1). Finally, while ammonium sulfate salts are better recognized in organic solvents, **XtubeTU** is able to selectively extract ammonium nitrate salts from water to chloroform. This remarkable result can be rationalized by the weaker hydration of the nitrate anion and its good geometrical complementarity with the tris-thioureido binding site. Under the same conditions, no extraction is observed with **XtubeU**, highlighting the reinforced complexation properties of the tris-thiourea-based host **XtubeU**.

## 6.5 Calix[6]azacryptands as Neutral Guest Receptors

**Polar Neutral Guests** The tris-amide host **XCA** is reluctant to small alcohols or amines in chloroform. However, this receptor strongly binds amides and ureas (G), with a preference for imidazolidinones or imidazolones (Fig. 6.10) [24]. Such

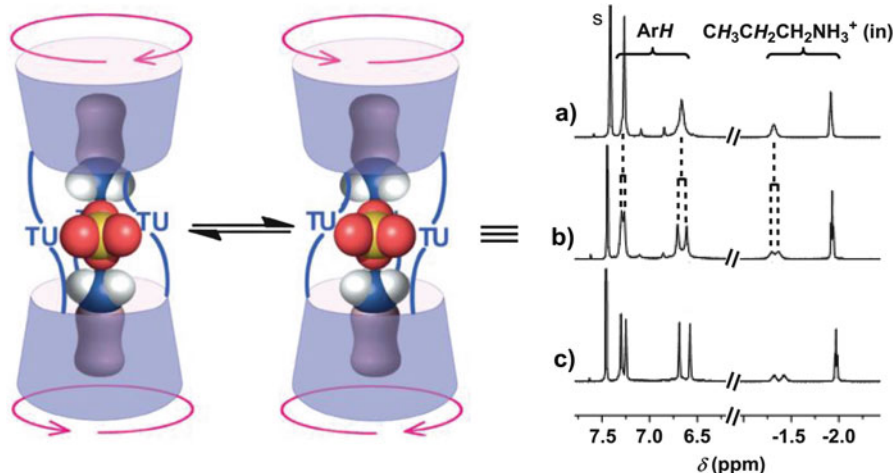


**Fig. 6.9** *Left*: schematic representation of the conformational equilibrium between the  $D_3$ -symmetrical helical enantiomers of  $\text{XtubeTU} \supset (\text{Ammo}^+)_2\text{SO}_4^{2-}$ . *Right*:  $^1\text{H}$  NMR spectra ( $\text{CDCl}_3$ , 600 MHz) of  $\text{XtubeTU} \supset (\text{PrNH}_3^+)_2\text{SO}_4^{2-}$  at: (a) 328 K; (b) 298 K; (c) 268 K. *s* residual solvent

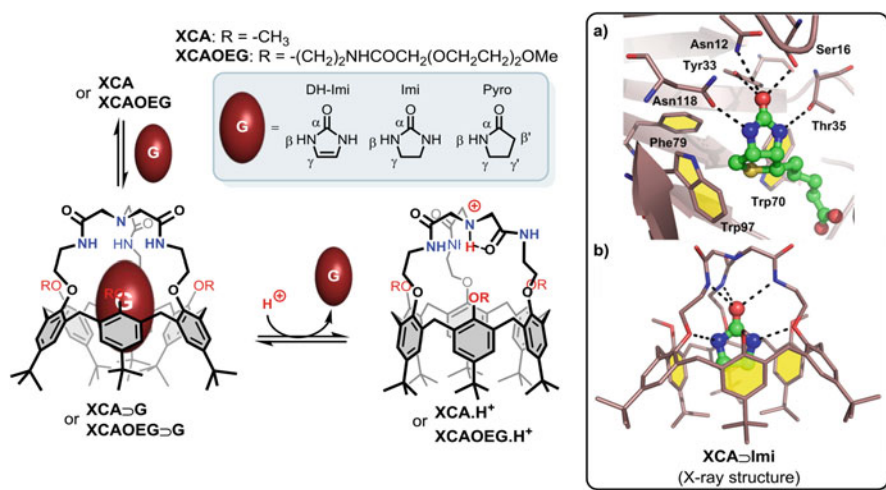


**Fig. 6.10** Host-guest properties of XCA and XCAOEG toward neutral guests ( $G$ ). *Inset*: (a) X-ray diffraction structure of avidin-biotin complex (PDB accession 2AVI); (b) X-ray diffraction structure of complex  $\text{XCA} \supset \text{Imi}$ . H-bonds are indicated by *dashed lines*

ureido heterocycles constitute attractive targets [48] since they are pharmacophores of many pharmaceutical drugs. The complexation induced shifts (CISs) clearly show that all the neutral guests are deeply included in the calixarene cavity (Table 6.2). The relative affinities (rel. aff.) decrease significantly according to the sequence 1,3-dihydro-2H-imidazol-2-one (DH-Imi) > imidazolidin-2-one (Imi)

**Table 6.2** Relative affinities ( $K_{G/Pyro}$ ) and  $^1\text{H}$  NMR complexation induced shifts (CISs) in the case of hosts **XCA** and **XCAOEG** with neutral guests

Guest G ( $\text{p}K_{\text{a1}}$ ) <sup>a</sup>	<b>XCA</b> ⊃G in $\text{CDCl}_3$		<b>XCAOEG</b> ⊃G in $\text{CDCl}_3$		<b>XCAOEG</b> ⊃G in $\text{D}_2\text{O}/\text{CD}_3\text{OD}$ (1:2)	
	$K_{G/Pyro}$ <sup>b</sup>	CIS (ppm) <sup>c</sup>	$K_{G/Pyro}$ <sup>b</sup>	CIS (ppm) <sup>c</sup>	$K_{G/Pyro}$ <sup>b</sup>	CIS (ppm) <sup>c</sup>
DH-Imi (12.2)	130	−3.43 ( $\text{H}_\gamma$ )	110	−3.37 ( $\text{H}_\gamma$ )	0.46	−3.51 ( $\text{H}_\gamma$ )
Imi (14.6)	17	−3.35 ( $\text{H}_\gamma$ )	19	−3.31 ( $\text{H}_\gamma$ )	3.0	−3.27 ( $\text{H}_\gamma$ )
Pyro (16.6)	1	−3.54 ( $\text{H}_\gamma$ ) −3.19 ( $\text{H}_\gamma$ )	1	−3.60 ( $\text{H}_\gamma$ ) −3.16 ( $\text{H}_\gamma$ )	1	−3.45 ( $\text{H}_\gamma$ ) −3.29 ( $\text{H}_\gamma$ )
AcNH <sub>2</sub> (16.6)	nd <sup>d</sup>	–	$4.8 \times 10^{-2}$	−2.13 ( $\text{H}_\beta$ )	Not detected	–
EtCONH <sub>2</sub> (16.6)	nd <sup>d</sup>	–	$3.2 \times 10^{-3}$	−3.13 ( $\text{H}_\gamma$ )	Not detected	–

<sup>a</sup>The  $\text{p}K_{\text{a1}}$  values were calculated using the Advanced Chemistry Development (ACD/Labs) software V11.02 (© 1994–2015 ACD/Labs)

<sup>b</sup>Relative affinities determined by NMR at 298 K and defined as  $([\text{G}_{\text{in}}] \times [\text{Pyro}_{\text{free}}])/([\text{G}_{\text{free}}] \times [\text{Pyro}_{\text{in}}])$  where the subscript “in” stands for “included”. Errors estimated  $\pm 15\%$

<sup>c</sup>CIS measured at 298 K and defined as  $\Delta\delta = \delta(\text{G}_{\text{in}}) - \delta(\text{G}_{\text{free}})$ . The  $\beta$  and  $\gamma$  positions are defined in Fig. 6.10

<sup>d</sup>Not determined

> pyrrolidin-2-one (Pyro) (Table 6.2). On the one hand, the affinity depends on the number of H-bonding interactions that the guest can form; ureas are thus better recognized than amides. On the other hand, the affinity increases with the acidity of the guest (Table 6.2). Hence, with such a synergistic effect, DH-Imi behaves as the best “key” for this type of receptor. An X-ray structure analysis shows that the complex **XCA**⊃**Imi** is stabilized by a complementary DAAAD-ADDDA quintuple H-bonding array between the cyclic ureido guest and its host. Besides, the guest establishes multiple CH– $\pi$  interactions with the aromatic walls of the calixarene cavity (Fig. 6.10). On a biomimetic point of view, this host–guest complex shows remarkable similarities with complexes formed between biotin and biotin-binding proteins such as avidin. As a representative example, the XRD structure of one of the two subunits of a homodimeric avidin-biotin complex is given in Fig. 6.10 [49]. The avidin and biotin interact through a complementary H-bonding network between the ureido imidazolidin-2-one ring and the polar side chains of amino acid residues. Moreover, the hydrophobic part of the biotin resides in a polyaromatic pocket of the binding site.

The recognition properties of the hydrophilic **XCAOEG** in chloroform are very similar to those of **XCA** (Table 6.2) [32]. However, in an aqueous medium ( $\text{D}_2\text{O}/\text{CD}_3\text{OD}$ , 1:2), a weak discrimination is observed and DH-Imi is now the worst guest. Such a discrepancy between the results obtained in chloroform and in an aqueous medium is ascribable to the greater solvation in water of the more polar and acidic molecules. An apparent association constant of  $300 \text{ M}^{-1}$  could be estimated for Imi in this aqueous medium. Similarly to natural systems, this

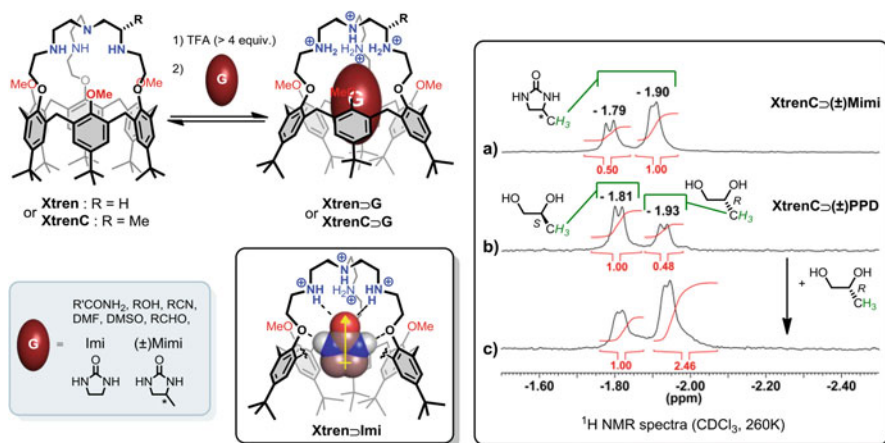


**Fig. 6.11** Host-guest properties of **Xtren** and **XtrenC** toward neutral guests. *Inset:*  $^1\text{H}$  NMR spectra (guest region, 300 MHz,  $\text{CDCl}_3$ , 260 K) of (a) 1:2 mixture of the two diastereomeric *endo*-complexes obtained upon the addition of ( $\pm$ )-Mimi (*ca.* 9 equiv.) to **XtrenC.4H<sup>+</sup>**; (b) 2:1 mixture of the two diastereomeric *endo*-complexes obtained upon the addition of ( $\pm$ )-PPD (*ca.* 17 equiv.) to **XtrenC.4H<sup>+</sup>**; (c) after the subsequent addition of *R*-(-)-PPD (*ca.* 23 equiv.) to the previous mixture

efficient binding of neutral guests through H-bonding interactions in a competing aqueous medium is likely due to the encapsulation of the guest which, consequently, is protected from the solvent.

Surprisingly, the protonated tris-amido hosts **XCA.H<sup>+</sup>** and **XCAOEG.H<sup>+</sup>** are insensitive to polar neutral molecules. This reluctance is rationalized by the competing formation of a stable five-membered intramolecular H-bonded ring between  $^+\text{NH}$  and an introverted  $\text{C}=\text{O}$  (Fig. 6.10). In other words, the  $^+\text{NH}$  proton can be considered as an allosteric inhibitor that induces a conformational reorganization of the tris-amido recognition site into an insensitive form of the receptor.

In strong contrast to the tris-amido receptors, the **Xtren** host can recognize polar neutral molecules (G) only in its protonated form. [42] The tetra-cationic derivative **Xtren.4H<sup>+</sup>**, obtained through protonation with an excess of a strong acid (e.g. > 4 equiv. of trifluoroacetic acid, TFA), can accommodate alcohols, nitriles, amides, ureas and even aldehydes in chloroform (Fig. 6.11). The driving force of the recognition event consists of a combination of charge-dipole and H-bonding interactions between the protonated cap and the guest. With such a mode of recognition, apolar molecules are not complexed and the following sequence of relative affinities (rel. aff.) is obtained: Imi (imidazolidin-2-one,  $\mu = 3.9$  D; rel. aff. = 500)  $\gg$  DMF (3.9 D; 1) >  $\text{AcNH}_2$  (3.7 D; 0.6) > EtOH (1.7 D; 0.15). The chiral recognition properties of the enantiopure **XtrenC** toward chiral neutral guests were evaluated by NMR spectroscopy in chloroform. The addition of chiral racemic guests [i.e. ( $\pm$ )-propane-1,2-diol (PPD) or ( $\pm$ )-4-methylimidazolidin-2-one (Mimi)] to **XtrenC** in presence of an excess of TFA leads, in both cases, to a *ca.* 2:1 mixture

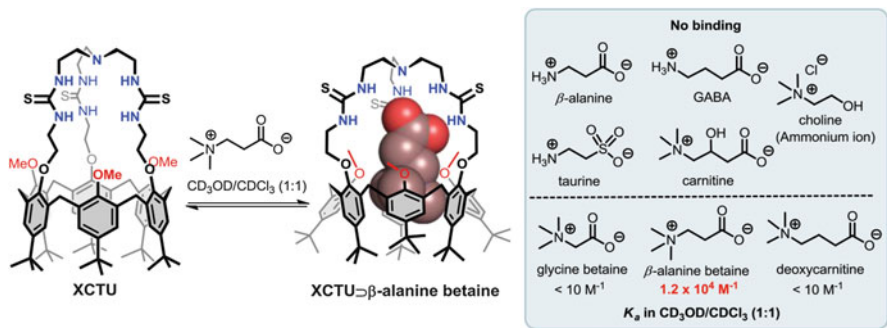
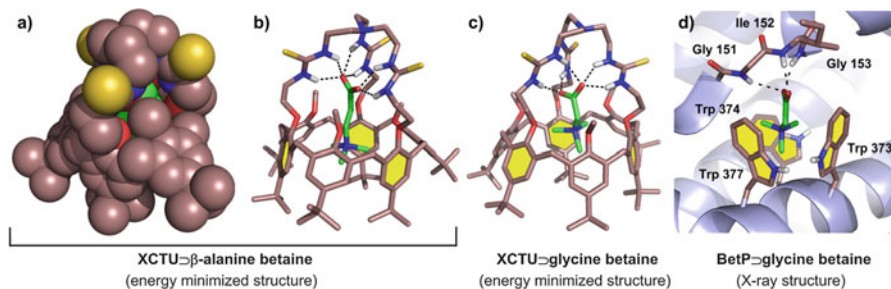


Fig. 6.12 Host-guest properties of **XCTU** toward zwitterionic species

of two diastereomeric *endo*-complexes **XtrenC.4H<sup>+</sup>⊃(-)-G** and **XtrenC.4H<sup>+</sup>⊃(+)-G** (Fig. 6.11) [17]. In the case of (±)-PPD, the subsequent addition of the enantiomer *R*-(-)-PPD leads to an inversion of the ratio, allowing the identification of the enantiomeric guests. These results clearly show that a discrimination process between two enantiomers is possible in the hydrophobic cavity of a calix[6]arene.

**Zwitterionic Species** Zwitterions are of central importance in many biological processes [50]. In particular, those containing a quaternary trimethylammonium group are an important class of biological compounds: [51] carnitine is involved in the transport of fatty acids, major phospholipids found in biological membranes display a zwitterionic phosphocholine headgroup and many naturally occurring betaines (e.g. glycine betaine or β-alanine betaine) serve as organic osmoregulatory solutes [52]. As a consequence, the binding and sensing of zwitterions by artificial receptors has emerged as a research field of significant importance [4, 53].

NMR studies show that the tris-thiourea receptor **XCTU** is able to bind small biologically relevant zwitterions in a competing protic medium (CD<sub>3</sub>OD/CDCl<sub>3</sub>, 1:1) [23]. A high binding constant, at least three orders of magnitude higher than all the other ones, is observed for β-alanine betaine in comparison to all the other zwitterions (Fig. 6.12). A high-field singlet corresponding to <sup>+</sup>N(CH<sub>3</sub>)<sub>3</sub> protons (δ<sub>N(CH<sub>3</sub>)<sub>3</sub></sub> = 0.13 ppm) indicates that the cationic part of this betaine is located in the heart of the aromatic cavity. The zwitterion is further stabilized through H-bonding interactions between its anionic moiety and the thioureido groups. The absence of binding of choline and zwitterions bearing a NH<sub>3</sub><sup>+</sup> group shows that both an anionic group and a quaternary ammonium group are mandatory for the recognition process. Besides, optimal encapsulation is obtained with an ethylene spacer between the two charged groups of the zwitterion (see the *K<sub>a</sub>* for glycine betaine, β-alanine betaine and deoxycarnitine, Fig. 6.12). The optimized structure of **XCTU⊃β-alanine betaine** shows that the guest is completely encapsulated by its receptor, the <sup>+</sup>N(CH<sub>3</sub>)<sub>3</sub> group being located in the poly-aromatic cavity



**Fig. 6.13** (a) and (b) Energy minimized structure of **XCTU**⊃**β-alanine betaine**; (c) Energy minimized structures of **XCTU**⊃**glycine betaine**; (d) XRD structure of **BetP**⊃**glycine betaine** (PDB accession 4AIN). H-bonds are indicated by *dashed lines*

for optimal CH– $\pi$  and  $\pi$ –cationic interactions (Fig. 6.13). In comparison, the optimized structure of **XCTU**⊃**glycine betaine** reveals that the  $^+\text{N}(\text{CH}_3)$  group of the glycine betaine is less buried into the cavity forcing the calixarene skeleton to adopt an unfavorable more straight conformation with one of the aromatic moieties filling the cavity in order to interact with the cationic group. Conversely, a steric clash between the cationic  $^+\text{N}(\text{CH}_3)_3$  group and the introverted *t*Bu groups of the calixarene results in the case of the longer deoxycarnitine. In other words, the remarkable selectivity for  $\beta$ -alanine betaine is likely due to a high complementarity in terms of size, shape, and electronic structure between the two heteroditopic partners. These results highlight the crucial importance of the distance between the binding units in the case of multipoint recognition. Interestingly, the calixarene-based host-guest complexes show remarkable similarities with the complexes of glycine betaine encountered in natural systems such as betaine-choline-carnitine transporter (BCCT, i.e. betaine transporter BetP from *Corynebacterium glutamicum*) proteins (see for example the X-ray structure of **BetP**⊃**glycine betaine** displayed in Fig. 6.13d). Indeed, the three aromatic moieties directed toward the inside of the calixarene cavity and the tris-thioureido cap of **XCTU** nicely mimic respectively the so-called tryptophan prism and the amido backbone found in the transport site of such proteins.

It was recently shown that **XtubeU** and **XtubeTU** behave as unique heteroditopic receptors for phosphatidylcholines (PCs), one of the most abundant classes of zwitterionic phospholipids in membranes [54]. NMR studies show that these hosts efficiently bind 1,2-dioleoyl-*sn*-glycero-3-phosphocholine (DOPC) in apolar solvents ( $K_a > 10^5 \text{ M}^{-1}$  in  $\text{CDCl}_3$ ) (Fig. 6.14). Similarly to **XCTU**, the recognition proceeds through the establishment of specific interactions with the zwitterionic head of the lipid. In a protic environment, **XtubeTU** binds DOPC much more strongly than **XtubeU** thanks to the higher acidity of its H-bonding thiourea groups. Moreover, **XtubeTU** is completely reluctant to the corresponding phosphatidylethanolamine (PE), highlighting a unique selectivity for PCs over PEs. A high selectivity for DOPC over dodecylphosphocholine (DPC), another PC, is also observed. An energy minimized structure of **XtubeTU**⊃**DOPC** suggests that



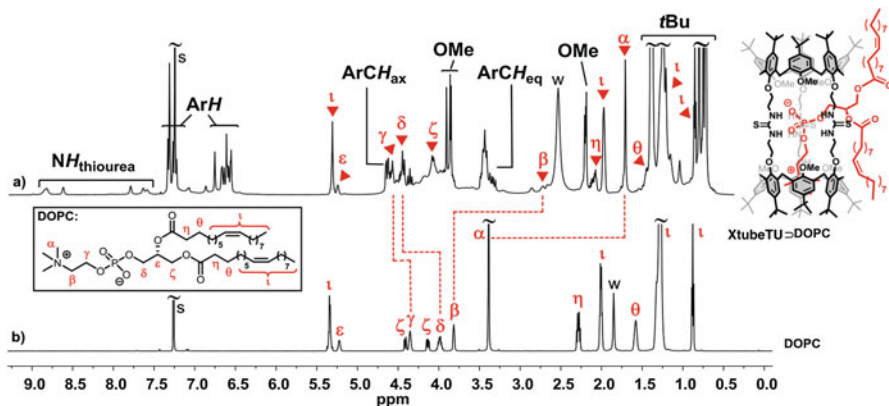


**Fig. 6.14**  $^1\text{H}$  NMR ( $\text{CDCl}_3$ , 600 MHz, 298 K) spectra of (a) **XtubeTU** + 1 equiv. of DOPC; (b) DOPC;  $\blacktriangledown$ : DOPC<sub>in</sub>; s solvent, w water. *Inset*: structure of DOPC

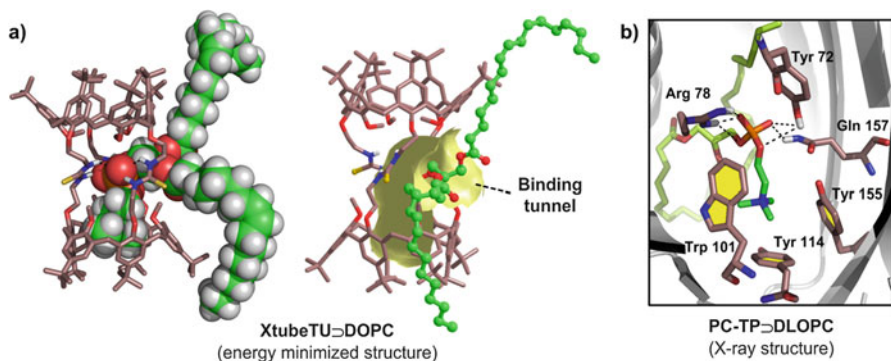


**Fig. 6.15** (a) Energy minimized structures of **XtubeTU**⊃DOPC; (b) XRD structure of PC-TP⊃DLOPC (PDB accession 1LN1). H-bonds are indicated by *dashed lines*

this selectivity likely originates from the unique curved shape of the tubular recognition site of **XtubeTU** which is well-adapted to the native conformation of DOPC (Fig. 6.15a). From a biomimetic point of view, this complex shows remarkable similarities with a natural complex formed between a PC and the human phosphatidylcholine transfer protein (PC-TPs) (Fig. 6.15b).

## 6.6 Calix[6]azacryptands as Funnel Complexes

A coordination bond can be used as a driving force for guest binding into a host, provided the following prerequisites are fulfilled: (i) the host must present a primary donor core for metal ion coordination, typically a  $N_3$  or  $N_4$  environment; (ii) a labile

site must be maintained for guest binding at the metal center; (iii) this labile site must be sterically protected by the macrocyclic structure and oriented inward in order to favor guest-ligand hosting and disfavor *exo*-coordination. From an architectural point of view, these prerequisites led to the following design: covalent linkage through a two-atom spacer of three *N*-donors to the phenol moieties of the calix[6]arene, in alternate position. When coordinated to the  $N_3$  site, the metal ion can sit in a tetrahedral (Td) environment with *endo*-coordination of a guest. Since the metal ion closes the small rim of the calixarene, guest exchange is possible only through the large rim. The corresponding complexes are thus called “funnel complexes”. A fifth coordination link in *exo* position remains however accessible to small ligands. Based on this design, three generations of calix[6]-ligands have been developed [4]:

- The first one proposes three *N*-donors, each one being covalently linked, independently from each other, to a phenol unit. When the guest ligand is a neutral molecule, the corresponding complexes undergo selective *endo* binding. However, poly-nuclear metal complexes can be formed through bridging anions bound in *exo* position, which inhibits their hosting properties;
- The second generation of ligand presents an additional donor that caps the system in *exo* position. However, due to the weak chelate effect, presence of anions still leads to polynuclear complexes;
- The third generation of ligands, the calix[6]azacryptands, allows to better control the host-guest properties as *exo*-coordination is restricted by the covalent capping of the calixarene. Some properties of the first three members of this generation of ligands (i.e. **Xtren**, **XPN<sub>3</sub>** and **Xtmpa**) are described below.

**Example of the Xtren-Zn<sup>II</sup> Complex** This complex is classically obtained by addition of a stoichiometric quantity of Zn(TfO)<sub>2</sub> to the **Xtren** ligand. It displays a 5-coordinate Zn<sup>II</sup> center where the *endo* binding site is either occupied by a solvent molecule (in coordinating solvents such as MeCN) or residual water (e.g. in chlorinated solvents) [42]. As a result of the metal ion coordination to the tren cap, the calixarene core is rigidified and displays stronger guest binding properties compared to those displayed by the Zn<sup>II</sup> complexes based on the first or second generation of calix[6]-ligands. The selectivity however is relatively similar [14], and is based on:

- (i) The donor properties of the guest ligand: amines > amides > alcohols > nitriles;
- (ii) The shape of the guest that must not be bulky at the level of the coordinating atom due to its positioning at the level of the small rim of the calixarene;
- (iii) The establishment of H-bonding interactions with the lone pairs of the phenoxy moieties of the calixarene small rim when the guest presents H-bonding donor sites (e.g. amines, amides and alcohols);
- (iv) The presence of an alkyl chain on the guest that can stabilize the host-guest complex by CH- $\pi$  interactions with the cavity aromatic walls. However, alkyl



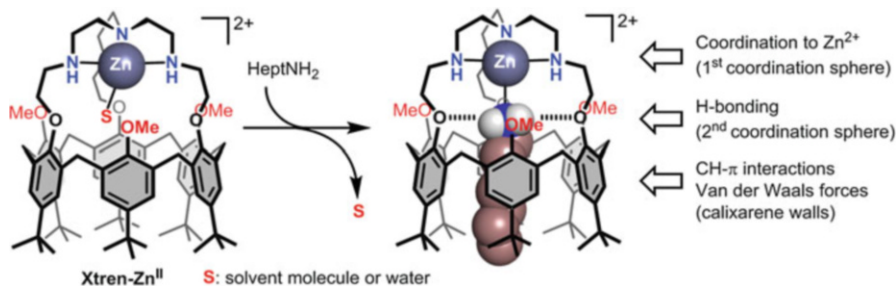


**Fig. 6.16** Binding properties of the Xtren-Zn<sup>II</sup> complex

chains longer than propyl have to push out the *t*Bu door, which has a cost in terms of host-guest affinity;

- (v) The inward orientation of the oxygen lone pairs of the phenoxy units of the calixarene that completely precludes anion binding in these complexes (*vide infra*). This is very unusual for metal complexes as anions (such as hydroxide and halides) are intrinsically much better donors than neutral ligands.

Finally, it is important to mention that in these systems, the guest is in competition with either the coordinating solvent or residual water, which makes its affinity strongly dependent on the solvent, not so much from a polarity point of view, but from a coordination point of view. The overall properties of these complexes are illustrated in Fig. 6.16.

### Comparison of Guest Hosting Properties of Cu<sup>II</sup> Complexes Based on Three Different Calix[6]Azacryptands, Presenting Three Different Coordination Cores

Such a controlled environment allows the evaluation of the impact of the first (the donor cap) and second coordination spheres (the oxygen-rich calixarene small rim providing H-bonding sites and dipolar interactions), as well as cavity effects (CH- $\pi$  interactions within the cavity, shape selectivity). Hence, the competitive binding of three different guest ligands (DMF, EtOH, MeCN) was evaluated for complexes presenting the same metal ion (Cu<sup>II</sup>, but embedded to a different cap: tren [55], PN<sub>3</sub> [56] or tmpa [18, 57]). XRD structures illustrating the three different complexes are displayed in Fig. 6.17. The first very surprising property is the reluctance of the Xtren and XPN<sub>3</sub> systems for anion binding, which stands in contrast to Xtmpa-ligand. Actually, a careful analysis of the calix conformation showed a major difference with the systems capped by the flexible tren or PN<sub>3</sub> units and the tmpa ligand. In the first two cases, the calixarene adopts a flattened cone conformation with the phenoxy units connected to the nitrogenous arms pointing their lone pair toward the donor atom of the guest ligand. In contrast, the more rigid tmpa core imposes to the same three phenol units to stand in the opposite direction, the corresponding oxygen atoms orienting their dipoles toward the outside. As a result, the electron-rich environment provided by the small rim of Xtren and XPN<sub>3</sub>

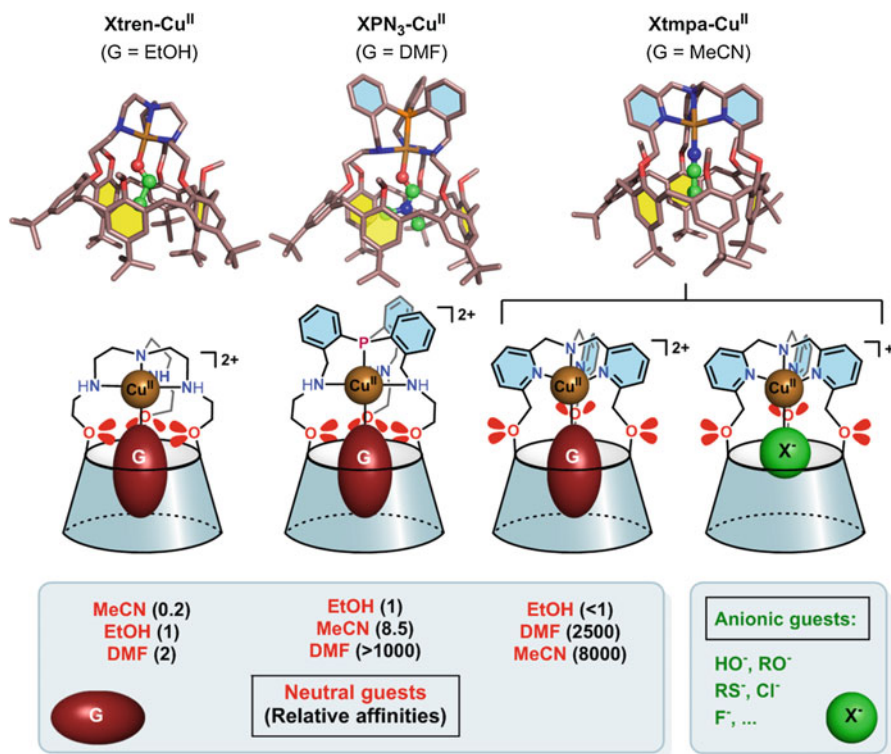


**Fig. 6.17** XRD structures of Cu<sup>II</sup>-funnel complexes with various guests and supramolecular control of guest binding

prevents coordination of anions, whereas the **Xtmpa-Cu<sup>II</sup>** complex readily binds hydroxide, alkoxides, azide, and halides. With neutral guest ligands, the **Xtren**-based complexes display relative affinities that are essentially directed by the donor strength ability of these small guests, in the same order as described above with Zn<sup>II</sup>: amides > alcohols > nitriles. The same study with the **XPN<sub>3</sub>** system highlighted a first surprising behavior with its very high affinity for DMF (and relatively high affinity for MeCN vs. EtOH). This is rationalized by the  $\pi$ -acceptor ability of the apical P(Ar)<sub>3</sub> donor core imposed to the Cu<sup>II</sup> center. Even more spectacular is the tremendous affinity of the **Xtmpa**-based Cu complex for the weakest donor MeCN. This gives evidence of a strong effect of the cavity leading to selectivity based on guest shape. Such contrasted behaviors illustrate the importance of the second coordination sphere generated by the macrocyclic environment. It also highlights the dramatic impact of a conformational change of the molecular microenvironment on the metal ion properties, which echoes the regulatory role of proteic conformational changes for many biochemical processes.

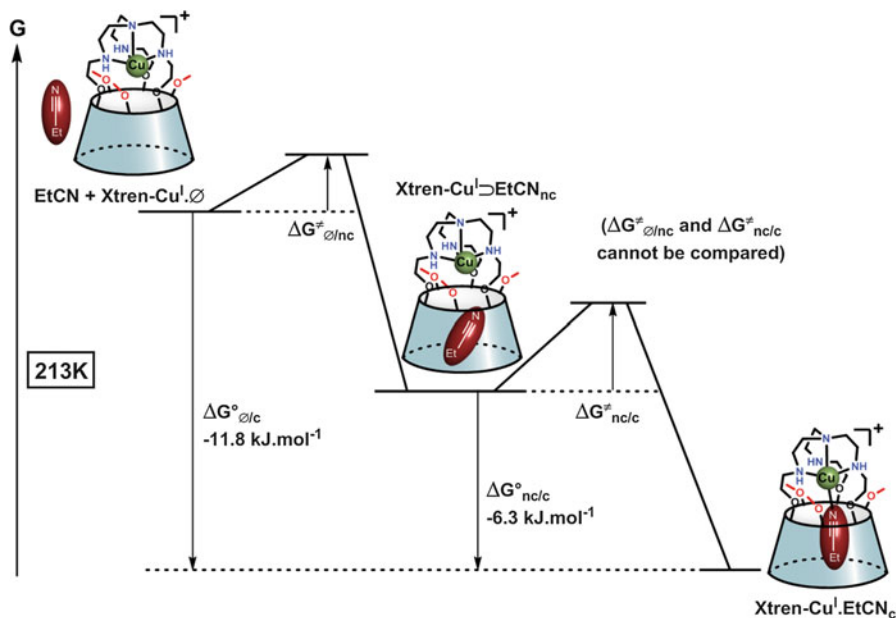


**Fig. 6.18** Two-step dissociation of nitrilo guests with  $\text{Xtren-Cu}^{\text{I}}$  complexes

**Trapping an Intermediate: Guest Binding at a Soft Metal Ion ( $\text{Cu}^{\text{I}}$ )** Due to its  $d^{10}$  configuration and soft character, the  $\text{Cu}^{\text{I}}$  demand is very different from that of  $\text{Cu}^{\text{II}}$  or other divalent metal ions. Because it is electron rich, it readily binds  $\pi$ -acceptors such as CO or nitriles. This confers different affinities for guest molecules compared to  $\text{Cu}^{\text{II}}$  that does not coordinate CO. Due to its low Lewis acidity, the coordination bond is weak and labile. As a result, guest ligand exchange is faster at  $\text{Cu}^{\text{I}}$  than at  $\text{Cu}^{\text{II}}$ . Monitored by  $^1\text{H}$  NMR spectroscopy, variable T study relative to ligand exchange with RCN guests revealed the transient formation of a host-guest complex where the nitrilo guest is not coordinated. This highlights an interesting case of a two-step dissociative pathway due to the entrapment of an intermediate (Fig. 6.18) [58].

**Redox Switch** The very different electronic and geometric demands of  $\text{Cu}^{\text{II}}$  and  $\text{Cu}^{\text{I}}$  was exploited for obtaining redox switches. Indeed, guest ligand interconversion during the  $\text{Cu}^{\text{II/I}}$  redox process is nicely illustrated by competitive experiments with DMF and MeCN. The  $\text{Cu}^{\text{II}}$  state displays a higher affinity for the better  $\sigma$ -donor (DMF), while  $\text{Cu}^{\text{I}}$  favors  $\pi$ -acceptor (MeCN) binding. With classical complexes deprived of cavity, the competitive guests are exchanged through an associative mechanism at  $\text{Cu}^{\text{II}}$  and a dissociative mechanism at  $\text{Cu}^{\text{I}}$ , both of which are fast processes. As a result, a Nernstian potential shift is observed, responding thermodynamically to the composition of the solution. With calix[6]

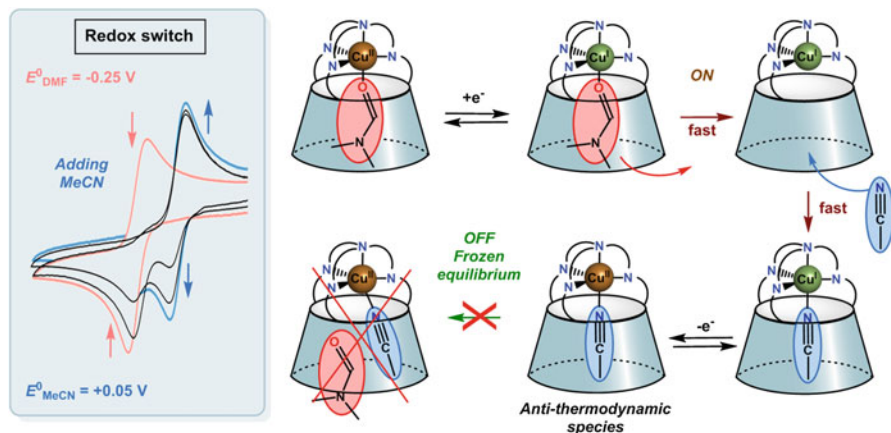


**Fig. 6.19** Electrochemically driven interchange of guest ligand with **Xtmpa**-Cu complexes

azacryptands such as **Xtmpa**, the associative exchange at  $\text{Cu}^{\text{II}}$  is frozen, because two guests cannot fit into the cavity simultaneously. At the  $\text{Cu}^{\text{I}}$  state, the dissociative ligand exchange is fast, and the more stable  $\text{Cu}^{\text{I}}(\text{MeCN})$  is the only observed species. After reoxidation to the  $\text{Cu}^{\text{II}}$  state, the transient  $\text{Cu}^{\text{II}}(\text{MeCN})$  complex is “trapped” on the electrochemical time scale, although thermodynamically less stable than  $\text{Cu}^{\text{II}}(\text{DMF})$ : the redox sequence  $\text{Cu}^{\text{II}} \rightarrow \text{Cu}^{\text{I}} \rightarrow \text{Cu}^{\text{II}}$  switches a good ligand for  $\text{Cu}^{\text{II}}$  for a weak one (Fig. 6.19). The redox potential hence no more corresponds to the thermodynamic equilibrium in the solution but to the guest nature. This can be seen as an “anti-thermodynamic” process [59].

Such a redox-switch mechanism results from the blocking of the associative process at the  $\text{Cu}^{\text{II}}$  state, imposed by the calixarene funnel. All of this suggests that the embedment of a reactive redox metal ion in a funnel-like cavity can play a crucial role in catalysis, particularly for metallo-enzymes associating electron transfer and ligand exchange.

**Water-Solubilization Through Incorporation into Micelles** Water is a unique solvent and the design of selective artificial hosts that can efficiently work in an aqueous medium is a challenging task. It is known that the **Xtren**- $\text{Zn}^{\text{II}}$  complex can recognize neutral guests in organic solvents. This complex was incorporated into dodecylphosphocholine micelles and studied by  $^1\text{H}$  NMR. The incorporated complex is able to extract selectively primary amines from the aqueous environment driven by an important hydrophobic effect, which also affects the selectivity of the complex for these amines (Fig. 6.20). Hence, the incorporation of organo-soluble receptors in micelles is an elegant and very efficient strategy to obtain water compatible nano-sized supramolecular recognition devices that can be prepared *via* a straightforward self-assembly process [4].

## 6.7 Versatile and Acid/Base Controllable Receptors

As shown above, calix[6]azacryptands are particularly versatile in terms of binding properties. For example, the tris-ureido receptor **XCU** binds polar neutral guests such as ureas, zwitterionic species such as betaines, small anions and organic contact ion-pairs with a high selectivity within each class of guests [37]. Another interesting feature of most of these hosts lies in the presence of proton sensitive site(s) at the level of the polar aza-cap. The protonation of the basic cap leads to positively cationic hosts whose binding properties are either reinforced or inhibited. If combined, these two properties of calix[6]azacryptands (i.e. versatility and acid-base control) make possible the reversible interconversion of different modes of recognition. For instance, a three-way supramolecular switch was obtained with **XCU** (Fig. 6.21). The protonation of the apical nitrogen of the cap acts as an effector that allows the switch from one mode of recognition to

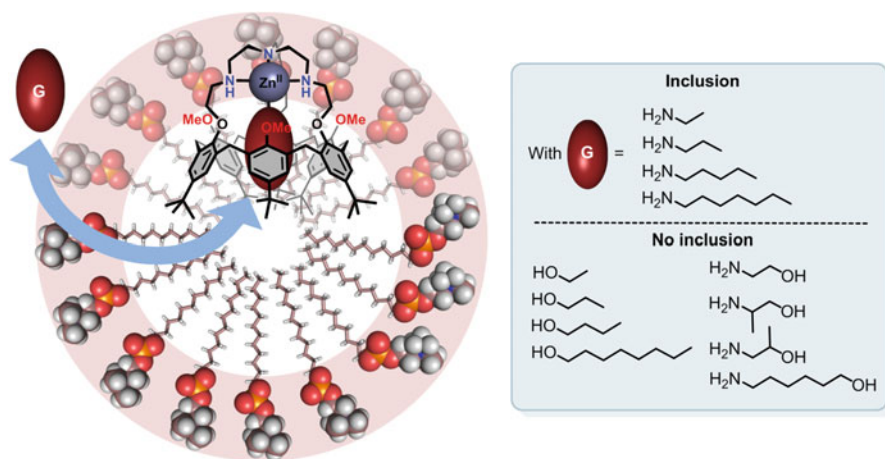


Fig. 6.20 Binding properties of funnel complexes incorporated into micelles

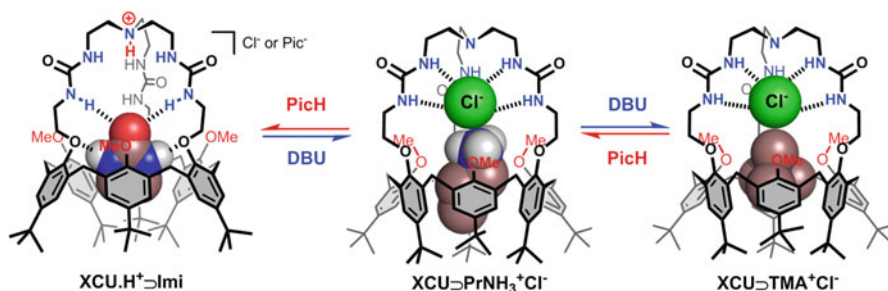


Fig. 6.21 Three-way supramolecular switch triggered by the addition of acid or base to **XCU**

another and a remarkable guest selection from a complex mixture. In other words, these receptors nicely illustrate how the host properties of a hydrophobic cavity can be tuned by the environment, which is reminiscent of natural systems and their propensity to pH control.

## 6.8 Conclusion

The results described herein highlight the unique binding properties of the calix[6]azacryptands:

- These heteroditopic receptors display high affinities for either neutral guests, zwitterions, anions, contact ion-pairs and metal ions. However, despite this versatility, remarkable selectivity is obtained within each class of guests;
- Their channel-like calixarene cavity controls the access to the polyaza recognition site. As a result, the bound guest is protected from the external medium and recognition is possible even in competitive media such as water;
- The high, but controlled, flexibility of their calixarene framework allows induced-fit processes. This stands in contrast to rigid concave receptors which exhibit strong binding only when there is a good fit between the size of the guest and of the cavity;
- When displaying a basic polyaza cap, their binding properties can be allosterically controlled by the addition of acids and bases, allowing the design of supramolecular switches based on the interconversion of different host-guest systems.

All in all, this work validates the biomimetic approach that consists of combining in close proximity a buried polar site to a polyaromatic pocket for the elaboration of efficient and sophisticated host-guest systems.

## References

1. (a) Lehn, J.-M. *Supramolecular Chemistry*. Wiley-VCH: Weinheim, 1995; (b) Steed, J. W.; Turner, D. R.; Wallace, K. J. *Core concepts in supramolecular chemistry and nanochemistry*. John Wiley: Chichester, United Kingdom; Hoboken, NJ, 2007; (c) Hartley, J. H.; James, T. D.; Ward, C. J. *J. Chem. Soc., Perkin Trans. 1* **2000**, 3155–3184.
2. (a) Valeur, B.; Brochon, J.-C. *New Trends in Fluorescence Spectroscopy: Applications to Chemical and Life Sciences*. Springer: Berlin, 2001; (b) Nguyen, B. T.; Anslyn, E. V. *Coord. Chem. Rev.* **2006**, 250, 3118–3127; (c) Schneider, H.-J. *Applications of Supramolecular Chemistry*. CRC Press, Taylor & Francis group: Boca Raton, 2012; Vol. 3; (d) Lehn, J.-M. *Science* **2002**, 295, 2400–2403.
3. Dugas, H. *Bioorganic Chemistry: A Chemical Approach to Enzyme Action*. 3rd ed.; Springer-Verlag: New-York, 1996.
4. (a) Coquière, D.; Le Gac, S.; Darbost, U.; Sénèque, O.; Jabin, I.; Reinaud, O. *Org. Biomol. Chem.* **2009**, 7, 2485–2500; (b) Perraud, O.; Robert, V.; Gornitzka, H.; Martinez, A.; Dutasta,

- J.-P. *Angew. Chem. Int. Ed.* **2012**, *51*, 504–508; (c) Daze, K. D.; Ma, M. C. F.; Pineux, F.; Hof, F. *Org. Lett.* **2012**, *14*, 1512–1515; (d) Le Poul, N.; Le Mest, Y.; Jabin, I.; Reinaud, O. *Acc. Chem. Res.* **2015**, *48*, 2097–2106; (e) Gramage-Doria, R.; Armspach, D.; Matt, D. *Coord. Chem. Rev.* **2013**, *257*, 776–816; (f) Rebilly, J.-N.; Colasson, B.; Bistri, O.; Over, D.; Reinaud, O. *Chem. Soc. Rev.* **2015**, *44*, 467–489; (g) Bistri, O.; Reinaud, O. *Org. Biomol. Chem.* **2015**, *13*, 2849–2865; (h) Zelder, F. H.; Salvio, R.; Rebek Jr, J. *Chem. Commun.* **2006**, 1280–1282; (i) Ma, Y.; Xue, M.; Zhang, Z.; Chi, X.; Huang, F. *Tetrahedron* **2013**, *69*, 4532–4535; (j) Cuevas, F.; Di Stefano, S.; Magrans, J. O.; Prados, P.; Mandolini, L.; de Mendoza, J. *Chem. Eur. J.* **2000**, *6*, 3228–3234; (k) Brunetti, E.; Inthasot, A.; Keymeulen, F.; Reinaud, O.; Jabin, I.; Bartik, K. *Org. Biomol. Chem.* **2015**, *13*, 2931–2938; (l) Kunsági-Máté, S.; Szabó, K.; Bitter, I.; Nagy, G.; Kollár, L. *J. Phys. Chem. A* **2005**, *109*, 5237–5242; (m) Corbellini, F.; Knegt, R. M. A.; Grootenhuis, P. D. J.; Crego-Calama, M.; Reinhoudt, D. N. *Chem. Eur. J.* **2005**, *11*, 298–307.
- (a) Gutsche, C. D. *Calixarenes revisited*. The Royal Society of Chemistry: Cambridge, 1998; (b) Asfari, Z.; Böhmer, V.; Harrowfield, J.; Vicens, J. In *Calixarenes 2001*, Kluwer Academic Publishers (Springer): Dordrecht, The Netherlands, 2001.
  - (a) Lavendomme, R.; Zahim, S.; De Leener, G.; Inthasot, A.; Mattiuzzi, A.; Luhmer, M.; Reinaud, O.; Jabin, I. *Asian J. Org. Chem.* **2015**, *4*, 710–722; (b) Martino, M.; Neri, P. *Mini-Rev. Org. Chem.* **2004**, *1*, 219–231; (c) Gutsche, C. D. *Calixarenes: An Introduction*, 2nd ed.; The Royal Society of Chemistry: Cambridge, United Kingdom, 2008; (d) Sliwa, W.; Deska, M. *Arkivoc* **2011**, *1*, 496–551.
  - Szejtli, J. *Chem. Rev.* **1998**, *98*, 1743–1754.
  - Lagona, J.; Mukhopadhyay, P.; Chakrabarti, S.; Isaacs, L. *Angew. Chem. Int. Ed.* **2005**, *44*, 4844–4870.
  - (a) Timmerman, P.; Verboom, W.; Reinhoudt, D. N. *Tetrahedron* **1996**, *52*, 2663–2704; (b) Jain, V. K.; Kanaiya, P. H. *Russ. Chem. Rev.* **2011**, *80*, 75–102.
  - (a) Quinlan, E.; Matthews, S. E.; Gunnlaugsson, T. *J. Org. Chem.* **2007**, *72*, 7497–7503; (b) Bu, J.-H.; Zheng, Q.-Y.; Chen, C.-F.; Huang, Z.-T. *Org. Lett.* **2004**, *6*, 3301–3303.
  - (a) Redshaw, C. *Coord. Chem. Rev.* **2003**, *244*, 45–70; (b) Ikeda, A.; Shinkai, S. *Chem. Rev.* **1997**, *97*, 1713–1734.
  - Chen, Y.; Gong, S. *J. Inclusion Phenom. Macrocyclic Chem.* **2003**, *45*, 165–184.
  - (a) Le Gac, S.; Marrot, J.; Reinaud, O.; Jabin, I. *Angew. Chem. Int. Ed.* **2006**, *45*, 3123–3126; (b) Arduini, A.; Ferdani, R.; Pochini, A.; Secchi, A.; Ugozzoli, F.; Sheldrick, G. M.; Prados, P.; González, J. J.; de Mendoza, J. *J. Supramol. Chem.* **2002**, *2*, 85–88; (c) González, J. J.; Ferdani, R.; Albertini, E.; Blasco, J. M.; Arduini, A.; Pochini, A.; Prados, P.; de Mendoza, J. *Chem. Eur. J.* **2000**, *6*, 73–80; (d) de Mendoza, J. *Chem. Eur. J.* **1998**, *4*, 1373–1377.
  - (a) Hamon, M.; Ménand, M.; Le Gac, S. p.; Luhmer, M.; Dalla, V.; Jabin, I. *J. Org. Chem.* **2008**, *73*, 7067–7071; (b) Sénéque, O.; Rager, M.-N.; Giorgi, M.; Reinaud, O. *J. Am. Chem. Soc.* **2000**, *122*, 6183–6189.
  - Spek, A. *Acta Cryst. D* **2009**, *65*, 148–155.
  - Jabin, I.; Reinaud, O. *J. Org. Chem.* **2003**, *68*, 3416–3419.
  - Garrier, E.; Gac, S.; Jabin, I. *Tetrahedron: Asymmetry* **2005**, *16*, 3767–3771.
  - Zeng, X.; Coquière, D.; Alenda, A.; Garrier, E.; Prangé, T.; Li, Y.; Reinaud, O.; Jabin, I. *Chem. Eur. J.* **2006**, *12*, 6393–6402.
  - Darbost, U.; Giorgi, M.; Reinaud, O.; Jabin, I. *J. Org. Chem.* **2004**, *69*, 4879–4884.
  - Zeng, X.; Hucher, N.; Reinaud, O.; Jabin, I. *J. Org. Chem.* **2004**, *69*, 6886–6889.
  - Ménand, M.; Jabin, I. *Org. Lett.* **2009**, *11*, 673–676.
  - Cornut, D.; Marrot, J.; Wouters, J.; Jabin, I. *Org. Biomol. Chem.* **2011**, *9*, 6373–6384.
  - Cornut, D.; Moerkerke, S.; Wouters, J.; Bruylants, G.; Jabin, I. *Chem. Asian J.* **2015**, *10*, 440–446.
  - Lascaux, A.; Le Gac, S.; Wouters, J.; Luhmer, M.; Jabin, I. *Org. Biomol. Chem.* **2010**, *8*, 4607–4616.
  - Moerkerke, S.; Ménand, M.; Jabin, I. *Chem. Eur. J.* **2010**, *16*, 11712–11719.

26. Moerkerke, S.; Le Gac, S.; Topić, F.; Rissanen, K.; Jabin, I. *Eur. J. Org. Chem.* **2013**, 5315–5322.
27. (a) Casnati, A.; Minari, P.; Pochini, A.; Ungaro, R. *J. Chem. Soc., Chem. Commun.* **1991**, 1413–1414; (b) Janssen, R. G.; Verboom, W.; Reinhoudt, D. N.; Casnati, A.; Freriks, M.; Pochini, A.; Ugozzoli, F.; Ungaro, R.; Nieto, P. M.; Carramolino, M.; Cuevas, F.; Prados, P.; de Mendoza, J. *Synthesis* **1993**, 380–386.
28. Danjou, P.-E.; De Leener, G.; Cornut, D.; Moerkerke, S.; Mameri, S.; Lascaux, A.; Wouters, J.; Brugnara, A.; Colasson, B.; Reinaud, O.; Jabin, I. *J. Org. Chem.* **2015**, *80*, 5084–5091.
29. Lejeune, M.; Picron, J.-F.; Mattiuzzi, A.; Lascaux, A.; De Cesco, S.; Brugnara, A.; Thiabaud, G.; Darbost, U.; Coquière, D.; Colasson, B.; Reinaud, O.; Jabin, I. *J. Org. Chem.* **2012**, *77*, 3838–3845.
30. Thiabaud, G.; Brugnara, A.; Carboni, M.; Le Poul, N.; Colasson, B.; Le Mest, Y.; Reinaud, O. *Org. Lett.* **2012**, *14*, 2500–2503.
31. Le Gac, S.; Ménand, M.; Jabin, I. *Org. Lett.* **2008**, *10*, 5195–5198.
32. Lascaux, A.; De Leener, G.; Fusaro, L.; Topic, F.; Rissanen, K.; Luhmer, M.; Jabin, I. *Org. Biomol. Chem.* **2016**, *14*, 738–746.
33. (a) Themed issue on anions: Supramolecular Chemistry of Anionic Species, *Chem. Soc. Rev.* **2010**, *39*, 3597–4003; (b) Busschaert, N.; Caltagirone, C.; Van Rossom, W.; Gale, P. A. *Chem. Rev.* **2015**, *115*, 8038–8155.
34. Beer, P. D. *Acc. Chem. Res.* **1998**, *31*, 71–80.
35. Matthews, S. E.; Beer, P. D. Calixarene-Based Anion Receptors. In *Calixarenes 2001*, Asfari, Z.; Böhmer, V.; Harrowfield, J.; Vicens, J., Eds. Kluwer Academic Publishers (Springer): Dordrecht, The Netherlands, 2001; pp 421–439.
36. (a) Scheerder, J.; Engbersen, J. F. J.; Casnati, A.; Ungaro, R.; Reinhoudt, D. N. *J. Org. Chem.* **1995**, *60*, 6448–6454; (b) Zhang, S.; Palkar, A.; Echegoyen, L. *Langmuir* **2006**, *22*, 10732–10738.
37. Ménand, M.; Jabin, I. *Chem. Eur. J.* **2010**, *16*, 2159–2169.
38. Svec, J.; Necas, M.; Sindelar, V. *Angew. Chem. Int. Ed.* **2010**, *49*, 2378–2381.
39. Bordwell, F. G.; Algrim, D. J.; Harrelson, J. A. *J. Am. Chem. Soc.* **1988**, *110*, 5903–5904.
40. Dannecker, W.; Kopf, J.; Rust, H. *Cryst. Struct. Commun.* **1979**, *8*, 429–432.
41. (a) Gaeta, C.; Troisi, F.; Neri, P. *Org. Lett.* **2010**, *12*, 2092–2095; (b) Talotta, C.; De Simone, N. A.; Gaeta, C.; Neri, P. *Org. Lett.* **2015**, *17*, 1006–1009.
42. Darbost, U.; Rager, M.-N.; Petit, S.; Jabin, I.; Reinaud, O. *J. Am. Chem. Soc.* **2005**, *127*, 8517–8525.
43. For recent reviews on ion-pair receptors, see: (a) Kim, S. K.; Sessler, J. L. *Chem. Soc. Rev.* **2010**, *39*, 3784–3809; (b) McConnell, A. J.; Beer, P. D. *Angew. Chem. Int. Ed.* **2012**, *51*, 5052–5061.
44. Selected references: (a) Arduini, A.; Ferdani, R.; Pochini, A.; Secchi, A.; Ugozzoli, F. *Angew. Chem. Int. Ed.* **2000**, *39*, 3453–3456; (b) Credi, A.; Dumas, S.; Silvi, S.; Venturi, M.; Arduini, A.; Pochini, A.; Secchi, A. *J. Org. Chem.* **2004**, *69*, 5881–5887; (c) Boccia, A.; D’Orazi, F.; Carabelli, E.; Bussolati, R.; Arduini, A.; Secchi, A.; Marrani, A. G.; Zanon, R. *Chem. Eur. J.* **2013**, *19*, 7999–8006; (d) Arduini, A.; Bussolati, R.; Credi, A.; Secchi, A.; Silvi, S.; Semeraro, M.; Venturi, M. *J. Am. Chem. Soc.* **2013**, *135*, 9924–9930.
45. (a) Davies, C. W. *Ion Association*. Butterworths: London, 1962; (b) Kubik, S. J. *Am. Chem. Soc.* **1999**, *121*, 5846–5855; (c) Mahoney, J. M.; Davis, J. P.; Beatty, A. M.; Smith, B. D. *J. Org. Chem.* **2003**, *68*, 9819–9820; (d) Lankshear, M. D.; Dudley, I. M.; Chan, K.-M.; Cowley, A. R.; Santos, S. M.; Felix, V.; Beer, P. D. *Chem. Eur. J.* **2008**, *14*, 2248–2263; (e) Atwood, J. L.; Szumna, A. *Chem. Commun.* **2003**, 940–941.
46. Hossain, M. A.; Morehouse, P.; Powell, D.; Bowman-James, K. *Inorg. Chem.* **2005**, *44*, 2143–2149.
47. Hossain, M. A.; Llinares, J. M.; Mason, S.; Morehouse, P.; Powell, D.; Bowman-James, K. *Angew. Chem. Int. Ed.* **2002**, *41*, 2335–2338.



48. (a) María, D. S.; Farrán, M. Á.; García, M. Á.; Pinilla, E.; Torres, M. R.; Elguero, J.; Claramunt, R. M. *J. Org. Chem.* **2011**, *76*, 6780–6788; (b) Herranz, F.; Santa María, M. D.; Claramunt, R. M. *J. Org. Chem.* **2006**, *71*, 2944–2951; (c) Hegde, V.; Hung, C. Y.; Madhukar, P.; Cunningham, R.; Hopfner, T.; Thummel, R. P. *J. Am. Chem. Soc.* **1993**, *115*, 872–878.
49. Livnah, O.; Bayer, E. A.; Wilchek, M.; Sussman, J. L. *P. Natl. Acad. Sci. U.S.A.* **1993**, *90*, 5076–5080.
50. Tzianabos, A. O.; Finberg, R. W.; Wang, Y.; Chan, M.; Onderdonk, A. B.; Jennings, H. J.; Kasper, D. L. *J. Biol. Chem.* **2000**, *275*, 6733–6740.
51. Peden, A. S.; Mac, P.; Fei, Y.-J.; Castro, C.; Jiang, G.; Murfitt, K. J.; Miska, E. A.; Griffin, J. L.; Ganapathy, V.; Jorgensen, E. M. *Nat. Neurosci.* **2013**, *16*, 1794–1801.
52. Hanson, A. D.; Rathinasabapathi, B.; Rivoal, J.; Burnet, M.; Dillon, M. O.; Gage, D. A. *P. Natl. Acad. Sci. U.S.A.* **1994**, *91*, 306–310.
53. Cochrane, J. R.; Schmitt, A.; Wille, U.; Hutton, C. A. *Chem. Commun.* **2013**, *49*, 8504–8506.
54. Moerkerke, S.; Wouters, J.; Jabin, I. *J. Org. Chem.* **2015**, *80*, 8720–8726.
55. Izzet, G.; Douziech, B.; Prange, T.; Tomas, A.; Jabin, I.; Le Mest, Y.; Reinaud, O. *P. Natl. Acad. Sci. U.S.A.* **2005**, *102*, 6831–6.
56. (a) Izzet, G.; Zeng, X.; Over, D.; Douziech, B.; Zeitouny, J.; Giorgi, M.; Jabin, I.; Mest, Y. L.; Reinaud, O. *Inorg. Chem.* **2007**, *46*, 375–377; (b) Over, D.; de la Lande, A.; Zeng, X.; Parisel, O.; Reinaud, O. *Inorg. Chem.* **2009**, *48*, 4317–4330.
57. Izzet, G.; Zeng, X.; Akdas, H.; Marrot, J.; Reinaud, O. *Chem. Commun.* **2007**, 810–812.
58. Izzet, G.; Rager, M.-N.; Reinaud, O. *Dalton Trans.* **2007**, 771–780.
59. Le Poul, N.; Douziech, B.; Zeitouny, J.; Thiabaud, G.; Colas, H.; Conan, F.; Cosquer, N.; Jabin, I.; Lagrost, C.; Hapiot, P.; Reinaud, O.; Le Mest, Y. *J. Am. Chem. Soc.* **2009**, *131*, 17800–17807.

# Chapter 7

## Large Calixarenes

Carmen Talotta, Carmine Gaeta, Annunziata Soriente,  
Margherita De Rosa, Corrada Geraci, and Placido Neri

### 7.1 Introduction

To date the calix[ $n$ ]arene family consists of 17 cyclooligomers, ranging from the tetramer to the eicosamer [1]. Those constituted by 4, 6, and 8 phenolic units are called “*major*” because they are obtainable in good yields with typical one-pot procedures, differently by the “*minor*” calixarenes, with odd phenolic units ( $n = 5, 7$ ), only obtainable in lower yields. Usually, the cyclic oligomers with a number of phenolic units  $\geq 7$  are termed “*large*” [2] and they have in common a number of features, such as the high conformational mobility and the large variety of possible conformations.

Notwithstanding their low yielding synthesis [3], large calixarenes are of particular interest in supramolecular chemistry thanks to their ability to host medium-sized organic molecules [4] or metal clusters [5] into their large cavities. Interestingly, thanks to the presence of a greater number of functionalizable phenolic units, large calixarenes can act as multivalent ligands or receptors possessing two or more complexing sites, which may act cooperatively or allosterically [6]. For these and others reasons, the study of large calixarenes is of particular interest and represents a future challenge in the field of macrocyclic and supramolecular chemistry (Fig. 7.1).

---

C. Talotta • C. Gaeta • A. Soriente • M. De Rosa • P. Neri (✉)  
Dipartimento di Chimica e Biologia “A. Zambelli”, Università di Salerno, Via Giovanni Paolo II, 132, 84084 Fisciano, Salerno, Italy  
e-mail: [neri@unisa.it](mailto:neri@unisa.it)

C. Geraci (✉)  
Istituto di Chimica Biomolecolare, Consiglio Nazionale delle Ricerche, Via Paolo Gaifami 18, 95126 Catania, Italy  
e-mail: [corrada.geraci@icb.cnr.it](mailto:corrada.geraci@icb.cnr.it)

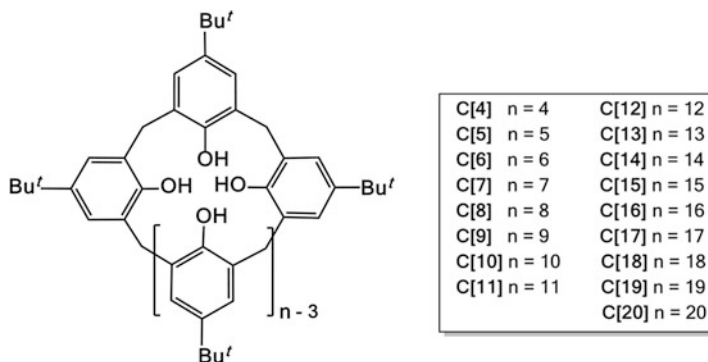


Fig. 7.1 Family of *p*-*tert*-butylcalix[4–20]arene C[4–20]

## 7.2 Synthesis of Calix[7–20]arene Macrocycles

In the last three decades, many efforts have been made to improve the synthesis of large calixarenes. Between the two basic and general synthetic procedures, the so called “one-pot” [7] and “fragment condensation” [8], the former is surely the best way to obtain a given calixarene macrocycle starting from *p*-*tert*-butylphenol. In the following paragraphs, the best yielding synthesis reported for each large calix [*n*]arene macrocycle are listed.

**Calix[7]arenes** Gutsche and Stewart reported the acid-catalyzed synthesis (*p*-TsOH) of *p*-*tert*-butylcalix[7]arene **C[7]** in a 25 % yield, using CHCl<sub>3</sub> as the solvent and *s*-trioxane as the HCHO source [7a]. By using a KOH-catalyzed procedure with paraformaldehyde in tetralin, *p*-methyl- **1a** [9], *p*-ethyl- **1b** [9], and *p*-benzylcalix [7]arene **1c** [10] (Fig. 7.2) were obtained in 22 %, 27 %, and 21 % yield, respectively.

**Calix[8]arenes** *p*-*tert*-Butylcalix[8]arene **C[8]** has been obtained with yield up to 60 % by a base-catalyzed synthesis using NaOH and paraformaldehyde in xylene as the solvent [3]. By using *p*-phenylphenol in diphenylether as solvent and NaOH as base, it was possible to obtain the deep-cavity *p*-phenylcalix[8]arene **2a** (Fig. 7.2) [11]. Izatt and coworkers have reported the synthesis of the *p*-*tert*-pentyl octamer **2b** (Fig. 7.2) (yield up to 35 %) from *p*-*tert*-pentylphenol, paraformaldehyde, in the presence of KOH in tetralin [12]. Ungaro [10a] and coworkers, synthesized *p*-(benzyloxy)calix[8]arene derivative **2c** in 48 % yield by a one-pot procedure using *p*-benzyloxyphenol, paraformaldehyde, and NaOH in xylene [13]. Kovalev [14] and coworkers reported the synthesis of **2j** in excellent yield (71 %) starting from *p*-1-adamantylphenol using KOH as base, and diphenyl ether as solvent [14]. Recently, Falana and coworkers [15] used a similar convergent strategy to synthesize *p*-*tert*-butylcalix[8]arene in excellent yields. A “7 + 1” reaction type at ambient temperature, using trifluoroacetic acid (TFA) as catalyst, provides quantitatively the cyclic octamer as crystalline precipitate (overall yield 58 %) (Fig. 7.2).

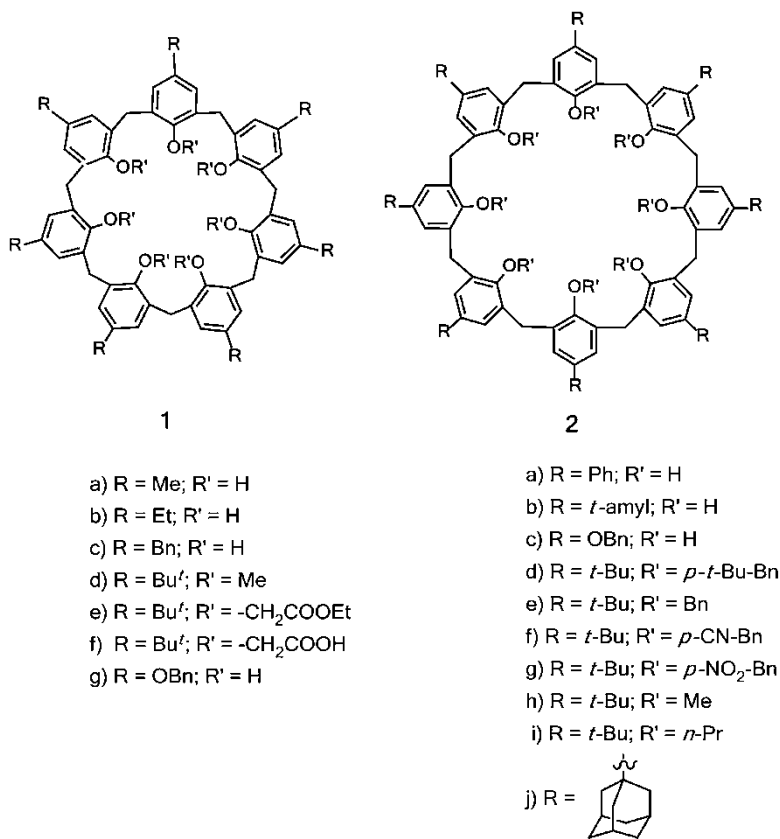


Fig. 7.2 Examples of functionalized calix[7,8]arene derivatives

**Calix[9]arenes** Bew and Sharma reported a SnCl<sub>4</sub>-promoted synthesis of *p*-*tert*-butylcalix[9]arene **C[9]** (36% yield) using *s*-trioxane as formaldehyde source in CH<sub>2</sub>Cl<sub>2</sub> as the solvent [16]. Besides to **C[9]**, a good amount of *p*-*tert*-butylcalix[8]arene (58%) was also obtained. Recently, Bonnamour and coworkers [16] have reported a large scale synthesis of *p*-*tert*-butylcalixarenes **C[7]** and **C[9]**. The procedure, involves the use of 1,2-dichloroethane, *p*-*tert*-butylphenol, TsOH and *s*-trioxane, and it is performed on a semi-industrial scale reactor. From 1,000 g of *p*-*tert*-butylphenol it is possible to obtain 96 g **C[7]** and 25 g of **C[9]** with a simplified workup procedure. The cost of two macrocycles from this synthesis are very inexpensive (15\$/g and 60\$/g, respectively) [16].

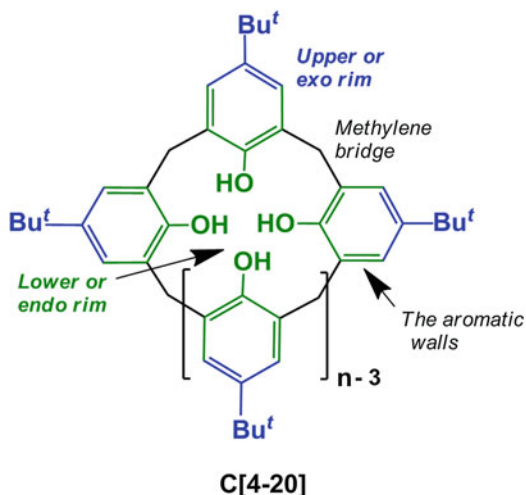
**Calix[10–12]arenes** Lamartine and coworkers [17] have obtained the *p*-*tert*-butylcalix[10 and 12]arenes **C[10]** and **C[12]**, through a cyclocondensation of linear phenolic oligomers (a 6+3 procedure), under basic conditions. These macrocycles were isolated even up to half-gram scale by usual work-up (several crystallizations and purifications by column chromatography).

**Calix[13–20]arenes** *p*-*tert*-Butylcalix[13–20]arenes **C[13]–C[20]** were originally synthesized by Gutsche and Stewart via their general “one pot” acid-catalyzed procedure [3]. From the reaction mixture, usual work-up (gradient flash chromatography and selective precipitation) allows to obtain **C[13]–C[20]** in a very low yield. The Gutsche’s procedure is still the only used to obtain these macrocycles. More recently, Huc [18] and coworkers has reported a procedure in which starting by *p*-(benzyloxy)phenol is possible to obtain in good yields (between 30 % and 70 %) calix[13–20]arene macrocycles through a simple crystallization-based purification procedure [18]. Interestingly, following this purification process reported by Huc [18], the giant calixarenes with a number of phenols until 200 were isolated in good yields [18].

### 7.3 Functionalization of Calix[7–20]arene Macrocycles

Since their first isolation, the chemical modification of calix[*n*]arenes has been actively investigated with the main aim to obtain macrocyclic hosts with novel supramolecular properties [1]. The most common functionalizations regard the *endo* rim (phenolic hydroxyl groups, also called *lower* or *small* rim) [1], and the *exo* rim (*para* position of the aromatic rings, also called *upper* or *wide* rim) [1], but more recently a certain interest has been also devoted to the modification of the methylene bridges [19a] and of the aromatic walls [19b–f] of the calix cavity (Fig. 7.3).

**Fig. 7.3** Parts of the *tert*-butylcalix[*n*]arene macrocycles susceptible to functionalization



### 7.3.1 Lower Rim Functionalization of Large Calixarenes

The preferred way to append new groups at the endo rim of calixarene macrocycles is the *O*-alkylation of the phenolic ring by a base-promoted Williamson's reaction to give partially or fully alkylated derivatives [1]. Another less popular route is provided by any esterification reaction [20].

Exhaustive methylation of *p*-*tert*-butylcalix[7]arene **C[7]** has been obtained upon treatment with MeI in the presence of Cs<sub>2</sub>CO<sub>3</sub> as the base to give heptamethoxycalix[7]arene **1d** [21] (Fig. 7.2) in 90 % yield. Treatment of **C[7]** with ethyl bromoacetate and K<sub>2</sub>CO<sub>3</sub> in acetone afforded **1e** [22] in high yield, which was then converted to heptacarboxylic acid **1f** [23].

Exhaustive alkylation [24] of *p*-*tert*-butylcalix[8]arene **C[8]** has been performed by treatment with strong bases such as NaH or BaO/Ba(OH)<sub>2</sub> and a large excess of alkylating agent, obtaining derivatives **2d–i** (Fig. 7.2) in excellent yield [24, 25].

Regarding the exhaustive alkylation of *p*-*tert*-butylcalix[9]arene **C[9]** [26], it has been obtained by treatment with a large excess of K<sub>2</sub>CO<sub>3</sub> (3 equiv./OH) and alkylating agent (14 equiv./OH). Thus, calix[9]arene derivatives **3a–f** (Fig. 7.4), have been obtained in good yields (from 48 % to 78 %) [26]. Dynamic NMR studies have shown a high conformational mobility for all calix[9]arene derivatives, even at low temperatures.

**Selective Functionalization** The possibility to selectively append substituents at the *endo* rim is of prime interest for the synthesis of new hosts based on large calixarenes. In the selective modification of large calixarenes, the number of the possible partially substituted derivatives (16, 28, and 46 for calix[7]-, -[8]-, and -[9]arenes, respectively) increases exponentially by increasing the number of phenol rings. Notwithstanding this inherent difficulty, the regioselective functionalization at the *endo* rim of *p*-*tert*-butylcalix[7]arene **C[7]** has been obtained [21] through a

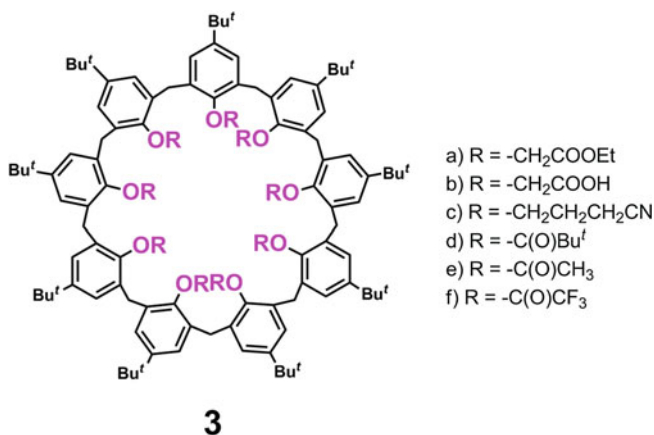
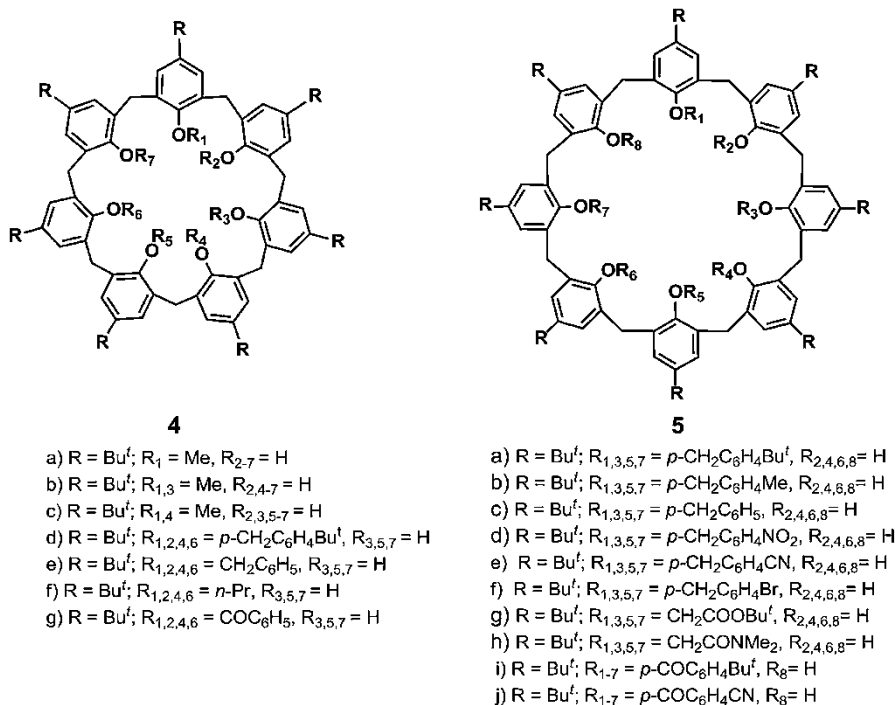


Fig. 7.4 Examples of calix[9]arene derivatives functionalized at the lower rim



**Fig. 7.5** Examples of functionalized *p*-*tert*-butylcalix[7,8]arene derivatives

weak-base promoted *O*-alkylation or *O*-benzylation. It is noteworthy that the 1,2,4,6-tetrasubstitution (derivatives **4d–g** in Fig. 7.5) has been obtained with high selectivity (50–88 % yield) by using K<sub>2</sub>CO<sub>3</sub> as the base [21].

Analogously, the use of weak bases such as K<sub>2</sub>CO<sub>3</sub> or CsF allowed the synthesis of partially *O*-substituted calix[8]arenes **5a–h** (Fig. 7.5) [24, 25]. Regarding the partial acylation of **C[8]**, heptaesters such as **5i–j** [27c] have been obtained in 40–80 % yields. These compounds can be regarded as “protected” calix[8]arenes in the synthesis of mono-functionalized derivatives.

No examples of partially substituted (unbridged, *vide infra*) calix[9–20]arenes are currently known.

### 7.3.2 Shaping Large Calixarenes by Intramolecular Bridging

As it is known “the more highly hosts are preorganized and more stable will be their host-guest complexes” [28]. In the last decades, many reports have showed that the

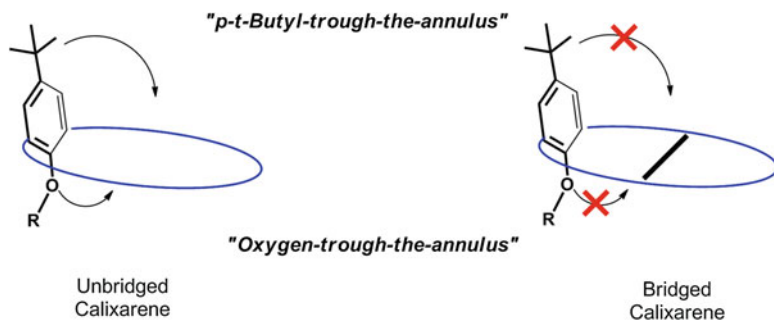


**Fig. 7.6** Possible pathways for conformational interconversion in *p-tert*-butylcalix[*n*]arenes and their blockage following intramolecular bridging [2a]

intramolecular bridging at the lower rim of large calixarenes is an useful way toward their preorganization [2a]. In fact, large calix[*n*]arenes undergo conformational interconversion by means of the “oxygen-trough-the-annulus” or “*p*-substituent-trough-the-annulus” routes (Fig. 7.6) [2a, 29]. Consequently, the shaping of their molecular skeleton can only be achieved by blocking both mechanisms through an appropriate intramolecular bridging (Fig. 7.6) [2a, 29].

**Calix[7]arenes** The first examples of singly bridged calix[7]arenes (Fig. 7.7) have been obtained by direct *O*-alkylation [30a] of *p-tert*-butylcalix[7]arene **C[7]** with bis-electrophiles such as BrCH<sub>2</sub>Cl, oligoethylene glycol ditosylates, and 1,4-bis(bromomethyl)benzene, in the presence of a base (K<sub>2</sub>CO<sub>3</sub> or Cs<sub>2</sub>CO<sub>3</sub>) [30a]. The proximal 1,2-bridging was favored with “short bridging-element” such as dioxamethylene or crown-2, while the bridging with the longer tri(ethylene glycol) ditosylate in the presence of Cs<sub>2</sub>CO<sub>3</sub> in acetone gave the 1,4-calix[7]crown-4 **7a** (Fig. 7.7) in good yield (72 %). Finally, the bridging of **C[7]** with an aromatic unit was also obtained by Cs<sub>2</sub>CO<sub>3</sub>-promoted alkylation with 1,4-bis(bromomethyl)benzene, which afforded the corresponding 1,4-(*p*-xylylene)-bridged calix[7]arene **7d** in 40 % yield [30a].

Interestingly, Chen [30b] and coworkers have shown that the treatment of *p-tert*-butylcalix[7]arene **C[7]** with *N,N'*-bis(chloroacetyl)trimethylene diamine afforded the 1,4-bridged calix[7]arene derivative **7f** (Fig. 7.7) in 45 % yield in the presence of Cs<sub>2</sub>CO<sub>3</sub> as the base. Differently, using a shorter spacer such as *N,N'*-bis(chloroacetyl)ethylene diamine the 1,3-bridged calix[7]arene was obtained in 54 % yield in the presence of K<sub>2</sub>CO<sub>3</sub> as the base. Interestingly, it has been shown that the use of a large excess of alkylating agent and base led directly to 1,4:2,3-doubly bridged calix[7]arene derivatives **8** (Fig. 7.8) [31].

Li and coworkers [32] showed that the treatment of **C[7]** with phosphorus pentachloride afforded the first example of phosphorus multiply-bridged calix[7]arene derivative **9** (Fig. 7.9).

**Calix[8]arenes** The mono-bridging reaction of calix[8]arene macrocycle **C[8]** could give rise to four regioisomeric products, namely the 1,2-, 1,3-, 1,4-, or



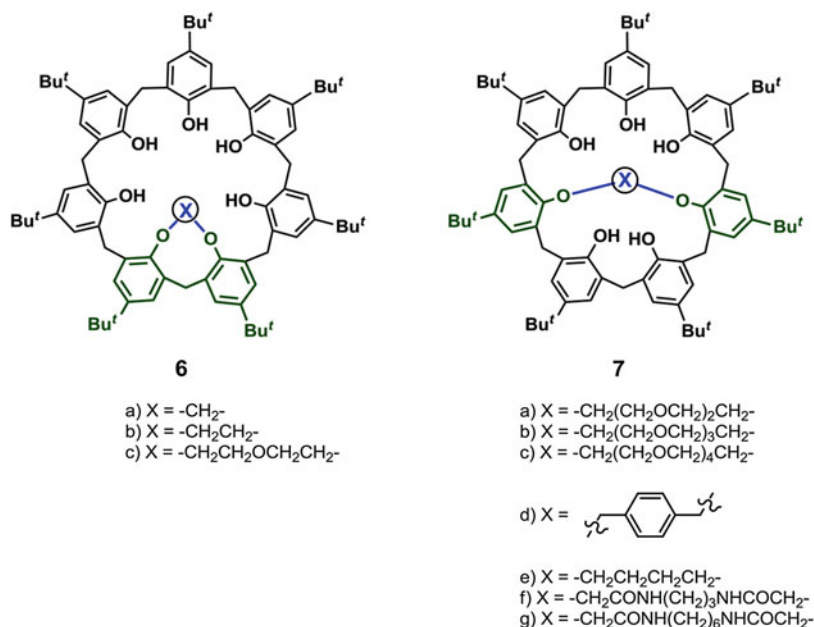


**Fig. 7.7** Singly-bridged *p*-*tert*-butylcalix[7]arene derivatives [30]

**Fig. 7.8** Doubly-bridged *p*-*tert*-butylcalix[7]arene derivatives [31]

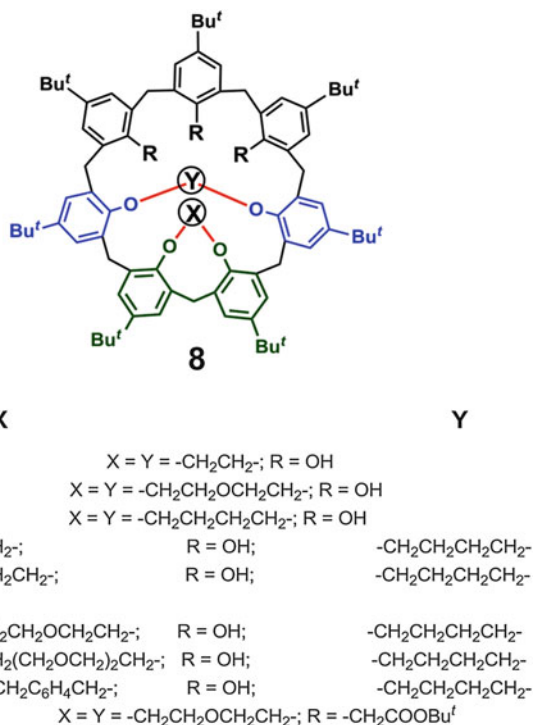
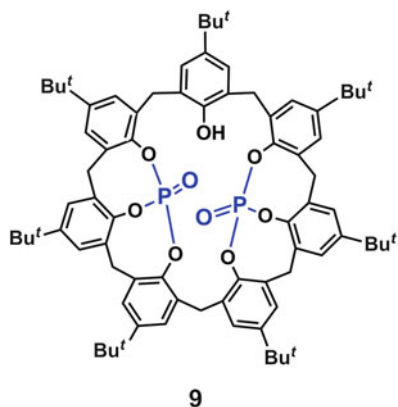


**Fig. 7.9** Phosphorus multiple bridged calix[7]arene derivative **9** [32]



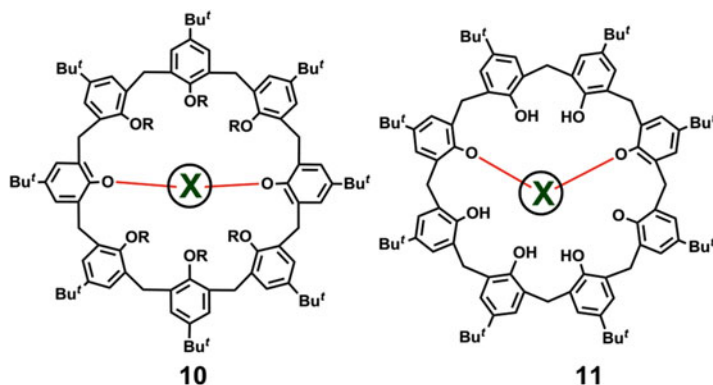
1,5-bridged compounds. Surprisingly, the strength of the base and the length and nature of the bridge allow a good control of the regioselectivity of the reaction [33]. In fact, it has been shown [33] that the treatment of **C[8]** with  $\text{Cs}_2\text{CO}_3$  as the base and aromatic shorts bridges such as *ortho*, *meta* or *para*-bis(bromomethyl) benzene, affords 1,5-bridged calix[8]arenes **10d–f** (Fig. 7.10) in high yields (80–90 %) [34].

The functionalization of calixarene lower rim with crown ether bridges gives rise to compounds termed *calixcrown* [33, 35], which have shown interesting recognition properties towards cationic guests. Regarding calix[8]crowns, the four possible singly-bridged derivatives have been obtained by direct regioselective alkylation of *p*-*tert*-butylcalix[8]arene under various conditions [33, 35]. Thus crown-2 and crown-3 bridges have been introduced between phenolic rings at 1,5-positions by treatment of **C[8]** in the presence of  $\text{Cs}_2\text{CO}_3$  to give derivatives **10b** and **10c** in high yields (88 % and 78 %, respectively) [33, 35]. Alkylation of **C[8]** with longer chains, such as tri-, tetra-, or penta(ethylene glycol) ditosylate in the presence of strong bases such as NaH, afforded crown-4 derivatives **11a–c** in 20–35 % yields, while the use of  $\text{K}_2\text{CO}_3$  as the base afforded 1,3- and 1,2-crowned calix[8]arenes in lower yields [33, 35].

The 1,5-regioselectivity observed in the bridging reaction of **C[8]** in the presence of  $\text{Cs}_2\text{CO}_3$  has been confirmed by Castillo and coworkers [36] who reported the regioselective introduction of the 2,6-dimethylpyridyl bridge to those positions upon treatment with  $\text{Cs}_2\text{CO}_3$  in DMF in the presence of 2,6-bis(chloromethyl) pyridine (derivative **10i**, Fig. 7.10) as the alkylating agent. Under analogous conditions, the 2,9-bis(methylene)-1,10-phenanthroline-bridged calix[8]arene **10j** was obtained in high yields [37].

In all of the above instances, the regiochemistry of the mono-bridging reactions of **C[8]** can be explained mainly in terms of strength of the base [33].

With the aim to shape to the calix[8]arene macrocycle, the functionalization with large alkyl groups of the lower rim of 1,5-tetramethylene-bridged calix[8]



- a) X =  $-\text{CH}_2(\text{CH}_2)_2\text{CH}_2-$ ; R = H  
 b) X =  $-\text{CH}_2\text{CH}_2-$ ; R = H  
 c) X =  $-\text{CH}_2\text{CH}_2\text{OCH}_2\text{CH}_2-$ ; R = H  
 d) X =  $o\text{-CH}_2\text{C}_6\text{H}_4\text{CH}_2-$ ; R = H  
 e) X =  $m\text{-CH}_2\text{C}_6\text{H}_4\text{CH}_2-$ ; R = H  
 f) X =  $p\text{-CH}_2\text{C}_6\text{H}_4\text{CH}_2-$ ; R = H  
 g) X =  $-\text{CH}_2(\text{CH}_2\text{OCH}_2)_2\text{CH}_2-$ ; R = H  
 h) X =  $-\text{CH}_2(\text{CH}_2\text{OCH}_2)_3\text{CH}_2-$ ; R = H

- a) X =  $-\text{CH}_2(\text{CH}_2\text{OCH}_2)_2\text{CH}_2-$   
 b) X =  $-\text{CH}_2(\text{CH}_2\text{OCH}_2)_3\text{CH}_2-$   
 c) X =  $-\text{CH}_2(\text{CH}_2\text{OCH}_2)_4\text{CH}_2-$

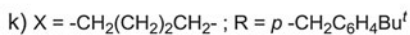
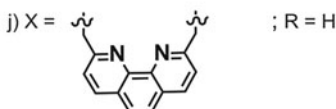
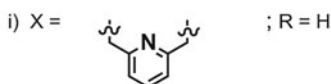
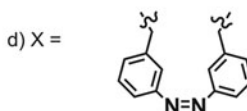


**Fig. 7.10** Singly-bridged *p*-*tert*-butylcalix[8]arene derivatives

arene **10a** was studied [6a]. Thus, the reaction of **10a** with *p*-*tert*-butylbenzylbromide afforded two conformational isomers **10** and **10k'** (Fig. 7.11) having two 3/4-cone halves oriented *syn* or *anti* with respect to the tetramethylene bridge [6a]. VT NMR studies clearly indicated that the *O*-through-the-annulus passage was inhibited by the *tert*-butylbenzyl groups at the *endo* rim of **10k**, while the presence of the 1,5-tetramethylene bridge allowed an effective inhibition of the *tert*-butyl-through-the-annulus route [6a]. The crystal structure of **10k** showed the presence of a cone-shaped calix[8]arene skeleton with an extended tetramethylene bridge almost coplanar to the mean molecular plane [6a].

The calix[8]arene macrocycle can be additionally shaped through the introduction of two bridging elements at the lower rim, to obtain doubly-bridged calix[8]

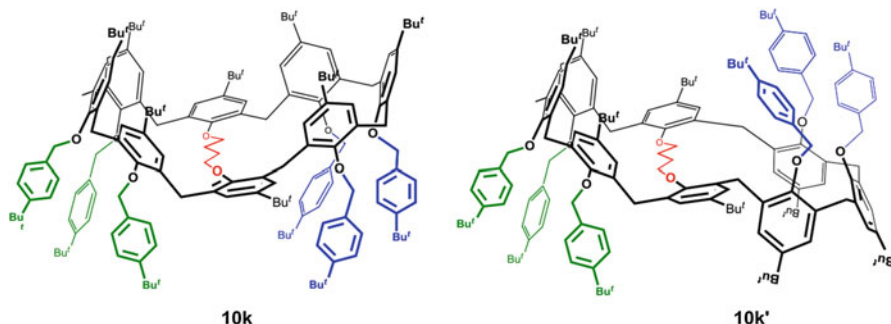


Fig. 7.11 Structures of the two atropoisomers **10** and **10 k'** [6]

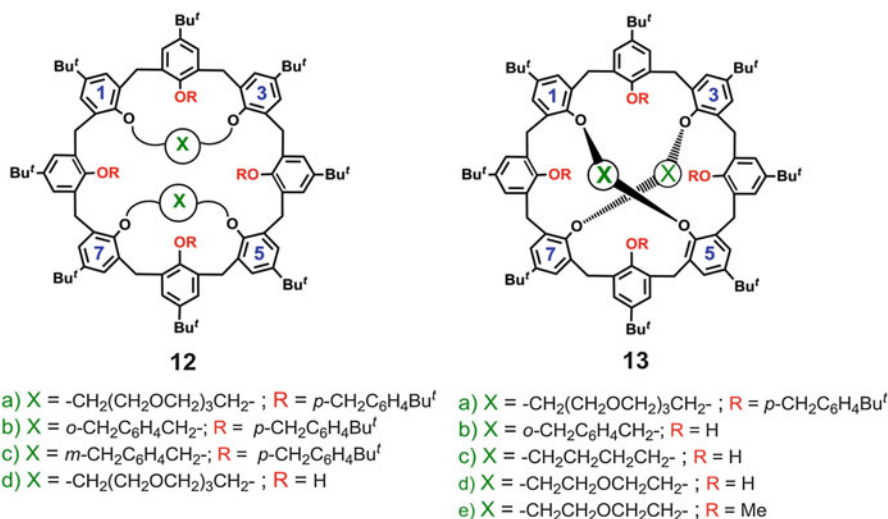
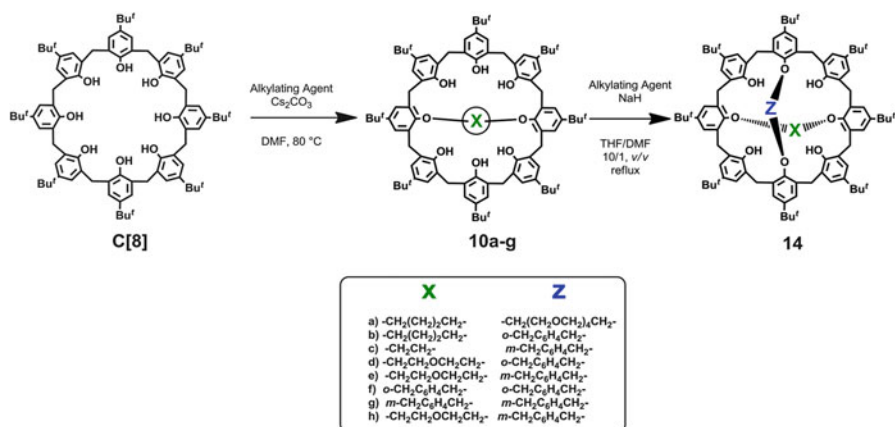
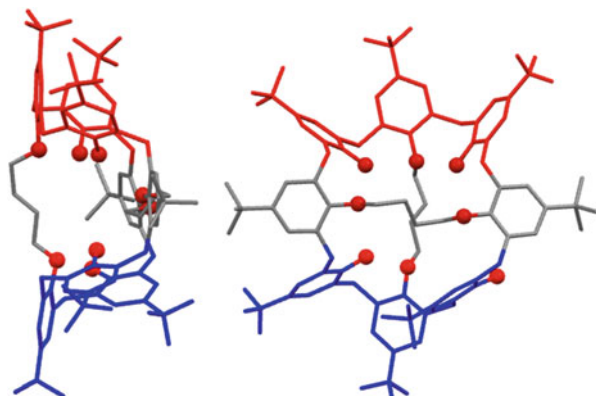


Fig. 7.12 Doubly-bridged *p*-tert-butylcalix[8]arene derivatives

arene derivatives (Fig. 7.12), which present a higher degree of preorganization with respect to the singly-bridged ones above discussed. The 1,3:5,7-doubly-bridged calix[8]arene **12a** was obtained by direct *O*-alkylation of the 1,3,5,7-tetrakis(*p*-tert-butylbenzyl) calix[8]arene ether **5a** (Fig. 7.5) with tetraethyleneglycol ditosylate in the presence of Cs<sub>2</sub>CO<sub>3</sub> as the base [38]. Under these conditions, the direct alkylation of **5a** with *ortho* or *para*-bis(bromomethyl)benzene afforded derivatives **12b–c** in high yields (80%) [39]. Interestingly, the direct alkylation of **C[8]** with 1,2-bis(bromomethyl)benzene in the presence of NaH afforded 1,5:3,7-doubly-bridged derivative **13b** (Fig. 7.12) [40], while derivatives **13a** and **13c** were obtained by a two step reaction (Cs<sub>2</sub>CO<sub>3</sub> followed by NaH) [41] in the presence of diethylene glycol ditosylate and 1,4-diiodobutane, respectively.

**Fig. 7.13** Different views of the X-ray crystal structure of **13c** (H atoms, have been omitted for clarity) [41]



**Scheme 7.1** Synthesis of the 1,5:3,7-doubly-bridged calix[8]arenes with mixed spanning elements [42]

X-ray [41] studies of **13c** showed a intriguing structure in which four  $\frac{3}{4}$ -cone clefts (Fig. 7.13) were present with seven calixarene oxygen atoms converging toward the central polyhedral cavity, while the bridged oxygens at the 1,3,5,7 positions adopted a tetrahedral arrangement.

The two-step procedure for the synthesis of 1,5:3,7-doubly-bridged calix[8]arenes was then extended to derivatives **14a–h** (Scheme 7.1) bearing two different bridges at the lower rim. The first step makes use of  $\text{Cs}_2\text{CO}_3$  to obtain 1,5-monobridged calix[8]arenes **10a–g** [42]. In the second step, the introduction of the other 3,7-bridge was promoted by NaH in anhydrous THF/DMF at reflux to give derivatives **14a–g**.

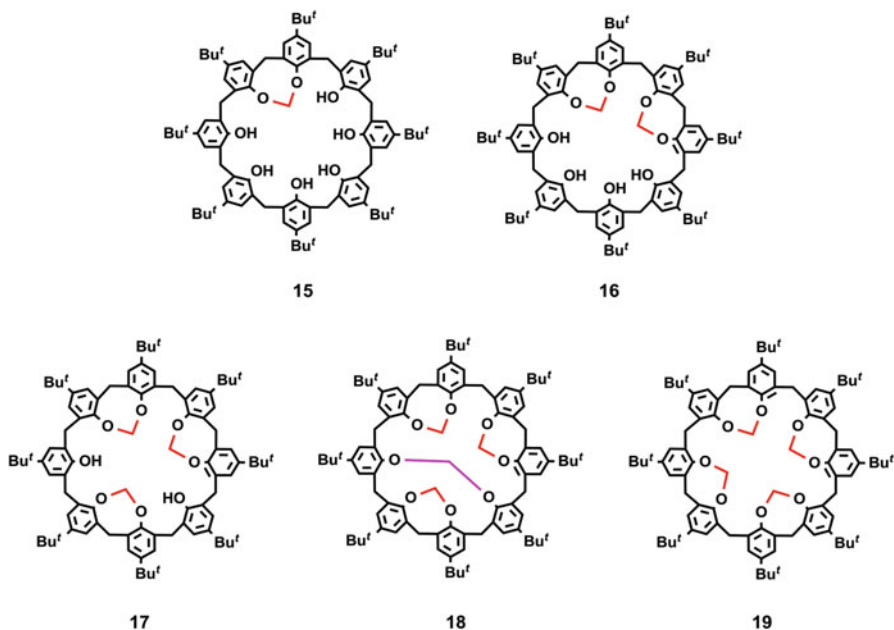


Fig. 7.14 Multiply-bridged calix[8]arenes **15–19** [44]

The high yield observed in the second bridging reaction could be explained by the cation templation previously [43] described for 1,5-bridged derivatives, which folds the calix[8]arene skeleton in a tub-shaped conformation well suitable to bridging with short spacers.

Several examples of various OCH<sub>2</sub>O-bridged calix[8]arenes **15–19** (Fig. 7.14) were obtained by treatment of **C[8]** with Cs<sub>2</sub>CO<sub>3</sub> and BrCH<sub>2</sub>Cl [44]. Dynamic <sup>1</sup>H NMR studies and MM3 calculations indicated that the dioxocine subunits adopt a boat–chair conformation, which is well compatible with the geometrical requirements of a calix[8]arene *pleated-loop* conformation [44].

As reported by Gloede [45] and coworkers the treatment of **C[8]** with PCl<sub>5</sub>, followed by hydrolysis, gave derivative **20**, which was converted to a 1:1 mixture of two stereoisomeric triphosphate derivatives **21a** and **21b**, by treatment with triethyl orthoformate [45] (Fig. 7.15).

**Calix[9–10]arenes** The bridging of calix[9–10]arene macrocycles has been studied only recently (Fig. 7.16). Thus, the first example of a calix[9]arene containing three bridged phosphoryl groups **22** (Fig. 7.16) was obtained by Gloede [46] and coworkers upon treatment of **C[9]** with phosphorus pentachloride.

Li and Zhan [47] have reported a series of crowned-calix[10]arenes **23a–c** (Fig. 7.16) obtained by intramolecular bridging of **C[10]**. The regiochemistry of these bridging reactions can be controlled by the strength of the base analogously to the results previously reported for calix[8]arene macrocycle.

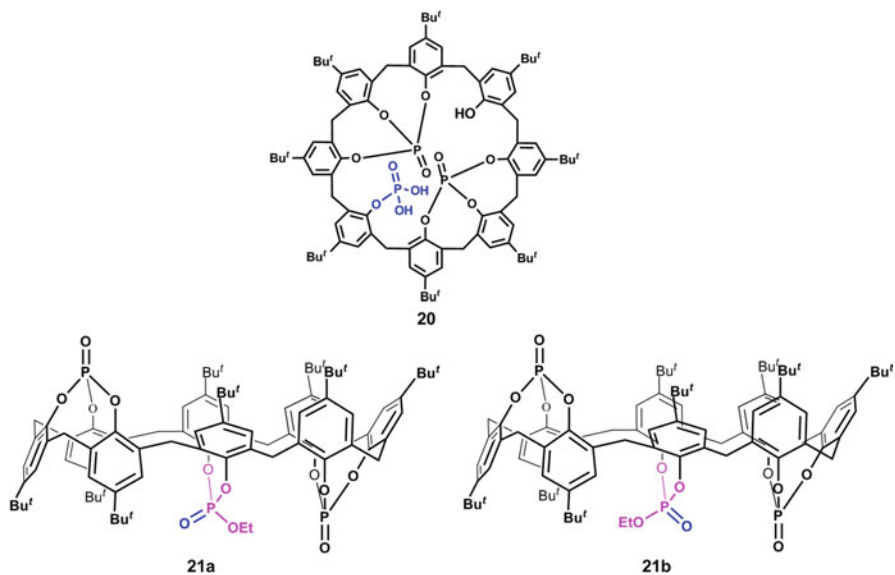


Fig. 7.15 Phosphate-bridged *p*-*tert*-butylcalix[8]arene derivatives [45]

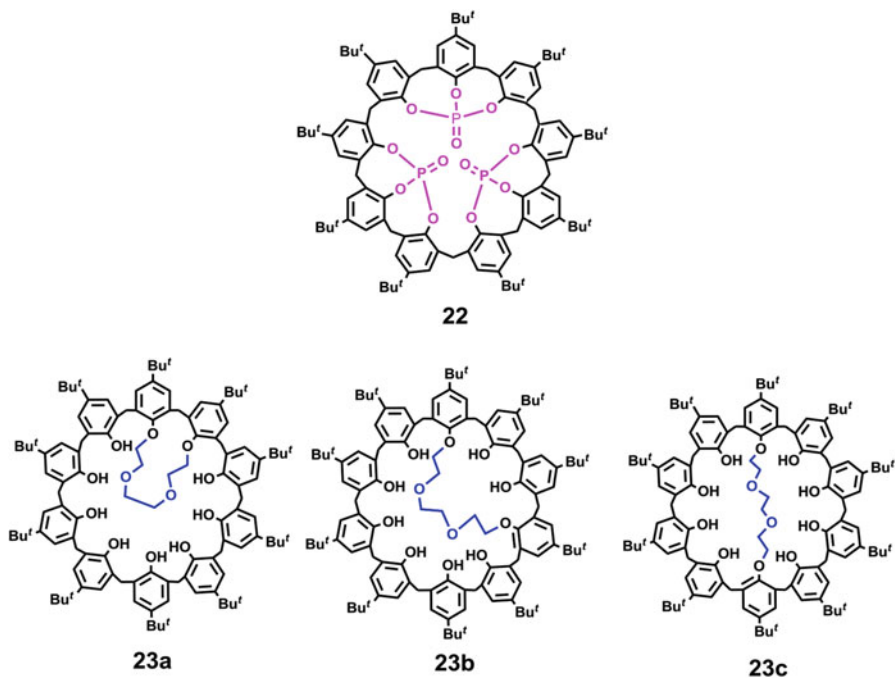


Fig. 7.16 Single- and multiple-bridged calix[9,10]arene derivatives



### 7.3.3 Exo Rim Functionalization of Large Calixarenes

The widespread diffusion of calixarene hosts in several areas of supramolecular chemistry is mainly due to the possibility to introduce a range of functionalities at both rims of the macrocycle. Regarding the *exo* rim functionalization [1, 48], many procedures have been developed to introduce new groups based on a direct electrophilic aromatic substitution [1], which include nitration [49], halogenation [50], acylation [51], sulfonation [52]. The standard way starts with a complete removal of the *para*-substituents followed by the aromatic electrophilic substitution. The *tert*-butyl group is easily removed by  $\text{AlCl}_3$ -mediated *trans-tert*-butylation to give the corresponding *p*-H-calixarenes **24a** and **25a** (Fig. 7.17) [53].

**Calix[7]arenes** Water soluble calix[7]arenes bearing dialkylamino **24b** or carboxylic **24c** groups were obtained (Fig. 7.17) [54] by functionalization of *p*-H-calix[7]

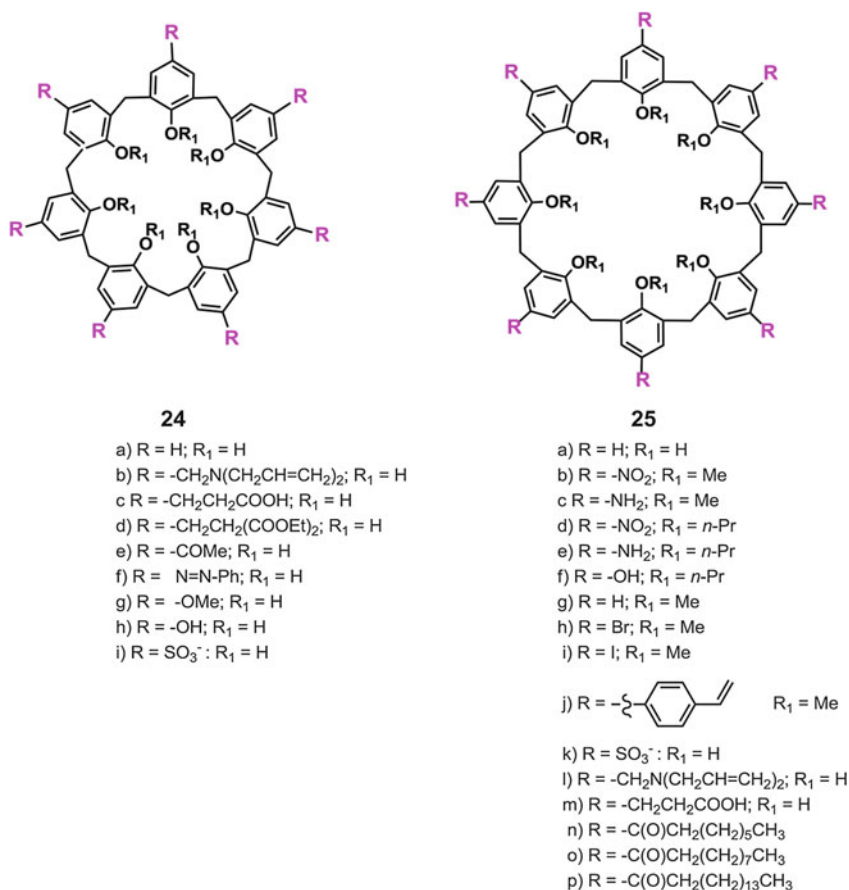


Fig. 7.17 Calix[7,8]arene derivatives functionalized at the *exo* rim

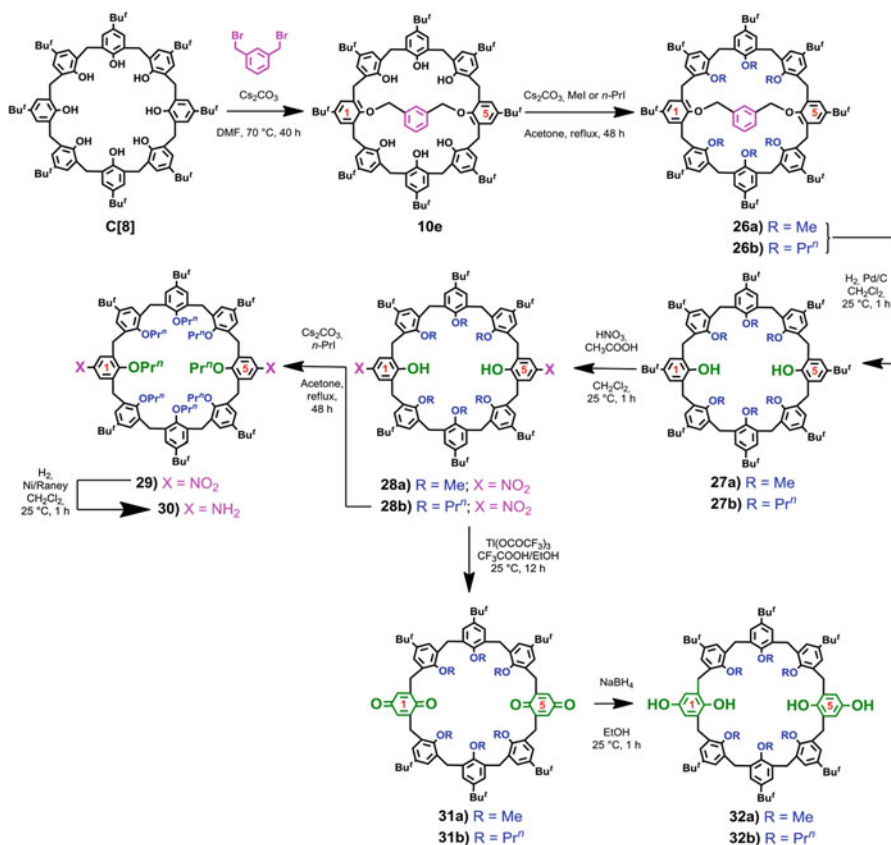


arene **24a** via the Mannich/*p*-quinone-methide route [55], which involves the treatment of **24a** with formaldehyde and a secondary amine to give the Mannich base, quaternarization, and nucleophilic substitution (via the putative *p*-quinone-methide intermediate). The functionalization with acetyl groups has been obtained in a one-pot procedure in which **C[7]** was first de-*tert*-butylated to give **24a** as an intermediate (Fig. 7.17) and then acylated *in situ* by slow addition of  $\text{CH}_3\text{COCl}$  to give **24e** (49 % overall yield) [54]. The treatment of *p*-H-calix[7]arene **24a** with benzenediazonium tetrafluoroborate in THF in the presence of pyridine afforded phenylazocalix[7]arene **24f** in 21 % yield [56]. The  $\text{BBR}_3$ -mediated demethylation of the parent *p*-methoxycalix[7]arene **24g** gave calix[7]arene heptahydroquinone derivative **24h** which was also obtained by palladium-catalyzed debenzoylation of **2g** [57].

Water-soluble *p*-sulfonatocalix[7]arene derivative **24i** was obtained [58] by treatment of *p*-H-calix[7]arene **24a** with  $\text{H}_2\text{SO}_4$  at 80 °C for 3 h. The following stepwise dissociation constants of **24i** were obtained by potentiometric titration:  $\text{p}K_{\text{a}1} = 3.19$ ;  $\text{p}K_{\text{a}2} = 5.40$ ,  $\text{p}K_{\text{a}3} = 9.41$ ,  $\text{p}K_{\text{a}4} = 12.0$  [58].

**Calix[8]arenes** The nitration of calixarene *exo* rim and the successive reduction of the nitro to amino-group is considered an useful synthetic way to introduce on the calixarene skeleton hydrogen-bond acceptor/donor groups such as urea, thiourea, amide, and peptido groups. Böhmer [59a] reported the exhaustive *ipso*-nitration of octamethoxycalix[8]arene **2h** by treatment with  $\text{HNO}_3/\text{AcOH}$  at 0 °C in  $\text{CHCl}_3$  to obtain **25b** (50 %). Successively, **25b** was reduced to the corresponding octamine **25c** with hydrazine in the presence of Pd/C. In a previous work, the *ipso*-nitration of octapropoxycalix[8]arene **2i** was performed in  $\text{CH}_2\text{Cl}_2$  at room temperature to obtain **25d** (Fig. 7.17) in 40 % yield, which was converted to give **25e** by hydrogenation with Pd/C [59b]. The functionalization of the calix[8]arene *exo* rim with OH groups has been obtained by hydrogenolysis of the octa(*p*-benzyloxy)calix[8]arene **2c** to give **25f** in 85 % yield [60]. Bromination of the calix[8]arene *exo* rim was reported [61] in 75 % yield upon treatment of **25g** (Fig. 7.17) with  $\text{Br}_2$  and  $\text{Fe}^0/\text{AcOH}$  as catalyst to give derivative **25h**. Analogously, the fully iodinated derivative **25i** was obtained by treatment of **25g** with  $\text{I}_2$ ,  $\text{CF}_3\text{COOAg}$  in refluxing  $\text{CH}_2\text{Cl}_2$  (57 % yield). The fully *para*-brominated and -iodinated calix[8]arenes **25h-i** (Fig. 7.17) were used for a Suzuki or Negishi type, respectively, cross-coupling reaction, to give calix[8]arene **25j** bearing styryl groups at the *exo* rim [11b]. Interestingly, de-*tert*-butylated *p*-H-calix[8]arene derivative **25a** was reacted with  $\text{H}_2\text{SO}_4$  to afford water soluble *p*-sulfonatocalix[8]arene **25k** (Fig. 7.17) [62].

Calix[8]arenes derivatives bearing dialkylamino **25l** or carboxylic **25m** groups (Fig. 7.17) were obtained by a Mannich/*p*-quinone-methide route analogously to the above discussed calix[7]arenes **24b-d** [54, 55]. The first examples of *para*-acylcalix[8]arene derivatives were reported by Shinkai in 1993 [62]; more recently, Coleman [63a, b] reported a series of amphiphilic *para*-acyl-calix[8]arenes **25n-p**, having acyl chains of eight or more carbon atoms, and their self-assembly



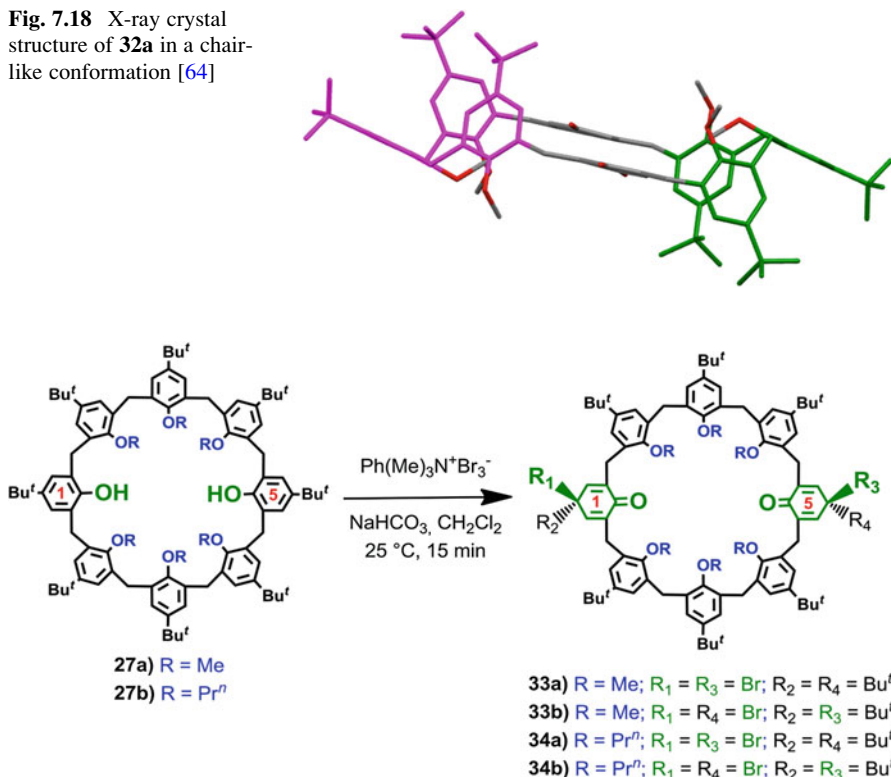
**Scheme 7.2** Selective *exo*-rim functionalization of *p*-*tert*-butylcalix[8]arene

properties. They were obtained in 61–81 % yield by Friedel–Crafts acylation of *p*-H-calix[8]arene **25a** in the presence of AlCl<sub>3</sub> [63].

Some years ago, a simple and convenient route to selectively functionalize the calix[8]arene *exo* rim was introduced [34]. The easily accessible 1,5-xylylene-bridged derivatives **26a–b**, can be easily deprotected by hydrogenolysis to give **27a–b** which can be selectively functionalized at the free phenolic rings because of their higher reactivity with respect to the *O*-alkylated ones. In this way, the first examples of calix[8]arenes partially substituted with *p*-nitro, *p*-amino, quinone, and hydroquinone functionalities have been obtained (Scheme 7.2) [34, 64].

A successive X-ray study [64] showed that in the solid state calix[8]arene 1,5-diquinone **32a** adopts a ‘pseudo-chair-like’ conformation (Fig. 7.18). In this structure, two anti-oriented 3/4-cone moieties can be seen (in magenta and green in Fig. 7.18) while the two quinone rings (in grey) are on parallel planes. Two quinone oxygens point towards the centre of the molecule with a short distance of 3.27 Å [64].

**Fig. 7.18** X-ray crystal structure of **32a** in a chair-like conformation [64]



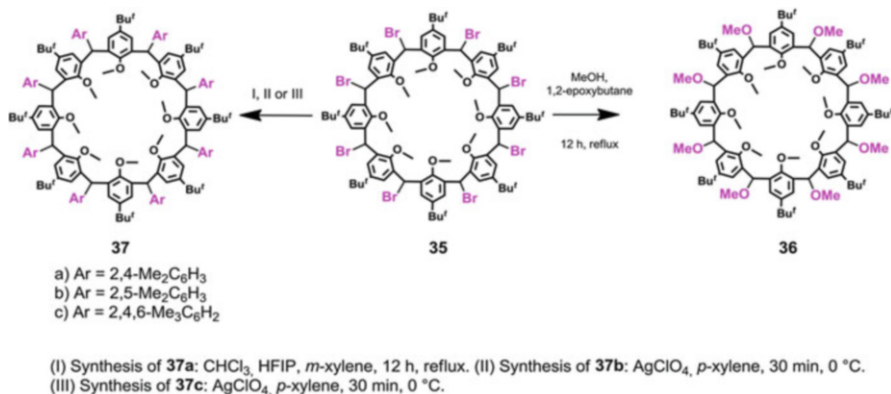
**Scheme 7.3** Synthesis of calix[8]arene *p*-bromodienone derivatives [65]

Successively, it was shown that the reaction of 1,5-dihydroxycalix[8]arenes **27a–b** with trimethylphenylammonium tribromide and a saturated solution of NaHCO<sub>3</sub> results in the formation of derivatives **33–34** (Scheme 7.3) bearing at the 1,5-positions of the calix[8]arene skeleton two 4-*tert*-butyl-4-bromo-2,5-cyclohexadienone moieties (shortly, the *p*-bromodienone moieties) [65].

The serendipitous discovery of calixarene *p*-bromodienone derivatives has then led to the development of the novel “*p*-bromodienone route” [66] in which nucleophilic agents can be directly linked to the *para*-position of a calixarene aromatic ring in a sort of “aromatic ring umpolung” [66].

### 7.3.4 Methylene Bridge Functionalization of Large Calixarenes

Recently, Biali and coworkers reported the functionalization of the calixarene methylene bridges [67] as a novel route to modify the properties of the calixarene



**Scheme 7.4** Synthesis of calix[8]arene derivatives functionalized at the methylene bridges [67]

scaffold (see Chap. 4). This structural modification can alter the intrinsic conformational preferences of the scaffold and increase the rigidity and preorganization of the calix macrocycle [67].

Typically (Scheme 7.4) [67], the easily accessible octabromocalix[8]arene **35** was reacted under S<sub>N</sub>1 conditions in the presence of methanol to obtain the complete substitution product **36** in a nonstereoselective fashion [68a]. Interestingly, all-*cis* octaryl derivatives **37** are the main products in the reaction with arenes, and the incorporation of aryl substituents at the bridges rigidifies the calix[8]arene skeleton [68a].

## 7.4 Supramolecular Features of Large Calixarenes

**Calix[7]arenes** The first studies on the recognition abilities of a calix[7]arene derivative towards alkali-metal cations were reported by Hirata [69] and coworkers in 1988. They showed that *p*-*tert*-butylcalix[7]arene heptaester **1e** was able to transport alkali-metal ions across a soybean phospholipid bilayer membrane, displaying a Cs<sup>+</sup> selectivity. Very recently, it has been shown [70] that heptaester **1e** is able to form Langmuir and LB films [70]. Interestingly, calix[7]arene heptaacid derivative **1f** [23] was used to extract trivalent lanthanides and actinides from water to chloroform/xylene organic phase with the following order of extractability: Am<sup>3+</sup> > Nd<sup>3+</sup> > Eu<sup>3+</sup> > Tb<sup>3+</sup> > Dy<sup>3+</sup> > Er<sup>3+</sup> > Yb<sup>3+</sup> [30]. More recently, it was shown that singly-bridged calix[7]arene **8a** is able to bind K<sup>+</sup> and Rb<sup>+</sup> cations [71], which give rise to a conformational templation of the macrocycle.

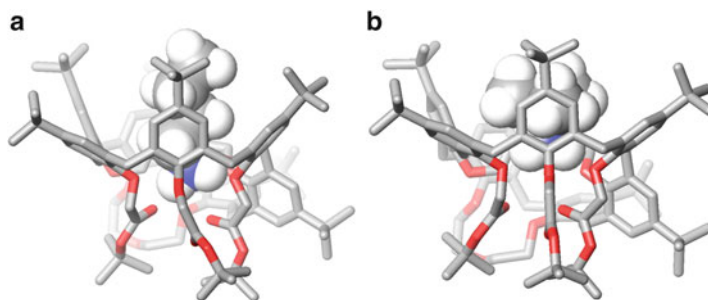


**Fig. 7.19** Lowest OPLS-energy structures of: (a)  $n\text{-BuNH}_3^+\text{C}8\mathbf{i}$ , (b)  $t\text{-BuNH}_3^+\text{C}8\mathbf{i}$  complexes obtained by Monte Carlo conformational searches

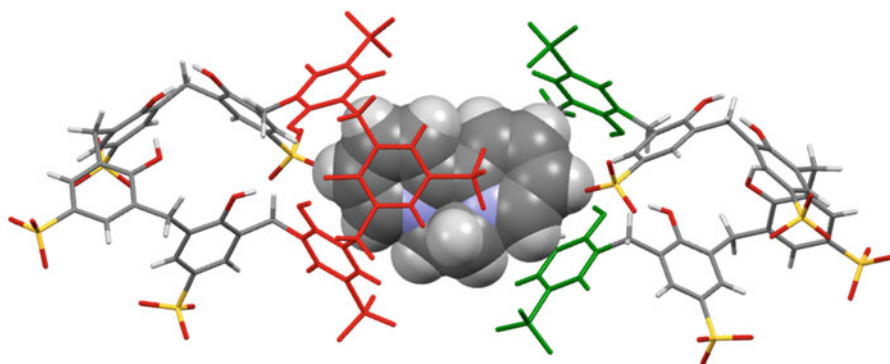
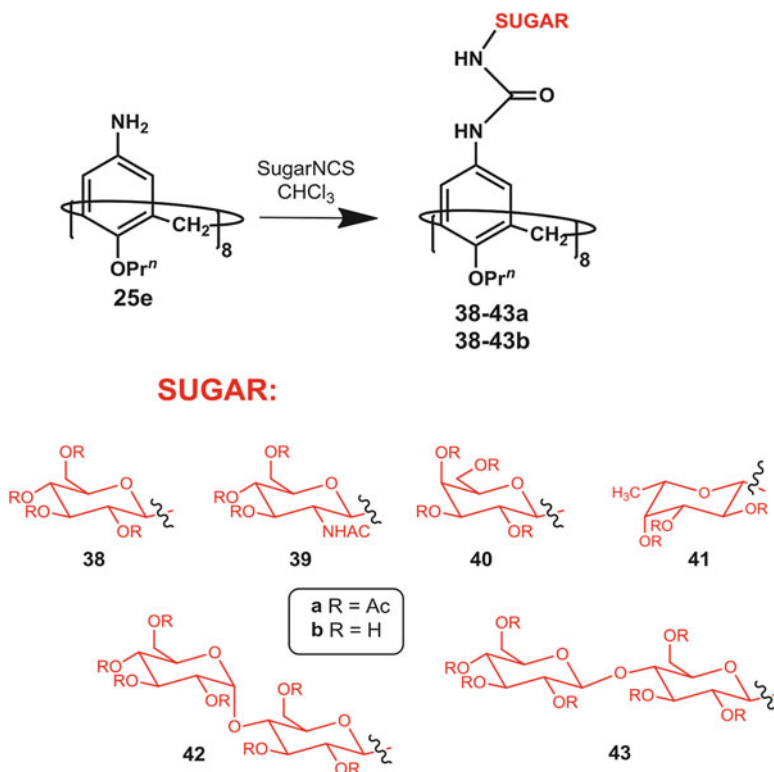


**Fig. 7.20** Representation of the molecular capsule between  $p$ -sulfonatocalix[7]arene **25i** (stick) and diquat (space-filling) guest [72]

Recently, interesting recognition abilities toward both sodium and potassium cations were reported for cone-shaped 1,4:2,3-doubly-bridged calix[7]arene **8i** [6b] by using the corresponding Tetrakis[3,5-bis(triFluoromethyl)Phenyl]Borate (TFPB<sup>-</sup>) salts. In particular, a selectivity of 94 for sodium over potassium was found [6b]. Derivative **8i** also showed interesting recognition abilities toward linear and branched alkyl ammonium cations with which forms *endo*-cavity complexes (Fig. 7.19).

Recent studies [58] on  $p$ -sulfonatocalix[7]arene **24i** evidenced interesting recognition abilities toward organic cationic guests such as paraquat, diquat, and chlormequat, known herbicides highly toxic toward humans. ROESY and DOSY experiments [58] indicated that both diquat<sup>2+</sup> and paraquat<sup>2+</sup> are sandwiched between the aromatic walls of the calix cavity with N<sup>+</sup>-atoms close to SO<sub>3</sub><sup>-</sup> groups to maximize electrostatic interactions. These binding modes were also confirmed by molecular mechanics and X-ray studies (Fig. 7.20) [72]. In particular, in the solid state one cationic diquat guest is encapsulated inside two trimeric  $\frac{3}{4}$ -cone subunits (red and green in Fig. 7.20) of two different  $p$ -sulfonatocalix[7]arene caps



**Scheme 7.5** Synthesis of calix[8]arene-based glycoconjugate derivatives [74]

[73]. The molecular capsules are sealed electrostatically by means of interactions between anionic  $\text{SO}_3^-$  groups and  $\text{Ba}^{2+}$  cations. The *p*-sulfonatocalix[7]arene adopts a distorted double-cone pinched conformation.

**Calix[8]arenes** Thanks to their high degree of preorganization,  $D_{2d}$ -symmetrical 1,5:3,7-calix[8]bis-crown-3 derivatives **13d,e** were able to complex  $\text{Na}^+$ ,  $\text{K}^+$ ,  $\text{Rb}^+$ ,  $\text{Cs}^+$ , and  $\text{NH}_4^+$  cations with a size dependent selectivity [73]. In fact, these compounds adopt a  $D_{2d}$  structure composed by four  $3/4$ -cone clefts with the oxygen atoms converging toward the central polyhedral cavity and able to fit spherical cationic guests (see, also the X-ray structure of the  $\text{Cs}^+ \subset \mathbf{11a}$  complex in Fig. 7.28) [73]. On this basis, more recently, the 1,5:3,7-doubly-bridged calix[8]arenes **14a–h** bearing mixed spanning elements (Scheme 7.1) were also studied for alkali cation recognition [42].

Calix[8]arene-based glycoconjugate derivatives **38–43** (Scheme 7.5) were obtained by glycosylation of octamino-calix[8]arene **25e** using isothiocyanate glycosyl donors [74]. 1D NMR experiments showed that octagalactosyl-**40b** and octacellobiosyl-calix[8]arene **42b** are able to complex ionic guests, such as

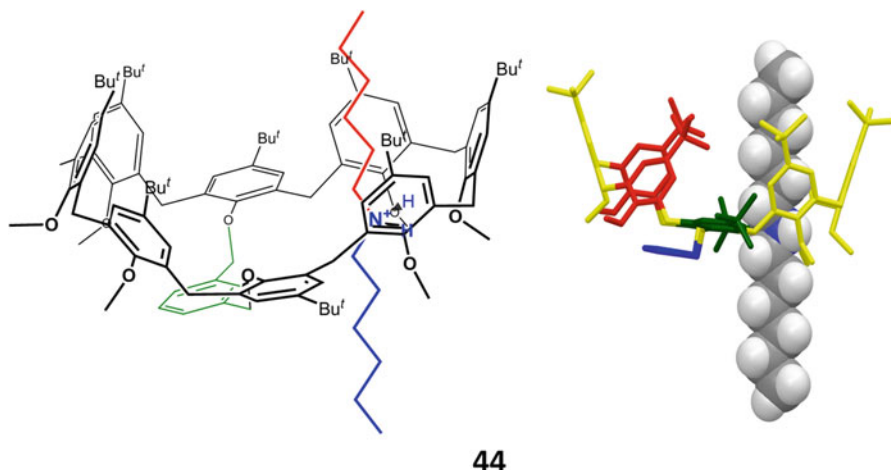


**Fig. 7.21** Drawing representation (*left*) and DFT-energy-minimized structure (*right*) of pseudo[2]rotaxane **44** [4c]

histidine hydrochloride, D-glucosamine hydrochloride, pyromellitic acid tetrasodium salt, and adenosine-5'-triphosphate disodium salt [74].

Calix[8]arene-based pseudorotaxane architectures (e.g. **44**) have been recently obtained [4c] by *through-the-annulus* threading with dialkylammonium axle of 1,5-bridged calix[8]arene **26a**. It was shown that the threading is only effective when the cationic axle is coupled with the weakly coordinating Tetrakis[3,5-bis(triFluoromethyl)Phenyl]Borate (TFPB<sup>-</sup>) “superweak anion” [75] which gives free “naked” cations in solution (see Chap. 30). 1D and 2D NMR experiments in accordance with DFT calculations indicated that the threading process was driven by the formation of stabilizing H-bonds between the R<sub>2</sub>NH<sub>2</sub><sup>+</sup> protons of the axle and the ethereal O-atoms of calix[8]-wheel (Fig. 7.21) [4c].

Water soluble *p*-sulfonatocalix[8]arene **25k** has shown interesting complexation abilities toward inhibitors of cholinesterases (ChEs) **45a–c** (Fig. 7.22) [4]. The recognition process occurs through an interesting induced fit mechanism driven by electrostatic interactions.

*p*-Sulfonatocalix[8]arene **25k** was also able to detect by fluorometric analysis the neurotransmitter acetylcholine (ACh) in water [76]. In particular, the fluorescent ACh analogue dansylcholine (DANCh) forms a 1:1 DANCh<sup>+</sup>⊂**25k** complex with *p*-sulfonatocalix[8]arene. Recently, *p*-sulfonatocalix[8]arene was immobilized in a gold-electrode, which showed good reproducibility and high selectivity toward tryptophane [77].

In 1994, Atwood [78] and Shinkai [79] independently reported that *p*-*tert*-butylcalix[8]arene **C[8]** was able to include selectively fullerene C<sub>60</sub> from carbon soot and to form a precipitate with a 1:1 stoichiometry. This precipitation constituted an useful method to obtain pure C<sub>60</sub> in large quantity (see Chap. 33).



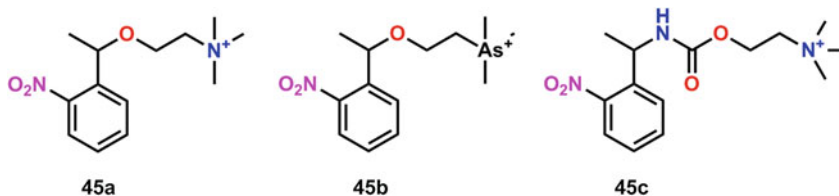


Fig. 7.22 Structure of inhibitors of cholinesterases (ChEs) **45a–c** [4]

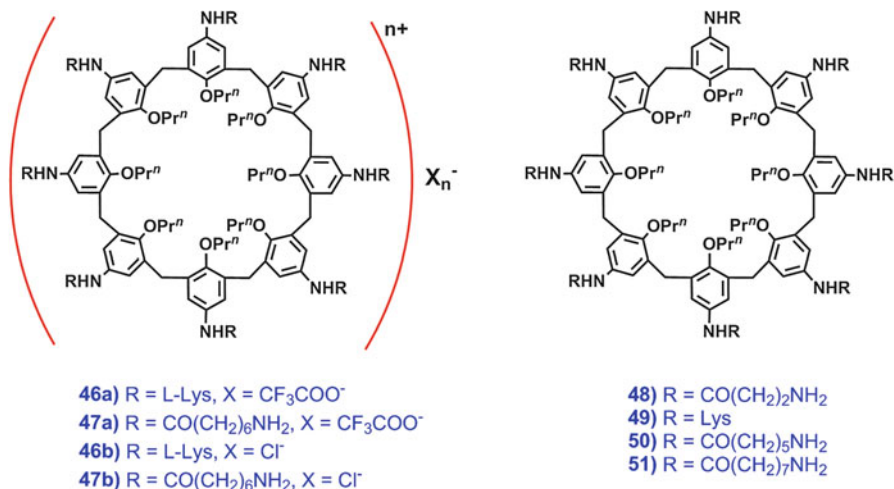


Fig. 7.23 Polycationic calix[8]arene derivatives

Recently [78b], the solid-state structure of the C<sub>60</sub>/p-Bu<sup>+</sup>-calix[8]arene complex has been studied through characterization techniques such as: SEM, TEM, AFM, XRD, and Raman spectroscopy. Interestingly, these studies evidenced the existence of a layered tetragonal array of fullerenes encapsulated by calixarenes [78b].

Very recently, Castillo and coworkers [80], have reported a Cu(I) complex of calix[8]arene-1,5-phenanthroline-bridged derivative **10j** (Fig. 7.10) which was able to act as nanoreactor for the C–S catalytic coupling.

### 7.4.1 Biomolecular Applications of Large Calixarenes

In the last decades, recognition of molecules of biological interest and more in particular of druggable target(s) by calixarenes has received a considerable attention [81]. Regarding the larger macrocycles, polycationic calix[8]arenes **46–47** (Fig. 7.23) bearing ammonium groups were able to interact with and to neutralize heparin [82]. This sulfated anionic polysaccharide is known as one of the most



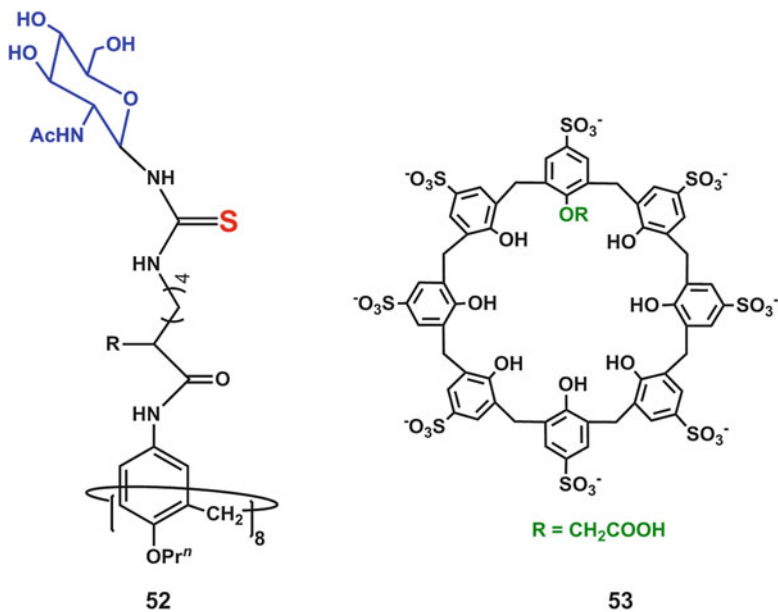


**Fig. 7.24** (Left) Calix[8]arene-based glycoconjugate derivative **52** [85] and (right) *p*-sulfonatocalix[8]arene derivative **53**

powerful anticoagulant drugs; therefore, to avoid risk of bleeding, the excess of heparin needs to be balanced and, if necessary, carefully neutralized [82].

Interestingly, calix[8]arene derivatives **48–51** bearing amino acid (Fig. 7.23) moieties at the *exo* rim were able to inhibit trypsin enzyme by surface recognition upon interaction with the negatively charged active sites of the enzyme [83].

Glycoconjugate calix[8]arene derivatives bearing terminal *N*-acetyl-D-glucosamine moieties (e.g.: **52**, Fig. 7.24) [84], showed lectin-binding abilities and amplified inhibitory effects on erythrocyte agglutination induced by wheat germ (*Triticum vulgare*) agglutinin (WGA) [84]. The inhibitory ability depends on the presence of an appropriate spacer between the carbohydrate moieties and the calixarene scaffold and on the shape and rigidity of the calixarene macrocycle.

Large negatively charged supramolecular hosts such as water-soluble *p*-sulfonatocalix[*n*]arenes have shown an increasing interest because of their biomedical potentialities as antiviral anti-thrombotic activities, enzyme blocking, and protein/amino acids complexation [85]. Very recently, Coleman showed that *p*-sulfonatocalix[8]arene is able to inhibit endonuclease [85c], an enzyme able to digest DNA and as such plays a role in human cell repair; this enzyme represents a valid target in drug design for anti-cancer, anti-viral, and antibiotic treatments.

The anti-microbial activity of a series of water-soluble *p*-sulfonatocalix[8]arene derivatives has been studied by Lamartine et al. [86]. An anti-microbial activity against corynebacterium, *fusarium solani*, *rosellinia necatrix*, and *colletotrichum dematium* was found. Finally, *p*-sulfonatocalixarenes have shown recognition

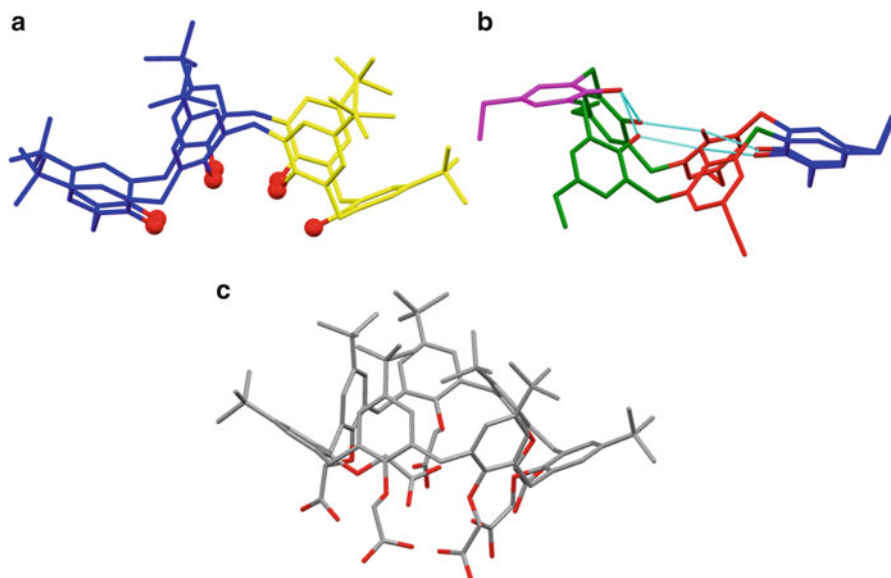


**Fig. 7.25** Most common X-ray structures found for calix[7]arene macrocycle. (a) Double-cone pinched conformation of *p*-*tert*-butylcalix[7]arene **C[7]**. (b) X-ray structure of *p*-ethylcalix[7]arene **1b**. (c) X-ray structure of heptacarboxylic acid **1f**

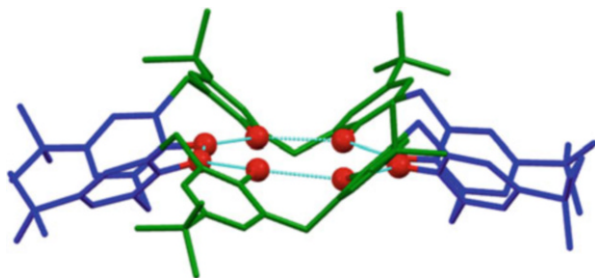
properties towards arginine and lysine [87] which are the major constituents of the heparin recognition peptide sequences. Therefore, their antithrombotic activity has been studied more deeply evidencing, in particular, that mono-substituted *p*-sulfonatocalix[8]arene **53**, bearing one carboxylic group at the *endo* rim, possesses anti-coagulant properties [88].

#### 7.4.2 Coordination and Solid State Supramolecular Architectures Based on Large Calixarenes

In the last decades many reports [2, 89] on the solid state structures of the larger calixarenes have shown intriguing self-assembling properties. A special attention has been also devoted to the solid state structure of their metal complexes.

Different solid state structures of *p*-*tert*-butylcalix[7]arene **C[7]** have been determined by X-ray crystallography. The most common conformation found was the so-called *double-cone-pinched* [90] one (Fig. 7.25a) in which a tetrameric cone-like (blu in Fig. 7.25a) and a trimeric  $\frac{3}{4}$ -cone-like (yellow in Fig. 7.25a) substructures were stabilized by the strong intramolecular H-bonds between OH groups. The structure reported by Perrin et al. [91] for *p*-ethylcalix[7]arene **1b** (Fig. 7.25b) is characterized by a more flattened  $\frac{3}{4}$ -cone-like trimeric subunit and by a tetrameric subunit with the two central phenolic rings inverted with respect to

**Fig. 7.26** X-ray structure of *p*-*tert*-butylcalix[8]arene in the *pleated-loop* conformation



the others. In the solid state structure of heptacarboxylic acid **1f** [23], all calixarene oxygens are on the same side of the molecule with the two distal aryls of tetrameric portion “outward” oriented, while the distal rings of the trimeric subunit are “inward” inclined. A recent solid state structure of 1,4:2,3-double-bridged calix[7]arene **8i** evidenced a cone-shaped conformation (Fig. 7.25c) very similar to that adopted by **1f** [6b].

The most common conformations found for *p*-*tert*-butylcalix[8]arene are the *pleated-loop* [92] (Fig. 7.26) and the *chair-like* (for an example of *chair-like* conformation, see Fig. 7.18) [93]. In particular, some reports [65] showed that the *chair-like* solid state conformation is preferred when the intramolecular hydrogen bonding at the lower rim is absent.

The *pleated loop* conformation was also found in the solid state structures of a monopotassium salt of **C[8]** reported by Fromm [94a] and obtained by its treatment with  $K_2CO_3$  in a two-phase  $H_2O/THF$  system. The macrocycles are supramolecularly stacked one over the other to give a one-dimensional system with an inner “coaxial” channel (Fig. 7.27). A 10-molecule water cluster with a distorted cubane core is sandwiched between two consecutive calixarenes [94a].

The solid state structure of a  $Cs^+ \cdot C[8]$  complex evidenced a folded ‘tub-shaped’ calix[8]arene conformation composed by four 3/4-cone clefts (Fig. 7.28) [43]. The  $Cs^+$  cation was ‘electrostatically’ coordinated by the eight calix[8]arene oxygens [43]. A similar solid state structure was reported for a dicesium complex of 1,5-bridged derivative **10i** [36].

Zhang and coworkers [95] reported an intriguing solid state architecture in which two calix[8]arene macrocycles in a *double-cone* conformation were coordinated to a  $[Ce^{IV}_6]$  octahedron while ligated DMF molecules were inside the cavities (Fig. 7.29) [95].

Among the solid state structures of the larger calix[*n*]arenes, Raston [96] and coworkers reported the first inclusion complex of *p*-*tert*-butylcalix[9]arene **C[9]** with *o*-carborane (Fig. 7.30). In this structure, the calix[9]arene macrocycle adopts a conformation composed by three 3/4-cone clefts and a *pleated-loop* portion. Perrin et al. [97] showed that *p*-*tert*-butylcalix[10]arene **C[10]** adopts in the solid state a *pinched cone* conformation stabilized by a circular H-bond between OH groups and very similar to that found for calix[6]arene macrocycle [98].

**Fig. 7.27** Channel structure of the monopotassium salt of **C**[**8**] [94a]

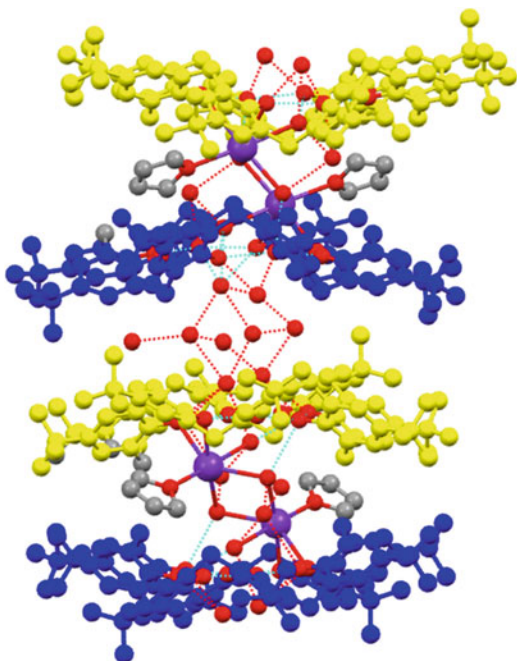


**Fig. 7.28** X-ray structure of  $\text{Cs}^+\text{C}10\text{a}$  complex [43]

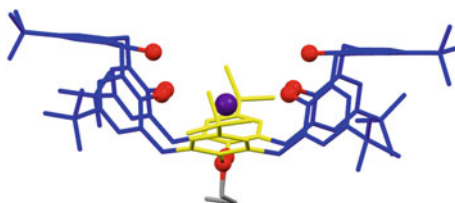


**Fig. 7.29** Double-cone conformation adopted by **C**[**8**] in its solid state complex with  $\text{Ce(IV)}$  [95]

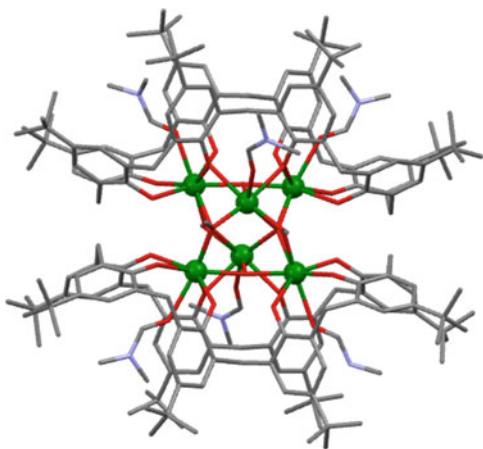


**Fig. 7.30** X-ray structure of *p*-*tert*-butylcalix[9]arene

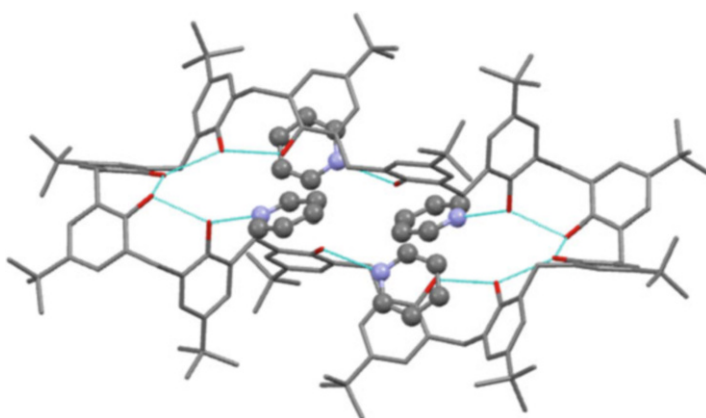
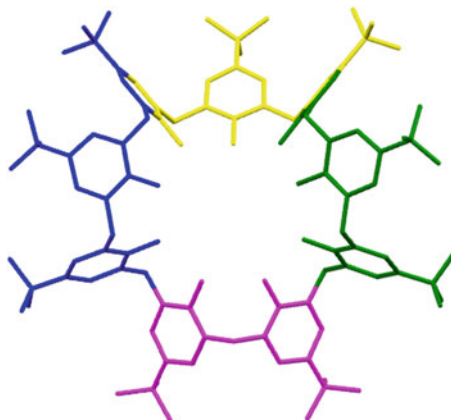


**Fig. 7.31** X-ray structure of *p*-*tert*-butylcalix[12]arene **C[12]**

In the solid state, *p*-*tert*-butylcalix[12]arene **C[12]**, crystallized from pyridine–acetonitrile, gives an all-in conformation which is reminiscent of the *chair-like* conformation of **C[8]** [97]. The typical circular H-bond array between OH groups is here interrupted by H-bonding interactions with four pyridine solvent molecules (Fig. 7.31).

An intriguing solid state structure of *p*-*tert*-butylcalix[16]arene **C[16]** has been reported by Perrin and coworkers [99]. The conformation adopted by calix[16]arene macrocycle can be described as two superimposed celtic torcs with a large pleated-loop geometry. Each torc is connected to the other one by a pseudo-calix[4]arene cone moiety. This conformation confirms the Gutsche’s postulate [7a] stating that ‘calixarenes incorporate as many cone-like and/or pleated-loop-like conformational segments as possible’ because they are “the best conformation stabilizing structures in the calixarene family”.

## 7.5 Conclusions

The chemistry of the larger calix[*n*]arenes is certainly less explored than that of the smaller homologues and has not yet reached a comparable level of sophistication. This can be partly ascribed to the lack of efficient large-scale syntheses for the basic macrocycles; however, the main reason is likely linked to their intricate chemistry and to their high conformational mobility, which imply many possible regioisomers with floppy three-dimensional shapes. On the other hand, they are somewhat attractive for the synthesis of hosts for medium-sized organic molecules or metal clusters. In addition, di- or polytopic receptors can be also derived which may present cooperativity or allostery typical of biological systems. Clearly, such targets can only be reached by gaining an appropriate control of the above features to give suitably functionalized and preorganized host molecules. The feasibility of this approach is demonstrated by the work here reviewed, which describes very interesting examples obtained by exploiting the current chemical knowledge for each member of this family. Differently from other more mature areas of calixarene chemistry, much work is here still necessary to further advance the supramolecular and practical applications in this field.

## References

1. For comprehensive reviews on calixarene macrocycles, see: (a) Gutsche, C. D. *Calixarenes, An Introduction*; Royal Society of Chemistry: Cambridge, UK, 2008. (b) Böhmer, V. *Angew. Chem., Int. Ed. Engl.* **1995**, *34*, 713–745. (c) Gutsche, C. D. *Calixarenes Revisited*; Royal Society of Chemistry: Cambridge, 1998. (d) *Calixarenes 2001*; Asfari, Z.; Böhmer, V.; Harrowfield, J.; Vicens J.; Eds.; Kluwer: Dordrecht, 2001. (e) Böhmer, V. In *The Chemistry of Phenols*; Rappoport, Z., Ed.; Wiley: Chichester, UK, 2003; Chapter 19. (f) *Calixarenes in the Nanoworld*; Vicens J.; Harrowfield, J.; Eds.; Springer, Dordrecht, 2007.
2. For reviews on the chemistry of large calixarenes, see: (a) ref. 1d; Neri, P.; Consoli, G. M. L.; Cunsolo, F.; Geraci, C.; Piattelli, M.; Chapter 5, p. 89–109. (b) Martino, M.; Neri, P. *Mini-Rev. Org. Chem.* **2004**, *1*, 219–231.
3. Munch, J. H.; Gutsche, C. D. *Org. Synth.* **1990**, *68*, 243–246.
4. (a) Specht, A.; Bernard, P.; Goeldner, M.; Peng, L. *Angew. Chem. Int. Ed.* **2002**, *41*, 4706–4708. (b) Martínez-Alanis, P. R.; Castillo, I. *Tetrahedron Lett.* **2005**, *46*, 8845–8848. (c) Gaeta, C.; Talotta, C.; Margarucci, L.; Casapullo, A.; Neri, P. *J. Org. Chem.* **2013**, *78*, 7627–7638.
5. (a) Bergougnant, R. D.; Robin, A. Y.; Fromm, K. M. *Tetrahedron* **2007**, *63*, 10751–10757. (b) Redshaw, C. *Coord. Chem. Rev.* **2003**, *244*, 45–70.
6. (a) Consoli, G. M. L.; Cunsolo, F.; Geraci, C.; Gavuzzo, E.; Neri, P. *Org. Lett.* **2002**, *4*, 2649–2652. (b) Gaeta, C.; Talotta, C.; Farina, F.; Camalli, M.; Campi, G.; Neri, P. *Chem. Eur. J.* **2012**, *18*, 1219–1230.
7. (a) For the synthesis of *p*-*tert*-butylcalix[7]arene by a one-pot procedure, see: Stewart, D. R.; Gutsche, C. D. *J. Am. Chem. Soc.* **1999**, *121*, 4136–4146. (b) For the synthesis of *p*-*tert*-butylcalix[8]arene by a one-pot procedure, see reference 3.
8. (a) Kämmerer, H.; Happel, G. *Makromol. Chem.* **1980**, *181*, 2049–2062. (b) Hayes, B. T.; Hunter, R. F. *J. Appl. Chem.* **1958**, *8*, 743–748. (c) Zetta, L.; Wolff, A.; Vogt, W.; Platt, K. L.;

- Böhmer, V. *Tetrahedron* **1991**, *47*, 1911–1924. (d) Tabatabai, M.; Vogt, W.; Böhmer, V. *Tetrahedron Lett.* **1990**, *31*, 3295–3298.
9. Asfari, Z.; Vicens, J. *Makromol. Chem.- Rapid* **1989**, *10*, 181–183.
  10. (a) Casnati, A.; Ferdani, R.; Pochini, A.; Ungaro, R. *J. Org. Chem.* **1997**, *62*, 6236–6239. (b) Atwood, J. L.; Hardie, M. J.; Raston, C. L.; Sandoval, C. A. *Org. Lett.* **1999**, *1*, 1523–1526.
  11. (a) Gutsche, C. D.; Pagoria P. F. *J. Org. Chem.* **1985**, *50*, 5795–5802. (b) Baudry, R.; Felix, C.; Bavoux, C.; Perrin, M.; Vocanson, F.; Dumazet-Bonnamour, I.; Lamartine, R. *New J. Chem.*, **2003**, *27*, 1540–1543.
  12. Izatt, S. R.; Hawkins, R. T.; Christensen, J. J.; Izatt, R. M. *J. Am. Chem. Soc.* **1985**, *107*, 63–66.
  13. Recently the procedure for the synthesis of **2c** has been revised by: Huc, V.; Npetgat, E.; Guérineau, V.; Bourcier, S.; Dos Santos, A.; Guillot, R.; Baltaze, J.-P.; Martini, C. *Eur. J. Org. Chem.* **2010**, 6186–6192.
  14. Lubitov, I. E.; Shokova, E. A.; Kovalev, V. V. *Synlett* **1993**, 647–648.
  15. Falana, O. O.; Keehn, F. M.; Stevenson, R. *Tetrahedron Lett.* **2015**, 3240–3242.
  16. Ferchichi, M.; Jeanneau, E.; Sollier, J.-C.; Meganem, F.; Darbost, U.; Bonnamour, I. *Chem* **2011**, *1*, 27–35.
  17. Dumazet, I.; Regnouf De-Vains, J.-B.; Lamartine, R. *Synthetic Commun.* **1997**, *27*, 2547–2555.
  18. Huc, V. G.; Martini, C. PCT Int. Appl. **2014**, WO2014033406A120140306.
  19. (a) Columbus, I.; Biali, S. E. *Org. Lett.* **2007**, *9*, 2927–2929. (b) Gaeta, C.; Troisi, F.; Martino, M.; Gavuzzo, E.; Neri, P. *Org. Lett.* **2004**, *6*, 3027–3030. (c) Troisi, F.; Mogavero, L.; Gaeta, C.; Gavuzzo, E.; Neri, P. *Org. Lett.* **2007**, *9*, 915–918. (d) Troisi, F.; Citro, L.; Gaeta, C.; Gavuzzo, E.; Neri, P. *Org. Lett.* **2008**, *10*, 1393–1396. (e) Gaeta, C.; Troisi, F.; Gavuzzo, E.; Camalli, M.; Campi, G.; Neri, P. *CrystEngComm* **2010**, *12*, 880–887. (f) Gaeta, C.; Troisi, F.; Spagna, R.; Camalli, M.; Campi, G.; Neri, P. *CrystEngComm* **2011**, *13*, 467–473.
  20. Shu, C.-M.; Liu, W.-C.; Ku, M.-C.; Tan, F.-S.; Yeh, M.-L.; Lin, L.-G. *J. Org. Chem.* **1994**, *59*, 3730–3733. No, K.; Koo, H. J. *Bull. Korean Chem. Soc.* **1994**, *15*, 483–488. Stewart, D. R.; Krawiec, M.; Kashyap, R. P.; Watson, W. H.; Gutsche, C. D. *J. Am. Chem. Soc.* **1995**, *117*, 586–601. Rogers, J. S.; Gutsche, C. D. *J. Org. Chem.* **1992**, *57*, 3152–3159. Gutsche, C. D.; Dhawan, B.; No, K. H.; Muthukrishnan, R. *J. Am. Chem. Soc.* **1981**, *103*, 3782–3792.
  21. Martino, M.; Gregoli, L.; Gaeta, C.; Neri, P. *Org. Lett.* **2002**, *4*, 1531–1534.
  22. Jin, T.; Kinjo, M.; Kobayashi, Y.; Hirata, H. *J. Chem. Soc., Faraday Trans.* **1998**, *94*, 3135–3140.
  23. Ludwing, R.; Lentz, D.; Nguyen, T. K. D. *Radiochim. Acta* **2000**, *88*, 335–343.
  24. Neri, P.; Battoccolo, E.; Cunsolo, F.; Geraci, C.; Piattelli, M. *J. Org. Chem.* **1994**, *59*, 3880–3889.
  25. Cunsolo, F.; Consoli, G. M. L.; Piattelli, M.; Neri, P. *J. Org. Chem.* **1998**, *63*, 6852–6858.
  26. Ferchichi, M.; Jeanneau, E.; Fenet, B.; Meganem, F.; Darbost, U.; Bonnamour, I. *Tetrahedron Lett.* **2012**, *53*, 4047–4050.
  27. (a) Neri, P.; Geraci, C.; Piattelli, M. *Tetrahedron Lett.* **1993**, *34*, 3319–3322. (b) Neri, P.; Geraci, C.; Piattelli, M. *J. Org. Chem.* **1995**, *60*, 4126–4135. (c) Consoli, G. M. L.; Cunsolo, F.; Piattelli, M.; Neri, P. *J. Org. Chem.* **1996**, *61*, 2195–2198.
  28. Cram, D. J. *Angew. Chem. Int. Ed. Engl.* **1988**, *27*, 1009–1020.
  29. Cunsolo, F.; Piattelli, M.; Neri, P. *J. Chem. Soc., Chem. Commun.* **1994**, 1917–1918.
  30. For examples of singly bridged calix[7]arene derivatives, see: (a) Martino, M.; Gaeta, C.; Gregoli, L.; Neri, P. *Tetrahedron Lett.* **2002**, *43*, 9521–9525. (b) Luo, Z.; Gong, S.; Zhang, C.; Zheng, Q.; Chen, Y. *Synlett* **2006**, *5*, 795–797.
  31. Martino, M.; Gaeta, C.; Neri, P. *Tetrahedron Lett.* **2004**, *45*, 3387–3391.
  32. Li, H.; Xiong, D.; Chen, Y.; Xie, P.; Wan, J. J. *Incl. Phenom. Macrocycl. Chem.* **2008**, *60*, 169–172.
  33. Geraci, C.; Piattelli, M.; Chessari, G.; Neri, P. *J. Org. Chem.* **2000**, *65*, 5143–5151.
  34. Gaeta, C.; Gregoli, L.; Martino, M.; Neri, P. *Tetrahedron Lett.* **2002**, *43*, 8875–8878.

35. (a) Neri, P.; Geraci, C.; Piattelli, M. In: *Recent Research Developments in Organic Chemistry*; Pandalai, S. G. Ed.; Transworld Research Network, Trivandrum 1997; Vol. 1, p. 285. (b) Geraci, C.; Consoli, G. M. L.; Piattelli, M.; Neri, P. *Collect. Czech. Chem. Commun.* **2004**, *69*, 1345–1361. (c) Geraci, C.; Piattelli, M.; Neri, P. *Tetrahedron Lett.* **1996**, *37*, 3899–3902.
36. Hernández, D. J.; Castillo, I. *Tetrahedron Lett.* **2009**, *50*, 2548–2551.
37. Hernández, D. J.; Vázquez-Lima, H.; Guadarrama, P.; Martínez-Otero, D.; Castillo, I. *Tetrahedron Lett.* **2013**, *54*, 4930–4933.
38. Geraci, C.; Piattelli, M.; Neri, P. *Tetrahedron Lett.* **1995**, *36*, 5429–5432.
39. Cunsolo, F.; Consoli, G. M. L.; Piattelli, M.; Neri, P. *Tetrahedron Lett.* **1996**, *37*, 715–718.
40. Ikeda, A.; Akao, K.; Harada, T.; Shinkai, S. *Tetrahedron Lett.* **1996**, *37*, 1621–1624.
41. Geraci, C.; Bottino, A.; Piattelli, M.; Gavuzzo, E.; Neri, P. *J. Chem. Soc., Perkin Trans. 2* **2000**, 185–187.
42. Gregoli, L.; Russo, L.; Stefio, I.; Gaeta, C.; Arnaud-Neu, F.; Hubscher-Bruder, V.; Khazaeli-Parsa, P.; Geraci, C.; Neri, P. *Tetrahedron Lett.* **2004**, *45*, 6277–6281.
43. (a) Consoli, G. M. L.; Cunsolo, F.; Geraci, C.; Neri, P. *Org. Lett.* **2001**, *3*, 1605–1608. (b) Consoli, G. M. L.; Cunsolo, F.; Geraci, C.; Gavuzzo, E.; Neri, P. *Tetrahedron Lett.* **2002**, *43*, 1209–1211.
44. Troisi, F.; Gaeta, C.; Neri, P. *Tetrahedron Lett.* **2005**, *46*, 8041–8045.
45. Gloede, J.; Ozegowski, S.; Matt, D.; De Cian, A. *Tetrahedron Lett.* **2001**, *42*, 9139–9142.
46. Gloede, J.; Ozegowski, S.; Costisella, B.; Gutsche, C. D. *Eur. J. Org. Chem.* **2003**, 4870–4873.
47. Li, H.; Zhan, J. *J. Incl. Phenom. Macrocycl. Chem.* **2008**, *60*, 379–382.
48. Gutsche, C. D. *Acc. Chem. Res.* **1983**, *16*, 161–170.
49. Verboom, W.; Durie, A.; Egberink, R. J. M.; Asfari, Z.; Reinhoudt, D. N. J. *Org. Chem.* **1992**, *57*, 1313–1316.
50. Gutsche, C. D.; Pagoria, P. F. *J. Org. Chem.* **1985**, *50*, 5795–5802.
51. Gutsche, C. D.; Lin, L.-G. *Tetrahedron* **1986**, *42*, 1633–1640.
52. Shinkai, S.; Koreishi, H.; Ueda, K.; Arimura, T.; Manabe, O. *J. Am. Chem. Soc.* **1987**, *109*, 6371–6375.
53. (a) Cornforth, J. W.; Morgan, E. D.; Potts, K. T.; Rees, R. J. W. *Tetrahedron* **1973**, *29*, 1659–1667. (b) Yao, B.; Bassus, J.; Lamartine, R. *An. Quim. Int. Ed.* **1998**, *94*, 65–66.
54. Gutsche, C. D.; Alam, I. *Tetrahedron* **1988**, *44*, 4689–4694.
55. Gutsche, C. D.; Nam, K. C. *J. Am. Chem. Soc.* **1988**, *110*, 6153–6162.
56. Bouoit, S.; Bassus, J.; Lamartine, R. *An. Quim. Int. Ed.* **1998**, *94*, 342–344.
57. Dozol, J. F.; Ungaro, R.; Casnati, A. PCT Int. Appl. WO 0112586, 2001 [Chem. Abstr. 2001, 134, 193226].
58. Gaeta, C.; Caruso, T.; Mincoletti, M.; Troisi, F.; Vasca, E.; Neri, P. *Tetrahedron* **2008**, *64*, 5370–5378.
59. (a) Podoprygorina, G.; Zhang, J.; Brusko, V.; Bolte, M.; Janshoff, A.; Böhmer, V. *Org. Lett.* **2003**, *5*, 5071–5074. (b) Consoli, G. M. L.; Cunsolo, F.; Geraci, C.; Mecca, T.; Neri, P. *Tetrahedron Lett.* **2003**, *44*, 7467–7470.
60. Leverd, P. C.; Huc, V.; Palacin, S.; Nierlich, M. *J. Incl. Phenom. Macrocycl. Chem.* **2000**, *36*, 259–266.
61. Makha, M.; Raston, C. L. *Tetrahedron Lett.* **2001**, *42*, 6215–6217.
62. Aoki, M.; Nakashima, K.; Kawabata, H.; Tsutsui, S.; Shinkai, S. *J. Chem. Soc., Perkin Trans. 2* **1993**, 347–354.
63. (a) Jebors, S.; Ananchenko, G. S.; Coleman, A. W.; Ripmeester, J. A. *Tetrahedron Lett.* **2007**, *48*, 5503–5506. (b) Jebors, S.; Fache, F.; Balme, S.; Devoige, F.; Monachino, M.; Cecillon, S.; Coleman, A. W. *Org. Biomol. Chem.* **2008**, *6*, 319–329.
64. Ferro, R.; Tedesco, C.; Gaeta, C.; Neri, P. *J. Incl. Phenom. Macrocycl. Chem.* **2008**, *60*, 115–122.
65. Gaeta, C.; Martino, M.; Neri, P. *Tetrahedron Lett.* **2003**, *44*, 9155–9159.



66. (a) Troisi, F.; Pierro, T.; Gaeta, C.; Neri, P. *Org. Lett.* **2009**, *11*, 697–700. (b) Troisi, F.; Pierro, T.; Carratù, M.; Gaeta, C.; Neri, P. *Tetrahedron Lett.* **2009**, *50*, 4416–4419. (c) Talotta, C.; Gaeta, C.; Troisi, F.; Monaco, G.; Zanasi, R.; Mazzeo, G.; Rosini, C.; Neri, P. *Org. Lett.* **2010**, *12*, 2912–2915. (d) Chena, S.; Webster, R. D.; Talotta, C.; Troisi, F.; Gaeta, C.; Neri, P. *Electrochim. Acta* **2010**, *55*, 7036–7043. (e) Gaeta, C.; Troisi, F.; Talotta, C.; Pierro, T.; Neri, P. *J. Org. Chem.* **2012**, *77*, 3634–3639. (f) De Rosa, M.; Soriente, A.; Concilio, G.; Talotta, C.; Gaeta, C.; Neri, P. *J. Org. Chem.* **2015**, *80*, 7295–7300. (g) For an exhaustive review on the *p*-bromodienone route, see: Gaeta, C.; Talotta, C.; Neri, P. *J. Incl. Phenom. Macrocycl. Chem.* **2014**, *79*, 23–46.
67. (a) Kuno, L.; Seri, N.; Biali, S. E. *Org. Lett.* **2007**, *9*, 1577–1580. (b) Columbus, I.; Biali, S. E. *J. Org. Chem.* **2008**, *73*, 2598–2606. (c) Kogan, K.; Columbus, I.; Biali, S. E. *J. Org. Chem.* **2008**, *73*, 7327–7335. (d) Kuno, L.; Biali, S. E. *J. Org. Chem.* **2011**, *76*, 3664–3675.
68. (a) Kogan, K.; Biali, S. E. *J. Org. Chem.* **2011**, *76*, 7240–7244. (b) Itzhak, N.; Kogan, K.; Biali, S. E. *Eur. J. Org. Chem.* **2011**, 6581–6585.
69. Jin, T.; Kinjo, M.; Kobayashi, Y.; Hirata, H. *J. Chem. Soc., Faraday Trans.* **1998**, *94*, 3135–3140.
70. Torrent-Burgues, J.; Vocanson, F.; Perez-Gonzalez, J. J.; Errachid, A. *Colloids and Surfaces A: Physicochem. Eng. Aspects* **2012**, *401*, 137–147.
71. Gaeta, C.; Martino, M.; Neri, P. *Org. Lett.* **2006**, *8*, 4409–4412.
72. Erra, L.; Tedesco, C.; Vaughan, G.; Brunelli, M.; Troisi, F.; Gaeta, C.; Neri, P. *CrystEngComm* **2010**, *12*, 3463–3466.
73. Geraci, C.; Chessari, G.; Piattelli, M.; Neri, P. *Chem. Commun.* **1997**, 921–922.
74. Consoli, G. M. L.; Cunsolo, F.; Geraci, C.; Mecca, T.; Neri, P. *Tetrahedron Lett.* **2003**, *44*, 7467–7470.
75. (a) Gaeta, C.; Troisi, F.; Neri, P. *Org. Lett.* **2010**, *12*, 2092–2095. (b) Pierro, T.; Gaeta, C.; Talotta, C.; Casapullo, A.; Neri, P. *Org. Lett.* **2011**, *13*, 2650–2653. (c) Talotta, C.; Gaeta, C.; Pierro, T.; Neri, P. *Org. Lett.* **2011**, *13*, 2098–2101. (d) Talotta, C.; Gaeta, C.; Neri, P. *Org. Lett.* **2012**, *14*, 3104–3107. (e) Gaeta, C.; Talotta, C.; Mirra, S.; Margarucci, L.; Casapullo, A.; Neri, P. *Org. Lett.* **2013**, *15*, 116–119. (f) Talotta, C.; Gaeta, C.; Qi, Z.; Schalley, C. A.; Neri, P. *Angew. Chem. Int. Ed.* **2013**, *52*, 7437–7441. (g) Ciao, R.; Talotta, C.; Gaeta, C.; Margarucci, L.; Casapullo, A.; Neri, P. *Org. Lett.* **2013**, *15*, 5694–5697. (h) Ciao, R.; Talotta, C.; Gaeta, Neri, P. *Supramol. Chem.* **2014**, *26*, 569–578. (i) Gaeta, C.; Talotta, C.; Neri, P. *Chem. Commun.* **2014**, *50*, 9917–9920. (j) Gaeta, C.; Talotta, C.; Farina, F.; Teixeira, F. A.; Marcos, P. A.; Ascenso, J. R.; Neri, P. *J. Org. Chem.* **2012**, *77*, 10285–10293.
76. Jin, T. *J. Incl. Phenom. Macrocyclic Chem.* **2003**, *45*, 195–201.
77. Pang, T.-T.; Cai, Z.-F.; Liu, H.-L.; Du, L.-M.; Guo, M.-G.; Fu, Y.-L. *Anal. Lett.* **2014**, *47*, 1808–1820.
78. (a) Atwood, J. L.; Koutsantonis, G. A.; Raston, C. L. *Nature* **1994**, *368*, 229–231. (b) Chen, X.; Boulos, R. A.; Slattery, A. D.; Atwood, J. L.; Raston, C. L. *Chem. Commun.* **2015**, *51*, 11413–11416.
79. Suzuki, T.; Nakashima, K.; Shinkai, S. *Chem. Lett.* **1994**, 699–702.
80. Guzmán-Percástegui; Hernández, D. J.; Castillo, I. *Chem. Commun.* **2016**, *52*, 3111–3114.
81. (a) Peczu, M. W.; Hamilton, A. D. *Chem. Rev.* **2000**, *100*, 2479–2493. (b) Baldini, L.; Casnati, A.; Sansone, F.; Ungaro, R. *Chem. Soc. Rev.* **2007**, *36*, 254–266. (c) Casnati, A.; Sansone, F.; Ungaro, R. *Acc. Chem. Res.* **2003**, *36*, 246–254. (d) Chini, M. G.; Terracciano, S.; Riccio, R.; Bifulco, G.; Ciao, R.; Gaeta, C.; Troisi, F.; Neri, P. *Org. Lett.* **2010**, *12*, 5382–5385. (e) Francese, S.; Cozzolino, A.; Caputo, I.; Esposito, C.; Martino, M.; Gaeta, C.; Troisi, F.; Neri, P. *Tetrahedron Lett.* **2005**, *46*, 1611–1615.
82. (a) Mecca, T.; Consoli, G. M. L.; Geraci, C.; La Spina, R.; Cunsolo, F. *Org. Biomol. Chem.* **2006**, *4*, 3763–3768. (b) Consoli, G. M. L.; Cunsolo, F.; Geraci, C.; Mecca T. U.S. Patent 7,465,820, **2008**.
83. Mecca, T.; Consoli, G. M. L.; Geraci, C.; Cunsolo, F. *Bioorg. Med. Chem.* **2004**, *12*, 5057–5062.

84. Consoli, G. M. L.; Cunsolo, F.; Geraci, C.; Sgarlata, V. *Org. Lett.* **2004**, *6*, 4163–4166.
85. For exhaustive reviews, see: (a) Perret, F.; Lazar, A. N.; Coleman, A. W. *Chem. Commun.* **2006**, 2425–2438. (b) Guo, D.-S.; Liu, Y. *Acc. Chem. Res.* **2014**, *47*, 1925–1934. (c) For a recent report, see: Tauran, Y.; Anjard, C.; Kim, B.; Rhimi, M.; Coleman, A. W. *Chem. Commun.* **2014**, *50*, 11404–11406.
86. Lamartine, R.; Tsukadab, M.; Wilson, D.; Shirata, A. *C. R. Chimie* **2002**, *5*, 163–169.
87. (a) Kalchenko, O. I.; Perret, F.; Morel-Desrosiers, N.; Coleman, A. W. *J. Chem. Soc., Perkin Trans. 2* **2001**, 258–263. (b) Arena, G.; Contino, A.; Gulino, F. G.; Magri, A.; Sansone, F.; Sciotto, D.; Ungaro, R. *Tetrahedron Lett.* **1999**, *40*, 1597–1600.
88. Da Silva, E.; Ficheux, D.; Coleman, A. W. *J. Incl. Phenom. Macrocyclic Chem.* **2005**, *52*, 201–206.
89. See Ref. 1f: Gaeta, C.; Tedesco, C.; Neri, P.; Chapter 16, p. 335–354.
90. Andreetti, G. D.; Ugozzoli, F.; Nakamoto, Y.; Ishida, S.-I. *J. Incl. Phenom. Macrocyclic Chem.* **1991**, *10*, 241–253.
91. Perrin, M.; Lecocq, S.; Asfari, Z. *C. R. Acad. Sci. Ser. 2* **1990**, *310*, 515–520.
92. Gutsche, C. D.; Gutsche, A. E.; Karaulov, A. I. *J. Inclusion Phenom.* **1985**, *3*, 447–451.
93. Czugler, M.; Tisza, S.; Speier, G. *J. Inclusion Phenom. Mol. Recognit. Chem.* **1991**, *11*, 323–331.
94. (a) Bergougnant, R. D.; Robin, A. Y.; Fromm, K. M.; Katharina, M. *Cryst. Growth Des.* **2005**, *5*, 1691–1694. (b) Dalgarno, S. J.; Hardie, M. J.; Atwood, J. L.; Warren, J. E.; Raston, C. L. *New J. Chem.* **2005**, *29*, 649–652. (c) Perret, F.; Bonnard, V.; Danylyuk, O.; Suwinski, K.; Coleman, A. W. *New J. Chem.* **2006**, *30*, 987–990.
95. Liu, Y.; Liao, W.; Bi, Y.; Wang, M.; Wu, Z.; Wang, X.; Su, Z.; Zhang, H. *CrystEngComm* **2009**, *11*, 1803–1806.
96. Clark, T. E.; Makha, M.; Sobolev, A. N.; Raston, C. L. *Dalton Trans.* **2008**, 4855–4859.
97. Perrin, M.; Ehlinger, N.; Viola-Motta, L.; Lecocq, S.; Dumazet, I.; Bouoitmontesinos, S.; Lamartine, R. *J. Incl. Phenom. Macrocycl. Chem.* **2001**, *39*, 273–276.
98. Leverd, P. C.; Dumazet-Bonnamour, I.; Lamartine, R.; Nierlich, M. *Chem. Commun.* **2000**, 493–494.
99. Bavoux, C.; Baudry, R.; Dumazet-Bonnamour, I.; Lamartine, R.; Perrin, M. *J. Incl. Phenom. Macrocycl. Chem.* **2001**, *40*, 221–224.

# Chapter 8

## Resorc[4]arenes as Preorganized Synthons for Surface Recognition and Host-Guest Chemistry

Ilaria D'Acquarica, Francesca Ghirga, Cinzia Ingallina, Deborah Quaglio, Giovanni Zappia, Gloria Uccello-Barretta, Federica Balzano, and Bruno Botta

### 8.1 The Construction of the Resorc[4]arene Scaffold by Lewis Acid-Mediated Tetramerization of 2,4-Dimethoxycinnamates

The acid-catalyzed condensation between resorcinol and an aliphatic or aromatic aldehyde (Scheme 8.1) represents the classical approach to the preparation of the resorc[4]arene nucleus [1–3]. Although the reaction is carried out by heating the reagents to reflux, each aldehyde requires different optimal conditions, while unsubstituted resorcinol is the mostly used counterpart.

---

I. D'Acquarica • D. Quaglio • B. Botta (✉)  
Dipartimento di Chimica e Tecnologie del Farmaco, Sapienza Università di Roma, P.le Aldo Moro 5, 00185 Rome, Italy  
e-mail: [bruno.botta@uniroma1.it](mailto:bruno.botta@uniroma1.it)

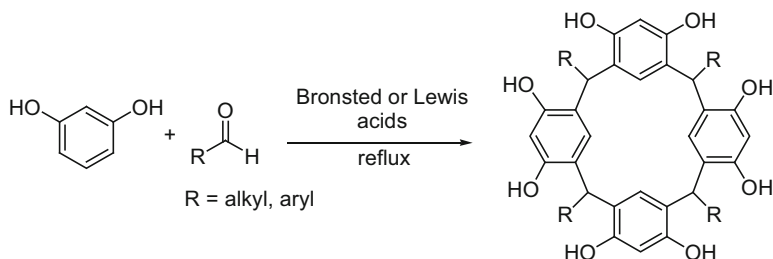
F. Ghirga  
Center for Life Nano Science@Sapienza, Istituto Italiano di Tecnologia, Viale Regina Elena 291, 00161 Rome, Italy

C. Ingallina  
Dipartimento di Chimica e Tecnologie del Farmaco, Sapienza Università di Roma, P.le Aldo Moro 5, 00185 Rome, Italy

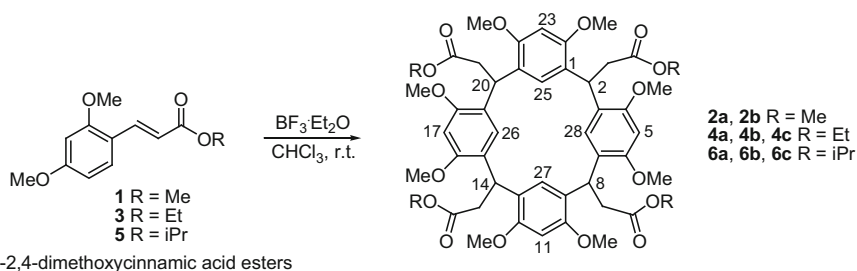
Center for Life Nano Science@Sapienza, Istituto Italiano di Tecnologia, Viale Regina Elena 291, 00161 Rome, Italy

G. Zappia  
Dipartimento di Scienze Biomolecolari, Università degli Studi di Urbino “Carlo Bo”, Via Aurelio Saffi 2, 61029 Urbino, Italy

G. Uccello-Barretta • F. Balzano  
Dipartimento di Chimica e Chimica Industriale, Università di Pisa, Via G. Moruzzi 3, 56124 Pisa, Italy



**Scheme 8.1** The acid-catalyzed condensation between resorcinol and an aliphatic or aromatic aldehyde



**Scheme 8.2** Tetramerization of (*E*)-2,4-dimethoxycinnamic acid esters

Additional discussions on the chemistry of resorc[4]arene scaffold can be found in Chaps. 9–11.

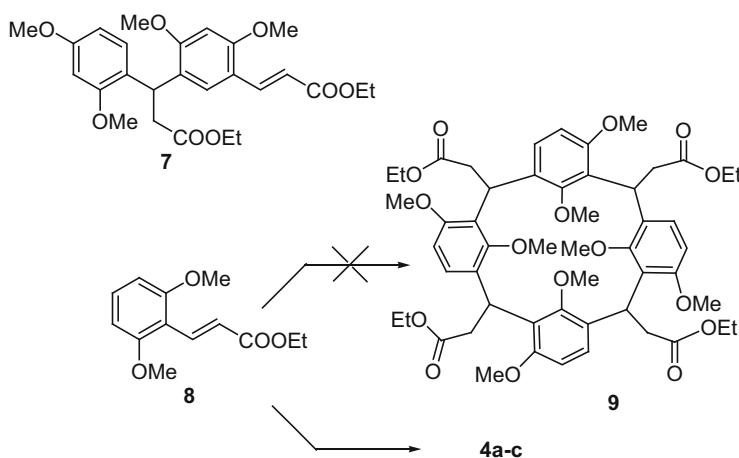
Our group became interested in the synthesis of these macrocycles, when the resorc[4]arene octamethyl ether **2** (R = Me) was produced by a tetramerization reaction (Scheme 8.2) of (*E*)-2,4-dimethoxycinnamic acid ester **1** (R = Me) under carefully controlled reaction conditions employing  $\text{BF}_3 \cdot \text{Et}_2\text{O}$  as a Lewis acid catalyst [4, 5]. Indeed, this simple reaction allows the design and preparation of several new structures, each one with new physical-chemical features that opened up new research avenues in the field of molecular recognition.

Depending on the reaction conditions and the nature of the ester side chain in the cinnamates, the resorc[4]arenes can adopt different conformational states, namely, 1,2-alternate, 1,3-alternate, or flattened-cone). In particular, when (*E*)-2,4-dimethoxycinnamic acid methyl ester **1** was reacted with  $\text{BF}_3 \cdot \text{Et}_2\text{O}$  at room temperature, only the 1,2-alternate **2a** and flattened-cone **2b** stereoisomers were obtained in a 2:3 ratio and 75% overall yield. In the 1,2-alternate conformation, the assignment of the 12- and 16-OMe signals, by INEPT experiments in conjunction with DIF NOE measurements, allowed to establish the correct stereochemistry at C(14). On the other hand, the presence in the  $^1\text{H}$ - and  $^{13}\text{C}$ -NMR spectra of only one signal for both external (H-5) and internal (H-28) aromatic protons and the related carbons, as well as a similar pattern for the methoxy group and the aliphatic

moiety, respectively, required a  $C_{4v}$  symmetry for compound **2b**. DIF NOE measurements revealed the proximity of the methine and the aromatic methoxy groups, as well as that of the  $CH_2$  and internal aromatic protons. Thus, a flattened-cone conformation was assigned to compound **2b**, with an all-*cis* arrangement of the pseudoaxial substituents.

A different pattern of reaction products was obtained with the ethyl **3** and isopropyl **5** cinnamic esters. In both cases, comparable chemical yields were obtained, but in addition to the 1,2-alternate (**4a**, **6a**, respectively) and the flattened-cone (**4b**, **6b**, respectively), a third type of stereoisomers (namely, **4c** and **6c**) emerged from the reaction mixture. An accurate analysis of  $^1H$  and  $^{13}C$  NMR spectra pointed out the existence of two symmetry planes. DIF NOE experiments revealed the proximity of the methine and the methylene groups with the aromatic protons. Therefore, on the basis of only NMR evidences, **4c** and **6c** were assigned the 1,3-alternate conformation with the pseudoequatorial side chains in an all-*cis* position. Later, thanks to the obtainment of suitable crystals for X-ray analysis, the stereoisomer **4c** was definitively reassigned the chair conformation [6].

The role of temperature and of substrate/Lewis acid ratio in the distribution of the conformations was investigated for the ethyl 2,4-dimethoxycinnamate **3**. In summary, at low temperature (namely,  $-20\text{ }^\circ\text{C}$ ) the distribution of the three stereoisomers did not change significantly; but, increasing the amount of  $BF_3 \cdot Et_2O$ , the yield of **4b** (flattened-cone stereoisomer) improved at the expense of **4a** (1,2-alternate stereoisomer), while the concentration of **4c** initially did not change. At room temperature, and with 1:0.75 and 1:1 substrate/ $BF_3 \cdot Et_2O$  ratios, compound **3** afforded, albeit in low yield, the dimeric product **7** (Scheme 8.3), while with ratios greater than 1:1.5 the reaction proceeded again to afford tetrameric products. In general, shorter reaction times were required, although the ratios of **4a** to **4b** never reached the values obtained in the previous experiments. Finally, at



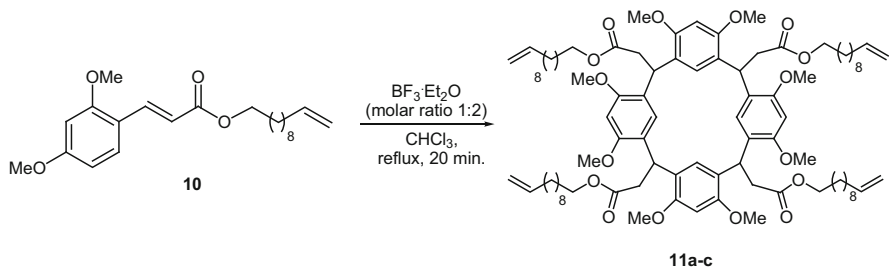
**Scheme 8.3** Dimeric and tetrameric products from **8**

reflux temperature, the same trend was observed. That is, **4b** is the major product, even with very short reaction times, for example, 8 min. According to these results, the 1,2-alternate stereoisomers **2a**, **4a**, and **6a** proved to be the first to form (kinetic products) whereas **2b**, **4b**, and **6b** develop with time (thermodynamic products). The above-reported results are substantiated by a series of reactions of the pure tetramers with  $\text{BF}_3 \cdot \text{Et}_2\text{O}$  at increasing temperatures and substrate/ $\text{BF}_3 \cdot \text{Et}_2\text{O}$  ratios. The 1,2-alternate stereoisomers **4a** and **6a** gave increasing quantities of **4b** and **6b**, respectively. For example, after 6 h at a 1:3 substrate/ $\text{BF}_3 \cdot \text{Et}_2\text{O}$  ratio, the conversion into the flattened-cone stereoisomers is complete. These experiments clearly established that the flattened-cone conformation is the more thermodynamically stable. Finally, X-ray studies and molecular modeling for compounds **6a** and **6b** confirmed the above conclusions.

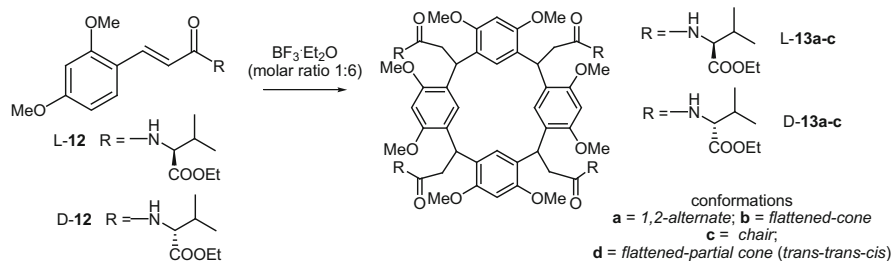
Interestingly, the three products **4a–c** were obtained, rather than the expected structure **9** (Scheme 8.3) [7], even starting from the (*E*)-2,6-dimethoxycinnamic acid ethyl ester **8** in chloroform with  $\text{BF}_3 \cdot \text{Et}_2\text{O}$  (1.5 mol) at reflux for 2 h. The three stereoisomers were obtained in an overall yield of 67 % and in a relative ratio 1:1:1. Also isolated were the (*E*)-2,4-dimethoxycinnamic acid ethyl ester **3** and the dimeric compound **7**. Experimental data and product distribution suggested an initial rearrangement of **8** to **3**, followed by tetramerization as in the case of (*E*)-2,4-dimethoxycinnamic ethyl ester.

In 2013, the tetramerization of (*E*)-2,4-dimethoxycinnamic acid  $\omega$ -undecenyl ester **10** has been reported by our group (Scheme 8.4). The reaction afforded, under usual reaction conditions, the three stereoisomers **11a**, **11b**, and **11c**, which were assigned as the 1,2-alternate, cone and chair conformations, respectively [8]. The conformation in solution of resorc[4]arenes **11a** (1,2-alternate with  $C_s$  symmetry) and **11b** (cone with  $C_{4v}$  symmetry) were assigned by the distribution pattern of the NMR spectral data, whereas the chair conformation of **11c** was confirmed by X-ray diffraction analysis, which also showed a peculiar self-assembly behavior in the crystal lattice, forming intercalated hydrophilic and hydrophobic layers (6–7 Å thickness) as a consequence of strong CH- $\pi$  interactions.

The undecenyl resorc[4]arene **11c**, which featured the simplest pattern of substituents, was afterward submitted to olefin metathesis reactions (see Sect. 8.4).



**Scheme 8.4** Tetramerization of (*E*)-2,4-dimethoxycinnamic acid  $\omega$ -undecenyl ester **10**

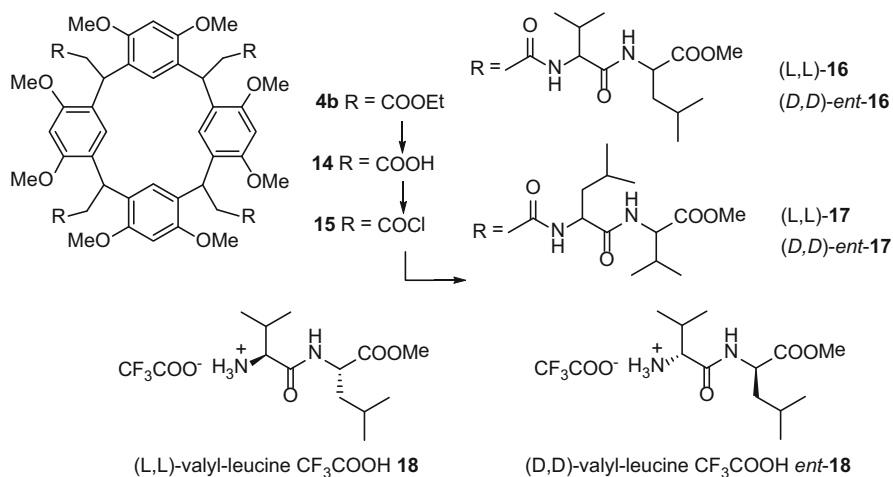


**Scheme 8.5** Amido-resorc[4]arenes **13a-c** from 2,4-dimethoxycinnamic acid amides such as **12**

Notably, not only the 2,4-dimethoxycinnamates underwent the  $\text{BF}_3 \cdot \text{Et}_2\text{O}$  mediated tetramerization reaction, and this has proved the versatility of the reaction. In fact, also 2,4-dimethoxycinnamic acid amides such as **12** (Scheme 8.5), derived from the mixed anhydride of 2,4-dimethoxycinnamic acid with l- or d-valine ethyl ester, upon treatment with  $\text{BF}_3 \cdot \text{Et}_2\text{O}$  yielded the amido-resorc[4]arenes **13a-c** which proved to be chiral for the presence of four axial pendants containing the chiral valine residue [9]. A novel flattened-partial cone conformation was isolated for the first time from the reaction mixture, together with three other stereoisomers (namely, 1,2-alternate, flattened-cone, and chair). The flattened-cone stereoisomer, which was identified by molecular modeling as the most stable, proved to form as minor product in kinetic conditions, and to become the main component of the reaction mixture under more drastic conditions (namely, substrate/ $\text{BF}_3 \cdot \text{Et}_2\text{O}$  = 1:400 M ratio). The chiral amido-resorc[4]arenes **13a-c** were obtained in enantiomerically pure forms, as checked by enantioselective HPLC.

The intrinsic enantioselectivity of the valinamido-resorc[4]arene **13b** was the starting point to investigate recognition phenomena performed by resorc[4]arenes in the gas phase towards a series of amino acids, both natural and non natural. Comprehensive ESI-FT-ICR-MS studies on the displacement of such small molecules from the chiral amido-resorc[4]arene were extensively engaged [10, 11]. The general concept is that the resorc[4]arene incorporates an amino acid in solution by forming a proton-bonded complex that persists when the solution is electrosprayed into the heated capillary of a Fourier-transform mass spectrometer; then, the complex is quenched by collisions with an inert gas pulsed into the analyzer, isolated by broad-band ejection of the accompanying ions and allowed to react with a neutral alkylamine. The amino acid is displaced by the amine in a guest exchange reaction, where the amine replaces the guest to produce a new proton-bound complex with the host. The rate constant of the guest exchange reaction is extracted based on the decay of the isolated proton-bonded diastereoisomeric complex as a function of time.

When the alkylamine is chiral too (e.g., 2-aminobutane is used as reactant), a comparison of the different rates of the guest exchange reaction can yield an authentic picture of the enantioselectivity exhibited by the resorc[4]arene hosts. Furthermore, the support of MM calculations and MD simulations may provide



**Scheme 8.6** *N*-linked peptidoresorc[4]arene **16** in both the enantiomeric forms, and its regioisomer **17**

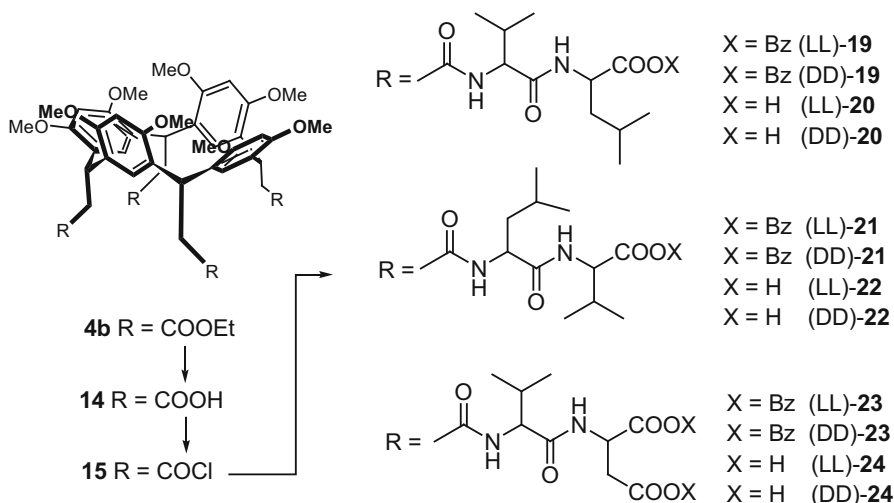
significant information on the spatial orientation of the resorc[4]arene host and a given pair of enantiomeric guests.

Later on [12], we decided to lengthen the chiral pendant by one further amino acid (that is, leucine) by preparing *N*-linked peptidoresorc[4]arene **16** (Scheme 8.6) in both the enantiomeric forms, and its regioisomer **17**. The compounds were prepared starting from resorc[4]arene tetraester **4b** which was hydrolyzed to tetracarboxylic acid **14** and quantitatively converted into the corresponding acid chloride **15** by reaction with thionyl chloride in THF. Coupling with the appropriate dipeptides (namely, valine-leucine and leucine-valine methyl esters), prepared under standard peptide conditions, was achieved by adding an excess of DIPEA in dry THF.

*N*-linked peptidoresorc[4]arenes **16** and **17**, obtained in 48–51 % yield, proved capable of recognizing the homologue dipeptides as guests, both in solution and in the gas phase, by forming relatively stable host-guest complexes, resistant to chromatographic purification but not to heating. Complexation phenomena between peptidoresorc[4]arene **16** and dipeptides **18** and *ent*-**18** in solution were investigated by NMR methods, including NMR DOSY experiments, for the detection of translational diffusion. Heteroassociation constants of 2030 and 186 M<sup>-1</sup> were obtained by the Foster-Fyfe method for the complexes [**16**·**18**] and [**16**·*ent*-**18**], respectively, the latter being comparable to the self-association constant of the dipeptide itself. Therefore, we concluded that the interaction between **16** and its homologous dipeptide occurs at the external surface of the resorcarene host by means of attractive hydrogen bonds.

Additional experiments aimed at measuring the kinetics of the dipeptide guests (G) release from the diastereoisomeric [M·H·G]<sup>+</sup> complexes induced by (*R*)- and (*S*)-2-aminobutane were performed by ESI-FT-ICR-MS [13]. In most of the cases





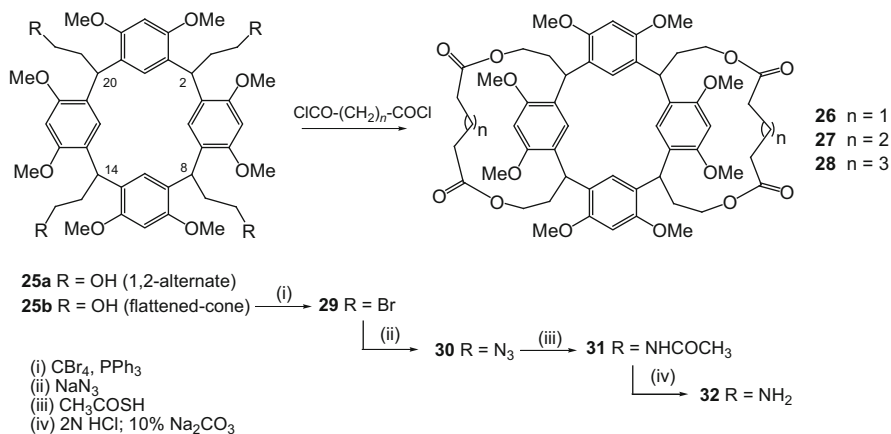
**Scheme 8.7** Anionically functionalized *N*-linked peptidoresorc[4]arenes **20**, **22**, and **24**

investigated, the heterochiral  $[M \cdot H \cdot G]^+$  complexes, namely those wherein the configuration of the guest is opposite to that of the host *M* pendants, proved to react faster (up to five times) than the homochiral analogues, wherein the guest *G* has the same configuration.

The kinetic results indicate that both the efficiency and the enantioselectivity of the guest exchange reaction depend essentially on the structure and the relative stability of the diastereoisomeric  $[M \cdot H \cdot G]^+$  complexes. These, in turn, depend on the functional groups and the configuration of both the guest and the host pendants. The lack of any significant effects of the configuration of 2-aminobutane confirmed the earlier investigation in solution, which had pointed out that the dipeptide guest is predominantly located outside the host chiral cavity.

More recently, according to the synthetic methodology above-mentioned, we designed, prepared and tested a new series of receptors for protein surface recognition [14], namely, anionically functionalized *N*-linked peptidoresorc[4]arenes **20**, **22**, and **24** (Scheme 8.7), obtained by Pd/C-catalyzed hydrogenation of the corresponding benzyl esters **19**, **21**, and **23**. From this family of receptors we have identified noncompetitive inhibitors of  $\alpha$ -chymotrypsin (ChT), which function by binding to the surface of the enzyme in the neighborhood of the active site cleft ( $K_i$  values ranging from  $12.4 \pm 5.1 \mu\text{M}$  for free carboxylate (DD)-**20** to  $0.76 \pm 0.14 \mu\text{M}$  for benzyl ester (LL)-**23**).

Computational docking experiments pointed out that for anionically functionalized receptors, the inhibition of ChT is based essentially on electrostatic interaction, and the bound enzyme can be released from the resorc[4]arene surface by increasing the ionic strength, with its activity almost completely restored. On the contrary, for peptidoresorc[4]arenes with terminal benzyl ester groups a



**Scheme 8.8** Insertion of methylene bridges led to a cavity shaped architecture resembling a basket

hydrophobic network was suggested as the main source for enzyme inhibition. For a deeper discussion of the inhibition of ChT by peptidoresorc[4]arenes, see Sect. 8.2.

When the substituents cannot be modulated by choosing the proper cinnamic acid derivative as starting monomer or by coupling reactions, new resorc[4]arenes can be obtained by more drastic modifications of the ester groups in the lower rim. In this way, the properties, mainly the cavity size and the rigidity, of the new macrocycles can be altered to address specific application requirements. Thus, reduction of tetraesters **2a**, **4a**, and **6a** (1,2-alternate conformation) with LiAlH<sub>4</sub>, as well as of **2b**, **4b**, and **6b** (flattened-cone conformation) gave the corresponding tetraalcohols **25a** and **25b**, respectively (Scheme 8.8). By contrast, the reaction of **4c** and **6c** (chair conformation) with LiAlH<sub>4</sub> afforded a mixture of **25a** and **25b**, the former being predominant [5].

Treatment of tetraalcohol **25b** with glutaroyl, adipoyl and pimeloyl dichlorides in the presence of Et<sub>3</sub>N gave the corresponding double-spanned resorcarenes **26** (*n* = 1), **27** (*n* = 2), and **28** (*n* = 3) [15], in which the insertion of the methylene bridges led to the formation of a cavity shaped architecture resembling a basket (Scheme 8.8). <sup>1</sup>H- and <sup>13</sup>C-NMR spectra, X-ray analysis, as well as molecular dynamic studies agreed that the basket derivative had a frozen flattened-cone conformation.

Compound **6b** (R = *i*Pr) was chosen to investigate complexation phenomena of resorc[4]arenes with Fe(III) cation in organic media [15, 16], in comparison with the corresponding methyl ester (**2b**, R = Me). As suggested by <sup>1</sup>H-NMR studies carried out with the diamagnetic Ga(III) instead of Fe(III), resorcarene bearing carbonyl groups either in a freely rotating side chain (as in **6b**) or in the polymethylene bridge of the basket compound **27**, have two sites of interaction with the cation: the first is located at the aromatic upper rim, and the other one is in the vicinity of the side chain carbonyl groups. On the contrary, resorcarenes lacking

carbonyl groups in the side chains have been found to exhibit only one interaction site towards Fe(III).

Tetraalcohol **25b** was the starting reagent for the synthesis of a wide range of other resorc[4]arene derivatives, namely tetrabromide **29** [16], tetraazide **30**, tetraaminoacetyl **31**, and finally tetraamine **32** [17, 18], obtained by standard cascade reactions (Scheme 8.8). Notably, tetraamine **32** proved able to strongly interacting with Cu(II) cations by forming a complex with octahedral geometry, as suggested by the EPR spectrum obtained.

An interesting example of lower rim selective functionalization is the regioselective acylation of the C(2) side chain of tetraalcohol **25b**, obtained using immobilized lipase from *Mucor miehei* in organic solvents and vinyl acetate as acylating agent. The enzyme also proved capable of partially acetylating the prochiral side chains at C(8) and C(20), but did not produce the desired dissymmetrization [19].

## 8.2 Surface Recognition Made by Resorc[4]arene Receptors

A wide variety of techniques have been applied to measure drug-macromolecule binding constants and to characterize drug interactions at the binding site, namely, biochemical binding assays [20], high-performance affinity chromatography, capillary electrophoresis, and fluorescence spectroscopy [21].

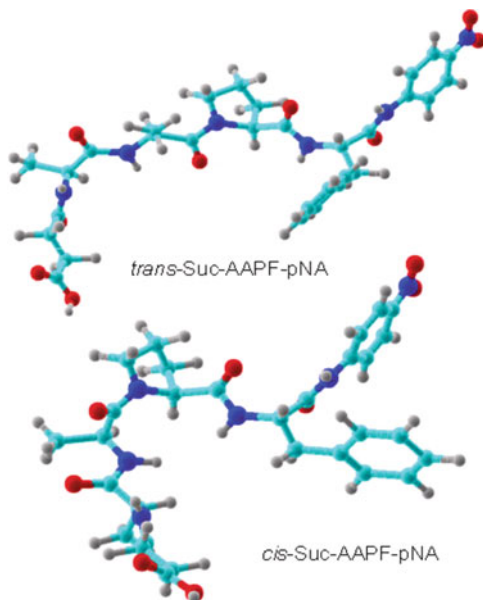
Nuclear Magnetic Resonance (NMR) spectroscopy is an attractive technique for studying ligand-macromolecule interactions because a single kind of analysis can yield a vast amount of structural information without destroying the sample [22–25].

In principle, both ligand and macromolecule NMR parameters may be measured: for low-molecular weight proteins, the chemical shift of a protein nucleus is monitored in solution, and increasing amounts of the ligand are added till saturation of protein binding sites (receptor-base approach). For high-molecular weight proteins, the small molecule is preferentially observed (ligand-based approach), without upper limitation of the protein molecular weight.

Chymotripsin (ChT) is a serine protease which was already shown to be inhibited by a specific family of calix[4]arene receptors [26, 31]. P NMR diffusion methods were exploited to probe the molecular interaction of ChT with organophosphorus compounds which are known to block the enzyme. In such cases, covalent conjugates with the serine active site were detected on the basis of the relevant decreases of diffusion coefficients of the enzyme bound species, simultaneously enabling the determination of the diffusion coefficient of the enzyme [27].

In order to point out the stereochemical basis of the inhibitory activity shown by *N*-linked peptidoresorc[4]arenes **19–24** towards ChT (see Sect. 8.1), we investigated by NMR spectroscopy the molecular interactions of peptidoresorc[4]arene

**Fig. 8.1** Three-dimensional representation of the two isomers of Suc-AAPF-*p*NA according to NMR data



(DD)-**22** with ChT and with the enzyme substrate *N*-Succinyl-Ala-Ala-Pro-Phe-*p*-nitroanilide (Suc-AAPF-*p*NA; Fig. 8.1), both in D<sub>2</sub>O and DMSO-*d*<sub>6</sub> solution [28].

1D and 2D NMR experiments, such as ROESY and DOSY allowed us to define the conformation assumed by macrocycle **22** and by the model Suc-AAPF-*p*NA substrate in solution. In the latter case, the coexistence of *trans* and *cis* stereoisomers due to the constrained rotation around the Pro-Ala peptide bond was pointed out, with a large prevalence of the *trans* one (namely, 90:10). Notably, any of the two species (**22** and Suc-AAPF-*p*NA) showed propensity to self-assemble, which could, instead, compete with aggregation processes with the enzyme. In this respect, the determination of diffusion coefficients by DOSY in progressively diluted solutions was fundamental.

We measured the selective relaxation rates of some protons nuclei of **22** and by extrapolation of the normalized affinity indices for these protons we were able to highlight the <sup>1</sup>H nuclei mainly involved in the interaction between receptor **22** and ChT, which is at the basis of the inhibition. Unlike what we expected, most of the interaction affects protons which belong to the resorcarene core rather than to the dipeptide side chain, thus suggesting that the hydrophobic portion of the macrocycle mainly stabilizes the [**22**•ChT] complex, causing the loss of the proteolytic ChT activity.

Finally, being known the catalytic triad of ChT (namely, Ser-195, His-57 and Asp-102), the ability of **22** to interact with the above amino acids was also evaluated by analyzing the diffusion coefficients of the individual amino acids, their binary and ternary mixtures. In this way, the capability of aspartate to

promoting the interaction of Ser-195 with the resorc[4]arene **22** was assessed, but with the cooperation of His-57.

Molecular modeling studies confirmed that the resorc[4]arene core interacts within a hydrophobic region of the ChT catalytic groove, whereas the dipeptide chains and, particularly, the C-terminal carboxyl groups, are docked within positively charged regions of ChT.

### 8.3 Interaction of Nitrosonium Cation with Resorc[4]arenes

Nitrogen dioxide ( $\text{NO}_2$ ) belongs to the family of  $\text{NO}_x$  gases [29, 30], where  $\text{NO}_x$  is the general formula used to describe a mixture of  $\text{NO}_2$ , nitrogen monoxide (NO), and other nitrogen oxides.

The unpaired electron on the nitrogen atom confers to  $\text{NO}_2$  paramagnetic properties, an intense brown-orange color and the capability of reacting with itself, to form a colorless dimer, namely dinitrogen tetroxide ( $\text{N}_2\text{O}_4$ ) [31].  $\text{N}_2\text{O}_4$  may disproportionate to ionic  $\text{NO}^+\text{NO}_3^-$  upon reacting with aromatic compounds [32]. The reacting species is the nitrosonium cation ( $\text{NO}^+$ ) and the final products are nitroso and nitro derivatives. Nitrosonium salts can serve effectively either as oxidants or as electrophiles toward different aromatic substrates [33, 34].

Very stable complexes between calix[4]arenes and  $\text{NO}^+$  cation have been described in the literature, both in solution and in the solid state, under conditions of host-to-guest excess [35–39]. Under conditions of guest-to-host excess, both complexes with stoichiometry greater than 1:1 and covalent nitration products have been obtained [40]. Such calixarene-based systems are now considered as supramolecular materials for generation, detection, storage, and release of NO [41–43].

Resorc[4]arenes **29** (flattened-cone conformation), **4b** and **4c** were treated with  $\text{NOBF}_4$  salt using a tenfold host-to-guest excess in chloroform, and proved to form stable 1:1 complexes deeply colored with  $\text{NO}^+$  cation [6]. Kinetic and spectral UV-visible analysis (300–800 nm wavelength range at 298 K) showed two absorption patterns for the above-mentioned complexes growing at different rates, one featuring high-energy bands (HEB) within the near-UV zone, and the other one low-energy bands (LEB), attributed to charge-transfer interactions. The complexation process proved to be reversible, and the complexes dissociate and bleach upon addition of methanol or water, to give the starting macrocycles.

Semiempirical calculations evidenced three optimized geometries for **29**- $\text{NO}^+$  complexes: two very stable and highly populated geometries, featuring the guest inside the cavity, and a third less-stable geometry, with the guest located outside, under the convex side of the resorcarene in the lower rim defined by the tetrabromide side chains. In the case of the resorcarenes **4b** and **4c**, the presence of ester carbonyl groups in the side chains strongly drives the  $\text{NO}^+$  cation outside the resorcarene, in agreement with the observed UV-visible spectral profile in the

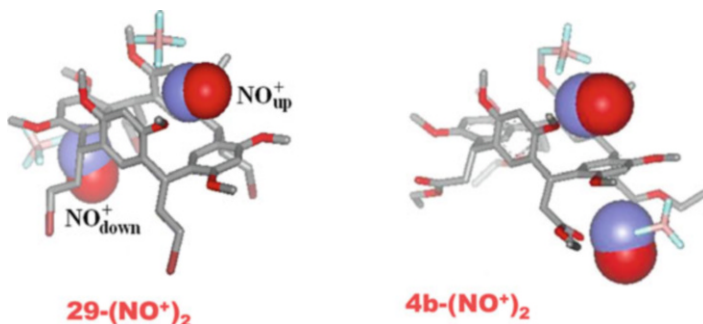


**Fig. 8.2** Structures of the three-body **29**-(NO<sup>+</sup>)<sub>2</sub> and **4b**-(NO<sup>+</sup>)<sub>2</sub> adducts obtained by DFT calculations for the interaction of resorc[4]arenes **29** and **4b** with NO<sup>+</sup> cation, respectively. The counterion BF<sub>4</sub><sup>-</sup> was added to keep the adducts neutral

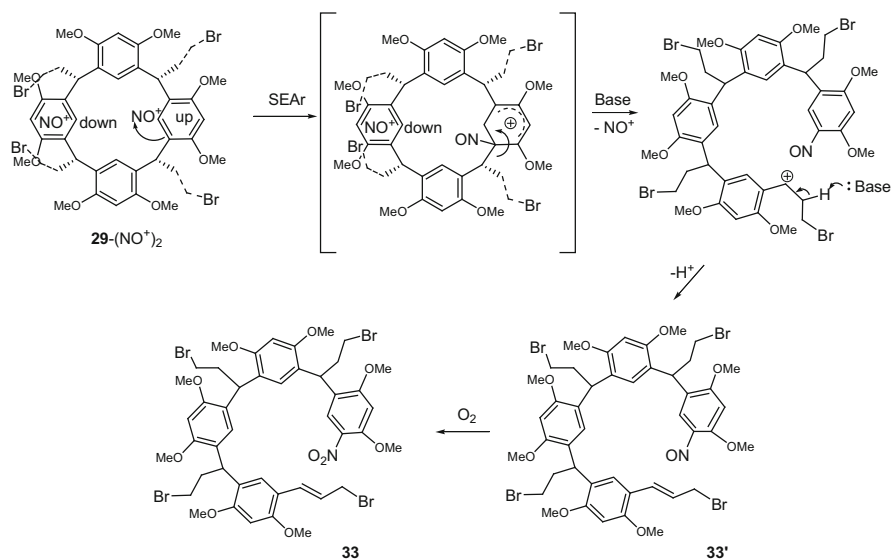
HEB zone. Such behaviour proved to be independent on the type of conformation assumed by the macrocycle.

To clarify whether complexes with a stoichiometry greater than 1:1 could be formed in the presence of a guest-to-host excess, resorc[4]arenes **29** and **4b** were treated with NOBF<sub>4</sub> salt using a threefold guest-to-host excess in chloroform [44]. Kinetic and spectral UV-visible analyses were in agreement with the formation of isomeric 1:2 complexes as a direct evolution of the previously observed event. Accordingly, three-body **29**-(NO<sup>+</sup>)<sub>2</sub> and **4b**-(NO<sup>+</sup>)<sub>2</sub> adducts were built by MM and fully optimized by DFT calculations at the B3LYP/6-31G(d) level of theory (Fig. 8.2). Such adducts proved to be the prereactive supramolecular species capable of undergoing an electrophilic attack by the NO<sup>+</sup> cation which led to the formation of specific nitration products according to a postulated S<sub>E</sub>Ar mechanism.

For resorc[4]arene **29**, it was assumed that a first NO<sup>+</sup> unit accommodated inside the cone cavity (namely, NO<sup>+</sup><sub>up</sub>) performs an ipso-electrophilic attack on the resorcinol ring (Scheme 8.9), catalyzed by a second NO<sup>+</sup> unit located outside the macrocycle and leaning against one aromatic ring (namely, NO<sup>+</sup><sub>down</sub>). Displacement of the methine carbon from the Wheland intermediate, which leads to the ring-opening of macrocycle, yields a benzylic carbocation on the other side of the ruptured bond. Removal of the adjacent proton by a base provides alkene intermediate **33'**, which evolves to the final *trans*-olefin **33** by spontaneous oxidation of NO to NO<sub>2</sub>.

Taking into account the large excess of NOBF<sub>4</sub> used in the reaction and the well-known reactivity of NO<sup>+</sup> cation towards carbon-carbon double bonds, a further progress of the reaction was hypothesized, starting from olefin precursor **33** and leading to aldehyde **34** after addition of water, according to at least two plausible mechanisms (namely, a and b pathways in Scheme 8.10).

Not surprisingly, resorc[4]arene **4b** gave rise to the same kind of products in the reaction with NO<sup>+</sup> cation, although in different yields. In other words, the same typology of structures was assigned to the two products **35** and **36** recovered from the reaction (Fig. 8.3), i.e., **35** proved to be a *trans*-olefin, and **36** the corresponding aldehyde.



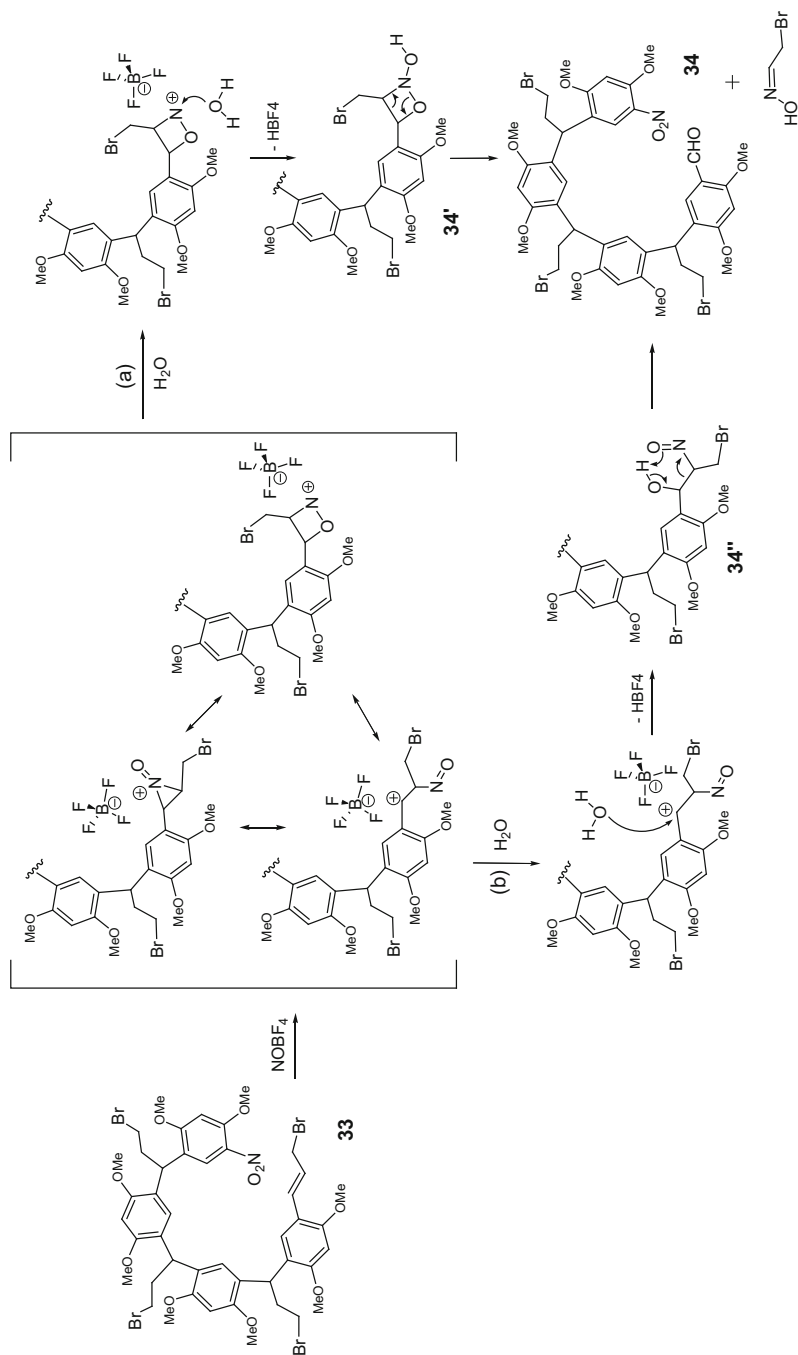
**Scheme 8.9** Prereactive supramolecular species capable of undergoing an electrophilic attack by the NO<sup>+</sup> cation according to a postulated S<sub>E</sub>Ar mechanism

## 8.4 Intriguing Resorc[4]arene Architectures Built Up by Olefin Metathesis Reaction

As an extension of our studies on NO<sup>+</sup> guest entrapment, with the aim of combining the entrapping properties of resorc[4]arenes with the possible anchorage to a solid support, we synthesized resorc[4]arenes **11a–c** (Scheme 8.4) featuring 11-carbon aliphatic side chains ending with a vinylidene group [8]. The presence of the ω-unsaturated function on the long alkyl chains, in fact, was thought to allow the attachment of the host to an opportunely functionalized silica gel by either hydrosilylation or radical thiol-ene addition. However, looking at the terminal double bonds of the four alkyl chains, we had the serendipitous idea to submit the above-mentioned resorc[4]arenes to a metathesis reaction, in order to incorporate the macrocycles into polymeric architectures with intriguing mechanical properties. Olefin metathesis indeed currently represents a powerful tool in the formation of carbon-carbon bonds, attracting a vast amount of interest both in industry and academia [45–49].

Undecenyl resorc[4]arene **11c** (see Scheme 8.4), which featured the simplest pattern of substituents, was chosen as a suitable substrate for different versions of the olefin metathesis reaction.

To ascertain the optimal reaction conditions, several experiments were run, in which a series of substrate concentrations and catalyst loadings were used



**Scheme 8.10** Two plausible mechanisms for a further progress of the reaction of  $\text{NO}^+$  cation



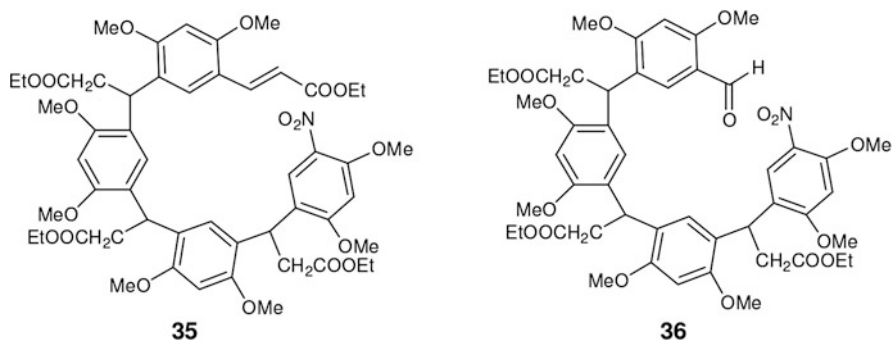


**Fig. 8.3** Structures of compounds **35** and **36** obtained by olefin metathesis of resorc[4]arene **4b**

**Table 8.1** Optimization of reaction conditions for olefin metathesis on undecenyl resorc[4]arene **11c**

Substrate conc. $3 \times 10^{-3}$ M	Catalyst (loading)	Yield (%)		
		<b>37</b>	<b>38</b>	<b>11a</b>
$3 \times 10^{-3}$ M	Grubbs 2nd (10 %)	46	5	44
	Grubbs-Hoveyda 2nd (10 %)	30	Trace	50
	Grubbs 2nd (1 %)	43	Trace	n.f.
	Grubbs-Hoveyda 2nd (1 %)	30 <sup>a</sup>	Trace	n.f.
	Grubbs 2nd (10 %)	60	n.f.	n.f.
$3 \times 10^{-4}$ M	Grubbs-Hoveyda 2nd (10 %)	40 <sup>a</sup>	n.f.	n.f.
	Grubbs 2nd (1 %)	30 <sup>a</sup>	n.f.	n.f.
	Grubbs-Hoveyda 2nd (1 %)	10 <sup>a</sup>	n.f.	n.f.
	Grubbs-Hoveyda 2nd (1 %)	10 <sup>a</sup>	n.f.	n.f.

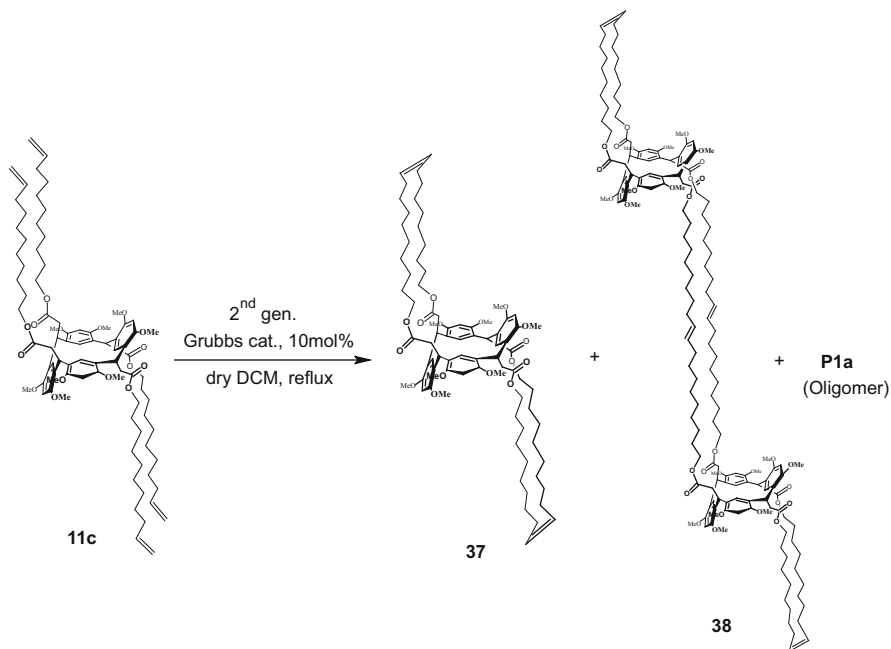
Reactions in DCM at reflux temperature and 20 min reaction time

<sup>a</sup>Starting material **11c** was present. *n.f.* not formed

(Table 8.1). Second-generation Grubbs and Hoveyda-Grubbs catalysts proved to be almost equally effective. After some trials under TLC plate checking, we observed that under high substrate concentration (i.e.,  $1.0 \times 10^{-2}$  M in DCM), a large quantity of oligomer products, presumably, was obtained, as revealed by the thickness of the baseline in the TLC plate system. Under high dilution conditions (i.e.,  $3.0 \times 10^{-4}$  M), a less complicated TLC pattern was obtained; the starting material did not completely disappear, except in the case of second-generation Grubbs catalyst at 10 mol%.

An intermediate substrate concentration (namely,  $3.0 \times 10^{-3}$  M) and a second-generation Grubbs catalyst loading of 10 mol% were chosen, since they allowed the formation of a series of interesting compounds (Scheme 8.11).

Two independent ring-closing metathesis reactions between two adjacent side chains of **11c** gave bicyclic alkene **37** in 46 % yield and with an E:Z = 3:1 ratio. Such a relatively low yield was attributed to a co-occurring ADMET-like polymerization, which, although under unfavourable conditions, gave an oligomer product



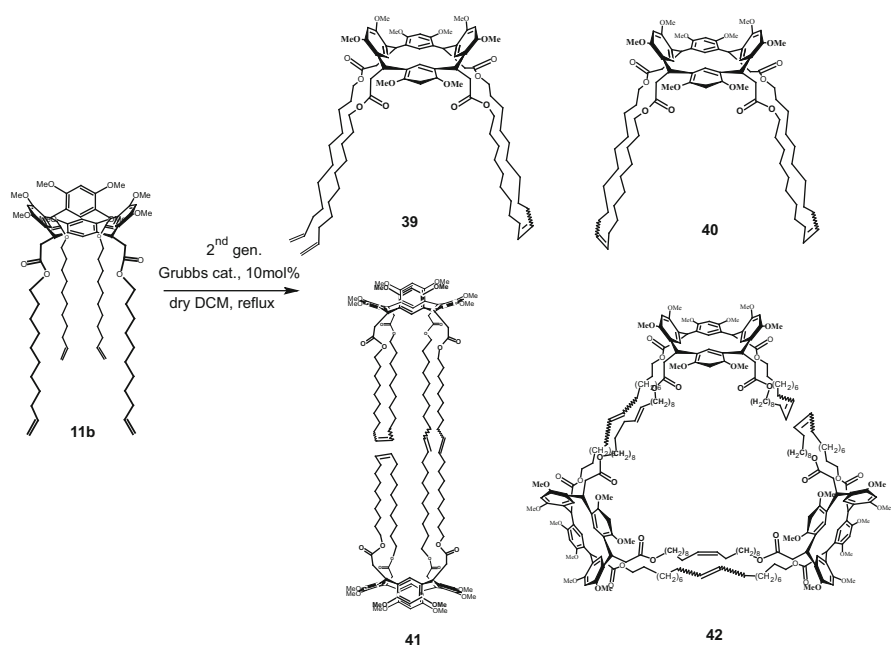
**Scheme 8.11** Intriguing resorc[4]arene architectures built up by olefin metathesis reaction

**P1a** in comparable yield (44%). A second product was obtained in 5% yield, namely the linear dimer **38**, where the two units are linked by two intermolecular eleven carbon chains. The dimer has still two reactive alkenes, which could likely result in the formation of similar trimers or tetramers, but the presence of such compounds, due to the expected lower yield, was not supported by isolation. Notably, bicyclic alkene **37** proved to be a key intermediate in the pathway leading to **38**, through a hypothesized series of reversible equilibrium reactions.

The same investigation was done on the cone stereoisomer **11b**, featuring a different arrangement of the four undecenyl side chains [50]. Under the same experimental conditions, resorc[4]arenes **39–42** were obtained (Scheme 8.12) and any detectable polymer was recovered.

The major metathesis product (50% yield) was resorc[4]arene **40**, which showed a cavity-shaped architecture resembling a basket, endowed with a large intramolecular space (~10 Å) measured by X-ray diffraction analysis. The macrocycle showed also a strong propensity to self-assemble in the solid state as a supramolecular trio of heterochiral dimers (Fig. 8.4).

To investigate the hydrophilic-hydrophobic balance of basket **40**, we monitored its tendency to self-assemble in solution (namely, THF/water) by UV-visible spectroscopy, following a procedure already reported [51]. A set of physical descriptors were developed, namely, the aggregation polarity index (API), the



**Scheme 8.12** Olefin metathesis reaction performed on the cone stereoisomer **11b**

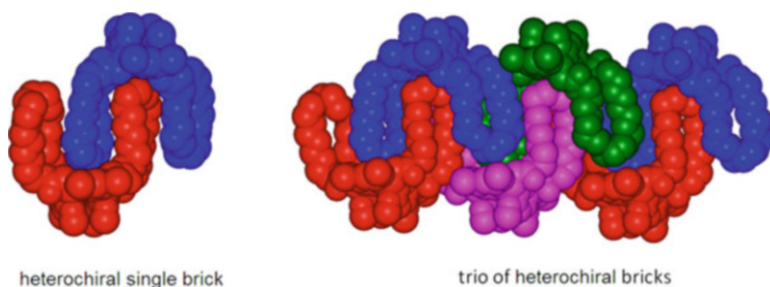


**Fig. 8.4** CPK models of basket resorc[4]arene **40** in crystal lattice. Supramolecular dimer (*left*) and zigzag 1D ribbon (*right*) as a trio of heterochiral dimers

cavitation Gibbs free-energy change ( $\Delta\Delta G_{\text{cav}}$ ) and the decrease of the molecular surface A ( $\% \Delta A$ ). API is the solvent polarity which indicates that a 50% self-aggregation is achieved.  $\Delta\Delta G_{\text{cav}}$  is the change of free energy occurring for the insertion of a cavity into a solvent, in response to the change of solvent composition before and after the self-assembly phenomena in a given solute.  $\% \Delta A$  refers to the molecular surface that a given solute exposes to the solvent upon aggregation, to minimize the free energy.

The hydrophilic-hydrophobic balance for basket **40**, calculated by the above-mentioned descriptors, proved comparable to that previously observed for some amphiphilic C60 fullerene derivatives in the same solvent system. A particular similarity was found with a fulleropyrrolidine functionalized with a hydrophilic pendant [51]. Such similarity suggests that if the C60 fullerene sphere was accommodated inside the hydrophobic cage of a resorc[4]arene, a reversible manipulation of the chemical properties of fullerenes could take place, which might have an interesting impact on the wide field of applications of fullerenes, such as materials technology, microelectronics, biology, and medicinal chemistry [52, 53].

## References

1. Sliwa, W.; Kozłowski, C. (Eds) *Calixarenes and Resorcinarenes. Synthesis, Properties and Applications*. Wiley-VCH: Weinheim, Germany, **2009**.
2. Botta, B.; Cassani, M.; D'Acquarica, I.; Misiti, D.; Subissati, D.; Delle Monache, G. *Curr. Org. Chem.* **2005**, *9*, 337–355.
3. Botta, B.; Cassani, M.; D'Acquarica, I.; Subissati, D.; Zappia, G.; Delle Monache, G. *Curr. Org. Chem.* **2005**, *9*, 1167–1202.
4. Botta, B.; Iacomacci, P.; Di Giovanni, M.C.; Delle Monache, G.; Gacs-Baitz, E.; Botta, M.; Tafi, A.; Corelli, F.; Misiti, D. *J. Org. Chem.* **1992**, *57*, 3259–3261.
5. Botta, B.; Di Giovanni, M.C.; Delle Monache, G.; De Rosa, M.C.; Baitz, E.G.; Botta, M.; Corelli, F.; Tafi, A.; Santini, A.; Benedetti, E.; Pedone, C.; Misiti, D. *J. Org. Chem.* **1994**, *59*, 1532–1541.
6. Botta, B.; D'Acquarica, I.; Delle Monache, G.; Nevola, L.; Tullo, D.; Ugozzoli, F.; Pierini, M. *J. Am. Soc. Chem.* **2007**, *129*, 11202–11212.
7. Botta, B.; Delle Monache, G.; De Rosa, M.C.; Carbonetti, A.; Baitz, E.G.; Botta, M.; Corelli, F.; Misiti, D. *J. Org. Chem.* **1995**, *60*, 3657–3662.
8. Ghirga, F.; D'Acquarica, I.; Delle Monache, G.; Toscano, S.; Mannina, L.; Sobolev, A.P.; Ugozzoli, F.; Crocco, D.; Antiochia, R.; Botta, B. *RSC Adv.* **2013**, *3*, 17567–17576.
9. Botta, B.; Delle Monache, G.; Salvatore, P.; Gasparrini, F.; Villani, C.; Botta, M.; Corelli, F.; Tafi, A.; Gacs-Baitz, E.; Santini, A.; Carvalho, C.F.; Misiti, D. *J. Org. Chem.* **1997**, *62*, 932–938.
10. Botta, B.; Botta, M.; Filippi, A.; Tafi, A.; Delle Monache, G.; Speranza, M. *J. Am. Chem. Soc.* **2002**, *124*, 7658–7659.
11. Tafi, A.; Botta, B.; Botta, M.; Filippi, A.; Delle Monache, G.; Speranza, M. *Chem. Eur. J.* **2004**, *10*, 4126–4135.
12. Botta, B.; D'Acquarica, I.; Nevola, L.; Sacco, F.; Valbuena Lopez, Z.; Zappia, G.; Frascchetti, C.; Speranza, M.; Tafi, A.; Caporuscio, F.; Letzel, M.C.; Mattay, J. *Eur. J. Org. Chem.* **2007**, 5995–6002.
13. Botta, B.; Frascchetti, C.; D'Acquarica, I.; Speranza, M.; Novara, F.R.; Mattay, J.; Letzel, M.C. *J. Phys. Chem. A* **2009**, *113*, 14625–14629.
14. D'Acquarica, I.; Cerreto, A.; Delle Monache, G.; Subrizi, F.; Boffi, A.; Tafi, A.; Forli, S.; Botta, B. *J. Org. Chem.* **2011**, *76*, 4396–4407.
15. Botta, B.; Delle Monache, G.; De Rosa, M. C.; Seri, C.; Benedetti, E.; Iacovino, R.; Botta, M.; Corelli, F.; Masignani, V.; Tafi, A.; Gacs-Baitz, E.; Santini, A.; Misiti, D. *J. Org. Chem.* **1997**, *62*, 1788–1794.
16. Botta, B.; Delle Monache, G.; Ricciardi, P.; Zappia, G.; Seri, C.; Gacs-Baitz, E.; Csokasi, P.; Misiti, D. *Eur. J. Org. Chem.* **2000**, 841–847.

17. [17] Botta, B.; Delle Monache, G.; Ricciardi, P.; Zappia, G.; Misiti, D.; Baratto, M.C.; R. Pogni, R.; Gacs-Baitz, E.; Botta, M.; F. Corelli, F.; Manetti, F.; Tafi, A. *J. Org. Chem.* **2002**, *67*, 1178–1183.
18. Botta, B.; Delle Monache, G.; Subissati, D.; Subrizi, F.; Zappia, G. *Synthesis* **2008**, 2110–2116.
19. Botta, B.; Zappia, G.; Tafi, A.; Botta, M.; Manetti, F.; Cernia, E.; Milana, G.; Palocci, C.; Soro, S.; Delle Monache, G. *J. Mol. Catal., B Enzym.* **2002**, *16*, 241–247.
20. Cohen, L. H.; Nicoll-Griffith, D. A. In: *Encyclopedia of Drug Metabolism and Interactions* **2012**, *5*, 657–674. Lyubimov, A. V.; Rodrigues, A. D.; Sinz, M. A. (Eds.)
21. Oravcovà, J.; Boehs, B.; Lindner, W. *J. Chromatogr. B* **1996**, *677*, 1–28.
22. Davis, B. In: *Methods in Molecular Biology* (New York, NY, United States) **2013**, *1008* (Protein-Ligand Interactions), 389–413.
23. Cala, O.; Guillièrre, F.; Krimm, I. *Anal. Bioanal. Chem.* **2014**, *406*, 943–956.
24. Ramirez, B. E.; Antanasijevic, A.; Caffrey, M. In: *Methods in Molecular Biology* (New York, NY, United States) **2014**, *1140* (Structural Genomics and Drug Discovery), 305–313.
25. Unione, L.; Galante, S.; Diaz, D.; Canada, F. J.; Jimenez-Barbero, J. *MedChemComm.* **2014**, *5*, 1280–1289.
26. Park, H. S.; Lin, Q.; Hamilton, A. D. *J. Am. Chem. Soc.* **1999**, *121*, 8–13.
27. Segev, O.; Columbus, I.; Ashani, Y.; Cohen, Y. *J. Org. Chem.* **2005**, *70*, 309–314.
28. Uccello-Barretta, G.; Balzano, F.; Aiello, F.; Vanni, L.; Mori, M.; Menta, S.; Calcaterra, A.; Botta, B. *Org. Biomol. Chem.* **2015**, *13*, 916–924.
29. Lerdau, M. T.; Munger, J. W.; Jacob, D. *J. Science* **2000**, *289*, 2291–2293.
30. Kirsch, M.; Korth, H.-G.; Sustmann, R.; de Groot, H. *Biol. Chem.* **2002**, *383*, 389–399.
31. Addison, C. C. *Chem. Rev.* **1980**, *80*, 21–39.
32. Bosch, E.; Kochi, J. K. *J. Org. Chem.* **1994**, *59*, 3314–3325 and references cited therein.
33. Kim, E. K.; Kochi, J. K. *J. Org. Chem.* **1989**, *54*, 1692–1702.
34. Kim, E. K.; Kochi, J. K. *J. Am. Chem. Soc.* **1991**, *113*, 4962–4974.
35. Zyryanov, G. V.; Kang, Y.; Stampf, S. P.; Rudkevich, D. M. *Chem. Commun.* **2002**, 2792–2793.
36. Zyryanov, G. V.; Kang, Y.; Rudkevich, D. M. *J. Am. Chem. Soc.* **2003**, *125*, 2997–3007.
37. Rudkevich, D. M. *Angew. Chem., Int. Ed.* **2004**, *43*, 558–571.
38. Rathore, R.; Lindeman, S. V.; Rao, K. S. S. P.; Sun, D.; Kochi, J. K. *Angew. Chem., Int. Ed.* **2000**, *39*, 2123–2128.
39. Rathore, R.; Abdelwahed, S. H.; Guzei, I. A. *J. Am. Chem. Soc.* **2004**, *126*, 13582–13583.
40. Borodkin, G. I.; Elanov, I. R.; Andreev, R. V.; Shakirov, M. M.; Shubin, V. G. *Russ. J. Org. Chem.* **2006**, *42*, 406–411.
41. Wanigasekara, E.; Leontiev, A. V.; Organo, V. G.; Rudkevich, D. M. *Eur. J. Org. Chem.* **2007**, 2254–2256.
42. Wanigasekara, E.; Gaeta, C.; Neri, P.; Rudkevich, D. M. *Org. Lett.* **2008**, *10*, 1263–1266.
43. Hines, J. H.; Wanigasekara, E.; Rudkevich, D. M.; Rogers, R. D. *J. Mater. Chem.* **2008**, *18*, 4050–4055.
44. Ghirga, F.; D’Acquarica, I.; Monache, G.; Mannina, L.; Molinaro, C.; Nevola, L.; Sobolev, A. P.; Pierini, M.; Botta, B. *J. Org. Chem.* **2013**, *78*, 6935–6946.
45. Chauvin, Y. *Angew. Chem., Int. Ed.* **2006**, *45*, 3740–3747.
46. Schrock, R. R. *Angew. Chem., Int. Ed.* **2006**, *45*, 3748–2759.
47. Grubbs, R. H. *Angew. Chem., Int. Ed.* **2006**, *45*, 3760–3765.
48. Vougioukalakis, G. C.; Grubbs, R. H. *Chem. Rev.* **2010**, *110*, 1746–1787.
49. Nicolaou, K. C.; Bulger, P. G.; Sarlah, D. *Angew. Chem., Int. Ed.* **2005**, *44*, 4490–4527.
50. Ghirga, F.; Quaglio, D.; Iovine, V.; Botta, B.; Pierini, M.; Mannina, L.; Sobolev, A. P.; Ugozzoli, F.; D’Acquarica, I. *J. Org. Chem.* **2014**, *79*, 11051–11060.
51. Angelini, G.; Cusan, C.; De Maria, P.; Fontana, A.; Maggini, M.; Pierini, M.; Prato, M.; Schergna, S.; Villani, C. *Eur. J. Org. Chem.* **2005**, 1884–1891.
52. Prato, M. *J. Mater. Chem.* **1997**, *7*, 1097–1109.
53. Da Ros, T.; Prato, M. *Chem. Commun.* **1999**, 663–669.

# Chapter 9

## A Chronology of Cavitands

Anthony Wishard and Bruce C. Gibb

### 9.1 Introduction

In 1982, Donald J. Cram coined the term “cavitand” to refer to synthetic organic molecules with an enforced cavity to accommodate molecules or ions [1]. This coinage was in the context of resorcinarene-based hosts, but the term is occasionally expanded to include other classes of hosts. In the spirit of this book however, we remain true to the context of Cram’s definition and discuss here the diverse family of resorcinarene-based hosts that have been created and studied to date. This is an incredibly expansive field and we have not attempted to be comprehensive. However, we hope that our selection of the literature gives some idea of the breadth of opportunity the field provides.

### 9.2 Resorcinarenes

Resorcinarenes (see the companion chapter by Bruno Botta) date back nearly 150 years when Baeyer discovered that the mixing of aldehydes with resorcinol in the presence of strong acid produced a red resin [2]. Over a decade later, Michael successfully determined the correct chemical composition of the product, but proposed the incorrect structure [3]. The correct structure of resorcin[4]arene (**1**, Scheme 9.1) was first proposed by Niederl [4], but it was almost 100 years after Baeyer’s initial work that Erdtman and Högberg obtained a definitive structure [5]. Twelve years after that, Högberg fully documented resorcinarene synthesis,

---

A. Wishard • B.C. Gibb (✉)  
Department of Chemistry, Tulane University, New Orleans, LA 70118, USA  
e-mail: [bgibb@tulane.edu](mailto:bgibb@tulane.edu)

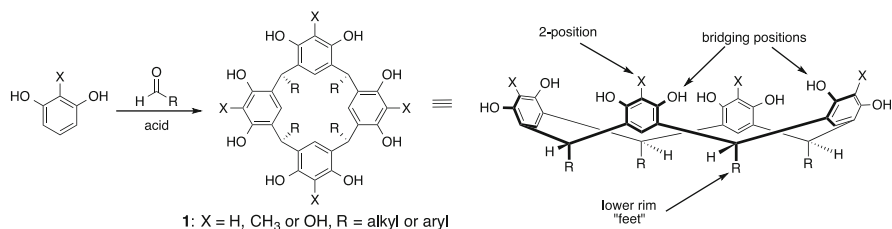
opening the field to many new possibilities [6], including the development of cavitands.

Resorcinarenes are typically synthesized from the acid-catalyzed condensation of resorcinol and an aldehyde (Scheme 9.1). Brønsted acids, such as HCl, are most common [6, 7], but Cabaleiro showed that a range of Lewis acids also work [8], and allow acid-sensitive aldehydes to be used in this macrocyclization [9]. Unlike their calixarene cousins, resorcinarenes are primarily available as cyclic tetramers. This macrocycle is the thermodynamic product, and their relative insolubility means that they can be precipitated as the sole product of a condensation process producing a multitude of acyclic and cyclic oligomers. By inducing precipitation early on in the reaction, higher resorcinarenes as kinetic products can be isolated, albeit in low yields [10].

Resorcinarenes can exist in a number of stereoisomers each with their own conformational forms [7, 11], but with very few exceptions [12] cavitand research has focused on the all-*cis* form (Scheme 9.1).

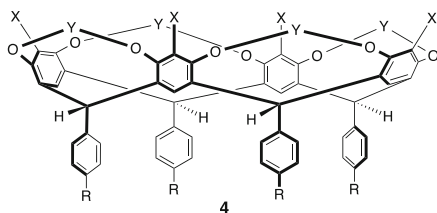
Functionalization of resorcinarenes involves three primary routes: (1) At the R-groups or “feet” of the resorcinarene by choice of aldehyde in the resorcinarene reaction, and/or post-macrocyclization modification; (2) the 2-position (X, Scheme 9.1) can be controlled by choice of the starting resorcinol derivative or modification of the resorcinarene product; (3) functionalized through utilization of the phenolic groups at the upper rim. A variation of this strategy, using *bis*-electrophiles that “bridge” the phenolic pairs, leads to the cavitands discussed here.

Note that a review of cavitands biases the view of the literature away from the R-groups or feet; those interested in cavitand research necessarily focus on the upper-rim of the host and mostly consider the feet as a means of solubilization or attachment to surfaces. Noted exceptions include the host shown in Fig. 9.1 (below)



**Scheme 9.1** The synthesis and structure of resorcinarenes

**Fig. 9.1** Phenyl-footed cavitand containing two guest-binding sites



and work by Dalcanale and Diederich examining phosphate footed cavitands as salt binders [13]. Thus, the emphasis here is on the structural diversity possible simply by considering the two-position and the bridges in cavitands; unless important to do so, when we refer to specific structures in the text we do not specify the nature of the R-groups or feet of the cavitand.

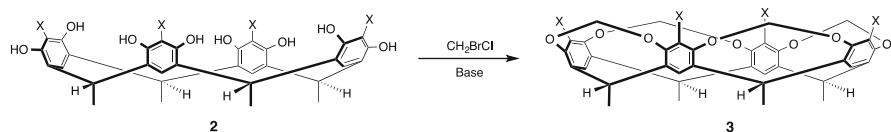
## 9.3 The Cram Years: The First Cavitands

### 9.3.1 Cavitands

It was Donald Cram who reported the synthesis of the first cavitands just 2 years after Högberg's landmark paper [14]. The synthesis involved covalently linking adjacent oxygens of neighboring resorcinol moieties of **2** (Scheme 9.2) with  $\text{BrCH}_2\text{Cl}$  as bridging material [14, 15]. Cram's synthesis gave a low 14% yield of **3** ( $X = \text{H}$ ), but bridging of the corresponding 2-Br-resorcinarene (**2**,  $X = \text{Br}$ ) improved the yield to 42%. A decade and a half later the Kaifer group reported a modification to this reaction that gave near quantitative yields [16].

Cram subsequently reported on the synthesis and crystal structures of simple cavitands in which the length of the polymethylene bridge varied [17]. While 1-carbon bridges yielded the most rigid cavitand, even three-carbon bridges maintained a permanently enforced cavity. Cram also found that with **2** ( $X = \text{Br}$ , Scheme 9.2), the fourth bridge was harder to insert than the first three. This allowed the isolation of *tris*-bridged cavitands. As we will see, this ease of synthesis has provided access to a broad range of lower-symmetry molecules. Subsequent work revealed that the bromine substituent was not always necessary for the isolation of cavitands with fewer than three bridges, and that with *bis*-bridging the major product possessed bridges adjacent to one another (*A,B*-) rather than on opposite sides of the cavitand (*A,C*-) [18].

Many of the early cavitands were insoluble or only sparingly so. Because this resulted in reduced utility, Cram invested considerable effort into synthesizing resorcinarenes with increased solubility [19]. This work focused on increasing the size/length of the feet of the cavitand. A byproduct of this was that larger feet could engender a second binding site. For example, benzaldehyde derivatives led to cavitands such as **4** ( $X$ , R and Y (bridges) = various, Fig. 9.1) [20]. In general, these hosts were found to bind guests more strongly to the enforced upper "bowl" than the less preorganized lower "box".



**Scheme 9.2** Synthesis of cavitands



### 9.3.2 (Hemi)Carcerands and (Hemi)Carceplexes

Based on his very early cavitand work, Cram envisioned a new class of molecule, [1, 14] but it was 6 years later before the report of the first example of what he named carcerands (**5**, Fig. 9.2), from the Latin *carcer*, or prison [21]. Cram chose this name because these hosts could permanently imprison guests inside their shell of covalent bonds. Unless one or more covalent bond is broken, the guest could not escape. He would later coin the term “carceplex” to refer to this complex of a carcerand containing an imprisoned guest.

The synthesis of carcerand **5** involved the formation of two novel precursor cavitands **3** (Scheme 9.2, X = CH<sub>2</sub>Cl<sub>2</sub> and CH<sub>2</sub>SH respectively) which were subsequently joined in 29 % yield. However, the product was insoluble in all tested solvents, making purification and full characterization difficult.

Cram modified **5** by replacing methyl feet with phenethyl or pentyl feet to form soluble hosts [22]. The studies of these carceplexes indicated that their formation was templated by the guest.

A further step forward was reported the subsequent year when Cram and Sherman revealed carcerand **6** (Fig. 9.2) [23]. The introduction of more solubilizing feet, and the change in the “dimerization” strategy to joining two tetrol cavitands (**7**, Scheme 9.3) using CH<sub>2</sub>BrCl, led to three soluble carceplexes containing DMSO, DMF, and DMA [23, 24].

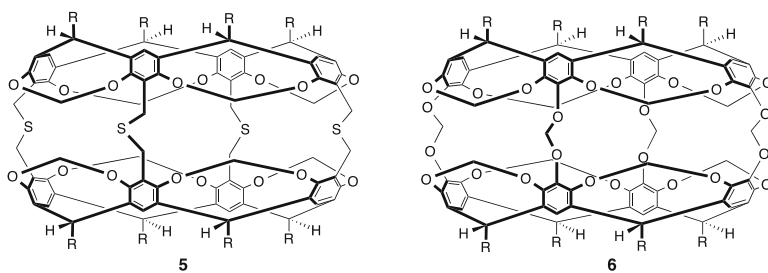
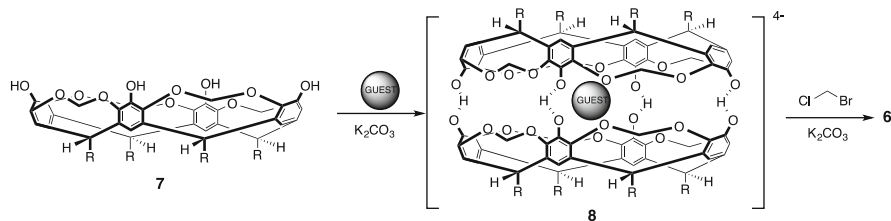
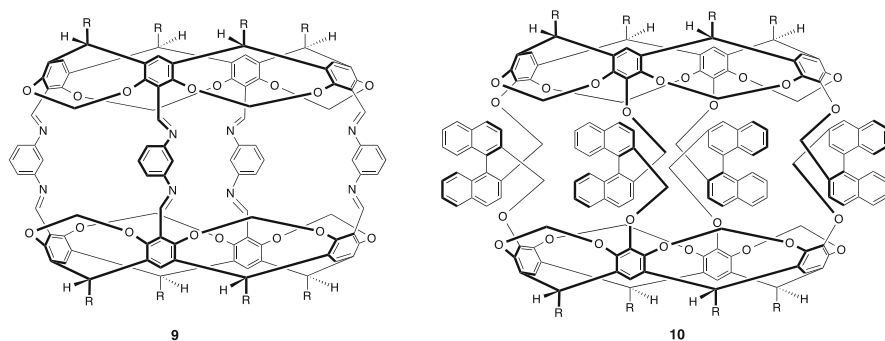


Fig. 9.2 The first and second-generation carcerands **5** and **6**



Scheme 9.3 Templation and carceplex formation



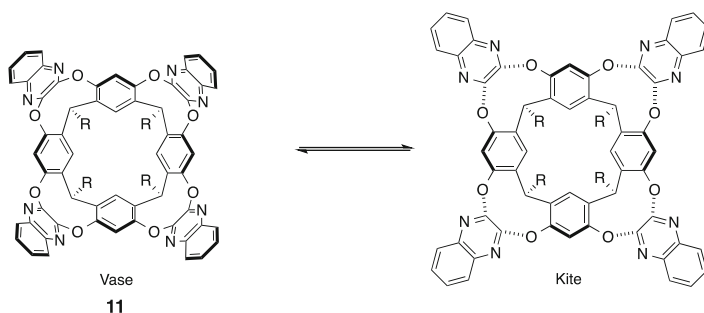
**Fig. 9.3** The first hemicarcerand **9** and chiral hemicarcerand **10**

The efficient formation of carceplexes involving **7** opened the way to one of the most graphic examples of supramolecular chemistry in the early 1990s; the idea of trapping highly reactive intermediates, most exquisitely demonstrated by the “Taming of Cyclobutadiene.”[25]. Tanner and Cram trapped  $\alpha$ -pyrone within **6** and photolytically induced the elimination of  $\text{CO}_2$  to form the elusive cyclobutadiene. Indefinitely stable at room temperature, an NMR analysis of the entrapped guest confirmed its anti-aromaticity.

Although Cram continued to work with carcerands and carceplexes, he also looked for ways to make the spacer units between the two hemispheres of the carcerand bigger and/or more flexible. In doing so, in 1991 he synthesized the first hemicarcerand **9** and chiral hemicarcerand **10** (Fig. 9.3); [26] hosts that can trap a guest within their interior but possess sufficiently large portals for guests to enter or egress. As anticipated, hemicarcerand **10** and its enantiomer showed enantioselective guest binding. Over the subsequent years many variations of the hemicarcerand concept were realized, including examples where two different cavitands were conjoined [27], hemicarcerands with redox-active linkers [28], and hemicarcerands with less than the maximal number of linker units between cavitand subunits [29]. Theoretical modeling of the mechanisms of guest entry and egress were also investigated [30].

### 9.3.3 The Velcrand Nucleation

A related family of hosts that Cram first synthesized were the velcrands [14, 31]. In the most general of terms, velcrands are cavitands in which the bridges between resorcinol moieties are comprised of *ortho*-substituted aromatic rings. Scheme 9.4 shows the first velcrand with quinoxaline walls (**11**). As we will see in Sect. 9.5, a wide variety of velcrands have since been synthesized, but in general these hosts exist in two forms: the vase and the kite.



**Scheme 9.4** Vase and kite forms of quinoxaline velcrand **11**

## 9.4 The Post-Cram Renaissance: Exploiting the Two-Position

### 9.4.1 Containing Chemistry with Covalent Bonds

In early independent work John Sherman's group published a pair of papers in 1994 investigating the ability of templates to promote carceplex formation (Scheme 9.3) [32]. Subsequent studies combining two different cavitands, or joining two copies of the corresponding mono-ol, diol and triol variants of **7**, revealed much about assemblies such as **8** and the synthesis of carceplexes [33]. Parallel computational studies also shed light on this matter [34]. Similarly, in 2000 the Sherman group also probed the effects of adding large linkers between the ternary complex **8** to form hemi-carceplexes [35].

Although the Sherman group's burgeoning expertise in the carceplex reaction would pave the way for the synthesis of some exceedingly large (hemi)carceplexes, the bar was raised somewhat in 1995 by David Reinhoudt's group when they reported on the synthesis of a new type of hemicarcerand in which calixarenes were used as the bridging units between the cavitands (**12**, Fig. 9.4) [36]. Moreover, open structures composed of one cavitand and two calixarenes were shown to complex steroids [37]. Reinhoudt also functionalized this class of host with thioether feet so as to form monolayers on gold surfaces possessing enhanced steroid binding properties [38].

Shortly thereafter, using their carceplex reaction knowledge the Sherman group constructed macrocyclic (methylene-linked) tetramers of **7**, which under carceplex conditions formed the corresponding *bis*-carceplex **13** (Fig. 9.5) [39]. The corresponding charged hydrogen-bonded intermediate showed very strong cooperativity; one template in each "hemisphere" is required for its formation and hence two templates are found trapped in the carceplex [40]. An analogous situation applies to the formation of *tris*-carceplexes created from macrocycles composed of six cavitand subunits [41]. Moreover, the corresponding cyclic trimer

**Fig. 9.4** “Holand” **12**  
synthesized by the  
Reinhoudt group

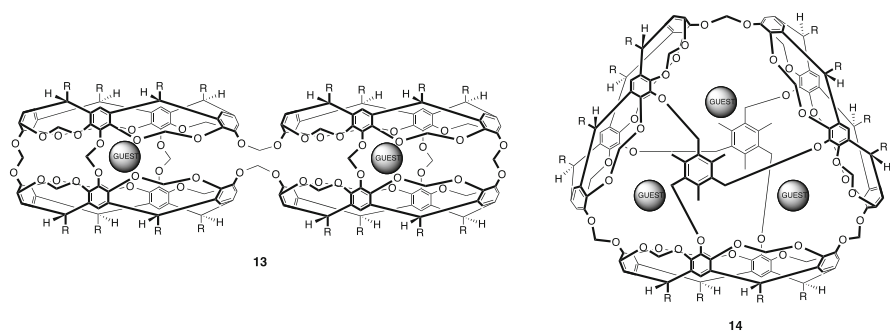
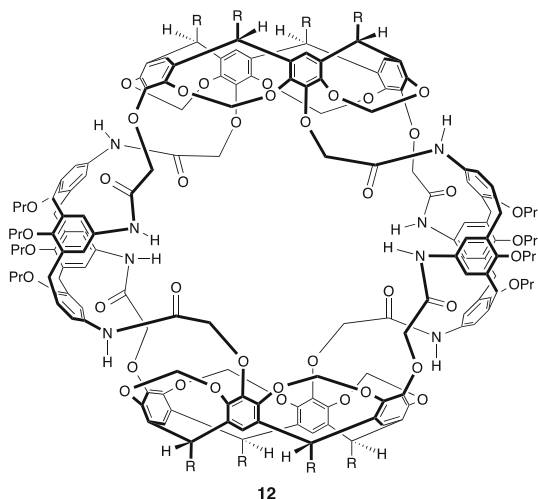


**Fig. 9.5** Bis-carceplex **13** and large carceplex **14**

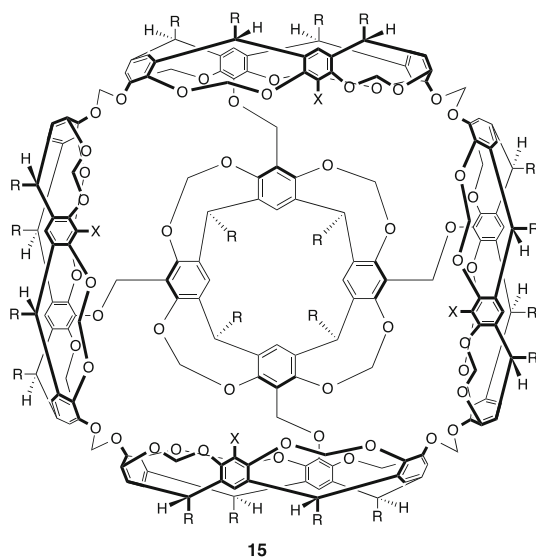
of **7** could also be isolated and capped top and bottom to form large carceplexes such as **14** (Fig. 9.5) that entrapped three guests [42]. Understanding how to form carceplexes such as **13** also allowed the Sherman group to generate a trapped enol that, unable to react with a proton, couldn't tautomerize to its more stable keto form [43].

In the late 1990s and at the beginning of his own independent career, Ralf Warmuth expanded on Cram's idea of carceplexes as storage media for highly reactive species. For example, he used a hemicarcerand formed by linking two equivalents of **7** with butylene groups to isolate and characterize benzyne in the solution state [44]. This feat was accomplished by photolytically generating benzyne within the hemicarcerand of benzocyclobutenedione. He later showed that the entrapped benzyne slowly reacted with the carcerand host [45]. Shortly thereafter he formed the corresponding cycloheptatetraene hemicarcerand [46], and

used NMR to determine the enantiomerization barrier of related chiral guests [47]. Warmuth continued to work with this idea, publishing on the effect of a hemicarcerand on the transition state of encapsulated diazirines [48], how to isolate stable *anti*-Bredt bicyclic octenes [49] or fluorophenoxy (singlet) carbenes [50], and how to study the ring expansion of aryl azides [51]. The Warmuth group later studied a series of thirty-two guests within a hemicarcerand to analyze what effects the nature of a guest molecule plays with regards to chromatography of the hemicarcerand [52]. Warmuth's recent work has largely focused on the formation of dynamic covalent molecular capsules.

The introduction of the four phenol groups in cavitand **7** was accomplished by lithiation of the corresponding *tetra*-bromide, followed by quenching with trimethyl borate and oxidative workup [23]. This lithiation has proven to be an invaluable tool for synthesizing two-functionalized cavitands, and the work from the Sherburn group just after the turn of the millennium has proven to be invaluable in this regard. They determined protocols for the mono-lithiation of *tetra*-bromo cavitands and quenching with electrophiles (E) to form a wide range of reduced symmetry derivatives [53], before going on to reveal how to control *bis*-lithiation and quenching [54]. The former protocol has been used to synthesize hosts that demonstrate atropisomerism controlled by guest binding [55], whilst the latter was subsequently utilized to form specific boronic acid cavitands for selective fructose transport [56]. Building on these lithiation studies, in 2004 the Sherburn group published the synthesis of “super bowl” **15** (Fig. 9.6); arguably the largest covalent container molecule published to date [57]. Relatedly, the following year the Sherman group synthesized a hexameric (octahedral) closed-shell equivalent of **15**

Fig. 9.6 “Super bowl” **15**



[58]. NMR demonstrated that with a volume of approximately  $\sim 1,300 \text{ \AA}^3$  this shell-like host could bind up to seven DMSO molecules.

Although tetrol **7** was proving to be an invaluable tool for large host synthesis, other approaches to hemicarcerands were being investigated at the end of the 1990s. For example, early work from the Paek group involved the coupling of two *tetra*-thiomethylcavitands with two equivalents of 1,2,4,5-*tetra*-bromomethylbenzene [59], whilst in 2014 a one-pot synthesis of disulfide-linked carceplexes was achieved by treating the corresponding *tetra*-2-bromomethyl cavitand with potassium thioacetate and methanolysis [60].

As discussed in Sect. 9.2, almost all resorcinarene-based cavitand chemistry is based on the thermodynamically most stable resorcin[4]arenes. However, the kinetic products of resorcinarene reactions using 2-methyl resorcinol and dialkoxy-methanes are macrocyclic resorcin[5/6/7]arenes that can be isolated in low yield [10]. The Sherman and Kaifer groups were the first to wade into the field of larger cavitands based on these resorcinarenes [61]. While [5]cavitands adopt the typical cone conformation, [6/7]cavitands are more conformationally flexible. Further investigations into both functionalization of the upper rim methyl and the lower rim methylene groups of [6]cavitand were also carried out [62]. Around the same time, a [5]cavitand was investigated for its ability to form the corresponding carceplex [63]. The larger resorcin[5]arene-based cavitands readily bind two guests. Extensive templation studies weren't performed, but the authors did demonstrate that two DMF molecules template the reaction better than two DMA molecules.

### 9.4.2 Enveloping with Metal Ion Coordination

In 1998 Harrison reported the synthesis and characterization of water-soluble, dynamic, cobalt-coordinated carcerand **16** (Fig. 9.7) [64]. A follow-on study 7 years later found that **16** can entrap a range of guests [65]. Competition studies revealed that anisole and *p*-xylene were the strongest binders; both had an encapsulation preference  $\sim 20,000$  times stronger than the poorest guest, *m*-xylene. Harrison extended this work using the same cavitand complexed with Fe (II) [66]. The resulting carcerands were also water-soluble and were found to contain six waters. In the presence of bromobenzene-saturated water, the aromatic preferentially bound.

The early 2000s were an intense time for metal coordination via the two-position and the assembly of cavitands into dimeric capsules. Work in the Kobayashi group focused on using palladium coordination to assemble capsules from **17**, **18**, and **19** (Fig. 9.8) [67]. Around the same time the Reinhoudt group examined the assembly of **20** on gold surfaces [68]. Kobayashi's further work examining assemblies with two different cavitands showed that self-sorting into either homo- or hetero-cavitand hemicarcerands was controlled by a balance of factors such as

**Fig. 9.7** Cobalt-coordinated carcerand **16**

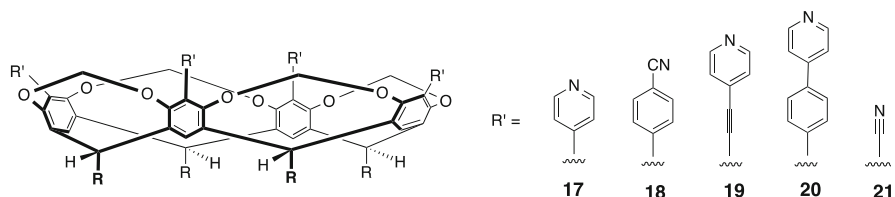
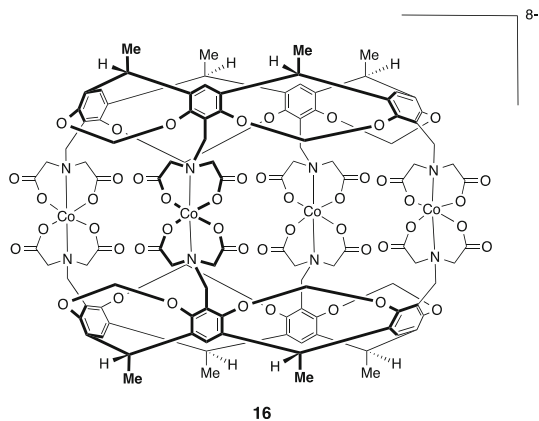


**Fig. 9.8** Select cavitaands for metal-coordinated dimeric capsules (hemicarcerands)

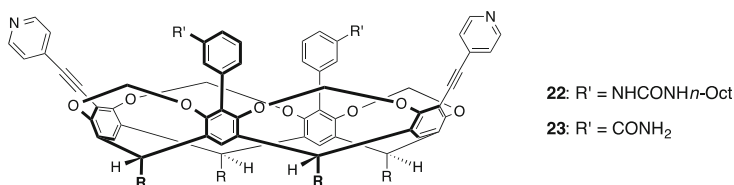


**Fig. 9.9** Hybrid cavitaands for metal-coordinated and hydrogen bonded dimeric capsules

coordination ability and steric demand. Analogous hosts have been reported by Paek using assembly around Pt complexes [69].

The Dalcanale group was also involved in this kind of hemicarcerand formation. For example, cavitaand **21** was shown to coordinate with palladium or platinum and form the corresponding hemicarceplex containing either a solvent molecule or a single triflate counter-ion [70]. Additionally, taking advantage of their cavitaand lithiation expertise, similar hosts were also synthesized by the Sherburn group. For example, they synthesized an *A,C*-bis-pyridyl derivative and showed that reaction with platinum complexes led to cyclic dimers and trimers [71].

A few years later the Kobayashi group reported on cavitaands with two metal-coordinating and two hydrogen-bonding sites [72]. The capsule formed from **22** (Fig. 9.9) was shown to envelop neutral guests with the assistance of an anion.

A similar hybrid host **23** was examined and found to undergo host-structure changes upon guest binding [73]. Furthermore, the authors determined that while hydrogen bonding in the capsule has only a small influence on the thermodynamic properties of guest binding, it has a much more pronounced effect on the kinetics of encapsulation.

### 9.4.3 Hemicarcerands Held Together by Hydrogen Bonding

Also in the early 2000s, analogous capsules held together by hydrogen bonding were being investigated. In particular, the Kobayashi group reported on a number of examples. Initial work examined cavitands such as **24** (Fig. 9.10) forming dimeric capsules via an equatorial belt of four copies of 2-aminopyrimidine [74]. Extending this, 2-aryl cavitands such as **25** were also synthesized and found to undergo an analogous assembly [75]. A range of guests have been qualified to bind to these capsules.

More recently, hetero-capsules were reported by Kobayashi by combining the aforementioned *tetra*-acids with cavitand such as **26** [76]. Guests that bound included 1,4-diiodobenzene derivatives, which were shown to form C-H...X hydrogen bonds with the host. The orientational preferences in bound guests have been studied [77].

In 2007 it was shown that cavitand **17** (Fig. 9.8) and *tetra*-(4-phenol)-cavitands **27** (Fig. 9.10) also form hetero-dimeric-capsules [78]. The lack of symmetry in these capsules led to highly specific guest orientations [79]. NMR studies have revealed that suitably low symmetry guests allow the capsular complex to function as a supramolecular gyroscope [80]. Subsequently, these hetero-capsules were studied by *ab initio* calculations showing that electrostatic interactions between oxygen atoms in the guests and the hydrogen atoms of the aromatic rings and methylene-bridge rim of the capsule are key complex stabilizers [81].

Building on these assemblies, in the late 2000s the Paek group revealed a number of supramolecular capsules assembled through hydrogen bonds. For example, **28** (Fig. 9.11) forms stable capsules in nonpolar solvents via the formation of eight intermolecular N-H...O = C hydrogen bonds [82]. Likewise, cavitand **29** forms dimeric capsular assemblies that entrap small aromatic guests [83]. More recently, the same group revealed host **30**, a chromogenic self-assembling host that opened the way to naked eye detection of encapsulation [84]. The Paek group also

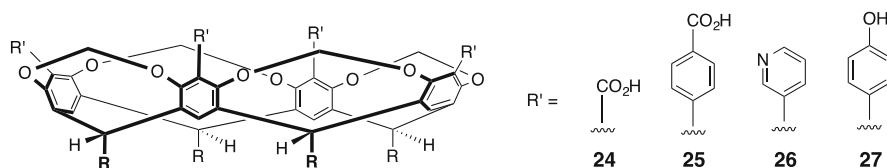
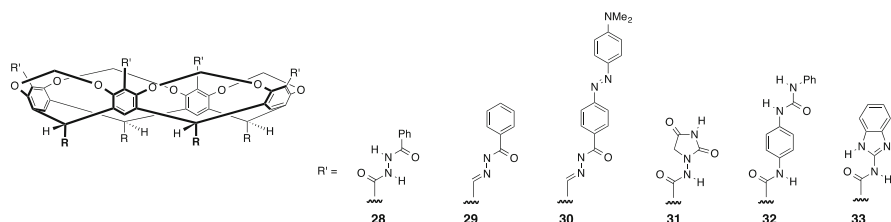


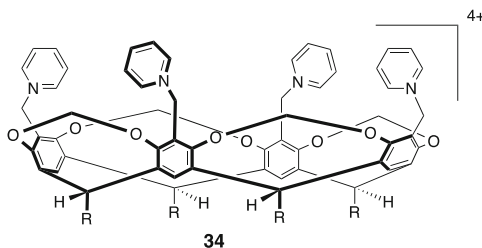
Fig. 9.10 Cavitand for hydrogen-bonded dimeric capsules from the Kobayashi group





**Fig. 9.11** Cavitand for hydrogen-bonded dimeric capsules from the Paek group

**Fig. 9.12** A pyridinium cavitand for assembly around anions



found that cavitand **31** forms a stable supramolecular capsule in the presence of suitable anionic guests [85]. Not all designs go according to plan however. Urea cavitands such as **32** failed to form dimeric capsules, but instead formed 1:1 complexes with anions [86].

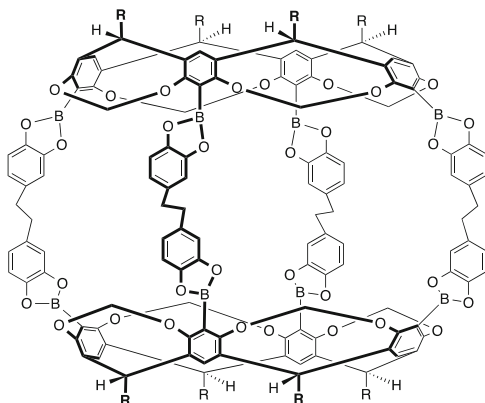
Along a similar design vein, cavitand **33** does not dimerize to form a capsule but instead forms a well-defined vase-form in the presence of methanol. This “methanol-mediated cavitand” weakly binds *n*-alkanes [87].

#### 9.4.4 Other Means Toward Reversible Dimeric Capsules

Although metal coordination and hydrogen bonding have been popular approaches for the assembly of cavitands, other strategies were considered during the first decade of the new millennium. The Reinhoudt group has, for example, shown how the dimerization of **34** is influenced by anion complexation into the interior of the assembly [88]. It is interesting to note that given sufficiently short R groups these cavitands are water-soluble and mono-dispersed [89] (Fig. 9.12).

The Kobayashi group has also reported on two-substituted *tetra*-(dihydroxyboryl) cavitands and how they assemble in the presence of linkers such as 1,2-*bis*-(3,4-dihydroxyphenyl)ethane to form dynamic boronic acid ester capsules (e.g., **35**, Fig. 9.13) [90]. Guest binding has also been reported in these assemblies [91]. Additionally, these capsules have been shown to function as both photosensitizers and as a guard against photochemically-induced dimerization of anthracene guests [92]. Most recently, the scope of the *bis*-catechol linker that joins the cavitands together has been expanded [93].

**Fig. 9.13** A container formed by boronic acid ester bond formation



35

### 9.4.5 *Mimetics, Hosts, Separators and Catalysts*

Although containers have figured prominently in the research of those studying cavitands, the architecture of these hosts lends itself to a variety of other applications. We highlight some of these in the following paragraphs.

In 1995 Sherman introduced the cavitein, a hybrid of a cavitand and a protein (**36** Fig. 9.14) [94]. In the first examples, the formation of a template-stabilized four-helix bundle was investigated by the coupling of chloroacetate *N*-terminated peptide strands to 2-thiol cavitands. CD spectroscopy demonstrated that the prototype possessed helicity, and second generation derivatives included water-soluble feet in the cavitand to minimize aggregation issues [95], and considered the effect of linker type and length on the properties of the four-helix bundles [96]. Building on this, further work exploring the effects of peptide sequence and linker type led to the most stable and native-like of caviteins [97], and caviteins composed of two different peptides [98]. An X-ray analysis revealed further details about the structure of these conjugates [99]. Subsequent studies showed that in solution, formation of a dimeric eight-helix bundle could be favored via either histidine metal-ion chelation or disulfide incorporation [100]. Yang *et al.* later showed that a monomeric histidine-containing cavitein could catalyze ester hydrolysis [101]. Lastly, the Sherman group has also studied three-, five-, and six-helix bundles [102].

Building upon his work with caviteins, Sherman has also designed cavitand-based, template-assembled synthetic G-quartets (TASQs, **37** Fig. 9.14) [103]. Unlike most systems, these G-quartets do not require cation coordination to form. Subsequently, they were shown to be excellent chelators of cations [104]. While  $\text{Na}^+$  and  $\text{Sr}^{2+}$  left the G-quartet intact,  $\text{K}^+$  induced the formation of an asymmetric dimer in addition to a unimolecular G-quartet, while  $\text{Cs}^+$  showed only the presence of an asymmetric dimer. Sherman was later able to modify these G-quartet TASQs to make them water-soluble [105].

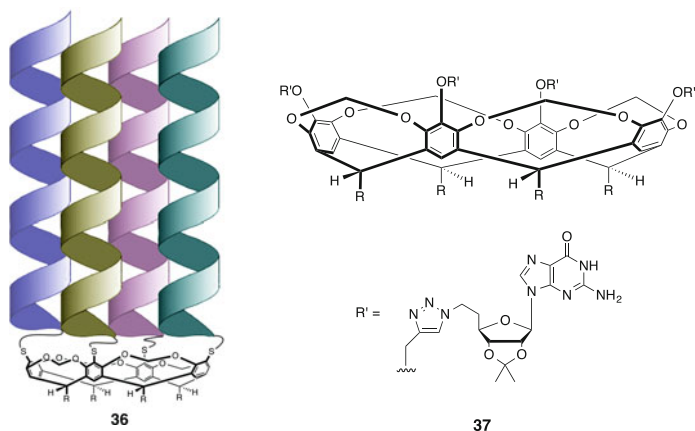
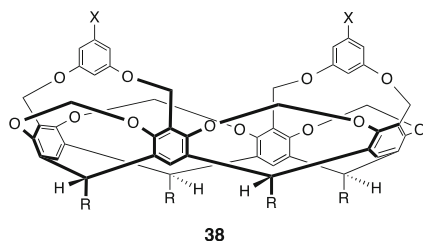


**Fig. 9.14** (Left) Generic structure of a cavitein (**36**). (Right) A template-assembled synthetic G-quartet **37**

**Fig. 9.15** Cavitand **38** from the Paek group



In 2012 the Sherman group also reported on U-quartets that did not require cation templation [106]. Most recently, the Sherman group reported on cavitands containing thymine moieties attached through phosphate linkages, and demonstrated their ability to form T-tetrad assemblies [107].

Functionalization at the 2-position has also been utilized for host-guest complexations. For example, in 2000 the Diederich group reported ethylene-bridged cavitands appended with guanidinium-substituted two-aryl groups [108]. These have been shown to bind dicarboxylates and nucleotides/phosphates in methanol and water. More recently, the Paek group has utilized the two-position of cavitands to synthesize velcrand-like, *tetra*-ether **38** (Fig. 9.15). A crystal structure revealed that the two second-row aromatic rings partially fold into the pocket to form a small but well-defined binding site. As a result, in water-saturated chloroform the host binds both small anions such as  $\text{Cl}^-$  and water [109]. An attempt to form the corresponding *tetra*-amide led instead to the formation of a hemicarcerand capable of binding small anions [110].

Around the turn of the millennium, Harrison described ligand **39** (Fig. 9.16) [111]. Upon addition of  $\text{Cu(II)}$  ions the cavitand formed the corresponding *tetra*-nuclear complex. Harrison then showed that the cavitand also coordinated  $\text{Zn(II)}$  and  $\text{Fe(III)}$  [112]. The anion transport properties of these hosts were studied,

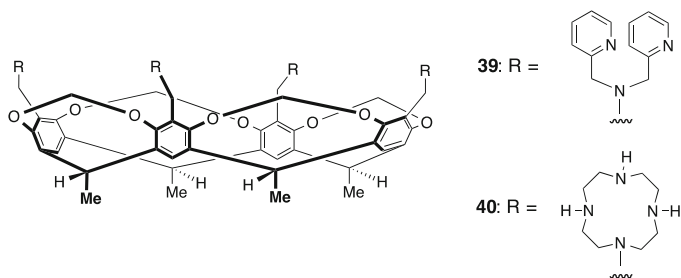


**Fig. 9.16** Structures of ligands **39** and **40**

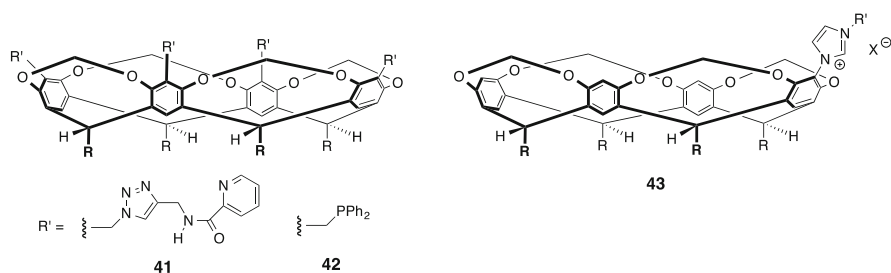


**Fig. 9.17** Three cavitands for catalysis

and in their examination of oxo-anions ( $\text{SO}_4^{2-}$ ,  $\text{SeO}_4^{2-}$ ,  $\text{NO}_3^-$ ,  $\text{ReO}_4^-$ ) it was found that  $\text{ReO}_4^-$  was consistently transported more effectively. Harrison continued to work with this cavitand design but switched to using protic media in order to bind anions in the absence of coordinating metal ions [113]. The authors found that the protonated host bound two anions simultaneously.

Subsequently, near the end of the decade Lamb and Harrison investigated the anion binding properties of the zinc complex of cavitand **40** [114]. ITC revealed that the four cyclens of each cavitand could bind two or more anions. In methanol the complex had high affinity for dihydrogen phosphate, acetate, and halide ions, and weak affinity for nitrate and perchlorate. Further work revealed that the protonated, metal-free ligand could also bind anions, and when loaded on a hydrophobic stationary phase could bring about much higher ion separation than the corresponding *N*-undecyl cyclen monomer [115]. Most recently, Lamb and Harrison screened the same ligand (**40**) for its selectivity and separation powers of transition metal-ions [116]. The preconcentration of  $\text{Cu}^{2+}$  at the ppb level from a high concentration matrix of five, divalent transition metals was readily achieved. Furthermore, the subsequent recovery of  $\text{Cu}^{2+}$  was greater than 98%. Further column development using cavitands is ongoing in the Lamb and Harrison groups [117].

A number of papers focusing on catalytic cavitands have appeared in the previous 5 years. For example, the Hooley group has synthesized pyridine-appended cavitands such as **41** (Fig. 9.17) [118]. These cavitands coordinate

metal ions on either the inside or outside of the cavity, depending on the particular ligand [118]. The resulting metal complexes proved to be water-soluble and were used as catalysts to oxidize the C-H bonds of fluorene. The group followed up this work by grafting the metal-coordinated host to a silica surface and showing that the system can catalytically oxidize cyclic alkanes [119].

The Matt group has also investigated cavitands as catalysts. For example, cavitand **42** is a catalyst for Heck reactions [120]. Conversion percentages were highest when the cavitand was present in a 1:1 ratio with the Pd ligand. Sémeril and Matt have also examined *mono*- and *di*-phosphine cavitands. The *A,B*- and *A,C*-*di*-phosphines formed complexes with ruthenium [121], but the properties of these bulky ligands have to our knowledge not yet been reported.

The Sémeril and Matt groups have more recently reported on catalysts of the Suzuki-Miyaura cross-coupling reaction. The authors reported on three cavitands such as **43**. These were readily converted to their *mono*- and *bis*-carbene Pd complexes, all three of which were highly successful catalysts displaying high turn-over frequencies [122].

## 9.5 The Velcrand Explosion

The first velcrands were pyrazine- and quinoxaline-based (e.g., **11**, reproduced in Fig. 9.18) [14] and tended to form dimeric kites (Scheme 9.4). By the end of the 1980s and beginning of the 1990s, these hosts represented the extent of the field, with the Cram and Dalcanale groups examining both solution- and gas-phase guest binding [31b, 123]. It wasn't until the mid- to late 1990s that the field began to expand rapidly. Already well versed in calixarene chemistry and supramolecular chemistry in general, Julius Rebek and his group were poised beautifully to lead the charge [124], and together with Francois Diederich, Enrico Dalcanale, Pablo Ballester and others they have grown the field exponentially.

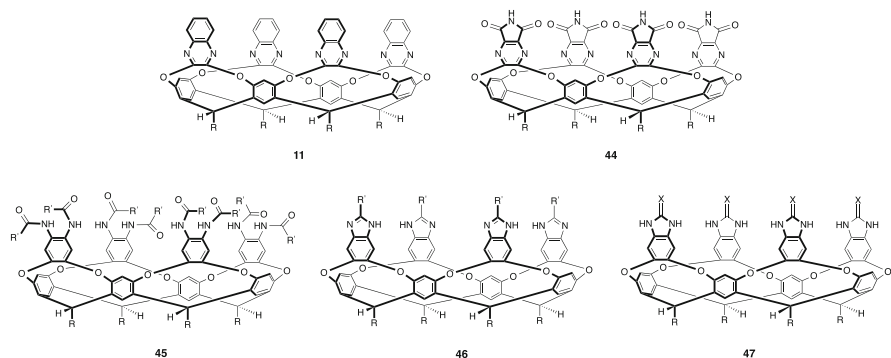


**Fig. 9.18** Representative velcrands

The breadth of velcrand derivatives stems from the type of bridging unit (and of course the nature of the R group, Fig. 9.18). There are two broad classes: those that are bridged with suitably activated benzene derivatives such as 1,2-difluoro-4-6-dinitrobenzenes, and those bridged with activated pyrazine derivatives such as *tetra*-chloropyrazine or 2,3-dichloroquinoxalines. The breadth of velcrands with just these two approaches is very large, so to highlight this area we focus primarily on the five general classes of velcrand **11**, **44–47**, (Fig. 9.18), discussing them from oldest to youngest.

### 9.5.1 Quinoxaline Velcrands

Quinoxaline velcrands date back to 1982 [14], but further work by Cram [31b] and Dalcanale [123] apparently stimulated little in the way of interest. In large part this can be attributed to solubility issues and a tendency to dimerize. These handicaps notwithstanding, the Diederich group has over the last 15 years or so been instrumental in building an understanding of what exogenous factors control the vase-kite equilibrium of these hosts, and in doing so has identified new velcrands that respond to changes in environment.

In 2001 it was determined that protonation of quinoxaline-bridged velcrands (**11**) switches the vase form to the kite form [125]. Similarly, it was demonstrated that reversible switching from the vase to the kite conformation of an amphiphilic quinoxaline-bridged velcrand could be induced by zinc ions [126]. Measurements of the monolayers of both conformers show that the area per molecule increases from 120 Å<sup>2</sup> in the vase form to 270 Å<sup>2</sup> for the kite.

To gain a better understanding of the vase-kite transition the Diederich group subsequently synthesized quinoxaline-bridged velcrands bearing one or two (**48**, Fig. 9.19) fluorescent (BODIPY) labels for single molecule spectroscopic studies [127]. The introduction of the BODIPY labels had little effect on the switching

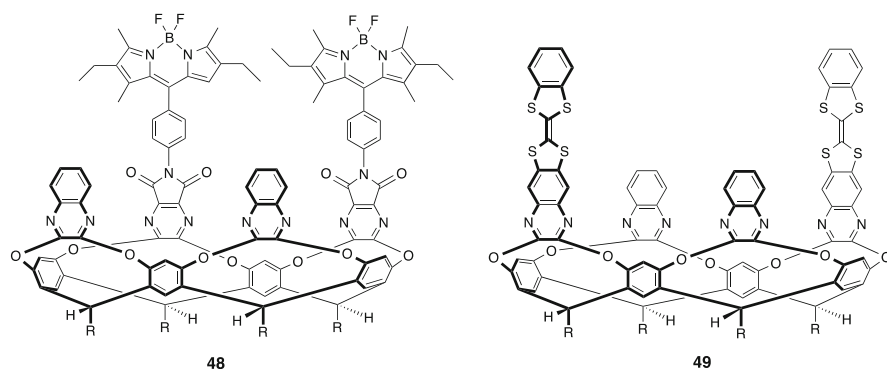


Fig. 9.19 Select quinoxaline-based velcrands from the Diederich group

between forms. Relatedly, more recently a velcrand similar to **48** but with donor and acceptor BODIPY dyes was studied by FRET to probe the vase-kite equilibrium as a function of temperature [128]. The observed FRET efficiencies revealed an average opening angle of  $16^\circ$  for the vase. Further work involving a combined experimental and molecular dynamics study was carried out with velcrands possessing different length linkers between bowl and dye [129]. Furthermore, the dynamics of these types of velcrands has also been probed by *A,C*-bis-quinoxaline-bridged velcrands with *B,D*-bis-bridges functionalized with anthracene or pyrene groups [130].

In the last decade, a variety of other mixed-bridged velcrands based on **11** have been reported by Diederich [131]. For example, *A,C*-bis-quinoxaline-bridged velcrands with (linked) *B,D*-groups that provide a “roof” to the pocket were synthesized and their binding properties studied [132]. Relatedly, Diederich and Dalcanale have expanded on the pyrazine-bridged cavitands first reported by Cram and formed a range of pyrazine/quinoxaline mixed-bridged cavitands [133].

Most recently, the Diederich group has examined redox-active velcrands [134]. For example, the vase-kite equilibrium of *bis*-tetrathiafulvalene (TTF) cavitands such as **49** (Fig. 9.19) can be shifted depending on redox environment. In the neutral form these cavitands adopt principally the vase form, whereas upon oxidation Coulombic repulsion leads to the kite [135]. The same group has also recently synthesized redox-active velcrands possessing quinone/hydroquinone bridges (Fig. 9.20). Cavitands with four quinone units exist only in the kite conformation, but those containing two quinone and two quinoxaline units – such as the roofed example **50** – can access both the kite and the vase forms depending on its redox state and the nature of the solvent [136]. NMR showed that host **50** was a weak binder of guests, but also that it bound guests more strongly in the oxidized quinone form.

A different family of diquinone-based resorcin[4]arene cavitands, **51** is an example, were found to bind guests more strongly in the reduced form where hydrogen bonds could form between the bridges of the velcrand [137]. The study of a range of these hosts allowed design guidelines for successful hydrogen bond acceptors to be ascertained. Thus, a carboxamide acceptor was shown to be the best candidate, and based on this moiety a redox-switchable triptycene-derived host that completely encapsulated a guest in its closed vase conformation was prepared [138].

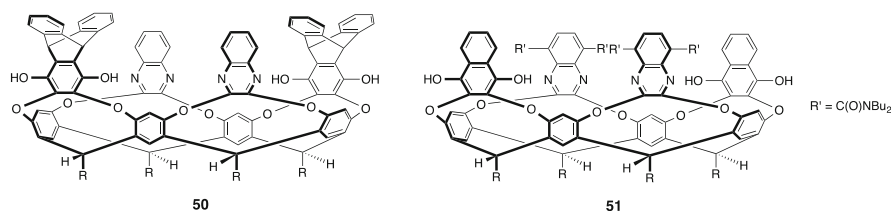


Fig. 9.20 Quinone/hydroquinone velcrands from the Diederich group

Finally, very recently Ballester and Llobet modified the feet of a quinoxaline velcrand to incorporate thio-ether groups. This allowed their grafting onto gold-nanoparticle coated (AuNP) multiwall carbon nanotubes. The system was used to detect benzene with a limit of detection close to 600 ppt [139].

### 9.5.2 Imide Velcrands

In 1998 the Rebek group demonstrated that *tetra*-imide velcrand **44** formed dimeric, hydrogen-bonded, supramolecular capsules containing one or more guests within their nano-spaces [140]. Such encapsulations have been shown to lead to many interesting phenomena including: helical guest conformations [141], isomerism based on the arrangements of molecules in space [142], supramolecular isotopic effects [143], chiral discrimination [144], and controlling reversible reactions of guests [145]. Furthermore, in the past 6 years the Rebek group has studied the subtleties of guest conformation and packing [146], the thermodynamics and kinetics of guest entrapment [147], and used the capsules to amplify halogen bonding between guests [148]. Variations whereby one of the bridges of **44** have been replaced with a unique bridge have been used to study the properties of capsules with holes in their side [149], and the supramolecular properties of a cavitand-capsule “chimera” [150].

Velcrands such as **44** don't just self-associate. Under suitable conditions they can be capped with resorcinarene and *bis*-glycoluril derivatives [151]. Moreover, four copies of glycoluril derivatives have been shown to insert into the hydrogen bond seam of the dimer of **44** to form extended capsules [124b, 124d, 152] in which the precise hydrogen bond network between the subunits is controlled by the internalized guest(s) [153]. These extensions enlarge the cavity of the capsule by  $\sim 200 \text{ \AA}^3$ . NMR and computational studies of the stability of encapsulated carboxylic acid and amide homo- and hetero-guests pairs have revealed details about why a normal or extended capsule forms [154]. This notion of an elongated capsule can be taken further. For example, eight glycolurils can be inserted into the equator of the capsule formed by **44** to form a longer host capable of entrapping four guests molecules [155]. Remarkably, in just the last few years it has been shown that even 12 glycoluril subunits can be incorporated between two copies of **44** to generate hyperextended capsules [156]. Furthermore, a switch to propanediurea spacer units leads to extended assemblies that lead to a whole host of S- and banana-shaped containers [156a, 157].

### 9.5.3 Octa-Amide Velcrands

In the same year as imide velcrands were introduced, Rebek also reported on “self-folding” cavitands **45** [158]. These *octa*-amide hosts form a seam of hydrogen



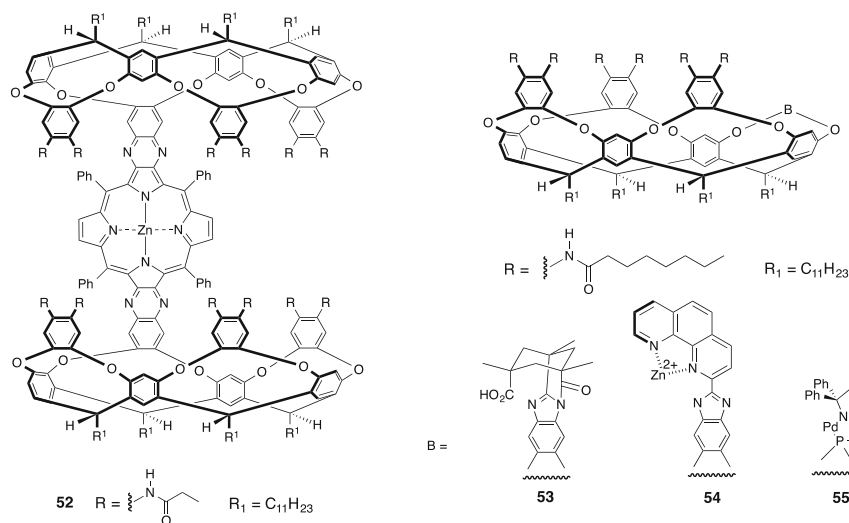


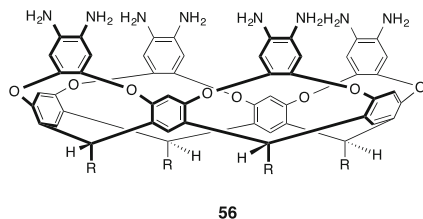
**Fig. 9.21** Selected early examples of self-folding velcra from the Rebek group

bonds around their rim to stabilize the vase form and enhance their binding properties. This has opened up the possibility of these hosts as being used as sensors, and as a means to bring about shape-selective reactions with bound guests.

Although derivatives of **45** without added functionality have been investigated for their ability to bring about selective reactions on bound guests, [159] prior to this work a significant effort was expended replacing one bridge of these hosts with a unique group that brings greater functionality to the inner pocket. Examples from the early 2000s include the velcra dimer linked by a porphyrin moiety (**52**, Fig. 9.21) [160]. Another *endo*-functionalized host, **53**, dangles a carboxylic acid group from a Kemp's *tri*-acid-based bridge [161]. Intriguingly, through steric and chemical effects from the carboxylic acid, **53** can freeze *N*-inversion of amine guests. This racemate host was also shown to diastereoselectively recognize chiral guests [162]. Using a similar framework, the Rebek group also synthesized the *mono*-functionalized Zn-phenanthroline velcra **54**. It was shown that the zinc ion could interact with the bound guest [163]. Keeping on this theme, the Rebek group also developed velcra **55** possessing a fourth bridge with a phosphite group appended with a diphenyl-substituted oxazoline moiety. Addition of a palladium complex allowed the host to catalyze allylic alkylations with unusual substrate selectivity [164].

Furthering this idea of reactions in velcra and using them as catalysts, the middle of the last decade saw a significant number of papers on this topic [165]. Furthermore, recently the Ballester group has also considered velcra such as **45** as shape-selective catalysts by examining the reactivity of the cationic guest *bis*-norbornadiene rhodium(I) [166]. Ballester has expanded this work by repeating it with a modified cavitand which included a single pyridyl unit at the rim designed to increase the binding affinity of the rhodium complex to the pocket [167].

**Fig. 9.22** *Octa*-amine velcrand **56**



All this noted, there is still much to learn about guest selection however, and reflecting this, very recent work has examined unique-bridge velcrands controlling guest association and the guest binding motif [168], and how “dimer” derivatives can have photochemically controlled hosting behavior [169]. Furthermore, the binding properties of hosts such as **45** have also been explored by rendering them water soluble [124f]. This brings into the picture the Hydrophobic effect, which can be exploited to promote incorporation into micelles [170], or enhance the binding of complex, biologically relevant guests such as unsaturated  $\omega$ -3, -6, and -9 fatty acids and their derivatives [171].

These types of velcrands have also been used as sensors, and one such early example came from the Rebek and Ballester groups who examined the *octa*-amine **56** (Fig. 9.22) as a selective choline and carnitine sensor [172]. By virtue of the well-defined binding pocket the host examined showed good selectivity for trimethylammonium guests, but particularly tetramethylammonium and the two aforementioned biochemical species. Sensor development has relied on improving our understanding of the binding properties of these types of hosts, and in this respect Ballester and Sarmentero have considered *tris*-bridged velcrand derivatives of **56** as hosts for trimethylalkylammonium guests [173]. The free phenols of this host bestow it with pH-modulated binding affinities toward trimethylalkylammonium ions, whilst the walls of the velcrand bestow it with good selectivity.

Later, the Ballester and Rius groups took this one step further by devising a new solid-contact, ion-selective electrode for sensing choline and its derivatives. Based on a velcrand of type **45** and carbon nanotubes, the electrode was shown to detect choline at concentrations as low as  $10^{-6}$  M, and possessed sufficient selectivity that choline could be successfully detected in biological samples [174]. Using similar hosts, Sarmentero and Ballester have identified and rationalized effective and selective binding of positively charged organometallic sandwich complexes with the aid of DFT calculations [175].

#### 9.5.4 Benzimidazole Velcrands

In 2002 Rebek reported that although velcrand **46** ( $R' = \text{H, Me, and Ph}$  etc.) is poorly soluble in organic media, the addition of hydroxyl-containing co-solvents such as water and alcohols bridge the gap between the four walls of the host to

solubilize the cavitand and generate a stable vase monomer [176]. Under such conditions it is therefore able to bind small guests; even when the host is bound to a micelle [177].

Shortly after their initial report on this type of host, velcrand **46** was rendered water-soluble [178], and indeed water solubility can be obtained with a number of polar R groups [124f]. These hosts bind guests in a 1:1 fashion, with amphiphilic guests adopting distinct helical motifs when bound [178], and non-amphiphiles tumbling rapidly within the pocket [179]. A few years after the initial report of water-solubilization, the attachment of doors to the portal of the cavity was found to control entry and egress [180], and as a consequence of their general binding properties these hosts have been shown to act as phase-transfer catalysts [181], and influence the redox chemistry of electroactive guests [182].

In 2010, one of Hooley's first independent papers focused on the development of a novel supramolecular switch based on the specific host-guest interactions of these kinds of velcrand [183]. The authors loaded fluorescein inside nano-porous silica and trapped them inside by capping the pores with gold nano-particles. The nano-particles were themselves coated with trimethylammonium groups, and so upon introducing the velcrand it bound to the ammonium groups, released the gold nano-particles from the silica, and hence allowed release of the encapsulated fluorescein.

A collaboration between the Hooley and Cheng groups has examined the properties of velcrands incorporated into lipid membrane bilayers [184]. Surface Plasmon Resonance and Fluorescence Microscopy revealed that by and large the host properties of velcrands such as **46** remain intact in the membrane, and this allowed molecules with trimethylammonium "handles" to bind to the membrane-bound hosts leaving their tails displayed at the surface. Any trimethylammonium derivative could be incorporated into the membrane, and as an example the authors bound a modified biotin that could be used to immobilize the protein avidin on the membrane. Theoretically, this system could be used to bind any protein, assuming that the protein target is known and strongly associates with it [185]. An analogous system built on a gold-surface, self-assembled monolayer was also reported [186]. Most recently, the same velcrand has been shown to embed in a supported lipid bilayer, anchor an ATRP initiator, and allow the synthesis of primary amine-containing polymethacrylate patches at the water-membrane interface [187]. Moreover, these polymers can be derivatized in situ to introduce fluorescent reporters, allow the selective recognition of proteins, and could be applied to the immobilization of non-adherent cells at the interface.

The same velcrand has also been shown to engender cavitand-mediated endocytosis [188]. The authors demonstrated selective, controlled endocytosis of a trimethylammonium-tagged fluorescein to several types of living human cells with little observed cytotoxicity. This approach therefore represents a novel method of small-molecule trans-membrane transport controlled by host-guest complementarity.

Very recently the Hooley group has modified the general velcrand structure **46** at the upper rim to incorporate metal-coordinating ligands ( $R' =$  various)

**Fig. 9.23** R' groups of **46** (Fig. 9.18) for halogen-bonded capsules

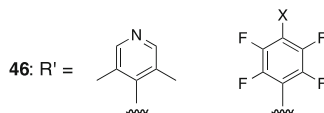
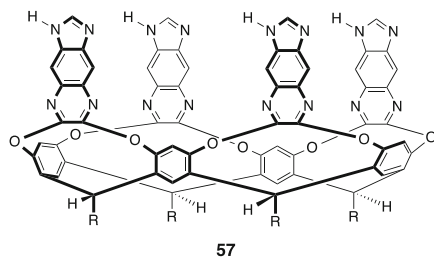


**Fig. 9.24** A recent velcrand from the Choi group



[189]. Metal-mediated self-folding can then be induced by coordination to control gating at the entrance and limit target binding.

Recently, the Diederich group has also adapted velcrands **46** with the R' groups shown in Fig. 9.23 [190]. Mixing these two hosts forms halogen-bonded capsules, with the pyridyl derivative acting as the acceptor and the fluorinated aryl derivative acting as the donor (X = F, Cl, Br, and I). As anticipated, it was the iodo-donor that afforded the most stable capsule. Only limited host-guest binding results have been so far presented.

Finally, Heung-Jin Choi and his group have made a preliminary report on the synthesis and binding properties of imidazoquinoxaline velcrand **57** (Fig. 9.24) [191]. An NMR analysis revealed that normal alkane guests bound weakly but exchanged relatively slowly.

### 9.5.5 Benzimidazolone Velcrands

Of the velcrands shown in Fig. 9.18, De Mendoza's benzimidazolone (*tetra*-carbamide) velcrand **47** (R = *n*-C<sub>11</sub>H<sub>23</sub>, X = O) is perhaps the least explored. In large part this can be attributed to its poor solubility. This point notwithstanding, **47** has been shown to dimerize in organic solvents and entrap guests within the corresponding nano-capsule [154b, 192].

The Rebek group has very recently revisited this type of host. They have shown that the solubility of this host can be improved by having tetraethylene glycol R groups [193]. Moreover, judicious choice of R group can render the host water soluble, allowing such examples to dimerize in water and trap a variety of guests within their inner spaces [194]. Interestingly, replacing the benzimidazolone oxygen with a sulfur atom results in a wider thiourea derivative with distinctly different hosting and assembly properties [124c, 195]. This intense flurry of papers in the past 4 years suggests that there is still much to learn about these hosts.

## 9.6 The Rise of Stereoselective Bridging

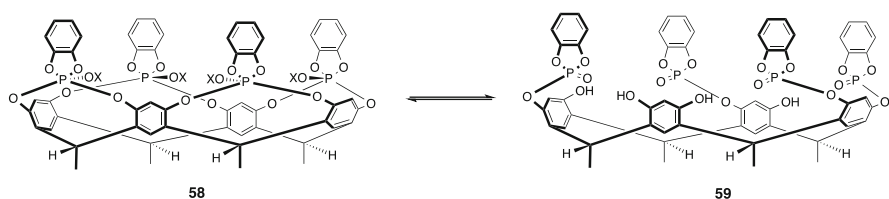
### 9.6.1 Phosphorus Bridging

In 1992 Markovsky and his group were the first to publish work concerning bridging with phosphorus when they introduced spirophosphorane moieties to the resorcinarene framework (Scheme 9.5) [196]. Cavitand **58** is itself in equilibrium with the unbridged form **59**; an equilibrium controlled by both solvent and temperature. There was no discussion concerning the stereochemistry of these reversibly formed bridges (only one isomer shown in **58**).

Extending this line of thought, Puddephatt's group reported in 1993 cavitands bridged with P(III) moieties. They demonstrated the formation of several *tetra*-gold (I) and *tetra*-copper(I) complexes and showed that they were capable of the size-selective binding of halide ions [197]. Molecular mechanics and NMR data were consistent with the stereochemistry of the free ligand in which the lone pairs on the phosphorus point towards the center of the pocket (**60**).

Dalcanale and Mann entered the field a year later with work centered around using P(V) moieties for bridging [198]. The authors observed all six possible isomers of phosphate cavitands with the P = O bond pointing either into or out of the pocket; compound **61** is the all in-isomer, a trace product in the original synthesis. Dalcanale's group extended their initial foray into this with a variety of mixed cavitands comprised of methylene and phosphate bridges [199]. Again the variability of the stereogenicity of the phosphorus bridges led to multiple isomers, and although these could be readily isolated and characterized, [199] this particular branch of cavitand chemistry has not grown significantly (Fig. 9.25).

Shortly after Dalcanale's initial exploration of phosphate bridging was reported, the Dutasta group published a synthesis of *tetra*-phosphonate cavitand **62** [200]. In



**Scheme 9.5** Reversible phosphorus bridging and the formation of spirophosphorane cavitands (**58**)

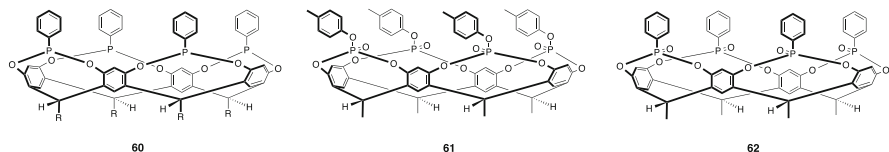


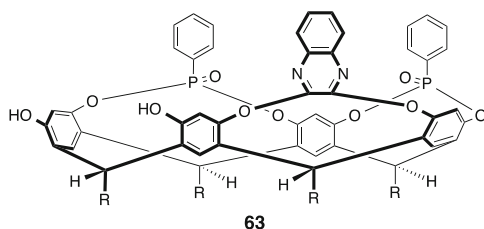
**Fig. 9.25** Select phosphorus-bridged cavitands

contrast to phosphate bridging, the major product reported was the all in-isomer with its strong hydrogen bond acceptors all pointing towards the center of the pocket. As a result, Dutasta was able to report strong binding of alkali metal and ammonium ions. The ease of synthesis of compounds such as **62**, with their deepened pockets and converging array of hydrogen bond acceptor groups has undoubtedly played a major role in the success of these types of cavitands relative to other phosphorous-bridged hosts.

Many variations to the structure of **62** have been published since 1998. In that year a team led by Dalcanale reported further structural characterization [201], and in 2003 the Dutasta group reported on the synthesis of the thio-phosphonate equivalent of **62** and its ability to complex (soft) metal ions [202]. A few years later, Dalcanale reported the synthesis of partially-bridged phosphonate and thio-phosphonate cavitands [203]. Both *bis*- and *tris*-bridged cavitands were successfully isolated, and in each case the P = O or P = S bonds faced inwards. Shortly thereafter, Dutasta and Dalcanale built on this work by synthesizing a *tris*-phosphonate bridged cavitand of which the fourth bridge was an *N*-methylpyridinium moiety [204]. The complementarity of the three inward pointing P = O groups and the charged pyridinium group on the fourth bridge resulted in a self-complimentary cavitand that formed dimers in all phases. Subsequently, mixed cavitands composed of different numbers of phenyl- and 4-(4-pyridyl)aryl (thio) phosphonates and their corresponding rhenium-linked hemicarceplexes were studied for methylpyridinium guest binding [205]. In this regard the number of inward pointing phosphonate groups was crucial to binding; for example, the removal of a single P = O bridge from each cavitand in the hemicarceplex was sufficient to reduce the binding constant of some guests by ~3-orders of magnitude. The same year the Dutasta group also reported on the synthesis of inherently chiral phosphonate-cavitands. Thus, the (*tris*-bridged) cavitand **63** (Fig. 9.26) and its enantiomer possessing a single quinoxaline bridge were synthesized and resolved, and their chiroptical properties investigated [206].  $^1\text{H}$  and  $^{31}\text{P}$  NMR were used to investigate their enantioselective guest complexation. Analogous studies with cavitands possessing two phosphonate and one quinoxaline bridge have also been studied [207].

Other reported phosphonate cavitands include a *tetra*-methyl phosphonate that has been shown to template, via its rigidly preorganized P = O acceptor groups, a unique cyclic water tetramer of  $C_4$  symmetry [208]. The same host has also been shown to bind zinc, barium, and calcium salts in a dimeric 2:1 host-guest complex

**Fig. 9.26** Inherently chiral cavitand **63** from the Dutasta group



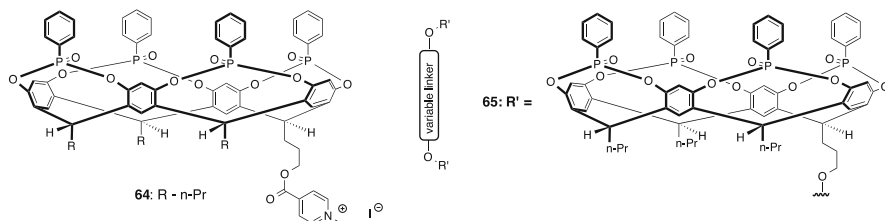


**Fig. 9.27** Phosphonate-bridged cavitands for supramolecular polymers

[209]. The assemblies incorporate multiple water molecules, with the metal ion coordinating to the waters and stabilized by interactions with the P = O bonds.

Phosphonate cavitands such as **62** are strong binders of ammonium ions, and the Dalcanale group have taken advantage of this to control the methylation of amines [210]. A reaction that is usually plagued by over-methylation, treatment of amines with methyl iodide was found to halt at mono-methylation because the ammonium form of this product was such a strong binder to the host that it was sequestered from the reaction milieu. A comparison with the simple methylene-bridged cavitant and the *tetra*-thio-phosphonate cavitant revealed that again the four phosphonate groups were essential.

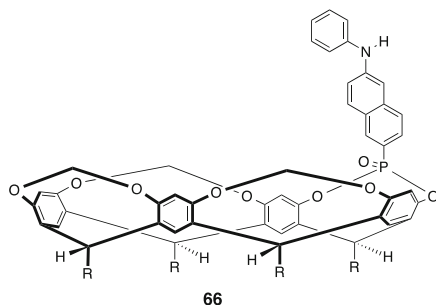
More recently, a number of mixed-bridged (thio)phosphonate cavitands, where for example the cavitant contains three P = O bridges and one P = S bridge, have also been investigated for their ammonium binding properties [211].

The Dalcanale group has taken advantage of the strong affinity of *tetra*-phosphonate bridged cavitands for methylpyridiniums [212] to form supramolecular polymers from cavitant **64** (Fig. 9.27) [213]. Furthermore, using a pyridinium-modified porphyrin core, the authors were able to also form star polymers using this cavitant. Through similar methods, Dalcanale developed a *tetra*-phosphonate cavitant system for forming linear and cyclic AABB supramolecular polymers using *bis*-cavitands linked through their feet (e.g., **65**) and *bis*-methylpyridyls [214]. The propensity of these to form acyclic or cyclic polymers depended on the nature of the linkers between the cavitands and the pyridines, but both linear polymeric chains and concentration-dependent rings were demonstrated using respectively X-ray analysis and solution viscosity measurements.

The aforementioned work has been a foundation for more recent sensor development. Dalcanale has demonstrated the utility of phosphonate cavitands for sensing water and alcohols in the gas phase [215]. In this work a number of mixed-bridged (methylene and phosphonate) cavitands were studied by X-ray crystallography, Mass Spectrometry and Quartz Crystal Microbalance that revealed the importance of cooperativity among the different host-guest interactions to engender selective sensing. A next-generation sensor (**66**, Fig. 9.28) loaded onto a PVC film was subsequently shown to be highly selective in sensing alcohol vapors [216].

Continuing on the theme of sensor development, the same group has built nano-mechanical silicon micro-cantilevers functionalized by a film of *tetra*-phosphonate cavitands that responded (flexed) to the presence of methyl pyridinium analytes

**Fig. 9.28** A *mono*-phosphonate bridged cavitand for alcohol sensing



[217]. The devised system was able to discriminate between guests differing by only 15 Daltons and could thereby be used to differentiate between sarcosine and glycine. Additionally, single-walled carbon nanotubes have been functionalized with the same *tetra*-phosphonate cavitand receptors and the binding of *N*-methylammonium guests analyzed by X-ray photoelectron spectroscopy and  $^{31}\text{P}$  MAS NMR [218]. These derivatized nano-tubes were shown to function as chemi-resistive sensory materials for sarcosine and its ethyl ester hydrochloride in water; in contrast to a decreased conductance response for competitors such as glycine ethyl ester hydrochloride, exposure to these guests resulted in increased conductance. Combining the idea of cavitand-functionalized nano-mechanical silicon micro-cantilevers for detection, and the supreme ability of *tetra*-phosphonate cavitand receptors to bind methyl ammonium guests, has led to the important development of universal probes for detecting illicit and designer drugs in aqueous solution [219]. Interestingly, even *tris*-bridged phosphonate cavitands provide good recognition. For example, they can bring about the selective complexation of acetylcholine and choline [220].

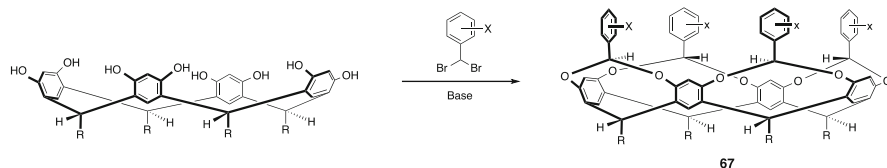
Massera has also turned to phosphonate cavitand **62** in an effort to separate ephedrine and pseudoephedrine [221]. While the cavitand was shown to bind both epimers, the host can discriminate against pseudoephedrine in a mixture of the guests by selectively binding ephedrine.

Finally, and most recently, phosphonate-cavitands have been used as catalysts [222]. Taking advantage of the strong affinity *tetra*-alkylammoniums have for these cavitands, Dutasta and Dufaud showed that bound *tetra*-alkylammonium halides catalytically oxidize epoxides in the presence of  $\text{CO}_2$  to form cyclic carbonates in excellent yields. Catalytic activity was improved dramatically over a system lacking the host cavitand, implying a cooperative effect in the catalytic host-guest system [222].

### 9.6.2 Benzal Bridging

In 1998 the Gibb group reported the first example of stereoselective bridging with carbon (**67**, Scheme 9.6) [223]. Shortly thereafter it was demonstrated that a range





**Scheme 9.6** Synthesis of benzal-bridged cavitands **67**

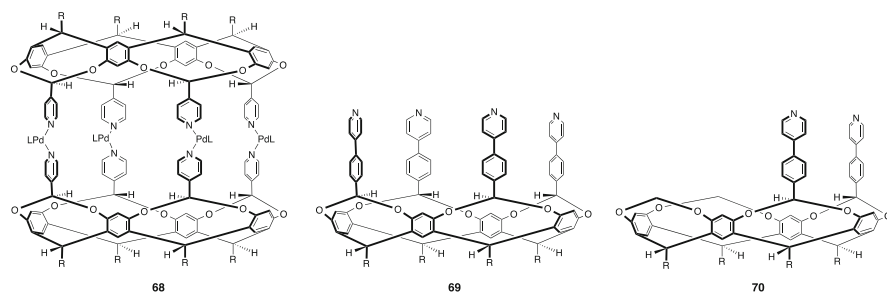
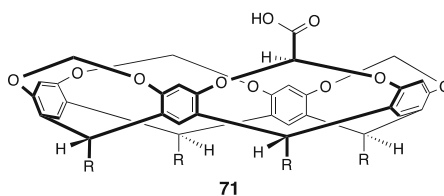


**Fig. 9.29** Selected benzal-bridged cavitands

**Fig. 9.30** A stereoselective bridged cavitaol from the Dalcanale group

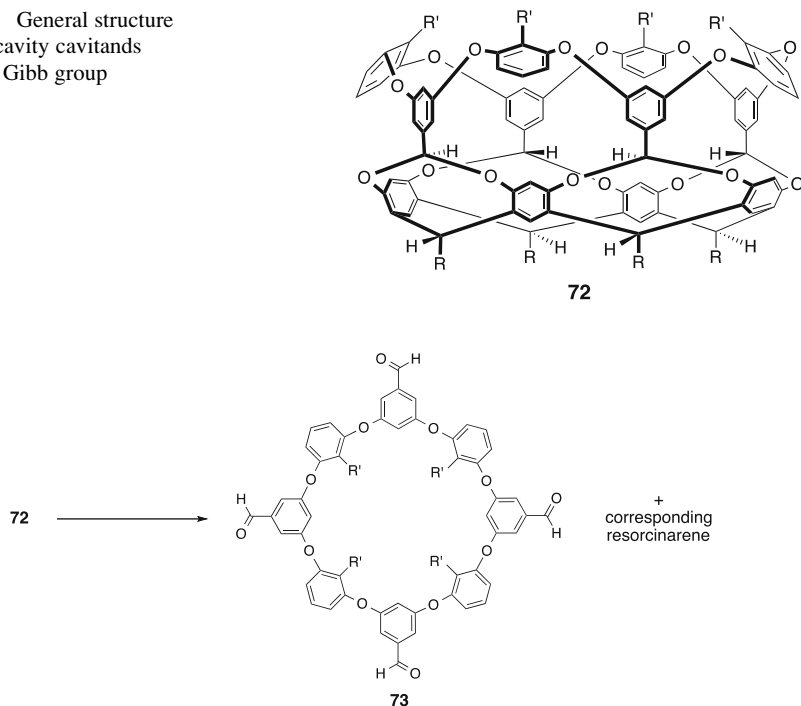


of functional groups (X) are tolerated by this reaction [224], and if desired it is possible to insert two different kinds of bridge to generate lower symmetry deep-cavity cavitands [225].

Guest binding to these hosts is inhibited by free rotation of the “second row” of aromatic rings. However in 2006 Dalcanale and Diederich reported that host **68** (Fig. 9.29) can bind fullerenes [226]. Around the same time, the Dalcanale group also reported on the metal-coordination driven assembly of deep-cavity cavitaol **69** [227], as well as mixed (*A,B*-) bridged cavitaol **70** and its corresponding *A,C*-bridged isomer [228]. Regarding **70** and its *A,C*-bridged isomer, in the presence of coordinating metals the former led to cyclic dimer, trimer and tetramer, whilst the latter only gave dimer.

In the guise of cavitaol **71** (Fig. 9.30) and its corresponding “in” isomer, the Dalcanale group have also demonstrated a second kind of stereoselective bridging with carbon [229]. Although diastereoselectivity was low, the two isomers could be isolated in good yield starting from the corresponding *tris*-methylene bridged cavitaol. These hosts were synthesized in the context of the detection of organophosphorus vapors.

**Fig. 9.31** General structure of deep-cavity cavitands from the Gibb group



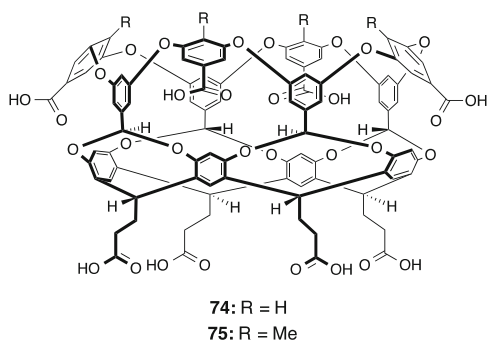
**Scheme 9.7** Synthesis of macrocycle **73** via resorcinarene templation

In 2001 the Gibb group demonstrated that instilling greater rigidity in molecules of general structure **67** could be accomplished by “weaving” with an eightfold Ullman ether reaction to generate cavitands, such as **72** (Fig. 9.31) [230]. These show well-defined host-guest chemistry driven in large part by shape complementarity and the possibility of C-H $\cdots$ X hydrogen bonds between host and (halogenated) guest [230, 231]. Lower symmetry examples followed, and it was shown that if one R' group is a strong hydrogen-bonding group then both the thermodynamics and kinetics of complexation can be greatly effected [232]. Such less symmetric derivatives can be formed by either a two-step Ullman ether final step, or by using the  $C_{4v}$  symmetric host such as **72** and carrying out either directed *ortho*-lithiation protocols or electrophilic aromatic substitution [233].

As well as serving as useful hosts and precursors to extended carceplexes [234]. Gibb showed in 2003 that cavitands such as **72** can be cleaved to form large macrocycles (e.g., **73** Scheme 9.7) [235].

In 2004 the Gibb group then demonstrated that these types of cavitand could be rendered water-soluble by the addition of eight carboxylic acid groups to their exterior surface [236]. This so-called “*octa-acid*” **74** (Fig. 9.32) [237]. is sparingly soluble at pH 7, but highly soluble and monomeric under basic conditions. Four years later other water-soluble derivatives, including neutral, dendrimer- or polymer-coated examples were reported by Gibb and Grayson [238].

**Fig. 9.32** Structures of *octa-acid* (OA) **74** and *tetra-endo-methyl octa-acid* (TEMOA) **75** cavitands



In 2004 it was demonstrated that, driven by the Hydrophobic effect, **74** dimerized around guest molecules such as steroids [236a]. Moreover, shortly thereafter it was shown that this dimerization occurred for much smaller and/or more flexible guests [239] and even moderately polar molecules [240]. Building on this work it was shown recently that highly flexible guests such as *n*-alkanes adopt distinct packing motifs within the capsule [241].

The capsule formed by **74** has been examined by the Gibb group as a novel technology for purification, and as a nano-scale (yocto-liter) reactor. Regarding the former, in 2006 solutions of the capsule formed by **74** were shown to bring about the physical separation of propane and butane from gas-phase mixtures [242]. Four years later it was demonstrated that kinetic resolutions of mixtures of constitutional isomers of esters could similarly be carried out [243]. As very recently highlighted however, the success of separating small molecules is dependent on whether a mixture forms homo-guest or hetero-guest complexes [244].

On the topic of the capsules formed by **74** as yocto-liter reaction vessels, beginning in 2004 the Gibb and Ramamurthy groups published a series of papers on how confinement within the capsule affects the photochemical reactivity of stored guests [245]. The Ramamurthy group have since expended considerable effort on this topic to demonstrate that the capsules formed by **74** are unique confining media for controlling photochemical reactions [246].

Also in the last decade, the Kaifer group has studied the properties of redox active guests within the dimer of **74** [247]. Interestingly, the encapsulation of ferrocene results in the complete elimination of any voltammetric response. In contrast, viologen guests do not bind to the inside of the capsule but instead bind to the four carboxylate feet of **74**. Hence simultaneous binding of both guests is possible. Investigating the encapsulation of ferrocene further revealed that the capsule suppresses direct electron transfer between the guest and the electrode surface [248]. Furthermore, the addition of suitable mediators that bind to the surface of the capsule leads to effective electron transfer and disassembly of the resulting ferrocenium-containing capsule. Kaifer later appended ferrocenes with amine- and amide-functionalized adamantanes and demonstrated their ability to be encapsulated within an *octa-acid* dimeric capsule [249].

Recently, Bohne and Gibb have probed the real-time kinetics of capsule assembly and disassembly to reveal a rapid ( $<1$  ms) formation of the 1:1 complex, a slower capping to form the 2:1 host-guest complex, as well as a microsecond “breathing” of the capsule that is five orders of magnitude faster than the disassembly rate [250].

*Octa-acid* **74** has been shown to also form 1:1 complexes with amphiphiles [251]. More intriguingly, in 2011 a study of how salts affect the complexation of amphiphile binding to **74** revealed that relatively hydrophobic anions (e.g.,  $I^-$  and  $ClO_4^-$ ) have an affinity for the hydrophobic pocket of the host, and that as a consequence the thermodynamics of amphiphile binding follows the Hofmeister effect [252]. Moreover, even the binding of the anions themselves is influenced by other salts in a Hofmeister-like manner because of cation condensation to the exterior of the host and potential anion binding to the pocket [253].

A subtle variant on **74** is the *tetra-endo-methyl octa-acid* (TEMOA) **75**. The presence of four methyl groups at the rim of the pocket has a dramatic effect on the binding and assembly properties of this host. For example, in 2011 it was demonstrated that whereas the relationship between guest size and the assembly state of **74** is monotonic, the assembly profile for **75** is non-monotonic; very small and medium sized guests form 1:1 complexes, whereas small and large guests form capsular complexes composed of two hosts [254]. This unusual property is also reflected in the self-sorting of mixtures of **74** and **75**; whether homo-host capsules or hetero-host capsules are formed depends on the guest being encapsulated [255]. Moreover, cavitand **75** is not only capable of forming dimeric capsules, but also containers composed of four ( $D_{2d}$  or pseudo tetrahedral  $T_d$ ) and six ( $O_h$ ) subunits [256]. The assembly state is dependent on the nature of the *n*-alkane guest, relatively small guests ( $< C_{14}$ ) form 2:1 capsules, medium sized guests ( $C_{17}$ – $C_{22}$ ) form 4:2 assemblies, whilst the largest guests examined ( $> C_{24}$ ) form 6:3 host-guest complexes ( $> C_{24}$ ).

## 9.7 Conclusions

This review of state-of-the-art cavitand chemistry demonstrates that after being initiated by Cram, the field has expanded considerably in large part because of the ease of functionalizing the two-position of resorcinarenes and cavitands, and because of the wide nature of the bridging group used to form these hosts. In particular, the last decade has seen a veritable explosion of variety and hence application of cavitands, from the very fundamental to the wholly applied. One is forced to conclude that the future is very bright for this unique type of host.

**Acknowledgements** BCG acknowledges the generous support of the NSF (CHE 1507344) for assistance in writing this review. AW similarly acknowledges the Louisiana Board of Regents for a graduate student fellowship (LEQSF(2013-18)-GF-13).

## References

1. Cram, D. J. *Science* **1983**, *219*, 1177–83.
2. Baeyer, A. *Chemische Berichte* **1872**, *5*, 280–282.
3. Michael, A. *American Chemical Journal* **1883**, *4*, 339–349.
4. Niederl, J. B.; Vogel, H. J. *J. Am. Chem. Soc.* **1940**, *62*, 2512–2514.
5. Erdtman, H.; Högberg, S.; Abrahamsson, S.; Nilsson, B. *Tetrahedron Lett.* **1968**, *9*, 1679–1682.
6. Högberg, A. G. S. *J. Org. Chem.* **1980**, *45*, 4498–4500.
7. Timmerman, P.; Verboom, W.; Reinhoudt, D. N. *Tetrahedron* **1996**, *52*, 2663–2704.
8. Pieroni, O. I.; Rodriguez, N. M.; Vuano, B. M.; Cabaleiro, M. C. *J. Chem. Res., Synop.* **1994**, 188–9.
9. Curtis, A. D. M. *Tetrahedron Lett.* **1997**, *38*, 4295–4296.
10. (a) Konishi, H.; Ohata, K.; Morikawa, O.; Kobayashi, K. *Chem. Commun.* **1995**, 309–310; (b) Konishi, H.; Nakamura, T.; Ohata, K.; Kobayashi, K.; Morikawa, O. *Tetrahedron Lett.* **1996**, *37*, 7383–7386.
11. Weinelt, F.; Schneider, H.-J. *J. Org. Chem.* **1991**, *56*, 5527–5535.
12. Middel, O.; Verboom, W.; Hulst, R.; Kooijman, H.; Spek, A. L.; Reinhoudt, D. N. *J. Org. Chem.* **1998**, *63*, 8259–8265.
13. Tancini, F.; Gottschalk, T.; Schweizer, W. B.; Diederich, F.; Dalcanale, E. *Chem. Eur. J.* **2010**, *16*, 7813–7819.
14. Moran, J. R.; Karbach, S.; Cram, D. J. *J. Am. Chem. Soc.* **1982**, *104*, 5826–5828.
15. Cram, D. J.; Cram, J. M., *Container Molecules and Their Guests*. The Royal Society of Chemistry: London, 1994.
16. Roman, E.; Peinador, C.; Mendoza, S.; Kaifer, A. E. *J. Org. Chem.* **1999**, *64*, 2577–2578.
17. Cram, D. J.; Karbach, S.; Kim, H.-E.; Knobler, C. B.; Maverick, E. F.; Ericson, J. L.; Helgeson, R. C. *J. Am. Chem. Soc.* **1988**, *110*, 2229–2237.
18. Cram, D. J.; Tunstad, L. M.; Knobler, C. B. *J. Org. Chem.* **1992**, *57*, 528–535.
19. Tunstad, L. M.; Tucker, J. A.; Dalcanale, E.; Weiser, J.; Bryant, J. A.; Sherman, J. C.; Helgeson, R. C.; Knobler, C. B.; Cram, D. J. *J. Org. Chem.* **1989**, *54*, 1305–1312.
20. Tucker, J. A.; Knobler, C. B.; Trueblood, K. N.; Cram, D. J. *J. Am. Chem. Soc.* **1989**, *111*, 3688–3699.
21. Cram, D. J.; Karbach, S.; Kim, Y. H.; Baczynskyj, L.; Marti, K.; Sampson, R. M.; Kallemeyn, G. W. *J. Am. Chem. Soc.* **1988**, *110*, 2554–2560.
22. (a) Bryant, J. A.; Blanda, M. T.; Vincenti, M.; Cram, D. J. *J. Chem. Soc., Chem. Commun.* **1990**, 1403; (b) Bryant, J. A.; Blanda, M. T.; Vincenti, M.; Cram, D. J. *J. Am. Chem. Soc.* **1991**, *113*, 2167–2172.
23. Sherman, J. C.; Cram, D. J. *J. Am. Chem. Soc.* **1989**, *111*, 4527–4528.
24. Sherman, J. C.; Knobler, C. B.; Cram, D. J. *J. Am. Chem. Soc.* **1991**, *113* (6), 2194–2204.
25. Cram, D. J.; Tanner, M. E.; Thomas, R. *Angew. Chem. Int. Ed.* **1991**, *30*, 1024–1027.
26. (a) Quan, M. L. C.; Cram, D. J. *J. Am. Chem. Soc.* **1991**, *113*, 2754–2755; (b) Judice, J. K.; Cram, D. J. *J. Am. Chem. Soc.* **1991**, *113*, 2790–2791.
27. Helgeson, R. C.; Paek, K.; Knobler, C. B.; Maverick, E. F.; Cram, D. J. *J. Am. Chem. Soc.* **1996**, *118*, 5590–5604.
28. Mendoza, S.; Godinez, L. A.; Kaifer, A. E. *Supramol. Chem.* **2004**, *16*, 165–169.
29. Timmerman, P.; Van Mook, M. G. A.; Verboom, W.; Van Hummel, G. J.; Harkema, S.; Reinhoudt, D. N. *Tetrahedron Lett.* **1992**, *33*, 3377–80.
30. Houk, K. N.; Nakamura, K.; Sheu, C.; Keating, A. E. *Science* **1996**, *273*, 627–629.
31. (a) Cram, D. J.; Choi, H. J.; Bryant, J. A.; Knobler, C. B. *J. Am. Chem. Soc.* **1992**, *114*, 7748–7765; (b) Moran, J. R.; Ericson, J. L.; Dalcanale, E.; Bryant, J. A.; Knobler, C. B.; Cram, D. J. *J. Am. Chem. Soc.* **1991**, *113*, 5707–5714.
32. (a) Chapman, R. G.; Chopra, N.; Cochien, E. D.; Sherman, J. C. *J. Am. Chem. Soc.* **1994**, *116*, 369–370; (b) Chapman, R. G.; Sherman, J. C. *J. Am. Chem. Soc.* **1995**, *117*, 9081–9082.

33. (a) Fraser, J. R.; Borecka, B.; Trotter, J.; Sherman, J. C. *J. Org. Chem.* **1995**, *60*, 1207–1213; (b) Chapman, R. G.; Olovsson, G.; Trotter, J.; Sherman, J. C. *J. Am. Chem. Soc.* **1998**, *120*, 6252–6260; (c) Chapman, R. G.; Sherman, J. C. *J. Am. Chem. Soc.* **1998**, *120*, 9818–9826; (d) Chapman, R. G.; Sherman, J. C. *J. Am. Chem. Soc.* **1999**, *121*, 1962–1963; (e) Chapman, R. G.; Sherman, J. C. *J. Org. Chem.* **2000**, *65*, 513–516.
34. Nakamura, K.; Sheu, C.; Keating, A. E.; Houk, K. N.; Sherman, J. C.; Chapman, R. G.; Jorgensen, W. L. *J. Am. Chem. Soc.* **1997**, *119*, 4321–4322.
35. Makeiff, D. A.; Pope, D. J.; Sherman, J. C. *J. Am. Chem. Soc.* **2000**, *122*, 1337–1342.
36. Timmerman, P.; Nierop, K. G. A.; Brinks, E. A.; Verboom, W.; van Veggel, F. C. J. M.; van Hoorn, W. P.; Reinhoudt, D. N. *Chem. Eur. J.* **1995**, *1*, 132–43.
37. Higler, I.; Timmerman, P.; Verboom, W.; Reinhoudt, D. N. *J. Org. Chem.* **1996**, *61*, 5920–5931.
38. Friggeri, A.; Van Veggel, F. C. J. M.; Reinhoudt, D. N. *Chem. Eur. J.* **1999**, *5*, 3595–3602.
39. Chopra, N.; Sherman, J. C. *Angew. Chem. Int. Ed.* **1997**, *36*, 1727–1729.
40. Chopra, N.; Naumann, C.; Sherman, J. C. *Angew. Chem. Int. Ed.* **2000**, *39*, 194–196.
41. Mungaroo, R.; Sherman, J. C. *Chem. Commun.* **2002**, 1672–1673.
42. Chopra, N.; Sherman, J. C. *Angew. Chem. Int. Ed.* **1999**, *38*, 1955–1957.
43. Makeiff, D. A.; Vishnumurthy, K.; Sherman, J. C. *J. Am. Chem. Soc.* **2003**, *125*, 9558–9559.
44. Warmuth, R. *Angew. Chem. Int. Ed. Engl.* **1997**, *36*, 1347–1350.
45. Warmuth, R. *Chem. Commun.* **1998**, 59–60.
46. Warmuth, R.; Marvel, M. A. *Angew. Chem. Int. Ed.* **2000**, *39*, 1117–1119.
47. Warmuth, R. *J. Am. Chem. Soc.* **2001**, *123*, 6955–6956.
48. Warmuth, R.; Kerdelhué, J.-L.; Sánchez Carrera, S.; Langenwalter, K. J.; Brown, N. *Angew. Chem. Int. Ed.* **2002**, *41*, 96–99.
49. Roach, P.; Warmuth, R. *Angew. Chem. Int. Ed. Engl.* **2003**, *42*, 3039–42.
50. Liu, X.; Chu, G.; Moss, R. A.; Sauers, R. R.; Warmuth, R. *Angew. Chem. Int. Ed. Engl.* **2005**, *44*, 1994–7.
51. (a) Warmuth, R.; Makowiec, S. *J. Am. Chem. Soc.* **2005**, *127*, 1084–1085; (b) Warmuth, R.; Makowiec, S. *J. Am. Chem. Soc.* **2007**, *129*, 1233–41.
52. Liu, Y.; Warmuth, R. *Angew. Chem. Int. Ed. Engl.* **2005**, *44*, 7107–10.
53. Irwin, J. L.; Sherburn, M. S. *Org. Lett.* **2001**, *3*, 225–227.
54. Barrett, E. S.; Irwin, J. L.; Turner, P.; Sherburn, M. S. *J. Org. Chem.* **2001**, *66*, 8227–8229.
55. Nguyen, T. V.; Sinclair, D. J.; Willis, A. C.; Sherburn, M. S. *Chem. Eur. J.* **2009**, *15*, 5892–5895.
56. Altamore, T. M.; Barrett, E. S.; Duggan, P. J.; Sherburn, M. S.; Szydzik, M. L. *Org. Lett.* **2002**, *4*, 3489–3491.
57. Barrett, E. S.; Irwin, J. L.; Edwards, A. J.; Sherburn, M. S. *J. Am. Chem. Soc.* **2004**, *126*, 16747–16749.
58. Makeiff, D.; Sherman, J. C. *J. Am. Chem. Soc.* **2005**, *127*, 12363–12367.
59. (a) Lee, J.; Choi, K.; Paek, K. *Tetrahedron Lett.* **1997**, *38*, 8203–8206; (b) Paek, K.; Ihm, C.; Ihm, H. *Tetrahedron Lett.* **1999**, *40*, 4697–4700.
60. Shin, J.; Paek, K. *Bull. Korean Chem. Soc.* **2014**, *35*, 2205–2206.
61. Naumann, C.; Roman, E.; Peinador, C.; Ren, T.; Patrick, B. O.; Kaifer, A. E.; Sherman, J. C., *Chem. – Eur. J.* **2001**, *7*, 1637–1645.
62. Naumann, C.; Patrick, B. O.; Sherman, J. *Chem. Eur. J.* **2002**, *8*, 3717.
63. Naumann, C.; Place, S.; Sherman, J. C. *J. Am. Chem. Soc.* **2002**, *124*, 16–17.
64. Fox, O. D.; Dalley, N. K.; Harrison, R. G. *J. Am. Chem. Soc.* **1998**, *120*, 7111–7112.
65. Harrison, R. G.; Burrows, J. L.; Hansen, L. D. *Chemistry* **2005**, *11*, 5881–8.
66. Fox, O. D.; Dalley, N. K.; Harrison, R. G. *Inorg. Chem.* **1999**, *38*, 5860–5863.
67. (a) Kobayashi, K.; Yamada, Y.; Yamanaka, M.; Sei, Y.; Yamaguchi, K. *J. Am. Chem. Soc.* **2004**, *126*, 13896–13897; (b) Yamanaka, M.; Yamada, Y.; Sei, Y.; Yamaguchi, K.; Kobayashi, K. *J. Am. Chem. Soc.* **2006**, *128*, 1531–1539.

68. Menozzi, E.; Pinalli, R.; Speets, E. A.; Ravoo, B. J.; Dalcanale, E.; Reinhoudt, D. N. *Chem. Eur. J.* **2004**, *10*, 2199–2206.
69. Ihm, C.; Lah, M. S.; Paek, K. *Bull. Korean Chem. Soc.* **2005**, *26*, 184–186.
70. Zuccaccia, D.; Pirondini, L.; Pinalli, R.; Dalcanale, E.; Macchioni, A. *J. Am. Chem. Soc.* **2005**, *127*, 7025–7032.
71. Jude, H.; Sinclair, D. J.; Das, N.; Sherburn, M. S.; Stang, P. J. *J. Org. Chem.* **2006**, *71*, 4155–4163.
72. Yamanaka, M.; Toyoda, N.; Kobayashi, K. *J. Am. Chem. Soc.* **2009**, *131*, 9880–9881.
73. Yamanaka, M.; Kawaharada, M.; Nito, Y.; Takaya, H.; Kobayashi, K. *J. Am. Chem. Soc.* **2011**, *133*, 16650–16656.
74. Kobayashi, K.; Shirasaka, T.; Horn, E.; Furukawa, N.; Yamaguchi, K.; Sakamoto, S. *Chem. Commun.* **2000**, 41–42.
75. Yamanaka, M.; Ishii, K.; Yamada, Y.; Kobayashi, K. *J. Org. Chem.* **2006**, *71*, 8800–8806.
76. Kobayashi, K.; Ishii, K.; Sakamoto, S.; Shirasaka, T.; Yamaguchi, K. *J. Am. Chem. Soc.* **2003**, *125*, 10615–10624.
77. Kobayashi, K.; Ishii, K.; Yamanaka, M. *Chem. Eur. J.* **2005**, *11*, 4725–4734.
78. Kobayashi, K.; Kitagawa, R.; Yamada, Y.; Yamanaka, M.; Suematsu, T.; Sei, Y.; Yamaguchi, K. *J. Org. Chem.* **2007**, *72*, 3242–3246.
79. Kitagawa, H.; Kawahata, M.; Kitagawa, R.; Yamada, Y.; Yamanaka, M.; Yamaguchi, K.; Kobayashi, K. *Tetrahedron* **2009**, *65*, 7234–7239.
80. Kitagawa, H.; Kobori, Y.; Yamanaka, M.; Yoza, K.; Kobayashi, K. *Proc. Natl. Acad. Sci.* **2009**, *106*, 10444–10448.
81. Tsuzuki, S.; Uchimar, T.; Mikami, M.; Kitagawa, H.; Kobayashi, K. *J. Phys. Chem. B* **2010**, *114*, 5335–5341.
82. Park, Y. S.; Paek, K. *Org. Lett.* **2008**, *10*, 4867–4870.
83. Park, Y. S.; Park, J.; Paek, K. *Chem. Commun.* **2013**, 49, 6316–6318.
84. Park, Y. S.; Park, J.; Paek, K. *Chem. Commun.* **2015**, *51*, 6006–6009.
85. Park, Y. S.; Seo, S.; Kim, E.-H.; Paek, K. *Org. Lett.* **2011**, *13*, 5904–5907.
86. (a) Park, H. S.; Paek, K. *Bull. Korean Chem. Soc.* **2009**, *30*, 505–508; (b) Park, Y. S.; Seo, S.; Paek, K. *Tetrahedron Lett.* **2011**, *52*, 5176–5179.
87. Park, Y. S.; Paek, K. *Tetrahedron Lett.* **2013**, *54*, 6291–6295.
88. Oshovsky, G. V.; Reinhoudt, D. N.; Verboom, W. *J. Org. Chem.* **2006**, *71*, 7441–7448.
89. (a) Gansey, M. H. B. G.; Bakker, F. K. G.; Feiters, M. C.; Geurts, H. P. M.; Verboom, W.; Reinhoudt, D. N. *Tetrahedron Lett.* **1998**, *39*, 5447–5450; (b) Middel, O.; Verboom, W.; Reinhoudt, D. N. *Eur. J. Org. Chem.* **2002**, 2587–2597.
90. Nishimura, N.; Kobayashi, K. *Angew. Chem., Int. Ed.* **2008**, *47*, 6255–6258.
91. Nishimura, N.; Yoza, K.; Kobayashi, K. *J. Am. Chem. Soc.* **2010**, *132*, 777–790.
92. Nishimura, N.; Kobayashi, K. *J. Org. Chem.* **2010**, *75*, 6079–6085.
93. Tamaki, K.; Ishigami, A.; Tanaka, Y.; Yamanaka, M.; Kobayashi, K. *Chem. Eur. J.* **2015**, *21*, 13714–13722.
94. (a) Gibb, B. C.; Mezo, A. R.; Causton, A. S.; Fraser, J. R.; Tsai, F. C. S.; Sherman, J. C. *Tetrahedron* **1995**, *51*, 8719–8732; (b) Gibb, B. C.; Mezo, A. R.; Sherman, J. C. *Tetrahedron Lett.* **1995**, *36*, 7587–7590.
95. Mezo, A. R.; Sherman, J. C. *J. Org. Chem.* **1998**, *63*, 6824–6829.
96. Mezo, A. R.; Sherman, J. C. *J. Am. Chem. Soc.* **1999**, *121*, 8983–8994.
97. Seo, E. S.; Scott, W. R.; Straus, S. K.; Sherman, J. C. *Chemistry* **2007**, *13*, 3596–605.
98. Huttunen-Hennelly, H. E.; Sherman, J. C. *Org. Biomol. Chem.* **2007**, *5*, 3637–50.
99. Freeman, J. O.; Lee, W. C.; Murphy, M. E. P.; Sherman, J. C. *J. Am. Chem. Soc.* **2009** *131*, 7421–7429.
100. (a) Freeman, J. O.; Sherman, J. C. *Chemistry* **2011**, *17*, 14120–8; (b) Freeman, J. O.; Murphy, M. E.; Sherman, J. C. *Chemistry* **2012**, *18*, 11409–16.
101. Yang, H.; Sherman, J. C. *Bioorg. Med. Chem. Lett.* **2013**, *23*, 1752–3.

102. (a) Causton, A. S.; Sherman, J. C. *J. Pept. Sci.* **2002**, *8*, 275–82; (b) Seo, E. S.; Sherman, J. C. *Biopolymers* **2007**, *88*, 774–9.
103. Nikan, M.; Sherman, J. C. *Angew. Chem. Int. Ed. Engl.* **2008**, *47*, 4900–2.
104. Nikan, M.; Sherman, J. C. *J. Org. Chem.* **2009**, *74*, 5211–8.
105. Bare, G. A.; Liu, B.; Sherman, J. C. *J. Am. Chem. Soc.* **2013**, *135*, 11985–9.
106. Hui, B. W.; Sherman, J. C. *Chem. Commun.* **2012**, *48*, 109–11.
107. Bare, G. A.; Sherman, J. C. *J. Org. Chem.* **2013**, *78*, 8198–202.
108. Sebo, L.; Diederich, F.; Gramlich, V. *Helv. Chim. Acta* **2000**, *83*, 93–113.
109. Ihm, C.; Cho, S.; Paek, K. *Bull. Korean Chem. Soc.* **2007**, *28*, 1867–1870.
110. Jung, N. S.; Lee, J.; Suh, S.; Paek, K. *Bull. Korean Chem. Soc.* **2009**, *30*, 2782–2784.
111. Fox, O. D.; Dalley, N. K.; Harrison, R. G. *Inorg. Chem.* **2000**, *39*, 620–622.
112. Gardner, J. S.; Conda-Sheridan, M.; Smith, D. N.; Harrison, R. G.; Lamb, J. D. *Inorg. Chem.* **2005**, *44*, 4295–300.
113. Gardner, J.; Peterson, Q.; Walker, J.; Jensen, B.; Adhikary, B.; Harrison, R.; Lamb, J. *J. Membr. Sci.* **2006**, *277*, 165–176.
114. Wang, J.; Lamb, J. D.; Hansen, L. D.; Harrison, R. G. *J. Incl. Phenom. Macrocycl. Chem.* **2009**, *67*, 55–61.
115. Wang, J.; Harrison, R. G.; Lamb, J. D. *J. Chromatogr. Sci.* **2009**, *47*, 510–515.
116. Li, N.; English, C.; Eaton, A.; Gillespie, A.; Ence, T. C.; Christensen, T. J.; Segó, A.; Harrison, R. G.; Lamb, J. D. *J. Chromatogr. A* **2012**, *1245*, 83–9.
117. (a) Li, N.; Harrison, R. G.; Lamb, J. D. *J. Incl. Phenom. Macrocycl. Chem.* **2013**, *78*, 39–60; (b) Panahi, T.; Weaver, D. J.; Lamb, J. D.; Harrison, R. G. *J. Chromatogr. A* **2015**, *1376*, 105–11.
118. Djernes, K. E.; Moshe, O.; Mettry, M.; Richards, D. D.; Hooley, R. J. *Org. Lett.* **2012**, *14*, 788–91.
119. Hong, J.; Djernes, K. E.; Lee, I.; Hooley, R. J.; Zaera, F. *ACS Catalysis* **2013**, *3*, 2154–2157.
120. El Moll, H.; Semeril, D.; Matt, D.; Youinou, M.-T.; Toupet, L. *Org. Biomol. Chem.* **2009**, *7*, 495–501.
121. El Moll, H.; Semeril, D.; Matt, D.; Toupet, L. *Eur. J. Org. Chem.* **2010**, 1158–1168.
122. Sahin, N.; Semeril, D.; Brenner, E.; Matt, D.; Oezdemir, I.; Kaya, C.; Toupet, L. *ChemCatChem* **2013**, *5*, 1116–1125.
123. (a) Dalcanele, E.; Soncini, P.; Bacchilega, G.; Ugozzoli, F. *J. Chem. Soc., Chem. Commun.* **1989**, 500; (b) Vincenti, M.; Dalcanele, E.; Soncini, P.; Guglielmetti, G. *J. Am. Chem. Soc.* **1990**, *112*, 445–447.
124. (a) Ma, S.; Rudkevich, D. M.; Rebek, J., Jr. *J. Am. Chem. Soc.* **1998**, *120*, 4977–4981; (b) Ajami, D.; Liu, L.; Rebek, J., Jr. *Chem. Soc. Rev.* **2015**, *44*, 490–9; (c) Ajami, D.; Rebek, J. Jr. *Acc. Chem. Res.* **2013**, *46*, 990–999; (d) Ajami, D.; Rebek, J., Jr. *Top. Curr. Chem.* **2012**, *319*, 57–78; (e) Ajami, D.; Rebek, J., Jr. *J. Org. Chem.* **2009**, *74*, 6584–6591; (f) Biros, S. M.; Rebek, J., Jr. *Chem. Soc. Rev.* **2007**, *36*, 93–104.
125. Skinner, P. J.; Cheetham, A. G.; Beeby, A.; Gramlich, V.; Diederich, F. *Helv. Chim. Acta* **2001**, *84*, 2146–2153.
126. Frei, M.; Marotti, F.; Diederich, F. *Chem. Commun.* **2004**, 1362–1363.
127. (a) Azov, V. A.; Diederich, F.; Lill, Y.; Hecht, B. *Helv. Chim. Acta* **2003**, *86*, 2149–2155; (b) Azov, V. A.; Skinner, P. J.; Yamakoshi, Y.; Seiler, P.; Gramlich, V.; Diederich, F. *Helv. Chim. Acta* **2003**, *86*, 3648–3670.
128. Pochorovski, I.; Breiten, B.; Schweizer, W. B.; Diederich, F. *Chem. Eur. J.* **2010**, *16*, 12590–12602.
129. Pochorovski, I.; Knehans, T.; Nettels, D.; Müller, A. M.; Schweizer, W. B.; Caflisch, A.; Schuler, B.; Diederich, F. *J. Am. Chem. Soc.* **2014**, *136*, 2441–2449.
130. (a) Pochorovski, I.; Diederich, F. *Isr. J. Chem.* **2012**, *52*, 20–29; (b) Shirtcliff, L. D.; Xu, H.; Diederich, F. *Eur. J. Org. Chem.* **2010**, 846–855.
131. (a) Azov, V. A.; Beeby, A.; Cacciarini, M.; Cheetham, A. G.; Diederich, F.; Frei, M.; Gimzewski, J. K.; Gramlich, V.; Hecht, B.; Jaun, B.; Lатыchevskaia, T.; Lieb, A.; Lill, Y.;



- Marotti, F.; Schlegel, A.; Schlittler, R. R.; Skinner, P. J.; Seiler, P.; Yamakoshi, Y. *Adv. Funct. Mater.* **2006**, *16*, 147–156; (b) Azov, V. A.; Jaun, B.; Diederich, F. *Helv. Chim. Acta* **2004**, *87*, 449–462.
132. Hornung, J.; Fankhauser, D.; Shirtcliff, L. D.; Praetorius, A.; Schweizer, W. B.; Diederich, F. *Chem. Eur. J.* **2011**, *17*, 12362–12371.
133. Roncucci, P.; Pirondini, L.; Paderni, G.; Massera, C.; Dalcanale, E.; Azov, V. A.; Diederich, F. *Chemistry* **2006**, *12*, 4775–84.
134. Pochorovski, I.; Diederich, F. *Acc. Chem. Res.* **2014**, *47*, 2096–2105.
135. Frei, M.; Diederich, F.; Tremont, R.; Rodriguez, T.; Echegoyen, L. *Helv. Chim. Acta* **2006**, *89*, 2040–2057.
136. Pochorovski, I.; Boudon, C.; Gisselbrecht, J.-P.; Ebert, M.-O.; Schweizer, W. B.; Diederich, F. *Angew. Chem. Int. Ed.* **2012**, *51*, 262–266.
137. Pochorovski, I.; Ebert, M.-O.; Gisselbrecht, J.-P.; Boudon, C.; Schweizer, W. B.; Diederich, F. *J. Am. Chem. Soc.* **2012**, *134*, 14702–14705.
138. Pochorovski, I.; Milic, J.; Kolarski, D.; Gropp, C.; Schweizer, W. B.; Diederich, F. *J. Am. Chem. Soc.* **2014**, *136*, 3852–3858.
139. Clément, P.; Korom, S.; Struzzi, C.; Parra, E. J.; Bittencourt, C.; Ballester, P.; Llobet, E. *Adv. Funct. Mater.* **2015**, *25*, 4011–4020.
140. (a) Rebek, J., Jr.; Heinz, T.; Rudkevich, D. M. *Nature* **1998**, *394*, 764–766; (b) Heinz, T.; Rudkevich, D. M.; Rebek, J., Jr. *Angew. Chem. Int. Ed.* **1999**, *38*, 1136–1139.
141. (a) Scarso, A.; Trembleau, L.; Rebek, J., Jr. *J. Am. Chem. Soc.* **2004**, *126*, 13512–13518; (b) Scarso, A.; Trembleau, L.; Rebek, J., Jr. *Angew. Chem. Int. Ed.* **2003**, *42*, 5499–5502.
142. Shivanyuk, A.; Rebek, J., Jr. *Angew. Chem. Int. Ed.* **2003**, *42*, 684–686.
143. Rechavi, D.; Scarso, A.; Rebek, J., Jr. *J. Am. Chem. Soc.* **2004**, *126*, 7738–7739.
144. Amaya, T.; Rebek, J., Jr. *J. Am. Chem. Soc.* **2004**, *126*, 6216–6217.
145. Iwasawa, T.; Mann, E.; Rebek, J., Jr. *J. Am. Chem. Soc.* **2006**, *128*, 9308–9309.
146. Ams, M. R.; Ajami, D.; Craig, S. L.; Yang, J.-S.; Rebek, J., Jr. *J. Am. Chem. Soc.* **2009**, *131*, 13190–13191.
147. Jiang, W.; Ajami, D.; Rebek, J., Jr. *J. Am. Chem. Soc.* **2012**, *134*, 8070–8073.
148. Sarwar, M. G.; Ajami, D.; Theodorakopoulos, G.; Petsalakis, I. D.; Rebek, J., Jr. *J. Am. Chem. Soc.* **2013**, *135*, 13672–13675.
149. Jiang, W.; Rebek, J., Jr. *J. Am. Chem. Soc.* **2012**, *134*, 17498–17501.
150. Lledo, A.; Kamioka, S.; Sather, A. C.; Rebek, J., Jr. *Angew. Chem. Int. Ed.* **2011**, *50*, 1299–1301.
151. Ajami, D.; Hou, J.-L.; Dale, T. J.; Barrett, E.; Rebek, J., Jr. *Proc. Natl. Acad. Sci., Early Ed.* **2009**, 1–5.
152. (a) Ajami, D.; Rebek, J., Jr. *J. Am. Chem. Soc.* **2006**, *128*, 5314–5315; (b) Ajami, D.; Rebek, J., Jr. *J. Am. Chem. Soc.* **2006**, *128*, 15038–15039; (c) Tzeli, D.; Theodorakopoulos, G.; Petsalakis, I. D.; Ajami, D.; Rebek, J., Jr. *J. Am. Chem. Soc.* **2012**, *134*, 4346–4354.
153. Ajami, D.; Rebek, J., Jr. *Nat. Chem.* **2009**, *1*, 87–90.
154. (a) Tzeli, D.; Petsalakis, I. D.; Theodorakopoulos, G.; Ajami, D.; Jiang, W.; Rebek, J., Jr. *Chem. Phys. Lett.* **2012**, *548*, 55–59; (b) Jiang, W.; Tiefenbacher, K.; Ajami, D.; Rebek, J., Jr. *Chem. Sci.* **2012**, *3*, 3022–3025.
155. (a) Taira, T.; Ajami, D.; Rebek, J., Jr. *J. Am. Chem. Soc.* **2012**, *134*, 11971–11973; (b) Ajami, D.; Rebek, J., Jr. *Proc. Natl. Acad. Sci.* **2007**, *104*, 16000–16003.
156. (a) Tiefenbacher, K.; Ajami, D.; Rebek, J., Jr. *Angew. Chem. Int. Ed.* **2011**, *50*, 12003–12007; (b) Ajami, D.; Rebek, J., Jr. *Angew. Chem. Int. Ed.* **2007**, *46*, 9283–9286.
157. Tiefenbacher, K.; Rebek, J., Jr. *J. Am. Chem. Soc.* **2012**, *134*, 2914–2917.
158. Rudkevich, D. M.; Hilmersson, G.; Rebek, J., Jr. *J. Am. Chem. Soc.* **1998**, *120*, 12216–12225.
159. (a) Hooley, R. J.; Rebek, J., Jr. *J. Am. Chem. Soc.* **2005**, *127*, 11904–11905; (b) Purse, B. W.; Gissot, A.; Rebek, J., Jr. *J. Am. Chem. Soc.* **2005**, *127*, 11222–11223.
160. Starnes, S. D.; Rudkevich, D. M.; Rebek, J., Jr. *J. Am. Chem. Soc.* **2001**, *123*, 4659–4669.
161. Wash, P. L.; Renslo, A. R.; Rebek, J., Jr. *Angew. Chem. Int. Ed.* **2001**, *40*, 1221–1222.

162. Renslo, A. R.; Rebek, J., Jr. *Angew. Chem. Int. Ed.* **2000**, *39*, 3281–3283.
163. Lücking, U.; Chen, J.; Rudkevich, D. M.; Rebek, J., Jr. *J. Am. Chem. Soc.* **2001**, *123*, 9929–9934.
164. Gibson, C.; Rebek, J., Jr. *Org. Lett.* **2002**, *4*, 1887–1890.
165. (a) Restorp, P.; Rebek, J., Jr. *J. Am. Chem. Soc.* **2008**, *130*, 11850–11851; (b) Iwasawa, T.; Hooley, R. J.; Rebek, J., Jr. *Science* **2007**, *317*, 493–496; (c) Hooley, R. J.; Iwasawa, T.; Rebek, J., Jr. *J. Am. Chem. Soc.* **2007**, *129*, 15330–15339; (d) Butterfield, S. M.; Rebek, J., Jr. *J. Am. Chem. Soc.* **2006**, *128*, 15366–15367; (e) Gissot, A.; Rebek, J., Jr. *J. Am. Chem. Soc.* **2004**, *126*, 7424–7425; (f) Richeter, S.; Rebek, J., Jr. *J. Am. Chem. Soc.* **2004**, *126*, 16280–16281; (g) Purse, B. W.; Ballester, P.; Rebek, J., Jr. *J. Am. Chem. Soc.* **2003**, *125*, 14682–3; (h) Shenoy, S. R.; Pinacho Crisostomo, F. R.; Iwasawa, T.; Rebek, J., Jr. *J. Am. Chem. Soc.* **2008**, *130*, 5658–5659.
166. Sarmentero, M. A.; Fernandez-Perez, H.; Zuidema, E.; Bo, C.; Vidal-Ferran, A.; Ballester, P. *Angew. Chem. Int. Ed. Engl.* **2010**, *49*, 7489–92.
167. Korom, S.; Ballester, P. *Eur. J. Org. Chem.* **2014**, *2014*, 4276–4282.
168. Degardin, M.; Busseron, E.; Kim, D.-A.; Ajami, D.; Rebek, J., Jr. *Chem. Commun.* **2012**, *48*, 11850–11852.
169. Busseron, E.; Lux, J.; Degardin, M.; Rebek, J., Jr. *Chem. Commun.* **2013**, *49*, 4842–4844.
170. Javor, S.; Rebek, J., Jr. *J. Am. Chem. Soc.* **2011**, *133*, 17473–17478.
171. Mosca, S.; Ajami, D.; Rebek, J., Jr. *Proc. Natl. Acad. Sci.* **2015**, *112*, 11181–11186.
172. Ballester, P.; Shivanyuk, A.; Far, A. R.; Rebek, J., Jr. *J. Am. Chem. Soc.* **2002**, *124*, 14014–14016.
173. Ballester, P.; Sarmentero, M. A. *Org. Lett.* **2006**, *8*, 3477–80.
174. Ampurdanes, J.; Crespo, G. A.; Maroto, A.; Sarmentero, M. A.; Ballester, P.; Rius, F. X. *Biosens. Bioelectron.* **2009**, *25*, 344–9.
175. Zuidema, E.; Sarmentero, M. A.; Bo, C.; Ballester, P. *Chemistry* **2008**, *14*, 7285–95.
176. (a) Far, A. R.; Shivanyuk, A.; Rebek, J., Jr. *J. Am. Chem. Soc.* **2002**, *124*, 2854–2855; (b) Choi, H.-J.; Park, Y. S.; Song, J.; Youn, S. J.; Kim, H.-S.; Kim, S.-H.; Koh, K.; Paek, K. *J. Org. Chem.* **2005**, *70*, 5974–5981.
177. Schramm, M. P.; Hooley, R. J.; Rebek, J., Jr. *J. Am. Chem. Soc.* **2007**, *129*, 9773–9.
178. Trembleau, L.; Rebek, J., Jr. *Science* **2003**, *301*, 1219–1221.
179. (a) Biroš, S. M.; Ullrich, E. C.; Hof, F.; Trembleau, L.; Rebek, J., Jr. *J. Am. Chem. Soc.* **2004**, *126*, 2870–2876; (b) Hooley, R. J.; Gavette, J. V.; Mettry, M.; Ajami, D.; Rebek, J., Jr. *Chem. Sci.* **2014**, *5*, 4382–4387.
180. Hooley, R. J.; Van Anda, H. J.; Rebek, J., Jr. *J. Am. Chem. Soc.* **2006**, *128*, 3894–3895.
181. Hooley, R. J.; Biroš, S. M.; Rebek, J., Jr. *Angew. Chem. Int. Ed.* **2006**, *45*, 3517–3519.
182. Podkoscielny, D.; Hooley, R. J.; Rebek, J., Jr.; Kaifer, A. E. *Org. Lett.* **2008**, *10*, 2865–2868.
183. Liu, R.; Liao, P.; Zhang, Z.; Hooley, R. J.; Feng, P. *Chem. Mater.* **2010**, *22*, 5797–5799.
184. Liu, Y.; Liao, P.; Cheng, Q.; Hooley, R. J. *J. Am. Chem. Soc.* **2010**, *132*, 10383–90.
185. (a) Ghang, Y. J.; Lloyd, J. J.; Moehlig, M. P.; Arguelles, J. K.; Mettry, M.; Zhang, X.; Julian, R. R.; Cheng, Q.; Hooley, R. J. *Langmuir* **2014**, *30*, 10161–6; (b) Ghang, Y. J.; Perez, L.; Morgan, M. A.; Si, F.; Hamdy, O. M.; Beecher, C. N.; Larive, C. K.; Julian, R. R.; Zhong, W.; Cheng, Q.; Hooley, R. J. *Soft Matter* **2014**, *10*, 9651–6.
186. Liu, Y.; Taira, T.; Young, M. C.; Ajami, D.; Rebek, J., Jr.; Cheng, Q.; Hooley, R. J. *Langmuir* **2012**, *28*, 1391–1398.
187. Perez, L.; Ghang, Y. J.; Williams, P. B.; Wang, Y.; Cheng, Q.; Hooley, R. J. *Langmuir* **2015**, *31*, 11152–7.
188. Ghang, Y. J.; Schramm, M. P.; Zhang, F.; Acey, R. A.; David, C. N.; Wilson, E. H.; Wang, Y.; Cheng, Q.; Hooley, R. J. *J. Am. Chem. Soc.* **2013**, *135*, 7090–3.
189. Mettry, M.; Moehlig, M. P.; Hooley, R. J. *Org. Lett.* **2015**, *17*, 1497–500.
190. Dumele, O.; Trapp, N.; Diederich, F. *Angew. Chem. Int. Ed.* **2015**, *54*, 12339–12344.
191. Choi, H.-J.; Nguyen, Q.-T.; Park, Y. S.; Choi, C.-H.; Paek, K.; Kim, E.-H., *Chem. Commun.* **2009**, 4971–4973.

192. (a) Ebbing, M. H.; Villa, M. J.; Valpuesta, J. M.; Prados, P.; de Mendoza, J. *Proc. Natl. Acad. Sci.* **2002**, *99*, 4962–6; (b) Choi, H. J.; Park, Y. S.; Cho, C. S.; Koh, K.; Kim, S.-H.; Paek, K. *Org. Lett.* **2004**, *6*, 4431–4433.
193. Tiefenbacher, K.; Zhang, K.-d.; Ajami, D.; Rebek, J., Jr., *J. Phys. Org. Chem.* **2015**, *28*, 187–190.
194. (a) Zhang, K.-D.; Ajami, D.; Gavette, J. V.; Rebek, J., Jr. *J. Am. Chem. Soc.* **2014**, *136*, 5264–5266; (b) Zhang, K.-D.; Ajami, D.; Rebek, J., Jr. *J. Am. Chem. Soc.* **2013**, *135*, 18064–18066; (c) Gavette, J. V.; Petsalakis, I. D.; Theodorakopoulos, G.; Zhang, K.-D.; Yu, Y.; Rebek, J., Jr. *Chem. Commun.* **2015**, Ahead of Print.
195. Asadi, A.; Ajami, D.; Rebek, J., Jr. *J. Am. Chem. Soc.* **2011**, *133*, 10682–4.
196. Markovsky, L. N.; Kal'chenko, V. I.; Rudkevich, D. M.; Shivanyuk, A. N. *Mendeleev Commun.* **1992**, *2*, 106–108.
197. (a) Xu, W.; Rourke, J. P.; Vittal, J. J.; Puddephatt, R. J. *J. Chem. Soc., Chem. Commun.* **1993**, 145; (b) Xu, W.; Vittal, J. J.; Puddephatt, R. J. *J. Am. Chem. Soc.* **1993**, *115*, 6456–6457.
198. (a) Lippmann, T.; Dalcanale, E.; Mann, G. *Tetrahedron Lett.* **1994**, *35*, 1685–1688; (b) Lippmann, T.; Wilde, H.; Dalcanale, E.; Mavilla, L.; Mann, G.; Heyer, U.; Spera, S. *J. Org. Chem.* **1995**, *60*, 235–242.
199. Dalcanale, E.; Jacopozi, P.; Ugozzoli, F.; Mann, G. *Supramol. Chem.* **1998**, *9*, 305–316.
200. (a) Delangle, P.; Dutasta, J.-P., *Tetrahedron Lett.* **1995**, *36*, 9325–9328; (b) Delangle, P.; Mulatier, J.-C.; Tinant, B.; Declercq, J.-P.; Dutasta, J.-P., *Eur. J. Org. Chem.* **2001**, *2001*, 3695.
201. Jacopozi, P.; Dalcanale, E.; Spera, S.; Chrisstoffels, L. A. J.; Reinhoudt, D. N.; Lippmann, T.; Mann, G., *J. Chem. Soc., Perkin Trans. 2* **1998**, 671–678.
202. Bibal, B.; Declercq, J.-P.; Dutasta, J.-P.; Tinant, B.; Valade, A.-G. *Tetrahedron* **2003**, *59*, 5849–5854.
203. Cantadori, B.; Betti, P.; Boccini, F.; Massera, C.; Dalcanale, E. *Supramol. Chem.* **2008**, *20*, 29–34.
204. Dubessy, B.; Harthong, S.; Aronica, C.; Bouchu, D.; Busi, M.; Dalcanale, E.; Dutasta, J. P. *J. Org. Chem.* **2009**, *74*, 3923–6.
205. Busi, M.; Cantadori, B.; Boccini, F.; De Zorzi, R.; Geremia, S.; Dalcanale, E. *Eur. J. Org. Chem.* **2011**, *2011*, 2629–2642.
206. Vachon, J.; Harthong, S.; Jeanneau, E.; Aronica, C.; Vanthuyne, N.; Roussel, C.; Dutasta, J.-P. *Org. Biomol. Chem.* **2011**, *9*, 5086–5091.
207. Vachon, J.; Harthong, S.; Dubessy, B.; Dutasta, J.-P.; Vanthuyne, N.; Roussel, C.; Naubron, J.-V. *Tetrahedron: Asymmetry* **2010**, *21*, 1534–1541.
208. Massera, C.; Melegari, M.; Ugozzoli, F.; Dalcanale, E. *Chem. Commun.* **2010**, *46*, 88–90.
209. Melegari, M.; Massera, C.; Ugozzoli, F.; Dalcanale, E. *CrystEngComm* **2010**, *12*, 2057.
210. Yebeutchou, R. M.; Dalcanale, E. *J. Am. Chem. Soc.* **2009**, *131*, 2452–3.
211. Menozzi, D.; Pinalli, R.; Massera, C.; Maffei, F.; Dalcanale, E. *Molecules* **2015**, *20*, 4460–72.
212. (a) Biavardi, E.; Battistini, G.; Montalti, M.; Yebeutchou, R. M.; Prodi, L.; Dalcanale, E. *Chem. Commun.* **2008**, 1638–40; (b) Menozzi, D.; Biavardi, E.; Massera, C.; Schmidtchen, F.-P.; Cornia, A.; Dalcanale, E. *Supramol. Chem.* **2010**, *22*, 768–775.
213. Yebeutchou, R. M.; Tancini, F.; Demitri, N.; Geremia, S.; Mendichi, R.; Dalcanale, E. *Angew. Chem. Int. Ed. Engl.* **2008**, *47*, 4504–8.
214. Tancini, F.; Yebeutchou, R. M.; Pirondini, L.; De Zorzi, R.; Geremia, S.; Scherman, O. A.; Dalcanale, E. *Chemistry* **2010**, *16*, 14313–21.
215. Melegari, M.; Suman, M.; Pirondini, L.; Moiani, D.; Massera, C.; Ugozzoli, F.; Kalenius, E.; Vainiotalo, P.; Mulatier, J. C.; Dutasta, J. P.; Dalcanale, E. *Chemistry* **2008**, *14*, 5772–9.
216. Maffei, F.; Betti, P.; Genovese, D.; Montalti, M.; Prodi, L.; De Zorzi, R.; Geremia, S.; Dalcanale, E. *Angew. Chem. Int. Ed. Engl.* **2011**, *50*, 4654–7.
217. Dionisio, M.; Oliviero, G.; Menozzi, D.; Federici, S.; Yebeutchou, R. M.; Schmidtchen, F. P.; Dalcanale, E.; Bergese, P. *J. Am. Chem. Soc.* **2012**, *134*, 2392–8.

218. Dionisio, M.; Schnorr, J. M.; Michaelis, V. K.; Griffin, R. G.; Swager, T. M.; Dalcanale, E. *J. Am. Chem. Soc.* **2012**, *134*, 6540–3.
219. Biavardi, E.; Federici, S.; Tudisco, C.; Menozzi, D.; Massera, C.; Sottini, A.; Condorelli, G. G.; Bergese, P.; Dalcanale, E. *Angew. Chem. Int. Ed.* **2014**, *53*, 9183–9188.
220. (a) Abdoul-Carime, H.; Harb, M. M.; Montano, C. G.; Teyssier, C.; Farizon, B.; Farizon, M.; Vachon, J.; Harthong, S.; Dutasta, J.-P.; Jeanneau, E.; Maerk, T. D. *Chem. Phys. Lett.* **2012**, *533*, 82–86; (b) Abdoul-Carime, H.; Farizon, B.; Farizon, M.; Mulatier, J.-C.; Dutasta, J.-P.; Chermette, H. *Phys. Chem. Chem. Phys.* **2015**, *17*, 4448–4457; (c) Mettra, B.; Bretonniere, Y.; Mulatier, J.-C.; Bibal, B.; Tinant, B.; Aronica, C.; Dutasta, J.-P. *Supramol. Chem.* **2013**, *25*, 672–681.
221. Biavardi, E.; Ugozzoli, F.; Massera, C. *Chem. Commun.* **2015**, *51*, 3426–3429.
222. Mirabaud, A.; Mulatier, J.-C.; Martinez, A.; Dutasta, J.-P.; Dufaud, V. *ACS Catal.* **2015**, *5*, 6748–6752.
223. Xi, H.; Gibb, C. L. D.; Stevens, E. D.; Gibb, B. C. *Chem. Commun.* **1998**, 1743–1744.
224. Xi, H.; Gibb, C. L. D.; Gibb, B. C. *J. Org. Chem.* **1999**, *64*, 9286–9288.
225. Green, J. O.; Baird, J.-H.; Gibb, B. C. *Org. Lett.* **2000**, *2*, 3845–3848.
226. Pirondini, L.; Bonifazi, D.; Cantadori, B.; Braiuca, P.; Campagnolo, M.; De Zorzi, R.; Geremia, S.; Diederich, F.; Dalcanale, E. *Tetrahedron* **2006**, *62*, 2008–2015.
227. Pinalli, R.; Cristini, V.; Sottili, V.; Geremia, S.; Campagnolo, M.; Caneschi, A.; Dalcanale, E. *J. Am. Chem. Soc.* **2004**, *126*, 6516–6517.
228. Menozzi, E.; Busi, M.; Massera, C.; Ugozzoli, F.; Zuccaccia, D.; Macchioni, A.; Dalcanale, E. *J. Org. Chem.* **2006**, *71*, 2617–2624.
229. Tudisco, C.; Betti, P.; Motta, A.; Pinalli, R.; Bombaci, L.; Dalcanale, E.; Condorelli, G. G. *Langmuir* **2012**, *28*, 1782–1789.
230. Gibb, C. L. D.; Stevens, E. D.; Gibb, B. C. *J. Am. Chem. Soc.* **2001**, *123*, 5849–5850.
231. (a) Gibb, C. L. D.; Xi, H.; Politzer, P. A.; Concha, M.; Gibb, B. C. *Tetrahedron* **2002**, *58*, 673–681; (b) Laughrey, Z. R.; Gibb, C. L.; Senechal, T.; Gibb, B. C. *Chemistry* **2003**, *9*, 130–9.
232. Gibb, C. L. D.; Li, X.; Gibb, B. C. *Proc. Natl. Acad. Sci.* **2002**, *99*, 4857–4862.
233. (a) Laughrey, Z. R.; Gibb, B. C. *J. Org. Chem.* **2006**, *71*, 1289–1294; (b) Srinivasan, K.; Laughrey, Z. R.; Gibb, B. C. *Eur. J. Org. Chem.* **2008**, 3265–3271; (c) Srinivasan, K.; Gibb, B. C. *Org. Lett.* **2007**, *9*, 745–8.
234. Srinivasan, K.; Gibb, B. C. *Chem. Commun.* **2008**, 4640–2.
235. (a) Li, X.; Upton, T. G.; Gibb, C. L.; Gibb, B. C. *J. Am. Chem. Soc.* **2003**, *125*, 650–1; (b) Gibb, B. C. *Chem. Eur. J.* **2003**, *9*, 5180–5187.
236. (a) Gibb, C. L.; Gibb, B. C. *J. Am. Chem. Soc.* **2004**, *126*, 11408–9; (b) Liu, S.; Whisenhunt-Ioup, S. E.; Gibb, C. L.; Gibb, B. C. *Supramol. Chem.* **2011**, *23*, 480–485.
237. Jordan, J. H.; Gibb, B. C. *Chem. Soc. Rev.* **2015**, *44*, 547–85.
238. (a) Giles, M. D.; Liu, S.; Emanuel, R. L.; Gibb, B. C.; Grayson, S. M. *J. Am. Chem. Soc.* **2008**, *130*, 14430–1; (b) Giles, M. D.; Liu, S.; Emanuel, R. L.; Gibb, B. C.; Grayson, S. M. *Isr. J. Chem.* **2009**, 31–40; (c) Li, Y.; Giles, M. D.; Liu, S.; Gibb, B. C.; Grayson, S. M. *Polym. Prepr.* **2010**, *51*, 526–527; (d) Li, Y.; Giles, M. D.; Liu, S.; Laurent, B. A.; Hoskins, J. N.; Cortez, M. A.; Sreerama, S. G.; Gibb, B. C.; Grayson, S. M. *Chem. Commun.* **2011**, 47, 9036–8.
239. Gibb, C. L.; Gibb, B. C. *Chem. Commun.* **2007**, 1635–7.
240. Gibb, C. L.; Gibb, B. C. *Tetrahedron* **2009**, *65*, 7240–7248.
241. Liu, S.; Russell, D. H.; Zinnel, N. F.; Gibb, B. C. *J. Am. Chem. Soc.* **2013**, *135*, 4314–24.
242. Gibb, C. L.; Gibb, B. C. *J. Am. Chem. Soc.* **2006**, *128*, 16498–9.
243. Liu, S.; Gan, H.; Hermann, A. T.; Rick, S. W.; Gibb, B. C. *Nat. Chem.* **2010**, *2*, 847–52.
244. Sullivan, M. R.; Gibb, B. C. *Org. Biomol. Chem.* **2015**, *13*, 1869–77.
245. (a) Kaanumalle, L. S.; Gibb, C. L.; Gibb, B. C.; Ramamurthy, V. *J. Am. Chem. Soc.* **2004**, *126*, 14366–7; (b) Gibb, C. L.; Sundaresan, A. K.; Ramamurthy, V.; Gibb, B. C. *J. Am. Chem. Soc.* **2008**, *130*, 4069–80; (c) Kaanumalle, L. S.; Gibb, C. L.; Gibb, B. C.; Ramamurthy, V.

- J. Am. Chem. Soc.* **2005**, *127*, 3674–5; (d) Kaanumalle, L. S.; Gibb, C. L.; Gibb, B. C.; Ramamurthy, V. *Org. Biomol. Chem.* **2007**, *5*, 236–8; (e) Natarajan, A.; Kaanumalle, L. S.; Jockusch, S.; Gibb, C. L.; Gibb, B. C.; Turro, N. J.; Ramamurthy, V. *J. Am. Chem. Soc.* **2007**, *129*, 4132–3; (f) Sundaresan, A. K.; Gibb, C. L.; Gibb, B. C.; Ramamurthy, V. *Tetrahedron* **2009**, *65*, 7277–7288; (g) Sundaresan, A. K.; Kaanumalle, L. S.; Gibb, C. L.; Gibb, B. C.; Ramamurthy, V. *Dalton Trans.* **2009**, 4003–11.
246. Ramamurthy, V. *Acc. Chem. Res.* **2015**.
247. Podkoscielny, D.; Philip, I.; Gibb, C. L. D.; Gibb, B. C.; Kaifer, A. E. *Chem. Eur. J.* **2008**, *14*, 4704–4710.
248. Podkoscielny, D.; Gadde, S.; Kaifer, A. E. *J. Am. Chem. Soc.* **2009**, *131*, 12876–12877.
249. Qiu, Y.; Yi, S.; Kaifer, A. E. *J. Org. Chem.* **2012**, *77*, 4622–4627.
250. Tang, H.; de Oliveira, C. S.; Sonntag, G.; Gibb, C. L.; Gibb, B. C.; Bohne, C. *J. Am. Chem. Soc.* **2012**, *134*, 5544–7.
251. (a) Sun, H.; Gibb, C. L. D.; Gibb, B. C. *Supramol. Chem.* **2008**, *20*, 141–147; (b) Gibb, C. L.; Gibb, B. C. *J. Comput. Aided Mol. Des.* **2014**, *28*, 319–25; (c) Wanjari, P. P.; Gibb, B. C.; Ashbaugh, H. S. *J. Chem. Phys.* **2013**, *139*, 234502.
252. (a) Gibb, C. L.; Gibb, B. C. *J. Am. Chem. Soc.* **2011**, *133*, 7344–7; (b) Gibb, C. L.; Oertling, E. E.; Velaga, S.; Gibb, B. C. *J. Phys. Chem. B* **2015**, *119*, 5624–38.
253. Carnegie, R. S.; Gibb, C. L.; Gibb, B. C. *Angew. Chem. Int. Ed. Engl.* **2014**, *53*, 11498–500.
254. Gan, H.; Benjamin, C. J.; Gibb, B. C. *J. Am. Chem. Soc.* **2011**, *133*, 4770–3.
255. Gan, H.; Gibb, B. C. *Chem. Commun.* **2012**, *48*, 1656–8.
256. Gan, H.; Gibb, B. C. *Chem. Commun.* **2013**, *49*, 1395–7.

# Chapter 10

## Calix[4]arenes and Resorcinarenes Bridged at the Wider Rim

Daniel A. Tan and Mauro Mocerino

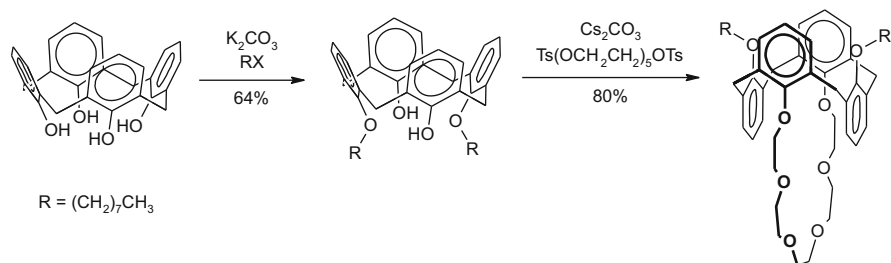
The versatile ability of calixarene derivatives to act as hosts for a variety of smaller guest species has been widely demonstrated in the literature [1–6]. This is because calixarenes are relatively large bowl-shaped molecules that are readily synthesised and functionalised. The wider rim of a calixarene bowl may be selectively and variously functionalised to enable the calixarene cavity to engage in a range of binding interactions with smaller guest molecules. This range of interactions can be adjusted to be charged or neutral, and may lead to the cavity being selective for a particular type of guest molecule, depending on the configuration and the type of functional groups on the wider rim. An interesting type of functionalisation would be a bridge that spans over the cavity of the calixarene. Such a bridge could partially enclose the calixarene cavity, and perhaps lead to enhanced containment of guest molecules inside the cavity.

Calixarenes that are distally-bridged on the narrower rim are common in the literature [7–11]. The crown ether bridged calixarene synthesised by Ungaro and co-workers in 1995 is one of many examples [12]. Selective distal functionalisation of a calixarene on the narrower rim was first achieved by treating tetrahydroxycalixarene with 1.1 equivalents of potassium carbonate base with an octyl halide (Scheme 10.1). Simple alkylation of the remaining two distal phenols by pentaethylene glycol ditosylate furnished the crown ether-bridged calixarene in the 1,3-alternate conformation. The calixarene crown ether was then shown to be a membrane transport agent selective for caesium ions over sodium ions. Such a system has been utilised by the U.S. Department of Energy to remove caesium ions from more than 11 million litres of radioactive waste [13, 14].

Distal selectivity is a key requirement for selective distal-bridging of calixarenes. The simple two-step procedure developed by Ungaro and co-workers

---

D.A. Tan • M. Mocerino (✉)  
Department of Chemistry, Curtin University, U1987, Perth, WA 6845, Australia  
e-mail: [m.mocerino@curtin.edu.au](mailto:m.mocerino@curtin.edu.au)

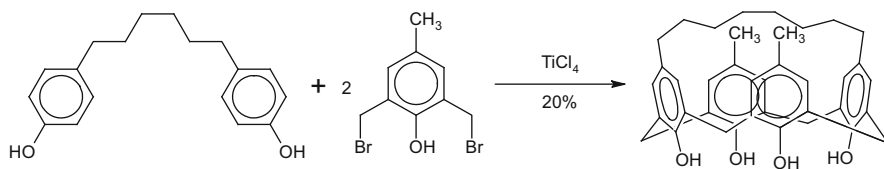
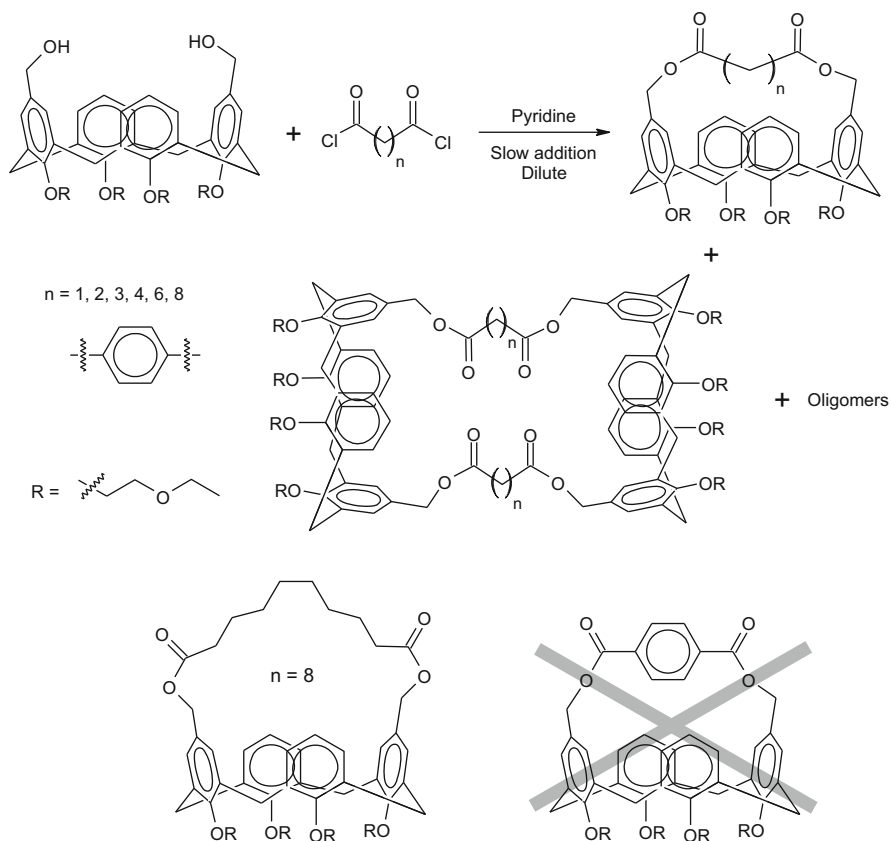


**Scheme 10.1** Selective distal bridging of calixarene at the narrower rim

has been responsible for the many narrow-rim, distally-bridged calixarenes reported in the literature. However, this mechanism of distal selectivity is only applicable to the narrower rim of calixarenes where the hydrogen bonding stabilisation is enabled by the phenols being in proximity to each other. Therefore, the popular method for distal bridging calixarenes does not directly apply to the wider rim of calixarenes. Unfortunately, a bridge at the narrower rim of calixarenes in the cone conformation does not make use of the cavity, which is a key attribute of a calixarene. Generally, the calixarene portion in these narrow-rim bridged calixarenes simply serves as a scaffold. Nevertheless, distal bridging over the wider rim has been accomplished by transferring the distal selectivity from the narrower rim to the wider rim via the stronger para-activating effect of the remaining two phenols [15], as reported in the literature [16, 17].

The first characterisation of calixarenes with a distal bridge at the wider rim was reported by Böhmer and co-workers in 1988 [18]. In their pioneering work, distally-bridged calixarenes were synthesised by the  $\text{TiCl}_4$ -catalysed Friedel-Crafts alkylation of  $\alpha,\omega$ -(*p*-hydroxyphenyl)alkanes with bis(bromomethyl)phenols (Scheme 10.2).  $\text{TiCl}_4$  was thought to also act as a template for the cyclisation. Calixarenes with various aliphatic bridge lengths were synthesised, but with lower yields. Calixarenes with bridges of eight carbons and longer were observed to be in the cone conformation, but shorter bridges resulted in the cone conformation becoming pinched. The cyclisation reaction with a shorter bridge of four carbons was not successful.

To study the effect of the bridge length and rigidity on the synthesis of a distally-bridged calixarene, Zeng et al. have tried various diacid chlorides to form diester linkages with a distal-diol calixarene (Scheme 10.3) [19]. Each experiment was conducted at dilute concentrations and produced multiple products which were separated by column chromatography into three main fractions. The yields of the three fractions of the various trials are shown in (Table 10.1). At these conditions, it is evident that the longer bridge with an eight-carbon chain gives the highest proportion of distally-bridged calixarene. This could be attributed to the increasing flexibility of the longer chain [19], and perhaps the reduction of strain on the calixarene cone conformation. It is also evident that the distally-bridged calixarene was the predominant product for all tests, except for the terephthalate, which may have suffered from steric strain/hindrance due to its rigidity. The reactions were

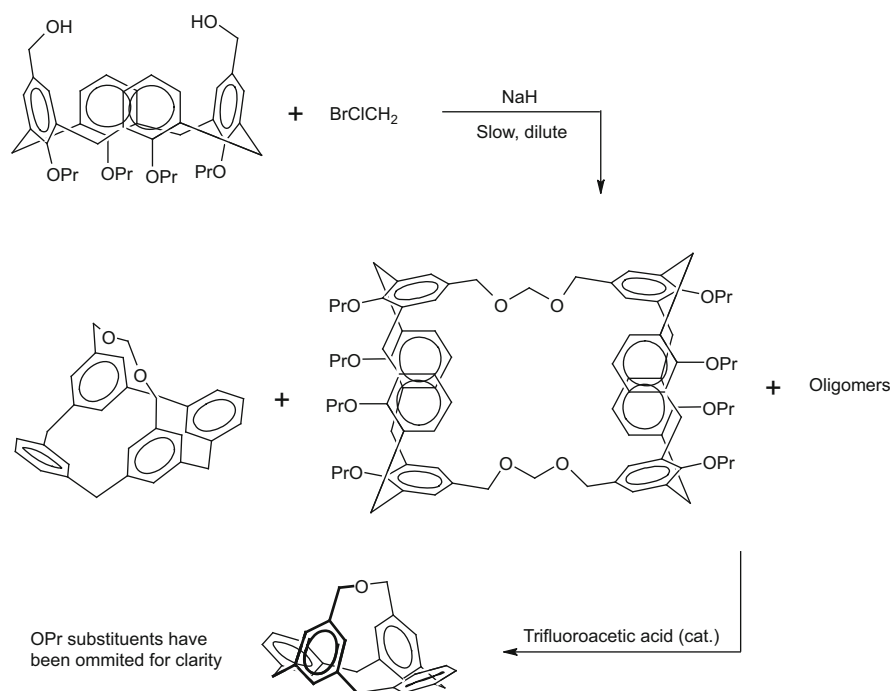
**Scheme 10.2** Pioneering synthesis of distally-bridged calixarene**Scheme 10.3** Synthesis of distally-bridged calixarenes via diester linkages. Experiments to explore the impact of bridge length and rigidity

also attempted at higher concentrations, producing a greater proportion of calixarene oligomer products, as well as trace amounts of shorter-bridged calixarene dimers. Thus as expected, a higher concentration of the reactants increases the chance of intermolecular reactions between calixarenes at the expense of intramolecular reactions within calixarenes.



**Table 10.1** Yields of the three main fractions from various calixarene bridging experiments

Bridge	Yield determined by HPLC (%)		
	Distally-bridged calixarene	Calixarene dimer	Calixarene oligomer mixture
1	55.6	0	41.0
2	39.8	17.4	42.8
3	41.3	23.7	35.0
4	42.2	25.5	32.3
6	66.5	0	33.5
8	82.2	0	17.8
phenyl	0	34.5 <sup>a</sup>	45.4 <sup>a</sup>

<sup>a</sup>Isolated yield (not determined by HPLC)**Scheme 10.4** Synthesis of acetal-bridged calixarenes and their decomposition into distally-bridged ether calixarene upon treatment with acid

In a related reaction, Cacciapaglia et al. constructed a distally-bridged calixarene with acetal linkages (Scheme 10.4) [20]. The outcome of this reaction was also similar to Zheng et al. in that the reaction produced multiple calixarene products that included a distally-bridged calixarene, a calixarene dimer and a mixture of calixarene oligomers. This work was part of an investigation into the synthesis of dynamic ‘living’ polymers which could be manipulated by concentration, to

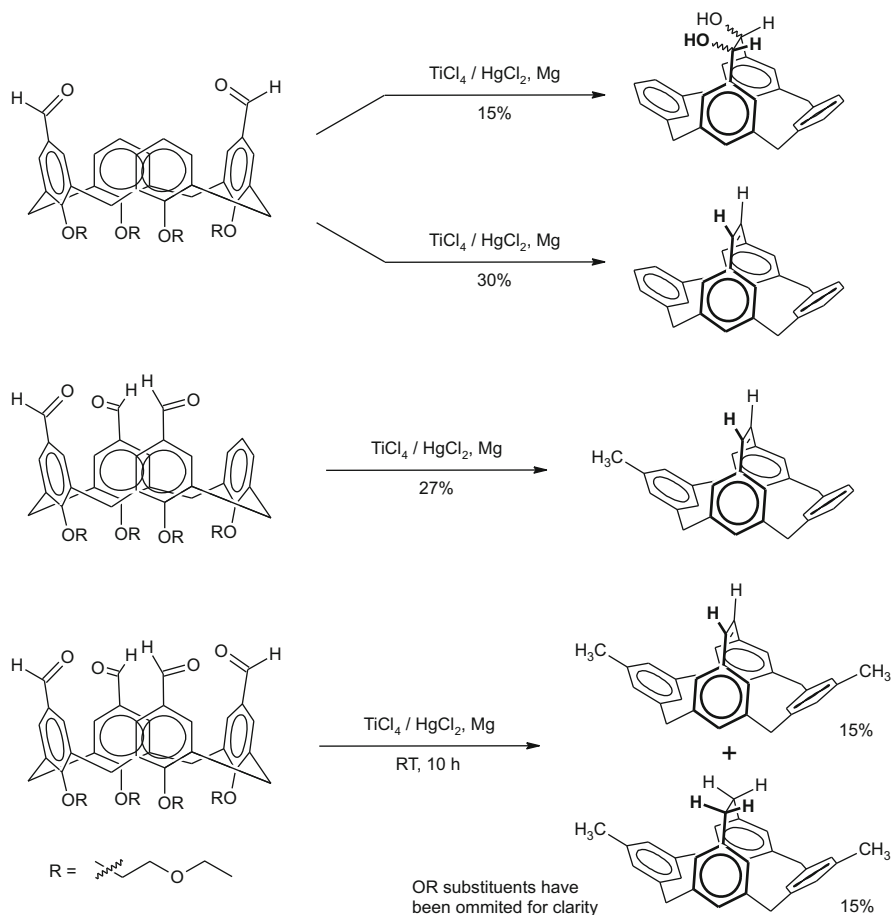
selectively give a particular product or oligomer at equilibrium. This work envisioned the creation of a dynamic family of cyclic calixarene oligomers linked together by formaldehyde acetal linkages, which could be reversibly interchanged by the addition of a catalytic amount of acid. However, when a catalytic amount of trifluoroacetic acid was added to all three acetal calixarene fractions, a distally-bridged ether calixarene formed instead. This was thought to proceed via a benzylic carbocation on the calixarene that could be formed by the acid-catalysed cleavage of one of the acetal bonds. The resultant hemiacetal and stabilised *p*-propoxy benzyl carbocation would then react in an intramolecular reaction, eliminating formaldehyde and forming the unreactive distal ether bridge. This mechanism would explain the observation that all acetal calixarenes, regardless of the type of acetal linkage, resulted in the same distal ether bridge when treated with acid.

A very similar calixarene with the same short distal ether bridge has also been synthesised by Arduini et al. Beginning with a distal diol calixarene, but with ethoxyethylether substituents on the narrow rim, reaction with NaH and tosyl chloride gave the distal ether bridged calixarene in 30 % yield [21]. The <sup>1</sup>H NMR spectrum of the product provided evidence that the ether-bridged calixarene was rigid, adopting a highly-distorted flattened-cone conformation. The protons of the aromatic rings involved in the bridge appeared at a significantly lower chemical shift (~ $\delta$  5.7), which suggested their shielding by the un-bridged proximal aromatic rings. The intermolecular bridging product, a calixarene pair linked by two ether bridges, was also produced, but as a minor product. Interestingly, the intermolecular reaction could be favoured by reacting the distal diol calixarene with a distal dichloromethyl calixarene with caesium hydroxide as base, to give the calixarene pair product in 50 % yield.

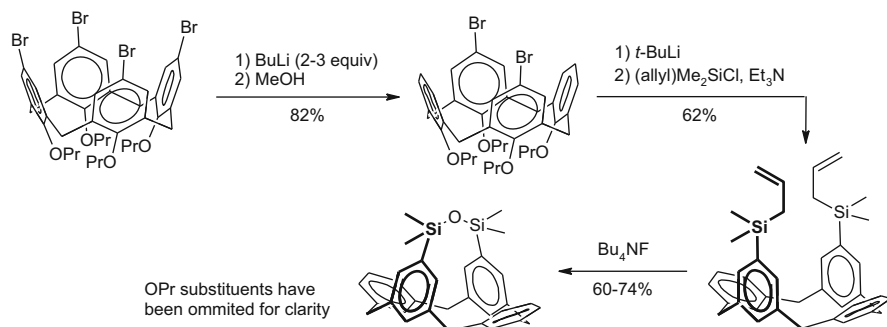
The intramolecular bridging on the wider rim of the calixarenes was further studied by Arduini et al. with a McMurry reductive coupling between the formyl groups of various formyl calixarenes (Scheme 10.5) [22]. The reductive coupling of distal diformyl calixarene afforded a distally-bridged calixarene with a diol bridge, after 5 h, which could be further reduced to an alkene after 16 h. A similar result was also reported by Lhoták and Shinkai in separate work [23]. Arduini et al. also explored the possibility for the coupling to occur between formyl groups on proximal aromatic rings of tri and tetra formyl calixarenes. With both these calixarenes, only the distal formyl groups showed coupling, while the remaining formyl groups were reduced to methyl groups.

Another calixarene with a short distal bridge is the siloxane-bridged calixarene synthesised by Hudrlík et al. [24]. The synthesis of this calixarene was accomplished in four steps, as described in Scheme 10.6. The distal selectivity on the wider rim of the calixarene was obtained through a selective bromine to lithium exchange, followed by quenching with methanol, as described by Larsen and Jørgensen [25].

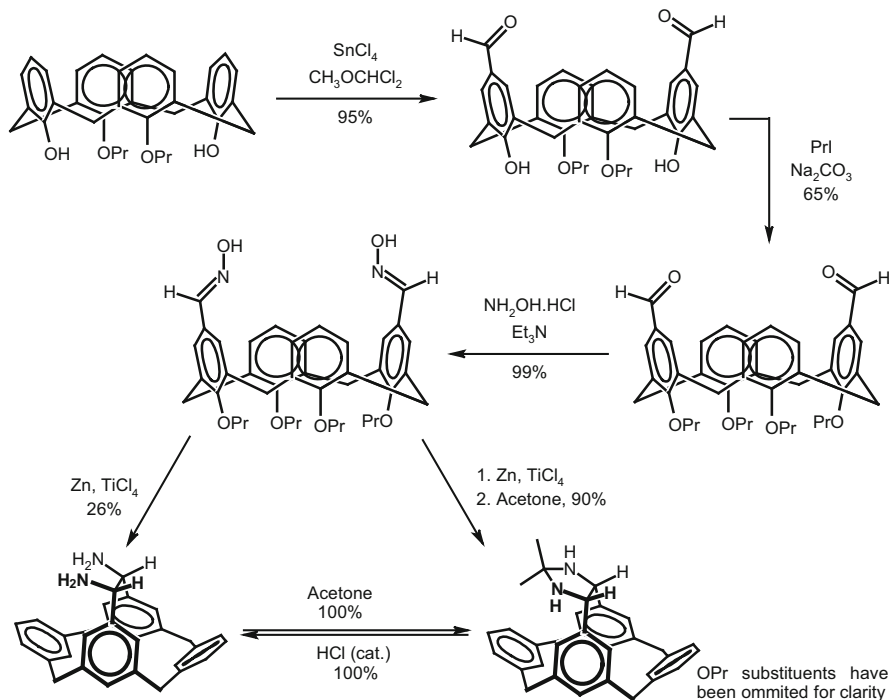
In recent work, Zajíčková et al. reported a distally-bridged calixarene obtained from the reductive coupling of a distal dialdoxime calixarene (Scheme 10.7) [16]. The distal selectivity of the starting dialdoxime calixarene was obtained by the stronger activating effect of distal phenols at the narrower rim. The reductive



**Scheme 10.5** Distal bridging of formyl calixarenes via intramolecular McMurry reductive coupling



**Scheme 10.6** Synthesis of distally-bridged siloxane calixarene



**Scheme 10.7** Distal bridging of dialdoxime calixarene via reductive coupling

coupling afforded the diamine product in a rather low yield of 26%, which was attributed to decomposition of the product under aerobic conditions. However, it was discovered that the product easily formed a stable aminal with acetone. Therefore, immediate chromatography of the diamine product with acetone afforded the aminal of the distally-bridged diamine calixarene in 90% yield. The scope of the reductive coupling was investigated with a number of dialdoxime calixarene derivatives with various substituents at both rims of the calixarene, as well as a calixarene in the 1,3-alternate conformation (Fig. 10.1). In all these cases, no distally-bridged calixarene was detected, alluding to the sensitivity of the reductive coupling to the conformation of the starting dialdoxime calixarene. A crystal structure of an amide derivative of the distally-bridged calixarene showed that the short bridge, of two carbons, forced the supporting aromatic rings to be bent into the cavity, causing the calixarene to take the pinched cone conformation.

While investigating the synthesis of phenanthrene calixarenes via photochemical cyclisation, Barton [26] synthesised a distally-bridged calixarene with a cyclobutane bridge (Scheme 10.8). The photolysis of tetra-stilbene calixarenes produced a highly complex mixture of cyclisation products including the distally-bridged cyclobutane calixarene, which was isolated in 1% yield by HPLC. Deducing that the bridging does not occur on the proximal aromatic rings, Hüggenberg et al. attempted the same photochemical cyclisation on proximal di-stilbene

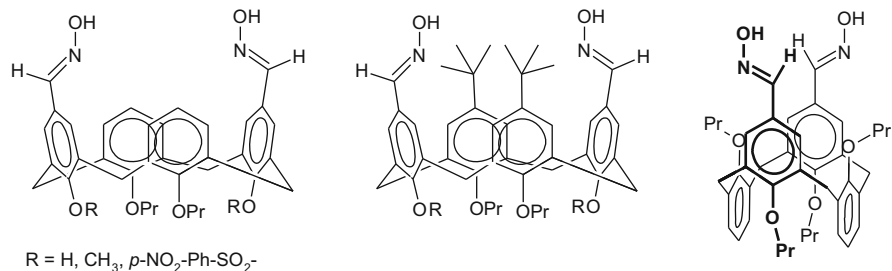
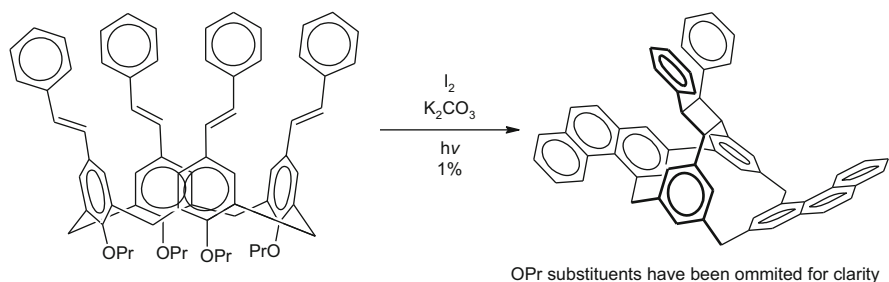


**Fig. 10.1** Reductive coupling with other dialdoxime calixarene derivatives failed to give the distally-bridged product



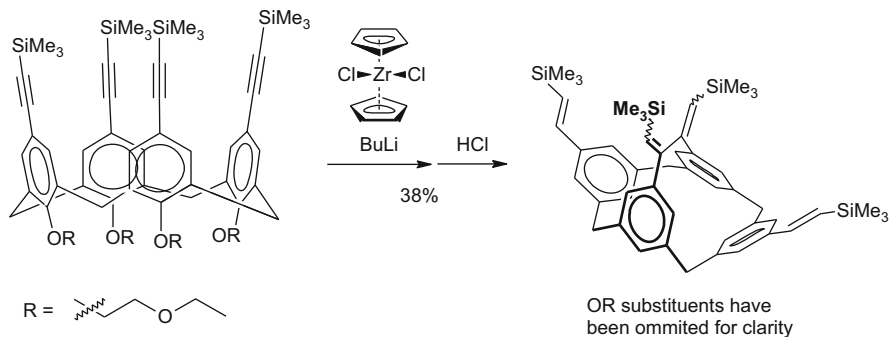
**Scheme 10.8** Photochemical [2+2] cycloaddition of tetra-stilbene calixarene to give distal cyclobutane-bridged diphenanthrene calixarene

calixarene [27]. As anticipated, the proximal di-phenanthrene calixarene was produced as three diastereomers in 67% yield, without any bridged calixarene. It is interesting that the bridging only occurred on the distal aromatic rings, rather than on proximal.

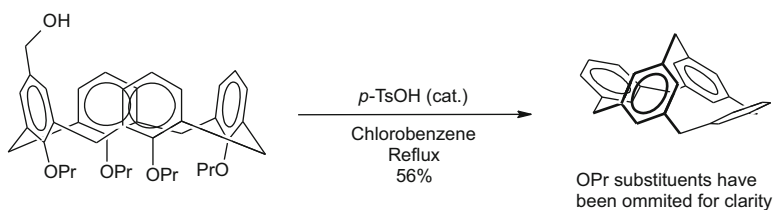
Liu et al. while exploring the synthesis of cage-like compounds, reported another unexpected distal bridging of calixarenes by intramolecular coupling [28]. The aim was to couple two tetraalkynyl calixarenes via a reversible intermolecular zirconocene coupling to form a cage-like structure. However, the intramolecular coupling was prevalent, and a two-carbon distally bridged calixarene formed instead (Scheme 10.9).

A distally bridged calixarene with the shortest possible bridge has been synthesised by Struck et al. [29]. The distal methylene-bridged calixarene was reported to be exclusively formed by the reaction shown in Scheme 10.10. The ‘collapsed’ cone conformation of the product was evident by signals at  $\delta$  5.6 in the <sup>1</sup>H NMR spectrum. These signals were attributed to the protons of the bridging aromatic ring, which had become shielded by the neighbouring non-bridging aromatic rings.

It is noteworthy from the preceding examples that it is possible to span across the wider rim of the calixarene with short bridges. This is possible because the



**Scheme 10.9** Zirconocene coupling of tetra tetraalkynyl calixarene leads to distal bridging of calixarene

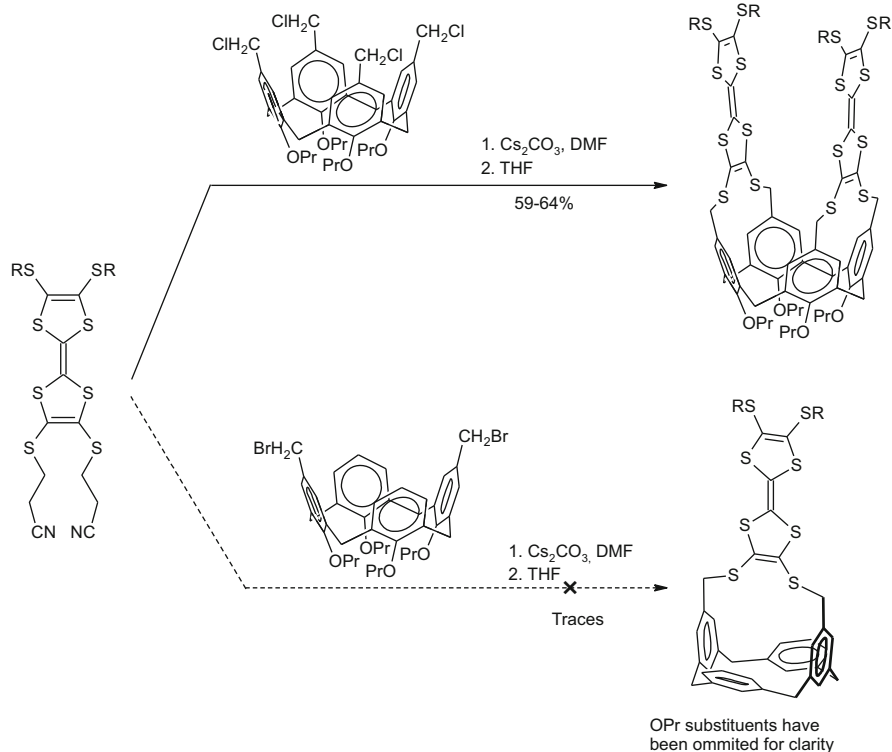


**Scheme 10.10** Synthesis of distal methylene bridged calixarene

calixarene in the cone conformation is not entirely rigid, despite the steric bulk of the four substituents on the narrower rim. In such a scenario, the cone calixarene oscillates between two pinched-cone conformers, enabling the calixarene to adopt a highly-distorted, pinched cone conformation where the pair of distal aromatic rings involved in bridging are pinched close enough together to form the short bridge. The vibrational motion also allows the other pair of unbridged distal aromatic rings to be forced outwards from the cavity.

Düker and co-workers have synthesised, in good yields, dual tetrathiafulvene proximal bridges across the wider rim of calixarenes for the construction of redox-active molecular architectures (Scheme 10.11) [30]. However bridging the tetrathiafulvene across distal aromatic rings was unsuccessful for calixarene derivatives in both the 1,3-alternate and cone conformations. The lack of success may be due to the conditions used as the bridging reactions were carried out at room temperature. Under these conditions, there may not be sufficient oscillation energy to bring the distal rings close enough to be bridged. Interestingly, distal bridging was possible by using a longer tetrathiafulvene bridging unit, although a calixarene dimer was also produced (Scheme 10.12).

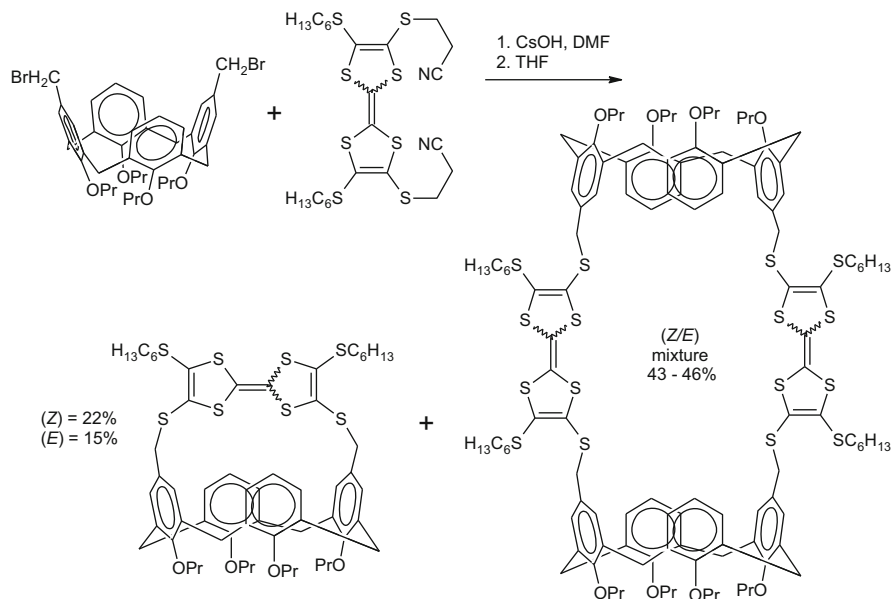
The potential application of calixarenes to function as biomimetic receptors has led Casnati et al. to design distally-bridged calixarenes with peptide bridges. The aim was to use the hydrophobic cavity of the calixarene in conjunction with the



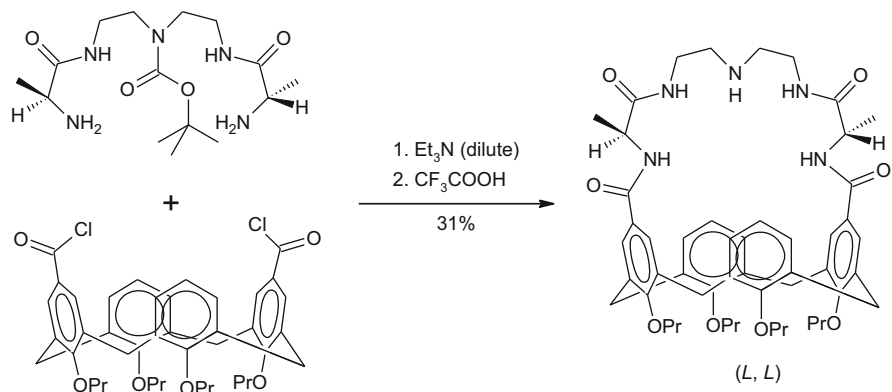
**Scheme 10.11** Synthesis of bridged calixarenes with tetrathiafulvene derivatives

hydrogen bonding of the peptide bridge to enable binding of guest molecules. Starting with a distally-functionalised diacid chloride calixarene, the cavity of the calixarene was bridged over by two alanine residues linked together by a nitrogen atom (Scheme 10.13) [31]. The distally-bridged *N*-linked peptidocalixarene was shown to bind D-Ala-D-Ala (Fig. 10.2), thus mimicking the mode of binding of the vancomycin group of antibiotics. Studies indicated that a proton transfer from the carboxylic acid group of the guest to the amino group of the calixarene pseudopeptide bridge generated a salt which was thought to be the key binding interaction, besides the hydrogen bonding between NH and CO groups. It was speculated that the hydrophobic calixarene cavity may host the methyl group of the non-terminal alanine residue [4].

However, some peptidocalixarenes are poor receptors due to intramolecular hydrogen bonding between amino acid residues within the molecule. This is caused by the peptidocalixarene being conformationally flexible. Therefore, to increase conformational rigidity, Sansone et al. have placed a rigid aromatic spacer between the two amino acid residues in a distally-bridged peptidocalixarene that adopted a pinched cone conformation (Scheme 10.14) [32]. This peptidocalixarene was shown to bind anionic guests, having the best affinity for benzoate. From



**Scheme 10.12** Distal bridging of calixarene with tetrathiafulvene



**Scheme 10.13** Synthesis of distally-bridged (L, L) peptidocalixarene

investigations, it appeared again that a proton transfer had occurred, and that the resultant carboxylate anion was electrostatically attracted to the amide protons of the bridge of the peptidocalixarene (Fig. 10.3).  $\pi$ - $\pi$  Stacking between the aromatic rings also appeared to contribute to the binding [4].

Distal bridging of calixarenes has also been performed on resorcinarenes. An interesting example is the thiocrown resorcinarenes synthesised by Konishi et al. by the bridging of distal dibromoresorcinarene with 2-mercaptoethyl ether, propane-1,3-dithiol, and ethane-1,2-dithiol (Scheme 10.15) [33]. The octahydroxythiacrown



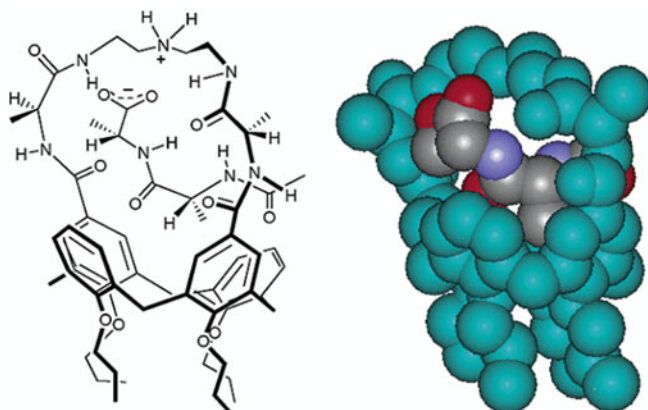
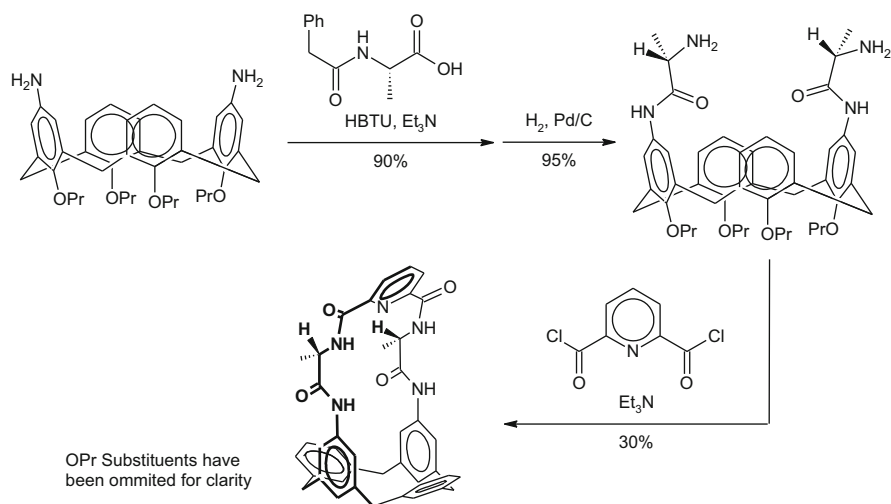


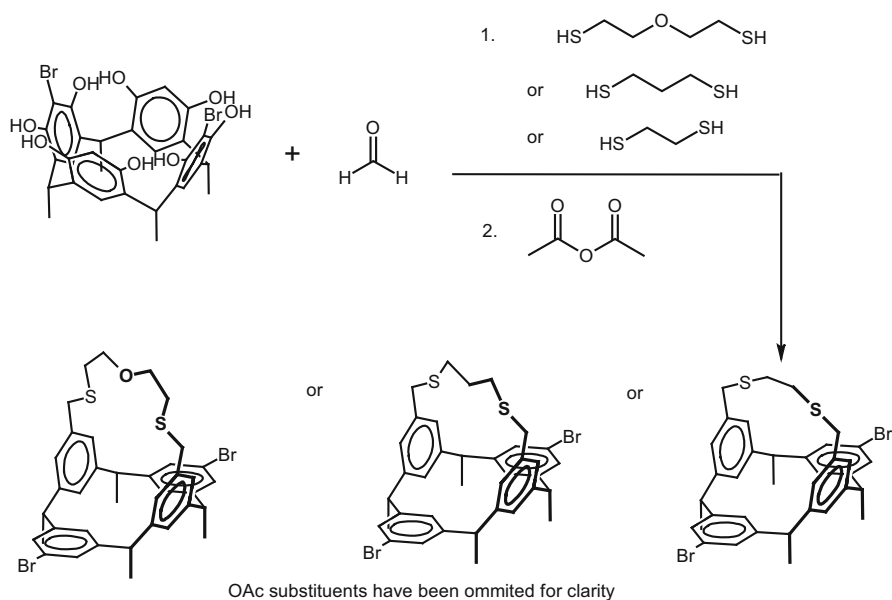
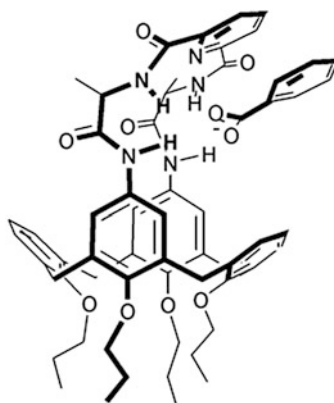
**Fig. 10.2** Distally-bridged peptidocalixarene mimics the mode of binding of vancomycin antibiotics by binding D-Ala-D-Ala by the suggested binding mechanism (Image from Casnati et al. [4])



**Scheme 10.14** Synthesis of distally-bridged peptidocalixarene linked with a rigid aromatic spacer

resorcinarene product was reportedly difficult to purify, hence the conversion to octaacetates for characterisation. Despite the various bridge lengths, all the thiocrown resorcinarenes were determined to be in the pinched cone conformation, by analysis of the  $^1\text{H-NMR}$  chemical shifts and molecular modelling. The bridging was also attempted with rigid dithiols such as 2,6-dimercaptomethylpyridine or *m*-xylylenedithiol, but to no success. The distal dibromoresorcinarene starting

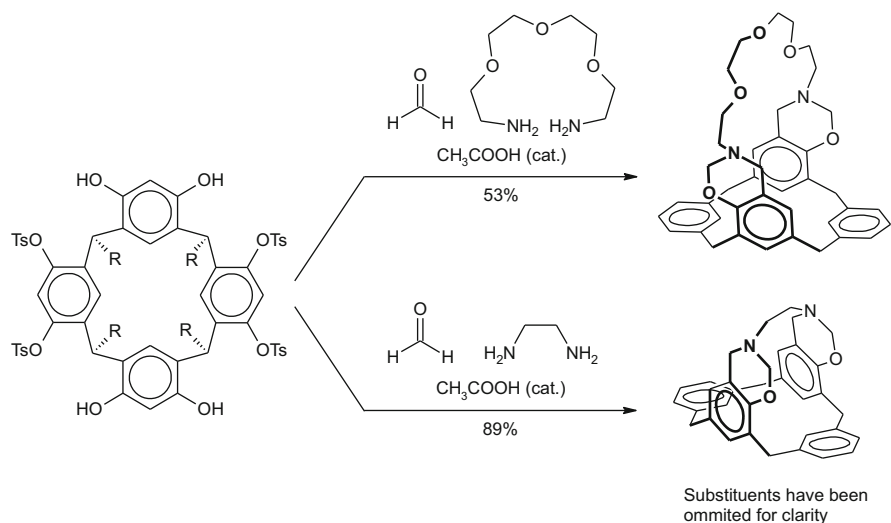
**Fig. 10.3** Proposed binding of benzoate by distally-bridged peptidocalixarene (Image from Casnati et al. [4])



**Scheme 10.15** Synthesis of distally-bridged thiacycrown resorcinarenes with three bridges of varying length

material was obtained by the careful, direct bromination of octahydroxyresorcinarene with limited *N*-bromosuccinimide [34].

Other distally-bridged resorcinarenes have been synthesized by Shivanyuk et al. who used aliphatic diamines to bridge distal tetraosylate resorcinarenes by the formation of benzoxazine linkages from a Mannich condensation with formaldehyde (Scheme 10.16) [35]. The cavity of the crown ether-bridged resorcinarene was actually chiral due to the positions of the two benzoxazine linkages. However,

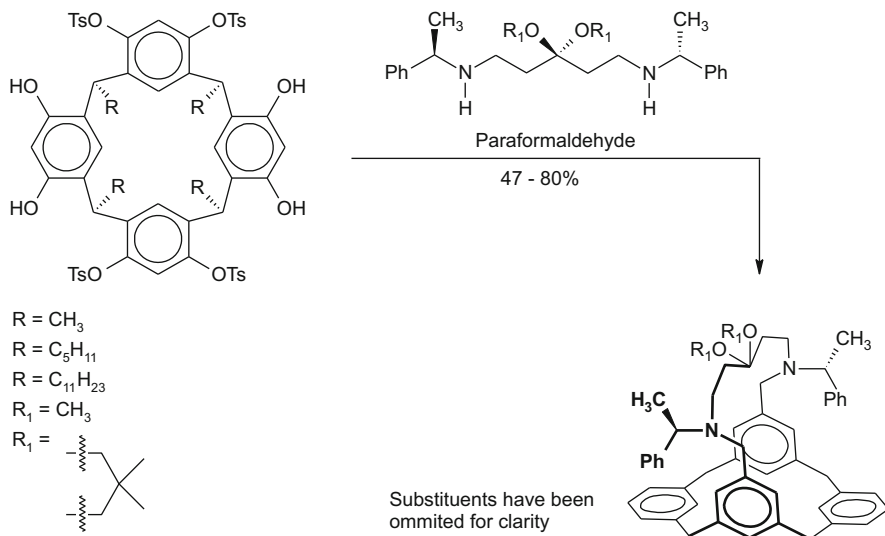


**Scheme 10.16** Synthesis of axially-chiral distally-bridged tetratosylate resorcinarene via benzoxazine linkages

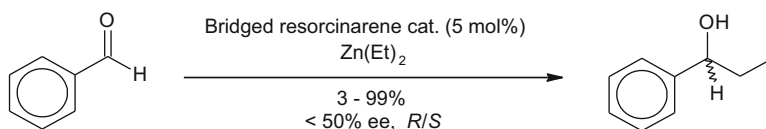
no attempt was made to separate the enantiomers. The impact of a shorter bridge on the distal-bridging Mannich condensation was also investigated. Based on the conformation from the crystal structures of the previous chiral benzoxazine resorcinarenes, bridging should not be possible with shorter diamines. Contrary to expectation, the distal bridging was accomplished with ethylene diamine, but the shorter bridge forced the benzoxazine linkages to form on the phenols that were closer together producing the other possible regioisomer which is not chiral. Both these distally-bridged resorcinarene regioisomers took on the pinched cone conformation.

In similar work, the Mannich condensation was also used by Arnott et al. to distally-bridge tetratosylate resorcinarene with various diamines in good yields of 47–80 % (Scheme 10.17) [36]. Various derivatives of these distally-bridged resorcinarenes were then tested for potential to act as enantioselective asymmetric catalysts for the alkylation of benzaldehyde with dimethyl zinc (Scheme 10.18) [37, 38]. Addition of functionality to the bridge, in the form of a dioxane and dimethoxy acetals, was explored for potential coordination to zinc. The different acetals and/or changing the length of the bridge caused a reversal in enantioselectivity. These reversals of enantioselectivity were indicative that the modifications were causing a significant change in conformation of the bridged resorcinarene. In all these cases, the enantioselectivity of the bridged resorcinarene was limited to about 50 % ee. Arnott et al. have suggested a hypothetical mechanism based on Noyori's model to explain this limitation [38].

In almost all the examples presented so far in this review, the distal-bridging of calixarenes at the wider rim has been accomplished on calixarenes that have already



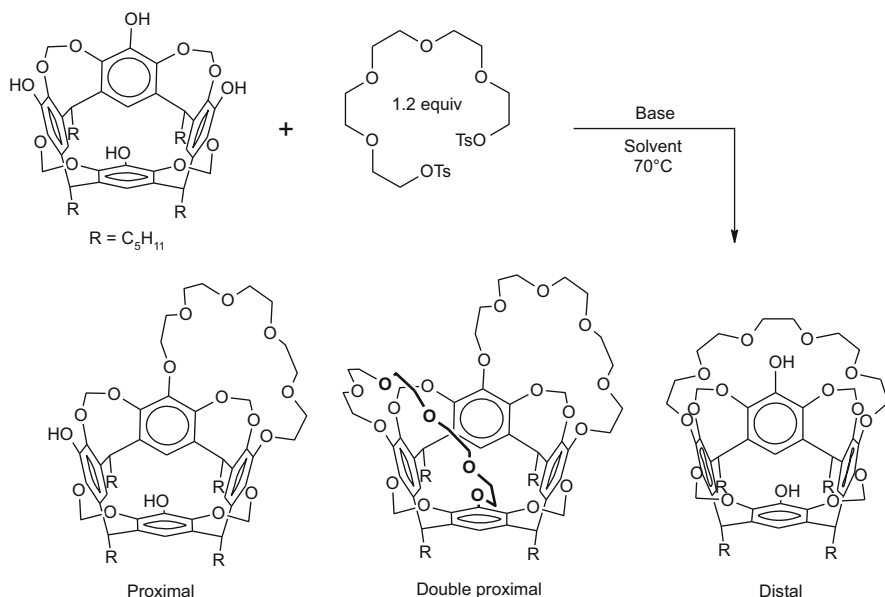
**Scheme 10.17** Distal bridging of tetratosylate resorcinarene



**Scheme 10.18** Studies into the potential enantioselective alkylation of benzaldehyde with diethylzinc in the presence of distally-bridged resorcinarene derivatives

been distally functionalised. However, if bridging were to be performed on a non-distally-functionalised calixarene with four equally-reactive subunits, multiple bridged-calixarene products are possible. Reinhoudt and coworkers have demonstrated this with flexible crown ether bridges on a cavitand (resorcinarene derivative) [39]. In this work, a cavitand with four equally-reactive phenol subunits was treated with 1.2 equivalents of pentaethyleneglycol ditosylate to give three differently-bridged crown-cavitand products (Scheme 10.19). The bridging reaction was performed with various solvents and bases, and the yields of each crown-cavitand are shown in Table 10.2. It is evident that the proximally-bridged crown-cavitand can be selectively produced in 33% yield, but with a significant amount of unreacted starting cavitand. The distally-bridged crown-cavitand could only be obtained in trace yields of 2–3% as part of a mixture of all three crown-cavitand products. These results show that directly bridging a calixarene with four equally-reactive subunits, with a flexible bridge, will most likely produce either a proximally-bridged calixarene, or a mixture of bridged calixarene products.

Bridging calixarenes on the wider rim with crown ethers has also been explored by Nissinen and coworkers in their synthesis of tetramethoxy resorcinarene crown

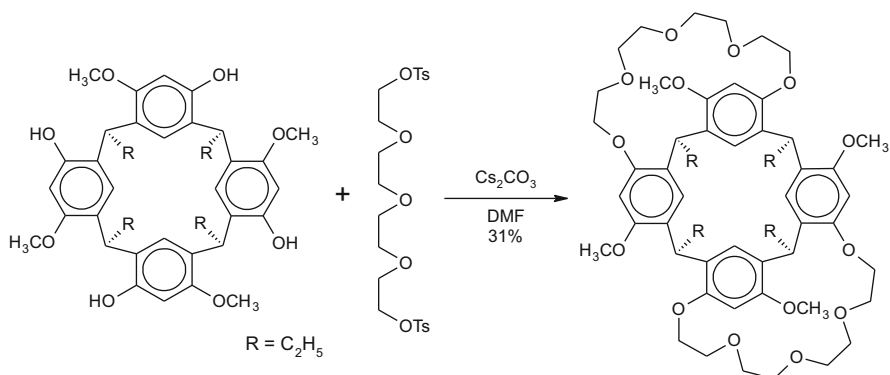


**Scheme 10.19** Bridging of tetrol cavitand with pentaethyleneglycol ditosylate to form three different crown-cavitand products

**Table 10.2** Reaction with various solvents and bases, and the yields of each crown-cavitand product

Solvent	Base	Yield (%)			
		Starting cavitand	Proximal	Double proximal	Distal
DMF	NaH	21	33	0	0
DMF	Na <sub>2</sub> CO <sub>3</sub>	22	18	0	0
DMF	K <sub>2</sub> CO <sub>3</sub>	22	2	8	2
DMF	Cs <sub>2</sub> CO <sub>3</sub>	40	2	10	2
CH <sub>3</sub> CN	NaH	3	13	0	3

ethers [40]. Tetramethoxy resorcinarene was treated with caesium carbonate base for 15 min, followed by two equivalents of the tetraethylene glycol ditosylate to produce proximally-bridged bis-crown tetramethoxy resorcinarene in 31% yield (Scheme 10.20). When the deprotonation time with caesium carbonate was extended to 60 min, the bis-crown tetramethoxy resorcinarene was produced in 10% yield along with the proximally-bridged mono-crown by-product in 13% yield [41]. Both the mono-crown and this bis-crown tetramethoxy resorcinarenes adopted the flattened cone conformation. The bis-crown tetramethoxy resorcinarene was shown to bind potassium, rubidium, caesium, and silver ions [42–44]. The binding of silver ions was reversible, and was utilised to deliver silver ions to bacteria resulting in cell death and an anti-bacterial effect [43]. The mono-crown tetramethoxy resorcinarene, having a larger cavity, was not able to bind



**Scheme 10.20** Synthesis of proximally-bridged crown ether tetramethoxy resorcinarenes

alkali metal cations. Nevertheless, the mono-crown was an optimal host for an acetylcholine (neurotransmitter) guest, binding through interactions between the crown ether with the ammonium portion, as well as hydrogen bonding between the two phenols with the acetate group of the guest.

The distal mono-crown tetramethoxy resorcinarene was not reported, signalling a tendency for flexible bridges to form on proximal aromatic rings of a calixarene with equally-reactive subunits.

## 10.1 Conclusion

As evident from the examples, distally-bridged calixarenes can be obtained from tetra, mono and distally-functionalised calixarenes through a variety of coupling methods. It is also evident that these methods are not applicable to the whole range of different calixarene derivatives, and that achieving selective distal bridging can be challenging. A common issue appears to be the competition between intra and intermolecular coupling. In fact, the examples of distal bridging from tetra and mono functionalised calixarenes were a rather accidental result of dominant intramolecular coupling. The reports of short distal bridged calixarenes demonstrates that the cone conformation of some calixarenes may be more flexible than expected. This flexible cone conformation enables the calixarene to adopt a cone conformation that is pinched, which is characteristic of the distally-bridged calixarenes reported here.

## References

1. Tero, T.-R.; Nissinen, M. *Tetrahedron* **2014**, *70*, 1111–1123.
2. Adhikari, B. B.; Fujii, A.; Schramm, M. P. *Eur. J. Org. Chem.* **2014**, 2972–2979.

3. Adhikari, B. B.; Roshandel, S.; Fujii, A.; Schramm, M. P. *Eur. J. Org. Chem.* **2015**, 2683–2690.
4. Casnati, A.; Sansone, F.; Ungaro, R. *Acc. Chem. Res.* **2003**, *36*, 246–254.
5. Mutihac, L.; Lee, J. H.; Kim, J. S.; Vicens, J. *Chem. Soc. Rev.* **2011**, *40*, 2777–2796.
6. Nimse, S. B.; Kim, T. *Chem. Soc. Rev.* **2013**, *42*, 366–386.
7. Arduini, A.; Fabbi, M.; Mantovani, M.; Mirone, L.; Pochini, A.; Secchi, A.; Ungaro, R. *J. Org. Chem.* **1995**, *60*, 1454–1457.
8. Yang, Y.; Cao, X.; Surowiec, M.; Bartsch, R. A. *Tetrahedron* **2010**, *66*, 447–454.
9. Asfari, Z.; Wenger, S.; Vicens, J. *Supramol. Sci.* **1994**, *1*, 103–110.
10. Joseph, R.; Rao, C. P. *Chem. Rev.* **2011**, *111*, 4658–4702.
11. He, Y.; Xiao, Y.; Meng, L.; Zeng, Z.; Wu, X.; Wu, C.-T. *Tetrahedron Lett.* **2002**, *43*, 6249–6253.
12. Casnati, A.; Pochini, A.; Ungaro, R.; Ugozzoli, F.; Arnaud, F.; Fanni, S.; Schwing, M.-J.; Egberink, R. J. M.; de Jong, F.; Reinhoudt, D. N. *J. Am. Chem. Soc.* **1995**, *117*, 2767–2777.
13. Casnati, A. *Chem. Commun.* **2013**, *49*, 6827–6830.
14. Duncan, N. C.; Roach, B. D.; Williams, N. J.; Bonnesen, P. V.; Rajbanshi, A.; Moyer, B. A. *Sep. Sci. Technol.* **2012**, *47*, 2074–2087.
15. Van Loon, J. D.; Arduini, A.; Coppi, L.; Verboom, W.; Pochini, A.; Ungaro, R.; Harkema, S.; Reinhoudt, D. N. *J. Org. Chem.* **1990**, *55*, 5639–5646.
16. Zajíčková, M.; Eigner, V.; Budka, J.; Lhoták, P. *Tetrahedron Lett.* **2015**, *56*, 5529–5532.
17. Kanamathareddy, S.; Gutsche, C. D. *J. Org. Chem.* **1995**, *60*, 6070–6075.
18. Goldmann, H.; Vogt, W.; Paulus, E.; Böhmer, V. *J. Am. Chem. Soc.* **1988**, *110*, 6811–6817.
19. Zeng, C.-C.; Yuan, H.-S.; Huang, Z.-T. *Chin. J. Chem.* **2002**, *20*, 795–802.
20. Cacciapaglia, R.; Di Stefano, S.; Mandolini, L. *J. Phys. Org. Chem.* **2008**, *21*, 688–693.
21. Arduini, A.; Fanni, S.; Manfredi, G.; Pochini, A.; Ungaro, R.; Sicuri, A. R.; Ugozzoli, F. *J. Org. Chem.* **1995**, *60*, 1448–1453.
22. Arduini, A.; Fanni, S.; Pochini, A.; Sicuri, A. R.; Ungaro, R. *Tetrahedron* **1995**, *51*, 7951–7958.
23. Lhoták, P.; Shinkai, S. *Tetrahedron Lett.* **1996**, *37*, 645–648.
24. Hudrlik, P. F.; Hudrlik, A. M.; Zhang, L.; Arasho, W. D.; Cho, J. *J. Org. Chem.* **2007**, *72*, 7858–7862.
25. Larsen, M.; Jørgensen, M. *J. Org. Chem.* **1996**, *61*, 6651–6655.
26. Barton, O. G., Dissertation, Universität Bielefeld, **2008**, <https://pub.uni-bielefeld.de/publication/2302017> (accessed 16 May 2016).
27. Hüggenberg, W.; Seper, A.; Oppel, I. M.; Dyker, G. *Eur. J. Org. Chem.* **2010**, 6786–6797.
28. Liu, F.-Q.; Harder, G.; Tilley, T. D. *J. Am. Chem. Soc.* **1998**, *120*, 3271–3272.
29. Struck, O.; van Duynhoven, J. P. M.; Verboom, W.; Harkema, S.; Reinhoudt, D. N. *Chem. Commun.* **1996**, 1517–1518.
30. Düker, M. H.; Kutter, F.; Dülcks, T.; Azov, V. A. *Supramol. Chem.* **2014**, *26*, 552–560.
31. Casnati, A.; Fabbi, M.; Pelizzi, N.; Pochini, A.; Sansone, F.; Ungaro, R.; Di Modugno, E.; Tarzia, G. *Bioorg. Med. Chem. Lett.* **1996**, *6*, 2699–2704.
32. Sansone, F.; Baldini, L.; Casnati, A.; Lazzarotto, M.; Ugozzoli, F.; Ungaro, R. *PNAS* **2002**, *99*, 4842–4847.
33. Morikawa, O.; Nakanishi, K.; Miyashiro, M.; Kobayashi, K.; Konishi, H. *Synthesis* **2000**, 233–236.
34. Konishi, H.; Nakamaru, H.; Nakatani, H.; Ueyama, T.; Kobayashi, K.; Morikawa, O. *Chem. Lett.* **1997**, *26*, 185–186.
35. Shivanyuk, A.; Schmidt, C.; Böhmer, V.; Paulus, E. F.; Lukin, O.; Vogt, W. *J. Am. Chem. Soc.* **1998**, *120*, 4319–4326.
36. Arnott, G.; Bulman Page, P. C.; Heaney, H.; Hunter, R.; Sampler, E. P. *Synlett* **2001**, 412–414.
37. Arnott, G.; Heaney, H.; Hunter, R.; Page, Philip C. B. *Eur. J. Org. Chem.* **2004**, 5126–5134.
38. Arnott, G.; Hunter, R. *Tetrahedron* **2006**, *62*, 992–1000.

39. Higler, I.; Boerrigter, H.; Verboom, W.; Kooijman, H.; Spek, A. L.; Reinhoudt, D. N. *Eur. J. Org. Chem.* **1998**, 1998, 1597–1607.
40. Salorinne, K.; Nissinen, M. *Org. Lett.* **2006**, 8, 5473–5476.
41. Salorinne, K.; Tero, T.-R.; Riikonen, K.; Nissinen, M. *Org. Biomol. Chem.* **2009**, 7, 4211–4217.
42. Salorinne, K.; Nissinen, M. *Tetrahedron* **2008**, 64, 1798–1807.
43. Helttunen, K.; Moridi, N.; Shahgaldian, P.; Nissinen, M. *Org. Biomol. Chem.* **2012**, 10, 2019–2025.
44. Helttunen, K.; Salorinne, K.; Barboza, T.; Barbosa, H. C.; Suhonen, A.; Nissinen, M. *New J. Chem.* **2012**, 36, 789–795.



# Chapter 11

## ***N*-Alkyl Ammonium Resorcinarene Salts: A Versatile Family of Calixarene-Related Host Molecules**

Ngong Kodiah Beyeh and Kari Rissanen

### 11.1 Introduction

The term “cavitand” was coined by Cram in the early 1980s to describe molecules possessing an enforced cavity large enough to accommodate other molecules, atoms or ions [1, 2]. Calixarenes and resorcinarenes are members of the cyclophane family which consists of bridged aromatic compounds [3]. These compounds are readily available and are considered as pillars of supramolecular chemistry. Their most characteristic feature is the hydrophobic electron-rich cavity formed by the aromatic rings. Additional binding sites such as the hydroxyl groups and restrained flexibility facilitate stronger interactions with guests. The ability of resorcinarenes to be easily functionalized makes them ideal building blocks and their ability to selectively bind specific guest species highlight their role in supramolecular chemistry [3–8]. Resorcinarenes can be modified at the two-position on the aromatic ring, lower rim chains and the phenol hydroxyl groups. Resorcinarenes are conformationally mobile macrocycles generally possessing ephemeral rather than permanent cavities. However, bridging the hydroxyl groups of the adjacent aromatic rings of such structures with covalent linkages leads to rigid, bowl-shaped cavitands capable of forming supramolecular host-guest complexes with many different guest species [3–7, 9]. Their potential in forming multifunctional compounds makes them important tools in the synthesis of various receptors [1, 2, 9],

---

N.K. Beyeh (✉)

School of Science, Department of Applied Physics, Aalto University,  
Puumiehenkuja 2, FI-02150 Espoo, Finland  
e-mail: [kodiah.beyeh@aalto.fi](mailto:kodiah.beyeh@aalto.fi)

K. Rissanen

Department of Chemistry, Nanoscience Center, University of Jyväskylä,  
35, FI-40014 Jyväskylä, Finland  
e-mail: [kari.t.rissanen@jyu.fi](mailto:kari.t.rissanen@jyu.fi)

dendrimers [10, 11] and in the construction of larger supramolecular and tubular assemblies [12, 13].

## 11.2 Resorcinarenes and Their Tetrabenzoxazines, the Starting Point to the *N*-Alkyl Ammonium Resorcinarene Salts

### 11.2.1 Resorcinarenes

The presence of free hydroxyl groups on the resorcinarenes that are involved in strong intramolecular hydrogen bonding is critical in the cyclisation step during the synthesis and subsequently maintaining the  $C_{4v}$  cone conformation (Fig. 11.1) [3, 4]. The disruption of the intramolecular hydrogen bonds leads to the collapse of the unique cone conformation. In order to achieve convergent arrangement of binding sites, the cone shape of resorcinarenes is utilized in the design of specific receptors for a variety of applications [14–16]. Resorcinarene receptors are particularly attractive due to their easy large scale preparations. They are commonly utilized as building blocks in supramolecular chemistry [3].

### 11.2.2 Resorcinarene Tetrabenzoxazines

#### 11.2.2.1 Synthesis

The two activating hydroxyl groups make the two-position of the resorcinarenes electron-rich and thus suitable for electrophilic substitutions. Mannich [17] condensation is arguably the most popular method of attaching functional groups at the

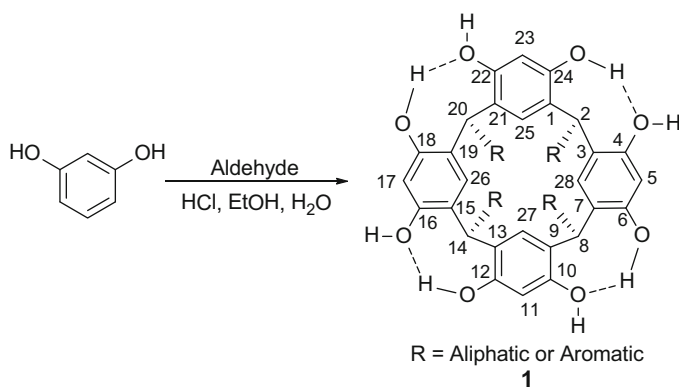


**Fig. 11.1** Resorcinarene, a cyclic tetramer from aldehyde and resorcinol [8]

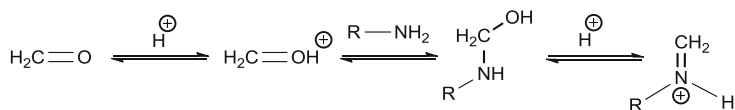


**Fig. 11.2** Acid catalyzed reaction of formaldehyde ( $\text{H}_2\text{C}=\text{O}$ ) and primary amine ( $\text{RNH}_2$ ) leading to the formation of an iminium ion [17–19]

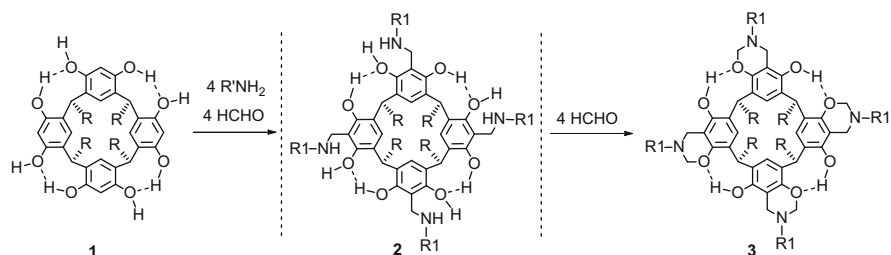


**Fig. 11.3** General scheme of the reaction between resorcinarene, a primary amine and formaldehyde. The formed intermediary amine **2** reacts further resulting in a tetrabenzoxazine **3** [20–22, 24]

two-position of the benzene rings of resorcinarenes. In a classical Mannich reaction, a carbonyl compound capable of keto-enol tautomerism and an amine condenses to form an iminium ion (Fig. 11.2) [18, 19].

A combination of resorcinarene, formaldehyde and secondary amines results to tertiary amines or tetrakis-aminoalkylated resorcinarenes through a Mannich condensation reaction. When primary amines are used, the resulting secondary amine **2** reacts intramolecularly with one of the phenolic hydroxyl groups and a second equivalent of formaldehyde, forming tetrabenzoxazines **3** (Fig. 11.3) [20–23].

Two different orientations of the new six-membered rings are possible which would translate into a mixture of 16 potential isomers for the tetrabenzoxazines. However, due to the pattern of the hydrogen bond seam connecting the free and adjacent hydroxyl groups, only two different isomers of **I** and **II** are formed (Fig. 11.4). The two isomers all bear the oxazines in a clockwise or all in a counter-clockwise orientation with respect to the resorcinarene scaffold. This element of chirality is not dynamic as is the hydrogen-bonding pattern in the parent resorcinarene. The regioselectivity can be explained in large part by the formation of maximum number of hydrogen bonds in this structure [20, 21, 23–25].

When aminoethanol starting compounds are used in the Mannich condensation reaction with resorcinarenes, the 2-aminoethanol does not lead to the formation of benzodihydro-1,3-oxazines. Under the same reaction conditions instead these reactants give 1,3-oxazolidines **4** (Fig. 11.5) in which the second formaldehyde molecule reacts with the hydroxyl group of aminoethanol instead of the phenolic hydroxyl group [20].

The condensation of resorcinarenes with certain long chain aliphatic diamines with an excess of formaldehyde under high dilution conditions lead to

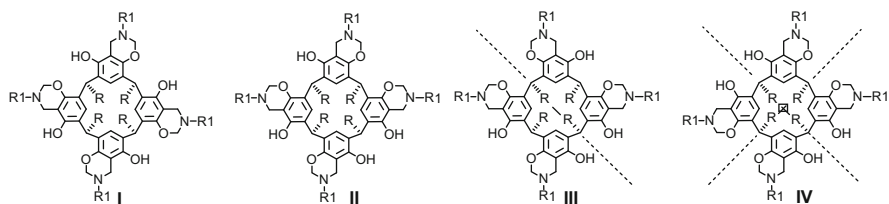


**Fig. 11.4** The 1,3-oxazine stereoisomer **I** (one of the two forms of **I** shown) is the exclusively formed tetrabenzoxazine. Other possible isomers **II–IV** are not observed [25] (Image adapted from [25] with permission from Elsevier)

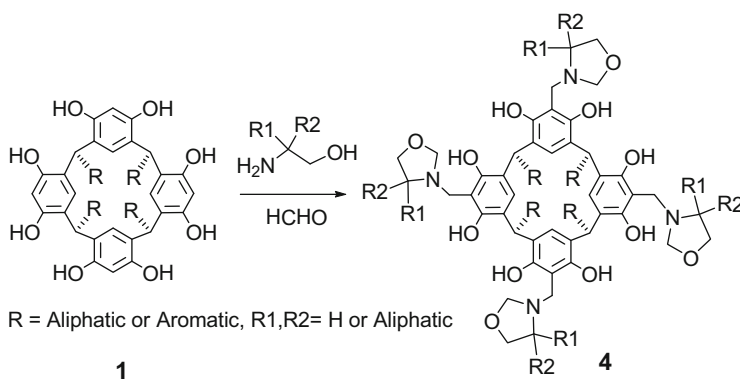


**Fig. 11.5** Reaction of resorcinarene and aminoethanol leading to 1,3-oxazolidine derivatives **4** [20]

tetrabenzoxazine derivatives **5–6** in which pairs of adjacent oxazine rings are covalently linked (Fig. 11.6) [25].

The hydroxyl groups of the resorcinarenes can be completely acylated and alkylated to esters and ethers, and regioselectively acylated via partial acylation [23, 26]. The tetraacylation and alkylation of resorcinarenes is regioselective and only the opposite ring hydroxyl groups are substituted. Mannich condensation of the tetraosylates **7** with primary amines and formaldehyde is also regioselective leading exclusively to tetrabenzoxazines **8** with  $C_4$ -symmetry due to their stabilisation by intramolecular O-H $\cdots$ O hydrogen bonding [25, 27]. In addition, in the case of chiral amines, the reaction is diastereoselective [28, 29]. Only the  $C_4$ -symmetrical isomer of tetrabenzoxazines is possible since it is the only form that enables the formation of four intramolecular O-H $\cdots$ O hydrogen bonds. For the tetraosylated bis-benzoxazines, two intramolecular O-H $\cdots$ O = S hydrogen bonds are possible in principle for both isomers **A** and **B** (Fig. 11.7). However, the starting tetraosylate prefers the conformation in which the tosylated resorcinol rings are oriented outwards and in which, by a slight  $C_2$ -symmetrical distortion of the resorcinarene skeleton, two distal hydrogen bonds are stronger [28, 29]. As such the orientation of the oxazine rings must be trans as in the  $C_2$ -symmetrical isomer **A** to avoid steric and electrostatic repulsion of the N-R' groups (Fig. 11.7).



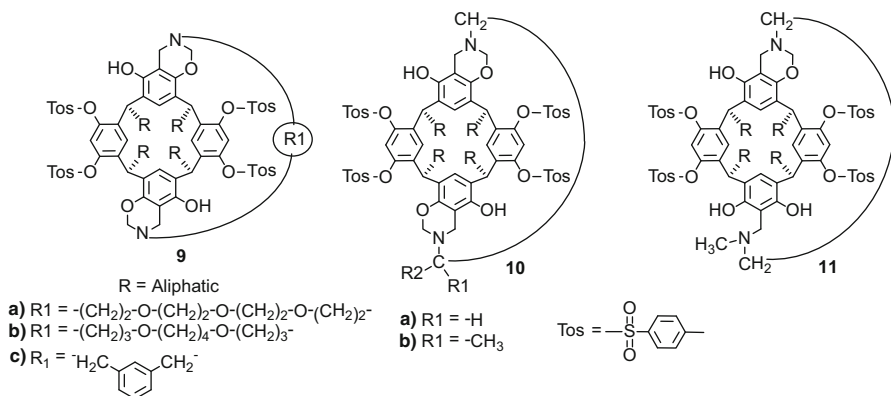


**Fig. 11.8** Bridged tetrabenzoxazines [22] (Image adapted from [22] with permission from The American Chemical Society)

derivatives **9–11** in which two opposite resorcinol units are connected with yields of 17–53 % (Fig. 11.8) [22]. Other diamines such as ethylenediamine, 1,1-dimethyl ethylenediamine, or *N*-methyl ethylenediamine gave exclusively the corresponding macrobicyclic dibenzoxazines and the monobenzoxazine in 75–90 % yields [22].

Similarly, covalently linked resorcinarene dimers **12–13** were synthesized from resorcinarene and ethylenediamine and an excess of formaldehyde catalyzed by a small amount of acetic acid in a moderate 15 % yield under high dilution conditions (Fig. 11.9) [30]. This procedure has been modified by using the more rigid piperazine as a linker to covalently connect two resorcinarene units via four piperazine units into a dimeric covalent cage **14** with yields ranging from 20 to 40 % (Fig. 11.9) [31]. These cage compounds were purified by flash chromatography. The <sup>1</sup>H NMR of the cages reveal a symmetrical compound with overlapping signals corresponding to the upper and lower part of the molecule.

### 11.2.2.2 Guest Binding Properties of Resorcinarene Tetrabenzoxazines

Resorcinarene tetrabenzoxazines, like their parent resorcinarenes, possess electron-rich cavities suitable for guest binding. During synthesis, the cavities of the resorcinarene tetrabenzoxazines are usually filled with solvent molecules. One example being a tetraoxazine host where the amine groups fold over the included dichloromethane guest molecule via intramolecular hydrogen bonding of the *N*-alkyl substituents forming a ‘hood’ over the guest molecule [32].

Whether the tetrabenzoxazines, the tetraoxazines, or tetraoxazolidines are formed, depended primarily, as mentioned above, on the structure of the amine or amino alcohol used. However, the relative energies of the isomeric products with five- or six-membered rings are very similar and both structural motifs can be observed simultaneously for 2- and 3-amino alcohols [20]. The X-ray structure of the

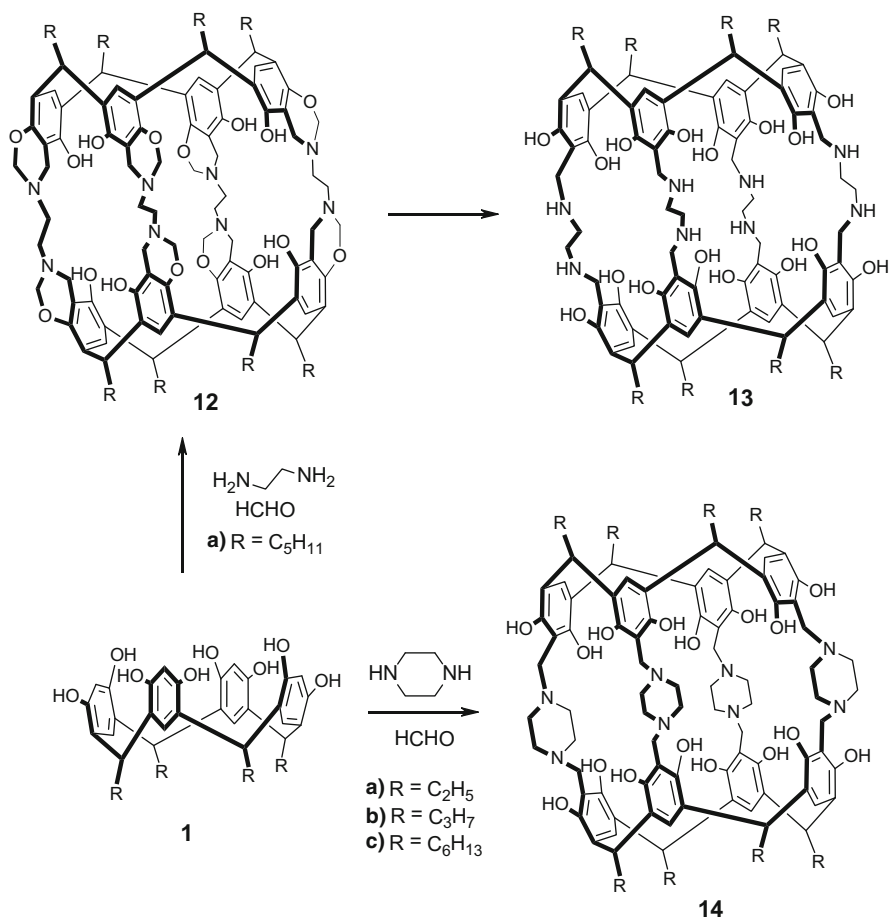


**Fig. 11.9** Covalently linked tetrabenzoxazine capsules [30, 31] (Image adapted from [30, 31] with permission from Elsevier and The American Chemical Society)

tetraoxazolidine e.g. **15** (Fig. 11.10) confirms the constitution of a tetraoxazolidine, and the  $C_4$ -symmetrical conformation with four intramolecular  $\text{OH} \cdots \text{OH} \cdots \text{N}$  hydrogen bonds, supported also by the NMR spectra. In the structure, the oxazolidine oxygens point away from the cavity, while the stereogenic centres are orientated towards the cavity. The nearly closed cavity is occupied by a molecule of dichloromethane, while a further molecule of acetonitrile is located on the twofold axis and embedded between the four pentyl chains of the resorcinarene skeleton.

Resorcinarene tetrabenzoxazines with amide side chains e.g. **16a–c** (Fig. 11.12), constitute a unique group of compounds with specific properties. The electron-rich interior cavity of the resorcinarene tetrabenzoxazines is suitable for trapping/inclusion of cationic species just like the regular resorcinarenes, while the terminal amide groups are suitable for binding anions (Fig. 11.11). As such, these receptors

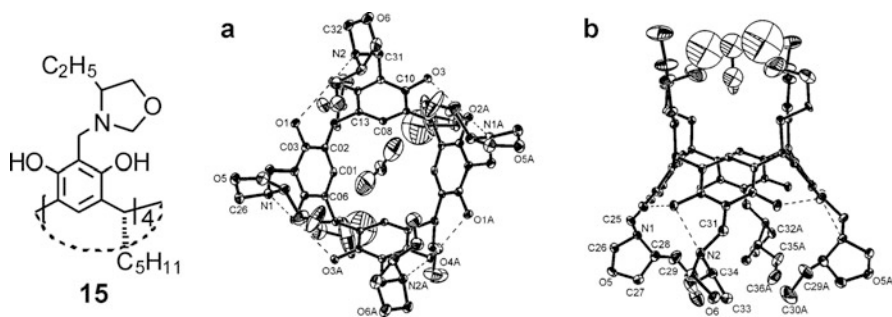


**Fig. 11.10** Molecular conformation of tetraoxazolidine **15** (a) top view and (b) side view. Hydrogen bonds are marked by *dotted lines*. The included  $\text{CH}_2\text{Cl}_2$  is shown only in (a) and the included  $\text{CH}_3\text{CN}$  only in (b) for clarity [20] (Image reproduced from [20] with permission from Wiley)

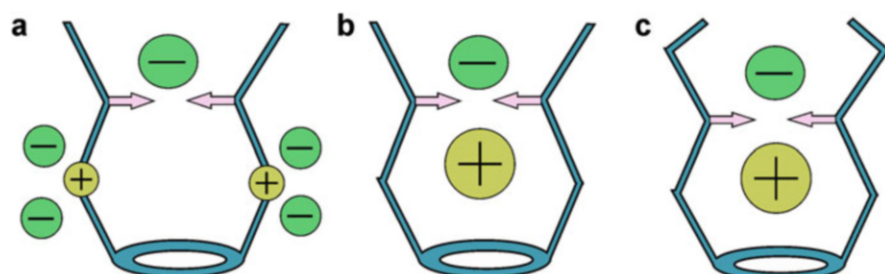


**Fig. 11.11** Receptors based on electrostatic (*yellow*) and hydrogen bonding interactions (*pink*): a Shows possible positions for the anions [34] (Image adapted from [34] with permission from Wiley)

where utilized as ditopic receptors through a combination of cation- $\pi$  and hydrogen bond interactions [33, 34].

The solvent interaction with the anion can be restricted by introducing bulky groups at the upper rim of the resorcinarene tetrabenzoxazine [34]. The  $^1\text{H}$  NMR spectra of 1:1 complexes e.g. **16b**•TMACl indicates the binding of the ion-pair (Fig. 11.12). With bulky groups such as the phenyl group in **16b**, the introduction of methanol (10–15 % v/v) does not remove the anion from its binding site contrary to the resorcinarene tetrabenzoxazines without the bulky groups such as in **16a** (Fig. 11.12) [33, 34]. This was also confirmed from comparative experiments where two different tetramethyl ammonium salts with different anions (TMACl and TMABr) were used **16b**•TMACl and **16b**•TMABr. In pure  $\text{CDCl}_3$ , the  $^1\text{H}$  NMR shows two set of signals corresponding to the two different complexes. One set of signals was observed when methanol (10 % v/v) was added, suggesting either anion release or fast anion exchange between the two complexes. The more methanol added, the lower the temperature required for the separation of the



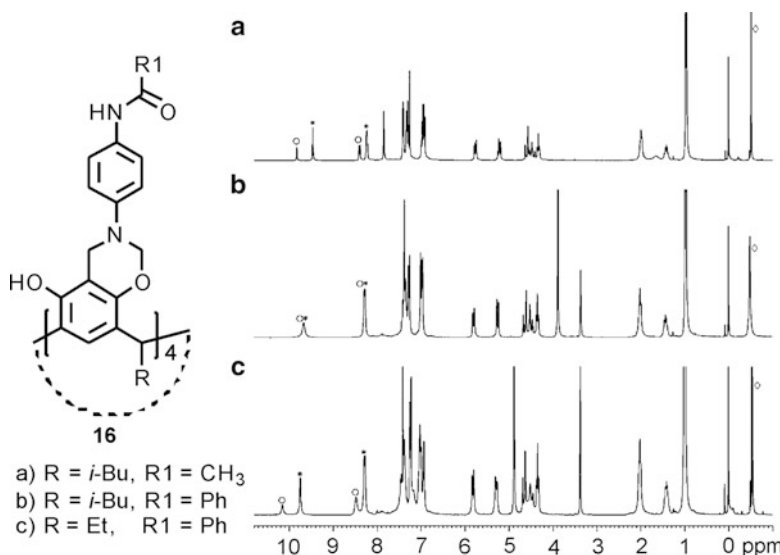


**Fig. 11.12**  $^1\text{H}$  NMR spectra of the 1:1 mixture of **16b**•TMA<sup>+</sup>Cl and **16b**•TMA<sup>+</sup>Br (300 MHz). ° Correspond to **16b**•TMA<sup>+</sup>Cl signals, \* correspond to **16b**•TMA<sup>+</sup>Br signals and ◇ correspond to TMA<sup>+</sup> ions. (a) In CDCl<sub>3</sub>, 300 K; (b) CDCl<sub>3</sub>/MeOH 9/1, 300 K; (c) CDCl<sub>3</sub>/MeOH 9/1, 1253 K [34] (Image reproduced from [34] with permission from The Royal Society of Chemistry)

peaks, implying the methanol accelerates the exchange of anions, but does not destroy the anion complex [34].

The anion confinement by the receptor was further confirmed by single crystal X-ray analyses in the solid state. In the structure, the anion remains in proximity to the TMA cation, and is symmetrically bound by all four –NH amide hydrogen bonds (Fig. 11.13). Additionally, from the top, four aromatic hydrogens (from *ortho*-positions) are in close proximity to the chloride (C–H···Cl distances are 2.7–3.1 Å). This weak interaction also adds to the overall binding efficiency and selectivity. Indeed, it is seen that the anion effectively seals this molecular capsule. The view from the top (Fig. 11.13) also reveals the space/void to which the anion is embedded and isolated from the environment by the bulky phenyl groups [34].

Tetrabenzoxazines with chiral groups have been utilized as receptors with the aim of binding specific chiral salts [35]. In the study, pseudo-racemates were prepared from one unlabelled guest enantiomer and the other deuterium labelled enantiomer. Electrospray ionization mass spectra (ESI-MS) of the pseudo-racemates yield intense signals for anion bridged dimers. When an exact 1:1 mixture of the guests is used, homo- and heterodimers of the ammonium ions appear at the statistical 1:2:1 ratio. These mass spectra were used as proof that both cations are present in exactly equal amounts. Since one of the host-guest complexes is labelled with a CD<sub>3</sub> group the two diastereomeric host-guest complexes overlap with their isotope patterns. Chiral selectivity was not observed with these receptors (Fig. 11.14) [35].

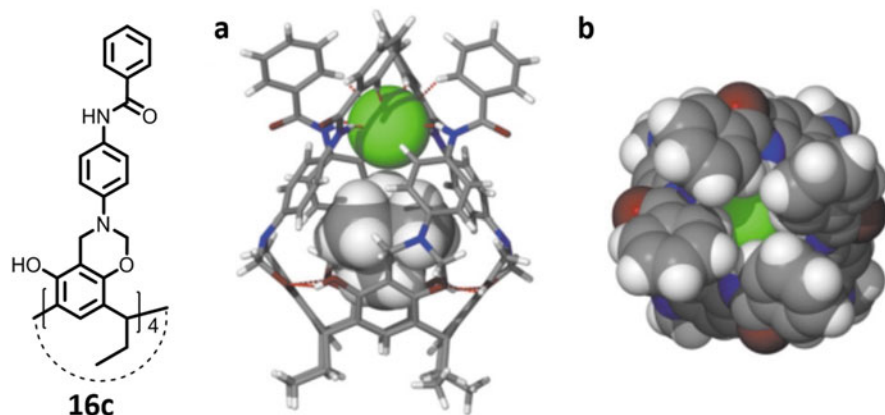


**Fig. 11.13** Crystal structure of **16c**•TMACl. (a) Side view with receptor molecule in capped stick representation and guests in CPK mode; (b) top view in CPK mode (Cl green) [34] (Image reproduced from [34] with permission from The Royal Society of Chemistry)

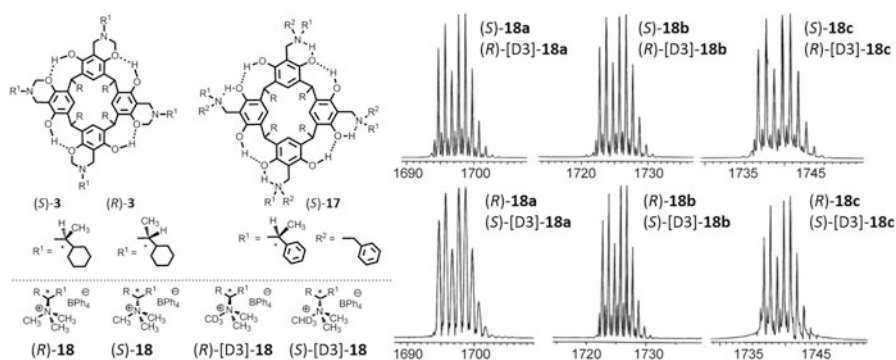


**Fig. 11.14** Tetrabenzoxazines (*R*)-**3** and (*S*)-**3** and tetrakis-aminomethylated resorcinarene (*S*)-**17**. Quaternary ammonium ions (**18**). Isotope pattern regions of the ESI-FTICR (*FTICR* Fourier transform ion cyclotron resonance) mass spectra of (*S*)-**17** with pseudo-racemates of the two guests. The *bottom* row represents control experiments with a reversed labelling of the two guest enantiomers as compared to the *top* row [35] (Image reproduced from [35] with permission from Springer)

### 11.3 The *N*-Alkyl Ammonium Resorcinarene Salts

The *N*-alkyl ammonium resorcinarene salts (NARSs) are easily prepared from the corresponding resorcinarene tetrabenzoxazines under refluxing conditions in the presence of mineral acids [36]. The hydrogen bonds between the ammonium moieties and halides form a strong circular hydrogen bond seam ( $\cdots\text{H}(\text{R}')\text{N}^+(\text{R}'')\text{H}\cdots\text{X}^-\cdots\text{H}(\text{R}')\text{N}^+(\text{R}'')\text{H}\cdots\text{X}^-\cdots$ )<sub>2</sub> leading to concave host molecules that can be considered as the hydrogen bond analogues of resorcinarene cavitands [1, 37] since they possess a similar shape and cavity size to covalent resorcinarene

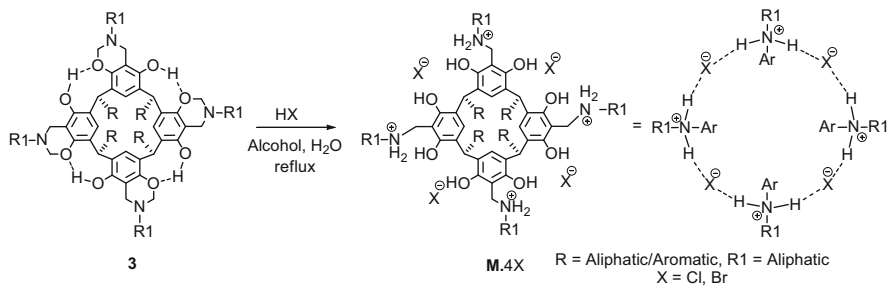


**Fig. 11.15** *N*-Alkyl ammonium resorcinarene halides (NARXs) with a strong circular hydrogen bond cation-anion seam [38]

cavitations. The NARSs have larger and deeper cavities as well as different binding behaviour than the parent resorcinarenes offering a possibility to use a larger set of guest molecules that can be bound into the cavity. In addition the *N*-alkyl ammonium resorcinarene salts, via the circular hydrogen bond seam, can interact with guests through hydrogen bond interactions [36].

### 11.3.1 Synthesis

The resorcinarene tetrabenzoxazines discussed in Sect. 11.2.2 undergo a ring opening in the presence of concentrated mineral acids (HCl, HBr) in alcoholic solvents with refluxing, resulting to the *N*-alkyl ammonium resorcinarene halides (NARXs) in yields ranging from 40 to 90 % (Fig. 11.15) [36, 38].

The NARXs are relatively symmetrical in solution as observed from their usually well-resolved  $^1\text{H}$  NMR spectra. Taking the cyclohexyl-NARCl as an example, in  $\text{CDCl}_3$  the protons of the resorcinarene skeleton appear as sharp signals which is in accord with a  $C_{4v}$  symmetrical structure. The diastereotopic nature of the protons of the methylene bridge connecting the aromatic ring of resorcinarene and the amino ( $\text{Ar-CH}_2\text{-N}$ ) are easily identified as a broad signal around 4.20 ppm. Two signals of the hydroxyl and the ammonium groups appear as broad signals around 9.3 ppm and 7.6 ppm respectively (Fig. 11.16) [36, 38].

Crystallization of the cyclohexyl analog **19•4Cl** from chloroform/diethyl ether mixture resulted in a 2:1 host-chloroform complex ( $2\text{CHCl}_3@19\bullet4\text{Cl}$ ) [39]. The first  $\text{CHCl}_3$  molecule is situated deep in the cavity slightly below the cation-anion belt (Fig. 11.17a) and is somewhat offset from the center of the cavity, while the second  $\text{CHCl}_3$  sits between cyclohexyl rings on the top of the first  $\text{CHCl}_3$  (Fig. 11.17b). The positions of the  $\text{CHCl}_3$  molecules are fixed by  $\text{N}(\text{NH}_2^+) - \text{H} \cdots \text{Cl}(\text{CHCl}_3)$ ,  $\text{C} - \text{H} \cdots \text{Cl}(\text{CHCl}_3)$  and  $\text{C}(\text{CHCl}_3) - \text{H} \cdots \text{Cl}^-$  hydrogen bonds and are situated between the hydrogen-bonded cation-anion seam and the seam formed by intramolecular  $\text{O} - \text{H} \cdots \text{O}$  hydrogen bonds (Fig. 11.17) [39].

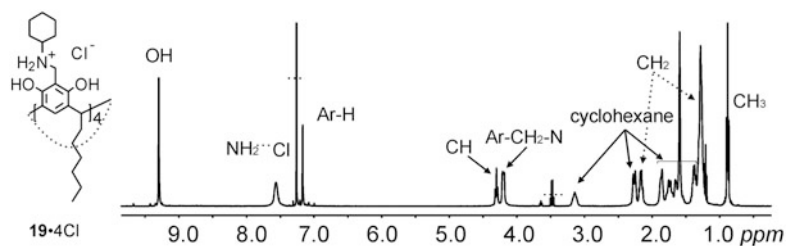


**Fig. 11.16**  $^1\text{H}$  NMR spectrum of cyclohexyl-NARCl in  $\text{CDCl}_3$  at 303 K, revealing a triplet for the CH of the resorcinarene skeleton, broad signals for the diastereotopic  $\text{ArCH}_2\text{N}$  and  $\text{NH}_2^+$  protons [38] (Image adapted from [31, 38] with permission from Taylor & Francis)

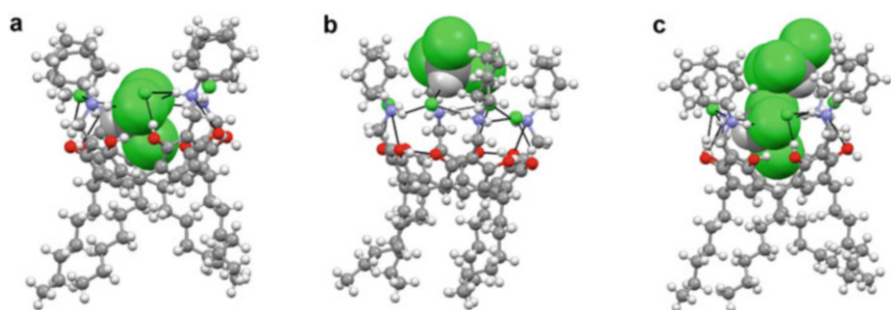


**Fig. 11.17** Ball and stick representation of the host-guest complex  $2\text{CHCl}_3@19\bullet 4\text{Cl}$ , showing chloroform molecule at (a) lower position, (b) at the upper position and (c) at both positions. Atoms of chloroform molecules are presented in CPK style [39] (Image adapted from [39] with permission from Wiley)

### 11.3.2 Self-Inclusion

The NARXs are charge-neutral with their rose-flower-like shape and deep electronic rich cavities and with short aliphatic *N*-propyl upper rim chains form self-included dimeric assemblies [38, 39]. In the structures, one of the upper rim propyl chains perfectly fits in the cavity of another molecule, leading to a self-included dimer via  $\text{NH}\cdots\text{X}^-$  hydrogen bonds (Fig. 11.18). The dimer is formed by two self-included resorcinarene tetracations and six halide anions. The two central anions are hydrogen bonded between six positively charged nitrogen atoms, and two self-included propyl ammonium chains share the remaining four anions, each of which being hydrogen bonded to two ammonium cations (Fig. 11.18c). The remaining two anions are located outside the dimer, linking the dimers via intermolecular hydrogen bonds. The nitrogen atoms form an almost perfect square, with the  $\text{N}\cdots\text{N}$  distance difference of 0.04 Å (Fig. 18.4c). The structures are nearly symmetrical whereas the upper rim propyl and lower rim alkyl chains are approximately related by an inversion center (Fig. 11.18) [39].

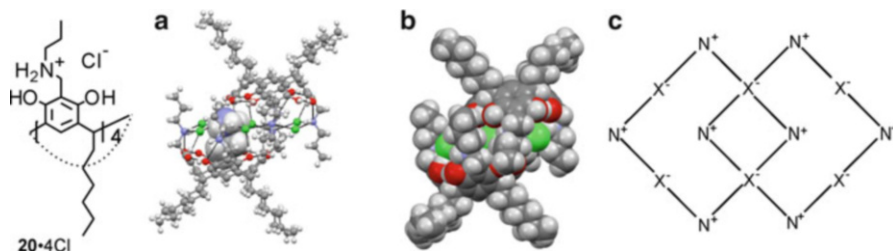


**Fig. 11.18** **a** Ball and stick representation of the self-inclusion dimer (**20•4Cl**)<sub>2</sub>. Atoms of one self-included *N*-propyl chain as well as nitrogen atom to which they are attached are presented in CPK style. **b** CPK plot of the dimer (**20•4Cl**)<sub>2</sub>, showing symmetrical disposition of cations that form the dimer. **c** Schematic representation of the orientation of the positively charged nitrogen atoms and halide anions in the self-included dimers [38, 39] (Image adapted from [39] with permission from Wiley)

The self-included dimers were also confirmed in solution via variable temperature <sup>1</sup>H NMR spectroscopy in CDCl<sub>3</sub>. Significant complexation-induced shielding of the <sup>1</sup>H NMR resonances corresponding to the protons of one *N*-propyl group encapsulated in the cavity of the resorcinarene second host were observed at lower temperatures (Fig. 11.19). The –NH<sub>2</sub><sup>+</sup> moieties of the propyl chain interact with the cation-anion hydrogen bond seam, thus the –OH and –NH<sub>2</sub> signals are also affected. This is observed from the new signals between 7 and 9 ppm. These new signals including the signals of the cavity-bound *N*-propyl group slowly disappear with increase in temperature. This is a clear indication that the self-included dimer dissociates to the isolated monomeric species at higher temperatures (Fig. 11.19) [39].

### 11.3.3 Neutral Guest Binding

The charge-neutral NARXs, possess two different binding motifs: (a) the electron-rich deep cavity; (b) the cation-anion seam.

The electron-rich cavity can interact with neutral guests mainly through CH- $\pi$  interaction while the cation-anion seam can interact with guests through hydrogen bonding. Small solvent molecules such as acetonitrile, short chain alcohols and 1,4-dioxane are suitable guests molecules for the NARXs and therefore interact through CH- $\pi$  and hydrogen bond interactions [36, 38, 39]. In the presence of these guests (Fig. 11.20), the *N*-propyl NARX **20•4Cl** that typically forms self-included dimers, forms 1:1 host-guest complexes. When NARXs with larger/rigid groups such as *N*-cyclohexyl **19•4Cl** are used, self-included dimers are not formed and host-guest complexes are observed.

Several different types of host-guest assemblies have been observed in the solid state and in solution. In one example, from a dichloromethane/acetonitrile mixture, **19•4Cl** crystallized as a 1:1 host-guest complex with disordered MeCN

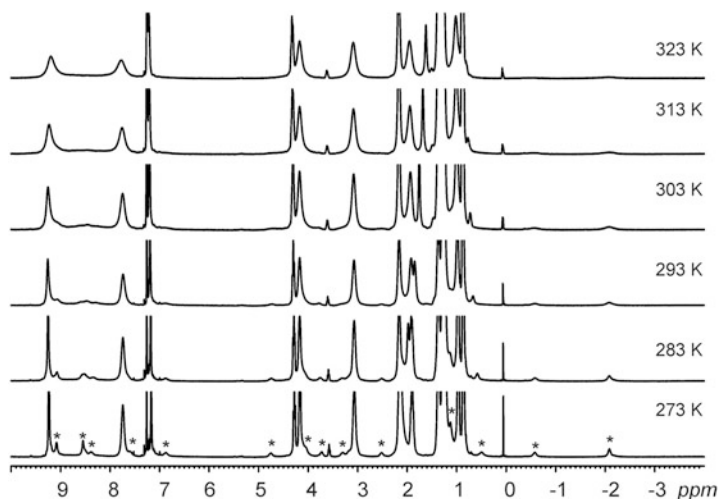


**Fig. 11.19** Variable temperature  $^1\text{H}$  NMR of  $20\cdot 4\text{Cl}$  in  $\text{CDCl}_3$  showing self-inclusion at low temperature. The self-inclusion dimer disassembles into monomeric species at higher temperatures. Asterisks correspond to signals resulting from the self-inclusion of the *n*-propyl groups [39] (Image reproduced from [39] with permission from Wiley)

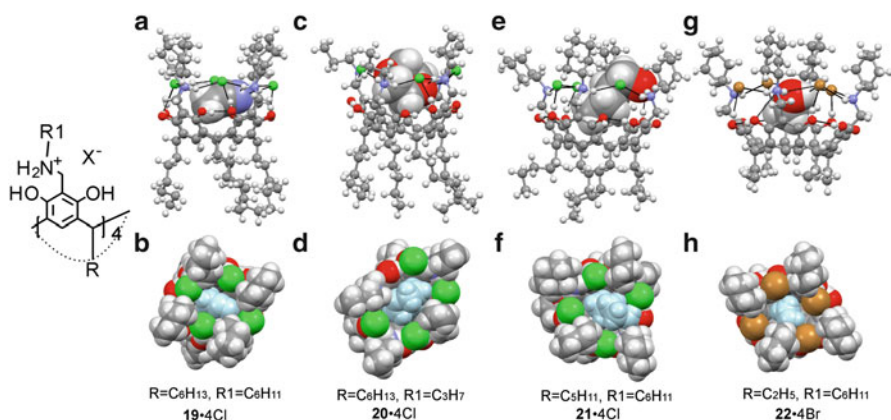


**Fig. 11.20** Ball and stick (*side view*) and CPK plot (*top view*) of: (a, b)  $\text{MeCN}@19\cdot 4\text{Cl}$ , (c, d)  $1,4\text{-dioxane}@20\cdot 4\text{Cl}$ , (e, f)  $\text{BuOH}@21\cdot 4\text{Cl}$  and  $\text{MeOH}@22\cdot 4\text{Br}$ . In the *side view*, the guest are presented in CPK. In the *top view*, the guest are presented in *light blue* for clarity [36, 38, 39] (Image adapted from [36, 38, 39] with permission from Wiley and Taylor & Francis)

and  $\text{CH}_2\text{Cl}_2$  molecules ( $\text{MeCN}@19\cdot 4\text{Cl}$ ). The MeCN is located deep in the cavity of  $19\cdot 4\text{Cl}$  interacting via  $\text{CH}\text{-}\pi$  and hydrogen bonds while the  $\text{CH}_2\text{Cl}_2$  molecule is located at the upper part of the cavity [38]. Other examples include host-guest complexes with methanol ( $\text{MeOH}@22\cdot 4\text{Br}$ ), butanol ( $\text{BuOH}@21\cdot 4\text{Cl}$ ) and 1,4-dioxane ( $1,4\text{-dioxane}@19\cdot 4\text{Cl}$ ) (Fig. 11.20) [36, 38, 39]. These host guest



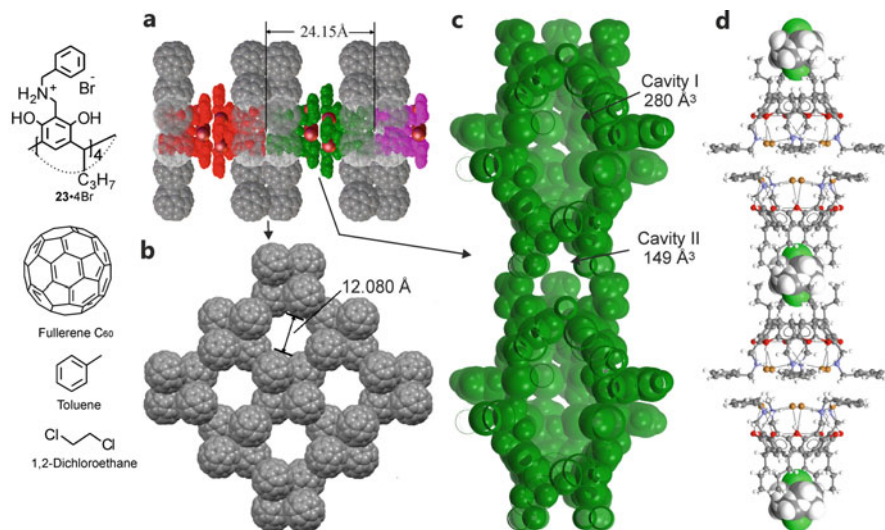


**Fig. 11.21** Selected packing plots. (a) The assembly of the **23•4Br** into the lattice of the hierarchical assembly, (b) The C<sub>60</sub> packing (all other molecules removed for clarity), (c) The space-filling model highlighting the cavities **I** and **II** in the packed **23•4Br** and (d) A ball-and-stick model showing the encapsulated 1,2-dichloroethane (CPK) in cavity **II** [40] (Image reproduced from [40] with permission from The American Chemical Society)

assemblies were also shown to exist in solution through a variety of <sup>1</sup>H NMR studies [36, 38, 39].

A completely different structure, such as hierarchical solid-state architectures can be constructed involving **23•4Br**, fullerene C<sub>60</sub>, toluene and 1,2-dichloroethane [40]. In this assembly, the fullerene C<sub>60</sub> organizes into a lattice with dimeric head-to-head and tail-to-tail **23•4Br** assemblies with two differently sized cavities containing 1,2-dichloroethane molecules (Fig. 11.21). The toluene molecules assisted the self-assembly process acting as adhesives to glue the C<sub>60</sub> molecules together through multiple  $\pi \cdots \pi$  and C-H  $\cdots \pi$  interactions while the 1,2-dichloroethane molecules are trapped into small cavities formed by the NARBr during the crystallization process. In the absence of C<sub>60</sub>, the **23•4Br** forms head-to-tail assemblies with solvent-filled cavities highlighting the importance of the fullerene C<sub>60</sub> in the growth of the hierarchical structure [40].

Small amides have both hydrogen-bond donor and acceptor groups and thus would be suitable guests for the NARX receptors. The NARXs have been shown to be suitable receptors for a series of *N*-alkyl- and *N*-aryl acetamides in solution, in the gas phase and in the solid state [39]. X-ray structure of the complex amide@**19•4Cl** shows the position of the amide and that it is bound in the cavity of the host mainly through strong hydrogen bonds N(amide)–H  $\cdots$  Cl<sup>-</sup> and N(NH<sub>2</sub><sup>+</sup>)–H  $\cdots$  O and by two C–H  $\cdots \pi$  interactions (Fig. 11.22). The <sup>1</sup>H NMR titration studies (Fig. 11.22) reveal the upper rim substituent to have an effect on the binding affinity. NARXs with rigid upper rims gave slightly higher association

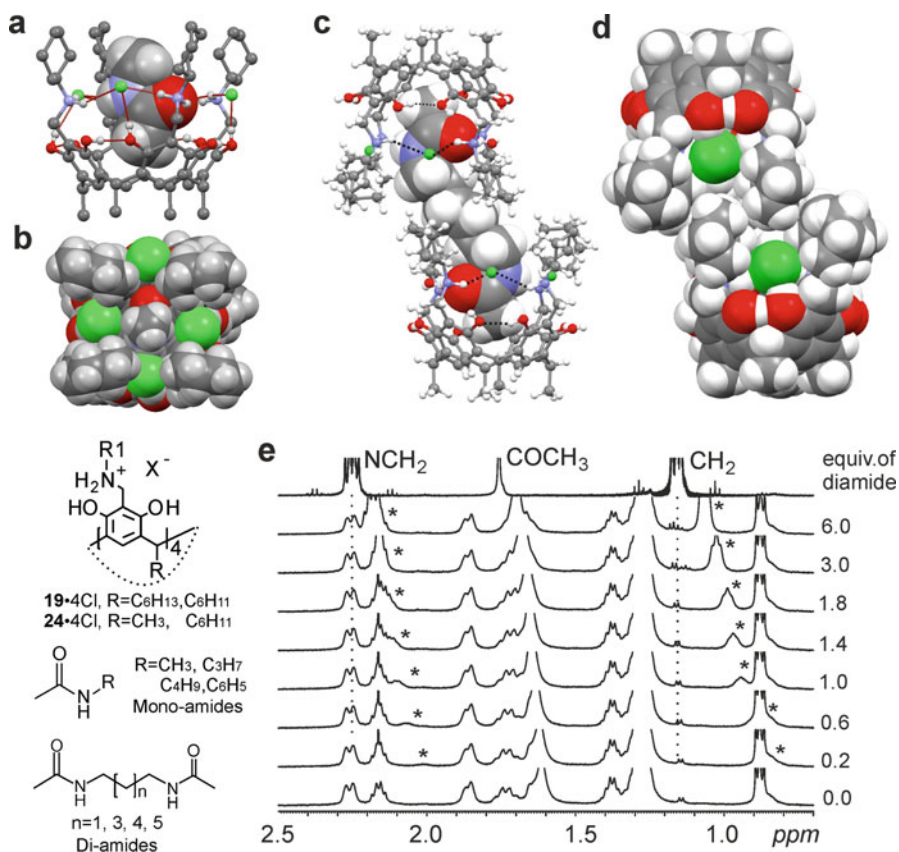


**Fig. 11.22** The mono-amide complex amide@**19•4Cl** (amide:  $\text{R} = \text{CH}_3$ ): (a) ball and stick with the mono-amide guest in CPK style, (b) CPK representation. The di-amide complex amide@**24•4Cl** (di-amide:  $n = 3$ , host:  $\text{R}^1 = \text{CH}_3$ ,  $\text{R}^2 = \text{C}_6\text{H}_{11}$ ): (c) Ball and stick representation with the di-amide guest in CPK mode, (d) CPK representation of the capsule. (e) Selected region of the  $^1\text{H}$  NMR spectra observed upon the titration of the di-amide guest to **19•4Cl** in  $\text{CDCl}_3$  at 303 K. Stars show the changes of the  $-\text{NCH}_2$  and  $-\text{COCH}_3$  signals [39, 41] (Image reproduced from [39, 41] with permission from Wiley)

constants [39]. The 1:1 host-guest assemblies were also observed in the gas phase via mass spectrometry studies [39]. The NARX receptors were shown to also bind diamides in a cooperative manner [41]. In the study, di-acetamides as homoditopic guests and the NARXs as monovalent receptors were utilized. The  $^1\text{H}$  NMR titration studies reveal that the lengths of the carbon-chain spacer have a profound effect on the binding event and stoichiometry, with a statistical distribution based on the length of the spacer. The optimum binding was observed with the six-carbon spacer between the amide moieties, confirming the best-fit scenario of the host. The three-carbon spacer was too short and led to 1:1 binding. In all cases in the 2:1 host-guest assemblies, the second binding constants  $K_2$  were larger than the first  $K_1$  values, confirming a positively cooperative binding process. Job plots,  $^1\text{H}$  NMR titration (Fig. 11.22) and DOSY NMR experiments were used to study the different



assemblies in solution and to confirm 2:1 complexes for the longer spacer diamide guests. In the solid state through single X-ray diffraction analyses, 2:1 host-guest assembly was also confirmed in the case of **24**•Cl (Fig. 11.22) [41].

### 11.3.4 *The NARXs as Halogen Bond Acceptors*

Hydrogen bonds are arguably the most frequently used weak interactions in the design of organic supramolecular architectures [42]. Recently, the “long lost brother” of the hydrogen bond, viz. the halogen bond (XB) has been defined [43] and been extensively used and studied in the solid state and in solution, as well as in material science [44–48]. The halogen bond is analogous to a hydrogen bond in both strength and directionality. Halogen bonds result from the interaction between a polarized halogen atom, sometimes supplemented with coordinative [49], or covalent character, and Lewis bases [43]. The polarized halogen atoms in halogen bond donors exhibit an anisotropic electron distribution leading to an electropositive region on the halogen, and this is named the  $\sigma$ -hole [50]. The strength of the halogen bond interactions ( $R-X \cdots A$ ) usually follow the trend:  $X = I > Br \gg Cl \gg F$ .

Anions are very good Lewis bases which makes them suitable XB acceptors. Halides are particularly excellent hydrogen bond and halogen bond acceptors due to their spherical, symmetrical and electronic nature. The cooperative utilization of both a hydrogen and a halogen bonds by receptors in host-guest systems are rare. Nonetheless, researchers have demonstrated the selective recognition of anions by a host showing both halogen and hydrogen bonds as a result of a “compromise” between the distinct preferences of the two interactions [51]. More recently, hydrogen and halogen bonds work in tandem and have been demonstrated in pre-organized concave cavitand system for host-guest binding [52]. Many 1-D, 2-D and 3-D halogen bond structures with halides have been reported [53].

The NARXs possess four spatially-fixed halogen-bond acceptor sites (the four anions) with deep cavities for guest binding. The resorcinarene skeleton and the strong hydrogen bond interactions from the ammonium ions shield the halide anions, so that in the presence of suitable halogen bond donors, the latter interactions can only form either parallel or perpendicular to the upper rim of the NARXs.

#### 11.3.4.1 Halogen Bonded Deep Cavity Cavitands

Bromotrichloromethane ( $CCl_3Br$ ), an inexpensive solvent was utilized as a halogen-bond donor. The bromine atom in this liquid at room temperature is substantially polarized by the three chlorine atoms. As such,  $CCl_3Br$  is a suitable solvent and building block for the construction of halogen-bonded architectures. In the presence of NARXs, single crystals of the halogen-bonded assembly NARX ( $CCl_3Br$ )<sub>4</sub> obtained via slow evaporation were analyzed. In the structure, four

$\text{CCl}_3\text{Br}$  molecules are halogen-bonded to the bromide anions, thereby extending the cavity height by approximately 2 Å, resulting in an analogue of deep cavity cavitands (Fig. 11.23) [54]. The halogen bonding ratio  $R_{\text{XB}}$  ( $R_{\text{XB}} = d_{\text{XB}}/(X_{\text{vdw}} + B_{\text{vdw}})$ ) can be used to roughly measure the strength of the halogen bond interactions [55, 56]. The four  $\text{CCl}_3\text{Br}$  molecules bond to the four bromide anions through moderate halogen bonds. The halogen bond ratio ( $R_{\text{XB}}$  for the four halogen bonds) observed in the structure varies between 0.85 and 0.90 (Fig. 11.23). The halogen-bonded  $\text{CCl}_3\text{Br}$  molecules form a wall together with the *N*-cyclohexyl rings, resulting in a deep cavity with a height of approximately 12 Å. The effective diameter of the cavity in the structure defined by the closest van der Waals surfaces between the opposite chlorine atoms of  $\text{CCl}_3\text{Br}$  molecules is approximately 7 Å which is large enough for the  $\text{CCl}_3\text{Br}$  to fit into the cavity (Fig. 11.23). The solvent-accessible cavity void volume was calculated to be approximately 550 Å<sup>3</sup> [54].

Perfluorinated iodo compounds are considered as iconic halogen-bond donors, due to the high electronegativity of the fluorines atoms and the ease of polarizability of the iodines at the periphery. Several NARXs with different upper rim substituents (cyclohexyl and propyl) as halogen-bond acceptors, in the presence of perfluorinated iodoalkanes and perfluorinated iodoarenes resulted in deep-cavity cavitands (Fig. 11.23) analogous in shape to the assembly formed with  $\text{CCl}_3\text{Br}$  [57, 58]. In the presence of a bis-halogen bond donor 1,4-diiodooctadecane ( $\text{I}-(\text{CF}_2)_4-\text{I}$ ), both *N*-propyl NARBr and *N*-cyclohexyl NARBr resulted in structures of the same packing, although the assembly involving *N*-propyl NARBr and *N*-cyclohexyl NARBr crystallizes in the orthorhombic space group *Ccce* and tetragonal *P4/ncc*, respectively. In the structures, the halogen-bond donor  $\text{IC}_4\text{F}_8\text{I}$  interacts with the NARBr via  $\text{I} \cdots \text{Br}$  halogen bonds. The  $\text{Br}^- \cdots \text{I}-(\text{CF}_2)_4-\text{I} \cdots \text{Br}^-$  halogen-bonded species forms as in the  $\text{CCl}_3\text{Br}$  assembly. In both structures a second NARBr sits in

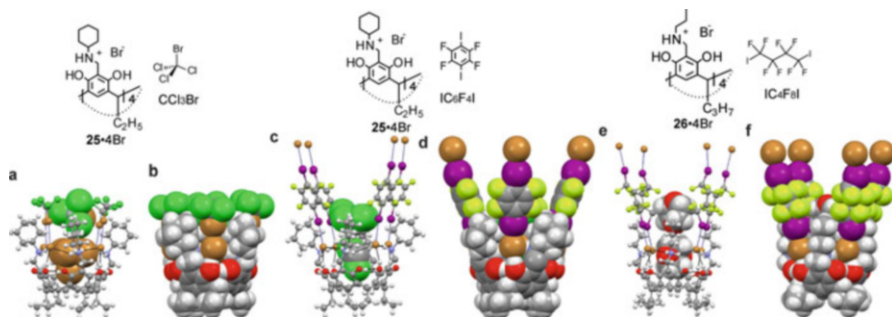


**Fig. 11.23** The halogen-bonded deep cavity cavitand  $[(25\cdot 4\text{Br})\cdot(\text{CCl}_3\text{Br})_4]$ : (a) ball-and-stick representation with two encapsulated  $\text{CCl}_3\text{Br}$  (one ordered and one disordered) molecules in CPK mode and (b) CPK representation. The halogen-bonded deep cavity cavitand  $[(25\cdot 4\text{Br})\cdot(\text{IC}_6\text{F}_4\text{I})_2]$ : (c) ball-and-stick representation with the encapsulated  $\text{CHCl}_3$  (disordered) in CPK mode and (d) CPK representation. The halogen-bonded deep-cavity cavitand  $[(26\cdot 4\text{Br})\cdot(\text{I}-(\text{CF}_2)_4-\text{I})_2]$ : (e) ball-and-stick representation with the two encapsulated 1,4-dioxane molecules in CPK mode and (f) CPK representation [54, 57, 58] (Image adapted from [54, 57, 58] with permission from The Royal Society of Chemistry and The American Chemical Society)

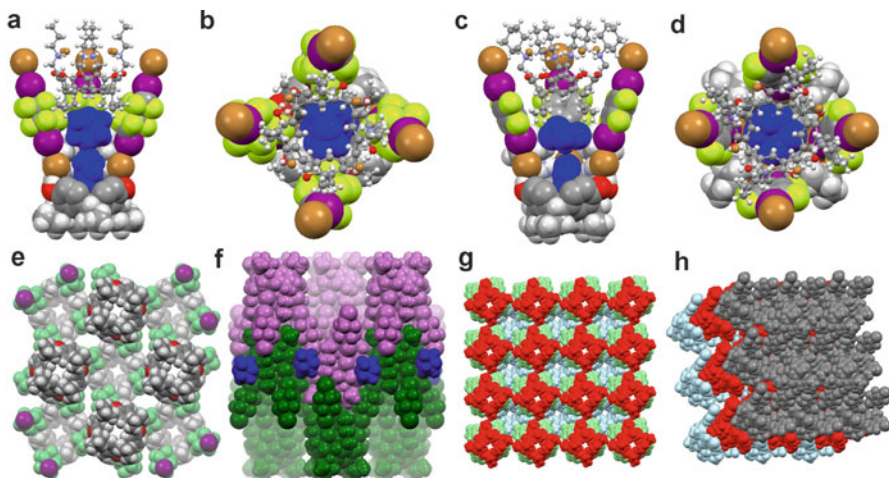


**Fig. 11.24** The sliced side (a) and top (b) view of the XB deep cavity cavitand [(dioxane)<sub>2</sub>@25•4Br]•(I-(CF<sub>2</sub>)<sub>4</sub>-I)<sub>2</sub> with two 1,4-dioxane molecules and one resorcinarene host within the cavity. The sliced side (c) and top (d) view of the XB deep-cavity cavitand [(CHCl<sub>3</sub>@25•4Br)•(IC<sub>6</sub>F<sub>4</sub>I)<sub>2</sub>]. The halogen-bonded layer with peaks and holes and the packing to show the fitting of the layers for the assemblies [(dioxane)<sub>2</sub>@26•4Br]•(I-(CF<sub>2</sub>)<sub>4</sub>-I)<sub>2</sub> (e, f) and [(CHCl<sub>3</sub>@26•4Br)•(IC<sub>6</sub>F<sub>4</sub>I)<sub>2</sub>] (g, h) respectively. The different colours portray the different components and layers for clarity [57, 58] (Image reproduced from [57, 58] with permission from The Royal Society of Chemistry and The American Chemical Society)

the upper cavity of the halogen bond assemblies, in a head-to-tail packing arrangement with 1,4-dioxane molecules filling up the deep cavities (Fig. 11.23).

Cocrystallization of cyclohexyl-NARBr with aromatic bishalogen-bond donor 1,4-diiodotetrafluorobenzene (IC<sub>6</sub>F<sub>4</sub>I), in CHCl<sub>3</sub> resulted in a similar halogen-bonded deep-cavity cavitand [58]. The four I⋯Br<sup>-</sup> halogen bonds are relatively short (3.25 Å) resulting in the halogen-bond ratio  $R_{XB} = 0.85$  with C-I⋯Br<sup>-</sup> angle of 170.28° thus demonstrating moderate halogen bond acceptor character. The solvent accessible cavity void volume was calculated to be *ca.* 644.16 Å<sup>3</sup> (Fig. 11.23) [57].

In all these structures, the other iodine ends of the four halogen-bond donors IC<sub>6</sub>F<sub>4</sub>I and I-(CF<sub>2</sub>)<sub>4</sub>-I, are each halogen-bonded to the bromides of the next assembly in the opposite direction forming Br<sup>-</sup>⋯IC<sub>6</sub>F<sub>4</sub>I⋯Br<sup>-</sup> and Br<sup>-</sup>⋯I-(CF<sub>2</sub>)<sub>4</sub>-I⋯Br<sup>-</sup> halogen bond systems and resulting in a 3-D polymeric arrangement (Fig. 11.24) [57, 58].

### 11.3.4.2 Halogen Bonded Dimeric Assemblies

The formation of container compounds with cavities for guest binding is an important and widely studied area of contemporary supramolecular chemistry. The above results have shown the NARXs to be suitable halogen-bond acceptors and forms deep cavity cavitands in the presence of suitable halogen-bond donors.

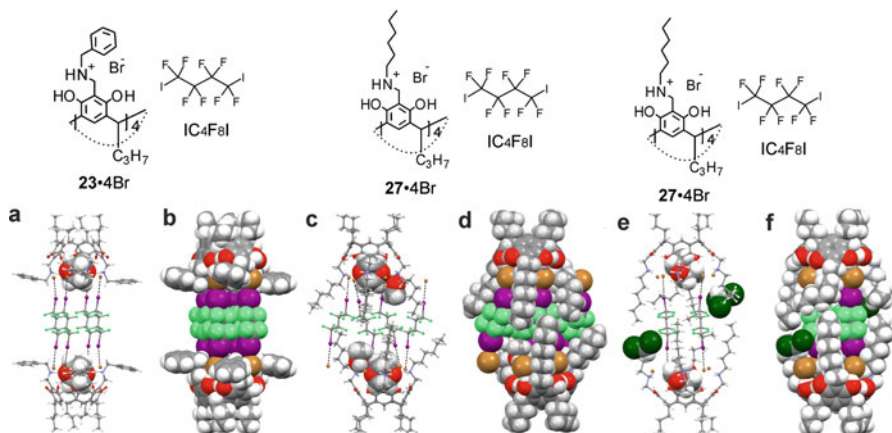


**Fig 11.25** The halogen-bonded dimeric dumbbell assembly [(dioxane@**23•4Br**)•(I-(CF<sub>2</sub>)<sub>4</sub>-I)<sub>5</sub>•(dioxane@**23•4Br**)]: (a) ball-and-stick model with the in-cavity 1,4-dioxane in CPK mode and (b) CPK mode. The 1-D halogen bond pseudo-capsular polymeric [(dioxane)<sub>1.5</sub> + MeOH@**27•4Br**]•(I-(CF<sub>2</sub>)<sub>4</sub>-I)<sub>3</sub>•(dioxane)<sub>1.5</sub> + MeOH@**27•4Br**]: (c) ball-and-stick model with the in-cavity guests in CPK mode and (d) CPK mode. The halogen dimeric capsule-like assembly [(dioxane + CHCl<sub>3</sub>@**27•4Br**)•(I-(CF<sub>2</sub>)<sub>4</sub>-I)<sub>2</sub>•(dioxane + CHCl<sub>3</sub>@**27•4Br**)]: (e) ball-and-stick model with the in-cavity guests in CPK mode and (f) CPK mode [58] (Image reproduced from [58] with permission from The American Chemical Society)

Changing the upper rim substituents of the NARXs to benzyl groups introduces a degree of flexibility (flexibility originating from the -CH<sub>2</sub>- group) to the NARX receptors. In the presence of a slight excess of the halogen-bond donor I-(CF<sub>2</sub>)<sub>4</sub>-I and 1,4-dioxane in chloroform, suitable single crystals corresponding to the assembly [(dioxane@**23•4Br**)•(I-(CF<sub>2</sub>)<sub>4</sub>-I)<sub>5</sub>•(dioxane@**23•4Br**)] were obtained (Fig. 11.25a, b) [58]. The molecules aggregate in a triclinic *P*-1 space group, with the unit cell containing a “dumbbell”-shaped halogen bond dimer. This dimer entraps 1,4-dioxane molecules in each cavity of **23•4Br**. Four halogen-bond donors, link two of the **23•4Br** molecules with Br ··· I halogen-bonds, forming the “dumbbell-shaped” dimeric assembly. A fifth halogen-bond donor molecule interacts with one of the bromide anions by halogen bond formation, providing the additional extension of the dimer along the crystallographic [0 1 1] direction leading to a 1-D polymer of dimers (Fig. 11.26a). The halogen bonding ratio R<sub>XB</sub> ranges from 0.86 to 0.88 [58].

Changing the upper rim of the NARBr from *N*-benzyl to *N*-hexyl groups removes the conformational twisting and π ··· π stacking of the benzyl groups. In methanol, a 1:4 mixture of **27•4Br** and the halogen-bond donor in the presence of 1,4-dioxane resulted in the dimeric assembly [(dioxane)<sub>1.5</sub> + MeOH@**27•4Br**]•(I-(CF<sub>2</sub>)<sub>4</sub>-I)<sub>3</sub>•(dioxane)<sub>1.5</sub> + MeOH@**27•4Br**]<sub>n</sub> (Fig. 11.25c, d). The same components in chloroform gave a different dimeric assembly corresponding to [(dioxane + CHCl<sub>3</sub>@**27•4Br**)•(I-(CF<sub>2</sub>)<sub>4</sub>-I)<sub>2</sub>•(dioxane + CHCl<sub>3</sub>@**27•4Br**)] (Fig. 11.25e, f) [58]. In methanol, only three of the four Br<sup>-</sup> anions in each host are involved in

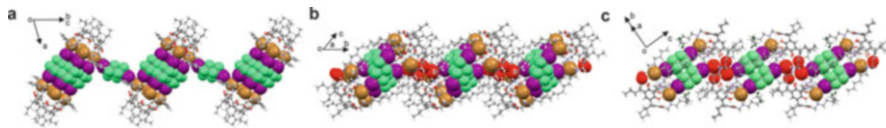


**Fig. 11.26** (a) A view of the 1-D chain of (a) the halogen-bonded dimeric dumbbell assembly [(dioxane@**23**•4Br)•(I-(CF<sub>2</sub>)<sub>4</sub>-I)<sub>5</sub>•(dioxane@**23**•4Br)], (b) the pseudo-capsular polymer [(dioxane)<sub>1.5</sub> + MeOH@**27**•4Br)•(I-(CF<sub>2</sub>)<sub>4</sub>-I)<sub>3</sub>•(dioxane)<sub>1.5</sub> + MeOH@**27**•4Br)]<sub>n</sub> showing the halogen bond donor I-(CF<sub>2</sub>)<sub>4</sub>-I within the capsule cavity and (c) the XB dimers [(dioxane + CHCl<sub>3</sub>@**27**•4Br)•(I-(CF<sub>2</sub>)<sub>4</sub>-I)<sub>2</sub>•(dioxane + CHCl<sub>3</sub>@**27**•4Br)] connected by OH⋯Br hydrogen bonds along [1 1 1] direction [58] (Image reproduced from [58] with permission from The American Chemical Society)

halogen bond formation, while the fourth Br<sup>-</sup> donates electrons to a methanol molecule which is located between the two *N*-hexyl arms. The *N*-hexyl **27**•4Br dimerises by two halogen-bond donor I-(CF<sub>2</sub>)<sub>4</sub>-I molecules with the other two stretching outside the dimer towards the neighbouring **27**•4Br, leading to a 1-D polymeric assembly along the crystallographic *a* axis direction. Along the *b* direction, OH⋯Br hydrogen bonds connect the 1-D halogen-bond polymers, resulting in a 2-D network in the *ab* plane (Fig. 11.26b). The three independent Br⋯I halogen bonding distances in this structure results in R<sub>XB</sub> ratios of 0.85, 0.88 and 0.89 [58].

In the assembly formed in chloroform, only two halogen-bond donors are involved in connecting the dimer. In the assembly [(dioxane + CHCl<sub>3</sub>@**27**•4Br)•(I-(CF<sub>2</sub>)<sub>4</sub>-I)<sub>2</sub>•(dioxane + CHCl<sub>3</sub>@**27**•4Br)], the dimer consists of two head-to-head eclipsed **27**•4Br molecules with a pseudo-center of inversion. Two adjacent Br<sup>-</sup> anions of each **27**•4Br molecule are involved in halogen bonding thus dimerising the assembly. Two 1,4-dioxane molecules are located with the assembly with one in each **27**•4Br cavity. Inter-dimeric hydrogen bonds between two adjacent resorcinarene along [1 1 1] direction, play an important role in the extension of the structure, thus generating a 2-D network in a (1 1 0) plane (Fig. 11.26c). The Br⋯I halogen bond interactions in this structure are comparable with those in the XB “dumbbell” and polymer assemblies with R<sub>XB</sub> ratios ranging from 0.86 to 0.88 [58].

It is very challenging to demonstrate halogen-bond formation in solution due to solvent interference. Nonetheless, NMR spectroscopy is a powerful and reliable tool to study such interactions in solution [46, 47, 59]. <sup>19</sup>F NMR spectroscopy is commonly used to study halogen bonds in solution involving perfluorinated hydrocarbons as halogen-bond donors [46, 47] while comparative monitoring [59] of <sup>1</sup>H NMR chemical shift changes is also utilized for the detection of halogen bonds. The different halogen-bonded assemblies were studied in solution via <sup>19</sup>F, <sup>1</sup>H and <sup>13</sup>C NMR. Changes in the -CF<sub>2</sub> protons of the halogen-bond donors, -NH<sub>2</sub> and -OH protons of the NARXs, clearly confirm the existence of

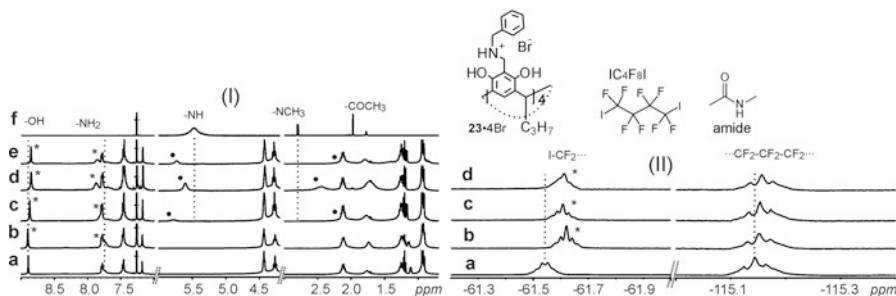


**Fig. 11.27** (I): <sup>1</sup>H NMR in CDCl<sub>3</sub> at 303 K of: (a) **23•4Br**, (b) 1:2 mixture of **23•4Br** and I-(CF<sub>2</sub>)<sub>4</sub>-I, (c) 1:2:1 mixture of **23•4Br**, I-(CF<sub>2</sub>)<sub>4</sub>-I and amide, (d) 1:2:excess mixture of **23•4Br**, I-(CF<sub>2</sub>)<sub>4</sub>-I and amide, (e) 1:1 mixture of **23•4Br** and amide, (f) amide (10 mM). (II) <sup>19</sup>F NMR in CDCl<sub>3</sub> at 303 K of: a I-(CF<sub>2</sub>)<sub>4</sub>-I (10 mM), (b) 1:2 mixture of **23•4Br** and I-(CF<sub>2</sub>)<sub>4</sub>-I, c) 1:2:1 mixture of **23•4Br**, I-(CF<sub>2</sub>)<sub>4</sub>-I and amide and (d) 1:2:1 mixture of **23•4Br**, I-(CF<sub>2</sub>)<sub>4</sub>-I and amide. Stars indicate shifts resulting from the formation of either halogen bonds and/or guest binding. Black dots indicate complexation induced shielding of the guest amide [58] (Image adapted from [58] with permission from The American Chemical Society)

halogen bond formation in solution (Fig. 11.27). Guest binding was also confirmed from the NMR studies [58].

### 11.3.4.3 Halogen-Bonded Dimeric Capsules

An important development in supramolecular chemistry is the construction of capsular assemblies with a single cavity large enough to encapsulated either larger or several guests. Attempts at constructing halogen-bond capsular assemblies mainly involved organic halogen-bond donor compounds. However, organic halogen-bond donors interact mainly by electrostatic interactions while charge-transfer interaction dominates inorganic XB donors. Molecular iodine I<sub>2</sub>, a divalent halogen-bond donor in the presence of **28•4Cl** resulted in the formation of a dimeric capsule held together solely by halogen bonds. The single cavity was large enough to encapsulate three ordered 1,4-dioxane guests (Fig. 11.28) [60]. The formed capsule has a cavity volume of 511 Å<sup>3</sup> which is perfectly sized for the entrapment of three 1,4-dioxane molecules. The assembly is held together via moderate Cl<sup>-</sup>...I-I...Cl<sup>-</sup> halogen bonds [60].

The <sup>1</sup>H NMR studies in chloroform confirm the existence of iodine-to-**28•4Cl** halogen-bond in solution (Fig. 11.29). The weakness of the second I<sup>+</sup>...Cl<sup>-</sup> halogen bond (in the solid state the R<sub>XB</sub> = 0.82 for the first I<sup>+</sup>...Cl<sup>-</sup> halogen bond and R<sub>XB</sub> = 0.94 for the second I<sup>+</sup>...Cl<sup>-</sup> halogen bond) implies the dimeric assembly could not be confirmed in solution. However, marked chemical shift changes in the -NH<sub>2</sub> signals with increase in I<sub>2</sub> concentration were observed (0.1–0.22 ppm) and are significantly larger than those reported for halogen-bonded deep-cavity cavitands with organic halogen-bond donors [60].



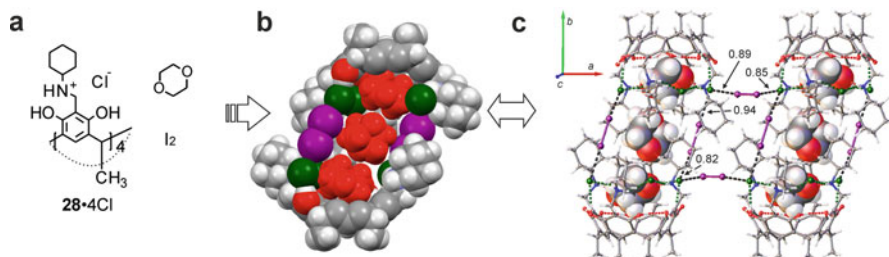


**Fig. 11.28** (a) Halogen-bond acceptor **28•4Cl**, halogen-bond donor  $I_2$  and guest 1,4-dioxane. (b) A sliced CPK plot of the halogen-bonded dimeric capsule  $[(1,4\text{-dioxane})_3@((\mathbf{28}\cdot\mathbf{4Cl})_2(I_2)_2)]$  with three 1,4-dioxane molecules (in red) in the cavity. (c) A ball-and-stick representation showing adjacent capsules connected by a  $[I-I\cdots Cl\cdots I-I\cdots Cl\cdots I-I\cdots Cl\cdots I-I]_2$  halogen bond network shown in the  $ab$  plane. The guests are shown in CPK mode [60] (Image reproduced from Ref. [60] with permission from Wiley)

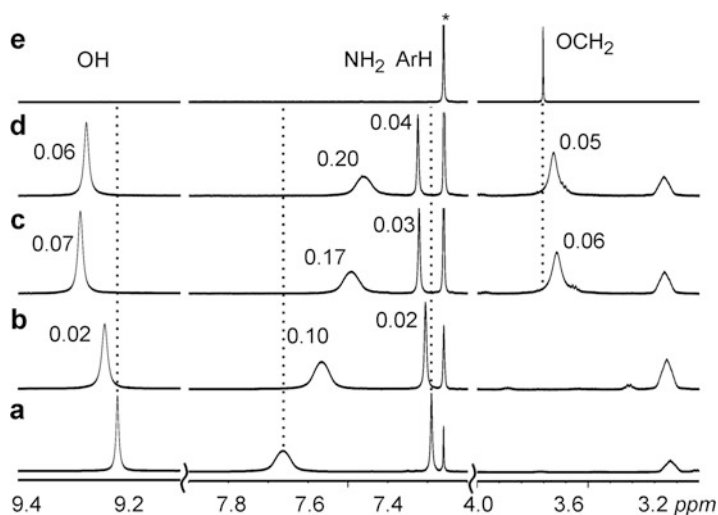


**Fig. 11.29** The  $^1H$  NMR spectra in  $CDCl_3$  at 303 K of: (a) **28•4Cl** (20 mM), (b) 1:1 mixture of **28•4Cl** and  $I_2$ , (c) 1:3:1.5 mixture of **28•4Cl**,  $I_2$  and 1,4-dioxane, (d) 1:excess:1.5 mixture of **28•4Cl**,  $I_2$  and 1,4-dioxane, (e) 1,4-dioxane (20 mM). Dashed lines give an indication of the spectral changes with values in ppm [60] (Image adapted from [60] with permission from Wiley)

### 11.3.5 The NARs with Non-spherical Anions (NARY)

The halides (Cl and Br) in the NARXs are of suitable size and nicely fit between the  $-NH_2$  cations. The compounds are symmetric both in solution and in the solid state. Non-spherical anions such as nitrate (*trigonal planar*), picrate (*aromatic planar*), triflate and trifluoroacetate (*ellipsoidal*) have been used to understand the effect on the conformation of the *N*-alkyl ammonium resorcinarene salts

(NARYs, Y = non-halide) which were synthesized either directly from the tetrabenzoxazine using the corresponding acids or from anion exchanges utilizing the corresponding silver salts [61, 62]. Although the non-spherical anion-based NAR's are less symmetrical, the main features such as the inherited "bowl" shape, the circular hydrogen bonded cation-anion seam, and the guest binding properties are expected to be retained. Compared to the spherical halides, the larger non-spherical anions broaden the opening of the "bowl", which enables the capture of either larger-sized or multiple guest molecules. This "opening" of the cavity allows new guest binding motifs to the resorcinarene family. These non-spherical anions possess several hydrogen-bond acceptor sites and manifest complex arrays of intra- and intermolecular hydrogen bonds resulting in twisted cavitand-like structures possessing cavities suited for binding neutral molecules through C-H $\cdots\pi$  and hydrogen bonding interactions (Fig. 11.30) [61, 62].

Single crystal X-ray crystallographic studies reveals that the conformations of the resorcinarene skeleton in NARYs vary greatly due to the nature and structure of the anion and the included guest molecules. For the picrate salt with *N*-propyl upper rim chains (**29**•4Pic), self-included dimers were observed. An extremely distorted resorcinarene skeleton was observed in the nitrate structure **31**•4NO<sub>3</sub>. Multiple hydrogen bonds hold the different assemblies together (Fig. 11.31) [61, 62].

Modulating the crystallization conditions of the triflate salts resulted in two distinct assemblies. From wet methanol, a six-component dimeric capsule (OTf•MeOH)<sub>2</sub>@(30•3OTf•MeOH)<sub>2</sub> encapsulating two triflate anions and two methanol molecules was isolated (Fig. 11.32). When wet 1,4-dioxane was used, a

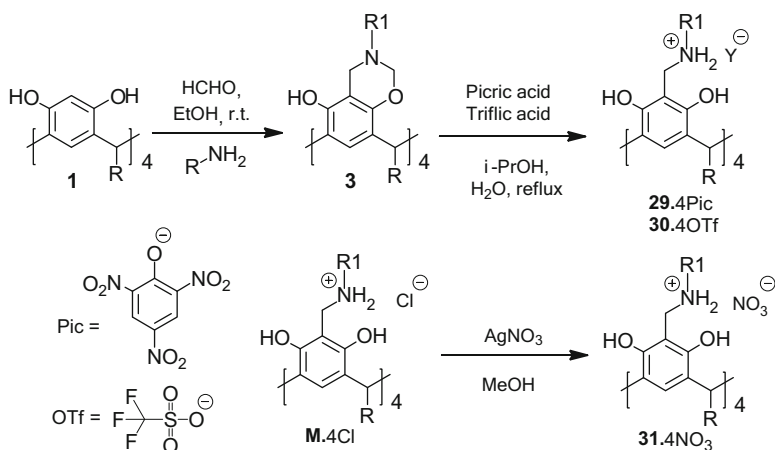
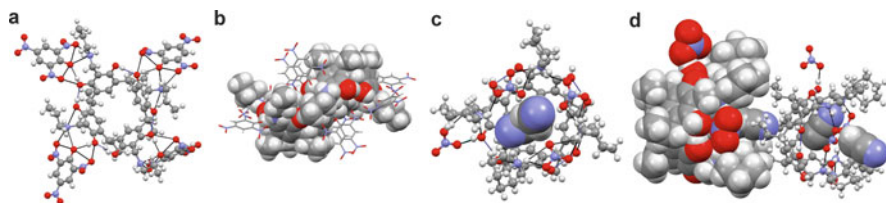


Fig. 11.30 *N*-Alkyl ammonium resorcinarene salts (NARYs, Y = non-halide)





**Fig. 11.31** The X-ray structure of **29•4Pic**: (a) ball-and-stick representation showing the multiple hydrogen bonds and the one picrate off the circular cation-anion seam. (b) CPK plot of the self-included dimer with the picrates in capped-stick mode. The X-ray structure of **31•4NO<sub>3</sub>**: (a) ball-and-stick representation showing the multiple hydrogen bonds and one nitrate off the circular cation-anion seam with the encapsulated acetonitrile molecules in CPK mode, (b) a head-to-tail packing of the assembly. The first **31•4NO<sub>3</sub>** in CPK mode and the second in ball-and-stick mode with all the acetonitrile in CPK mode [61] (Image adapted from [61] with permission from The American Chemical Society)

ten-component dimeric capsule ( $2 \times 1,4$ -dioxane  $\cdot 2 \times \text{H}_2\text{O}$ )<sub>2</sub>@(**30•4OTf**)<sub>2</sub> was isolated, showing a very tight encapsulation of four 1,4-dioxane and four water molecules (Fig. 11.32). One interesting property was the ability of the NARY to encapsulate a triflate anion with definite intermolecular hydrogen bonds. This was an unusual property and thus opens the possibility of the NARY to be modulated into anion receptors under certain conditions. Also, the extremely large cavity of the capsule encapsulated simultaneously eight neutral guests (four 1,4-dioxanes and four water molecules) [62].

The inclusion of the anion was investigated in solution by NMR studies in CDCl<sub>3</sub>. At 300 K, the <sup>1</sup>H NMR of **30•4OTf** shows two signals for the  $-\text{NH}_2$  protons of the host in a 1:3 ratio (Fig. 11.33). The  $-\text{NH}_2$  signals of the NARXs usually appear as a single broad signal under the same conditions [62]. This indicates that one  $-\text{NH}_2$  group has different hydrogen bonds with the triflate anion as compared to the other three  $-\text{NH}_2$  groups, suggesting that the symmetrical cation-anion hydrogen bond seam is broken and one of the triflates resides inside the cavity. Upon the addition of a small amount of 1,4-dioxane to this system, the <sup>1</sup>H NMR in CDCl<sub>3</sub> proves that 1,4-dioxane will readily occupy the resorcinarene cavity thus replacing the encapsulated triflate and driving it out from the cavity to re-form the normal circular cation-anion hydrogen bonded seam (Fig. 11.33) [62].

## 11.4 Zwitterionic Resorcinarenes from Amino Acids

Complementing our work on pure *N*-alkyl ammonium resorcinarene salts, Szumna and coworkers have prepared a series of zwitter-ionic resorcinarene molecules from amino acids through Mannich condensation reactions [63, 64, 65, 66]. These

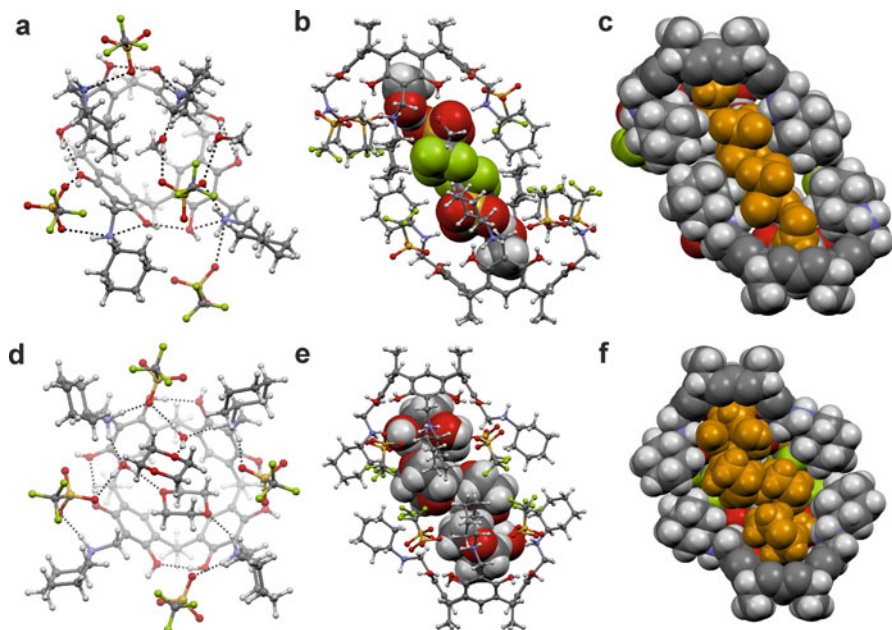


**Fig. 11.32** X-ray structure of the dimeric capsule  $(\text{OTf}\cdot\text{MeOH})_2@(\mathbf{30}\cdot\mathbf{30}\text{OTf}\cdot\text{MeOH})_2$ : (a) One half of the capsule with intramolecular hydrogen bonds shown in *black dotted lines*, (b) the dimeric capsule with encapsulated guests in CPK mode and (c) sliced CPK model to show the encapsulation of the guests in the dimeric capsule. The in-cavity guests are shown in *gold* colour. X-ray structure of the dimeric capsule  $(2 \times 1,4\text{-dioxane}\cdot 2 \times \text{H}_2\text{O})_2@(\mathbf{30}\cdot\mathbf{4}\text{OTf})_2$ : (d) one half of the capsule with intramolecular hydrogen bonds shown in *black dotted lines*, (e) the dimeric capsule with encapsulated guests in CPK mode and (f) sliced CPK model to show the encapsulation of the guests in the dimeric capsule. The in-cavity guests are shown in *brown* colour [62] (Image reproduced from [62] with permission from The Royal Society of Chemistry)

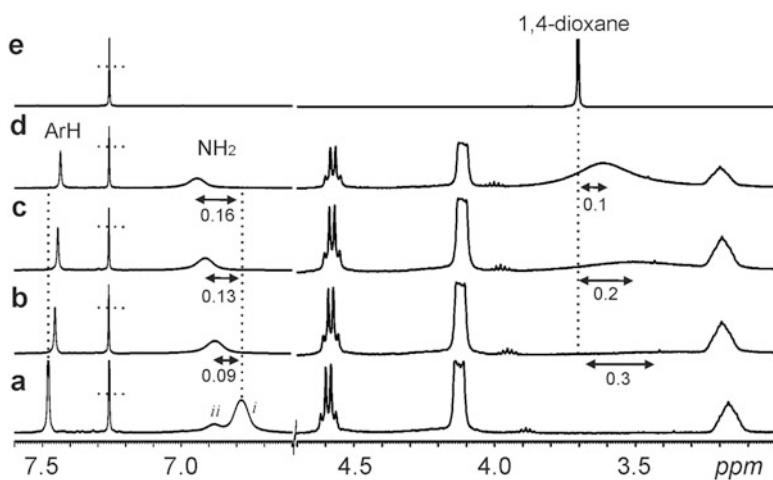


**Fig. 11.33** The  $^1\text{H}$  NMR spectra in  $\text{CDCl}_3$  at 300 K of: (a)  $\mathbf{30}\cdot\mathbf{4}\text{OTf}$  (10 mM), (b) 1:1, (c) 1:2, (d) 1:4 host-guest mixtures of  $\mathbf{30}\cdot\mathbf{4}\text{OTf}$  and 1,4-dioxane, (e) 1,4-dioxane (10 mM). *Dashed lines* give an indication of the spectra changes with values in ppm; *i* and *ii* reflects the different environment of the  $\text{NH}_2$  protons in a 3:1 ratio [62] (Image adapted from [62] with permission from The Royal Society of Chemistry)

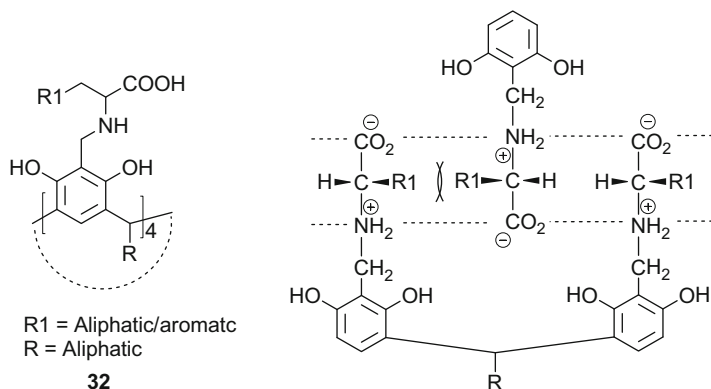


**Fig. 11.34** (a) Molecular structure of zwitterionic host, (b) binding motif with marked possible steric repulsions for homochiral capsule (**32**)<sub>2</sub> [63] (Image adapted from [63] with permission from The Royal Society of Chemistry)

compounds contain structurally self-complimentary zwitterionic upper rim substituents. These very intriguing compounds have been shown to form self-complementary dimeric homo- or heterochiral capsules based on deeply buried electrostatic interactions (salt bridges) with numerous polar and non-polar functionalities in their interiors available for interactions with encapsulated polar molecules (Fig. 11.33) [63, 64, 65, 66]. In spite of the synthetic similarities, these zwitterionic resorcinarene molecules are not salts and thus are not chemically related to the *N*-alkyl ammonium resorcinarene salts and are therefore not discussed in this chapter (Fig. 11.34).

## 11.5 Conclusion

The Mannich condensation between amines (primary and secondary) and resorcinarenes results in resorcinarene tetrabenzoxazines and tetra-azoxazines. Out of 16 potential isomers for the resorcinarene tetrabenzoxazines, only 2 isomers are formed. In the resorcinarene tetrabenzoxazines the adjacent and opposite oxazine rings can be covalently linked with diamines, and covalently-linked dimeric capsules can be formed via the oxazine ring. The resorcinarene tetrabenzoxazines have a deeper cavity than the parent resorcinarenes. This cavity is suitable for binding neutral and cationic guests. Resorcinarene tetrabenzoxazines with terminal amide groups offer a route to single molecule capsules for ion-pair binding.

In the presence of mineral acids, the six-membered oxazine ring in the resorcinarene tetrabenzoxazines is opened, resulting in *N*-alkyl ammonium resorcinarene salts (NARSs). The NARSs possess four spatially-fixed anions within

a circular cation-anion seam in between the ammonium moieties. The NARSs can be considered as hydrogen-bonded analogues of cavitands since they possess similar structural properties as covalent cavitands. The NARSs are shown to bind a series of neutral guests and anions. The four spatially-fixed halides in NARXs are also suitable halogen-bond acceptors. Multiple assemblies such as deep cavity cavitands, polymeric, dimeric and capsular assemblies are formed in the presence of organic and inorganic halogen-bond donors. The *N*-alkyl ammonium resorcinarene triflate (NAROTf) has been shown to possess larger cavities that can bind anions as well as several neutral guests at the same time. The resorcinarene tetrabenzoxazines and especially the *N*-alkyl ammonium resorcinarenes salts have yet a mostly unexplored potential in contemporary supramolecular chemistry as receptors for neutral molecules and anions.

## References

1. Moran, J. R.; Karbach, S.; Cram, D. J. *J. Am. Chem. Soc.* **1982**, *104*, 5826.
2. Cram, D. J. *Science* **1983**, *219*, 1177.
3. Tochtermann, W. *J. für Prakt. Chemie/Chemiker-Zeitung* **1994**, *336*, 474.
4. Timmerman, P.; Verboom, W.; Reinhoudt, D. N. *Tetrahedron* **1996**, *52*, 2663.
5. Böhmer, V. *Angew. Chem. Int. Ed. Engl.* **1995**, *34*, 713.
6. Grüner, B.; Mikulášek, L.; Báča, J.; Cisařová, I.; Böhmer, V.; Danila, C.; Reinoso-García, M. M.; Verboom, W.; Reinhoudt, D. N.; Casnati, A.; Ungaro, R. *Eur. J. Org. Chem.* **2005**, 2022.
7. Jasat, A.; Sherman, J. C. *Chem. Rev.* **1999**, *99*, 931.
8. Erdtman, H.; Högberg, S.; Abrahamsson, S.; Nilsson, B. *Tetrahedron Lett.* **1968**, *9*, 1679.
9. Tunstad, L. M.; Tucker, J. A.; Dalcanale, E.; Weiser, J.; Bryant, J. A.; Sherman, J. C.; Helgeson, R. C.; Knobler, C. B.; Cram, D. J. *J. Org. Chem.* **1989**, *54*, 1305.
10. Luostarinen, M.; Laitinen, T.; Schalley, C. A.; Rissanen, K. *Synthesis* **2004**, 255.
11. Luostarinen, M.; Nissinen, M.; Nieger, M.; Shivanyuk, A.; Rissanen, K. *Tetrahedron* **2007**, *63*, 1254.
12. Mansikkamäki, H.; Nissinen, M.; Rissanen, K. *Angew. Chem. Int. Ed.* **2004**, *43*, 1243.
13. Mansikkamäki, H.; Busi, S.; Nissinen, M.; Åhman, A.; Rissanen, K. *Chem. – Eur. J.* **2006**, *12*, 4289.
14. Atwood, J. L.; Koutsantonis, G. A.; Raston, C. L. *Nature* **1994**, *368*, 229.
15. Orr, G. W.; Barbour, L. J.; Atwood, J. L. *Science* **1999**, *285*, 1049.
16. Atwood, J. L.; Barbour, L. J.; Jerga, A. *Science* **2002**, *296*, 2367.
17. Mannich, C.; Krösche, W. *Arch. Pharm.* **1912**, *250*, 647.
18. Matsushita, Y.; Matsui, T. *Tetrahedron Lett.* **1993**, *34*, 7433.
19. Arnecke, R.; Böhmer, V.; Friebe, S.; Gebauer, S.; Krauss, G. J.; Thondorf, I.; Vogt, W. *Tetrahedron Lett.* **1995**, *36*, 6221.
20. Schmidt, C.; Straub, T.; Faläbu, D.; Paulus, E. F.; Wegelius, E.; Kolehmainen, E.; Böhmer, V.; Rissanen, K.; Vogt, W. *Eur. J. Org. Chem.* **2000**, 3937.
21. Luostarinen, M.; Shivanyuk, A.; Rissanen, K. *Org. Lett.* **2001**, *3*, 4141.
22. Shivanyuk, A.; Schmidt, C.; Böhmer, V.; Paulus, E. F.; Lukin, O.; Vogt, W. *J. Am. Chem. Soc.* **1998**, *120*, 4319.

23. Shivanyuk, A.; Paulus, E. F.; Rissanen, K.; Kolehmainen, E.; Böhmer, V. *Chem. – Eur. J.* **2001**, *7*, 1944.
24. Schmidt, C.; Paulus, E. F.; Böhmer, V.; Vogt, W. *New J. Chem.* **2001**, *25*, 374.
25. Airola, K.; Böhmer, V.; Paulus, E. F.; Rissanen, K.; Schmidt, C.; Thondorf, I.; Vogt, W. *Tetrahedron* **1997**, *53*, 10709.
26. Nummelin, S.; Falabu, D.; Shivanyuk, A.; Rissanen, K. *Org. Lett.* **2004**, *6*, 2869.
27. Arnecke, R.; Böhmer, V.; Paulus, E. F.; Vogt, W. *J. Am. Chem. Soc.* **1995**, *117*, 3286.
28. El Gihani, M. T.; Heaney, H.; Slawin, A. M. *Tetrahedron Lett.* **1995**, *36*, 4905.
29. Iwanek, W.; Frohlich, R.; Urbaniak, M.; Nather, C.; Mattay, J. *Tetrahedron* **1998**, *54*, 14031.
30. Schmidt, C.; Thondorf, I.; Kolehmainen, E.; Böhmer, V.; Vogt, W.; Rissanen, K. *Tetrahedron Lett.* **1998**, *39*, 8833.
31. Kodiah Beyeh, N.; Valkonen, A.; Rissanen, K. *Org. Lett.* **2010**, *12*, 1392.
32. Leigh, D. A.; Linnane, P.; Pritchard, R. G.; Jackson, G. *J. Chem. Soc., Chem. Commun.* **1994**, *4*, 389.
33. Atwood, J. L.; Szumna, A. *J. Am. Chem. Soc.* **2002**, *124*, 10646.
34. Atwood, J. L.; Szumna, A. *Chem. Commun.* **2003**, 940.
35. Beyeh, N. K.; Fehér, D.; Luostarinen, M.; Schalley, C. A.; Rissanen, K. *J. Incl. Phenom. Macrocycl. Chem.* **2006**, *56*, 381.
36. Shivanyuk, A.; Spaniol, T. P.; Rissanen, K.; Kolehmainen, E.; Böhmer, V. *Angew. Chem. Int. Ed.* **2000**, *39*, 3497.
37. Jordan, J. H.; Gibb, B. C. *Chem. Soc. Rev.* **2015**, *44*, 547.
38. Beyeh, N. K.; Cetina, M.; Löfman, M.; Luostarinen, M.; Shivanyuk, A.; Rissanen, K. *Supramol. Chem.* **2010**, *22*, 737.
39. Beyeh, N. K.; Ala-Korpi, A.; Cetina, M.; Valkonen, A.; Rissanen, K. *Chem. – Eur. J.* **2014**, *20*, 15144.
40. Beyeh, N. K.; Pan, F.; Rissanen, K. *Cryst. Growth Des.* **2014**, *14*, 6161.
41. Beyeh, N. K.; Ala-Korpi, A.; Pan, F.; Jo, H. H.; Anslyn, E. V.; Rissanen, K. *Chem. – Eur. J.* **2015**, *21*, 9556.
42. Conn, M. M.; Rebek, J. *Chem. Rev.* **1997**, *97*, 1647.
43. Desiraju, G. R.; Ho, P. S.; Kloo, L.; Legon, A. C.; Marquardt, R.; Metrangolo, P.; Politzer, P.; Resnati, G.; Rissanen, K. **2013**, *85*, 1711.
44. *Halogen Bonding: Fundamentals and Applications*; Metrangolo, P., Resnati, G., Eds.; Springer-Verlag: Berlin, 2008.
45. Gilday, L. C.; Robinson, S. W.; Barendt, T. A.; Langton, M. J.; Mullaney, B. R.; Beer, P. D. *Chem. Rev.* **2015**, *115*, 7118.
46. Erdelyi, M. *Chem. Soc. Rev.* **2012**, *41*, 3547.
47. Beale, T. M.; Chudzinski, M. G.; Sarwar, M. G.; Taylor, M. S. *Chem. Soc. Rev.* **2013**, *42*, 1667.
48. Priimagi, A.; Cavallo, G.; Metrangolo, P.; Resnati, G. *Acc. Chem. Res.* **2013**, *46*, 2686.
49. Koskinen, L.; Hirva, P.; Kalenius, E.; Jaaskelainen, S.; Rissanen, K.; Haukka, M. *CrystEngComm* **2015**, *17*, 1231.
50. Politzer, P.; Lane, P.; Concha, M.; Ma, Y.; Murray, J. *J. Mol. Model.* **2007**, *13*, 305.
51. Chudzinski, M. G.; McClary, C. A.; Taylor, M. S. *J. Am. Chem. Soc.* **2011**, *133*, 10559.
52. Dumele, O.; Trapp, N.; Diederich, F. *Angew. Chem. Int. Ed.* **2015**, *54*, 12339.
53. Liefbrig, J.; Jeannin, O.; Fourmigué, M. *J. Am. Chem. Soc.* **2013**, *135*, 6200.
54. Beyeh, N. K.; Cetina, M.; Rissanen, K. *Chem. Commun.* **2014**, *50*, 1959.
55. Lommerse, J. P. M.; Stone, A. J.; Taylor, R.; Allen, F. H. *J. Am. Chem. Soc.* **1996**, *118*, 3108.
56. Brammer, L.; Bruton, E. A.; Sherwood, P. *Cryst. Growth Des.* **2001**, *1*, 277.
57. Beyeh, N. K.; Valkonen, A.; Bhowmik, S.; Pan, F.; Rissanen, K. *Org. Chem. Front.* **2015**, *2*, 340.
58. Pan, F.; Beyeh, N. K.; Rissanen, K. *J. Am. Chem. Soc.* **2015**, *137*, 10406.
59. Bertrán, J. F.; Rodríguez, M. *Org. Magn. Reson.* **1980**, *14*, 244.
60. Beyeh, N. K.; Pan, F.; Rissanen, K. *Angew. Chem. Int. Ed.* **2015**, *54*, 7303.

61. Beyeh, N. K.; Cetina, M.; Rissanen, K. *Cryst. Growth Des.* **2012**, *12*, 4919.
62. Pan, F.; Beyeh, N. K.; Rissanen, K. *RSC Adv.* **2015**, *5*, 57912.
63. Kuberski, B.; Szumna, A. *Chem. Commun.* **2009**, 1959.
64. Szumna, A. *Chem. Commun.* **2009**, 4191.
65. Wierzbicki, M.; Gilski, M.; Rissanen, K.; Jaskolski, M.; Szumna, A. *CrystEngComm* **2014**, *16*, 3773.
66. Jędrzejewska, H.; Wierzbicki, M.; Cmoch, P.; Rissanen, K.; Szumna, A. *Angew. Chem., Int. Ed.* **2014**, *53*, 13760.

# Chapter 12

## Functionalized Calixpyrroles: Building Blocks for Self-Assembly

Gabriela I. Vargas-Zúñiga, Jonathan L. Sessler, and Steffen Bähring

### 12.1 Introduction

The use of supramolecular systems for the complexation of anions and cations is an area of chemistry that has been explored since the 1970s [1]. In recent years, this line of investigation has evolved from isolated syntheses of few receptors to the development of a wide range of molecules that can function as sensors, extractants, anion-responsive materials, and more recently the use of supramolecular systems as transmembrane ion carriers. Within the context of these broad trends, so-called calixpyrroles have received particular attention due to their potential use as receptors for anions, cations, and ion pairs. They have proved to be important complements to their namesakes, the calixarenes.

Octamethylcalix[4]pyrrole (OMCP), first synthesized by Baeyer in 1886 [2] and characterized by Chelintzev and Tronov [3] in 1916, is a colorless compound consisting of four pyrrole subunits linked by fully substituted  $sp^3$  hybridized *meso* carbon atoms. This parent system and a number of related compounds are obtained via acid-catalyzed condensation reactions of pyrrole and a ketone [2]. Unlike, porphyrinogens, the non-aromatic precursors to porphyrins, most calixpyrroles are resistant to oxidation due to the presence of the fully substituted *meso* carbons. Moreover, they are not inherently effective ligands. Perhaps as a consequence of these two attributes, calix[4]pyrroles remained largely unstudied during most of the twentieth century until the early 1990s, when Floriani and coworkers explored the

---

G.I. Vargas-Zúñiga • J.L. Sessler (✉)

Department of Chemistry, The University of Texas at Austin, 105 E 24th St. Stop A5300,  
Austin, TX 78712-1224, USA

e-mail: [seessler@cm.utexas.edu](mailto:seessler@cm.utexas.edu)

S. Bähring

Department of Physics, Chemistry and Pharmacy, University of Southern Denmark,  
Campusvej 55, 5230 Odense M, Denmark

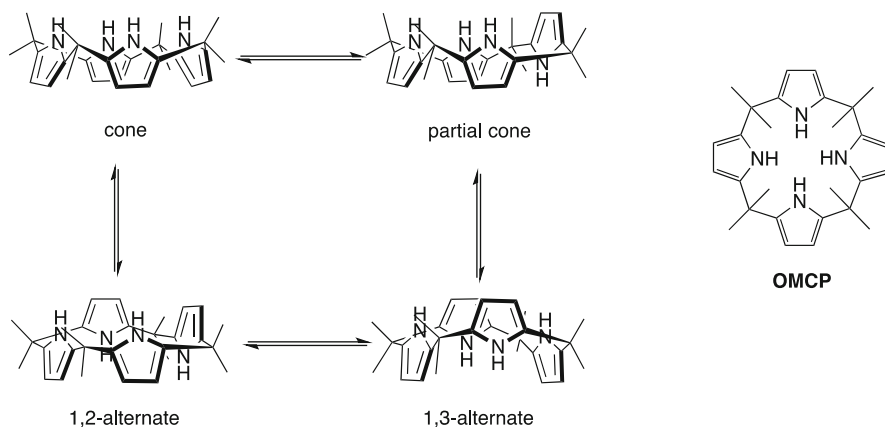


**Fig. 12.1** Possible conformations of octamethylcalix[4]pyrrole (OMCP), 1,3-alternate, 1,2-alternate, partial cone, and cone conformation [5, 6]

metallation of deprotonated calix[4]pyrroles [4]. In 1996, Sessler and coworkers reported the anion recognition properties of OMCP and showed that they could bind halide anions effectively in dichloromethane via receptor-anion hydrogen bonding interactions involving the pyrrolic NH protons [5]. In a follow-up study, it was found that OMCP undergoes a structural change from 1,2-alternate, 1,3-alternate, or partial cone to a cone conformation upon anion binding [6]. This prompted Sessler and coworkers to introduce the name calix[4]pyrrole to identify OMCP and its analogues. In 2005, the same research group reported the ability of OMCP to complex cesium salts (and other salts of charge diffuse cations) in the form of ion pairs [5, 6] (Fig. 12.1).

## 12.2 Synthesis

The discovery of the anion recognition properties of calix[4]pyrrole in the mid-1990s attracted considerable attention and inspired many research groups to develop modified calixpyrroles. The initial goal of this work was to develop new calix[4]pyrrole motifs wherein the anion selectivity and specificity were tuned. To modulate the anion-binding properties of OMCP, two main strategies have been employed. These involve, respectively, adding synthetic substituents on the  $sp^3$  carbon constituting the *meso*-bridges and modifications of the  $\beta$ -pyrrolic positions. Sometimes both modifications strategies have been employed in concert.

Functionalization of the *meso*-positions has been achieved most commonly via an acid-catalyzed condensation of a dipyrromethane, containing the group or moiety that is designed to assist in ion binding, with an excess of acetone [1, 7]. One elegant embodiment of this approach involves so-called strapped calix[4]pyrroles; here, a tethered bispyrromethane, the precursor to the “strap”, is used in the synthesis [8].



Separate from these cryptand-type systems, the attachment of functional groups on the *meso*-positions has led to the development of deep cavity systems, capsules, strapped calix[4]pyrroles, and calix[4]pyrroles with pendant arms.

Many of the  $\beta$ -substituted calix[4]pyrroles known in the literature were likewise synthesized via a condensation strategy. Typically, a functionalized pyrrole bearing substituents on one or both of the  $\beta$ -pyrrolic positions is condensed with a ketone under acid catalyzed conditions. However, a number of mono-substituted calix[4]pyrroles have been prepared by a post-synthetic strategy. Here, a functional group, such as an ester, formyl, or iodine substituent, is introduced onto one of the  $\beta$ -pyrrolic positions within OMCP. In many cases, this is done by subjecting the calix[4]pyrrole to deprotonation with a strong base (e.g., *n*-butyl lithium), followed by the addition of the appropriate electrophile [9, 10]. On the other hand, iodination has typically been achieved by reacting calix[4]pyrrole with iodine-[bis(trifluoroacetoxy)iodo]benzene [11]. These functionalized systems have been elaborated further to create, *inter alia*, anion sensors or materials that may be attached to solid or polymeric supports.

The purpose of this review is to highlight the most recent work involving calix[4]pyrroles wherein strategic modification of the basic OMCP core has resulted in more efficient ion recognition. Two excellent reviews discussing in depth the methods employed in the synthesis of functionalized calix[4]pyrroles have been published to which the interested reader is directed [3, 9]. Although some examples of systems used as sensors, liquid-liquid extractants, and transmembrane transporters will be described here, much of this chapter will focus on self-assembled systems based on calix[4]pyrrole. Some discussion of capsule systems will be included, although a separate chapter, authored by the Tarragona group covering this aspect of calixpyrrole chemistry is slated for inclusion in this book. Expanded calixpyrroles and hybrids porphyrin-calix[4]pyrrole, calixphyrin will not be covered in the present chapter [12].

### 12.3 Anion Recognition Using Functionalized Calix[4]pyrroles

As implied above, considerable effort has been devoted to the preparation of new systems by means of *meso*-bridge modification. Much of this work has centered around the development of strapped calix[4]pyrroles. The first such system, compound **1** (cf. Fig. 12.2), was reported by Lee and coworkers in 2002 [13, 14]. The strapped macrocycle **1** and its congener **2** contain benzene and pyrrole moieties, respectively, within the strap. These calix[4]pyrrole derivatives were found to display higher anion binding affinities in acetonitrile than the parent macrocycle OMCP. For instance, as inferred from isothermal calorimetry titration (ITC) analyses the affinities of **1** and **2** for chloride (studied as the tetrabutylammonium, TBA, salt) in acetonitrile were  $K_a = 2.2 \times 10^6$  and  $1.8 \times 10^7$ , respectively, vs.  $2.2 \times 10^5$  and  $1.4 \times 10^5 \text{ M}^{-1}$  for **3** and OMCP, respectively [15]. These

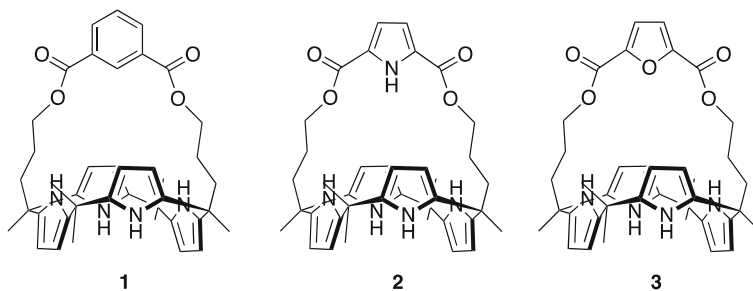
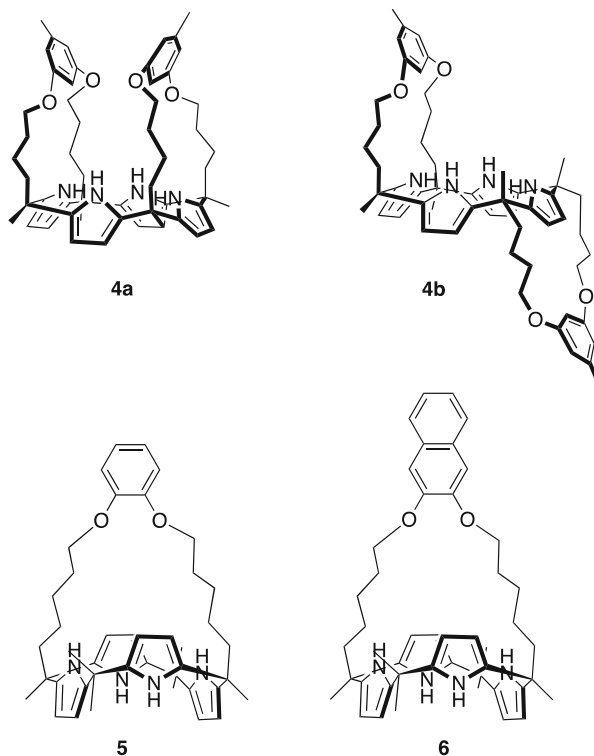


**Fig. 12.2** Structures of the strapped calix[4]pyrroles **1**, **2**, and **3**

**Fig. 12.3** Structures of the *cis*- and *trans*-calix[4]pyrrole isomers **4a** and **4b** and the ether strapped calix[4]pyrroles **5** and **6**



enhanced anion affinities relative to OMCP were ascribed to the presence of hydrogen bond donors in the strap, as well as an ability to isolate the anion from the medium more efficiently than the unstrapped parent system. Since the time of these initial reports, many strapped calix[4]pyrroles, including several containing yet additional hydrogen binding motifs, have been reported.

In a subsequent report, Lee and coworkers reported the *cis*- and *trans*-strapped receptors **4a** and **4b**. These systems contain two straps adjacent to the *meso* positions of OMCP (cf. Fig. 12.3) [16]. The anion binding properties analyzed by

$^1\text{H}$  NMR spectroscopy revealed that the *cis*-isomer **4a** displayed strong affinities for  $\text{F}^-$  and  $\text{Cl}^-$  in deuterated chloroform, whereas no appreciable affinities were seen for the other anions considered in this test series ( $\text{Br}^-$ ,  $\text{I}^-$ ,  $\text{H}_2\text{PO}_4^-$ , and  $\text{SO}_4^{2-}$ ; all anions studied as their TBA salts). In the case of the *trans* isomer **4b**, the binding results led the authors to suggest that the straps do not participate in the binding of anionic species. Relatively higher affinities are seen in the case of **4a** as compared to **4b** (e.g., the  $K_a$  values for  $\text{Cl}^-$  are  $2.65 \times 10^5$  and  $2.31 \times 10^4 \text{ M}^{-1}$  in the case of **4a** and **4b**, respectively). This was ascribed to the combination of C–H–X and N–H–X hydrogen bonding interactions that serve to stabilize the resulting complex [**4a**•X] ( $X = \text{F}^-$  or  $\text{Cl}^-$ ) [16].

Panda and coworkers investigated the anion binding properties of the ether-strapped calix[4]pyrroles **5** (cf. Fig. 12.3) [17]. The anion binding constants calculated by ITC using their respective TBA salts, provided support for the conclusion that in dry acetonitrile at  $30^\circ\text{C}$  receptor **5** displays a relatively high affinity for  $\text{Cl}^-$  ( $K_a = 2.12 \times 10^6 \text{ M}^{-1}$ ) but only a modest affinity for  $\text{Br}^-$  ( $K_a = 1.95 \times 10^4 \text{ M}^{-1}$ ) [17]. This difference was attributed to a more constrained cavity and lack of additional hydrogen bond donors within the strap. Later on, the same research group reported the naphthalene-incorporated receptors **6** (cf. Fig. 12.3) [18]. This system displayed binding affinities for chloride and bromide anions that were similar to those seen in the case of **5** when studied under analogous conditions (e.g.,  $K_a = 2.96 \times 10^6 \text{ M}^{-1}$  and  $2.40 \times 10^4 \text{ M}^{-1}$  for chloride and bromide anion, respectively) [18]. Although the constrained cavity present in **6** was expected to favor the binding of fluoride anion, surprisingly the anion affinity for this relatively small anion was found to about one order of magnitude less than that seen in the case of chloride as determined from ITC studies ( $K_a = 2.42 \times 10^5 \text{ M}^{-1}$ ) under analogous conditions [18]. DFT computational analysis led the authors to suggest that in the presence of the  $\text{F}^-$  anion, the naphthalene moiety resides parallel to the calix[4]pyrrole average plane and that this orientation militates against fluoride binding as the result of repulsive anion- $\pi$  interactions. In contrast, in the case of  $\text{Cl}^-$  the naphthalene moiety remains almost orthogonal; this is thought to favor the binding of this particular anion.

The incorporation of more complex binding sites within the strap has been pursued as a strategy to enhance ion binding. Although most of these efforts have been focused on anion binding, it has become increasingly appreciated that the counteraction plays a critical role in mediating anion recognition in the case of calix[4]pyrroles. This has led to the consideration that it could be beneficial to design receptors that can bind both an anion and a cation concurrently. This line of investigation was inspired in part by the finding that under certain conditions OMCP will bind to both an anion and a cation, leading to net ion pair recognition within the same overall calix[4]pyrrole receptor system [19].

In 2010 Kim and Sessler described three limiting ion pair association modes for a two site, ditopic receptor corresponding to (a) host-guest separated ion pair, (b) contact ion pair, and (c) solvent-separated ion pair, (cf. Fig. 12.4) [20]. This intellectual construct has facilitated the design of ion pair calix[4]pyrrole-based receptors in recent years.

**Fig. 12.4** Schematic representation of ion pair interactions mediated by a receptor (a) contact ion pair, (b) solvent separated ion pair, and (c) host-guest separated ion pair. This figure was redrawn based on one that originally appeared in ref [20]

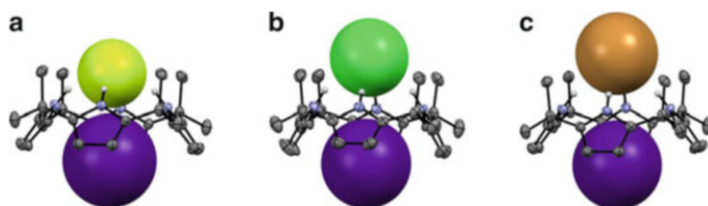
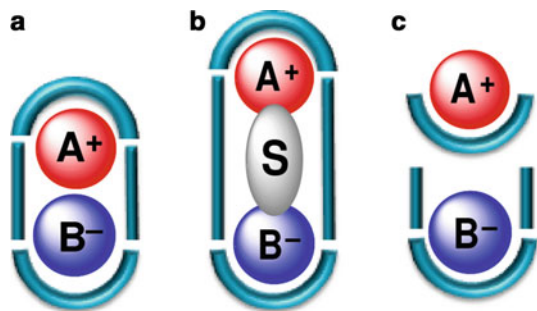
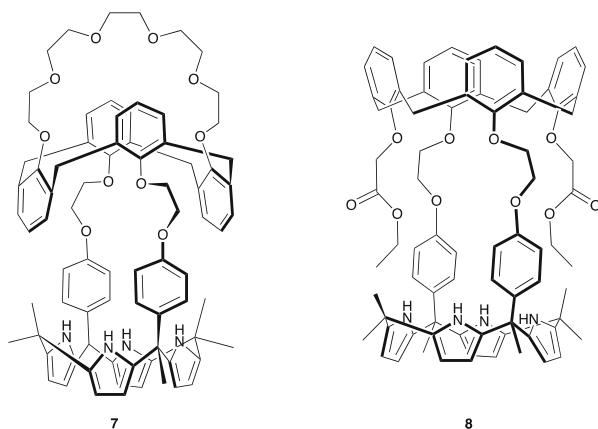


**Fig. 12.5** Single crystal X-ray diffraction structures of (a) the CsF, (b) CsCl, and (c) CsBr complexes of OMCP. These X-ray figures were reproduced using the data downloaded from the Cambridge Crystallographic Data Centre. Solvent molecules were removed for the sake of clarity

Initial evidence that OMCP can act as ion pair receptor came from the 2005 report of Moyer, Sessler, Gale and coworkers mentioned above [21]. On the basis of single crystal structures of complexes such as  $[\text{Cs}\cdot\text{OMCP}\cdot\text{X}]$  (where  $\text{X} = \text{F}, \text{Cl},$  or  $\text{Br}$ ; cf. Fig. 12.5), it was inferred that OMCP could bind ion pairs [21]. Many of these complexes were analyzed by X-ray diffraction methods. The resulting structures revealed that the calix[4]pyrrole core in recognizing cesium halide salts adopts a cone conformation wherein the halide anion is bound via four pyrrole NH-anion hydrogen bonding interactions while the cesium cation is complexed on the opposite side of the macrocycle via a combination of cation- $\pi$  and ion-dipole interactions. Further proton spectroscopic studies in acetone- $d_6$  (containing 2%  $\text{D}_2\text{O}$ ) provided evidence in support of the notion that this binding mode is also operative in solution. However, it was also inferred from these studies that the calix [4]pyrrole-cation interactions were relatively weak. This provided an incentive to create systems wherein cation recognition elements were incorporated into the calix [4]pyrrole-based receptor framework.

The synthesis of functionalized calix[4]pyrroles able to accommodate ion pairs within their cavities was first approached by using crown ether-like polyether straps to link two of the four *meso*-carbon atoms of the calix[4]pyrrole framework. The first of such ditopic systems, receptor **7**, reported by Kim, Sessler, and coworkers, was designed to contain a the calix[4]arene crown-6-moiety for cesium cation recognition, while retaining a calix[4]pyrrole subunit for anion recognition (cf. Fig. 12.6) [22]. In the solid state, the individual ions within the CsF ion pair complex, which are bound to **7**, are separated from one another by a single methanol molecule that was presumably “captured” during crystallization. Proton NMR spectroscopic analyses, carried out in deuterated methanol/chloroform (1:9 v/v),

**Fig. 12.6** Strapped calix[4]arene-6-crown calix[4]pyrrole **7**, strapped calix[4]arene diethyl ester calix[4]pyrrole **8** (top), and single crystal X-ray structure of the  $[\mathbf{8}\cdot\text{TEAF}\cdot\text{H}_2\text{O}]$  complex, where TEA = tetraethylammonium cation (bottom). The X-ray figure was reproduced using data downloaded from the Cambridge Crystallographic Data Centre



provided support for the conclusion that the binding mode observed in the solid state is retained in solution [22]. Furthermore, it was inferred that the  $\text{Cs}^+$  cation serves to enhance the binding of  $\text{F}^-$  by the calix[4]pyrrole unit. This supposition came from the finding that reduced fluoride anion binding was observed when the  $\text{Cs}^+$  cation was replaced by  $\text{TBA}^+$  [22].

Subsequently, the same research group reported a calix[4]pyrrole containing a calix[4]arene diethyl ester bearing two phenyl pickets (i.e., macrocycle **8**; cf. Fig. 12.6). [23]  $^1\text{H}$  NMR spectroscopic titrations, carried out in deuterated chloroform, served to reveal that **8** binds  $\text{F}^-$  selectively with good affinity ( $K_a \geq 10^4 \text{ M}^{-1}$ ) to form a monohydrated complex ( $[\mathbf{8}\cdot\text{F}\cdot\text{H}_2\text{O}]^-$ ) even in the presence of competing anions such as  $\text{Cl}^-$ ,  $\text{Br}^-$ ,  $\text{I}^-$ ,  $\text{AcO}^-$ ,  $\text{NO}_3^-$ ,  $\text{SO}_4^{2-}$ ,  $\text{H}_2\text{PO}_4^-$ , and  $\text{HP}_2\text{O}_7^-$  (as their TBA salts) [23]. In the solid state, the complex  $[\mathbf{8}\cdot\text{TEAF}\cdot\text{H}_2\text{O}]$  (where TEA = tetraethylammonium), obtained from a saturated chloroform solution, revealed that  $\text{F}^-$  is

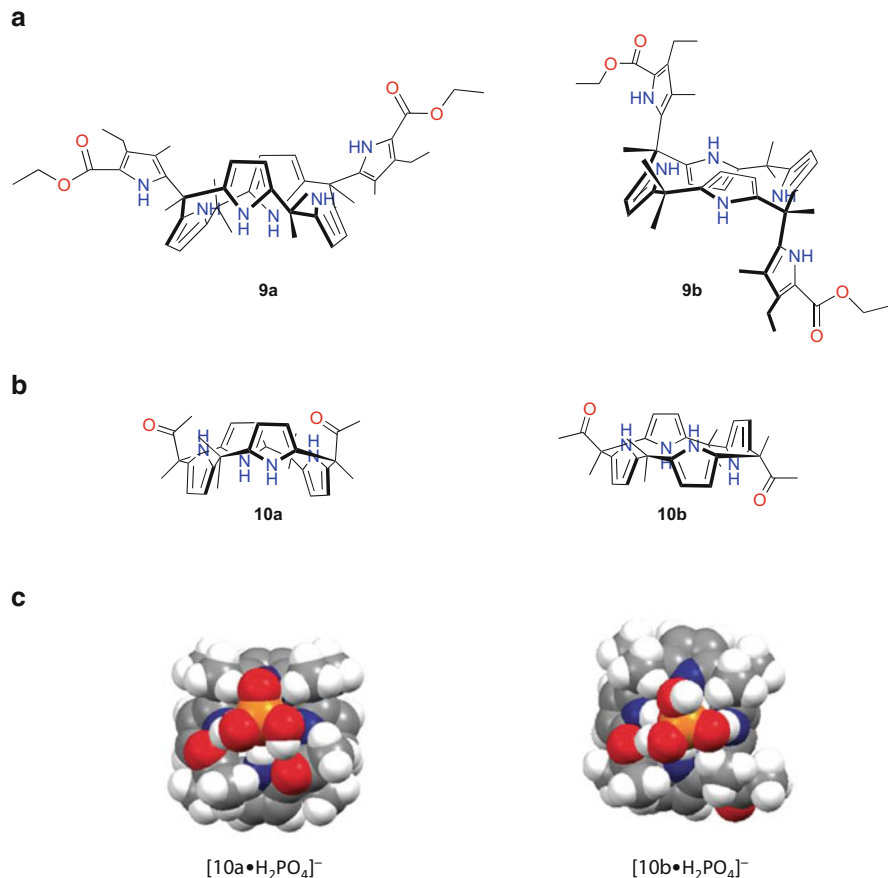


**Fig. 12.7** Structures of the *cis*- and *trans*-isomers of (a) the hexapyrrolic calix[4]pyrroles **9a** and **9b** reported by Anzenbacher and coworkers, [24] (b) the dicacyl calix[4]pyrroles *cis*- and *trans*-isomers **10a** and **10b**, and (c) the space filling model DFT-optimized structures of the complexes **[10a•H<sub>2</sub>PO<sub>4</sub>]<sup>-</sup>** and **[10b•H<sub>2</sub>PO<sub>4</sub>]<sup>-</sup>** reported by Panda and coworkers [26]. (Reprinted from *Org. Biomol. Chem.* **2014**, *12*, 278–285, with the permission from the Royal Society of Chemistry)

bonded to the four pyrrolic NH groups via hydrogen bonding, as well as bonded to a molecule of water, whereas a TEA cation is bound within the electron-rich side of the calix[4]pyrrole moiety (cf. Fig. 12.6) [23]. The high selectivity of **8** was ascribed to the rigidity of the binding cavity created by the presence of the bulky calix[4]arene cap.

Good fluoride anion binding affinities were observed in the case of the two hexapyrrolic calix[4]pyrrole receptors **9** reported in 2014 by Anzenbacher and coworkers [24]. The incorporation of two additional carbonyl ester pyrrole units on either side of the macrocycle produced the *cis*- and *trans*-configurational isomers, **9a** and **9b**, respectively (cf. Fig. 12.7). In acetonitrile solution, a  $K_a$  value of  $1.0 \times 10^6 \text{ M}^{-1}$  for fluoride anion binding was estimated for both **9a** and **9b** on the

basis of UV/Vis and proton spectroscopy studies. However, in the case of other anions, such as  $\text{Cl}^-$ ,  $\text{AcO}^-$ ,  $\text{BzO}^-$ , and  $\text{H}_2\text{PO}_4^-$  (all anions studied as their TBA salts), a difference in affinities is seen between the two isomers. For instance, in acetonitrile **9a** is a better chloride anion receptor than **9b**, with  $K_a = 2.2 \times 10^5 \text{ M}^{-1}$  and  $1.9 \times 10^3 \text{ M}^{-1}$  for **9a** and **9b**, respectively [24]. The difference in affinities was attributed to the combination of stabilizing hydrogen bonding and  $\pi$  interactions involving both pyrrolic “arms” and the anion in the case of **9a**, whereas only one arm is involved in the binding events in the case of **9b**.

A conformationally flexible structure and the presence of hydrogen bond donors units has been a successful strategy for the design of receptors able to bind halide anions. However, the effective binding of oxoanions, such as sulfate and phosphate, has proved to be more challenging, particularly in polar media. This is due mainly to the higher hydration energies and high charge densities associated with anions (e.g.,  $\Delta G_h = -1080 \text{ kJ mol}^{-1}$  and  $-2765 \text{ kJ mol}^{-1}$  for  $\text{SO}_4^{2-}$  and  $\text{PO}_4^{3-}$ , respectively, where  $\Delta G_h$  refers to hydration energies) [25]. Additionally, many oxoanions are susceptible to protonation at lower pH values. As a consequence, they participate in protonation equilibria in aqueous media. In the limit, these anions lose their negative charge, which generally precludes strong binding to a receptor. One approach to creating receptors for anions with more complex geometries involves appending ancillary recognition units to the *meso* positions of calix[4]pyrrole core. In accord with this general strategy, Panda and coworkers reported the isomeric *cis*- and *trans*-diacylated calix[4]pyrrole derivatives **10** (cf. Fig. 12.7) [26]. The *cis*-bisacyl-calix[4]pyrrole receptor **10a** was found to display binding affinities for several anions including  $\text{F}^-$ ,  $\text{Cl}^-$ ,  $\text{Br}^-$ , and  $\text{H}_2\text{PO}_4^{2-}$  (as their TBA salts), in acetonitrile at 30 °C that are higher than those observed with OMCP. Microcalorimetry titrations revealed that **10a** binds  $\text{H}_2\text{PO}_4^{2-}$  anions  $\approx 4.8$  times strongly than OMCP, whereas the *trans*-isomer **10b** showed weak affinities for all the anions analyzed [26]. The high dihydrogen phosphate affinity exhibited by **10a** was ascribed to the cooperative interactions between the carbonyl group and the bound phosphate anion. Support to these additional interactions came from density functional theory (DFT) calculations.

## 12.4 Anion Sensors

Anion sensors are molecules that display a change in their physico-chemical properties when exposed to an anionic analyte. The induced change can be spectroscopic (either a color or fluorescence change), electrochemical, or involve a sol-gel transition. All of these changes can be used to monitor the presence and in some cases the concentration of the anionic guest [27]. Anion sensors based on calix[4]pyrroles have typically consisted of OMCP derivatives onto which an appropriate signaling probe has been attached that undergoes an easy-to-monitor response upon anion binding. As noted above, most chemosensors of this ilk have been synthesized via post-synthetic functionalization of the core OMCP macrocycle at one or

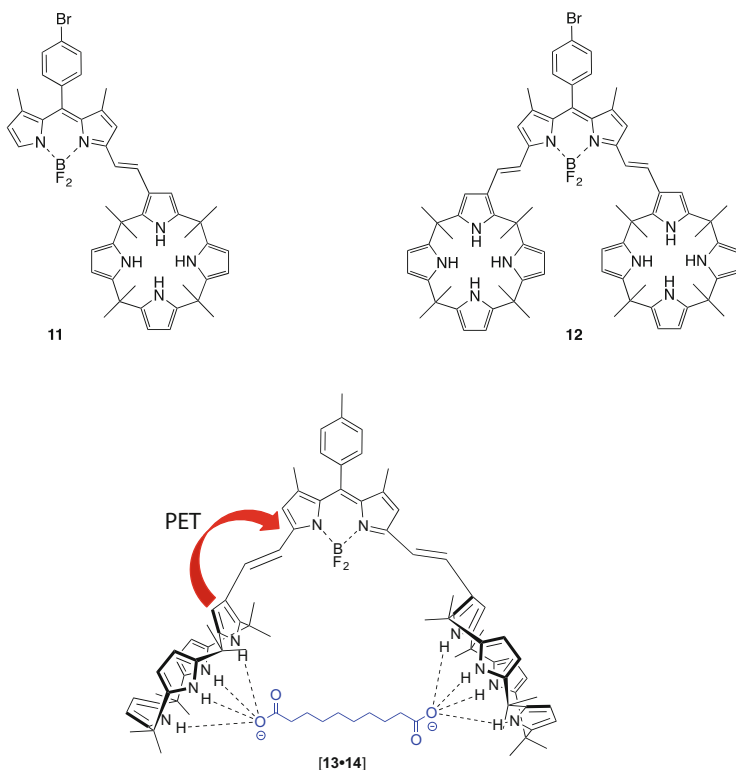


**Fig. 12.8** Structures of the BODIPY calix[4]pyrroles **11**, **12**, and the complex **[13•14]**

more  $\beta$ -pyrrolic positions. However, new systems with functional groups attached to the *meso*-positions, including strapped systems containing a chromophore, have been reported. Examples of calix[4]pyrrole systems used as anion sensors will be discussed in this section.

The attachment of a boron-dipyrrromethene (BODIPY) fluorescent reporter group to calix[4]pyrrole via styrene linker to produce receptors **11** and **12** was reported by Shao and coworkers (cf. Fig. 12.8) [28]. These optical chemosensors displayed selective recognition and sensing of diverse anions, such as  $F^-$ ,  $AcO^-$ ,  $H_2PO_4^-$ ,  $Cl^-$ , and  $Br^-$  (as the TBA salts) in acetonitrile in the order  $F^- > AcO^- > H_2PO_4^- > Cl^- >> Br^-$ ,  $I^-$ , and  $ClO_4^-$  [28]. It was found that the intramolecular charge transfer (ICT) band in the absorption spectra of **11** is red-shifted in the presence of  $F^-$ ,  $AcO^-$ ,  $H_2PO_4^-$ , and  $Cl^-$ , with the most pronounced shift from 587 nm (fuchsia) to 602 nm (blue) being seen when **11** is exposed to the fluoride anions. No absorption changes were observed in the presence of  $I^-$ ,  $ClO_4^-$ , and  $HSO_4^-$ .

Similar behavior under analogous experimental conditions was observed for **12**; however, slightly higher affinities for anions were observed. This was attributed to

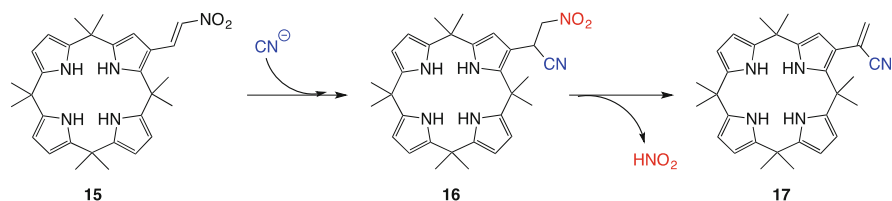


the formation of a sandwich complex between the two calix[4]pyrroles and the anion. In separate work, Costero and coworkers reported in 2013 a similar BODIPY-calix[4]pyrrole conjugate **13** that recognizes dicarboxylate anions (cf. Fig. 12.8) [29].

In this latter case, the analysis of the spectroscopic titrations and speciation diagrams calculated using SPECFIT program provided support for the notion that at low concentrations of anion (i.e., 1 equiv. of anion and a host concentration of  $10^{-5}$  M, in THF) appropriately chosen TBA-dicarboxylate salts bind to **13** with a 1:1 (**13**/dicarboxylate) complex stoichiometry [29]. At higher anion concentrations, 1:2 complexes dominate. Different absorption responses were observed upon addition of aliphatic and aromatic dicarboxylates. Specifically, a visual color change from green to greenish blue was seen upon exposure to a long chain aliphatic dicarboxylate (e.g., decanedionate **14**). In contrast, a change from bright pink to purple-blue was seen with shorter chain aliphatic dicarboxylates, such as glutarate. These changes in color were ascribed to increases in the extent of intramolecular charge transfer (ICT) process from the electron-rich calix[4]pyrrole moiety to the electron-withdrawing BODIPY unit in the excited state [29]. The emission spectra in the presence of the test anions were characterized by a bathochromic shift and a dramatic decrease in intensity. Such findings are consistent with a photoinduced electron transfer (PET) process occurring upon coordination of the anion, while the emission maxima shift was ascribed to the change of donor-acceptor properties of the system.

In 2012, Lee and coworkers reported the  $\beta$ -nitrovinyl-substituted calix[4]pyrrole **15** and showed that it acted as a sensitive ratiometric cyanide anion sensor [30]. The nitrovinyl group on the  $\beta$ -pyrrolic position of the calix[4]pyrrole in **15** is susceptible to nucleophilic attack, which results in the formation of adduct **16** upon exposure to TBACN. Evidence collected from infrared and proton spectroscopies, as well mass spectrometry, confirmed that adduct **16** undergoes elimination of the nitro group to form **17** and release  $\text{HNO}_2$  (cf. Scheme 12.1) [30]. Furthermore, the addition of TBACN to a solution containing **15** (40  $\mu\text{M}$  in  $\text{CH}_3\text{CN}/\text{DMSO}$  97/3 % v/v) produced a color change from yellow to colorless, even when other anions such as chloride and fluoride were present as competitive guests. The color change was ascribed to the Michael-type addition shown in Scheme 12.1. The underlying nucleophilic attack was not observed in the presence of other anions such as  $\text{F}^-$ ,  $\text{Cl}^-$ ,  $\text{AcO}^-$ , and  $\text{H}_2\text{PO}_4^-$  (as their respective TBA salts). Rather, anion binding to calix[4]pyrrole core was observed, as inferred from ITC and UV/Vis studies [30].

Fluorescent probes that give rise to ratiometric fluorescence responses are valuable in the design of chemosensors. They are particularly attractive when the concentration of the analytes is limited since many of the problems associated with direct intensity-based methods, such as dye bleaching, medium-induced fluctuations in absorbance or emission intensity, and interference from the medium are avoided [31]. This class of chemosensors also offers the advantages of being less likely to be biased by non-specific interactions or impurities, while the signal-to-noise ratio is improved [31].



**Scheme 12.1** Transformations involving the nitrovinyl calix[4]pyrrole **15** observed upon exposure to cyanide anions (as the TBA salt) in organic media

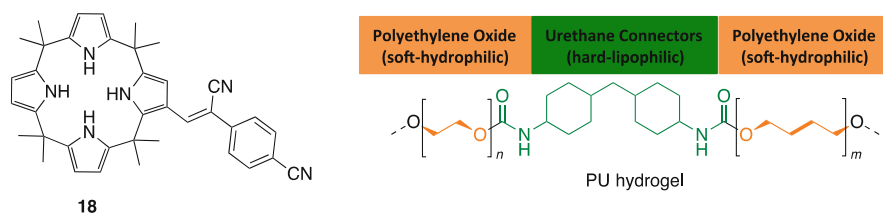
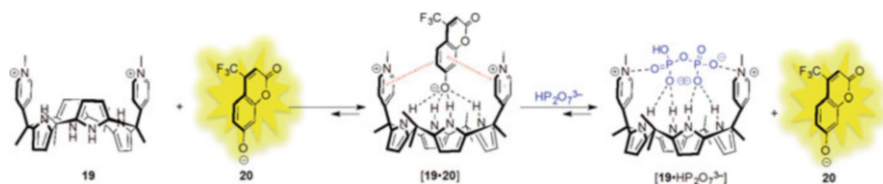


**Fig. 12.9** Structures of calix[4]pyrrole **18** and the polyurethane polymers (PU) employed

Azenbacher and coworkers designed and prepared the fluorescent calix[4]pyrrole probe **18** presented in Fig. 12.9. Fluorescence titrations carried out using a diverse set of anions, including  $F^-$ ,  $Cl^-$ ,  $AcO^-$ ,  $BzO^-$ , and  $H_2PO_4^-$  (as the TBA salts) in two solvents with different polarities ( $CH_2Cl_2$  and  $CH_3CN$ ), revealed an anion-dependent decrease in the emission intensity at 470 nm and the appearance of a new emission band at 570 nm [32]. Such findings are consistent with a turn-on ratiometric response, wherein a binding-induced ICT between the calix[4]pyrrole and the fluorophore takes place. Unlike OMCP, receptor **18** displays strong affinity for anions in wet polar organic solvents (i.e., containing 1% water). The relative affinities calculated from UV/Vis titrations in both  $CH_2Cl_2$  and  $CH_3CN$  were found to be in the following order:  $F^- \gg AcO^- > BzO^- > Cl^- > H_2PO_4^-$  [32]. Probes embedded into hydrogel polymers of poly(ether-urethane) (PU) and polybutene oxide (PBO) or polyethylene oxide (PEO) (Fig. 12.9) were found to be efficient in the detection of various anions, including  $AcO^-$ ,  $BzO^-$ ,  $F^-$ ,  $Cl^-$ ,  $H_2PO_4^-$ ,  $HP_2O_7^{3-}$ ,  $CN^-$ , and  $HS^-$  in aqueous media. A linear discriminant analysis (LDA) led to the suggestion that **18** within the polymeric matrix can discriminate anions with 90% accuracy and a detection limit of 0.1 ppm [32].

Pyrophosphate ( $HP_2O_7^{3-}$ ) is a very important anion in biology [33]. The biological roles of  $HP_2O_7^{3-}$  include ATP hydrolysis, [33] energy storage, [33] DNA synthesis, [34] and a number of other enzymatic reactions [33]. Thus, the development of synthetic receptors for the selective recognition and sensing of  $HP_2O_7^{3-}$  has been a recognized goal within the supramolecular community for a number of years. In 2012 Sessler, Lee, and coworkers reported the functionalized calix[4]pyrrole sensor **19** bearing two pyridinium moieties on the *meso*-positions

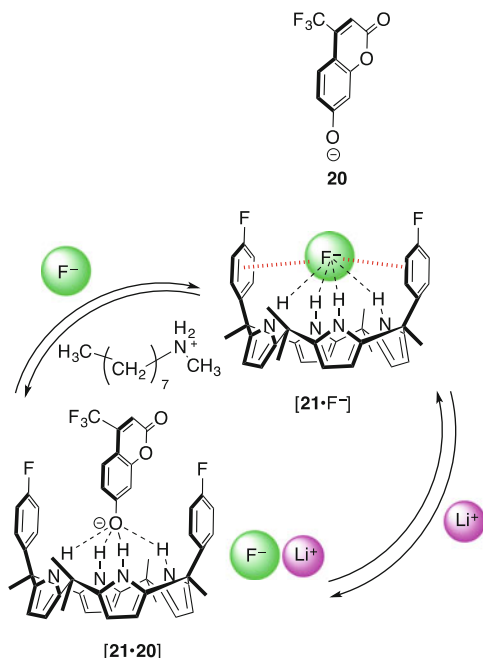


**Scheme 12.2** A schematic representation of pyrophosphate detection by receptor **19** achieved by means of a fluorescence dye displacement (FDDA) assay

(cf. Scheme 12.2) [35]. This dicationic receptor was found to bind the  $\text{HP}_2\text{O}_7^{3-}$  and 2-oxo-4-(trifluoromethyl)-2H-chromen-7-olate **20** anions via electrostatic interactions, hydrogen bonding, and presumed anion- $\pi$  interactions. The sensing properties of **19** for pyrophosphate anions were studied using the fluorescence dye displacement assay (FDDA) method introduced by Anslyn and coworkers [36]. The FDDA approach method relies on the restoration of the fluorescence signal of an added guest (fluorophore) that is pre-bound weakly to the receptor and thus quenched. Ideally, upon the addition of a competitive analyte the bound fluorophore is displaced from its bound position, allowing for a restoration of its emissive properties. In the case of **19**, an FDDA analysis using the chromenolate anion **20** as the fluorophore and acetonitrile as solvent, revealed that the system acts as a specific sensor for  $\text{HP}_2\text{O}_7^{3-}$ , even in the presence of competing anions such as  $\text{F}^-$  and  $\text{H}_2\text{PO}_4^-$  (both as their respective TBA salts). This successful FDDA detection was ascribed to the fact that the  $[\mathbf{19}\cdot\text{HP}_2\text{O}_7^{3-}]$  complex is thermodynamically more stable than the complex **19•20** ( $K_a = 2.55 \pm 0.12 \times 10^7$  and  $7.25 \pm 0.12 \times 10^6 \text{ M}^{-1}$  for the binding of  $\text{HP}_2\text{O}_7^{3-}$  and **20**, respectively, by **19** in acetonitrile) [35]. In fact, the calculated affinities of various anions (calculated from separate fluorescence titration experiments) follow the order  $\text{HP}_2\text{O}_7^{3-} > \text{F}^- \approx \text{H}_2\text{PO}_4^- > \text{AcO}^- \approx \text{Cl}^- \gg \text{HSO}_4^- \approx \text{Br}^-$  (all anions studied as their TBA salts). Even in the presence of wet solvent, receptor **19** proved to be selective for pyrophosphate over the other anions studied. Binding studies carried out in  $\text{CH}_3\text{CN}/\text{H}_2\text{O}$  (70/30 % v/v mixture) revealed an affinity constant value ( $K_a = 3.63 \pm 0.23 \times 10^6 \text{ M}^{-1}$ ) for  $\text{HP}_2\text{O}_7^{3-}$  binding that was approximately 1/7 of that measured in pure acetonitrile [35]. This change in solvent served to decrease the affinities of receptor **19** for  $\text{F}^-$  and  $\text{H}_2\text{PO}_4^-$  by  $\sim 1/276$  and  $\sim 1/140$ , respectively [35]. The relatively increased selectivity of **19** for the pyrophosphate anion seen in wet acetonitrile was attributed to the cooperative effect of hydrogen bonding and Coulombic interactions within a pre-organized binding domain.

The development of sensors and extractants for the fluoride anion has been a subject of particular interest due to the beneficial role that this anion plays in preventing dental caries at appropriate low concentrations, as well as its effects on bone health [37]. At high concentrations, the fluoride anion acts as a G-protein activator [38] and as a Ser/Thr phosphatase inhibitor, [39] thus affecting essential cell signaling processes.

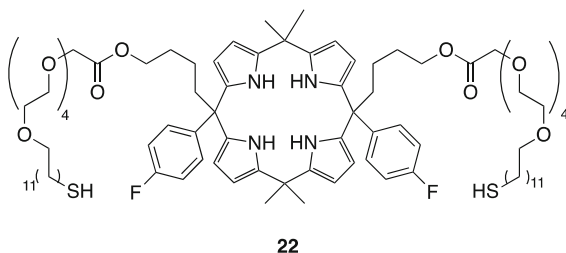
**Fig. 12.10** Schematic representation of fluoride sensing by receptor **21** as achieved using an FDDA assay



To address the challenge of fluoride anion sensing Lee and coworkers used an FDDA assay in conjunction with the *meso*-aryl picket calix[4]pyrrole receptor **21**. [40] The same coumarin chromenolate fluorophore was used as exploited by this group previously (see above). In the absence of a displacement-inducing analyte, the emission of coumarin-based chromenolate **20** is quenched, presumably as the result of a PET process that involves a direct interaction between the *meso-p*-fluorophenyl substituents and the coumarin anion (cf. Fig. 12.10) [40]. On exposure to fluoride anion (as the TBA salt) in acetonitrile a fluorescence emission at  $\lambda = 500$  nm ( $\lambda_{ex} = 410$  nm) is observed [40]. This turn-on in fluorescence emission is ascribed to the larger stability constant for the formation of  $[21 \cdot F^-]$  as compared to  $[21 \cdot 20]$  ( $K_a = 5.96 \times 10^6$  and  $K_a = 4.69 \times 10^6$  M $^{-1}$  for  $F^-$  and **20**, respectively) and the release of the chromenolate fluorophore [40]. The detection limit calculated for fluoride anions was calculated to be 2.3 ppb [40]. The turn-on in fluorescence was found to be limited to the fluoride anions, with exposure to other anions, including  $Cl^-$ ,  $Br^-$ ,  $I^-$ ,  $HSO_4^-$ ,  $PF_6^-$ ,  $H_2PO_4^-$ ,  $HP_2O_7^{3-}$ ,  $AcO^-$ ,  $BzO^-$ ,  $SCN^-$ ,  $CN^-$ , and  $NO_3^-$ , failing to displace the chromenolate dye or to produce a turn-on FDDA response [40]. Interestingly, the displacement of the chromenolate dye was found to be a reversible process. For instance, the addition of lithium or sodium perchlorate leads to the formation of LiF or NaF and restoration of the original chromenolate complex  $[21 \cdot 20]$  complex is restored and MF is formed ( $M = Li$  or Na).

In a further study, Sessler, Lee, and coworkers reported the thiol-containing double-armed calix[4]pyrrole derivative **22** attached to gold nanoparticles (AuNPs)

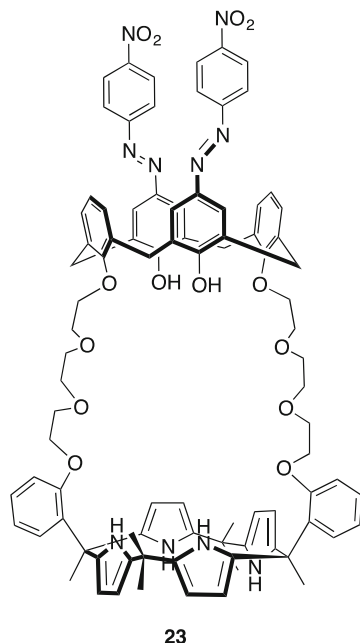
**Fig. 12.11** Structure of the double-armed calix[4]pyrrole **22**



(cf. Fig. 12.11) [41]. This receptor-nanoparticle conjugate was designed to take advantage of the selective anion recognition properties of calix[4]pyrrole as well as the high molar absorptivity of AuNPs in the visible region so as to obtain nanoprobes for anionic species. Although calix[4]pyrroles have been widely studied due to their selective affinities for anions such as  $F^-$  and  $Cl^-$  in organic media, their ability to recognize anionic species effectively under aqueous conditions remains limited. Some systems in which calix[4]pyrrole are incorporated to polymeric scaffolds have been developed to address this deficiency [42–44]. These polymeric systems have proved to be useful for extraction. However, they are inherently incapable of producing an optical signal upon exposure to various anions and hence not suitable for use in sensing. The high absorptivity of AuNPs makes calix[4]pyrrole-based molecular probes of potential interest for anion sensing in aqueous media. The creation of the calix[4]pyrrole AuNPs were obtained by anchoring the fluoride receptor **22** bearing thiol alkyl chains to AuNPs [41]. Similar to what was observed with receptor **21** (*vide supra*), receptor **22** exhibits a strong affinity for the fluoride anions. In this case, a UV/Vis titration of **22** with TBAF in  $CH_2Cl_2$  resulted in a  $\sim 20$ – $25\%$  enhancement in the intensity of the absorption band at 228 nm, a finding that is in agreement with anion complexation by the calix[4]pyrrole [41]. Gratifyingly, the addition of aliquots of other anions, such as chloride and bromide (as their corresponding TBA salts), produced relatively small changes in the absorption spectra. Moreover, the addition of other anions ( $CN^-$ ,  $AcO^-$ ,  $NO_3^-$ ,  $HSO_4^-$ ,  $H_2PO_4^-$ , and  $HP_2O_7^{3-}$ , as their TBA salts) only produced negligible changes in the absorption spectral features [41]. A fluorescent dye displacement assay using the same chromenolate fluorophore (**20**) as used above, revealed that the initial complex ( $[22 \cdot 20]$ ) would act as a highly sensitive fluorescent sensor for the fluoride anions. Thus, the receptor-AuNP conjugate can be used as a sensitive dual mode sensor (i.e., both colorimetric and fluorometric) for the fluoride anions. The fluoride anion affinity of the AuNP-bound system **22**, determined in dichloromethane, was found to be considerably higher than that for the free receptor **21** ( $K_a = 1.43 \pm 0.16 \times 10^8$  and  $9.84 \pm 0.25 \times 10^6 M^{-1}$  for **22** and **21**, respectively) [41]. This could reflect the effect of multivalency.

Extraction experiments were conducted employing a solution of TBAF in  $D_2O$  that was contacted with a solution of **22** (1.42 mM) in deuterated chloroform.  $^1H$  NMR spectral analyses revealed that **22** is able to extract  $F^-$  anions along with the tetrabutylammonium counteranion into the organic phase. This stands in contrast

**Fig. 12.12** Structure of the chromogenic fluoride sensor **23**



to what was observed with receptor **21**, which acted as a rather ineffective TBAF extractant under similar conditions.

The azocalix[4]arene-strapped calix[4]pyrrole **23** reported by Pulpoka and coworkers in 2012 displayed selective sensing properties for fluoride anions (cf. Fig. 12.12) [45]. A color change from orange to blue was observed when receptor **23** was exposed to  $F^-$ , which was reflected in distinctive UV/vis absorption changes. A spectroscopic analysis revealed a bathochromic shift in the absorption band of **23** absorption  $\lambda_{max}$  395–600 nm in  $CH_3CN$  upon the addition 6 equivalents of  $F^-$ , whereas smaller absorption changes were observed upon the addition of other test anions, such as  $AcO^-$ ,  $BzO^-$ , and  $H_2PO_4^-$  (all anions studied as their TBA salts). Negligible changes in the electronic spectrum were observed in the presence of  $NO_3^-$ ,  $PF_6^-$ , and  $ClO_4^-$  under the same experimental conditions [45]. The spectroscopic changes were ascribed to a charge transfer interactions involving the oxygen of the azophenol unit acting as a donor and the nitro ( $-NO_2$ ) group of the chromophore acting as an acceptor that are modulated upon anion complexation. The significant color changes led the authors to conclude that a greater stabilization of the excited state is achieved when anions are bound to receptor **23** [45]. Thus, the greater stability of the complex  $[23 \cdot F^-]$  is expected to correlate with a stronger absorption feature, as observed by experiment. In addition, spectroscopic analyses led to the suggestion that **23** forms two types of complexes with  $F^-$  characterized by relative stoichiometries of 1:1 and 1:2 (ligand/anion). These are formed in solution with  $\log\beta$  values of  $3.07 \pm 0.08$  and  $11.09 \pm 0.07$ . All other anions that bind to **23** do so with a 1:1 stoichiometry. The affinities were found to follow

the order:  $\text{BzO}^- > \text{AcO}^- > \text{F}^- > \text{H}_2\text{PO}_4^-$  (with cumulative binding constants reported of  $\log\beta_{1:1 \text{ complex}} = 5.64 \pm 0.09$ ,  $\log\beta_{1:1 \text{ complex}} = 4.81 \pm 0.06$ ,  $\log\beta_{1:1 \text{ complex}} = 3.07 \pm 0.08$  and  $\log\beta_{2:1 \text{ complex}} = 11.09 \pm 0.07$ , and  $\log\beta_{1:1 \text{ complex}} = 2.55 \pm 0.02$ , for  $\text{BzO}^-$ ,  $\text{AcO}^-$ ,  $\text{F}^-$ , and  $\text{H}_2\text{PO}_4^-$ , respectively) [45]. The relatively high affinity for benzoate was ascribed to the preorganization of the receptor, which allows it to accommodate the benzoate without a need for significant reorganization. Recovery of the free receptor **23** could be achieved in acetonitrile by adding  $\text{Ca}(\text{NO}_3)_2$  into a solution containing the fluoride anion complexes. The recovery of the original light orange solution was indicative of salting out of  $\text{F}^-$  in the form of  $\text{CaF}$  [42]. In contrast, when two equivalents of  $\text{Ca}(\text{NO}_3)_2$  were added to the benzoate and acetate complexes, ion pair complexes of **23** were formed (i.e.,  $\mathbf{23} \cdot \text{BzO}^- \cdot \text{Ca}^{2+}$  and  $\mathbf{23} \cdot \text{AcO}^- \cdot \text{Ca}^{2+}$ ) [42].

## 12.5 Extraction

The extraction of ions in organic solvents is a process that relies on the transfer of ionic species present in from the aqueous phase into the organic phase [46, 47]. This transfer process generally involves a multitude of noncovalent phenomena, including solvation, [48] association, [49] and interfacial phenomena, [50] as well as hydrophobic-hydrophilic interactions [51]. In the case of idealized liquid-liquid extraction process where a receptor functions as an extractant, the charged species in the aqueous phase are initially solvated by water molecules while the receptor is solvated by organic solvent molecules. In order to maximize the interactions with the anionic species at the liquid-liquid interface and avoid ancillary interactions, the receptor is generally designed to be hydrophobic enough to minimize interactions with the aqueous phase. Hydrophobicity also plays a critical role in the extraction of ions in that a more hydrophobic anion easier to extract. This bias towards extraction in the case of more hydrophobic anion is reflected in the Hofmeister series, which roughly parallels the degree of hydration (cf. Fig. 12.13) [52].

Effective transfer of charged species from an aqueous phase into an organic milieu requires charge neutrality. This has been achieved using one of four limiting strategies. These rely, respectively, on the use of: (a) A positively charged extracting agent that can act as the countercation for the targeted anion, (b) a ditopic ligand capable of binding concurrently both a target anion and its countercation, (c) two separate receptors, one with affinity for anions and other for cations, that act in concert and (d) an anion receptor and a lipophilic cation in the organic phase that facilitates the transfer of the anion from the aqueous phase (cf. Fig. 12.14) [46]. In this section we provide an overview of receptors that have been used as extractants for anions and ion pairs under liquid-liquid extraction conditions. Although kinetic and thermodynamic effects are beyond the scope of this chapter, multiple reports can be found in the literature that discuss these aspects in depth [25, 46, 47, 53].

The use of extractants to transfer anionic species from water to a non-polar medium represents a nontrivial task. Calix[4]pyrrole-based receptors are very

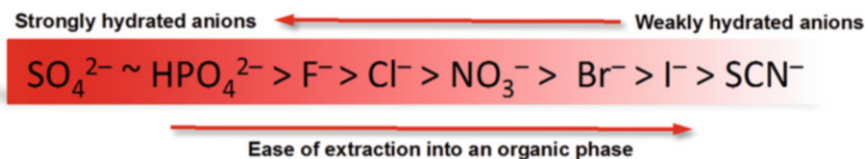


Fig. 12.13 Hofmeister series

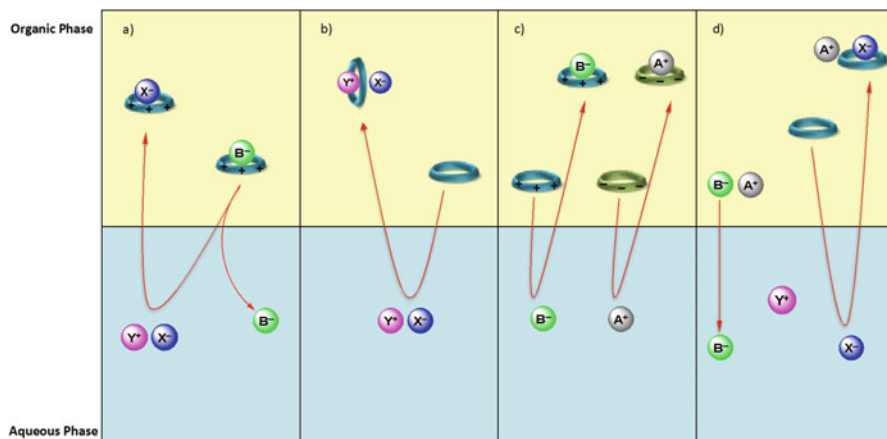
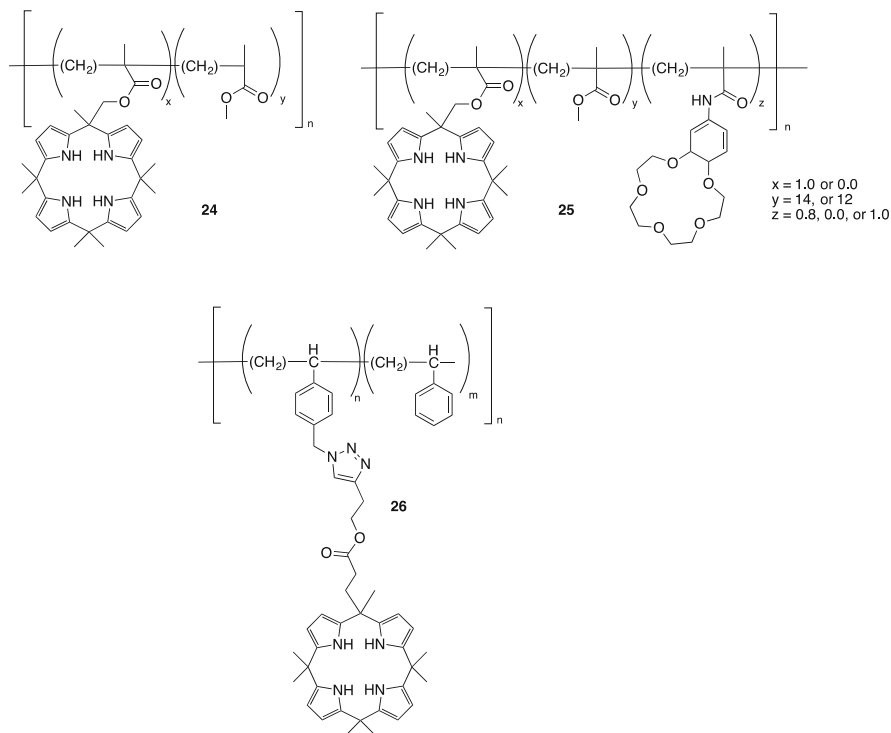


Fig. 12.14 Limiting extraction approaches that maintain charge neutrality. These involve, respectively, the use of: (a) A positively charged receptor, (b) a ditopic receptor, (c) two different receptors, and (d) an anion receptor assisted by a lipophilic cation [47]. This diagram is a redrawing of a scheme first reported by Gale and coworkers and which appeared in [47]

attractive agents for extraction. They provide hydrogen bond donor groups in their cavities that may interact with the targeted anionic species. In favorable cases, this leads to encapsulation of the anion at a level that serves to overcome hydration effects, thus allowing extraction into the organic phase. In the case of neutral receptors, the effect of the counteranion is paramount since charge considerations require that it too be carried into the organic phase in the absence of some other compensating effect.

In 2008, Akar, Bielawski, Sessler, and coworkers reported an organic solvent soluble methyl methacrylate (MMA) copolymer of calix[4]pyrrole **24** (cf. Fig. 12.15) [42]. <sup>1</sup>H NMR spectroscopic and thermogravimetric studies revealed that compound **24** is capable of extracting halide anions from aqueous D<sub>2</sub>O solutions containing tetrabutylammonium salts (TBACl and TBAF) into a CD<sub>2</sub>Cl<sub>2</sub> phase [42]. Polymer **24** was found to extract halide anions from aqueous solutions more efficiently than OMCP [42]. Greater efficacy was seen for chloride over fluoride. This anion selectivity is in accord with the Hofmeister series.





**Fig. 12.15** Structures of three different calix[4]pyrrole copolymers, namely the calix[4]pyrrole copolymer **24** reported by Akar et al. [42] the ditopic copolymer **25** containing a calix[4]pyrrole and a crown-5 ether [43], and the polystyrene polymer **26** bearing pendant calix[4]pyrroles of Aydoğan [44]

Subsequently, the poly(methyl methacrylate), PMMA, copolymer **25** was reported by Kim, Sessler and coworkers (cf. Fig. 12.15) [43]. This macromolecule contains both calix[4]pyrrole and crown-5 ether subunits incorporated into the copolymer. These subunits were designed to function as anion and cation recognition moieties, respectively [43]. Extraction studies using potassium halide salts in aqueous solutions revealed that copolymer **25** promotes the extraction of both KCl and KF into dichloromethane. Control extraction assays under identical experimental conditions using separately PMMA and OMCP revealed no appreciable extraction of alkali salts into the organic phase. These findings led the authors to suggest that incorporation of receptors in a polymeric backbone could provide a means of enhancing the extraction ability of simple receptors as the result of enhanced multivalency effects, improved solubility of the individual extracting agents, and facilitated recovery and reuse [43].

In a recent report, Aydoğan reported a polystyrene backbone bearing pendant calix[4]pyrroles. The system in question, polymer **26**, was found capable of extracting TBA halide salts (cf. Fig. 12.15) [44]. Extraction efficacy was monitored

by proton spectroscopy and typically involved experiments wherein a solution of **26** (7.9 mM based on repeat units) in  $\text{CD}_2\text{Cl}_2$  was contacted with TBAX (60 mM, X = F, Cl, Br, I, and  $\text{H}_2\text{PO}_4$ ) in  $\text{D}_2\text{O}$ . All anions were extracted to some extent [44]. However, no transfer of TBAF or  $\text{TBAH}_2\text{PO}_4$  was observed in the presence of TBACl. These findings are in accord with the Hofmeister bias in that a more hydrophobic anion (chloride) is extracted to the organic phase in preference to more hydrated anions (e.g.,  $\text{F}^-$  or  $\text{H}_2\text{PO}_4^-$ ). They were thus not deemed remarkable. However, in contrast to what would be expected based on the Hofmeister bias, **26** proved to be a relatively better extractant for the  $\text{Cl}^-$  anions when tested in the presence of TBABr and TBAI. This reversal in the expected trend was attributed to a better fit of chloride anion into the calix[4]pyrrole cavity. Control experiments revealed that the extraction efficiency of **26** was  $\approx 40\%$  higher than that of the parent system, OMCP [44].

Sulfate anion is highly hydrated (i.e.,  $\Delta G_{\text{h}} = -1080 \text{ kJ mol}^{-1}$ ) [25]. This makes its extraction from an aqueous phase into an organic phase particularly challenging. This challenge reflects not only its high hydration energy but also the fact that there is a high inherent charge density associated with this polyanion. Formation of a so-called third phase, wherein the phase partition between the aqueous and organic phases is not complete under conditions of extraction, is also common. In order to facilitate the transfer of the sulfate anion into an organic phase and hence overcoming to some extent the Hofmeister bias, phase-transfer catalysts, such as Aliquat 336 (a quaternary ammonium salt), are often employed [54].

In 2010, Fowler, Moyer, Sessler, and coworkers studied OMCP and its octafluorinated derivative as possible extractants of  $\text{SO}_4^{2-}$  [55]. The organic phase consisted of chloroform containing the putative extractant (0.1–10 mM) along with 10 mM of Aliquat nitrate (A336N) used as a lipophilic phase-transfer catalyst. The organic mixtures were contacted with an aqueous layer containing  $\text{Na}_2\text{SO}_4$  (0.1 mM) and  $\text{NaNO}_3$  (10 mM). In the case of OMCP,  $\text{SO}_4^{2-}$  was extracted into the organic phase more efficiently than  $\text{NO}_3^-$  (cf. Fig. 12.17) [55]. In fact, the extraction of  $\text{SO}_4^{2-}$  is enhanced over  $\text{NO}_3^-$ , even when  $\text{NaNO}_3$  is present in excess in the aqueous phase. The effective phase transfer of sulfate anions from aqueous phase into the organic phase mediated by OMCP was rationalized in terms of the receptor acting as an effective receptor for both the anion and the methylammonium head group of A336N (cf. Fig. 12.16). Support for this conclusion came from the observation that when A336N was replaced by a symmetrical long-chain quaternary ammonium cation, the extent of sulfate ion was reduced.

Functionalized calixpyrroles able to accommodate ion pairs within their cavities were synthesized by Kim, Sessler, Lee, Moyer, and coworkers using crown ether-like polyether straps to link two of the four *meso*-carbon atoms of the calix[4]pyrrole core. One example is the calix[4]arene crown-5-strapped calix[4]pyrrole **27** (cf. Fig. 12.17) [56]. This ditopic receptor was designed to control cation binding and release via cation metathesis. Receptor **27** was found to bind  $\text{K}^+$  selectively relative to  $\text{Cs}^+$ . Both cations can be recognized. In the absence of  $\text{K}^+$ , the  $\text{Cs}^+$  cation is accommodated. However, addition of  $\text{K}^+$  serves to displace the  $\text{Cs}^+$  cation. This cation metathesis release mechanism, it was suggested, could prove useful in

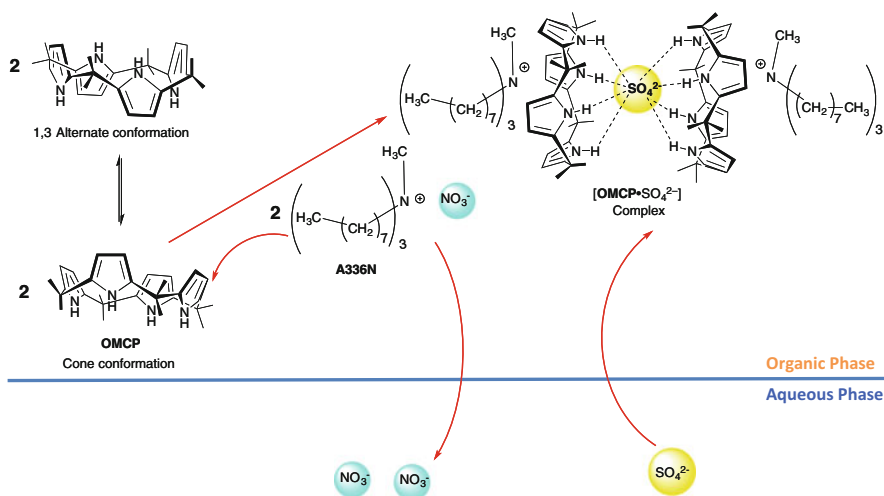


**Fig. 12.16** Proposed mechanism of sulfate anion extraction mediated by OMCP [55]

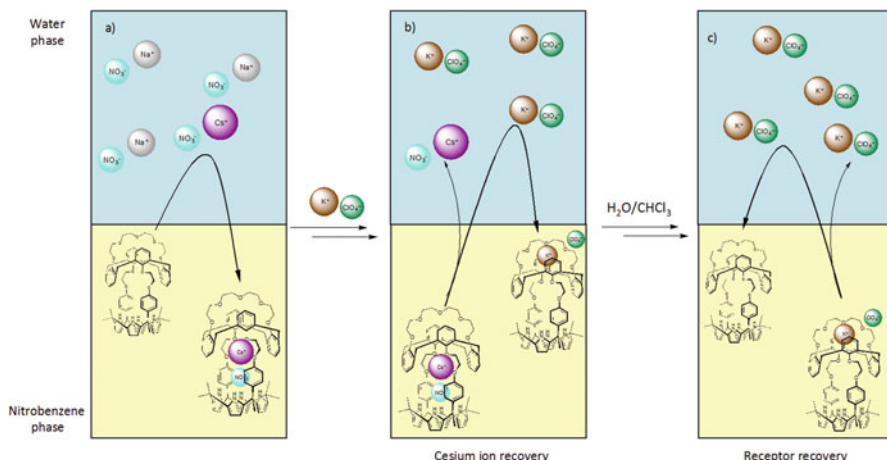
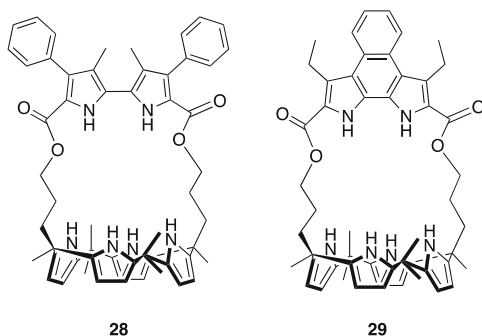


**Fig. 12.17** Schematic representation of the two phase  $\text{CsNO}_3$  extraction and recovery events promoted by using the strapped calix[4]arene-5-crown calix[4]pyrrole **27**

application scenarios wherein release of cesium is desirable, such as those involving the remediation of  $^{137}\text{Cs}$ .

Extraction experiments with **27** were performed using a two-phase water-nitrobenzene setup [57]. The results were consistent with the design expectation in that  $\text{CsF}$  could be extracted into the organic phase. Stripping of the  $\text{Cs}^+$  cation could be achieved via exposure of the cesium complex to an aqueous solution containing  $\text{K}^+$  cations (in the form of  $\text{KClO}_4$ ). This produces a new complex,  $[\text{27}\cdot\text{K}]^+\text{ClO}_4^-$ , and

**Fig. 12.18** Structures of the bipyrrrole strapped calix [4]pyrroles **28** and **29**



is accompanied by the transfer of the free cesium cation into the aqueous phase. The use of perchlorate, a weakly bound anion, prevents the stabilization of an ion pair complex, and presumably, this allows the recovery of free receptor **27** upon exposure of  $[27 \cdot K]^+ ClO_4^-$  to water [57]. Operationally, the three-step process of cesium salt complexation, potassium cation-induced decomplexation, and a water wash allows the overall cesium extraction process to be repeated and the receptor recycled.

The extraction of  $SO_4^{2-}$  by the bipyrrrole strapped calix[4]pyrrole receptors **28** and **29** was reported by Sessler and coworkers in 2014 (cf. Fig. 12.18) [58]. The strap containing two additional hydrogen-bond donors in the bipyrrrole subunits. In accord with design expectations, receptors **28** and **29** were found to extract  $SO_4^{2-}$  from water more effectively than the control system OMCP [58]. In particular, receptor **29** in the presence of the co-extractant Aliquat 336 chloride (A336Cl) extracted sulfate anions into the chloroform phase much more effectively than either OMCP or its congener **28** under identical experimental conditions ( $[SO_4^{2-}] = 1.0$  mM, in the presence of NaCl at 10 mM). Distribution ratios ( $D_{sulfate} [SO_4^{2-}]_{org}/[SO_4^{2-}]_{aq}$ ) of 0.013, 0.00614, and 0.00055 were observed for receptors **29**, **28**, and OMCP, respectively [58]. In this case, analysis of synergistic factors led to the conclusion that sulfate extraction in the presence of A336Cl results from the stabilization of higher order sulfate–receptor–co-extractant complexes in the organic phase, which serve to enhance the extraction process.

## 12.6 Transport

The phospholipid membrane surrounding the cell serves as a semi-permeable barrier in living organisms, allowing a limited diffusion of large molecules and small charged species. For the correct functioning of cells it is important that proper concentrations of ions are maintained both inside and outside of the cell. The through-membrane transport of charged species in mammalian systems is with few exceptions, regulated by specialized proteins, known as ion channels. These are embedded in the membrane and provide a localized polar environment that

allows a controlled passage of ions through the hydrophobic membrane. Inappropriate functioning of these ion channels and more specifically an inability to maintain appropriate intra- and extracellular chloride anion concentrations can lead to a variety of well-recognized disease states, including cystic fibrosis (CF) [59a], Bartter's syndrome [59b], Dent's disease [59c], congenital chloride diarrhea [59d], and idiopathic epilepsy. [59e] These diseases are characterized by higher than normal intracellular chloride anion concentrations that also affect the transmembrane flow of other ions, including bicarbonate [60] (for which intra- and extracellular concentrations of 12 and 29 mM, respectively [61], are typical). Dysregulation of the mechanisms that maintain intracellular chloride anion concentrations at relatively low levels relative to the extracellular matrix (ca. 6 mM and 115 mM, for intracellular and extracellular chloride concentrations, respectively) has been shown to correlate closely with the onset of programmed cell death (i.e., apoptosis) [62–64]. Thus, the creation of supramolecular systems that work as ion carriers able to transport anions or ion pairs across phospholipid membranes is a fast growing area of research. The particular properties of calix[4]pyrrole and related ion pair receptors have attracted interest as synthetic transmembrane transporter. Some of these systems have been tested in model membrane systems, including liposomes, and recently in vitro. While the field is still in its infancy a correlation between carrier capability in model membranes and in vitro efficacy is beginning to emerge.

The use of small molecules to mediate the transport of charged species through phospholipid membranes has for the most part followed two main strategies, namely the use of mobile carriers and synthetic channels [47]. Unlike synthetic channels, mobile carriers display slower diffusion rates. The advantages of the use of mobile carriers for transport of ions are that the mobile carriers are easier to synthesize and are less prone to be involved in complex equilibria than synthetic channels. To date, calix[4]pyrroles have only been used as carriers.

Coulombic considerations dictate that transport processes needs to be electroneutral, or nearly so. Therefore, in the case of carriers the diffusion of ions across the membrane is expected to occur via two limiting mechanism referred to as symport or co-transport, and antiport or exchange. Symport/co-transport occurs when both cations and anions (with the exact relative stoichiometry determined by charge considerations) are transported concurrently and in the same direction. In contrast, antiport/exchange processes involve the simultaneous transport of two ions in opposite directions (cf. Fig. 12.19). To date, most work has focused on anion transporters that do not allow for the concurrent complexation of a counteranion. However, recently a few reports have appeared wherein ditopic receptors were employed as transporters.

Recently, it was discovered that calixpyrroles are effective extractants and carriers under mixed aqueous-organic interfacial conditions [65]. For instance, Sessler, Gale, and coworkers showed that OMCP [66] and its octafluoro derivative, **30**, [67] could be used to transport chloride anions across both liposomal (unilamellar POPC vesicles) and U-tube type (i.e., Aq. 1/CH<sub>2</sub>Cl<sub>2</sub>/Aq. 2, where Aq. = aqueous) model membranes. Not surprisingly, the fluorinated carrier **30**

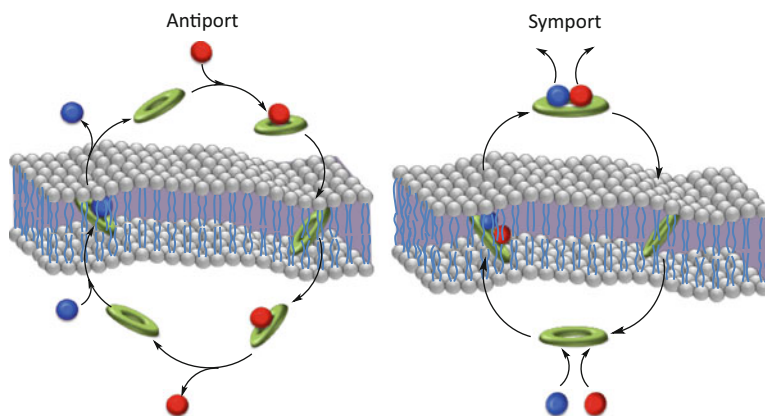
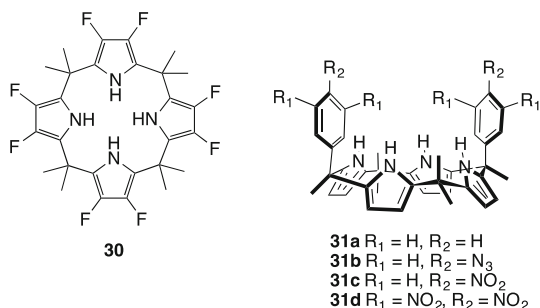


**Fig. 12.19** Schematic representation of (a) antiport/exchange and (b) symport/co-transport processes

**Fig. 12.20** Structures of octafluorocalix[4]pyrrole **30** and two-wall calix[4]pyrroles **31**



proved much more effective than OMCP under conditions of  $\text{Cl}^-/\text{HCO}_3^-$  antiport [67]. This was attributed to an enhanced anion affinity of **30** relative to OMCP as a consequence of the electron withdrawing fluoride groups present on the  $\beta$ -pyrrolic positions (cf. Fig. 12.20). However, no real control over the counteraction is achieved with either of these systems.

A series of modified calix[4]pyrroles, containing two aryl groups (termed “walls”) attached to the *meso*-carbon atoms, were studied as nitrate carriers by Matile, Ballester and coworkers [68]. These “two-wall” calixpyrroles were found to be capable of transporting the nitrate anion. Presumably, the nitrate anion forms a complex with these macrocycles that is stabilized in part by interaction with the electron deficient aryl groups (i.e., **31c–d**; cf. Fig. 12.20). Detailed  $^1\text{H}$  NMR spectroscopic analyses provided support for the notion that receptor **31** interacts with the bound  $\text{NO}_3^-$  anion via NH hydrogen bonding and aryl- $\pi$  interactions. Transport studies, carried out using **31** in large unilamellar vesicles (LUVs) in the presence of competitive anions, such as  $\text{Br}^-$  or  $\text{Cl}^-$  (as their alkali metal salts), served to confirm that compound **31** functions as a selective nitrate anion

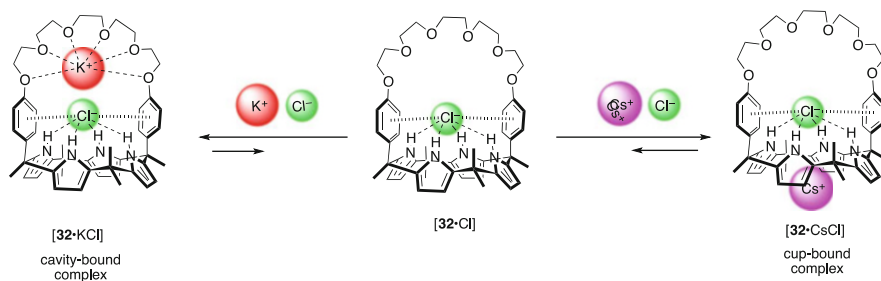


**Fig. 12.21** Structures of the ditopic receptor **32** and its ion pair complexes. These are referred to as cup-bound (seen for  $[32 \cdot CsCl]$ ) and cavity-bound (seen for  $[32 \cdot KCl]$ ) species, respectively

transporter under these conditions [68]. Interestingly, it was observed that **31a** and **31b** containing electron rich walls transport via a cation/anion symport mechanism  $CsNO_3$  and with selectivity relative to other alkali metal salts [68]. In contrast, calixpyrroles **31c** and **31d**, containing electron deficient walls, displayed no preference for  $CsNO_3$  salts. These differences were rationalized in terms of nitrate transport with **31c** and **31d** occurring via an anion/anion antiport mechanism [68].

The hybrid system **32** reported by Sessler, Gale, Lee and coworkers was designed to provide two recognition motifs, namely an oligoether strap for cation binding and a calix[4]pyrrole macrocycle for anion recognition [69]. The oligoether-strapped ion pair receptor **32** forms complexes with  $CsCl$  and  $KCl$  in two different binding modes, a cup-bound ion pair and a cavity-bound ion pair, respectively (cf. Fig. 12.21). Liposomal model membrane transport studies provided support for the conclusion that macrocycle **32** functions as a cotransporter for alkali chloride salts, as well as a  $Cl^-/NO_3^-$  ion exchanger [69].

Functionalized calix[4]pyrrole **33** bearing a mono *meso*-aminophenyl-*trans*-Pt(II) moiety was reported by Kohnke and coworkers in 2013 as a potential anticancer prodrug (cf. Fig. 12.22) [70]. Compound **33** was prepared by reacting *cis*- $[PtCl_2(DMSO)_2]$  with **34** in acetonitrile. A change in the Pt(II) configuration from *cis* to *trans* was proposed to occur during the complexation reaction. The configurational isomerization was confirmed by the single crystal X-ray diffraction analysis of the Pt(II) complex **33** where a distorted square planar coordination geometry was observed for the Pt(II) center with two chloride anions occupying the *trans* positions [70]. Stability studies performed in both  $CD_2Cl_2$  and  $D_2O/CD_2Cl_2$  (20/80 % v/v) revealed that only 30 % of the Pt(II) in **33** is released after 24 h, even in the presence of high concentrations of chloride anions (i.e., 50 mM of TBACl salt, ~5 times the chloride concentration found in plasma) [70]. The viability of **33** as a prodrug was studied by using  $^1H$  NMR spectroscopy in  $CD_3CN$  to follow the transfer of the Pt(II) center to adenosine monophosphate (AMP). This spectroscopic analysis revealed that the Pt(II) metal center is indeed transferred to AMP, but also that other platinum species are formed, as inferred from negative ion mode ESI-MS analyses.

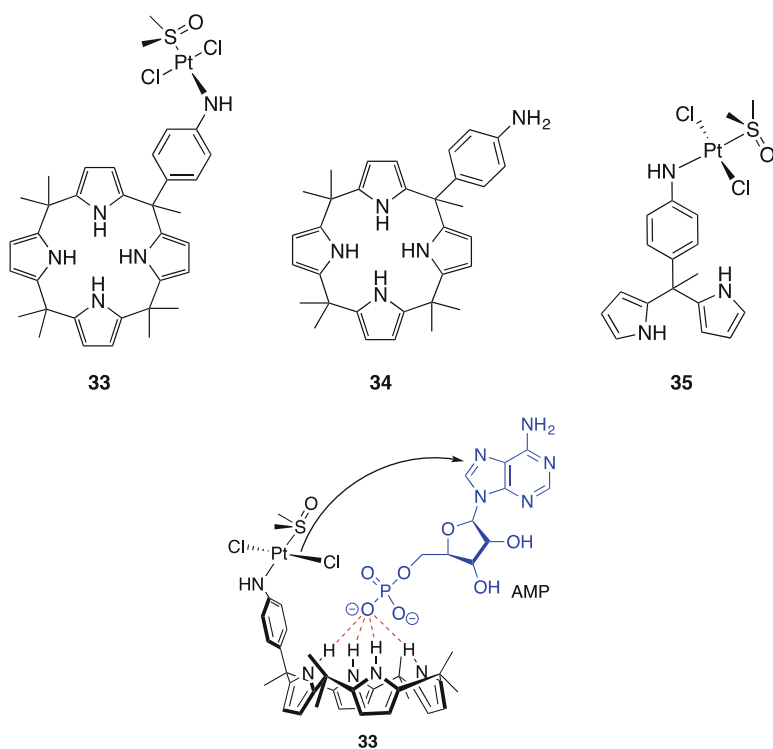


**Fig. 12.22** Structures of calix[4]pyrroles **33**, **34**, and **35** (above). Representation of the transfer of Pt(II) center from **33** to adenosine monophosphate (AMP)

The antiproliferative activity of **33** was explored using a standard MTT assay with the A2774, OVCAR-3, and SKOV-3 ovarian carcinoma cell lines [70]. The results from this assay provided evidence that both the calix[4]pyrrole skeleton and the Pt(II) coordinated to the macrocycle play a key role in modulating the reactivity of the Pt(II) center. Support for this conclusion came from control antiproliferative studies carried out using the dipyrromethane-*trans*-Pt(II) complex **35**, OMCP, and *trans*-[PtCl<sub>2</sub>(NH<sub>3</sub>)<sub>2</sub>]. For the A2774 cell line, IC<sub>50</sub> values of 23 ± 3, 32 ± 8, and >100 μM were found for **33**, **35**, and *trans*-[PtCl<sub>2</sub>(NH<sub>3</sub>)<sub>2</sub>], respectively, whereas the OMCP control did not exhibit any activity [70].

The use of an external cationic transporter to assist in the transport of anions by certain carriers has been explored by Gale and others recently. This was demonstrated by Gale in the case the triazole-strapped calix[4]pyrrole **36**, which was combined with the potassium carrier valinomycin. The combination led to enhanced transport of chloride anions across POPC membranes (cf. Fig. 12.23) [71]. The overall transport process was consistent with a K<sup>+</sup>/Cl<sup>-</sup> symport mechanism. This “dual host” approach was employed by Sessler, Gale, Shin, and coworkers in the case of the pyridine-diamide strapped calix[4]pyrrole Cl<sup>-</sup> transporter **37** (cf. Fig. 12.23) [72]. It was found that the combination of **37** and



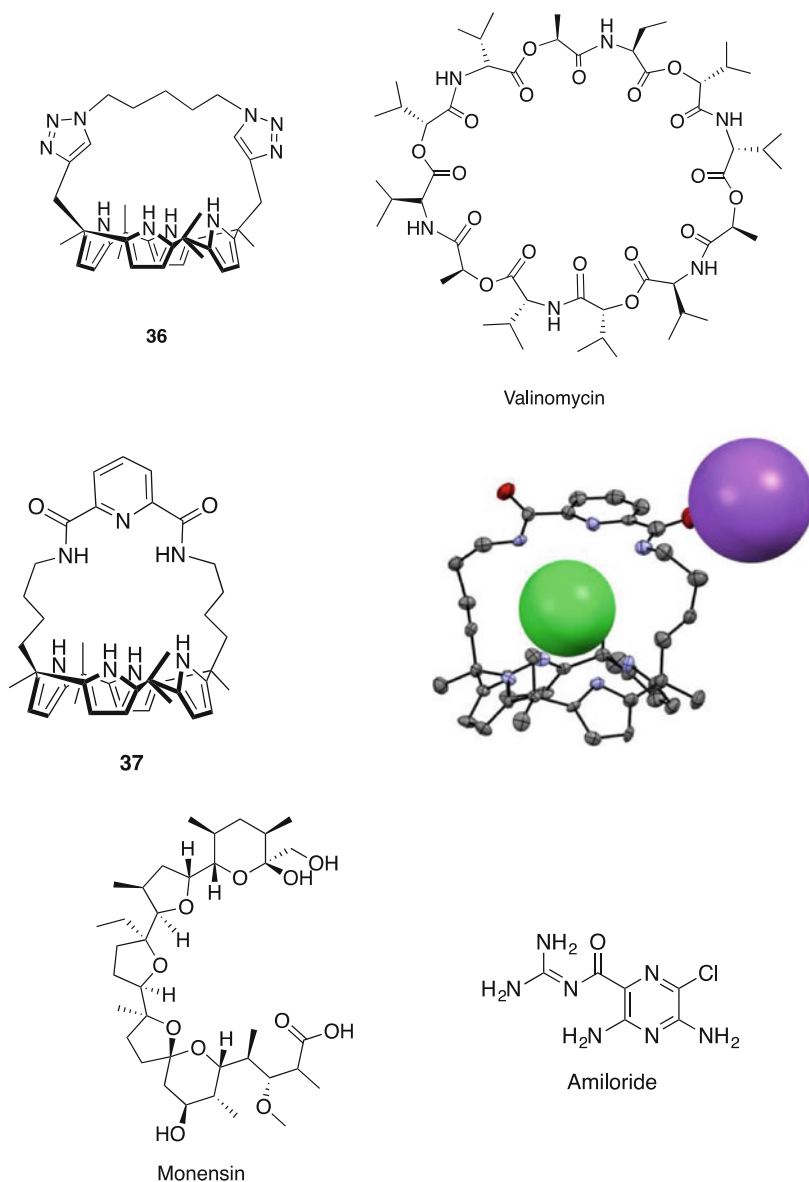


**Fig. 12.23** Structure of strapped calix[4]pyrroles **36** and the potassium cation carrier valinomycin (*top*), the pyridine amide strapped calix[4]pyrrole **37**, and single crystal structure of its [37•NaCl] complex (*middle*). TBA cation, water, and hexane molecules in the crystal structure were omitted for clarity. This X-ray figure was reproduced using the data downloaded from the Cambridge Crystallographic Data Centre. The Na<sup>+</sup> transporter monensin, and the Na<sup>+</sup> channel blocker amiloride (*bottom*)

monensin induces coupled chloride anion and sodium cation transport in liposomal models. In vitro, **37** exhibited apoptotic activity in the HeLa and A549 cancer cell lines as the direct consequence of increasing intracellular sodium chloride concentrations inside the cell [72]. This apoptotic activity was ascribed to the ability of **37** to carrier  $\text{Cl}^-$  across the cell membrane as the result of coupled  $\text{Na}^+$  transport mediated via natural sodium channels. Carrier **37** thus functions through a formal dual-host mechanism. Support for this conclusion came from studies wherein the natural  $\text{Na}^+$  channels were blocked with amiloride; under these conditions, the antiproliferative activity of **37** was significantly reduced [72].

## 12.7 Capsules and High Order Aggregates

Molecular arrangements where one or more molecules accommodate other molecules or ions within a confined space have received the name of molecular containers. To date molecular containers of various sizes and shapes have been reported, as have those containing interior recognition sites [73]. The nature of the molecular container can be permanent, in which the architecture of the container is constituted by covalent bonds, [74] or temporary with the structures being spontaneously self-assembled via weaker interactions, such as metal-ligand interactions [75], hydrogen bonds [76], or hydrophobic forces [77]. Containers that self-assemble through supramolecular interactions are typically referred to as capsules.

The interest in molecular containers reflects in large measure the fact that molecules and ions contained within the interior of containers exhibit different behavior from those surrounded by bulk solvent molecules. Molecules held inside containers can adopt new conformations, undergo reactions at an accelerated pace, or be stabilized as reactive intermediates [73–77]. Most of these features resemble those observed in enzymes where the isolation from the bulk solvent allows a diversity of reactions that otherwise would not occur in solution. However, inside of synthetic containers phenomena unknown to biology or solution chemistry have been observed, which is providing an incentive to study molecular containers in greater depth. Calix[4]pyrroles have a role to play in advancing this effort.

The flexible structure of calix[4]pyrrole possess coupled with their relative ease of synthesis and inherent affinities for anions have made this core structure a key building block in the creation of containers and capsules [76, 78]. Examples of calix [4]pyrroles capsules and self-assembled systems are presented in a separate chapter in this book that is authored by the Tarragona group. Thus, only a brief description will be provided here to avoid redundancy.

An early example of a self-assembled calix[4]pyrrole system was reported in 1996 by Sessler and coworkers [79]. Solid state analysis of the calix[4]pyrrole monoacid **38** revealed that it forms a homoditopic complex both in the solid state (cf. Fig. 12.24) and in organic media upon deprotonation. This dimer could be broken (i.e., disassembled) by exposure to a source of fluoride anions. However, it is only in recent years that calix[4]pyrroles have been explored for the creation of capsule-like systems that can be responsive to a specific stimulus [79].

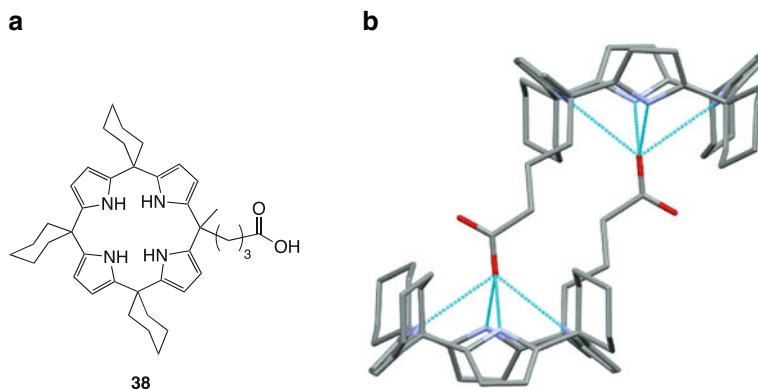


**Fig. 12.24** Structure of calix[4]pyrrole **38** and the homoditopic complex observed in the solid state upon deprotonation. This X-ray figure was produced using data downloaded from the Cambridge Crystallographic Data Centre. Solvent molecules, counter cations, and hydrogen atoms have been omitted for clarity

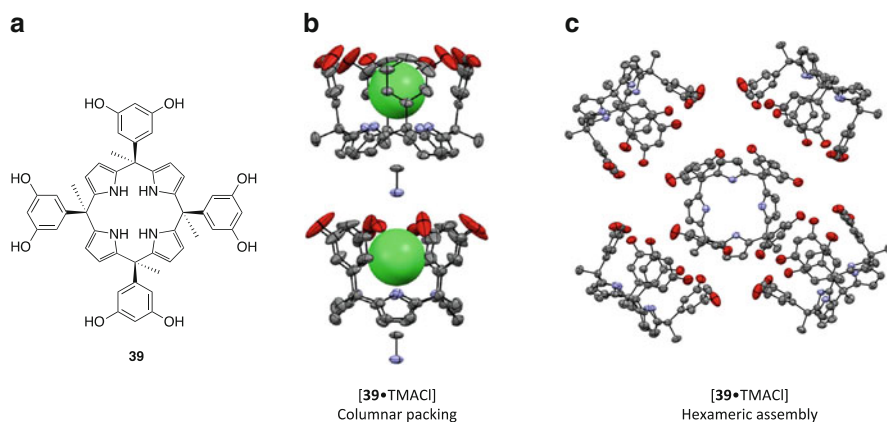


**Fig. 12.25** (a) Chemical structure of resorcinol-functionalized calix[4]pyrrole **39**. (b) Single crystal X-ray structure of the columnar packing of the *endo* cavity complex [39•TMACl]. In this crystal structure, the methyl groups of the tetramethylammonium (TMA) counteranion were disordered. Three methyl groups of the TMA cation were removed for clarity. (c) Single crystal X-ray structure of a hexameric ensemble containing complex [39•TMACl]. TMA cations, chloride anions, and solvent molecules have been omitted for clarity. These X-ray figures were reproduced using data downloaded from the Cambridge Crystallographic Data Centre

One of the pioneers in the area of calix[4]pyrrole container research is Ballester. In 2007, he and his coworkers reported the use of resorcinol-functionalized calix[4]pyrroles **39** to create hexameric cages (cf. Fig. 12.25) [80]. Solid-state analyses revealed that the formation of the hexameric molecular assembly was controlled by the relative stoichiometry of the tetramethylammonium chloride (TMACl) salt and

macrocycle **39** in the solutions used for crystallization. For instance, a solid state structure characterized by columnar packing of the *endo* cavity complex [**39**•TMACl] is obtained when an equimolar mixture of TMACl and **39** is subject to crystallization [80]. In contrast, a separate single crystal X-ray analysis revealed that a hexameric structure containing [**39**•TMACl] is obtained when an excess of TMACl salt is added to the crystallization solution (cf. Fig. 12.27) [80].

*N*-Tosylpyrrolidine functionalized calix[4]pyrrole **40**, containing a cationic binding site on the  $\beta$ -pyrrolic positions of the calix[4]pyrrole, was reported by Sessler and coworkers in 2011 (cf. Fig. 12.27) [81]. Isothermal titration calorimetry (ITC) analysis in chloroform revealed that receptor **40** displays enhanced affinities for tetraalkyl ammonium halide ion pairs (i.e., TBACl, TBABr, and TBAI) relative to what is observed for OMCP. For instance, **40** exhibited an affinity for TBACl of  $2.4 \times 10^6 \text{ M}^{-1}$ , which is significantly greater than the affinity obtained for the same chloride salt bound to OMCP ( $K_a < 10^2 \text{ M}^{-1}$ ) under analogous conditions [81]. This enhancement in affinities was ascribed to additional stabilizing interactions between the tetrabutylammonium cation and the four tosyl groups on the  $\beta$ -pyrrolic positions as inferred from a single crystal X-ray diffraction analysis of the complex [**40**•TBACl] (cf. Fig. 12.26) [81]. The effective encapsulation of the

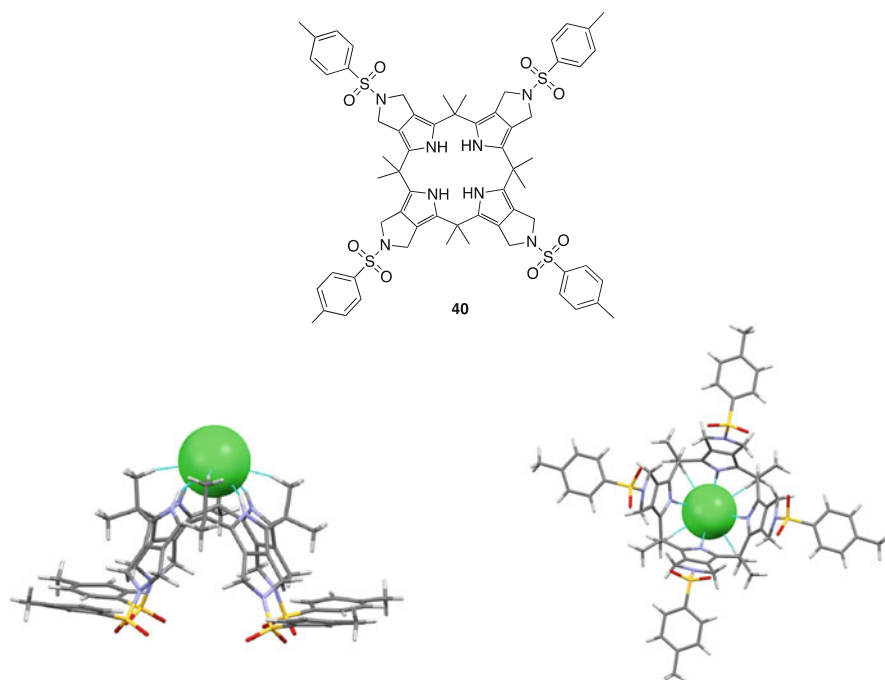








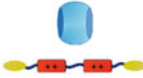
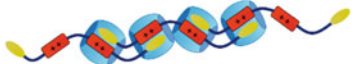
**Fig. 12.26** Structure of the *N*-tosylpyrrolidine calix[4]pyrrole **40** (top) and two views of the single crystal structure of its TBA complex, [**40**•TBACl]. The TBA cation sitting in the cavity of **40** was disordered and not shown. These X-ray figures were reproduced using data downloaded from the Cambridge Crystallographic Data Centre

TBA cation deep within the cavity of **40** is thought to reflect the co-complexation of the chloride anion by the –NH pyrrolic groups, which results in the formation of a tighter ion pair. The presumably stabilizing interactions observed in the solid state were preserved in solution as evidenced by  $^1\text{H}$  NMR spectroscopic analyses carried out in  $\text{CDCl}_3$  [81].

## 12.8 Self-Assembled Materials

Supramolecular polymers or oligomers are a class of materials that are attractive due to their inherent dynamic nature and the fact that they can generally be prepared easily via self-assembly. These macromolecules are stabilized via non-covalent interactions that allow them to sense their surrounding environment in such a way that stimuli-induced reversible assembly and disassembly may often be triggered. In nature, there are several examples of supramolecular oligomers, which can undergo stimuli-induced assembly and disassembly [82]. This responsive behavior is used to alter their physical properties depending on the external environment. One goal of supramolecular chemists in recent years has been to mimic this essential function, while creating systems that have no precedent in nature. In this section, we will discuss synthetic systems based on calix[4]pyrrole and its derivatives.

There are several types of synthetic supramolecular polymers derived from different types of monomeric units (cf. Fig. 12.27). In the literature, there are few examples of hetero-complementary AA/BB type monomers that aggregate into supramolecular polymers [83].

Type	Monomer	Supramolecular polymers
AB		
AA/BB		
Host/BB		
Host/ABBA		

**Fig. 12.27** Representative types of host-guest monomers and their corresponding supramolecular polymers. (Adapted from *Chem. Rev.* **2015**, *115*, 7196–7239)

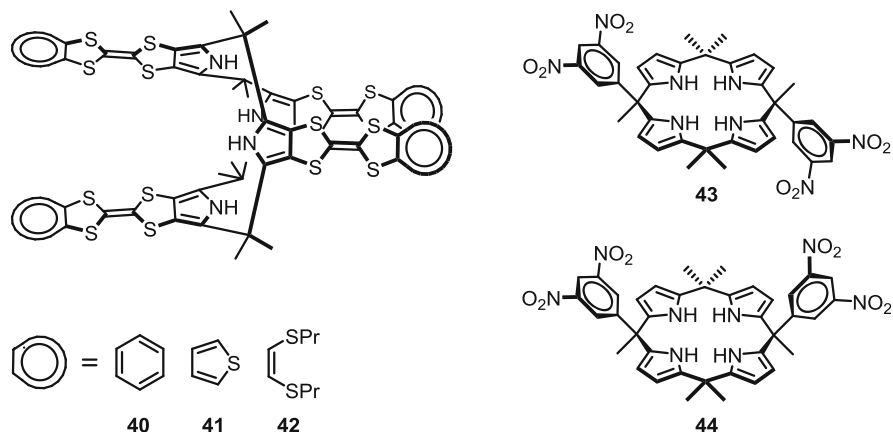


**Fig. 12.28** Chemical structures of TTF-C4P monomers **40–42** (hosts) and DNP-C4P monomers **43** and **44** (guests)

Calix[4]pyrroles bearing fused tetrathiafulvalene (TTF) subunits, abbreviated as TTF-C4Ps, have been extensively exploited over the last decade as receptors for electron-deficient substrates. In their native 1,3-alternate conformations, they act as receptors for planar electron-deficient, hydrogen bond-acceptor guests [84]. In the presence of strongly bound anions, TTF-C4Ps undergo a conformational change to the so-called cone conformation in analogy to what is seen for OMCP. This anion-bound conformation provides a larger cavity that may be used for the recognition of  $C_{60}/C_{70}$  both in solution and in the solid state [85]. In both cases, there are two recognition sites that may be exploited, namely two electron-rich clefts in the 1,3-alternate conformation and an electron-rich pocket and an anion recognition site in the cone conformation. This led to the consideration that TTF-C4Ps could be exploited to create self-assembled materials. This potential was first demonstrated in 2011 by Sessler and collaborators [86] who designed ditopic guests consisting of *cis*- and *trans*-bis(3,5-dinitrophenyl)-*meso*-substituted calix[4]pyrroles (DNP-C4Ps). In this study, six different heterocomplementary supramolecular polymers were constructed based on the TTF-C4Ps **40–42** [83] and DNP-C4Ps **43** and **44** (cf. Fig. 12.28) [86, 87]. Solid-state analysis of two of the resulting systems revealed the formation of long needle-like fibers (Fig. 12.30a, c). Single-crystal X-ray analyses provided insight into the binding modes and revealed the formation of 1-dimensional, directionally oriented linear supramolecular polymers (cf. Fig. 12.29b, d). The formation of oligomeric species in organic solution (chloroform) was established on the basis of dynamic light scattering (DLS), as well as NOESY and DOSY  $^1\text{H}$  NMR and absorption-based spectroscopies.

DLS analysis of the supramolecular aggregates based on  $[\mathbf{40}\cdot\mathbf{43}]_n$ ,  $[\mathbf{40}\cdot\mathbf{44}]_n$ ,  $[\mathbf{42}\cdot\mathbf{43}]_n$  and  $[\mathbf{42}\cdot\mathbf{44}]_n$ , at total monomer concentration of 0.6 mM revealed a diversity of size-distributions. In the case of  $[\mathbf{40}\cdot\mathbf{43}]_n$  and  $[\mathbf{40}\cdot\mathbf{44}]_n$ , hydrodynamic radii of 60 nm and 95 nm, respectively, were recorded (cf. Fig. 12.29d). For  $[\mathbf{43}\cdot\mathbf{44}]_n$  and  $[\mathbf{42}\cdot\mathbf{43}]_n$ , hydrodynamic radii were estimated to be 10 nm and 30 nm,

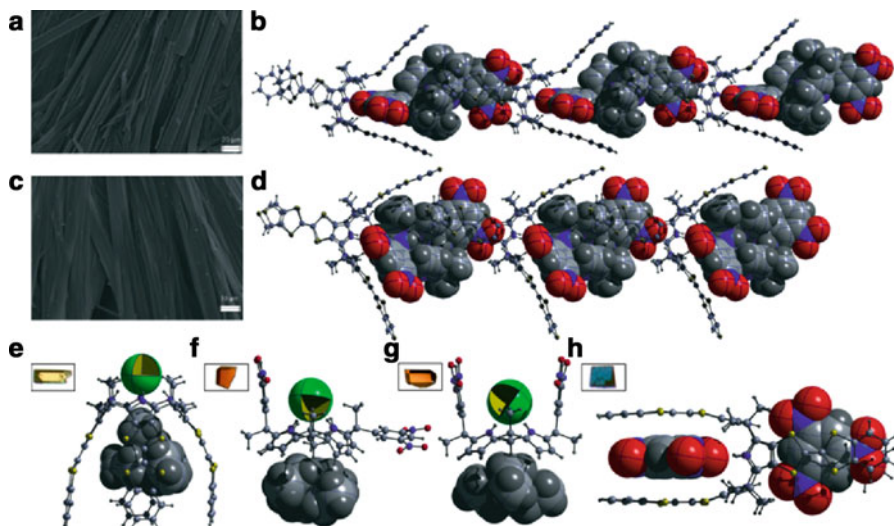


**Fig. 12.29** Solid-state analyses of several of the heterocomplementary supramolecular polymers built up from combinations of TTF-C4P and DNP-C4P, as well as those of several of the guest-bound monomers. (a) SEM image of  $[40\cdot43]_n$ ; (b) crystal structure of  $[40\cdot43]_n$ ; (c) SEM image of  $[41\cdot44]_n$ ; (d) crystal structure of  $[41\cdot45]_n$ ; (e) crystal structure of  $40\cdot\text{TEACl}$ ; (f) crystal structure of  $43\cdot\text{TEACl}$ ; (g) crystal structure of  $44\cdot\text{TEACl}$ , and (h) crystal structure of  $\text{TNB}_2\cdot40$ . Inset boxes show photographs of the corresponding crystals. Note: TNB = 1,3,5-trinitrobenzene (This figure is reproduced with permission from Ref. [86]. Copyright 2011, National Academy of Sciences)

respectively (cf. Fig. 12.29d). The discrepancy in aggregate size was rationalized in terms of two structural differences. First, the *trans*-isomer of DNP-C4P is thought to preclude unfavorable steric clashes between the two neighboring host TTF-C4P units, something that cannot be avoided in the case of the *cis*-isomer. Secondly, the benzo-annulated TTF moieties **40** provides a larger  $\pi$ -surface than that provided by the corresponding thiopropyl system **42**. The latter may also be subject to unfavorable steric effects under conditions of binding to DNP-C4P.

The NOESY  $^1\text{H}$  NMR spectra ( $\text{CDCl}_3$ ) of the supramolecular polymer  $[40\cdot43]_n$  (cf. Fig. 12.30a) are characterized by features consistent with coupling between the *meso*-methyl protons of **40** and the aromatic dinitrophenyl protons of **43**. Such observations are taken as evidence of proximity between the two heterocomplementary monomers under the solution phase conditions of the experiment. Absorption spectroscopic-based continuous variation plots of the systems comprising  $[40\cdot43]_n$  and  $[40\cdot44]_n$  (cf. Fig. 12.29b) revealed maxima at 0.5, a finding consistent with a 1:1 binding stoichiometry. Taken in concert, these spectroscopic analyses lend support to the proposal that a well-defined aggregate is produced in solution upon mixing appropriately chosen DNP-C4P and TTF-C4P monomers.

The presumed supramolecular oligomers were subjected to concentration-dependent absorption spectroscopic analysis in solution. Fits of the extinction coefficients obtained as a function of concentration to an isodesmic model allowed association constants to be derived (cf. Table 12.1). On this basis, it was noted that



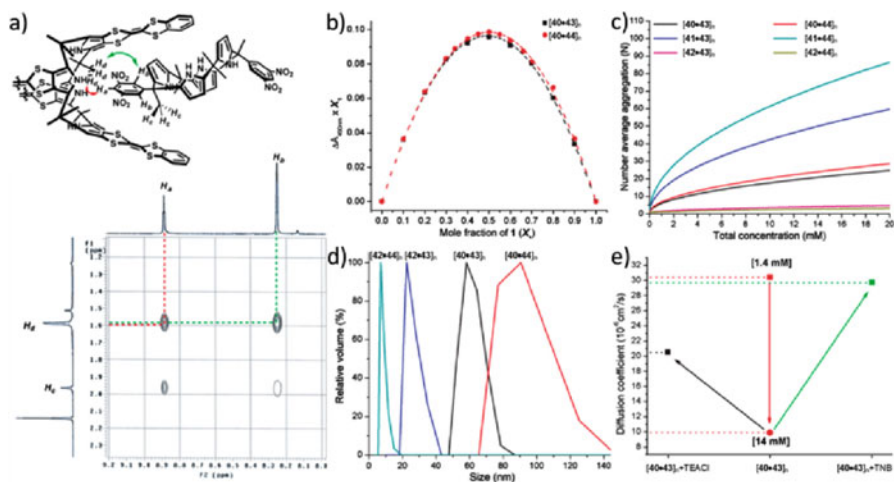


**Fig. 12.30** Solution-based analyses of the heterocomplementary binding interactions between TTF-C4P and DNP-C4P monomers. (a) Expanded region of the 2D NOESY NMR spectrum of  $[40\bullet43]_n$  showing couplings between the *meso*-methyl protons of **40** and the dinitrophenyl protons of **43**; (b) continuous variation Jobs plots of  $[40\bullet43]_n$  (black squares) and  $[40\bullet44]_n$  (red circles); (c) estimated number average aggregation ( $N$ ) as a function of total monomer concentration; (d) dynamic light scattering spectra recorded at a total monomer concentration of 0.6 mM, and (e) change in diffusion coefficients of  $[40\bullet43]_n$  seen upon varying the total monomer concentration (red square) and upon addition of external guest species (TNB and TEACl, black and green squares, respectively), as determined from DOSY-NMR spectroscopic analyses. (This figure is reproduced with permission from Ref. [86]. Copyright 2011, National Academy of Sciences)

**Table 12.1** Association constants for the supramolecular oligomers built up from TTF-C4Ps and DNP-C4Ps, as inferred from fits of concentration-dependent absorption spectroscopic data to an isodesmic model [86]

Supramolecular polymer	Association constant [ $M^{-1}$ ]
$[40\bullet43]_n$	$5.9 \times 10^4$
$[40\bullet44]_n$	$7.9 \times 10^4$
$[41\bullet43]_n$	$3.5 \times 10^5$
$[41\bullet44]_n$	$7.9 \times 10^5$
$[42\bullet43]_n$	$1.8 \times 10^3$
$[42\bullet44]_n$	$6.9 \times 10^2$

using TTF-C4P **41** and DNP-C4P **44** produced the highest degree of polymerization.

When the supramolecular oligomers built up from TTF-C4Ps and DNP-C4Ps were subjected to stimuli, in the form of added substrates such as trinitrobenzene (TNB) or chloride anion, changes in the physical properties were observed. For instance, solutions of the supramolecular aggregates are light green, but change to clear yellow upon addition of tetraethylammonium chloride (TEACl). This color change is reflected in the absorption spectrum of  $[40\bullet43]_n$ , where a weak broad band



centered at  $\lambda = 670$  nm decreases with a subsequent increase in the absorption feature observed near 500 nm upon the addition of TEACl. This change is rationalized in terms of the TEACl inducing a conformational change in both **40** and **43** from the 1,3-alternate to the corresponding cone conformation. When TTF-C4Ps adopt the cone conformation, the stabilizing charge transfer interactions between the electron-rich TTFs and the electron-deficient DNP moieties of the DNP-C4P guests are disrupted. This results in breakup of the oligomeric aggregate. Adding DNP or reducing the concentration also led to breakup of the supramolecular oligomer initially present in solution.

NMR spectroscopic measurements provide support for these conclusions. Specifically, the diffusion coefficient of a mixture of **40** and **43** was first measured at low monomer concentration (total monomer concentration = 1.4 mM). Under these conditions, a relatively large diffusion coefficient is obtained (cf. Fig. 12.30e). On the other hand, at a 10 $\times$  higher monomer concentration (total monomer concentration = 14 mM), a diffusion coefficient of roughly 0.33 of that recorded at low concentration is obtained (cf. Fig. 12.30e). Such a finding is consistent with the formation of larger aggregates ( $[\mathbf{40}\cdot\mathbf{43}]_n$ ) in solution, which are less free to diffuse in solution.

Adding TEACl (14 mM) to  $[\mathbf{40}\cdot\mathbf{43}]_n$  at a total monomer concentration of 14 mM, causes the diffusion coefficient to increase (cf. Fig. 12.30e). This is consistent with disaggregation of the supramolecular polymer and formation of monomeric chloride anion C4P complexes.

The addition of TNB to the same initial solution of  $[\mathbf{40}\cdot\mathbf{43}]_n$  results in a visual color change from light green to dark green. This color change is again reflected in the absorption spectrum where the intensity of the weak broad band centered at  $\lambda = 670$  nm increases considerably. This increase is thought to reflect enhanced charge transfer interactions, presumably as the result of a substrate containing three nitro groups (TNB) displacing one with only two (DNP-C4P). This displacement, which is expected to be a competitive equilibrium process, leads to partial breakup of the oligomeric species  $[\mathbf{40}\cdot\mathbf{43}]_n$ . DOSY NMR spectroscopic analyses revealed that the addition of TNB (28 mM) to  $[\mathbf{40}\cdot\mathbf{43}]_n$  (total monomer concentration = 14 mM) led to a substantial increase in the diffusion coefficient (cf. Fig. 12.30e). This is consistent with breakup of the aggregate and formation of monomeric complexes (i.e.,  $\text{TNB}_2\subset\mathbf{40}$ ).

Overall, this initial report by Sessler and collaborators served to demonstrate that TTF-C4Ps could be used to create heterocomplementary supramolecular oligomers, both in solution and in the solid state, and that stimulus-induced responsive behavior was an inherent feature of the resulting self-assembled systems.

In 2013 Sessler and collaborators reported the formation of heterocomplementary supramolecular aggregates derived from TTF-C4P **40** and two electron-deficient 4-(1-methylpyridinium)-*meso*-functionalized C4Ps, namely **45** and **46** (cf. Fig. 12.31) [88]. These latter positively charged species (referred to as Pyr-CP4s) are able to complex with **40** via different modes depending on the counter anions used and the nature of the added salts, if any. Interaction between **40** and the *tetrakis*-[bis(3,5-trifluoromethyl)-phenyl]borate ( $\text{BArF}^-$ ) salt of

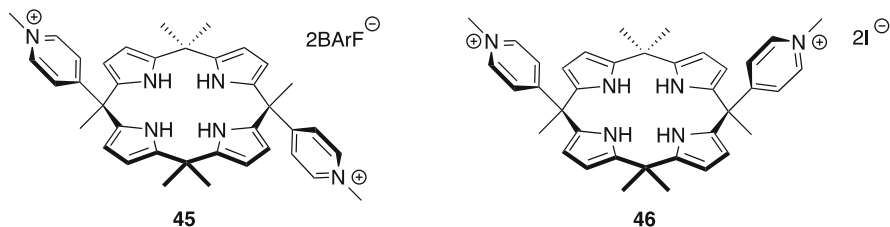


**Fig. 12.31** Chemical structures of the *cis/trans* 4-(1-methylpyridinium)-*meso*-substituted calix[4]pyrroles of **45** and **46**, respectively, and the corresponding counter-anions

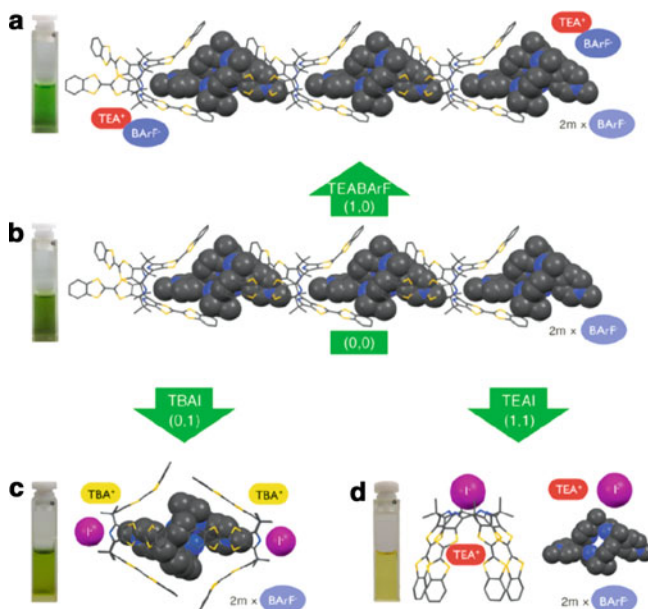


**Fig. 12.32** Schematic representation of the three limiting equilibrium states produced from **40** and **46** seen upon treatment with appropriate ions. (Reprinted with permission from Kim, D. S.; Lynch, V. M.; Park, J. S.; Sessler, J. L. Three Distinct Equilibrium States via Self-Assembly: Simple Access to a Supramolecular Ion-Controlled NAND Logic Gate. *J. Am. Chem. Soc.* **2013**, *135*, 14889–14894 [88]. Copyright 2013 American Chemical Society)

Pyr-C4P **45** in chloroform results in the formation of a linear alternating supramolecular oligomer (cf. Fig. 12.32b). A corresponding color-change from yellow to green is observed, a change reflected in the formation of a CT band at 650 nm. This color change was not observed when **45** was mixed with TTF. Therefore, on this basis it was inferred that the electron-deficient positively charged pyridinium

moieties of **45** interact with the electron-rich TTF arms of **40** in the 1,3-alternate conformation to form a stabilized complex.

Solution phase studies of the putative  $[\mathbf{40}\cdot\mathbf{45}]_n$  complex carried out in  $\text{CDCl}_3$  revealed NOESY coupling interactions between the aromatic benzo-TTF-protons of **40** and the *meso*-methyl protons of **45**. DOSY-NMR spectra of  $[\mathbf{40}\cdot\mathbf{45}]_n$  recorded at varying total monomer concentrations revealed a non-linear decrease in diffusion coefficient with increasing total monomer concentration. This is consistent with the concentration-dependent behavior typically observed for supramolecular polymers.

Absorption spectroscopic analyses were used to determine that the complex stoichiometry of  $[\mathbf{40}\cdot\mathbf{45}]_n$  was 1:1 and to probe the concentration-dependent behavior. Applying an isodesmic binding isotherm, a complexation constant of  $1.1 \times 10^5 \text{ M}^{-1}$  could be derived. Translating the complexation constant into a number average degree of polymerization ( $\text{DP}_N$ ) yielded an average oligomer size of  $\sim 7$  at a total monomer concentration of 1 mM. The average oligomer size increased to  $\sim 23$  when the total monomer concentration was 10 mM.

This study was supported by solid-state analyses in the form of single-crystal X-ray analyses (cf. Fig. 12.32). The counter anion of **45** is sterically bulky and unable to bind to TTF-C4P **40** strongly enough to induce a conversion from the 1,3-alternate conformation to the corresponding cone conformation. Therefore, there is no competition between **45** and its counteranion for **40**.  $\text{TEA}^+$  is well-known [85, 89] to occupy the cavity of the cone, however the complexation is too weak to induce a conformational change. Consequently, when the  $\text{TEA}^+$  salt of  $\text{BArF}^-$  ( $\text{TEABArF}$ ) is added to a  $\text{CHCl}_3$  solution of  $[\mathbf{40}\cdot\mathbf{45}]_n$ , it does not induce disaggregation. Conversely, the addition of the TEA-salt of  $\text{I}^-$  ( $\text{TEAI}$ ) results in a conformational change of **40** to the cone conformation wherein the  $\text{I}^-$  anion is bound to the pyrrole NH protons. The  $\text{TEA}^+$  cations are bound inside the cavity of the calix[4]pyrrole cone (cf. Fig. 12.32d). Remarkably, when TBAI is added to a solution of  $[\mathbf{40}\cdot\mathbf{45}]_n$ , a conformational change to the cone conformation is induced for **40** and the  $\text{I}^-$  anions are again bound to the NH protons. However, the pyridinium moieties of **45** occupy the cavity in preference to the relatively bulky  $\text{TBA}^+$  cations. The result is a capsule-like 2:1 complex (cf. Fig. 12.32c).

Overall, mixtures of **40** and **45** define a system that is characterized by three limiting equilibrium states that may be accessed as a function of four chemical scenarios depending on the nature of the external stimuli. Absorption spectroscopic analysis of the four scenarios (cf. Fig. 12.33a) shows varying degrees of CT band absorption intensities in the 550–800 nm spectral region. Analyzing the absorbance at 690 nm gives almost equal absorption intensities for  $[\mathbf{40}\cdot\mathbf{45}]_n$ ,  $[\mathbf{40}\cdot\mathbf{45}]_n + \text{TEABArF}$  and  $[\mathbf{40}\cdot\mathbf{45}]_n + \text{TBAI}$ . For the mixture consisting of  $[\mathbf{40}\cdot\mathbf{45}]_n + \text{TEAI}$ , the lack of strong CT interactions yields a low absorbance at 690 nm. The net result is a chemical system that displays NAND logic gate (cf. Fig. 12.33b). Specifically, only the combination of  $[\mathbf{40}\cdot\mathbf{45}]_n$  and TEAI produces an “off” or “0” output. Under all other test conditions, including the use of test salts other than TEAI, the output is “1” or “on”.

Building on the studies described above, [86, 88] in 2014 the Sessler and Jeppesen groups reported a study wherein the sterically rigid DNP-C4Ps **43** and

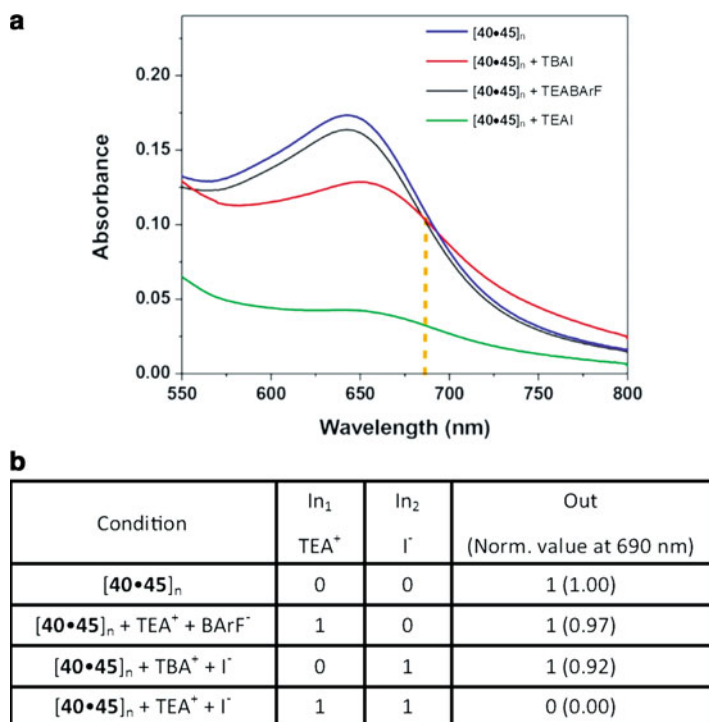
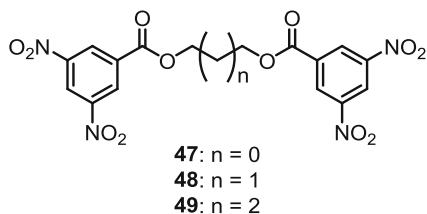


**Fig. 12.33** Logic operations that may be generated using mixtures of **40** and **45**. **(a)** CT response of the self-assembled NAND gate  $[40\cdot45]_n$  seen when the iodide anion ( $I^-$ ) and the tetraethylammonium cation ( $TEA^+$ ) are added as inputs. **(b)** Truth table. Note that both  $I^-$  and  $TEA^+$  are required to produce a “0” output. (Reproduced with permission from Kim, D. S.; Lynch, V. M.; Park, J. S.; Sessler, J. L. Three Distinct Equilibrium States via Self-Assembly: Simple Access to a Supramolecular Ion-Controlled NAND Logic Gate. *J. Am. Chem. Soc.* **2013**, *135*, 14889–14894 [88]. Copyright 2013 American Chemical Society)

**Fig. 12.34** Chemical structures of the flexible *bis*-3,5-dinitrophenyl esters **47–49**



**44** were replaced by a set of flexible *bis*-3,5-dinitrophenyl esters of varying length **47–49** (cf. Fig. 12.34) [90]. This work was undertaken so as to identify the factors that control self-assembly in calix[4]pyrrole-based systems.

Initial evidence of supramolecular self-assembly came from absorption spectroscopic analysis of **42** and **47**. The individual monomers did not show features over the 550–900 nm spectral region (cf. Fig. 12.35a). However, an equimolar mixture of

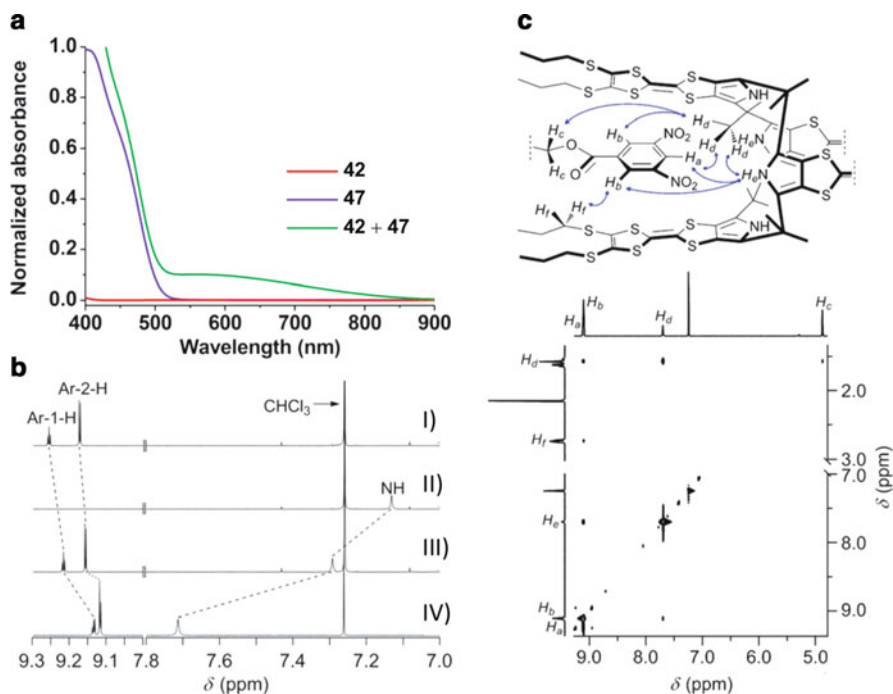


**Fig. 12.35** Solution-based analyses of the supramolecular oligomeric system  $[42\cdot 47]_n$ . (a) UV-vis-NIR absorption spectra of **42**, **47**, and **42 + 47** recorded in chloroform at 298 K. (b) Partial  $^1\text{H}$  NMR spectra (600 MHz, 298 K) of I) **42** (0.7 mM), II) **42** (0.7 mM), III) **42 + 47** (0.7 mM of **42** and **47**, respectively) and IV) **42 + 47** (7.0 mM in both **42** and **47**) all in  $\text{CDCl}_3$ . c 2D NOESY NMR spectroscopic analysis of a mixture of **42** (7 mM) and **47** (7 mM) in  $\text{CDCl}_3$ . (Reproduced from Bähring, S.; Kim, D. S.; Duedal, T.; Lynch, V. M.; Nielsen, K. A.; Jeppesen, J. O.; Sessler, J. L. Use of solvent to regulate the degree of polymerisation in weakly associated supramolecular oligomers. Reprinted from *Chem. Commun.* **2014**, 50, 5497–5499 [90], with the permission from the Royal Society of Chemistry)

**42** and **47** displays a CT absorption band centered at  $\lambda = 566$  nm that extends out to 900 nm (cf. Fig. 12.35a).  $^1\text{H}$  NMR spectral analyses of the putative supramolecular self-assembly process provided support for the expected concentration-dependent behavior characteristic of a supramolecular oligomer. Specifically, the aromatic NH proton signals of **42** shift to lower field (from 7.13 to 7.29 ppm) when 1 equivalent of **47** was added to a 0.7 mM  $\text{CDCl}_3$  solution of **42** (cf. Fig. 12.35b). When the total monomer concentration was increased to 14 mM (7 mM in each monomer), the NH protons were further shifted downfield to 7.70 ppm (cf. Fig. 12.35b). The aromatic protons of **47** underwent shift upon exposure to **42** (cf. Fig. 12.35b). This is explained in terms of the pyrrolic NH protons interacting with the hydrogen bond acceptor  $\text{NO}_2$ -groups of **47** causing a shift to lower field. However, the aromatic protons become shielded within the cleft formed by the TTF subunits in the 1,3-alternate conformation of **42**, thus undergoing a shift to higher field.

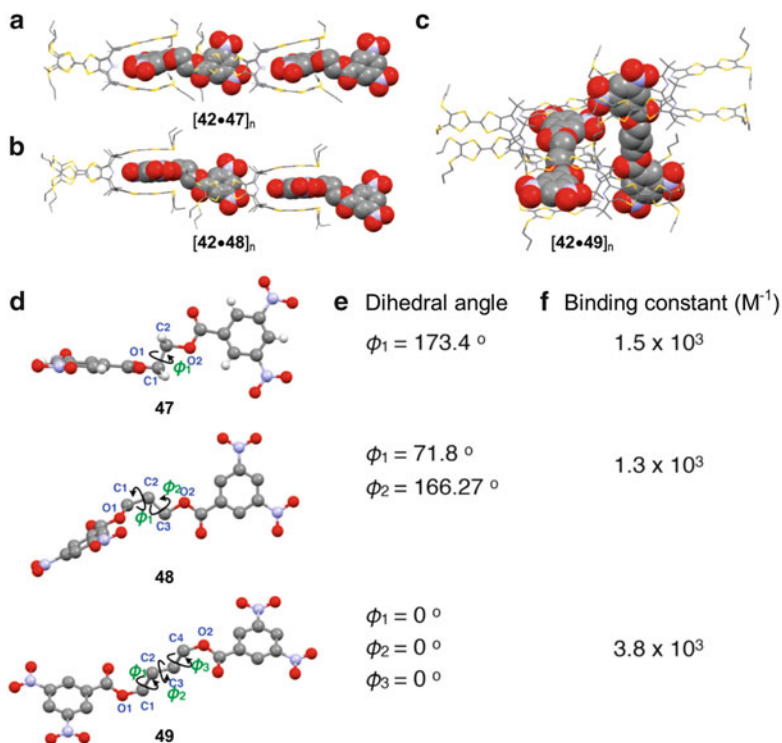
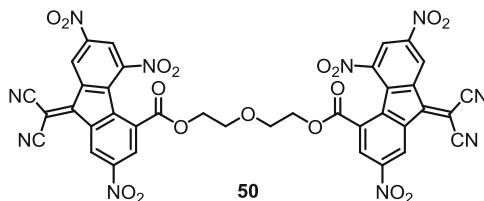


**Fig. 12.36** Solid-state analyses of the supramolecular oligomeric systems  $[42\cdot47]_n$ ,  $[42\cdot48]_n$ , and  $[42\cdot49]_n$ . (a)–(c) Single crystal X-ray diffraction structures of  $[42\cdot47]_n$ ,  $[42\cdot48]_n$ , and  $[42\cdot49]_n$ . (d), (e) Dihedral angles for the linkers present in monomers **47**–**49** as deduced from the solid state structural parameters. (f) Binding constants calculated from dilution-based UV vis-NIR spectroscopic titrations carried out in chloroform (Reproduced from Bähring, S.; Kim, D. S.; Duedal, T.; Lynch, V. M.; Nielsen, K. A.; Jeppesen, J. O.; Sessler, J. L. Use of solvent to regulate the degree of polymerisation in weakly associated supramolecular oligomers. Reprinted from *Chem. Commun.* **2014**, *50*, 5497–5499 [90], with the permission from the Royal Society of Chemistry)

2D NOESY NMR spectral analyses (cf. Fig. 12.35c) revealed cross peaks between the aromatic DNP-protons of **47** and the *meso*-methyl protons of **42**, as well as coupling between the pyrrole NH protons of **42** and the 4-H proton of the aromatic DNP moiety of **47**. Such findings are consistent with the formation of a supramolecular oligomer in solution.

Concentration-dependent studies of the aggregates formed between **42** and each of the three DNP monomers were carried out using absorption spectroscopy. The data were then fit to an isodesmic model as above. The complexation constants derived from these analyses (cf. Fig. 12.36f) revealed association constants for the interaction with **42** in the order  $49 > 47 > 48$ . This led to the suggestion that the length of the linker between the DNP moieties plays a role in modulating the binding events; however, it does not fully explain these findings. More complex

**Fig. 12.37** Chemical structure of TNDCF **50**



features, such as the ability of the linkers to adopt conformations favorable for binding or steric effects may be important. Support for this latter supposition came from solid state structural analyses.

Diffraction grade single crystals were obtained via the slow-diffusion of *n*-pentane into  $\text{CH}_2\text{Cl}_2$  or  $\text{CHCl}_3$  solutions of  $[\mathbf{42}\cdot\mathbf{47}]_n$ ,  $[\mathbf{42}\cdot\mathbf{48}]_n$  and  $[\mathbf{42}\cdot\mathbf{49}]_n$ . The solid-state structures (cf. Fig. 12.36a–c) revealed that 1D alternate polymers are formed between **42** and both **47** and **48**, whereas with **49** a twisted linear supramolecular polymer is found. Analysis of the conformational arrangements in the aggregates formed from the DNP monomers **47–49** revealed a correlation between the solution phase complexation strength and both the inferred steric hindrance of interaction with **42** and the dihedral angles within the DNP monomer linker chains (cf. Fig. 12.36e).

Further solvent-dependent studies were carried out on the supramolecular complex of  $[\mathbf{42}\cdot\mathbf{47}]_n$ . Here, variable temperature absorption spectroscopic analyses in 1,2-dichloroethane (DCE, total monomer concentration = 0.40 mM) and methylcyclohexane (MCH, total monomer concentration = 0.10 mM) in conjunction with isodesmic analyses were used to estimate the binding interactions between the constituent monomers. At 293 K these were calculated to be  $3.9 \times 10^2 \text{ M}^{-1}$  and  $4.8 \times 10^5 \text{ M}^{-1}$  for DCE and MCH, respectively. The higher affinity seen in MCH was ascribed to its relative lower polarity and enhanced ability to promote hydrogen bonding interactions.

The desire to create additional TTF-C4P-based stimuli-responsive supramolecular oligomers has led to the design of new ditopic guest monomers. Recently, the groups of Jeppesen, Sastre-Santos, and Sessler have reported a supramolecular oligomer based on TTF-C4P **42** and a ditopic guest based on the 2,5,7-trinitrodicyanomethylene-fluorene [**91**] moiety, namely a glycol diester-linked *bis*-2,5,7-trinitrodicyanomethylene-fluorene-4-carboxylate (TNDCF) monomer **50** (cf. Fig. 12.37) [**92**].

The monomeric subunits in **50**, esters of 2,5,7-trinitrodicyanomethylene-fluorene-4-carboxylate, has previously been used to create complexes with TTF-C4P **42** [**91**]. This led to the consideration that ditopic systems, such as **50**, that incorporates an adequate glycol-linker between the two moieties would promote the formation of supramolecular oligomers when exposed to **42**. Initial evidence of a supramolecular oligomer formation came from  $^1\text{H}$  NMR spectroscopic studies (cf. Fig. 12.38a). As expected based on the previous studies described above, the proton resonances of the aromatic TNDCF moiety **50** were shifted upfield, while the NH proton resonances of **42** were shifted to lower field.



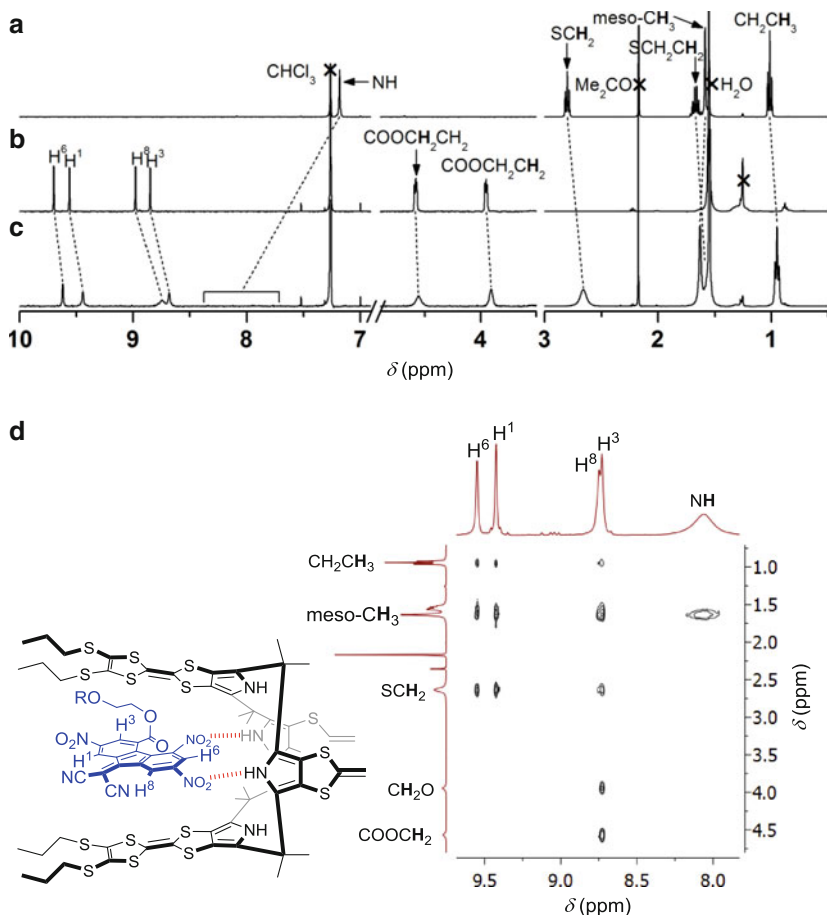


**Fig. 12.38**  $^1\text{H}$  NMR spectroscopic analyses of **42** and **50** carried in  $\text{CDCl}_3$  at 298 K. (a) Partial  $^1\text{H}$  NMR spectrum of **42** (1 mM), (b) Partial  $^1\text{H}$  NMR spectrum of **50** (<1 mM), (c) Partial  $^1\text{H}$  NMR spectrum of the proposed supramolecular aggregate  $(\mathbf{42}\cdot\mathbf{50})_n$  produced from an equimolar mixture of **42** and **50** (both 1 mM). The spectral regions between 3 and 3.5 ppm, as well as between 4.9 and 6.9 ppm, contain no signals and are not shown. Note: The intensity scales for the two spectral regions displayed in this figure have been adjusted for clarity. (d) Expanded view of the 2D NOESY NMR spectrum of a mixture of TTF-C4P **42** (7 mM) with TNDCF **50** (7 mM), showing the NOE interactions between the aromatic protons of **50** and the *meso*- $\text{CH}_3$  and  $\text{SCH}_2\text{CH}_2\text{CH}_3$  protons of **42** in the aliphatic region. (This figure was reproduced with permission from Bähring, S.; Martín-Gomis, L.; Olsen, G.; Nielsen, K. A.; Kim, D. S.; Duedal, T.; Sastre-Santos, Á.; Jeppesen, J. O.; Sessler, J. L. Design and Sensing Properties of a Self-Assembled Supramolecular Oligomer. Reprinted from *Chem. Eur. J.* **2016**, *22*, 1958–1967 [92]. Copyright 2016, Chem. Soc. Europe)

Increased broadening of the proton resonances ascribed to both **42** and **50** was also observed. 2D NOESY NMR spectroscopic analyses of equimolar mixtures of **42** and **50** revealed evidence of through-space coupling between the aromatic protons of **50** and the *meso*-methyl and thiopropyl protons of **42** (cf. Fig. 12.38d). Density



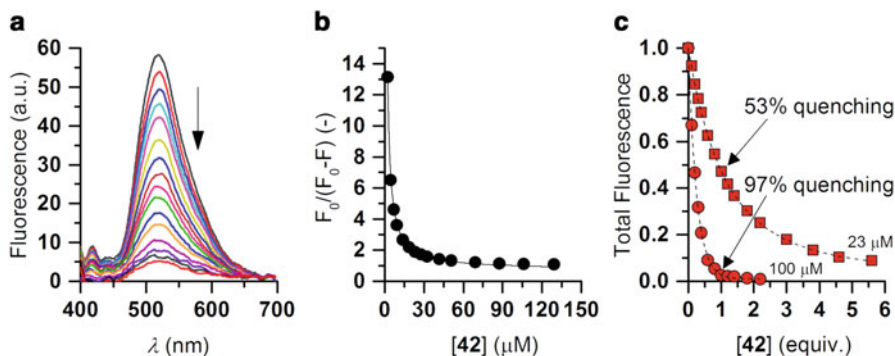


**Fig. 12.39** Fluorescence spectroscopic-based studies of the interaction between **42** and **50**. (a) Fluorescence emission spectra ( $\text{CH}_2\text{ClCH}_2\text{Cl}$ , 293 K,  $\lambda_{\text{ex}} = 374$  nm) of TNDCF **50** ( $23 \mu\text{M}$ ) recorded upon titrating with increasing quantities of **42** (0–5.6 equiv.). (b) Benesi-Hildebrand plot of the fluorescence quenching observed at 520 nm during the course of the titration shown in (a). Panel (c) shows the relative fluorescence of **50** ( $23 \mu\text{M}$  and  $100 \mu\text{M}$ ) recorded at 520 nm upon treating with increasing equivalents of **42**. (This figure was reproduced with permission from Bähring, S.; Martín-Gomis, L.; Olsen, G.; Nielsen, K. A.; Kim, D. S.; Duedal, T.; Sastre-Santos, Á.; Jeppesen, J. O.; Sessler, J. L. *Design and Sensing Properties of a Self-Assembled Supramolecular Oligomer*. Reprinted from *Chem. Eur. J.* **2016**, *22*, 1958–1967 [92]. Copyright 2016, Chem. Soc. Europe)

functional theory (DFT) calculations were performed and supported the proposed formation of supramolecular oligomers.

Solution-based analyses of the supramolecular complexation process were carried out by monitoring changes in the absorption spectral features as a function of concentration and temperature. Both methods gave data that could be fit to an isodesmic self-assembly model. The complexation constants derived in this way for the concentration- and temperature dependent analyses are  $1.76 \times 10^4 \text{ M}^{-1}$  (in DCE at 298 K) and  $5.6 \times 10^3 \text{ M}^{-1}$  (in DCE at 293 K and  $C_T = 125 \mu\text{M}$ ), respectively.

A salient feature of the TNDCF monomer **50** is its fluorescence. When excited at  $\lambda = 308$  nm an emission band centered around 520 nm is observed (cf. Fig. 12.39a). The fluorescence emission of **50** is quenched upon the addition of **42**. For instance, the fluorescence emission intensity of a  $23 \mu\text{M}$  solution of **50** in  $\text{CH}_2\text{ClCH}_2\text{Cl}$  is quenched by 53 % when 1 equivalent of **42** is added (cf. Fig. 12.39c). Likewise, the fluorescence emission of **50** is quenched by 97 % when 1 equivalent of **42** is added to a solution of **50** at  $100 \mu\text{M}$  (cf. Fig. 12.39c). The quenching mechanism is assumed to reflect charge transfer interactions, as well as possibly competitive photon absorption by **42**. Analyzing the fluorescence quenching (cf. Fig. 12.39b) by the Benesi-Hildebrand equation gave a complexation constant of  $2.6 \times 10^4 \text{ M}^{-1}$  [93].

The supramolecular aggregate  $(\mathbf{42} \cdot \mathbf{50})_n$  proved chemoresponsive to external stimuli, including both TNB and TEACl (cf. Fig. 12.40) as proved true in the case of previous systems [86, 88]. However, in contrast to the earlier systems, the fluorescence emission of **50** could be used to evaluate the degree of aggregation at low concentrations. In the case of TNB, the addition of TNB to a solution of

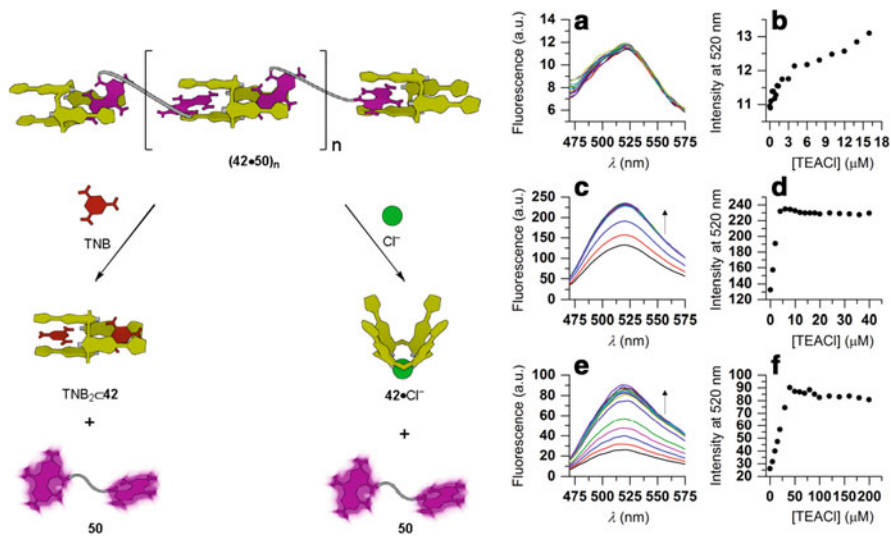


**Fig. 12.40** Graphical representation of the proposed disaggregation of the supramolecular oligomer  $(42\cdot50)_n$  and release of a fluorescent monomer induced by TNB (*left*) or chloride ion (*right*). (a)–(f) Fluorescence spectroscopic study (298 K,  $\text{CH}_2\text{ClCH}_2\text{Cl}$ ,  $\lambda_{\text{ex}} = 308$  nm) of the supramolecular aggregate  $(42\cdot50)_n$  in the presence of TEACl. (a) Fluorescence emission spectra of the supramolecular ensemble  $(42\cdot50)_n$  (4.0  $\mu\text{M}$ ) recorded at differing concentrations of TEACl (0–16  $\mu\text{M}$ ). (b) Fluorescence intensity of the supramolecular oligomer  $(42\cdot50)_n$  (4.0  $\mu\text{M}$ ) recorded at 520 nm vs. the concentration of TEACl (0–16  $\mu\text{M}$ ), (c) Fluorescence emission spectra of the supramolecular aggregate  $(42\cdot50)_n$  (40  $\mu\text{M}$ ) recorded in the presence of increasing concentrations of TEACl (0–40  $\mu\text{M}$ ). (d) Fluorescence intensity at 520 nm of the supramolecular ensemble  $(42\cdot50)_n$  (40  $\mu\text{M}$ ) vs. the concentration of TEACl (0–40  $\mu\text{M}$ ). (e) Fluorescence emission spectra of the supramolecular ensemble  $(42\cdot50)_n$  (200  $\mu\text{M}$ ) recorded in the presence of increasing concentrations of TEACl (0–200  $\mu\text{M}$ ). (f) Fluorescence intensity at 520 nm of the supramolecular ensemble  $(42\cdot50)_n$  (200  $\mu\text{M}$ ) plotted vs. the concentration of TEACl (0–200  $\mu\text{M}$ ). (This figure was reproduced with permission from Bähring, S.; Martín-Gomis, L.; Olsen, G.; Nielsen, K. A.; Kim, D. S.; Duedal, T.; Sastre-Santos, Á.; Jeppesen, J. O.; Sessler, J. L. Design and Sensing Properties of a Self-Assembled Supramolecular Oligomer. Reprinted from *Chem. Eur. J.* **2016**, *22*, 1958–1967 [92]. Copyright 2016, Chem. Soc. Europe)

$(42\cdot50)_n$  at three different total concentrations (4.0  $\mu\text{M}$ , 40  $\mu\text{M}$  and 200  $\mu\text{M}$ ) resulted in three very different scenarios. At low concentrations (e.g., 4.0  $\mu\text{M}$ ) the degree of association between the monomers is small. Thus, the addition of TNB does not induce disaggregation of  $(42\cdot50)_n$ . Nor, does it lead to a notable increase in fluorescence intensity. Instead, the fluorescence remains unaffected. When the concentration of  $(42\cdot50)_n$  is increased to 40  $\mu\text{M}$ , a 35 % increase in the fluorescence emission intensity is seen upon exposure to 2 equivalents of TNB (4 equivalents relative to  $42$ ). Increasing the TNB concentration does not affect the fluorescence output further. At a total  $(42\cdot50)_n$  concentration of 200  $\mu\text{M}$ , the addition of TNB results in a gradual increase in the fluorescence intensity with an 80 % relative increase being seen in the presence of 25 equivalents of TNB. This increase is

rationalized in terms of a competition between TNB and **50**, which leads to breakup of  $(\mathbf{42}\cdot\mathbf{50})_n$  and release of the fluorescent TNDCF monomer.

A similar experiment carried out using TEACl (cf. Fig. 12.40a–f) under otherwise identical experimental conditions revealed a slight fluorescence increase at a total (**42** + **50**; 1:1 ratio) concentration of 4.0  $\mu\text{M}$  upon the addition of TEACl. Increasing the total concentration of **42** + **50** to 40  $\mu\text{M}$  resulted in an abrupt fluorescence increase upon exposure to TEACl, with a relative fluorescence increase of 74 % seen in the presence of 0.1 molar equivalent of TEACl. At total concentration  $(\mathbf{42}\cdot\mathbf{50})_n$  of 200  $\mu\text{M}$ , addition of TEACl results in a maximum relative fluorescence increase of 245 %.

The differences in fluorescence response seen upon the addition of either TNB or TEACl reflect in part the fact that the underlying mechanisms of interaction are different. Whereas complexation of TNB involves the 1,3-alternate conformation, that of TEACl occurs in the cone conformation. As a result, different affinity constants are operational and the degree of disaggregation for the two external stimuli are different. Ultimately, this type of differential response could prove useful in the construction of sensors with increased sensitivity and selectivity.

A number of studies of the self-association features of TTF-C4P-based systems are ongoing presently in the Sessler and Jeppesen laboratories. The interested reader is advised to consult the current literature for updates that may arise as the result of these efforts. Based on what has been reported to date, it is clear that functionalized calixpyrroles have a role to play in the design and synthesis of stimulus-responsive supramolecular constructs, including capsules and self-assembled polymers.

**Acknowledgement** Support for this work was provided by the Office of Basic Energy Sciences, U.S. Department of Energy (DOE) (grant number DE-FG02-01ER15186 to J.L.S.) and the National Science Foundation (grant CHE CHE-1402004 to J.L.S.).

## References

1. a) Shriver, D. F.; Biallas, M. J. *J. Am. Chem. Soc.* **1967**, *89*, 1078–1081. b) Park, C. H.; Simmons, H. E. *J. Am. Chem. Soc.* **1968**, *90*, 2431–2432. c) Graf, E.; Lehn, J.-M. *J. Am. Chem. Soc.* **1976**, *98*, 6403–6405.
2. Baeyer, A. *Ber. Dtsch. Chem. Ges.* **1886**, *19*, 2184–2185.
3. Chelintzev, V. V.; Tronov, B. V. *J. Russ. Phys. Chem. Soc.* **1916**, *48*, 105–155.
4. a) Benech, J.-M.; Bonomo, L.; Solari, E.; Scopelliti, R. Floriani, C. *Angew. Chem. Int. Ed.* **1999**, *38*, 1957–1959. b) Floriani, C. and Floriani-Mono, R. In *The Porphyrin Handbook*, Vol. 3, Eds.: Kadish, K.; Smith, M.; Guillard, R.; Academic Press, San Diego, 2000, Chapter 24, pp. 385–420.
5. Gale, P. A.; Sessler, J. L.; Král, V.; Lynch, V. *J. Am. Chem. Soc.* **1996**, *118*, 5140–5141.
6. Gale, P. A.; Sessler, J. L.; Král, V. *Chem. Commun.* **1998**, 1–8.
7. Mamarashvili, G. M.; Mamardashvili, N. Z.; Koifman, O. I. *Chem. Rev.* **2015**, *84*, 275–287.
8. a) Lee, C.-H., Miyaji, H.; Toon, D.-W.; Sessler, J. L. *Chem. Commun.* **2008**, 24–34. b) Lee, C.-H.; Na, H.-K.; Yoon, D.-W.; Won, D.-H.; Cho, W.-S., Lynch, V. M.; Shevchuk, S. V.;

- Sessler, J. L. *J. Am. Chem. Soc.* **2003**, *125*, 7301–7306. c) Miyaji, H.; Kim, H.-K.; Sim, E.-K.; Lee, C.-K.; Cho, W.-S. Sessler, J. L.; Lee, C.-H. *J. Am. Chem. Soc.* **2005**, *127*, 12510–12512.
9. Gale, P. A.; Azenbacher Jr., P.; Sessler, J. L. *Coord. Chem. Rev.* **2001**, *222*, 57–102.
10. Azenbacher Jr., P.; Jursiková, K.; Shriver, J. A.; Miyaji, H.; Lynch, V. M.; Sessler, J. L.; Gale, P. A. *J. Org. Chem.* **2000**, *65*, 7641–7645.
11. Miyaji, H.; Sato, W.; Sessler, J. L.; Lynch, V. M. *Tetrahedron Lett.* **2000**, *41*, 1369–1373.
12. a) Dehaen, W. In *Anion Recognition in Supramolecular Chemistry*; Gale, P. A.; Dehaen, W., Eds.; Springer: New York, NY, 2010; pp. 75–103. b) Bucher, C.; Seidel, D.; Lynch, V.; Král, V.; Sessler, J. L. *Org. Lett.* **2000**, *2*, 3103–3106. c) Sessler, J. L.; Zimmerman, R. S.; Bucher, C.; Král, V.; Andrioletti, B. Calixphyrins. *Pure Appl. Chem.* **2001**, *73*, 1041–1057.
13. Yoon, D. W.; Hwang, H.; Lee, C. H. *Angew. Chem. Int. Ed.* **2002**, *41*, 1751–1759.
14. Lee, C.-H.; Miyaji, H.; Yoon, D.-W., Sessler, J. L. *Chem. Commun.* **2008**, *1*, 24–34.
15. Yoon, D.-W.; Gross, D. E.; Lynch, V. M.; Sessler, J. L.; Hay, B. P.; Lee, C.-H. *Angew. Chem. Int. Ed.* **2008**, *47*, 5038–5042.
16. Park, J.-Y., Skonieczny, K.; Aratani, N.; Osuka, A.; Gryko, D. T.; Lee, C.-H. *Chem. Commun.* **2012**, *122*, 9350–9351.
17. Mahanta, S. P.; Kumar, S. P.; Panda, P. K. *Chem. Commun.* **2011**, *47*, 4496–4498.
18. Samanta, R.; Mahanta, S. P.; Chaudhuri, S.; Panda, P. K.; Narahi, A. *Inorg. Chim. Acta* **2011**, *372*, 281–285.
19. a) Lee, C.-H.; Miyaji, H.; Yoon, D.-W.; Sessler, J. L. *Chem. Commun.* **2008**, 24–34. b) Gale, P. A.; Lee, C.-H. *Top. Heterocycl. Chem.* **2010**, *24*, 39–73.
20. Kim, S. K.; Sessler, J. L. *Chem. Soc. Rev.* **2010**, *39*, 3784–3809.
21. Custelcean, R.; Delmau, L. H.; Moyer, B. A.; Sessler, J. L.; Cho, W.-S.; Gross, D.; Bates, G. W.; Brooks, S. J.; Light, M. E.; Gale, P. A. *Angew. Chem. Int. Ed.* **2005**, *44*, 2537–2542.
22. Sessler, J. L.; Kim, S. K.; Gross, D. E.; Lee, C.-H.; Kim, J. S.; Lynch, V. M. *J. Am. Chem. Soc.* **2008**, *130*, 13162–13166.
23. Kim, S. K.; Lynch, V. M.; Sessler, J. L. *Org. Lett.* **2014**, *16*, 6128–6131.
24. Chang, K.-C.; Minami, T.; Koutnik, P.; Savechenkov, P. Y. Liu, Y.; Azenbacher Jr. P. *J. Am. Chem. Soc.* **2014**, *136*, 1520–1525.
25. Moyer, B. A.; Bonnesen, P. V. In *Supramolecular Chemistry of Anions*; Bianchi A.; Bowman-James K.; and García-España E., Eds.; Wiley-VCH: New York, NY, 1997; pp. 4–9.
26. Mahanta, S. P.; Panda, P. K. *Org. Biomol. Chem.* **2014**, *12*, 278–285.
27. Gale, P. A.; Caltagirone, C. *Chem. Soc. Rev.* **2015**, *44*, 4212–4227.
28. Lv, Y.; Xu, J.; Guo, Y.; Shao, S. *J. Inclusion Phenom. Macrocyclic Chem.* **2012**, *72*, 95–101.
29. Gotor, R.; Costero, A. M.; Gaviña, P. Gil, S.; Parra, M. *Eur. J. Org. Chem.* **2013**, 1515–1520.
30. Hong, S.-J.; Lee, C.-H. *Tetrahedron Lett.* **2012**, *53*, 3119–3122.
31. a) Lakowicz, J. R. Fluorophores. In *Principles of Fluorescence Spectroscopy*; 3<sup>rd</sup>. Edition, Springer: Verlag US, 2006; pp. 63–95. b) Demchenko, A. P. *J. Fluoresc.* **2010**, *20*, 1099–1128. c) Hilderbrend, S. S.; Lim, M. H.; Lippard, S. J. In *Advanced Concept in Fluorescence Sensing: Small Molecule Sensing*, Topics in Fluorescence Spectroscopy; Vol. 9; Geddes, C. D.; Lakowicz, J. R., Eds.; Springer: New York, NY, 2005; pp. 163–188.
32. Azenbacher Jr., P.; Liu, Y.; Palacios, M. A.; Minami, T.; Wang, Z.; Nishiyabu, R. *Chem. Eur. J.* **2013**, *19*, 8497–8506.
33. a) Mathews, C. P.; van Hold, K. E. In *Biochemistry*; The Benjamin/Cummings Publishing Company, Inc.: Redwood City, CA, 1990. b) Ronaghi, M. Karamohamed, S.; Petterson, B.; Uhlén, M.; Nyrén, P. *Anal. Biochem.* **1996**, *242*, 84–89. c) Tabary, T.; Ju, L. *J. Immunol. Methods.* **1992**, *156*, 55–60. d) Saenger, W. In *Principles of Nucleic Acid Structure*; Cantor, C. R., Ed.; Springer-Verlag, New York, 1998; pp. 81–88.
34. Xu, S.; He, M.; Yu, H.; Cai, X.; Tan, X.; Lu, B.; Shu, B. *Anal. Biochem.* **2001**, *299*, 188–193.
35. Sokkalingam, P.; Kim, D. S.; Hwang, H.; Sessler, J. L.; Lee, C.-H. *Chem. Sci.* **2012**, *3*, 1819–1824.
36. a) Wiskur, S. L.; Ait-Haddou, H.; Lavigne, J. L.; Anslyn, E. V. *Acc. Chem. Res.* **2001**, *34*, 963–972. b) Nguyen, B. T.; Anslyn, E. V. *Coord. Chem. Rev.* **2006**, *250*, 3118–3127. c) Zhang, T.; Anslyn, E. V. *Org. Lett.* **2007**, *9*, 1627–1629.
37. Phipps, K. *J. Public Health Dent.* **1995**, *55*, 53–56.

38. Vincent, S.; Brouns, M.; Hart, M. J.; Setleman, J. *Proc. Nat. Acad. Sci. (USA)* **1997**, *95*, 2210–2215.
39. Pinkse, M. W. H.; Merk, M.; Averill, B. A. *Biochem.* **1999**, *38*, 9926–9936.
40. Sokkalingam, P.; Yoo, J.; Hwang, H.; Lee, P. H.; Jung, Y. M.; Lee, C.-H. *Eur. J. Org. Chem.* **2011**, 2911–2915.
41. Sokkalingam, P.; Hong, S.-J.; Aydogan, A.; Sessler, J. L.; Lee, C.-H. *Chem. Eur. J.* **2013**, *19*, 5860–5867.
42. Aydogan, A.; Coady, D. J.; Lynch, V. M.; Akar, A. Marquez, M. Bielawski, C.W.; Sessler, J. L. *Chem. Commun.* **2008**, 1455–1457.
43. Aydogan, A.; Coady, D. J.; Kim, S. K.; Akar, A.; Bielawski, C. W.; Marquez, M.; Sessler, J. L. *Angew. Chem. Int. Ed.* **2008**, *120*, 9794–9798.
44. Aydogan, A. *Supramol. Chem.* **2015**, 1–8.
45. Thiapanya, P.; Muangsin, N.; Pulpoka, B. *Org. Lett.* **2012**, *14*, 4050–4053.
46. a) Gloe, K.; Gloe, K.; Wenzel, M.; Lindoy, L. F.; Li, F. In *Ion Exchange and Solvent Extraction Supramolecular Aspects of Solvent Extraction*; Moyer B., Ed.; Ion Exchange and solvent Extraction Series; CRC: Boca Raton, FL, 2014; pp. 1–49. b) Kubik, S. Anion recognition in water. *Chem. Soc. Rev.* **2010**, *39*, 3648–3663. Gloe, K.; Stephan, H.; Grotjahn, M. *Chem. Eng. Technol.* **2003**, *26*, 1107–1117.
47. Busschaert, N.; Caltagirone, C.; Van Rossom, W.; Gale, P. A. *Chem. Rev.* **2015**, *115*, 8038–8155.
48. Wu, J. G.; Zhou, N. F.; Shi, N.; Zhou, W. J.; Gao, H. C.; Xi, G. X. *Prog. Nat. Sci.* **1997**, *7*, 257–264.
49. Friberg, S. E.; Qamheye, K. In *The structure dynamics and equilibrium properties of colloidal systems*; NATO ASI Series C, Vol. 234; Bloor, D. M. and Wyn-Jones, E., Ed; Kluwer Academic, Dordrecht, The Netherlands.
50. Diss, R.; Wipff, G. *Phys. Chem. Chem. Phys.* **2005**, *7*, 264–272.
51. Fourre, P.; Bauter, D.; Lemerle, J. *Anal. Chem.* **1983**, *55*, 662–667.
52. Hofmeister, F. Zur Lehre Von Der Wirkung Der Salze. *Arch. Exp. Pathol. Pharmacol.* **1888**, *24*, 247–260.
53. Levitskaia, T. G.; Maya, L.; Van Berkel, G. J.; Moyer, B. A. *Inorg. Chem.* **2006**, *46*, 261–272. b) Borman, C. J.; Bonnesen, P. V.; Moyer, B. A. *Anal. Chem.* **2012**, *84*, 8214–8221.
54. a) Menon, S. V. G.; Kelkar, V. K.; Manohar, C. *Phys. Rev. A.* **1991**, *43*, 1130–1133. b) Chiarizio, R.; Stepinski, D.; Antonio, M. R. *Sep. Sci. Technol.* **2010**, *45*, 1668–1678.
55. Moyer, B. A.; Sloop, F. V.; Fowler, C. J.; Haverlock, T. J.; Kang, H.-A.; Delmau, L. H.; Bau, D. M.; Hossain, M. A.; Bowman-James, K.; Shriver, J. A.; Bill, N. L.; Gross, D. E.; Marquez, M.; Lynch, V. M.; Sessler, J. L. *Supramol. Chem.* **2010**, *22*, 653–671.
56. Kim, S. K.; Lynch, V. M.; Young, N. J.; Hay, B. P.; Lee, C.-H.; Kim, J. S.; Moyer, B. A.; Sessler, J. L. *J. Am. Chem. Soc.* **2012**, *134*, 20837–20843.
57. a) Kim, S. K.; Vargas-Zúñiga, G. I.; Hay, B. P.; Young, N. J.; Delmau, L. H.; Masselin, C.; Lee, C.-H.; Kim, J. S.; Moyer, B. A.; Lynch, V. M.; Sessler, J. L. *J. Am. Chem. Soc.* **2012**, *134*, 1782–1792. b) Kim, S. K.; Hay, B. P.; Kim, J. S.; Moyer, B. A.; Sessler, J. L. *Chem. Commun.* **2013**, *49*, 2112–2114.
58. Kim, S. K.; Lee, J.; Williams, N. J.; Lynch, V. M.; Hay, B. P.; Moyer, B. A.; Sessler, J. L. *J. Am. Chem. Soc.* **2014**, *136*, 15079–15085.
59. (a) Welsh, M.; Smith, A. E. *Cell* **1993**, *73*, 1251–1254. (b) Simmon, D. B.; Bindra, R. S.; Mansfield, T. A.; Nelson-Williams, C.; Mendonca, E.; Stone, R.; Schuman, S.; Nayir, A.; Alpaya, H.; Bakaloglu, A.; Rodriguez-Soriano, J.; Morales, J. M.; Sanjad, S. A.; Taylor, C. M.; Pliz, D.; Brem, A.; Trachtman, H.; Griswold, W.; Richard, G. A.; John, E.; Lifton, R. P. *Nat. Genet.* **1997**, *17*, 171–178. (c) Loyd, S. E.; Pearce, S. H. S.; Fisher, S. E.; Steinmeyer, K.; Schwappach, B.; Scheinman, S. J.; Harding, B.; Bolino, A.; Devoto, M.; Goodyer, P.; Rigden, S. P. S.; Wrong, O.; Jentsch, T. J.; Craig, I. W.; Thakker, R. V. A. *Nature* **1996**, *379*, 445–449. (d) Moseley, R. H.; Höglund, P.; Wu, G. D.; Silberg, D. G.; Haila, S.; De La Chapelle, A.; Holmberg, C.; Kere, J. *Am. J. Physiol., Gastrointest. Liver Physiol.* **1999**, *276*, G185-G192. (e) Miller, C. *Nature* **2006**, *440*, 484–489.

60. a) Choi, J. Y.; Muallem, D.; Kiselyov, K.; Lee, M. G.; Thomas, P. J.; Muallem, S. *Nature* **2001**, *410*, 94–97. b) Ishiguro, H.; Steward, M. C.; Naruse, S.; Ko, S. B. H.; Goto, H.; Case, R. M.; Kondo, T.; Yamamoto, A. *J Gen Physiol* **2009**, *133*, 315–326.
61. Lodish, H.; Berk, A.; Masudaira, P.; Kaiser, C. A.; Krieger, M.; Scott, M. P.; Zipursky, S. L.; Darnell, J. *Molecular Cell Biology*. 5th ed.; W. H. Freeman and Company: New York, 2003.
62. a) Li Yu, L.; Jiang, X. H. Zhou, Z.; Tsang, L. L.; Yu, M. K.; Chung, Y. W.; Zhang, X. H.; Wang, A. M.; Tang, H.; Chan, H. C. *PLoS ONE* **2011**, *6*, e17322. b) Tsukimoto, M.; Harada, H.; Ikari, A.; Takagi, K. *J. Biol. Chem.* **2005**, *280*, 2653–2658.
63. Wang, H. Z.; Zhang, Y. Q.; Cao, L. W.; Han, H.; Wang, J. X.; Yang, B. F.; Nattel, S.; Wang, Z. G. *Cancer Res* **2002**, *62*, 4843–4848.
64. Arcangeli, A.; Crociani, O.; Lastraioli, E.; Masi, A.; Pillozzi, S.; Bechetti, A. *Curr. Med. Chem.* **2009**, *16*, 66–93.
65. Wintergerst, M. P.; Levitskaia, T. G.; Moyer, B. A.; Sessler, J. L.; Delmau, L. H. *J. Am. Chem. Soc.* **2008**, *130*, 4129–4139.
66. Tong, C. C.; Quesada, R.; Sessler, J. L.; Gale, P. A. *Chem. Commun.* **2008**, *47*, 6321–6323.
67. Gale, P. A.; Tong, C. C.; Haynes, C. J. E.; Adeosun, O.; Gross, D. E.; Karnas, E.; Sedenberg, E. M.; Quesada, R.; Sessler, J. L. *J. Am. Chem. Soc.* **2010**, *132*, 3240–3241.
68. Adriaenssens, L.; Estarellas, C.; Vargas Jentzh, A.; Martinez Bartolome, M.; Matile, S.; Ballester, P. *J. Am. Chem. Soc.* **2013**, *135*, 8324–8330.
69. Park, I.-W.; Yoo, J.; Kim, B.; Adhikari, S.; Kim, S. K.; Yeon, Y.; Gale, P. A.; Lee, C.-H. *Chem.–Eur. J.* **2012**, *18*, 2514–2523.
70. Cafeo, G.; Carbotti, G.; Cuzzola, A.; Fabbri, M.; Ferrini, S.; Kohnke, F. H.; Papanikolaou, G.; Plutino, M. R.; Rosano, C.; White, A. J. P. *J. Am. Chem. Soc.* **2013**, *135*, 2544–2551.
71. a) Moore, S. J.; Fischer, M. G.; Yano, M.; Tong, C. C.; Gale, P. A. *Dalton Trans.* **2011**, *40*, 12017–12020.
72. Ko, S.-K.; Kim, S. K.; Share, A.; Lynch, V. M.; Park, J.; Namkung, W.; Rossom, W. V.; Busschaert, N.; Gale, P. A.; Sessler, J. L.; Shin, I. *Nat. Chem.* **2014**, *6*, 885–892.
73. Ballester, P.; Fujita, M.; Rebek Jr., J. *Chem. Soc. Rev.* **2015**, *44*, 392–393.
74. Kobayashi, K.; Yamanaka, M. *Chem. Soc. Rev.* **2015**, *44*, 449–466.
75. a) Leenders, S. H. A. M.; Gramage-Doria, R.; de Bruin, B.; Reek, J. N. H. *Chem. Soc. Rev.* **2015**, *44*, 433–448. b) Rebilly, J.-N.; Colasson, B.; Bistri, O.; Over, D.; Reinaud, O. *Chem. Soc. Rev.* **2015**, *44*, 467–489.
76. a) Adriaenssens, L.; Ballester, P. *Chem. Soc. Rev.* **2013**, *42*, 3261–3277. b) Kim, D. S.; Sessler, J. L. *Chem Soc. Rev.* **2015**, *44*, 532–546.
77. Jordan, J. H.; Gibb, B. *Chem. Soc. Rev.* **2015**, *44*, 547–585.
78. Ballester, P. *Isr. J. Chem.* **2011**, *51*, 710–724.
79. Sessler, J. L.; Andrievsky, A.; Gale, P. A.; Lynch, V. *Angew. Chem. Int. Ed. Engl.* **1996**, *35*, 1154–1196.
80. Gil-Ramírez, G.; Benet-Buchholz, J.; Escudero-Adán, E. C.; Ballester, P. *J. Am. Chem. Soc.* **2007**, *129*, 3820–3821.
81. a) Kim, S. K.; Gross, D. E.; Cho, D.-G.; Lynch, V. M.; Sessler, J. L. *N. J. Org. Chem.* **2011**, *76*, 1005–1012. b) Kim, S. K.; Sessler, J. L. *Acc. Chem. Res.* **2014**, *47*, 2525–2536.
82. a) Goldstein, J. L.; Brown, M. S. *Nature* **1990**, *343*, 425–430. b) Lehn, J. M. *Angew. Chem. Int. Ed.* **1990**, *29*, 1304–1319. c) Lehn, J.-M. *Angew. Chem.* **1990**, *102*, 1347–1362. d) Cravatt, B. F.; Giang, D. K.; Mayfield, S. P.; Boger, D. L.; Lerner, R. A.; Gilula, N. B. *Nature* **1996**, *384*, 83–87. e) Pawson, T.; Scott, J. D. *Science* **1997**, *278*, 2075–2080. f) Cohen, G. M. *Biochem. J* **1997**, *326*, 1–16. g) Green, D.; Kroemer, G. *Trends Cell Biol.* **1998**, *8*, 267–271. h) Feiters, M. C.; Nolte, R. J. M. *Adv. Supramol. Chem.* **2000**, *6*, 41–156. i) Bertozzi, C. R.; Kiessling, L. L. *Science* **2001**, *291*, 2357–2364.
83. a) Niu, Z.; Huang, F.; Gibson, H. W. *J. Am. Chem. Soc.* **2011**, *133*, 2836–2839. b) Wang, K.-P.; Guo, D.-S.; Zhao, H.-X.; Liu, Y. *Chem. Eur. J.* **2014**, *20*, 4023–4031.

84. a) Nielsen, K. A.; Cho, W. S.; Jeppesen, J. O.; Lynch, V. M.; Becher, J.; Sessler, J. L. *J. Am. Chem. Soc.* **2004**, *126*, 16296–16297. b) Park, J. S.; Le Derf, F.; Bejger, C. M.; Lynch, V. M.; Sessler, J. L.; Nielsen, K. A.; Johnsen, C.; Jeppesen, J. O. *Chem. Eur. J.* **2010**, *16*, 848–854.
85. Davis, C. M.; Lim, J. M.; Larsen, K. R.; Kim, D. S.; Sung, Y. M.; Lyons, D. M.; Lynch, V. M.; Nielsen, K. A.; Jeppesen, J. O.; Kim, D.; Park, J. S.; Sessler, J. L. *J. Am. Chem. Soc.* **2014**, *136*, 10410–10417.
86. Park, J. S.; Yoon, K. Y.; Kim, D. S.; Lynch, V. M.; Bielawski, C. W.; Johnston, K. P.; Sessler, J. L. *Proc. Natl. Acad. Sci. U. S. A.* **2011**, *108*, 20913–20917.
87. Adriaenssens, L.; Estarellas, C.; Vargas Jentzsch, A.; Martinez Belmonte, M.; Matile, S.; Ballester, P. *J. Am. Chem. Soc.* **2013**, *135*, 8324–8330.
88. Kim, D. S.; Lynch, V. M.; Park, J. S.; Sessler, J. L. *J. Am. Chem. Soc.* **2013**, *135*, 14889–14894.
89. Park, J. S.; Karnas, E.; Ohkubo, K.; Chen, P.; Kadish, K. M.; Fukuzumi, S.; Bielawski, C. W.; Hudnall, T. W.; Lynch, V. M.; Sessler, J. L. *Science* **2010**, *329*, 1324–1327.
90. Bähring, S.; Kim, D. S.; Duedal, T.; Lynch, V. M.; Nielsen, K. A.; Jeppesen, J. O.; Sessler, J. L. *Chem. Commun.* **2014**, *50*, 5497–5499.
91. a) Nielsen, K. A.; Sarova, G. H.; Martín-Gomis, L.; Stein, P. C.; Sanguinet, L.; Levillain, E.; Sessler, J. L.; Guldi, D. M.; Sastre-Santos, Á.; Jeppesen, J. O. *J. Am. Chem. Soc.* **2008**, *130*, 460–462. b) Nielsen, K. A.; Martín-Gomis, L.; Sarova, G. H.; Sanguinet, L.; Gross, D. E.; Fernández-Lázaro, F.; Stein, P. C.; Levillain, E.; Sessler, J. L.; Guldi, D. M.; Sastre-Santos, Á.; Jeppesen, J. O. *Tetrahedron* **2008**, *64*, 8449–8463.
92. Bähring, S.; Martín-Gomis, L.; Olsen, G.; Nielsen, K. A.; Kim, D. S.; Duedal, T.; Sastre-Santos, Á.; Jeppesen, J. O.; Sessler, J. L. *Chem. Eur. J.* **2016**, *22*, 1958–1967.
93. Benesi, H. A.; Hildebrand, J. H. A. *J. Am. Chem. Soc.* **1949**, *71*, 2703–2707.

# Chapter 13

## Thiacalixarenes

Nobuhiko Iki

### 13.1 Introduction

#### 13.1.1 *In the Beginning Was Thiacalixarene*

Chemists dream of creating new compounds with original molecular motifs and contributing to the long history of evolution, which started with the big bang, followed by the evolution in elementary particles, elements, molecules, life, and then, artificial molecules. If any compound is truly useful for humankind, it will co-exist with humans forever. Calixarene is one such motif, which provides opportunities for versatile modifications leading to useful functions as already described in the previous chapters of this book. During the development of this area, some chemists had wondered about replacing the bridging methylene groups with heteroatoms like sulfur. These thoughts remained in their imagination. The first synthesis was reported by Prof. Sone, who connected *p*-*tert*-butylphenol with sulfur in a stepwise manner followed by cyclization to afford *p*-*tert*-butylthiacalix[4]arene (TC4A, with Y. 1.6 %) [1]. The synthesis was laborious and hindered the exploratory study on the function. In the meanwhile, Prof. Miyano was consulted by a company, COSMO Research Institute, about an additive for lubricants used in the internal-combustion engine. He noticed a slightly intense peak, corresponding to the cyclic tetramer of alkylphenol linked by sulfur, in a mass spectrum of a fraction from preparative chromatography of the reaction product. Later, they optimized the reaction conditions and established the one-step protocol to synthesize TC4A (Y. 54 %) [2]. This was the beginning. They did not design nor intend to obtain the molecule or even expect its profuse functions surpassing conventional

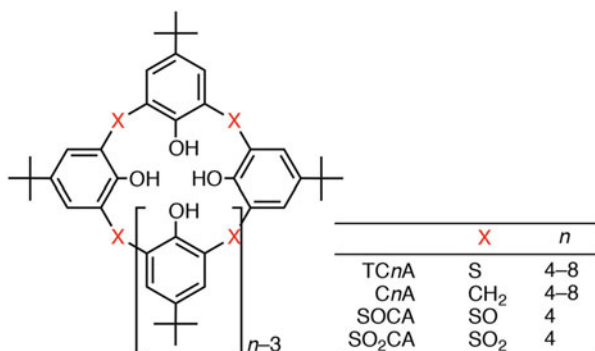
---

N. Iki (✉)

Graduate School of Environmental Studies, Tohoku University, 6-6-07 Aramaki-Aoba,  
Aoba-ku, Sendai 980-8579, Japan  
e-mail: [iki@tohoku.ac.jp](mailto:iki@tohoku.ac.jp)



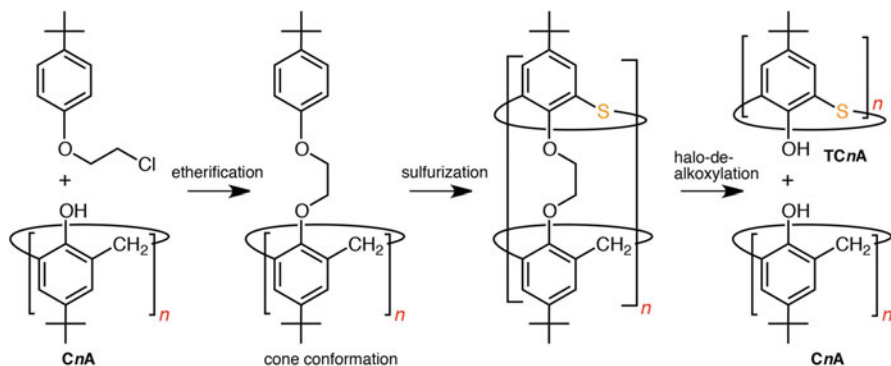
calixarenes as described in this chapter. Interestingly, thiacalixarene was discovered in the industrial field rather than in academia as exemplified by the discovery of “classical” calixarene [3]. The advent of thiacalixarene immediately caught the attention of chemists, who always dream of new chemical functions. Since then, a large number of thiacalixarene research papers have been published [4–10]. In this review, we focus on research that wisely utilizes the bridging sulfur (including sulfinyl and sulfonyl) to derive novel structure, property, reactivity, and function. The author strongly believes that the originality in thiacalixarene research comes from the sulfur. Studies that routinely apply the same chemistry already established for calixarenes, such as modifications of the phenol oxygen and using it, for example, as a ligand for metal ions, are omitted from this review. Dealing with thiacalixarene, chemists should keep in mind whether the chemical function could be achieved with the conventional calixarene or not.



## 13.2 Covalent Strategy

### 13.2.1 Synthesis

Before diving into the vast expanse of functions of sulfur-bridged calixarenes, the marked progress achieved in the covalent bond formation in this area should be dealt with. The difficulties encountered in the synthesis of extended thiacalixarenes such as TC6A and TC8A have been rather frustrating and hinder the exploration of their expected functions. Rare thiacalixarenes like TC6A exhibit interesting functions such as inclusion [11, 12], complex formation [13, 14], and metal-clustering ability [15, 16]. In the base-catalyzed oligomerization/cyclization of *p*-*tert*-butylphenol, TC4A is the predominant species in the presence of NaOH [2, 17]. In a strategy designed to utilize the template effects of alkali metal cations previously observed in the synthesis of *p*-*tert*-butylcalix[*n*]arene (CnA), CsOH was employed for the synthesis of thiacalix[6]arene, but unfortunately, the reaction gave a complex mixture of linear oligomers with a very small amount of TC6A (isolated Y. 0.8 %) [12]. This result suggests that the template effect by cations is not very

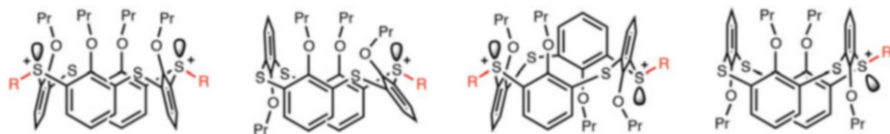


**Scheme 13.1** Calix[*n*]arene-templated synthesis of thiacalix[*n*]arene ( $n = 4-8$ )

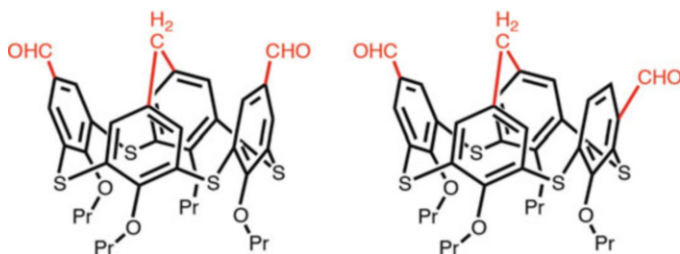
effective in the case of TC<sub>n</sub>A. Recently, Patel et al. employed a new strategy based on the principles of pre-organization for the synthesis of these thiacalixarenes (Scheme 13.1) [18]. Here, the individual phenol units are covalently attached to C<sub>n</sub>A ( $n = 4-8$ ) in the required geometry, which are then joined together by sulfur bridges to form the TC<sub>n</sub>A skeleton. Although additional steps such as the removal and separation of the ether tethers and C<sub>n</sub>A are required, the method provides TC<sub>n</sub>A in good yields especially the thiacalixarenes with odd  $n$  values (38, 32, 23, and 8% for  $n = 5, 6, 7,$  and  $8,$  respectively, from C<sub>n</sub>A to the corresponding TC<sub>n</sub>A). An attractive feature of this methodology is that it could be adapted for the synthesis of other types of heteroatom-bridged calix[*n*]arenes. The strategy also tolerates a variety of functional groups on the phenol units. Although there is a lot of scope for further research in the synthesis of thiacalixarenes, these significant developments should open the way for exploring the latent functions of TC<sub>n</sub>A with  $n > 4$  as well as of heterocalix[*n*]arenes.

### 13.2.2 Modification

Modification of TC<sub>4</sub>A is certainly a direct and useful way to extend the list of functions of these thiacalixarenes. In many cases, the modification methods developed for C<sub>4</sub>A can be readily adapted to TC<sub>4</sub>A. However, in this section, we will restrict ourselves to a discussion on the modification methods specific to thiacalixarenes. In some interesting modifications so far, the bridging sulfide has been converted into sulfoxide, sulfone, and sulfimides [7]. A recently reported modification was the *S*-alkylation to a sulfonium moiety, which was attempted by Lhoták et al. [19, 20] Using alkyl triflates as strong alkylating reagents for *O*-propylated TC<sub>4</sub>As, they succeeded in the preparation of mono- and di-*S*-alkylated thiacalixarenes with controlled regio- and stereoselectivity (Scheme 13.2). These results nicely illustrate the rules governing the alkylation as follows. (i) An



**Scheme 13.2** S-Alkylated products of tetra(propoxy)thiacalix[4]arene in various conformations



**Scheme 13.3** Intramolecularly bridged products of Duff reaction of cone-shaped tetra(propoxy)thiacalix[4]arene

equatorial orientation of the S-alkyl group is strongly preferred over the axial. (ii) Proximal sulfur bridges are not alkylated; only distally dialkylated compounds can be formed. (iii) Sulfur connecting phenyl rings in mutually *syn* positions is preferred over one in an *anti* position. (iv) *Anti* position is alkylated only if the molecule does not contain any bridge possessing the *syn* stereochemistry. Consequently, the selectivity seems to be controlled by the steric and electrostatic repulsion in the system. Calixarenes with a cationic moiety in the skeleton would be interesting candidates for anion receptors, in particular for chiral anions, since inherently chiral TC4A could be synthesized by the controlling the configuration of the S-alkylated center and the conformation of the O-alkylated phenol units.

Chemists have been puzzled by the fact that the reactions used to modify classical calixarenes sometimes cannot be applied to thiacalixarenes seemingly because of the reactivity of the phenol is altered by the sulfur bridges. For example, Lhoták et al. revealed that the formylation [21] and nitration [22] ended up with *meta* rather than *para* substitution in the phenol moiety. Also, during the formylation (Gross and/or Duff conditions) of 1,3-alternate TC4A, two formyl groups were introduced exclusively into the *meta* positions of the thiacalixarene skeleton [23]. DFT calculations revealed that the high electron density at the *meta* position might be responsible for the *meta* substitution. Interestingly, in the case of cone-shaped TC4A, intramolecularly methylene-bridged derivatives (Scheme 13.3) were obtained under Duff conditions. Thus, an interesting interplay between the conformation and the reaction conditions determines the outcome of the formylation reaction of TC4A.

### 13.3 Molecular Functions

Whether as a host or a ligand, the basic function of the sulfur-bridged calixarenes is the recognition of molecules and ions by inclusion and coordination, respectively. The resulting complexes may then exhibit higher functions, which will be described in the subsequent sections, but herein we focus on recent progress in such molecular functions.

#### 13.3.1 Inclusion

Inclusion is the most fundamental function in host-guest chemistry. As soon as TC4A was synthesized, its inclusion properties were studied in the solid state [1, 17, 24]. Recently, the inclusion of alcohols and carboxylic acid guests into TC4A was studied by Morohashi et al. by suspending the powdery crystals of TC4A in the mixture of the guest liquids [25]. The crystals were suspended in a 1:1 mixture of MeOH-EtOH. After recovering the crystals from the alcohol mixture, the average number ( $n$ ) of guest molecules bound by TC4A was determined by NMR as  $n_{\text{MeOH}} = 0.07$  and  $n_{\text{EtOH}} = 0.78$ . In the case of EtOH-PrOH the numbers were  $n_{\text{EtOH}} = 0.90$  and  $n_{\text{PrOH}} = 0.11$ . These results suggest a highly selective recognition of EtOH by the TC4A crystals. X-ray diffraction studies of the single crystals of TC4A obtained from each alcoholic solution revealed the hydrogen bonding between the alcoholic and phenolic OH groups and a CH- $\pi$  interaction between the alkyl and phenyl groups. These interactions resulted in a one-dimensional columnar arrangement of the TC4A molecules in a head-to-tail fashion while connected by the included alcohols (Fig. 13.1). A scrutiny of the distances of the interactions clarified that the EtOH molecules had the strongest interactions with the TC4A, which could be responsible for the high selectivity of the inclusion.

Recently they reported that the inclusion selectivity can be controlled by the conditions such as temperature and polarity of the solvents [26]. For example, from a solution containing 0.43 M Me<sub>2</sub>NH and 0.43 M Me<sub>3</sub>N in a 1:1 mixture of EtOH/H<sub>2</sub>O, Me<sub>2</sub>NH was selectively included in the crystals of TC4A (1 M  $\equiv$  1 mol dm<sup>-3</sup>). On the other hand, Me<sub>3</sub>N was selectively included from the solution with the same concentrations of the guests in 1:1 *N*-methylformamide/H<sub>2</sub>O. Moreover, they demonstrate a smart method to control the guest inclusion by using a metastable crystal of TC4A instead of the thermodynamically most stable one (Fig. 13.2) [27]. The crystal of TC4A in the most stable form adopting a self-inclusion structure (1) was immersed in an aqueous solution of Me<sub>2</sub>NH to include the amine as the crystal guest (2). The crystal was then suspended in methanol and heated to provide the metastable crystal having a 1D columnar arrangement of TC4A in the head-to-tail manner without any guest molecules (3). The metastable crystal exhibited an enhanced ability to include organohalogens from aqueous solutions and switching of the selectivity between HCOOH/EtCOOH by temperature. These results point towards a new strategy to control the inclusion ability and

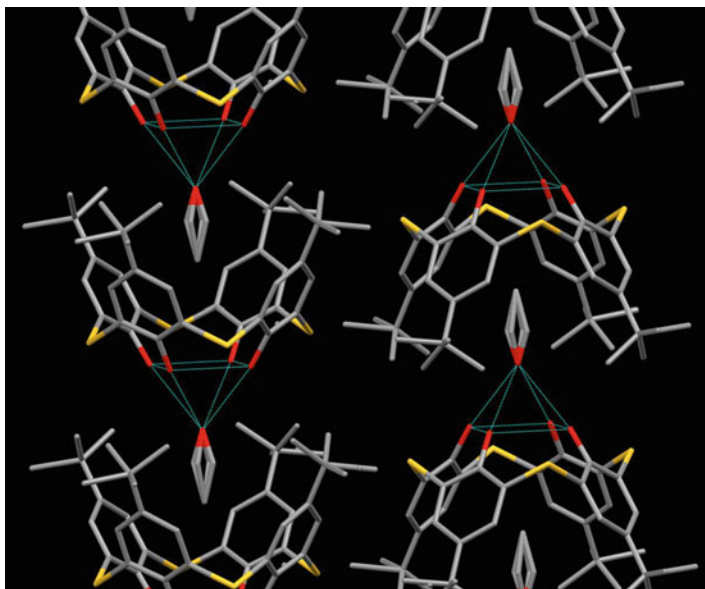


**Fig. 13.1** X-ray crystallographic structure of TC4A-EtOH. The *tert*-butyl groups and guest molecules are disordered

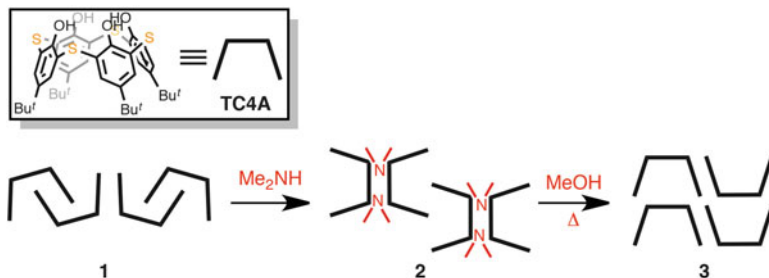
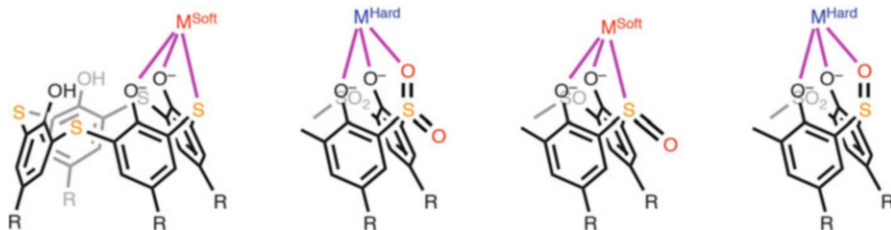


**Fig. 13.2** Transformation of thermodynamically stable crystal **1** of TC4A to metastable **3** via **2** including dimethyl amine

selectivity of TC4A by changing the conditions or crystal morphology without modifying the molecule.

### 13.3.2 Coordination

The most characteristic feature of thiacalixarene is its binding ability towards metal ions by coordination with the bridging sulfur as well as with the adjacent phenol



**Scheme 13.4** *Exo*-coordination fashion of sulfur-bridged calix[4]arenes. Partial structure is drawn for sulfonyl- and sulfinylcalix[4]arenes

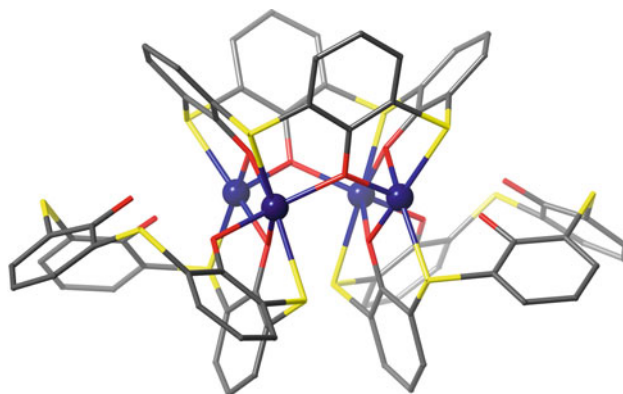


**Fig. 13.3** X-ray crystallographic structure of  $[\text{Zn}^{\text{II}}_3(\text{H}_2\text{tca})_2(\text{tca})]$ . The blue sphere represents  $\text{Zn}^{\text{II}}$  ion. The *tert*-butyl groups are not drawn for clarity

oxygen atoms, i.e., O,S,O *exo*-binding (Scheme 13.4). The striking difference in metal binding in thiacalixarenes compared to the classical calixarene was first revealed by solvent extraction [28]. Besides the binding ability, the selectivity can be controlled by the oxidation states of the bridging sulfur [29]. The thia form prefers so-called soft metal ions to hard ones, but the sulfonylcalix[4]arene prefers the hard metal ions. Interestingly, the sulfinylcalix[4]arene binds to both by switching the ligating atom according to the hardness/softness of the metal ion. The coordination of the bridging sulfur was first revealed for the  $\text{Zn}^{\text{II}}$ -TC4A complex by X-ray diffraction of a single crystal obtained from the organic phase of the solvent extraction of  $\text{Zn}^{\text{II}}$  with TC4A (Fig. 13.3) [30]. Surprisingly, the one of the TC4A ligands assembled  $\text{Zn}^{\text{II}}_4$  cluster in the crystal to form  $[\text{Zn}^{\text{II}}_4(\text{H}_2\text{tca})_2(\text{tca})]$ , suggesting that all of the four O,S,O donor sets can accommodate four metal ions at the same time to lead to cluster complexes ( $\text{H}_4\text{tca} = \text{TC4A}$ ). Later on, a number of crystallographic structures were revealed for sulfur-bridged calixarenes including *p-tert*-butylsulfinylcalix[4]arene (SOCA) and *p-tert*-butylsulfonylcalix[4]arene ( $\text{SO}_2\text{CA}$ ), which emphasize their ability to form metal cluster complexes due to the large number of donor atoms present as  $\text{O}_4\text{X}_4$  ( $\text{X} = \text{S}$  or  $\text{O}$ ) [31, 32]. A systematic

investigation of TC4A-metal complexes was carried out by Harrowfield et al. [33–35] Furthermore, TC6A was revealed to bind to metal ions with selectivity similar to TC4A [14]. In the solid state, TC6A assembled transition metal clusters of  $\text{Cu}^{\text{II}}_{10}$  and  $\text{Co}^{\text{II}}_5$ ,  $\text{Ni}^{\text{II}}_4$ , and  $\text{M}^{\text{II}}\text{Ni}^{\text{II}}_4$  ( $\text{M}^{\text{II}} = \text{Mn}^{\text{II}}, \text{Co}^{\text{II}}, \text{and Cu}^{\text{II}}$ ), owing to the O,S,O tridentate fashion [15, 16].

## 13.4 Supramolecular Functions

As a result of the recognition of molecules and metal ions by calixarene, functions of a higher level (secondary function) than simple binding (primary function) may arise. This can be conveniently described by a mathematical formulation as:

$$f(x + y) > f(x) + f(y) \quad (13.1)$$

where  $x$  and  $y$  are calixarene and other entities, respectively, and  $f(x)$  is the function (of the component  $x$ ) such as structure, properties, and chemical functions. In other words, the components  $x$  and  $y$  show a synergistic effect to generate a new function  $f(x + y)$ . In many cases, however, functionalizing of the calixarene  $x$  relies on covalently attaching functional groups  $y$  to afford sophisticated molecules  $x + y$ , which are sometimes referred as supramolecules (super molecule, correctly). As a result, the resulting functions are expressed by Eq. (13.2).

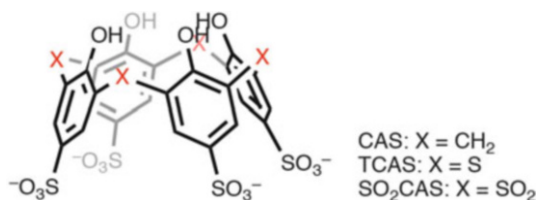
$$f(x + y) = f(x) + f(y) \quad (13.2)$$

On the one hand, this means a success in molecular design where the resulting function  $f(x + y)$  is exactly what is expected from  $f(x) + f(y)$ . For example, when  $x = \text{calix}[4]\text{arene}$  and  $y = \text{ligating group}$ , then  $f(x + y) = \text{coordination}$ . On the other hand, this is strictly different from the definition of a supramolecule, because the word “supra” means “*beyond*” and therefore supramolecular function should be greater than what is expected from the individual functions of each components as expressed by Eq. (13.1). Hereafter, truly supramolecular functions defined by Eq. (13.1) such as separation, catalysis, cage formation, magnetism, luminescence, and sensing will be described.

### 13.4.1 Separation

As mentioned above, the sulfur-bridged calixarenes have been revealed as ligands, and the most direct application of these molecules should be the separation of metal ions. To separate different metal ions, the ligand must be in a medium such as an organic phase or a solid support. The latter is currently preferred from an environmental point of view. Matsumiya used a strong anion-exchange resin as a

convenient support to immobilize thiocalix[4]arene-*p*-tetrasulfonate (TCAS) through the noncovalent electrostatic interaction between the  $\text{SO}_3^-$  group and trimethylammonium group of the resin [36]. The resulting composite can be used as a chelating resin to separate and preconcentrate metal ions without leaking the TCAS. It can also be applied to the speciation of free  $\text{Cu}^{\text{II}}$  and  $\text{Cu}^{\text{II}}$ -humate in natural water [37]. Hydrophobic interactions can also be used for the noncovalent immobilization. SOCA-impregnated XAD resins can separate Nb(V) from Ta(V) [38]. Furthermore, Kikuchi et al. reported the preparation of  $\text{SO}_2\text{CA}$ -impregnated silica adsorbents for the actinides [39, 40] that showed excellent performance in the separation of trivalent actinides such as Am, from a high-level radioactive liquid waste in a weakly acidic solution. The adsorbent was chemically stable under irradiation and the amount of dissolution of  $\text{SO}_2\text{CA}$  was only 1% by gamma-ray irradiation at a total dose of 1 MGy. The value of the distribution coefficient of Am at pH 4 by the adsorbent was constant even at the high irradiation dose. Moreover, the separation factor of Am to lanthanides showed a high value. These successes in the separation of metal ions are attributed to the *exo*-binding mode with the O,X,O donor set ( $X = \text{S}$  or  $\text{O}$ ) present in these molecules and its compatibility with the solid support via a noncovalent immobilization. These characteristic properties of the sulfur-bridged calix[4]arene lead to the emergence of the separation function upon combination with the solid support.

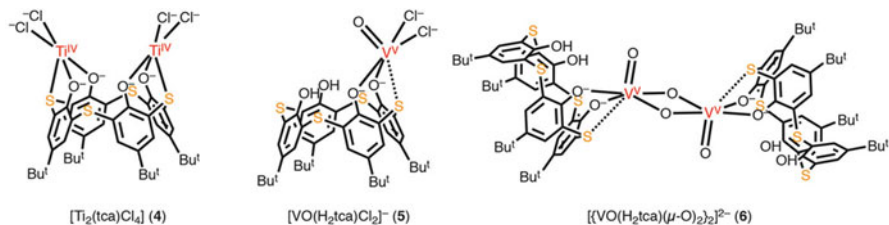


### 13.4.2 Catalysis

Owing to the controllable Lewis acidity and/or redox potential of the metal center as well as selective binding to a substrate arising from the stereochemistry of ligands, molecular catalysts have been designed based on metal complexes. The *exo*-coordination ability with the O,X,O atoms ( $X = \text{S}$  or  $\text{O}$ ) to leave the metal center coordinatively unsaturated as well as the ability to assemble a multiple-metal core, the sulfur-bridged calixarenes can provide molecular catalysts with high activity. The first example was a cone-shaped  $[\text{Ti}^{\text{IV}}_2(\text{tca})\text{Cl}_4]$  (**4**), which has high catalytic activity in the Mukaiyama-aldol reaction of aromatic aldehydes with silyl enol ethers [41]. Owing to the cone conformation, which brings the two Lewis acid centers to the same sides of the calix, the aldehyde oxygen coordinates to both simultaneously and is activated enough leading to a facile condensation. The



cone-shaped **4** can also be used as a catalyst for the regioselective [2 + 2 + 2] cycloaddition of terminal alkynes [42] and to the polymerization of ethylene [43].

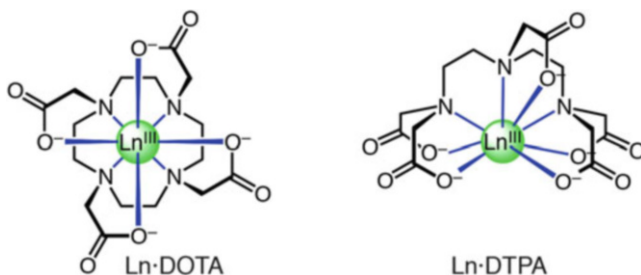


As has been reported, a classical calixarene forms a complex with metal ions with high valency by the coordination of the phenolic O<sup>-</sup> group [44]. A wide variety of metal complexes showed catalytic activity, where the phenolic O<sup>-</sup> of calix behaves as an oxosurface [45]. For example, the oxovanadium(V)-C4A complex can catalyze the oxidation of alcohols and the polymerization/copolymerization of olefins [46]. Seeking higher catalytic activity, Hoppe et al. prepared mono- and dinuclear oxovanadium(V)-TC4A complexes PPh<sub>4</sub>[VO(H<sub>2</sub>tca)Cl<sub>2</sub>] (**5**) and (PPh<sub>4</sub>)<sub>2</sub>[(VO(H<sub>2</sub>tca)(μ-O)<sub>2</sub>)]<sup>2-</sup> (**6**) and assessed their activity to catalyze the oxidation of alcohols with O<sub>2</sub> at 80 °C. X-ray analyses confirmed the *exo*-O,S,O coordination to the V(V) center in both **5** and **6**. The latter showed a somewhat weaker S–V interaction as judged by the distance (2.9446(11) Å) as compared to the one in **5** (2.7553(16) Å). Both **5** and **6** efficiently catalyze the oxidation of benzyl alcohol, crotyl alcohol, 1-phenyl-1-propanol, and fluorenol with turnover frequencies up to 83 h<sup>-1</sup>. In most cases, the dinuclear complex **6** is more active than the mononuclear complex **5**. Interestingly, the thiacalixarene complexes **5** and **6** are in many instances more active than oxovanadium(V) complexes containing “classical” calixarene ligands. Although a detailed mechanistic study of the observed higher catalytic activity is still awaited, the authors suspect that the acceleration of the rate-determining step (probably the alcohol conversion) is due to the electronic effect of the bridging sulfur.

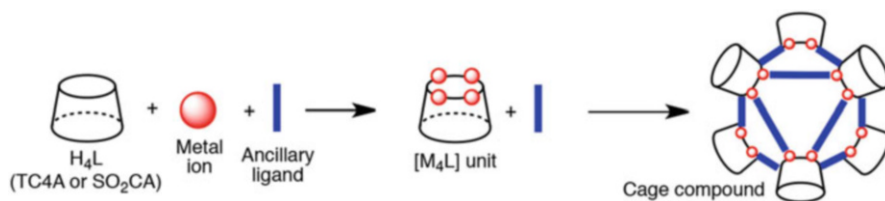
Thus, taking advantage of the peculiar coordination fashion of TC4A, some success in the application of these molecules as catalysts has been achieved. However, it seems that the development of molecular catalysts of this class is still in its infancy, which may be due to the difficulty in the prediction of catalytic function as shown by Eq. (13.1). Therefore, the rational design of catalysts based on these molecules is still a challenge for chemists who have to rely on empirical studies on structure-activity relationships.

### 13.4.3 Cage Formation

Owing to the structural beauty and latent functions based on magnetism and luminescence, cluster complexes with high nuclearity is one of the active areas of



**Scheme 13.5** *Endo*-coordination fashion of DOTA and DTPA to lanthanide



**Scheme 13.6** Self-assembly of sulfur-bridged calix[4]arene with a metal ion and ancillary ligand to a cage compound via the tetranuclear unit  $[M_4L]$

research in coordination chemistry. It is a common tactic to design ligands having a large number of donor atoms to accommodate multimetal cores, because use of an excess amount of ligands having low denticity tends to end up forming mononuclear complexes. Another factor, which affects the nuclearity, is the stereochemistry of the ligating atoms to array several metal cores. Even when the denticity is high as in the cases of DOTA and DTPA with 8 donor atoms, they encapsulate a single metal ion inside the molecule (i.e. *endo*-coordination, see Scheme 13.5, DOTA = 1,4,7,10-tetraazacyclododecane-*N,N',N'',N'''*-tetraacetic acid and DTPA = 1,1,4,7,7-diethylenetriamine pentaacetic acid). As described above, early studies have revealed that the sulfur-bridged calixarenes per se behave as the cluster forming ligands owing to the large number of donating atoms and the *exo*-binding fashion. However, the presence of ancillary ligands and their effects had been greatly unknown. The recent explosive growth in the exploration of giant cage-type complexes with sulfur-bridged calix[4]arenes mainly led by Chinese groups is noteworthy. They focus on molecular cages by assembling the calixarene complexes. The strategy is to react a sulfur-bridged calix[4]arene ( $H_4L$ ) and a metal salt in the presence of an ancillary ligand under solvothermal conditions (Scheme 13.6). The calix assembles four transition metal ions ( $M^{n+}$ ) to form  $M_4L$  subunits, which are bridged by the ancillary ligand to form a wide variety of cage or polyhedral structures. The variety of the 3D-structures of the cage-shaped complexes can be regarded as the results of supramolecularity between the calix, metal, and ancillary ligand as expressed by Eq. (13.1).

For instance, Su et al. reported the synthesis of coordination cages with high-nuclearity ( $M_{4n}$  where  $M = Ni$  or  $Co$ ;  $n = 2-6$ ) using inorganic phosphate or

**Fig. 13.4** Coordination cages **7–14** obtained from sulfur-bridged calix[4]arenes,  $M^{II}$ , and ancillary phosphate ligands (© 2014 American Chemical Society)

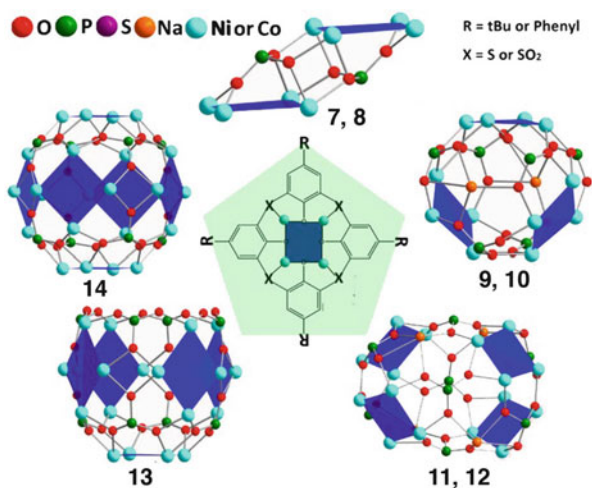
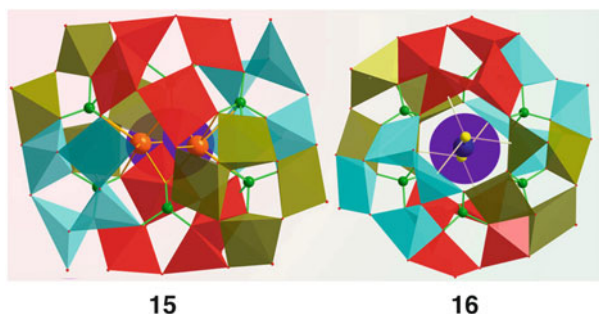


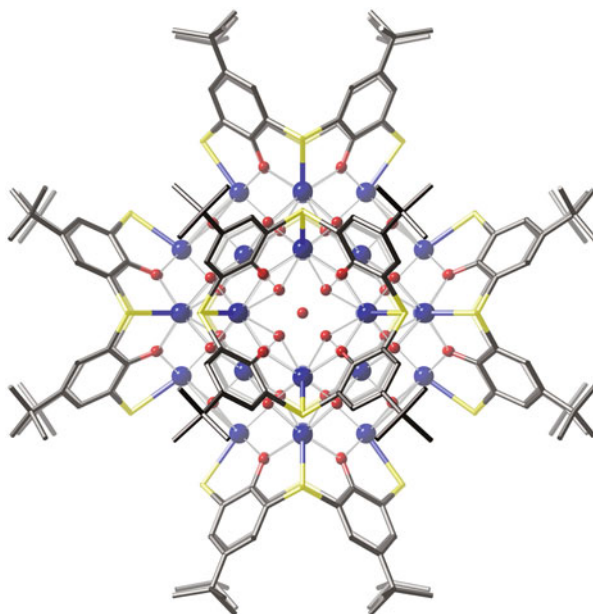
**Fig. 13.5** Coordination cages **15** and **16** obtained from TC4A,  $Co^{II}$ , and alkali hydrogen phosphates. Polyhedron: Co, green sphere: P, orange: Na, blue: K, yellow: Cl (© 2014 American Chemical Society)



organic phosphonate ligands as the ancillary ligands [47]. Varying the calix ligand (TC4A, *p*-phenylthiacalix[4]arenes (PTCA), and  $SO_2CA$ ) and the metal:calix: ancillary ligand ratio gave five types of clusters (Fig. 13.4). Dimeric clusters **7** and **8** ( $n=2$ ) have a  $Ni_8$  core, which was arranged in a chair conformation. The clusters with sphere-shaped  $M_{12}$  ( $M = Ni$ (**9**) and  $Co$ (**10**),  $n=3$ ) and capsule-like  $M_{16}$  ( $M = Ni$ (**11**) and  $Co$ (**12**),  $n=4$ ) have closed-shell structures, where their ports are sealed by sodium ions. The helmet-like  $Co_{20}$  (**13**) is the only one in this family with an open-shell structure, which can be regarded as a truncated octahedral  $Co_{24}$  (**14**) nanocage cutting one face.

More recently two kinds of coordination cages including alkali metal ions were formed by the solvothermal reaction of TC4A,  $Co(NO_3)_3$ , and  $Na_2HPO_4/K_2HPO_4$  in DMF-MeOH (Fig. 13.5) [48]. On one hand, the disodium salt gave the oval-shaped capsule,  $[Na_2Co_{24}(tca)_6(PO_4)_6(HCOO)_6(DMC)_2(DMF)_2(dma)_4]$  (**15**), inside which two sodium ions were included (DMC = *N,N'*-dimethylcarbamate, dma = dimethylamine). The capsule was capped by six  $[Co_4(tca)]^{4+}$  units and six phosphate linkers and other different auxiliary anions, possessing a  $Co_{24}$  core

**Fig. 13.6** X-ray crystallographic structure of coordination cage  $[\text{Co}^{\text{II}}_{24}\text{Co}^{\text{III}}_8(\mu_3\text{-O})_{24}(\text{H}_2\text{O})_{24}(\text{tca})_6]$ . Blue sphere:  $\text{Co}^{\text{II/III}}$  ion



templated by two  $\text{Na}^+$  ions. On the other hand, a dipotassium salt gave spherical cages of cationic  $[\text{KCo}_{24}(\text{tca})_6(\text{PO}_4)_6\text{Cl}_2(\text{HCOO})_4(\text{DMF})_8]^+$  (**16**) and anionic  $[\text{KCo}_{24}(\text{tca})_6(\text{PO}_4)_6\text{Cl}_2(\text{HCOO})_6(\text{DMF})_4(\text{CH}_3\text{OH})_2]^-$ , sharing the same subunits with **15** but including only one  $\text{K}^+$  ion in each capsule.

In terms of nuclearity, the highest reported so far is  $\text{M}_{32}$  clusters. The first example was a giant spherical cage,  $[\text{Co}^{\text{II}}_{24}\text{Co}^{\text{III}}_8(\mu_3\text{-O})_{24}(\text{H}_2\text{O})_{24}(\text{tca})_6]$ , prepared by the solvothermal reaction of  $\text{Co}(\text{AcO})_2$  and TC4A in a 1:1 mixture of  $\text{MeOH}/\text{CHCl}_3$  (Fig. 13.6) [49]. The  $[\text{Co}^{\text{III}}\text{O}_6]_8$  cube was formed in situ to act as an ancillary ligand and bridged six  $[\text{Co}^{\text{II}}_4(\text{tca})]^{4+}$  units located at the vertices of the octahedron to form a giant sphere. The peripheral diameter defined by the distance between two *tert*-butyl carbons of two distal TC4A molecules on the sphere was about 2.3 nm. In addition, the diameter of the inner cavity was estimated to be 4.8 Å. Other examples reported so far are  $[\text{Ni}^{\text{II}}_{32}(\text{OH})_{40}(\text{tca})_6]$  [35] and  $[\text{M}^{\text{II}}_{32}\text{O}_{16}(\text{OH})_8(\text{CH}_3\text{OH})_6(\text{tca})_6]$  ( $\text{M} = \text{Co}, \text{Ni}$ ) [50], which were prepared by a reaction between the metal salts and TC4A in DMF at room temperature. These share a few common features such as bridging of the six  $[\text{M}_4\text{tca}]^{4+}$  units by eight  $\text{MO}_6$  units and the resulting giant spherical form. Surprisingly, such highly ordered molecular edifices were readily constructed by simply mixing the components under solvothermal or nonsolvothermal conditions, suggesting that the  $[\text{M}_4\text{tca}]^{4+}$  cluster units seemingly sought a bridging  $\text{MO}_6$  unit to assemble together to form the giant sphere.

Using high-valence oxometalates as ancillary components, heterometallic cluster complexes can be formed by a one-step synthesis. The solvothermal reaction of  $\text{Co}(\text{OAc})_2$ , TC4A, and  $\text{Na}_2\text{M}^{\text{VI}}\text{O}_4$  in  $\text{EtOH}/\text{CHCl}_3$  readily afforded

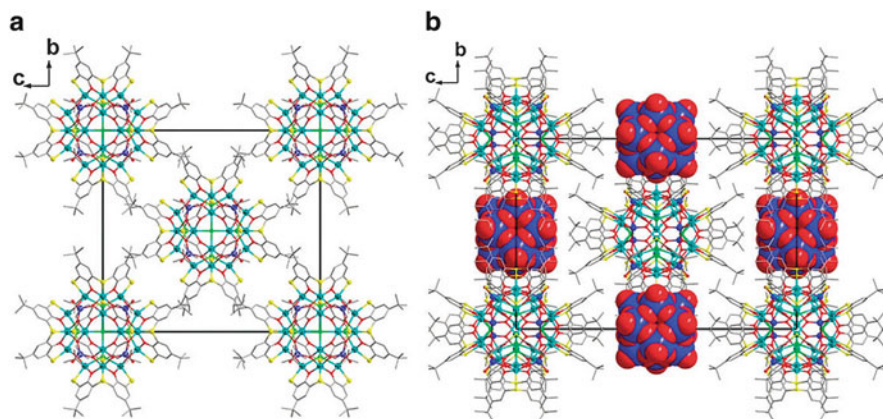


**Fig. 13.7** Packing diagrams of (a)  $[\text{Co}_{24}(\text{tca})_6(\text{MoO}_4)_8\text{Cl}_6](\text{OH})_2(\text{CHCl}_3)_{12}(\text{CH}_3\text{CH}_2\text{OH})_{12}$  and (b)  $[\text{Co}_{24}(\text{tca})_6(\text{MoO}_4)_8\text{Cl}_6][\text{HPM}_{12}\text{O}_{40}](\text{CHCl}_3)_{12}(\text{CH}_3\text{CH}_2\text{OH})_7$  © 2011 Royal Society of Chemistry

$[\text{Co}_{24}(\text{tca})_6(\text{MO}_4)_8\text{Cl}_6]^{2+}$  ( $\text{M} = \text{Mo}$  or  $\text{W}$ , Fig. 13.7a) [51]. It has a spherical shape with a diameter being of *ca.* 2.3 nm, which is quite similar to that observed in the  $[\text{Co}^{\text{II}}_{24}\text{Co}^{\text{III}}_8(\mu_3\text{-O})_{24}(\text{H}_2\text{O})_{24}(\text{tca})_6]$  nanosphere except that the  $[\text{Co}^{\text{III}}\text{O}_6]$  sites have been replaced by the  $[\text{MO}_4]$  groups and the water molecules in the lower rim of the  $[\text{Co}_4\text{tca}]^{4+}$  units have been substituted by the  $\text{Cl}^-$  anions. The cubic  $(\text{MO}_4)_8$  assemblies in the cationic nanospheres penetrate through the  $\text{Co}^{\text{II}}_{24}$  sodalite cages while the  $\text{Co}^{\text{III}}_8$  cube in the  $[\text{Co}_{32}]$  nanosphere is located inside the sodalite cage. Interestingly, in the case using  $\text{H}_3\text{PM}_{12}\text{O}_{40}$  as the ancillary component, the cationic nanosphere formed hybrids with Keggin polyoxometalates  $[\text{HPM}_{12}\text{O}_{40}]^{2-}$  to result in a superstructure in which  $[\text{HPM}_{12}\text{O}_{40}]^{2-}$  is surrounded by six nanospheres occupying the vertices of an octahedron (Fig. 13.7b). The success of this method relies on the complexation selectivity of TC4A, which does not react with  $\text{Mo}^{\text{VI}}$  and  $\text{W}^{\text{VI}}$ .

Organic ligands can also serve as the ancillary bridging ligand. Liao et al. used aromatic di- or tricarboxylic acids, bifunctional carboxylic acids, and azoles as the ancillary ligands to bridge the  $\text{M}_4\text{L}$  units ( $\text{H}_4\text{L} = \text{TC4A}$  or  $\text{SO}_2\text{CA}$ ) [52]. Clusters of octahedral cage  $[(\text{M}_4\text{L})_6(\text{tc})_8]$  ( $\text{tc} =$  aromatic tricarboxylates), octahedral cage  $[(\text{M}_4\text{L})_6(\text{dc})_{12}]$ , square  $[(\text{M}_4\text{L})_4(\text{dc})_8]$ , tetragonal  $[(\text{M}_4\text{L})_4(\text{dc})_4]$  ( $\text{dc} =$  aromatic dicarboxylates), wheel  $[(\text{M}_4\text{L})_6(\text{trz})_{12}]$  ( $\text{trz} = 1,2,4\text{-triazole}$ ) [53], wheel  $[(\text{M}_4\text{L})_4(\text{tta})_8]$  ( $\text{tta} = 5\text{-Me-tetrazolate}$ ) [54], and tetragonal prismatic  $[(\text{M}_4\text{L})_8(\text{btz})_4(\text{N}_3)_8]$  ( $\text{btz} = 1,3\text{-bis}(2\text{H-tetrazol-5-yl})\text{benzene}$ ) [55] were constructed. More recently, an extra-large octahedral coordination cage (overall peripheral diameter of 5.4 nm and an internal cavity of 2.7 nm) was prepared with  $[\text{Co}_4(\text{so}_2\text{ca})]^{4+}$  units ( $\text{H}_4(\text{so}_2\text{ca}) = \text{SO}_2\text{CA}$ ) and extended tricarboxylate, 4,4',4''-(benzene-1,3,5-triyl-tris(benzene-4,1-diyl))tribenzoate ligands [56]. In addition, the same modular approach by using  $[\text{M}_4(\text{so}_2\text{ca})]^{2+}$  and di- and tricarboxylates has been reported by Wang et al. [57–59].

Although these systematic studies have demonstrated the usefulness of the combination of the components such as metal, calix, and the additional ligand in the construction of the large cluster cages, they also have indicated some limitations of the resulting cluster systems. Firstly, the rational design of these cages is still difficult because the outcome of the components are often affected by the in situ generated ligand such as  $\text{MO}_6$ , tri- and tetrazole or even  $\text{Cl}^-$  from the  $\text{CHCl}_3$  solvent. Secondly, the physicochemical properties and functional characteristics of the giant cages still need to be uncovered. For example, the magnetic properties of these cages were often studied but they only show the properties of the  $[\text{M}_4\text{L}]^{x+}$  units, which is typically the antiferromagnetic coupling between the metal centers. Finally, the giant space created by the assembly of  $[\text{M}_4\text{L}]^{x+}$  units cannot be accessed from outside because of the closed structure of these cages. These are significant weaknesses compared to metal-organic frameworks and cluster complexes with other types of ligands. Nonetheless, the beauty of the resulting structures should provide enough motivation to calixarene chemists for pursuing studies on these cages.

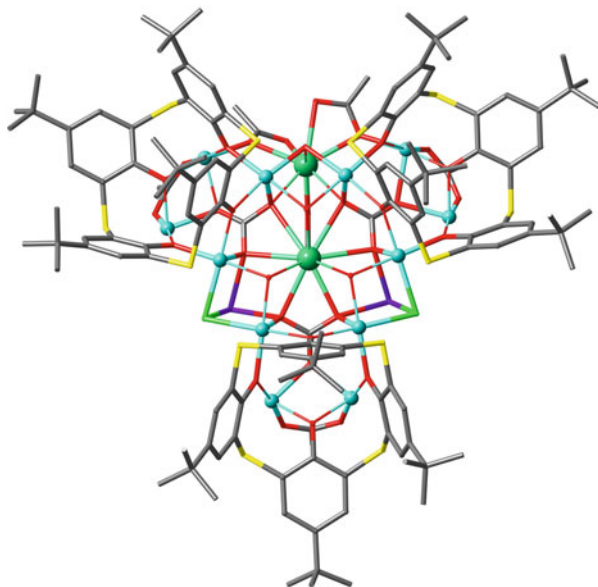
### 13.4.4 Magnetism

One of the characteristic properties of the metal complexes is the molecular magnetism depending on the number of unpaired electrons at the metal center. Recently, single molecule magnets (SMMs), which exhibit superparamagnetic behavior below a blocking temperature, have attracted a lot of attention for applications in memory devices with high density. The magnetic properties of the complexes of thia- and sulfonyl calixarenes with 3d and 4f transition metal ions have been investigated. In some cases, SMM behavior can be found. In an early example, Kajiwara et al., reported that di- $\text{Tb}^{\text{III}}$  complex of  $\text{SO}_2\text{CA}$  shows superparamagnetic behavior due to the slow magnetic relaxation at low temperatures [60]. They took advantage of  $\text{Tb}^{\text{III}}$  having a large angular momentum and strong magnetic anisotropy in the ground multiplet state. In addition, the  $\text{SO}_2\text{CA}$  has *exo*-O,O,O donor sets with negative charges in a narrow area to stabilize the ground sublevel, which leads to a strong easy-axis anisotropy. The results of these studies suggest that the sulfur-bridged calixarenes can be a platform to obtain SMMs. Using PTCA ( $\text{H}_4\text{ptca}$ ), Bi et al. solvothermally synthesized  $[\text{Dy}^{\text{III}}_4(\text{ptca})_2(\mu_4\text{-OH})\text{Cl}_3(\text{CH}_3\text{OH})_2(\text{H}_2\text{O})_3]$ , which showed a slow magnetic relaxation behavior characteristic of SMM behavior [61].

The 3d transition metal ions can also give SMMs. For example, Desroches et al. have studied the magnetic properties of polynuclear complexes of the calixarenes with 3d transition metal ions [62, 63]. Recently, they reported the formation of a series of  $\text{Co}^{\text{II}}\text{-SO}_2\text{CA}$  complexes by a one-pot solvothermal reaction and succeeded in preparation of a variety of polynuclear complexes: three dinuclear  $[\text{Co}^{\text{II}}_2(\text{so}_2\text{ca})\text{X}_n]$  in 1,2-alternate form ( $\text{X}_n = \text{py}_4$ ,  $\text{bpy}_2$ , or  $\text{en}_2$ ),  $[\text{Co}^{\text{II}}_{14}(\text{so}_2\text{ca})_3(\mu_4\text{-OH})_3(\mu_6\text{-O})_3(\text{OCH}_3)_6]^+[\text{Co}^{\text{II}}_4(\text{so}_2\text{ca})_2(\mu_4\text{-OH})]^-$  cluster salt, and



**Fig. 13.8** X-ray crystallographic structure of heterometallic cluster  $[\text{Na}_2\text{Ni}^{\text{II}}_{12}\text{Tb}^{\text{III}}_2(\text{tca})_3(\mu_7\text{-CO}_3)_3(\mu_3\text{-OH})_4(\mu_3\text{-Cl})_2(\text{OAc})_6(\text{dma})_4]^{2+}$ . Dark green:  $\text{Tb}^{\text{III}}$ , light blue:  $\text{Ni}^{\text{II}}$ , purple:  $\text{Na}^{\text{I}}$

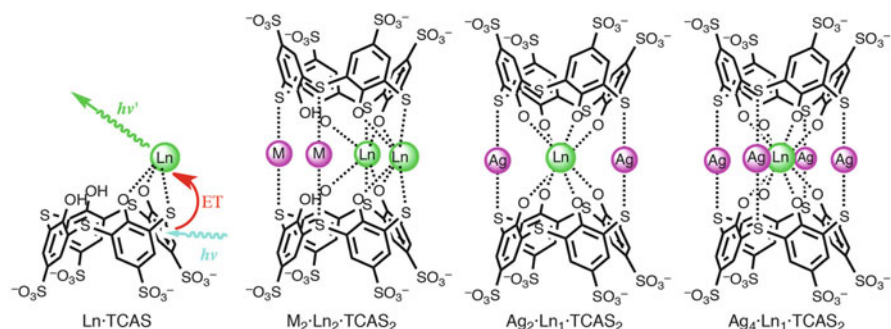


tetranuclear  $[\text{Co}^{\text{II}}_4(\text{so}_2\text{ca})_2(\mu_3\text{-OH}_2)]$  cluster [64]. The addition of the chelating ligands X was shown to be a critical factor to stabilize the dinuclear complexes  $[\text{Co}^{\text{II}}_2(\text{so}_2\text{ca})\text{bpy}_2]$  and  $[\text{Co}^{\text{II}}_2(\text{so}_2\text{ca})\text{en}_2]$ , which showed slow relaxation of magnetization at small magnetic fields.

Introducing both 3d and 4f elements in the molecule is another way to design SMMs. In thiacalixarene territory, Xiong et al. reported the preparation of the heterometallic cluster  $[\text{Na}_2\text{Ni}^{\text{II}}_{12}\text{Ln}^{\text{III}}_2(\text{tca})_3(\mu_7\text{-CO}_3)_3(\mu_3\text{-OH})_4(\mu_3\text{-Cl})_2(\text{OAc})_6(\text{dma})_4]^{2+}$  ( $\text{Ln} = \text{Dy}$  or  $\text{Tb}$ ,  $\text{dma} = \text{dimethylamine}$ , Fig. 13.8) [65]. In the complex, three  $[\text{Ni}^{\text{II}}_4\text{tca}]^{4+}$  units are linked together in an up-to-up fashion through two  $\text{Na}^+$  ions and two  $\text{Ln}^{\text{III}}$  ions, along with other anions, leading to a pseudo-trigonal planar entity. Within this entity, there is a ternary-cubane core composed of one  $[\text{Ni}_2\text{Ln}_2]$  cubane unit and two  $[\text{NaNi}_2\text{Ln}]$  cubane units sharing a  $\text{Ln}^{\text{III}}$  ion. Magnetic studies reveal that the  $\text{Dy}^{\text{III}}$  complex shows the slow relaxation of the magnetization expected for SMM behavior. Regrettably, however, the cooperativity between the 3d–4f metal ions was not observed. Su et al. reported the synthesis of  $[\text{Zn}^{\text{II}}\text{Ln}^{\text{III}}_3(\mu_4\text{-OH})(\text{tca})_2(\text{OAc})_2(\text{CH}_3\text{OH})(\text{H}_2\text{O})(\text{DMA})_2] \cdot 3\text{H}_2\text{O}$  in which a  $\text{Zn}^{\text{II}}\text{Ln}^{\text{III}}_3$  heterometallic cluster is sandwiched by two cone-shaped TC4A ligands ( $\text{Ln} = \text{Gd}$ ,  $\text{Tb}$ ,  $\text{Dy}$ ,  $\text{Ho}$ ,  $\text{DMA} = N,N'$ -dimethylacetamide) [66]. Some antiferromagnetic interactions between the  $\text{Ln}^{\text{III}}$  ions are observed in the complexes. The *ac* susceptibility measurement on the  $\text{Dy}^{\text{III}}$  complex reveals an obvious frequency-dependent in- and out-of-phase signal, indicating the slow magnetization relaxation typical for SMMs. Thus, the quest for thiacalix-based SMMs having higher blocking temperatures and also reducing the probability of quantum tunneling is still on.

### 13.4.5 Luminescence

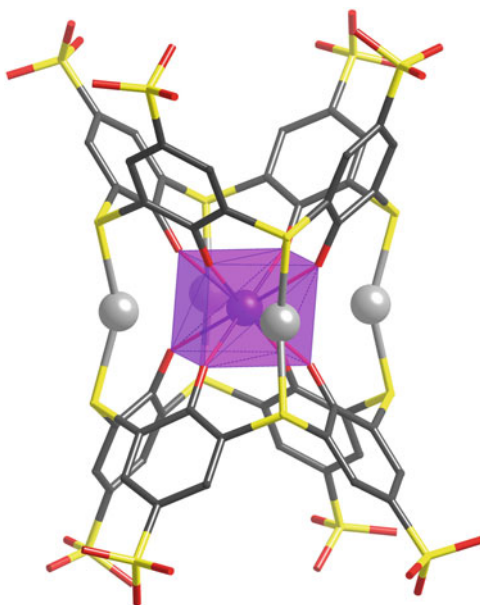
Molecular-based luminescence materials are used in luminescent display devices, inks, and bio-analysis and imaging [67–70]. Because the calixarenes are not fluorescent, they cannot be used as luminescent materials without introducing a luminescent center. Introducing a fluorophore is not ideal unless the calix part plays an essential role in the fluorescent function. A more rational approach is to introduce a luminescent metal center such as a lanthanide(III) ion, which can be excited by energy transfer from the antenna group in the ligand in its  $T_1$  state. Attached with auxiliary ligand(s), classical calixarenes have been proven to be good ligands for the energy-transfer luminescence of  $\text{Ln}^{\text{III}}$  [71]. Here, the calix[4]arene skeleton acts as the platform to attach the ligating group and as a light-absorbing antenna to excite the  $\text{Ln}^{\text{III}}$  center. An auxiliary antenna group should also be introduced if the  $T_1$  state of the calix does not match the excitation of  $\text{Ln}^{\text{III}}$ . By using the inherent coordination ability of the sulfur-bridged calixarenes, we studied the formation of  $\text{Ln}^{\text{III}}$  complexes with water-soluble calixarenes TCAS and sulfonylcalix[4]arene-*p*-tetrasulfonate ( $\text{SO}_2\text{CAS}$ ) in aqueous solutions [72]. Among the  $\text{Ln}^{\text{III}}$  species,  $\text{Tb}^{\text{III}}$  exhibited strong luminescence with the calixarenes. TCAS formed a 1:1 complex ( $\text{Tb}^{\text{III}} \cdot \text{TCAS}$ , Scheme 13.7) at  $\text{pH} \geq 8.5$ , exhibiting the  $\text{Tb}^{\text{III}}$ -centered luminescence with a quantum yield  $\Phi = 0.15$  and a lifetime  $\tau = 0.71$  ms. Reflecting the high acidity of the ligand [73], the sulfonyl counterpart ( $\text{Tb}^{\text{III}} \cdot \text{SO}_2\text{CAS}$ ) at  $\text{pH} \geq 5.5$  also showed luminescence ( $\Phi = 0.13$ ,  $\tau = 0.70$  ms). By contrast the classical calixarene, calix[4]arene-*p*-tetrasulfonate (CAS), formed a 1:2 luminescence complex,  $\text{Tb}^{\text{III}} \cdot \text{CAS}_2$ , at very high pH ( $\text{pH} > 12$ ,  $\Phi = 0.12$ ,  $\tau = 0.61$  ms), indicating that the coordination only by the phenol oxygen is very weak in aqueous solution. These results endorse the usefulness of the sulfur-bridged calixarenes in terms of formation of the luminescent  $\text{Tb}^{\text{III}}$  complex, owing to the inherent *exo*-coordination ability of the ligand and the  $T_1$  level suitable for the excitation.



**Scheme 13.7** Structures of the  $\text{Ln}^{\text{III}}$ -TCAS complexes. For  $\text{Ln}$ -TCAS, energy-transfer luminescence is schematically drawn



**Fig. 13.9** X-ray crystallographic structure of  $\text{Ag}^{\text{I}}_4\text{Tb}^{\text{III}}\cdot\text{TCAS}_2$ . Chemical formula:  $\text{Na}_9[\text{Ag}_4\text{Tb}(\text{tcas})_2\text{dmf}_2](\text{dmf})_6(\text{H}_2\text{O})_6(\text{H}_4\text{tcas}^{4-} = \text{TCAS})$ . The purple cube depicts the  $\text{O}_8$ -cubic coordination geometry of  $\text{Tb}^{\text{III}}$  provided by two TCAS ligands

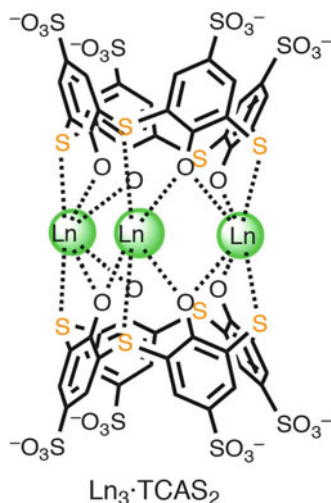


During efforts to study the effect of diverse ions coexisting in the solution on the luminescence intensity of  $\text{Tb}^{\text{III}} \cdot \text{TCAS}$ , Horiuchi unexpectedly found that  $\text{Ag}^{\text{I}}$  enhanced the luminescence intensity. The scrutiny of the  $\text{Ag}^{\text{I}}\text{-Tb}^{\text{III}}\text{-TCAS}$  system by electrospray ionization mass spectrometry (ESI-MS) and molar ratio methods clarified that at pH 6 a ternary complex  $\text{Ag}^{\text{I}}_2\text{Tb}^{\text{III}}_2\text{TCAS}_2$  was formed [74]. Moreover, in the presence of excess amount of  $\text{Ag}^{\text{I}}$  and TCAS to  $\text{Tb}^{\text{III}}$  at pH 10,  $\text{Ag}^{\text{I}}_2\text{Tb}^{\text{III}}\text{TCAS}_2$  formed as the main luminescent species. The structures of  $\text{Ag}^{\text{I}}_2\text{Tb}^{\text{III}}_2\text{TCAS}_2$  and  $\text{Ag}^{\text{I}}_2\text{Tb}^{\text{III}}\text{TCAS}_2$  was proposed on the basis of the crystal structure of  $\text{Ag}^{\text{I}}_4\text{Tb}^{\text{III}}\text{TCAS}_2$  (Fig. 13.9), in which two TCAS ligands are linked by four S–Ag(I)–S linkages [75]. Among the photophysical properties, the exceptionally long-lived luminescence of  $\text{Ag}^{\text{I}}_2\text{Tb}^{\text{III}}\text{TCAS}_2$  (4.6 ms) should be noted, which could be due to the  $\text{O}_8$ -cubic coordination environment provided to  $\text{Tb}^{\text{III}}$  to expel coordinating water from  $\text{Tb}^{\text{III}}$ . In fact, the number of coordinating water molecules to  $\text{Tb}^{\text{III}}$  was estimated to be 0.1 using Horrocks' equation. Taking advantage of the  $\text{O}_8$  coordination environment of  $\text{Tb}^{\text{III}}$  provided by  $\text{Ag}^{\text{I}}_4\text{Tb}^{\text{III}}\text{TCAS}_2$ , the analogous  $\text{Nd}^{\text{III}}$  complex  $\text{Ag}^{\text{I}}_4\text{Nd}^{\text{III}}\text{TCAS}_2$  was formed via self-assembly [76]. This complex exhibited efficient near infrared (NIR) luminescence ( $\Phi = 4.8 \times 10^{-4}$ ) even in water, which is usually a strong quencher of the excited states of  $\text{Nd}^{\text{III}}$  via the coupling to the overtone of the O–H vibration. The  $\text{Ag}^{\text{I}}\text{-Ln}^{\text{III}}\text{-TCAS}$  system provides a good example of the supramolecularity: the resulting structure and function (such as the  $\text{O}_8$ -cubic coordination geometry, the long-lived luminescence of  $\text{Tb}^{\text{III}}$ , and efficient NIR luminescence of  $\text{Nd}^{\text{III}}$ ) are beyond that predicted from the individual properties of each component (Eq. (13.1)). Among the components, the most valuable player is undoubtedly

TCAS, which selectively provides the S and O donor atoms to the ions in the complexes  $\text{Ag}^{\text{I}}_2\cdot\text{Tb}^{\text{III}}\cdot\text{TCAS}_2$  and  $\text{Ag}^{\text{I}}_4\cdot\text{Ln}^{\text{III}}\cdot\text{TCAS}_2$ .

Besides  $\text{Ag}^{\text{I}}$ , other metal species that form luminescent ternary complexes with  $\text{Tb}^{\text{III}}$  and TCAS were examined [77]. Among  $\text{Fe}^{\text{III}}$ ,  $\text{Ni}^{\text{II}}$ ,  $\text{Zn}^{\text{II}}$ ,  $\text{Pd}^{\text{II}}$ ,  $\text{Cd}^{\text{II}}$ ,  $\text{Hg}^{\text{II}}$ ,  $\text{Tl}^{\text{I}}$ , and  $\text{Pb}^{\text{II}}$ , only  $\text{Cd}^{\text{II}}$  gave more intense luminescence than a  $\text{Tb}^{\text{III}}\text{-TCAS}$  binary system. The luminescence occurs at a pH around 6.5 with the formation of a ternary complex. The ESI-MS results revealed that the species formed at pH 6.5 was  $\text{Cd}^{\text{II}}_2\cdot\text{Tb}^{\text{III}}_2\cdot\text{TCAS}_2$  ( $\phi=0.15$ ,  $\tau=1.12$  ms, very similar to the case of  $\text{Ag}^{\text{I}}_2\cdot\text{Tb}^{\text{III}}_2\cdot\text{TCAS}_2$ ). However, the  $\text{Cd}^{\text{II}}$  system did not form the 2:1:2 ternary complexes like  $\text{Ag}^{\text{I}}_2\cdot\text{Tb}^{\text{III}}\cdot\text{TCAS}_2$  at higher pH values. This is because the S– $\text{Cd}^{\text{II}}$ –S linkages are shorter than S– $\text{Ag}^{\text{I}}$ –S, which brings the two TCAS ligands closer together and ejects  $\text{Tb}^{\text{III}}$  from the center of the complex. These results suggest that the formation of the ternary complex relies on precise recognition of ionic radii of  $\text{Ln}^{\text{III}}$  and  $\text{Ag}^{\text{I}}/\text{Cd}^{\text{II}}$  by the TCAS ligand.

One of the potential applications of the luminescence complexes is in molecular probes for bio-imaging and bio-analysis [78]. A large luminescence quantum yield and long lifetime are desirable for the sake of highly sensitive and time-resolved detection with a high signal-to-background ratio. Another indispensable property is the kinetic stability, because the probes are used in a situation where the free components (ligand and metal ion) are removed. To obtain high kinetic stability, ligands with high denticity to encapsulate  $\text{Ln}^{\text{III}}$  inside the molecule by *endo*-coordination fashion are used as exemplified by DOTA and DTPA (Scheme 13.5). Quite recently, we noticed a gradual change in the absorption spectra of  $\text{Ln}^{\text{III}}\text{-TCAS}$  binary systems. The monitoring of the aqueous mixture of TCAS and  $\text{Ln}^{\text{III}}$  (=  $\text{Nd}^{\text{III}}$  or  $\text{Yb}^{\text{III}}$ ) with HPLC revealed that the composition changes from  $\text{Ln}^{\text{III}}\cdot\text{TCAS}$  to  $\text{Ln}^{\text{III}}_3\cdot\text{TCAS}_2$  occur to form a cluster-type complex over a long period of time (1 d) [79]. Because of the  $\text{Ln}^{\text{III}}_3$  core sandwiched between the two TCAS ligands, the  $\text{Ln}^{\text{III}}_3\cdot\text{TCAS}_2$  complex is not only luminescent but also kinetically stable. For example, the observed dissociation rate constant of  $\text{Yb}^{\text{III}}_3\cdot\text{TCAS}_2$  is  $1.26 \times 10^{-4} \text{ s}^{-1}$  (25 °C, at pH 1.16), which corresponds to the  $t_{1/2}$  value of 1.53 h. This was not expected from the *exo*-coordination fashion of TCAS with the O,S,O donors found in  $\text{Ln}^{\text{III}}\cdot\text{TCAS}$ , and thus, this feature was attributed to the multiple bonds between the  $\text{Ln}^{\text{III}}_3$  core and TCAS. Here, the kinetic inertness is another example of supramolecularity of the components, where multidenticity of TCAS plays an essential role. Thus, the  $\text{Ln}^{\text{III}}_3\cdot\text{TCAS}_2$  complex opens an exciting possibility of designing kinetically stable  $\text{Ln}^{\text{III}}$  complexes by using *exo*-type ligands as scaffolds to sandwich a multi- $\text{Ln}^{\text{III}}$  core rather than *endo*-type ones to encapsulate a  $\text{Ln}^{\text{III}}$  core. Extensions of the  $\text{Ln}^{\text{III}}_3\cdot\text{TCAS}_2$  in two directions are now underway. The first is not luminescence probe but the design of a magnetic resonance imaging (MRI) contrast agent ( $\text{Gd}^{\text{III}}_3\cdot\text{TCAS}_2$ ) [80]. The second is a heterolanthanide assembly  $\text{Tb}^{\text{III}}_{3-x}\cdot\text{Yb}^{\text{III}}_x\cdot\text{TCAS}_2$  ( $x=1, 2$ ) to realize f-f communication between the two different lanthanide centers that will lead to enhanced  $\text{Yb}^{\text{III}}$  luminescence or down-conversion [81].



### 13.4.6 Sensing

Sensing has been one of the main applications of calixarenes owing to its facile modification with binding and reporter groups to enable optical or electrochemical signaling [82–86]. Sharing the same phenol moiety, TC4A can be modified and used in the same fashion as exemplified by the literature cited in the recent review [10]. However, such modification without using the bridging sulfur is a typical *mottainai* (wasteful) way of application of TC4A and will not be described here.

Sensing can be divided into two major modes: electrochemical and optical. In the former, an analyte is detected by the electrochemical potential generated at the membrane surface as seen in potentiometry, or by current upon oxidation (or reduction) of the accumulated analyte in the reduced (or oxidized) form as seen in stripping voltammetry. Therefore, in electrochemical sensing, TC4A does not have to be modified with any reporter moiety. For example, TC4A was used as the ionophore for  $\text{Cu}^{\text{II}}$  sensors based on field-effect transistor and electrolyte-insulator-semiconductor sensor. The TC4A was used as thin films (thickness: 20–100 nm) formed by thermal sublimation ( $10^{-6}$  Torr, 270–280 °C) [87, 88]. The sensor enabled the detection of  $\text{Cu}^{\text{II}}$  at low ( $10^{-5}$  M) levels by the complexation of  $\text{Cu}^{\text{II}}$  with the TC4A layer, which should be due to the coordination ability of the bridging sulfur.

In the voltammetric scheme, Zheng et al. reported the simultaneous determination of  $\text{Pb}^{\text{II}}$  and  $\text{Cd}^{\text{II}}$  by a glassy carbon electrode (GCE) modified with a Langmuir–Blodgett (LB) film of TC4A [89]. In the accumulation step, the TC4A film seemed to form a complex with  $\text{Pb}^{\text{II}}$  and  $\text{Cd}^{\text{II}}$  to preconcentrate these metal ions. After reduction, the metal ions were measured by differential pulse stripping voltammetry, enabling their ultratrace determination with the detection limits

$2 \times 10^{-8}$  M ( $\text{Cd}^{\text{II}}$ ) and  $8 \times 10^{-9}$  M ( $\text{Pb}^{\text{II}}$ ), respectively. The method can be successfully applied to real samples (river, lake and tap water), where the selectivity of TC4A to the heavy metal ions over other hard metal ions in the samples should play a key role.

Recently, Wang et al. covalently attached TC4A to multiwalled carbon nanotubes (MWCNT) to obtain chemically modified electrodes for anodic stripping voltammetry to detect ultratrace  $\text{Pb}^{\text{II}}$  [90]. The stripping response is highly linear ( $R = 0.999$ ) over a  $\text{Pb}^{\text{II}}$  concentration range of  $2 \times 10^{-10}$  to  $1 \times 10^{-8}$  M, and the limit of detection is  $4 \times 10^{-11}$  M. The improved sensitivity seems to originate from the high surface area and excellent conductivity of the MWCNT.

As can be seen in the electrochemical methods, the analyte itself can act as the reporter. Therefore, it was not necessary for TC4A to be modified with electrochemical reporters. In the case of luminescence sensing for metal ions, the metal ions per se do not usually show luminescence because of the poor ability in the absorption of photon, quenching by solvent, and the forbidden d-d and f-f transition for the luminescence. An easy method to detect metal ions by luminescence is to design a fluorescence sensor having both ion-binding and fluorescent moieties, which was seen in both calix- and thiacalixarene research. There are many examples for thiacalixarenes in which the auxiliary binding moiety nicely binds to metal ions as intended but at the same time the bridging sulfur has no role to play. Combining with reporter materials in a noncovalent fashion, TC4A will behave as the signal-transducing unit by virtue of its intrinsic binding ability towards a metal ion. For example, a quantum dot (QD), which is a nanocolloidal particle of semiconductors, can be a luminescent probe owing to its attractive features such as narrow and tunable emission band, high quantum efficiency, high durability to photobleaching, and broad excitation band. For these reasons, the application of QDs to bioanalytical chemistry is a hot area of research. However, QD per se does not possess the ability to respond to certain analyte ions or molecules. Jin et al. coated CdSe/ZnS quantum dots with 25,26,27,28-tetra(carboxymethoxy)-2,8,14,20-tetrathiacalix[4]arene (TCC) by simply mixing them in THF followed by the deprotonation of TCC with *t*-BuOK (Fig. 13.10) [91]. The coating proceeded

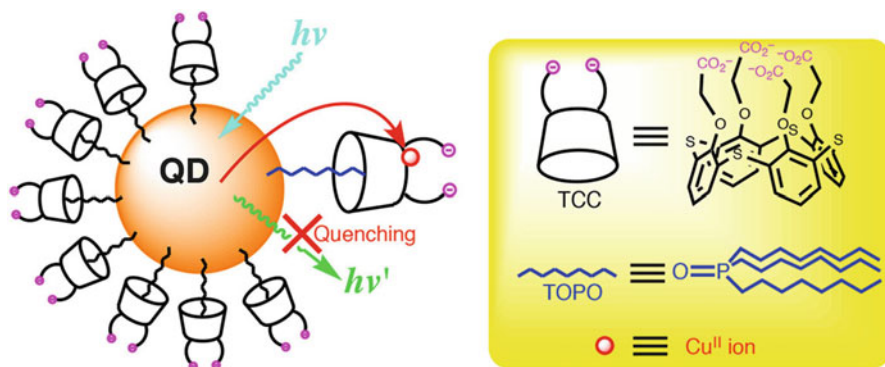
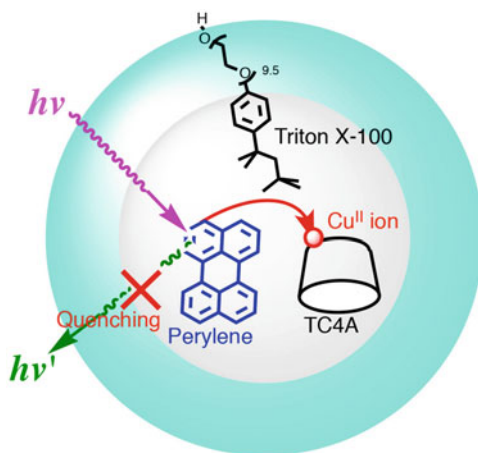


**Fig. 13.10** Sensing of  $\text{Cu}^{\text{II}}$  with a QD/TOPO/TCC supramolecular system

by self-assembly of TCC onto trioctylphosphine oxide (TOPO) on the QD via hydrophobic interactions. This converts the QD into a water-soluble supramolecular fluorescent sensor for  $\text{Cu}^{\text{II}}$ , in which the TC4A moiety acts as the signal transducer to bind to  $\text{Cu}^{\text{II}}$  to quench the luminescence of the QD. In the absence of  $\text{Cu}^{\text{II}}$ , the luminescence quantum yield was higher (0.21) than that achieved with QDs surface-modified with mercaptoacetic acid and mercaptoundecanoic acid. The fluorescence of the TCC-coated QDs was selectively quenched by  $\text{Cu}^{\text{II}}$  ions even in the presence of other transition metal ions such as  $\text{Cd}^{\text{II}}$ ,  $\text{Zn}^{\text{II}}$ ,  $\text{Co}^{\text{II}}$ ,  $\text{Fe}^{\text{II}}$ , and  $\text{Fe}^{\text{III}}$  in the same solution. The quenching mechanism followed a static manner, implying that a selective complexation of TCC moiety to  $\text{Cu}^{\text{II}}$  is responsible for the observed selectivity. The fluorescence of TCC-coated QDs was almost insensitive to other physiologically important ions such as  $\text{Na}^{\text{I}}$ ,  $\text{K}^{\text{I}}$ ,  $\text{Mg}^{\text{II}}$ , and  $\text{Ca}^{\text{II}}$ , suggesting that the TCC-coated QDs can be used as a fluorescent  $\text{Cu}^{\text{II}}$  ion probe for biomedical samples. Here the TCC is the key multifunctional material as the QD coating to make it water soluble, ion-selective ligand, and transducer to quench the luminescence of the QD.

Recently, Hu et al. prepared a  $\text{Cu}^{\text{II}}$ -selective self-assembled fluorescent chemosensor by solubilizing both TC4A as the ion-binding moiety and perylene as the fluorescent reporter in a micelle of a nonionic surfactant Triton X-100 (Fig. 13.11) [92]. Upon addition of  $\text{Cu}^{\text{II}}$  to the micelle solution, the fluorescence emission of perylene inside the micelles was quenched. The authors attributed this to intramolecular electron-transfer or energy-transfer from perylene to  $\text{Cu}^{\text{II}}$ -TC4A complex induced by the complexation of TC4A with  $\text{Cu}^{\text{II}}$  ion. Copper(II) ions can be detected selectively in the presence of other metal ions ( $\text{Zn}^{\text{II}}$ ,  $\text{Pb}^{\text{II}}$ ,  $\text{Cd}^{\text{II}}$ ,  $\text{Mn}^{\text{II}}$ ,  $\text{Ni}^{\text{II}}$ ,  $\text{Al}^{\text{III}}$ ,  $\text{Na}^{\text{I}}$ ,  $\text{K}^{\text{I}}$ ,  $\text{Ca}^{\text{II}}$ , and  $\text{Mg}^{\text{II}}$ ) and its concentration in the submicromolar range can be determined based on the fluorescence quenching. The micelle provides water-solubility to both TC4A and perylene, and confined space to facilitate the complex-fluorophore interaction, where TC4A acted as the signal transducer for  $\text{Cu}^{\text{II}}$ .

**Fig. 13.11** Quenching sensing of  $\text{Cu}^{\text{II}}$  with Triton X-100 micelle containing TC4A and perylene. The large blue sphere represents hydrophilic region of the micelle, while white sphere does the hydrophobic core



Since the resulting function of the TC4A-erythrin-micelle ternary sensor exceeds the expected individual function from the component, the sensor can be regarded as a supramolecular system.

Metal ions having luminescence function can be used in molecular-based chemosensors without using colloidal materials such as QD and micelles. As mentioned above,  $\text{Ln}^{\text{III}}$  can emit visible to NIR light with high efficiency if the excited energy can be transferred from the  $T_1$  state of an antenna ligand such as TCAS and  $\text{SO}_2\text{CAS}$  [72, 79]. The formation of  $\text{Tb}^{\text{III}}\cdot\text{TCAS}$  can be readily applied for the luminescence detection of  $\text{Tb}^{\text{III}}$  at sub-ppb levels [93]. From the viewpoint of multifunctionality of thiocalixarene,  $\text{Tb}^{\text{III}}\cdot\text{TCAS}$  still has sites to interact with ions and molecules: the remaining O,S,O binding sites and the hydrophobic cavity.

For the latter, we studied the luminescence quenching of  $\text{Tb}^{\text{III}}\cdot\text{TCAS}$  by a cationic guest such as the quaternary ammonium ion [94]. For example, 1-ethylquinolinium quenched the luminescence of  $\text{Tb}^{\text{III}}\cdot\text{TCAS}$  most efficiently, affording a very low detection limit (D.L. =  $6.71 \times 10^{-10}$  M, S/N = 3). The agreement of the Stern-Volmer (SV) coefficients obtained with luminescent intensity ( $K_{\text{SV,all}} = 6.74 \times 10^6 \text{ M}^{-1}$ ) and lifetime ( $K_{\text{SV,Tb}} = 6.50 \times 10^6 \text{ M}^{-1}$ ) implied that dynamic quenching of the  $^5\text{D}_4$  excited state of  $\text{Tb}^{\text{III}}$  was predominant in the quenching processes. The quenching rate is  $k_{\text{q,Tb}} = 9.94 \times 10^9 \text{ M}^{-1} \text{ s}^{-1}$ , which was as fast as the diffusion-limited rate. Unexpectedly, the classical  $\text{Tb}^{\text{III}}\cdot\text{CAS}_2$  also showed luminescence quenching by 1-ethylpyridinium (D.L. =  $5.94 \times 10^{-8}$  M) and nicotinamide adenine dinucleotide (NAD, D.L. =  $2.78 \times 10^{-7}$  M). These results clearly indicate that luminescence chemosensors can be constructed not only by using covalent attachment of fluorophore to CAS and TCAS, but also in a noncovalent, supramolecular fashion.

For the remaining O,S,O sites, the formation of  $\text{Ag}^{\text{I}}_2\cdot\text{Tb}^{\text{III}}_2\cdot\text{TCAS}_2$  can be regarded as such because the ternary complex utilizes the full donor sets. The formation of complex  $\text{Ag}^{\text{I}}_2\cdot\text{Tb}^{\text{III}}_2\cdot\text{TCAS}_2$  was applied to the supramolecular luminescent detection of  $\text{Ag}^{\text{I}}$  ion at nanomolar levels [95]. As mentioned above,  $\text{Ag}^{\text{I}}_2\cdot\text{Tb}^{\text{III}}_2\cdot\text{TCAS}_2$  formed at pH = 6, whereas in the absence of  $\text{Ag}^{\text{I}}$  ions, TCAS scarcely complexed with  $\text{Tb}^{\text{III}}$  ions. The dependence of the luminescence intensity of  $\text{Ag}^{\text{I}}_2\cdot\text{Tb}^{\text{III}}_2\cdot\text{TCAS}_2$  on the  $\text{Ag}^{\text{I}}$  concentration was measured for  $[\text{Ag}^{\text{I}}] = 0.5\text{--}100 \times 10^{-8}$  M with  $[\text{Tb}^{\text{III}}] = 1.0 \times 10^{-6}$  M and  $[\text{TCAS}] = 2.0 \times 10^{-6}$  M at pH = 6.1. The system exhibited an almost linear response to  $[\text{Ag}^{\text{I}}]$  and yielded a D.L. of  $3.2 \times 10^{-9}$  M (0.35 ppb) for  $\text{Ag}^{\text{I}}$  at S/N = 3. Addition of fivefold amount of transition metal ions to  $1.0 \times 10^{-7}$  M  $\text{Ag}^{\text{I}}$  did not interfere except in the following cases:  $\text{Cu}^{\text{II}}$  and  $\text{Fe}^{\text{III}}$  caused negative interference due to the concomitant formation of nonluminescent  $\text{Tb}^{\text{III}}\text{-TCAS}$  ternary complex that decreased the availability of  $\text{Tb}^{\text{III}}$  ions.  $\text{Cd}^{\text{II}}$  caused a positive deviation due to the formation of the luminescent  $\text{Cd}^{\text{II}}_2\cdot\text{Tb}^{\text{III}}_2\cdot\text{TCAS}_2$ . Among halide ions, a fivefold amount of iodide caused negative interference due to its high complexation ability with  $\text{Ag}^{\text{I}}$  ions. Besides the analytical performance, the emergence of the function of this system should be noted (Fig. 13.12). The components  $\text{Tb}^{\text{III}}$  and TCAS do not have signaling function (i.e. luminescence) at pH = 6. However, in the presence of analyte  $\text{Ag}^{\text{I}}$  ions, two TCAS ligands were linked by  $\text{Ag}^{\text{I}}$  and coordinated to the  $\text{Tb}^{\text{III}}$  ions to form  $\text{Ag}^{\text{I}}_2\cdot\text{Tb}^{\text{III}}_2\cdot\text{TCAS}_2$  to provide the signaling function as indicated by

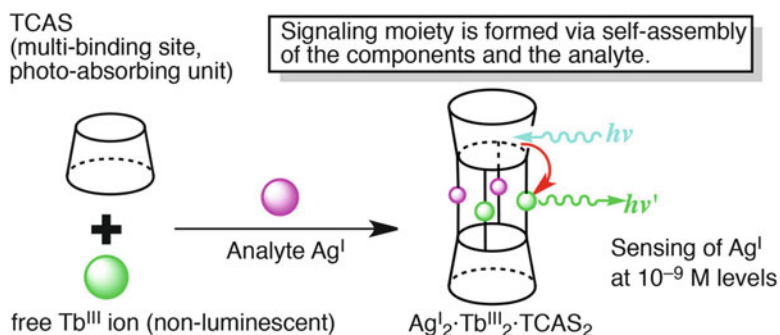


Fig. 13.12 Supramolecular sensing of Ag<sup>I</sup> ion by the ternary complex formation

Eq. (13.1). Thus, this system demonstrates the supramolecular strategy to develop luminescent sensors for metal ions.

By using the self-assembly of Cd<sup>II</sup><sub>2</sub>·Tb<sup>III</sup><sub>2</sub>·TCAS<sub>2</sub>, a determination method for nanomolar levels of Cd<sup>II</sup> was developed similar to the Ag<sup>I</sup> determination with the formation of Ag<sup>I</sup><sub>2</sub>·Tb<sup>III</sup><sub>2</sub>·TCAS<sub>2</sub> [96]. At pH 6.5 where the difference in the luminescence intensities between Cd<sup>II</sup>·Tb<sup>III</sup>·TCAS and Tb<sup>III</sup>·TCAS systems was the largest, the calibration curve for Cd<sup>II</sup> was linear to give a detection limit of ( $S/N = 3$ ) 2.08 nM. The method was applicable to the determination of sub-ppm levels of Cd in rice, which is one of the major sources of Cd exposure. The interference by Cu<sup>II</sup> and phosphate in the acid digests of rice samples were removed by masking Cu<sup>II</sup> with iminodiacetate and separation of the phosphate using chelate disk, respectively. The detection limit for 1 g of a rice sample was 12.2 ppb ( $S/N = 3$ ), which cleared the standard of cadmium in rice based on the Food Sanitation Act, Japan (0.4 ppm). Recovery for 1.007 g brown rice spiked with 3.56 nmol Cd<sup>II</sup> and 2.002 g brown rice spiked with 7.12 nmol Cd<sup>II</sup> were 101.0% and 100.3%, respectively. In addition, in the standard rice sample (certified value of Cd 0.548 ppm) measurement, result was 0.564 ppm. Thus, despite the fact that TCAS lacks the reporter group in the molecule, it was successfully applied to the practical determination of Cd<sup>II</sup> by the formation of the luminescence ternary complex.

Inspired by metalloenzymes having two Lewis acid centers, and by the catalytic action of the dinuclear complex, cone-[Ti<sup>IV</sup><sub>2</sub>(tca)Cl<sub>4</sub>], Matsumiya devised a dinuclear complex, Ce<sup>IV</sup><sub>2</sub>·TCAS mimicking the phosphatase enzyme [97, 98]. This complex can promote the hydrolysis of *p*-nitrophenyl phosphate with a turnover frequency of 6.8 h<sup>-1</sup> at 50 °C. Moreover, the dinuclear complex can be electrostatically immobilized onto an antibody by simply mixing them together in water. The antibody labeled with the catalyst provides immunoassay of an antigen by detecting the color-development reaction (Fig. 13.13). Thus, 10 ng mL<sup>-1</sup> of a tumor marker, Bence-Jones protein (BJP), in urine sample was detected by using this sensor. Here, TCAS plays an essential role not only as the ligand assembling two Ce<sup>IV</sup> centers to realize the enzymatic function, but also as a platform to attach the artificial enzyme to the antibody in a noncovalent fashion.



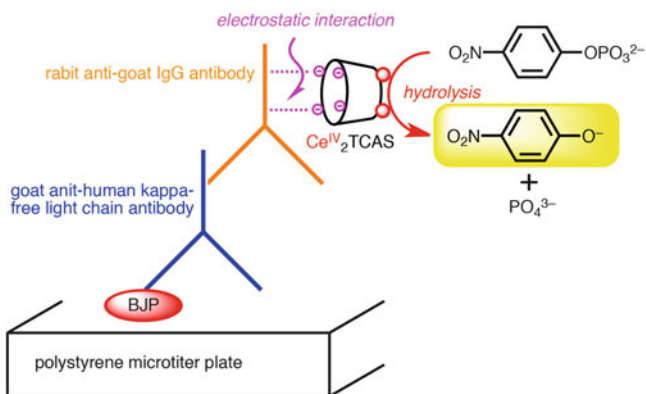


**Fig. 13.13** Immunoassay for BJP using antibody labeled with  $\text{Ce}^{\text{IV}}$ -TCAS complex having hydrolysis activity

The facile conjugation of TCAS suggests the possibility of application of the diverse reporter functions of TCAS complexes, such as catalysis, energy transfer luminescence, and relaxivity, to bioanalysis and bioimaging. In combination with other components, TCAS thus provides supramolecular sensing functions, which rely on the multifunctionality of thiocalixarene.

## 13.5 Conclusion

As we have seen in the preceding discussion, thiocalixarene and its derivatives with oxidized sulfur bridges have unique properties and functions arising from the sulfur such as reactivity, inclusion, selective binding to the metal ions, and metal-cluster formation. Moreover, with its synergistic combination with other entities such as metal ions, profuse functions beyond prediction have emerged: separation of metal ions, Lewis acid and oxidation catalysis, giant-cage formation by self-assembly of the metal-cluster unit, molecular magnetism to lead to SMMs, energy-transfer luminescence for probes, and sensing through the formation of supramolecular metal complexes. In each case, the bridging sulfur plays an indispensable role in the emergence of the function. Some of the examples showed practical applicability, but the remaining are still on the way to the level of real situations. The supramolecular strategy to develop the function as formulated by Eq. (13.1) suggests that there is no limitation of the outcome of the function  $f(x + y)$  derived from the combination of thiocalixarene  $x$  with other entity  $y$ . In addition, the number of combinations with  $y$  is unlimited, which leads to unlimited possibilities in function. To draw the nautical chart to sail the vast expanse of the thiocalix ocean, we chemists must still pursue exploratory but systematic research while expecting the discovery of novel functions.



**Acknowledgements** The author acknowledges with thanks Profs. S. Miyano, T. Hattori, and N. Morohashi, Tohoku University for their great suggestions, discussions, and contributions.

## References

1. Sone, T.; Ohba, Y.; Moriya, K.; Kumada, H.; Ito, K. *Tetrahedron* **1997**, *53*, 10689–10698.
2. Kumagai, H.; Hasegawa, M.; Miyanari, S.; Sugawa, Y.; Sato, Y.; Hori, T.; Ueda, S.; Kamiyama, H.; Miyano, S. *Tetrahedron Lett.* **1997**, *38*, 3971–3972.
3. Gutsche, C. D. *Calixarenes*; Royal Society of Chemistry: Cambridge, 1989.
4. Iki, N.; Miyano, S. *J. Inclusion Phenom. Macrocyclic Chem.* **2001**, *41*, 99–105.
5. Morohashi, N.; Iki, N.; Miyano, S. *Yuki Gosei Kagaku Kyokaiishi* **2002**, *60*, 550–562.
6. Lhoták, P. *Eur. J. Org. Chem.* **2004**, 1675–1692.
7. Morohashi, N.; Narumi, F.; Iki, N.; Hattori, T.; Miyano, S. *Chem. Rev.* **2006**, *106*, 5291–5316.
8. Iki, N. *J. Inclusion Phenom. Macrocyclic Chem.* **2009**, *64*, 1–13.
9. Iki, N. *Supramol. Chem.* **2011**, *23*, 160–168.
10. Kumar, R.; Lee, Y. O.; Bhalla, V.; Kumar, M.; Kim, J. S. *Chem. Soc. Rev.* **2014**, *43*, 4824–4870.
11. Iki, N.; Ogawa, S.; Matsue, T.; Miyano, S. *J. Electroanal. Chem.* **2007**, *610*, 90–95.
12. Iki, N.; Morohashi, N.; Suzuki, T.; Ogawa, S.; Aono, M.; Kabuto, C.; Kumagai, H.; Takeya, H.; Miyanari, S.; Miyano, S. *Tetrahedron Lett.* **2000**, *41*, 2587–2590.
13. Kondo, Y.; Ulzii, M.; Itoh, S.; Yamada, M.; Hamada, F. *Int. J. Soc. Mater. Eng. Resour.* **2014**, *20*, 103–108.
14. Morohashi, N.; Iki, N.; Aono, M.; Miyano, S. *Chem. Lett.* **2002**, *31*, 494–495.
15. Kajiwara, T.; Kon, N.; Yokozawa, S.; Ito, T.; Iki, N.; Miyano, S. *J. Am. Chem. Soc.* **2002**, *124*, 11274–11275.
16. Kajiwara, T.; Shinagawa, R.; Ito, T.; Kon, N.; Iki, N.; Miyano, S. *Bull. Chem. Soc. Jpn.* **2003**, *76*, 2267–2275.
17. Iki, N.; Kabuto, C.; Fukushima, T.; Kumagai, H.; Takeya, H.; Miyanari, S.; Miyashi, T.; Miyano, S. *Tetrahedron* **2000**, *56*, 1437–1443.
18. Patel, M. H.; Shrivastav, P. S. *Chem. Commun.* **2009**, 586–588.
19. Kundrat, O.; Eigner, V.; Dvorakova, H.; Lhoták, P. *Org. Lett.* **2011**, *13*, 4032–4035.
20. Kundrat, O.; Dvorakova, H.; Bohm, S.; Eigner, V.; Lhoták, P. *J. Org. Chem.* **2012**, *77*, 2272–2278.
21. Kundrat, O.; Dvorakova, H.; Eigner, V.; Lhoták, P. *J. Org. Chem.* **2010**, *75*, 407–411.
22. Kundrat, O.; Kroupa, J.; Bohm, S.; Budka, J.; Eigner, V.; Lhoták, P. *J. Org. Chem.* **2010**, *75*, 8372–8375.
23. Kundrat, O.; Cisarova, I.; Bohm, S.; Pojarova, M.; Lhoták, P. *J. Org. Chem.* **2009**, *74*, 4592–4596.
24. Akdas, H.; Bringel, L.; Graf, E.; Hosseini, M. W.; Mislin, G.; Pansanel, J.; De Cian, A.; Fischer, J. *Tetrahedron Lett.* **1998**, *39*, 2311–2314.
25. Morohashi, N.; Noji, S.; Nakayama, H.; Kudo, Y.; Tanaka, S.; Kabuto, C.; Hattori, T. *Org. Lett.* **2011**, *13*, 3292–3295.
26. Morohashi, N.; Miyoshi, I.; Tonosaki, A.; Ohsugi, K.; Kitamoto, Y.; Hattori, T. In *The 13th Host-Guest Chemistry Symposium, Japan Sendai*, 2015, B-16.
27. Ebata, K.; Morohashi, N.; Hattori, T. In *The 13th Host-Guest Chemistry Symposium, Japan Sendai*, 2015, 1P-12.
28. Iki, N.; Morohashi, N.; Narumi, F.; Miyano, S. *Bull. Chem. Soc. Jpn.* **1998**, *71*, 1597–1603.
29. Morohashi, N.; Iki, N.; Sugawara, A.; Miyano, S. *Tetrahedron* **2001**, *57*, 5557–5563.
30. Iki, N.; Morohashi, N.; Kabuto, C.; Miyano, S. *Chem. Lett.* **1999**, *28*, 219–220.

31. Harrowfield, J.; Koutsantonis, G. In *Calixarenes in the Nanoworld*; Vicens, J., Harrowfield, J., Baklouti, L., Eds.; Springer: Netherlands, 2007, p 197–212.
32. Kajiwara, T.; Iki, N.; Yamashita, M. *Coord. Chem. Rev.* **2007**, *251*, 1734–1746.
33. Bilyk, A.; Hall, A. K.; Harrowfield, J. M.; Hosseini, M. W.; Skelton, B. W.; White, A. H. *Inorg. Chem.* **2001**, *40*, 672–686.
34. Bilyk, A.; Dunlop, J. W.; Fuller, R. O.; Hall, A. K.; Harrowfield, J. M.; Hosseini, M. W.; Koutsantonis, G. A.; Murray, I. W.; Skelton, B. W.; Sobolev, A. N.; Stamps, R. L.; White, A. H. *Eur. J. Inorg. Chem.* **2010**, 2127–2152.
35. Bilyk, A.; Dunlop, J. W.; Fuller, R. O.; Hall, A. K.; Harrowfield, J. M.; Hosseini, M. W.; Koutsantonis, G. A.; Murray, I. W.; Skelton, B. W.; Stamps, R. L.; White, A. H. *Eur. J. Inorg. Chem.* **2010**, 2106–2126.
36. Matsumiya, H.; Iki, N.; Miyano, S.; Hiraide, M. *Anal. Bioanal. Chem.* **2004**, *379*, 867–871.
37. Matsumiya, H.; Hiraide, M. *Bull. Chem. Soc. Jpn.* **2005**, *78*, 1939–1943.
38. Matsumiya, H.; Yasuno, S.; Iki, N.; Miyano, S. *J. Chromatogr. A* **2005**, *1090*, 197–200.
39. Kikuchi, T.; Goto, I.; Suzuki, K. *J. Nucl. Sci. Technol.* **2006**, *43*, 690–693.
40. Kikuchi, T.; Suzuki, K. *J. Alloys Compd.* **2006**, *408–412*, 1287–1290.
41. Morohashi, N.; Hattori, T.; Yokomakura, K.; Kabuto, C.; Miyano, S. *Tetrahedron Lett.* **2002**, *43*, 7769–7772.
42. Morohashi, N.; Yokomakura, K.; Hattori, T.; Miyano, S. *Tetrahedron Lett.* **2006**, *47*, 1157–1161.
43. Proto, A.; Giugliano, F.; Capacchione, C. *Eur. Polym. J.* **2009**, *45*, 2138–2141.
44. Floriani, C.; Floriani-Moro, R. In *Calixarenes 2001*; Kluwer Academic Publishers: 2001, p 536–560.
45. Yilmaz, M. In *Calixarenes and Beyond*; Neri, P., Ed.; Springer: 2016.
46. Limberg, C. *Eur. J. Inorg. Chem.* **2007**, 3303–3314.
47. Su, K.; Jiang, F.; Qian, J.; Gai, Y.; Wu, M.; Bawaked, S. M.; Mokhtar, M.; Al-Thabaiti, S. A.; Hong, M. *Cryst. Growth Des.* **2014**, *14*, 3116–3123.
48. Su, K.; Jiang, F.; Qian, J.; Pang, J.; Al-Thabaiti, S. A.; Bawaked, S. M.; Mokhtar, M.; Chen, Q.; Hong, M. *Cryst. Growth Des.* **2014**, *14*, 5865–5870.
49. Bi, Y.; Wang, X.-T.; Liao, W.; Wang, X.; Wang, X.; Zhang, H.; Gao, S. *J. Am. Chem. Soc.* **2009**, *131*, 11650–11651.
50. Gehin, A.; Ferlay, S.; Harrowfield, J. M.; Fenske, D.; Kyritsakas, N.; Hosseini, M. W. *Inorg. Chem.* **2012**, *51*, 5481–5486.
51. Bi, Y.; Du, S.; Liao, W. *Chem. Commun.* **2011**, *47*, 4724–4726.
52. Bi, Y.; Du, S.; Liao, W. *Coord. Chem. Rev.* **2014**, *276*, 61–72.
53. Bi, Y.; Xu, G.; Liao, W.; Du, S.; Wang, X.; Deng, R.; Zhang, H.; Gao, S. *Chem. Commun.* **2010**, *46*, 6362–6364.
54. Xiong, K.; Jiang, F.; Gai, Y.; He, Z.; Yuan, D.; Chen, L.; Su, K.; Hong, M. *Cryst. Growth Des.* **2012**, *12*, 3335–3341.
55. Bi, Y.; Wang, S.; Liu, M.; Du, S.; Liao, W. *Chem. Commun.* **2013**, *49*, 6785–6787.
56. Du, S.; Yu, T.-Q.; Liao, W.; Hu, C. *Dalton Trans.* **2015**, *44*, 14394–14402.
57. Dai, F.-R.; Wang, Z. *J. Am. Chem. Soc.* **2012**, *134*, 8002–8005.
58. Dai, F.-R.; Becht, D. C.; Wang, Z. *Chem. Commun.* **2014**, *50*, 5385–5387.
59. Dai, F.-R.; Sambasivam, U.; Hammerstrom, A. J.; Wang, Z. *J. Am. Chem. Soc.* **2014**, *136*, 7480–7491.
60. Kajiwara, T.; Hasegawa, M.; Ishii, A.; Katagiri, K.; Baatar, M.; Takaishi, S.; Iki, N.; Yamashita, M. *Eur. J. Inorg. Chem.* **2008**, 5565–5568.
61. Bi, Y.; Wang, X.-T.; Liao, W.; Wang, X.; Deng, R.; Zhang, H.; Gao, S. *Inorg. Chem.* **2009**, *48*, 11743–11747.
62. Desroches, C.; Pilet, G.; Borshch, S. A.; Parola, S.; Luneau, D. *Inorg. Chem.* **2005**, *44*, 9112–9120.
63. Desroches, C.; Pilet, G.; Szilagyi, P. A.; Molnar, G.; Borshch, S. A.; Bousseksou, A.; Parola, S.; Luneau, D. *Eur. J. Inorg. Chem.* **2006**, 357–365.

64. Lamouchi, M.; Jeanneau, E.; Novitchi, G.; Luneau, D.; Brioude, A.; Desroches, C. *Inorg. Chem.* **2014**, *53*, 63–72.
65. Xiong, K.; Wang, X.; Jiang, F.; Gai, Y.; Xu, W.; Su, K.; Li, X.; Yuan, D.; Hong, M. *Chem. Commun.* **2012**, *48*, 7456–7458.
66. Su, K.; Jiang, F.; Qian, J.; Wu, M.; Xiong, K.; Gai, Y.; Hong, M. *Inorg. Chem.* **2013**, *52*, 3780–3786.
67. Eliseeva, S. V.; Bünzli, J. C. *Chem. Soc. Rev.* **2010**, *39*, 189–227.
68. Eliseeva, S. V.; Bünzli, J.-C. G. *New J. Chem.* **2011**, *35*, 1165–1176.
69. Zhu, X.-H.; Peng, J.; Cao, Y.; Roncali, J. *Chem. Soc. Rev.* **2011**, *40*, 3509–3524.
70. Liu, Z.; Zhang, G.; Zhang, D. *Chem. – Eur. J.* **2016**, *22*, 462–471.
71. Sabbatini, N.; Guardigli, M.; Manet, I.; Ziessel, R. In *Calixarenes 2001*; Kluwer Academic Publishers: 2001, p 583–597.
72. Iki, N.; Horiuchi, T.; Oka, H.; Koyama, K.; Morohashi, N.; Kabuto, C.; Miyano, S. *J. Chem. Soc. Perkin Trans.* **2001**, *2*, 2219–2225.
73. Matsumiya, H.; Masai, H.; Terazono, Y.; Iki, N.; Miyano, S. *Bull. Chem. Soc. Jpn.* **2003**, *76*, 133–136.
74. Iki, N.; Ohta, M.; Horiuchi, T.; Hoshino, H. *Chem. – Asian J.* **2008**, *3*, 849–853.
75. Tanaka, T.; Iki, N.; Kajiwara, T.; Yamashita, M.; Hoshino, H. *J. Inclusion Phenom. Macrocyclic Chem.* **2009**, *64*, 379–383.
76. Iki, N.; Hiro-oka, S.; Tanaka, T.; Kabuto, C.; Hoshino, H. *Inorg. Chem.* **2012**, *51*, 1648–1656.
77. Iki, N.; Tanaka, T.; Hoshino, H. *Inorg. Chim. Acta* **2013**, *397*, 42–47.
78. Bünzli, J.-C. G. *J. Lumin.* **2016**, *170*, 866–878.
79. Iki, N.; Hiro-oka, S.; Nakamura, M.; Tanaka, T.; Hoshino, H. *Eur. J. Inorg. Chem.* **2012**, 3541–3545.
80. Iki, N.; Boros, E.; Nakamura, M.; Baba, R.; Caravan, P. *Inorg. Chem.* **2016**, *55*, 4000–4005.
81. Karashimada, R.; Iki, N. *Chem. Commun.* **2016**, *52*, 3139–3142.
82. Tang, W.; Su, M. *Appl. Mech. Mater.* **2014**, *687–691*, 4223–4227.
83. Song, M.; Sun, Z.; Han, C.; Tian, D.; Li, H.; Kim, J. S. *Chem. – Asian J.* **2014**, *9*, 2344–2357.
84. Patra, S.; Maity, D.; Gunupuru, R.; Agnihotri, P.; Paul, P. *J. Chem. Sci.* **2012**, *124*, 1287–1299.
85. Kim, H. N.; Ren, W. X.; Kim, J. S.; Yoon, J. *Chem. Soc. Rev.* **2012**, *41*, 3210–3244.
86. Sharma, K.; Cragg, P. J. *Chem. Sens.* **2011**, *1*, 1–18.
87. Ben Ali, M.; Bureau, C.; Martelet, C.; Jaffrezic-Renault, N.; Lamartine, R.; Ben Ouada, H. *Mater. Sci. Eng., C* **2000**, *C7*, 83–89.
88. Ben Ali, M.; Jaffrezic-Renault, N.; Martelet, C.; Ben Ouada, H.; Davenas, J.; Charbonnier, M. *Mater. Sci. Eng., C* **2001**, *C14*, 17–23.
89. Zheng, H.; Yan, Z.; Dong, H.; Ye, B. *Sens. Actuators, B* **2007**, *120*, 603–609.
90. Wang, L.; Wang, X.; Shi, G.; Peng, C.; Ding, Y. *Anal. Chem.* **2012**, *84*, 10560–10567.
91. Jin, T.; Fujii, F.; Yamada, E.; Nodasaka, Y.; Kinjo, M. *Comb. Chem. High Throughput Screen.* **2007**, *10*, 473–479.
92. Hu, X.-J.; Li, C.-M.; Song, X.-Y.; Zhang, D.; Li, Y.-S. *Inorg. Chem. Commun.* **2011**, *14*, 1632–1635.
93. Horiuchi, T.; Iki, N.; Oka, H.; Miyano, S. *Bull. Chem. Soc. Jpn.* **2002**, *75*, 2615–2619.
94. Horiuchi, T.; Iki, N.; Hoshino, H. *Anal. Chim. Acta* **2009**, *650*, 258–263.
95. Iki, N.; Ohta, M.; Tanaka, T.; Horiuchi, T.; Hoshino, H. *New J. Chem.* **2009**, *33*, 23–25.
96. Abe, N.; Hoshino, H.; Iki, N. *Bunseki Kagaku* **2015**, *64*, 493–499.
97. Matsumiya, H.; Nakamura, H.; Hiraide, M. *Anal. Bioanal. Chem.* **2009**, *394*, 1471–1476.
98. Nagai, S.; Matsumiya, H.; Hiraide, M. *Bunseki Kagaku* **2012**, *61*, 723–726.

# Chapter 14

## Azacalixaromatics

De-Xian Wang and Mei-Xiang Wang

### 14.1 Introduction

Calix[n]arenes are known as one type of the privileged macrocyclic host molecules in the study of supramolecular chemistry [1]. Replacement of the carbon bridges by heteroatoms, and the phenol moiety by heteroaromatic rings such as pyridine, pyrimidine, pyrazine, triazine, etc. engenders a new family of macrocycles which are named as heteracalixaromatics or heteroatom-bridged calix(het)arenes. In comparison to conventional calix[n]arenes, heteracalixaromatics enjoy much richer molecular diversity and complexity as the different combinations of various heteroatoms and heteroaromatic rings afford almost limitless macrocyclic compounds. Moreover, heteracalixaromatics give unique conformation and cavity structures and, more importantly, they exhibit versatile property of molecular recognition and self-assembly. This is attributable to the fact that the bridging heteroatoms can adopt different electronic configurations and form variable conjugations with their adjacent aromatic rings. The interplay between linking heteroatoms and aromatic rings therefore plays a key role in regulating the bond lengths and angles of bridging segments and ultimately the electronic features of macrocyclic cavity.

Though the first nitrogen- [2] and oxygen-bridged calix[4]arenes [3] may date back to 1960s, they had not drawn attention from chemists for nearly the next 40 years due to most probably the formidable obstacles of synthesis. Miyano and

---

D.-X. Wang (✉)

Beijing National Laboratory for Molecular Sciences, CAS Key Laboratory of Molecular Recognition and Function, Institute of Chemistry, Chinese Academy of Sciences, Beijing 100190, China

e-mail: [dxwang@iccas.ac.cn](mailto:dxwang@iccas.ac.cn)

M.-X. Wang (✉)

Key Laboratory of Bioorganic Phosphorus Chemistry and Chemical Biology (Ministry of Education), Tsinghua University, Beijing 100084, China

e-mail: [wangmx@mail.tsinghua.edu.cn](mailto:wangmx@mail.tsinghua.edu.cn)

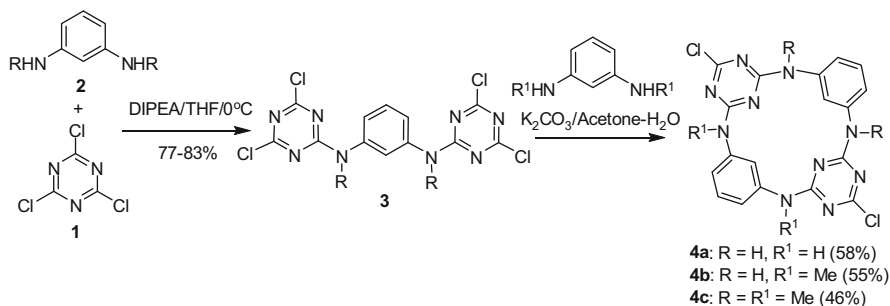
co-workers [4] reported in 1997 the facile synthesis of thiacalix[4]arene in 54 % yield from the reaction of *p*-*tert*-butylphenol with elemental sulfur in the presence of sodium hydroxide. The easy preparation of thiacalix[4]arene has led to extensive investigation of its application in molecular recognition. It was not until the beginning of this century when efficient methods were established for the synthesis of nitrogen- and oxygen-bridged calixaromatics the new era of the chemistry and supramolecular chemistry of heterocalixaromatics started to emerge. Gratifyingly, the past decade has witnessed a significant development of the field [5–13]. In this chapter we will focus briefly on the synthesis, structure, molecular recognition and application of azacalixaromatics. Readers are referred to Chaps. 13 and 15–17 and excellent review articles for sulfur- [9, 10], oxygen- [11], and other heteroatom-linked calix(het)arenes [5–8, 12, 13].

## 14.2 Synthesis

Being different from conventional calix[*n*]arenes and thiacalix[4]arenes, azacalix[*n*]arenes cannot be constructed from condensation of *p*-*tert*-butylphenol with nitrogen sources. Fortunately, C-N bonds can be readily formed by means of nucleophilic aromatic substitution reaction ( $S_NAr$ ) and transition metal-catalyzed cross coupling reaction between amines and haloarenes. Indeed, almost all reported strategies to construct macrocyclic skeletons of azacalix[*n*]aromatics rely on these bond forming reactions as the key steps. To synthesize azacalix[*n*]aromatics, methods including (1) fragment coupling protocol, (2) one-pot reaction approach and (3) step-by-step non-convergent synthesis have been developed using cheap and commercially available aromatic compounds as starting materials. The fragment coupling protocol provides an efficient and diversity-orientated synthetic method while one-pot reaction gives an operationally convenient access to symmetric azacalix[*n*]aromatics. The employment of pre-functionalized reactants in syntheses leads conceivably to the functionalized azacalix[*n*]aromatics. Moreover, post-macrocyclization chemical manipulations constitute an alternative and useful route to functionalized azacalix[*n*]aromatics that are not easily obtained by other methods.

### 14.2.1 Fragment Coupling Synthesis

In 2004 Wang and Yang [14] reported a fragment coupling synthesis of heterocalix[4]aromatics. Taking the advantage of high reactivity of cyanuric acid chloride **1**, authors first prepared linear trimers **3** from two-directional  $S_NAr$  reaction of 1,3-phenylenediamines **2** at 0 °C. They subsequently conducted the further  $S_NAr$  reaction of the resulting linear trimer intermediates **3** with 1,3-phenylenediamine at room temperature, achieving the synthesis of a number of nitrogen-bridged calix[2]



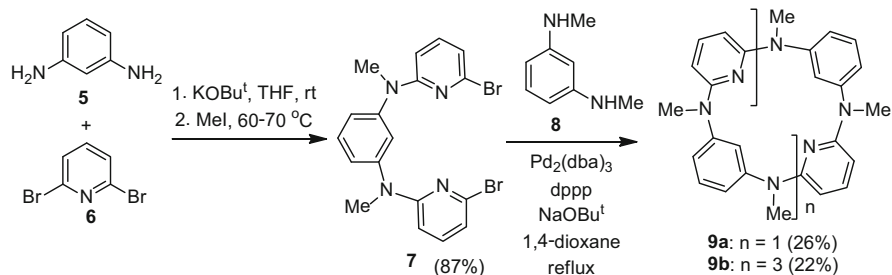
**Scheme 14.1** Fragment coupling synthesis of azacalix[2]arene[2]triazines [14]

arene[2]triazines **4** (Scheme 14.1) [14]. It is noteworthy that the fragment coupling approach to azacalix[2]arene[2]triazines is straightforward and cost-effective as the synthesis does not consume any expensive reactants, reagents and catalysts, and the reactions proceed smoothly under very mild conditions. In addition, the synthesis is efficient, scalable and high yielding. In many cases, good chemicals are obtained in multi-gram scale synthesis. Furthermore, the method is very general and diversity-orientated, insuring the construction of calix[2]arene[2]triazines bridged by nitrogen and other heteroatoms in different combinations.

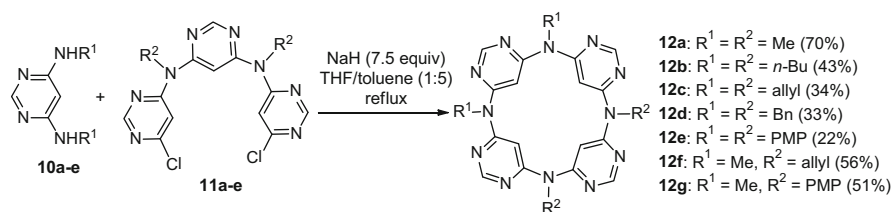
During the meantime, Wang and his coworkers also demonstrated a fragment coupling method for the synthesis of azacalix[m]arene[n]pyridines [15]. In the synthesis, the linear trimeric fragment **7** is prepared in a good yield from S<sub>N</sub>Ar reaction of 1,3-phenylenediamine **5** with two equivalents of 2,6-dibromopyridine **6** followed by *N*-methylation reaction in a one-pot fashion. In the presence of 1,3-bis(diphenylphosphino)propane (dppp) as a ligand, Pd<sub>2</sub>(dba)<sub>3</sub>-catalyzed [3+1] macrocyclic cross coupling reaction between **7** and *N,N*-dimethyl-1,3-phenylenediamine **8** produces azacalix[2]arene[2]pyridine **9a** in 26%. A larger macrocyclic ring homolog azacalix[4]arene[4]pyridine **9b** is also generated in 22% yield. The latter macrocycle is obviously formed from [3+1+3+1] fragment coupling reactions involving two equivalents of linear trimer **7** and diamine **8** (Scheme 14.2).

The fragment coupling protocol has ever since been extensively studied, becoming the most frequently used method in the preparation of azacalix[n]aromatics. Scheme 14.3 shows the fragment coupling synthesis of azacalix[4]pyrimidines. Macrocyclic condensation of **11**, which are obtained from S<sub>N</sub>Ar reaction of 4,6-diaminopyrimidines and 4,6-dichloropyrimidine, with 4,6-diaminopyrimidines **12** in the presence of an excess amount of NaH affords the desired products [16]. The same fragment coupling strategy has been applied in the efficient synthesis of tetra(*o*-methoxyphenyl)azacalix[4]arene [17] and azacalix[2]pyrimidine[2]triazines [18].

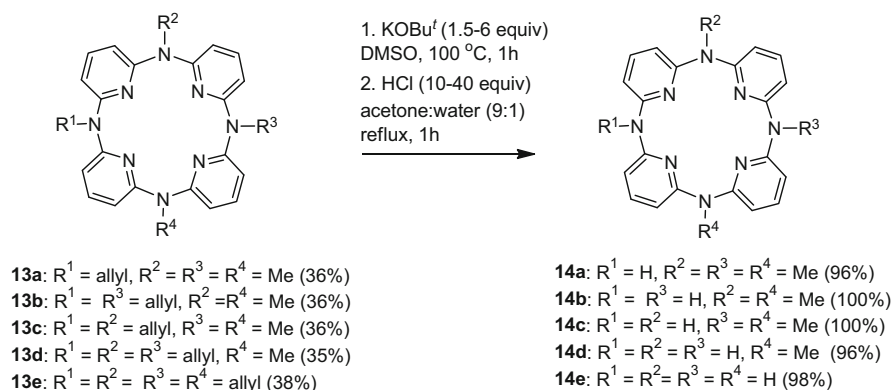
The fragment coupling approach has been successfully applied in the preparation of azacalix[4]pyridines bearing different substituents on the bridging nitrogen atoms [19, 20]. Illustrated in Scheme 14.4 are examples of (NAllyl)<sub>m</sub>(NMe)<sub>4-m</sub>-



**Scheme 14.2** Synthesis of azacalix[m]arene[n]pyridines ( $m = n = 2, 4$ ) [15]



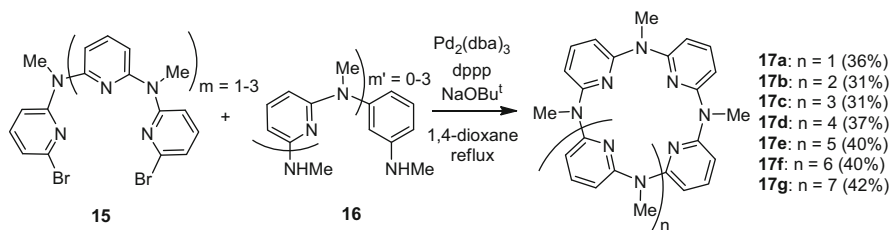
**Scheme 14.3** Fragment coupling synthesis of azacalix[4]pyrimidines [16]



**Scheme 14.4** Synthesis of  $(\text{NH})_m(\text{NMe})_{4-m}$ -bridged calix[4]pyridines [19]

bridged calix[4]pyridines **13** ( $m = 1-4$ ) that are obtained in moderate yields by macrocyclic [3 + 1] and [2 + 2] coupling reactions between simple diamino- and dibromo-substituted fragments. Deallylation through isomerization of C-C double bond under alkaline condition followed by acidic hydrolysis gives  $(\text{NH})_m(\text{NMe})_{4-m}$ -bridged calix[4]pyridines **14** ( $m = 1-4$ ) in excellent yields.

In addition to the synthesis of azacalix[4]aromatics that are composed of either identical or varied aromatic rings and substituents on nitrogen linkages, the fragment coupling method is also powerful in the construction of azacalixaromatics of



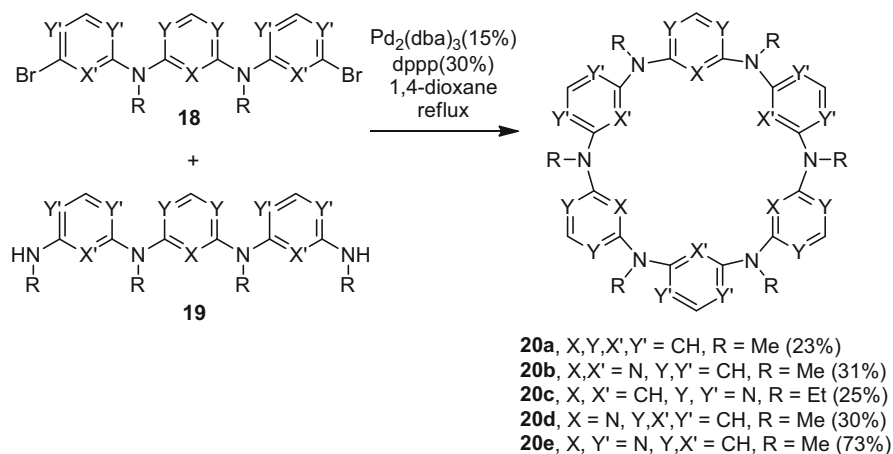
**Scheme 14.5** Fragment coupling synthesis of azacalix[ $n$ ]pyridines ( $n = 4-10$ ) [21–23]

large macrocyclic ring sizes. Shown in Scheme 14.5 is the synthesis of azacalix[ $n$ ]pyridines that contain up to ten pyridine units [21–23]. The linear dielectrophilic and dinucleophilic fragments **15** and **16** are easily prepared by iterative  $S_NAr$  reactions between 2,6-dibromopyridine and 2,6-diaminopyridine derivatives. The Pd-catalyzed macrocyclic [ $m + m'$ ] fragment cross-coupling reactions furnish the formation of azacalix[ $n$ ]pyridines **17** ( $n = 4-10$ ) in good yields. It is worth noting that the azacalix[ $n$ ]pyridines bearing both odd and even numbers of pyridine units are available by the fragment coupling approach. The smallest macrocyclic analog, namely, azacalix[3]pyridine, has been efficiently synthesized by means of a [2 + 1] fragment coupling approach [24]. Other fascinating examples include Tsue's synthesis of azacalix[6]- and -[7]arenes from [5 + 1] and [5 + 2] fragment coupling reactions, respectively [25–27].

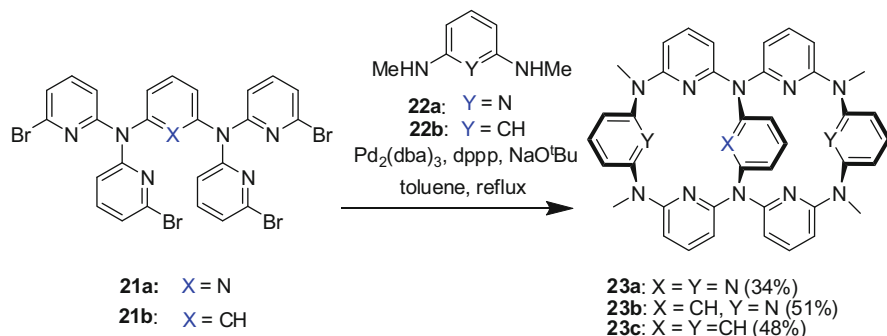
The versatility of fragment coupling synthesis has been further highlighted recently in the construction of azacalix[6]aromatics containing different combinations of benzene, pyridine and pyrimidine rings. Applying  $S_NAr$  reaction or transition-metal promoted C-N formation reaction,  $\alpha,\omega$ -dibromo and diamino trimeric fragments **18** and **19** are synthesized efficiently from cheap and commodity chemicals. By the cross-coupling reaction between **18** and **19** under palladium catalysis, azacalix[6]arene, azacalix[6]pyridine, azacalix[6]pyrimidine, azacalix[3]arene[3]pyridine and azacalix[3]pyridine[3]pyrimidine are obtained respectively. The chemical yields for macrocyclization are in the range of 23–73 % depending on the constitutional aromatic segments (Scheme 14.6) [28].

It is important to address that the fragment coupling approach is not merely confined to the simple (hetero)aromatic rings aforementioned. Other aromatic nuclei such as naphthalene, triptycenes and terphenylenes have also been employed, which lead to the construction of a few intriguing and unique azacalixarene derivatives [29–33]. Significantly, the fragment coupling synthesis has also found its application in the fabrication of sophisticated azacalixarene derivatives. Depicted in Scheme 14.7 is the facile synthesis of 1,3-arylene-bridged azacalix[6]aromatics **23** by the Pd-catalyzed macrocyclic fragment coupling reaction between brominated pentamers **21** and  $N^2,N^6$ -dimethylpyridine-2,6-diamine **22a** or  $N^1,N^3$ -dimethylbenzene-1,3-diamine **22b** [34]. Another attractive example is the construction of a fused azacalix[4]arene compound **26** through a [3 + 1 + 3]





**Scheme 14.6** [3+3] Fragment coupling synthesis of azacalix[6]aromatics [28]

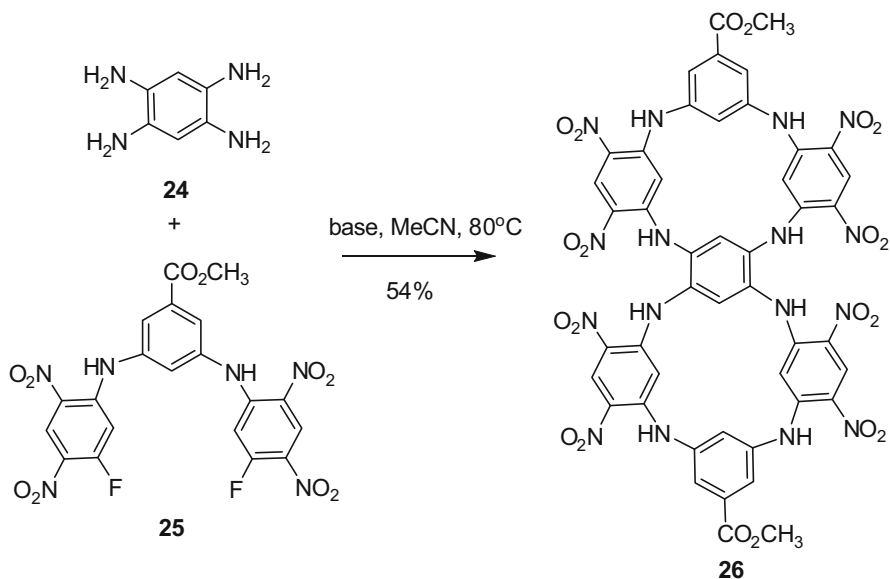


**Scheme 14.7** Synthesis of 1,3-arylene-bridged azacalix[6]aromatics [34]

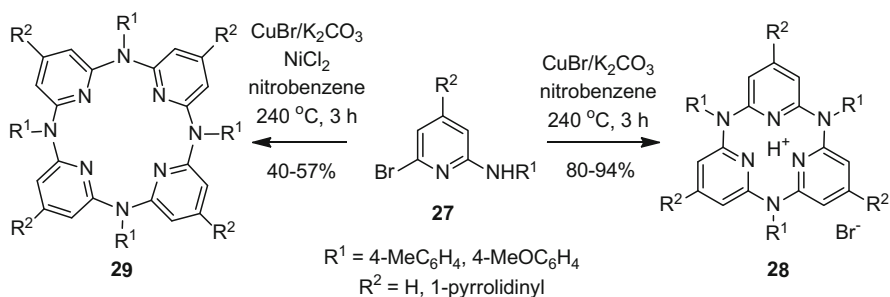
fragment coupling reaction between 1,2,4,5-tetraaminobenzene **24** and two equivalents of trimer **25** (Scheme 14.8) [35].

## 14.2.2 One-Pot Synthesis

For the synthesis of symmetric heteracalixaromatics, a one-pot reaction method appears advantageous in terms of simplicity of practical operation. Many of the attempts, especially those reported in early time, however, do not give satisfactory results. Low chemical yields and appallingly poor selectivity are the major flaws, leading the one-pot synthesis less useful in practice [36–39]. For example, the Pd-catalyzed cross-coupling reactions of 3-bromo-*N*-methylaniline [36] and of 2,6-dibromopyridine with 2,6-bis(methylamino)pyridine [38] produce,



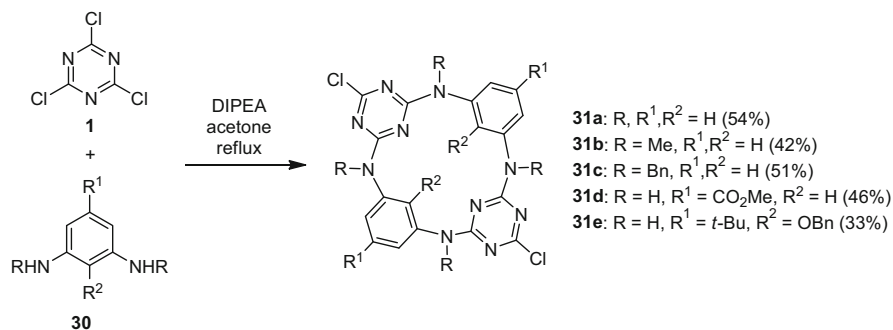
**Scheme 14.8** Synthesis of fused azacalix[4]arene [35]



**Scheme 14.9** One-pot synthesis of azacalix[3] and [4]pyridine derivatives [41]

respectively, a mixture of azacalix[ $n$ ]arenes ( $n = 3-8$ ) and azacalix[ $n$ ]pyridines ( $n = 4, 6$ ) with the chemical yield for each macrocycle being lower than 13%. Only in the case of the Pd-catalyzed reaction of 6-bromo-*N*-(*p*-tolyl)pyridin-2-amine, *N*-(*p*-tolyl)-substituted azacalix[3]- and -[4]pyridines are generated in 38% and 31% yield, respectively, along with the formation of small amounts of other larger macrocyclic homologs [40].

A practically useful one-pot synthesis has been reported very recently by Kanbara and co-workers [41]. Using proton and nickel ion as templates, authors have achieved selective synthesis of azacalix[3]- and -[4]pyridine derivatives in very good yields. As illustrated in Scheme 14.9, the Cu-catalyzed Ullmann reaction of 2-anilino-6-bromopyridines **27** proceeds smoothly to afford the monoprotonated



**Scheme 14.10** One-pot synthesis of azacalix[2]arene[2]triazines [43]

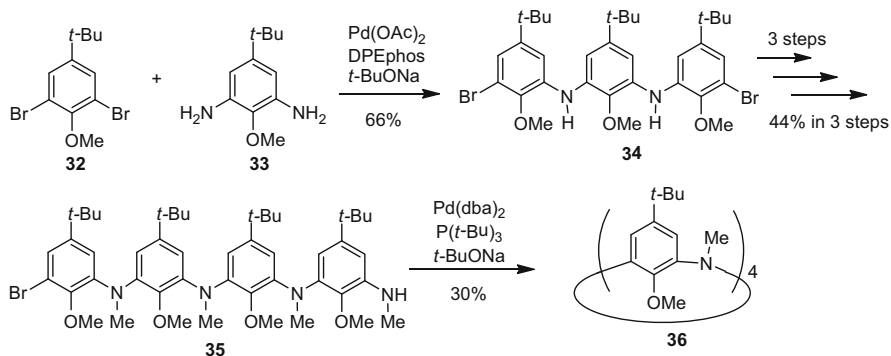
azacalix[3]pyridines **28** in 80–94 % yields albeit a very high temperature (240 °C) is necessary. In the presence of NiCl<sub>2</sub>, however, azacalix[4]pyridines **29** are obtained as the main products in 40–57 % yields. Upon the treatment with a base, the monoprotonated azacalix[3]pyridines are transformed into azacalix[3]pyridines that are superbases species [24, 42].

In 2014, the one-pot synthesis was successfully developed by Wang and co-workers in synthesis of nitrogen-bridged calix[2]arene[2]triazines [43], which had only been obtained by a fragment coupling approach as reported in their previous report [14]. In the presence of DIPEA as a base, the macrocyclic condensation between cyanuric acid chloride **1** and 1,3-phenylene diamines **30** proceeds effectively under very mild conditions to produce the corresponding azacalix[2]arene[2]triazines **31** in 33–54 % yields. It is noteworthy that the one-pot reaction works well for the synthesis of functionalized azacalix[2]arene[2]triazines when pre-functionalized *m*-phenylenediamines are employed (Scheme 14.10).

One-pot macrocyclic condensation reaction between 4,6-dichloropyrimidine and 4,6-bis(amino)pyrimidines has been reported to take place in the presence of sodium hydride giving azacalix[4]pyrimidines **12a–d** in 7–35 % yields [16]. Another metal free one-pot example has been demonstrated by Chen and co-workers [29], who prepared triptycene-bearing azacalixarenes in 8–27 % yield through the nucleophilic aromatic substitution reaction of 2,7-diaminotriptycene with cyanuric acid chloride or 1,5-difluoro-2,4-dinitrobenzene in the presence of DIPEA as a base.

### 14.2.3 Stepwise Synthesis

In theory the step-by-step synthesis allows the synthesis of diverse azacalix-aromatics that are composed of different numbers of completely varied aromatic segments and bridging units though the synthetic procedures appear tedious and frustrating in some cases. Nevertheless, Tsue and co-workers at Kyoto University



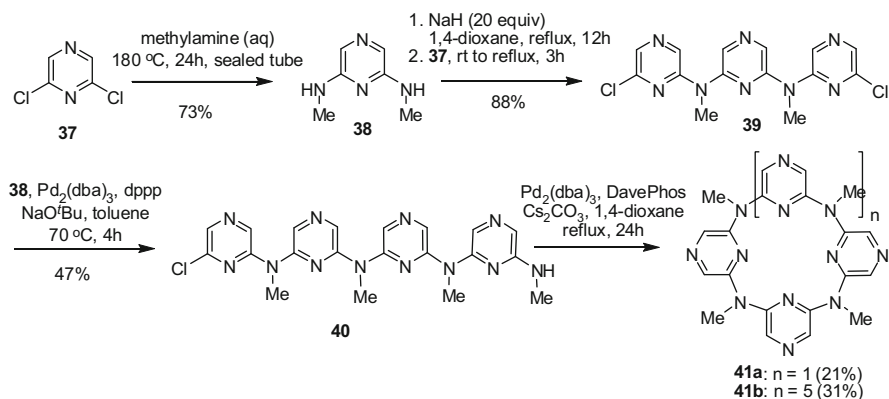
**Scheme 14.11** Stepwise synthesis of azacalix[4]arene [44]

reported the stepwise approach to obtain azacalix[4]arenes [44]. As depicted in Scheme 14.11, Buchwald-Hartwig aryl amination reaction of dibromoanisole **32** with *m*-phenylenediamine **33** afforded a linear trimer **34**. Surprisingly, a fragment coupling reaction between **34** and **33** under various Pd-catalyzed C-N bond forming reaction conditions does not produce azacalix[4]arene [45]. Authors then prepared a linear tetramer **35** from trimer **34** in three steps. Intramolecular cyclization reaction of **35** under the catalysis of  $\text{Pd}(\text{dba})_2$  in refluxing anhydrous toluene gave the desired azacalix[4]arenes **36** in 30% yield (Scheme 14.11) [44]. By using the same stepwise strategy, syntheses of inherently chiral azacalix[4]arene [46] and larger macrocyclic azacalix[5]arenes [47] have also been reported by the same group.

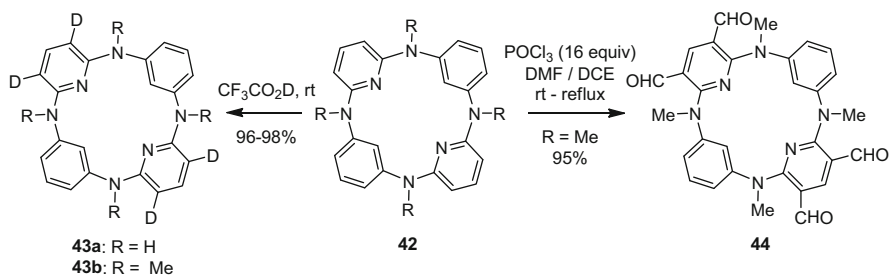
Scheme 14.12 shows another example of the stepwise synthesis of azacalix[*n*]pyrazines that has been reported by Zhao and Wang [48]. Reaction of 2,6-bis(methylamino)pyrazine **38** and 2,6-dichloropyrazine **37** produced trimer **39** effectively. Attempted convergent macrocyclic cross coupling reaction of **39** with **38** failed to afford the targeted azacalix[4]pyrazine. Instead, a linear tetramer **40** was produced in 47% yield along with the recovery of 31% yield of reactant **39**. Catalyzed by  $\text{Pd}_2(\text{dba})_3$ , moderate yields of azacalix[4]pyrazine (21%) and its macrocyclic octamer, namely, azacalix[8]pyrazine (31%) were achieved from **40** when the reaction was carried out in 1,4-dioxane in the presence of DavePhos as a ligand and  $\text{Cs}_2\text{CO}_3$  as a base (Scheme 14.12). Following the same strategy, the same authors reported very recently the preparation of azacalix[3*n*]pyrazine[*n*]pyridines (*n* = 1, 2) when the linear trimer **39** was reacted with 2,6-bis(methylamino)pyridine [49].

### 14.2.4 Post-Macrocyclization Functionalization

In general, the aforementioned fragment coupling strategy, one-pot reaction method and step-by-step non-convergent synthesis provide useful and



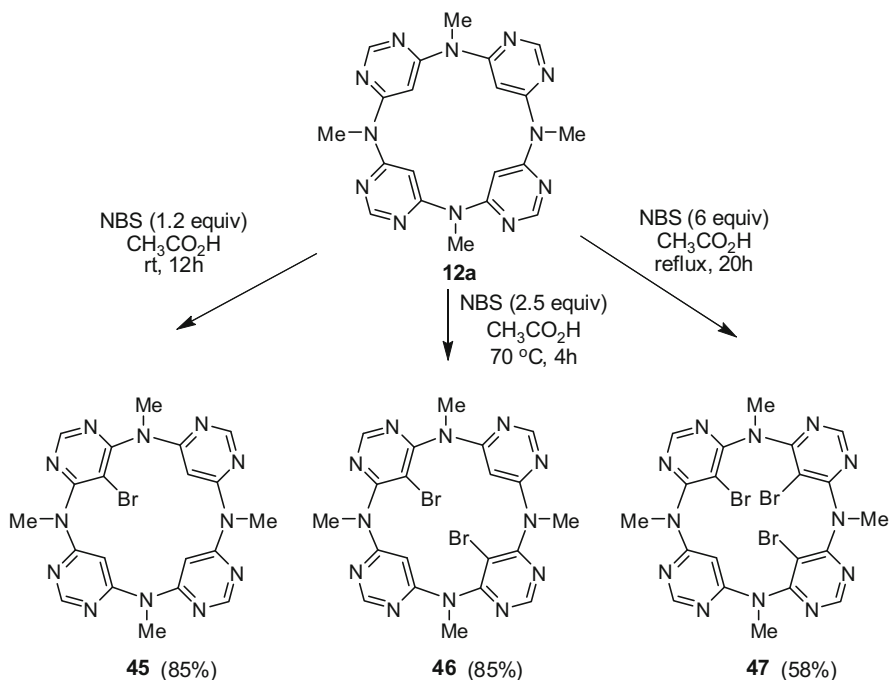
**Scheme 14.12** Stepwise synthesis of azacalix[n]pyrazines (n = 4, 8) [48]



**Scheme 14.13** Site-specific deuteration and formylation of azacalix[2]arene[2]pyridines [20, 50]

straightforward access to functionalized azacalixaromatics if appropriate pre-functionalized reactants are utilized. Indeed, a large number of functionalized azacalixaromatics have been synthesized using these methods. Admittedly, however, when the required pre-functionalized starting materials are not easily available and the function groups are not compatible with the reaction conditions, synthesis of functionalized azacalixaromatics becomes a great challenge. Gratifyingly, post-macrocyclization functionalization provides a unique and powerful alternative. Site-selective and facile chemical manipulations on constitutional aromatic rings and bridging nitrogen atoms enable the construction of diverse functionalized azacalixaromatics.

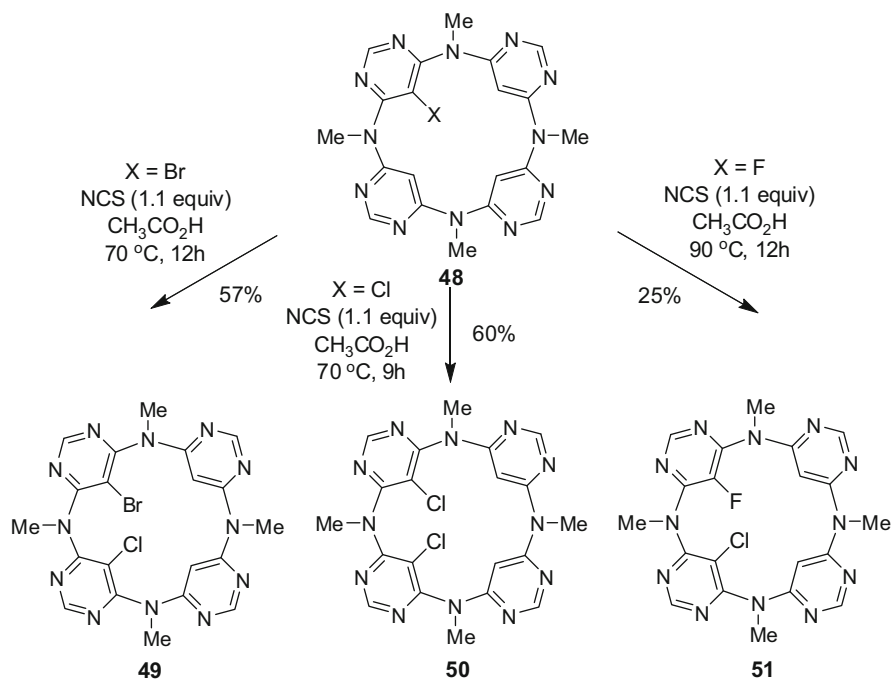
Wang and co-workers have extensively studied electrophilic aromatic substitution reactions of azacalixaromatics, providing various functionalized macrocycles that are otherwise difficult to obtain by other means. It has been found that NH- and NMe-bridged calix[2]arene[2]pyridines undergo deuteration gradually and exclusively on 3- and 5-position of pyridine rings of the macrocycles when treated with  $\text{CF}_3\text{CO}_2\text{D}$ . No deuteration occurs on the benzene rings (Scheme 14.13). The site-specificity of the deuteration is originated from the 1,3-alternate conformational



**Scheme 14.14** Selective bromination of azacalix[4]pyrimidines [16]

structures in which the nitrogen linkages form conjugation with pyridine ring rather than the benzene ring, resulting in the dramatic enhancement of the electron density of pyridine units [20]. Predictably, electrophilic aromatic bromination reaction and the Vilsmeier-Haack formylation reaction take place preferentially on the pyridine rings. For example, mono- and di-bromination and formylation reactions are achieved under controlled conditions. When an excess amount of formylating reagent is employed, azacalix[2]arene[2]pyridine **42** (R = Me) is transformed into tetra-formylated azacalix[2]arene[2]pyridine **44** (Scheme 14.13). Compound **44** is an invaluable intermediate in the construction of functional and structurally sophisticated architectures. Taking advantage of the close proximity of aldehyde groups in the macrocycle, for instance, a McMurry reductive coupling reaction has been accomplished to afford a unique semicage molecule [50].

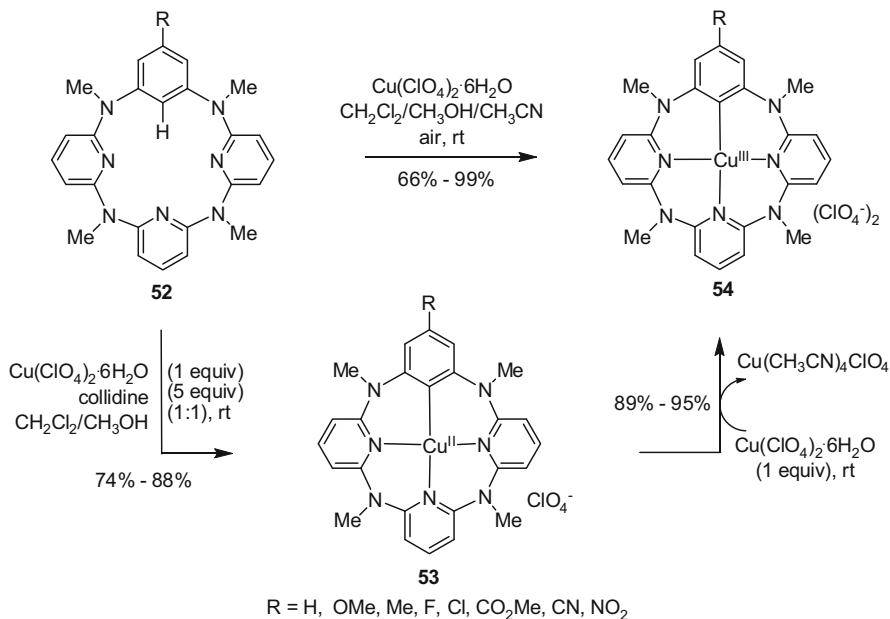
Azacalix[4]pyrimidines are able to undergo chlorination and bromination on the lower rim positions using NCS and NBS, respectively. Simply by varying the ratio of azacalix[4]pyrimidines over halogenating reagents and by controlling the reaction temperature, azacalix[4]pyrimidines bearing mono- to tri- or even tetra-halo substituents are synthesized. Exemplified in Scheme 14.14 are selective bromination reactions [16]. Intriguingly, chlorination of mono-halogenated azacalix[4]pyrimidines with NCS gives rise to the selective formation of proximally di-halogenated products (Scheme 14.15). The site-selectivity is most probably resulted from a conformation in which the proximal pyrimidine ring is strongly



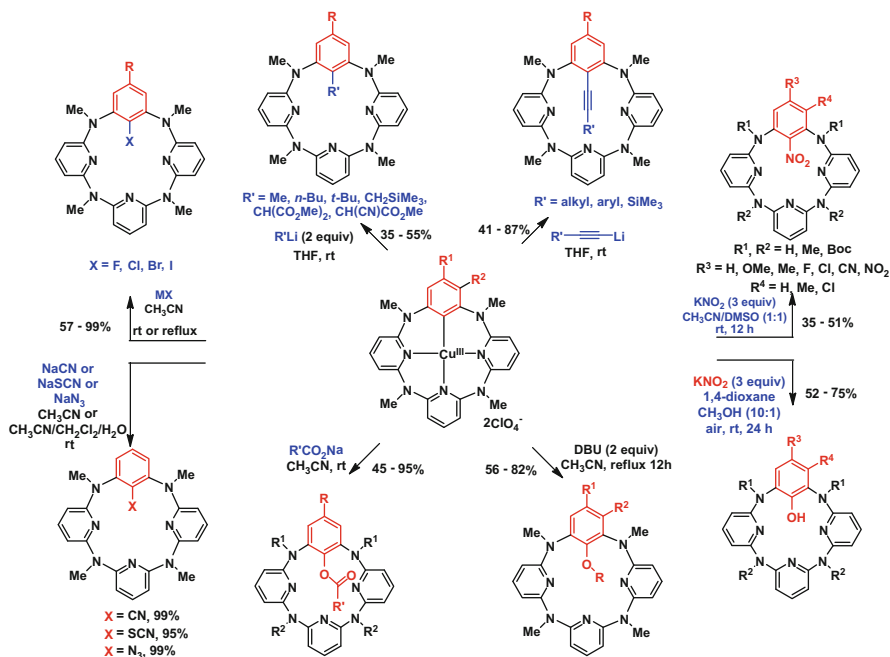
**Scheme 14.15** Selective chlorination of mono-halogenated azacalix[4]pyrimidines [51]

conjugated by electron-donating amino groups. The obtained compounds are actually inherently chiral macrocycles in a racemic form. Resolution by HPLC method using a column coated with chiral stationary phase affords enantiomeric pure di-halogenated azacalix[4]pyrimidines [51].

To install the functionality regioselectively on azacalixarenes, Wang and co-workers have recently established very powerful copper-mediated or -catalyzed aryl C-H transformation reactions [52–59]. They discovered that azacalix[1]arene [3]pyridines reacted efficiently with  $\text{Cu}(\text{ClO}_4)_2 \cdot 6\text{H}_2\text{O}$  under aerobic condition at room temperature to form shelf-stable Ar-Cu(III) complexes almost quantitatively [52]. The formation of the unusual high-valent organocopper(III) species has been revealed later by the authors to proceed through direct electrophilic metalation to initially form aryl-Cu(II) complexes followed by oxidation by free copper(II) ion (Scheme 14.16) [53]. The structures of both Ar-Cu(II) and Ar-Cu(III) compounds, particularly the oxidative state of metal centers, are well characterized unambiguously by X-ray crystallography, XPS, EPR and NMR spectroscopic data. Ar-Cu(III) complexes exhibit excellent reactivity towards a wide variety of nucleophiles under very mild conditions to form functionalized azacalix[1]arene[3]pyridine derivatives. As summarized in Scheme 14.17, treatment of Ar-Cu(III) complexes with cheap alkali metal halides [54] or tetraalkylammonium halides, sodium acetates, cyanide and thiocyanate [52] leads to the introduction of the corresponding

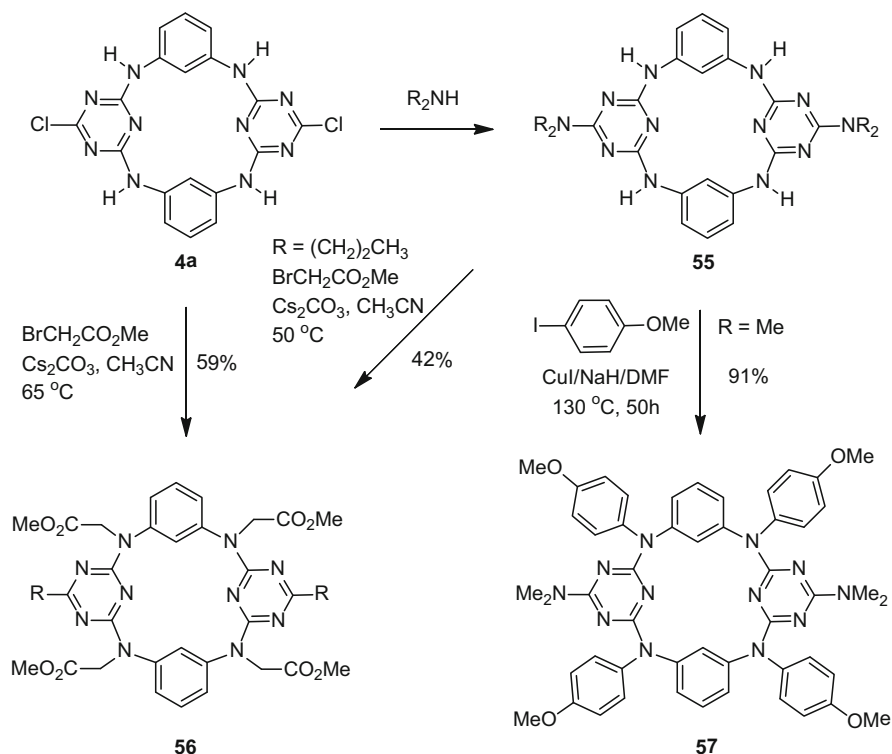


**Scheme 14.16** Synthesis of Ar-Cu(II) and Ar-Cu(III) complexes [52, 53]



**Scheme 14.17** Regiospecific functionalization of azacalix[1]arene[3]pyridine [52, 54–59]

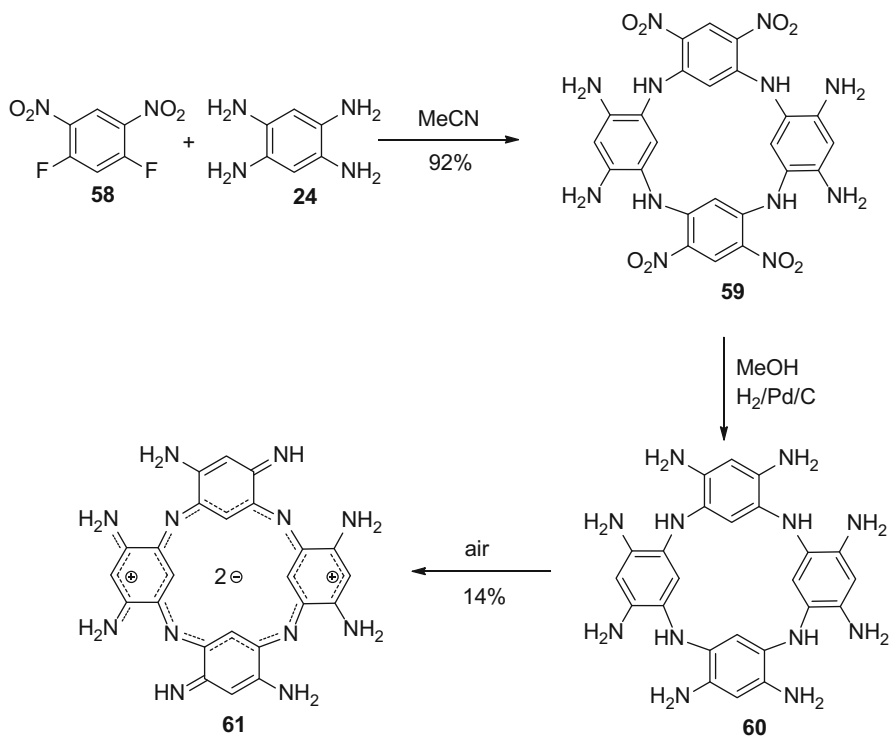




**Scheme 14.18** Functionalization of azacalixarenes on the bridging nitrogen atoms [60, 61]

functional groups in high yields. Alkoxy and aryloxy are readily introduced when alkyl and aryl alcohol derivatives are utilized as nucleophiles in the presence of a base [55]. The cross-coupling reactions with alkyl and alkynyl lithium reagents result in the  $\text{C}_{\text{aryl}}-\text{C}_{\text{sp}^3}$  and  $\text{C}_{\text{aryl}}-\text{C}_{\text{sp}}$  bonds, respectively [56, 57]. In many cases, isolation of pure  $\text{Ar}-\text{Cu}(\text{III})$  intermediates are not necessary in synthesis. For instance, a one-pot copper(II)-mediated reaction of azacalix[1]arene[3]pyridines with  $\text{KNO}_2$  in a mixture of  $\text{CH}_3\text{CN}$  and  $\text{DMSO}$  (1:1) at ambient temperature yields selectively nitrobenzene-bearing macrocyclic products in moderate yields. Interestingly, when the reaction media is replaced by a mixture of 1,4-dioxane and methanol (10:1), copper(II)-catalyzed hydroxylation reaction proceeds smoothly under atmospheric conditions to furnish the formation of phenol products [58]. Very recently, an azido group is conveniently installed at the lower rim position regioselectively via a highly efficient copper(II)-catalyzed aryl C-H bond activation using sodium azide as azido source under acidic condition [59].

In addition to electrophilic aromatic substitution reaction and copper salts-mediated or -catalyzed C-H bond functionalization, nucleophilic aromatic substitution reaction has also been explored to introduce the functional groups [60, 61]. One of successful examples is the amination reaction of dichloro-substituted azacalix[2]arene[2]triazine with various amines based on the reactivity of chlorotriazine moiety (Scheme 14.18) [60].



**Scheme 14.19** Synthesis of a bis-zwitterionic tetraazacalixarene [65]

It is particularly worth emphasizing that the uniqueness of azacalixarenes in stark contrast to conventional calixarenes is the straightforward functionalization on the bridging nitrogen atoms as the NH linkages provide chemical handles to execute arylation [60, 62, 63], alkylation [61, 63] and acylation [20] reactions. Illustrated in Scheme 14.18 are representative examples. Under the Ullmann reaction conditions, NH-bridged calix[2]arene[2]triazine **55** undergoes exhaustive coupling reaction with 4-methoxyphenyl iodide to afford the product **57** in an excellent yield [61]. The same strategy has been used to introduce triarylamine moieties into NH-bridged calix[4]arene to synthesize molecular spin materials [62]. Complete *N*-alkylation of azacalix[2]arene[2]triazines with methyl bromoacetate furnishes the formation of *N*-ligand-pended azacalixaromatics, that are useful selective receptors for copper(II) ion [61].

The functional group transformations of functional azacalixaromatics further diversify the structures of macrocycles. For example, lithiation of monobrominated azacalix[4]pyrimidine **45** with *n*BuLi followed by the interaction with HCO<sub>2</sub>Et produces mono-formyl-substituted azacalix[4]pyrimidine [64] while an intramolecular McMurry reductive coupling reaction of **44** affords a highly rigid molecular semi-cage [50]. Siri and coworkers reported recently the synthesis of a bis-zwitterionic tetraazacalixarene **61** [65]. As depicted in Scheme 14.19,

tetranitro-substituted azacalix[4]arene **59**, that is obtained from the condensation reaction of tetraaminobenzene **24** and 1,5-difluoro-2,4-dinitrobenzene **58** in 92 % yield, undergoes catalytic hydrogenation reaction with Pd/C to give octaamino-substituted azacalix[4]arene intermediate **60**. Subsequent oxidation by air at room temperature furnishes a stable bis-zwitterionic tetraazacalixarene **61** as a green solid in 14 % yield. As it is a NIR-absorbing organic material with a very low gap ( $E_g = 1.01$  eV), potential applications of the compound can be anticipated [65].

## 14.3 Structure

### 14.3.1 Structure in the Solid State

Most of the azacalixaromatics reported to date are crystalline compounds, and many of them give high-quality single crystals from recrystallization from suitable solvents. X-ray crystallography provides therefore detailed structural information, particular the conformational structures of these novel macrocycles in the solid state.

#### 14.3.1.1 Azacalix[3]pyridine

As a smallest macrocyclic member in azacalix[n]aromatics family, tri[(*p*-tolyl)aza]calix[3]pyridine **62** adopts a highly pinched alternate conformation (Fig. 14.1) [40]. While one of the pyridine rings lies on the plane defined by three bridging nitrogen atoms, the other two pyridine rings are oriented to different directions. Three *p*-tolyl moieties on the linking nitrogen atoms, on the other hand, tend to be perpendicular to the plane of bridging nitrogens. The convergence of lone-pair

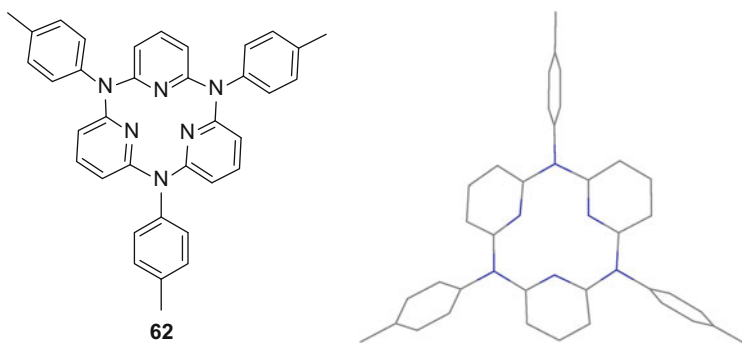


**Fig. 14.1** Crystal structure of azacalix[3]pyridine **62**. All hydrogen atoms are omitted for clarity [40]

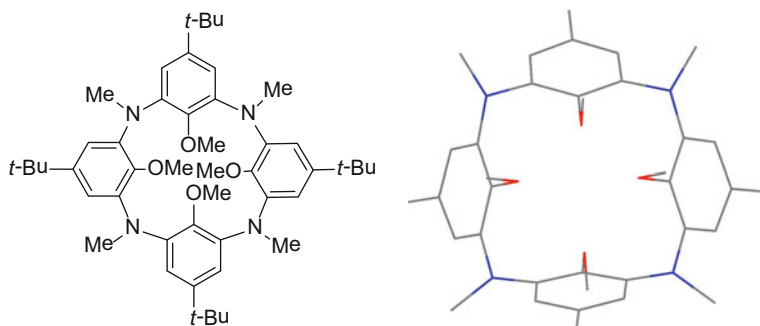


**Fig. 14.2** Crystal structure of azacalix[4]arene **35**. All *t*-butyl groups and hydrogen atoms are omitted for clarity [44]

electrons of three pyridine nitrogen atoms forms a small cavity, engendering azacalix[3]pyridine a strong receptor for one proton [24, 42].

### 14.3.1.2 Azacalix[4]aromatics

In contrast to conventional calix[4]arenes that form mainly four major different conformations, azacalix[4]aromatics give dominant 1,3-alternate conformation in the solid state. Noticeably, judging from the bond lengths and angles of azacalix[4]aromatics, all bridging nitrogen atoms tend to adopt  $sp^2$  configuration. However, they are able to form different degrees of conjugation with their adjacent aromatic rings depending on the nature of constitutional aromatic rings and of substituents on the nitrogen atoms. As a consequence, 1,3-alternate conformational structures with different symmetries and of various cavity sizes are formed.

Being a very similar analog to conventional *p-t*-butylcalix[4]arene *O*-tetramethyl ether, azacalix[4]arene **35**, for example, forms a 1,3-alternate conformation with an approximate  $D_{2d}$  symmetry (Fig. 14.2). The distances from each bridging nitrogen atom to the carbon atoms of the adjacent benzene rings are in the range from 1.407 to 1.425 Å ( $d_{N-C}$ ), indicating a weak conjugation effect between all linking nitrogen atoms and their two connecting benzene rings [44].

Azacalix[4]pyridine **17a** adopts a highly symmetric 1,3-alternate conformational structure. In contrast to azacalix[4]arene **35**, the molecule bears a  $C_{2v}$  rather than a  $D_{2d}$  symmetry [21]. As illustrated clearly in Fig. 14.3, two distal pyridine rings are face-to-face orientated while the other two tend to be procumbent to the plane defined by four bridging nitrogen atoms. Nitrogen linkages are electronically  $sp^2$ -configured, forming conjugation with procumbent pyridine rings. Therefore the cavity could be viewed as a result of a cyclic array of two pieces of planar conjugated aromatic segments and two isolated aromatic rings in a 1,3-alternate fashion (Fig. 14.3). Interestingly, similar 1,3-alternate conformation and conjugation system have been observed from X-ray crystal structures of many other azacalix[4]aromatics albeit some structures are distorted or twisted leading to the

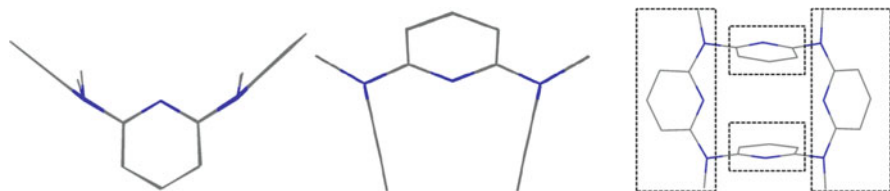


**Fig. 14.3** Crystal structure of azacalix[4]pyridine **17a**. All hydrogen atoms are omitted for clarity [21]

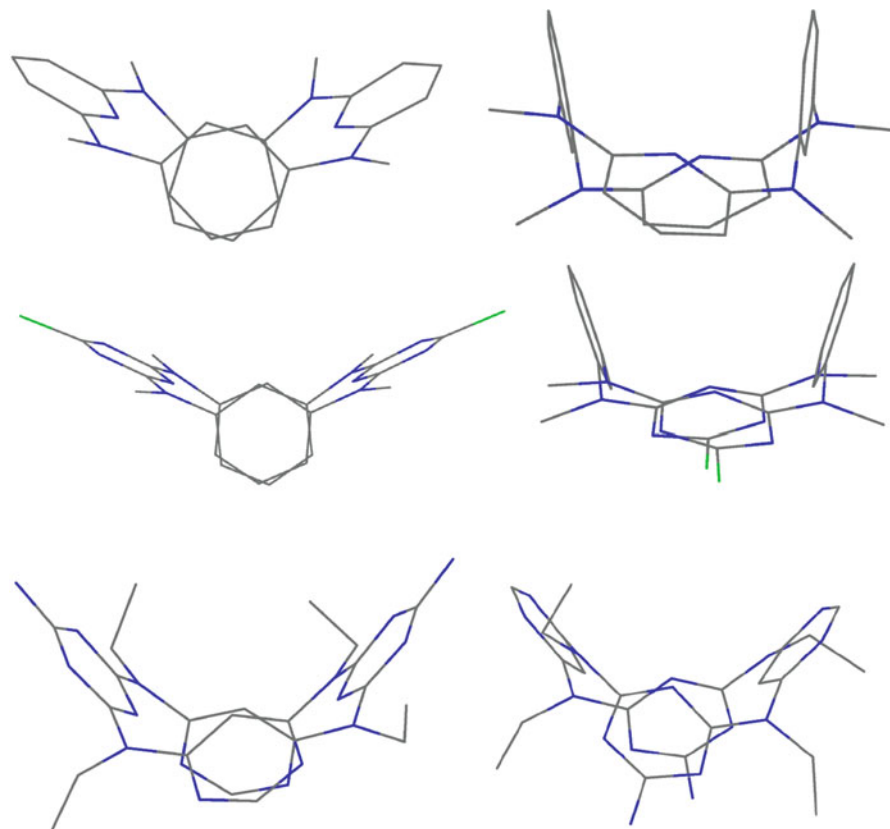


**Fig. 14.4** Crystal structure of azacalix[2]arene[2]pyridine **9a** (top) [15], azacalix[2]arene[2]triazine **4c** (middle) [14] and azacalix[2]pyridine[2]triazine (bottom) [18]. Alkyl groups and hydrogen atoms are omitted for clarity

loss of symmetry. Examples shown in Fig. 14.4 include azacalix[2]arene[2]pyridine [15], azacalix[2]arene[2]triazine [14] and azacalix[2]pyrimidine[2]triazine [18]. It is interesting to point out that all nitrogen atoms in bridging positions form stronger conjugation with the more electron-deficient aromatic units in the macrocycles. It best explains the selective electrophilic aromatic substitution

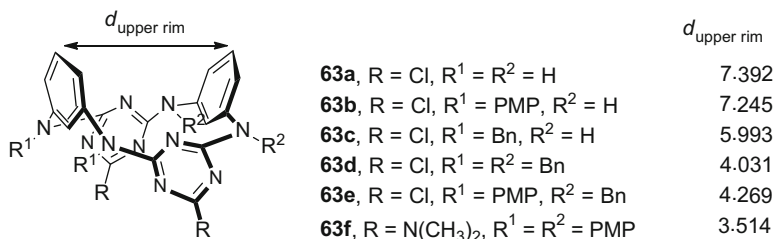


**Fig. 14.5** Cavity size of azacalix[2]arene[2]triazines [60]

reaction on pyridine rather than benzene ring when azacalix[2]arene[2]pyridine reacts with electrophiles (vide supra).

One remarkable structural feature of 1,3-alternate azacalix[4]aromatics is the tuning of the size of the V-shaped cavity by the steric effect of the substituents on the bridging nitrogen linkages. This has been manifested by a series of azacalix[2]arene[2]triazine macrocycles **63** (Fig. 14.5). With the increase of the number and the bulkiness of *N*-substituents, the cavity size, which is defined by the upper-rim distance between two benzene rings, shrinks gradually from 7.39 to 4.03 Å. An extreme example is tetra(*p*-methoxyphenylaza)-linked calix[2]arene[2]triazine **63f** that gives the shortest upper rim distance as 3.51 Å [60]. Since the cavity size plays an essential role in molecular recognition, self-assembly and molecular crystal engineering, the cavity regulation of azacalix[2]arene[2]triazines simply through the variation of substituent on the linking nitrogen atoms appears unique and practically useful.

It is probably more important to address that the azacalix[4]aromatics are capable of self- and fine-tuning the conformation and cavity due to the easy alteration of conjugation systems between bridging nitrogen atoms and their neighboring aromatic rings under different conditions. One of the fascinating examples documented in literature is azacalix[4]pyridine **17a** [21]. Titration of **17a** with an acid results in the formation of mono-, di-, and triprotonated azacalix[4]pyridine species. Their X-ray crystal structures reveal the formation of a saddle-shape structure with an approximate  $S_4$  symmetry from the parent highly symmetric 1,3-alternate conformer with a  $C_{2v}$  symmetry. Noticeably, the similar saddle-shaped macrocycles give cavities of varied sizes, with the distances between two upper-rim carbon atoms of pyridine rings being 7.345 Å, 8.213 Å and 7.406 Å, respectively. The cavities accommodate respectively one DMF,  $\text{ClO}_4^-$ , and  $\text{HO}_2\text{CCO}_2^-$  guest species via the hydrogen bonding (Fig. 14.6). From the host-guest chemistry viewpoint, it could be the guest species that induce the change of macrocyclic conformation and cavity. Nevertheless, it is the intrinsic nature of nitrogen atoms to form various conjugation systems with pyridine rings that account for the conformation and cavity self-adaption to best fit the guest species. In this regard, azacalix[4]pyridine is truly a “smart” macrocycle, an always-pursued unique and invaluable feature of macrocyclic host molecules.

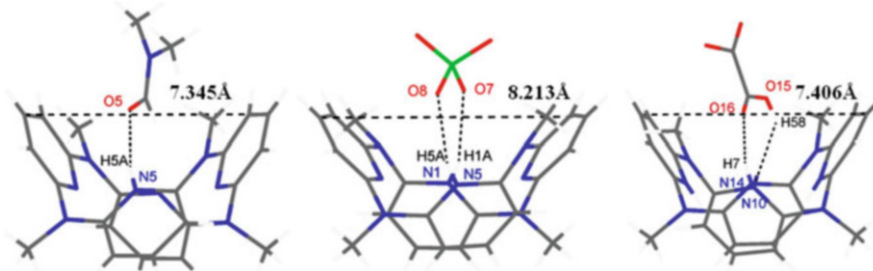


**Fig. 14.6** Cavity structures of mono- (*left*), di- (*middle*) and tri-protonated (*right*) azacalix[4]pyridines [21]

### 14.3.1.3 Azacalix[n]aromatics ( $n = 5-10$ )

As expected, the enlargement of the size of azacalix[n]aromatics ( $n > 4$ ) leads to increased macrocyclic flexibility. Generally, azacalix[n]aromatics bearing odd numbers of aromatic rings, such as azacalix[5]- and azacalix[7]pyridines, give drastically distorted alternate conformations in the solid state [22, 23, 27]. Among all larger macrocyclic azacalix[n]aromatics, the conformational structures of azacalix[6]aromatics in the solid state have been systematically investigated [28]. Azacalix[6]arene **20a** adopts a 1,3,5-alternate conformation with a  $C_3$  symmetry. The macrocycle is composed of three different segments including conjugated *meta*-bis(methylamino)benzene, (methylamino)benzene and isolated benzene [28]. When *t*-Bu and methoxyl groups are introduced onto the larger and lower rims, respectively, azacalix[6]arene shows a 1,2,3-alternate conformation due to the formation of intramolecular bifurcated  $\text{MeO} \cdots \text{NH} \cdots \text{MeO}$  hydrogen bonds [25]. In the case of azacalix[6]pyridine **20b** and azacalix[6]pyrimidine **20c**, heavily distorted 1,3,5-alternate conformers are observed in the crystalline state [28]. Interestingly, azacalix[6]aromatics bearing two different aromatic rings adopt a much more symmetric 1,3,5-alternate conformation. Illustrated in Fig. 14.7 are typical examples of azacalix[3]arene[3]pyridine **20d** and azacalix[3]pyridine[3]pyrimidine **20e**, which give similar bowl-shaped structures. All bridging nitrogen atoms tend to form conjugation with pyrimidine rings on a basal plane leading to the increase of the electron-density of molecular bowls, rendering azacalix[3]pyridine[3]pyrimidines excellent receptors for fullerenes (*vide infra*) [28, 66].

The dependence of conformation on the nature of constitutional aromatic rings is also evidenced in the case of azacalix[8]aromatics. Azacalix[8]arene, for example, possesses a roughly ellipsoidal conformation with a  $C_2$  symmetry as a result of the formation of intramolecular hydrogen bonds which is similar to azacalix[6]arene [45]. Being composed by four conjugated 2,6-bis(methylamino)pyridine planar segments, and four isolate benzene rings, azacalix[4]arene[4]pyridine shows a 1,2,3-partial cone conformation, resembling a double-ended spoon [15]. Azacalix[8]pyridine, however, gives pleated loop-like conformation with a  $C_i$  symmetry as a result of various conjugations between the bridging nitrogen atoms and their

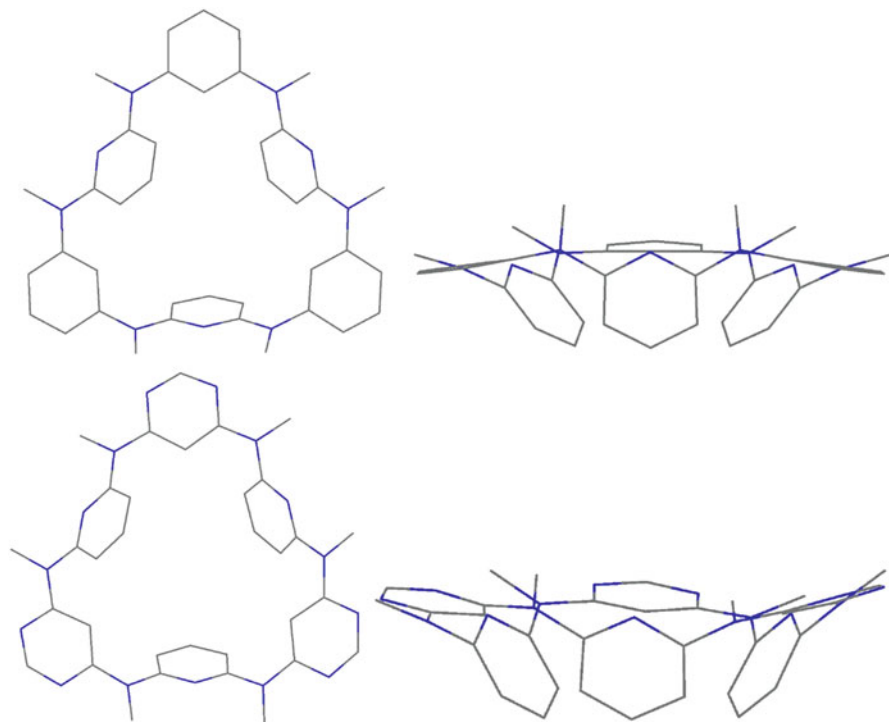


**Fig. 14.7** Crystal structures of azacalix[3]arene[3]pyridine (*top*) and azacalix[3]pyridine[3]pyrimidine (*bottom*). All hydrogen atoms are omitted for clarity [28, 66]

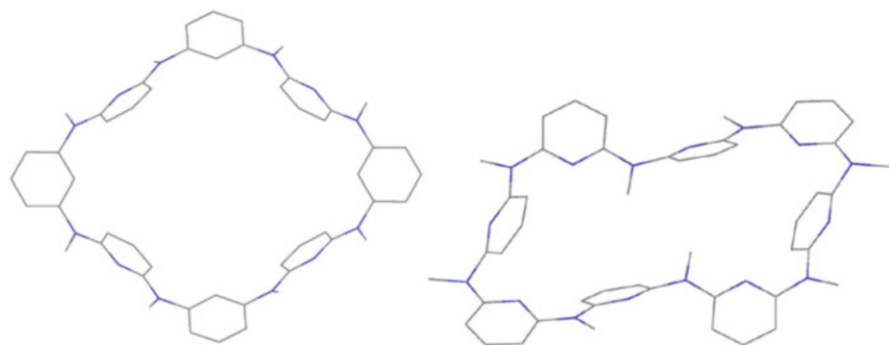


**Fig. 14.8** Crystal structures of azacalix[4]arene[4]pyridine (*left*) [15] and azacalix[8]pyridine (*right*) [21]. All hydrogen atoms are omitted for clarity

adjacent pyridine rings (Fig. 14.8) [21]. Similar to azacalix[8]pyridine, the larger macrocyclic homolog azacalix[10]pyridine also adopts a parallelogram structure with a  $C_2$  symmetry [22].



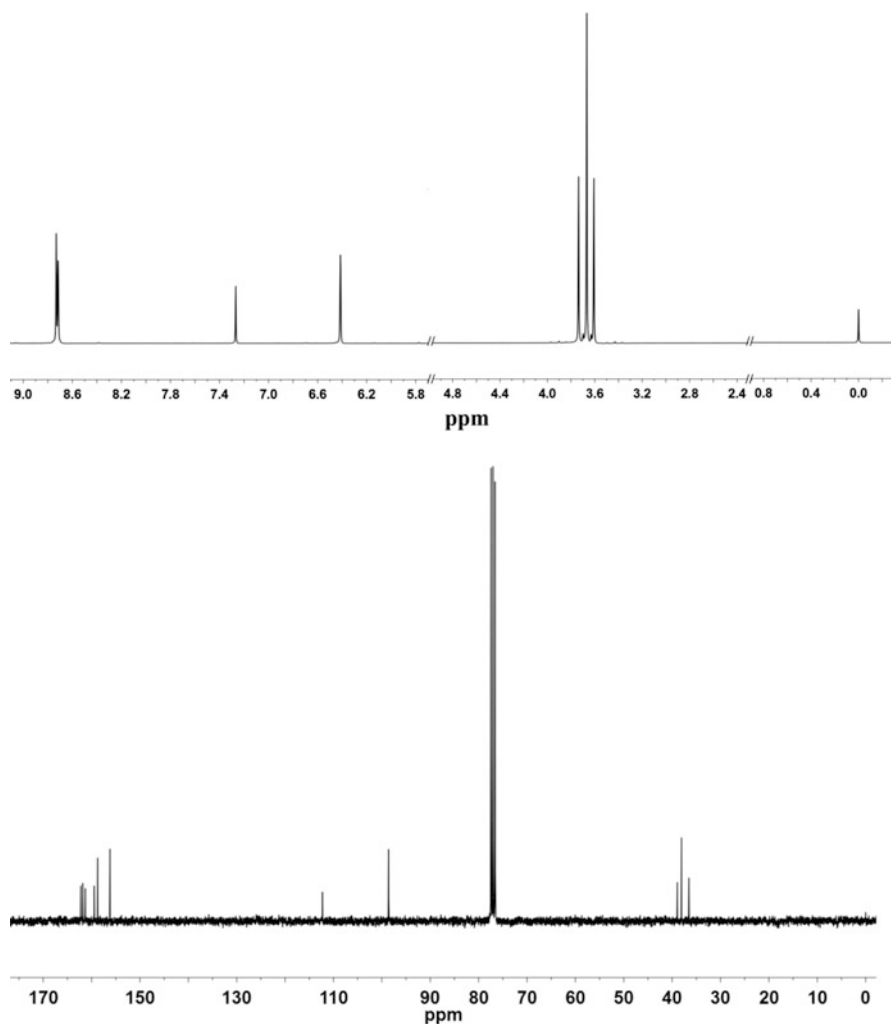
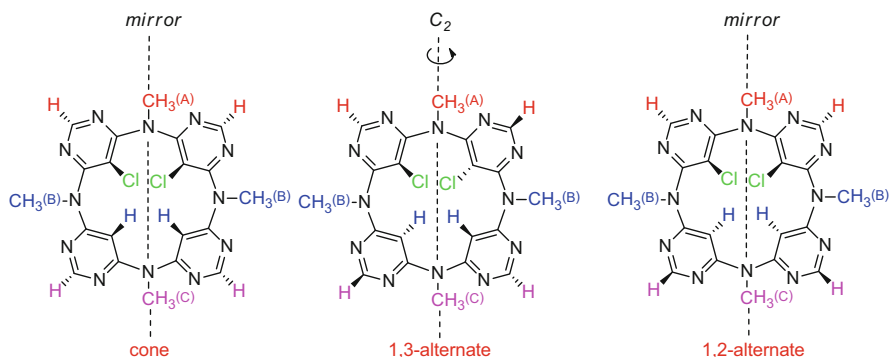


Fig. 14.9  $^1\text{H}$  and  $^{13}\text{C}$  NMR spectra of azacalix[4]pyrimidine **50** [51]

### 14.3.2 Structure in Solution

For a long time the elucidation of conformational structure of azacalixaromatics in solution had remained a formidable challenge [37, 44, 67–69]. Because of the lack of diagnostic methylene linkages, while their proton signals in  $^1\text{H}$  NMR tell explicitly the conformational structures of conventional calixarenes, the assignment of and the differentiation of conformational structures of azacalixaromatics are impossible based solely on NMR spectra [51, 69]. For instance, both  $^1\text{H}$  and  $^{13}\text{C}$  NMR spectra of **50** give a simple and single set of proton and carbon signals, respectively (Fig. 14.9). The set of proton signals with intensity of 3H, 6H, and 3H



**Fig. 14.10** Cone, 1,3- and 1,2-alternate conformational structures of **50** [51]

at 3.60–3.75 ppm and carbon signals with intensity of 1C, 2C, and 1C at 36–39 ppm can be assigned to one of the cone, 1,3- and 1,2-alternate conformational structures (Fig. 14.10). Because of the difficulty and frustration, the solid state 1,3-alternate conformation of azacalix[4]aromatics had always been tentatively extrapolated to solution.

The quandary has been solved elegantly by Wang and co-workers by the study of inherently chiral azacalix[4]pyrimidines [51]. Scrutiny of the structures of cone, 1,3- and 1,2-alternate conformers of **50** reveals that both cone and 1,2-alternate conformers are *meso* compounds whereas 1,3-alternate conformer has a  $C_2$  symmetry. If azacalix[4]pyrimidine **50** adopts stable 1,3-alternate conformation, optical resolution would afford a pair of enantiomerically pure inherently chiral macrocycles. Pleasingly, resolution of a racemic mixture of **50** using chiral HPLC gives indeed *P*- and *M*-macrocycles. Perfect mirror images are observed in their CD spectra. Authors have further investigated the quantification of conformational mobility of 1,3-alternate structure in solution by measuring the kinetics and activation free energy of racemization of a number of enantiopure inherently chiral azacalix[4]pyrimidines. It has been concluded that 1,3-alternate conformations are the most populated structures of azacalix[4]pyrimidines in solution. As summarized in Fig. 14.11, without any substitution or with sterically small substituents on the lower rim, 1,3-alternate azacalix[4]pyrimidines undergo very rapid macrocyclic ring inversion at ambient temperature relative to the time scale of analytical methods. In the case of proximally disubstituted azacalix[4]pyrimidines, the presence of two substituents larger than the van der Waals radii  $r_w = 1.75 \text{ \AA}$  (such as chlorine) and  $r_w = 1.47 \text{ \AA}$  (such as fluorine), respectively, at the lower rim is able to immobilize conformational mobility at room temperature. A minimum activation free energy of 30 kcal/mol is required when these macrocycles undergo conformation interconversions. A combination of two groups larger than the van der Waals radii  $r_w = 1.75 \text{ \AA}$  (such as chlorine) and  $r_w = 1.85 \text{ \AA}$  (such as bromine), respectively, is necessary to prevent the macrocyclic ring inversion, yielding a shape-persistent 1,3-alternate conformer in solution up to 180 °C.

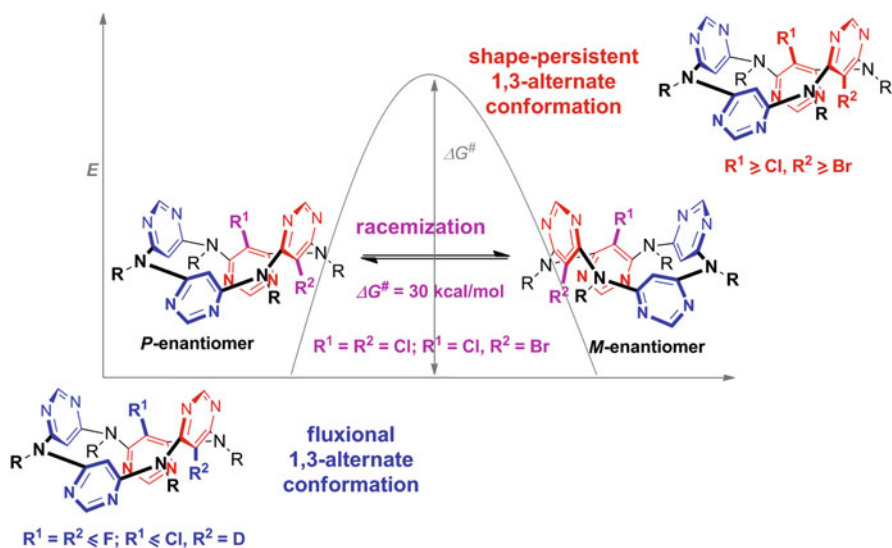


**Fig. 14.11** Racemization of inherently chiral azacalix[4]pyrimidines [51]

It should be noted that detailed conformational structures of larger azacalix[ $n$ ] aromatics ( $n > 4$ ) in solution still remain unknown. For example, the single sets of resonance signals are recorded in NMR spectra for azacalix[ $n$ ]pyridines ( $n = 5-10$ ) and azacalix[ $n$ ]arenes ( $n = 5-8$ ). The outcomes can probably only suggest the formation of a mixture of conformers which are able to undergo very rapid interconversions at the probe temperature in relative to NMR time scale. Further studies, especially, new strategy and physical methods, are needed to solve the problem.

## 14.4 Molecular Recognition and Application

The easy availability, unique conformation and fine-tunable cavity render functionalized azacalixarenes useful macrocycles in supramolecular chemistry. Investigations have demonstrated indeed that azacalixaromatics are new generation macrocyclic host molecules. Based on various non-covalent interactions, they are able to recognize a wide variety of guests ranging from cations, organometallic clusters to neutral molecules including fullerenes. Azacalixaromatics have also been utilized as macrocyclic units in the fabrications of materials such as  $\text{CO}_2$  absorbents, metal-organic coordination networks and liquid crystals.

## 14.4.1 Complexation with Cations

### 14.4.1.1 Protonation

The small cavity formed by pyridines of functionalized azacalix[3]pyridines acts ideally as a host to accommodate one proton. As revealed by Kanbara and co-workers, pyrrolidinyl-substituted azacalix[3]pyridines are superbases with basicity up to  $pK_{\text{BH}^+} = 29.5$  in  $\text{CD}_3\text{CN}$  [24]. Treatment of azacalix[3]pyridines with acids results readily in the formation of complexes **28**. No multiple protonation occurs on azacalix[3]pyridine derivatives. Azacalix[4]pyridine, on the contrary, undergoes selective mono- to tetra-protonation reactions due to its unique 1,3-alternate conformation. Multiple protonation reaction such as octa-protonation has also been observed when azacalix[8]pyridine is treated with a strong acid. As aforementioned, X-ray single crystal structures of mono-, di- and tri-protonated azacalix[4]pyridines are obtained (Scheme 14.6). The resulting cavity of each protonated azacalix[4]pyridines interacts guest species of different size and different geometry through the formation of hydrogen bonds (vide supra) [21].

### 14.4.1.2 Complexation with Transition Metal Ions

When incorporating heteroaromatic units such as pyridine, pyrimidine and pyrazine, the acquired azacalixarenes behave as powerful host molecules to recognize transition metal ions based on ion-dipole interaction [19, 34, 48, 49, 63, 70, 71]. One of the remarkable examples is tetramethylazacalix[4]pyridine, which forms 1:1 complexes selectively with transition and heavy metal ions including  $\text{Cr}^{3+}$ ,  $\text{Fe}^{2+}$ ,  $\text{Co}^{2+}$ ,  $\text{Cu}^{2+}$ ,  $\text{Zn}^{2+}$ ,  $\text{Ag}^+$ ,  $\text{Hg}^{2+}$ ,  $\text{Pb}^{2+}$  and  $\text{Pd}^{2+}$  in a mixture of water and acetonitrile. The binding constants ( $\log K_{1:1}$ ) are in the range of 2.7–8.2 [71]. Noticeably, tetramethylazacalix[4]pyridine acts as a highly  $\text{Zn}^{2+}$  – selective fluorescent sensor. Interacting with  $\text{Zn}^{2+}$  leads to a threefold enhancement of fluorescence intensity [70]. Later on,  $(\text{NH})_2(\text{NMe})_2$ -bridged azacalix[4]pyridine **14b** has been found to be a more strong and selective host for  $\text{Zn}^{2+}$ , with a more than 13-fold enhancement of fluorescence intensity being observed when it forms 1:1 complex with  $\text{Zn}^{2+}$  in the presence of a large amount of alkali and other transition metal ions [19]. Further modification on a bridging nitrogen of azacalix[4]pyridine generates a number of the lariat azacalix[4]pyridines that contain a fifth chelating group such as pyridine and thiophene on the lariat arm. The fifth binding site installed on the lariat arm of azacalix[4]pyridines contributes significantly to the enhanced binding as the resulting lariat azacalix[4]pyridines exhibit powerful capability of binding transition metal ions with binding constants ( $\log K_{1:1}$ ) up to 10.6 [63]. It is notable that azacalix[4]pyridines change their 1,3-alternate conformation into a saddle-like one after complexation with metal ions. As depicted in Fig. 14.12, the four pyridine nitrogen atoms probably undergo pre-organization into a square planar tetradentate ligand during the course of metal complexation [19, 63, 70, 71].

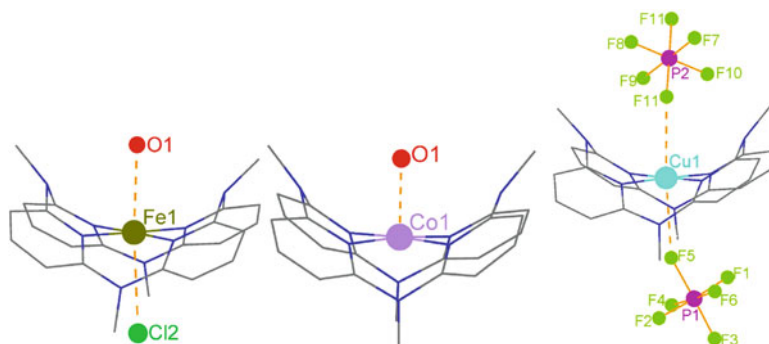


**Fig. 14.12** Crystal structures of azacalix[4]pyridine-metal ion complexes. All hydrogen atoms are omitted for clarity. [71]

Being different from azacalix[4]pyridines that have convergent or inner binding sites on the smaller rim, azacalix[4]pyrimidine **12a** contains multiple divergent binding sites on the larger rim. The coordination self-assembly between azacalix[4]pyrimidines with cubane-like copper halides has been reported to produce coordination polymers of different topologies [72]. Tetramethylazacalix[4]pyrazines **41a**, on the other hand, has both convergent and divergent binding sites on the smaller and larger rims respectively. The convergent and divergent binding sites are orthogonal to each other because of the 1,3-alternate conformational structure. It acts as a unique multimodal ligand to form versatile self-assembled networks with metal and cluster centers orchestrated by the nature of coordination chemistry [48]. Illustrated in Fig. 14.13 are appealing coordination network structures such as honeycomb, Kagomé,  $\alpha$ -quartz, and cavity-involved two dimensional layers that are conducted by different combination modes between the chelation bonding sites of tetramethylazacalix[4]pyrazines and silver triflate, silver tetrafluoroborate, zinc triflate and  $\text{Cu}_x\text{I}_x$ , respectively.

#### 14.4.2 Complexation with Organosilver Clusters

Azacalix[n]pyridines ( $n = 6, 8$ ) are utilized as macrocyclic multidentate ligands of a larger cavity to complex organosilver clusters. In combination of anionic directing ligands, cluster-centered metallocuprasupramolecular architectures are produced [73–76]. For example, the interaction of azacalix[6]pyridine with  $\text{Ag}_2\text{C}_2$  results in the formation of a supramolecular capsule that contains a closed silver cage with a  $\text{C}_2^{2-}$  anion trapped inside (Fig. 14.14) [73]. The encapsulation method provides a promising practical means to stabilize reactive and unstable organosilver clusters, thereby making their existing applications more feasible and potentiating some new applications. On the other hand, an unprecedented and sophisticated organosilver cluster-centered pseudo-rotaxane supramolecular structure is constructed by

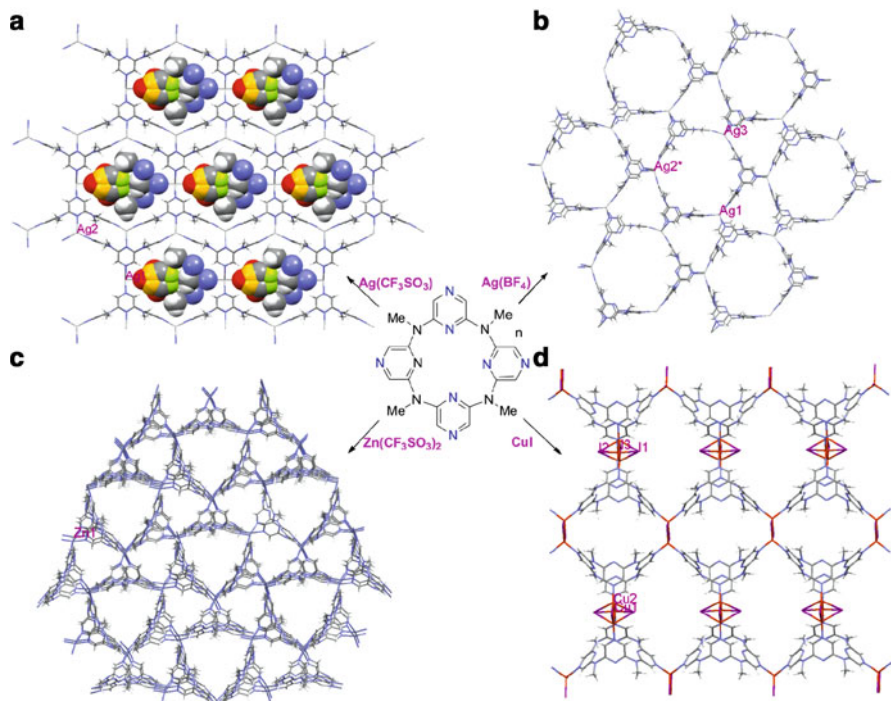
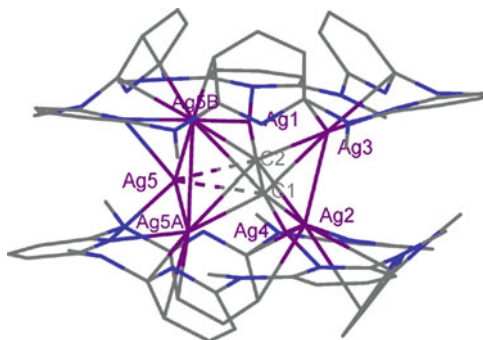


**Fig. 14.13** Coordination self-assembled honeycomb (a), Kagomé (b),  $\alpha$ -quartz (c), and cavity-involved two dimensional layers (d) from **41a** and different metal salts [48]

**Fig. 14.14** X-ray crystal structure of organosilver cluster-centered supramolecular capsule. All hydrogen atoms are omitted for clarity [73]



reacting azacalix[8]pyridine with silver triflate and silver acetylide complex derived from 1,3-bis((3-ethynylphenyl)ethynyl)benzene [74]. In the crystal structure, which is illustrated in Fig. 14.15, the two terminal acetylide anions each bonds to an approximately planar  $\text{Ag}_4$  aggregate. Each  $\text{Ag}_4$  aggregate is encircled by a azacalix[8]pyridine ligand through the coordination of six pyridyl nitrogen atoms. The study opens a new avenue to fabricate new types of (pseudo)-rotaxanes employing organometal cluster as a threading component.

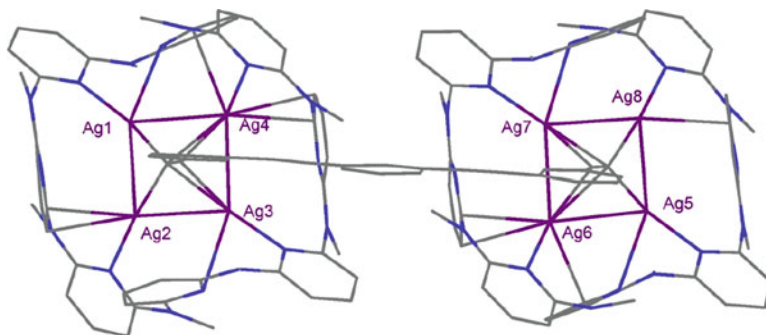


**Fig. 14.15** X-ray crystal structures of organosilver cluster-centered pseudo-rotaxane. All hydrogen atoms are omitted for clarity [74]

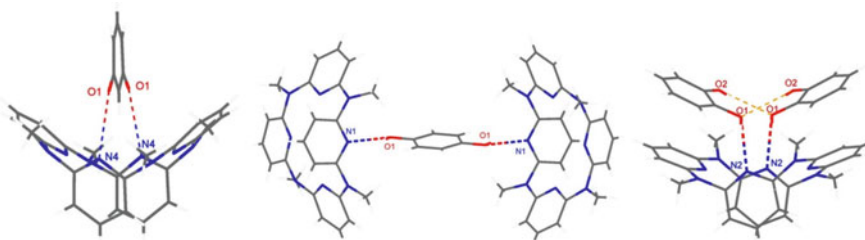


**Fig. 14.16** Crystal structures of complexes of **17a** with resorcinol, hydroquinone and catechol [77]

### 14.4.3 Complexation with Neutral Molecules

As a multiple pyridine-containing macrocycle, azacalix[4]pyridine is a good hydrogen bond receptor. By means of  $^1\text{H}$  NMR titrations, Wang and co-workers have demonstrated azacalix[4]pyridine **17a** is able to recognize benzene diols, aliphatic diols and alcohols [77]. Depending on the structure, especially the geometry of guests, azacalix[4]pyridine forms complexes with varied stoichiometries in the solid state. For example, **17a** forms 1:1 inclusion complexes with ethanol, ethylene glycol, 1,3-dihydroxypropane, and resorcinol. In the case of catechol and hydroquinone, the 1:2 and 2:1 complexes are obtained, respectively. It is very interesting to note that with the help of hydrogen bonding, along with weak C-H/ $\pi$  and  $\pi/\pi$  interactions, **17a** forms sandwich-type, capsule-like and butterfly-layered complexes with resorcinol, hydroquinone and catechol, respectively (Fig. 14.16). The binding constants, measured by the  $^1\text{H}$  NMR titration method in  $\text{CDCl}_3$  show the excellent selectivity for resorcinol ( $K_{1:1} = 6,000 \text{ M}^{-1}$ ). Since the binding to other diols and alcohols is weak with the stability constants hardly exceeding  $200 \text{ M}^{-1}$ , and because the interaction between **17a** with resorcinol leads to considerable chemical shift of proton signals,  $^1\text{H}$  NMR provides a useful method to detect

1,3-phenylene diol component from a mixed sample owing to the strong and selective recognition of 1,3-phenylene diol structure by azacalix[4]pyridine.

#### 14.4.4 Complexation with Fullerenes

Molecular recognition property of azacalixaromatics toward fullerenes is also noteworthy. In their very first study, Wang and co-workers demonstrated that fullerene  $C_{60}$  changes its color from characteristic purple to light brown when mixing with azacalix[4]arene[4]pyridine. Spectroscopic titration substantiates convincingly that azacalix[4]arene[4]pyridine is able to complex  $C_{60}$  and  $C_{70}$ , giving high binding constants ( $K_{1:1}$ ) of  $70,680 \pm 2,060$ , and  $136,620 \pm 3,770 \text{ M}^{-1}$ , respectively. The smaller homologue azacalix[2]arene[2]pyridine, however, does not show affinity to fullerenes [15]. Systematic studies conducted by the same research group indicate that azacalix[n]pyridines ( $n > 5$ ) with different cavities form 1:1 complexes with  $C_{60}$  and  $C_{70}$ , with binding constants around  $10^4$ – $10^5 \text{ M}^{-1}$ . As the mono-macrocyclic species in comparison to other synthetic receptors, azacalix[n]pyridines ( $n > 5$ ) appear most probably the strongest hosts in binding with fullerenes [21–23]. Although being not significant, selectivity of complexation with  $C_{70}$  by azacalix[n]pyridines ( $n > 5$ ) is generally higher than with  $C_{60}$ .

To seek for stronger fullerene receptors and also to shed light on the nature of azacalixaromatics-fullerene interactions, a number of shape-persistent 1,3,5-alternate azacalix[3]pyridine[3]pyrimidines with various substituents on the bridging nitrogen atoms along with other azacalix[6]aromatics containing different combinations of benzene, pyridine, and pyrimidine rings are investigated [28, 66]. Similar to azacalix[n]pyridines ( $n > 5$ ), azacalix[3]pyridine[3]pyrimidines and all other azacalix[6]aromatics form 1:1 complexes with  $C_{60}$  and  $C_{70}$  in solution. Surprisingly, although the formation of 1:1 complexes between azacalix[6]aromatics in solution is evidenced by Job's plot experiments, most of azacalix[3]pyridine[3]pyrimidines complex  $C_{60}$  and  $C_{70}$  in the solid state in a 2:1 stoichiometric ratio. Figure 14.17 shows the X-ray crystal structures of the complexes between hexaallylazacalix[3]pyridine[3]pyrimidine and  $C_{60}$  and  $C_{70}$ . In both cases, a fullerene molecule is encapsulated by two interdigitated azacalix[3]pyridine[3]pyrimidine hosts. The shorter distances of the surface of fullerenes to pyrimidine rings and to *N*-substituents indicate explicitly multiple  $\pi/\pi$  stacking and C-H/ $\pi$  interactions are the driving forces to form host-guest complexes [28].

#### 14.4.5 Selective $CO_2$ Absorbents

Tsue and co-workers have discovered that  $(NH)_n$ -azacalix[n]arenes ( $n = 5$ – $7$ ) are solid materials able to absorb carbon dioxide selectively [25, 27, 78, 79]. The desolvated polycrystalline powder of azacalix[6]arene, which is obtained after





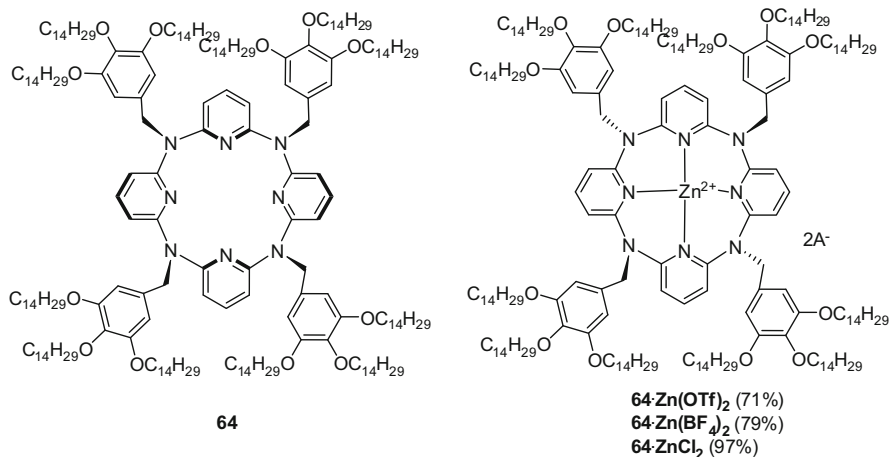


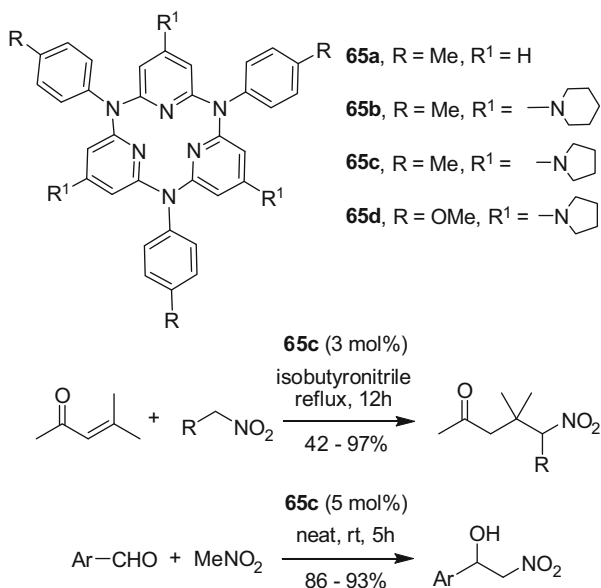
**Fig. 14.18** Structure of liquid crystalline azacalix[4]pyridine derivative **64** and its zinc complexes [80]

complexation with zinc ion leads to a significant expansion of the LC range. For instance, the  $\text{ZnCl}_2$ -**64b** complex presents the texture of Col at around 100 °C upon cooling the samples from the isotropic state. The birefringence becomes stronger when cooling to ambient temperature. It is worth addressing that it is the first example of LC materials constructed by saddle-shaped macrocycles. Moreover, change of macrocyclic conformation from 1,3-alternate to a pinched one by zinc ion through complexation enables facile regulation of phase behavior of macrocyclic liquid crystals (Fig. 14.18) [80].

#### 14.4.7 Catalysis

Kabara and co-workers have shown that azacalix[3]pyridines **65** act as superbases to catalyze some synthetic organic reactions. As expected, the catalytic activity is enhanced with the increase of basicity of the macrocycles. The 1-pyrrolidinyl-bearing azacalix[3]pyridine **65c** of  ${}^{\text{MeCN}}pK_{\text{BH}^+}$  28.1 is found to catalyze efficiently the Michael addition of nitroalkanes and alcohols to enones. Significantly, azacalix[3]pyridine **65c** also appears as an excellent catalyst to effect 1,2-addition of nitromethane to various aromatic and heterocyclic aldehyde substrates that are not accepted by other base catalysts (Scheme 14.20).

**Scheme 14.20** Azacalix[3] pyridine-catalyzed reactions [24, 81]



### 14.4.8 Miscellaneous

Applications of azacalixaromatics in various other fields have been documented in literature. Zhang and co-workers have prepared azacalix[2]arene[2]triazine-based silica gel as the solid-phase extraction sorbent to purify a trace amount of arylamide in starchy foodstuffs. It has also been used as HPLC stationary phase to separate polycyclic aromatic compounds and inorganic anions [82, 83]. Ito, Tsue and co-workers have demonstrated the feasibility of using azacalixarenes as high-spin materials [62, 84]. Employing Se···N non-covalent bond interactions, Xu and co-workers have fabricated well-defined azacalix[6]arene nanosheets in aqueous solution in the presence of a selenium-containing amphiphile [85].

## 14.5 Concluding Remarks

As a new generation of synthetic macrocyclic host molecules, azacalixaromatics have gained attention at the onset of the twenty-first century when general and convenient methods for their synthesis were established. Owing to the formation of variable conjugational systems between bridging nitrogen atoms and their adjacent aromatic rings, the unique conformational structures and fine-tunability of cavity and electronic feature render azacalixaromatics powerful and versatile synthetic hosts to form a wide variety of complexes with different guest species through non-covalent bond interactions. Admittedly, the study of application of

azacalixaromatics in supramolecular chemistry is still in its infancy in comparison to conventional calix[n]arenes. However, the easy accessibility to diverse designable functionalized azacalixaromatics by means of efficient and straightforward synthetic methods, and substantiated versatility of azacalixaromatics in host-guest interactions will attract growing interest of supramolecular chemists in future. A new era of azacalixaromatics centering on the application in non-covalent bond interactions and self-assembly, catalysis, functional materials and life science is expected in the years to come.

**Acknowledgments** We thank National Natural Science Foundation of China 佛如 financial support.

## References

1. Gutsche, C. D. *Calixarenes: An Introduction*, Cambridge, The Royal Society of Chemistry, **2008**.
2. Smith, G. W. *Nature* **1963**, *198*, 879.
3. Sommer, N.; Staab, H. A. *Tetrahedron Lett.* **1966**, 2837.
4. Kumagai, H.; Hasegawa, M.; Miyanari, S.; Sugawa, Y.; Sato, Y.; Hori, T.; Ueda, S.; Kamiyama, H.; Miyano, S. *Tetrahedron Lett.* **1997**, *38*, 3971–3972.
5. Wang, M.-X. *Chem. Commun.* **2008**, 4541–4551.
6. Wang, M.-X. *Acc. Chem. Res.* **2012**, *45*, 182–195.
7. Tsue, H.; Ishibashi, K.; Tamura, R. *Top Heterocycl. Chem.* **2008**, *17*, 73–96.
8. König, B.; Fonseca, M. H. *Eur. J. Inorg. Chem.* **2000**, 2303–2310.
9. Morohashi, N.; Narumi, F.; Iki, N.; Hattori, T.; Miyano, S. *Chem. Rev.* **2006**, *106*, 5291–5316.
10. Lhoták, P. *Eur. J. Org. Chem.* **2004**, 1675–1692.
11. Maes, W.; Dehaen, W. *Chem. Soc. Rev.* **2008**, *37*, 2393–2402.
12. Thomas, J.; Van Rossom, W.; Van Hecke, K.; Van Meervelt, L.; Smet, M.; Maes, W.; Dehaen, W. *Chem. Commun.* **2012**, *48*, 43–45.
13. Ma, Y.-X.; Han, Y.; Chen C.-F. *J. Incl. Phenom. Macrocycl. Chem.* **2014**, *79*, 261–281.
14. Wang, M.-X.; Yang, H.-B. *J. Am. Chem. Soc.* **2004**, *126*, 15412–15422.
15. Wang, M.-X.; Zhang, X.-H.; Zheng, Q.-Y. *Angew. Chem. Int. Ed.* **2004**, *43*, 838–842.
16. Wang, L.-X.; Wang, D.-X.; Huang, Z.-T.; Wang, M.-X. *J. Org. Chem.* **2010**, *75*, 741–747.
17. Bushby, R. J.; Kilner, C. A.; Taylor, N.; Vale, M. E. *Tetrahedron* **2007**, *63*, 11458–11466.
18. Wang, L.-X.; Wang, D.-X.; Wang, M.-X. *Chin. J. Chem.* **2013**, *32*, 1033–1038.
19. Zhang, E.-X.; Wang, D.-X.; Huang, Z.-T.; Wang, M.-X. *J. Org. Chem.* **2009**, *74*, 8595–8603.
20. Yao, B.; Wang, D.-X.; Gong, H.-Y.; Huang, Z.-T.; Wang, M.-X. *J. Org. Chem.* **2009**, *74*, 5361–5368.
21. Gong, H.-Y.; Zhang, X.-H.; Wang, D.-X.; Ma, H.-W.; Zheng, Q.-Y.; Wang, M.-X. *Chem. Eur. J.* **2006**, *12*, 9262–9275.
22. Liu, S.-Q.; Wang, D.-X.; Zheng, Q.-Y.; Wang, M.-X. *Chem. Commun.* **2007**, 3856–3858.
23. Zhang, E.-X.; Wang, D.-X.; Zheng, Q.-Y.; Wang, M.-X. *Org. Lett.* **2008**, *12*, 2565–2568.
24. Uchida, N.; Kuwabara, J.; Taketoshi, A.; Kanbara, T. *J. Org. Chem.* **2012**, *77*, 10631–10637.
25. Tsue, H.; Ishibashi, K.; Tokita, S.; Takahashi, H.; Matsui, K.; Tamura, R. *Chem. Eur. J.* **2008**, *14*, 6125–6134.
26. Ishibashi, K.; Tsue, H.; Takahashi, H.; Tokita, S.; Matsui, K.; Tamura, R. *Heterocycles* **2008**, *76*, 541–550.
27. Tsue, H.; Matsui, K.; Ishibashi, K.; Takahashi, H.; Tokita, S.; Ono, K.; Tamura, R. *J. Org. Chem.* **2008**, *73*, 7748–7755.

28. Fa, S.-X.; Wang, L.-X.; Wang, D.-X.; Zhao, L.; Wang, M.-X. *J. Org. Chem.* **2014**, *79*, 3559–3571.
29. Xue, M.; Chen, C.-F. *Org. Lett.* **2009**, *11*, 5294–5297.
30. Xue, M.; Chen, C.-F. *Chem. Commun.* **2011**, *47*, 2318–2320.
31. Hu, W.-J.; Ma, M.-L.; Zhao, X.-L.; Guo, F.; Mi, X.-Q.; Jiang, B.; Wen, K. *Tetrahedron* **2012**, *68*, 6071–6078.
32. Yuan, J.; Zhu, Y.; Gao, Q.; Liu, M.; Jia, F.; Wu, A. *Tetrahedron Lett.* **2012**, *53*, 1222–1226.
33. Clayden, J.; Rowbottom, S. J. M.; Hutchings, M. G.; Ebenezer, W. J. *Tetrahedron Lett.* **2009**, *50*, 3923–3925.
34. Fang, Y.-X.; Zhao, L.; Wang, D.-X.; Wang, M.-X. *J. Org. Chem.* **2012**, *77*, 10073–10082.
35. Haddoub, R.; Touil, M.; Chen, Z.; Raimundo, J.-M.; Marsal, P.; Elhabiri, M.; Siri, O. *Eur. J. Org. Chem.* **2014**, 745–752.
36. Ito, A.; Ono, Y.; Tanaka, K. *J. Org. Chem.* **1999**, *64*, 8236–8241.
37. Fukushima, W.; Kanbara, T.; Yamamoto, T. *Synlett* **2005**, 2931–2934.
38. Miyazaki, Y.; Kanbara, T.; Yamamoto, T. *Tetrahedron Lett.* **2002**, *43*, 7945–7948.
39. Vale, M.; Pink, M.; Rajca, S.; Rajca, A. *J. Org. Chem.* **2008**, *73*, 27–35.
40. Suzuki, Y.; Yanagi, T.; Kanbara, T.; Yamamoto, T. *Synlett* **2005**, 263–266.
41. Uchida, N.; Zhi, R.; Kuwabara, J.; Kanbaraj, T. *Tetrahedron Lett.* **2014**, *55*, 3070–3072.
42. Despotović, I.; Kovačević, B.; Maksić, Z.B. *Org. Lett.* **2007**, *9*, 1101–1104.
43. Wang, X.-D.; Wang, D.-X.; Huang, Z.-T.; Wang, M.-X. *Supromol. Chem.* **2014**, *26*, 601–606.
44. Tsue, H.; Ishibashi, K.; Takahashi, H.; Tamura, R. *Org. Lett.* **2005**, *7*, 2165–2168.
45. Ishibashi, K.; Tsue, H.; Tokita, S.; Matsui, K.; Takahashi, H.; Tamura, R. *Org. Lett.* **2006**, *8*, 5991–5994.
46. Ishibashi, K.; Tsue, H.; Takahashi, H.; Tamura, R. *Tetrahedron: Asymmetry* **2009**, *20*, 375–380.
47. Tsue, K.; Miyata, K.; Takahashi, D.; Takahashi, H.; Sasaki, K.; Tamura, R. *Heterocycles* **2012**, *86*, 159–164.
48. Wu, J.-C.; Zhao, L.; Wang, D.-X.; Wang, M.-X. *Inorg. Chem.* **2012**, *51*, 3860–3867.
49. Wu, J.-C.; Zhao, L.; Wang, D.-X.; Wang, M.-X. *Chin. J. Chem.* **2013**, *31*, 589–597.
50. Ren, W.-S.; Zhao, L.; Wang, M.-X. *J. Org. Chem.* **2015**, *80*, 9272–9278.
51. Li, J.-T.; Wang, L.-X.; Wang, D.-X.; Zhao, L.; Wang, M.-X. *J. Org. Chem.* **2014**, *79*, 2178–2188.
52. Yao, B.; Wang, D.-X.; Huang, Z.-T.; Wang, M.-X. *Chem. Commun.* **2009**, 2899–2901.
53. Zhang, H.; Yao, B.; Zhao, L.; Wang, D.-X.; Xu, B.-Q.; Wang, M.-X. *J. Am. Chem. Soc.* **2014**, *136*, 6326–6332.
54. Yao, B.; Wang, Z.-L.; Zhang, H.; Wang, D.-X.; Zhao, L.; Wang, M.-X. *J. Org. Chem.* **2012**, *77*, 3336–3340.
55. Wang, Z.-L.; Zhao, L.; Wang, M.-X. *Org. Lett.* **2011**, *13*, 6560–6563.
56. Wang, Z.-L.; Zhao, L.; Wang, M.-X. *Chem. Commun.* **2012**, *48*, 9418–9420.
57. Wang, Z.-L.; Zhao, L.; Wang, M.-X. *Org. Lett.* **2012**, *14*, 1472–1475.
58. Zhang, H.; Zhao, L.; Wang, D.-X.; Wang, M.-X. *Org. Lett.* **2013**, *15*, 3836–3839.
59. Yao, B.; Liu, Y.; Zhao, L.; Wang, D.-X.; Wang, M.-X. *J. Org. Chem.* **2014**, *79*, 11139–11145.
60. Wang, Q.-Q.; Wang, D.-X.; Ma, H.-W.; Wang, M.-X. *Org. Lett.* **2006**, *8*, 5967–5970.
61. Caio, J. M.; Esteves, T.; Carvalho, S.; Moiteiro, C.; Félix, V. *Org. Biomol. Chem.* **2014**, *12*, 589–599.
62. Ito, A.; Inoue, S.; Hirao, Y.; Furukawa, K.; Kato, T.; Tanaka, K. *Chem. Commun.* **2008**, 3242–3244.
63. Fang, Y.-X.; Ao, Y.-F.; Wang, D.-X.; Zhao, L.; Wang, M.-X. *Tetrahedron* **2015**, *71*, 2105–2112.
64. Li, J.-T.; Wang, D.-X.; Zhao, L.; Wang, M.-X. *Tetrahedron Lett.* **2014**, *55*, 3259–3262.
65. Chen, Z.; Giorgi, M.; Jacquemin, D.; Elhabiri, M.; Siri, O. *Angew. Chem. Int. Ed.* **2013**, *52*, 6250–6254.
66. Wang, L.-X.; Zhao, L.; Wang, D.-X.; Wang, M.-X. *Chem. Commun.* **2011**, *47*, 9690–9692.

67. Tsue, H.; Ishibashi, K.; Tokita, S. Matsui, K.; Takahashi, H.; Tamura, R. *Chem. Lett.* **2007**, *36*, 1374–1375.
68. Touil, M.; Lachkar, M.; Siri, O. *Tetrahedron Lett.* **2008**, *49*, 7250–7252.
69. Konishi, H.; Hashimoto, S.; Sakakibara, T.; Matsubara, S.; Yasukawa, Y.; Morikawa, O.; Kobayashi, K. *Tetrahedron Lett.* **2009**, *50*, 620–623.
70. Gong, H.-Y.; Zheng, Q.-Y.; Zhang, X.-H.; Wang, D.-X.; Wang, M.-X. *Org. Lett.* **2006**, *8*, 4895–4898.
71. Gong, H.-Y.; Wang, D.-X.; Zheng, Q.-Y.; Wang, M.-X. *Tetrahedron* **2009**, *65*, 87–92.
72. Wang, L.-X.; Zhao, L.; Wang, D.-X.; Wang, M.-X. *J. Solid State Chem.* **2010**, *183*, 3010–3016.
73. Gao, C.-Y.; Zhao, L.; Wang, M.-X. *J. Am. Chem. Soc.* **2012**, *134*, 824–827.
74. Gao, C.-Y.; Zhao, L.; Wang, M.-X. *J. Am. Chem. Soc.* **2011**, *133*, 8448–8451.
75. He, X.; Gao, C.-Y.; Wang, M.-X.; Zhao, L. *Chem. Commun.* **2012**, *48*, 10877–10879.
76. Gao, C.-Y.; He, X.; Zhao, L.; Wang, M.-X. *Chem. Commun.* **2012**, *48*, 8368–8370.
77. Gong, H.-Y.; Wang, D.-X.; Xiang, J.-F.; Zheng, Q.-Y.; Wang, M.-X. *Chem. Eur. J.* **2007**, *13*, 7791–7802.
78. Tsue, H.; Ono, K.; Tokita, S.; Ishibashi, K.; Matsui, K.; Takahashi, H.; Miyata, K.; Takahashi, D.; Tamura, R. *Org. Lett.* **2011**, *13*, 490–493.
79. Tsue, H.; Takahashi, H.; Ishibashi, K.; Inoue, R.; Shimizu, S.; Takahashi, D.; Tamura, R. *CrystEngComm.* **2012**, *14*, 1021–1026.
80. Fa, S.-X.; Chen, X.-F.; Yang, S.; Wang, D.-X.; Zhao, L.; Chen, E.-Q.; Wang, M.-X. *Chem. Commun.* **2015**, *51*, 5112–5115.
81. Uchida, N.; Taketoshi, A.; Kuwabara, J.; Yamamoto, T.; Inoue, Y.; Watanabe, Y.; Kanbara, T. *Org. Lett.* **2010**, *12*, 5242–5245.
82. Zhang, W.; Deng, Z.; Zhao, W.; Guo, L.; Tang, W.; Du, H.; Lin, L.; Jiang, Q.; Yu, A.; He, L.; Zhang, S. *J. Agric. Food Chem.* **2014**, *62*, 6100–6107.
83. Zhao, W.; Wang, W.; Chang, H.; Cui, S.; Hu, K.; He, L.; Lu, K.; Liu, J.; Wu, Y.; Qian, J.; Zhang, S. *J. Chromatogr. A* **2012**, *1251*, 74–81.
84. Ishibashi, K.; Tsue, H.; Sakai, N.; Tokita, S.; Matsui, K.; Yamauchi, J.; Tamura, R. *Chem. Commun.* **2008**, 2812–2814.
85. Yi, Y.; Fa, S.-X.; Cao, W.; Zeng, L.; Wang, M.-X.; Xu, H.; Zhang, X. *Chem. Commun.* **2012**, *48*, 7495–7497.

# Chapter 15

## Oxacalixarenes

Reuben Hudson and Jeffrey L. Katz

### 15.1 Overview

Oxacalix[n]arenes **1**, or oxa[1<sub>n</sub>]metacyclophanes, are systems in which the bridging carbon atoms in the calix[n]arene framework have been replaced by oxygen atoms (Fig. 15.1) [1–5]. While oxacalixarenes have been known in the literature for almost half a century, [6–10] it is only since 2002 that research into the synthesis and applications of oxacalixarenes has become active and rich. This chapter will focus on oxa[1<sub>n</sub>]cyclophanes that are *meta*-linked across each arene, as well as on systems that combine *meta*-linkages with an alternative attachment type (e.g., *meta*-linkages mixed with one or more *ortho*- or *para*-linkages). Calixarenes with bridges containing more than one atom (such as homooxacalixarenes [11]) will not be covered, nor will oxacyclophanes that do not contain any *meta*-linkages between arenes (e.g., oxaparacyclophanes, [12, 13] or *ortho*-linked oxacrown [14] compounds).

### 15.2 Oxacalixarene Synthesis

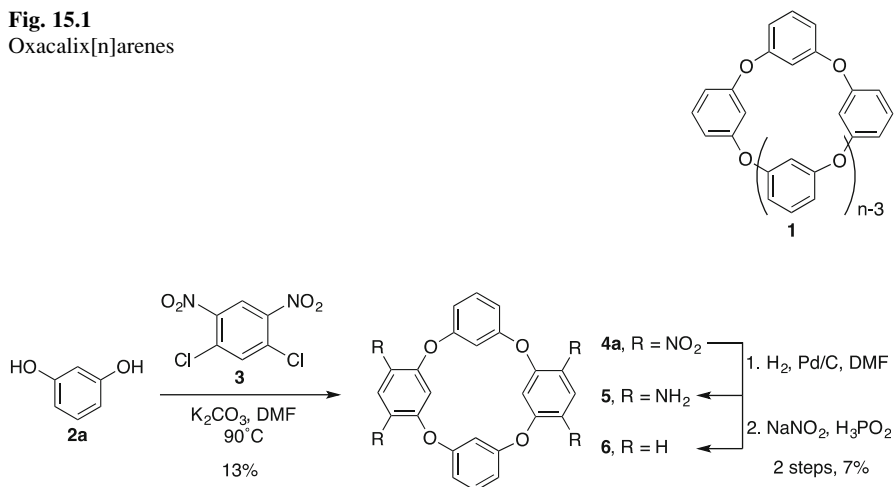
#### 15.2.1 Early Synthesis of Tetranitro-Oxacalix[4]arenes

Oxacalix[4]arenes were first synthesized in 1966 by Sommer and Staab by nucleophilic aromatic substitution ( $S_NAr$ ) reaction of resorcinol **2a** and 1,5-dichloro-2,4-dinitrobenzene **3** using  $K_2CO_3$  base in DMF (Scheme 15.1) [6]. A 13 % yield of the

---

R. Hudson • J.L. Katz (✉)  
Department of Chemistry, Colby College, 5754 Mayflower Hill Drive,  
Waterville, ME 04901, USA  
e-mail: [jlkatz@colby.edu](mailto:jlkatz@colby.edu)

**Fig. 15.1**  
Oxocalix[n]arenes



**Scheme 15.1** Oxocalix[4]arenes synthesized in 1966 by Sommer and Staab

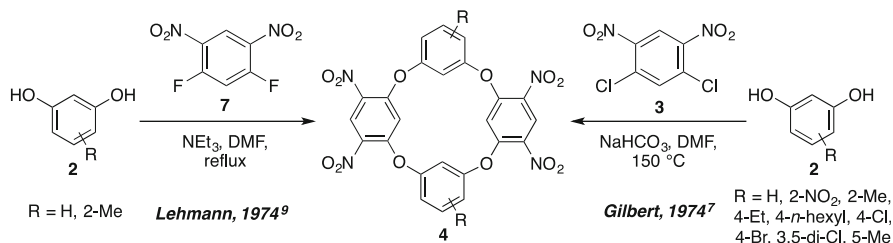
tetranitro-oxocalix[4]arene **4a** was isolated and subsequently deaminated in two steps (7% yield).

Over the decade that followed, several other groups revisited this  $\text{S}_{\text{N}}\text{Ar}$ -based synthesis of tetranitro-oxocalix[4]arenes **4**. In 1974, Lehmann reacted 1,5-difluoro-2,4-dinitrobenzene **7** with resorcinols **2** ( $\text{NEt}_3$ , DMF, reflux) and isolated oxocalix[4]arenes **4** by precipitation in 23–77% yields (Scheme 15.2) [9]. Seeking a platform for the production of thermostable high energy materials, Gilbert reported revised reaction and purification conditions ( $\text{NaHCO}_3$ , DMF,  $150^\circ\text{C}$ , 2 h; purified by recrystallization) in the condensation of 1,5-dichloro-2,4-dinitrobenzene **3** with a range of substituted resorcinols **2**, producing the corresponding oxocalix[4]arenes **4** in good to excellent yields (60–95%) [7, 8]. Two years later, Bottino used slightly altered conditions ( $\text{KOH}$ , DMF, reflux) to react electrophile **3** and resorcinols **2** to produce several previously reported oxocalix[4]arenes **4** in 25–70% yield [10].

Several attributes of these early oxocalixarene syntheses are notable. First, many of the formed products had very low solubility, which hindered purification and characterization. Second, oxocalix[4]arenes were selectively produced over higher cyclic oligomers or linear oligomers, and in certain cases in exceptionally high yield. Finally, all of the early syntheses of oxocalixarenes relied on  $\text{S}_{\text{N}}\text{Ar}$  reactions of a nucleophilic diphenol and an electrophilic dihalobenzene, and this simple and effective synthetic strategy still pervades to current day.

Modern investigations into oxocalixarene synthesis and applications did not begin in earnest until publications by Chambers in 2002, [15–17] M.-X. Wang in 2004, [18] and Katz in 2005 [19]. Substitution reactions between nucleophilic dihydroxy arenes and dihalogenated aromatic electrophiles remain the primary method for creation of oxocalixarenes. The functional group tolerance and modularity of  $\text{S}_{\text{N}}\text{Ar}$ -based ring formations has facilitated the synthesis of diverse collections of oxocalixarenes by structure modification of the nucleophilic and





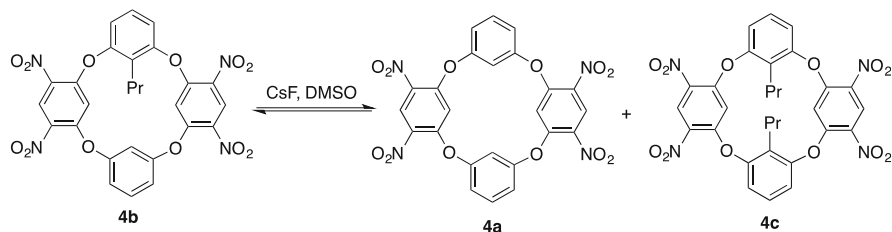
**Scheme 15.2** Oxacalix[4]arenes synthesized by Lehmann and Gilbert in 1974

electrophilic building blocks. This flexibility in oxacalixarene design has in turn enabled increasingly sophisticated applications investigations.

### 15.2.2 Modern Synthesis of Tetranitro-Oxacalix[4]arenes

Based on the early work of Sommer and Staab, [6] Gilbert, [8] and Lehmann, [9] in 2005 Katz reported the synthesis of tetranitro-oxacalix[4]arenes **4** by the short (15 min) room temperature reaction of equimolar amounts of resorcinols **2** with 1,5-difluoro-2,4-dinitrobenzene **7** in DMSO using  $\text{K}_2\text{CO}_3$  base [19]. Under these exceptionally mild conditions, high yields (75–92%) of diversely functionalized oxacalix[4]arenes **4** were obtained ( $\text{R} = \text{H}, 2\text{-OH}, 5\text{-OH}, 5\text{-Me}, 5\text{-}n\text{-pentyl}, 5\text{-}t\text{-Bu}, 5\text{-CHO}, 5\text{-CO}_2\text{Me}, 5\text{-CO}_2\text{Et}$ ). Katz suggested the oxacalix[4]arene formation was taking place under equilibrating conditions, and that the high yields and selectivities observed were due to the oxacalix[4]arenes **4** being the thermodynamically favored products [19]. This proposal for a thermodynamically controlled process was later verified on related oxacalix[2]arene[2]hetarenes [20].

Konishi measured the ability of tetranitro-oxacalix[4]arenes **4** to undergo thermodynamic equilibration. Oxacalix[4]arene **4b** bearing a single lower-rim propyl group was subjected to nucleophilic reaction conditions ( $\text{CsF}$ , DMF,  $80^\circ\text{C}$ ), and it was possible to observe by  $^1\text{H}$  NMR the disproportionation of **4b** into symmetric oxacalix[4]arenes containing either zero (**4a**) or two (**4c**) lower-rim propyl groups (Scheme 15.3). This demonstrated that under the nucleophilic conditions the linking ether bonds are not static, and that the oligomeric mixture exists in a state of dynamic equilibrium in which the thermodynamically favored product is the oxacalix[4]arene [21]. The authors also found that reversible C-O bond formation of this type by *ipso* substitution could be mitigated by the inclusion of sterically bulky *t*-Bu groups on the upper rim [22].



**Scheme 15.3** Disproportionation of monoprolylated oxacalix[4]arene **4b**

### 15.2.3 Diversity of Building Blocks and Approaches for Oxacalix[4]arene Synthesis

While early work showed that structural diversity on the oxacalixarene framework was possible by use of differentially functionalized nucleophilic diphenols (Schemes 15.2 and 15.3), [6–10] use of azaheterocyclic electrophiles to form oxacalix[2]arene[2]hetarenes was first realized by Chambers [15–17] and Wang [18]. Chambers initially reacted two equivalents of a tetrafluoropyridine **8** (see Fig. 15.2) with a 1,3-bis((trimethylsilyl)oxy)benzene **9** (CsF, DME, reflux) to form an electrophilic linear “trimer” species (70–90 % yield). Subsequent cyclization via a 3+1 fragment coupling with a second equivalent of **9** then yielded the corresponding oxacalix[2]arene[2]pyridines (19–64 % yield).

Two years later, M.-X. Wang showed that cyanuric chloride **10** could be used as the electrophile to produce oxacalix[2]arene[2]triazines **12** by a 3+1 fragment coupling strategy that does not require pre-silylation of the diphenol nucleophile (Scheme 15.4) [18]. The researchers also optimized a single step approach to macrocycles **12**, although 3+1 fragment coupling tends to be higher yielding [23]. The mild reaction conditions and high functional group tolerance of the procedures to access both tetranitro-oxacalix[4]arenes **4** and oxacalix[2]arene[2]triazines **12** makes these macrocycles popular and important synthetic platforms for applications development in the oxacalixarene field.

In the years that followed, many other azaheterocyclic electrophiles including 2,6-dihalopyridines **13**, [20] 2,6-dichloropyrazine **14**, [20] 4,6-dihalogenated pyrimidines **15**, [20, 24] 2,4-dichloropyrimidines [25] and quinazolines [25] **16**, 2,7-dichloro-1,8-naphthyridines **17**, [26] and 2,3-dichloroquinoxalines **18** [27] have been coupled with diphenols for oxacalixarene synthesis using either single step or 3+1 fragment coupling methods (Fig. 15.2). As an alternative carbocyclic electrophile to nitrated systems **3** and **7**, 1,5-diethynyl-2,4-difluorobenzenes **19** [28, 29] have also been used to directly form tetraethynyl-oxacalix[4]arenes [30].

The nucleophilic reactant in S<sub>N</sub>Ar-based oxacalixarene formation has been modified and functionalized to impart a great deal of structural diversity to the resulting macrocycles. Vicente used porphyrin-substituted diphenol **2b** for the construction of conformationally constrained multiporphyrin-[31] and monoporphyrin [32]-oxacalixarene systems (Fig. 15.3). Zn-complexes of

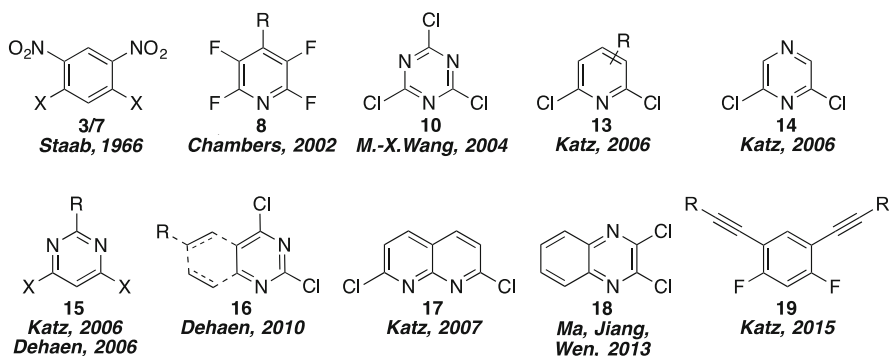
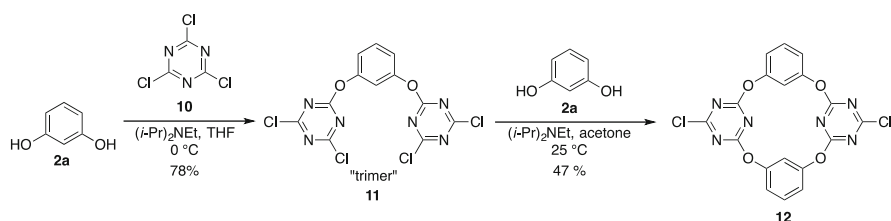


**Fig. 15.2** Electrophile diversity for oxalixarene synthesis



**Scheme 15.4** Synthesis of oxalix[2]arene[2]triazines via 3+1 fragment coupling

porphyrin-substituted oxalixarenes were later studied toward the development of fluorometric probes for wastewater analysis [33, 34]. Oxalixarene synthesis using 2,7-dihydroxynaphthalene **20** is an early example of how an extended nucleophile, where reacting hydroxyl groups are not attached to the same benzene ring, allows modulation of macrocycle topology. For the creation of even larger and more elaborate oxalixarene-like scaffolds, other extended nucleophiles have been utilized such as terphenyl systems **21**, [27, 35] bisphenol A derivatives **22**, [36, 37] adamantane-bridged bisphenols **23**, [38] triptycenes **24**, [39–42] and tetraphenylethylene units **25** [43, 44].

Oxa[1<sub>n</sub>]cyclophanes analogous to oxalix[n]arenes but containing one or more *ortho*- or *para*-linked aromatic rings have been synthesized by several research groups following the general methodology developed for their all-*meta* oxalix[4]arene counterparts. For S<sub>N</sub>Ar-based syntheses, the *ortho*-[9, 26, 37, 45–48] or *para*-linkage [7, 9, 48] is generally established from the nucleophilic component by changing the resorcinol to either a catechol or hydroquinone, but incorporation of an *ortho*-[27] (**18**) or *para*-dihalide electrophile [13] is also possible.

While S<sub>N</sub>Ar chemistry has shaped both early and contemporary routes for the synthesis of oxalixarenes, the Ullmann ether reaction has also been used successfully as an alternative approach to access selected oxalixarene targets using both single pot, [49] or two step, 3 + 1 fragment coupling [50]. While generally lower yielding and with reduced substrate scope, Ullmann ether reaction-based

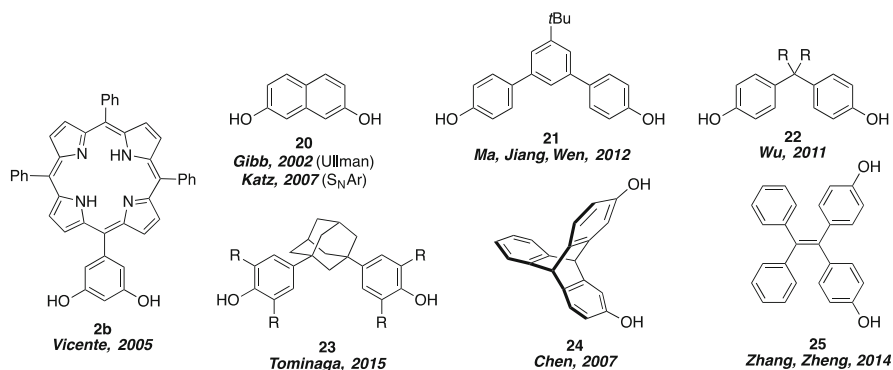


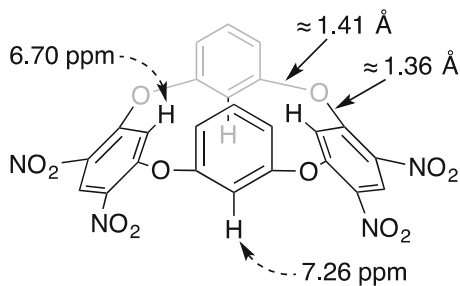
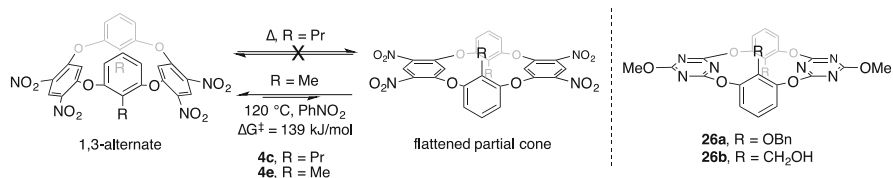
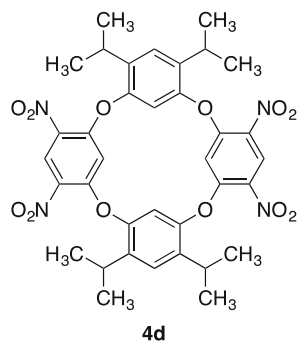
**Fig. 15.3** Diphenol diversity for oxacalixarene synthesis

routes to oxacalixarenes provide a straightforward means to systems in which all aromatic rings are identical, and to oxacalixarenes bearing arene and functional group profiles that may be difficult to access using  $S_NAr$  methods.

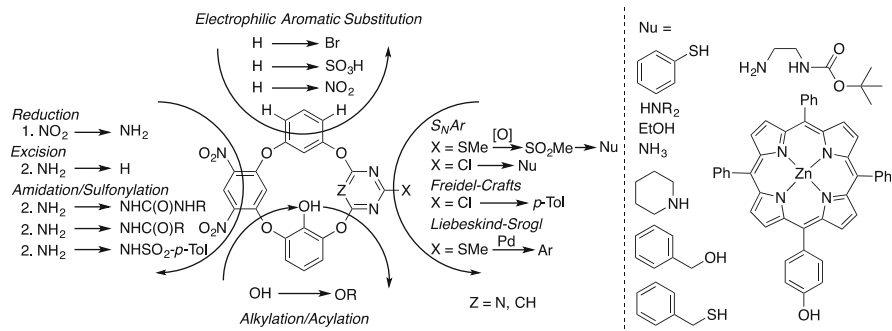
### 15.2.4 Oxacalix[4]arene Conformation and Dynamics

Lehmann was first to propose that oxacalix[4]arenes adopt lowest energy saddle conformations (now generally referred to as a 1,3-alternate conformation using calixarene terminology [51]). Particularly instructive were the low field chemical shifts of the lower rim protons on the dinitrobenzene rings due to the anisotropic shielding of the adjacent aromatic rings, 6.70 ppm for the all *meta*-linked system and 5.67 ppm for the analogous *ortho*-linked system derived from catechol (Fig. 15.4) [9]. Solid-state and solution phase studies confirm that the vast majority of oxacalix[4]arenes adopt distorted 1,3-alternate conformations that maximize the conjugation between the  $sp^2$ -like bridging oxygen atoms and the aromatic rings, while also minimizing transannular steric repulsive effects. The more electron deficient rings of the electrophilic reactant usually slant outwards forming a V-shaped cleft. In contrast, the more electron rich aromatic rings from the nucleophilic reactant are often found to align in a nearly parallel and coplanar arrangement, and receive far less conjugative donation of electron density from the oxygen bridges, as evinced by differences in C-O bond lengths [1, 2, 5]. This 1,3-alternate conformational preference has also been confirmed computationally [52].

The solution-phase conformational dynamics of oxacalix[4]arenes **4** have been studied experimentally by Konishi. Using the diastereotopic methyl resonances of **4d** as a spectroscopic probe (Fig. 15.5), VT  $^1H$  NMR methods revealed a through-the-annulus inversion barrier of 69.5 kJ/mol ( $4.0\text{ s}^{-1}$  at 298 K). In contrast, a higher barrier and slower inversion rates were measured for structurally analogous aza- and thiacalix[4]arenes [53].

**Fig. 15.4** 1,3-alternate conformation**Fig. 15.5** Spectroscopic probe to measure through-the-annulus inversion barrier**Scheme 15.5** Conformational dynamics

Although almost all oxocalix[4]arenes prefer to adopt 1,3-alternate conformations, examples of oxocalix[4]arenes in flattened partial cone [51] (chair [54]) conformations have been reported. Konishi isolated mixtures of two conformational isomers in forming oxocalix[4]arenes with *n*-propyl (**4c**) or methyl (**4e**) groups on the lower rim (Scheme 15.5). The lower rim propyl groups on **4c** prevented through-the-annulus ring conformational equilibration, [55] while thermal interconversion of methyl substituted **4e** could be accomplished in PhNO<sub>2</sub> at 120 °C ( $\Delta G^\ddagger = 139$  kJ/mol) [56]. *O*-benzyl substitution on the lower rim of oxocalix[2]arene[2]triazines such as **26a** (R = OBn) was similarly found by M.-X. Wang to furnish conformational mixtures resistant to thermal interconversion



**Scheme 15.6** Post-cyclization derivatization

[57]. The same group found that oxacalix[2]arene[2]triazines **26b** ( $R = \text{CH}_2\text{OH}$ ) with one or two lower-rim hydroxymethyl groups energetically prefer to adopt flattened partial cone and distorted partial cone conformations. This unusual conformational preference was confirmed by both solid-state structural analysis and VT  $^1\text{H}$  NMR experiments, but analogous systems bearing lower-rim carboxylic acid, ester, or aldehyde functional groups preferred to adopt 1,3-alternate structures [58].

### 15.2.5 Further Derivatization of Oxacalixarenes

While a diverse collection of oxacalixarenes can be accessed through choice of nucleophilic or electrophilic reaction components, many groups have explored post-cyclization derivatization methods for further macrocycle elaboration. In his 1974 work, Gilbert subjected tetranitro-oxacalix[4]arenes **4** to electrophilic aromatic substitution reactions and achieved near-quantitative bromination, sulfonation and nitration at positions *ortho* and *para* to the oxygen bridges (Scheme 15.6) [7, 8]. Sommer and Staab performed nitro group reduction on tetranitro-oxacalix[4]arene **4a**, and then fully excised the resulting amino groups [6]. Tetraamino-oxacalix[4]arenes **5** have also been reacted with isocyanates, [59] acid chlorides, [60] or tosyl chloride, [60] to produce urea, amide, or sulfonamide substituted oxacalix[4]arenes.

Nucleophilic aromatic substitution on oxacalix[2]arene[2]triazines [58, 61] (e.g. **12**) bearing pendant chlorines or oxacalix[2]arene[2]pyrimidines [62] bearing methylsulfonyl groups has enabled post-macrocyclization derivatization with a range of nucleophiles including alcohols, [62] thiols, [62] (thio [62]) phenols, [61–63] and amines [61, 62, 64] (Scheme 15.6). Chloro-triazine rings on the oxacalixarene backbone have also been subjected to Friedel-Crafts arylation, [65] while thiomethyl groups on pyrimidine rings have been utilized for Liebeskind-

Srogl coupling reactions [62]. Both alkylation and acylation of phenols appended to oxacalix[4]arenes has also been achieved [65].

### 15.2.6 *Synthesis of Larger Oxacalix[n]arenes*

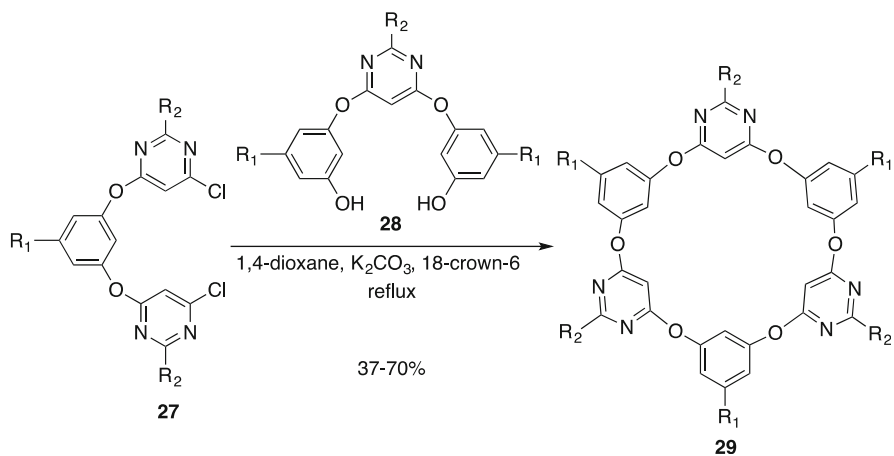
The strong thermodynamic and kinetic preference for formation of oxacalix[4]arenes under  $S_NAr$  conditions hinders access to larger oxacalix[n]arenes with  $n > 4$ . Isolation of larger oxacalix[n]arenes by  $S_NAr$  chemistry typically relies on choosing conditions that minimize macrocycle equilibration and chromatographically separating the resulting cyclooligomeric product mixture. Examples of such syntheses include investigations by Vicente, [31, 33] Konishi, [55] Katz, [20, 28] Dehaen, [24] Wen, [46] and D.-X. Wang and M.-X. Wang [65].

Toward the goal of selective formation of larger oxacalix[n]arenes, Dehaen developed a stepwise, fragment coupling strategy (Scheme 15.7). Linear fragments containing three or five aromatic rings and bearing either nucleophilic or electrophilic end groups were preformed and isolated. Combination of nucleophilic and electrophilic linear fragments could be accomplished under high dilution conditions (dioxane,  $K_2CO_3$ , 18-crown-6, reflux) to furnish oxacalix[6]arenes in 37–70 % yield and an oxacalix[8]arene in 77 % yield [66]. This approach was later elaborated upon for the formation of oxacalix[n]arenes where  $n = 5$  or 7 by coupling one even numbered linear fragment with one odd numbered fragment (41–75 % yields) [67].

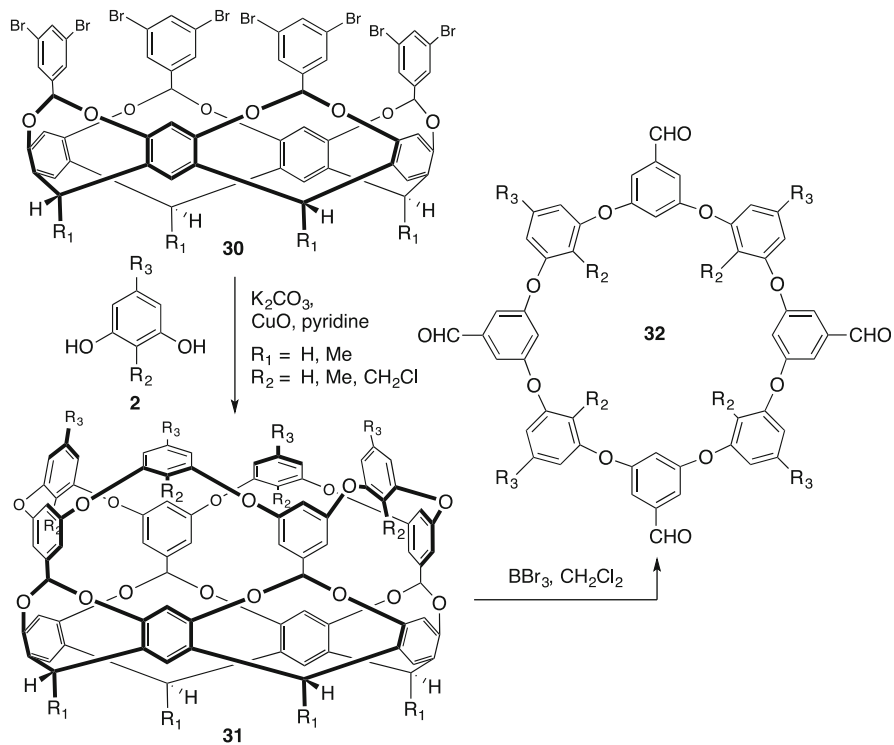
The Gibb group has published an alternative strategy for the selective synthesis of several oxacalix[8]arenes **32** using resorcinarenes as molecular templates (Scheme 15.8) [68]. Formation of cavitand **30** was first accomplished via acetal formation using four equivalents of 3,5-dibromobenzaldehyde (resorcinarene, DBU, DMA, 60 °C, 43 % yield) [69–71]. Macrocyclization to form **31** was then achieved by Ullman coupling between the aryl bromides on the cavitand and four equivalents of diphenol **2** or **20** ( $K_2CO_3$ , CuO, pyridine, reflux, 45–70 % yield). Cleavage from the resorcinarene template ( $BBr_3$ ,  $CH_2Cl_2$ ; then aq. HCl) then furnished a series of lower-rim tetraformylated oxacalix[8]arenes **32** [68]. - Non-templated Ullmann ether coupling reactions of preformed linear fragments have also been used to form oxacalix[n]arenes with  $n = 5–10$  in yields of 8–54 % [50].

### 15.2.7 *Bicyclic and Tricyclic Oxacalixarenes*

Traditional single step  $S_NAr$  approaches to oxacalixarene synthesis rely on reacting equimolar quantities of a nucleophilic diphenol and a dihalide electrophile. By using the triphenolic phloroglucinol **33** as the nucleophile and altering the reaction stoichiometry (2:3 equiv, nucleophile:electrophile), Katz has synthesized several

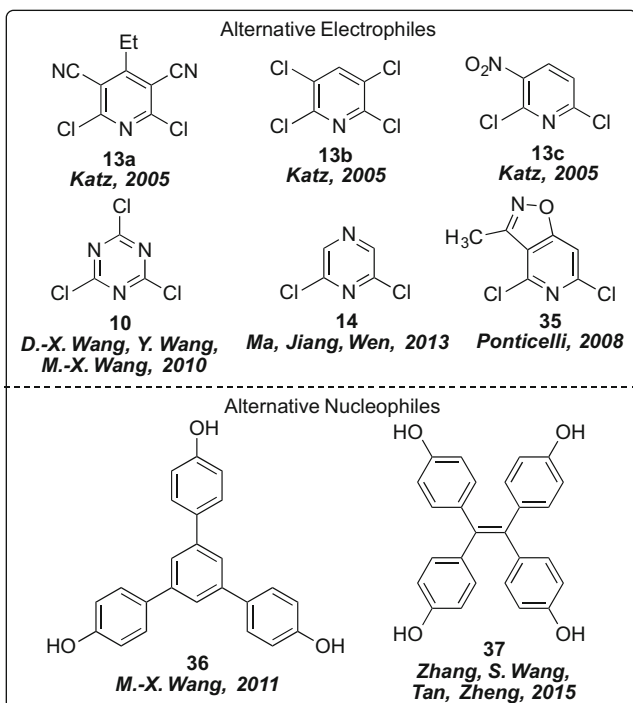
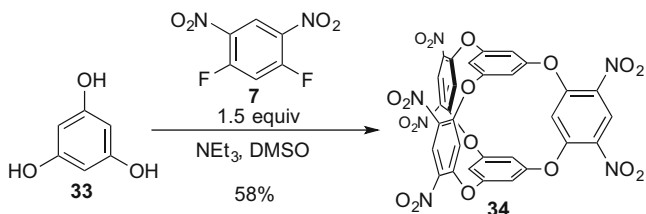


**Scheme 15.7** Synthesis of oxacalix[3]arene[3]pyrimidines via 3+3 fragment coupling



**Scheme 15.8** Synthesis of oxacalix[8]arenes using resorcinarenes as molecular templates





**Scheme 15.9** Multicyclic oxocalixarenes and possible monomers for their preparation

bicyclic oxocalixarenes **34** from either 1,5-difluoro-2,4-dinitrobenzene **7** ( $\text{NEt}_3$ , DMSO, 58% yield), or various 2,6-dichloropyridine electrophiles **13** ( $\text{Cs}_2\text{CO}_3$ , DMSO, 45–95% yield) (Scheme 15.9). The bicyclooxocalixarenes **34** displayed  $D_{3h}$ -symmetry in solution and in the solid state, projecting either the concave-surface hydrogen atoms on **34** or azaheterocyclic nitrogen atoms on **13** into the center of the cavity formed by the bicyclic structure [72]. Related bicycles that incorporate the electrophiles cyanuric chloride **10**, [73] isoxazolopyridines **35**, [74] or 2,6-dichloropyridazine **14**, [75] have been accessed by several groups using either one-pot, or two-pot fragment coupling approaches. The abilities of **34** and several related structures to bind  $\text{F}^-$  ion have also been explored computationally [76].

Bicyclic cage structures with expanded internal volumes have been synthesized by M.-X. Wang using the nucleophile 1,3,5-tri(*p*-hydroxyphenyl)benzene **36** in

reaction with cyanuric chloride **10** [77, 78]. Further enlargement of the internal cavity volumes to approximately  $980 \text{ \AA}^3$  was also accomplished by using an aza-bridged trimeric electrophilic linker similar to **11** [78]. The single step synthesis of a tricyclic cage compound was reported by Zhang, Wang, Tan, and Zheng by reacting tetrahydroxy-tetraphenylethylene **37** with 2,6-dichloropyridine-3,5-dicarbonitrile **13d** [79]. The grid-like microporous solid-state structure of the resulting square-shaped tricyclicoxacalixarene exhibited gas absorption capability including a high capacity to uptake  $\text{CO}_2$  and good  $\text{CO}_2/\text{N}_2$  selectivity [79].

### 15.2.8 Chiral Oxacalixarenes

Oxacalixarenes can be rendered chiral by attachment of stereogenic functionality to one or more of the aromatic rings, or by appending functionality that removes symmetry planes, yielding inherently chiral [80, 81] macrocycles. Inherently chiral oxacalixarenes undergo enantiomerization via through-the-annulus conformational inversion unless this macrocyclic inversion process is prevented by sterically bulky substituents or transannular tethering. M.-X. Wang first formed inherently chiral oxacalix[2]arene[2]triazines **38** by incorporating one resorcinol unit substituted in the 4-position followed by tethering via formation of an azacrown bridge (Fig. 15.6). Enantiomeric structures **38** ( $\text{R}^* = \text{OBn}$ ) were inseparable by chiral HPLC methods, but diastereomerically pure analogues **38** ( $\text{R}^* = (-)\text{-menthol}$ ,  $(+)\text{-}\alpha\text{-phenylethylamine}$ ) were isolable [82]. The same group has synthesized inherently chiral oxacalix[2]arene[2]pyridines in a single step using the non-symmetric electrophile 2,6-dichloro-3-nitropyridine **13c**. The corresponding macrocycles were formed with high selectivity for the  $\text{C}_2$ -symmetric (*anti*) regioisomer, and then conformationally constrained either by adding lower-rim allyloxy groups (**39**) or via tethering using olefin metathesis (**40**). Resolution using chiral HPLC yielded enantiomerically pure inherently chiral oxacalix[2]arene[2]pyridines **39–40** [83]. The formation of chiral cage structures with large internal cavities has been achieved by M.-X. Wang through upper-rim linking of two oxacalix[2]arene[2]triazines with diamino or diphenol units. Use of a chiral diamino linker enabled the authors to impart asymmetry to the internal cavity surface [84].

Oxacalixarenes containing axially chiral elements have been synthesized using BINOL and the electrophiles 1,5-difluoro-2,4-dinitrobenzene **7** or cyanuric chloride **10**. Likely due to increased macrocycle flexibility, the  $(\pm)$ -BINOL-derived oxacalixarenes **41** (mixture of stereoisomers) are formed kinetically, but equilibration experiments reveal that they are not the thermodynamically favored products (Fig. 15.6) [85]. The analogous macrocycles derived from enantiopure BINOL and cyanuric chloride **10** demonstrated high enantioselective fluorescence responses to  $\alpha$ -amino acids [86].

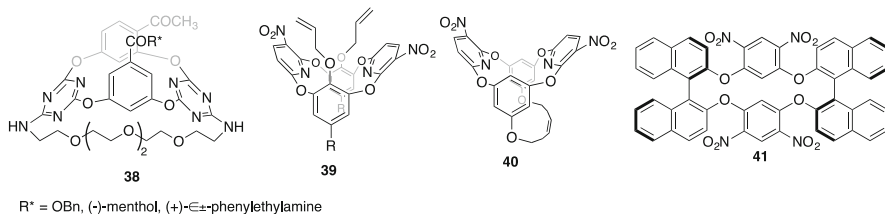


**Fig. 15.6** Chiral oxocalixarenes

## 15.3 Applications of Oxocalixarenes

### 15.3.1 Ion Binding

Oxocalixarenes are versatile platforms for the design of synthetic receptors due to the ease of their synthesis and functionalization, and predictable 1,3-alternate conformations. Strategies for cation binding/extraction have thus far relied on oxocalix[4]crowns tethered to either the lower [87] or upper [88] rim. In contrast, anion binding, [89, 90] has been explored in far greater detail, and has been accomplished both by appending additional interacting functional groups to the macrocycles, and through interactions of anions directly with the macrocyclic arenes.

Toward the synthesis of pincer-type anion receptors, Dehaen and Maes appended ureido and thioureido groups to oxocalix[2]arene[2]pyrimidines **42** (Fig. 15.7). A binding preference for oxyanionic guests  $\text{H}_2\text{PO}_4^-$ ,  $\text{AcO}^-$  and  $\text{BzO}^-$  was observed over the alternative anions  $\text{Cl}^-$ ,  $\text{Br}^-$ ,  $\text{NO}_3^-$ , and  $\text{HSO}_4^-$ . Association constants of 200–400  $\text{M}^{-1}$  were measured in wet DMSO, indicating that the oxocalixarene hosts have the potential to act as neutral receptors for anions even in highly competitive media [64].

Oxocalix[2]arene[2]triazines have been developed by M.-X. Wang into a versatile platform for studying anion- $\pi$  interactions with the highly electron deficient triazine rings. Oxocalix[2]arene[2]triazines **12** were found to form an unusual ternary  $\pi$ -complex with chloride or bromide and water in the solid state (Fig. 15.7), and binding of **12** to chloride and fluoride was measured in acetonitrile solution ( $K_a = 4246 \text{ M}^{-1}$  for  $\text{Cl}^- \cdot \mathbf{12}$  and  $4036 \text{ M}^{-1}$  for  $\text{F}^- \cdot \mathbf{12}$ ). The solid-state structure of the ternary  $\mathbf{12} \cdot \text{Cl}^- \cdot \text{H}_2\text{O}$  complex revealed that the chloride ion interacts with **12** via anion- $\pi$  attraction to one triazine ring, while also hydrogen bonding to the water molecule. The water molecule, in turn, interacts with the second triazine ring on the oxocalixarene host via a lone pair- $\pi$  interaction [91, 92]. Computational [93, 94] and photoelectron spectroscopy [94] studies have corroborated the preference for this binding mode. The system **12** was also found to bind polyatomic anions, with a strong preference for  $\text{NO}_3^-$  ( $16950 \text{ M}^{-1}$ ) over  $\text{BF}_4^-$ ,  $\text{PF}_6^-$ , and  $\text{NCS}^-$  ( $239\text{--}673 \text{ M}^{-1}$ ) [95].

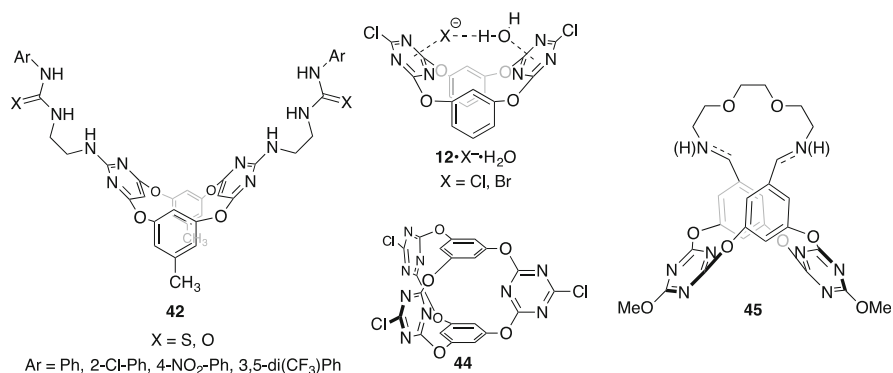


**Fig. 15.7** Anion receptors

Modifications to oxacalix[2]arene[2]triazine **12** and the effects of the changes on anion binding have been heavily researched. By appending ester or amide functionality to the lower rim of **12**, D.-X. Wang and M.-X. Wang designed macrocycles **43** capable of selective H<sub>2</sub>PO<sub>4</sub><sup>-</sup> ion recognition through cooperative anion- $\pi$  and hydrogen bonding interactions (Fig. 15.8) [96]. Alternately, appending additional electron deficient aromatic binding sites to the lower rim was shown to increase solution phase complex formation, [97] while installation of electron donating groups on the triazine ring hindered anion- $\pi$  interactions [98]. Inclusion of an upper-rim azacrown bridge, as in **45**, afforded ditopic ion pair receptors that bound metal cations in acetonitrile. Addition of F<sup>-</sup> led to decomplexation with most metals, except Pb<sup>+2</sup> and Zn<sup>+2</sup>. In the case of Pb<sup>+2</sup>, addition of one equivalent of F<sup>-</sup> resulted in a 23-fold binding enhancement, which was attributed to simultaneous binding of metal ion by the azacrown linkage and anion- $\pi$  binding of the F<sup>-</sup> between the two triazine rings [99]. Anion- $\pi$  interactions have also been used to influence the morphology of supramolecular aggregates generated from upper-rim functionalized amphiphilic oxacalix[2]arene[2]triazines **46** (Fig. 15.8) [100, 101]. Bicyclooxacalix[2]arene[3]triazine **44** (Fig. 15.7), which serves as a more structurally rigid analogue of **12**, was found to form a ternary solid-state complex **44**·Cl<sup>-</sup>·H<sub>2</sub>O with a fundamentally different Cl<sup>-</sup>·triazine binding mode. Rather than a non-covalent anion- $\pi$  interaction, the interaction of Cl<sup>-</sup> with bicyclooxacalixarene **44** was instead characterized as a weak  $\sigma$ -complex, although the triazine·H<sub>2</sub>O interaction remained similar to that found for **12** [73].

### 15.3.2 Molecular Recognition

Oxacalixarenes have been explored as host molecules for guest species beyond simple anions and cations. The development of oxacalix[2]arene[2]naphthyridines **47** as molecular receptors was first investigated by Katz (Fig. 15.9). In the preferred

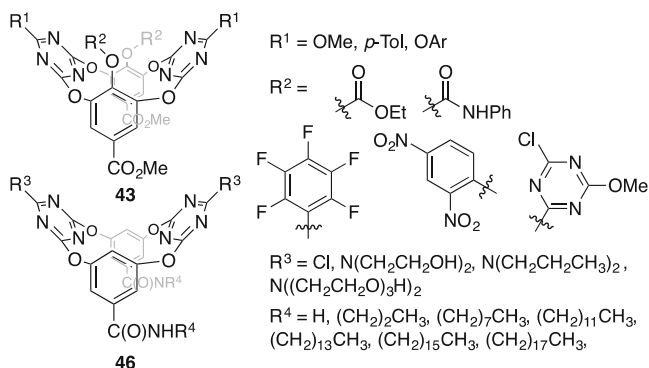


Fig. 15.8 Anion receptors

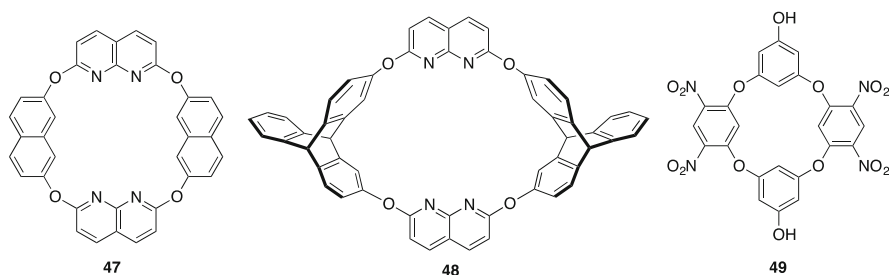


Fig. 15.9 Oxcalixarenes for molecular recognition

1,3-alternate conformation, incorporation of the extended electrophile 2,7-dichloro-1,8-naphthyridine **17** creates a spacing in the resulting macrocycles of approximately 7 Å between opposing nucleophile-derived arenes. The U-shaped cavity in **47** was found to selectively interact with *o*-salicylic acid in  $\text{CH}_2\text{Cl}_2$  over alternative aromatics (benzonitrile, benzoic acid, phenol) [26]. Reacting the same electrophile **17** with dihydroxytryptcene **24**, Chen has generated macrocycles **48** capable of forming solution phase complexes with fullerenes  $\text{C}_{60}$  and  $\text{C}_{70}$  in organic solvents [102]. Fluorescence titration carried out in toluene revealed formation of 1:1 complexes with  $K_s = 7.54 \times 10^4$  for  $\text{C}_{60}$  and  $K_s = 8.96 \times 10^4$  for  $\text{C}_{70}$  in toluene [42]. In a separate study, it was also found that the fluorescence profile of **48** could be modulated by  $\text{Hg}^{+2}$  ion; addition of  $\text{Hg}^{+2}$  caused a dramatic reduction in host fluorescence intensity while little or no such change was observed upon addition of alternative metal ions ( $\text{Mn}^{+2}$ ,  $\text{Co}^{+2}$ ,  $\text{Ni}^{+2}$ ,  $\text{Cu}^{+2}$ ,  $\text{Zn}^{+2}$ ,  $\text{Cd}^{+2}$ ,  $\text{Pb}^{+2}$ , alkali, alkaline earth) [103].

The host behavior of oxcalixarene **49** with the electrochemically active guests ferrocene (**F**) and cobaltocene (**C**) has been studied by Shimizu. A host-guest complex results from cation- $\pi$  interactions between the hydroxyl-substituted aromatic rings of **49** with the positively charged ferrocenium ( $\text{F}^+$ ) in  $\text{CH}_2\text{Cl}_2$ . Binding

was analyzed to proceed through a tweezer-like arrangement of the opposing hydroxyl-substituted aromatic rings with the  $F^+$  guest in a 1:1 stoichiometry [104].

Aqueous phase molecular recognition of tetraamino-oxacalix[4]arene **5** (see Scheme 15.1) has been studied by Gattuso. Macrocycle **5** was found to form complexes with paraquat dication in water that were highly sensitive to the protonation state of the oxacalixarene host [105].

### 15.3.3 Supramolecular Structures

The ease of incorporating functional groups capable of hydrogen bonding [106] or  $\pi$ -stacking [107] interactions makes oxacalixarenes excellent scaffolds for the design of supramolecular metal complexes and solid-state networks. Wen has reported the self assembly of discrete molecular cages or polymeric coordination networks upon complexation of  $Ag^+$  or  $Cu^{+2}$  ions with both *ortho*-linked (**50**) and *meta*-linked (**51**) oxacalix[2]arene[2]pyrazines (Fig. 15.10) [108–110]. The hydrogen-bond driven solid-state self assembly of carboxylic acid-functionalized derivatives of **50–51** has also been explored [106, 111]. Bicyclooxacalix[2]arene[3]pyrazine **52** has also been used by Jiang and Wen for the creation of metal coordination polymers wherein modulation of the topology could be achieved through complexation with different metals ( $Ag^+$ ,  $Cu^{+2}$ , and  $Zn^{+2}$ ) or by variation of solvent and counterion [112].

### 15.3.4 Catenanes and Rotaxanes

Several catenanes and rotaxanes have been synthesized using either oxacalix[2]tritycene[2]naphthyridines **48** or oxacalixcrowns (Fig. 15.11). Chen has formed [2]rotaxanes based on macrocycles **48** and dicationic paraquat derivatives [102]. The solution phase threading and unthreading of the [2]pseudorotaxanes **53** could be controlled either by modulation of pH or by addition/sequestration of  $Hg^{+2}$  ion. Esterification of [2]pseudorotaxanes **53** ( $R = (CH_2)_4CH_2OH$ ) with 3,5-di-*t*-butylbenzoic anhydride provided [2]rotaxane **54** (56% yield). Oxacalix[2]arene[2]pyrazine-oxacrowns have been used by Li, Jiang, and Wen to make both [2]rotaxanes and [2]catenanes. [2]Catenane **55** was synthesized by complexing an oxacalix[2]arene[2]pyrazine-oxacrown to a xylyl-linked diparaquat dication, followed by cyclization to the catenated tetrapyrindinium (Fig. 15.11) [113]. [2]Rotaxane **56** was generated instead by threading of an ammonium guest and stoppering it via carbamylation. Subsequent Boc derivatization of the amine allowed translocation down the axel [114].

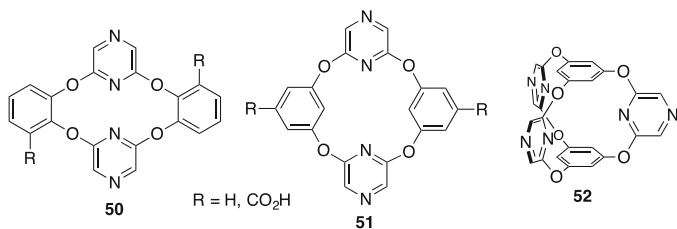
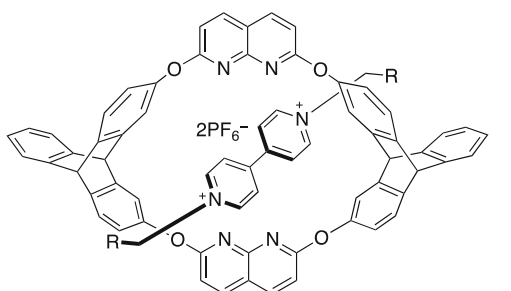


**Fig. 15.10** Oxacalixarenes for the formation of supramolecular structures and solid state networks

**Fig. 15.11** Oxacalixarene-derived catenanes and rotaxanes



53, R = H, CH<sub>2</sub>CH<sub>2</sub>, CH<sub>2</sub>OH, (CH<sub>2</sub>)<sub>4</sub>CH<sub>2</sub>OH, CH<sub>2</sub>OCH<sub>3</sub>, CH<sub>3</sub>OCH<sub>2</sub>CH=CH<sub>2</sub>, CH<sub>2</sub>OCH<sub>2</sub>CCH  
 54, R = (CH<sub>2</sub>)<sub>4</sub>CH<sub>2</sub>OC(O)NH-3,5-di-*t*-Bu-Ph

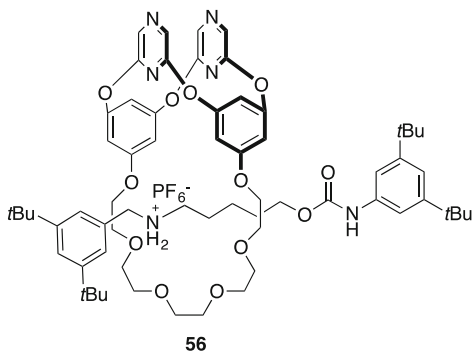
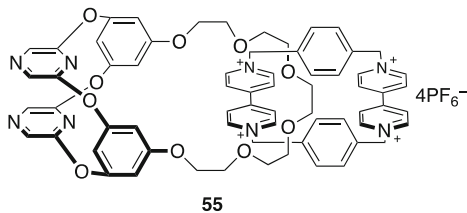
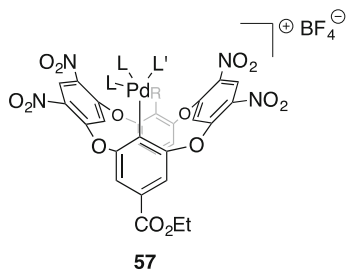


**Fig. 15.12** Palladium-oxacalixarene complexes



R = H, OH, PdL<sub>2</sub>L'

L = DMAP, 1/2 TMEDA

L' = DMAP, PhCN, pyridine, PPh<sub>3</sub>, acetone

### 15.3.5 Further Applications

The utility of oxacalixarenes for molecular design continues to be demonstrated through diverse applications investigations. The switching behavior of oxacalix[4]arenes bearing an azobenzene group has been studied by Gattuso toward photoresponsive molecular receptors [115]. Organometallic mono-palladium and bis-palladium-oxacalixarene complexes **57** have been synthesized and characterized by Vigalok (Fig. 15.12). In the observed 1,3-alternate conformations, opposing lower-rim hydroxyl functionality (R = OH) did not interact transannularly with the Pd center, but an iodine ligand was found to bridge the Pd atoms across the lower rim in a bimetallic complex (R = PdL<sub>2</sub>L'; L' = I) [116].

Toward the fabrication of new solid-state data storage systems, Xu and Zhang have synthesized oxacalixarenes from 1,5-difluoro-2,4-dinitrobenzene **7** and 2,3-dihydroxyphenazine for the formation of stable high-density memory devices [117]. Devices fabricated from these oxacalix[4]arenes showed excellent ternary memory behavior with promising switching and stability characteristics.

## 15.4 Conclusion and Outlook

In less than 15 years, oxacalixarenes have emerged from relative obscurity to become an actively investigated class of macrocycles. The simplicity and modularity of modern methods to access diverse oxacalixarene systems, as well as the ability to tailor appended functional groups both pre- and post-cyclization, makes the compounds ideal for applications-focused molecular design. Enabled by synthetic advances and a deeper understanding of conformational preferences and dynamics, oxacalixarenes are now being designed into ion receptors, supramolecular assemblies, chemical sensors, and hosts for molecular recognition, among other applications. Future research in the oxacalixarene field will undoubtedly continue to reveal increasingly sophisticated applications for this developing macrocyclic platform.



## References

1. Maes, W.; Dehaen, W. *Chem. Soc. Rev.* **2008**, *37*, 2393–2402.
2. Wang, M.-X. *Chem. Commun.* **2008**, *38*, 4541–4551.
3. König, B.; Fonseca, Maria H. *Eur. J. Inorg. Chem.* **2000**, *11*, 2303–2310.
4. Semenov, V. *J. Incl. Phenom. Macrocycl. Chem.* **2013**, *77*, 1–22.
5. Mehta, V.; Panchal, M.; Modi, K.; Kongor, A.; Panchal, U.; K Jain, V. *Curr. Org. Chem.* **2015**, *19*, 1077–1096.
6. Sommer, N.; Staab, H. A. *Tetrahedron Lett.* **1966**, *7*, 2837–2841.
7. Gilbert, E. E. *J. Heterocycl. Chem.* **1974**, *11*, 899–904.
8. Gilbert, E. E., Thermally stable octanitro macrocyclic explosives. US Patent. Appl. No. 566,848, 1976.
9. Lehmann, F. P. A. *Tetrahedron.* **1974**, *30*, 727–733.
10. Bottino, F.; Foti, S.; Pappalardo, S. *Tetrahedron.* **1976**, *32*, 2567–2570.
11. Cottet, K.; Marcos, P. M.; Cragg, P. J. *Beilstein J. Org. Chem.* **2012**, *8*, 201–226.
12. Takeuchi, D.; Asano, I.; Osakada, K. *J. Org. Chem.* **2006**, *71*, 8614–8617.
13. Guo, Q. H.; Fu, Z. D.; Zhao, L.; Wang, M.-X. *Angew. Chem. Int. Ed.* **2014**, *53*, 13548–13552.
14. Kime, D. E.; Norymberski, J. K. *J. Chem. Soc., Perkin Trans. 1.* **1977**, *9*, 1048–1052.
15. Chambers, R. D.; Hoskin, P. R.; Kenwright, A. R.; Khalil, A.; Richmond, P.; Sandford, G.; Yufit, D. S.; Howard, J. A. K. *Org. Biomol. Chem.* **2003**, *1*, 2137–2147.
16. Chambers, R. D.; Hoskin, P. R.; Khalil, A.; Richmond, P.; Sandford, G.; Yufit, D. S.; Howard, J. A. K. *J. Fluorine Chem.* **2002**, *116*, 19–22.
17. Chambers, R. D.; Khalil, A.; Richmond, P.; Sandford, G.; Yufit, D. S.; Howard, J. A. K. *J. Fluorine Chem.* **2004**, *125*, 715–720.
18. Wang, M.-X.; Yang, H.-B. *J. Am. Chem. Soc.* **2004**, *126*, 15412–15422.
19. Katz, J. L.; Feldman, M. B.; Conry, R. R. *Org. Lett.* **2005**, *7*, 91–94.
20. Katz, J. L.; Geller, B. J.; Conry, R. R. *Org. Lett.* **2006**, *8*, 2755–2758.
21. Konishi, H.; Mita, T.; Morikawa, O.; Kobayashi, K. *Tetrahedron Lett.* **2007**, *48*, 3029–3032.
22. Akagi, S.; Yasukawa, Y.; Kobayashi, K.; Konishi, H. *Tetrahedron.* **2009**, *65*, 9983–9988.
23. Wang, X.-D.; Wang, D.-X.; Huang, Z.-T.; Wang, M.-X. *Supramol. Chem.* **2014**, *26*, 601–606.
24. Maes, W.; Van Rossom, W.; Van Hecke, K.; Van Meervelt, L.; Dehaen, W. *Org. Lett.* **2006**, *8*, 4161–4164.
25. Van Rossom, W.; Kishore, L.; Robeyns, K.; Van Meervelt, L.; Dehaen, W.; Maes, W. *Eur. J. Org. Chem.* **2010**, *21*, 4122–4129.
26. Katz, J. L.; Geller, B. J.; Foster, P. D. *Chem. Commun.* **2007**, *10*, 1026–1028.
27. Hu, W.-J.; Liu, L.-Q.; Ma, M.-L.; Zhao, X.-L.; Liu, Y. A.; Mi, X.-Q.; Jiang, B.; Wen, K. *Tetrahedron.* **2013**, *69*, 3934–3941.
28. Bizier, N. P.; Wackerly, J. W.; Braunstein, E. D.; Zhang, M.; Nodder, S. T.; Carlin, S. M.; Katz, J. L. *J. Org. Chem.* **2013**, *78*, 5987–5998.
29. Hudson, R.; Bizier, N. P.; Esdale, K. N.; Katz, J. L. *Org. Biomol. Chem.* **2015**, *13*, 2273–2284.
30. Wackerly, J. W.; Zhang, M.; Nodder, S. T.; Carlin, S. M.; Katz, J. L. *Org. Lett.* **2014**, *16*, 2920–2922.
31. Hao, E.; Fronczek, F. R.; Vicente, M. G. H. *J. Org. Chem.* **2006**, *71*, 1233–1236.
32. Jiao, L.; Hao, E.; Fronczek, F. R.; Smith, K. M.; Vicente, M. G. H. *Tetrahedron* **2007**, *63*, 4011–4017.
33. Wu, L.; Jiao, L.; Lu, Q.; Hao, E.; Zhou, Y. *Spectrochim Acta A.* **2009**, *73*, 353–357.
34. Jiao, L.; Fang, Y.; Zhou, Y.; Wang, S.; Hao, E.; Vicente, M. G. H. *J. Porphyrins Phthalocyanines.* **2010**, *14*, 523–530.
35. Hu, W.-J.; Zhao, X.-L.; Ma, M.-L.; Guo, F.; Mi, X.-Q.; Jiang, B.; Wen, K. *Eur. J. Org. Chem.* **2012**, *2012*, *7*, 1448–1454.

36. Yuan, J.; Zhu, Y.; Lian, M.; Gao, Q.; Liu, M.; Jia, F.; Wu, A. *Tetrahedron Lett.* **2012**, *53*, 1222–1226.
37. Zhu, Y.; Yuan, J.; Li, Y.; Gao, M.; Cao, L.; Ding, J.; Wu, A. *Synlett* **2011**, *1*, 52–56.
38. Tominaga, M.; Kunitomi, N.; Katagiri, K.; Itoh, T. *Org. Lett.* **2015**, *17*, 786–789.
39. Chen, C.-F. *Chem. Commun.* **2011**, *47*, 1674–1688.
40. Ma, Y.-X.; Han, Y.; Chen, C.-F. *J. Incl. Phenom. Macrocycl. Chem.* **2014**, *79*, 261–281.
41. Zhang, C.; Chen, C.-F. *J. Org. Chem.* **2007**, *72*, 3880–3888.
42. Hu, S.-Z.; Chen, C.-F. *Chem. Commun.* **2010**, *46*, 4199–4201.
43. Zhang, C.; Wang, Z.; Song, S.; Meng, X.; Zheng, Y.-S.; Yang, X.-L.; Xu, H.-B. *J. Org. Chem.* **2014**, *79*, 2729–2732.
44. Wang, Z.; Cheng, H.; Zhai, T.-L.; Meng, X.; Zhang, C. *RSC Adv.* **2015**, *5*, 76670–76674.
45. Kleyn, A.; Jacobs, T.; Barbour, L. J. *Cryst. Eng. Comm.* **2011**, *13*, 3175–3180.
46. Ma, M.; Wang, H.; Li, X.; Liu, L.; Jin, H.; Wen, K. *Tetrahedron* **2009**, *65*, 300–304.
47. Li, M.; Ma, M.-L.; Li, X.-Y.; Wen, K. *Tetrahedron* **2009**, *65*, 4639–4643.
48. Yang, C.; Chen, Y.; Wang, D.-X.; Zhao, L.; Wang, M.-X. *Org. Lett.* **2013**, *15*, 4414–4417.
49. Yang, F.; Yan, L.; Ma, K.; Yang, L.; Li, J.; Chen, L.; You, J. *Eur. J. Org. Chem.* **2006**, *5*, 1109–1112.
50. Zhou, Q.; Su, L.; Jiang, T.; Zhang, B.; Chen, R.; Jiang, H.; Ye, Y.; Zhu, M.; Han, D.; Shen, J.; Dai, G.; Li, Z. *Tetrahedron* **2014**, *70*, 1125–1132.
51. Thondorf, I., Conformations and Stereodynamics. In *Calixarenes 2001*, Asfari, Z.; Böhmer, V.; Harrowfield, J.; Vicens, J.; Saadioui, M., Eds. Springer Netherlands: 2001; p 280–295.
52. Zuo, C.-S.; Wiest, O.; Wu, Y.-D. *J. Phys. Org. Chem.* **2011**, *24*, 1157–1165.
53. Yasukawa, Y.; Kobayashi, K.; Konishi, H. *Tetrahedron Lett.* **2009**, *50*, 5130–5134.
54. The oxacalixarene literature often assigns the term *flattened partial cone* to what the calixarene literature describes as a *chair* conformation (see reference 51). In an attempt to minimize confusion, this chapter observes oxacalixarene convention in using the *flattened partial cone* nomenclature.
55. Konishi, H.; Tanaka, K.; Teshima, Y.; Mita, T.; Morikawa, O.; Kobayashi, K. *Tetrahedron Lett.* **2006**, *47*, 4041–4044.
56. Konishi, H.; Mita, T.; Yasukawa, Y.; Morikawa, O.; Kobayashi, K. *Tetrahedron Lett.* **2008**, *49*, 6831–6834.
57. Wang, Q.-Q.; Wang, D.-X.; Zheng, Q.-Y.; Wang, M.-X. *Org. Lett.* **2007**, *9*, 2847–2850.
58. Pan, S.; Wang, D.-X.; Zhao, L.; Wang, M.-X. *Tetrahedron* **2012**, *68*, 9464–9477.
59. Capici, C.; Garozzo, D.; Gattuso, G.; Messina, A.; Notti, A.; Parisi, M. F.; Pappalardo, S. *ARKIVOC.* **2009**, *8*, 199–211.
60. Kong, L.; Ma, M.; Zhao, X.; Liu, Y.; Mi, X.; Jiang, B.; Wen, K. *Chin. J. Chem.* **2013**, *31*, 684–688.
61. Yang, H.-B.; Wang, D.-X.; Wang, Q.-Q.; Wang, M.-X. *J. Org. Chem.* **2007**, *72*, 3757–3763.
62. Van Rossom, W.; Maes, W.; Kishore, L.; Ovaere, M.; Van Meervelt, L.; Dehaen, W. *Org. Lett.* **2008**, *10*, 585–588.
63. Van Rossom, W.; Kandrát, O.; Ngo, T. H.; Lhoták, P.; Dehaen, W.; Maes, W. *Tetrahedron Lett.* **2010**, *51*, 2423–2426.
64. Van Rossom, W.; Caers, J.; Robeyns, K.; Van Meervelt, L.; Maes, W.; Dehaen, W. *J. Org. Chem.* **2012**, *77*, 2791–2797.
65. Wang, Q.-Q.; Wang, D.-X.; Yang, H.-B.; Huang, Z.-T.; Wang, M.-X. *Chem. Eur. J.* **2010**, *16*, 7265–7275.
66. Van Rossom, W.; Ovaere, M.; Van Meervelt, L.; Dehaen, W.; Maes, W. *Org. Lett.* **2009**, *11*, 1681–1684.
67. Van Rossom, W.; Robeyns, K.; Ovaere, M.; Van Meervelt, L.; Dehaen, W.; Maes, W. *Org. Lett.* **2011**, *13*, 126–129.
68. Li, X.; Upton, T. G.; Gibb, C. L. D.; Gibb, B. C. *J. Am. Chem. Soc.* **2003**, *125*, 650–651.
69. Xi, H.; Gibb, C. L. D.; Gibb, B. C. *J. Org. Chem.* **1999**, *64*, 9286–9288.
70. Xi, H.; L. D. Gibb, C. *Chem. Commun.* **1998**, *16*, 1743–1744.

71. Green, J. O.; Baird, J.-H.; Gibb, B. C. *Org. Lett.* **2000**, *2*, 3845–3848.
72. Katz, J. L.; Selby, K. J.; Conry, R. R. *Org. Lett.* **2005**, *7*, 3505–3507.
73. Wang, D.-X.; Wang, Q.-Q.; Han, Y.; Wang, Y.; Huang, Z.-T.; Wang, M.-X. *Chem. Eur. J.* **2010**, *16*, 13053–13057.
74. Ferrini, S.; Fusi, S.; Giorgi, G.; Ponticelli, F. *Eur. J. Org. Chem.* **2008**, *2008*, 5407–5413.
75. Li, X.-Y.; Hu, C.; Ma, M.-L.; Liu, Y. A.; Mi, X.-Q.; Jiang, B.; Wen, K. *Chin. Chem. Lett.* **2013**, *24*, 279–282.
76. Zuo, C.-S.; Quan, J.-M.; Wu, Y.-D. *Org. Lett.* **2007**, *9*, 4219–4222.
77. Naseer, M. M.; Wang, D.-X.; Zhao, L.; Huang, Z.-T.; Wang, M.-X. *J. Org. Chem.* **2011**, *76*, 1804–1813.
78. Naseer, M. M.; Wang, D.-X.; Zhao, L.; Wang, M.-X. *Eur. J. Org. Chem.* **2014**, *2014*, 7895–7905.
79. Zhang, C.; Wang, Z.; Tan, L.; Zhai, T.-L.; Wang, S.; Tan, B.; Zheng, Y.-S.; Yang, X.-L.; Xu, H.-B. *Angew. Chem. Int. Ed.* **2015**, *54*, 9244–9248.
80. Böhmer, V.; Kraft, D.; Tabatabai, M. J. *Incl. Phenom. Macrocycl. Chem.* **1994**, *19*, 17–39.
81. Dalla Cort, A.; Mandolini, L.; Pasquini, C.; Schiaffino, L. *New J. Chem.* **2004**, *28*, 1198–1199.
82. Hou, B.-Y.; Zheng, Q.-Y.; Wang, D.-X.; Wang, M.-X. *Tetrahedron* **2007**, *63*, 10801–10808.
83. Pan, S.; Wang, D.-X.; Zhao, L.; Wang, M.-X. *Org. Lett.* **2012**, *14*, 6254–6257.
84. Hou, B.-Y.; Zheng, Q.-Y.; Wang, D.-X.; Huang, Z.-T.; Wang, M.-X. *Chem. Commun.* **2008**, *33*, 3864–3866.
85. Capici, C.; Gattuso, G.; Notti, A.; Parisi, M. F.; Bruno, G.; Nicolò, F.; Pappalardo, S. *Tetrahedron Lett.* **2011**, *52*, 1351–1353.
86. Xu, K.; Jiao, S.; Yao, W.; Xie, E.; Tang, B.; Wang, C. *Chirality.* **2012**, *24*, 646–651.
87. Csokai, V.; Kulik, B.; Bitter, I. *Supramol. Chem.* **2006**, *18*, 111–115.
88. Hou, B.-Y.; Wang, D.-X.; Yang, H.-B.; Zheng, Q.-Y.; Wang, M.-X. *J. Org. Chem.* **2007**, *72*, 5218–5226.
89. Wang, M.-X. *Acc. Chem. Res.* **2012**, *45*, 182–195.
90. Gamez, P. *Inorg. Chem. Front.* **2014**, *1*, 35–43.
91. Wang, D.-X.; Zheng, Q.-Y.; Wang, Q.-Q.; Wang, M.-X. *Angew. Chem. Int. Ed.* **2008**, *47*, 7485–7488.
92. Wang, D.-X.; Wang, M.-X. *J. Am. Chem. Soc.* **2013**, *135*, 892–897.
93. Zheng, X.; Shuai, Z.; Wang, D. *J. Phys. Chem. A.* **2013**, *117*, 3844–3851.
94. Zhang, J.; Zhou, B.; Sun, Z.-R.; Wang, X.-B. *Phys. Chem. Chem. Phys.* **2015**, *17*, 3131–3141.
95. Alberto, M. E.; Mazzone, G.; Russo, N.; Sicilia, E. *Chem. Commun.* **2010**, *46*, 5894–5896.
96. Li, S.; Wang, D.-X.; Wang, M.-X. *Tetrahedron Lett.* **2012**, *53*, 6226–6229.
97. Li, S.; Fa, S.-X.; Wang, Q.-Q.; Wang, D.-X.; Wang, M.-X. *J. Org. Chem.* **2012**, *77*, 1860–1867.
98. Wang, D.-X.; Fa, S.-X.; Liu, Y.; Hou, B.-Y.; Wang, M.-X. *Chem. Commun.* **2012**, *48*, 11458–11460.
99. Chen, Y.; Wang, D.-X.; Huang, Z.-T.; Wang, M.-X. *Chem. Commun.* **2011**, *47*, 8112–8114.
100. He, Q.; Han, Y.; Wang, Y.; Huang, Z.-T.; Wang, D.-X. *Chem. Eur. J.* **2014**, *20*, 7486–7491.
101. He, Q.; Huang, Z.-T.; Wang, D.-X. *Chem. Commun.* **2014**, *50*, 12985–12988.
102. Hu, S.-Z.; Chen, C.-F. *Chem. Eur. J.* **2011**, *17*, 5424–5431.
103. Hu, S.-Z.; Chen, C.-F. *Org. Biomol. Chem.* **2011**, *9*, 5838–5844.
104. Sobransingh, D.; Dewal, M. B.; Hiller, J.; Smith, M. D.; Shimizu, L. S. *New J. Chem.* **2008**, *32*, 24–27.
105. Manganaro, N.; Lando, G.; Gargiulli, C.; Pisagatti, I.; Notti, A.; Pappalardo, S.; Parisi, M. F.; Gattuso, G. *Chem. Commun.* **2015**, *51*, 12657–12660.
106. Li, X.-Y.; Yu, K.-Y.; Zhao, X.-L.; Ma, M.-L.; Guo, F.; Mi, X.-Q.; Jiang, B.; Wen, K. *Cryst. Eng. Comm.* **2012**, *14*, 7869–7871.
107. Yang, Y.; Xue, M.; Chen, C.-F. *Cryst. Eng. Comm.* **2010**, *12*, 3502–3505.

108. Ma, M.-L.; Li, X.-Y.; Wen, K. *J. Am. Chem. Soc.* **2009**, *131*, 8338–8339.
109. Li, X.-Y.; Liu, L.-Q.; Ma, M.-L.; Zhao, X.-L.; Wen, K. *Dalton Trans.* **2010**, *39*, 8646–8651.
110. Ma, M.-L.; Li, X.-Y.; Zhao, X.-L.; Guo, F.; Jiang, B.; Wen, K. *Cryst. Eng. Comm.* **2011**, *13*, 1752–1754.
111. Kong, L.-W.; Ma, M.-L.; Wu, L.-C.; Zhao, X.-L.; Guo, F.; Jiang, B.; Wen, K. *Dalton Trans.* **2012**, *41*, 5625–5633.
112. Hu, W.-J.; Liu, L.-Q.; Ma, M.-L.; Zhao, X.-L.; Liu, Y. A.; Mi, X.-Q.; Jiang, B.; Wen, K. *Inorg. Chem.* **2013**, *52*, 9309–9319.
113. Liu, H.; Li, X.-Y.; Zhao, X.-L.; Liu, Y. A.; Li, J.-S.; Jiang, B.; Wen, K. *Org. Lett.* **2014**, *16*, 5894–5897.
114. Liu, H.; Hu, W.-J.; Liu, Y. A.; Li, J.-S.; Jiang, B.; Wen, K. *Eur. J. Org. Chem.* **2015**, *28*, 6270–6277.
115. Gargiulli, C.; Gattuso, G.; Notti, A.; Pappalardo, S.; Parisi, M. F.; Puntoriero, F. *Tetrahedron Lett.* **2012**, *53*, 616–619.
116. Visitaev, Y.; Goldberg, I.; Vigalok, A. *Inorg. Chem.* **2013**, *52*, 6779–6781.
117. Gu, P.-Y.; Gao, J.; Lu, C.-J.; Chen, W.; Wang, C.; Li, G.; Zhou, F.; Xu, Q.-F.; Lu, J.-M.; Zhang, Q. *Mater. Horiz.* **2014**, *1*, 446–451.

# Chapter 16

## Homoheteracalix[*n*]arenes (X = S, Se, N)

Joice Thomas, Aliya S. Gusak, and Wim Dehaen

### 16.1 Overview

Homoheteracalix[*n*]arenes are macrocyclic systems in which the bridging carbons in the well known calix[*n*]arene framework are replaced by a polyatomic bridge of which at least one connecting atom is a heteroatom. In this Chapter, we will discuss the macrocycles that have sulfur, selenium or nitrogen as one of the connecting heteroatoms. The related (homo)oxacalix[*n*]arenes will be discussed elsewhere in this volume. The first results on homothiocalix[*n*]arenes were reported in the 1970s, while aza-analogs took until the 1990s or seleno analogs even until recently (2009) to be introduced. We will focus on systems that have *n*-fold symmetry, i.e. having all the same bridging polyatomic unit, although less symmetrical compounds have also been described. The aromatic units are mostly *meta*-connected, but we will for comparison also introduce work on alternative aryl (e.g. 1,4-coupled benzene or naphthalene) or hetaryl units.

---

J. Thomas • W. Dehaen (✉)  
Department of Chemistry, KU Leuven, Celestijnenlaan 200F, 3001 Leuven, Belgium  
e-mail: [Wim.Dehaen@chem.kuleuven.be](mailto:Wim.Dehaen@chem.kuleuven.be)

A.S. Gusak  
Department of Chemistry, KU Leuven, Celestijnenlaan 200F, 3001 Leuven, Belgium  
Ural Federal University, 19 Mira Str, Ekaterinburg 620002, Russia

## 16.2 Homothiacalixarenes

### 16.2.1 Historical Perspective

In 1970, two reports appeared, first by Boekelheide et al. [1] and later in the year by Neumann and Vögtle [2] on macrocycles **2** and **3** that now can be perceived as belonging to the family of homothiacalixarenes. This research was made in the context of the synthesis of [3,3]metacyclophanes **1** (two isomers *syn* and *anti*) from 1,3-xylylene dithiol and dibromide building blocks, or from dibromide and sulfide. The macrocycles **2a** and **3a** were only formed as side products in low yield (<10%).

The interest at that time was focused on the conformational aspects of the [3,3]metacyclophanes **1**, or in their conversion to dihydropyrene **4** via methylation reactions followed by Stevens rearrangement and Hofmann elimination (Fig. 16.1). Also in later work, compounds analogous to **2** and **3** were observed as side products [3, 4].

The first targeted synthesis of a homothiacalixarene analogue was reported by Tsuge et al. in 1977. High dilution reaction of 2,6-bis(bromomethyl)pyridine **5** and dithiol **6** under basic conditions lead to a 51% yield of pyridine-containing macrocycle **7** (Scheme 16.1) [5].

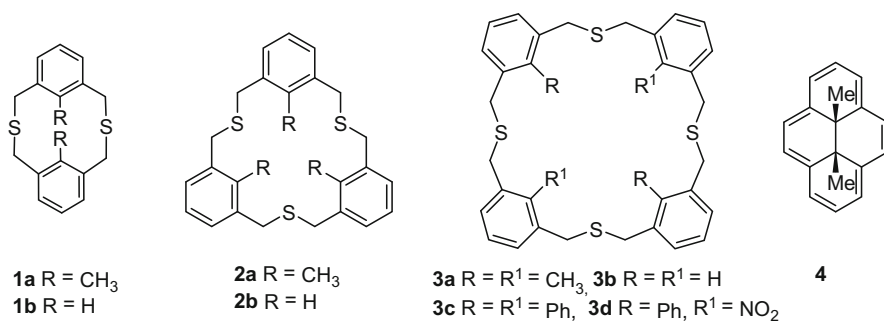
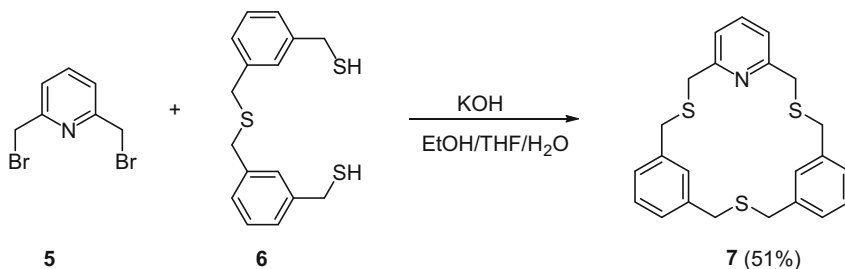
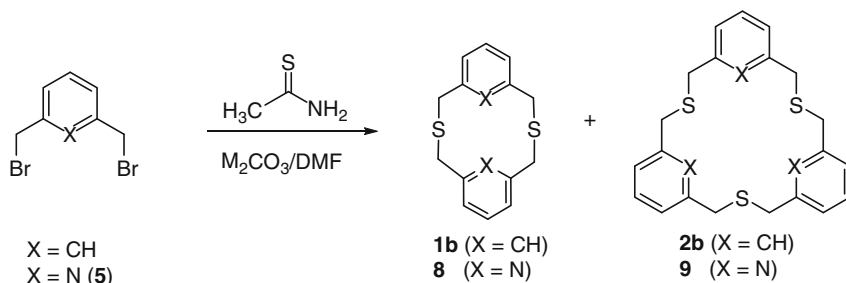


Fig. 16.1 Structures 1–4



Scheme 16.1 Synthesis of pyridine macrocycle **7**



**Scheme 16.2** Formation of dimers and trimers from 1,3-bis(bromomethyl)benzene and 2,6-bis(bromomethyl)pyridine building blocks, respectively

The selectivity of the formation of “dimer” [3,3]metacyclophanes **1b** and **8** versus “trimer” 18-membered macrocycles **2b** and **9** which were perceived as crown ether analogues, was discussed by Vögtle in 1983 [6]. Both 1,3-bis(bromomethyl)benzene and 2,6-bis(bromomethyl)pyridine building blocks were used, with thioacetamide as the source of sulfur. Increasing the size of the counterion of the carbonate base raises the amount of trimers. Apparently, no higher oligomers were formed (Scheme 16.2).

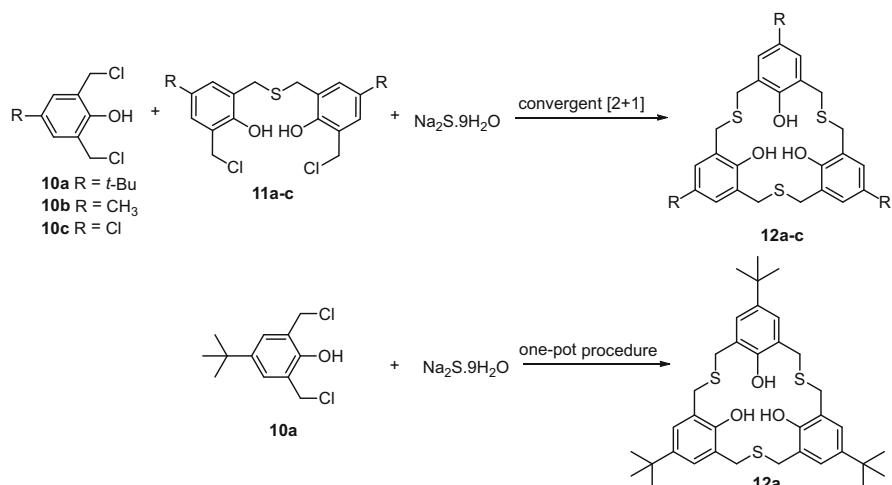
Sterically demanding groups at the intraannular positions also favor the formation of larger macrocycles. Vögtle reported the formation of a tetramer **3c** as the only product in 33 % yield from the corresponding 2-phenyl-1,3-xylylene dibromide and -dithiol. In the same way, the dinitro macrocycle **3d** was obtained in 25 % yield without any formation of the [1 + 1] adduct (Fig. 16.1) [7, 8].

The first “true” hexahomotrihialix[n]arenes **12a–c**, with both inter- and intraannular substituents, similar to the ones encountered in regular calixarene chemistry, were reported by Ashram in 2006 [9]. He used either a straightforward condensation of 2,6-bis(chloromethyl)-*p*-*tert*-butylphenol **10a** with sodium sulfide nonahydrate under high-dilution conditions to give **12a**, or a more convergent but longer [2 + 1] cyclization reaction of 2,6-bis(chloromethyl)phenols **10a–c** and dimeric dichloride units **11a–c**. The latter strategy gave higher yields. No higher oligomers, such as homothialix[4]arenes were observed (Scheme 16.3).

Preliminary data were given on binding properties of **12a–c** towards alkali- and heavy metal ions, determined by extraction experiments, but no promising results were obtained.

## 16.2.2 Synthetic Strategies and Postmodifications

The most common reaction used in the synthesis of these macrocyclic sulfides is the nucleophilic substitution of thiols (in the presence of base), inorganic sulfide, or a sulfide analog such as thioacetamide onto electrophilic benzylic bromides or chlorides **13**. The reaction is normally carried out under high dilution and inert atmosphere, the latter to avoid disulfide by-products. Working with inorganic sulfide (or analogs) and a single aromatic dihalide **13** has the advantage of

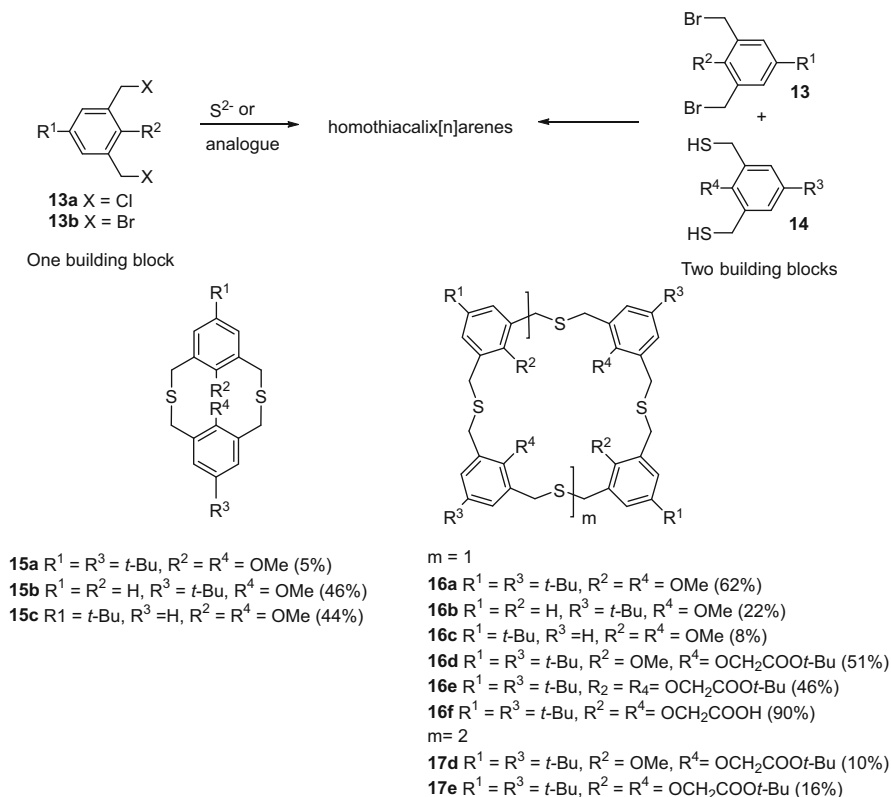


**Scheme 16.3** Hexahomotriacalix[3]arenes **12a–c** reported by Ashram

simplicity and good availability of the building blocks but could in principle give mixtures of [2+2]-, [3+3]-, [4+4]- and other higher cyclic oligomers as the reaction products. This method was the one used by Ashram, and the trimers **12a–c** seem to be highly favored in this case over other macrocycles [9].

The two-building block approach involves previous synthesis of a dithiol **14**, normally starting from the dihalide building block **13**. In one modification, the isolation of the dithiol **14** may be avoided by generating it *in situ* from the dihalide and thioacetamide [10]. With two monoaryl building blocks **13** and **14**, only macrocycles with an even number of aryl rings are expected to be formed, which has a positive effect on the yield. Dehaen et al. did a study on the factors that influence the formation of [3,3]metacyclophanes **15** versus homothiocalix[4]arenes **16**, using the two building block approach. Several factors influence the ratio of the products, such as the solvent, the counterion of the base used, and the substituents at the two-position of the aryl ring (the intraannular position). Substituents at the two-position (the extraannular position) did not have a significant effect. From the point of view of obtaining the maximum yield (62%) of homothiocalix[4]arene **16a**, it was best to work in a solvent of moderate polarity and with potassium carbonate as the base. In this case the product **15a** was only formed as a side product in 5% yield. When using EtOH or DMF as the solvent, 50% or 54% respectively of **15a** are formed together with a minor amount (22% or 15% respectively) of the larger macrocycle **16a**. Other counterions (Na<sup>+</sup>, Cs<sup>+</sup>) or the use of organic base such as *N,N*-diisopropylethylamine led to a lower total yield or failure of the reaction. When some of the intraannular methoxy groups are omitted, as in the reaction of 1,3-xylylene dibromide with 1,3-(bis)mercaptomethyl-4-*t*-butyl-2-methoxybenzene, the ratio of the products changes back to favor **15b**. Omitting



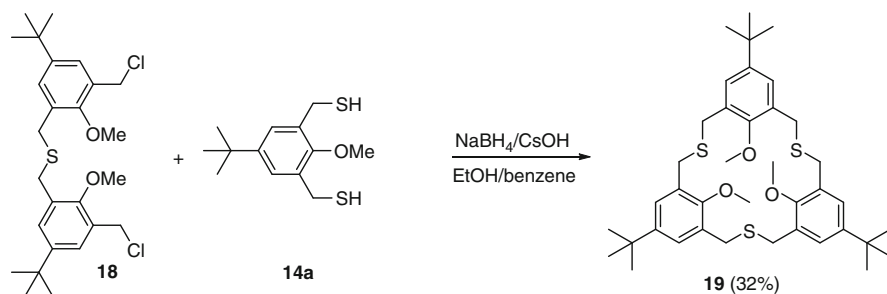


**Scheme 16.4** Exploration of the thiacyclophane size

the 4-*t*-butyl substituents seems to have no significant effect, the major product is **16c** (Scheme 16.4) [4, 11].

Interestingly, when the intraannular substituent was expanded from a methoxy to a *t*-butyloxycarbonylmethoxy substituent, no [3,3]metacyclophane **15** was obtained and next to the expected macrocycles **16d** and **16e**, significant amounts (up to 16%) of the homothiocalix[6]arenes **17d** and **17e** were isolated (Scheme 16.4) [11].

Strategies towards homothiocalix[3]arenes using a two building block approach also exist. Previous to the macrocyclization, a synthesis of a bisaryl building block needs to be carried out, which usually takes a number of steps. Two examples have been reported, one described by Ashram et al. [9] (see Scheme 16.3) and the other by Kohno et al. [12]. Dichloride **18** was prepared in a few steps from dibromide **13** and used in a macrocyclization with dithiol **14a**, affording a fair yield (32%) of the macrocycle **19**. The latter compound was found to bind  $\text{Ag}^+$  with high selectivity [12]. Although it has not been used in this way so far, this method has the potential to lead to unsymmetrically substituted homothiocalix[3]arenes by combining the appropriate building blocks (Scheme 16.5).



**Scheme 16.5** Two building block approach towards homothiacalix[3]arenes

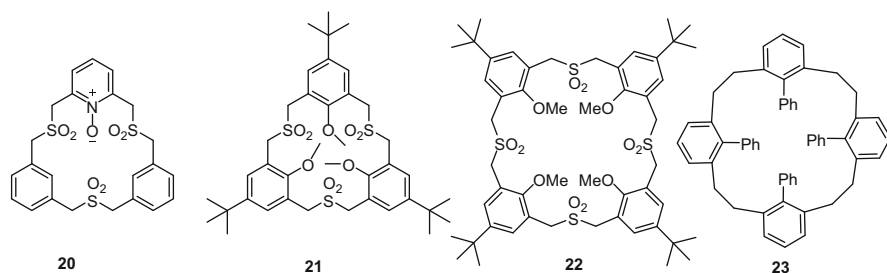


**Fig. 16.2** Oxidized (sulfone) homothiacalixarenes **20–22** and homocalix[4]arene **22**

Not many postmodifications of the formed homothiacalixarene rings have been reported. Tetracarboxyl derivative **16f** (Scheme 16.4) was obtained in high yield (90 %) after deprotection with trifluoroacetic acid and was soluble in water. This compound **16f** can be further transformed by coupling various functional groups to the carboxyl functions as it has been done previously for homooxalix[*n*]arenes [11].

Attempted demethylation of macrocycles such as **16a** with  $\text{BBr}_3$  or trimethylsilyl iodide led to extensive decomposition, probably due to the sensitivity of the benzylic sulfides.

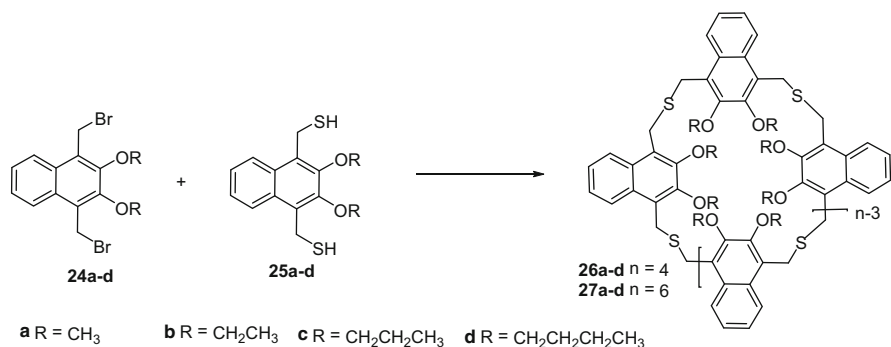
Oxidation of the sulfide groups to sulfones is another possibility for postfunctionalization. This was already tried for the pyridine thiacalix[3]arene **7**, giving the tris-sulfone N-oxide **20** quantitatively on treatment with peracid [5]. Kohno did a similar oxidation of homothiacalix[3]arene **19** to the trisulfone **21** [12]. Dehaen and co-workers prepared tetrasulfone **22** in 84 % yield starting from **16a** and an excess of *m*-CPBA [11]. An interesting ring contraction of the tetraphenylhomothiacalix[4]arene **3c** to the desulfurized homocalixarene **23** was reported by Vögtle et al. and involved oxidation of **3c** to the corresponding sulfone and pyrolysis at  $600\text{ }^\circ\text{C}/10^{-6}$  Torr (Fig. 16.2) [7].

### 16.2.3 Conformational and Structural Aspects

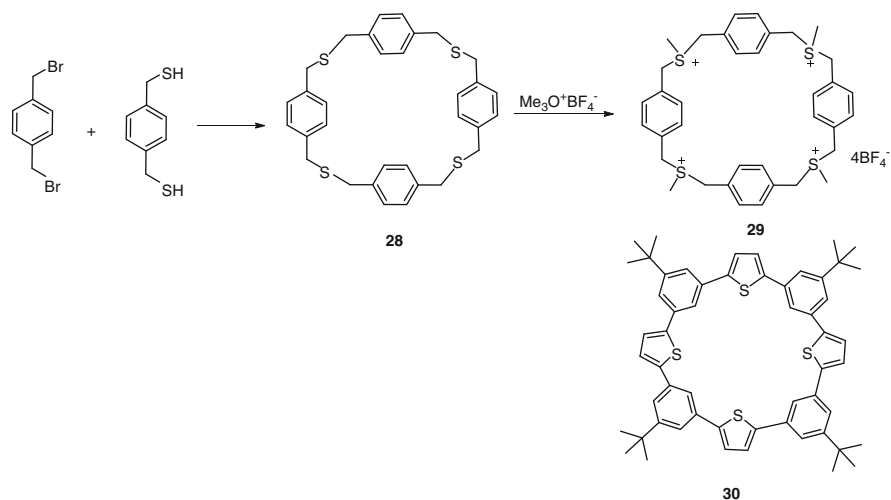
NMR characterization of compounds **16a**, **16d** and **17d** was done and showed relatively flexible structures [11]. The  $^1\text{H}$  NMR spectrum of **16a** showed sharp singlet signals for all the hydrogens. The absence of geminal coupling for the benzylic  $\text{CH}_2\text{SCH}_2$  protons points to fast interconformational conversion at the NMR time scale. Interestingly, the signals for the methoxy protons in  $\text{CDCl}_3$  ( $\delta = 3.15$  at room temperature) are significantly upfield compared to the usual value ( $\delta = 3.85$ ). This shift is in agreement with a 1,2- or 1,3-alternate conformation in which the methoxy groups are pointing towards neighboring aromatic groups. Cooling down the NMR experiment to 230 K further shifted the methoxy signal to 2.87 ppm, without any splitting of the benzylic methylenes. The solid-state structure of **16a**, determined by X-ray crystallography, was indeed shown to be the 1,2-alternate. The analog **16d**, with two much larger intraannular *t*-butoxycarbonylmethyl substituents, showed a 1,2-alternate conformation in the solid state. However, the  $^1\text{H}$  NMR spectrum at room temperature displayed eight AB doublets for the benzylic protons and individual singlets for each of the *t*-butyl, methoxy (at  $\delta = 3.16$  and 3.11 ppm) and acetate methylenes. Clearly, the larger intraannular substituents prevented fast conformational exchange as seen for **16a**. When the spectrum of **16d** was recorded at 353 K, most of the signals sharpened to clear singlets. The larger macrocycle **17d** showed only singlet signals in its  $^1\text{H}$  NMR spectrum at room temperature, indicating its greater flexibility. The analog **16e** with four large substituents shows very broad  $^1\text{H}$  NMR spectra at lower or room temperature indicative of multiple 1,2-alternate or 1,3-alternate conformations. At 353 K however, only sharp signals were observed for **16e**. The solid state structure of **16e** proved to correspond to the 1,3-alternate conformation. The larger tetraacetate analogue **17e** displayed enhanced flexibility as apparent from the  $^1\text{H}$  NMR spectra [11].

### 16.2.4 Homothiocalixarenes with Other Arene Units

Georghiou et al. described the synthesis of the homothiaisocalix[4]naphthalenes **26a–d** in 17–13 % yield, starting from 1,4-linked 2,3-dialkoxynaphthalenes **24a–d** and **25a–d** in a two building block approach (Scheme 16.6). The larger calix[6]naphthalene analogues **27b** and **c** were also isolated [13]. Notably, the one building block approach starting from **24** and sodium sulfide/alumina did not give any macrocycles (Scheme 16.6). The new macrocycles **26a–d** were tried as hosts for  $\text{C}_{60}$  and  $\text{C}_{70}$  fullerenes, or tetramethylammonium cation, without success. Binding studies with silver(I)triflate and mercuric chloride showed effective binding of silver, and only moderate affinity to the mercuric cation [13].



**Scheme 16.6** Synthesis of homothiacalix[4]- and -[6]naphthalenes **26** and **27**, respectively



**Scheme 16.7** Structures **28–29** related to homothiacalix[n]arenes

In a previous work, the 1,4-connected homothiacalix[4]arene isomer **28** had been prepared from two 1,4-xylylene building blocks (dibromide and dithiol) and converted to a water-soluble tetracationic host **29** by permethylation with Meerwein's salt [3]. This molecule **29** acted as a host to sodium 1-anilinoanthracene-8-sulfonate, as shown by fluorescence enhancement [14]. After 1976, no further binding studies appeared on this promising host, possibly due to its chemical instability.

The remarkable shape persistent metacyclophane **30** with 2,5-thiophene units prepared from the butadiyne linked analogues by treatment with sodium sulfide, is a rigid analogue of homothiacalix[4]arene (Scheme 16.7) [15].

### 16.3 Homothiocalix[*n*]arene Analogues

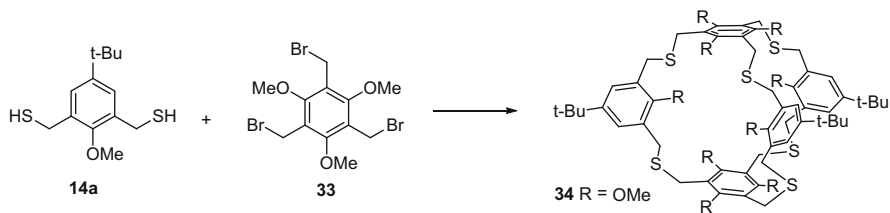
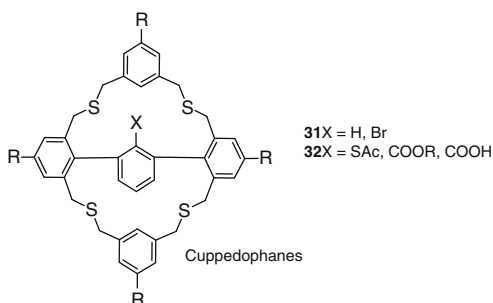
Several macrobicyclic systems were prepared using building blocks similar to the ones used for calixarenes. Cuppedophanes **31** and the concave reagents **32** having terphenyl units in their structures besides the *meta*-connected building blocks were described by Hart et al. [16] and Lüning et al. [17, 18], respectively (Fig. 16.3). Other work includes isomeric pyridinophanes and thiacyclophanes described by Rajakumar [19].

Macrobicyclic cage compound **34** was prepared in 23 % yield, starting from dithiol **14a** and 1,3,5-tris(bromomethyl)2,4,6-trimethoxybenzene **33** in a 3:2 molecular ratio, using high dilution conditions (Scheme 16.8) [11]. The NMR spectrum of **34** was extremely simple, in accordance with the highly symmetrical structure. The methoxy groups that are placed intraannularly ( $\delta = 3.07$  ppm) are shifted upfield in comparison to the six methoxy groups ( $\delta = 3.76$  ppm) on the “roof” and the “floor” of the cage compound. The solid-state structure of **34** showed only one of the four intraannular methoxy groups self-included in the cavity (Scheme 16.8) [11].

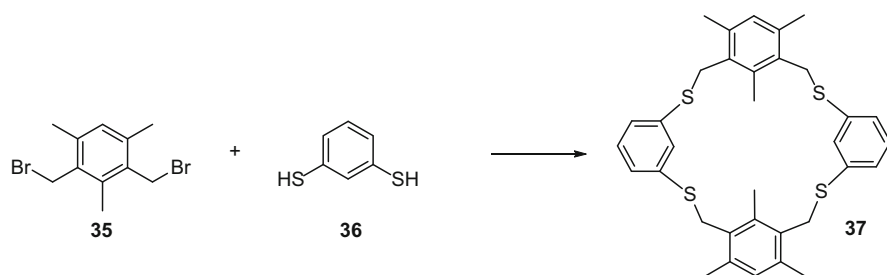
Vögtle reported for the first time on [2<sub>4</sub>]calixarenes with CH<sub>2</sub>S-bridges, that were formed in small amount as side products from dithioresorcinol and 1,3-xylylene dibromide or dibromide **5** [20]. The main products were in this case the [2,2]cyclophanes. Better yields of tetraaryl macrocycle **37** were reported by Pappalardo et al. when methylated dibromide **35** and dithioresorcinol **36** were used (Scheme 16.9) [21, 22].

Using building blocks available from earlier studies, such as the thiol **14a** and 4,6-dichloropyrimidine **38** (R = S-Pr), Dehaen et al. succeeded to prepare [2<sub>4</sub>]tetrathiocalix[2]arene[2]pyrimidines **39a** in up to 57 % isolated yield. Small amounts (less than 10 %) of the higher cyclic oligomers **40** and **41** ( $n = 6, 8,$

**Fig. 16.3** Macrobicyclic structures 33–32



**Scheme 16.8** Synthesis of macrobicyclic cage compound **34**



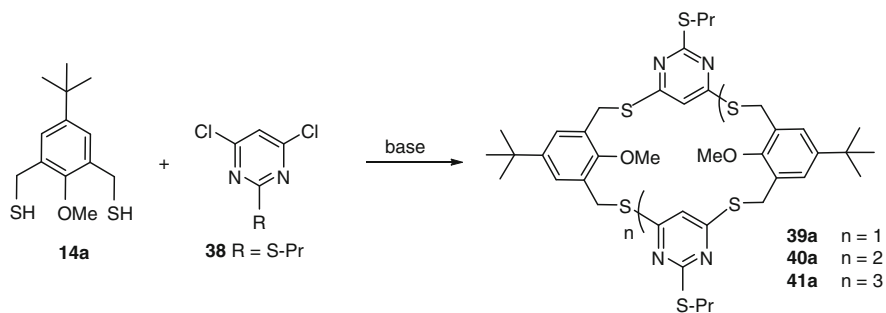
**Scheme 16.9** [2<sub>4</sub>]cyclophanes related to homothiacalixarenes

respectively) were also isolated and after changing the reaction conditions (MeCN instead of DMF) the [2<sub>8</sub>]cyclooligomer **41a** even becomes the major compound (41 %). The major compound is the [2<sub>6</sub>] analogue **40a** (27 % yield) when Cs<sub>2</sub>CO<sub>3</sub> is used as the base in DMF. Building blocks **14** lacking two-substituents in combination with analogs of **38** with different two-substituents (R = H, SMe, SBz) gave lower amounts (15–26 % isolated) of the [2<sub>4</sub>]tetrathiacalixarenes **39** (Scheme 16.10) [23].

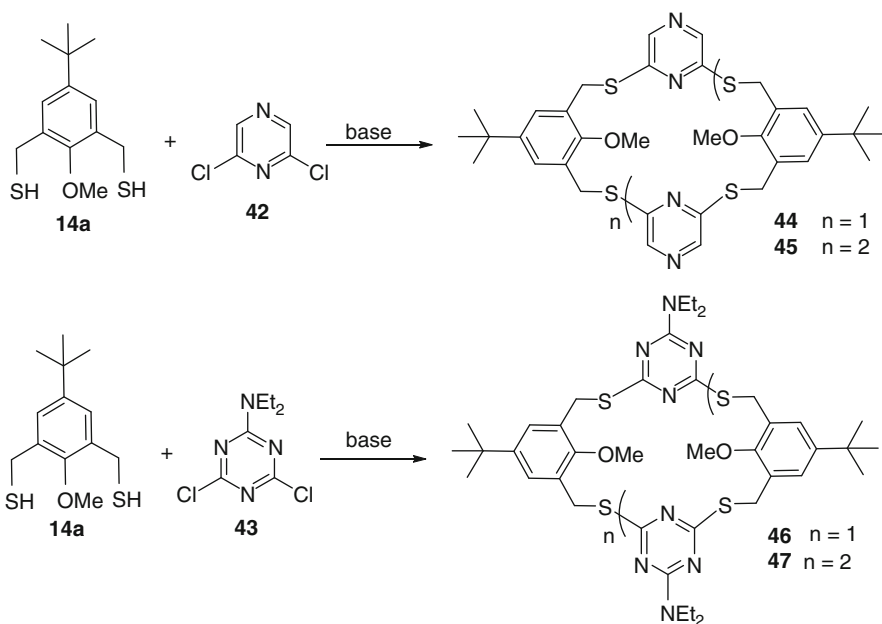
The analogous [2<sub>4</sub>] and [2<sub>6</sub>] cyclophanes (**44–47**) derived from 2,6-substituted pyrazines and 2,4-disubstituted triazines were prepared in low yields with a two building approach, combining dithiol **14a** with electrophilic dichloro heterocycles **42** and **43**. Moderate affinity of the [2<sub>6</sub>] macrocycles **45** and **47** for Cu(I), Cu(II) and Ag (I) was observed (Scheme 16.11) [24].

Thioresorcinols oxidize to macrocyclic disulfides that also can be seen as analogs of homothiacalixarenes. The first example of these compounds was reported by Aryian and Wiles [25]. The result of the reaction of 1,3-dimethoxybenzene with sulfur monochloride was a product for which the structure was tentatively assigned as the trimer **49** (Schemes 16.12 and 16.13). The same compound **49** was obtained when the corresponding dithioresorcinol **48** was oxidized with iodine [26]. The 1,3,5-trimethylbenzene-2,4-dithiol derived from mesitylene gives the tetramer on oxidation rather than the trimer, probably due to the intraannular methyl groups [21, 22]. An NMR study has been carried out on these tetrameric compounds, showing that either a saddle or crown conformation may be preferred, depending on the substituents [27]. Trimer compound **49** shows a propeller-like conformation [28]. The unsubstituted dithioresorcinol trimeric oxidation product has been described by Marvel et al. as a polymer crosslinking reagent [29].

Recently, a lot of attention has gone to dynamic combinatorial chemistry (DCC), in which dithiols are oxidized to libraries of disulfide macrocycles that can reversibly ring open. Different stimuli can influence the composition of the dynamic libraries. Thus, 3,5-mercaptobenzoic acid **50** or its derivatives can be converted after oxidation to such disulfide libraries containing macrocycles of different sizes, with mainly the trimer **51** and tetramer **52** [30–38]. For a thorough discussion of this



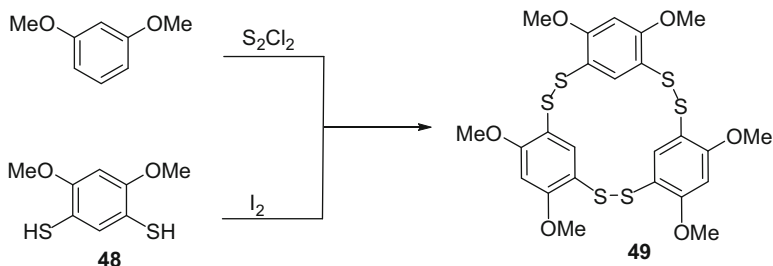
**Scheme 16.10** Synthesis of [24]tetrathiacalix[2]arene[2]pyrimidines and higher oligomers



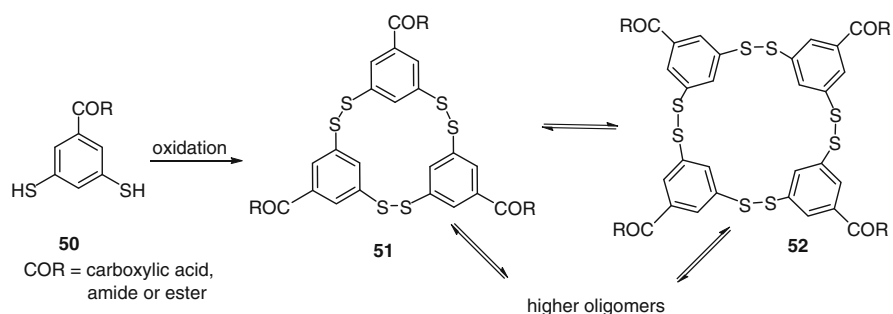
**Scheme 16.11** Pyrazine and 1,3,5-triazine [2<sub>4</sub>] and [2<sub>6</sub>] cyclophanes **44–47**

very active field of chemistry the reader is referred to the review articles of Otto and Stefankiewicz [39, 40].

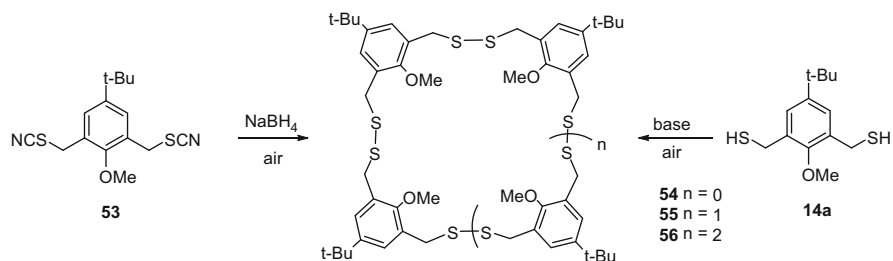
By oxidation of dithiolate precursors generated from dithiol **14a** or by reduction of the corresponding bis(thiocyanate) **53**, Dehaen et al. have prepared several macrocyclic disulfides. Remarkably, the dithiol **14a** when oxidized in basic conditions initially gives a complicated mixture of trimer, tetramer, pentamer and acyclic oligomers, that slowly (over 5 days) evolves to a mixture from which 45 % tetramer **55** could be isolated, next to 13 % trimer **54** and 9 % pentamer **56**. The reduction/reoxidation of the bis(thiocyanate building block gave only the tetramer **55** (91 % isolated), when the reaction was left for 3 days (Scheme 16.14) [41]. In the <sup>1</sup>H NMR



**Scheme 16.12** Disulfide macrocycles



**Scheme 16.13** Dynamic combinatorial libraries starting from 3,5-dimercaptobenzoic acid derivatives



**Scheme 16.14** Homodithiacalix[n]arenes

spectrum of the macrocycles **54–56**, the methoxy signals ( $\delta = 3.71$  for the tetramer **55**) are not shielded, so conformations where the methoxy group is pointing to the aryl groups are not favored in this case. We have observed reversible, solvent-induced conformational switching in the single crystals of homodithiacalix[4]arene **55**. This compound crystallizes as a THF solvate, adopting a 1,3-alternate conformation. The methoxy groups are outside the folded macrocycle. The packing



reveals undulated continuous 1D channels. Interstitial space is filled with disordered THF molecules. The THF molecules can be completely removed by heating the single crystal at 120 °C and the single crystals analysis was done again. This revealed that **55** was now in a different phase with 1,2-alternate conformation. The single-crystal-to-single-crystal process can be reversed by immersing the crystals for 3 min in a THF solution. This process could also be monitored by solid-state  $^{13}\text{C}$  NMR spectroscopy and also occurs with other solvents such as acetonitrile and ethyl acetate [42].

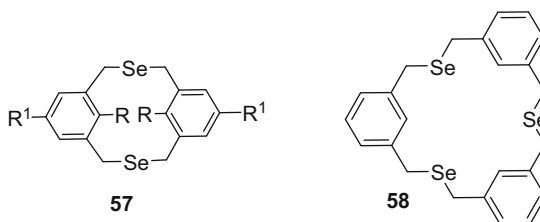
## 16.4 Homoselenacalix[n]arenes

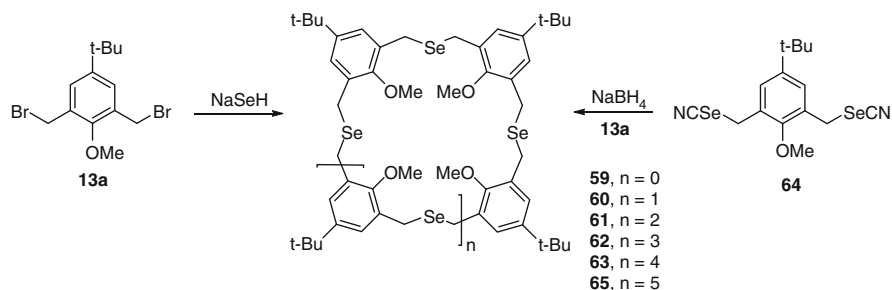
Several reports were made of diselena[3,3]metacyclophanes **57**, which was prepared by the addition of  $\text{Na}_2\text{Se}$  to a solution of 1,3-bis(bromomethyl)benzene. Mitchell has also isolated byproducts in this reaction, the higher macrocycles **58** (8 %) that can be seen as homoselenacalix[3]arene derivatives (Figs. 16.4) [43].

Dehaen et al. described homoselenacalix[n]arenes ( $n = 3-8$ ), that may be prepared using two different strategies using nucleophilic selenium species [44]. The one building block approach starting from **13a** and sodium hydroselenide gave a mixture of macrocycles **59-63** in 86 % total yield, with a respective 37:20:14:8:7 product ratio. These selenacalixarenes could be separated by column chromatography. A more selective synthesis of homoselenacalix[4]arene is achieved using a two building block approach. Reductive coupling of bisbromide **13a** and bis(selenocyanate **64** afforded tetramer **60** in 67 % yield, together with 18 % hexamer **62** and 9 % octamer **65** (Scheme 16.15).

The homoselenacalix[n]arenes **59-65** were characterized by  $^1\text{H}$ ,  $^{13}\text{C}$  and  $^{77}\text{Se}$ -NMR spectroscopy. In the  $^1\text{H}$  NMR spectra of these macrocycles only singlets were observed, and the absence of methylene geminal couplings again points to conformational flexibility. Especially in the spectrum of the homoselenacalix[4]arene **60** an upfield shift of the methoxy groups ( $\delta = 3.22$ ) was seen, showing that these groups are pointing towards aryl moieties. The  $^{77}\text{Se}$  NMR spectra showed only one signal for each macrocycle, again confirming the high symmetry and flexibility. A minor shift of the  $^{77}\text{Se}$  signal to downfield is observed on increasing the size of the macrocycles from **59** to **65**. X-ray crystallographic analysis of **60** showed a heavily twisted 1,3-alternate conformation, with the bridging selenium atoms inside of the

**Fig. 16.4** Diselena[3,3]metacyclophanes **57** and homoselenacalix[3]arenes **58**





**Scheme 16.15** Two strategies to synthesise homoselenacalix[ $n$ ]arenes **59–65**

cavity. The larger macrocycle **62** had a 1,3,5-alternate conformation with the seleniums outside the cavity and facing aryl rings directed in an antiparallel manner. Omitting the intraannular methoxy substituents from the building blocks **13a** or **64** had the effect of leading mainly to diselena[3,3]metacyclophanes of type **57** [44].

Further work with bisbromide-acetate building block **13d** ( $R^1 = t\text{-Bu}$ ,  $R^2 = \text{OCH}_2\text{COO}t\text{-Bu}$ ) and bis-selenocyanate **64** led to the formation of a mixture of bis- and trisacetate homoselenacalix[ $n$ ]arenes **66** and **67** ( $n = 4, 6$ ). Substitution at the outer rim was also possible, with bisester homoselenacalix[ $n$ ]arene **68**, formed in 42% yield by macrocyclisation of **13a** and the corresponding bis(selenocyanate) benzoate, or bisalcohol homoselenacalix[ $n$ ]arene **69**, formed in 85% yield by reduction of **68**. The homoselenacalix[4]arenes **60** formed complexes with Ag [I] that showed bonding to the four selenium atoms in the solid state structure [45] (Fig. 16.5).

The bis-selenocyanates **64a–c** when reduced with  $\text{NaBH}_4$  and allowed to oxidize gave within 12 h exclusively the homodiselenacalix[4]arenes **70a–c** in excellent yields (Scheme 16.16). GPC traces of the macrocyclization reaction leading to **70a** showed after 10 min a rather complex reaction mixture with a large fraction of oligomeric material. After 1 h the macrocycle **70a** is the major product, and after 6 h the conversion is practically quantitative. Several reducing agents were used in combination with **64a**, but the main factor controlling the yield was the thermodynamic stability of the tetramer **70**, together with the reversibility of the diselenide bond formation. The equilibration process towards **70** was seen to be much faster in comparison with the corresponding disulfides **55**. Theoretical calculations confirmed the higher thermodynamic stability of **70** in comparison to the trimer and pentamer homologues, and gave insight in the conformational behavior. Single crystal X-ray analysis of THF solvates of **70a, b** revealed high similarity between both. The methoxy substituted **70a** underwent a single-crystal-to-single-crystal transformation from 1,3-alternate (the THF solvate) to 1,2-alternate (the apohost) conformations [46].

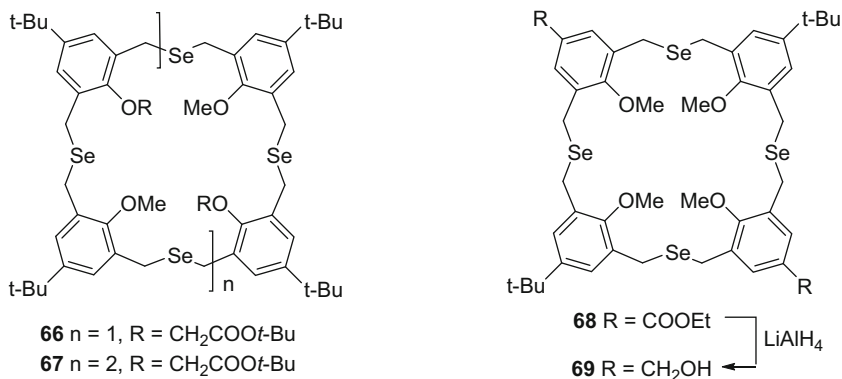
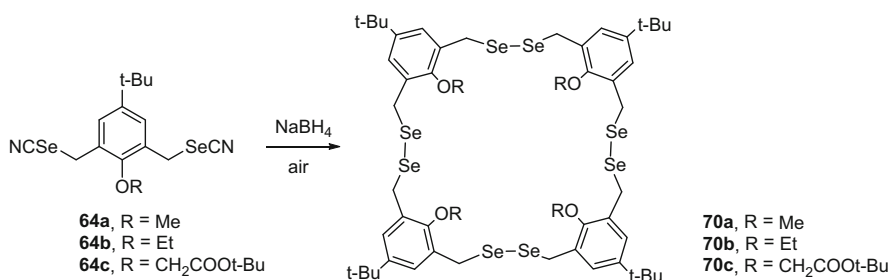


Fig. 16.5 Substituted homoselenacalix[n]arenes

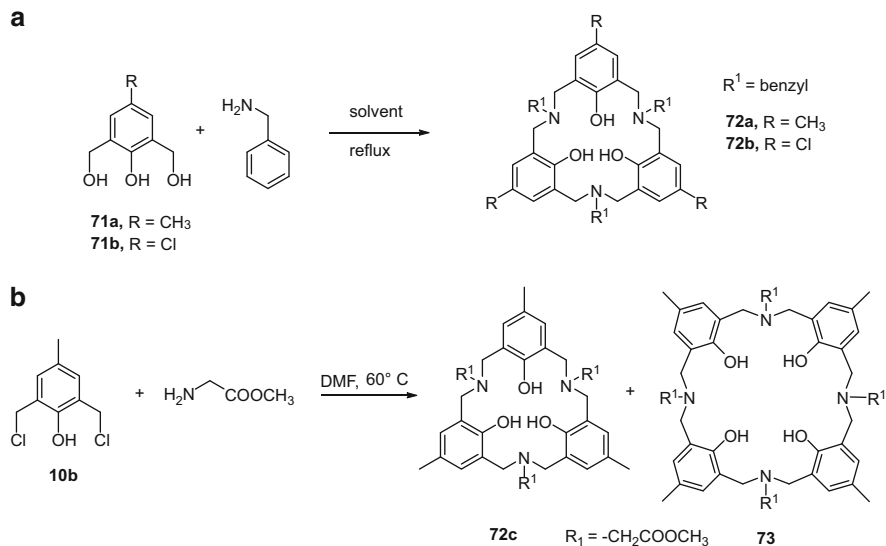


Scheme 16.16 Formation of diselenide calixarenes 70a–c

## 16.5 Homoazacalix[n]arenes

### 16.5.1 Synthetic Strategies

Takemura was the first in 1992 to prepare hexahomotriazacalix[3]arenes (in short homoazacalix[3]arenes) **72** starting from 2,6-bis(hydroxymethyl)phenol derivatives **71** and amines by reflux in toluene for 1 day followed by an additional heat treatment (for an additional day) at 120–135 °C of the oily residue after evaporation (Scheme 16.17a). The yield is very variable, and dependent on the amine and R-substituent. Benzylamines gave rather good yields, but anilines and simple alkylamines gave complicated reaction mixtures from which no macrocycles could be isolated [47–49]. In some cases, the amines themselves may template the formation of **72**, in such way that high dilution conditions are not needed. Therefore, the solvents used are apolar to maximize the hydrogen bonding interactions. With electron withdrawing substituents, e.g.  $R = \text{Cl}$ , xylene was used instead of toluene to get the azacalix[3]arene **72b** [50].



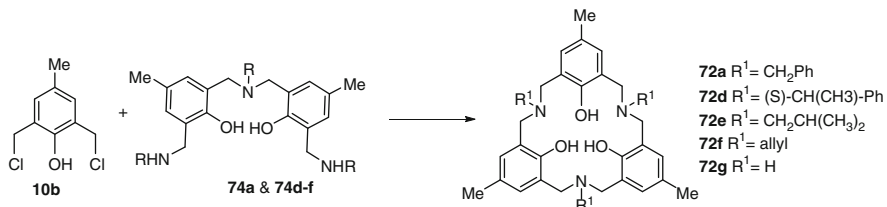
**Scheme 16.17** Homoazacalix[*n*]arenes **72** and **73**

Hampton et al. have claimed that the method of Takemura gave mixtures of the homoazacalix[3]arene **72c** and the tetrameric analogue **73**, which are difficult to separate [51]. When the more reactive 2,6-bis(chloromethyl)-*p*-methylphenol **10b** is used as the starting material in the condensation reaction with glycine methyl ester hydrochloride and K<sub>2</sub>CO<sub>3</sub> in DMF at 60 °C, a mixture of **72c** and **73** (6:1) is formed in 43 % yield, from which 19 % pure **72c** could be isolated by selective crystallization (Scheme 16.17b) [52].

Hampton et al. described a more convergent, but longer synthesis towards analogues homoazacalix[3]arenes (**72a** and **72d–f**), starting from two building blocks, dichlorides **10b** and trisamines **72a** and **72d–f**. The latter were prepared from **71** and different amines in a number of steps. The macrocyclization step itself towards **72a** and **72d–f** was highly effective (up to 95 % yield) and selective, and the resulting products were of high purity (Scheme 16.18) [51].

Nucleophilic substitution of O-protected dibromide **13a** with tosylamide and NaH base gave a 13 % yield of the homoazacalix[4]arene **75**, next to 10 % yield of the [3,3]cyclophane **76** [48]. On the other hand, 2-fluoro-*m*-xylylene dibromide under similar circumstances gave 25 % [3,3]cyclophane **77** and only 3.7 % of the homoazacalix[3]arene **78** (Fig. 16.6) [53]. In the same way, starting from cyanamide and **13a**, mixtures of the corresponding [3,3]cyclophane **76** (R = CN) and homoazacalix[4]arene **75** (R = CN) were formed (Fig. 16.6) [54].

Dialkylation in basic conditions of cyanamide with xylylene dibromide or the diaryl dibromide building block **79** gave mixtures of [3,3]cyclophane **80** (17 %) and **81** (56 %) and the homoazacalix[3]arene **82** (13 %) and homoazacalix[4]arene **83** (28 %), respectively (Fig. 16.7) in a single reaction [54].



**Scheme 16.18** Convergent synthesis of macrocycles **72a** and **72d-f**

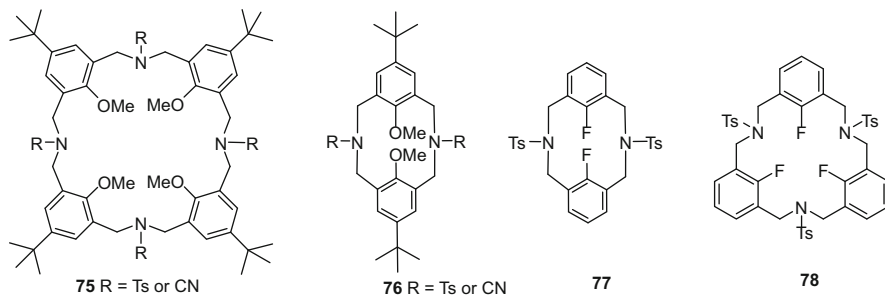


**Fig. 16.6** Structures **75-78**

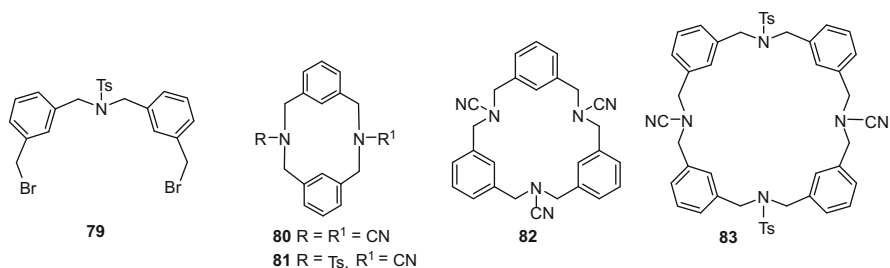
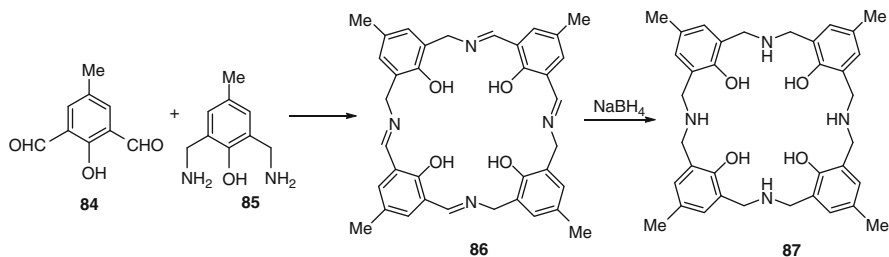


**Fig. 16.7** Structures **79-83**

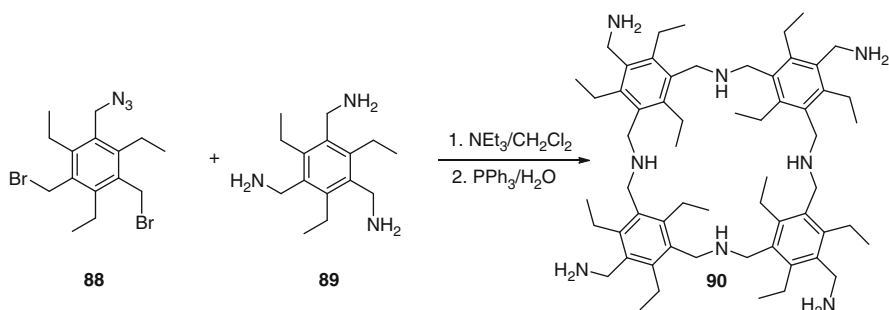
A two-building block approach towards homoazacalix[4]arenes has been applied by Robson et al. [55, 56]. Condensation of 2,6-diformyl-4-methylphenol **84** with 2,6-bis(aminomethyl)-4-methylphenol **85** gave the imine **86**, that could be reduced with sodium borohydride to afford the N-unsubstituted macrocycle **87** in 79% yield at a multigram scale (Scheme 16.19).

Similar reductive coupling of unsubstituted m-phenylenedi(methylamine) and m-phenylenedicarboxaldehyde also gave the corresponding cyclic tetramer in 47% yield; however, this was accompanied by the higher cyclic oligomers such as hexamer (18%) and octamer (3%) (Scheme 16.19) [57].

Anslyn et al. reported the formation of the water-soluble homoazacalix[4]arene analogue **90** in a reasonable yield (40%) from a two-building block approach with



**Scheme 16.19** Synthesis of N-unsubstituted calix[4]arene **87**



**Scheme 16.20** Water soluble homoazacalix[4]arene **90**

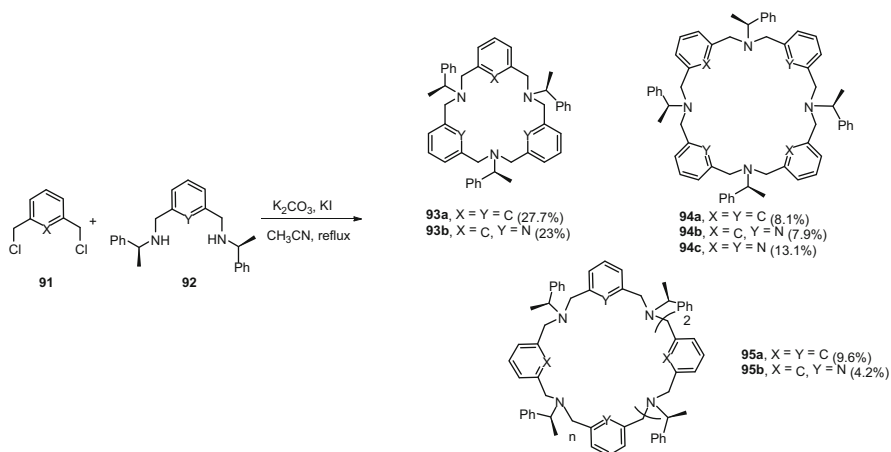
dibromide **88** and trisamine **89**, followed by reduction of the azide functions of the intermediate bisazide with triphenylphosphine/water (Scheme 16.20) [58].

A similar two building block approach, but with 1,3-xylylene or 2,6-pyridinemethylene moieties **91** and **92** that lack 2-substituents led to a mixture of the [3,3]cyclophanes **93a, b**, the homoazacalix[4]arenes **94a–c** and the homoazacalix[6]arenes **95a–b** with the former compounds in the majority, except in the case when both building blocks are pyridine derivatives, when only the [2 + 2] cyclization product **94c** is isolated (Scheme 16.21) [59].

### 16.5.2 Postfunctionalization and Conformational Aspects

The most obvious place for functionalization of homoazacalix[3]arenes of type **72** is on the phenol functionalities. The triphenols **72** have two possible conformations, the cone and partial cone, which are in fact in fast equilibrium in solution at room temperature. The cone conformation normally is the more stable one due to intramolecular hydrogen bonding. Hampton et al. were the first to report a solid state structure of **72** ( $\text{R} = \text{Me}$ ,  $\text{R}^1 = \text{CH}_2\text{COOMe}$ ) [52].

Etherification of the phenols can lead to different isomers if the substituent  $\text{R}^1$  is large enough to prevent partial cone/cone conversion. O-Silyl ethers were prepared



**Scheme 16.21** Cyclization products **93a–b**, **94a–c** and **95a–b**

from compounds **72** and 1-(trimethylsilyl)imidazole, hexamethyldisilazane or bis(trimethylsilyl)trifluoroacetamide (BSTFA). The first two reagents gave the cone isomer selectively as confirmed by X-ray crystallography, on the other hand BSTFA gave a mixture of partial cone and cone isomers (3:2 ratio based on the  $^1\text{H}$  NMR spectra of the mixture) [60].

Functionalization of **72** with bromoacetate groups gave a mixture of cone and partial cone isomers **96a, b** and **97a, b**, respectively, with yield and ratio dependent on the R group of the ester. The cone-triester **96a** could be condensed with tris(aminoethyl)amine (tren) to an interesting cryptand-like compound that is an efficient receptor for halide anions [61]. Interestingly, both isomers of the ethyl triester **96b** and **97b** gave the partial cone trisamide **98** on condensation with 1-naphthylmethylamine, proving that on heating at reflux in a 1:1 toluene/methanol mixture the energy barrier for partial-cone to cone conversion can be overcome [62].

Pulpoka et al. reported alkylation of **72** (R = Cl, R<sup>1</sup> = benzyl) with N-(4-bromobutyl)carbazole, apparently leading exclusively to the partial cone isomer in low yield (10%) [63].

Hampton et al. have described the deallylation of **72f** to the N-unsubstituted **72g**, but no further reactions were done with this interesting compound [51].

Robson et al. have converted their N-unsubstituted homoazacalix[4]arene **87** with formaldehyde into tetrabenzoxazine **99** (Figs. 16.8) [56].

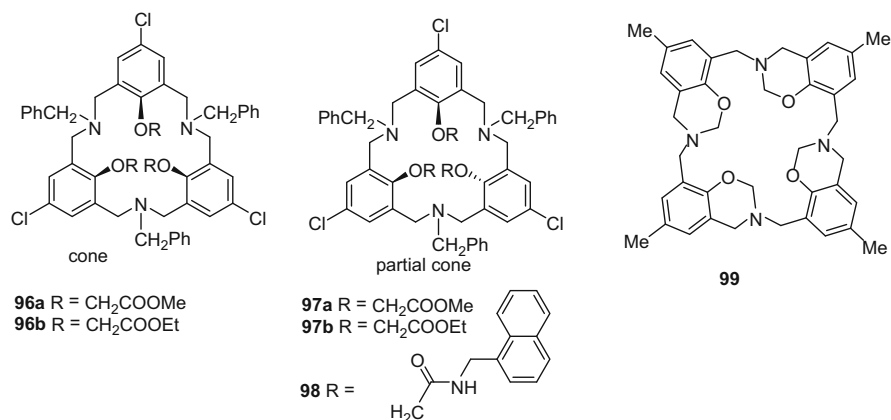


**Fig. 16.8** Functionalization of homoazacalix[n]arenes

### 16.5.3 Molecular Recognition Properties

The homoazacalix[3]arenes **72** showed only low affinity for alkali and alkaline-earth metal cations as shown already in 1992 by Takemura [47] and later confirmed by Hampton [52], using picrate extraction experiments.

For the picolyl derivatives of **72** (R = Me, R<sup>1</sup> = 2-pyridylmethyl), the extraction rates became 50–60 times greater as compared to the tribenzyl derivative of **72**, but the ion selectivity for potassium decreased markedly, which was due to the flexibility of the picolyl side arms [48].

Binding of macrocycles **72** to uranyl ions was already reported by Takemura [47] and confirmed in a number of other papers [64–66]. The extraction of the uranyl cation by **72a** from the aqueous phase into chloroform is optimal at neutral pH. The uranyl complex was prepared from the ligand **72b** and uranyl nitrate without the addition of base and was crystallized. The uranyl unit is external to the macrocycle and bound to only two of the phenoxide units in the solid state structure obtained by X-ray analysis. Together with the two nitrate ligands this means a six-coordinate complex, which is unusual for uranyl calixarene complexes [64]. Singh et al. described compounds **72** with arylchalcogens (ArSe, ArTe) appended to the three nitrogens via two or three methylene spacers. Naked eye detection of uranyl (yellowish green to red on complexation) was possible by these receptors in the presence of a large range of other metal cations [65, 66]. This was confirmed by UV Vis, <sup>1</sup>H, and <sup>77</sup>Se NMR spectra. A PVC membrane ion selective membrane containing these chalcogen derivatives of **72** showed selective Nernstian response for uranyl cations over a variety of other metal ions, including alkali, alkali earth, and p- and d-block metal cations.

Lanthanide ions also form complexes with the homoazacalix[2]arenes. Neodymium nitrate forms a 1:1 complex with **72b** in which the lanthanide ion is bound external to the macrocycle, involving all three phenoxide ions and three nitrates,



while the amine groups are transformed to ammonium ions [50]. The crystal structure of the uncomplexed ligand **72b** was determined for comparison, and shown to have also the cone conformation stabilized by intramolecular hydrogen bonds.

Thuéry et al. reported about ytterbium (III) complexes of **72b**. A 1:1 complex is formed starting from the metal nitrate, that is similar in structure to the Nd(III) complex. The replacement of the nitrate counterion by less coordinating triflate ion results in the formation of a 2:1 sandwich complex between **72b** and ytterbium(III) which is hexacoordinated to six phenoxides of two ligands [67].

The partial cone naphthalene trisamide **98** described by Pulpoka et al. showed molecular recognition for Cd<sup>2+</sup>, Pb<sup>2+</sup> and Co<sup>2+</sup> as indicated by changes in its monomer and excimer emission happening upon binding. Compound **98** also binds anions, with the highest binding constant for fluoride (1:1 complexation) [62]. A highly selective and sensitive chemical sensor for Zn<sup>2+</sup> was prepared by electrochemical linking of the O-carbazolylbutyl functionalized partial cone compound **98** to ultrathin films by cyclic voltammetry. The size of the macrocycle together with the dipole specificity is the reason for the high selectivity and sensitivity [67].

Robson et al. reported the synthesis and solid state structures of tetrazinc (II) and tri(cobalt (III)) cluster complexes of the homoazacalix[4]arene ligands **87** [55, 56].

Anslyn showed by variable temperature NMR that the homoazacalix[4]arene **90** at room temperature had several conformations, with the more stable cone conformation freezing out at -70 °C. Anionic guests were shown to bind to **90** by a fluorescence displacement assay [58].

### 16.5.4 Similar Structures

Structures in which one or two of the methylene groups CH<sub>2</sub> of every bridge have been replaced by carbonyl groups CO have been reported recently. Hamilton et al. have generated a set of macrocycles **100** from a solid phase synthesis of linear trimers of 5-aminoacyl-3-aminomethyl benzoates. These macrocycles are large area scaffolds useful in molecular recognition studies [68].

Hjelmggaard has reported on meta-arylopeptoids **101** without five-substituent that were prepared in excellent yields (83–88 %) via the cyclization of an open chain trimer. No cyclohexamer was formed in this case, differently than for the *ortho*- or *para* substituted isomers [69]. Gale et al. were the first to prepare [4+4] macrocycles **103e** and **103f** from tetra- or pentafluoroaniline and isophthaloyl dichloride in relatively low yields (3, respectively 13 %). X-ray crystallographic analysis showed that these macrocycles adopt saddle-like conformations in the solid state [70].

Almost a decade later, Gallagher et al. reported the synthesis of trezimides (**102a** and **102b**) and tennimides (**103a** and **103b**) from aminoheterocycles and isophthaloyl chloride. Both macrocycles are formed in low yields. Halogen bonding

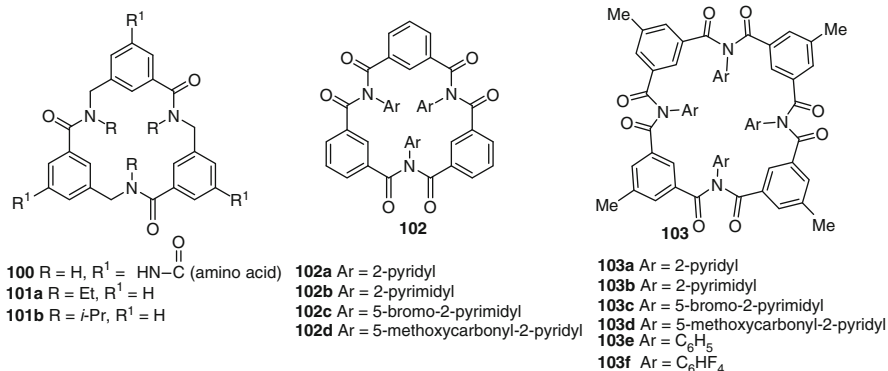


**Fig. 16.9** Structures **100–103** related to homoazacalix[*n*]arenes

has been observed in macrocycles that were prepared from 4-bromosubstituted aminoheterocycles [71–73].

A vast literature exists on the synthesis and properties of cryptand-like 3D analogs of the homoazacalixarenes, but a discussion is out of the scope of this book on calixarenes (Fig. 16.9).

## 16.6 Conclusion

Homothia-, homoselena and homoazacalix[*n*]arenes of different sizes and substitution patterns have become available via a number of straightforward synthetic methods. These molecules complement the better known calix[*n*]arenes and have additional features due to the presence of the heteroatoms and their larger conformational flexibilities, allowing them to be more than just platforms but also to act as host. It is hoped that this review could stimulate further research in this interesting class of macrocycles, for instance towards applications in molecular recognition studies and as chemical sensors.

## References

- Mitchell R. H.; Boekelheide, V. *Tetrahedron Lett.* **1970**, *11*, 1197–1202.
- Vögtle, F.; Neumann, P. *Tetrahedron* **1970**, *26*, 5299–5318.
- Mitchell R. H.; Boekelheide, V. *J. Am. Chem. Soc.* **1974**, *96*, 1547–1557.
- Tashiro, M.; Yamato, T. *J. Org. Chem.* **1981**, *46*, 1543–1552.
- Tsuge, O.; Okumura, M. *Heterocycles* **1977**, *6*, 5–12.
- Vögtle, F.; Ley, F. *Chem. Ber.* **1983**, *116*, 3000–3002.
- Boeckmann, K.; Vögtle, F. *Chem. Ber.* **1981**, *114*, 1048–1064.
- Boeckmann, K.; Vögtle, F. *Chem. Ber.* **1981**, *114*, 1065–1073.

9. Ashram, M. J. *Inclusion Phenom. Macrocycl. Chem.* **2006**, *54*, 253–259.
10. Takido, T.; Toriyama, M.; Ogura, K.; Kamijo, H.; Motohashi, S.; Seno, M. *Phosphorus, Sulfur and Silicon*, **2003**, *178*, 1295–1301.
11. Thomas, J.; Van Hecke, K.; Robeyns, K.; Van Rossom, W.; Sonawane, M. P.; Van Meervelt, L.; Smet, M.; Maes, W.; Dehaen, W. *Chem. Eur. J.* **2011**, *17*, 10339–10349.
12. Kohno, K.; Takeshita, M.; Yamato, T. *J. Chem. Res.* **2006**, 251–253.
13. Tran, H.-A.; Georghiou, P. E. *New J. Chem.* **2007**, *31*, 921–926.
14. Tabushi, I.; Sasaki, H.; Yasuhisa, K. *J. Am. Chem. Soc.* **1976**, *98*, 5727–5728.
15. Tobe, Y.; Utsumi, N.; Nagano, A.; Sonoda, M.; Naemura, K. *Tetrahedron* **2001**, *57*, 8075–8083.
16. Vinod, T.; Hart, H. J. *Org. Chem.* **1990**, *55*, 881–890.
17. Lüning, U.; Wangnick, C.; Peters, C.; Von Schnering, H. G. *Chem. Ber.* **1991**, *124*, 397–402.
18. Lüning, U.; Baumgartner, H. *Synlett* **1993**, 571–572.
19. Rajakumar, P.; Dhanasekaram, M.; Selvanayagam, S.; Rajakannan, V.; Velmurugan, D.; Ravikumar, K. *Tetrahedron Lett.* **2005**, *46*, 995–999.
20. Vögtle, F. *Tetrahedron Letters* **1968**, *9*, 3623–3626.
21. Bottino, F.; Pappalardo, S.; Foti, S. *Chimica e l'Industria* **1976**, *58*, 379–80.
22. Bottino, F.; Foti, S.; Pappalardo, S. *Tetrahedron* **1976**, *32*, 2567–2570.
23. Sonawane, M. P.; Van Hecke, K.; Jacobs, J.; Thomas, J.; Van Meervelt, L.; Dehaen, W.; Van Rossom, W. *J. Org. Chem.* **2012**, *77*, 8444–8450.
24. Sonawane, M. P.; Boodts, S.; Thomas, J.; Dehaen, W. *Supramol. Chem.* **2014**, *26*, 547–551.
25. Ariyan, Z. S.; Wiles, L. A. *J. Chem. Soc.* **1962**, 4709–4712.
26. Bottino, F.; Foti, S.; Pappalardo, S. *J. Chem. Soc., Perkin Trans 1*, **1979**, 1712–1715.
27. Ronsisvalle, G.; Bottino, F.; Pappalardo, S. *Org. Magn. Reson* **1980**, *14*, 344–348.
28. Pappalardo, S.; Bottino, F.; Ronsisvalle, G. *J. Chem. Soc. Perkin Trans 2*, **1984**, 1001–1004.
29. Wong, D. T. M.; Marvel, C. S. *J. Polymer Sci., Polymer Chem. Ed.* **1976**, *14*, 1637–1644.
30. Leclaire, J.; Vial, L.; Otto, S.; Sanders, J. K. M. *Chem. Commun.* **2005**, *41*, 1959–1961.
31. Perez-Fernandez, R.; Pittelkow, M.; Belenguer, A. M.; Sanders, J. K. M. *Chem. Commun.* **2008**, 1738–1740.
32. Carnall, J. M. A.; Waudby, C. A.; Belenguer, A. M.; Stuart, M. C. A.; Peyralans, J. J.-P.; Otto, S. *Science* **2010**, *327*, 1502–1506.
33. Li, J.; Carnall, J. M. A.; Stuart, M. C. A.; Otto, S. *Angew. Chem. Int. Ed.* **2011**, *50*, 8384–8386.
34. Stefankiewicz, A. R.; Sambrook, M. R.; Sanders, J. K. M. *Chem. Sci.* **2012**, *3*, 2326–2329.
35. Malakoutikhah, M.; Peyralans, J. J.-P.; Colomb-Delsuc, M.; Fanlo-Virgos, H.; Stuart, M. C. A.; Otto, S. *J. Am. Chem. Soc.* **2013**, *135*, 18406–18417.
36. Rasmussen, B.; Sorensen, A.; Gotfredsen, H.; Pittelkow, M. *Chem. Commun.* **2014**, *50*, 3716–3718.
37. Leonetti, G.; Otto, S. *J. Am. Chem. Soc.* **2015**, *137*, 2067–2072.
38. Pal, A.; Malakoutikhah, M.; Leonetti, G.; Tezcan, M.; Colomb-Delsuc, M.; Nguyen, V. D.; van der Gucht, J.; Otto, S. *Angew. Chem. Int. Ed.* **2015**, *54*, 7852–7856.
39. Corbett, P. T.; Leclaire, J.; Vial, L.; West, K. R.; Wietor, J. L.; Sanders, J. K. M.; Otto, S. *Chem. Rev.* **2006**, *106*, 3652–3711.
40. Black, S. P.; Sanders, J. K. M.; Stefankiewicz, A. R. *Chem. Soc. Rev.* **2014**, *43*, 1861–1872.
41. Thomas, J.; Dobrzanska, L.; Sonawane, M. P.; Smet, M.; Maes, W.; Dehaen, W. *Supramol. Chem.* **2014**, *26*, 591–596.
42. Thomas, J.; Reekmans, G.; Adriaensens, P.; Van Meervelt, L.; Smet, M.; Maes, W.; Dehaen, W.; Dobrzanska, L. *Angew. Chem. Int. Ed.* **2013**, *52*, 10237–10240.
43. Mitchell, R. H. *Can. J. Chem.* **1980**, *58*, 1398–406.
44. Thomas, J.; Maes, W.; Robeyns, Ovaere, M.; Van Meervelt, L.; Smet, M.; Dehaen, W. *Org. Lett.* **2009**, *11*, 3040–3043.
45. Thomas, J.; Dobrzanska, L.; Van Hecke, K.; Sonawane, M. P.; Robeyns, K.; Van Meervelt, L.; Wozniak, K.; Smet, M.; Maes, W.; Dehaen, W. *Org. Biol. Chem.* **2012**, *10*, 6526–6536.

46. Thomas, J.; Dobrzanska, Van Meervelt, L.; Quevedo, M. A.; Wozniak, K.; Stachowicz, M.; Smet, M.; Maes, W.; Dehaen, W. *Chem. Eur. J.* **2016**, *22*, 979–987.
47. Takemura, H.; Yoshimura, K.; Khan, I. U.; Shinmyouzu, T.; Inazu, T. *Tetrahedron Lett.* **1992**, *33*, 5775–5778.
48. Takemura, H.; Shinmyouzu, T.; Miyura, H. *J. Inclusion Phenom. Molec. Recognit. Chem.* **1994**, *19*, 193–206.
49. Takemura, H. *J. Inclusion Phenom. Macrocycl. Chem.* **2002**, *42*, 169–186.
50. Thuéry, P.; Nierlich, M.; Vicens, J.; Takemura, H. *J. Chem. Soc., Dalton Trans.* **2000**, 279–283.
51. Chirakul, P.; Hampton, P. D.; Bencze, Z. *J. Org. Chem.* **2000**, *65*, 8297–8300.
52. Hampton, P. D.; Tong, W.; Wu, S.; Duesler, E. N. *J. Chem. Soc.; Perkin Trans. 2*, **1996**, 1127–1130.
53. Takemura, H.; Karyazono, H.; Yasutake, M.; Kon, N.; Tani, K.; Sako, K.; Shinmyouzu, T.; Inazu, T. *Eur. J. Org. Chem.* **2000**, 141–148.
54. Wen, G.; Matsunaga, M.; Matsunaga, T.; Takemura, M.; Shinmyuzo, T. *Synlett* **1995**, 947–948.
55. Grannas, M. J.; Hoskins, B. F.; Robson, R. *J. Chem. Soc., Chem. Commun.* **1990**, 1644–1646.
56. Grannas, M. J.; Hoskins, B. F.; Robson, R. *Inorg. Chem.* **1994**, *33*, 1071–1079.
57. Honzawa, S.; Chiba, S.; Okubo, H.; Yamaguchi, M. *Heterocycles* **2002**, *57*, 1091–1099.
58. Niikura, K.; Anslyn, E. V. *J. Chem. Soc.; Perkin Trans. 2* **1999**, 2769–2775.
59. Ai, L.; Xiao, J.; Shen, X.; Zhang, C. *Tetrahedron Lett.* **2006**, *47*, 2371–2375.
60. Chirakul, P.; Hampton, P. D.; Duesler, E. N. *Tetrahedron Lett.* **1998**, *39*, 5473–5476.
61. Kaewtong, C.; Fuangswasdi, S.; Muangsin, N.; Chaichit, N.; Vicens, J.; Pulkova, B. *Org. Lett.* **2006**, *8*, 1561–1564.
62. Kaewtong, C.; Muangsin, N.; Chaichit, N.; Pulpoka, B. *J. Org. Chem.* **2008**, *73*, 5574–5577.
63. Kaewtong, C.; Jiang, G.; Park, Y.; Fulghum, T.; Baba, A.; Pulpoka, B.; Advincula, R. *Chem. Mat.* **2008**, *20*, 4915–4924.
64. Thuéry, P.; Nierlich, M.; Vicens, J.; Marci, B.; Takemura, H. *Eur. J. Inorg. Chem.* **2001**, 637–643.
65. Khan, S.; Singh, J. D.; Mahajan, R. K.; Sood, P. *Tetrahedron Lett.* **2007**, *48*, 3605–3608.
66. Khan, S.; Maheshwari, M.; Singh, J. D. *Phosphorous Sulfur Silicon Rel. Elem.* **2008**, *183*, 961–965.
67. Thuéry, P.; Nierlich, M.; Vicens, J.; Takemura, H. *Polyhedron* **2000**, *19*, 2673–2678.
68. Jain, R. K.; Tsou, L. K.; Hamilton, A. D. *Tetrahedron Lett.* **2009**, *50*, 2787–2789.
69. Hjelmgaard, T.; Roy, O.; Nauton, L.; El-Ghozzi, M.; Avignant, D.; Didierjean, C.; Taillefumier, C.; Faure, S. *Chem. Commun.* **2014**, *50*, 3564–3567.
70. Evans, L. S.; Gale, P. A. *Chem. Commun.* **2004**, 1286–1287.
71. Mocilac, P.; Gallagher, J. F. *J. Org. Chem.* **2013**, *78*, 2355–2361.
72. Mocilac, P.; Gallagher, J. F. *Acta Cryst B.* **2013**, *69*, 62–69.
73. Mocilac, P.; Gallagher, J. F. *CrystEngCommun* **2014**, *18*, 1893–1903.

# Chapter 17

## Functionalization and Properties of Homooxacalixarenes

Paula M. Marcos

### 17.1 Introduction

Homooxacalixarenes are calixarene analogues in which the  $\text{CH}_2$  bridges are partly or completely replaced by  $\text{CH}_2\text{OCH}_2$  groups [1]. The prefix homooxa implies the presence of additional atoms in the calixarene cyclic framework, of which at least one of them is oxygen. These macrocycles are members of the heteracalixarene class, in which heteroatoms are inserted between the methylene bridges or replace them entirely. The incorporation of oxygen atoms and the higher conformational mobility resulting from the dimethyleneoxa bridges affect the host–guest properties of these compounds compared to their all-carbon analogues.

This chapter presents the developments made in the homooxacalixarene chemistry for the last 15 years (2000–2015), focusing mainly on the functionalization and properties of hexahomotrioxacalix[3]- (**I**), dihomooxacalix[4]- (**II**) and tetrahomodioxacalix[4]arenes (**III**), which have been the most exploited compounds. Examples of bridged homooxacalixarenes are also reported. Studies prior to 2000 were described by Masci [2], and other good reviews are those from Shokova and Kovalev in 2004 [3, 4], and Cragg and coworkers in 2012 [5].

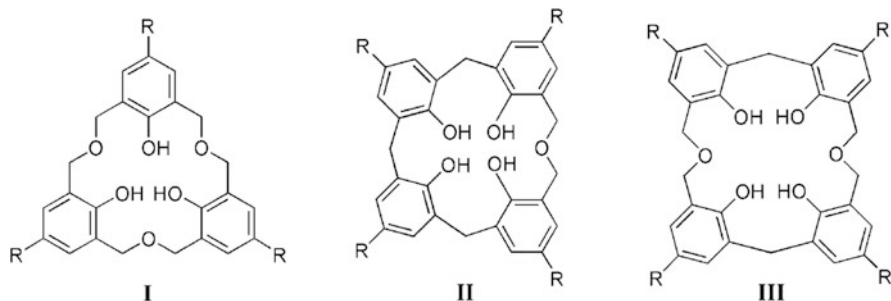
---

P.M. Marcos (✉)

Faculdade de Farmácia da Universidade de Lisboa, Av. Prof. Gama Pinto, 1649-003 Lisbon, Portugal

Centro de Química Estrutural, Faculdade de Ciências da Universidade de Lisboa, Edifício C8, 1749-016 Lisbon, Portugal

e-mail: [pmmarcos@fc.ul.pt](mailto:pmmarcos@fc.ul.pt)

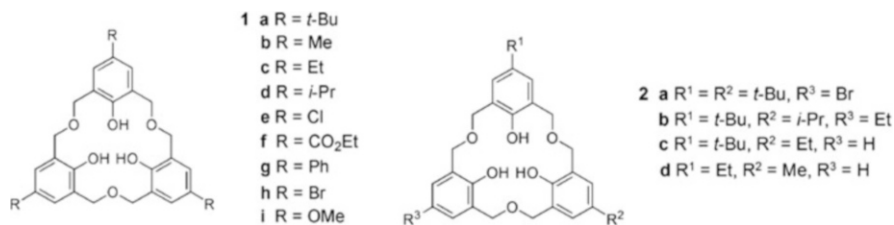


## 17.2 Homooxalix[*n*]arenes (*n* = 3, 4)

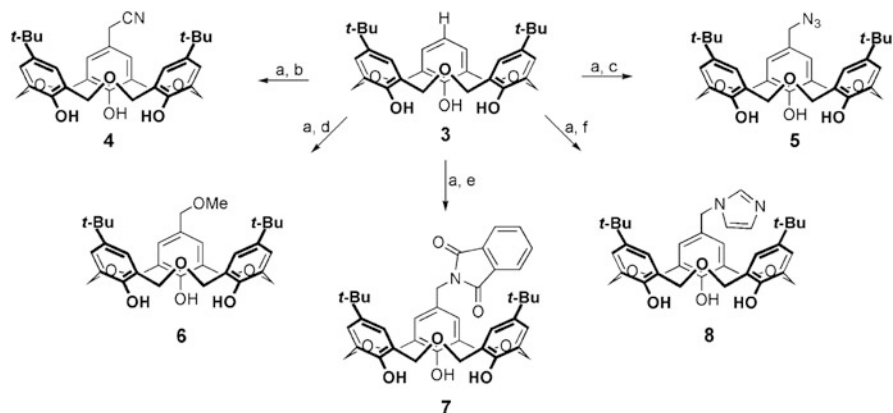
### 17.2.1 Functionalization of the Upper Rim

Removal of the *tert*-butyl groups by a reverse Friedel–Crafts reaction is not applicable to *p*-*tert*-butylhomooxalixarenes due to the fragility of the dibenzyl ether bonds in strongly acidic conditions. The introduction of different functional groups at the upper rim must therefore be done by varying the *p*-substituent in the starting phenol.

Besides the large number of symmetrical hexahomotrioxacalix[3]arene upper rim derivatives (**1a–i**) previously reported [2], asymmetric analogues of **1** were obtained by Fuji and coworkers [6, 7]. Compounds **2** (a few examples are illustrated below), bearing different substituents on their upper rims, were prepared by a stepwise synthesis based on the cyclization of the corresponding linear trimers under acidic high-dilution conditions. This procedure was later improved [7], involving a condensation reaction between *p*-substituted phenol dimers and a monomer. These methods have been useful in the preparation of chiral homooxalix[3]arenes.



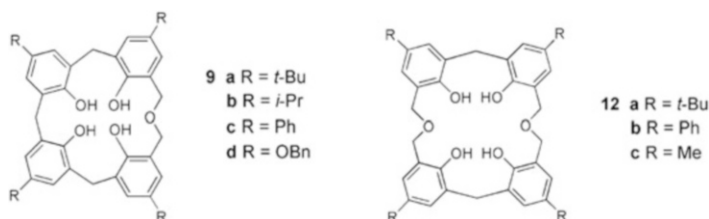
As an extension of the previous work, the Fuji group [8] introduced several functional groups on the upper rim of hexahomotrioxacalix[3]arenes. Selective debromination of **2a** under formic acid reduction conditions yielded the mono-unsubstituted derivative **3**, which allowed the direct introduction of several new groups in the vacant *para*-position (Scheme 17.1). Through a four step synthesis



**Scheme 17.1** Reaction conditions: (a)  $\text{Me}_2\text{NH}$ ,  $\text{CH}_2\text{O}$ ,  $\text{AcOH}$ ,  $80^\circ\text{C}$ , then  $\text{MeI}$ ,  $\text{DMSO}$ ; (b)  $\text{NaCN}$ ; (c)  $\text{NaN}_3$ ; (d)  $\text{NaOMe}$ ; (e) potassium phthalimide; (f) imidazole

(the Mannich reaction, methylation, *p*-quinonemethide formation and nucleophilic substitution) **3** was converted to the cyano (**4**), azide (**5**), methoxide (**6**), phthalimide (**7**) and imidazole (**8**) derivatives in reasonable yields (45–59%).

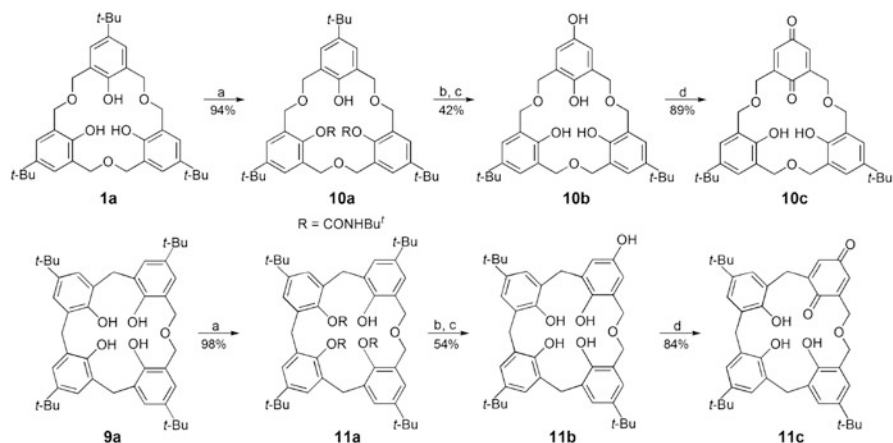
In the case of dihomooxalix[4]arenes (**9**), *tert*-butyl, *isopropyl* [**9**], phenyl [**10**] and benzyloxy [**11**] upper rim substituents have been reported. Recently, the “all-but-one” carbamatation methodology was successfully applied to homooxa compounds **1a** and **9a** [**12**], allowing the introduction of a single *para*-OH group (monohydroquinones **10b** and **11b**, respectively) and its subsequent transformation into the corresponding monoquinones (**10c** and **11c**), as shown in Scheme 17.2.



Tetrahomodioxalix[4]arenes (**12**) bearing *tert*-butyl, phenyl [**10**] and methyl [**13**] groups have been the only upper rim derivatives reported.

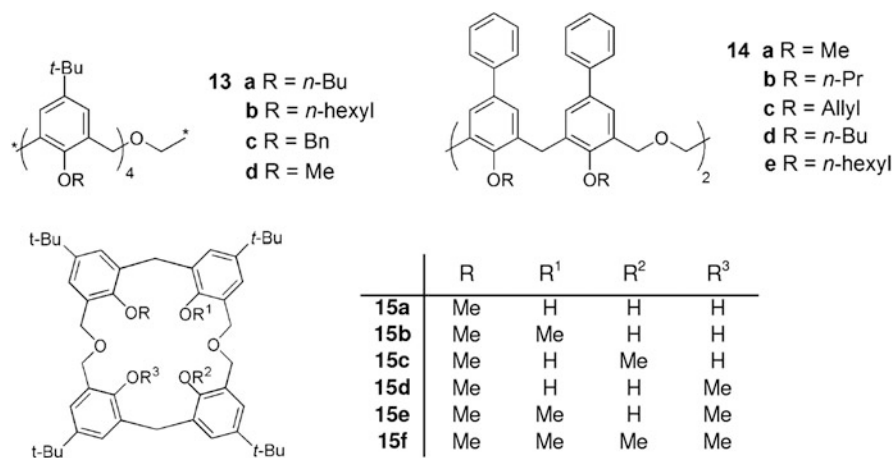
### 17.2.2 Functionalization of the Lower Rim

Modification of the homooxalixarene lower rim has been achieved by alkylation reactions with simple alkyl halides or functionalized alkylating agents.



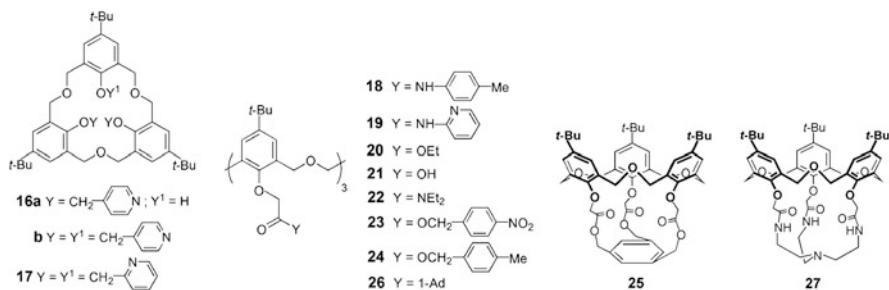
**Scheme 17.2** Reaction conditions: (a) *t*-BuNCO, Ba(OH)<sub>2</sub>·8H<sub>2</sub>O, CH<sub>2</sub>Cl<sub>2</sub>, rt; (b) PbO<sub>2</sub>, HClO<sub>4</sub> (aq) 70%, CH<sub>2</sub>Cl<sub>2</sub>/acetone, rt; (c) LiAlH<sub>4</sub>, THF<sub>anh</sub>/CH<sub>2</sub>Cl<sub>2anh</sub>, rt; (d) Activated MnO<sub>2</sub>, CH<sub>2</sub>Cl<sub>2</sub>, rt, 1 h

Since 2000, only dihomooxa and tetrahomodioxas alkyl ether derivatives have been reported. Treatment of **9a** with an excess of the corresponding alkyl iodide in THF/DMF in the presence of NaH yielded *n*-butyl (**13a**) [14] and *n*-hexyl (**13b**) [15] ethers mainly in the cone conformation [16]. By a similar NaH promoted alkylation reaction, tetrahomodioxas tetra alkyl ethers **14a–e** in the 1,4-alternate conformation were obtained [17]. The whole set of partially *O*-methylated derivatives (**15a–f**) of tetrahomodioxas **12a** was obtained by Masci and coworkers [18]. Four of the five compounds presented the 1,4-alternate conformation in the solid state (**15b** assumed a partial cone conformation), and in solution the cone/1,4-alternate ratio decreased on increasing the number of methoxy groups.

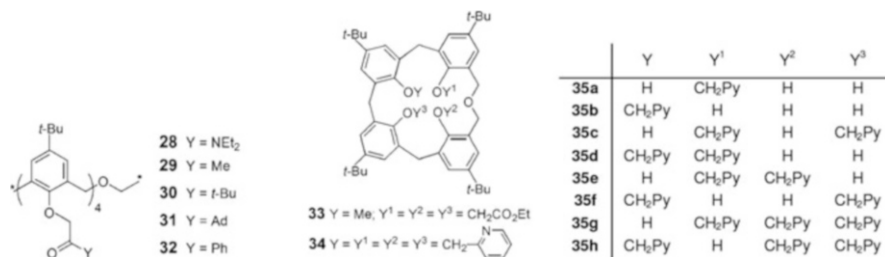




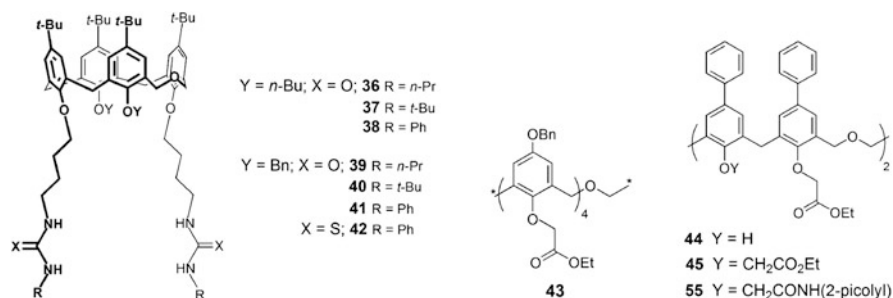
Alkylating agents of the type  $XCH_2Y$  (where X is a leaving group and Y is a functional group) have also been used to introduce different groups into the lower rim of homooxalixarenes. The reaction of **1a** with 4-(chloromethyl)pyridine gave di- (**16a**) and tri-substituted (**16b**) compounds in cone or partial cone conformations, depending on the base used [19], a similar result to the one described for the alkylation reaction with 2-(chloromethyl)pyridine (compound **17**) [20]. Hexahomotrioxa derivatives containing the carbonyl group, namely amide, ester and ketone, have been reported. Toluidinylamide **18** and 2-pyridylamide **19** were prepared in both conformations through the intermediate products partial cone ethyl ester **20** and partial cone carboxylic acid **21** or cone diethylamide **22** and cone carboxylic acid, respectively [21]. The *p*-nitrobenzyl ester **23** was synthesised in the partial cone conformation [22], while *p*-methylbenzyl ester **24** [23], a triply bridged capped analogue **25** [23] and 1-adamantyl ketone **26** [24] were obtained with  $C_3$ -symmetry. Recently, a hexahomotrioxacalix[3]cryptand (**27**) was synthesised from the cone ethyl ester **20** and *tris*-(2-amino-ethylamine), and its crystal structure was determined indicating a cone conformation [25].



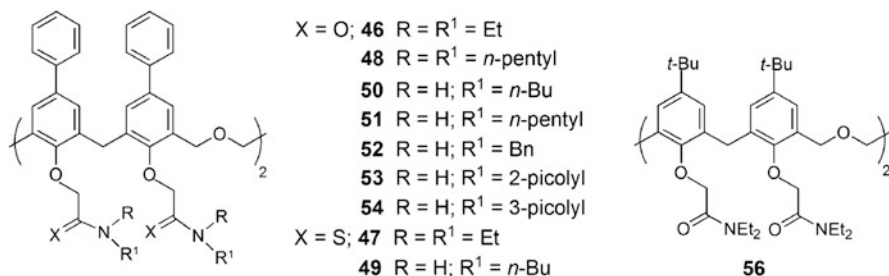
Besides dihomooxalix[4]arenes bearing carbonyl groups at their lower rims (**28–32**) reported before 2000 [26, 27], **9a** has been used to prepare the inherently chiral triethyl ester **33** [28] and the tetra(2-pyridyl) **34** [29] derivatives. Depending on the reaction conditions (use of 80 % NaH instead of 95 % NaH and less reaction time), partial *O*-alkylation of **9a** with 2-(chloromethyl)pyridine hydrochloride was also achieved by Marcos and coworkers [29]. Five of the eight possible partially alkylated compounds **35** (mono-substituted **35b** and di-substituted **35c–f**) were obtained in the cone conformation. Recently, the same group reported the preparation of a series of bidentate urea (**36–41**) and thiourea (**42**) derivatives in a four step synthesis from the parent compound **9a** [30, 31]. Their structure determination in solution by NMR spectroscopy (and in the solid state for compounds **38** and **41** by single crystal X-ray crystallography) indicated the cone conformation for all the compounds. The cone tetraethyl ester **43** was also described [11].



Alkylation reactions of the tetrahomodioxacalix[4]arene **12b** with polyfunctional reagents have been extensively studied by No and coworkers. Selective 1,3-di-*O*-alkylation gave the asymmetrically substituted ester **44** in the cone conformation [32]. Total modification of the lower rim of **12b** afforded ethyl ester **45** [33], diethyl (thio)amides **46** [34] and **47** [35], dipentyl amide **48** [36] and monobutyl thioamide **49** [35], all in the 1,4-alternate conformation, while monobutyl- and monopentyl-amides **50** [35] and **51** [36] presented the 1,3-alternate conformation (the latter was also obtained in the 1,4-alternate conformation). According to No and coworkers [35], the 1,3-alternate conformation is more stable due to intramolecular hydrogen bonding between the NH group and the facing oxygen atom of the carbonyl group. X-ray crystallographic data corroborated this conformation in the case of **50**. A series of benzyl, 2-picolyl and 3-picolyl amides (**52–54**) in the 1,4-alternate conformation were reported, as well as a di-substituted compound **55** with two 2-picolyl amides and two ethyl ester groups [37].



In 2007, Yamato and coworkers [38] obtained the 1,4-alternate conformer of the diethyl amide **56** as the major product of the alkylation reaction of tetrahomodioxacalix[4]arene **12a** and *N,N*-diethylchloroacetamide in the presence of NaH.



## 17.2.3 Binding Properties

### 17.2.3.1 Ammonium Cations

The structural features of hexahomotrioxacalix[3]arenes, namely a cavity formed by a 18-membered ring, only two basic conformations and  $C_3$ -symmetry, make them suitable macrocycles to bind ammonium cations. The binding properties of amide derivatives **18** and **19** towards butylammonium ions have been investigated using the picrate extraction method [21]. Cone-**19** showed a higher affinity for  $n\text{-BuNH}_3^+$  (38 %) than cone-**18** (19 %), while both compounds exhibited no binding ( $\leq 2\%$ ) to  $i\text{-BuNH}_3^+$  and  $t\text{-BuNH}_3^+$ . Partial cone amides also displayed no affinity to these three cations. These amides showed low efficiency compared to diethylamide **22** (98 % and 93 % with  $n\text{-BuNH}_3^+$  for cone and partial cone, respectively). Extraction experiments with  $n\text{-BuNH}_3^+$  picrate were carried out and showed very high extractabilities ( $>90\%$ ) for ester ligand **24** and its capped analogue **25** [23]. Association constants for the 1:1 complexes in  $\text{CH}_2\text{Cl}_2/\text{THF}$  gave a higher value for the capped and more preorganized **25** than to the uncapped **24** ( $7.64 \times 10^4$  and  $2.21 \times 10^4 \text{ M}^{-1}$ , respectively). Ammonium cations carrying fluorescent groups such as pyrene, fluorene, naphthalene or anthracene were bound to ester ligand **23**, resulting in quenching of the fluorescence [22].

Complexation studies of linear ( $n\text{-BuNH}_3^+$ ) and branched ( $t\text{-BuNH}_3^+$ ,  $s\text{-BuNH}_3^+$  and  $i\text{-PrNH}_3^+$ ) alkylammonium cations by the conformationally blocked cone dihomooxa benzyl ether **13c** in the presence of the weakly coordinating tetrakis [3,5-bis(trifluoromethyl)phenyl]-borate ( $\text{TFPB}^-$ ) anion were reported [15]. The *endo*-cavity complexation was evidenced by the alkyl group resonances in the negative region of the  $^1\text{H}$  NMR spectrum. For the branched and chiral  $s\text{-BuNH}_3^+$  guest, the complex formed was asymmetric, indicating chirality transfer from the guest to the host, and resulting in a chiral supramolecule. Association constants for all the guests with **13c** were determined in  $\text{CDCl}_3$ :  $5.5 \times 10^6$ ,  $3.1 \times 10^4$ ,  $3.6 \times 10^4$  and  $7.6 \times 10^4 \text{ M}^{-1}$ , respectively. The binding of di-*n*-alkylammonium- $\text{TFPB}$  salts (di- $\text{EtNH}_2^+$ , di- $\text{PrNH}_2^+$  and di-pentyl $\text{NH}_2^+$ ) with **13b** and **13c** was also evaluated and showed that the 18-membered dihomooxalix[4]arene macrocycle cannot give the *through-the-annulus* threading with them because of its small dimensions

[15]. However, these cations gave rise to a fast exchange *endo*-cavity complexation driven by hydrogen bonding between the nitrogen atom of the guests and the oxa bridge of the hosts. Association constants in  $\text{CDCl}_3$  were also obtained for the complexes with **13b**:  $6.0 \times 10^5$ ,  $3.4 \times 10^3$  and  $4.5 \times 10^3 \text{ M}^{-1}$ , respectively. In a related study [39], the conformationally mobile dihomooxa methyl ether **13d** was able to form *endo*-complexes with the linear  $n\text{-BuNH}_3^+$  and branched  $s\text{-BuNH}_3^+$  and  $i\text{-PrNH}_3^+$  cations preferentially in a cone conformation through an induced fit process, mainly driven by H-bonds between the guest ammonium group and the host oxa bridge, and cation- $\pi$  interactions. In addition, 1D and 2D NMR studies revealed the existence of other minor complexes with **13d** in conformations different than the cone.

Binding studies in  $\text{CDCl}_3$  of quaternary ammonium ions ( $\text{Me}_4\text{N}^+$ ,  $\text{Et}_4\text{N}^+$ , *N*-methylpyridinium and acetylcholine) with tetrahomodioxo parent **12a** and all the methyl ether derivatives **15** showed the importance of intramolecular hydrogen bonding on the conformation of the free and complexed ligands [18]. As mentioned before, on increasing the number of methoxy groups and decreasing the number of hydrogen bonds, the cone conformation becomes relatively less stable but deeper, thus more effectively surrounding the small organic cations. The highest association constants were obtained with  $\text{Me}_4\text{N}^+$ , ranging from  $7.4 \times 10^2 \text{ M}^{-1}$  for **15c** to  $15 \text{ M}^{-1}$  for **12a**. Two-phase ammonium picrate extraction studies carried out with ligands **45–55** exhibited very low affinity for  $\text{NH}_4^+$  (<8%), except for dipentyl amide **48** (21%) [36] and 2-picolyl amide **53** (28%) [37]. In the case of diethyl amide **46** contradictory values (3–4% [34, 35] and 64% [36]) were found in the literature.

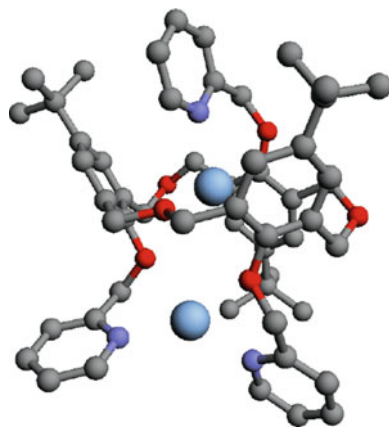
### 17.2.3.2 Metal Cations

The ionophoric properties of derivatives **18**, **19**, **24** and **25** towards alkali and transition metal cations were evaluated by extraction experiments from alkaline aqueous picrate solutions to  $\text{CH}_2\text{Cl}_2$ . Both cone and partial cone **18** showed no affinity to any of the cations due to intramolecular hydrogen bonding between the neighbouring NH and CO groups [21]. The same lack of affinity was observed for ligand **19**, although it displayed high extraction percentage for transition metal ions  $\text{Al}^{3+}$ ,  $\text{Cu}^{2+}$  and mainly  $\text{Ag}^+$  (77% for cone and 31% for partial cone), suggesting the interaction of the pyridyl nitrogen atoms with the soft cation. Capped compound **25** showed higher extractability than its uncapped analogue **24** [23]. Association constants of  $6.71 \times 10^4$  and  $2.20 \times 10^4 \text{ M}^{-1}$  were obtained in  $\text{CH}_2\text{Cl}_2/\text{THF}$  for **25** and **24** with  $\text{K}^+$ , respectively. Liquid-liquid extraction data of alkali, alkaline earth, transition, heavy and lanthanide metal cations with ligands **22** [40, 41] and **26** [24] were reported. These studies, performed with neutral aqueous picrate solutions, indicated that both ligands show similar extraction profiles, although **22** is a much stronger extractant than **26**. Both exhibit a selectivity peak for  $\text{Na}^+$  (50 and 20% for **22** and **26**, respectively) and **22** displays also high percentages for  $\text{Ba}^{2+}$  (55%),  $\text{Ni}^{2+}$  (45%),  $\text{Ag}^+$  (40%) and  $\text{Pb}^{2+}$  (80%). Concerning lanthanide ions, ketone **26** is a

poor extractant ( $\leq 7\%$ ), while amide **22** clearly discriminates between the light and heavy lanthanides, with the former (34 % for  $\text{Ce}^{3+}$ ,  $\text{Pr}^{3+}$  and  $\text{Nd}^{3+}$ ) preferred over the latter (13 % for  $\text{Er}^{3+}$  and  $\text{Yb}^{3+}$ ). In methanol, using chloride salts, 1:1 stability constants gave the same positive discrimination for the light lanthanides ( $\log \beta = 5.5$  and 3.4 for  $\text{La}^{3+}$  and  $\text{Yb}^{3+}$ , respectively) [41]. The complexation process was shown to be governed by entropy changes only. The metal cation binding ability of the cone tricarboxylic acid **21** was evaluated by NMR and UV-visible spectrometry [42]. Proton NMR studies indicated that **21** strongly interacts with  $\text{Na}^+$ ,  $\text{K}^+$ ,  $\text{Ag}^+$  and  $\text{Pb}^{2+}$  and that the cations should be encapsulated in the cavity defined by the phenoxy and carbonyl oxygen atoms [42]. Transport experiments involving an aqueous/chloroform/aqueous system demonstrated that **21** actively transports  $\text{Cr}^{3+}$ ,  $\text{Fe}^{3+}$ ,  $\text{Co}^{2+}$  and  $\text{Cu}^{2+}$  through the organic phase.

Cone and partial cone derivatives **17** bearing nitrogen donor atoms on the lower rim have also been tested as ionophores towards a large variety of metal cations [43, 44]. Extraction studies from neutral aqueous picrate solutions to  $\text{CH}_2\text{Cl}_2$  showed that the partial cone conformer is the best phase transfer agent for all the cations studied, although the cone is a slightly better binder. Both conformers displayed very high stability constants for the soft and intermediate cations  $\text{Pb}^{2+}$ ,  $\text{Cd}^{2+}$ ,  $\text{Zn}^{2+}$  and  $\text{Ni}^{2+}$ , as well as for the heavy lanthanide  $\text{Yb}^{3+}$  (ML species,  $\log \beta \geq 7$  in MeCN). High  $\log \beta$  values were also reported for  $\text{Ca}^{2+}$  (6.76 and 6.2 for cone and partial cone, respectively). Proton NMR and DFT studies indicated that, for binding between partial cone **17** and  $\text{Ag}^+$ , the  $\text{M}_2\text{L}$  complex was more stable than the ML complex [43]. According to these results, one  $\text{Ag}^+$  ion is encapsulated into the upper rim cavity composed by two benzene rings and one pyridyl group of the inverted phenyl unit that is turned inward, through metal–nitrogen and cation– $\pi$  interactions, while the second  $\text{Ag}^+$  ion is bound into the lower rim cavity through metal–nitrogen and metal–oxygen interactions, as illustrated in Fig. 17.1.

**Fig. 17.1** Optimized DFT structure for the partial cone-**17**·( $\text{Ag}^+$ )<sub>2</sub> metal complex. All hydrogens were removed for clarity [43]



The complexing ability of dihomooxa compounds containing the carbonyl group (**28–33**) towards a large variety of metal cations has been reported. Extraction studies using the same conditions as described above showed that triester **33** possessing only six donating sites is a weak extractant, while transport experiments with metal picrates through a  $\text{CH}_2\text{Cl}_2$  membrane indicated that **33** is a good carrier for the alkali cations, for  $\text{Ba}^{2+}$  and mainly for  $\text{Ag}^+$ , exhibiting the highest transport rate ( $4.7 \mu\text{mol h}^{-1}$ ) among all the cations studied [28, 45]. Extraction and stability constant data indicated that partial cone methylketone **29** is a poor binder for all the cations studied [46, 47]. In contrast, cone ketones **30–32** are good binders, showing a selectivity plateau for  $\text{Na}^+$  and  $\text{K}^+$  (%  $E$  ranges from 68 to 85;  $\log \beta$  in MeOH ranges from 5.00 to 6.53) and a selectivity peak for  $\text{Ba}^{2+}$  [46]. Concerning transition metal cations, these derivatives are reasonable binders, displaying preference for  $\text{Cu}^{2+}$ , while towards heavy metal cations they are stronger, showing a high affinity for  $\text{Ag}^+$  (%  $E$  ranges from 74 to 80;  $\log \beta$  in MeOH ranges from 3.4 to 5.36) and  $\text{Pb}^{2+}$  [47]. The nature of the substituents attached to the ketone function evidenced some influence on their binding properties, with phenyl ketone **32** being a slightly weaker binder than *tert*-butyl ketone **30** and adamantyl ketone **31**, according to the basicity of their carbonyl oxygens. Transport data [46, 47] indicated that ketones **30–32** are reasonable neutral carriers displaying, in general, transport rate sequences reversed of those shown in extraction and complexation. As observed for calix[4]arene derivatives, the presence of the tertiary amide group in dihomooxa ligand **28** also enhances its binding ability compared to the previous ketones. Cone amide **28** showed very high affinities for several cations, including  $\text{Na}^+$ ,  $\text{K}^+$ ,  $\text{Ca}^{2+}$ ,  $\text{Ba}^{2+}$ ,  $\text{Mn}^{2+}$ ,  $\text{Ag}^+$ ,  $\text{Cd}^{2+}$  and  $\text{Pb}^{2+}$  (%  $E$  ranges from 76 to 99;  $\log \beta$  in MeOH ranges from 5.0 to 7.23) [48]. Concerning lanthanides, **28** is a very strong binder, displaying some preferences in extraction for the lighter cations from  $\text{La}^{3+}$  to  $\text{Eu}^{3+}$  (%  $E$  = 69–75) and the highest stability constants ever found with this ligand ( $\log \beta$  = 8.6 for  $\text{Yb}^{3+}$  and 9.2 for  $\text{Pr}^{3+}$ , in MeOH) [41].

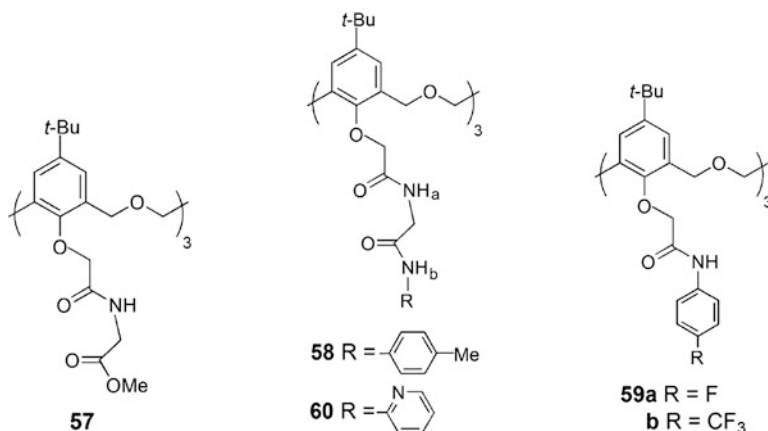
The binding properties of cone 2-pyridylmethoxy derivative **34** were also established by extraction studies and stability constants measurements in MeOH and MeCN. The results indicated that **34** is a weak binder towards the hard alkali and alkaline earth metal ions, although a high  $\log \beta$  value ( $\geq 7$ ) in MeCN was reported for  $\text{Ca}^{2+}$  [49]. In the case of transition and heavy metal cations, **34** displayed a high affinity for the soft metal ions  $\text{Ag}^+$  (%  $E$  = 90;  $\log \beta$  = 4.79 in MeCN) and  $\text{Hg}^{2+}$ , but also for those of intermediate nature,  $\text{Pb}^{2+}$  (%  $E$  = 40;  $\log \beta$  = 5.3 in MeCN) and  $\text{Cu}^{2+}$  [49], while it showed the highest stability constants for the heavy lanthanides as  $\text{Yb}^{3+}$  ( $\log \beta \geq 7$  in MeCN) [44].

Extraction data for some alkali, alkaline earth,  $\text{Ag}^+$  and  $\text{Pb}^{2+}$  cations with tetrahomodioxo derivatives **45–51** were reported [34–36]. The results showed no metal cation affinity for ester **45** and the monoamides **50** and **51**. In the latter case, the presence of intramolecular hydrogen bonding between NH and CO groups decreases the metal ion binding ability. Tertiary amides **46** and **48** are better

extractants, mainly for  $\text{Ag}^+$  and  $\text{Pb}^{2+}$ , and thioamides **47** and **49** showed selectivity for the soft  $\text{Ag}^+$  ion. Extraction results obtained with amide derivatives **52–54** [37] indicated that 2-picolyl amide **53** is the best phase transfer agent for most metal cations, showing some preference for  $\text{Pb}^{2+}$ ,  $\text{Sr}^{2+}$  and  $\text{Ba}^{2+}$  and a selectivity peak for  $\text{Ag}^+$ . In the case of diethylamide **56** [38], two-phase solvent extraction data indicated a strong affinity for the alkali metal cations and  $\text{Ag}^+$ , but no significant selectivity among them.

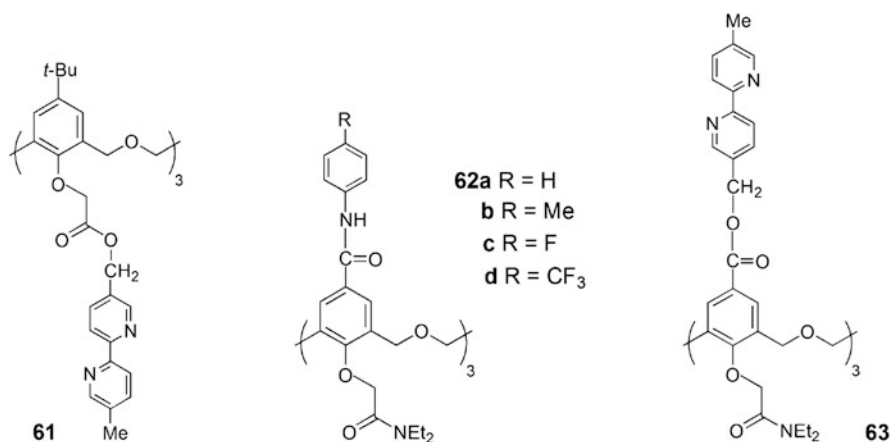
### 17.2.3.3 Ditopic Receptors for Anions and Ion Pairs

To obtain anion recognition, many neutral receptors take advantage of hydrogen bond donor groups, such as amides, ureas and thioureas. Some of these receptors are able to simultaneously bind the cation and the anion of a given ion pair. This ion pair recognition is a cooperative process, as the binding of one ion enhances the binding of the other. The anion complexation of receptor **18** and of the related compounds **57–59** was studied by  $^1\text{H}$  NMR titration experiments in  $\text{CDCl}_3$  [21, 50, 51]. These amides bind halides ( $\text{Cl}^-$  and  $\text{Br}^-$ ) through hydrogen bonding interactions, but only in the presence of the *n*-butylammonium cation. The complexation of  $n\text{-BuNH}_3^+$  through the  $\pi$ -cavity induces conformational changes of the host, which will break the intramolecular hydrogen bonding between the neighbouring NH and CO groups, allowing the anion complexation by the amide NH hydrogens. These compounds behave as heteroditopic receptors, as they complex simultaneously  $\text{X}^-$  and  $n\text{-BuNH}_3^+$ . The binding data indicated a preference for  $\text{Cl}^-$  over  $\text{Br}^-$  with the highest association constants for electron-withdrawing substituents **59** ( $K_{\text{ass}} = 10,655$  and  $13,450 \text{ M}^{-1}$  for  $\text{Cl}^-$ , and  $2450$  and  $3120 \text{ M}^{-1}$  for  $\text{Br}^-$  with **59a** and **59b**, respectively). The smallest  $K_{\text{ass}}$  values ( $536$  and  $230 \text{ M}^{-1}$  for  $\text{Cl}^-$  and  $\text{Br}^-$ , respectively) shown by receptor **58** may be due to reduced electrostatic interactions between  $n\text{-BuNH}_3^+$  and  $\text{X}^-$  ions arising from the longer distance, as anion complexation occurs at the *p*-methylphenyl amide moiety ( $\text{NH}_b$  group).



Due to strong intramolecular hydrogen bonding between NH and CO groups the affinity of receptor **19** and of the related **60** to metal cations was weakened, as mentioned before. However, both derivatives can bind  $n\text{-BuNH}_3^+$  and  $\text{Ag}^+$  cations through cation– $\pi$  interactions and the pyridyl groups, respectively. In a recent study [52], it was reported that they can act as heteroditopic receptors, binding both cations at the same time. In addition, the results indicated that cone-**60** can simultaneously bind  $\text{Ag}^+$ ,  $n\text{-BuNH}_3^+$  and  $\text{Cl}^-$  (or  $\text{Br}^-$ ) ions and that  $n\text{-BuNH}_3^+$  complexation, inducing conformational changes in the macrocycle, is a prerequisite for the anion complexation. Compound **61**, bearing the 2,2'-bipyridyl moiety, was also reported as a ditopic receptor [53]. One nitrogen atom in the bipyridine rings turns from outside to the inside of the cavity to interact with  $\text{Ag}^+$ , while the  $n$ -butylammonium ion is bound through the  $\pi$ -cavity.

The binding properties of cone receptors **62a–d**, containing secondary amides on the upper rim and tertiary amides on the lower rim, towards chloride, bromide, acetate and benzoate anions were investigated by  $^1\text{H}$  NMR experiments in  $\text{CDCl}_3/\text{CD}_3\text{CN}$  (10:1) using TBA salts [54]. The highest association constants were obtained for **62d**, which showed preference for the trigonal planar oxoanions  $\text{BzO}^-$  and  $\text{AcO}^-$  over the spherical halides  $\text{Cl}^-$  and  $\text{Br}^-$  ( $K_{\text{ass}} = 3307, 1085, 396$  and  $168 \text{ M}^{-1}$  for  $\text{BzO}^-$ ,  $\text{AcO}^-$ ,  $\text{Cl}^-$  and  $\text{Br}^-$ , respectively). A significant increase in the anion binding ability was observed when the  $\text{Li}^+$  cation was complexed at the lower rim ( $K_{\text{ass}} = 5123$  and  $3289 \text{ M}^{-1}$  for  $\text{Cl}^- + \text{Li}^+$  and  $\text{Br}^- + \text{Li}^+$ , respectively). This positive cooperative binding was attributed to allosteric and electrostatic effects. Receptor **63**, bearing the 2,2'-bipyridyl moiety at the upper rim linked by a carbonyl group and  $N,N$ -diethylacetamide unit at the lower rim, was obtained and showed the ability to bind two alkali metal cations and a transition metal cation in a cooperative mode [55].  $^1\text{H}$  NMR studies in  $\text{CDCl}_3/\text{CD}_3\text{CN}$  indicated that this heterotritopic receptor binds  $\text{Li}^+$  at the lower rim, and  $\text{Na}^+$  and  $\text{Ag}^+$  at the upper rim.





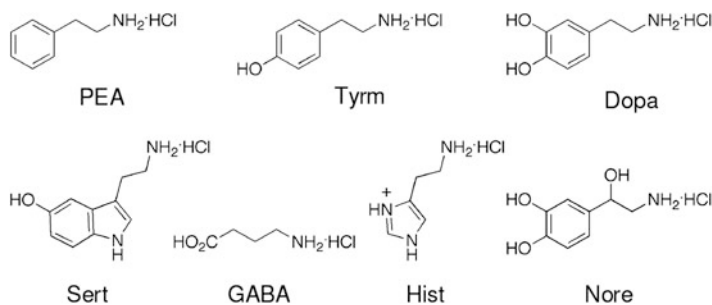


**Fig. 17.2** Structures of the monoamine neurotransmitters and trace monoamines tested as the corresponding hydrochlorides: 2-phenylethylamine (*PEA*), tyramine (*Tyrm*), dopamine (*Dopa*), serotonin (*Sert*),  $\gamma$ -aminobutyric acid (*GABA*), histamine (*Hist*) and norepinephrine (*Nore*)

The binding properties of dihomooxa receptors **36–42** towards spherical, linear, trigonal planar and tetrahedral anions were assessed by <sup>1</sup>H NMR titrations in CDCl<sub>3</sub> and using TBA salts [30, 31]. The results showed that the association constants strongly depend on the nature of the substituent (alkyl/aryl) at the urea moiety and decrease with decreasing anion basicity. Ph-urea **38** [30] is the best anion receptor, showing the strongest complexation for F<sup>-</sup> (log  $K_{\text{ass}} = 3.10$ ) and also high binding affinity for the carboxylates AcO<sup>-</sup> and BzO<sup>-</sup> (log  $K_{\text{ass}} = 2.88$  and 2.93, respectively). F<sup>-</sup>, AcO<sup>-</sup>, BzO<sup>-</sup> and H<sub>2</sub>PO<sub>4</sub><sup>-</sup> were the best bound anions by Ph-urea **41** and Ph-thiourea **42** [31]. Despite the increased acidity of its NH groups, thiourea **42** was in general a weaker receptor than urea **41**. Steric interactions between the large sulfur atom and the phenyl group destabilize the cis geometry required for the anion chelation [56]. Thioureas are thus less preorganized than ureas and consequently energetically less favourable.

Bidentate ureas **38** and **41** were tested as heteroditopic receptors for *n*-butylammonium halides (Cl, Br and I) by <sup>1</sup>H NMR titrations in CDCl<sub>3</sub> [57]. The *n*-BuNH<sub>3</sub><sup>+</sup> cation inclusion inside the dihomooxa cavity was demonstrated by the appearance of the alkyl group resonances at negative chemical shifts, while simultaneous anion halide binding to the urea moiety was shown by the downfield shifts observed for the NH resonances. All host-guest ternary systems studied displayed very high percentages of complexation ( $\geq 95\%$  corresponding to  $K_{\text{ass}} > 10^9 \text{ M}^{-2}$ ). These derivatives were also evaluated as heteroditopic receptors for monoamine neurotransmitter and trace amine hydrochlorides (Fig. 17.2). <sup>1</sup>H NMR experiments in CDCl<sub>3</sub>/CD<sub>3</sub>OD (10:1) at 233 K indicated that **38** is slightly more efficient than **41**, but both show selectivity towards phenylethylamine and tyramine over the other amines, by five to tenfold (Table 17.1). The lower association constants observed in the case of the aliphatic neurotransmitter  $\gamma$ -aminobutyric acid (GABA) suggest that  $\pi$ - $\pi$  interactions play a key role in the binding process between these receptors and those guests.

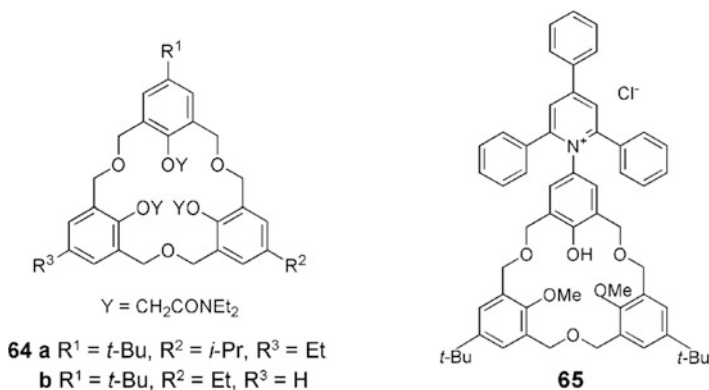
**Table 17.1** Percentages of complex formation and corresponding  $K_{\text{ass}}$  ( $\text{M}^{-2}$ )<sup>a</sup>

	PEA	Tyrm	Dopa	Sert	GABA	Hist.	Nore
38	86.0 %	85.0 %	67.3 %	61.2 %	62.7 %	— <sup>b</sup>	— <sup>b</sup>
	41,000	36,000	6300	4100	4500		
41	83.4 %	81.0 %	62.7 %	59.7 %	59.9 %	— <sup>b</sup>	— <sup>b</sup>
	30,000	23,000	4500	3700	3700		

<sup>a</sup> $\text{CDCl}_3/\text{CD}_3\text{OD}$  (10:1, v/v), 233 K<sup>b</sup>No complexation observed

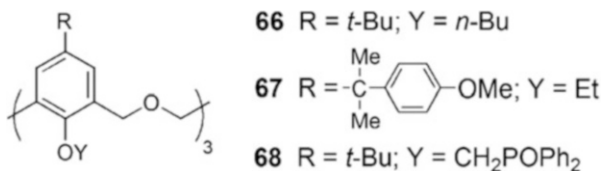
### 17.2.4 Other Applications

Besides the well-known applications of hexahomotrioxacalix[3]arenes as effective hosts for fullerenes [5, 58], other relevant applications have been reported since 2000. Chiral cones **64a–b** were prepared from the corresponding triphenol **2b** and **2c**, and in the case of **64b** both of its enantiomeric forms were separated using a chiral HPLC column [59]. <sup>1</sup>H NMR studies suggested that optically active **64b** can discriminate the enantiomers of phenylalanine ethyl ester hydrochloride. Another asymmetric derivative (**65**), bearing a pyridinium *N*-phenolate dye on the upper rim, was synthesised [60]. Compound **65** contains a proton-ionizable phenol group that acts as a chemical switch to generate colour change in the presence of alkali cations and amines. Small association constants were obtained with various types of amines, although **65** was able to differentiate among primary, secondary and tertiary amines ( $K_{\text{ass}} = 135.7, 43.8$  and  $7.6 \text{ M}^{-1}$  for *n*-hexNH<sub>2</sub>, (*i*-Pr)<sub>2</sub>NH and Et<sub>3</sub>N, respectively).



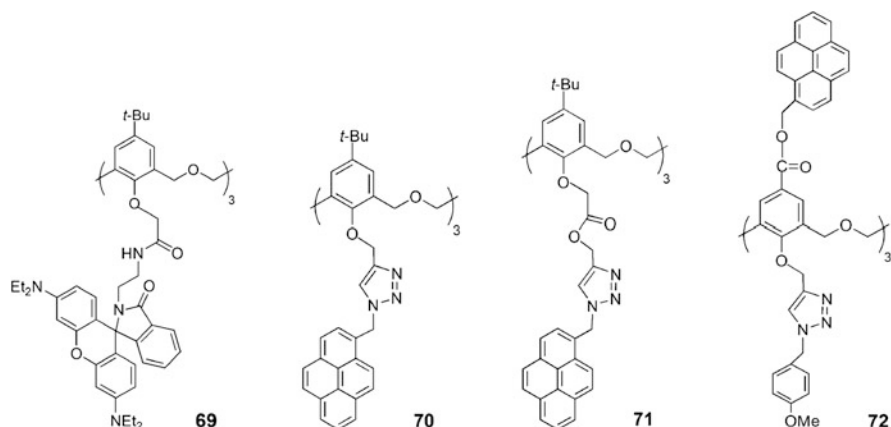
In the field of analytical sensors, homooxacalixarenes have been used in the preparation of ion-selective electrodes. Among hexahomotrioxa derivatives, *n*-butyl ether **66** [61] was incorporated into a PVC liquid membrane resulting a

very selective electrode for dopamine against other catecholamines, such as adrenaline and noradrenaline and also against  $\text{Na}^+$  and  $\text{K}^+$  cations. Subsequently, an electrode based on an ionophore (**67**) containing an ether group at the lower rim and a lipophilic moiety at the upper rim, displayed greater selectivity for serotonin than for other biogenic amines, as well as for organic and inorganic cations [62]. Moreover, this electrode was used to monitor in situ the accumulation of serotonin in liposomes induced by a proton gradient. Lead-selective electrodes based on phosphorylated derivative **68** [63] and diethylamides **22** and **28** [64] were reported. **68** gave a good Nernstian response of 29.7 mV/decade over a concentration range of  $1 \times 10^{-8}$  M to  $1 \times 10^{-4}$  M, showed high selectivity for  $\text{Pb}^{2+}$  when tested in mixtures containing several mono-, di-, tri- and tetra-valent ions and was successfully used as an indicator electrode for a potentiometric titration of a lead solution with a standard solution of EDTA. The performances of ISEs incorporating the ionophores **22** and **28** and using different plasticizers (DEHA, *o*-NPOE and BBPA) towards a large variety of cations were tested [64]. Both compounds displayed the best results for  $\text{Pb}^{2+}$  and in the presence of DEHA (30.5 and 28.8 mV/decade for **22** and **28**, respectively).

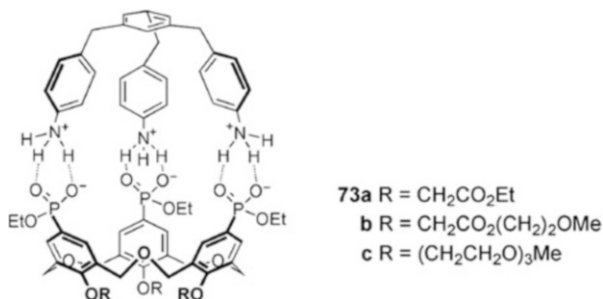


Fluorescent chemosensors based on hexahomotrioxacalix[3]arenes have been reported, mainly by Yamato and coworkers. The fluorescent sensor **69**, incorporating a rhodamine amide moiety and presenting a cone conformation, was tested towards several metal ions by UV-vis and fluorescence spectroscopies [65]. Significant fluorescent enhancement was observed upon the addition of  $\text{Sb}^{3+}$ ,  $\text{Fe}^{3+}$  and  $\text{Ni}^{2+}$  to **69**, as well as strong colorimetric changes. The cone chemosensors **70** and **71** bearing pyrene moieties attached to the calixarene scaffold by triazole groups, showed high selectivity for  $\text{Pb}^{2+}$  in comparison to most other competitive ions tested [66]. Large differences in the fluorescence intensity of the monomer emission were observed in the presence of  $\text{Pb}^{2+}$  for receptor **71**, which gave an 1:1 association constant of  $2.6 \times 10^5 \text{ M}^{-1}$  in  $\text{CH}_3\text{CN}/\text{H}_2\text{O}/\text{DMSO}$  (1000:50:1). Compound **71** also exhibited an increased fluorescence intensity upon the addition of a large amount of  $\text{Zn}^{2+}$ , forming a 1:1 complex ( $K_{\text{ass}} = 2.81 \times 10^4 \text{ M}^{-1}$ ). In another paper [67], the **71**- $\text{Zn}^{2+}$  complex was reported to have a high selectivity for the  $\text{H}_2\text{PO}_4^-$  anion by enhancement of the excimer emission of pyrene. Receptor **71** seems to have the capacity to detect and recognize both  $\text{Zn}^{2+}$  and  $\text{H}_2\text{PO}_4^-$  ions with different optical signals. A ditopic chemosensor **72** was prepared by introducing an ionophore (1,2,3-triazole moiety) at the lower rim of the calixarene and a

fluorophore (pyrene) at the upper rim [68]. Addition of  $\text{Cu}^{2+}$ ,  $\text{Zn}^{2+}$ ,  $\text{Hg}^{2+}$  and  $\text{Pb}^{2+}$  ions caused monomer emission of the pyrene accompanied by excimer quenching, while addition of  $\text{Fe}^{3+}$  placed the pyrene units closer to each other, producing an increase in the emission intensity of the static excimer. The ditopic scaffold of the calixarene acts as a molecular spacer, creating a long distance between the metal cation and the fluorophore, thus blocking the heavy metal ion effect.

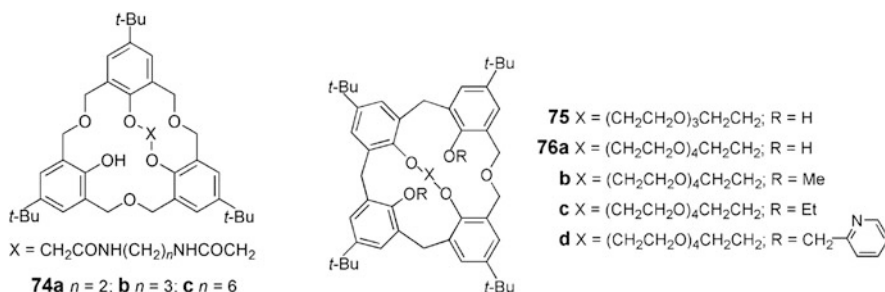


The formation of water-soluble hetero-capsules (**73**) from hexahomotrioxacalix [3]arenes containing negatively charged phosphonate groups at the upper rim and a positively charged flexible anilinium unit was reported [69]. A significant increase in the water solubility was observed for capsules **73b** and **73c**, with ethylene glycol substituents on the calixarene lower rim. The binding properties of capsule **73a** towards 1-methylpyrazinium iodide or 1,4-dimethylpyridinium iodide were evaluated by  $^1\text{H}$  NMR titrations (1:1 complex,  $K_{\text{ass}} \approx 10^2 \text{ M}^{-1}$  in  $\text{D}_2\text{O}$ ), although this quantitative analysis was difficult as the capsules exist in equilibrium with the free building blocks.



### 17.3 Homooxalix-Crowns

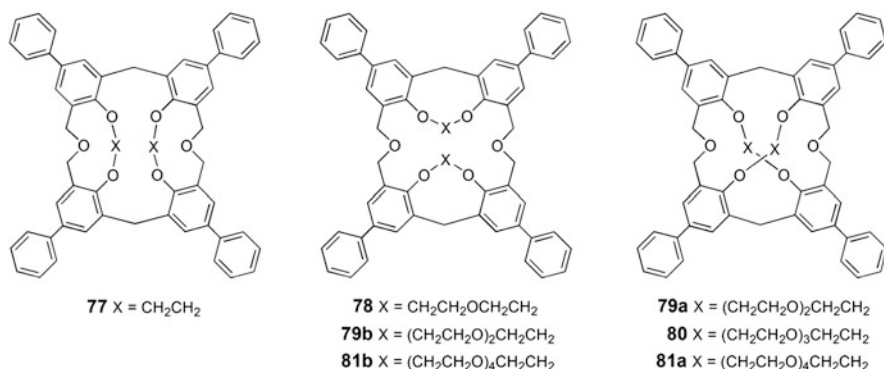
A few examples of bridged homooxalixarenes, mainly bearing crown ether units, have been described since 2000. Diamido *O*-bridged hexahomotrioxalix[3]arenes **74** [70] were prepared by the reaction of **1a** with *N,N'*-bis(chloroacetyl)- $\alpha,\omega$ -alkylenediamine and  $K_2CO_3$  in refluxing acetone and their binding properties towards alkylammonium ions were evaluated by NMR. Ligands **74a** and **74b** showed selectivity for the longer alkylammonium ions, such as *n*-BuNH<sub>3</sub><sup>+</sup>, *n*-pentylNH<sub>3</sub><sup>+</sup> and *n*-hexylNH<sub>3</sub><sup>+</sup> ( $K_{\text{ass}} = 602, 609$  and  $611 \text{ M}^{-1}$  in  $CDCl_3/CD_3CN, 3:1$ , for **74b**, respectively) compared to the shorter chain ions as EtNH<sub>3</sub><sup>+</sup> and *n*-PrNH<sub>3</sub><sup>+</sup> ( $K_{\text{ass}} = 36.8$  and  $75.0 \text{ M}^{-1}$  for **74b**, respectively). Although there was not enough evidence to assign a cone or partial cone conformation to the free ligands **74a** and **b**, a cone conformation was adopted upon 1:1 complexation.



Following the synthesis of the first dihomooxalix[4]-crowns-*n* (**75**, **76a** with  $n = 5, 6$ , respectively) before 2000 [71], Marcos and coworkers [72–74] obtained the 1,3-dialkoxy- and 1,3-di(2-pyridylmethoxy)dihomooxalix[4]-crowns-6 (**76b–d**) and reported their cation binding properties. Extraction studies from water to  $CH_2Cl_2$  of ligands **75–76d** with alkali, alkaline earth, transition and heavy metal picrates indicated negligible ability of both unsubstituted calixcrowns **75** and **76a** to bind these cations, except in the case of **75** with  $Rb^+$  where a modest value of 14 % was obtained [72]. Partial cone 1,3-dialkoxy-calixcrowns **76b** and **76c** were found to be much better extractants, displaying selectivity for  $Cs^+$  (%  $E = 40$  and  $47$ , respectively) and also some preference for  $Ag^+$  (18 %  $E$ ) [73]. The cone crown-6 derivative **76d**, bearing two picolyl groups, displayed moderate percentages of extraction for the alkali cations (22–34 %) with a slight preference for  $Cs^+$ . Smaller percentages were found for the alkaline earth cations (14–17 %), but it showed a strong affinity for the soft metal cations  $Ag^+$  (87 %) and  $Hg^{2+}$  (44 %), and also for some cations of intermediate nature such as  $Cu^{2+}$  and  $Pb^{2+}$  (37 %). [74] Ligands **76c** and **76d** form 1:1 complexes with  $K^+$ ,  $Ca^{2+}$ ,  $Ag^+$  and  $Pb^{2+}$ . No complexation with  $Zn^{2+}$  was shown by **76c**, while a  $ML_2$  complex was obtained

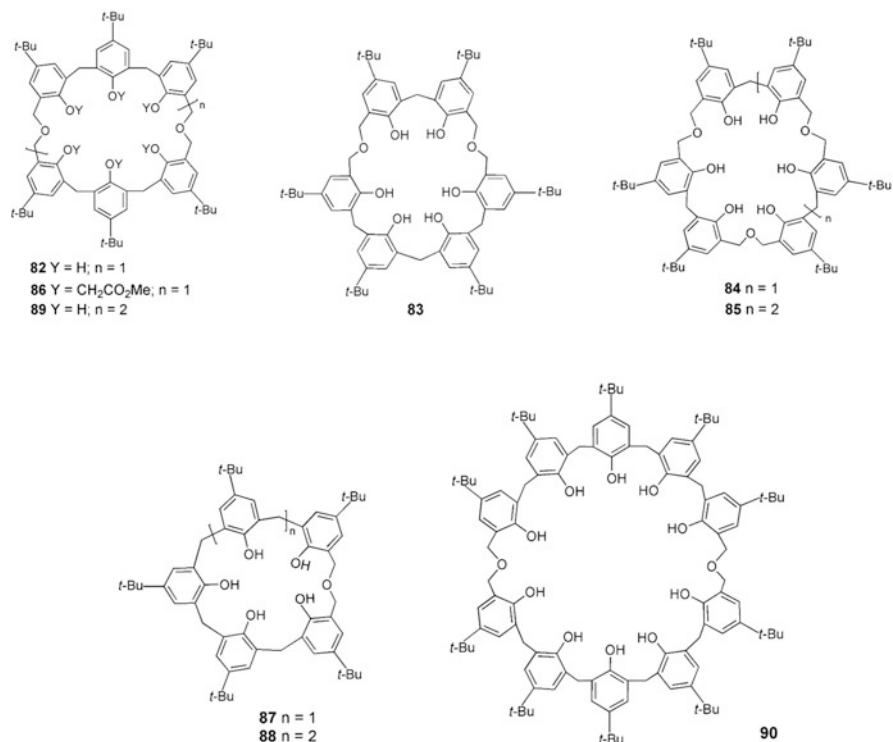
for **76d**. The 1:1 complex structures deduced by NMR experiments showed the cations encapsulated into the cavity composed by the crown ether unit, the ethoxy group and the inverted aryl ring or the crown ether and the two pyridyl groups, respectively.

A series of tetrahomodioxacalix[4]-biscrowns **77–81** with crown ether units varying from crown-2 to crown-6 were obtained in different conformations, according to the NMR spectra and X-ray crystal structures [75, 76]. The results from the two-phase picrate extraction method indicated that 1,3-alternate biscrown-4 (**79a**) showed preference for  $K^+$ , while both 1,3-alternate biscrown-5 (**80**) and biscrown-6 (**81a**) showed preference for  $Cs^+$ . The cone biscrown-2 (**77**) and the 1,4-alternate conformers **78**, **79b** and **81b** displayed no affinity for any of the cations studied.



## 17.4 Large Homooxacalix[n]arenes ( $n \geq 5$ )

Besides homooxacalix[3, 4]arenes, larger macrocyclic compounds such as the homooxacalix[6]arenes with two (**82**, **83**) or three (**84**) CH<sub>2</sub>OCH<sub>2</sub> bridges and the octahomotetraoxacalix[8]arene **85** were reported by Masci in reference 2. Only the synthesis and the structural analysis of these parent compounds have been described. One rare example of lower rim functionalization of a large homooxa compound is the tetrahomodioxacalix[6]arene hexamethyl ester **86** [77]. Its X-ray crystal structure was determined and <sup>1</sup>H NMR studies indicated that it is a poor extractant for the alkali metal ions. Dihomooxacalix[5]- (**87**) [78] and -[6]arene (**88**) [79], hexahomotrioxacalix[9]arene (**89**) [79] and tetrahomodioxacalix[10]arene (**90**) [78] were also reported.



## References

- (a) Gutsche, C. D. *Calixarenes*; Royal Society of Chemistry: Cambridge, 1989; Chapter 2.  
(b) Gutsche, C. D. *Calixarenes, An Introduction*; Royal Society of Chemistry: Cambridge, 2008; Chapter 2.
- Masci, B. In *Calixarenes 2001*; Asfari, Z.; Böhmer, V.; Harrowfield, J.; Vicens, J. Eds.; Kluwer Academic: Dordrecht, 2001; pp 235–249.
- Shokova, E. A.; Kovalev, V. V. *Russ. J. Org. Chem.* **2004**, *40*, 607–643.
- Shokova, E. A.; Kovalev, V. V. *Russ. J. Org. Chem.* **2004**, *40*, 1547–1578.
- Cottet, K.; Marcos, P. M.; Cragg, P. J. *Beilstein J. Org. Chem.* **2012**, *8*, 201–226.
- Tsubaki, K.; Otsubo, T.; Tanaka, K.; Fuji, K. *J. Org. Chem.* **1998**, *63*, 3260–3265.
- Tsubaki, K.; Mukoyoshi, K.; Otsubo, T.; Fuji, K. *Chem. Pharm. Bull.* **2000**, *48*, 882–884.
- Tsubaki, K.; Otsubo, T.; Morimoto, T.; Maruoka, H.; Furukawa, M.; Momose, Y.; Shang, M.; Fuji, K. *J. Org. Chem.* **2002**, *67*, 8151–8156.
- Suzuki, K.; Armah, A. E.; Fujii, S.; Tomita, K.; Asfari, Z.; Vicens, J. *Chem. Lett.* **1991**, 1699–1702.
- No, K. *Bull. Korean Chem. Soc.* **1999**, *20*, 33–34.
- Huc, V.; Npétgat, E.; Guérineau, V.; Bourcier, S.; Santos, A.; Guillot, R.; Baltaze, J.-P.; Martini, C. *Eur. J. Org. Chem.* **2010**, 6186–6192.
- Lavendomme, R.; Cragg, P. J.; Marcos, P. M.; Luhmer, M.; Jabin, I. *Org. Lett.* **2015**, *17*, 5690–5693.

13. Masci, B.; Gabrielli, M.; Mortera, S. L.; Nierlich, M.; Thuéry, P. *Polyhedron* **2002**, *21*, 1125–1131.
14. Marcos, P. M.; Teixeira, F. A.; Ascenso, J. R. unpublished results.
15. Gaeta, C.; Talotta, C.; Farina, F.; Teixeira, F. A.; Marcos, P. M.; Ascenso, J. R.; Neri, P. *J. Org. Chem.* **2012**, *77*, 10285–10293.
16. According to the  $^1\text{H}$  NMR spectrum, two conformations were obtained: cone (75 %) and 1,4-alternate (25 %). Due to the lower symmetry introduced by the oxa bridges, homooxacalix [4]arenes can assume a higher number of basic conformations than calix[4]arenes. For this subject see: (a) Marcos, P. M.; Ascenso, J. R.; Lamartine, R.; Pereira, J. L. C. *Tetrahedron* **1997**, *53*, 11791–11802. (b) Masci, B.; Finelli, M.; Varrone, M. *Chem. Eur. J.* **1998**, *4*, 2018–2030.
17. No, K.; Park, Y. J. *Bull. Korean Chem. Soc.* **2002**, *23*, 1629–1634.
18. Masci, B.; Mortera, S. L.; Persiani, D.; Thuéry, P. *J. Org. Chem.* **2006**, *71*, 504–511.
19. Yamato, T.; Zhang, F.; Sato, T.; Ide, S. *J. Chem. Research (S)* **2000**, 10–12.
20. Yamato, T.; Haraguchi, M.; Nishikawa, J. I.; Ide, S.; Tsuzuki, H. *Can. J. Chem.* **1998**, *76*, 989–999.
21. Yamato, T.; Zhang, F. *J. Incl. Phenom. Macrocyclic Chem.* **2001**, *39*, 55–64.
22. Kang, J.; Cheong, N. *Bull. Korean Chem. Soc.* **2002**, *23*, 995–997.
23. Yamato, T.; Zhang, F.; Tsuzuki, H.; Miura, Y. *Eur. J. Org. Chem.* **2001**, 1069–1075.
24. Marcos, P. M.; Ascenso, J. R.; Segurado, M. A. P.; Bernardino, R. J.; Cragg, P. J. *Tetrahedron* **2009**, *65*, 496–503.
25. Jiang, X. K.; Deng, M.; Mu, L.; Zeng, X.; Zhang, J. X.; Yamato, T. *Asian J. Chem.* **2013**, *25*, 515–517.
26. Félix, S.; Ascenso, J. R.; Lamartine, R.; Pereira, J. L. C. *Tetrahedron* **1999**, *55*, 8539–8546.
27. Marcos, P. M.; Ascenso, J. R.; Segurado, M. A. P.; Pereira, J. L. C. *J. Phys. Org. Chem.* **1999**, *12*, 695–702.
28. Marcos, P. M.; Ascenso, J. R.; Segurado, M. A. P.; Pereira, J. L. C. *Tetrahedron* **2001**, *57*, 6977–6984.
29. Marcos, P. M.; Ascenso, J. R.; Pereira, J. L. C. *Eur. J. Org. Chem.* **2002**, 3034–3041.
30. Marcos, P. M.; Teixeira, F. A.; Segurado, M. A. P.; Ascenso, J. R.; Bernardino, R. J.; Michel, S.; Hubscher-Bruder, V. *J. Org. Chem.* **2014**, *79*, 742–751.
31. Marcos, P. M.; Teixeira, F. A.; Segurado, M. A. P.; Ascenso, J. R.; Bernardino, R. J.; Brancatelli, G.; Geremia, S. *Tetrahedron* **2014**, *70*, 6497–6505.
32. No, K.; Lee, J. H. *Bull. Korean Chem. Soc.* **2000**, *21*, 1055–1164.
33. No, K.; Park, Y. J.; Choi, E. J. *Bull. Korean Chem. Soc.* **1999**, *20*, 905–09.
34. No, K.; Kim, J. S.; Shon, O. J.; Yang, S. H.; Suh, I. H.; Kim, J. G.; Bartsch, R. A.; Kim, J. Y. *J. Org. Chem.* **2001**, *66*, 5976–5980.
35. No, K.; Lee, J. H.; Yang, S. H.; Yu, S. H.; Cho, M. H.; Kim, M. J.; Kim, J. S. *J. Org. Chem.* **2002**, *67*, 3165–3168.
36. No, K.; Lee, J. H.; Yang, S. H.; Noh, K. H.; Lee, S. W.; Kim, J. S. *Tetrahedron* **2003**, *59*, 2403–2407.
37. No, K.; Lee, J. H.; Yang, S. H.; Noh, K. H.; Kim, S. K.; Seo, J.; Lee, S. S.; Kim, J. S. *J. Incl. Phenom. Macrocyclic Chem.* **2003**, *47*, 167–171.
38. Takimoto, M.; Aramaki, T.; Xi, Z.; Yamato, T. *J. Chem. Research* **2007**, 400–403.
39. Talotta, C.; Gaeta, C.; De Rosa, M.; Ascenso, J. R.; Marcos, P. M.; Neri, P. *Eur. J. Org. Chem.* **2016**, 158–167.
40. Marcos, P. M.; Ascenso, J. R.; Cragg, P. J. *Supramol. Chem.* **2007**, *19*, 199–206.
41. Marcos, P. M.; Ascenso, J. R.; Segurado, M. A. P.; Cragg, P. J.; Michel, S.; Hubscher-Bruder, V.; Arnaud-Neu, F. *Supramol. Chem.* **2011**, *23*, 93–101.
42. Griffiths, K.; Sharma, K.; Marcos, P. M.; Ascenso, J. R.; Nind, J.; Cottet, K.; Cragg, P. J. *Supramol. Chem.* **2015**, *27*, 167–173.



43. Marcos, P. M.; Teixeira, F. A.; Segurado, M. A. P.; Ascenso, J. R.; Bernardino, R. J.; Cragg, P. J.; Michel, S.; Hubscher-Bruder, V.; Arnaud-Neu, F. *J. Phys. Org. Chem.* **2013**, *26*, 295–305.
44. Marcos, P. M.; Teixeira, F. A.; Segurado, M. A. P.; Ascenso, J. R.; Bernardino, R. J.; Cragg, P. J.; Michel, S.; Hubscher-Bruder, V.; Arnaud-Neu, F. *Supramol. Chem.* **2013**, *25*, 522–532.
45. Marcos, P. M.; Ascenso, J. R.; Segurado, M. A. P.; Pereira, J. L. C. *J. Incl. Phenom. Macrocyclic Chem.* **2002**, *42*, 281–288.
46. Marcos, P. M.; Félix, S.; Ascenso, J. R.; Segurado, M. A. P.; Mellah, B.; Abidi, R.; Hubscher-Bruder, V.; Arnaud-Neu, F. *Supramol. Chem.* **2006**, *18*, 285–297.
47. Marcos, P. M.; Félix, S.; Ascenso, J. R.; Segurado, M. A. P.; Thuéry, P.; Mellah, B.; Michel, S.; Hubscher-Bruder, V.; Arnaud-Neu, F. *New J. Chem.* **2007**, *31*, 2111–2119.
48. Marcos, P. M.; Félix, S.; Ascenso, J. R.; Segurado, M. A. P.; Pereira, J. L. C.; Khazaeli-Parsa, Hubscher-Bruder, V.; Arnaud-Neu, F. *New J. Chem.* **2004**, *28*, 748–755.
49. Marcos, P. M.; Mellah, B.; Ascenso, J. R.; Michel, S.; Hubscher-Bruder, V.; Arnaud-Neu, F. *New J. Chem.* **2006**, *30*, 1655–1661.
50. Yamato, T.; Rahman, S.; Xi, Z.; Kitajima, F.; Gil, J. T. *Can. J. Chem.* **2006**, *84*, 58–64.
51. Ni, X. L.; Rahman, S.; Zeng, X.; Hughes, D. L.; Redshaw C.; Yamato, T. *Org. Biomol. Chem.* **2011**, *9*, 6535–6541.
52. Takimoto, M.; Ni, X. L.; Rahman, S.; Xi, Z.; Yamato, T. *J. Incl. Phenom. Macrocyclic Chem.* **2011**, *70*, 69–80.
53. Ni, X. L.; Takimoto, M.; Xi, Z.; Yamato, T. *J. Incl. Phenom. Macrocyclic Chem.* **2011**, *71*, 231–237.
54. Ni, X. L.; Tahara, J.; Rahman, S.; Zeng, X.; Hughes, D. L.; Redshaw C.; Yamato, T. *Chem. Asian J.* **2012**, *7*, 519–527.
55. Jin, C. C.; Cong, H.; Ni, X. L.; Zeng, X.; Redshaw C.; Yamato, T. *RSC Adv.* **2014**, *4*, 31469–31475.
56. Bryantsev, V. S.; Hay, B. P. *J. Phys. Chem. A* **2006**, *110*, 4678–4688.
57. Gattuso, G.; Notti, A.; Parisi, M. F.; Pisagatti, I.; Marcos, P. M.; Ascenso, J. R.; Brancatelli, G.; Geremia, S. *New J. Chem.* **2015**, *39*, 817–821.
58. Zhong, Z. L.; Ikeda, A.; Shinkai, S. In *Calixarenes 2001*; Asfari, Z.; Böhmer, V.; Harrowfield, J.; Vicens, J. Eds.; Kluwer Academic: Dordrecht, 2001; pp 476–495.
59. Tsubaki, K.; Otsubo, T.; Kinoshita, T.; Kawada, M.; Fujii, K. *Chem. Pharm. Bull.* **2001**, *49*, 507–509.
60. Tsubaki, K.; Morimoto, T.; Otsubo, T.; Fujii, K. *Org. Lett.* **2002**, *4*, 2301–2304.
61. Odashima, K.; Yagi, K.; Tohda, T.; Umezawa, Y. *Bioorg. Med. Chem. Lett.* **1999**, *9*, 2375–2378.
62. Katsu, T.; Ido, K.; Sagara, S.; Tsubaki, K.; Fujii, K. *Electroanalysis* **2003**, *15*, 287–293.
63. Yaftian, M. R.; Parinejad, M.; Matt, D. J. *Chin. Chem. Soc.* **2007**, *54*, 1535–1542.
64. Bocheńska, M.; Cragg, P. J.; Guziński, M.; Jasiński, A.; Kulesza, J.; Marcos, P. M.; Pomečko, R. *Supramol. Chem.* **2009**, *21*, 732–737.
65. Wu, C.; Zhang, W. J.; Zeng, X.; Mu, L.; Xue, S. F.; Tao, Z.; Yamato T. *J. Incl. Phenom. Macrocyclic Chem.* **2010**, *66*, 125–131.
66. Ni, X. L.; Wang, S.; Zeng, X.; Tao, Z.; Yamato, T. *Org. Lett.* **2011**, *13*, 552–555.
67. Ni, X. L.; Zeng, X.; Redshaw, C.; Yamato, T. *J. Org. Chem.* **2011**, *76*, 5696–5702.
68. Wu, Y.; Ni, X. L.; Mou, L.; Jin, C. C.; Redshaw, C.; Yamato, T. *Supramol. Chem.* **2015**, *27*, 501–507.
69. Kusakawa, T.; Katano, C.; Kim, C. *Tetrahedron* **2012**, *68*, 1492–1501.
70. Liu, S. L.; Gong, S. L.; Chen, Y. Y. *Chin. J. Chem.* **2005**, *23*, 1651–1654.
71. Félix, S.; Ascenso, J. R.; Lamartine, R.; Pereira, J. L. C. *Synth. Commun.* **1998**, *28*, 1793–1799.
72. Marcos, P. M.; Félix, S.; Ascenso, J. R.; Santos, M. A.; Segurado, M. A. P.; Pereira, J. L. C. *Tetrahedron* **2002**, *58*, 9223–9230.
73. Marcos, P. M.; Ascenso, J. R. *Supramol. Chem.* **2009**, *21*, 61–67.
74. Marcos, P. M.; Ascenso, J. R. *Tetrahedron* **2006**, *62*, 3081–3088.

75. No, K.; Chung, H. J.; Yu, H. J.; Yang, S. H.; Noh, K. H.; Thuéry, P.; Vicens, J.; Kim, J. S. *J. Incl. Phenom. Macrocyclic Chem.* **2003**, *46*, 97–103.
76. No, K.; Bok, J. H.; Suh, H.; Kang, S. O.; Ko, J.; Nam, K. C.; Kim, J. S. *J. Org. Chem.* **2004**, *69*, 6938–6941.
77. Oueslati, I.; Abidi, R.; Asfari, Z.; Vicens, J.; Masci, B.; Thuéry, P.; Nierlich, M. *J. Incl. Phenom. Macrocyclic Chem.* **2001**, *39*, 353–355.
78. Masci, B.; Thuéry, P. *New J. Chem.* **2005**, *29*, 493–498.
79. Masci, B. *J. Org. Chem.* **2001**, *66*, 1497–1499.

# Chapter 18

## Triptycene-Derived Calixarenes, Heteracalixarenes and Analogues

Chuan-Feng Chen, Han-Xiao Wang, Ying Han, and Ying-Xian Ma

### 18.1 Introduction

As “the third generation of host molecules” after crown ethers and cyclodextrins, calixarenes [1] are a class of well-defined phenol-derived cyclic oligomers bridged by methylene groups. Due to their convenient preparation, unique structural features and easy functionalization on both lower and upper rims, calixarenes have become one of the most important macrocyclic hosts and finds applications in wide areas like molecular recognition [2], sensing [3], self-assembly [4], catalysis [5] and drug discovery [6]. Similar to calixarenes, heteracalixarenes [7] with heteroatoms as the linkages between the aromatic units have also attracted much attention in recent years for their ready availability, unique conformation and cavity tunability. However, the small cavities of classic (hetera)calix[4]arenes and the flexible conformations of (hetera)calix[6]arenes and their larger analogues make their cavities actually difficult to be utilized and thus limit their applications in supramolecular chemistry.

As the first and simplest member of triptycene [8] family, triptycene has three arene units fused to bicyclo[2.2.2]octatriene bridgehead system with  $D_{3h}$  symmetry. In this unique Y-shaped rigid structure, the three phenyl ring “panels” are connected by the bridgehead carbon atoms. Taking advantage of its three-dimensional rigid structure and rich reactive sites, we have succeeded in developing several kinds of novel triptycene-derived hosts with specific structures and properties, including triptycene-derived macrotricyclic polyethers [9] and tweezer-like triptycene-derived crown ethers [10]. We supposed that if a proper triptycene moiety with 3D rigid structure took place of one or more phenol groups in classic (hetera)calixarenes, a class of novel calixarenes, heteracalixarenes and analogues

---

C.-F. Chen (✉) • H.-X. Wang • Y. Han • Y.-X. Ma  
Institute of Chemistry, Chinese Academy of Sciences, Beijing 100190, China  
e-mail: [cchen@iccas.ac.cn](mailto:cchen@iccas.ac.cn)

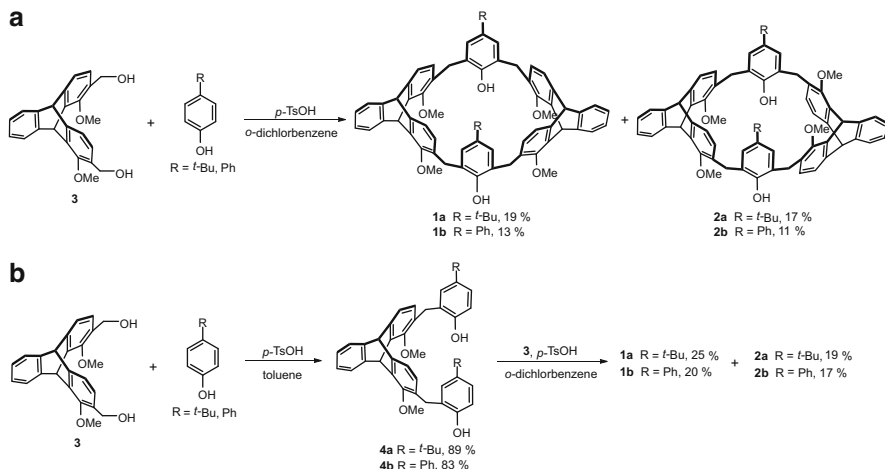
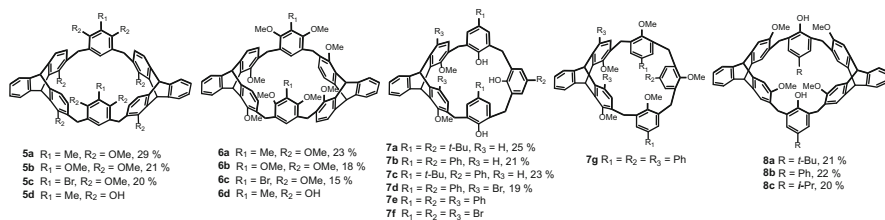
with fixed conformations and expanded cavities could be constructed. As could be envisaged, the introduction of triptycene moieties will bring novel properties in structure, molecular recognition and assembly due to the rigidity and electron-richness of triptycene.

In this chapter, we will summarize our advances in studies on the synthesis, structures, molecular recognition and assembly of triptycene-derived calixarenes, heteracalixarenes and analogues.

## 18.2 Triptycene-Derived Calixarenes and Analogues

### 18.2.1 *Synthesis of Triptycene-Derived Calixarenes and Analogues*

By replacing one or two of the phenol groups in the classic calixarenes with rigid triptycene moieties, we [11, 12] obtained a series of novel triptycene-derived calixarenes. Through a one-pot reaction of *p*-substituted phenol with one equivalent of 1,8-dimethoxy-2,7-dihydroxymethyl- triptycene **3** in *o*-dichlorobenzene in the presence of *p*-methylbenzenesulfonic acid, a pair of triptycene-derived calixarenes **1** and **2** were obtained (Scheme 18.1a) [11a]. They could also be synthesized by a two-step approach. [11b] As shown in Scheme 18.1b, trimer **4** was obtained in above 80 % yield by the reaction of **3** with an excess of *p*-substituted phenol in the presence of *p*-toluenesulfonic acid, which then reacted with **3** in *o*-dichlorobenzene to give the target macrocycles **1** and **2** (Scheme 18.1b). Utilizing the similar synthetic strategy, we synthesized dialkoxytriptycene-derived calix[6]arenes **5a–c** and **6a–c** (Fig. 18.1a) [11c]; and the reactions of corresponding dihydroxymethyl *p*-substituted phenol with **4** or its derivatives gave triptycene-derived calix[5]arenes **7a–d** in about 20 % yields, and with reactive sites on it, **7d** further reacted to give **7e** and **7g** (Fig. 18.1b) [11d, e]. Moreover, we [12] also obtained a class of novel triptycene-derived calixresorcinarene-like hosts **8** containing two dimethoxy-triptycene moieties and two *p*-substituted phenol moieties via a similar approach (Fig. 18.1c). The corresponding demethylated or debutylated products of these triptycene-derived calixarenes and analogues could be further obtained in high yields by the treatment with BBr<sub>3</sub> in dry CH<sub>2</sub>Cl<sub>2</sub> or with AlCl<sub>3</sub> in toluene, respectively. Generally, however, the high rigidity of triptycene made the macrocyclization not easy to proceed, leading to the relatively low yields of the products, which was also the main challenge in constructing both triptycene-derived calixarenes and heteracalixarenes.

Scheme 18.1 Synthesis of triptycene-derived calixarenes **1** and **2**Fig. 18.1 Structures of triptycene-derived calixarenes and analogues **5**, **6**, **7** and **8**

### 18.2.2 Structures of Triptycene-Derived Calixarenes and Analogues

With NMR spectroscopy, we investigated the structures and conformations of these triptycene-derived calixarenes and analogues in solution. In the case of triptycene-derived calixarenes **1a** and **2a** [11a, b], there was one singlet for the *tert*-butyl protons, one singlet for the methoxy protons, and two singlets for the bridgehead protons of the triptycene moieties in the <sup>1</sup>H NMR spectra with no obvious changes observed by increasing the temperatures, and there was only one signal for the methylene carbons in their <sup>13</sup>C NMR spectra, all of which suggested that both **1a** and **2a** had highly symmetric structures and fixed conformations. However, the signals for the methylene protons of **1a** and **2a** showed a large difference: a pair of doublet signals at 3.35 and 4.25 ppm ( $\Delta\delta = 0.90$  ppm) were observed in the <sup>1</sup>H NMR spectrum of **1a**, whereas that of **2a** showed a pair of doublet signals at 3.67 and 3.86 ppm with a  $\Delta\delta$  value of 0.19 ppm. These results

implied that macrocycles **1a** and **2a** were a pair of diastereomers, in which **1a** had a *cis*-orientation of the two triptycene moieties, while **2a** had a *trans*-orientation. Similarly, **5** and **6** had symmetric structures and fixed conformations as well, in which **5** were *syn*-isomers while **6** were *trans*-isomers [11c]. In the case of triptycene-derived calix[5]arenes **7a–d** [11d, e], two pairs of doublets for the bridged methylene protons were observed in the  $^1\text{H}$  NMR spectra, which were quite similar to those of the classical calix[4]arene with a cone conformation [13], indicating that they had  $C_s$  symmetric structures with a fixed cone conformation in solution. Notably, though **7e** also adopted a fixed cone conformation, the full methyl etherified **7g** adopted a 1,2-alternate conformation evidenced by the up-field shift of the methoxy of triptycene moiety, suggesting the occurrence of conformational transformation [11e]. The NMR signals for calixresorcinarene-like hosts **8a–c** [12] also showed that they were all *cis*-isomers with highly symmetric structures and fixed cone conformations in solution. The presence of the triptycene moieties added to the rigidity of the whole macrocycle, solving the deep-rooted problem of the highly mobile conformation of conventional calixarenes, and thus might bring new properties in recognition and assembly.

The corresponding X-ray crystal structures of these triptycene-derived calixarenes and analogues were also obtained. As shown in Fig. 18.2a, b, macrocycle **1a** adopted a typical cone conformation with a highly symmetric structure, while *trans*-isomer **2a** adopted a chair conformation with two opposite phenol rings in the same plane [11a, b]. Similar structural features were also found in the crystals of their derivatives **5** and **6** [11c]. In the case of **7a, b** and **e** [11d, e] (Fig. 18.2c) and **8a** [12] (Fig. 18.2d), the crystal structures showed that they adopted cone conformations with fixed cavities while **7g** [11e] was in a 1,2-alternate conformation.

### 18.2.3 Molecular Recognition and Assembly of Triptycene-Derived Calixarenes and Analogues

As stated above, the rigid triptycene moieties led to a relatively fixed cavity in the triptycene-derived calixarenes; more than that, the triptycene was quite electron-rich, which further facilitated host-guest complexation via non-covalent interactions including hydrogen bonds,  $\text{C–H}\cdots\pi$  and  $\pi\cdots\pi$  stacking interactions.

With large cavities and fixed conformations, triptycene-derived calixarenes could easily encapsulate small organic molecules inside their cavities in the solid state [11]. It was found that **1a** could encapsulate two  $\text{CH}_3\text{OH}$  molecules in its cavity via a pair of  $\text{O–H}\cdots\text{O}$  hydrogen bonds between the phenolic oxygen atoms and the hydroxyl protons of  $\text{CH}_3\text{OH}$ ; while *trans*-isomer **2a** could also accommodate two  $\text{CH}_3\text{OH}$  molecules via multiple non-covalent interactions, including  $\text{O–H}\cdots\text{O}$  hydrogen bonds,  $\text{C–H}\cdots\text{O}$  hydrogen bonds, and  $\text{C–H}\cdots\pi$  interactions (Fig. 18.3a) [11b]. For the *trans*-isomer **2b**, one  $\text{CH}_2\text{Cl}_2$  molecule was encapsulated

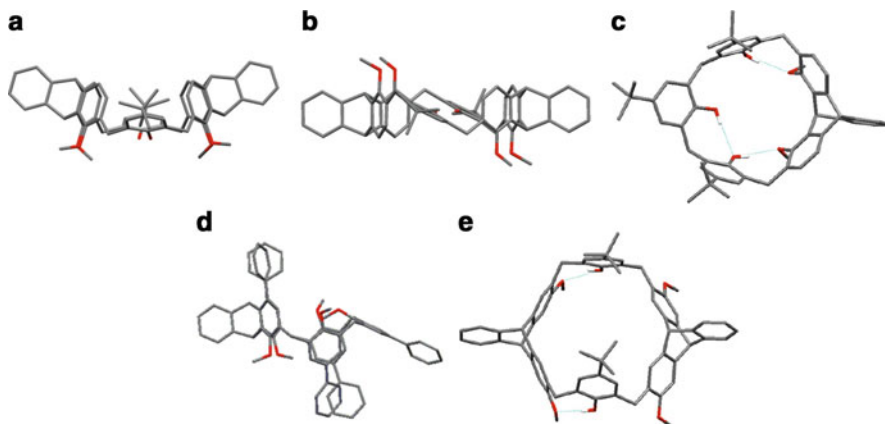


**Fig. 18.2** Crystal structures of (a) **1a**, (b) **2a**, (c) **7a**, (d) **7g** and (e) **8a**. Solvents and hydrogen atoms not involved in the hydrogen bonding interactions are omitted for clarity

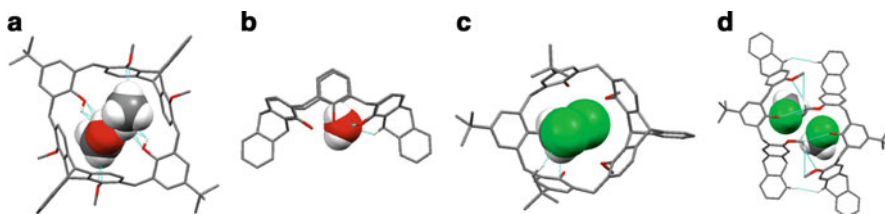


**Fig. 18.3** Crystal structures of (a)  $2\text{CH}_3\text{OH}@2\mathbf{a}$ , (b)  $\text{H}_2\text{O}@9$ , (c)  $\text{CH}_2\text{Cl}_2@7\mathbf{a}$ , and (d)  $2\text{CH}_2\text{Cl}_2@(8\mathbf{a})_2$ . Other solvent molecules and hydrogen atoms are omitted for clarity

by multiple  $\text{O}-\text{H}\cdots\text{Cl}$  and  $\text{C}-\text{H}\cdots\text{O}$  hydrogen-bonding, and  $\text{C}-\text{H}\cdots\pi$  interactions. The demethylated macrocycle of **1a** could encapsulate one  $\text{CHCl}_3$  molecule, while the demethylated and debutylated product **9** of **1a** could accommodate one water molecule via multiple hydrogen-bonding interactions (Fig. 18.3b). Moreover, **5d** could even form 1:1 complexes with linear guests such as paraquat derivatives and a [2]rotaxane was subsequently synthesized [11c]. For triptycene-derived calix[5]arenes, small neutral guest molecules were easily encapsulated in their cavities as well [11d, e]. With a pair of  $\text{C}-\text{H}\cdots\pi$  interactions, **7a** could encapsulate a  $\text{CH}_2\text{Cl}_2$  molecule (Fig. 18.3c), while for **7b** and **7e**, one methanol molecule and one chloroform molecule could be encapsulated inside their cavities, respectively. Moreover, calixresorcinarene-like host **8a** tended to form a head-to-head dimeric capsule by virtue of two pairs of  $\text{C}-\text{H}\cdots\text{O}$  hydrogen bonds between the methyl protons of one triptycene moiety and the methoxy groups of its adjacent macrocycle; and two  $\text{CH}_2\text{Cl}_2$  molecules were positioned inside the dimeric cavity by  $\text{C}-\text{H}\cdots\text{Cl}$  interaction between the methyl protons of one macrocycle and each dichloromethane molecule (Fig. 18.3d) [12].

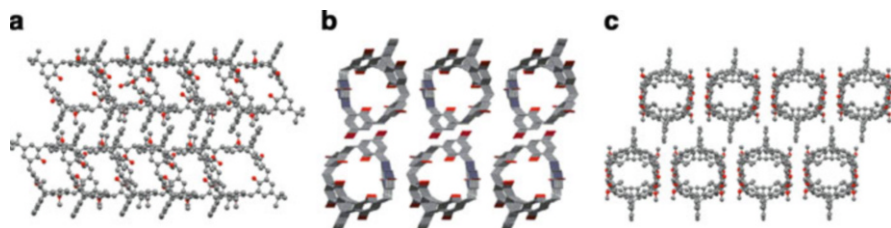


**Fig. 18.4** Packing structures of (a) **1a**, (b) **7f** and (c) **8a**

By means of fluorescence method, we tested the complexation of the triptycene-derived calix[6]arenes with fullerenes [11b]. It was found that **1b** and **2b** could form 1:1 stable complexes with both  $C_{60}$  and  $C_{70}$ , which was different from classical calix[6]arene derivatives [14]. The association constants ( $K_a$ ) for the complexes formed by **1b-2b** and  $C_{60}$  were determined to be more than  $5 \times 10^4 M^{-1}$  by the fluorescence titration experiments, which were significantly higher than the complexes formed by  $C_{60}$  and the classical calix[5]arene and calix[6]arene derivatives (only 9–1,300  $M^{-1}$ ) [15]. These results suggested that the introduction of the triptycene moieties not only fixed the conformations of the calixarenes, but also increased the electron density of the cavities, leading to much higher affinities towards  $C_{60}$  and  $C_{70}$ .

The rigidity of those novel calixarenes brought by triptycene moieties made them promising candidates to self-assemble into supramolecular structures. Both the *cis*-isomer **1a** with a cone conformation and the *trans*-isomers **2a-b** and **6a-c** with a chair conformation could self-assemble into tubular structures with the aromatic rings as the walls and phenolic oxygen atoms situated in their cavities [11a-c]. These tubular assemblies could further stack into 2D superstructures and 3D microporous architectures with solvent molecules situated inside the channels (Fig. 18.4a). Interestingly, calixarene **7f** could also form a tubular assembly with a diameter of approximately 6 Å (Fig. 18.4b) [11e]. As mentioned above, calix[6]resorcinarene-like host **8a** could form a dimeric capsule via multiple non-covalent interactions. These dimers could be stacked to form a tubular structure, and then further assembled into a 3D microporous architecture [12]. Its demethylated macrocycle, with multiple non-covalent interactions including hydrogen bonding between the macrocycle and its adjacent molecules, could self-assemble into the 3D microporous architecture (Fig. 18.4c).

## 18.3 Triptycene-Derived Heteracalixarenes

### 18.3.1 Synthesis of Triptycene-Derived Heteracalixarenes

Apart from methylene-bridged calixarenes, we [16, 17] also designed and synthesized a series of triptycene-derived oxacalixarenes **10-13** starting from

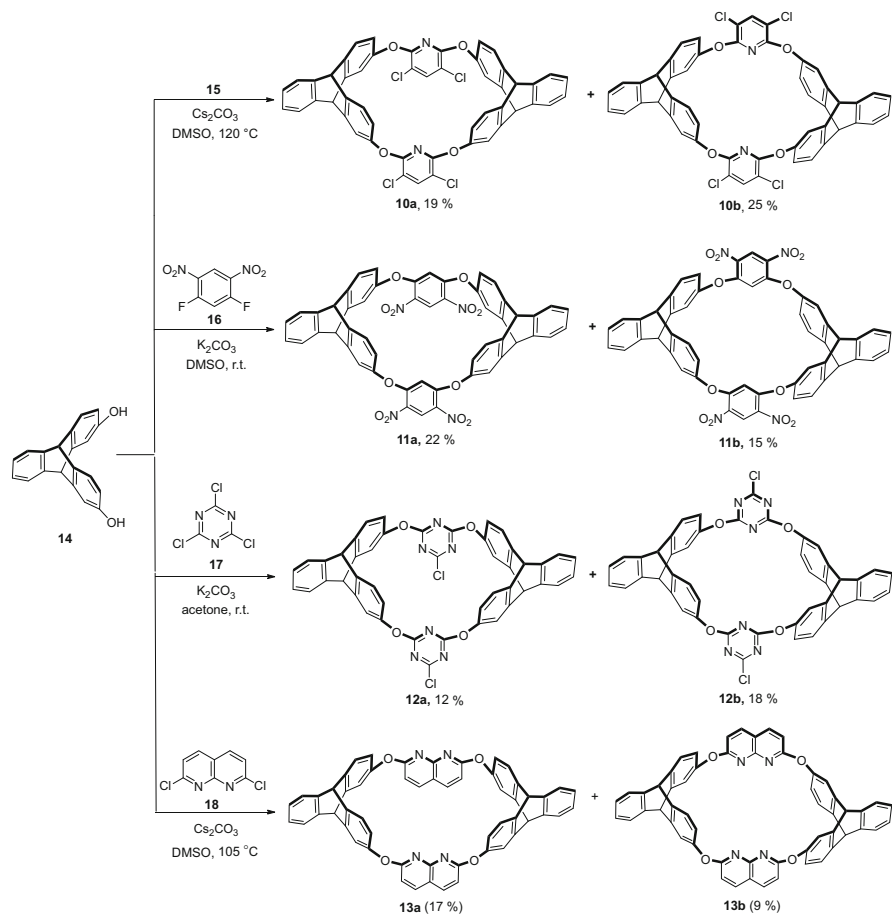


2,7-dihydroxytriptycene **14**. The one-pot reaction of 2,7-dihydroxytriptycene **14** and 2,3,5,6-tetrachloropyridine **15** in DMSO with  $\text{Cs}_2\text{CO}_3$  as the base gave oxacalixarenes **10a** and **10b** in 19 % and 25 % yields, respectively. In the presence of  $\text{K}_2\text{CO}_3$ , macrocycles **11a** and **11b** could be obtained in 22 % and 15 % yields, respectively, by  $\text{S}_{\text{N}}2$  reaction of **14** with 1,5-difluoro-2,4-dinitrobenzene **16** (Scheme 18.2). However, it was found that oxacalixarenes **12a** and **12b** could not be obtained in similar conditions probably due to their instabilities therein. Under various conditions examined, we found that the one-pot reaction of **14** with cyanuric chloride **17** could afford the target oxacalixarenes **12a** and **12b** in acetone in the presence of  $\text{K}_2\text{CO}_3$  in 12 % and 18 % yield, respectively. Actually, they could also be synthesized by a two-step method: we firstly obtained the linear trimer formed by **14** and two equivalents of **17** in 58 % yield, which further reacted with **14** in acetone with DIPEA as the base at room temperature to give **12a** and **12b** in 12 % and 15 % yields, respectively [16]. Moreover, we [17] synthesized **13a** containing two triptycene subunits and two naphthyridine subunits in 37 % yield by the one-pot reaction of 2,7-dihydroxy-triptycene **14** and 2,7-dichloro-1,8-naphthyridine **18** in refluxed 1,4-dioxane with  $\text{Cs}_2\text{CO}_3$  as the base. However, a pair of triptycene-derived oxacalixarenes **13a** and **13b** were obtained in 17 % and 9 % yield, respectively, if the reaction was carried out in DMSO at 105 °C with  $\text{Cs}_2\text{CO}_3$  as the base (Scheme 18.2).

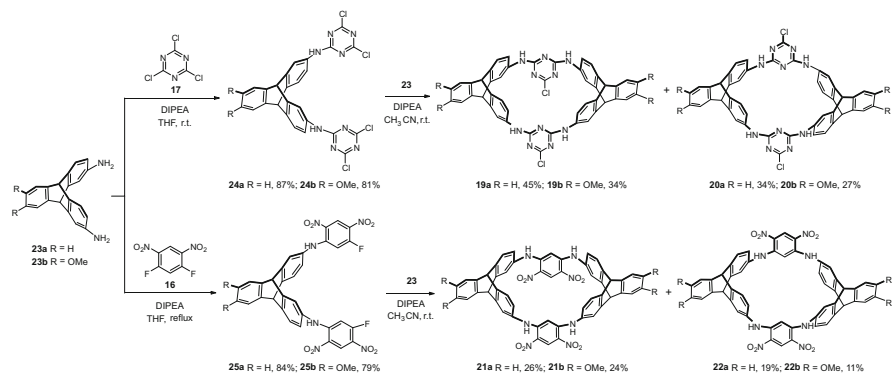
According to the similar synthetic strategy, we [18] also synthesized a series of novel triptycene-derived *N(H)*-bridged azacalixarenes **19–22** starting from 2,7-diaminotriptycene **23a** and its analogue **23b** containing an *o*-dimethoxybenzene subunit. **19–22** could be obtained in moderate yields by one-pot reactions of 2,7-diaminotriptycenes **23** with 1,5-difluoro-2,4-dinitrobenzene **16** or cyanuric chloride **17** in dry THF in the presence of DIPEA. In another synthetic route, we could synthesize linear trimers **24** and **25** in high yields by the reaction of **23** with corresponding electrophilic reagents, and then **24** and **25** further reacted with **23** in  $\text{CH}_3\text{CN}$  in the presence of DIPEA to afford the target macrocycles (Scheme 18.3). In addition, we [19] also synthesized a series of triptycene-derived diazadioxacalixarenes **26a–c** and **27a–c** by a two-step  $\text{S}_{\text{N}}\text{Ar}$  reaction of triptycene derivatives **23** or **14** with proper electrophilic reagents (Fig. 18.5).

### 18.3.2 Structures of Triptycene-Derived Heteracalixarenes

Due to the different linking modes of the triptycene moieties, triptycene-derived oxacalixarenes **10a–b**, **11a–b**, **12a–b** and **13a–b** were pairs of diastereomers [16, 17], respectively. It was found that **10a–b** were in a  $\text{C}_2$  symmetry, showing only two singlets for the bridgehead protons and one singlet for the protons of pyridine moieties in the  $^1\text{H}$  NMR spectra, and only two signals for the bridgehead carbons in the  $^{13}\text{C}$  NMR spectra. Moreover, *cis*-isomer **10a** showed close chemical shifts for the aromatic protons, and slightly different shifts for the bridgehead protons ( $\Delta\delta = 0.15$  ppm), but for *trans*-isomer **10b**, it was found that the aromatic



**Scheme 18.2** Synthesis of triptycene-derived oxacalixarenes **10–13**



**Scheme 18.3** Synthesis of triptycene-derived azacalixarenes **19–22** via a two-step method.

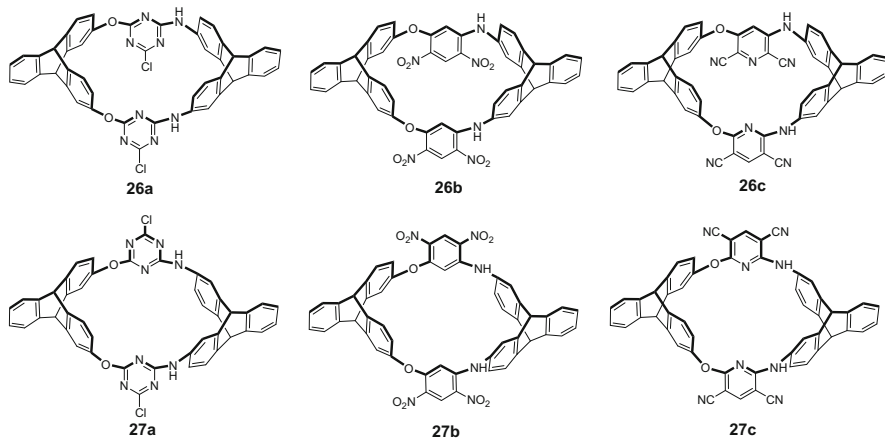
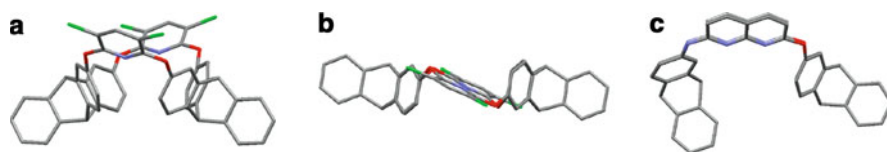


Fig. 18.5 Structures of triptycene-derived diazadioxacalixarenes **26** and **27**

proton signals of the triptycene moieties split well, and the two bridgehead protons also showed significantly different chemical shifts with  $\Delta\delta$  of 0.79 ppm. **11a** and **12a** showed similar split modes of triptycene protons to those of **10a** which confirmed their *cis*-configurations, and **11b** was a *trans*-isomer with a split mode similar to that of **10b**. However, **12b** was probably in a dynamic interconversion between the chair and boat conformations, which showed broadened proton signals at room temperature. The variable-temperature  $^1\text{H}$  NMR experiments suggested that **12b** might adopt a stable boat conformation at low temperature. At 328 K, the broadened triptycene signals split distinctly and became only one set of signals due to rapid interconversion of different conformations on the NMR timescale [16]. The similar features in NMR spectra also showed that **13a** was a *cis*-isomer while **13b** was a *trans*-isomer, both with fixed conformations [17].

The  $^1\text{H}$  NMR spectra of triptycene-derived *N(H)*-bridged azacalixarenes **19** with **20**, and **20** with **21** [18] showed a big difference from each other, which revealed that they were pairs of diastereomers. It was found that the  $^1\text{H}$  NMR spectra of *cis*-isomers **19a–b** and **21a–b** showed close chemical shifts of the aromatic protons and slightly different shifts for the benzylic protons, implying a highly symmetric boat conformation. However, the four singlets with significantly different chemical shifts for the bridgehead protons and two singlets for the protons of N–H bridged groups of the *trans*-isomers **20a–b** and **22a** suggested that they adopted fixed curved-boat conformation without high symmetry at room temperature, while **22b** exhibited high symmetry in its  $^1\text{H}$  NMR spectrum implying its normal chair conformation. Similarly, triptycene-derived diazadioxacalixarenes **26a–c** and **27a–c** were also pairs of diastereomers [19]. Their NMR spectra revealed that *cis*-isomers **26a–c** adopted twisted boat conformation, while *trans*-isomers **27a–c** were in a symmetric chair conformation.

X-ray crystal structural analysis showed that **10a**, **12a** and **13a** were *cis*-isomers with a 1,3-alternate conformation (Fig. 18.6a) while **10b** and **13b** were *trans*-



**Fig. 18.6** Crystal structures of (a) **10a**, (b) **10b** and (c) **13b**. Solvent molecules and hydrogen atoms are omitted for clarity

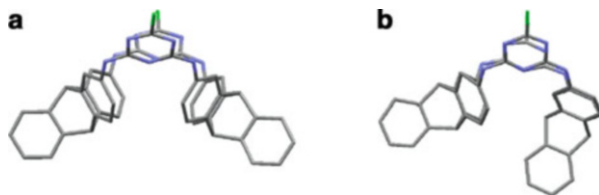
isomers [16, 17]. But in contrast with **10b** which adopted a chair formation, **13b** adopted a curved-boat conformation probably due to the solvent effect (Fig. 18.6b, c).

In the case of triptycene-derived *N(H)*-bridged azacalixarenes, the X-ray crystal structures showed that *cis*-isomers **19** and **21** adopted the similar boat conformation with a  $C_2$  axis (Fig. 18.7a), which indicated that the boat conformations could be maintained with different aromatic subunits and derivatization on the triptycene due to the rigidity brought by triptycene moieties [18]. This unique structural feature made the wider rim of triptycenes and the wider rim of the heteroaromatics point to the same direction, which was strikingly different from that of the reported azacalixarenes [7a]. *Trans*-isomer **20a** adopted a curved-boat conformation without a highly symmetric structure (Fig. 18.7b). For the triptycene-derived diazadioxalixarenes, the crystal structure showed that *cis*-isomer **26c** [19] was in a high symmetry with boat conformation, in which the two pyridine rings were located in different positions with respect to the triptycene moieties for the different hybrid orbitals and electronic effects of nitrogen atom and oxygen atom.

### 18.3.3 Molecular Recognition and Assembly of Triptycene-Derived Heteracalixarenes

Since oxacalixarenes **16a–b** had large cavities with fixed conformations, we [17a] studied its recognition capabilities towards fullerenes. By means of spectrophotometric experiments, we found that **13a** could form 1:1 complexes with both  $C_{60}$  and  $C_{70}$ , the stability constants  $K_s$  determined to be over  $1 \times 10^4 \text{ M}^{-1}$ , which represented the first example of complexation of the oxacalixarene with fullerenes. The binding properties of **13a** and **13b** towards metal ions were also investigated [20a]. It was found that the *cis*-isomer showed a highly selective response towards  $\text{Hg}^{2+}$  and thus could serve as a fluorescent probe for  $\text{Hg}^{2+}$ . Moreover, both **13a** and **13b** showed complexation capabilities towards electron-deficient linear guests and could form 1:1 complexes with paraquat derivatives **28a–g** (Fig. 18.8a) containing different functional groups in solution [17b]. By virtue of the  $^1\text{H}$  NMR spectroscopic titration experiments, the association constants for the 1:1 constants in solution were determined to be about  $1 \times 10^3 \text{ M}^{-1}$  for host **16a**, and  $1 \times 10^2 \text{ M}^{-1}$  for **16b**. The obviously smaller value of the latter might result from the bulky inward orientation

**Fig. 18.7** Crystal structures of (a) **19a** and (b) **20a**. Hydrogen atoms are omitted for clarity



with the chair conformation of **16b**. The X-ray crystal structures of complexes **13a@28a** and **13a@28f** further confirmed the formation of the complexes, in which it was found that the linear guests threaded through the cavity of **13a** and the bipyridinium units were distorted probably owing to the nonsymmetric environment provided by host **13a** (Fig. 18.8b). There existed multiple C–H···N hydrogen-bonding, C–H··· $\pi$  and  $\pi$ ··· $\pi$  stacking interactions between the host and the guests, which played an important role in formation of the stable [2]pseudorotaxane-type complexes [17b]. It was also found that the dethreading/rethreading processes of the [2]pseudorotaxanes could be easily controlled by acid/base stimuli or  $\text{Hg}^{2+}$  association/ dissociation. To exploit the potential of **13a** and **13b** to construct mechanically interlocked molecules, we further synthesized a pair of isomeric [2]rotaxanes by the reactions of [2]pseudorotaxanes with 3,5-di-*tert*-butylbenzoic anhydride in the presence of a catalytic amount of tri(*n*-butyl)phosphane, in which for the first time oxacalixarenes were used as wheels for the synthesis of mechanically interlocked molecules. The subsequent single-crystal structural analysis confirmed the formation of the [2]rotaxanes based on **13a**, in which the paraquat axle **28d** was bent, and one stopper group was positioned close to the 1,8-naphthyridine unit of the wheel with scorpion-like mode (Fig. 18.8c).

The two different semi-cavities of the 1,3-alternate oxacalixarene **13a** encouraged us to further investigate whether the discrepancies in size and electron density between the two semi-cavities of **13a** would exert different induction upon the threading of guests. Interestingly, it was found that the electron densities of axles **29a–c** (Fig. 18.9) greatly affected the threading direction, unequivocally demonstrated by NMR spectra and single crystal structures [20b]. Actually, the threading direction of a (bi)pyridinium guest pre-stoppered at one of its ends could be dominated by the electrostatic effect and finely tuned by the steric effect. Consequently, with elaborate design, unidirectional threading was achieved, resulting in an oriented rotaxane based on axle **29c**. Therefore, we provided a new approach in which the threading direction as well as the final orientation might be finely controlled by adjusting the structures of the guests based on triptycene-derived oxacalixarene with a fixed conformation and 3D unsymmetric structure.

In the case of triptycene-derived *N(H)*-bridged azacalixarenes, *cis*-isomers **19** and **21** with fixed boat conformations and large cavities also showed the capability of encapsulating solvent molecules inside their cavities [18]. Macrocyclic **19a** could encapsulate one methanol molecule via the O–H···N hydrogen bond between the hydroxyl group of methanol and N atoms in the triazine rings, and the O–H··· $\pi$  hydrogen bond between the hydroxyl group of methanol and one phenyl ring in

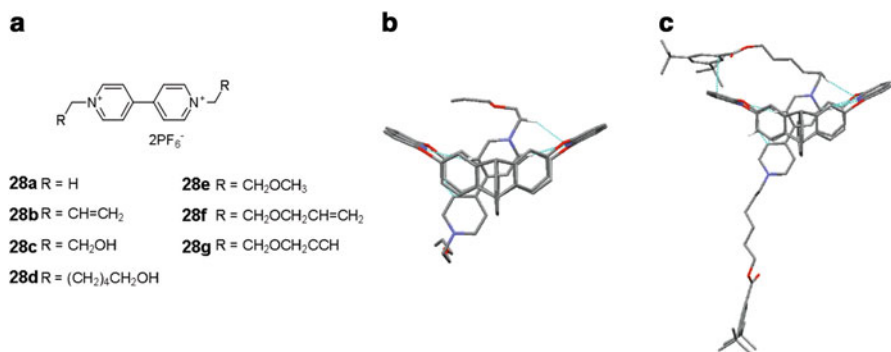


**Fig. 18.8** (a) Chemical structures of guests **28a–g**; (b) Crystal structure of complex **13a@28f**; (c) Crystal structure of [2]rotaxane formed by **13a** and **28d**. Solvent molecules, PF<sub>6</sub><sup>−</sup> counterions, and hydrogen atoms are omitted for clarity

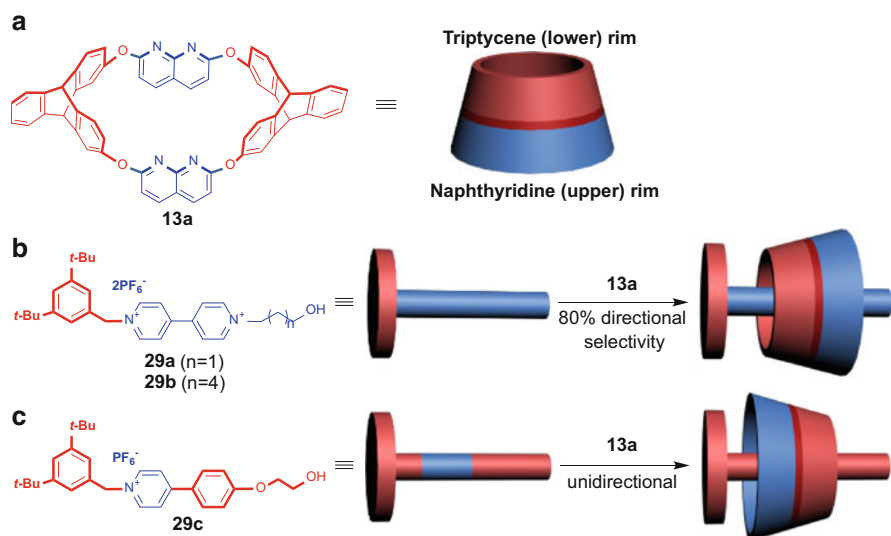


**Fig. 18.9** (a) Structure and representation of **13a**; (b) Structures and representation of guests **29a–b** and their directional threading into **13a**; (c) Structure and representation of **29c** and its unidirectional threading into **13a**

triptycene moieties. Similarly, **21a** could encapsulate one acetone molecule in its cavity with C–H···O hydrogen bond and two pairs of C–H··· $\pi$  interactions. In addition, it was found that two molecules of **21a** could form a dimer through the O<sup>δ−</sup>···N<sup>δ+</sup> and O<sup>δ−</sup>···C<sup>δ+</sup> interactions with two acetone molecules and two dichloromethane molecules inside its cavity (Fig. 18.10).

Similar to the triptycene-derived calixarenes, expanded oxalixarene **10a** with a fixed conformation could assemble into a tubular structure by virtue of C–Cl··· $\pi$ , C–H··· $\pi$  and  $\pi$ ··· $\pi$  interactions (Fig. 18.11) [16]. **10b** could also stack into a tubular

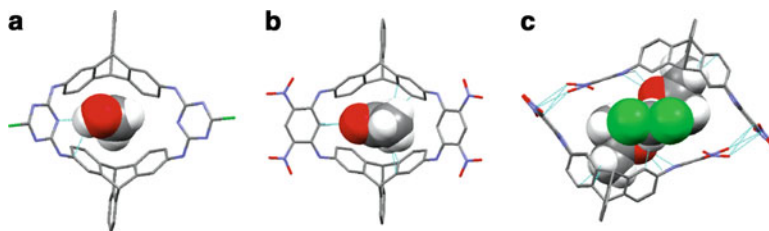


**Fig. 18.10** Crystal structures of (a)  $\text{CH}_3\text{OH}@19\text{a}$ , (b)  $\text{acetone}@21\text{a}$ , and (c)  $(\text{CH}_2\text{Cl}_2)_2 \cdot (\text{acetone})_2 @21\text{a}_2$

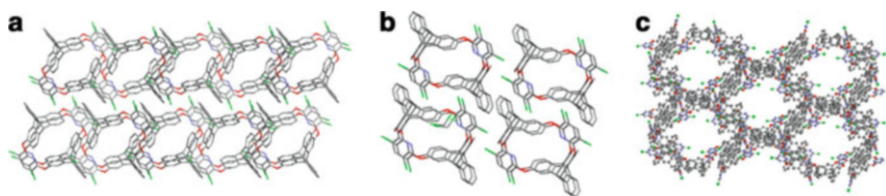


**Fig. 18.11** Packing structure of (a) **10a**, (b) **10b** and (c) **12a**

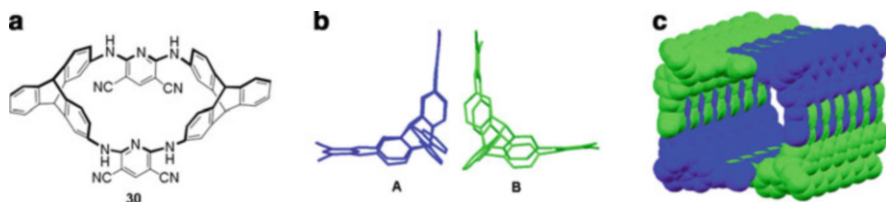


**Fig. 18.12** (a) Molecular structure of **30**, (b) crystal structure with the asymmetric unit of **30**, and (c) space-filling representation of a **30**-based nanotube

structure where the aromatic rings acted as the wall, and the nitrogen atoms of the pyridine rings all pointed inward towards the tube. In the tubular superstructure assembled by **12a**, the three adjacent molecules were connected to form an arc-like structure, and then connected with two molecules of **12a** in different orientations, finally resulting in the tubular assembly.

By replacing the phenyl rings with cyano-substituted pyridine rings in the triptycene-derived azacalixarene **21a**, azacalixarene **30** (Fig. 18.12a) obtained by similar synthetic strategy showed very interesting characteristics of aggregation in the solid state [21]. It was found that **30** could self-assemble into a novel aromatic single-walled organic nanotube with two molecules (denoted as **A** and **B**, Fig. 18.12b) in the boat-like conformation with similar cavity in one unit cell. Moreover, two molecules of **A** were located in opposite positions and generated a rectangular geometry with the four cyano groups and four NH sites in the same direction; while two molecules of **B** were also located face to face and generated a rectangular geometry rotated with respect to the former one by  $90^\circ$ . Then, with four



pairs of hydrogen bonds, they further assembled into two zigzags H-bonding chains and with four infinite one-dimensional H-bonding chains they further self-assembled into an aromatic single-walled square organic nanotube with diameters in excess of 15 Å, along with THF molecules located in each corner of the square channels (Fig. 18.12c). Moreover, this organic nanotube could retain its 3D honeycombed architecture upon the exchange of THF-methanol guests with acetone-methanol.

## 18.4 Other Triptycene-Derived Macrocyclic Arenes

Homoheterocalixarenes are expanded analogues of calixarenes in which the methylene bridges are partly or completely replaced by  $(\text{CH}_2)\text{XCH}_2$  ( $\text{X} = \text{O}, \text{NR}, \text{etc.}$ ) groups, resulting in bigger cavity sizes, different recognition properties and a wide field of applications [22]. Recently, we [23] utilized one-pot reactions of 2,7-dihydroxytriptycene **14** with 1,3-bisbromobenzene derivatives in DMF in the presence of  $\text{Cs}_2\text{CO}_3$  to obtain several pairs of triptycene-derived homooxalixarene analogues **31a–d** and **32a–d** in moderate yields, and further synthesized two pairs of “basket-like” triptycene-derived homooxalixarene analogues **33a–b** and **34a–b** in which the two *p*-phenyl-substituted benzene rings were linked together by crown ether chains (Fig. 18.13). In the  $^1\text{H}$  NMR spectra of **31a–c**, there were two singlets for the bridgehead protons with small  $\Delta\delta$  value showing that they were *cis*-isomer with a highly symmetric structure, while **32a–d** were *trans*-isomers with significantly different chemical shifts for bridgehead protons. In the case of **32c**, the two sets of doublet signals of the methylene groups gradually merged into one set of doublet signals above 370 K, which meant that at very high temperature the rigid conformation of it was no longer maintained. However, for **31c**, the methylene proton signals exhibited no obvious changes even up to 380 K. The conformations of macrocycles **34** and **33** could be fixed up to 380 K, since their two *p*-phenyl-substituted benzene rings were linked together by crown ether chains and could not rotate freely. With crystal structural analysis, it was further confirmed that *trans*-isomers **32b** and **32d** had chair-like conformations, while **31b** was a *cis*-isomer with a boat-like conformation.

Triptycene-derived homooxalixarene analogues with larger and fixed electron-rich cavities showed efficient complexation abilities towards fullerenes  $\text{C}_{60}$  and  $\text{C}_{70}$  [23]. **31a–d** and **32a–d** could all form 1:1 complexes with both  $\text{C}_{60}$  and  $\text{C}_{70}$ , in which most of the *cis*-isomers exhibited a little larger affinity towards  $\text{C}_{60}$ , while the *trans*-isomers have larger affinity towards  $\text{C}_{70}$ . This observation might be resulted from the symmetric cavities of the *cis*-isomers and the relatively flat cavities of the *trans*-isomers which fitted well with the sphere  $\text{C}_{60}$  and the oval  $\text{C}_{70}$ , respectively.

Tetralactam macrocycles as a class of hosts with special ability to include anions and organic molecules have been widely applied to construct a variety of interlocked supramolecular assemblies, develop new molecular machines, and



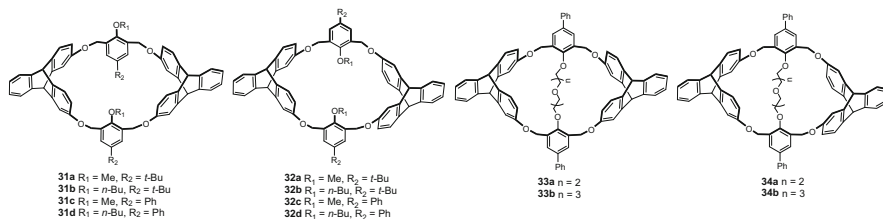


**Fig. 18.13** Structures of triptycene-derived homooxalixarene analogues **31–34**

improve the properties of organic dyes by molecular encapsulation [24]. Starting from 2,7-diaminotriptycene **23a**, we [25] conveniently synthesized macrocycles **35a–b** in 26% and 20% yield, respectively, by a one-pot [2 + 2] cyclization reaction with pyridine-2,6-dicarbonyl dichloride in dry THF in the presence of Et<sub>3</sub>N. This pair of macrocycles showed greatly different signals on the NMR spectra from each other, which suggested they were a pair of diastereomers. The only one signal for the NH protons and two singlets for the bridgehead protons of the triptycene moieties in their <sup>1</sup>H NMR spectra revealed that both of them were in highly symmetric structures. In addition, X-ray crystal structures of **35a–b** further confirmed that they were a pair of diastereomers, in which **35a** was a *cis*-isomer adopting a cone conformation with four carbonyl groups attached to the wider rim and the four amide NH protons defining the narrower rim. And the two triptycene moieties of **35b** were *trans*-connected by the pyridyl amide subunits in a chair conformation. Moreover, we also found intramolecular hydrogen bonds in both **35a** and **35b** which played an important role in the formation of their specific conformation (Fig. 18.14).

Similar to other triptycene-derived macrocyclic arenes, triptycene-derived tetralactam macrocycles also had fixed conformations with large electron-rich cavities, which made them promising candidates as the host for some electron-deficient guests with comparatively large sizes. Squaraines [26] were a family of fluorescent dyes with specific near-IR photophysical properties, which had wide potential applications. However, their instability limited the utilization of them, and thus improving their chemical stability and the photophysical properties were the key to applications of squaraines [27]. Consequently, we [25, 28] found that macrocycles **35a–b** could form a new kind of stable pseudorotaxane-type complexes with the squaraine in both solution and solid state. We further studied the chemical stability of squaraine in these complexes, and found that free guest **35b** underwent hydrolytic decomposition to turn colorless in polar THF-water solvent in 4 days, but for squaraine **36b** (Fig. 18.15) in complexation with **35a–b**, its blue colors could be retained for several weeks. This observation revealed that the formation of complexes could efficiently protect the squaraine dyes from polar solvents.

With further studied on the complexation of the macrocycles and the squaraine dyes with different terminal groups (Fig. 18.15), we found that these complex exhibited the complexation-induced asymmetry of the guest, which might result

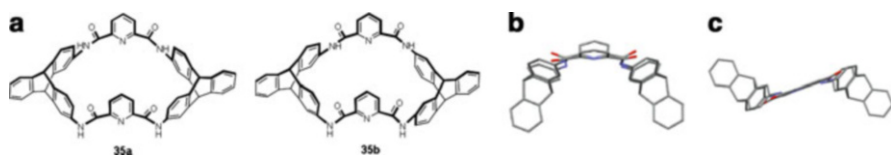


**Fig. 18.14** (a) Chemical structures of **35a–b**, and crystal structures of (b) **35a** and (c) **35b**. Solvent molecules and hydrogen atoms are omitted for clarity

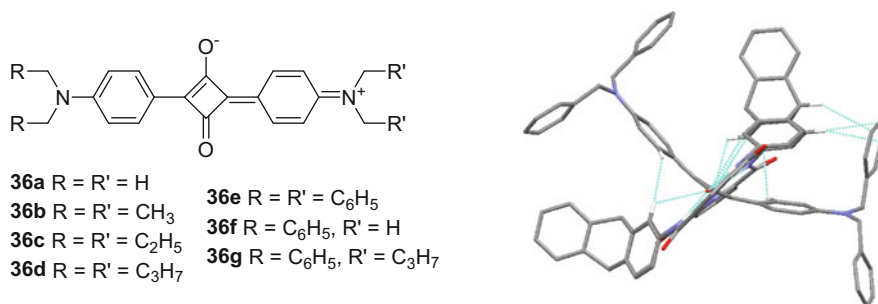


**Fig. 18.15** Chemical structures of squaraines **36a–g** and crystal structure of complex **35a@36e**

from the 3D cone conformation of **35a** [25, 28]. Meanwhile, the terminal groups of squaraine could influence the complexation mode. Guests **36a–b** containing small terminal groups could thread the wheels **35a–b** to form [2]pseudorotaxane complexes. However, for **36c**, we found that it could penetrate through macrocycle **35b** to form a [2]pseudorotaxane complex, but the similar insertion process could not be observed between **35a** and **36c** until the temperature was raised to 333 K, indicating a slippage mechanism. In addition, no threading processes between **35a/35b** and squaraines **36d** and **36e** were observed, even at 333 K for several days. These results revealed that the bulkier *N,N*-bis(*n*-butyl) and *N,N*-bis(benzyl) groups could act as the stopper for the [2]rotaxanes formed by triptycene-derived macrocycles **35a–b**. Interestingly, two new sets of resonances with different intensities could be found in the <sup>1</sup>H NMR spectrum of mixtures of **35a** and **36f**, suggesting that two isomeric [2]pseudorotaxanes based on **35a** and **36f** were obtained with a slight selectivity. According to the above results, we chose **36d–g** containing stopper groups that were bulky enough as the templates to synthesize [2]rotaxanes through clipping reactions. With the condensation reactions between pyridine-2,6-dicarbonyl dichloride and 2,7-diaminotriptycene in the presence of appropriate squaraine derivatives, a series of squaraine-based [2]rotaxanes were obtained. As expected, with symmetric guests as the template, two isomeric [2]rotaxanes were obtained due to the different linking modes of triptycene derivatives; but with asymmetric guests as the template, three isomeric [2]rotaxanes would be obtained due to not only the different linking modes of triptycene, but also different directions of the guest insertion process with partial selection. Further studies showed that these rotaxane-type complexes showed higher chemical stabilities than those of

free squaraines. In addition, with the typical hydrogen bonds between the amide protons of the hosts and the carbonyl oxygen atoms of the guests, and the multiple  $\pi\cdots\pi$  stacking interactions and  $C-H\cdots\pi$  interactions between triptycene subunits and the aromatic rings of the guests, [2]rotaxane with nonsymmetric macrocycles could self-assemble into an oriented non-symmetric channel-like structure.

## 18.5 Conclusion and Outlook

Based on triptycene building block with unique 3D rigid structure, we have designed and synthesized several kinds of novel macrocyclic arenes including triptycene-derived calixarenes, heteracalixarenes, homooxalixarene analogues and tetralactam macrocycles by one-pot or two-step methods. These macrocyclic arenes have the expanded 3D cavities, and also show fixed conformations in even high temperatures. These specific structural features made them be used as a new kind of host molecules, and exhibited well molecular recognition abilities towards small neutral organic molecules, paraquat derivatives, fullerenes and organic dyes. Moreover, these macrocycles can also be utilized as useful building blocks for the self-assembling into various supramolecular structures by multiple non-covalent interactions. Since different functionalized triptycenes including chiral triptycene derivatives can be conveniently achieved, various other novel triptycene derived macrocyclic arenes besides those ones presented in this chapter could be designed and synthesized as well. These macrocycles with specific structural features will find wide potential applications in molecular recognitions and self-assemblies, and even other research areas. Although studies on the synthesis and applications of the triptycene-derived macrocyclic hosts are still in the infancy, we believe that they will attract more and more attention, and thus become one of the important and hot research areas in both supramolecular chemistry and triptycene chemistry in the near future.

## References

1. (a) Gutsche, C. D. *Calixarenes Revisited, Monographs in Supramolecular Chemistry*. Royal Society of Chemistry: Cambridge, 1998; (b) Thondorf, I. *Calixarenes 2001*. Kluwer Academic Publishers: Dordrecht, The Netherlands, 2001.
2. (a) Mutihac, L.; Lee, J. H.; Kim, J. S.; Vicens, J. *Chem. Soc. Rev.* **2011**, *40*, 2777; (b) Ikeda, A.; Shinkai, S. *Chem. Rev.* **1997**, *97*, 1713.
3. (a) Kim, J. S.; Quang, D. T. *Chem. Rev.* **2007**, *107*, 3780; (b) Kim, J. S.; Lee, S. Y.; Yoon, J.; Vicens, J. *Chem. Commun.* **2009**, 4791.
4. (a) Wei, A. *Chem. Commun.* **2006**, 1581; (b) Haino, T.; Matsumoto, Y.; Fukazawa, Y. *J. Am. Chem. Soc.* **2005**, *127*, 8936.
5. Homden, D. M.; Redshaw, C. *Chem. Rev.* **2008**, *108*, 5086.

6. (a) Amrhein, P.; Shivanyuk, A.; Johnson, D. W.; Rebek, J. *J. Am. Chem. Soc.* **2002**, *124*, 10349; (b) de Fatima, A.; Fernandes, S. A.; Sabino, A. A. *Curr. Drug. Discov. Technol.* **2009**, *6*, 151.
7. (a) Wang, M.-X. *Chem. Commun.* **2008**, 4541; (b) Wang, M.-X. *Acc. Chem. Res.* **2011**, *45*, 182; (c) Maes, W.; Dehaen, W. *Chem. Soc. Rev.* **2008**, *37*, 2393. (d) Ma, Y.-X.; Han, Y.; Chen, C.-F. *J. Incl. Phenom. Macrocycl. Chem.* **2014**, *79*, 261.
8. (a) Ma, Y.-X.; Chen, C.-F. *Iptycene Chemistry: from Synthesis to Applications*. Springer-Verlag: Berlin Heidelberg, 2013; (b) Chen, C.-F. *Chem. Commun.* **2011**, *47*, 1674; (c) Jiang, Y.; Chen, C.-F. *Eur. J. Org. Chem.* **2011**, 6377; (d) Han, Y.; Meng, Z.; Ma, Y.-X.; Chen, C.-F. *Acc. Chem. Res.* **2014**, *47*, 2026.
9. (a) Han, Y.; Lu, H.-Y.; Zong, Q.-S.; Guo, J.-B.; Chen, C.-F. *J. Org. Chem.* **2012**, *77*, 2422; (b) Zhu, X.-Z.; Chen, C.-F. *J. Am. Chem. Soc.* **2005**, *127*, 13158; (c) Zong, Q.-S.; Chen, C.-F. *Org. Lett.* **2006**, *8*, 211; (d) Han, T.; Chen, C.-F. *Org. Lett.* **2007**, *9*, 4207.
10. (a) Han, T.; Chen, C.-F. *Org. Lett.* **2006**, *8*, 1069; (b) Peng, X.-X.; Lu, H.-Y.; Han, T.; Chen, C.-F. *Org. Lett.* **2007**, *9*, 895; (c) Jiang, Y.; Cao, J.; Zhao, J.-M.; Xiang, J.-F.; Chen, C.-F. *J. Org. Chem.* **2010**, *75*, 1767.
11. (a) Tian, X.-H.; Hao, X.; Liang, T.-L.; Chen, C.-F. *Chem. Commun.* **2009**, 6771; (b) Tian, X.-H.; Chen, C.-F. *Chem. Eur. J.* **2010**, *16*, 8072; (c) Xia, Y.-X.; Xie, T.; Han, Y.; Chen, C.-F. *Org. Chem. Front.* **2014**, *1*, 140; (d) Tian, X.-H.; Chen, C.-F. *Org. Lett.* **2010**, *12*, 524; (e) Xia, Y.-X.; Han, Y.; Chen, C.-F. *Eur. J. Org. Chem.* **2014**, *9*, 1976.
12. Li, P.-F.; Chen, C.-F. *Chem. Commun.* **2011**, *47*, 12170.
13. Gutsche, C. D. *Acc. Chem. Res.* **1983**, *16*, 161.
14. Atwood, J. L.; Barbour, L. J.; Raston, C. L.; Sudria, I. B. N. *Angew. Chem. Int. Ed.* **1998**, *37*, 981.
15. Wang, J.; Gutsche, C. D. *J. Am. Chem. Soc.* **1998**, *120*, 12226.
16. Zhang, C.; Chen, C.-F. *J. Org. Chem.* **2007**, *72*, 3880.
17. (a) Hu, S.-Z.; Chen, C.-F. *Chem. Commun.* **2010**, 46, 4199; (b) Hu, S.-Z.; Chen, C.-F. *Chem. Eur. J.* **2011**, *17*, 5423.
18. Xue, M.; Chen, C.-F. *Org. Lett.* **2009**, *11*, 5294.
19. Xue, M.; Hu, S.-Z.; Chen, C.-F. *Acta Chim. Sinica.* **2012**, *70*, 1697.
20. (a) Hu, S.-Z.; Chen, C.-F. *Org. Biomol. Chem.* **2011**, *9*, 5838; (b) Wang, H.-X.; Meng, Z.; Xiang, J.-F.; Xia, Y.-X.; Sun, Y.; Hu, S.-Z.; Chen, H.; Yao, J.; Chen, C.-F. *Chem. Sci.* **2016**, *7*, 469.
21. Xue, M.; Chen, C.-F. *Chem. Commun.* **2011**, *47*, 2318.
22. (a) Chen, Y.; Wang, D. X.; Huang, Z. T.; Wang, M. X. *J. Org. Chem.* **2010**, *75*, 3786; (b) Thomas, J.; Van Hecke, K.; Robeyns, K.; Van Rossom, W.; Sonawane, M. P.; Van Meervelt, L.; Smet, M.; Maes, W.; Dehaen, W. *Chem. Eur. J.* **2011**, *17*, 10339.
23. Xie, T.; Hu, S.-Z.; Chen, C.-F. *J. Org. Chem.* **2012**, *78*, 981.
24. (a) Vögtle, F.; Dunnwald, T.; Schmidt, T. *Acc. Chem. Res.* **1996**, *29*, 451; (b) Kay, E. R.; Leigh, D. A.; Zerbetto, F. *Angew. Chem. Int. Ed.* **2007**, *46*, 72.
25. Xue, M.; Chen, C.-F. *Chem. Commun.* **2008**, 6128.
26. Sreejith, S.; Carol, P.; Chithra, P.; Ajayaghosh, A. *J. Mater. Chem.* **2008**, *18*, 264.
27. (a) Chen, H.-J.; Farahat, M. S.; Law, K. Y.; Whitten, D. G. *J. Am. Chem. Soc.* **1996**, *118*, 2584; (b) Johnson, J. R.; Fu, N.; Arunkumar, E.; Leevy, W. M.; Gammon, S. T.; Pivnicka-Worms, D.; Smith, B. D. *Angew. Chem. Int. Ed.* **2007**, *46*, 5528.
28. Xue, M.; Su, Y.-S.; Chen, C.-F. *Chem. Eur. J.* **2010**, *16*, 8537.

# Chapter 19

## Pillar[*n*]arenes: Easy-to-Make Pillar-Shaped Macrocyclic Hosts for Supramolecular Chemistry

Tomoki Ogoshi and Tada-aki Yamagishi

### 19.1 Introduction

The search for novel macrocyclic host molecules with unique structural features, host-guest properties and functionalities represents a challenging but very important area of supramolecular chemistry, where discoveries made during the last decade have led to a period of significant growth [1]. Macrocyclic compounds have symmetrical ring-shaped structures with a diameter of about 1 nm. The building up of these materials may therefore lead to the construction of new supramolecular materials with highly controlled structures. Furthermore, macrocyclic compounds have intrinsic pores, which can be used to capture guest molecules via the formation of various physical interactions. Another important feature of macrocyclic compounds is that they contain a wide variety of functional groups, which can be readily modified to tune their properties, including their solubility, guest-recognition ability and self-assembly characteristics. Several compound classes have been reported in the literature as typical host molecules, including crown ethers [2], cyclodextrins [3], cucurbit[*n*]urils [4] and calix[*n*]arenes [5], as well as several structurally related scaffolds [6].

In 2008, we reported the discovery of a new class of pillar-shaped macrocyclic host compounds, known as “pillar[*n*]arenes” [7]. Compared with typical host molecules, there are several unique advantages associated with pillar[*n*]arenes

---

T. Ogoshi (✉)

Graduate School of Natural Science and Technology, Kanazawa University, Kakuma-machi, Kanazawa 920-1192, Japan

Japan Science and Technology Agency, Kawaguchi, Saitama 332-0012, Japan

e-mail: [ogoshi@se.kanazawa-u.ac.jp](mailto:ogoshi@se.kanazawa-u.ac.jp)

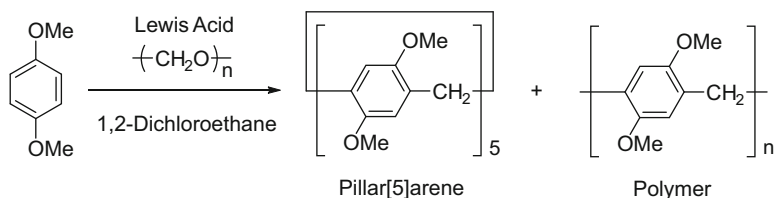
T.-a. Yamagishi

Graduate School of Natural Science and Technology, Kanazawa University, Kakuma-machi, Kanazawa 920-1192, Japan

such as their unique pillar-shape, one-pot synthesis, versatile functionality and superior host-guest properties resulting from their pillar-shaped structures. Based on their unique properties, pillar[ $n$ ]arenes are currently recognized as key players in supramolecular chemistry [8]. In this chapter, we have provided a brief description of the different methods available for the synthesis of pillar[ $n$ ]arenes. Furthermore, we have explained why cyclic pentamers (i.e., pillar[5]arenes) and cyclic hexamers (i.e., pillar[6]arenes) are selectively obtained in high yields under optimized conditions, and discussed the difficulties associated with the synthesis of higher pillar [ $n$ ]arene homologs ( $n > 7$ ). Second, we have provided some discussion of the difficulties associated with the functionalization of pillar[ $n$ ]arenes. Third, we have discussed the unique pillar-shaped structure of pillar[ $n$ ]arenes and compared it with the structures of several other typical host molecules. We have also provided a brief description of the unique host-guest properties of pillar[ $n$ ]arenes resulting from their pillar-shaped structures. Finally, we have provided several examples of one-, two- and three-dimensional supramolecular assemblies constructed from pillar[ $n$ ]arenes.

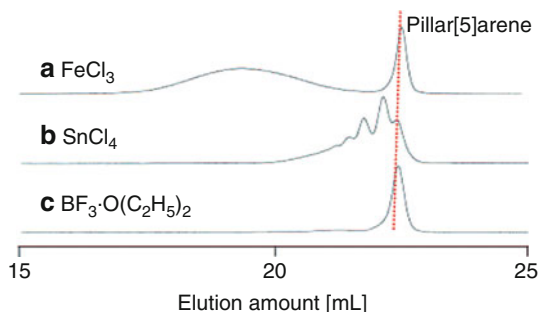
## 19.2 Synthesis of Pillar[ $n$ ]arenes

Pillar[ $n$ ]arenes were accidentally produced as an unexpected byproduct during our investigation towards the synthesis of new phenolic polymers via the reaction of 1,4-dimethoxybenzene with paraformaldehyde in the presence of a Lewis acid (Scheme 19.1 and Fig. 19.1) [7].

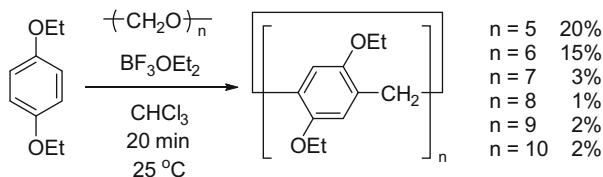


**Scheme 19.1** Condensation of 1,4-dimethoxybenzene and paraformaldehyde with Lewis acids

**Fig. 19.1** GPC traces of the products obtained using (a)  $\text{FeCl}_3$ , (b)  $\text{SnCl}_4$  and (c)  $\text{BF}_3\text{OEt}_2$  as a Lewis acid (Reprinted with permission from Ref. [7]. Copyright 2008 American Chemical Society)



**Scheme 19.2** Synthesis of pillar[*n*]arene homologs (*n* = 5–10) from 1,4-diethoxybenzene reported by Hou et al. [11]



When  $\text{FeCl}_3$  (Fig. 19.1a) or  $\text{SnCl}_4$  (Fig. 19.1b) was used as the Lewis acid, we obtained the desired phenolic polymer as the major product, along with pillar[5]arene as a minor product. Surprisingly, however, when  $\text{BF}_3\text{OEt}_2$  was used as the Lewis acid (Fig. 19.1c), the major product became pillar[5]arene. Furthermore, by tuning the feed ratios of 1,4-dialkoxybenzene and paraformaldehyde, we successfully improved the yield of pillar[5]arene from 26 % to 73 % [9]. However, it remained unclear at this stage why pillar[5]arene was obtained in such a high yield from this reaction. Szumna et al. reported a solvent effect for the synthesis of pillar[5]arene [10]. When 1,2-dichloroethane was used as a solvent, pillar[5]arene was produced as the major product (up to 81 % under the optimized conditions). In contrast, the yields were low when dichloromethane (26 %), chloroform (15 %) or 1,1,2,2-tetrachloroethane (7 %) was used as the solvent. Although chloroform and 1,1,2,2-tetrachloroethane only afforded low yields of pillar[5]arene, they can be used as solvents for the synthesis of higher pillar[*n*]arene homologs under kinetically controlled conditions. Based on these observations, Hou et al. reported the synthesis of several higher pillar[*n*]arene homologs using chloroform (Scheme 19.2) [11].

The conditions for this reaction have to be carefully optimized because this process is conducted under kinetically control. The optimized reaction conditions were determined to be 20 min at 25 °C for the synthesis of higher pillar[*n*]arene homologs. Under these optimized conditions, the reaction of 1,4-diethoxybenzene with paraformaldehyde in the presence of  $\text{BF}_3\text{OEt}_2$  in chloroform not only afforded pillar[5]arene and pillar[6]arene as the major products, but also gave several larger pillar[*n*]arene homologs as minor products, including pillar[7]arene, pillar[8]arene, pillar[9]arene and pillar[10]arene in 3 %, 1 %, 2 % and 2 % yields, respectively.

The type of solvent used for the preparation of pillar[*n*]arenes can have a pronounced impact on the number of the repeating units incorporated in pillar[*n*]arene structure. With this in mind, we envisioned that bulky hydrocarbon molecules could be used as template solvents to produce pillar[6]arene because these compounds are good guest molecules for pillar[6]arenes. When chlorocyclohexane was used as a solvent (Scheme 19.3), pillar[6]arene was produced as the major product (87 %), together with a small amount of pillar[5]arene (3 %) [12].

Based on these experiential results, it was possible to elucidate the mechanism responsible for the formation of pillar[*n*]arenes (Fig. 19.2). Cyclic pentamers (i.e., pillar[5]arenes) and hexamers (i.e., pillar[6]arenes) can be selectively prepared based on the choice of an appropriate template solvent, which also acts as good guests for pillar[5]arene and pillar[6]arene, respectively. For example, linear

**Scheme 19.3** Selective synthesis of pillar[6]arene using chlorocyclohexane as a template solvent

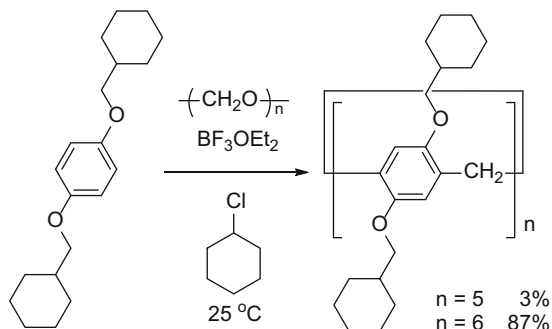
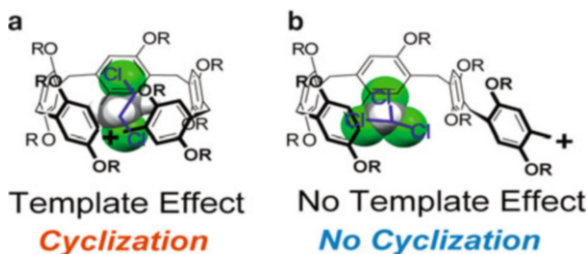


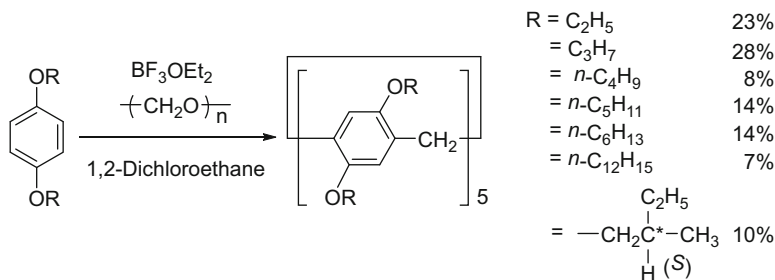
**Fig. 19.2** (a) Linear 1,2-dichloroethane acts as template solvents for the formation of pillar[5]arene, whereas (b) branched chloroform failed as a template for the synthesis of specific pillar[ $n$ ]arene homologs



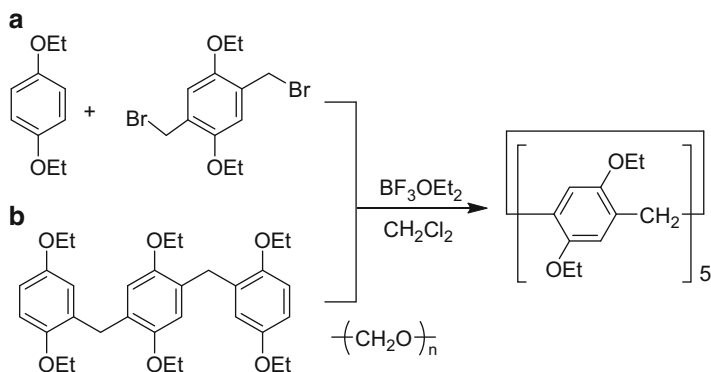
solvents, such as 1,2-dichloroethane are suitable solvents for the synthesis of pillar[5]arene (Fig. 19.2a). In contrast, bulky solvents such as chlorocyclohexane are useful for the selective synthesis of pillar[6]arene. However, the use of an unsuitable template solvent such as chloroform generally results in the formation of a mixture of pillar[ $n$ ]arene homologs and polymers (Fig. 19.2b). Under the optimized reaction conditions, higher pillar[ $n$ ]arene homologs can be obtained in low yields. One of the major bottle-necks associated with the synthesis of macrocyclic compounds is their low yields. Pillar[5]arene can be produced in high yield via a one-pot synthesis using commercially available reagents. The facile synthesis of pillar[5]arene therefore represents a significant advantage to this host system compared with other host molecules. Furthermore, based on the ease with which these compounds can be synthesized, Tokyo Chemical Industry (TCI) commercialized pillar[5]arene in 2014 [13]. The solvent template synthesis of pillar[5]arene can be used for the synthesis of the other pillar[5]arene derivatives. Pillar[5]arenes bearing linear alkyl chains of different lengths and branched alkyl groups, such as ethoxy, propoxy, butoxy, pentyloxy, hexyloxy, dodecanoxy and 2(*S*)-methylbutoxy groups, can also be prepared from the corresponding 1,4-dialkoxybenzene monomers using 1,2-dichloroethane as a template solvent (Scheme 19.4) [14].

Nierengarten et al. discovered that the formation of pillar[ $n$ ]arenes proceeded under dynamic covalent bond formation during their investigation towards the development of selective synthetic procedures for the formation of pillar[6]arenes (Scheme 19.5) [15]. During their investigation, Nierengarten's group investigated the co-cyclization of two different monomers, namely 2,5-bis(bromomethyl)-1,4-diethoxybenzene and 1,4-diethoxybenzene, with a Lewis acid (Scheme 19.5a).





**Scheme 19.4** Simple pillar[5]arenes bearing a variety of different linear alkyl and branched chains



**Scheme 19.5** Formation of pillar[5]arene via the (a) co-cyclization of different monomers and (b) a trimer

However, the major product obtained from these reactions was pillar[5]arene rather than pillar[6]arene. The macrocyclization of the trimer by the reaction of paraformaldehyde with Lewis acid also afforded pillar[5]arene (Scheme 19.5b). In both of these cases, it would be necessary for the methylene bridge bonds to be cleaved during the reaction to explain the formation of the cyclic pentamer pillar[5]arene. Our groups have also reported the occurrence of dynamic covalent bond formation via the ring opening reaction of pre-formed pillar[5]arene. The reaction of pillar[5]arene with BF<sub>3</sub>OEt<sub>2</sub> in chlorocyclohexane, which is a good template solvent for the synthesis of pillar[6]arenes, led to the formation of pillar[6]arene (Fig. 19.3a) [12].

In contrast, the reaction of pillar[6]arene with BF<sub>3</sub>OEt<sub>2</sub> in 1,2-dichloroethane, which is a template solvent for pillar[5]arenes, resulted in formation of pillar[5]arene (Fig. 19.3b). Based on this ring-opening reaction, we developed a new synthetic route for the preparation of higher pillar[*n*]arene homologs (Scheme 19.6) [16].

We also investigated the use of chloroform, which could not be used as a template solvent, as a solvent for these reactions. The ring-opening reaction of

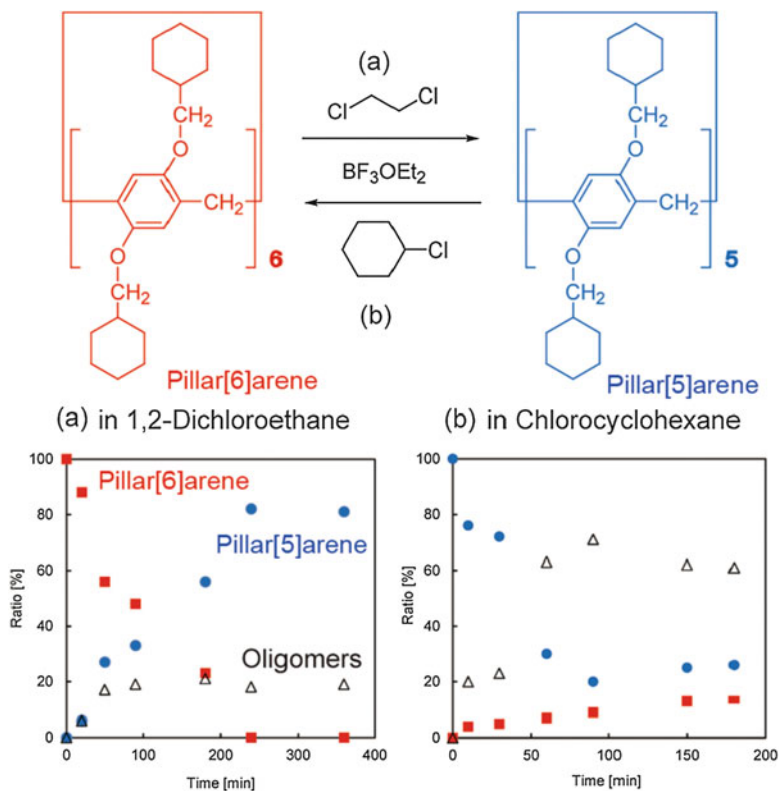
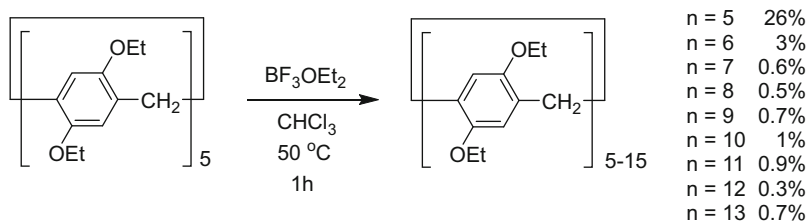


**Fig. 19.3** Inversion between pillar[5]arene and pillar[6]arene. Ratios of pillar[5]arene (*blue circles*) and pillar[6]arene (*red squares*) and oligomers (*black triangles*) resulting from the ring-opening reactions of (a) pillar[6]arene in 1,2-dichloroethane and (b) pillar[5]arene in chlorocyclohexane at 80 °C, both of which were monitored by the  $^1\text{H}$  NMR analysis of the reaction mixtures over time (Reproduced with permission from Ref. [12]. Copyright 2014 Royal Society of Chemistry)



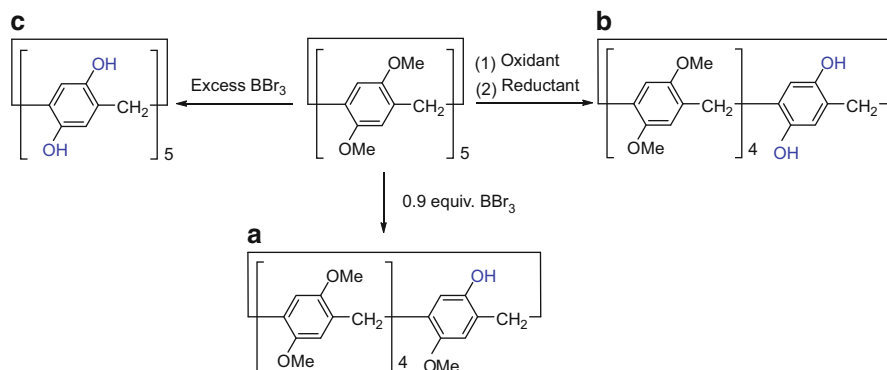
**Scheme 19.6** Synthesis of pillar[*n*]arene homologs (*n* = 5–13) via the ring-opening reactions of pillar[5]arene

pillar[5]arene with  $\text{BF}_3\text{OEt}_2$  in chloroform did not proceed at 25 °C. However, this reaction did proceed at 50 °C, indicating that heating was necessary to promote the ring-opening reaction. Furthermore, this reaction resulted in the formation of a mixture of pillar[*n*]arene homologs ( $n = 5-15$ ) when it was conducted under the optimized reaction conditions (1 h). Several new higher pillar[*n*]arene homologs ( $n = 11-13$ ) were also obtained from known pillar[*n*]arene homologs ( $n = 5-10$ ) in this way. Notably, this method avoids the formation of soluble byproducts such as linear polymers and oligomers because it uses a pre-formed pillar[*n*]arene ring as a starting compound. The lack of soluble byproducts enabled us to separate several new pillar[*n*]arene homologs ( $n = 11-13$ ). In addition, these experiments provided a clear demonstration of the dynamic nature of the covalent bond formation process of pillar[*n*]arenes.

### 19.3 Functionalization of Pillar[*n*]arenes

The installation of different functional groups on the rims of macrocyclic compounds is an important area of research because these changes can have a dramatic effect on the solubility, host-guest and self-assembly properties of the resulting macrocyclic compounds. Based on their versatile functionality, cyclodextrins and calix[*n*]arenes represent superior macrocyclic platforms compared with other known macrocyclic host molecules because they contain numerous reactive OH groups, which can be readily converted to a wide range of other functional groups by means of etherification. To achieve a similar level of functional diversity, our group recently investigated the de-protection of the methoxy groups to produce pillar[*n*]arenes bearing reactive OH groups [7].

Pillar[5]arenes bearing ten OH moieties can be readily produced in a quantitative manner by the treatment of pre-formed pillar[5]arene bearing ten alkoxy groups with an excess of  $\text{BBr}_3$  (Scheme 19.7c). Our group and Stoddart's group successfully synthesized pillar[5]arenes bearing one, two and three OH moieties by optimizing the reaction conditions used for the cleavage of the alkoxy groups with  $\text{BBr}_3$  [17]. The amount of  $\text{BBr}_3$  and reaction temperature used in these deprotection reactions are important factors in terms of obtaining pillar[5]arenes with OH groups at specific positions (Scheme 19.7a). Another useful method for the introduction of reactive OH moieties into pillar[*n*]arenes is the sequential oxidation/reduction method (Scheme 19.7b) [18]. The oxidation of one of the 1,4-dialkoxybenzene units in pillar[5]arene afforded a pillar[5]arene bearing a benzoquinone unit. The subsequent reduction of this material afforded a pillar[5]arene bearing 2 OH groups on the same unit by the reduction of the benzoquinone unit. The main advantage of this sequential oxidation/reduction method is that it can be used to selectively produce pillar[5]arenes bearing two phenolic groups on the same unit. The use of  $\text{BBr}_3$  for the deprotection of the alkoxy groups in pillar[5]arenes generally results in the formation of a mixture of multi-deprotected pillar[5]arenes, making the separation of the desired dihydroxylated pillar[5]arene isomers from the mixture quite

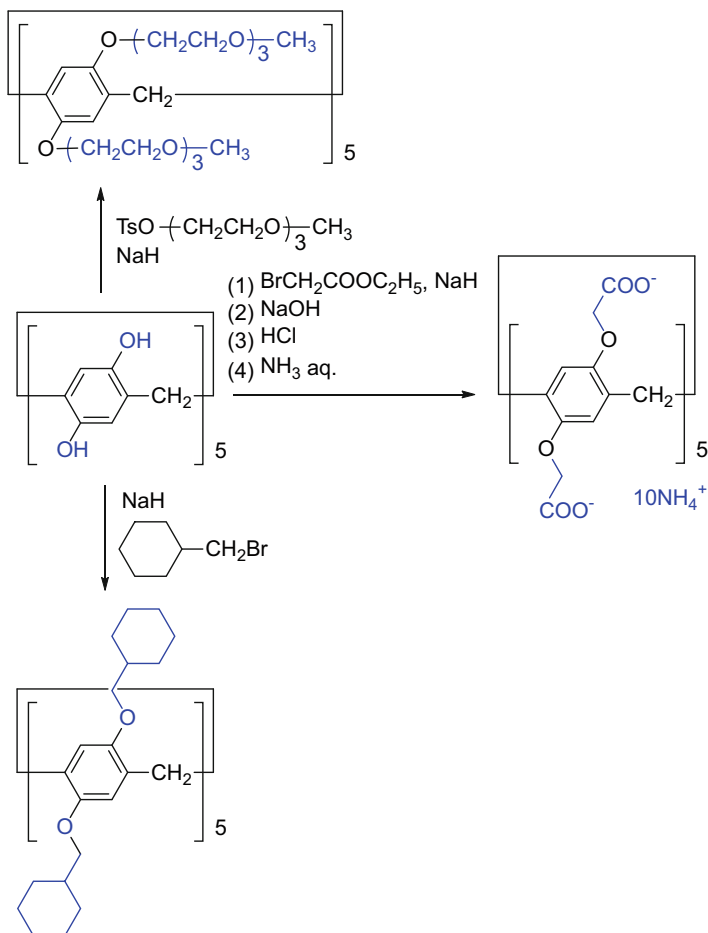


**Scheme 19.7** Synthesis of (a) mono- or (b) di- and (c) per-hydroxylated pillar[5]arenes using deprotection strategies using BBr<sub>3</sub> and sequential oxidation and reduction reactions, respectively

difficult. The sequential oxidation/reduction method is therefore useful for the synthesis of pillar[5]arenes bearing two OH moieties on the same unit. Further oxidation of pre-formed pillar[5]arenes afforded pillar[5]arenes containing two benzoquinone units. The subsequent reduction of these pillar[5]arenes afforded pillar[5]arenes bearing four OH moieties at specific positions [18a]. The deprotection of alkoxy moieties with BBr<sub>3</sub> and the subsequent sequential oxidation/reduction of the resulting alkoxy moieties can therefore provide access to pillar[5]arenes bearing one, two, three, four and ten OH moieties, which can be used for the synthesis of higher pillar[*n*]arene homologs with reactive OH moieties. A wide variety of pillar[5]arene derivatives can be produced by the etherification of pillar[*n*]arenes bearing OH moieties with alkyl halides in the presence of an appropriate base. Scheme 19.8 shows the functionalization of per-hydroxylated pillar[5]arene.

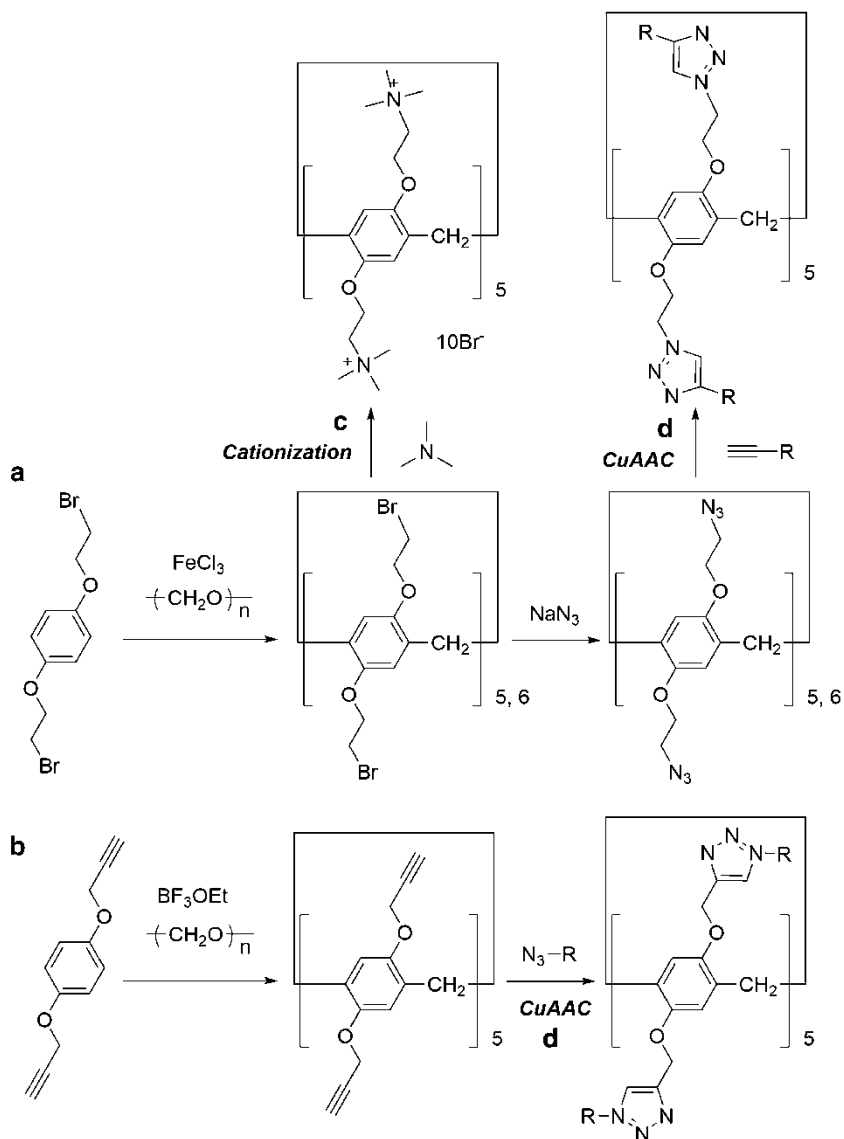
We reported the first ever synthesis of a water-soluble pillar[5]arene bearing ten carboxylate moieties by an etherification method [19]. Water-soluble pillar[5]arenes bearing ten amino and tri(ethylene oxide) moieties can also be prepared using an etherification method [20]. This method can also be used for the introduction of bulky substituents such as cyclohexylmethyl groups [21]. Etherification therefore represents a straightforward and reliable process that can be readily applied to the functionalization of pillar[5]arenes bearing one to four OH moieties, which can themselves be prepared by the deprotection of the corresponding alkoxy groups using the methods described above. Etherification has also been used for the functionalization of larger pillar[*n*]arene homologs with OH groups [22].

Another powerful protocol for the synthesis of functionalized pillar[*n*]arenes involves the cyclization of 1,4-dialkoxybenzenes bearing a variety of different functional groups. Nierengarten et al. reported the formation of pillar[5]- and pillar[6]arenes bearing bromo moieties in moderate yields using 1,4-dialkoxybenzene monomers containing two bromide moieties (Scheme 19.9a) [23].



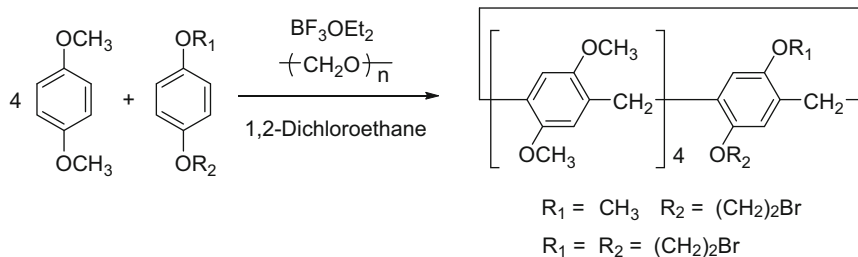
**Scheme 19.8** Synthesis of per-functionalized pillar[5]arenes from pre-formed per-hydroxylated pillar[5]arene

Deca- and dodecabromides are good building blocks for the preparation of various functionalized pillar[5]- and pillar[6]arenes. Water-soluble cationic pillar[5]- and pillar[6]arenes can be synthesized by the reaction of deca- and dodecabromides with amino compounds, as well as pyridine and triazole groups (Scheme 19.9c) [24]. The etherification of decabromides with coumarin derivatives bearing a phenolic moiety gave a pillar[5]arene with ten coumarin moieties [25]. Another useful method for the synthesis of functionalized pillar[*n*]arenes involves the reaction of azides and alkynes with copper (I), namely the copper (I)-catalyzed Huisgen alkyne-azide 1,3-dipolar cycloaddition reaction (CuAAC reaction). Pillar[*n*]arenes with azide moieties such as decaazide and dodecaazide can be readily prepared from the corresponding deca- and dodecabromides, respectively [23]. The CuAAC reaction of these azides with alkyne derivatives can be



**Scheme 19.9** Cyclization of 1,4-dialkoxybenzenes bearing (a) two bromide or (b) two alkyne moieties to produce deca- and dodecabromides or decaalkyne, respectively. Functionalization of deca- and dodecabromides by (c) cationization, as well as deca- and dodecaazides or decaalkyne by (d) CuAAC reactions

used to provide facile access to pillar[*n*]arenes bearing a wide range of functional groups such as mesogens, mannose and ferrocene moieties (Scheme 19.9d) [23, 26]. Pillar[5]arenes bearing ten alkyne moieties can not only be accessed by



**Scheme 19.10** Co-cyclization of two different 1,4-dialkoxybenzene monomers with paraformaldehyde to produce pillar[5]arenes bearing one and two bromide moieties

the etherification of decanol with propargyl bromide [27] but can also be prepared by the cyclization of a suitable dialkoxybenzene monomer with two alkyne groups (Scheme 19.9b) [28]. The CuAAC reaction of a decaalkyne substrate with numerous azide derivatives afforded pillar[*n*]arenes with various functional groups such as hexyl, benzyl, phenyl and pyrenyl moieties, as well as oligo(ethylene oxide) groups and cationic dendrons (Scheme 19.9d) [28].

Pillar[5]arenes bearing one or two bromide moieties have also been prepared by the co-cyclization of different 1,4-dialkoxybenzene monomers. The co-cyclization method, which was first reported by Huang et al., involves the cyclization of one 1,4-dialkoxybenzene molecule with another 1,4-dialkoxybenzene bearing different alkoxy groups [29]. The first example of a pillar[5]arene with one bromide group was reported by Stoddart et al., who prepared the material using a co-cyclization method [30]. Stoddart's group also reported the preparation of a similar pillar[5]arene containing one bromide group by the co-cyclization of 1,4-dimethoxybenzene with a dialkoxybenzene substrate containing one bromide group (Scheme 19.10).

Wang et al. reported the preparation of a pillar[5]arene bearing two bromide moieties on the same unit by the co-cyclization of 1,4-bis(2-bromoethoxy)benzene with 1,4-dimethoxybenzene [31]. In a similar manner to the decabromide, the mono- and dibromides were readily functionalized by cationization, etherification and CuAAC reactions.

## 19.4 Structure of Pillar[*n*]arenes

The structure of pillar[*n*]arenes is the most important feature of their chemistry and has a significant impact on their reactivity, as well as their behavior as host systems. We reported the first X-ray crystal structure of a pillar[*n*]arene in 2008 when we solved the structures of pillar[5]arene bearing ten methoxy groups (Fig. 19.4a) [7].

The X-ray crystal structure of pillar[5]arene revealed that this compound existed in a highly symmetric cylindrical form when viewed from its side, and a regular pentagon when viewed from the top. The difference in these two perspectives may

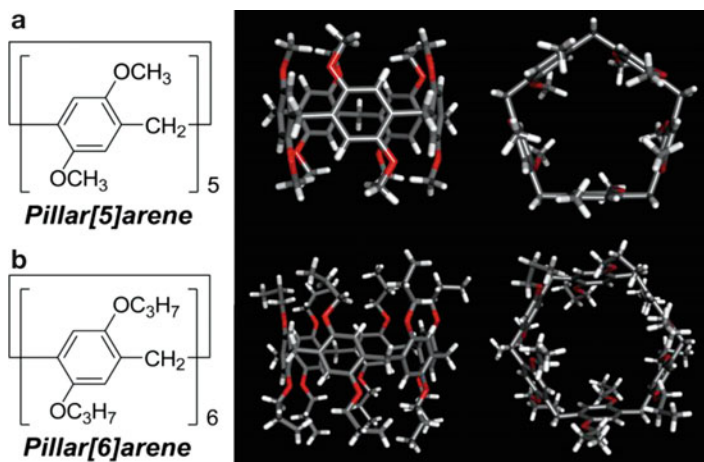


**Fig. 19.4** Chemical and X-ray crystal structures of (a) pillar[5]-, (b) pillar[6]arenes

be attributed to differences in the position of the methylene bridges. The 1,4-dimethoxybenzene units were connected through methylene linkages at their *para*-positions. The positioning of these methylene linkages at the *para*-positions of the phenyl rings resulted in these highly symmetrical structures. In contrast, calix [*n*]arenes and their derivatives, including calix[*n*]resorcinarenes and cyclotrimer-arylene, are vase-shaped structures because their units are connected by methylene or methine bridges located at the *ortho*- and *meta*-positions of their phenyl rings. It is noteworthy that the highly symmetrical pillar-shaped structure of pillar[*n*]arenes was the reason that we named these paracyclophanes as “pillar[*n*]arenes” in the first place. The first X-ray crystal structure of a pillar[6]arene was reported by Huang and co-workers in 2010 (Fig. 19.4b) [32]. As with pillar[5]arene, the X-ray crystal structure of pillar[6]arene revealed that it existed as a highly symmetrical structure. For example, pillar[6]arene appears as a hexagonal-like cyclic structure when viewed from the top, and a highly symmetrical cylindrical structure when viewed from its side. The X-ray crystal structures of larger pillar[*n*]arene homologs, including pillar[8]-, pillar[9]- and pillar[10]arenes were reported by Hou et al. in 2012 [11]. The results revealed that pillar[5]- and pillar[6]arenes have one cavity each, whereas the higher pillar[*n*]arenes (*n* = 8, 9 and 10) have two pentagonal, one pentagonal and one hexagonal, and two hexagonal cavities, respectively, when viewed from the top. The presence of two cavities in these higher pillar[*n*]arenes leads to a reduction in the level of ring strain in these systems. A similar trend to this has also been reported in calix[*n*]arene chemistry, where calix[8]-, calix[12]- and calix[16]arenes gave lower levels of ring strain compared with other the calix[*n*]arene homologs because calix[4]arenes have low ring strain structures [33]. When viewed from the side, these larger pillar[*n*]arenes appeared to be highly symmetrical pillar-shaped structures in the same way as the pillar[5]- and pillar[6]arenes.



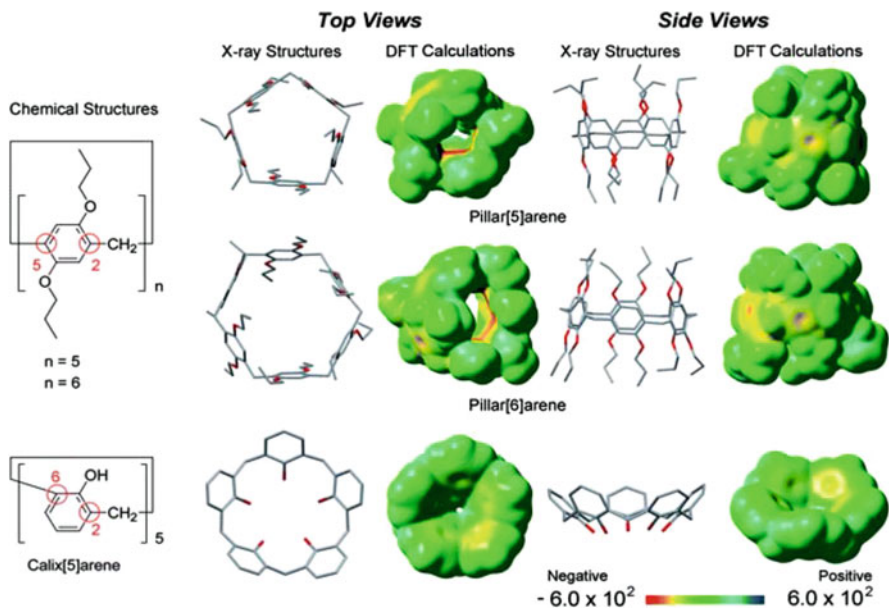


**Fig. 19.5** Calculated electron potential profiles (DFT calculations, B3LYP/6-31G(d,p)) of pillar [5]arene, pillar[6]arene and calix[5]arene (Reproduced with permission from Ref. [8i]. Copyright 2014 Royal Society of Chemistry)

## 19.5 Host-Guest Property of Pillar[*n*]arenes

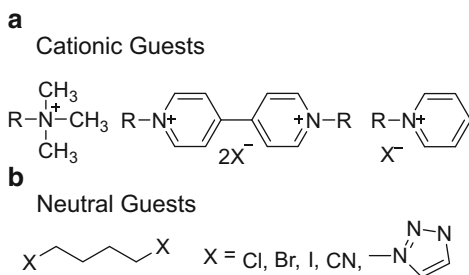
The electrostatic potentials of macrocyclic compounds play an important role in their molecular recognition properties. The electrostatic potentials of pillar[5]- and pillar[6]arenes are unique because of their pillar-shaped structures. Figure 19.5 shows the electrostatic potentials of pillar[5]- and pillar[6]arenes [8i]. The electrostatic potential of calix[5]arene is also shown as a reference for comparison.

In case of calix[5]arene, the cavity was found to be almost neutral because of its vase-shaped structure. In contrast, the cavities in pillar[5]arene and pillar[6]arene possessed negative charges. Because of their pillar-shaped structures, the  $\pi$ -electrons in these systems were condensed into the tubular-shaped cavities. The negative cavities in these pillar[*n*]arene systems therefore prefer to bind to positively charged molecules.

### 19.5.1 Host-Guest Property of Pillar[5]arenes

Pillar[5]arenes have a cavity of approximately 4.7 Å in diameter, allowing simple per-alkylated pillar[5]arenes to form complexes with linear molecules containing a

**Fig. 19.6** (a) Cationic and (b) neutral guests for simple per-alkylated pillar[5]arenes



cationic moiety, such as ammonium, viologen and pyridinium compounds (Fig. 19.6a) [29, 34].

Natural linear hydrocarbons can also be encapsulated in the cavity of pillar[5]arenes [30, 35]. The driving force for complexation processes of this type is the formation of multiple CH/ $\pi$  interactions between the linear alkane guests and the pillar[5]arene host. However, the association constants for the formation of host-guest complexes between simple, neutral linear alkanes such as *n*-hexane and *n*-heptane are generally low. The introduction of electron-withdrawing groups at either end of an *n*-alkane guest was reported by Li and co-workers as an effective strategy for enhancing the host-guest complexation ability of neutral guests. Li's group reported that neutral linear alkanes bearing electron-withdrawing groups (e.g., cyano or halogen groups) at either end of their structure were good guests for pillar[5]arenes (Fig. 19.6b) [36]. They also demonstrated that the length of the alkane chain between the two electron-withdrawing groups had a pronounced effect on the complexation ability of the guest molecule. Among the many linear alkanes tested with a variety of different chain lengths and electron-withdrawing groups at either end of their chain, C4 linear alkanes were identified as the best guests for pillar[5]arenes because the length of the hydrophobic C4 linker was a good fit to the pillar[5]arene cavity. The other interesting aspect of the host-guest chemistry of pillar[5]arenes is their good alkane-shape selectivity. For example, pillar[5]arenes formed host-guest complexes with linear hydrocarbons, but did not form complexes with branched or cyclic hydrocarbons [35b].

The complexation abilities of pillar[5]arenes can be enhanced via the installation of appropriate functional groups on both rims of their macrocyclic structures. For example, a simple pillar[5]arene bearing ten methoxy moieties on its rims formed host-guest complexes with linear alkanes with an amine group at either end of the chain, although the general stability of these complexes was quite low. Furthermore, the introduction of one or two carboxylic acid moieties led to a considerable increase in the host-guest complexation abilities of the resulting pillar[5]arenes towards linear alkanes bearing amino moieties. For example, Xia and Xue reported a pillar[5]arene bearing a monocarboxylic acid moiety, which formed a very stable host-guest complex with a monoamine derivative [ $K = (1.52 \pm 0.075) \times 10^5 \text{ M}^{-1}$ ] [37]. Yu et al. reported the formation of host-guest complexes between a pillar[5]

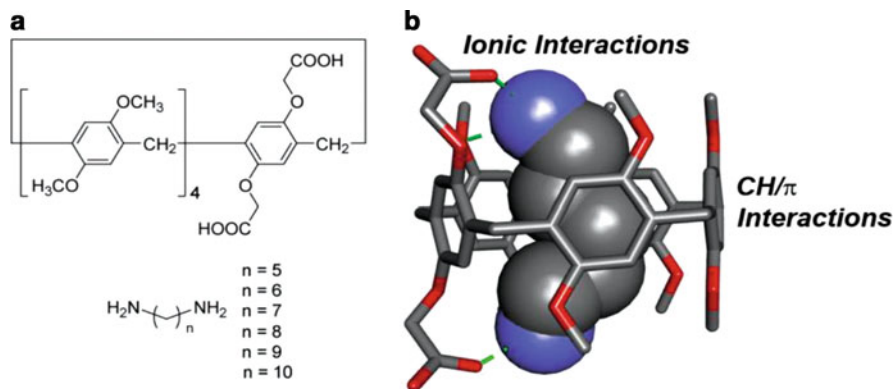


**Fig. 19.7** (a) Host-guest complexes based on the formation of ionic interactions between a pillar [5]arene bearing two di-carboxylic groups and diamines. (b) X-ray crystal structure of the host-guest complex between pentaethylenediamine and the diacid

arene host bearing two carboxylic acid groups and alkane diamines [38]. The  $K$  values for these complexes were all in the vicinity of  $10^5 \text{ M}^{-1}$  (Fig. 19.7).

The high binding constants of these host-guest complexes were attributed to the formation of electrostatic interactions between the ammonium cations of the guest molecules and the carboxylate anions on the rims of the pillar[5]arenes, together with the formation of multiple CH/ $\pi$  interactions between the alkyl chains of the alkyldiamine guests and the pillar[5]arenes.

The introduction of appropriate functional groups to the rims of pillar[5]arenes also can allow for the host-guest complexation media to be changed from an organic solvent to aqueous media. We first reported the preparation of a water-soluble pillar[5]arene via the installation of ten carboxylate moieties on both rims of pillar[5]arene (Fig. 19.8a) [19]. This pillar[5]arene formed very stable host-guest complexes with molecules bearing cationic moieties and amino acids with two or more amino groups in aqueous media (Fig. 19.8b) [39].

Pillar[5]arenes bearing ten neutral amino groups or cationic ammonium, pyridinium and imidazolium moieties have also been prepared and found to be soluble in aqueous media, where they were used to capture linear mono- and diacid guests [24a, b]. In both of these cases, the driving force for the formation of the complexes was the formation of electrostatic interactions between the host and the guest molecules. Hydrophobic-hydrophilic interactions also occur in these systems to stabilize the complexation process because they are conducted in aqueous media.

### 19.5.2 Host-Guest Property of Pillar[6]arenes

Pillar[6]arenes have a cavity size of approximately 6.7 Å in diameter, as shown by X-ray crystallography, which is larger than that of pillar[5]arenes. Based on their

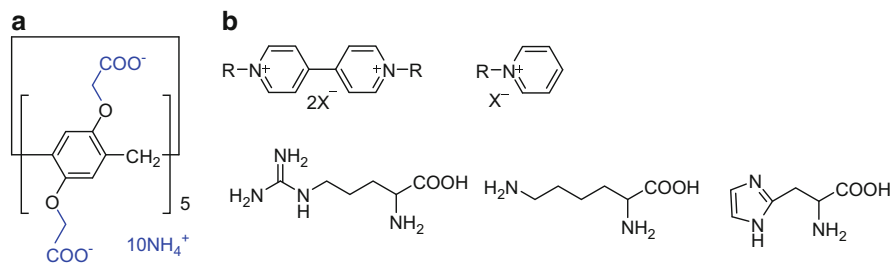


**Fig. 19.8** Chemical structures of (a) water-soluble anionic pillar[5]arene and (b) its guests

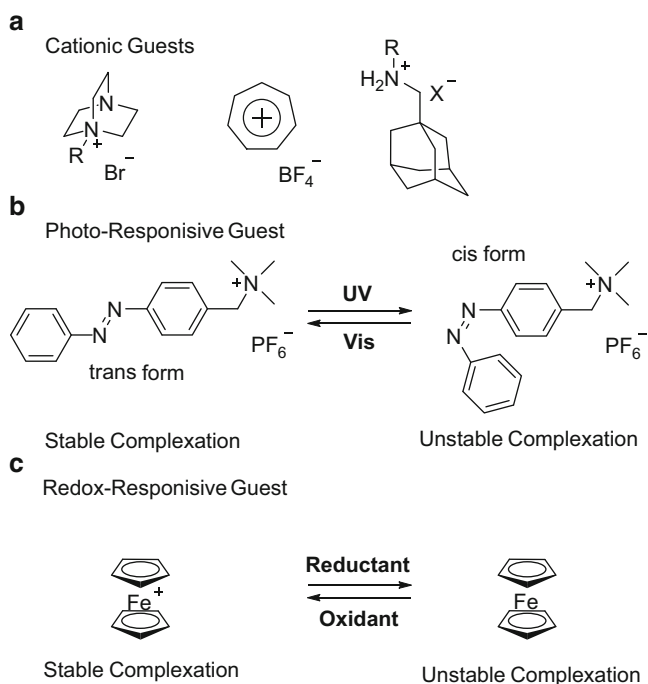


**Fig. 19.9** (a) Cationic guests, (b) photo- and (c) redox-responsive guests for simple per-alkylated pillar[6]arenes

larger cavity size, pillar[6]arenes can form host-guest complexes with polyaromatic compounds and bulky hydrocarbons bearing positive charges (Fig. 19.9) [40].

It is noteworthy that polyaromatic *trans*-azobenzene derivatives bearing cationic moieties are size-suitable guest molecules for simple pillar[6]arenes bearing 12 alkoxy groups [ $K = (2.2 \pm 0.3) \times 10^3 \text{ M}^{-1}$ ] [40c]. In contrast, the corresponding *cis*-azobenzene derivatives are too bulky to form stable host-guest complexes with simple pillar[6]arenes [ $K = (2.6 \pm 0.3) \times 10^2 \text{ M}^{-1}$ ]. Huang et al. reported that the differences in the association constants between the *trans* and *cis* forms of these compounds could be used to prepare photo-responsive host-guest systems. Pillar[6]

arene can form a host-guest complex with the oxidized form of the ferrocenium cation [ $K = (2.0 \pm 0.1) \times 10^4 \text{ M}^{-1}$ ], but barely undergo any complexation with the reduced form of ferrocene ( $K = 18 \pm 0.5 \text{ M}^{-1}$ ) [41]. This system can therefore be used as redox-responsive host-guest system. Pillar[6]arene can also form complexes with bulky hydrocarbons bearing cationic groups such as 1,4-diazabicyclo [2.2.2]octane ( $K = 552 \pm 65 \text{ M}^{-1}$ ) [40b], adamantyl cations [ $K = (3.4 \pm 0.2) \times 10^3 \text{ M}^{-1}$ ] [40a] and carbonium tropylium ion tetrafluoroborate [ $K = (1.8 \pm 0.3) \times 10^3 \text{ M}^{-1}$ ] [42].

In a similar manner to pillar[5]arenes, the rims of pillar[6]arenes can also be modified with water-soluble moieties to give water-soluble pillar[6]arenes. The first reported water-soluble pillar[6]arene was synthesized by Huang et al. via the introduction of 12 carboxylate anions to a simple pillar[6]arene system [22b]. The resulting water-soluble pillar[6]arene was subsequently used to capture paraquat in water with a higher association constant than that of the corresponding water-soluble pillar[5]arene [43]. The failure of the water-soluble pillar[5]arene in this case was attributed to the size of paraquat (ca. 6.3 Å), which is much larger than the cavity of pillar[5]arene (ca. 4.7 Å), but slightly smaller than the cavity of pillar [6]arene (ca. 6.7 Å). Water-soluble pillar[6]arene also formed very stable host-guest complexes with several cationic molecules, including a series of pyridinium derivatives ( $K > 10^5 \text{ M}^{-1}$ ) [44]. In a similar manner to simple pillar[6]arene systems bearing 12 alkoxy moieties, anionic water-soluble pillar[6]arene also accommodated *trans*-azobenzene guests with reasonable ease but failed to form complexes with the corresponding *cis*-azobenzene guests [45]. Anionic water-soluble pillar[6]arene also formed a very stable host-guest complex with an oxidized ferrocenium cation bearing a hydrophobic tail, but failed to form a complex with the corresponding reduced form of this ferrocene derivative [46]. Photo- and redox-responsive host-guest systems capable of acting in this way in aqueous media could also be applied as drug responsive systems. Cationic pillar[6]arenes can also form host-guest complexes with naphthalene derivatives bearing sulfonate moieties [24d]. Notably, the association constant of a cationic pillar[6]arene host with a naphthalene guest bearing two sulfonate groups was found to be 5.5 times higher than that of the corresponding host-guest complex formed with a naphthalene guest bearing only one sulfonate group. Multiple electrostatic interactions between the ammonium groups on the rims of the pillar[6]arene host and the anionic sulfonate groups of the naphthalene guest were determined to be the main driving force for these complexation processes, which explains the difference in the two results.

## 19.6 Pillar[*n*]arene-Based Supramolecular Assemblies

Pillar[*n*]arenes appear as highly symmetrical structures when they are viewed from the side, and appear as regular polygons when they are viewed from the top. For this reason, it was envisaged that individual pillar[*n*]arene molecules would interact

with each other to form regularly ordered supramolecular assemblies. The highly symmetrical structures of pillar[*n*]arenes can form three different kinds of assembled structure, including (i) one-dimensional tubular assemblies; (ii) - two-dimensional sheets; and (iii) three-dimensional assembled structures.

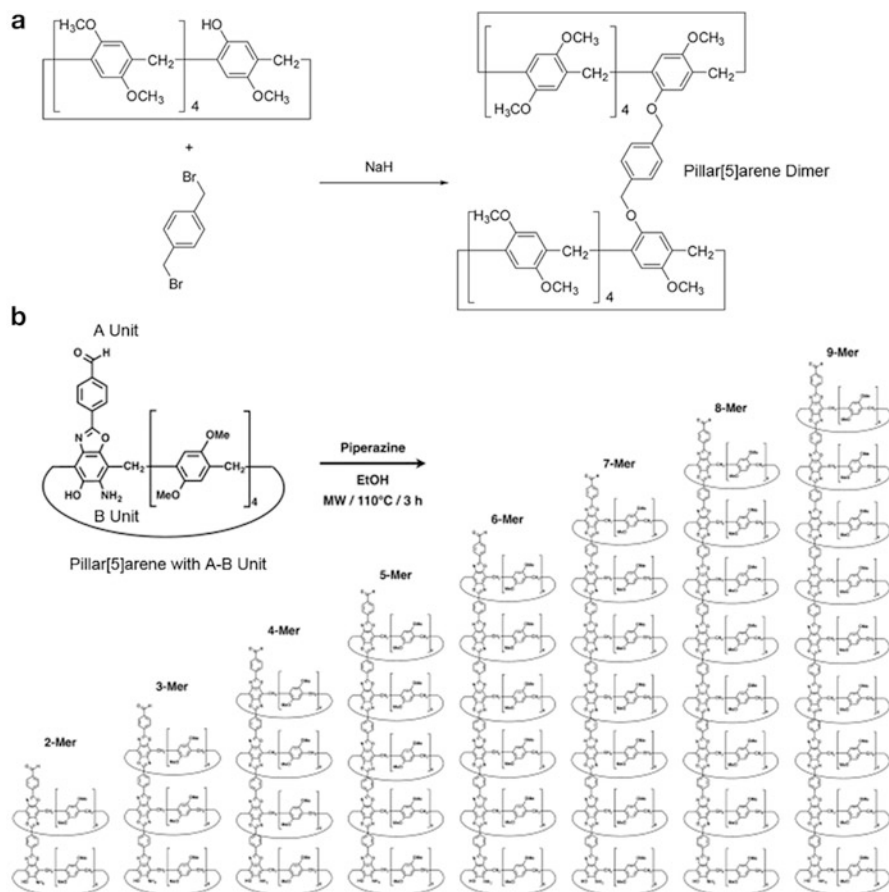
### 19.6.1 Pillar[*n*]arene-Based 1D Supramolecular Assemblies

The highly regular structures of pillar[*n*]arenes make them good candidates for the construction of one-dimensional channels. The construction of one-dimensional channel structures based on pillar[*n*]arenes can be achieved by the formation of covalent bonds between the constituent pillar[*n*]arene molecules. We first synthesized pillar[5]arene dimers by linking two molecules of pillar[5]arene bearing one OH group each with 1,4-bis(bromomethyl)benzene (Fig. 19.10a) [35b].

The pillar[5]arene dimer described above formed relatively strong host-guest complexes with linear alkanes, whereas the complexation ability of the corresponding monomeric pillar[5]arene towards linear alkanes was too weak to determine the association constants or stoichiometry of any potential interactions. The dimerization of this pillar[5]arene system therefore enhanced its host-guest ability. Stoddart et al. synthesized one-dimensional tubular assemblies by the polycondensation reaction of pillar[5]arene with A-B units [47]. It is noteworthy that this strategy allowed for the successful formation of one-dimensional tubular arrays containing between two and nine pillar[5]arene molecules (i.e., 2-mer to 9-mer) (Fig. 19.10b).

Hou et al. investigated the use of pillar[5]arene dimers as artificial proton channels (Fig. 19.11a). The results revealed that a simple pillar[5]arene bearing ten ester groups worked effectively as a proton channel following the incorporation of its dimer into the lipid bilayer [48]. The dimer was necessary in this case because the thickness of a lipid bilayer is approximately 3.7 nm, which is over twice the width of a single pillar[5]arene molecule (1.6 nm). It is noteworthy that this decaester dimer also showed higher channel stability than the corresponding monomeric decaester.

The same group also synthesized a rigid tubular pillar[5]arene structure by installing hydrazine subunits (Fig. 19.11b) [49]. In this case, the introduction of hydrazine subunits on the rims led to the formation of intramolecular hydrogen bonds with the adjacent hydrazine subunits, which contributed to the stabilization of the tubular structure. Furthermore, the height of the resulting pillar[5]arene with its expanded hydrazine subunits was approximately 5 nm, which is greater than the thickness of the lipid bilayer. Pillar[5]arene systems of this type could therefore be used as single molecular channels to transport water molecules (Fig. 19.11c). The same group also reported the preparation of chiral selective transport channels using peptide-appended pillar[6]arenes (Fig. 19.11d) [50]. In a similar manner to the hydrazine appended pillar[5]arene described above, the peptide-appended pillar [6]arenes formed rigid tubular structures via the formation of intermolecular



hydrogen bonding interaction between the peptide chains. These peptide-appended pillar[6]arenes have been used as chirality-selective transport channels for the transportation of amino acids from the inside to the outside of lipid bilayers, with D-amino acids generally moving faster than L-amino acids.

### 19.6.2 Pillar[*n*]arene-Based 2D Supramolecular Assemblies

We previously reported the construction of 2D supramolecular assemblies based on pillar[*n*]arenes using a method known as molecular tailing, which involves the ordering of molecules with regular polygons. The assembly of hexagonal molecules



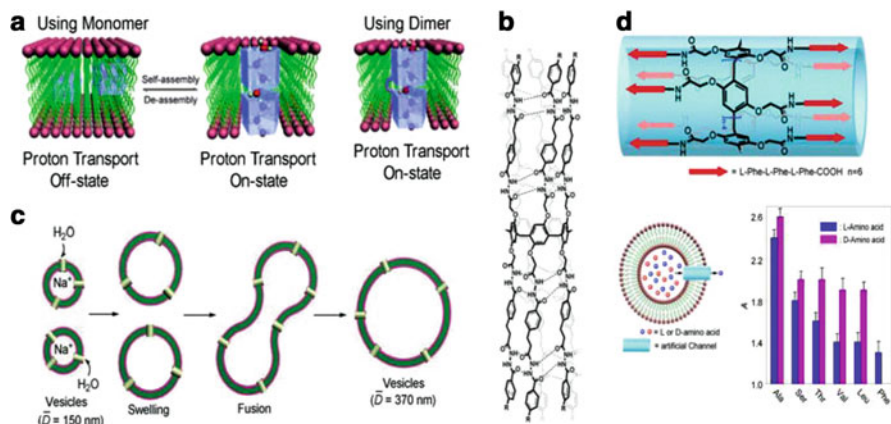


**Fig. 19.11** Artificial channels using pillar[*n*]arenes. **(a)** Proton channels using a pillar[5]arene dimer. **(c)** Water transport channels using **(b)** a pillar[5]arene with expanded hydrazine subunits. **(d)** Chirality-selective transport channels for transporting amino acids using a peptide-appended pillar[5]arene (**a** Reproduced with permission from Ref. [48]. Copyright 2011 Wiley-VCH Verlag GmbH & Co. KGaA. **c** Reproduced with permission from Ref. [49]. Copyright 2012 American Chemical Society. **d** Reproduced with permission from Ref. [50]. Copyright 2013 American Chemical Society)

represents a good method for the production of densely packed 2D sheet structures. With this in mind, we used pillar[6]arene as a suitable monomer to produce 2D supramolecular sheet structures (Fig. 19.12) [51].

The two-dimensional supramolecular polymerization of pillar[6]arene can be induced by the oxidation of its hydroquinone moieties to benzoquinone units because the CT complexation process between these units results in the formation of intermolecular connections between the hexagonal pillar[6]arene molecules (Fig. 19.12b). In contrast, the CT complexation-induced 2D supramolecular polymerization of pentagonal pillar[5]arene molecules generally results in the formation of amorphous assembled structures. Studies in this area have shown that the hexagonal structure of pillar[6]arene contributed to the formation of 2D supramolecular sheet structures, which were converted to carbons following 2 h of calcination at 900 °C under an inert atmosphere (Fig. 19.12c). It is noteworthy that the fibrous structure of the 2D sheets remained intact even after the calcination process. Furthermore, the fibrous carbon structure contained pores that were similar in size to the original starting compound pillar[6]arene assembly (4.09 Å). This method for the creation of porous carbon does not require inorganic templates, and therefore represents a simple process for the synthesis of porous carbons with angstrom-sized pores.



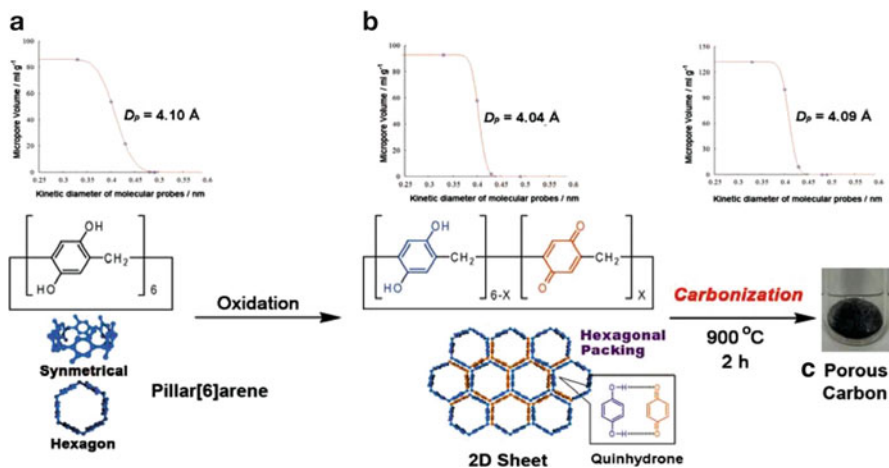


**Fig. 19.12** Two-dimensional supramolecular polymerization via the oxidation of the hydroquinone units of (a) per-hydroxylated pillar[6]arene, (b) the resulting two-dimensional sheet and (c) the porous carbon prepared by the carbonization of (Reprinted with permission from ref. [51]. Copyright 2015 Wiley-VCH Verlag GmbH & Co. KGaA)

### 19.6.3 Pillar[*n*]arene-Based 3D Supramolecular Assemblies

In their crystalline state, pillar[5]arenes mainly form three different kinds of assembled structure, including 3D structures (e.g., herringbone), 1D channels and slipped-stack structures. The ring size, nature of the substituents on the rims of the pillar[*n*]arene structure and type of solvent used for the crystallization all play a critical role in dictating the assembled structures of pillar[*n*]arenes.

We previously reported that a pillar[5]arene bearing ten ethoxy groups on its rims could form two different assembled structures depending on the type of solvent used for the crystallization (Fig. 19.13) [52].

The crystallization of pillar[5]arene from an acetone solution afforded one-dimensional channel structures, whereas the crystallization of the same material from chloroform under *n*-hexane vapor afforded herringbone type assemblies. These crystals were activated by heating to give crystals without any solvent molecules in both cases. After removing the solvent molecules from these crystals, they changed from herringbone and one-dimensional channel structures to give a different crystal structure. The activated crystals quantitatively adsorbed *n*-hexane, with the uptake of *n*-hexane inducing changes in the crystal structure to give a herringbone structure. The activated crystals also adsorbed acetone in the presence of acetone vapor, which resulted in a significant change in the crystal structure to give a one-dimensional channel structure. Notably, these processes were completely reversible.

We also investigated the construction of 1D crystal-like channel structures on the substrate using a Layer-by-Layer (LbL) assembly approach (Fig. 19.14) [53].

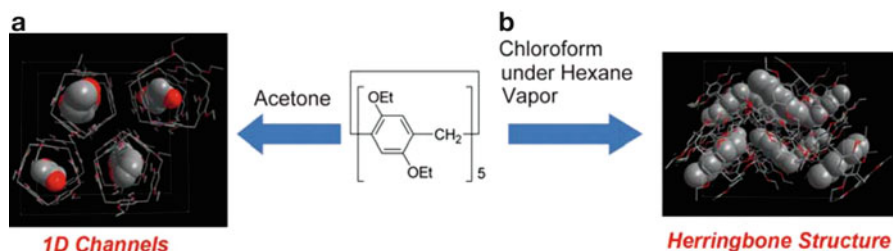


**Fig. 19.13** (a) One-dimensional channel and (b) herringbone crystal structures by crystallization of per-ethylated pillar[5]arene from its acetone and chloroform under *n*-hexane vapor, respectively

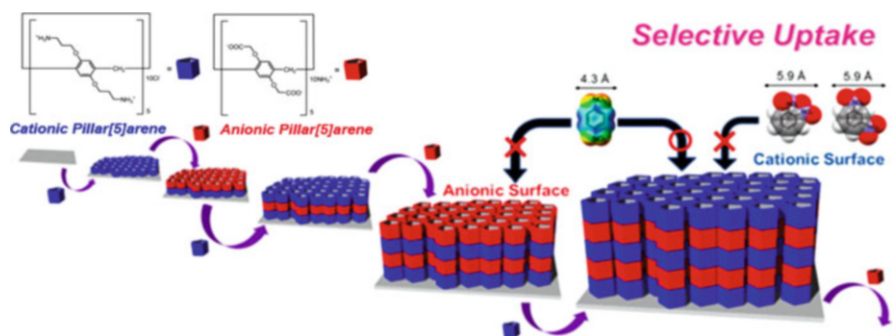


**Fig. 19.14** Layer-by-Layer assembly by the consecutive adsorption of cationic and anionic pillar[5]arenes. The multi-layered film showed size-selective and surface potential-dependent molecular recognition properties (Reprinted with permission from ref. [53]. Copyright 2015 American Chemical Society)

LbL assembly is generally used to construct polymer-based thin films by the consecutive adsorption of oppositely charged polyelectrolytes on a solid substrate. The use of an LbL assembly technique for the construction of multi-layered materials using low molecular weight molecules can be challenging because of the lack of multiple interaction points in low molecular weight molecules. However, the formation of multi-layered structures can be achieved by the consecutive aspiration of pillar[5]arenes bearing ten cations and ten anions. The resulting multi-layered materials possess the original pores of the constituent pillar[5]arene, allowing them to take up guest molecules with shape selectivity. For example, one multi-layered pillar[5]arene adsorbed *para*-dinitrobenzene but could not adsorb *ortho*- or *meta*-dinitrobenzene.

## 19.7 Concluding Remarks

In this chapter, we have described the fundamental properties of pillar[*n*]arenes, including their synthesis, structure and host-guest properties. The most important feature of pillar[*n*]arenes compared with calix[*n*]arenes is their unique pillar-shaped structure, which contributes to their highly selective and unique neutral guest recognition properties. Second, we have discussed one-, two- and three dimensional pillar[*n*]arene-based supramolecular assemblies. The highly symmetrical and regular polygonal structures of pillar[*n*]arenes are also very important for the construct of highly ordered supramolecular assemblies. The creation of supramolecular assemblies based on the highly symmetrical pillar-shaped structure of pillar[*n*]arenes is an important area of research. The combination of pillar[*n*]arenes with different areas of chemistry such as physical, biomedical, material and polymer chemistry could also provide important opportunities for the creation of new supramolecular assemblies that cannot be achieved by other macrocyclic hosts. Reaching these goals will lead to further developments in pillar[*n*]arene chemistry, which could contribute to the development of new supramolecular materials. We believe that pillar[*n*]arenes have unlimited potential, and look forward to further discoveries in pillar[*n*]arene chemistry.

## References

1. *Synthesis of macrocycles. The Design of Selective Complexing Agents. Progress in Macrocyclic Chemistry*; R. M. Izatt; J. J. Christensen Eds.; John Wiley and Sons: New York, 1987.
2. Pedersen, C. J. *J. Am. Chem. Soc.* **1967**, *89*, 7017–7036.
3. (a) Rekharsky, M. V.; Inoue, Y. *Chem. Rev.* **1998**, *98*, 1875–1918; (b) Harada, A.; Hashidzume, A.; Yamaguchi, H.; Takashima, Y. *Chem. Rev.* **2009**, *109*, 5974–6023; (c) Harata, K. *Chem. Rev.* **1998**, *98*, 1803–1828; (d) Nepogodiev, S. A.; Stoddart, J. F. *Chem. Rev.* **1998**, *98*, 1959–1976; (e) Uekama, K.; Hirayama, F.; Irie, T. *Chem. Rev.* **1998**, *98*, 2045–2076; (f) Engeldinger, E.; Armspach, D.; Matt, D. *Chem. Rev.* **2003**, *103*, 4147–4174; (g) Khan, A. R.; Forgo, P.; Stine, K. J.; D'Souza, V. T. *Chem. Rev.* **1998**, *98*, 1977–1996; (h) Crini, G. *Chem. Rev.* **2014**, *114*, 10940–10975.
4. (a) Kaifer, A. E. *Acc. Chem. Res.* **2014**, *47*, 2160–2167; (b) Lee, J. W.; Samal, S.; Selvapalam, N.; Kim, H.-J.; Kim, K. *Acc. Chem. Res.* **2003**, *36*, 621–630; (c) Lagona, J.; Mukhopadhyay, P.; Chakrabarti, S.; Isaacs, L. *Angew. Chem. Int. Ed.* **2005**, *44*, 4844–4870; (d) Ko, Y. H.; Kim, E.; Hwang, I.; Kim, K. *Chem. Commun.* **2007**, 1305–1315; (e) Freeman, W. A.; Mock, W. L.; Shih, N. Y. *J. Am. Chem. Soc.* **1981**, *103*, 7367–7368; (f) Jon, S. Y.; Selvapalam, N.; Oh, D. H.; Kang, J.-K.; Kim, S.-Y.; Jeon, Y. J.; Lee, J. W.; Kim, K. *J. Am. Chem. Soc.* **2003**, *125*, 10186–10187; (g) Kim, J.; Jung, I.-S.; Kim, S.-Y.; Lee, E.; Kang, J.-K.; Sakamoto, S.; Yamaguchi, K.; Kim, K. *J. Am. Chem. Soc.* **2000**, *122*, 540–541.
5. (a) Gutsche, C. D. *Calixarenes*; The Royal Society of Chemistry: Cambridge, 1989; (b) J. Vicens, V. B. *Calixarenes: a Versatile Class of Macrocyclic Compounds*. Kluwer Academic: Dordrecht, 1991; (c) Guo, D. S.; Liu, Y. *Acc. Chem. Res.* **2014**, *47*, 1925–1934.
6. (a) Ajami, D.; Rebek, J. *Acc. Chem. Res.* **2012**, *46*, 990–999; (b) Kim, S. K.; Sessler, J. L. *Acc. Chem. Res.* **2014**, *47*, 2525–2536; (c) Morohashi, N.; Narumi, F.; Iki, N.; Hattori, T.; Miyano,

- S. Chem. Rev.* **2006**, *106*, 5291–5316; (d) Brotin, T.; Dutasta, J.-P. *Chem. Rev.* **2009**, *109*, 88–130; (e) Omachi, H.; Segawa, Y.; Itami, K. *Acc. Chem. Res.* **2012**, *45*, 1378–1389.
7. Ogoshi, T.; Kanai, S.; Fujinami, S.; Yamagishi, T.; Nakamoto, Y. *J. Am. Chem. Soc.* **2008**, *130*, 5022–5023.
8. (a) Ogoshi, T. *Pillararene*; The Royal Society of Chemistry: Cambridge, 2015; (b) Ogoshi, T. *J. Inclusion Phenom. Macrocycl. Chem.* **2012**, *72*, 247–262; (c) Ogoshi, T.; Yamagishi, T. *J. Syn. Org. Chem. Jpn.* **2012**, *70*, 842–851; (d) Xue, M.; Yang, Y.; Chi, X. D.; Zhang, Z. B.; Huang, F. *Acc. Chem. Res.* **2012**, *45*, 1294–1308; (e) Cragg, P. J.; Sharma, K. *Chem. Soc. Rev.* **2012**, *41*, 597–607; (f) Zhang, H.; Zhao, Y. *Chem. –Eur. J.* **2013**, *19*, 16862–16879; (g) Ogoshi, T.; Yamagishi, T. *Bull. Chem. Soc. Jpn.* **2013**, *86*, 312–332; (h) Ogoshi, T.; Yamagishi, T. *Eur. J. Org. Chem.* **2013**, 2961–2975; (i) Ogoshi, T.; Yamagishi, T. *Chem. Commun.* **2014**, *50*, 4776–4787; (j) Strutt, N. L.; Zhang, H. C.; Schneebeli, S. T.; Stoddart, J. F. *Acc. Chem. Res.* **2014**, *47*, 2631–2642; (k) Si, W.; Xin, P.; Li, Z. T.; Hou, J. L. *Acc. Chem. Res.* **2015**, *48*, 1612–1619.
9. Ogoshi, T.; Aoki, T.; Kitajima, K.; Fujinami, S.; Yamagishi, T.; Nakamoto, Y. *J. Org. Chem.* **2011**, *76*, 328–331.
10. Boinski, T.; Szumna, A. *Tetrahedron* **2012**, *68*, 9419–9422.
11. Hu, X. B.; Chen, Z. X.; Chen, L.; Zhang, L.; Hou, J. L.; Li, Z. T. *Chem. Commun.* **2012**, *48*, 10999–11001.
12. Ogoshi, T.; Ueshima, N.; Akutsu, T.; Yamafuji, D.; Furuta, T.; Sakakibara, F.; Yamagishi, T. *Chem. Commun.* **2014**, *50*, 5774–5777.
13. CAS Number: 1188423-16-6, Product Number: D4471
14. (a) Ogoshi, T.; Kitajima, K.; Aoki, T.; Fujinami, S.; Yamagishi, T.; Nakamoto, Y. *J. Org. Chem.* **2010**, *75*, 3268–3273; (b) Ogoshi, T.; Shiga, R.; Yamagishi, T.; Nakamoto, Y. *J. Org. Chem.* **2011**, *76*, 618–622.
15. (a) Holler, M.; Allenbach, N.; Sonet, J.; Nierengarten, J. F. *Chem. Commun.* **2012**, *48*, 2576–2578; (b) Ma, Y.; Zhang, Z.; Ji, X.; Han, C.; He, J.; Abliz, Z.; Chen, W.; Huang, F. *Eur. J. Org. Chem.* **2011**, 5331–5335.
16. Ogoshi, T.; Ueshima, N.; Sakakibara, F.; Yamagishi, T.; Haino, T. *Org. Lett.* **2014**, *16*, 2896–2899.
17. (a) Ogoshi, T.; Demachi, K.; Kitajima, K.; Yamagishi, T. *Chem. Commun.* **2011**, *47*, 7164–7166; (b) Han, J.; Hou, X.; Ke, C.; Zhang, H.; Strutt, N. L.; Stern, C. L.; Stoddart, J. F. *Org. Lett.* **2015**, *17*, 3260–3263.
18. (a) Ogoshi, T.; Yamafuji, D.; Kotera, D.; Aoki, T.; Fujinami, S.; Yamagishi, T. *J. Org. Chem.* **2012**, *77*, 11146–11152; (b) Han, C. Y.; Zhang, Z. B.; Yu, G. C.; Huang, F. *Chem. Commun.* **2012**, *48*, 9876–9878. (c) Wei, P.; Yan, X.; Huang, F. *Chem. Commun.* **2014**, *50*, 14105–14108.
19. Ogoshi, T.; Hashizume, M.; Yamagishi, T.; Nakamoto, Y. *Chem. Commun.* **2010**, *46*, 3708–3710.
20. Ogoshi, T.; Shiga, R.; Yamagishi, T. *J. Am. Chem. Soc.* **2012**, *134*, 4577–4580.
21. Ogoshi, T.; Masaki, K.; Shiga, R.; Kitajima, K.; Yamagishi, T. *Org. Lett.* **2011**, *13*, 1264–1266.
22. (a) Ogoshi, T.; Kida, K.; Yamagishi, T. *J. Am. Chem. Soc.* **2012**, *134*, 20146–20150; (b) Yu, G.; Xue, M.; Zhang, Z.; Li, J.; Han, C.; Huang, F. *J. Am. Chem. Soc.* **2012**, *134*, 13248–13251; (c) Chi, X. D.; Xue, M. *Chem. Commun.* **2014**, *50*, 13754–13756; (d) Yang, J.; Chi, X.; Li, Z.; Yu, G.; He, J.; Abliz, Z.; Li, N.; Huang, F. *Org. Chem. Front.* **2014**, *1*, 630–633; (e) Chi, X. D.; Xue, M. *RSC Adv.* **2014**, *4*, 37786–37789; (f) Li, Z. T.; Yang, J.; Yu, G. C.; He, J. M.; Abliz, Z.; Huang, F. *Chem. Commun.* **2014**, *50*, 2841–2843; (g) Shao, L.; Zhou, J.; Hua, B.; Yu, G. *Chem. Commun.* **2015**, *51*, 7215–7218; (h) Li, Z. T.; Yang, J.; Yu, G. C.; He, J. M.; Abliz, Z.; Huang, F. *Org. Lett.* **2014**, *16*, 2066–2069. (i) Ma, Y.; Chi, X.; Yan, X.; Liu, J.; Yao, Y.; Chen, W.; Huang, F.; Hou, J. L. *Org. Lett.* **2012**, *14*, 1532–1535.
23. Nierengarten, I.; Guerra, S.; Holler, M.; Karmazin-Brelot, L.; Barbera, J.; Deschenaux, R.; Nierengarten, J. F. *Eur. J. Org. Chem.* **2013**, 3675–3684.

24. (a) Ma, Y. J.; Ji, X. F.; Xiang, F.; Chi, X. D.; Han, C. Y.; He, J. M.; Abliz, Z.; Chen, W. X.; Huang, F. *Chem. Commun.* **2011**, 47, 12340–12342; (b) Hu, X. B.; Chen, L.; Si, W.; Yu, Y. H.; Hou, J. L. *Chem. Commun.* **2011**, 47, 4694–4696; (c) Yao, Y.; Xue, M.; Chi, X. D.; Ma, Y. J.; He, J. M.; Abliz, Z.; Huang, F. *Chem. Commun.* **2012**, 48, 6505–6507; (d) Chen, W.; Zhang, Y.; Li, J.; Lou, X.; Yu, Y.; Jia, X.; Li, C. *Chem. Commun.* **2013**, 49, 7956–7958.
25. Zhang, F.; Cao, X. L.; Tian, D. M.; Li, H. B. *Chin. J. Chem.* **2015**, 33, 368–372.
26. (a) Nierengarten, I.; Guerra, S.; Holler, M.; Nierengarten, J. F.; Deschenaux, R. *Chem. Commun.* **2012**, 48, 8072–8074; (b) Nierengarten, I.; Nothisen, M.; Sigwalt, D.; Biellmann, T.; Holler, M.; Remy, J. S.; Nierengarten, J. F. *Chem. –Eur. J.* **2013**, 19, 17552–17558; (c) Chang, Y.; Yang, K.; Wei, P.; Huang, S.; Pei, Y.; Zhao, W.; Pei, Z. *Angew. Chem. Int. Ed.* **2014**, 53, 13126–13130.
27. Zhang, H.; Ma, X.; Nguyen, K. T.; Zhao, Y. *ACS Nano* **2013**, 7, 7853–7863.
28. (a) Ogoshi, T.; Shiga, R.; Hashizume, M.; Yamagishi, T. *Chem. Commun.* **2011**, 47, 6927–6929; (b) Deng, H. M.; Shu, X. Y.; Hu, X. S.; Li, J.; Jia, X. S.; Li, C. *Tetrahedron Lett.* **2012**, 53, 4609–4612.
29. (a) Zhang, Z. B.; Xia, B. Y.; Han, C. Y.; Yu, Y. H.; Huang, F. *Org. Lett.* **2010**, 12, 3285–3287; (b) Han, C.; Yu, G.; Zheng, B.; Huang, F. *Org. Lett.* **2012**, 14, 1712–1715.
30. Strutt, N. L.; Forgan, R. S.; Spruell, J. M.; Botros, Y. Y.; Stoddart, J. F. *J. Am. Chem. Soc.* **2011**, 133, 5668–5671.
31. Duan, Q. P.; Xia, W.; Hu, X. Y.; Ni, M. F.; Jiang, J. L.; Lin, C.; Pan, Y.; Wang, L. *Chem. Commun.* **2012**, 48, 8532–8534.
32. Han, C. Y.; Ma, F. Y.; Zhang, Z. B.; Xia, B. Y.; Yu, Y. H.; Huang, F. *Org. Lett.* **2010**, 12, 4360–4363.
33. Stewart, D. R.; Gutsche, C. D. *J. Am. Chem. Soc.* **1999**, 121, 4136–4146.
34. Ogoshi, T.; Yamafuji, D.; Aoki, T.; Kitajima, K.; Yamagishi, T.; Hayashi, Y.; Kawauchi, S. *Chem. –Eur. J.* **2012**, 18, 7493–7500.
35. (a) Zhang, Z.; Luo, Y.; Chen, J.; Dong, S.; Yu, Y.; Ma, Z.; Huang, F. *Angew. Chem. Int. Ed.* **2011**, 50, 1397–1401; (b) Ogoshi, T.; Demachi, K.; Kitajima, K.; Yamagishi, T. *Chem. Commun.* **2011**, 47, 10290–10292. (c) Xia, B.; Heb, J.; Abliz, Z.; Yu, Y.; Huang, F. *Tetrahedron Lett.* **2011**, 52, 4433–4436. (d) Zhang, Z.; Yu, G.; Han, C.; Liu, J.; Ding, X.; Yu, Y.; Huang, F. *Org. Lett.* **2011**, 13, 4818–4821; (e) Gao, L.; Han, C.; Zheng, B.; Dong, S.; Huang, F. *Chem. Commun.* **2013**, 49, 472–474; (f) Ma, Y.; Xue, M.; Zhang, Z.; Chi, X.; Huang, F. *Tetrahedron* **2013**, 69, 4532–4535.
36. (a) Shu, X.; Chen, S.; Li, J.; Chen, Z.; Weng, L.; Jia, X.; Li, C. *Chem. Commun.* **2012**, 48, 2967–2969; (b) Shu, X. Y.; Fan, J. Z.; Li, J.; Wang, X. Y.; Chen, W.; Jia, X. S.; Li, C. *Org. Biomol. Chem.* **2012**, 10, 3393–3397; (c) Li, C.; Chen, S.; Li, J.; Han, K.; Xu, M.; Hu, B.; Yu, Y.; Jia, X. *Chem. Commun.* **2011**, 47, 11294–11296; (d) Han, K.; Zhang, Y.; Li, J.; Yu, Y.; Jia, X.; Li, C. *Eur. J. Org. Chem.* **2013**, 2013, 2057–2060.
37. Xia, B. Y.; Xue, M. *Chem. Commun.* **2014**, 50, 1021–1023.
38. Yu, G. C.; Hua, B.; Han, C. Y. *Org. Lett.* **2014**, 16, 2486–2489.
39. (a) Li, C.; Shu, X.; Li, J.; Chen, S.; Han, K.; Xu, M.; Hu, B.; Yu, Y.; Jia, X. *J. Org. Chem.* **2011**, 76, 8458–8465; (b) Li, C. J.; Ma, J. W.; Zhao, L.; Zhang, Y. Y.; Yu, Y. H.; Shu, X. Y.; Li, J.; Jia, X. S. *Chem. Commun.* **2013**, 49, 1924–1926.
40. (a) Li, C.; Shu, X.; Li, J.; Fan, J.; Chen, Z.; Weng, L.; Jia, X. *Org. Lett.* **2012**, 14, 4126–4129; (b) Ogoshi, T.; Kayama, H.; Yamafuji, D.; Aoki, T.; Yamagishi, T. *Chem. Sci.* **2012**, 3, 3221–3226; (c) Yu, G.; Han, C.; Zhang, Z.; Chen, J.; Yan, X.; Zheng, B.; Liu, S.; Huang, F. *J. Am. Chem. Soc.* **2012**, 134, 8711–8717.
41. Xia, W.; Hu, X. Y.; Chen, Y.; Lin, C.; Wang, L. *Chem. Commun.* **2013**, 49, 5085–5087.
42. Fan, J. Z.; Deng, H. M.; Li, J.; Jia, X. S.; Li, C. *Chem. Commun.* **2013**, 49, 6343–6345.
43. Yu, G. C.; Zhou, X. R.; Zhang, Z. B.; Han, C. Y.; Mao, Z. W.; Gao, C. Y.; Huang, F. *J. Am. Chem. Soc.* **2012**, 134, 19489–19497.
44. (a) Wang, P.; Yan, X. Z.; Huang, F. *Chem. Commun.* **2014**, 50, 5017–5019; (b) Yang, J.; Yu, G. C.; Xia, D. Y.; Huang, F. *Chem. Commun.* **2014**, 50, 3993–3995.

45. Xia, D. Y.; Yu, G. C.; Li, J. Y.; Huang, F. *Chem. Commun.* **2014**, *50*, 3606–3608.
46. Duan, Q. P.; Cao, Y.; Li, Y.; Hu, X. Y.; Xiao, T. X.; Lin, C.; Pan, Y.; Wang, L. *J. Am. Chem. Soc.* **2013**, *135*, 10542–10549.
47. Strutt, N. L.; Zhang, H. C.; Schneebeli, S. T.; Stoddart, J. F. *Chem. –Eur. J.* **2014**, *20*, 10996–11004.
48. Si, W.; Chen, L.; Hu, X. B.; Tang, G.; Chen, Z.; Hou, J. L.; Li, Z. T. *Angew. Chem. Int. Ed.* **2011**, *50*, 12564–12568.
49. Hu, X. B.; Chen, Z.; Tang, G.; Hou, J. L.; Li, Z. T. *J. Am. Chem. Soc.* **2012**, *134*, 8384–8387.
50. Chen, L.; Si, W.; Zhang, L.; Tang, G. F.; Li, Z. T.; Hou, J. L. *J. Am. Chem. Soc.* **2013**, *135*, 2152–2155.
51. Ogoshi, T.; Yoshikoshi, K.; Sueto, R.; Nishihara, H.; Yamagishi, T. *Angew. Chem. Int. Ed.* **2015**, *54*, 6466–6469.
52. Ogoshi, T.; Sueto, R.; Yoshikoshi, K.; Sakata, Y.; Akine, S.; Yamagishi, T. *Angew. Chem. Int. Ed.* **2015**, *54*, 9849–9852.
53. Ogoshi, T.; Takashima, S.; Yamagishi, T. *J. Am. Chem. Soc.* **2015**, *137*, 10962–10964.

# Chapter 20

## Function-Directed Supramolecular Assembly Based on Water Soluble Calixarenes

Yu Liu, Pei-Yu Li, and Yong Chen

### 20.1 Introduction

Calix[*n*]arenes(CAs) are widely regarded as the third generation of macrocyclic molecules. It is well known that water is the solvent where most biological processes happened. In the earlier researches, studies about the biomedical applications of CAs were relatively limited due to their hydrophobic property and poor water solubility. To solve this problem, researchers focused their attention on the design and synthesis of water-soluble CAs, and thereafter several synthetic methods including sulfonation at the upper rims, esterification or etherification at the lower rim, and functionalization of polar groups onto the edge of CAs were developed [1]. Shinkai et al. reported a water-soluble calixarene derivatives named *p*-sulfonatocalix[*n*]arenes (SCnAs *n* = 4–8, Fig. 20.1) [2]. From then on, SCnAs have shown many advantageous features as compared with other calixarene derivatives as (1) SCnAs can be prepared easily through the direct sulfonation of calixarenes at the upper rim; (2) the cavities of SCnAs have strong binding ability towards guests through hydrophobic and  $\pi$ -stacking interactions which are more effective in aqueous media than in organic media; (3) the sulfonate groups on the upper rim can provide the binding site towards cations through electrostatic interaction that further increase the binding interactions; [3, 5] (4) SCnAs also possess

---

Y. Liu (✉)

Department of Chemistry, State Key Laboratory of Elemento-Organic Chemistry, Nankai University, Tianjin 300071, People's Republic of China

Collaborative Innovation Center of Chemical Science and Engineering (Tianjin), Nankai University, Tianjin 300071, People's Republic of China

e-mail: [yuliu@nankai.edu.cn](mailto:yuliu@nankai.edu.cn)

P.-Y. Li • Y. Chen

Department of Chemistry, State Key Laboratory of Elemento-Organic Chemistry, Nankai University, Tianjin 300071, People's Republic of China

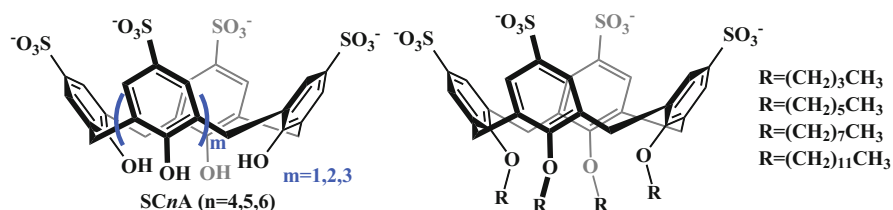


**Fig. 20.1** Structure of water-soluble CAs

good water-solubility and biocompatibility that are necessary properties for their potential biological and pharmaceutical applications. Because of the unique features of different cavity structure, framework rigidity, and complexation affinity, SCnAs afford distinguishable recognition and assembly behaviors in building responsive host-guest systems. A typical example for the potential applications of *p*-sulfonatocalix[*n*]arenes was the treatment of viologen poisoning, where *p*-sulfonatocalix[*n*]arenes were capable of inhibiting the viologen toxicity owing to high binding abilities to viologens, negative shifts in the reduction potentials of viologens, hydrogen transfer to (toxic) radicals, and coordination of transition metal ions [4].

Generally, many amphiphilic calixarenes are strictly non-water-soluble. However, after the introduction of sulfonate groups, the obtained amphiphilic SCnAs (Fig. 20.1) bearing the hydrophilic macrocyclic skeleton and several hydrophobic alkyl chains at the lower rim will become water soluble. Compared with traditional SCnA, these water-soluble amphiphilic SCnAs possess several characters as (1) self-assembly ability; (2) the hydrophilic and ionizable phenolic hydroxyl groups are replaced by the hydrophobic alkyl chains, which provide hydrophobic interactions in the assemble process; (3) through the modification at the lower rim, the cavity of SCnAs gains more rigidity, [5] which enhances the binding ability towards planar cationic guests and decreases the binding ability towards spherical cationic guests. These features make this kind of water-soluble amphiphilic SCnAs a feasible host molecule in building nano-carrier.

This chapter mainly summarizes the recent endeavors on the SCnA-based supramolecular assemblies, with a special emphasis on their construction, structural characters and their applications in biological and material fields.

## 20.2 Construction Methods and Applications of Supramolecular Assembly Based on Sulfonatocalixarenes

In the early study, calixarenes were reported as hydrophilic molecules and unable to form self-assemble, while amphiphilic sulfonato-calixarene could only form small micelles, in water [6]. Recently, SCnAs were found able to improve the aggregation



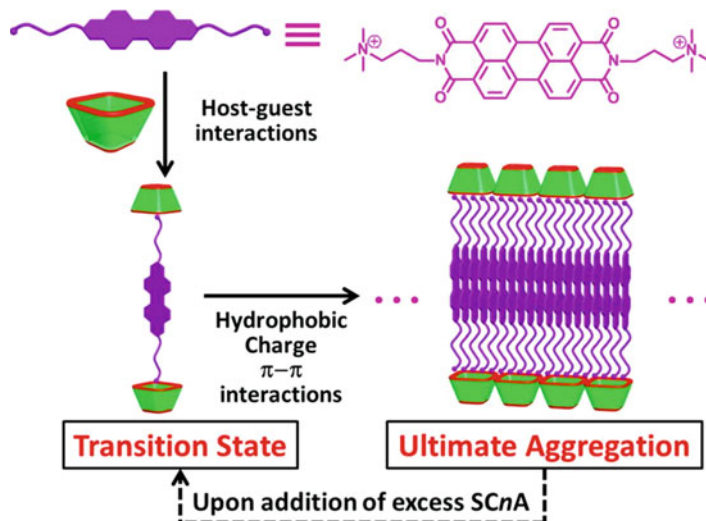


**Fig. 20.2** Schematic illustration of the “calixarene-induced aggregation (CIA)”

ability of guest molecules through the strong binding between host and guest, which was defined as “calixarene-induced aggregation (CIA)” (Fig. 20.2) [7]. Guest molecules used in the CIA aggregation since 2009 could be divided into four categories as aromatic fluorescent dyes [7, 8, 13, 16, 17] amphiphilic surfactants, [9, 18, 19] drugs, [10] and proteins [11]. Following the concept of CIA, several new methods to construct SCnA-based supramolecular assembly such as “guest-induced SCnA aggregation” and “SCnA/guest co-assembly” were developed, and their applications were also extended to the scope of stimuli-responsive material, drug delivery system and supramolecular catalysis.

### 20.2.1 *Supramolecular Assembly Constructed from Calixarene-Induced Aggregation*

Among the various water-soluble macrocycles, cyclodextrins and cucurbiturils tend to form the threading structures including rotaxanes and catenanes with guest molecules, and the inclusion of guest molecules in cyclodextrin and cucurbituril cavities prevent the self-aggregation of guests to some extent [12]. However, SCnAs can promote the self-aggregation of aromatic or amphiphilic guest molecules by lowering the critical aggregation concentration (CAC), enhancing the aggregate stability and compactness, and regulating the degree of order in the aggregates [13]. This unique phenomenon was called “calixarene-induced aggregation (CIA)”. The early prototype of CIA was reported by Randaccio, Purrello, and Sciotto. They found that the complexation between a SC4A derivative, of

which the lower-rim was modified with tetrakis-acetates, and a cationic porphyrin led to the formation of aggregates with pH-tunable host/guest stoichiometries ranging from 4:1 to 4:7 [14].

In the process of CIA, there are two major weak interactions working for the formation of the highly ordered assemblies: hydrophobic/ $\pi$ -stacking interactions and electrostatic interactions. Hydrophobic and/or  $\pi$ -stacking interactions drive the aggregation of alkyl chains and aromatic moieties in water, which provides the impetus of self-organization. Without SCnA, the organic ammonium cations as the polar head groups have the electrostatic repulsion between each other, which will be a negative effect on the formation of large three-dimensional assemblies. Upon complexation with SCnA, the electrostatic repulsion between the ammonium cations is replaced by the electrostatic attraction between the cationic head groups and the anionic sulfonate groups of the SCnAs, which is a favorable effect on the guest aggregation. A simple speculation of the CIA can be explained as two processes. First, the host and guest molecules instantaneously form a complex. The model of host-guest interactions was a 2:1 capsule-like complex with the two head groups of the guest are captured by the cavities of two host molecules. Second, more guest molecules participate into the complex which results in a new model of 2:n complexes and lead to the formation of large three-dimensional aggregates. The ultimate aggregates were stabilized by several non-covalent interactions including host-guest, charge-charge,  $\pi$ -stacking, and hydrophobic interactions. Most importantly, the prerequisite for CIA is strong host-guest interactions. In summary, three important effect of CIA: (1) strong binding affinities between SCnAs and the ammonium cations of guests, (2) charge compensation between hosts and guests, (3) the pre-assembly ability of the SCnAs scaffold [14].

The size of CIA assembly was often larger than that of the self-assembly formed by guest molecules alone, and these supramolecular assemblies constructed through supramolecular host-guest interactions have the responsive ability towards external stimuli [15]. Thus, the CIA method may be a useful tool in constructing stimuli-responsive materials and controlled release drug carriers.

A typical example is the construction of supramolecular binary vesicles with *p*-sulfonatocalix[5]arene (SC5A) as host and 1-pyrenemethylaminium (PMA) as guest (Fig. 20.3) [16]. The CAC of PMA is 0.27 mM, and it did not form any organized assembly. However, when sulfonato-calixarene was introduced into the solution, the CAC of PMA lowered three times due to the formation of CIA assembly. Interestingly, the obtained CIA assembly as a vesicle showed good thermal reversibility that could disassemble when the temperature increased to 35–40 °C. This temperature-responsive character made this kind of vesicle a potential delivery system for special cargos. Furthermore, when mono-*p*-sulfonatocalix[*n*]arenes were replaced by bis-*p*-sulfonatocalix[*n*]arenes as the host molecules, bis-*p*-sulfonatocalix[*n*]arene/PMA assembly was found to exist as nanorods instead of vesicles [17].

In addition to PMA, 1-methyl-10-dodecyl-4,40-bipyridinium(MVC12) was also employed as the guest to construct the self-assembled nanosupramolecular binary vesicle with *p*-sulfonatocalix[4]arene (SC4A) as the host (Fig. 20.4) [18]. In the

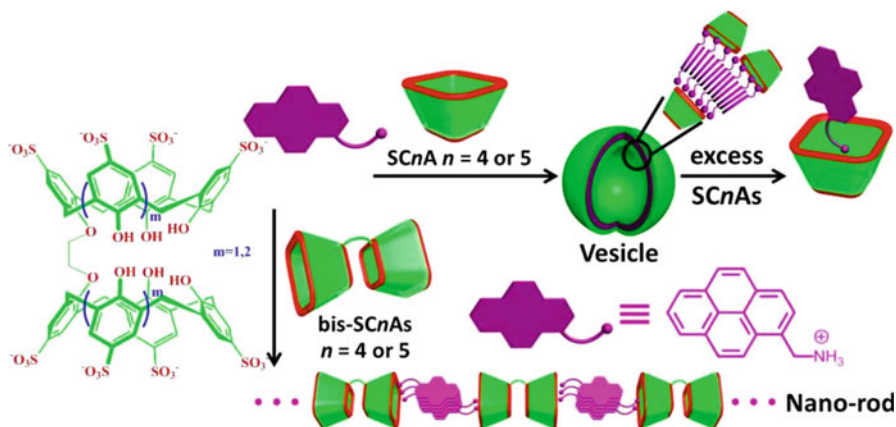
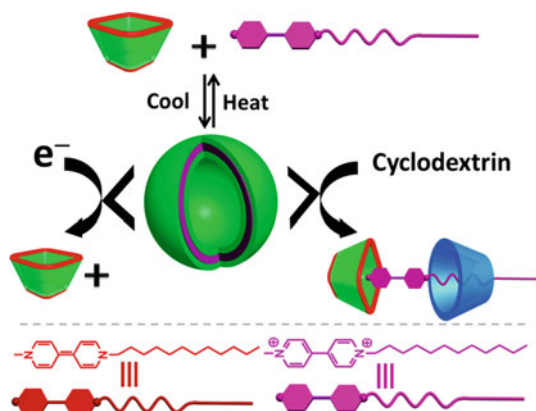


**Fig. 20.3** Different architectures of PMA aggregates in the presence of SCnAs or bis-SCnAs

**Fig. 20.4** Formation of a multistimulus-responsive supramolecular binary vesicle composed of SC4A and an asymmetric viologen



presence of SC4A, the CAC value of MVC12 decreased by three orders of magnitude. More noticeably, the obtained vesicle was responsive towards several external stimuli such as temperature, redox and competitive agents, owing to the intrinsic advantages of supramolecular interactions. That is, MVC12 can be reduced to a radical cation state which could be used to control the morphology of assembly. More interestingly, by reduction to neutral form, increasing temperature, and inclusion of CDs, the vesicle could be completely disrupted. These external stimuli could be effective switches that triggered the release of the loaded cargos. Furthermore, cell experiments showed that the loading of doxorubicin (DOX) by a vesicle did not affect the therapeutic effect of DOX for cancer cells but reduced the damage for normal cells. This material may have substantial application in the fields of controlled release and drug delivery.

Enzyme-responsive supramolecular assemblies were always used as passive drug delivery systems. Through the method of CIA, an enzyme-responsive

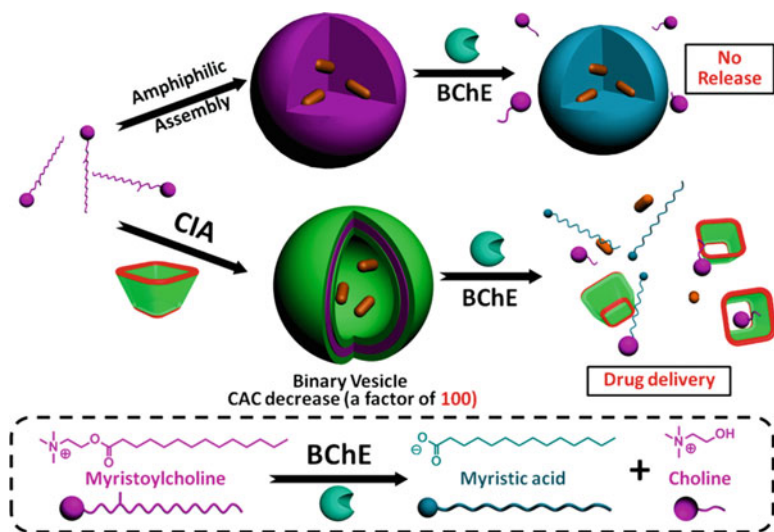


**Fig. 20.5** Enzymatic responsiveness of amphiphilic assemblies of myristoylcholine fabricated in the absence or presence of SC4A

supramolecular vesicle with SC4A as the host and myristoylcholine, which could be specially hydrolyzed by butyrylcholine esterase (BChE), as guest was constructed (Fig. 20.5) [19]. The CAC of myristoylcholine and its hydrolysis product choline had a respective CAC of 2.5 and 4.5 M. However, with the introduction of SC4A, the CAC of choline decreased by two orders of magnitude. Cholinesterase was a key protein over-expressed in Alzheimer's disease. This supramolecular vesicle thus could be used as a targeted delivery system for anti-Alzheimer's disease drug tacrine, which will find the potential application in treating Alzheimer's disease.

Tetraphenylethylene (TPE) was a kind of dye molecules that exhibited the aggregation induced emission (AIE) property. That is, these molecules were non-fluorescent as isolated species but emitted the fluorescence upon aggregation due to the restriction of intramolecular rotations [20]. To further explore the application of AIE and CIA, SC4A and quaternary ammonium-modified TPE (QA-TPE) were selected as host and as guest respectively to construct a fluorescent supramolecular nano-particle (Fig. 20.6) [21]. Compared with QA-TPE alone, the SC4A/QA-TPE aggregate became tightly compacted, leading to a great increase of the fluorescence. Significantly, the fluorescence of free QA-TPE and the self-assembled SC4A/QA-TPE nanoparticles could be photo-switched. These can be expected to pave the way for the construction of organic nanoparticle systems with fluorescence that can be modulated by multiple stimuli. Such systems are expected to find practical applications as fluorescent probes, memory devices, and logic gates.

Anthracenes are highly reactive upon light irradiation with the ability of singlet oxygen detection [22]. Moreover, the reversible dimerization character also made

**Fig. 20.6** Schematic illustration of the photocyclization of free QA-TPE and the SC4A/QA-TPE nanoparticles

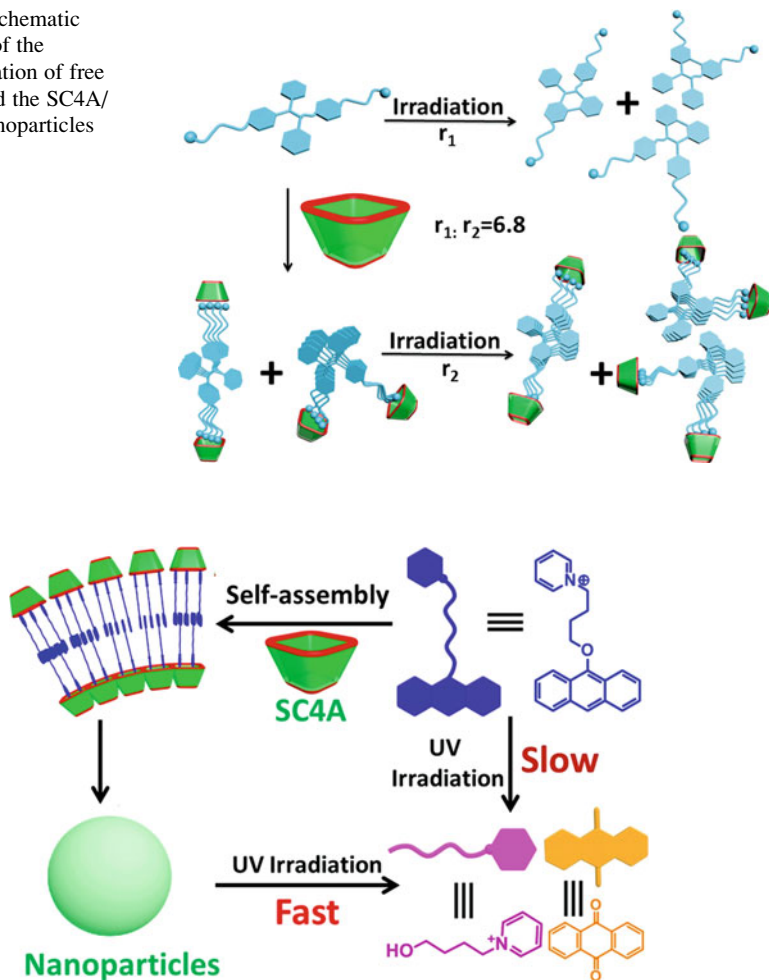


**Fig. 20.7** Schematic illustration of photolyzable supramolecular amphiphilic assembly

anthracene a photo-crosslinking functional material. By combining these advantages, a photolyzable assembly was constructed by using SC4A as host and amphiphilic 9-alkoxy-substituted anthracene (AnPy) as guest (Fig. 20.7) [23]. Herein, SC4A not only induced the compact packing among anthracenes but also inhibited the fluorescence quenching of AnPy, which was favorable for the photosensitization. Interestingly, the photodecomposition of aggregated AnPy was significantly promoted. Previous studies demonstrated that the fluorescence of photosensitizers could be generally self-quenched after aggregation, resulting in the greatly reduced ability for singlet oxygen generation and lower photoreactivity. Therefore, such a photolyzable system promoted by supramolecular aggregation

made CIA a promising strategy in the fields of photodynamic therapy and the photodegradation of pollutants.

Alkynylated surfactants have been used to construct a series of cross-linked micelles to realize light-harvesting, drug delivery and catalysis function [24]. Recently, a cross-linked vesicle was constructed by combining the CIA method with a “click” reaction [25]. In this work SC4A and (dodecyloxybenzyl) tripropargylammonium (TPA) were respectively employed as host and guest. Firstly, SC4A induced the aggregation of TPA to form a CIA vesicle. Then by introducing azides into the system, the cross-linking polymerization process was achieved by the “click” reaction between the terminal alkynes and azides (Fig. 20.8). Free TPA could only self-assembled into micelles with a higher surface curvature whereas the complexation between SC4A and TPA resulted in a reduced head group area and a lower surface curvature in order to form vesicles. The stability of the dynamic vesicles was enhanced with the cross-linking polymerization method and this kind of vesicles which may have further applications mainly because the availability in diverse and complex surroundings. This kind of vesicles also had the stimulus-triggered disassembly ability which can be applied to controlled release the loaded cargos. With these properties mentioned above, the combination of CIA and cross-linking strategy may become a promising universal nanocarrier.

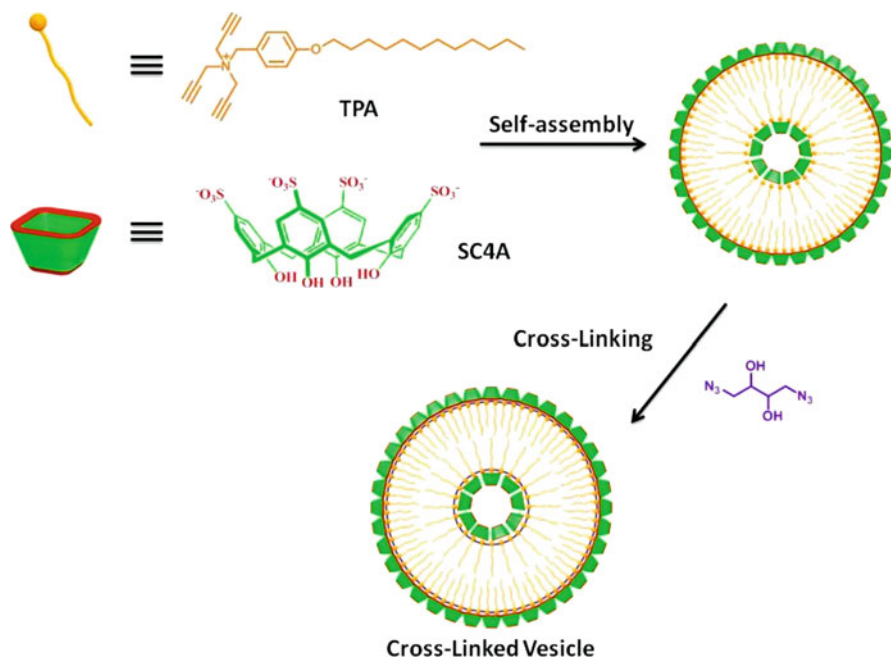


**Fig. 20.8** Schematic illustration of the SC4A–TPA cross-linked vesicle



## 20.2.2 Supramolecular Assembly Constructed from Guest-Induced Aggregation of Calixarene

Amphiphilic macrocyclic molecules with a hydrophilic skeleton and hydrophobic alkyl chains was a new kind of building blocks to construct functional materials. Compared to non-cyclic molecules, amphiphilic macrocyclic molecules exhibited a better aggregation performance [26]. More importantly, after forming the assembly with amphiphilic molecules, the hydrophilic macrocyclic host tended to spread of the surface of assembly which provided binding sites for different kinds of guest molecules [27]. Among the various amphiphilic macrocyclic molecules, amphiphilic calixarene was easily prepared through the simple modification of calixarene. The cone-type rigid skeleton of calixarene was also a useful character to improve the stability of amphiphilic assembly [28].

In a typical example, the anionic amphiphilic sulfonatocalixarene was used as the host and the selenocystamine dihydrochloride (Se-Cys) was used as the guest (Fig. 20.9) [29]. Through the host-guest interaction, the positive charge of Se-Cys partly neutralized the negative charge of sulfonatocalixarene, which reduced the hydrophilicity of sulfonatocalixarene. In addition, the charge compensation weakened the electrostatic repulsion of hydrophilic head groups and changed the morphology of assembly. Benefiting from the redox activity of Se-Se bond, the binary assembly could respond to the addition of oxidant ( $\text{H}_2\text{O}_2$ ) or reductant (GSH) and release the loaded dye molecule. Due to the over expressing of GSH in cancer cells,

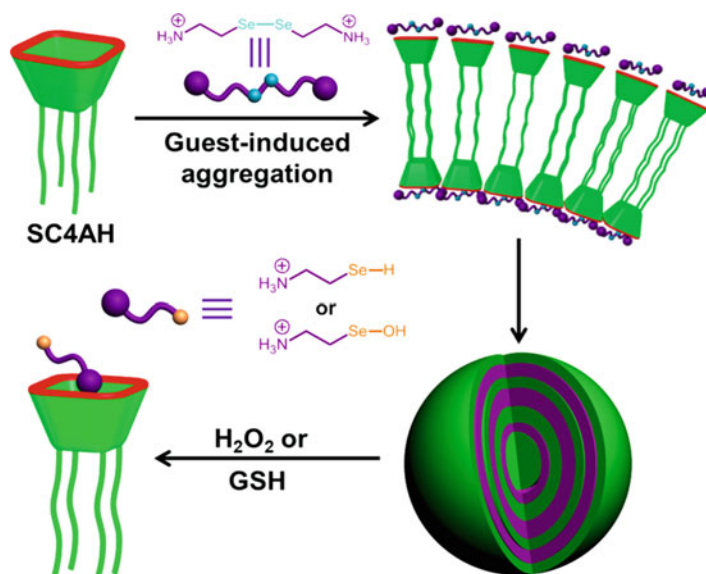


Fig. 20.9 Schematic illustration of the SC4AH–Se-Cys assembly and its redox-response

this nano-assembly could be used as a potential drug delivery system for cancer therapy.

### 20.2.3 *Supramolecular Host-Guest Co-assembly of Amphiphilic Calixarene*

Except the amphiphilic guest molecules, SC4A could also assembled with polycations. In this case, neither the host nor the guest had the possibility of self-aggregation under the experimental condition. Therefore, this kind of assembly behavior was defined as “host-guest co-assembly”. The supramolecular assembly of SC4A with a cationic polyelectrolyte chitosan produced a multistimuli-responsive supramolecular vesicle that could disassemble upon increasing pH or adding a competitive guest but tended to form a larger one upon increasing temperature (Fig. 20.10) [30]. A possible reason may be that chitosan with a higher deacetylation degree could form a more stable assembly with SC4A because it afforded stronger multivalent electrostatic interactions with SC4A. Subsequently, DOX was loaded into the vesicles, and the loading of DOX could not affect the stability of the supramolecular polymeric vesicle. Furthermore, natural biological

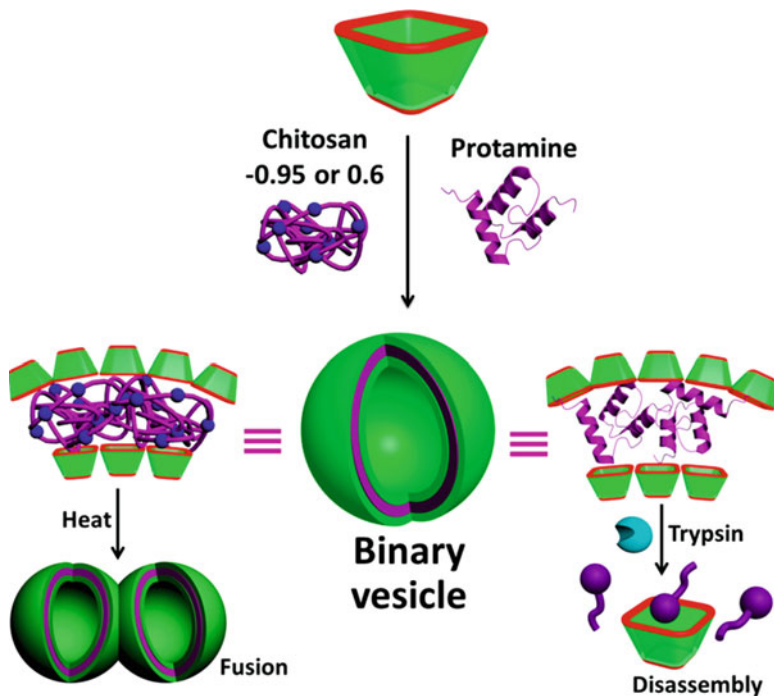


Fig. 20.10 Formation of supramolecular co-assembly composed of SC4A and polycations



cationic protein protamine was used as the enzyme-cleavable guest to construct a serine protease trypsin-responsive supramolecular vesicle with SC4A as the host, and this assembly could be disaggregated at trypsin-overexpressed sites to realize site-controlled release [9]. This trypsin-triggered controllable release model is reasonably promised in improving the drug efficacy and minimizing the undesired side effects.

In addition to polysaccharide and protein, amphiphilic drugs were also employed in the co-assembly with calixarenes, and this approach could improve the drug loading efficiency (Fig. 20.11) [31]. In a typical example, chlorpromazine hydrochloride (CPZ) was used as a building subunit to construct the supramolecular assembly with the desired high loading efficiencies for irinotecan·HCl and mitoxantrone·HCl. Due to the host-guest binding site of SC4A on the outer-layer surface, trimethylated chitosan (TMC) as a targeting agent could be non-covalently modified on the SC4A-CPZ nanoparticles. This strategy of calixarene-drug co-assembly provided a new direction for the development of nano-carriers with high drug loading and easily constructing. The versatility of the envisaged nanostructures, simply by changing the drug molecule and the exposed ligand, may be a highly desirable advantage for engineering a universal nanocarrier.

Liposomes, which could load hydrophilic substrates in the internal hydrophilic environment and hydrophobic one in the membrane structure, gain a lot of interests [32]. Many functional molecules including imaging probes, targeting ligands, and treating modules, were covalently or non-covalently modified to the liposomes to construct drug delivery systems with the diagnostic and therapeutic function [33]. In such a drug delivery system by embedding amphiphilic SC4A on the outer shell of liposomes (Fig. 20.12), [34] the vesicle displayed a good long-term stability in aqueous solution. The fluorescence image probe and targeting ligand were further modified to the vesicle through host-guest interactions. The confocal

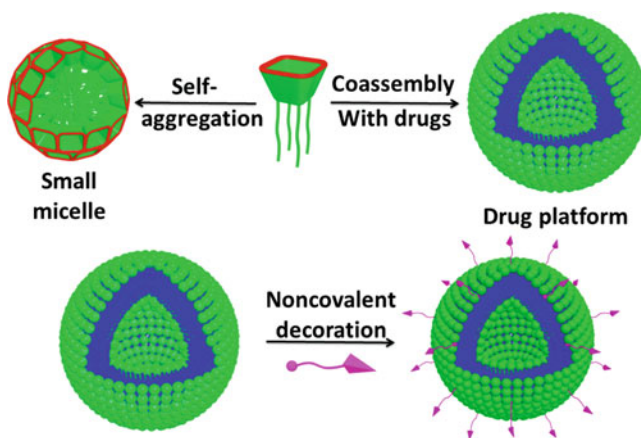
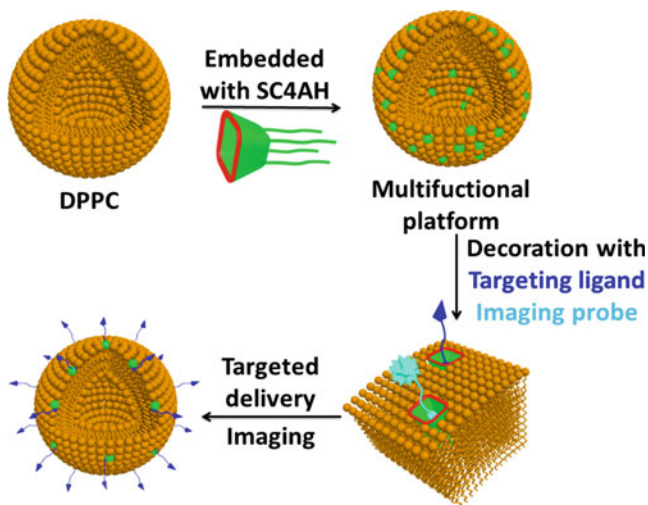


Fig. 20.11 Functionalization protocol of the "drug chaperone" strategy



**Fig. 20.12** Schematic illustration of multifunctional liposome and the noncovalent surface modification via host-guest interaction

laser scanning microscopic experiments showed that the functionalized lipids could be transferred into cancer cells through the receptor-mediated internalization.

### 20.3 Conclusions and Expectation

Combined with various guest molecules, supramolecular assemblies based on water-soluble calixarenes have become a hotspot in the fields of stimuli-response material, drug delivery system, multifunctional nano-platform for the delivery of biological substrates and the treatment of pesticide poisoning, as well as supramolecular catalysis. However, with the further understanding there still remain several questions on the development of water-soluble calixarenes including (1) how to enrich the main skeleton of sulfonato-calixarenes; (2) how to employ more the host-guest interactions other than mainly utilizing electrostatic interactions; (3) how to extend the scope of stimuli-responsive method. It could be expected that the further functionalization of sulfonato-calixarene hosts and the finding of more guest molecules with new stimuli-responsive ability will bring the supramolecular assemblies based on sulfonato-calixarene more prospect.

**Acknowledgments** We thank NNSFC (21432004, 21272125, and 91527301) for financial support.

## References

1. (a) Perret, F.; Lazar, A. N.; Coleman, A. W. *Chem. Commun.* **2006**, 2425–2438. (b) Arduini, A.; Pochini, A.; Raverberri, S.; Ungaro, R. *J. Chem. Soc., Chem. Commun.* **1984**, 981–982. (c) Kalchenko, V. I.; Visotsky, M. A.; Shivanyuk, A. N.; Pirozhenko, V. V.; Markovsky, L. N. *Phosphorus, Sulfur Silicon Relat. Elem.* **1996**, *109*, 513. (d) Perret, F.; Coleman, A. W. *Chem. Commun.* **2011**, *47*, 7303–7319.
2. Shinkai, S.; Mori, S.; Tsubaki, T.; Sone, T.; Manabe, O. *Tetrahedron Lett.* **1984**, *25*, 5315–5318.
3. (a) Shinkai, S.; Araki, K.; Matsuda, T.; Nishiyama, N.; Ikeda, H.; Takasu, I.; Iwamoto, M. *J. Am. Chem. Soc.* **1990**, *112*, 9053–9058. (b) Liu, Y.; Guo, D.-S.; Zhang, H.-Y.; Ma, Y.-H.; Yang, E.-C. *J. Phys. Chem. B* **2006**, *110*, 3428–3434. (c) Zhao, H.-X.; Guo, D.-S.; Liu, Y. *J. Phys. Chem. B* **2013**, *117*, 1978–1987.
4. Wang, K.; Guo, D.-S.; Zhang H.-Q.; Li D.; Zheng X.-L.; Liu Y. *J. Med. Chem.* **2009**, *52*, 6402–6412.
5. Cui, J.; Uzunova, V. D.; Guo, D.-S.; Wang, K.; Nau, W. M.; Liu, Y. *Eur. J. Org. Chem.* **2010**, 1704–1710.
6. Kellermann, M.; Bauer, W.; Hirsch, A.; Schade, B.; Ludwig, K.; Böttcher, C. *Angew. Chem. Int. Ed.* **2004**, *43*, 2959–2962.
7. Guo, D.-S.; Chen, K.; Zhang, H.-Q.; Liu, Y. *Chem. Asian J.* **2009**, *4*, 436–445.
8. (a) Guo, D.-S.; Jiang, B.-P.; Wang, X.; Liu, Y. *Org. Biomol. Chem.* **2012**, *10*, 720–723. (b) Varga, O.; Kubinyi, M.; Vidoczy, T.; Baranyai, P. Bitter, I.; Kallay, M. *J. Photochem. Photobiol., A* **2009**, *207*, 167–172. (c) Lau, V.; Heyne, B. *Chem. Commun.* **2010**, *46*, 3595–3597. (d) Megyesi, M.; Biczok, L. *J. Phys. Chem. B* **2010**, *114*, 2814–2819.
9. (a) Basílio, N.; Piñeiro, Á.; Silva, J. P. D.; García-Río, L. *J. Org. Chem.* **2013**, *78*, 9113–9119. (b) Basilio, N.; García-Río, L. *Chem. Eur. J.* **2009**, *15*, 9315–9319. (c) Francisco, V.; Basilio, N.; García-Río, L.; Leis, J. R.; Maques, E. F.; Vazquez-Vázquez, C. *Chem. Commun.* **2010**, *46*, 6551–6553. (d) Basilio, N.; Gomez, B.; García-Río, L.; Francisco, V. *Chem. Eur. J.* **2013**, *19*, 4570–4576. (e) Basilio, N.; Martín-Pastor, M.; García-Río, L. *Langmuir* **2012**, *28*, 6561–6568. (f) Li, Z. Q.; Hu, C. X.; Chen, Y. Q.; Xu, H.; Cao, X. L.; Song, X. W.; Zhang, H. Y.; Liu, Y. *Sci. China Chem.* **2012**, *55*, 2063–2068. (g) Cao, Y.; Wang, Y.-X.; Guo, D.-S.; Liu, Y. *Sci. China Chem.* **2014**, *57*, 371–378. (h) Wintgens, V.; Coeur, C. L.; Amiel, C.; Guigner, J.-M.; Harangozo, J. G.; Miskolczy, Z.; Biczók, L. *Langmuir* **2013**, *29*, 7682–7688.
10. Qin, Z.; Guo, D.-S.; Gao, X.-N.; Liu, Y. *Soft Matter* **2014**, *10*, 2253–2263.
11. Wang, K.; Guo, D.-S.; Zhao, M.-Y.; Liu, Y. *Chem. Eur. J.* **2016**, *22*, 1475–1483.
12. (a) Biedermann, F.; Elmalem, E.; Ghosh, I.; Nau, W. M.; Scherman, O. A. *Angew. Chem., Int. Ed.* **2012**, *51*, 7739–7743. (b) Dsouza, R. N.; Pischel, U.; Nau, W. M. *Chem. Rev.* **2011**, *111*, 7941–7980.
13. D.-S. Guo, Y. Liu, *Acc. Chem. Res.* **2014**, *47*, 1925–1934.
14. Costanzo, L. D.; Geremia, S.; Randaccio, L.; Purrello, R.; Lauceri, R.; Sciotto, D.; Gulino, F. G.; Pavone, V. *Angew. Chem., Int. Ed.* **2001**, *40*, 4245–4247.
15. Rowan, S. J.; Cantrill, S. J.; Cousins, G. R. L.; Sanders, J. K. M.; Stoddart, J. F. *Angew. Chem. Int. Ed.* **2002**, *41*, 898–952.
16. Wang, K.; Guo, D.-S.; Liu, Y. *Chem. Eur. J.* **2010**, *16*, 8006–8011.
17. Wang, K.; Guo, D.-S.; Liu, Y. *Chem. Eur. J.* **2012**, *18*, 8758–8764.
18. Wang, K.; Guo, D.-S.; Wang, X.; Liu, Y. *ACS Nano* **2011**, *5*, 2880–2894.
19. Guo, D.-S.; Wang, K.; Wang, Y.-X.; Liu, Y. *J. Am. Chem. Soc.* **2012**, *134*, 10244–10250.
20. Luo, J.; Xie, Z.; Lam, J.; Cheng, L.; Chen, H.; Qiu, C.; Kwok, H. S.; Zhan, X.; Liu, Y.; Zhu, D.; Tang, B. *Z. Chem. Commun.* **2001**, 1740–1741.
21. Jiang, B.-P.; Guo, D.-S.; Liu, Y.-C.; Wang, K.-P.; Liu, Y. *ACS Nano* **2014**, *8*, 1609–1618.
22. Liu, K.; Liu, Y.; Yao, Y.; Yuan, H.; Wang, S.; Wang, Z.; Zhang, X. *Angew. Chem. Int. Ed.* **2013**, *52*, 8285–8289.
23. Wang, Y.-X.; Zhang, Y.-M.; Liu, Y. *J. Am. Chem. Soc.* **2015**, *137*, 4543–4549.

24. (a) Peng, H.-Q.; Chen, Y.-Z.; Zhao, Y.; Yang, Q.-Z.; Wu, L.-Z.; Tung, C.-H.; Zhang, L.-P.; Tong, Q.-X. *Angew. Chem., Int. Ed.*, **2012**, *51*, 2088; (b) Zhang, S.; Zhao, Y. *J. Am. Chem. Soc.*, **2010**, *132*, 10642; (c) Zhang, S.; Zhao, Y. *Chem. Commun.*, **2012**, *48*, 9998; Li, X.; Zhao, Y. *Bioconjugate Chem.*, **2012**, *23*, 1721.
25. Peng, S.; Gao, J.; Liu, Y.; Guo, D.-S. *Chem. Commun.*, **2015**, *51*, 16557–16560.
26. Voskuhl, J.; Ravoo, B. *J. Chem. Soc. Rev.* **2009**, *38*, 495–505.
27. Shinkai, S.; Mori, S.; Koreishi, H.; Tsubaki, T.; Manabe, O. *J. Am. Chem. Soc.* **1986**, *108*, 2409–2416.
28. Wang, Y.-X.; Guo, D.-S.; Cao, Y.; Liu, Y. *RSC Adv.* **2013**, *3*, 8058–8063.
29. Hu, X.-Y.; Chen, Y.; Liu, Y. *Chin. Chem. Lett.* **2015**, *26*, 862–866.
30. Peng, S.; Wang, K.; Guo, D.-S.; Liu, Y. *Soft Matter* **2015**, *11*, 290–296.
31. Wang, Y.-X.; Guo, D.-S.; Duan, Y.-C.; Wang, Y.-J.; Liu, Y. *Sci. Rep.* **2015**, *5*, 9019.
32. Rösler, A.; Vandermeulen, G. W. M.; Klok, H.-A. *Adv. Drug Delivery Rev.* **2001**, *53*, 95–108.
33. Gu, F.; Zhang, L.; Teply, B. A.; Mann, N.; Wang, A.; Radovic-Moreno, A. F.; Langer, R.; Farokhzad, O. C. *Proc. Natl. Acad. Sci. USA* **2008**, *105*, 2586–2591.
34. Wang, Y.-X.; Zhang, Y.-M.; Liu, Y. *Chem. Mat.* **2015**, *27*, 2848–2854.

# Chapter 21

## Water-Soluble Cryptophanes: Design and Properties

Thierry Brotin, Alexandre Martinez, and Jean-Pierre Dutasta

### 21.1 Introduction

The cryptophanes constitute an important class of molecular hosts with remarkable binding properties, known for nearly 35 years since the pioneering works of Collet et al. [1–3]. They still play a prominent role in molecular recognition phenomena and during these last decades their chemistry has evolved to novel domains of supramolecular chemistry such as bio-sensing and chemistry within confined space [4]. Cryptophane derivatives are made of two cyclotribenzylene units (CTB) connected together by three linkers whose length and nature can be varied (Fig. 21.1). The bowl-shaped rigid structure and the presence of an inner molecular cavity make these compounds easily recognizable and of high interest. Indeed, they are particularly well suited to accommodate small molecules or ions. For instance, cryptophane-A (Fig. 21.1),<sup>1</sup> one of the best-known members of this family exhibits strong affinities for a large range of guests such as halogenomethanes, CH<sub>4</sub> or xenon. Most of the cryptophane molecules reported in the literature are soluble in organic solvents.

---

<sup>1</sup>The A, B, C... nomenclature of cryptophanes was established based on the chronological order of their discovery. Later on, a nomenclature more appropriate to the growing complexity of the molecules has been proposed, taking into account the nature of the linkers. However, it is often necessary to describe each structure if we wish to avoid the use of complex IUPAC nomenclature. In this review, we have tried to make this terminology as explicit as possible.

T. Brotin (✉) • J.-P. Dutasta (✉)  
Laboratoire de Chimie, École Normale Supérieure de Lyon, CNRS, UCBL, 46 Allée d'Italie,  
69364 Lyon, France  
e-mail: [thierry.brotin@ens-lyon.fr](mailto:thierry.brotin@ens-lyon.fr); [jean-pierre.dutasta@ens-lyon.fr](mailto:jean-pierre.dutasta@ens-lyon.fr)

A. Martinez  
Aix Marseille Université, Centrale Marseille CNRS iSm2 UMR 7313, 13397 Marseille, France

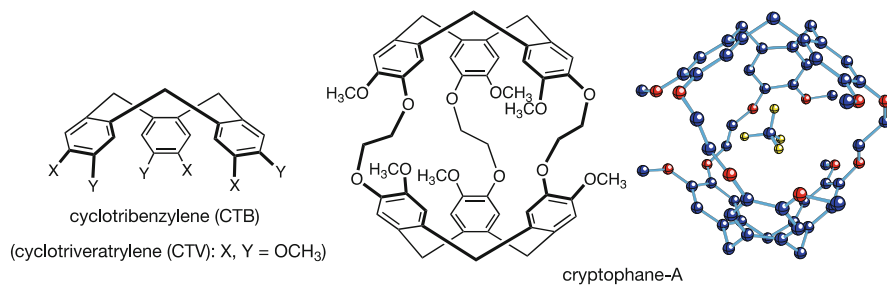


**Fig. 21.1** Cyclotribenzylene and cryptophane-A (*right*: energy minimized structure of the CH<sub>4</sub>@cryptophane-A inclusion complex) [5]

Only very few studies concern derivatives soluble in aqueous solution. Probably the difficulties to modify the chemical structure of the cryptophanes delayed the production of water-soluble compounds and the study of their binding properties in the aqueous phase. A reason, which has stimulated the development of water-soluble cryptophanes, is the discovery that xenon and cryptophane-A form a strong host-guest complex in solution [6]. This finding has been rapidly exploited to design NMR contrast agents using hyperpolarized xenon, and recent studies suggest that magnetic resonance imaging (MRI) applications could be envisaged in the near future [7–10]. However, this requires the development of new synthetic strategies to produce sizable amounts of water-soluble cryptophanes with reliable biocompatibility. Several research groups are currently developing different strategies to improve the solubility of cryptophanes in water.

This review is dedicated to the synthesis of water-soluble cryptophanes and of the closely related hemicyptophane derivatives that were developed more recently. The study of their binding properties with different species and some peculiar properties related to their chiral structure are also described. A particular attention is given to xenon-cryptophane complexes since, as above mentioned, these complexes have played a major role in the development of water-soluble cryptophane derivatives. We describe in a concise manner the different approaches, which have been reported in the literature to introduce hydrophilic moieties onto the cryptophane structure. Finally, we report some physical properties of the water-soluble cryptophane complexes. This mainly concerns the study of their binding properties with neutral molecules or charged species. The preparation of enantiopure cryptophanes has also contributed to the development of this field. Indeed, it was stressed that cryptophanes exhibit remarkable chiroptical and binding properties in water [11]. These properties are also described. The last part of this review is devoted to hemicyptophane derivatives, which are closely related to the cryptophane structure and which allow the functionalization of the inner space of the molecular cavity. These show a renewed interest in their applications in chiral recognition and supramolecular catalysis.

## 21.2 Synthesis of Water-Soluble Cryptophanes

### 21.2.1 Preparation of Cryptophane Derivatives Soluble in Aqueous Phase

In recent time the number of water-soluble cryptophanes reported in the literature has increased substantially. The main reason for this arises from the rapid development of the xenon-cryptophane complexes aimed at designing biosensors for MRI applications. Nevertheless, it seems important to distinguish between two types of water-soluble cryptophanes. The first series of water-soluble cryptophanes are made from a cryptophane skeleton, which has been properly modified in order to significantly enhance its solubility in water. For instance, the hexa-carboxylate cryptophane **1** (Fig. 21.2), whose synthesis is reported below (Scheme 21.1), is sparingly soluble in neutral water and very soluble in basic solution (NaOH/H<sub>2</sub>O). The second class of water-soluble cryptophanes is made of lipophilic cryptophane cores, which have been adequately functionalized in order to make the whole molecule soluble in water. For example, cryptophanol-A **2**, when suitably substituted by hydrosoluble moiety at the phenol function, belongs to this second class of molecule (Fig. 21.2). Original cryptophane biosensors have been prepared by this way and will be described in more detail below.

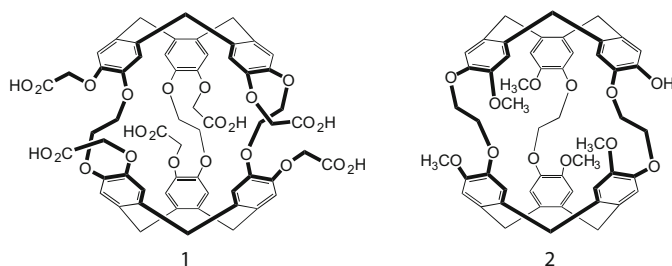
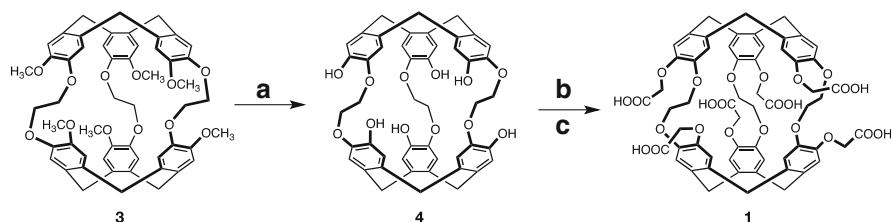


Fig. 21.2 Water-soluble hexa-acid cryptophane **1**, and lipophilic cryptophanol-A **2**



Scheme 21.1 Synthesis of hexa-carboxylate cryptophane **1** [reaction conditions: (a) Ph<sub>2</sub>PLi (1 M), THF, 60 °C, 70–80%; (b) methyl bromoacetate, Cs<sub>2</sub>CO<sub>3</sub>, DMF, 60 °C, 75–80%; (c) KOH/H<sub>2</sub>O-THF, 60 °C, then conc. HCl, 0 °C; 95 %]

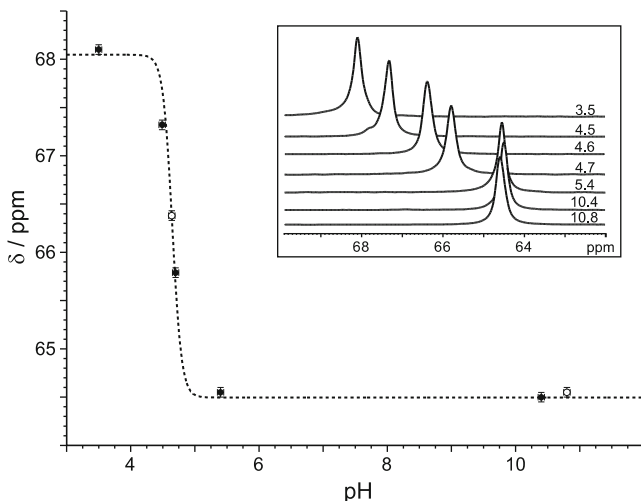
The ring closure reaction to form the CTB moieties requires strong activated benzene rings such as 3,4-dialkoxybenzylalcohol derivatives, which are the most commonly used starting materials to prepare cryptophanes. In addition, even though the nature of the linkers can be easily varied, dialkoxyalkane chains are those most commonly used to connect the two CTB units. This makes the cryptophane skeleton strongly lipophilic and the solubilization in aqueous phase is only possible after adding appropriate hydrophilic substituents to the benzene rings. The higher the substitution, the better the solubility in water. For example, cryptophane-A **3**, which possesses six methoxy groups, can be modified to design the water soluble, hexa-functionalized cryptophane **1** (Scheme 21.1) [12]. This requires the removal of the six methyl groups with lithium diphenylphosphide to give rise to the hexa-phenol derivative **4**. This derivative is soluble in water under basic condition and possesses interesting binding properties towards cationic species. A  $\text{S}_{\text{N}}2$  substitution reaction of the six phenol groups with bromomethyl acetate followed by hydrolysis of the ester groups in  $\text{KOH}/\text{H}_2\text{O}$  provides compound **1** in good yield. This compound is sparingly soluble in water at neutral pH and very soluble under basic conditions. Collet et al. used a similar approach to design water-soluble  $D_3$ -symmetry cryptophanes with larger cavities. For instance, water-soluble congeners of cryptophane-E, comprising three propylenedioxy linkers and cryptophane-O with three butanedioxy linkers have been prepared. These compounds show good molecular recognition properties towards ammonium species (see Sect. 21.3.4) [13].

Cryptophane **1** has been prepared as both a racemate and optically active molecule, and the formation of complexes with neutral species in water has been thoroughly investigated by several spectroscopic techniques (see Sect. 21.3.2). The  $\text{Xe}@\mathbf{1}$  complex has also been used as a model system for several fundamental studies. For instance, it has been shown that the  $^{129}\text{Xe}$  chemical shift of the  $\text{Xe}@\mathbf{1}$  complex is very sensitive to a small variation in pH [14], which is characterized by a significant shift of the  $^{129}\text{Xe}$  NMR signal (Fig. 21.3).

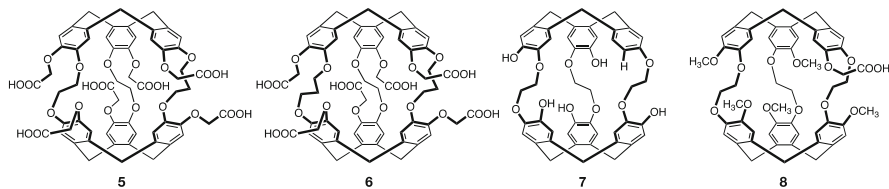
Recently, other studies aimed at rapidly detecting the  $^{129}\text{Xe}$  NMR signal of this complex at low concentration have been reported [15]. This host compound, used either as a racemate or optically active molecule, is also a key compound for the elaboration of more complex derivatives which are described in the following sections. A similar strategy was applied to design cryptophanes with  $C_2$  or  $C_1$  symmetry depending on the nature of the linkers. For instance, cryptophanes **5** and **6** bearing six carboxylic acid moieties and linkers of different length within each molecule have been prepared from the so-called *template method* (Fig. 21.4). This approach requires the formation of the two CTB caps at different stage of the synthesis [4, 16].  $C_1$ -Symmetry cryptophane **7** bearing five hydroxyl groups has been synthesized in a similar manner in four steps from cryptophanol-A **2** [17]. This compound is soluble in  $\text{NaOH}/\text{H}_2\text{O}$  solution and shows interesting enantioselective recognition properties towards chiral oxirane derivatives (see Sect. 3.3).

The sparingly water-soluble carboxylic acid cryptophane **8** was prepared from cryptophanol-A **2**. Although its solubility is very limited in water, the  $\text{Xe}@\mathbf{8}$  complex can be easily detected in water thanks to high sensitivity laser-polarized





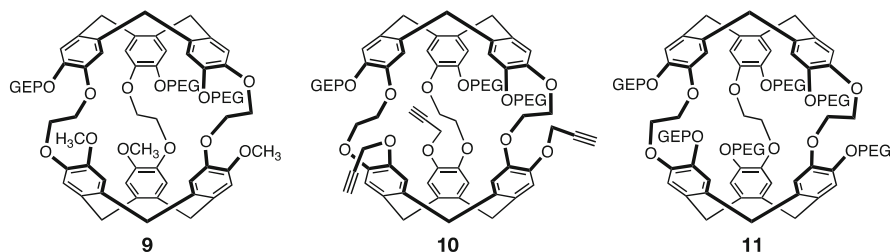
**Fig. 21.3** pH Sensitive Xe@1 NMR probe: Plot of  $^{129}\text{Xe}$  chemical shift vs. pH ( $\square$  KOD/ $\text{D}_2\text{O}$ ;  $\blacksquare$ : NaOD/ $+\text{D}_2\text{O}$ ) (Reprinted from Ref. [14], Copyright 2010, with permission from Wiley-VCH)



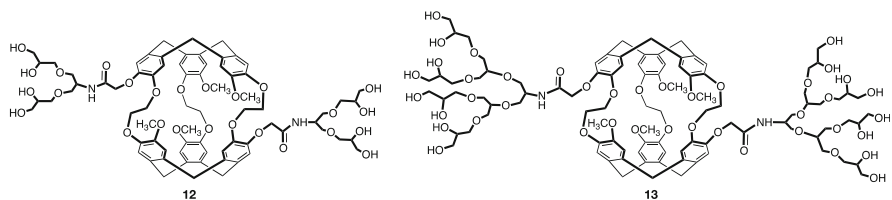
**Fig. 21.4** Structures of  $C_2$ -symmetry cryptophanes **5–6** and  $C_1$ -symmetry cryptophanes **7–8**

(LP)  $^{129}\text{Xe}$  NMR techniques at or even below the micromolar scale. For instance, compound **8** has been used to demonstrate that the xenon *in-out* exchange process with **8** occurs via a degenerate process [18]. Schröder et al. also reported the study of Xe@**8** as a sensor to study membrane fluidity and membrane composition [19, 20]. Independently, Fréchet et al. demonstrated that the introduction of several Xe@**8** cryptophane complexes inside a PAMAM dendritic structure allowed a significant gain (by a factor 8) in sensitivity of the  $^{129}\text{Xe}$  NMR signal [21].

The need for cryptophane derivatives soluble at neutral pH or under physiological conditions is a prerequisite for the construction of efficient xenon-biosensors. In order to improve solubility of the cryptophane-A skeleton at neutral pH, Rousseau et al. suggested replacing the six carboxylic acid moieties in **1** by polyethylene glycol (PEG) substituents [22]. The PEG units strongly enhance the solubility at neutral pH without significantly modifying the *in-out* xenon guest exchange dynamics. The same authors reported the synthesis of several cryptophane-A congeners bearing three (**9** and **10**) and six (**11**) PEG moieties respectively (Fig. 21.5). The strategy used to introduce the PEG substituents depends on the nature of the cryptophane. Thus, the synthesis of cryptophanes **9** and **10** requires the



**Fig. 21.5** Structures of the water-soluble cryptophanes **9–11**

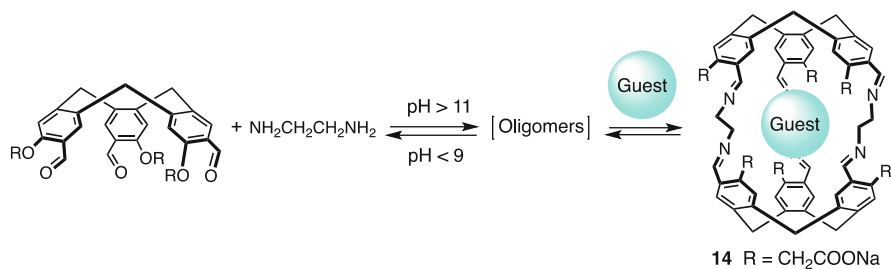
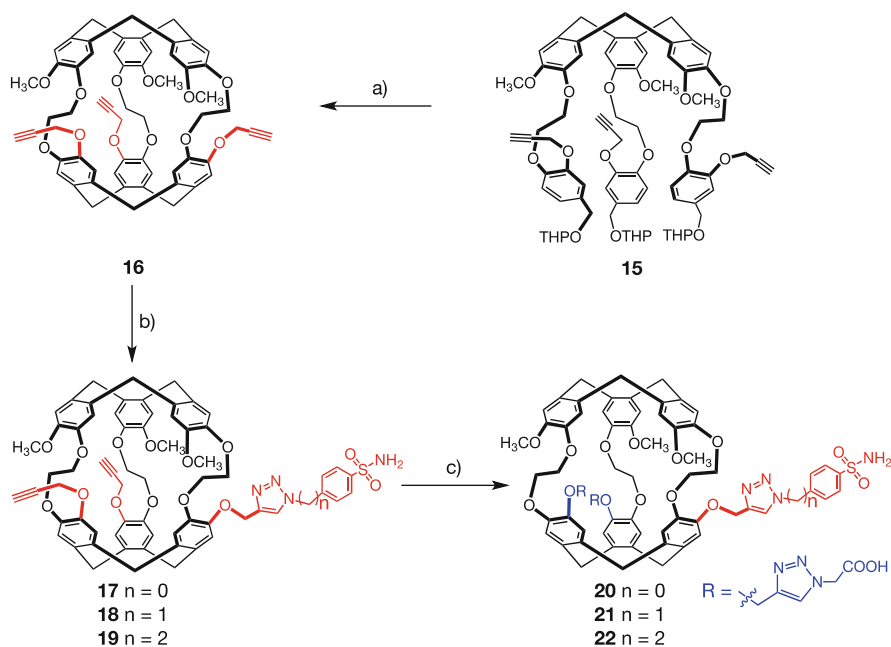


**Fig. 21.6** Dendronized cryptophanes **12** and **13**

introduction of three PEG<sub>550</sub> moieties at an early stage of the synthesis. The second ring closing reaction is performed at a later stage and allows for the introduction of other chemical functions such as methyl or propargyl groups. The synthesis of cryptophane **11** is different as the six PEG<sub>550</sub> are introduced during the last synthetic step by reacting tosyl-functionalized PEG monomethyl ether ( $M_n$  550) moieties with cryptophane **4**.

Schröder et al. synthesized the two dendronized cryptophanes, **12** and **13**, to enhance the solubility of the host in water at neutral pH [23]. They are formed from a bis-functionalized cryptophane containing two carboxylic acid groups, each of which are located on a distinct CTB unit (Fig. 21.6). Polyglycerol substituents were then added to afford water-soluble cryptophanes that are expected to show high biocompatibility and to provide multi-functionality on the outer surface of the molecules for subsequent reactions. This approach appears promising for the design of new xenon-biosensors for biological studies. It is noteworthy that the synthesis of the cryptophane precursor has never been fully described.

Warmuth et al. reported the synthesis of a series of water-soluble cryptophanes via a self-association process. The strategy used by the authors involves the formation of six imine bonds in a single step by reacting two triformyl-cyclotribenzylene units with three diamino-linkers [24]. When mixed together the reaction evolves spontaneously to give rise to the formation of a unique cryptophane derivative in almost quantitative yield. The formation of the cryptophane derivative can be easily followed by <sup>1</sup>H NMR spectroscopy. This approach appears as a facile way to prepare new water-soluble cryptophanes in high yields. An example is given in Scheme 21.2 with the water-soluble cryptophane **14** bearing six carboxylic acid moieties.

**Scheme 21.2** Templated synthesis of a dynamic cryptophane**Scheme 21.3** Synthesis of a water-soluble cryptophanes for the complexation of human carbonic anhydrase [reaction conditions: (a) HClO<sub>4</sub>, MeOH, rt, 14 h, 48 %; (b) Sulfonamide linker, CuSO<sub>4</sub>, 2,6-lutidine, sodium ascorbate, DMSO/H<sub>2</sub>O (10/1), 41–57 %; (c) 3-azido propanoic acid, CuSO<sub>4</sub>, 2,6-lutidine, sodium ascorbate, DMSO/H<sub>2</sub>O (10/1), 12 h, 41–63 %]

Dmochowski et al. used the *template method* to synthesize a series of water-soluble tri-acetic acid cryptophane derivatives aimed at complexing human carbonic anhydrase. The binding site of this protein contains a zinc cation, which is well recognized by the *p*-benzene-sulfonamide moiety grafted on the cryptophane backbone. Reaction of the cryptophane precursor **15** under acidic conditions gave rise to the tri-functionalized cryptophane **16** bearing three propargylic functions (Scheme 21.3). First, a single propargylic moiety was used to introduce a benzene-sulfonamide recognition site tethered with links of different length, aimed at

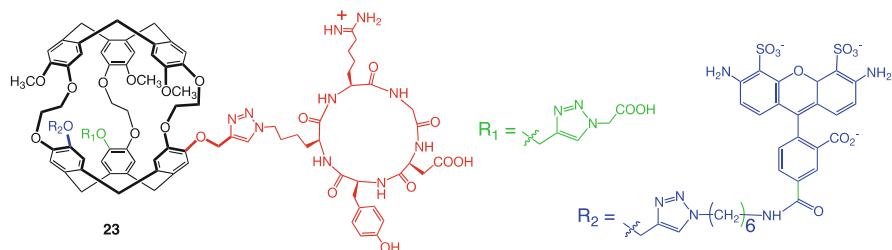


**Fig. 21.7** Chemical structure of biosensor **23** with a bimodal detection mode for the detection of  $\alpha_v\beta_3$  integrin proteins

complexing the protein. This gave rise to compounds **17–19**, which were later allowed to react to introduce water-solubilizing carboxylic acid substituents, affording host molecules **20–22** (Scheme 21.3). Xenon-biosensors Xe@**20**, Xe@**21** and Xe@**22** have been studied in presence of human carbonic anhydrase. The stability of the complexes ( $K_d = 20\text{--}110$  nM) was measured by isothermal titration calorimetry experiments (ITC). Laser polarized  $^{129}\text{Xe}$  NMR spectroscopy of the complexes reveals the presence of several downfield shifted signals with respect to the unbound biosensors [25]. The same group followed a similar route to prepare water-soluble cryptophanes showing high affinity for xenon and radon gases [26, 27].

A similar strategy to that reported in Scheme 21.3 allowed for the preparation of tri-functionalized cryptophane **23** with three suitable linkers aimed at detecting  $\alpha_v\beta_3$  integrin proteins (Fig. 21.7). These proteins are of high interest since they are usually overexpressed in many human cancers [28]. Starting from cryptophane **16**, a small cyclic peptide containing an arginine-glycine-aspartic acid (RGD) sequence was first introduced as the protein recognizing site. In a second step, a linker bearing a fluorophore (Alexa Fluor® 488) was used to localize the biosensor in cells more easily. Finally, a short hydrophilic arm was tethered at the third position. Cryptophane **23** is only sparingly soluble in water and *in-cellulo* experiments have been performed in a water-DMSO mixture (9:1). Thanks to the presence of the fluorophore moiety attached to the cryptophane structure, confocal laser scanning microscopy could be used to investigate cell uptake. Additional *in vitro* experiments have shown that the Xe@**23** gives rise to a downfield shifted  $^{129}\text{Xe}$  NMR signal in presence of  $\alpha_{\text{IIb}}\beta_3$  integrin proteins [29].

These authors recently used a similar strategy to design the pH sensitive cryptophane biosensor **24**. Cryptophane **14** bearing three propargylic moieties on the same CTB cap was successively functionalized by a peptide, whose sequence is described in Fig. 21.8. Then, two hydrophilic moieties aimed at solubilizing the whole structure were introduced via a click chemistry reaction to give the water-soluble host molecule **24**. A conformational change of the peptide occurs upon acidification, which in turn impacts the chemical shift of the  $^{129}\text{Xe}$ @**24** complex. This effect can be easily detected at low concentration in water by using LP  $^{129}\text{Xe}$  NMR spectroscopy. A  $^{129}\text{Xe}$  chemical shift difference  $\Delta\delta = 13.5$  ppm was observed

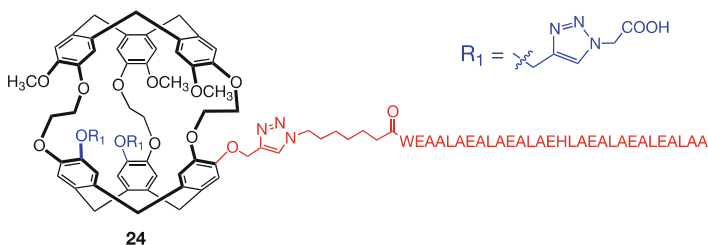


**Fig. 21.8** Structure of the pH sensitive water-soluble cryptophane biosensor **24**

between the two Xe@**24** complexes, which differ by the pH dependent conformation of the peptidic chain.

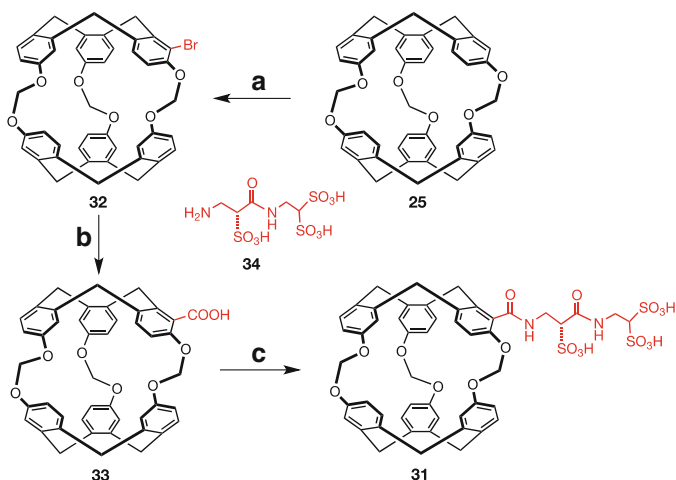
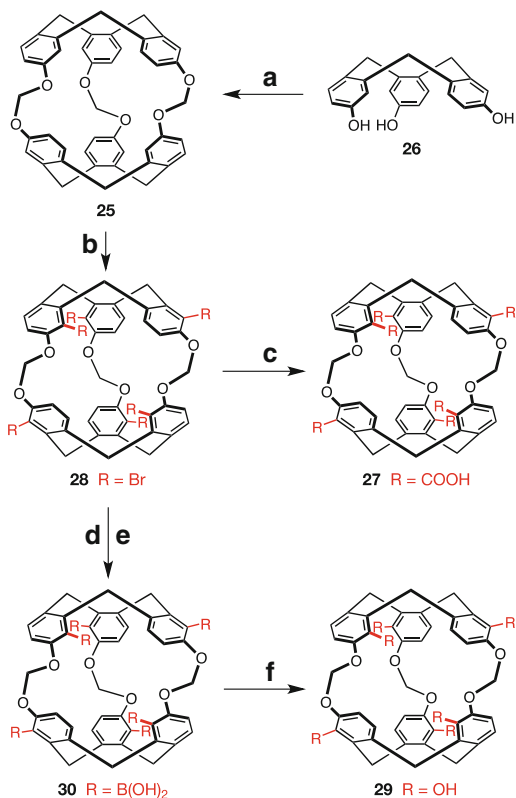
Cryptophanes-111, whose structures are depicted in Scheme 21.4, have been suitably functionalized in order to enhance their solubility in water. Rousseau et al. have developed an interesting strategy to functionalize cryptophane-111 **25**, which shows remarkable binding properties with xenon in organic solution. This compound was prepared in a single step from cyclotriphenolene **26** (Scheme 21.4). The water-soluble cryptophane-111 **27** was obtained in three steps from the naked cryptophane-111 **25**. Bromination with *N*-bromosuccinimide allowed for the introduction of six bromine atoms in the ortho-position relative to the methylene bridge to afford compound **28**. Surprisingly, this position seems to be privileged with respect to the other less hindered one available. Subsequent halogen-metal exchange followed by reaction with ethyl chloroformate afforded the cryptophane-111 bearing six ester groups in moderate yield. Finally, a hydrolysis step under basic condition gave rise to the water-soluble compound **27**, whose xenon binding properties have been investigated [30].

In a similar way, the same authors reported the synthesis of the hexa-phenol cryptophane-111 **29** from compound **28** according to the synthetic pathway depicted in Scheme 21.4 [31]. It is interesting to note that the hexa-boronic acid derivative **30** showed good solubility in water. This reaction proceeded very slowly at room temperature and could be monitored by  $^{129}\text{Xe}$  NMR spectroscopy. When xenon was added to the reaction mixture the formation of Xe@cryptophane(OH)<sub>x</sub> complexes ( $x = 0-6$ ) gave rise to a specific  $^{129}\text{Xe}$  NMR chemical shift. The most high-field shifted  $^{129}\text{Xe}$  NMR signal is observed with Xe@**29** ( $\delta = 30$  ppm). DFT calculations were able to predict the  $^{129}\text{Xe}$  NMR chemical shifts of the different Xe@cryptophane complexes generated during the reaction with high precision. An energy-decomposition analysis suggested that the phenyl-xenon interactions are predominant in the stabilization of the xenon-cryptophane complexes [31].

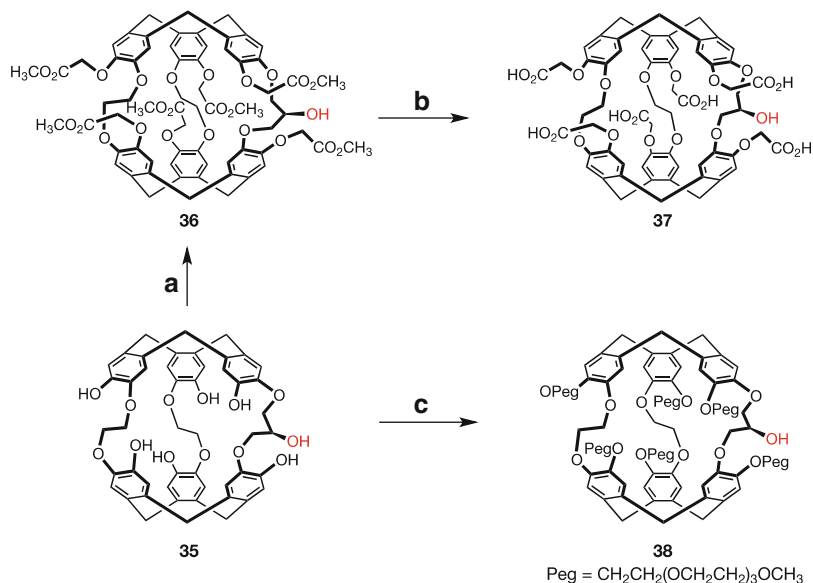
Rousseau et al. reported the preparation of the water-soluble cryptophane-111 **31** for xenon biosensing application [32]. The synthesis of this compound (Scheme 21.5) first requires the introduction of a reactive function on compound **25** that can be used for subsequent reactions. Thus, a single bromine atom was introduced on the cryptophane-111 skeleton to give rise to cryptophane **32**. In turn, a halogen-metal exchange reaction allowed for the introduction of a carboxylic acid

**Scheme 21.4** Synthesis of the water-soluble cryptophane-111 (**29**) from compound (**25**)

(reaction conditions: (a)  $\text{CH}_2\text{ClBr}$  (excess), DMF,  $80^\circ\text{C}$ , 46%; (b) NBS (excess),  $\text{CHCl}_3$ , rt, 13 days, 60%; (c) *n*-BuLi (2.19 M in hexane), benzyl chloroformate,  $-15^\circ\text{C}$  then  $\text{H}_2$ , Pd/C, THF/MeOH (1/1), 18%; (d) *n*-BuLi (2.5 M, excess), THF,  $-15^\circ\text{C}$ , 2-isopropoxy-4,4,5,5-tetramethyl-1,3,2-dioxaborolane (excess); (e) KOH/ $\text{H}_2\text{O}$ ,  $\text{CH}_3\text{CN}$ , rt, 1 night, 12%; HPLC purification ( $\text{CH}_3\text{CN}$ ,  $\text{H}_2\text{O}$ , TFA 0.1%, 0:100–70:30). (f)  $\text{H}_2\text{O}_2$  (30%),  $\text{H}_2\text{O}$ , rt)



**Scheme 21.5** Synthesis of the water-soluble cryptophane-111 **31** from **25** (reaction conditions: (a) NBS,  $\text{CHCl}_3$ , 24 h, rt, 64%; (b) THF, *n*-BuLi,  $\text{CO}_2$ , 1 h, 27%; (c) DMSO, **34**, PyBOP, DIEA in NMP then TFA 0.1%, 43%)



**Scheme 21.6** Synthesis of the chemical platforms **37** and **38** for xenon biosensing (reaction conditions: (a) Methyl bromoacetate, DMF, rt, 53 %. (b) KOH/H<sub>2</sub>O (0.5 M), THF, 60 °C, 85 %. (c) K<sub>2</sub>CO<sub>3</sub>, Ts-peg-3, DMF, 60 °C, 82 %)

group to give compound **33** in two steps. Finally, a Schotten-Baumann reaction with **33** allowed the grafting of the highly hydrophilic  $\alpha$ -sulfo- $\beta$ -alanine group **34**, making the resulting cryptophane-111 **31** soluble in water. The  $\alpha$ -sulfo- $\beta$ -alanine residue contains a stereogenic center and two diastereomeric species are generated in the reaction with *rac*-**33**. The formation of the two diastereomeric complexes Xe@**31** was easily detected by LP <sup>129</sup>Xe NMR spectroscopy and a difference of chemical shifts  $\Delta\delta = 3.0$  ppm has been measured between the two Xe@**31** diastereomers (54.0 and 51.4 ppm).

To date, cryptophane-111 derivatives are the best molecular hosts for xenon with unprecedentedly high binding constants. However, their use as xenon carriers for MRI application is questionable since the exchange dynamics of xenon is much slower than for cryptophane-A based biosensors. This point is crucial for designing efficient xenon biosensor since small quantities of biosensor have to be detected in solution in a very short time.

Recently, Brotin et al. reported the synthesis of novel water-soluble cryptophanes based on the cryptophane-223 skeleton (Scheme 21.6) [33]. The design of such new cryptophane hosts was motivated by the need for fast and easy preparation of cryptophane biosensors and the critical requirement for producing sizable amounts of compounds if future in-vivo experiments are envisaged. The cryptophane-223 skeleton has been used as starting material and new functionalities were introduced on the central carbon atom of the propylenedioxy linker. The authors have described two different approaches to cryptophane-223 **35**

bearing six phenol hydroxyl groups and one secondary alcohol function located on the propylenedioxy linker (Scheme 21.6). Reaction of cryptophane **35** with methylbromoacetate gave the hexa-ester derivative **36** in moderate yield. In turn, hydrolysis of **36** in KOH/H<sub>2</sub>O-THF led to the water-soluble cryptophane **37**. Similarly, **35** was allowed to react with functionalized polyethylene glycol chains to give cryptophane **38** in good yield. In both examples the secondary alcohol is left unreacted and can be used for subsequent reactions. Complexation studies with xenon guest in aqueous solution performed with **37** and **38** exemplified the potential of these new structures for the design of xenon-biosensors.

## 21.2.2 Metallated Cryptophanes

As mentioned above, the synthesis of water soluble cryptophanes often requires the attachment of solubilizing groups to the molecular backbone. A new and original approach based on the preparation of metallated cryptophanes has been reported by Holman et al. to prepare water-soluble compounds. The first example was reported in 2005 with the preparation of the metallated cryptophane-E **39**. Cryptophane-E readily reacts with ruthenium metal complex  $[\text{Cp}^*\text{Ru}(\text{CH}_3\text{CN})]^+ [\text{SbF}_6]^-$  in  $\text{CH}_2\text{Cl}_2$  to give the hexa-metallated derivative **39** [34]. Interestingly, a simple change of counter-ion facilitates solubilization in water. For instance, the replacement of hexafluoroantimonate anions by chlorides gives a compound that is very soluble in water at neutral pH. The introduction of a  $\text{Cp}^*\text{Ru}$  unit on each benzene ring produces a cryptophane with unique properties. For instance, it has been observed that the inner cavity of the permetallated species is more acidic and can accommodate different anionic guests such as a triflate anion. This work has been extended to the synthesis of the permetallated cryptophane-111 **40** (Fig. 21.9). This compound exhibits very high affinity for xenon, with a measured binding constant  $K = 29,000 \text{ M}^{-1}$  at 298 K in water. A remarkable  $^{129}\text{Xe}$  NMR chemical shift of nearly 300 ppm for the  $\text{Xe}@\mathbf{40}$  complex is observed compared to the non-metallated xenon complex [35].

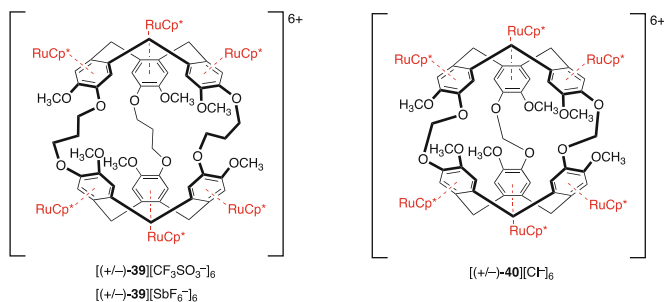


**Fig. 21.9** Synthesis of the permetallated cryptophanes  $(+/-)\text{-}[(\text{Cp}^*\text{Ru})_6\text{Cryptophane-E}]^{6+}$  **39** and  $(+/-)\text{-}[(\text{Cp}^*\text{Ru})_6\text{Cryptophane-111}]^{6+}$  **40** (counter-ions are indicated below each structure)



### 21.2.3 Enantiopure Water-Soluble Cryptophanes

Although access to optically active cryptophanes was reported some time ago, the synthesis of enantiopure water-soluble compounds has only recently been investigated [11]. Their preparation is often a difficult synthetic challenge and the number of covalently bound chiral capsules reported in the literature is very limited. However, useful information on the molecular recognition properties of these derivatives towards various species in water can be reached from the study of their chiroptical properties. The synthesis of these compounds is also motivated by the recent study of the xenon@cryptophane complexes used as xenon carrier for MRI applications. For instance, our group and others have shown that  $^{129}\text{Xe}$  NMR spectroscopy can easily distinguish between several diastereomeric xenon complexes. The identification and characterization of each diastereomer is thus pivotal for a better understanding of the interactions between the biosensor and the biological target. Thus, the preparation of cryptophanes in their enantiopure form is strongly desired.

Cryptophanes **1** and **4**, described in Sect. 21.2.1, are the two first optically active water-soluble compounds synthesized from cryptophanol-A **2**. The single phenol function in **2** can easily react with a small chiral auxiliary (e.g., camphanic acid chloride) to provide the two diastereomeric species **41** and **42** (Fig. 21.10) [36]. The two diastereomers can be isolated by crystallization in toluene, and the two enantiomers of **2** can then be recovered after hydrolysis under basic solution and then re-used for subsequent reactions. The interest of this strategy is twofold: (i) it provides fair quantities of optically active cryptophanol-A **2** with high enantiomeric excess ( $ee = 98\text{--}100\%$ ); (ii) it allows the preparation of new optically active cryptophanes without any loss of enantiomeric excess. Thus, starting from

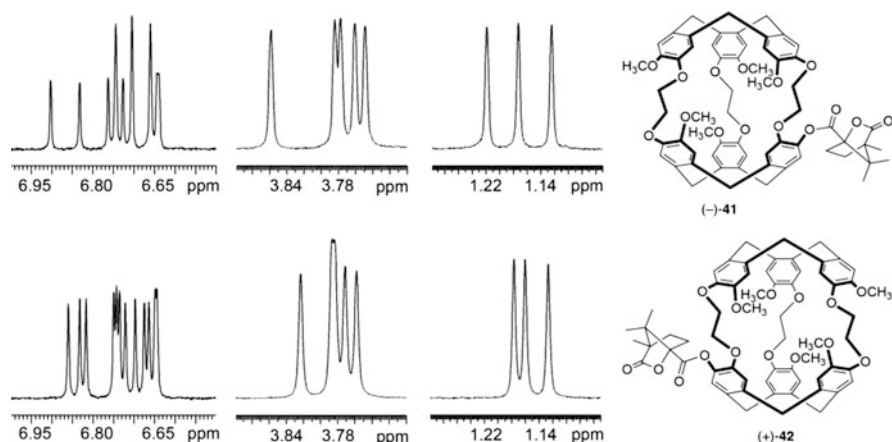
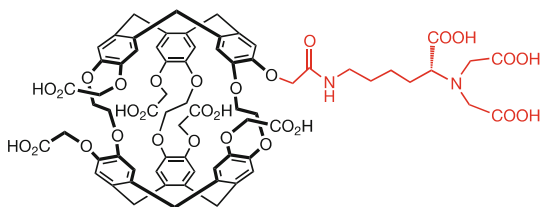


**Fig. 21.10** Selected parts of the  $^1\text{H}$  NMR spectra of the two diastereomers **41** and **42** recorded in  $\text{CDCl}_3$  at 298 K; *left*: aromatic region; *middle*: methoxy region; *right*: methyl region (Reprinted from ref [36], Copyright 2003, with permission from Wiley-VCH)

**Fig. 21.11** Structure of enantiopure cryptophane *MM*-**43** used for the detection of metal cations ( $\text{Zn}^{2+}$ ,  $\text{Cd}^{2+}$ ,  $\text{Pb}^{2+}$ ) in water

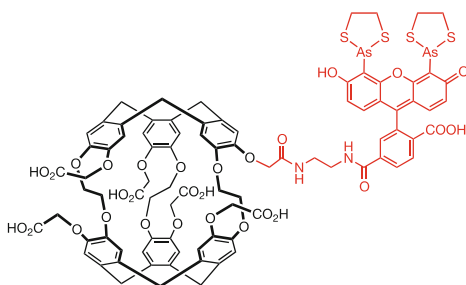


enantiopure compound **2**, following a multi-step procedure, the two enantiomers of cryptophanes **1** and **4** were obtained with enantiomeric excess  $ee = 100\%$ . A similar approach was used to prepare the two enantiomers of optically active derivative **7** (Fig. 21.4), which shows interesting molecular recognition properties in water with chiral neutral guests and cationic species [17].

Enantiopure cryptophane **1** has been used to design more sophisticated chemical structures for magnetic resonance imaging. For instance, compound **43** (Fig. 21.11) has been prepared to detect zinc cations in aqueous phase and biological fluids [37]. A substituent with a nitriloacetic moiety has been conjugated to the two enantiomers of compound **1**. This chemical function binds different cationic species such as  $\text{Zn}^{2+}$  very efficiently in water. In the presence of  $\text{Zn}^{2+}$  cations, the  $\text{Xe}@MM\text{-}43$  complex gives rise to a downfield shifted  $^{129}\text{Xe}$  NMR signal ( $\Delta\delta = 1.6$  ppm). A different signal is observed for the second diastereomeric complex. The complexation of  $\text{Zn}^{2+}$  cations occurs via a 1:2 complex as demonstrated by diffusion experiments. Interestingly, it was shown that LP  $^{129}\text{Xe}$  NMR spectroscopy allows for the detection of  $\text{Zn}^{2+}$  cations at concentration as low as 100 nM, the spectrum being acquired in a very short time. The quite large  $^{129}\text{Xe}$  chemical shift difference observed between  $\text{Xe}@43$  and  $\text{Zn}^{2+}\text{Xe}@43$  is sufficient to perform MRI experiments. This work was then extended to the study of other cationic species such as  $\text{Pb}^{2+}$  and  $\text{Cd}^{2+}$ . It was demonstrated that multiplexing experiments could be achieved. In these experiments a single biosensor is used to target several cationic species at the same time. Thus, it was shown that each  $\text{M}^{2+}\text{Xe}@43$  (with  $\text{M}^{2+} = \text{Zn}^{2+}$ ,  $\text{Cd}^{2+}$ ,  $\text{Pb}^{2+}$ ) species gives rise to a specific  $^{129}\text{Xe}$  NMR chemical shift. This chemical shift is not affected upon addition of other cationic species into the solution. Hence, concentration of metal cation in the nanomolar range can be detected in a single experiment and in a very short time in water or in biological fluids [38].

Rousseau et al. have designed the optically active water-soluble cryptophane **44** for the detection of Cys4-tagged peptide. Thus, a CrAsH probe, which has the particularity to emit a strong fluorescent signal when bound to cysteine residues, has been conjugated to enantiopure compound **1** to give **44** (Fig. 21.12). Even though the CrAsH probe does not contain stereogenic centers, different association between the biosensor and the peptide can occur. These different diastereomeric assemblies can be detected by  $^{129}\text{Xe}$  NMR spectroscopy and can produce several signals that should be eliminated if an enantiopure biosensor is used. Compound **44** presents the advantage to combine both  $^{129}\text{Xe}$  NMR sensitivity and fluorescence properties. Upon binding with a Cys4-tagged peptide, a large  $^{129}\text{Xe}$  NMR chemical

**Fig. 21.12** Compound **44** comprising a CrAsH probe conjugated to the optically active *MM*-cryptophane **1**



shift was detected ( $\Delta\delta = 6.4$  ppm) in water and a significant enhancement of the fluorescence (by a factor 24) was observed [39].

In a similar approach Dmochowski et al. reported the synthesis of the two enantiomers of cryptophane **20** (Scheme 21.3). Using LP  $^{129}\text{Xe}$  NMR spectroscopy they showed that both Xe@**20** enantiomers respond differently upon binding to the carbonic anhydrase II [40].

## 21.3 Physical Properties of Water-Soluble Cryptophanes

### 21.3.1 Xenon-Biosensors from Mono-functionalized Cryptophane-A

Over the last few years, the design of xenon-based biosensors has strongly contributed to the development of water-soluble cryptophane derivatives [8, 10]. Indeed, cryptophanes are known to bind strongly xenon either in organic solution or in aqueous solution, and compared to other molecular hosts showing good affinity, they present several advantages. For instance, varying the length of the linkers can change the cavity size. Consequently, the association constant, the in-out xenon exchange and the  $^{129}\text{Xe}$  chemical shift can be easily tuned by changing the nature of the linkers, making these compounds the molecules of choice for the elaboration of laser-polarized xenon carriers for MRI applications. For biological application, good host solubility is a prerequisite condition to investigate molecular events in biological media and, as viewed in the previous sections, many efforts have been made in this direction to prepare water-soluble cryptophanes with a strong affinity for xenon. One of the most common approaches is to leave the cryptophane skeleton intact and to attach a single solubilizing group that also contains a biological receptor. Cryptophane biosensors **45–57**, depicted in Figs. 21.13 and 21.14, have been obtained by this way and have been used for in-vitro and *in-cellulo* studies. However, the solubility of these molecules usually remains much lower than that observed for the above-mentioned systems. It is noteworthy that biosensors exhibiting an important lipophilic character can develop undesired interactions with cells. This can be detrimental for in-vivo experiments.

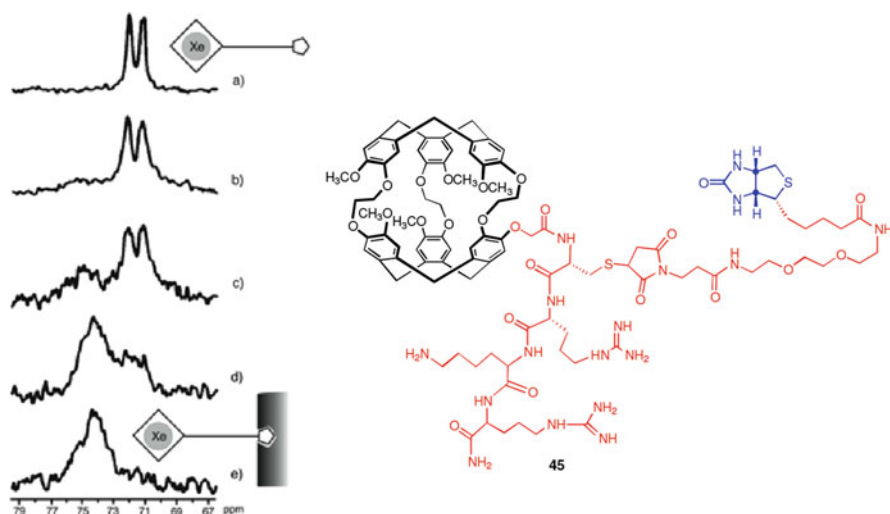


**Fig. 21.13** Structure of the cryptophane biosensor **45** and laser-polarized  $^{129}\text{Xe}$  NMR spectra of  $\text{Xe}@45$  in the presence of different relative amounts of avidin: (a) 0 %, (b) 10 %, (c) 20 %, (d) 60 %, (e) 120 % (Reprinted from Ref. [42], Copyright 2004, with permission from American Chemical Society)

Pines et al. were the first to design a cryptophane-biosensor from a water-soluble functionalized cryptophane-A derivative [41, 42]. Molecule **45** is made of a cryptophanol-A skeleton, whose phenol function has been allowed to react with a hydrophilic linker (Fig. 21.13). This linker contains a small solubilizing group (peptide) and a biologically active group (biotin residue). The biotin moiety is attached at the extremity of the linker and shows a great affinity for the avidin protein. The biotin-avidin binding process has been evidenced by LP  $^{129}\text{Xe}$  NMR spectroscopy. As shown in Fig. 21.13, the two NMR signals initially present on the  $^{129}\text{Xe}$  NMR spectrum of the free biosensor are slowly replaced by a broader signal located at higher frequency as the concentration of protein present in the solution increases. The presence of several stereogenic centers on the linker explains the different signals initially observed for the unbound biosensor. Indeed, several xenon-biosensor diastereomers are present in solution and each of them exhibits a specific  $^{129}\text{Xe}$  chemical shift [43]. Several groups have made similar observations with different systems in organic or aqueous solution [44, 45]. The synthesis of optically active cryptophanes can thus be an advantage in the present case.

Later, several other cryptophane biosensors with linkers of different lengths were designed (for example host molecule **46** in Fig. 21.14). Laser polarized  $^{129}\text{Xe}$  NMR spectroscopy reveals that the length of the linker has a strong influence on the overall shape of the  $^{129}\text{Xe}$  signals of the different complexes. A long linker possesses a high flexibility, which in turn produces a narrow  $^{129}\text{Xe}$  NMR signal and a small chemical shift difference between the unbound biosensor and the biosensor-protein complex. In contrast, a broader signal is observed when a short and more

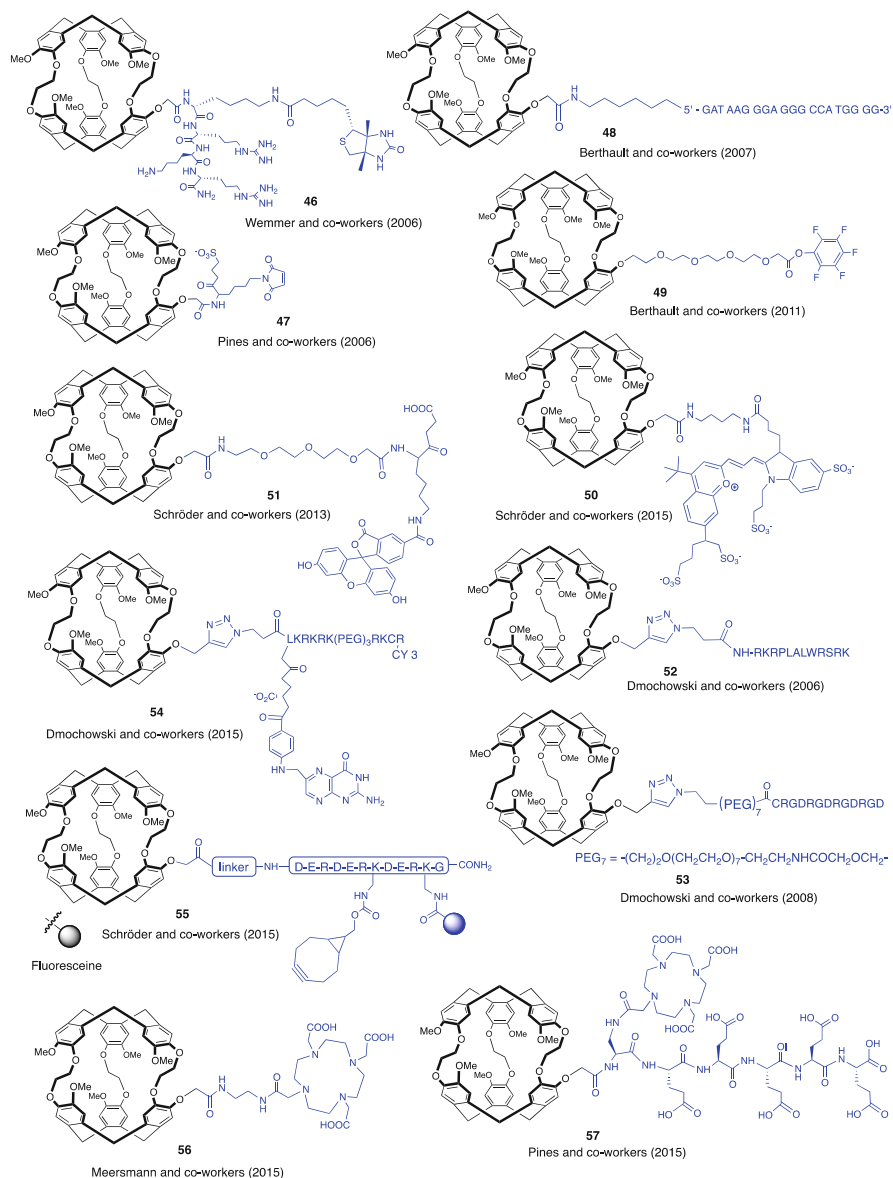


**Fig. 21.14** Structure of biosensors 46–57 used as xenon carrier for *in-vitro* or *in-cellulo* studies

rigid linker is conjugated to the cryptophane skeleton. Thus, a linker of moderate length with a good flexibility is a good compromise in this case [46]. In another study Pines and co-workers have reported that the cryptophane biosensor does not necessarily need to be covalently bound to the target to produce a signal detectable by <sup>129</sup>Xe NMR spectroscopy [47].

Thanks to LP  $^{129}\text{Xe}$  NMR spectroscopy, the detection of small quantities of biosensors (in the micromolar range) can be easily achieved in aqueous solution. In particular, the hyper-CEST method (chemical exchange saturation transfer) is very promising for MRI applications, and xenon biosensors present in solution can now be easily detected at nanomolar range. Pines et al. were the first to exploit this concept to produce a MRI signal using the  $^{129}\text{Xe}@45$  complex [48]. Since then, several studies aimed at improving signal acquisition have been reported using water-soluble cryptophane derivatives as xenon carriers [49–52]. Increasing spin density in the proximity of the biological target also improves the  $^{129}\text{Xe}$  NMR signal. For instance, cryptophane **47** is one of the compounds used to aggregate numerous cryptophane hosts onto a viral capsid or a bacteriophage structure. This approach allows a significant enhancement of the  $^{129}\text{Xe}$  NMR signal. Indeed, combined with hyper-CEST the detection limit is strongly decreased to a concentration level as low as 230 femtomol [53, 54].

Cryptophane biosensor **48** has been designed by Berthault et al. to recognize a specific DNA strand [55]. A DNA strand with a known sequence has been conjugated to an enantiopure cryptophanol-A **2**. At low concentration in water, the  $^{129}\text{Xe}$  NMR spectrum of the biosensor reveals a unique signal located at 68.5 ppm. In presence of the complementary strand this signal is shifted toward low frequencies by 1.5 ppm. In contrast, upon addition of a non-complementary DNA strand into the solution, the position of the  $^{129}\text{Xe}$  NMR signal remains unchanged and no molecular recognition occurs. The same group reported the first cell uptake detection of a xenon-cryptophane biosensor by  $^{129}\text{Xe}$  NMR spectroscopy. The mono-functionalized cryptophane derivative **49** capable of recognizing lysine residues located at the surface of the transferrin protein has been synthesized. The cell uptake of the biosensor-transferrin system occurring via an endocytosis process has been then investigated with LP  $^{129}\text{Xe}$  NMR spectroscopy. The experiments have revealed a strong interaction between cell membranes and the lipophilic skeleton of the cryptophane [56]. Schröder et al. have exploited the strong interaction of the cryptophane skeleton of **50** with vesicles to design specific bimodal biosensors that exhibit  $^{129}\text{Xe}$  NMR chemical shift and fluorescence properties [57]. Other bimodal systems such as **51** have been reported by the same group to study cell uptake of several xenon carriers [58].

The group of Dmochowski has contributed significantly to the field of enzyme-responsive  $^{129}\text{Xe}$  NMR biosensors. For instance, the peptide-cryptophane conjugate **52** was prepared via a click chemistry reaction between a mono-propargyl cryptophane-A and a peptide residue. The peptide sequence can be easily cleaved by the matrix metalloproteinase MMP-7 at very low concentration of protease (picomolar concentration). Taking advantage of this property the authors monitored the cleavage of this peptide by HPLC. Independently, LP  $^{129}\text{Xe}$  NMR experiments have revealed a small chemical shift difference (0.5 ppm) between the unreacted biosensor in solution and the cleaved biosensor [59]. Several peptide sequences such as a HIV-1 TAT (residues 48–60), a nonamer of D-arginine and a (RGD)<sub>4</sub> dodecamer (conjugate **53** in Fig. 21.14) have been attached to the cryptophane-A skeleton [60]. Similarly, the water-soluble cryptophane-folate biosensor **54**

containing a fluorescent moiety was developed to investigate the endocytosis process of the folate receptor protein-bound biosensor by KB and HT-1080 cells [61]. The cell uptake of these biosensors was monitored by confocal laser scanning microscopy and quantified by flow cytometry experiments. The biosensors developed in these studies show low toxicity at micromolar concentration, which is usually the concentration required for recording LP  $^{129}\text{Xe}$  NMR spectra.

Freund et al. reported the synthesis of a xenon-cryptophane biosensor aimed at recognizing Major Histocompatibility Complex (MHC) class II protein present on cell surfaces. As a model system a functionalized cryptophanol-A derivative bearing a hemagglutinin peptide at its extremity was specifically prepared to bind a human leukocyte antigen (HLA) DR1 [62]. A LP  $^{129}\text{Xe}$  NMR study of this system shows a small chemical shift difference between the free biosensor and the MHC-bound biosensor. In addition, *in-cellulo* experiments highlight the non-toxicity of the biosensor prepared for this study. Freund and Schröder reported another complex for the detection of the cell surface protein CD14. Several functionalized cryptophanes conjugated to an antibody have been prepared, which in turn efficiently bind CD14 proteins located on cell surfaces. This recognition process was detected by LP  $^{129}\text{Xe}$  NMR spectroscopy with unprecedented sensitivity [63]. Schröder and Hackenberger have designed a complex bimodal biosensor for detecting tagged-proteins present on cell surfaces. The cryptophane biosensor **55** possesses both a fluorescence probe and a bicyclo[6.1.0]nonyne moiety, and has been prepared to recognize metabolically labelled sialic acid via a click chemistry reaction. MRI imaging has then been used as a tool for detecting the cells treated with the synthetic sugar containing a reactive azide group. Thanks to the hyper-CEST approach, a clear contrast has been observed between the cell-containing compartment with tagged proteins (higher hyper-CEST effect) and the reference compartment. Fluorescence spectroscopy was used as a second method to quantify the amount of biosensor attached to the cell surface [64]. Recently, Meersmann et al. reported the synthesis of cryptophane **56** comprising a DOTA macrocyclic unit that shows good affinity for  $\text{Gd}^{3+}$  cations. Upon complexation of the DOTA moiety with a  $\text{Gd}^{3+}$  cation a significant increase of the  $^{129}\text{Xe}$  relaxivity occurs with complex  $\text{Gd}^{3+}\text{-Xe@56}$ . The relaxivity process was found to be better with biosensor **56** than with  $\text{Gd}^{3+}\text{-DOTA}$  complex alone (used as a reference), suggesting that the close proximity of these two components is important. This concept could be aimed at designing new efficient contrast agents for  $^{129}\text{Xe}$  MRI [65]. The xenon complex of DOTA-conjugated Cryptophane **57** was also used to discriminate between several metal cations by showing distinct  $^{129}\text{Xe}$  chemical shifts in aqueous solution [66].

### 21.3.2 Recognition of Neutral Molecules

Neutral guests were the first organic species to be studied with water-soluble cryptophanes. In 1987 Collet et al. reported the complexation of chloroform and



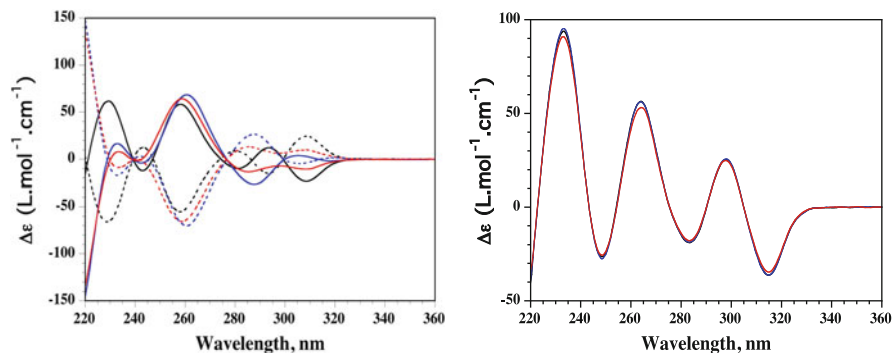


**Fig. 21.15** Left, ECD spectra of *MM-4* and *PP-4* in NaOH/H<sub>2</sub>O solution (0.1 M): empty cage (black), CH<sub>2</sub>Cl<sub>2</sub>@*MM-4* and CH<sub>2</sub>Cl<sub>2</sub>@*PP-4* (blue), CHCl<sub>3</sub>@*MM-4* and CHCl<sub>3</sub>@*PP-4* (red). Dashed lines correspond to the *PP*-enantiomers. Right, ECD spectra of *MM-4* in CsOH/H<sub>2</sub>O solution (0.1 M): empty cage (black), CH<sub>2</sub>Cl<sub>2</sub>@*MM-4* (blue), CHCl<sub>3</sub>@*MM-4* (red)

dichloromethane in aqueous solution by cryptophane **1** (Fig. 21.2, Sect. 21.2.1) [12]. The CHCl<sub>3</sub>@(*rac*)-**1** complex was characterized by the highfield <sup>1</sup>H NMR signal of the encapsulated chloroform molecule due to the shielding effect of the six aromatic rings surrounding the guest molecule. A similar effect was observed with CH<sub>2</sub>Cl<sub>2</sub> and cryptophane **1** in water. In both cases the hydrophobic effect favors the host-guest association, and consequently a significant enhancement of the binding constants for these two guests is observed in water, when compared to the experiments run with the parent cryptophane-A **3** (Scheme 21.1, Sect. 21.2.1) in organic solution.

Brotin and Buffeteau investigated the recognition of methane and halogenomethane derivatives (CH<sub>3</sub>Cl, CH<sub>2</sub>Cl<sub>2</sub>, CHCl<sub>3</sub>, CH<sub>3</sub>I, CH<sub>2</sub>Br<sub>2</sub>) with enantiopure compounds *MM-4* and *PP-4* under basic conditions (LiOH/H<sub>2</sub>O and NaOH/H<sub>2</sub>O) [67]. Chiroptical techniques were employed to study the binding process with the two enantiomers of **4** (Scheme 21.1, Sect. 21.2.1). Electronic circular dichroism (ECD) spectroscopy is very convenient to study the conformational changes occurring during complexation. For instance, when small guest molecules such as CH<sub>4</sub> or xenon are present inside the cavity of *MM-4* only small modifications are observed on the ECD spectrum. In contrast, larger guest molecules such as CHCl<sub>3</sub> or CH<sub>2</sub>Br<sub>2</sub> induce important spectral modifications of the ECD spectrum of *MM-4* (Fig. 21.15). These spectral changes are especially visible at low wavelength and are characteristic of the rearrangement of the three linkers that modify their conformation to allow the cryptophane to maximize interactions with the guest molecules. Thus, for the two small guest CH<sub>4</sub> and Xe, with Van der Waals volumes ( $V_{\text{vdw}}$ ) of 24 Å<sup>3</sup> and 42 Å<sup>3</sup> respectively, the linkers of the host predominantly adopt the *all-gauche* (*ggg*) conformation allowing the molecular cage to reduce the size of its cavity. In contrast the three linkers predominantly adopt an *all-trans* (*ttt*) conformation when larger guest molecules are encapsulated. Other chiroptical techniques such as polarimetry and vibrational circular dichroism



(VCD) spectroscopy reveal important modifications upon binding with guest molecules. Polarimetry measurements show large modifications of the optical rotation values depending on the nature of the aqueous solvent (LiOH/H<sub>2</sub>O, NaOH/H<sub>2</sub>O) or the molecular volume of the guest trapped in the cavity.

The use of a CsOH/H<sub>2</sub>O solution instead of NaOH/H<sub>2</sub>O solution has a dramatic effect on the binding of neutral molecules. As evidenced by ECD spectroscopy and polarimetric measurements, the addition of a CH<sub>2</sub>Cl<sub>2</sub> or CHCl<sub>3</sub> guest molecule does not induce any spectral modifications (Fig. 21.15). This surprising result suggests that the guest molecules cannot enter the cavity of the host. A similar result was also observed with the two enantiomers of **7** (Fig. 21.4, Sect. 21.2.1), even though this compound has a larger portal [17]. Further investigation performed with these two host molecules led to the conclusion that the Cs<sup>+</sup> cation acts as a strong competitor and forms a very stable complex with hosts **4** and **7**. In addition, the difference of affinity between the neutral molecules (CH<sub>2</sub>Cl<sub>2</sub>, CHCl<sub>3</sub>) and the Cs<sup>+</sup> cation is so large that even a small amount of the latter is sufficient to displace the equilibrium toward the formation of the Cs<sup>+</sup>@**4** and Cs<sup>+</sup>@**7** complexes. Thus, in CsOH/H<sub>2</sub>O solution, the presence of a large amount of Cs<sup>+</sup> cation prevents any neutral molecules to be encapsulated into hosts **4** and **7**.

A different situation is observed with enantiopure **1**. For instance, the chiroptical properties of **1** remain unchanged whatever the nature of the guest molecule inside the host cavity. As an example, in NaOH/H<sub>2</sub>O solution, enantiopure compound **1** shows superimposable ECD spectra for the empty cryptophane and the CH<sub>2</sub>Cl<sub>2</sub>@**1** and CHCl<sub>3</sub>@**1** complexes. In contrast, <sup>1</sup>H NMR spectra are very sensitive to the nature of the guest molecules present inside the cavity and a linear relationship was observed between the molecular volume of guest molecules and the chemical shift of an aromatic proton localized near the carboxylic acid group. Cryptophane **1** does not bind alkali cations and the complexation of neutral molecules is observed in LiOH/H<sub>2</sub>O and CsOH/H<sub>2</sub>O solutions as well.

### 21.3.3 Recognition of Chiral Molecules

To date, very few studies concerning the complexation of chiral molecules by cryptophanes have been reported in the literature. One of the reasons for this is the limited size of the cavity of the cryptophane-A **3** and its water-soluble congeners, whose cavity size is in the range 80–100 Å<sup>3</sup> as estimated from single crystal X-ray structures [68]. Thus, the range of chiral guests that can fit the cavity is strongly limited. The enantioselective complexation of methyl-oxirane with the two enantiomers of compound **7** was investigated using <sup>1</sup>H NMR and ECD spectroscopy [69]. The <sup>1</sup>H NMR and ECD spectra of **7** show different signals depending on the absolute configuration (AC) of the *R*- or *S*-methyloxirane used. The ECD bands of the <sup>1</sup>L<sub>b</sub> region (280–330 nm) are affected by the nature of the AC of the methyloxirane, and the spectral differences observed between these two

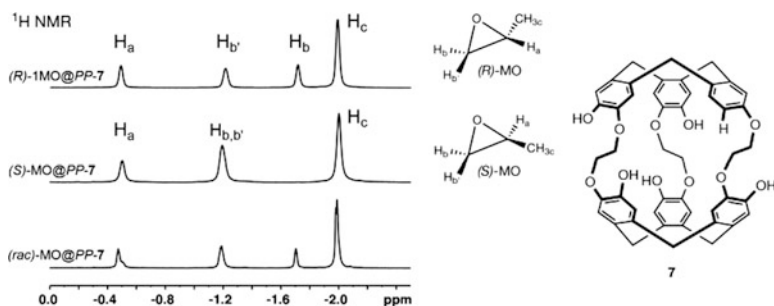


**Fig. 21.16**  $^1\text{H}$  NMR spectra (NaOD/D<sub>2</sub>O, 275 K) of bound methyloxirane (MO) in *PP-7*

diastereomeric species are sufficient to establish that enantiomer *PP-7* better recognizes (*R*)-methyloxirane. This result is confirmed by the  $^1\text{H}$  NMR analysis of the two diastereomers formed in NaOD/D<sub>2</sub>O solution. The shielding effect of the six benzene rings produces several highfield signals for the encapsulated methyloxirane between 0.0 and  $-2.0$  ppm that can be easily distinguished from the NMR signals of the host (Fig. 21.16). The affinity of host **7** strongly depends on the nature of the solution used to perform the measurement. Thus, in LiOD/D<sub>2</sub>O and NaOD/D<sub>2</sub>O the enantioselectivity is preserved. For instance, in NaOD/D<sub>2</sub>O solution, binding constants  $K_a = 309 \text{ M}^{-1}$  and  $K_a = 146 \text{ M}^{-1}$  have been measured for (*S*)-methyloxirane and the (*R*)-methyloxirane with *MM-7*, respectively. However, no binding was observed in CsOD/D<sub>2</sub>O solution.

Enantioselectivity has been also observed for the two enantiomers of **1** with methyloxirane, chloromethyloxirane and ethyloxirane as guests [70]. In NaOD/D<sub>2</sub>O solution at 275 K, moderate binding constants  $K_a = 128 \text{ M}^{-1}$  and  $K_a = 99 \text{ M}^{-1}$  have been measured with *PP-1* for (*R*)-methyloxirane and (*S*)-methyloxirane, respectively. In the same solvent, a similar enantioselectivity was measured with the two enantiomers of chloromethyloxirane. Surprisingly, ethyloxirane showed the highest enantioselectivity but also the lowest affinity for compound **1**. It is noteworthy, that in contrast to compounds **4** and **7**, the recognition of oxirane derivatives is independent on the nature of the basic solution and similar results are observed in NaOD/D<sub>2</sub>O and CsOD/D<sub>2</sub>O solutions.

### 21.3.4 Complexation of Ionic Species

In 1993 Collet et al. reported the first examples of the binding of a cationic species in water [13]. They showed that water-soluble cryptophanes possessing larger internal cavities could efficiently bind ammonium salt in aqueous solution. For instance, the water-soluble congener **58** of cryptophane-E (Fig. 21.17), possessing three propylenedioxy linkers and six carboxylic acid moieties binds tetramethyl ammonium salts efficiently. The molecular recognition between ammonium

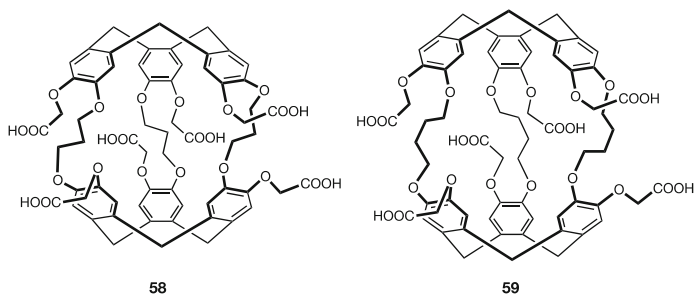


Fig. 21.17 Structure of water-soluble cryptophanes **58** and **59**

species and cryptophane host is strongly dependent on the molecular volume of the guest. Thus, the stability of the complexes significantly decreases when the molecular volume of the guest increases. The water-soluble congener **59** of cryptophane-O (Fig. 21.17), which possesses a larger inner cavity, shows a higher affinity for the same ammonium salts. This host also shows good binding properties for choline and acetylcholine, which are important molecules of biological interest. The high affinity of ammonium@**59** complexes was enthalpically driven due to the existence of strong  $\pi$ -cation interactions. It was also assumed that loose association is necessary to observe strong binding between the ammonium salts and cryptophane **59**.

Until recently the recognition of ammonium salts by water-soluble cryptophanes were the only examples of cationic guests reported in the literature. It was found that water-soluble cryptophanes **4** and **7** bind  $K^+$ ,  $Rb^+$  and  $Cs^+$  cations efficiently in LiOH/H<sub>2</sub>O or NaOH/H<sub>2</sub>O solutions [71]. The interaction between the cations and the two enantiopure compounds **4** and **7** was evidenced by ECD Spectroscopy. The addition of small amounts of cations into the solution resulted in a dramatic change of their ECD spectra in the 220–330 nm spectral region. These spectral modifications were particularly important with  $Rb^+$  and  $Cs^+$  cations. Interestingly, larger spectral modifications were observed in the presence of a competitor initially present inside the cavity of the host **4** and **7**. This suggests that the modifications observed in the ECD spectra are the result of strong conformational rearrangement of the three linkers, which in turn modifies the cavity size of the host. Titration experiments (ITC) reveal a large difference in the binding constants for these cationic species, with an increasing order in the association constants  $K_a(Cs^+) > K_a(Rb^+) > K_a(K^+)$  (Fig. 21.18). For instance, a very high binding constant  $K_a = 2.7 \times 10^9 \text{ M}^{-1}$  was measured for  $Cs^+$ @**4** in LiOH/H<sub>2</sub>O (0.1 M) at 298 K.

<sup>133</sup>Cs NMR Spectroscopy also reveals a strong downfield shifted NMR signal for this complex ( $\delta = -250$  ppm) in LiOD/D<sub>2</sub>O (Fig. 21.19). It is noteworthy that the lack of efficient complexation with the hexacarboxylic acid derivative **1** suggests that both  $\pi$ -cation and coulombic interactions are pivotal to observe binding between  $Cs^+$  and host **4**.

Further investigation also revealed that  $Tl^+$  cations bind strongly with these two hosts in LiOH/H<sub>2</sub>O or NaOH/H<sub>2</sub>O solutions [72, 73]. The ECD Spectral

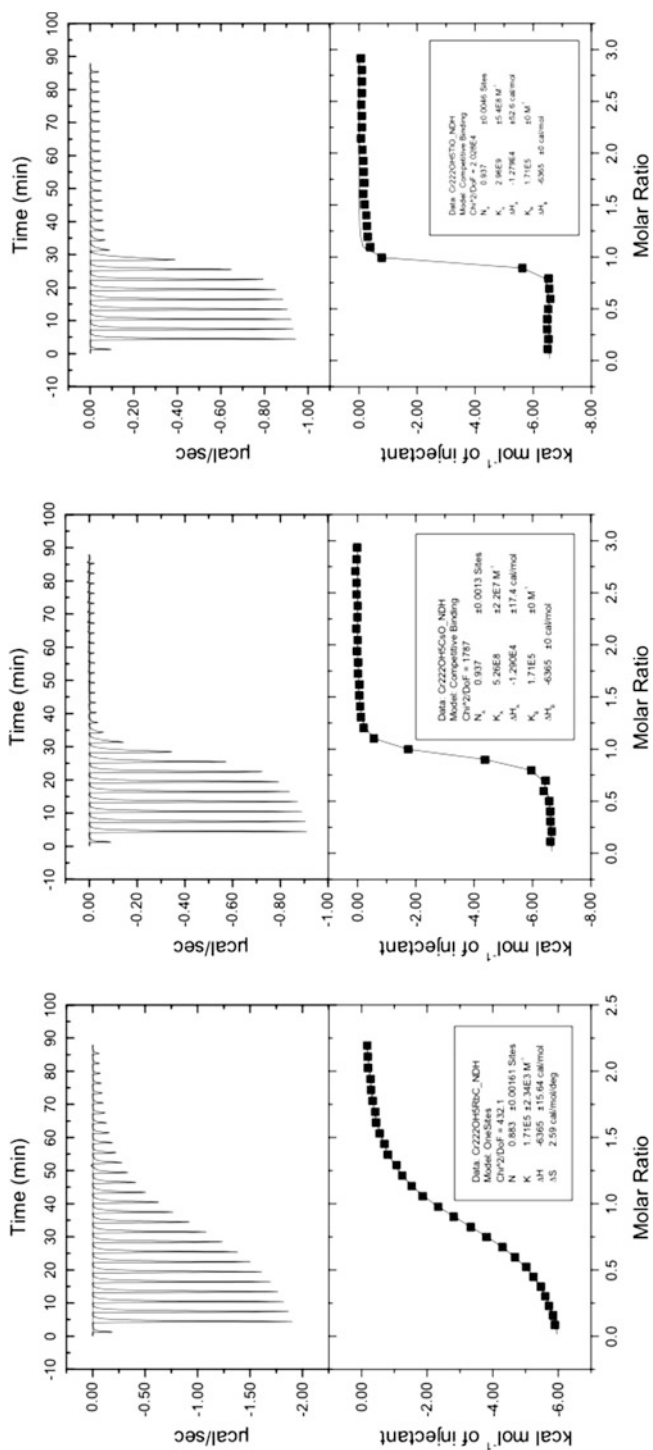


**Fig. 21.18** ITC Titration experiments with water-soluble cryptophane **7** in NaOH/H<sub>2</sub>O at 298 K in presence of RbCl (*left*), CsOH (*middle*) and TIOAc (*right*) solutions

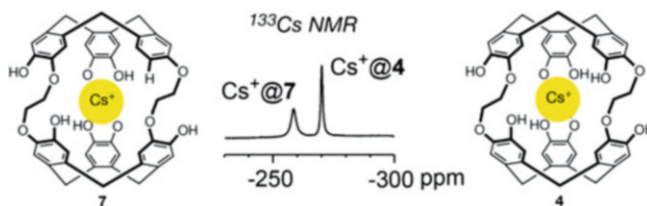


**Fig. 21.19**  $^{133}\text{Cs}$  NMR spectrum of compounds **4** and **7** in presence of small amount of CsOH,  $1\text{H}_2\text{O}$ . Spectrum recorded at 298 K in  $\text{LiOD}/\text{D}_2\text{O}$

modifications are even more important especially for the ECD bands corresponding to the  $^1\text{L}_b$  transition region. The association constant between  $\text{Ti}^+$  and these water-soluble cryptophanes is larger than the  $\text{Cs}^+@4$  and  $\text{Cs}^+@7$  complexes measured under the same conditions. For instance, a binding constant  $K_a = 5.0 \times 10^{10} \text{ M}^{-1}$  ( $\Delta G^0 = -14.6 \text{ kcal/mol}$  at 298 K) has been measured in  $\text{LiOH}/\text{H}_2\text{O}$  (0.1 M) by ITC experiments. The binding constant decreases as the LiOH concentration increases but still remains very high, and in 1 M  $\text{LiOH}/\text{H}_2\text{O}$  solution the binding constants are  $K_a = 3.8 \times 10^8 \text{ M}^{-1}$  ( $\Delta G^0 = -11.6 \text{ kcal/mol}$  at 298 K) and  $K_a = 7.0 \times 10^7 \text{ M}^{-1}$  ( $\Delta G^0 = -10.8 \text{ kcal/mol}$  at 298 K) for compounds **4** and **7** respectively. Efficient binding was also observed with  $\text{Ti}^+$  and  $\text{Cs}^+$  cations in  $\text{KOH}/\text{H}_2\text{O}$  (0.1 M). A very high selectivity is thus observed for these two cationic species and other alkali metals ( $\text{Li}^+$ ,  $\text{Na}^+$  and  $\text{K}^+$ ).

Cryptophanes **5** and **6** (Fig. 21.4) with larger internal cavities have also demonstrated their ability to bind  $\text{Cs}^+$  and  $\text{Ti}^+$  cations in water efficiently under analogous experimental conditions ( $\text{LiOH}/\text{H}_2\text{O}$  (0.1 M)). The  $^{133}\text{Cs}$  NMR spectra of  $\text{Cs}^+@5$  and  $\text{Cs}^+@6$  in 0.1 M  $\text{NaOD}/\text{D}_2\text{O}$  solutions are characterized by two highfield-shifted signals located at  $-270$  and  $-290$  ppm respectively. However, these two complexes behave differently when the temperature increases. The association constants measured by titration experiments at 298 K are still very high for **5**:  $K_a = 3.1 \times 10^9 \text{ M}^{-1}$  for the  $\text{Cs}^+@5$  complex ( $\Delta G^0 = -13.2 \text{ kcal/mol}$ ) and  $K_a = 2.2 \times 10^{10} \text{ M}^{-1}$  for  $\text{Ti}^+@5$  ( $\Delta G^0 = -14.1 \text{ kcal/mol}$ ). In contrast, the association constants measured with compound **6** are lower by several orders of magnitude.

Altogether these results demonstrate that cryptophanes **4–7** show remarkable binding properties towards  $\text{Cs}^+$  and  $\text{Ti}^+$  cations in water over a wide range of experimental conditions (nature and concentration of the basic solution, temperature). These complexes have been thoroughly studied by several spectroscopic techniques (ITC, UV-vis,  $^{133}\text{Cs}$  NMR,  $^{205}\text{Tl}$  NMR). An important change of the physical properties of these complexes with respect to the empty cages has been observed. Chiroptical spectroscopic techniques (ECD and VCD) have also been employed for the study of these complexes thanks to the optical resolution of compounds **4** and **7**. A dramatic change of these spectra is observed upon complexation with the two cations suggesting strong host-guest interactions. Such derivatives could find some application in environmental chemistry e.g., for extracting these two (toxic) cations from soil and groundwater.

## 21.4 Water-Soluble Hemicryptophanes

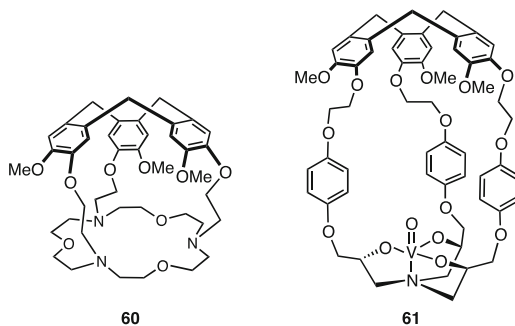
Hemicryptophanes are molecular containers, constructed on the cryptophane structure, but where one CTB unit is changed for another  $C_3$  symmetry group. Compounds **60** [74], and **61** [75], (Fig. 21.20) are representative of this new class of host molecules. They have been designed to allow the endohedral functionalization of the inner molecular cavity. They were found to be efficient and selective receptors for cations, anions, ion pairs, zwitterions and carbohydrates.

### 21.4.1 Hemicryptophanes for the Recognition of Neurotransmitters

The selectivity in the recognition process by hemicryptophane hosts is driven by the specific size and shape of the molecular cavity. Indeed, fine-tuning of the confined space of the cavity can dramatically change the recognition properties of the host molecule. For instance, hemicryptophane **62** was found to bind efficiently taurine neurotransmitter with a binding constant of  $1.4 \times 10^4 \text{ M}^{-1}$  in a 9:1 mixture of acetonitrile and water [76], whereas compound **63** selectively recognizes choline phosphate with respect to choline with binding constants of  $4.2 \times 10^5 \text{ M}^{-1}$  and  $7.0 \times 10^3 \text{ M}^{-1}$ , respectively, in a 98:2 DMSO/water mixture (Fig. 21.21) [77]. Interestingly, host **63** was not able to complex taurine whereas **62** displayed no affinity for choline.

Given the high selectivity and efficiency of these host compounds for the recognition of molecules of biological interest in competitive solvent containing water, the complexation of taurine in pure water was investigated in our laboratory to more accurately mimic biological systems. The water-soluble hemicryptophane **64** (Fig. 21.21) was synthesized by following a strategy similar to that used for the hexacarboxylic acid cryptophanes **1**, **5** or **6** (see Sect. 2.1): carboxylate units were grafted on the CTB unit after deprotection of the methoxy groups with trimethylsilyl iodide (TMSI) followed by reaction with tert-butyl-bromoacetate in the presence of  $\text{CsCO}_3$  and the subsequent deprotection of the carboxylic functions

**Fig. 21.20** Structures of hemicryptophane hosts **60** and **61**



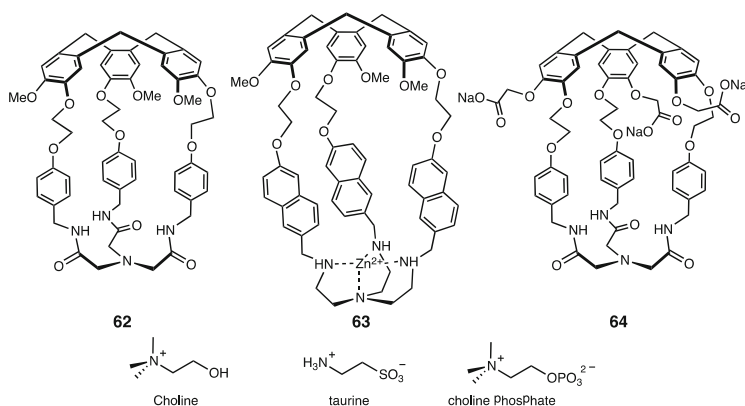


**Fig. 21.21** Structures of hemicryptophanes **62–64** and guest compounds that have been engaged in their molecular cavity

with trifluoroacetic acid (TFA) [78]. The resulting hemicryptophane **64** was found to be water soluble under physiological conditions (pH = 7.4, phosphate buffer). However, neither NMR titrations nor ITC experiments were able to unambiguously demonstrate the complexation of taurine by host **64** in water. Thus, although the related hemicryptophane **62** binds taurine very efficiently in a mixture of acetonitrile and water, its water-soluble counterpart **64** failed to perform such recognition in water. In the present case, water appears too competitive as a solvent, preventing any complexation process [79].

However, hemicryptophanes were found to have good recognition properties towards zwitterionic neurotransmitters such as taurine and choline phosphate in acetonitrile or DMSO/water mixtures. Ammonium neurotransmitters represent a second class of guests that can bind efficiently hemicryptophane hosts as shown above with choline and host **63** [77]. Thus, the recognition properties of hemicryptophanes toward this other class of neurotransmitters were further studied, first in organic solvents. For instance, host **65** (Fig. 21.22) was found to complex norephedrine and ephedrine in CDCl<sub>3</sub>/CD<sub>3</sub>OD 95:5 (v.v.) with modest enantioselectivity but high binding constants (up to  $2.5 \times 10^5 \text{ M}^{-1}$ ) depending on the configuration of the chiral host [80]. This high affinity of hemicryptophane **64** toward ammonium guests in organic solution was further explored in water, expecting that some affinity could be retained in this highly competitive solvent. The parent water-soluble hemicryptophane was synthesized from compound **66** by first protecting the amine functions with tert-butoxycarbonyl (Boc), followed by deprotection of the methoxy groups with lithium diphenylphosphide (Ph<sub>2</sub>PLi) and subsequent removal of the Boc protecting groups using TFA, to afford hemicryptophane **67** soluble in basic water (Fig. 21.22). This molecular receptor efficiently encapsulates the ammonium neurotransmitter choline as evidenced both by NMR and ITC experiments, and a binding constant of  $2.3 \times 10^3 \text{ M}^{-1}$  was measured. Moreover, hemicryptophane **67** was found to be highly selective since

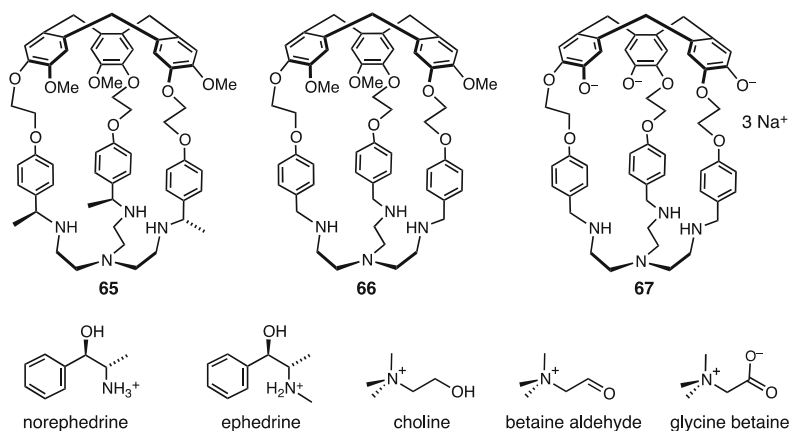


**Fig. 21.22** Structures of hemicryptophanes **65–67** and ammonium neurotransmitters

neither betaine aldehyde nor glycine betaine (two metabolites of choline; Fig. 21.22) were recognized by the host molecule. This was the first example of the recognition of a guest molecule by a hemicryptophane cage in water. Although these results were obtained in a strongly basic aqueous medium (pH = 12), this nevertheless constitutes an important step towards the development of sensors for ammonium neurotransmitters in biological media, based on the hemicryptophane structure [81].

#### 21.4.2 *Water-Soluble Metal@Hemicryptophane Complexes: Towards Supramolecular Catalysis in Water*

Beside their recognition properties, hemicryptophanes were also found to act as efficient and selective supramolecular catalysts. For instance a phosphorus atom has been trapped inside the molecular cavity of a hemicryptophane ligand, leading to the encapsulated Verkade superbase **68** (Fig. 21.23) [82]. The confinement dramatically affects the thermodynamics and kinetics of proton transfer, leading to species up to 100 times more basic than their model counterpart **69**. Compound **68** was also tested as a supramolecular organocatalyst in a basico-catalyzed Diels Alder reaction. Interestingly, the diastereomeric excess was strongly improved by the specific shape of the inner space induced by the cage structure [83].

Vanadium was also complexed in the cavity of a hemicryptophane providing the cage compound **61** (Fig. 21.23), which proved to be an efficient supramolecular catalyst for the oxidation of sulfide into sulfoxide with turnover number up to 180 [84]. Moreover, an improvement of the reaction rate by a factor of 6 was observed when compared to the model molecule **70** that lacks a cavity.



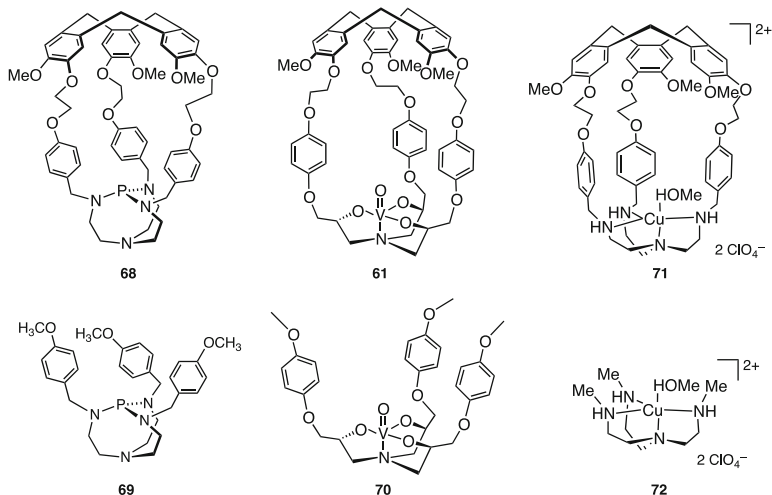


**Fig. 21.23** Structure of hemicryptophanes acting as supramolecular catalysts and their model counterparts

Hemicryptophane **71** (Fig. 21.23) containing a copper trapped in a hemicryptophane core was synthesized and tested as catalyst in the oxidation of cyclohexane into cyclohexanol and cyclohexanone in the presence of H<sub>2</sub>O<sub>2</sub> as stoichiometric oxidant [85]. The Cu@hemicryptophane complex **71** displays a yield twice higher than that obtained with the related model compound **72**. A kinetic study demonstrates that confinement protects the catalytic site from decomposition; hence higher yields can be reached. Furthermore, this supramolecular catalyst was able to more efficiently discriminate cyclohexane from adamantane than the model complex, likely because this latter substrate is too large to efficiently enter the cavity [86]. The C-H oxidation reaction plays an important role for instance in the valorization of alkanes. Martinez et al. have shown that the effect of encapsulation greatly improves the catalytic activity of the copper complex, and to improve the confinement, they perform the reaction in water. Indeed, an important hydrophobic effect should force the alkane to enter the hydrophobic cavity of the hemicryptophane in the vicinity of the catalytic center. Hence, strong changes in the catalytic activity and selectivity should be expected. To this end the water-soluble Cu@hemicryptophane complex **73** (Fig. 21.24) was synthesized in four steps from ligand **66** and was fully characterized [87].

The Near-IR/vis absorption spectrum of complex **73** in water-NaOH solution was fully consistent with a trigonal-bipyramidal geometry of the copper(II) ion and the EPR spectrum is in agreement with a five-coordination sphere with the cation bound to the four nitrogen atoms of the *tren* unit and to one solvent molecule, a structure similar to that proposed for the parent complex **71** soluble in organic solvents. Thus it appears that the water solubilization retains the geometry of the complex around the metal center, but it was found that the redox properties were

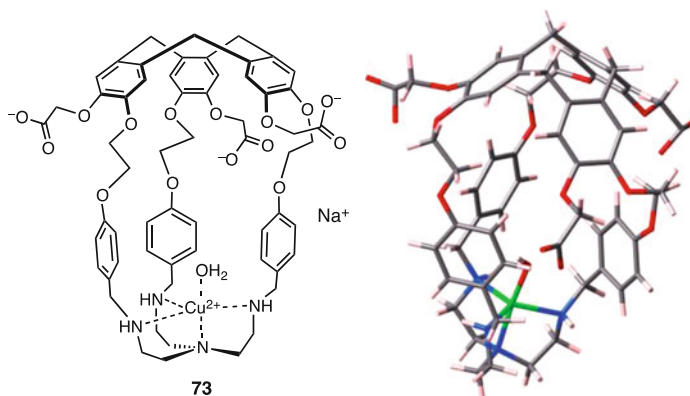


**Fig. 21.24** Cu@hemicryptophane complex **73** and its DFT calculated structure

strongly affected. The cyclic voltammograms of Cu(II)@**73** and Cu(II)@**71** exhibit an irreversible process with the reduction wave and the associated re-oxidation being observed under these conditions at  $E_{pc} = -0.59$  and  $-0.91$  V/SCE and  $E_{pa} = 0.14$  and  $0.45$  V/SCE, respectively. This novel water-soluble metallo-enzyme model featuring a Cu(II) site encaged in a closed-shell cavity opens up an avenue to new bio-inspired catalytic systems.

## 21.5 Conclusion

In the present chapter we have described the most recent progress concerning the synthesis of water-soluble cryptophanes and their hemicryptophane congeners. The physical properties of these molecules in aqueous solution as well as the properties of their complexes have been thoroughly reported. It is noteworthy that the overwhelming majority of these results have been reported only very recently in the literature. We have emphasized the renewed attention given to the preparation of water-soluble cryptophanes and the study of their binding properties that is strongly related to the development of xenon biosensors. Cryptophanes may exhibit a suitable solubility in biological fluids and the use of laser-polarized xenon paves the way to future in-vivo studies for MRI applications. However, this still requires the development of new synthetic approaches to design these biosensors more easily and to produce larger quantities of molecules. Some recent studies aimed at solving this problem have been recently published in the literature and seem promising. Chemists now have in hand several cryptophanes to design a wide range of water-soluble cryptophane derivatives suitable for biosensing applications. As underlined by several groups, the possibility to perform multiplexing experiments is another important characteristic of these systems. Hence, several cryptophane biosensors can be used in a single experiment for targeting multiple biological

molecules or tissues. It has been frequently observed that in aqueous solution enantiopure cryptophanes exhibit remarkable chiroptical properties (ECD, VCD, optical rotation), which upon binding are strongly affected. Enantioselectivity has also been evidenced with enantiopure water-soluble cryptophanes. Similar development of water-soluble hemicryptophanes has only recently been reported. The possibility to functionalize the inner cavity of the host molecules affords new tools for the design of original chiral receptors and supramolecular catalysts. Altogether, these studies suggest that water-soluble cryptophanes and hemicryptophanes in their racemic or enantiopure form should continue to develop rapidly in the future.

## References

1. Gabard, J.; Collet, A. *J. Chem. Soc. Chem. Commun.* **1981**, 1137–1139.
2. Collet, A. *Tetrahedron* **1987**, *43*, 5725–5759.
3. Collet, A.; Dutasta, J.-P.; Lozach, B.; Canceill, J. *Top. Curr. Chem.* **1993**, *165*, 103–129.
4. Brotin, T.; Dutasta, J.-P. *Chem. Rev.* **2009**, *109*, 88–130.
5. Garel, L.; Dutasta, J.-P.; Collet, A. *Angew. Chem. Int. Ed. Engl.* **1993**, *32*, 1169–1171.
6. Bartik, K.; Luhmer, M.; Dutasta, J.-P.; Collet, A.; Reisse, J. *J. Am. Chem. Soc.* **1998**, *120*, 784–791.
7. Harel, E.; Schröder, L.; Xu, S. *Annu. Rev. Anal. Chem.* **2008**, *1*, 133–163.
8. Berthault, P.; Huber, G.; Desvaux, H. *Prog. NMR Spectrosc.* **2009**, *55*, 35–60.
9. Schröder, L. *Physica Medica*, **2011**, *29*, 3–16.
10. Witte, C.; Schröder, L. *NMR Biomed.* **2013**, *26*, 788–802.
11. Brotin, T.; Guy, L.; Martinez, A.; Dutasta, J.-P. *Top. Curr. Chem.* **2013**, *341*, 177–230.
12. Canceill, J.; Lacombe, L.; Collet, A. *J. Chem. Soc. Chem. Commun.* **1987**, 219–221.
13. Garel, L.; Lozach, B.; Dutasta, J.-P.; Collet, A. *J. Am. Chem. Soc.* **1993**, *115*, 11652–11653.
14. Berthault, P.; Desvaux, H.; Wendlinger, T.; Gyejacquot, M.; Stopin, A.; Brotin, T.; Dutasta, J.-P.; Boulard, Y. *Chem. Eur. J.* **2010**, *16*, 12941–12946.
15. Boutin, C.; Léonce, E.; Brotin, T.; Jerschow, A.; Berthault, P. *J. Phys. Chem. Lett.* **2013**, *4*, 4172–4176.
16. Brotin, T.; Dutasta, J.-P. *Eur. J. Org. Chem.* **2003**, 973–984.
17. Bouchet, A.; Brotin, T.; Linares, M.; Agren, H.; Cavagnat, D.; Buffeteau, T. *J. Org. Chem.* **2011**, *76*, 1372–1383.
18. Korchak, S.; Kilian, W.; Mitschang, L. *Chem. Commun.* **2015**, *51*, 1721–1724.
19. Schnurr, M.; Witte, C.; Schröder, L. *Phys. Chem. Chem. Phys.* **2013**, *15*, 14178–14181.
20. Schnurr, M.; Witte, C.; Schroder, L. *Biophysical journal*, **2014**, *106*, 1301–1308.
21. Mynar, J. L.; Lowery, T. J.; Wemmer, D. E.; Pines, A.; Fréchet, J. M. J. *J. Am. Chem. Soc.* **2006**, *128*, 6334–6335.
22. Delacour, L.; Kotera, N.; Traoré, T.; Garcia-Argote, S.; Puente, C.; Leteurtre, F.; Gravel, E.; Tassali, N.; Boutin, C.; Léonce, E.; Boulard, Y.; Berthault, P.; Rousseau, B. *Chem. Eur. J.* **2013**, *19*, 6089–6093.
23. Tyagi, R.; Witte, C.; Haag, R.; Schröder, L. *Org. Lett.* **2014**, *16*, 4436–4439.
24. Givélet, C.; Sun, J.; Xu, D.; Emge, T. J.; Dhokte, A.; Warmuth, R. *Chem. Commun.* **2011**, 47, 4511–4513.
25. Chambers, J. M.; Aru Hill, P.; Aaron, J. A.; Han, Z.; Christianson, D. W.; Kuzma, N. N.; Dmochowski, I. J. *J. Am. Chem. Soc.* **2009**, *131*, 563–569.
26. Jacobson, D. R.; Khan, N. S.; Collé, R.; Fitzgerald, R.; Laureano-Pérez, L.; Bai, Y.; Dmochowski, I. J. *PNAS*, **2011**, *108*, 10969–10973.

27. Laureano-Perez, L.; Collé, R.; Jacobson, D. R.; Fitzgerald, R.; Khan, N. S.; Dmochowski, I. J. *Appl. Radiat. Isotopes* **2012**, *70*, 1997–2001.
28. Desgrosellier, J. S.; Cheresch, D. A. *Nature Rev. Cancer* **2010**, *10*, 9–22.
29. Seward, K. G.; Bai, Y.; Khan, N. S.; Dmochowski, I. J. *Chem. Sci.* **2011**, *2*, 1103–1110.
30. Dubost, E.; Kotera, N.; Garcia-Argote, S.; Boulard, Y.; Léonce, E.; Boutin, C.; Berthault, P.; Dugave, C.; Rousseau, B. *Org. Lett.* **2013**, *15*, 2866–2868.
31. Dubost, E.; Dognon, J.-P.; Rousseau, B.; Milanole, G.; Dugave, C.; Boulard, E.; Léonce, E.; Boutin, C.; Berthault, P. *Angew. Chem. Int. Ed.* **2014**, *53*, 9837–9840.
32. Traoré, T.; Clavé, G.; Delacour, L.; Kotera, N.; Renard, P.-Y.; Romieu, A.; Berthault, P.; Boutin, C.; Tassali, N.; Rousseau, B. *Chem. Commun.*, **2011**, *47*, 9702–9704.
33. Chapellet, L. L.; Cochrane, J. R.; Mari, E.; Boutin, C.; Berthault, P.; Brotin, T. *J. Org. Chem.* **2015**, *80*, 6143–6151.
34. Fairchild, R. M.; Holman, K. T. *J. Am. Chem. Soc.* **2005**, *127*, 16364–16365.
35. Fairchild, R. M.; Akil, I. J.; Holman, K. T.; Fogarty, H. A.; Brotin, T.; Dutasta, J.-P.; Boutin, C.; Huber, G.; Berthault, P. *J. Am. Chem. Soc.* **2010**, *132*, 15505–15507.
36. Brotin, T.; Barbe, R.; Darzac, M.; Dutasta, J.-P. *Chem. Eur. J.* **2003**, *9*, 5784–5792.
37. Kotera, N.; Tassali, N.; Léonce, E.; Boutin, C.; Berthault, P.; Brotin, T.; Dutasta, J.-P.; Delacour, L.; Traoré, T.; Buisson, D.-A.; Taran, F.; Coudert, S.; Rousseau, B. *Angew. Chem. Int. Ed.* **2012**, *124*, 4176–4179.
38. Tassali, N.; Kotera, N.; Boutin, C.; Léonce, E.; Boulard, Y.; Rousseau, B.; Dubost, E.; Taran, F.; Brotin, T.; Dutasta, J.-P.; Berthault, P. *Anal. Chem.* **2014**, *86*, 1783–1788.
39. Kotera, N.; Dubost, E.; Milanole, G.; Doris, E.; Gravel, E.; Arhel, N.; Brotin, T.; Dutasta, J.-P.; Cochrane, J.; Mari, E.; Boutin, C.; Léonce, E.; Berthault, P.; Rousseau, B. *Chem. Commun.* **2015**, *51*, 11482–11484.
40. Taratula, O.; Bai, Y.; D'antonio, E. L.; Dmochowski, I. J. *Supramol. Chem.* **2014**, *27*, 65–71.
41. Spence, M. M.; Rubin, S. M.; Dimitrov, I. E.; Ruiz, E. J.; Wemmer, D. E.; Pines, A. Yao, S. Q.; Tian, F.; Shultz, P. G. *Proc. Natl. Acad. Sci. U. S. A.* **2001**, *98*, 10654–10657.
42. Spence, M. M.; Ruiz, E. J.; Rubin, S. M.; Lowery, T. J.; Wissinger, N.; Schultz, P. G.; Wemmer, D. E.; Pines, A. *J. Am. Chem. Soc.* **2004**, *126*, 15287–15294.
43. Ruiz, E. J.; Sears, D. N.; Pines, A.; Jameson, C. J. *J. Am. Chem. Soc.* **2006**, *128*, 16980–16988.
44. Huber, J. G.; Dubois, L.; Desvaux, H.; Dutasta, J.-P.; Brotin, T.; Berthault, P. *J. Phys. Chem. A*, **2004**, *108*, 9608–9615.
45. Taratula, O.; Kim, M. P.; Bai, Y.; Philbin, J. P.; Riggle, B. A.; Haase, D.; Dmochowski, I. J. *Org. Lett.* **2012**, *14*, 3580–3583.
46. Lowery, T. J.; Garcia, S.; Chavez, L.; Ruiz, E. J.; Wu, T.; Brotin, T.; Dutasta, J.-P.; King, D. S.; Schultz, P. G.; Pines, A.; Wemmer, D. E. *ChemBioChem* **2006**, *7*, 65–73.
47. Garimella, P. D.; Meldrum, T.; Witus, L. S.; Smith, M.; Bajaj, V. S.; Wemmer, D. E.; Francis, M. B.; Pines, A. *J. Am. Chem. Soc.* **2014**, *136*, 164–168.
48. Schröder, L.; Lowery, T.; Hilty, C.; Wemmer, D. E.; Pines, A. *Science* **2006**, *314*, 446–449.
49. Garcia, S.; Chavez, L.; Lowery, T. J.; Han, S.-I.; Wemmer, D. E.; Pines, A. *J. Magn. Reson.* **2007**, *184*, 72–77.
50. Meldrum, T.; Bajaj, V. S.; Wemmer, D. E.; Pines, A. *J. Magn. Reson.* **2011**, *213*, 14–21.
51. Bai, Y.; Hill, P. A.; Dmochowski, I. J. *Anal. Chem.* **2012**, *84*, 0035–9941.
52. Döpfert, J.; Witte, C.; Kunth, M.; Schröder, L. *Contrast Media Mol. Imaging* **2014**, *9*, 100–107.
53. Meldrum, T.; Seim, K. L.; Bajaj, V. S.; Palaniappan, K. K.; Wu, W.; Francis, M. B.; Wemmer, D. E.; Pines, A. *J. Am. Chem. Soc.* **2010**, *132*, 5936–5937.
54. Stevens, T. K.; Palaniappan, K. K.; Ramirez, R. M.; Francis, M. B.; Wemmer, D. E.; Pines, A. *Magn. Reson. Med.* **2013**, *69*, 1245–1252.
55. Roy, V.; Brotin, T.; Dutasta, J. P.; Charles, M.-H.; Delair, T.; Mallet, F.; Huber, G.; Desvaux, H.; Boulard, Y.; Berthault, P. *ChemPhysChem*, **2007**, *8*, 2082–2085.
56. Boutin, C.; Stopin, A.; Lenda, F.; Brotin, T.; Dutasta, J.-P.; Jamin, A.; Sanson, A.; Boulard, Y.; Leteurtre, G.; Huber, G.; Bogaert-Buchmann, A.; Tassali, N.; Desvaux, H.; Carrière, M.; Berthault, P. *Bioorg. Med. Chem.*, **2011**, *19*, 4135–4143.

57. Sloniec, J.; Shnurr, M.; Witte, C.; Resch-Genger, U.; Schröder, L.; Hennig, A. *Chem. Eur. J.* **2013**, *19*, 3110–3118.
58. Klippel, S.; Dopfert, J.; Jayapaul, J.; Kunth, M.; Rossella, F.; Schnurr, M.; Witte, C.; Freund, C.; Schröder, L. *Angew. Chem. Int. Ed.* **2014**, *126*, 503–506.
59. Wei, Q.; Seward, G. K.; Hill, A.; Patton, B.; Dimitrov, I. E.; Kuzma, N. N.; Dmochowski, I. J. *J. Am. Chem. Soc.* **2006**, *128*, 13274–13283.
60. Seward, G. K.; Wei, Q.; Dmochowski, I. J. *Bioconjugate Chem.* **2008**, *19*, 2129–2135.
61. Khan, N. S.; Riggle, B. A.; Seward, G.; Bai, Y.; Dmochowski, I. J. *Bioconjugate Chem.* **2015**, *26*, 101–109.
62. Schlundt, A.; Kilian, W.; Beyermann, M.; Sticht, J.; Günther, S.; Höpner, S.; Falk, K.; Roetzschke, O.; Mitschang, L.; Freund, C. *Angew. Chem. Int. Ed.* **2009**, *48*, 4142–4145.
63. Rose, H. M.; Witte, C.; Rossella, F.; Klippel, S.; Freund, C.; Schröder, L. *PNAS*, **2014**, *111*, 11697–11702.
64. Witte, C.; Martos, V.; Rose, H. M.; Reinke, S.; Klippel, S.; Schröder, L.; Hackenberger, C. P. *R. Angew. Chem. Int. Ed.* **2015**, *54*, 2806–2810.
65. Zamberlan, F.; Lesbats, C.; Rogers, N. J.; Krupa, J. L.; Pavlovskaya, G. E.; Thomas, N. R.; Fass, H. M.; Meersmann, T. *ChemPhysChem* **2015**, *16*, 2294–2298.
66. Jeong, K.; Slack, C. C.; Vassiliou, C. C.; Dao, P.; Gomes, M. D.; Kennedy, D. J.; Truxal, A. E.; Sperling, L. J.; Francis, M. B.; Wemmer, D. E.; Pines, A. *ChemPhysChem* **2015**, *16*, 3573–3577.
67. Bouchet, A.; Brotin, T.; Cavagnat, D.; Buffeteau, T. *Chem. Eur. J.* **2010**, *16*, 4507–4518.
68. Taratula, O.; Hill, P. A.; Khan, N. S.; Carroll, P. J.; Dmochowski, I. J. *Nature Comm.* **2010**, *1*, 148.
69. Bouchet, A.; Brotin, T.; Linares, M.; Agren, H.; Cavagnat, D.; Buffeteau, T. *J. Org. Chem.* **2011**, *76*, 4178–4181.
70. Bouchet, A.; Brotin, T.; Linares, M.; Cavagnat, D.; Buffeteau, T. *J. Org. Chem.* **2011**, *76*, 7816–7825.
71. Brotin, T.; Montserret, R.; Bouchet, A.; Cavagnat, D.; Linares, M.; Buffeteau, T. *J. Org. Chem.* **2012**, *77*, 1198–1201.
72. Brotin, T.; Cavagnat, D.; Berthault, P.; Montserret, R.; Buffeteau, T. *J. Phys. Chem. B*, **2012**, *116*, 10905–10914.
73. Brotin, T.; Goncalves, S.; Berthault, P.; Cavagnat, D.; Buffeteau, T. *J. phys. Chem. B*, **2013**, *117*, 12593–12601.
74. Canceill, J.; Collet, A.; Gabard, J.; Kotzyba-Hibert, F.; Lehn, J.-M. *Helv. Chim. Acta.* **1982**, *65*, 1894–1897.
75. Gautier, A.; Mulatier, J.-C.; Crassous, J.; Dutasta, J.-P. *Org. Lett.* **2005**, *7*, 1207–1210.
76. Perraud, O.; Robert, V.; Martinez, A.; Dutasta, J.-P. *Chem. Eur. J.* **2011**, *17*, 13405–13408.
77. Zhang, D.; Gao, G.; Guy, L.; Robert, V.; Dutasta, J.-P.; Martinez, A. *Chem. Comm.* **2015**, *51*, 2679–2682.
78. Schmitt, A.; PhD thesis, University of Lyon, 2014.
79. Schmitt, A.; Martinez, A. unpublished results.
80. Schmitt, A.; Chatelet, B.; Collin, S.; Dutasta, J.-P.; Martinez, A. *Chirality*, **2013**, *25*, 475–479.
81. Schmitt, A.; Robert, V.; Dutasta, J.-P.; Martinez, A. *Org. Lett.* **2014**, *16*, 2374–2377.
82. Dimitrov-Raytchev, P.; Martinez, A.; Gornitzka, H.; Dutasta, J.-P. *J. Am. Chem. Soc.* **2011**, *133*, 2157–2159.
83. Chatelet, B.; Dufaud, V.; Dutasta, J.-P.; Martinez, A. *J. Org. Chem.* **2014**, *79*, 8684–8688.
84. Martinez, A.; Dutasta, J.-P. *J. Catal.* **2009**, *267*, 188–192.
85. Perraud, O.; Tommasino, J.-B.; Robert, V.; Albela, B.; Khrouz, L.; Bonneviot, L.; Dutasta, J.-P.; Martinez, A. *Dalton Trans.* **2013**, *42*, 1530–1535.
86. Perraud, O.; Sorokin, A.; Dutasta, J.-P.; Martinez, A. *Chem. Comm.* **2013**, *49*, 1288–1290.
87. Schmitt, A.; Collin, S.; Bucher, C.; Maurel, V.; Dutasta, J.-P.; Martinez, A. *Org. Biomol. Chem.* **2015**, *13*, 2157–2161.

# Chapter 22

## Calixsugars: Finally Reaching Their Therapeutic Potential?

Susan E. Matthews

### 22.1 Introduction

The calixarene family has proved to be an attractive scaffold for the development of both therapeutic molecules and delivery systems [1]. Applications in a wide range of areas including cancer treatments, [2, 3] antivirals, [4] antibacterials, [5] and delivery of genes [6] and drugs [7] have been proposed. Of these, it is the calixsugars that have attracted the most attention where the combination of the carbohydrate and its presentation as a cluster lead to a variety of biological applications.

One of the most important observations in understanding sugar-protein and sugar-DNA interactions *in vivo* was the identification of multivalency or the ‘glycoside cluster’ effect [8]. Multivalency can be defined as the non-linear increase in binding strength on multiple interactions of binding motifs on the same scaffold with a biological molecule with multiple binding sites. This enables excellent binding, despite the promiscuity of the sugars between targets and the relatively weak binding affinity of the single molecules. A wide range of glycoside clusters based on polymers, dendrimers and macrocyclic scaffolds have been developed to exploit this property [9–11].

A number of different binding modes have been proposed to account for the increased activity observed in these systems. In particular, the ability of a multivalent vector to bind to multiple biological molecules and enable aggregation (Fig. 22.1a), to bind to multiple sites on a single biological molecule to give chelates (Fig. 22.1b) and the possibility of binding being enhanced by an increase

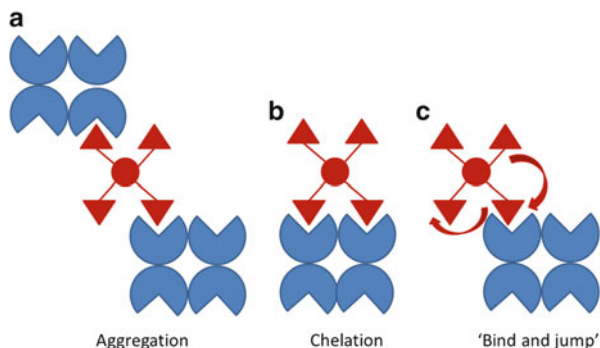
---

S.E. Matthews (✉)

School of Pharmacy, University of East Anglia, Norwich Research Park, Norwich NR4 7TJ, UK

e-mail: [susan.matthews@uea.ac.uk](mailto:susan.matthews@uea.ac.uk)

**Fig. 22.1** Binding modes of multivalent ligands



in local concentration, which facilitates a ‘bind and jump’ mechanism (Fig. 22.1c) have been demonstrated [11].

The calixarene family, including resorcin[4]arenes and, most recently, the pillar [5]arenes and pillar[6]arenes, offer a highly attractive coherent family for evaluation of multivalent interactions. The role of topology in the presentation of ligands can be effectively analysed through using the fixed conformations (cone, partial cone, 1,3-alternate and 1,2-alternate) of the calix[4]arenes in the preparation of isomeric glycoclusters. Equally, valency can be readily addressed through partial functionalisation of a single scaffold or through using a combination of identically functionalised calix[4],[6] and [8]arenes. Valency matching is also possible, due to the ready preparation of calixarenes featuring between three and eight aromatic residues. Additionally, the flexibility of the core and how it can affect binding can be investigated through the preparation of both conformationally fixed and flexible analogues.

The early development of calixsugars was relatively slow, often requiring highly elegant synthetic routes for their preparation, and this story has been expertly reviewed elsewhere [8]. However, it should be noted that significant advances, particularly in biological evaluation, have been achieved since the introduction of click chemistry. In particular the development of copper-catalysed azide alkyne cycloaddition (CuACC) [12] by Sharpless and Meldal, has allowed ready synthetic access to a wider variety of glycoclusters and has had a particularly marked effect on the development of enzyme inhibitors and functionalisation with iminosugars [11].

In this chapter, we ask the question ‘after almost two decades of research, are calixsugars finally reaching their therapeutic potential?’

## 22.2 Gene Delivery

Gene therapy, with its ability to halt the development of a disease rather than merely treat the symptoms, remains one of the most attractive therapeutic targets in modern medicinal chemistry. To-date, only one gene therapeutic treatment has been approved in the EU; alipogene tiparvovec (Glybera), for the treatment of lipoprotein lipase deficiency [13]. The major stumbling block in achieving effective gene therapy is in the design of vectors that can deliver the active gene cell selectively. Whilst early research focused on manipulation of viral capsids, more recently the use of synthetic vectors *e.g.* polymers and dendrimers featuring high levels of protonated amines has gained momentum [14].

From 1999, the group of Aoyama introduced an alternative approach to the design of a synthetic vector based on sugar-derivatised resorcin[4]arenes. From an amino-functionalised resorcin[4]arene featuring four undecyl tails, they developed a facile approach to derivatisation with a range of oligosaccharides through reaction with a terminal lactone, resulting in the first sugar residue being ring-opened (Fig. 22.2). The octa-functionalised derivatives **2–4** (Fig. 22.2) were shown to act as neutral amphiphiles, with the large sugar clusters acting as the head group whilst

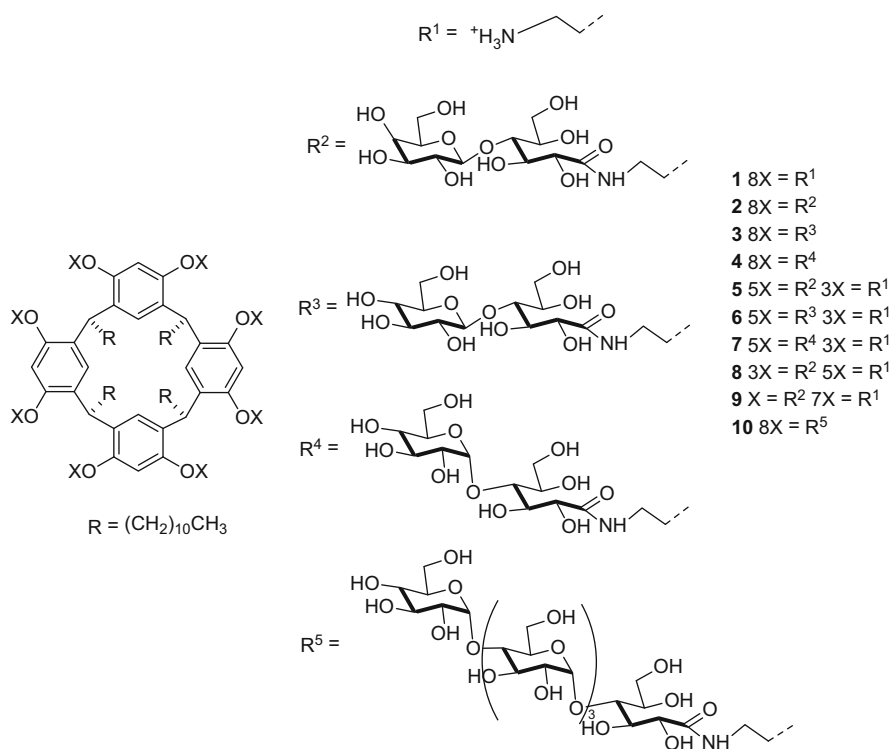


**Fig. 22.2** Resorcin[4]arene sugar clusters



the long alkyl chains gave rise to the classical conical shaped structure required for self-assembly [15, 16]. Stable micelles, or glyconanoparticles, of 4–5 nm diameter, were observed using dynamic light scattering (DLS). Purification of the micelles, using gel permeation chromatography (GPC), indicated that the micellisation process was irreversible and that the particles were not in equilibrium with single molecules. From size analysis, an estimate of molecules per micelle could be made, which was between five and six resorcin[4]arenes per particle. Based on preliminary research [17] which indicated that the assemblies from **4** to **10** were able to bind and undergo agglutination with phosphate and nucleotides through hydrogen bonding, the glyconanoparticles were additionally investigated for their ability to bind DNA and transfect cells.

An initial evaluation [18] of the potential to bind to DNA was undertaken using biophysical techniques with the maltoheptaose derivative **10** and the plasmid pBR322. Electrophoresis demonstrated strong binding to DNA that was enhanced by using longer chain sugars as in **10** compared with maltose **4**. This effect was confirmed by DNA melting experiments where **10** showed stabilisation of double stranded DNA by an increase of 27° in the melting temperature compared to 9° for **4**. In both cases, aggregation of the resorcin[4]arenes was clearly seen by DLS, where particles of up to 550 nm were observed.

This was taken further through investigation of transfection ability, [19] using the cellobiose-derivatised resorcin[4]arene **3**, in which the terminal sugar residue is a  $\beta$ -glucose, and a 7,040 base pair plasmid (pCMVluc) featuring a firefly protein luciferase reporter. Gel electrophoresis studies showed compaction of the DNA reached saturation at a ratio of 1:1.2 for **3**:base pair indicating that two glyconanoparticles were bound per helical pitch of the DNA, probably in the major groove in a manner similar to the glycoside antibiotics. This binding was achieved not through charge neutralisation, as in the case of amine-based vectors, but simply through hydrogen-bonding interactions between the phosphates of DNA and the sugar clusters; it gave rise to discrete particles of ~50 nm diameter. These particles can be likened to an artificial virus, where each glyconanoparticle is equivalent to a capsid protein. Transfection, through measurement of expression of luciferase and chemoluminescence, was achieved in a range of cells, including HeLa, CHO and HepG2, and was enhanced by the presence of foetal bovine serum. In all cases, transfection was more effective than with the cationic lipid, lipofectin, by an order of magnitude and, at operating concentrations, the particles showed limited toxicity.

From this foundation, a comparative study looked at the potential for these glyconanoparticles to achieve cell-selective delivery through alteration of the terminal sugar residue [20]. Surprisingly, alteration of the terminal sugars to  $\alpha$ -glucose **4** or  $\beta$ -galactose **2**, led to a significant change in self-assembly. Organisation into the glyconanoparticle occurred with all three derivatives but, subsequently, additional clustering occurred with both the  $\alpha$ -glucose and  $\beta$ -galactose derivatives, resulting in aggregates of up to 300 nm diameter. Transfection ability in HeLa cells showed a distinct correlation with the size of aggregate, with the  $\alpha$ -glucose derivative **4**, at 300 nm, being least effective, the  $\beta$ -glucose **3** being the most and the  $\beta$ -galactose **2**, at 200 nm, showing intermediate behaviour. This

suggested that transfection was operating through size-dependent non-specific endocytosis or pinocytosis processes, which have been shown to favour uptake of particles of below 100 nm. This uptake mechanism was confirmed through performing transfection at 4 °C, where endocytosis is halted, and by the use of endocytosis inhibitors, cytochalasin B and wortmannin. Additional co-localisation studies using fluorescently labelled plasmids showed the presence of the plasmid within endosomes. Interestingly, the size-dependency of the pinocytosis can also be observed with smaller aggregates, [21] where particles <50 nm also show low uptake; for example a 15 nm resorcin[4]arene glycocluster-coated CdSe quantum dot is taken up by cells less effectively than the 50 nm glycoviruses but more effectively than a single 5 nm glyconanoparticle.

Variation in response was observed when transfection in HepG2 cells was investigated. HepG2 cells express on their surface the asialoglycoprotein which is specific for binding galactose and offers the possibility of achieving transfection through receptor mediated endocytosis (RME) [22]. In this case, whilst  $\beta$ -glucose-derivatised glyconanoparticles continued to perform well through non-targeted endocytosis, the previous size limitations for  $\beta$ -galactose derivatives were overcome and comparable transfection activity was observed. The role of RME in achieving this was confirmed by using asialofelutin, as a competitive inhibitor of binding to the asialoglycoprotein, in which case transfection levels dropped to those observed with HeLa cells having no specific surface receptors. Two questions still remain with these clusters; why is such a significant difference in aggregation occurring with a change in the terminal sugar? What is their release mechanism from the endosome? It is unlikely to be through the proton sponge mechanism [23] proposed for-amine based vectors.

The observation of a level of cell-selectivity with lactose-derivatised resorcin[4]arenes was further investigated through the preparation of partly functionalised macrocycles [24]. Resorcin[4]arenes bearing, on average, one (**9**), three (**8**) or five (**5**) lactose units were prepared and compared with **2** and the octa-amino derivative **1**. Unsurprisingly, the octa-amino derivative is the most effective in condensation through charge neutralisation and this was the dominant effect, above hydrogen-bonding interactions, for the mixed derivatives. Whilst the pentasugar derivative, as with **2**, shows aggregation of the glyconanoparticles to 100 nm clusters, **1**, **8** and **9** exist as the monomeric assemblies of 40–50 nm. Measurement of the zeta potential also indicates that assemblies formed of **1** and **9** are overall positive, whereas those from **2**, **5** and **8** are neutral. Transfection studies in HeLa cells revealed the importance of both size and charge of aggregates in affording uptake, with the octa-amino compound being the most effective, followed by **9**, **8** and then **5** and **2**. In HepG2 cells, **2**, **5** and **8** all show good cell-selective uptake, in line with the understanding that a three-point interaction is required for interaction with the asialoglycoprotein [22]. Although enhancement of activity is highest in HepG2 with **2**, derivative **8**, by virtue of its smaller sized aggregates and underlying transfection ability, can be considered to be the ideal vector; however it remains to be further optimised through the regioselective functionalisation of the resorcin[4]arene core. It should be noted that the most effective transfection agent, **1** is highly toxic.

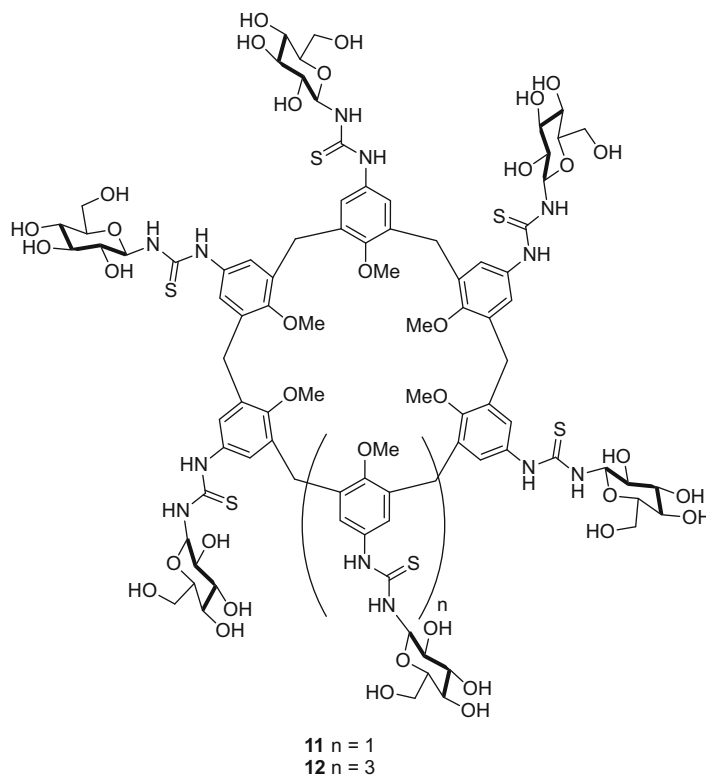


**Fig. 22.3** Thiourea calix[6,8]arene clusters

In contrast to these promising results with resorcin[4]arene-based clusters, glucosyl-functionalised calix[6]arene **11** and calix[8]arene **12** (Fig. 22.3) are unable to condense DNA, despite being able to interact with phosphate anions [25]. AFM studies of their interaction with plasmid DNA gave evidence of binding and the formation of aggregates but not of the formation of the compact particles required for transfection.

## 22.3 Inhibition of Binding to Lectins

The biological activity of calixsugars has been most extensively studied in lectin-binding systems. Lectins are proteins that recognise cell-surface carbohydrates, through non-covalent interactions, and play a wide range of biological roles in both healthy and disease states [26, 27]. The altered expression of cell-surface sugars in diseases such as cancer and the prevalence of lectin binding as a precursor to

infectivity for both viruses and bacteria make inhibition of lectin-binding an attractive therapeutic target.

### 22.3.1 Preliminary Lectin Studies

The majority of early calixsugar papers, on the potential of achieving multivalent lectin inhibition, focused on biological studies with plant lectin models rather than with a long-term human biological target. These studies gave important preliminary data and understanding for the design of clusters and also led to the development of excellent biological tools, including surface plasmon resonance (SPR), [10] that could later be exploited in more human biologically relevant studies.

The lectins used in these studies included wheat-germ agglutinin (WGA), peanut agglutinin (PNA), *Vicia villosa* agglutinin (VVA) and concanavalin A (ConA). WGA from *Triticum vulgare* is a homodimer with eight carbohydrate binding sites that is selective for sialosides and *N*-acetyl-D-galactosamine and is thus useful in assessing antiviral activity. For investigating galactose binding capability, PNA, which binds  $\beta$ -galactose, *N*-acetyl-D-galactosamine and T antigen and VVA which is selective for galactose, have been used extensively. In contrast, ConA, featuring four binding sites selective for  $\alpha$ -mannose and  $\alpha$ -glucose is generally used for determining binding of glucose clusters [26, 27].

#### 22.3.1.1 Sialic Acid Calixsugars

In 1996, Roy and co-workers [28] described the first biological application of calixsugars by evaluating a calixarene functionalised at the lower-rim with  $\alpha$ -sialosides **13** (Fig. 22.4) and its ability to bind to WGA as a model plant lectin. Using turbidity studies, **13** was shown to bind the lectin highly effectively and a

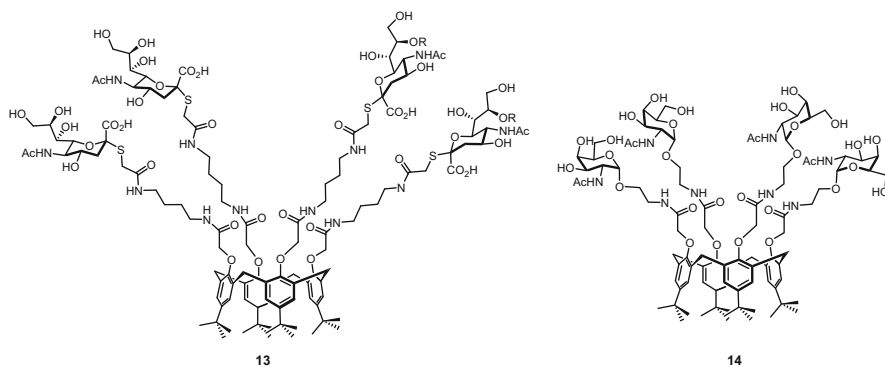
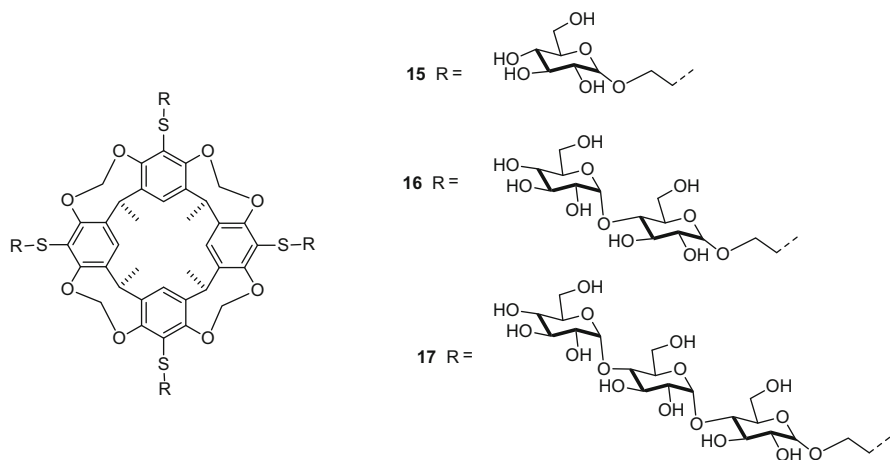


Fig. 22.4 Roy's calix[4]arene clusters



**Fig. 22.5** Macrocyclic sugar clusters

significant excess of the mono-sialoside, phenylthio  $\alpha$ -sialoside, was required to disrupt this binding.

### 22.3.1.2 Glucose Calixsugars

Using the same resorcin[4]arene based glycoclusters as investigated for DNA binding, the group of Aoyama examined lectin selectivity based on sugar structure and pioneered the use of SPR [29] as an effective model of competing biological interactions. Comparative binding studies with **2** and **4** (Fig. 22.2) and ConA and PNA confirmed that the clusters could interact selectively with the complementary lectins and that the strength of the binding was high, requiring elevated concentrations of single sugars for disruption. Using the SPR approach, unlike with turbidity, it was possible to see that there are, however, some non-specific binding interactions, albeit of low strength, and thus a cluster bound to a non-complementary lectin to the same extent as it binds to bovine serum albumin.

This group has also prepared a series of macrocyclic sugar clusters, [30] featuring four sugar units of varying length, including glucose **15**, maltose **16** and maltotriose **17** (Fig. 22.5). These bind selectively to ConA, with the maltose and maltotriose being most effective, and are unable to interact with PNA, confirming that the turbidity involved is due to the presence of the specific sugar rather than the platform.

The introduction of sugars to the upper rim of calixarenes *via* a thiourea is an attractive and readily accessible synthetic approach. The group of Ungaro [31] first exploited this for the introduction of two (**18**) or four (**19**) glucose or galactose residues and evaluated their binding with their partnered lectins, ConA and PNA, through turbidity studies (Fig. 22.6). In both cases, strong binding was seen that

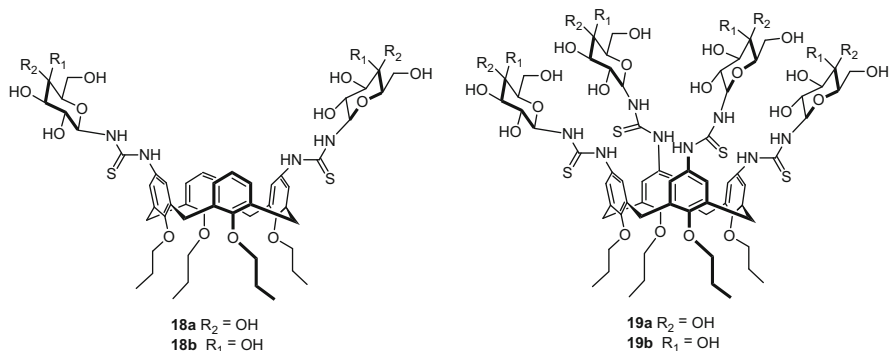


**Fig. 22.6** Upper-rim thiourea calix[4]arene clusters

could only be partially disrupted by adding large excesses (400-fold) of monomeric sugars.

The interaction of larger calixarenes with ConA has also been studied [25]. Calix [6]arene **11** and [8]arenes **12** functionalised through thioureas at the upper rim with  $\beta$ -glucose moieties were found to readily self-assemble in water into small aggregates (Fig. 22.3). These were believed to be micelles, of 10–15 nm diameter in AFM studies and 3–5 nm in DLS. This is somewhat unexpected as the calixarenes do not exhibit the classical V-shaped structure having short chains at the lower-rim and being conformationally flexible. Despite the preference of ConA for  $\alpha$ -anomers of glucose and mannose, both of these compounds are able to agglutinate the lectin, as shown by turbidity studies, with the calix[8]arene **12** being the most effective, whilst no effect is seen with PNA. AFM of the lectin in the presence and absence of **12** shows the progression to larger aggregates from monomeric lectins over time.

### 22.3.1.3 GalNAc Calix Sugars

An early study [32] into the potential of calixsugars to inhibit interactions with cancer specific lectins, *e.g.* Tn Antigen, an epitope of human adenocarcinoma mucin, was undertaken using calixarenes decorated with  $\alpha$ -GalNAc *e.g.* **14** (Fig. 22.4). Analysis of inhibition, with the model plant lectin VVA showed that, whilst all calixarene molecules induced turbidity through aggregation, a hexadecavalent dendritic calixsugar was the most effective ligand in an enzyme linked lectin assay (ELLA) [10] of inhibition of binding of asialoglycophorin to VVA.

### 22.3.1.4 GlcNAc Calix Sugars

The importance of high valency in achieving good inhibition of lectin binding has been further investigated by the Consoli group [33, 34], who have focused on *N*-

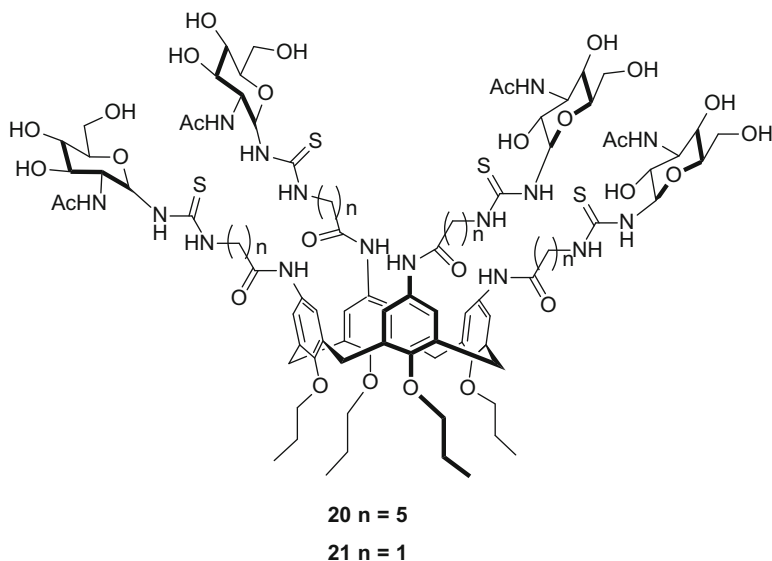


**Fig. 22.7** N-acetyl-D-glucosamine functionalised calix[4]arene

acetyl-D-glucosamine (GlcNAc) derivatives of calix[4]arene and calix[8]arene (Fig. 22.7). GlcNAc has been shown to be bound effectively by a wide range of lectins involved in cell processes, including replication and migration. GlcNAc was attached to the upper rim of cone calix[4]arene and conformationally mobile calix[8]arene, either directly through a urea [33] or through an amino-acid spacer [34]. Turbidity studies with WGA and PNA confirmed that the calixarene derivatives were selective for *N*-acetyl- $\alpha$ -D-glucosamine-binding proteins and the requirement of a large excess of competitive monosaccharide demonstrated the enhancement of binding through multivalency. Inhibition of WGA haemagglutination of human erythrocytes was higher for all the glycoclusters, compared with monovalent sugar. The most effective ligands were **20**, a calix[4]arene featuring a five-carbon spacer, which showed a 312-fold relative improvement and **21** with a shorter spacer, which gave a 250-fold improvement. The smaller rigid clusters are more effective than the conformationally mobile calix[8]arenes, which show a maximum of an 62-fold improvement.

Interestingly, the clusters without spacers showed considerably lower binding, as did those featuring higher numbers of sugars introduced through a branched lysine spacer. This latter result is unexpected as generally an increase in valency would be expected to enhance inhibition of lectin binding; however, the authors suggest that crowding of the residues on the calix surface may be reducing accessibility to binding.

### 22.3.2 Antivirals

Influenza virus A has two surface glycoproteins that offer potential for the development of competitive multivalent sugar clusters featuring 5-*N*-acetyl neuraminic acid (Neu5Ac) units [35]. Haemagglutinin (HA) binds to sialic acid receptors and fuses the cell membranes of the virus and host and neuraminidase (NA), an enzyme, cleaves sialic acid residues and is involved in release of new virus by the host cell. Whilst small molecule inhibitors of NA, such as oseltamivir (Tamiflu) and zanamavir (Relenza), are now available, no therapy based on inhibition of binding of HA has reached the clinic.

An early study into the potential of sialo clusters in inhibiting human influenza A infection, featured *N*-acetylneuraminic acid resorcin[4]arene clusters **22** (Fig. 22.8) [36]. Unlike previous clusters of this type, the sugar cannot be introduced through lactonisation and thus a thioglycoside was used. SPR studies with a model lectin, Japanese horseshoe crab lectin from *Tachypleus tridentatus* (TTA), which shows high selectivity for amino-sugars and sialic acid, indicated strong binding of the glycocluster which was difficult to displace with high concentrations of competitive sialic acid. The specificity of the interaction with TTA was shown by the absence of binding when a SPR chip coated in glucose terminated resorcin[4]arene was used. Two more biologically relevant studies showed that these clusters can effectively inhibit the interaction of influenza A virus with cells. Thus **22**, inhibits both haemagglutination of human erythrocytes in the presence of a variety of influenza A strains and also shows some neutralisation of cytopathic effects on Madine-Darby canine kidney cells (MDKC).

A more extensive study on selectivity between sialic acid-binding viral proteins was undertaken by the group of Marra and Dondoni, [37] through comparing the activity of a series of calixsugars functionalised at the lower **23a, b**, upper **24** or both rims **25** with Neu5Ac residues against BK and Influenza A viruses (Fig. 22.9). The BK virus [38] is implicated in nephropathy and organ loss in transplant

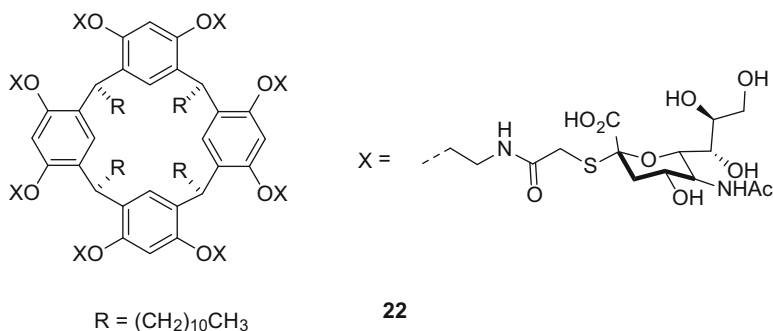
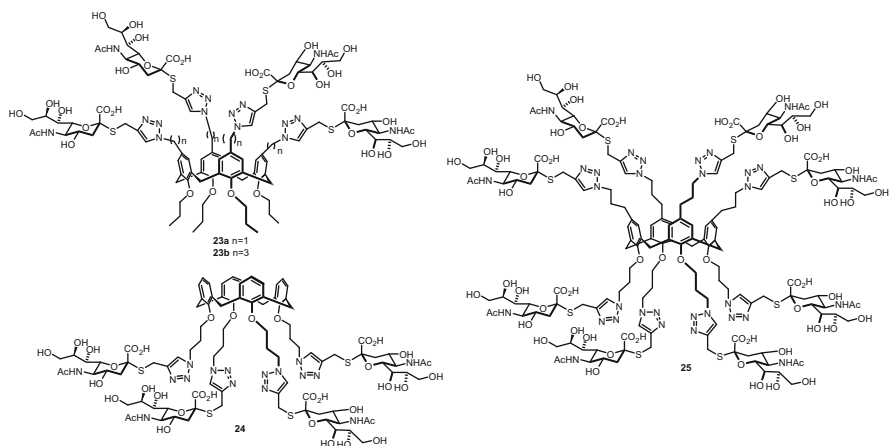


Fig. 22.8 Resorcin[4]arene sialosides





**Fig. 22.9** Antiviral glycoclusters

patients, heightened by their immunocompromised state, and its binding to cells and thus its infectivity, are facilitated by Neu5Ac.

Haemagglutination assays with the BK virus gave unexpected results as, whilst all the clusters were able to inhibit agglutination of group O human erythrocytes, with **24** being especially active, no enhancement of activity was observed between the glycoclusters and monomeric controls. It was proposed to be due to low expression of the Neu5Ac-binding lectin on the viral cell surface; however, this has not been verified. However, neutralisation of infection experiments in Vero cells showed that, whereas after 8 days incubation of BK virus alone a cytopathic effect was seen on cells, pre-incubation with the glycoclusters resulted in protection from infection. Immunofluorescence studies in the pre-treated cells demonstrated that no viral proteins were present in the nucleus and thus that the adsorption step had been halted by preferential interaction of the virus with the calixsugar clusters.

In contrast, studies with Influenza A showed that the glycoclusters **23b**, **24** and **25** were all substantially more effective in the haemagglutination assay than the monomeric ligand, giving a 50–83-fold increase per sugar residue. Steric effects in presenting the ligands to the virus were clear from the absence of activity of the less flexible **23a**, even at 50 mM concentration and the similar activity of **25** to **23b** and **24** suggested that in the octavalent cluster, only some of the residues are involved in binding. **23b**, **24** and **25** were all able to inhibit the cytopathic effect normally observed on infection of MDKC.

### 22.3.3 Antibacterials

One of the most highly explored areas of carbohydrate:protein binding is the investigation of how bacterial cells adhere to sugar residues on human cell surfaces



calorimetry (ITC) [9] studies were not possible for **26–28**, owing to solubility problems with clusters containing fewer sugar residues. A 24-fold increase, per galactose residue, in binding was observed for the tri-substituted calixarene **29** compared with a monomeric model **33** ( $K_d$  2  $\mu\text{M}$  cf. 150  $\mu\text{M}$ ). However, this was greatly surpassed by all of the tetravalent derivatives, which give nanomolar activities, confirming that valency plays an important role in binding to LecA. The role of topology is also clear, the 1,3-alternate being the most effective with a  $K_d$  of 176 nM. The same trend was observed in SPR studies, where the ability of the calixarenes to inhibit binding of LecA to a galactosylated chip was assessed. The stoichiometry calculated from ITC for **31** shows that the calixarene is interacting with four galactose binding sites. It is not possible for a single calixarene to span all the binding sites on LecA and this, combined with an absence of aggregation which would be expected if binding to four separate lectins was to occur, led to a proposed chelate binding mode where a calixarene binds to two neighbouring binding sites on two different lectins. Molecular modelling of **31** gave distances between sugars on the same side of the calixarene as 28 Å and on opposite sides as 39 Å, with the latter arrangement being able to span two binding sites on the short face of LecA. Additionally, modelling showed that it was possible for the chelate to be formed without any steric interactions between the two lectins.

A subsequent study [43] considered the nature of the linker and how it could be rigidified to reduce entropy on binding but still retain flexibility to allow multiple interactions. Building on the most effective ligand, the 1,3-alternate **31**, glycoclusters were prepared with five other linkers varying in length and rigidity (Fig. 22.11). A combination of ELLA, SPR and ITC studies were used and, as has been seen previously, mixed results were observed with some molecules performing better in a single model of binding. Molecule **37** with the most rigid phenyl spacer gave good binding constants in ELLA and SPR studies but was not sufficiently water-soluble for ITC studies and induced haemolysis in the haemagglutination assay HIA. However, for this ligand, due to the exceptional high affinity of the corresponding monomer, there was little advantage of incorporation onto the calixarene. Incorporating the highly flexible but shorter diethyleneglycol linker in **34** resulted in slightly reduced binding compared with the original triethyleneglycol linker. The cluster containing a semi-rigidified spacer **35** showed particularly good binding in ITC; however, further rigidification **36** altered the stoichiometry of binding.

In order to understand the binding arrangement between the 1,3-alternate calixarene **31** and LecA further, an AFM study [44] was undertaken in which a 1:1 mixture of both was visualised. Self-assembly into rectilinear filaments of 90–500 nm length (between 10 and 50 lectin molecules) occurred. Height measurements of the filaments were consistent with single lectin molecules and, at high resolution, regular variations in brightness of adjacent lectins was observed. This is consistent with the chelate model proposed in which neighbouring proteins are perpendicular to each other due to the two binding interactions coming from different faces of the calix[4]arene. Occasional bifurcations, and thus branches were seen which can be rationalised as being due to a failure in the chelate

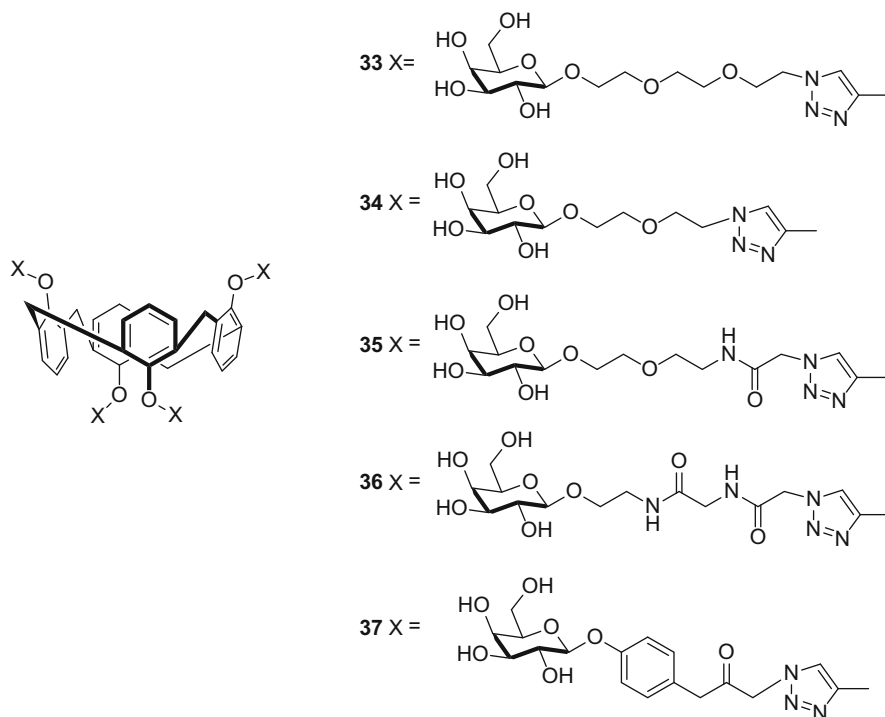


**Fig. 22.11** Comparison of spacers in LecA binding calix[4]arenes

formation where one sugar binds to an additional lectin and sets up a new strand for chelate formation. The concentration of the solution used, as well as the ratio of lectin:glycoclusters, strongly affects the aggregates seen in AFM [45]. Disruption of the lectin:lectin interactions observed with pure lectin samples can be seen even for ratios of 20,000:1, showing the importance of the sugar-lectin binding in how lectins interact.

The use of these calix[4]arene scaffolds has recently been extended to the inhibition of LecB by the preparation of fucosyl glycoclusters (Fig. 22.12) [41]. A reduction in the  $K_d$  value, measured by ITC, for the 1,3-alternate glycoclusters **38** was observed compared to monomeric ligands. However the relative increase in potency is modest, pointing to a ‘bind and jump’ mechanism, and the stoichiometry also suggests that the calixarene is interacting with a single binding site on three lectins as the spacer length is insufficient to allow binding of multiple sites on the same lectin. The mannose derivative **39** was also able to bind but, as expected, owing to the lower affinity of mannose for LecB [46] this was 50-fold lower.

With effective ligands for both LecA and LecB available based on the 1,3-alternate core, a comprehensive study combining evaluation on whole bacteria

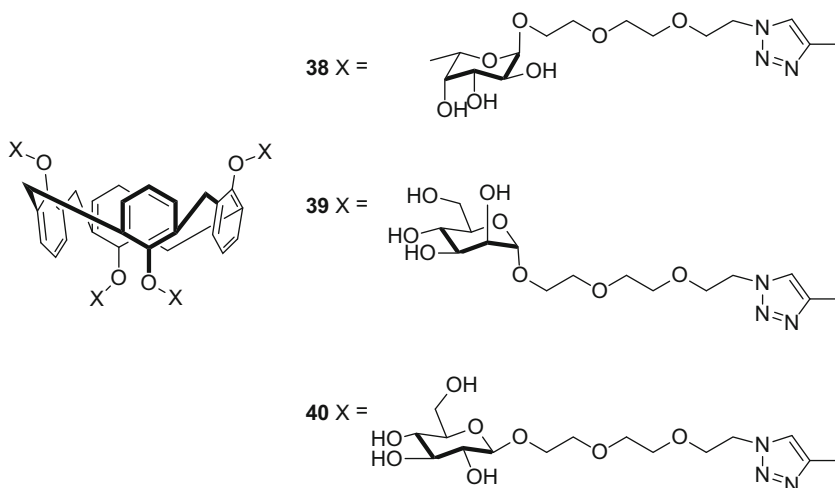
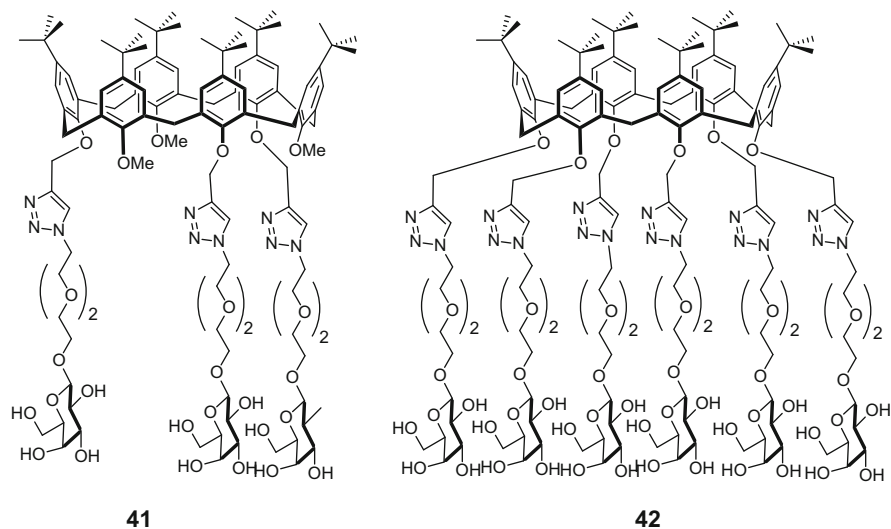


Fig. 22.12 Calix[4]arenes for evaluation of LecB binding

and mouse models *in vivo* was undertaken [41]. Aggregation of wild type PAO1 *Pseudomonas aeruginosa* was observed with both galactose **31** and fucose **38** derivatives, although a stronger effect was seen with the fucose ligand. Mutants with deleted LecA and LecB demonstrated the specificity of the interaction, as no aggregation was seen for the **31** with the LecA mutant and reduced aggregation was observed with **38** and the LecB mutant. This latter observation highlights an important aspect of bacterial studies as other surface fucose binding lectins may be present in the whole organism allowing interaction with the ligand even in the mutant. Similar results were seen with cell-adhesion studies, where **38** was able to inhibit up to 90 % of adhesion and **31** up to 70 % as a consequence of the much higher affinity of fucose to LecB than galactose to LecA. Although the mutant strains showed reduction in inhibition, it was not abolished, again pointing to the role of additional lectins. Formation of biofilm in the wild type bacteria was reduced for both **31** and **38** and was confirmed to be a consequence of specific sugar interactions as neither the glucose **40** or mannose **39** ligands were effective.

The molecules also proved effective in a lung infection model *in vivo*, in which leakage of fluorescein-labelled albumin from the serum into the lungs, as a result of *Pseudomonas* induced damage to the alveolar capillary, can be measured. Infection with *Pseudomonas aeruginosa* causes a 4 % rise in permeability, however pre-incubation of the bacteria with either **31** or **38** leads to a significant reduction of permeability to 2 % and an associated reduction in bacterial load in the spleen showing that these molecules have real therapeutic potential. However, it is important to note that despite being highly effective ligands for the simple lectins, the studies with bacteria and mice require much higher levels of ligand for an effect to be seen, probably due to the more complex biological system and the presence of competing processes.



**Fig. 22.13** Calix[6]arenes for LecA binding

The system has been extended to consider derivatives of calix[6]arene [47] resulting in a slightly more active LecA inhibitor. Whilst both the tri- and hexa-functionalised calix[6]arenes (**41** and **42**) were prepared, only **42** was of sufficient solubility to undergo biological evaluation (Fig. 22.13). A comparator lectin was also studied to allow an understanding of the role of topology in binding. ECA the agglutinin from *Erythrina cristagalli* is able to bind both galactose and lactose but at lower affinity than LecA and provides two binding sites which are approximately 100 Å apart [26]. Inhibition of lectin-induced erythrocyte agglutination was more effective for LecA (MIC 63 μM) than for ECA (1,250 μM). SPR studies, using a galactose-functionalised chip, gave IC<sub>50</sub> values of 0.8 and 5.2 μM, respectively, for LecA and ECA and thus relative potencies of 80 and 40, compared to a monovalent control. ITC gave a measure of stoichiometry for **42** with LecA of 1:3 and it was proposed that the binding may involve a chelate where two binding sites on one lectin are complexed by the calix[6]arene whilst a second lectin is bound through a single sugar group and this may be exchanged through a ‘bind and jump’ mechanism.

Altering the scaffold further to a resorcin[4]arene [48] in either the *rccc* boat or *rctt* chair configuration gave surprising results on the effect of topology (Fig. 22.14). Both lactose and galactose derivatives of the diastereoisomers were prepared using CuACC, having first incorporated an alkyne during the condensation reaction. Whilst haemagglutination inhibition assays were not possible with these ligands owing to haemolysis, ELLA experiments with LecA were undertaken and very similar IC<sub>50</sub> values were observed: 0.7 μM for *rctt* **43** and 0.9 μM for the *rccc* **44** (a 314-fold and 244-fold relative potency, respectively). This apparent absence of topology effects between the diastereoisomer presenting two ligands on one side

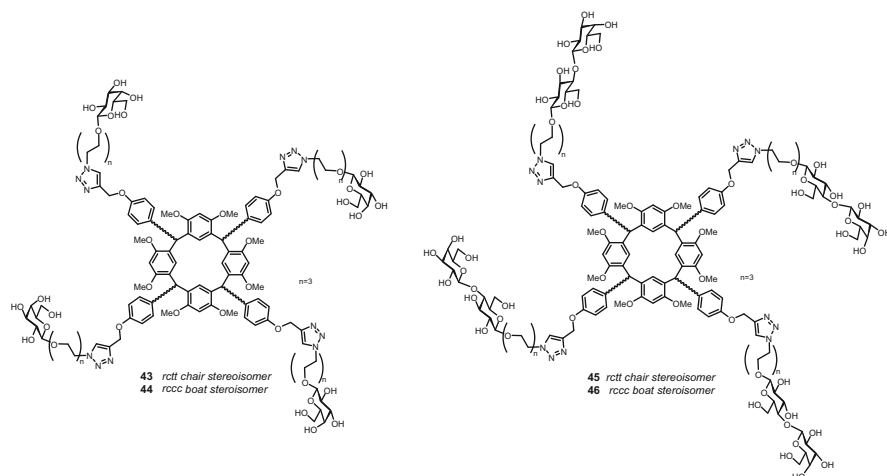


**Fig. 22.14** Resorcin[4]arenes for LecA binding

(*rctt*) and that which clusters all four on the same side (*rccc*) can be rationalised by molecular modelling. Although the core is of fixed shape, the spacer arms in these molecules are long and for both molecules it is possible for a chelate arrangement in which two sugars bind to neighbouring galactose binding site on LecA, as seen for the 1,3 alternate calix[4]arene **31**, to be adopted by both ligands. Unfortunately, the low solubility of the lactose ligands **45** and **46** precluded any binding studies with galectin 1.

The development of the pillar[5]arenes, [49] resulted in an interesting new flexible scaffold for the investigation of multivalent interactions and larger glycoclusters, as it can bear up to ten sugar residues without additional derivatisation. In two recent studies, [50, 51] sugar functionalised pillar[5]arenes have been investigated for their ability to bind to both LecA and LecB.

A series of decavalent and icosavalent fucose functionalised pillar[5]arenes **48**–**52** were evaluated against LecB (Fig. 22.15) [50]. From ELLA studies, nanomolar activity was observed for **48**–**52**; however, this represented only a moderate multivalent effect, compared with the high-affinity monomeric sugar, methyl  $\alpha$ -L-fucosepyranoside. Binding to LecB was shown to be enhanced with increase of spacer length between the core and sugar residue (**48** IC<sub>50</sub> 90 nM, **50** IC<sub>50</sub> 30 nM). More complex results were seen when increasing the valency, with **51** showing the highest activity of the series (IC<sub>50</sub> 6 nM), whilst this was reduced for the more flexible **52**. ITC gave an indication of binding stoichiometry, with the decavalent molecules interacting with seven to eight LecB monomers and the icosavalent derivatives interacting with ten. This may indicate aggregation of LecB monomers rather than multivalent clustering interactions.

The two galactosylated pillar[5]arenes **47** and **53** were both submicromolar inhibitors of LecA, when evaluated by ITC, with the more flexible **53** (featuring

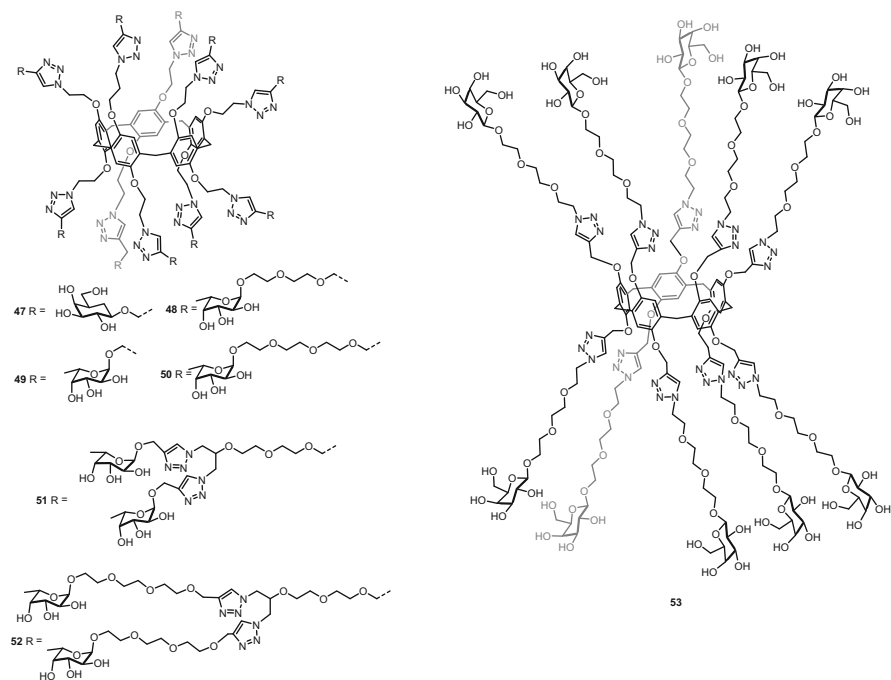


**Fig. 22.15** Pillar[5]arenes for LecA and Lec B binding

long spacer arms) showing higher binding affinity. Analysis of the stoichiometry of binding showed that the pillar[5]arene derivatives were interacting with five LecA monomers in both cases.

In a truly innovative approach, Nierengarten and co-workers [51] exploited the inclusion properties of pillar[5]arenes to prepare self-assembled rotaxane heteroglycoclusters, with the aim of inhibiting LecA and LecB concurrently. Two systems were investigated; a rotaxane featuring pillar[5]arene functionalised with galactose and threaded with an alkyl chain stoppered with fucose **54** and a fucose pillar[5]arene with galactose stoppers **55**. ITC studies indicated that simultaneous binding to both of the lectins was possible for each assembly; however, **54** proved the most effective. This can be rationalised by considering the different binding modes of the two lectins. Thus, when the stopper features galactose residues, these are unable to interact with the same LecA monomer, due to the presence of the wheel prohibiting folding of the alkyl chain, and no enhancement of binding due to multivalency can be achieved. In contrast, LecB is considerably less affected by multivalent binding and thus the single binding interaction of a fucose stopper still results in high-affinity binding. Additionally, the presence of ten galactose residues on the wheel in **54** favours multiple binding interactions to LecA, whereas no improvement, based on multivalency, is seen with the fucose wheel in **55** (Fig. 22.16).



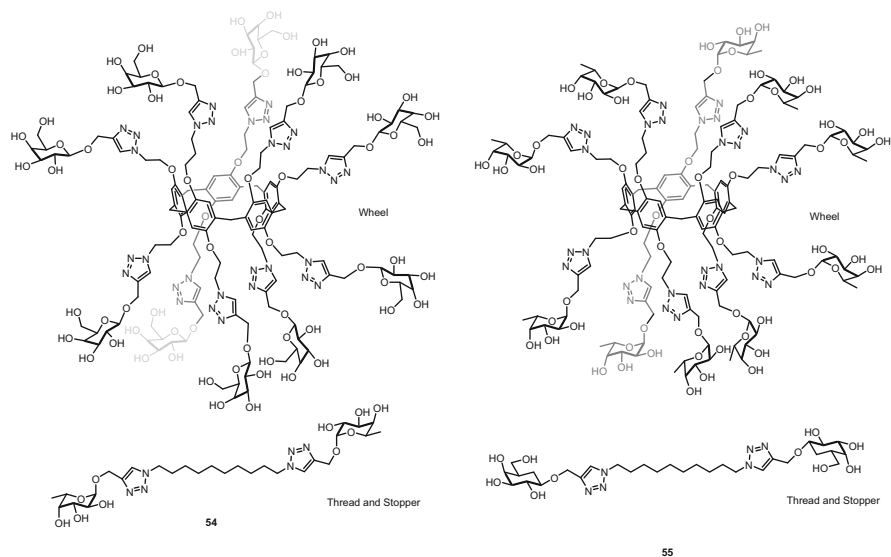
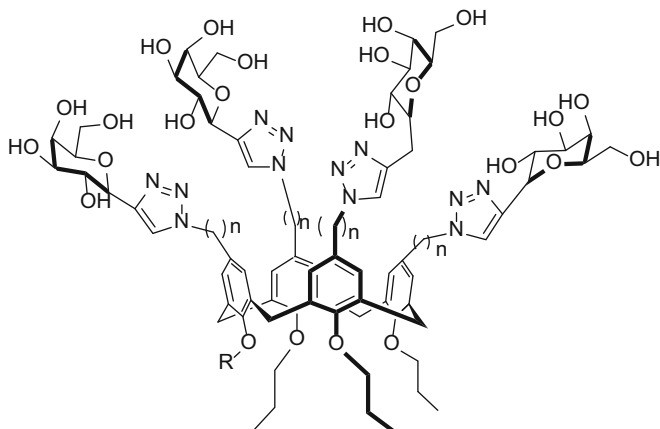


**Fig. 22.16** Pillar[5]arene rotaxanes for LecA and Lec B binding

LecA has also been used as a target in a study for assessing binding of lectins to sugar clusters using a DNA microarray [52]. Oligonucleotides, functionalised with either one or two alkynes to enable incorporation of monoazido functionalised calixsugars *via* CuACC were prepared and hybridised with complementary sequences adsorbed on a glass surface. Exposure of the slide to fluorescently labelled lectins then allowed an assessment of binding through fluorescence intensity. Two calixarenes **56** and **57** functionalised at the upper rim but varying in the spacer length to the oligonucleotide (Fig. 22.17), were evaluated along with a series of unclustered ligands for binding to LecA. Surprisingly, given the other results observed with galactose functionalised calixarenes, no binding of LecA was observed for either of these glycoclusters, which could be due to their clustering at the upper-rim and the shortness of the spacer, giving rise to steric issues in binding. In contrast, when the same array was exposed to RCA<sub>120</sub> a dimeric lectin, from *Ricinus communis*, featuring only two carbohydrate binding sites, [26] arrays functionalised with both **56** and **57** bound the lectin, although there was not a great difference in binding between the array containing one cluster and that containing two. Inhibition studies with lactose allowed an evaluation of relative binding enhancement per galactose residue compared to single ligands and showed a moderate enhancement of five to sevenfold.

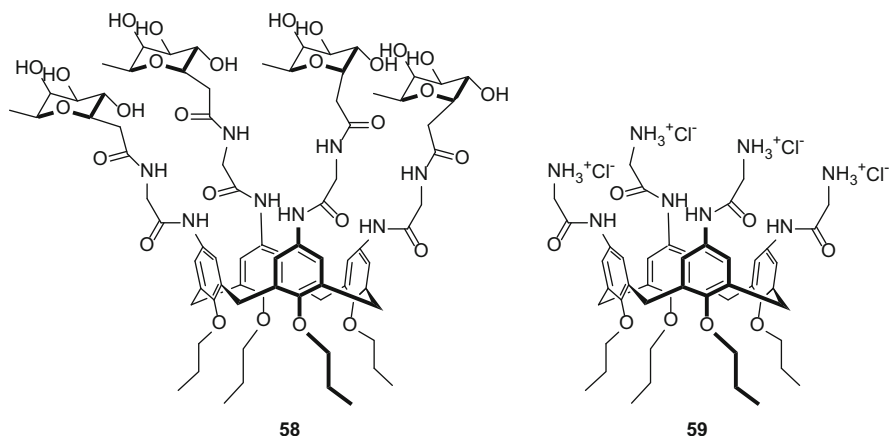
The potential to inhibit binding of cell surface fucose to LecB and thus disrupt biofilms has also been investigated by the group of Consoli and Geraci, [53] using a calix[4]arene fixed in the cone conformation with four  $\alpha$ -L-C-fucosyl units at the upper rim **58** (Fig. 22.18). Cell viability assays with planktonic *Pseudomonas aeruginosa* (wild type PAOI) confirmed the molecule has no direct antimicrobial



**56**  $n=3$ ,  $R = \text{CH}_2\text{CH}_2\text{N}_3$

**57**  $n=3$ ,  $R = \text{CH}_2\text{CONHCH}_2\text{CH}_2\text{OCH}_2\text{CH}_2\text{OCH}_2\text{CH}_2\text{OCH}_2\text{CH}_2\text{N}_3$

**Fig. 22.17** Calix[4]arenes for DNA array functionalisation



**58**

**59**

**Fig. 22.18** Calix[4]sugars for LecB biofilm disruption

activity. However, following pre-incubation, **58** was able to inhibit 73 % of biofilm formation at 200  $\mu\text{M}$  and 35 % at 12.5  $\mu\text{M}$ . Additionally, a control calixarene **59**, in which the sugar was absent, but bearing a charge was also effective at inhibiting the biofilm, probably as a result of cationic interactions, but to a lesser extent and only at higher concentrations. This offers up the interesting possibility of combining specific sugar binding interactions with non-specific charge-based interactions within a single molecule to enhance reduction of biofilm.

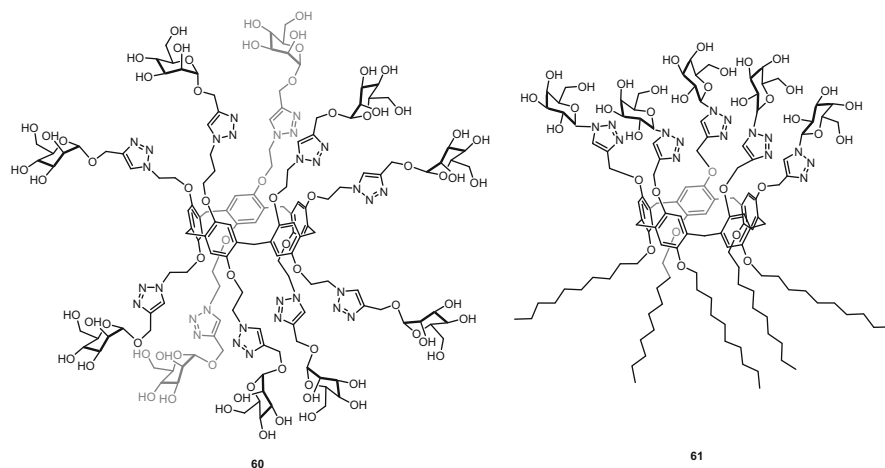


**Fig. 22.19** Pillar[5]arene sugar clusters

### 22.3.3.2 *Escherichia coli*

Nierengarten [54] first examined the potential of pillar[5]arenes as scaffolds for sugar clusters in a preliminary study on FimH, an adhesin lectin from *Escherichia coli* involved in binding to host cells. Whilst FimH is a monomeric lectin [55] and thus binding should not be enhanced by the ‘cluster effect’, it has been shown that multivalent ligands do give substantially better binding than monomeric ones potentially owing to the higher local concentration allowing a ‘bind and jump’ mechanism.

Haemagglutination inhibition assays with guinea pig erythrocytes using the decavalent mannose derivative **60** (Fig. 22.19) gave low  $\mu\text{M}$  values for the minimum inhibitory concentration ( $5.91 \mu\text{M}$ ), a 6.7-fold enhancement per mannose unit, compared to a monomeric control confirming the potential of multivalent ligands to aid binding even with monomeric lectins.

A complementary study by Huang [56], using galactose-functionalised pillar[5]arenes compared the activities of penta- and deca-valent glycoclusters in aggregating *Escherichia coli*. An interesting aspect of this study was the observation that self-assembly of **61** occurred in water. Whilst, it first assembled into vesicles of around 150 nm diameter, capable of including calcein, with a bilayer pillararene membrane, these reorganised, over 1 week, into nanotubes of 100–200 nm diameter and micrometer lengths. Both of the glycoclusters were non-toxic in lung cell lines but only **61** could cause agglutination of *E. coli* and thus inhibit its replication and growth, presumably through interaction of the galactose ligands with a range of lectins on the bacterial surface. Surprisingly, no aggregation effect was seen with the decavalent galactose cluster, which the authors proposed to be due to higher water-solubility.

### 22.3.3.3 *Burkholderia ambifaria*

BambL is a fucose selective lectin from *Burkholderia ambifaria*, which self-assembles into a trimeric  $\beta$ -propeller fold presenting six binding sites. Whilst the exact role of the lectin in infection has not been ascertained, it is believed to be of therapeutic relevance, as the bacterium is a component of the *Burkholderia cepacia* complex associated with acute and chronic respiratory disease [57].

ELLA studies of a series of fucose-functionalised pillar[5]arenes **48–52** (Fig. 22.15) with BambL revealed picomolar binding affinities and a large multivalent effect for all the ligands, compared with methyl  $\alpha$ -L-fucosepyranoside, with **52** being the most effective. When ITC and SPR were used, these results were diminished although the series still showed nanomolar  $K_D$  values demonstrating the importance of using multiple techniques in evaluating the biological activity of sugar clusters.

### 22.3.3.4 Cholera Toxin

The main physical symptoms of cholera infection are caused by the interaction of the pentavalent cholera toxin [58] produced by the *Vibrio cholerae* with intestinal epithelial cells and subsequent internalisation of the toxin. This sugar-protein interaction is between the cholera toxin B subunit (CTB), through both galactose and sialic acid residues of the oligosaccharide portion of the GM1 gangliosides; thus presentation of an alternative sugar cluster with higher binding strength will allow inhibition and stop internalisation. The group of Ungaro [59] first considered a non-topologically complementary calix[4]arene **62** functionalised at the upper-rim with just two sugar clusters as a potential inhibitor (Fig. 22.20). This cluster featured long spacers to enable interaction with non-adjacent binding sites on the protein and a modified sugar cluster featuring a pseudo-trisaccharide which had

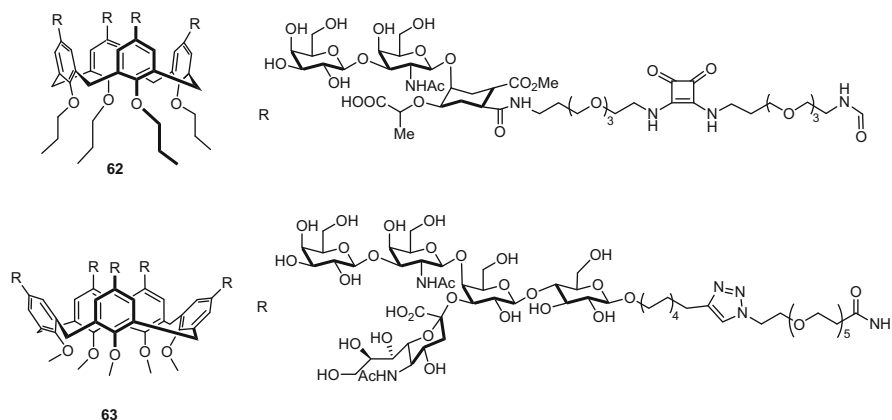


Fig. 22.20 Calixsugar ligands for cholera toxin

been shown to have very high affinity [58]. Fluorescence spectroscopy with CTB showed a 4,000-fold improvement in binding of the calixsugar compared with the single pseudo-trisaccharide, an improvement of 2,000-fold per binding arm, suggesting a role for multivalency. However, other platforms featuring two units have not shown such remarkable improvements and thus it appears that the properties of the calixarene scaffold are also playing a part.

A picomolar inhibitor [60] has subsequently been prepared based on a conformationally mobile calix[5]arene, which offers the ideal spatial arrangement for interaction with all five binding sites on the protein. The importance of both the galactose and sialic acid residues in binding was confirmed by evaluating glycoclusters featuring GM1os, a galactose deleted GM2os and two much simpler molecules featuring either galactose or lactose residues in an ELISA study with horseradish peroxidase labelled CTB. Whilst GM1os alone has an  $IC_{50}$  of 44  $\mu$ M, the pentavalent cluster **63** produced an exceptional  $IC_{50}$  of 450 pM, which rose significantly to 9  $\mu$ M when the galactose was deleted and to mM values with the simple sugars.

### 22.3.4 Cancer Chemotherapy

Lectins also play a significant role in the development of cancer, being implicated in processes including cell replication, migration and formation of metastases. Thus inhibiting these cell surface interactions offers an alternative approach to classical chemotherapy in the treatment of cancer.

In particular, the galactose- and lactose- binding galectins provide an interesting and difficult series of targets. Fifteen different human galectins have been identified which can be categorised as one of three types; the prototypes that feature a single carbohydrate binding domain but capable of dimerization *e.g.* galectin 1, the tandem repeat type with two binding sites on one chain *e.g.* galectin 4 and the chimera type *e.g.* galectin 3 [61]. Whilst some galectins are involved in progression of cancer, others can play protective roles, making selectivity in binding between the family a significant factor in using galectin inhibition in therapy.

These issues were addressed in a 2008 report [62] using a series of thiourea calixsugars featuring galactose or lactose residues (Fig. 22.21) (Table 22.1). By comparing calix[4]arenes in the cone and 1,3-alternate conformations and calix[6]arenes and calix[8]arenes, structural features for selectivity between VAA, galectin 1, galectin 3 and galectin 4 could be identified. In competitive studies, where the interaction of the lectin with solid-supported asialofetuin was challenged by addition of the glycoclusters, both VAA and galectin 4 showed good ability to selectively bind some clusters with strong affinity whilst galectin 1 and 3 were much less able to discriminate between the clusters. Thus for galectin 4, 300-fold improvements in binding could be seen over monomeric sugars. Interestingly, the two most effective ligands **64** and **65** showed little structural similarity, being based on a fixed

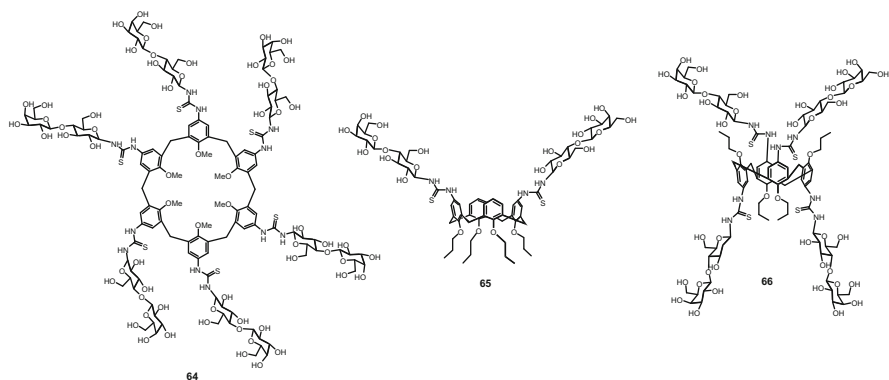


**Fig. 22.21** Galectin binding calixsugars

**Table 22.1** Inhibition of galectins by calixsugars

	IC <sub>50</sub> (μM)			
	VAA (0.5 μg mL <sup>-1</sup> )	Galectin 1 (10 μg mL <sup>-1</sup> )	Galectin 3 (5 μg mL <sup>-1</sup> )	Galectin 4 (5 μg mL <sup>-1</sup> )
<b>64</b>	15	600	400	5
<b>65</b>	1000	n.i.	2000	5
<b>66</b>	200	1250	500	80

<sup>a</sup>*n.i.* no inhibition

cone calix[4]arene or a conformationally mobile calix[6]arene, or density of presenting ligands, having either two or six lactose groups.

Flow cytometry studies with a range of human tumour cells lines allowed an assessment of the inhibition properties of the glycoclusters in a more realistic biological environment. In these studies, interactions with galectin 1 and galectin 3 were more readily observed and enhanced activities were observed compared to the solid-supported studies. Importantly, **66** was identified as a molecule that could inhibit binding of both galectin 1 and 4 to the cancer cell surface, whereas selectivity for galectin 4 was achieved with the conformationally mobile large calixarenes *e.g.* **64** in pancreatic cancer cells. For galectin 3, in colon cancer, the lactose-derivatised fixed cone calix[4]arene **65** was found to be the most effective ligand.

One way of enhancing selectivity further is the incorporation of designed high-affinity unnatural sugars onto the multivalent platform. This approach was exploited by the group of Ungaro [63], who introduced *N*-acetyllactosamine modified at the 2'-N, to enhance affinity, and 3' position, to impart some selectivity to galectin 3, to the upper-rim of both cone locked calix[4]arene and conformationally mobile calix[6]arene (Fig. 22.22). In solid supported studies, substantial gains could be observed for galectin 3, where introduction of the 3'-derivative resulted

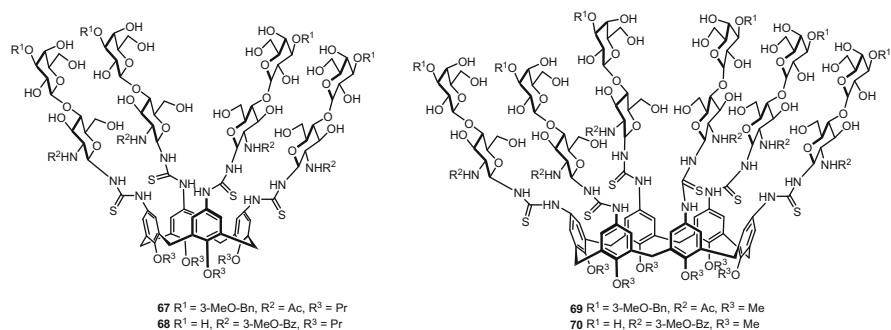


**Fig. 22.22** Galectin binding calixarenes featuring unnatural sugars

in a reduction of  $\text{IC}_{50}$  from 200  $\mu\text{M}$  [62] to 0.15  $\mu\text{M}$  for the calix[4]arene **67**; less effect was observed with molecules modified at the 2'-N position. Less variation in activity was seen for galectin 4 and 9, where all molecules showed good inhibition, in contrast to galectin 1 and 8, confirming that structural alterations in the sugar combined with varied presentation can provide highly selective ligands.

Calixarene **67** was confirmed as the best inhibitor of galectin 3 binding, using flow cytometry across a panel of cells, including colon carcinoma, but does not readily bind to galectin 1. This is an important result, given their opposing roles in pancreatic cancer, where galectin 3 is known to inhibit the actions of galectin 1 in promoting cell death. In contrast, for galectin 4 and 9, the hexavalent ligands **69–70** are the most effective.

A later study, [64] using click assembled glycoclusters, focused solely on galectin 3 inhibition. SPR studies with both lactose- and galactose-functionalised molecules in the cone and 1,3-alternate conformations confirmed that lactose was a more effective ligand for the galectin than galactose and that presentation of the lactose on a fixed-cone calixarene **71** gave the most activity (Fig. 22.23).

Galectin-1 binding has also been investigated for a family of conformationally fixed calix[4]arene ligands bearing lactose binding groups, to investigate whether binding is affected by topology [65]. Binding of **72–74** (Fig. 22.24) was studied both against galectin 1 and ECA using a combination of haemagglutination inhibition assays, ELLA and SPR. A modest effect of topology was observed for ECA with the cone **72** exhibiting no positive multivalent rise in binding whereas the 1,3-alternate **73** with an  $\text{IC}_{50}$  (ELLA) of 8.5  $\mu\text{M}$  showed a relative potency increase of 30. In contrast, as often seen when investigating interactions with multiple techniques, the results with galectin 1 are more complex. In the haemagglutination assay, there is marked preference for binding of the cone conformation **72** which showed a relative potency of 625, compared with a monomeric ligand whilst the partial cone **74** and 1,3 alternate **73** are poor ligands. However, these data were not replicated in SPR, which may be a consequence of the different presentation of galactose groups between the cell surface and the SPR slide. The distinct difference in the haemagglutination assay between the two lectins demonstrates once again

**Fig. 22.23** Galectin-3 binding calixsugar

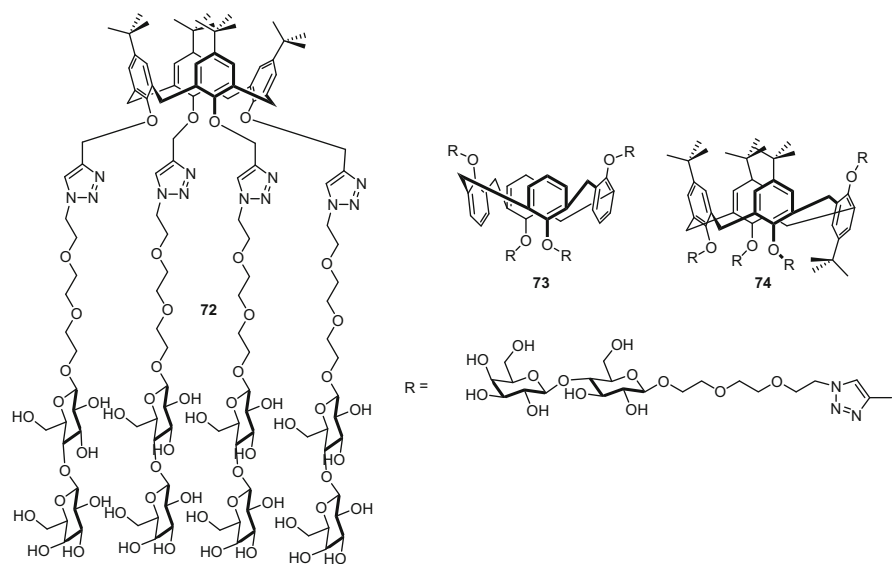
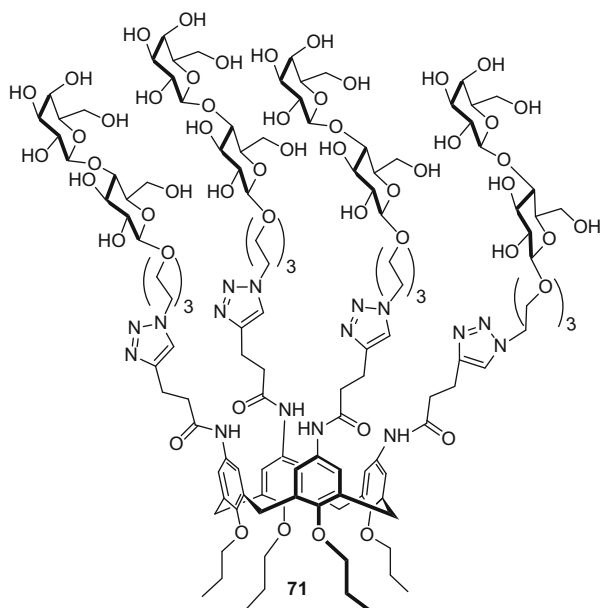


**Fig. 22.24** Galectin 1 binding calixsugars



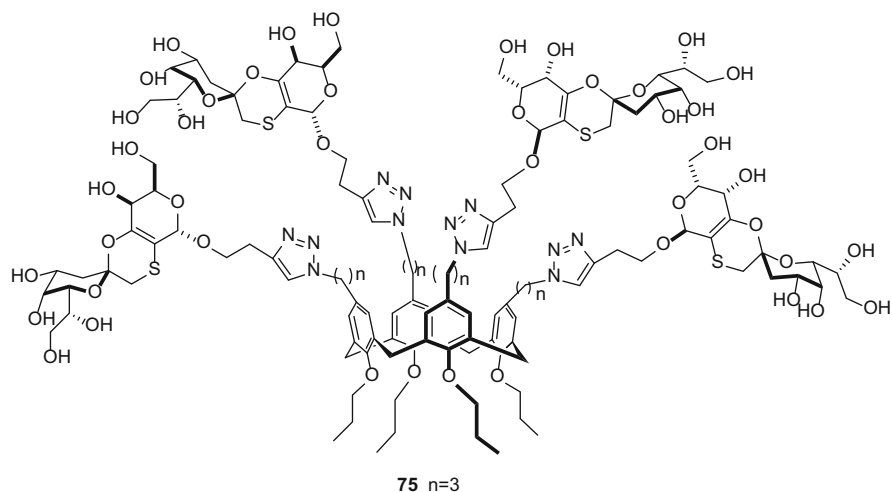


**Fig. 22.25** Calix[4]sugar for inhibition of metastases

that very similar lectins, in this case dimers presenting two lactose binding sites, can show a wide range of shape selectivity for multivalent ligands.

In a different approach, Nativi and co-workers [66] have examined the potential of calixarene glycoclusters to mimic tumour-associated antigens and thus reduce the adherence and migration of malignant melanoma cells, key roles in the formation of metastases. Whilst healthy melanocytes display gangliosides, in particular GM<sub>3</sub>, as part of their glycocalyx, in tumour cells an additional GM<sub>3</sub> lactone derivative is also observed. Building on their previous report on the development of a stable version of the lactone which, whilst being substantially chemically altered retained the shape and antibody raising characteristics of the lactone [67] they incorporated this modified unit onto the upper rim of a calix[4]arene to give calixsugar **75** (Fig. 22.25). This construct was able to interfere with adhesion of A375 malignant melanoma cells to endothelium cell matrix, showing a 33 % adherence after 24 h compared with 61 % in untreated cells. Similar results were seen in a model of cell migration, where a 60 % reduction was observed. Induction of apoptosis or anoikis was achieved with 32 % cell death, compared to 15 % for untreated cells. The importance of multivalency was demonstrated by comparison with monovalent molecules which showed no effect on adhesion, migration or cell death. Equally, the role of sugar specific structural interactions was confirmed by the absence of any biological activity in a calix[4]arene presenting four β-C-glucosides.

An important aspect of cell division and replication, features of development of cancer, is cell matrix adhesion, in which extracellular proteins interact with cell-surface integrins [68]. Chondroitin sulfate, a class of proteoglycans, has been shown to interfere with cell adhesion and thus mimics could offer a therapeutic intervention. Using their established resorcin[4]arene platform, Aoyama and

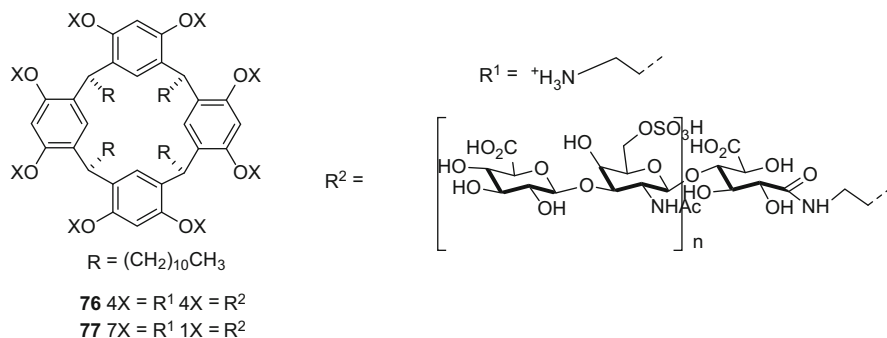


**Fig. 22.26** Resorcin[4]arene based chondroitin clusters

co-workers [69] have prepared clusters featuring these large, 40,000–80,000 Da MW chondroitin sulfate residues. Unsurprisingly, probably due to steric reasons, it is not possible to introduce eight of these residues to a single resorcin[4]arene, rather clusters featuring either one or four ligands can be prepared (Fig. 22.26). Whilst baby hamster kidney cells normally adhere well to a fibronectin pate and undergo adhesion-related expansion, no expansion is observed in the presence of **76** indicating that adhesion is inhibited. The monofunctionalised resorcin[4]arene **77** is not effective, nor are the proteoglycan precursors, suggesting that multivalency is of importance in inhibiting cell-fibronectin interactions. Interestingly, **76** is more effective than previously prepared polymeric derivatives, demonstrating a positive effect due to structural clustering.

At this point, it is also appropriate to discuss a paper published in 2007 [70] but which has subsequently been retracted, which evaluated the ability of calix[4]arenes derivatised with GlcNAc to stimulate natural killer cells through activation of CD69 receptors. Whilst the synthesis of the compounds is not in any way disputed, the biological claims, binding of the ligands to the CD69, have been deemed to be falsified.

### 22.3.5 Drug Delivery

The preparation of calixsugars which are able to interact specifically with cell-surface receptors, which internalise on binding, raises the possibility of using the clusters to aid drug delivery to certain cell types either through formation of inclusion complexes or covalent attachment of the drug.

Aoyama investigated the inclusion potential of resorcin[4]arenes through encapsulation of fluorescent dyes. In a preliminary study, [71] it was shown that the glucose cluster **4** and galactose cluster **2** (Fig. 22.2) were able to encapsulate eosin Y in a 1:1 manner. Cluster **4** could readily bind to sepharose gel-supported ConA as a model of a surface cell and thus present the ‘drug’ for uptake. Taking this further,

[72] they showed, through fluorescence imaging, that the galactose clusters **2**, encapsulating phloxin B or calcein, can specifically interact with rat hepatoma cells expressing the galactose-binding asialoglycoprotein. Delivery of the fluorescent dyes does not occur in mouse spleen cells that do not express a galactose binding lectin or with the glucose cluster in either the rat hepatoma or mouse spleen cells, showing the importance of the specific lectin-sugar interaction.

The group of Casnati, has evaluated a number of different approaches to achieving sugar-mediated site-specific drug delivery with calixarene scaffolds. In a proof-of-concept study [73] using the 1,3-alternate glucosylcalixarene **78**, liposomes were prepared in which the bola-amphiphile (Fig. 22.27), with its two hydrophilic head groups, was incorporated in the bilayer with 1,2-dioleoyl-*sn*-glycero-3-phosphocholine (DOPC). These liposomes could efficiently incorporate calcein and, in comparison to liposomes formed from DOPC alone, a reduced rate of release, to *ca.* 50%, was observed, raising the possibility of development of a sustained release formulation. Enhanced lectin interactions, compared to those observed for single molecules, were observed both in binding of fluorescein labelled ConA, where the liposome incorporating calixarene inhibited fluorescence of the lectin at low concentrations, and in turbidity studies which showed full aggregation and precipitation after 24 h. It will be interesting to see whether this system can be developed further and assessed in cellular experiments.

Gold nanoparticles, like liposomes, have also drawn attention for selective cell delivery; however, there has only been a single report of using calixsugars as the targeting moiety for the particles [74]. Gold nanoparticles coated in dodecanethiol could additionally be functionalised with the mannose calix sugar **79** through non-covalent hydrophobic intercalation with the calixarene lower-rim alkyl chain (Fig. 22.28). Interestingly it was possible, through using the calixarene scaffold to incorporate higher surface levels of mannose than with a single sugar ligand **80**. Uptake into mannose receptor expressing HeLa cells was enhanced for the coated

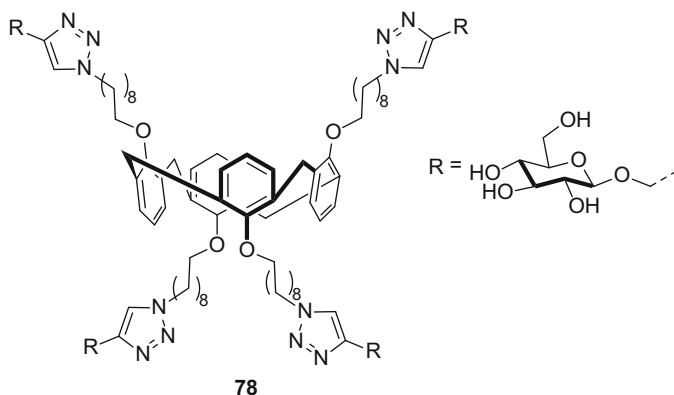
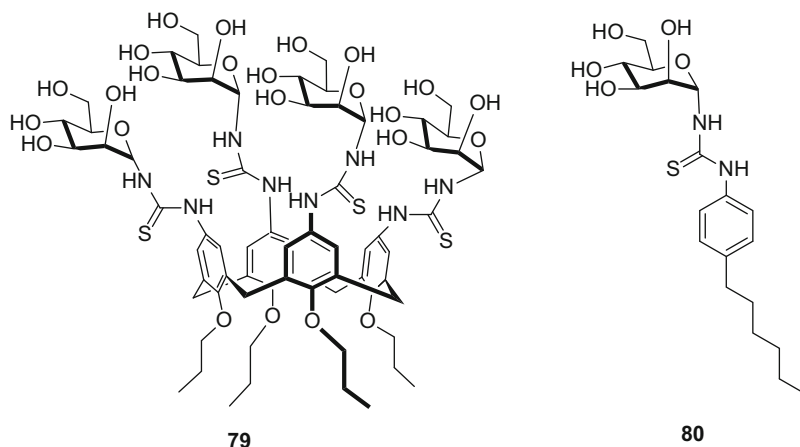


Fig. 22.27 Calix[4]sugar bola-amphiphile



**Fig. 22.28** Mannose calix[4]arene for functionalisation of nanoparticles

nanoparticles. A threefold increase was observed between those coated with **79** over those with **80**. This cannot be accounted for by the difference in loading raising the possibility of this being aided by the effective high local concentration allowing a ‘bind and jump’ mechanism.

Interestingly, the uptake is significantly reduced in the presence of dextran, which inhibits binding to the mannose receptor, suggesting that the nanoparticles are only readily taken up by RME and thus a high level of cell-specificity could be achieved in cells where only passive endocytosis mechanisms were available. A significant issue with using all nanoparticle systems is their interaction, and thus coating, with body proteins which can lead to deactivation of targeting moieties; [75] however, in this case significantly fewer interactions with bovine serum albumin are seen compared with nanoparticles with other surface targeting agents and thus it can be considered to be a ‘stealth’ system.

Preparing dimers of calixarenes and cyclodextrins **81** (Fig. 22.29) offers the potential to develop self-assembled nanoparticles in which a drug could be incorporated within the calixarene nanoparticle core and targeting could be achieved by exploiting the strong inclusion properties of cyclodextrins for adamantane terminated ligands [76]. Gallego-Yerga et al. [77] described such a system using docetaxel, an anti-mitotic chemotherapeutic, as a model drug and a tri-antennary mannosepyranosyl ligand as a targeting moiety and investigated its binding with the macrophage mannose receptor. DLS and AFM studies suggested that the dimers first associated into small nanospheres containing 17–25 units and subsequently aggregated into particles of over 100 nm diameter, containing around 60 nanospheres. Incorporation of docetaxel resulted in a bimodal drug release profile that could be accounted for by the drug not only incorporating in the calixarene core, giving a sustained release character, but also being bound by the surface cyclodextrins, from which it could be released more readily. This release

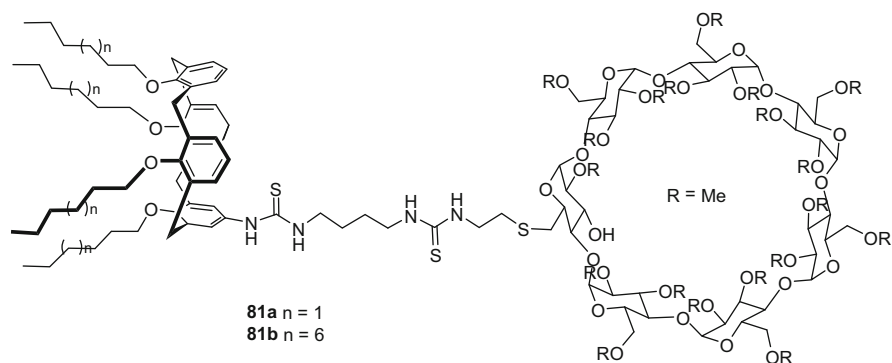


**Fig. 22.29** Calix[4]arene:cyclodextrin dimers

was also modulated by the nature of the calixarene lower-rim substituent, offering the possibility of tailoring release rate. ELLA assays with the mannose receptor showed the expected enhanced binding of particles with the mannosepyranosyl ligands over those without, as high as 46-fold for **81b**.

### 22.3.6 Vaccines

The ability of a calixarene-based glycocluster to stimulate the immune system and thus to act as an anti-cancer vaccine was investigated by Geraci [78]. In a range of epithelial cells cancers, the mucin glycoprotein profile is changed due to incomplete glycosylation and chain termination [79]. These changes affect both cell adhesion and migration and thus are important in the spread of cancer. The altered glycoproteins are able to act as antigens, *e.g.* Tn antigen; however, they are insufficiently strong to allow a full immune response. By preparing glycoclusters that mimic these antigens, antibodies can be more effectively raised to the antigens and thus a therapeutic immune response could be possible. Glycoclusters are particularly attractive as higher affinity is seen between antibodies and clusters than with simple monomers.

Calixsugar **82** (Fig. 22.30) featuring a cluster of S-Tn residues at the upper rim to mimic the antigen and a tripalmitoyl-S-glycerylcysteinylserine at the lower rim, as an immunoadjuvant to stimulate activation of cytokines and chemokines was tested for the ability to raise antibodies in mice. Both the cluster and a monomeric molecule were effective in raising antibodies, however **82** was active at a twofold higher dilution than the same concentration of sugar ligands as in the monomeric system indicating a major role for the clustering of the Tn residues onto the calixarene core.

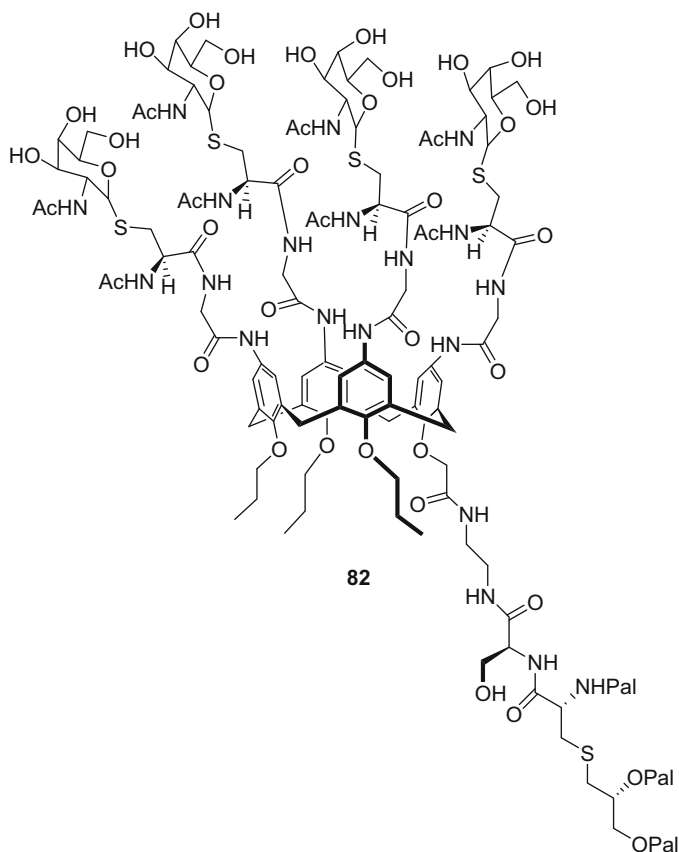


Fig. 22.30 Calixarene vaccine

## 22.4 Enzyme Inhibition

Enzymes have only recently been considered as targets for multivalent ligands due to their single, usually inaccessible, binding sites; and thus most research has focused on the preparation of small molecule monovalent inhibitors. Recently, however, [11] considerable interest has arisen in the use of multivalent probes for sugar-binding enzymes including glycosidases and glycosyltransferases. Improvements in inhibitory binding have been seen, but also enhancements of selectivity especially for glycosidases.

Whilst it is possible that the enhancement in binding is a result of chelation or a combination of an increased local concentration facilitating a 'bind and jump' mechanism as seen with lectins, specific binding modes for glycosidases have been proposed. In particular, the presence of non-catalytic carbohydrate binding sites on the enzyme may allow a multivalent cluster to bind at more than one site [10].

### 22.4.1 Anti-parasitic Drugs

Trypanosomal infection is responsible for a range of tropical diseases, with *Trypanosoma cruzi* being the cause of Chaga's disease (American trypanosomiasis), a major course of morbidity and mortality in Latin America. Inhibition of the cell surface transialidase TcTS by lactose-containing molecules has been proposed as a mechanism of limiting infection and its multiple expression suggested that the use of multivalent ligands could be beneficial [80]. A family of lactose-containing calixsugars **83–86** was prepared using CuAAC, [81] functionalised at the lower or upper rim or both, fixed in the cone or partial cone conformation and with variable spacer lengths (Fig. 22.31). Of these the most effective, showing  $\mu\text{M}$  activity ( $\text{IC}_{50}$  68  $\mu\text{M}$ ) comparable with the current prescription treatment benznidazole, was the cone derivative **85** in whole trypanosome experiments with the host infectious trypomastigote form of *T. cruzi* Y strain. Activity was clearly related to topology as the isomeric partial cone showed very low activity even at the highest concentration (1 mM) giving an apparent  $\text{IC}_{50}$  of 1.60 mM.

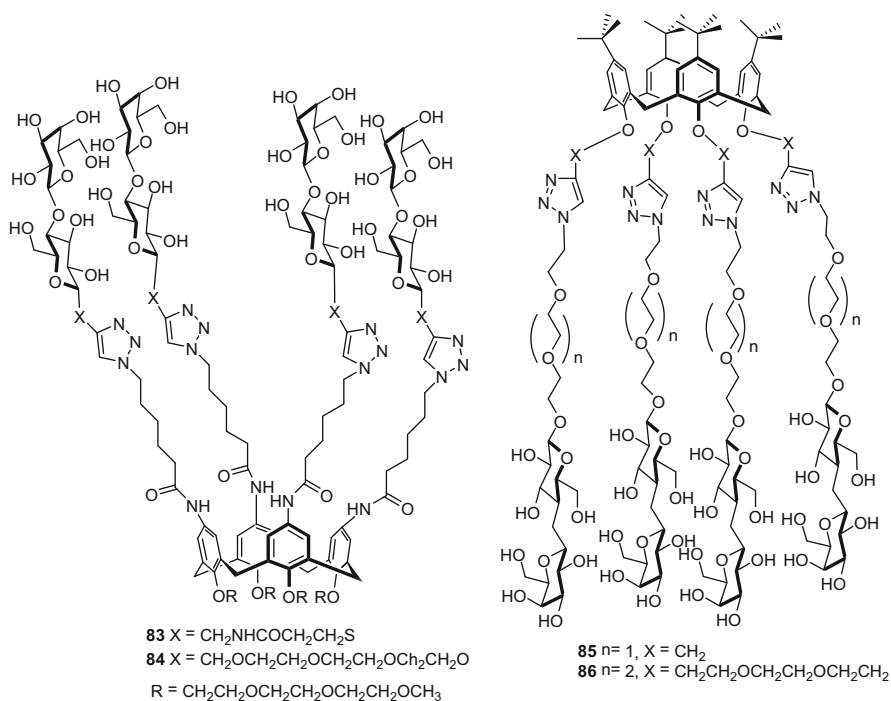


Fig. 22.31 Anti-trypanosomal calixsugars

## 22.4.2 Cancer Therapy

Consoli and co-workers have probed the potential of calixsugars in cancer through an investigation into the inhibition of  $\beta$ -1,4-galactosyltransferases, cell-surface enzymes that have been shown to be overexpressed in glioma and involved in cell migration [82]. Specifically, their role is to galactosylate GlcNAc residues on branched oligosaccharides and evidence of their activity can be obtained through the extent of phosphorylation of focal adhesion kinase (FAK), part of the cell signalling pathway. The previously described calix[8]arene GlcNAc cluster **87** (Fig. 22.32) was effective in reducing wound closure and hence cell migration in a wound model, whilst no effect was seen for a simple butylureido calixarene. Additionally, it was shown through Western blot and immunocytochemistry, to reduce the rate of FAK phosphorylation and thus it has an effect on downstream cell signalling. A surprising result from this and subsequent studies [83] is that both the sugar-functionalised and the urea-functionalised calixarene have an effect on cell proliferation, measured through MTT assays, where, rather than inducing apoptosis, cells are halted in the S phase through affecting growth factor signalling. This cannot be achieved by high concentrations of GlcNAc or by a calixarene without upper-rim ureas and thus must be related to the presence of the ureas and not to a specific binding interaction of the sugars.

The effects observed may also be due to additional aggregation at biologically relevant pH. A DLS study [84] on calix[8]arenes **87** and **88** showed that both formed stable vesicles between pH 4.5 and pH 12 of between 100 and 200 nm mean hydrodynamic radius which collapsed at pH 3–5 nm into micellar structures.

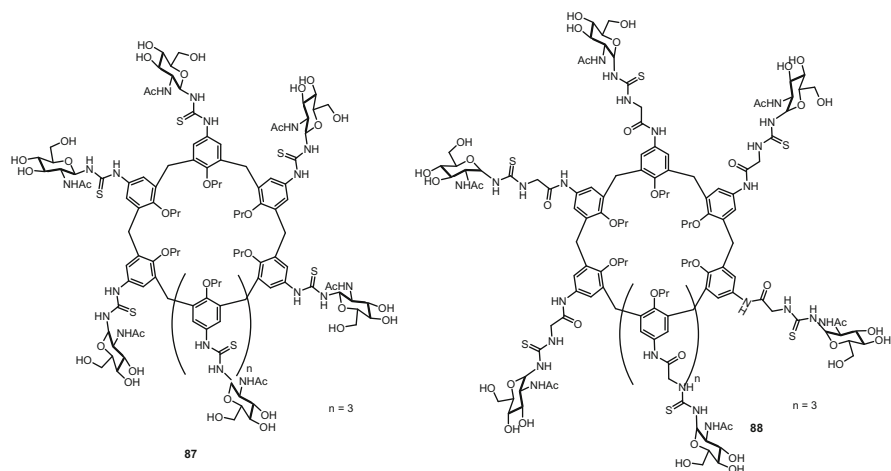


Fig. 22.32 Calix[8]sugars for inhibition of cell migration



### 22.4.3 Iminosugars

Whilst some early studies [85, 86] focused only on the difficult synthesis of iminosugar calixarene clusters, more recently preparation by CuAAC [87, 88] has allowed access to derivatives that could be assessed for their biological activity.

Iminosugar inhibitors of glycosidases [89] offer a very attractive target for the development of drugs for a range of diseases, including cancer, viral infections and inherited lysosomal storage disorders. Currently, two derivatives of the natural product, 1-deoxynojirimycin (DNJ), have been licenced, [90] miglitol for type II diabetes, through inhibiting intestinal  $\alpha$ -1,4-glycosidases and thus carbohydrate degradation and miglustat [91] for type 1 Gaucher's disease and Niemann-Pick type C, lysosomal storage disorders, where it prevents build-up of glucosylceramide by inhibiting glucosylceramide synthase. Additionally, migalastat, [89] a treatment for Fabry's disease, where it stabilises inherited mutant  $\alpha$ -galactosidase A, is undergoing currently licensing procedures in the EU and US following successful clinical trials.

A particularly relevant target in cancer chemotherapy is the Golgi  $\alpha$ -mannosides family, where inhibition has been shown to reduce tumour growth and inhibit the formation of metastases [89]. However, most early candidate molecules, including the plant natural product swainsonine also inhibit lysosomal  $\alpha$ -mannosides resulting in an unacceptable mannosidosis. Two calixsugars functionalised with DNJ, [87] one in the cone conformation **89** and one in the 1,3-alternate conformation **90**, were compared with conjugates prepared from other platforms including porphyrin, cyclodextrin and mono- and di-saccharides in their ability to inhibit a range of glycosidases (Fig. 22.33). Substantial differences were seen between different glycosidases and also between the same glycosidase from different species (Table 22.2). The jack bean  $\alpha$ -mannoside has been used extensively as a model enzyme for therapeutically relevant mannosides and, in this binding screen, **80** was highly effective in binding showing a relative enhancement per sugar of 67, exceeded only by a tetraporphyrin derivative at 200. Jack bean  $\alpha$ -galactosidase has previously been shown to be inhibited by copper and, as these clusters are prepared by CuACC, some residual copper may still be included; however, under the assay conditions used, control experiments with high concentrations of copper did not affect activity and thus it could be confirmed that the inhibition observed is from the specific sugar-binding events.

An understanding of how the clusters bind with the enzymes was obtained through AFM studies, whilst the 1,3-alternate **90** assembles the protein into rectilinear arrays as seen previously with the galactose functionalised analogue and LecA, the cone conformer **89** instead results in the formation of large open circular arrays. The role of sugar binding in formation of the array was confirmed by the absence of assembled structures in the AFM of  $\alpha$ -glucosidase and  $\beta$ -galactosidase treated with the calixarenes.

Unfortunately, despite the good result with jack bean  $\alpha$ -mannoside, **89** showed no inhibitory activity on either Golgi  $\alpha$ -mannoside or lysosomal  $\alpha$ -mannosides

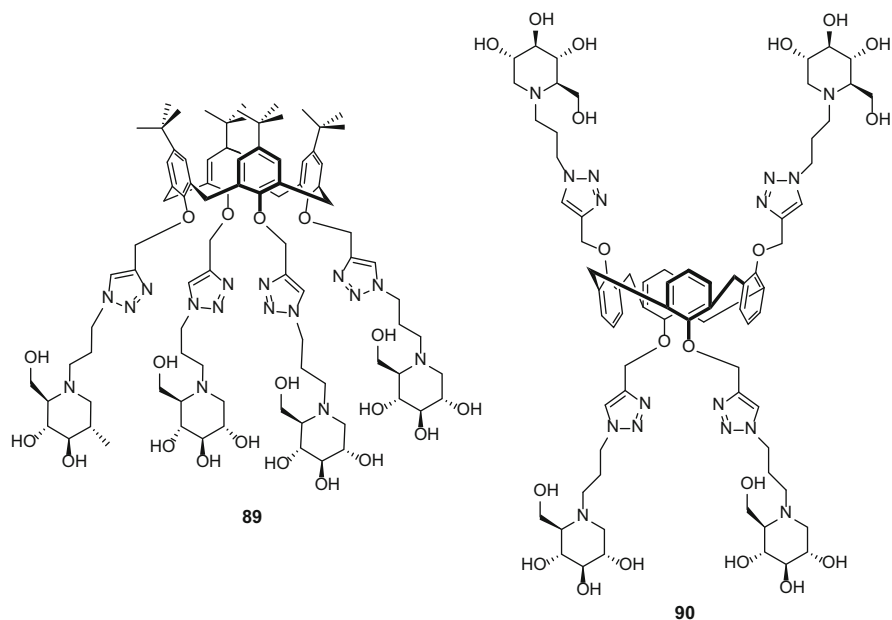


Fig. 22.33 Calixsugars for inhibition of glycosidases

from *Drosophila melanogaster*, confirming the high specificity and selectivity of enzymes of this type despite high sequence homology.

Following from this work, Marra and co-workers [88] described the synthesis of tetra DNJ substituted cone calix[4]arene conjugates at the upper-rim and lower-rim (Fig. 22.34). These were assessed for their ability to inhibit turnover of *p*-nitrophenol glycoside by a panel of glycosidases. Again, marked selectivity, compared with the monovalent iminosugar was observed. **91**, **93** were able to inhibit  $\alpha$ -mannosidase,  $\alpha$ -galactosidase and  $\alpha,\alpha$ -trehalase, although significant enhancement (sevenfold) based on the multivalency was only seen for **93**, but were unable to inhibit  $\alpha$ -glucosidase and  $\beta$ -glucosidase.

## 22.5 Conclusion

Calixsugars show promise in a wide range of therapeutic applications, increasing the likelihood of a successful treatment or delivery system reaching the clinic within the next 10 years. The recent expansion in the range of therapeutic targets, such as the development of enzyme inhibitors, opens up new avenues for biological evaluation. However, recent experiments *in vivo* have highlighted that even ligands with high specificity *in vitro* require higher than expected concentrations to exert

**Table 22.2** Glycosidase inhibitory activities

	<i>K<sub>i</sub></i> ( $\mu$ M)							
	$\beta$ -galactosidase (bovine liver)	$\beta$ -galactosidase ( <i>E. coli</i> )	$\alpha$ -galactosidase (green coffee)	$\beta$ -glucosidase (almonds)	$\alpha$ -glucosidase (baker's yeast)	$\alpha$ -mannosidase (jack bean)	$\beta$ -mannosidase (helix pomatia)	
<b>89</b>	38 $\pm$ 4	n.i.	24 $\pm$ 2	n.i.	585 $\pm$ 59	1.5 $\pm$ 0.2	n.i.	
<b>90</b>	58 $\pm$ 6	n.i.	36 $\pm$ 4	729 $\pm$ 87	45 $\pm$ 4	20 $\pm$ 2	n.i.	

*n.i.* no inhibition

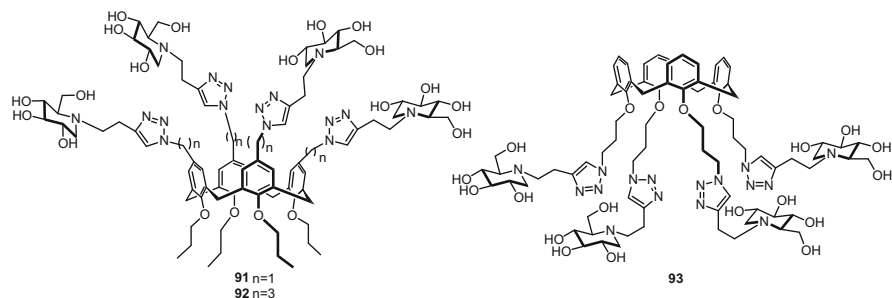


**Fig. 22.34** Iminosugar calixarenes

therapeutic responses, owing to the complex competing processes in animals and thus selection of appropriate candidates will be key for this to be achieved.

## References

1. Yousaf, A.; Abd Hamid, S.; Bunnori, N. M.; Ishola, A. A. *Drug Des. Dev. Ther.* **2015**, *9*, 2831–2838.
2. Sun, J.; Blaskovich, M. A.; Jain, R. K.; Delarue, F.; Paris, D.; Brem, S.; Wotoczek-Obadia, M.; Lin, Q.; Coppola, D.; Choi, K.; Mullan, M.; Hamilton, A. D.; Sebtí, S. M. *Cancer Res.* **2004**, *64*, 3586–3592.
3. Astorgues-Xerri, L.; Riveiro, M. E.; Tijeras-Raballand, A.; Serova, M.; Rabinovich, G. A.; Bieche, I.; Vidaud, M.; de Gramont, A.; Martinet, M.; Cvitkovic, E.; Faivre, S.; Raymond, E. *Eur. J. Cancer* **2014**, *50*, 2463–2477.
4. Tsou, L. K.; Dutschman, G. E.; Gullen, E. A.; Telpoukhovskaia, M.; Cheng, Y.-C.; Hamilton, A. D. *Bioorg. Med. Chem. Lett.* **2010**, *20*, 2137–2139.
5. Mourer, M.; Massimba Dibama, H.; Fontanay, S.; Grare, M.; Duval, R. E.; Finance, C.; Regnouf-de-Vains, J.-B. *Bioorg. Med. Chem.* **2009**, *17*, 5496–5509; Mourer, M.; Massimba Dibama, H.; Constant, P.; Daffé, M.; Regnouf-de-Vains, J.-B. *Bioorg. Med. Chem.* **2012**, *20*, 2035–2041.
6. Bagnacani, V.; Sansone, F.; Donofrio, G.; Baldini, L.; Casnati, A.; Ungaro, R. *Org. Lett.* **2008**, *10*, 3953–3956; Bagnacani, V.; Franceschi, V.; Bassi, M.; Lomazzi, M.; Donofrio, G.; Sansone, F.; Casnati, A.; Ungaro, R. *Nature Comm.* **2013**, *4*, 1721; Rodik, R. V.; Klymchenko, A. S.; Jain, N.; Miroshnichenko, S. I.; Richert, L.; Kalchenko, V. I.; Mély, Y. *Chem. Eur. J.* **2011**, *17*, 5526–5538.
7. Consoli, G. M. L.; Granata, G.; Fragassi, G.; Grossi, M.; Sallese, M.; Geraci, C. *Org. Biomol. Chem.* **2015**, *13*, 3298–3307; Guo, D.-S.; Wang, K.; Wang, Y.-X.; Liu, Y. *J. Am. Chem. Soc.* **2012**, *134*, 10244–10250.
8. Dondoni, A.; Marra, A. *Chem. Rev.* **2010**, *110*, 4949–4977; Fulton, D. A.; Stoddart, J. F. *Bioconjug. Chem.* **2001**, *12*, 655–672; Sansone, F.; Casnati, A. *Chem. Soc. Rev.* **2013**, *42*, 4623–4639.
9. Kiessling, L. L.; Gestwicki, J. E.; Strong, L. E. *Curr. Opin. Chem. Biol.* **2000**, *4*, 696–703; Lee, Y. C.; Lee, R. T. *Acc. Chem. Res.* **1995**, *28*, 321–327; Mammen, M.; Choi S.-K., Whitesides, G. M. *Angew. Chem. Int. Ed.* **1998**, *37*, 2754–2794.
10. Lundquist, J. J.; Toone, E. J. *Chem. Rev.* **2002**, *102*, 555–578.
11. Gouin, S. G. *Chem. Eur. J.* **2014**, *20*, 11616–11628; Compain, P.; Bodlenner, A. *ChemBioChem* **2014**, *15*, 1239–1251

12. Kolb, H. C.; Finn, M. G.; Sharpless, K. B. *Angew. Chem. Int. Ed.* **2001**, *40*, 2004–2021; Tornøe, C. W.; Christensen, C.; Meldal, M. *J. Org. Chem.* **2002**, *67*, 3057–3064.
13. Büning, H. *EMBO Mol Med.* **2013**, *5*, 1–3.
14. Seow, Y.; Wood, M. J. *Mol. Ther.* **2009**, *17*, 767–777; Yin, H.; Kanasty, R. L.; Eltoukhy, A. A.; Vegas, A. J.; Dorkin, J. R.; Anderson, D. G. *Nat. Rev. Genet.* **2014**, *15*, 541–555.
15. Hayashida, O.; Mizuki, K.; Akagi, K.; Matsuo, A.; Kanamori, T.; Nakai, T.; Sando, S.; Aoyama, Y. *J. Am. Chem. Soc.* **2003**, *125*, 594–601.
16. Aoyama, Y. *Chem. Eur. J.* **2004**, *10*, 588–593.
17. Hayashida, O.; Kato, M.; Akagi, K.; Aoyama, Y. *J. Am. Chem. Soc.* **1999**, *121*, 11597–11598.
18. Hayashida, O.; Matso, A.; Aoyama, Y. *Chem. Lett.* **2001**, 272–273.
19. Aoyama, Y.; Kanamori, T.; Nakai, T.; Sasaki, T.; Horiuchi, S.; Sando, S.; Niidome, T. *J. Am. Chem. Soc.* **2003**, *125*, 3455–3457.
20. Nakai, T.; Kanamori, T.; Sando, S.; Aoyama, Y. *J. Am. Chem. Soc.* **2003**, *125*, 8465–8475.
21. Aoyama, Y. *Trends Glycosci. Glycotech.* **2005**, *17*, 39–47.
22. Yamazakia, N.; Kojima, S.; Bovin, N.V.; André, S.; Gabius, S.; Gabius, H.-J. *Adv. Drug Del. Rev.* **2000**, *43*, 225–244.
23. Boussif, O.; Lezoualch, F.; Zanta, M. A.; Mergny, M. D.; Scherman, D.; Demeneix, B.; Behr, J.-P. *Proc. Natl. Acad. Sci. U.S.A.* **1995**, *92*, 7297–7301; Behr, J.-P. *Chimia*, **1997**, *51*, 34–36.
24. Horiuchi, S.; Aoyama, Y. *J. Cont. Rel.* **2006**, *116*, 107–114.
25. Sansone, F.; Baldini, L.; Casnati, A.; Ungaro, R. *Supramol. Chem.* **2008**, *20*, 161–168.
26. Wittmann, V.; Pieters, R. J. *Chem. Soc. Rev.* **2013**, *42*, 4492–4503.
27. Ambrosi, M.; Cameron, N. R.; Davis, B. G. *Org. Biomol. Chem.* **2005**, *3*, 1593–1608.
28. Meunier, S. J.; Roy, R. *Tetrahedron Lett.* **1996**, *37*, 5469–5472.
29. Hayashida, O.; Shimizu, C.; Fujimoto, T.; Aoyama, Y. *Chem. Lett.* **1998**, 13–14.
30. Hayashida, O.; Nishiyama, K.; Matsuda, Y.; Aoyama, Y. *Tetrahedron Lett.* **1999**, *40*, 3407–3410.
31. Sansone, F.; Chierici, E.; Casnati, A.; Ungaro, R. *Org. Biomol. Chem.* **2003**, *1*, 1802–1809.
32. Roy, R.; Kim, J. M. *Angew. Chem. Int. Ed.* **1999**, *38*, 369–372.
33. Consoli, G. M. L.; Cunsolo, F.; Geraci, C.; Mecca, T.; Neri, P. *Tetrahedron Lett.* **2003**, *44*, 7467–7470.
34. Consoli, G. M. L.; Cunsolo, F.; Geraci, C.; Sgarlata, V. *Org. Lett.* **2004**, *6*, 4163–4166.
35. Yang, J.; Li, M.; Shen, X.; Liu, S. *Viruses* **2013**, *5*, 352–373; Air, G. M. *Curr. Op. Virology* **2014**, *7*, 128–133.
36. Fujimoto, K.; Hayashida, O.; Aoyama, Y.; Guo, C.-T.; Jwa Hidari, K. I.-P.; Suzuki, Y. *Chem. Lett.* **1999**, 1259–1260.
37. Marra, A.; Moni, L.; Pazzi, D.; Corallini, A.; Bridi, D.; Dondoni, A. *Org. Biomol. Chem.* **2008**, *6*, 1396–1409.
38. Dalianis, T.; Hirsch, H. H. *Virology* **2013**, *437*, 63–72.
39. Cecioni, S.; Imberty, A.; Vidal, S. *Chem. Rev.* **2015**, *115*, 525–561; Bernardi, A.; Jiménez-Barbero, J.; Casnati, A.; De Castro, C.; Darbre, T.; Fieschi, F.; Finne, J.; Funken, H.; Jaeger, K.-E.; Lahmann, M.; Lindhorst, T. K.; Marradi, M.; Messner, P.; Molinaro, A.; Murphy, P. V.; Nativi, C.; Oscarson, S.; Penadés, S.; Peri, F.; Pieters, R. J.; Renaudet, O.; Reymond, J.-L.; Richichi, B.; Rojo, J.; Sansone, F.; Schäffer, C.; Turnbull, W. B.; Velasco-Torrijos, T.; Vidal, S.; Vincent, S.; Wennekes, T.; Zuillhof, H.; Imberty, A. *Chem. Soc. Rev.* **2013**, *42*, 4709–4727; Audfray, A.; Varrot, A.; Imberty, A. *Comp. Rend. Chimie* **2013**, *16*, 482–490.
40. Loris, R.; Tielker, D.; Jaeger, K.-E.; Wyns, L. *J. Mol. Biol.* **2003**, *331*, 861–870.
41. Boukerb, A. M.; Rousset, A.; Galanos, N.; Méar, J.-B.; Thépaut, M.; Grandjean, T.; Gillon, E.; Cecioni, S.; Abderrahmen, C.; Faure, K.; Redelberger, D.; Kipnis, E.; Dessein, R.; Havet, S.; Darblade, B.; Matthews, S. E.; de Bentzmann, S.; Guéry, B.; Cournoyer, B.; A. Imberty, S. Vidal, *J. Med. Chem.* **2014**, *57*, 10275–10289.
42. Cecioni, S.; Lalor, R.; Blanchard, B.; Praly, J.-P.; Imberty, A.; Matthews, S. E.; Vidal, S. *Chem. Eur. J.* **2009**, *15*, 13232–13240.

43. Cecioni, S.; Praly, J.-P.; Matthews, S. E.; Wimmerová, M.; Imberty, A.; Vidal, S. *Chem. Eur. J.* **2012**, *18*, 6250–6263.
44. Sicard, D.; Cecioni, S.; Iazykov, M.; Chevolut, Y.; Matthews, S. E.; Praly, J.-P.; Souteyrand, E.; Imberty, A.; Vidal, S.; Phaner-Goutorbe, M. *Chem. Commun.* **2011**, *47*, 9483–9485.
45. Sicard, D.; Chevolut, Y.; Souteyrand, E.; Imberty, A.; Vidal, S.; Phaner-Goutorbe, M. *J. Mol. Recognit.* **2013**, *26*, 694–699.
46. Garber, N.; Guempel, U.; Gilboa-Garber, N.; Doyle, R. J. *FEMS Micro. Lett.* **1987**, *48*, 331–334.
47. Cecioni, S.; Faure, S.; Darbost, U.; Bonnamour, I.; Parrot-Lopez, H.; Roy, O.; Taillefumier, C.; Wimmerová, M.; Praly, J.-P.; Imberty, A.; Vidal, S. *Chem. Eur. J.* **2011**, *17*, 2146–2159.
48. Soomro, Z. H.; Cecioni, S.; Blanchard, H.; Praly, J.-P.; Imberty, A.; Vidal, S.; Matthews, S. E. *Org. Biomol. Chem.* **2011**, *9*, 6587–6597.
49. Strutt, N. L.; Zhang, H.; Schneebeli, S. T.; Stoddart, J. F. *Acc. Chem. Res.* **2014**, *47*, 2631–2642; Cao, D.; Meier, H. *Asian J. Chem.* **2014**, *3*, 244–262; Ogoshi, T.; Yamagishi, T. *Eur. J. Org. Chem.* **2013**, 2961–2975.
50. Buffet, K.; Nierengarten, I.; Galanos, N.; Gillon, E.; Holler, M.; Imberty, A.; Matthews, S. E.; Vidal, S.; Vincent, S. P.; Nierengarten, J.-F. *Chem. Eur. J.* **2016**, *22*, 2955–2963.
51. Vincent, S. P.; Buffet, K.; Nierengarten, I.; Imberty, A.; Nierengarten, J.-F. *Chem. Eur. J.* **2016**, *22*, 88–92.
52. Moni, L.; Pourceau, G.; Zhang, J.; Meyer, A.; Vidal, S.; Souteyrand, E.; Dondoni, A.; Morvan, F.; Chevolut, Y.; Vasseur, J.-J.; Marra, A. *ChemBioChem* **2009**, *10*, 1369–1378.
53. Consoli, G. M. L.; Granata, G.; Cafiso, V.; Stefani, S.; Geraci, C. *Tetrahedron Lett.* **2011**, *52*, 5831–5834.
54. Nierengarten, I.; Buffet, K.; Holler, M.; Vincent, S. P.; Nierengarten, J.-F. *Tetrahedron Lett.* **2013**, *54*, 2398–2402.
55. Parera Pera, N.; Pieters, R. J. *Med. Chem. Commun.* **2014**, *5*, 1027–1035.
56. Yu, G.; Ma, Y.; Han, C.; Yao, Y.; Tang, G.; Mao, Z.; Gao, C.; Huang, F. *J. Am. Chem. Soc.* **2013**, *135*, 10310–10313.
57. Audfray, A.; Claudinon, J.; Abounit, S.; Ruvoën-Clouet, N.; Larson, G.; Smith, D. F.; Wimmerová, M.; Le Pendu, J.; Römer, W.; Varrot, A.; Imberty, A. *J. Biol. Chem.* **2012**, *287*, 4335–4347.
58. Bernardi, A.; Arosio, D.; Manzoni, L.; Monti, D.; Posteri, H.; Potenza, D.; Mari, S.; Jiménez-Barbero, J. *Org. Biomol. Chem.* **2003**, *1*, 785–792.
59. Arosio, D.; Fontanella, M.; Baldini, L.; Mauri, L.; Bernardi, A.; Casnati, A.; Sansone, F.; Ungaro, R. *J. Am. Chem. Soc.* **2005**, *127*, 3660–3661.
60. Garcia-Hartjes, J.; Bernardi, S.; Weijers, C. A. G. M.; Wenekes, T.; Gilbert, M.; Sansone, F.; Casnati, A.; Zuilhof, H. *Org. Biomol. Chem.* **2013**, *11*, 4340–4339.
61. Pieters, R. J. *ChemBioChem* **2006**, *7*, 721–728.
62. André, S.; Sansone, F.; Kaltner, H.; Casnati, A.; Kopitz, J.; Gabius, H.-J.; Ungaro, R. *ChemBioChem* **2008**, *9*, 1649–1661.
63. André, S.; Grandjean, C.; Gautier, F.-M.; Bernardi, S.; Sansone, F.; Gabius, H.-J.; Ungaro, R. *Chem. Commun.* **2011**, *47*, 6126–6128.
64. Bernardi, S.; Fezzardi, P.; Rispoli, G.; Sestito, S. E.; Peri, F.; Sansone, F.; Casnati, A. *Beilstein J. Org. Chem.* **2014**, *10*, 1672–1680.
65. Cecioni, S.; Matthews, S. E.; Blanchard, H.; Praly, J.-P.; Imberty, A.; Vidal, S. *Carbohydr. Res.* **2012**, *356*, 132–141.
66. Richichi, B.; Comito, G.; Cerofolini, L.; Gabrielli, G.; Marra, A.; Moni, L.; Pace, A.; Pasquato, L.; Chiarugi, P.; Dondoni, A.; Toma, L.; Nativi, C. *Bioorg. Med. Chem.* **2013**, *21*, 2756–2763.
67. Toma, L.; Di Cola, E.; Ienco, A.; Legnani, L.; Lunghi, C.; Moneti, G.; Richichi, B.; Ristori, S.; Dell’Atti, D.; Nativi, C. *ChemBioChem* **2007**, *8*, 1646–1649; Arcangeli, A.; Toma, L.; Contiero, L.; Crociani, O.; Legnani, L.; Lunghi, C.; Nesti, E.; Moneti, G.; Richichi, B.; Nativi, C. *Bioconj. Chem.* **2010**, *21*, 1432–1438.

68. Iida, J.; Meijne, A. M. L.; Knutson, J. R.; Furch, L. T.; McCarthy, J. B. *Sem. Cancer Biol.* **1996**, *7*, 155–162.
69. Tomita, N.; Sando, S.; Sera, T.; Aoyama, Y. *Bioorg. Med. Chem. Lett.* **2004**, *14*, 2087–2090.
70. Křenek, K.; Kuldová, M.; Hulíková, K.; Stibor, I.; Lhoták, P.; Dudič, M.; Budka, J.; Pelantová, H.; Bezouška, K.; Fišerová, A.; Křena, V. *Carbohydr. Res.* **2007**, *342*, 1781–1792.
71. Fujimoto, T.; Shimizu, C.; Hayashida, O.; Aoyama, Y. *J. Am. Chem. Soc.* **1998**, *120*, 601–602.
72. Fujimoto, K.; Miyata, T.; Aoyama, Y. *J. Am. Chem. Soc.* **2000**, *122*, 3558–3559.
73. Aleandri, S.; Casnati, A.; Fantuzzi, L.; Mancini, G.; Rispoli, G.; Sansone, F. *Org. Biomol. Chem.* **2013**, *11*, 4811–4817.
74. Avvakumova, S.; Fezzardi, P.; Pandolfi, L.; Colombo, M.; Sansone, F.; Casnati, A.; Prosperi, D. *Chem. Commun.* **2014**, *50*, 11029–11032.
75. Salvati, A.; Pitek, A. S.; Monopoli, M. P.; Prapainop, K.; Baldelli Bombelli, F.; Hristov, D. R.; Kelly, P. M.; Åberg, C.; Mahon, E.; Dawson, K. A. *Nat. Nanotech.* **2013**, 137–145.
76. Harrison, J. C.; Eftink, M. R. *Biopolymers* **1982**, *21*, 1153–1166.
77. Gallego-Yerga, L.; Lomazzi, M.; Sansone, F.; Ortiz Mellet, C.; Casnati, A.; Garcia Fernandez, J. M. *Chem. Commun.* **2014**, *50*, 7440–7443.
78. Geraci, C.; Consoli, G. M. L.; Galante, E.; Bousquet, E.; Pappalardo, M.; Spadaro, A. *Bioconj. Chem.* **2008**, *19*, 751–758.
79. Kim, Y. J.; Varki, A. *Glycoconjugate J.* **1997**, *14*, 569–576; Peri, F. *Chem. Soc. Rev.* **2013**, *42*, 4543–4556; Shiao, T. C.; Roy, R. *New. J. Chem.* **2012**, *36*, 324–339.
80. Giorgi, M. E.; de Lederkremer, R. M. *Carbohydr. Res.* **2011**, *346*, 1389–1393; Neres, J.; Brewer, M. L.; Ratier, L.; Botti, H.; Buschiazzo, A.; Edwards, P. N.; Mortenson, P. N.; Charlton, M. H.; Alzari, P. M.; Frasc, A. C.; Bryce, R. A.; Douglas, K. T. *Bioorg. Med. Chem. Lett.* **2009**, *19*, 589–596.
81. Galante, E.; Geraci, C.; Sciuto, S.; Campo, V. L.; Carvalho, I.; Sesti-Costa, R.; Guedes, P. M. M.; Silva, J. S.; Hill, L.; Nepogodiev, S. A.; Field, R. A. *Tetrahedron* **2011**, *67*, 5902–5912.
82. Viola, S.; Consoli, G. M. L.; Merlo, S.; Drago, F.; Sortino, M. A.; Geraci, C. *J. Neurochem.* **2008**, *107*, 1047–1055.
83. Viola, S.; Merlo, S.; Consoli, G. M. L.; Drago, F.; Geraci, C.; Sortino, M. A. *Pharmacology* **2010**, *86*, 182–188.
84. Micali, N.; Villari, V.; Consoli, G. M. L.; Cunsolo, F.; Geraci, C. *Phys. Rev. E* **2006**, *73*, 051904.
85. Cardona, F.; Isoldi, G.; Sansone, F.; Casnati, A.; Goti, A. *J. Org. Chem.* **2012**, *77*, 6980–6988.
86. Marradi, M.; Cicchi, S.; Sansone, F.; Casnati, A.; Goti, A. *Beilstein J. Org. Chem.* **2012**, *8*, 951–957.
87. Brissonnet, Y.; Ortiz Mellet, C.; Morandat, S.; Garcia Moreno, M. I.; Deniaud, D.; Matthews, S. E.; Vidal, S.; Šesták, S.; El Kirat, K.; Gouin, S. G. *J. Am. Chem. Soc.* **2013**, *135*, 18427–18435.
88. Marra, A.; Zelli, R.; D’Orazio, G.; La Ferla, B.; Dondoni, A. *Tetrahedron* **2014**, *70*, 9387–9393.
89. Horne, G.; Wilson, F. X.; Tinsley, J.; Williams, D. H.; Storer, R. *Drug Discovery Today* **2011**, *16*, 107–118.
90. Nash, R. J.; Kato, A.; Yu, C.-Y.; Fleet, G. W. J. *Future Med. Chem.* **2011**, *3*, 1513–1521.
91. Ficcioglu, C. *Therapeutics and Clinical Risk Management* **2008**, *4*, 425–431.

# Chapter 23

## New Technologies Powered by Protein-Binding Calixarenes

Meagan A. Beatty and Fraser Hof

### 23.1 Introduction

Calixarenes present a unique three-dimensional topology that is unlike that of most other drugs, probes, or supramolecular hosts. The cup-shaped cavity can act as a discrete recognition pocket, while their ease of synthetic modification means that they can also be used as a symmetric scaffold for outward display of recognition elements. This Chapter deals with the creation and study of calixarenes that bind to amino acid, peptide, and protein targets. The size of the targets dictates which binding mode might be used. Targets suited to being bound in ‘host-guest’ mode could be amino acids, small elements on peptides, or individual residues projecting from a protein surface (Fig. 23.1). Large patches of protein surface are well suited to being bound by calixarenes in ‘scaffold’ mode — especially if they consist of multiple, symmetry-related binding sites (Fig. 23.1).

Calixarenes are the most easily derivatized of the common supramolecular host systems, and tens of thousands of calixarene derivatives have been synthesized. In order to focus this discussion, Sect. 23.2 of this chapter will present selected examples of calixarenes binding to amino acids, peptides, and proteins, with some examples that provide general lessons in calixarene chemistry and biomolecular recognition. A Table that serves as an index for all reported equilibrium constants, including solution conditions, is presented at the end of Sect. 23.2. Section 23.3 of the Chapter will report on recent efforts to use calixarenes in both ‘host-guest’ and ‘scaffold’ modes as the basis for new biomolecular technologies.

The choice of biological targets implicitly creates a challenge — it is consistently harder to encode molecular recognition in pure water than in common organic solvents. But this challenge is also an opportunity for learning new lessons

---

M.A. Beatty • F. Hof (✉)

Department of Chemistry, University of Victoria, Victoria V8W 3V6, BC, Canada

e-mail: [fhof@uvic.ca](mailto:fhof@uvic.ca)



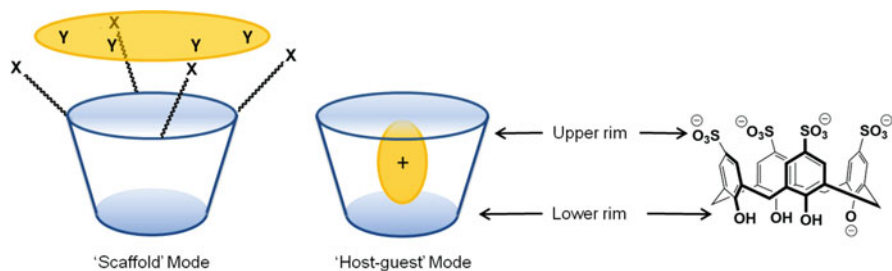


**Fig. 23.1** Cartoon depiction illustrating 'scaffold' and 'host-guest' mode to encapsulate a guest and defining upper and lower rims on the calix[4]arene

and for driving new directions in research. There are essentially no binding studies relevant to the targets in this chapter that have been done with the parent, undecorated or *t*-butyl substituted calix[*n*]arenes. The aromatic core of a calixarene is inherently hydrophobic, but needs to be rendered soluble in a biological medium in order to be useful for targeting biologically active molecules. One of the most common methods is to introduce charges by sulfonating the upper rim. In this focused set of topics, therefore, one of the most common 'parent' structure that is used for diverse purposes is the *para*-sulfonatocalix[4]arene, **PSC4**. The charged elements are rarely innocent — they cooperate with the hydrophobic pocket and/or appended binding elements and play an active role in target binding. Accordingly, decorating with other groups like carboxylates, guanidinium, or ammonium groups is also common and will also be discussed below.

### 23.1.1 Calixarene-Derived Binders of Amino Acids, Peptides, and Proteins

#### 23.1.1.1 Amino Acid Recognition

Amino acids are small guests that generally bind within the pockets of calixarenes. Amino acids have diverse side chain structures, and the nature of the side chain has large influence on the interactions of these guests with different calixarenes. In the late 1990s, *para*-sulfonatocalix[*n*]arenes ( $n = 4, 6, 8$ ; **PSC4**, **PSC6**, and **PSC8**) were tested extensively as hosts for neutral and positively charged amino acids. The intermolecular interactions that participate in these binding events are representative of the forces that are always found to be important in calixarene-based biomolecular recognition. They include and are illustrated in Fig. 23.2:

1. Electrostatic interactions between negatively charged sulfonato groups and positively charged guests. A simple, abiological example that proves the concept is the binding of trivalent lanthanide cations at the sulfonate rim of **PSC4** [1].

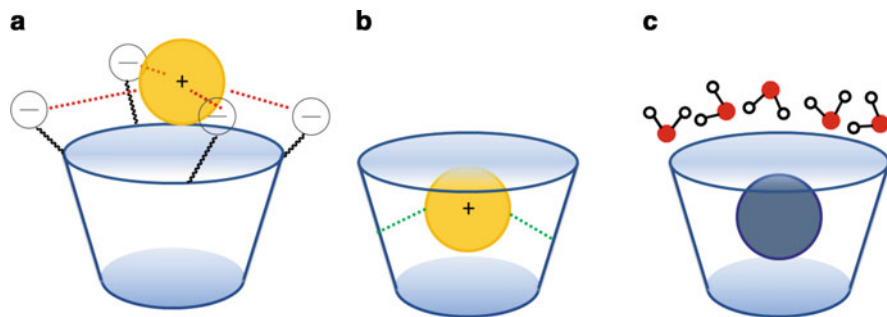


**Fig. 23.2** (a) Electrostatic interactions, (b) Cation- $\pi$  interaction, and (c) Hydrophobic effects as they frequently occur in calixarene-derived systems

2. Cation- $\pi$  interactions between the cation and the cyclic array of quadruples from the aromatic macrocycle [2]. Again, picking an abiological example, this kind of interaction is evident upon complexation of softer monovalent alkali cations inside the aromatic cavity of **PSC4** [3].
3. Hydrophobic effects between non-polar portions of each guest and the hydrophobic pocket provided by the aromatic macrocycle. In calixarene-based systems this is typically driven by the non-classical hydrophobic effect, where  $\Delta H < 0$  [4]. Examples that prove the concept here come from neutral hydrophobic guests such as alcohols [4], and also from the fact that tetraalkylated ammonium guests are driven deeper into the cavity and show a more favourable enthalpy of complexation than related, less hydrophobic monoalkylated ammonium guests. Small neutral guests such as acetone, acetonitrile, and butanone bind to **PSC4** [5] with small but noticeable binding affinities, as do larger neutral guests such as iodobenzene, toluene and biphenyl [6].

The pre-organization of calixarenes is another important feature of their programmed molecular recognition. The detailed conformational preferences of calixarenes are discussed in other Chapters in this book. It is generally true that host-type binding of small amino acid, peptide, or protein guests by calixarenes is favored by the cone conformation. The cone conformation of calix[4]arenes is stabilized by a network of intramolecular hydrogen bonds among the lower rim phenols. In aqueous solutions, this network is intact and stabilizing when all four phenols are protonated ( $\text{pH} < 3.26$ ) [7], and when a single phenol is deprotonated ( $3.26 < \text{pH} < 11.80$ ), but becomes unstable and disorganized at high pH when more than one of the lower-rim phenols is deprotonated (Fig. 23.3) [8]. Calixarenes bearing more than four repeating units are generally more flexible and can more easily adopt diverse conformations even at neutral pH values, normally providing for poorer host-type binding affinities. An example of this is provided by the fact that amino acids like lysine and arginine are more strongly bound by **PSC4** ( $735 \text{ M}^{-1}$  lysine;  $1520 \text{ M}^{-1}$  arginine) than by **PSC6** ( $94 \text{ M}^{-1}$  lysine;  $186 \text{ M}^{-1}$  arginine) or **PSC8** ( $400 \text{ M}^{-1}$  lysine;  $350 \text{ M}^{-1}$  arginine) in spite of the greater charge

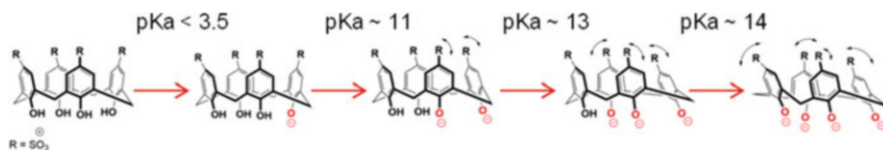
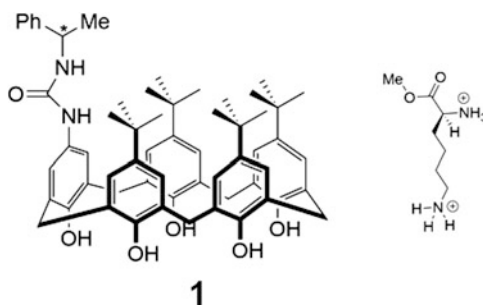


**Fig. 23.3** Changes in cavity conformation of a calix[4]arene with respect to pH

**Fig. 23.4** A calix[5]arene, **1**, able to bind with LysOMe with  $K_{\text{assoc.}}$  of  $2240 \text{ M}^{-1}$  in  $\text{C}_2\text{D}_2\text{Cl}_4/\text{CD}_3\text{OH}$  (2:1)



and larger hydrophobic surface areas that are offered by the larger calixarenes [9]. There is relatively less research on **PSC5** as a potential host for amino acids in water, but one reported calix[5]arene recognizes lysine methyl ester (LysOMe) in a mixture of methanol and tetrachloroethane (1:2) with  $K_{\text{assoc.}}$   $2240 \text{ M}^{-1}$  (Fig. 23.4) [10].

The influence of pre-organization is less easy to predict for scaffold-type recognition systems than for host-guest systems, but it remains true even in the scaffold family that most studies of protein binding by calixarenes have involved functionalized calix[4]arenes rather than their higher analogs.

**PSC4** has been tested as a host for all neutral and cationic natural amino acids. Neutral side chain amino acids, such as valine, leucine, phenylalanine, and tryptophan, form weak complexes with **PSC4**. The binding affinities in pH  $\sim 7$  buffers are  $15\text{--}63 \text{ M}^{-1}$ , with the strongest neutral side chain guest being phenylalanine [11, 12]. Histidine, lysine and arginine form complexes with **PSC4** in water at neutral pH measured at  $20 \text{ M}^{-1}$  (histidine),  $520\text{--}740 \text{ M}^{-1}$  (lysine) and  $330\text{--}1780 \text{ M}^{-1}$  (arginine) [4, 5, 9, 11, 13]. Guests like lysine bind in a side-on mode: the  $\epsilon\text{-NH}_3^+$  is engaged along the upper rim with the sulfonates but not included in the cavity, while the side-chain beta, gamma, and delta methylenes (Fig. 23.5) are bound within the hydrophobic cavity. This binding mode was confirmed with an X-ray crystal structure [14]. It has been suggested that the cationic part of the arginine side chain penetrates deeper into the aromatic pocket than does lysine, as the guanidinium is involved with  $\pi\text{-}\pi$  stacking [9].

Methylated lysines and arginines are amino acid guests that combine two favourable properties for binding sulfonato calixarenes: electrostatic attraction (as in their parent cationic amino acids), and additional hydrophobic contacts.

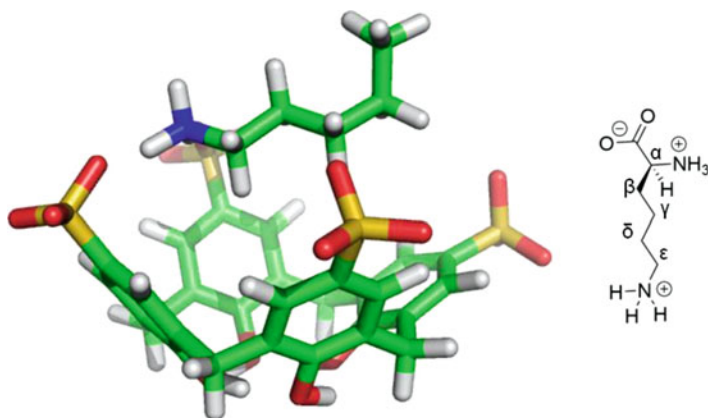


Fig. 23.5 X-ray structure of lysine complexed side-on with PSC4

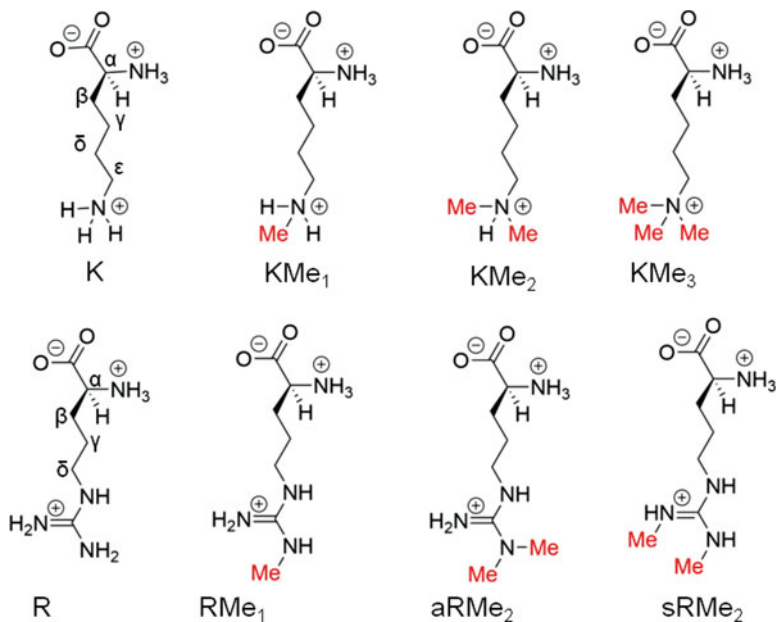


Fig. 23.6 Notation used for lysine (K) and arginine (R) side chain carbons and the different methylation states

Multiple methylation states are relevant to biology, including mono, di, and trimethyllysine (KMe<sub>1</sub>, KMe<sub>2</sub>, and KMe<sub>3</sub>), monomethyl arginine (RMe<sub>1</sub>), symmetric dimethylarginine (sRMe<sub>2</sub>) and asymmetric dimethylarginine (aRMe<sub>2</sub>) (Fig. 23.6) [15, 16]. KMe<sub>3</sub> is the single strongest guest for PSC4 with  $K_{\text{assoc}} =$

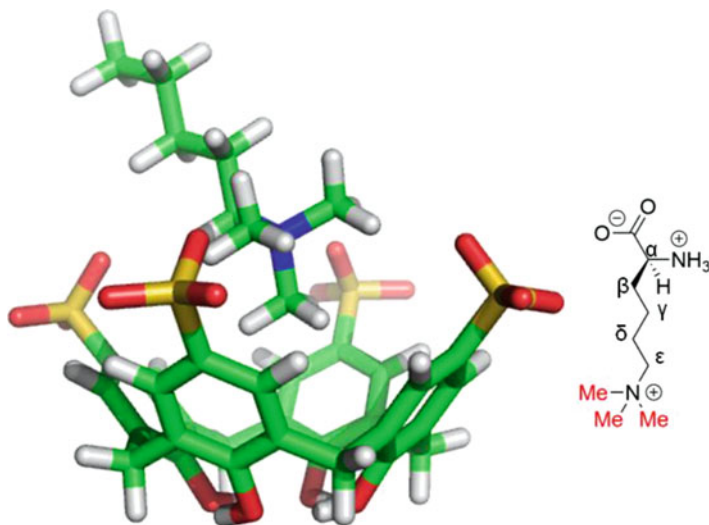
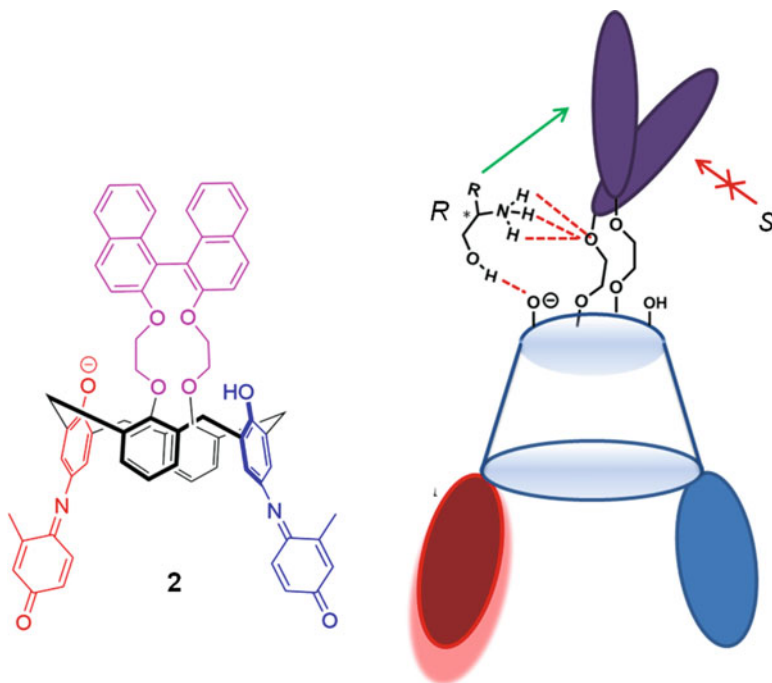


Fig. 23.7 Energy-minimized complex illustrating deep inclusion of trimethyllysine in PSC4 [13]

$37,000 \text{ M}^{-1}$  (by NMR). This host has a 70-fold selectivity for  $\text{KMe}_3$  over  $\text{K}$ , but only a threefold selectivity for  $\text{aRMe}_2$  or  $\text{sRMe}_2$  over  $\text{R}$ . NMR data shows how  $\text{KMe}_3$  adopts a different binding geometry than does unmethylated lysine. The methylenes remain relatively unchanged upon binding, while the methyl groups and the  $\epsilon\text{-CH}_2$  move strongly upfield. This is indicative of methyl inclusion deep within the pocket rather than a side-on interaction (Fig. 23.7).

Enantioselective recognition of amino acids by chiral calixarene hosts is a feature of calixarene-amino acid chemistry that has been extensively investigated [17, 18]. In most cases the calixarene acts as a scaffold to append chiral functional groups about the lower and/or upper rim. This book provides examples in other chapters of chiral calixarenes hosting other kinds of chiral guests. Most of the chiral calixarene systems relevant to this Chapter target amino acid methyl esters and/or amino alcohols selective between the *S/R*-amino acid methyl esters while operating in organic solvents [19, 20]. One interesting example is of an enantioselective fluorescent sensor (Fig. 23.8). The lower rim is strapped by a macrocyclic appendage, (*S*)-1,1'-bi-2-naphthol, via ether linkers, while the upper rim contains two indophenol chromophores, **2** [21]. The selectivity of the *R*-isomer of tryptophanol (one of the amino alcohol guests tested) was favoured with an association constant of  $159,000 \text{ M}^{-1}$  in ethanol, whereas the *S* enantiomer complexation was undetected. The amino group of the tryptophanol hydrogen bonds to the ether straps while the carboxylate group deprotonates one of the indophenols. This produces a long-wavelength absorbance from the deprotonated indophenol at 625 nm, turning the solution from red to blue. This contact is not possible for the *S* enantiomer, giving rise to the observed selectivities (Fig. 23.8).



**Fig. 23.8** Cartoon depiction of **2** and the “turn-on” fluorescence mechanism of enantioselectivity

### 23.1.1.2 Peptide Recognition

Studies on free amino acids routinely show binding for lysine or arginine in neutral water. The next step is to explore the binding abilities of different calixarenes when lysine or arginine are incorporated within peptide sequences. There have been studies with both **PSC4** and **PSC6** binding to dipeptides and tripeptides containing lysine and arginine [22]. ITC results are summarized in Table 23.1. The most noteworthy observation is stronger binding with increase number of residues, for arginine and lysine binding to both **PSC4** and **PSC6**. This increased binding affinity correlates to higher charge state and more potential recognition sites – a promising step toward more complex systems.

The parent sulfonated calix[4]arene **PSC4** mimics the aromatic cage and was shown to bind methyllysines more strongly than any other amino acid (modified or not). The next questions explored were: can binding selectivity and affinity be retained when trimethyllysine is incorporated in a peptide or protein? Can selectivity and affinity improve with functionalization of the upper or lower rims of the calixarene? The peptides tested were a string of eight residues that are found normally on histone 3 around lysine 27. The results of these studies showed that the most successful modifications were to leave the lower rim as unalkylated phenols, and to monofunctionalize along the upper rim in a way that modified the

**Table 23.1**  $K_{\text{assoc.}}$  of lysine- and arginine-containing peptides with **PSC4** and **PSC6**

	$K_{\text{assoc.}}$ ( $M^{-1}$ ) with PSC4	$K_{\text{assoc.}}$ ( $M^{-1}$ ) with PSC6 <sup>a</sup>
K	740	94
KK	3800	2300
KKK	30,000	3100
R	1520	186
RR	7700	1200
RRR	35,000	1600

<sup>a</sup>Values determined for 1:1 complexes. 10 mM phosphate buffer (pH 8)

**Table 23.2**  $K_{\text{assoc.}}$ , selectivity and  $IC_{50}$  values of H3K27Me<sub>3</sub> with **3** and **4**

	$K_{\text{assoc.}}$ for H3K27Me <sub>3</sub> ( $M^{-1}$ )	Selectivity over unmethylated <sup>a</sup>	$IC_{50}$ for H3K27Me <sub>3</sub> -reader protein disruption <sup>b</sup> ( $\mu M$ )
<b>PSC4</b>	190,000	40	2500
<b>4</b>	540,000	12	590
<b>3</b>	1,300,000	26	360

<sup>a</sup>Ratio of  $K_{\text{assoc.}}$  of H3K27Me<sub>3</sub>/H3K27 unmethylated, as measured by indicator displacement assays

<sup>b</sup> $IC_{50}$  measured in a competitive fluorescence polarization assay. 10 mM phosphate buffer (pH 7.4)

binding pocket itself [23]. From several calixarene derivatives, two aryl derivatives, **3** and **4**, showed the highest  $K_{\text{assoc.}}$  and lowest  $IC_{50}$ , outlined in Table 23.2. The small library of calixarenes provides a toolbox for probing the protein-protein interactions of reader proteins that engage post-translationally methylated histone tails (Fig. 23.9).

Hydrophobic residues in dipeptides like alanine, glycine, and tyrosine (Fig. 23.10) were recognized by a diphosphorylated calix[4]arene, **5**. Thermodynamic data showed that **5** recognized and included the protonated N-terminus of the small peptides [12]. More favourable binding energies exist for dipeptides relative to the amino acids, as the charge-charge repulsion between the phosphonates and carboxylates decreased, as their mutual separation distance increased (Table 23.3).

### 23.1.1.3 Protein Recognition

The ultimate goal for much of bio-targeted supramolecular chemistry is the selective binding of proteins. Some early studies proved that calixarenes like **PSC4** bind to proteins, but without providing structural information [24]. As previously discussed (Sect. 23.1), calixarenes can be designed to be either symmetric structures to which other recognition elements can be appended (the scaffold approach), or to participate in the binding event using their binding pocket (the host approach). The scaffolding approach was the first method used for calixarenes binding to proteins.

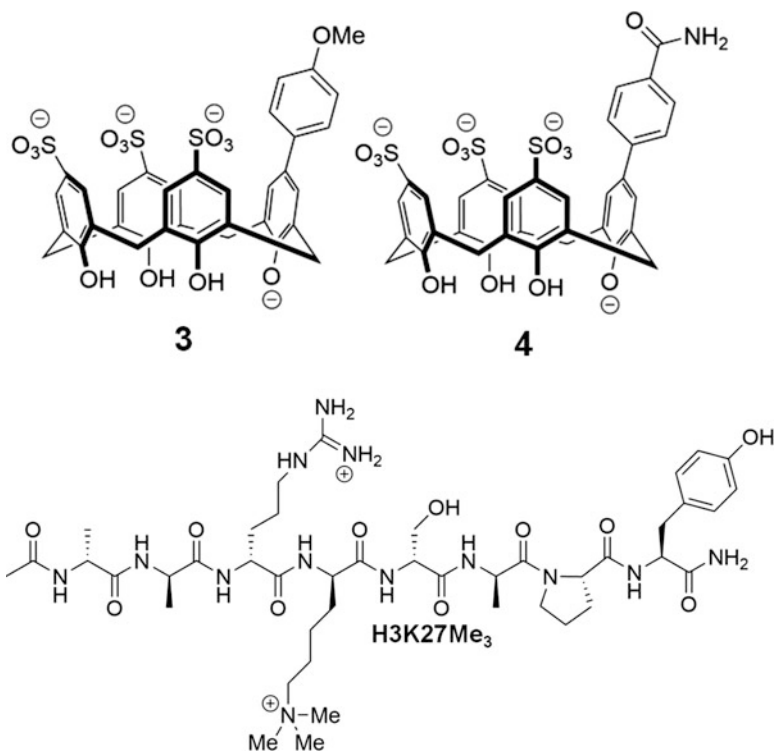


**Fig. 23.9** Calixarenes 3 and 4, two calixarenes that bind with strong affinity to the H3K27Me<sub>3</sub> peptide shown

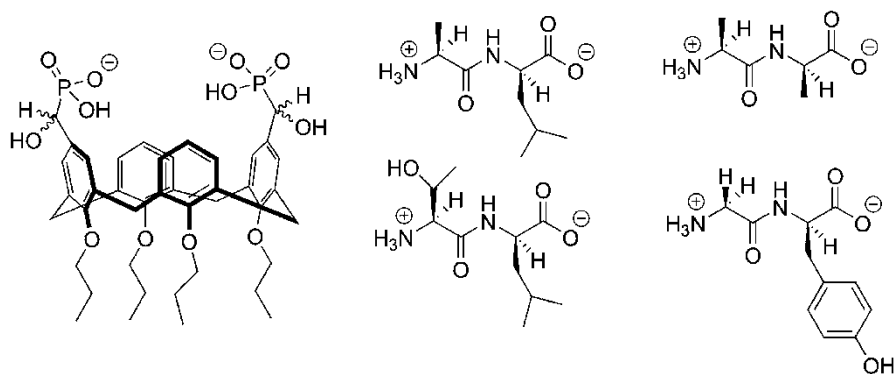


**Fig. 23.10** Calixarene 5 binds to hydrophobic dipeptides



**Table 23.3** Index of  $K_{\text{assoc.}}$  and solution conditions for all host-guest complexes in this section

Host	Guest	$K_{\text{assoc.}}$ ( $\text{M}^{-1}$ )	Solvent conditions	Ref.
PSC4	Lysine	734	Unbuffered $\text{H}_2\text{O}/\text{D}_2\text{O}$	9
PSC4	Arginine	1520	Unbuffered $\text{H}_2\text{O}/\text{D}_2\text{O}$	9
PSC6	Lysine	94	Unbuffered $\text{H}_2\text{O}/\text{D}_2\text{O}$	9
PSC6	Arginine	186	Unbuffered $\text{H}_2\text{O}/\text{D}_2\text{O}$	9
PSC8	Lysine	400	Unbuffered $\text{H}_2\text{O}/\text{D}_2\text{O}$	9
PSC8	Arginine	350	Unbuffered $\text{H}_2\text{O}/\text{D}_2\text{O}$	9
PSC4	Valine	15	0.1 M PBS	11
PSC4	Phenylalanine	63	0.1 M PBS	11
PSC4	Histidine	19	0.1 M PBS	5, 11
PSC4	Lysine	520	40 mM phosphate buffer	13
PSC4	Arginine	330	40 mM phosphate buffer	13
PSC4	Lysine	741	Water	4
PSC4	Arginine	1778	Water	4
PSC4	$\text{KMe}_3$	37,000	40 mM phosphate buffer	13
2	R-tryptophanol	159,000	Ethanol	21
5	Ala-Leu	43,651	Methanol	12
5	Thr-Leu	39,810	Methanol	12
5	Ala-Ala	42,657	Methanol	12
5	Gly-Tyr	43,651	Methanol	12

Protein-protein disruption by multivalent scaffolded binding is a method used to pursue a potential HIV-1 therapy. The proteomimetic calix[4]arene **6** prevents fusion and entry of the HIV-1 virus by antibody mimicry. It disrupts protein-protein interaction between the cell membrane's CD4 cell receptor and gp120 viral envelope. The cone conformation was fixed with alkyl groups and the upper rim was fashioned with aromatic diacids to create **6**. It is proposed that **6** interacts with gp120 by electrostatic interactions from the diacids and positively charged residues, and hydrophobic interactions with the calixarene's core [25, 26] (Fig. 23.11).

Tetraguanidiniomethylcalix[4]arene, **7**, was designed to bind in a central cleft formed in a multi-protein tetramer, with the guanidinium groups presented in a way that complements groups on each of the four assembled protein monomers. The protein target is p53 R337H, a common mutant of p53. Normally p53 is a key tumor suppressor protein, responsible for detecting aberrant growth in a cell. With this single mutation, an essential salt bridge is lost between Arg337 and Asp352 and the functional p53 homotetramer becomes unstable. Compound **7** wedges in between two of the four monomers, interacting by hydrogen bonds, salt bridges and hydrophobic interactions as a 2:1 complex (two **7** for one homotetramer). A pinched cone conformation is necessary to achieve those electrostatic interactions on either side of the calixarene. The design is unique as **7** opens up like a flower and makes extensive contacts with the *outside* surface of the calixarene's aromatic core [27] (Fig. 23.12).

**Fig. 23.11** Calixarene **6** blocks important protein-protein interaction to prevent cell infection of HIV-1

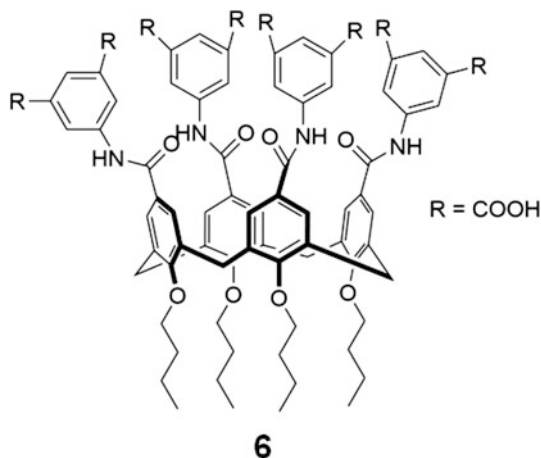
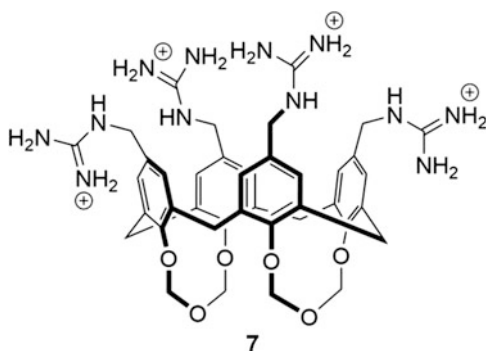


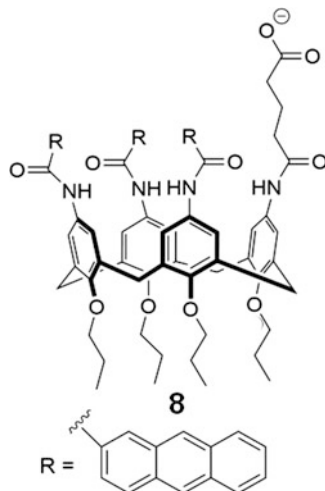
**Fig. 23.12** Calixarene **7**, stabilizes tetrameric mutant p53



Enzymes are also a target for scaffold based calix[4]arene. Histone deacetylase (HDAC) was investigated as it is an essential enzyme in removing the epigenetic mark, acetyllysine, from the histone tails of chromatin. The general criterion for HDAC inhibitors is to contain both a hydrophobic region and a Zn(II) chelator, separated by five to seven heavy atoms. A few known HDAC inhibitors also contain cyclic tetrapeptides as the hydrophobic element, and calix[4]arenes with converging hydrophobic elements were explored as an alternative [28]. Unlike **7** where the same functionality was found on all four units, **8** has three units of alkyl or aryl amido groups to provide the hydrophobic region, while the fourth unit is functionalized with a carboxylate to bind the Zn(II) (Fig. 23.13). The most promising calixarenes in this study presented aromatic substituents, and the 2-anthracenyl derivative **8** proved to have the lowest IC<sub>50</sub> value of 0.14 μM. Modeling of **8** with HDAC suggested that the 2-anthracenyl interacts with surface tyrosines via π-π stacking and also participated in cation-π interactions with a nearby lysine side chain.

In a different set of examples, calixarenes are used as hosts that bind protruding recognition elements on protein surfaces within their concave binding pocket. Both

**Fig. 23.13** Calixarene **8**, is a potent inhibitor for histone deacetylase



solution and solid-state data have been obtained for such complexes between **PSC4** and different sites on the lysine-rich surface of cytochrome C [29]. The crystal structure showed three lysine sites, 4, 22, 89, bound by **PSC4**. Water-mediated salt bridges and hydrogen bonds form between calixarene sulfonates and the lysine side chains, while the lysines methylenes are included in the aromatic cage in a side-on manner, similar to the binding mode shown for the free amino acid (above). The NMR data revealed two clusters of binding activity, centered around two lysine residues, 4 and 87, both with  $\sim$  mM binding affinities. The same group subsequently were able to obtain co-crystal structures of lysozyme — another highly cationic protein — with **PSC4**. In this example, **PSC4** was observed engaging arginine residues while bridging adjacent monomers in the crystal structure, acting like “protein-glue” [30].

Based on the results with post-translationally methylated amino acids and peptides (above), it was postulated there would be improved host-type binding with dimethyllysine (KMe<sub>2</sub>) residues projecting from the surface of an intact, folded protein. A proof of concept of **PSC4** binding to a methylated protein involved comparing lysozyme and an artificially dimethylated lysozyme construct bearing six dimethyllysine residues on the surface (lysozyme-KMe<sub>2</sub>) [31]. NMR data showed upfield shift of only one site (K116Me<sub>2</sub>) dependent on the concentration of **PSC4**, demonstrating site-selectivity induced by structural features on the surface of the protein. Unfortunately, due to the insolubility of the protein upon addition of the calixarene, the binding affinity could only estimated to be in the  $\mu$ M region — improved relative to unmethylated proteins, but not easily quantified. In the co-crystal structure K116Me<sub>2</sub> was encapsulated by **PSC4**, and both X-ray and molecular dynamics studies showed that the environment around K116Me<sub>2</sub> was better suited to host binding because it protruded away from the surface, while also allowing additional sulfonate-based salt bridges to neighboring residues (Fig. 23.14).

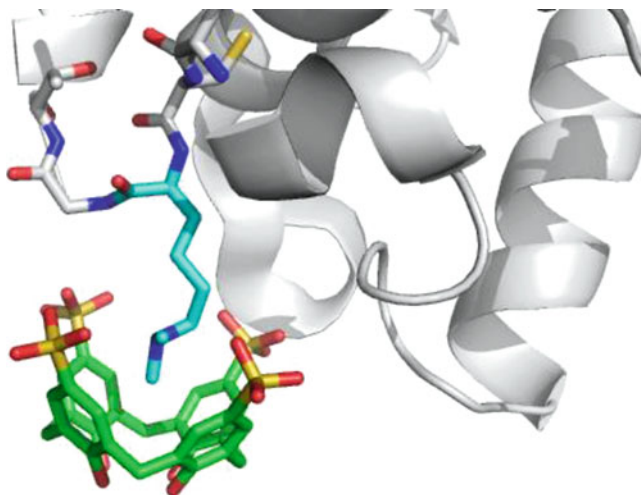
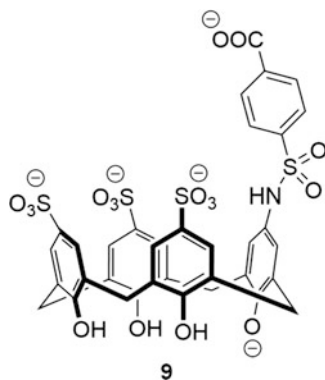


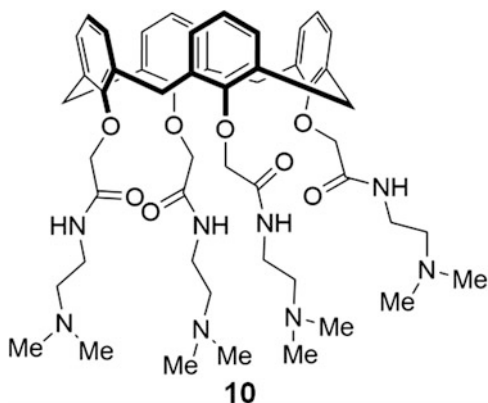
**Fig. 23.14** PSC4 encapsulating K116Me<sub>2</sub> on dimethylated lysozyme

**Fig. 23.15** Calixarene **9**, disrupts protein interactions with trimethyllysine histone tails



Previously discussed, **3** and **4** showed promising results with competitive recognition with chromodomain reader proteins for peptides of H3K27Me<sub>3</sub>. Other trimethyllysine residues exist in the proteome, and they too are flags for protein-protein interactions with their complementary reader proteins. In one specific example, the methyl mark H3K4Me<sub>3</sub> recruits proteins containing PHD (plant homeodomain) fingers. **PSC4** and calixarene **9** (Fig. 23.15) each disrupted protein-protein interactions between a PHD finger containing protein called ING2 and H3K4Me<sub>3</sub> with low  $\mu\text{M}$  dissociation constants. Selectivity among different methylated targets was studied, showing that **9** was selective for H3K4Me<sub>3</sub> over H3K27Me<sub>3</sub>, as well as being selective over H3K4 (unmethylated) and H3K4Me<sub>2</sub> [32, 33]. This compound disrupted a different PHD finger-driven pathway in living cells, presumably also by targeting the relevant trimethyllysine binding partner. The functional cellular disruption of a protein-protein interaction by a calixarene is an

**Fig. 23.16** Calixarene **10**, prevents blood vessel formation in tumor cells by inhibiting galectin-1



uncommon result that pushes the boundaries for calixarenes as agents for chemical biology.

A fragment based approach succeeded in creating a calixarene host mimicking a known peptidic-like inhibitor of galectin-1. Galectin-1's function is to promote blood vessel production within tumours, and the proposal is that its inhibitors would slow or stop tumour growth. Most of the substrates of galectin-1 share a hydrophobic region and a positively charged face. The undecorated upper rim of **10** was designed to act as the hydrophobic region while the lower rim provided the positively charged face (Fig. 23.16). **10** yielded lower microvessel density in basic fibroblast growth factor (bFGF)-stimulated human umbilical vein-derived endothelial cell (HUVEC) cultures than previously reported non-calixarene galectin-1 inhibitors. Interestingly, NMR data indicated that the calixarene does not bind with the carbohydrate active site but on various allosteric regions; the aromatic hydrophobic pocket (non-functionalized upper rim) participated in hydrophobic interactions with aliphatic and aromatic residues along the surface, whereas the cationic arms participated in long-range electrostatics. Compound **10** showed such promising results that in 2012 it started phase I clinical trials as an antiangiogenic drug. Unfortunately, when the radio-labeled derivative was synthesized and injected into mice with a tumour, the calixarene did not accumulate at the tumour site [34–36].

## 23.2 New Technologies

### 23.2.1 Solution-Phase Enzyme Assays and Related Technologies

To monitor a reaction in real-time, there needs to be a “turn-on” or “turn-off” response correlated to the reaction progress. This is achieved with a calixarene-

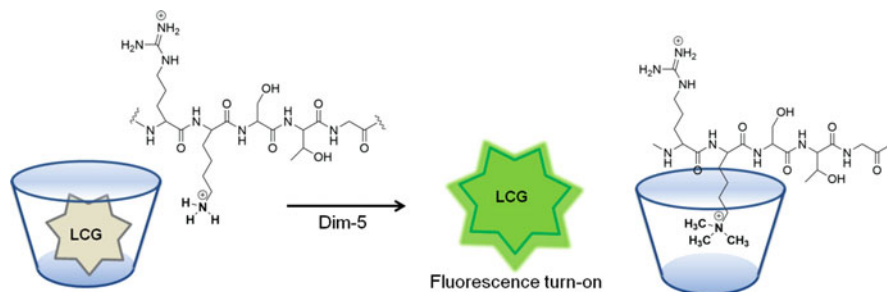


**Fig. 23.17** Cartoon depiction of monitoring an enzymatic reaction of a methylase with IDA

based indicator displacement assay (IDA). When the dye lucigenin (LCG), is bound within the cavity of a calixarene, the dye's fluorescence is quenched. A stronger-binding guest can displace the dye from the cavity and restore fluorescence. An early application of this technology toward enzyme assays relied on calixarenes binding post-translational methylation sites (see above). The enzymatic reaction in which a histone lysine methyltransferase (HKMT) adds methyl groups to a lysine substrate is, therefore, a candidate for the supramolecular IDA described above. As highlighted previously, **PSC4** has a higher binding affinity for trimethyllysine over unmethylated lysine in the context of peptides, so this was used to monitor the real-time production of trimethyllysine by the HKMT Dim-5, Fig. 23.17. This assay provided real-time data on reaction progress that allowed characterization of the enzyme's kinetics as well as the determination of IC<sub>50</sub> and K<sub>i</sub> values of a known Dim-5 inhibitor, 1,10-phenanthroline [37, 38].

The same sensing principle was useful for enzyme reactions with non-peptidic substrates when deployed in a coupled enzyme assay format. One example involves the enzymes acetylcholinesterase (AChE) and choline oxidase (ChO). AChE converts acetylcholine to choline, while ChO oxidizes choline to betaine. Choline and acetylcholine are both good guests for **PSC4**, which means that the aforementioned IDA scheme would not give a strong change upon progress of the initial enzymatic reaction of AChE. But betaine — produced by the action of ChO — has a lower affinity for **PSC4** and therefore the coupled enzyme assay produces a fluorescence switch-off response when both enzymes are present. The kinetics of ChO and AChE reaction progress were measurable using these calixarene-based sensors deployed in different experiments [39].

IDA was also shown to work well in live cells by incubating the **PSC4**-LCG complex with Chinese hamster ovary (CHO) and fibroblast (V79) cells. The fluorescence “turn-on” response was visualized in both cells when introducing known, cell-permeable biological analytes that displace LCG from **PSC4** (e.g. acetylcholine) [41]. In separate experiments, the same group also visualized transmembrane translocation of cationic species via transporter proteins. In this set of experiments, the IDA complex was incubated with lipid particles containing the outer membrane protein F (OmpF) — a selective channel for transport of organic cations [40]. The “turn-on” response occurs when cationic protamine was able to

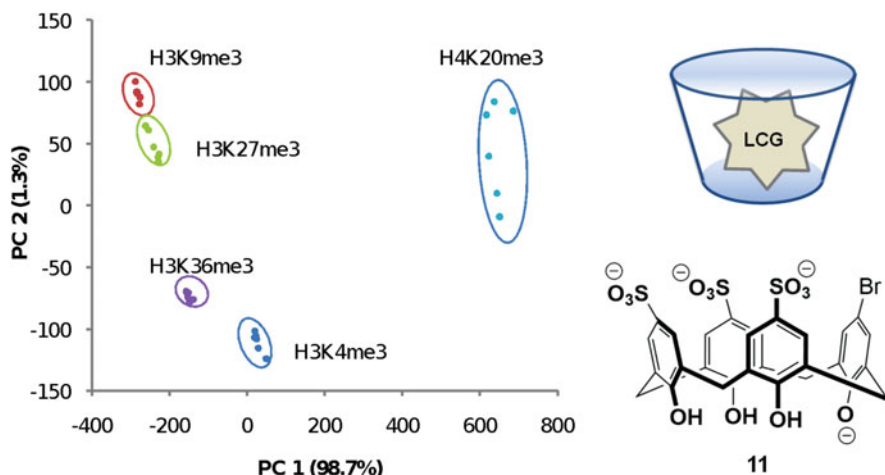


**Fig. 23.18** Example of a fingerprint generated from chemical sensor array of histone peptides bearing trimethyllysine within different biologically relevant peptide sequences. The basic readout of each sensor uses the LCG-based IDA as in Fig. 23.17, but using two different calixarenes **PSC4** and **11** to generate a fingerprint pattern of responses

pass the membrane via OmpF and displace LCG from **PSC4**. The ability of **PSC4** to bind its cognate dye and its targets selectively within cells, and to provide real-time feedback on a chemical process, is a powerful demonstration of supramolecular programming within complex solutions [40, 41].

Each example until now has focused on a single, targeted complexation event. The nature of post-translational modification is that it generates a huge number of possible modified proteins combinatorially by installing many kinds of modifications, alone or in combination with other modifications at nearby sites. In order to tackle the diversity of analytes, the same calixarene-LCG indicator displacement assay was expanded into a small array of two to three chemical sensors wherein each sensor was composed of a different calixarene (**PSC4**, **PSC6**, and/or **11**) bound to LCG. The resulting array generated multivariate data that could be used to discriminate between multiple PTM histone analytes to generate a unique fingerprint. The data was converted to easily readable maps through the use of principal component analysis (PCA) or linear discriminant analysis (LDA) (Fig. 23.18). The greater the spatial difference between the ellipse enclosing each analyte's replicate measurements, the greater the ability of the array to discriminate between guests. These sensor arrays offer a chemical alternative to the use of antibodies for discriminating among post-translationally modified analytes [42].

Although not strictly contained within the protein-focused scope of this Chapter, it is worth providing an example of calixarene-based nucleic acid binding technologies such as biscalixarenes able to recognize and bind with the major-groove of DNA. Multiple cationic (**12–15**) calixarenes were tethered together and linked by alkyl chains on the upper rim (Fig. 23.19). UV/Vis melting curves showed increased melting temperature with dimers, indicating complexation and

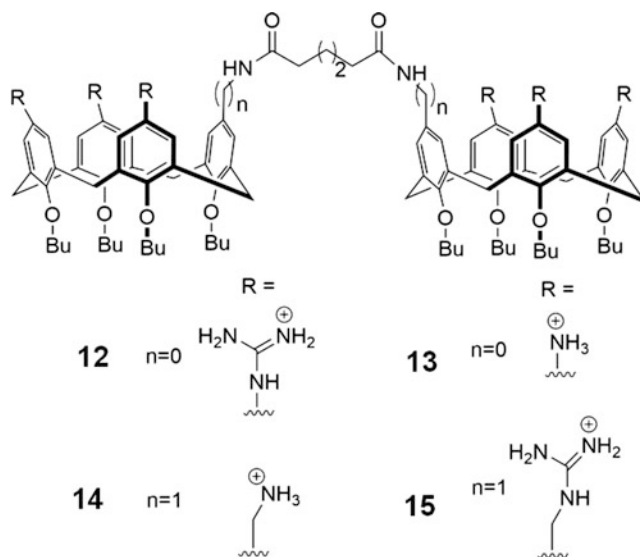


**Fig. 23.19** Biscalixarenes (12–15) that complex to the major-groove of DNA

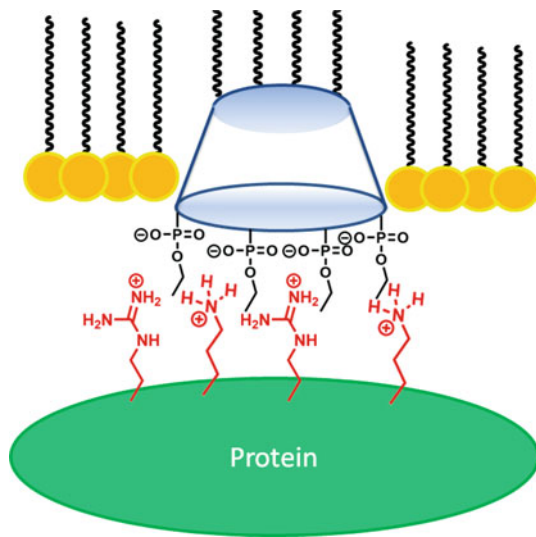
stabilization of a DNA oligomer when bound with the dimers. Binding constants were found through fluorescent titrations with a string of nucleotides revealed binding constants to be around  $10 \mu\text{M}$  and specificity for DNA over RNA. To confirm that the biscalixarenes were indeed binding to the major-groove, they performed circular dichroism (CD) spectroscopy experiments and found the molar ellipticities decreased with increasing concentrations of biscalixarene, corresponding to helix unwinding with respect to groove widening. This can be interpreted as spatial rearrangement within the major-groove induced by the biscalixarene, which offers hope for future applications in the control of gene function through the use of calixarene-based agents [43, 44].

### 23.2.2 Calixarene-Based Technologies Based on Self-Assembly and/or Lipid Phases

A unique technology involving calixarenes as the centrepieces yields a novel supramolecular method for protein surface recognition. Amphiphilic calixarenes insert into a lipid monolayer, with their lower-rim alkanes in the lipid phase and upper-rim tetraphosphonates pointing into the aqueous solution. In the presence of a protein in the adjacent aqueous phase, the anionic groups on the calixarene arrange themselves to form maximum electrostatic interactions and anchor the newly formed calixarene-protein complex in the monolayer (Fig. 23.20) [45, 46]. Pressure and area changes of the thin film allowed monitoring of the complexation



**Fig. 23.20** Amphiphilic calixarenes bind to protein surfaces while anchored non-covalently to a lipid layer



processes. The method was insensitive to salt and buffer types, and the binding strength was similar to those of protein-protein interactions. The method was also extended to use mixtures of acidic and basic calixarenes, which provided different pressure and area changes than found for individual calixarenes in the same monolayer. This generated a unique surface fingerprint of the protein that corresponded to the charge topology.

Another family of amphiphilic calixarenes has been used to stabilize integral membrane proteins. Many membrane proteins are targets for therapeutics, but their study *in vitro* is complicated by the fact that extracting them from a lipid bilayer can destabilize their three-dimensional structures and functions. A solution to this problem is found in anionic amphiphilic calixarene surfactants that stabilize membrane proteins. The anionic calixarene surfactants provide stabilizing interactions to positively charged protein surface residues while creating a stabilizing micelle around the more hydrophobic region of the protein (Fig. 23.21). It is proposed that the ordered structure and multiple charges of the calixarene headgroup offer better, more-stabilizing contacts with the folded protein than conventional surfactants. The calixarene surfactant that worked best for extracting the transmembrane protein BmrA contained tetracarboxyl groups along the upper rim and a heptyl chain on only one of the lower-rim phenols (**16**). NMR studies and surface tension measurements at various pH values verified **16** as a stabilizing surfactant. Purification and extraction of BmrA was achieved by implementing a series of extractions: first removing smaller contaminating proteins with a shorter-chain calixarene amphiphile, then extracting with **16** to yield pure functional BmrA [47].

Another family of self-assembly driven technologies arises from the creation of calixarene-derived self-assembled polymers.

One example of a dynamic system arising from calixarene self-assembly is a redox-responsive, host-guest polymer material. The basic structure is an alternating

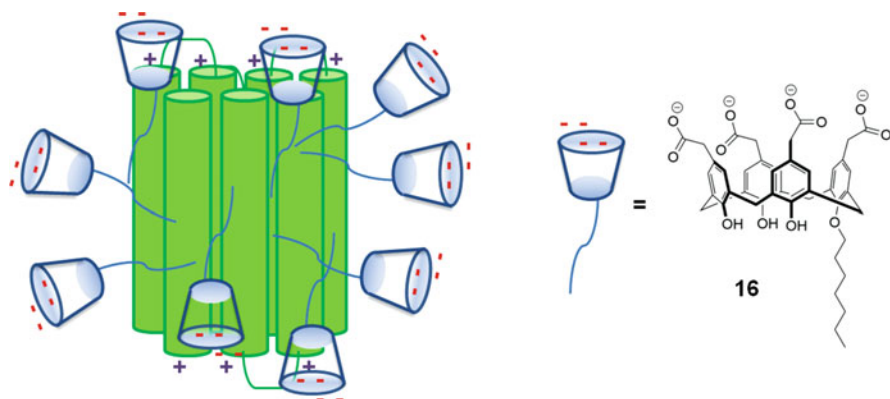


**Fig. 23.21** Cartoon depiction of an amphiphilic calixarene, **16**, serving as a structured detergent that stabilizes transmembrane proteins

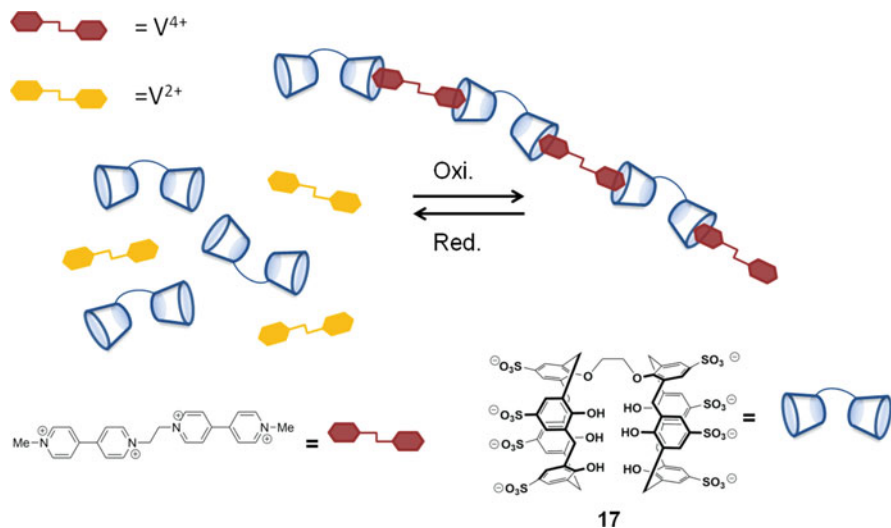


**Fig. 23.22** Cartoon depiction of the reversible non-covalent polymerization of a divergent divalent calixarene, **17**, and a divalent bis-viologen

non-covalent co-polymer of a bis-calixarene (ditopic host) and bis-viologen (ditopic guest). The linear polymer is formed by two **PSC4** units tethered at the lower rim with ether linkages, **17**, each binding one unit of the dicationic bis-viologen guest. Upon stimulus via electrochemical redox reaction of bis-viologen (4+) to the diradical dication and finally to the neutral form, **17** loses affinity for the guest and the polymer disassembles. The redox chemistry of the guest can be cycled, rendering a reversible material potentially capable of self-healing and self-repair [48] (Fig. 23.22).

In another example, supramolecular polymers were used in the context of multi-stimuli vesicular drug delivery. The combination of **PSC4** and partially acetylated chitosan (a cationic glucosamine-based polysaccharide) self-assembled into 200 nm diameter vesicles in water. Multiple stimuli were tested to probe the integrity of the vesicles. The first was pH — as the pH of the system increased, some amines became deprotonated and the vesicles lost integrity due to loss of electrostatic interactions between the cationic polymer and the anionic calixarene. The vesicles were able to re-form under acidic pH. Another stimulus tested was the addition of a competitive guest. 1,4-diazabicyclo[2.2.2]octane (DBO) was previously shown to have strong binding affinities with **PSC4**. It took a significantly higher concentration of DBO (50 eq.) to disassemble the vesicles than would have been expected for simple host-guest binding in free solution. But still, this provides a unique example in which host-guest chemistry exerts programmed control of macromolecular assemblies and their bulk properties. The vesicles were also successfully loaded with an anticancer drug, doxorubicin hydrochloride, to prove that for future work, these calixarene based vesicles could act as drug delivery technology [49].

### 23.2.3 *Calixarenes Operating on Solid Supports*

Protein microarrays are used frequently in biochemistry to scan the binding ability of a given analyte over a large library of proteins. A small aliquot of protein is immobilized on a glass chip: normally using streptavidin-biotin interactions, or a variety of related, irreversible covalent linkages. Both the streptavidin-biotin interactions and covalent linkages are valued for their high reproducibility and versatility, but they share a common disadvantage: some of the immobilized protein no longer adopts the native, active conformation that is needed to measure binding with an analyte. Some non-covalent linkages have been introduced as softer/reversible options that might avoid this problem, but in some cases have shown poor reproducibility. A balance of both covalent and non-covalent immobilization methods to us calixarenes as “surface glue” to append proteins — noncovalently — to the surface without distorting their native conformations (Fig. 23.23) [50]. To enable two distinct experiments (SPR and fluorescence), two different calixarenes were designed. The solution for SPR was a dithiolated calixarene that covalently attaches to the gold chips used in the technique. The solution for the glass chips used in fluorescence experiments was a calixarene tetrafunctionalized with formyl groups to react with amine-functionalized glass by reductive amination. Both handles present a bridging calix-crown ether on the lower rim that binds ammonium groups (lysine side chains) present on the surface of all proteins. The proposed mode of binding was supported by pH-dependence, as well as competition experiments with other ammonium ions. Non-specific binding — proteins adsorbing directly onto the substrate — is another factor that interferes with protein

### 3C) Calixarenes operating on solid supports

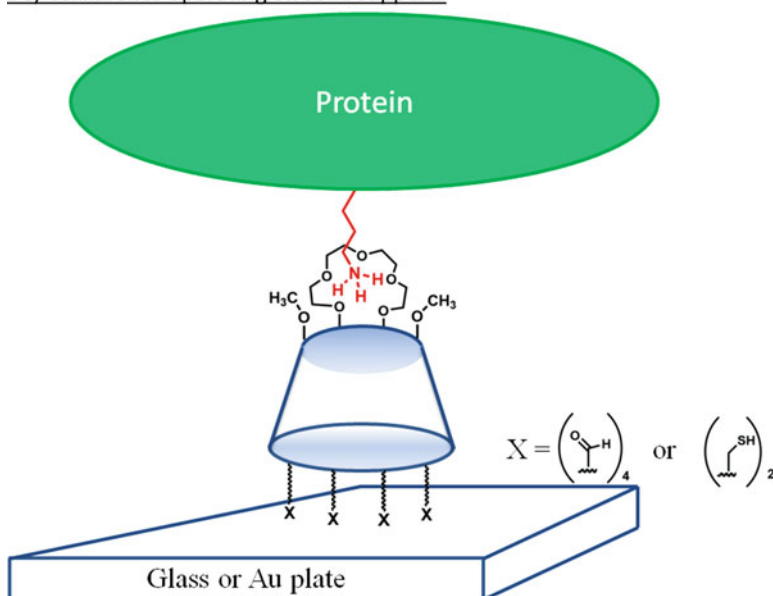


**Fig. 23.23** Cartoon depiction of calixarene “surface glue” to adhere proteins for protein microarray assays

microarray chips. AFM experiments on the above systems show that the calixarene “surface glue” provides significant coverage and minimizes non-specific adsorption.

Where the above application required calixarenes that could bind essentially all proteins with equal affinity, there is also interest in the use of substituted calixarenes as specific binding agents for certain protein partners. An unbiased approach to this problem starts with a specific calixarene and interrogates the whole proteome for specific binding partners. Tetraacetoamidocalixarene (**18**) was linked by its lower rim to solid support. The functionalized matrix was used to pull down partners from cell lysate. In order to identify positive targets, the pulled down fraction was processed and analyzed by conventional LC-MS/MS-driven proteomics (Fig. 23.24). One specific partner, protein disulfide isomerase (PDI) was then subject to further confirmation and independent experiments that proved that the calixarene could bind and modulate its biochemical activity. This novel protein-fishing technique could easily be expanded to differently functionalized calixarenes [51].

The idea of selectively binding a *class* of proteins represents a middle ground between the two examples above. The aforementioned trisulfonate hosts like **4** had a demonstrated ability to bind to trimethyllysine sites, and to cationic proteins in general. The connection of host **4** to a scaffold provided a multivalent affinity reagent, **19**, that was used in a series of experiments focused on the class of

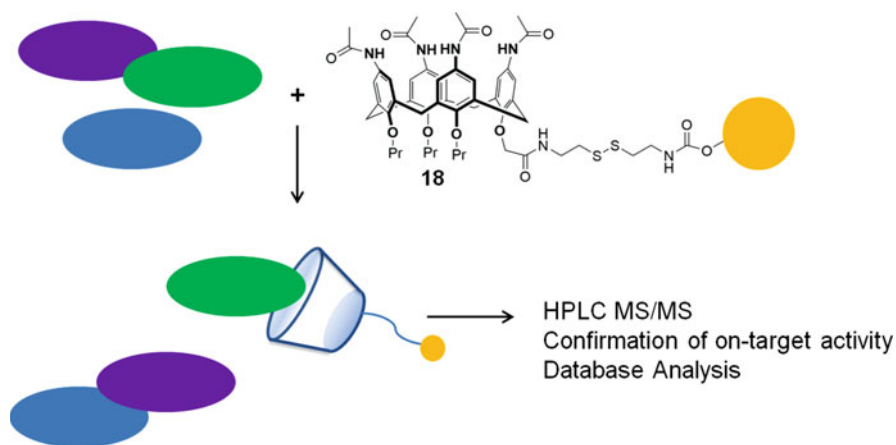


**Fig. 23.24** Calixarene **18**, tethered to solid support and mixed with proteins from cell lysate to identify those proteins having strong interactions with **18**

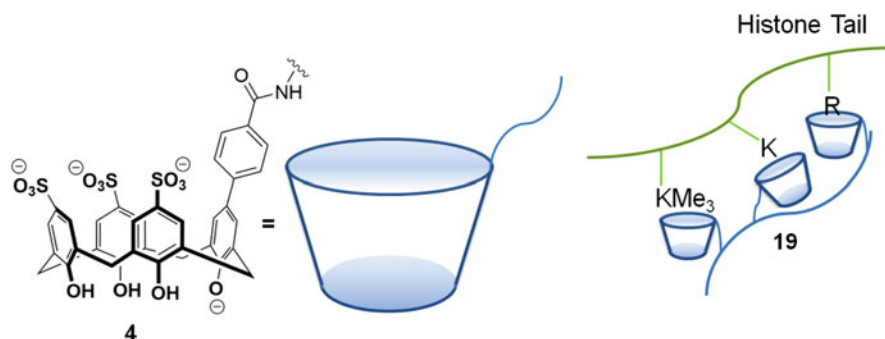


**Fig. 23.25** Multivalent calixarene ligand, **19**, recognizing multivalent residues on a histone tail

DNA-packaging proteins called histones. The strongly anionic and polyvalent nature of the affinity reagent was well suited to the binding of multiple residues on the lysine- and arginine-rich histone tails (Fig. 23.25). The binding affinity, measured with SPR, increased with increasing valency from mono- to tri-valent calixarene ligands. Additionally, selectivity for trimethylated versions of histone tail peptides over the unmethylated counterparts was observed, as expected from the properties of the parent host molecule. Pulldowns showed the ability to bind and enrich histones from cell lysates, demonstrating the goal of enriching for a class of proteins from the proteome [52].

The above three examples offer complementary approaches to the different kinds of selectivities and specificities in protein binding. Together they show that, with suitable functionalization, calixarenes can achieve high specificity for a single target, selectivity for a class of targets, or general binding of all proteins. These

ligands each establish new technologies that are based on their respective selectivities, and demonstrate the potential of calixarenes as affinity reagents that enable a wide variety of biomolecular technologies.

### 23.3 Conclusions and Outlook

This chapter provides illustrative, diverse examples of the use of peptide- or protein-binding calixarenes as the basis for new technologies. Recurrent themes include reliable, chemically driven assays of biomolecules, self-assembly into vesicles or as detergents, and attachment to varied solid supports. In many of the examples, calixarenes replace antibodies or other biomolecular affinity tools. It is unlikely that any calixarene will ever achieve the high specificity of such affinity reagents, but each class of supramolecular hosts have their own distinct advantages. These include chemical stability, batch reproducibility, and different patterns of binding selectivities and valencies that might not be accessible by antibodies and related reagents. All of the applications discussed here are made possible by the easy synthetic functionalization of calixarenes at multiple positions. We think that the synthetic flexibility of calixarenes is unequalled by any other supramolecular scaffold, that this advantage is part of the reason for their past fundamental successes as supramolecular reagents, and that it makes them especially promising for future work on diverse technological applications. We look forward to seeing more new technologies developed through the creative design, synthesis, and targeted application of calixarenes.

### References

1. Bonal, C.; Israëli, Y.; Morel, J.P.; Morel-Desrosiers, N. *J. Chem. Soc., Perkin Trans. 2* **2001**, 1075–1078.
2. Dougherty, D. A. *J. Nutr.* **2007**, *137*, 1504S–1508S.
3. Morel, J. P.; Morel-Desrosiers, N. *Org. Biomol. Chem.* **2006**, *4*, 462–5.
4. Perret, F.; Morel, J.P.; Morel-Desrosiers, N. *Supramol. Chem.* **2003**, *15*, 199–206.
5. Arena, G.; Contino, A.; Giuseppe Gulino, F.; Magri, A.; Sansone, F.; Sciotto, D.; Ungaro, R. *Tetrahedron Lett.* **1999**, *40*, 1597–1600.
6. Baur, M.; Frank, M.; Schatz, J.; Schildbach, F. *Tetrahedron* **2001**, *57*, 6985–6991.
7. Shinkai, S. *Tetrahedron* **1993**, *49*, 8933–8968.
8. Daze, K. D.; Jones, C. E.; Lilgert, B. J.; Beshara, C. S.; Hof, F. *Can. J. Chem.* **2013**, *91*, 1072–1076.
9. Douteau-Gueval, N.; Coleman A. W.; Morel, J.P.; Morel-Desrosiers, N. *J. Phys. Org. Chem.* **1998**, *11*, 693–696.
10. Ballistreri, F. P.; Notti, A.; Pappalardo, S.; Parisi, M. F.; Pisagatti, I. *Org. Lett.* **2003**, *5*, 1071–1074.
11. Arena, G.; Casnati, A.; Contino, A.; Magri, A.; Sansone, F.; Sciotto, D.; Ungaro, R. *Org. Biomol. Chem.* **2006**, *4*, 243–9.

12. Zielenkiewicz, W.; Marcinowicz, A.; Cherenok, S.; Kalchenko, V. I.; Poznański, J. *Supramol. Chem.* **2006**, *18*, 167–176.
13. Beshara, C. S.; Jones, C. E.; Daze, K. D.; Lilgert, B. J.; Hof, F. *ChemBioChem* **2010**, *11*, 63–6.
14. Selkti M.; Coleman A. W.; Nicolis I.; Douteau-Guevel N.; Villain F.; Tomas A.; de Rango C. *Chem. Commun.* **2000**, 161–162.
15. Ruthenburg, A. J.; Allis, C. D.; Wysocka, J. *Mol. Cell.* **2007**, *25*, 15–30.
16. Chi, P.; Allis, C. D.; Wang, G. G. *Nat. Rev. Cancer* **2010**, *10*, 457–69.
17. Erdemir, S.; Tabakci, M.; Yilmaz, M. *J. Inclusion Phenom. Mol. Recognit. Chem.* **2007**, *59*, 197–202.
18. Arimura, T.; Kawabata, H.; Matsuda, T.; Muramatsu, T.; Satoh, H.; Fujio, K.; Manabe, O.; Shinkai, S. *J. Org. Chem.* **1991**, *56*, 301–306.
19. Demirtas, H. N.; Bozkurt, S.; Durmaz, M.; Yilmaz, M.; Sirit, A. *Tetrahedron* **2009**, *65*, 3014–3018.
20. Kocabas, E.; Durmaz, M.; Alpaydin, S.; Sirit, A.; Yilmaz, M. *Chirality* **2008**, *20*, 26–34.
21. Kubo Y.; M. S.; Tokita S.; Kubo M. *Nature* **1996**, *382*, 522–524.
22. Douteau-Guével, N.; Perret, F.; Coleman, A. W.; Morel, J.P.; Morel-Desrosiers, N. *J. Chem. Soc., Perkin Trans. 2* **2002**, 524–532.
23. Tabet, S.; Douglas, S. F.; Daze, K. D.; Garnett, G. A.; Allen, K. J.; Abrioux, E. M.; Quon, T. T.; Wulff, J. E.; Hof, F. *Bioorg. Med. Chem.* **2013**, *21*, 7004–10.
24. Memmi, L.; Lazar, A.; Brioude, A.; Ball, V.; Coleman, A. W. *Chem. Commun.* **2001**, 2474–2475.
25. Tsou, L. K.; Dutschman, G. E.; Gullen, E. A.; Telpoukhovskaia, M.; Cheng, Y. C.; Hamilton, A. D. *Bioorg. Med. Chem. Lett.* **2010**, *20*, 2137–9.
26. Tsou, L. K.; Chen, C. H.; Dutschman, G. E.; Cheng, Y. C.; Hamilton, A. D. *Bioorg. Med. Chem. Lett.* **2012**, *22*, 3358–61.
27. Gordo, S.; Martos, V.; Santos, E.; Menendez, M.; Bo, C.; Giralt, E.; de Mendoza, J. *Proc. Natl. Acad. Sci. U.S.A* **2008**, *105*, 16426–31.
28. Chini, M. G.; Terracciano, S.; Riccio, R.; Bifulco, G.; Ciao, R.; Gaeta, C.; Troisi, F.; Neri, P. *Org. Lett.* **2010**, *12*, 5382–5385.
29. McGovern, R. E.; Fernandes, H.; Khan, A. R.; Power, N. P.; Crowley, P. B. *Nat. Chem.* **2012**, *4*, 527–33.
30. McGovern, R. E.; McCarthy, A. A.; Crowley, P. B. *Chem. Commun.* **2014**, *50*, 10412–5.
31. McGovern, R. E.; Snarr, B. D.; Lyons, J. A.; McFarlane, J.; Whiting, A. L.; Paci, I.; Hof, F.; Crowley, P. B. *Chem. Sci.* **2015**, *6*, 442–449.
32. Allen, H. F.; Daze, K. D.; Shimbo, T.; Lai, A.; Musselman, C. A.; Sims, J. K.; Wade, P. A.; Hof, F.; Kutateladze, T. G. *J. Biochem.* **2014**, *459*, 505–12.
33. Ali, M.; Daze, K. D.; Strongin, D. E.; Rothbart, S. B.; Rincon-Arano, H.; Allen, H. F.; Li, J.; Strahl, B. D.; Hof, F.; Kutateladze, T. G. *J. Biol. Chem.* **2015**, *290*, 22919–30.
34. Dings, R. P.; Chen, X.; Hellebrekers, D. M.; van Eijk, L. I.; Zhang, Y.; Hoye, T. R.; Griffioen, A. W.; Mayo, K. H. *J. Natl. Cancer Inst.* **2006**, *98*, 932–6.
35. Dings, R. P.; Miller, M. C.; Nesmelova, I.; Astorgues-Xerri, L.; Kumar, N.; Serova, M.; Chen, X.; Raymond, E.; Hoye, T. R.; Mayo, K. H. *J. Med. Chem.* **2012**, *55*, 5121–9.
36. Lappchen, T.; Dings, R. P.; Rossin, R.; Simon, J. F.; Visser, T. J.; Bakker, M.; Walhe, P.; van Mourik, T.; Donato, K.; van Beijnum, J. R.; Griffioen, A. W.; Lub, J.; Robillard, M. S.; Mayo, K. H.; Grull, H. *Eur. J. Med. Chem.* **2015**, *89*, 279–95.
37. Florea, M.; Kudithipudi, S.; Rei, A.; Gonzalez-Alvarez, M. J.; Jeltsch, A.; Nau, W. M. *Chem. Eur. J.* **2012**, *18*, 3521–8.
38. Ghale, G.; Nau, W. M. *Acc. Chem. Res.* **2014**, *47*, 2150–9.
39. Guo, D.S.; Uzunova, V. D.; Su, X.; Liu, Y.; Nau, W. M. *Chem. Sci.* **2011**, *2*, 1722.
40. Norouzy, A.; Azizi, Z.; Nau, W. M. *Angew. Chem. Int. Ed.* **2015**, *54*, 792–5.
41. Ghale, G.; Lanctot, A. G.; Kreissl, H. T.; Jacob, M. H.; Weingart, H.; Winterhalter, M.; Nau, W. M. *Angew. Chem. Int. Ed.* **2014**, *53*, 2762–5.
42. Minaker, S. A.; Daze, K. D.; Ma, M. C.; Hof, F. *J. Am. Chem. Soc.* **2012**, *134*, 11674–80.

43. Hu, W.; Blecking, C.; Kralj, M.; Suman, L.; Piantanida, I.; Schrader, T. *Chem. Eur. J.* **2012**, *18*, 3589–97.
44. Breitzkreuz, C. J.; Zadmard, R.; Schrader, T. *Supramol. Chem.* **2008**, *20*, 109–115.
45. Kolusheva, S.; Zadmard, R.; Schrader, T.; Jelinek, R. *J. Am. Chem. Soc.* **2006**, *128*, 13592–13598.
46. Zadmard, R.; Schrader, T. *J. Am. Chem. Soc.* **2005**, *127*, 904–915.
47. Matar-Merheb, R.; Rhimi, M.; Leydier, A.; Huche, F.; Galian, C.; Desuzinges-Mandon, E.; Ficheux, D.; Flot, D.; Aghajari, N.; Kahn, R.; Di Pietro, A.; Jault, J. M.; Coleman, A. W.; Falson, P. *PLoS One* **2011**, *6*, e18036.
48. Guo, D.S.; Chen, S.; Qian, H.; Zhang, H.Q.; Liu, Y. *Chem. Commun.* **2010**, *46*, 2620.
49. Peng, S.; Wang, K.; Guo, D. S.; Liu, Y. *Soft Matter* **2015**, *11*, 290–6.
50. Lee, Y.; Lee, E. K.; Cho, Y. W.; Matsui, T.; Kang, I. C.; Kim, T. S.; Han, M. H. *Proteomics* **2003**, *3*, 2289–304.
51. Tommasone, S.; Talotta, C.; Gaeta, C.; Margarucci, L.; Monti, M. C.; Casapullo, A.; Macchi, B.; Prete, S.; Ladeira De Araujo, A.; Neri, P. *Angew. Chem. Int. Ed.* **2015**, *54*, 15405–15409.
52. Kimura, Y.; Saito, N.; Hanada, K.; Liu, J.; Okabe, T.; Kawashima, S. A.; Yamatsugu, K.; Kanai, M. *ChemBioChem* **2015**, *16*, 2599–2604.



# Chapter 24

## Calix[*n*]arenes and Nucleic Acids

Max Sena Peters and Thomas Schrader

### 24.1 Introduction

Calixarenes are regular macrocyclic aromatic systems, whose conformation can be largely controlled between the extremes of rigid defined molecular shapes and entirely flexible architectures. Upper and lower rim of *cone*-shaped calixarenes can be equipped with a large variety of functional groups, which may carry multiple charges. These features qualify calixarenes to be potential ligands for biomacromolecules such as proteins and nucleic acids.

Early prototypes mainly exploited Coulomb attraction between the polyanionic phosphate backbone and permanent cations on the calixarenes. Later more sophisticated ligands were developed which used hydrogen bonding,  $\pi$ -stacking, metal coordination and the hydrophobic effect to recognize the shape and charge state of nucleic acids. The field of calixarene-DNA chemistry has vastly expanded in recent years, and many excellent reviews appeared with almost comprehensive coverage, some of them including calixarenes under a broader selection of artificial DNA binders.

Thus, macrocyclic amphiphiles are reviewed by Huang et al. with respect to cyclodextrins, calixarenes, cucurbiturils and pillararenes [1]. Similarly, Ma and Zhao present biomedical applications of supramolecular systems based on host-guest interactions, with a focus on cyclodextrins, calixarenes and cucurbiturils [2]. Sansone et al. published a review on calixarenes as multivalent ligands for biomolecular recognition [3].

A large body of information has been accumulated about calixarenes with attached sugars, the so-called glycolcalixarenes; Dondoni and Marra present the

---

M.S. Peters (✉) • T. Schrader  
Faculty of Chemistry, Institute for Organic Chemistry, University of Duisburg-Essen,  
Universitätsstr. 7, 45117 Essen, Germany  
e-mail: [max.peters@uni-due.de](mailto:max.peters@uni-due.de); [thomas.schrader@uni-due.de](mailto:thomas.schrader@uni-due.de)

synthesis and biological applications of calixarene and calixresorcarene glycosides [4]. Casnati and Sansone describe the potential of these glycocalyx mimics for the recognition of biological macromolecules [5].

Two excellent reviews with the same focus appeared recently: biological applications of calixarenes were compiled by Nimse and Kim, followed very recently by a feature article by Casnati et al. about “moulding” calixarenes for biomolecule targeting [6, 7].

With a more application-oriented emphasis Ludwig earlier summarized the use of calixarenes for biochemical recognition and separation, whereas Loftsson et al. gave a recent survey about the encapsulation of drug molecules into calix[n]arene nanobaskets [8, 9].

## 24.2 Nucleic Acids as Supramolecular Targets

Supramolecular interactions with nucleic acids are fundamental for biological processes like replication, transcription and translation. With regard to biomedical applications there is a general demand for artificial DNA binders, e. g., in order to interfere with natural binders such as transcription factors or to perform gene transfer into cell nuclei by transfection. Therefore a detailed view on the DNA structure and its potential binding sites is essential. In this context Schneider et al. present a valuable book chapter with the same title as this chapter, summarizing the possible binding modes and the scope of research in the field of interactions with nucleic acids [10]. A detailed review on the interactions of calix[n]arenes with nucleic acids along with several applications is given by Schrader et al. [11].

Based on their structural regularity, nucleic acids represent perfect targets for supramolecular complexation. In double-stranded B-DNA two polymeric strands, consisting of nucleic bases connected to a negatively charged deoxyribose phosphodiester backbone, form a right-handed double helix. The purine bases adenine (A) / guanine (G) and the pyrimidine bases thymine (T) / cytosine (C) form hydrogen-bonded base pairs (AT and GC). These planar arrangements are steadily piled up upon each other, stabilized by  $\pi$ -stacking interactions. Due to the non-diametral arrangement of the strands, two grooves of different size are formed, termed minor and major groove (Fig. 24.1).

These structural features bring along four different avenues for nucleic acid recognition. Ligands can either exploit electrostatic interactions with the negative charges of the phosphates present in the backbone, insert between the base pairs by (bis)intercalation, or set up attractive contacts by occupying the minor or major groove. Of these different avenues groove binding represents the sole possibility for sequence selective recognition and is therefore utilized by many biological DNA-binders. In the physiologically prevailing B-DNA the major groove has a width of 11.6 Å and a depth of 8.5 Å providing a large contact area. The minor groove possesses a similar depth of 8.2 Å but a much smaller width of 6.0 Å, which

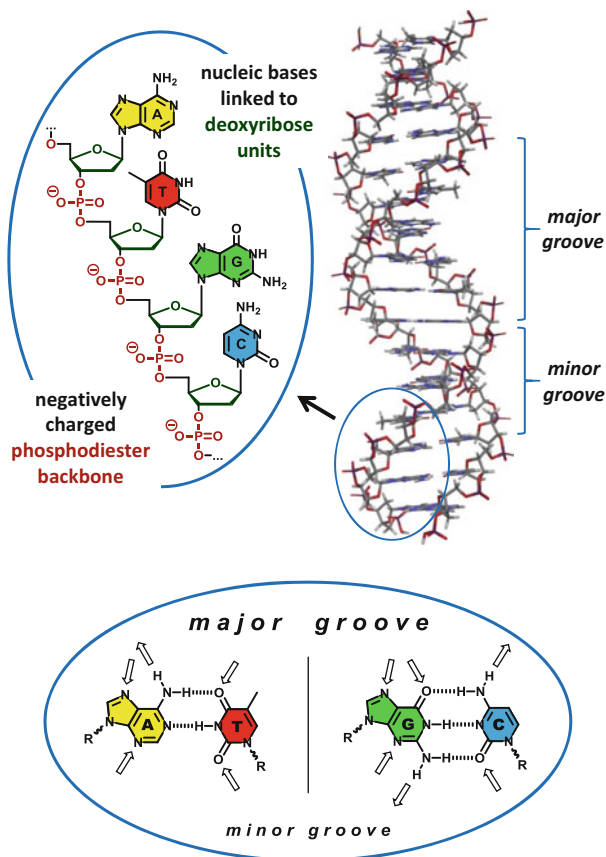


**Fig. 24.1** Structure of the B-DNA double helix. Enlarged Lewis structures depict the single strand and the canonical base pairs (AT and GC) with their hydrogen bond donor/acceptor pattern inside the minor and major groove indicated by arrows

determines its narrow shape. In view of these characteristics the major groove can be seen as the “hotspot” for larger biomolecules such as transcription factors or other regulatory proteins, whereas smaller ligands of predominantly crescent shape bind in the minor groove, e.g. distamycin or netropsin. Both of them bind to AT-rich regions owing to the higher density of negative charge and the absence of a sterically hindering amino group as in case of the GC base pair [10].

The anionic character of nucleotides and nucleic acid strands makes them easily accessible via electrostatic interactions, therefore many DNA binding ligands exhibit cationic sites. This structural feature is also commonly provided by protonated polyamines as known from biogenic amines such as spermine, which strongly binds to the negatively charged phosphate groups via its ammonium groups. Since nucleic acids embody polyanions it is obvious that the concept of multivalency generates synthetic ligands with enhanced affinities towards nucleic acids [12].



NMR titrations of the amino-calixarene derivatives **1** and **2** with adenine nucleotides in D<sub>2</sub>O revealed that complexation free energies and binding constants of the 1:1 complexes increase from AMP ( $18 \pm 1$  kJ/mol;  $K_a \approx 1.4 \times 10^3$  M<sup>-1</sup>), over ADP ( $20 \pm 1$  kJ/mol;  $K_a \approx 3.2 \times 10^3$  M<sup>-1</sup>) to ATP ( $22 \pm 1$  kJ/mol;  $K_a \approx 7.1 \times 10^3$  M<sup>-1</sup>), indicating a large contribution of salt bridging consistent with weak adenosine binding. Extension to other nucleotides (GMP, UMP, CMP and TMP) confirmed electrostatic attraction as the major driving force. It is interesting to see that the larger flexible ligands ( $n = 6, 8$ ) bind ATP in aqueous solution much better than the conformationally defined *cone* and *1,3-alternate* derivatives **1** and **2**, with association constants of  $7 \times 10^4$  M<sup>-1</sup> for the calix[8]arene **4** [13].

In addition to isolated nucleotides the amino-calixarene derivatives also bind to nucleic acids, stabilized by ion pairing and supplementary van der Waals-type contributions. Their binding properties were investigated on calf thymus (CT) DNA with established methods such as thermal melting studies and fluorometric ethidium bromide displacement assays. In contrast to nucleotide binding, where the affinity increases with the number of positive ligand charges, now the *cone*-shaped calix[4]arene **1** shows the strongest effect. Remarkably it is even more effective than the DNA-binder spermine, indicating further interactions with the calixarene phenol groups. The larger and inherently more flexible derivatives **3** and **4** exhibit only little increase in affinity suggesting that the distances between the phosphates in the B-DNA (7 Å or 11 Å) and between the ammonium cations of the calixarenes are important. Molecular modeling studies indicate that up to eight simultaneous salt bridges are possible with *cone*-shaped calix[4]arenes owing to the appropriate distances of the ammonium N<sup>+</sup>-atoms (9 Å and 12 Å) [13].

In 2004 Ungaro et al. introduced a series of water soluble calix[*n*]arenes ( $n = 4, 6, 8$ ) with upper rim guanidinium groups and different alkyl groups at the lower rim for the recognition of plasmid DNA (Fig. 24.2). The calixarene derivatives **5**, **7** and **8** display good water solubility indicated by sharp peaks in the <sup>1</sup>H-NMR spectra (D<sub>2</sub>O) and underlined by maximal solubilities ( $c_{\max}$ ) in the millimolar range, determined by UV-vis spectroscopic experiments. On top the compounds display very low cytotoxicity. Combining these features the guanidinium calixarenes appear suitable for biological applications. **6** on the other side forms a gelatinous macroscopic aggregate in water, surprisingly even at very low concentrations [14].

The soluble derivatives were subjected to binding studies on plasmid DNA monitored by agarose gel Electrophoresis Mobility Shift Assays (EMSA). Here **5** displays the best recognition potential, with the band shift beginning at 12.5 μM and complete plasmid complexation between 100 and 200 μM [14]. Over the years Ungaro et al. developed a number of different guanidinium calixarene derivatives with the main purpose of transporting nucleic acids over cell membranes into the nucleus (transfection, see also Chap. 22).

Schrader et al. utilized aminocalixarenes to construct dimers which are able to recognize double stranded nucleic acids. Butoxy groups at the lower rim lock the calixarene moieties in the *cone* conformation so that the NH<sub>2</sub>/NH<sub>3</sub><sup>+</sup> groups all point in the same direction in order to generate multivalent interactions to the target (Fig. 24.3) [15].

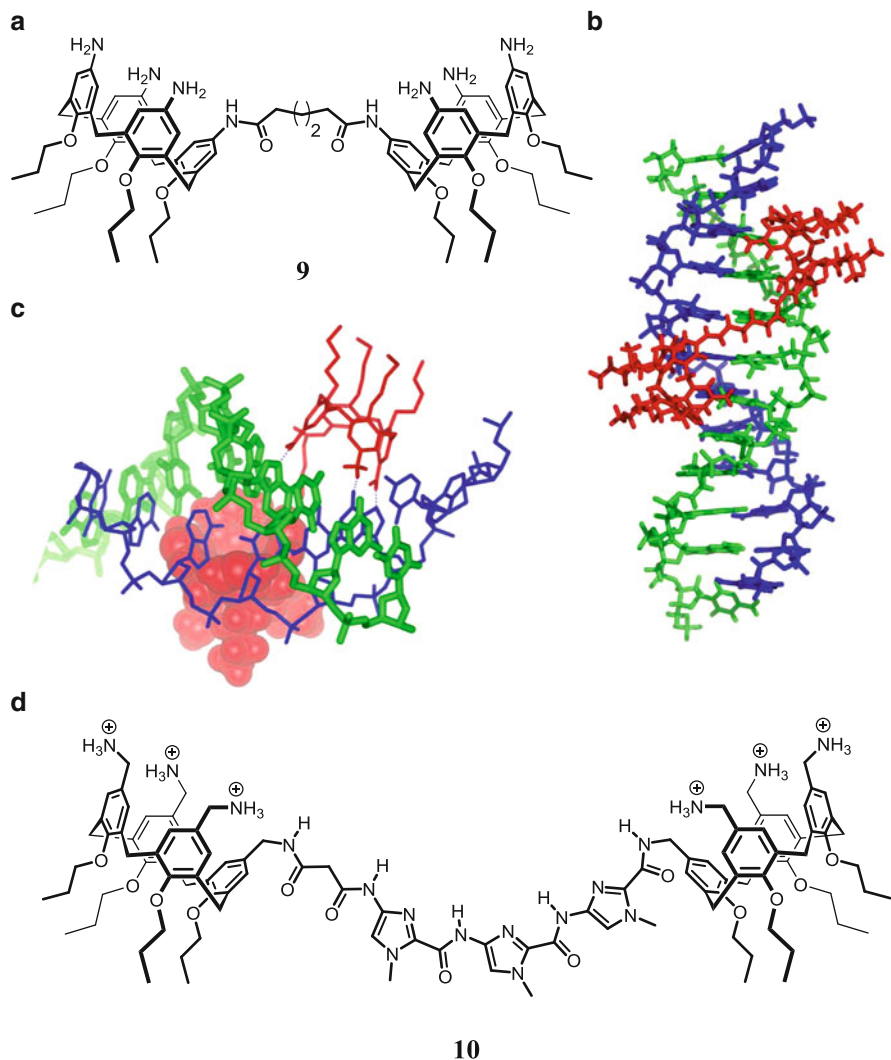


**Fig. 24.3** (a) Anilinalocalix[4]arene dimer **9** with a flexible aliphatic bridge. (b) B-DNA (12 bp, green and blue) with tightly bound dimer **9** (red) [15]. (c) View along the major groove, revealing three hydrogen bond contacts between  $\text{NH}_2/\text{NH}_3^+$  groups of each calixarene and various nucleic bases at the groove floor (MacroModel 7.0, MMFFs, water, 1000 steps) [15]. (d) Calix[4]arene dimer with benzylammonium groups at the upper rims and a trimethylimidazolyl bridge for attempted sequence-selective binding. (Reprinted from Ref. [15])

Experimental evidence gained from a synopsis of established DNA binding experiments, such as melting curves, displacement assays and circular dichroism (CD) studies, suggests major groove insertion as the main binding mode. This is further supported by the dimer size of about  $3 \times 1$  nm which excludes intercalation or minor groove insertion and by molecular modeling studies which find multiple

contacts between the calixarene amino/ammonium groups and the phosphate backbone as well as the nucleobases in the major groove (Fig. 24.3) [15].

Comparison to a weakly binding derivative with a rigid aromatic linker (terephthalic acid) reveals the necessity of a flexible bridging unit that allows the dimer to adjust to the curvature of the major groove. Fluorescence titration of **9** with fluorescein-labeled DNA strands produces association constants of  $\sim 10^5 \text{ M}^{-1}$ . UV melting curves and ethidium bromide displacement assays indicate a preference of (GC)*n*- over (AT)*n*-DNA strands. Interestingly  $C_{50}$  values remained modest whereas the determined charge excess ratio ( $CE_{50}$ ) is among the lowest ever reported for DNA binders – even at high salt loads [15].

The concept of polycationic calix[4]arene dimers was further investigated by the Schrader group who created a number of dimers with varying bridges that differ in length and charge. Elongation of the bridging unit does not lower dimer affinity towards DNA. This is of great importance, as for promotor specificity linkers must be suitable to span and recognize at least six base pairs, as a prerequisite for sequence-selective binding. The new dimers display a stabilizing effect on short DNA strands (12 bp) indicated by a melting point increase of up to 20 °C. CD spectroscopic measurements support the postulated binding mode inside DNA's major groove. Complexation of double stranded RNA is accompanied by drastic conformational changes in line with an expansion of its narrow major groove (A-DNA conformation) towards a B-DNA geometry, which offers a wider major groove to accommodate the calixarene body [16].

Dimer **9** and its rigid analogue have also been tested for their ability to bind biologically important diphosphates- and oligonucleotides such as ATP, FAD, NADH, NADPH and triadenosine as well as single stranded DNA strands (ssDNA). Binding studies point to Coulomb interactions as the major source of attraction. For reasons of comparison, a nonpolar analogue of dimer **9** with *tert*-butyl groups instead of the amino groups was synthesized and investigated; here hydrophobic forces dominate the binding event [17].

The Schrader group pursued the ultimate goal of interference with gene expression; thus calixarene dimers were synthesized with elongated bridges, designed to read the base sequence on the floor of its major groove. Inspired by natural DNA binding heterocyclic oligoamides and the minor groove binding polyamides of the Dervan group, *N*-methyl pyrrole and *N*-methyl imidazole units were integrated into the calixarene dimers [18]. Their crescent shape matches the curved major groove floor, enabling in principle a set of directed hydrogen bonds towards nucleic base pairs via their amide protons and imidazole nitrogen lone pairs. In addition to the linker variation, the calixarenes' upper rim ammonium ions were replaced by guanidinium ions or benzylammonium ions for increased water solubility.  $pK_a$  titrations performed on the amino derivatives revealed, that at pH 7 the aniline groups only generate a maximal dimer charge of +2, whereas the benzylamine calixarene dimer has a charge of +6. One representative of the benzylamine series with a trimeric imidazole bridging unit (**10**) showed a significant preference for polydG-polydC duplexes, and reached association constants of about  $10^7 \text{ M}^{-1}$  (Fig. 24.3). The distinction between AT- and GC-strands most probably arises

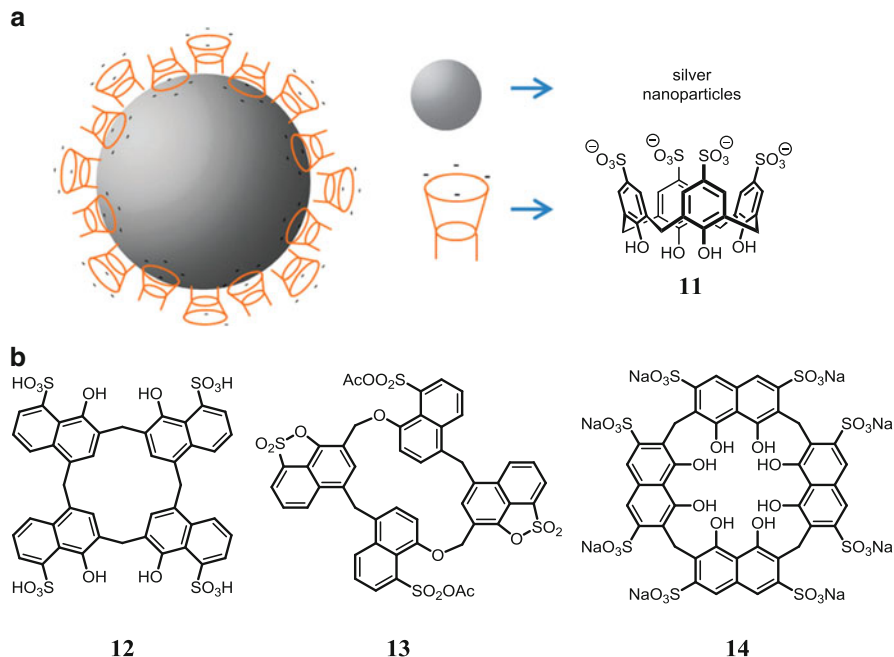


**Fig. 24.4** (a) Schematic representation of the self-organization of Coleman's *para*-sulfonato-calix[4]arene capped silver nanoparticles [23] (b) Lewis structures of different calixnaphthalenes (**12**–**14**). The exact protonation state of **14** is uncertain but a full deprotonation of the sulphonate groups is suggested [24]. (Reprinted from Ref. [23])

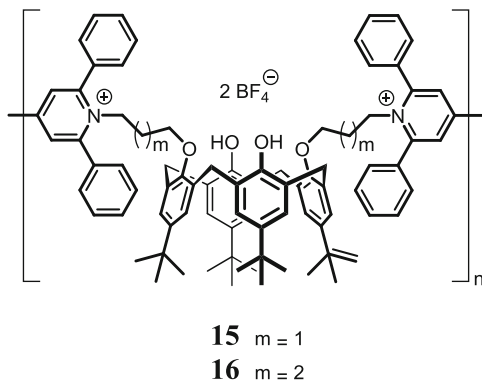
from the steric hindrance of thymine's methyl group in AT-rich DNA in combination with strong N-H...N hydrogen bridges formed between the imidazole lone pair and guanine's NH proton [19, 20].

Zadmard et al. carried on the dimer concept by introducing amino acid or peptide bridges in order to increase hydrogen bonding to the nucleic acid bases [21]. In another approach calixarene derivatives were equipped with acridine moieties, and high affinities were detected between acridine-functionalized calix[4]arenes and CT-DNA by fluorescence titration [22].

Other groups have also applied calixarenes to address DNA and related compounds. Coleman et al. used *para*-sulfonato-calix[4]arene (**11**) capped silver nanoparticles for the colorimetric and spectroscopic discrimination between pyrimidine and purine based analytes (Fig. 24.4). For pyrimidine bases new absorbances around 530 nm appear along with drastic color changes from yellow to orange red and pink that are based on nanoparticle aggregation [23]. The group also investigated different naphthalene based calixarene-like macrocycles (calixnaphthalenes) on their ability to form nanoparticles applicable for specific DNA interaction. All three derivatives (**12**–**14**) are suited for capping and stabilizing silver nanoparticles, but differences in behavior suggest individual capping mechanisms indicating that only oxalix[4]naphthalenesultone **13** presents a large cavity for complexation (Fig. 24.4) [23, 24].



**Fig. 24.5** Calix[4]arene-based polymeric pyridinium salts [25]



Li, Lu and Zeng et al. present the synthesis of fluorescent poly(pyridinium) salts (**15** and **16**) by condensation of 4,4'-(1,4-phenylene)bis(2,6-diphenylpyrylium tetrafluoroborate) with calix[4]arene diamines (Fig. 24.5). The interaction of the polymer with label free *Pseudomonas fluorescens* DNA has been investigated by fluorescence titration methods and TEM, demonstrating strong interactions, predominantly relying on electrostatic interactions [25].

In 2008 Shahgaldian et al. introduced a *para*-amino calix[4]arene with dodecyl groups at the lower rim (**17**), that self-assembles into positively charged solid lipid nanoparticles (SLNs) with DNA binding properties. These SLNs were used for the transfection of mammalian cells, which will be discussed later in Sect. 24.7.1. The amphiphilic calixarene was also used to form well-defined Langmuir monolayers at the air water interface with relatively high dynamic stability, presented in the following Sect. 24.3.2 [26].

These nanoparticles were produced by applying the solvent displacement method on derivative **17**, bringing forward SLNs of about 190 nm diameter. In AFM images the particles appear as round-shaped objects (Fig. 24.6). In the self-assembled particles the polar upper rim head groups most likely spread over the particle surface. To investigate their interaction with DNA, the SLNs were incubated with plasmid DNA and centrifuged. Complex formation, most likely via Coulomb interactions was proven using gel chromatography on the supernatant, where no DNA was detected, concluding that all the DNA material was centrifuged down with the nanoparticles (Fig. 24.6) [26].

Later Shagaldian et al. investigated the related amphiphilic calix[4]arene derivative **18**, equipped with four guanidinium groups at the upper rim. In spite of the structural similarity to Ungaro's guanidino calixarenes **5** and **6**, this amphiphile forms stable SLNs in water just as **17**. It was shown that the solubility decrease caused by the long dodecyl chains enables the molecule to self-assemble as SLNs rather than micelles. Experimental data from fluorescence displacement experiments, CD spectra and isothermal titration calorimetry (ITC) studies indicate that the nanoparticles are able to recognize DNA in a base-selective manner. It is argued that electrostatic interactions are accompanied by a groove binding mechanism: the

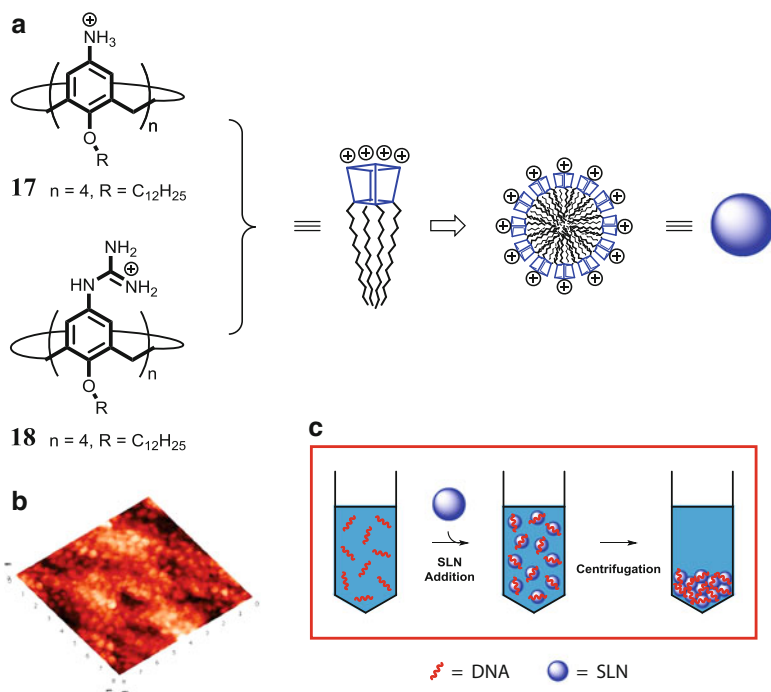


**Fig. 24.6** (a) Structure of the amphiphilic aminododecyloxy-calix[4]arene (**17**) and its guanidinium analogue (**18**) [26, 27]. (b) AFM image of **17**-based SLNs spread on mica and imaged in air in noncontact mode [26]. (c) DNA complexation with SLN and centrifugation [26]. (Reprinted from Ref. [26])

SLNs display a preference for AT sequences, probably via minor groove insertion as suggested from ITC investigations, while GC strands are bound in their major groove [27].

More recently Rescifina and Neri et al. presented calixarene derivatives equipped with polycyclic aromatic hydrocarbons (PAHs). More precisely, the conjugates consisted of one or two pyrenylisoxazolidine moieties at the upper rim of a *cone*-shaped lower rim propyl calix[4]arene. Experimental investigations revealed intercalating abilities, most probably from the minor groove side, suggesting the conjugates as suitable tools for cooperative DNA complexation. The *in vitro* cytotoxic activity of the most potent agent (mono-substituted analogue to **19** with a free acid, not displayed) reached an  $IC_{50}$  value of 95 nM which is more than 50 times lower than that of the pyrenylisoxazolidinyl alcohols alone. Further, molecular docking and CD-spectroscopic studies support the proposed binding mode and hint to a certain discrimination between nucleobases. An MD simulation experiment on a (dA–dT)<sub>2</sub> dodecamer for the investigation of the (bis)intercalation properties of **19** is depicted in Fig. 24.7 [28].

Rao et al. synthesized an anthracenyl calix[4]arene conjugate with two positive charges (**20**). The cationic nature was implemented by *N*-methylation of the

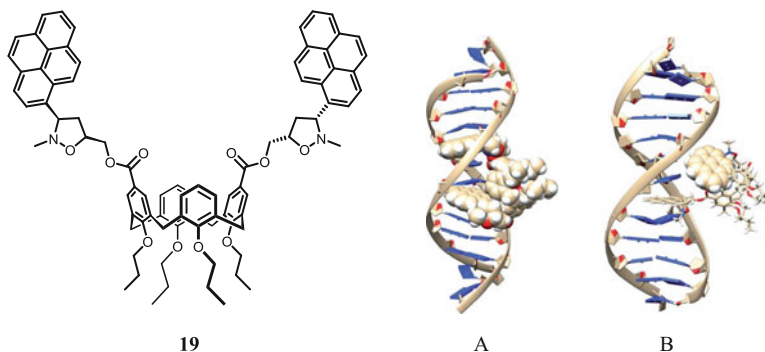
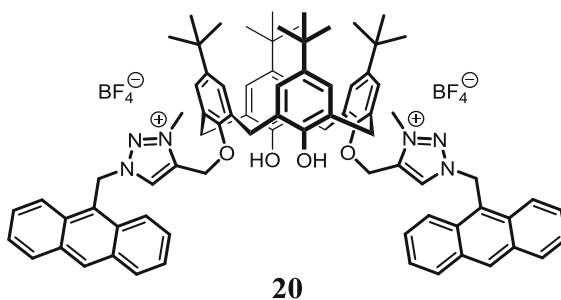


**Fig. 24.7** *Left:* PAH-calixarene derivative **19** with two pyrenylisoxazolidine moieties at the upper rim. *Right:* Plot representing **19** intercalated into the (dA–dT)<sub>2</sub> dodecamer from the major groove. After 1 ns of MD simulation, the two pyrene moieties are both intercalated (A). After 5 ns, only one pyrene moiety is still intercalated, the other one is completely deintercalated and the corresponding pocket is closed (B) [28]. (Reprinted from Ref. [28])

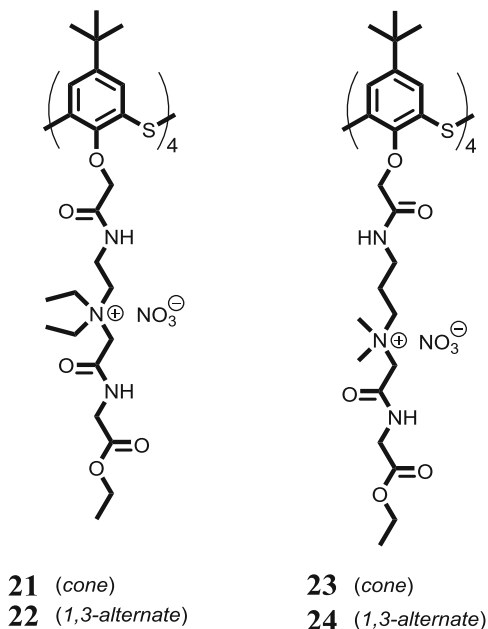
**Fig. 24.8** Lower rim 1,3-bis(anthracenyl-triazolium) calix[4]arene conjugate (**20**) [29]



precursor triazole derivative. Fluorescence titrations showed preference for NTPs (nucleoside triphosphates) over NDPs and NMPs. Among the nucleotide triphosphates the fluorescence enhancement follows the order: ATP  $\approx$  UTP > CTP  $\approx$  TTP > GTP, while the corresponding association constant for ATP, the most strongly bound guest, is about  $4 \times 10^4 \text{ M}^{-1}$  and the minimal detectable concentration is  $2.3 \mu\text{M}$ . These results suggest that the binding event not only relies on the electrostatic interactions between the cationic triazolium arms and the anionic phosphates, but also on attraction between the nucleic bases and the anthracenyl moiety. Furthermore, a Job's plot experiment revealed a complex stoichiometry of 1:2 (calixarene:NTP). Association constants gained from absorption studies confirm ATP as the strongest bound guest, GTP as the weakest. Observations from <sup>1</sup>H-NMR studies suggest ionic as well as hydrogen bond interactions. ESI-MS titrations, molecular mechanics computations as well as AFM and SEM studies contributed to the elucidation of the binding mode [29] (Fig. 24.8).

Stoikov et al. synthesized water-soluble *para-tert*-butylthiacalix[4]arenes with peptide and quaternary ammonium fragments at the lower rim in *cone* and *1,3-alternate* conformation that are able to complex DNA (**21–24**, Fig. 24.9).

**Fig. 24.9** Quaternary ammonium salts based on peptide fragment containing *para-tert*-butylthiacalix[4]arenes [30]



Experimental data obtained from UV spectroscopy, dynamic light scattering and TEM prove the formation of aggregates with hydrodynamic diameters between 70 and 140 nm at millimolar concentration in aqueous solution. The thiacalix[4]arenes interact with salmon sperm by the formation of monodisperse nanoparticles with polydispersity index of 0.09–0.21 [30].

### 24.3.2 Interactions at the Air-Water Interface

Control of the appropriate substitution pattern on the calixarene scaffold provides a convenient route to amphiphilic macrocycles. One application of these calixarene-based amphiphiles is their use as binding agents at the air-water interface.

Lu et al. used calix[4]arene derivatives with two ammonium (**25**) or guanidinium functionalities (**26**) at opposite sides of the lower rim to form stable monolayers. Inside the layer the amphiphiles are orientated orthogonal to the air-water interface (Fig. 24.10). With their cationic moieties immersed in the water phase the calixarene derivatives are able to recognize nucleotides in the subphase. The properties of the monolayer along with the recognition potential for 5'-AMP<sup>-</sup> and 5'-GMP<sup>-2</sup> were analyzed at the film balance by means of surface pressure–area ( $\pi$ -A) isotherms and relaxation experiments as well as UV, CD, TR-IR spectra and X-ray photoelectron spectra. Due to their strong molecular interactions nucleotides can even be transferred onto solid substrates along with the monolayers. The

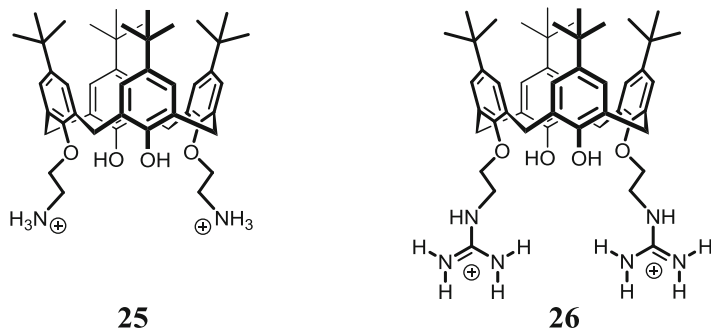


**Fig. 24.10** 1,3-Aminoethoxy- (**25**) and 1,3-guanidinoethoxycalix[4]arenes (**26**) in their protonated states [31, 32]

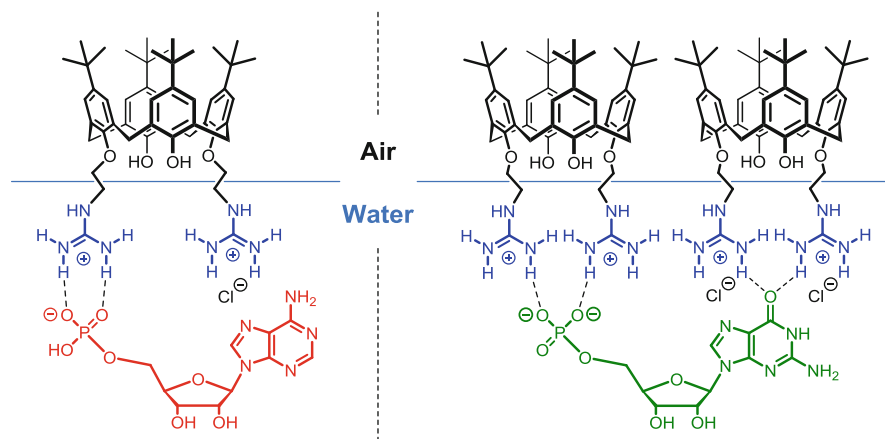


**Fig. 24.11** Interaction patterns of 1,3-substituted lower rim guanidinoethoxy calix[4]arene (**26**) with different nucleotides: 5'-AMP<sup>-</sup> (left) and 5'-GMP<sup>2-</sup> (right) [32]

binding event is proposed to rely on multiple hydrogen bonding reinforced by electrostatic attraction. Binding constants are in the range of  $10^5$ – $10^6$  M<sup>-1</sup> with a molar ratio of 1:1 for the adenosine and 1:2 for the guanosine guest (Fig. 24.11). It is proposed that complex stoichiometry depends on the difference in nucleobase and charge state of the nucleotides that cause different supramolecular interaction patterns at the air-water interface [31, 32].

Hereafter Lu et al. replaced the cationic functionality at the lower rim by a nucleobase. Hybrids between calixarenes and nucleic acid derived compounds have attracted more and more attention and will be presented in Sect. 24.4 in more detail. Equally to the amino and guanidino derivatives the uracil calixarene conjugate was used for the interfacial interaction, now specifically via base pairing to the complementary nucleoside adenine in the subphase rather than by electrostatic attraction. The same principle was used for the reverse arrangement: An adenine calixarene

conjugate that recognizes the matching nucleosides uridine and thymidine in the subphase. The nucleosides were efficiently bound to the monolayers at the interface by multiple hydrogen bonding, again making it possible to transfer them onto solid substrates along with the monolayers [33–35].

Similar to the nucleobase-calixarene conjugates described above, Shi et al. designed a calix[4]arene derivative with a uracil moiety at the upper rim by coupling uracil acetic acid directly to a mono-anilino calix[4]arene. The obtained  $\pi$ -A isotherms again indicate the formation of supramolecular complexes at the air-water interface, that rely on the base pairing between uracil and adenine moieties. Furthermore ESI-MS experiments showed that the uracil calixarene conjugate is able to recognize adenine and adenosine from other nucleotides and bases [36].

Shahgaldian et al. used the previously described *para*-amino-tetradecyloxy-calix[4]arene (**17**) also for interactions at the air-water interface. Similar to the other interface amphiphiles, upon compression the molecule adopts an orthogonal orientation to the surface. It was pointed out that the positive charges of the amine groups do not cause significant repulsive interactions within the monolayer. Moreover, the matrix-like arrangement of the particles was confirmed by atomic force microscopy measurements as illustrated previously (Fig. 24.6). Compression isotherms revealed that interaction with DNA molecules in the subphase causes an expansion of the monolayer and a phase transition from a liquid-condensed to a liquid-expanded phase. This is indicated by an increasing apparent molecular area: from 105 Å<sup>2</sup>/molecule for monolayers on pure water to 140 Å<sup>2</sup>/molecule for DNA concentrations of 100 mg/L. The attractive interactions between the positively charged surface and the negatively charged DNA are accompanied by a slight decrease in the stability of the monolayers [26] (Fig. 24.12).

The Shahgaldian group also investigated guanidiniocalix[4]arene analogue **18** in view of its potential for interactions at the air-water interface. In accordance with

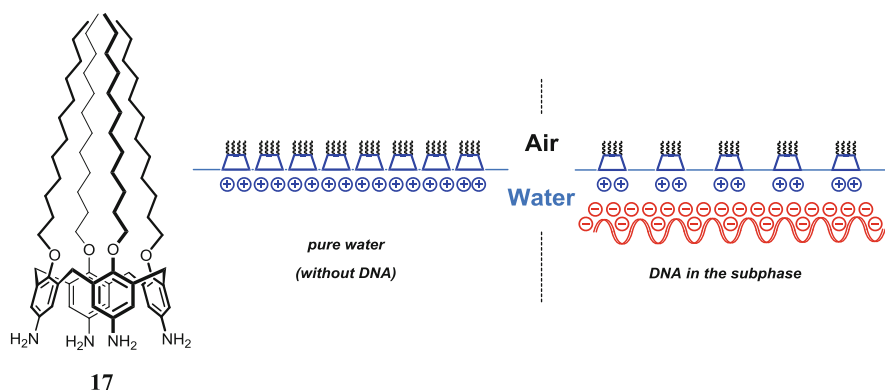


**Fig. 24.12** Structure of dodecyl anilino-calix[4]arene **17** and schematic representation of monolayers based on **17** compressed on a subphase with or without DNA [26]

the findings presented in Sect. 24.3.1 the expansion of the monolayer was found to be larger in the presence of AT- compared to GC-DNA, indicating a certain discrimination potential [37].

## 24.4 Hybrids of Calixarenes with Nucleic Acid Derivatives

Conjugates of nucleic acid related compounds (nucleobases, nucleosides and nucleotides) and calixarene scaffolds are potential candidates for the formation of well-defined supramolecular structures. Nucleobases are structurally predetermined to mediate non-covalent interactions, e.g. base pairing via hydrogen bonds and  $\pi$ -stacking to aromatic moieties. The versatile nature of the calixarene corpus provides a convenient entry to multiple pre-oriented functionalities. By this combination a broad range of supramolecular architectures becomes accessible. Over the years a number of calixarene DNA hybrids have been constructed and investigated in their complexation properties towards nucleic acid related compounds. A valuable summary on this topic is given by Kumar et al. in “Advances in Heterocyclic Chemistry” [38].

In the late 1990s de Mendoza et al. designed hybrids between calix[4]arene compounds and two cytosine-like amino-pyrimidinone derivatives (**27** and **28**) which are attached to the scaffold at the 1,3-positions. The resulting hybrids adopt a *1,3-alternate* conformation and form non-covalent dimers with two sets of four intermolecular DDAA hydrogen bonds (Fig. 24.13). The dimeric complexes

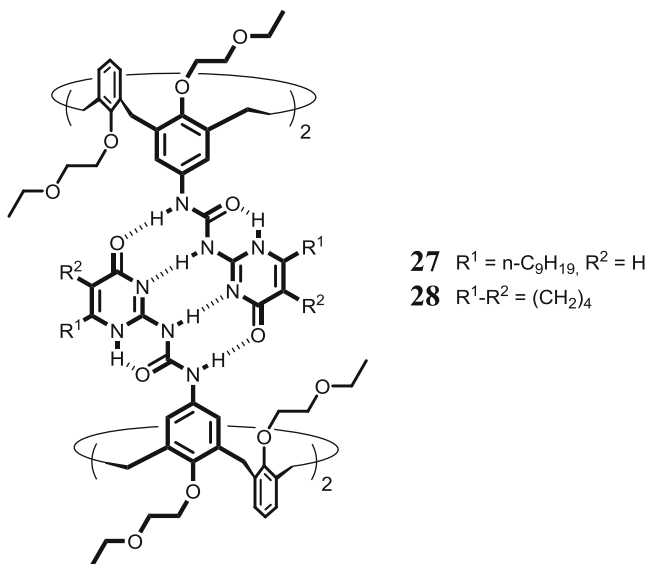


**Fig. 24.13** *1,3-alternate* ureidopyrimidin-4(1H)-one calix[4]arene dimers **27** and **28** [39]

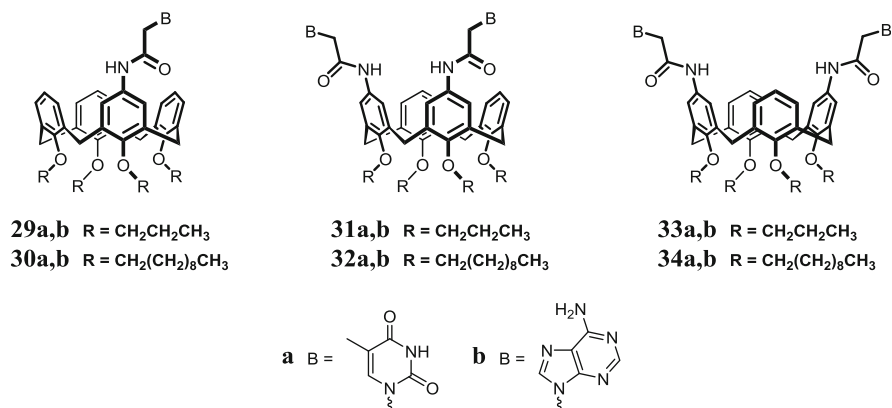


**Fig. 24.14** Cone shaped mono-, 1,2- and 1,3-disubstituted upper rim adenine and thymine calixarene derivatives [40, 41]

are soluble in nonpolar solvents like benzene and toluene, but exhibit poor or almost no solubility in DMSO or acetone. Evidence for the dimer assembly was obtained from mass spectrometry and vapor pressure osmometry (VPO) [39].

Similar to the lower rim nucleobase calixarene conjugates by Lu et al., presented previously in Sect. 24.3.1, Huang et al. synthesized *cone*-shaped calixarene derivatives with an adenine or thymine moiety at the upper rim and propyl or decyl groups at the lower rim (**29** and **30**). In contrast to the conjugates used for interfacial interaction, here the distance between the calixarene scaffold and the nucleobases is designed to be rather short: acetic acid derivatives of the nucleobases are directly connected to the aniline calixarene. <sup>1</sup>H-NMR and ESI-MS studies revealed self-association of the hybrids in solution, indicating Watson-Crick A-T base pair recognition as the main binding event [40]. Furthermore, the group extended the number of hybrids by introducing two nucleobase moieties on one calixarene scaffold (**31–34**) either in a 1,2- or a 1,3-substitution [41] (Fig. 24.14).

In 2002 Kim et al. presented similar hybrids, containing nucleosides instead of the plain nucleobases, by coupling carboxylic acid derivatives of the thymine nucleoside to *para*-1,3-diaminocalix[4]arene (**35–38**, Fig. 24.15). X-ray crystallography revealed a preference for the *pinched cone* conformation which is supposedly favored due to hydrogen bonding between amide linkages and the thymine base, resulting in an assembly of four calixnucleoside molecules coordinated by a two dimensional network with eight intermolecular hydrogen bonds (N-H...O). Furthermore, an NMR Job plot between a hybrid and an acetylated adenosine derivative revealed 1:1 complex formation [42].

These calixnucleosides were designed as a scaffold for DNA hairpin structure mimics. Hairpin type oligonucleotides enable the recognition of complementary strands through triplex formation. Infact, incorporation into oligonucleotides effected a V-shape of the calix[4]arene-oligonucleotide hybrids, indicated by



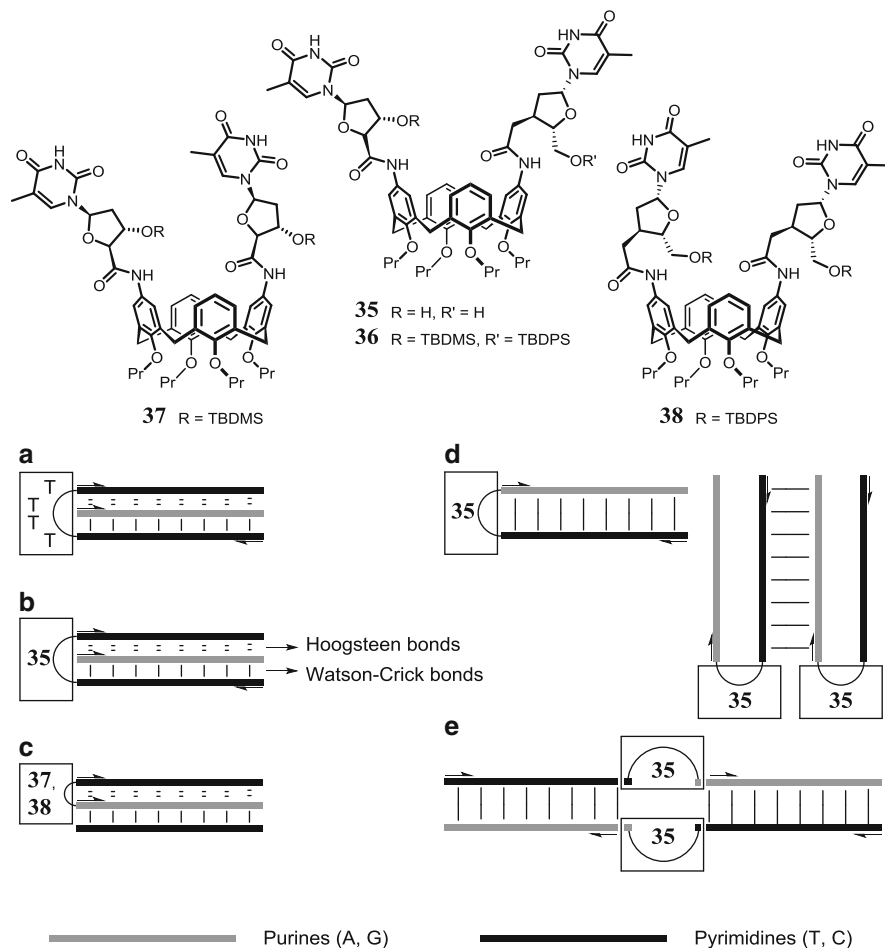


**Fig. 24.15** Above: Thymidine calix[4]nucleosides [42, 43]. Possible triplex formation patterns with hairpin structures: (a) natural type, (b) hairpin moiety replaced by calixnucleoside **35**, (c) hairpin moiety replaced by calixnucleoside **37** or **38** [42]. Possible intra- and intermolecular structures adopted by calixnucleotides: (d) Hairpin structure: intramolecular base pairing; (e) bulged duplex: intermolecular base pairing; (f) V-shaped aggregate: intermolecular base pairing [43]

UV-monitored thermal denaturation experiments and CD spectra. Further experimental data obtained from melting curves point out that intermolecular base pairing is more favorable than intramolecular H-bond formation. Possible triplex formation patterns and structures with intra- and intermolecular base pairing are illustrated in Fig. 24.15. In this context the hybrid compounds may serve as versatile building blocks for the construction of oligonucleotide nanostructures [42, 43].

Davis et al. presented a *1,3-alternate* calix[4]arene equipped with four guanosine units at the lower rim (**39**) that is able to form self-assembled nanotubes. In the

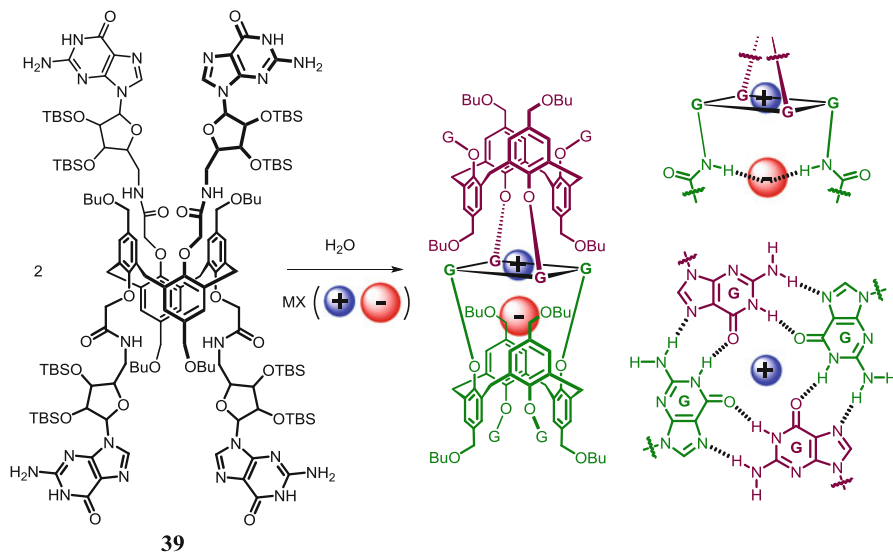


**Fig. 24.16** Structure of the tetrakis(guanosine)calix[4]arene (**39**) and the schematic representation of the G-quartet self-assembled dimer. Anion binding by the amide protons and cation complexation by the G-quartet are presented separately. Water molecules in the complex core necessary for the self-assembly are omitted for clarity [45]

presence of sodium cations two guanosine moieties on one side of the calixarene form intermolecular G-quartets with two guanosine moieties from the next calixarene unit. In practice, the nanostructures are formed upon addition of  $\text{NaBPh}_4$  to a solution of **39** in a binary MeCN/water mixture (1:1) effecting instantaneous and quantitative precipitation of the nanotubes as a white solid. TEM images illustrate that the precipitate consists of single or bundled micrometer-long strands, confirming the proposed tube-like structure [44].

Later it was shown that the above-presented calix[4]arene-guanosine conjugate is able to form water-stabilized dimers with a central intermolecular G-quartet assembly that may act as a cation binding site. In addition, the neighboring 5'-amide NH-groups provide an anion complexation site turning the dimeric assembly into an ion pair receptor (Fig. 24.16). These findings were elucidated by thorough NMR experiments and CD spectroscopic investigations. Interestingly, a modest selectivity for extracting  $\text{K}^+$  over  $\text{Na}^+$  and  $\text{Br}^-$  over  $\text{Cl}^-$  was indicated. Furthermore, the type of anion determines the association process. Whereas chloride complexation results in the formation of a soluble, discrete dimer, addition of the large non-coordinating  $\text{BPh}_4^-$  anion creates a noncovalent polymer with extensive aggregation and precipitation [45].

Shi et al. synthesized a lower rim uridine-substituted *para-tert*-butylcalix[4]arene derivative and examined its recognition potential for ATP, GMP and adenine as well as  $\text{KH}_2\text{PO}_4$ . UV-vis spectroscopic studies revealed a hypochromic effect only for adenine and ATP, implying molecular recognition by the uridine

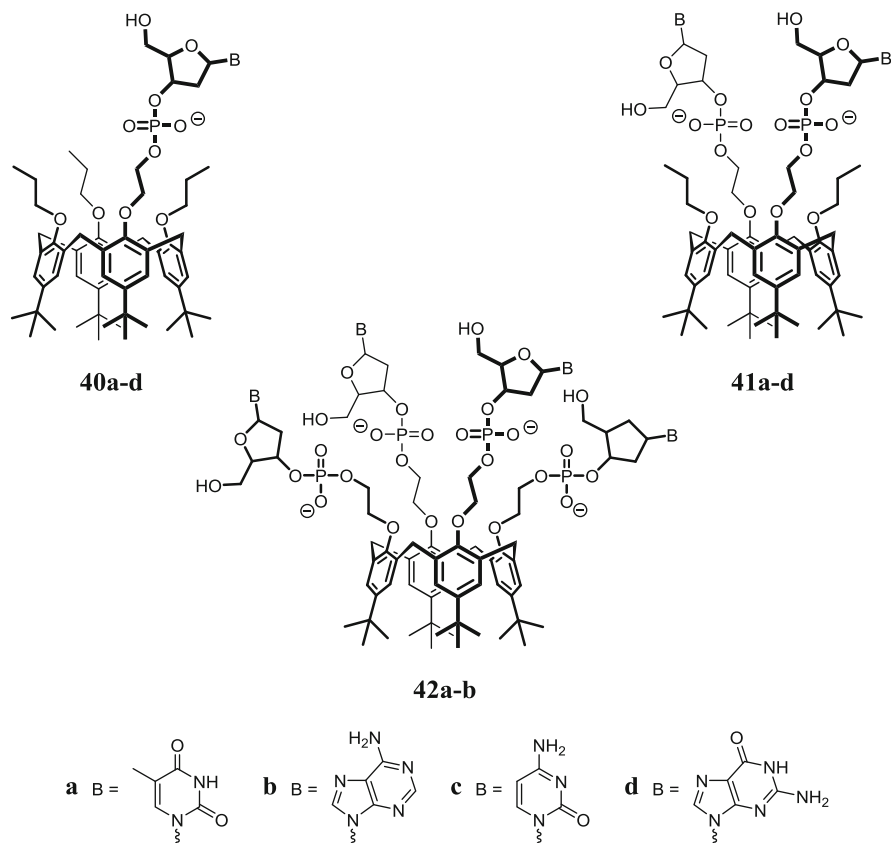


**Fig. 24.17** Nucleotide calix[4]arene conjugates [47–50]

calixarene conjugate. This is underlined by an association constant for adenine of  $2 \times 10^4 \text{ M}^{-1}$  [46].

Consoli and Geraci et al. presented calix[4]arene conjugates bearing either one (**40a–d**) or two nucleotides (**41a–d**) at the lower and *tert*-butyl groups at the upper rim (Fig. 24.17). These hybrid compounds were the first examples of nucleotides attached to the lower rim by a phosphodiester bond [47].

Subsequently the group further examined the self-assembly of the thymine-containing compound **41a** in  $\text{CDCl}_3$ . FT-IR, ESI-MS,  $^1\text{H}$ - and DOSY-NMR spectra provided experimental evidence for a dimeric assembly as well as triangular trimeric supramolecular assemblies by hydrogen bonding between the thymine moieties. Furthermore, it was shown that switching between the two aggregate types can be triggered by simple protonation/deprotonation of the nucleotide phosphate groups [48].

Later Consoli and Geraci et al. generated water-soluble calixarene derivatives (**42a–d**) bearing four nucleotide moieties (Fig. 24.17). These hybrids do not only show a high tendency for self-assembly in polar solvents, but they are also able to

interfere with DNA replication *in vitro*, shown by a polymerase chain reaction assay (PCR). Compared to analogous nucleotide compounds lacking the macrocyclic calixarene template, the observed inhibitory effect is unique. Most probably, tight binding to the DNA polymerase is accomplished by the multivalent presentation of the nucleotide moieties, along with electrostatic interactions between basic residues on the polymerase and the anionic nucleotide phosphate groups that draw both molecules close to each other [49, 50].

Recently Chawla et al. designed lower rim nucleobase calix[4]arene conjugates with two adenine moieties in a 1,3-substitution connected via a short alkyl chain and *tert*-butyl groups at the upper rim. The other two phenol functionalities were previously masked by the reaction with bromo ethyl acetate. Although lacking anionic phosphate groups, the hybrid is able to recognize biologically important cations like  $\text{Zn}^{2+}$  and  $\text{Mn}^{2+}$  ions in a 1:1 stoichiometry. Experimental data was obtained by UV, IR, NMR and ESI-MS analyses. UV-vis titrations in methanol/acetonitrile (1:1, v/v) revealed association constants of  $3.6 \times 10^5 \text{ M}^{-1}$  for  $\text{Zn}^{2+}$  and  $1.6 \times 10^5 \text{ M}^{-1}$  for  $\text{Mn}^{2+}$ . The stronger binding of zinc(II) cations is suggested to be a consequence of the cavity size of the adenine calixarene conjugate [51].

## 24.5 Hetero-Calixarenes

Hetero-calixarenes represent another interesting group of calixarene-related compounds that can be used for the interaction with nucleic acids and related compounds. Due to their constitutional variation their structural features significantly differ from the corresponding original calixarene scaffolds. Still there is a number of examples worth considering in the broad context of calixarenes and nucleic acids.

In 2002 Sessler et al. designed two cytosine-substituted calix[4]pyrrole conjugates with a cytosine moiety attached either at a  $\beta$ - or *meso*-pyrrolic position (**43** and **44**, Fig. 24.18). These hetero-calix[4]arene nucleobase conjugates were tested as nucleotide-selective carriers and as active components of nucleotide-sensing ion-selective electrodes [52].

Whereas the *meso*-linked derivative exhibited promising selectivity for the complementary nucleotide 5'-guanosine monophosphate (5'-GMP), the  $\beta$ -linked analogue transports the cytosine monophosphate nearly five times faster than the matching guanosine nucleotide. Furthermore it was shown that the calix[4]pyrrole hybrid with *meso*-substituted cytosine is able to bind the anionic phosphate group and the guanidine moiety simultaneously, acting as a neutral ditopic receptor [52].

Based on a calix[4]pyrrol Kohnke et al. designed a *meso-para*-aniline derivative *trans*-coordinated to a Pt(II) centre (**45**). Platin complexes are commonly used as anticancer drugs and have recently received renewed attention. In this context the presented calix[4]pyrrole-*trans*-Pt(II) complex was designed as a drug delivery vehicle. In order to evaluate the potential for the assisted Pt-delivery to DNA nucleobases the complex was tested with adenosine monophosphate as a model

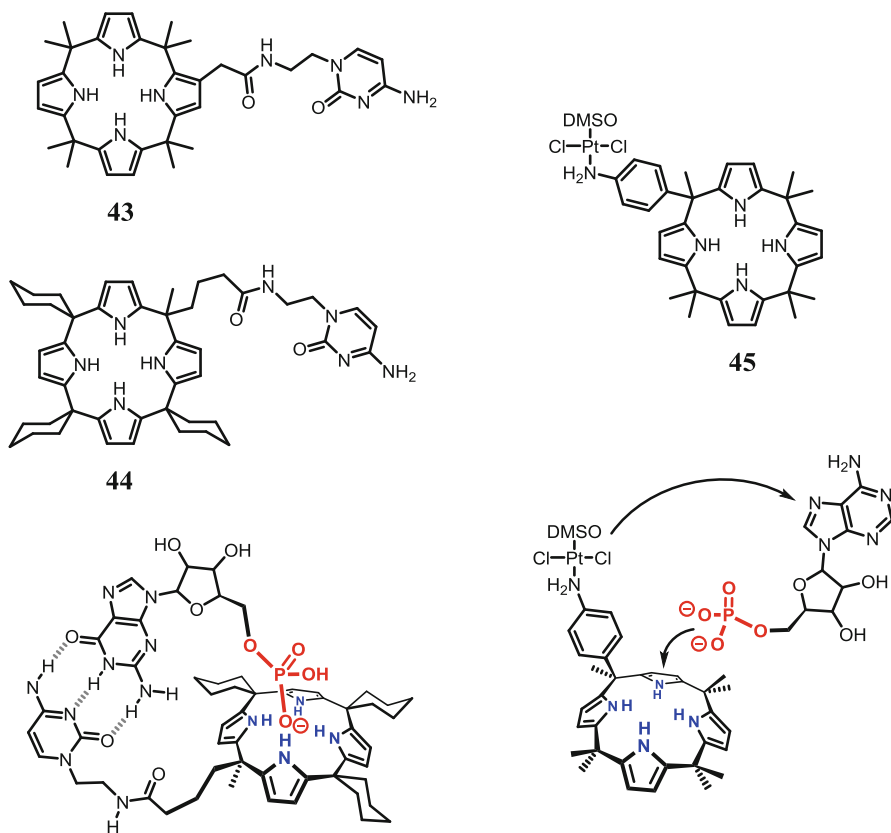


**Fig. 24.18** *Left*: cytosine calix[4]pyrrole conjugates with a connection either at the  $\beta$ - or *meso*-pyrrolic position (**43** and **44**) and complex formation of **44** with guanosine monophosphate [52]. *Right*: “drug delivery vehicle”; calix[4]pyrrole-*trans*-Pt(II) complex (**45**) and schematic representation of the interaction with adenosine monophosphate as a model compound [53]

compound. NMR experiments in dry  $\text{CD}_3\text{CN}$  indicate that the complexation of the phosphate anion of the calix[4]pyrrole is a main feature of the assisted delivery. The presence of water on the other hand prevented the calix[4]pyrrole/phosphate interaction. This hypothesis is further supported by molecular modeling and docking simulations with the dodecamer sequence CGCGAATTCGCG. Here, hydrogen bonds between the pyrrole rings and two phosphate oxygen atoms are displayed, effecting an orientation of the *trans*-Pt towards or into the minor groove, respectively [53].

Wang and Tang et al. created a flexible methylazacalix[6]pyridine (**46**) which is able to interact with G-quadruplexes (Fig. 24.19). This azacalixarene is also capable of discriminating between G-quartets and double stranded DNA as well as between different types of quadruplexes. It is argued that the distinction relies on the preferred binding to the loops, where different types of nucleotides are present [54]. In a reverse concept Tang and Xiang et al. were able to induce chirality in the

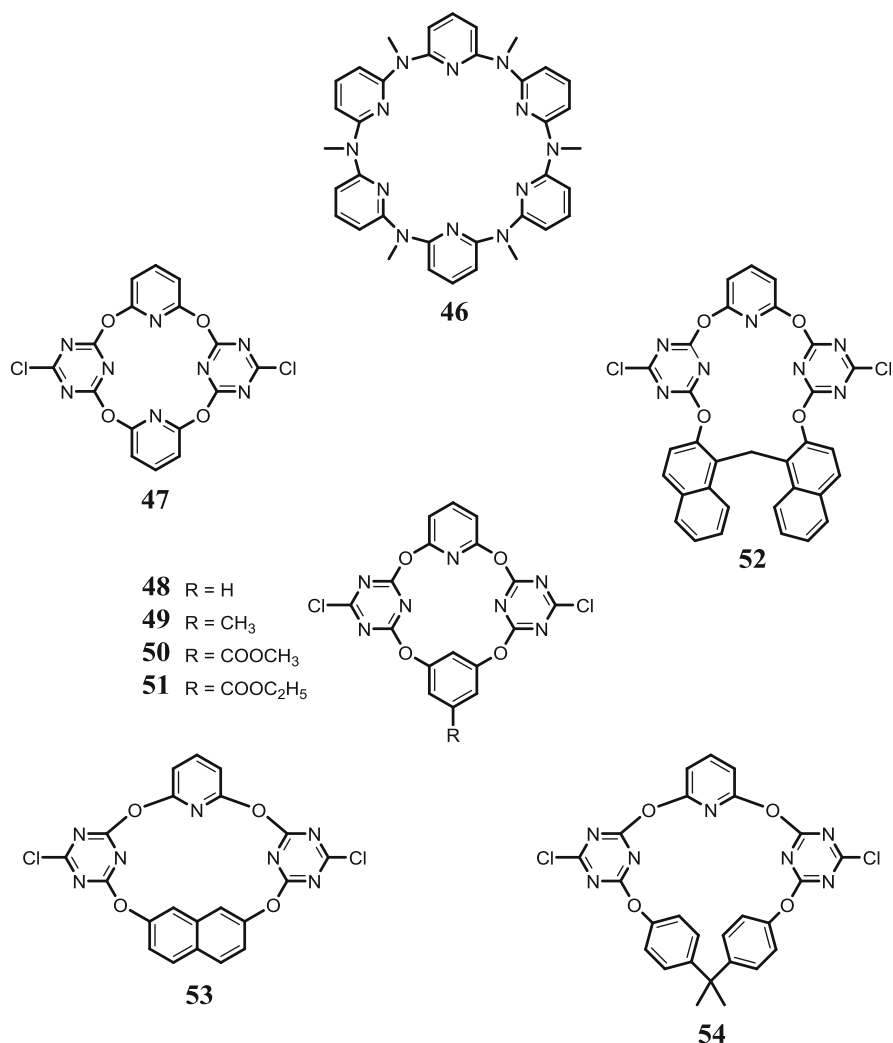


**Fig. 24.19** Methylazacalix[6]pyridine (**46**) and various oxacalix[2]arene[2]triazines (**47–54**) [54, 56]

azacalixarene **46** by template-effects of DNA. In detail, methylazacalix[6]pyridines with two opposite chiralities have been realized by templating with a G-quadruplex or an oligonucleotide. It was proven that the applied method provides a possible approach to construct chiral calixaromatics by the template-effect of G-quadruplexes [55].

Recently, Rajakumar et al. presented a set of oxygen bridged calix[2]arene[2]triazine derivatives (**47–54**) bearing pyridine and triazine moieties (Fig. 24.19). The binding properties of the oxacalixarenes towards CT-DNA were investigated by

viscosity measurements, UV-VIS and CD studies. Experimental data revealed a binding constant of  $3.4 \times 10^5 \text{ M}^{-1}$  for the best candidate (**53**). Binding of the presented oxacalixarenes to DNA is also supported by supplementary docking studies. Finally, all oxacalixarenes show a comparable antibacterial activity [56].

## 24.6 Metallacalixarenes

Heterocycles that contain ligating nitrogens are valuable compounds for metal coordination. In this respect, pyrimidine as well as purine nucleobases are well suited for the metal driven self-assembly into macrocyclic structures. The resulting unique class of compounds is referred to as metallacalixarenes, the inorganic analogues of calixarenes (Fig. 24.20). Although these display a certain similarity

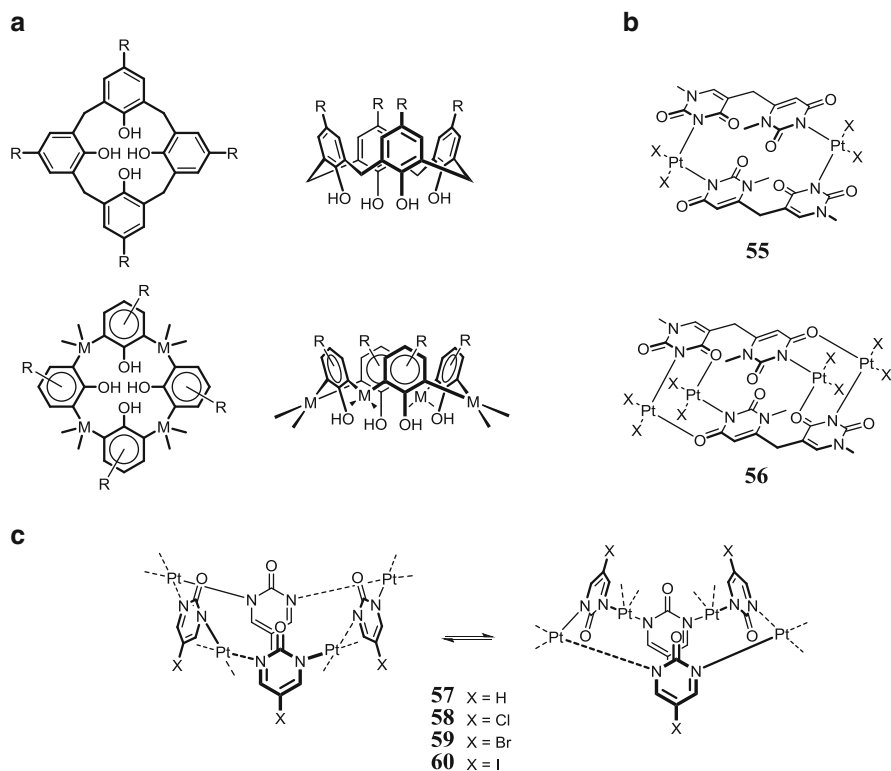


**Fig. 24.20** (a) Analogy between calix[4]arenes and metallacalix[4]arenes [60]. (b) Hybrids between organic (hetero)calix[4]arenes and Pt(II)-coordinated metalla-calix[4]arenes (**55** and **56**) [62]. (c) Platinum(II)-based metallacalix[4]arenes (**57**–**60**) interconverting between *1,3-alternate* conformation at low temperatures and *cone* conformation at higher temperatures [66]

to the classical calixarenes, substantial structural differences remain, when methylene bridges and phenol rings are replaced by metal cations and nitrogen heterocycles. 2015 marks the 50th anniversary of the discovery of cisplatin, followed by successors such as carboplatin and oxaliplatin. In the light of the enormous success of these metal-based DNA binding anticancer agents, the development of metallacalixarenes seems a logical consequence, perhaps with the expectation, that these might expand the established repertoire [57]. Kumar et al. recently presented a valuable compilation concerning metallacalixarenes derived from nucleobases in “Advances in Heterocyclic Chemistry” [58]. A thorough review on the synthesis and applications of metallacalixarenes is given by Kulesza et al. [59].

A great deal of pioneering work comes from the Lippert group. In 2003, they were among the first groups that introduced chiral pyrimidine metallacalixarenes. They synthesized a set of enantiomerically pure cyclic polynuclear complexes consisting of 2-hydroxypyrimidine, 4(3H)-pyrimidone or 4,6-dimethyl-2-hydroxypyrimidine heterocyclic ligating compounds on the one hand and palladium cations on the other hand. The complexes were studied by  $^1\text{H-NMR}$  spectroscopy and X-ray crystallography, elucidating structural features like crystal system and size. Furthermore, the virtue of the complexes as molecular receptors of mononucleotides was investigated by NMR experiments in aqueous solution, indicating that indeed two metallacalixarenes exhibit recognition potential for AMP, with a potential application as metal-based DNA-binding drugs. As a general insight regarding the stability of metallacalixarenes, it was shown that tetranuclear species are entropically favoured over the corresponding hexanuclear derivatives. This was experimentally proven by slow conversion of calix[6]- to calix[4]arenes at higher temperatures [60].

The Lippert group further investigated the field of pyrimidine metallacalixarenes and synthesized a series of multinuclear mixed-metal (Pt, Pd), mixed-nucleobase (uracil, cytosine) complexes, which were characterized by X-ray crystallography. The nucleobases adopt an *1,3-alternate* conformation in the solid state, regardless of the nucleobase connectivity. Hence, the structures lack a void for inclusion of anions or solvent molecules, unlike the hydrophobic cavity present in many non-metallic *cone*-shaped calix[4]arene derivatives [61]. By combining bis(1-methyluracil-5-yl)-methane with square-planar  $\text{Pt}^{\text{II}}$  entities Lippert et al. introduced a kind of hybrid between classical organic calix[4]arenes and metallacalix[4]arenes. Assemblies with two or four metal ions are formed, depending on the nature of the co-ligands bound to the  $\text{Pt}^{\text{II}}$ -atom. This self-assembly process results in either neutral or positively charged complexes (55 and 56, Fig. 24.20) [62].

Furthermore, the Lippert group designed two isomeric cyclic octanuclear complexes with four bridging cytosins, in which the nucleobases act as tetradentate ligands [63]. Additional investigations on the assembly of metallacalix[*n*]arenes with pyrimidine ligands were carried out in order to further elucidate the basic principles that govern the formation of metallacycles, consisting of Pt- and/or Pd-cations and the pyrimidine nucleobases [64, 65].



Similar to the complexes presented by the Lippert group, Hannon et al. developed a series of platinum(II)-based metallacalix[4]arenes (**57–60**), that are able to interact with DNA in a non-covalent fashion (Fig. 24.20). UV-Vis binding studies exclude intercalation and insights from CD and LD spectra indicate a DNA binding mode in a specific orientation, most likely inside the major groove. The four metallacalix[4]arenes displayed significant differences in their fluorescence and NMR spectra. Furthermore gel electrophoresis experiments and AFM images indicate strong interactions between the metal-coordinated macrocycles and DNA [66].

Finally, De Munno et al. reported the one-pot synthesis of a stable polynuclear copper(II)-cytidine complex, entitled as the “nucleoside-wheel”. Surprisingly, despite the positive charges from eight copper(II) centers the complex is able to act as a host for  $[\text{Cu}(\text{H}_2\text{O})_6]^{2+}$  cations. These unique complexes provide new opportunities for specific molecular recognition in the broad field of host-guest chemistry [67].

## 24.7 Applications

### 24.7.1 Condensation, Aggregation and Transfection

Gene therapy was introduced to substitute defective genes or to disrupt their expression. Its success depends largely on efficient gene delivery vehicles. As an alternative to viral systems, mild non-viral gene transfer into cells has been explored in recent years with artificial delivery vectors. These must bind to DNA and thereby greatly reduce its volume, without carrying high positive charges. In addition, the resulting aggregates must be taken up efficiently by cells, but must not lead to elevated cytotoxicity. In recent years, calixarenes have been discovered as ideal preorganized platforms, which can be equipped with cationic groups on their upper rim and with alkyl tails at their lower rim. Programmed hierarchical self-assembly often occurs in the presence of plasmid DNA and produces promising new materials for gene delivery into cells.

Multivalent presentation of guanidinium groups on calixarene scaffolds has been exploited very successfully to deliver genetic material into cells. The Ungaro group discovered the ability of calix[4]arenes with guanidinium groups at the upper rim and hydrophobic tails at the lower rim to bind, condense and transport DNA across cell membranes. In a systematic study, it was found that small rigid calixarenes in the *cone* conformation form tight complexes with the phosphodiester backbone, followed by hydrophobic interaction between their lipophilic tails, which lead to very compact collapsed DNA plasmids. On the contrary, conformationally flexible larger ring sizes lead to extended interstrand aggregates, which do not collapse, as evidenced by AFM studies. Interestingly, only the first species promotes cell

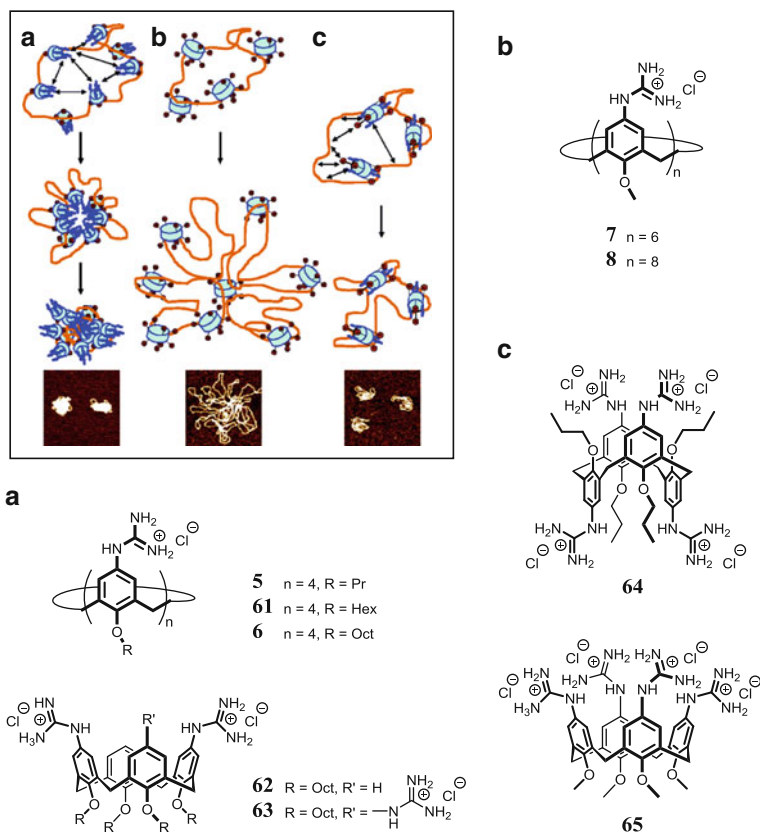


**Fig. 24.21** Schematic representation of possible condensation processes induced by (a) the *cone* guanidinium calix[4]arenes, (b) the conformationally mobile calix[6]- and calix[8]arenes, and (c) the 1,3-alternate and the mobile calix[4]arene and AFM images of the aggregates [68]. (Reprinted from Ref. [68])

transfection, indicating a subtle interplay of hydrophobic and electrostatic interactions (5–8 and 61–65, Fig. 24.21) [68].

Shortly afterwards a new class of cytofectins was synthesized with guanidinium ions attached to the phenolic oxygens of a calix[4]arene core by way of a C<sub>3</sub>-linker (66–68, Fig. 24.22). Again compact DNA material was formed which could be used for efficient transfection of GFP in combination with helper lipid DOPE (2,3-di-(oleolyloxy)propyl phosphatidyl ethanolamine). This time, however, the cell toxicity was negligible. Macrocyclic vectors were found to be superior to linear Gemini-type analogues, with the best systems outperforming the commercially available lipofectamine LTX [69, 70].

Recently, the calix[4]arene scaffold could be used to achieve arginine clustering when four basic amino acid residues were attached via peptide bond formation to the upper or lower rim of amphiphilic *cone* calix[4]arenes (69 and 70). These new

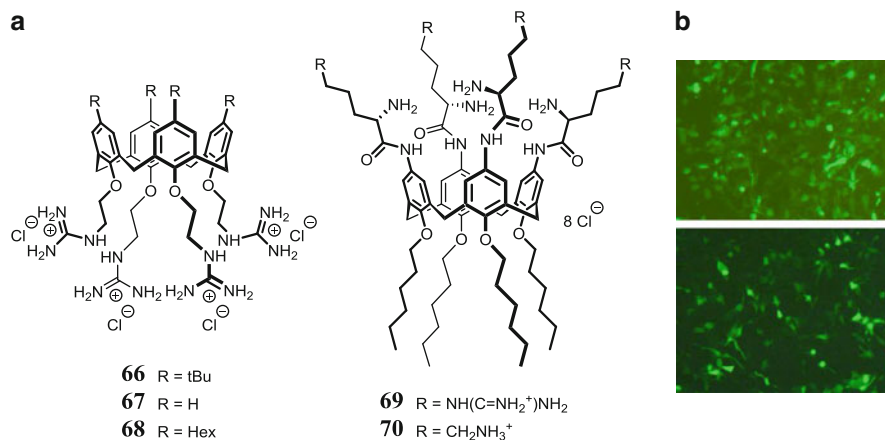


**Fig. 24.22** (a) Lower rim guanidinocalixarenes **66**–**68** and upper rim peptidocalix[4]-arenes **69** and **70** [69, 71]. (b) Cell transfection experiments. Images by fluorescence microscopy of human Rhabdomyosarcoma cells transfected (in green) upon treatment (at 48 h) with EGFP-C1 plasmid 1 nM formulated with (top) 10 mM calixarene **69** and (bottom) LTX [69]. (Reprinted from Ref. [71])

materials boosted the cell penetrating properties of conventional oligoarginine fragments by convergent presentation of only four arginine residues in an amphiphilic environment. Most likely, the presence of unprotected  $\alpha$ -amines helps to protect the vector-DNA complex from lysosomal degradation and facilitates cargo release from the endosomes into the cytosol [71].

In a comparative study, Fernandez et al. created an oriented library of  $\beta$ -cyclodextrin ( $\beta$ -CD) and calix[4]arene (CA<sub>4</sub>) vectors which displayed various head groups (aminothiourea, arginine or guanidinium) and the same lipophilic tails. DLS, TEM and AFM experiments revealed a new mechanism of monomeric DNA condensation by initial electrostatic attraction and subsequent formation of ( $\beta$ -CD) and (CA<sub>4</sub>) bilayers between the DNA filaments. The resulting spherical transfectious nanoparticles display superior levels of transfection when aminothiourea groups are attached to  $\beta$ -cyclodextrins or arginines are linked to calixarenes (vide supra). Surprisingly, the optimal platform strongly depends on the cell type, justifying diversity-oriented strategies in gene therapy [72] (Fig. 24.23).

The guanidinium calix[4]arene conjugates are also able to transport chloride ions across phospholipid bilayers, in various membrane models. Here the calixarene works as an anion shuttle concomitant with OH<sup>-</sup> antiport in liposomes; a selectivity sequence inverse is observed with chloride transported faster than bromide [73].

The Klymchenko group introduced a hierarchical assembly protocol between amphiphilic calixarenes such as **71** and DNA to generate virus-sized nanoparticles for gene delivery (Fig. 24.24). In a two-step process cationic calix[4]arenes with choline headgroups at the upper and long alkyl tails at the lower rim were subjected

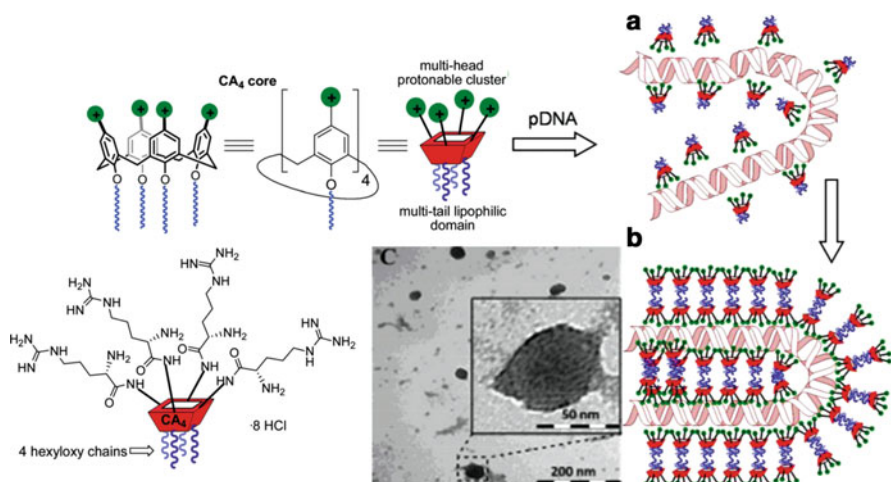


**Fig. 24.23** Schematic representation of the CA<sub>4</sub> vector **69** in the optimal upper-rim protonable *cone* arrangement. Schematic representation of the proposed mechanism for pDNA complexation by polycationic amphiphilic macrocycles involving electrostatically- driven templating (**a**) and bilayer zipping/nanocondensation (**b**). The TEM micrograph corresponding to the nanocomplexes formulated with compound **69** at N/P 10, is also presented (**c**). The typical snake-like ultra-thin structure can be appreciated in the insert [72]. (Reprinted from Ref. [72])

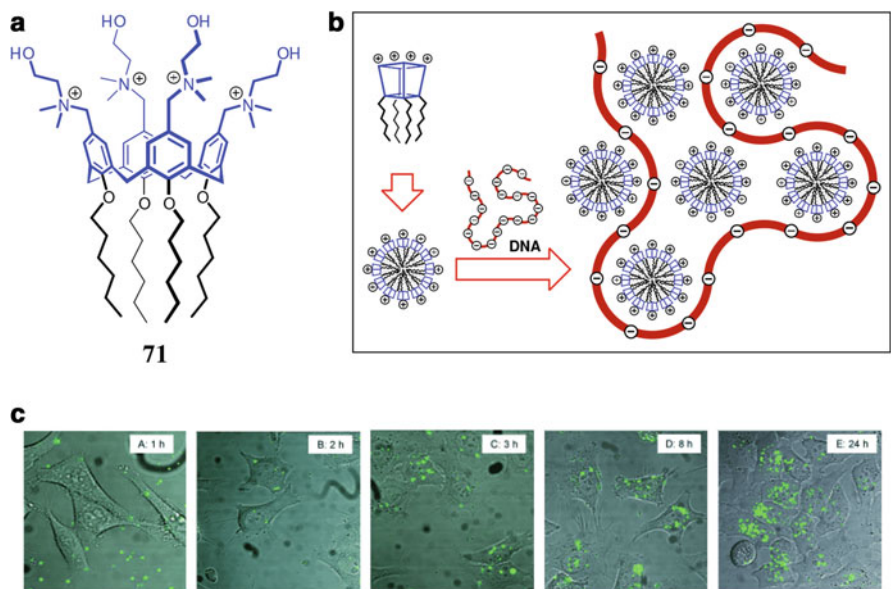


**Fig. 24.24** (a) Chemical structure of the choline calix[4]arene **71**. (b) Simplified scheme for self-assembly of **71** into micelles and further formation of the DNA complex. (c) Fluorescence imaging of HeLa cells incubated for different times with **69**/DOPE/pDNA complexes (N/P = 5) stained with YOYO-1 [74]. (Reprinted from Ref. [74])

to micelle formation (6 nm diameter), followed by electrostatically-driven DNA coassembly into nanoparticles (50 nm diameter). Fluorescence imaging of DNA-stained nanoparticles demonstrated efficient uptake into HeLa cells [74].

In a systematic study, these large calixarene-DNA nanoparticles could be optimized. It was found, that longer alkyl tails lead to smaller nanoparticles with low polydispersity, promoted gene transfection and lowered cytotoxicity. On the other hand, the introduction of additional amine head groups only altered the stoichiometry of the calixarene-DNA complexes [75].

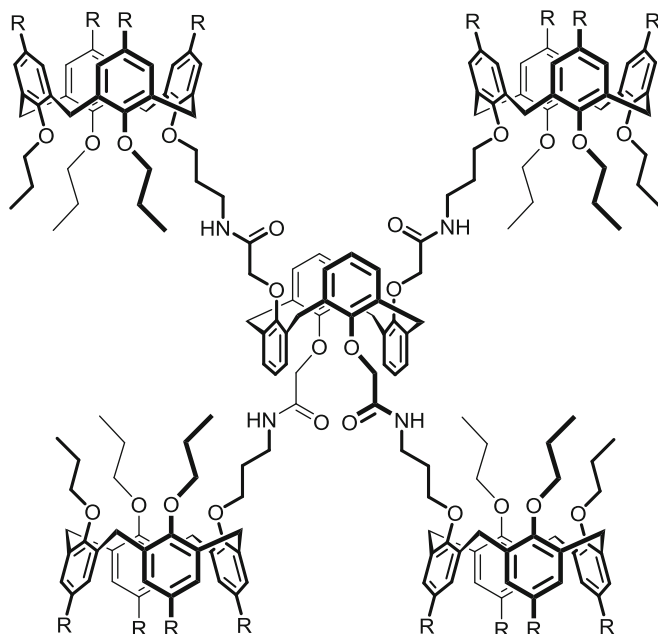
In order to achieve cooperativity between multiple preoriented groups Matthews et al. prepared amine-functionalized multicalixarenes (72–74, Fig. 24.25). A central calix[4]arene unit was used as the scaffold, and four additional calix[4]arenes were attached to it via short polar spacers. Each terminal calixarene carried a glycine extension with a free aliphatic amine on its upper rim. Only for multimeric calixarenes DNA binding was observed at very low concentrations, pointing to cooperativity effects. Cytotoxicity against various cell lines was found to be negligible, and gene transfection was confirmed in CHO cells at standard conditions [76].

The first example of a calixarene-based SLN, layer-by-layer coated with DNA cargo, was recently published by the Shahgaldian group: The authors prepared the SLNs by the nanoprecipitation method, starting from the well known tetraaminocalix[4]arene with dodecyl tails at the lower rim. Plasmid DNA was coated on the SLN surface, followed by alternating coatings with plasmid DNA and polycationic labeled chitosan. MDCK cells were transfected with the new DNA carrying materials, and no decrease in cell viability was observed. Uptake into the cell was confirmed by confocal microscopy and GFP expression [77].

A complete biophysical and biological study was very recently conducted by Junquera et al., who used lipoplexes from tetracationic calixarene TMAC4 (75) and the helper lipid DOPE (Fig. 24.26). The resulting nanoaggregates were investigated by zeta potential measurements (PALS), agarose gel electrophoresis, small angle scattering (SAXS), cryo-TEM, AFM, fluorescence microscopy and cytotoxicity assays. Various populations of nanoaggregates were found, which become all organized in  $L_{\alpha}$  multilamellar structures in the presence of p-DNA. The bound plasmid DNA seems to make the lipid bilayer more deformable, thus enhancing the capability of penetrating the cells [78].

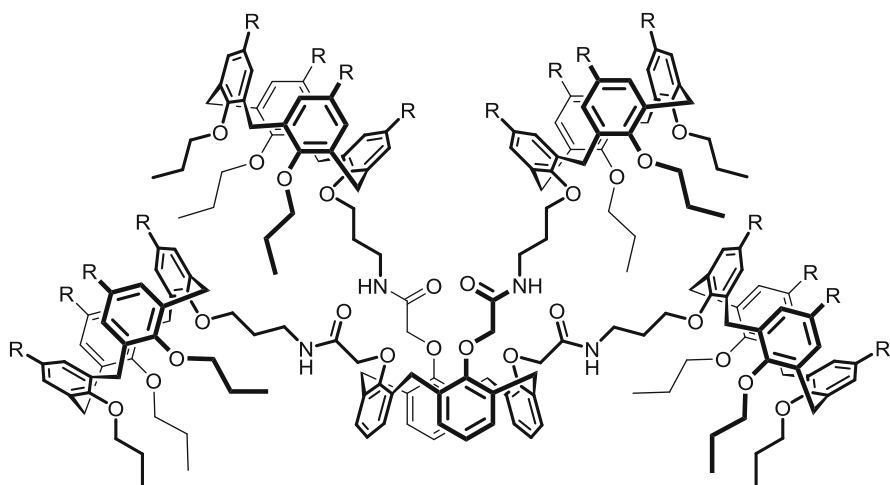
Another more structural study was conducted with a special dinitrodiester calix[4]arene. Lopez-Cornejo et al. describe significant changes in the conformation of CT-DNA. At low macrocycle concentration denaturation and polynucleotide condensation into a globular structure was observed. Conversely at higher molar ratios of the calixarene, decondensation into an extended DNA state occurs, most likely due to calixarene stacking. The implications on gene transfection are mentioned, but not studied experimentally [79].

Several reviews appeared in recent years, which covered in part the use of calixarene derivatives as non-viral vectors for gene transfection. Mellet and Fernandez summarized preorganized macromolecular systems such as cyclodextrins, fullerenes and cavitands which self-assemble into transfectious nanoparticles



**72** R =  $\text{NH}_3^+\text{Cl}^-$

**73** R =  $\text{NHCOCH}_2\text{NH}_3^+\text{Cl}^-$



**74** R =  $\text{NH}_3^+\text{Cl}^-$

Fig. 24.25 Multicalixarenes **72**, **73** and **74**; only **73** shows transfection [76]

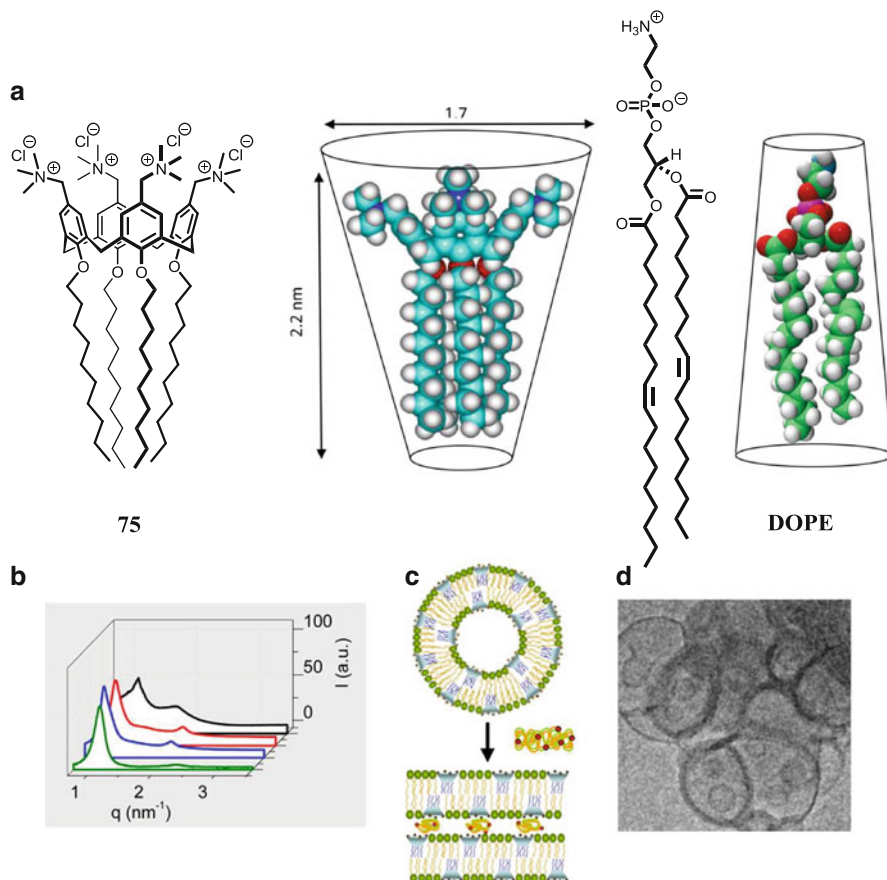


**Fig. 24.26** (a) Molecular Structures of **75** and DOPE. (b) SAXS diffractograms of **75**/DOPE-pDNA lipoplexes at several various CxCL (Calixarene Cationic Lipid) molar fractions. (c) Mixed liposome from **75**/DOPE at  $\alpha=0.5$  and a lamellar  $L_{\alpha}$  phase, derived thereof. (d) Cryo-TEM micrograph showing a general view of the **75**/DOPE-pDNA lipoplex nanoaggregates at CxCL molar fractions of  $\alpha=0.2$  [78]. (Reprinted from Ref. [78])

[80]. With a focus on the DNA condensation event, Xu and Yang compiled nanostructure-based agents and highlighted structure elucidation of their DNA complexes with AFM and other microscopic techniques [81]. Very recently, Kalchenko et al. gave an overview of calixarenes and related macrocycles as gene delivery vehicles, with an emphasis on the preorganized scaffold, amphiphilic substitution pattern and well-defined architecture of calixarenes. In their outlook, they challenge the community to proceed to animal testing as ultimate validation of these novel materials for gene therapy [82].



## 24.7.2 *Cleavage of Nucleic Acids and Oligonucleotides*

The convergent arrangement of four functional groups at the upper rim of calix[4]arenes has also been used to place transition metal cations in a well-defined spatial environment, and thereby promote catalysis, mostly of ester forming and cleaving reactions.

In an early paper, Shinkai et al. celebrate the “first man-made catalyst” for the regioselective cleavage of ribonucleoside 2',3'-cyclic phosphate. At pH 2, the well known parent calix[4]arene tetrasulfonate was shown to cleave the P-O (2') bond of cytidine 2',3'-cyclic phosphate. This outcome was rationalized by formation of a network of largely ionic hydrogen bonds between the calixarene anion and the protonated nucleotide [83].

Reinhoudt et al. later designed dinuclear Cu(II) complexes and used the cone-shaped calix[4]arene scaffold as a convenient platform for preorganization (Fig. 24.27). Thus, two chelating bisimidazolyl ligands were introduced at the distal positions of the upper rim, creating after addition of Cu<sup>2+</sup> ions a dinuclear cis-diaqua complex which was intended to mimic dinuclear metalloenzymes. Intriguingly, transesterification of RNA model 2-hydroxypropyl-*para*-nitrophenyl phosphate (HPNP) as well as hydrolysis of the DNA model ethyl-*para*-nitrophenyl phosphate (EPNP) were catalyzed with turnover conversion and 10,000-fold rate accelerations. Mononuclear reference complexes had much lower activity, pointing to synergism between both metal centers. Michaelis-Menten kinetics suggested double Lewis acid activation of a bridging phosphate ester, and a remarkable pK decrease of the coordinated water ligands, turning them into powerful OH<sup>-</sup> nucleophiles, similar to hydrophobic enzyme active sites [84].

In a related study, the Reinhoudt group examined di- and trinuclear Zn(II) calix[4]arene complexes. Two or three zinc cations were bound by 2,6-bis(aminomethyl)pyridyl groups at the upper rim in the distal 1,3- or 1,2,3-positions. HPNP transesterification (RNA model) was even more efficient than with the dinuclear Cu(II) complexes, and occurred at neutral conditions. Mononuclear reference complexes performed much more poorly, and thus supported cooperative effects in the hydrophobic environment of the aromatic macrocycle. Interestingly, a very similar, but rigid calixarene produced a lowered catalytic rate, while the flexible trinuclear complex exhibited weaker substrate binding but superior rate acceleration. In a tentatively proposed mechanism, two zinc cations activate the phosphate ester and another activates the 2-hydroxyl group of the substrate [85, 86].

The first dinucleotide cleavage with the trinuclear zinc complex was reported shortly afterwards; pseudo-first order rate constants were determined and a pronounced selectivity for the 3',5'-GpG RNA homodinucleotide was discovered [87]. These new dinuclear metallo-phosphodiesterase models were reviewed in 2000, and compared with other less efficient existing models [88].

A new design was published in 2006, featuring calix[4]arenes functionalized in the 1,2-, 1,3- and 1,2,3-positions of the upper rim with [12]ane-N<sub>3</sub> ligating units. In this case, only the 1,2-vicinal bimetallic complexes with Cu(II) ions exhibited high



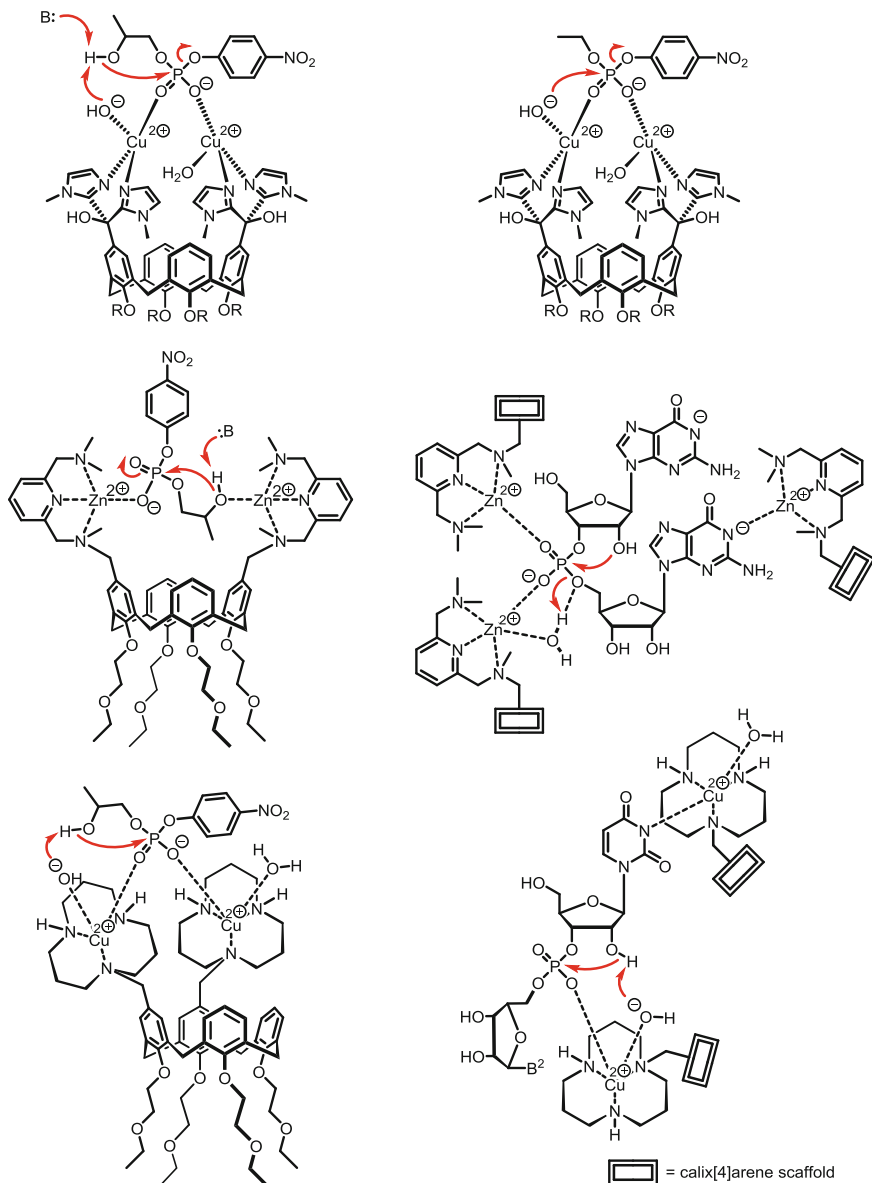


**Fig. 24.27** (a, b) Mechanism for catalytic phosphate diester cleavage by the synergistic action of two Cu(II) centers in a dinuclear *cis*-diaqua Cu(II) calix[4]arene enzyme model. (c, d) Schematic representation of possible mechanisms for Zn(II)-mediated HPNP and GpG cleavage. (e, f) Proposed mechanism of HPNP cleavage by 1,2-vicinal bimetallic copper(II) complex and model for cooperative binding and selective cleavage of UpU and UpG by a 1,2-vicinal copper(II) complex [84–89]

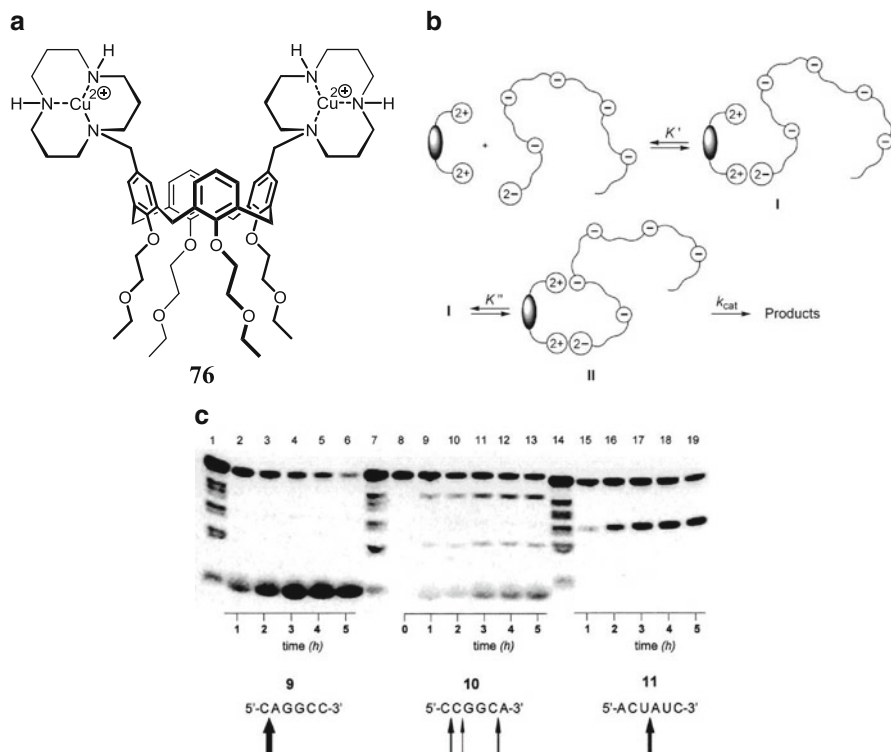


**Fig. 24.28** (a) Chemical structure of dinuclear Cu(II) calix[4]arene complex **76**. (b) Tentative mechanistic model for hexanucleotide cleavage with a  $^{32}\text{P}$ -labeled 5' terminus. (c) Gel electrophoretic autoradiograms corresponding to the cleavage of oligoribonucleotides **9–11** promoted by 50  $\mu\text{M}$  **76**. Lanes 1, 7, and 14 correspond to the aspecific hydrolysis in 0.1 M NaOH. Note the high CA- and UA-cleavage preference [90]. (Reprinted from Ref. [90])

catalytic efficiency and powerful cooperativity, both in the cleavage of HPNP and diribonucleoside monophosphates: However, here no nucleobase preference was observed [89].

Finally, in 2007, the Reinhoudt and Ungaro groups made the step to RNA oligonucleotide cleavage by their di- and trinuclear Cu(II) complexes of [12]aneN<sub>3</sub> macrocycles anchored at the upper rim of calix[4]arenes (e.g., **76**, Fig. 24.28). All complexes were found to cleave 6-, 7-, and 17-meric oligonucleotides. Enzyme-like kinetics were established in electrophoretic assays with  $^{32}\text{P}$ -labeled phosphates in the terminal 5'-position. Remarkably, all metal complexes strongly preferred the CpA sequence over other dinucleotides, similar to ribonuclease A. The trinuclear Cu(II) complex almost reached a million-fold rate enhancement [90].

Very recently, the Ungaro group replaced the transition metal cations by guanidinium groups (**77**) and switched from Lewis acid to Brønsted acid catalysis

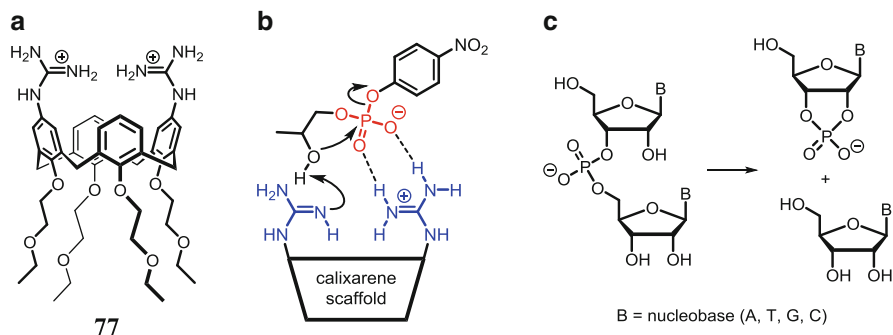


**Fig. 24.29** (a) Chemical structure of 1,3-guanidinocalix[4]arene **77**. (b) Bifunctional general acid–base catalysis of monoprotonated guanidinocalix[4]arene in the transesterification of HPNP. (c) Diribonucleotide phosphate cleavage [91, 92]

(Fig. 24.29). pH preferences in the calixarene-catalyzed HPNP cyclization (RNA model) unequivocally provided experimental evidence for the fact, that a central requirement for catalysis is the simultaneous presence of a guanidine acting as a general base and a guanidinium ion for electrophilic phosphate activation [91].

This concept was now transferred very successfully to diribonucleotide phosphate cleavage by Salvio et al. Rate accelerations approach 100,000-fold with the most favorable substrate catalyst combinations 1,2-diguanidinocalixarene and CpA as well as GPU [92].

### 24.7.3 Chromatography and Extraction

Since calixarenes can be functionalized almost at will at their upper or lower rim, they represent good candidates for new stationary phases. Similar to cyclodextrins, guests can in principle be inserted into the hydrophobic interior of the *cone*-shaped macrocycles. To this end, calixarenes of different ring sizes have been immobilized on silica gel and were studied with respect to their discrimination between nucleosides and nucleobases in HPLC separations.

Early attempts to use calixarenes as new stationary phases in the HPLC of biomolecules focussed on silica gel materials with a short hydrophilic linker between the silanol groups and the phenolic OH groups at the lower rim (Fig. 24.30). However, the new materials behaved more or less like reversed phases, and separated nucleobases according to their polarity increase [93].

Very well defined calixarenes bonded on silica gel were later prepared from distal 1,3-chloroacetate derivatives of *tert*-butyl calix[4]arene and  $\gamma$ -(ethylenediamino)-propyl-triethoxyl-silane.  $^{29}\text{Si}$  cross-polarization magic angle spinning (CP-MAS) NMR spectroscopy furnished evidence on the postulated crosslinking of a large portion of the trifunctional alkylsilyl groups to the surface of the silica gel. Retention times increased when sodium counterions were added to

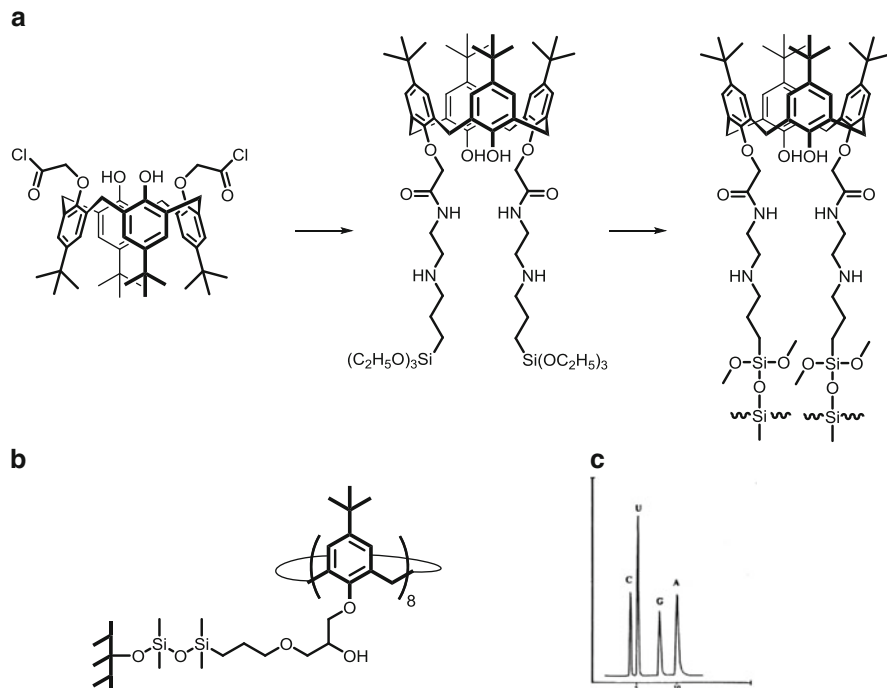


**Fig. 24.30** (a) Synthetic steps towards a *para-tert-butyl-calix[4]arene*-bonded silica stationary phase [94]. (b) Chemical structure of *para-tert-butyl-calix[8]arene*-bonded silica gel stationary phase [95]. (c) Isocratic separation of nucleosides cytidine, uridine, guanosine and adenosine on an Aren Si 60 column with 0.02 M  $\text{NaH}_2\text{PO}_4$  (pH 3.5) as mobile phase (x-axis: time in min; y-axis: absorbance at 254 nm) [93]. (Reprinted from Ref. [93])

the mixture, and almost baseline separation was achieved on coated HPLC phases for nucleosides and nucleobases [94].

When *tert-butyl calix[8]arenes* were immobilized on silica gel from a 3-glycidoxypopyl-bonded stationary phase (GBS) precursor, nucleosides and bases were strongly retained inside the mobile calixarene cavity and led to much better separation on the advanced stationary phases, especially in mobile phases with a large water content [95].

Calixarenes have also been used to extract nucleobases from aqueous solutions into chloroform (Goto et al.). In this respect, a *tert-octyl-calix[6]arene* equipped with six acetic acid moieties on its lower rim was found to form a strong 1:1 complex with adenine, and was indeed able to extract 80 % of adenine with high preference from mixtures with other nucleobases [96, 97].

Similarly, the same calixarene hexacarboxylic acid together with two equivalents of bis-(2-ethylhexyl)phosphoric acid (D2EHPA) formed a synergistic coextractant pair for adenine and cytosine from neutral aqueous buffer into isooctanol, most likely because a favorable 1:1:2 complex was formed [98].

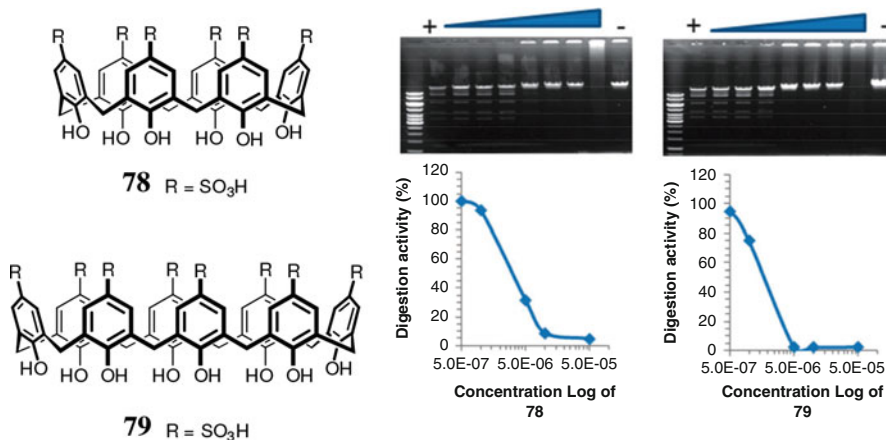


**Fig. 24.31** *Left*: Chemical structures of calix[6]- and calix[8]-arene sulfonates **78** and **79**. *Right*: IC<sub>50</sub> values for **78** and **79** acting on the restriction enzyme NruI. Gel electrophoresis was used to determine the activity of the enzyme in the presence of increasing concentrations of inhibitor [99]. (Reprinted from Ref. [99])

#### 24.7.4 Other Applications

Apart from the above-described established areas of calixarene applications, several very interesting new fields have been opened in recent years, which all rely on calixarene-DNA interactions.

After identifying the presence of multiple basic amino acids in the DNA binding site and the cleavage site of endonucleases, Coleman et al. selected three large macrocyclic host molecules, namely  $\beta$ -cyclodextrin heptasulfate, calix[6]-arene-hexasulfonate **78** and calix[8]-arene-octasulfonate **79** as potential inhibitors (Fig. 24.31). All three molecules are characterised by a combination of high negative charge and a size capable of spanning both functional sites in influenza PA endonuclease. In a typical digestion assay, IC<sub>50</sub> values in the low micromolar range were identified for all compounds, a promising starting point for further therapeutic development [99].

In a conceptual paper, Matile et al. described that CT-DNA can be activated by amphiphilic cations such as guanidiniocalixarenes **7** to act as a cation transporter in bulk and lipid bilayer membranes and showed that this unusual activity of DNA can be of interest for the development of biosensors (Fig. 24.32). In light of the charge-balancing effect of cell-penetrating peptides as anion transporters across lipid membranes, this discovery demonstrates that the multifunctionality of polyion-counterion complexes is general and occurs with low-basicity polyanions exactly as with low-acidity polycations [100].

Platinum-based DNA intercalators are important anticancer drugs, but suffer from degradation by reduced L-glutathione. Aldrich-Wright et al. hence

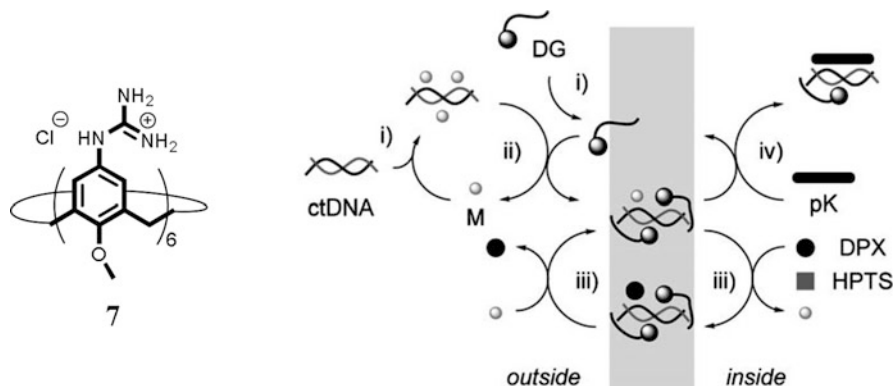


**Fig. 24.32** *Left:* Structure of guanidinium calix[6]arene **7**. *Right:* Vesicle experiments: (i) Addition of polyions (e.g., ctDNA) and counterion activators (e.g., DG, guanidiniocalixarenes) to vesicles with internal reporter ions (e.g., DPX, HPTS) and counterion inactivators (e.g., pK) triggers (ii) the formation of membrane-active polyion-counterion complexes (e.g., ctDNA-DG), (iii) DPX export, (iv) the formation of internal polyion-counterion complexes (e.g., ctDNA-DG-pK), etc; M = Na [100]. (Reprinted from Ref. [100])

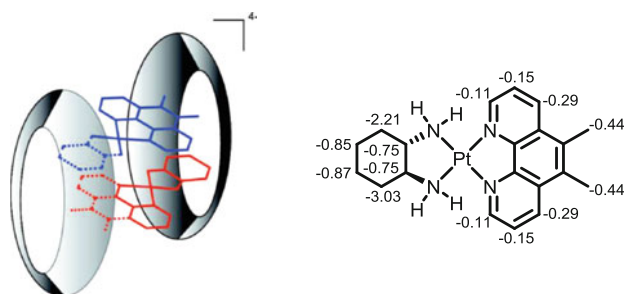


**Fig. 24.33** *Left:* Anionic 2:2 host-guest complex of [(5,6-dimethyl-1,10-phenanthroline)(1S,2S-diaminocyclohexane)platinum(II)]<sup>2+</sup> (**56MESS**) with calix[4]arene tetrasulfonate: two metal complex molecules associate in a head-to-tail fashion and carry a calixarene molecule encapsulated over either end. *Right:* Large upfield shifts experienced by the proton resonances of **56MESS** after the formation of the 2:2 host-guest complex with the tetrasulfonate calix[4]arene [101]. (Reprinted from Ref. [101])

investigated the potential protection inside self-assembled complexes with carboxylated  $\beta$ -cyclodextrins or sulfonated calix[4]arenes (Fig. 24.33). The authors indeed found that  $\beta$ -cyclodextrins formed 1:1 complexes with phenanthroline inclusion, whereas the calixarenes produced 2:2 complexes with head-to-tail stacked metal complexes capped by the macrocycles. The assemblies were structurally characterized by NMR-spectroscopic techniques and used as encapsulation vehicles in growth inhibition assays with human cancer cell lines. No decrease in cytotoxicity was observed for the protected metal complexes, rendering both macrocycles promising for in-vitro trials as drug delivery agents [101].

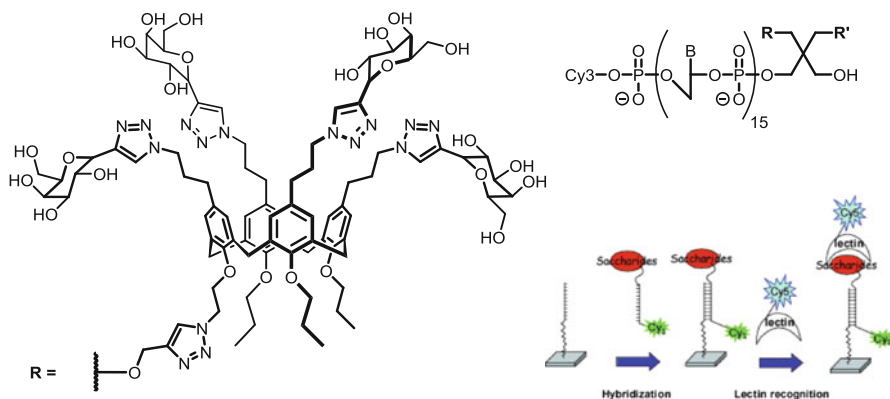


**Fig. 24.34** *Left:* Calixarene-based glycocluster (R = H, R) oligonucleotide derivatives. Cy3 = fluorescent dye. *Right:* Schematic representation of the hybridization assay for the investigation of lectin–carbohydrate interactions [102]. (Reprinted from Ref. [102])

Calixarenes have been used to spatially arrange glycoclusters in a defined predictable way (Fig. 24.34). Covalent attachment of small oligonucleotides allowed hybridization of these recognition elements for lectins on solid support (DNA chips). FRET experiments indeed demonstrated that the spatial arrangement is more important than the number of galactose residues to reach maximum lectin affinity [102].

Further applications of calixarene–DNA interactions include acridine-calix[4]arenes as anionophores, whose electrochemical signal is diminished in the presence of DNA, as a potential DNA hybridization detection using electrochemistry at the interface between two immiscible electrolyte solutions [103]. Calix[4]arene derivatives with electron-donating heterocycles at their lower rim have also been used as ionophores in polymeric membrane electrodes for Ag(I), likewise applied in a DNA hybridization assay [104]. A calix[4]crown-5-ether with aldehyde groups at its upper rim was covalently bound to an amino-coated glass slide and used for the immobilisation of proteins with arginine tags. Alternatively, short DNA strands with G<sub>9</sub> tags were immobilized by the crown ether moiety, and used for the hybridization of complementary fluorescence-labeled DNA. The calixcrown chip was able to detect single nucleotide polymorphism (one base pair mismatch) [105].

Inclusion of Solvent Violet 9 inside sulfonated calix[4–6]arenes was employed for altering its interaction with DNA [106]. Supramolecular complexes between calixarenes and nucleobases were formed as single cocrystals and shown to confine the nucleic bases inside self-assembled calixarene containers [107].

Glycoclusters have been prepared from conformationally mobile glucosylthiouracil-calix[6]- and calix[8]arenes. These interact with plasmid DNA but do not condense it, until a glucose-specific lectin is added [108]. Finally, a water-soluble carbohydrate-containing nonionic homooxalix[3]arene was synthesized; it could solubilize fullerene C<sub>60</sub> into water and the resulting complex acted as an efficient DNA photocleavage reagent [109].

## 24.8 Conclusion and Outlook

The field of calixarene nucleic acid interactions is highly attractive for chemists and biologists. Numerous new functional calixarene derivatives have been prepared in recent years which bind to nucleic acids in a predictable way and are able to interfere with biological functions. Although calixarenes are now available for intercalation, insertion in the major groove and for backbone binding, the dream of sequence-specific recognition of nucleic acids by designed calixarene derivatives has not yet been fulfilled.

A large number of detection and sensor systems has been designed with built-in DNA/RNA calixarene interactions. Important new applications have also evolved, e.g. in the area of endonuclease inhibition, cation transport across membranes, drug delivery from self-assembled calixarene capsules, immobilisation linkers for DNA, and DNA photocleavage. However, the most promising field for calixarenes still remains their use as transfection agents. Condensation, aggregation and transport of nucleic acids across membranes is stimulated by multiple preorganized cations, further supported by self-assembly into micelles or immobilization on nanoparticles. Thus, calixarene chemistry is mature for the development of drugs, diagnostics, sensors and advanced materials based on molecular recognition of nucleic acids.

## References

1. Jie K.; Zhou Y.; Yao Y.; Huang F. *Chem. Soc. Rev.* **2015**, *44*, 3568–3587.
2. Ma X.; Zhao Y. *Chem. Rev.* **2015**, *115*, 7794–7839.
3. Sansone F.; Baldini L.; Casnati A.; Ungaro R. *New J. Chem.* **2010**, *34*, 2715–2728.
4. Dondoni A.; Marra A. *Chem. Rev.* **2010**, *110*, 4949–4977.
5. Sansone F.; Casnati A. *Chem. Soc. Rev.* **2013**, *42*, 4623–4639.
6. Nimse S. B.; Kim T. *Chem. Soc. Rev.* **2013**, *42*, 366–386.
7. Giuliani M.; Morbioli I.; Sansone F.; Casnati A. *Chem. Commun.* **2015**, *51*, 14140–14159.
8. Ludwig R. *Microchim. Acta*, **2005**, *152*, 1–19.
9. Ukhatskaya E. V.; Kurkov S. V.; Matthews S. E.; Loftsson T. *J. Pharm. Sci.* **2013**, *102*, 3485–3512.
10. García-España E.; Piantanida I.; Schneider H.-J. *Monographs in Supramolecular Chemistry: Supramolecular Systems in Biomedical Fields*, **2013**, *13*, 213–259.
11. Peters M. S.; Li M.; Schrader T. *Nat. Prod. Commun.* **2012**, *7*, 409–417.
12. Baldini L.; Casnati A.; Sansone F.; Ungaro R. *Chem. Soc. Rev.* **2007**, *36*, 254–266.
13. Shi Y.; Schneider H.-J. *J. Chem. Soc., Perkin Trans. 2*, **1999**, 1797–1803.
14. Dudic M.; Colombo A.; Sansone F.; Casnati A.; Donofrio G.; Ungaro R. *Tetrahedron*, **2004**, *60*, 11613–11618.
15. Zadmart R.; Schrader T. *Angew. Chem. Int. Ed.* **2006**, *45*, 2703–2706.
16. Breitzkreuz C.; Zadmart R.; Schrader T. *Supramol. Chem.* **2008**, *20*, 109–115.
17. Zadmart R.; Taghvaei-Ganjali S.; Gorji B.; Schrader T. *Chem. Asian J.* **2009**, *4*, 1458–1464.
18. Dervan P. B. *Bioorgan. Med. Chem.* **2001**, *9*, 2215–2235.
19. Blecking C. J.; Hu W.; Zadmart R.; Dasgupta A.; Schrader T. *Synthesis*, **2011**, *8*, 1193–1204.



20. Hu W.; Blecking C.; Kralj M.; Šuman L.; Piantanida I.; Schrader T. *Chem. Eur. J.* **2012**, *18*, 3589–3597.
21. Zadmand R.; Hajiramezanali M. *Lett. Org. Chem.* **2013**, *10*, 590–593.
22. Mirza-Aghayan M.; Yarmohammadi M.; Zadmand R.; Boukherroub R. *Supramol. Chem.* **2014**, *26*, 442–449.
23. Tauran Y.; Grosso M.; Brioude A.; Kassab R.; Coleman A. W. *Chem. Commun.* **2011**, *47*, 10013–10015.
24. Valluro G.; Georghiou P. E.; Slee, H. F.; Perret F.; Montasser I.; Grandvoinet A.; Brolles L.; Coleman A. W. *Supramol. Chem.* **2014**, *26*, 561–568.
25. Lu Y.; Xiao C.; Yu Z.; Zeng X.; Ren Y.; Li C. *J. Mater. Chem.* **2009**, *19*, 8796–8802.
26. Shahgaldian P.; Sciotti M. A.; Pieles U. *Langmuir*, **2008**, *24*, 8522–8526.
27. Rullaund V.; Siragusa M.; Cumbo A.; Gygax D.; Shahgaldian P. *Chem. Commun.* **2012**, *48*, 12186–12188.
28. Rescifina A.; Zagni C.; Mineo P. G.; Giofrè S. V.; Chiacchio U.; Tommasone S.; Talotta C.; Gaeta C.; Neri P. *Eur. J. Org. Chem.* **2014**, 7605–7613.
29. Sreenivasu Mummdivarapu V. V.; Kumar Hinge V.; Samanta K.; Yarramala D. S.; Rao C. P. *Chem. Eur. J.* **2014**, *20*, 14378–14386.
30. Padnya P. L.; Andreyko E. A.; Mostovaya O. A.; Rizvanov I. Kh.; Stoikov I. I. *Org. Biomol. Chem.* **2015**, *13*, 5894–5904.
31. Liu F.; Lu G.-Y.; He W.-J.; Liu M.-H.; Zhu L.-G. *Thin Solid Films*, **2002**, *414*, 72–77.
32. Liu F.; Lu G.-Y.; He W.-J.; Liu M.-H.; Zhu L.-G. Wu H.M. *New J. Chem.* **2002**, *26*, 601–606.
33. Wang Z.-S.; Lu G.-Y.; Guo X.; Wu H.-M. *Supramol. Chem.* **2003**, *15*, 327–334.
34. Wang Z.-S.; Lu G.-Y.; Sheng X.; Guo X.; Jin C.-M. *Chin. J. Chem.* **2003**, *21*, 600–603.
35. Guo X.; Lu G.-Y.; Li Y. *Thin Solid Films*, **2004**, *460*, 264–268.
36. Shi H.-J.; Shi X.-F. Yao T.-M.; Ji L.-N. *Chin. J. Chem.* **2008**, *26*, 170–174.
37. Rullaund V.; Moridi N.; Shahgaldian P.; *Langmuir*, **2014**, *30*, 8675–8679.
38. Kumar S.; Luxami V.; Singh H. *Adv. Heterocycl. Chem.* **2009**, *97*, 219–290.
39. González J. J.; Prados P.; de Mendoza J. *Angew. Chem. Int. Ed.* **1999**, *38*, 525–528.
40. Zeng C.-C.; Tang Y.-L.; Zheng Q.-Y.; Huang L.-J.; Xin B.; Huang Z.-T. *Tetrahedron Letters*, **2001**, *42*, 6179–6181.
41. Zeng C.-C.; Zheng Q.-Y.; Tang Y.-L.; Huang Z.-T. *Tetrahedron*, **2003**, *59*, 2539–2548.
42. Kim S. J.; Kim B. H. *Tetrahedron Lett.* **2002**, *43*, 6367–6371.
43. Kim S. J.; Kim B. H. *Nucleic Acids Res.* **2003**, *31*, 2725–2734.
44. Sidorov V.; Kotch F. W.; El-Kouedi M.; Davis J. T. *Chem. Commun.* **2000**, 2369–2370.
45. Kotch F. W.; Sidorov V.; Lam Y.-F.; Kayser K.-J.; Li H.; Kaucher M. S.; Davis J. T. *J. Am. Chem. Soc.* **2003**, *125*, 15140–15150.
46. Liang J.; Fu H.; Liu Y.; Wang L.; Ye Z.; Shi X. *Can. J. Chem.* **2003**, *81*, 1019–1024.
47. Consoli G. M. L.; Granata G.; Galante E.; Cunsolo F.; Geraci C. *Tetrahedron Lett.* **2006**, *47*, 3245–3249.
48. Consoli G. M. L.; Granata G.; Garozzo D.; Mecca T.; Geraci C. *Tetrahedron Lett.* **2007**, *48*, 7974–7977.
49. Consoli G. M. L.; Granata G.; Galante E.; Di Silvestro I.; Salafia L.; Geraci C. *Tetrahedron*, **2007**, *63*, 10758–10763.
50. Consoli G. M. L.; Granata G.; Lo Nigro R.; Malandrino G.; Geraci C. *Langmuir*, **2008**, *24*, 6194–6200.
51. Chawla H. M.; Kar J. R.; Siddiqui W. A.; Kumar N.; StC Black D. *Tetrahedron Lett.* **2014**, *55*, 4517–4520.
52. Sessler J. L.; Král V.; Shishkanova T. V.; Gale P. A. *P. Natl. Acad. Sci. USA*, **2002**, *99*, 4848–4853.
53. Cafeo G.; Carboti G.; Cuzzola A.; Fabbi M.; Ferrini S.; Kohnke F. H.; Papanikolaou G.; Plutino M. R.; Rosano C.; White A. J. P. *J. Am. Chem. Soc.* **2013**, *135*, 2544–2551.
54. Guan A.-J.; Zhang E.-X.; Xiang J.-F.; Li Q.; Yang Q.-F.; Li L.; Tang Y.-L.; Wang M.-X. *J. Phys. Chem. B*, **2011**, *115*, 12584–12590.

55. Guan A.-J.; Zhang E.-X.; Xiang J.-F.; Yang Q.-F.; Li Q.; Sun H.-X.; Wang D.-X.; Zheng Q.-Y.; Xu G.-Z.; Tang Y.-L. *J. Phys. Chem. Lett.* **2012**, *3*, 131–135.
56. Rajavelu K.; Rajakumar P. *J. Mater. Chem. B*, **2015**, *3*, 3340–3350.
57. Apps M. G.; Choi E. H. Y.; Wheate N. J. *Endocr.-Rel. Cancer*, **2015**, *22*, 219–233.
58. Kumar S.; Kaur N.; Singh H. *Adv. in Heterocycl. Chem.* **2008**, *96*, 123–173.
59. Kulesza J.; Barros B. S.; Alves Junior S. *Coordin. Chem. Rev.* **2013**, *257*, 2192–2212.
60. Barea E.; Navarro J. A. R.; Salas J. M.; Quiro M.; Willermann M.; Lippert B. *Chem. Eur. J.* **2003**, *9*, 4414–4421.
61. Bardají E. G.; Freisinger E.; Costisella B.; Schalley C. A.; Brüning W.; Sabat M.; Lippert B. *Chem. Eur. J.* **2007**, *13*, 6019–6039.
62. Das N.; Sanz Miguel P. J.; Khutia A.; Lazar M.; Lippert B. *Dalton Trans.* **2009**, 9120–9122.
63. Khutia A.; Sanz Miguel P. J.; Lippert B. *Inorg. Chem.* **2010**, *49*, 7635–7637.
64. Khutia A.; Sanz Miguel P. J.; Lippert B. *Chem. Eur. J.* **2011**, *17*, 4195–4204.
65. Khutia A.; Sanz Miguel P. J.; Lippert B. *Chem. Eur. J.* **2011**, *17*, 4205–4216.
66. Galindo M. A.; Olea D.; Romero M. A.; Gómez J.; Del Castillo P.; Hannon M. J.; Rodger A.; Zamora F.; Navarro J. A. R. *Chem. Eur. J.* **2007**, *13*, 5075–5081.
67. Armentano D.; Mastropietro T. F.; Julve M.; Rossi R.; Rossi P.; De Munno G. *J. Am. Chem. Soc.* **2007**, *129*, 2740–2741.
68. Sansone F.; Dudič M.; Donofrio G.; Rivetti C.; Baldini L.; Casnati A.; Cellai S.; Ungaro R. *J. Am. Chem. Soc.* **2006**, *128*, 14528–14536.
69. Bagnacani V.; Sansone F.; Donofrio G.; Baldini L.; Casnati A.; Ungaro R. *Org. Lett.* **2008**, *10*, 3953–3956.
70. Bagnacani V.; Franceschi V.; Fantuzzi L.; Casnati A.; Donofrio G.; Sansone F.; Ungaro R. *Bioconjugate Chem.* **2012**, *23*, 993–1002.
71. Bagnacani V.; Franceschi V.; Bassi M.; Lomazzi M.; Donofrio G.; Sansone F.; Casnati A.; Ungaro R. *Nature Commun.* **2013**, 1–7.
72. Gallego-Yerga L.; Lomazzi M.; Franceschi V.; Sansone F.; Ortiz Mellet C.; Donofrio G.; Casnati A.; García Fernández J. M. *Org. Biomol. Chem.* **2015**, *13*, 1708–1723.
73. Licen S.; Bagnacani V.; Baldini L.; Casnati A.; Sansone F.; Giannetto M.; Pengo P.; Tecilla P. *Supramolecular Chemistry*, **2013**, *25*, 631–640.
74. Rodik R. V.; Klymchenko A. S.; Jain N.; Miroshnichenko S. I.; Richert L.; Kalchenko V. I.; Mély Y. *Chem. Eur. J.* **2011**, *17*, 5526–5538.
75. Rodik R. V.; Anthony A.-S.; Kalchenko V. I.; Mély Y.; Klymchenko A. S. *New J. Chem.* **2015**, *39*, 1654–1664.
76. Lalor R.; DiGesso J. L.; Mueller A.; Matthews S. E. *Chem. Commun.* **2007**, 4907–4909.
77. Nault L.; Cumbo A.; Pretôt R. F.; Sciotti M. A.; Shahgaldian P. *Chem. Commun.* **2010**, *46*, 5581–5583.
78. Barrán-Berdón A. L.; Yélamos B.; García-Río L.; Domènech Ò.; Aicart E.; Junquera E. *ACS Appl. Mater. Interfaces*, **2015**, *7*, 14404–14414.
79. Ostos F. J.; Lebron J. A.; Moyá M. L.; Deasy M.; López-Cornejo P. *Colloids and Surfaces B: Biointerfaces*, **2015**, *127*, 65–72.
80. Ortiz Mellet C.; Benito J. M.; García Fernández J. M. *Chem. Eur. J.* **2010**, *16*, 6728–6742.
81. Zhou T.; Llizo A.; Wang C.; Xu G.; Yang Y. *Nanoscale*, **2013**, *5*, 8288–8306.
82. Rodik R. V.; Klymchenko A. S.; Mély Y.; Kalchenko V. I. *J. Incl. Phenom. Macrocycl. Chem.* **2014**, *80*, 189–200.
83. Komiyama M.; Isaka K.; Shinkai S. *Chem. Lett.* **1991**, 937–940.
84. Molenveld P.; Engbersen J. F. J.; Kooijman H.; Spek A. L.; Reinhoudt D. N. *J. Am. Chem. Soc.* **1998**, *120*, 6726–6737.
85. Molenveld P.; Stikvoort W. M. G.; Kooijman H.; Spek A. L.; Engbersen J. F. J.; Reinhoudt D. N. *J. Org. Chem.* **1999**, *64*, 3896–3906.
86. Cacciapaglia R.; Casnati A.; Mandolini L.; Reinhoudt D. N.; Salvio R.; Sartori A.; Ungaro R. *J. Org. Chem.* **2005**, *70*, 624–630.

87. Molenveld P.; Engbersen J. F. J.; Reinhoudt D. N. *Angew. Chem. Int. Ed.* **1999**, *38*, 3189–3192.
88. Molenveld P.; Engbersen J. F. J.; Reinhoudt D. N. *Chem. Soc. Rev.* **2000**, *29*, 75–86.
89. Cacciapaglia R.; Casnati A.; Mandolini L.; Reinhoudt D. N.; Salvio R.; Sartori A.; Ungaro R. *J. Am. Chem. Soc.* **2006**, *128*, 12322–12330.
90. Cacciapaglia R.; Casnati A.; Mandolini L.; Peracchi A.; Reinhoudt D. N.; Salvio R.; Sartori A.; Ungaro R. *J. Am. Chem. Soc.* **2007**, *129*, 12512–12520.
91. Baldini L.; Cacciapaglia R.; Casnati A.; Mandolini L.; Salvio R.; Sansone F.; Ungaro R. *J. Org. Chem.* **2012**, *77*, 3381–3389.
92. Salvio R.; Cacciapaglia R.; Mandolini L.; Sansone F.; Casnati A. *RSC Adv.* **2014**, *4*, 34412–34416.
93. Friebe S.; Gebauer S.; Krauss G. J. *J. Chromatogr. Sci.* **1995**, *33*, 281–284.
94. Xiao X.-Z.; Feng Y.-Q.; Da S.-L.; Zhang Y. *Chromatographia*, **1999**, *49*, 643–648.
95. Li L.-S.; Liu M.; Da S.-L.; Feng Y.-Q. *Talanta*, **2004**, *63*, 433–441.
96. Shimojo K.; Oshima T.; Goto M. *Anal. Chim. Acta*, **2004**, *521*, 163–171.
97. Shimojo K.; Oshima T.; Goto M. *Solvent Extr. Res. Dev.* **2004**, *11*, 85–92.
98. Shimojo K.; Goto M. *Sep. Purif. Technol.* **2005**, *44*, 175–180.
99. Tauran Y.; Anjard C.; Kim B.; Rhimi M.; Coleman A. W. *Chem. Commun.* **2014**, *50*, 11404–11406.
100. Takeuchi T.; Bagnacani V.; Sansone F.; Matile S. *ChemBioChem*, **2009**, *10*, 2793–2799.
101. Krause-Heuer A. M.; Wheate N. J.; Tilby M. J.; Pearson D. G.; Ottley C. J.; Aldrich-Wright J. R. *Inorg. Chem.* **2008**, *47*, 6880–6888.
102. Moni L.; Pourceau G.; Zhang J.; Meyer A.; Vidal S.; Souteyrand E.; Dondoni A.; Morvan F.; Chevotot Y.; Vasseur J.-J.; Marra A. *ChemBioChem*, **2009**, *10*, 1369–1378.
103. Kivlehan F.; Lefoix M.; Moynihan H. A.; Thompson D.; Ogurtsova V. I.; Herzog G.; Arrigan D. W. M. *Electrochim. Acta*, **2010**, *55*, 3348–3354.
104. Janrungroatsakul W.; Vilaivan T.; Vilaivan C.; Watchasit S.; Suksai C.; Ngeontae W.; Aeungmaitrepirom W.; Tuntulani T. *Talanta*, **2013**, *105*, 1–7.
105. Kim H. J.; Oh S. W.; Kim S. J.; Amiri A.; Wang H. T.; Choi E. Y. *BioChip J.* **2012**, *6*, 1–9.
106. Chao J.; Wang H. F.; Zhang Y.; Huo F.; Yin C. *Spectrochim. Acta A*, **2013**, *103*, 73–78.
107. Nichols P. J.; Makha M.; Raston C. L. *Cryst. Growth Des.* **2006**, *6*, 1161–1167.
108. Sansone F.; Baldini L.; Casnati A.; Ungaro R. *Supramol. Chem.* **2008**, *20*, 161–168.
109. Ikeda A.; Ejima A.; Nishiguchi K.; Kikuchi J.-I.; Matsumoto T.; Hatano T.; Shinkai S.; Goto M. *Chem. Lett.* **2005**, *34*, 308–309.

# Chapter 25

## Structural Trends in Calix[4]arene-Supported Cluster Chemistry

Marco Coletta, Euan K. Brechin, and Scott J. Dalgarno

### 25.1 Introduction

Polynuclear clusters of paramagnetic metal ions that display interesting magnetic phenomena, species also known as Molecular Magnets (MMs), continue to attract strong interest due to their potential application in fields such as information storage, spintronics, magnetic resonance imaging (MRI), magnetic refrigeration and thermotherapy [1]. Understanding or controlling the synthesis and construction of these (often highly) complex assemblies from multi-component mixtures is a challenging goal, and one that is frequently tackled through targeted/smart ligand design. As cone conformers, calix[4]arenes (denoted  $H_4C[4]s$  and  $C[4]s$  herein to represent the extremes of fully protonated or deprotonated forms respectively) are excellent synthetic platforms for both the complexation of metal ions and, due to the bridging capability of their lower-rim oxygen atoms, subsequent cluster formation. Cluster formation is of course the main thrust of this contribution, but before continuing to detailed discussion it should be noted that metal ions can be complexed by the lower-rim phenolic oxygens such that the ion resides either *endo* or *exo* to the calix[4]arene cavity [2]. In cases involving *endo* binding the metal ion interacts simultaneously with both the  $\pi$  systems of the macrocycle and the lower-rim oxygen atoms (Fig. 25.1a). In contrast, *exo* binding involves complexation of the metal ion to the lower-rim phenolic oxygens such that it resides just below the macrocycle plane (Fig. 25.1b). It is noteworthy that a limited number of

---

M. Coletta • S.J. Dalgarno (✉)

Institute of Chemical Sciences, Heriot-Watt University, Riccarton, Edinburgh EH14 4AS, UK  
e-mail: [s.j.dalgarno@hw.ac.uk](mailto:s.j.dalgarno@hw.ac.uk)

E.K. Brechin (✉)

EaStCHEM School of Chemistry, The University of Edinburgh, David Brewster Road,  
Edinburgh EH9 3FJ, UK  
e-mail: [ebrechin@ed.ac.uk](mailto:ebrechin@ed.ac.uk)

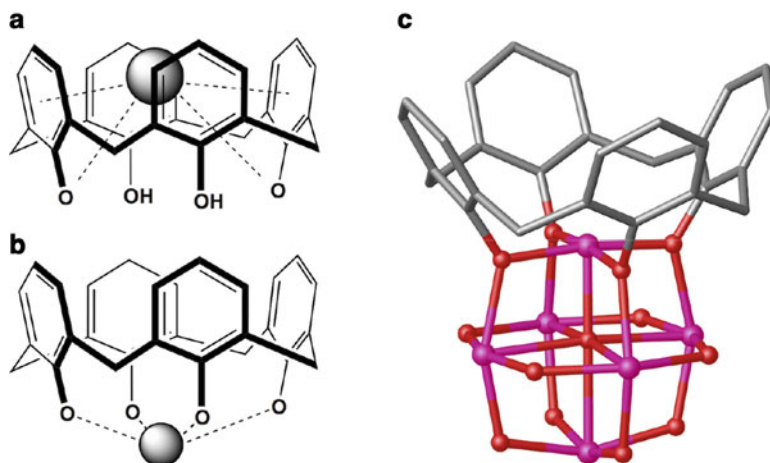


**Fig. 25.1** (a) Schematic of *endo*-C[4] metal ion binding. (b) Schematic of *exo*-C[4] metal ion binding at the lower-rim oxygens. (c) C[4]-supported polyoxovanadate cluster showing the core and bridging atoms [3]. H atoms, C[4] *t*Bu groups and other atoms of bridging groups are omitted for clarity in C. Figures not to scale. Colour code: C – grey, O – red, V – pink

cations (e.g. alkaline and alkaline-earth metal ions) are sufficiently small to allow them to participate in *endo* complexation involving simultaneous cation- $\pi$  interactions, rendering this type of interaction far less common in the literature. Moreover, *exo* complexation will always be preferred over *endo* if there are ligated solvent molecules present [2]. The remainder of this chapter deals almost exclusively with *exo* metal ion binding.

To our knowledge the first high-nuclearity C[4]-supported transition metal (TM) cluster was reported by Luneau and co-workers in 2008, this being a mixed valence polyoxovanadate species shown in Fig. 25.1c [3]. Recent times have witnessed an expansion in C[4]-supported cluster synthesis, but before that is reviewed in detail it is worth noting that significant attention has been devoted to analogous coordination chemistry with thia-, sulfinyl- and sulfonyl-bridged calix[4] arenes; these molecules possess S, SO and SO<sub>2</sub> bridging atoms/groups respectively [4]. This chemistry is discussed prior to that of methylene-bridged C[4]s.

### 25.1.1 Thia-, Sulfinyl- and Sulfonyl-Bridged Calix[4]arenes in Cluster Synthesis

While methylene-bridged C[4]s are able to bind one metal ion centrally at the lower-rim, the presence of heteroatoms or heteroatom-containing groups at the bridging positions (rather than CH<sub>2</sub>) presents additional binding sites that markedly affect the complexation of metal ions, and thus the resulting cluster topologies.

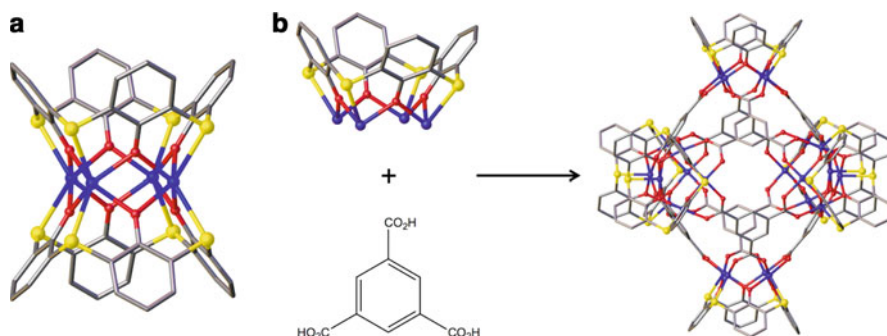


**Fig. 25.2** (a) Structure of a tC[4]-supported tetranuclear TM ion cluster showing coordination to the bridge donor atoms as well as lower-rim oxygens [4]. (b) Directed assembly of a metal-organic octahedron through the use of a topologically directing linker and a [TM<sub>4</sub>tC[4]] building block [16]. Figures not to scale. Colour code: C – grey, O – red, S – yellow, TM – dark blue

Given that the C-S bonds in thia-C[4] (H<sub>4</sub>tC[4]) are longer than the corresponding C-C bonds in H<sub>4</sub>C[4], each heteroatom generates an alternative binding site containing one soft sulphur and two proximal hard oxygen donors. Several H<sub>4</sub>tC[4]-supported alkali metal clusters in the literature display cation binding akin to that of H<sub>4</sub>C[4]s, examples of which include [Na<sub>6</sub>(tC[4])<sub>2</sub>(dmf)<sub>2</sub>]<sup>2-</sup>, [K<sub>2</sub>(H<sub>3</sub>tC[4])<sub>2</sub>(OEt<sub>2</sub>)<sub>2</sub>H<sub>2</sub>O] and [Rb<sub>4</sub>(H<sub>3</sub>tC[4])<sub>4</sub>(H<sub>2</sub>O)(dmf)<sub>10</sub>] [5, 6]. Although this is the case, H<sub>4</sub>tC[4] behaves very differently in comparison to H<sub>4</sub>C[4] with respect to the coordination of first row transition metal (TM) ions such as Mn<sup>II</sup>, Co<sup>II</sup>, Cu<sup>II</sup> and Zn<sup>II</sup> [7–9]. The same is true for heavier TM as well as lanthanide metal (Ln) ions (e.g. Hg<sup>II</sup> and Nd<sup>III</sup> respectively) [10, 11], and this behaviour is also common to both sulfanyl- and sulfonyl-C[4]s. In the vast majority of cases these components form trinuclear or tetranuclear metal clusters, an example of the latter being shown in Fig. 25.2a. The coordination pattern is similar in all cases, with TM or Ln ions sandwiched between two partially or fully deprotonated tC[4]s. In this arrangement the four phenolic oxygens and four sulphur atoms are near co-planar, with complexation occurring in the alternative binding sites described above. The ubiquity of [TM<sub>4</sub>tC[4]] moieties has recently led to them being used as structural building units in the assembly of large metal-organic polyhedra (MOPs) [12–21]. A number of groups have demonstrated the ability to assemble a range of stable (and in some cases porous) MOPs through linking [TM<sub>4</sub>tC[4]] moieties with topologically directing ligands such as benzene tricarboxylic acid (Fig. 25.2b) [16, 17]. The ability to control MOP volume/shape and pore size is particularly attractive, as these stable assemblies have potential for application as gas storage materials or hosts for dye molecules [21] (amongst other species).

The fact that C[4] predictably binds one metal ion at the lower-rim gives rise to a different type of metal-organic building unit, one that we (amongst others) have used to assemble a range of new cluster species [3, 22–31]. In the absence of additional donor atoms at the bridge positions, a single TM or Ln ion can be bound

in the polyphenolic pocket and these oxygen atoms are well suited to bridge to additional metal ions (for example see bridging between vanadium centres in Fig. 25.1c). The remainder of Sect. 25.1 deals with (a) exploratory cluster synthesis with  $H_4C[4]s$ , (b) the effects of varying ambient reaction conditions, (c) the establishment of empirical metal ion binding rules for  $H_4C[4]s$  and (d) synthetic modification at the methylene bridge position. Sections 25.2 and 25.3 are concerned with the use of bis- $H_4C[4]s$  tethered either directly at, or with a spacer via the methylene bridge, with a particular emphasis on extension of metal ion binding principles established here for  $H_4C[4]s$ .

### 25.1.2 Methylene-Bridged Calix[4]arenes in Cluster Synthesis

Attempts at C[4]-supported cluster synthesis with first row TM ions under ambient conditions gave rise to the formation of two new assembly types. The first of these was found to be a family of mixed valence  $[Mn^{III}_2Mn^{II}_2(C[4])_2(\mu_3-OH)_2(dmf)_6]$  clusters (**1**, Fig. 25.3a), the metallic skeleton of which has a planar diamond- or butterfly-like topology (Fig. 25.4a) [22, 23]. The (Jahn-Teller distorted)  $Mn^{III}$  and (distorted octahedral)  $Mn^{II}$  ions occupy the wing-tip and body positions respectively and these are bridged via the C[4] lower-rim oxygens and  $\mu_3$ -hydroxides. This cluster motif is not unusual in Mn cluster chemistry but, in this case, the oxidation states are reversed relative to those previously reported [24]. A notable feature of **1** is that the  $[Mn^{III}(C[4])]^-$  moiety caps the cluster core, a feature observed in all clusters containing manganese ions.

The second general type of assembly isolated was a pair of enneanuclear  $Cu^{II}$  clusters. These were formed from different  $Cu^{II}$  salts and have formulae  $[Cu^{II}_9(C[4])_3(\mu-OH)_3Cl_2(dmsO)_6][Cu^{II}Cl_2]$  (**2**, Fig. 25.3b) and  $[Cu^{II}_9(C[4])_3(\mu-OH)_3(NO_3)_2(dmsO)_6](NO_3)$  (**3**); the only significant difference between these clusters is the nature of the anions present [25]. The common metallic skeleton has a tri-capped trigonal prismatic topology (Fig. 25.4b), the central core of which has three hydroxides bridging the  $Cu^{II}$  ions at the prism vertices. Chloride or nitrate anions occupy the triangular faces of the prism and additional counterions are present in the crystal lattice. Cluster core capping occurs on each of the rectangular faces of the prism with  $[Cu^{II}(C[4])]^{2-}$  moieties, showing the versatility of C[4] in its ability to accommodate TM ions in either the second or third oxidation state. Other structurally analogous  $TM^{II}_9$  clusters have followed (e.g.  $Co^{II}_9$ ), all of which have similar cluster topologies but that possess variations in the anions present [26].

Similar screening of cluster formation with Ln ions resulted in the formation of a series of clusters with general formula  $[Ln^{III}_6(C[4])_2(\mu-OH)_4(\mu_4-O)_2(HCO_2)_2(dmf)_8][Cu^I Cl_2]$  (**4**, Ln = Gd, Tb or Dy, Fig. 25.3c); [27] there is disorder in the bridging anions within these clusters but only one combination is described and shown for

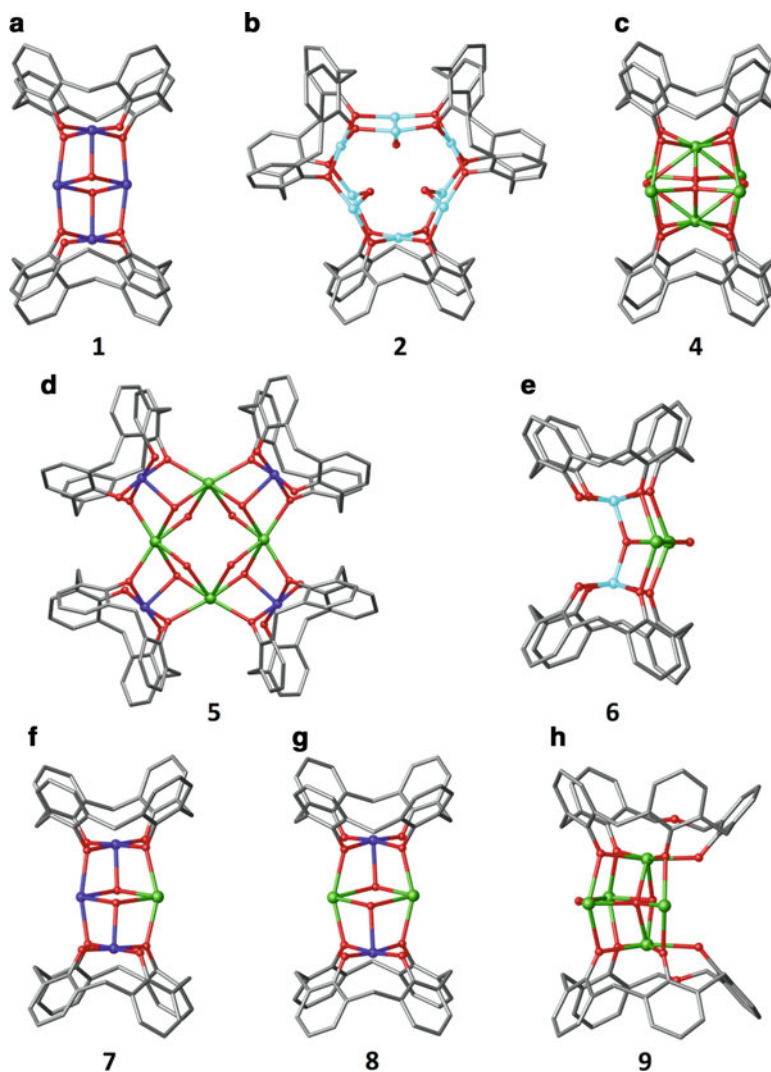


**Fig. 25.3** Partial single crystal X-ray structures of clusters **1** (a) [22, 23], **2** (b) [25], **4** (c) [27], **5** (d) [29], **6** (e) [30], **7** (f) [31], **8** (g) [31], and **9** (h) [32]. H atoms, C[4] *t*Bu groups, ligated and co-crystallised solvent molecules omitted for clarity. Figures not to scale. Colour code: C – grey, O – red, TM – dark/pale blue, Ln – green

clarity. The core topology in **4** is markedly different to those discussed above for TM clusters, with the Ln ions arranged at the vertices of an octahedron (Fig. 25.4c). The cavity bound Ln ions sit slightly out of the plane defined by the C[4] lower-rim oxygens, and the four remaining ions define the central square of the octahedron. Capping behaviour is again observed, in this case as a  $[\text{Ln}^{\text{III}}(\text{C}[4])^-]$  moiety, and this core topology can also be achieved through solvothermal synthesis [28].



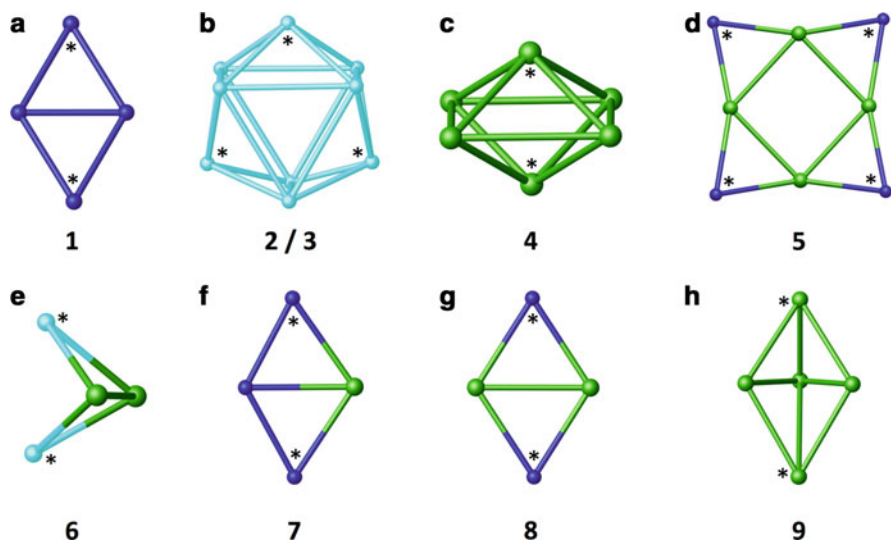


**Fig. 25.4** Topologies of clusters 1–9 with asterisks indicating core capping by either [TM<sup>II</sup>C[4]]<sup>2-</sup>, [TM<sup>III</sup>C[4]]<sup>-</sup> or [Ln<sup>III</sup>C[4]]<sup>-</sup> moieties [22–31]. Figures not to scale. Colour code: TM – dark/pale blue, Ln – green

Given the versatility of H<sub>4</sub>C[4] towards cluster formation with TM or Ln ions we thought it reasonable to expect that, with tuning of the reaction conditions/stoichiometries, it would be possible to synthesise mixed 3d/4f assemblies. Addition of Ln<sup>III</sup> ions to the reaction used to form **1** afforded the first series of C[4]-supported 3d/4f clusters that were found to be of general formula [Mn<sup>III</sup><sub>4</sub>Ln<sup>III</sup><sub>4</sub>(C[4])<sub>4</sub>(μ<sub>3</sub>-OH)<sub>4</sub>(NO<sub>3</sub>)<sub>2</sub>(dmf)<sub>6</sub>(H<sub>2</sub>O)<sub>6</sub>(OH)<sub>2</sub> (**5**, Ln = Gd, Tb or Dy, Fig. 25.3d) [29]. These are best described as a square of Ln ions, each edge of which is capped by a [Mn<sup>III</sup>(C[4])]<sup>-</sup> moiety (Fig. 25.4d). The library of 3d/4f clusters was expanded by synthesis of a series of C[4]-supported Fe<sup>III</sup><sub>2</sub>Ln<sup>III</sup><sub>2</sub> clusters of general formula [Fe<sup>III</sup><sub>2</sub>Ln<sup>III</sup><sub>2</sub>(C[4])<sub>2</sub>(μ<sub>4</sub>-O)(μ-OH)(dmf)<sub>4</sub>(MeOH)<sub>2</sub>(H<sub>2</sub>O)<sub>2</sub>]Cl (**6**, Ln = Gd, Tb or Dy, Fig. 25.3e) [30]. The metallic skeleton is a distorted tetrahedron in which all of the metal ions are connected via a μ<sub>4</sub>-O<sup>2-</sup> anion (Fig. 25.4e). The pentacoordinate Fe<sup>III</sup> ions (distorted square pyramidal geometry) are bound by the C[4] lower-rim oxygens, capping the core in a manner akin to [Mn<sup>III</sup>(C[4])]<sup>-</sup> in **1**.

By tuning the reaction conditions it was possible to interchange one or both of the body Mn<sup>II</sup> ions in **1** for Ln<sup>III</sup> ions. As a result we isolated clusters of general formulae [Mn<sup>III</sup><sub>2</sub>Mn<sup>II</sup>Ln<sup>III</sup>(C[4])<sub>2</sub>(μ<sub>3</sub>-OH)<sub>2</sub>(NO<sub>3</sub>)(dmsO)<sub>6</sub>] (**7**, Ln = Gd, Tb or Dy, Fig. 25.3f) and [Mn<sup>III</sup><sub>2</sub>Ln<sup>III</sup><sub>2</sub>(C[4])<sub>2</sub>(μ<sub>3</sub>-OH)<sub>2</sub>(dmsO)<sub>8</sub>]Cl<sub>2</sub>, (**8**, Ln = Gd, Tb or Dy, Fig. 25.3g), and through structural studies observed small structural changes due to difference in ion size [31]. The presence of the larger, more highly-coordinated Ln ion in **7** has the effect of distorting the formerly co-planar orientation of C[4]s in **1** (Fig. 25.4f). Co-planarity is restored upon the introduction of the second Ln ion

(**8**, Fig. 25.4g) and, from these exploratory studies, it is possible to make the following empirical rules for binding and structural assembly behaviour:

- TM(II)/TM(III) ions will be bound by C[4] to produce  $[\text{TM}(\text{C}[4])]^{-/2-}$  capping moieties
- Ln(III) ions will be bound by C[4] to produce  $[\text{Ln}(\text{C}[4])]^{-}$  capping moieties
- TM ions will be preferentially bound by C[4] in any *3d/4f* mixture
- Clusters are always capped on faces and or edges by the aforementioned moieties

With respect to this section, one final cluster of interest is that formed by reaction of Ln ions with homooxalix[4]arene (hoC[4]) and which has the formula  $[\text{Ln}^{\text{III}}_5(\text{hoC}[4])_2(\text{NO}_3)_3(\mu\text{-MeO})(\mu_4\text{-O})(\mu_3\text{-OH})(\text{dmf})_7(\text{H}_2\text{O})]$  (**9**, Ln = Gd, Tb or Dy, Fig. 25.3h) [32]. Inspection of the structure shows that the introduction of one etheral linker in the  $\text{H}_4\text{C}[4]$  framework alters the size and shape of the lower-rim binding pocket, the result of which is expulsion of one metal ion from the C[4]-supported  $\text{Ln}^{\text{III}}_6$  cluster motif (**4**, Fig. 25.3c). In this case  $[\text{Ln}^{\text{III}}(\text{hoC}[4])]^{-}$  moieties cap a triangle to produce a distorted square pyramidal metallic skeleton (Fig. 25.4h). These subtle effects therefore represent another viable route to influencing cluster composition through understandable structure capping behaviour.

### 25.1.3 Calix[4]arenes Functionalised at the Methylene Bridge

While functionalisation of the calix[4]arene framework at both the upper- and lower-rims leads to a myriad of useful supramolecular building blocks, synthetic alteration at the methylene bridge also represents a viable synthetic route to obtain novel platforms that can be exploited in cluster formation; modification at the bridge leaves the lower-rim polyphenolic pocket free for metal ion binding [33]. In this regard Böhmer showed that it is possible to include new functionalities within the calixarene scaffold through convergent synthetic routes involving fragment condensation and subsequent cyclisation. Work by the Biali group explored direct functionalisation at the methylene bridge, producing an impressive number of new derivatives bearing different functionalities (including double bonds [34], alkyl chains and aryl groups [35]). Fantini and co-workers developed an alternative synthetic strategy to directly modify the methylene bridge, affording a series of C[4] derivatives with alkyl, benzyl, carboxylic acid and halide functionalities [36]. All of these developments are important in the context of C[4]-supported cluster formation as they present opportunities to introduce additional functionality that may, in turn, influence or direct both lower-rim coordination chemistry and cluster topology.

In addition to this, Fantini also recently developed a synthetic route to 2,2'-biscalix[4]arene (bis-H<sub>4</sub>C[4]) [37], an important new building block in which the two macrocycles are directly linked via the methylene bridge. Single crystal X-ray diffraction data supported molecular modelling studies and demonstrated that the two H<sub>4</sub>C[4] moieties are arranged *anti* with respect to one another, thus minimising interactions between bulky <sup>t</sup>Bu groups. Having established binding rules for H<sub>4</sub>C[4]s, it was of interest to explore the coordination chemistry of bis-H<sub>4</sub>C[4], with the expectation that it (a) would exhibit characteristic behaviour towards the complexation of TM and Ln ions and (b) allow one to increase and or control the nuclearity of the resulting polymeric clusters.

## 25.2 Methylene-Bridge Linked Bis-calix[4]arene in Cluster Synthesis

Exploratory cluster formation experiments with bis-H<sub>4</sub>C[4] began by mirroring conditions found to be successful in C[4]-supported cluster synthesis. Formation of bis-H<sub>4</sub>C[4]-supported clusters would involve incorporation of two TM or Ln ions (one *per* C[4] pocket), coupled with inversion of one of the constituent C[4] rings from an *anti*- to *syn*- conformation [38]. Structural inversion was also expected to generate additional binding sites for TM/Ln ions as a result of four proximal lower-rim oxygens, two from each C[4] moiety. Bis-H<sub>4</sub>C[4] behaved as one would expect, affording a series of clusters that are structurally related to their C[4]-supported analogues. Systematic increasing of cluster nuclearity, as well as double capping behaviour was also observed, all of which is discussed below.

### 25.2.1 Monometallic Systems

Reaction of bis-H<sub>4</sub>C[4] with Mn<sup>II</sup> chloride under analogous conditions used to form **1** afforded a new cluster of formula [Mn<sup>III</sup><sub>4</sub>Mn<sup>II</sup><sub>4</sub>(bis-C[4])<sub>2</sub>(μ<sub>3</sub>-OH)<sub>2</sub>(μ-OH)(μ-Cl)(H<sub>2</sub>O)(MeOH)(dmf)<sub>4</sub>] (**10**, Fig. 25.5a) [39]. Comparison of **1** and **10** shows that the mixed valence Mn<sup>III</sup><sub>4</sub>Mn<sup>II</sup><sub>4</sub> metallic skeleton in the latter (Fig. 25.6a) is closely related to the Mn<sup>III</sup><sub>2</sub>Mn<sup>II</sup><sub>2</sub> butterfly obtained with H<sub>4</sub>C[4]. The metal ions in **10** are connected by phenolates, bridging hydroxide and chloride, with the ligand undergoing inversion as expected. In this *syn*-conformation the region between the two C[4]s has accommodated two additional Mn<sup>II</sup> ions, and as a result the entire assembly is best described as two fused (and distorted) Mn<sup>III</sup><sub>2</sub>Mn<sup>II</sup><sub>2</sub> butterflies. Finally, bis-H<sub>4</sub>C[4] has formed a [Mn<sup>III</sup><sub>2</sub>(bis-C[4])]<sup>2-</sup> capping moiety as anticipated, further highlighting the related structural features observed upon linking H<sub>4</sub>C[4]s directly via the methylene bridge.

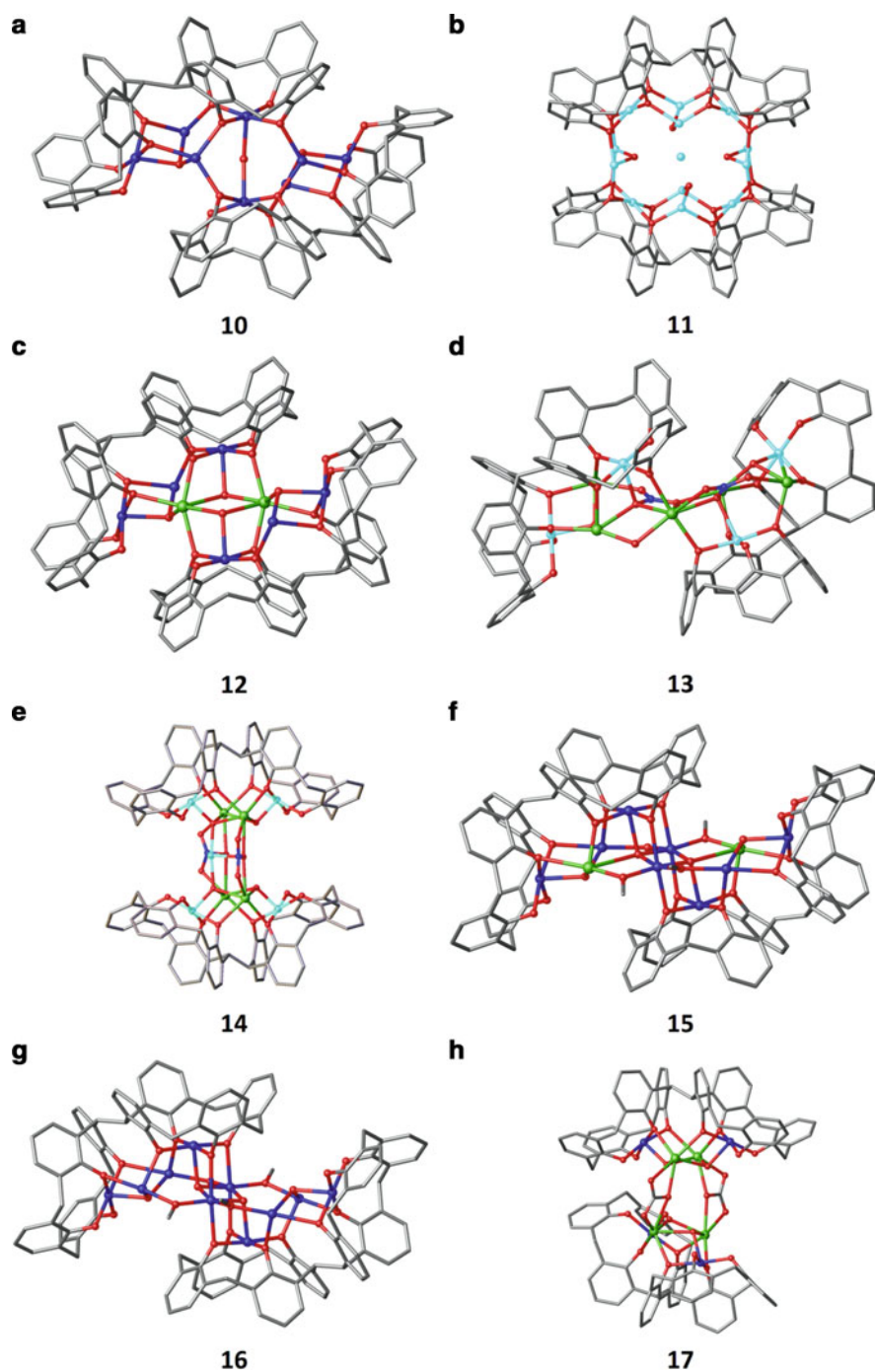


**Fig. 25.5** Partial single crystal X-ray structures of clusters **10** (a) [39], **11** (b) [39], **12** (c) [39], **13** (d) [40], **14** (e) [40], **15** (f) [41], **16** (g) [41], and **17** (h) [41]. H atoms, C[4] 'Bu groups, ligated and co-crystallised solvent molecules omitted for clarity. Figures not to scale. Colour code: C – grey, N – navy blue, O – red, TM – dark/pale blue, Ln – green

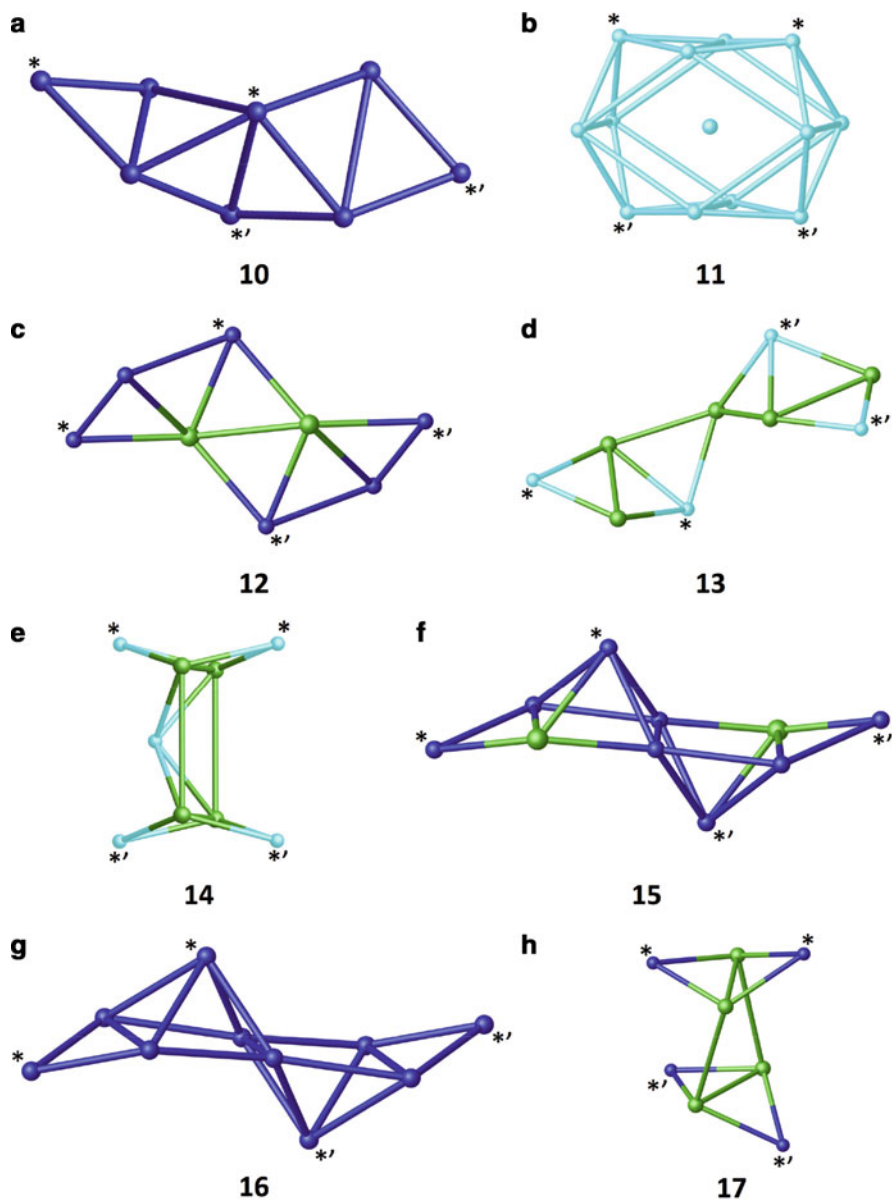


**Fig. 25.6** Topologies of clusters **10–17** with asterisk/primed asterisk pairs indicating double core capping with either  $[\text{TM}^{\text{II}}_2\text{bisC}[4]]^{4-}$  or  $[\text{TM}^{\text{III}}_2\text{bisC}[4]]^{2-}$  moieties [39–41]. Figures not to scale. Colour code: TM – dark/pale blue, Ln – green

Reaction of bis- $\text{H}_4\text{C}[4]$  with  $\text{Cu}^{\text{II}}$  nitrate under analogous conditions used to form **3** afforded a second structurally related cluster of formula  $[\text{Cu}^{\text{II}}_{13}(\text{bis-C}[4])_2(\text{NO}_3)(\mu\text{-OH})_8(\text{dmf})_7](\text{OH})$  (**11**, Fig. 25.5b) [39]. The metallic skeleton can be described as a tetracapped square prism (Fig. 25.6b), the central core of which has hydroxides bridging the  $\text{Cu}^{\text{II}}$  ions at the prism vertices, as well as the final  $\text{Cu}^{\text{II}}$  ion that resides in the centre of the assembly. This cluster shows striking similarity to the tri-capped trigonal prismatic  $\text{Cu}^{\text{II}}_9$  species (**2** and **3**, Fig. 25.3b), with capping of the metallic core occurring with  $[\text{Cu}^{\text{II}}_2(\text{bis-C}[4])]^{4-}$  moieties. This further validates binding rules observed for C[4], and the principle of their extension through  $\text{H}_4\text{C}[4]$  methylene bridge linking. Furthermore, it also demonstrates equivalent versatility towards accommodation of TMs in both the second and third oxidation states.

### 25.2.2 Bimetallic Systems

Screening cluster formation with bis- $\text{H}_4\text{C}[4]$  and  $3d/4f$  ions afforded several interesting results, all of which display structural trends observed for  $\text{H}_4\text{C}[4]$ . The first of the new clusters obtained was formed upon reaction of bis- $\text{H}_4\text{C}[4]$  with  $\text{Mn}^{\text{II}}$  and  $\text{Gd}^{\text{III}}$  chlorides and has the formula  $[\text{Mn}^{\text{III}}_4\text{Mn}^{\text{II}}_2\text{Gd}^{\text{III}}_2(\text{bis-C}[4])_2(\text{Cl})_2(\mu_3\text{-OH})_4(\text{MeOH})_2(\text{dmf})_8]$  (**12**, Fig. 25.5c). Compound **11** has clear similarities with **10** (Fig. 25.5a), the main difference being replacement of two  $\text{Mn}^{\text{II}}$  with two  $\text{Gd}^{\text{III}}$  ions [39]. The central butterfly in the metallic skeleton of **10** is retained to some extent, now being present as a central  $\text{Mn}^{\text{III}}_2\text{Gd}^{\text{III}}_2$  analogue (Fig. 25.6c); this arises from the fusing of two distorted  $\text{Mn}^{\text{III}}_2\text{Mn}^{\text{II}}\text{Gd}^{\text{III}}$  butterflies, with capping occurring through the expected  $[\text{Mn}^{\text{III}}_2(\text{bis-C}[4])]^{2-}$  moieties.

Reaction of bis- $\text{H}_4\text{C}[4]$  with  $\text{Cu}^{\text{II}}$  and  $\text{Ln}^{\text{III}}$  nitrates yielded a series of new clusters with general formula  $[\text{Cu}^{\text{II}}_4\text{Ln}^{\text{III}}_5(\text{bis-C}[4])_2(\mu_3\text{-OMe})(\mu\text{-OMe})(\mu_3\text{-OH})(\mu_4\text{-NO}_3)(\mu_5\text{-NO}_3)(\text{MeOH})(\text{dmf})_6(\text{H}_2\text{O})_4](\text{OH})_2$  (**13**,  $\text{Ln} = \text{Gd}, \text{Tb}$  or  $\text{Dy}$ , Fig. 25.5d) [40]. The metallic skeleton is best described as two  $\text{Cu}^{\text{II}}_2\text{Ln}^{\text{III}}_2(\text{bis-C}[4])$  butterflies tethered by a central  $\text{Ln}^{\text{III}}$  ion that is of square antiprismatic geometry (Fig. 25.6d). The core also contains a mixture of bridging anions, including  $\mu_4$ - and  $\mu_5$ -nitrates. As in the case of **11**, capping occurs through the expected  $[\text{Cu}^{\text{II}}_2(\text{bis-C}[4])]^{4-}$  moieties.

A series of new  $\text{Fe}^{\text{III}}/\text{Ln}^{\text{III}}$  clusters was successfully isolated under analogous conditions used to synthesise **6** [40]. This new cluster type has a general formula of  $[\text{Fe}^{\text{III}}_5\text{Ln}^{\text{III}}_4(\text{bis-C}[4])_2(\mu_4\text{-O})_2(\mu_3\text{-OH})_2(\mu_4\text{-NO}_3)_2(\text{dmf})_8(\text{H}_2\text{O})_6](\text{OH})_3$  (**14**,  $\text{Ln} = \text{Gd}, \text{Tb}$  or  $\text{Dy}$ , Fig. 25.5e). The metallic skeleton is best described as a square of Ln ions doubly-capped on distal edges by  $[\text{Fe}^{\text{III}}_2(\text{bis-C}[4])]^{4-}$  moieties (Fig. 25.6e). The fifth  $\text{Fe}^{\text{III}}$  ion caps one side of the square, with two  $\mu_4$ -nitrates and a  $\mu_4$ -oxygen bridging the central metal ions. The capped square of  $\text{Ln}^{\text{III}}$  cations is another common structural feature observed upon moving from  $\text{H}_4\text{C}[4]$  (cluster **5**, Fig. 25.3d) to bis- $\text{H}_4\text{C}[4]$ , and is also found in one other series of bis-C

[4]-supported 3d/4f clusters described below (and that are formed under stoichiometric control).

### 25.2.3 Stoichiometric Control Over Cluster Synthesis

Like H<sub>4</sub>C[4], bis-H<sub>4</sub>C[4] has proved to be a highly versatile ligand for the synthesis of 3d and 3d/4f polynuclear clusters; a polynuclear Ln cluster is yet to be formed, but should be achievable based on the chemistry of H<sub>4</sub>C[4]. As variation in reaction stoichiometries facilitated ion interchange within the C[4]-supported butterfly-like cluster, we explored analogous chemistry with bis-H<sub>4</sub>C[4] and found that it was in fact possible to ‘expand’ clusters through variation in both reactant ratios and crystallisation conditions [41].

The first cluster isolated from this study was found to have a general formula of [Mn<sup>III</sup><sub>6</sub>Mn<sup>II</sup><sub>2</sub>Ln<sup>III</sup><sub>2</sub>(bis-C[4])<sub>2</sub>(μ<sub>4</sub>-O)<sub>2</sub>(μ<sub>3</sub>-OH)<sub>2</sub>(μ-OCH<sub>3</sub>)<sub>4</sub>(MeOH)<sub>4</sub>(dmf)<sub>8</sub>](NO<sub>3</sub>)<sub>2</sub> (**15**, Ln = Tb or Dy, Fig. 25.5f) and represents an ‘expansion’ of the Mn<sup>III</sup><sub>4</sub>Mn<sup>II</sup><sub>2</sub>Ln<sup>III</sup><sub>2</sub> core in cluster **12** [41]. The metallic skeleton in **15** is best described as three fused butterflies (Fig. 25.6f). Comparison of both structures shows the presence of two additional Mn<sup>III</sup> ions in the body positions of the new central butterfly in **15**; μ-OMe anions are also incorporated and represent a significant difference between **12** and **15**. Cluster **15** is capped at either end by [Mn<sup>III</sup><sub>2</sub>(bis-C[4])]<sup>2-</sup> moieties, as is the case in **12**.

Variation in the stoichiometries used to isolate **10** resulted in isolation of a cluster of formula [Mn<sup>III</sup><sub>6</sub>Mn<sup>II</sup><sub>4</sub>(bis-C[4])<sub>2</sub>(μ<sub>3</sub>-OH)<sub>4</sub>(μ-OCH<sub>3</sub>)<sub>4</sub>(H<sub>2</sub>O)<sub>4</sub>(dmf)<sub>8</sub>] (**16**, Fig. 25.5g) that is structurally related to **15** [41]. The metallic skeleton in **16** (Fig. 25.6g) can be described as three fused butterflies, with the only major difference being that Mn<sup>II</sup> ions have taken up the Ln<sup>III</sup>-occupied positions in **15**, mirroring the coordination behaviour of bis-H<sub>4</sub>C[4] in cluster **12**. As in **15**, cluster **16** is capped at either end by [Mn<sup>III</sup><sub>2</sub>(bis-C[4])]<sup>2-</sup> moieties.

The final cluster obtained from stoichiometric control resulted from variation in the reaction conditions used to form cluster **15**, and has a general formula of [Mn<sup>III</sup><sub>4</sub>Ln<sup>III</sup><sub>4</sub>(bis-C[4])<sub>2</sub>(μ<sub>3</sub>-OH)<sub>4</sub>(μ-CO<sub>3</sub>)<sub>2</sub>(dmf)<sub>8</sub>(H<sub>2</sub>O)<sub>4</sub>] (**17**, Ln = Gd, Tb or Dy, Fig. 25.5h) [41]. The metallic skeleton is a distorted square of Ln<sup>III</sup> ions that is doubly-capped on distal edges by [Mn<sup>III</sup><sub>2</sub>(bis-C[4])]<sup>4-</sup> moieties (Fig. 25.6h), a structural feature observed in the Fe<sup>III</sup><sub>5</sub>Ln<sup>III</sup><sub>4</sub> cluster described above (**14**, Fig. 25.5e). Each half of the assembly can be considered a distorted Mn<sup>III</sup><sub>2</sub>Ln<sup>III</sup><sub>2</sub> butterfly-like cluster, with these being connected by μ-carbonates that arise from atmospheric CO<sub>2</sub> fixation, a relatively common phenomenon in Ln coordination cluster chemistry and one that we have also seen with C[4]-supported systems.



## 25.3 Methylene-Bridge Tethered Bis-calix[4]arenes in Cluster Synthesis

Tethering H<sub>4</sub>C[4]s at the methylene bridge with organic spacers varying in chemical nature, shape and size represents an exciting new way to control or direct the coordination chemistry of bis-H<sub>4</sub>C[4]s, but most importantly, cluster composition and or nuclearity. Preliminary cluster forming studies with H<sub>4</sub>C[4]s substituted at one methylene bridge with small alkyl chains (methyl and ethyl) resulted in the isolation of Mn<sup>III</sup><sub>2</sub>Mn<sup>II</sup><sub>2</sub> butterfly-like clusters analogous to those formed with H<sub>4</sub>C[4] (**1**, Fig. 25.3a) [22] clearly demonstrating that lower-rim coordination chemistry is unperturbed by the presence of groups at the methylene bridge.

### 25.3.1 Flexibly Tethered Bis-calix[4]arenes

With the above in mind a series of bis-H<sub>4</sub>C[4]s containing flexible alkyl tethers (propyl to decyl) were synthesised and their coordination chemistry explored [42]. Full characterisation of these new ligands was carried out as standard, but it was only possible to isolate single crystals that were suitable for X-ray diffraction studies in one case, this being the acetonitrile solvate of H<sub>4</sub>C[4]-(CH<sub>2</sub>)<sub>3</sub>-H<sub>4</sub>C[4] (Fig. 25.7a). The asymmetric unit (ASU) comprises one molecule of H<sub>4</sub>C[4]-(CH<sub>2</sub>)<sub>3</sub>-H<sub>4</sub>C[4] and four MeCN of crystallisation, two of which occupy H<sub>4</sub>C[4] cavities, forming CH- $\pi$  interactions with the aromatic rings.

Four new clusters resulted from preliminary cluster forming studies involving this series of molecules. Three of these were formed with bis-H<sub>4</sub>C[4]s tethered by octyl (H<sub>4</sub>C[4]-(CH<sub>2</sub>)<sub>8</sub>-H<sub>4</sub>C[4]), nonyl (H<sub>4</sub>C[4]-(CH<sub>2</sub>)<sub>9</sub>-H<sub>4</sub>C[4]) and decyl (H<sub>4</sub>C[4]-(CH<sub>2</sub>)<sub>10</sub>-H<sub>4</sub>C[4]) alkyl chains, and structural studies found these to be isostructural with formulae of [Mn<sup>III</sup><sub>2</sub>Mn<sup>II</sup><sub>2</sub>(C[4]-(CH<sub>2</sub>)<sub>8</sub>-C[4])( $\mu_3$ -OH)<sub>2</sub>(DMF)<sub>6</sub>] (**18**, Fig. 25.7b), [Mn<sup>III</sup><sub>2</sub>Mn<sup>II</sup><sub>2</sub>(C[4]-(CH<sub>2</sub>)<sub>9</sub>-C[4])( $\mu_3$ -OH)<sub>2</sub>(MeOH)(dmf)<sub>5</sub>] (**19**) and [Mn<sup>III</sup><sub>2</sub>Mn<sup>II</sup><sub>2</sub>(C[4]-(CH<sub>2</sub>)<sub>10</sub>-C[4])( $\mu_3$ -OH)<sub>2</sub>(dmf)<sub>6</sub>] (**20**) [42]. In each case the butterfly-like Mn<sup>II</sup><sub>2</sub>Mn<sup>III</sup><sub>2</sub> metallic skeleton is analogous to that of cluster **1** shown in Fig. 25.3a. The only difference in **18–20** is the length of the alkyl chain tethering the H<sub>4</sub>C[4]s, thereby demonstrating that a sufficiently long tether will allow for formation of known structural motifs established in analogous C[4]-supported cluster chemistry.

The fourth cluster was obtained by reaction of H<sub>4</sub>C[4]-(CH<sub>2</sub>)<sub>10</sub>-H<sub>4</sub>C[4] with Mn<sup>II</sup> and Ln<sup>III</sup> chlorides under typical reaction conditions and has a formula of [Mn<sup>III</sup><sub>4</sub>Ln<sup>III</sup><sub>4</sub>(C[4]-(CH<sub>2</sub>)<sub>10</sub>-C[4])<sub>2</sub>( $\mu_3$ -CO<sub>3</sub>)<sub>2</sub>( $\mu_3$ -OH)<sub>4</sub>(dmf)<sub>6</sub>(H<sub>2</sub>O)<sub>6</sub>] (**21**, Ln = Gd, Tb or Dy, Fig. 25.7c). This cluster bears a striking resemblance to the C[4]-supported Mn<sup>III</sup><sub>4</sub>Ln<sup>III</sup><sub>4</sub> cluster, **5**, the metallic skeleton of which is a square of Ln<sup>III</sup> ions capped on each edge by a [Mn<sup>III</sup>(C[4])]⁻ moiety. The only significant difference between **21** and **5** is that  $\mu_3$ -nitrates in the latter are replaced by  $\mu_3$ -carbonates. From inspection



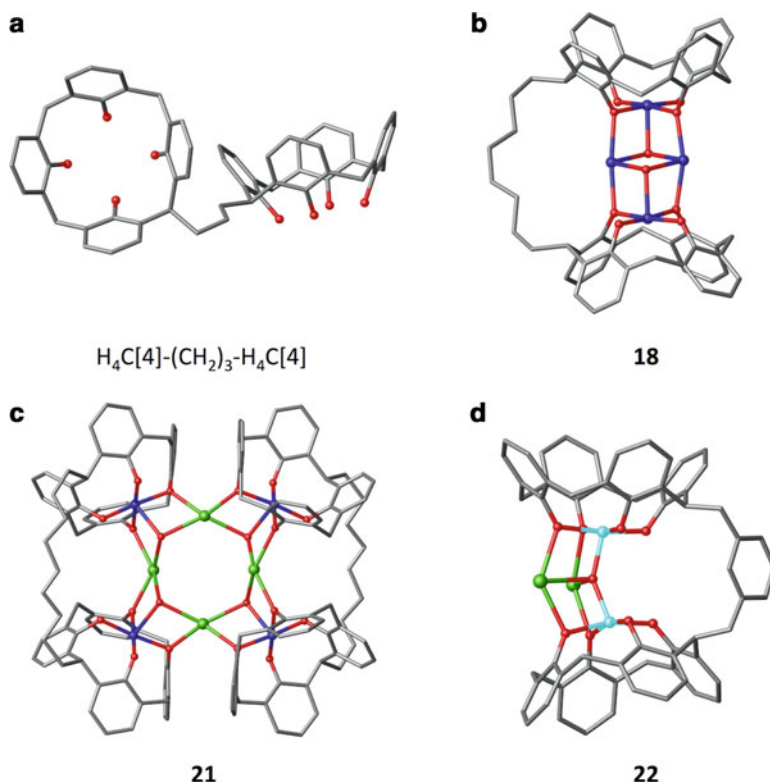


**Fig. 25.7** Partial structures of  $\text{H}_4\text{C}[4]-(\text{CH}_2)_3-\text{H}_4\text{C}[4]$  (a) and clusters **18** (b), **21** (c) and **22** (d) [42, 43]. Cluster core capping in **18**, **21** and **22** occurs, as is the case in C[4]-supported analogues, through  $[\text{TM}^{\text{II}}_2\text{bisC}[4]]^{4-}$  or  $[\text{TM}^{\text{II}}_2\text{bisC}[4]]^{2-}$  moieties. H atoms, C[4] 'Bu groups, ligated solvent and solvent of crystallisation omitted for clarity. Figures not to scale. Colour code: C – grey, O – red, TM – dark/pale blue, Ln – green

it is again clear that sufficiently long alkyl tethers allow for formation of analogous C[4]-supported cluster types.

Although it has not yet been possible to isolate single crystals from reactions involving shorter tethers, it is reasonable to expect that these will preclude the formation of known cluster types/structural motifs, necessarily giving rise to new species that will be of interest due to disparate metal ion composition/coordination environments.

### 25.3.2 Rigidly Tethered Bis-calix[4]arenes

The use of more rigid tethers in the synthesis of bis- $\text{H}_4\text{C}[4]$ s is potentially the most interesting route towards controlling or directing cluster formation; this can be

achieved by facile introduction of directionality through the tether. Initial efforts in this area have focused on the use of *ortho*-, *meta*- and *para*-xylyl tethers. Proof of concept DFT calculations were performed on these new ligands to rationalise if the constituent H<sub>4</sub>C[4]s would be favourably positioned in space to either allow for or direct the formation of existing and or new clusters from the known library of structures, all of which will take place through established core capping behaviour established for H<sub>4</sub>C[4] and bis-H<sub>4</sub>C[4] [43].

The H<sub>4</sub>C[4] moieties in both the *ortho*- and *meta*- derivatives are necessarily convergent due to constraints imposed by the spacer and the presence of the methylene groups between the aromatic ring of the tether and the methylene bridges. Calculations showed these to adopt a lower-rim eclipsed arrangement with separation between phenolic pockets being at a distance of ~3 Å. Given these constraints, these ligands would only be suitable to form metal clusters from the structural library in which the lower-rim to lower-rim separation was close to this distance. For example, inspection of the library of known clusters showed that formation of an analogue to the Mn<sup>III</sup><sub>2</sub>Mn<sup>II</sup><sub>2</sub>(C[4])<sub>2</sub> (**1**) cluster would not be possible for both *ortho*- and *meta*-bis-H<sub>4</sub>C[4], as lower-rim separation is measured to be ~5.7 Å. Analysis of all known C[4]-supported clusters did, however, suggest that it would be possible to form a bis-C[4]-supported analogue of the Fe<sup>III</sup><sub>2</sub>Ln<sup>III</sup><sub>2</sub>(C[4])<sub>2</sub> cluster (**6**, Fig. 25.3e). In contrast, gas phase structure calculations for the *para*- derivative show that the H<sub>4</sub>C[4] moieties are (as expected) divergent and positioned far from one another, with a lower-rim to lower-rim distance (centroid to centroid) of more than 12 Å. From inspection it is clear that, due structural constraints, formation of an analogue to any known C[4]-supported cluster is impossible.

Tolerance in cluster formation was tested prior to the synthesis of these ligands through the use of a methylene bridge benzyl substituted H<sub>4</sub>C[4]. This was carried out in order to assess any effects of the bulky substituent on cluster formation with the series of xylyl-bis-H<sub>4</sub>C[4]s. Given that it was possible to form Mn<sup>III</sup><sub>2</sub>Mn<sup>II</sup><sub>2</sub> butterfly-like clusters with H<sub>4</sub>C[4]s substituted at one methylene bridge with either methyl or ethyl groups, the same reaction conditions were used to test the benzyl analogue. This reaction was successful and a structure of the Mn<sup>III</sup><sub>2</sub>Mn<sup>II</sup><sub>2</sub>(benzyl-C[4])<sub>2</sub> cluster was obtained, clearly demonstrating that formation is tolerant to a wide range of groups at the methylene bridge. Subsequent synthesis of the aforementioned ligands was then undertaken and cluster formation explored; this resulted in the isolation and characterisation of two new xylyl-bis-C[4]-supported clusters.

Computational studies, coupled with inspection of the C[4]-supported cluster library, predicted that *ortho*- and *meta*-xylyl-bis-H<sub>4</sub>C[4] would be well suited to support formation of a Fe<sup>III</sup><sub>2</sub>Ln<sup>III</sup><sub>2</sub> cluster. Single crystals were isolated upon reaction of *meta*-xylyl-bis-H<sub>4</sub>C[4] under conditions used to form cluster **6** (Fig. 25.3e), and structure analysis showed these to be of formula [Fe<sup>III</sup><sub>2</sub>Gd<sup>III</sup><sub>2</sub>(*meta*-xylyl-bis-C[4])(μ<sub>4</sub>-O)(μ-OH)(dmf)<sub>7</sub>(MeOH)(H<sub>2</sub>O)<sub>2</sub>][*meta*-xylyl-bis-H<sub>4</sub>C[4]-H] (**22**, Fig. 25.7d). The metallic skeleton is analogous to that found in **6**, and a mono-deprotonated *meta*-xylyl-bis-H<sub>4</sub>C[4] is present as a counterion to the cationic

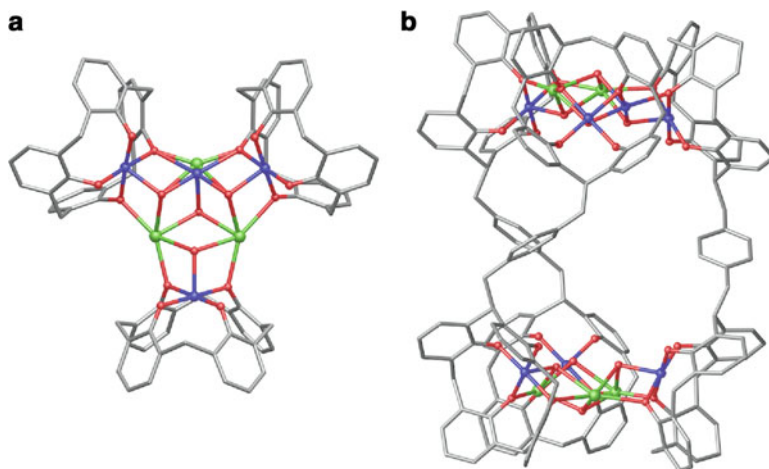


**Fig. 25.8** Partial single crystal X-ray structure of **23** [43]. (a) Triangular cluster capped on each edge by a  $[\text{Mn}^{\text{III}}\text{C}4]^-$  moiety within the ASU. (b) Symmetry expansion showing the metal-organic trigonal antiprism. Bridge linking *para*-xylyl units are omitted in A. H atoms, C[4] <sup>t</sup>Bu groups, ligated solvent, anions and solvent of crystallisation omitted for clarity in both A and B. Figures not to scale. Colour code: C – grey, O – red, Mn – dark blue, Ln – green

cluster. Although this does not represent a new structural motif, it does validate the approach of restricting cluster types through tether/ligand design.

As stated above, *para*-xylyl-bis- $\text{H}_4\text{C}[4]$  is predicted to have a divergent structure in the gas phase. Reaction of this ligand with  $\text{Mn}^{\text{II}}$  and  $\text{Ln}^{\text{III}}$  chlorides under ambient reaction conditions resulted in formation of a cluster with general formula  $[\text{Mn}^{\text{III}}_6\text{Mn}^{\text{II}}\text{Dy}_5(\textit{para}\text{-xylyl-bis-C}[4])_3(\mu_3\text{-OH})_8(\text{dmf})_8(\text{MeCN})_4(\text{H}_2\text{O})_9](\text{OH})_3$  (**23**). The ASU consists of three half molecules of *para*-xylyl-bis- $\text{H}_4\text{C}[4]$ , all of which house a  $\text{Mn}^{\text{III}}$  ion at the constituent C[4] lower-rims as expected. The lower-rim oxygens of each C[4] moiety bridge to  $\text{Ln}^{\text{III}}$  and  $\text{Mn}^{\text{II}}$  ions (two of which are disordered) that define a central triangle, which is also held together by  $\mu_3$ -hydroxides (Fig. 25.8a). As such the ASU is best described as a triangular cluster capped on each edge by a  $[\text{Mn}^{\text{III}}(\text{C}[4])]^-$  moiety, again stressing that structural trends carry through upon modification of the general  $\text{H}_4\text{C}[4]$  scaffold; there are some similarities between cluster **23** and the enneanuclear  $\text{Cu}^{\text{II}}$  cluster, **2**, shown in Fig. 25.3b.

Symmetry expansion of the ASU results in formation of a metal-organic polyhedron (MOP) that has trigonal antiprismatic topology (Fig. 25.8b), and which is clearly influenced by the directing nature of *para*-xylyl-bis- $\text{H}_4\text{C}[4]$ . Given the presence of a solvent/anion occupied space in the centre of the assembly, it was of interest to investigate if cluster **23** would be robust towards desolvation. Thermal studies found this to be the case and the assembly was capable of taking up gases ( $\text{N}_2$  and  $\text{H}_2$ ). Although the cavity in **23** is relatively small, these experiments represent a good proof of concept that bis- $\text{H}_4\text{C}[4]$  ligand design is a viable route towards the controlled assembly of supramolecular architectures containing

magnetically interesting building units. Such assemblies would have great potential to act as hosts for smaller, magnetically interesting species and is an avenue of future investigation with these new molecules.

## 25.4 Conclusions

C[4]-supported cluster synthesis is a truly burgeoning area of supramolecular coordination chemistry. The ease with which the H<sub>4</sub>C[4] scaffold can be functionalised at the upper-rim generates potentially limitless opportunities for the synthetic chemist. Moreover, understanding of the empirical ion binding rules for H<sub>4</sub>C[4]s towards 3*d*, 4*f* and 3*d*/4*f* ion mixtures allows one to predict, to a certain extent, the minimum number of metal ions to be incorporated into a cluster, as well as the structural capping behaviour of a C[4] derivative during design, and prior to synthesis. This represents a powerful tool in structural chemistry, especially when the formation of a cluster may be targeted for the incorporation of specific numbers of paramagnetic metal ions toward the construction of magnetically interesting entities. Functionalisation of the H<sub>4</sub>C[4] methylene bridge presents a new avenue to explore cluster formation, with the possibility to introduce a plethora of functional groups that do not impinge on lower-rim coordination chemistry.

Moving from H<sub>4</sub>C[4] to bis-H<sub>4</sub>C[4] via direct methylene bridge tethering gives an equally versatile molecular platform for cluster synthesis. Results obtained with this new molecule conform to the binding rules for H<sub>4</sub>C[4], thereby allowing one to enhance nuclearity of the resulting cluster. As was the case for H<sub>4</sub>C[4], stoichiometric control in reactions involving bis-H<sub>4</sub>C[4] also had the effect of altering the cluster core. Tethering H<sub>4</sub>C[4]s with simple flexible or rigid linkers has already resulted in fascinating new clusters/assemblies. Rigidly tethered bis-H<sub>4</sub>C[4]s provide the chemist with yet another route to control structure, either by dictating formation of one cluster type, or directing assembly of a nanoscale MOP. All of these developments bode well for the future of C[*n*]-supported cluster chemistry, and all of these principles will likely be applicable to larger ring sizes.

## References

1. For example see: Gatteschi, D.; Sessoli, R.; Villain, J. *Molecular Nanomagnets*, Oxford University Press, 2006.
2. Petrella, A. J.; Raston, C. L. *J. Organomet. Chem.* **2004**, 689, 4125–4136.
3. Aronica, C.; Chastanet, C.; Zueva, E.; Borshch, S. A.; Clemente-Juan, J. M.; Luneau, D. *J. Am. Chem. Soc.* **2008**, 130, 2365–2371.
4. Kajiwara, T.; Iki, N.; Yamashita, M. *Coord. Chem. Rev.* **2007**, 251, 1734–1746.
5. Fischer, R.; Görls, H.; Walther, D. *Eur. J. Inorg. Chem.* **2004**, 6, 1243–1252.

6. Bilyk, A.; Hall, K. A.; Harrowfield, J. M.; Hosseini, M. W.; Skelton, B. W.; White, A. H. *Inorg. Chem.* **2001**, *40*, 672–686.
7. Desroches, C.; Pilet, G.; Borshch, S. A.; Parola, S.; Luneau, D. *Inorg. Chem.* **2005**, *44*, 9112–9120.
8. Bilyk, A.; Hall, K. A.; Harrowfield, J. M.; Hosseini, M. W.; Mislin, G.; Skelton, B. W.; Taylor, C.; White, A. H. *Eur. J. Inorg. Chem.* **2000**, 823–826.
9. Mislin, G.; Graf, E.; Hosseini, M. W.; Bilyk, A.; Hall, A. K., Harrowfield, J. M.; Skelton, B. W.; White, A. H. *Chem. Commun.* **1999**, 373–374.
10. Akdas, H.; Graf, E.; Hosseini, M. W.; De Cian, A.; Bilyk, A.; Skelton, B. W.; Koutsantonis, G. A.; Murray, I.; Harrowfield, J. M.; White, A. H. *Chem. Commun.* **2002**, 1042–1043.
11. Bilyk, A.; Hall, A. K., Harrowfield, J. M.; Hosseini, M. W.; Skelton, B. W.; White, A. H. *Aust. J. Chem.* **2000**, *53*, 895–898.
12. Bi, Y.; Wang, X.-T.; Liao, W.; Wang, X.; Wang, X.; Zhang, H.; Gao, S. *J. Am. Chem. Soc.* **2009**, *131*, 11650–11651.
13. Xiong, C.; Jiang, F.; Gai, Y.; Yuan, D.; Han, D.; Ma, J.; Zhang, S.; Hong, M. *Chem. Eur. J.* **2012**, *18*, 5536–5540.
14. Su, K.; Jiang, F.; Qian, J.; Pang, J.; Al-Thabaiti, S. A.; Bawaked, S. M.; Mokhtar, M.; Chen, Q.; Hong, M. *Cryst. Growth Des.* **2014**, *14*, 5865–5870.
15. Su, K.; Jiang, F.; Qian, J.; Pang, J.; Hu, F.; Bawaked, S. M.; Mokhtar, M.; Al-Thabaiti, S. A.; Hong, M.; *CrystEngComm*, **2015**, *17*, 1750–1753.
16. Liu, M.; Liao, W.; Hu, C.; Du, S.; Zhang, H. *Angew. Chem. Int. Ed.* **2012**, *51*, 1585–1588.
17. Dai, F.-R.; Wang, Z. *J. Am. Chem. Soc.* **2012**, *134*, 8002–8005.
18. Xiong, K.; Jiang, F.; Gai, Y.; Yuan, D.; Chen, L.; Wu, M.; Su, K.; Hong, M. *Chem. Sci.* **2012**, *3*, 2321–2325.
19. Bi, Y.; Du, S.; Liao, W. *Coord. Chem. Rev.* **2014**, *276*, 61–72.
20. Su, K.; Jiang, F.; Qian, J.; Chen, L.; Pang, J.; Bawaked, S. M.; Mokhtar, M.; Al-Thabaiti, S. A.; Hong, M. *Inorg. Chem.* **2015**, *54*, 3183–3188.
21. Dai, F.-R.; Becht, D. C.; Wang, Z. *Chem. Commun.* **2014**, *50*, 5385–5387.
22. Karotsis, G.; Teat, S. J.; Wernsdorfer, W.; Piligkos, S.; Dalgarno, S. J.; Brechin, E. K. *Angew. Chem. Int. Ed.* **2009**, *48*, 8258–8288.
23. Taylor, S. M.; Karotsis, G.; McIntosh, R. D.; Kennedy, S.; Teat, S. J.; Beavers, C. M.; Wernsdorfer, W.; Piligkos, S.; Dalgarno, S. J.; Brechin, E. K. *Chem. Eur. J.* **2011**, *17*, 7521–7530.
24. Brechin, E. K.; Yoo, J.; Nakano, M.; Huffman, J. C.; Hendrickson, D. N.; Christou, G. *Chem. Commun.* **1999**, 783–784.
25. Karotsis, G.; Kennedy, S.; Dalgarno, S. J.; Brechin, E. K. *Chem. Commun.* **2010**, *46*, 3884–3886.
26. Su, K.; Jiang, F.; Qian, J.; Zhou, K.; Pang, J.; Basahel, S.; Mokhtar, M.; Al-Thabaiti, S. A.; Hong, M. *Inorg. Lett.* **2014**, *1*, 1–8.
27. Sanz, S.; McIntosh, R. D.; Beavers, C. M.; Teat, S. J.; Evangelisti, M.; Brechin, E. K., Dalgarno, S. J. *Chem. Commun.* **2012**, *48*, 1449–1451.
28. Bi, Y.; Xu, G.; Liao, W.; Du, S.; Deng, R.; Want, B. *Sci. China Chem.* **2012**, *55*, 967–972.
29. Karotsis, G.; Kennedy, S.; Teat, S. J.; Beavers, C. M.; Fowler, D. A.; Morales, J. J.; Evangelisti, M.; Dalgarno, S. J.; Brechin, E. K. *J. Am. Chem. Soc.* **2010**, *132*, 12983–12990.
30. Sanz, S.; Ferreira, K.; McIntosh, R. D.; Dalgarno, S. J.; Brechin, E. K. *Chem. Commun.* **2011**, *47*, 9042–9044.
31. Palacios, M. A.; McLellan, R.; Beavers, C. M.; Teat, S. J.; Weihe, H.; Piligkos, S.; Dalgarno, S. J.; Brechin, E. K. *Chem. Eur. J.* **2015**, *21*, 11212–11218.
32. Fairbairn, R. E.; McLellan, R.; McIntosh, R. D.; Taylor, S. M.; Brechin, E. K.; Dalgarno, S. J. *Chem. Commun.* **2012**, *48*, 8493–8495.
33. Scully, P. A.; Hamilton, T. M.; Bennett, J. L. *Org. Lett.* **2001**, *17*, 2741–2744.
34. Poms, D.; Itzhak, N.; Kuno, L.; Biali, Silvio E. *J. Org. Chem.* **2014**, *79*, 538–545.
35. Kogan, K.; Biali, Silvio E. *J. Org. Chem.* **2011**, *76*, 7240–7244.

36. Hertel M. P.; Behrle A. C.; Williams S. A.; Schmidt J. A.R.; Fantini J. L. *Tetrahedron*, **2009**, *65*, 8657–8667.
37. Carroll, L. T.; Hill, P. A.; Ngo, C. Q.; Klatt, K. P.; Fantini J. L. *Tetrahedron*, **2013**, *69*, 5002–5007.
38. Murphy, P.; Dalgarno, S. J.; Paterson, M. J. *J. Phys. Chem. A*, **2014**, *118*, 7986–8001.
39. McLellan, R.; Palacios, M. A.; Beavers, C. M.; Teat, S. J.; Piligkos, S.; Brechin, E. K.; Dalgarno, S. J. *Chem. Eur. J.* **2015**, *21*, 2804–2812.
40. Coletta, M.; McLellan, R.; Sanz, S.; Teat, S. J., Gagnon, K.; Brechin, E. K.; Dalgarno, S. J., **2015**, *submitted*.
41. Coletta, M.; McLellan, R.; Sanz, S.; Teat, S. J., Gagnon, K.; Brechin, E. K.; Dalgarno, S. J. **2015**, *submitted*.
42. Coletta, M.; McLellan, R.; Cols, J.-M.; Gagnon, K.; Teat, S. J., Brechin, E. K.; Dalgarno, S. J. **2016**, *28*, 557–566.
43. Coletta, M.; McLellan, R.; Murphy, P.; Leube, B.; Sanz, S.; Clowes, R.; Gagnon, K.; Teat, S. J.; Cooper, A. I.; Paterson, M. J.; Brechin, E. K.; Dalgarno, S. J. *Supramol. Chem.* **2016**, *22*, 8791–8795.

# Chapter 26

## Calixarenes as Supramolecular Catalysts Endowed with Esterase and Phosphodiesterase Activity

Riccardo Salvio, Roberta Cacciapaglia, and Alessandro Casnati

### 26.1 Introduction

An efficient supramolecular catalyst must be able to (i) recognize the substrate (s) and/or reactant(s); (ii) promote the conversion of the bound substrate(s) into products; (iii) promptly release the product(s) and restore the catalytically active form, thus assuring turn over [1].

The rational design of catalysts capable of achieving significant results in terms of selectivity and acceleration of reaction rates has been inspired by the remarkable properties of enzymes, which have provided chemists with outstanding examples to emulate.

The wide employment of calixarenes derivatives as supramolecular catalysts rests on the extreme versatility of these cyclophanes. They are able to act both as hosts, with the involvement of their molecular cavity in the recognition step, and as molecular platforms for the arrangement of well organized catalytic/binding groups. The extensive use of calixarenes as molecular platforms has been possible thanks to the accessibility to the selective derivatization at either rims of the macrocycle, with the introduction of a countless variety of ligating moieties and functional groups, in diverse mutual geometrical arrangements. Another important distinctive feature of this class of cyclophanes is the possibility of a fine control of their conformational properties, sometimes accompanied by a residual flexibility of

---

R. Salvio • R. Cacciapaglia  
Dipartimento di Chimica and IMC – CNR Sezione Meccanismi di Reazione,  
Università La Sapienza, 00185 Rome, Italy  
e-mail: [riccardo.salvio@uniroma1.it](mailto:riccardo.salvio@uniroma1.it); [roberta.cacciapaglia@uniroma1.it](mailto:roberta.cacciapaglia@uniroma1.it)

A. Casnati (✉)  
Dipartimento di Chimica, Università degli Studi di Parma, Parco Area delle Scienze 17/A,  
43124 Parma, Italy  
e-mail: [alessandro.casnati@unipr.it](mailto:alessandro.casnati@unipr.it)

the calixarene scaffold, even when it is suitably preorganized in a fixed *cone* conformation.

Reinhoudt et al. [2] developed one of the first examples of efficient calixarene-based artificial nuclease and introduced the concept of ‘dynamic preorganization’ to describe the capability of calixarenes to secure a good compromise between a suitable preorganization of a set of catalytic and/or recognition moieties in reciprocal close proximity and a residual flexibility in the molecular scaffold that greatly helps in the dynamic fit of the catalyst to the bound substrate through the reaction path.

Altogether, the several features of calixarenes, notably their ability to form host–guest complexes and the ease of introducing a large variety of active units by means of selective derivatization, make this class of compounds most useful for the purpose of multifunctional catalysis, and excellent candidates as platforms for the design of artificial catalysts.

In this chapter we will focus the readers’ attention on the reactions of acyl and phosphoryl transfer catalyzed and/or promoted by calixarenes, since these are the transformations which mostly took advantage of the preorganization of active sites on the calixarene with the highest degree of cooperation.

## 26.2 Metal Complexes of Calixarenes as Artificial Esterases or Phosphodiesterases

Ligated metal cations, typically  $\text{Zn}^{\text{II}}$  and  $\text{Cu}^{\text{II}}$ , are active units in many enzyme mimics capable of solvolytic activity [3]. Different mode of actions have been proposed [4] to explain the role of metal cations in the acceleration of the reaction: (1) *Lewis acid activation*: the metal ion can interact with the oxygen atoms of the substrate reacting group and increase its electrophilicity; (2) *nucleophile delivery*: the metal cation increases the acidity of a coordinated protic solvent molecule, assuring a high concentration of the active nucleophile (the conjugate base of the solvent) even at relatively low pH values; (3) *bifunctional mechanism*: takes place when both the activating processes described in (1) and (2) are active and the reaction proceeds via a four-membered cyclic transition state; and (4) *leaving group activation*: the metal ion coordinates to the leaving group and facilitates its release. This last operation mode can act synergically with the other three modes of action described before.

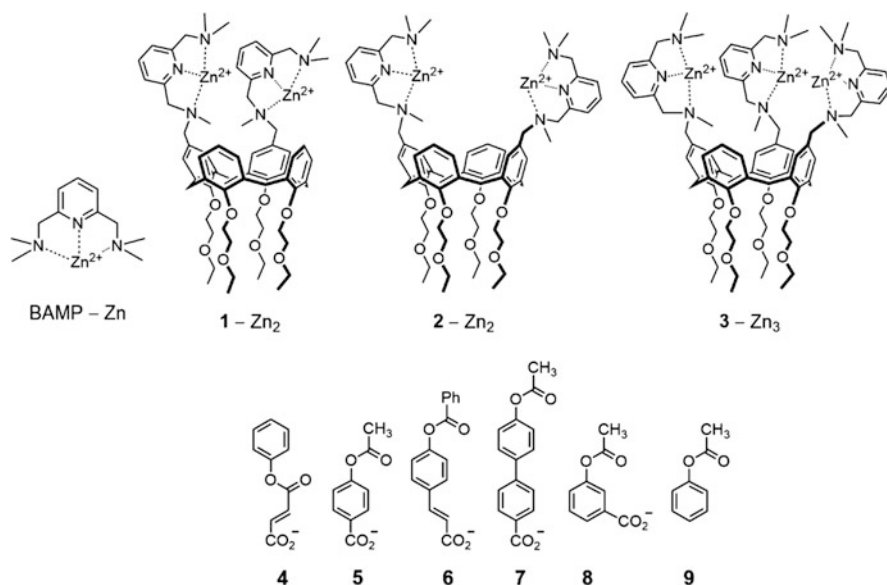
There has been a wide interest in the biomimetic hydrolytic activity of bimetallic and trimetallic catalysts [5]. In the frame of this research line, calixarenes have been extensively used as molecular scaffolds to connect ligands for metal cations.

In this section we present an overview of metal complexes of calixarenes acting as enzyme mimics in acyl and phosphoryl transfer.



### 26.2.1 $Zn^{II}$ Complexes as Artificial Esterases

Regioisomeric dinuclear complexes **1**- $Zn_2$  and **2**- $Zn_2$  are shape- and size-selective catalysts of the methanolysis of esters **5**-**8** provided with a carboxylate anchoring group, (MeOH, pH 10.4, 25 °C) [6, 7]. At variance with the reactivity picture obtained with phenyl acetate **9**, the reactions of the esters **5**-**8** functionalized with a distal carboxylate ( $-COO^-$ ) are catalyzed by dinuclear complexes **1**- $Zn_2$  and **2**- $Zn_2$  much more efficiently than by the monometallic control BAMP- $Zn$ . The activity of the bimetallic catalyst is more than two orders of magnitude larger than that of the monometallic model in the most favorable cases. This evidence is consistent with a bifunctional catalytic mechanism in which the two metal ions work in a cooperative manner (Fig. 26.1a). One of the metal ions acts as an anchoring site for the negatively charged carboxylate and the other cation intramolecularly delivers an activated methoxide ion to the carbonyl function of the complexed substrate. Rate enhancements larger than four orders of magnitude were observed in the methanolysis of **8** catalyzed by the 1,2-vicinal metal complex **1**- $Zn_2$ .



The role of the anchoring step is manifold: it selects the substrate, provides electronic activation to the ester undergoing the nucleophilic attack by conversion of a moderately electron-releasing substituent into an electron-withdrawing one (with a resulting increase of reactivity) and, more importantly, it turns an otherwise intermolecular delivery of the methoxide to the ester function into an intramolecular (intracomplex) delivery.

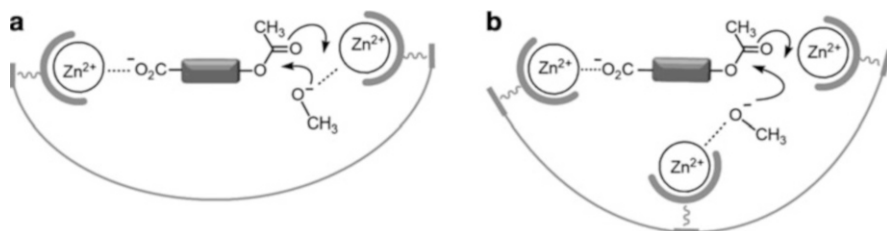


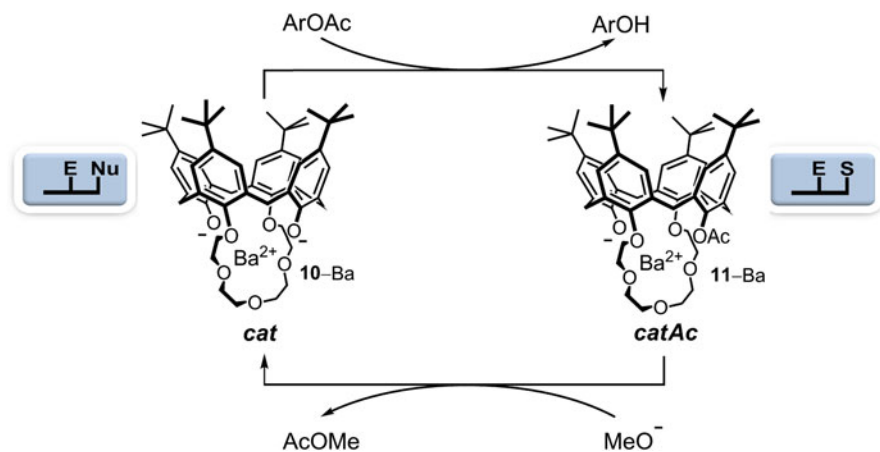
**Fig. 26.1** Bimetallic (a), and trimetallic (b) catalytic mechanism for the basic methanolysis of esters functionalized with a distal carboxylate anchoring group

The superiority of 1,2-vicinal bimetallic catalysts over their distal regioisomers has been also confirmed in the methanolysis of esters catalyzed by the zinc (II) complexes of calix[4]arenes decorated with 1,5,9-triazacyclododecane ([12] aneN<sub>3</sub>) ligands **24–26** [8].

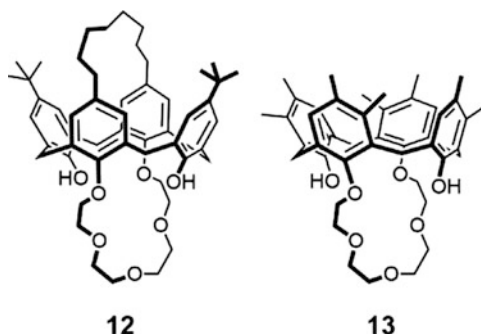
Clear evidence of trifunctional catalysis in ester cleavage is obtained in the investigation of the catalytic activity of the trinuclear complexes **3–Zn<sub>3</sub>** in the cleavage of esters provided with a carboxylate anchoring group [6, 7]. The superiority of the trimetallic catalyst **3–Zn<sub>3</sub>** over the 1,2-bimetallic catalyst **1–Zn<sub>2</sub>** in the cleavage of ester **5** is higher than the calculated statistical advantage of the trimetallic complex over its bimetallic analogues [7]. Some evidence of trifunctional catalysis is also obtained in the cleavage of ester **6** catalyzed by **1–Zn<sub>3</sub>**, and of ester **8** catalyzed by the trimetallic complex **26–Cu<sub>3</sub>** of the [12] aneN<sub>3</sub> series. In Fig. 26.1b are illustrated the three different activation modes performed by the metal ions in the proposed catalytic mechanism: (i) substrate anchoring through binding to carboxylate, (ii) Lewis-acid activation of the ester carbonyl, and (iii) nucleophile activation and delivery.

## 26.2.2 Ba<sup>II</sup> Complexes as Artificial Esterases

A fairly efficient nucleophile catalyst with transacylase activity (**10–Ba**; *cat*) was developed by us [9]. Previous investigations indicated that alkaline-earth metal ions complexed by crown ethers are efficient promoters of acyl transfer reactions from esters to anionic nucleophiles [10]. The barium complex **10–Ba** acts as a turnover catalyst in the methanolysis of aryl acetates, (diisopropylethylamine buffer in MeCN–MeOH 9:1, (v/v), 25 °C). Experimental evidence points to the operation of a *ping-pong* mechanism as outlined in Scheme 26.1.



**Scheme 26.1** Turnover nucleophilic catalysis of **10**-Ba in the methanolysis of aryl acetates

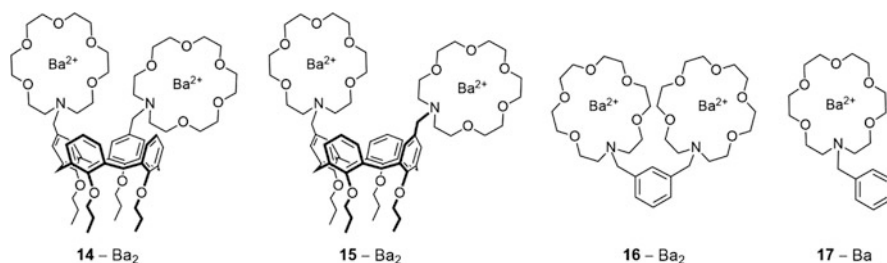


The catalytic activity of **10**-Ba relies on the effective preorganization on the calixarene molecular platform of the electrophile (**E**) and the nucleophile (**Nu**) in the acylation step, and of the substrate (**S**; the ester function of *catAc*) and the electrophile (**E**) in the deacylation step (cfr. Scheme 26.1).

The lack of any catalytic activity of the barium complexes of rigidified structures **12** and **13** [11] indicates that a certain degree of flexibility of the macrocyclic backbone is a fundamental requisite for catalysis.

Calix[4]arene-based bimetallic complexes **14**-Ba<sub>2</sub> and **15**-Ba<sub>2</sub> are efficient catalysts of the ethanolysis of esters **4**-**7** provided with a distal carboxylate anchoring group [12]. The barium ion plays a crucial role both in the recognition and catalytic event of these esterases. The marked affinity of the carboxylate unit for the complexed barium ion ensures efficient binding of substrates **4**-**7** to the catalyst. Upon complexation, in analogy with zinc(II) catalysts, a moderately rate retarding (electron-releasing) carboxylate substituent is converted into a rate enhancing (electron-withdrawing) one, and the otherwise intermolecular ethoxide addition to the ester carbonyl is transformed into an intramolecular (intracomplex)

delivery of an ethoxide ion complexed to the second barium(II) ion. The latter ion also promotes the reaction by electrophilic activation of the ester function. The observed rate enhancements range from one to more than four orders of magnitude, depending on the substrate-catalyst combination.

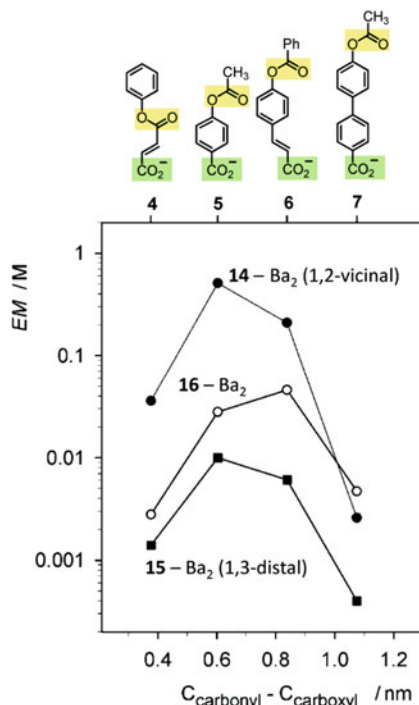


The marked superiority shown by dinuclear catalysts over the mononuclear model **17**–Ba confirms that the two metal ions act cooperatively. In the cleavage of **5**, for example, the reaction rate in the presence of 0.1 mM **14**–Ba<sub>2</sub> is more than three orders of magnitude higher than the rate observed in the presence of 0.2 mM **17**–Ba.

Overall, the reactivity picture obtained with catalysts **1**–Zn<sub>2</sub>, **2**–Zn<sub>2</sub>, **24**–Zn<sub>2</sub>, **25**–Zn<sub>2</sub>, **14**–Ba<sub>2</sub>, and **15**–Ba<sub>2</sub> in the basic alcoholysis of esters, shows that the order of catalytic efficiency 1,2-vicinal  $\gg$  1,3-distal is a substrate-independent feature of upper rim calix[4]arene-based bimetallic catalysts in the cleavage of esters provided with an anchoring group, which is unaffected by the nature of the metal ion and of the ligating unit.

High catalytic efficiency is observed when the target substrate and the catalyst match in terms of size and geometrical features. Catalytic performances of isomeric **14**–Ba<sub>2</sub> and **15**–Ba<sub>2</sub>, and that of the complex **16**–Ba<sub>2</sub> based on a *m*-xylylene spacer have been compared in terms of effective molarities (*EMs*) [13, 14]. The *EM* parameter, defined by the ratio  $k_{\text{intra}}/k_{\text{inter}}$ , provides a measure of the advantage coming from the intramolecularity in the process catalyzed by the bifunctional catalyst. The *EM* value is independent of the chemical activation provided by the catalytic units, solely depending on the way the molecular scaffold arranges reactants in a geometry suitable for the transformation. The *EM* value, unlike the advantage of dinuclear over mononuclear catalyst and the catalytic rate enhancement, is independent of reactant concentrations. The plot of *EM* vs the carbonyl-carboxylate distances in ester substrates, taken as a gross estimate of their size, is reported in Fig. 26.2. This plot indicates that a good match of ester size to the distance between the two metal ions is an important prerequisite for catalysis. The dinuclear 1,2-vicinal **14**–Ba<sub>2</sub> catalyst is not only far superior to its 1,3-regioisomer **15**–Ba<sub>2</sub> in all cases, but it is also remarkably superior to the dinuclear catalyst based on the *m*-xylylene scaffold **16**–Ba<sub>2</sub> [15] in the reactions of esters **4**–**6**.

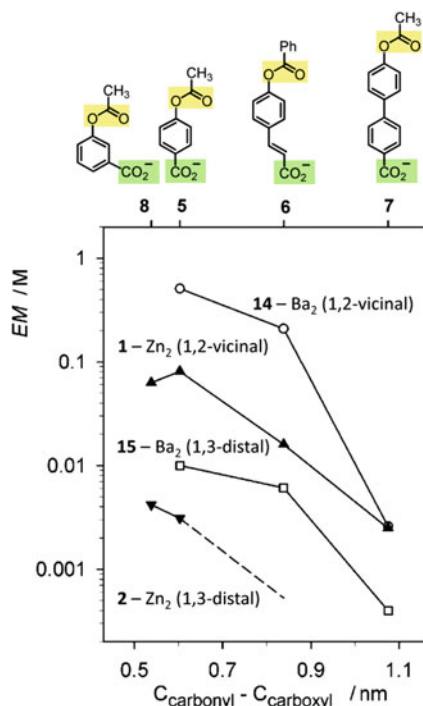
**Fig. 26.2** *EM* values for the basic ethanolysis of esters **4–7** catalyzed by the barium complexes of calix[4]arene ligands **14** and **15** and of the *p*-xylylene ligand **16** (Data from Refs. [12, 15])



The efficiency of the intramolecular process involving the bifunctional catalyst and reactants is dramatically influenced by the number of skeletal single bonds involved in the formation of the (pseudo)cyclic transition state. This effect is due to a partial loss of the torsional entropy in a cyclic arrangement. A general extrathermodynamic treatment [13b] relates the entropy loss upon cyclization to the number of rotatable bonds in the open chain reactant undergoing cyclization, and provides a set of predicted *EM* values. Under the assumption that the carboxylate–metal–(crown ether) and ethoxide–metal–(crown ether) moieties can be treated as pseudo-single bonds, in the productive complex involving **14**–Ba<sub>2</sub> and esters **5** and **6**, there are nine and ten rotatable bonds, respectively. The predicted values of *EM* 0.67 M and 0.47 M, in the given order, are in good agreement with the experimental *EM* values. A reasonably good match between the bimetallic catalyst and the transition state is thus apparent in these systems. With the same substrates the catalytic performances of the 1,3-distal isomer **15**–Ba<sub>2</sub> and of the *p*-xylylene system **16**–Ba<sub>2</sub> are definitely lower, indicating the existence of a mismatch between transition state and the bimetallic catalyst.

A comparison in terms of effective molarities between the catalytic performance of complexes **14**–Ba<sub>2</sub> and **15**–Ba<sub>2</sub> in the ethanolysis of esters provided with a carboxylate anchoring group, with that of complexes **1**–Zn<sub>2</sub> and **2**–Zn<sub>2</sub> in the methanolysis of the same substrates, is reported in Fig. 26.3. The plot shows a

**Fig. 26.3** Comparison of the catalytic performance of the zinc(II) complexes of calix[4]arene ligands **1** and **2** and barium(II) complexes of **14** and **15** in the basic alcoholysis of esters **5–8** (Data from Refs. [7, 12])



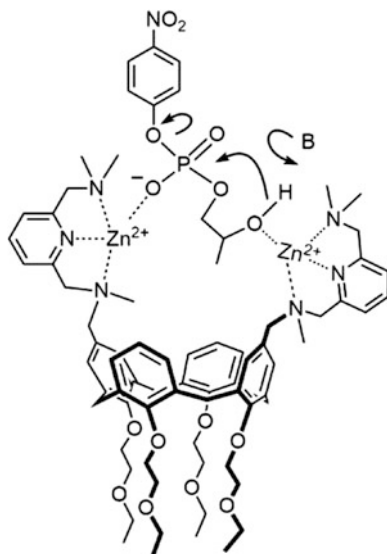
marked superiority of **14**-Ba<sub>2</sub> and **15**-Ba<sub>2</sub> over the structurally related **1**-Zn<sub>2</sub> and **2**-Zn<sub>2</sub>, pointing to a lower adaptability of the zinc(II) complexes to the altered substrates in the transition state. This picture is consistent with the more stringent geometrical coordination requirements of a *d*-block metal ion compared with an *s*-block metal ion.

### 26.2.3 Zn<sup>II</sup> and Cu<sup>II</sup> Complexes as Artificial Phosphodiesterases

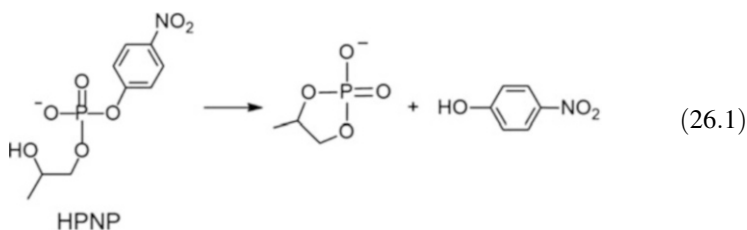
A set of effective metal based enzyme mimics with phosphodiesterase activity were developed by Reinhoudt and coworkers [2], pioneering the use of calix[4]arenes as scaffolds for the dynamic arrangement of multiple catalytic groups.

The bimetallic complex **2**-Zn<sub>2</sub> is a highly efficient turnover catalyst of the transesterification of the RNA model compound 2-hydroxypropyl *p*-nitrophenyl phosphate (HPNP) (Eq. 26.1). A 23,000-fold rate enhancement is observed in the presence of **2**-Zn<sub>2</sub> (0.48 mM catalyst concentration, 50% MeCN-20 mM aqueous buffer, pH 7, 25 °C) [16]. The two metal ions in **2**-Zn<sub>2</sub> efficiently cooperate both in

**Fig. 26.4** Proposed catalytic mechanism for the cleavage of HPNP catalyzed by **2**-Zn<sub>2</sub>



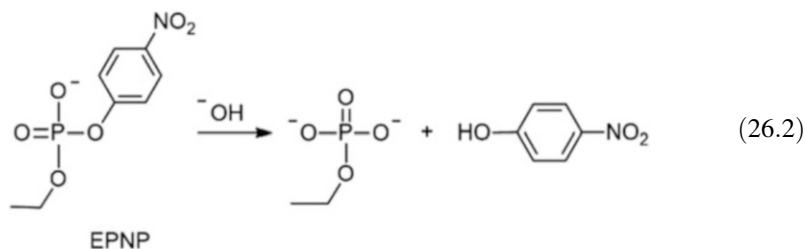
the binding and in the catalytic conversion of the substrate (Fig. 26.4). The catalytic activities of the monometallic model compounds, the calix[4]arene **18**-Zn and BAMP-Zn, are 50- and 300-fold lower, respectively [17]. The sixfold higher activity of **18**-Zn over BAMP-Zn was ascribed to a favourable role of the hydrophobic cavity of the calix[4]arene moiety. In contrast to what observed in the catalytic cleavage of carboxylic esters, the 1,2-vicinal complex **1**-Zn<sub>2</sub> is significantly less effective than its 1,3-distal regioisomer **2**-Zn<sub>2</sub> in the cleavage of HPNP [6].



The crown ether bridge in calix[4]arene **19** freezes the calixarene structure in a rigid *flattened-cone* conformation also pushing the two metal ions apart. The bimetallic complex **19**-Zn<sub>2</sub> cleaves HPNP eight times less effectively than the flexible **2**-Zn<sub>2</sub> [17], thus confirming that a certain degree of flexibility is beneficial and is an important requisite in a supramolecular catalyst.



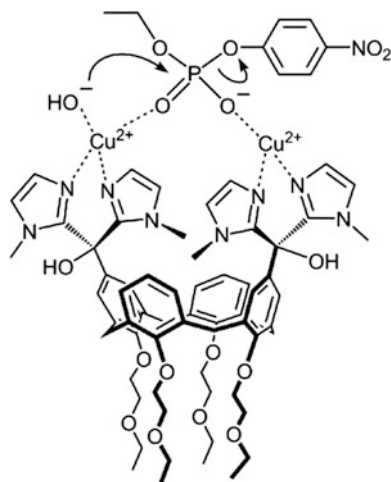




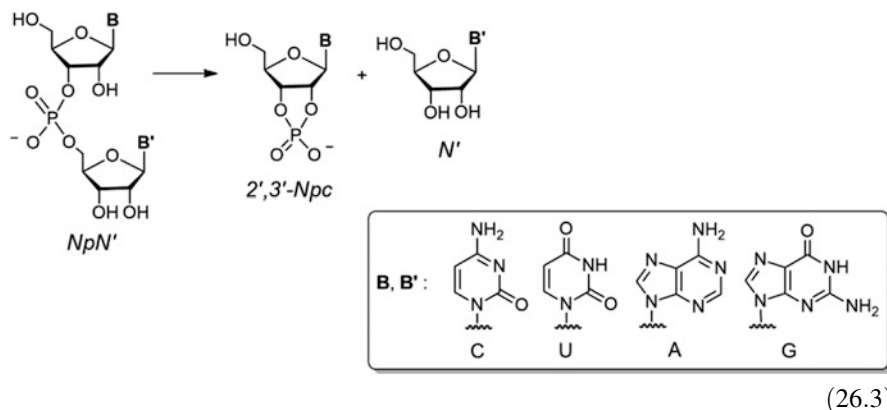
The close spatial proximity of the two metal ions in **20**-Cu<sub>2</sub> allows double Lewis acid activation of the phosphoryl moiety of HPNP and EPNP by the two copper(II) centers. Liberation of *p*-nitrophenol occurs by nucleophilic attack of the  $\beta$ -hydroxy group in the case of HPNP, and of the metal bound hydroxide ion in the case of EPNP (Fig. 26.5).

A further increase in the catalytic activity is obtained upon introduction of a third metal center [17]. The trimetallic zinc(II) complex of calix[4]arene **3** shows a three-fold increase over **2**-Zn<sub>2</sub> in the specific rate of HPNP transesterification (50 % MeCN-20 mM aqueous buffer pH 7, at 25 °C). Actually three metal ions operate synergically also in the active site of a number of families of metallo-phosphodiesterases such as nuclease P1 and phospholipase C, involved in the hydrolytic cleavage of phosphate diester bonds in phosphatidylcholine and phosphatidylinositol and in RNA and DNA, respectively [19]. The high catalytic power of **3**-Zn<sub>3</sub> allows efficient cleavage of diribonucleoside monophosphates (Eq. 26.3) [20]. Catalytic turnover and rate accelerations in the order of 10<sup>4</sup>-10<sup>5</sup> are obtained with **3**-Zn<sub>3</sub> in the cleavage of UpU and GpG, that are processed 19- and 160-fold faster than ApA, respectively, (0.9 mM catalyst concentration, 35 % EtOH-20 mM HEPES, pH 8.0). Michaelis-Menten saturation profiles obtained in the cleavage of GpG and UpU vs the linear dependency on the catalyst concentration obtained with ApA, suggest the formation of a productive substrate-catalyst complex with UpU and GpG, and a

**Fig. 26.5** Proposed catalytic mechanism for the cleavage of EPNP catalyzed by **20**-Cu<sub>2</sub>



small affinity for ApA. The enhanced binding has been ascribed to coordination of a metal center to a deprotonated amide ( $-\text{C}(\text{O})\text{N}^-$ ) group in uridine and guanosine.



## 26.2.4 Water Soluble Artificial Metallonucleases

In order to achieve catalysts which are soluble enough in water, thus avoiding the use of organic cosolvents, bifunctional and trifunctional calixarenes **24**–**26** decorated with [12]aneN<sub>3</sub> ligand units were developed [21]. The high affinity of this ligand moiety for copper(II) and zinc(II) ions also ensures extensive formation of the metal complexes of [12]aneN<sub>3</sub>-based ligands in water and at submillimolar concentrations. On the other hand, the relatively low affinity of the BAMP ligand for zinc(II) in water at pH 7.0 ( $\text{Log } K = 3.0$ ) prevents the investigation of the RNAase activity of any BAMP functionalized catalyst under physiological conditions.

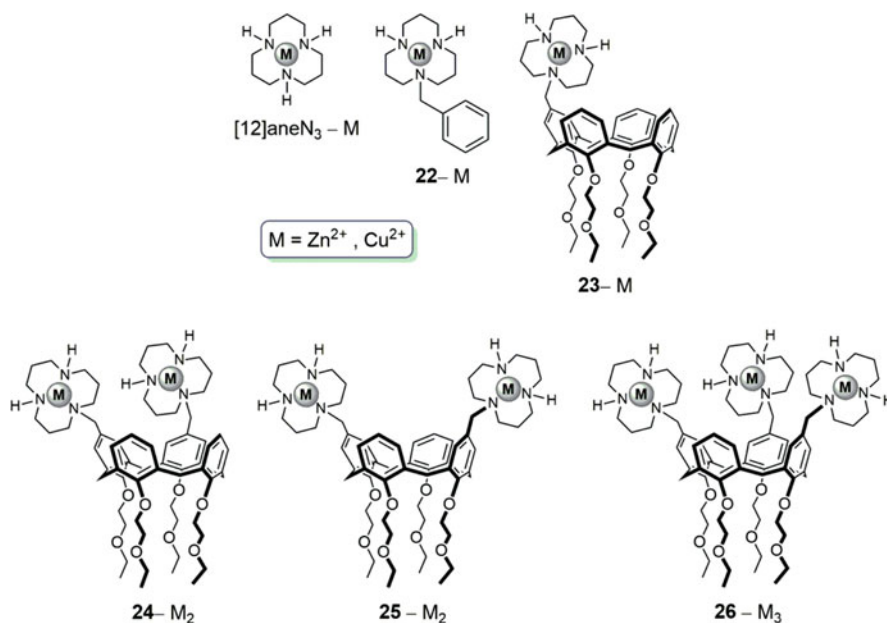
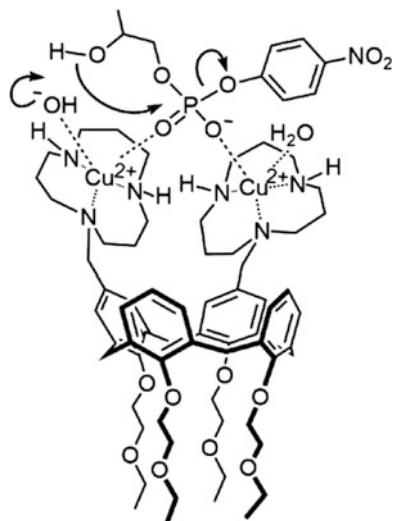


**Fig. 26.6** HPNP transesterification catalyzed by **24**-Cu<sub>2</sub>

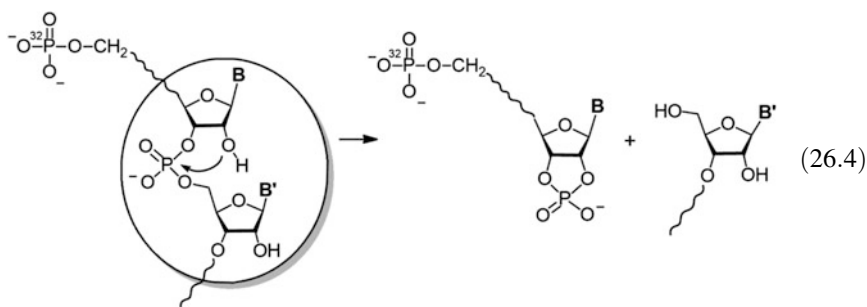


Unlike the corresponding zinc(II) complexes, the copper(II) complexes of ligands **23**–**26** are soluble enough in water for catalytic measurements, the highest solubility being experienced by the trimetallic complex **26**-Cu<sub>3</sub>. Cooperation between metal centers is fairly high in the case of the 1,2-vicinal dinuclear complex **24**-Cu<sub>2</sub> in the cleavage of HPNP (0.2 mM catalyst concentration, water, pH 7, 25 °C) with a  $>10^3$  rate acceleration over the reaction carried out in the presence of buffer alone. Accelerations of 42- and 73-fold over **23**-Cu and [12]aneN<sub>3</sub>-Cu, respectively, are observed [21]. On the other hand, the catalytic efficiency of 1,3-distal bimetallic regioisomer **25**-Cu<sub>2</sub> is about twice as great as that of monometallic **22**-Cu, with no rate acceleration per metal center. The Michaelis-Menten profile indicates the reversible formation of a HPNP · (**24**-Cu<sub>2</sub>) complex ( $K = 1/K_M = 500 \text{ M}^{-1}$ ). A possible transition state of the reaction is given in Fig. 26.6. A two-point interaction of the negatively charged phosphate moiety to the two metal ions with double Lewis-acid activation and the possible involvement of a metal-bound hydroxide acting as a general base is proposed. The trimetallic complex **26**-Cu<sub>3</sub> turns out to behave essentially as a 1,2-vicinal dinuclear catalyst, indicating that a trimetallic catalytic mechanism is not operative.

Trimetallic complex **26**-Cu<sub>3</sub> at 1 mM concentration efficiently cleaves diribonucleoside monophosphates (UpU, UpG, GpU, GpG, ApG, CpG, GpA, CpA) with rate accelerations in the order of  $10^4$  compared to background reaction in most cases [21]. Rate enhancements are as high as  $10^5$  in the cleavage of UpU and UpG. The presence of an additional binding site arising from the copper-assisted deprotonation of the uracyl moiety at the 5'-terminus of the diribonucleoside has been proposed. Unexpectedly, CpA is not cleaved by **26**-Cu<sub>3</sub>. This is not due to the inherently low reactivity of this substrate, nor to its insensitivity to copper(II) catalysis, as demonstrated by the finding that CpA is cleaved by [12]aneN<sub>3</sub>-Cu and **25**-Cu<sub>2</sub> about three times more rapidly than UpU. The activity of

**26**–Cu<sub>3</sub> in the cleavage of UpU is similar to that of **24**–Cu<sub>2</sub>. Only two 1,2-vicinal metal centers are apparently involved in the catalysis by **26**–Cu<sub>3</sub>, with the third metal ion acting as an innocent spectator.

The copper(II) complexes of triazacyclododecane decorated calix[4]arenes **24**–**26** also show high phosphodiesterase activity in the cleavage of oligoribonucleotides (water, pH 7.4, 50 °C; Eq. 26.4) [22]. This substrates (ACCAUC, CGCUGA, AGGUUAA, CAGGCC, CCGGCA, ACUAUC) have a radioactive phosphate label at the 5'-terminal position that allows the detection of the reagents and of the <sup>32</sup>P containing products (Eq. 26.4) in the gel electrophoresis analyses. Rate constants for the cleavage of all of the scissile bonds of the investigated substrates are obtained in a detailed kinetic analysis. There is an evident tendency for the catalytic efficiency to increase with the number of metal units, suggesting an effective cooperation between the metal centers in the bimetallic and trimetallic complexes. In a number of cases the 1,2-vicinal complex **24**–Cu<sub>2</sub> is more efficient than its distal regioisomer **25**–Cu<sub>2</sub>. This is in line with what observed in the reactions of UpU and HPNP, but in other cases the reverse behaviour is observed. A similar situation holds for the relative efficiency of trinuclear vs dinuclear complexes, with a reactivity order strongly depending on the identity of the oligoribonucleotide. The trinuclear complex is the best cleaving agent in the lot, nevertheless a clear evidence of the operation of a trimetallic catalytic mechanism is lacking, since the advantage due to the presence of the third metal ion hardly exceeds a factor of 2.

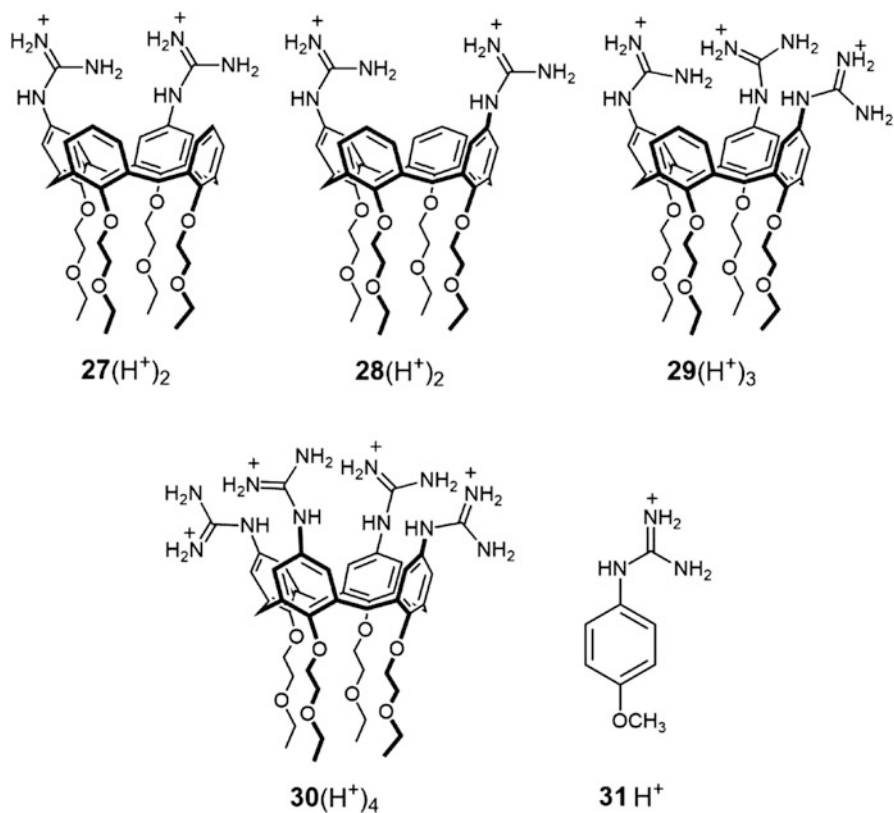


In marked contrast to the selectivity observed in the reactions of diribonucleoside monophosphates, a noteworthy preference for cleavage of the CpA sequence of oligoribonucleotides is observed for all the catalysts. For example, in the cleavage of the CpA bond in the hexamer CAGGCC by **26**–Cu<sub>3</sub>, the rate enhancement over the background of ca.  $5 \times 10^5$ -fold is one of the highest values observed for the cleavage of oligoribonucleotides by artificial metallonucleases. This picture is also confirmed in the reaction of a longer oligoribonucleotide (5'-GCAAGCACAGACAUCAG-3'), in which all CpA bonds are efficiently cleaved by **24**–Cu<sub>2</sub>, whereas the cleavage of the other sequences has not been detected. A similar behaviour is observed with the 1,3-distal regioisomer **25**–Cu<sub>2</sub>.

## 26.3 Calixarene Catalysts Containing Brønsted Acid/Base Moieties

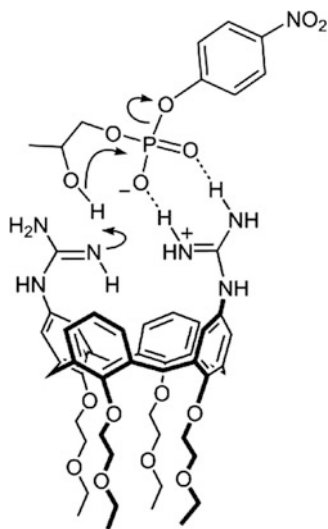
### 26.3.1 Guanidinocalix[4]arenes as Artificial Phosphodiesterases and ATPases

The guanidinium unit plays a crucial role in the activity of some enzymes such as staphylococcal nuclease [23] and has been used as an activating and/or anchoring group in the design of supramolecular catalysts [24–28]. Artificial phosphodiesterases **27**–**30** were developed by introducing from two to four guanidinium units at the upper rim of a *cone* calix[4]arene scaffold [26].



The catalytic activity of **27**–**30** in the transesterification of HPNP (Eq. 26.1) was investigated in 80 % DMSO-H<sub>2</sub>O, 25 °C, at pH 9–12. These pH values correspond to neutral to moderately basic solutions in the investigated reaction medium ( $pK_w = 18.4$  in 80 % DMSO-H<sub>2</sub>O, at 25 °C) [26].

**Fig. 26.7** General-acid/general-base catalytic mechanism in HPNP transesterification in the presence of  $28\text{H}^+$



Combination of the pH-dependence of catalytic rates with potentiometric acidity measurements shows that a necessary requisite for effective catalysis is the presence, on the same molecular scaffold, of the guanidine-guanidinium pair. This finding suggests the operation of a mechanism in which the neutral guanidine acts as a general base and a protonated guanidine as an electrophilic activator (Fig. 26.7). In this set of measurements the most effective catalyst is the 1,3-distal derivative  $28\text{H}^+$ , that is slightly more efficient than the 1,2-vicinal regioisomer  $27\text{H}^+$ . On the other hand, no clear evidence of trifunctional catalysis is observed with **29**, indicating that the additional guanidinium unit is acting as an innocent spectator. The tetrasubstituted calix[4]arene **30** is slightly less effective than **27**–**29**, most likely on account of steric interferences caused by overcrowding.

The kinetic picture obtained shows that a high level of synergism results from the preorganization of the guanidine-guanidinium catalytic dyad at the upper rim of the *cone* calix[4]arene scaffold. The transesterification rate of HPNP catalyzed by 1 mM  $27\text{H}^+$  or  $28\text{H}^+$  is three orders of magnitude higher than that obtained when the two active units are disconnected, i.e. in a buffer composed by equimolar amounts of **31** and  $31\text{H}^+$  at millimolar catalyst concentration.

The diguanidinocalix[4]arenes **27** and **28** have been also tested as catalysts in the cleavage of diribonucleoside monophosphates [27]. They exhibit a remarkable selectivity for some sequences (GpU, GpG and UpU) and accelerate this reaction much more effectively than the transesterification of HPNP. Rate accelerations relative to the background reaction range from  $10^3$  to  $10^4$ -fold, and approach  $10^5$ -fold with the best substrate-catalyst combinations. The 1,2-vicinal isomer  $27\text{H}^+$  is slightly more efficient than its 1,3-distal regioisomer  $28\text{H}^+$  in the cleavage of most of the substrates.

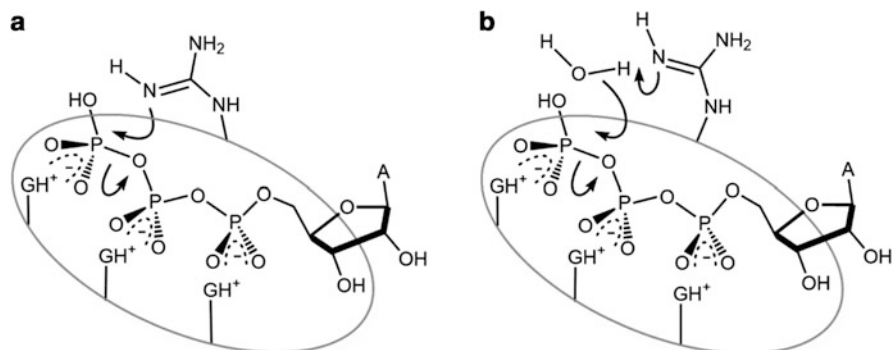


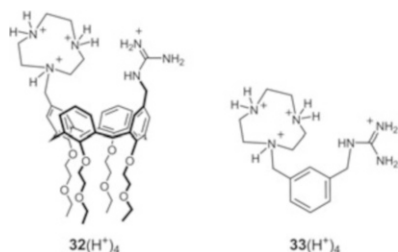
**Fig. 26.8** ATP cleavage promoted by  $30(\text{H}^+)_3$ . Possible operating mechanisms: (a) nucleophilic catalysis; (b) general-base catalysis

The triprotonated species  $30(\text{H}^+)_3$  has proved to be a highly efficient and selective turnover catalyst of the cleavage of adenosine triphosphate (ATP) (Eq. 26.5) [28]. In the reaction medium (80 % DMSO, 0.1 M  $\text{Me}_4\text{NClO}_4$ , 80 °C) at pH 9.8 the dominant species is  $30(\text{H}^+)_3$ . At this pH value, the cleavage rate of 10 mM ATP in the presence of 0.2 mM guanidinocalix[4]arene **30** is at least three orders of magnitude higher than in the absence of catalyst. In the active species  $30(\text{H}^+)_3$ , the synergic action of three guanidinium units and a neutral guanidine results in a catalytic activity comparable to that of  $[\text{24}]\text{N}_6\text{O}_2$  and of similar macrocyclic polyamines developed by Lehn, Mertes, and their co-workers [29]. The three guanidinium groups in  $30(\text{H}^+)_3$  bind and activate ATP, while the neutral guanidine behaves as a nucleophilic catalyst or as a general base catalyst, yielding adenosine diphosphate (ADP) (Fig. 26.8).



### 26.3.2 Heterobifunctional Guanidinium-Metal Ion Calix[4]arene Catalysts

Excellent performances have been obtained in the reaction of HPNP and of diribonucleoside monophosphates with the heterobifunctional catalyst  $32\text{H}^+-\text{Cu}$  featuring a triazacyclononane 9[ane] $\text{N}_3$  (TACN) and a guanidinium moiety [30].



The unsymmetrically substituted calix[4]arene **32** was designed with the aim at mimicking a common feature of many phosphatases, nucleases, and ribonucleases based on the arginine guanidinium moiety, i.e. the additional presence of one or more metal cations in the active site of the enzyme [3c]. A noteworthy example of metal ion – guanidinium cooperation is given by alkaline phosphatase, which accelerates the cleavage of phosphate monoesters through a mechanism involving two Zn<sup>II</sup> centers, a serine, and an arginine residue.

The development of a synthetic strategy [31] allowing the implantation of different functionalities at the upper rim of calix[4]arene **32** has opened the way to the achievement of versatile multifunctional catalysts featuring the fruitful cooperation of specialized active units and of supramolecular catalysts of increased molecular diversity.

Kinetic and potentiometric measurements carried out in 80% DMSO-H<sub>2</sub>O support the operation of a general-base/general-acid mechanism involving the hydroxo-form of the ligated metal ions (Zn<sup>II</sup> or Cu<sup>II</sup>), and the guanidinium moiety, as depicted in Fig. 26.9. Best results are obtained with Cu<sup>II</sup> ions, both in terms of rate enhancements and effective cooperation of the two active moieties. Rate enhancements relative to the background hydrolysis reaction at 1 mM **32H<sup>+</sup>**-Cu concentration are  $6 \times 10^5$ -fold for HPNP and cluster around an unprecedented  $10^7$ -fold value with the most favorable catalyst-NpN' combinations. The catalytic activity of **32H<sup>+</sup>**-Cu in the reaction of HPNP is 1000-fold higher than that of the monofunctional control TACN-Cu, and significantly higher than that of the corresponding Cu<sup>II</sup> complex based on the *m*-xylylene scaffold **33H<sup>+</sup>**-Cu.<sup>25h</sup> The upper rim of *cone*-calix[4]arenes once again proves to be a very convenient platform for the construction of bifunctional catalysts, here strongly enhancing the extent of cooperation between the guanidinium moiety and the ligated Cu<sup>II</sup> ion. Furthermore, both in the reaction of HPNP and of diribonucleoside monophosphates, the catalytic activity obtained with the heterobifunctional catalyst **32H<sup>+</sup>**-Cu is also definitely higher than that of **28H<sup>+</sup>** featuring the guanidine-guanidinium catalytic dyad [26].



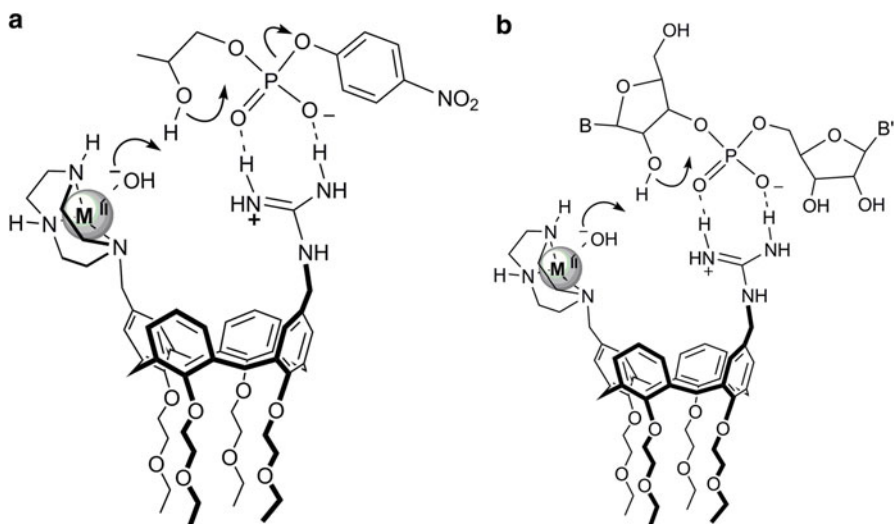


**Fig. 26.9** Proposed catalytic mechanism in the transesterification of HPNP (a) and of NpN' (b) in the presence of the heterobifunctional catalyst  $32\text{H}^+-\text{Cu}$

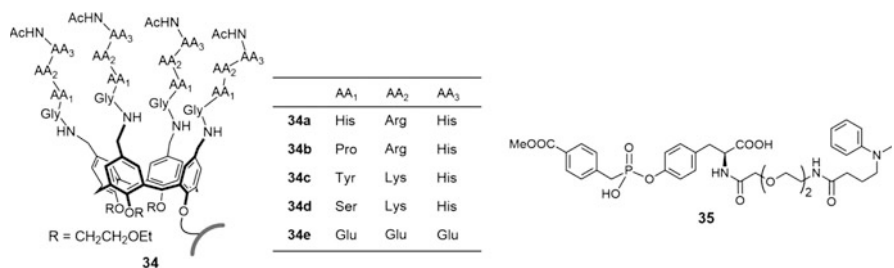
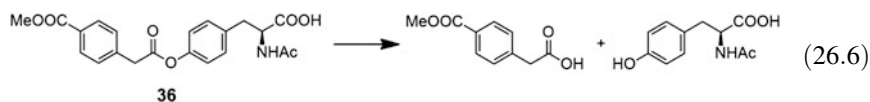


**Fig. 26.10** Resin-bound library of 1000 peptidocalix[4]arenes **34** (AA<sub>1</sub>, AA<sub>2</sub>, AA<sub>3</sub> = Arg, Asn, Glu, His, Leu, Lys, Pro, Ser, Trp, Tyr) screened and the candidates (**34a–e**) selected as catalysts for the hydrolysis of ester **36** by binding assay with **35**

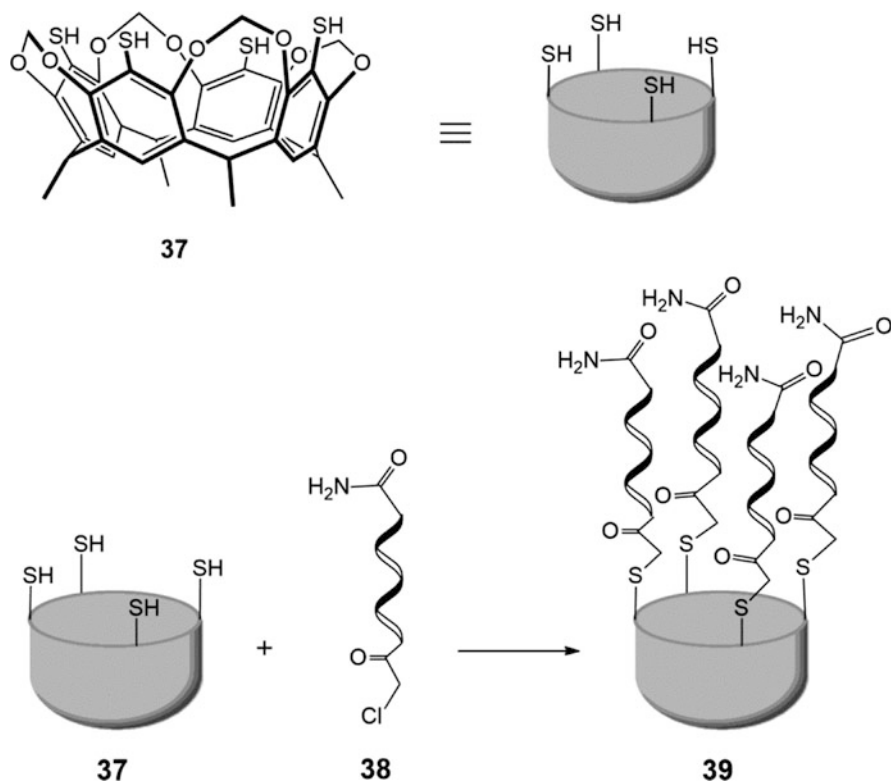
### 26.3.3 Peptidoderivatives

The library of resin-bound peptidocalix[4]arenes **34** (Fig. 26.10) was developed by Hioiki et al. [32] to select potentially active catalysts of the hydrolysis of ester **36**, (Eq. 26.6). The potentially most efficient structures (**34a–e**) were selected among the components of this library by using a binding assay with a mimic **35** of the tetrahedral transition state of the hydrolysis reaction. The aniline group in **35** allows to quantify, via a colorimetric assay, the amount of **35** bound to the resin beads and to select the members showing the highest affinity.



From hydrolysis experiments (1.25 mM substrate concentration, 0.2 molar equiv. candidate catalyst, aqueous phosphate buffer, pH 6.86, 30 °C), peptidocalix[4]arene **34a** turns out to be the most effective catalyst, with a rate enhancement at saturation 53-fold higher than that of the uncatalyzed reaction and a Michaelis constant  $K_M = 1.59 \times 10^{-3}$  M.

The cavitein (cavitand-protein) **39** developed by Sherman et al. [33] has been tested as a catalyst in the hydrolysis of *p*-nitrophenyl butanoate in phosphate buffer, pH 7, at room temperature. The four polypeptide chains attached on the resorcinarene scaffold of the arylthiol cavitand **37**, (Scheme 26.2), form a four-helix bundle with a hydrophobic core that could host the hydrophobic moiety of the substrate. The histidine residue close to the C-terminus of the peptide chains (GG EQLL KQLE QLLK QHG) in **39** is believed to play a key role in the catalytic

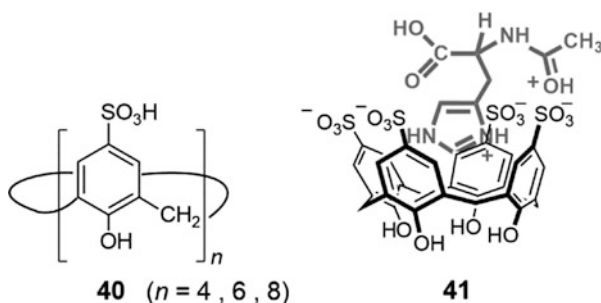


**Scheme 26.2** Preparation of the template-assembled synthetic protein **39** from cavitand **37** and chloroacetylated peptide **38**

activity. The rate enhancement observed in the presence of 0.10 mM cavitein **39** is 18-fold over the background, while that of 0.40 mM free peptide is only fourfold.

### 26.3.4 Sulfonato Derivatives

The *p*-sulfonatocalix[*n*]arenes **40** previously developed by Shinkai et al. [34] have been reported by Ueoka et al. [35] as water soluble catalysts of the specific acid catalyzed methanolysis of the acetamido group of *N*-Ac-L-amino acids (Phe, Tyr, Trp, His, Lys, Arg).

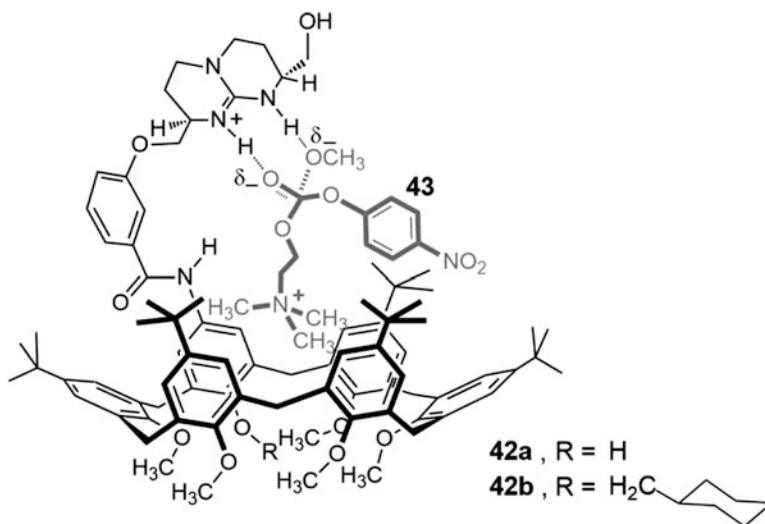


The catalytic efficiency of the calix[*n*]arene catalysts **40**, normalized per sulfonic group, is compared with the results obtained in the presence of the noncyclic analogue *p*-hydroxybenzenesulfonic acid. In the methanolysis of basic amino acid (His, Lys, Arg) derivatives, rate enhancements observed in the presence of *p*-sulfonatocalix[*n*]arenes **40**, are from 12- to 86-fold compared to the noncyclic control. On the other hand, in the reaction of neutral *N*-Ac-L-amino acids (Phe, Tyr, Trp), rate enhancements obtained in the presence of cyclic and noncyclic catalysts are within the experimental errors. <sup>1</sup>H NMR evidences and Michaelis-Menten kinetics suggest complexation of the protonated form of basic amino acid derivatives to *p*-sulfonatocalix[*n*]arenes **40**, as shown in **41** for the *N*-Ac-L-His–(**40**, *n* = 4) combination.

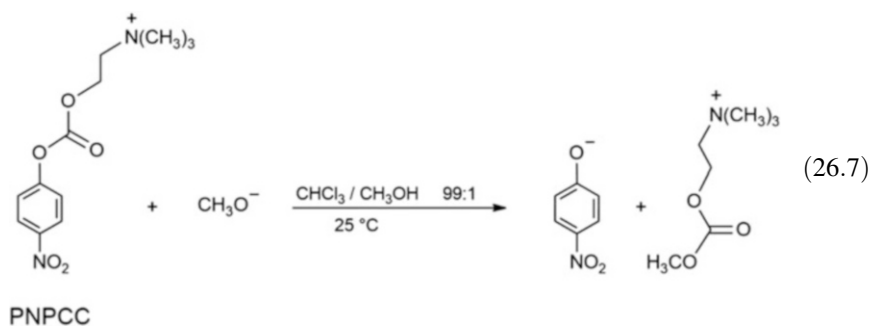
Effective transesterification reactions of Passiflora seed oil with methanol or ethanol in the presence of solid *p*-sulfonic acid calix[4]arene catalyst (**40**, *n* = 4) was reported by Le Hyaric et al. [36] The calixarene catalyst is described as non-corrosive, easily recoverable from the reaction medium and reusable. High and fast conversions into desired products are reported.

## 26.4 Calixarene Catalysts Exploiting the Cavity for Substrate Recognition

A remarkable example of the use of the calixarene cavity for substrate recognition is provided by calix[6]arenes **42** developed by de Mendoza et al. [37] These ditopic receptors, featuring a guanidinium unit at the catalytic site, have been reported as effective turnover catalysts of the basic methanolysis of *p*-nitrophenylcholine carbonate (PNPCC), (Eq. 26.7).



Anionic phosphodiesteres have been widely used as transition state analogues of the basic hydrolysis of carboxylic esters. Accordingly, ditopic receptors **42** were designed [37a] as mimics of the phosphocholine binding site of the McPC603 antibody. Recognition of dioctanoyl-L- $\alpha$ -phosphatidylcholine by **42** is effective ( $K = 73,000 \text{ M}^{-1}$  for **42a**, and  $95,000 \text{ M}^{-1}$  for **42b**;  $\text{CHCl}_3$ ,  $25^\circ\text{C}$ ), as a result of combined interactions of the anionic phosphodiester group to the guanidinium unit through electrostatic and hydrogen bonding interactions, and of the choline trimethylammonium moiety within the calix[6]arene cavity through cation- $\pi$  interactions.

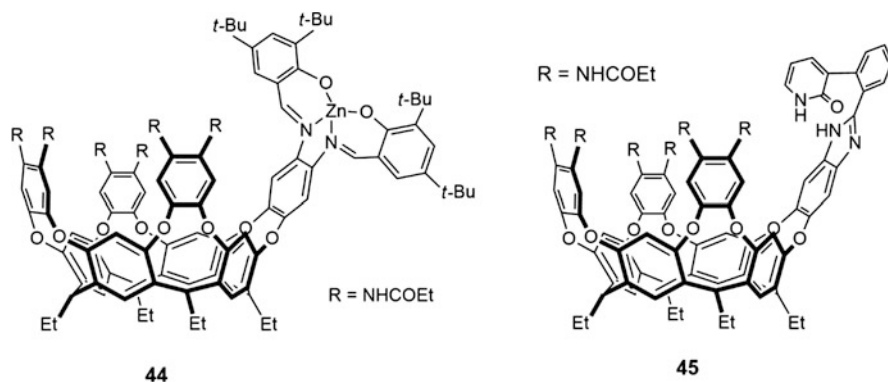


A rate enhancement of 76-fold over the background is observed in the basic methanolysis of PNPCC in the presence of **42a**, and of 149-fold in the presence of **42b**, (1 mM catalyst concentration;  $\text{CHCl}_3/\text{MeOH}$  99:1, diisopropylethylamine buffer, 25 °C). Significantly lower rate enhancements are observed in the presence of the two disconnected subunits of the catalyst at 1 mM concentration, pointing towards a marked degree of synergism in the operation of the two subunits in the ditopic catalyst.

While the cavity of calix[4]arenes is not suitable for substrate inclusion, unless suitably rigidified by the bridging of adjacent oxygen atoms at the lower rim with short linkers or possibly expanded with the introduction of additional moieties at the upper rim [38], the cavity of bridged resorcin[4]arene cavitands is conveniently preorganized in a suitable arrangement for substrate inclusion. Accordingly, the resorcin[4]arene scaffold has been successfully exploited in the design of the recognition site of diverse supramolecular catalysts for the productive inclusion of the substrate (or more properly of part of the substrate), typically the trimethylammonium head of a choline derivative.

Rebek et al. developed a number of cavitand derived from resorcinol as ditopic catalysts featuring distinct recognition elements for the reacting and nonreacting parts of the substrates. In many of these reaction systems, choline derivatives are involved and the trimethylammonium head of the substrate is complexed in the cyclophane cavity of the catalyst.

Receptor **44** is an artificial esterase featuring a zinc(II)-salophen unit appended to a resorcinarene scaffold [39]. The basic hydrolysis of PNPCC in buffered  $\text{CH}_2\text{Cl}_2$  containing 0.01 % water (Eq. 26.8) is more than 50 times faster in the presence of the catalyst. The substrate shows a very high affinity for **44**. The trimethylammonium head is hosted deep in the receptor cavity and the ester function is properly oriented towards the metal electrophile of the catalytic site.



The ditopic catalyst **44** is five times more effective than the monotopic zinc(II)-salophen model lacking the cavity binding site, at the same concentration.

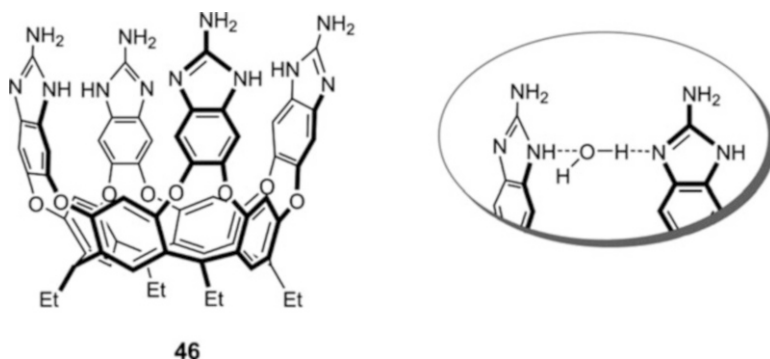
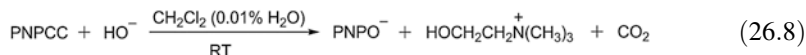
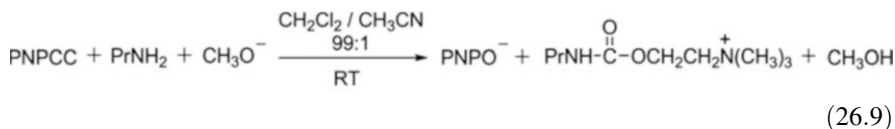


**Fig. 26.11** Hydrogen-bonded water molecules bridging adjacent 2-ABI units (*right*) of cavitant **46** preorganized in a vase-like conformation



The catalytic core of ditopic receptor **45** [40] features a 2-pyridone unit, that is a known bifunctional catalyst for the rate limiting breakdown of the tetrahedral intermediate involved in the aminolysis of active esters in aprotic solvents. Turn-over catalysis is observed in the presence of receptor **45** in the reaction between propylamine and PNPCC (Eq. 26.9) in  $\text{CH}_2\text{Cl}_2/\text{CH}_3\text{CN}$  99:1. It is estimated that the reaction in the interior of **45** is 6000 times faster than in the bulk solvent.



Cavitant **46**, decorated with four 2-aminobenzimidazole (2-ABI) units is a metal-free catalyst for the hydrolysis of PNPCC in  $\text{MeCN}:\text{H}_2\text{O}$  99:1 (v/v), (10 mM  $\text{EtN}(\text{i-Pr})_2$  and 5 mM  $\text{CF}_3\text{CO}_2\text{H}$  buffer; 25 °C) [41]. The substrate is extensively complexed by cavitant **46** that is preorganized in a vase-like conformation by hydrogen-bonded water molecules bridging adjacent 2-ABI units (Fig. 26.11). Fast carbamylation step of one of the amino function of the catalyst by the complexed substrate is followed by rate-determining hydrolysis of the carbamoylcholine-cavitant intermediate. The latter process is extremely slow, since restoration of the active form of the catalyst is complete after 30 days. From kinetic data reported in the paper it appears that the formation of the carbamate derivative by intracomplex reaction of PNPCC included in the cavitant with the amino function of a 2-ABI moiety of **46** is not significantly faster than the intermolecular model reaction of PNPCC with 2-ABI, when the comparison is carried out at the same concentration of 2-ABI units. The rate-determining hydrolysis of the cholinecarbamate derivative of the cavitant is on the other hand much faster than hydrolysis of the cholinecarbamate derivative of 2-ABI, that under the

given reaction conditions is totally inert towards hydrolysis, even after extended time periods. Hydrolysis of the carbamate intermediate by intracomplex nucleophilic reaction of water molecules bridging adjacent 2-ABI moieties of the cavitand has been proposed by the authors.

## 26.5 Conclusions

In this chapter, focussing on the catalytic solvolysis of carboxylate and phosphate esters controlled by calixarenes we have shown examples of high levels of cooperation among recognition and catalytic sites preorganized on a calixarene platform.

Dynamic preorganization on the calixarene scaffold of two or more active units is highly convenient in the design of effective supramolecular catalysts. A certain level of residual flexibility seems to be crucial in the dynamic fit of the catalyst to the bound substrate throughout its transformation into the transition state, and reduces the risk of failure connected to the design of tailored, perfectly “fitting” rigid receptors for the recognition of the transition state.

## References

1. (a) Breslow, R., Ed. *Artificial Enzymes*; Wiley-VCH Verlag GmbH & Co. KGaA: Weinheim, Germany, 2005; (b) van Leeuwen, P. W. N. M., Ed. *Supramolecular Catalysis*; Wiley-VCH Verlag GmbH & Co. KGaA: Weinheim, Germany, 2008; (c) Brinker, U. H., Mieusset, J.-L., Eds. *Molecular Encapsulation – Organic Reactions in Constrained Systems*; John Wiley & Sons, Ltd.: New York, 2010. (d) Raynal, M.; Ballester, P.; Vidal – Ferran, A.; Van Leeuwen, P. W. N. M. *Chem. Soc. Rev.* **2014**, *43*, 1734–1787.
2. Molenveld, P.; Engbersen, J. F. J.; Reinhoudt, D. N. *Chem. Soc. Rev.* **2000**, *29*, 75–86.
3. (a) Weston, J. *Chem. Rev.* **2005**, *105*, 2151–2174; (b) Cowan, J. A. *Chem. Rev.* **1998**, *98*, 1067–1087; (c) Wilcox, D. E. *Chem. Rev.* **1996**, *96*, 2435–2458.
4. (a) Williams, N. H.; Takasaki, B.; Wall, M.; Chin, J. *Acc. Chem. Res.* **1999**, *32*, 485–493; (b) Mancin, F.; Scrimin, P.; Tecilla, P. *Chem. Commun.* **2012**, *48*, 5545–5559; and references therein.
5. (a) Gruber, B.; Kataev, E.; Aschenbrenner, J.; Stadlbauer, S.; König, B. *J. Am. Chem. Soc.* **2011**, *133*, 20704–20707; (b) Panja, A.; Matsuo, T.; Nagao, S.; Hirota, S. *Inorg. Chem.* **2011**, *50*, 11437–11445; (c) Linjalahti, H.; Feng, G. Q.; Mareque-Rivas, J. C.; Mikkola, S.; Williams, N. H. *J. Am. Chem. Soc.* **2008**, *130*, 4232–4233; (d) Nwe, K.; Andolina, C. M.; Morrow, J. R. *J. Am. Chem. Soc.* **2008**, *130*, 14861–14871; (e) Wang, Q.; Lönnberg, H. *J. Am. Chem. Soc.* **2006**, *128*, 10716–10728; (f) O’Donoghue, A.; Pyun, S. Y.; Yang, M. Y.; Morrow, J. R.; Richard, J. P. *J. Am. Chem. Soc.* **2006**, *128*, 1615–1621; (g) Neverov, A. A.; Lu, Z. -L.; Maxwell, C. I.; Mohamed, M. F.; White, C. J.; Tsang, J. S. W.; Brown, R. S. *J. Am. Chem. Soc.* **2006**, *128*, 16398–16405.
6. Cacciapaglia, R.; Casnati, A.; Mandolini, L.; Reinhoudt, D. N.; Salvio, R.; Sartori, A.; Ungaro, R. *J. Org. Chem.* **2005**, *70*, 624–630.
7. Cacciapaglia, R.; Casnati, A.; Mandolini, L.; Reinhoudt, D. N.; Salvio, R.; Sartori, A.; Ungaro, R. *J. Org. Chem.* **2005**, *70*, 5398–5402.

8. Cacciapaglia, R.; Casnati, A.; Mandolini, L.; Reinhoudt, D. N.; Salvio, R.; Sartori, A.; Ungaro, R. *Inorg. Chim. Acta* **2007**, *360*, 981–986.
9. (a) Cacciapaglia, R.; Casnati, A.; Mandolini, L.; Ungaro, R. *J. Am. Chem. Soc.* **1992**, *114*, 10956–10958; (b) Baldini, L.; Bracchini, C.; Cacciapaglia, R.; Casnati, A.; Mandolini, L.; Ungaro, R. *Chem. Eur. J.* **2000**, *6*, 1322–1330.
10. Cacciapaglia, R.; Mandolini, L. *Chem. Soc. Rev.* **1993**, *22*, 221–231.
11. Kraft, D.; Böhmer, V.; Cacciapaglia, R.; Mandolini, L.; Vogt, W. *unpublished results*.
12. Cacciapaglia, R.; Casnati, A.; Di Stefano, S.; Mandolini, L.; Paolemili, D.; Reinhoudt, D. N.; Sartori, A.; Ungaro, R. *Chem. Eur. J.* **2004**, *10*, 4436–4442.
13. (a) Kirby, A. J. *Adv. Phys. Org. Chem.* **1980**, *17*, 183–278; (b) Mandolini, L. *Adv. Phys. Org. Chem.* **1986**, *22*, 1–111.
14. (a) Cacciapaglia, R.; Di Stefano, S.; Mandolini, L. *Acc. Chem. Res.* **2004**, *37*, 113–122; (b) Di Stefano, S.; Cacciapaglia, R.; Mandolini, L. *Eur. J. Org. Chem.* **2014**, 7304–7315.
15. Cacciapaglia, R.; Di Stefano, S.; Kelderman, E.; Mandolini, L. *Angew. Chem. Int. Ed.* **1999**, *38*, 348–351.
16. Molenveld, P.; Kapsabelis, S.; Engbersen, J. F. J.; Reinhoudt, D. N. *J. Am. Chem. Soc.* **1997**, *119*, 2948–2949.
17. Molenveld, P.; Stikvoort, W. M. G.; Kooijman, H.; Spek, A. L.; Engbersen, J. F. J.; Reinhoudt, D. N. *J. Org. Chem.* **1999**, *64*, 3896–3906.
18. Molenveld, P.; Engbersen, J. F. J.; Kooijman, H.; Spek, A. L.; Reinhoudt, D. N. *J. Am. Chem. Soc.* **1998**, *120*, 6726–6737.
19. Sträter, N.; Lipscomb, W. N.; Klabunde, T.; Krebs, B. *Angew. Chem. Int. Ed.* **1996**, *35*, 2024–2055.
20. Molenveld, P.; Engbersen, J. F. J.; Reinhoudt, D. N. *Angew. Chem. Int. Ed.* **1999**, *38*, 3189–3192.
21. Cacciapaglia, R.; Casnati, A.; Mandolini, L.; Reinhoudt, D. N.; Salvio, R.; Sartori, A.; Ungaro, R. *J. Am. Chem. Soc.* **2006**, *128*, 12322–12330.
22. Cacciapaglia, R.; Casnati, A.; Mandolini, L.; Peracchi, A.; Reinhoudt, D. N.; Salvio, R.; Sartori, A.; Ungaro, R. *J. Am. Chem. Soc.* **2007**, *129*, 12512–12520.
23. Cotton, F. A.; Hazen, E. E., Jr.; Legg, M. J. *Proc. Natl. Acad. Sci. U.S.A.* **1979**, *76*, 2551–2555.
24. For a recent review article see: Salvio, R. *Chem. Eur. J.* **2015**, *21*, 10960–10971.
25. (a) Suh, J.; Moon, S. -J. *Inorg. Chem.* **2001**, *40*, 4890–4895; (b) Ait-Haddou, H.; Sumaoka, J.; Wiskur, S. L.; Folmer-Andersen, J. F.; Anslyn, E. V. *Angew. Chem., Int. Ed.* **2002**, *41*, 4014–4016; (c) Piatek, A. M.; Gray, M.; Anslyn, E. V. *J. Am. Chem. Soc.* **2004**, *126*, 9878–9879; (d) Scheffer, U.; Strick, A.; Ludwig, V.; Peter, S.; Kalden, E.; Göbel, M. W. *J. Am. Chem. Soc.* **2005**, *127*, 2211–2217; (e) Gnaccarini, C.; Peter, S.; Scheffer, U.; Vonhoff, S.; Klussmann, S.; Göbel, M. W. *J. Am. Chem. Soc.* **2006**, *128*, 8063–8067; (f) Lindgren, N. J. V.; Lars Geiger, J.R.; Schmuck, C.; Baltzer, L. *Angew. Chem., Int. Ed.* **2009**, *48*, 6722–6725; (g) Corona-Martinez, D. O.; Taran, O.; Yatsimirsky, A. K. *Org. Biomol. Chem.* **2010**, *8*, 873–880; (h) Salvio, R.; Cacciapaglia, R.; Mandolini, L. *J. Org. Chem.* **2011**, *76*, 5438–5443; (i) Salvio, R.; Mandolini, L.; Savelli, C. *J. Org. Chem.* **2013**, *78*, 7259–7263; (j) Savelli, C.; Salvio, R. *Chem. Eur. J.* **2015**, *21*, 5856–5863; (k) Salvio, R.; Cincotti, A. *RSC Adv.* **2014**, *4*, 28678–28682.
26. Baldini, L.; Cacciapaglia, R.; Casnati, A.; Mandolini, L.; Salvio, R.; Sansone, F.; Ungaro, R. *J. Org. Chem.* **2012**, *77*, 3381–3389.
27. Salvio, R.; Cacciapaglia, R.; Mandolini, L.; Sansone, F.; Casnati, A. *RSC Adv.* **2014**, *4*, 34412–34416.
28. Salvio, R.; Casnati, A.; Mandolini, L.; Sansone, F.; Ungaro, R. *Org. Biomol. Chem.* **2012**, *10*, 8941–8943.
29. (a) Hosseini, M. W.; Lehn, J. -M.; Jones, K. C.; Plute, K. E.; Mertes, K. B.; Mertes, M. P. *J. Am. Chem. Soc.* **1989**, *111*, 6330–6335; (b) Hosseini, M. W.; Lehn, J. -M.; Maggiora, L.; Mertes, K. B.; Mertes, M. P. *J. Am. Chem. Soc.* **1987**, *109*, 537–544; (c) Hosseini, M. W.; Lehn, J. -M.; Mertes, M. P. *Helv. Chim. Acta* **1983**, *66*, 2454–2466.



30. Salvio, R.; Volpi, S.; Cacciapaglia, R.; Casnati, A.; Mandolini, L.; Sansone, F. *J. Org. Chem.* **2015**, *80*, 5887–5893.
31. For the desymmetrization of calix[4]arenes, see also: (a) Ciaccia, M.; Tosi, I.; Cacciapaglia, R.; Casnati, A.; Baldini, L.; Di Stefano, S. *Org. Biomol. Chem.* **2013**, *11*, 3642–3648. (b) Galli, M.; Berrocal, J. A.; Di Stefano, S.; R. Cacciapaglia; L. Mandolini; L. Baldini; A. Casnati; F. Ugozzoli *Org. Biomol. Chem.* **2012**, *10*, 5109–5112.
32. Hioki, H.; Nishimoto, R.; Kawaguchi, K.; Kubo, M.; Harada, K.; Fukuyama, Y. *Chem. Commun.* **2009**, 7194–7196.
33. Yang, H.; Sherman, J. C. *Bioorg. Med. Chem. Lett.* **2013**, *23*, 1752–1753
34. Shinkai, S.; Mori, S.; Koreishi, H.; Tsubaki T.; Manabe, O. *J. Am. Chem. Soc.* **1986**, *108*, 2409–2416.
35. Goto, K.; Yano, Y.; Okada, E.; Liu, C. -W.; Yamamoto, K.; Ueoka, R. *J. Org. Chem.* **2003**, *68*, 865–870.
36. Almeida, C. G.; Souza, I. F.; Liberto, N. A.; Da Silva, M. J.; Fernandes S. A.; Le Hyaric M. *Monatsh. Chem.* **2015**, *146*, 1927–1934.
37. (a) Magrans, J.O.; Ortiz, A.R.; Molins, A.; Lebouille, P.H.P.; Sánchez-Quesada, J.; Prados, P.; Pons, M.; de Mendoza, J. *Angew. Chem. Int. Ed.* **1996**, *35*, 1712–1715; (b) Cuevas, F.; Di Stefano, S.; Magrans, J. O.; Prados, P.; Mandolini, L.; de Mendoza, J. *Chem. Eur. J.* **2000**, *6*, 3228–3234.
38. See for example: (a) Arduini, A.; Brindani, E.; Giorgi, G.; Pochini, A.; Secchi, A. *J. Org. Chem.* **2002**, *67*, 6188–6194; (b) Arduini, A.; Brindani, E.; Giorgi, G.; Pochini, A.; Secchi, A. *Tetrahedron* **2003**, *59*, 7587–7594; and references therein.
39. (a) Richeter, S.; Rebek, J., Jr. *J. Am. Chem. Soc.* **2004**, *126*, 16280–16281; (b) Zelder, F. H.; Salvio, R.; Rebek, J., Jr. *Chem. Commun.* **2006**, 1280–1282.
40. Gissot, A.; Rebek, J., Jr. *J. Am. Chem. Soc.* **2004**, *126*, 7424–7425.
41. Soberats, B.; Sanna, E.; Martorell, G.; Rotger, C.; Costa, A. *Org Lett.* **2013**, *16*, 840–843.

# Chapter 27

## Calixarenes in Organo and Biomimetic Catalysis

Mustafa Yilmaz and Serkan Sayin

### 27.1 Introduction

Calixarenes possessing tunable 3D-scaffolds along with their easy syntheses and versatile functionalization are known as the third generation supramolecules after cyclodextrin and crown ether. In addition, substitution from each positions “upper and lower rim” of calixarenes with different groups gives them significant challenge (see Fig. 27.1). These advantages lead a great deal of attention on them in supramolecular chemistry. So far, calixarenes bearing diverse functional groups have been introduced and successfully applied in several areas such as extraction, separation science, sensors, nanotechnology, drug delivery, and catalysis etc. However, in this chapter the catalytic affinities of calixarene-based organo- and biomimetic catalysts have been discussed.

### 27.2 Calixarenes as Organocatalysts

Organocatalysis is basically the reactions require an organic-based metal free catalyst in order to accelerate chemical reactions, and provide operational simplicity and low toxicity [1–3]. Owing to the metal free organic compounds contaminant, organocatalysts attracted much attention in many fields of green chemistry associating food, pharmaceutical, and cosmetic industries [4].

---

M. Yilmaz (✉)

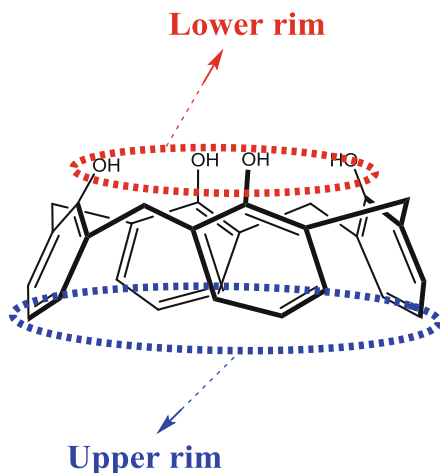
Department of Chemistry, Selcuk University, Konya 42075, Turkey

e-mail: [myilmaz@selcuk.edu.tr](mailto:myilmaz@selcuk.edu.tr)

S. Sayin

Department of Environmental Engineering, Giresun University, Giresun 28200, Turkey

**Fig. 27.1** Lower and upper rim positions of calix[4]arene



Up to now, a great deal of attention on catalytic applications of calixarenes has been paid to achieve a promising catalyst which efficiently catalyzes the specific reactions in a faster and an easy way. It has been reported that some of calixarene-based organocatalysts exhibited efficient catalytic properties for some organic reactions [5–7].

Some research groups addressed proline-substituted calixarene derivatives as effective asymmetric catalysts for the direct aldol reaction of cyclohexanone and aromatic aldehydes (see Fig. 27.2 and Table 27.1) [5–7]. They have mentioned the nature of these chiral calixarenes such as their hydrophobic/hydrophilic properties for their catalytic activities. Table 27.1 clearly indicates that proline-substituted calixarene derivatives exhibited higher catalytic activity and enantioselectivity than their mono-analogues. This attributes that cooperative and cavity skeleton affinities of calixarenes affects catalytic and enantioselective properties of the catalysts in direct aldol reactions. In addition, it was reported that **Clx-Pr-4** showed the highest conversion, diastereoselectivity and enantioselectivity among the other calixarene catalysts, whereas the catalytic ability of **Clx-Pr-4** decreased when DMF added into the reaction instead of water. The results have indeed brought much attention on calixarene-based catalysts in terms of green chemistry which require water usage instead of toxic and hazard solvents in the catalytic reactions.

Inspired by the strong ability of **calix[6]arene 1** in complexation of alkali metal ions [4, 8–10], Nomura et al. (1991, 1993) reported that calix[6]arene derivative **1** was an effective catalyst for the esterification reaction of alkyl halide and alkali metal carboxylates (see Fig. 27.3, and Table 27.2) [11, 12]. In order to assess the role of calix[6]arene in the reaction, it needs to take a look the skeleton of **calix[6]arene 1**. **Calix[6]arene 1** contains a hydrophobic aromatic groups and a hydrophilic trioxadecyl functionality. These groups commit **calix[6]arene 1** into an octopus-type shape, and indeed this shape provides conformational and structural mobility that brings out a highly efficient catalyst. Similar phase-transfer catalysts

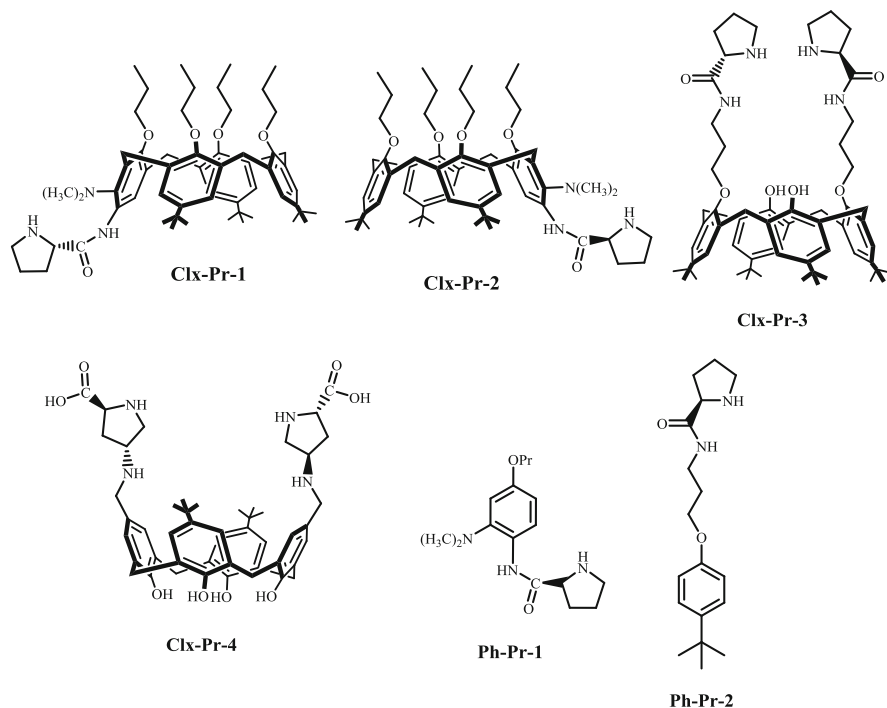


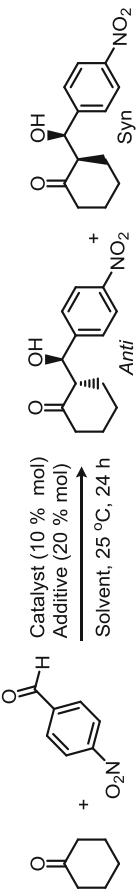
Fig. 27.2 Proline-substituted calixarenes as asymmetric catalysts

devoted calixarene/calix[6]arene usage were also reported (see Figs. 27.4 and 27.5) [13–18].

So, catalyst “**calix[4]arene 1**” would not act like as a catalyst in the same way of **calix[6]arene 1** due to their different molecular skeleton. The catalytic affinity of **calix[4]arene 1** might ascribe the nature of the proton-switchable groups of the corresponding quaternary ammonium ions. Therefore, the quaternary ammonium capped calix[4]arene could complex with carboxylate ions as an ion pair leading to a faster reaction rate and better yield (see Fig. 27.4 and Table 27.2) [19].

Another calixarene-based phase-transfer catalyst was designed by Srivastava and Srivastava [20]. In that study, two different quaternary ammonium salts of calix[4]arene (**Calix[4]arene 2a** and **2b**) were employed as a catalyst in the Darzens condensation to synthesize  $\alpha,\beta$ -epoxy carbonyl compounds (see Fig. 27.5). It was found that these phase-transfer catalysts exhibited significant catalytic activity, especially when the calix[4]arene with long alkyl chain (*n*-butyl) was chosen (see Table 27.3).

An imidazole-substituted **calix[4]arene 3** was designed as a phase-transfer catalyst for aromatic nucleophilic substitution reaction in water [21]. The stable conformation associating cavities of calixarene skeleton and the synergistic effect of imidazolium groups of **calix[4]arene 3** expressed the excellent catalytic ability (see Fig. 27.6). Taking into account the results represented in Table 27.4, **calix[4]**

**Table 27.1** Direct aldol reaction of cyclohexanone and aromatic aldehydes in the presence of proline-substituted organo-catalysts (**Cix-Pr-1-4**, **Ph-Pr-1** and **-2**)


Additive	Catalyst	Solvent	Conv. <sup>d</sup> (%)	Anti/syn <sup>e</sup>	ee <sup>f</sup> (%)
–	Cix-Pr-1 <sup>a</sup>	–	98	78:22	44
–	Cix-Pr-2 <sup>a</sup>	–	99	81:19	44
CF <sub>3</sub> CO <sub>2</sub> H	Cix-Pr-1 <sup>a</sup>	–	34	54:44	37
CF <sub>3</sub> CO <sub>2</sub> H	Cix-Pr-2 <sup>a</sup>	–	26	64:36	48
CH <sub>3</sub> CO <sub>2</sub> H	Cix-Pr-1 <sup>a</sup>	–	99	73:27	58
CH <sub>3</sub> CO <sub>2</sub> H	Cix-Pr-2 <sup>a</sup>	–	99	76:24	63
ClCH <sub>2</sub> CO <sub>2</sub> H	Cix-Pr-3 <sup>b</sup>	H <sub>2</sub> O	95	64:36	90
–	Cix-Pr-3 <sup>b</sup>	H <sub>2</sub> O	93	67:33	48
–	Cix-Pr-4 <sup>c</sup>	H <sub>2</sub> O	98	96:4	77
–	Cix-Pr-4 <sup>c</sup>	DMF	97	86:14	84
CH <sub>3</sub> CO <sub>2</sub> H	Ph-Pr-1 <sup>a</sup>	–	70	76:24	68
–	Ph-Pr-2 <sup>b</sup>	H <sub>2</sub> O	<10	56:42	n.d.

Reaction conditions: cyclohexanone (2 mmol), aldehyde (0.125 mmol), solvent (1 mL)

<sup>a</sup>[5]

<sup>b</sup>[6]

<sup>c</sup>[7]

<sup>d</sup>Determined by <sup>1</sup>H-NMR

<sup>e</sup>The ee value was determined by chiral HPLC analysis

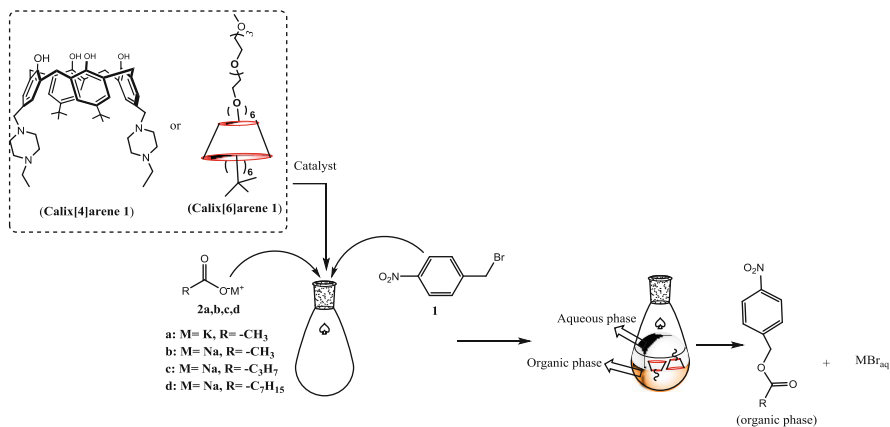


**Fig. 27.3** Esterification of metal acetate in the presence of calix[n]arene 1 catalysts [11, 12, 19]

**Table 27.2** Esterification of alkali metal acetate with *p*-nitrobenzyl bromide in the presence of calix[n]arene 1 catalyst

Catalyst	Nucleophile	Temp (°C)	Reaction time (h)	Yield (%)
Calix[6]arene 1	2a <sup>a</sup>	40	24	100
Calix[6]arene 1	2b <sup>a</sup>	40	24	12
none	2a <sup>a</sup>	60	24	0
none	2c <sup>b</sup>	60	30	Trace
Calix[4]arene 1	2c <sup>b</sup>	60	30	99
None	2d <sup>b</sup>	25	30	3
Calix[4]arene 1	2d <sup>b</sup>	25	30	80

<sup>a</sup>[11, 12]

<sup>b</sup>[19]

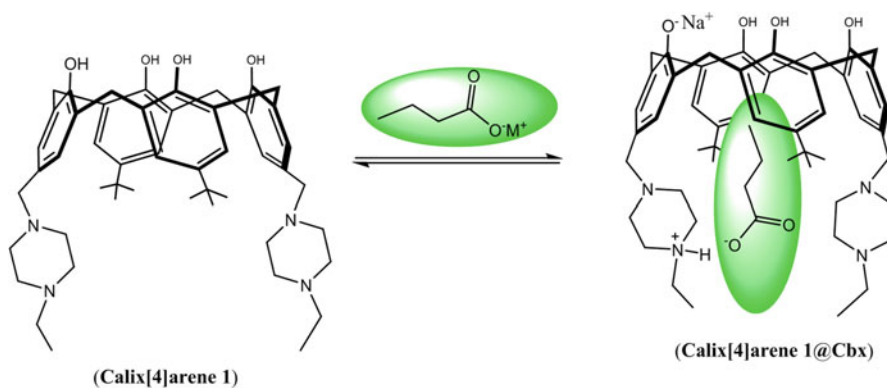


**Fig. 27.4** Complexation of calix[4]arene with carboxylate ions

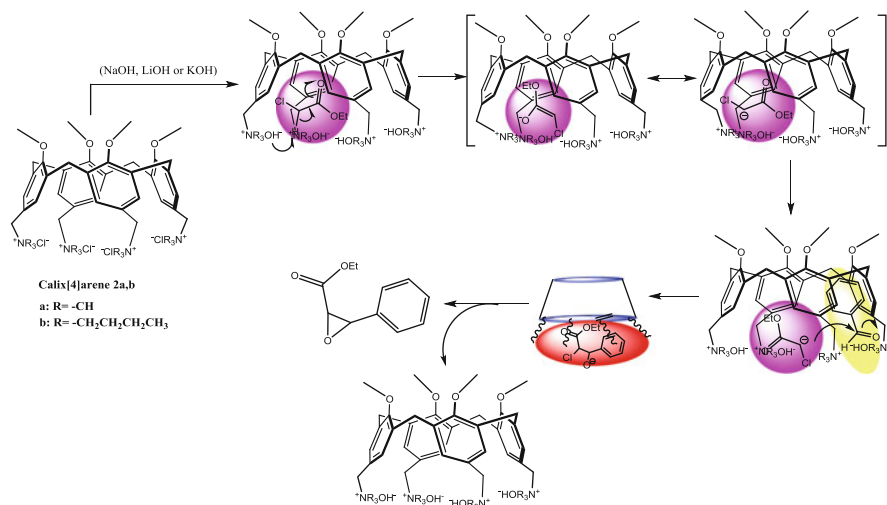


**Fig. 27.5** The Darzens condensation in the presence of calixarene organocatalysts

**Table 27.3** Catalytic efficacy of calix[4]arene **2a** and **2b** in Darzens condensation [20]

Catalyst	Base	Solvent	Yield <sup>a</sup> (%)	Cis/trans
None	KOH	THF	9.0	8:1
Calix[4]arene <b>2a</b>	KOH	THF	43.9	8:1
Calix[4]arene <b>2b</b>	KOH	THF	72.0	7:1
Calix[4]arene <b>2b</b>	NaOH	THF	65.2	7.5:1
Calix[4]arene <b>2b</b>	LiOH	THF	35.9	14:1
Calix[4]arene <b>2b</b>	KOH	CH <sub>2</sub> Cl <sub>2</sub>	39.5	4.5:1
Calix[4]arene <b>2b</b>	KOH	(C <sub>2</sub> H <sub>5</sub> ) <sub>2</sub> O	59.2	6.7:1
Calix[4]arene <b>2b</b>	KOH	C <sub>6</sub> H <sub>6</sub>	54.2	6.4:1
Calix[4]arene <b>2b</b>	KOH	THF	35.8 <sup>b</sup>	6.5:1 <sup>b</sup>

<sup>a</sup>Reaction condition: benzaldehyde (5 mmol),  $\alpha$ -chloroester (6.0 mmol), base (6.0 mmol), catalyst (2.0 mol %), solvent (10 mL), reaction temperature (298 K), run time (24 h)

<sup>b</sup>Reactions were carried out for 8 h

**arene 3** was addressed as an excellent phase-transfer catalyst for nucleophilic substitution in green chemistry.

In our discussion, many calixarens have been mentioned in number of chemical reactions as catalyst, however out of these, quaternary ammonium-terminated calixarenes “calix[4]arene **4** and calix[6]arene **2** catalysts” were used in one-pot Mannich reaction of benzaldehyde, acetophenone and aniline in aqueous media to produce  $\beta$ -aminocarbonyl compounds (see Fig. 27.7) [19]. These calix[*n*]arene catalysts emphasized not only the high catalytic activity but also have an outstanding reusability with high yield, at low loading amount. Advantages of that were, short reaction times, high yields, and easy work-up that make them great candidate for Mannich-type reactions (see Table 27.5).

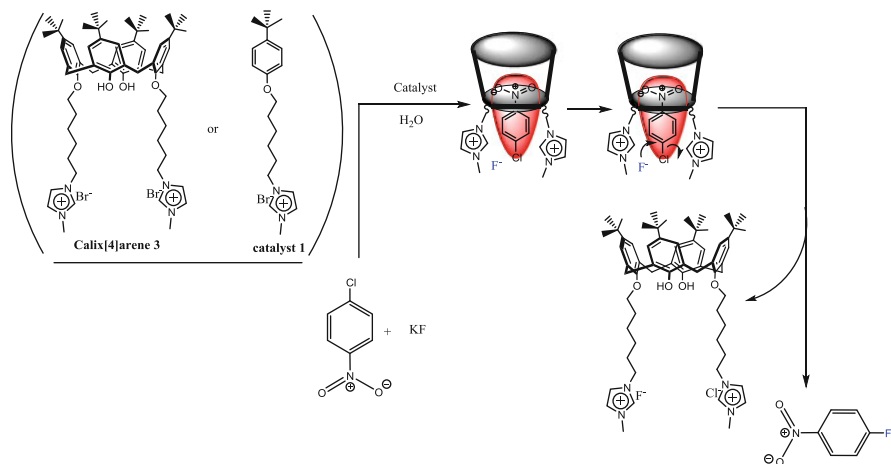


**Fig. 27.6** Aromatic nucleophilic substitution reaction in the presence of phase-transfer catalysts [21]

**Table 27.4** Aromatic nucleophilic substitution reaction in the presence of organo-catalysts

Catalyst	Reax. time (h)	Tem. (°C)	Catalyst mol(%)	Yield (%) <sup>a</sup>
None	12	50	None	0.5
Catalyst 1	12	30	3.0	4.5
Catalyst 1	12	50	3.0	7.4
Catalyst 1	12	80	3.0	8.3
Catalyst 1	12	80	5.0	9.2
Calix[4]arene 3	12	30	2.0	68.8
Calix[4]arene 3	12	30	3.0	88.9
Calix[4]arene 3	12	50	3.0	96.6
Calix[4]arene 3	12	50	5.0	94.2
Calix[4]arene 3	12	80	3.0	96.7
Calix[4]arene 3	6	50	3.0	90.4
Calix[4]arene 3	18	50	3.0	97.2

Reaction condition: *p*-nitrochlorobenzene (5 mmol), KF (15 mmol), water (10 mL)

<sup>a</sup>[21]

Some of calix[*n*]arene sulfonic acids were also developed as Brønsted acid catalysts for Mannich-type reactions [23]. Because of their water-solubility, the reaction can be performed in water with obvious advantages from an environmentally point of view. As depicted in Fig. 27.8, two water soluble calixarene bearing a sulphonic acid group are suitably employed in the Mannich reaction in water as a catalyst.

Because of the water solubility of calixarene sulfonic acids, they have been used in many organic reactions other than Mannich reaction outlined in above. In a study, *p*-sulfonic acid calix[4]arene (**calix[4]arene 5**) was employed as



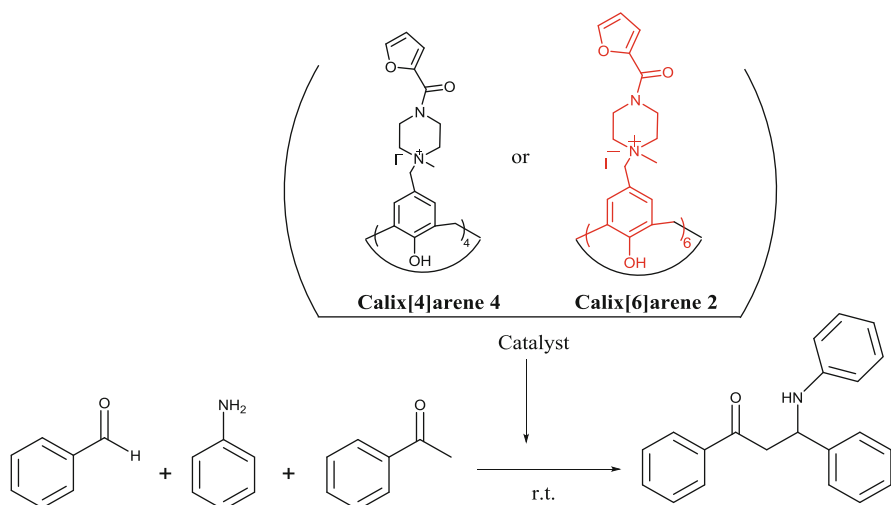


**Fig. 27.7** Three component Mannich reaction in the presence of **calix[*n*]arene** catalysts

**Table 27.5** Mannich reaction in the presence of **calix[4]arene 4** or **calix[6]arene 2** catalyst [22]

Catalyst	Catalyst amount	Time/h	H <sub>2</sub> O/mL	Yield (%) <sup>a</sup>
None	–	168	2	Trace
Clx[4] <b>4</b>	0.288 mol%	2	2	95.4
Clx[4] <b>4</b>	0.576 mol%	2.3	2	99.6
Clx[6] <b>2</b>	0.288 mol%	2.1	2	99.9
Clx[6] <b>2</b>	0.288 mol%	2.1	2	99.3 <sup>b</sup>
Clx[6] <b>2</b>	0.288 mol%	2.1	2	98.9 <sup>c</sup>
Clx[4] <b>4</b>	0.144 % mol	3	2	84.9
Clx[4] <b>4</b>	0.144 % mol	24	8	99.9
Clx[6] <b>2</b>	0.288 % mol	2.1	2	99.9
Clx[6] <b>2</b>	0.288 % mol	9	8	88.8

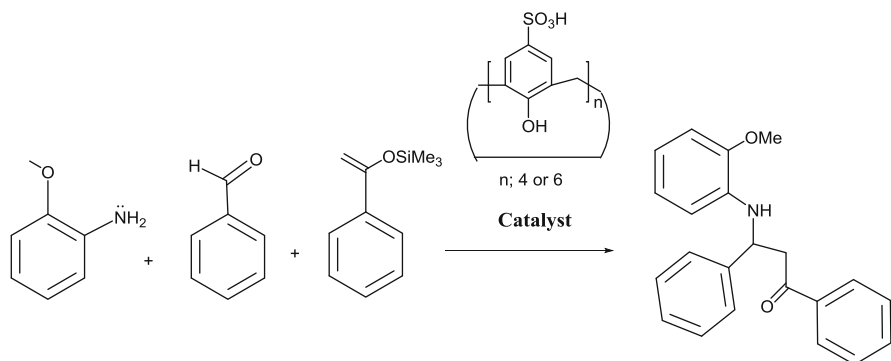
<sup>a</sup>Reaction conditions: benzaldehyde (0.23 g), aniline (0.20 g), acetophenone (0.53 g), NaOH (21.5 mmol), 500 rpm at rt

<sup>b</sup>Second reuse of calixarene-based catalysts

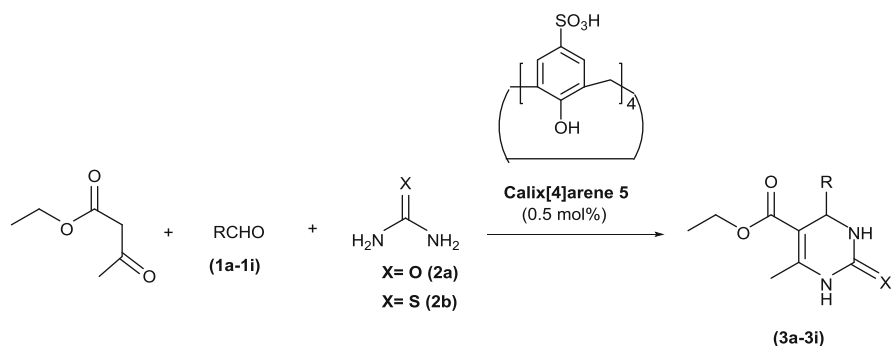
<sup>c</sup>Third reuse of calixarene-based catalysts

organocatalyst in multicomponent Biginelli reactions (see Fig. 27.9) [1]. In that reaction, *p*-sulfonic acid calix[4]arene exhibited high catalytic activity to form 3,4-dihydropyrimidin-2(1*H*)-ones/thiones of pharmacological interest (see Table 27.6).

In an outstanding study, calix[6]arene sulfonic acids (**Calix[6]arene 3a-3d**) were employed as efficient surfactant-type acid catalysts for Michael reactions of indoles with  $\alpha,\beta$ -unsaturated ketones in water [24]. It was pointed out that calix[6]arene sulfonic acids were efficient inverse phase-transfer catalysts, and performed a significant catalytic activity in water (see Fig. 27.10). This remarkable activity in



**Fig. 27.8** Three component Mannich reaction in the presence of Brønsted-type **calix[n]arene** catalysts

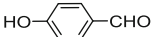
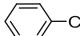
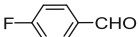
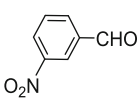
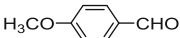
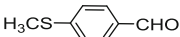
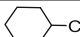




**Fig. 27.9** Synthesis of 3,4-dihydropyrimidin-2(1*H*)-ones/thiones in the presence of **calix[4]arene 5** catalyst

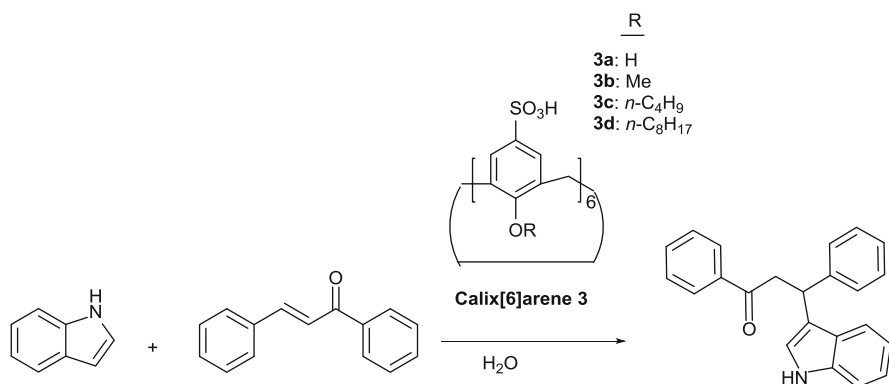
water expresses the fact that calix[6]arene sulfonic acids would open new room in catalysis using an environmentally friendly solvent.

Beside employment of calixarene based organocatalyst in many organic reactions, their separation from the reaction mixture might be difficult and time consuming task. Therefore, the attention has been paid on the usage of calixarene-grafted magnetic nanoparticles to facilitate their separation and recovery [25]. Because calixarene-grafted magnetic nanoparticles have a vast surface area, they are easily dispersed into solvents, their separation from the reaction mixture is quite easy due to their magnetic properties. In this case, Sayin and Yilmaz [25] designed three magnetic recoverable Brønsted-type calix[n]arene organocatalysts to catalyze aromatic substitution reaction for the first time (see Fig. 27.11). It was emphasized that calixarene-grafted magnetic nanoparticle organocatalysts not only were efficient catalysts for the coupling of electron-rich arenes with some alcohols in water but they could be easily separated from the reaction mixture by using a simple magnet (see Table 27.7) [25].

**Table 27.6** Biginelli reaction in the presence of calixarene-based organo catalyst [1]

Product	Aldehydes (1a–1i)	X	Yield (%)
<b>3a</b>		O	81
<b>3b</b>		O	69
<b>3c</b>		O	91
<b>3d</b>		O	62
<b>3e</b>		O	89
<b>3f</b>		O	92
<b>3g</b>		O	38
<b>3h</b>		S	78
<b>3i</b>		S	78

Reagents; aldehyde/ethyl acetoacetate/urea/thiourea (1/1.5/1.5)

**Fig. 27.10** Michael reaction of indole with chalcone in the presence of calix[6]arene sulfonic acids

Given the effective usability of calixarene-grafted magnetic nanoparticles in catalysis, a chiral calix[4]arene-grafted magnetic nanoparticle organocatalyst was developed [26]. Its catalytic activity, enantioselectivity/diastereoselectivity, reusability was investigated in aldol reaction of cyclohexanone and aromatic aldehydes in water (see Fig. 27.12). It was indicated that the chiral organocatalyst exhibited high catalytic activity and enantioselectivity/diastereoselectivity (see Table 27.8). From the results, it was concluded that **Calix-Pro-MN** provided the highest conversion (97%) of the corresponding aldol product with excellent diastereoselectivity (97:3, anti/sin) and high enantioselectivity (93%).

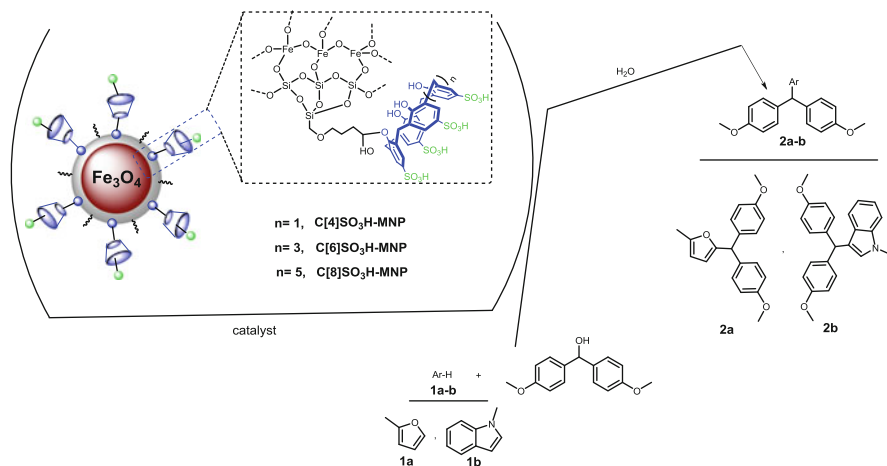


**Fig. 27.11** The coupling of electron-rich arenes with some alcohols in water

### 27.3 Calixarenes as Biomimetic Catalyst

Owing to their highly chemical selectivity behavior relying on the shapes, enzymes are mostly preferred as catalyst in specific reactions. However, various shapes of the enzyme molecules have been observed at various pHs and temperatures this differentiation in the shape validates them in several specific reactions. However, during an enzyme-catalyzed reaction, suddenly differentiation in the shape (configuration of the enzyme) by changing medium pH or temperature may trigger side reaction (unwanted product) or may take the reaction down.

Because of their unique molecular structure, calixarenes have been used as promising materials which could take a prominent place such as development of mimic biocatalysts, enhancing catalytic activity and enantioselectivity of enzymes, and providing organic/water solubility to the reagents for several enzyme-dependent biological reactions [27–29].

Actually, enzyme based reaction proceeds in an aqueous media, which brings out the water-insoluble substrates in the reaction. The rest of the enzyme based reactions, we may call the homogeneous enzymatic reaction, occur in a non-aqueous medium. In the homogeneous enzymatic reaction, the enzyme is forced to be dissolved by applying method including covalent or noncovalent interaction, and solubilization into reversed micelles in a non-aqueous medium [30–33].

The researchers working on calixarene chemistry realized that calixarenes would be a perfect candidate which may interact with enzyme by means of covalent or noncovalent interaction thanks to either their unique scaffold bearing hydrophobic and hydrophilic sites, and also their easy and limitless functionalization.

Oshima et al. (2007) achieved to dissolve cytochrome c in an organic solvent by using a macrocyclic compound “calix[6]arene carboxylic acid” [34]. They

**Table 27.7** The coupling reaction of **1a–b** in H<sub>2</sub>O in the presence of C[n]SO<sub>3</sub>H-MN catalysts

Catalyst	Catalyst amount	Ar-H	Time /h	H <sub>2</sub> O /mL	Product	Yield (%)
None	–	<b>1a</b>	48	1 or 2	<b>2a</b>	0
C[4]SO <sub>3</sub> H-MN	5 mg	<b>1a</b>	48	1	<b>2a</b>	62.8
C[4]SO <sub>3</sub> H-MN	5 mg	<b>1a</b>	48	2	<b>2a</b>	85.2
C[6]SO <sub>3</sub> H-MN	5 mg	<b>1a</b>	48	1	<b>2a</b>	73.3
C[6]SO <sub>3</sub> H-MN	5 mg	<b>1a</b>	48	2	<b>2a</b>	67.1
C[8]SO <sub>3</sub> H-MN	5 mg	<b>1a</b>	48	1	<b>2a</b>	82.3
C[8]SO <sub>3</sub> H-MN	5 mg	<b>1b</b>	48	2	<b>2a</b>	86
None	–	<b>1b</b>	48	1 or 2	<b>2b</b>	0
C[4]SO <sub>3</sub> H-MN	5 mg	<b>1b</b>	6	1	<b>2b</b>	98.1
C[4]SO <sub>3</sub> H-MN	5 mg	<b>1b</b>	24	1	<b>2b</b>	99.9
C[6]SO <sub>3</sub> H-MN	5 mg	<b>1b</b>	24	1	<b>2b</b>	96.6
C[8]SO <sub>3</sub> H-MN	5 mg	<b>1b</b>	24	1	<b>2b</b>	96.3
C[4]SO <sub>3</sub> H-MN	5 mg	<b>1b</b>	24	1	<b>2b</b>	99.8 <sup>a</sup> , 99.8 <sup>b</sup> , 98.9 <sup>c</sup>
C[6]SO <sub>3</sub> H-MN	5 mg	<b>1b</b>	24	1	<b>2b</b>	96.6 <sup>a</sup> , 96.4 <sup>b</sup> , 95.8 <sup>c</sup>
C[8]SO <sub>3</sub> H-MN	5 mg	<b>1b</b>	24	1	<b>2b</b>	96.2 <sup>a</sup> , 95.4 <sup>b</sup> , 95.5 <sup>c</sup>

[25]

<sup>a</sup>Second reuse of catalysts<sup>b</sup>Third reuse of catalysts<sup>c</sup>Fourth reuse of catalysts

suggested that calix[6]arene carboxylic acid derivative was complexed with cytochrome c so that it makes the enzyme soluble in an organic solvent. The formed cytochrome c@calixarene complex was used as a biocatalyst in the enzymatic oxidation reaction of *o*-phenylenediamine in the presence of hydrogen peroxide in chloroform or hexane (see Fig. 27.13). Noncovalent complexation between protein and artificial compounds, which was reported by Oshima et al. [34], would be the best method for bio-catalyzed polymer synthesis in vitro. Because noncovalent complexation depends upon reaction parameters such as pH and solvent, when the pH of the medium was changed, the complex broke down as presented in Fig. 27.14.

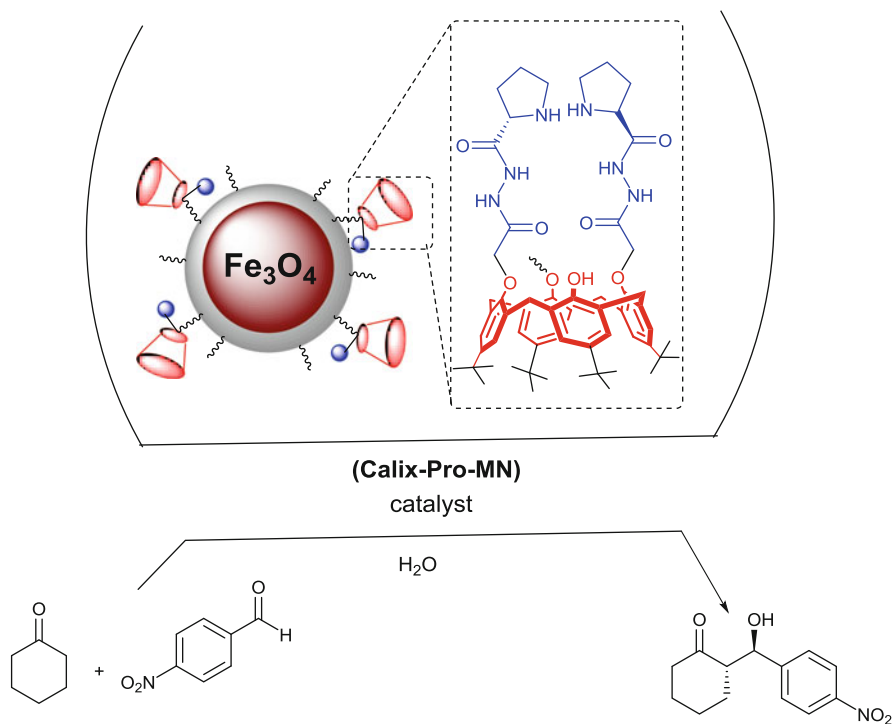


**Fig. 27.12** Aldol reaction of cyclohexanone and aromatic aldehydes in water

**Table 27.8** Aldol reaction of cyclohexanone and *p*-nitrobenzaldehyde in the presence of **Calix-Pro-MN** [26]

Entry	H <sub>2</sub> O (mL)	Additive	Conversion (%) <sup>a</sup>	anti:syn <sup>c</sup>	ee (%) <sup>d</sup>
1	0.5	–	97	97:3	93
2	0.25	–	96	78:22	92
3	0.125	–	70	88:12	92
4 <sup>a</sup>	0.5	–	66	84:16	90
5 <sup>b</sup>	0.5	–	38	82:18	37
6	0.25	ClCH <sub>2</sub> COOH	94	88:12	84
7	0.25	CH <sub>3</sub> COOH	93	86:14	81
8	0.25	PhCOOH	97	79:21	86

<sup>a</sup>5 % mol catalyst

<sup>b</sup>2.5 % mol catalyst

<sup>c</sup>Obtained by <sup>1</sup>H NMR spectroscopy

<sup>d</sup>Obtained by chiral HPLC analysis in comparison with authentic racemic material

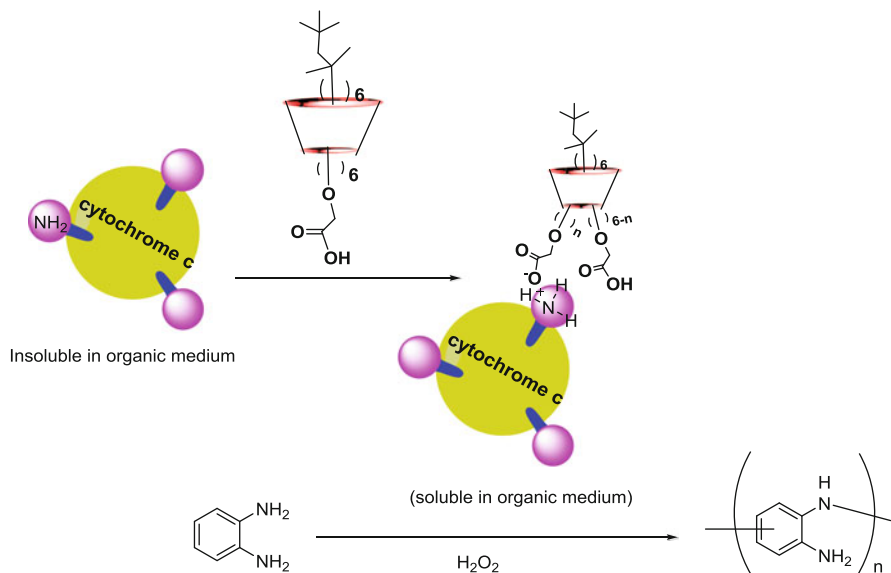


Fig. 27.13 The enzymatic oxidation reaction of *o*-phenylenediamine in organic medium [34]

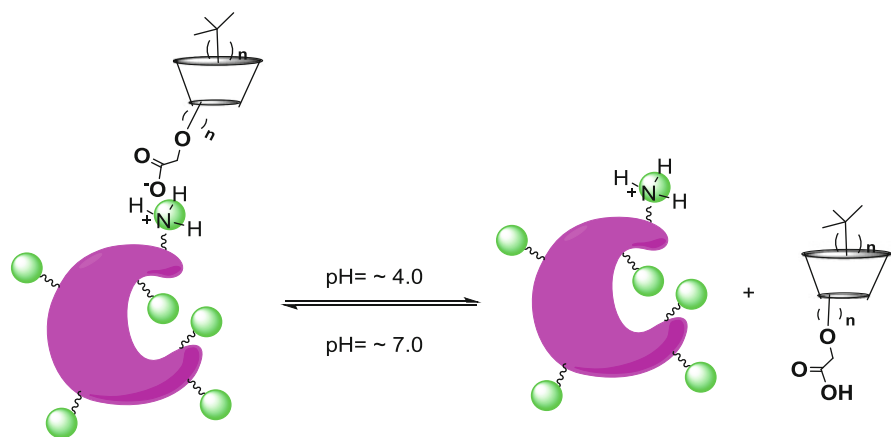
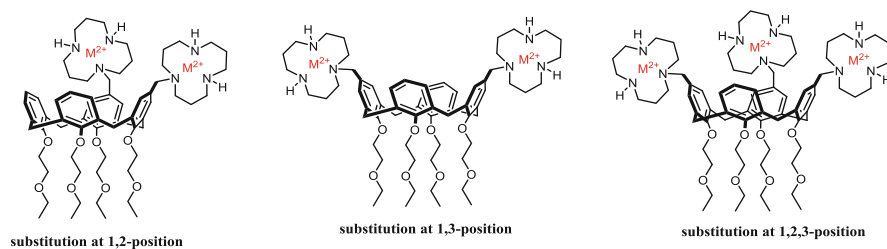


Fig. 27.14 pH depended complexation of the biomolecules and calixarene-carboxylic acid derivative

### 27.3.1 Calixarenes as Pseudo-biomimetic Catalysts

Investigations on calixarene-based pseudo-biomimetic catalyst has received considerable attention because calixarenes can be functionalized on this purpose, and particularly they are nonpeptidic molecules that mimic structural and substitution aspect of the biomolecules [35, 36]. In principle, calixarene-based pseudo-biocatalysts



**Fig. 27.15** Pseudo-biocatalyst oriented with the substituted at 1,2-, 1,3-, and 1,2,3-positions of the upper rim of calix[4]arene and Zinc(II) or copper(II) [37]

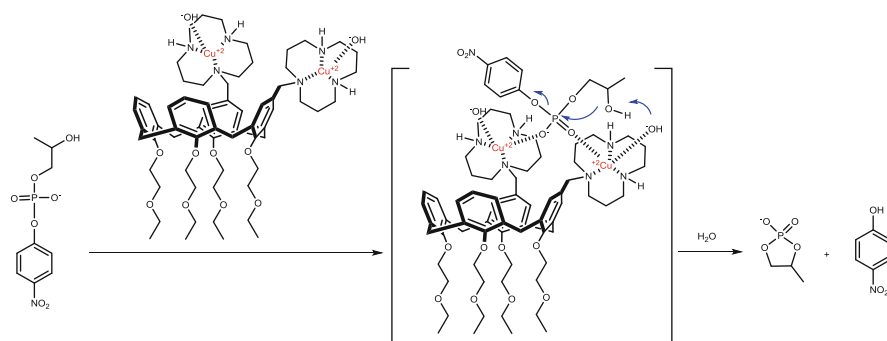


**Fig. 27.16** The cleavage reaction of phosphodiester by using calixarene@Cu biocatalysts

provide an efficient hole that keep the active groups of substrates at the correct distance in order to produce the corresponding products in the fast and good yields.

In a study, Cacciapaglia et al. (2006) successfully synthesized a pseudo-biomimetic catalyst that worked as a phosphodiesterase enzyme [37]. For that purpose, 1,2-, 1,3-, and 1,2,3-positions of the upper rim of calix[4]arene were functionalized with 1,5,9-triazacyclododecane ([12]ane- $N_3$ ) moieties, which were able to coordinate with several metals (see Fig. 27.15). These calix[4]arene derivatives were complexed with Zinc(II) and copper(II) to produce effective catalysts for the cleavage reaction of phosphodiester as RNA models. As seen in Fig. 27.16, the reaction takes place over the calixarene-metal complexes that indeed clarifies the importance of the substitution pattern of ligated metal ions (1,2-vicinal or 1,3-distal) along with calix[4]arene skeleton.

Another outstanding study on the usage of an effective calixarene derivative as a biomimetic catalyst for the cleavage of the RNA model compound, 2-hydroxypropyl *p*-nitrophenyl phosphate was reported by Baldini et al. [35]. They prepared four calix[4]arene derivatives substituted with two to four guanidinium moieties at the upper rim of calixarenes, and investigated their catalytic affinities in the cleavage of the RNA model compound 2-hydroxypropyl *p*-nitrophenyl phosphate in water (see Figs. 27.17 and 27.18). They found that the



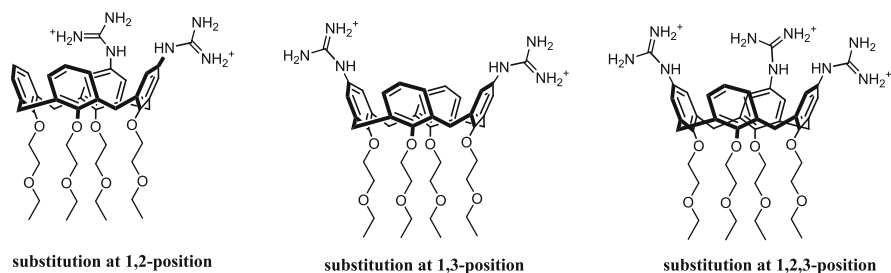


**Fig. 27.17** Prepared four calix[4]arene derivatives that substituted with two to four guanidinium moieties at the upper rim of calixarenes [35]

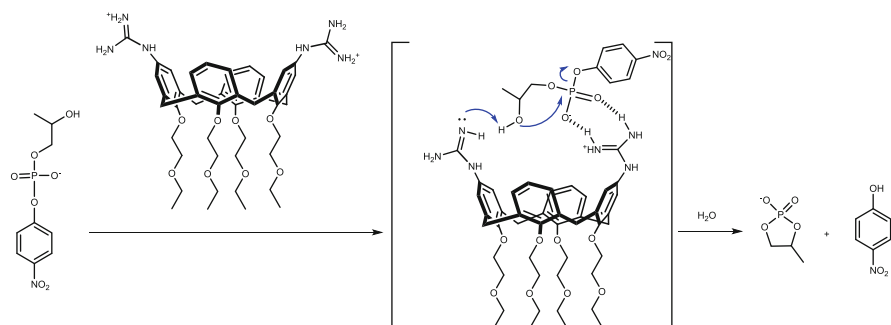


**Fig. 27.18** Cleavage of the RNA model compound 2-hydroxypropyl *p*-nitrophenyl phosphate in the presence of calixarene-based pseudo-biocatalyst [35]

catalytic activity of the calixarene biocatalyst relied on the pH values of the reaction medium. When the pH was decreased, the guanidinium moieties of the biocatalyst was protonated (Fig. 27.19).

In another study, Salvia et al. (2012) successfully synthesized tetraguadinocalix[4]arene in order to use as a biocatalyst in transformation of adenosine triphosphate (ATP) [38]. The catalytic mechanism for ATP hydrolysis lays on the protonation of three guanidinium units of the biocatalyst, followed by the formation of a 1:1 substrate-calixarene biocatalyst complex, and proceeds by nucleophilic attack of the unprotonated guanidinium unit of the biocatalyst in order to produce a phosphoramidate intermediate and adenosine diphosphate (ADP) [38]. Upon hydrolysis, of the phosphoramidate intermediate gives the biocatalyst by completing the catalytic cycle (see Fig. 27.20). They concluded that the triprotonated tetraguadinocalix[4]arene had more substantial catalytic efficacy than the other catalysts.

To obtain better catalytic reactivity in the enzyme-based highly selective and demanding reactions, calixarenes are employed as an enzyme-mimic vehicle which introduce hydrophobic environment and residues in the enzyme pocket to stabilize intermediates. The substrate binding pocket, having a substantial role in the reaction kinetics, basically locates next to the metal ion in order to lead substrate to

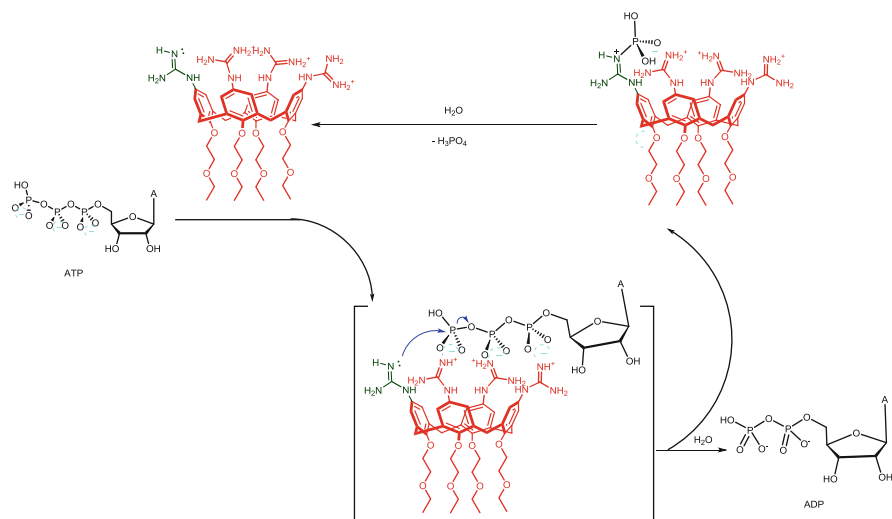


Fig. 27.19 Proposed mechanism for the catalytic cleavage of ATP [38]

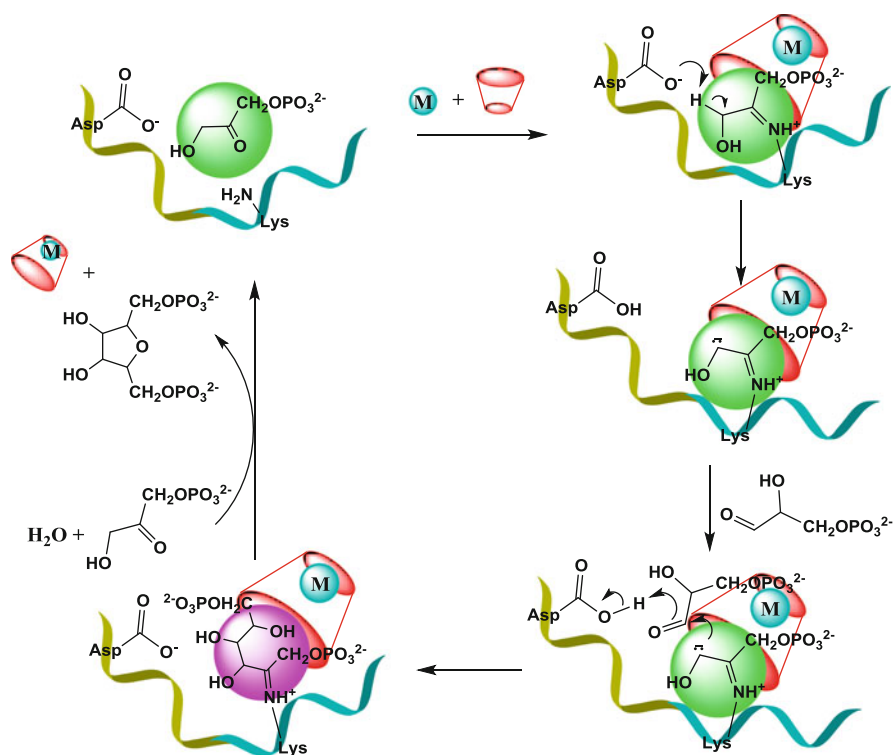


Fig. 27.20 Suggested mechanism for aldolase reaction [40]

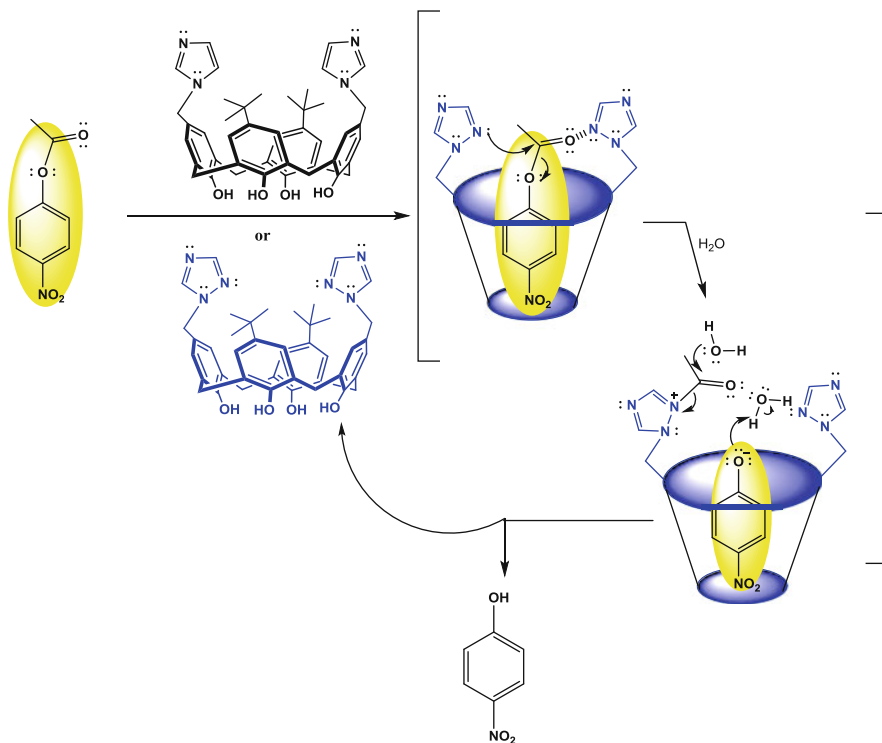


Fig. 27.21 Proposed mechanism for hydrolysis reaction [41]

defined positions [39]. Thanks to the selective metal binding abilities of calixarenes, in 1983, a calixarene derivative bearing both amino and carboxylic acid groups was synthesized for a hypothetical model of aldolase (see Fig. 27.20) [40].

In another enzyme-mimics study invested by Yilmaz et al. [41], calix[4]arenes bearing imidazole or triazole groups were synthesized in order to investigate their enzymatic performance by applying the Michaelis-Menten kinetics in the catalytic hydrolysis of *p*-nitrophenyl acetate (see Fig. 27.21). It was found that the imidazole-functionalized monomeric mimic exhibited higher acyltransferase mimics efficacy than the triazole-functionalized mimic. It was also found that H-bonding sites of calixarenes had a significant effect on catalytic activity.

### 27.3.2 Calixarenes as Additive for Enzyme-Associated Biocatalyst

Enzymes comprising of a bunch of linear chains of amino acids are known as macromolecular biocatalysts in most chemical/biological reactions such as

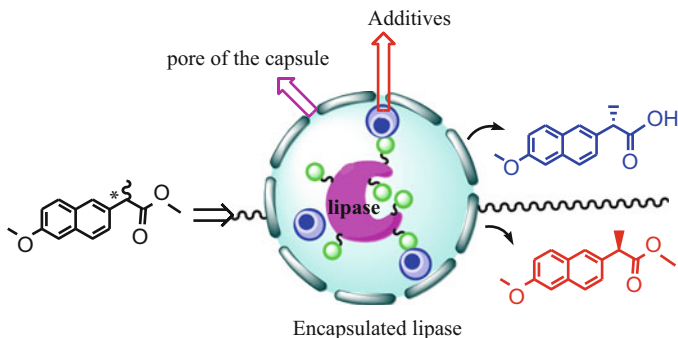


**Fig. 27.22** Enantioselective hydrolysis of racemic-Naproxen methyl ester by the encapsulated lipase in the presence of an additive

esterification, hydrolysis, epoxidation and interesterification etc. [42]. As a biocatalyst, enzymes can accelerate the product formation process by lowering the activation energy like all chemical catalysts. However, unlike most chemical catalysts, enzymes can separate stereoisomers of substrate molecules due to their complementary shapes such as charge and hydrophilic/hydrophobic characteristics [43]. Lipase enzymes are widely employed as biocatalysts in organic/bioorganic chemistry for kinetic resolution reactions of a broad range of substrate [44–46]. Nevertheless, lipase structures unfold (denature) when heated affected reproducibility in yield and also losing the bio-catalytic and stereoselectivity attitudes [47]. To overcome these issue and to enhance their bio-catalytic and stereoselective behaviors, lipases have been encapsulated in the presence of various carriers such as celite, glass beads,  $\text{Fe}_3\text{O}_4$ , chitosan, organic/bio-polymers, cyclodextrins, kaolin, and calixarenes (see Fig. 27.22) [27–29, 48–54]. Because of the scope of this book, we will describe the usage of calixarenes in the encapsulation process of lipases, and elucidate how they affect the catalytic and enantioselective behavior of lipases.

### 27.3.2.1 Calixarenes as Additive

To enhance catalytic and enantioselective behaviors of lipase in the kinetic resolution of some racemic anti-inflammatory drugs, Calix[n]arene, Calix[n]- $\text{NH}_2$ , Calix [n]- $\text{COOH}$  ( $n = 4, 6, 8$ ), 5-CRL and 6-CRL were used as additives for the encapsulation of lipase by using sol-gel techniques compensating of polycondensation by tetraethoxysilane and octyltriethoxysilane (see Fig. 27.23) [27, 28]. The sol-gel encapsulation method is mostly applied for lipase immobilization owing to the many advantages such as entrapment of a large amount of biological molecules, thermal and chemical stabilities [44]. Calixarene-encapsulated lipases were used as catalysts for hydrolysis reactions of *p*-nitrophenylpalmitate and Naproxen methyl ester. It has been elucidated that not only free  $-\text{NH}_2$  and  $-\text{COOH}$  groups but also heteroaromatic substituents play substantial role on the conversion and

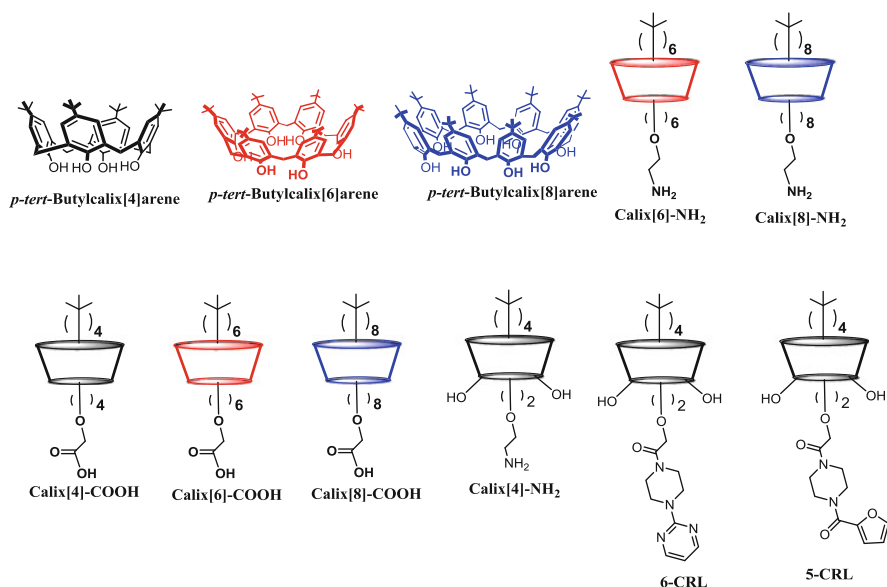


**Fig. 27.23** Calix[ $n$ ]arene additives used in sol-gel encapsulation [27, 28]

**Table 27.9** Enantioselective efficacy of the encapsulated lipases in the hydrolysis reaction of ( $R/S$ )-Naproxen methyl ester

Lipase	Conversion (x, %)	$ee_p$ (%)	$E^d$
Enc-Lipase <sup>a,b</sup>	37.9	>98	166
Calix[4]arene <sup>b</sup>	34.8	>98	166
Calix[6]arene <sup>b</sup>	33.0	>98	149
Calix[8]arene <sup>b</sup>	36.7	>98	173
Calix[4]-NH <sub>2</sub> <sup>b</sup>	45.4	>98	>200
Calix[6]-NH <sub>2</sub> <sup>b</sup>	46.3	>98	>200
Calix[8]-NH <sub>2</sub> <sup>b</sup>	36.5	>98	170
Calix[4]-COOH <sup>b</sup>	28.0	>98	163
Calix[6]-COOH <sup>b</sup>	41.2	>98	>200
Calix[8]-COOH <sup>b</sup>	32.9	>98	168
5-CRL <sup>c</sup>	49.5	>98	392
6-CRL <sup>c</sup>	50.0	>98	525

<sup>a</sup>Encapsulated lipase without additives

<sup>b</sup>[27]

<sup>c</sup>[28]

<sup>d</sup>Enantiomeric ratio

enantioselectivity of racemic Naproxen methyl ester. The results clearly suggest that the heteroaromatic units of calix[4]arene increased both catalytic and enantioselective capability of lipase (see Table 27.9).

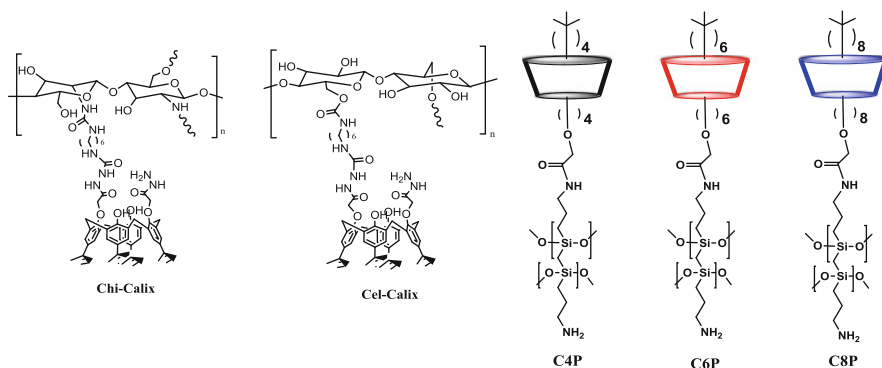


**Fig. 27.24** Calix[n]arene-immobilized polymer as additives used in sol-gel encapsulation [44, 55]

### 27.3.2.2 Calixarenes-Immobilized onto Polymers as Additives for Lipase Encapsulation

Immobilization of calixarenes onto polymer supports such as chitosan, cellulose, silica based or organic based polymers has been extensively studied in terms of not only stacking a great number of calixarenes onto the surface of the polymers but also to obtain rigid scaffolds to the calixarenes. In addition, it is well known that the catalytic and enantioselective activity of lipase are enhanced if the proteins of lipase are held as much strength as into a stable catalytic conformation. Regarding that, some of the calixarene-grafted polymers were employed for the encapsulation of lipase (see Fig. 27.24) [44, 55]. It was emphasized that the type of the polymers and position of substituents which bond to calixarenes and even cavity sizes of calixarenes are important parameters in order to design an effective biocatalyst associating with enzyme (see Table 27.10).

### 27.3.2.3 Calixarene-Grafted $\text{Fe}_3\text{O}_4$ as Additive for Lipase Encapsulation

In most enzyme-catalyzed reactions, it is hard to separate catalysts from, excess of substrates and products, and indeed to reuse. To overcome this issues,  $\text{Fe}_3\text{O}_4$  magnetic nanoparticles have been introduced biomimetic and organocatalysis. When a bio-catalyst was encapsulated/immobilized in the presence of  $\text{Fe}_3\text{O}_4$ / $\text{Fe}_3\text{O}_4$ -based magnetic nanoparticles, separation and reusable processes of the bio-catalyst from the reaction mixture became an easy task due to their magnetic behaviour. A couple of calixarene-grafted  $\text{Fe}_3\text{O}_4$  magnetic nanoparticles was driven as an additive for the encapsulation of lipase in order to investigate their effects on the catalytic activity and enantioselectivity of lipase in the hydrolysis of racemic Naproxen methyl ester (see Fig. 27.25) [56–58, 59]. From these studies (see Table 27.11), it appeared that encapsulated lipase in the presence of calixarene-

**Table 27.10** Enantioselective hydrolysis of racemic Naproxen methyl ester with the encapsulated lipases

Lipase	x (%)	ee <sub>p</sub> (%)	E <sup>g</sup>
Free E <sup>a,b</sup>	20.3	>98	137
Chi-Calix-E <sup>b,c</sup>	41.6	>98	241
Cel-Calix-E <sup>b,c</sup>	46.7	>98	300
Cel-E <sup>b,d</sup>	41.0	>98	189
Chi-E <sup>b,e</sup>	38.3	>98	178
C4P <sup>f</sup>	24.6	>98	142
C6P <sup>f</sup>	39.5	>98	195
C8P <sup>f</sup>	27.5	>98	131

Enantiomeric excess (ee) as obtained by Chiral HPLC, Agilent 1200 Series -chiral column (Chiralcel OD-H); n-hexane/2 propanol/trifluoroacetic acid (100/1/0.1, v/v/v) for the Naproxen as mobile phase; 24 h; 20 mM of substrate

<sup>a</sup>Encapsulated free lipase without calixarene

<sup>b</sup>[44]

<sup>c</sup>Encapsulated lipase with calixarene-immobilized biopolymers

<sup>d</sup>Encapsulated lipase with cellulose

<sup>e</sup>Encapsulated lipase with chitosan

<sup>f</sup>Encapsulated lipase with calixarene-immobilized polymers [55]

<sup>g</sup>Enantiomeric ratio

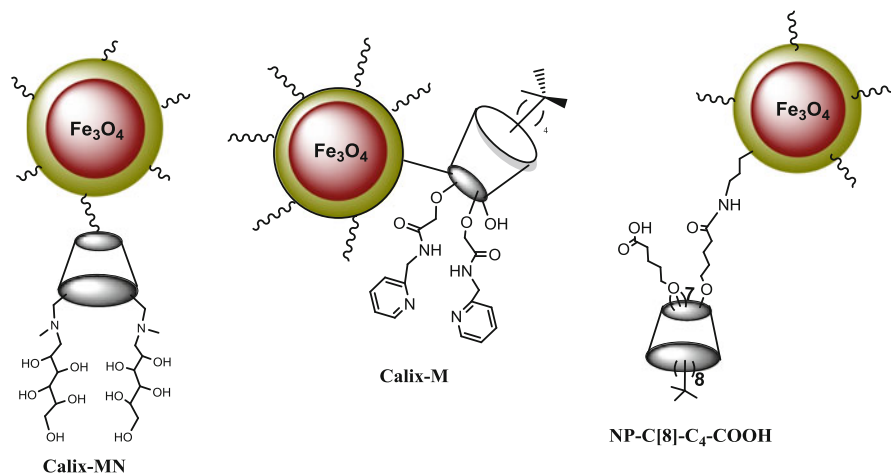


**Fig. 27.25** Calix[n]arene-grafted Fe<sub>3</sub>O<sub>4</sub>magnetic nanoparticles as additives used in sol-gel encapsulation[56–58]

**Table 27.11** The enantioselective hydrolysis of Naproxen methyl ester of using encapsulated lipases as catalysts

Bio-catalysts	X (%)	ee <sub>p</sub> (%)	E
Calix-MN <sup>a</sup>	50.0	>98	460
Free Lipase <sup>a,b</sup>	37.9	>98	166
Calix-M <sup>c</sup>	49	>98	>400
NP-C[8]-C4-COOH <sup>d</sup>	46	>98	265

<sup>a</sup>[56]<sup>b</sup>Encapsulated free lipase without magnetic calixarene nanoparticles<sup>c</sup>[57].<sup>d</sup>[58]. Where E, ee<sub>p</sub>, X, enantiomeric ratio for irreversible reactions, enantiomeric excess of product, racemate conversion, respectively

grafted Fe<sub>3</sub>O<sub>4</sub> magnetic nanoparticles not only exhibited highly catalytic and enantioselective efficacy but also brought the separation process easy via simple magnetic decantation, and increased reusability of bio-catalysts without significant loss of their catalytic activity and enantioselectivity.

## References

- Da Silva, D.L.; Fernandes, S.A.; Sabino, A.A.; de Fatima, A. *Tetrahedron Lett.* **2011**, *52*, 6328–6330.
- Dalko, P.I.; Moisan, L. *Angew. Chem. Int. Ed.* **2004**, *43*, 5138–5175.
- Berkessel, A.; Gröger, H. Chapter 8: Cycloaddition Reactions. *Asymmetric Organocatalysis: From Biomimetic Concepts to Applications in Asymmetric Synthesis*. Weinheim: Wiley-VCH. **2005**, p. 256–268. ISBN 3-527-30517-3.
- Amarante, G.W.; Coelho, F. *Quim. Nova* **2009**, *32*, 469–481.
- Eymur, S.; Akceylan, E.; Sahin, O.; Uyanik, A.; Yilmaz, M. *Tetrahedron* **2014**, *70*, 4471–4477.
- Xu, Z.-X.; Li, G.-K.; Chen, C.-F.; Huang, Z.-T. *Tetrahedron* **2008**, *64*, 8668–8675.
- (a) Uyanik, A.; Bayrakci, M.; Eymur, S.; Yilmaz, M. *Tetrahedron* **2014**, *70*, 9307–9313.; (b) Durmaz, M.; Sirit, A. *Tetrahedron: Asymmetry* **2013**, *24*, 1443–1448.
- Bocchi, V.; Foina, D.; Pochini, A.; Ungaro, R.; Andreotti, G.D. *Tetrahedron* **1982**, *38*, 373–378.
- Ungaro, R.; Pochini, A.; Andreotti, G.D.; Domiano, P. *J. Inclusion Phenom.* **1985**, *3*, 35–42.
- Ungaro, R.; Pochini, A.; Andreotti, G.D.; Ugozzoli, F. *J. Inclusion Phenom.* **1985**, *3*, 409–420.
- Nomura, E.; Taniguchi, H.; Kawaguchi, K.; Otsuji, Y. *Chem. Lett.* **1991**, *20*, 2167–2170.
- Nomura, E.; Taniguchi, H.; Kawaguchi, K.; Otsuji, Y. *J. Org. Chem.* **1993**, *58*, 4709–4715.
- Shimizu, S.; Shirakawa, S.; Sasaki, Y.; Hirai, C. *Adv. Synth. Catal.* **2002**, *344*, 370–378.
- Shimizu, S.; Shirakawa, S.; Suzuki, T.; Sasaki, Y. *Tetrahedron* **2001**, *57*, 6169–6173.
- Shirakawa, S.; Shimizu, S. *Eur. J. Org. Chem.* **2009**, 1916–1924.
- Yilmaz, M, Sayin, S. Chapter 2: Organic based magnetic nanoparticles-polymers and various calixarene based magnetic nanoparticles. *Magnetic Nanoparticles: Properties, Synthesis and Applications*. Nova Science Publishers, Inc. New York. **2012**, p. 95–134. ISBN 978-1-61942-424-1.
- Araki, K.; Yanagi, A.; Shinkai, S. *Tetrahedron* **1993**, *49*, 6763–6772.



18. Shimizu, S.; Kito, K.; Sasaki, Y.; Hirai, C. *Chem. Commun.* **1997**, 1629–1630.
19. Akceylan, E.; Yilmaz, M. *Tetrahedron* **2011**, *67*, 6240–6245.
20. Srivastava, P.; Srivastava, R. *Tetrahedron Lett.* **2007**, *48*, 4489–4493
21. Yang, F.; Guo, H.; Jiao, Z.; Li, C.; Ye, J. *J. Iran Chem. Soc.* **2012**, *9*, 327–332.
22. Sayin, S.; Yilmaz, M. *RSC Adv.* **2014**, *4*, 2219–2225
23. Shimizu, S.; Shimada, N.; Sasaki, Y. *Green Chem.* **2006**, 608–614
24. Xie, Y.; Mao, L.; Li, L. *J. Chem. Res.* **2013**, 476–479.
25. Sayin, S.; Yilmaz, M. *Tetrahedron* **2014**, *70*, 6669–6676
26. Akceylan, E.; Uyanik, A.; Eymur, S.; Sahin, O.; Yilmaz, M. *Appl. Catal. A: Gen.* **2015**, *499*, 205–212
27. Sahin, O.; Erdemir, S.; Uyanik, A.; Yilmaz, M. *Appl. Catal. A: Gen.* **2009**, *369*, 36–41.
28. Akceylan, E.; Akoz, E.; Sahin, O.; Yilmaz, M. *J Incl Phenom Macrocycl Chem* **2015**, *81*, 237–243.
29. Akoz, E.; Akbulut, O.Y.; Yilmaz, M. *Appl. Biochem. Biotechnol.* **2014**, *172*, 509–523.
30. Okahata, Y.; Ijuro, K. *J. Chem. Soc., Chem. Commun.* **1988**, 1392–1394.
31. Goto, M.; Sumura, H.; Abe, K.; Nakashio, F. *Biotechnol. Tech.* **1995**, *9*, 101–104.
32. Pires, M.J.; Aires-Barros, M.R.; Cabral, J.M.S. *Biotechnol. Prog.* **1996**, *12*, 290–301.
33. Inada, Y.; Takahashi, K.; Yoshimoto, T.; Ajima, A.; Matsushima, A.; Saito, Y. *Trends Biotechnol.* **1986**, *4*, 190–194.
34. Oshima, T.; Sato, M.; Shikaze, Y.; Ohto, K.; Inoue, K.; Baba, Y. *Biochem. Eng. J.* **2007**, *35*, 66–70.
35. Baldini, L.; Cacciapaglia, R.; Casnati, A.; Mandolini, L.; Salvio, R.; Sansone, F.; Ungaro, R. *J. Org. Chem.* **2012**, *77*, 3381–3389
36. Hollenstein, M.; Hipolito, C.J.; Lam, C.H.; Perrin, D.M. *ChemBioChem* **2009**, *10*, 1988–1992.
37. Cacciapaglia, R.; Casnati, A.; Mandolini, L.; Reinhoudt, D.N.; Salvio, R.; Sartori, A.; Ungaro, R. *J. Am. Chem. Soc.* **2006**, *128*, 12322–12330.
38. Salvio, R.; Casnati, A.; Mandolini, L.; Sansone, F.; Ungaro, R. *Org. Biomol. Chem.* **2012**, *10*, 8941–8943.
39. Rebilly, J.-N.; Reinaud, O. *Supramol. Chem.* **2014**, *26*, 454–479.
40. (a)Choi, K.H.; Shi, J.; Hopkins, C.E.; Tolan, D.R.; Allen, K.N. *Biochemistry* **2001**, *40*, 13868–13875. (b) Gutsche, C.D. *Acc. Chem. Res.* **1983**, *16*, 161–170.
41. Tabakci, B.; Yilmaz, M.; Beduk, A.D. *J. Appl. Polym. Sci.* **2012**, *125*, 1012–1019.
42. Sayin, S.; Yilmaz, E.; Yilmaz, M. *Org. Biomol. Chem.* **2011**, *9*, 4021–4024.
43. Jaeger, K.E.; Eggert, T. *Curr. Opin. Biotechnol.* **2004**, *15*, 305–313.
44. Ozyilmaz, E.; Sayin, S. *Appl. Biochem. Biotechnol.* **2013**, *170*, 1871–1884.
45. Gotor-Fernández, V.; Brieva, R.; Gotor, V. *J. Mol. Catal. B: Enzym.* **2006**, *40*, 111–120.
46. Koeller, K.M.; Wong, C.H. *Nature* **2001**, *409*, 232–240.
47. Petsko, G.A.; Ringe, D. Chapter 1: From sequence to structure. *Protein structure and function*. London: New Science. **2003**, p. 27. ISBN 978-1405119221.
48. Yilmaz, E.; Sezgin, M.; Yilmaz, M. *Biocatal. Biotransform.* **2009**, *27*, 360–366
49. Yilmaz, E.; Can, K.; Sezgin, M.; Yilmaz, M. *Bioresource Technol.* **2011**, *102*, 499–506
50. Tutar, H.; Yilmaz, E.; Pehlivan, E.; Yilmaz, M. *Inter. J. Biological Macromol.* **2009**, *45*, 315–320.
51. Erdemir, S.; Yilmaz, M. *J. Mol. Catal. B: Enzym.* **2009**, *58*, 29–35.
52. Ozyilmaz, E.; Sayin, S.; Arslan, M.; Yilmaz, M. *Colloid Sur. B: Biointer.* **2014**, *113*, 182–189.
53. Akoz, E.; Sayin, S.; Kaplan, S.; Yilmaz, M. *Bioprocess Biosyst Eng.* **2015**, *38*, 595–604.
54. Pereira, E.B.; De Castro, H.F.; De Moraes, F.F.; Zanin, G.M. *Appl. Biochem. Biotechnol.* **2001**, *93*, 739–752.
55. Erdemir, S.; Yilmaz, M. *J. Incl. Phenom. Macrocycl. Chem.* **2012**, *72*, 189–196
56. Sayin, S.; Yilmaz, E.; Yilmaz, M. *Org. Biomol. Chem.* **2011**, *9*, 4021–4024.
57. Ozyilmaz, E.; Sayin, S. *Bioprocess Biosyst Eng.* **2013**, *36*, 1803–1806
58. Sayin, S.; Akoz, E.; Yilmaz, M. *Org. Biomol. Chem.* **2014**, *12*, 6634–6642.
59. Ozyilmaz, E.; Bayrakci, M.; Yilmaz, M. *Bioorganic Chemistry.* **2016**, *65*, 1–8.

# Chapter 28

## Fluorescent Calixarene Hosts

Rajesh Kumar, Yujin Jung, and Jong Seung Kim

### 28.1 Introduction

#### 28.1.1 Calixarene as Host

Calixarenes are among the most efficient macrocyclic scaffolds for investigating host-guest interactions [1]. They are cyclic oligomers synthesized from *p*-*tert*-butyl phenol and formaldehyde, linked through methylene groups [2]. Compared with other macrocyclic scaffolds such as cyclodextrins, cucurbiturils, cryptands, and crown ethers, calixarenes have many advantages, including (i) well-defined hydrophobic calix cavity, (ii) interesting conformational behavior, (iii) functional modification of upper and lower rims, and (iv) strong inclusion of different guest molecules. Calixarenes have two rims: an upper rim (or wider rim) and a lower rim (or narrow rim), consisting of the para substituents and phenolic hydroxyl groups of the phenolic units, respectively. Depending on the orientation and on the substituents of the phenolic units at the lower or upper rim, calixarenes assume different conformations, including cone, partial cone, 1,2-alternate, and 1,3-alternate. These conformations can be interconverted in the presence of specific metal ions [3]. The benzene ring preorganization in the hydrophobic cavity of calixarenes enhances the inclusion of various metal ions through cation- $\pi$  interactions [4].

Calix[4]arene and its derivatives, among various calix[*n*]arenes, have attracted tremendous interest and have been extensively explored in various fields, including chemistry, biology, medicine, and environmental processes. Because of their inherent versatility [5] and numerous possibilities of functionalization, calix[4]arene derivatives have been widely used for different applications such as molecular

---

R. Kumar • Y. Jung • J.S. Kim (✉)  
Department of Chemistry, Korea University, Seoul 136-701, South Korea  
e-mail: [jongskim@korea.ac.kr](mailto:jongskim@korea.ac.kr)

recognition of various ions [6], ion extraction [7] and transportation [8], biomimetics of enzymes [9], biomolecular interactions [10], and catalysis [11]. The pre-organized core of calix[4]arene is well-known for the complexation of ions and molecules of particular size and shape. The lower and upper rim modification of calix[4]arene with various ligating sites, such as N, O, S, and P, further tune and improve the binding efficiency and selectivity toward different guest molecules (hard or soft). These modifications make calix[4]arene derivatives more flexible for efficient binding with guest species. The change in conformation upon derivatization from mono- to tetra-substitution also alters their binding behavior. Thus, the binding ability of calix[4]arene derivatives toward specific guest molecules can be affected by various factors, including the conformation of calix[4]arene, lower or upper rim substituents, the nature of the ligating sites, and the type of guest molecule. Numerous calix[4]arene derivatives exhibiting different binding properties have been developed for the sensitive and selective detection of anions, cations, and other biologically relevant species. Because of their numerous applications, calix[n]arene scaffolds are regarded as ‘third generation’ [12] hosts, along with other macrocyclic hosts including crown ethers [13] and cyclodextrins [14].

### 28.1.2 Fluorescence Detection of Binding Events

In general, the binding of a guest molecule to calix[4]arene ligands can be monitored by NMR, redox, UV-vis, and fluorescence spectroscopies. Because of its very high sensitivity and simplicity, fluorescence spectroscopy, in which the molecular recognition event of a specific analyte is converted into a detectable fluorescence signal, is particularly attractive [15]. Basically, a fluorogenic probe consists of two significant units i.e. an ionophore (guest recognition unit) and a fluorophore (optical signaling unit, Fig. 28.1) [16]. The binding of specific analyte to the ionophore results in the change of optical signal of fluorophore (Fig. 28.1). Therefore, design of ionophore is very significant in the efficient binding and fluorogenic detection of the analytes.

Various fluorogenic moieties, such as pyrene, dansyl, anthracene, 7-nitrobenzofurazan (NBD), coumarin, quinoline, and naphthalimide, have been used alone or in combination with other fluorophores for an efficient detection of

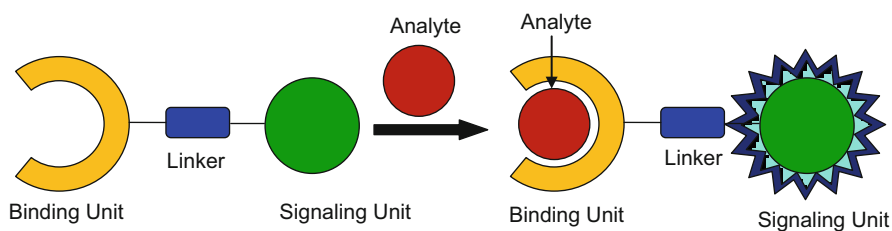


**Fig. 28.1** Illustration of a fluorescence-based chemosensor for a specific analyte

guests. Upon interaction with guest molecules, fluorogenic receptors trigger various signaling mechanisms including competitive binding [17], photoinduced electron transfer (PET) [18], intramolecular charge transfer [19], excimer/exciple [20], metal-to-ligand charge transfer (MLCT) [21], and intermolecular excited state proton transfer (ESPT) [22]. These signaling mechanisms result in different fluorogenic behaviors, such as fluorescence quenching, fluorescence enhancement, or ratiometric response on interaction with anions. In the presence of the specific guest, the change in the photophysical properties is directly correlated to the detection efficiency of the probe. Thus, fluorescence spectroscopy provides a unique and sensitive approach for the rapid detection of a particular analyte.

The development of synthetic receptors for the detection of environmentally or biologically important cations, anions, and other analytes, such as amino acids, thiols, and reactive oxygen species, is highly desirable due to their involvement in various fields of science including chemical, biological, and environmental sciences [23]. These species are involved in various biochemical processes and, therefore, a variation in their concentration causes many adverse effects on human health. On the other hand, exposure of transition metal ions have enormous toxic impact on the environment, therefore fluorogenic detection of these metal ions is highly desirable [24]. Compared with the sensing of cationic species, anion recognition has been a great challenge because, unlike for metal cations, anion complexation to the receptor is complicated by their varying size, shape, and charge, and by their pH-dependent nature [25].

## 28.2 Fluorescent Calixarene Hosts

### 28.2.1 Pyrene-Appended Calixarene Hosts

Pyrene, among the various fluorogenic units available [26], is one of the most useful as it displays both monomer emission (370–430 nm) and excimer emission (around 480 nm). The conformational change of the recognition and signaling units upon binding with specific guest ion results in variable intensity ratio of excimer to monomer emission ( $I_E/I_M$ ) that provides sensitive informative about the detection of different analytes. The development of fluorogenic chemosensors for metal ions based on fluorescence changes is particularly attractive due to their quick and fast detection with very high sensitivity [27].

#### 28.2.1.1 Receptors for Cations

Pyrene-appended fluorogenic calix[4]arenes **1** and **2** (Fig. 28.2) bearing two amide units were developed, and their cation recognition behavior was evaluated [28]. The different orientation of the pyrene units in probes **1** and **2** determine the selectivity

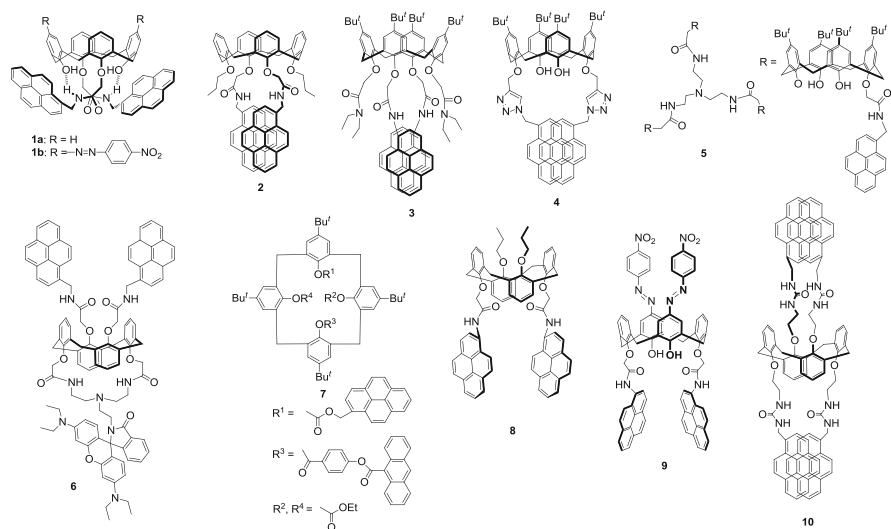


**Fig. 28.2** Structures of pyrene-appended receptors for cations (1–7) and anions (8–10)

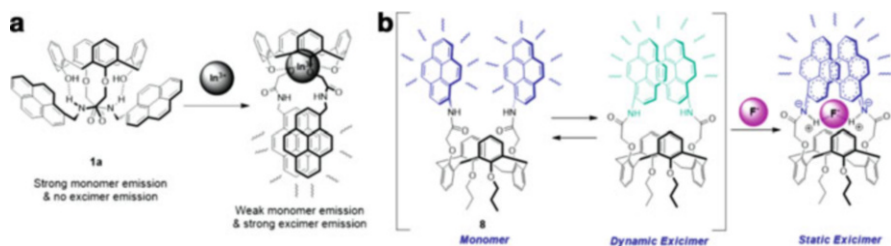


**Fig. 28.3** Binding modes of probes **1a** and **8** toward  $In^{3+}$  and  $F^-$  ions, respectively

and the binding affinity to different cationic species. The amide hydrogen atoms and phenolic OH groups of probes **1a** and **1b** are involved in intramolecular hydrogen bonding, which results in divergent orientation and monomer emission of the pyrene units (Fig. 28.3a). Among the various metal ions examined, probe **1a** showed the highest selectivity for  $In^{3+}$ . Upon binding with  $In^{3+}$ , in probes **1a** and **2**, phenolic OH groups deprotonate and inhibit the hydrogen bonding that leads to ratiometric fluorescence changes (Fig. 28.3a). The initial addition of  $In^{3+}$  caused an increase in excimer emission and a decrease in monomer emission of probes **1a** and **2**, indicating the destruction of hydrogen bonding and the formation of a 1:1 metal complex. However, with excess addition of  $In^{3+}$ , the opposite tendency was observed, i.e., excimer emission decreases and monomer emission increases, due to the 1:2 (L:  $In^{3+}$ ) stoichiometry of the complex. On the other hand, probe **1b** showed less selectivity between  $In^{3+}$ ,  $Pb^{2+}$ , and  $Ca^{2+}$ . This unusual pyrene

orientation and fluorogenic changes by  $\text{In}^{3+}$  could be a good model system for high selectivity.

Fluorescent probe **3** (Fig. 28.2) also showed face-to-face stacking of pyrene molecules, revealed by excimer emission at 480 nm [29]. Among the alkali and alkaline earth metals, probe **3** showed significant binding to  $\text{Sr}^{2+}$  and  $\text{Ca}^{2+}$  ions. Quenching of the excimer emission at 480 nm and enhancement of the monomer emission at 397 nm was observed upon addition of  $\text{Sr}^{2+}$  and  $\text{Ca}^{2+}$  ions, which showed similar complexation behavior. As compared with fluorescence spectroscopy, polyvinyl chloride (PVC) membrane developed by using probe **3** showed better selectivity for  $\text{Sr}^{2+}$ .

A ratiometric sensor **4** for  $\text{Cd}^{2+}$  and  $\text{Zn}^{2+}$  based on calix[4]arene bearing 1,2,3-triazole-linked pyrene units has been reported (Fig. 28.2) [30]. Probe **4** showed strong excimer and weak monomer emissions, due to face-to-face  $\pi$ -interactions. Addition of  $\text{Cd}^{2+}$  or  $\text{Zn}^{2+}$  produced a ratiometric fluorescence change, with a decrease in excimer emission and an increase in monomer emission. This ratiometric behavior is due to the complexation of  $\text{Cd}^{2+}$  and  $\text{Zn}^{2+}$  by the triazole nitrogen atoms, which causes a change in the conformation of the pyrene arms. No other metal ions produced such ratiometric response, confirming the high selectivity of probe **4**.

Another fluorogenic probe **5** (Fig. 28.2), tren-N-tricalix[4]arene, bearing three pyrene-amide units at the periphery of the tren-calix[4]arene unit, has strong complexation ability with  $\text{Al}^{3+}$ : [31] addition of small amounts of  $\text{Al}^{3+}$  ions results in a ratiometric response, with a decrease in the excimer emission at 480 nm and an increase in the monomer emission at 394 nm, attributed to reduced  $\pi$ - $\pi$  interactions due to the complexation of  $\text{Al}^{3+}$  by the tren part. Further addition of  $\text{Al}^{3+}$  leads to an overall increase in the monomer and excimer fluorescence emissions attributed to the CHEF (chelation-enhanced fluorescence) effect observed upon complexation. Mono- and difunctionalized derivatives were not suitable for fluorogenic detection of  $\text{Al}^{3+}$  ions.

A Förster Resonance Energy Transfer (FRET) system consisting of chemosensor **6**, based on calix[4]arene containing pyrene and rhodamine, was developed (Fig. 28.2) [32]. The excimer emission of pyrene at 470 nm was used as excitation wavelength of rhodamine. In the absence of  $\text{Hg}^{2+}$ , no FRET was observed. The complexation of  $\text{Hg}^{2+}$  opens the rhodamine ring and a fluorescence at 576 nm appears with a concomitant decrease in excimer emission at 470 nm. The ratiometric fluorescence change indicates the efficient energy transfer from the excimer emission to the opened-ring rhodamine. Similar intramolecular fluorescence energy transfer was observed for probe **7** (Fig. 28.2), containing pyrene as donor and anthroyloxy as acceptor [33] and has been used to monitor the complexation of  $\text{Na}^+$  ions. Upon complexation of  $\text{Na}^+$ , the energy transfer from pyrene to anthroyloxy increased and, hence, the fluorescence intensity of the anthroyloxy group was enhanced as compared with that of pyrene or anthroyloxy monomers alone.

### 28.2.1.2 Receptors for Anions

Anions play an important role in our daily life: they are crucial for physiological functions as well as for various industrial processes [34]. In the environment, anionic species are either essential to sustain growth or act as harmful pollutants. In addition, they are important for many biological processes, being involved in the regulation of cellular pH, cell volume, and osmotic balance and serving as cellular signals. Anion receptors can be neutral or positively charged molecules. Neutral anion receptors, containing amide, (thio)urea, and pyrrole groups, bind anions via favorable hydrogen bonding interactions [35]. However, in some cases, in the presence of highly basic anions, such as fluoride and cyanide, deprotonation of the acidic functionalities occurs. On the other hand, positively charged molecules interact with anions through electrostatic forces.

Calix[4]arene has also been used for specific recognition of anions because of its pre-organized cavity, which provides a suitable environment for anion complexation. Kim et al. developed a pyrene-conjugated fluorogenic calix[4]arene **8** in the 1,3-alternate conformation, bearing amide units for anion complexation (Fig. 28.2) [36]. Among all the anions examined, probe **8** showed high selectivity for  $F^-$  with interesting optical properties. Upon interacting with  $F^-$ , probe **8** exhibit a formation of new red shifted absorption band at 400 nm. In the fluorescence spectra, significant quenching of monomer and excimer emissions were observed with 600 equivalents of  $F^-$  due to strong PET effect. With further addition of  $F^-$  (>600 equivalents), a new fluorescence peak at 470 was observed. The new emission band at 470 was also found on excitation of probe **8** at 400 nm in the presence of excess  $F^-$  ions. The blue shifted band at 470 nm is due to strong interactions between  $F^-$  and NH units of probe **8** that lead to the formation of static excimer. Probes **9** and **1b** (Fig. 28.2), based on calix[4]arene in the cone conformation and bearing two pyrene and amide units, showed similar static excimer formation and enhanced fluorescence intensity in the presence of  $F^-$  ions [37].

A urea-based optical sensor **10** (Fig. 28.2) for chloride ions, based on pyrene-appended tetrasubstituted calix[4]arene in the 1,3-alternate conformation, has been reported by Diamond et al. [38] Urea has ability to donate two parallel H-bonds to a spherical anion in a bifurcate mode compared to the amide group which can donate only a single hydrogen bond. A strong intramolecular excimer emission at 452 nm was observed for probe **10** with a weak monomer emission. Among all the anions tested, high selectivity was observed for chloride ions. The addition of chloride caused a ratiometric response with quenching of excimer emission and simultaneous enhancement in monomer emission. For chloride ions, a binding constant of  $2.4 \times 10^4 M^{-1}$ , limit of detection (LOD) of  $8 \times 10^{-6} M$ , and response time <3 s were observed. Thus, directionality and preorganization of the hydrogen bonds of receptors can differentiate anions of different size, shape, and geometry.

In conclusion, suitably designed calix[4]arene scaffolds in cone and 1,3-alternate conformations with specific binding units could provide an interesting platform for the detection of anions of biological interest.

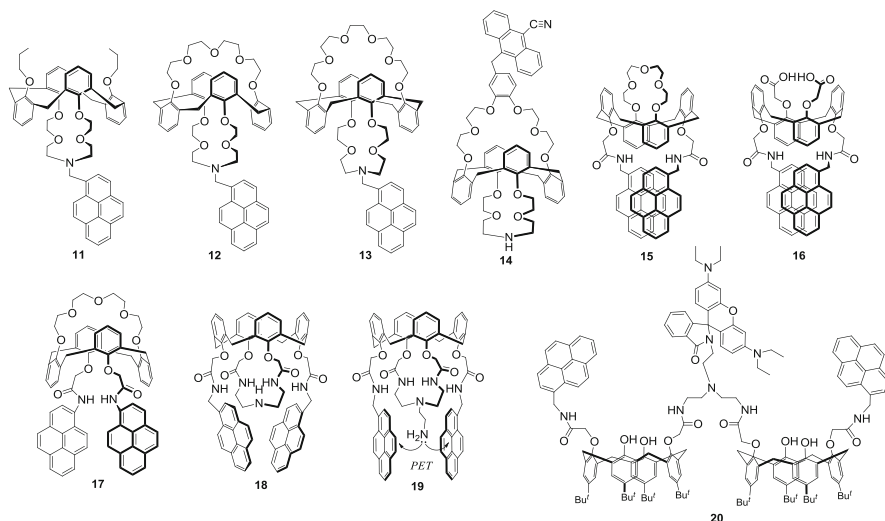


Fig. 28.4 Pyrene-appended bifunctional receptors 11–20

### 28.2.1.3 Bifunctional Receptors

Multi-ion detection by a single optical sensor bearing different binding sites are very interesting in terms of their applications. Because of the versatile derivatization and conformations of calix[4]arenes, optical receptors for the simultaneous detection of various ions, including cations, anions, and other species, have been developed.

PET fluorescent probes **11–13**, bearing a pyrenyl unit and an (aza)crown ether, were reported to be suitable for multi-ion detection (Fig. 28.4) [39]. The fluorescence of these probes was quenched due to PET from the nitrogen atom of the azacrown to the pyrenyl unit. However, in the presence of  $K^+$ ,  $Rb^+$ ,  $Cu^{2+}$ , and  $Pb^{2+}$  ions, which bind to the nitrogen atom of the azacrown unit, PET is inhibited and fluorescence is enhanced due to the CHEF effect. Probes **12** and **13** with an azacrown ether and a crown ether as two different binding sites displayed a CHEF effect upon binding of  $Ag^+$ ,  $Co^{2+}$ ,  $Cu^{2+}$ , and  $Pb^{2+}$  ions to the azacrown ring. On the other hand,  $K^+$ ,  $Rb^+$ , and  $Cs^+$  are preferentially bound to the crown ether ring. Interestingly, the addition of  $K^+$  to probe **12** dislodges the  $Ag^+$  ions from the azacrown ring, leading to quenching of the fluorescence emission (Fig. 28.5a). Similarly, addition of  $Cs^+$  to the in situ complex **13**- $Ag^+$  leads to quenching of the fluorescence emission, indicating the ejection of  $Ag^+$  ions. This “entry-ejection” process, called “molecular taekwondo”, has been observed upon protonation of the azacrown ether, which causes the removal of  $Ag^+$  ions from the ring. These fluorogenic receptors are quite useful for the multiple detection of different analytes.



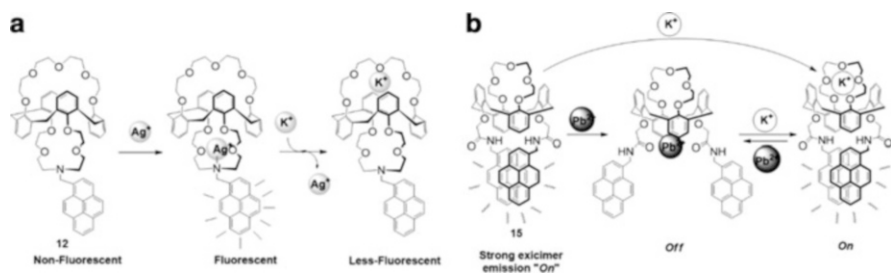


**Fig. 28.5** Binding modes of pyrene-appended bifunctional receptors **12** and **15**

Another molecular taekwondo sensor **14** (Fig. 28.4), bearing an anthracenyl unit on one side of the crown ether ring, showed opposite complexation tendencies to that of probe **13** [40]. Probe **14** exhibits weak fluorescence due to PET from the dialkoxybenzene unit to the 9-cyanoanthracene moiety. The complexation of  $\text{Cs}^+$  inhibits the PET process, thus enhancing the fluorescence intensity. The addition of  $\text{Cu}^{2+}$  to the in situ **14**- $\text{Cs}^+$  complex leads to decomplexation of  $\text{Cs}^+$  and quenching of fluorescence. Similar fluorescence behavior was observed for  $\text{Ag}^+$  and  $\text{Cs}^+$  ions.

Fluorescent chemosensor **15** based on the 1,3-alternate calix[4]arene possesses two different binding sites, i.e., amide groups and a polyether unit, for different cationic species (Fig. 28.4) [41]. The choice of binding locations depends on the nature of the metal ion. Probe **15** showed strong monomer and excimer emissions, attributed to the face-to-face  $\pi$ -interactions of the pyrene units. Among all the metal ions examined, probe **15** exhibits the highest selectivity for  $\text{Pb}^{2+}$ , which binds to the oxygen atoms of the amide groups (Fig. 28.5b). The binding of  $\text{Pb}^{2+}$  quenches both monomer and excimer emissions due to reverse PET to the carbonyl oxygen atoms from pyrene units and to conformational changes, respectively. In order to facilitate  $\text{Pb}^{2+}$  binding, the amide carbonyl units of probe **15** turn inward, causing a conformational change and quenching of the excimer emission (Fig. 28.5b). Another binding site, the polyether unit, preferentially binds  $\text{K}^+$  ions, as shown by  $^1\text{H}$  NMR titrations. The addition of  $\text{K}^+$  to the **15**- $\text{Pb}^{2+}$  complex leads to revival of monomer and excimer emissions, indicating the decomplexation of  $\text{Pb}^{2+}$  from **15** due to electrostatic repulsions and allosteric effects (Fig. 28.5b). Further addition of  $\text{Pb}^{2+}$  to **15**- $\text{K}^+$  complex caused quenching of the monomer and excimer emissions. The **15**- $\text{K}^+$  complex produced a strong emission corresponding to the “On” state, which is converted into the “Off” state upon addition of  $\text{Pb}^{2+}$  ions. Thus, an on-off optical sensor switchable by two metal ions was developed (Fig. 28.5b). Probe **16** (Fig. 28.4) containing dicarboxylate and pyrenyl amide groups showed strong binding with  $\text{Ca}^{2+}$  and  $\text{Pb}^{2+}$  and displays interesting On-Off switchable fluorescent properties, similarly to probe **17** [42].

Another PCT-based calix[4]crown, probe **17** (Fig. 28.4), containing pyrene amide groups, shows different fluorescent behaviors with  $\text{Pb}^{2+}$  and  $\text{Cu}^{2+}$  ions [43]. In the presence of  $\text{Pb}^{2+}$ , fluorescence properties similar to those of probes **15** and **16** were observed. Unlike the binding of  $\text{Pb}^{2+}$  to the carbonyl oxygen atoms,

$\text{Cu}^{2+}$  binds to the nitrogen atoms of the pyrene amide units resulting in a wavelength shift in the absorption and fluorescence spectra. Compared with the excitation spectra at 80 nm, a red shift in the excitation spectra of the **17**- $\text{Cu}^{2+}$  complex was observed at 470 nm, suggesting the formation of a static excimer. Moreover, On-Off switching between **17**- $\text{Pb}^{2+}$  and **17**- $\text{K}^+$  complexes was observed, due to the strong binding capacity of  $\text{K}^+$  to the crown part of the probe. Such switching was not detected in the case of the **17**- $\text{Cu}^{2+}$  complex, because of the strong binding of  $\text{Cu}^{2+}$  ions.

Fluorogenic calix[4]triazacrown-5 **18** (Fig. 28.4), bearing two pyrene amide units in the cone conformation, was designed for the bifunctional detection of  $\text{Pb}^{2+}$  and  $\text{F}^-$  ions [44]. Because of the proximal triazacrown ring, the overlapping of the two pyrene units is partially reduced. Among all the cations and anions examined, probe **18** showed the highest selectivity for  $\text{Pb}^{2+}$  or  $\text{Co}^{2+}$  and  $\text{F}^-$  ions. Upon addition of  $\text{Pb}^{2+}$  or  $\text{Co}^{2+}$ , quenching of the monomer and excimer emissions was observed, due to conformational changes, reverse PET, and heavy metal effect. On the other hand, upon addition of  $\text{F}^-$  ions, the decrease in monomer emission was more significant than that in excimer emission, due to PET to the pyrene units from  $\text{F}^-$ , which indicate its binding to the azacrown ring. The interaction between  $\text{F}^-$  and the azacrown ring was further supported by  $^1\text{H}$  NMR spectroscopy.

Calix[4]arene probe **19** with an ethyleneamine-appended triazacrown ring and pyrene pendent groups (Fig. 28.4) showed similar selectivity to probe **18** [45]. Because of the strong PET to the pyrene groups from the amine unit ( $-\text{CH}_2\text{CH}_2\text{NH}_2$ ), probe **19** showed relatively weak fluorescence emission. In the presence of  $\text{Pb}^{2+}$  ions, the excimer emission is quenched whereas the monomer emission is enhanced because of conformational changes. On the other hand, upon binding with  $\text{Li}^+$ , an increase in monomer and excimer emissions was observed, due to the CHEF effect. The metal exchange experiment indicates that the  $\text{Pb}^{2+}$  ions added to the **19**- $\text{Li}^+$  complex replace the  $\text{Li}^+$  ions, thereby causing quenching of the excimer emission and an increase of the monomer emission. Among the anions examined, probe **19** showed the strongest binding with  $\text{F}^-$  ions, because of its hydrogen bonding with the amide NH of the triazacrown ring, resulting in a decrease of monomer and excimer emissions due to PET from  $\text{F}^-$  to the pyrene units.

FRET-based optical probe **20** containing a rhodamine B unit conjugated to a N-tripodal molecule and two pyrene-appended calix[4]arene units was designed (Fig. 28.4) [46]. The excimer emission of probe **20** was used as energy donor and rhodamine B as energy acceptor. Upon excitation at 343 nm, the binding of  $\text{Hg}^{2+}$  to probe **20** results in enhanced fluorescence at 575 nm through a FRET-ON phenomenon. In contrast, a strong excimer emission of pyrenyl units was observed upon addition of  $\text{Al}^{3+}$  without FRET. This indicates that probe **20** has different binding modes for  $\text{Al}^{3+}$  and  $\text{Hg}^{2+}$ . On the basis of these results, it was postulated that  $\text{Hg}^{2+}$  binds to the tren-spirolactam unit, thereby inducing the ring opening of rhodamine, whereas  $\text{Al}^{3+}$  coordinates with the tren-diamide unit, which bringing the two pyrenyl units close to each other to form excimer emission.

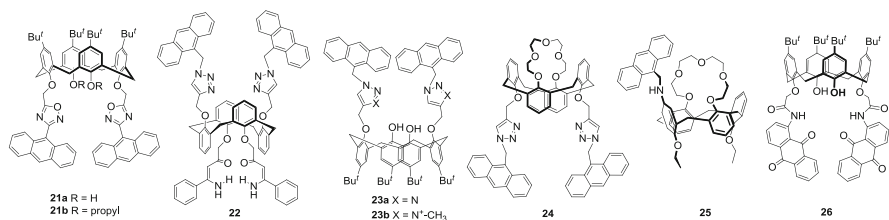


**Fig. 28.6** Anthracene-appended receptors **21–26**

### 28.2.2 Anthracene-Appended Calix[4]arene Hosts

In host guest chemistry, anthracene fluorophore is of special interest in both inorganic and biological systems, because of its availability, derivatization, and fluorescence sensitivity [47]. Numerous anthracene-appended calix[4]arene hosts have been developed for the fluorogenic recognition of cations and anions.

Calix[4]arene-based fluorescent chemodosimeters **21a** and **b** (Fig. 28.6) in the cone conformation bearing two anthryl groups and a 1,2,4-oxadiazole moiety have been developed for the detection of Fe<sup>3+</sup> ions [48]. The strong fluorescence of **21a** at 440 nm is quenched by addition of Fe<sup>3+</sup> and Cu<sup>2+</sup> whereas **21b** was selective for Fe<sup>3+</sup> only. This is due to the oxidation of the phenolic OH groups of calix[4]arene to form phenoxy radicals upon binding with Cu<sup>2+</sup> ion and PET of oxadiazole-derivatized anthracene. The addition of excess Fe<sup>3+</sup> ions to probe **21a** and **21b** leads to the initial oxidation of calix[4]quinone, and the 3-(9-anthryl)-1,2,4-oxadiazolyl groups are then further oxidized to mono- and bis-oxantrones. These oxidative transformations of calix[4]arene and anthracene are potentially useful in host guest chemistry.

Fluorescent probe **22** [49] (Fig. 28.6) in the 1,3-alternate conformation of calix[4]arene bearing different cation binding sites, distal bis-enaminone and bis-triazole groups, have been used as homobinuclear ditopic chemosensors with high selectivity for Ag<sup>+</sup> ions, revealed by enhanced anthracene fluorescence. The association constant of the second Ag<sup>+</sup> complexation was higher ( $9.20 \times 10^4 \text{ M}^{-1}$ ) than that of the first complexation ( $4.46 \times 10^3 \text{ M}^{-1}$ ), indicating a positive allosteric effect between the two Ag<sup>+</sup> ions. The binding of two Ag<sup>+</sup> ions induces rigidity in the complex structure, which results in enhancement of fluorescence emission. After addition of one equivalent of Ag<sup>+</sup> ions, no significant changes were observed in the absorption spectra of triazole-linked anthracene, whereas absorbance of the enaminone group increases. This shows that the first Ag<sup>+</sup> ion binds to the triazole site and the second to the bis-enaminone.

Contrary to probe **22**, triazole-linked anthracene bearing calix[4]arene in the cone conformation **23a** [50] (Fig. 28.6) showed selectivity for Co<sup>2+</sup> ions, with a detection limit of 55 ppb (0.92 μM). The selectivity is favored by the hexacoordination of Co<sup>2+</sup> by two ether oxygens, two phenolate oxygens, and two triazole nitrogen atoms of probe **23a**. Alkylation of **23a** results in the triazolium-anthracenyl calix[4]arene probe **23b** (Fig. 28.6) [51]. The fluorescence titrations with various nucleosides showed high selectivity for nucleoside triphosphates

(NTPs), such as ATP, UTP, CTP, TTP, and GTP, over mono- and diphosphates (NMPs and NDPs, respectively), with enhancement of the fluorescence emission. In addition, it was postulated that, in the presence of probe **23b**, NTPs induce aggregation, leading to an increase in fluorescence emission called aggregation-induced emission.

Anthracene-appended calix[4]arene chemosensor **24** in 1,3-alternate conformation containing two different binding sites, i.e., triazole and crown units, was developed (Fig. 28.6) [52]. Among the metal ions examined, probe **24** showed highest selectivity for  $\text{Hg}^{2+}$ ,  $\text{Cu}^{2+}$ ,  $\text{Cr}^{3+}$ , and  $\text{Pb}^{2+}$ , which bind to the triazole nitrogen atoms, resulting in quenching of the fluorescence emission. The calix[4]arene subunit is necessary for  $\text{Pb}^{2+}$  binding but not for  $\text{Hg}^{2+}$ ,  $\text{Cu}^{2+}$ , and  $\text{Cr}^{3+}$ , because a single triazole arm also binds to these cations, as evidenced by the fluorescence spectra. The crown ether unit of probe **24** preferentially binds  $\text{K}^+$  ions. An interesting fluorescent “on-off” switch was observed by addition of  $\text{K}^+$  to the **24**- $\text{Pb}^{2+}$  complex, which revives the fluorescence emission by dislodging the  $\text{Pb}^{2+}$  ion.

Fluorescent chemosensor **25** [53] (Fig. 28.6) with calix[4]arene in the 1,3-alternate conformation, a conjugated crown ether unit, and an anthracenyl amine showed strong fluorescence under acidic conditions but very weak emission in neutral and basic media. The strong fluorescence is due to the inhibition of PET to the anthracene moiety from the amine units. The addition of  $\text{K}^+$  ions leads to the formation of complexes with the crown ether moiety, which induce deprotonation of ammonium ion, causing resumption of the PET process. This metal ion-induced deprotonation is interesting for the design of improved receptors for specific cations.

Another fluorescent probe **26**, based on 1-amidoanthraquinone and with calix[4]arene in the cone conformation, was developed (Fig. 28.6) [54]. Probe **26** exhibits very weak fluorescence because of the excited state intramolecular proton transfer (ESIPT) between the amide NH and the quinone oxygen. The addition of  $\text{F}^-$  significantly enhances the fluorescence emission due to inhibition of the ESIPT process. The  $\text{F}^-$  ions interact with the amide NH groups on the two arms, thereby inhibiting the ESIPT process and thus increasing the fluorescence emission.

### 28.2.3 Dansyl-Appended Calix[4]arene Hosts

Calix[4]arene in the cone conformation bearing two **27a** and four dansyl groups **27b** were developed by Valeur et al. for the selective detection of  $\text{Hg}^{2+}$  and  $\text{Pb}^{2+}$  ions, respectively (Fig. 28.7) [55]. Probe **27a** exhibits strong fluorescence emission, which is quenched upon addition of  $\text{Hg}^{2+}$  because of electron transfer from the fluorophore to  $\text{Hg}^{2+}$ . On the other hand, addition of  $\text{Pb}^{2+}$  to probe **27b** containing four dansyl groups resulted in enhancement of fluorescence emission with a blue shift of 52 nm, attributed to the deprotonation of the sulfonamide group upon complexation of  $\text{Pb}^{2+}$ . The detection limit of  $\text{Hg}^{2+}$  (0.3  $\mu\text{M}$ ) and  $\text{Pb}^{2+}$  (20 nM) is

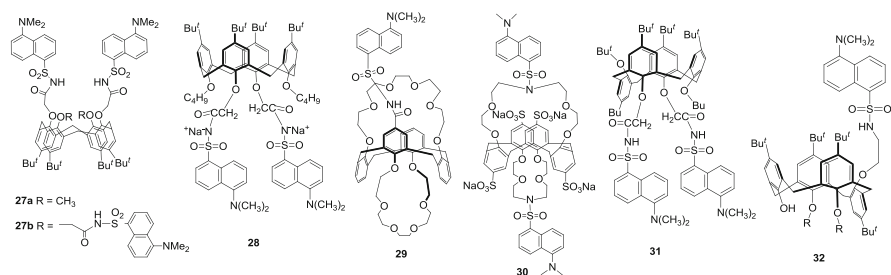


**Fig. 28.7** Dansyl-appended receptors **27–32**

in the range of approved level by world health organization. Another dansyl-conjugated calix[4]arene fluorophore **28** [56] (Fig. 28.7) in its disodium salt also showed high selectivity for Hg<sup>2+</sup> with quenching of fluorescence emission. Among other metal ions, including Na<sup>+</sup>, the detection of Hg<sup>2+</sup> (detection limit:  $8.0 \times 10^{-7}$  M) is highly desirable for practical applications.

Calix[4]arene probe **29** [57] (Fig. 28.7), in 1,3-alternate conformation and containing bis(crown-6-ether) and a dansyl group, showed selectivity for thallium (I). The fluorescence titrations of **29** with thallium(I) were performed at pH 3.5, at which the probe is in its undissociated form. The complexation of thallium(I) to probe **29** results in slight quenching and blue shift of the fluorescence emission. This behavior was attributed to both PET in the complex and NH-proton displacement by thallium(I).

Water-soluble probe **30** [58] (Fig. 28.7), based on *p*-sulfonato calix[4]arene bearing dansyl units, was developed and showed selective detection of Al<sup>3+</sup>, among other cations examined. The complexation of Al<sup>3+</sup> induces the aggregation of negatively charged probe **30**, due to the electrostatic interactions between them, as shown by the absorption spectra, anisotropy, and DLS measurements. The change in the micro-environment of the dansyl units of probe **30** results in the blue shift and enhancement of fluorescence due to aggregation-induced emission. In general, in their aggregated state, dansyl fluorophores exhibit quenched fluorescence due to the formation of H-aggregates. Thus, this behavior is quite interesting and could be useful for gaining insight into the environmental properties of specific fluorophores.

To enhance the sensitivity and selectivity of Pb<sup>2+</sup> detection, a dansyl appended fluorescent probe **31** based on *partial cone (paco)* conformation of calix[4]arene was reported (Fig. 28.7) [59]. Probe **31** showed high selectivity toward Pb<sup>2+</sup> via a proton displacement mechanism, which enhances the fluorescence emission of the dansyl unit; the interference of Hg<sup>2+</sup> ions is disfavored because of the preorganization of calix[4]arene in the *paco* conformation. On the other hand, probe **27a** possessing two dansyl units in the cone conformation was more selective for Hg<sup>2+</sup> over Pb<sup>2+</sup>. This indicates that preorganization of the calix[4]arene cavity plays a significant role in the selectivity of metal ion recognition.

Moreover, in case of fluorescent probe **32** (Fig. 28.7), *paco* conformer in which a single dansyl unit is attached to the benzene moiety, the selectivity pattern is

different from that observed for probe **30** [60]. The crystal structure of **32** reveals an intramolecular hydrogen bond between the oxygen atom of the adjacent benzene ring containing a propyl unit and the phenolic OH group, which limits the rotation of the phenolic ring through annulus, thus resulting in the *paco* conformation. Addition of  $\text{Hg}^{2+}$  ions leads to ratiometric response in the fluorescence spectrum, with a decrease in emission at 502 nm and simultaneous formation of blue-shifted emission bands at 435 and 412 nm. The blue-shifted bands were also observed upon titration with trifluoroacetic acid, due to protonation of the dansyl group. This indicates that the presence of  $\text{Hg}^{2+}$  ions induces proton transfer from the phenolic to the dansyl moiety, resulting in the formation of blue-shifted bands. These studies highlight the versatile properties of the calix[4]arene scaffold, which can be tailored by appropriate control of its conformation and derivatization.

### 28.2.4 Discrete Fluorescent Calix[4]arene Hosts

BODIPY (4,4-difluoro-4-bora-3a,4a-diaza-s-indacene) fluorophore has many advantages, such as high quantum yield, high photochemical stability, and intense absorbance and emission. These properties can be tuned by appropriate derivatization at specific positions. Thus, BODIPY derivatives have been widely used for various applications, including sensing, bioimaging, and labeling of proteins. The calix[4]arene scaffold has been used to exploit the interesting properties of BODIPY. Calix[4]arene diethyl ester conjugated with BODIPY was used as fluorogenic sensor **33** for the detection of  $\text{Ca}^{2+}$  ions (Fig. 28.8) [61]. Probe **33**

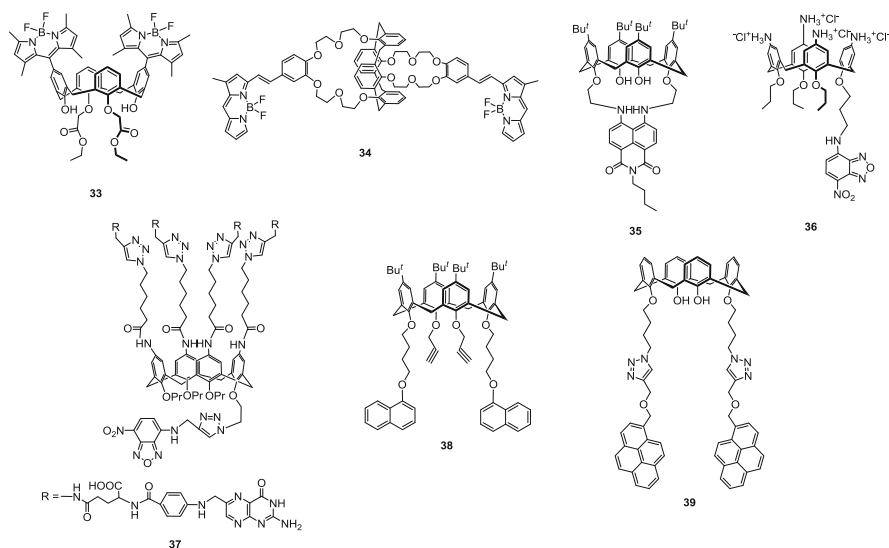


Fig. 28.8 Discrete-appended receptors

showed strong fluorescence at 502 nm.  $\text{Ca}^{2+}$  complexation led to quenching of the fluorescence emission, because of a reverse PET from BODIPY to the carbonyl oxygen atoms. The high selectivity of probe **33** toward  $\text{Ca}^{2+}$  over other cations is due to the participation of two proximal hydroxy groups and carbonyl oxygen atoms.

Probe **34** (Fig. 28.8), a calix[4]biscrown-6 ether conjugated with BODIPY units, exhibits high selectivity for  $\text{Cs}^+$ , among several cations examined [62]. Substitution at the  $\alpha$ -position of BODIPY improves the photophysical sensitivity. In the presence of  $\text{Cs}^+$  ions, a hypsochromic shift was observed in the fluorescence and absorption spectra. This shift is due to binding of the crown ether to  $\text{Cs}^+$ , which decreased the electron-donating ability of the oxygen atoms.

Naphthalimide-appended calix[4]arene probe **35** acts as a two-faced fluorophore for the detection of  $\text{Cu}^{2+}$  and  $\text{F}^-$  ions (Fig. 28.8) [63]. It exhibits strong fluorescence attributed to the naphthalimide unit. The addition of  $\text{Cu}^{2+}$  or  $\text{F}^-$  ions result in quenching of the fluorescence emission. The decrease in emission intensity is attributed to the naphthalimide NH deprotonation in the presence of  $\text{Cu}^{2+}$  and  $\text{F}^-$ .

Calix[4]arene-based fluorescent probes have been widely investigated for the detection of various cations, anions, and other analytes. In addition, their bio-applications were thoroughly examined. In order to evaluate the cellular uptake of calixarene conjugates, probes **36** [64] and **37** [65], containing a NBD group, were developed (Fig. 28.8). Probe **36**, possessing four ammonium groups on the upper rim of the calix[4]arene, was used for the investigation of the cellular uptake, cytotoxicity, and imaging of Chinese Hamster Ovary (CHO) cells (Fig. 28.9). The cellular uptake of probe **36** was very fast, as shown by the CHO cell images after 10 min of incubation; however, the mechanism of its uptake was not clear. Various uptake inhibitors including filipin, sucrose, and  $\beta$ -cyclodextrin have little

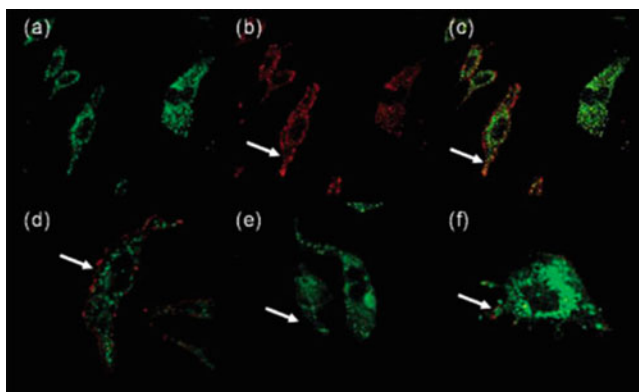


**Fig. 28.9** Cellular uptake of probe **36**. Colocalization studies of **36** (15 mM) and anti CCR5 receptor IgG (HEK/1/85a/7a) counterstain in CHO (a) **36**, (b) HEK/1/85a/7a, (c) overlay of **36** and HEK/1/85a/7a, and (d) preincubation with filipin, e sucrose, and f  $\beta$ -cyclodextrin. *Arrows* indicate receptor in membrane (Reprinted with permission from [64]. Copyright 2008, American Chemical Society)



effect on the cellular uptake of probe **36** (Fig. 28.9). After internalization, probe **36** mainly found in the cytoplasm. As demonstrated by viability experiments, probe **36** exhibits low toxicity, with an  $IC_{50}$  value of 82 mM and 8 mM for CHO and HL cell lines, respectively, indicating its potential utility for bioinvestigation.

On the other hand, the cellular uptake of probe **37** (Fig. 28.8) occurred via folate receptor-mediated endocytosis due to cancer targeting units, folic acids. It is well-known that cancer cells express more receptors for folic acid as compared with normal cells. HeLa cells, expressing more folate receptors as compared with fibroblast NIH3T3 cells, showed better internalization of probe **37**. Co-localization studies revealed endo-lysosomal accumulation of probe **37**. This suggests that cellular uptake and visualization of calix[4]arene can be enhanced using a cancer targeting unit.

In agriculture, pesticides including carbosulfan, pirimicarb, metolcarb, carbaryl, carbofuran, and isoprocarb have significant impact in controlling the growth of unwanted insects, weeds, rodents, and fungus and thereby enhance the production of crops. However, excessive and regular use of these pesticides raised huge concern for the environmental and human health [66]. Therefore, sensitive detection of these pesticides is of high importance.

The calix[4]arene based hosts **38** [67] and **39** [68] were employed for the detection of metolcarb and carbaryl, respectively by observing change in the fluorescence and contact angle measurements (as wettability sensors). Probe **38**, containing naphthol, was conjugated to microstructured Au surface and showed high selectivity for metolcarb over other pesticides by observing increase in fluorescence emission. This is due its host-guest interaction of metolcarb with upper rim of probe **38**. On the other hand, pyrene appended calix[4]arene probe **39** and its conjugation with graphene oxide using non-covalent interactions exhibit high selectivity for carbaryl, particular in serum samples among other pesticides. The detection was monitored by quenching in fluorescence emission of probe **39** with carbaryl and macroscopic recognition by the contact angle. The significant intermolecular  $\pi$ - $\pi$  interactions between naphthyl ring of carbaryl and benzene rings of calix results in strong host-guest complex and selective detection of carbaryl. Thus, calix[4]arene based fluorescent probes could be suitable could be suitable hosts for monitoring for the pesticide level in the environmental.

### 28.3 Conclusions

Calixarenes are one of the most interesting scaffolds for molecular recognition in host guest chemistry. The versatility of calixarene macrocycles includes modification of their upper and lower rims, different conformation behavior, and hydrophobic cavity for the inclusion of guest molecules. The conformational preference of calixarene derivatives depends on the substitution at the upper and lower rim. Numerous attractive receptors have been developed for the detection of various guest molecules. The molecular recognition can be characterized by various



spectroscopic techniques, including UV-vis, fluorescence, redox, and NMR. Among these, fluorescence spectroscopy has several advantages, such as high sensitivity, selectivity, and spontaneous response. Fluorescent calixarene receptors bearing different fluorophores have been used for various applications, e.g., detection of cations, anions, and other biologically important analytes. Thus, the development of fluorescent calixarene probes for various applications serves as a useful strategy for the determination of different analytes in environmental and biological systems.

## References

1. (a) Gutsche, C. D. *Calixarenes*; Royal Society of Chemistry: Cambridge, U.K., 1989. (b) Mandolini, L.; Ungaro, R. *Calixarenes in Action*; Imperial College Press: London, 2000.
2. (a) Gutsche, C. D.; Muthukrishnan, R. *J. Org. Chem.* **1978**, *43*, 4905. (b) Gutsche, C. D.; Iqbal, M.; Stewart, D. *J. Org. Chem.* **1986**, *51*, 742.
3. Vicens, J.; Bohmer, V. *Calixarenes, a Versatile Class of Macrocyclic Compounds*; Kluwer Academic Publishers: Dordrecht, The Netherlands, 1991.
4. (a) Ikeda, A.; Shinkai, S. *Chem. Rev.* **1997**, *97*, 1713. (b) Inokuchi, F.; Miyahara, Y.; Inazu, T.; Shinkai, S. *Angew. Chem., Int. Ed. Engl.* **1995**, *34*, 1364. (c) Ma, J. C.; Dougherty, D. A. *Chem. Rev.* **1997**, *97*, 1303. (d) Ikeda, A.; Tsuzuki, H.; Shinkai, S. *J. Chem. Soc., Perkin Trans. 2* **1994**, 2073.
5. (a) Vicens, J.; Harrowfield, J. *Calixarenes in the Nanoworld*; Springer: Dordrecht, The Netherlands, 2007. (b) Bohmer, V. *Angew. Chem., Int. Ed. Engl.* **1995**, *34*, 713.
6. (a) Kim, J. S.; Quang, D. T. *Chem. Rev.* **2007**, *107*, 3780. (b) Creaven, B. S.; Donlon, D. F.; McGinley, J. *Coord. Chem. Rev.* **2009**, *253*, 893.
7. Casnati, A.; Barbosa, S.; Rouquette, H.; Schwing-Weill, M.-J.; Arnaud-Neu, F.; Dozol, J.-F.; Ungaro, R. *J. Am. Chem. Soc.* **2001**, *123*, 12182.
8. Iqbal, K. S. J.; Cragg, P. J. *Dalton Trans.* **2007**, 26.
9. Molenveld, P.; Engbersen, J. F. J.; Reinhoudt, D. N. *Chem. Soc. Rev.* **2000**, *29*, 75.
10. (a) Dondoni, A.; Marra, A. *Chem. Rev.* **2010**, *110*, 4949. (b) Baldini, L.; Casnati, A.; Sansone, F.; Ungaro, R. *Chem. Soc. Rev.* **2007**, *36*, 254.
11. Homden, D. M.; Redshaw, C. *Chem. Rev.* **2008**, *108*, 5086.
12. Shinkai, S. Calixarenes as Third Supramolecular Host. In *Advances in Supramolecular Chemistry*; JAI Press, 1993; vol. 3, p. 97.
13. *Cation Binding by Macrocycles*; Inoue, Y., Gokel, G. W., Eds.; Marcel Dekker: New York, 1990.
14. Szejtli, J. *Cyclodextrins and their Inclusion Complexes*; Akademiai Kiado: Budapest, 1982.
15. Valeur, B.; Bourson, J.; Pouget, J.; Czarnik, A. W. *Fluorescent Chemosensors for Ion and Molecule Recognition*; ACS Symposium Series 538; American Chemical Society: Washington, DC, 1993.
16. (a) Nohta, H.; Satozono, H.; Koiso, K.; Yoshida, H.; Ishida, J.; Yamaguchi, M. *Anal. Chem.* **2000**, *72*, 4199. (b) Okamoto, A.; Ichiba, T.; Saito, I. *J. Am. Chem. Soc.* **2004**, *126*, 8364.
17. (a) Wiskur, S. L.; Ait-Haddou, H.; Anslyn, E. V.; Lavigne, J. J. *Acc. Chem. Res.* **2001**, *34*, 963. (b) Fabbri, L.; Marcotte, N.; Stomeo, F.; Taglietti, A. *Angew. Chem., Int. Ed.* **2002**, *41*, 3811.
18. (a) Kim, S. K.; Yoon, J. *Chem. Commun.* **2002**, 770. (b) Gunnlaugsson, T.; Davis, A. P.; O'Brien, J. E.; Glynn, M. *Org. Lett.* **2002**, *4*, 2449.
19. (a) Wu, F. Y.; Jiang, Y. B. *Chem. Phys. Lett.* **2002**, *355*, 438. (b) Xu, Z. C.; Xiao, Y.; Qian, X. H.; Cui, J. N.; Cui, D. W. *Org. Lett.* **2005**, *7*, 889.

20. (a) Nishizawa, S.; Kato, Y.; Teramae, N. *J. Am. Chem. Soc.* **1999**, *121*, 9463. (b) Wu, J. S.; Zhou, J. H.; Wang, P. F.; Zhang, X. H.; Wu, S. K. *Org. Lett.* **2005**, *7*, 2133.
21. Beer, P. D. *Acc. Chem. Res.* **1998**, *31*, 71.
22. (a) Choi, K.; Hamilton, A. D.; *Angew. Chem., Int. Ed.* **2001**, *40*, 3912. (b) Tolbert, L. M.; Solntsev, K. M. *Acc. Chem. Res.* **2002**, *35*, 19.
23. (a) Holm, R. H.; Kennepohl, P.; Solomon, E. I. *Chem. Rev.* **1996**, *96*, 2239. (b) Lippard, S. J.; Berg, J. M. *Principles of Bioinorganic Chemistry*; University Science Books: Mill Valley, CA, 1994.
24. Nolan, E. M.; Lippard, S. J. *Chem. Rev.* **2008**, *108*, 3443.
25. Sessler, J. L.; Gale, P. A.; Cho, W.-S. *Anion Receptor Chemistry*; Royal Society of Chemistry: Cambridge, 2006.
26. (a) Birks, J. B. *Photophysics of Aromatic molecules*; Wiley Inter-Science: London, 1970. (b) Winnik, F. M. *Chem. Rev.* **1993**, *93*, 587.
27. (a) Que, E. L.; Domaille, D. W.; Chang, C. J. *Chem. Rev.* **2008**, *108*, 1517. (e) Nolan, E. M.; Lippard, S. J. *Acc. Chem. Res.* **2009**, *42*, 193.
28. Kim, S. K.; Kim, S. H.; Kim, H. J.; Lee, S. H.; Lee, S. W.; Ko, J.; Bartsch, R. A.; Kim, J. S. *Inorg. Chem.* **2005**, *44*, 7866.
29. Ji, H.-F.; Yang, Y.; Xu, X.; Brown, G. *Org. Biomol. Chem.* **2006**, *4*, 770.
30. Park, S. Y.; Yoon, J. H.; Hong, C. S.; Souane, R.; Kim, J. S.; Matthews, S. E.; Vicens, J. J. *Org. Chem.* **2008**, *73*, 8212.
31. Othman, A. B.; Lee, J. W.; Huh, Y.-D.; Abidi, R.; Kim, J. S.; Vicens, J. *Tetrahedron* **2007**, *63*, 10793.
32. Lee, Y. H.; Lee, M. H.; Zhang, J. F.; Kim, J. S. *J. Org. Chem.* **2010**, *75*, 7159.
33. Jin, T. *Chem. Commun.* **1999**, 2491.
34. Sessler, J. L.; Davis, J. M. *Acc. Chem. Res.* **2001**, *34*, 989.
35. (a) Caltagirone, C.; Gale, P. A. *Chem. Soc. Rev.*, **2009**, *38*, 520. (b) Gale, P. A. *Acc. Chem. Res.* **2006**, *39*, 465. (f) Gale, P. A.; Quesada, R. *Coord. Chem. Rev.* **2006**, *250*, 3219.
36. Kim, S. K.; Bok, J. H.; Bartsch, R. A.; Lee, J. Y.; Kim, J. S. *Org. Lett.* **2005**, *7*, 4839.
37. Kim, H. J.; Kim, S. K.; Lee, J. Y.; Kim, J. S. *J. Org. Chem.* **2006**, *71*, 6611.
38. Schazmann, B.; Alhashimy, N.; Diamond, D. *J. Am. Chem. Soc.* **2006**, *128*, 8607.
39. Kim, J. S.; Shon, O. J.; Rim, J. A.; Kim, S. K.; Yoon, J. J. *Org. Chem.* **2002**, *67*, 2348.
40. Kim, J. S.; Noh, K. H.; Lee, S. H.; Kim, S. K.; Kim, S. K.; Yoon, J. J. *Org. Chem.* **2003**, *68*, 597.
41. Kim, S. K.; Lee, S. H.; Lee, J. Y.; Lee, J. Y.; Bartsch, R. A.; Kim, J. S. *J. Am. Chem. Soc.* **2004**, *126*, 16499.
42. Kim, S. H.; Choi, J. K.; Kim, S. K.; Sim, W.; Kim, J. S. *Tetrahedron Lett.* **2006**, *47*, 3737.
43. Choi, J. K.; Kim, S. H.; Yoon, J.; Lee, K.-H.; Bartsch, R. A.; Kim, J. S. *J. Org. Chem.* **2006**, *71*, 8011.
44. Lee, J. Y.; Kim, S. K.; Jung, J. H.; Kim, J. S. *J. Org. Chem.* **2005**, *70*, 1463.
45. Lee, S. H.; Kim, S. H.; Kim, S. K.; Jung, J. H.; Kim, J. S. *J. Org. Chem.* **2005**, *70*, 9288.
46. Othman, A. B.; Lee, J. W.; Wu, J.-S.; Kim, J. S.; Abidi, R.; Thuery, P.; Strub, J. M.; Dorselaer, A. V.; Vicens, J. J. *Org. Chem.* **2007**, *72*, 7634.
47. de Silva, A. P.; Gunaratne, H. Q. N.; Gunnlaugsson, T.; Huxley, A. J. M.; McCoy, C. P.; Rademacher, J. T.; Rice, T. E. *Chem. Rev.* **1997**, *97*, 1515.
48. Chen, Y.-J.; Yang, S.-C.; Tsai, C.-C.; Chang, K.-C.; Chuang, W.-H.; Chu, W.-L.; Kovalev, V.; Chung, W.-S. *Chem. Asian J.* **2015**, *10*, 1025.
49. Ho, I.-T.; Haung, K.-C.; Chung, W.-S. *Chem. Asian J.* **2011**, *6*, 2738.
50. Mummidivarapu, V. V. S.; Hinge, V. K.; Tabbasum, K.; Gonnade, R. G.; Rao, C. P. *J. Org. Chem.* **2013**, *78*, 3570.
51. Mummidivarapu, V. V. S.; Hinge, V. K.; Samanta, K.; Yarramala, D. S.; Rao, C. P. *Chem. Eur. J.* **2014**, *20*, 14378.
52. Chang, K.-C.; Su, I.-H.; Senthilvelan, A.; Chung, W.-S. *Org. Lett.* **2007**, *9*, 3363.
53. Bu, J.-H.; Zheng, Q.-Y.; Chen, C.-F.; Huang, Z.-T. *Org. Lett.* **2004**, *6*, 3301.

54. Jung, H. S.; Kim, H. J.; Vicens, J.; Kim, J. S. *Tetrahedron Lett.* **2009**, *50*, 983.
55. (a) Metivier, R.; Leray, I.; Valeur, B. *Chem. Commun.* **2003**, 996. (b) Metivier, R.; Leray, I.; Valeur, B. *Chem. Eur. J.* **2004**, *10*, 4480.
56. Dinake, P.; Prokhorova, P. E.; Talanov, V. S.; Butcher, R. J.; Talanova, G. G. *Tetrahedron Lett.* **2010**, *51*, 5016.
57. Talanova, G. G.; Roper, E. D.; Buie, N. M.; Gorbunova, M. G.; Bartsch, R. A.; Talanov, V. S. *Chem. Commun.* **2005**, 5673.
58. Ruan, Y.-B.; Depauw, A.; Leray, I. *Org. Biomol. Chem.* **2014**, *12*, 4335.
59. Buie, N. M.; Talanov, V. S.; Butcher, R. J.; Talanova, G. G. *Inorg. Chem.* **2008**, *47*, 3549.
60. Dhir, A.; Bhalla, V.; Kumar, M. *Org. Lett.* **2008**, *10*, 4891.
61. Kim, H. J.; Kim, J. S. *Tetrahedron Lett.* **2006**, *47*, 7051.
62. Depauw, A.; Kumar, N.; Ha-Thi, M.-H.; Leray, I. *J. Phys. Chem. A* **2015**, *119*, 6065.
63. Xu, Z.; Kim, S.; Kim, H. N.; Han, S. J.; Lee, C.; Kim, J. S.; Qiand, X.; Yoon, J. *Tetrahedron Lett.* **2007**, *48*, 9151.
64. Lalor, R.; Baillie-Johnson, H.; Redshaw, C.; Matthews, S. E.; Mueller, A. *J. Am. Chem. Soc.* **2008**, *130*, 2892.
65. Consoli, G. M. L.; Granata, G.; Fragassi, G.; Grossi, M.; Sallese, M.; Geracia, C. *Org. Biomol. Chem.* **2015**, *13*, 3298.
66. (a) Ni, X. L.; Zeng, X.; Redshaw, C. *J. Org. Chem.* **2011**, *76*, 5696. (b) Chawla, H.; Sahu, S.; Shrivastava, R. *Tetrahedron Lett.* **2007**, *48*, 6054. (c) Lee, J.; Kim, S.; Jung, J. *J. Org. Chem.* **2005**, *70*, 1463.
67. Zeng, X.; Ma, J.; Luo, L.; Yang, L.; Cao, X.; Tian, D.; Li, H. *Org. Lett.* **2015**, *17*, 2976.
68. Sun, Y.; Mao, X.; Luo, L.; Tian, D.; Li, H. *Org. Biomol. Chem.*, **2015**, *13*, 9294.

# Chapter 29

## Calixarene Threading by Viologen-Based Axles

Arturo Arduini, Guido Orlandini, Andrea Secchi, Alberto Credi, Serena Silvi, and Margherita Venturi

### 29.1 Introduction

During these last decades the interest in calixarene chemistry gradually turned from their selective and stereocontrolled functionalization to the transfer of their binding properties to the development of calixarene-based functional devices like switches, sensors, supramolecular catalysts or active coating of solid surfaces [1–4]. In spite of the remarkable achievements gained in these topics by employing the calix[4]arene platform, relatively less explored has been the possibility to exploit the larger members of the calixarene series; this is probably due to the low yielding selective (partial) functionalization procedures and to the difficulties to fix their conformation through functionalization. Nevertheless, calix[5]- and calix[6]arene are recently overbearingly emerging as very convenient platforms to further expand the scopes of calixarene chemistry also towards nanoscience and nanotechnology. It is a fact that their larger size, for some decades considered somehow a drawback for their employment in molecular recognition processes, is instead the reason for the growing interest in their chemistry. In fact, recent is the discover that a guest having an axle-type shape and suitable chemical properties can thread their annulus to yield interwoven supramolecular complexes belonging to the class of pseudorotaxanes, which can be successively converted into interlocked systems like rotaxanes and catenanes. These achievements disclose the possibility to use

---

A. Arduini (✉) • G. Orlandini • A. Secchi  
Dipartimento di Chimica, Università di Parma, Parco Area delle Scienze 17/a, 43124 Parma, Italy  
e-mail: [arturo.arduini@unipr.it](mailto:arturo.arduini@unipr.it)

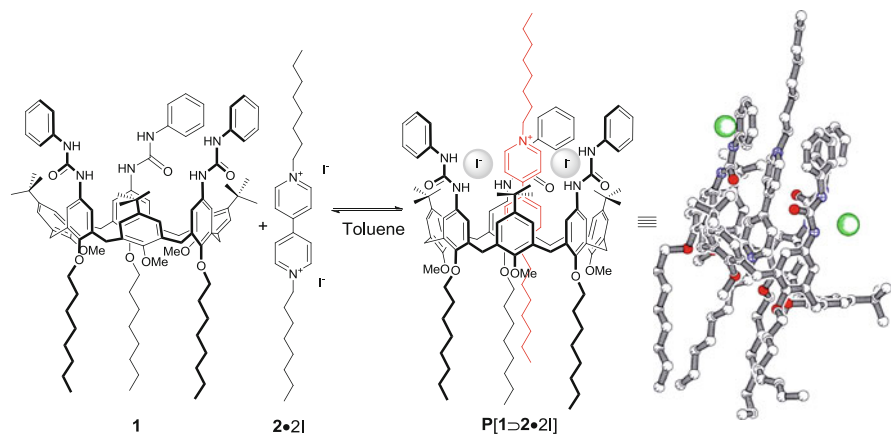
A. Credi • S. Silvi • M. Venturi  
Dipartimento di Chimica “G. Ciamician”, Università di Bologna, Via Selmi 2, 40126 Bologna, Italy

these larger members of the calixarene series for the construction of new generation of calixarene-based devices and prototypes of molecular machines. The discussion that follows deals with the achievements gained over the last two decades on the binding properties of calix[6]arene derivatives towards viologen-based salts for the construction of prototypes of molecular devices and machines [5] based on pseudorotaxane or rotaxane species [6]. Readers interested to obtain further insight into pseudorotaxanes or rotaxanes synthesis and properties or highlights concerning calixarenes or their use for the preparation of supramolecular devices are encouraged to consult the several other books [3, 7], books chapters [8, 9], and reviews [10–18] which have appeared in the recent literature, in addition to the other chapters of this book.

In simple instances a  $[n]$ pseudorotaxane can be defined as a supramolecular complex composed of a macrocycle (*rota*) that acts as the host for a guest having an axial shape (*axle*) [5].  $[n]$ Rotaxanes are interlocked systems [5, 6, 19, 20] in which *two or more species become connected each other, not via chemical bonds but rather they are threaded through or around one another to form a single entity* [21]. The number of molecular components is indicated between square brackets before the name. The nature and magnitude of the non-covalent interactions usually drive their formation and are also responsible of the relative spatial arrangement of their components. The modulation of these interactions through external stimuli can promote the reversible (and cyclic) dethreading-reeading of the axle from/into the wheel in pseudorotaxanes or the shuttling motion of the wheel along the dumbbell in rotaxanes. These movements can thus mimic the functioning of a mechanical switch or a molecular machine [5].

## 29.2 Calix[6]arene as Wheels for Pseudorotaxane and Rotaxane Synthesis

The discovery that a calixarene binds a guest and form a complex having the structure of a pseudorotaxane was published almost 15 years ago [22], when it was demonstrated that the tris-(*N*-phenylureido)-calix[6]arene derivative **1** is able to take up dioctylviologen diiodide (**2**•2I) in apolar solvents, forming the pseudorotaxane complex **P**[**1** ⊃ **2**•2I] (Scheme 29.1), whose structure was inferred in solution through NMR measurements and established in the solid state by single crystal X-ray diffraction experiments. The X-ray structure clearly showed that the dicationic viologen **2**<sup>2+</sup> threads the calix[6]arene annulus and that the two iodide counteranions are hydrogen bonded to the phenylureido NH of the calix upper rim. In this complex all the components – namely the di-cationic viologen-based axle **2**, its two counteranions and the calix[6]arene wheel **1** – are held together by a combination of several non-covalent interactions. Of particular importance was the observation that all the domains of the wheel participate in stabilizing the complex (Scheme 29.1). These findings, together with the trigonal prism structure



**Scheme 29.1** Self-assembly in toluene of calix[6]arene-based wheel **1** and viologen-based axle **2•2I** and solid-state structure of the resulting pseudorotaxane **P[1 ⊃ 2•2I]**

adopted by **1** in solution and the observation that (i) the  $\pi$ -rich calixarene rims are spanned by a lipophilic region represented by the three alkyl chains present at the lower rim of the macrocycle, and (ii) the three polar phenylureido groups at the upper rim can coordinate anions via hydrogen bonding, allowed us to consider **1** as an asymmetric hetero-polytopic and three-dimensional wheel to design new generations of devices and molecular machines models endowed with functions governed by a wider set of control elements.

The ability of **1** to form pseudorotaxanes was verified in dichloromethane, where these complexes are endowed with fairly high thermodynamic stability ( $\Delta G^\circ = -8 \text{ Kcal}\cdot\text{mol}^{-1}$ ). It was also evidenced that the counteranions of the viologen-based axle play an important role in the formation of the pseudorotaxane complex as they affect both the stability of the complex and the rate of the threading process [23]. This role was interpreted in terms of ion-pair recognition, suggesting that coordination of the two counteranions of the axle by the ureido units at the upper rim is crucial for the loosening and breaking of the tight ion pairs, before axle threading [24]. Cyclic voltammetry (CV) measurements carried out in  $\text{CH}_2\text{Cl}_2$  on a series of pseudorotaxanes showed that a fast (submicrosecond time-scale) dethreading takes place upon mono-electronic electrochemical reduction of the axle (Fig. 29.1). Such a dethreading, of course, is not possible in **R[3•2PF<sub>6</sub>]**, as confirmed by the CV pattern. In addition, the heterogeneous electron-transfer kinetics for the reduction of the viologen unit is slowed down upon encapsulation into the calixarene cavity walls, in the case of both **P[1 ⊃ 2•2PF<sub>6</sub>]** and **R[3•2PF<sub>6</sub>]**. Similarly, it was observed that inclusion of the viologen unit into the calixarene host slows down the homogeneous electron-transfer process from photoexcited Ru(II) tris(2,2'-bipyridine) by four times [25].

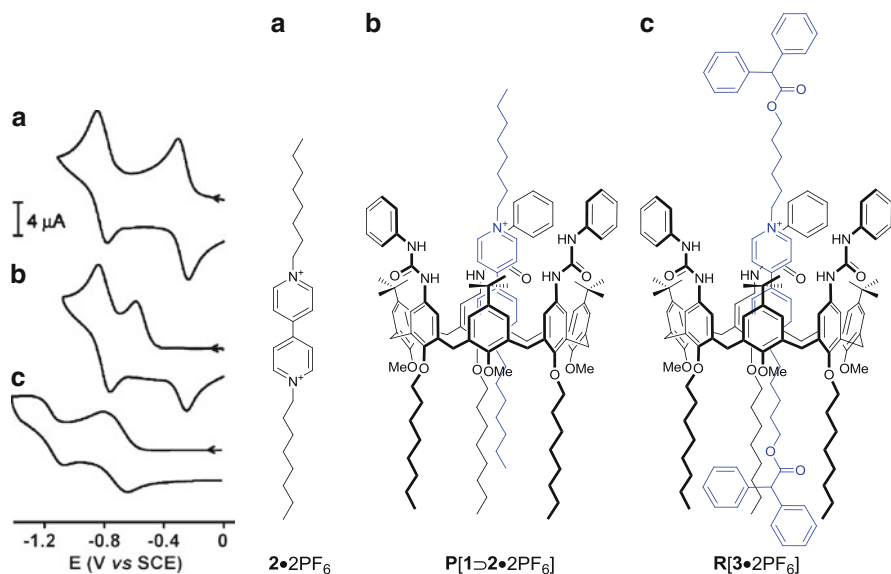
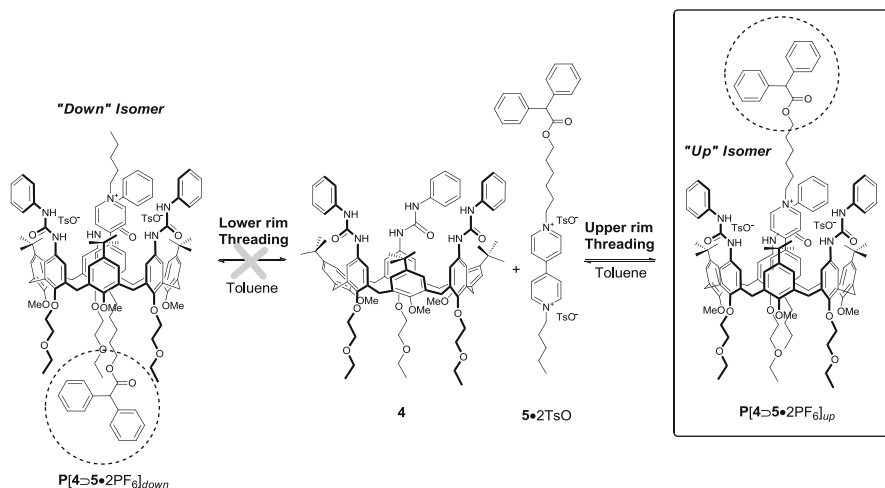


**Fig. 29.1** Cyclic voltammetric curves ( $2 \times 10^{-4}$  M in  $\text{CH}_2\text{Cl}_2$ , 0.05 M TBAPF<sub>6</sub>, 293 K; scan rate  $200 \text{ mV} \cdot \text{s}^{-1}$ ) for the first and second reduction of the viologen unit in **a**  $2 \cdot 2\text{PF}_6$ , **b** pseudorotaxane  $\text{P}[1 \supset 2 \cdot 2\text{PF}_6]$  and **c** rotaxane  $\text{R}[3 \cdot 2\text{PF}_6]$

A very peculiar property of calix[6]arene-based wheels is that pseudorotaxane orientational isomers can be selectively obtained when a non-symmetric axle is used as the guest. For example wheel **4**, having three ethylethoxy chains at its lower rim to simplify the NMR spectra, acts as a host for a non-symmetric dicationic axle consisting of a viologen-based unit bearing two alkyl side chains, one of which is stoppered at one terminus (**5•2TsO**), forming exclusively the oriented pseudorotaxane in which the stopper of the axle is positioned in proximity of the upper rim of the wheel (Scheme 29.2) [26]. This strict unidirectional threading mode was explained considering that: (a) in apolar media, the three methoxy groups present at the lower rim of **4** are oriented inside the cavity, occupying it and thus disfavoring, by repulsive intermolecular interactions, the access of the axle through this rim; (b) the size and binding ability of the wheel inner volume are suitable only for the inclusion of the cationic portion of the axle; (c) in the apolar  $\text{C}_6\text{D}_6$ , axle **5•2TsO** is present as tight ion pairs and, therefore, it is reasonable to assume that at least a partial separation of the viologen dication from its counterions should take place before threading; (d) the ureido groups present at the upper rim are potent hydrogen bonding donor groups and participate in the overall binding process by coordinating the two anions of the axle and favoring the formation of a ligand-separated ion pair. On these bases, it can be hypothesized that hydrogen bonding interactions between the two anions of the viologen salt and the ureido NH moieties



**Scheme 29.2** Formation of the two possible pseudorotaxane orientational isomers derived from the calix[6]arene wheel **4** and the non-symmetric axle **5•2TsO** carrying only one stopper

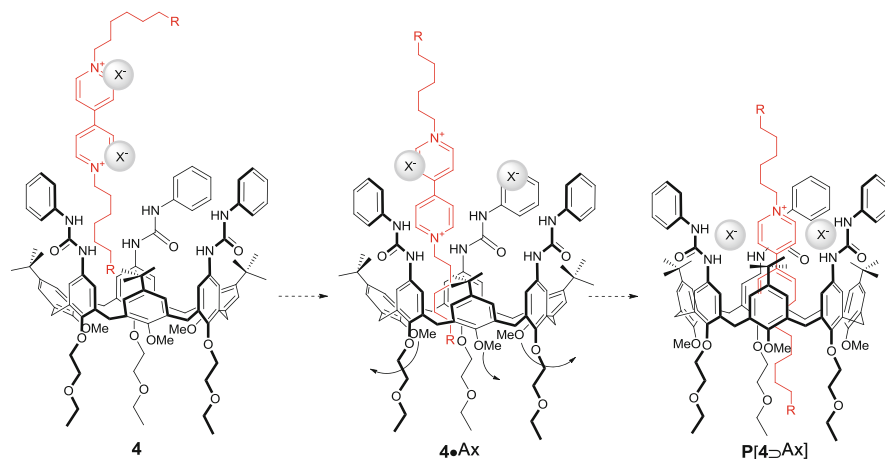
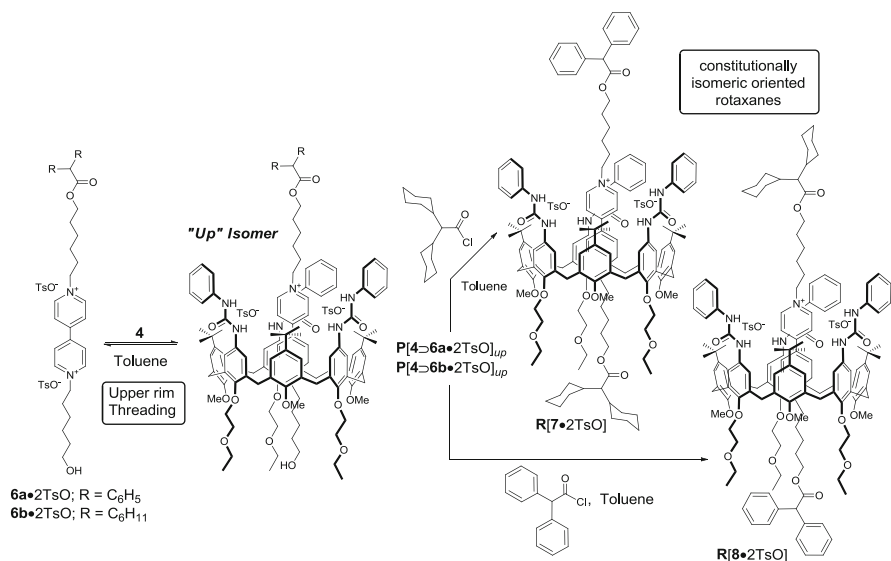


**Fig. 29.2** Possible threading mechanism of a viologen-based non-symmetric axle in a triphenylureido calix[6]arene-based wheel (**4**): the three phenylurea moieties present on the calix[6]arene aromatic cavity coordinate the viologen counteranions by hydrogen bonding, thus pivoting threading of the dicationic axle from the upper rim of the wheel (see text)

pivot the direction of axle insertion from the upper rim of the calixarene wheel (Fig. 29.2).

The possibility to gain full control on the unidirectional threading of a viologen salt through the upper rim of **4**, was utilized for the synthesis of the first example of two constitutionally isomeric oriented calix[6]arene-based rotaxanes (Scheme 29.3) [27]. It was also observed that the orientational control of the threading process





**Scheme 29.3** Self-assembly of oriented pseudorotaxanes  $P[4 \supset 6a \cdot 2TsO]_{up}$  and  $P[4 \supset 6b \cdot 2TsO]_{up}$  in weakly polar solvents and their transformation in the corresponding constitutionally isomeric oriented rotaxanes  $R[7 \cdot 2TsO]$  and  $R[8 \cdot 2TsO]$

involving wheel **4** and non-symmetric axles **6a** and **6b** is strongly affected by the polarity of the solvent employed during the threading step. Indeed, when acetonitrile was used instead of toluene or benzene, the higher polarity of the medium affects both the concentration of the active guest available in solution and the binding ability of the calixarene wheel, by changing the extent of ion pairing and the pivoting role of the urea moieties of the host, respectively. Moreover, in acetonitrile the three methoxy groups at the lower rim of **4** reside outside the cavity in the NMR time-scale, thus decreasing the crowding at this rim. As a result, both axles can thread the wheel either from the upper and the lower rim yielding a mixture of pseudorotaxane orientational isomers (Fig. 29.3).

To evidence possible effects of the structural information of the axle on these threading processes, a series of pseudorotaxanes composed of **4** and rivet-like non-symmetric axles (**5**•2TsO, **9**–**10**•2TsO and **11**•2TsO•TFA, Fig. 29.4) containing the viologen unit as a common feature was synthesized [28]. It was examined that at rt, in apolar media, all the axles thread the wheel from the upper rim for kinetic reasons. At higher temperature, the threading of axles bearing uncharged head groups, **5** and **9**–**10**, is still kinetically controlled and yields the "up" pseudorotaxane isomer as the sole threading product. Conversely, axle **11** that bears an ammonium terminus is capable of entering the calixarene cavity from the lower rim at 340 K. In this latter case, the threading process is under thermodynamic control and the "down" isomer is the favored orientational pseudorotaxane isomer [28].

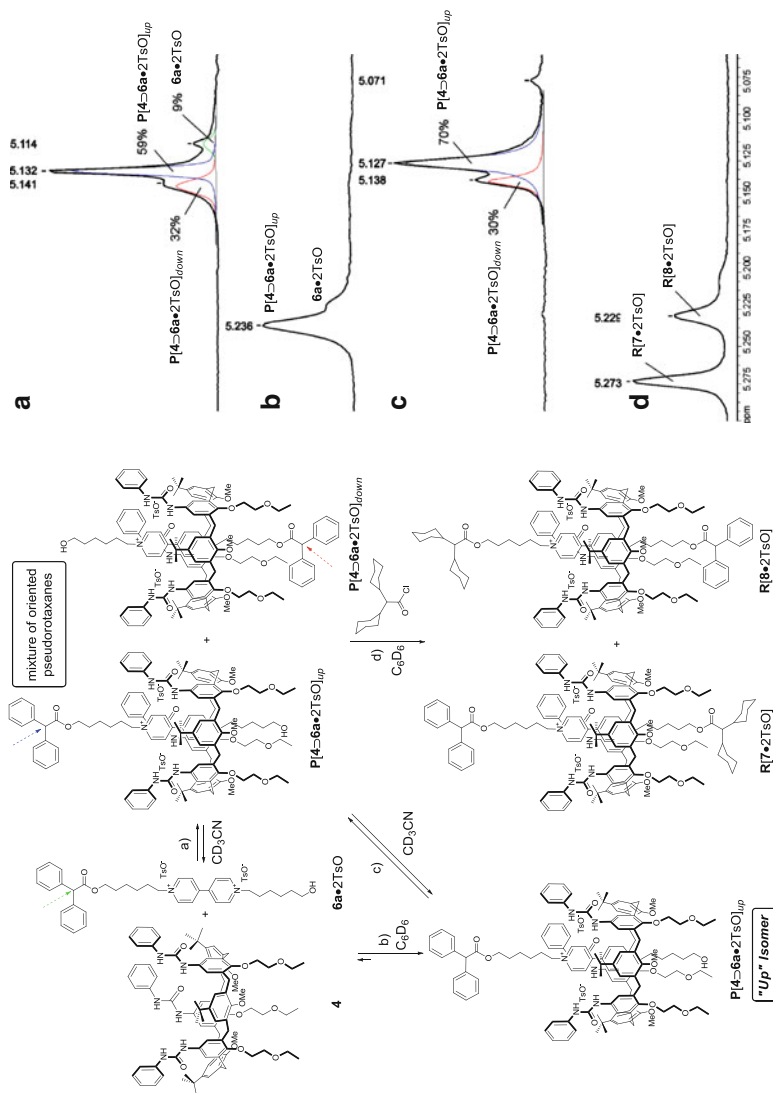


**Fig. 29.3** (Left) Effect of the solvent polarity on the self-assembly processes between wheel **4** and non-symmetric axle **6a•2TsO**; (right) 5.3–5.0 ppm <sup>1</sup>H NMR expansion showing the resonance region of the diphenylacetic methine proton of **a** pseudorotaxane mixture **P[4-6a•2TsO]<sub>lup</sub>** and **P[4-6a•2TsO]<sub>down</sub>** in CD<sub>3</sub>CN; **b** pseudorotaxane **P[4-6a•2TsO]<sub>lup</sub>** and **P[4-6a•2TsO]<sub>down</sub>** in C<sub>6</sub>D<sub>6</sub>; **c** pseudorotaxane **P[4-6a•2TsO]<sub>lup</sub>** dissolved in CD<sub>3</sub>CN, and **d** mixture of the two isomeric oriented rotaxanes **R[7•2TsO]** and **R[8•2TsO]** in C<sub>6</sub>D<sub>6</sub>

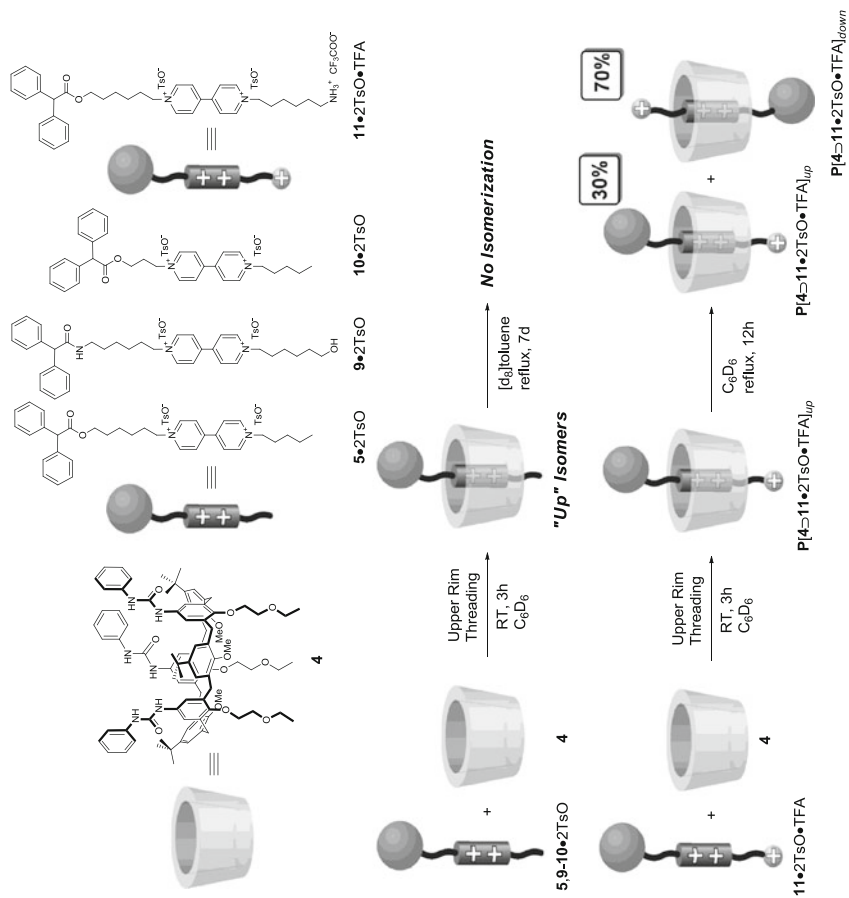


**Fig. 29.4** (Top) Representation of the two pseudorotaxane orientational isomers, "up" and "down", that can form through the threading of the non-symmetric wheel **4** with monostoppered rivet-like non-symmetric axes **5•2TsO**, **9•10•2TsO** and **11•2TsO•TFA**



**Table 29.1** Thermodynamic and kinetic data for the association of the non-symmetric axles **C5Cn** with wheel **4** (CH<sub>2</sub>Cl<sub>2</sub>, 293 K)

Axle	logK <sup>a</sup>	k <sub>in</sub> (M <sup>-1</sup> ·s <sup>-1</sup> ) <sup>b</sup>	k <sub>out</sub> (s <sup>-1</sup> ) <sup>c</sup>
<b>C5C5</b>	6.7	2 × 10 <sup>8</sup>	40
<b>C18C18</b>	5.1	1.5 × 10 <sup>2</sup>	1 × 10 <sup>-3</sup>
<b>C5C8</b>	>7	2 × 10 <sup>8</sup>	<20
<b>C5C12</b>	>7	2 × 10 <sup>8</sup>	<20
<b>C5C18</b>	>7	2 × 10 <sup>8</sup>	<20

The data corresponding to the symmetric axles **C5C5** and **C18C18** are also reported for comparison

<sup>a</sup>Determined by spectrophotometric titrations: the value reported for the non-symmetric axles refers to the individual *short* and *long* oriented pseudorotaxane isomers;  $K = K_{\text{short}} = K_{\text{long}}$

<sup>b</sup>Determined by stopped-flow experiments

<sup>c</sup> $k_{\text{out}} = k_{\text{in}}/K$

wheel and axle components, they can give rise to two orientational pseudorotaxane isomers following four different pathways (Fig. 29.5). For example, **P** [**4** ⊃ **C5Cn**·2TsO]<sub>short</sub> can be originated either by piercing **4** from its upper rim with the shorter alkyl chain of the axle or by passing the longer alkyl chain through the lower rim of the wheel. Nevertheless, in apolar media threading occurs only through the upper rim (vide supra). For the same reasons the viologen unit should pass through the upper rim also on dethreading. Hence, in apolar solvents, the upper rim of the wheel can be threaded by axles **C5Cn**·2TsO either through their shorter or longer chain, forming “short” and “long” oriented pseudorotaxane isomers (Fig. 29.5). The investigated system exhibits both intra- and intermolecular self-sorting capabilities, as a result of the kinetic selectivity toward alkyl chains of different lengths. In fact, NMR structural investigation together with stopped-flow measurements of the threading rate constants ( $k_{\text{in}}$ , Table 29.1) for pseudorotaxane assembly demonstrated that when the non-symmetric axles are mixed with the inherently non-symmetric **4** under appropriate conditions, only one out of the two equally stable pseudorotaxane isomers was obtained. The rate constant for threading of the symmetric axles **C5C5**·2TsO and **C18C18**·2TsO into **4** strongly depends on the length of the alkyl chain (lines 1–2 in Table 29.1); as expected, the threading is much slower for the axle bearing the longer octadecyl chains. The data obtained for the **C5Cn**·2TsO nonsymmetric axles (lines 3–5 in Table 29.1) show that they thread the wheel with the same rate constant, which agrees with  $k_{\text{in}}$  measured for **C5C5**·2TsO. These data clearly point to a common threading mode, involving the slipping of the shorter chain of the non-symmetric axles through the upper rim of the wheel; in other words, the observed  $k_{\text{in}}$  (Table 29.1) corresponds precisely to  $k_{\text{in,short}}$  in Fig. 29.5.

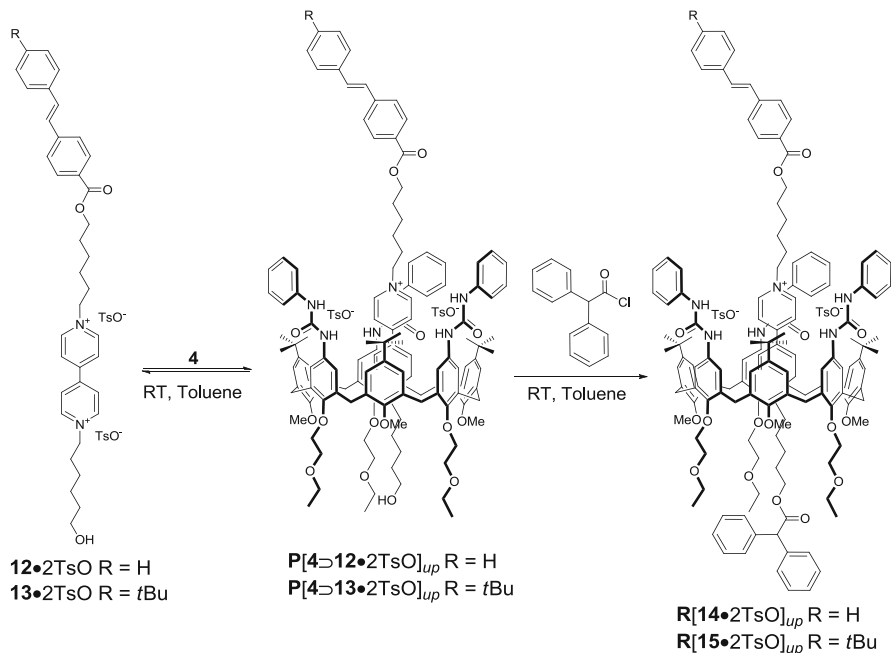
This strict kinetic control guides the self-assembly process through one of the four possible threading-dethreading mechanisms (Fig. 29.5). This behavior represents the first case of host-guest self-assembly that exhibit selectivity for both the host face and the guest side. It was also evidenced that when symmetric axles endowed with side chains of different length are mixed with **4**, the wheel can sort the guest with the shorter chains, forming only the pseudorotaxane with this latter axle.

## 29.4 Unidirectional Transit of Non-symmetric Axles Through the Calixarene Wheel

By playing around the structural features of the groups anchored at the viologen-based unit and the experimental conditions, the solvent and light- controlled unidirectional transit of non-symmetric axles through wheel **4** was also achieved [30]. In separate experiments, axles **12•2TsO** and **13•2TsO**, containing a photoisomerizable stilbene moiety at one end, were equilibrated with **4**, in apolar media, to yield the two oriented pseudorotaxanes **P[4 ⊃ 12•2TsO]<sub>up</sub>** and **P[4 ⊃ 13•2TsO]<sub>up</sub>**, respectively. Stoppering reaction of these pseudorotaxanes with diphenylacetyl chloride gave the corresponding semi-rotaxanes **R[14•2TsO]<sub>up</sub>** and **R[15•2TsO]<sub>up</sub>** (Scheme 29.4).

By means of NMR and UV-Vis measurements it was demonstrated that in the highly polar DMSO these complexes disassemble. Because of the presence of the bulky diphenylacetyl stopper, this process must take place through the slippage of the stilbene unit from the lower rim of the wheel. The fact that the dethreading rate constants depend on the stilbene bulkiness unambiguously evidences that these groups, positioned in proximity of the upper rim of both complexes, should pass through the lower calixarene annulus during the slippage (Fig. 29.6).

To explore the possibility of photocontrolling the dethreading rate, **R[14•2TsO]<sub>up</sub>** and **R[15•2TsO]<sub>up</sub>** were submitted to UV radiation in CH<sub>2</sub>Cl<sub>2</sub> at



**Scheme 29.4** Synthesis of oriented “semi-rotaxanes” **R[14•2TsO]<sub>up</sub>** and **R[15•2TsO]<sub>up</sub>**

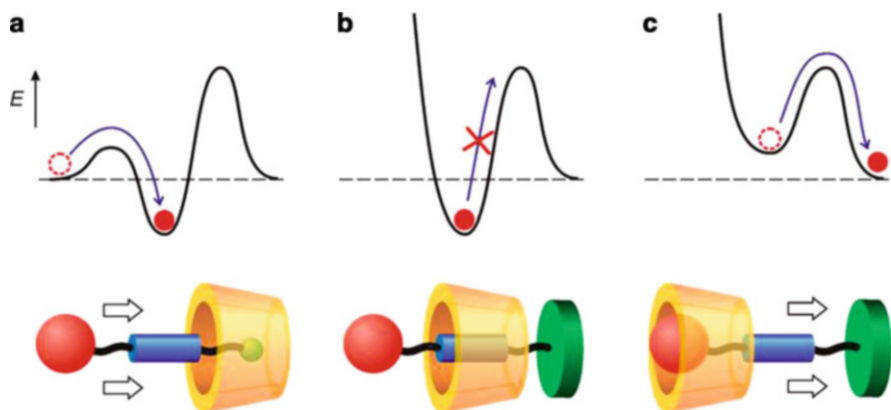


**Fig. 29.6** Simplified potential energy curves representing the steps that account for the unidirectional transit of the axle through the wheel. The horizontal coordinate of the diagrams represents the axle–wheel distance when they approach one another along the direction and with the orientation shown in the cartoons. **(a)** Threading of the axle through the upper rim of the wheel in apolar solvents. **(b)** The stoppering reaction to convert the pseudorotaxane into a rotaxane-like species. **(c)** Dethreading of the axle from the lower rim of the wheel occurring in polar solvents (Reprinted with permission from [30]. Copyright © 2012 WILEY-VCH Verlag GmbH & Co. KGaA, Weinheim)

$\lambda = 334$  or  $313$  nm to promote the  $E \rightarrow Z$  isomerization of the stilbene end groups of the axles. It was found that after irradiation for 90 min, 70 % conversion of the stilbene units from the  $E$  to the  $Z$  takes place. The photoisomerized complexes were then dissolved in DMSO and the visible absorption bands ( $\lambda_{\text{max}} = 460$  nm) of **R** [**14**•2TsO]<sub>up</sub> and **R** [**15**•2TsO]<sub>up</sub>, originating from charge-transfer (CT) interactions between the  $\pi$ -electron poor bipyridinium and the  $\pi$ -electron rich calixarene walls, were monitored over time. In the case of **R** [**14**•2TsO]<sub>up</sub> the disappearance of the CT band occurs in agreement with two superimposed first-order kinetics with rate constants of  $5.9 \times 10^{-3}$  and  $2.3 \times 10^{-5} \text{ s}^{-1}$ , respectively (Fig. 29.7a). The faster process, which accounts for 30 % of the total decay, was attributed to the slippage of the stilbene in the  $E$  configuration, as the rate constant coincides with that of the non-irradiated **R** [**14**•2TsO]<sub>up</sub>. Consequently, the slower process was attributed to the dethreading of the axle bearing the stilbene in the  $Z$  configuration. This slower dethreading is in agreement with the higher hampering effect of the  $Z$  isomer compared with the  $E$  isomer, which results in a more difficult slippage of this unit through the calixarene annulus. In the case of **R** [**15**•2TsO]<sub>up</sub>, a decrease of the CT absorption band of only 30 % was observed (Fig. 29.7b). The measured first-order kinetics rate constant ( $4 \times 10^{-5} \text{ s}^{-1}$ ) is similar to that determined for the dethreading of the non-irradiated **R** [**15**•2TsO]<sub>up</sub> and was thus attributed to dethreading of the 30 % of the rotaxane molecules having stilbene in the  $E$  configuration. It was then concluded that the photoisomerized species do not undergo dethreading, accounting for the fact that 70 % of the CT absorption intensity does not disappear in DMSO. These observation showed that the  $Z$  isomer of the  $p$ -<sup>t</sup>Bu-stilbene unit present in **R**

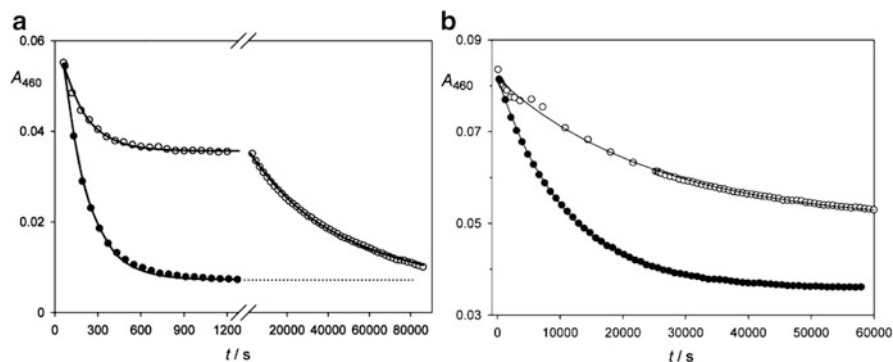


**Fig. 29.7** Absorbance decrease at  $\lambda = 460$  nm upon dissolution in DMSO of rotaxanes at room temperature **a**  $\mathbf{R}[14\cdot 2\text{TsO}]_{up}$  and **b**  $\mathbf{R}[15\cdot 2\text{TsO}]_{up}$  ( $2.2 \times 10^{-4}$  M) before (*full circles*) and after (*open circles*) exhaustive irradiation at  $\lambda = 334$  nm. The first-order fitting curves are also shown (Reprinted with permission from Ref. [30]. Copyright © 2012 WILEY-VCH Verlag GmbH & Co. KGaA, Weinheim)

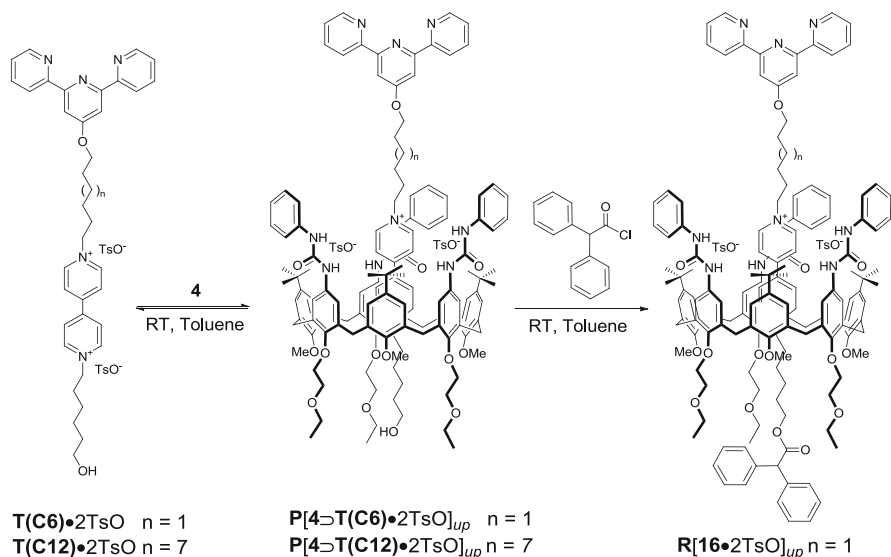
$\mathbf{R}[15\cdot 2\text{TsO}]_{up}$  is too bulky to pass through the calixarene lower rim, and that  $\mathbf{R}[15\cdot 2\text{TsO}]_{up}$  in its *Z* configuration behaves as a real rotaxane.

## 29.5 Metal-Directed Assemblies of Oriented Calix[6]arene-based Pseudorotaxanes and Rotaxanes

Interlocked systems bearing a terpyridine in the axle were synthesized with the aim to verify whether the orientation of the calix[6]arene wheel rims toward one particular stopper in rotaxanes could be employed as further structural information element to subtly tune the properties and/or the working mode of oriented pseudorotaxanes and rotaxanes. The functioning mode of these new systems was studied through NMR, UV/Vis spectroscopy and cyclic voltammetry [31]. The equilibration of wheel **4** with axles  $\mathbf{T}(\mathbf{C6})\cdot 2\text{TsO}$  or  $\mathbf{T}(\mathbf{C12})\cdot 2\text{TsO}$  in toluene gave, as expected, the corresponding oriented pseudorotaxanes  $\mathbf{P}[4 \supset \mathbf{T}(\mathbf{C6})\cdot 2\text{TsO}]$  and  $\mathbf{P}[4 \supset \mathbf{T}(\mathbf{C12})\cdot 2\text{TsO}]$  (Scheme 29.5), where the terpyridine unit of the axial component is in positioned at the calixarene upper rim.

The reaction of  $\mathbf{P}[4 \supset \mathbf{T}(\mathbf{C6})\cdot 2\text{TsO}]$  with diphenylacetyl chloride gave the corresponding oriented rotaxane  $\mathbf{R}[16\cdot 2\text{TsO}]_{up}$ . To establish whether the binding behavior of the terpyridine unit in axle  $\mathbf{T}(\mathbf{C6})\cdot 2\text{TsO}$  toward metal cations was influenced by the presence of the cationic viologen-based unit,  $\text{Zn}(\text{TsO})_2$  was selected because of its well documented preference to adopt an octahedral coordination geometry and its ability to form either 1:1 or 2:1 complexes with terpyridine ligands [32]. NMR measurements taken in  $\text{CDCl}_3/\text{CD}_3\text{OD}$  (6/4) showed that, in agreement with literature data,  $\mathbf{T}(\mathbf{C6})\cdot 2\text{TsO}$  forms either 1:1 or 2:1  $\text{Zn}/\mathbf{T}(\mathbf{C6})$  complexes, depending on the ratio between the analytes and that these complexes





**Scheme 29.5** Self-assembly of pseudorotaxanes  $\text{P}[4 \supset \text{T}(\text{C6})\cdot 2\text{TsO}]$  and  $\text{P}[4 \supset \text{T}(\text{C12})\cdot 2\text{TsO}]$  and stoppering reaction of the former complex to yield rotaxane  $\text{R}[16\cdot 2\text{TsO}]_{up}$

are in slow exchange in the NMR timescale. On the contrary, the spectra recorded upon addition of an excess of solid  $\text{Zn}(\text{TsO})_2$  to a  $\text{C}_6\text{D}_6$  solution of  $\text{P}[4 \supset \text{T}(\text{C6})\cdot 2\text{TsO}]$  showed the formation of the 1:2  $\text{Zn}/\text{P}[4 \supset \text{T}(\text{C6})\cdot 2\text{TsO}]$  complex as the unique adduct present in solution (Fig. 29.8), as also verified through DOSY experiments that confirmed the stoichiometry of complexation around the  $\text{Zn}^{2+}$  ion. This 1:2 stoichiometry was observed also when  $\text{R}[16\cdot 2\text{TsO}]_{up}$  was employed as ligand for  $\text{Zn}(\text{TsO})_2$ . CV measurements carried out on the metal free  $\text{T}(\text{C6})\cdot 2\text{TsO}$ ,  $\text{P}[4 \supset \text{T}(\text{C6})\cdot 2\text{TsO}]$  and  $\text{R}[16\cdot 2\text{TsO}]_{up}$  in  $\text{CH}_2\text{Cl}_2$  showed, as expected, the reduction processes of the viologen unit (Fig. 29.8a–c), with a behavior similar to that already measured for related previously studied systems. [23] Quite remarkably, in the case of the 1:2  $\text{Zn}/\text{P}[4 \supset \text{T}(\text{C6})\cdot 2\text{TsO}]$ , the presence of the metal cation induces a negative shift of the first reduction wave of the viologen unit (–20 to –30 mV), suggesting that the dethreading of the axle is more difficult when  $\text{Zn}^{2+}$  is bound to the terpyridine units (Fig. 29.8b). These results, together with UV/Vis data, indicate that the viologen core of the axle “communicates” through the calixarene component with the Zn-terpyridine domain. On the contrary, in the case of 1:2  $\text{Zn}/\text{R}[16\cdot 2\text{TsO}]_{up}$ , a positive shift (up to +50 mV) of the two reversible waves was observed suggesting the redox potential of the viologen unit is affected, although in the opposite direction, by the presence of the  $\text{Zn}^{2+}$  ion bound to the terpyridine units (Fig. 29.8c). To verify whether these reduction potential changes of the axle are a consequence of the proximity of the upper rim of the calix with respect to the terpyridine units, pseudorotaxane  $\text{P}[4 \supset \text{T}(\text{C12})\cdot 2\text{TsO}]$  in which the span between the terpyridine domain and the viologen unit is now twelve carbon atoms was synthesized and its electrochemical behavior was studied with and without Zn ions. The observation

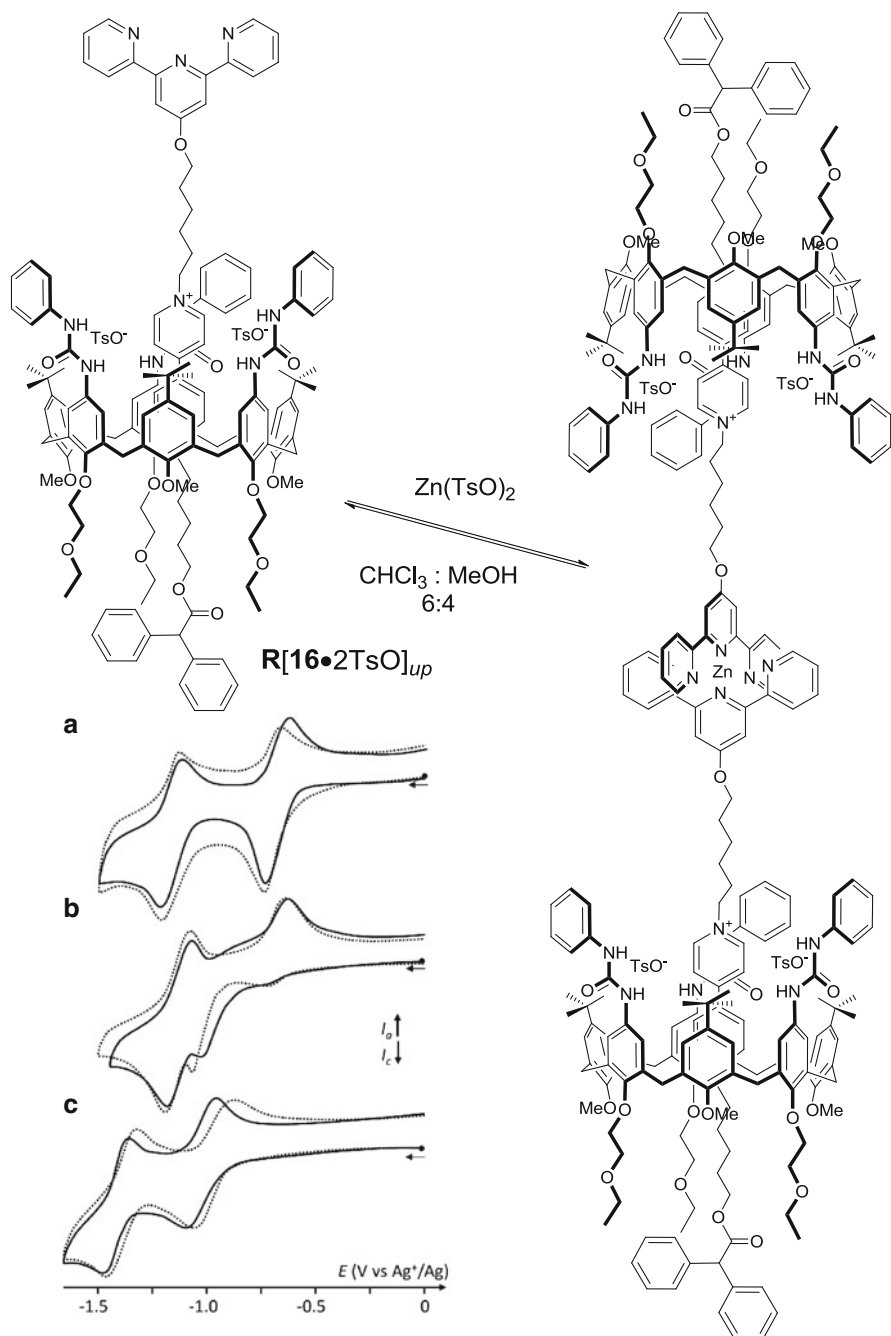


**Fig. 29.8** (Top) Complexing behavior of rotaxane **R[16•2TsO]<sub>up</sub>** in presence of an excess of  $\text{Zn}(\text{TsO})_2$ . (Bottom, left) Cyclic voltammograms of **a** **T(C6)•2TsO**, **b** **P[4 ⊃ T(C6)•2TsO]**, and **c** **R[16•2TsO]<sub>up</sub>** in  $\text{CH}_2\text{Cl}_2$ , 0.5 M TBAPF<sub>6</sub> [scan rate:  $100 \text{ mV} \cdot \text{s}^{-1}$ ]. Full line: no  $\text{Zn}^{2+}$ , dashed line: 1 equiv. of  $\text{Zn}^{2+}$  added] (Adapted with permission from Ref. [31]. Copyright © 2012 WILEY-VCH Verlag GmbH & Co. KGaA, Weinheim)

that the CV curves for both systems are almost superimposable, clearly indicates that the viologen and the Zn-terpyridine units no longer interact because of the increased distance determined by the dodecyl spacer.

## 29.6 Calix[6]arene-based Molecular Machines Operated by Photoinduced Proton Transfer

A very simple calix[6]arene-based molecular machine operated by intermolecular photoinduced proton transfer was realized by employing wheel **1**, N-decyl pyridylpyridinium axle-like  $[17]^+$ , that upon protonation could act as a viologen-type guest, and the spiropyran photochrome **SP** (Fig. 29.9) [33]. This latter component has been selected because its acid-base properties can be photocontrolled so that it can

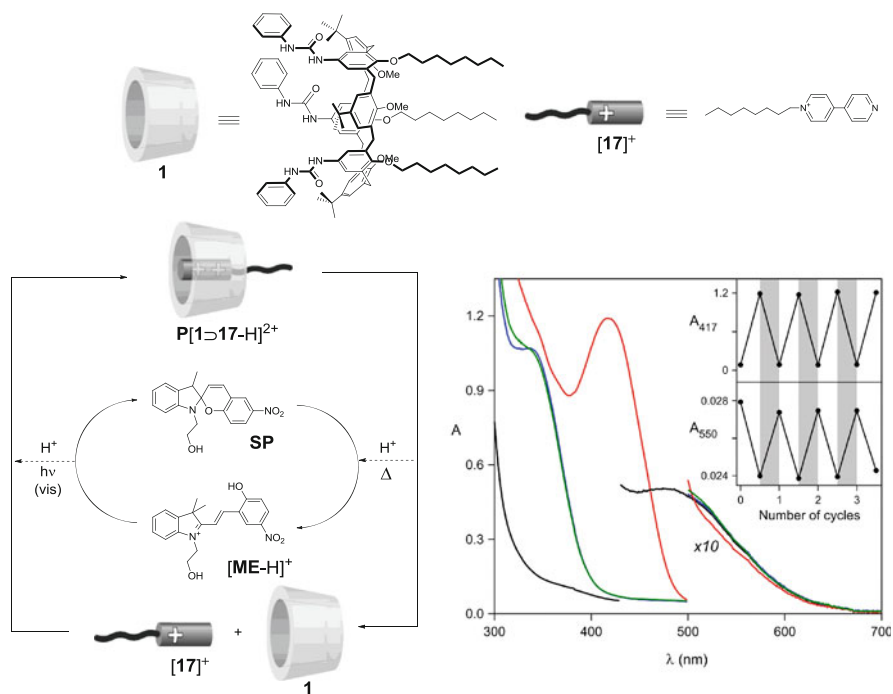


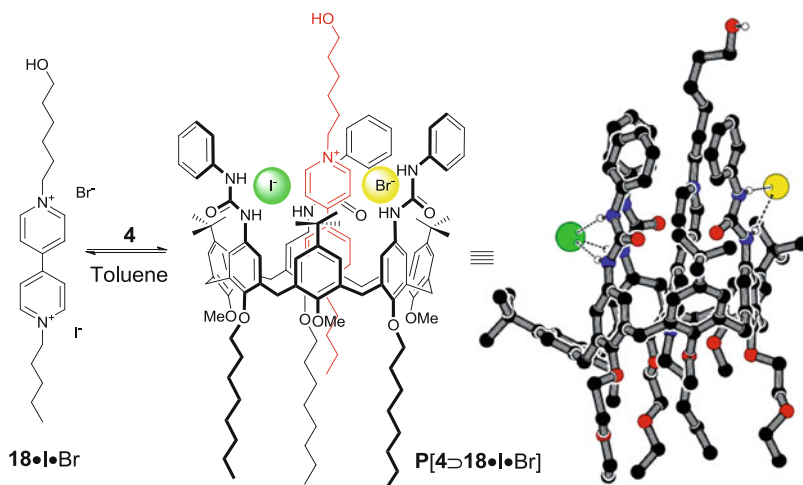
**Fig. 29.9** (Left) Control of threading-dethreading processes in pseudorotaxane  $P[1 \supset 17-H]^{2+}$  by means of light-induced proton exchange with a spiropyran (**SP**)/merocyanine  $[ME-H]^+$  photochromic system. (Right) absorption spectra in  $CH_2Cl_2$  at RT of (i)  $P[1 \supset 17-H]^{2+}$  (black curve); (ii)  $P[1 \supset 17-H]^{2+}$  and **SP**, immediately after the addition of the latter (blue curve); (iii) solution (ii) after 7 days of rest in the dark (red curve); (iv) solution (iii) after 10 min of irradiation at  $\lambda > 450$  nm (green curve). Inset: absorbance changes at 417 and 550 nm of  $10^{-4}$  M solution of **P**  $[1 \supset 17-H]^{2+}$  and **SP** in  $CH_2Cl_2$  taken upon several thermal equilibration cycles (white bars) and visible light irradiation (gray bars) (Adapted with permission from [33]. Copyright © 2007 American Chemical Society)

be converted into two forms by light irradiation, exhibiting smaller and larger acid strength than that of  $[17\text{-H}]^{2+}$ . In particular, in the presence of an acid, the **SP** is converted into the protonated merocyanine form  $[\text{ME-H}]^+$ . Upon irradiation with visible light  $[\text{ME-H}]^+$  releases a proton, isomerizing back to the spiropyrane form **SP**.

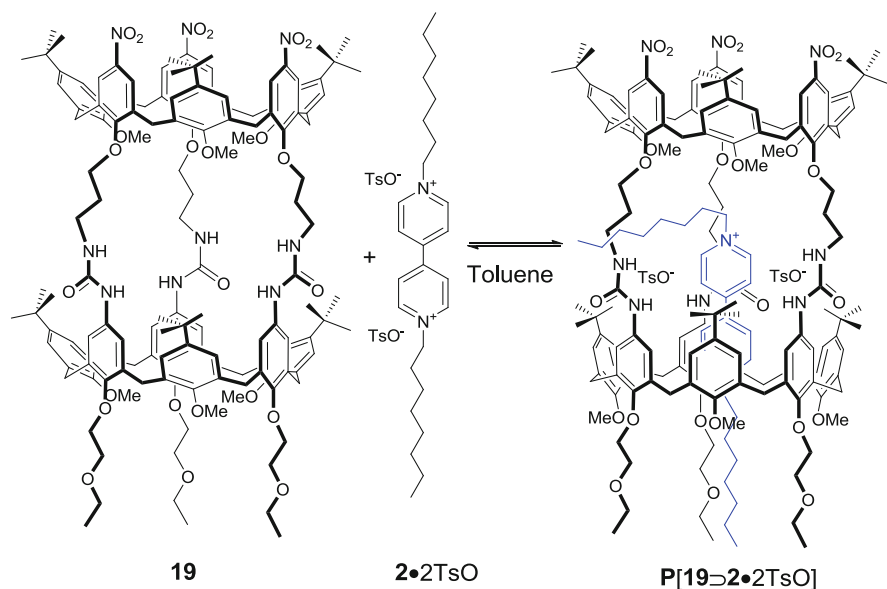
The functioning mode of such a multicomponent machine can be briefly summarized as follows: by mixing in  $\text{CH}_2\text{Cl}_2$  **SP** and the pseudorotaxane obtained from the threading of  $[17\text{-H}]^{2+}$  with **1**, a thermal proton transfer from  $[17\text{-H}]^{2+}$  to the **SP** takes place, yielding the merocyanine  $[\text{ME-H}]^+$  and the deprotonated axle  $[17]^+$ , which is not appreciably complexed by **1**. As a consequence, in the dark, a dethreading process of  $[17]^+$  from **1** occurs. Subsequent light irradiation of  $[\text{ME-H}]^+$  in the visible region causes an opposite proton transfer converting  $[17]^+$  into  $[17\text{-H}]^{2+}$  which rethreads **1**. Since the reset of the system takes place thermally, its operation under continuous light irradiation can give rise to autonomous behavior. Because of the large difference in the time scale of the dark and light parts of the cycle, the photostationary state is strongly displaced toward the **SP**- $[17\text{-H}]^{2+}$  state, unless irradiation is carried out with very low intensity and/or the temperature is increased.

## 29.7 Solid State Studies on Calix[6]arene-Based Pseudorotaxanes

From the analysis of the solid-state structure of the pseudorotaxane formed by **4** and a non-symmetric axle **18•I•Br** (Scheme 29.6), it emerged that the calixarene wheel possesses a trigonal prism structure 1.65 nm in length with an internal width of about 0.75 nm [34].



**Scheme 29.6** (Left) Self-assembly process between calix[6]arene wheel **4** and axle **18•I•Br**; (right) perspective view of pseudorotaxane **P[4 ⊃ 18•I•Br]** showing the intramolecular hydrogen bonding between the urea groups and the two anions



**Scheme 29.7** Synthesis of pseudorotaxane **P[19 ⊃ 2•2TsO]**

This finding suggested the idea to construct an oriented non-symmetric channel-like structure **19** that was thus obtained through the head-to-tail three points covalent connection of two calix[6]arene units (Scheme 29.7) [35]. The “calixtube” **19** maintains its ability to complex viologen-type guests such as dioctylviologen as shown by UV/Vis and voltammetric measurements. In the solid state (Fig. 29.10), this complex, that is 2.6 nm long and 1.6 nm wide, undergoes a further stage of self-assembly, giving rise to extended oriented tubular structures. The position of the viologen dication  $2^{2+}$  inside the double calixarene is determined by a complicate pattern of cooperative non covalent interactions that involve only the calixarene host, whereas the remaining and more polar half creates long-range structural order which leads to a secondary structure of extended supramolecular channels that, in turn, self-assemble in the lattice, thus giving rise to a “tertiary” structure of parallel sandwiches of nanotubes (Fig. 29.10).

## 29.8 Conclusion

In the last two decades calix[6]arene derivatives have proved to be very convenient platforms to further expand the scopes of calixarene chemistry also towards nanoscience and nanotechnology. Because of the relatively large size of their cavity they are capable to accommodate guests with an axle-type shape giving rise to pseudorotaxane and rotaxane systems. Furthermore, upon the functionalization of

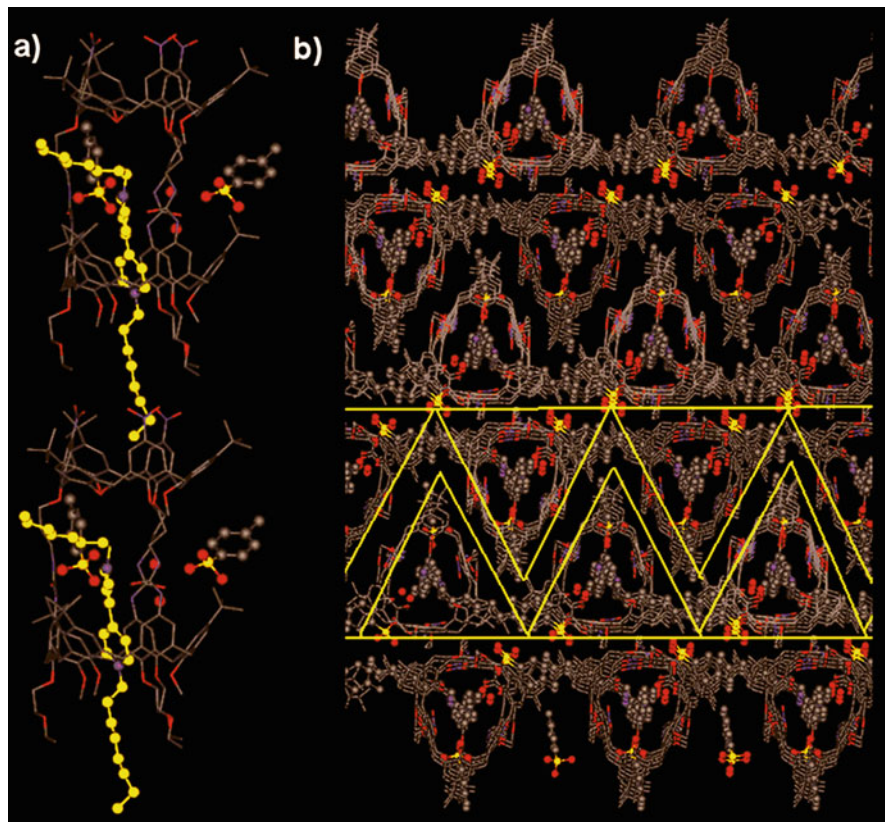


**Fig. 29.10** X-rays structures of pseudorotaxane **P[19]C<sub>2.2</sub>TsO** complex: **(a)** columnar arrangement in a nanotube-like “secondary” structure (for clarity, the  $2^{2+}$  dicationic axial component is represented in yellow) and **(b)** “tertiary” structure of sandwiched bilayers of nanotubes (hydrogen atoms have been omitted for clarity; a bilayer is evidenced between the two horizontal yellow lines) (Adapted with permission from [35] Copyright © 2008 WILEY-VCH Verlag GmbH & Co. KGaA, Weinheim)

their upper and lower rims by appropriately selecting the nature and the spatial arrangement of the binding sites, they act as heteroditopic wheels that, in apolar media, can also recognize charged axle-type guests. As reported in the present chapter viologen-based axles are particularly interesting in this regard enabling the construction of a new generation of calixarene-based prototypes of molecular machines. Exploiting the special features of the calix[6]arene-based wheels and using non-symmetric viologen-based axles it is possible to obtain pseudorotaxanes that are characterized by the univocal orientation of the axle with respect to the distinct rims of the calixarene and exhibit very peculiar behaviors. Indeed, by means of the interplay of thermodynamic and kinetic elements such oriented pseudorotaxanes can (i) display both intra- and inter-molecular self-sorting

capabilities and (ii) undergo the solvent and light controlled unidirectional transit of the axle component through the wheel. These studies are still in their infancy, but it can be easily foreseen that the principles and methods of Supramolecular Chemistry and the almost limitless synthetic possibilities for the functionalization of calyx[6] arene platforms will lead to the development of molecular machines and motors with an operation mode controlled by a wider set of elements. Surely these calixarene-based systems are in the cutting-edge research topics: the imagination and ingenuity of researchers together with their ability to take inspiration by nature will open the way to the construction of devices that in a not too distant future can find useful and fascinating applications in several fields.

**Acknowledgments** This work was supported by the Italian MIUR (PRIN 2010CX2TLM “InfoChem”) and the Universities of Bologna and Parma.

## References

1. *Calixarenes 2001*; Asfari, Z.; Böhmer, V.; Harrowfield, J.; Vicens, J., Eds.; Kluwer Academic Publishers: New York, 2001.
2. *Calixarenes in Action*; Mandolini, L.; Ungaro, R., Eds.; Imperial College Press: London, 2000.
3. *Calixarenes in the Nanoworld*; Vicens, J.; Harrowfield, J., Springer: Dordrecht, 2007.
4. Giuliani, M.; Morbioli, I.; Sansone, F.; Casnati, A. *Chem. Commun.* **2015**, *51*, 14140–14159.
5. Balzani, V.; Credi, A.; Venturi, M. *Molecular Devices and Machines: Concepts and Perspectives for the Nanoworld*; Wiley: Weinheim, 2008.
6. *Molecular Catenanes, Rotaxanes and Knots: A Journey Through the World of Molecular Topology*; Sauvage, J. P.; Dietrich-Buchecker, C., Eds. Wiley: Weinheim, 2008.
7. Sliwa, W.; Kozłowski, C. *Calixarenes and Resorcinarenes*; Wiley: Weinheim, 2009.
8. Baldini, L.; Sansone, F.; Casnati, A.; Ungaro, R. Calixarenes in Molecular Recognition. In *Supramolecular Chemistry: From Molecules to Nanomaterials*; Steed, J. W.; Gale, P. A., Eds.; John Wiley & Sons, Ltd: Weinheim, 2012; pp 863–894.
9. Davis, F.; Higson, S. Heterocalixarenes and Calixnaphthalenes. In *Macrocycles*; John Wiley & Sons, Ltd: Chichester (UK), 2011; pp 126–189.
10. Homden, D. M.; Redshaw, C. *Chem. Rev.* **2008**, *108*, 5086–5130.
11. Sameni, S.; Jeunesse, C.; Matt, D.; Harrowfield, J. *Chem. Soc. Rev.* **2009**, *38*, 2117–2146.
12. Creaven, B. S.; Donlon, D. F.; McGinley, J. *Coord. Chem. Rev.* **2009**, *253*, 893–962.
13. Dondoni, A.; Marra, A. *Chem. Rev.* **2010**, *110*, 4949–4977.
14. Joseph, R.; Rao, C. P. *Chem. Rev.* **2011**, *111*, 4658–4702.
15. Muthiac, L.; Lee, J. H.; Kim, J. S.; Vicens, J. *Chem. Soc. Rev.* **2011**, *40*, 2777–2796.
16. Chinta, J. P.; Ramanujam, B.; Rao, C. P. *Coord. Chem. Rev.* **2012**, *256*, 2762–2794.
17. Wang, M.-X. *Acc. Chem. Res.* **2012**, *45*, 182–195.
18. Harrowfield, J. *Chem. Commun.* **2013**, *49*, 1578–1580.
19. *Topology in Chemistry: Discrete Mathematics of Molecules*; Rouvray, D. H., King, R. B., Eds.; Horwood series in chemical science; Horwood Publishing Ltd.: Cambridge (UK), 2002.
20. Breault, G. A.; Hunter, C. A.; Mayers, P. C. *Tetrahedron* **1999**, *55*, 5265–5293.
21. Steed, J. W.; Turner, D. R.; Wallace, K. *Core Concepts in Supramolecular Chemistry and Nanochemistry*; John Wiley & Sons, Ltd: Chichester (UK), 2007.
22. Arduini, A.; Ferdani, R.; Pochini, A.; Secchi, A.; Ugozzoli, F. *Angew. Chem. Int. Ed.* **2000**, *39*, 3453–3456.

23. Credi, A.; Dumas, S.; Silvi, S.; Venturi, M.; Arduini, A.; Pochini, A.; Secchi, A. *J. Org. Chem.* **2004**, *69*, 5881–5887.
24. Semeraro, M.; Arduini, A.; Baroncini, M.; Battelli, R.; Credi, A.; Venturi, M.; Pochini, A.; Secchi, A.; Silvi, S. *Chem. Eur. J.* **2010**, *16*, 3467–3475.
25. Semeraro, M.; Secchi, A.; Silvi, S.; Venturi, M.; Arduini, A.; Credi, A. *Inorg. Chim. Acta* **2014**, *417*, 258–262.
26. Arduini, A.; Calzavacca, F.; Pochini, A.; Secchi, A. *Chem. Eur. J.* **2003**, *9*, 793–799.
27. Arduini, A.; Ciesa, F.; Fragassi, M.; Pochini, A.; Secchi, A. *Angew. Chem. Int. Ed.* **2005**, *44*, 278–281.
28. Arduini, A.; Bussolati, R.; Credi, A.; Faimani, G.; Garaudee, S.; Pochini, A.; Secchi, A.; Semeraro, M.; Silvi, S.; Venturi, M. *Chem. Eur. J.* **2009**, *15*, 3230–3242.
29. Arduini, A.; Bussolati, R.; Credi, A.; Secchi, A.; Silvi, S.; Semeraro, M.; Venturi, M. *J. Am. Chem. Soc.* **2013**, *135*, 9924–9930.
30. Arduini, A.; Bussolati, R.; Credi, A.; Monaco, S.; Secchi, A.; Silvi, S.; Venturi, M. *Chem. Eur. J.* **2012**, *18*, 16203–16213.
31. Arduini, A.; Bussolati, R.; Masseroni, D.; Royal, G.; Secchi, A. *Eur. J. Org. Chem.* **2012**, 1033–1038.
32. Shunmugam, R.; Gabriel, G. J.; Aamer, K. A.; Tew, G. N. *Macromol. Rapid Commun.* **2010**, *31*, 784–793.
33. Silvi, S.; Arduini, A.; Pochini, A.; Secchi, A.; Tomasulo, M.; Raymo, F. M.; Baroncini, M.; Credi, A. *J. Am. Chem. Soc.* **2007**, *129*, 13378–13379.
34. Ugozzoli, F.; Massera, C.; Arduini, A.; Pochini, A.; Secchi, A. *Crystengcomm* **2004**, *6*, 227–232.
35. Faimani, G.; Massera, C.; Pochini, A.; Secchi, A.; Semeraro, M.; Silvi, S.; Ugozzoli, F. *Chem. Eur. J.* **2008**, *14*, 98–106.



# Chapter 30

## Calixarene Threading via Superweak Anion

Carmine Gaeta, Carmen Talotta, Margherita De Rosa,  
Annunziata Soriente, and Placido Neri

### 30.1 Introduction

In the last two decades interpenetrated molecules such as (pseudo)rotaxanes and catenanes [1], have shown peculiar properties as molecular machines [2], sensors [3], and more recently as catalysts [4]. Rotaxanes can be defined as interlocked supramolecular systems in which a linear molecular axle bearing two bulky groups (stoppers) at the ends is threaded through a macrocyclic-wheel [1]. In the last two decades, numerous examples of rotaxane-based molecular shuttle in which the macrocyclic wheel was able to traslocate over two or more sites on the axle under the influence of an external stimulus have been reported [2]. These controlled movements have been recently exploited for the release of pharmacological active molecules [5] or in the switching of the organocatalytic function of rotaxane systems. [4] Differently, catenanes [1] are interlocked architectures constituted by two or more interpenetrated macrocycles. Catenane-based molecular architectures has found interesting applications in the field of the molecular electronics as solid state switching device [2b] and as unidirectional motors. Interpenetrated molecules can be easily synthesized through a template-directed procedure [1] exploiting the threading of a linear molecular axle through a macrocyclic wheel to give a pseudorotaxane supramolecule, which can be considered as the most direct synthetical precursor of both rotaxanes and catenanes. Following this strategy, different kinds of macrocycles, including crown-ethers [6], cyclodextrins [7], cucurbiturils [8], macrolactams [9], and most recently pillararenes [10], have been used as the basic wheel undergoing threading with a complementary axle and exploiting various preorganizing supramolecular interactions.

---

C. Gaeta (✉) • C. Talotta • M. De Rosa • A. Soriente • P. Neri (✉)  
Dipartimento di Chimica e Biologia "A. Zambelli", Università di Salerno, Via Giovanni Paolo  
II 132, I-84084 Fisciano, Salerno, Italy  
e-mail: [cgaeta@unisa.it](mailto:cgaeta@unisa.it); [neri@unisa.it](mailto:neri@unisa.it)

Thanks to their synthetic and conformational versatility, calixarene macrocycles [11] have become one of the most important host systems, with peculiar properties in the context of anion [12] and cation [13] recognition, gas storage [14], and self-assembly both in solution and in the solid state [11]. Differently, their use as basic wheels in the building of rotaxane and catenane architectures has been relatively limited [15], probably because of the lack of an efficient and general cavity-threading method [15]. In fact, the reported examples regard the threading of viologen derivatives through the annulus of calix[6]arene hosts [15f] in which the anion coordinating ability of their ureido groups is exploited to favor the ion-pair dissociation (see Chap. 29). In these studies, Arduini and coworkers showed that the separation of a tight ion-pair is fundamental to induce the threading of a viologen cation through a calix[6]arene annulus [15f]. In addition, it has been shown that the use of either tosylate or hexafluorophosphate as counterions of bipyridinium-based threads affects both the stability of the complex and the rate of the threading process.

Regarding the threading with dialkylammonium ions, simple ethers of calixarenes can be seen as modified crown ethers and in principle they should be able to give *endo*-complexation of such organic cations in a similar way [6]. Unfortunately, with the notable exception of some calix[5]arene derivatives [16], simple ethers of calix[*n*]arenes do not complex halide, hexafluorophosphate or tetraphenylborate salts of dialkylammonium cations.

## 30.2 Calixarene/Dialkylammonium-Based Pseudo[2]rotaxane Architectures

A few years ago, [17] our group showed that the threading of simple calix[6]arene ethers **1a,b** with dialkylammonium axles **2-3a<sup>+</sup>** (Fig. 30.1) occurs in CDCl<sub>3</sub> when the cationic axle is coupled with the weakly coordinating Tetrakis[3,5-bis(tri-Fluoromethyl)Phenyl]Borate (TFPB<sup>-</sup>) “superweak anion” [18] (Fig. 30.2). This anion gives very loose ion-pairs with free “naked” dialkylammonium cations in solution and thus induces their *through-the-annulus* threading through the large calix[6]arene macrocycle.

In addition, we showed that the scarcely preorganized, conformationally mobile, hexamethoxy-*p-tert*-butylcalix[6]arene **1a** can be threaded by the TFPB<sup>-</sup> salts of dipentylammonium and dibenzylammonium cations **2<sup>+</sup>** and **3a<sup>+</sup>** in CDCl<sub>3</sub> (Fig. 30.3) [17]. 1D and 2D NMR studies revealed that the conformationally mobile macrocycle **1a** was blocked in a cone conformation upon threading with a dialkylammonium axle, as indicated by the presence of an AX system relative to ArCH<sub>2</sub>Ar groups (Fig. 30.4b). As a consequence of the directionality of the cone calix-wheel **1a**, two different pentyl chains were observed in the <sup>1</sup>H NMR spectrum of the pseudo[2]rotaxane **2<sup>+</sup>⊂1a**, one strongly shielded, inside the cavity, and resonating between -1.20 and 0.53 ppm, and the other, at more normal values of chemical shift outside the cavity.

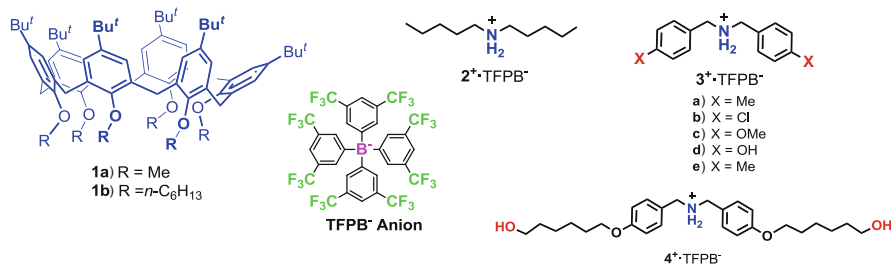


**Fig. 30.1** Calix[6]arene ethers, TFPB anion, and dialkylammonium threads

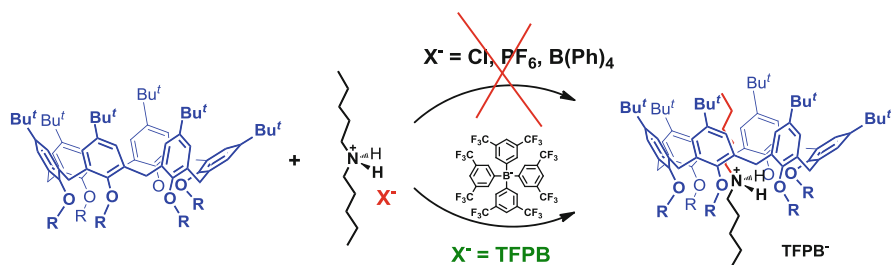


**Fig. 30.2** Anion influence on the *through-the-annulus* threading of calix[6]arene macrocycle

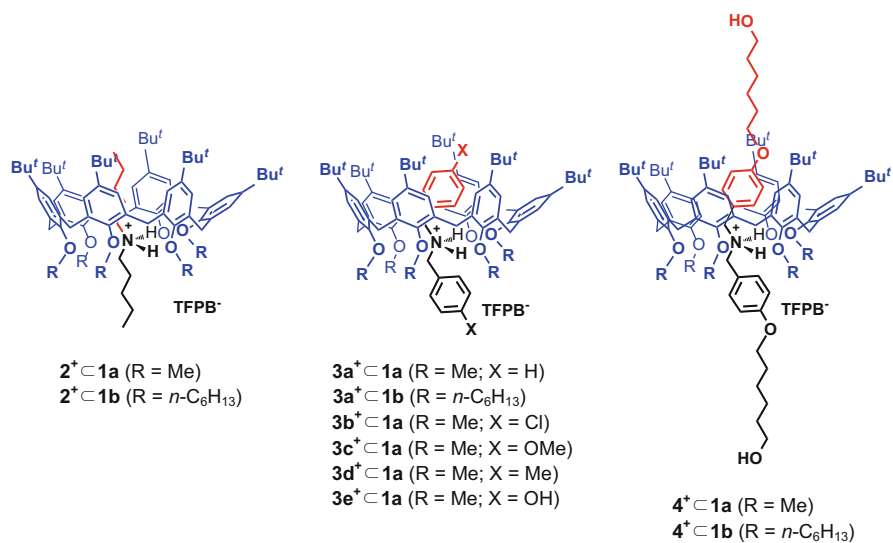


**Fig. 30.3** Dialkylammonium-based calix-pseudo[2]rotaxanes

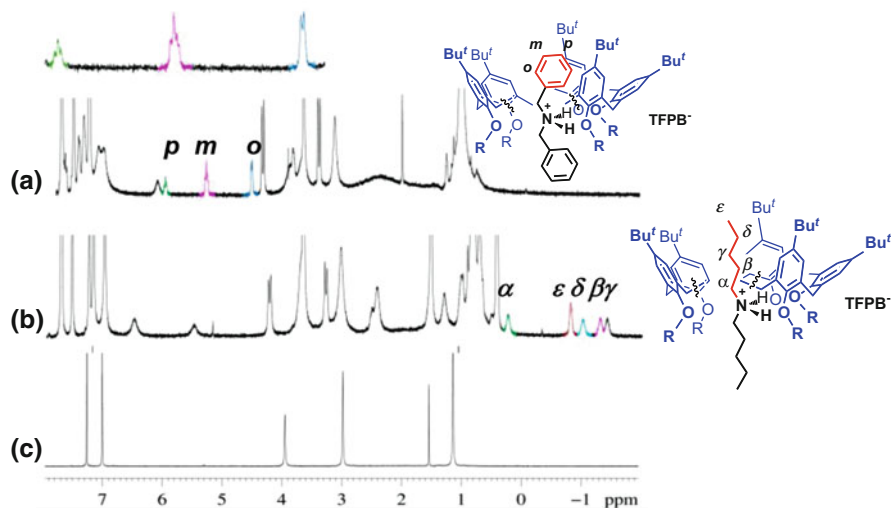


**Fig. 30.4**  $^1\text{H}$  NMR spectra (400 MHz,  $\text{CDCl}_3$ , 298 K) of: (c) **1a**; (b) 1:1 mixture (3 mM each one) of **1a** and  $2^+\cdot\text{TFPB}^-$ ; (a) 1:1 mixture (3 mM each one) of **1a** and  $3^+\cdot\text{TFPB}^-$ . The coloring corresponds to the portion of the axle hosted inside the cavity of the calix, as indicated in Fig. 30.5

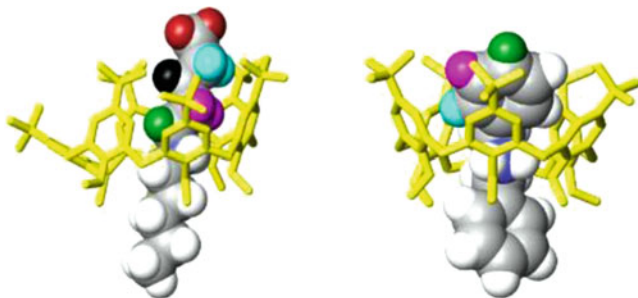


**Fig. 30.5** Optimized structures at the B3LYP/6-31G(d,p) level of theory of the  $2^+\subset\mathbf{1a}$  and  $3a^+\subset\mathbf{1a}$  pseudo[2]rotaxane structures

DFT calculations at the B3LYP/6-31G(d,p) level of theory confirmed the presence in the  $2^+\subset\mathbf{1a}$  pseudorotaxane structure of two  $\text{NH}\cdots\text{O}$  hydrogen bonds (Fig. 30.5, left). Analogously, in the  $^1\text{H}$  NMR spectrum of the  $3a^+\subset\mathbf{1a}$  pseudo[2]rotaxane structure two sets of shielded and unshielded benzyl signals can be always observed (Fig. 30.4a) corresponding to their *exo*- or *endo*-cavity disposition.

The apparent association constants, obtained by integration of the slowly exchanging  $^1\text{H}$  NMR signals, showed that the dibenzylammonium-based pseudorotaxane  $3a^+\subset\mathbf{1a}$  was more stable ( $K_{\text{ass}} = 2.5 \times 10^3 \text{ M}^{-1}$ ) than the dipentylammonium analogue  $2^+\subset\mathbf{1a}$  ( $K_{\text{ass}} = 4.4 \times 10^2 \text{ M}^{-1}$ ) [17].

Interestingly, when longer hexyloxy chains were appended at the *endo* rim of the calix[6]arene macrocycle the two dipentyl/dibenzylammonium pseudorotaxane  $2^+ \subset 1b$  ( $K_{\text{ass}} = 3.5 \times 10^4 \text{ M}^{-1}$ ) and  $3a^+ \subset 1b$  ( $K_{\text{ass}} = 1.2 \times 10^5 \text{ M}^{-1}$ ) were more stable than the corresponding hexamethoxy-*p-tert*-butylcalix[6]arene analogues  $2^+ \subset 1a$  and  $3a^+ \subset 1a$ , because of the greater preorganization of the calixarene wheel induced by the longer hexyl-chains [17].

A close inspection of the DFT-optimized structure (Fig. 30.5) of the dibenzylammonium  $3a^+ \subset 1a$  pseudorotaxane complex revealed that  $\pi$ - $\pi$  interactions play an essential role in the stabilization of the complex [19] as evidenced by the face-to-face stacked geometry between the benzyl ring of  $3a^+$  and one anisole ring of  $1a$ . These considerations led us to envision that the presence of electron-withdrawing (EW) or electron-donating (ED) substituents on the aromatic rings of dibenzylammonium axles could modulate the affinity of the calixarene-wheel toward the axle. Prompted by these considerations, we studied the threading equilibrium between calix[6]arene  $1a$  and disubstituted axles  $3b-e^+$  (Figs. 30.1 and 30.3) [19]. Thus, we have evidenced that the *p*-chloro-substituted axle  $3b^+$  forms pseudo[2]rotaxane  $3b^+ \subset 1a$  (Fig. 30.3) in  $\text{CDCl}_3$  with an apparent association constant of  $4.5 \times 10^3 \text{ M}^{-1}$ , a value higher than that previously observed for the *p*-H-substituted  $3a^+ \subset 1a$  analogue ( $K_{\text{ass}} = 2.5 \times 10^3 \text{ M}^{-1}$ ). This result, in addition to the modification of the H-bond donating ability of the  $^+\text{NH}_2$  group, can be primarily explained in terms of the substituent-induced changes in the aryl  $\pi$ -system according to the electrostatic model of Hunter and Sanders [20] or the “polar/ $\pi$ ” model of Cozzi and Siegel [21]. Thus, the presence of an EW-substituent (*p*-Cl) at the *para*-position of dibenzylammonium axle  $3a^+$ , lowers the  $\pi$ -electron density on its aromatic rings and increases the affinity toward the  $\pi$ -electron rich calix cavity of  $1a$  [19]. Unsurprisingly, the stability constants of complexes  $3c^+ \subset 1a$ ,  $3d^+ \subset 1a$ , and  $3e^+ \subset 1a$  are decreased by the presence of ED-substituents (*p*-OMe, *p*-OH, and *p*-Me, respectively), which increase the  $\pi$ -electron density on the aromatic rings of the corresponding dibenzylammonium axle [19]. Finally, through a Hammett-type plot, a linear free-energy relationship (LFER) between the  $K_{\text{ass}}$  values and the electronic nature of the X substituents on the aryl rings of the dibenzylammonium axles (Hammett’s constant) was evidenced, which may be mainly ascribed to the propensity of the substituted aromatic ring of the  $3a-e^+$  axles to become involved in  $\pi$ - $\pi$  interactions with the electron-rich aromatic cavity of  $1a$  [19].

Regarding the kinetic aspects of the threading process of calixarene-wheels with dialkylammonium cations, it was evidenced that the time necessary to reach the threading equilibrium are particularly sensitive to the length of the axle. Thus, while with short dipentyl/dibenzylammonium axles the threading equilibrium is reached immediately after mixing with both calix[6]arene wheels  $1a$  and  $1b$  [17], with a longer axle such as  $4^+$  72 h at 60 °C are necessary to reach the formation equilibrium of  $4^+ \subset 1a$  and  $4^+ \subset 1b$  pseudo[2]rotaxanes (Fig. 30.3) [22].

In a similar way, the threading abilities with dialkylammonium axles are also profoundly influenced by the dimension of the calix-wheel. In fact, differently by the 24-membered calix[6]arene-wheel, the 32-membered calix[8]arene macroring  $4^{23}$  does not give the *through-the-annulus* threading with TFPB salts of

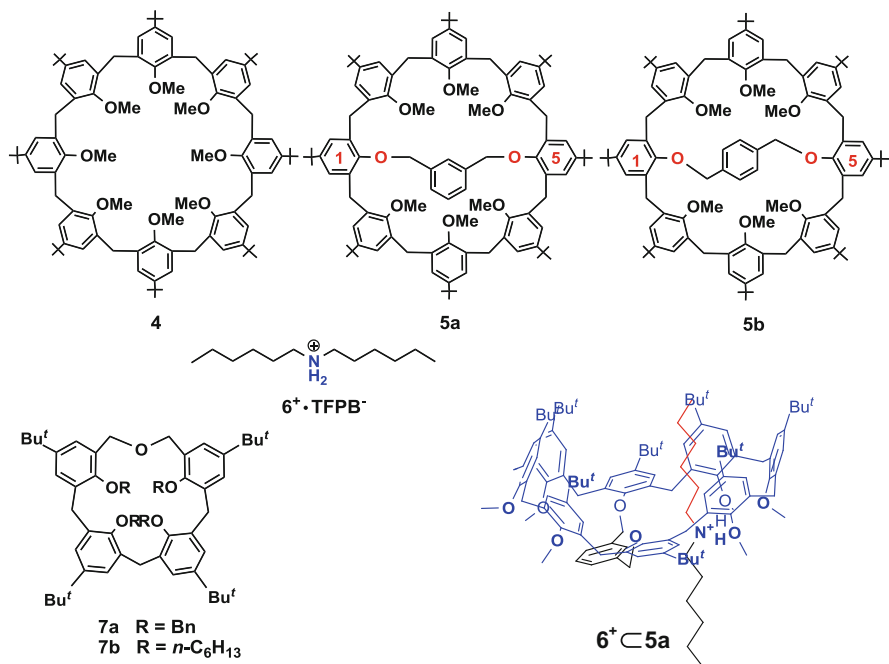


**Fig. 30.6** Calix[8]arene and dihomooxacalix[4]arene hosts

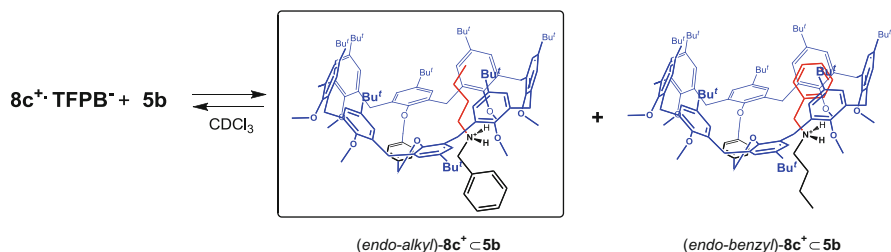
dialkylammonium cations likely because of the lower preorganization due to its larger dimension. To overcome this problem, a partial rigidification of the calix[8]arene skeleton by intramolecular bridging (e.g.: **5a** and **5b**) is necessary to favour the threading process with di-*n*-alkylammonium axes (Fig. 30.6).

Thus, 1D and 2D NMR studies indicated that 1,5-bridged calix[8]arenes with a *meta*-xylylene bridge **5a** gave a 1:1 wheel/thread stoichiometry [23], in which one dihexylammonium axle  $6^+$  was threaded into one of the two 24-membered subcavities of the calix[8]-wheel. Analogously, the *para*-xylylene bridged calix[8]arene **5b** was threaded by dialkylammonium axle  $6^+$  into one of the two 25-membered subcavities [23].

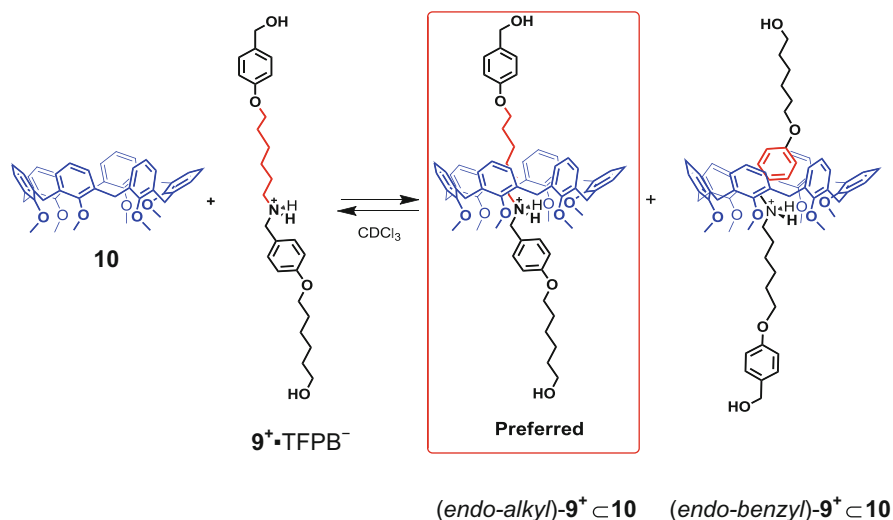
Finally, it was found that the smaller 18-membered dihomooxacalix[4]arene macrocycling (i.e.: **7a–b**) cannot give the *through-the-annulus* threading with dialkylammonium cations because of its small dimension [24]. However, the macrocycle is able to complex such ions into its cavity, which can only be accommodated in a hook-like conformation [24].

Interestingly, the applicability of the weakly coordinating TFPB anion in the induction of the threading of dialkylammonium cation with macrocycles is quite general. In fact, 2 years later with respect to our first report [17], Chiu and coworkers [25] showed that by replacing the counterion of dibenzylammonium cations from hexafluorophosphate to TFPB significantly increased the affinity of





**Scheme 30.1** Formation of the oriented  $(endo\text{-}alkyl)\text{-}8c^+ \subset 5b$  pseudo[2]rotaxane



**Scheme 30.2** Stereoprogrammed formation of the oriented  $(endo\text{-}alkyl)\text{-}9^+ \subset 10$  calix-pseudo[2]rotaxane

*threading of a directional alkylbenzylammonium axle through a hexaalkoxycalix[6]arene occurs with an endo-alkyl preference.*

The *endo-alkyl* rule was observed also with larger calix[8]arene hosts [23]. In fact, when the TFPB<sup>−</sup> salt of butylbenzylammonium **8c**<sup>+</sup> was added to a CDCl<sub>3</sub> solution of host **5b** (Scheme 30.1), the <sup>1</sup>H NMR spectrum of the mixture clearly indicated that the  $(endo\text{-}alkyl)\text{-}8c^+ \subset 5b$  pseudo[2]rotaxane stereoisomer (Scheme 30.1) had been exclusively formed [23]. Interestingly, *meta*-xylylene bridged host **5a** does not give threading with axle **8c**<sup>+</sup>, likely because of the smaller dimension of the two 24-membered sub-macrorings with respect to the *para*-bridged analogue **5b** [23].

Interestingly, the *endo-alkyl* rule was also observed for the longer alkylbenzylammonium axle **9**<sup>+</sup> which, in presence of the *de-tert*-butylated calix-wheel **10** in CDCl<sub>3</sub>, gave exclusively the *endo-alkyl* stereoisomer of **9**<sup>+</sup>⊂**10** pseudo[2]rotaxane (Scheme 30.2) [28].



**Fig. 30.8** Threads **11a–d** and **12a–c**

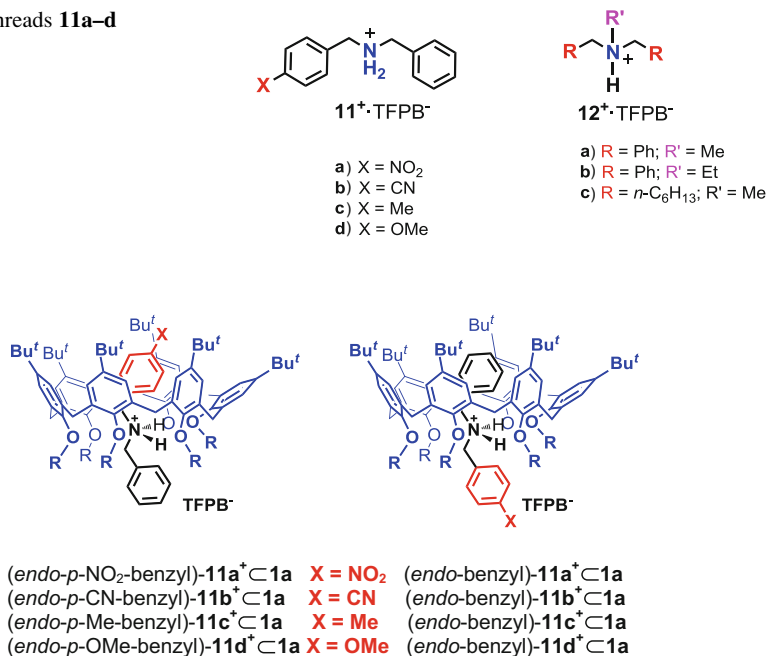
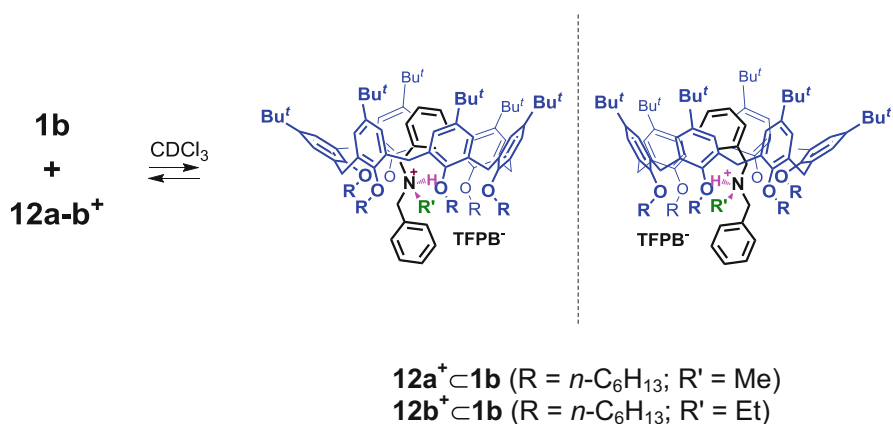


**Fig. 30.9** Dibenzylammonium-based calix-pseudo[2]rotaxane stereoisomers

As mentioned above, the affinity of the calix[6]arene-wheel **1a** toward dibenzylammonium axles is increased by increasing the EW nature of its X *para*-substituent (Figs. 30.1, 30.3, and 30.8) favoring  $\pi$ – $\pi$  interactions with the electron-rich calix-cavity of **1a** [19]. On the basis of these results, we have envisioned that the *endo*-cavity orientation of unsymmetrical axles **11a–d**<sup>+</sup> (Fig. 30.8), bearing only one *p*-X-substituted benzyl group, could be driven by the EW or ED nature of the X *para*-substituent [19].

In fact, the threading of dibenzylammonium axles **11a–d**<sup>+</sup> with calix-wheel **1a** can give rise to the two *endo*-benzyl and *endo-p*-X-benzyl orientational pseudorotaxane stereoisomers (Fig. 30.9) [19]. In particular, the threading of benzyl-*p*-NO<sub>2</sub>-benzylammonium **11a**<sup>+</sup> with calix-wheel **1a** in CDCl<sub>3</sub> led to the formation of the (*endo-p*-NO<sub>2</sub>-benzyl)-**11a**<sup>+</sup>⊂**1a** in a 95:5 ratio with respect to the (*endo*-benzyl)-**11a**<sup>+</sup>⊂**1a** stereoisomer [19].

Of course, the observed stereoselectivity can be justified on the basis of the greater aptitude of the electron-poor *p*-NO<sub>2</sub>-substituted aromatic ring of axle **11a**<sup>+</sup> to become involved in  $\pi$ – $\pi$  interactions with the electron-rich aromatic cavity of **1a** [19]. Interestingly, the corresponding *p*-CN-thread **11b**<sup>+</sup> gave the (*endo-p*-CN-benzyl)-**11b**<sup>+</sup>⊂**1a** pseudorotaxane in a 90:10 ratio with respect to the (*endo*-benzyl)-**11b**<sup>+</sup>⊂**1a** stereoisomer (Fig. 30.9) [19]. Thus, the presence of an EW-substituent (X = CN) with a Hammett's constant smaller than the nitro group ( $\sigma_{\text{CN}} = 0.71$ ,  $\sigma_{\text{NO}_2} = 0.78$ ) lowers the stereoselectivity of the threading



**Scheme 30.3** Formation of the chiral  $\mathbf{12a}^+ \subset \mathbf{1b}$  and  $\mathbf{12b}^+ \subset \mathbf{1b}$  pseudorotaxanes

process. On the other hand, the presence of ED-groups with a negative Hammett's constant should reverse the above observed preference for the *endo-p*-X-benzyl stereoisomer [19]. In fact, the *p*-Me-thread  $\mathbf{11c}^+$  preferentially gave the (*endo*-benzyl)- $\mathbf{11c}^+ \subset \mathbf{1a}$  pseudorotaxane in a 70:30 ratio with respect to the (*endo-p*-Me-benzyl)-stereoisomer ( $\sigma_{\text{Me}} = -0.14$ ). To corroborate this results, the presence of the OMe group in  $\mathbf{11d}^+$ , with a more negative Hammett's para constant ( $\sigma_{\text{OMe}} = -0.27$ ), increases the stereoisomeric ratio to 85:15 in favor of the *endo*-benzyl- stereoisomer [19].

A very peculiar stereochemical behaviour was found by threading  $\mathbf{1b}$  with tertiary *N*-alkyl-dibenzylammonium axles  $\mathbf{12a,b}^+$  (Scheme 30.3) [29]. It is worthy to note that the direct threading of such tertiary ammonium cations is scarcely investigated in the crown-ether series because of the very labile pseudorotaxanes, which can only be formed in very low yields (<3 %) [30]. Thanks to the induced effect of the superweak TFPB anion a surprising percentage of formation of 60% and an apparent association constant of  $1.1 \times 10^3 \text{ M}^{-1}$  was observed for  $\mathbf{12a}^+ \subset \mathbf{1b}$  pseudorotaxane. A close inspection of 1D and 2D NMR spectra of  $\mathbf{12a}^+ \subset \mathbf{1b}$  clearly evidenced the presence of a nitrogen stereogenic center, which makes chiral the entire pseudo[2]rotaxane architecture [29].

This peculiar chirality was generated by the directionality of the cone calix[6]arene wheel which upon threading with  $\mathbf{12a}^+$  differentiates the two benzylic units around the ammonium center (Scheme 30.3) [29]. It is here worth noting that while beautiful examples of dissymmetric supramolecules assembled from achiral molecules are known [31], to the best of our knowledge, this is the first example of a chiral supramolecule in which an atomic stereogenic center is generated supramolecularly.

Another interesting stereochemical feature was observed in the threading of  $\mathbf{1b}$  with tertiary *N*-methyldihexylammonium axle  $\mathbf{12c}^+$ , which, in addition to the usual  $\mathbf{12c}^+ \subset \mathbf{1b}$  pseudorotaxane with a cone calix[6]-wheel, gives also rise to the stereoisomeric  $\mathbf{12c}^+ \subset \mathbf{1b}^{1,2,3\text{-alt}}$  pseudorotaxane containing a calix[6]arene macrocycle in

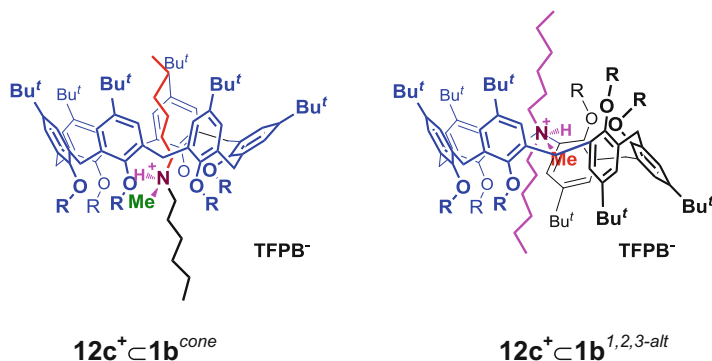


**Fig. 30.10** Stereoisomeric pseudorotaxanes containing a calix[6]arene macrocycle in the cone or in the 1,2,3-alternate conformation

the 1,2,3-alternate conformation (Fig. 30.10) [29]. To the best of our knowledge, this is the first example of a threaded calix[6]arene in a conformation different from the cone one and we can expect that the fine control of this isomerism could give rise to further yet unexplored stereochemical features.

### 30.4 Stereochemical Features of Calixarene/Ammonium-Based Pseudo[3]rotaxane

From the above discussion, it is easy to image that additional interesting stereochemical features can be obtained in the formation of calixarene-based pseudo[3]rotaxane architectures, in which two calix-wheels are threaded along one axle. In fact, because of the three-dimensional directional nature of the two calix[6]arene wheels, in these instances a stereoisomerism (Fig. 30.7) can be generated which is related to their different relative orientation. In particular, three different stereoisomers can be obtained, which have been termed as *head-to-head* (*H,H*), *head-to-tail* (*H,T*) and *tail-to-tail* (*T,T*) (Fig. 30.11a). We have demonstrated that the stereocontrolled direct preparation of any given stereoisomer can be obtained by the rational choice of the threading element exploiting the above mentioned **endo-alkyl rule**, that is the preference for the *endo*-alkyl complexation over the *endo*-benzyl one. Thus, we designed the bis-(alkylbenzylammonium) axle  $13^{2+}$  (Fig. 30.11) in which two alkylbenzylammonium motifs were connected by the alkyl ends to give a thread exposing benzyl units at the two extremities. 1D and 2D NMR studies of the 1:2 mixture of **10** and  $13^{2+}$  in  $CDCl_3$  showed that in accordance with the *endo*-alkyl rule, the *head-to-head* pseudo[3]rotaxane (*H,H*)- $13^{2+} \subset 10_2$  (Fig. 30.12), had been exclusively formed [32].

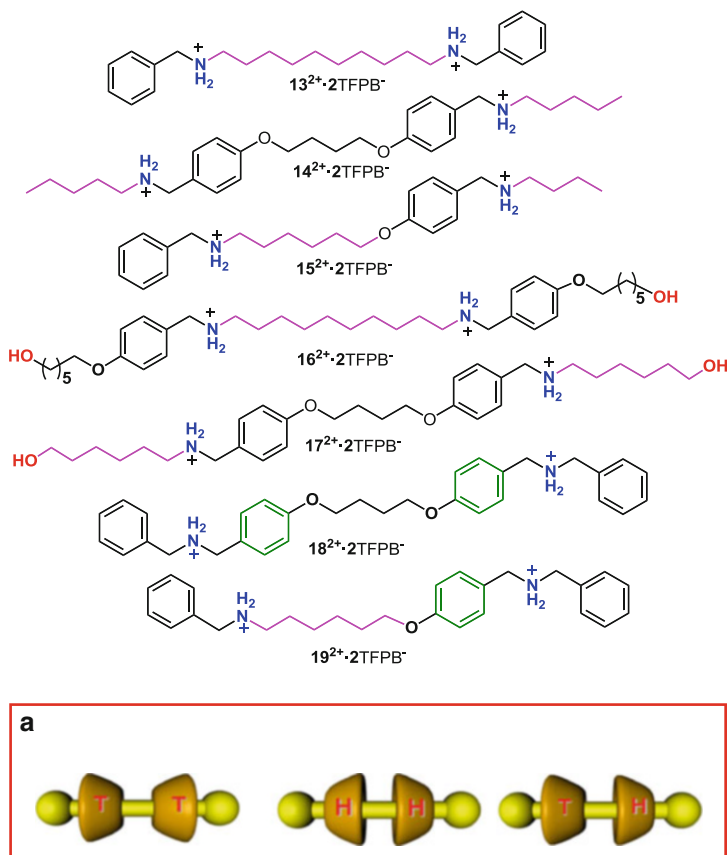


**Fig. 30.11** Structure of the bis-ammonium axles. (a) Cartoon representation of the three pseudo [3]rotaxane stereoisomers obtainable by threading of two directional wheels along a thread element

The formation of pseudo[3]rotaxane (*H,H*)-**13**<sup>2+</sup>⊂**10**<sub>2</sub> occurred with high efficiency. In fact, only a minimal amount of uncomplexed wheel **10** was present, while the singly threaded pseudo[2]rotaxane was below the detection limit [30].

Thus, by exploiting the *endo-alkyl rule*, the head/tail stereo-sequence of the two calix-wheels along a bis(alkylbenzylammonium) axle (Fig. 30.11a) can be controlled through the programmable connection of the two alkylbenzylammonium moieties of the axle [32]. In fact, when the two alkylbenzylammonium moieties were connected by the benzyl ends to give thread **14**<sup>2+</sup> exposing alkyl chains at the terminations, we observed the exclusive formation of the *tail-to-tail* stereosequence of the calix-wheels to give pseudo[3]rotaxane (*T,T*)-**14**<sup>2+</sup>⊂**10**<sub>2</sub> (Fig. 30.12). Finally, threading of the axle **15**<sup>2+</sup>, bearing an alkyl and a benzyl unit at the two extremities, with calix-wheel **10** led to the formation of the *head-to-tail* stereo-sequence (*H,T*)-**15**<sup>2+</sup>⊂**10**<sub>2</sub> (Fig. 30.12).

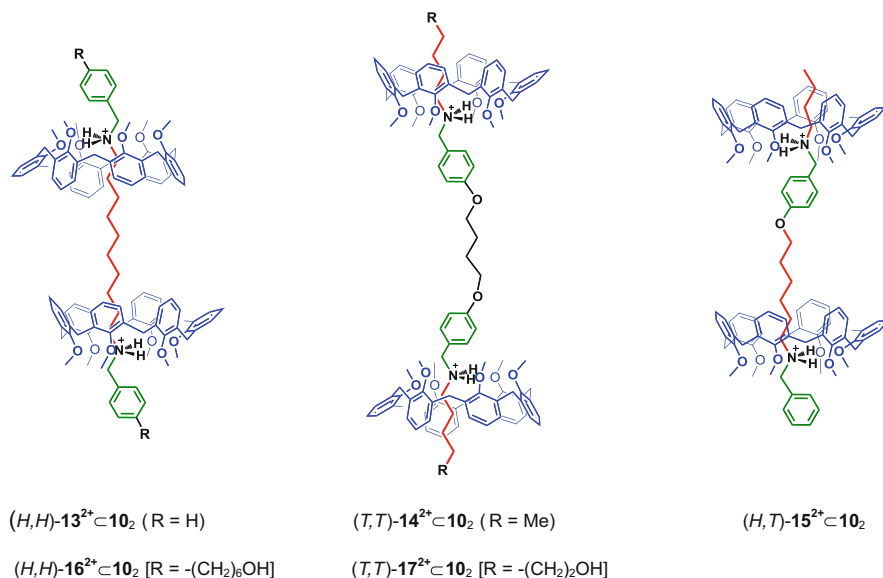


**Fig. 30.12** Structures of (*H,H*)-, (*T,T*)-, and (*H,T*)-pseudo[3]rotaxane stereoisomers obtained by threading of **10** with axles  $13^{2+}$ – $17^{2+}$

Interestingly, the stereosequence of the two calix-wheels was programmable also with longer and functionalized bis(alkylbenzylammonium) axles  $16^{2+}$  and  $17^{2+}$  which led to the formation of nanosized pseudo[3]rotaxanes (*H,H*)- $16^{2+} \subset 10_2$  and (*T,T*)- $17^{2+} \subset 10_2$  (Fig. 30.12) in which the *endo-alkyl rule* was again observed.

The extension of the *endo-alkyl rule* allowed the formation of the first examples of oriented handcuff pseudorotaxane architectures with a predefined stereochemistry [27]. With respect to the use of a single calixarene, a further synthetic challenge is represented by the use of a double-calixarene like **20** (Fig. 30.13), because of the inherent difficulty in controlling the relative orientation of the wheels within the entire pseudorotaxane system. In fact, the threading of **20** with a bis-ammonium axle (e.g.,  $14^{2+}$  and  $17^{2+}$ ) could give rise again to the three stereoisomeric handcuff pseudorotaxane structures, [27] with the two calix-wheels in three different relative orientations, *head-to-head* (*H,H*) (**I**), *tail-to-tail* (*T,T*) (**II**), and *head-to-tail* (*H,T*) (**III**) (Fig. 30.13).

Naturally, the linkage of the two calix-wheels in **20** through a short *m*-xylylene spacer could favor a different anomalous stereochemistry with respect to that predicted by the “*endo-alkyl rule*”. However, 1D and 2D NMR studies clearly evidenced the formation of pseudorotaxane (*T,T*)- $14^{2+} \subset 20$  (or (*T,T*)- $17^{2+} \subset 20$ ) in accordance with the stereochemistry predicted by the *endo-alkyl rule* [27] (Scheme 30.4).

The *endo-alkyl rule* was also confirmed in the formation of pseudo[3]rotaxane topologies in which two alkylbenzylammonium axles were threaded into the double-calix[6]arene system **20** (Fig. 30.14) [33]. In fact, among the three possible

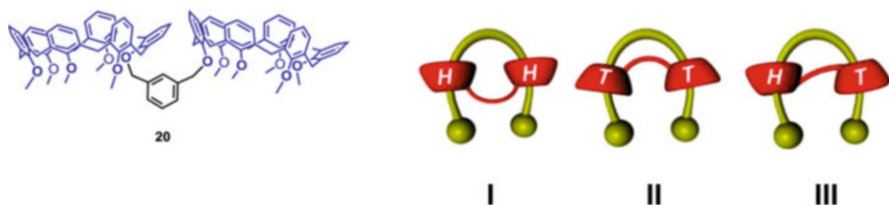
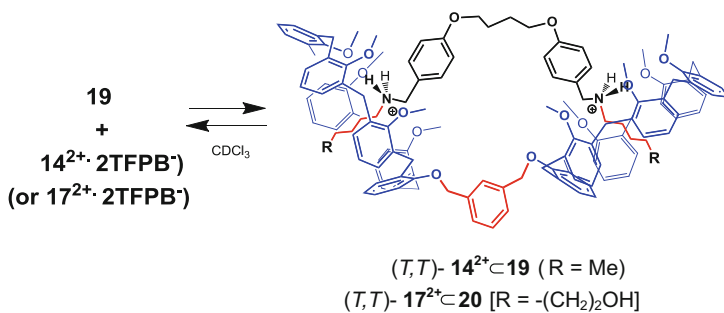


**Fig. 30.13** Structure of the double-calix[6]arene host **20**. (I–III) Cartoon representation of the three possible handcuff pseudorotaxane stereoisomers obtainable by threading of **20**



**Scheme 30.4** Formation of handcuff pseudorotaxanes  $(T,T)\text{-}14^{2+} \subset 20$  and  $(T,T)\text{-}17^{2+} \subset 20$

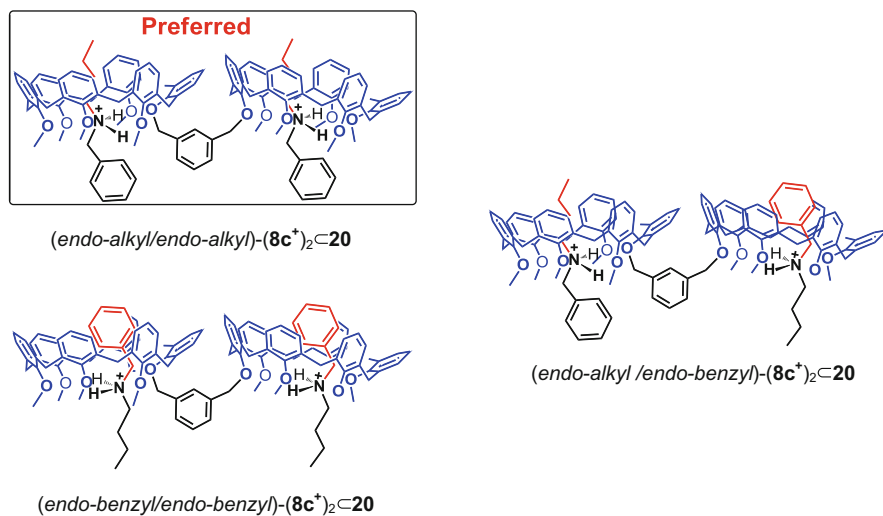


**Fig. 30.14** Structure of the three possible stereoisomers obtainable by threading of **20** with  $8\text{c}^+$

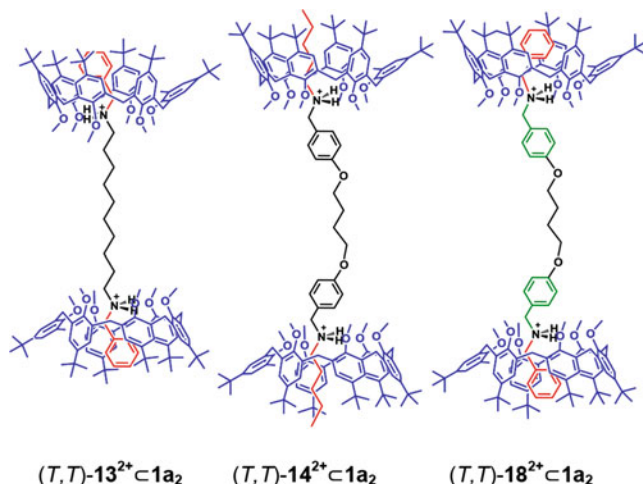


**Fig. 30.15** Structures of  $(T, T)$ -pseudo[3]rotaxanes stereoisomers obtained by threading of **1a** with axles  $\mathbf{13}^{2+}$ ,  $\mathbf{14}^{2+}$ , and  $\mathbf{18}^{2+}$

directional double-threaded pseudo[3]rotaxanes (Fig. 30.14), the  $(endo\text{-}alkyl/endo\text{-}alkyl)\text{-}(\mathbf{8c}^+)_2 \subset \mathbf{20}$  was exclusively formed [33].

The presence of *tert*-butyl groups at the *exo* rim of the calix-wheel strongly influence the stereochemistry of the formation of pseudo[3]rotaxanes. We have examined the threading of the *tert*-butylated calix-wheel **1a** with the benzyl-exposing thread  $\mathbf{13}^{2+}$ , which gives rise to an *head-to-head* stereo-sequence with hexamethoxycalix[6]arene **10** bearing H-atoms at the upper rim [32]. Unexpectedly, the 1D and 2D NMR analysis revealed the double *endo*-benzyl threading of  $\mathbf{13}^{2+}$  to give the *tail-to-tail* pseudo[3]rotaxane  $(T, T)\text{-13}^{2+} \subset \mathbf{1a}_2$  (Fig. 30.15) [32]. A total binding constant of  $2.5 \times 10^5 \text{ M}^{-2}$  was evaluated by signal integration, which was significantly lower than that reported for the  $(H, H)\text{-13}^{2+} \subset \mathbf{10}_2$  analogue ( $5.8 \times 10^6 \text{ M}^{-2}$ ) bearing two *de-tert*-butylated calix-wheels **10** on the same axle [32]. Clearly, the change from the *head-to-head* to the *tail-to-tail* stereo-sequence by replacing *p*-H-**10** with *p*-*t*-Bu-calix[6]-wheel **1a**, has to be attributed to the steric encumbrance of the *t*-Bu groups in **1a**. This conclusion was also confirmed by OPLS calculations (in  $\text{CHCl}_3$ , GB/SA model solvent), which favoured  $(T, T)\text{-13}^{2+} \subset \mathbf{1a}_2$  with respect to  $(H, H)\text{-13}^{2+} \subset \mathbf{1a}_2$  stereoisomer by an energy difference of 4 kcal/mol and evidenced a steric crowding between the facing calixarene *t*-Bu groups in the latter [32].

In a similar way, thread  $\mathbf{14}^{2+}$  preferred the *tail-to-tail* stereo-sequence with *p*-*t*-Bu-calix[6]-wheel **1a** to give  $(T, T)\text{-14}^{2+} \subset \mathbf{1a}_2$  with an apparent association constant of  $2.2 \times 10^3 \text{ M}^{-2}$ , which was again significantly lower than that observed for the formation of pseudo[3]rotaxane  $(T, T)\text{-14}^{2+} \subset \mathbf{10}_2$  with *de-tert*-butylated calix-wheels. These data clearly indicated the greater affinity of the bis(alkylammonium) axles  $\mathbf{13}^{2+}$  and  $\mathbf{14}^{2+}$  toward *de-tert*-butylated calix-wheel **10** with respect to the *tert*-butylated analogue **1a**. Regarding the behaviour of the bis(dibenzylammonium) thread  $\mathbf{18}^{2+}$  (Fig. 30.11), surprisingly no complexation was observed with *p*-H-

calix-wheel **10**, while with the tert-butylated analogue **1a** the pseudo[3]rotaxane architecture  $(T,T)$ -**13**<sup>2+</sup>⊂**1a**<sub>2</sub> (Fig. 30.15) was formed with a *tail-to-tail* stereochemistry and an apparent association constant of  $1.8 \times 10^4 \text{ M}^{-2}$ .

### 30.5 Pseudorotaxanes with Self-Sorted Sequence and Stereochemistry

Self-sorting is one of the most fundamental processes in living systems, which led complex mixtures of biomolecules (e.g., proteins, nucleic acids, oligosaccharides, lipids) to self-organize into larger biomacromolecular assemblies (e.g., DNA double-helix, multienzyme complexes, ribosomes) and finally into cellular compartments essential for the development of life on Earth.

Inspired by the living systems, over the last decade, artificial self-sorting systems have emerged as a high-interest research area in the field of supramolecular chemistry. Thus, like the natural ones, the artificial self-sorting systems are characterized by the selective formation of a defined and small number of supramolecular assemblies out of a significantly larger number of possible ones. Obviously, the efficiency of any artificial self-sorting systems can be related to its ability to discriminate between individual species with increased structural similarity. In this regard, a fundamental step toward mimicking the efficiency and complexity of natural systems is to define an artificial system able to sort species that, at the same time, are differing both at the sequence and stereochemical level.

Based on the stereochemical results exemplified by the pseudo[3]rotaxane structures reported in Figures 30.12 and 30.15, the question arises whether these pseudo[3]rotaxanes are also capable of self-sorting at the sequence and stereochemical level: does an axle choose a couple of identical or different wheels when they are competing for binding and what is then their relative orientation?

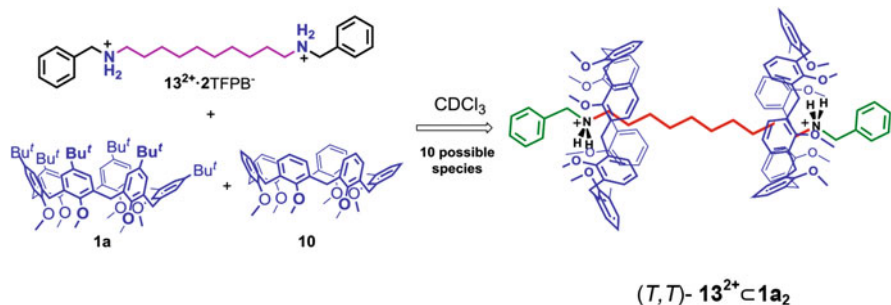
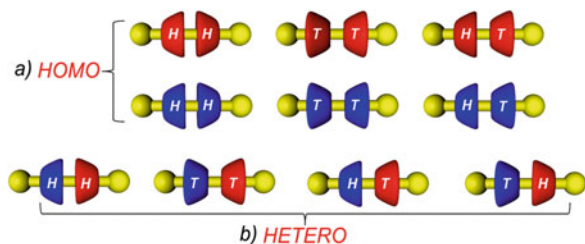
Starting with the simpler case of a [1+2] sorting system [34], the benzyl-exposing symmetrical axle **13**<sup>2+</sup> and two equivalents of each of *p*-H- **10** and *p*-*t*-Bu-wheel **1a** were mixed in CDCl<sub>3</sub>. By this sorting system ten different homo- and heteropseudo[3]rotaxanes can form (Fig. 30.16).

A close inspection of the <sup>1</sup>H NMR spectrum of the mixture clearly evidenced the absence of signals of the known  $(T,T)$ -**13**<sup>2+</sup>⊂**1a**<sub>2</sub> pseudo[3]rotaxane as well as that of any heteropseudorotaxane [34]. In contrast,  $(H,H)$ -**13**<sup>2+</sup>⊂**10**<sub>2</sub> (Scheme 30.5) was clearly present. In conclusion, from the ten possible pseudorotaxane structures, the *head-to-head* homo-pseudo[3]rotaxane  $(H,H)$ -**13**<sup>2+</sup>⊂**10**<sub>2</sub> was self-sorted as the only product (Scheme 30.5). This result is in good agreement with the 23-fold higher binding constant of  $(H,H)$ -**13**<sup>2+</sup>⊂**10**<sub>2</sub> with respect to that of  $(T,T)$ -**13**<sup>2+</sup>⊂**1a**<sub>2</sub> [34].

The above results can be generalized with a “molecular code” [34] (Fig. 30.17) which defines the affinities between axles and calix-wheels by means of the following rules. *Rule 1 (social behaviour)*: (Fig. 30.17a) benzylalkylammonium sites on diammonium axles (e.g. **13**<sup>2+</sup>) select the non-*tert*-butylated calix[6]arene



**Fig. 30.16** All species that can form in mixtures of two different wheels and one axle



**Scheme 30.5** A [1+2] sorting system: sorting of a *head-to-head* homo-pseudo[3]rotaxane

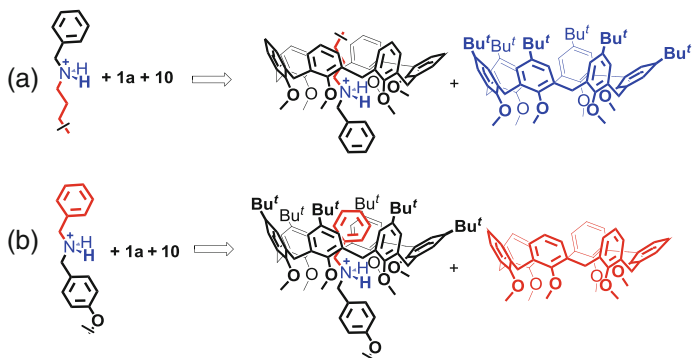
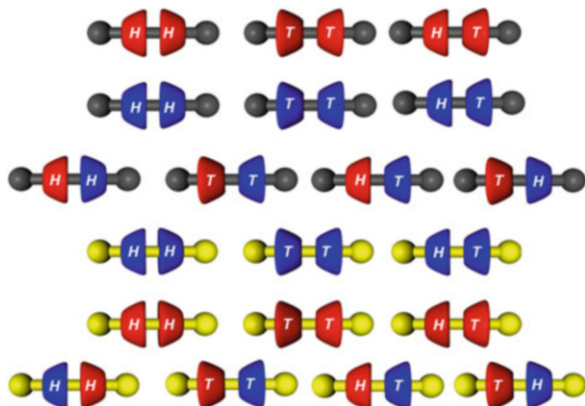


**Fig. 30.17** The “molecular code” [32] with respect to both benzylalkylammonium and benzyl-*p*-alkoxybenzylammonium sites

wheel (e.g. **10**) leaving uncomplexed the *tert*-butylated one (e.g. **1a**). *Rule 2* (*stereochemistry*): (Fig. 30.17a) threading of a directional alkylbenzylammonium station (e.g. in  $13^{2+}$ ) through a non-*tert*-butylated hexaalkoxycalix[6]arene (e.g., **10**) occurs with an *endo*-alkyl preference [34].

In a second [1+2] self-sorting experiment, bis(dibenzylammonium) axle  $18^{2+}$  and wheels **10** and **1a** were mixed in a 1:2:2 ratio in  $CDCl_3$ . The corresponding  $^1H$  NMR spectrum clearly showed *endo*-benzyl resonances in the 4–6 ppm region corresponding to  $(T, T)-18^{2+} \subset 1a_2$  pseudo[3]rotaxane (Fig. 30.15) ruling out the

**Fig. 30.18** All species that can form in mixtures of two different wheels and two different axles



presence of other homo- or heteropseudorotaxanes [34]. On the basis of this result, the molecular code was then expanded with two new rules. *Rule 3 (social behaviour)*: (Fig. 30.17b) benzyl-*p*-alkoxybenzylammonium sites on a diammonium axle (e.g.  $\mathbf{18}^{2+}$ ) select the *tert*-butylated calix[6]arene (e.g.  $\mathbf{1a}$ ) leaving uncomplexed the *de-tert*-butylated one (e.g.  $\mathbf{10}$ ). *Rule 4 (stereochemistry)*: (Fig. 30.17b) threading of a benzyl-*p*-alkoxybenzylammonium site (e.g., in  $\mathbf{18}^{2+}$ ) by a *tert*-butylated hexaalkoxycalix[6]arene (e.g.  $\mathbf{1a}$ ) occurs with an *endo*-benzyl preference [34].

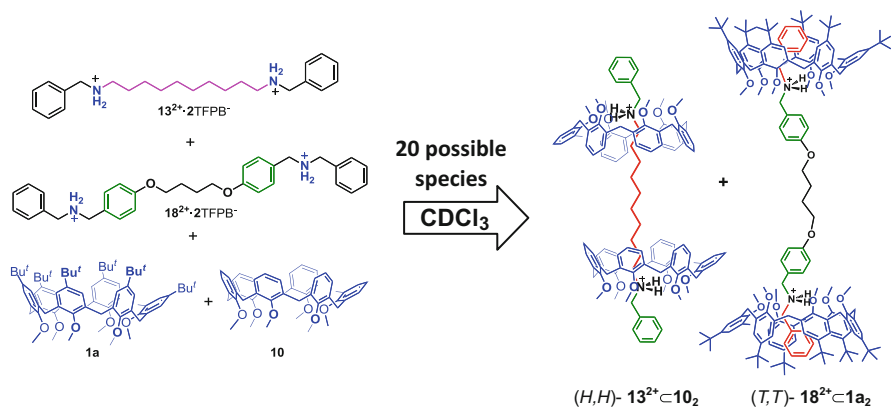
The validity of the complete molecular code was tested in a more complex [2 + 2] self-sorting experiment in which two different axles and two different wheels are mutually competing. As shown in Fig. 30.18, a total of 20 possible homo- and heteropseudo[3]rotaxanes can form with symmetrical axles.

In a [2 + 2] self-sorting experiment, axles  $\mathbf{13}^{2+}$  and  $\mathbf{18}^{2+}$  and wheels  $\mathbf{10}$  and  $\mathbf{1a}$  were mixed in a 1:1:2:2 ratio in  $\text{CDCl}_3$ . Analysis of the  $^1\text{H}$  NMR spectrum of this sorting mixture clearly indicated the presence of only two pseudo[3]rotaxane species, namely  $(H,H)\text{-}\mathbf{13}^{2+}\subset\mathbf{10}_2$  and  $(T,T)\text{-}\mathbf{18}^{2+}\subset\mathbf{1a}_2$  (Scheme 30.6) [34].

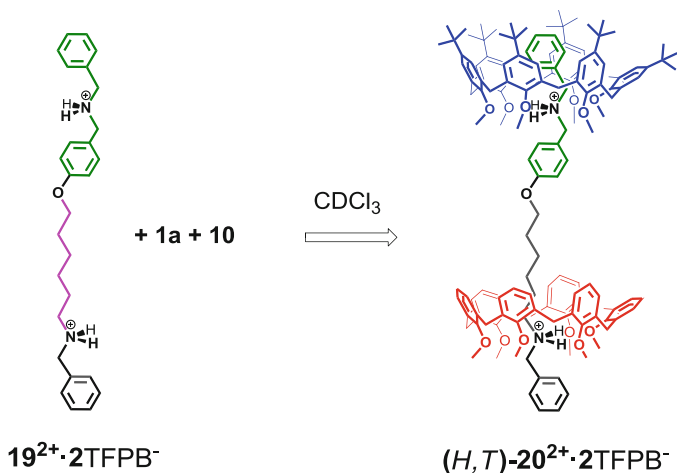
These results undoubtedly confirm the validity of the molecular code even for a more complex [2 + 2] self-sorting system, in which only 2 out of 20 possible pseudo[3]rotaxanes are stereospecifically formed [34].

In order to perform an integrative self-sorting between species that at the same time are differing both for the sequence and the stereochemistry of their components, the new constitutionally asymmetric axle  $\mathbf{19}^{2+}$  (Scheme 30.7) constituted by two different ammonium centers was designed and tested with two different calix-wheels  $\mathbf{1a}$  and  $\mathbf{10}$  [34]. In this instance, considering the possible relative orientation of the directional calix-wheels, a [1 + 2] system could give rise to a  $2 \times 4 = 8$  homopseudo[3]rotaxanes and  $2 \times 4 = 8$  hetero ones, with a total of 16 possible species (Fig. 30.19). Clearly, some of them are simultaneously isomeric at the sequence and stereochemical level [34].

Along the new thread  $\mathbf{19}^{2+}$  we “encoded” the sequence of alkylbenzylammonium and benzyl-*p*-alkoxybenzylammonium binding sites (Scheme 30.7). According to the above molecular code (Fig. 30.17), in the presence of  $\mathbf{10}$  and  $\mathbf{1a}$ ,

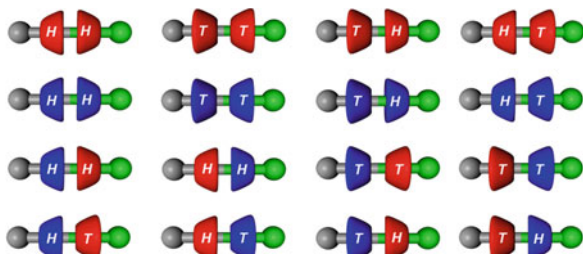


**Scheme 30.6** A [2+2] self-sorting experiment: sorting of only two pseudo[3]rotaxane species out of 20 possible ones



**Scheme 30.7** Integrative self-sorting. Formation of the (H,T)-20<sup>2+</sup> pseudo[3]rotaxane

**Fig. 30.19** All possible species that can be formed in the mixture constituted by two calix-wheels **1a** and **10** and the constitutionally asymmetrical axle **19<sup>2+</sup>**



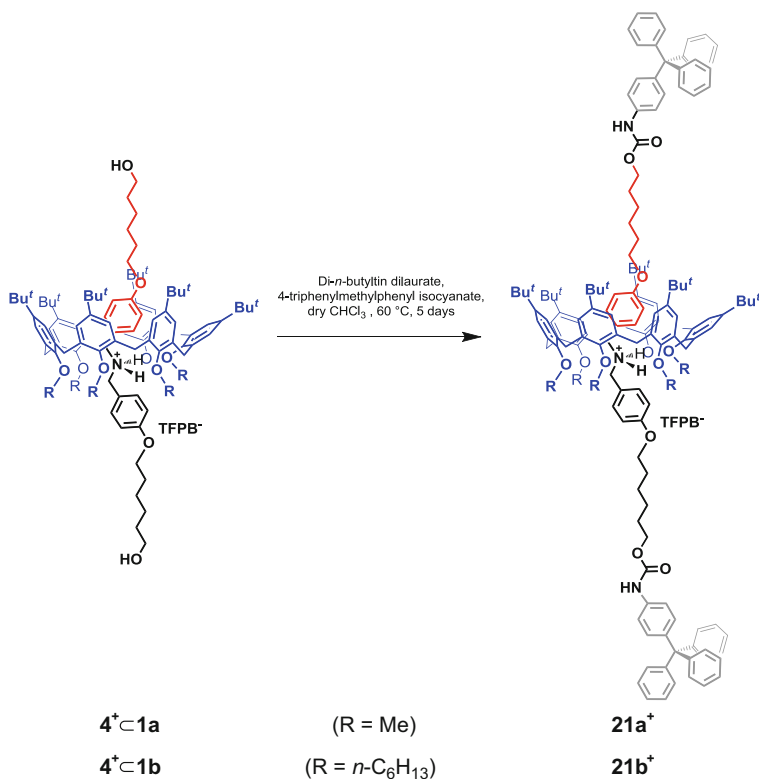
the first site should select the *endo*-alkyl binding of **10**, while the second site should prefer the *endo*-benzyl complexation of **1a**, which would result in the sorting of the sequence shown in Scheme 30.7 with the (*H,T*)-stereochemistry [34].

In accordance with this expectation, ESI(+) mass spectrum and 1D and 2D NMR spectroscopy clearly indicated the formation of the expected (*H,T*)-**20**<sup>2+</sup> pseudo[3]rotaxane [34].

### 30.6 Calixarene-Based Rotaxane Architectures

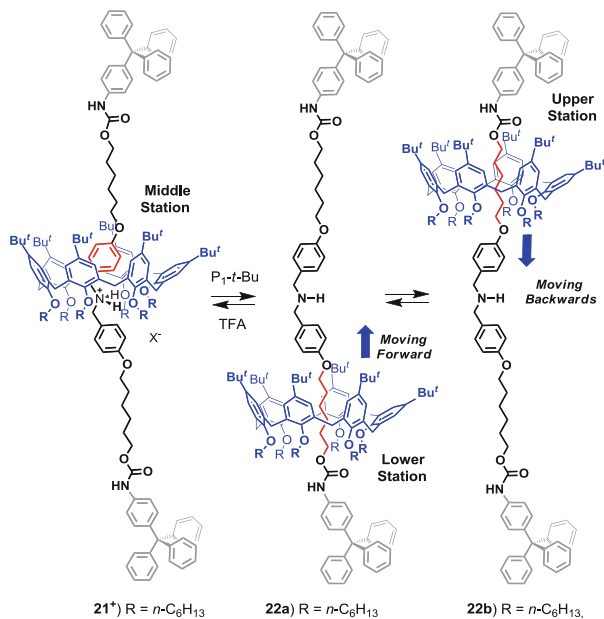
The first examples [22] of dialkylammonium-threaded calixarene rotaxanes **21a**<sup>+</sup> and **21b**<sup>+</sup> were obtained in 24 % and 32 % yields, respectively, by stoppering pseudo[2]rotaxanes **4**<sup>+</sup>⊂**1a** and **4**<sup>+</sup>⊂**1b** (Fig. 30.3 and Scheme 30.8) with 4-triphenylmethylphenyl isocyanate [22].

Upon deprotonation of **21b**<sup>+</sup>, by addition of phosphazene base P1-*t*-Bu, the hexahexyloxycalix[6]arene-wheel moves from the initial dibenzylammonium



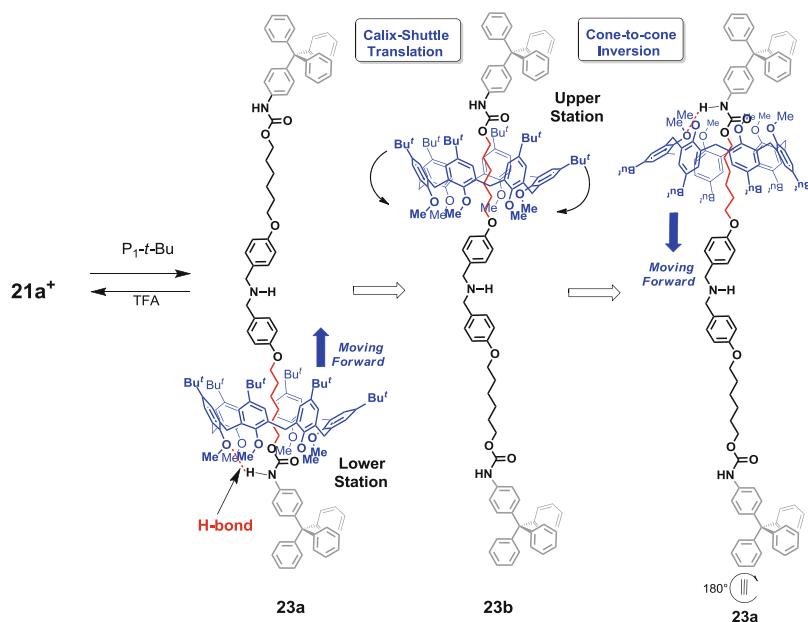
**Scheme 30.8** Synthesis of calix-rotaxanes **21a**<sup>+</sup> and **21b**<sup>+</sup>

**Scheme 30.9** Directional shuttling motion in cationic/neutral calix[6]arene-based [2]rotaxanes **21b<sup>+</sup>**/**22**



station (or middle station in Scheme 30.9) to a new position in which an aliphatic chain is inside the calix-cavity [22]. Because of the unsymmetrical nature of the calix[6]arene wheel, the two possible translational isomers (co-conformers), namely **22a** and **22b**, were both observed in a 6:4 ratio. In good accordance, MM3 calculations indicated that **22a** was only slightly more stable than **22b** by a small energy difference of 0.18 kcal/mol [22]. The acidic treatment of **22** fully restored the  $^1\text{H}$  NMR spectrum of cationic **21b<sup>+</sup>** (Scheme 30.9) demonstrating that this system acts as a molecular shuttle [22]. In fact, under acidic condition the calix-wheel encircles the benzylammonium unit (middle station in Scheme 30.9) of **21b<sup>+</sup>**, while in neutral **22** it travels back-and-forth between the lower and the upper station.

Interestingly, a peculiar behaviour was observed during the shuttling movement of the calix-wheel **1a** upon deprotonation of the calix-rotaxane **21a<sup>+</sup>** due to the presence of the small methoxy groups at its *endo* rim (Scheme 30.10) [22]. In fact, the corresponding neutral rotaxane **23** gave a broad  $^1\text{H}$  NMR spectrum which was ascribed to the **23a/23b** shuttling (Scheme 30.10), as described above for neutral **22**, which should be faster because of the smaller dimension of OMe groups [22]. 1D and 2D NMR studies of neutral **23** in  $\text{CDCl}_3$  at 253 K showed two sets of signals in a 97:3 ratio which were attributable to the slowly exchanging translational isomers **23a** and **23b**, respectively [22]. The most abundant isomer **23a** showed the calix-wheel at the lower station close to the urethane function engaging a strong H-bond between its NH and the calixarene oxygens (Scheme 30.10) [22]. Variable-temperature 1D and 2D NMR studies clearly evidenced the inversion of calix[6]



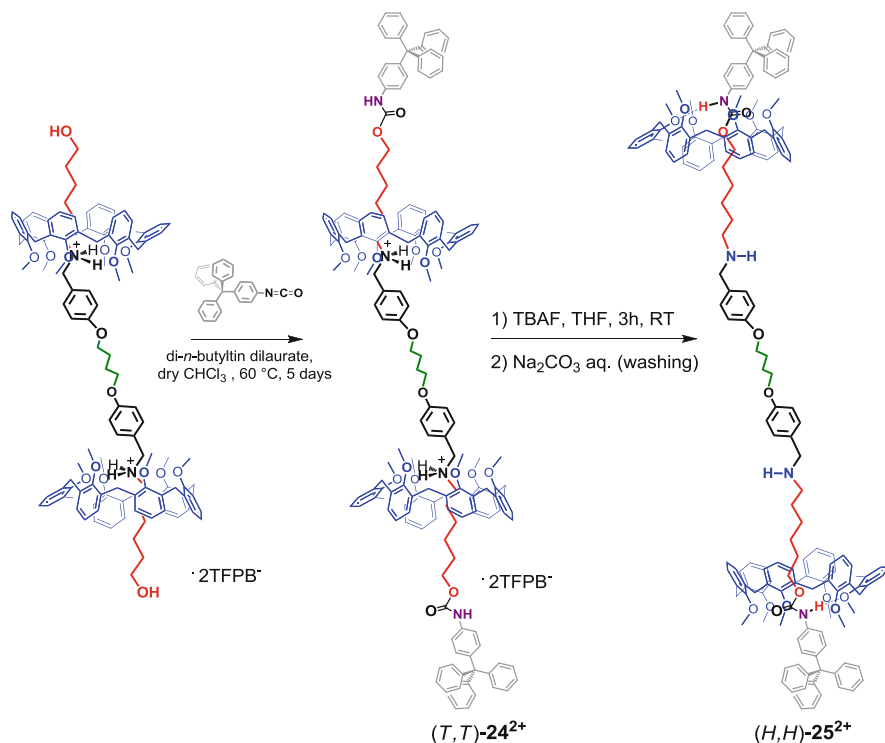
**Scheme 30.10** Combined translation/inversion motion of calix[6]-wheel in [2]rotaxane **21a<sup>+</sup>**

arene cone conformation of **23b**, which gives rise to a degenerate rotaxane system. This degeneration is the result of a combined motion of translation followed by a *cone-to-cone* inversion of the calix-shuttle, as represented in Scheme 30.10 [22].

A similar behaviour was observed for the nanosized [3]rotaxane architecture **24<sup>2+</sup>** obtained by stoppering of pseudo[3]rotaxane (*T,T*)-**17<sup>2+</sup>**⊂**10<sub>2</sub>** (Fig. 30.12 and Scheme 30.11) [35]. Upon neutralization of **24<sup>2+</sup>** to give **25**, the calix[6]arene wheels invert their original *tail-to-tail* orientation to a *head-to-head* one more suitable for the formation of stabilizing CONH⋯OR H-bonds between the N-H urethane groups and the calix-oxygens (Scheme 30.11) [22].

The acidic treatment of **25** fully restored the spectrum of cationic **24<sup>2+</sup>** (Scheme 30.11) demonstrating that this system acts as a molecular shuttle, which moves on a nanometer scale level.

The versatility of the threading of calixarene wheels with dialkylammonium and bis-ammonium threads prompted us to investigate the synthesis of more complex architectures such as an handcuff rotaxane [27]. As previously described, the threading of double-calix[6]arene **20** with bis-ammonium axle **17<sup>2+</sup>** led to the specific formation of the handcuff pseudorotaxane (*T,T*)-**17<sup>2+</sup>**⊂**20**, as predict by the *endo*-alkyl rule (Scheme 30.3). In order to permanently trap the handcuff architecture, this pseudorotaxane was then stoppered by reaction with 4-tritylphenyl isocyanate (Scheme 30.12) to give the first example of predefined orientational handcuff [2]rotaxane (*T,T*)-**26<sup>2+</sup>** in 28% yield [27].

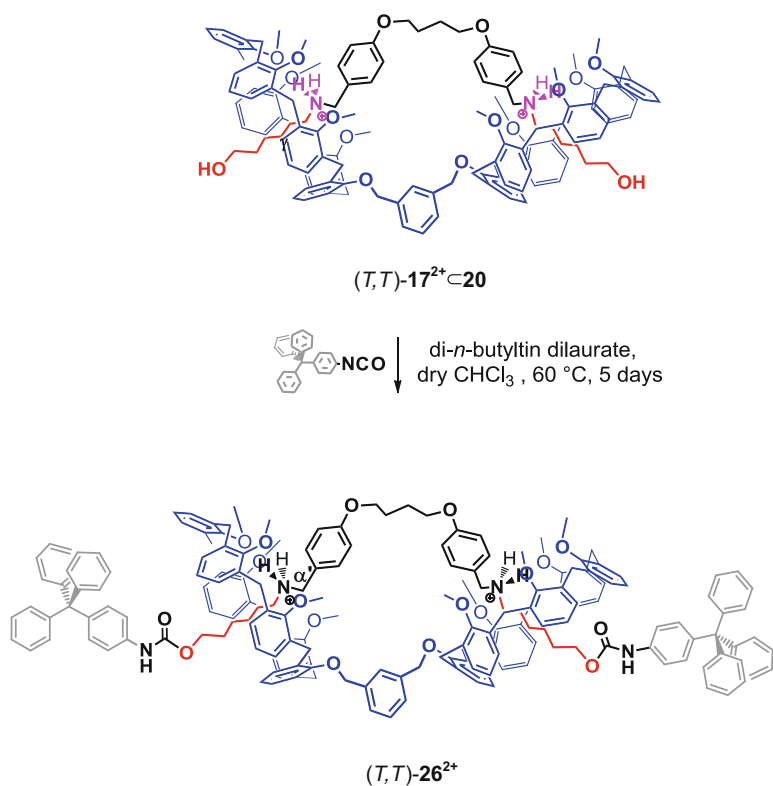


**Scheme 30.11** Stereoprogrammed synthesis of calix[3]rotaxane systems

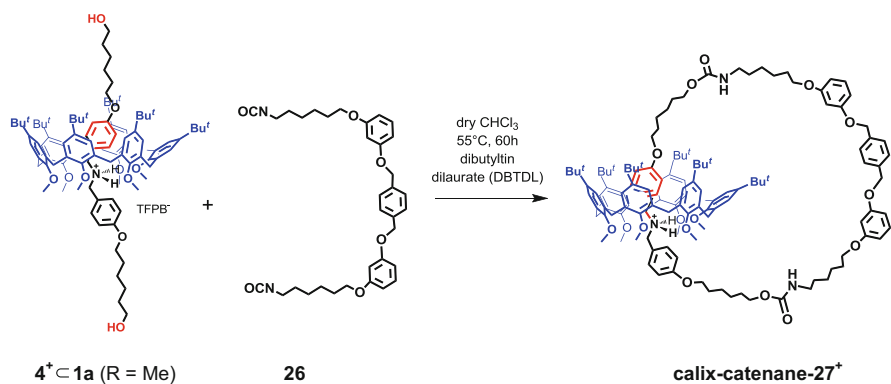
## 30.7 Calixarene-Based Catenane Architectures

The successful *through-the-annulus* threading of calix[6]arene macrocycle induced by the weakly coordinating TFPB anion could be exploited for the synthesis of the first example of a catenane obtained by catenation through the calixarene annulus [28]. In fact, only a few examples of catenanes have been previously reported, in which the calixarene annulus is not catenated at all, but simply acts as a “static” scaffold on which various catenated macrocycles are constructed, leaving the calix cavity completely unexploited [15a–e].

The previously described 4<sup>+</sup>⊂1a pseudo[2]rotaxane (Fig. 30.3) was the ideal candidate to attempt the synthesis of a calix-threaded [2]catenane by a [1 + 1] cyclocondensation clipping with the appropriate diisocyanate derivative **26** (Scheme 30.13). Therefore, pseudo[2]rotaxane 4<sup>+</sup>⊂1a, previously formed in dry CHCl<sub>3</sub> (starting from a 6 × 10<sup>−3</sup> M initial concentration of each precursor), and diisocyanate **3b** (6 × 10<sup>−3</sup> M in dry CHCl<sub>3</sub>) were added, at a rate of 0.6 mL/min from two distinct dropping reservoirs, to 2.0 mL of dry CHCl<sub>3</sub> under stirring in the presence of dibutyltin dilaurate (DBTDL) as the catalyst. Under these conditions

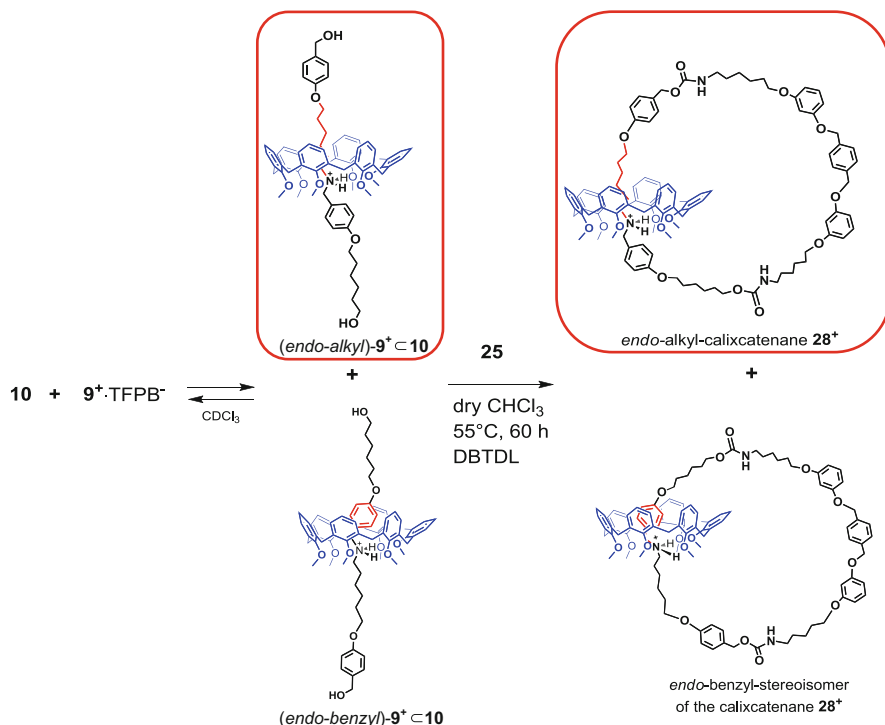


**Scheme 30.12** Stereoprogrammed synthesis of an handcuff calix-rotaxane



**Scheme 30.13** Synthesis of the calix-catenane  $27^+$





**Scheme 30.14** Stereoprogrammed synthesis of the oriented *endo*-alkyl-calixcatenane  $28^+$

the first example of *through-the-annulus*-threaded calix[2]catenane  $27^+$  (Scheme 30.13) was formed and isolated by semi-preparative HPLC in 30 % yield [28].

The macroring formed in the synthesis of calix-catenane  $27^+$  was constitutionally symmetrical (non-oriented), therefore, no stereochemical problems were present there. A new stereochemical feature can arise if one of the above macroring components is constitutionally nonsymmetrical (oriented); in fact, this orientation coupled to the directional nature of the cone-shaped calix-wheel would give rise to two possible catenane orientational isomers (Scheme 30.14) [28]. The first stereoprogrammed synthesis of one of them was possible by exploiting the directionality of threading of calix[6]-wheel  $10$  by alkylbenzylammonium axle  $9^+$  in the formation of the *(endo-alkyl)*- $9^+ \subset 10$  pseudo[2]rotaxane (Schemes 30.2). Thus, having secured the stereocontrol of the intermediate pseudo[2]rotaxane (Scheme 30.14), the [1+1] cyclocondensation with diisocyanate derivative  $26$  was performed by its dropwise addition to a solution  $6 \cdot 10^{-3}$  M of *(endo-alkyl)*- $9^+ \subset 10$  in dry  $\text{CHCl}_3$  at  $55^\circ\text{C}$ , in the presence of dibutyltin dilaurate (DBTDL) as the catalyst. Under these conditions, the first example of oriented *endo*-alkyl-calix [2]catenane  $28^+ \cdot \text{TFPB}^-$  was isolated in 23 % yield (Scheme 30.14) [28].

## 30.8 Conclusions

The “superweak anion” approach here described allows the *through-the-annulus* threading of calixarene macrocycles with functionalized dialkylammonium axes by exploiting the inducing effect of the weakly coordinating TFPB anion, which gives free “naked” dialkylammonium cations in solution. The efficiency and generality of this method permits the preparation of pseudorotaxane systems starting from scarcely functionalized calixarene hosts. A fine control of the stereochemical features of these systems can be obtained by exploiting subtle electronic effects or the so-called *endo*-alkyl rule to give stereoprogrammed synthetical precursors of calixarene-based interlocked architectures. In this way, the first examples of oriented calix[2 and 3]rotaxane and catenane architectures have been obtained. Considering the current enormous interest for mechanically interlocked molecules (MIMs) and the large variety of shapes and dimensions obtainable with calix[*n*]arene scaffolds, it is conceivable that the “superweak anion” approach to calixarene-based MIMs will pave the way to a quickly expanding new area of research.

**Acknowledgment** We thank the Italian MIUR (PRIN 20109Z2XRJ\_006) for financial support and the Centro di Tecnologie Integrate per la Salute (Project PONA3\_00138), Università di Salerno, for the 600 MHz NMR instrumental time.

## References

1. Sauvage, J. P.; Dietrich-Buchecker, C. *Molecular Catenanes, Rotaxanes and Knots: A Journey Through the World of Molecular Topology*; Wiley, 2008.
2. (a) Balzani, V.; Credi, A.; Venturi, M. *Molecular Devices and Machines: Concepts and Perspectives for the Nanoworld*; Wiley: Weinheim, 2008. (b) Collier, C. P.; Mattersteig, G.; Wong, E. W.; Luo, Y.; Beverly, K.; Sampaio, J.; Raymo, F. M.; Stoddart, J. F.; Heath, J. R. *Science* **2000**, *289*, 1172–1175. (c) Leigh, D. A.; Wong, J. K.; Dehez, F.; Zerbetto, F. *Nature* **2003**, *424*, 174–179.
3. Mullaney, B. R.; Thompson, A. L.; Beer, P. D. *Angew. Chem. Int. Ed.* **2014**, *53*, 11458–11462.
4. Leigh, D. A.; Marcos, V.; Wilson, M. R. *ACS Catal.* **2014**, *4*, 4490–4497.
5. Barat, R.; Legigan, T.; Tranoy-Opalinski, I.; Renoux, B.; Peraudeau, E.; Clarhaut, J.; Poinot, P.; Fernandes, A. E.; Aucagne, V.; Leigh, D. A.; Papot, S. *Chem. Sci.* **2015**, *6*, 2608–2613.
6. Ashton, P. R.; Campbell, P. J.; Chrystal, E. J. T.; Glink, P. T.; Menzer, S.; Philp, D.; Spencer, N.; Stoddart, J. F.; Tasker, P. A.; Williams, D. J. *Angew. Chem. Int. Ed. Engl.* **1995**, *34*, 1865–1869.
7. Harada, A.; Takashima, Y.; Nakahata, M. *Acc. Chem. Res.* **2014**, *47*, 2128–2140.
8. Kim, K. *Chem. Soc. Rev.* **2002**, *31*, 96–107.
9. Alvarez-Perez, M.; Goldup, S. M.; Leigh, D. A.; Slawin, A. M. Z. *J. Am. Chem. Soc.* **2008**, *130*, 1836–1838.
10. Ogoshi, T.; Aoki, T.; Ueda, S.; Tamura, Y.; Yamagishi, T.-a. *Chem. Commun.* **2014**, *50*, 6607–6609.
11. Asfari, Z.; Böhmer, V.; Harrowfield, J.; Vicens, J. *Calixarenes 2001*; Springer, 2001.

12. Gaeta, C.; Talotta, C.; Della Sala, P.; Margarucci, L.; Casapullo, A.; Neri, P. *J. Org. Chem.* **2014**, *79*, 3704–3708.
13. Talotta, C.; Gaeta, C.; Neri, P. *J. Org. Chem.* **2014**, *79*, 9842–9846.
14. Tedesco, C.; Erra, L.; Brunelli, M.; Cipolletti, V.; Gaeta, C.; Fitch, A. N.; Atwood, J. L.; Neri, P. *Chem. Eur. J.* **2010**, *16*, 2371–2374.
15. Different reports have shown examples of calixarene-based interlocked architectures in which the calixarene annulus is unthreaded, and acts as scaffold on which the threaded macrocycle is constructed: (a) Schlesier, T.; Metzroth, T.; Janshoff, A.; Gauss, J.; Diezemann, G. *J. Phys. Chem. B* **2011**, *115*, 6445 – 6454. (b) Phipps, D. E.; Beer, P. D. *Tetrahedron Lett.* **2009**, *50*, 3454 – 3457. (c) Li, Z.-T.; Zhao, X.; Shao, X.-B. in *Calixarenes in the Nanoworld*; Harrowfield, J.; Vicens, J., Eds.; Springer Dordrecht, 2007, Chapter 3, pp. 47–62 and references cited therein. (d) Wang, L.; Vysotsky, M. O.; Bogdan, A.; Bolte, M.; Böhmer, V. *Science* **2004**, *304*, 1312 – 314. (e) Gaeta, C.; Vysotsky, M. O.; Bogdana, A.; Böhmer, V. *J. Am. Chem. Soc.* **2005**, *127*, 13136 – 13137. For examples of threading of the calixarene annulus, see: (f) Arduini, A.; Ferdani, R.; Pochini, A.; Secchi, A.; Ugozzoli, F. *Angew. Chem. Int. Ed.* **2000**, *39*, 3453–3456.
16. Gattuso, G.; Notti, A.; Parisi, M. F.; Pisagatti, I.; Amato, M. E.; Pappalardo, A.; Pappalardo, S. *Chem. Eur. J.* **2010**, *16*, 2381–2385.
17. Gaeta, C.; Troisi, F.; Neri, P. *Org. Lett.* **2010**, *12*, 2092–2095.
18. Strauss, S. H. *Chem. Rev.* **1993**, *93*, 927–942.
19. Gaeta, C.; Talotta, C.; Neri, P. *Chem. Commun.* **2014**, *50*, 9917–9920.
20. Hunter, C. A.; Sanders, J. K. M. *J. Am. Chem. Soc.*, **1990**, *112*, 5525–5534.
21. Cozzi, F.; Cinquini, M.; Annunziata, R.; Siegel, J. S. *J. Am. Chem. Soc.* **1993**, *115*, 5330–5331.
22. Pierro, T.; Gaeta, C.; Talotta, C.; Casapullo, A.; Neri, P. *Org. Lett.* **2011**, *13*, 2560–2563.
23. Gaeta, C.; Talotta, C.; Casapullo, A.; Margarucci, L.; Neri, P. *J. Org. Chem.* **2013**, *78*, 7627–7638.
24. Gaeta, C.; Talotta, C.; Farina, F.; Teixeira, F. A.; Marcos, P. M.; Ascenso, J. R.; Neri, P. *J. Org. Chem.* **2012**, *77*, 10285–10293.
25. Chen, N.-C.; Chuang, C.-J.; Wang, L.-Y.; Lai, C.-C.; Chiu, S.-H. *Chem. Eur. J.* **2012**, *18*, 1896–1900.
26. Li, C.; Shu, X.; Li, J.; Fan, J.; Chen, Z.; Weng, L.; Jia, X. *Org. Lett.* **2012**, *14*, 4126–4129.
27. Ciao, R.; Gaeta, C.; Talotta, C.; Casapullo, A.; Margarucci, L.; Neri, P. *Org. Lett.* **2013**, *15*, 5694–5697.
28. Gaeta, C.; Talotta, C.; Mirra, S.; Casapullo, A.; Margarucci, L.; Neri, P. *Org. Lett.* **2013**, *15*, 116–119.
29. Talotta, C.; De Simone, N. A.; Gaeta, C.; Neri, P. *Org. Lett.* **2015**, *15*, 116–119.
30. Nakazono, K.; Kuwata, S.; Takata, T. *Tetrahedron Lett.* **2008**, *49*, 2397–2401.
31. (a) Rivera, J. M.; Nartin, T.; Rebek, J., Jr. *Science* **1998**, *279*, 1021 – 1023. (b) Prins, L. J.; Huskens, J.; de Jong, F.; Timmerman, P.; Reinhoudt, D. N. *Nature* **1999**, *398*, 498–502. (c) Pop, A.; Vysotsky, M. O.; Saadioui, M.; Böhmer, V. *Chem. Commun.* **2003**, 1124–1125.
32. Talotta, C.; Gaeta, C.; Pierro, T.; Neri, P. *Org. Lett.* **2011**, *13*, 2098–2101.
33. Ciao, R.; Talotta, C.; Gaeta, C.; Neri, P. *Supramol. Chem.* **2014**, *26*, 569–578.
34. Talotta, C.; Gaeta, C.; Qi, Z.; Schalley, C.; Neri, P. *Angew. Chem. Int. Ed.* **2013**, *52*, 7437–7441.
35. Talotta, C.; Gaeta, C.; Neri, P. *Org. Lett.* **2012**, *14*, 3104–3107.

# Chapter 31

## Hydrogen Bond Hexameric Capsules: Structures, Host-Guest Interactions, Guest Affinities, and Catalysis

Yoram Cohen, Sarit Slovak, and Liat Avram

### 31.1 Introduction

Molecular cages and capsules have become a central theme in supramolecular chemistry in the last two decades [1–3], and molecular capsules based on calixarene derivatives have played a pivotal role [3, 4]. It was the seminal paper by Hogberg on the synthesis of resocin[4]arenes [5] that facilitated the development of the first covalent molecular container and cage molecules by the Cram group. These first cages were, in fact, based on two covalently linked resocin[4]arene units (**1**, see Fig. 31.1) [6, 7]. These covalent molecular cages and capsules are an intriguing class of molecules that can engulf guests practically isolating them from the bulk and thus can, in principle, be regarded as nano-reactors. Indeed the Cram covalent molecular containers, known also as carcerands, seal the guest practically forever and have been used to stabilize certain reactive intermediates [7]. Even Collet's cryptophane-A [8] and its derivatives, used to complex xenon, and which were extensively used for molecular magnetic resonance sensing [9], are in fact covalent container molecules made of two covalently linked cyclotrimeratrylene (CTV) units. In these systems, however, xenon encapsulation is reversible. Covalent molecular capsules are robust systems that can be structurally characterized relatively easily. The main disadvantages of covalent molecular cages and capsules are their lack of responsiveness to external stimuli and their limited ability to release the guests. Moreover, covalent containers must be tailored for each guest, and in many cases *de novo* syntheses are required when different guests need to be encapsulated. In addition, these covalent capsules and container molecules are generally obtained in low yields [4]. Therefore the self-assembly of molecular

---

Y. Cohen (✉) • S. Slovak • L. Avram  
The Raymond and Beverly Sackler Faculty of Exact Sciences, School of Chemistry,  
Tel Aviv University, Tel Aviv 69978, Israel  
e-mail: [ycohen@post.tau.ac.il](mailto:ycohen@post.tau.ac.il)

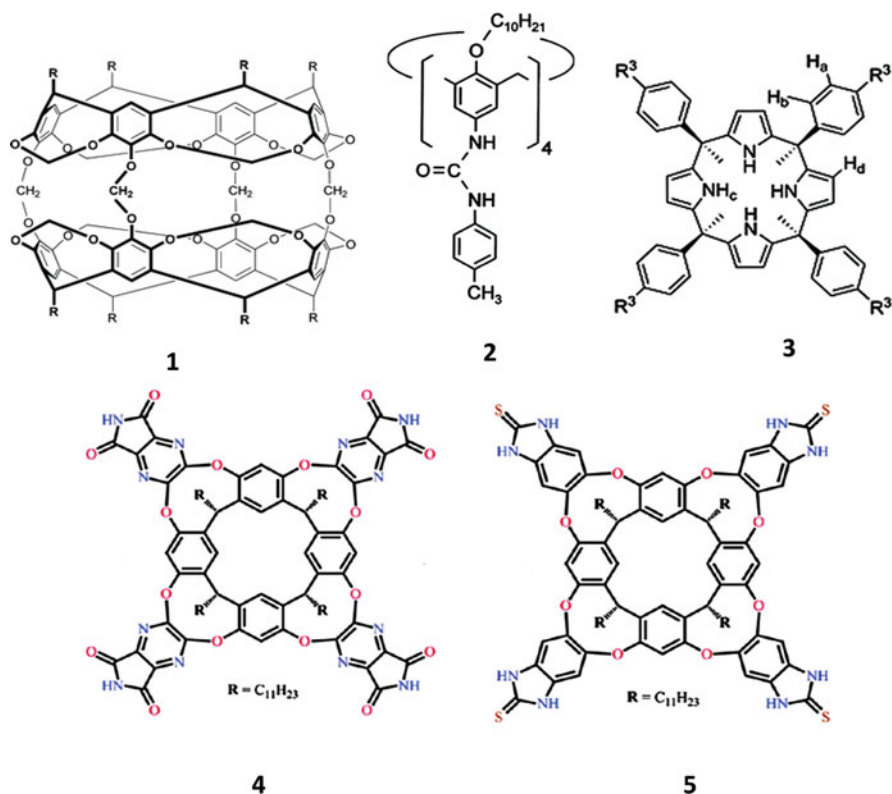


**Fig. 31.1** Structures of calix[4]arene-based molecular containers, cages, and capsules: Cram's carcerand (1), tetraureacalix[4]arene dimer (2), Ballester's tetraureacalix[4]pyrrole dimer (3), Rebek's imide containing calix[4]resorcinarene (4), and thiourea-containing calix[4]resorcinarene (5)

containers and capsules, which is a thermodynamic process by which two or more molecules form a more organized system, has become an important alternative approach for the preparation of molecular capsules and cages of different sizes [1–4].

This happened since self-assembled molecular cages and capsules seem to overcome many of the intrinsic disadvantages of covalent containers and cages. Indeed in the last two decades self-assembled molecular capsules based on several concave systems were prepared using a variety of non-covalent interactions [1–4]. In the early 1990s, a few examples of small self-assembled dimeric capsules stabilized by hydrogen bonds were reported by the Rebek group [10]; however, the real turning point in the field of self-assembled hydrogen-bonded capsules was the work by Shimidzu and Rebek which demonstrated that simple molecules like tetraureacalix[4]arenes (2) (see Fig. 31.1) spontaneously self-assemble in organic solvents into dimeric capsules [11]. As stated by Rebek this suggestion was first received with some skepticism but after monitoring guest encapsulation they indeed

published their finding [11b]. Soon after, Böhmer and his co-workers who were able to demonstrate the formation of heterodimers when two different tetraureacalix[4]arenes were mixed in solution; [11c] were able to crystallize and solve the x-ray structure of the dimer of **2** [11d].

Then dimeric capsules based on resorcin[4]arene derivatives (see **4** and **5** in Fig. 31.1) were prepared and used as tools in physical organic chemistry mostly by the Rebek group [3, 12]. Resorcin[4]arenes and pyrogallol[4]arenes were also found to form dimeric capsules [13], however it was the seminal paper of the Atwood group in 1997 [14] that triggered the research that is the subject matter of the present chapter which is devoted to the hexameric molecular capsules based on resorcin[4]arenes and pyrogallol[4]arenes [14, 15].

## 31.2 From Dimeric to the Larger Self-Assembled Hexameric Capsules

Figure 31.1 shows the structures of some of the calixarene and calixpyrrole derivatives that were found to self-assemble into dimeric capsules (see structures **2–5**). The tetraureacalix[4]arenes (**2**) were found to form dimeric capsules with internal volumes estimated to be in the range of 160–200 Å<sup>3</sup> [11b]. These dimeric capsules were found to encapsulate solvent molecules like chloroform and benzene and small ammonium salts [11]. In addition, it was demonstrated with the aid of diffusion NMR [16] that such dimers have a high affinity for charged systems, and it was found that tropylium cation and cobaltocenium cation have higher affinities than benzene and ferrocene, respectively, for the cavity of the dimer of **2** [17]. These and other studies demonstrated that indeed diffusion NMR is an excellent means to probe encapsulation [17, 18], a fact that was instrumental in the study of the large hexameric capsules of resorcin[4]arenes and pyrogallol[4]arenes as will be demonstrated below [18–20].

Based on the studies of the tetraureacalix[4]arene dimers [11, 17], Ballester and his colleagues postulated and demonstrated, many years later, that tetraureacalix[4]pyrroles (**3**) also form dimeric capsules [3d, 21]. These capsules have some differences compared to those that are formed by **2** and its analogues. Cavity sizes are larger by about 60 %, but their mode of organization were found to be not very different from that of the tetraureacalix[4]arene-based dimeric capsules. In the case of tetraureacalix[4]pyrroles, however, well-defined dimeric species are observed only after the addition of specific guests to the organic solutions [3d, 21].

An intriguing class of hydrogen-bonded self-assembled molecular capsule is that of the Rebek dimeric capsules based on deep cavitands prepared from resorcin[4]arene derivatives [3, 12, 22]. The importance of this class of dimeric capsules arises from their elongated shape which resulted in anisotropic unsymmetrical cavities which gave birth to several phenomena such as “social” and “constellational” isomerism, [23a–b] which could not be observed in the bulk or in other capsules

with more spherical cavities. In addition, Rebek and Ajami were able to increase the size of these capsules (from  $\sim 450$  to  $\sim 980 \text{ \AA}^3$ ) by reacting them with multiple glycoluril units, thus transforming these capsules into even more attractive tools for physical organic chemistry [3c,d, 22]. However, all these types of hydrogen-bonded self-assembled dimeric capsules [3, 4, 10–12, 22, 23], as well as the dimeric capsules of resorcin[4]arenes and pyrogallol[4]arenes [13], have significantly smaller cavities than the hexameric capsules of resorcin[4]arenes [14] and pyrogallol[4]arenes [15], which are the subject of this chapter.

### 31.3 Structural Studies of Hexameric Capsules

The structures of the hexameric capsules of resorcin[4]arenes and pyrogallol[4]arenes were studied in the solid state by x-ray crystallography [14, 15, 24] and in solution mostly by NMR [25], diffusion NMR [19, 20, 26, 27] and small angle neutron scattering (SANS) [28, 29]. Schalley and coworkers have used mass spectrometry (MS) to study such systems in the gas phase [30]. Note, however, that to form hexameric capsules of the kind discussed below based on hydrogen bonds between the hydroxyl groups of the resorcin[4]arenes and pyrogallol[4]arenes, the *rccc* macrocycles should be locked in a cone conformation projecting all OH groups on the wider rim of the macrocycle onto one face of the macrocycle. In contrast to covalent container molecules, self-assembled capsules, which provide mechanical barriers between the encapsulated guest and the guest in the bulk and which are based on weak non-covalent interactions, are much more labile systems. Such non-covalent systems form and dissociate constantly, affording reversible guest encapsulation, but making their characterization, in solution and even more so in the gas phase, challenging. Therefore to characterize some of these systems less conventional analytical methods had to be applied (diffusion NMR, SANS) and other methods (MS) had to be modified to be more suitable for the characterization of such labile, kinetically and thermodynamically less stable systems.

#### 31.3.1 Resorcin[4]arene-Based Hexamers

The eye-opening publication in the field of hydrogen-bonded hexameric capsules was the *Nature* paper by MacGillivray and Atwood that presented the fascinating structure of the hexamer of C-methyl resorcin[4]arene (**6a**) shown in Fig. 31.2a [14]. This structure shows that the hexamer of **6a** is held together by 60 hydrogen bonds between the six macrocycles. Each macrocycle forms the face of a virtual cube through interactions mediated by eight water molecules at the corners of this cube; the volume of the capsule is about  $1400 \text{ \AA}^3$  [14]. The hexamer was found to be both spherical and chiral (Fig. 31.2b). In this structure each resorcin[4]arene lies

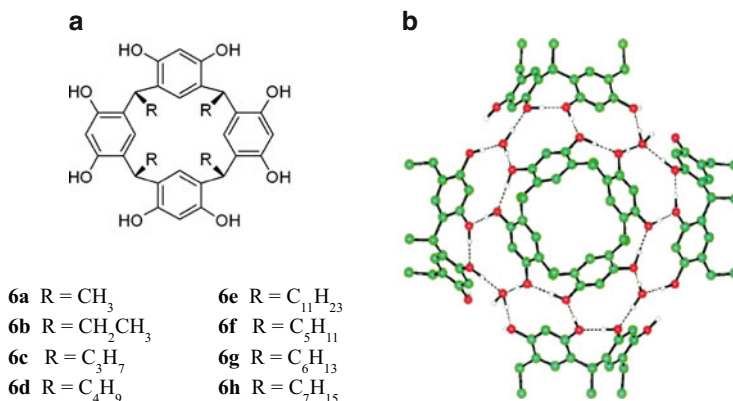


**Fig. 31.2** (a) The structures of different resorcin[4]arenes (**6**) and (b) the crystal structure of the hexamer of **6a** [14]

around a fourfold axis. Each hydroxyl points to the periphery and forms hydrogen bonds with two other macrocycles; the water molecules lie in a threefold axis on the surface of the hexamer, and each participates in three hydrogen bonds to three macrocycles.

When tetraethylammonium bromide (TEABr) was added to the solution of **6b**, dimer formation, mediated by water molecules, is observed in the solid state [13a]. Addition of Et<sub>3</sub>NH<sup>+</sup> to compound **6c** also affords a dimeric capsule in the solid state [13b]. The fact that hexameric capsule can indeed be observed in solution was again presented by the Rebek group who showed that addition tetrahexylammonium bromide (THABr) to water-saturated chloroform solution of **6e** results in separate sets of signals for the un-encapsulated and encapsulated THABr molecules, the later exhibiting large up-field shifts [25a]. Simple integration clearly showed that the **6e**:THABr ratio is 6:1. The ammonium salt is selectively encapsulated because of the partial negative charges of the concave macrocycle host and the partial positive charge on the hydrogen of the convex ammonium guest. Shivanyuk and Rebek then demonstrated that such hexamers are observed in solution when Bu<sub>4</sub>SbBr or Ph<sub>4</sub>SbBr (i.e., neutral guests) are added to the chloroform solution of **6e** [25b]. These examples demonstrate that the hexameric resorcin[4]arene capsules can be observed in solution provided that a proper guest, which occupies about 50 % of the inner volume of the capsule, is present in the solution [31].

The clear proof, however, that hexameric capsules are indeed the resting state of lipophilic resorcin[4]arenes in water-saturated organic solvents was provided by Avram and Cohen based on diffusion NMR measurements [19, 32]. Diffusion NMR revealed that chloroform and benzene can be the occupants in such hexameric capsules. Figure 31.3a shows the changes in the diffusion coefficients in chloroform solutions of **6e** encapsulating THABr and of **6e** in the absence of any guest upon addition of different amount of dimethyl-sulfoxide (DMSO); Fig. 31.3a shows that the results in both cases are essentially the same [19a]. It was found that the addition



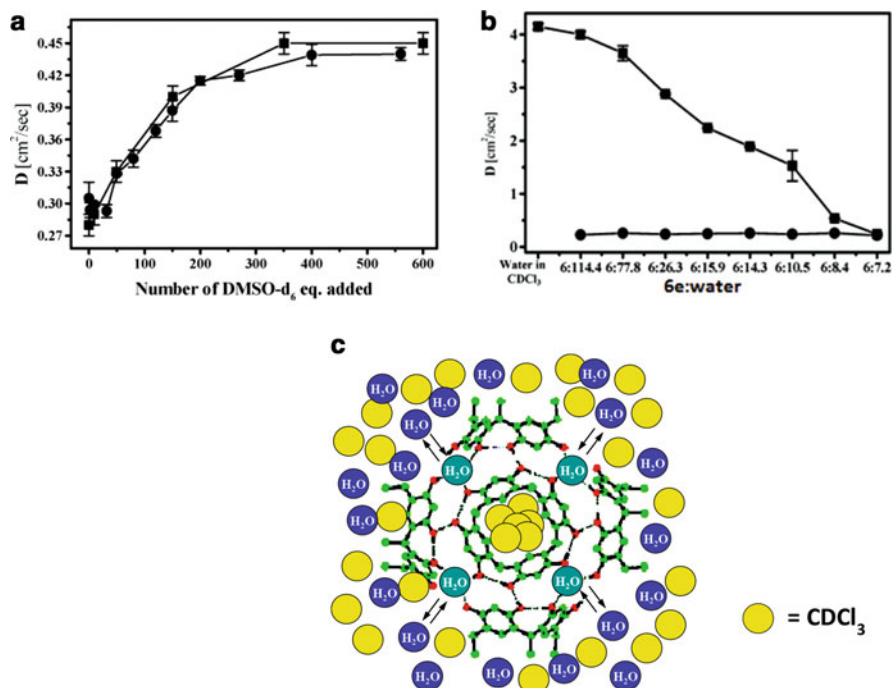


**Fig. 31.3** (a) Diffusion coefficient of **6e** in the absence and presence of THABr as a function of addition of DMSO to the  $\text{CDCl}_3$  solution [19a]. (b) Diffusion coefficients of **6e** and  $\text{H}_2\text{O}$  in  $\text{CDCl}_3$  solution at different **6e**: $\text{H}_2\text{O}$  ratios [19b]. (c) Schematic representation of the resorcin[4]arene hexamers in water-saturated  $\text{CDCl}_3$  solution

of DMSO that disrupts hydrogen bonds results in a similar increase in the diffusion coefficients in both cases up to asymptotic values of about  $0.4 \times 10^{-5} \text{ cm}^2/\text{s}$ , values expected for the monomer of **6e**. When **6e** is dissolved in  $\text{CHCl}_3$ , separate up-field shifted signals are observed for the encapsulated  $\text{CHCl}_3$  molecules. These high-field signals were found to have the same diffusion coefficient as the hexamer of **6e** [19a]. The only explanation for the above observations is that resorcin[4]arene **6e** self-assembles, spontaneously, into hexamers in both cases.

One of the main motivations for studying the hexameric capsules of resorcin[4]arenes using diffusion NMR was to evaluate the role, in solution, of the water molecules in the self-assembly of such hexameric capsules. Because of the large difference between water molecules in the bulk ( $M_w = 18 \text{ Da}$ ) and in the hexamer ( $M_w = 6624 \text{ Da}$ ) water in these two environments should have very different diffusion coefficients.

Therefore we postulated that diffusion NMR would be an extremely useful analytical method to evaluate the role of water in the self-assembly process. With this in mind, NMR diffusion measurements on solutions of **6e** over a range of **6e**: $\text{H}_2\text{O}$  ratios were collected (Fig. 31.3b) [19b]. These diffusion NMR measurements demonstrate that indeed resorcin[4]arenes form, in water-saturated chloroform

solution,  $[\mathbf{6}_6(\text{H}_2\text{O})_8]$ -type capsules [19b]. The diffusion coefficient of water was found to be much larger than that of the hexamer when the  $\text{H}_2\text{O}:\mathbf{6e}$  ratio was 8.4:6 or higher, however, when this ratio was 7.2:6 the same diffusion coefficient was found for both  $\text{H}_2\text{O}$  and  $\mathbf{6e}$ . Clearly these diffusion NMR results demonstrate that the hexameric capsules of resorcin[4]arenes are of the  $[\mathbf{6}_6(\text{H}_2\text{O})_8]$ -type both in solution and in the solid state [14, 19].

Interestingly, for the solutions of  $[\mathbf{6}_6(\text{H}_2\text{O})_8]$ -type capsules, the expected diffusion NMR results were obtained for the  $\text{H}_2\text{O}$  peak only when diffusion was measured with pulse-gradient spin-echo or stimulated-echo sequences (PGSE or PGSTE, respectively) [33]; however, when diffusion is measured by diffusion ordered spectroscopy (DOSY) [34], using the longitudinal eddy current (LED) or bi-polar LED (BPLED) sequences, different results are obtained. It was found that the origin for these differences is the extra eddy current delay ( $t_e$ ) in the LED sequence, which allows for exchange of magnetization between the bulk water, with a large diffusion coefficient, and the water molecules that are part of the capsule, which have a much smaller diffusion coefficient [33]. In fact it was argued that such a dependency of the diffusion NMR results on the  $t_e$  when the diffusion data is collected with the LED sequence can serve as an additional indication that the water molecules are located on the surface of the hexamer rather than encapsulated in it: Only from the surface of the hexamer could the water molecules exchange magnetization fast enough with bulk water. All these results imply that the structure of the hexameric capsule of resorcin[4]arene in water-saturated chloroform solution is as presented schematically in Fig. 31.3c. These diffusion NMR measurements also enable to map all the intramolecular interaction in these  $[\mathbf{6}_6(\text{H}_2\text{O})_8]$ -type hexameric capsules which in fact are supramolecular entities having 20 constituents (six macrocycles, eight water molecules, and six encapsulated  $\text{CHCl}_3$  molecules).

As it became apparent that water molecules play a crucial role in the self-assembly of the hexameric capsule of resorcin[4]arenes, Ogno and Holman [35] studied whether alcohols can replace the water molecules in such structures. They provided an x-ray structure that shows that, in fact, alcohol molecules can replace some of the water molecules in the structure of the self-assembled hexameric capsules of resorcin[4]arenes. Their findings in solution were much less conclusive than the analyses in solid state. This is probably due to the fact that, as shown by Slovak et al., some alcohols do replace the water molecules and are part of the structure of the hexameric capsules of  $\mathbf{6e}$  (these show peculiar diffusion behavior), while others act as guests, are encapsulated and have the expected diffusion characteristics [36].

### 31.3.2 Pyrogallol[4]arene-Based Hexamers

Mattay and his coworkers were the first to demonstrate that  $\mathbf{7b}$  can form hexamers in the solid state (Fig. 31.4) and estimated its cavity to be  $\sim 1520 \text{ \AA}^3$  [15].

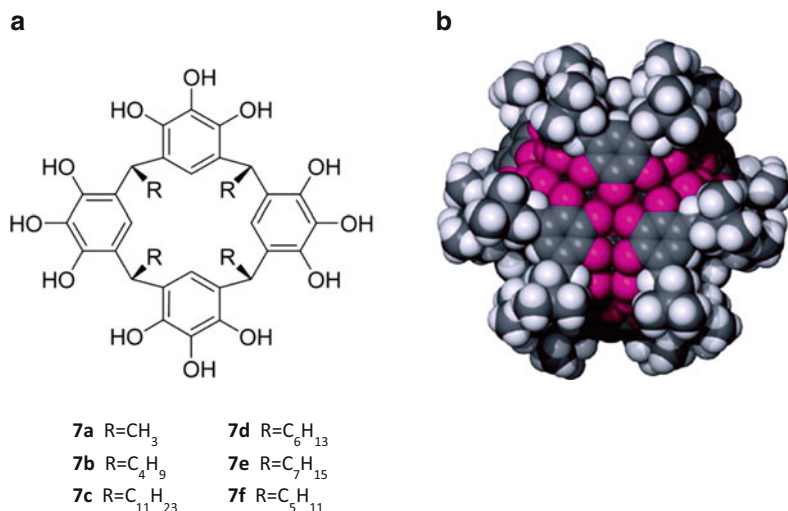


**Fig. 31.4** (a) The chemical structures of pyrogallol[4]arenes and (b) the crystal structure of the hexamer of **7b** [15, 24]

In this system it was found that all 72 hydrogen bonds are used to form the network that holds the capsule together (Fig. 31.4b). In this capsule there are 48 intermolecular hydrogen bonds and the capsule is formed without the mediation of water molecules. It was claimed that the fact that all the hydrogen bonds take part in the capsular network contribute to the observation that the guest is disordered in such capsules [24].

As it was found that resorcin[4]arenes form hexameric capsules in several non-polar organic solvents, Avram and Cohen have used diffusion NMR to verify that this is the situation also for the lipophilic pyrogallol[4]arenes **7b** and **7c** [20a]. Interestingly, it was found that the diffusion coefficient of **7c** is similar to that of **6e**. In addition, when prepared in CHCl<sub>3</sub> extra signals at about 5.0 ppm were observed having diffusion coefficients which were found to be similar to that of **7c**. Addition of methanol to the chloroform solutions of **7b** or **7c** results in an increase in the diffusion coefficients of **7b,c**. All of these results are consistent with the conclusion that both **7b** and **7c**, similarly to **6d** and **6e**, spontaneously self-assemble in organic solvents to form hexameric capsules [19, 20]. It was found that about six CHCl<sub>3</sub> molecules are encapsulated in each hexamer. For the hexamer of **7c**, as in the case of the hexamer of **6e**, only one signal is observed in the <sup>1</sup>H-NMR spectrum for the water molecules in the chloroform solution. Monitoring of the effect of the **7c**:H<sub>2</sub>O ratio on the diffusion coefficient of H<sub>2</sub>O in the solution led to the conclusion that the lipophilic pyrogallol[4]arenes form hexamers without the aid of water molecules in solution just as found in the solid state [15, 20]. As diffusion NMR showed unequivocally that pyrogallol[4]arenes form hexamers in water-saturated chloroform solution with no water involvement, the Rebek group postulated that such hexamers should be formed in hydrocarbon solutions. Indeed Palmer and Rebek

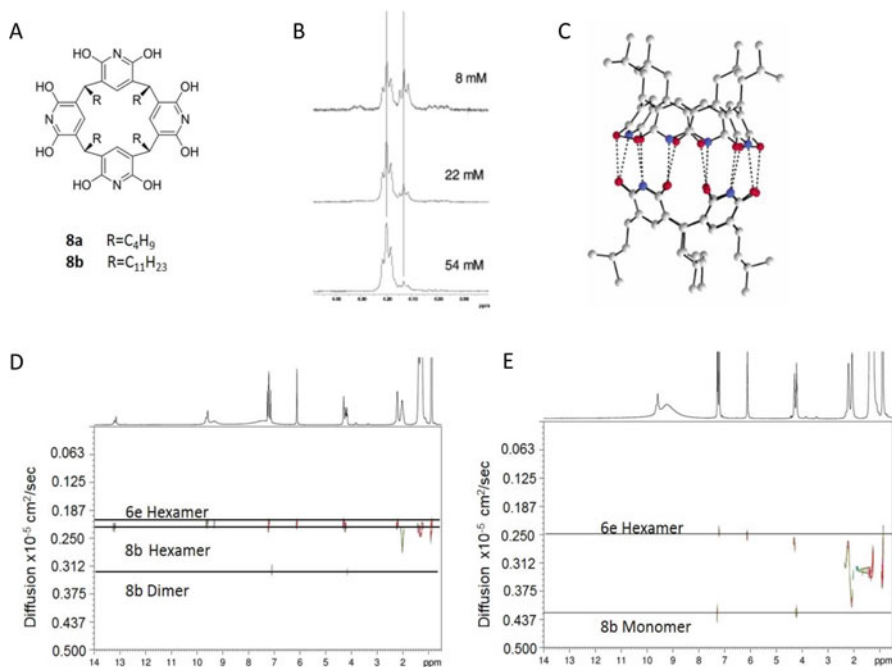


**Fig. 31.5** (a) The structures of octahydroxypyridine[4]arenes. (b)  $^1\text{H-NMR}$  signal of the bridge protons in **8a** at different concentrations [37b]. (c) The crystal structure of the dimer of **8a** [37b]. (d–e) DOSY spectra of 1:1 chloroform solutions of **8b**:**6d** (d) before and (e) after addition of 3  $\mu\text{l}$  of TFA [38]

showed exactly that [20d]. In addition, surprisingly it was found that the  $^1\text{H-NMR}$  spectra of solvent molecules encapsulated by pyrogallol[4]arene hexamers appear more structured than those in the resorcin[4]arene hexamers [20c].

### 31.3.3 Octahydroxypyridine[4]arene Hexamers

Mattay and coworkers were the first to synthesize compound **8a** in 2001 (Fig. 31.5a) [37a]. When the chloroform solutions of **8a** at different concentrations were examined by  $^1\text{H-NMR}$ , two different triplets were observed for the bridge protons of **8a** [37b]. One triplet increased at the expense of the other triplet when the concentration of **8a** was increased (Fig. 31.5b). Since Mattay and his co-workers were able to crystallize the dimer of **8a** (Fig. 31.5c) they assigned the  $^1\text{H-NMR}$  spectra to the monomer and dimer forms of **8a** [37b].

However when DOSY experiments were performed on the chloroform solution of **8b**, one set of signals had a low diffusion coefficient that was reminiscent of those of the hexamers of **6e** and **7c** [38]. As the molecular weight of **6e**, **7c**, and **8b**

are all similar, this result called for a more thorough diffusion NMR investigation of the species that prevail in the solution of **8b**. Therefore DOSY experiments were repeated on a 1:1 mixture of **6e:8b** [38]. In this diffusion NMR study, **6e**, known to form hexamers, was used as an internal reference. The diffusion coefficient of one set of signals of **8b** was nearly the same as that of the **6e** hexamers ( $\sim 0.24 \pm 0.01 \times 10^{-5} \text{ cm}^2/\text{s}$ , see Fig. 31.5d). The other set of signals had a higher diffusion coefficient ( $\sim 0.31 \pm 0.01 \times 10^{-5} \text{ cm}^2/\text{s}$ , Fig. 31.5d). However, when 3  $\mu\text{l}$  of trifluoroacetic acid (TFA) were added to this chloroform solution a new set of signals was observed for **8b** while no effect was observed on the  $^1\text{H-NMR}$  spectrum of **6e** [38]. These changes in the  $^1\text{H-NMR}$  spectrum of **8b** were accompanied by a further increase in the diffusion coefficient to approximately  $0.41 \pm 0.01 \times 10^{-5} \text{ cm}^2/\text{s}$  (Fig. 31.5e), a value reminiscent of the value obtained for the monomers of **6e** and **7c**. In addition, the addition of TFA had almost no effect on the diffusion coefficient of **6e** (Fig. 31.5e) [38]. These results show that, with diffusion NMR, it is possible to identify the hexamer, the dimer, and the monomer of **8b** in solution [38]. Despite the fact that a dimeric species is observed in the solid-state, in the solution the dimer is not the sole aggregate, and at high concentration the dimer is not the dominant species. The studies of this system clearly demonstrate that extrapolation of the findings from the solid-state to solution may lead to erroneous conclusions.

## 31.4 Self-Sorting and Guest Affinity in Resorcin[4]arene and Pyrogallol[4]arene Hexamers

### 31.4.1 Self-Sorting in Hexameric Capsules

Nature is capable of organizing intricate functional systems from a large “soup” of components [39]. It does so through self-assembly and self-sorting. Self-sorting, the ability to distinguish “self” from “non-self”, is crucial for obtaining specific systems in self-assembly processes of multi-components systems. As we found that both resorcin[4]arenes (**6**) and pyrogallol[4]arenes (**7**) form hexameric capsules [19, 20] and since diffusion NMR is such an efficient tool to probe the hexameric structures of these systems, mixtures of such systems that differ in their molecular weights, and hence in their diffusion coefficients, were prepared. These mixtures were followed over time using diffusion NMR [20b]. As shown in Fig. 31.6, when resorcin[4]arenes and pyrogallol[4]arenes having different molecular weights are mixed, we observe two distinct diffusion coefficients in the solution, and no change is observed for 5 weeks or 8 h of reflux implying that only homo-hexamers prevail in the solution [20b]. These results seem to suggest that resorcin[4]arenes and pyrogallol[4]arenes take the narcissistic self-sorting pathway by which only homo-hexamers are formed (Fig. 31.6a).

When such experiments were repeated with solutions of two resorcin[4]arenes or two pyrogallol[4]arenes that differ in their molecular weights, two distinct diffusion

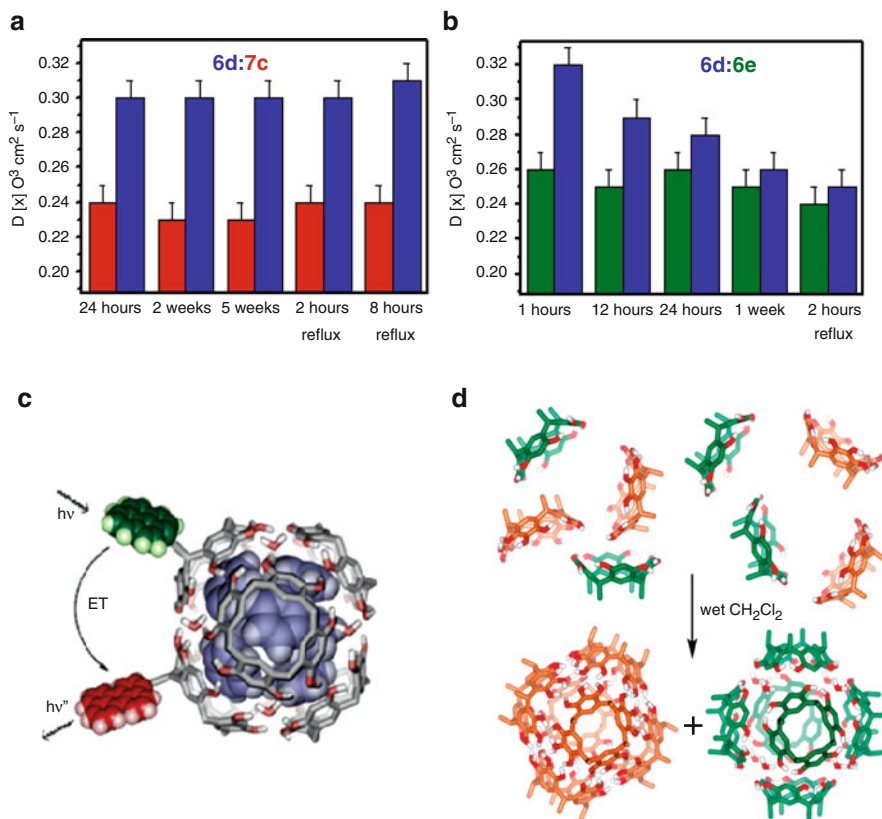


**Fig. 31.6** Self-sorting in hexameric capsules: Diffusion coefficients as a function of time and temperature for 1:1 mixtures of (a) **6d:7c**, (b) **6d:6e**, and (c) FRET pairs. (d) Schematic representation of the results showing that only homo-hexamers are formed when resorcin[4]arenes are mixed with pyrogallol[4]arenes [20d, 41]

coefficients are initially observed, which equilibrate with time, suggesting that with time hetero-hexamers are formed in these cases from the homo-hexamers (Fig. 31.6b) [20b]. Interestingly, in the NMR experiments performed at 10 mM concentrations, equilibration took many hours to days. When the Rebek group performed similar experiments after preparing fluorescence resonance energy transfer (FRET, Fig. 31.6c) pairs they reached very similar conclusions [41]. No hetero-hexamers are formed when resorcin[4]arenes and pyrogallol[4]arenes are mixed, whereas hetero-hexamers are observed when macrocycles of the same type are mixed.

In the Rebek self-sorting experiments, which were carried out at low concentrations because of the increased sensitivity of FRET compared to NMR and because of technical issues, equilibration took place faster than in the NMR experiments. For example, half-lives in the range of 10–16 min were found in these FRET

experiments for the macrocycle exchange in the resorcin[4]arene hexamers in water-saturated  $\text{CH}_2\text{Cl}_2$  solutions [41c]. In chloroform and benzene solutions half-lives of 46 and 3 min were found, respectively. For the pyrogallol[4]arene hexamers, however, longer half-lives in the range of 60 min were calculated for macrocycle exchange [41c].

These FRET half-lives were found to increase more dramatically with the increase in the concentration for pyrogallol[4]arene hexamers than for the resorcin[4]arene hexamers. In addition, the FRET experiments also corroborated what was previously known from diffusion NMR: Pyrogallol[4]arene hexamers are more stable than resorcin[4]arene hexamers and form both in dry and in water-saturated organic solvents, whereas resorcin[4]arene hexamers only form in water-saturated organic solvents [19, 20, 41]. These results showed that similar conclusions are reached from diffusion NMR [19, 20] and FRET experiments [41]. It should be noted that in the gas phase hetero-hexamers of resorcin[4]arenes and pyrogallol[4]arenes were found [30], a fact that is not easy to reconcile with solution data. In the gas phase, a charged ruthenium complex was added to the solution to allow detection of the hexameric capsule by the MS detector. This ruthenium complex could not be encapsulated in any of these hexamers in solution. In other dimeric capsules, however, hetero-capsules are observed in solution. For example, heterodimers are observed in which resorcin[4]arene is, in fact, one panel of the heterodimer [42].

### 31.4.2 Guest Affinity in Hexameric Capsules

The hexameric capsules of both resorcin[4]arenes and pyrogallol[4]arenes have large cavities that can, in principle, accommodate several medium-sized molecules. If one aims at using such molecular containers and capsules as nano-reactors, it is important to evaluate the affinity of different guests for the cavities of these capsules. However it should be noted that, at least in solution, the recorded affinity can be masked at least to some extent by the affinity of the solvent used. Interestingly, during the last decade it has become apparent that by direct dissolution of the components in organic solvents more guests can be encapsulated in the resorcin[4]arene hexamers [25–27, 36, 43] as compared to pyrogallol[4]arene hexamers [44]. In addition, based on analysis of  $^1\text{H-NMR}$  spectra, encapsulated solvent molecules appear generally more structured in the pyrogallol[4]arene hexamers than in the resorcin[4]arene hexamers [45]. As it has been found that very few non-liquid materials are encapsulated in  $(\mathbf{7c})_6$  compared with  $[\mathbf{6e}_6(\text{H}_2\text{O})_8]$ , for example, and in view of the fact that in the few such examples reported for  $(\mathbf{7c})_6$  the level of occupancy was low [44c–e], the Purse group suggested use of the melting approach to avoid competition from the solvents and increase guest loading in pyrogallol[4]arene hexamers [46]. Using this approach, Purse and co-workers were able to increase the repertoire of guests that can be encapsulated in  $(\mathbf{7c})_6$ . They prepared in fact a series of kinetically trapped hexameric capsule complexes [46],



demonstrating that both aliphatic and a large series of aromatic systems can indeed be encapsulated in (**7c**)<sub>6</sub>.

Ammonium salts were among the first guests to be encapsulated in the resorcin[4]arene hexamers in water-saturated chloroform solution [19, 20, 25]. Indeed in this solution both trialkylamines and tetraalkylammonium salts of different sizes were found to be encapsulated in hexamers of **6e**; under the same conditions, however, hexamers of **7c** encapsulate trialkylamines but not tetraalkylammonium salts [20a,b]. In fact in an early diffusion NMR study it was found that for **7c**<sub>6</sub> encapsulating trialkylamines slight acidification of the chloroform solution, which probably protonated the encapsulated trialkylamines, resulted in the disappearance of the <sup>1</sup>H-NMR signals of the encapsulated guest in (**7c**)<sub>6</sub> but not in the disruption of (**7c**)<sub>6</sub> [27]. Interestingly, even when using the melting approach, no encapsulation of Bu<sub>4</sub>N<sup>+</sup>X<sup>-</sup> (where X<sup>-</sup> = Cl<sup>-</sup>, Br<sup>-</sup>, and I<sup>-</sup>) in (**7c**)<sub>6</sub> was observed [46b]. This is even more surprising given that Kaifer and co-workers were able to encapsulate the cobaltocenium cation both in the resorcin[4]arene and pyrogallol[4]arene hexamers [43a, 44a]. Some preliminary results suggest that in benzene solution and under the appropriate conditions, tetraalkylammonium salts can be encapsulated in (**7c**)<sub>6</sub> [46d].

Yamanaka et al. studied the kinetics and thermodynamics of encapsulation of a series of tetraalkylammonium salts by the resorcin[4]arene hexameric capsules **6e** [43b]. There the C<sub>3</sub>–C<sub>8</sub> tetraalkylammonium salts were found to be encapsulated with their respective anion. Tetrapropyl and tetrabutyl are accompanied by three CHCl<sub>3</sub> molecules, tetrapentyl and tetrahexyl by two, and tetraheptyl and tetraoctyl each with only one molecule of CHCl<sub>3</sub>. There the maximal induced high-field shift was about 3 ppm [43b, 47a] and it was found for the methyl group in the hexyl chains of THABr. For the longer chains ammonium salts, however, the maximal high-field shifts were observed for C<sub>4</sub> (Fig. 31.7a). These <sup>1</sup>H-NMR spectra imply that hexyl chains are fully extended in the capsule, and the alkyl chains of the longer chain ammonium salts are probably bent in the capsules. Such phenomenon was observed also for long alkyl-chain alkanes encapsulated in the hexamer of **7c** [20d] and in open-water-soluble cavitand [47b]. In addition the exchange between the encapsulated and bulk tetraalkylammonium salts was slower for the bulkier ammonium salts, although less bulky R<sub>4</sub>N<sup>+</sup> salts were found to have higher apparent K<sub>a</sub>s for encapsulation [43b]. These results suggest that the mechanism of the exit of the encapsulated guests should involve a detachment of one resorcin[4]arene panel from the hexamer (as shown in Fig. 31.7b) rather than a complete disintegration of the hexamer [43b].

Which aggregate indeed prevail in a given solution is in fact a manifestation of a delicate equilibrium that may be affected by subtle experimental conditions. For example, when Et<sub>4</sub>N<sup>+</sup> salts are added to a solution of **6c**, dimers are observed in the solid-state [13]; however, when these guests were added to the chloroform solution of **6e** diffusion NMR analysis indicates that hexamers prevail in the solution. In these solutions each hexamer encapsulates, on the average, two ammonium salts [26b]. In this study the bis-calix[5]arene prepared by Parisi and co-workers was used as internal reference [48a]. This covalent dimer was selected as an internal



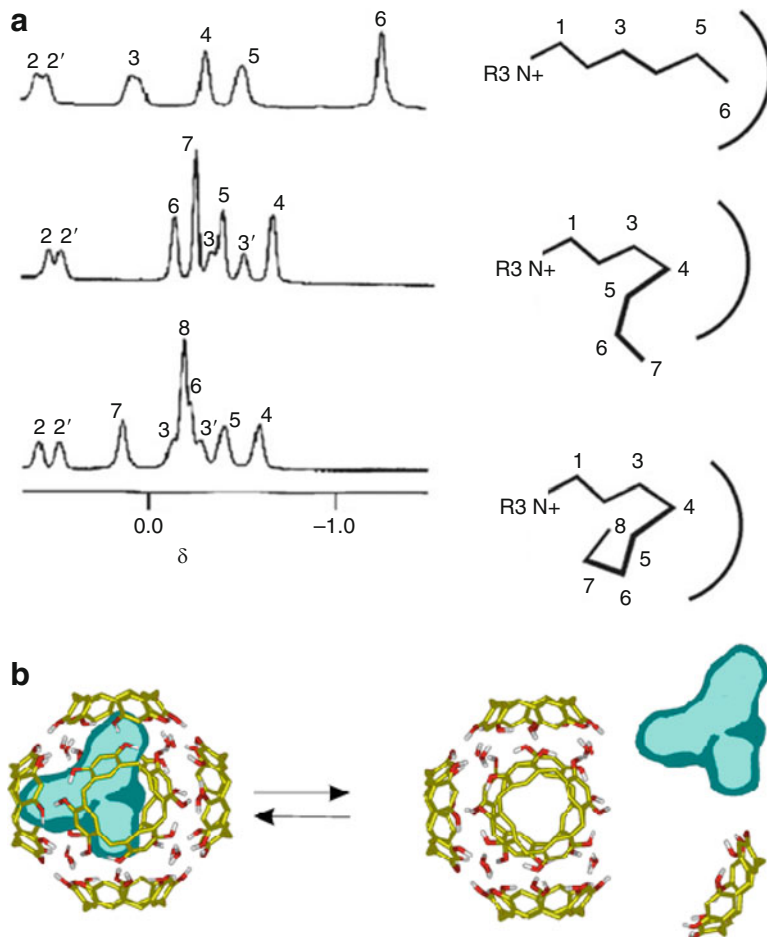


**Fig. 31.7** (a) Extracts of the <sup>1</sup>H-NMR spectra and assignment of the signals of the encapsulated ammonium salts in hexameric capsules of **6e** showing that in the cases of tetraheptylammonium and tetraoctylammonium the buckle of the chain is at C<sub>4</sub> [43b]. (b) Suggested mechanism for exit of  $R_4N^+$  from a hexameric capsule [43b]

reference since its molecular weight is slightly higher from that of the non-covalent dimer of **6e**. It was found that the diffusion coefficients of **6e** encapsulating different ammonium salts are very similar and significantly lower than the diffusion coefficient of the covalent dimer used as a reference. In addition, using the  $t_c$  dependency of the signal decay of the water peak in the LED diffusion NMR sequence it was possible to determine that in the case of  $Et_4N^+X^-$  salts, where  $X^-$  was  $Cl^-$ ,  $Br^-$  and  $I^-$ , **6e**<sub>6</sub>-type hexamers form; in contrast, when  $X$  is  $BF_4^-$  or  $PF_6^-$ , **6e**<sub>6</sub>(H<sub>2</sub>O)<sub>8</sub>-type hexamers seem to prevail [26b].

The interactions of trialkylamines (and tetraalkylammonium salts) with the hexamers of **6e** were studied in detail by diffusion NMR, and evidence for the

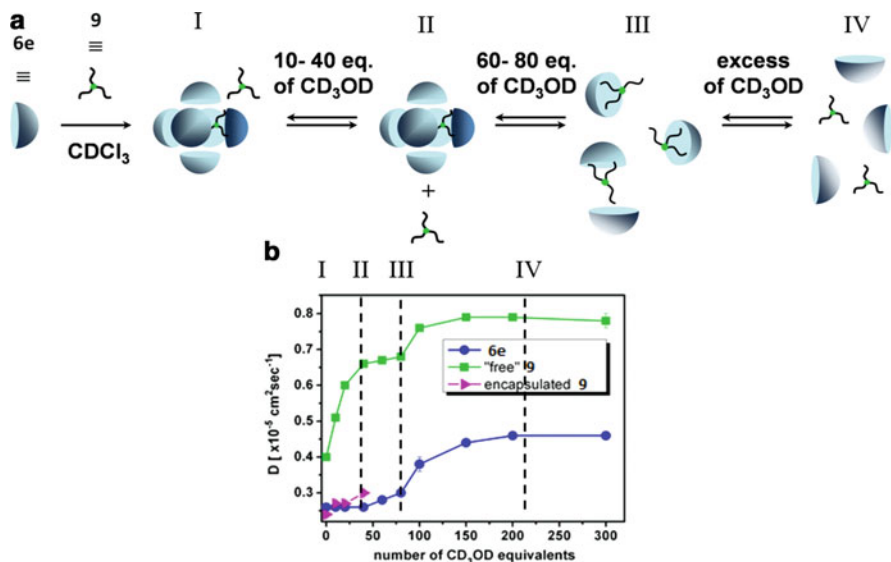


**Fig. 31.8** (a) Schematic mapping of the non-covalent interactions that prevail in a solution of the hexamers of **6e** and trioctylamine (**9**) and their disruption upon addition of methanol [43c]. (b) The diffusion coefficients associated with the molecular species that prevail in the solution at each stage [43c]

interaction of the non-encapsulated guests with the hexamers of **6e** were obtained [43c]. These results showed that trialkylamines interact with the hexamers of **6e** from the inside and from the outside. When methanol was added to the chloroform solution of trioctylamine (**9**) with the hexamer of **6e** it was possible to follow the disintegration of the capsule step by step as presented in Fig. 31.8 [43c]. These data demonstrate the added value of high-resolution diffusion NMR for characterizing supramolecular systems in solution since high-resolution diffusion NMR allows simultaneous measurement of the diffusion coefficients of the different components in the solution thus enabling one to map all the intermolecular interactions that prevail in the system in a single experiment.

The added value of diffusion NMR in the field of hexameric capsules was also demonstrated when the host-guest complexes of **6e** with glutaric acid (**10**) and the  $\beta$ -anomer of methyl-D-glucopyranoside (**11**) were revisited [43d]. The Aoyama group showed that **6e** forms a dimeric capsule with **11**, and a 1:1 complex with **10**; [48b, c] however, diffusion NMR unequivocally showed that in these cases the real complexes in solution are in fact hexameric capsules of **6e** encapsulating six and three molecules of **10** and **11**, respectively [43d]. The glutaric acid replaces the encapsulated chloroform molecules quite efficiently showing also that the symmetry of the encapsulated glutaric acid molecules is different than that in the bulk. Here again, a covalent dimer of biscalix[5]arene with a molecular weight higher than that of **6e** was used as an internal reference. These results clearly demonstrate that hexameric capsules are much more abundant than previously thought, [43d, e]

suggesting that much of the known host-guest chemistry of resorcin[4]arenes in organic solvents should be revisited.

Ogno and Holman were able to show that, at least in the solid state, alcohols can replace some of the water molecules in the  $[\mathbf{6}_6(\text{H}_2\text{O})_8]$  capsule [35]. With the aid of diffusion NMR, Slovak and Cohen studied the interaction of a series of alcohols with the hexamers of **6e** [36]. It was found that some of the alcohols are encapsulated, whereas others indeed replace the water molecules and are part of the hexameric superstructure. In chloroform solution of the hexamers of **6e**, alcohols were found to have two sets of peaks because of slow exchange on the chemical shift timescale between bulk alcohols and alcohols interacting with the hexamers of **6e**. Encapsulated alcohols, as expected, have only one diffusion coefficient, which was the same as that of the hexameric capsule and was not affected by length of the  $t_c$  used in the LED (and BPLED) sequences [36a, b]. In contrast, alcohols that replace the water and are part of the superstructure of the capsule can exchange magnetization with alcohols in the bulk, and these alcohols have diffusion coefficients that are higher than that of the hexameric capsule. The signal decay of these alcohols in the LED diffusion NMR experiments was found to be affected by the  $t_c$  values used in the LED sequence. At sufficiently long  $t_c$ s, two distinct diffusion coefficients are observed for the peaks of the alcohols at high field that are part of the structure of the hexameric capsules [36]. These studies demonstrated that guest signals at high field in the  $^1\text{H}$ -NMR spectra do not necessarily imply that the guest is encapsulated in the capsules. It should be noted, however, that in many cases slow exchange between the encapsulated guest and the guest in bulk is, in fact, a good criteria for guest encapsulation especially when the guest lack polar/charged functional group.

The smaller number of guests that were found to be encapsulated by direct dissolution in the pyrogallol[4]arene hexamers as compared with the resorcin[4]arene hexamers may be partially due to the higher affinity of solvent for the cavity of the pyrogallol[4]arene hexamers. Indeed the  $^1\text{H}$ -NMR spectra of different solvents encapsulated in the hexamers of **7c** appear very structured as shown in Fig. 31.9. The signals that appear as multiplets (heptets) are actually a series of singlets with very similar chemical shifts [45]. These observations seem to originate from the fact that each of the macrocycles in the hexamer can, in principle, have two different orientations resulting in seven slightly different capsules each inducing a slightly different averaged chemical shift for the encapsulated solvent molecules. It was even more striking to observe that for several halogenated solvents other than  $\text{CHCl}_3$ , the spectra consist of two signals each composed of seven singlets [45]. Different NMR experiments (COSY, 1D NOE, and NOESY) demonstrated, surprisingly, that the two signals originate from encapsulated molecules residing in two different chemical environments within a single capsule [45b]. The only solvent in which only one major set of signals is observed for the encapsulated solvent is  $\text{CHCl}_3$  for which a significantly lower percent occupancy was calculated compared to the other encapsulated solvents tested (Fig. 31.9a–d) [45b]. In the spectrum of the hexamer of **7c** in  $\text{CH}_2\text{Cl}_2$  solution in the presence of adamantane carboxylic acid (**12**), two additional sets of signals are observed (Fig. 31.9e). Based

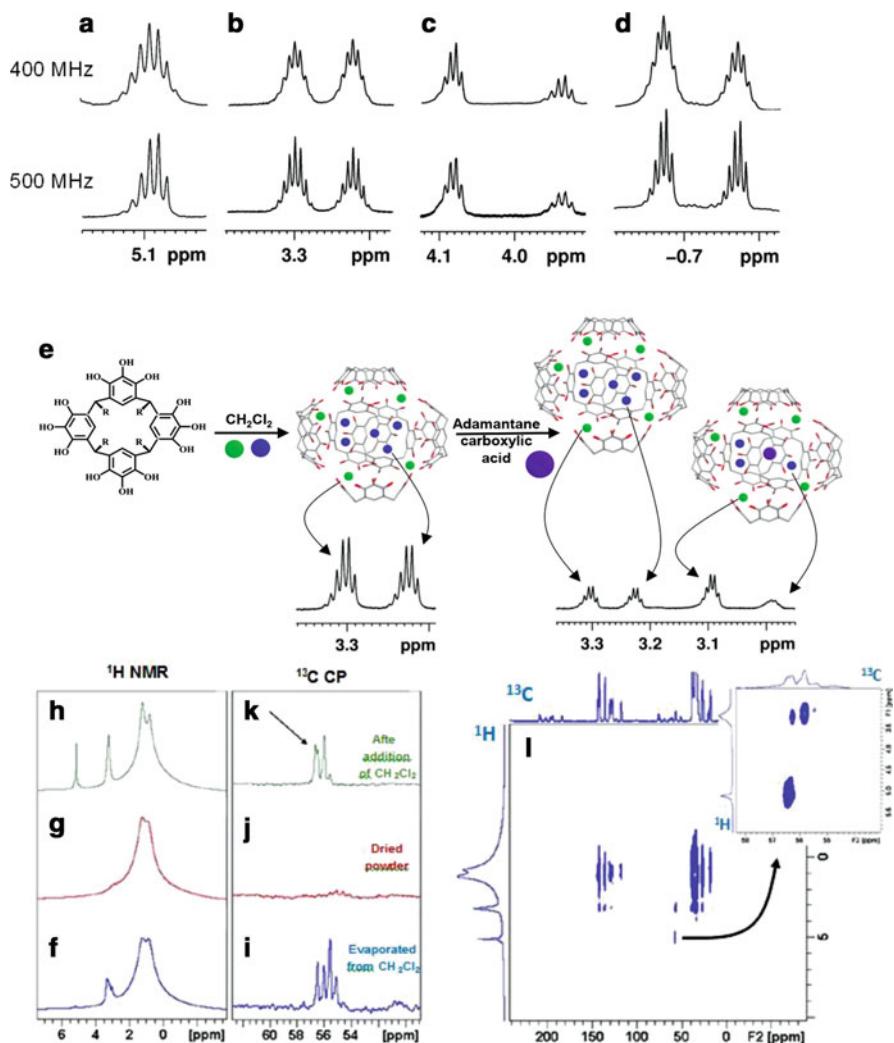


**Fig. 31.9** Extracts of the  $^1\text{H}$  NMR spectra (400 and 500 MHz, 298 K) showing only the peaks of the encapsulated solvent molecules in the hexamers of  $7\text{c}$  for (a)  $\text{CHCl}_3$ , (b)  $\text{CH}_2\text{Cl}_2$ , (c)  $\text{CHBr}_3$ , and (d)  $\text{CH}_3\text{I}$ . (e) Schematic representation of the systems that prevail in solution and assignment of the signals of the encapsulated  $\text{CH}_2\text{Cl}_2$  molecules [45b]. (f–l) MAS ssNMR spectra of the  $7\text{c}$  powder obtained by evaporation of the  $\text{CH}_3\text{I}$  solution. (f–g)  $^1\text{H}$  NMR spectra and (i–k) regions of  $^{13}\text{C}$  CPMAS spectra (f), (g), (i), (j) before and (h), (k) after exposure to  $\text{CH}_2\text{Cl}_2$  vapor. (l) The  $^1\text{H}/^{13}\text{C}$  HETCOR spectrum of the powder of  $7\text{c}$  after exposure to  $\text{CH}_2\text{Cl}_2$  vapor [45c]

on NOE NMR experiments it was possible to assign the peaks to an inner and an outer belt of encapsulated solvent molecules within a single capsule since only the low-field set of signals showed NOEs with the hexamer walls. In addition, in the

presence of **12** the high-field set of signals has a much lower integration because the encapsulated molecule **12** replaces the inner belt of  $\text{CH}_2\text{Cl}_2$  molecules [45b]. This  $^1\text{H}$ -NMR study shows that in the  $\text{CH}_2\text{Cl}_2$  solution of **7c** in the presence of **12** two types of hexameric capsules are formed. The systems that prevail in solution along with schematic assignment of the peaks of the encapsulated  $\text{CH}_2\text{Cl}_2$  molecules are presented in Fig. 31.9e [45b].

It was also shown that slow evaporation of organic solution of **7c** allow to selectively remove the non-encapsulated solvent molecules leaving powders of stable hexameric capsules that contain solvent molecules; these were studied by magic angle spinning solid-state NMR (MAS ssNMR) [45c]. The use of different  $^1\text{H}$  and  $[13]\text{C}$  MAS ssNMR experiments as well as 2D  $^1\text{H}/^{13}\text{C}$  hetero-nuclear correlation (HETCOR) both before and after exposure of the samples to solvent vapor allowed assignment of the signals of the external and the encapsulated solvent molecules. Figure 31.9f–i shows such data for capsule obtained from  $\text{CH}_2\text{Cl}_2$  solution. This first MAS ssNMR study of the hexameric capsule of **7c** demonstrated that the capsules in the powders are stable for months and that the process of solvent encapsulation is reversible. These MAS ssNMR experiments led to the conclusion that at least the encapsulated  $\text{CH}_2\text{Cl}_2$  and  $\text{CH}_3\text{I}$  molecules occupy, as they do in solution, different sites in the powdered capsule and that the encapsulated solvents in the different sites have different mobilities.

The fact that simple evaporation affords powders of such hexamers paves the way for studying guest exchange, guest affinity and gas storage in such hexamer in the solid-state [45c].

The Atwood group studied the solid state structures of different pyrogallol[4]arenes quite extensively [24] and found, in many cases, that the inner space is generally not very ordered thus limiting the information that one can get from crystallography on the organization of the encapsulated guests [24]. For **7f** in the solid state, however, it was found six ethyl acetates are encapsulated and six such molecules interact with the capsule from the outside through the alkyl chains [44b]. Based on the results from C5-C7-pyrogallol[4]arene hexamers, it was concluded that, in the solid state, the side chains may affect the organization of guest in the cavity.

To address the issue of guest organization in hexamer cavities further, the Atwood group studied several chromophores in such hexamers [44c–e]. For example, using fluorescence spectroscopy it was shown that pyrene butyric acid (PBA, **14**) is indeed encapsulated in the hexamer of C-hexyl-pyrogallol[4]arene (**7g**) thereby exhibiting much higher fluorescence than PBA in the bulk in the presence of a quencher like dimethylaniline (DMA). The guest loading in these studies was not very high, making the NMR characterization of the complexes in solution difficult; however, crystals suitable for x-ray analysis were obtained [44c]. Solid-state crystallography showed that indeed two PBA molecules are encapsulated in each capsule as shown in Fig. 31.10a [44c]. The hexamer has an estimated volume of approximately  $1,250 \text{ \AA}^3$ , and the distance between the two PBA molecules is about  $7.8 \text{ \AA}$ . Using the quencher DMA, it was possible to determine that only 10 %

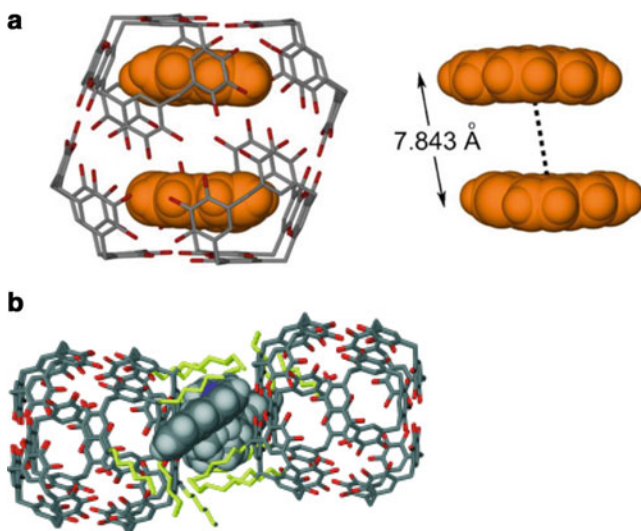


**Fig. 31.10** (a) Diagram of PBA encapsulated in a hexameric PgC<sub>6</sub> nano-capsule [44c]. (b) View of the ADMA channels (space-filling representation: C gray, N blue) formed by fluorophore intercalation between walls of neighbouring nano-capsules (stick representation: C gray, O red). The PgC<sub>6</sub> hexyl chains proximate to the ADMA channels are shown in yellow, whilst all others were removed for clarity [44d]

of the PBA leached during a period of 30 days. Interestingly when a larger probe with a built-in quencher moiety (i.e., [3-(9-anthryl)propyl]-N,N-dimethylaniline, **15**, ADMA) was used, **15** was found to occupy the interior of the hexameric capsules of **7g** or occasionally the exterior of the capsule forming ADMA channels that seem to push apart the neighboring nano-capsules (Fig. 31.10b) [44d].

To evaluate the limits of encapsulation in these hexameric capsules benzo[a]pyrene (**16**) and pentacene (**17**) were added to the saturated acetonitrile solution of **7g** under sonication [44e]. Spectroscopic evidence demonstrated that these two guests are encapsulated; however, since the occupancy was very low, the encapsulated guests could not be observed by NMR or even by X-ray crystallography. Therefore, over the years several approaches to increase guest occupancy have been suggested including spinning disk processing [49]. The most efficient method for this purpose, however, is the melting approach presented by the Purse group [46]. By eliminating the solvent that competes for the capsule cavity, this method results in high yield of encapsulation of a series of aliphatic and aromatic compounds [46]. Using the melting approach many guests that could not be encapsulated by direct dissolution were encapsulated in the hexameric capsule **7e** thus forming a series of kinetically trapped capsular complexes as shown in Fig. 31.11a. Three pyrene, fluoranthene, or anthracene molecules can be trapped in **7e**, whereas four smaller molecules like biphenyl, fluorene, and norbornene are encapsulated in each capsule. Six of the much smaller naphthalenes are observed in each capsule. Calculations assuming an average volume of 1,300 Å<sup>3</sup> indicate that in these

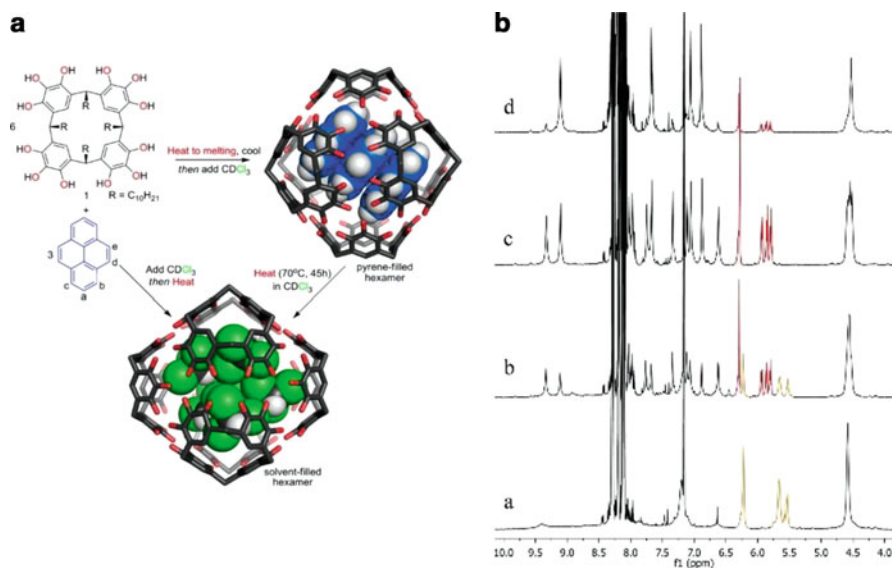


**Fig. 31.11** (a) Experimental conditions for the formation of kinetically trapped capsular complexes by the melting approach and for obtaining such complexes in solution. By the melting approach, three molecules of pyrene are encapsulated in the hexameric capsules. (b)  $^1\text{H}$  NMR spectra tracking the pyrene-filled (Oh)→pyrene filled (D3)→ $\text{CCl}_4$ -filled hexamer process: (a) prior to heating; (b) 2 h at 343 K; (c) 24 h at 343 K; (d) 4 h at 393 K, at this temperature equilibrium is established after 4 h [46a,b]

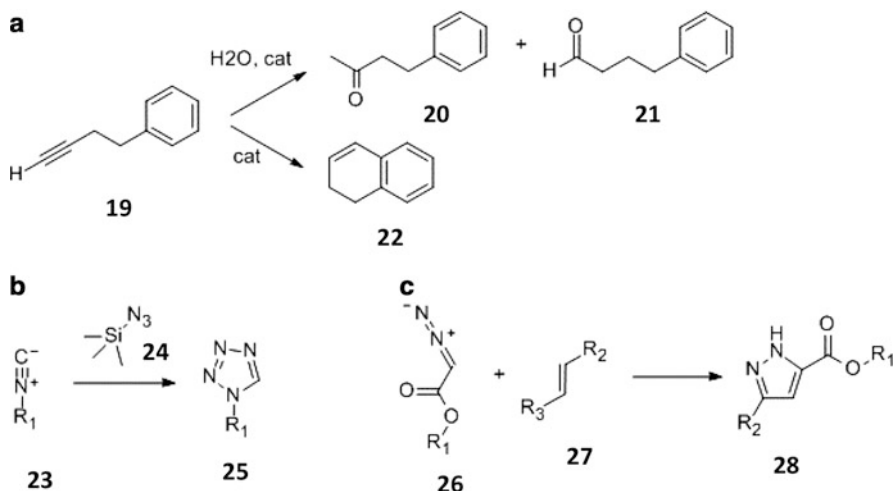
complexes the packing coefficients are in the range of 0.35–0.67. For these kinetically trapped capsular complexes, half-lives for solvent guest exchange at ambient temperature are in the range of 8–150 h. For pyrene at 343 K, a total life time of 45 h was found for the solvent guest exchange; at ambient temperature, however, no significant exchange was observed [46a, b].

Interestingly, when the more bulky solvent  $\text{CCl}_4$  was used instead of  $\text{CDCl}_3$  longer total lifetimes of guest encapsulated in **7e<sub>6</sub>** were observed. For encapsulated pyrene both the rearrangement and guest-solvent exchange were monitored as shown in Fig. 31.11b. Very recently it was shown that some of these kinetically trapped complexes are stable enough to be separated from the guest in the bulk by column chromatography [46c]. This opens the way for the use of such complexes as molecular storage and on-command release systems [46 c].

### 31.5 Catalysis in Hydrogen-Bonded Hexameric Capsules

Enzymes are in fact supramolecular catalysts; these proteins translate supramolecular interactions between targets and active sites into substrate selection, reactant orientation, and promotion of selective covalent bond formation into selective





**Scheme 31.1** (a) The products obtained from the catalytic reaction of 4-phenylbutyne (**19**) with **18** both in the presence and absence of water [53a]. (b) Addition of TMSN<sub>3</sub> to isonitriles to obtain a series of substituted 1*H*-tetrazoles [53d]. (c) 1,3-Cycloaddition reaction between diazoacetate esters (**26**) and electron-poor alkene (**27**) to obtain 4,5-dihydro-1*H*-pyrazole derivatives (**28**) [53e]

reactions [50]. Since one of the most important features of molecular capsules is their ability to serve as nano-reactors where new chemistry and catalysis may occur it is not surprising that efforts were made to harness molecular cages and capsules to this task. Despite the fact that supramolecular catalysis has received much attention in the last decade, and examples of catalysis were reported for metal-organic cages [51] and in the Sherman and Gibb octaacids [52], catalysis with hexameric capsules were reported only very recently [53, 54]. Even today the number of examples are miniscule and all reported examples to date were performed with the aid of the resorcin[4]arene hexamers and not in pyrogallol[4]arene hexamers. In contrast to cationic metal-ligand cages and Gibb capsules, which were shown to act as nano-reactors and catalytic systems in aqueous solutions [52], hydrogen-bonded hexameric capsule-mediated catalysis has been performed, to date, in organic solutions [53, 54].

The first example in which resorcin[4]arene hexamers were used to obtain modest chemo- and region-selectivity of a reaction was reported for the hexamer of **6e** encapsulating a gold catalyst (i.e., [chloro[1,3-bis(2,6-diisopropylphenyl)imidazole-2-ylidene]gold(I)], **18**) [53a]. In this study, <sup>1</sup>H-NMR clearly indicated that **18** is encapsulated in the hexamers of **6e** [53a]. The reaction in hexamers of **6e**, shown in Scheme 31.1a, is slower than in the bulk, and the product distribution is different in the presence of **18@6e** than in its absence. Interestingly, it was also found that **19** has no affinity for **6e** in the absence of **18**.

It was also demonstrated that addition of Et<sub>4</sub>N<sup>+</sup>, a better guest of **6e** than **18**, results in a dramatic increase in the formation of **20**, the major product obtained when the reaction is catalyzed by **18** in the bulk. In this study, however, the product

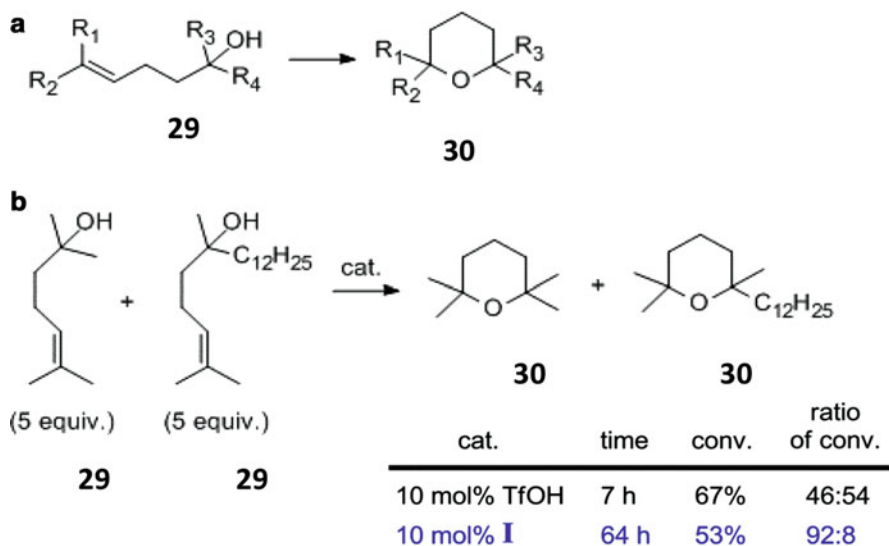


distribution was altered by the presence of the encapsulated catalyst but altogether the reaction was slower in the presence of capsule than in the bulk [53a].

In a more recent study, Scarso and co-workers demonstrated that encapsulation of a cationic carbodiimide condensing agent in the hexameric capsule of **6e** favors the formation of shortest amide from a series of carboxylic acids and amines by favoring co-encapsulation of the short reactants (acids, amines) with the cationic carbodiimide [53c]. The same hexamers were also used to catalyze the reaction shown in Scheme 31.1b between a series of aliphatic and aromatic isonitriles (**23**) and trimethylsilylazide (TMSN<sub>3</sub>, **24**) to obtain a series of 1-substituted 1H-tetrazoles (**25**). The reaction is rapid and efficient and is inhibited by a competing guest as an enzymatic reaction is [53d]. In this case, the competing guest was TEABF<sub>4</sub>, which is known to have high affinity for the capsule cavity. The Scarso group also demonstrated that hexamers of **6e** are capable of catalyzing 1,3-dipolar cycloaddition [53c]. The catalyzed cycloaddition reaction between diazoacetate esters (**26**) and electron-poor alkenes (**27**) yields 4,5-dihydro-1H-pyrazole derivatives (**28**) as shown in Scheme 31.1c. Here again TEABF<sub>4</sub> was used to demonstrate that blocking the cavity of the hexamers indeed nulls the effect of the hexamer on the reaction [53e].

Zhang and Tiefenbacher showed that resorcin[4]arene hexamers act as relatively strong Brønsted acids with pK<sub>a</sub> values in the range of 5.5–6.0 units [54a]. They suggested that this fact may explain the tendency of such hexameric capsules to encapsulate tertiary amines, which can be protonated imparting π-cation interactions inside the cavity of the resorcin[4]arene hexamers [54a]. Using this information it was possible to affect the course of a Wittig reaction but more importantly to catalyze the acidic hydrolysis of diethyl acetal [54a]. Based on the fact that alcohols are encapsulated in the hexamers of **6e** [36] and that positive charged compounds like quaternary ammonium salts have high affinity for hexamer cavity, the same group was able to show that these hexamers can be used to catalyze the intramolecular hydroalkoxylation of inactivated unsaturated alcohols (**29**) affording cyclic ethers (**30**) (Scheme 31.2a) [54b].

The hydroalkoxylation reaction is catalyzed by strong acids like triflic acid (TfOH), but considerable side reactions and poor compatibility of functional groups limit the scope of the reaction. With the aid of the hexamer **6e**(H<sub>2</sub>O)<sub>8</sub> such transformations can be achieved efficiently and under mild conditions (30 °C, 3.5 days) [54b]. The reaction rate increases dramatically as the amount of water is decreased, and moving from water-saturated chloroform solution to ordinary chloroform solution results in generally higher yields (up to 85 %). Here again addition of a small amount of good guest (i.e., 1.5 equivalent of Bu<sub>4</sub>NBr) blocked the catalytic activity of the hexamer of **6e** reducing yields considerably to below 7 % [54b]. In a second control experiment when the reaction was performed with no addition of **6e** no conversion was observed for 7 days. These results demonstrate that the reaction is taking place in the cavity of the hexamer of **6e**. Zhang and Tiefenbacher suggested that the catalytic activity is due to the stabilization of the positively charged intermediates or transition states by π-cation interaction in the cavity of the hexamers. The catalytic cycle is completed after the product is released from the



**Scheme 31.2** (a) General scheme for the intramolecular hydroalkoxylation of inactivated hydroxyl olefins and (b) substrate selectivity imposed by the **6e** hexamer on the reaction [54b]

cavity of the hexamer since the obtained ethers have a low affinity to the hexamer cavity. The hexamer can also impose substrate selectivity as shown in Scheme 31.2b [54b].

However the most important example to date for the use of the hexamer of **6e** as a catalytic nano-vessel was provided very recently by Zhang and Tiefenbacher. They studied the so-called tail-to-head terpene (THT) cyclization (Fig. 31.12a), which in Nature is accomplished by multiple enzyme systems [55] including terpene cyclase [54c]. Zhang and Tiefenbacher noted that the hexamers of **6e**: (1) are large enough to accommodate acyclic terpene; (2) encapsulate positively charged species and due to their aromatic walls can, as terpene cyclase does, stabilize positively charged cationic intermediates, (3); can function as mild Bronstead acids, and (4) allow facile guest exchange. Zhang and Tiefenbacher speculated and indeed found that the hexamers activate a THT cyclization cascade inside their cavities [54c].

By judicious characterization of the kinetics of the different intermediates and products in the reactions of different substrates and by comparing the results from alcohols and acetates, the mechanism for the formation of a series of terpenes from unsaturated alcohols in the presence of the hexamers of **6e** was elucidated [54c]. For example, Fig. 31.12b shows the kinetics of one of the reactions performed in the presence of  $[\mathbf{6e}_6(\text{H}_2\text{O})_8]$ . This analysis showed that direct rotation of the *transoid* allylic cation to a *cisoid* cation, previously thought to be impossible, does occur [54c, d]. In this study it was shown that the hexameric capsule can encapsulate the terpene, stabilize the formed carbocations in a lipophilic environment (like in an enzyme pocket) which presumably increase their lifetimes (excluding water and

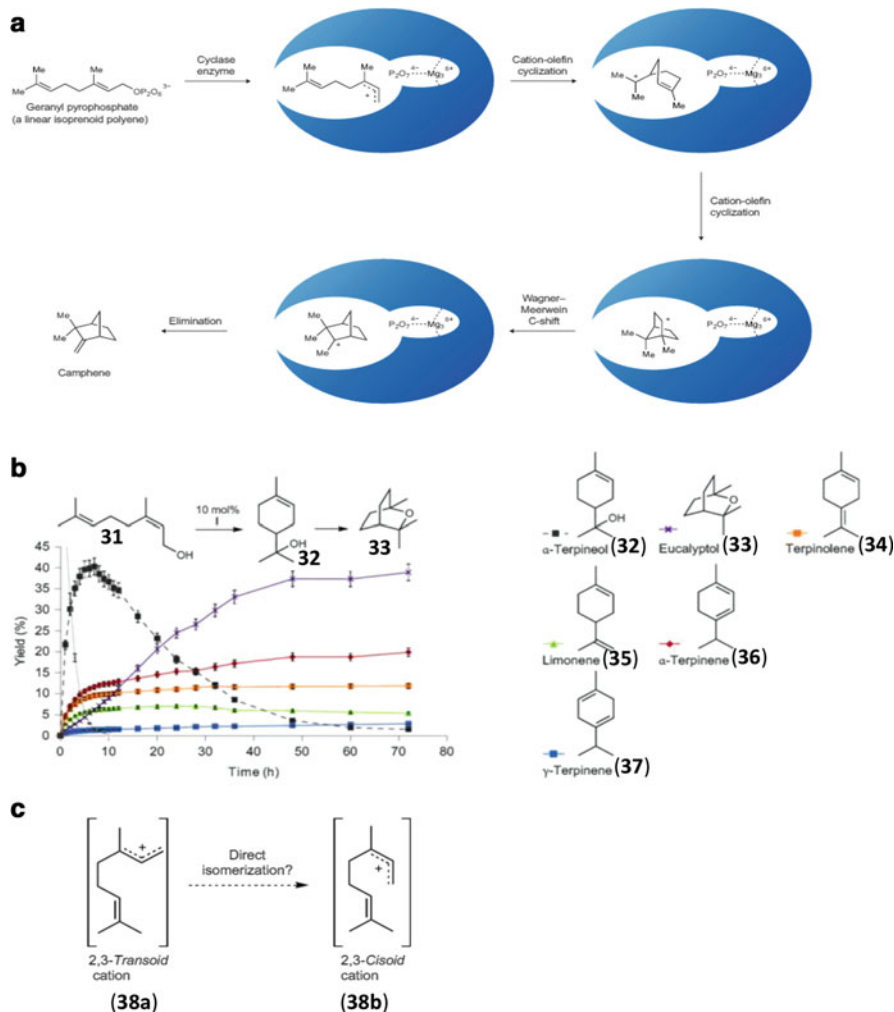


**Fig. 31.12** (a) Non-stop polycyclization/rearrangement controlled by terpene cyclase enzymes [54d]. The enzyme folds the polyene chain, ionizes the polyene, sequesters the pyrophosphate anion, and stabilizes the highly reactive carbocation formed. (b) Results of the THT cyclization of alcohol substrates performed in  $[\mathbf{6e}_6(\text{H}_2\text{O})_8]$ . Compound (31) is first cyclized mainly to  $\alpha$ -terpineol (32), which is then converted into eucalyptol (33); other products are also shown (34–37) [54c]. (c) Isomerization of *transoid* cation (38a) to *cisoid* form (38b) [54c]

anion) and allowing a cascade of reactions (i.e., rotations and rearrangements) to occur. Finally, the product, which has a lower affinity for the cavity of the hexamer than the reactants, is released (Fig. 31.12). This operation catalyzed by the hexamer, which was carried in organic solvents, parallels enzyme action [54d]. These results show that in the confined space of the capsules the isomerization of a *transoid* carbocation **38a** to the *cisoid* carbocation **38b** is possible although for many years it

was accepted that such transformation has a too high activation energy (55 KJ/mol) [55] to be probable (Fig. 31.12c) [54c, d].

In another example of catalysis by the hydrogen-bonded hexamers, Shimizu et al. prepared “Teflon-footed” resorcin[4]arenes [56] (i.e., resorcin[4]arenes with per-fluorinated side chains) that form hexameric capsules in wet fluoruous solvents. These capsules, several years later, were used to accelerate a Diels-Alder reaction in a biphasic system [56b].

### 31.6 Metal Mixed Organic Hexameric Capsules

An intriguing class of hexameric capsules are the hybrid systems based on metal organic pyrogallol[4]arene nano-capsules (MONCs) [57, 58]. These systems were recently the subject of several reviews [57] but in recent years the field have witness a tremendous advancement, mostly by the group of Atwood. The first example of a MONC system was obtained by reacting *C*-proyl-3-ol-pyrogallol[4]arene obtained using the reaction shown in Fig. 31.13a with copper(II) nitrate [58a]. From the

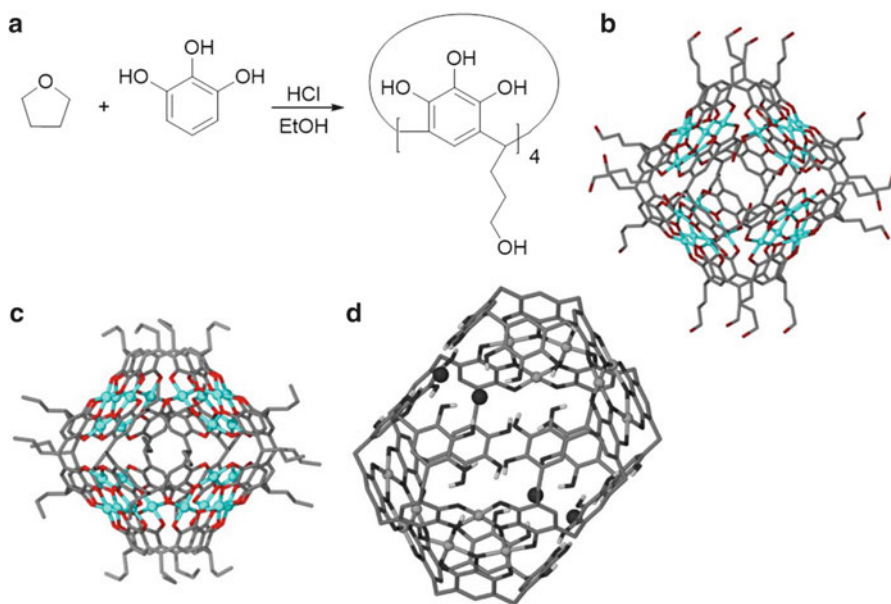


**Fig. 31.13** (a) The synthesis of *C*-propan-3-ol-pyrogallol[4]arene [58a]. (b) The metal-organic nano-capsule formed by combining *C*-propan-3-ol-pyrogallol[4]arene with copper(II) nitrate [58a]. Hydrogen atoms, solvent molecules, and apical copper ligands are omitted for clarity. (c) Partial structure of the metal-organic nano-capsule formed by combining *C*-propyl-pyrogallol[4]arene with copper(II) nitrate in methanol [58b]. (d) The Ga-*C*-propyl-pyrogallol[4]arene capsule showing the distorted ‘rugby-ball’ shape of the assembly and the water molecules occupying the surface voids [58d]. The propyl chains, as well as hydrogen atoms (except for OH) are omitted for clarity

structure of the obtained nano-capsules (Fig. 31.13b), it is apparent that the OH groups on the alkyl side chains do not participate in the formation of the capsular assembly.

When the *C*-propyl pyrogallol[4]arene was reacted with copper(II) nitrate, the obtained hexamers were found to have a very similar capsular structure (see Fig. 31.13c) [58b]. In these Cu-MONC systems the 24 copper atoms replace 48 protons affording nearly spherical capsules with a very similar geometries (Fig. 31.13b, c). Then after such systems containing nickel were also prepared and found to have similar structures [58c]. Interestingly, when different *C*-alkylpyrogallol[4]arenes are reacted with gallium (III) nitrate, hexameric Ga-MONC systems are obtained in which 12 gallium atoms replace 36 protons affording, in the solid state, a “rugby-ball” shaped hexameric capsule in which four water molecules are embedded in the seam of the capsular framework (Fig. 31.13d) [58d–f]. Efforts to increase the number of gallium atoms beyond 12 in such MONC systems failed. As these intriguing Ga-MONC systems are diamagnetic, it is possible to study these systems by NMR. It was found that these Ga-MONCs have entries allowing transport of other metals in and out the capsules [58e–f]. As several protons remain in these systems, the idea of using Ga-MONC as starting materials for the preparation of mixed-metal MONCs was suggested [57b]. Indeed Cu/Ga-MONCs and Zn/Ga-MONCs were prepared, and more recently large metals have been incorporated into these systems thus forming, for example, Cd/Ga MONCs hexameric capsules [57, 58g]. The Cd/Ga MONCs are also nearly spherical and there it was possible, for the first time, to distinguish between disparate metal center positions [59]. Interestingly, the addition of Cu, Zn, or Cd to the Ga-MONC results in the structural changes from a “rugby-ball” shape to nearly spherical structures [57–59].

Determining the actual shape of the formed MONC systems in solution is more difficult than in the solid state, especially for paramagnetic species [29]. Atwood and Deakne have used small-angle neutron scattering (SANS) to address this issue [28, 29]. Using this methodology it was shown that upon dissolution the “rugby-ball” shape of the Ga-MONC changes to a toroidal shaped structure. Interestingly, Ga/Zn-MONCs, which are nearly spherical in the solid state, also form toroidal shaped structures with different dimensions in solution (Fig. 31.14) [28b]. Recently, it was shown that addition of Zn to a Ga-MONC system encapsulating Cs changes the solid-state “rugby-ball” structure to a toroidal structure solution while keeping the Cs cation encapsulated in the structure, thus forming, in fact, a tri-metallic hybrid MONC system [60a]. Tri-metallic MONC systems can be formed also by addition of K/Rb to the Ga-MONC encapsulating Cs where the K or Rb replaces the portal water leaving the Cs encapsulated in the Ga-K-MONC or Ga-Rb-MONC structures [28a].

Very recently it was shown that Ga-K- and Ga-Zn-MONCs encapsulating Tl can be prepared [60b]. In addition to the capsular MONC systems of different shapes it was found that these systems can form tubular and bilayer structures. To appreciate the wealth of possibilities of MONCs, the reader is advised to consult recent reviews on the subject [29, 60b].

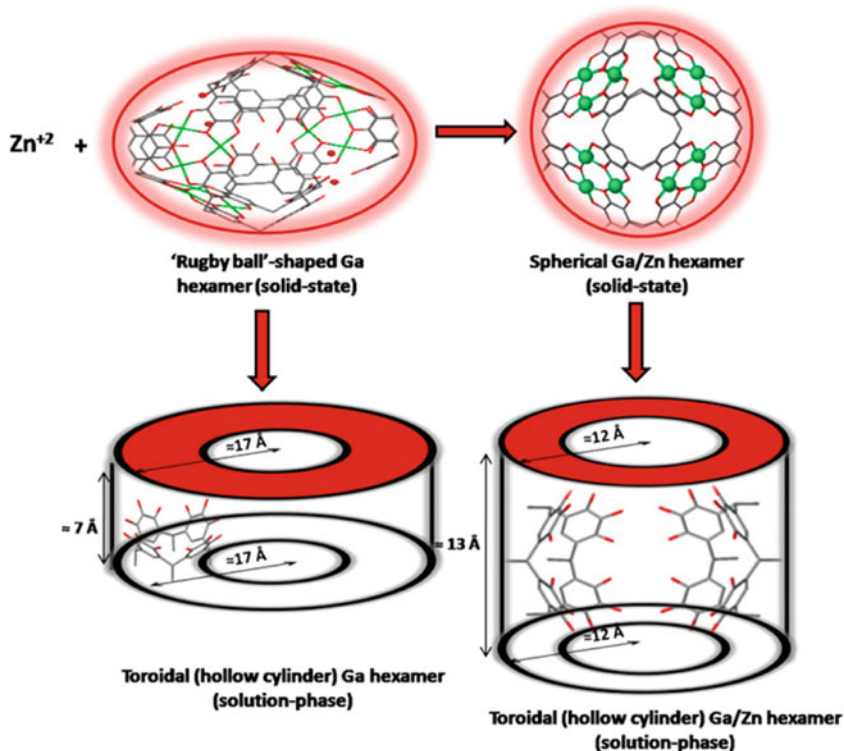


**Fig. 31.14** Graphical representations of the geometries of gallium-seamed and gallium/zinc-seamed pyrogallol[4]arene MONCs as a function of change in phase (solid to solution or solid to solid) [29].

## 31.7 Summary

Self-assembled molecular capsules are an intriguing class of molecules that are expected to find applications as nanomeric reaction vessels where new chemistry and catalysis may occur. Molecular capsules may, in principle, be used as drug delivery systems, as transport systems, and for storage purposes. Arguably resorcin [4]arene and pyrogallol[4]arenes are simple concave shaped molecules which tendency to form, spontaneously, giant molecular capsules is remarkable. Such hexameric capsules are observed in all three phases, in the solid-state, in solution, and even in the gas phase. Diffusion NMR demonstrated unequivocally that the hexameric capsules are in fact the resting state of resorcin[4]arenes and pyrogallol [4]arenes in organic solvents implying that these systems are indeed more abundant than previously thought. Despite the apparent similarities, these hexamers do differ: Diffusion NMR demonstrated that resorcin[4]arenes form  $[6_6(H_2O)_8]$ -type

hexamers, whereas pyrogallol[4]arenes form 7<sub>6</sub>-type hexamers in solution as found in the solid-state by x-ray crystallography. This may be the one of the reasons that, as found by diffusion NMR and FRET, the self-assembly process in these systems proceeds via narcissist self-sorting.

In the case of resorcin[4]arene hexamers, alcohols can replace the water molecules, and, in fact, alcohols can be either encapsulated or can be part of structure of the hexamers. In addition, the <sup>1</sup>H-NMR signals of the encapsulated solvent molecules were found to be much more structured in the pyrogallol[4]arene hexamers compared to resorcin[4]arene hexamers. This seems to provide a partial explanation for the fact that, by direct dissolution, the resorcin[4]arene hexamers encapsulate a much larger repertoire of guests than do the pyrogallol[4]arene hexamers. Recent use of the melting approach showed that one can increase considerably the number of guests that can be encapsulated in the pyrogallol[4]arene hexamers. Interestingly the solvent-free approach provides a mean to obtain kinetically trapped capsular complexes that may be used for controlled release, and these systems will be interesting to study even further in the future. Today, more than a decade after they were first described, hexameric capsules are indeed the best example in the literature for the added values of diffusion NMR in assisting in structural determination of supramolecular systems in solution.

An important development in the field in the last decade is the preparation of the hexameric pyrogallol[4]arene MONCs, some of which are based on mixed metals with properties that are only now being explored. These MONCs change shapes in solution as demonstrated by SANS. The MONCs that allow entrapment and transport of metal cations could well be found useful in the future as molecular storage devices and even as drug delivery systems due to their high stability. It will be of interest to determine whether such systems are sufficiently stable in aqueous solutions.

One of the most recent developments in the field is the use of the self-assembled hexameric resorcin[4]arene capsules as reaction vessels or nano-reactors where new chemistry and catalysis may occur. There are only few such examples however in the past year or so several convincing and interesting examples were reported. The most interesting to date is the terpenes synthesis from unsaturated alcohols, which seems to mimic the action of cyclase enzymes. Clearly there is more chemistry to discover with these nano-vessels.

Resorcin[4]arenes and pyrogallol[4]arenes forms spectacular hexameric capsules quite easily, and their study has supplied several surprises regarding their narcissist self-assembly and their guest affinity. At least in the pyrogallol[4]arene capsules, guest affinity is still largely a subject of trial and error. Therefore methods to partially circumvent this limitation were developed affording kinetically trapped capsules which by themselves are interesting systems, which may have some potential applications as storage and delivery systems. The fact that powders of such hexameric capsules can be prepared quite easily may open new avenues of research regarding guest exchange and guest affinity in such systems and their use as storage systems.

A large variety of MONCs have been prepared in recent years, and there is now convincing evidence that such hexameric capsules can be used as molecular containers and nano-vessels. The fact that resorcin[4]arenes and pyrogallol[4]arenes are simple molecules that can be synthesized in large quantities with little effort indicate that new exciting findings and developments with these systems and derivatives thereof are still to be unfolded.

**Acknowledgement** Yoram Cohen wishes to thank the Israel Science Foundation (ISF, Jerusalem, Israel) for financial support.

## References

1. (a) Fujita, M.; Umemoto, K.; Yoshizawa, M.; Fujita, T. *Chem. Commun.* **2001**, 509–518. (b) Inokuma, Y.; Kawano, M.; Fujita, M. *Nat. Chem.* **2011**, *3*, 349–358. (c) Yoshizawa, M.; Klosterman, J. K.; Fujita, M. *Angew. Chem., Int. Ed.* **2009**, *48*, 3418–3438. (d) Klosterman, J. K.; Yamaguchi, Y.; Fujita, M. *Chem. Soc. Rev.* **2009**, *38*, 1714–1725.
2. (a) Fiedler, D.; Leung, D. H.; Bergman, R. G.; Raymond, K. N. *Acc. Chem. Res.* **2005**, *38*, 349–358. (b) Raymond, K. N.; Brown, C. J. *Top. Curr. Chem.* **2012**, *323*, 1–18. (c) Pluth, M. D.; Bergman, R. G.; Raymond, K. N. *Acc. Chem. Res.* **2009**, *42*, 1650–1659. (d) Adriaenssens, L.; Ballester, P. *Chem. Soc. Rev.* **2013**, *42*, 3261–3277. (e) Breiner, B.; Clegg, J. K.; Nitschke, J. R. *Chem. Sci.* **2011**, *2*, 51–56.
3. (a) Hof, F.; Craig, S. L.; Nuckolls, C.; Rebek, J., Jr. *Angew. Chem. Int. Ed.* **2002**, *41*, 1488–1508. (b) Berryman, O. B.; Dube, H.; Rebek, J., Jr. *Isr. J. Chem.* **2011**, *51*, 700–709. (c) Rebek, J. Jr. *Angew. Chem. Int. Ed.* **2005**, *44*, 2068–2078. (c) Rebek, J. Jr. *Acc. Chem. Res.* **2009**, *42*, 1660–1668.
4. (a) Rebek, J. Jr. *Chem. Commun.* **2007**, 2777–2789. (b) Schröder, T.; Sahu, S. N.; Anselmetti, D.; Mattay, J. *Isr. J. Chem.* **2011**, *51*, 725–742. (c) Kobayashi, K.; Yamanaka, M. *Chem. Soc. Rev.* **2015**, *44*, 449–466. (d) Gangemi, C. M. A.; Pappalardo, A.; Sfrazzetto, G. T. *RSC Adv.* **2015**, *5*, 51919–51933. (e) Gangemi, C. M. A.; Pappalardo, A.; Sfrazzetto, G. T. *Current Org. Chem.* **2015**, *19*, 2281–2308. (f) Rebek, J. Jr. *Hydrogen-Bonded Capsules: Molecular Behavior in Small Spaces*, World Scientific Publishing Co. Pte. Ltd. Singapore **2016**.
5. Högberg, A. G. S. *J. Am. Chem. Soc.* **1980**, *102*, 6046–6050.
6. (a) Cram, D. J.; Karbach, S.; Kim, Y. H.; Baczyński, L.; Kallemeyn, G. W. *J. Am. Chem. Soc.* **1985**, *107*, 2575–2576. (b) Tanner, M. E.; Knobler, C. B.; Cram, D. J. *J. Am. Chem. Soc.* **1990**, *112*, 1659–1660. (c) Cram, D. J. *Nature* **1992**, *356*, 29–36.
7. (a) Jasat, A.; Scherman, J. C. *Chem. Rev.* **1999**, *99*, 931–967. (b) Warmuth, R. *Acc. Chem. Res.* **2001**, *34*, 95–105. (c) Rue, M. R.; Sun, J.; Warmuth, R. *Isr. J. Chem.* **2011**, *51*, 743–768.
8. (a) Bartik, K.; Luhmer, M.; Dutasta, J.-P.; Collet, A.; Reisse, J. J. *J. Am. Chem. Soc.* **1998**, *120*, 784–791. (b) Brotin, T.; Dutasta, J.-P. *Chem. Rev.* **2009**, *109*, 88–130.
9. (a) Schröder, L. *Physica Medica*, **2013**, *29*, 3–16. (b) Palaniappan, K. K.; Francis, M. B.; Pines, A.; Wemmer, D. E. *Isr. J. Chem.* **2014**, *54*, 104–112 (c) Taratula, O.; Dmochowski, I. J. *Curr. Opin. Chem. Biol.* **2010**, *14*, 97–104.
10. (a) Branda, N.; Wyler, R.; Rebek, J. Jr. *Science* **1994**, *263*, 1267–1268. (b) Wyler, R.; Mendoza, Rebek, J. Jr. *Angew. Chem. Int. Ed. Engl.* **1993**, *32*, 1699–1701.
11. (a) Shimizu, K. D.; Rebek, J. Jr. *Proc. Natl. Acad. Sci. USA* **1995**, *92*, 12403–12407. (b) Rebek, J. Jr. *Chem. Commun.* **2000**, 637–643. (c) Mogck, O.; Böhmer, V.; Vogt, W. *Tetrahedron* **1996**, *52*, 8489–8496. (d) Mogck, O.; Paulus, E. F.; Böhmer, V.; Thondorf, I.; Vogt, W. *Chem. Commun.* **1996**, 2533–2434.



12. (a) Heintz, T.; Rudkevich, D.; Rebek, J. Jr. *Nature* **1998**, *394*, 764–766. (b) Heintz, T.; Rudkevich, D. M.; Rebek, J. Jr. *Angew. Chem. Int. Ed. Engl.* **1999**, *38*, 1136–1139. (c) Rechavi, D.; Scarso, A.; Rebek, J. Jr. *J. Am. Chem. Soc.* **2004**, *126*, 7738–7739. (d) Asadi, A.; Ajami, D.; Rebek, J. Jr. *J. Am. Chem. Soc.* **2011**, *133*, 10682–10684.
13. (a) Murayama, K.; Aoki, K. *Chem. Commun.* **1998**, 607–608. (b) Shivanyuk, A.; Rissanen, K.; Kolehmainen, E. *Chem. Commun.* **2000**, 1107–1108.
14. MacGillivray, L. R.; Atwood, J. L. *Nature* **1997**, *389*, 469–472.
15. Gerkenmeier, T.; Iwanek, W.; Agena, C.; Fröhlich, R.; Kotila, S.; Näther, C.; Mattay, J. *Eur. J. Org. Chem.* **1999**, 2257–2262.
16. (a) Stejskal, O. E.; Tanner, J. E. *J. Chem. Phys.* **1965**, *42*, 288–292. (b) Stilbs, P.J. *Prog. NMR Spectrosc.* **1987**, *19*, 1–45. (c) Pregosin, P. S.; Kumar, G. A.; Fernandez, I. *Chem. Rev.* **2015**, *105*, 2977–2998.
17. (a) Frish, L.; Matthews, S. E.; Böhmer, V.; Cohen, Y. *J. Chem. Soc. Perkin Trans 2* **1999**, 669–671. (b) Frish, L.; Vysotsky, M. O.; Matthews, S. E.; Böhmer, V.; Cohen, Y. *J. Chem. Soc. Perkin Trans 2* **2002**, 88–93. (c) Frish, L.; Vysotsky, M. O.; Böhmer, V.; Cohen, Y. *Org. Biomol. Chem.* **2003**, *1*, 2011–2014.
18. (a) Cohen, Y.; Avram, L.; Frish, L. *Angew. Chem., Int. Ed.* **2005**, *44*, 520–556. (b) Avram, L.; Cohen, Y. *Chem. Soc. Rev.* **2015**, *44*, 586–602. (c) Cohen, Y.; Avram, L.; Evan-Salem, T.; Slovak, S.; Shemesh, N.; Frish, L. in *Analytical Methods in Supramolecular Chemistry*, Ed. Schalley, C. A., **2012**, Vol 1, pp. 197–285.
19. (a) Avram, L.; Cohen, Y. *J. Am. Chem. Soc.* **2002**, *124*, 15148–15149. (b) Avram, L.; Cohen, Y. *Org. Lett.* **2002**, *4*, 4365–4368.
20. (a) Avram, L.; Cohen, Y. *Org. Lett.* **2003**, *5*, 3329–3332. (b) Avram, L.; Cohen, Y. *J. Am. Chem. Soc.* **2004**, *126*, 11556–11563. (c) Avram, L.; Rebek, J. Jr.; Cohen, Y. *Chem. Commun.* **2011**, *47*, 5368–5373. (d) Palmer, L. C.; Rebek, J. Jr. *Org. Lett.* **2005**, *7*, 787–789.
21. (a) Ballester, P.; Gil-Ramirez, G. *Proc. Natl. Acad. Sci. U.S.A.* **2009**, *106*, 10455–10459. (b) Ballester, P. *Isr. J. Chem.* **2011**, *51*, 710–724. (c) Galan, A.; Valderrey, V.; Ballester, P. *Chem. Sci.* **2015**, *6*, 6325–6333.
22. Ajami, D.; Rebek, J. Jr. *Acc. Chem. Res.* **2013**, *46*, 990–999.
23. (a) Shivanyuk, A.; Scarso, A.; Rebek, J. Jr. *Chem. Commun.* **2003**, 1230–1231. (b) Shivanyuk, A.; Rebek, J. Jr. *Angew. Chem. Int. Ed.* **2003**, *42*, 684–686. (c) Yamanka, M.; Rebek, J. Jr. *Chem. Commun.* **2004**, 1690–1691.
24. (a) Atwood, J. L.; Barbour, L. J.; Jerga, A. *Proc. Natl. Acad. Sci. U.S.A.* **2002**, *99*, 4837–4841. (b) Atwood, J. L.; Barbour, L. J.; Jerga, A. *Chem. Commun.* **2001**, 2376–2377.
25. (a) Shivanyuk, A.; Rebek, J. Jr. *Proc. Natl. Acad. Sci. U.S.A.* **2001**, *98*, 7662–7665. (b) Shivanyuk, A.; Rebek, J. Jr. *Chem. Commun.* **2001**, 2424–2425.
26. (a) Avram, L.; Cohen, Y. *Org. Lett.* **2003**, *5*, 1099–1102. (b) Avram, L.; Cohen, Y. *Org. Lett.* **2008**, *10*, 1505–1508.
27. Avram, L.; Cohen, Y. *J. Am. Chem. Soc.* **2003**, *125*, 16180–16181.
28. (a) Kumari, H.; Jin, P.; Teat, S. J.; Barnes, C. L.; Dalgarno, S. J.; Atwood, J. L. *J. Am. Chem. Soc.* **2014**, *136*, 17002–17005. (b) Kumari, H.; Kline, S. R.; Wycoff, W. G.; Paul, R. L.; Mossine, A. V.; Deakyne, C. A.; Atwood, J. L. *Angew. Chem., Int. Ed.* **2012**, *51*, 5086–5091.
29. Kumari, H.; Deakyne, C. A.; Atwood, J. L. *Acc. Chem. Res.* **2014**, *47*, 3080–3088.
30. (a) Beyeh, N. K.; Kogej, M.; Ahman, A.; Rissanen, K.; Schalley, C. A. *Angew. Chem., Int. Ed.* **2006**, *45*, 5214–5218.
31. Mecozzi, S.; Rebek, J. Jr. *Chem. Eur. J.* **1998**, *4*, 1016–1022.
32. Cohen, Y.; Evan-Salem, T.; Avram, L. *Supramol. Chem.* **2008**, *20*, 71–79.
33. Avram, L.; Cohen, Y. *J. Am. Chem. Soc.* **2005**, *127*, 5714–5719.
34. Johnson, C. S. *Jr. Prog. NMR Spectrosc.* **1999**, *34*, 203–256.
35. Ugono, O.; Holman, K. T. *Chem. Commun.* **2006**, 2144–2146.
36. (a) Slovak, S.; Avram, L.; Cohen, Y. *Angew. Chem. Int. Ed.* **2010**, *49*, 428–431. (b) Slovak, S.; Cohen, Y. *Chem. Eur. J.* **2012**, *18*, 8515–8520.

37. (a) Gerkenmeier, T.; Mattay, J.; Näther, C. *Chem. Eur. J.* **2001**, *7*, 465–474. (b) Letzel, M. C.; Decker, B.; Rozhenko, A. B.; Schoeller, W. W.; Mattay, J. *J. Am. Chem. Soc.* **2004**, *126*, 9669–9674.
38. Evan-Salem, T.; Cohen, Y. *Chem. Eur. J.* **2007**, *13*, 7659–7663.
39. (a) Safont-Sempere, M. M.; Fernandez, G.; Würther, F. *Chem. Rev.* **2011**, *111*, 5784–5814. (b) Lal Saha, M.; Schmittel, M. *Org. Biomol. Chem.* **2012**, *10*, 4651–4684.
40. (a) Kramer, R.; Lehn, J.-M.; Marquis-Rigault, A. *Proc. Natl. Acad. Sci. USA.* **1993**, *90*, 5394–5398. (b) Wu, A.; Isaacs, L. *J. Am. Chem. Soc.* **2003**, *125*, 4831–4835.
41. (a) Barrett, E.; Dale, T. J.; Rebek, J. Jr. *J. Am. Chem. Soc.* **2007**, *129*, 3818–3819. (b) Barrett, E.; Dale, T. J.; Rebek, J. Jr. *Chem. Commun.* **2007**, 4224–4226. (c) Barrett, E.; Dale, T. J.; Rebek, J. Jr. *J. Am. Chem. Soc.* **2008**, *130*, 2344–2350.
42. (a) Ajami, D.; Hou, J.-L.; Dale, T. J.; Barrett, E.; Rebek, J., Jr. *Proc. Natl. Acad. Sci. USA* **2009**, *106*, 10430–10434. (b) Ajami, D.; Schramm, M. P.; Volonterio, A.; Rebek, J., Jr. *Angew. Chem., Int. Ed.* **2007**, *46*, 242–244.
43. (a) Philip, I.; Kaifer, A. E. *J. Am. Chem. Soc.* **2002**, *124*, 12678–12679. (b) Yamanaka, M.; Shivanyuk, A.; Rebek, J., Jr. *J. Am. Chem. Soc.* **2004**, *126*, 2939–2943. (c) Slovak, S.; Cohen, Y. *Supramol. Chem.* **2010**, *22*, 803–807. (d) Evan-Salem, T.; Baruch, I.; Avram, L.; Cohen, Y.; Palmer, L. C.; Rebek, J., Jr. *Proc. Natl. Acad. Sci. U. S. A.* **2006**, *103*, 12296–12300. (e) Cohen, Y.; Evan-Salem, T.; Avram, L. *Supramol. Chem.* **2008**, *20*, 71–79.
44. (a) Philip, I.; Kaifer, A. E. *J. Org. Chem.* **2005**, *70*, 1558–1564. (b) Cave, G. W. V.; Antesberger, J.; Barbour, L. J.; McKinlay, R. M.; Atwood, J. L. *Angew. Chem. Int. Ed.* **2004**, *43*, 5263–5266. (c) Dalgarno, S. J.; Tucker, S. A.; Bassil, D. B.; Atwood, J. L. *Science* **2005**, *309*, 2037–2039. (d) Dalgarno, S. J.; Bassil, D. B.; Tucker, S. A.; Atwood, J. L. *Angew. Chem. Int. Ed.* **2006**, *45*, 7019–7022. (e) Dalgarno, S. J.; Szabo, T.; Siavosh-Haghighi, A.; Deakynne, C. A.; Adams, J. E.; Atwood, J. L. *Chem. Commun.* **2009**, 1339–1341.
45. (a) Avram, L.; Cohen, Y. *Org. Lett.* **2006**, *8*, 219–222. (b) Guralnik, V.; Avram, L.; Cohen, Y. *Org. Lett.* **2014**, *16*, 5592–5595. (c) Avram, L.; Goldbourt, A.; Cohen, Y. *Angew. Chem. Int. Ed.* **2016**, *52*, 904–907.
46. (a) Kvasnica, M.; Chapin, J. C.; Purse, B. W. *Angew. Chem. Int. Ed.* **2011**, *50*, 2244–2248. (b) Chapin, J. C.; Kvasnica, M.; Purse, B. W. *J. Am. Chem. Soc.* **2012**, *134*, 15000–15009. (c) Chapin, J. C.; Purse, B. W. *Supramol. Chem.* **2014**, *26*, 517–520. (d) Shoushan-Yariv, S.; Cohen Y. *Org. Lett.* **2016**, *18*, 936–939.
47. (a) Note that larger high-field shift of about 4.0 ppm were observed in tightly packed dimeric capsules, see: Shivanyuk, A.; Rebek, J. Jr. *Chem. Commun.* **2002**, 2326–2327. (b) Trambleu, L.; Rebek, J. Jr.; *Science* **2003**, *301*, 1219–1220.
48. (a) Garozzo, D.; Gattuso, G.; Kohnke, F. H.; Notti, A.; Pappalardo, S.; Parisi, M. F. *Org. Lett.* **2003**, *5*, 4025–4028. (b) Tanaka, Y.; Kato, Y.; Aoyama, Y. *J. Am. Chem. Soc.* **1990**, *112*, 2807–2808. (c) Kikuchi Y.; Tanaka, Y.; Sutarto, S.; Kobayashi, K.; Toi, H.; Aoyama, Y. *J. Am. Chem. Soc.* **1992**, *114*, 1351–1358.
49. (a) Dalgarno, S. J.; Power, N. P.; Antesberger, J.; McKinlay, R. M.; Atwood, J. L. *Chem. Commun.* **2006**, 3803–3805. (b) Antesberger, J.; Cave, G. W. V.; Ferrarelli, M. C.; Heaven, M. W.; Raston, C. L.; Atwood, J. L. *Chem Commun.* **2005**, 892–894. (c) Iyer, K. S.; Norret, M.; Dalgarno, S. J.; Atwood, J. L.; Raston, C. L. *Angew. Chem. Int. Ed.* **2008**, *47*, 6362–6366.
50. Christianson, D. W. *Chem. Rev.* **2006**, *106*, 3412–3442.
51. (a) Brown, C. J.; Toste, F. D.; Bergman, R. G.; Raymond, K. N. *Chem. Rev.* **2015**, *115*, 3012–3035. (b) Raynal, M.; Ballester, P.; Vidal-Ferran, A.; van Leeuwen, Piet W. N. M. *Chem. Soc. Rev.* **2014**, *43*, 1660–1733. (c) Raynal, M.; Ballester, P.; Vidal-Ferran, A.; van Leeuwen, Piet W. N. M. *Chem. Soc. Rev.* **2014**, *43*, 1734–1787.
52. (a) Jordan, J. H.; Gibb, B. C. *Chem. Soc. Rev.* **2015**, *44*, 547–585.
53. (a) Cavarzan, A.; Scarso, A.; Sgarbossa, P.; Strukul, G.; Reek, N. H. *J. Am. Chem. Soc.* **2011**, *133*, 2848–2853. (b) Cavarzan, A.; Reek, J. N. H.; Trentin, F.; Scarso, A.; Strukul, G. *Catal. Sci. Technol.* **2013**, *3*, 2898–2901. (c) Giust, S.; Sorella, G. L.; Sporni, L.; Strukul, G.; Scarso, A. *Chem. Commun.* **2015**, *51*, 1658–1661. (d) Giust, S.; Sorella, G. L.; Sporni, L.; Fabris, F.;

- Strukul, G.; Scarso, A. *Asian J. Org. Chem.* **2015**, *4*, 217–220. (e) Sorella, G. L.; Sperti, L.; Strukul, G.; Scarso, A. *ChemCatChem.* **2015**, *7*, 291–296.
54. (a) Zhang, Q.; Tiefenbacher, K. *J. Am. Chem. Soc.* **2013**, *135*, 16213–16219. (b) Catti, L.; Tiefenbacher, K. *Chem Commun.* **2015**, *51*, 892–894. (c) Zhang, Q.; Tiefenbacher, K. *Nature Chem.* **2015**, *7*, 197–202. (d) Roach, J. J.; Shevni, R. A. *Nature Chem.* **2015**, *7*, 187–189.
55. Croteau, R. *Chem. Rev.* **1987**, *87*, 929–954.
56. (a) Shimizu, S.; Kiuchi, T.; Pan, N. *Angew. Chem. Int. Ed.* **2007**, *46*, 6442–6445. (b) Shimizu, S.; Usui, A.; Sugai, M.; Suematsu, Y.; Shirakawa, S.; Ichikawa, H. *Eur. J. Org. Chem.* **2013**, 4734–4737.
57. (a) Dalgarno, S. J.; Power, N. P.; Atwood, J. L. *Coord. Chem. Rev.* **2008**, *252*, 825–841. (b) Jin, P.; Dalgarno, S. J.; Atwood, J. L. *Coord. Chem. Rev.* **2010**, *254*, 1760–1768.
58. (a) McKinlay, R. M.; Cave, G. W. V.; Atwood, J. L. *Proc. Natl. Acad. Sci. U.S.A.* **2005**, *44*, 5944–5948. (b) Dalgarno, S. J.; Power, N. P.; Warren, J. E.; Atwood, J. L. *Chem. Commun.* **2008**, 1539–1541. (c) Kumari, H.; Dennis, C. L.; Mossine, C. V.; Deakyne, C. A.; Atwood, J. L. *ACSNano* **2012**, *6*, 272–275. (d) McKinlay, R. M.; Thallapally, P. K.; Cave, G. W. V.; Atwood, J. L. *Angew. Chem. Int. Ed.* **2005**, *44*, 5733–5736. (e) McKinlay, R. M.; Thallapally, P. K.; Atwood, J. L. *Chem. Commun.* **2006**, 2956–2958. (f) Dalgarno, S. J.; Power, N. P.; Atwood, J. L. *Chem. Commun.* **2007**, 3447–3449. (g) Jin, P.; Dalgarno, S. J.; Warren, J. E.; Teat, S. J.; Atwood, J. L. *Chem. Commun.* **2009**, 3348–3350.
59. Jin, P.; Kumari, H.; Kennedy, S.; Barnes, C. L.; Teat, S. J.; Dalgarno, S. J.; Atwood, J. L. *Chem. Commun.* **2015**, *50*, 4508–4510.
60. (a) Kumari, H.; Jin, P.; Teat, S. J.; Barnes, C. L.; Dalgarno, S. J.; Atwood, J. L. *Angew. Chem. Int. Ed.* **2014**, *53*, 13088–13092. (b) Kumari, H.; Jin, P.; Deakyne, C. A.; Atwood, J. L. *Curr. Org. Chem.* **2013**, *17*, 1481–1488.

# Chapter 32

## Self-Assembled Dimeric Containers Based on Calix[4]arene, Resorcin[4]arene and Calix[4]pyrrole Scaffolds

G. Aragay and P. Ballester

### 32.1 Introduction

The isolation of molecules from the bulk solution through confinement in the inner cavity of molecular containers represented an important breakthrough in the field of Supramolecular Chemistry. The origin of molecular encapsulation dates back to the stimulating work of Collet (cryptophanes) and Cram (carcerands) in the mid 1980s and early 1990s [1–3]. The first containers had a purely covalent structure and their binding was based on mechanical forces that prevented guest escape. At a later date, non-covalent interactions were also used to construct the container's frameworks. This strategy generally referred as molecular self-assembly of cage or capsular containers constitutes a key concept in supramolecular chemistry. The self-assembly of container structures requires the use of multiple copies of identical or not-identical flat or concave molecules that fit together yielding a supramolecule. Supramolecular containers bind guests reversibly and, in most cases, by simply surrounding most of their surface. That is, the encapsulated guest establishes weak interactions with the inner surface of the container. The synthetic economy featured by molecular self-assembly is remarkable but it is also associated with practical limitations. Supramolecular encapsulation/inclusion complexes have a dynamic nature owing to the use of reversible interactions holding together the container's

---

G. Aragay

Institute of Chemical Research of Catalonia (ICIQ), The Barcelona Institute of Science and Technology, Avda. Països Catalans 16, 43007 Tarragona, Spain

P. Ballester (✉)

Institute of Chemical Research of Catalonia (ICIQ), The Barcelona Institute of Science and Technology, Avda. Països Catalans 16, 43007 Tarragona, Spain

Catalan Institution for Research and Advanced Studies (ICREA), Passeig Lluís Companys 23, 08010 Barcelona, Spain

e-mail: [pballester@icq.es](mailto:pballester@icq.es)

components. In short, they form and dissociate reversibly. In solution, container assemblies and their complexes usually reach thermodynamic equilibria rapidly under mild conditions. Supramolecular containers with high thermodynamic stability are present in solution as exclusive species in a suitable range of concentrations. However, their kinetic stability is significantly reduced compared to the covalent counterparts. For reversible capsular aggregates lacking portals large enough to allow the in-out guest's exchange, the lifetime of the encapsulation complex may not be a direct indication of the affinity of the container for the bound guest but of the affinity of the capsular components for each other.

In solution and in gas phase, the characterization of self-assembled cages/capsules requires analytical methods operating in timescales that are in accordance with their lifetimes (milliseconds to hours). NMR spectroscopy and mass spectrometry using soft methods (ESI, MALDI) for vaporization and ionization are appropriate. In some cases, the containers' structures and their complexes have also been characterized in the solid state by X-ray diffraction. Generally, the purification of supramolecular containers and their encapsulation complexes using chromatography is not feasible owing to dynamic features of the reversible self-assembly process that led to their formation.

The inner space of the molecular containers represents a unique environment for molecules. In fact, Cram referred to it as a new phase of matter. The confinement of molecules in supramolecular nanocontainers affects their chemical-physical properties. In this sense, molecules in enforced cavities often modify their chemical reactivity. Likewise, encapsulation of two reacting partners can promote the formation of unusual products, modify the regioselectivity of the reaction, and stabilize short-lived species and high-energy intermediates. Molecular encapsulation has also been used to accelerate reaction rates and to dissolve molecules in solvents where they were non-soluble. Supramolecular encapsulation complexes have been used in the development of new functional materials and cargo delivery systems with potential applications in biomedicine among others.

As stated above, reversible encapsulation was achieved by the use of multiple molecular components self-assembled through non-covalent interactions. Hydrogen bonding interactions have been widely used for the construction of interesting supramolecular container structures. It is worth noting that the thermodynamic stability of self-assembled capsular structures based on hydrogen bonding interactions is highly dependent on the nature of the solvent.

Coordination bonds constitute another reversible interaction used to produce a great variety of self-assembled container structures displaying a wide range of geometries. Coordination bonds are highly directional and offer greater binding strength than hydrogen bonds. Consequently, the self-assembly of molecular containers using coordination bonds yielded thermodynamically more robust architectures. However, many coordination bonds are reversible in the human timescale endowing the self-assembly process with the possibility of self-correction. Because molecular self-assembly driven by coordination bonds provided the most thermodynamically favorable metal-mediated structure, reaching the thermodynamic

equilibrium usually required longer times and higher temperatures than for hydrogen-bonded driven counterparts.

Metal complexes have attractive optical, magnetic, redox and catalytic properties, expanding the application of metal-mediated self-assembled containers in research areas such as supramolecular catalysis, development of redox and photoactive capsular systems, etc.

The preparation of molecular containers using self-assembly processes facilitated the control of size, shape and the chemical surface of their inner cavities. The inner volumes of self-assembled molecular containers are in the range of few hundreds to few thousand cubic angstroms [4]. The encapsulation of guest molecules is dependent on the complementarity of guest's size, shape and functional groups with the cavity of the container. In solution, the assembly of thermodynamically stable encapsulation complexes for guests that interact weakly with the container's inner cavity required filling approximately half of the cavity's volume (55 % rule) [5]. Encapsulated guests that do establish polar/strong interactions with the container lining form stable encapsulation complexes having packing coefficient (PC) values larger and smaller than 55 %. A PC value of 75 % was estimated as the maximum expected for reversible encapsulation complexes. Dense molecular solids have also packing coefficients of 75 % [6].

Stoichiometrically well-defined molecular containers (monodispersed molecular flasks) are suitable for the study of the thermodynamic and kinetic properties of molecular encapsulation processes. On the other hand, the use of polydispersed molecular containers (i.e. vesicles, liposomes [7] and polymeric microcapsules [8] etc.) is not recommended for this purpose. Learning the basic rules and principles governing reversible encapsulation processes is necessary for further development and improvement of the uses and applications of synthetic molecular containers.

There are many reports in recent literature describing the self-assembly of molecular containers and a great variety of molecular scaffolds have been used as container's components. Among them, molecular units featuring a concave shape are very useful to cover and complement the convex surface of the encapsulated guests. Calix[4]arenes, resorcin[4]arenes and aryl-extended calix[4]pyrrole are privileged subunits for the self-assembly of molecular containers (Fig. 32.1). All of them are conformationally flexible but, through appropriate elaboration, can be fixed in bowl-shaped conformations featuring aromatic cavities of different depths. The prefix "*calix-*" (from the Greek chalice) is used to remark this characteristic.

Interestingly, the concave cavity in all these subunits is exclusively shaped by aromatic panels. Functional groups can be introduced at the upper or lower rims of these subunits. The introduced functional groups serve to tune the inner space of the resulting capsular assemblies, the assembling properties of the subunits and their solubility in non-polar or aqueous solvents. Modifications at their upper rims are crucial in controlling the reversible self-assembly of the monomers into more complex container aggregates. Examples of the assembly of container aggregates driven by non-covalent interactions, such as hydrogen bonds or metal/ligand coordination bonds and even combinations of both are known. Examples of molecular containers based on derivatized scaffolds held together by halogen bonding

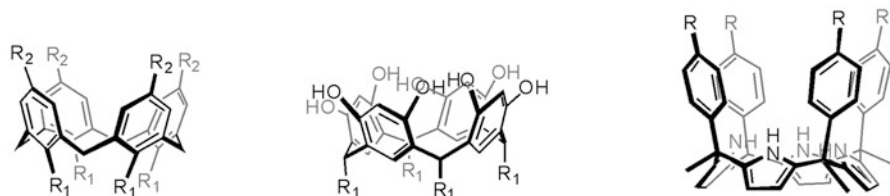


**Fig. 32.1** Line drawing structures of privileged units for the self-assembly of dimeric molecular containers (from *left to right*): calix[4]arene, resorcin[4]arene and aryl-extended calix[4]pyrrole

interactions have appeared recently in the literature [9, 10]. The different strength of the reversible forces, used to maintain together the capsule's components, confer the assemblies with distinct properties suitable for diverse potential applications.

Calix[4]arene and calix[4]pyrroles derivatives display quite different binding properties. Calix[4]arene derived containers are typically deprived of inwardly oriented polar groups that could be presented to the encapsulated guest. These assemblies are known to encapsulate non-polar aliphatic and aromatic neutral molecules through a combination of weak Van der Waal interactions, CH- $\pi$  and  $\pi$ - $\pi$  interactions for the latter. Organic cations are also suitable encapsulation guests for these containers featuring a non-polar but electron-rich lining and cation- $\pi$  interactions are important for the stabilization of these complexes. Supramolecular containers soluble in aqueous media use the hydrophobic effect to drive not only their assembly but also to encapsulate guests. One of the main differences between calix[4]arene and calix[4]pyrrole units resides in the hydrogen bonding ability of the tetrapyrrolic core of the later. Containers based on calix[4]pyrrole scaffolds display high affinities for electron rich neutral molecules and anions, which form hydrogen bonds with the pyrrole NHs and stabilize the cone conformation.

This chapter does not intend to be an exhaustive review of self-assembled dimeric containers based on the privileged units described above. In fact, a very recent review on self-assembled containers based on calix[4]resorcinarene cavitands has been published [11]. Instead, we simply try to provide the reader with a general overview of the different strategies used in the self-assembly of dimeric containers derived from these three types of molecular components. We also highlight some of the interesting features displayed by the encapsulation complexes of the assembled containers. Owing to space constraints, dimeric containers self-assembled through the hydrophobic effect [12] and charge-charge interactions [13] were not covered in the present report.

## 32.2 Self-Assembly of Dimeric Containers Driven by Hydrogen Bonding Interactions

### 32.2.1 Containers Based on Calix[4]arene Units

The first example of self-assembled dimeric molecular containers based on calix[4]arene scaffolds was described by Shimizu and Rebek in 1995 [14]. Tetraurea calix[4]arene **1** formed a dimeric capsular assembly in non-polar solvents through interdigitation of eight urea groups (Fig. 32.2). The homodimer was stabilized by a circular array of 16 intermolecular  $\text{NH}\cdots\text{O}=\text{C}$  hydrogen bonds established between four urea groups belonging to one of the capsule's half and other four urea groups in the other half. The seam of hydrogen bonds present in the capsule's equator required that the eight urea groups were unidirectionally oriented. This defined that the sense of rotation of the four urea groups in each of the two halves was complementary (clockwise (*P*) and counterclockwise (*M*) when viewed from the top of the cavity). Evidence of capsule formation was derived from the number of signals observed in the  $^1\text{H}$  NMR spectrum of the assembly. Thus, in non-polar solvents, the number of proton signals of the tetraurea calix[4]arene units was consistent with a  $C_4$  symmetry, instead of the  $C_{4v}$  symmetry displayed in hydrogen bonding competitive solvent (i.e. DMSO). In addition, in  $\text{CDCl}_3$  solution, the aryl and benzyl proton signals of the calix[4]arene units resonated as diastereotopic signals. The authors attributed the origin of the magnetic asymmetry to the unidirectional orientation of urea groups being kinetically stable on the NMR timescale. The complementary arrangement of urea groups rendered the two tetraurea halves cyclochiral conformers. However, the hemispheres were forced to have an opposite cyclochirality, they were cycloenantiomers, and the overall assembly **1•1** was *meso* and displayed a  $S_8$  symmetry.

The observation of highly upfield shifted signals for the protons of solvent molecules encapsulated in the cavity of the **1•1** container provided further evidence

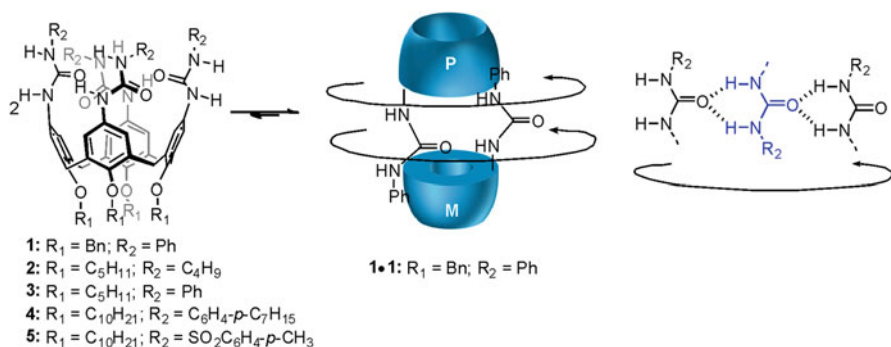


**Fig. 32.2** (Left) Equilibrium involved in the self-assembly of calix[4]arene **1** into a homodimeric capsular container **1•1**. (Right) Schematic representation of the hydrogen-bonding pattern of urea groups present in the capsule's equator



of capsule formation. Encapsulated fluorobenzene was directly observed in the  $^{19}\text{F}$  NMR spectrum of **1** dissolved in a mixture of 1% of fluorobenzene in *p*-xylened<sub>10</sub>. A new fluorine signal, upfield shifted compared to that of the free fluorobenzene, appeared in the  $^{19}\text{F}$  NMR spectrum of the mixture. This signal was assigned to the fluorine atoms of encapsulated fluorobenzene. The size and shape of the solvent determined its encapsulation preferences. While chloroform and benzene were shown to be excellent guests, ethyl benzene and *p*-xylene were considered poor guests for encapsulation in dimeric containers based on tetraurea calix[4]arene units like **1** [14].

Just 1 year later, in 1996, Böhmer and co-workers demonstrated, using  $^1\text{H}$  NMR spectroscopy, that combining two different tetraurea calix[4]arenes (**2** and **3** from Fig. 32.2) in benzene-*d*<sub>6</sub> provided a mixture of homodimers **2**•**2** and **3**•**3** in addition to the heterodimeric capsular assembly **2**•**3**. The ratio of the three self-assembled containers was very close to the statistical distribution expected for three isoenergetic dimers (25:25:50 for **2**•**2**, **3**•**3**, and **2**•**3** respectively) [15]. Immediately, following this report, Böhmer and co-workers described the first X-ray structure of a tetraurea calix[4]arene homodimeric container. This finding was perceived by the community of Supramolecular Chemists as the definitive proof of the self-assembly of tetraurea calix[4]arenes in dimeric capsular assemblies held together by hydrogen bonds [16].

Rebek and co-workers demonstrated that the statistical disproportionation equilibrium involving two tetraurea homodimers and their heterodimer, which was initially reported by Böhmer, could be altered by the introduction of other terminal substituents in the urea groups installed at the upper rim of the calix[4]arene scaffold [17, 18]. For example, a chloroform solution containing an equimolar mixture of tetratolyl urea **4** and tetratosyl urea **5** afforded the exclusive and quantitative formation of the heterocapsular assembly **4**•**5** (Fig. 32.2). The two hemispheres of the heterocapsular assembly **4**•**5** were different and induced its existence in solution as a pair of enantiomers (*M*-**4**•*P*-**5** and *P*-**4**•*M*-**5**) owing to the unidirectional orientation of urea groups that was kinetically stable on the chemical shift timescale. More recently, Böhmer, Rebek and co-workers revealed the structural reasons that governed the highly diastereoselective self-sorting process observed in the self-assembly of tetraurea calix[4]arenes **4** and **5** [19].

Covalent connection of two tetraurea calix[4]arene units through their lower rims with a *p*-disubstituted benzene spacer held the tetraurea functions of both calixarene apart (molecules **6** and **7**, Fig. 32.3). Consequently, in this case the formation of a unimolecular capsule was not allowed. Alternatively, supramolecular polymerization took place under adequate conditions forming functional polymeric capsules, the so-called “polycaps” [20, 21]. Gel permeation chromatography was used for the physical characterization (i.e. aggregate stability and molecular weight) of these polymeric capsules. Moreover, encapsulation studies of adequate guests (e.g. *p*-difluorobenzene) were performed to study further the self-assembly behavior of polycaps [22].

Not surprisingly, polycaps were shown to be highly sensitive to their chemical environment. In the presence of competitive solvents (e.g. DMSO), the polymeric

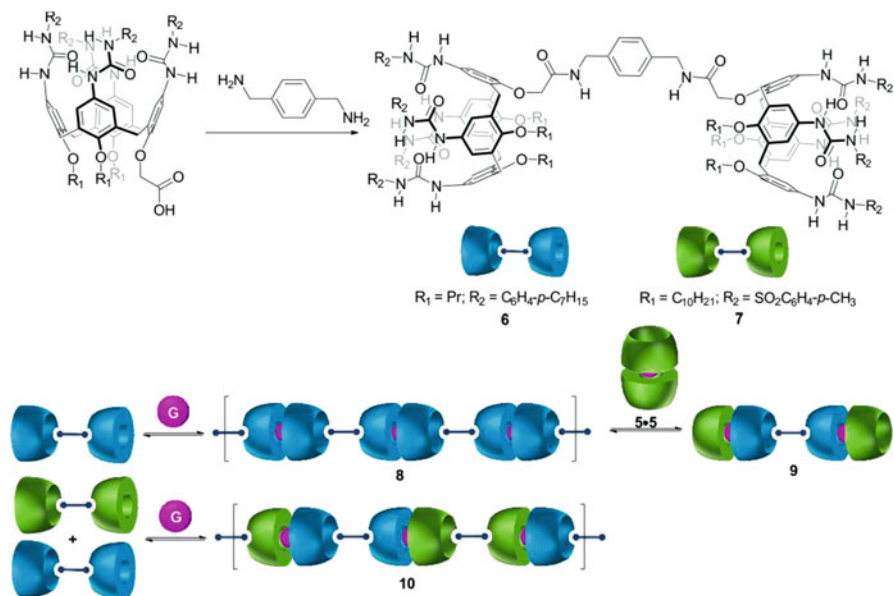


**Fig. 32.3** *Top*: Structure and synthesis of polycap modules. *Bottom*: Schematic representation of different self-assemblies of polycaps in the presence of a guest G

assemblies were disrupted (partially or totally depending on the amount of competitive solvent) to yield their monomeric form. The dissociation of the polymeric capsules was also evaluated through the formation of dumbbell-shaped heteroassemblies comprising three hosts and two guests (Fig. 32.3) [21]. When a stoichiometric amount of tetratosyl urea **5** was added to a chloroform solution of tetratosyl based polycap **8**, the polymeric assembly was disrupted to form the dumbbell heterosystem **9**. This already-known heterodimerization preference offered by tetratosyl and tetratosyl urea calix[4]arenes was also exploited for the formation of polycaps with alternating subunits such as **10** of interest in materials science.

The volume of the inner cavity of dimeric containers was slightly increased, from  $\sim 200$  to  $310 \text{ \AA}^3$ , using resorcin[4]arene building blocks substituted with four amino acids at the upper rim, in particular at the 2-position of the resorcinol aromatic rings i.e. **D-11** (Fig. 32.4). In 2009, Szumna and co-workers described, in a series of papers, the self-assembly and binding properties of homo- and heterodimeric containers based on resorcin[4]arene derivatives substituted with four *D* or *L* phenylalanines at the upper rim (Fig. 32.4a) [23–25]. The two hemispheres of the dimeric containers were held together by deeply buried salt bridges formed between the amine and carboxyl groups of the aminoacids substituents. Polar hydrogen bond interactions were also established between the hydroxyl groups of the resorcinarene and the carboxylic groups of the phenylalanine residues, which tightened the capsule's core (Fig. 32.4b). The homodimers (**D-11**)<sub>2</sub> or (**L-11**)<sub>2</sub> were chiral, however the heterodimer **D-11**•**L-11** was *meso* and *S*<sub>8</sub> symmetric. Both types of

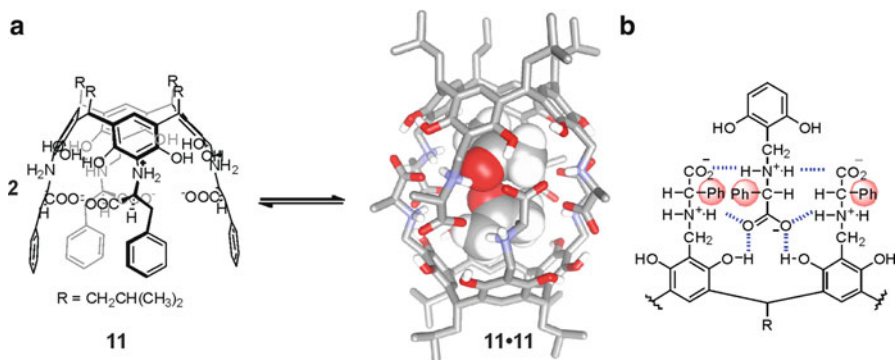


**Fig. 32.4** (a) Self-assembly of **11** into a dimeric capsule **11•11**. In the model of **11•11** the terminal phenyl groups of the phenyl alanine moieties have been omitted for clarity. (b) Binding motif of the dimeric assembly indicating the possible steric clashes with a red sphere

containers displayed polar groups (amino and carboxyl groups) inwardly oriented with respect to their inner aromatic cavity. The polar groups were isolated from the environment (solvent molecules) by the hydrophobic phenylalanine side chains. The polar functionalization of the inner cavity allowed the encapsulation of polar guests such as alcohols, carboxylic acids, *N*-protected amino acids and even carboxylic acid salts. Interestingly, the typical guests encapsulated in tetraureacalix[4]arene based dimeric containers like **1•1** were not included in the inner cavity of **11•11**. Most likely, the polar walls of the resorcin[4]arene **11•11** containers, which are constituted by aminoacid backbones, were responsible for the switch observed in their complexation preferences towards more hydrophilic guests. Because the homodimeric (*D*-**11**)<sub>2</sub> or (*L*-**11**)<sub>2</sub> containers are chiral, Szumna and co-workers also investigated their recognition properties towards chiral guests. The (*D*-**11**)<sub>2</sub> container showed moderate level of chiral discrimination in the encapsulation of chiral hydroxyacids producing the two diastereomeric encapsulation complexes in different extent (up to *de* = 59 %).

Recently, Szumna and coworkers used tetraformyl resorcin[4]arene as the concave scaffold for the self-assembly of dimeric containers. The tetraformyl derivative reacted very easily with primary amines to form imines. It is known that the resulting imines tautomerized to their enamine forms. For the reaction of the tetraformyl resorcin[4]arene derivative with an optically pure chiral amine, six diastereoisomers can be produced owing to the double bond isomerism and the inherent chirality of the macrocycle. However, the establishment of a preferred network of intramolecular hydrogen bonds in the resulting ketoenamines drives the equilibrium towards two diastereoisomers produced in similar proportions (Fig. 32.5) [26]. Short peptides of variable lengths (1–4 aminoacids) and typically alternating D-Phe or L-Phe with Gly aminoacids were used as the amine component for imine formation. The interdigitation of the peptide backbones covalently connected to the concave macrocyclic scaffold producing self-assembled dimeric

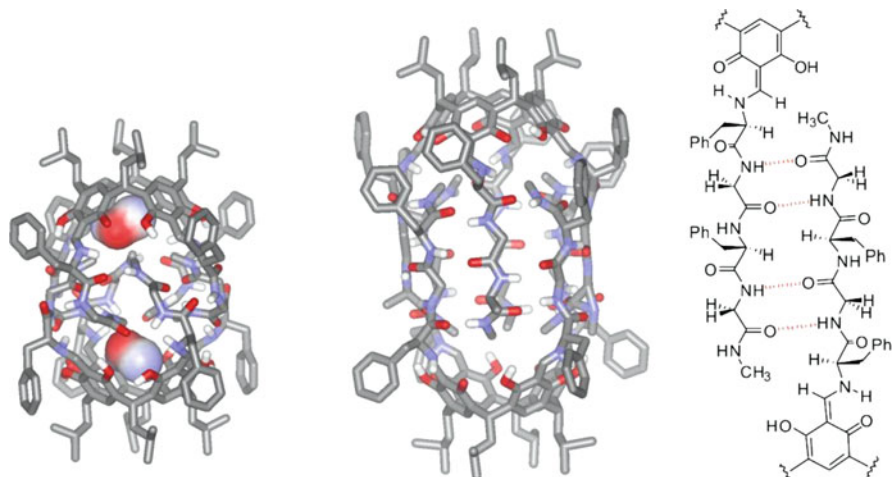


**Fig. 32.5** X-ray structures of two peptidic dimeric containers described by Szumna and coworkers [26]. A detailed scheme of the hydrogen bonding interactions established between the interdigitated peptide backbones is also depicted for one of them

containers stabilized by a seam of intermolecular hydrogen bonds (Fig. 32.5). The authors also observed interesting self-sorting phenomena not only between peptides of different chirality but also of different length. The obtained result highlighted the importance of hydrogen bonding complementarity for effective self-sorting processes. In general, chiral peptides with an even number of aminoacids preferentially provided homodimeric aggregates (Daa)<sub>2</sub> or (Laa)<sub>2</sub> (narcissistic self-sorting) while odd numbered amino acids tend to dimerize in hetero aggregates (Daa•Laa) (social self-sorting). In several cases, the capsular structures of the containers and the details of the binding motifs between the aminoacids backbone residues were confirmed in the solid state by X-ray crystallography (Fig. 32.5). The data in the solid state also corroborated the presence of two non-identical hemispheres observed in solution, as the imine linkers in each of them were present in different tautomeric forms.

Resorcin[4]arene cavitand scaffolds have also been used for the self-assembly of molecular containers displaying inner cavities with even large volumes [27]. Rebek and co-workers reported the self-assembly of a molecular container formed by two units of tetraimide derived resorci[4]narene cavitand **12a** that featured an inner cavity of 425 Å<sup>3</sup> (Fig. 32.6) [28, 29]. The two components were held together by establishing a network of eight self-complementary bifurcated hydrogen bonds between the imide functionalities at their upper rims. The assembly of the container required the appropriate filling of its inner volume. For example, in chloroform solution, three molecules of solvent were encapsulated to fill the container's inner volume adequately [28].

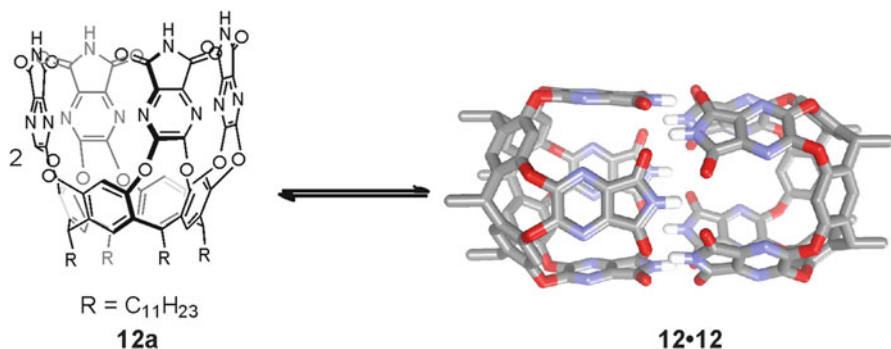


**Fig. 32.6** Equilibrium involved in the self-assembly of the dimeric container **12a•12a** stabilized by a cyclic seam of 8 bifurcated hydrogen bonds. Cavitand **12** is shown in line-drawing representation. The **12a•12a** dimeric container is depicted as energy minimized structure in stick representation. Non-polar hydrogen atoms were omitted for clarity

The single or pairwise reversible encapsulation of many different guests in the cavity of the dimeric container **12a•12a** has been described [30–32]. For instance, the encapsulation of a homologous series of normal alkanes in the cavity of the **12a•12a** container was described to take place in mesitylene-*d*<sub>12</sub> solution [33]. The mesitylene solvent cannot fit in the cavity of the container or in that of its cavitand precursors. The authors demonstrated that for short chain alkanes such as *n*-pentane or *n*-hexane, two guests were encapsulated inside the container and moved freely within. The resulting encapsulation complexes displayed packing coefficient values of the order of 40–48%. In the particular case of *n*-heptane, no clear encapsulation was observed. Most probably, the container's cavity was too large to accept one molecule alone (packing coefficient = 28%) but too small to accommodate two molecules of *n*-heptane. The guest that fitted best the inner cavity of the **12a•12a** container was *n*-undecane, which adopted an extended conformation with minimal coiling at the extremities. Longer alkanes unable to be encapsulated in its fully extended form, such as *n*-tetradecane, adopted helical conformations within capsule **12a•12a**. This guest coiling resulted in a number of unfavorable gauche interactions that could be detected by 2D NOESY experiments. In the case of *n*-tetradecane, NOE cross-peaks were observed between the hydrogens located at C1 and the ones at C3 and C4 indicating the presence of gauche conformations in the extremes of the alkane. However, hydrogens at C2, C3 and C4 only presented NOE cross peaks with the ones at C4, C5 and C6, respectively. This was a clear indication that the central part of the guest displayed an extended conformation. The guest coiling had an energetic cost (i.e. 0.55 kcal/mol per gauche interaction in the liquid state) that was partially compensated by the favorable CH- $\pi$  interactions between the guest and the aromatic walls of the host [33]. In this work, Rebek and coworkers also demonstrated the dynamic nature of the helical conformation featured by long alkanes encapsulated within capsule **12a•12a**. For example, for *n*-C<sub>14</sub>H<sub>30</sub> coiled within the capsule, one could expect that geminal coupling between the penultimate methylene protons could be observed due to their diastereotopic nature. However, a

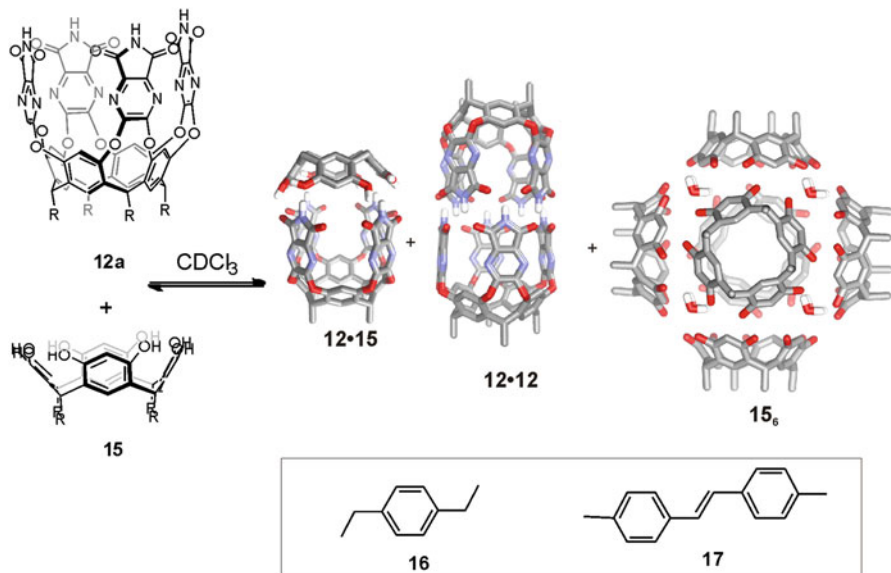


**Fig. 32.7** Resorcinarene **15** and tetraimide cavitant **12a** self-assemble in three different capsules in  $\text{CDCl}_3$ : hexameric capsule **15<sub>6</sub>**, homodimeric capsule **12•12** and heterodimeric capsule **12•15**.  $\text{R} = \text{C}_{11}\text{H}_{23}$

well-defined sextet was observed in the  $^1\text{H}$  NMR instead. These observations were explained by dynamic processes in the coiling (i.e. helix-helix interconversion between two enantiomeric forms) that occurred fast on the NMR time scale. A reasonable mechanism was proposed by the authors for the racemization process occurring inside the capsule. It involves the untwisting from (+) gauche conformation to antiperiplanar and then twisting again to (−) gauche resembling the geometry of the *trans*-alkene, 7-tetradecene.

The inner cavity provided by the symmetrical and cylindrical capsule **7•7** was exploited as reaction flask in multiple studies. For example, it was shown that the 1,3-dipolar cycloaddition reaction between phenylazide **13** and phenylacetylene **14** (Huisgen reaction) was 20,000-fold accelerated when the **12a•12a** container was used as molecular vessel compared to the reaction in bulk solution. Likewise, the regioselectivity of the reaction was modified affording one single region-isomer, exclusively the 1,4-adduct [34, 35]. These observations were explained by the increase in local concentration and the close and correct disposition of molecules **13** and **14** experienced in the capsule's cavity. Many other studies related to the use of the cylindrical **12a•12a** capsule as molecular reactor have been reported [36–38] but for the sake of brevity, they will not be discussed in this chapter.

Rebek and co-workers also prepared hybrid dimeric capsules based on resorcin[4]arene **15** and tetraimide cavitant **12** (Fig. 32.7) [39, 40]. In  $\text{CDCl}_3$  solution, mixtures of resorcinarene **15** and cavitant **12** at different molar ratios produced three different containers in varying amounts: the two homocapsular assemblies (**15<sub>6</sub>** and **12•12**) and the heterodimeric assembly (**12•15**) [39]. Interestingly, in the



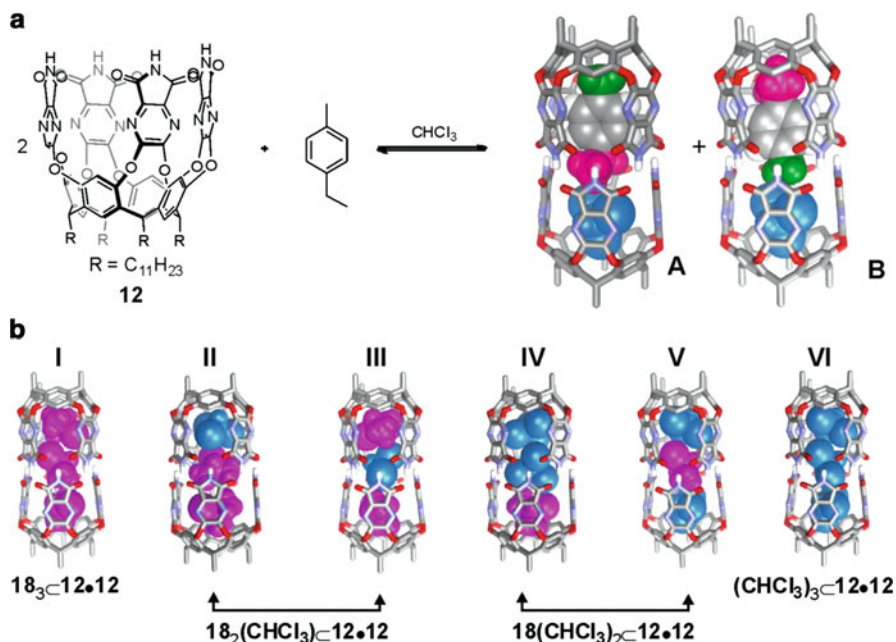


**Fig. 32.8** (a) Social isomers (A and B) generated from the self-assembly of dimeric capsule **12•12** in  $\text{CHCl}_3$  (blue) in the presence of *p*-ethyltoluene. Both extremes of *p*-ethyltoluene (ethyl and methyl groups) are highlighted in different colors (pink and green, respectively). (b) Possible arrangements for co-encapsulated  $\text{CHCl}_3$  (blue) and isopropyl chloride **18** (pink) within capsule **12•12**. Complexes **II** and **III** (and **IV** and **V**) are isomeric constellations

presence of an excess of 1,4-diethylbenzene **16** (Fig. 32.7), an ideal guest for the cavity of the hybrid containers, the equilibrium between the three different containers was driven to the exclusive formation of the heterodimeric **16C12•15** assembly. The dynamic nature of the hybrid container was demonstrated by addition of 4,4'-dimethyl-*trans*-stilbene **17**, which was known to fit perfectly in the cavity of the dimeric **12•12** container. The addition of guest **17** in excess drove the equilibrium away from the formation of the hybrid container **16C12•15**.

Cylindrical capsule **12•12** was exploited to study new forms of isomerism coming from the limited mobility of encapsulated guests in a confined environment. When *p*-ethyltoluene was used as guest for **12•12** capsule in chloroform, two isomeric complexes were detected by the  $^1\text{H}$  NMR spectra (A and B from Fig. 32.8) differing on the spatial arrangement of the two molecules within the capsule. Sharp and well-separated signals were observed for each isomer indicating slow exchange on the NMR chemical shift time scale between the two isomers and suggesting a high energy barrier for their interconversion. In brief, the two guests were too large to squeeze past each other and tumbling of *p*-ethyltoluene was also limited inside the capsule. These isomers were termed as social isomers by Rebek and coworkers [41]. The two isomers were present in different concentrations

indicating that they were not isoenergetic. The energetic differences between the social isomers came from the lining and shape of the inner space of the capsule and from the interactions established between the co-encapsulated guests (i.e. chloroform and *p*-ethyltoluene). For example, a methyl group is better accommodated in the tapered cavity ends than ethyl groups, and thus, complex A was more favored in solution than B.

Another form of isomerism, constellational isomerism, was also described by Rebek 1 year later. Constellational isomerism was related to the diastereomeric arrangement of guests enforced by the cylindrical space of the tetraimide-based capsule **12•12**. Constellational isomers resulted from the restricted motion featured by three small guest molecules encapsulated within capsule **12•12** [42, 43]. Encapsulation of three molecules of isopropyl chloride **18** in **12•12** capsule produced two different sets of <sup>1</sup>H NMR signals: one for the centrally located isopropyl chloride and another of twice the intensity more upfield shifted corresponding to the two isopropyl chloride molecules located at the extremes of the capsule. Addition of small amounts of CHCl<sub>3</sub> to a mesitylene solution of **18**<sub>3</sub>⊂**12•12** complex, resulted in four additional resonances appearing in the upfield region of the <sup>1</sup>H NMR spectra. These results were attributed to the coexistence in solution of six different arrangements of the guests inside the capsule: two capsules with three of the same guest inside, **18**<sub>3</sub>⊂**12•12** and (CHCl<sub>3</sub>)<sub>3</sub>⊂**12•12** and two sets of constellational isomers **18**<sub>2</sub>(CHCl<sub>3</sub>)⊂**12•12** and **18**(CHCl<sub>3</sub>)<sub>2</sub>⊂**12•12** complexes (with terminal or central CHCl<sub>3</sub> or isopropyl chloride, respectively) (Fig. 32.8).

The cylindrical capsule was also employed by Rebek and co-workers for the study of supramolecular chiral spaces [44]. The cylindrical space inside capsule **12•12** is achiral. However, when a chiral guest was encapsulated, a chiral space was generated (Fig. 32.9). Co-encapsulation of isopropyl chloride **18** and styrene oxide **19** in capsule **12•12** displayed the epoxide group of **19** near the hydrogen bond seam. This particular disposition presented the chiral center of **19** confronted to the co-encapsulated partner **18**. The chiral epoxide center generated an effective magnetic and spatial anisotropy that provoked the observation of the methyl groups of isopropyl chloride **18** as diastereotopic signals. When a racemic co-guest (i.e. 2-chlorobutane, 2-butanol) was used for the co-encapsulation of epoxide **19** within capsule **12•12**, two different diastereomeric complexes were observed. However, no diastereoselection was observed in these cases. Most likely, the weak intermolecular interactions and the shape complementarity (space between both guests) were not enough to result in a preferential arrangement of the guests. Better results regarding diastereoselectivity were obtained in the co-encapsulation of (*S*)-mandelic acid **20** and 2-butanol. The diastereomeric complex formed by co-encapsulation of **20** and (*R*)-2-butanol was preferred over the one with (*S*)-2-butanol. Hydrogen bond interactions between the acid and the alcohol moieties of **20** and 2-butanol, respectively, were established near the capsule's center bringing the asymmetric centers close.

In a different attempt to generate chiral spaces, Rebek and co-workers decided to study the influence of a chiral element placed outside the inner space of the cylindrical capsule (Fig. 32.9) [45]. Even with a high number of chiral centers



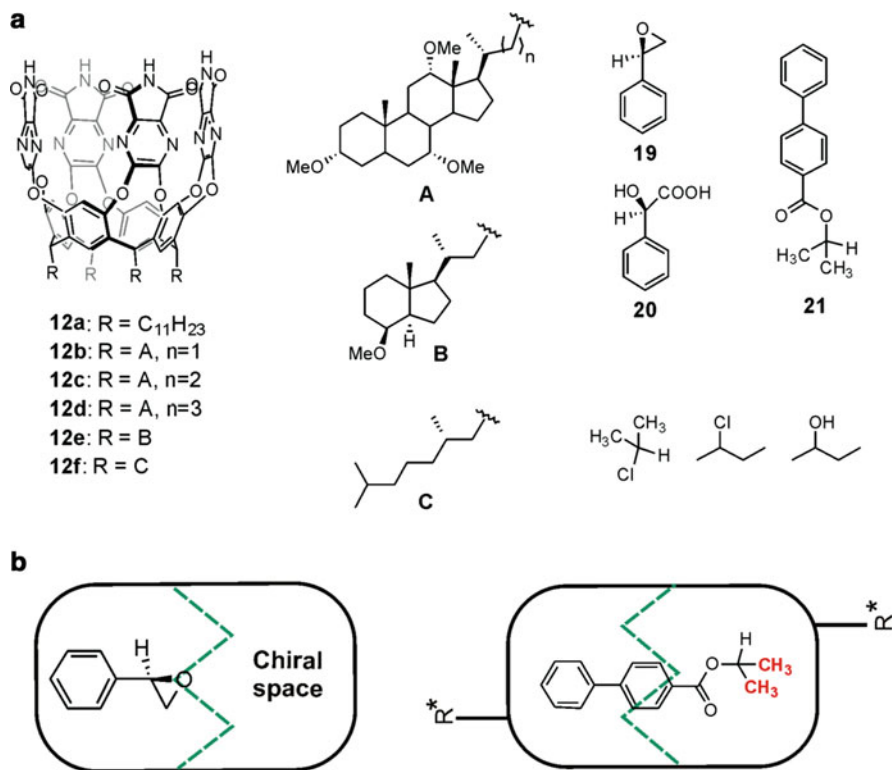


**Fig. 32.9** (a) Cylindrical capsules bearing chiral centers in their lower rim and guests used for chirality studies. (b) *Left*: when a chiral guest was placed the non-chiral cylindrical capsule **12a**•**12a**, a chiral space was generated. *Right*: The isopropyl groups of ester **21** sense the asymmetric magnetic environment generated by the chiral centers outside the capsule (*R*\*) and show diastereotopic methyl signals in the <sup>1</sup>H NMR spectra

placed on the capsule ends, the inner space remained achiral. However, guest **21**, which was rigidly fixed inside the cavity, could experiment in some cases the magnetic anisotropy exerted by the asymmetric centers located at the lower rim. Concretely, when the chiral centers are separated no more than two – CH<sub>2</sub> units from the cavity ends (**12b**, **12c**, **12e** and **12f**) the methyl groups of guest **21** were shown as diastereotopic.

The electron-deficient pyrazine panels of resorcin[4]arene **12** enhanced the vulnerability of imide carbonyls to suffer a nucleophilic attack. Consequently, in the presence of strong organic bases the cylindrical capsule decomposes. De Mendoza and coworkers proposed benzimidazolone panels as an alternative binding motif that led to a dimeric capsule displaying very similar geometric features than **12**•**12** capsule but with higher stability to nucleophilic attack (Fig. 32.10) [46]. Depending on the length of the alkyl chains located in the lower rim of resorcinarenes **22**, these capsules tend to aggregate in large structures such as

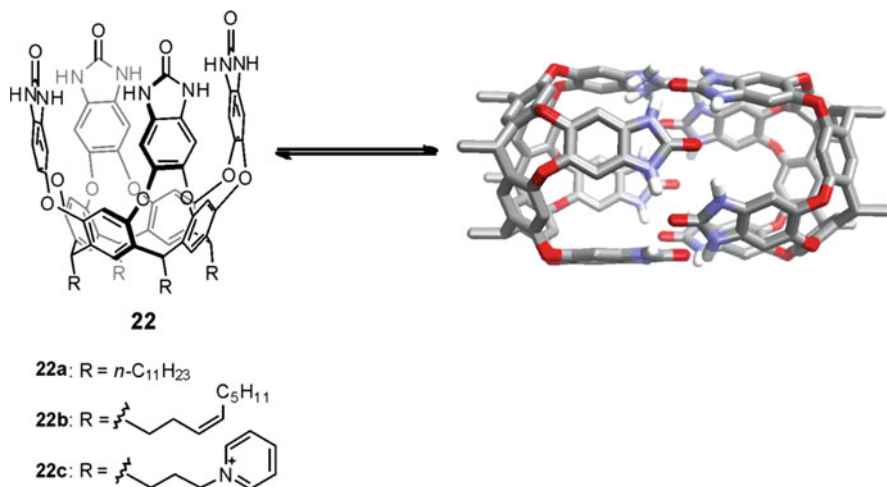


**Fig. 32.10** Line-drawing structure of tetra-benzimidazole calix[4]arenes **22** and equilibrium involved in the self-assembly of the dimeric container **22•22** depicted as an energy minimized structure in stick representation. Non-polar hydrogen atoms and peripheral groups were omitted for clarity

vesicles and filaments in chloroform solution. A solution to this aggregation problem was described by Choi and coworkers by loading the guests at high temperatures in mesitylene [47].

The strong network of hydrogen bonds featured by **22•22** capsules rendered them good aspirants to operate in aqueous solution. Rebek and collaborators managed to make resorcinarene **22** reasonably soluble in  $\text{D}_2\text{O}$  by introducing pyridinium groups at the lower rim (**22c** from Fig. 32.10) [48]. The water-soluble resorcinarene showed typical dimerization behavior in  $\text{D}_2\text{O}$  in the presence of long hydrophobic guests despite the competitive nature of the solvent thanks to the robust network of hydrogen bonds stabilizing the capsule. Capsule formation might be entropy driven. The release of high energy water molecules from the surface of benzimidazolone moieties to the bulk solution and the complete desolvation of the encapsulated hydrophobic guests resulted in an entropy gain that most likely assisted the dimerization process. The observed binding behavior with alkanes was shown to be similar to the one described by related capsules in mesitylene [33].

### 32.2.2 Containers Based on $\alpha,\alpha,\alpha,\alpha$ -aryl Extended Calix[4]pyrrole Units

$\alpha,\alpha,\alpha,\alpha$ -Aryl extended calix[4]pyrrole macrocycles functionalized with four urea groups at their upper rims were used to self-assemble dimeric containers with polar interiors [49]. The resulting assembled containers displayed an increased internal

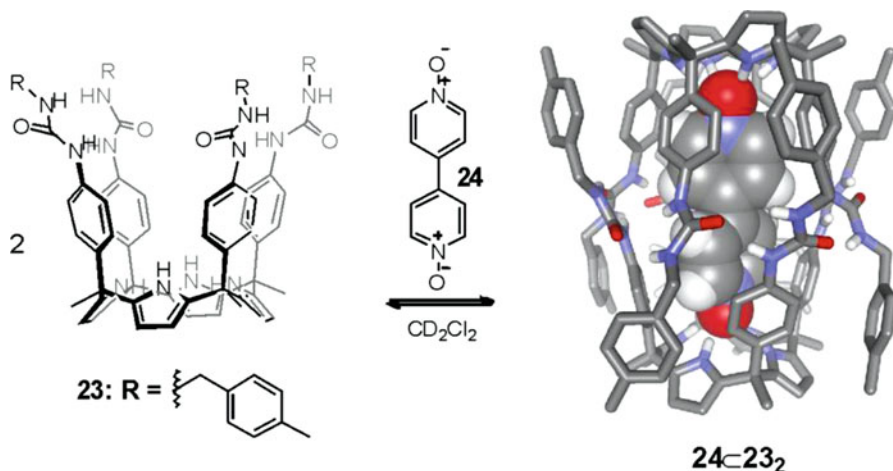


**Fig. 32.11** Equilibrium involved in the reversible self-assembly of tetraurea calix[4]pyrrole **23** into a dimeric container induced by encapsulation of one molecule of bis-*N*-oxide **24**

cavity volume ( $>300 \text{ \AA}^3$ ) compared to their counterparts assembled from tetraureacalix[4]arenes ( $200\text{--}250 \text{ \AA}^3$ ). In addition, the tetrapyrrole cores offered endohedral binding sites suitably oriented to be presented to electron rich groups of encapsulated guests. The establishment of hydrogen bonding intermolecular interactions between the guests and the container lining served, not only to orientate the guests but also to restrict their internal motions. These polar interactions were also responsible for the large packing coefficient values featured by some encapsulation complexes deriving from calix[4]pyrrole-based containers and their unprecedented selectivity relying on functional groups complementarity. All these features made calix[4]pyrrole-based molecular containers interesting additions to the well-known calix[4]arene based containers. Molecular containers based on aryl-extended calix[4]pyrrole units combined a deep hydrophobic cavity with the presence of polar groups, that were located at its closed end. This arrangement of functions reminded the binding sites of enzymes, in which polar and hydrophobic groups converge and establish multiple intermolecular forces with the bound substrate.

Our group reported the synthesis of tetraurea calix[4]pyrrole **23** as molecular component for the self-assembly of containers with polar interiors (Fig. 32.11) [50]. In  $\text{CD}_2\text{Cl}_2$  solution, the  $^1\text{H}$  NMR spectrum of tetraurea-calixpyrrole **23** showed broad and unresolved proton signals. Most likely, ill-defined aggregates were formed in solution as a result of intermolecular hydrogen bonding between urea groups in the arms of **23**. Conversely, in DMSO solution, the tetraurea **23** showed a  $^1\text{H}$  NMR spectrum with sharp proton signals that were assigned to the monomer. It's well established that the assembly of a dimeric molecular container based on **23** required suitable guests capable of switching the calix[4]pyrrole core from an alternate conformation, typically observed in non-polar solvents, to the cone conformation. In the cone conformation, the four urea substituents installed at

the upper rim of **23** are positioned in a perfect arrangement to induce a dimerization process driven by interdigitation of these residues. In this manner, the energetic cost associated with the conformational locking of the calix[4]pyrrole components that demands the assembly of the container is substantially reduced. Molecular modeling suggested that the 4,4'-bipyridine bis-*N*-oxide **24** was a suitable guest to induce the conformational locking of the calix[4]pyrrole units by placing them at an appropriate distance to establish a circular seam of 16 hydrogen bonds between the NHs and COs of the eight unidirectionally oriented urea groups. Experimentally, we observed that the addition of an excess of 4,4'-bipyridine bis-*N*-oxide **24** to a CD<sub>2</sub>Cl<sub>2</sub> solution of **23** produced a <sup>1</sup>H NMR spectrum displaying sharp and well-defined proton signals. The multiplicity and number of observed signals were diagnostic of the quantitative assembly of the homodimeric molecular container encapsulating one molecule of the *N*-oxide, **24**⊂**23**•**23** (Fig. 32.11).

The hydrogen bonding pattern that held together the two hemispheres of the **23**•**23** container was reminiscent to the one described above for the tetraurea-calix[4]arene **1**•**1** container. In complete analogy with the tetraurea calix[4]arene dimers, the unidirectional orientation of the eight urea groups in the calix[4]pyrrole dimer **23**•**23** forced a complementary sense of rotation of the urea groups in each hemisphere, that is the two hemispheres of the container were cycloenantiomeric conformers. Each hemisphere was inherently chiral but the entire assembly **23**•**23** was *meso* and displayed *S*<sub>8</sub> symmetry. The <sup>1</sup>H NMR signature characteristic for the **23**•**23** capsular container included: (a) the benzylic protons resonating as diastereotopic signals, (b) the two aromatic protons *ortho* to the urea groups also resonating as separate signals. In the case of the container encapsulating bis-*N*-oxide **24** the observation of diastereotopic signals for the aromatic protons *ortho* to the urea groups in the *meso*-phenyl substituents was only observed lowering the temperature of the solution to 200 K. This observation was attributed to the existence at r.t. of a fast rotation on the chemical shift time scale for the *meso*-phenyl groups around the C<sub>meso</sub>-C<sub>p-phenyl</sub> bond. The pairwise encapsulation of the aliphatic trimethyl *N*-oxide **25** in the dimeric container **23**•**23** allowed the observation of diastereotopic signals for the aromatic protons *ortho* to the urea, even at room temperature. It was hypothesized that the encapsulation of a three dimensional *N*-oxide instead of the planar aromatic increased the energy barrier for the C<sub>meso</sub>-C<sub>p-phenyl</sub> bond rotation.

Interestingly, the modulation of the inner cavity dimension of supramolecular container **23**•**23** was evidenced through the study of the encapsulation of a series of *N,N,N',N'*-tetramethylalkyl-*N,N'*-dioxide guests displaying different alkyl spacers ranging from three to seven methylene groups [51]. The cyclic hydrogen bonding array of urea groups also adapted to the dimensions of the guest. In turn, the longest guests had to adopt coiled conformations to fit in the container's volume by bridging the gap between the two opposite tetrapyrrole binding sites. The resulting compressed bis-*N*-oxides applied some pressure on the side walls and ends of the container forcing the tetraureas to slip partially. As the urea groups were separated, the hydrogen bonds between the carbonyl ureas and the benzyl NHs shortened and became more linear. On the other hand, the hydrogen bonds of the carbonyl ureas

and the phenylic NHs experienced the opposite effect. It is worthy to note that some protons of the included non-chiral guests were observed as diastereotopic signals in the  $^1\text{H}$  NMR spectrum of the encapsulation complex. This was attributed to the asymmetric magnetic environment produced by the kinetically stable unidirectional orientation of urea groups on the chemical shift time scale.

The described self-assembled container **23**•**23** was recently used in our group for the study of the co-encapsulation of chloride with polar neutral guests such as trimethyl *N*-oxide **25** or  $\beta$ -alanine betaine **26**. In most of the examples, the chloride precursor was the methyltrioctylammonium chloride salt (MTOACl) **27** owing to the known heteroditopic nature of the calix[4]pyrrole receptors in ion-pair binding and the perfect fit of the methyl group for methyltrialkylammonium cations in the shallow and electron rich cavity defined by the pyrrole rings opposite to the bound chloride [52]. The self-assembly process of the capsular container was stoichiometrically controlled. Thus, five particles assemblies with closed container topology were produced  $[(\text{Cl}^- \cdot \mathbf{25}) \subset \mathbf{23} \cdot \mathbf{23}] \text{MTOA}^+$  or  $[(\text{Cl}^- \cdot \mathbf{26}) \subset \mathbf{23} \cdot \mathbf{23}] \text{MTOA}^+$  when working under strict stoichiometric control, 2:1:1 molar ratios of **23**:**25**:MTOACl and **23**:**26**:MTOACl).

The addition of an excess of the tetraalkylammonium salt induced the disassembly of the container. Using equimolar amounts of the three components (1:1:1 molar ratio of **23**:**25**:MTOACl or **23**:**26**:MTOACl) resulted in the exclusive assembly of four particle inclusion complexes  $[\mathbf{25} \subset \mathbf{23}] \text{MTOACl}$  or  $[\mathbf{26} \subset \mathbf{23}] \text{MTOACl}$ . In them, the neutral polar compound formed  $\text{NH} \cdots \text{O}$  hydrogen bonds with the four pyrrole NHs and was included in the aromatic cavity of the calix[4]pyrrole unit. The chloride interacted with the urea groups forming  $\text{NH} \cdots \text{Cl}^-$  charged hydrogen bonds. Finally, the organic cation was bound by placing its methyl group in the electron rich cavity defined by the pyrrole rings. Thus, the resulting complex showed a receptor-separated binding mode for the ion-pair.

The chiral tetraurea calix[4]pyrrole **28** was obtained by substituting one of the hydrogen atoms at the four benzylic methylenes of **23** by a methyl group (Fig. 32.12).

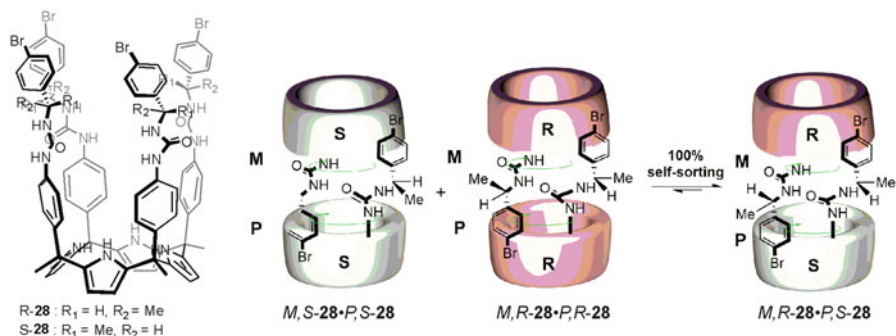


**Figure 32.12** (Left) Line-drawing structure of chiral tetraurea calix[4]pyrrole **28**. (Right) Schematic representation of the diastereoselective self-sorting process that takes place by mixing equimolar amount of chiral homocontainers  $M, S\text{-}28 \cdot P, S\text{-}28$  and  $M, R\text{-}28 \cdot P, R\text{-}28$

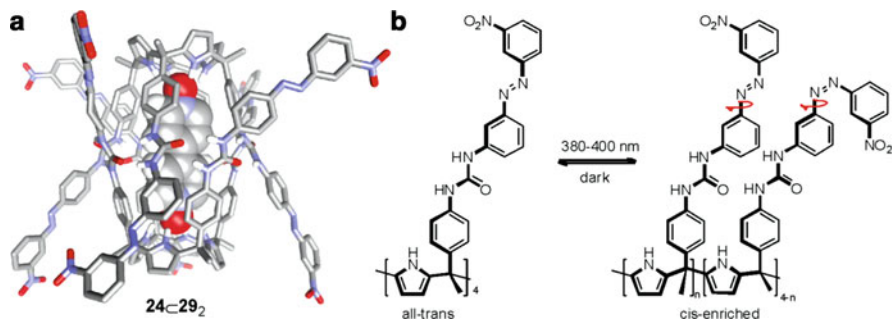


**Fig. 32.13** (a) Side view of the energy minimized structure of the *all-trans* **24C29** assembly. Non-polar protons of the host have been omitted for clarity. (b) Equilibrium of the photoisomerization process of *all-trans*-**29** to *cis*-enriched **29**

The substitution created four stereogenic carbon atoms with the same absolute configuration. The dimeric assembly of enantiopure tetraurea calix[4]pyrrole **S-28** in the presence of the bis-*N*-oxide **24** produced a single capsular container with two diastereomeric halves *P,S*-**28** and *M,S*-**28**. The diastereoselectivity of the dimerization process starting from a racemic mixture of tetraurea calix[4]pyrrole **28** was also studied [52]. A  $\text{CH}_2\text{Cl}_2$  solution containing an equimolar mixture of preformed enantiopure homocontainers, **24C<sub>P,R</sub>-28**•*M,R*-**28** and **24C<sub>P,S</sub>-28**•*M,S*-**28**, rapidly equilibrated to yield exclusively the single heterodimeric diastereoisomer **24C<sub>P,S</sub>-28**•*M,R*-**28** upon addition of a 10 % of  $\text{THF-}d_8$ . The same equilibration process was observed for the mixture of chiral homocontainers featuring pairwise encapsulation of trimethyl-*N*-oxide without the need of THF addition. Using MM3 calculations, the other possible diastereoisomer, *P,R*-**28**•*M,S*-**28** was shown to be higher in energy and experimentally it was not observed in solution to a measurable extent.

More recently, our group described a tetraurea calix[4]pyrrole decorated with four terminal azobenzene groups at the upper rim (**29** from Fig. 32.13) [54]. Tetraurea **29** self-assembled quantitatively into a dimeric container in the presence of 0.5 equiv. of bis-*N*-oxide **24** when all azobenzene groups were in *trans*-form. Irradiation of the  $\text{CD}_2\text{Cl}_2$  solution containing the assembly **24C<sub>all-trans</sub>-29**•**29** with 400 nm light triggered the *trans*-to-*cis* isomerization of the azo-groups (Fig. 32.13). The irradiated samples at different times were analyzed using  $^1\text{H}$  NMR spectroscopy. The photoisomerization process provoked the disappearance of the proton signals assigned to the *all-trans* capsular container and the appearance of broad and unresolved signals. Most likely, the steric hindrance caused by the terminal azo-groups in *cis*-enriched components destabilized the assembly of dimeric aggregates with container topology. However, the formation of a complex mixture of dimeric containers based on *cis*-enriched units could not be ruled out. The *all-trans* dimeric container was reversibly assembled by thermal relaxation of the irradiated mixture in the dark. These findings augur well for applications of these or related containers in light-controlled cargo delivery processes.

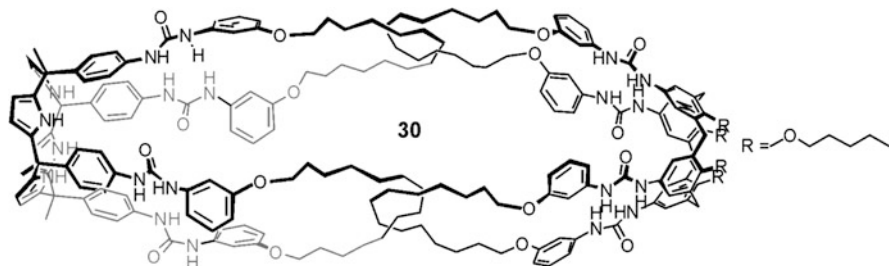


**Fig. 32.14** Line drawing of calix[4]arene-calix[4]pyrrole biscatenane **30**

Limitations on the application of hydrogen bonded capsular assemblies come from the poor stability of these assemblies in polar media compared to those held by covalent bonds. In an attempt to overcome these limitations, Böhmer described the synthesis of a mechanically locked chiral bis-catenane based on calixarene capsules [55]. Inspired by this pioneering work, our group produced a mechanically locked hybrid tetraurea calix[4]arene-calix[4]pyrrole capsule **30** (Fig. 32.14) [56]. This catenated capsule displayed reversible encapsulation (i.e. reversible assembly of the urea belt). The two hemispheres of the capsule never dissociate completely due to the bis-catenated topology.

### 32.3 Self-Assembled Capsules Based on Metal Coordination Interactions

Many thermodynamically robust and kinetically stable molecular containers have been assembled using reversible coordination bonds. Both directionality and high thermodynamic stability features exhibited by the metal-ligand bonds allowed the rapid, efficient and reversible self-assembly of complex structures starting from very simple building blocks. Cavitand structures derived from calix[4]arenes, owing to their conformational rigidity, are particularly suitable for the construction of metal-mediated self-assembled containers. Consequently, many of the metal-mediated containers described in the literature and, in particular, all the examples described in this section are based on calix[4]arene cavitand units. In general, these bowl-shaped host molecules are functionalized at their upper rim with appropriate donor atom ligands that can be bound to a metal center. The metal center ends up coordinatively saturated and become embedded in the structure of the container. In other words, it is not catalytically active. For the sake of brevity, in this section we will only describe dimeric containers. Information on the self-assembly of metal-mediated containers based on more than two components can be found in the following references [57, 58].



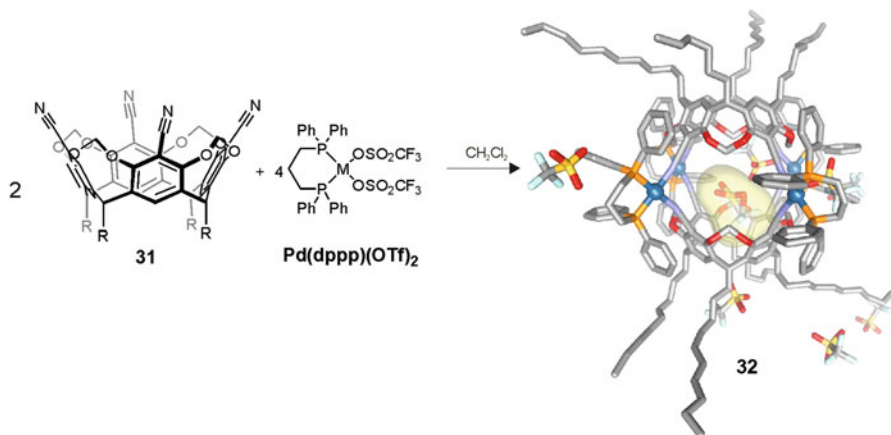


**Fig. 32.15** Equilibrium involved in the self-assembly of metal-coordinated capsule **32** from a 1:2 molar ratio mixture of  $\text{Pd}(\text{dppp})(\text{OTf})_2$  and the tetracyano cavitaand **31**

### 32.3.1 Homodimeric Capsules

The first examples of metal-mediated molecular containers based on resorcin[4]arene cavitaand scaffolds were published a few years later than the ones involving hydrogen bond interactions. Dalcanale et al. used the tetracyano cavitaand derivative **31** to assemble the homodimeric container **32** (Fig. 32.15) [59]. The two hemispheres of container **32** were held together by four square-planar Pd(II) centers. Two upper rim cyano substituents in different cavitaand units formed two  $\text{N}\cdots\text{Pd}$  coordination bonds with the metal. The other two coordination sites of the Pd(II) were occupied by a chelated bisphosphine that forced the *cis*-coordination of the cyano substituents. An analogous container based on Pt(II) metal center was also assembled. In solution, the assembly of the supramolecular container was confirmed using  $^{19}\text{F}$  NMR spectroscopy. The  $^{19}\text{F}$  NMR spectrum displayed two signals resonating at  $\delta = -81$  and  $-75$  ppm and showing a 1:7 integral ratio. The upfield shifted fluorine signal was assigned to an included triflate counterion. The other seven triflate anions were located outside the cavity's container and acted as simple counterions of the cationic metal centers.

The assembly-disassembly-reassembly process of the container was also studied in solution. Addition of eight equivalents of a competitive metal-ligand such as triethylamine induced the disassembly of the container affording the free cavitaand and the  $[\text{Pd}(\text{dppp})(\text{NEt}_3)_2(\text{OTf})_2]$  complex. The subsequent addition of eight equivalents of triflic acid to the above mixture restored the initial  $\text{Pd}(\text{dppp})(\text{OTf})_2$ , which immediately reassembled the dimeric container by coordination with two copies of cavitaand **31**. A few years later, the assembly of the container **32** in the solid-state was evidenced using X-ray diffraction analysis of a single crystal [60].



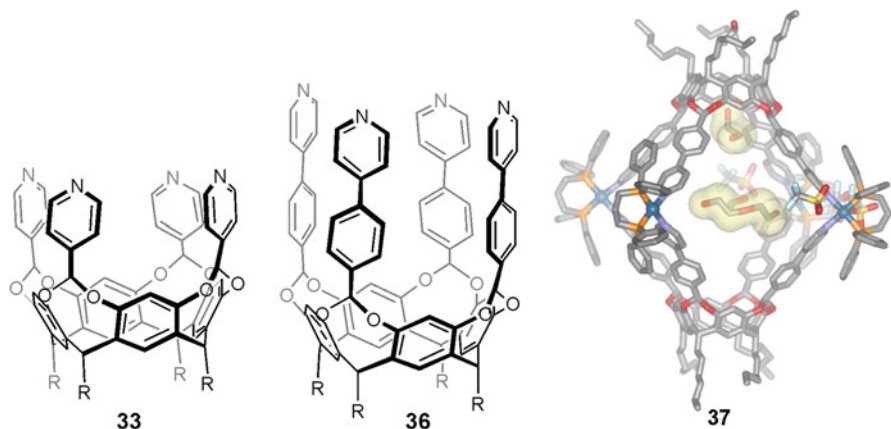


**Fig. 32.16** Chemical structure of cavitands **33** and **36** and X-ray structure of the cage-like container **37** assembled from cavitand **36**

The incorporation of four pyridyl bridging substituents at the upper rim of a resorcin[4]arene cavitand scaffold **33** (Fig. 32.16) produced closely related coordination containers using Pd(II) and Pt(II) *cis*-protected complexes as metal precursors [61]. The four bridging pyridyl ligands were adequately preorganized and directed outwardly with respect to the cavity of cavitand **33**. The arrangement of the pyridyl substituents and the conformational rigidity of the cavitand were crucial for the quantitative self-assembly of the dimeric containers, **34** and **35**, through the intermediacy of strainless square-planar metal complexes of Pd(II) and Pt(II), respectively. The pyridyl protons *ortho* to the nitrogen atom experienced a significant downfield shift upon container assembly. This result was indicative of the coordination of the pyridyl nitrogen to the metal center. Additional evidence of capsule formation was derived from the upfield shift experimented by the bridging methine groups that pointed towards the container's cavity. In this particular case, the  $^{19}\text{F}$  NMR spectrum did not provide any signal that could be assigned to the existence of an encapsulated triflate anion. Most likely, because the Pd(II) and Pt(II) homocontainers **34** and **35** assembled from cavitand **33** have larger portals than **32**, the in-out exchange of the bulky triflate anions was fast on the chemical shift time scale.

It is worthy to note that in  $\text{CD}_2\text{Cl}_2$  solution the Pd(II) coordination homocontainer **34** was able to encapsulate methano[60]fullerenes derivatives bearing dimethyl and diethyl malonate residues. The association constants of the resulting 1:1 encapsulation complexes were experimentally determined to be in the order of  $150\text{ M}^{-1}$  [62].

In 2004, Dalcanale's group reported and expanded version of resorcin[4]arene cavitand **33**. Cavitand **36** possessed a deeper aromatic cavity that was provided by four bridging phenylpyridyl groups but maintained the same relative orientation of the pyridyl moieties and the conformational rigidity of the cavitand unit. The out, out, out, out desired isomer with the four bridging groups pointing away from the

cavity was obtained in good yield and without traces of any other isomer having one of more phenylpyridyl groups directed towards the cavity's interior [63]. The assembly of container **37** in acetone and  $\text{CH}_2\text{Cl}_2$  solutions was evidenced by the chemical shift changes experienced by the diagnostic protons in the complex (aromatics *ortho* to the nitrogen atom and methane bridges). The structure of the container **37** was also characterized by X-ray crystallography in the solid state. A self-sorting experiment was performed by adding to an equimolar mixture of the pyridyl bridged cavitands **33** and **36** the stoichiometric amount of the metal precursor. The obtained solution was analyzed by  $^1\text{H}$  NMR spectroscopy and showed exclusively the proton signals belonging to the homocontainers **32** and **37** (narcissistic self-sorting). Probably, a bite angle mismatch of the ligands in the assembly of the putative heterocontainer favored the exclusive assembly of the homocontainers.

Haino and coworkers synthesized the octadentate resorcin[4]arene cavitand **38** by installing four bridging phenylbipyridyl units at the upper rim of the parent methylene bridged resorcin[4]arene cavitand [64]. Addition of two equivalents of  $\text{AgBF}_4$  to a nitromethane solution of **38** resulted in the quick assembly of container **39** with four silver(I) ions coordinated with tetrahedral geometry. Surprisingly, the  $^1\text{H}$  NMR spectrum of **39** showed that the eight phenylbipyridyl ligands were magnetically equivalent. This observation indicated the assembly of **39** as a unique diastereoisomer featuring  $D_4$  symmetry. Molecular mechanic calculations showed that the assembled diastereoisomer of the container was indeed the most stable energetically. The coordination container **39** was highly stable thermodynamically and kinetically as a result of a cooperative complexation of the eight phenylbipyridyl ligands to the four silver(I) metal centers. In chloroform solution, the  $^1\text{H}$  NMR spectrum of the mixture showed separate proton signals for the free cavitand and the container units. However, a 2D ROESY spectrum revealed the existence of a dynamic exchange between the free cavitand and the container units that was fast on the time scale of the experiment.

Container **39** was able to accommodate large and rigid aromatic guests in its aromatic cavity i.e. 4,4'-diacetoxybiphenyl. The addition of a 1:1 mixture of two different carboxylic acids (e.g. 4-acetoxybenzoic acid **40** with acetic acid or propionic acid) to a chloroform solution of the container resulted in the enhancement of the heterodimer complex of the two acids that were selectively encapsulated (Fig. 32.17). At 216 K, the proton signals diagnostic of the asymmetrically filled container complex  $40 \cdot \text{HOOCCH}_3 \subset 39$  were observed exclusively. When a 1:1:1 mixture of the three carboxylic acids (**40**, acetic acid and propionic acid) was added to a solution of **39**, only the co-encapsulation complex of **40** and acetic acid was formed. The authors attributed the observed selectivity to the higher acidity of the methyl protons in acetic acid compared to those of the propionic acid, which resulted in stronger  $\text{CH}/\pi$  interactions with one of the tapered ends of the cavity. However, a better fit of the cavity size by the  $40 \cdot \text{HOOCCH}_3$  heterodimer cannot be ruled out.

The functionalization of the methylene bridged resorcin[4]arene upper rim with four bis(iminodiacetato) substituents allowed the assembly of a water soluble and

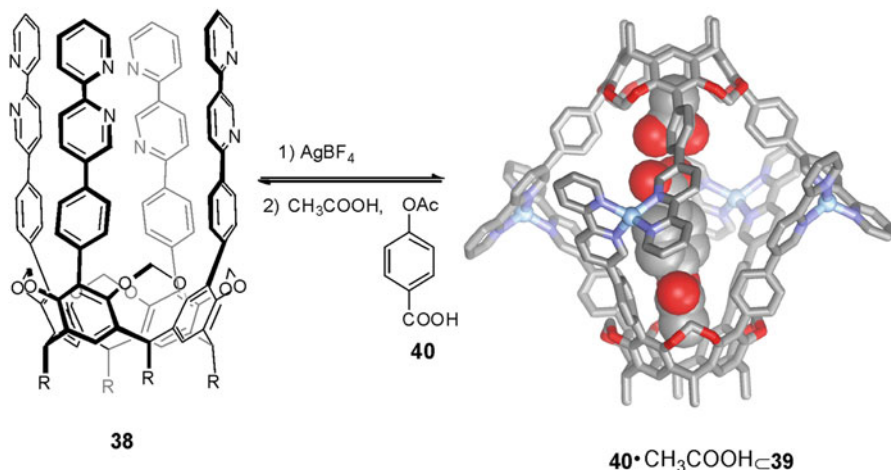


**Fig. 32.17** Line drawing structure of cavitaand **38** and energy minimized structure of the self-assembled homodimeric capsule **39** encapsulating the heterodimer **40**:acetic acid

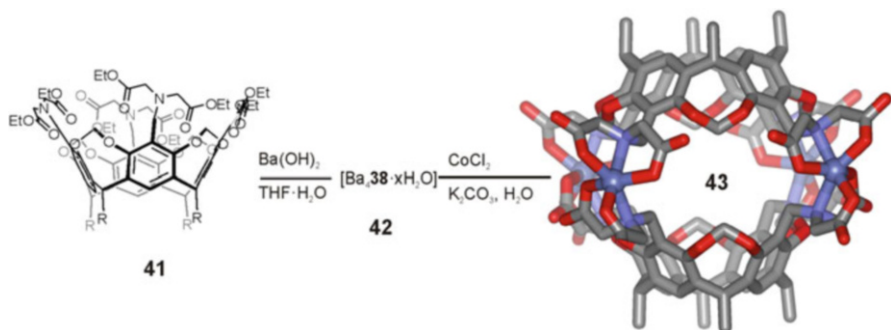


**Fig. 32.18** Line drawing structure of cavitaand unit **41** and energy minimized structure of the self-assembled homodimeric capsule **43**

pH dependent metal-mediated container [65]. Addition of  $\text{Ba}(\text{OH})_2$  to a THF:water solution of resorcinarene **41** produced a barium complex **42**. The subsequent addition of  $\text{CoCl}_2$  and  $\text{K}_2\text{CO}_3$  to the solution of **42** in dilute HCl induced the assembly of the coordination container **43**. The structure of **43** was confirmed in the solid state by X-ray diffraction analysis (Fig. 32.18). The X-ray structure confirmed a distorted octahedral geometry for the cobalt ions embedded in the container's structure. Each cobalt ion was coordinated to two doubly deprotonated iminodiacetate groups belonging two different resorcin[4]arene units producing overall an octaanionic container. In a sequel, the authors demonstrated the ability of cage **43** to bind and release a variety of organic guests (e.g. alkanes, haloalkanes, alcohols or aromatic guests) in water solution as a function of the pH [66]. The

selectivity in the guest's encapsulation was restricted to size and shape complementarities. Evidence of guest encapsulation was derived from the large upfield shifts ( $-30$  to  $-40$  ppm) experienced by the proton signals of the encapsulated molecules in the paramagnetic container.

### 32.3.2 Heterodimeric Capsules

Examples of self-assembly of metal-mediated dimeric containers based on two different resorcin[4]arene cavitand components are scarce compared to related counterparts containing two identical units, which were briefly revised in the previous section. The main difficulty to control the self-sorting of the two different components towards the exclusive formation of a heterodimer (social self-sorting) resided in overcoming the intrinsic metal coordination ability of two kinds of upper rim substituents for a single metal center. Containers equipped with non-symmetrical inner volumes provided new and interesting recognition features for molecular encapsulation. Examples of heterodimeric containers stabilized by metal coordination bonds have been reported mainly by Kobayashi and co-workers [67, 68]. The authors combined the coordination ability of two different substituent ligands appended at the upper rims of resorcin[4]arene cavitand components with the steric demand required for their assembly in different metal-mediated containers. Three different resorcin[4]arene deep cavitands bearing either four pyridyl **44**, four pyridylethynyl **45** and four cyanophenyl **46** groups at the upper rim were synthesized by using the Suzuki or Sonogashira coupling reactions. The selected cavitands were evaluated as molecular components in the metal-assisted assembly of heterodimeric containers (Fig. 32.19) [67]. A mixture of the tetrapyridyl derivative **44**, with Pd(dppp)(OTf)<sub>2</sub> in a 2:4 molar ratio did not result in the formation of a capsular assembly. The analysis of the mixture, using <sup>1</sup>H NMR spectroscopy, showed broad signals that were indicative of multiple and ill-defined aggregated species. The palladium assisted heterodimeric container **49** was quantitatively assembled in a CDCl<sub>3</sub> solution of tetrapyridyl and tetrakis(cyanophenyl) cavitand derivatives **44** and **46**, containing Pd(dppp)(OTf)<sub>2</sub> in a 1:1:4 molar ratio. The authors rationalized the exclusive assembly of the hetero-coordination container as the result of different factors. Firstly, the steric hindrance exerted by the *cis*-coordination of two tetrapyridyl cavitands **44** on the dppp protected Pd(II) centers and the restricted rotation of the coordinated pyridyl groups strongly disfavored the assembly of the corresponding homodimeric container. Secondly, pyridyl ligands are known to exhibit higher affinity for coordination to Pd(II) atoms centers than cyanophenyl ligands. Probably, the incorporation of a loosely bound cyano ligand in the *cis*-coordinated Pd(II) metal centers that stabilized the heterodimeric container **49** significantly reduced the steric hindrance present in the assembly. An alternative explanation may consist on a better match of the ligands' bite angle for the structure heterocontainer assembly.

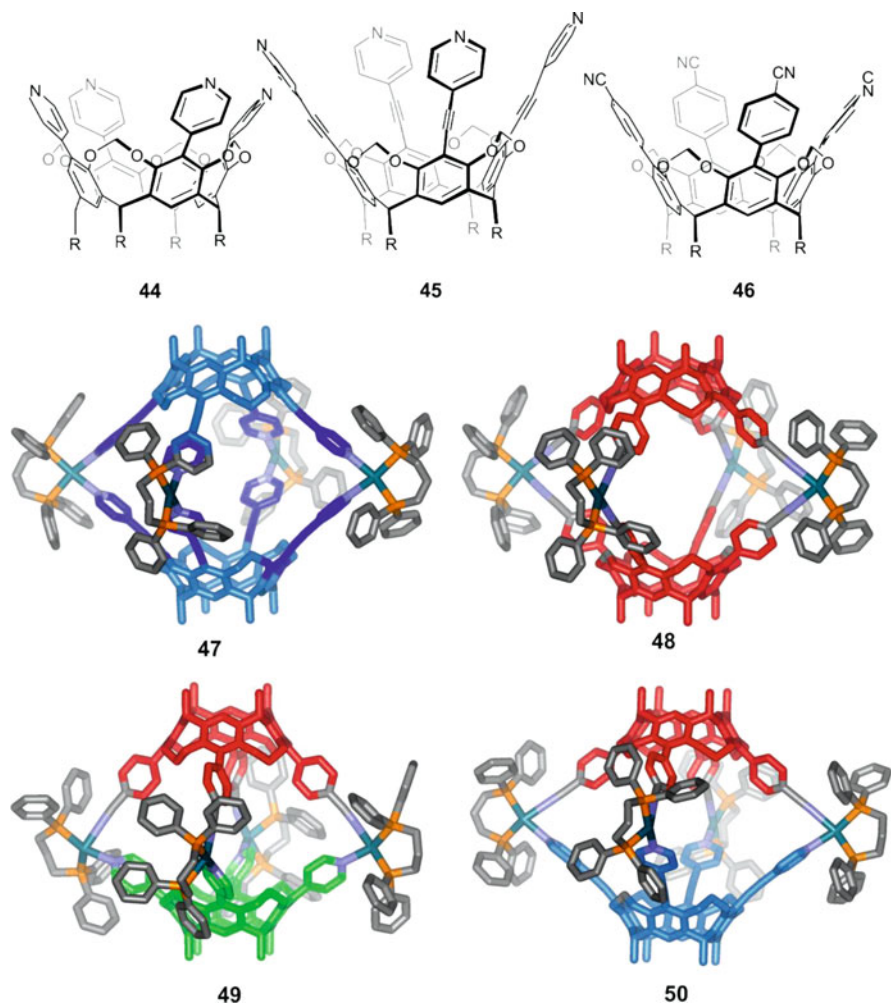


**Fig. 32.19** Line drawing structure of cavitanid units **44**, **45** and **46**, energy minimized structures of self-assembled homodimeric capsules **47** and **48** and self-assembled heterodimeric capsule **49** and **50**. A color code was used for the cavitanid core, **44** (green), **45** (blue) and **46** (red)

Interestingly, the addition of 4 equiv. of dppp *cis*-protected Pd(II) complex to a 1:1 mixture of tetrakis(4-pyridylethynyl) and tetrakis(cyanophenyl) cavitanid derivatives, **45** and **46**, resulted in the kinetically controlled formation of the two homocontainers **47** and **48** (narcissistic self-sorting). However, heating the mixture at 50 °C produced the diagnostic proton signals of the heterocontainer **50**. In a different experiment, a 1:1 mixture of pre-assembled homocontainers **47** and **48** was also shown to produce the heterocontainer **50**. In this latter case, the thermodynamic equilibrium was reached by heating the mixture at 50 °C for 2 h and produced a [50]/[47] ratio of 1.0 [68]. The heterocontainer **50** was also assembled

under kinetic control by adding 1 equiv. of the tetrakis(4-pyridylethynyl) cavitand **45** to a solution containing the preassembled homocontainer **47**. In the initial stages the ratio  $[50]/[47]$  reached a value of 3.0. The thermodynamic equilibrium of the above mixture was achieved after standing for 1 week at room temperature and showed a  $[50]/[47]$  ratio of 1.0. Similar self-sorting experiments were performed using a dppp Pt(II) complex as metal precursor. The obtained results were in line with those obtained in the self-assembly of the Pd(II) mediated containers. Owing to the well-known higher kinetic and thermodynamic stability of the Pt(II)-pyridyl coordination bonds, the heterodimer assembly prepared under kinetic control (homodimer  $47 \cdot [Pt(II)]_4 + 1$  equiv. of cavitand **45**) took more than a week to equilibrate with the corresponding heterodimer container  $50 \cdot [Pt(II)]_4$ .

### 32.4 Homodimeric Containers Stabilized by Combining Hydrogen-Bonds and Metal-Coordination Interactions

The use of different intermolecular interactions working in concert for the stabilization of reversibly assembled containers played a key role in the controlled release and uptake of its molecular cargo. Strong intermolecular interactions can be used to hold together the container components and define its inner cavity. On the other hand, mutual weaker interactions were implemented in the container's structure to control the kinetics of the encapsulation and release of the bound guests.

Examples of resorcin[4]arene cavitand scaffolds that combine hydrogen-bonding and metal-ligand binding sites for the self-assembly of molecular containers have been reported by Kobayashi and co-workers [69–71]. The authors described the synthesis of the resorcin[4]arene cavitand **51** displaying  $C_{2v}$  symmetry, and having two octylureido and two pyridylethynyl substituents at its upper rim. The urea groups provided hydrogen bonding sites while the pyridyl residues functioned as metal coordination sites (Fig. 32.20) [69]. Upon addition of the Pt(dppp)(OTf)<sub>2</sub> complex to a CDCl<sub>3</sub> solution of **51**, the homodimeric container **52** was assembled through the combined effect of hydrogen bonds and metal coordination interactions (Fig. 32.20). Evidence of capsule formation was derived from the <sup>1</sup>H NMR spectrum of the mixture. The aromatic protons  $\alpha$  to the pyridine nitrogen shifted downfield in response to nitrogen coordination with the metal center. Curiously, the alkyl groups of the ureido units appeared upfield shifted. This was indicative of their partial inclusion in the capsule's inner cavity. In addition, the observation of fluorine signals in the upfield region of the <sup>19</sup>F NMR spectrum of the container supported the co-encapsulation of triflate anions. The encapsulation of the ureido alkyl chains and a triflate anion were key elements for capsule's stabilization by the proper filling of its inner volume. Accordingly, the encapsulation of neutral guests required the exchange of the triflates by other anions. The exchanged anions had reduced affinity for the cavity and were prone



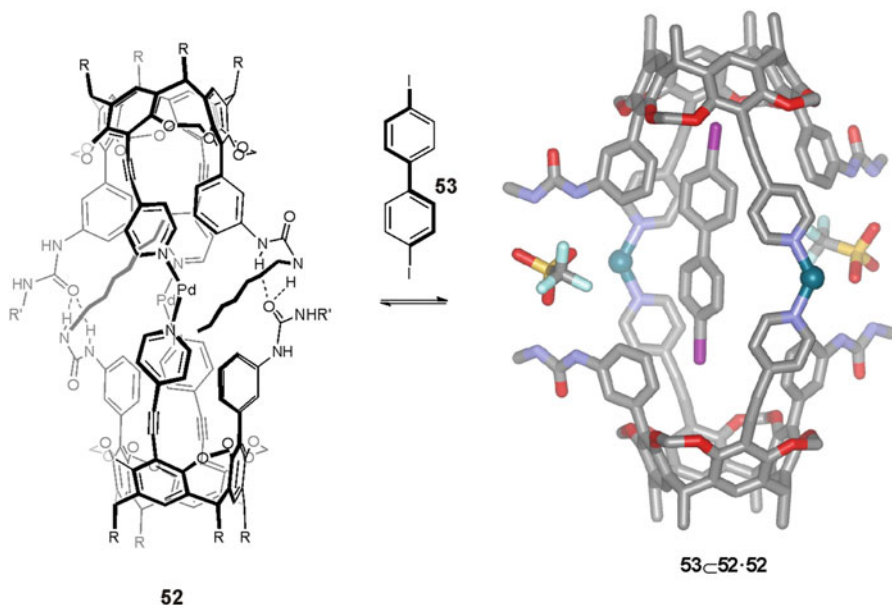


**Fig. 32.20** Encapsulation of guest **53** in the cavity of the self-assembled container **52** stabilized using a combination of hydrogen-bonds and metal-ligand interactions. The phosphine ligand dppp (1,3-bis(diphenylphosphino)-propane) of the palladium metal center has been omitted for clarity

to establish hydrogen bonds with the urea groups. This latter characteristic promoted a conformational change that released the octyl chains from the capsule's interior. In short, the anion exchange compensated the enthalpy loss associated with guest encapsulation in containers having triflate counterions and allowed the binding of neutral guests such as 4,4'-diiodobiphenyl **53**. A series of anions were used to study the anion exchange process (i.e.  $\text{PF}_6^-$ ,  $\text{NO}_3^-$ ,  $\text{TsO}^-$ ). The diverse employed anions produced different kinetic behaviors for the in-out guest exchange process, which were mainly related to their hydrogen bonding acceptor characteristics.

The substitution of phenylureido substituents in cavitand **52** by 3-carbomoylphenyl groups produced cavitand **54**. Cavitand **54** was shown to quantitatively assemble into homodimeric container **55** upon addition of *cis*-protected Pd(II) or Pt(II) complex (Fig. 32.21a). Again the resulting container was stabilized by a combination of hydrogen bonding and metal-ligand coordination interactions [70]. *Trans*-4,4'-dimethylstilbene **56** was a perfect guest for container **55** producing the **56@55** encapsulation complex. The  $^1\text{H}$  NMR spectrum of a mixture of container **55** and stilbene derivative **56** showed separated proton signals for the free and bound container **55**. This observation indicated that the in/out guest exchange process was slow on the NMR timescale. Sharp and well-defined proton signals were observed for the encapsulated guest **56**. Its proton signals were upfield shifted with respect to those of the free guest. Conversely, at

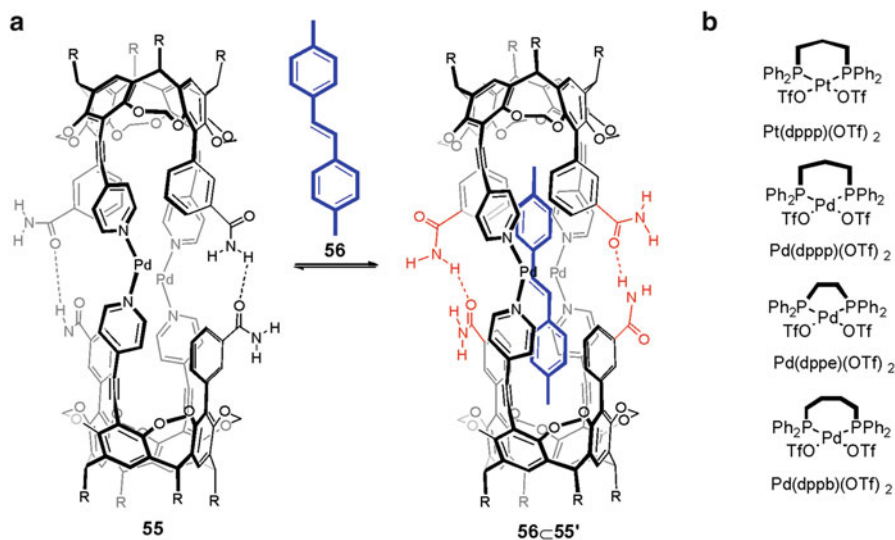


**Fig. 32.21** (a) Guest encapsulation in the hybrid capsule **55**. Notice the alteration in the cage structure highlighted in red. (b) Biphosphine metal complexes used for the study of the bite angle influence in ion-out exchange of the guest using hybrid cages. dppp = 1,3-bis(diphenylphosphino)-propane, dppe = 1,3-bis(diphenylphosphino)-ethane and dppb = 1,4-bis(diphenylphosphino)-butane

room temperature, the container's proton signals in the encapsulation complex **56⊂55** were broad. Upon lowering the temperature the signals of the bound cavitaund split while those of the bound guest did not experience any noticeable change. Likewise, the proton signals of the free cavitaund did not split on lowering the temperature. The authors concluded that the guest encapsulation modified the symmetry of the container. Using 1D and 2D NMR experiments they demonstrated that the container's symmetry changed from  $C_{2v}$  in the free state to  $C_{2h}$  in the complex. It is worthy to note that in the encapsulation complex **56⊂55** the bound guest maintained its  $C_2$  symmetry. This finding indicated that the two hemispheres of the  $C_{2h}$  bound container were equivalent. The kinetic and thermodynamic properties of the container and the encapsulation complex **56⊂55** were also evaluated. The authors found that the hydrogen bonding interactions holding together the two halves of the container had little influence in its thermodynamic stability but affected the kinetics of the in-out exchange process of the guest.

In a sequel, Kobayashi et al. reported the influence that the structure of the chelated phosphine ligand of the container's metal centers (i.e. dppp, dppe, dppb from Fig. 32.21b) had on the kinetics of the in-out exchange process of the guest [71]. Using a series of dimeric self-assembled containers stabilized by combining hydrogen-bonding and metal-ligand interactions, it was possible to correlate the kinetics of the in-out exchange processes of the guests with the bite angle of the chelated biphosphine ligand in the *cis*-coordinated Pd(II) and Pt(II) metal centers.



The widest bite angle of the chelated ligand corresponded to dppp ligand and resulted in the smallest N-M-N bond angle for the cavitand units. This geometrical arrangement produced the smallest inner cavity of the container assembly in the studied series and the concomitant reduction in the rate constant for guest release. Conversely, the smallest bite angle for the chelated biphosphine derived from the dppe ligand and translated into the largest inner space for the container and the largest rate of guest exchange. The kinetics of the guest release was also modified by the addition of a co-solvent like DMSO. Addition of DMSO provoked the weakening of the hydrogen bonding interactions that hold the flaps of the portals of the containers. Consequently, a faster release of the guest was observed with increasing concentration of DMSO without compromising the metal-ligand coordination bonds that were associated with the container's thermodynamic stability.

## 32.5 Halogen Bonded Capsules

In recent years, the study of halogen bonding interactions (XB), the interaction of a covalently-bonded halogen atom with a nucleophile (electron rich atom), has attracted considerable interest [71]. Halogen bonds were successfully applied in crystal engineering as alternative or complementary intermolecular forces to hydrogen bonding interactions [73]. Moreover, recently some reports involving halogen bonding interactions both in the area of supramolecular chemistry [74, 75] and drug design have also appeared [76, 77].

The application of halogen bonding interactions for the self-assembly of dimeric containers in solution is quite new. In 2015, Dumele and coworkers reported a molecular container held together by four halogen bonding interactions [9]. Two resorcin[4]arene cavitand scaffolds having four 2,3,5,6-tetrafluoro-4-halophenyl and four lutidyl substitutes, respectively, at their upper rims (**57** and **58** from Fig. 32.22) were selected as halogen bond donor and acceptor hemispheres of a self-assembled dimeric container. The assembly of the container in solution was demonstrated for the bromo **57c** and iodo tetrafluorophenyl **57d** substituted cavitands. On the other hand, the fluoro **57a** and chloro-phenyl **57b** cavitand derivatives did not produce the expected container assembly when mixed with equimolar amounts of the tetralutidyl counterpart. The thermodynamically most stable container was assembled from the interaction of the cavitand derivatives having a tetrakis-tetrafluoroiodophenyl substitution with the tetralutidine counterpart. The association constant experimentally determined for the heterodimeric container **57d**•**58** was  $5370 \text{ M}^{-1}$  in a solvent mixture of  $\text{C}_6\text{D}_6/(\text{CD}_3)_2\text{CO}/\text{CD}_3\text{OD}$  70:30:10 at 283 K. The obtained results were in complete agreement with the expected trend of strengths for halogen bonding interaction ( $\text{I} > \text{Br} > \text{Cl} > \text{F}$ ). Halogen bonding is just a particular case of  $\sigma$ -hole interactions and the key factors governing the interaction are electrostatic/polarization and dispersion. The authors described the substantial amplification of binding strength observed in the four-point halogen bonding interactions, which drive the container assembly, in

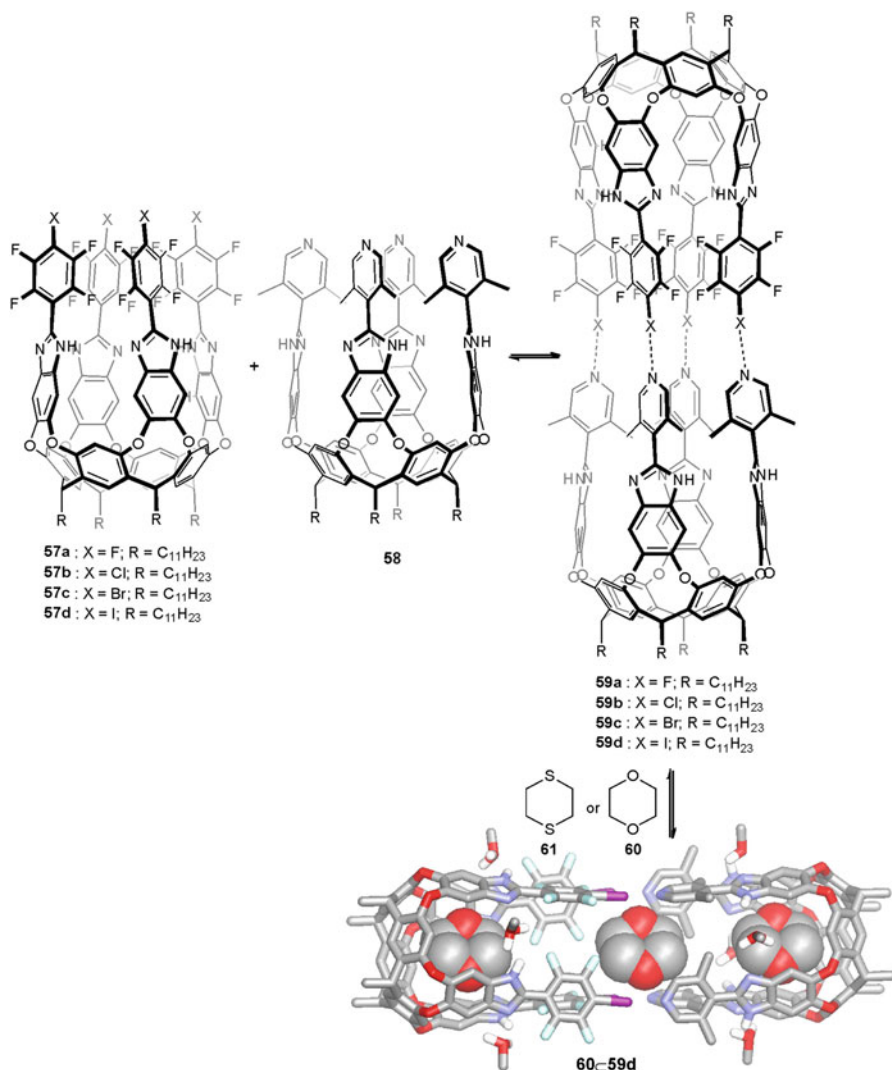


**Fig. 32.22** Line drawing structure of cavitaund units **57** and **58**, and self-assembled heterodimeric capsules **59**. The energy minimized structure of the encapsulation complex formed by three guests **60** in the cavity of the self-assembled container **59d** (**57d**•**58**) stabilized by four halogen bond interactions is also shown

comparison to a monodentated interaction, to the favorable decrease of entropy brought together by multivalency binding, also referred as effective molarity.

The authors also studied the encapsulation of guests in the halogen-bonded container **59** (Fig. 32.22). 1,4-dioxane **60** and 1,4-dithiane **61** were assayed as guests using a non-competitive solvent (mesytilene) and 2% of 3,5-dimethylbenzyl alcohol, to stabilize the cavitaund's vase conformation by

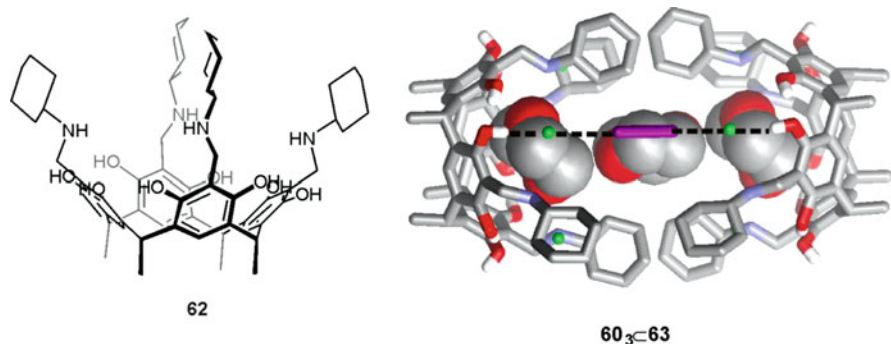


**Fig. 32.23** Line drawing structure of cavitand unit **62** and X-ray structure of the self-assembled capsule **63** including three molecules of dioxane in its interior. The halogen bonds of the bifunctional  $I_2$  molecule with two chloride anions are shown as a *dashed line*. Also *dashed line* represents the hydrogen bonds of the chloride atoms with the hydroxyl groups at the upper rim of **62**

forming a circular array of hydrogen bonds bridging the imidazole residues and not occupying the cavity. The molecular container **57d**•**58** did not feature a single cavity but to separate binding compartments. Four methyl groups of the lutidine moieties converged into the cavity and imposed steric barriers to the communication between the two hemispheres. The guests were bound into both hemispheres in a 1:2 complex and showed different  $^1H$  NMR signals depending on the hemisphere they were bound. Higher association constants were obtained for 1,4-dithiane compared to those for 1,4-dioxane. The higher binding was attributed to dispersive  $S \cdots \pi$  and  $S \cdots N$  interactions present in the 1,4-dithiane guest.

Also in 2015, Beyeh, Rissanen and coworkers reported the structure of a dimeric container based solely on XB interactions in the solid state [10]. The molecular container **63** was assembled from two units of the tetra-*N*-cyclohexylammonium resorcin[4]arene tetrachloride **62** and two iodine molecules (Fig. 32.23). The resorcin[4]arene derivatives showed a closed contact ion-paired circular structure stabilized by hydrogen bonds established between the ammonium substituents and the chloride anions. In addition, they functioned as XB acceptors using two of the four chloride anions. On the other hand, the molecular iodine  $I_2$  components of the container acted as bifunctional halogen bond donor bridging the two hemispheres in a distal arrangement (Fig. 32.23). Thus, the structure of the container was stabilized by both HB and XB interactions acting in concert. In the solid state, the container encapsulated three ordered 1,4-dioxane molecules. The authors commented that the bifunctional assembly involving molecular  $I_2$  was impossible to detect at the low concentrations used in  $^1H$  NMR experiments. However, the  $^1H$  NMR experiments did reveal the existence of iodine to ion-paired resorcin[4]arene interactions in solution and a strong binding with 1,4-dioxane. They claimed that after the formation of the first XB,  $(Cl^- \cdots I(a)-I(b))$ , the second iodine atom diminished its XB donor ability. Molecular iodine acting as bifunctional XB donors was only detected at high concentrations in solution or more typically in the solid state.

## 32.6 Conclusions and Outlook

In this chapter, we have described several methodologies typically used in the assembly of dimeric containers based on calix[4]arene, resorcin[4]arene and aryl extended calix[4]pyrrole derivatives as molecular components. These three molecular scaffolds share in common the presence of an aromatic cavity in their structures. However, only the calix[4]pyrrole units incorporate polar groups in the interior of their aromatic cavities which can establish strong hydrogen-bonding interactions with the bound guests. The assembly of the containers required the previous functionalization of the components upper rims with hydrogen-bonding groups or other substituents able to engage in metal-ligand interactions. The assembly process was favored by using conformationally locked components i.e. resorcin[4]arene cavitand derivatives. In general, the discussed self-assembly strategies rely on the dimerization of the components induced by the formation of intermolecular hydrogen bonds or by metal-coordination bonds (metal-mediated). Examples, of containers assembled by combining both types of intermolecular forces have also been shown. Finally, very recent examples of the use of halogen bonds for the assembly of dimeric containers have been briefly mentioned. The assembly of the dimeric containers required a proper filling of its inner space (55 % packing coefficient rule) together with shape, size and functionality complementarity between host and guest. For containers deprived of polar cavities, the encapsulated guest interacted with the lining of the cavity through weak polar interactions or van der Waals interactions (dispersion). On the other hand, for containers having polar groups inwardly directed stronger host-guest interactions were established i.e. hydrogen bonds. One or multiple guests were encapsulated in the containers' cavities and became totally isolated from the solvent molecules in the bulk. The confined guests experienced a new phase of matter that conveyed them with unique properties. Reversible encapsulation unveiled new reactivities of molecules and unexpected stabilizations of reactive species. We expect that the continued study of reversible encapsulation processes will provide, in a not so distant future, unprecedented examples and applications in the specialized areas of physical organic chemistry, material science and host-guest chemistry. The potential application of self-assembled capsules and their encapsulation complexes for the delivery and light controlled release of drugs has also been hinted.

**Acknowledgements** We thank Gobierno de España MINECO (projects CTQ2014-56295-R, Severo Ochoa Excellence Accreditation 2014–2018 SEV-2013-0319), FEDER funds (CTQ2014-56295-R) and the Catalan Institute of Chemical Research (ICIQ) Foundation for continuous financial support of our research. We also thank our co-workers whose names appear in the reference section.

## References

1. Gabard, J.; Collet, A. *J. Chem. Soc., Chem. Commun.* **1981**, 1137–1139.
2. Cram, D. J.; Karbach, S.; Kim, Y. H.; Baczynskij, L.; Kalleymeyn, G. W. *J. Am. Chem. Soc.* **1985**, *107*, 2575–2576.
3. Cram, D. J. *Nature* **1992**, *356*, 29–36.
4. Gan, H. Y.; Gibb, B. C. *Chem. Commun.* **2013**, *49*, 1395–1397.
5. Mecozzi, S.; Rebek, J. J. *Chem. Eur. J.* **1998**, *4*, 1016–1022.
6. Gavezzotti, A. *J. Am. Chem. Soc.* **1983**, *105*, 5220–5225.
7. Carter, K. A.; Shao, S.; Hoopes, M. I.; Luo, D.; Ahsan, B.; Grigoryants, V. M.; Song, W.; Huang, H.; Zhang, G.; Pandey, R. K.; Geng, J.; Pfeifer, B. A.; Scholes, C. P.; Ortega, J.; Karttunen, M.; Lovell, J. F. *Nat. Commun.* **2014**, *5*, 4546.
8. Erokina, S.; Benassi, L.; Bianchini, P.; Diaspro, A.; Erokhin, V.; Fontana, M. P. *J. Am. Chem. Soc.* **2009**, *131*, 9800–9804.
9. Dumele, O.; Trapp, N.; Diederich, F. *Angew. Chem., Int. Ed.* **2015**, n/a-n/a.
10. Beyeh, N. K.; Pan, F.; Rissanen, K. *Angew. Chem., Int. Ed.* **2015**, n/a-n/a.
11. Kobayashi, K.; Yamanaka, M. *Chem. Soc. Rev.* **2015**, *44*, 449–466.
12. Jordan, J. H.; Gibb, B. C. *Chem. Soc. Rev.* **2015**, *44*, 547–585.
13. Oshovsky, G. V.; Reinhoudt, D. N.; Verboom, W. *J. Am. Chem. Soc.* **2006**, *128*, 5270–5278.
14. Shimizu, K. D.; Rebek, J. *Proc. Natl. Acad. Sci. U. S. A.* **1995**, *92*, 12403–12407.
15. Mogck, O.; Bohmer, V.; Vogt, W. *Tetrahedron* **1996**, *52*, 8489–8496.
16. Mogck, O.; Paulus, E. F.; Bohmer, V.; Thondorf, I.; Vogt, W. *Chem. Commun.* **1996**, 2533–2534.
17. Castellano, R. K.; Kim, B. H.; Rebek, J. *J. Am. Chem. Soc.* **1997**, *119*, 12671–12672.
18. Castellano, R. K.; Nuckolls, C.; Rebek, J. *J. Am. Chem. Soc.* **1999**, *121*, 11156–11163.
19. Rudzевич, Y.; Vysotsky, M. O.; Bohmer, V.; Brody, M. S.; Rebek, J.; Broda, F.; Thondorf, I. *Org. Biomol. Chem.* **2004**, *2*, 3080–3084.
20. Castellano, R. K.; Rudkevich, D. M.; Rebek, J. *Proc. Natl. Acad. Sci.* **1997**, *94*, 7132–7137.
21. Castellano, R. K.; Rebek, J. *J. Am. Chem. Soc.* **1998**, *120*, 3657–3663.
22. Castellano, R. K.; Nuckolls, C.; Eichhorn, S. H.; Wood, M. R.; Lovinger, A. J.; Rebek, J. *J. Angew. Chem., Int. Ed.* **1999**, *38*, 2603–2606.
23. Kuberski, B.; Szumna, A. *Chem. Commun.* **2009**, 1959–1961.
24. Szumna, A. *Chem. Commun.* **2009**, 4191–4193.
25. Szumna, A. *Chem. Eur. J.* **2009**, *15*, 12381–12388.
26. Jedrzejewska, H.; Wierzbicki, M.; Cmoch, P.; Rissanen, K.; Szumna, A. *Angew. Chem., Int. Ed.* **2014**, *53*, 13760–13764.
27. Chapman, R. G.; Sherman, J. C. *J. Am. Chem. Soc.* **1998**, *120*, 9818–9826.
28. Heinz, T.; Rudkevich, D. M.; Rebek, J. *Nature* **1998**, *394*, 764–766.
29. Korner, S. K.; Tucci, F. C.; Rudkevich, D. M.; Heinz, T.; Rebek, J. *Chem. Eur. J.* **2000**, *6*, 187–195.
30. Amaya, T.; Rebek, J. *J. Am. Chem. Soc.* **2004**, *126*, 14149–14156.
31. Hof, F.; Rebek, J. *Proc. Natl. Acad. Sci. U. S. A.* **2002**, *99*, 4775–4777.
32. Korner, S. K.; Tucci, F. C.; Rudkevich, D. M.; Heinz, T.; Rebek, J. *Chem. Eur. J.* **2000**, *6*, 187–195.
33. Scarso, A.; Trembleau, L.; Rebek, J. *J. Am. Chem. Soc.* **2004**, *126*, 13512–13518.
34. Chen, J.; Korner, S.; Craig, S. L.; Rudkevich, D. M.; Rebek, J. *Nature* **2002**, *415*, 385–386.
35. Chen, J.; Rebek, J. *Org. Lett.* **2002**, *4*, 327–329.
36. Hou, J. L.; Ajami, D.; Rebek, J. *J. Am. Chem. Soc.* **2008**, *130*, 7810–+.
37. Sather, A. C.; Berryman, O. B.; Ajami, D.; Rebek Jr, J. *Tetrahedron Lett.* **2011**, *52*, 2100–2103.
38. Iwasawa, T.; Mann, E.; Rebek, J. *J. Am. Chem. Soc.* **2006**, *128*, 9308–9309.
39. Ajami, D.; Schramm, M. P.; Volonterio, A.; Rebek, J. *Angew. Chem., Int. Ed.* **2007**, *46*, 242–244.

40. Ajami, D.; Hou, J. L.; Dale, T. J.; Barrett, E.; Rebek, J. *Proc. Natl. Acad. Sci. U. S. A.* **2009**, *106*, 10430–10434.
41. Shivanyuk, A.; Rebek, J. *J. Am. Chem. Soc.* **2002**, *124*, 12074–12075.
42. Shivanyuk, A.; Rebek, J. *J. Angew. Chem., Int. Ed.* **2003**, *42*, 684–686.
43. Yamanaka, M.; Shivanyuk, A.; Rebek, J. *Proc. Natl. Acad. Sci. U. S. A.* **2004**, *101*, 2669–2672.
44. Scarso, A.; Shivanyuk, A.; Hayashida, O.; Rebek, J. *J. Am. Chem. Soc.* **2003**, *125*, 6239–6243.
45. Amaya, T.; Rebek, J. *J. Am. Chem. Soc.* **2004**, *126*, 6216–6217.
46. Ebbing, M. H. K.; Villa, M.-J.; Valpuesta, J.-M.; Prados, P.; de Mendoza, J. *Proc. Natl. Acad. Sci. U.S.A.* **2002**, *99*, 4962–4966.
47. Choi, H.-J.; Park, Y. S.; Cho, C. S.; Koh, K.; Kim, S.-H.; Paek, K. *Org. Lett.* **2004**, *6*, 4431–4433.
48. Zhang, K.-D.; Ajami, D.; Rebek, J. *J. Am. Chem. Soc.* **2013**, *135*, 18064–18066.
49. Adriaenssens, L.; Ballester, P. *Chem. Soc. Rev.* **2013**, *42*, 3261–3277.
50. Ballester, P.; Gil-Ramirez, G. *Proc. Natl. Acad. Sci. U. S. A.* **2009**, *106*, 10455–10459.
51. Espelt, M.; Ballester, P. *Org. Lett.* **2012**, *14*, 5708–5711.
52. Galan, A.; Valderrey, V.; Ballester, P. *Chem. Sci.* **2015**.
53. Chas, M.; Gil-Ramirez, G.; Escudero-Adan, E. C.; Benet-Buchholz, J.; Ballester, P. *Org. Lett.* **2010**, *12*, 1740–1743.
54. Osorio-Planes, L.; Espelt, M.; Pericas, M. A.; Ballester, P. *Chem. Sci.* **2014**, *5*, 4260–4264.
55. Wang, L.; Vysotsky, M. O.; Bogdan, A.; Bolte, M.; Böhmer, V. *Science* **2004**, *304*, 1312–1314.
56. Chas, M.; Ballester, P. *Chem. Sci.* **2012**, *3*, 186–191.
57. Ugono, O.; Moran, J. P.; Holman, K. T. *Chem. Commun.* **2008**, 1404–1406.
58. Schroder, T.; Brodbeck, R.; Letzel, M. C.; Mix, A.; Schnatwinkel, B.; Tonigold, M.; Volkmer, D.; Mattay, J. *Tetrahedron Lett.* **2008**, *49*, 5939–5942.
59. Jacopozi, P.; Dalcanale, E. *Angew. Chem., Int. Ed.* **1997**, *36*, 613–615.
60. Fochi, F.; Jacopozi, P.; Wegelius, E.; Rissanen, K.; Cozzini, P.; Marastoni, E.; Fisisaro, E.; Manini, P.; Fokkens, R.; Dalcanale, E. *J. Am. Chem. Soc.* **2001**, *123*, 7539–7552.
61. Pirondini, L.; Bertolini, F.; Cantadori, B.; Ugozzoli, F.; Massera, C.; Dalcanale, E. *Proc. Natl. Acad. Sci. U. S. A.* **2002**, *99*, 4911–4915.
62. Pirondini, L.; Bonifazi, D.; Cantadori, B.; Braiuca, P.; Campagnolo, M.; De Zorzi, R.; Geremia, S.; Diedrich, F.; Dalcanale, E. *Tetrahedron* **2006**, *62*, 2008–2015.
63. Pinalli, R.; Cristini, V.; Sottili, V.; Geremia, S.; Campagnolo, M.; Caneschi, A.; Dalcanale, E. *J. Am. Chem. Soc.* **2004**, *126*, 6516–6517.
64. Haino, T.; Kobayashi, M.; Chikaraishi, M.; Fukazawa, Y. *Chem. Commun.* **2005**, 2321–2323.
65. Fox, O. D.; Dalley, N. K.; Harrison, R. G. *J. Am. Chem. Soc.* **1998**, *120*, 7111–7112.
66. Fox, O. D.; Leung, J. F. Y.; Hunter, J. M.; Dalley, N. K.; Harrison, R. G. *Inorg. Chem.* **2000**, *39*, 783–790.
67. Kobayashi, K.; Yamada, Y.; Yamanaka, M.; Sei, Y.; Yamaguchi, K. *J. Am. Chem. Soc.* **2004**, *126*, 13896–13897.
68. Yamanaka, M.; Yamada, Y.; Sei, Y.; Yamaguchi, K.; Kobayashi, K. *J. Am. Chem. Soc.* **2006**, *128*, 1531–1539.
69. Yamanaka, M.; Toyoda, N.; Kobayashi, K. *J. Am. Chem. Soc.* **2009**, *131*, 9880–9881.
70. Yamanaka, M.; Kawaharada, M.; Nito, Y.; Takaya, H.; Kobayashi, K. *J. Am. Chem. Soc.* **2011**, *133*, 16650–16656.
71. Nito, Y.; Adachi, H.; Toyoda, N.; Takaya, H.; Kobayashi, K.; Yamanaka, M. *Chem. Asian J.* **2014**, *9*, 1076–1082.
72. Politzer, P.; Murray, J. S.; Clark, T. *Phys. Chem. Chem. Phys.* **2013**, *15*, 11178–11189.
73. Metrangolo, P.; Meyer, F.; Pilati, T.; Resnati, G.; Terraneo, G. *Angew. Chem., Int. Ed.* **2008**, *47*, 6114–6127.
74. El-Sheshtawy, H. S.; Bassil, B. S.; Assaf, K. I.; Kortz, U.; Nau, W. M. *J. Am. Chem. Soc.* **2012**, *134*, 19935–19941.

75. Gilday, L. C.; Robinson, S. W.; Barendt, T. A.; Langton, M. J.; Mullaney, B. R.; Beer, P. D. *Chem. Rev.* **2015**, *115*, 7118–7195.
76. Scholfield, M. R.; Vander Zanden, C. M.; Carter, M.; Ho, P. S. *Protein Sci.* **2013**, *22*, 139–152.
77. Wilcken, R.; Zimmermann, M. O.; Lange, A.; Joerger, A. C.; Boeckler, F. M. *J. Med. Chem.* **2013**, *56*, 1363–1388.

# Chapter 33

## Calixarenes and Fullerenes

Paris E. Georghiou

### 33.1 Introduction

In Chap. 26 of *Calixarenes 2001* Zhong, Ikeda and Shinkai [1] introduced the historical development of the supramolecular chemistry of calixarenes with fullerenes and extensively reviewed the literature to what had been reported to the end of 2000. Their review concerned mainly interactions of various calixarenes with non-derivatized or “pristine” C<sub>60</sub> and C<sub>70</sub>. More recent reviews [2, 3] and a monograph [4] have dealt with other studies in which calixarenes, but not exclusively, have been used, mainly with fullerenes C<sub>60</sub> and C<sub>70</sub>. The present review summarizes the literature which has appeared since the publication of the Zhong, Ikeda and Shinkai review and may also contain overlapping references to what has appeared in the more recent reviews cited above. The present review will also only focus mostly on examples in which calix[n]arenes, related molecules and their functionalized derivatives have been mainly associated with pristine C<sub>60</sub> and C<sub>70</sub> fullerenes only. For convenience, and for the sake of continuity, the sections presented herein will follow the general sub-headings that appeared in *Calixarenes 2001* and will be presented in chronological order within each of the sub-headings.

---

P.E. Georghiou (✉)

Department of Chemistry, Memorial University of Newfoundland, St. John's, NL, Canada,  
A1B 3X7

e-mail: [parisg@mun.ca](mailto:parisg@mun.ca)



## 33.2 Complexation in the Solid State

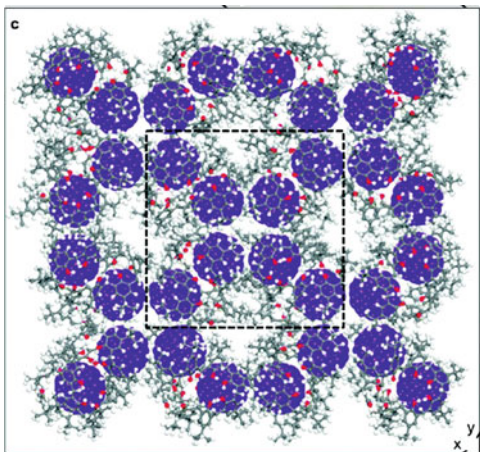
### 33.2.1 With Calix[8]arenes

Two of the earliest reports of a calixarene:fullerene solid state complex were those of Atwood [5a] and Shinkai [5b] who both independently discovered that the 1:1 complex formed between *p*-*tert*-butyl-calix[8]arene (**1**) and C<sub>60</sub> could be used to selectively separate and thus purify C<sub>60</sub> from carbon soot or fullerite mixture. Raston and coworkers [6] recently re-investigated the solid state structure of the C<sub>60</sub> and C<sub>70</sub> complex of **1** using a variety of methodologies, including AFM, SEM, TEM, XRD and Raman spectroscopy, and have coupled the data with advanced molecular simulations. They concluded that the complex was “a unique tetragonal structure of the complex between C<sub>60</sub> and *p*-Bu<sup>t</sup>-calix[8]arene” (Fig. 33.1). An earlier proposed structure [7] had been based on a triangular array of fullerenes and had been modeled for including a C<sub>70</sub> molecule with two C<sub>60</sub> molecules. That predicted structure was based on the calixarenes being in the double cone conformation, with three calixarenes shrouding a triangular array of fullerenes in a micelle-like structure. The latest study suggested instead that a less-restricted arrangement incorporating up to approximately 11 % of C<sub>70</sub> in place of C<sub>60</sub> could still retain the same structure.

### 33.2.2 With Calix[6]arenes

Makha et al. [8] reported the synthesis and structure elucidation by X-ray diffraction studies, powder XRD and TGA, of a C<sub>60</sub>-rich inclusion complex with

**Fig. 33.1** The structure of the C<sub>60</sub>:*p*-*tert*-butylcalix[8]arene complex generated by molecular simulations (Reproduced in part from Ref. [6] with permission of The Royal Society of Chemistry)



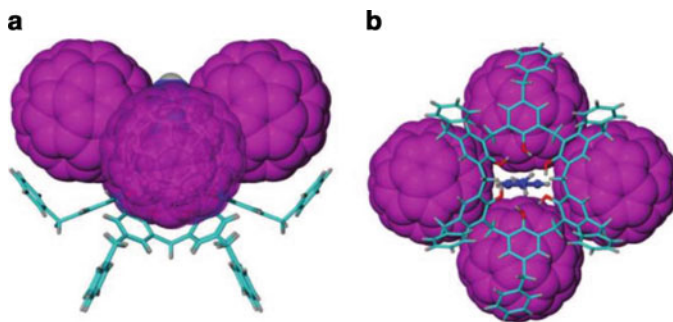


**Fig. 33.2** (a) Structure of the  $C_{60}:2$  complex (disordered parts removed for clarity), and (b) the same structure with the calixarene and toluene molecules (Figure adapted with permission from Ref. [8], Copyright 2008, American Chemical Society)

*p*-benzylcalix[6]arene (**2**). The composition of the complex (Fig. 33.2) which was formed from toluene was determined to be  $[2:(C_{60})_3] \cdot (toluene)_{4.25}$ . This structure was distinctly different from that for the complex of  $C_{60}$  with calix[6]arene (**3**) which forms a 1:2:1 complex with  $C_{60}$  and toluene, and as previously reported, has continuous three-dimensional arrays of the fullerene, and is isostructural with the analogous  $C_{70}$  complex [9]. In these complexes the calix[6]arenes adopt the double cone conformation, resembling a pincer acting on two fullerenes, one in each of its two shallow cavities.

According to Makha et al. [8], treatment of the solid complex of  $C_{60}$  and the *p*-benzylcalix[6]arene with dichloromethane resulted in a dethreading of the calixarene from the complex, without dissolution of the fullerene, thereby affording an all-carbon  $C_{60}$  structure. The ease of the dethreading is due to the mode of the association of **2** within the molecular crystal, consisting of interlocked calixarenes in linear arrays. Similar association has also been seen in the solid-state structure of **2**, itself, where one calixarene is associated with another through two modes, a frontal host-guest association involving inclusion of the pendent benzyl arms and a back-to-back stacking arrangement. The authors further concluded that prediction of the nature of  $C_{60}$  complexes with the larger calixarenes can present difficulties and that simply establishing the stoichiometry of a complex is not necessarily indicative of the nature of the association of the fullerenes and their interactions with calixarenes [8].

Raston's group has also examined the crystal structure using a synchrotron source X-ray diffraction data of a 2:1 complex of  $C_{70}$  and *p*-*tert*-butylcalix[6]arene (**3**) which formed from a toluene solution [10]. The crystallographic data for the complex showed that the fullerene was not included in the cavity of the calixarene. The  $C_{70}$  fullerenes shroud the *exo* surface of the calixarene at the van der Waals limit, with the  $C_{70}$  molecules arranged into "corrugated sheets", with each calixarene interdigitated at the upper rim, with the upper rim of two other calixarenes with the calixarenes forming a bilayer separating the sheets of the

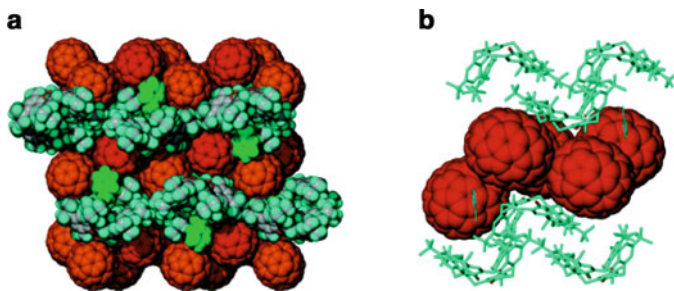


**Fig. 33.3** (a) Space-filling packing diagram showing the corrugated sheets of the  $C_{70}$  separated by layers of self-associated calixarenes. (b) Projection showing the interdigitation of the calixarenes relative to the fullerenes (Figure adapted with permission from Ref. [10], Copyright 2006, American Chemical Society)

fullerenes (Fig. 33.3). The authors then analyzed the X-ray structures of 26 complexes of  $C_{70}$  using the Cambridge Crystallographic Data Base. The closest contacts between fullerenes can involve different combinations of five- and six-membered rings facing each other, a ring edge facing a ring face or two ring edges facing each other. Seven arrangements of  $C_{70}$  molecules were identified: (i) encapsulated and isolated fullerenes, (ii) dimers, (iii) zigzag columns, (iv) columns, (v) close and pseudo-close packed layers, (vi) corrugated sheets, and (vii) 3-D networks. They further concluded that the type of organization of the fullerenes was influenced by the nature and the geometry of the ligand and/or the solvent used.

For comparison, in the structure of  $[(\text{calix}[6]\text{arene})(C_{70})_2]$  the  $C_{70}$  molecules are bound noncovalently to the pseudo-cavities of calix[6]arene in the double cone conformation [9]. The overall structure is complicated and is isostructural with  $[(\text{calix}[6]\text{arene})(C_{60})_2]$ , despite the anisotropic shape of  $C_{70}$ . The calixarenes are in the double-cone conformation, and each of the associated shallow cavities is occupied by a fullerene. The overall arrangement according to the authors “resembles the jaws of a pincer acting on two adjacent ellipsoids”, and the principal axis of the ellipsoidal  $C_{70}$  molecule is not directed toward the calixarene cavity (Fig. 33.4).

### 33.2.3 With Calix[5]arenes

Lhotak and coworkers [11] produced the mono-nitrated tetramethylcalix[5]arene (**4**) which had been designed to study fullerene complexation using cyclic voltammetry. Although this method was ultimately unsuccessful, complexes between **4** and  $C_{60}$  or  $C_{70}$  in solution were proven by mass spectrometry: an equimolar mixture of **4**,  $C_{60}$  and  $C_{70}$  in toluene was subjected to mass spectrometry screening using electrospray ionization in the negative mode. The peaks corresponding to the formation of complexes **4**: $C_{60}$  ( $m/z = 1351.25534$ ) and **4**: $C_{70}$

**Fig. 33.4** The  $C_{70}$  molecules reside in the pseudo-cavities of calix[6]arene **3** in the double cone conformation (Figure adapted with permission from Ref. [10], Copyright 2006, American Chemical Society)

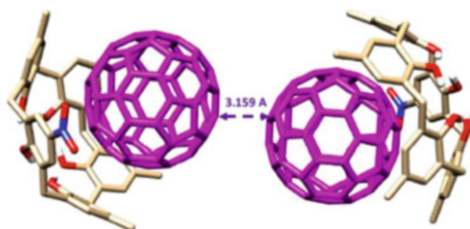
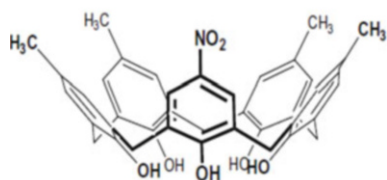
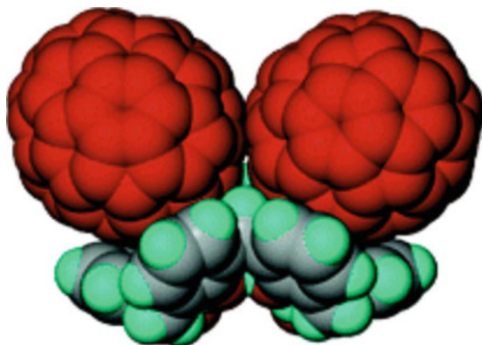


**Fig. 33.5** *Left*: structure of **4**; *Right*: x-ray structure of complex **4**: $C_{60}$ :toluene: $CS_2$ : showing the dimeric arrangement of fullerene moieties with closest contact distances of 3.159 Å (Figures taken from Ref. [11] Copyright 2015, with permission from Elsevier)

(1471.25693) were observed in a 4:1 ratio. X-ray crystallography of a **4**: $C_{60}$ :toluene: $CS_2$  complex was also reported (Fig. 33.5), showing the closest  $C_{60}$  convex-convex van der Waals distance of 3.159 Å.

Hubble and Raston [12] reported that mixing solutions of *p*-tert-butylcalix[5]arene (**5**) and  $C_{60}$  in toluene formed a 1:1  $C_{60}$ :**5** complex which precipitates out as nanofibers. The principal structural unit was based on a host-guest ball-and-socket nanostructure of the two components, with an extended structure comprising zigzag/helical arrays of fullerenes as determined by powder XRD data coupled with molecular modeling (Fig. 33.6) [12]. Under argon, at temperatures  $>309$  °C, the fibers undergo selective volatilization of the calixarenes to afford  $C_{60}$ -core nanostructures encapsulated in a graphitic material sheath, which exhibits a dramatic increase in surface area. Above 650 °C the material exhibits an ohmic conductance response, due to the encapsulation process.

A previous paper from Raston's group [13], established that calix[5]arene (**6**) and  $C_{70}$  in *p*-xylene formed a 1:1 **6**: $C_{70}$  ball-and-socket supramolecular complex whose single-crystal X-ray structure could be determined using synchrotron radiation. The C5 axis of the fullerene was found to be tilted 40° relative to the symmetry axis of the calixarene. Furthermore, the extended structure is comprised of well-separated zigzag sheets of the  $C_{70}$  molecules (Fig. 33.7) [13]. Powder

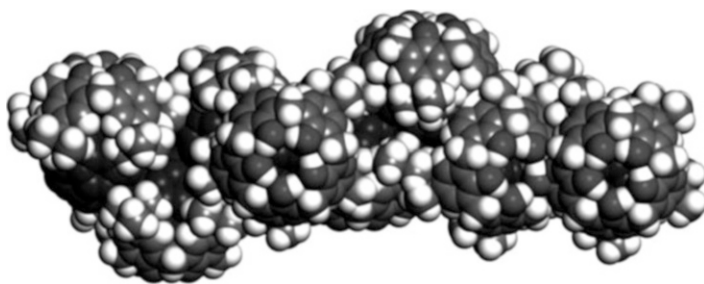


**Fig. 33.6** Proposed calixarene **5** packing arrangement around a  $C_{60}$  column (Figure taken from Ref. [12] with the permission of John Wiley & Sons Inc, Copyright 2010)

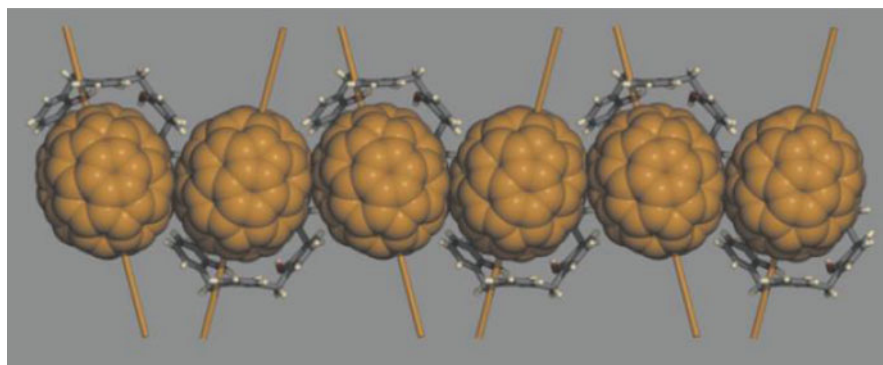


**Fig. 33.7** A single column of calix[5]arene: $C_{70}$  complexes aligned parallel to [001]. The fivefold axes of the fullerenes are shown in orange (Reproduced in part from Ref. [13] with permission of The Royal Society of Chemistry)

diffraction studies showed that the crystals obtained from toluene solution (which did not yield suitable crystals for X-ray crystallography) were not the same as those from the *p*-xylene. Thus, the authors concluded that although neither toluene nor *p*-xylene had a structural role in the solid state complexes of **6** with  $C_{70}$ , the solvent influences the form of the resultant structures. The authors further speculated that the ability to control the close contact-van der Waals complexes of the fullerenes could ultimately lead to being able to covalently link these fullerenes in a controlled manner, the calixarenes thereby playing a facilitating role.

In 2003 Atwood et al. [14] showed that the presence of  $C_{70}$  acts a mediator in the formation of different complexes of calix[5]arene (**6**) and  $C_{60}$ , as defined by the arrangements of the fullerenes. With different  $C_{60}$  to  $C_{70}$  ratios, different crystal types of solid-state structures are formed, ranging from a Z-array to a new 1:1:1  $C_{60}$ :**6**:toluene complex structure, as compared to the **6**:( $C_{60}$ )<sub>5</sub>:(toluene)<sub>2</sub> structure reported previously in 2002 [15]. This new complex crystallized from toluene with the fullerenes organized in a 1-dimensional zigzag array shrouded by a sheath of



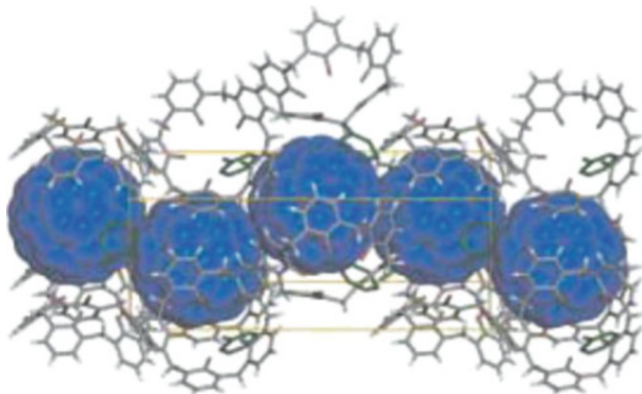


**Fig. 33.8** X-ray crystal structure of the 1:1:1  $C_{60}$ :**6**:toluene complex projected at right angles to the zigzag array of fullerenes (Reproduced in part from Ref. [14] with permission of The Royal Society of Chemistry)

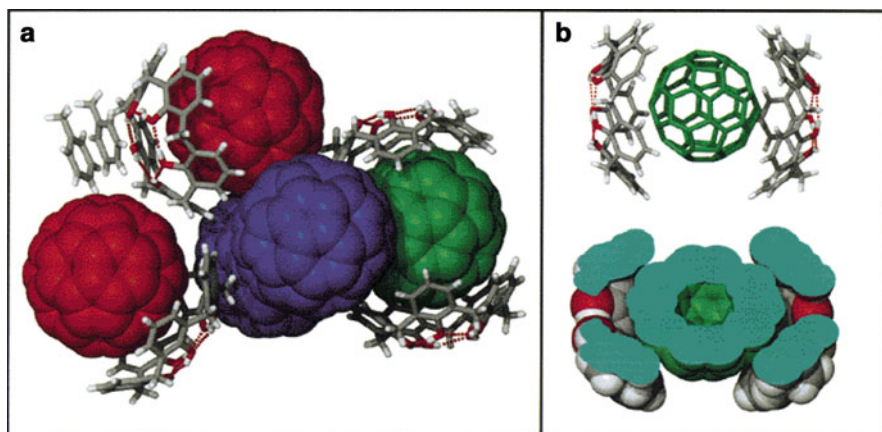


**Fig. 33.9** (a) The asymmetric unit consisting of five  $C_{60}$ , four **6**, and two toluene molecules. The  $C_{60}$  guest molecules are coloured according to their modes of interaction with the calix[5]arene host cavities (*green*: ball-and-dual-socket, *red*: ball-and-socket, *blue*: not interacting). (b) Cut-away section (*bottom*) of the space filling metaphor for ball-and-dual-socket nanostructure (*top*) showing the complementarity of curvature of the fullerene with the calixarene (Figure adapted with permission from Ref. [15], Copyright 2002, American Chemical Society)

calixarenes (Figs. 33.8 and 33.9). This complex is formed from an approximately 4.5:1 up to a 10:1 molar ratio of  $C_{60}$  to  $C_{70}$  with 1.4 mol equivalents of **6**. The authors concluded that the control of the assembly of fullerenes depending on the presence of a third component (in this case, the  $C_{70}$ ), “which does not form part of the assembly is an important development in the materials science of fullerenes” [14].

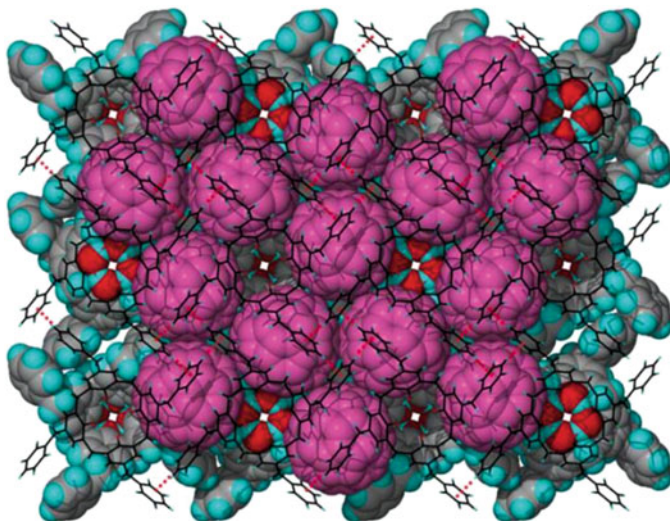


**Fig. 33.10** Top view projection down the  $c$  axis of the fullerene and calixarene layers in  $(C_{60})_2:9$ , with red dotted lines showing the CH- $\pi$  interactions (Reproduced in part from Ref. [16] with permission of The Royal Society of Chemistry)

Atwood, Barbour and Raston [15] showed that crystals grown by slow evaporation, from a 1:1 mixt. of **6** and  $C_{60}$  in toluene formed a  $6:(C_{60})_5:(\text{toluene})_2$  structure. The calix[5]arene and  $C_{60}$  arrange to form linear, fivefold, Z-shaped columns consisting of mol. spheres that are in van der Waals contact with one another. The  $C_{60}$  molecules are present in three completely different environments with regard to their supramolecular associations with the calixarene molecules.

### 33.2.4 With Calix[4]arenes

In contrast to the larger calix[ $n$ ]arenes ( $n > 4$ ) the cavities of calix[4]arene (**7**) or *p*-*tert*-butylcalix[4]arene (**8**), whether in the *cone* conformation or not, are generally too small to accommodate a  $C_{60}$  fullerene molecule. Makha et al. [16] however showed that with  $C_{60}$ , *p*-benzylcalix[4]arene (**9**) forms a 2:1  $(C_{60})_2:9$  complex in which the fullerenes are packed into flat sheets with each calixarene nestled *exo* to the cavity of the calixarene but into a cavity created by a square array of fullerenes (Fig. 33.10) [16]. The X-ray structure determination of this complex which was formed by slow evaporation of an equimolar solution of both components, required synchrotron radiation to provide suitable structural data refinement. The authors compared the X-ray data from this  $(C_{60})_2:9$  complex with that from the corresponding 1:1 complex formed with the smaller van der Waals diameter ( $\sim 8.1$  vs  $\sim 10.0$  Å) *o*-carborane which resided *endo* within the cavity with the

lower rim benzyl groups flattened out. They concluded that the diameter threshold for *endo* vs *exo* binding needed to be between 8.1 vs  $\sim 10.0$  Å [16].

### 33.3 Films and Self-Assembled Monolayers of Calixarene- $C_{60}$ Complexes

#### 33.3.1 With Calix[8]arenes

Busolo et al. [17] immobilized  $C_{60}$  onto silicon surfaces via the *p-tert*-butylcalix[8]arene (**10**) which was esterified at the lower-rim with 10-undecenoyl chloride. The grafting of the calix onto the flat Si(100) surface was conducted by a thermal hydrosilylation process. The resulting Si-substrates were then treated with  $C_{60}$  in toluene solutions. Grafting of **10** onto the silicon substrates was studied by XPS spectra, and the host-guest immobilization of fullerene was demonstrated by AFM and sessile drop-water contact angle measurements. The data they obtained from the surface topographical variations, modeled on the basis of the calix[8]arene and  $C_{60}$  geometrical parameters, were consistent with a Si surface-functionalization and to supramolecular binding of the  $C_{60}$ . Since  $C_{60}$  has a tendency to aggregate on the functionalized surface, forming tall pillars in some areas (Fig. 33.11, *left*), the calix [8]arene layer was diluted with 1-octene in order to keep the docked fullerenes away from one another and to discourage clustering (Fig. 33.11, *right*). This reduced the amount of oxidized areas observed on the surface, indicating that the aliphatic chains were taking up spaces between the calix[8]arene hosts. When the diluted calix[8]arene layer was treated with the  $C_{60}$ , the observed clustering was reduced, with flatter morphologies and no pillar structures being observed. The authors postulated that from their results, calix[8]arene-functionalized silicon chips can be used as a host surface, toward fullerenes and other electronically and structurally unique molecules [17].

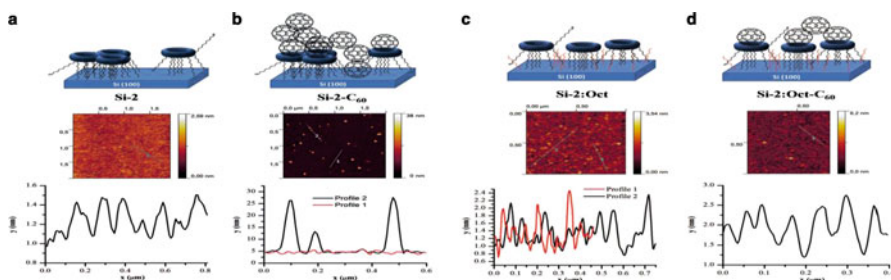


**Fig. 33.11** AFM image of samples *left*: (a) Si-2 and (b) Si-2- $C_{60}$ ; and *right*: samples (a) Si-2:Oct and (b) Si-2:Oct- $C_{60}$ . Profiles collected along the blue lines are reported at the bottom (Figure reprinted with permission from Ref. [17]. Copyright *J. Chem. Phys.*, 2013, AIP Publishing LLC)



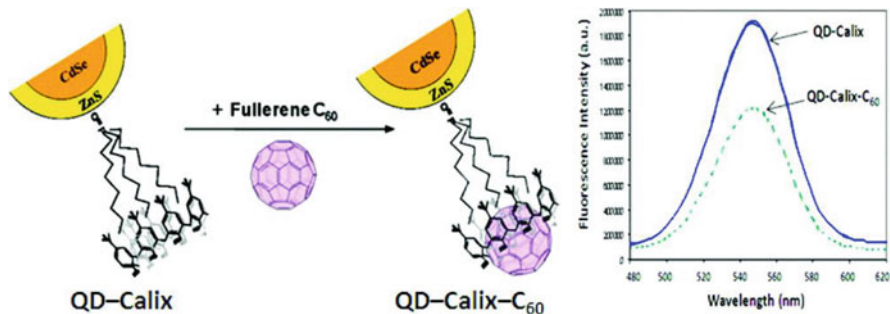


**Fig. 33.12** The supramolecular association between the quencher ( $C_{60}$  fullerene) and the receptor (QD-Calix). The fluorescence change observed when the ternary QD-Calix- $C_{60}$  complex is formed is shown on the right (Figure adapted with permission from Ref. [18], Copyright 2011, American Chemical Society)

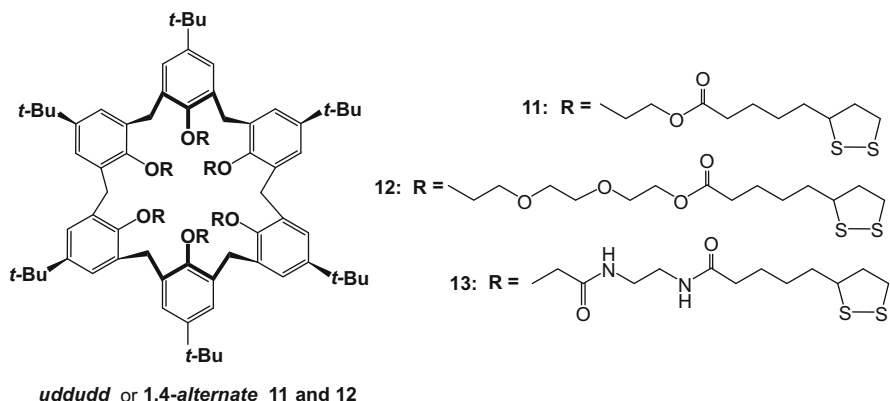


**Fig. 33.13** Structures of *p*-*tert*-butylcalix[8]arene thioctic ester derivatives **11–13** [20, 21]

Carrillo-Carrion et al. [18] reported on the preparation and application of *p*-*tert*-butylcalix[8]arene-coated CdSe/ZnS quantum dots (QD) as a  $C_{60}$ -nanosensor. The highly fluorescent calixarene-coated quantum dots were prepared according to a procedure by Jin et al. [19] by treating trioctylphosphine oxide (TOPO)-capped CdSe/ZnS QDs, by sonication with a toluene solution of **1** and centrifugation of the resulting QDs. The nanosensor is based on the selective host-guest interaction between  $C_{60}$  fullerene and the **1**-CdSe/ZnS complex quenches the original fluorescence of calix-QDs (Figs. 33.12 and 33.13). The potential application of the designed nanosensor for detection of  $C_{60}$  in spiked environmental river water samples is demonstrated. For the analysis of river samples, the authors proposed a liquid-liquid extraction multistep pre-concentration procedure. The method allowed for the detection of  $5 \mu\text{g L}^{-1}$  of  $C_{60}$ . The authors proposed that this sensor could be a useful tool for environmental and toxicological studies [18].

To explore their ability to immobilize  $C_{60}$  non-covalently onto Au surfaces, Zhang and Echegoyen [20, 21] synthesized several thioctic ester derivatives including *p*-*tert*-butylcalix[6]arene **11** and **12**, and a *p*-*tert*-butylcalix[8]arene thioctic ester derivative **13**. The conformations of **11** and **12** were found to be in *1,4-anti* conformations but the conformation of **13** could not be unequivocally assigned.

Self-assembled monolayers (SAMs) of these compounds formed on Au bead electrode surfaces were used to incorporate  $C_{60}$  onto the Au surfaces as judged by observation of its first two reduction potentials. Only the SAM of *p*-*tert*-butylcalix[8]arene thioctic ester **13** was found to be reasonably effective at immobilizing  $C_{60}$  on the surfaces (Fig. 33.14). Cyclic voltammetry with  $Ru(NH_3)_6^{3+/2+}$  as a redox probe, together with impedance spectroscopy and reductive desorption, indicated that SAMs of **13** had a higher coverage than those of **11** and **12** [21].

Pan et al. [22] studied the octakis(carboxymethoxy)calix[8]arene **14** derivative and showed that its inclusion complex with  $C_{60}$  in solution could be adsorbed onto a Au(111) surface to yield self-organized highly ordered arrays (Fig. 33.15). The

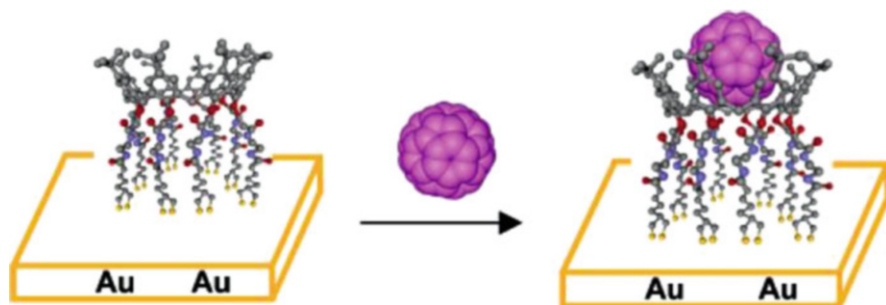


**Fig. 33.14** The proposed supramolecular immobilization of  $C_{60}$  onto a SAM of *p*-*tert*-butylcalix[8]arene thioctic ester derivative **13** (Figure adapted with permission from Ref. [20], Copyright 2005, American Chemical Society)

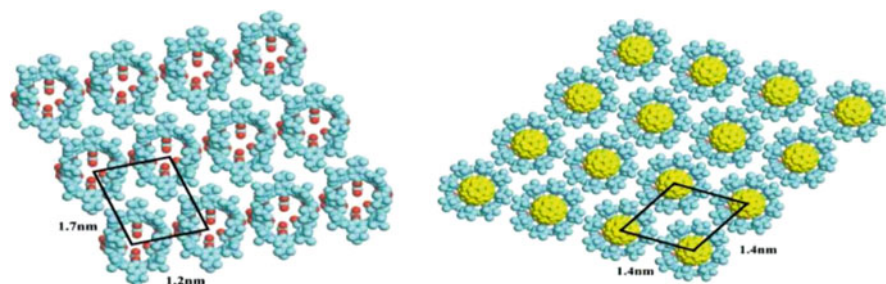


**Fig. 33.15** *Left*: the proposed structural model for the ordered array, seen in the STM, of **14**; *Right*: proposed structural model for the ordered array of  $C_{60}/\mathbf{14}$ . The bias voltage and tunneling current were  $-140$  mV and  $1.0$  nA, respectively. The scales are given in nm (Figure adapted from Ref. [22] with the permission of John Wiley & Sons Inc, Copyright 2003)

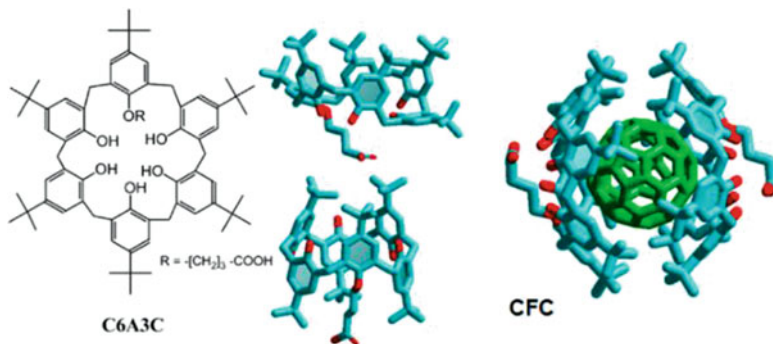


**Fig. 33.16** *Left*: molecular structure of **15**; *center*: two geometry-optimized molecular mechanics structures corresponding to the cone (*top*) and alternate-OH (*bottom*) conformations; *Right* optimized molecular mechanics structure for the (15)<sub>2</sub>:C<sub>60</sub> (CFC) complex (Figure adapted with permission from Ref. [23], Copyright 2012, American Chemical Society)

structures of the two arrays were investigated by scanning tunnelling microscopy, which showed clear evidence of the inclusion of the C<sub>60</sub> molecules.

### 33.3.2 With Calix[6]arenes

Gonzalez-Delgado et al. [23] synthesized a monosubstituted asymmetric derivative of *p*-*tert*-butylcalix[6]arene (**15**), in which a single hydroxyl group has been replaced with a  $-O(CH_2)_3COOH$  group. Langmuir monolayers of **15** were formed on pure water at the air-water interface, in which **15** adopts a flat-like orientation. The structure of **15** gives its amphiphilic character, while allowing the control of both the degree of dissociation its conformation at the air-water interface. When **15** is combined with pristine C<sub>60</sub> in toluene it forms the supramolecular complex “CFC” in a 2:1 molar ratio. The (15)<sub>2</sub>:C<sub>60</sub> complex forms Langmuir monolayers at the air/water interface. The interfacial molecular arrangement of the CFC complex was shown by UV-Vis reflection spectroscopy and synchrotron X-ray reflectivity measurements; charge transfer between the C<sub>60</sub> and the calixarenes was also found to occur. Computer simulations complemented the experimental data, confirming a perpendicular orientation of the calixarene units of CFC with respect to the air-water interface (Fig. 33.16) [23]. The authors proposed this interfacial monolayer of the CFC supramolecular complex as a useful model for the well-defined self-assembly of recognition and functional building blocks.

## 33.4 Calixarene-C<sub>60</sub> and Calixarene-C<sub>70</sub> Solution Binding Studies

### 33.4.1 With “classical” Calix[n]arenes and Their Derivatives

Since the initial overview of solution state studies of fullerene supramolecular complexation studies with calixarenes, some of their derivatives and other related macrocycles, by Zhong, Ikeda and Shinkai in *Calixarenes 2001*, there continues to be on-going interest and increased understanding in this area. The information pertaining to gauging the strength of the host-guest interactions is still by-and-large determined by measurement of their binding or association constants. Several reports have appeared in the intervening years, of new calixarene derivatives which have been subjected to such solution state studies with both C<sub>60</sub> and C<sub>70</sub>. The most common approach has been to use UV-Vis absorbance titration determinations, although caution is required when interpreting the experimental data derived by this method, as was pointed out by Georghiou et al. [24a]. Other solution studies have employed fluorescence spectroscopic titration methods and once again, caution needs to be exercised in interpreting the experimental data [25]. Several of the studies were augmented by mainly <sup>1</sup>H NMR titration chemical shift changes [26]. Most use the “classical” Benesi-Hildebrand [27] analysis or variants thereof, although its limitations have been addressed recently by Thordarson [28] and others. A few studies to 2010 were reviewed in Reference 3 but other studies are summarized in Tables 33.1 and 33.2 which are arranged in chronological order and according to their reference citations. It should be noted that some papers used the terms “stability”, “formation”, “binding” or “association” constant to represent the apparent equilibrium constants for the supramolecular complexation of the fullerenes in solution. In this review “binding constant”, i.e. “*K*” will be used to avoid confusion.

Bhattacharya et al. [29] studied the C<sub>60</sub> and C<sub>70</sub> 1:1 supramolecular complexes formed with octamethoxy-*p*-*tert*-butylcalix[8]arene (**16**), hexamethoxy-*p*-*tert*-butylcalix[6]arene (**17**) and 37,39,41-trimethoxy-38,40,42-trihydroxy-*p*-*tert*-butylcalix[6]arene (**18**) by UV-Vis absorption spectroscopy in three different solvents, CCl<sub>4</sub>, toluene and *o*-xylene. Binding constants for the complexes were determined at four different temperatures from which the enthalpies and entropies of formation of the complexes were also obtained. *K* values were greater for C<sub>60</sub>:**18** than for C<sub>60</sub>:**17** or C<sub>60</sub>:**16** at all of the temperatures studied. The authors rationalized this finding in terms of a higher degree of preorganization of **18** through the intramolecular hydrogen-bonding at its lower rim. The same authors [30] examined the complexation behaviour in CCl<sub>4</sub> with C<sub>70</sub> for three mono-*O*-substituted *p*-*tert*-butylcalix[6]arenes, **3a-c** (**3a**: mono-*O*-CH<sub>2</sub>Ph; **3b**: mono-*O*-CH<sub>2</sub>CO<sub>2</sub>Et; **3c**: mono-*O*-CH<sub>2</sub>CH=CH<sub>2</sub>) by UV-Vis absorption spectroscopy, and determined thermodynamic parameters for the supramolecular complex formations. The authors concluded that although 1:1 complexes were formed with all three receptors, the relatively high *K* value for the C<sub>70</sub>:**3b** complex suggested that **3b** formed an

**Table 33.1** Binding constants (*K*) for calixarene-*C*<sub>60</sub>- and/or *C*<sub>70</sub> complexation studies as determined by UV-Vis titrations in various solvents at 298 K unless otherwise noted

Compound	Calix[ <i>n</i> ]arene (Solvent)	Upper rim substituent	Lower rim substituent (s)	<i>K</i> · <i>M</i> <sup>-1</sup> · <i>C</i> <sub>60</sub>	<i>K</i> · <i>M</i> <sup>-1</sup> · <i>C</i> <sub>70</sub>	Reference
<b>3a</b>	<b>6</b> (CCl <sub>4</sub> )	<i>tert</i> -Butyl	(-OCH <sub>2</sub> Ph) <sub>1</sub> (-OH) <sub>5</sub>	1389 ± 78	<i>nr</i> <sup>b</sup>	[30] <sup>a</sup> , [31] <sup>a</sup>
<b>3b</b>			(-OCH <sub>2</sub> CO <sub>2</sub> Et) <sub>1</sub> (OH) <sub>5</sub>	3661 ± 110	1350 ± 65	
<b>3c</b>			(-OCH <sub>2</sub> CH=CH <sub>2</sub> ) <sub>1</sub> (-OH) <sub>5</sub>	623 ± 56	<i>nr</i> <sup>bb</sup>	
<b>3d</b>			(-OCH <sub>3</sub> ) <sub>1</sub> (-OH) <sub>5</sub>	3077 ± 204		[31] <sup>a</sup>
<b>3e</b>			(-OCH <sub>2</sub> COPh) <sub>1</sub> (-OH) <sub>5</sub>	1588 ± 95		
<b>3f</b>	<b>6</b> (Toluene)	<i>tert</i> -Butyl	(-OH) <sub>6</sub>	3.2 × 10 <sup>4</sup> ± 432	11 × 10 <sup>4</sup> ± 5,700	[37]
<b>5</b>	<b>5</b> (Toluene)	<i>tert</i> -Butyl	(-OH) <sub>5</sub>	23,600	94,460	[35] <sup>b</sup>
<b>16</b>	<b>8</b> (Toluene)	<i>tert</i> -Butyl	(-OMe) <sub>8</sub>	16,610	15,810	[29] <sup>a</sup>
<b>17</b>	<b>6</b> (Toluene)		(-OMe) <sub>6</sub>	14,470	6,490	
<b>18</b>	<b>6</b> (Toluene)		(-OMe) <sub>3</sub> ;(-OH) <sub>3</sub>	12,420	<i>nr</i> <sup>b</sup>	
<b>18</b>	<b>6</b> (CCl <sub>4</sub> )	<i>tert</i> -Butyl	(-OMe) <sub>3</sub> ;(-OH) <sub>3</sub>	<i>nr</i> <sup>b</sup>	4290 ± 86	[32] <sup>a</sup>
<b>19</b>	<b>4</b> (CCl <sub>4</sub> )		(-OMe) <sub>2</sub> ;(-OH) <sub>2</sub>	2430 ± 108 (308 K)	1093 ± 153 (305 K)	
<b>20</b>	<b>4</b> (CHCl <sub>3</sub> )	H	(-OMe) <sub>2</sub> ;(-OH) <sub>2</sub>	865 ± 25	4500 ± 225	[34] <sup>a</sup>
<b>21</b>	<b>4</b> (CHCl <sub>3</sub> + toluene+Ethanol)			540 ± 25	300 ± 15	
	<b>4</b> (Toluene)	Isopropyl	(-OH) <sub>4</sub>	1.6 × 10 <sup>4</sup> ± 325	8.2 × 10 <sup>4</sup> ± 1,100	[38]
	<b>4</b> (Benzonitrile)			6.1 × 10 <sup>4</sup> ± 933	1.03 × 10 <sup>5</sup> ± 600	
<b>22</b>	Trihomocalix[6] (Toluene)	<i>tert</i> -Butyl	(-OCH <sub>2</sub> CO <sub>2</sub> Et) <sub>6</sub>	47,540	86,360	[39]
<b>23a</b>	Thiacrown	<i>tert</i> -Butyl	(OH) <sub>2</sub>	1.0 × 10 <sup>4</sup>	<i>nr</i> <sup>b</sup>	[40] <sup>a</sup>
<b>23b</b>	Thiaoxacrown			0.3 × 10 <sup>4</sup>		
<b>23c</b>	Thiacrown			1.3 × 10 <sup>4</sup>		
<b>24</b>	Crown-5		(-CH <sub>2</sub> Ph) <sub>2</sub>	0.12 × 10 <sup>4</sup>		

<b>26</b>	Calix[4]naphthalene (Benzene)	H	(-OH) <sub>4</sub>	457 ± 40	m <sup>b</sup>	[24] <sup>a,b</sup>
<b>26a</b>		<i>tert</i> -Butyl		295 ± 13		
<b>26</b>	Calix[4]naphthalene (Toluene)	H		631 ± 51		
<b>26a</b>		<i>tert</i> -Butyl		676 ± 28		
<b>26</b>	Calix[4]naphthalene (CS <sub>2</sub> )	H		390 ± 180		
<b>26a</b>		<i>tert</i> -Butyl		6920 ± 330		
<b>38</b>	OctaMeCalix[4]pyrrole (Toluene)			4.37 × 10 <sup>4</sup>	2.47 × 10 <sup>5</sup>	[62]
	OctaMeCalix[4]pyrrole (CHCl <sub>3</sub> )			3.04 × 10 <sup>5</sup>	1.43 × 10 <sup>6</sup>	
	OctaMeCalix[4]pyrrole (1,2-Dichlorobenzene)			8.50 × 10 <sup>4</sup>	5.87 × 10 <sup>5</sup>	
	OctaMeCalix[4]pyrrole (Benzonitrile)			1.53 × 10 <sup>5</sup>	4.79 × 10 <sup>5</sup>	

The data are as presented from the references and have not been corrected for significant figures/precision

<sup>a</sup>This study included a thermodynamic study with different temperatures

<sup>b</sup>Not reported or determined

**Table 33.2** Binding constants (**K**) for calixarene-C<sub>60</sub>- and/or C<sub>70</sub> complexation studies as determined by NMR titrations at 298 K in the solvents noted

Compound	Calix[n]arene (Solvent)	Upper rim substituent	Lower rim substituent(s)	K·M <sup>-1</sup> C <sub>60</sub>	K·M <sup>-1</sup> C <sub>70</sub>	Reference
<b>3c</b>	<b>6</b> (CCl <sub>4</sub> )	<i>tert</i> -Butyl	(-OCH <sub>2</sub> CH=CH <sub>2</sub> ) <sub>1</sub> (-OH) <sub>5</sub>	1600 ± 110	2435 ± 75	[36] <sup>a</sup>
<b>16</b>	<b>8</b> (CCl <sub>4</sub> )	<i>tert</i> -Butyl	(OMe) <sub>8</sub>	2800 ± 50	4700 ± 200	[33] <sup>a</sup>
<b>17</b>	<b>6</b> (CCl <sub>4</sub> )		(OMe) <sub>6</sub>	100 ± 10	2100 ± 150	
<b>18</b>	<b>6</b> (CCl <sub>4</sub> )		(-OMe) <sub>3</sub> :(-OH) <sub>3</sub>	5700 ± 950	4500 ± 500	
<b>19</b>	<b>4</b> (CCl <sub>4</sub> )		(-OMe) <sub>2</sub> :(-OH) <sub>2</sub>	1350 ± 50	2150 ± 50	
<b>24</b>	<b>3</b> + (-CH <sub>2</sub> O-) <sub>3</sub> (Toluene- <i>d</i> <sub>8</sub> )	H	(-OH) <sub>3</sub>	150 ± 5	nr <sup>b</sup>	[41]
<b>24a</b>		<i>tert</i> -Butyl		296 ± 9		
<b>24</b>	<b>3</b> + (-CH <sub>2</sub> O-) <sub>3</sub> (Benzene- <i>d</i> <sub>6</sub> )	H		116 ± 6		
<b>24a</b>		<i>tert</i> -Butyl		441 ± 23		

The data are as presented from the references and have not been corrected for significant figures/precision

<sup>a</sup>K values cited in the paper were in units of kg mol<sup>-1</sup>

<sup>b</sup>Not reported or determined

inclusion-type complex with  $C_{70}$ . Following up on this study with calixarenes **3a-c**, another UV-Vis study in  $CCl_4$  this time, with  $C_{60}$  [31] included two additional mono-*O*-substituted *p-tert*-butylcalix[6]arenes derivatives, **3d** (mono-*O*- $CH_3$ ) and **3e** (mono-*O*- $CH_2COPh$ ). They found charge transfer (CT) transitions, although the degree of the CT was very low ( $\sim 0.15\%$ ). In each case, 1:1 complex formation apparently occurs. The thermodynamic parameters were also reported and they concluded that under the conditions used for the study, only **3d** and **3b** formed inclusion complexes with  $C_{60}$  and supported this conclusion with a limited PM3 computational determination. The presence and nature of the single substituent group on the lower rim of the calix[6]arene molecule therefore the authors proposed, appeared to govern the host-guest complexation process.

Bhattacharya and coworkers [32] in 2005 followed up their previously-reported  $C_{60}$  and  $C_{70}$   $^1H$ -NMR complexation study [33] with two of the methoxy-*p-tert*-butylcalixarene derivatives, namely **18** and 24,26-dimethoxy-*p-tert*-butylcalix[4]arene (**19**) and which had been used in that earlier study (Table 33.2). In the 2005 study using UV-Vis absorption spectroscopy they reported that  $C_{60}$  and  $C_{70}$  formed 1:1 complexes with **18** and **19** in  $CCl_4$ . They were able to determine CT absorption bands of the complexes in each of the cases, except for the  $C_{70}$ :**18** complex. Binding constants of the complexes were determined at four different temperatures from which they calculated thermodynamic parameters for the supramolecular complex formations. The authors showed that  $K$  of the  $C_{70}$ :**18** complex was higher than that of the corresponding  $C_{60}$ :**18** and also of the  $C_{60}$ :**19** complexes at all four temperatures. They concluded that this was due to both the larger cavity size, and higher degree of pre-organisation due to intramolecular hydrogen-bonding in the lower rim of **18**. Another UV-Vis absorption spectroscopic complexation study with  $C_{60}$  and  $C_{70}$  [34] this time was conducted with 24,26-dimethoxy-25,27-dihydroxycalix[4]arene (**20**), the *de-tert*-butylated analogue of **19** in two different solvent systems. The solvent systems used were (i) chloroform alone and (ii) a ternary system consisting of chloroform, ethanol and toluene although their relative proportions were not defined. They explained their experimental results using a model that took into account the interaction between electronic subsystems of **20** and the fullerene. They observed a preference for  $C_{60}$  over  $C_{70}$  for **20** in the ternary solvent mixture, as determined by the higher  $K$  value for the  $C_{60}$ :**20** complex.

Another absorption spectrophotometric complexation study with  $C_{60}$  and  $C_{70}$  in toluene using *p-tert*-butylcalix[5]arene **5** by Bhattacharya and coworkers [35] included  $^1H$  NMR data and a PM3 computational study. CT absorption bands were located for the complexes of  $C_{60}$  and  $C_{70}$  with **5** and yielded physicochemical parameters including oscillator strength, resonance energy and electronic coupling elements for the fullerene:**5** complexes. From the binding constant data, **5** was found to bind preferentially with  $C_{70}$  over  $C_{60}$ .  $^1H$  NMR also provided good support in favor of strong complexation between  $C_{70}$  and **5**. The PM3 calculations suggested that the binding pattern of  $C_{70}$  towards **5** was *end-on* rather than *side-on* as  $C_{70}/1$  complex gained  $2.43\text{ kJ mol}^{-1}$  of extra stabilization energy in case of its *end-on* orientation rather than a *side-on* approach.



A follow up  $^1\text{H}$  NMR titration study of mono-*O*-allyl-substituted *p*-*tert*-butylcalix[6]arene, **3c** [30] with  $\text{C}_{60}$  and  $\text{C}_{70}$  was conducted in  $\text{CCl}_4$ . [36] The 1:1 complexes of **3c**: $\text{C}_{60}$  and **3c**: $\text{C}_{70}$  were found to be stable and the measured binding constant data suggested that  $\text{C}_{70}$  binds more strongly to the calixarene than  $\text{C}_{60}$  (Table 33.2). PM3 and ab initio calculations were also reported. Halder et al. [37] conducted a UV-Vis titration study in toluene using *p*-*tert*-butylcalix[6]arene (**3f**) with  $\text{C}_{60}$  and  $\text{C}_{70}$ . Charge transfer transitions in the visible region between the fullerenes and the calixarene were used to determine parameters such as the oscillator strength, resonance energy, transition dipole strength of the fullerene:**3f** complexes and the ionization potential of **3f**. Both  $\text{C}_{60}$  and  $\text{C}_{70}$  were reported to form stable 1:1 complexes with **3f** with  $\text{C}_{70}$  showing the larger ( $1.1 \times 10^5 \text{ M}^{-1}$ ) binding constant than  $\text{C}_{60}$  ( $3.2 \times 10^4 \text{ M}^{-1}$ ). The authors cited only a 200 MHz  $^1\text{H}$  NMR single-point study which they claim provided “good support in favor of strong binding between  $\text{C}_{70}$  and **3f**” but the authors did not provide sufficient experimental titration data to support this. Halder et al. [38] also reported on a  $\text{C}_{60}$  and  $\text{C}_{70}$  UV-Vis host-guest complexation study with *p*-isopropylcalix[4]arene (**21**), in toluene and benzonitrile solutions. As in their previous studies, charge-transfer (CT) absorption bands were located for the ground states of the 1:1  $\text{C}_{60}$  and  $\text{C}_{70}$  complexes of **21**. The binding constant data showed that **21** complexed  $\text{C}_{70}$  more strongly than  $\text{C}_{60}$ . Larger binding constant values (Table 33.1) were observed with the benzonitrile solutions. Molecular mechanics MMMF force-field calculations in the gas-phase suggested that the  $\text{C}_{70}$  molecule in the  $\text{C}_{70}$ :**21** complex is directed in an *end-on* rather than *side-on* manner. Another UV-Vis absorption spectrophotometric, NMR and theoretical study on the ground state 1:1 supramolecular complexation of  $\text{C}_{60}$  and  $\text{C}_{70}$  with a trihomocalix[6]arene (**22**) in toluene was also described by Halder et al. [39] Binding constant data from the UV-Vis study indicated that **22** bound both  $\text{C}_{60}$  and  $\text{C}_{70}$ , ( $8.6 \times 10^4 \text{ M}^{-1}$  vs  $4.7 \times 10^4 \text{ M}^{-1}$ , respectively). The authors suggested that the  $^1\text{H}$  NMR data supported “strong binding between  $\text{C}_{70}$  and **22**”, however, only a single-point experiment was conducted.

Mizyed et al. [40] conducted a UV-Vis study in toluene solution of the CT complexes of  $\text{C}_{60}$  with *tert*-butylcalix[4]crowns **23a-c** and **24** (Fig. 33.17) and also measured the thermodynamic data of the resulting 1:1 complexes. The *K* values were found to decrease with increasing size of the crown moiety of the calixcrown **23c** ~ **23a** > **23b** > **24**. Most of the complexes were reportedly found to be enthalpy stabilized but entropy disfavoured.

### 33.4.2 With Calix[n]arene-Like Analogues

There are several basket- or bowl-shaped analogues of the “classical” calix[*n*]arenes which have been used in supramolecular complexation studies with the fullerenes. These have included mainly cyclotrimeratrylenes (“CTV”), cavitands and their derivatives, and but these will not be dealt with here. Instead this review

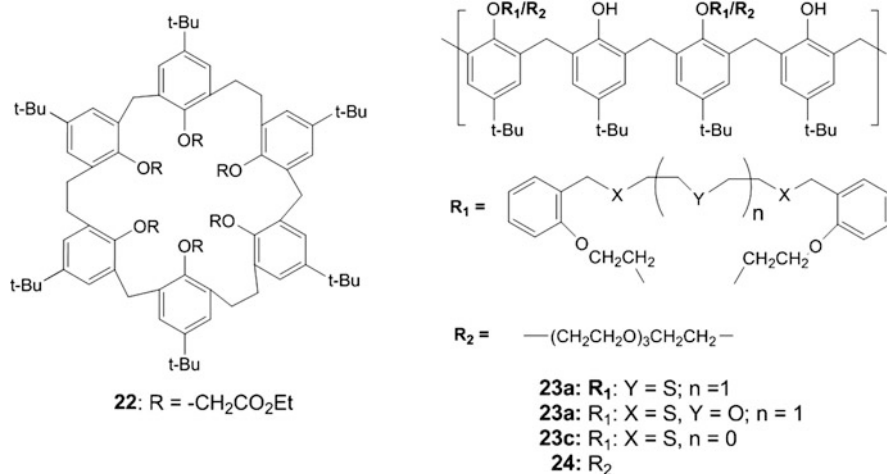


**Fig. 33.17** Left: *p*-*tert*-butyltrihomocalix[6]arene ester **22** [39] and right: bridged *p*-*tert*-butylcalix[4]arenes **23a–c** and crown **24** [40]

will summarize other analogues which more closely resemble calixarenes, and which were reported since 2001–2015. Their inclusion is presented in an approximately chronological order.

### 33.4.2.1 Calix[*n*]naphthalenes

The supramolecular complexation study of C<sub>60</sub> with two inherently chiral naphthyl ring-based hexahomotrioxacalix[3]naphthalenes **25** and **25a** was reported by Mizyed et al. [41] in 2006. The <sup>1</sup>H NMR titration study was conducted in benzene-*d*<sub>6</sub> and toluene-*d*<sub>8</sub> and only modest *K* values were obtained (Table 33.2) but the value of the *tert*-butylated **25a** was higher than that of **25**. The X-ray structure of a 2:1 (**26a**)<sub>2</sub>:C<sub>60</sub> crystal was obtained and disorder in the fullerene was clearly evident in the structure obtained (Fig. 33.18). Georghiou et al. [24a] conducted a re-investigation of the previously-reported supramolecular complexation study [24b, c] of C<sub>60</sub> with two *endo*-type calix[4]naphthalenes, **26** and **26a**. A strong solvent-dependent trend with *K* values had previously been seen, with values ranging e.g. from 295 ± 13 to 676 ± 28 to 6920 ± 330 for the 1:1 complexation behaviour of C<sub>60</sub> with **26a** going from benzene to toluene to CS<sub>2</sub>. Although a similar trend was seen with **26** no similar trend could be discerned with the same solvents using fullerite mixture. The analysis of the newly obtained data was evaluated in light of recent advances and understanding published by others of the limitations of, in particular, the absorption spectroscopic method showing that multiple equilibrium processes may be occurring which could lead to inaccurate binding constant determinations.

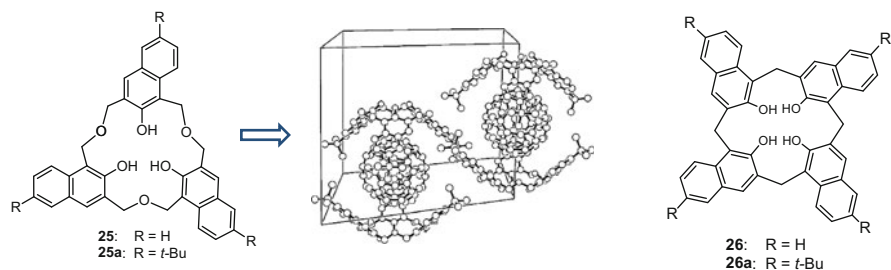
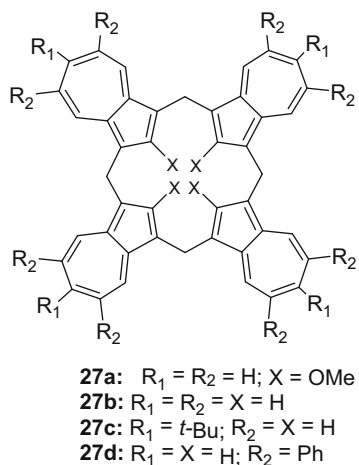


**Fig. 33.18** *Left and centre:* **25/25a** and X-ray structure of  $C_{60}:(25a)_2$  and *right:* calix[4]naphthalenes **26/26a** (Reproduced in part from Ref. [41] with permission of The Royal Society of Chemistry)

**Fig. 33.19** Calix[4]azulenes **27a–d** [43–45]



Closely-related fullerene hosts to the calixnaphthalenes are the calix[4]azulenes in which azulene moieties are linked via methylene group bridges, the first of which, **27a** ([1.1.1.1] (1,3)-2-methoxyazuleneophane) was reported by Asao [42] in 1988 but its potential supramolecular chemistry was never reported. The all-hydrocarbon analogues **27b** [43] and the *tert*-butylated **27c**, [44] however, which were reported by Lash and co-workers were recently tested for their fullerene binding potential. Due to the solubility limitations of **27b** or **27c**, a solid-state mechanochemically-generated study [45a] instead, was undertaken, in which equimolar amounts of  $C_{60}$  were hand-ground together with **27b** or **27c** and the resulting admixtures analyzed by solid-state  $^{13}C$  SP-MAS NMR. Only the *tert*-butylated **27c** showed clear evidence for the formation of a 1:1 supramolecular complex, and the experimental evidence was supported by a  $\omega B97xD/6-31G(d)$  - DFT-computational study (Fig. 33.19). A recent similar study [45b] with octaphenylcalix[4]azulene **27d** showed a similar mechanochemically-generated solid-state 1:1 complexation with  $C_{60}$ .

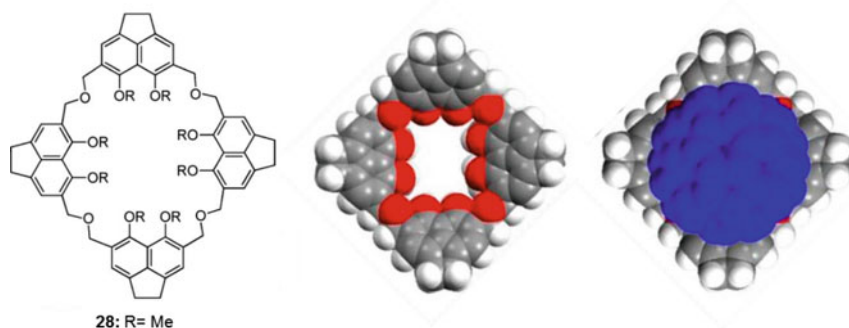


**Fig. 33.20** Octahomotetraoxacalix[4]acenaphthene (**28**) and space-filling molecular modeling structures of the top views of **28** with and without an embedded  $C_{60}$  (Figure adapted with permission from Ref. [46], Copyright 2012, American Chemical Society)

A different ‘naphthyl’-ring moiety-containing analogue is one based upon acenaphthene a molecule whose C-1 and C-10 *peri*-positions are connected by an ethylene bridge. AlHujran et al. [46] reported the synthesis of the octahomotetraoxacalix[4]acenaphthene (**28**) which was found to be capable of forming a 1:1 supramolecular complex with  $C_{60}$  (Fig. 33.20) as determined by  $^1\text{H}$  NMR titration, with a reported average  $K = 616 \pm 102 \text{ M}^{-1}$  using a “classical” fitting program based upon a 1:1 binding isotherm. [26, 47] and subjecting each of the three proton signals which had the largest chemical shift changes. However, when the same data was re-calculated using Thordarson’s global-analysis program [28] with all three of the observed chemical shift changes used above, an eightfold higher value of  $4600 \text{ M}^{-1}$  (cov. 0.0134)!

### 33.4.2.2 Triptycene-Derived Calix[6]arenes

Experimental and theoretical studies have shown that calix[6]arenes exhibit considerable conformational flexibility due to the ease of ring inversion of their aromatic units. Thus, various strategies [48] have been reported to restrict this conformational flexibility. A novel approach by Chen and coworkers have been the development of “trptycene-derived” calix[6]arenes [49–51] which incorporates two triptycene units and two phenolic groups to form what could essentially be viewed as a rigidly-enforced calix[6]arene since six phenolic groups which are joined by methylene bridging groups form an analogous cyclic array. Two pairs of triptycene-derived diastereoisomeric calix[6]arenes i.e. **29a** and **30a**; and **29b** and **30b** (**a**: R = *t*-Bu; **b**: R = Ph) were produced (Fig. 33.21). These rigid calix[6]arenes formed 1:1 complexes with  $C_{60}$  and  $C_{70}$ .  $K$  values for **29b**: $C_{60}$  of  $(6.9 \pm 0.18) \times 10^4 \text{ M}^{-1}$  and for **29b**: $C_{70}$  of  $5.2 \pm 0.20 \times 10^4 \text{ M}^{-1}$ ; and **30b**: $C_{60}$  of  $8.6 \pm 0.30 \times 10^4 \text{ M}^{-1}$  and for **30b**: $C_{70}$  of  $5.9 \pm 0.38 \times 10^4 \text{ M}^{-1}$  were determined by fluorescence quenching studies in toluene solutions.

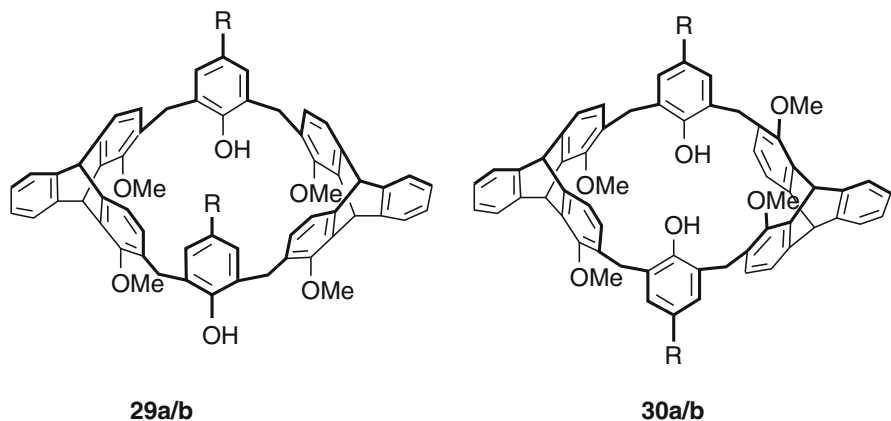


**Fig. 33.21** Triptycene-derived calix[6]arenes **29a/b** and **30a/b** (Figure adapted from Ref. [49] with the permission of John Wiley & Sons Inc, Copyright 2010)

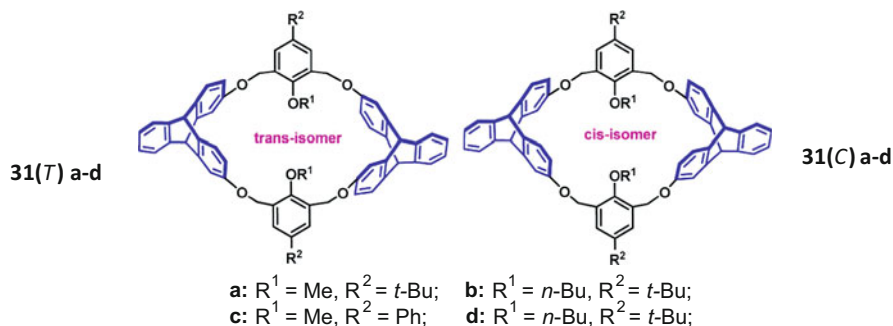
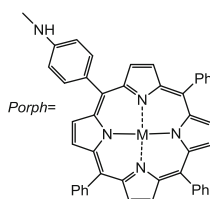
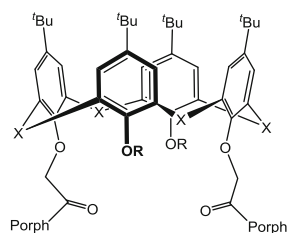
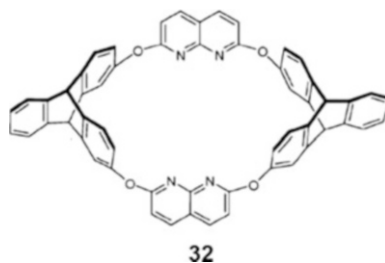


**Fig. 33.22** Triptycene-derived octahomotetraoxacalix[6]arene analogues “trans” **31(T)a–d** and “cis” **31(C)a–d** (Figure adapted with permission from Ref. [52], Copyright 2013, American Chemical Society)

Chen’s group [52] reported the synthesis and complexation studies using fluorescence quenching studies for a series of four pairs of triptycene-derived octahomotetraoxacalix[6]arene analogues, “trans” **31(T)a–d** and “cis” **31(C)a–d** (Fig. 33.22). They found that the different substituents of the macrocycles seemed to have no obvious influence on the affinity and selectivity toward fullerenes, and concluded that the fluorescence changes mainly resulted from the interaction between the macrocyclic skeleton and the fullerenes. Furthermore, in most cases, the “cis”-isomers showed a little larger affinity toward  $C_{60}$  while the “trans”-isomers had larger affinity toward  $C_{70}$ , which might be due to the relatively symmetrical cavities of the cis-isomers to fit well with the spherical  $C_{60}$  and the relative flat cavities of the trans-isomers to fit well with the oval  $C_{70}$ .

An expanded cavity triptycene-derived oxacalixarene **32** (Fig. 33.23) in which each of the central phenyl groups were replaced by 1,8-naphthyridine linking

**Fig. 33.23** Triptycene/naphthyridine-derived oxacalixarene **32** (Reproduced in part from Ref. [53] with permission of The Royal Society of Chemistry)



- 33a:** X = CH<sub>2</sub>, R = H, M = 2H  
**33b:** X = S, R = H, M = 2H  
**33c:** X = CH<sub>2</sub>, R = -CH<sub>2</sub>CO-Porph, M = 2H  
**33d:** X = S, R = -CH<sub>2</sub>CO-Porph, M = 2H  
**33a:Zn:** X = CH<sub>2</sub>, R = H, M = Zn  
**33b:Zn:** X = S, R = H, M = Zn  
**33c:Zn:** X = CH<sub>2</sub>, R = -CH<sub>2</sub>CO-Porph, M = Zn  
**33d:Zn:** X = S, R = -CH<sub>2</sub>CO-Porph, M = Zn

**Fig. 33.24** Structures of **33a–d** and **33a–d:Zn** synthesized by the Lhotak group [55]

groups to afford a single “cis” (with respect to the naphthyridine groups) isomer, was reported by Hu and Chen [53]. Stability constant values for 1:1 complexes of **32** with C<sub>60</sub> and C<sub>70</sub> by a fluorescence titrations were determined to be  $7.54 \pm 0.29 \times 10^4 \text{ M}^{-1}$ . and  $8.96 \pm 0.31 \times 10^4 \text{ M}^{-1}$ , respectively. The authors proposed that the stronger binding observed with C<sub>70</sub> could be due to a better complementarity between the “giant boat-like cavity” shape of the host and the oval shaped C<sub>70</sub> [53].

### 33.4.2.3 Thiocalix[4]arene- and Calix[4]arene-porphyrin Conjugates

Although thiacalix[4]arenes [54] are among the earliest of calixarene analogues to have been reported, a search on *SciFinder* has revealed only four recent papers dealing with solution-state binding constant studies with fullerenes. Lhotak’s group synthesized several *p-tert*-butylthiacalix[4]arene-porphyrin molecular tweezers and studied their complexation properties with C<sub>60</sub> and C<sub>70</sub>. They also compared these thiacalix[4]arenes with the corresponding calix[4]arenes (**33a–d** and corresponding zinc-porphyrins **33a–d:Zn**, Fig. 33.24). In the first report, [55] they showed that showed that 1:1 complexes with C<sub>60</sub> and C<sub>70</sub> were formed in toluene solutions and exhibited selectivity towards C<sub>70</sub> in almost all cases. When either *p-tert*-butylthiacalix[4]arene or *p-tert*-butylcalix[4]arene itself carried only a single porphyrin group much weaker association constants were observed when compared with those that contained two porphyrin groups, thus indicating a cooperative behavior of the two closely separated porphyrin units towards binding with C<sub>60</sub> or

**Table 33.3** Binding constants of  $C_{60}$  and  $C_{70}$  complexes with **33a–d** and **33a–d:Zn** Conjugates reported in Ref. [55]

Receptor	$C_{60}$	$C_{70}$
<b>33a</b>	4920	21,100
<b>33b</b>	2340	15,600
<b>33a:Zn</b>	$8600 \pm 1800$	$27,950 \pm 7,100$
<b>33b:Zn</b>	$2710 \pm 1800$	$37,400 \pm 1800$
<b>33c</b>	3510	3330
<b>33d</b>	3420	6350
<b>33c:Zn</b>	nd	nd
<b>33d:Zn</b>	$2300 \pm 470$	nd

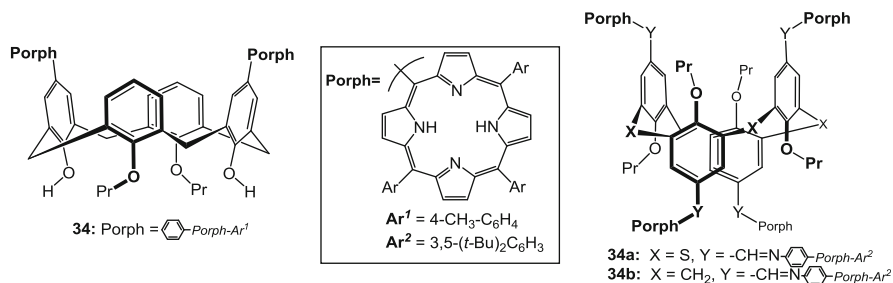


**Fig. 33.25** Structures of **34** and **34a** synthesized by the Lhotak group [57]

$C_{70}$ . Measurements were conducted by  $^1\text{H-NMR}$  titrations (Table 33.3), UV-Vis absorption spectroscopy and fluorescence quenching studies.

In their second paper dealing with the synthesis and  $C_{60}$  and  $C_{70}$  binding ability of calixarene-porphyrin conjugate receptors, [56] Lhotak reported a *cone*-conformation *bis*-porphyrin-calix[4]arene conjugate **34** (Fig. 33.25) and a corresponding mono-porphyrin. The 1:1 complexation between **34** and the mono-porphyrin-calixarene was studied in toluene and also benzene solutions by  $^1\text{H NMR}$ . Although the chemical shift changes with  $C_{60}$  were too small to allow accurate  $K_{\text{assoc}}$  determinations, a fourfold increase in the binding constants ( $4500 \pm 600$  vs  $1100 \pm 200 \text{ M}^{-1}$ ) could be determined with  $C_{70}$  for the *bis*-porphyrin **34** versus the mono-porphyrin analogue in benzene, thus showing a selectivity of the *bis*-porphyrin deriv. towards  $C_{70}$ . In toluene, no corresponding significant difference could be discerned ( $1000 \pm 200$  vs  $1300 \pm 500 \text{ M}^{-1}$ ). Solubility limitations however, precluded accurate determinations by UV-Vis spectroscopy.

A third contribution [57] from Lhotak's group dealing with thiacalixarene-porphyrin and also their corresponding calix[4]arene-porphyrin conjugate molecular tweezers, reported the synthesis of four new receptors. These receptors were produced starting from tetraformyl calixarenes and aminoporphyrin moieties which led to upper-rim *1,3*-alternate tetraporphyrin derivatives of the corresponding *O*-

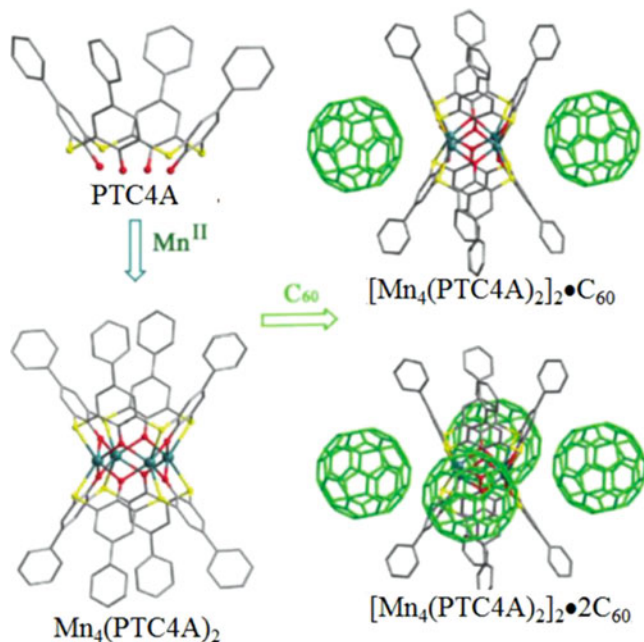


**Fig. 33.26** The structures of *p*-phenylthiacalix[4]arene (“PTC4A”, **35**) its “Mn<sub>4</sub>-hinged” Mn<sub>4</sub>(PTC4A)<sub>2</sub>, and X-ray structures of ([Mn<sub>4</sub>(PTC4A)<sub>2</sub>]<sub>2</sub>•C<sub>60</sub>), ([Mn<sub>4</sub>(PTC4A)<sub>2</sub>]<sub>2</sub>•2C<sub>60</sub>) complexes with C<sub>60</sub> (Figure adapted in part from Ref. [58] with permission of The Royal Society of Chemistry)

propoxythia- and calix[4]arenes, **34a** and **34b**, respectively (Fig. 33.25). All three of the phenyl moieties in the porphyrin derivatives of this group consisted of the corresponding 3,5-di-*tert*-butylated analogue of the porphyrin group shown previously in Fig. 33.22. Using both <sup>1</sup>H-NMR and UV/vis titration experiments (which were in good agreement), these compounds were shown to form 1:1 complexes with C<sub>60</sub> and C<sub>70</sub> in both benzene and toluene solution. The binding abilities of **34a** and **34b** towards C<sub>60</sub> were modest (~2300 vs 3600 M<sup>-1</sup> in benzene, and 2000 vs 2200 in toluene) but with C<sub>70</sub>, the binding constants were tenfold higher (36,000 vs 55,000 in benzene, and 20,000 vs 10,000 M<sup>-1</sup> in toluene). The *bis*-porphyrin-functionalized receptors therefore were highly selective for C<sub>70</sub>, as was also noted with their other receptors.

Bi et al. [58] obtained X-ray structures of three “Mn<sub>4</sub>-hinged” bi-tetra-*p*-phenylthiacalix[4]arenes (“PTC4A” **35**, Fig. 33.26) which could accommodate C<sub>60</sub> and C<sub>70</sub> in the solid state. The noncovalent assemblies ([Mn<sub>4</sub>(PTC4A)<sub>2</sub>]<sub>2</sub>•C<sub>60</sub>), ([Mn<sub>4</sub>(PTC4A)<sub>2</sub>]<sub>2</sub>•2C<sub>60</sub>) and ([Mn<sub>4</sub>(PTC4A)<sub>2</sub>]<sub>2</sub>•C<sub>70</sub>), involve π–π interactions between the “dumbbell-like” Mn<sub>4</sub>(PTC4A)<sub>2</sub> units and fullerenes (Fig. 33.26). The “host” Mn<sub>4</sub>(PTC4A)<sub>2</sub> has a small “waist” formed by the -O-Mn-O- units, and four curved surfaces as the fullerene binding sites.



### 33.4.2.4 Calixpyrroles

Among the earliest discovered nitrogen-containing calixarene analogues are the calixpyrroles which were reviewed by Vysotsky, Saadiou and Böhmer in Chap. 13 of *Calix 2001* [59]. The anion-binding properties of calix[4]pyrrole (**36**) itself has been extensively studied, but not with fullerenes. Sessler and Jeppesen [60] and coworkers however in 2006, have shown that the octa-*S*-propylated tetrathiafulvalene-(TTF) functionalized calixpyrrole **37** (PrS-TTF-CAP) undergoes a change in conformation from the 1,3-alternate form normally found with **36** itself to a cone conformation when chloride ion is added. As a result, it was shown that when  $C_{60}$  is added to a solution of **37**: $Cl^-$  as its tetrabutylammonium (TBA) salt, in dichloromethane (DCM), a color change and a strong CT band centred at around  $\lambda_{max} = 725$  nm formed. Subsequent UV-Vis titration experiments established that a 2:1 complex i.e.  $C_{60}:(37a:Cl^-)_2$  formed in the DCM solution. Binding constants for the two-step equilibria at 298 K were calculated as  $K_1 = 2.3 \times 10^3 M^{-1}$  and  $K_2 = 1.3 \times 10^4 M^{-1}$  (Fig. 33.27).

Since  $Li^+ @ C_{60}$  has been shown to be a more effective electron acceptor than pristine  $C_{60}$  Fukuzumi et al. [61] reported their study with the TTF-calix[4]pyrroles PrS-TTF-C4P (**37**) and Benzo-TF-C4P (**37a**) with  $Li^+ @ C_{60}$ . They showed that a careful choice of added cations or anions enabled the control of the direction of the

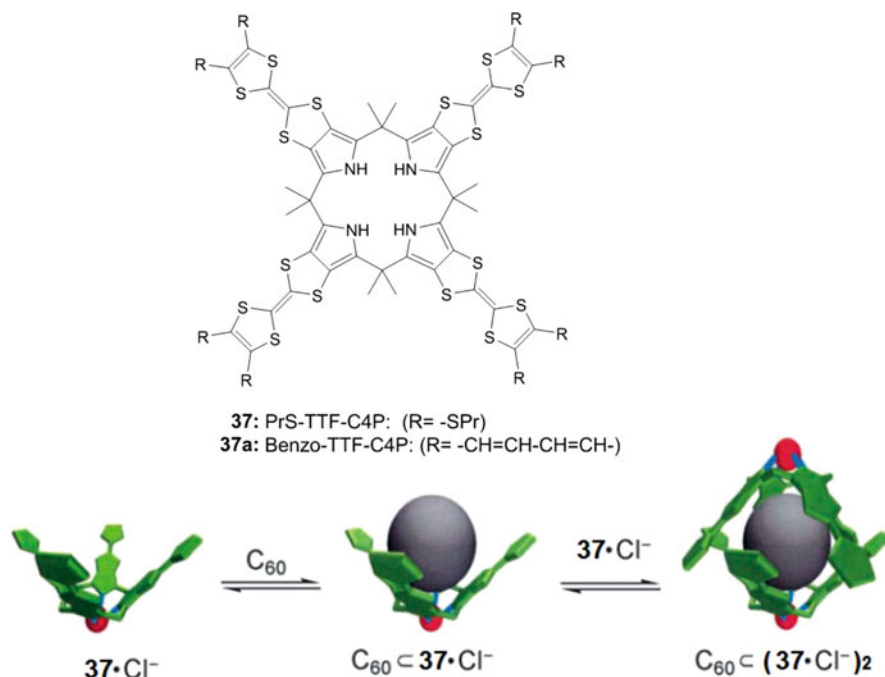


**Fig. 33.27** Top: structures of **37** and **37a** [61]. Bottom: representation of the equilibria for the encapsulation of  $C_{60}$  by the cone conformer **37**· $Cl^-$  /TBA salt in DCM at 298 K (Figure adapted with permission from Ref. [60], Copyright 2011, American Chemical Society)

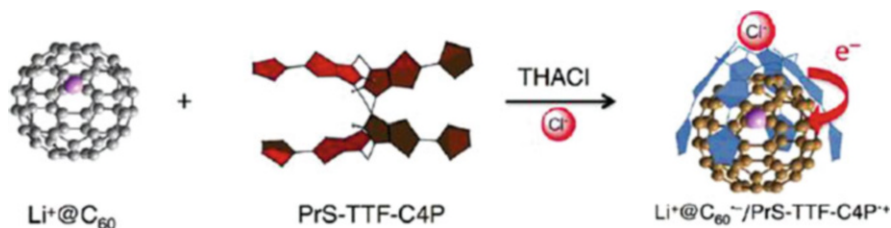


**Fig. 33.28** Representation of the stabilization of the radical ion pair involving the [PrS-TTF-CAP<sup>•+</sup>] host and [Li<sup>+</sup> @ C<sub>60</sub><sup>•-</sup>] guest by the addition of the Cl<sup>-</sup> (from THACl) (Figure adapted with permission from Ref. [61], Copyright 2011, American Chemical Society)

resulting ground-state thermal electron-transfer (ET) process. Thus, when **37** in benzonitrile was mixed with [Li<sup>+</sup> @ C<sub>60</sub>]PF<sub>6</sub> there was no evidence of any ET. Upon the addition of tetra-*n*-hexylammoniumchloride (THACl) however, the appearance of an absorption band at  $\lambda_{\text{max}} = 1035 \text{ nm}$  appeared which was ascribed to the reduced neutral [Li<sup>+</sup> @ C<sub>60</sub><sup>•-</sup>] radical ion species. The role of the Cl<sup>-</sup> was presumably, as shown above, to change the conformation of the host molecule to a cone conformer which enabled the radical ion pair involving the [PrS-TTF-CAP<sup>•+</sup>] host and [Li<sup>+</sup> @ C<sub>60</sub><sup>•-</sup>] guest to be stabilized (Fig. 33.28). A 1:1 binding constant in benzonitrile for the Cl<sup>-</sup> titration was  $\sim 1.9 \times 10^4 \text{ M}^{-1}$ . Addition of tetraethylammonium chloride (TEACl) caused the absorbance at 1035 nm to decrease as a function of increasing TEACl, presumably the TEA cation displaced the [Li<sup>+</sup> @ C<sub>60</sub><sup>•-</sup>] from the cavity. A similar set of observations were made with the corresponding Benzo TTF-C4P complexes. A single-crystal X-ray structure of the 1:1 complex of **37** with C<sub>60</sub>@Li<sup>+</sup> was also reported.

The supramolecular binding and CT properties from a detailed spectroscopic and computational (PM3) study of C<sub>60</sub> and C<sub>70</sub> with *meso*-octamethylcalix[4]pyrrole (**38**) and with several other non-macrocyclic electron acceptors, was conducted by the Bhattacharya group in different solvents (toluene, chloroform, 1,2-dichlorobenzene and benzonitrile) [62]. In all of the solvents tested, selectivity for 1:1 complexation of **38** with C<sub>70</sub> over C<sub>60</sub> was seen:  $K_{\text{C70}}/K_{\text{C60}}$  ratios ranged from low to high values of 3.10 (in benzonitrile) to 6.90 in 1,2-ODCB (see Table 33.1). The authors concluded among other points (i) that the CT complexation between **38** and C<sub>60</sub> and C<sub>70</sub> was facilitated in the solvent having the highest dielectric constant; (ii) that the ground states of the complexes were neutral; and (iii) that the higher binding constants with C<sub>70</sub> compared to C<sub>60</sub> suggested a size-selective and *side-on* interaction between C<sub>70</sub> and **38**, and (iv) that the CT interaction resulting between **38** and C<sub>70</sub> in chloroform plays a very important role.

### 33.4.2.5 Azacalix[*n*]pyridines

Azacalix[*m*]arene[*n*]pyridines and calix[*n*]pyridines are relative newcomers to the list of macrocycles that are analogues of the classic calix[*n*]arenes and which have

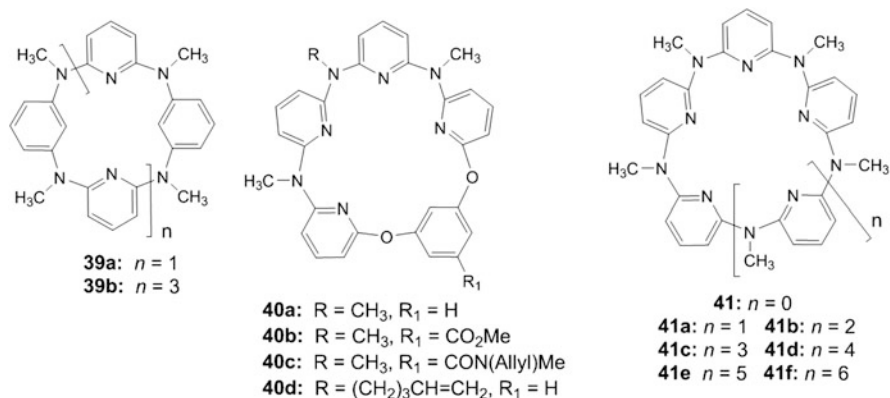


Fig. 33.29 Azacalix[ $m$ ]arene[ $n$ ]pyridines **39a/b** (left); **40a–d** (centre) and **41a–f** [64–67]

been shown to form supramolecular complexes with fullerenes. Mei-Xiang Wang and coworkers [63] synthesized azacalix[2]arene[2]pyridine ( $n = 1$ ) (**39a**) and azacalix[4]arene[4]pyridine ( $n = 3$ ) (**39b**) (Fig. 33.29). They found that whereas **39b** formed a 1:1 complex in toluene with  $\text{C}_{60}$ , the smaller **39a** did not. From a detailed analysis of the data from the fluorescence titration in toluene, a high stability constant ( $K_s$ ) value of  $70,680 \pm 2060 \text{ M}^{-1}$  was determined for the **39b**: $\text{C}_{60}$  complex. A similar treatment for the **39b**: $\text{C}_{70}$  complex formation gave an even higher  $K_s$  value of  $136,620 \pm 3770 \text{ M}^{-1}$ . The authors calculated their stability constants assuming both static and dynamic quenching of the fluorescence. No significant chemical shift changes however could be detected by either  $^1\text{H}$ - or  $^{13}\text{C}$ -NMR. Single-crystal X-ray structures revealed a “heavily twisted” 1,3-alternate conformation for **39a** and a “double-ended spoon-shaped” 1,2,3-partial cone conformation for **39b**. Since no new absorption or emission signals were observed in either case, no CT was presumed to account for the strong complexation seen with these fullerenes.

A series of  $N,O$ -bridged calix[1]arene[4]pyridines e.g. **40a–d** (Fig. 33.29) which adopted distorted 1,3-alternate conformations in the solid state were also synthesized by Wang’s group by a [2 + 3] fragment coupling approach [64]. These new macrocyclic compounds which adopted distorted 1,3-alternate conformations in the solid state, were powerful host molecules which were able to form 1:1 complexes with  $\text{C}_{60}$  in toluene. Binding constants were measured by fluorescence titrations and ranged from:  $35,113 \pm 106$  (**40b**);  $40,963 \pm 757$  (**40a**);  $44,342 \pm 1479$  (**40c**) to  $49,494 \pm 1581 \text{ M}^{-1}$  for (**40d**). The presence of an electron-withdrawing ester group on the upper rim decreased the electron density of the benzene ring, leading to the weakest binding toward  $\text{C}_{60}$ . These calix[1]arene[4]pyridine compounds were the first examples of the odd-numbered calixaromatics with mixed heteroatom bridges and mixed aromatic components.

The all-pyridine  $N$ -methyl-bridged azacalix[ $n$ ]arenes **41–41 g** ( $n = 4–10$ ) [65–67] were synthesized by Wang’s group in good yields, by Pd-catalyzed

**Table 33.4** Binding constants ( $K$ ) reported in Refs. [63–68], for calixarene- $C_{60}$ - and/or  $C_{70}$  complexation studies as determined by fluorescence titrations in toluene at 298 K

Compound	Azacalix[ $m$ ]-arene[ $n$ ] pyridine (solvent)	$KM^{-1} C_{60}$	$KM^{-1} C_{70}$	Reference
<b>39a</b>	$m = 2; n = 2$	No complexation	No complexation	[63]
<b>39b</b>	$m = 4; n = 4$	$70,680 \pm 2060$	$136,620 \pm 3770$	
<b>40a</b>	$m = 1; n = 4^a$	$40,963 \pm 757$	Not reported	[64]
<b>40b</b>	$m = 1; n = 4^a$	$35,113 \pm 106$		
<b>40c</b>	$m = 1; n = 4^a$	$44,342 \pm 1479$		
<b>40d</b>	$m = 1; n = 4^a$	$49,494 \pm 1581$		
<b>41</b>	$n = 0$ (azacalix[4]pyridine)	No complexation	No complexation	[65–67]
<b>41a</b>	$n = 1$ (azacalix[5]pyridine)	$(2.60 \pm 0.11) \times 10^4$	$(11.7 \pm 0.02) \times 10^4$	
<b>41b</b>	$n = 2$ (azacalix[6]pyridine)	$(6.62 \pm 0.22) \times 10^4$	$(6.24 \pm 0.19) \times 10^4$	
<b>41c</b>	$n = 3$ (azacalix[7]pyridine)	$(3.30 \pm 0.08) \times 10^4$	$(7.23 \pm 0.19) \times 10^4$	
<b>41d</b>	$n = 4$ (azacalix[8]pyridine)	$(4.60 \pm 0.16) \times 10^4$	$(10.9 \pm 0.02) \times 10^4$	
<b>41e</b>	$n = 5$ (azacalix[9]pyridine)	$(3.10 \pm 0.08) \times 10^4$	$(8.23 \pm 0.25) \times 10^4$	
<b>41f</b>	$n = 6$ (azacalix[10]pyridine)	$(3.03 \pm 0.08) \times 10^4$	$(13.0 \pm 0.03) \times 10^4$	
<b>43a</b>	$(n = 4)_2$ (bisazacalix[4]pyridine) <sup>a</sup>	$(5.52 \pm 0.16) \times 10^4$	$(5.37 \pm 0.11) \times 10^4$	[68]
<b>43b</b>	$(n = 7)_2$ (bisazacalix[7]pyridine) <sup>a</sup>	$(7.94 \pm 0.22) \times 10^4$	$(10.7 \pm 0.38) \times 10^4$	

<sup>a</sup>Structures are shown in Figs. 33.30 and 33.31

macrocyclic fragment coupling reactions between  $\alpha,\omega$ -dibrominated and  $\alpha,\omega$ -diaminated linear oligomers. The binding properties of these new macrocycles with  $C_{60}$  and  $C_{70}$  in toluene were determined by detailed fluorescence titration studies. Strong 1:1 complexes with  $C_{60}$  and  $C_{70}$  were formed with these new macrocyclic hosts in a size-selective manner and their binding constant data is summarized in Table 33.4.

Starting from the mono-*N*-allyl azacalix[4]- and azacalix[7]pyridines **42a** and **42b**, the corresponding bisazacalix[4]pyridine **43a** and bisazacalix[7]pyridine **43b** respectively were each synthesized by including a disulfide linker (Fig. 33.30) [68]. These bis-macrocyclic compounds were also strong receptors and formed 1:1 complexes with  $C_{60}$  and  $C_{70}$ , with binding constants up to  $107,000 M^{-1}$  determined by fluorescence quenching titrations (see Table 33.4). The authors concluded that the cooperation of the two mono-macrocycles improved their binding affinity to the fullerenes.

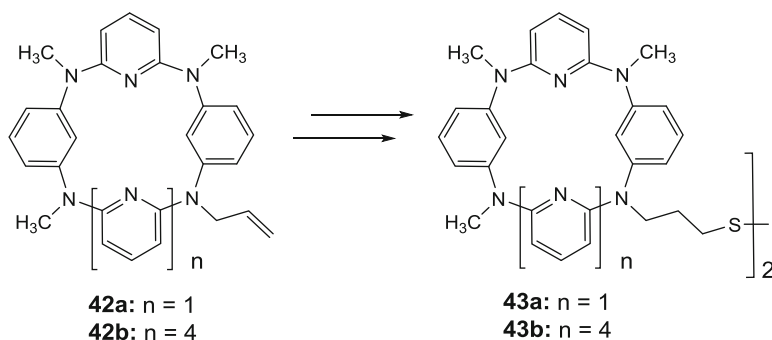


**Fig. 33.30** Structures of bisazacalix[ $n$ ]pyridines **43a** and **43b** and their synthetic precursor compounds **42a** and **42b**, respectively [68]

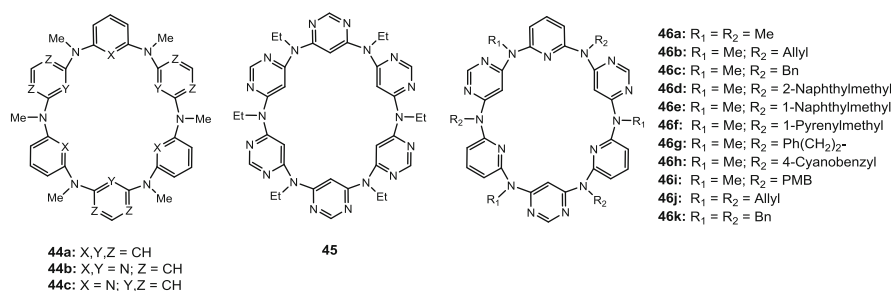


**Fig. 33.31** Structures of azacalix[6]aromatics **44a-c**, azacalix[6]pyrimidine **45**, and azacalix[3]pyridine[3]pyrimidines **46a-k** [69]

### 33.4.2.6 Azacalix[ $n$ ]pyridine[ $m$ ]pyrimidines

Wang's group has also synthesized a series of different azacalix[6]aromatic compounds **44a-c**; **45**, and **46a-k** (Fig. 33.31) [69] containing different combinations of benzene, pyridine, and pyrimidine rings, and various substituents on the bridging nitrogen atoms. These compounds, including 1,3,5-alternate-azacalix[3]pyridine [3]-pyrimidines [70], were synthesized conveniently in moderate to good yields. Single-crystal X-ray structures show that these macrocycles adopt symmetric and highly distorted 1,3,5-alternate conformations in the solid state depending on the aromatic ring building units. In solution, they exist as a mixture of conformers that undergo rapid interchanges relative to the NMR time scale. All macrocycles formed 1:1 complexes with  $\text{C}_{60}$  and  $\text{C}_{70}$  in toluene with binding constants up to  $7.28 \times 10^4 \text{ M}^{-1}$  (Table 33.5). Single-crystal X-ray 1:1, 1:2, and 2:1 host:guest complexes **46f**: ( $\text{C}_{60}$ ); **44c**:( $\text{C}_{60}$ )<sub>2</sub>; (**46b**)<sub>2</sub>: $\text{C}_{60}$ ; (**46j**)<sub>2</sub>: $\text{C}_{60}$  and (**46j**)<sub>2</sub>: $\text{C}_{70}$  were obtained which revealed that multiple  $\pi$ - $\pi$  and CH- $\pi$  interactions between the concave host molecules and convex fullerenes were presumed to both contribute a joint driving force to the formation of the complexes.

**Table 33.5** Binding constants for the 1:1 complexation of azacalix[6]aromatics **44a–c**, azacalix[6]pyrimidine **45**, and azacalix[3]pyridine[3]pyrimidines **46a–k** with C<sub>60</sub> and C<sub>70</sub> at 298 K in toluene<sup>a</sup>

Entry	Macrocyclic host	$K_a$ (1:1 complexation with C <sub>60</sub> )	$K_a$ (1:1 complexation with C <sub>70</sub> )
1	<b>44a</b>	$(3.05 \pm 0.06) \times 10^4$	$(7.06 \pm 0.15) \times 10^4$
2 <sup>b</sup>	<b>44b</b>	$(6.62 \pm 0.22) \times 10^4$	$(6.24 \pm 0.19) \times 10^4$
3	<b>45</b>	$(4.44 \pm 0.13) \times 10^4$	$(6.96 \pm 0.19) \times 10^4$
4	<b>44c</b>	$(5.22 \pm 0.11) \times 10^4$	$(7.27 \pm 0.02) \times 10^4$
5 <sup>c</sup>	<b>46a</b>	$(4.93 \pm 0.10) \times 10^4$	$(6.66 \pm 0.17) \times 10^4$
6	<b>46b</b>	$(6.36 \pm 0.09) \times 10^4$	$(6.52 \pm 0.15) \times 10^4$
7	<b>46c</b>	$(5.86 \pm 0.11) \times 10^4$	$(5.86 \pm 0.18) \times 10^4$
8	<b>46d</b>	$(6.56 \pm 0.15) \times 10^4$	$(6.08 \pm 0.16) \times 10^4$
9	<b>46e</b>	$(5.70 \pm 0.11) \times 10^4$	$(5.79 \pm 0.11) \times 10^4$
10	<b>46f</b>	$(7.28 \pm 0.21) \times 10^4$	$(6.56 \pm 0.20) \times 10^4$
11	<b>46g</b>	$(5.59 \pm 0.15) \times 10^4$	$(6.26 \pm 0.14) \times 10^4$
12	<b>46h</b>	$(6.28 \pm 0.15) \times 10^4$	$(6.55 \pm 0.11) \times 10^4$
13	<b>46i</b>	$(6.26 \pm 0.14) \times 10^4$	$(5.92 \pm 0.11) \times 10^4$
14	<b>46j</b>	$(6.29 \pm 0.07) \times 10^4$	$(6.72 \pm 0.10) \times 10^4$
15	<b>46k</b>	$(6.15 \pm 0.09) \times 10^4$	$(6.25 \pm 0.12) \times 10^4$

Table adapted with permission from Ref. [69], Copyright 2014, American Chemical Society  
Association constants were calculated on the fluorescence titration data with the Hyperquad 2000 program

<sup>a</sup>Structures shown in Figs. 33.30 and 33.31

### 33.4.2.7 Calix[*n*]imidazolium Salts

A new class of nitrogen heterocyclic ring based calixarene analogues, the calix[4]imidazolium **47a** and calix[5]imidazolium **47b** salts has been reported by Chun et al. [71]. When an aqueous solution of the pentabromide salt of **47b** was boiled with C<sub>60</sub> for 2 h the <sup>13</sup>C- NMR signal at 167.8 ppm in the resulting solution showed the presence of C<sub>60</sub>. The fluorescence emission spectrum of the C<sub>60</sub> in an aqueous solution of **47b** showed enhancement due to the calix[5]imidazolium π<sup>+</sup> to the C<sub>60</sub> π system. The protons of **47b** except for the imidazolium (C-H)<sup>+</sup> are shifted down-field. Therefore, the authors concluded, the interaction with the fullerene occurs at the double bond of the imidazolium ring, as shown from the resolution identity DFT calculated optimized structure shown in Fig. 33.32.

### 33.4.2.8 Ag(I) N-Heterocyclic Carbene-Bridged Calixarene

The highest reported binding constant to date for a mono-macrocyclic calixarene or calixarene analogue receptor and C<sub>60</sub> is  $3.48 \times 10^5 \text{ M}^{-1}$  which was ascribed to the Ag(I) N-heterocyclic carbene-bridged calixarene **48** synthesized by Quin et al. [72]. This binding constant for the 1:1 complexation was determined by fluorescence quenching titration study of in acetonitrile at 298 K (Fig. 33.33).

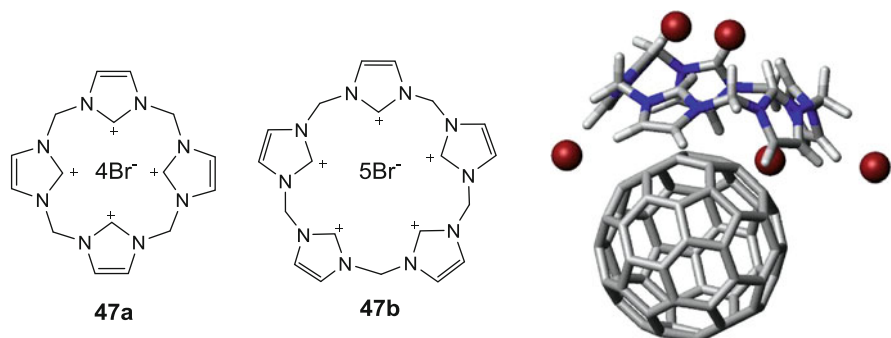
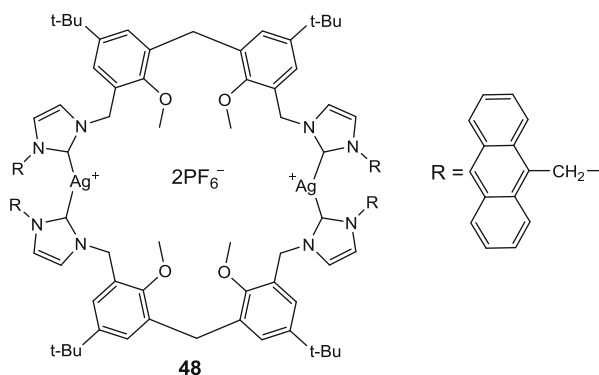


**Fig. 33.32** *Left and centre*: structures of calix[4]- and calix[5]imidazolium bromide salts **47a** and **47b** (Figure of the DFT optimized structure of **47b** reprinted by permission from Macmillan Publishers Ltd: from *Nature Communications*, Ref. [71], Copyright (2013))

**Fig. 33.33** Structure of the Ag<sup>+</sup>-NHC bridged calixarene **48** [72]



### 33.5 Complexation by Calixarene Dimers: Towards Complete Inclusion of Fullerenes

Following up on their previous work [73] with covalently-linked double calix[5]arenes, Fukazawa and coworkers [74] reported the fullerene complexation of other related double calix[5]arene receptors in a series of studies published in 2001–2010. A fullerene (Fig. 33.34) receptor which they produced was based on a silver-cation assisted self-assembled pair of upper-rim mono-2,2'-bispyridyl-functionalized tetra-*p*-methylcalix[5]arenes **49**. The cavity thus produced formed quaternary complexes C<sub>60</sub>@**49**:Ag<sup>+</sup>:**49** and C<sub>70</sub>@**49**:Ag<sup>+</sup>:**49** with the respective fullerenes in 1,1,2,2-tetrachloroethane (“TCE”) and which were established by using ESI MS. The relative intensities of the mass signals also suggested a preference for C<sub>60</sub> over C<sub>70</sub>. Later, these authors prepared a “double” calix[5]arene derivative **50** which was based upon linking two molecules of **49** covalently via their bipyridines. As measured by UV-Vis titration, treatment of C<sub>60</sub> with the complex of **50** with [Cu

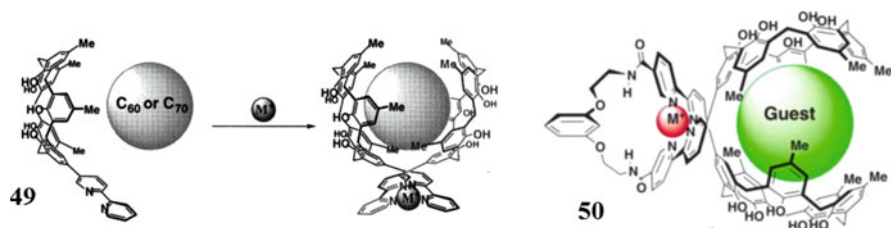


**Fig. 33.34** (a) The formation of the  $\text{Ag}^+$ -assisted ternary self-assembled receptor of two molecules of **49** with  $\text{C}_{60}$  or  $\text{C}_{70}$ . (b) Formation of  $\text{C}_{60}@\mathbf{50}\cdot[\text{Cu}^+]$  complex (Figures taken from Ref. [73] (left) Copyright 2000 and Ref. [74] (right), Copyright 2001 with permission from Elsevier)

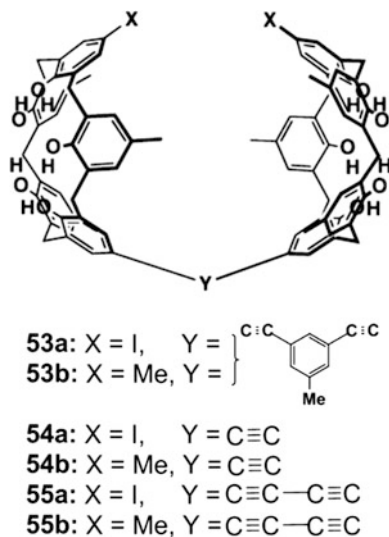
$^+\text{Me}(\text{CN})_4\text{PF}_6^-$  formed the  $\text{C}_{60}@\mathbf{50}\cdot[\text{Cu}^+]\text{PF}_6^-$  complex preferentially compared with the corresponding complex formed with  $\text{C}_{60}$  ( $K = 3800$  vs  $950 \text{ M}^{-1}$ ). The reverse was found when **50** itself was treated with  $\text{C}_{60}$  or  $\text{C}_{70}$  ( $K = 250$  vs  $98 \text{ M}^{-1}$ ).

Fukazawa's group synthesized a highly sensitive double calix[5]arene fullerene sensor [75] using a different linking group. The linking was formed via a Suzuki-Miyaura coupling of methyl-3,5-diethynylbenzoate to the same mono-*p*-iodo-tetra-*p*-methylcalix[5]arene which was used previously to form **49**. The double calix[5]arene thus formed was then elaborated at the carboxylate moiety with 4-methyl-4-methylamino-2,2'-bispyridyl and subsequent reaction with  $\text{Re}(\text{CO})_4\text{Cl}$ . The resulting  $\text{Re}(\text{CO})_3\text{Cl}(\text{bpy})$  **51** product and another formed with a  $\text{Re}(\text{CO})_3\text{Cl}(\text{bpy})$ -functionalized single calix[5]arene **52** were soluble in toluene and both showed strong orange luminescence when subjected to 365 nm light and which was quenched immediately when  $\text{C}_{60}$  or  $\text{C}_{70}$  was added to the respective solutions. Detailed analysis of the quenching of the steady-state luminescence at 400 nm using Stern-Volmer plots and the measured luminescence lifetimes with  $\text{C}_{60}$  and  $\text{C}_{70}$  gave binding constants, respectively, of  $7.1 \times 10^4 \text{ M}^{-1}$  and  $3.6 \times 10^5 \text{ M}^{-1}$  for **51** and only  $1100 \text{ M}^{-1}$  for **52** with  $\text{C}_{60}$  [75]. Mechanisms for the quenching processes occurring were also described by the authors.

The synthesis of a series of six other covalently-linked double calix[5]arenes i.e. **53a/b**; **54a/b** and **55a/b** (Fig. 33.35) and their complexation properties with  $\text{C}_{60}$  and  $\text{C}_{70}$  in different organic solvents and by UV-Vis spectroscopy were reported in 2006 by Haino et al. [76]. The binding abilities of the double calixarenes were much greater than the corresponding single calix[5]arenes. A solvent effect on the fullerene complexation was also clearly observed. The  $K$  values decreased in all cases with the highest values for both  $\text{C}_{60}$  and  $\text{C}_{70}$  being observed in the following order of solvents toluene  $>$   $\text{CS}_2$   $>$  ODCB which is in the same order for the highest to lowest solubilities of  $\text{C}_{60}$ . The binding abilities of **53a** and **53b** in which the two calix[5]arenes were covalently linked via a Suzuki-Miyaura coupling with 3,5-diethynyltoluene, for both  $\text{C}_{60}$  and  $\text{C}_{70}$  were  $7.60 \times 10^4$  and  $16.3 \times 10^5 \text{ M}^{-1}$  toluene solution respectively. The other double calixarenes reported in this study had much lower  $K$  values which were in the  $9 \times 10^3$  to  $3 \times 10^3 \text{ M}^{-1}$  range for  $\text{C}_{60}$  and in a broader range of  $9.1 \times 10^4$  to  $5.5 \times 10^3 \text{ M}^{-1}$  range for  $\text{C}_{70}$ . Higher binding selectivity toward  $\text{C}_{70}$  was observed for all of the double-calix[5]arenes, with a



**Fig. 33.35** Structures of double calix[5]arenes **53a/b-54a/b** and **55/55a** from the Fukazawa group (Figure adapted taken from Ref. [77] Copyright 2006 with permission from Elsevier)



tenfold selectivity for the  $C_{70}$  to  $C_{60}$  being highest in toluene. The structures of the complexes formed were investigated using  $^1\text{H}$ - and  $^{13}\text{C}$ -NMR and molecular mechanics calculations studies [76].

A new double *syn* isomer calix[5]arene **56** linked by a pair of 1,3-diyne linking groups was shown to [77] successfully extract higher fullerenes and with high  $K$  values i.e.  $9.0 \times 10^4 \text{ M}^{-1}$ ,  $11 \times 10^4 \text{ M}^{-1}$  and  $2 \times 10^4 \text{ M}^{-1}$ , for  $C_{76}$ ,  $C_{78}$  and  $C_{84}$  respectively, from fullerene mixtures in 1,1,2,2-tetra-chloroethane (TCE). By comparison, lower binding constants of  $9.7 \times 10^3 \text{ M}^{-1}$  and  $2.9 \times 10^4 \text{ M}^{-1}$  were measured for  $C_{60}$  and  $C_{70}$  respectively, in this solvent. A much lower binding ability for **55b** with all five of these fullerenes in the same solvent were also noted. Elevation of the temperature to  $>100^\circ\text{C}$  stimulates the conformational change of **56** to its *anti* isomer, **56a** which results in the liberation of the captured higher fullerenes (Fig. 33.36). Another study by the same authors [78] reported comparisons of the binding abilities of double calix[5]arenes **53b**, **54b** and **55b** with the same suite of fullerenes, this time in toluene and  $\text{CS}_2$ . Higher association constants were seen in toluene than in  $\text{CS}_2$ . In particular, with  $C_{76}$  and  $C_{78}$  in toluene, binding constants were, according to the authors “extremely high” and were of the order of  $\sim 2$  to  $3 \times 10^5 \text{ M}^{-1}$ . However, in the earlier study in TCE, double calix[5]arene **55b** had higher binding constants for  $C_{76}$  and  $C_{78}$  ( $9.0 \times 10^4$  and  $1.1 \times 10^5 \text{ M}^{-1}$ , respectively) than the corresponding binding constants for  $C_{76}$  and  $C_{78}$  ( $4.2 \times 10^4$  and  $2.8 \times 10^4 \text{ M}^{-1}$ , respectively) with **56b** in toluene. As with the previous study, the binding abilities of simple calix[5]arenes also decreased with increasing fullerene size. The authors concluded that linking two calix[5]arenes with the covalent bonds created the larger cavities which could accommodate the higher fullerenes. The structure of the host-guest complex of **53b** and  $C_{76}$  was interpreted based upon the  $^{13}\text{C}$ -NMR CIS values seen. The carbons of the polar end of  $C_{76}$  shifted upfield more

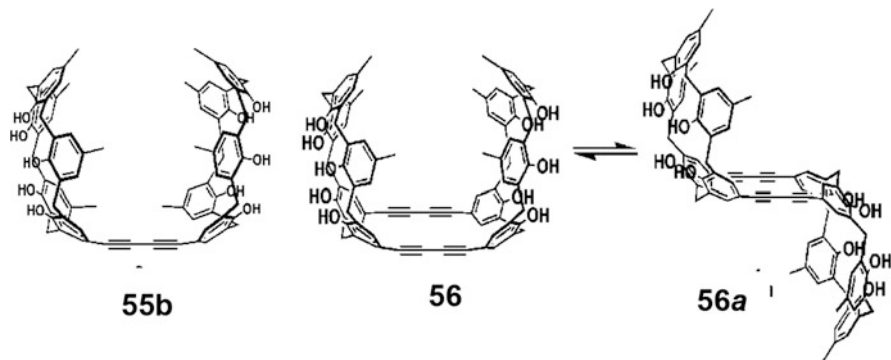
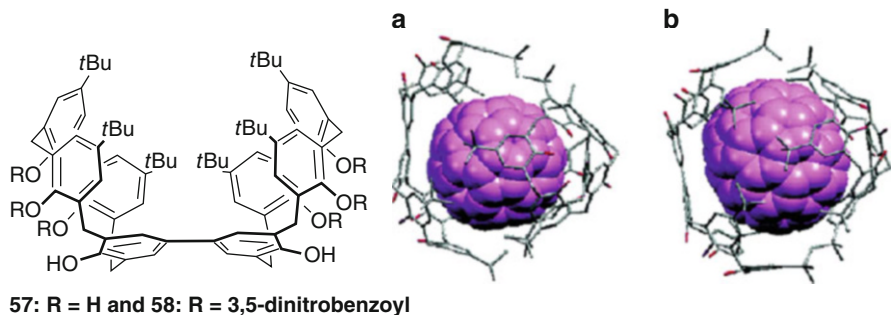


**Fig. 33.36** Structures of double calix[5]arenes **55b** and **56-56a** from the Fukazawa group (Figures of **56** and **56a** adapted with permission from Ref. [77], Copyright 2006, American Chemical Society)

than the other carbons in the host-guest complex, indicating that these polar carbons reside most deeply inside the cavity of **53b**.

Another wide-rim “head-to-head” molecular tweezer **57** was synthesized via **58** and studied for  $C_{60}$  and  $C_{70}$  complexation by Prados and coworkers [79] (Fig. 33.36). The only other examples of such “head-to-head” bicalix[ $n$ ]arenes ( $n = 4, 5, 6, 8$ ) directly connected through their wide rims, were reported previously by Neri et al. [80] and Gutsche and coworkers [81]. Among those receptors, only the *de-tert*-butylated bicalix[5]arene described by Gutsche [81] formed 1:1 fullerene complexes with relatively weak  $K$  values as determined by UV – vis titrations of  $43 \text{ M}^{-1}$  for  $C_{60}$  and  $233 \text{ M}^{-1}$  for  $C_{70}$  in  $\text{CS}_2$ , with a lower selectivity toward  $C_{70}$ . The UV – vis titration data of **57** with  $C_{60}$  and  $C_{70}$  in toluene solution was analyzed using a global multivariate factor analysis [82a–c] for a guest/host stoichiometry of 1:2 and considering the parent fullerene and its complex as a coloured species. The  $K$  values for the formation of a 1:2 complex were determined to be  $\log K_{12} = 4.2 \pm 0.2$  and  $5.1 \pm 0.4$  for  $C_{60}$  and  $C_{70}$ , respectively. If based upon a 1:1 binding model, the corresponding  $K$  values would only be  $\log K_{11} = 1.9 \pm 0.2$  and  $2.3 \pm 0.3$  for  $C_{60}$  and  $C_{70}$ . Thus, the authors concluded that **57** bound  $C_{70}$  about eight times more strongly than  $C_{60}$ . This behavior differs markedly from that reported by Gutsche’s group for their bicalix[5]arene, however, it should be noted that they used  $\text{CS}_2$  as solvent whereas with **57** toluene was used. Prados proposed that the selectivity toward  $C_{70}$  could arise from a better fit of the oval-shaped  $C_{70}$  into the “dimeric cage made from two bicalix[4]arenes orthogonally oriented in a ‘tennis-ball’ fashion, with intertwining *tert*-butyl groups” (Fig. 33.37).

Mizyed et al. [83] synthesized three new *p-tert*-butylcalix[4]arene “semitubes” **59a–c** (Fig. 33.38), in which a pair of *p-tert*-butylcalix[4]arenes were linked “tail to tail” via their lower rim phenolic hydroxyl groups. The linking groups used were *o*-, *m*- and *p*- $\alpha, \alpha'$ -dibromoxylenes. Binding constants of 15, 203 and  $525 \text{ M}^{-1}$  for the 1:1 complexes of **59a–c** with  $C_{60}$  respectively were determined by UV-Vis absorption spectroscopy but the solvent was not specified. The binding energies of the  $C_{60}$



**57: R = H and 58: R = 3,5-dinitrobenzoyl**

**Fig. 33.37** Left: the structures of **57** and **58**; Right: side views of optimized structures of the 1:2 complexes of **57** with (a) C<sub>60</sub> and (b) C<sub>70</sub> (Figure adapted with permission from Ref. [79], Copyright 2006, American Chemical Society)

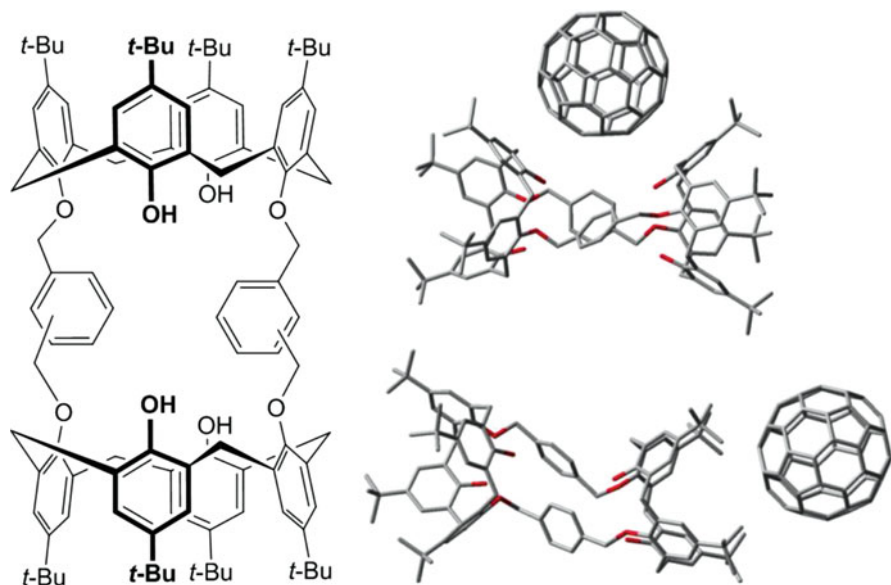


**Fig. 33.38** Left: the structures of **59a-c** (*o,m,p* respectively). Right: top: "centered" structure for the C<sub>60</sub>:**59c** complex, and bottom: the "side" structure of the C<sub>60</sub>:**59c** complex (Figure adapted from Ref. [83])

complexes were calculated using PM6 and DFT methods. Two possible geometries were considered "centered" and "side"-arrangements (Fig. 33.38 top and bottom). The calculated interaction energies revealed that with the exception of the *ortho*-linked ligand which has the shortest distance between the two calixarenes, the centered complexes were more stable than the side complexes. The PM6 calculations showed that the stability of the centered complexes is in the order  $m > p > o$ , which is the same as that obtained by experiments. The calculated energies using

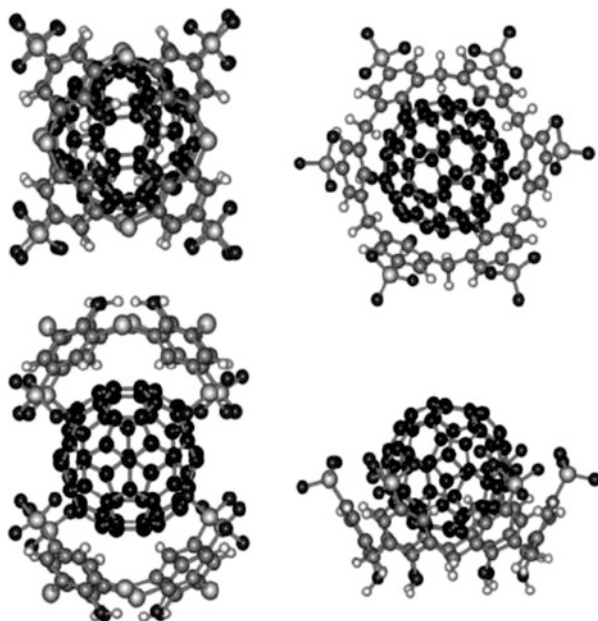
the DFT method however showed that the stability of both centered and side complexes is in the order  $p > m > o$  [83].

A UV-Vis complexation study in  $\text{CHCl}_3$  solution of  $\text{C}_{60}$  and  $\text{C}_{70}$  and a biscalix [6]arene **60** in which a pair of *p-tert*-butylcalix[6]arenes are linked via the lower-rim hydroxyls of the pair of calixarenes by a single  $-\text{CH}_2\text{CH}_2-$  linker was reported by Ghosh et al. [84] although synthetic details were not described. They also compared their results with a crown[4]calix[6]arene **61**.  $\text{C}_{60}$  and  $\text{C}_{70}$  formed 1:1 complexes with both host molecules. The highest  $K_{\text{assoc}}$  value ( $5900 \text{ M}^{-1}$ ) was measured for the  $\text{C}_{60}$ :**60** complex which the authors concluded was indicative of formation of an inclusion complex.

### 33.6 Water Soluble Calixarene-Fullerene Complexes

Kunsagi-Mate et al. [85] studied the inclusion complexes of  $\text{C}_{60}$  with the sodium salts of *p*-sulfonato-thiacalix[4]arene (**62**) and *p*-sulfonato-calix[6]arene (**63**) by photoluminescence and a semi-empirical AM1 followed by an HF/6-31G\* computational study. The stoichiometries of the calixarene: $\text{C}_{60}$  complexes are determined to be 2:1 for **63** with  $K$  values of  $1.20 \times 10^5 \text{ M}^{-1}$  and  $9.55 \times 10^4 \text{ M}^{-1}$  for each of the two steps; and  $K = 3.02 \times 10^5 \text{ M}^{-1}$  for the 1:1 complex of  $\text{C}_{60}$  with **64**. The computational studies showed the  $\text{C}_{60}$  to be included in a cavity composed of two molecules of **62**. In the other complex, the  $\text{C}_{60}$  is located deep within the cavity of **63** (Fig. 33.39) and consequently, the authors suggested that the negatively charged

**Fig. 33.39** Computed top and side views of the equilibrium conformations of: *left*:  $\text{C}_{60}$ :(**52**)<sub>2</sub> and *right*:  $\text{C}_{60}$ :(**63**) complexes (Figures taken from Ref. [85] Copyright 2004 with permission from Elsevier)



sulfonate groups probably inhibited the formation of a similar bowl-shaped capsule that was observed for the complex formed with **62**.

Ling et al. [86]. showed that stable colloidal suspensions of  $C_{60}$  and  $C_{70}$  in water were easily formed by mechanical grinding a mixture of  $C_{60}$  or  $C_{70}$  with *p*-sulfonatocalix[4]arene (**64**) alone and/or with the zwitterionic 3-(1-methylimidazolium-3-yl)propane-1-sulfonate, or 3-(1-methylimidazolium-3-yl)butane-1-sulfonate, followed by ultrasonication after the addition of water. Yellow and brown solutions formed with  $C_{60}$  and  $C_{70}$  respectively, were found to contain nano-arrays of the fullerenes (40–130 nm in diam.) covered by a sheath of sulfonated calixarene, sulfonated imidazolium zwitterions or supermolecules of these two components.

### 33.7 Conclusions

Since the discovery of the  $C_{60}$  and  $C_{70}$  fullerenes in September 1985, these aesthetic and symmetric allotropic forms of carbon have continued to generate much interest and fascination amongst scientists of various stripes. After the initial discovery of their existence in interstellar space, subsequent large-scale availability of these two fullerenes on Earth as the carbon soot or “fullerite” mixture via the carbon electron-arc process led to the need to purify the individual fullerenes. Atwood’s and Shinkai’s independently discovered in 1994 that *p-tert*-butylcalix[8]arene could sequester  $C_{60}$  from fullerite and that thereby purify it by its selective complexation and subsequent de-complexation from organic solutions led to the interest by synthetic organic chemists who have designed fascinating new calixarenes and related molecules to improve on the affinities for these fullerenes. Besides the intrinsic fundamental interest in the supramolecular processes that occur when calixarenes and other cavity-containing molecules bind to these fullerenes, the fact that  $C_{60}$  shows important photophysical and electrochemical properties has added to the on-going interest.

Since the publication of *Calixarenes 2001* which covered the interaction of calixarenes and fullerenes to that date, this review has examined approximately 80 papers. In some cases, especially with the more “classical” calixarenes whose syntheses have been made conveniently available through the pioneering contributions of C. David Gutsche and his coworkers, new insights have been gleaned. The X-ray and related work of Raston et al. have shed fascinating new insights into the solid state structures of several of the classical calixarenes with  $C_{60}$  and  $C_{70}$ . Fukazawa and Haino’s development of double calix[5]arenes, Lhotak’s incorporation of porphyrins onto calixarenes and thiacalixarenes, the triptycene-modified calix[6]arenes of Chen and the solution studies of others have all led to enhancements in the understanding of the structural and thermodynamic factors involved in the supramolecular binding process, as well as the meaningful and accurate analyses from spectroscopic studies. The Ag(I)-imidazolium-carbene-bridged calixarene of Quin et al. is another fine example of the imaginative and creative

ways that researchers have tackled fullerene binding challenges. Mei-Xian Wang's synthetic development of the series of nitrogen-containing heterocyclic calixarene analogues and their C<sub>60</sub> and C<sub>70</sub> binding properties also stand out as testaments to creativity, as of course do so many other contributions which were covered in this review.

## References

1. Zhong, Z.-L.; Ikeda A.; S. Shinkai, In *Calixarenes 2001* pp 476–495; Eds. Asfari, Z.; Böhmer, V.; Harrowfield, J.; Vicens, J., Kluwer Academic Publishers, Dordrecht, 2001.
2. Lhotak, P.; Kundrat, O. In *Artificial Receptors for Chemical Sensors* pp 249–272; Eds. Mirsky, V. M.; Yatsimirsky, A. K. Wiley-VCH, Weinheim, 2011.
3. Georghiou, P. E., pp 391–403, In *Handbook of Carbon Nanotubes, 1st Ed.*, Eds.: D'Souza, F.; Kadish, K. M., World Scientific, Singapore, 2011.
4. Kawase, T., In *Supramolecular chemistry of fullerenes and carbon nanotubes*, pp 55–78 Eds. Martin, N.; Nierengarten, J.-F. Wiley-VCH Weinheim, 2012.
5. (a) Atwood, J. L.; Koutsantonis, G. A.; Raston, C. L. *Nature* **1994**, *368*, 229. (b) Suzuki, T. Nakashima, K.; Shinkai, S. *Chem. Lett.* **1994**, 699.
6. Chen, X.; Boulos, R. A.; Slattery, A. D.; Atwood, J. L.; Raston, C. L. *Chem. Commun.* **2015**, *51*, 11413–11416.
7. Raston, C. L.; Atwood, J. L.; Nichols, P. J.; Sudria, I. B. N. *Chem. Commun.* **1996**, 2615–2616.
8. Makha, M.; Evans, C. W.; Sobolev, A. N.; Raston, C. R. *Cryst. Growth Des.* **2008**, *8*, 2929–2932.
9. Atwood, J. L.; Barbour, L. J.; Raston, C. L.; Sudria, I. B. N. *Angew. Chem. Int. Ed.* **1998**, *37*, 981.
10. Makha, M.; Raston, C. L.; Sobolev, A. N.; Turner, P. *Cryst. Growth Des.* **2006**, *6*, 224–228.
11. Flidrova, K.; Liska, A.; Ludvik, J.; Eigner, V.; Lhotak, P. *Tetrahedron Lett.* **2015**, *56*, 1535–1538.
12. Hubble, L. J.; Raston, C. L. *Chem Eur J.* **2007**, *13*, 6755–6760.
13. Hubble, L. J.; Barbour, L. J.; Heaven, M. W.; Raston, C. L. *Chem. Commun.* **2003**, *18*, 2270–2271.
14. Atwood, J. L.; Barbour, L. J.; Heaven, M. W.; Raston, C. L. *Angew. Chem. Int. Ed.* **2003**, *42*, 3254–3257.
15. Atwood, J. L.; Barbour, L. J.; Raston, C. L. *Cryst. Growth Des.* **2002**, *2*, 3–6.
16. Makha, M.; Raston, C. L.; Sobolev, A. N.; Barbour, L. J.; Turner, P. *Cryst. Eng. Comm.* **2006**, *8*, 306–308.
17. Busolo, F.; Silvestrini, S.; Armelao, L.; Maggini, M. *J. Chem. Phys.* **2013**, *139*, 164715–164718.
18. Carrillo-Carrion, C.; Lendl, B. M.; Simonet, B. M.; Valcarcel, M. *Anal. Chem.* **2011**, *83*, 8093–8100.
19. Jin, W. J.; Fernández-Argüelles, M. T.; Costa-Fernández, J. M.; R. Pereiro, Sanz-Medel, A. *Chem. Commun.* **2005**, 883–885.
20. Zhang, S.; Echegoyen, L. *J. Org. Chem.* **2005**, *70*, 9874–9881.
21. Zhang, S.; Echegoyen, L. *C. R. Chimie* **2006**, *9*, 1031–1037.
22. Pan, G.-B.; Liu, J.-M.; Zhang, H.-M.; Wan, L.-J.; Zheng, Q.-Y.; Bai, C.-L. *Angew. Chem. Int. Ed. Engl.* **2003**, *42*, 2747–2751.
23. Gonzalez-Delgado, A. M.; Giner-Casares, J. J.; Brezesinski, G.; Regnouf-de-Vains, J.-B.; Camacho, L. *Langmuir*, **2012**, *28*, 12114–12121.
24. 24(a) Georghiou, P. E.; Tran, A.-H.; Stroud, S. S.; Thompson, D. W. *Tetrahedron*, **2006**, *62*, 2036–2044. (b) Mizyed, S.; Tremaine, P. R.; Georghiou, P. E. *J. Chem. Soc. Perkin Trans. 2*,

- 2001, 3-6. (c) Mizyed, S.; Chowdhury, S.; Georghiou, P. E.; Mizyed, S.; Chowdhury, S. *Tetrahedron Lett.* **1999**, *40*, 611–614.
25. See for example: Stella, L.; Capadilupo, A. L.; Bietti, M. *Chem. Commun.* **2008**, *39*, 4744–4746.
26. Fielding, L. *Tetrahedron* **2000**, *56*, 6151–6170.
27. Benesi, H. A.; Hildebrand, J. H. *J. Am. Chem. Soc.* **1949**, *71*, 2703–2707.
28. Thordarson, P. *Chem. Soc. Rev.* **2011**, *40*, 1305–1323; and for an alternative on-line non-linear computational method see <http://www.supramolecular.org>.
29. Bhattacharya, S.; Nayak, S. K.; Chattopadhyay, S.; Banerjee, M.; Mukherjee, A. K. *J. Chem. Soc., Perkin Trans. 2* **2001**, *12*, 2292–2297.
30. Bhattacharya, S.; Nayak, S. K.; Semwal, A.; Chattopadhyay, S.; Banerjee, M. *J. Phys. Chem. A* **2004**, *108*, 9064–9068.
31. Bhattacharya, S.; Nayak, S. K.; Semwal, A.; Banerjee, M. *Spectrochim. Acta, A* **2005**, *61*, 595–606.
32. Bhattacharya, S.; Nayak, S. K.; Chattopadhyay, S.; Banerjee, M.; Mukherjee, A. K. *Spectrochim. Acta, A* **2005**, *61*, 321–329.
33. Bhattacharya, S.; Nayak, S. K.; Chattopadhyay, S.; Banerjee, M.; Mukherjee, A. K. *J. Phys. Chem. B*, **2003**, *107*, 11830–11834.
34. Bhattacharya, S.; Nayak, S. K.; Chattopadhyay, S.; Banerjee, M. *Spectrochim. Acta, A* **2006**, *63*, 200–206.
35. Halder, A.; Goswami, D.; Nayak, S. K.; Chattopadhyay, S.; Bhattacharya, S. *J. Mol. Struct.* **2009**, *936*, 112–117.
36. Bhattacharya, S.; Chattopadhyay, S.; Nayak, S. K.; Banerjee, M. *Spectrochim. Acta, A: Mol. Biomol. Spect.* **2005**, *62*, 729–735.
37. Halder, A.; Nayak, S. K.; Chattopadhyay, S.; Bhattacharya, S. *J. Mol. Liquids* **2010**, *151*, 125–129.
38. Halder, A.; Sandip; S. K.; Chattopadhyay, S.; Bhattacharya, S. *J. Solution Chem.* **2012**, *41*, 223–240.
39. Halder, A.; Kundu, K.; Nayak, S. K.; Chattopadhyay, S.; Bhattacharya, S. *Spectrochim. Acta, A: Mol. Biomol. Spect.* **2012**, *93*, 384–389.
40. Mizyed, S. A.; Al-Jarrah E.; Deeb, M.; Muhammad, A. *Spectrochim. Acta, A: Mol. Biomol. Spect.* **2007**, *68A*, 1274–1277.
41. Mizyed, S.; Ashram, M.; Miller, D. O.; Georghiou, P. E. *J. Chem. Soc. Perkin Trans. 2* **2001**, *10*, 1916–1919.
42. Asao, T.; Ito, S.; Morita, N. *Tetrahedron Lett.* **1988**, *29*, 2839–2842.
43. Colby D. A.; Lash, T. D. *J. Org. Chem.* **2002**, *67*, 1031–1033.
44. Lash, T.D.; El-Beck J.A.; Colby, D.A. *J. Org. Chem.* **2009**, *74*, 8830–8833.
45. Georghiou, P. E.; Schneider, C.; Shamov, G.; Lash, T. D.; Rahman S.; Giddings, S. *Supramol. Chem.* **2016**, *28*, 396–402 . b) Unpublished results.
46. Al Hujran, T. A.; Dawe, L.N.; Georghiou, P. E. *Org. Lett.* **2012**, *14*, 3530–3533.
47. Connors, K. A. *Binding Constants*, John Wiley & Sons, New York, 1987.
48. a) Iglesias-Sanchez, J. C.; Souto, B.; Pastor, C. J.; de Mendoza, J.; Prados, P. *J. Org. Chem.* **2005**, *70*, 10400–10407; b) Galan, H.; de Mendoza, J.; Prados, P. *Eur. J. Org. Chem.* **2005**, 4093–4097; c) Liu, J.-M.; Zheng, Q.-Y.; Chen, C.-F.; Huang, Z.-T. *Tetrahedron* **2007**, *63*, 9939–9946; d) Menand, M.; Jabin, I. *Org. Lett.* **2009**, *11*, 673–676.
49. Tian, X.-H.; Chen, C.-F. *Chem. Eur. J.* **2010**, *16*, 8072–8079.
50. Chen C.-F. *Chem. Commun.* **2011**, *47*, 1674–1688.
51. Ma, Y.-X.; Han, Y.; Chen, C.-F. *J. Incl. Phenom. Macro. Chem.* **2014**, *79*, 261–281, and references cited therein.
52. Xie, T.; Hu, S.-Z.; Chen C.-F. *J. Org. Chem.* **2013**, *78*, 981–987.
53. Hu, S.-Z.; Chen, C.-F. *Chem. Commun.* **2010**, *46*, 4199–4201.
54. For a recent review on thiacalixarenes, see: Kumar, R.; Lee, Y. O.; Bhalla, V.; Kumar, M.; Kim, J. S. *Chem. Soc. Rev.* **2014**, *43*, 4824–4870.



55. Dudic, M.; Lhotak, P.; Stibor, I.; Petrickova, H.; Lang, K. *New J. Chem.* **2004**, *28*, 85–90.
56. Kas, M.; Lang, K.; Stibor, I.; Lhotak, P. *Tetrahedron Lett.* **2007**, *48*, 477–481.
57. Kundrat, O.; Kas, M.; Tkadlecova, M.; Lang, K.; Cvacka, J.; Stibor, I.; Lhotak, P. *Tetrahedron Lett.* **2007**, *48*, 6620–6623.
58. Bi, Y.; Liao, W.; Wang, X.; Wang, X.; Zhang, H. *Dalton Trans.* **2011**, *40*, 1849–1851.
59. Vysotsky, M.; Saadioui, M.; Böhmer, V. In *Calixarenes 2001* pp 250–252; Eds. Asfari, Z.; Böhmer, V.; Harrowfield, J.; Vicens, J., Kluwer Academic Publishers, Dordrecht, 2001.
60. Nielsen, K. A.; Cho, W.-S.; Sarova, G. H.; Petersen, B. M.; Bond, A. D.; Becher, J.; Jensen, F.; Guldi, D. M.; Sessler, J. L.; Jeppesen, J. O. *Angew. Chem. Int. Ed.* **2006**, *45*, 6848–6853.
61. Fukuzumi, S.; Ohkubo, K.; Kawashima, Y.; Kim, Dong S.; Park, J. S.; Jana, A.; Lynch, V. M.; Kim, D.; Sessler, J. L. *J. Am. Chem. Soc.* **2011**, *133*, 15938–15941.
62. Pal, D.; Goswami, D.; Nayak, S. K.; Chattopadhyay, S.; Bhattacharya, S. *J. Phys. Chem. A* **2010**, *114*, 6776–6786.
63. Wang, M.-X.; Zhang, X.-H.; Zheng, Q.-Y. *Angew. Chem. Int. Ed.* **2004**, *43*, 838–842.
64. Wu, J.-C.; Wang, D.-X.; Huang, Z.-T.; Wang, M.-X. *Tetrahedron Lett.* **2009**, *50*, 7209–7212.
65. Liu, S.-Q.; Wang, D.-X.; Zheng, Q.-Y.; Wang, M.-X. *Chem. Commun.* **2007**, *37*, 3856–3858.
66. Zhang, E.-X.; Wang, D.-X.; Zheng, Q.-Y.; Wang, M.-X. *Org. Lett.* **2008**, *10*, 2565–2568.
67. Gong, H.-Y.; Zhang, X.-H.; Wang, D.-X.; Ma, H.-W.; Zheng, Q.-Y.; Wang, M.-X. *Chem. Eur. J.* **2006**, *12*, 9262–9275.
68. Zhang, E.; Wang, D.-X.; Huang, Z.; Wang, M.-X. *Chin. J. Chem.* **2010**, *28*, 1690–1696.
69. Fa, S.-X.; Wang, L.-X.; Wang, D.-X.; Zhao, L.; Wang, M.-X. *J. Org. Chem.* **2014**, *79*, 3559–3571.
70. Wang, L.-X.; Zhao, L.; Wang, D.-X.; Wang, M.-X. *Chem. Commun.* **2011**, *47*, 9690–9692.
71. Chun, Y.; Singh, N. J.; Hwang, I.-C.; Lee, J. W.; Yu, S. U.; Kim, K. S. *Nature Commun.* **2013**, *4*, 1797–1797.
72. Quin, D.; Zeng, X.; Li, Q.; Xu, F.; Song, H.; Zhang, Z.-Z. *Chem. Commun.* **2007**, 147–149.
73. Yanase, M.; Matsuoka, M.; Tatsumi, Y.; Suzuki, M.; Iwamoto, H.; Haino, T.; Fukazawa, Y. *Tetrahedron Lett.* **2000**, *41*, 493–497.
74. Haino, T.; Araki, H.; Yamanaka, Y.; Fukazawa, Y. *Tetrahedron Lett.* **2001**, *42*, 3203–3206.
75. Haino, T.; Yamanaka, Y.; Araki, H.; Fukazawa, Y. *Chem. Commun.* **2002**, 402–403.
76. Haino, T.; Yanase, M.; Fukunaga, C.; Fukazawa, Y. *Tetrahedron*, **2006**, *62*, 2025–2035.
77. Haino, T.; Fukunaga, C.; Fukazawa, Y. *Org. Lett.* **2006**, *8*, 3545–3548.
78. Haino, T.; Fukunaga, C.; Fukazawa, Y. *J. Nanosci. Nanotechnol.* **2007**, *7*, 1386–1388.
79. Iglesias-Sanchez, J. C.; Fragoso, A.; de Mendoza, J.; Prados, P. *Org. Lett.* **2006**, *8*, 2571–2574.
80. “Head-to-head” bicalix[4]arenes: (a) Neri, P.; Bottino, A.; Cunsolo, F.; Piattelli, M.; Gavuzzo, E. *Angew. Chem., Int. Ed.* **1998**, *37*, 166–169. (b) Bottino, A.; Cunsolo, M. F.; Piattelli, M.; Gavuzzo, E.; Neri, P. *Tetrahedron Lett.* **2000**, *41*, 10065–10069. Bicalix[6] and [8]arenes: (c) Bottino, A.; Cunsolo, F.; Piattelli, M.; Garozzo, D.; Neri, P. *J. Org. Chem.* **1999**, *64*, 8018–8020.
81. “Head-to-head” bicalix[5]arenes: Wang, J.; Borige, S. G.; Watson, W. H.; Gutsche, C. D. *J. Org. Chem.* **2000**, *65*, 8260–8263.
82. a) *SPECFIT*, version 3.0; Spectra Software Associates. (b) Gampp, H.; Maeder, M.; Meyer, C. J.; Zuberbühler, A. D. *Talanta* **1985**, *32*, 95–101. (c) Gampp, H.; Maeder, M.; Meyer, C. J.; Zuberbühler, A. D. *Talanta* **1986**, *33*, 943–951.
83. Mizyed, S.; Marji, D.; Rawashdeh, A. M.; Foudeh, A. *J. Incl. Phenom. Macrocycl. Chem.* **2013**, *76*, 113–118. For many other examples of narrow-rim bridged calix[*n*]arenes see Saadioui, M.; Böhmer, V., In *Calixarenes 2001*, pp130–154, Eds. Asfari, Z.; Böhmer, V.; Harrowfield, J.; Vicens, J., Kluwer Academic Publishers, Dordrecht, 2001.
84. Ghosh, K.; Semwal, A.; Nayak, S. K.; Banerjee, S. Bhattacharya; Banerjee, M. *Spectrochim. Acta, A* **2007**, *66*, 1122–1125.
85. Kunsagi-Mate, S.; Szabo, K.; Bitter, I.; Nagy, G.; Kollar, L. *Tetrahedron Lett.* **2004**, *45*, 1387–1390.
86. Ling, I.; Alias, Y.; Raston, C. L. *New J. Chem.* **2011**, *35*, 1549–1555.



# Chapter 34

## Calixarene-Encapsulated Nanoparticles: Synthesis, Stabilization, and Self-Assembly

Alexander Wei

### 34.1 Introduction

Supramolecular chemistry and nanotechnology are synergistic disciplines. The former is guided by principles of structural complementarity, enabling one to design complex molecular architectures assembled from relatively simple building blocks [1]. The latter requires an appreciation of nanoscale forces, some of which are nondirectional (long-range van der Waals (vdW) attraction, entropic steric repulsion) while others are driven by potentials generated by local field gradients [2]. Anisotropic molecules like calixarenes provide a gateway between the realms of supramolecular science and nanoscience: Their macrocyclic headgroups are famous for molecular encapsulation, whereas their tailgroups support the solvation or dispersion stability of the encapsulated complexes (Fig. 34.1). Furthermore, both ends of the calixarene can be structurally modified, permitting encapsulated nanomaterials to be systematically optimized and integrated with other materials in various environments. This also means that calixarenes can serve as platforms for nanoscale synthesis, complementing their supramolecular capacities. The sizes of such complexes are virtually limitless, ranging from Cram's seminal report on carcerands (covalent calixarene dimers) [3] to nanoparticles engaged in shells of polymerized calixarene capsules [4] to submicron vesicles comprised of crosslinked calixarenes [5].

In this chapter we offer a personalized perspective on the roles that calixarenes can play at the interface of chemistry and nanoscience, with an emphasis on metal nanoparticles (NPs). Synthesis, solvation and dispersion control, and self-assembly all contribute toward the creation of well-defined nanostructures and the emergence

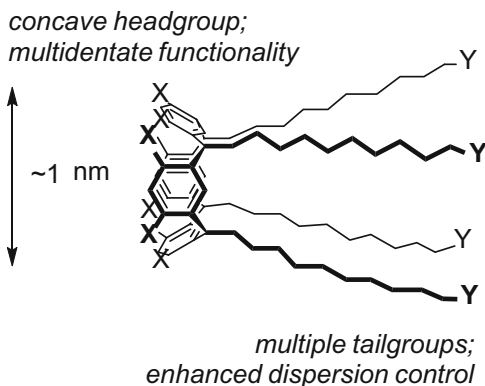
---

A. Wei (✉)

Department of Chemistry, Purdue University, 560 Oval Drive, West Lafayette, IN 47907-2084,  
USA

e-mail: [alexwei@purdue.edu](mailto:alexwei@purdue.edu)

**Fig. 34.1** Calixarenes as interfacial molecules between supramolecular chemistry and nanomaterials



of collective materials properties. In this regard, we have found calixarenes to be versatile templates for NP nucleation and growth, encapsulation, stabilization, and self-assembly. We apologize in advance for not providing a comprehensive coverage of all works related to calixarenes and nanoparticles, but refer instead to a complementary chapter in this monograph.

## 34.2 Calixarenes in Nanoparticle Synthesis: Separate Control Over Nucleation and Growth

Size-controlled nanoparticle (NP) synthesis in solution is an essential practice in nanotechnology, but has remained a largely empirical process, guided mostly by rudimentary models to describe the kinetics of nucleation and growth. These phenomena can be subdivided into four categories: (1) rapid “burst” nucleation under supersaturated conditions, a classic model first defined by LaMer and Dinegar; [6] (2) slow, continuous nucleation with fast, autocatalytic addition of monomers, as described by Watsky and Finke; [7] (3) postnuclear coalescence of metastable clusters; [8] and (4) size refinement by digestive “ripening,” mediated primarily by surfactants [9] (Fig. 34.2). Templated NP synthesis has been achieved mostly by pre-encapsulation of reactive monomers; for example, the reduction of metal salts within dendrimers, inverse micelles, or block copolymers can result in metal NPs from 1 to 10 nm in diameter. However, solvothermal methods remain the most common and scalable approach to NP synthesis.

Are calixarenes useful nucleating agents for NP synthesis? This hypothesis has been explored and partially validated; select examples include CdS nanocrystals within Langmuir-Blodgett layers of amphiphilic calix[8]arenes ( $d_{av} = 2$  nm); [10] colloidal Ag using thiolated cavitands in DMF ( $d_{av} = 83$  nm) [11], smaller Ag NPs by reduction in aqueous solutions of phosphonated calix[ $n$ ]arenes ( $d = 2$ –5 nm) [12], and subnanometer transition-metal clusters using calix[8]arene thioesters [13]. In all cases except one, the calixarene headgroup appears to serve as a

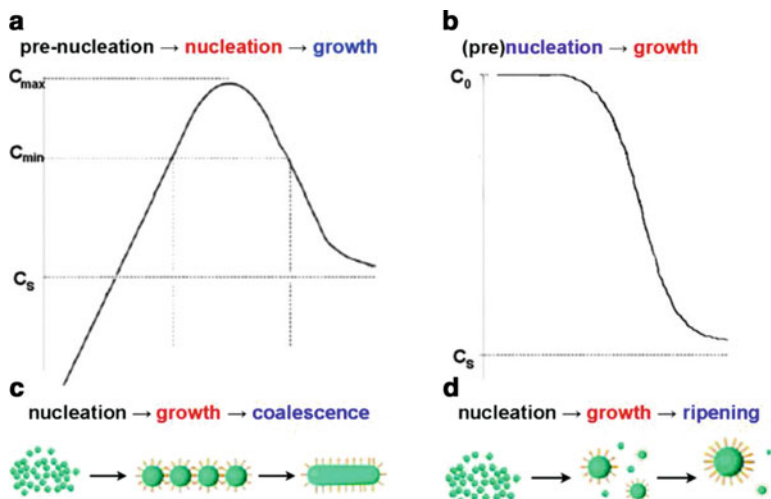


**Fig. 34.2** Models for NP growth behavior. (a) Rapid nucleation above a minimum level of monomer ( $C_{min}$ ), with growth until monomer depletion ( $<C_s$ ); (b) slow, gradual nucleation with rapid, autocatalytic growth; (c) coalescence or oriented aggregation after initial nucleation/growth; (d) digestive (Ostwald) ripening, with mass transfer mediated by surfactants

multidentate capping ligand that promotes nucleation but limits further growth or coalescence.

We raised the question whether solvothermal conditions could be designed to permit NP nucleation and growth as separate phases, each mediated by different types of ligands or organometallic species. Calixarenes appear to be excellent candidates for NP nucleation and stabilization, but are less suited for sustained growth. On the other hand, reactive monomers such as metal carbonyls ( $M(CO)_n$ ) are obvious candidates for NP growth, but are prone to spontaneous nucleation leading to size polydispersity. Both nucleation and growth reagents thus require fine tuning of their chemical reactivity: Capping ligands on the NP should provide sufficient stability yet permit surface reactions to occur, whereas growth reagents should have a low autonucleation profile but react readily with the nucleating species.

To confirm whether multidentate calixarenes could limit NP growth under solvothermal conditions, we prepared hexadecanuclear cobalt complexes **1** and **2** from  $Co_2(CO)_8$ , a common precursor for Co NP synthesis, and octa-*O*-propargyl derivatives of C1 and C11 resorcinarene (**3** and **4** respectively) [14, 15].  $Co_{16}$ -calixarenes **1** and **2** were stable under ambient conditions, but decomposed rapidly above 90 °C. An x-ray crystal structure of **1** shows all eight pendant  $Co_2(CO)_6$  units to be on the same face of the calixarene platform [14], and MALDI-MS analysis of **2** indicates facile decarbonylation into zerovalent  $Co_{16}$  clusters [15], implying formation of a metastable “capped-cluster” intermediate (Fig. 34.3).

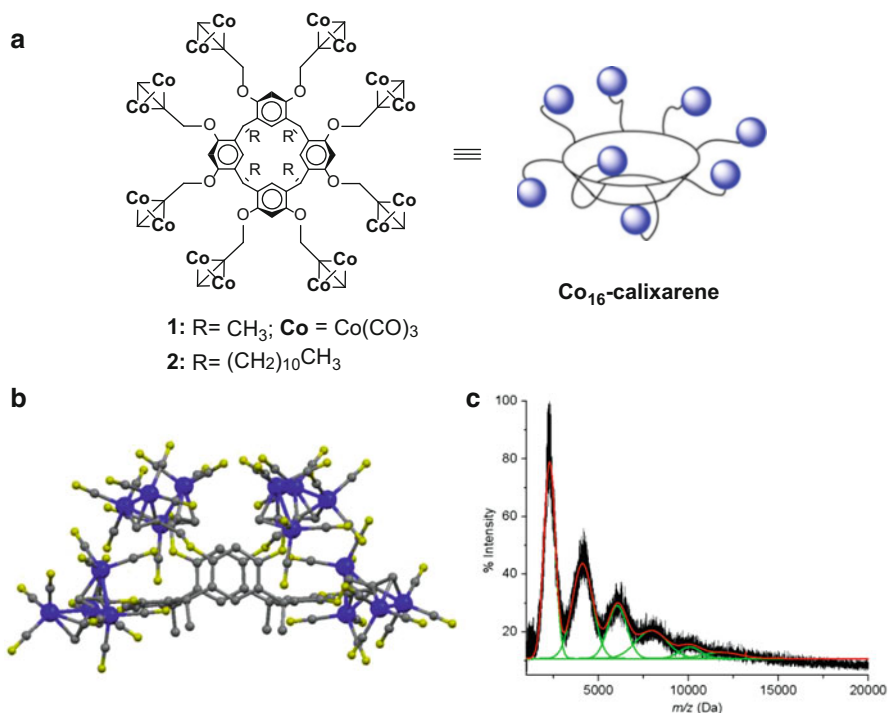


**Fig. 34.3** (a) Co<sub>16</sub>-calixarene complexes **1** and **2**; (b) x-ray crystal structure of **1** [14]; (c) MALDI-TOF mass spectrum of **2** [15]. Mode peak analysis corresponds with oligomers of decarbonylated **2**, presumably generated by condensation in the gas phase (Reprinted with permissions from the Royal Society of Chemistry and the American Chemical Society)

The MS analysis of **2** also revealed the formation of dimers, trimers, and other oligomers, suggesting that Co<sub>16</sub>-calixarenes have a strong propensity to coalesce into well-defined nanoclusters (Fig. 34.4a). This indeed proved to be the case: Solutions of **2** in hot *o*-dichlorobenzene (ODCB) produced Co nanocrystals with narrow size distributions, based on transmission electron microscopy (TEM) analysis ( $2.9 \pm 0.4$  nm or  $3.6 \pm 0.4$  nm; Fig. 34.4b, c); similar results were obtained for solutions of **1**. These NP size distributions were constant over time; by comparison, the thermolysis of PhOCH<sub>2</sub>C $\equiv$ CH–Co<sub>2</sub>(CO)<sub>6</sub> **3** (the monovalent equivalent of **1**) yielded Co NPs whose mean size slowly increased over time (Fig. 34.4d). These studies confirmed that the calixarene-encapsulated Co NPs were thermally stable and resistant to digestive ripening.

To determine whether Co NPs generated from Co<sub>16</sub>-calixarenes could support further (seeded) growth, complexes **1** and **2** were heated in the presence of other zerovalent Co species with the objective of stoichiometric control over particle size. Co<sub>2</sub>(CO)<sub>8</sub> proved to be too reactive and exhibited a high degree of autonucleation, regardless of activation temperature; in contrast, simple alkyne–Co<sub>2</sub>(CO)<sub>6</sub> complexes were insufficiently reactive and failed to produce NPs under solvothermal

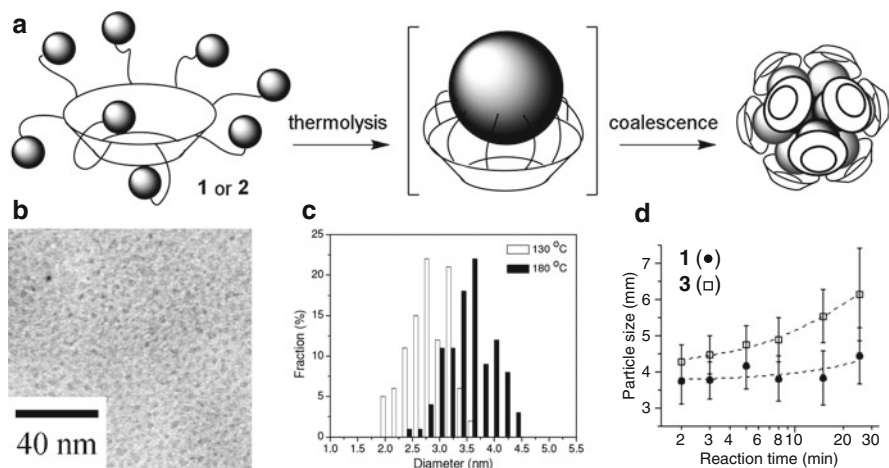


**Fig. 34.4** (a) Thermolysis of  $\text{Co}_{16}$ -calixarene complexes into capped-cluster intermediates, with rapid coalescence into Co nanocrystals; (b) TEM image of Co nanocrystals formed by thermolysis of **2** at 130 °C [15]; (c) size analysis of Co NPs generated from **2**; (d) stability of NPs generated from **1** (black squares) versus **3** (white squares) [14] (Reprinted with permissions from the Royal Society of Chemistry and the American Chemical Society)

conditions in ODCB. Fortunately, we found the thermal reactivity of pentyne- $\text{Co}_4(\text{CO})_{10}$  (PTC) to be between that of  $\text{Co}_2(\text{CO})_8$  and pentyne- $\text{Co}_2(\text{CO})_6$ . Thermogravimetric analysis indicated rapid degradation at 135 °C, but TEM analysis revealed the initial decomposition product to be amorphous, signifying a low autonucleation potential. Indeed, thermolysis of **2** in the presence of PTC produced cubelike, crystalline Co NPs with low size distributions, whose volumes correlated linearly with the mole ratio of growth and nucleating agents (i.e. PTC and **2**). Autonucleation of PTC could be further suppressed by slow addition via syringe pump, allowing the linear relationship to be extended up to mole ratios of 100:1, with Co NP sizes up to 40 nm (Fig. 34.5a).

In the course of this work, it became evident that crystalline Co NP growth was accompanied by the formation of an amorphous matrix, or accretion, which could be observed upon isolating NPs at an intermediate stage of growth (Fig. 34.5b). Indeed, this accretion may persist at the expense of NP growth, which implies its role in the rate-limited diffusion of Co to NP surfaces. Growth or crystallization within the accretion could be enhanced by spiking PTC with small amounts of octapropargyl calixarene **4**, whose multiple alkyne units can promote Co diffusion. At the end of the growth period, the residual accretion was dissipated with oleic acid to yield well-dispersed NPs. The growth of crystalline NPs within the accretion presents an entirely different model from growth by direct addition of monomers, which is commonly assumed in the solvothermal synthesis of NPs (Fig. 34.5c).

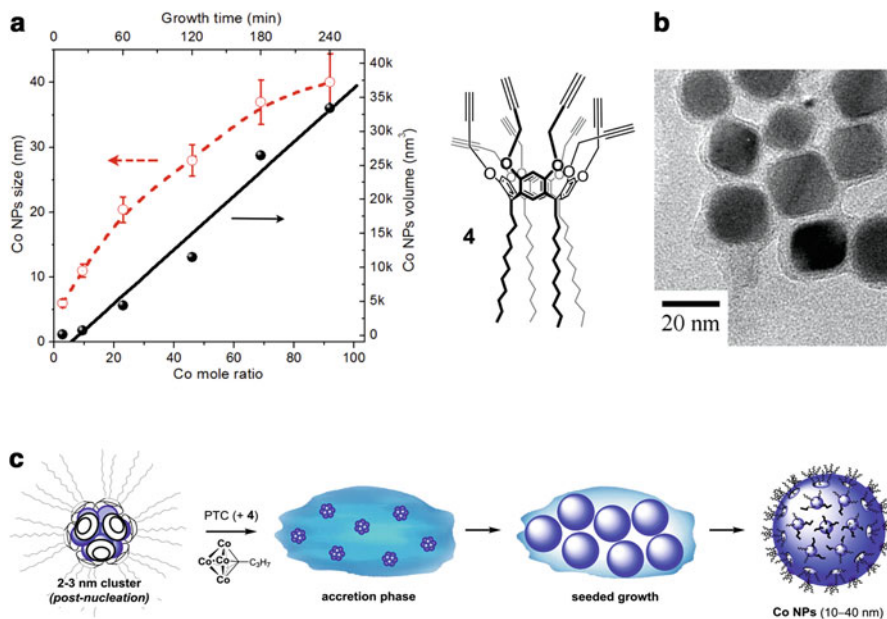


**Fig. 34.5** (a) Co NP synthesis using  $\text{Co}_{16}$ -calixarene **2** and PTC as nucleating and growth agents, and calixarene **4** as an additive. NP size was determined by the mole ratio of PTC to **2**, with a linear relationship to volume (●, right axis) and diameters up to 40 nm (O, left axis) [15]. (b) Appearance of an amorphous matrix (accretion) during NP growth. (c) Model of seeded growth within an accretion phase; crystalline NPs are released upon digestion of the residual matrix (Reprinted with permission from the the American Chemical Society)

### 34.3 Calixarenes in Nanoparticle Stabilization

With respect to NP synthesis, calixarenes are hardly unique; countless methods have been developed for preparing nanoparticles of various shapes, sizes, and composition. However, appropriately designed calixarenes may offer significant advantages over other low molecular weight surfactants for dispersing metal NPs in organic solvents. In the examples below, we demonstrate how a specific class of calixarenes (resorcinarenes) provides superior control over standard surfactants or amphiphiles for NP stabilization in nonpolar media.

The issue of NP stabilization is a practical one, *en route* to a desirable function or processing outcome. In that regard, colloidal dispersion stability is simply the nanoscale analog of solubility: For ideal solutions, one wishes to assume that species of interest are fully solvated with minimum aggregation. However, most solutions are far from ideal, with solutes (molecules as well as NPs) existing in complex equilibria between isolated and aggregated states. The finer details of dispersion control are best discussed elsewhere; for the sake of instruction, NP stabilization will be characterized here by optical density (OD) or extinction at specific wavelengths, at concentrations that support a linear relationship using the

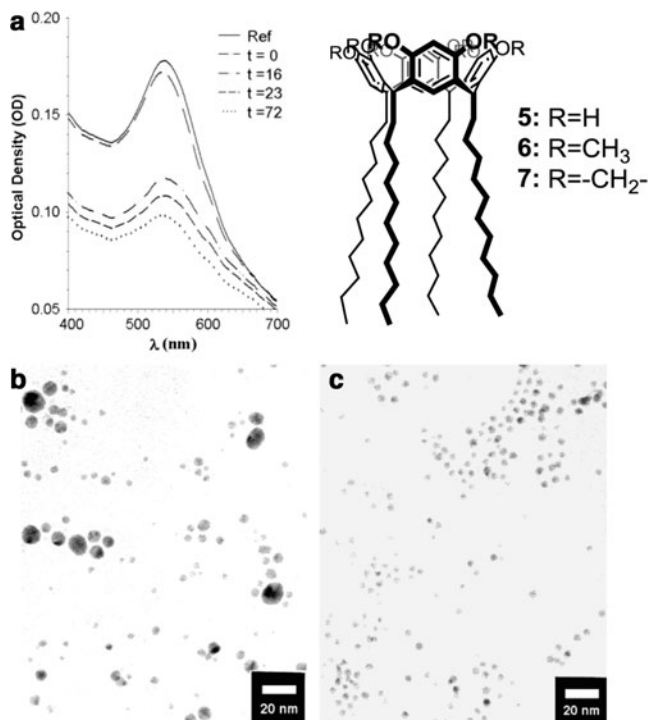


**Fig. 34.6** (a) Optical absorption spectra of Au NPs in mesitylene stabilized by resorcinarene **6** (Ref.), following treatment with 1 mM C12SH over 72 h; (b, c) TEM images of Au NPs stabilized by **6**, before and 72 h after C12SH treatment (Reprinted with permission from the American Chemical Society)

Beer–Lambert law. This approach is particularly germane to metal NPs such as Au and Ag, which support localized plasmon resonances at visible wavelengths [16].

Early evidence for the remarkable NP-stabilizing properties of calixarenes was obtained by using tetra-*C*-undecylcalix[4]resorcinarene **5** and its octa-*O*-methyl derivative **6** to capture Au nanocrystals in mesitylene [17]. These nanocrystals were produced as aerosols without any surfactants, and subsequently passed through solutions containing **5**, **6** or dodecanethiol (C12SH). Dispersions stabilized by **5** or **6** exhibited a distinct resonance characteristic of Au NPs, with ODs several times greater than those obtained using equimolar solutions of C12SH. Furthermore, calixarene-stabilized dispersions were stable if left undisturbed, but treatment with C12SH caused a substantial drop in OD within hours (Fig. 34.6a). Most tellingly, TEM analysis revealed that solutions with **5** or **6** contained Au NPs up to 20 nm in size, whereas those treated with C12SH contained NPs < 5 nm (Fig. 34.6b, c). Lastly, attempts to capture Au NPs with cavitand **7** were unsuccessful.

These simple but informative studies established the following: (i) under surface saturation conditions in nonpolar solvents (generally assumed to be the case), the presentation of multi-tailed ligands such as calixarenes **5** and **6** is more effective at



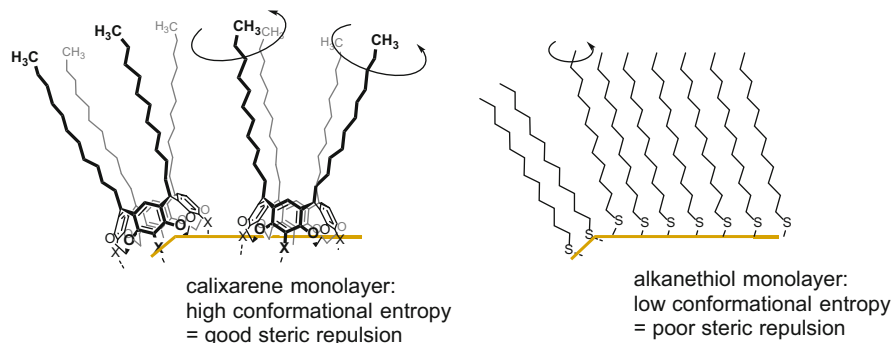


**Fig. 34.7** *Left*, calixarene-based monolayers with chains at intermediate packing density, creating high entropic steric repulsion between NP surfaces; *right*, alkanethiol monolayers at high packing density offer only limited steric repulsion, and decreases further with NP size

stabilizing large ( $>5$  nm) NPs than single-chain surfactants like C12SH; (ii) the presentation of multiple oxygen atoms on the macrocyclic headgroup of **5** and **6** is sufficient to stabilize Au NPs in the absence of competing surfactants; and (iii) the adsorption of polyols or polyethers on Au NPs is relatively weak, and easily disrupted by chemisorptive surfactants such as thiols.

With respect to the first observation, macrocyclic amphiphiles such as calixarenes are excellent dispersants because their tailgroups are projected at fixed positions around the ring, which ensures a high degree of conformational mobility after their adsorption onto NP surfaces (Fig. 34.7a) [18]. Conformational entropy is a critical factor in short-range steric repulsion for countering long-range vdW attraction between NPs, and for preventing subsequent loss of dispersion stability (Fig. 34.7b). Single-chain surfactants such as fatty acids and alkanethiols offer only limited steric repulsion, as they tend to form densely packed monolayers upon surface adsorption. As NPs increase in size their long-range vdW interactions also increase while their curvatures decrease, further reducing steric repulsion between monolayer-coated surfaces. The net effect is a loss of dispersion stability for NPs above a threshold size.

The latter two observations are enthalpic in nature, allowing us to design calixarene-based surfactants with multiple coordinating functional groups. This led to encapsulation studies with tetra(*O,O*-phosphonito)resorcinarene **8** [19], tetrathiol cavitand **9** [20], tetramethylthiol cavitand **10** [19], tetramethyl(*N*-methyl)dithiocarbamate cavitand **11** [21], and pyridinearene **12** [22] (Fig. 34.8). All of these calixarenes proved to be highly chemisorptive and capable of encapsulating Au NPs; furthermore, derivatives **9–11** were able to extract electrolyte-stabilized Au NPs from aqueous solutions. Compound **11** was the most effective at passivating Au NP surfaces, and could even be used to extract anisotropic NPs like Au nanorods into organic solvents, enabling us to measure significant solvatochromic effects [23].



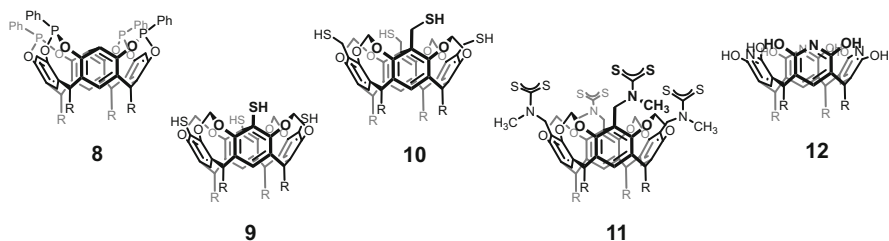


**Fig. 34.8** Chemisorptive calixarenes for stabilizing Au NPs in organic solvents ( $R = C_{11}H_{23}$ )

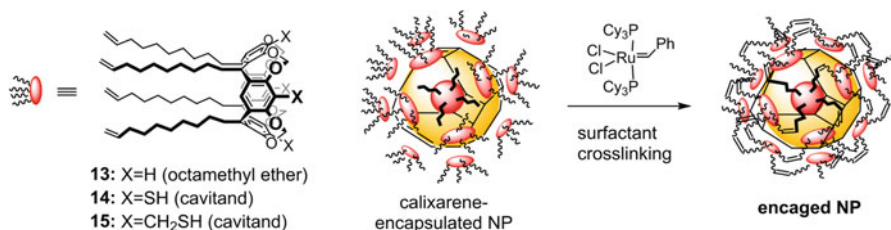


**Fig. 34.9** Au NPs encaged in nondescriptive shells of crosslinked calixarenes [24, 25]

The stable dispersion of calixarene-encapsulated NPs in organic solvents offered opportunities to perform additional reaction on the NP surface. However, the scope was restricted by the robustness of the chemisorptive ligands. For example, Au NPs encapsulated by **10** were susceptible to oxidation or surface exchange with competing thiols, resulting in ligand desorption loss of NP stability [20]. This limitation could be removed by encaging NPs within covalent shells of crosslinked calixarenes, to support a wider range of chemical reactions. We thus prepared tetra-*C*-(9-decenyl)resorcinarenes **13–15** to encapsulate Au NPs in organic solvents, followed by crosslinking using Grubb's first-generation olefin metathesis catalyst (Fig. 34.9). Gold nanocrystals encaged in crosslinked shells of octa-*O*-methyl ether **13** were found to be resistant to thiol-induced precipitation, and could be isolated by size-exclusion chromatography [24]. Tetrathiol and tetramethylthiol cavitand **14** and **15** were able to extract 20-nm Au NPs from water into THF–toluene mixtures, and were also amenable to crosslinking by olefin metathesis using 30 mol% catalyst without significant loss of dispersion stability [4]. Again, the crosslinked cavitand shells were resistant to surface desorption as well as heating; in addition, NPs encaged in shells of crosslinked **15** could withstand multiple rounds of centrifugation and redispersion, with less than 10% attrition in OD after ten cycles.

Nanoparticles encaged in shells of crosslinked **15** were then subjected to further synthetic modifications, taking advantage of the high density of *cis*-alkenes on the crosslinked monolayer (Fig. 34.10). Treatment with excess dimethyldioxirane

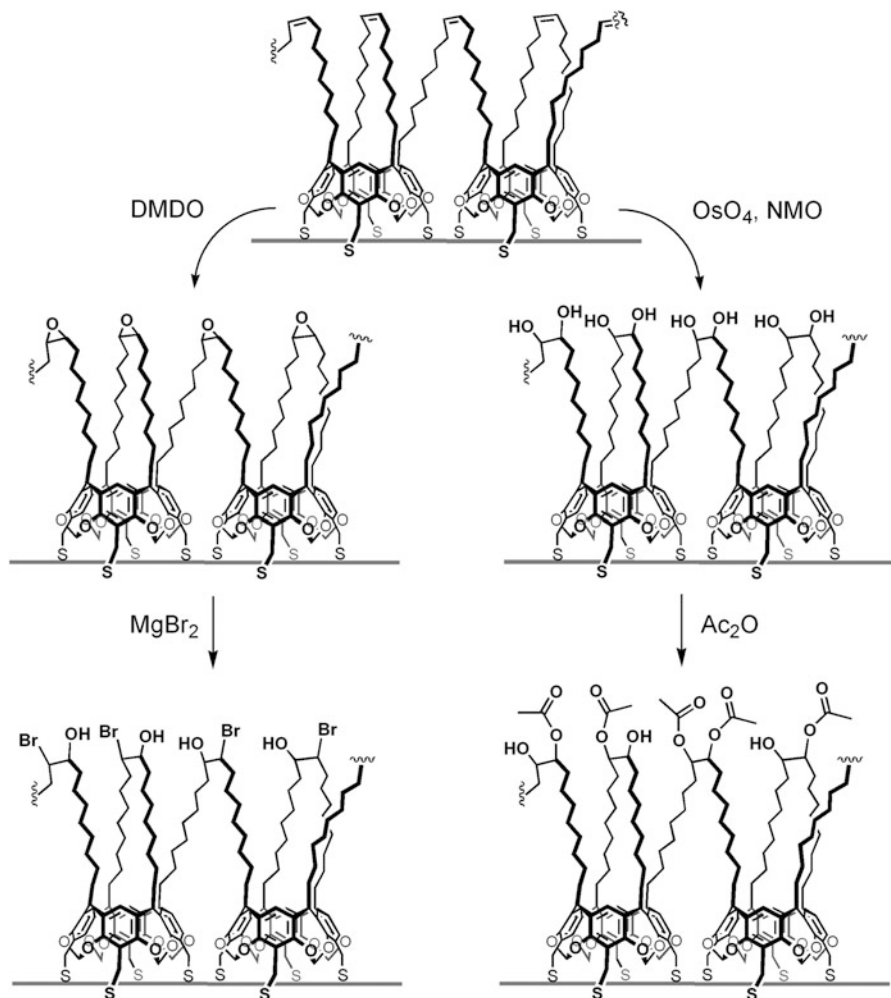


**Fig. 34.10** Synthetic modifications of Au NPs encaged in shells of crosslinked **15** (Reprinted with permission from the Royal Chemical Society)

(DMDO) yielded epoxidized cages; over 60% of the NPs could be recovered, despite the presumed oxidation of the adsorbed thiolates. Redispersion of the encaged NPs into  $\text{Et}_2\text{O}$  and treatment with  $\text{MgBr}_2$  yielded poly(1,2-bromohydrin) coatings that permitted NPs to be stably dispersed in MeOH. In a similar vein, NPs in crosslinked **15** were treated with  $\text{OsO}_4$  and excess *N*-methylmorpholine oxide (NMO) to generate polyhydroxylated cages, and could be acetylated with good recovery of encaged NPs.

## 34.4 Calixarenes in Nanoparticle Self-Assembly

Dispersion control is essential for ordered self-assembly, which involves a balance between enthalpic and entropic forces. Methods for achieving such equilibria vary considerably: For metal NPs less than 10 nm, vdW forces are typically at or below thermal energies ( $k_B T$ ), allowing self-assembly to be driven by supramolecular interactions such as hydrogen bonding or the interdigitation between hydrocarbon chains [18]. For these cases, NPs can self-organize into close-packed 2D arrays by simply casting dispersions onto wettable substrates followed by solvent evaporation under controlled conditions [25], or by deposition onto air–water interfaces followed by compression using Langmuir–Blodgett techniques [26, 27]. Surfactant-coated NPs can also self-organize into 3D superlattices using molecular crystal growth techniques [28, 29].

For metal NPs much larger than 10 nm, interparticle attraction can overwhelm short-range steric repulsion, leading to kinetically driven aggregation instead of self-organization. Simply increasing the length of the surfactant tailgroup does not necessarily increase entropic steric repulsion, as chain reptation remains restricted under close-packed conditions. Conformational entropy can be enhanced instead by adjusting surfactant chain density (cf. Fig. 34.7), analogous to the polymer brush model developed by Alexander and DeGennes [30]. The brush model can be extended qualitatively to surfactant monolayers if the chains are separated by a distance  $s$  such that  $X < s < L$ , where  $X$  represents the effective surfactant cross section (i.e. chain thickness) and  $L$  represents the length of the extended chain. Surfactant layers supporting an appropriate degree of short-range entropic repulsion can then effectively counter long-range attraction during self-assembly; the net result is a secondary minimum that defines the distance  $\delta$  between NP surfaces (Fig. 34.11).

Surfactants based on calixarenes are ideally suited for mediating NP self-assembly, for the reasons described above. In the case of the resorcinarene framework, the four hydrocarbon tails on each macrocyclic headgroup are grafted several angstroms apart, which ensures a high degree of conformational freedom per chain in the surfactant monolayer, even at maximum packing density on the NP surface (cf. Fig. 34.7).

### 34.4.1 Self-Organization of Calixarene-Encapsulated Au NPs into 2D Arrays

Initial studies were performed using toluene solutions of tetrathiol cavitand **9**, which was capable of extracting colloidal Au NPs from aqueous solutions. Passivation of Au NPs by **9** was in fact incomplete, resulting in their trapping at the biphasic solvent interface [31]. The calixarene-encapsulated NPs could be fully extracted into toluene by exchanging residual alkali counterions with

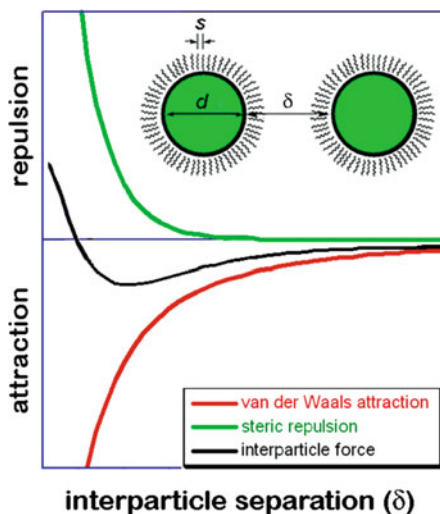


**Fig. 34.11** Force-distance curves between two NPs with diameter  $d$ , coated with surfactant layers having separation  $s$  between chains of length  $L$  [18]. Thermodynamic self-assembly can be achieved when long-range vdW attraction (*red*) is countered by short-range steric repulsion (*green*), which gives rise to a secondary minimum that defines the optimum distance between NPs in their self-assembled state (Reprinted with permission from the Royal Society of Chemistry)

tetraoctylammonium salts;[20] this was however unnecessary, as removal of the toluene layer permitted NP self-assembly at the air–water interface, and facile film transfer under Langmuir–Schaefer conditions. These conditions could be applied to a range of Au NP sizes, from 16 to 170 nm; TEM analysis revealed all self-organized NP films to have monoparticulate thickness with a high degree of local 2D order (Fig. 34.12).

TEM analysis of 2D arrays at high digital resolution (1200 dpi) enabled us to directly measure interparticle spacings ( $\delta$ ) to the first degree of approximation (Fig. 34.13). This revealed an inverse correlation between  $\delta$  and particle size ( $d$ ), corresponding with the size-dependent increase in van der Waals attraction (pressure) between NPs. The limited precision of these measurements precludes analysis of the surfactant thickness in absolute terms; nevertheless, they suggest that the calixarene chains are highly compressed rather than radially extended.

The 2D arrays of calixarene-encapsulated Au NPs also exhibit collective optical properties that vary with NP size and interparticle spacing [31, 32]. These structure–property relationships lie outside the scope of this chapter and are discussed in detail elsewhere;[16, 18] only a few highlights are presented here. In brief, Au NPs within the 2D arrays are strongly coupled, causing their plasmon resonances to broaden and shift by hundreds of nanometers into the near-infrared region (Fig. 34.14). The Au NP arrays also give rise to intense but highly localized electromagnetic (EM) field enhancements, concentrated at the cusps between NPs [33]. These near-field effects can support a variety of plasmon-enhanced

**Fig. 34.12** TEM image of self-organized 2D array of Au NPs ( $70 \pm 5$  nm) encapsulated by tetrathiol calixand **9**. FFT image (lower left) shows several harmonics, indicative of good local 2D order (Reprinted with permission from the American Chemical Society)

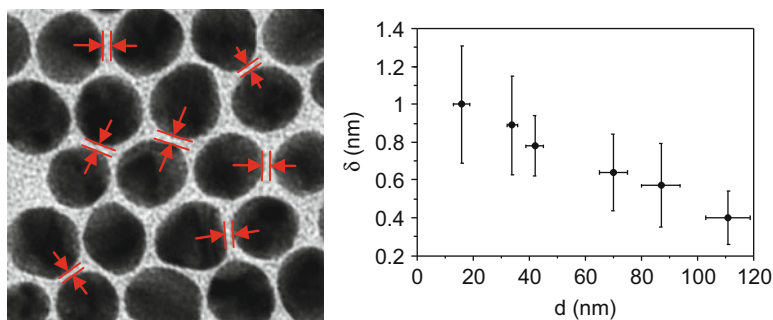
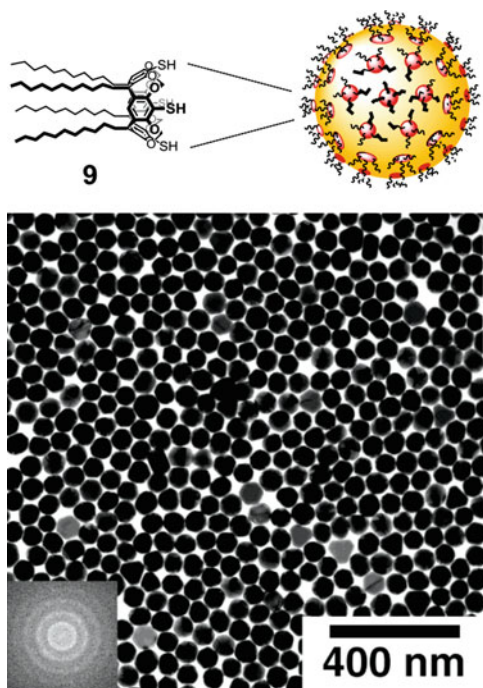


**Fig. 34.13** Left, TEM image analysis of interparticle spacings at high digital resolution (1200 dpi); right, inverse correlation between mean spacings ( $\delta$ ) and NP diameters ( $d$ ). Errors are equal to one standard deviation (Reprinted with permission from the American Chemical Society)

spectroscopies including surface-enhanced Raman scattering (SERS), which can enhance the vibrational bands of adsorbed molecules by many orders of magnitude. For the case of Au NP arrays encapsulated by **9**, SERS signals were produced from approximately 1 fmol of adsorbate, corresponding to surface-averaged enhancements up to  $10^7$ -fold [32], and several more orders of magnitude for localized peak enhancements [33].

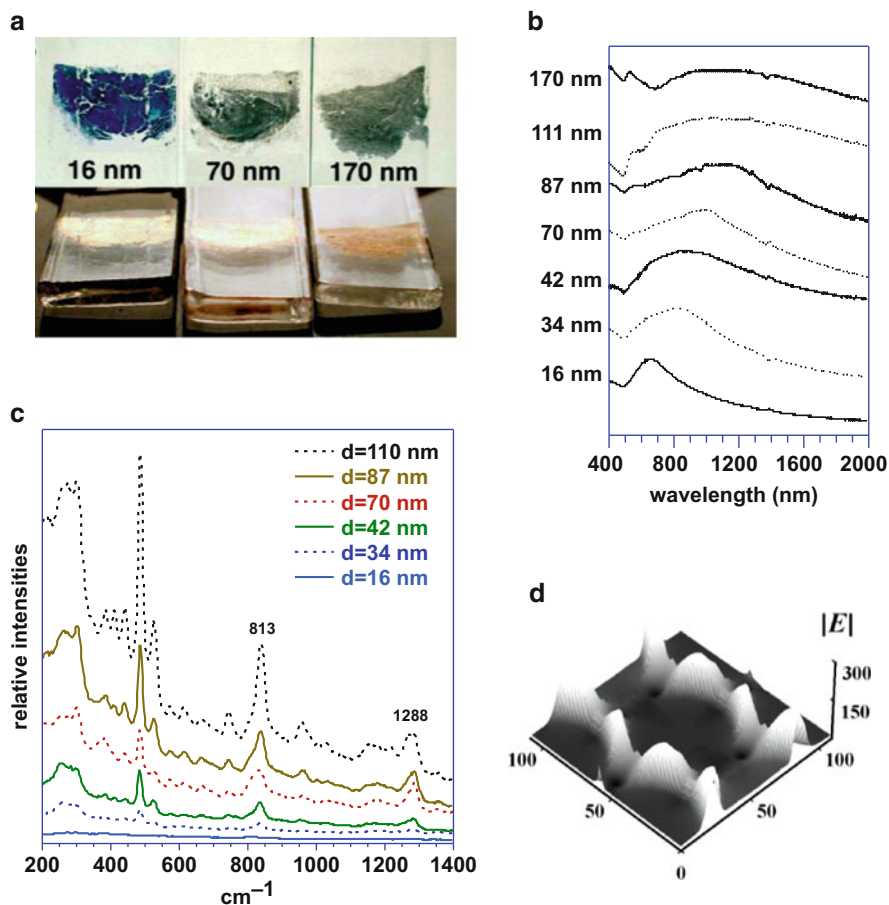


**Fig. 34.14** (a) 2D arrays of 16-, 70-, and 170-nm Au NPs on quartz, photographed at 0 and 60° angles of incidence [32]. Substrate width = 1 cm. (b) Visible–NIR extinction spectra of Au NP arrays [31]. (c) SERS spectra of Au NP arrays encapsulated by **9** (~1 fmol) using 785 nm excitation [32]. (d) Numerical simulation of EM field enhancements between Au NPs [33] (Reprinted with permission from the American Chemical Society and Wiley-VCH)

### 34.4.2 Self-Assembly of Calixarene-Encapsulated Co NP Rings

Up to now, we have considered self-assembly conditions driven by nondirectional, long-range vdW forces; however, NPs can also be directed by electric or magnetic dipoles, which can give rise to anisotropic assemblies. We wished to determine whether calixarenes could influence the self-assembly of NPs with remanent magnetic dipoles at room temperature. Magnetic NPs are characterized by an anisotropy energy that is proportional to  $K_u V/k_B T$ , where  $K_u$  represents a material-dependent,

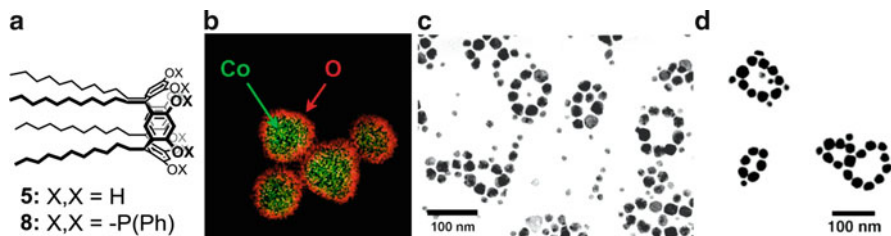


**Fig. 34.15** (a) Calixarenes **5** and **8** used in the synthesis and self-assembly of Co NP rings; (b) energy-filtered TEM image of Co NPs with CoO shells [37]; (c) initial mixture of Co NPs stabilized with **5** in toluene deposited onto TEM substrate, with larger ( $>20$  nm) NPs assembled into nanorings [18]; (d) size-refined Co NPs ( $27 \pm 4$  nm) stabilized by **5** in toluene, deposited onto TEM substrate [37] (Reprinted with permissions from the American Chemical Society and the Royal Society of Chemistry)

uniaxial anisotropy constant and  $V$  is the NP (domain) volume. The magnetic (Néel) relaxation time that defines remanence in the absence of a magnetic field increases exponentially with  $K_u V$ , making NP size a critical factor in ferromagnetic behavior at room temperature [34, 35]. Ferromagnetic NPs are thus subject to medium-range dipolar attractions that increase as a function of  $1/D^3$ , where  $D$  is the distance between NP centers (i.e.  $d + \delta$ ), in addition to long-range vdW forces that scale as an approximate function of  $1/D^2$ .

Our initial studies were based on weakly ferromagnetic (thermoremanent) Co NPs, which were synthesized by the thermal decomposition of  $\text{Co}_2(\text{CO})_8$  in toluene solutions containing tetra-*O,O*-phosphonite resorcinarene **8**, followed by exposure to air and magnetically induced precipitation [36, 37]. This produced polycrystalline Co NPs having a wide size range, with each NP coated by a thin but stable CoO shell based on energy-filtered TEM analysis (Fig. 34.15a, b). TEM also revealed a remarkably high count of self-assembled nanorings, each comprised of five to ten NPs. Most particles in these rings were at least 20 nm in size; smaller NPs ( $<15$  nm) did not participate directly in ring self-assembly due to the size-dependent transition between superparamagnetism and ferromagnetism. Further refinement by size-selective precipitation ( $d_{\text{av}} = 27 \pm 4$  nm) and redispersion in toluene solutions of C11 resorcinarene (**5**) recreated self-assembled Co nanorings at high density (Fig. 34.15d).

Magnetic NPs with cooperative dipolar interactions are well known to assemble into chains, which provide the basis for field-induced changes in viscosity of ferrofluids [38]. However, in situations where the dipolar couplings are weak (on the order of  $k_B T$ ), ring assembly is entropically favored over chains in the absence of applied magnetic fields. To prove this point, we prepared TEM samples in which calixarene-encapsulated Co NPs dispersed in toluene were exposed to a uniaxial magnetic field during deposition and drying, which resulted in a mixture of NP chains and rings (Fig. 34.16a). However, removing the magnetic field allowed the Co NP dispersions to equilibrate which restored the high number of self-assembled nanorings, demonstrating their thermodynamic preference to chain formation (Fig. 34.16b). Parallel studies performed with  $\text{CH}_2\text{Cl}_2$  dispersions



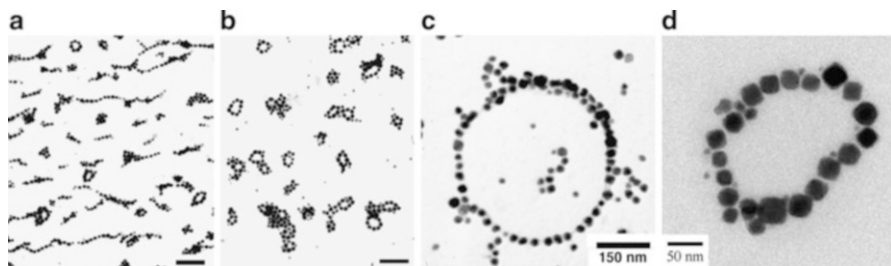


**Fig. 34.16** (a) Calixarene-encapsulated Co NPs exposed to a linear magnetic field during evaporative self-assembly from toluene (bar = 200 nm); (b) NPs deposited in the same manner in the absence of magnetic field (bar = 200 nm); (c) NP dispersions deposited under rapid evaporation (dissipative) conditions from  $\text{CH}_2\text{Cl}_2$ , resulting in larger, kinetically formed rings [37]. (d) Self-assembly of “macrocycles” from calixarene-encapsulated Co NPs [15] (Reprinted with permission from the American Chemical Society)

showed that larger, radially symmetric rings could be formed due to dissipative effects driven by rapid solvent evaporation (Fig. 34.16c); however, close inspection of these rings revealed multiple gaps between Co NPs, unlike the close-packed NP rings deposited from toluene. This illustrates how a change in the balance of forces can dictate the final structures of the self-assembled nanorings. It is worth noting that calixarene **5** is again essential for the controlled self-assembly of CoNPs into nanorings; replacing it with an equimolar amount of oleic acid resulted in close-packed aggregates by TEM analysis [15].

Subsequent studies have shown that the median size of nanorings (formed by dipolar self-assembly) can be reduced by diluting the dispersion prior to deposition, producing rings less than 100 nm across [39], or expanded into necklace-like NP “macrocycles” by exposing the calixarene-encapsulated Co NPs to uniaxial magnetic field shortly before (but not during) deposition (Fig. 34.16d) [15, 40]. Experimental control over nanoring size permitted us to explore its influence on magnetic flux closure (FC), a collective state with a net zero dipole that could be visualized by a specialized TEM technique known as off-axis electron holography (Fig. 34.17) [39, 41]. FC states are bistable and can possibly serve as nonvolatile memory bits, given a reliable switching mechanism; the structure–property relationships of Co nanorings and their potential technological applications are discussed elsewhere [40, 42]. In brief, self-assembled nanorings comprised of five to ten Co NPs support FC states at room temperature, which exist as racemic mixtures of clockwise (CW) and counterclockwise (CCW) states [39]. The polarizations of individual nanorings exhibit significant resistance to field-induced switching, but the FC states can be reversed by applying out-of-plane magnetic fields of sufficient strength. The critical field strength for FC switching at room temperature is 2.0–2.5 kOe for rings comprised of polycrystalline NPs, and 3–4 kOe for rings comprised of single-crystal fcc-Co NPs [43]. Interestingly, larger NP rings also favor FC formation, but can also support other remanent states with nonzero magnetic dipoles, an observation that remains to be further characterized.



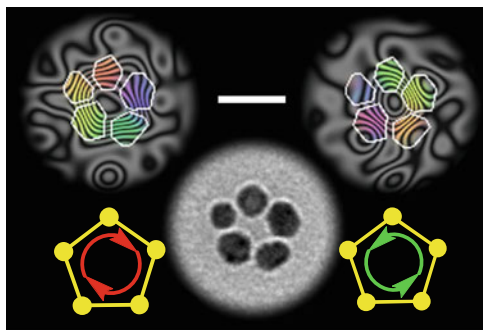


**Fig. 34.17** Self-assembled Co NP ring imaged by brightfield TEM (*center*) and by off-axis electron holography (*top*); bar = 50 nm. The latter reveals bistable flux-closure (FC) states, polarized either CW (*left*) or CCW (*right*). FC polarization can be switched by applying an out-of-plane magnetic “pulse” with a peak strength of 2–4 kOe. Line-bond representations for the Co NP ring and FC states are shown below for clarity [40] (Reprinted with permission from the Royal Society of Chemistry)

## 34.5 Conclusions

The supramolecular community has long been fascinated with molecular and nano-encapsulation with the prospects of novel chemical or material function. Calixarenes are truly versatile in this regard, and a variety of molecular interactions have been employed to form nanocapsules with endohedral cavities including hydrogen bonding [44, 45], metal-ion coordination [46], or dynamic covalent chemistry [47]. In the case of inorganic and metal NPs, encapsulation is templated and most readily achieved by surface chemisorption, but longer-range colloidal forces become dominant over short-range intermolecular forces as the particle size increases. Here, too, calixarenes can make a difference, by serving as a modular platform for stabilizing metal or magnetic NPs for their controlled self-assembly into 1D and 2D nanostructures. Calixarenes are also excellent templates for NP synthesis, and offer a novel approach for controlling pre- and post-nucleation processes that support stoichiometric control over NP size. Many opportunities remain for designing calixarene-based scaffolds as nanostructures, limited only by our understanding of the physical forces that direct the assembly of nanosized building blocks, and by our own creative drive.

## References

1. (a) Lehn, J.-M. *Supramolecular Chemistry: Concepts and Perspectives*. VCH Publishers: New York, NY, 1995. (b) Steed, J. W.; Atwood, J. L. *Supramolecular Chemistry*. 2nd ed.; John Wiley & Sons, Ltd: 2009.
2. (a) Evans, D. F.; Wennerström, H. *The Colloidal Domain: Where Physics, Chemistry, Biology, and Technology Meet*. 2nd ed.; Wiley-VCH: New York, 1999. (b) Ozin, G. A.; Arsenault, A.;

- Cademartiri, L. *Nanochemistry: A Chemical Approach to Nanomaterials*. 2nd ed.; RSC Publishing: 2009
- Cram, D. J. K., S.; Kim, Y. H.; Baczynskyj, L.; Kallemeyn, G. W. *J. Am. Chem. Soc.* **1985**, *107*, 2575–2576.
  - Balasubramanian, R.; Kwon, Y.-G.; Wei, A. *J. Mater. Chem.* **2007**, *17*, 105–112.
  - Peng, S.; Gao, J.; Liu, Y.; Guo, D.-S. *Chem. Commun.* **2015**, *51*, 16557–16560.
  - LaMer, V. K.; Dinegar, R. H. *J. Am. Chem. Soc.* **1950**, *72*, 4847–4854.
  - Watzky, M. A.; Finke, R. G. *J. Am. Chem. Soc.* **1997**, *119*, 10382–10400.
  - (a) Zheng, H.; Smith, R. K.; Jun, Y.-w.; Kisielowski, C.; Dahmen, U.; Alivisatos, A. P. *Science* **2009**, *324*, 1309–1312. (b) Liao, H.-G.; Niu, K.; Zheng, H. *Chem. Commun.* **2013**, *49*, 11720–11727.
  - Samia, A. C. S.; Schlueter, J. A.; Jiang, J. S.; Bader, S. D.; Qin, C.-J.; Lin, X.-M. *Chem. Mater.* **2006**, *18*, 5203–5212.
  - Nabok, A. V.; Richardson, T.; Davis, F.; Stirling, C. J. M. *Langmuir* **1997**, *13*, 3198–3201.
  - Liu, J.; Ong, W.; Kaifer, A. E.; Peinador, C. *Langmuir* **2002**, *18*, 5981–5983.
  - Hartlieb, K. J.; Saunders, M.; Raston, C. L. *Chem. Commun.* **2009**, 3074–3076.
  - Huc, V.; Pelzer, K. *J. Colloid Interface Sci.* **2008**, *318*, 1–4.
  - Liu, J.; Wei, A. *Chem. Commun.* **2009**, 4254–4256.
  - Chen, Z.; Liu, J.; Evans, A. J.; Alberch, L.; Wei, A. *Chem. Mater.* **2014**, *26*, 941–950.
  - (a) Wei, A., Plasmonic Nanomaterials: Enhanced Optical Properties From Metal Nanoparticles and their Ensembles. In *Nanoparticles: Scaffolds and Building Blocks*, Rotello, V. M., Ed. Kluwer Academic: New York, 2004; pp 173–200. (b) Wei, Q.; Wei, A., Signal Generation with Gold Nanoparticles: Photophysical Properties for Sensor and Imaging Applications. In *The Supramolecular Chemistry of Organic-Inorganic Hybrid Materials*, Rurack, K.; Martinez-Manez, R., Eds. John Wiley and Sons: New York, 2010; pp 319–49.
  - Stavens, K. B.; Puzstay, S. V.; Zou, S.; Andres, R. P.; Wei, A. *Langmuir* **1999**, *15*, 8337–8339.
  - Wei, A. *Chem. Commun.* **2006**, 1581–91.
  - Wei, A.; Stavens, K. B.; Puzstay, S. V.; Andres, R. P. *MRS Symp. Proc. Ser.* **1999**, *581*, 59–63.
  - (a) Balasubramanian, R.; Xu, J.; Kim, B.; Sadtler, B.; Wei, A. *J. Dispers. Sci. Tech.* **2001**, *22*, 485–489. (b) Balasubramanian, R.; Kim, B.; Tripp, S. L.; Wang, X.; Lieberman, M.; Wei, A. *Langmuir* **2002**, *18*, 3676–3681.
  - Zhao, Y.; Pérez-Segarra, W.; Shi, Q.; Wei, A. *J. Am. Chem. Soc.* **2005**, *127*, 7328–29.
  - Kim, B.; Balasubramanian, R.; Pérez-Segarra, W.; Wei, A.; Decker, B.; Mattay, J. *Supramol. Chem.* **2005**, *17*, 173–180.
  - Hansen, M. N.; Chang, L.-S.; Wei, A. *Supramol. Chem.* **2008**, *20*, 35–40.
  - Puzstay, S. V.; Wei, A.; Stavens, K. B.; Andres, R. P. *Supramol. Chem.* **2002**, *14*, 291–294.
  - Lin, X. M.; Jaeger, H. M.; Sorensen, C. M.; Klabunde, K. J. *J. Phys. Chem. B* **2001**, *105*, 3353–3357.
  - Narayanan, S.; Wang, J.; Lin, X.-M. *Phys. Rev. Lett.* **2004**, *93*, 135503.
  - Markovich, G.; Collier, C. P.; Henrichs, S. E.; Remacle, F.; Levine, R. D.; Heath, J. R. *Acc. Chem. Res.* **1999**, *32*, 415–423.
  - Murray, C. B.; Kagan, C. R.; Bawendi, M. G. *Science* **1995**, *270*, 1335–1338.
  - Talapin, D. V.; Shevchenko, E. V.; Kornowski, A.; Gaponik, N.; Haase, M.; Rogach, A. L.; Weller, H. *Adv. Mater.* **2001**, *13*, 1868–1871.
  - (a) Alexander, S. *J. Physique* **1977**, *38*, 977–981. (b) DeGennes, P.-G. *Macromolecules* **1980**, *13*, 1069–1071.
  - Kim, B.; Tripp, S. L.; Wei, A. *J. Am. Chem. Soc.* **2001**, *123*, 7955–7956.
  - Wei, A.; Kim, B.; Sadtler, B.; Tripp, S. L. *ChemPhysChem* **2001**, *2*, 743–745.
  - Genov, D. A.; Sarychev, A. K.; Shalaev, V. M.; Wei, A. *Nano Lett.* **2004**, *4*, 153–158.
  - Néel, L. *Adv. Phys.* **1955**, *4*, 191–243.
  - Dunlop, D. J. *J. Appl. Phys.* **2003**, *93*, 8236–8240.
  - Wei, A.; Kim, B.; Puzstay, S. V.; Tripp, S. L.; Balasubramanian, R. *J. Inclusion Phenom. Macrocyclic Chem.* **2001**, *41*, 83–86.

37. Tripp, S. L.; Puszta, S. V.; Ribbe, A. E.; Wei, A. *J. Am. Chem. Soc.* **2002**, *124*, 7914–7915.
38. Rosensweig, R. E. *Ferrohydrodynamics*. Cambridge University Press: Cambridge, 1985.
39. Tripp, S. L.; Dunin-Borkowski, R. E.; Wei, A. *Angew. Chem. Int. Ed.* **2003**, *42*, 5591–5593.
40. Wei, A.; Kasama, T.; Dunin-Borkowski, R. E. *J. Mater. Chem.* **2011**, *21*, 16686–16693.
41. Dunin-Borkowski, R. E.; Kasama, T.; Wei, A.; Tripp, S. L.; Hytch, M. J.; Snoeck, E.; Harrison, R. J.; Putnis, A. *Microsc. Res. Techn.* **2004**, *64*, 390–402.
42. Wei, A.; Tripp, S. L.; Liu, J.; Kasama, T.; Dunin-Borkowski, R. E. *Supramol. Chem.* **2009**, *21*, 189–195.
43. Kasama, T.; Dunin-Borkowski, R. E.; Scheinfein, M. R.; Tripp, S. L.; Liu, J.; Wei, A. *Adv. Mater.* **2008**, *20*, 4248–4252.
44. Dalgarno, S. J.; Tucker, S. A.; Bassil, D. B.; Atwood, J. L. *Science* **2005**, *309*, 2037–2039.
45. Avram, L.; Cohen, Y. *Chem. Soc. Rev.* **2015**, *44*, 586–602.
46. Kumari, H.; Deakyne, C. A.; Atwood, J. L. *Acc. Chem. Res.* **2014**, *47*, 3080–3088.
47. Liu, X.; Warmuth, R. *Nat. Protocols* **2007**, *2*, 1288–1296.

# Chapter 35

## Calixarenes and Nanoparticles

Francesco Vita, Arturo Arduini, and Andrea Secchi

### 35.1 Introduction

Atoms and molecules at the surfaces represent a fourth state of matter, where the gradients in properties are greatest. Self-assembled monolayers [1] (SAM) are organic assemblies formed by the adsorption of molecular constituents from solution or the gas phase onto solid surfaces. The organic ligands in such monolayer often possess a functional group, or “head-group”, with specific and high affinity for the material and allow their anchorage on the surface [2]. When the organic monolayer is self-assembled on the surface of a pseudo-spherical inorganic core, the resulting nano-sized structures are usually indicated as ligand-stabilized nanoparticles (NPs) [2–8]. The organic monolayer confers a steric protection to the inorganic core and is very effective in preventing aggregation phenomena, making these nanoparticles soluble in most organic solvents, stable in several conditions and with a relatively long shelf life [4, 5, 9]. They are also characterized by a low radius of curvature of their core that decreases the chain density of the organic shell, thus leading to a minimization of steric hindrance that could be instead present in SAMs on flat surfaces [10]. The most important feature of these small size organic-inorganic hybrid materials is the possibility to couple the unique and tunable properties of their inorganic core, with the chemistry of the protecting organic ligand. As a matter of fact, in the last three decades, nanoparticles bearing in their organic monolayer either natural or synthetic receptors have been synthesized and employed to study the supramolecular aspects of the monolayers as multivalent hosts or as new building blocks for self-assembly processes. This could finally enable the manufacturing of nanoscale devices with

---

F. Vita • A. Arduini • A. Secchi (✉)

Dipartimento di Chimica, Università di Parma, Parco Area delle Scienze 17/a, I-43124 Parma, Italy

e-mail: [andrea.secchi@unipr.it](mailto:andrea.secchi@unipr.it)

potential applications as sensors, waveguides, switches and for the preparation of novel functional materials [6, 11–14]. In this field, defined by Fitzmaurice as *hetero-supramolecular chemistry* [15], calixarene derivatives, are assuming also an increasing role as functional protecting layers of nanoparticles. In this perspective the present chapter will mainly describe recent literature examples which regard the synthesis and properties of two general classes of calixarene-capped NPs. This classification, based on the nature of the inorganic core and relative properties will cover noble metals nanoparticles, in particular of gold and silver. For larger (colloidal) metal nanoparticles stabilized by calixarene derivatives see Chap. 34 of this book. Calixarene-capped NPs whose cores are made of organic materials will not be treated at all.

## 35.2 Gold Nanoparticles

Thanks to the easy and reliable synthetic procedures devised by Brust and Schiffrin [16–18], it is nowadays possible the preparation of stable gold nanoparticles (AuNPs) of controllable size and reduced dispersity. The possibility to accomplish post-functionalization reactions on the organic monolayer and the particular optical properties of their gold core, the localized surface plasmon resonance (LSPR) [19–21], makes this class of nanomaterials one of the most studied. Indeed, in the last three decades, they have found applications in many fields, such as sensing, catalysis and drug delivery [22–24]. The functionalities present in the self-assembled monolayer can be directly inserted on the gold surface during the synthesis of the nanoparticles (see *infra*), but the most common strategy adopted is the displacement of one ligand for another in the organic shell after the formation of the nanoparticles [25–28]. These “ligand-exchange” methods are particularly useful, for example, if the ligand to be inserted is not compatible with the conditions used for the synthesis of the nanoparticles. This approach allows the possibility to insert ligands with different functionalities on the same inorganic surface [29]. Indeed, mixed-monolayer systems greatly enhance the versatility of these nanomaterials, allowing the construction of even more complicated and promising devices.

One of the first examples of calixarene-capped AuNPs employed for host-guest studies was published by Arduini and co-workers in 2005 [30]. The calixarene derivatives chosen for these studies were 1,3-dialkoxycalix[4]arenes, which were known to form endo-cavity inclusion complexes with tetraalkylammonium and *N*-alkyl pyridinium ion pairs in weakly polar solvents [31, 32].

To disclose a possible effect of the distance of the calixarene cavities from the gold core on the recognition efficiency, calix[4]arenes bearing two  $\omega$ -alkanethiol chains of eleven (**2a**) or six carbon (**2b**) atoms were prepared in a three-steps synthesis from the *p*-H-calix[4]arene (**1**) (see Fig. 35.1). The anchoring of these bidentate thiolate ligands on the gold surface was carried out through a ligand-exchange reaction on  $\sim$ 2-nm dodecanethiol-capped AuNP(C12), prepared

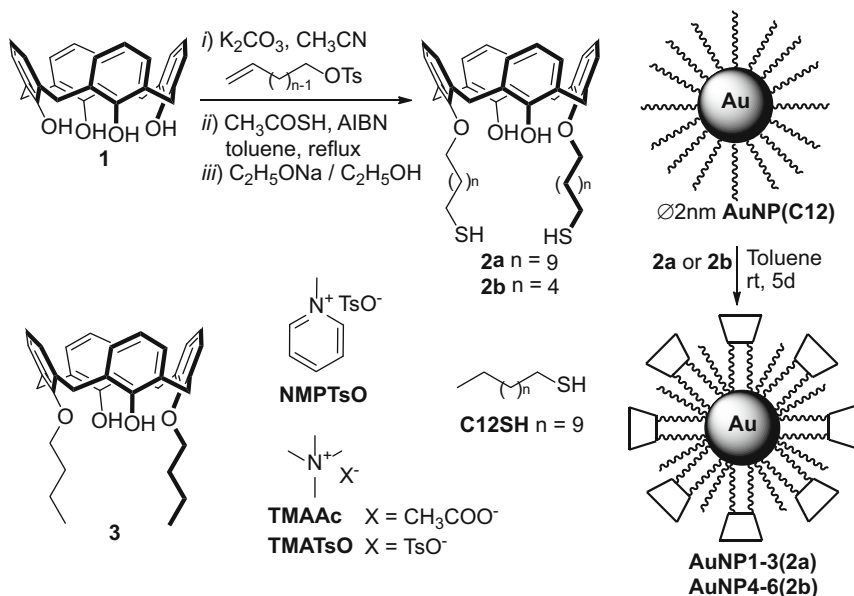


**Fig. 35.1** (Top, left) Synthesis of bidentate thiolate calix[4]arene **2a** and **2b**; (right) schematic representation of the synthesis of a series of AuNPs having a mixed organic monolayer of thiolate calix[4]arene (**2a** or **2b**) and dodecanthiol (**C12SH**) prepared by a ligand-exchange reaction from dodecanthiol-capped **AuNP(C12)**; (bottom, left) 1,3-dipropoxy calix[4]arene **3** and tetramethylammonium and *N*-methyl pyridinium salts

according to the Brust-Schiffrin method [16]. By this way, a series of nanoparticles, indicated as **AuNP1–6**, having a mixed-monolayer of calix[4]arene (**2a** or **2b**) and dodecanthiol (**C12SH**) in different molar ratios, were prepared and characterized. The binding ability of **AuNP1–6** vs. *N*-methylpyridinium tosylate (**NMPTsO**) was evaluated in chloroform solution through  $^1H$  NMR measurements, in terms of “average binding constant”  $\log K_{av}$  (see Table 35.1). This binding constant represents a measure of the strength of the noncovalent binding interaction between a single host moiety and a single guest in a multivalent host system.

The results reported in Table 35.1 show that the insertion of calix[4]arene binding elements on the surface of the nanoparticles increases the extent of binding of **NMPTsO** up to twice the value of the  $\log K$  calculated for the “free” 1,3-dipropoxy calix[4]arene host **3** (cf. entries 3 and 7, Table 35.1). The efficiency of binding further enhances as the number of calixarene units present in the monolayer of each series of AuNPs increases (cf. entries 1–3 and 4–6, Table 35.1). However, such enhancement is more marked for the **AuNP1–3** series, in which the organic monolayer contains calix[4]arene ligand having the longer C11  $\omega$ -thiolate alkyl chains (**2a**). This trend was also confirmed, although to a lesser extent, using tetramethylammonium acetate (**TMAAc**) and tosylate (**TMATsO**) ion pairs as guests [30].

**Table 35.1** Average binding constants ( $\log K_{av}$ ) for the complexation of **NMPTsO** by the series of calix[4]arene-capped **AuNP1–6** determined by  $^1\text{H}$  NMR titrations ( $\text{CDCl}_3$ ,  $T = 300\text{ K}$ )

Entry	AuNPs	2a or 2b/C12SH (%) <sup>a</sup>	$\log K_{av}$
1	<b>AuNP1</b>	10 ( <b>2a</b> )	3.5
2	<b>AuNP2</b>	50 ( <b>2a</b> )	4.0
3	<b>AuNP3</b>	100 ( <b>2a</b> )	5.0
4	<b>AuNP4</b>	15 ( <b>2b</b> )	3.2
5	<b>AuNP5</b>	75 ( <b>2b</b> )	3.4
6	<b>AuNP6</b>	100 ( <b>2b</b> )	3.7
7	<b>3</b> <sup>b</sup>	Not applicable	2.4

<sup>a</sup>Percentage of calix[4]arene ligand in the organic monolayer as determined by NMR measurements; <sup>b</sup>only the calix[4]arene ligand.

In later studies, the effect of the thiolate ligand denticity in the size-selective synthesis of a series of calixarene-capped AuNPs, decorated with monodentate (**4**), bidentate (**2a**) and tridentate (**5**) thiolate calix[n]arene ligands, was evaluated (Fig. 35.2) [33, 34]. To disclose the role of the ligand denticity on the size dispersion of the nanoparticles, the authors took advantage of the seminal paper published by Murray and co-workers for dodecanthiol-capped AuNPs [35]. For each ligand, three sets of AuNPs were prepared using different S: Au ratios (3:1, 1:3 and 1:6), where S indicates the equivalents of thiolate alkyl chains, present in the reaction mixture, regardless the nature of the calixarene used. In this way, the outcomes of the synthesis carried out become independent by the absolute amount of calixarene employed. For example, the TEM (transmission electron microscopy) micrographs of the series of nanoparticles obtained using a S: Au ratio = 3:1 are indicated in Fig. 35.2 next to the corresponding calix[n]arene used during the synthesis. The synthesized nanoparticles were characterized with NMR spectroscopy, elemental analysis, TEM and X-ray Photoelectron Spectroscopy (XPS). The latter two type of measurements evidenced as the particular multidentate structure of calix[4]arene **2a** and calix[6]arene **5** introduces a control element in the preparation of the nanoparticles. Very small (~1 nm) nanoparticles were obtained when a S: Au ratio of 3:1 was used during the synthesis (see Fig. 35.2b, c).

The high affinity for organic ion pairs of the calix[4]arene derivatives loaded in the organic monolayer of **AuNP1–3** was also exploited for the recognition of *N*-alkyl pyridinium moieties in aqueous solutions [36]. 14-nm Citrate-stabilized particles, **AuNP(citrate)**, prepared by the Turkevich synthesis [37], were functionalized with a 1:2 mixture of ligands **2a** and (1-sulfanylundec-11-yl) tetraethylene glycol (**6**) in a water/THF mixture (see Fig. 35.3). The resulting particles **AuNP(2a/6)** are stable thanks to the presence in the organic shell of ligands **6**, which acts also as solubilizer for the attached calix[4]arene units. The presence of host **2a** in the particles organic monolayer was verified by NMR measurements in  $\text{D}_2\text{O}$  solution. The recognition abilities in water solution of the unmodified calixarene cavities present in **AuNP(2a/6)** were then qualitatively demonstrated using two different chemically-modified substrates: (a) a SAM of *N*-(11-mercaptoundecyl)pyridinium tosylate ( $7 \times \text{TsO}$ ) on Au, and (b) silica molecular sieve beads loaded with the same ligand (see Fig. 35.4). In the former case

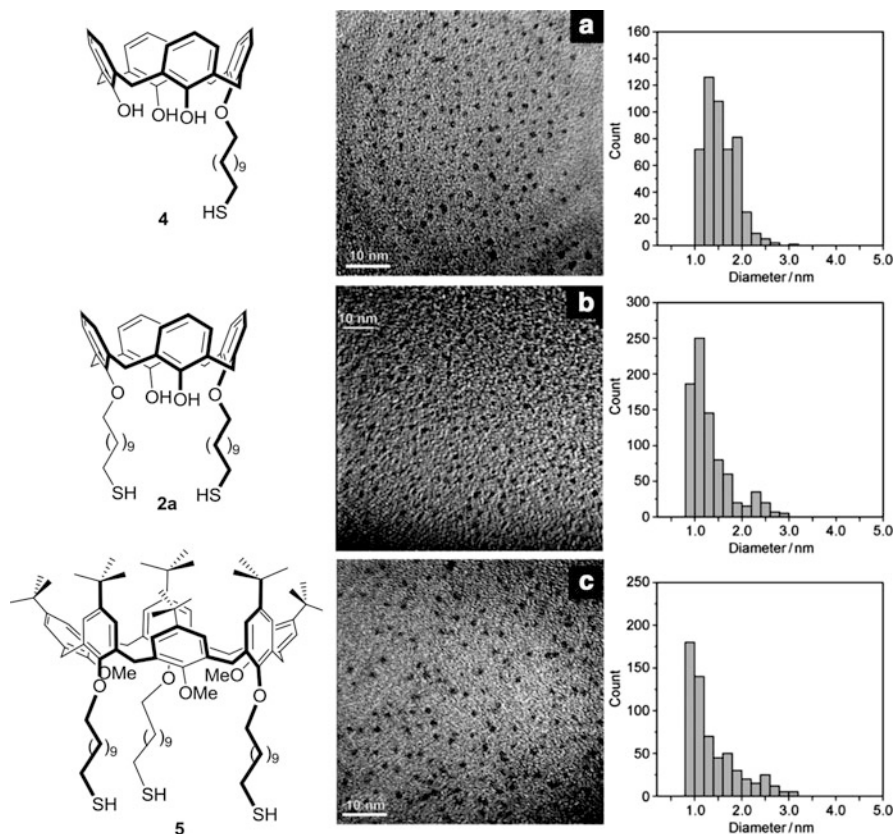


**Fig. 35.2** TEM images and core-size distribution diagrams (*right*) of calixarene-capped AuNPs prepared using S:Au = 3:1 (see text): (a) **AuNP(4)** ( $d_{\text{TEM}} = 1.5 \pm 0.3$  nm); (b) **AuNP(2a)** ( $d_{\text{TEM}} = 1.0 \pm 0.3$  nm), and (c) **AuNP(5)** ( $d_{\text{TEM}} = 1.0 \pm 0.2$  nm) (Adapted with permission from Ref. [33]. Copyright © 2010 WILEY-VCH Verlag GmbH & Co. KGaA, Weinheim)

(Fig. 35.4b) AFM measurements shows the **AuNP(2a/6)** bind selectively to the SAM from aqueous solution. In the second case (Fig. 35.4a), the calixarene-capped nanoparticles bind specifically to the molecular sieve beads primed with  $7 \times \text{TsO}$  from aqueous solution. Both experiments indicated that the cavity of **2a** exhibits its characteristic cation binding properties also in aqueous media.

The affinity in low polar media of the  $\pi$ -rich aromatic cavity of these 1,3-dialkoxy calix[4]arenes for the electron-poor aromatic moiety of *N*-alkyl pyridinium ion-pairs [38], was also exploited to obtain a guest-induced controlled aggregation of  $\sim 6$ -nm calix[4]arene-capped **AuNP(2a)** [39]. These nanoparticles were synthesized through a two-step procedure. First,  $\sim 6$ -nm tetraoctylammonium bromide-stabilized nanoparticles, **AuNP(TOABr)**, were prepared following the procedure reported by Schiffrin [40]. Then, the original charged bilayer was totally displaced by the addition of calix[4]arene **2a** (see Fig. 35.5).



**Fig. 35.3** Synthesis of water-soluble calix[4]arene-capped AuNP(2a/6)

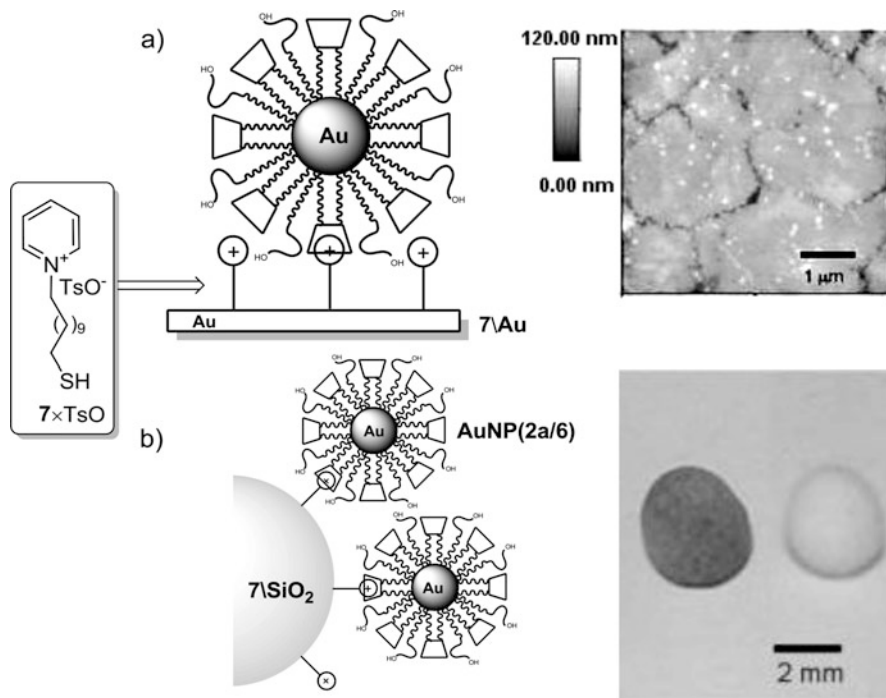
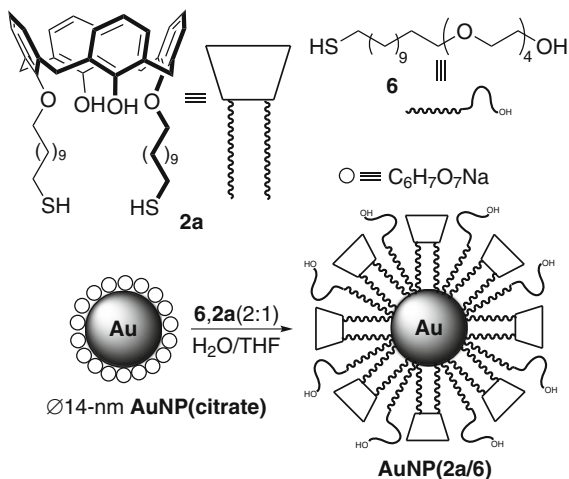


**Fig. 35.4** Schematic representation of the binding in aqueous solution of AuNP(2a/6) with two substrates primed with  $7 \times TsO$ : (a) in the AFM image (*right*) the bright spots represent nanoparticles bound to the gold substrate; (b) picture of two silica beads taken after their soaking in a aqueous solution of AuNP(2a/6): the silica bead on the left results darker than the one of the control experiment because, being previously primed with the  $7 \times TsO$ , it was able to bind AuNP(2a/6) from the solution (Adapted with permission from Ref. [36]. Copyright © 2005 WILEY-VCH Verlag GmbH & Co. KGaA, Weinheim)

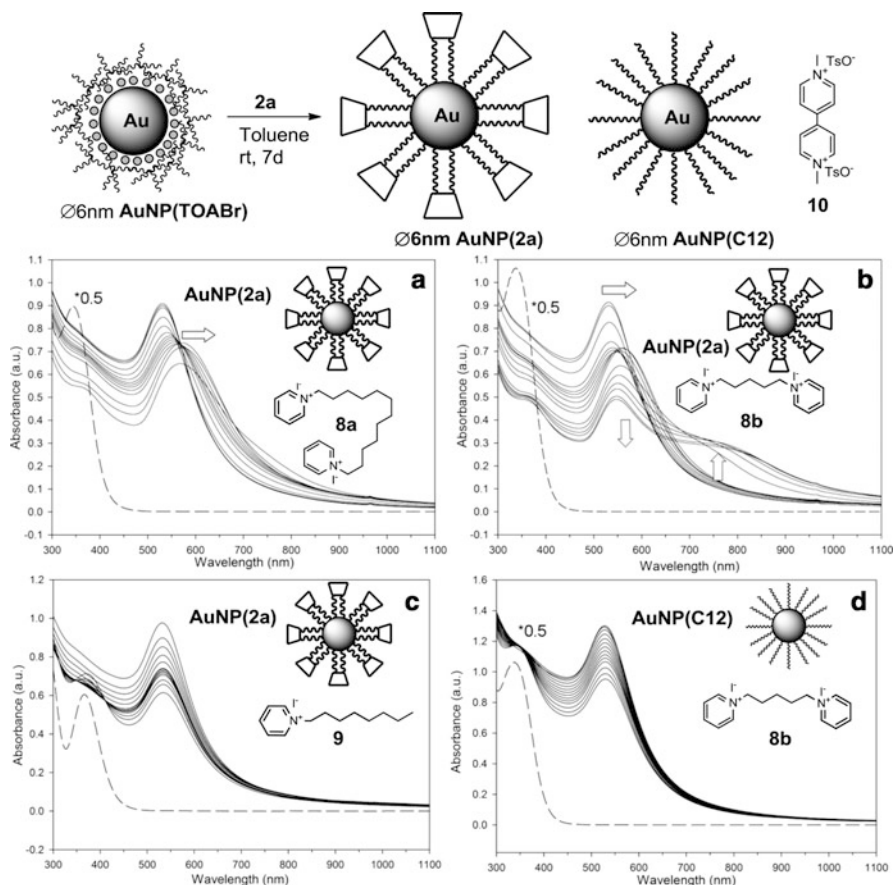


**Fig. 35.5** (Top) Schematic representation of the synthesis of calix[4]arene-capped  $\text{AuNP}(2a)$  and (bottom) collection of UV-Vis spectra in  $\text{CHCl}_3$  solution gathered during the titrations of nanoparticles  $\text{AuNP}(2a)$  with guests (a) **8a**, (b) **8b** and (c) **9**; and (d) of  $\text{AuNP}(\text{C12})$  with guest **8b**. The optical absorption of the free titrant has been depicted as a dashed line (Adapted with permission from Ref. [39]. Copyright © 2010 American Chemical Society)

To induce the guest-driven aggregation of  $\text{AuNP}(2a)$ , three “bifunctional supra-molecular linkers” were used: the “flexible”  $N,N'$ -alkyl dipyridinium diiodides **8a** and **8b**, in which the two pyridinium units are connected by an alkyl chain of ten and five carbon atoms, respectively; and the more rigid  $N,N$ -dimethyl viologen ditosylate **10** (Fig. 35.5). The ability of these nanoparticles to give rise to a superlattice through the complexation of bifunctional guests was evaluated in chloroform solution through UV-Vis and dynamic light scattering (DLS) titrations. As shown in Fig. 35.5a, b, the addition of the bifunctional guests **8a** or **8b** to the  $\text{AuNP}(2a)$  solution induces a large bathochromic shift of the nanoparticles surface plasmon band (SPB), originally centered at  $\lambda = 530$  nm. Using the shorter but still flexible bifunctional guest **8b**, a larger network of aggregated nanoparticles was

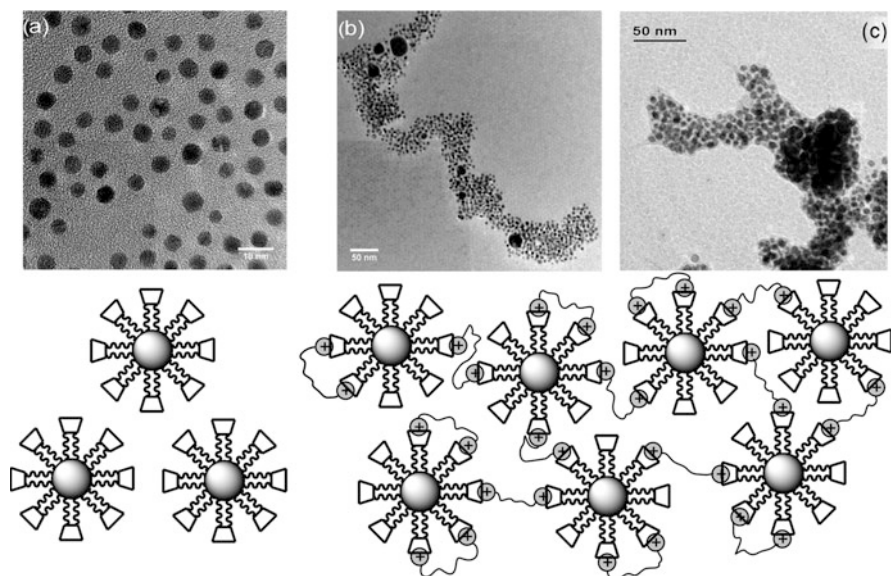


**Fig. 35.6** (Top) TEM micrographs of nanoparticles **AuNP(2a)** before (a) and after their aggregation with the bifunctional guests **8a** (b), and **8b** (c); (bottom) schematic representation of the guest-driven aggregation of the AuNPs (Adapted with permission from Ref. [39]. Copyright © 2010 American Chemical Society)

obtained, as shown by the formation of a broad low energy band at  $\lambda > 700$  nm (see Fig. 35.5b). The very rigid and directional viologen guest **10** led instead to an irreversible aggregation process with the precipitation of the nanoparticles from the solution.

To verify that these aggregation processes were effectively driven by host-guest interactions, the authors devised two control titrations: in the first one, nanoparticles **AuNP(2a)** were titrated with a monofunctional guest, i.e. the *N*-octyl pyridinium iodide (**9**), while in the second one, a solution of ~6-nm dodecanthiol-capped **AuNP** (**C12**) was titrated with a solution of guest **8b**. In both titrations, the maximum of the SPB did not undergo any shift to lower energy, indicating that aggregation did not occur (see Fig. 35.5c, d). The formation of super-aggregates of nanoparticles was then confirmed through TEM (see Fig. 35.6) and DLS measurements. The latter experiments, in particular, evidenced as the addition of **8a** and **8b** to a chloroform solution of **AuNP(2a)** induced the formation of aggregates having a hydrodynamic diameter of ca. 0.6 and 1  $\mu\text{m}$ , respectively.

In more recent studies, the fabrication of hybrid systems based on the reversible assembly of **AuNP(2a)** on a Si(100) surface was tackled [41]. This process was mediated by a series of hierarchical and reversible complexation steps involving a bifunctional guest (**12**), and two calix[n]arene-based hosts (**2a** and **11**) which were used to functionalize two inorganic components (Fig. 35.7). The thiolate calix[4]arene **2a** was covalently loaded on ~5 nm **AuNP(2a)**, while the novel tris(*N*-

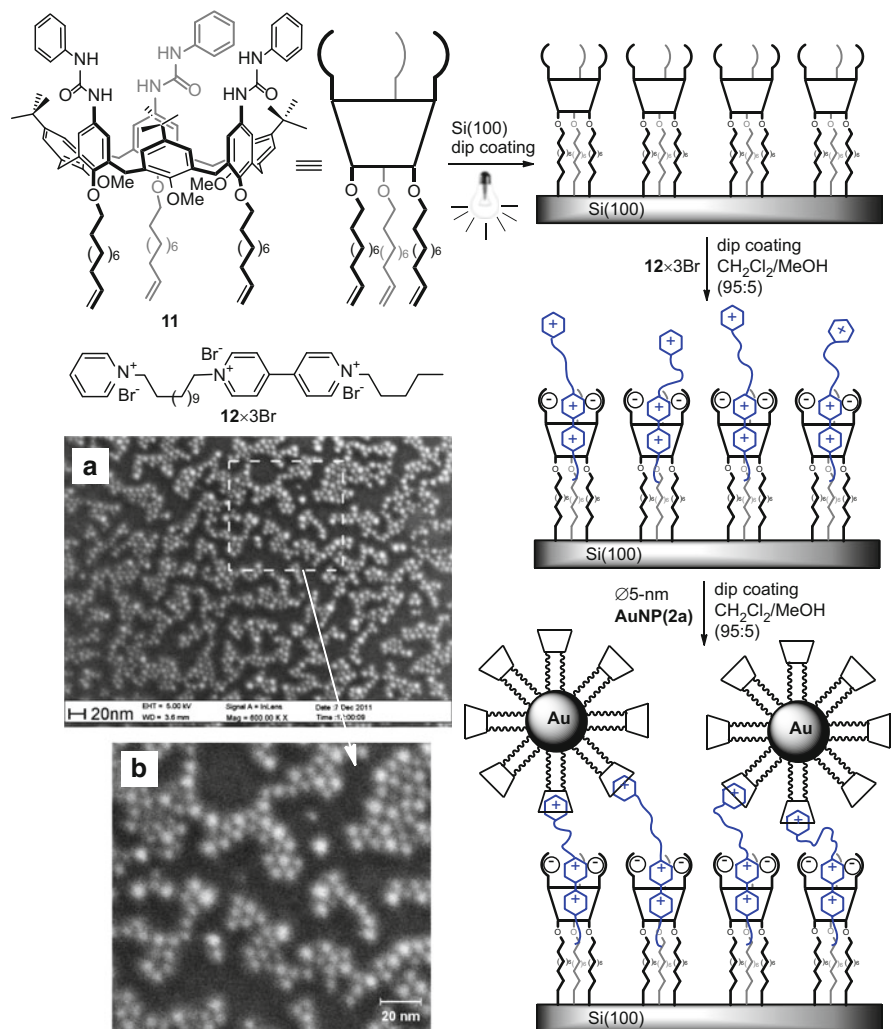


**Fig. 35.7** Schematic representation of the pseudorotaxane formation between a Si(100) surface coated with the tris(*N*-phenylureido)calix[6]arene “wheel” **11** and the bifunctional guest **12**, followed by the “supramolecular grafting” of AuNP(2a). FESEM image of (a) the Si(100) surface coated with the AuNPs (600 KX magnification,  $500 \times 375 \text{ nm}^2$ ), and (b) zoom ( $190 \times 190 \text{ nm}^2$ ) of the same area showing a hexagonal motif in the packing symmetry (Adapted with permission from Ref. [41]. Copyright © 2013 WILEY-VCH Verlag GmbH & Co. KGaA, Weinheim)

phenylureido)-calix[6]arene **11**, bearing three  $\omega$ -undecenyl chains on its lower rim, was employed to cover the silicon surface through a non-destructive approach successfully devised by Zanoni and co-workers [42]. The supramolecular linker **12** presents two binding sites separated by a flexible C12 spacer: a pyridinium unit and a redox-active bis-pyridinium core. This latter can give rise with calix[6]arene

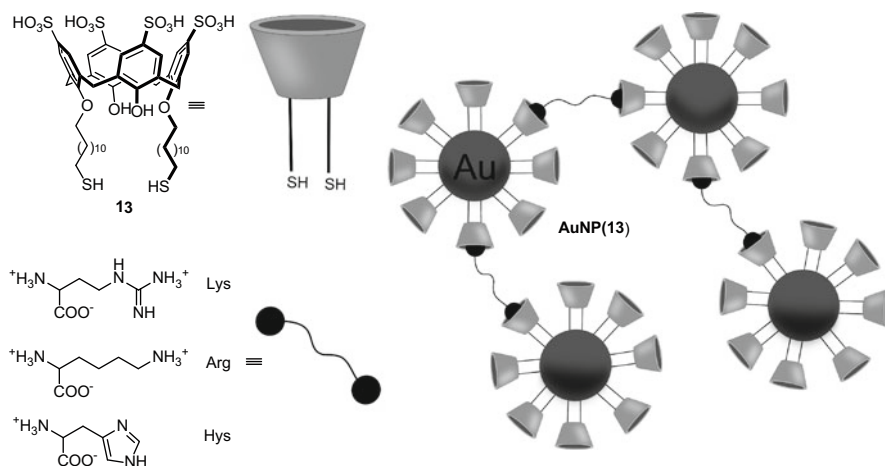


**Fig. 35.8** Schematic representation of water-soluble calix[4]arene-capped **AuNP(13)** used as colorimetric sensor for basic amino acids

**11** to very stable and electrochemically switchable pseudorotaxane complexes (see also Chap. 29 of this book) [43]. As previously seen, the electron poor pyridinium unit does form stable inclusion complexes with the aromatic cavity of **2a**. All the hierarchical surface-complexation reactions, accomplished as depicted in Fig. 35.7, were monitored by XPS, atomic force microscopy (AFM) and field-emission scanning electron microscopy (FESEM). An electrochemical stimulus was instead applied for the controlled release of the nanoparticles **AuNP(2a)** from the silicon surface.

Plasmonic calixarene-capped AuNPs can be potentially used for the construction of colorimetric sensors since the position of their SPB is strongly dependent on the distance between nanoparticles [44]. A ditopic guest, selectively recognized by the calixarene cavity, may induce the aggregation of the particles with consequent color change of the solution. For example, a colorimetric sensor for lysine (Lys), arginine (Arg) and histidine (His) based on calix[4]arene-capped AuNPs was developed in 2009 by Patel and Menon [45]. A tetra-*p*-sulfonato-calix[4]arene (**13**), bearing two ω-thiolate dodecyl chains at its lower rim (see Fig. 35.8), was anchored to water-soluble nanoparticles, previously prepared by the Turkevich method [37]. The resulting nanoparticles **AuNP(13)** were characterized by TEM measurements, UV-visible and IR spectroscopy. The latter technique was used to investigate the grafting of the calix[4]arene units on the particles surface. UV-vis titration were used to investigate the ability of **AuNP(13)** to act as a colorimetric sensor for a series of amino acids bearing amino functions in their side chain, by monitoring the shift of the SPB maximum. Indeed, the increasing additions of aqueous solutions of these basic amino acids to the solution of **AuNP(13)** resulted in nanoparticles aggregation. In particular, a red shift (from 524 to 550 nm) and broadening of the SPB occurs, which is accompanied by a color change of the

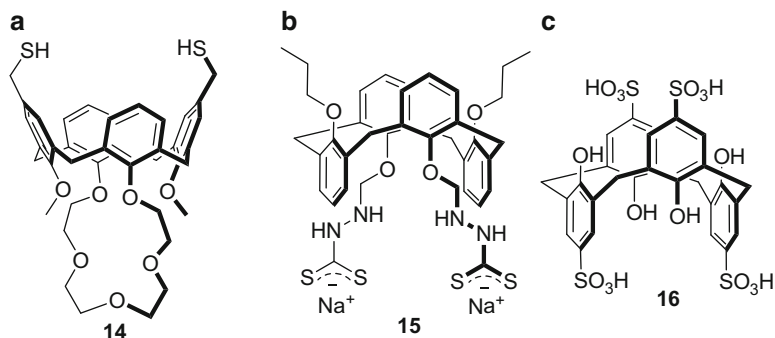


**Fig. 35.9** Calix[4]arene-based hosts used as functional capping agents for nanoparticles-based colorimetric sensors for the detection of: **(a)** diamine derivatives (see Ref. [46]); **(b)** Co(II) ion (see Ref. [47]); and **(c)** iodide anion (see Ref. [48])

suspension from red to purple. A control experiment was carried out titrating the nanoparticles solution with alanine, but any red-shift of the SPB was observed. These results demonstrated that two amino-functions are needed to obtain nanoparticles aggregation. Using a similar approach, Chen and co-workers recently employed the upper rim-methanthiolate calix[4]arene-crown-5 (**14**) (see Fig. 35.9a) in order to functionalize water-soluble ~5-nm AuNPs capable of sensing several diamine compounds [46]. Such colorimetric approach can be potentially exploited for the sensing of several species, provided that a suitable calixarene host is inserted in the organic monolayer of the nanoparticles. In this framework, several recent examples are present in the literature. For example, a colorimetric sensor for Co (II) in organic and aqueous media was developed by Paul and co-workers in 2014 [47]. They used the calix[4]arene derivative **15**, blocked in the 1,3-*alternate* conformation, bearing two thiocarbamate groups to promote its grafting on the Au surface (see Fig. 35.9b). The relative ~2-nm calix[4]arene-capped AuNPs were prepared using a modified Brust-Schiffrin method which requires the reduction of the Au(III) precursor in the presence of the thiolate calix[4]arene **15**. The resulting nanoparticles were characterized by IR, UV-vis, TEM and EDX techniques. The Co<sup>2+</sup> ion acts as bridging guest binding simultaneously two units of **15** by cation/ $\pi$  interactions. This host-guest interaction is responsible of a large aggregation of the nanoparticles, that leads to a red-shift of the original SBP from  $\lambda = 520$  up to 700 nm. This shift resulted in a visible color change of the suspension, from pink to blue. The aggregation of these nanoparticles was further confirmed by DLS and TEM measurements. Control experiments were carried out using several other mono- and divalent metal ions, and this nanoparticles-based colorimetric sensor resulted highly selective for the Co(II) species. In other studies, these authors developed a sensor for the iodide anion using the tetra *p*-sulfonato calix[4]arene **16**, blocked in the 1,3-*alternate* conformation (see Fig. 35.9c) [48]. This macrocycle was used for the electrostatic capping of ~13-nm water-soluble AuNPs prepared as reported by Frens [49]. As in the previous examples, the iodide



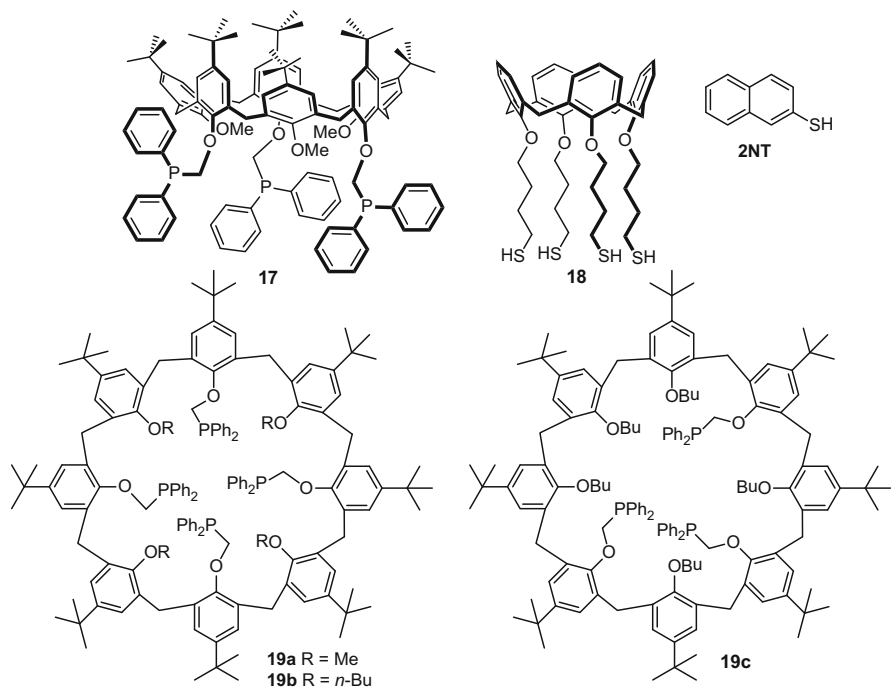


**Fig. 35.10** Diphenylphosphine-based calix[6]arene (**17**) and calix[8]arene (**19a–c**), tetrakis (4-mercaptobutyloxy) calix[4]arene (**18**) ligands used, together with 2-naphthalenethiol (**2NT**), to study the surface accessibility of AuNPs (see Ref. [50, 51])

sensing in aqueous solution was evidenced by a large red-shift and broadening of the nanoparticles SPB, with a color change of the solution from red to blue. The shift at lower energy was explained as due to the aggregation of nanoparticles driven by the simultaneous complexation of the anion by two calix[4]arene units placed on different particles. Control experiments were carried out using several different anions, demonstrating the high selectivity of this colorimetric sensor.

Metal nanoparticles bound with polymeric and oligomeric ligands are commonly employed in areas where the accessibility to the underlying metal is critical, such as in catalysis. Developing a fundamental understanding of molecular-scale factors that control accessibility to the metal surface in these systems would improve the ligand design. Starting from these considerations, Katz et al. developed an interesting way to study the accessibility of the nanoparticles surface [50]. The authors prepared a calix [6]arene derivative (**17**, see Fig. 35.10) alkylated with diphenylphosphinomethoxy groups which was used for the functionalization of ~5-nm nanoparticles (**AuNP(17)**). Aliquots of a solution of the fluorophore 2-naphthalenethiol (**2NT**) in  $\text{CH}_2\text{Cl}_2$  were added to solution of **AuNP(17)** and the fluorescence quenching was taken as a measure of the nanoparticles surface accessibility. For **AuNP(17)**, the surface accessibility was found to be sevenfold larger than nanoparticles **AuNP(18)**, which were capped with the smaller calix[4]arene **18**. Interestingly, the surface of nanoparticles

**AuNP(C12)**, capped with C12SH, was found completely inaccessible, since this ligand generates a packed monolayer. It is worth noting that the surface accessibility of nanoparticles functionalized with a higher amount of **17** is only fourfold larger than **AuNP(18)**. The reduced surface accessibility was explained considering that the increase of concentration changes the ligand denticity from three to two phosphine groups.

In a more recent study, the nanoparticles surface accessibility was found to be dependent also on the rigidity of the calixarene-based ligand [51]. To demonstrate this, ~4-nm AuNPs capped with three different calix[8]arene diphenylphosphine ligands (**19a–c**, Fig. 35.10) were prepared and investigated. The SPB of the nanoparticles was used to determinate the molecular footprints of the ligands, which resulted ~230 Å<sup>2</sup> per calix[8]arene unit. The ligands conformational flexibility was evaluated in CDCl<sub>3</sub> solution using variable-temperature <sup>1</sup>H NMR spectroscopy, and in the gas-phase as well as in the bound state (on the gold surface) through molecular modelling simulations. The latter calculations evidenced as in the bound state the most rigid ligand is the calix[8]arene **19a**. The surface accessibility was measured as described before [50], and the most rigid ligand in the bound state, **19a**, yielded no accessible surface, whereas the more flexible ligands **19b** and **19c** afforded a 5–7 % of the gold surface being accessible. In the same context, in 2010, these authors studied the synthesis of AuNPs using a series of Au(I)-calix[4]arene complexes as the precursor [52]. Three different calix[4]arene derivatives bearing alkyldiphenyl phosphine groups at their lower rim were synthesized (**20a–c**, Fig. 35.11). Their complexes with Au(I) were characterized

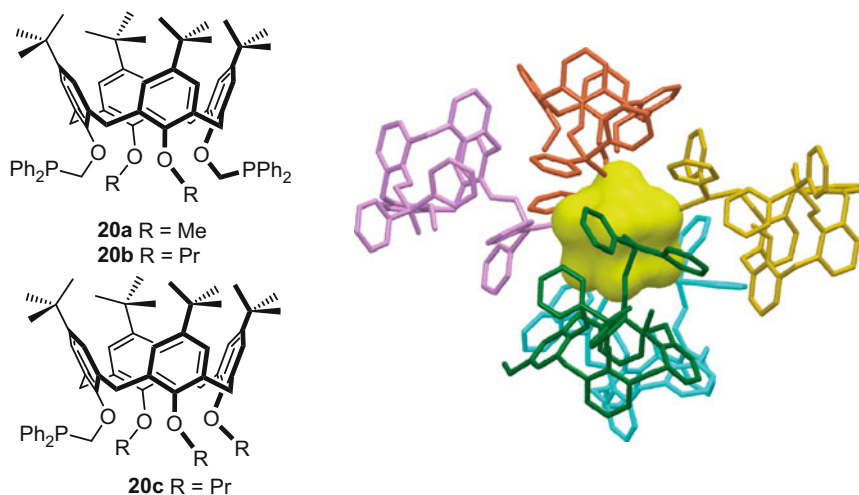


**Fig. 35.11** (Left) Calix[4]arene phosphine ligands **20a–c**; (right) Schematic representation of the 0.9-nm Au<sub>11</sub> cluster having five bound calixarene ligands **20a**. Two of these calixarene ligands are bound in a bidentate fashion and three are bound in a monodentate fashion. The monodentate ligands consist of bound phosphine and unbound phosphine-oxide substituents (Adapted with permission from Ref. [52]. Copyright © 2010 Macmillan Publishers Limited)



using  $^1\text{H}$ - and  $^{31}\text{P}$ -NMR spectroscopy, and single crystal X-Ray diffraction. The nanoparticles were prepared by  $\text{NaBH}_4$  reduction of ethanolic solution of the precursors, and characterized using UV-Vis spectroscopy, high-angle annular dark-field scanning transmission electron microscopy (HAADF-STEM), elemental analysis and XPS measurements. Accessible sites in the nanoparticles were titrated, as usual, with 2-naphthalenethiol (**2NT**) as a chemisorption probe [50]. The nanoparticles prepared using calix[4]arene **20a** as capping ligand resulted in undecagold ( $\text{Au}_{11}$ ) clusters, each stabilized by five units of **20a**, and for which the 25 % of the cluster surface was found to be accessible to **2-NT**. The surface accessibility dramatically decreases in 1.1-nm and 4-nm Au clusters, which were obtained using calix[4]arene ligands **20b** and **20c**, respectively.

Katz et al. also studied nanoparticles post-synthetically modified with the chiral calix[4]arene derivative **21** (see Fig. 35.12) [53], obtaining a system with a circular dichroism-active SPB. The two enantiomers **21a**-(*R,R*) and **21b**-(*S,S*) were synthesized and characterized by  $^1\text{H}$ -NMR and CD spectroscopy. They were used for the derivatization of  $\sim 5$ -nm AuNPs. The CD measurements on these nanoparticles demonstrated an ellipticity of the  $\pi$ - $\pi^*$  transition, in the 270–300 nm range, almost tenfold larger than the value of free calix[4]arenes **21** in solution, and an ellipticity of the SPB in the range 460–600 nm. Since the nanoparticles do not have a chiral gold core, and the presence of the bulky *tert*-butyl groups reasonably prevents any interaction between chiral centers that could induce a chiral pattern packing on the surface, the authors explained the origin of this CD-active behavior as probably due to an asymmetry induced by the chiral capping molecules. Because of the small distance between the chiral centers and the gold surface, it was reasonable to suppose an electronic communication between the capping ligands and the metal surface in a way that the chiral centers may influence the electronic states of the nanoparticles.

### 35.3 Silver Nanoparticles

In analogy with AuNPs, silver nanoparticles (AgNPs) present a strong SPB in the visible region of the electromagnetic spectrum that can be tuned and shifted up to the near-infrared (NIR) spectral region by varying the size and geometry of the nanoparticles [54]. For this reason, AgNPs have found applications in photothermal therapy and in sensing [55, 56], moreover they present peculiar antimicrobial properties [55, 57]. Although many synthetic methods have been developed [58, 59], the facile preparation of AgNPs endowed with a functional organic monolayer is still under active investigation by the scientific community. As described in the previous section, the design of ligands which plays an active role in controlling the shape and size of the nanoparticles, but capable also to confer certain functionalities would be extremely important. Properly functionalized calix[n]arene derivatives may satisfy one or both of these requirements. For example, Raston et al. have shown that the introduction of phosphonated groups on the

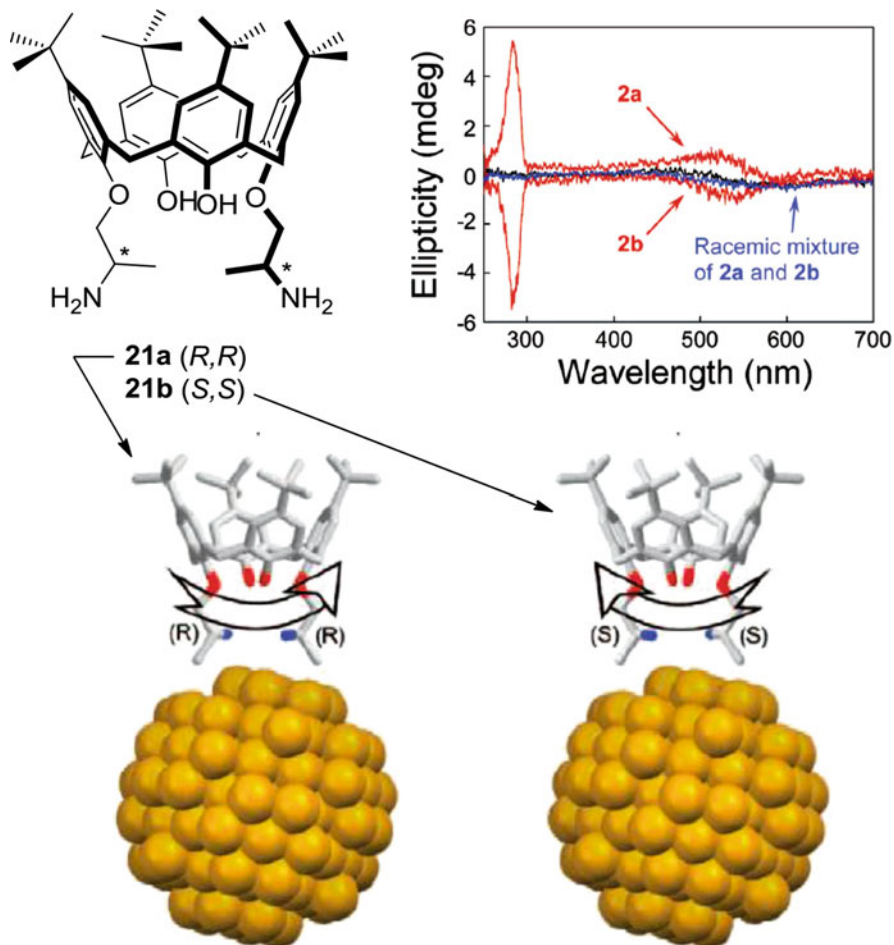


**Fig. 35.12** Schematic representation of AuNPs capped with the chiral calix[4]arene derivative **21** and selected CD spectra of TOABr-stabilized AuNP(TOABr) (black), AuNPs stabilized with **21a** and **21b** (red), and with a racemic mixture of the two enantiomers (blue) (Adapted with permission from Ref. [53] Copyright © 2009 American Chemical Society)

aromatic rings of a series of calix[*n*]arene (with *n* = 4, 5, 6 and 8) derivatives (**22a–d**, Fig. 35.13) makes these macrocycles ideal reagents for the preparation of water-soluble AgNPs with tunable size [60]. The nanoparticles were prepared by reducing the silver precursor (AgNO<sub>3</sub>) with hydrogen at 70 °C in the presence of the calix[*n*]arene derivative. The core size of these nanoparticles was analyzed through TEM measurements and resulted to be dependent on both the concentration and the nature, in terms of number of phenolic residues, of the calix[*n*]arene employed during the synthesis. Indeed, the biggest nanoparticles (up to 15-nm) were obtained using the larger calix[8]arene **22d**, while, by keeping constant the macrocycle size, smaller nanoparticles (2.4-nm) were obtained by rising the solution pH up to 12.

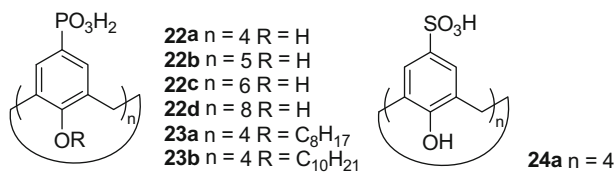


**Fig. 35.13** Phosphonated (**22–23**) and sulfonated (**24a**) calix[n]arene derivatives for the preparation of AgNPs

Although the phosphonated calixarenes **22a–d** themselves are capable to reduce  $Ag^+$  ions in presence of  $H_2$ , this reaction present several drawbacks such as the long reaction times, high temperature and, most important, the alkaline conditions which could not be compatible with all type of ligands to be placed on the nanoparticles. For this reason, the same authors, in 2010, have developed a photochemical synthesis of 3.6-nm AgNPs [61]. The nanoparticles were obtained by irradiating an aqueous solution containing  $AgNO_3$  and a phosphonated calix[n]arene (**22a** and **23a,b**, Fig. 35.13), maintained at room temperature and  $pH = 9$ , with a 100 W UV-lamp emitting 365-nm light. The resulting nanoparticles were characterized by TEM measurements and UV-vis spectroscopy. The optical properties of the colloidal solution showed that the intensity of the corresponding SPB increased with extended irradiation times. Unlike the aforementioned hydrogen-based reduction, the photochemical method works in a wide range of  $pH$  (from 2 to 9). The use of the *p*-sulfonato-calix[4]arene derivative **24a** (Fig. 35.13) instead of the phosphonated ones, led to much slower reaction rates, demonstrating that phosphonated groups have an active role in the silver ions reduction.

As seen for AuNPs, several examples of chemosensors based on calix[n]arene-capped AgNPs are present in the literature. Li and co-workers have developed a colorimetric sensor for histidine (His) based on  $\sim 8$ -nm AgNPs capped with the *p*-sulfonato-calix[4]arenes **24a** (Fig. 35.13) [62]. Nanoparticles **AgNP(24a)** were prepared by reducing  $AgNO_3$  at room temperature with  $NaBH_4$  in the presence of the calix[4]arene derivative. FT-IR measurements suggested an interaction between the sulfonato groups and the Ag surface. The stability of these colloids was evaluated by UV-vis spectroscopy and they resulted to be stable for at least 1 month. As previously seen for **AuNP(13)** (Fig. 35.8), the aggregation of **AgNP(24a)** can be promoted by a histidine that, thanks to its imidazole side chain and ammonium group, acts as bridging guest between two calix[4]arene cavities present on different nanoparticles. This phenomenon was investigated by monitoring the absorbance ratio at two different wavelengths ( $A_{493}/A_{394}$ ). Upon addition of a  $10^{-4}$  M solution of His, over 30 min, the color of the colloid changes from yellow to red and an increase of the  $A_{493}/A_{394}$  ratio was observed. The addition of other amino acids had no effect on the nanoparticles SPB, demonstrating the high selectivity of this colorimetric sensor.

The large increase of the electric field intensity near the surface of the nanoparticles is associated to local field enhancements, often called hot spots, which have attracted considerable attention from the scientific community because

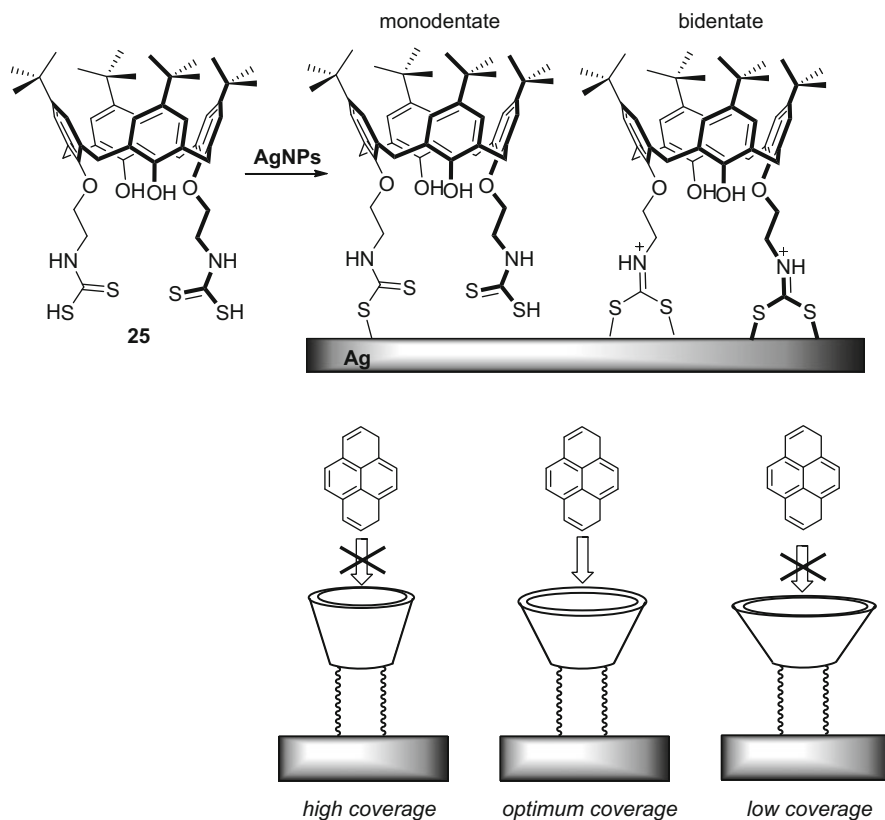


**Fig. 35.14** (Top) lower rim bis dithiocarbamate calix[4]arene **25** and interaction geometry adopted by **25** when adsorbed on particles AgNP(**25**); (bottom) schematic representation of the structure of **25** at different surface coverages and its interaction with pyrene

they can promote strong Raman scattering enhancement of molecules placed in their proximity. This allows the development of sensors based on the SERS effect [63]. In this context, Guerrini et al. studied a self-assembled monolayer of the dithiocarbamate calix[4]arene **25** (see Fig. 35.14) on AgNPs [64]. To investigate the effect of the reducing agent on the adsorption of the calix[4]arene derivative on the surface, the AgNPs were prepared from AgNO<sub>3</sub> using two different reducing agents: sodium citrate [65] and hydroxylamine [66]. The grafting of **25** on the surface of these two types of AgNPs was monitored through SERS measurements. In both cases, the SERS spectra are dominated by the dithiocarbamate bands at 1022 and 966 cm<sup>-1</sup>, ascribed to the  $\nu(\text{C}=\text{S})$  and to  $\nu(\text{C}-\text{S})$  modes, respectively. These bands are slightly shifted and broadened compared to the corresponding weak bands appearing in the Raman spectrum of the solid **25** at 1027 and 963 cm<sup>-1</sup>. Most important, the strong interaction of the dithiocarbamate group with the silver surface induces its isomerization into the corresponding thioureide form. As a result, a new band appears at 1514 cm<sup>-1</sup> which is assigned to the C=N<sup>+</sup> double

bond, because of the attraction of the lone pair electron on the nitrogen by the metal. Exploiting the position of the thioureide band,  $\nu(\text{C}=\text{N}^+)$ , the relative intensities of the  $\nu(\text{C}=\text{S})$  and  $\nu(\text{C}-\text{S})$  modes, and from an investigation on the  $\nu(\text{Ag}-\text{S})$  and  $\nu(\text{Ag}-\text{Cl})$  bands, the authors were able to estimate the concentration of **25** necessary to obtain a complete surface coverage, as well as the ligand denticity as a function of its concentration. The nanoparticles **AgNP(25)**, obtained from hydroxylamine, gave higher SERS peaks intensity than those obtained from citrate. This result was explained considering that in the latter nanoparticles, the citrate ions act as interferent reducing the SERS effects. The ability of the calix[4]arene cavity of **25** to form inclusion complexes with pyrene was then exploited for the realization of a sensor based on the SERS effect. Upon complexation by **25**, the pyrene molecule is easily recognized by the diagnostic peak at  $1404\text{ cm}^{-1}$  in the Raman spectrum. The efficiency of this sensor increases with the particles surface coverage because, as expected, also the number of the host cavities available for the pyrene complexation does increase. However, a further increase in the concentration of **25** during the synthesis determines the formation of nanoparticles in which the calix[4]arene cavity adopt a more closed conformation (see Fig. 35.14). This leads a reduced affinity for the pyrene molecule.

Thanks to the versatility of the Raman spectroscopy, nanoparticles **AgNP(25)** were used also to detect other polycyclic aromatic pollutants (PAHs), like benzo [c]phenanthrene, triphenylene, and coronene [67]. In this case, selectivity is not as important as in other sensors, because the pollutant molecule can be in principle identified by its Raman spectrum. The affinity constants and the limits of detection of PAHs were also determined. In 2012, Coleman and co-workers developed a method to determine the critical micellar concentration (CMC) of cationic surfactants exploiting the SPB of a series of sulfonato calix [n]arene-capped AgNPs [68]. The nanoparticles were synthesized by reducing  $\text{AgNO}_3$  with sodium borohydride in aqueous solution in the presence of the sulfonato calix[n]arene derivatives **24**, **26** and **27** (see Fig. 35.15) and characterized by TEM, DLS and UV-visible spectroscopy. Suspensions of the

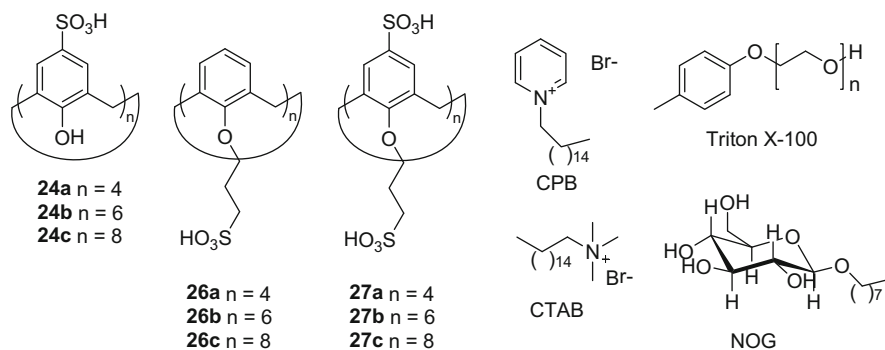


**Fig. 35.15** Structures of sulfonato calix[n]arene derivatives **24**, **26** and **27** and of cationic and neutral surfactants

nine synthesized calix[*n*]arene-capped nanoparticles at a concentration of  $10^{-3}$  M were titrated against five surfactants: cetyl pyridium bromide (CPB) and cetyl trimethyl ammonium bromide (CTAB) as cationics, Triton X-100 and *N*-octyl glucopyranoside (NOG) as neutral, and sodium dodecyl sulfate (SDS). Only the nanoparticles capped with the calix[4]arene derivatives **2a–c**, which are sulfonated in the *para* positions of the phenolic rings, showed changes in the corresponding UV-vis spectra. In particular, only with the two cationic surfactants CTB and CTAB the nanoparticles exhibit a minimum of the absorbance at  $\lambda_{\text{max}}$ . The minimum was reached at a surfactant concentration corresponding to the surfactant CMC.

Very recently, the possibility to exploit calix[4]arene-capped AgNPs to obtain a guest-controlled aggregation of plasmonic nanoparticles of different metals was demonstrated [69]. ~3-nm dodecanthiol-capped AgNP(**C12**), prepared with the method devised by Fitzmaurice [70], were functionalized in dichloromethane solution with an excess of calix[4]arene **2a**, through a ligand-exchange reaction (see Fig. 35.16). The resulting exchanged nanoparticles were characterized by UV-vis and XPS spectroscopy and TEM measurements. With the latter technique it was established the size monodispersity of their metallic core, while with the XPS measurements it was possible to determine the particles nuclearity and the coverage of their surface that resulted totally exchanged with calix[4]arene **2a**. A series of ~5-nm AuNPs capped with a mixed organic layers consisting of 1-dodecanethiol (**C12SH**) and the alkyl-pyridinium bromide (**7**×Br), in different molar ratios, were prepared and characterized (AuNP(**7**/**C12SH**), Fig. 35.16). Recognition in weakly polar solvents of the alkyl pyridinium moieties present on the surface of these nanoparticles by the calix[4]arene cavities of AgNP(**2a**) was demonstrated by UV-visible and DLS titrations. The extent of Au/Ag nanoparticles aggregation was evidenced through a bathochromic shift of their SPBs, and it was found to depend strongly on the loading of **7** in the organic monolayer of AuNP(**7**/**C12SH**). Extensive aggregation between dodecanethiol-capped AuNP(**C12**) and calix[4]arene-capped AgNP(**2a**) was also promoted by the action of a simple *N*-octyl pyridinium bifunctional supramolecular linker (**28**, see Fig. 35.17). This linker can interdigitate through its long fatty chain in the organic monolayer of AuNP(**C12**) and simultaneously interact through its pyridinium moiety with the calix[4]arene units at the surface of AgNP(**2a**).

## 35.4 Outlook

Calixarenes have been one of the most convenient platforms for the development of supramolecular chemistry. These macrocycles have facilitated the transition of this highly multidisciplinary branch of chemistry from the planar to the three-dimensional world. Given the efforts carried out during these last decades for

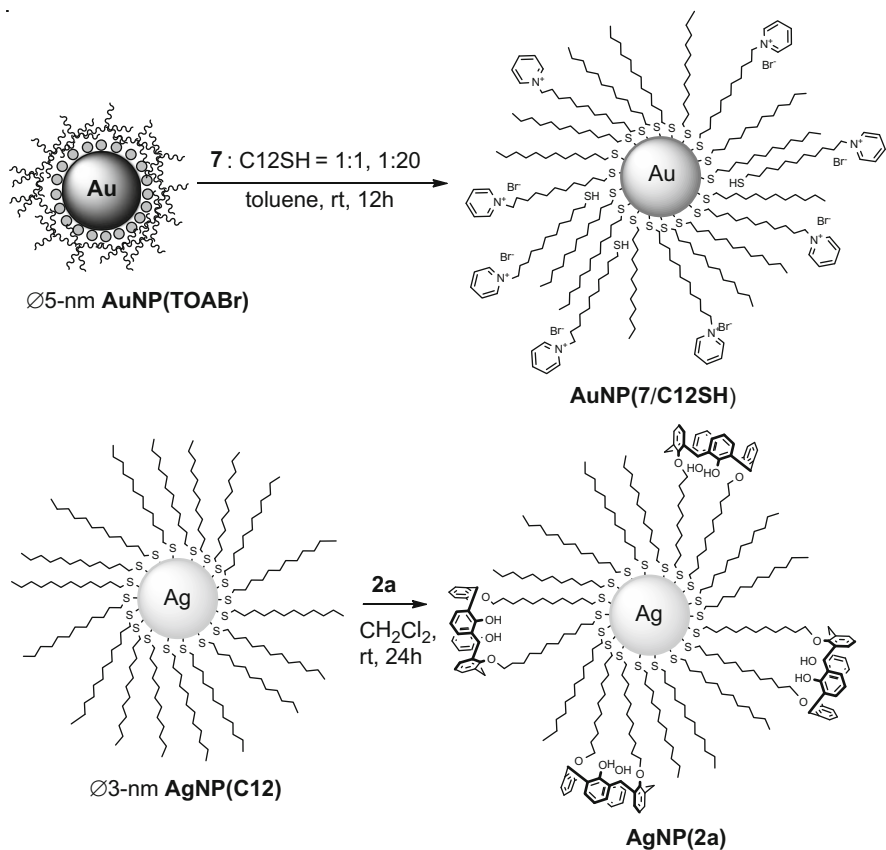


**Fig. 35.16** (Top) Schematic representation of the functionalization of AuNPs with a mixed-monolayer composed by the pyridinium ligand (7) and dodecanthiol (C12SH); (bottom) preparation of the calix[4]arene-capped AgNP(2a) from dodecanthiol-capped AgNP(C12) (Adapted with permission from Ref. [69]. Copyright © 2015 WILEY-VCH Verlag GmbH & Co. KGaA, Weinheim)

their regio- and stereoselective selective functionalization, it can be foreseen that the development of targeted and efficient procedures for the synthetic manipulation of all members of the calixarene series will contribute to the expansion of nanoscience and nanotechnology. The construction of calixarene-based working devices able to transfer their unique recognition properties to the nanometre scale and respond, in a programmable manner, to external stimuli will be the challenge of calixarene chemistry.

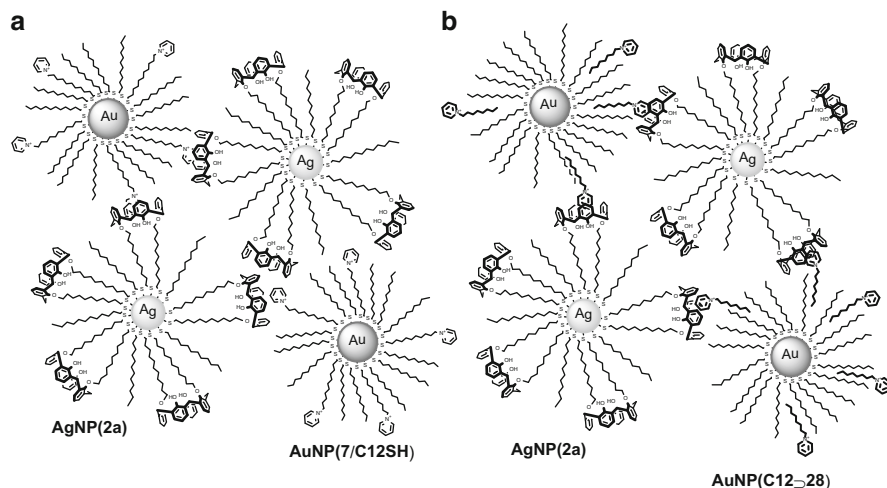


**Fig. 35.17** Schematic representations of the assembly between Au and AgNPs driven by supra-molecular interactions in (a) the two complementary binding sites are covalently linked on the NPs surface, whereas in (b) one binding site, the *N*-octyl pyridinium bromide **28**, is interdigitated in the dodecanethiol layer of AuNP(C12) (Adapted with permission from Ref. [69]. Copyright © 2015 WILEY-VCH Verlag GmbH & Co. KGaA, Weinheim)

## References

- Whitesides, G. M.; Boncheva, M. *Proc. Natl. Acad. Sci. U. S. A.* **2002**, *99*, 4769–4774.
- Love, J. C.; Estroff, L. a.; Kriebel, J. K.; Nuzzo, R. G.; Whitesides, G. M. *Chem. Rev.* **2005**, *105*, 1103–1169.
- Whetten, R. L.; Shafiqullin, M. N.; Khoury, J. T.; Schaaff, T. G.; Vezmar, I.; Alvarez, M. M.; Wilkinson, A. *Acc. Chem. Res.* **1999**, *32*, 397–406.
- Templeton, A. C.; Wuelfing, M. P.; Murray, R. W. *Acc. Chem. Res.* **2000**, *33*, 27–36.
- Badia, A.; Lennox, R. B.; Reven, L. *Acc. Chem. Res.* **2000**, *33*, 475–481.
- Daniel, M.-C. C.; Astruc, D. *Chem. Rev.* **2004**, *104*, 293–346.
- Nanoparticles*, 2<sup>nd</sup> ed.; Schmid, G., Ed.; Wiley-VCH Verlag GmbH & Co. KGaA: Weinheim, Germany, 2010.
- Nanoparticles: Building Blocks for Nanotechnology*; Rotello, V., Ed.; Nanostructure Science and Technology; Springer US: Boston, MA, 2004.
- Brust, M.; Kiely, C. J. Monolayer Protected Clusters of Gold and Silver. In *Colloids and Colloid Assemblies: Synthesis, Modification, Organization and Utilization of Colloid Particles*; Caruso, F., Ed. Wiley-VCH Verlag GmbH & Co. KGaA: Weinheim, 2003, pp 96–119.
- Boal, A. K.; Rotello, V. M. *J. Am. Chem. Soc.* **2002**, *124*, 5019–5024.
- Steed, J. W.; Turner, D. R.; Wallace, K. *Core Concepts in Supramolecular Chemistry and Nanochemistry*; John Wiley & Sons, Ltd: Chichester (UK), 2007.
- Montes-García, V.; Perez-Juste, J.; Pastoriza-Santos, I.; Liz-Marzan, L. M. *Chem. Eur. J.* **2014**, *20*, 10874–10883.
- Descalzo, A. B.; Martínez-Máñez, R.; Sancenón, F.; Hoffmann, K.; Rurack, K. *Angew. Chem. Int. Ed.* **2006**, *45*, 5924–5948.
- Shenhar, R.; Rotello, V. M. *Acc. Chem. Res.* **2003**, *36*, 549–561.
- Connolly, S.; Rao, S. N.; Rizza, R.; Zaccheroni, N.; Fitzmaurice, D. *Coord. Chem. Rev.* **1999**, *185–186*, 277–295.



16. Brust, M.; Walker, M.; Bethell, D.; Schiffrin, D. J.; Whyman, R. *J. Chem. Soc., Chem. Commun.* **1994**, 801–802.
17. Brust, M.; Fink, J.; Bethell, D.; Schiffrin, D. J.; Kiely, C. *J. Chem. Soc., Chem. Commun.* **1995**, 1655–1656.
18. Liz-Marzán, L. M. *Chem. Commun.* **2013**, 49, 16–18.
19. de Aberasturi, D. J.; Serrano-Montes, A. B.; Liz-Marzán, L. M. *Adv. Opt. Mater.* **2015**, 3, 602–617.
20. Lal, S.; Grady, N. K.; Kundu, J.; Levin, C. S.; Lassiter, J. B.; Halas, N. J. *Chem. Soc. Rev.* **2008**, 37, 898–911.
21. Hou, W.; Cronin, S. B. *Adv. Funct. Mater.* **2013**, 23, 1612–1619.
22. Kim, E. Y.; Kumar, D.; Khang, G.; Lim, D.-K. *J. Mater. Chem. B* **2015**, 3, 8433–8444.
23. Boisselier, E.; Astruc, D. *Chem. Soc. Rev.* **2009**, 38, 1759–1782.
24. Saha, K.; Agasti, S. S.; Kim, C.; Li, X.; Rotello, V. M. *Chem. Rev.* **2012**, 112, 2739–2779.
25. Guo, R.; Song, Y.; Wang, G.; Murray, R. W. *J. Am. Chem. Soc.* **2005**, 127, 2752–2757.
26. Woehrlé, G. H.; Warner, M. G.; Hutchison, J. E. *J. Phys. Chem. B* **2002**, 106, 9979–9981.
27. Brown, L. O.; Hutchison, J. E. *J. Am. Chem. Soc.* **1999**, 121, 882–883.
28. Brown, L. O.; Hutchison, J. E. *J. Am. Chem. Soc.* **1997**, 119, 12384–12385.
29. Hostetler, M. J.; Green, S. J.; Stokes, J. J.; Murray, R. W. *J. Am. Chem. Soc.* **1996**, 118, 4212–4213.
30. Arduini, A.; Demuru, D.; Pochini, A.; Secchi, A. *Chem. Commun.* **2005**, 645–647.
31. Arduini, A.; Brindani, E.; Giorgi, G.; Pochini, A.; Secchi, A. *J. Org. Chem.* **2002**, 67, 6188–6194.
32. Orda-Zgadaj, M.; Wendel, V.; Fehlinger, M.; Ziemer, B.; Abraham, W. *Eur. J. Org. Chem.* **2001**, 2001, 1549–1561.
33. Pescatori, L.; Boccia, A.; Ciesa, F.; Rossi, F.; Grillo, V.; Arduini, A.; Pochini, A.; Zaroni, R.; Secchi, A. *Chem. Eur. J.* **2010**, 16, 11089–11099.
34. Boccia, A.; Zaroni, R.; Arduini, A.; Pescatori, L.; Secchi, A. *J. Nanosci. Nanotechnol.* **2012**, 12, 8851–8855.
35. Hostetler, M. J.; Wingate, J. E.; Zhong, C. -J.; Harris, J. E.; Vachet, R. W.; Clark, M. R.; Londono, J. D.; Green, S. J.; Stokes, J. J.; Wignall, G. D.; Glish, G. L.; Porter, M. D.; Evans, N. D.; Murray, R. W. *Langmuir* **1998**, 14, 17–30.
36. Tshikhudo, T. R.; Demuru, D.; Wang, Z.; Brust, M.; Secchi, A.; Arduini, A.; Pochini, A. *Angew. Chem. Int. Ed.* **2005**, 44, 2913–2916.
37. Turkevich, J.; Stevenson, P. C.; Hillier, J. *Discuss. Faraday Soc.* **1951**, 11, 55–75.
38. Pescatori, L.; Arduini, A.; Pochini, A.; Secchi, A.; Massera, C.; Ugozzoli, F. *Org. Biomol. Chem.* **2009**, 7, 3698–3708.
39. Ciesa, F.; Plech, A.; Mattioli, C.; Pescatori, L.; Arduini, A.; Pochini, A.; Rossi, F.; Secchi, A. *J. Phys. Chem. C* **2010**, 114, 13601–13607.
40. Fink, J.; Kiely, C. J.; Bethell, D.; Schiffrin, D. J. *Chem. Mater.* **1998**, 10, 922–926.
41. Boccia, A.; D’Orazi, F.; Carabelli, E.; Bussolati, R.; Arduini, A.; Secchi, A.; Marrani, A. G.; Zaroni, R. *Chem. Eur. J.* **2013**, 19, 7999–8006.
42. Boccia, A.; Lanzilotto, V.; Zaroni, R.; Pescatori, L.; Arduini, A.; Secchi, A. *Phys. Chem. Chem. Phys.* **2011**, 13, 4444–4451.
43. Arduini, A.; Orlandini, G.; Secchi, A.; Credi, A.; Silvi, S.; Venturi, M. Calix-Based Molecular Machines and Devices. In *Reference Module in Chemistry, Molecular Sciences and Chemical Engineering*; Elsevier, 2014.
44. Ross, M. B.; Mirkin, C. A.; Schatz, G. C. *J. Phys. Chem. C* **2016**, 120, 816–830.
45. Patel, G.; Menon, S. *Chem. Commun.* **2009**, 3563–3565.
46. Chen, Y.; Zhang, J.; Gao, Y.; Lee, J.; Chen, H.; Yin, Y. *Biosens. Bioelectron.* **2015**, 72, 306–312.
47. Maity, D.; Gupta, R.; Gunupuru, R.; Srivastava, D. N.; Paul, P. *Sens. Actuators, B.* **2014**, 191, 757–764.
48. Maity, D.; Bhatt, M.; Paul, P. *Microchim. Acta* **2015**, 182, 377–384.

49. Frens, G. *Nature* **1973**, *241*, 20–22.
50. Ha, J.-M.; Solovyov, A.; Katz, A. *Langmuir* **2009**, *25*, 10548–10553.
51. Ha, J.-M.; Solovyov, A.; Katz, A. *J. Phys. Chem.* **2010**, *114*, 16060–16070.
52. de Silva, N.; Ha, J.-M.; Solovyov, A.; Nigra, M. M.; Ogino, I.; Yeh, S. W.; Durkin, K. A.; Katz, A. *Nat. Chem.* **2010**, *2*, 1062–1068.
53. Ha, J.-M.; Solovyov, A.; Katz, A. *Langmuir* **2009**, *25*, 153–158.
54. Noguez, C. *J. Phys. Chem. C* **2007**, *111*, 3806–3819.
55. Wei, L.; Lu, J.; Xu, H.; Patel, A.; Chen, Z.-S.; Chen, G. *Drug Discov. Today* **2015**, *20*, 595–601.
56. Murphy, M.; Ting, K.; Zhang, X.; Soo, C.; Zheng, Z. *J. Nanomater.* **2015**, *2015*, 1–12.
57. Singh, R.; Shedbalkar, U. U.; Wadhvani, S. A.; Chopade, B. A. *Appl. Microbiol. Biotechnol.* **2015**, *99*, 4579–4593.
58. Wiley, B.; Sun, Y.; Xia, Y. *Acc. Chem. Res.* **2007**, *40*, 1067–1076.
59. Rycenga, M.; Cogley, C. M.; Zeng, J.; Li, W.; Moran, C. H.; Zhang, Q.; Qin, D.; Xia, Y. *Chem. Rev.* **2011**, *111*, 3669–3712.
60. Hartlieb, K. J.; Saunders, M.; Raston, C. L. *Chem. Commun.* **2009**, 3074–3076.
61. Hartlieb, K. J.; Martin, A. D.; Saunders, M.; Raston, C. L. *New J. Chem.* **2010**, *34*, 1834–1837.
62. Xiong, D.; Chen, M.; Li, H. *Chem. Commun.* **2008**, 880–882.
63. Halas, N. J.; Lal, S.; Chang, W.-S. S.; Link, S.; Nordlander, P. *Chem. Rev.* **2011**, *111*, 3913–3961.
64. Guerrini, L.; Garcia-Ramos, J. V.; Domingo, C.; Sanchez-Cortes, S. *Phys. Chem. Chem. Phys.* **2009**, *11*, 1787–1793.
65. Lee, P. C.; Meisel, D. *J. Phys. Chem.* **1982**, *86*, 3391–3395.
66. Leopold, N.; Lendl, B. *J. Phys. Chem. B* **2003**, *107*, 5723–5727.
67. Guerrini, L.; Garcia-Ramos, J. V.; Domingo, C.; Sanchez-Cortes, S. *Anal. Chem.* **2009**, *81*, 953–960.
68. Tauran, Y.; Brioude, A.; Shahgaldian, P.; Cumbo, A.; Kim, B.; Perret, F.; Coleman, A. W.; Montasser, I. *Chem. Commun.* **2012**, *48*, 9483–9485.
69. Vita, F.; Boccia, A.; Marrani, A. G.; Zannoni, R.; Rossi, F.; Arduini, A.; Secchi, A. *Chem. Eur. J.* **2015**, *21*, 15428–15438.
70. Korgel, B. A.; Fitzmaurice, D. *Adv. Mater.* **1998**, *10*, 661–665.

# Chapter 36

## Calixarenes and Pillarenes on Surfaces

Li-Li Tan and Ying-Wei Yang

### 36.1 Introduction

Surface has seen a tremendous boost and is believed to be a fourth state of matter [1]. Comparing to molecules in bulk, molecules at the surface of a material constitute a different environment, thus own different free energies, reactivities, electronic states, mobilities, and structures. Meanwhile, the properties of hybrid materials, composited from two or more nano or molecularly different components, depend on their surface and interfacial environment. During the past decade, organic/inorganic hybrid nanostructures have been paid close attention and shown a wide application prospect in terms of their optical, mechanical, electrical, catalytic and electrochemical properties [2].

Calixarenes, as a typical type of supramolecular macrocycles capable of binding toward a variety of different guest molecules, have aroused great interest since their discovery, especially in smart sensing, controlled drug delivery, and smart responsive devices [3–6]. Calixarenes entered the surface-world. As an emerging class of calixarene analogues, pillarenes and their derivatives have been one of the hottest research topics in supramolecular chemistry during the past 8 years [7–12]. Different from conventional calixarenes, their unique symmetric rigid structures and superb host-guest properties inspire researchers to construct functional hybrid materials based on pillarenes and derivatives.

---

L.-L. Tan • Y.-W. Yang (✉)  
International Joint Research Laboratory of Nano-Micro Architecture Chemistry (NMAC),  
College of Chemistry, Jilin University, 2699 Qianjin Street, Changchun 130012,  
People's Republic of China  
e-mail: [ywyang@jlu.edu.cn](mailto:ywyang@jlu.edu.cn)

## 36.2 Calixarenes and Pillarenes on Solid Nanoparticles (NPs), Plate, Electrode and Devices

### 36.2.1 Gold-Supported Calixarenes and Pillarenes

The past decades have witnessed the revolutionary impact of gold (Au)-based materials on medicine, nanoelectronics, catalysis, drug delivery, imaging, sensing, detection, and surface-enhanced Raman scattering (SERS) spectroscopy [13]. Gold materials have proved to be powerful platforms for building novel hybrid nanomaterials owing to their high chemical stability, facile synthesis, and ease of surface functionalization [3]. Calixarenes and pillarenes have been playing important roles in the fields of supramolecular chemistry and materials science. Recently, tremendous progress has been made to the introduction of supramolecular concepts to the surface of Au-based materials, which combined and enhanced the electronic, thermal, and catalytic properties of gold materials with switchable molecular recognition, stimuli-responsiveness, and other unique properties of synthetic macrocycles [14]. These supramolecular macrocycles expand gold surfaces' potential applications for nanosensors, controlled drug delivery, electrode, and reversible controlled assembly for repeating usage in various occasions.

Resorcinarenes, as surfactants with multiple contact sites and large concave head groups, can stabilize Au nanoclusters for up to several months. SERS spectroscopy indicated that multiple Au-O interactions induced the chemisorption of resorcinarenes on the Au cluster surface [15]. Recognition of calix[4]arene towards pyridinium-based complexant or compound lead to the self-assembly or complexation-induced aggregation of these calix[4]arene or calix[4]arene/alkanethiol protected gold nanoparticles (AuNPs) [16, 17]. Synthetic procedures for monolayer protected clusters (MPC) were then obtained [18]. This MPC showed efficient recognition properties toward quaternary ammonium salts in a polar solvent due to the forming of endo-cavity inclusion complexes of 1,3-dialkoxycalix[4]arenes with quaternary ammonium cations. Accessible Au surface area in tripodal calix[6]arene phosphine protected AuNPs was first measured quantitatively through a newly developed fluorescence methodology (2-naphthalenethiol as a relevant chemisorption probe molecule) [19]. These nanoparticles are unusually stable, compared to precursor tetraoctylammonium bromide surfactant-stabilized AuNPs, in solution as well as when supported on the surface of TiO<sub>2</sub>. The high stability and accessible surface demonstrated here bodes well for applications in catalysis. Subsequently, surface plasmon resonance (SPR) band wavelength of AuNPs was also observed by direct synthesis with  $\pi$ -electron rich cavity contained thiol calixarene, because the presence of cavity influenced surface microenvironment upon adsorption [20]. Calorimetric nanoprobe for ionic recognition were obtained by tuning the guest access to the calixarene cone cavity [21]. *p*-Sulfonatocalix[6]arene (SC[6]A), thiol-modified *p*-sulfonatocalix[4]arene (SC[4]A), and calix[4]arene/phenyl boronic acid (CX-PBA) stabilized AuNPs were employed as colorimetric probes to detect diaminobenzenes

(DABs) isomer, lysine, arginine, histidine, and glucose [22–24]. And then, the targeting efficiency toward cancer cells was also improved by multivalent cone-glycocalixarenes-stabilized AuNPs [25].

In 2012, water-soluble pillar[5]arene with ten imidazolium groups (IP5) at its two rims were successfully synthesized by Huang and co-workers [26]. It provides a shell of imidazolium cations and bromide anions around the AuNPs, acting as the stabilizer for preparation of AuNPs due to the macrocyclic platform and the weak coordinating cations and anions of imidazolium groups. With increasing molar ratio of [pillar[5]arene]/[Au<sup>3+</sup>], the average particle size of the IP5-stabilized AuNPs decreased, and their standard deviations also became smaller. Comparing to the monomer of IP5, IP5-stabilized AuNPs are more stable and contain greater sensitive SPR, which provides a potential application in catalysis. They found that IP5-stabilized AuNPs could act as a catalyst for the borohydride reduction of 1,4-nitroaniline to 1,4-diaminobenzene following by the discoloration, while NaBH<sub>4</sub> itself was unable to reduce 1,4-nitroaniline.

In 2013, our group synthesized a new water-soluble macrocyclic receptor, sodium salts of carboxylatopillar[5]arene (CP5, we employ CP5 to represent the COO<sup>-</sup> version of carboxylatopillar[5]arene in this chapter) with five carboxylate groups on each rim, which proved to excel as a stabilizing ligand for in situ preparation of AuNPs with narrow size distributions ( $3.1 \pm 0.5$  nm, Fig. 36.1) [27]. Interestingly, we observed that the aggregation of CP5-modified AuNPs can be tuned by controlling the addition amount of viologen I, which can form a 1:1 host-guest complex with CP5 on Au surface, or by adjusting the incubation time. In 5 min, the aggregation of CP5-stabilized AuNPs was caused by small amounts of viologen I, related to the charge variations of AuNPs. After 24 h, monodisperse AuNPs were obtained. The samples became clear red, and correspondingly, their SPR main peaks became sharp. In the absence of stabilizing CP5 rings or in the presence of noncyclic monomers of CP5, the aggregation of AuNPs was induced, indicating the important role of macrocycle framework of CP5 on Au surfaces. Furthermore, 1D and 3D assembly of CP5-modified AuNPs were induced by adding viologen II (viologen I dimer). CP5-modified AuNPs were further shown to act as an optical probe to detect herbicide paraquat taking advantage of the guest-induced aggregation behavior of CP5-modified AuNPs.

In 2014, Huang group developed a new strategy to prepare organic/inorganic supramolecular hybrid micelles, onion-like disks and vesicles based on the self-assembly of water-soluble pillar[6]arene (CP6)-modified AuNPs and gold nanorods (AuNRs) with hydrophobic chain functionalized paraquat (Fig. 36.2) [28]. For preparing various hybrid nanostructures, it is easier to change the amount of paraquat than synthesize different amphiphilic stabilizers. Comparing to other hybrid structures, the disruption of these hybrid structures can be controlled, attributed to the operable host-guest interactions in response to pH changes or NIR irradiation.

Meanwhile, highly stable CP5-modified AuNPs against salts and pH were constructed via a facile one-pot hydrothermal process [29]. In the presence of silver cations, these CP5 coated AuNPs exhibited greater peroxidase-like activity than

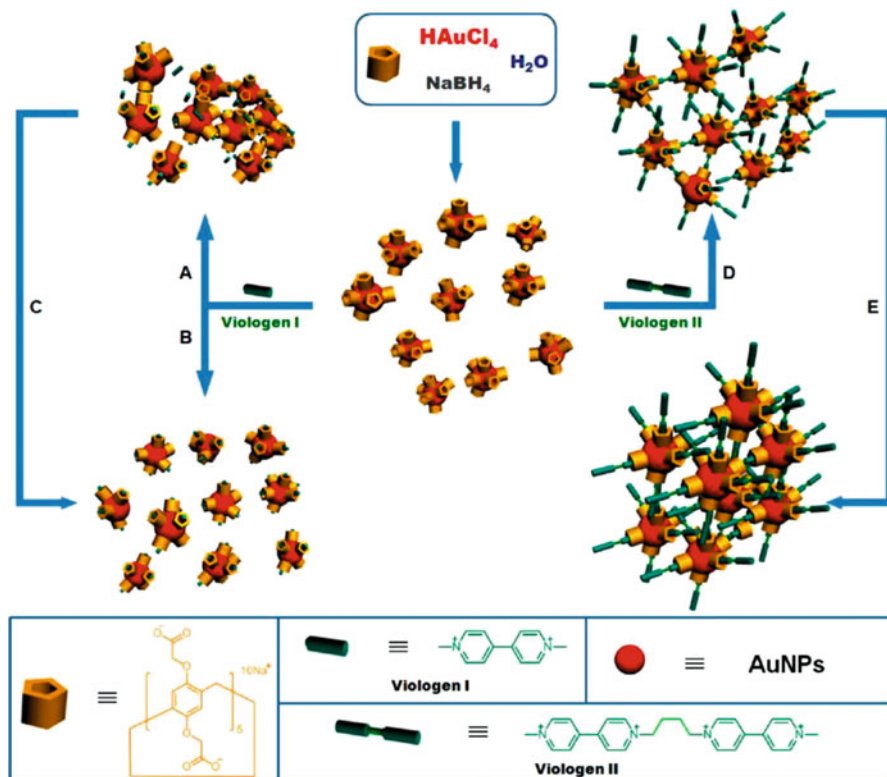


**Fig. 36.1** Schematic representation of the construction of CP5-stabilized AuNPs and their supramolecular self-assembly by adding viologen molecules (I and II): (a) 5 min and (c) 24 h after the addition of viologen I (10 mM) into a solution of CP5-modified AuNPs; (b) 5 min after the addition of viologen I (75 mM) into the solution of CP5-modified AuNPs; (d) 5 min and (e) 24 h after the addition of viologen II (3.8 mM) into a solution of CP5-modified AuNPs (Reprinted with permission from Ref. [27], Copyright 2013 American Chemical Society)

citrate-stabilized AuNPs. In addition, quasi-spherical ammonium pillar[5]arene-stabilized AuNPs were obtained via a seeded growth process [30]. SERS detection of 2-naphthoic acid and a polycyclic aromatic hydrocarbon, pyrene demonstrated that the marriage of metal NPs with supramolecular host-guest chemistry has promising synergetic effects.

In 2015, organic solvent soluble AuNPs stabilized by mono-sulfhydryl functionalized pillar[5]arene (SH-P5) were prepared by Zhou et al. [31] Quaternary ammonium salt functionalized anthracene has reversible noncovalent host-guest interactions with SH-P5, which can lead to reversible assembly of AuNPs. Based on photo [4 + 4] cycloaddition of anthracene, they can reversibly aggregate and disassemble by variation of the temperature and/or photo-irradiation, and can catalyze borohydride reduction of 2,6-dichloro-4-nitrophenol.

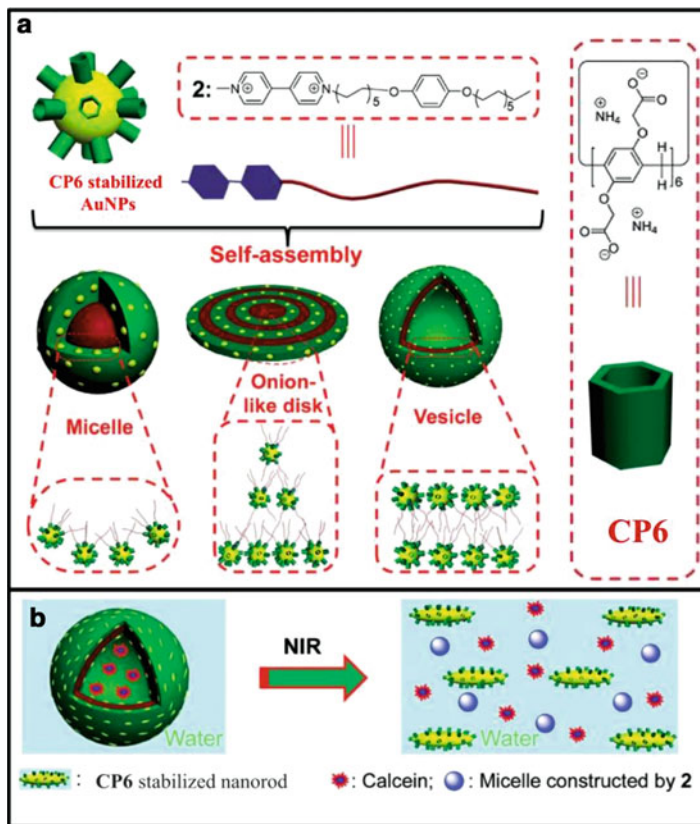


**Fig. 36.2** (a) Self-assembly of CP6 modified AuNPs with hydrophobic chain functionalized paraquat into various hybrid nanostructures. (b) Self-assembly of CP6 stabilized nanorod, NIR-triggered vesicle-to-micelle transition and release of the encapsulated calcein (Ref. [28], Copyright 2014 – Reproduced by permission of The Royal Society of Chemistry)

Au electrode stabilized by self-assembling monolayers (SAM) of resorcin[4]arenes derivatized with four flexible sulfide side chains was prepared at 60 °C, and the outer interface consists of receptor sites only [32]. Significantly, a monolayer of thiolated calix[6]arene self-assembled on Au electrode, which showed good performance for recognition of various kinds of bisphenols (BPs) as examined using cyclic voltammetry (CV) and localized SPR spectroscopy [33]. SAMs of calix[8]arene derivatives were also formed on Au bead electrodes, and characterized by CV blocking experiments, impedance spectroscopy, and reductive desorption [34]. As judged by the observation of first two reduction responses, only the calix[8]arene derivative was effective for immobilization of C<sub>60</sub> on Au surfaces. Calix[4]arene lipoic acid (C4LA) also self-assembled on Au surfaces to offer C4LA SAMs (Fig. 36.3) [35]. Attributing to the formation of inclusion complex between C4LA and methomyl, with highly sensitivity and selectivity, these C4LA SAMs

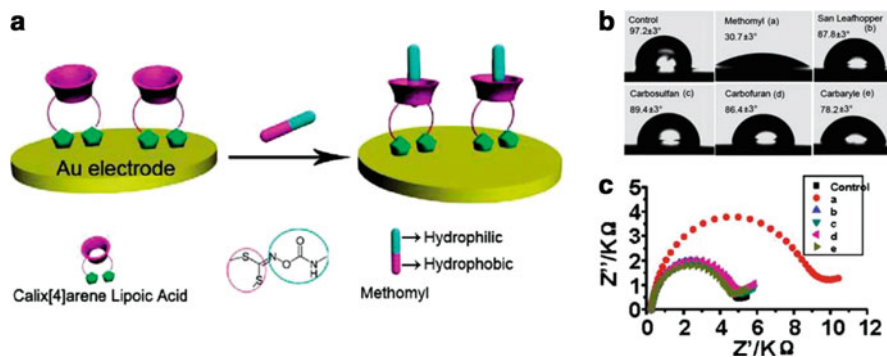


**Fig. 36.3** (a) The schematic recognition process of C4LA SAMs toward methomyl via host-guest complexation. (b) Contact angles relationship images of C4LA SAMs with different guests: methomyl, san leafhopper, carbosulfan, carbofuran, carbaryl. (c) Impedance response of  $\text{Fe}(\text{CV})_6^{3-/4-}$  at C4LA SAMs electrode in the presence of the five carbamates ( $1 \times 10^{-4}$  M) including blank as control, methomyl, san leafhopper, carbosulfan, carbofuran, and carbaryl (Reprinted with permission from Ref. [35], Copyright 2011 American Chemical Society)

exhibited remarkable wettability and impedance dual signal response to methomyl. The dual-signal responsiveness to methomyl suggests potential application to develop a chip or microelectrode.

Calix[4,6,8]arene derivatives were prepared for the fabrication of SAM redox-active ion, steroids, aromatic amines, metolcarb sensors on Au surfaces. SPR spectroscopy, CV and electrochemical impedance spectroscopy, contact angle measurements were used to monitor guest recognition of the SAM-modified gold electrodes [36–41]. Furthermore, multilayering calix[4]resorcinarene was also deposited on ordered Au, quartz and other substrates [42].

In 2003, Wan, Bai, and coworkers constructed well-ordered arrays of calix[8]arene derivative OBOCMC8 and  $\text{C}_{60}$ /OBOCMC8 on Au(111) surface, which can be clearly detected by scanning tunneling microscopy (STM) [43]. They also investigated conformation-related adlayer structures of calixarenes with specific conformations on Au(111) surface via in-situ STM and CV [44]. Then, Wang group, collaborated with the Wan group, investigated the adlayers of aza- and/or oxo-bridged calix[2]arene[2]triazines on Au(111) surfaces via STM and density functional theory (DFT) calculations [45]. The cavity sizes of these molecules, molecular orientation and conformation in the adlayers can be tuned by substituting the bridging atom and co-adsorption with 1,3,5-tris(5-carboxyamyl)oxy)benzene (TCAB). The electrochemically switchable  $\text{Cu}^{2+}$  complex of a 1,3-alternate bis(dipyridyl)calix[4]arene-based SAMs on Au(111) surfaces were then constructed via micro-contact printing procedures, and the resulting surface was imaged by SPR [46]. In 2007, under ultrahigh vacuum (UHV), calix[4]arene dimelamine derivatives were sublimated onto Au(111) surface equipped with variable-temperature Aarhus STM (Fig. 36.4) [47]. This is the first case that incorporation of coordinated metal atoms exhibited explicitly stabilizing effect. This work paves a new avenue to explore these large supramolecular complexes on the vacuum-solid interface.



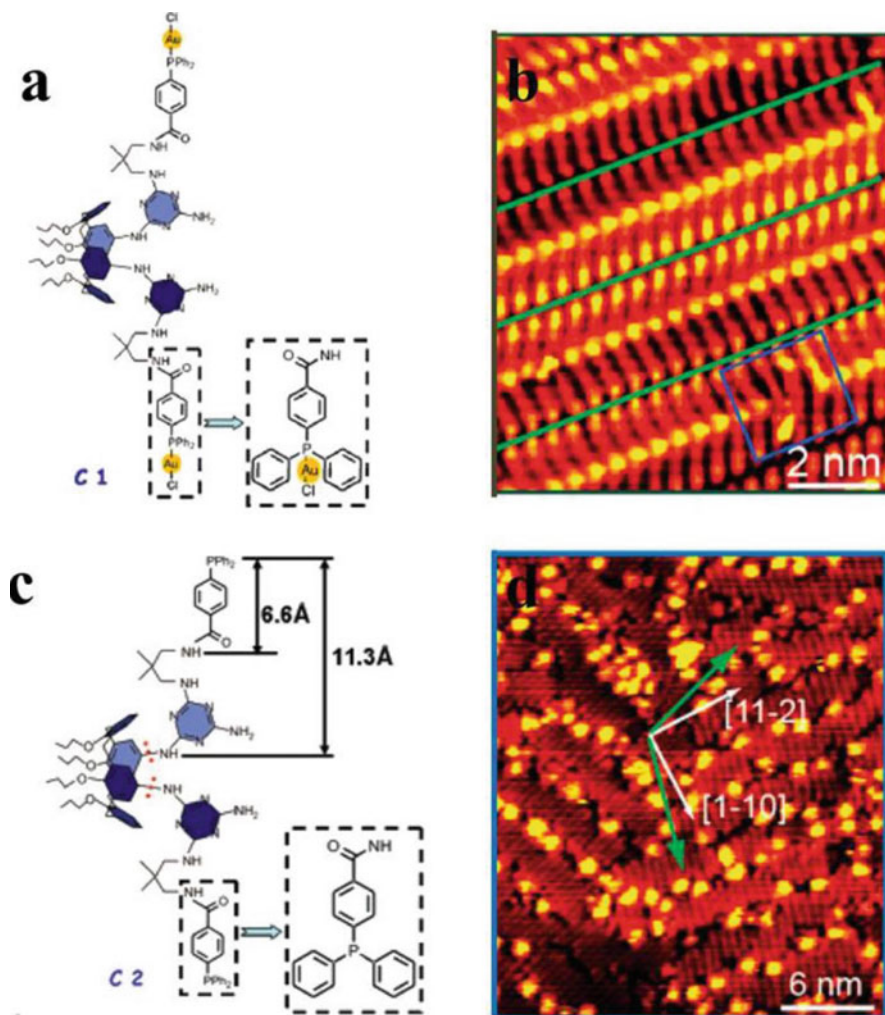


**Fig. 36.4** (a) Gold-functionalized compound (C1). (b) STM image of the well-ordered lamella structure of C1 (*green lines* stand for lamellae boundaries). (c) Triphenylphosphine calix[4]arene derivative (C2) deviating from C1 by the lack of coordinated gold atoms. Approximate molecular dimensions are indicated. (d) STM image of the surface morphology after deposition of C2 (Reprinted with permission from Ref. [47], Copyright 2007 American Chemical Society)

Interestingly, tetraguanidinium calix[4]arene was anchored, by Reinhoudt and coworkers, to a  $\beta$ -cyclodextrin ( $\beta$ -CD) SAM on Au surface (molecular printboard) through hydrophobic interactions of the adamantyl units with the surface-confined  $\beta$ -CD cavities [48]. The subsequent self-assembly of the molecular capsule with tetrasulfonate calix[4]arene on surface through ionic interactions was monitored by SPR spectroscopy. The tetrasulfonate calix[4]arene could be removed by rinsing of the surface with a high ionic strength aqueous solution, while the complete

desorption of the tetraguanidinium calix[4]arene from the  $\beta$ -CD SAM was achieved by rinsing with 2-propanol.

### 36.2.2 Silver-Supported Calixarenes and Pillarenes

Silver (Ag) is a soft, white, lustrous transition metal, it possesses the highest electrical conductivity, thermal conductivity and reflectivity of any metal [50]. Owing to broad plasmon resonance in the visible-near infrared region, high stability, and easy preparation, Ag is the most universal substrate among the possible metals (e.g., Ag, Au, and Cu) with applications in SERS. The benefit of using AgNPs is that the molar extinction coefficient is greater due to the difference in optical brightness, which increases sensitivity and leads to improved visibility [51].

In 2002, for the first time, by photon correlation spectroscopic measurements and visible spectrophotometry, Kaifer group reported the “macrocylic effect” on AgNPs formation in the presence of various macrocyclic thiol compounds in *N,N'*-dimethylformamide (DMF) solution [49]. AgNPs of <5 nm diameter were successfully obtained by photochemical reduction using *p*-phosphonated calix[4]arene and its *O*-alkyl derivatives as templates [52]. The aggregation of Au-AgNPs was monitored by supramolecular recognition of the pyridinium functionalized AuNPs by the calix[4]arene-modified AgNPs, which exhibited the low-energy shift of their SPR bands [53]. Trace concentrations of polycyclic aromatic hydrocarbons (PAHs) had been successfully detected using calix[4]arene-functionalized AgNPs by SERS [54–56]. SC[4]A derivatives-modified AgNPs could act as novel colorimetric histidine and organophosphorus pesticides probes, detector of surfactants, and electrochemical sensor of methyl parathion [50, 57–60]. Furthermore, pyridyl-appended calix[4]arene and thiolated-calix[4]arene functionalized Ag nanoprobe have been used as  $\text{Fe}^{3+}$  colorimetric sensors with nanomolar sensitivity [51, 61].

Reflection-absorption infrared spectroscopy (RAIRS), Monte Carlo simulation, and voltammetry were used to investigate the structures and redox-switching behaviors of  $\text{Ca}^{2+}$ /calix[4]quinone complexes on Ag surface [62]. The  $\text{Ca}^{2+}$  ions in the complexes locate near the quinone moieties and interact with the quinone moieties, offering the redox-switching properties of calix[4]quinones. Moreover, the  $\text{Ca}^{2+}$ /CTAQ and  $\text{Ca}^{2+}$ /CDAQ complexes on the Ag electrodes were extremely stable under electrochemical reactions, which is a practical and important advantage for applications.

In 2014, CP5 with five carboxylate groups on each rim was reported to be able to serve as a stabilizer for AgNPs preparation (Fig. 36.5) [63]. Moreover, the aggregation of CP5-stabilized AgNPs can be induced by adding a small amount of spermine or its analogues, which provides new opportunities for visual detection of spermine analogues in water through host-guest interactions.

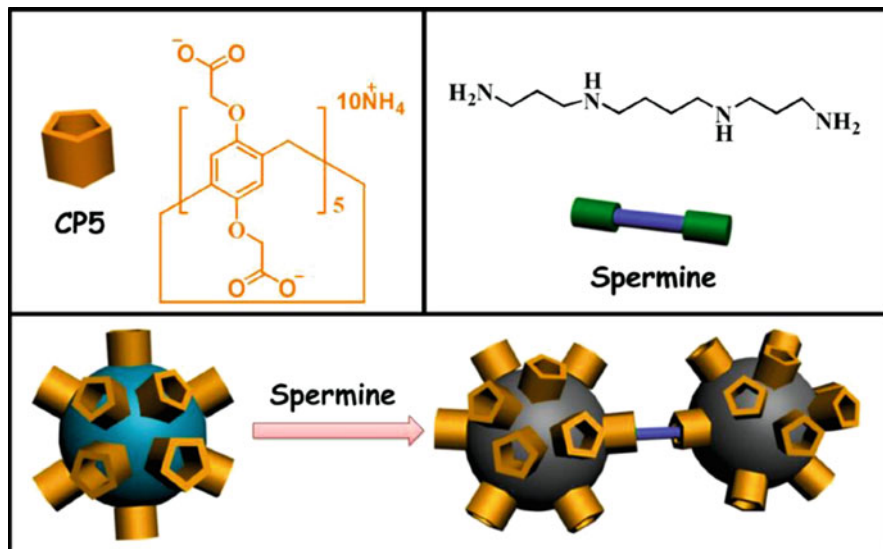


**Fig. 36.5** Visual detection of spermine by CP5-stabilized AgNPs (Ref. [63], Copyright 2014 – Adapted by permission of The Royal Society of Chemistry)

### 36.2.3 Quantum Dots-Supported Calixarenes and Pillarenes

Quantum dots (QDs) have been a research focus in recent years owing to their unique optical properties, such as high quantum yields, narrow and tunable emission spectra, strong fluorescence emission intensity, long fluorescence time, and reduced susceptibility to photobleaching. The fluorescence efficiency of QDs is sensitive to the presence and nature of adsorbates on their surfaces. The introduction of an organic ligand on QD surface affords not only the stability of these nanoentities in different solvents but also the desired surface functionality, which enables them to be used as chemosensors [64].

Combining the supramolecular host-guest properties of calixarenes, the optical properties of calixarene-modified CdSe/ZnS semiconductor QDs were controlled for the optical detection of neurotransmitter (acetylcholine), C<sub>60</sub> and mercury ions [65–70]. SC[4,6]A was selected to prepare highly fluorescent, stable and water-soluble CdSe QDs by simple, rapid ligand exchange route [71]. Then, this kind of QDs were used to construct Au electrode with enhanced photocurrents systems. [72] CdTe QDs in silica spheres coated with calix[4]arene were also synthesized as luminescent probes for pesticides and PAHs [64].

Due to the strong interaction of pre-organized multicarboxylated groups of CP5 sodium salts with CdTe QDs, CP5 was first used to stabilize CdTe QDs to give QD@CP5 via a ligand-exchange approach by our research group in 2013 (Fig. 36.6) [73]. CP5 rings improved the photophysical and photochemical properties of this organic-inorganic nanocomposite, and showed significant potential

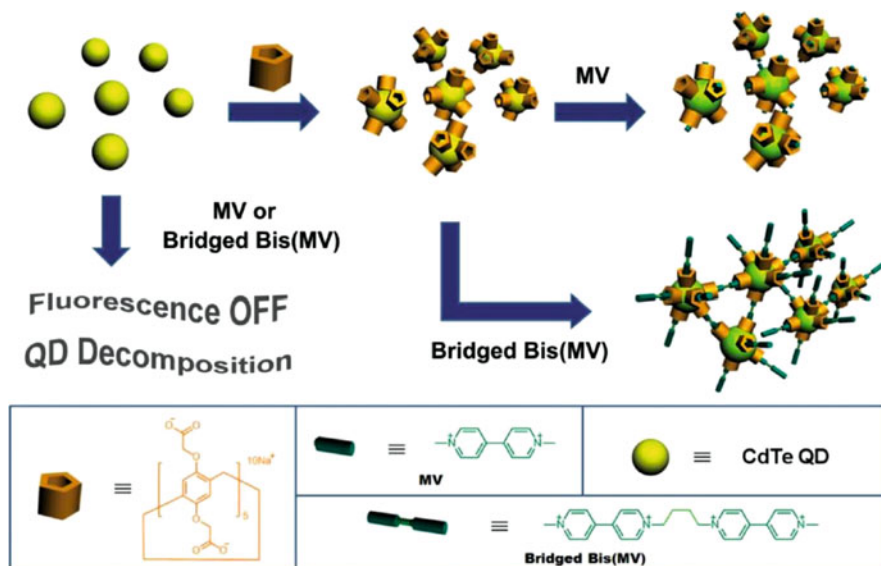


**Fig. 36.6** The formation of QD@CP5 and self-assembly behaviour of CP5-modified QDs by the addition of methyl viologen (MV) or bridged bis(MV) (Ref. [73], Copyright 2013 – Reproduced by permission of The Royal Society of Chemistry)

application for herbicide detection. Moreover, via host-guest interactions, an aggregated supramolecular network was constructed upon addition of bridged bis(methyl viologen)s guest.

### 36.2.4 Magnetic NPs-Supported Calixarenes and Pillarenes

Nanomaterials with unique magnetic and photonic properties possess a wide array of potential applications in biology such as magnetic storage media, MRI contrast agents, drug delivery carriers, biomarkers and separation of biomolecules, and catalyst [74–77]. In 2007, remarkably stable magnetite ferrofluids stabilized by sulfonatocalixarene macrocycles were constructed by rapid in situ co-precipitation, which exhibited superparamagnetic behaviour [78]. Furthermore, red-green emitting and superparamagnetic nanomarkers containing  $\text{Fe}_3\text{O}_4$  functionalized with calixarene and rare earth complexes were obtained [79]. These novel nanomaterials pave the potential applications in magnetic light-converting molecular devices.

Recently, collaborated with the Jia group, we first introduced carboxylatopillar[5]arene (CP[5]A, we employ CP5 to represent the  $\text{COO}^-$  version of carboxylatopillar[5]arene and CP[5]A to represent the original  $\text{COOH}$  form of carboxylatopillar[5]arene in this chapter) onto the surface of magnetic  $\text{Fe}_3\text{O}_4$  NPs (MNPs) via

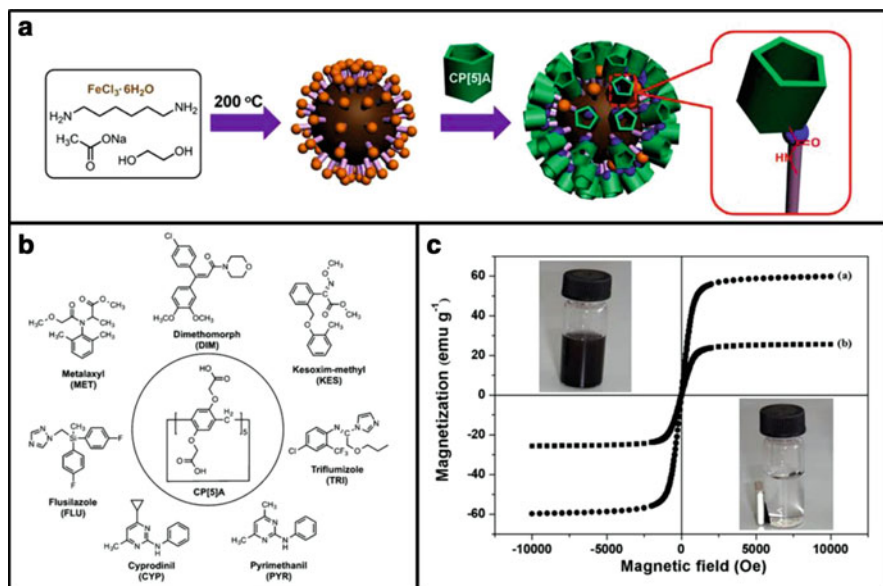


**Fig. 36.7** (a) Synthetic route to CP[5]A-functionalized MNPs. (b) Chemical structures of the target pesticides and CP[5]A. (c) Magnetic hysteresis loops of  $\text{Fe}_3\text{O}_4\text{-NH}_2$  (inset a) and  $\text{Fe}_3\text{O}_4/\text{CP}[5]\text{A}$  (inset b). Insets show the images of CP[5]A-functionalized MNP dispersions before and after exposing to an external magnet (Ref. [80], Copyright 2013 – Adapted by permission of The Royal Society of Chemistry)

covalent bonds (Fig. 36.7) [80]. Coupled with high-performance liquid chromatography (HPLC), these magnetic hybrid nanomaterials were used as magnetic solid phase extraction (MSPE) adsorbent for the determination of trace pesticides in commercial beverage samples, which exhibited good adsorption ability, strong superparamagnetism, high selectivity, high adsorption capacity and good recovery. This newly developed MSPE-HPLC method provided a new and efficient methodology in sample pretreatment and separation.

### 36.2.5 Ti, Si and Other Surfaces

Owing to the unique host-guest properties of calixarene macrocycles, calixarene-functionalized silica particles were used as cation-selective receptor colloids [81], and separator of lanthanides and actinides [82]. Calixarenes were also used for the syntheses of Ru, Pt and Pd NPs [83–85]. Furthermore, photoluminescence and charge-transfer complexes of calixarenes and calix[4]arene-based glycoclusters were grafted onto the surface of  $\text{TiO}_2$  NPs [64, 86].

The first single-step immobilization of calix[4]arene onto the surface of silica was successfully obtained by Katz and coworkers [87]. The lipophilic cavities of

the immobilized calixarenes can adsorb gas and neutral organic guests. SAMs of photofunctional siloxane-based calix[4]arenes on oxide surfaces, such as quartz and silicon wafers, were described by Wasielewski et al. [88]. Then, V(III)-calixarene as a sterically bulky chelating ligand enforced isolated pseudo-octahedral vanadium centers on silica [89], confined and site-isolated primary amine functionalized calixarenes were covalently immobilized on the surface of silica [90]. Calix[4]azacrown, tert-butylcalix[4]arene, and calix[5]arene were successfully grafted onto silica substrates and the silicon surface, which were used for switchable wettability sensor for ion pairs, recovery of n-butanol, recognition of n-butylammonium and 1,5-pentanediammonium picrates [91–93]. Perhydroxyl-pillar[5]arene and perhydroxyl-pillar[6]arene as new macrocycles of calixarene analogues, have been covalently attached to hydrophilic silica by our research group [94]. These two hybrid materials exhibited good adsorption ability toward typical herbicides. This new type of pillarene-based adsorbent materials has been proven to be good candidates for harmful substances removal from wastewaters.

Calixarene-Ti(IV) complexes were grafted onto SiO<sub>2</sub> for controlling epoxidation catalysis [95, 96]. SAMs of cavity-containing derivatives of calix[4]arene on noble metal surface served as molecular sieves for H<sub>2</sub> molecules and H<sup>+</sup> ions, which could have relevance for fuel cell applications [97, 98]. 3,4-(Ethylenedioxy)thiophene (EDOT)-functionalized calix[4]pyrrole were electropolymerized on an ITO electrode for an effective fluoride anion sensor in the solid state [99]. SPR method was used to probe the binding of calix[4]pyrroles to pyridine *N*-oxides [100]. Furthermore, supramolecular monolayers coated resonator could work as specific sensing interface for recognition of different volatile organic compounds (VOCs) which increases the sensor selectivity [101].

## 36.3 Calixarenes and Pillarenes on Porous Materials

### 36.3.1 Mesoporous Silica

Mechanized mesoporous silica nanoparticles (MSNs) with supramolecular nanovalves have attracted substantial attention owing to good biocompatibility, robust storage ability, tunable pore size, stimuli-responsiveness, and their excellent performance in drug delivery, sensing, imaging, and so on [102–106]. Compared with traditional release systems, attributing to the fine-tunable valve tightness, these supramolecular nanovalves exhibit negligible premature leakage before activation, and drug molecules can be transported to target cells or tissues accurately before they are released on demand. Water-soluble SC[n]As and CP5 are biocompatible and possess many advantages in molecular recognition and self-assembly, which hold great promise for the application in nanovalve systems.

For several years, our group have first worked on attaching calixarene and pillarene-based supramolecular switches onto the surface of MSNs. SC[4]As



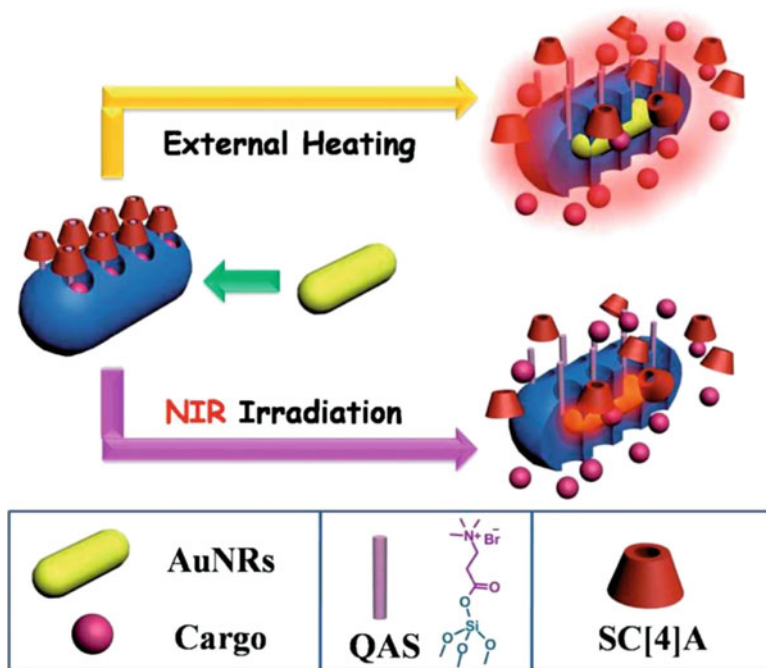


**Fig. 36.8** AuNR@MSN equipped with SC[4]A-QAS nanovalves. NIR light irradiation or external heating triggered the release of cargo from this platform (Ref. [109], Copyright 2013 – Reproduced by permission of The Royal Society of Chemistry)

were encircled around choline moieties-functionalized MSNs, and upon adding enzyme, competitive binding agent, or changing pH, the nanovalve can be opened and drug molecules can be released on command [107]. Comparing with that of normal people, the concentration of acetylcholine (ACh) in the synapses of Parkinson disease patients will increase remarkably, which can trigger drug release from calixarene or pillarene-gated MSNs by removing macrocycles from the stalks [108]. In the meantime, we first constructed a novel cancer theranostic hybrid platform by attaching SC[4]A on mesoporous silica-coated gold nanorods (AuNR@MSN, Fig. 36.8) [109]. Significantly, the plasmonic heating from the bio-friendly near-infrared (NIR) light-stimulated AuNR cores can efficiently kill cancer cells and decrease the ring-stalk binding affinity, allowing the dethreading of SC[4]A rings from the stalks on AuNR@MSNs to result in gate opening followed by drug release. The NIR light-responsive mechanized AuNR@MSN suggests a more effective and safer technique for non-invasive controlled drug delivery. In 2013, pillarene was first used by us as bulky rings to encircle stalks on MSNs to construct nanovalves [110]. The controlled release of drugs was achieved by changing pH or adding competitive binding agents. Afterwards, carboxylate-substituted pillar[6]arene (CP6)-valved MSNs were constructed for multi-

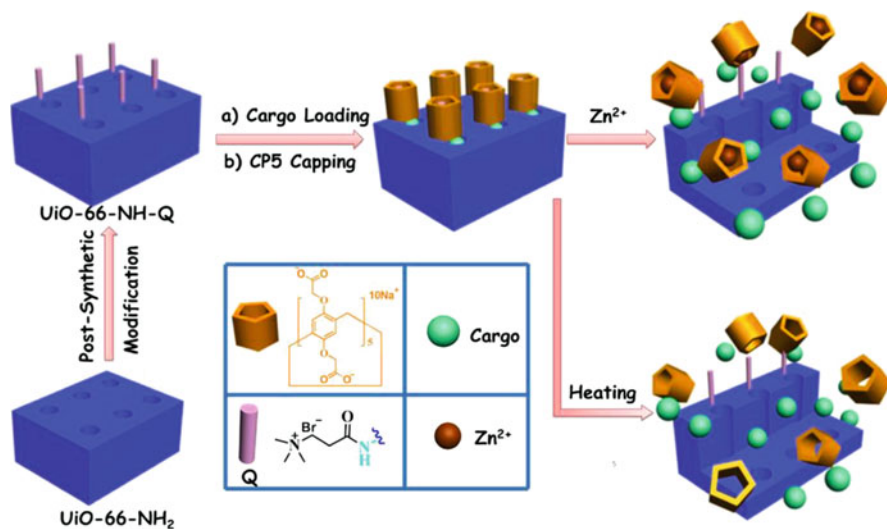


**Fig. 36.9** Mechanized UiO-66-NH<sub>2</sub> MOFs with quaternary ammonium salt (Q) and CP5 caps. Controlled release can be achieved by thermal heating or by competitive binding of Zn<sup>2+</sup> cations. Copyright 2013 Wiley (Adapted with permission from Ref. [116])

responsive controlled release, where acidic pH or competitive binding, and metal chelating with the carboxylate groups of CP6 triggered the opening of the nanovalves and the release of cargo [111].

### 36.3.2 Metal-Organic Frameworks

Metal-organic frameworks (MOFs) possess a wide array of potential applications in gas storage, catalysis, separation, drug delivery, imaging, sensors and detection, attributing to their tunable structural features and pore sizes, high surface areas, chemical/thermal stability, and versatile functionality [112–114]. Significantly, the first mechanized MOFs (MMOFs), composed of MOFs as scaffolds and CP5-based supramolecular switches as gates to prevent premature leakage, have been constructed to achieve targeted and controlled fashion of drug delivery. On-command drug release triggered by pH, bio-friendly Zn<sup>2+</sup> ions (abundant in synaptic vesicles) and auxiliary thermal stimulus is successfully realized (Fig. 36.9) [115, 116]. With large pore sizes for drug encapsulation, excellent biodegradability and biocompatibility, potential application in cell imaging, extremely low cytotoxicity and premature drug release, and superior multiple-stimuli responsiveness, this novel MMOFs open a new perspective in targeted drug delivery and controlled release of therapeutic agents, especially in the treatment of cancer and central nervous system (CNS) diseases.



## 36.4 Calixarenes and Pillarenes on Carbon Materials

### 36.4.1 Carbon Nanotubes

The past decades have seen an incredible boost of carbon nanotubes (CNTs) in both scientific research and commercial sectors since Iijima's discovery of CNTs [117]. CNTs have extraordinary and unique mechanical, optical and electrical properties and major research efforts were focused on areas including high performance electronics, scanning probe microscopy, fuel cells, composites, mechanical, chemical, biological and physical sensors, etc. [118]. However, the formation of insoluble large bundles, caused by the strong van der Waals interactions between individual hydrophobic nanotubes, limited the applications of CNTs. In order to harness the full potential of CNTs, their separation and dispersion are therefore an intense subject of scientific research.

Calixarenes and pillarenes are used for separating and dispersing CNTs in water [119–122]. These calixarenes and pillarenes functionalized CNTs were capable of detection of *N*-methylammonium [123], clear separation and accurate identification of VOCs [124]. A neutral guest with  $\pi$ -rich pyrenyl ring can attach to the surface of multiwalled nanotubes (MWNTs) through  $\pi$ – $\pi$  stacking interactions without destroying the structures of MWNTs (Fig. 36.10) [125]. CP6 can form host-guest complex (G2 $\subset$ CP6) with guest through hydrophobic interactions. In an aqueous solution of guest compound alone, MWNTs could not be dispersed. While, in an aqueous solution of G2 $\subset$ CP6, attributing to the formation of soluble surface with CP6, MWNTs were dispersed very well through simple sonication, and kept homogeneous and stable for over 1 month without significant change. Due to the reversible solubility of CP6 fragments depending on pH, the dispersion of MWNTs can be reversibly controlled by simply changing the solution pH. When the pH decreased to lower than 7.0, MWNTs precipitated from the solution, and when the pH was raised above 7.0, MWNTs dispersed well again. SEM, TEM, and fluorescence spectroscopy were used to visualize these phenomena. Overall, these phenomena suggest that G2 $\subset$ CP6 plays an important role in adjusting the solubility and dispersibility of MWNTs.

### 36.4.2 Graphene

In recent years, as a two-dimensional material (2D), graphene has garnered increasing attention on the horizon of materials science [126]. They possess remarkable and unique properties, such as unique planar structure, remarkable mechanical properties, extremely high specific surface area, exceptional optical properties, and fascinating electronic transfer at room temperature [127]. These outstanding

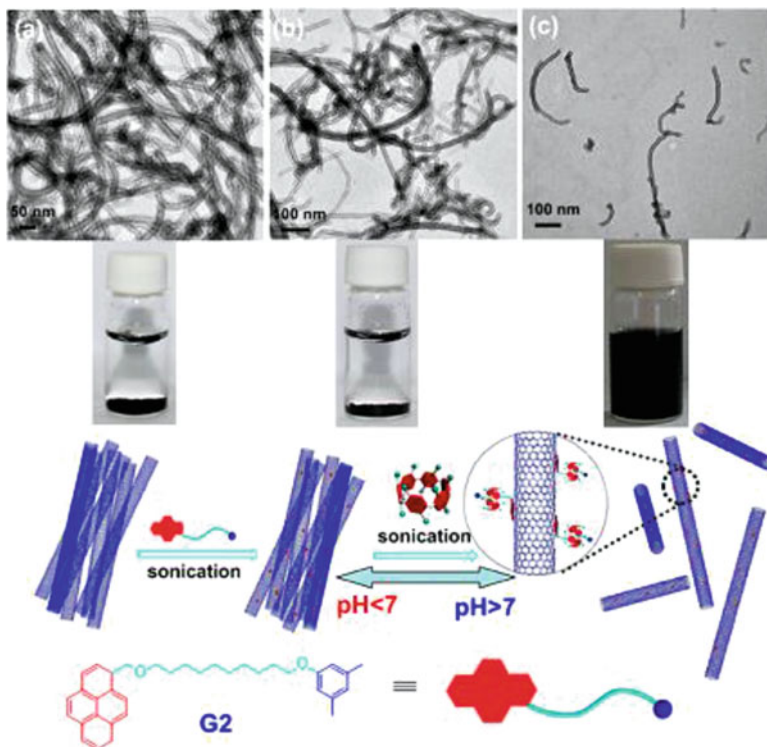


**Fig. 36.10** (top) TEM images of (a) MWNTs, (b) G2 and MWNTs, and (c) G2<sub>2</sub>CP6/MWNT complexes and photographs of the corresponding mixtures with water. (bottom) Illustration of the pH-responsive solubility of the MWNTs in the presence of G2<sub>2</sub>CP6 (Reprinted with permission from Ref. [125], Copyright 2012 American Chemical Society)

properties offer them a wide array of potential applications in nanocomposites and also make them attractive candidates for applications in many scientific fields such as catalysis, sensors, energy storages, electronics, and photonics.

*p*-Phosphonic acid calix[8]arene stabilized graphene was constructed for reversible nitrate uptake from aquatic effluents [128]. Then a fluorescent calix[4]arene triazole-linked pyrene modified graphene (CP-GO) exhibits very high supramolecular recognition for carbaryl, in particular in serum samples with a nanomolar concentration detection [129]. This was analyzed by electrochemical impedance spectroscopy or macroscopic recognition by contact angle measurements, and expands practical applications. Subsequently, Zhao and co-workers successfully prepared bola-amphiphilic pillar[5]arene and the tadpole-like amphiphilic pillar[5]arene-functionalized graphene [130], which was used for dual-mode Raman and fluorescence bioimaging *in vitro*. These hybrid materials are biocompatible and low cytotoxic, which can be stable in aqueous solution for a long time. Three kinds of

water-soluble SC[4,6,8]A sodium salts were also successfully grafted onto the surface of reduced graphene oxide (RGO) by using a simple wet chemical strategy. Significantly, SC[n]A-RGO composites exhibited high supramolecular recognition and enrichment capability, consequently displayed excellent electrochemical response toward four probe molecules (biological and organic dye molecules) [131]. Subsequently, RGO was modified with CP5 via covalent bonds [132]. Compared with native RGO, the obtained RGO-CP5 nanosheets own the ability of molecular recognition, good dispersibility in water, and exhibited enhanced fluorescence-quenching resistance. This novel sensing platform opens new perspectives in the sensing and detection of organic dye molecules and pesticides [132].

Ternary RGO-AP5-AuNPs nanocomposites were obtained by self-assembly of AuNPs onto the surface of amphiphilic pillar[5]arene (AP5) functionalized water-dispersive RGO nanocomposite. RGO-AP5 exhibited excellent selective supramolecular recognition and enrichment capability toward guest molecules. Furthermore, combining the excellent performances of RGO, selective molecular recognition, and catalytic property of AuNPs, ternary nanocomposites RGO-AP5-AuNPs exhibited synergistically enhanced electrochemical response of host-guest recognition [133]. Ultra-small Pd NPs nucleate on phosphonated calix[4]arenes stabilized graphenes (Pd-C4-G) [134]. High density 2D arrays of Pt NPs were obtained by using Pd-C4-G as galvanic reaction templates. Using a simple drop casting technique on interdigitated electrodes, electrocatalytic ternary Pd/Pt/Ru-phosphonic acid calix[8]arene (PC8)-G nanocomposite has been incorporated into a functional hydrogen sensing device [135–137].

## 36.5 Concluding Remarks

We described the development of calixarenes and pillarenes on surfaces and the applications of these hybrid materials. The selected surfaces include NPs, metal surface, Si surface, electrode, porous materials, and carbon materials. These multivariant hybrid materials combine the supramolecular host-guest properties of calixarene/pillarene hosts with the unique surface properties of other entities, expand the applications in recognition, stabilization, self-assembly, dispersion, electrode, controlled drug release, sensing, separation and absorption. This design principle holds great promise for the design and application of new desired materials in future.

**Acknowledgements** This work is supported by the National Natural Science Foundation of China (51473061, 21272093), the JLU Cultivation Fund for the National Science Fund for Distinguished Young Scholars, and the Fundamental Research Funds for the Central Universities (JCKY-QKJC05).

## References

1. Love, J. C.; Estroff, L. A.; Kriebel, J. K.; Nuzzo, R. G.; Whitesides, G. M. *Chem. Rev.* **2005**, *105*, 1103–1170.
2. Yang, Y.-W.; Sun, Y.-L.; Song, N. *Acc. Chem. Res.* **2014**, *47*, 1950–1960.
3. Wei, A. *Chem. Commun.* **2006**, 1581–1591.
4. Sameni, S.; Jeunesse, C.; Matt, D.; Harrowfield, J. *Chem. Soc. Rev.* **2009**, *38*, 2117–2146.
5. Mutihac, L.; Lee, J. H.; Kim, J. S.; Vicens, J. *Chem. Soc. Rev.* **2011**, *40*, 2777–2796.
6. Dondoni, A.; Marra, A. *Chem. Rev.* **2010**, *110*, 4949–4977.
7. Tan, L.-L.; Yang, Y.-W. *J. Incl. Phenom.* **2015**, *81*, 13–33.
8. Song, N.; Yang, Y.-W. *Sci. China Chem.* **2014**, *57*, 1185–1198.
9. Strutt, N. L.; Zhang, H.; Schneebeli, S. T.; Stoddart, J. F. *Acc. Chem. Res.* **2014**, *47*, 2631–2642.
10. Zhao, Q.; Dunlop, J. W. C.; Qiu, X.; Huang, F.; Zhang, Z.; Heyda, J.; Dzubiella, J.; Antonietti, M.; Yuan, J. *Nature Commun.* **2014**, *5*, 4293, doi: [10.1038/ncomms5293](https://doi.org/10.1038/ncomms5293).
11. Li, S.-H.; Zhang, H.-Y.; Xu, X.; Liu, Y. *Nature Commun.* **2015**, *6*, 7590, doi: [10.1038/ncomms8590](https://doi.org/10.1038/ncomms8590).
12. Ogoshi, T.; Kanai, S.; Fujinami, S.; Yamagishi, T.-a.; Nakamoto, Y. *J. Am. Chem. Soc.* **2008**, *130*, 5022–5023.
13. Li, H.; Yang, Y.-W. *Chin. Chem. Lett.* **2013**, *24*, 545–552.
14. Kim, H. J.; Lee, M. H.; Mutihac, L.; Vicens, J.; Kim, J. S. *Chem. Soc. Rev.* **2012**, *41*, 1173–1190.
15. Stavens, K. B.; Pusztay, S. V.; Zou, S.; Andres, R. P.; Wei, A. *Langmuir* **1999**, *15*, 8337–8339.
16. Ciesa, F.; Plech, A.; Mattioli, C.; Pescatori, L.; Arduini, A.; Pochini, A.; Rossi, F.; Secchi, A. *J. Phys. Chem. C* **2010**, *114*, 13601–13607.
17. Pulkkinen, P. M. S.; Wiktorowicz, S.; Aseyev, V.; Tenhu, H. *RSC Adv.* **2013**, *3*, 733–742.
18. Arduini, A.; Demuru, D.; Pochini, A.; Secchi, A. *Chem. Commun.* **2005**, 645–647.
19. Ha, J. M.; Solovyov, A.; Katz, A. *Langmuir* **2009**, *25*, 10548–10553.
20. Ha, J.-M.; Katz, A.; Drapailo, A. B.; Kalchenko, V. I. *J. Phys. Chem. C* **2009**, *113*, 1137–1142.
21. Yan, H.; Luo, J.; Xie, H.-M.; Xie, D. X.; Su, Q.; Yin, J.; Wanjala, B. N.; Diao, H.; An, D.-L.; Zhong, C.-J. *Phys. Chem. Chem. Phys.* **2011**, *13*, 5824–5830.
22. Han, C.; Zeng, L.; Li, H.; Xie, G. *Sensor. Actuat. B: Chem.* **2009**, *137*, 704–709.
23. Patel, G.; Menon, S. *Chem. Commun.* **2009**, 3563–3565.
24. Pandya, A.; Sutariya, P. G.; Menon, S. K. *Analyst* **2013**, *138*, 2483–2490.
25. Avvakumova, S.; Fezzardi, P.; Pandolfi, L.; Colombo, M.; Sansone, F.; Casnati, A.; Prospero, D. *Chem. Commun.* **2014**, *50*, 11029–11032.
26. Yao, Y.; Xue, M.; Chi, X.; Ma, Y.; He, J.; Abliz, Z.; Huang, F. *Chem. Commun.* **2012**, *48*, 6505–6507.
27. Li, H.; Chen, D. X.; Sun, Y. L.; Zheng, Y. B.; Tan, L. L.; Weiss, P. S.; Yang, Y. W. *J. Am. Chem. Soc.* **2013**, *135*, 1570–1576.
28. Yao, Y.; Wang, Y.; Huang, F. *Chem. Sci.* **2014**, *5*, 4312–4316.
29. Park, C.; Jeong, E. S.; Lee, K. J.; Moon, H. R.; Kim, K. T. *Chem. Asian J.* **2014**, *9*, 2761–2764.
30. Montes-García, V.; Fernández-López, C.; Gómez, B.; Pérez-Juste, I.; García-Río, L.; Liz-Marzán, L. M.; Pérez-Juste, J.; Pastoriza-Santos, I. *Chem. Eur. J.* **2014**, *20*, 8404–8409.
31. Zhou, Q.; Zhang, B.; Han, D.; Chen, R.; Qiu, F.; Wu, J.; Jiang, H. *Chem. Commun.* **2015**, *51*, 3124–3126.
32. Velzen, E. U. T. v.; Engbersen, J. F. J.; Reinhoudt, D. N. *J. Am. Chem. Soc.* **1994**, *116*, 3597–3598.
33. Nakaji-Hirabayashi, T.; Endo, H.; Kawasaki, H.; Gemmei-ide, M.; Kitano, H. *Environ. Sci. Technol.* **2005**, *39*, 5414–5420.

34. Zhang, S.; Echegoyen, L. *J. Org. Chem.* **2005**, *70*, 9874–9881.
35. Zhang, G.-F.; Zhan, J.-Y.; Li, H.-B. *Org. Lett.* **2011**, *13*, 3392–3395.
36. Cormode, D. P.; Evans, A. J.; Davis, J. J.; Beer, P. D. *Dalton Trans.* **2010**, *39*, 6532–6541.
37. Zhang, S.; Palkar, A.; Echegoyen, L. *Langmuir* **2006**, *22*, 10732–10738.
38. Valluru, G.; Rahman, S.; Georghiou, P. E.; Dawe, L. N.; Alodhayb, A. N.; Beaulieu, L. Y. *New J. Chem.* **2014**, *38*, 5868–5872.
39. Friggeri, A.; Veggel, F. C. J. M. v.; Reinhoudt, D. N. *Chem. Eur. J.* **1999**, *5*, 3595–3602.
40. Zhang, S.; Echegoyen, L. *Org. Lett.* **2004**, *6*, 791–794.
41. Zeng, X.; Ma, J.; Luo, L.; Yang, L.; Cao, X.; Tian, D.; Li, H. *Org. Lett.* **2015**, *17*, 2976–2979.
42. Davis, F.; Stirling, C. J. M. *J. Am. Chem. Soc.* **1995**, *117*, 10385–10386.
43. Pan, G.-B.; Liu, J.-M.; Zhang, H.-M.; Wan, L.-J.; Zheng, Q.-Y.; Bai, C.-L. *Angew. Chem. Int. Ed.* **2003**, *42*, 2747–2751.
44. Pan, G.-B.; Bu, J.-H.; Wang, D.; Liu, J.-M.; Wan, L.-J.; Zheng, Q.-Y.; Bai, C.-L. *J. Phys. Chem. B* **2003**, *107*, 13111–13116.
45. Yan, C.-J.; Yan, H.-J.; Xu, L.-P.; Song, W.-G.; Wan, L.-J.; Wang, Q.-Q.; Wang, M.-X. *Langmuir* **2007**, *23*, 8021–8027.
46. Arena, G.; Contino, A.; Longo, E.; Sgarlata, C.; Spoto, G.; Zito, V. *Chem. Commun.* **2004**, 1812–1813.
47. Xu, W.; Dong, M.; Vázquez-Campos, S.; Gersen, H.; Lægsgaard, E.; Stensgaard, I.; Crego-Calama, M.; Reinhoudt, D. N.; Linderoth, T. R.; Besenbacher, F. *J. Am. Chem. Soc.* **2007**, *129*, 10624–10625.
48. Corbellini, F.; Mulder, A.; Sartori, A.; Ludden, M. J. W.; Casnati, A.; Ungaro, R.; Huskens, J.; Crego-Calama, M.; Reinhoudt, D. N. *J. Am. Chem. Soc.* **2004**, *126*, 17050–17058.
49. Liu, J.; Ong, W.; Kaifer, A. E. *Langmuir* **2002**, *18*, 5981–5983.
50. Menon, S. K.; Modi, N. R.; Pandya, A.; Lodha, A. *RSC Adv.* **2013**, *3*, 10623–10627.
51. Pandya, A.; Sutariya, P. G.; Lodha, A.; Menon, S. K. *Nanoscale* **2013**, *5*, 2364–2371.
52. Hartlieb, K. J.; Martin, A. D.; Saunders, M.; Raston, C. L. *New J. Chem.* **2010**, *34*, 1834–1837.
53. Vita, F.; Boccia, A.; Marrani, A. G.; Zanoni, R.; Rossi, F.; Arduini, A.; Secchi, A. *Chem. Eur. J.* **2015**, *21*, 15428–15438.
54. Leyton, P.; Sanchez-Cortes, S.; Garcia-Ramos, J. V.; Domingo, C.; Campos-Vallette, M.; Saitz, C.; Clavijo, R. E. *J. Phys. Chem. B* **2004**, *108*, 17484–17490.
55. Guerrini, L.; Garcia-Ramos, J. V.; Domingo, C.; Sanchez-Cortes, S. *Langmuir* **2006**, *22*, 10924–10926.
56. Guerrini, L.; Garcia-Ramos, J. V.; Domingo, C.; Sanchez-Cortes, S. *Anal. Chem.* **2009**, *81*, 953–960.
57. Tauran, Y.; Brioude, A.; Shahgaldian, P.; Cumbo, A.; Kim, B.; Perret, F.; Coleman, A. W.; Montasser, I. *Chem. Commun.* **2012**, *48*, 9483–9485.
58. Xiong, D.; Chen, M.; Li, H. *Chem. Commun.* **2008**, 880–882.
59. Xiong, D.; Li, H. *Nanotechnology* **2008**, *19*, 465502.
60. Bian, Y.; Li, C.; Li, H. *Talanta* **2010**, *81*, 1028–1033.
61. Zhan, J.; Wen, L.; Miao, F.; Tian, D.; Zhu, X.; Li, H. *New J. Chem.* **2012**, *36*, 656–661.
62. Kang, S. K.; Lee, O.-S.; Chang, S.-K.; Chung, D. S.; Kim, H.; Chung, T. D. *J. Phys. Chem. C* **2009**, *113*, 19981–19985.
63. Yao, Y.; Zhou, Y.; Dai, J.; Yue, S.; Xue, M. *Chem. Commun.* **2014**, *50*, 869–871.
64. Li, H.; Qu, F. *Chem. Mater.* **2007**, *19*, 4148–4154.
65. Jin, T.; Fujii, F.; Sakata, H.; Tamura, M.; Kinjo, M. *Chem. Commun.* **2005**, 4300–4302.
66. Jin, T.; Fujii, F.; Sakata, H.; Tamura, M.; Kinjo, M. *Chem. Commun.* **2005**, 2829–2831.
67. Jin, T.; Fujii, F.; Yamada, E.; Nodasaka, Y.; Kinjo, M. *J. Am. Chem. Soc.* **2006**, *128*, 9288–9289.
68. Li, H.; Xiong, W.; Yan, Y.; Liu, J.; Xu, H.; Yang, X. *Mater. Lett.* **2006**, *60*, 703–705.
69. Li, H.; Zhang, Y.; Wang, X.; Xiong, D.; Bai, Y. *Mater. Lett.* **2007**, *61*, 1474–1477.

70. Carrillo-Carrión, C.; Lendl, B.; Simonet, B. M.; Valcárcel, M. *Anal. Chem.* **2011**, *83*, 8093–8100.
71. Wang, X.; Wu, J.; Li, F.; Li, H. *Nanotechnology* **2008**, *19*, 205501.
72. Sayin, S.; Azak, H.; Yildiz, H. B.; Camurlu, P.; Akkus, G. U.; Toppare, L.; Ersoz, M. *Phys. Chem. Chem. Phys.* **2015**, *17*, 19911–19918.
73. Chen, D.-X.; Sun, Y.-L.; Zhang, Y.; Cui, J.-Y.; Shen, F.-Z.; Yang, Y.-W. *RSC Adv.* **2013**, *3*, 5765–5768.
74. Ben-Ishay, M. L.; Gedanken, A. *Langmuir* **2007**, *23*, 5238–5242.
75. Sayin, S.; Yilmaz, E.; Yilmaz, M. *Org. Biomol. Chem.* **2011**, *9*, 4021–4024.
76. Qiu, X.-L.; Zhou, Y.; Li, Q.-L.; Jin, X.-Y.; Qi, A.-D.; Yang, Y.-W. *Chem. Commun.* **2015**, *51*, 4237–4240.
77. Qiu, X.-L.; Zhou, Y.; Jin, X.-Y.; Qi, A.-D.; Yang, Y.-W. *J. Mater. Chem. C* **2015**, *3*, 3517–3521.
78. Chin, S. F.; Makha, M.; Raston, C. L.; Saunders, M. *Chem. Commun.* **2007**, 1948–1950.
79. Khan, L. U.; Brito, H. F.; Holsa, J.; Pirota, K. R.; Muraca, D.; Felinto, M. C.; Teotonio, E. E.; Malta, O. L. *Inorg. Chem.* **2014**, *53*, 12902–12910.
80. Tian, M.-m.; Chen, D.-X.; Sun, Y.-L.; Yang, Y.-W.; Jia, Q. *RSC Adv.* **2013**, *3*, 22111–22119.
81. Nechifor, A. M.; Philipse, A. P.; de Jong, F.; van Duynhoven, J. P. M.; Egberink, R. J. M.; Reinhoudt, D. N. *Langmuir* **1996**, *12*, 3844–3854.
82. Böhmer, V.; Dozol, J.-F.; Grüttner, C.; Liger, K.; Matthews, S. E.; Rudershausen, S.; Saadioui, M.; Wang, P. *Org. Biomol. Chem.* **2004**, *2*, 2327–2334.
83. Yasin, F. M.; Boulos, R. A.; Hong, B. Y.; Cornejo, A.; Iyer, K. S.; Gao, L.; Chua, H. T.; Raston, C. L. *Chem. Commun.* **2012**, *48*, 10102–10104.
84. Zhou, R.; Srinivasan, M. P. *Langmuir* **2013**, *29*, 13042–13049.
85. Zang, W.; Chen, X.; Boulos, R. A.; Toster, J.; Raston, C. L. *Chem. Commun.* **2014**, *50*, 15167–15170.
86. Moni, L.; Rossetti, S.; Scoponi, M.; Marra, A.; Dondoni, A. *Chem. Commun.* **2010**, *46*, 475–477.
87. Katz, A.; Costa, P. D.; Lam, A. C. P.; Notestein, J. M. *Chem. Mater.* **2002**, *14*, 3364–3368.
88. van der Boom, T.; Evmenenko, G.; Dutta, P.; Wasielewski, M. R. *Chem. Mater.* **2003**, *15*, 4068–4074.
89. de Silva, N.; Hwang, S.-J.; Durkin, K. A.; Katz, A. *Chem. Mater.* **2009**, *21*, 1852–1860.
90. Solovyov, A.; Amundsen, T. J.; Daniels, J. J.; Kim, Y.-G.; Katz, A. *Chem. Mater.* **2008**, *20*, 6316–6318.
91. Lupo, F.; Capici, C.; Gattuso, G.; Notti, A.; Parisi, M. F.; Pappalardo, A.; Pappalardo, S.; Gulino, A. *Chem. Mater.* **2010**, *22*, 2829–2834.
92. Thompson, A. B.; Cope, S. J.; Swift, T. D.; Notestein, J. M. *Langmuir* **2011**, *27*, 11990–11998.
93. Feng, N.; Zhao, H.; Zhan, J.; Tian, D.; Li, H. *Org. Lett.* **2012**, *14*, 1958–1961.
94. Zhou, T.; Song, N.; Yu, H.; Yang, Y.-W. *Langmuir* **2015**, *31*, 1454–1461.
95. Notestein, J. M.; Solovyov, A.; Andrini, L. R.; Requejo, F. G.; Katz, A.; Iglesia, E. *J. Am. Chem. Soc.* **2007**, *129*, 15585–15595.
96. Notestein, J. M.; Andrini, L. R.; Kalchenko, V. I.; Requejo, F. G.; Katz, A.; Iglesia, E. *J. Am. Chem. Soc.* **2007**, *129*, 1122–1131.
97. Genorio, B.; He, T.; Meden, A.; Polanc, S.; Jamnik, J.; Tour, J. M. *Langmuir* **2008**, *24*, 11523–11532.
98. Santos, L.; Mattiuzzi, A.; Jabin, I.; Vandencastele, N.; Reniers, F.; Reinaud, O.; Hapiot, P.; Lhenry, S.; Leroux, Y.; Lagrost, C. *J. Phys. Chem. C* **2014**, *118*, 15919–15928.
99. Aydogan, A.; Koca, A.; Şener, M. K.; Sessler, J. L. *Org. Lett.* **2014**, *16*, 3764–3767.
100. Adriaenssens, L.; Sánchez, J. L. A.; Barril, X.; O’Sullivan, C. K.; Ballester, P. *Chem. Sci.* **2014**, *5*, 4210–4215.
101. Lu, Y.; Chang, Y.; Tang, N.; Qu, H.; Liu, J.; Pang, W.; Zhang, H.; Zhang, D.; Duan, X. *ACS Appl. Mater. Interfaces* **2015**, *7*, 17893–17903.

102. Li, Z.; Barnes, J. C.; Bosoy, A.; Stoddart, J. F.; Zink, J. I. *Chem. Soc. Rev.* **2012**, *41*, 2590–2605.
103. Li, Y.-J.; Wang, L.; Yan, B. *J. Mater. Chem.* **2011**, *21*, 1130–1138.
104. Li, Y. J.; Yan, B.; Wang, L. *Dalton Trans.* **2011**, *40*, 6722–6731.
105. Alahmadi, S.; Mohamad, S.; Maah, M. J. *Molecules* **2014**, *19*, 4524–4547.
106. Song, N.; Yang, Y.-W. *Chem. Soc. Rev.* **2015**, *44*, 3474–3504.
107. Sun, Y.-L.; Zhou, Y.; Li, Q.-L.; Yang, Y.-W. *Chem. Commun.* **2013**, *49*, 9033–9035.
108. Zhou, Y.; Tan, L.-L.; Li, Q.-L.; Qiu, X.-L.; Qi, A.-D.; Tao, Y.; Yang, Y.-W. *Chem. Eur. J.* **2014**, *20*, 2998–3004.
109. Li, H.; Tan, L.-L.; Jia, P.; Li, Q.-L.; Sun, Y.-L.; Zhang, J.; Ning, Y.-Q.; Yu, J.; Yang, Y.-W. *Chem. Sci.* **2014**, *5*, 2804–2808.
110. Sun, Y.-L.; Yang, Y.-W.; Chen, D.-X.; Wang, G.; Zhou, Y.; Wang, C.-Y.; Stoddart, J. F. *Small* **2013**, *9*, 3224–3229.
111. Huang, X.; Du, X. *ACS Appl. Mater. Interfaces* **2014**, *6*, 20430–20436.
112. Sumida, K.; Rogow, D. L.; Mason, J. A.; McDonald, T. M.; Bloch, E. D.; Herm, Z. R.; Bae, T.-H.; Long, J. R. *Chem. Rev.* **2012**, *112*, 724–781.
113. Lee, J.; Farha, O. K.; Roberts, J.; Scheidt, K. A.; Nguyen, S. T.; Hupp, J. T. *Chem. Soc. Rev.* **2009**, *38*, 1450–1459.
114. Li, J.-R.; Sculley, J.; Zhou, H.-C. *Chem. Rev.* **2012**, *112*, 869–932.
115. Tan, L.-L.; Li, H.; Qiu, Y.-C.; Chen, D.-X.; Wang, X.; Pan, R.-Y.; Wang, Y.; Zhang, S. X.-A.; Wang, B.; Yang, Y.-W. *Chem. Sci.* **2015**, *6*, 1640–1644.
116. Tan, L.-L.; Li, H.; Zhou, Y.; Zhang, Y.; Feng, X.; Wang, B.; Yang, Y.-W. *Small* **2015**, *11*, 3807–3813.
117. Iijima, S. *Nature* **1991**, *354*, 56–58.
118. Snow, E. S.; Perkins, F. K.; Robinson, J. A. *Chem. Soc. Rev.* **2006**, *35*, 790–798.
119. Hubble, L. J.; Clark, T. E.; Makha, M.; Raston, C. L. *J. Mater. Chem.* **2008**, *18*, 5961–5966.
120. Ling, I.; Alias, Y.; Makha, M.; Raston, C. L. *New J. Chem.* **2009**, *33*, 1583–1587.
121. Yang, J.; Yu, G.; Xia, D.; Huang, F. *Chem. Commun.* **2014**, *50*, 3993–3995.
122. Chen, X.; Gibson, C. T.; Britton, J.; Eggers, P. K.; Wahid, M. H.; Raston, C. L. *Chem. Commun.* **2015**, *51*, 239–2402.
123. Dionisio, M.; Schnorr, J. M.; Michaelis, V. K.; Griffin, R. G.; Swager, T. M.; Dalcanele, E. *J. Am. Chem. Soc.* **2012**, *134*, 6540–6543.
124. Wang, F.; Swager, T. M. *J. Am. Chem. Soc.* **2011**, *133*, 11181–11193.
125. Yu, G.; Xue, M.; Zhang, Z.; Li, J.; Han, C.; Huang, F. *J. Am. Chem. Soc.* **2012**, *134*, 13248–13251.
126. Kim, J.; Cote, L. J.; Huang, J. *Acc. Chem. Res.* **2012**, *45*, 1356–1364.
127. Luo, J.; Kim, J.; Huang, J. *Acc. Chem. Res.* **2013**, *46*, 2225–2234.
128. Eroglu, E.; Zang, W.; Eggers, P. K.; Chen, X.; Boulos, R. A.; Wahid, M. H.; Smith, S. M.; Raston, C. L. *Chem. Commun.* **2013**, *49*, 8172–8174.
129. Sun, Y.; Mao, X.; Luo, L.; Tian, D.; Li, H. *Org. Biomol. Chem.* **2015**, *13*, 9294–9299.
130. Zhang, H.; Ma, X.; Nguyen, K. T.; Zeng, Y.; Tai, S.; Zhao, Y. *ChemPlusChem* **2014**, *79*, 462–469.
131. Zhou, J.; Chen, M.; Diao, G. *ACS Appl. Mater. Interfaces* **2013**, *5*, 828–836.
132. Zhou, T.; Yu, H.; Liu, M.; Yang, Y.-W. *Chin. J. Chem.* **2015**, *33*, 125–130.
133. Zhou, J.; Chen, M.; Xie, J.; Diao, G. *ACS Appl. Mater. Interfaces* **2013**, *5*, 11218–11224.
134. Zou, J.; Martin, A. D.; Zdyrko, B.; Luzinov, I.; Raston, C. L.; Iyer, K. S. *Chem. Commun.* **2011**, *47*, 5193–5195.
135. Chen, X.; Yasin, F. M.; Eggers, P. K.; Boulos, R. A.; Duan, X.; Lamb, R. N.; Iyer, K. S.; Raston, C. L. *RSC Adv.* **2013**, *3*, 3213–3217.
136. Chen, X.; Zang, W.; Vimalanathan, K.; Iyer, K. S.; Raston, C. L. *Chem. Commun.* **2013**, *49*, 1160–1162.
137. Chen, X.; Vimalanathan, K.; Zang, W.; Slattery, A. D.; Boulos, R. A.; Gibson, C. T.; Raston, C. L. *Nanoscale* **2014**, *6*, 4517–4520.

# Chapter 37

## Calixarenes and Resorcinarenes at Interfaces

Ludovico Tulli and Patrick Shahgaldian

### 37.1 Introduction

The use of amphiphilic molecules extends well before the advent of modern chemical sciences and supramolecular chemistry as the first example of the use of amphiphiles traces back to 2200 B.C. when Babylonians were preparing soap-like materials by boiling fats with ashes. Mariners in antiquity were carrying barrels of oil on their ships to be dumped into the water in case of tempest, which had an immediate soothing effect on the waves. Benjamin Franklin studied this phenomenon that nowadays is known to be due to the formation of surface tension gradients in the oil film owing to the Gibbs–Marangoni effect [1–3]. In 1774, Franklin published “Of the Stilling of Waves by Means of Oil” that is an extract from letters between himself, William Brownrigg, and Mr. Reverend Farish [4]. Franklin reported that “*not more than a teaspoonful*” of oil on the surface of water had a wave attenuation effect over an area of “*perhaps half an acre*”. The pioneering works of Benjamin Franklin in the eighteenth century and Irving Langmuir in the twentieth century can be considered as major contributions to the rationalization of the behavior of amphiphiles at interfaces.

The main forces driving the self-assembly of amphiphiles in aqueous media and at interfaces are on the one hand the *hydrophobic effect* [5, 6] that is the tendency of the apolar portions of the amphiphile to stick together, and on the other hand the interactions of the polar part of the molecule with the aqueous phase [7]. Even if taken individually, these interactions are known in and of themselves, they interplay in such a complex, intricate and synergistic manner as to result in a tremendous

---

L. Tulli • P. Shahgaldian (✉)

School of Life Sciences, Institute of Chemistry and Bioanalytics, University of Applied Sciences and Arts Northwestern Switzerland, Gründenstrasse 40, CH-4132 Muttenz, Switzerland

e-mail: [patrick.shahgaldian@fhnw.ch](mailto:patrick.shahgaldian@fhnw.ch)



complexity. Amphiphilic self-assembly can lead to a variety of different nanometer-sized supramolecular architectures such as micelles, vesicles, mono- and multilayers, lyotropic liquid crystalline phases, twisted ribbons, helices, tubes, etc.

Besides natural amphiphiles, the design of artificial molecules possessing amphiphilic self-assembly properties is the focus of intensive research [8–10]. Besides the straightforward strategy that consists in directly attaching a polar headgroup to a lipophilic molecule, widely used for example to produce amphiphilic polymers, the approach using an intermediate molecule intercalated between these two poles of the amphiphile has been largely exploited. Nature is using this strategy to link apolar fatty acids to phosphorus-containing polar headgroups through a glycerol intermediate. This allows attaching more than one fatty acid to the resulting glycerophospholipid, which is crucial for the formation of the bilayered structure of biological membranes.

The calixarenes represent an attractive basis to design complex functional amphiphiles. Indeed, the relative rigidity of the macrocycle, along with the possibility to rim- and regio-selectively modify the parent macrocycle open a wealth of possibilities to produce designer amphiphiles able of self-assembly at interfaces and in water.

This chapter covers the most recent advances in the chemistry of calixarenes and resorcinarenes and their self-assembly at interfaces developed after the excellent book chapter of Lucke, Stirling and Böhmer published in 2001 [11]. We focus the present work on calixarene- and resorcinarene-based Langmuir monolayers, Langmuir-Blodgett films, self-assembled monolayers (SAMs) on planar surfaces and on nanoparticles. This book chapter is not intended to be an exhaustive review of all research works carried out on these topics; selected illustrative examples are chosen in the vast available literature and discussed. The self-assembly of amphiphilic calixarenes in water has been reviewed elsewhere and will not be treated herein [12, 13].

## 37.2 Amphiphilic Calixarenes

### 37.2.1 *Synthesis*

The use of calixarenes to design artificial amphiphiles is mainly motivated by the possibility given by these molecules to act as organizing entities (Fig. 37.1) [14]. The macrocycle allows introducing and orienting in the same molecule, in a three-dimensionally controlled fashion, hydrophobic and polar moieties. Because of its higher conformational rigidity, the calix[4]arene is generally preferred to the larger analogues to produce amphiphilic calixarenes.

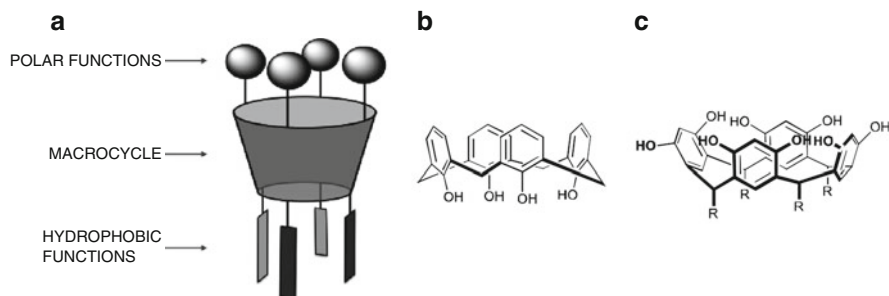


**Fig. 37.1** Schematic representation of a macrocyclic amphiphilic molecule (**a**) and chemical structures of the native calix[4]arene (**b**) and resorcin[4]arene (**c**). The calix[4]arene macrocycle, composed of four phenolic units, forms a fairly rigid truncated cone-shaped molecule when adequately modified to “lock” the structure to avoid conformational changes to partial cone conformations. The aromatic alcohol functions are exposed at the narrow rim, and the *para* phenolic positions at the wide rim. Applying different chemistries, the macrocycle can be selectively modified either on one rim or on the other. The regio-selectivity of the chemical modifications is not restricted to the selection of the modified rim; the number and the position within a rim could also be controlled

### 37.2.1.1 Enhancing the Lipophilic Character of the Macrocycle

Even if the parent *p*-*tert*-butyl derivatives of calixarenes and their de-alkylated analogues can be considered as amphiphiles, chemical modifications of the macrocycle allows enhancing the amphiphilic properties of the resulting derivatives. The synthetic routes to amphiphilic calixarenes are often initiated by the introduction of the lipophilic moieties of the molecule that are typically saturated hydrocarbon chains (Fig. 37.2). This is explained by the low chemical reactivity of these lipophilic moieties, which do not hinder the further chemical modification of the macrocycle to introduce the polar functions.

The facile removal of the *p*-*tert*-butyl groups from the upper rim of calixarenes by treatment with aluminum chloride as Lewis acid is typically carried out before the insertion of the lipophilic moieties either at the lower (phenolic) or the upper rim of the macrocycle (*para*- position).

At the lower rim, the grafting of lipophilic functions is typically achieved by a facile Williamson etherification using alkyl halides of the desired length. For the calix[4]arenes, the *per*-alkylation is typically accomplished by using a strong base such as NaH with a slight excess of the alkylating agent [15]. Varying the type of base and the stoichiometry of the alkylating agent allows for a partial regioselective substitution of the phenolic rim. For example, distal 1,3-dialkylation of *p*-*tert*-butylcalix[4]arene is favored using a weak base such as  $K_2CO_3$  with a limiting amount of the alkylating agent yielding the thermodynamically favored product of the di-alkylation reaction [16]. Proximal 1,2-dialkylation that yields the kinetically favored product can be achieved in the presence of a slight excess of NaH with an excess of the alkylating agent [17].

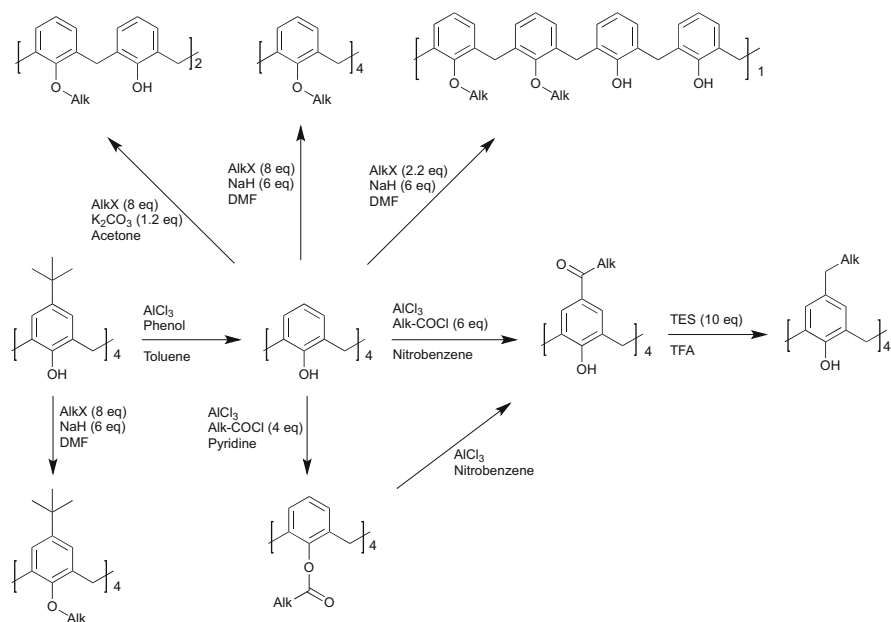


**Fig. 37.2** Chemical strategies to graft aliphatic functions onto calix[4]arenes

The attachment of lipophilic functions at the upper rim of the macrocycle was first achieved by Nakamoto et al.; the synthetic route reported was based on first an esterification of the lower rim of the calix[4]arene using octadecanoyl chloride in pyridine that yielded the pure tetraester calixarene derivative [18]. The Fries rearrangement of the acyl moieties using an excess of  $\text{AlCl}_3$  in nitrobenzene yielded the corresponding *para*-acyl derivative. The reduction of this tetra-ketone through a Wolff-Kishner reaction yielded the corresponding *para*-octadecylcalix[4]arene. We demonstrated that the direct acylation of the calix[4]arene was effective through a Friedel-Crafts acylation reaction in nitrobenzene using  $\text{AlCl}_3$  and a series of acyl chlorides with increasing chain lengths ( $C_6$ ,  $C_8$ ,  $C_{10}$  and  $C_{12}$ ) [19]. This procedure was subsequently adapted to calix[8]arene derivatives [20].

Resorcinarenes are macrocycles produced by the acid-catalyzed condensation of resorcinol with an aldehyde [21]. The lipophilic character of resorcinarenes is directly dependent on the structure of the aldehyde employed in the condensation reaction. Aldehydes with long aliphatic chains, e.g.  $C_{11}$ , confer strong lipophilic character to the so-produced macrocycle.

### 37.2.1.2 Grafting Hydrophilic Functions to the Calixarene Macrocycle

For the calixarenes that have been beforehand de-alkylated at the *para*- positions and alkylated at their lower rim to introduce aliphatic functions, a series of

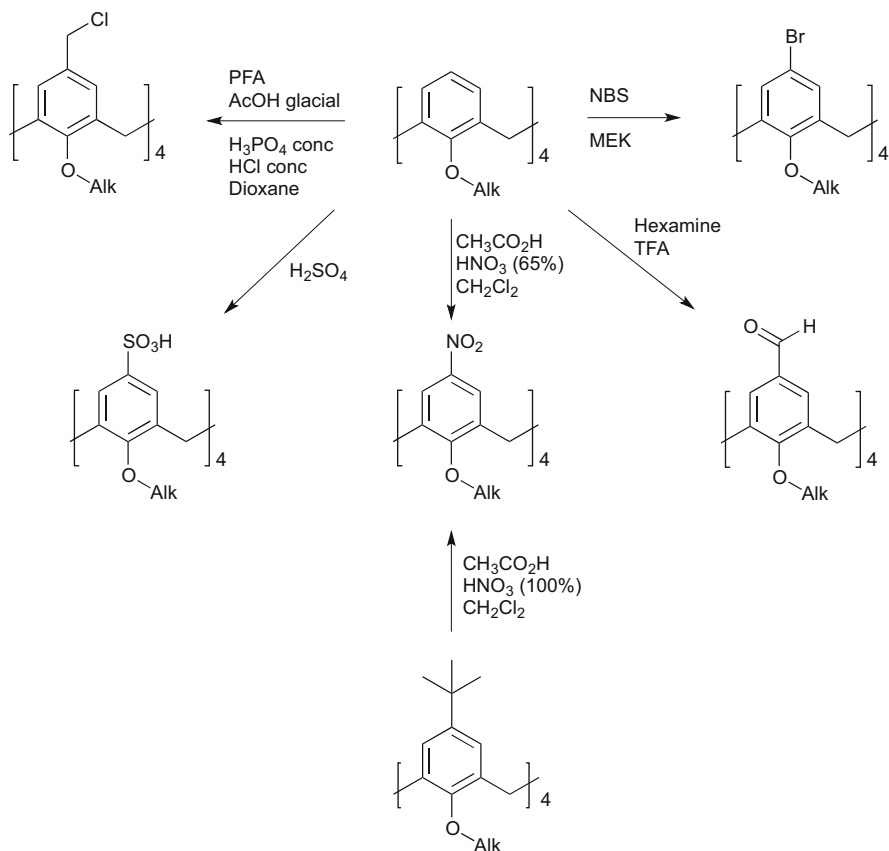


**Fig. 37.3** Selected examples of upper rim electrophilic aromatic substitutions of *O*-alkylated calix[4]arenes

electrophilic aromatic substitutions can be readily conducted. This allows introducing functional groups such as halogens [22], sulfonic acid [23], acyl [24], formyl [24], chloromethyl [25] and aminomethyl [26] on the *para* positions of the macrocycle (Fig. 37.3). The introduction of nitro groups is typically accomplished in excellent yields by *ipso*-nitration of *O*-alkylated *para*-*tert*-butyl derivatives [27]. Remarkably, the chemical moieties introduced at the *para*-positions can be further modified so as to make the synthesis of a vast number of calixarene derivatives possible.

For calixarenes bearing hydrophobic functions at the *para*-positions, the introduction of polar functions can be achieved by exploiting the reactivity of the phenolic functions. For example, the di-phosphorylation of the lower rim can be achieved regio-selectively by reaction with diethylchlorophosphate in basic conditions yielding the corresponding phosphoester [19]. The ethyl groups can be removed by consecutive treatment with trimethylbromosilane and methanol.

Coleman produced a series of different *para*-acyl-calix[8]arenes bearing at the phenolic rim carboxymethoxy, carboxypropoxy, 4-sulfonatobutoxy, ethoxycarboxymethoxy, ethoxycarboxypropoxy, 2-methoxyethoxy and 2-(2-methoxy)diethoxy functions [20].

Unlike calixarenes, resorcinarenes exhibit on their wide rim two distinct sites that can be chemically modified so as to introduce two different hydrophilic moieties. The hydrophilic character of resorcinarenes is conferred by eight hydroxyl functions. Their further functionalization can be readily conducted to introduce additional polar moieties. For example, Aoyama synthesized amphiphilic resorcinarenes bearing eight oligosaccharide moieties at the wide rim through the reaction of the alcohol groups with octamine followed by the reaction of the corresponding octamine derivative with maltooligosaccharide lactones [28]. In addition to the alcohol moieties, the *ortho*-positions of resorcinarenes can be functionalized with the introduction of four additional hydrophilic moieties. We described the synthesis of a tetra-undecylcalix[4]resorcinarene bearing four L-proline moieties at the *ortho*-positions via a Mannich-type reaction in the presence of L-proline and formaldehyde [29].

## 37.2.2 *Langmuir and Langmuir-Blodgett Films of Calixarenes and Resorcinarenes*

### 37.2.2.1 Langmuir Monolayers

A number of amphiphilic calixarenes have been shown to possess the ability to self-assemble in the form of insoluble monomolecular films at the air-water interface, which are called Langmuir monolayers. In order to exhibit the ability to form Langmuir monolayers, the amphiphilic derivative has to be designed so that it is not soluble in water. Indeed if the amphiphiles are partially water-soluble, they do not assemble at the air-water interface but (at least partially) in the water phase in the form of micelles [12, 30, 31]. Amphiphilic calixarenes, self-assembled as Langmuir monolayers at the air-water interface, typically “float” on the water surface with an orthogonal orientation with respect to the interface; the aliphatic chains point into air while the polar functions are immersed into the subphase (Fig. 37.4).

The macrocycles oriented in an orthogonal fashion with respect to the interface are stabilized by van der Waals interactions among the aliphatic chains and H-bonding between the calixarene head groups and water molecules. Unlike common aliphatic surfactants,  $\pi$ -stacking interactions among aromatic rings of neighboring calixarenes represent an additional driving force for the self-assembly process. Indeed, we recently demonstrated that two *p*-carboxycalix[4]arene derivatives, one bearing four  $C_{12}$  alkyl chains and the other four  $C_3$  aliphatic chains at the lower rim, form stable Langmuir monolayers at the air-water interface. While the interfacial self-assembly of the  $C_{12}$  derivative is mainly driven by van der Waals

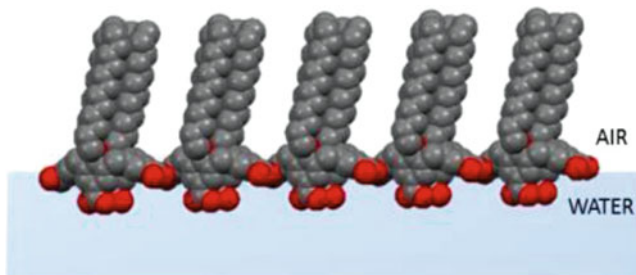


**Fig. 37.4** Graphical representation of Langmuir monolayers of amphiphilic calixarenes at the air-water interface. The polar groups are immersed into the aqueous subphase while the hydrophobic chains point in air

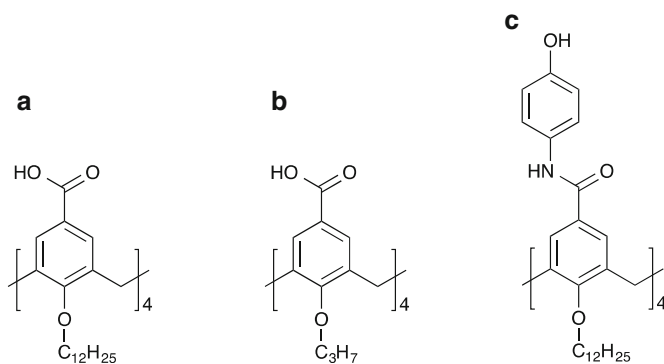


**Fig. 37.5** Chemical structures of  $C_{12}$ -*p*-carboxycalix[4]arene (a),  $C_3$ -*p*-carboxycalix[4]arene (b) and of  $C_{12}$ -*p*-amidophenolcalix[4]arene (c)

interactions among the aliphatic chains,  $\pi$ - $\pi$  interactions among aromatic rings of neighboring macrocycles favor the self-assembly of the  $C_3$  derivative [32, 33].

The cyclic skeleton of calixarenes significantly enhances their interfacial aggregation in comparison with that of their corresponding monomers. For example, a *p*-amidophenolcalix[4]arene derivative bearing four  $C_{12}$  chains on the lower rim (Fig. 37.5) does form stable monomolecular films at the air-water interface while the corresponding monomer does not [34].

The self-assembly properties of a large variety of amphiphilic calixarenes as Langmuir monolayers have been investigated [35–37]. The group of Coleman studied the self-assembly behavior of a series of *para*-acyl calix[4]arenes with different chain lengths (Fig. 37.6) [19, 38]. At the air-water interface, the apparent molecular area value of  $100 \text{ \AA}^2 \text{ molecule}^{-1}$  confirmed the orthogonal orientation of the macrocycles at the interface. The stability of the monolayers was demonstrated to linearly increase with the increase of the chain length. In 2005, the same group reported on the amphiphilic behavior of an apparently non-amphiphilic calix[4]arene [39]. The *p*-*H*-tetra-*O*-dodecyl calix[4]arene, bearing four  $C_{12}$  aliphatic

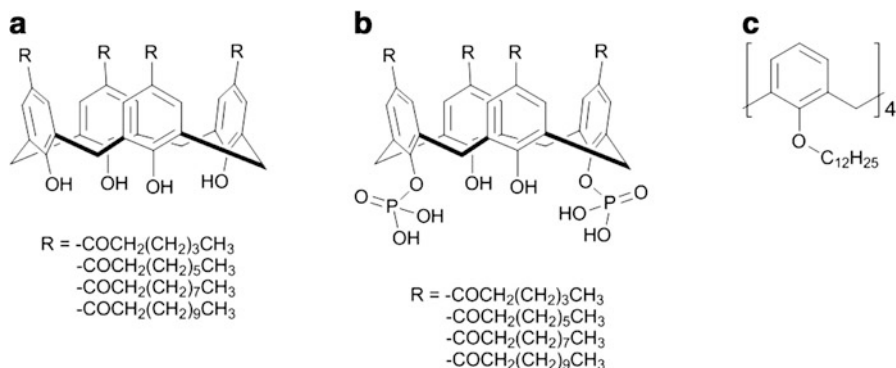


**Fig. 37.6** Chemical structures of a series of *p*-acyl calix[4]arenes (a, b) and of *p*-*H*-tetra-*O*-dodecyl-calix[4]arene (c)

chains at the lower rim and four H atoms at the *p*-positions (Fig. 37.6c), was demonstrated to form stable Langmuir monolayers at the air-water interface despite the absence of polar functions. In addition to van der Waals interactions among the aliphatic chains, the interfacial self-assembly process was attributed to H-bonding between the aromatic groups of the macrocycle and water molecules.

The interaction properties of Langmuir monolayers of amphiphilic calixarenes with ions [40–45], small organic molecules (e.g., aminoacids, nucleosides, pharmaceuticals) [29, 34, 46] and macromolecules (e.g., proteins and nucleic acids) [47–50] have been extensively investigated.

Shinkai first reported on the binding properties of Langmuir monolayers of amphiphilic calixarenes with ions in 1989 [43]. It was demonstrated that Langmuir monolayers of a calix[4]arene ester derivative are selectively interacting with Na<sup>+</sup> ions while monolayers of the corresponding cyclic hexamer preferentially bind K<sup>+</sup> ions. This binding selectivity was attributed to the size of the macrocycles cavity. Later reports showed that the binding affinity towards monovalent ions is also highly dependent on the type of polar functions at the *p*-position of the macrocycles and on their self-assembly state with a remarkable effect of the counterion [44, 51].

In 2015, we investigated the binding properties of Langmuir monolayers of a *p*-carboxycalix[4]arene derivative (Fig. 37.5a) towards a series of divalent transition metal cations, i.e. Co<sup>2+</sup>, Cu<sup>2+</sup>, Mn<sup>2+</sup> and Ni<sup>2+</sup> [45]. Synchrotron-based X-ray diffraction techniques, along with compression isotherms and Brewster angle microscopy, revealed that the macroscopic and microscopic properties of the monolayers are strongly affected by Cu<sup>2+</sup> ions with the formation of Cu<sup>2+</sup> clusters contiguous to the monolayer of **1**.

Lu et al. investigated the interaction of Langmuir monolayers of amphiphilic calix[4]arenes bearing two adenine units at the lower rim with the nucleosides uridine and thymidine at the air-water interface [46]. Surface pressure-area compression isotherms revealed that the monomolecular films interact specifically with uridine and thymidine at the interface.

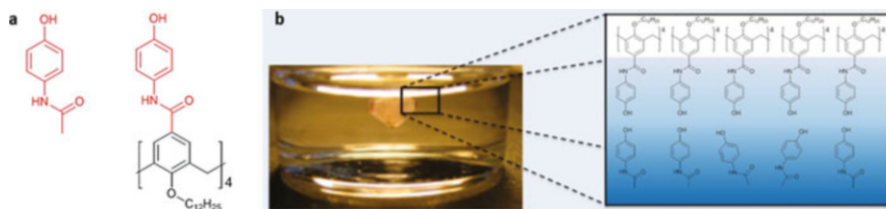


**Fig. 37.7** (a) Chemical structures of acetaminophen and *p*-amidophenol-modified calix[4]arene; (b) Snapshot of the interfacial crystallization of acetaminophen at the air-water interface (Reproduced with permission from Ref. [34], Copyright 2011, American Chemical Society)

Langmuir monolayers of calixarenes have also been studied for their ability to bind small organic molecules. Recently, we reported on the ability of Langmuir monolayers of an amphiphilic *p*-amidophenolcalix[4]arene derivative to interact with acetaminophen (APAP) [34, 49], an active pharmaceutical ingredient (API) widely used as analgesic and antipyretic, at the air-water interface. Interestingly, these calixarene-based surfaces act as templates for the interfacial crystallization of the pharmaceutical (Fig. 37.7) [34]. The similarity between the polar functions of the amphiphile and the structure of APAP were shown to favor the molecular recognition event.

In 2014, we demonstrated that a *p*-carboxycalix[4]arene derivative (Fig. 37.5a), self-assembled as Langmuir monolayers at the air-water interface, triggers the crystallization of an API, namely gabapentin, with a control over the crystalline polymorphism [52]. The modulation of the packing density of the amphiphiles allows controlling the crystal growth of two polymorphic forms of the same API. Indeed, while the partially compressed monolayer induced the crystallization of the GBP polymorph  $\gamma$ , the fully compressed monolayer kicks off the crystallization of the GBP polymorph  $\alpha$ .

Langmuir monolayers of amphiphilic calixarenes have been demonstrated to act as membranes for the selective recognition of proteins at the air-water interface. Schrader showed that mixed monolayers of stearic acid and an amphiphilic *p*-phosphonato-calix[4]arene derivative act as interfacial selective sensors for a series of proteins (Fig. 37.8) [53]. Compression isotherms revealed that, in the presence of the proteins dissolved in the subphase, the isotherms are shifted to significantly higher molecular area values. The authors explained such a shift by the presence of cooperative recognition events between the multivalent macrocycles and the binding sites of the proteins at the interface. The strong electrostatic interactions, in the form of ion pairing, between the host and the guest enhance the binding selectivity with a detection limit in the picomolar range.

### 37.2.2.2 Calixarene- and Resorcinarene-Based Langmuir-Blodgett Films

In the 1930s, Irving Langmuir and Katharine Blodgett developed the LB technique to fabricate mono and multilayer films on solid substrates. The LB transfer



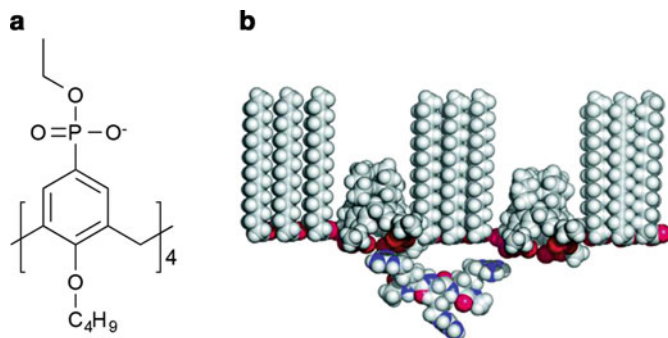


**Fig. 37.8** Chemical structure of the *p*-phosphonato-calix[4]arene (a) and suggested binding mode of the *p*-phosphonato-calix[4]arene embedded in a stearic acid monolayer with arginine residues of basic proteins dissolved in the aqueous subphase (b) (Reproduced with permission from Ref. [53], Copyright 2005, American Chemical Society)

technique was extensively exploited during the past 80 years to produce thin films with optical, semiconducting and sensing properties [54]. Nevertheless, the presence of defects typically encountered with the fabrication of LB films partially hampered their potential applications [55]. Despite that, during the last 30 years, progresses have been made to overcome this drawback. The first investigation on the stabilization of Langmuir films of calixarenes was carried out by Regen [56]. He introduced the concept of *perforated monolayers*, where mercurated-calix[6]arene derivatives were used to fabricate thin films with uniform and adjustable micropores. Malonic acid molecules act as molecular joints so as to link the macrocycles and increase the cohesiveness of the monolayer. In 2003, the same group reported on the concept of *gluing* calixarene-based LB films [57]. A calix[6]arene derivative, bearing six  $C_{15}$  chains on the upper rim and six quaternary ammonium groups at the *p*-positions, was used as self-assembling amphiphile at the air-water interface and a polyanionic polymer as supramolecular glue. Ellipsometry and X-ray photoelectron spectroscopy allowed demonstrating the incorporation of the polymer into the bilayer structure. The electrolyte increases the surface viscosity of the calix[6]arene monolayer and the glued LB bilayer shows a high He/N<sub>2</sub> selectivity.

Typically, the transfer of LB monolayers with the hydrophilic functional groups pointing outwards is a challenging task. Indeed, the transfer of a single LB layer of amphiphiles on a hydrophobic surface is classically performed by immersing the to-be-coated solid (i.e. substrate), through the monolayer, in the liquid phase. The substrate removal from the water surface causes, in the absence of monolayer at the interface, the amphiphiles to return at the interface resulting in a *naked* substrate. Oppositely, if the removal is carried out through the Langmuir monolayer present at the interface, a second layer is deposited. In 2012, we developed a strategy to deposit a single monomolecular layer of an amphiphilic *p*-guanidinocalix[4]arene derivative on a hydrophobic substrate, with the guanidine functions pointing into air, by using supramolecular clips of dicarboxylate molecules (Fig. 37.9) [58]. The stabilization of the monomolecular layer was achieved through electrostatic

interactions between the positively charged amphiphiles and the dicarboxylates at the air-water interface.

### 37.3 Calixarenes and Resorcinarenes at Solid-Liquid Interfaces

The design of organized molecular layers at solid interfaces represents a foremost research axis in surface science and nanotechnology. In this context, the development by Whitesides of self-assembled monolayers on metal surfaces represented a major breakthrough and SAMs are nowadays used in a broad range of applications [59, 60]. SAMs are surface coatings produced by the combined chemisorption and self-assembly of organic molecules onto the surface of solids (Fig. 37.10). The high order displayed by such monolayers is due to the self-assembly of the alkyl chains of the molecular components as the system approaches equilibrium. SAMs have

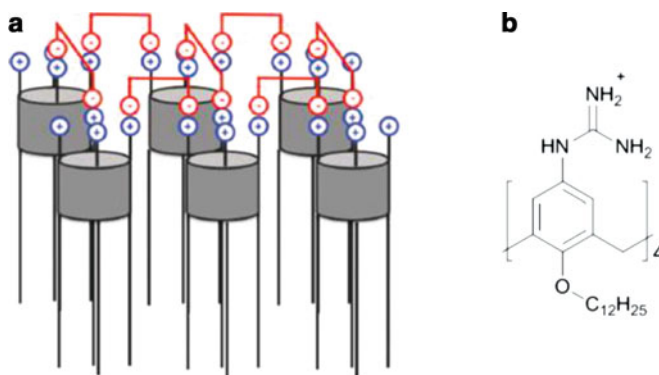
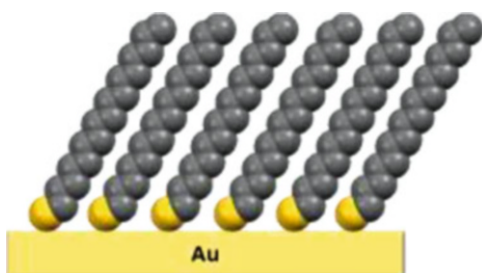


**Fig. 37.9** (a) Graphical representation of the monolayer stabilization by organic clips. Each organic clip (*red*) binds two macrocycles (*blue*) at the air-water interface through electrostatic interactions; (b) Chemical structure of the guanidinocalix[4]arene derivative (Reproduced with permission from Ref. [58], Copyright 2013, The Royal Society of Chemistry)

**Fig. 37.10** Graphical representation of SAMs of an alkanethiol on gold



been developed originally on planar surfaces but their application for engineering (nano)particles is now widespread. Reinhoudt first recognized the potential of transferring the recognition properties of calixarenes on solid surfaces; this pioneering work opened the way for the design of a variety of calixarenes possessing the ability to form SAMs on solid surfaces [61–63].

### 37.3.1 Synthetic Design

In order to confer the calixarenes the ability to form SAMs on metal surfaces, they have to be chemically modified to introduce chemical functions (e.g., thiol, thioether, disulfide) able of chemisorption on the surface. Reinhoudt published the synthesis of calix[4]arenes bearing four di-*n*-decyl sulfide chains at the lower rims. The synthesis proceeds via first the alkylation of the calix[4]arene-25,26,27,28-tetrol with 10-undecen-1-yl tosylate followed by the anti-Markovnikov addition of 1-dodecanthiol in the presence of 9-borabicyclo[3.3.1]nonane (9-BBN) (Fig. 37.11) [64]. Similarly to calix[4]arenes, resorcin[4]arenes tetrasulfides have been produced by the condensation reaction of resorcinol and 11-undecylenic aldehyde followed by the addition of 1-dodecanthiol to the terminal double bonds of the alkyl chains using catalytic amounts of 9-BBN [63].

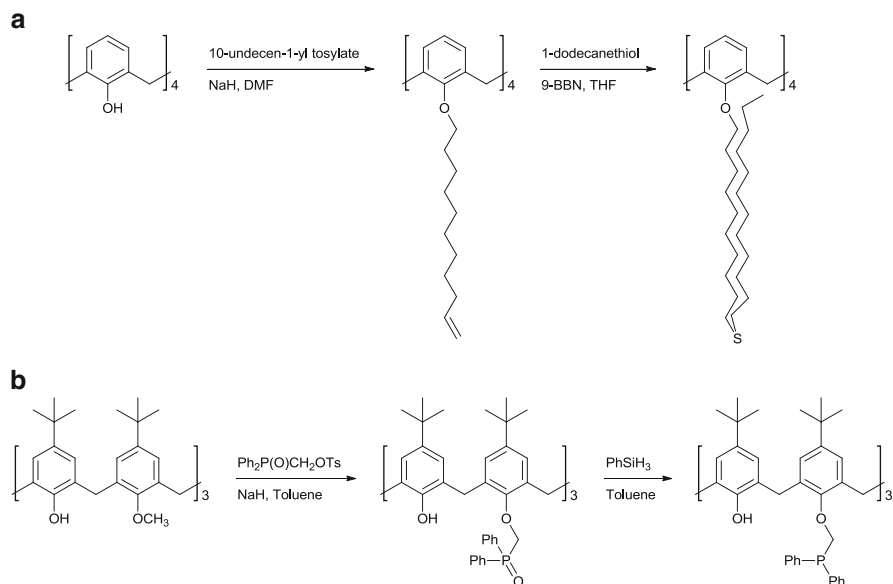


**Fig. 37.11** Synthesis of the calix[4]arene tetrasulfide (**a**) and of the tris(diphenylphosphino)methoxy-*p*-*tert*-butylcalix[6]arene derivative (**b**)

In addition to calixarene sulfides, macrocycles containing phosphine functions have been widely used to coat gold surfaces due to the strong interaction phosphine-gold. Tsuji reported on the synthesis of a *p-tert*-butylcalix[6]arene bearing three (diphenylphosphino)methyl moieties at the lower rim [65]. The reaction of the trimethoxy-*p-tert*-butylcalix[6]arene with tosyloxymethyldiphenylphosphine oxide in toluene yields the tris(diphenylphosphinoylmethoxy)-trimethoxy-*p-tert*-butylcalix[6]arene derivative. Further reaction of the macrocycle with  $\text{PhSiH}_3$  affords the desired product. The calix[6]arene phosphine derivative was demonstrated to strongly bind to gold nanoparticles, which were shown to successfully catalyze the reduction of 4-nitrophenol to 4-aminophenol [66].

### 37.3.2 Self-Assembly on Planar Surfaces

Reinhoudt reported on the first resorcinarene-based SAMs in 1994 [61, 63]. A resorcin[4]arene bearing four di-*n*-decyl sulfide chains was demonstrated to self-assemble on the surface of gold. The authors showed that both the size and shape of the resorcinarene headgroup are influencing the degree of order of the monolayer. When the headgroup cross-sectional area is smaller than the area occupied by the four di-sulfide chains, the monolayer is densely packed. On the other hand, the presence of functional groups forming a network of H-bonding causes the formation of disordered films. The alkyl chains also play an important role in the stability of the so-produced SAMs. Indeed, relatively long alkyl chains ( $C_{10}$ ) favor the generation of crystalline monolayers via van der Waals interactions when shorter aliphatic chains were demonstrated to hinder the order of the resulting SAMs. Thickness measurements showed that in the ordered monolayers the alkyl chains are oriented in an all-parallel fashion and perpendicular to the surface. More recently, Kim reported on the fabrication of mixed calixarene-based SAMs characterized at the molecular scale [67]. The mixed SAMs consist of mono-thiolated calix[4]crown-5, acting as molecular receptor, and thiolated alkylferrocene, as guest counterpart, immobilized on a gold electrode surface. The host-guest interaction between the calixarene derivative and ferrocene was demonstrated by cyclic voltammetry (Fig. 37.12).

In 2014, Demirkol et al. investigated the possibility to use calixarene-based SAMs to further immobilize enzymes on surfaces [68]. The calix[4]arene bearing two alkylthiol chains on the lower rim was shown to form ordered SAMs. The coupling reaction of the free hydroxyl groups of the macrocycle with the amine functions of the glucose oxidase enzyme via carbonyldiimidazole allowed for the covalent immobilization of the enzyme on the surface (Fig. 37.13). The authors demonstrated that the biosensor is sensitive towards glucose in the concentration range of 0.1–10 mM with a response time of 25 s.

**Fig. 37.12** Chemical structures of the monothiolated calix[4] crown-5 (1) and of thiolated alkylferrocene (3) and schematic diagram of the recognition process in the mixed SAMs (Reproduced with permission from Ref. [67], Copyright 2011, Royal Society of Chemistry)

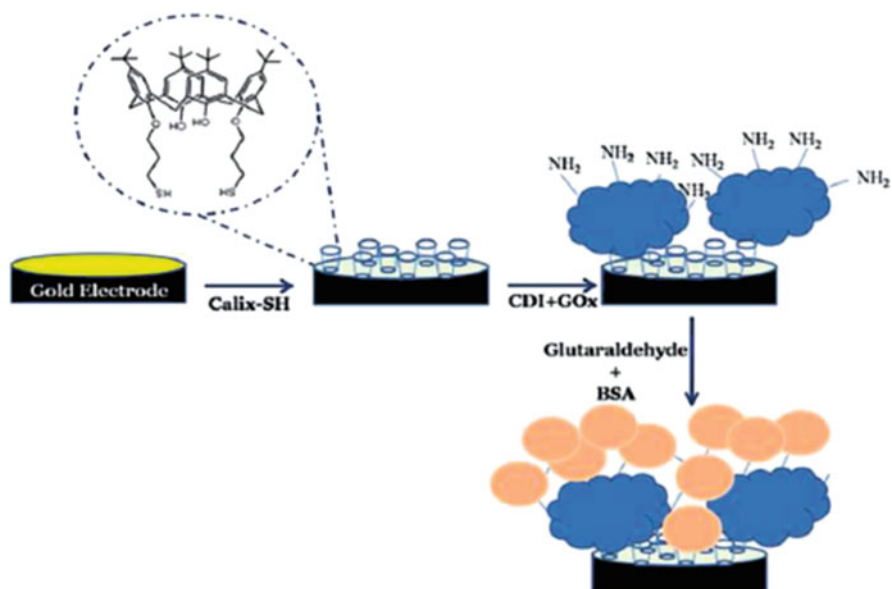
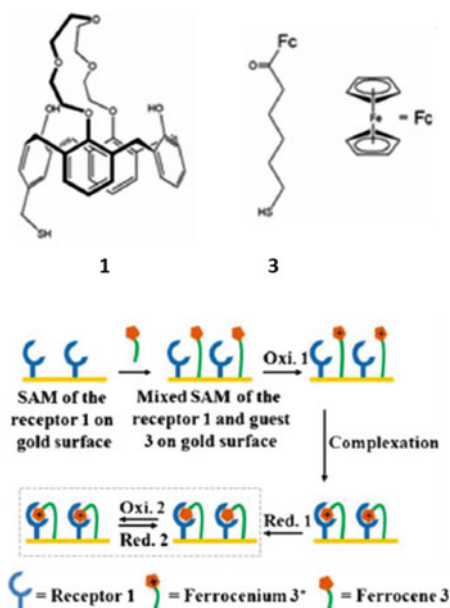


**Fig. 37.13** Schematic representation of the thiol calix[4]arene/glucose oxidase (GOx) biosensor (Reproduced with permission from Ref. [68], Copyright 2014, The Royal Society of Chemistry)

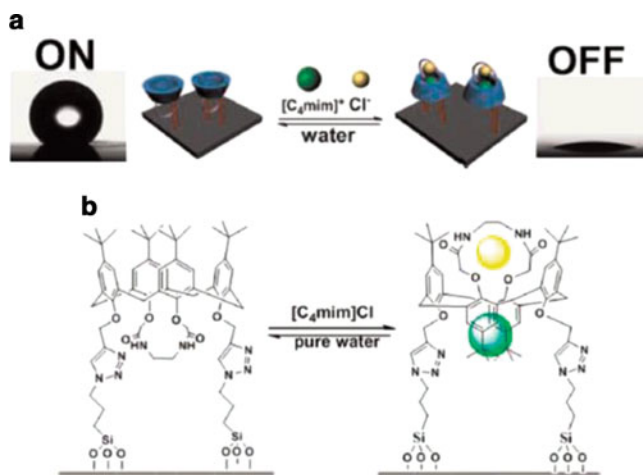


**Fig. 37.14** Schematic representation of the interaction of the calix[4]arene-based SAM with the ions (a) and proposed binding between the calix[4]arene derivative and the ion pair (b) (Reproduced with permission from Ref. [84], Copyright 2012, American Chemical Society)

SAMs of calixarene derivatives have been demonstrated to possess recognition properties towards ions [69–77] and small organic molecules [78–83]. For example, in 2012 Li reported on calix[4]azacrown-based SAMs that exhibit ion-pair recognition properties towards 1-butyl-3-methylimidazolium chloride [84]. The calixarene-based SAM was produced by a click reaction between the azido-modified silicon substrate and the calix[4]azacrown. The authors demonstrated by contact angle (CA) measurements that the calixarene-modified surface is superhydrophobic ( $CA = 154.6 \pm 3^\circ$ ). Upon immersion of the calixarene-based SAM in a 1-butyl-3-methylimidazolium chloride solution, the CA drops to  $10.1 \pm 3^\circ$  (Fig. 37.14). On the other hand, no changes in the CA of the surface are observed in the presence of 1-butyl-3-methylimidazolium bromide and 1-butyl-3-methylimidazolium hexafluorophosphate. The calix[4]azacrown modified SAM was therefore demonstrated to possess selective wettability response towards the 1-butyl-3-methylimidazolium chloride ion-pair.

Zanoni reported on the assembly of AuNPs on calixarene-based SAMs [85]. A silicon surface (Si) was functionalized with a calix[6]arene derivative bearing three undecenyl chains on the lower rim and three phenylurea moieties on the upper rim ( $C_6$ ). The so-produced SAMs form stable complexes with a redox-active molecule that consists of a 4,4'-bipyridinium unit linked by a dodecyl chain to another pyridinium ring (A). This surface showed binding towards AuNPs functionalized with a calix[4]arene derivative ( $C_4$ ) (Fig. 37.15). The presence of the di-topic guests allows for the reversible and hierarchical assembly of the AuNPs on the Si surface. Moreover, the nanoparticles were demonstrated to be electrochemically removed from the Si/ $C_6$ /A surface.

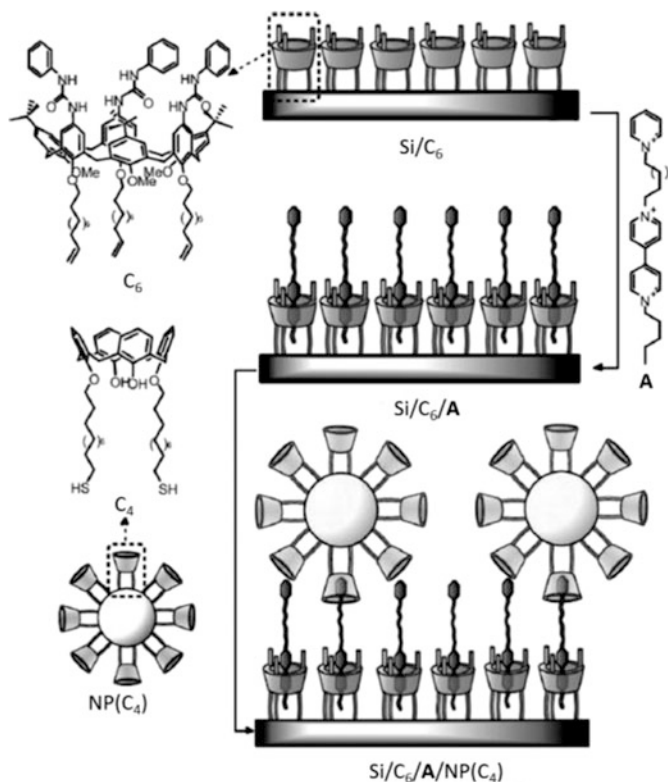


**Fig. 37.15** Schematic representation of the supramolecular interaction between the calix[6]arene-based SAM and the calix[4]arene modified AuNPs (Reproduced with permission from Ref. [85], Copyright 2013, John Wiley & Sons)

### 37.3.3 Calixarene and Resorcinarene Monolayers on Metal Nanoparticles (MNPs)

MNPs are the subject of extensive research due to their unusual plasmonic optical properties; the size, shape and surrounding environment of MNPs strongly influence such properties [86–88]. The presence of a coating monolayer at the surface of MNPs allows improving their functionalities and physicochemical properties [89]. Tailor-made calixarenes have shown the ability to chemi- or physisorb on MNPs. The choice of the proper functional groups attached on the calixarene skeleton favors its binding reaction on the MNPs surface, e.g. thiol functions on gold, and improves the dispersibility of the nanoparticles in the medium [90]. Calixarene-protected nanoparticles typically exhibit physico-chemical properties that significantly differ from those of the non-protected ones; and the macrocycle can be exploited for its molecular recognition properties [91–100]. Recently, Kim et al. have published a critical review on optical nanoparticles based on the

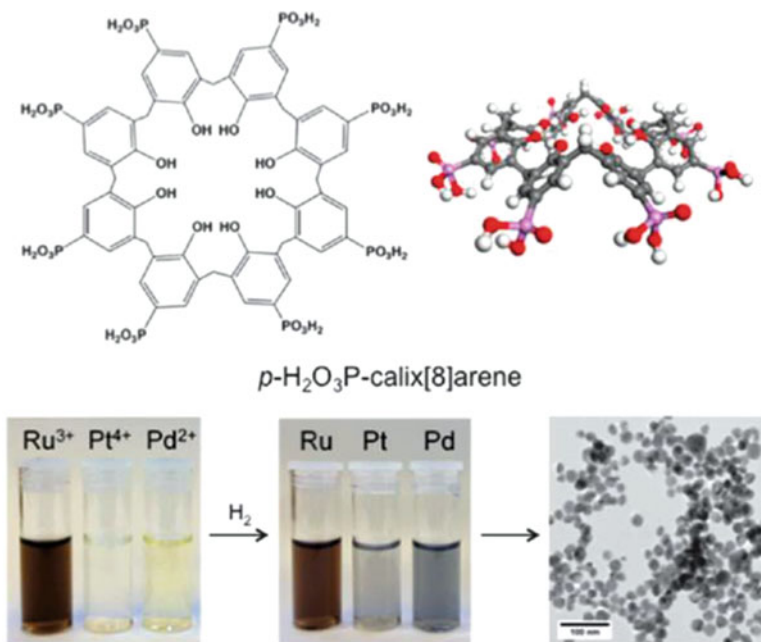


**Fig. 37.16** Chemical structure of the *p*-phosphonic acid calix[8]arene and graphical illustration of the synthesis of calix[8]arene capped Ru, Pt and Pd nanoparticles by hydrogen bubbling (Reproduced with permission from Ref. [105], Copyright 2014, The Royal Society of Chemistry)

association of gold, silver, silica and quantum dots and luminescent calixarenes [95]. Wei examined the ability of amphiphilic resorcinarenes to improve the dispersion of metal nanoparticles [101]. Particles with a size of 10–100 nm are amenable to spontaneously aggregate and give rise to collective optical and magnetic properties. The amphiphilic properties of amphiphilic calixarenes are ideal to form a shell around the nanoparticles so as to improve their dispersibility.

Calixarene derivatives have also been used to functionalize mesoporous silica nanoparticles (MSNs) [102–105]. The macrocycle acts as a gatekeeper for the loading and release processes of the selected molecule. Host-guest interactions between sulfonato-calixarenes and positively charged moieties attached on the surface of MSNs allow controlling drug encapsulation and release process.

Several reports in the literature show that calixarene derivatives play a crucial role in controlling the size and stability of MNPs [106–108]. For example, Raston reported on the synthesis of *p*-phosphonic acid calix[8]arene-modified Ru, Pt and Pd nanoparticles in aqueous solution (Fig. 37.16) [109]. The macrocycle was demonstrated to exert a control over the shape and size of the produced nanoparticles by acting as stabilizing agent. Molecular modeling revealed that 12 molecules of the macrocycle surround 2-nm Ru particles, where a H-bonding network among calix[8]arenes contribute to the interfacial self-assembly.



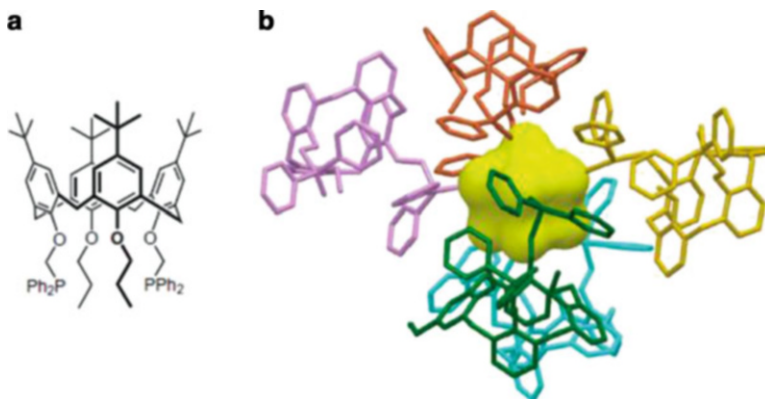


**Fig. 37.17** Chemical structure of the calixarene-phosphine ligand (a) and graphical representation of the macrocycle capped Au nanoparticle with the Au core diameter of 0.9 nm and five calixarenes bound to metal surface (b). Two calixarenes bind the metal core with two phosphines while the other three with only one phosphine. The monodentate ligand possesses one phosphine bound to the metal surface and one unbound phosphine oxide (Reproduced with permission from Ref. [106], Copyright 2010, Nature Publishing Group)

Inspired by the ability of enzymes to control the electronic and steric environment of their active sites, Katz and coworkers developed a biomimetic system where the calixarene macrocycles are mimicking the rigid backbone of proteins, cf. Fig. 37.17 [110]. This macrocycle, bearing phosphine moieties, is binding the AuNPs surface and allows controlling the accessibility of the metal core. The macrocycle-bound gold clusters show significantly higher surface accessibility when compared to the corresponding thiolate-bound gold clusters of analogous dimension. For the calixarene-capped AuNPs with a core diameter of 0.9 nm, up to 25 % of the gold atoms bind the probe molecule 2-naphthalenthioal (2-NT) while the accessibility drastically decreases for AuNPs of larger sizes. The increase in accessibility when the metal-core diameter is smaller than the size of the macrocyclic ligand has been proposed as general mechanism of accessibility in organic ligand-bound metal clusters.

In 2004, Arduini et al. demonstrated that gold nanoparticles, modified with a calix[4]arene derivative bearing two alkanethiol chains, possess a high binding affinity towards quaternary ammonium salts in apolar solvents [97]. The binding constant calculated for the macrocycle bearing two dodecanethiol chains on the lower rim is three orders of magnitude higher than that of its analogue bearing two propyl chains. This high binding efficiency was attributed to the presence of complexed cations and anions on the surface of the calix[4]arene-modified nanoparticles so as to decrease the interaction between the ions of the ion pair. Recently, Urban et al. designed a strategy for the decontamination of radioactive waste streams [111]. Calixarene-crown-6 derivatives containing terminal carboxylic groups attached on the surface of magnetoferritin were demonstrated to detect

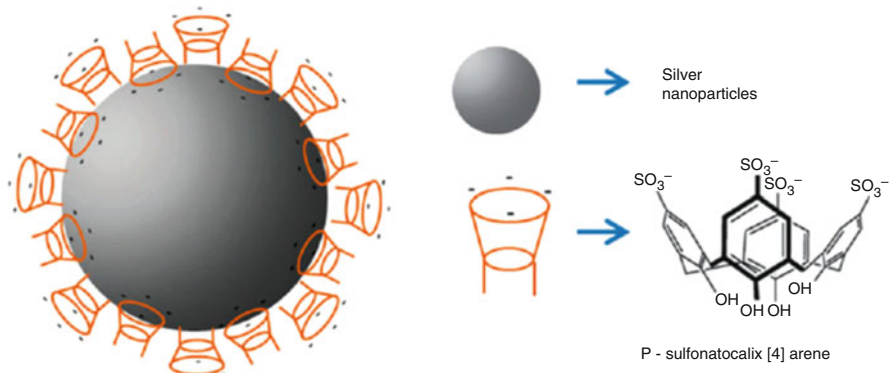


**Fig. 37.18** Schematic representation of the binding mode of *p*-sulfonatocalix[4]arenes on Ag nanoparticles (Reproduced with permission from Ref. [108], Copyright 2011, The Royal Society of Chemistry)

$\text{Cs}^+$  and promote its separation from aqueous solutions. The nanoparticles loaded with the ions can be readily removed from the solution by magnetic filtration and further concentrated by evaporation.

In 2011, Coleman demonstrated that *p*-sulfonatocalix[4]arene-capped AgNPs interact with nucleobases [112]. The nanoparticles discriminate between pyrimidine and purine-based derivatives. The binding efficiency was ascribed to the self-assembly of the macrocycles on the metal surface in an up-down fashion. Macrocycles with the sulfonate functions that bind the guest alternate with those with the sulfonate moieties attached to the silver nanoparticle (Fig. 37.18).

AuNPs modified with *p*-sulfonatocalix[4]arenes bearing two thiol chains at the lower rim were shown to act as colorimetric sensors for the detection of amino acids in water [100]. The addition of lysine, arginine and histidine in a solution containing the calixarene-capped NPs produces a red shift in the UV-visible spectrum and the broadening of the surface plasmon band. The other amino acids did not cause such changes. The authors explained these results in terms of nanoparticles aggregation induced by the three amino acids. The negatively charged upper rim of the *p*-sulfonatocalix[4]arene interacts with the positively charged moieties of the amino acids so as to form 1:2 complexes amino acid–nanoparticle (Fig. 37.19).

The ability of AgNPs functionalized with diethyl-dithiocarbamic-di-hydroxy-*p*-*tert*-butylcalix[4]arene to bind polycyclic aromatic hydrocarbons such as pyrene was investigated [113]. Surface-enhanced Raman spectroscopy revealed that the macrocycles interact with AgNPs due to the formation of the S–Ag bond. When the pyrene solution was added to the macrocycle-capped AgNPs, significant changes in the Raman spectra of both the ligand and the host were observed. These changes were attributed to the complexation of pyrene into the macrocycle cavity.

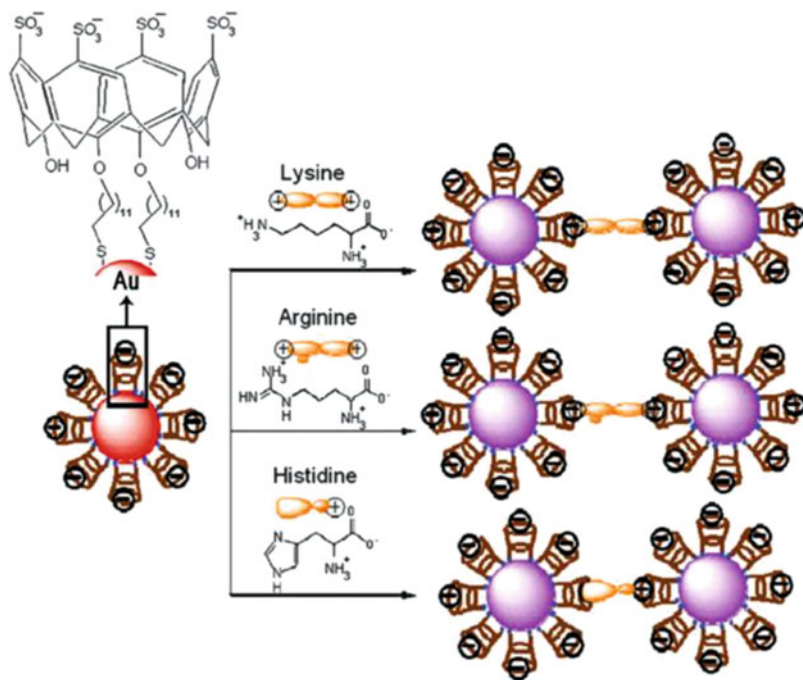


**Fig. 37.19** Graphical representation of the aggregation process of *p*-sulfonatocalix[4]arenes capped AuNPs caused by amino acid encapsulation (Reproduced with permission from Ref. [100], Copyright 2009, The Royal Society of Chemistry)

## 37.4 Conclusion

The tremendous versatility of the macrocyclic structure of the calixarenes represents an excellent basis to design complex macrocyclic receptors possessing the ability to self-assemble at interfaces. A large number of calixarenes have been demonstrated to form stable Langmuir monolayers at the air-water interface. These monolayers have been exploited as crystallization templates at the air-water interface, or transferred on solid substrates using the Langmuir-Blodgett technique. Suitably modified calixarenes have also been shown to self-assemble at the surface of metals to form stable and functional coatings.

With the advent of nanosciences and nanotechnology, a large number of elaborate and sophisticated scientific concepts are getting rapidly transferred from the research laboratory to the industrial application. As a consequence, the conventional gap between fundamental and applied sciences tends to shrink rapidly. In this context, the scientists involved in calixarene chemistry have the great responsibility to ensure that the potential of this class of macrocycles will not be restricted to fundamental sciences but will also be exploited at the industrial level.

## References

1. Wilde, P.; Mackie, A.; Husband, F.; Gunning, P.; Morris, V. *Adv. Colloid Interface Sci.* **2004**, *108*, 63–71.
2. MacRitchie, F. *Chemistry at interfaces*; Academic Press: San Diego, 1990.
3. Gaines, G. L. *Insoluble monolayers at liquid-gas interfaces*; Interscience Publishers: New York, 1966.
4. Franklin, B. *Philos. Trans.* **1774**, *64*, 445–460.
5. Tanford, C. *The Hydrophobic Effect, 2nd edition*; Wiley: New York, 1980.
6. Israelachvili *Intermolecular and Surface forces, 3rd ed.*; Academic Press: San Diego, 2011.
7. Velonia, K.; Cornelissen, J. J. L. M.; Feiters, M. C.; Rowan, A. E.; Nolte, R. J. M. In *Nanoscale assembly*; Huck, W. T. S., Ed.; Springer: New York.
8. Cui, H. G.; Webber, M. J.; Stupp, S. I. *Biopolymers* **2010**, *94*, 1–18.
9. *Amphiphiles: Molecular Assembly and Applications*; Nagarajan, R., Ed.; ACS Symposium Series: Washington DC, 2011.
10. Jie, K. C.; Zhou, Y. J.; Yao, Y.; Huang, F. H. *Chem. Soc. Rev.* **2015**, *44*, 3568–3587.
11. Lucke, A.; Stirling, C. J. M.; Böhmer, V. In *Calixarene 2001*; Asfari, Z., Böhmer, V., Harrowfield, J., Eds.; Kluwer Academic Publisher: Dordrecht.
12. Helttunen, K.; Shahgaldian, P. *New J. Chem.* **2010**, *34*, 2704–2714.
13. Montasser, I.; Shahgaldian, P.; Perret, F.; Coleman, A. W. *Int. J. Mol. Sci.* **2013**, *14*, 21899–21942.
14. Shahgaldian, P. *Chimia* **2010**, *64*, 427–427.
15. Gutsche, C. D.; Dhawan, B.; Levine, J. A.; Hyun No, K.; Bauer, L. J. *Tetrahedron* **1983**, *39*, 409–426.
16. Iwamoto, K.; Araki, K.; Shinkai, S. *Tetrahedron* **1991**, *47*, 4325–4342.
17. Groenen, L. C.; Ruël, B. H. M.; Casnati, A.; Timmerman, P.; Verboom, W.; Harkema, S.; Pochini, A.; Ungaro, R.; Reinhoudt, D. N. *Tetrahedron Lett.* **1991**, *32*, 2675–2678.
18. Nakamoto, Y.; Kallinowski, G.; Bohmer, V.; Vogt, W. *Langmuir* **1989**, *5*, 1116–1117.
19. Shahgaldian, P.; Coleman, A. W.; Kalchenko, V. I. *Tetrahedron Lett.* **2001**, *42*, 577–579.
20. Jebors, S.; Fache, F.; Balme, S.; Devoge, F.; Monachino, M.; Cecillon, S.; Coleman, A. W. *Org. Biomol. Chem.* **2008**, *6*, 319–329.
21. Hoegberg, A. G. S. *J. Org. Chem.* **1980**, *45*, 4498–4500.
22. Gutsche, C. D.; Pagoria, P. F. *J. Org. Chem.* **1985**, *50*, 5795–5802.
23. Shinkai, S.; Araki, K.; Tsubaki, T.; Arimura, T.; Manabe, O. *J. Chem. Soc., Perkin Trans. 1* **1987**, 2297–2299.
24. Dondoni, A.; Marra, A.; Scherrmann, M. C.; Casnati, A.; Sansone, F.; Ungaro, R. *Chem. Eur. J.* **1997**, *3*, 1774–1782.
25. Düker, M. H.; Gómez, R.; Vande Velde, C. M. L.; Azov, V. A. *Tetrahedron Lett.* **2011**, *52*, 2881–2884.
26. Gutsche, C. D.; Nam, K. C. *J. Am. Chem. Soc.* **1988**, *110*, 6153–6162.
27. Verboom, W.; Durie, A.; Egberink, R. J. M.; Asfari, Z.; Reinhoudt, D. N. *J. Org. Chem.* **1992**, *57*, 1313–1316.
28. Hayashida, O.; Mizuki, K.; Akagi, K.; Matsuo, A.; Kanamori, T.; Nakai, T.; Sando, S.; Aoyama, Y. *J. Am. Chem. Soc.* **2003**, *125*, 594–601.
29. Shahgaldian, P.; Pieles, U.; Hegner, M. *Langmuir* **2005**, *21*, 6503–6507.
30. Lee, M.; Lee, S. J.; Jiang, L. H. *J. Am. Chem. Soc.* **2004**, *126*, 12724–12725.
31. Rodik, R. V.; Klymchenko, A. S.; Jain, N.; Miroshnichenko, S. I.; Richert, L.; Kalchenko, V. I.; Mely, Y. *Chem. Eur. J.* **2011**, *17*, 5526–5538.
32. Strobel, M.; Kita-Tokarczyk, K.; Taubert, A.; Vebert, C.; Heiney, P. A.; Chami, M.; Meier, W. *Adv. Funct. Mater.* **2006**, *16*, 252–259.
33. Tulli, L. G.; Moradi, M.; Jung, T. A.; Shahgaldian, P. *Unpublished results*.
34. Moridi, N.; Elend, D.; Danylyuk, O.; Suwinska, K.; Shahgaldian, P. *Langmuir* **2011**, *27*, 9116–9121.

35. Markowitz, M. A.; Bielski, R.; Regen, S. L. *Langmuir* **1989**, *5*, 276–278.
36. Vollhardt, D.; Gloede, J.; Weidemann, G.; Rudert, R. *Langmuir* **2003**, *19*, 4228–4234.
37. Van der Heyden, A.; Regnoui-de-Vains, J.-B.; Warszyński, P.; Dalbavie, J.-O.; Żywociński, A.; Rogalska, E. *Langmuir* **2002**, *18*, 8854–8861.
38. Shahgaldian, P.; Cesario, M.; Goreloff, P.; Coleman, A. W. *Chem. Commun.* **2002**, 326–327.
39. Shahgaldian, P.; Coleman, A. W.; Kuduva, S. S.; Zaworotko, M. J. *Chem. Commun.* **2005**, 1968–1970.
40. Lonetti, B.; Lo Nostro, P.; Ninham, B. W.; Baglioni, P. *Langmuir* **2005**, *21*, 2242–2249.
41. Houel, E.; Lazar, A.; Da Silva, E.; Coleman, A. W.; Solovyov, A.; Cherenok, S.; Kalchenko, V. I. *Langmuir* **2002**, *18*, 1374–1379.
42. Korchowiec, B.; Orlof, M.; Sautrey, G.; Ben Salem, A.; Korchowiec, J.; Regnoui-de-Vains, J. B.; Rogalska, E. *J. Phys. Chem. B* **2010**, *114*, 10427–10435.
43. Ishikawa, Y.; Kunitake, T.; Matsuda, T.; Otsuka, T.; Shinkai, S. *J. Chem. Soc., Chem. Commun.* **1989**, 736–738.
44. Shahgaldian, P.; Coleman, A. W. *Langmuir* **2001**, *17*, 6851–6854.
45. Tulli, L. G.; Wang, W.; Lindemann, W. R.; Kuzmenko, I.; Meier, W.; Vaknin, D.; Shahgaldian, P. *Langmuir* **2015**, *31*, 2351–2359.
46. Guo, X.; Lu, G. Y.; Li, Y. *Thin Solid Films* **2004**, *460*, 264–268.
47. Zadmand, R.; Arendt, M.; Schrader, T. *J. Am. Chem. Soc.* **2004**, *126*, 7752–7753.
48. Shahgaldian, P.; Sciotti, M. A.; Pieleś, U. *Langmuir* **2008**, *24*, 8522–8526.
49. Moridi, N.; Danylyuk, O.; Suwinska, K.; Shahgaldian, P. *J. Colloid Interface Sci.* **2012**, *377*, 450–455.
50. Rullaud, V.; Moridi, N.; Shahgaldian, P. *Langmuir* **2014**, *30*, 8675–8679.
51. LoNostro, P.; Casnati, A.; Bossoletti, L.; Dei, L.; Baglioni, P. *Colloid Surface A* **1996**, *116*, 203–209.
52. Tulli, L. G.; Moridi, N.; Wang, W.; Helttunen, K.; Neuburger, M.; Vaknin, D.; Meier, W.; Shahgaldian, P. *Chem. Commun.* **2014**, *50*, 3938–3940.
53. Zadmand, R.; Schrader, T. *J. Am. Chem. Soc.* **2005**, *127*, 904–915.
54. Ariga, K.; Yamauchi, Y.; Mori, T.; Hill, J. P. *Adv. Mater.* **2013**, *25*, 6477–6512.
55. Hansma, H. G.; Gould, S. A. C.; Hansma, P. K.; Gaub, H. E.; Longo, M. L.; Zasadzinski, J. A. N. *Langmuir* **1991**, *7*, 1051–1054.
56. Markowitz, M. A.; Bielski, R.; Regen, S. L. *J. Am. Chem. Soc.* **1988**, *110*, 7545–7546.
57. Yan, X.; Janout, V.; Hsu, J. T.; Regen, S. L. *J. Am. Chem. Soc.* **2003**, *125*, 8094–8095.
58. Moridi, N.; Wackerlin, C.; Rullaud, V.; Schelldorfer, R.; Jung, T. A.; Shahgaldian, P. *Chem. Commun.* **2013**, *49*, 367–369.
59. Ulman, A. *Chem. Rev.* **1996**, *96*, 1533–1554.
60. Love, J. C.; Estroff, L. A.; Kriebel, J. K.; Nuzzo, R. G.; Whitesides, G. M. *Chem. Rev.* **2005**, *105*, 1103–1169.
61. Schierbaum, K. D.; Weiss, T.; Vanvelzen, E. U. T.; Engbersen, J. F. J.; Reinhoudt, D. N.; Gopel, W. *Science* **1994**, *265*, 1413–1415.
62. Schonherr, H.; Vancso, G. J. *Langmuir* **1999**, *15*, 5541–5546.
63. Vanvelzen, E. U. T.; Engbersen, J. F. J.; Delange, P. J.; Mahy, J. W. G.; Reinhoudt, D. N. *J. Am. Chem. Soc.* **1995**, *117*, 6853–6862.
64. Huisman, B. H.; Vanvelzen, E. U. T.; Vanveggel, F. C. J. M.; Engbersen, J. F. J.; Reinhoudt, D. N. *Tetrahedron Lett.* **1995**, *36*, 3273–3276.
65. Obora, Y.; Liu, Y. K.; Jiang, L. H.; Takenaka, K.; Tokunaga, M.; Tsuji, Y. *Organometallics* **2005**, *24*, 4–6.
66. Nigra, M. M.; Ha, J. M.; Katz, A. *Catal. Sci. Technol.* **2013**, *3*, 2976–2983.
67. Ta, V. T.; Nimse, S. B.; Song, K. S.; Kim, J.; Sayyed, D. R.; Nguyen, V. T.; Kim, T. *Chem. Commun.* **2011**, *47*, 11261–11263.
68. Demirkol, D. O.; Yildiz, H. B.; Sayin, S.; Yilmaz, M. *RSC Adv.* **2014**, *4*, 19900–19907.
69. Cormode, D. P.; Evans, A. J.; Davis, J. J.; Beer, P. D. *Dalton Trans.* **2010**, *39*, 6532–6541.
70. Zhang, S.; Echegoyen, L. *Org. Lett.* **2004**, *6*, 791–794.

71. Benounis, M.; Jaffrezic, N.; Martelet, C.; Dumazet-Bonnamour, I.; Lamartine, R. *Mater. Trans.* **2015**, *56*, 539–544.
72. de Oliveira, I. A. M.; Vocanson, F.; Uttaro, J. P.; Asfari, Z.; Mills, C. A.; Samitier, J.; Errachid, A. *J. Nanosci. Nanotechnol.* **2010**, *10*, 413–420.
73. Xu, S. B.; Podopygorina, G.; Moon, C.; Bohmer, V.; Ding, Z. F.; Mittler, S. *Electrochim. Acta* **2008**, *53*, 7981–7987.
74. Arena, G.; Contino, A.; Longo, E.; Sgarlata, C.; Spoto, G.; Zito, V. *Chem. Commun.* **2004**, 1812–1813.
75. Zhang, S.; Song, F. Y.; Echegoyen, L. *Eur. J. Org. Chem.* **2004**, 2936–2943.
76. Park, J. Y.; Kim, B. C.; Park, S. M. *Anal. Chem.* **2007**, *79*, 1890–1896.
77. Zhang, S.; Palkar, A.; Echegoyen, L. *Langmuir* **2006**, *22*, 10732–10738.
78. Zhang, G. F.; Zhu, X. L.; Miao, F. J.; Tian, D. M.; Li, H. B. *Org. Biomol. Chem.* **2012**, *10*, 3185–3188.
79. Friggeri, A.; van Veggel, F. C. J. M.; Reinhoudt, D. N. *Chem. Eur. J.* **1999**, *5*, 3595–3602.
80. Friggeri, A.; van Veggel, F. C. J. M.; Reinhoudt, D. N.; Kooyman, R. P. H. *Langmuir* **1998**, *14*, 5457–5463.
81. Chen, H. X.; Jia, S. S.; Gao, Y. M.; Liu, F. Z.; Chen, X. Y.; Koh, K.; Wang, K. M. *Microchim. Acta* **2015**, *182*, 1757–1763.
82. Snejdarkova, M.; Poturnayova, A.; Rybar, P.; Lhotak, P.; Himl, M.; Flidrova, K.; Hianik, T. *Bioelectrochemistry* **2010**, *80*, 55–61.
83. Nakaji-Hirabayashi, T.; Endo, H.; Kawasaki, H.; Gemmei-Ide, M.; Kitano, H. *Environ. Sci. Technol.* **2005**, *39*, 5414–5420.
84. Feng, N. M.; Zhao, H. Y.; Zhan, J. Y.; Tian, D. M.; Li, H. B. *Org. Lett.* **2012**, *14*, 1958–1961.
85. Boccia, A.; D’Orazi, F.; Carabelli, E.; Bussolati, R.; Arduini, A.; Secchi, A.; Marrani, A. G.; Zanoni, R. *Chem. Eur. J.* **2013**, *19*, 7999–8006.
86. Jain, P. K.; Huang, X. H.; El-Sayed, I. H.; El-Sayed, M. A. *Acc. Chem. Res.* **2008**, *41*, 1578–1586.
87. Yang, X.; Yang, M. X.; Pang, B.; Vara, M.; Xia, Y. N. *Chem. Rev.* **2015**, *115*, 10410–10488.
88. Zhou, W.; Gao, X.; Liu, D. B.; Chen, X. Y. *Chem. Rev.* **2015**, *115*, 10575–10636.
89. Prins, L. J. *Acc. Chem. Res.* **2015**, *48*, 1920–1928.
90. Tu, C. L.; Li, G. L.; Shi, Y. F.; Yu, X.; Jiang, Y.; Zhu, Q.; Liang, J. M.; Gao, Y.; Yan, D. Y.; Sun, J.; Zhu, X. Y. *Chem. Commun.* **2009**, 3211–3213.
91. Sutariya, P. G.; Pandya, A.; Lodha, A.; Menon, S. K. *Talanta* **2016**, *147*, 590–597.
92. Vita, F.; Boccia, A.; Marrani, A. G.; Zanoni, R.; Rossi, F.; Arduini, A.; Secchi, A. *Chem. Eur. J.* **2015**, *21*, 15428–15438.
93. Kaur, H.; Singh, J.; Chopra, S.; Kaur, N. *Talanta* **2016**, *146*, 122–129.
94. Maity, D.; Kumar, A.; Gunupuru, R.; Paul, P. *Colloid Surface A* **2014**, *455*, 122–128.
95. Kim, H. J.; Lee, M. H.; Mutihac, L.; Vicens, J.; Kim, J. S. *Chem. Soc. Rev.* **2012**, *41*, 1173–1190.
96. Tshikhudo, T. R.; Demuru, D.; Wang, Z. X.; Brust, M.; Secchi, A.; Arduini, A.; Pochini, A. *Angew. Chem. Int. Ed.* **2005**, *44*, 2913–2916.
97. Arduini, A.; Demuru, D.; Pochini, A.; Secchi, A. *Chem. Commun.* **2005**, 645–647.
98. Sokkalingam, P.; Hong, S. J.; Aydogan, A.; Sessler, J. L.; Lee, C. H. *Chem. Eur. J.* **2013**, *19*, 5860–5867.
99. Pandya, A.; Sutariya, P. G.; Menon, S. K. *Analyst* **2013**, *138*, 2483–2490.
100. Patel, G.; Menon, S. *Chem. Commun.* **2009**, 3563–3565.
101. Wei, A. *Chem. Commun.* **2006**, 1581–1591.
102. Li, H.; Tan, L. L.; Jia, P.; Li, Q. L.; Sun, Y. L.; Zhang, J.; Ning, Y. Q.; Yu, J. H.; Yang, Y. W. *Chem. Sci.* **2014**, *5*, 2804–2808.
103. Zhou, Y.; Tan, L. L.; Li, Q. L.; Qiu, X. L.; Qi, A. D.; Tao, Y. C.; Yang, Y. W. *Chem. Eur. J.* **2014**, *20*, 2998–3004.
104. Sun, Y. L.; Zhou, Y.; Li, Q. L.; Yang, Y. W. *Chem. Commun.* **2013**, *49*, 9033–9035.

105. Yang, Y. W. *Chemphyschem : a European journal of chemical physics and physical chemistry* **2015**.
106. Ciesa, F.; Plech, A.; Mattioli, C.; Pescatori, L.; Arduini, A.; Pochini, A.; Rossi, F.; Secchi, A. *J. Phys. Chem. C* **2010**, *114*, 13601–13607.
107. Chin, S. F.; Makha, M.; Raston, C. L.; Saunders, M. *Chem. Commun.* **2007**, 1948–1950.
108. Pescatori, L.; Boccia, A.; Ciesa, F.; Rossi, F.; Grillo, V.; Arduini, A.; Pochini, A.; Zanoni, R.; Secchi, A. *Chem. Eur. J.* **2010**, *16*, 11089–11099.
109. Zang, W. Z.; Chen, X. J.; Boulos, R. A.; Toster, J.; Raston, C. L. *Chem. Commun.* **2014**, *50*, 15167–15170.
110. de Silva, N.; Ha, J. M.; Solovyov, A.; Nigra, M. M.; Ogino, I.; Yeh, S. W.; Durkin, K. A.; Katz, A. *Nat. Chem.* **2010**, *2*, 1062–1068.
111. Urban, I.; Ratcliffe, N. M.; Duffield, J. R.; Elder, G. R.; Patton, D. *Chem. Commun.* **2010**, *46*, 4583–4585.
112. Tauran, Y.; Grosso, M.; Brioude, A.; Kassab, R.; Coleman, A. W. *Chem. Commun.* **2011**, *47*, 10013–10015.
113. Guerrini, L.; Garcia-Ramos, J. V.; Domingo, C.; Sanchez-Cortes, S. *Langmuir* **2006**, *22*, 10924–10926.

# Chapter 38

## Solid State Features of Calixarenes

Kinga Suwinska

### 38.1 Introduction

X-ray diffraction studies of crystalline samples provide direct information about molecular structure (atoms types and distribution, geometrical parameters, i.e. bond lengths, bond angles and torsion angles, molecular conformation and absolute configuration) and crystal structure (crystal composition, i.e. molecular ratio for complex crystals and/or presence of solvent(s) molecules, intermolecular interactions, especially determination of the networks of hydrogen bonds and short intermolecular contacts).

Solid state investigations are of great importance in particular in case of studying calixarene and calix-type compounds due to their great ability to form molecular inclusion complexes, co-crystals and supramolecular assemblies. In CSD (Cambridge Structural Database [1]) over 6000 structures of calix-type compounds are deposited so far. Approximately one-third of the entries are organometallic compounds and two-thirds are classified as organic compounds.

The analysis of over 4000 entries classified as organic compounds reveals that calixarene structures are in great majority (approx. 2900 entries). Among them about 2270 entries refers to calix[4]arenes. The number of entries referring to the number of aromatic residues in the macrocyclic ring is presented in Table 38.1.

Among calix-type compounds other than calixarenes represented in CSD the largest group consists of calixpyrroles. The number of entries in CSD for non-calixarene structures are listed in Table 38.2.

The very first crystal structure of calix-type compound was published in 1968 by B. Nilsson [2]. The reported compound was “obtained by acylation of a phenolic

---

K. Suwinska (✉)

Faculty of Mathematics and Natural Sciences, Cardinal Stefan Wyszyński University  
in Warsaw, K. Wóycickiego 1/3, PL-01 938 Warszawa, Poland  
e-mail: [k.suwinska@uksw.edu.pl](mailto:k.suwinska@uksw.edu.pl)



**Table 38.1** Distribution of entries in CSD for calix[n]arenes

Calixarene	No. of entries
Calix[3]arene	40
Calix[4]arene	2270
Thiacalix[4]arene	284
Oxacalix[4]arene	52
Calix[5]arene	127
Calix[6]arene	171
Calix[7]arene	8
Calix[8]arene	47
Calix[n]arene (n > 8)	7

**Table 38.2** Distribution of entries in CSD for calix-type compounds other than calix [n]arenes

Calix-type compounds	No. of entries
Calixresorcinarenes	518
Calixpyrogallolarenes	138
Calixpyrroles	212
Pillararenes	38
Calixquinones	26
Caliximidazoles	24
Calixphyrins	22
Calixnaphthalenes	11
Other	61

product obtained by condensation of resorcinol with *para*-bromobenzaldehyde in the presence of hydrogen chloride". It turns out to be the first resorcin[4]arene derivative (4,6,10,12,16,18,22,24-*O*-octabutanoyl-*C*-bromophenylcalix[4]resorcinarene) crystal structure (Fig. 38.1).

It took 8 years to publish another structure. In 1976 K. J. Palmer et al. reported two conformers of another resorcin[4]arene derivative, i.e. *cis*- and *trans*-*C*-*para*-bromophenyl-4,6,10,12,16,18,22,24-*O*-octaacetylcalix[4]resorcinarene [3]. Than in next 3 years G. D. Andreetti et al. published the first crystal structure of inclusion compound formed by *para-tert*-butylcalix[4]arene with toluene [4]. The calixarene molecule was found in cone conformation and the guest molecule could not be located within the host cavity due to its disorder (the molecular complex was located on a crystallographic fourfold axis). The Authors also noticed that the structure undergoes the order-disorder phase transition at 248 K. In 1996 the disorder high temperature phase was resolved with the aid of solid-state NMR data by E. B. Brouwer et al. [5] (unfortunately, the atoms coordinates are not deposited in CSD) and in 1998 the low temperature ordered phase was reported by A. Arduini et al. [6] (Fig. 38.2). The inclusion complex is stabilized by weak C–H... $\pi$  interaction. The crystal and molecular structure of this complex was also studied by other authors [7].

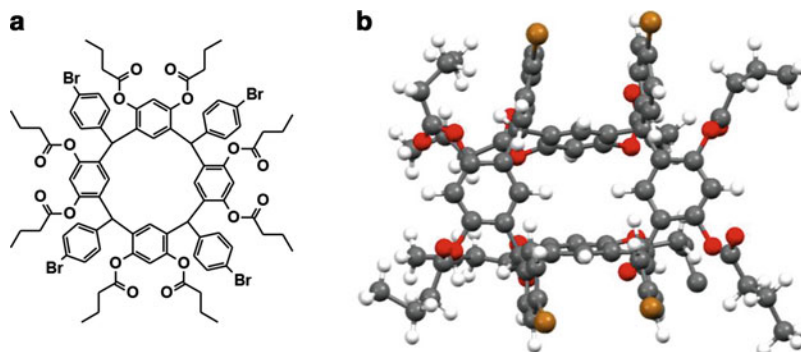


**Fig. 38.1** The very first published crystal structure of calix-type compound: (a) molecular formula; (b) molecular structure [2]

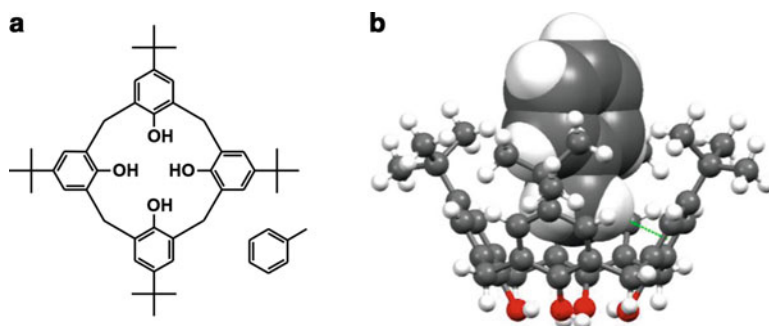


**Fig. 38.2** Inclusion complex of *para-tert-butylcalix[4]arene* with toluene: (a) molecular formula; (b) molecular structure, weak C–H $\cdots$  $\pi$  interaction stabilizing the inclusion complex shown in green (only one of the two independent complexes in the unit cell is shown) [6]

As mentioned above, the number of calixarene and calix-type compounds structures investigated and deposited so far in CSD is very big it is not possible to discuss all of them in this chapter. So the discussion will be limited mostly to organic inclusion compounds and co-crystals of course having in mind that the monomolecular crystal structures as well as the metalorganic complexes are also a rich source of valuable information about geometries, possible conformations, coordination types, intermolecular interactions, etc.

## 38.2 Calixarenes

### 38.2.1 *Calix[3]arenes*

One of the smallest in ring size calix[3]arenes reported in CSD is 2,2,8,8,14,14-hexamethyl-2,8,14-trisilicalix[3]arene [8] in which the aryl residues are linked by

**Fig. 38.3** 2,2,8,8,14,14-hexamethyl-2,8,14-trisilacalix[3]arene [8]

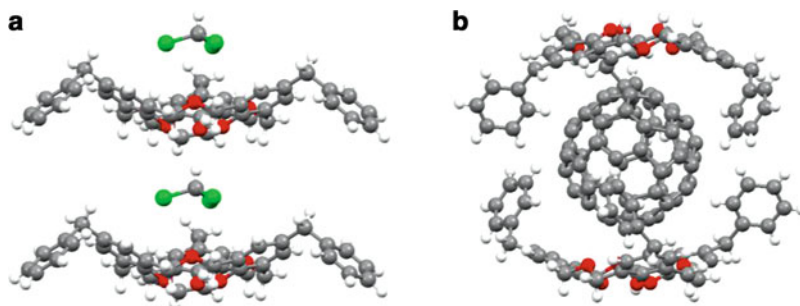
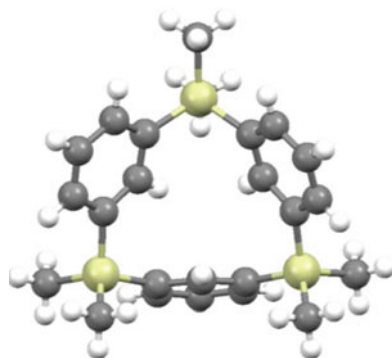


**Fig. 38.4** Inclusion complexes formed by 9-hexahomo-3,11,19-trioxacalix[3]arene: (a) with chloroform, two “stacking” 1:1 complexes are shown; (b) with fullerene, one 2:1 complex is shown [9]

only one silica atom (Fig. 38.3). In this molecule one aryl residue is oriented alternate in respect to the other two.

Majority of compounds in this group are oxacalixarenes where the aryl moieties are linked by  $-\text{CH}_2-\text{O}-\text{CH}_2-$  linkers. Some of these molecules are able to form molecular complexes with various solvent molecules but quite large species like fullerenes. One of such examples is 9-hexahomo-3,11,19-trioxacalix[3]arene which forms 1:1 (host:guest) molecular complexes with chloroform and 2:1 complex with fullerene [9] (Fig. 38.4). It must be stressed that the host 9-hexahomo-3,11,19-trioxacalix[3]arene molecule adjusts its conformation in order to best fit the guest molecules.

### 38.2.2 Calix[4]arenes

This is the largest, over 2000 entries, group of compounds investigated in solid state (see Table 38.1). In this group of compounds one finds simple unsubstituted

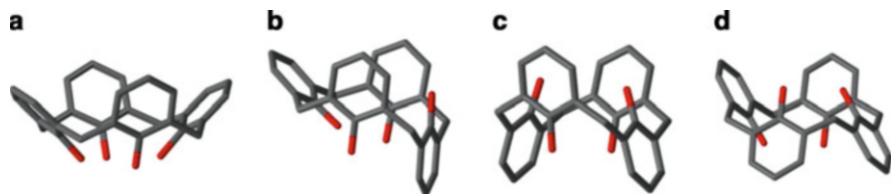


**Fig. 38.5** Basic conformations of calix[4]arenes: (a) cone; (b) partial cone; (c) 1,3-alternate; (d) 1,2-alternate

calixarenes and its complexes/co-crystals with variety of guest molecules and a great number of modified calixarenes and their complexes where the type of substituents and modifications is highly differentiated and so wide that it seems to be limited only by imagination of the chemists.

The calix[4]arene molecules may adopt four basic conformations which are known as cone, partial cone, 1,3-alternate and 1,2-alternate (Fig. 38.5).

In unsubstituted or substituted with relatively small substituents calixarenes the rotation around the methylene bridges are easy and the molecule may exist in different conformations or in dynamic equilibrium of different conformations. In solid state the conformation of calix[4]arene molecule depends also on the intermolecular interactions with other molecules of the same type and on the eventual presence of included guest molecule(s), not included guest molecules present in the structure and possible solvent molecules. The very popular cone conformation in unsubstituted at lower rim calixarenes is stabilized by hydrogen bond formation between hydroxyl groups. The desired conformation may be also locked in place by substitution of hydroxyl hydrogen with larger substituents and/or by insertion bulky substituents on the upper rim, i.e. in *para* position to the hydroxyl group. Alternative methods to protect the calixarene against the rotational change of the conformation is incorporating additional bridges providing cryptand-type molecules or metal complexation using as complexing centers the hydroxyl oxygen atoms (stabilizing the cone conformation). Insertion of proper substituents on the upper rim may also result in increasing the molecular cavity.

### 38.2.2.1 Cone Conformation

It is quite often observed for unsubstituted on upper rim calix[4]arenes in cone conformation that in solid state they form inclusion dimers by mutual inserting one aromatic ring into molecular cavity of the other one. Such a dimer formation prevents the inclusion of guest molecules into the host cavity and the co-crystals are formed instead. An example of such co-crystal formed by diphosphorylated on lower rim calix[4]arene with melaminium is shown in Fig. 38.6 [10]. Additionally in the co-crystal one ethanol and nine water molecules are present.

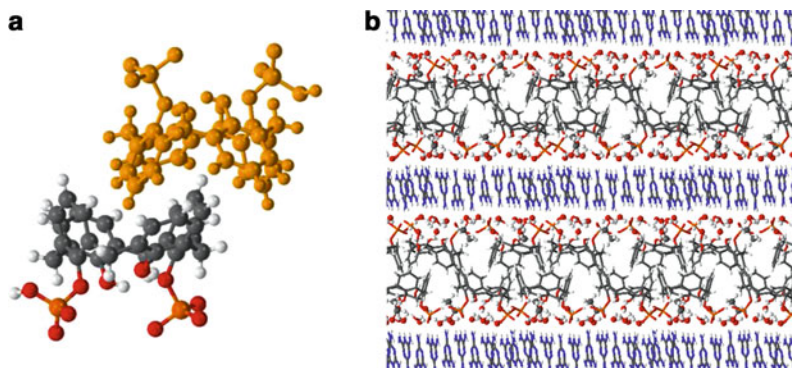


**Fig. 38.6** Diphosphorylated calix[4]arene/melaminium/ethanol/water co-crystal: (a) host inclusion dimer formation; (b) layer-type arrangement of molecules in the crystal structure [10]

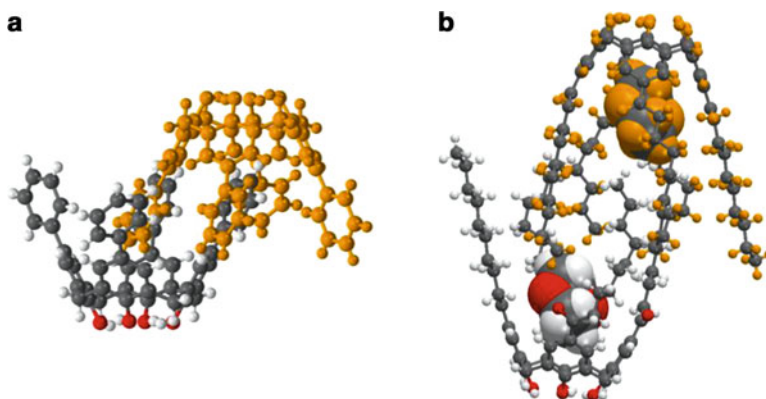


**Fig. 38.7** Inclusion dimer formation by calix[4]arenes substituted on upper rim: (a) mutual inclusion of phenyl substituent in *para*-phenylcalix[4]arene; [11] (b) mutual inclusion of one decanoyl substituent in decanoylcalix[4]arene/dioxane [12]

In this structure well defined layers of guest cations and bilayers of host anions are separated by layers of solvent (ethanol and water) molecules. The host bilayers are hydrophobic with hydrophilic surface.

Formation of inclusion dimers is not limited only to unsubstituted on upper rim calix[4]arenes. It is observed also for *para* substituted calixarenes and also, when the substituents are suitable, it may occur with already formed inclusion complex. Examples are shown in Fig. 38.7.

A wide range of calix[4]arenes derivatives having interesting chemical properties and capable to form inclusion complexes and co-crystals with different molecules and ions is known. It is not possible here to discuss all of them in this chapter. Looking after compounds which would have potential applications like molecular carriers for, e.g. drug molecules the researchers turn their attention to water-soluble

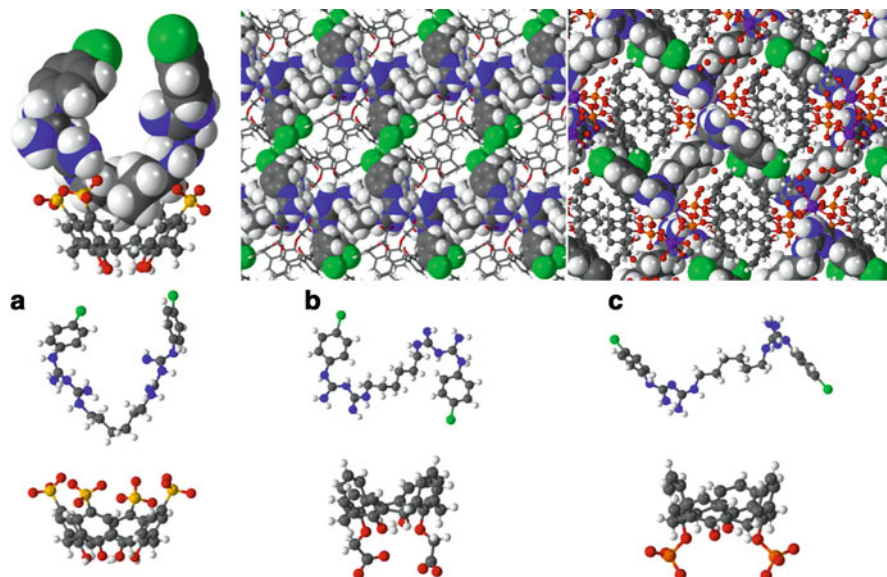


**Fig. 38.8** Chlorhexidine inclusion complex and co-crystals with anionic water-soluble calix[4]arenes: (a) inclusion complex with *para*-sulphonatocalix[4]arene; (b) co-crystal with calix[4]arene dimethoxycarboxylic acid; co-crystal with calix[4]arene dihydroxyphosphonic acid [13]

derivatives of calix[4]arenes such as sulphonated, carboxylated or phosphorylated ones. Depending on type of derivatization inclusion complexes or co-crystals may be obtained for the same guest molecule. The example is the guest chlorhexidine, a wide-spectrum antiseptic which does not crystallize, as evidenced by its absence from the CSD, preventing its use as a solid-state formulation.

Chlorhexidine forms an inclusion complex with *para*-sulphonatocalix[4]arene. In this complex chlorhexidine adopts V-shaped conformation (Fig. 38.8a). Two other derivatives of calix[4]arene, i.e. the dimethoxycarboxylic acid and dihydroxyphosphonic acid which are derivatized on lower rim the calixarenes form inclusion dimers and their internal cavities are protected against inclusion of guest molecule (Fig. 38.8b, c). The co-crystals are formed instead and the chlorhexidine molecule adopts S and Z-shaped conformations, respectively. This may suggest that the conformation of guest molecule may be controlled by appropriate selection of host molecule.

Sometime the guest molecule wins the competition for the access to the host cavity against the host inclusion dimer formation. This is the case in the complex of calix[4]arene dihydroxyphosphonic acid with piroxicam shown in Fig. 38.9 [14].

More about crystalline complexes of drug and other molecules of biological importance one may find in Chem. Commun. Feature Article [15].

An interesting feature of calix[4]arenes is formation of molecular capsules.

Two *p-tert*-butylcalix[4]arene oriented ‘head-to-head’ form molecular capsules by which may accommodate anisole molecule (Fig. 38.10a – guest molecule is



**Fig. 38.9** Inclusion complex of calix[4]arene dihydroxyphosphonic acid with piroxicam [14]

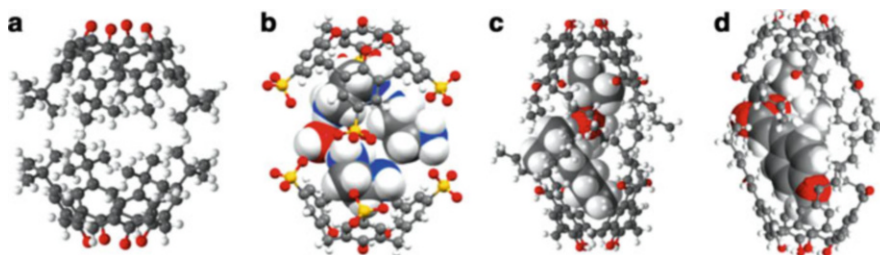
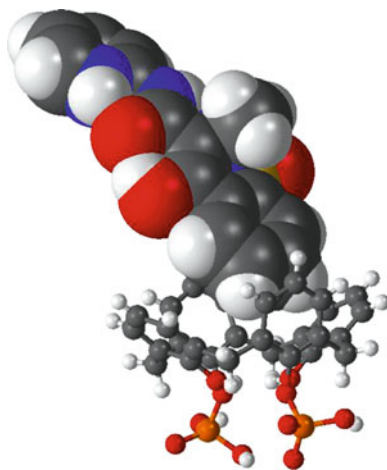


**Fig. 38.10** Molecular capsules formed by *para* substituted calix[4]arenes: (a) *t*-butylcalix[4]arene/anisole; [16] (b) *para*-sulphonatocalix[4]arene/ethylenediammonium/amidoethyleneammonium/H<sub>2</sub>O; [17] (c) *para*-hexanoylcalix[4]arene/(-)-menthone; [18] (d) *para*-hexanoylcalix[4]arene/octyl methoxycinnamate; [19]

disordered in the cavity over at least eight equivalent positions and is not shown in the picture). Molecular capsules are formed also by *para*-sulphonatocalix[4]arene. In this case the capsular complex is in form of organic salt. An example is given in Fig. 38.10b where within the capsule three ions (one ethylenediammonium and two amidoethyleneammonium) and one water molecule are located [17]. By introducing much longer hexanoyl substituents in *para* positions allows creation of larger cavity able to accommodate two medium size molecules like (Fig. 38.10c). Similar 2:2 capsular complexes formed by the same host are 1,4-dioxane, [20] tetrahydrofuran, [20] (+)-carvone, [20] 1-bromo-1-chloro-2,2,2-trifluoroethane [12], chloroform and 1,3-diphenylpropane-2-one, [21]. Larger molecules like octyl methoxycinnamate may also be included in (*para*-hexanoylcalix[4]arene)<sub>2</sub> capsules to form 2:1 complexes (Fig. 38.10d). Similar 2:1 complexes are reported, e.g. with *cis*-stilbene and *trans*-stilbene [22]. Also may form molecular capsules. In this case a 2:2 inclusion complex with (-)-menthone is reported [23].

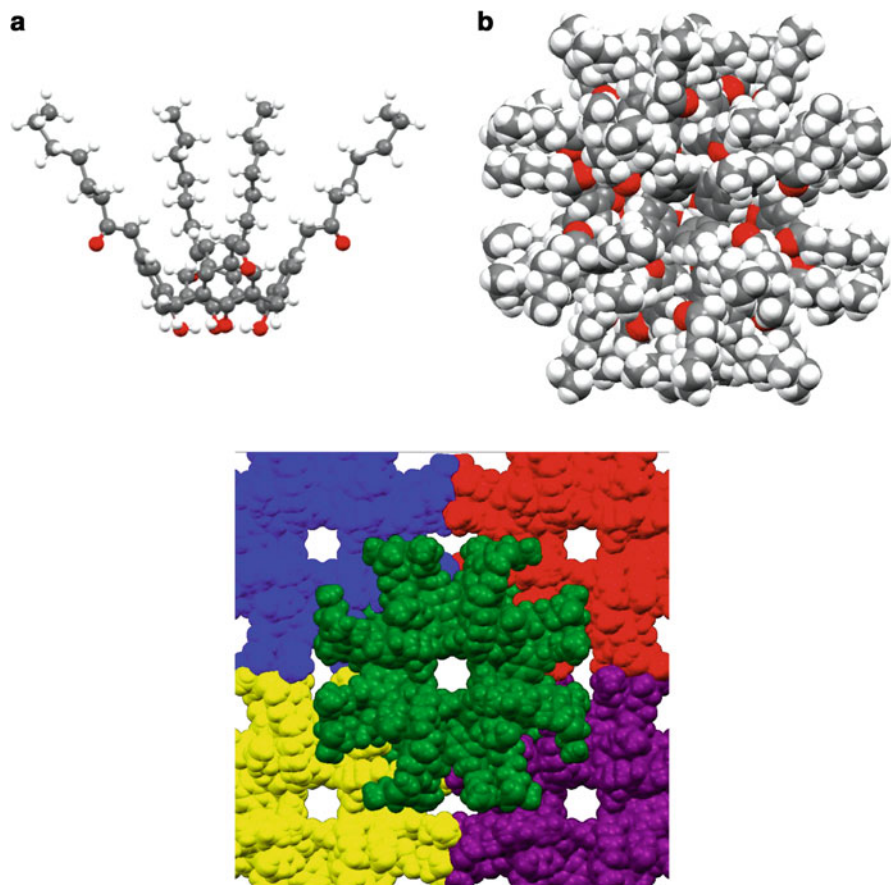


**Fig. 38.11** Self-assembly of  $\beta$ -carbonyl-*para*-octyl-calix[4]arene in solid state: (a) molecular structure; (b) dodecameric self-assembly; (c) packing of spherical self-assemblies in the crystal [24]

Interestingly, the  $\beta$ -carbonyl-*para*-octyl-calix[4]arene (Fig. 38.11a) which differs from the *para*-octanoylcalix[4]arene only by the position of carbonyl group instead of the capsule formation a different self-assembly mode is observed. Twelve molecules of the  $\beta$ -carbonyl-*para*-octyl-calix[4]arene self-assemble to micelle-like spherical aggregate with highly hydrophilic interior where 48 hydroxyl groups are accumulated and highly hydrophobic exterior with 48 aliphatic chains pointing out (Fig. 38.11b) [24].

### 38.2.2.2 Partial-Cone Conformation

In partial-cone conformation the calixarene cavity self-inclusion of a substituent belonging to the alternate aromatic moiety may occur. Such a situation is shown in



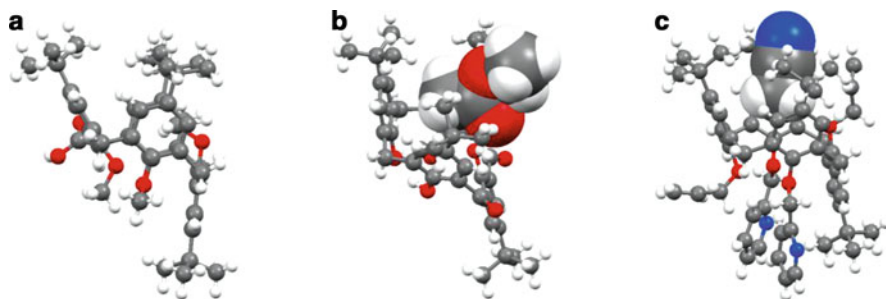


**Fig. 38.12** Calix[4]arenes in partial-cone conformation: (a) t-butylmethoxycalix[4]arene-2-carboxylic acid ethanol monohydrate clathrate; [25] (b) t-butyl-dioxocalix[4]arene/ethyl acetate inclusion complex; [26] (c) t-butyl-bis(2-pyridylmethoxy)-bis(allyloxy)calix[4]arene/acetonitrile inclusion complex [27]

Fig. 38.12a where the methyl replacing hydrogen in hydroxyl group is oriented towards the center of the cavity and instead of inclusion complex the co-crystal (ethanol monohydrate clathrate) is formed [25]. When the cavity is not blocked like in t-butyl-dioxocalix[4]arene the ethyl acetate enters the cavity and the inclusion complex is formed (Fig. 38.12b) [26]. When the substituent replacing hydrogen in hydroxyl group mimics the *para* substituent a cavity similar to the one in cone conformation is created and the inclusion is similar to that observed for calix[4]arenes in cone conformation (Fig. 38.12c) [27].

### 38.2.2.3 1,3-Alternate Conformation

In 1,3-alternate conformation the benzene rings of calix[4]arene are perpendicular or almost perpendicular to the main plane of the molecule defined by the four methylene bridges. As a consequence, the inclusion of guest molecules into the host cavity is much more difficult compared to the cone conformation and as general rather co-crystals than molecular inclusion complexes are observed. One of the exceptions is an inclusion/additive complex of *para*-bromomethyl-dodecamethylcalix[4]arene with 1,2-dichloroethane where one molecule of guest is included in shallow cavity on one side of the host molecule while the second guest molecule forms an additive complex (Fig. 38.13a) [28].

Already described *para*-sulphonatocalix[4]arene while crystallized with 4,4'-bipyridine adopts 1,3-alternate conformation (Fig. 38.13b) and forms co-crystal which appears to be an organic salt (Fig. 38.13c) [29].

### 38.2.2.4 1,2-Alternate Conformation

In 1,2-alternate conformation the in calix[4]arene molecules with unsubstituted OH group very often two shallow cavities are formed symmetrically on both sides of the

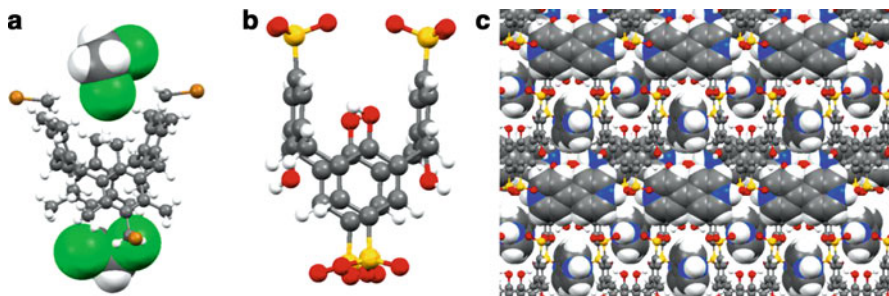


**Fig. 38.13** Calix[4]arenes in 1,3-alternate conformation: (a) *para*-bromomethyl-dodecamethylcalix[4]arene 1,2-dichloroethane inclusion/additive complex; (b) *para*-sulfonatocalix[4]arene in 1,3-alternate conformation; (c) *para*-sulfonatocalix[4]arene/4,4'-bipyridinium co-crystal

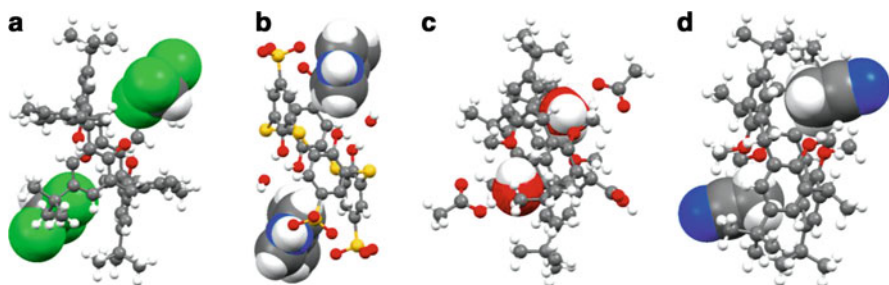


**Fig. 38.14** Molecular complexes of calix[4]arenes in 1,2-alternate conformation: (a) *t*-butyl-bis(mesityl)calix[4]arene/chloroform 1:2 complex; [30] (b) *para*-sulfonatocalix[4]arene/bipyridinium/water inclusion/additive complex; [31] (c) *t*-butyl-2-carboxy-14-methyl-methoxycalix[4]arene/hydronium/water acetic acid acetate inclusion/additive complex; [32] (d) *t*-butyl-2,14-dimethyl-methoxycalix[4]arene/acetonitrile inclusion complex [32]

macrocyclic ring. Small solvent molecules may be located in these cavities and molecular 1:2 (host:guest) complexes are created. An example of such a complex is that of *t*-butyl-bis(mesityl)calix[4]arene with chloroform presented in Fig. 38.14a [30]. *para*-Sulfonatocalix[4]arene was found to adopt 1,2-alternate conformation in its ionic inclusion/additive complex with two bipyridinium ions and two water molecule (Fig. 38.14b) [31]. Water molecules are hydrogen bonded to the calixarene anion.

Substitution of hydroxyl hydrogen with methyl group (methoxy derivative) in calix[4]arenes in 1,2-alternate conformation results in creation slightly deeper and better defined cavity similar to that characteristic for calix[4]arenes in cone conformation. Several of such molecular complexes was reported by C. Fischer et al. [32]. Two of them is shown in Fig. 38.14c, d.

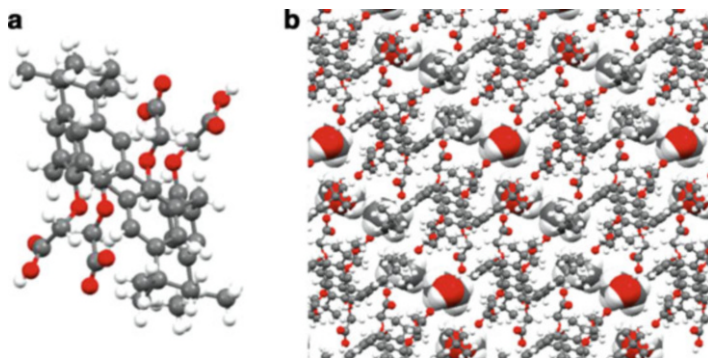


**Fig. 38.15** *p-tert*-Butylcalix[4]arene oxyacetic acid ethanol solvate: (a) calix[4]arenes in 1,2-alternate conformation; (b) crystal packing [33]

Substitution of the hydroxyl hydrogen with larger groups prevents the shallow cavities of calix[4]arene against inclusion of guest molecules and the co-crystals (clathrates, solvates) are formed (Fig. 38.15) [33].

### 38.2.3 Calix[5]arenes

The five-membered macrocyclic ring of calix[5]arenes is much more flexible compared to calix[4]arenes. Nevertheless, the majority of known calix[5]arenes in solid state adopts cone or distorted (pinched) cone conformations. The same host molecule is found in different conformations in complexes in different or even the same guest molecule. One of the examples is the complex of water-soluble anionic *para*-sulphonatocalix[5]arene with the 1,10-phenantroline cation in 1:1 (host: guest) inclusion complex and 2:2 inclusion complex [34], and with the 1,4-diazabicyclo(2.2.2)octanium cation in 2:2 inclusion complex [35]. In complexes with phenantroline cations the *para*-sulphonatocalix[5]arene is present in two distorted cone conformations. In the 1:1 complex three aromatic rings are almost perpendicular to the main plane of the macrocyclic ring and two are tilted outwards the center of the host molecule (Fig. 38.16a) while in the 2:2 complex the opposite is observed – two aromatic rings are almost perpendicular to the main plane of the macrocyclic ring and three are tilted outwards the center of the host molecule (Fig. 38.16b). This makes the internal cavity of the host big enough to form a dimeric capsule able to accommodate two phenantroline cations. In the third complex with 1,4-diazabicyclo(2.2.2)octanium cation the conformation of host molecule is such that four aromatic rings are almost parallel to the main plane of the macrocyclic ring and one are tilted inwards the center of the host molecule (Fig. 38.16c). As a consequence in the dimer formed by two host molecules there are two capsules present, each accommodating one guest cation.

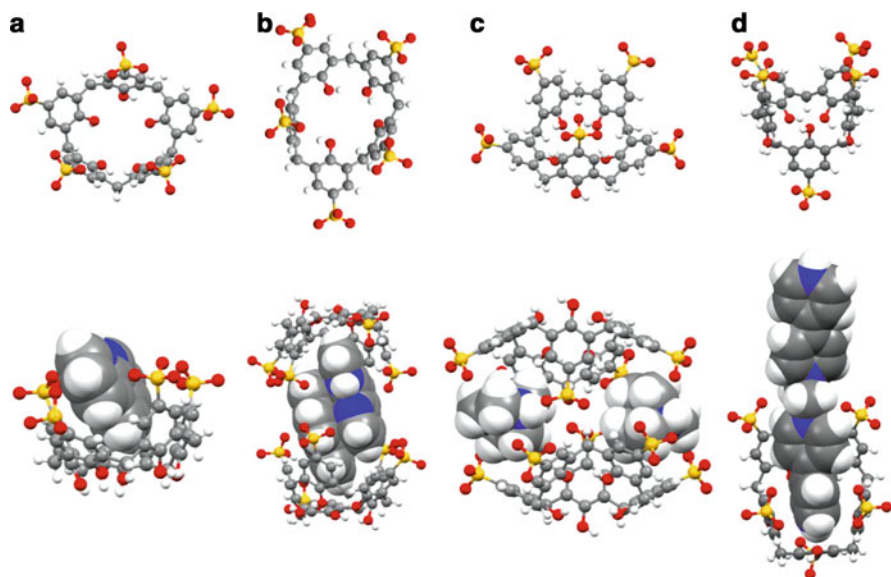


**Fig. 38.16** Flexibility of the *para*-sulphonatocalix[5]arene host: (a) host conformation (*top*) and 1:1 inclusion complex formation with 1,10-phenantrolium cation; [34] (b) host conformation (*top*) and 2:2 inclusion complex formation with 1,10-phenantrolium cation; [34] (c) host conformation (*top*) and 2:2 inclusion complex formation with 1,4-diazabicyclo(2.2.2)octanium cation; [35] (d) host conformation (*top*) and 1:1 inclusion complex formation with ethane-1,2-bis(4,4'-bipyridinium) cation [36]

In the last example of the *para*-sulphonatocalix[5]arene inclusion complex with ethane-1,2-bis(4,4'-bipyridinium) cation the host molecule adopts 1-alternate conformation (Fig. 38.16d). It is interesting that the part of the guest is not included into another calixarene cavity but it interacts with hydrophilic surrounding formed by water molecules and sulphonate group of the inverted ring of host molecule [36].

For calix[5]arenes, similarly to calix[4]arenes, formation of inclusion dimers is observed for unsubstituted at upper rim or substituted with small e.g. methyl groups calix[5]arenes. As an example *para*-methylated calix[5]arene is shown in Fig. 38.17a [37].

For more richly decorated calix[5]arenes the self-inclusion of one of the substituents may occur. This was observed for e.g. *para*-*t*-butyl-penta-alloxyalix[5]arenes (Fig. 38.17b) [38]. Interestingly, the self-inclusion of an allyl group was observed non-solvated *para*-*t*-butyl-penta-(propan-2-yl)oxyalix[5]arene and *para*-*t*-butyl-penta-propenyloxyalix[5]arene acetone solvate, while in *para*-*t*-butyl-penta-propoxyalix[5]arene hexane solvate the *t*-butyl group is self-included [38]. This suggests that the self-inclusion and inclusion of solvent into the macrocyclic cavity are competitive processes and in the above cases the solvent loses the competition.

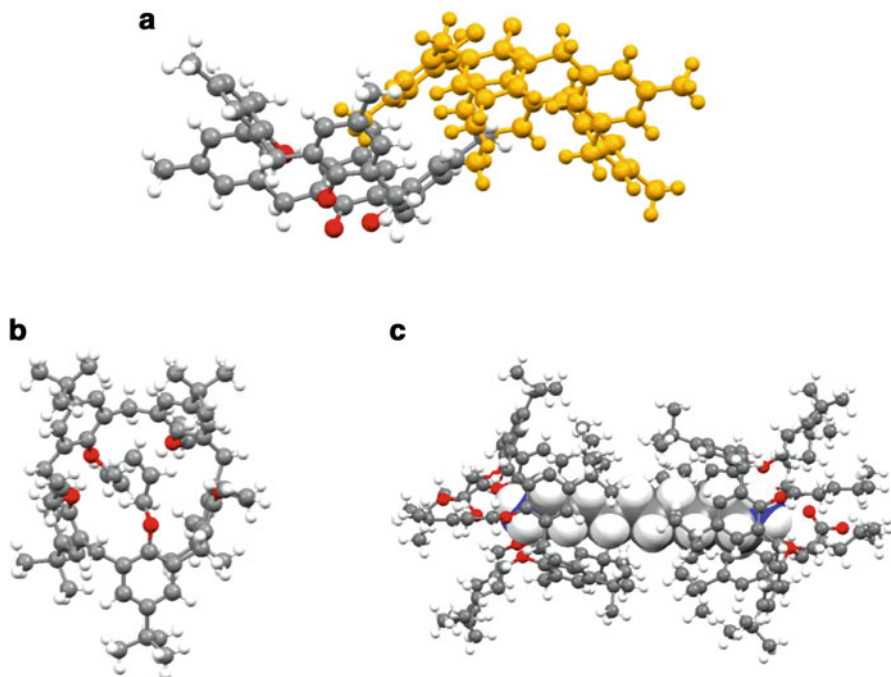


**Fig. 38.17** (a) Dimer formation by a mutual inclusion of one methyl group of one *para*-methylcalix[5]arene in the cavity of another one; [37] (b) self-inclusion of propenyloxy group in *para*-*t*-butyl-penta-propenyloxy-calix[5]arene; [38] (c) inclusion complex of carboxylcalix[5]arene with 1,12-dodecanediyldiammonium [39]

But it is not always a case. Similar carboxylcalix[5]arene forms inclusion complexes with 1,10-decanediyldiammonium (Fig. 38.17c) and 1,12-dodecanediyldiammonium [39]. But it must be noticed here that the latest complexes are organic salts with 2:1 host:guest stoichiometry as the calixarene host is a monoanion and the guest is a dication and additional, i.e. electrostatic interactions are playing important role in complex formation.

Calix[5]arenes are also suitable molecules for complexation of fullerene molecules [40]. An example of 2:1 host:guest molecular complex is shown in Fig. 38.18.

### 38.2.4 Calix[6]arenes

Extending the macrocycle ring to six-membered ring gives more flexibility to the calix[6]arene molecule compared to three- four- and five-membered calixarenes. For calix[6]arenes eight main (basic) conformations are defined: [41] distorted cone, compressed cone, pinched cone, double partial cone, winged, 1,2,3-alternate, 1,3,5-alternate and distorted 1,2,3-alternate. Other conformations are also observed

**Fig. 38.18** Molecular complex of *para*-benzylcalix[5]arene with  $C_{60}$  [40c]

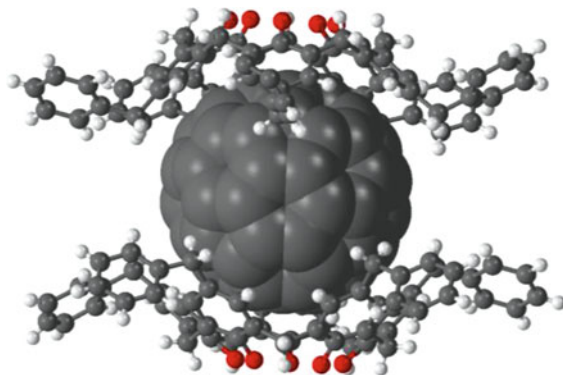
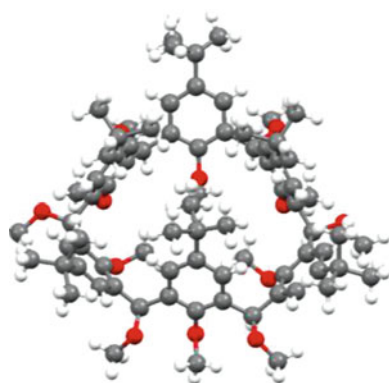


**Fig. 38.19** Self-inclusion in *para*-*t*-butyl-dodecamethoxycalix[6]arene molecule [42]



but they may be considered as intermediate or distorted conformations of the above defined ones.

Among about 200 structures deposited in CSD a large variation of calix[6]arenes derivatives is reported. The derivatization concerns the *para*-substitution on the upper rim, substitution of hydrogen atom of hydroxyl group on the lower rim, or both. Other derivatives are also reported.

Similarly to the calix[5]arenes, for the flexible calix[6]arenes the self-inclusion is observed. An example of self-inclusion is shown in Fig. 38.19 in case of *para*-*t*-butyl-dodecamethoxycalix[6]arene hydrate where two distal residues are turned one inside and the other one outside the calixarene cavity causing self-inclusion of *t*-butyl group on one side and the methoxy group on the other side of the molecule [42].

An example of 1:1 host:guest inclusion complex can be *para*-*t*-butyl-calix[6]arene with *n*-hexylammonium (the calixarene is in dianion form, one ammonium cation is included into the host cavity, second is located outside the cavity) [43]. The calix[6]arene adopts such a conformation, that the resulted cavity mimics the one of calix[4]arene (Fig. 38.20a). In 2:2 inclusion complex with pyridine of the *para*-*t*-butyltrihomocalix[6]arene in which every second methylene bridge is



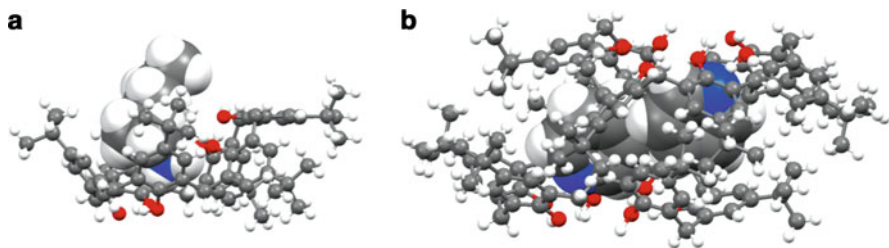


**Fig. 38.20** Host-guest complex formation by calix[6]arenes: (a) *para*-t-butyl-calix[6]arene/n-hexylammonium complex; [43] (b) *para*-t-butyltrihomocalix[6]arene/pyridine [44]

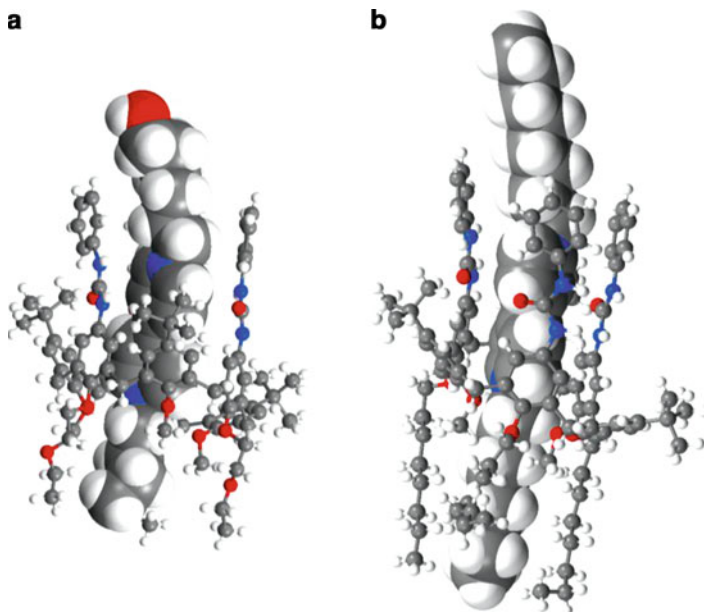


**Fig. 38.21** Pseudorotaxanes formed by calix[6]arenes: (a) 5,17,29-tri-t-butyl-11,23,35-tris(phenylureido)-38,40,42-trimethoxy-37,39,41-tris(ethoxyethoxy)calix[6]aren/N-hydroxyhexyl-N'-pentyl-4,4'-bipyridinium bromide iodide; [45] (b) 5,17,29-tri-t-butyl-11,23,35-tris(phenylureido)-38,40,42-trimethoxy-37,39,41-trioctyloxy-calix[6]arene/N,N'-dioctyl-4,4'-bipyridinium di-iodide [46]

substituted by ethylene group and the macrocyclic ring is enlarged the host molecule adopts flattened cone conformation and the guest molecules are located within a capsule formed by two calix[6]arene molecules (Fig. 38.20b) [44].

The calix[6]arene derivatives are capable to form pseudorotaxanes (Fig. 38.21) [45, 46]. In both complex the calixarene molecules are richly decorated with four types of substituents of different chemical properties enabling formation of C–H⋯O, C–H⋯N and C–H⋯ $\pi$  interactions between host and guest.

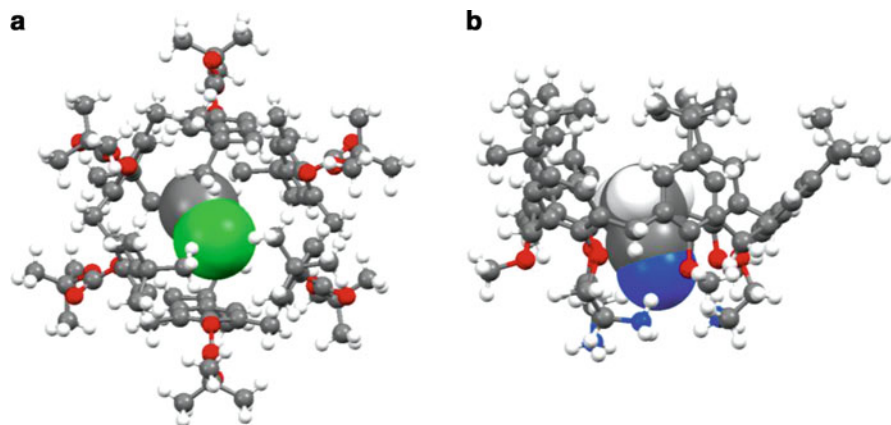


**Fig. 38.22** Capsules formed by derivatized calix[6]arenes: (a) *para*-t-butyl-t-butyoxycarboxylic acid calix[6]arene/chloroform; [47] (b) *para*-t-butyl-trimethoxy-tris(2-ammonioethyl) calix[6]arene/acetonitrile [48]

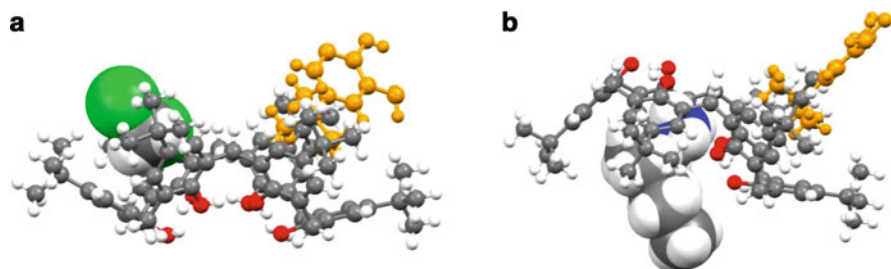


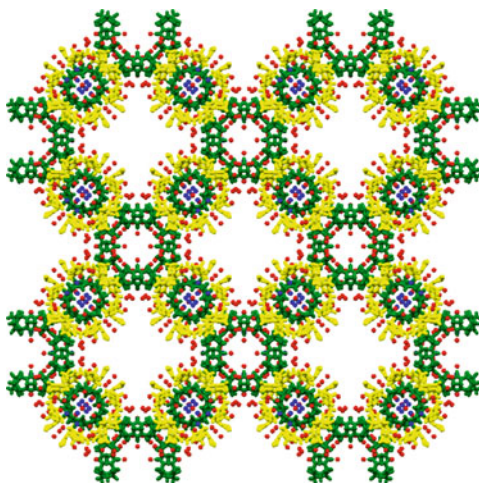
**Fig. 38.23** Simultaneous formation of host-guest inclusion complex and inclusion dimer: (a) *para*-t-butyl-calix[6]arene/dichloromethane complex; [50] (b) *para*-t-butyl-calix[6]arene/hexylammonium complex [43]. For clarity only part of the second calixarene molecules is shown (orange) to illustrate the t-butyl group inclusion in the partial cone pseudocalix[4]arene cavity

Derivatization of calix[6]arenes with bulky substituents like t-butyl groups provides molecular capsules suitable for complete inclusion of small guest molecules. The examples of such capsules are shown in Fig. 38.22. The capsule formed by *para*-t-butyl-t-butyoxycarboxylic acid calix[6]arene in 1,3,5-alternate conformation accommodates one chloroform molecule (Fig. 38.22) [47] and the capsule formed by *para*-t-butyl-trimethoxy-tris(2-ammonioethyl)calix[6]arene in cone conformation accommodates one acetonitrile molecule (Fig. 38.22b) [48].

Calix[6]arenes in partial double cone and inverted partial double cone conformation may adopt in each pseudocalix[4]arene a guest molecule [49]. But it is also observed that the guest molecule is located in one cavity while the second one is occupied by a one of the substituents of neighboring calixarene, similarly to inclusion dimer formation in calix[4]- and calix[5]arenes. The examples are shown in Fig. 38.23.



**Fig. 38.24** Packing of molecules and ions in *para*-sulphonatocalix[6]arene hexaammonium/cucurbit[6]uril co-crystal. View along *c* crystallographic axis (calix[6]arene hexaions – yellow, cucurbit[6]urils – green, ammonium cations – blue, water molecules – red) [51]



Besides the inclusion complexes, calix[6]arenes may form co-crystals with other molecules. An interesting example is a co-crystal formed by *para*-sulphonatocalix[6]arene hexaammonium with cucurbit[6]uril. As the Authors mention in the paper this structure “not only exhibit an intriguing topology but also show clearly the role of hydrophobic–hydrophobic and hydrophilic–hydrophilic interactions in directing the supramolecular assembly” [51]. It is interesting to notice a significant amount of free space in the crystal lattice (Fig. 38.24).

### 38.2.5 Calix[7]arenes

There is only eight crystal structures of calix[7]arenes deposited in CSD. The reason for this is much more difficult synthesis of seven-membered calixarenes and/or difficulties in obtaining monocrystals of this compounds and their complexes/co-crystals. Like for smaller calixarenes discussed above also here the self-inclusion of one of the substituent may occur like in *para*-*t*-butyl-carboxymethoxycalix[7]arene/deuteriochloroform clathrate (Fig. 38.25a) [52] or inclusion complexes are obtained. For the later, due to a great degree of flexibility, many conformations of calixarene host molecule is possible but the most observed is a double partial cone, e.g. 1:2 *para*-*t*-butyl-calix[7]arene/pyridine inclusion complex where one guest molecule is located in each partial cone cavity (Fig. 38.25b) [53]. In one case the flattened cone conformation was found where the (Fig. 38.25c). In this crystal structure one toluene and one disordered benzene/toluene molecule are involved in inclusion complex formation with one *para*-*t*-butyl-calix[7]arene molecule [54].

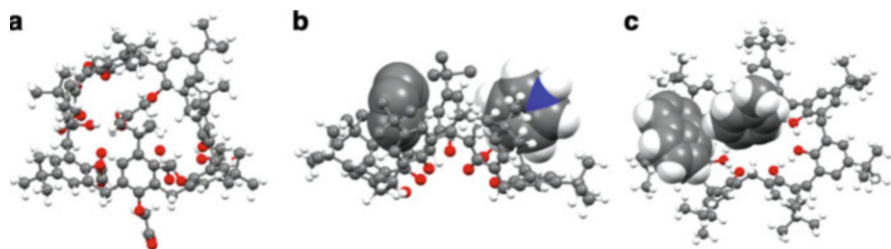


**Fig. 38.25** Calix[7]arenes: (a) self-inclusion of one t-butyl group in *para*-t-butyl-carboxymethoxycalix[7]arene; [52] (b) 1:2 *para*-t-butyl-calix[7]arene/pyridine inclusion complex – one pyridine molecule is disordered and neither the nitrogen atom position nor the hydrogen atoms were determined; [53] (c) 1:2 *para*-t-butyl-calix[7]arene/toluene (toluene/benzene) inclusion complex [54]

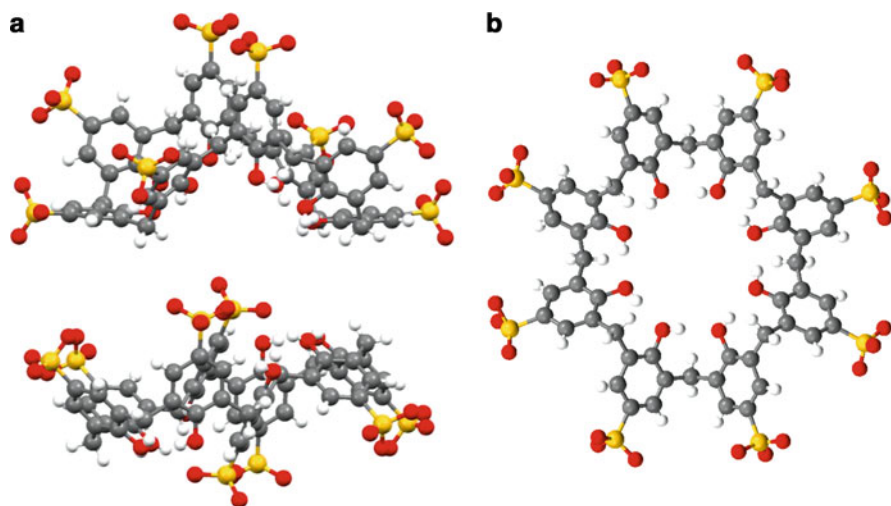


**Fig. 38.26** Extreme conformations of *para*-sulphonatocalix[8]arene: (a) compact double cone (top) [55] and inverted double cone (bottom); [56] (b) extended 'rosette' [56]

### 38.2.6 Calix[8]arenes

Calix[8]arenes may adopt 16 main (basic) conformations[41] and numerous intermediate or distorted conformations related to the main ones. There are two extreme conformations: the double cone or inverted double cone conformation which may be characterized as a compact one and mimics two joined together in parallel or antiparallel cones of calix[4]arenes and, at the other end, there is an extended nearly planar circular conformation which may be called 'rosette' or 'pleated loop'. This extreme conformations are exemplified by these found for *para*-sulphonatocalix[8]arene (Fig. 38.26).

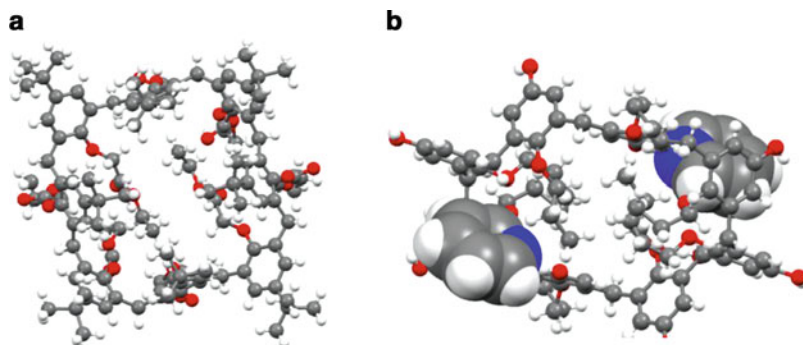


**Fig. 38.27** Self-inclusion in calix[8]arenes: (a) *para*-*t*-butyl-ethoxycarbonyl-methoxycalix[8]arene; [57] (b) *para*-hydroxy-propoxycalix[8]arene/pyridine molecular complex, the two pyridine molecules are located in shallow pockets formed on the surface of the host molecule [58]

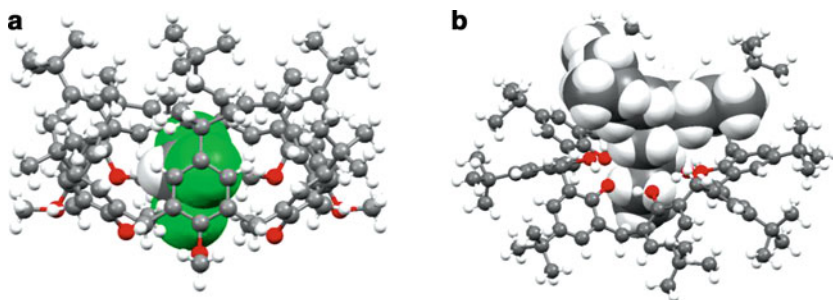


**Fig. 38.28** Inclusion complexes of calix[8]arenes: (a) *para*-*t*-butyl-methoxycalix[8]arene/chloroform complex; [59] (b) *para*-*t*-butyl-calix[8]arene/tetra-*n*-butylammonium complex [60]

In the CSD about 60 structures of calix[8]arenes are deposited. Many of them are decorated at hydroxyl group or/and at *para* position to the hydroxyl group. As it was already observed for smaller macrocycles, also here self-inclusion by rotating one or more aromatic rings and placing substituent(s) inside the macrocycle is observed. As a result the calix[8]arene crystallizes alone or is forming co-crystals with other molecular species, or only shallow binding sites are created in which the guest molecules are located. This is illustrated in Fig. 38.27.

In such cases like the molecular complex of *para*-hydroxy-propoxycalix[8]arene with pyridine it is difficult to classify such a molecular assembly as inclusion complex. It is rather an intermediate state between the inclusion and additive complex.

Nevertheless, the calix[8]arenes were found to form typical inclusion complexes as well. These were observed for the complex of *para*-*t*-butyl-methoxycalix[8]arene with chloroform where the guest molecule is located deeply inside the macrocycle (Fig. 38.28a) [59]. This is also the unique example of the conformation

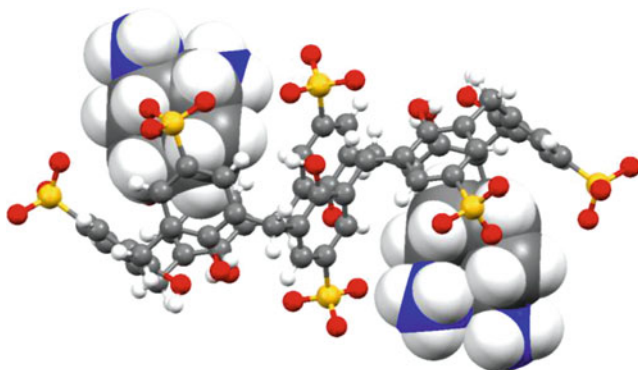


**Fig. 38.29** Inclusion complex of *para*-sulphonatocalix[8]arene in inverted double cone conformation with 1,2-cis-cyclohexanediammonium cations (host:guest stoichiometry 1:2) [56]

of the calix[8]arene where all the aromatic residues are oriented “up”, i.e. like in cone conformation in calix[4]arene.

The second known inclusion complex is formed by *para*-*t*-butyl-calix[8]arene with tetra-*n*-butylammonium but in this case the complex is an organic salt where the host is in form of dianion and the guest is monocation (Fig. 38.28b). The second monocation is located outside the cavity [60].

Inclusion complexes are also observed in organic salts formed by *para*-sulphonatocalix[8]arenes in double cone and inverted double cone conformations [55, 56]. In Fig. 38.29 an inclusion complex with 1,2-cis-cyclohexanediammonium cations is presented.

### 38.2.7 Calix[n]arenes, $n > 8$

In CSD there are deposited only seven structures of calixarenes with more than eight-membered macrocyclic ring. The reason for such a small number may be the difficulty in synthesis of such a big macrocycles (especially with odd-membered rings) and perhaps the difficulties in obtaining monocrystals suitable for X-ray diffraction analysis. Among these seven deposited crystal structures there is one calix[9]arene [55], two calix[10]arenes [61], one calix[12]arene [62], and one calix[16]arene [63]. The remaining two are one oxacalix[10]arene [64] and one azacalix[10]arene [65].

The *t*-butyl-calix[9]arene co-crystallizes with *o*-carborane, cyclohexane and water. It does not form inclusion complexes with either of these compounds. The conformation of the calixarene is basically similar to the ‘rosette’ one but it is highly folded (Fig. 38.30a). In case of the *t*-butyl-calix[10]arene inclusion of one acetone and one toluene molecule inside the macrocyclic ring occurs and two other toluene molecules take part in additive complex formation (Fig. 38.30b). In this

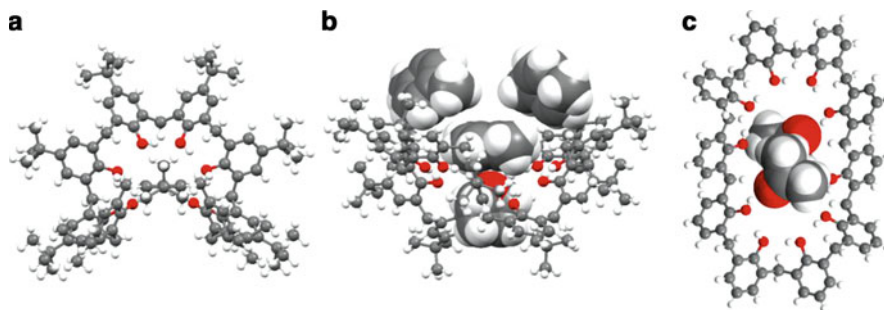
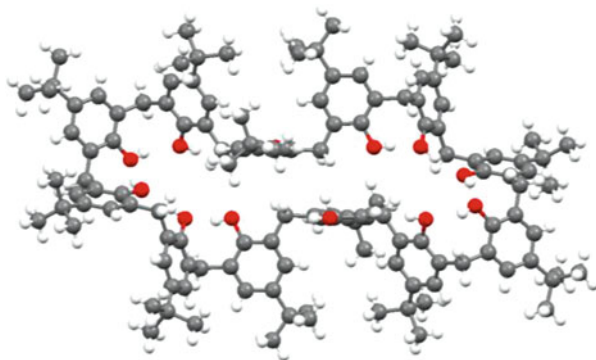


**Fig. 38.30** Large calixarenes: (a) t-butyl-calix[9]arene; [55] (b) inclusion/additive complex of t-butyl-calix[10]arene/tetrahydrofuran/toluene; [61] (c) calix[10]arene/acetone molecular complex [61]

**Fig. 38.31** t-Butyl-calix [12]arene molecule in its pyridine clathrate [62]



complex the calixarene conformation is similar to that of t-butyl-calix[9]arene. The second 12-membered calixarene is an unsubstituted calix[12]arene. Here the conformation of the molecule is almost planar like in ‘rosette’ conformation but the macrocyclic ring is elongated in one direction. Two acetone molecules are located on both sides of the macrocycle and are in contact on with the other. Acetone molecules are hold within the macrocycle by  $O-H_{\text{host}} \cdots O_{\text{guest}}$  hydrogen bond.

The t-butyl-calix[12]arene crystallizes with ten pyridine molecules and forms a clathrate [62]. The calixarene molecule adopts rather compact elongated conformation (Fig. 38.31) without distinct cavities to accommodate guest molecules.

Finally, the largest so far reported calixarene, i.e. t-butyl-calix[16]arene which conformation is defined by the Authors as “two superimposed Celtic torcs connected by their extremities” (Fig. 38.32b). The t-butyl-calix[16]arene forms an inclusion complex with two acetonitrile molecules and two dichloromethane molecules (Fig. 38.32a) [63].

Two acetonitrile molecules are located in the internal void created in the middle of the host molecule, while the two dichloromethane molecules occupy two pseudocalix[4]arene cavities formed at both ends of the double torc.

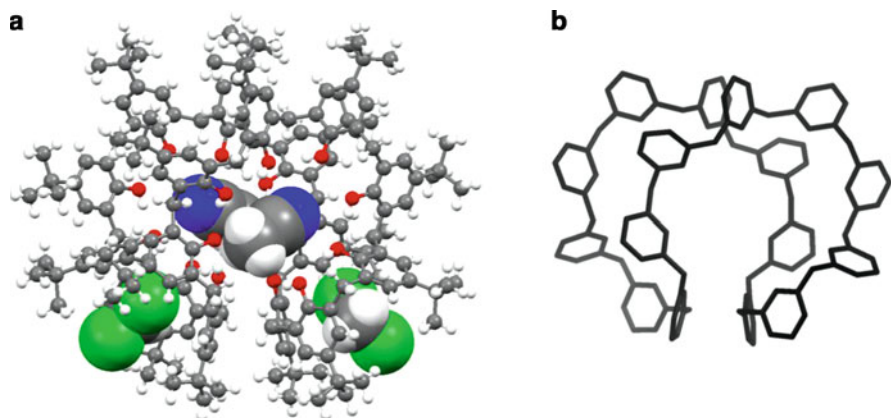


**Fig. 38.32** *t*-Butyl-calix[16]arene: (a) inclusion complex with two acetonitrile molecules and two dichloromethane molecules; (b) the backbone of the calixarene showing the two superimposed Celtic torcs [63]

### 38.3 Summary

Due to a limited length of the chapter only selected crystal structures of calixarenes, their inclusion complexes and co-crystals are presented (some structural information on calixarene inclusion compounds containing gases as guest molecules can be found in the Chap. 39 on gas storage and separation applications by Thallapally et al.). Unfortunately, many of very interesting, important and also very beautiful and exotic calixarenes and its derivatives are worth to be presented and the author apologizes here that so many entries had to be, for obvious reasons, omitted in this publication. All of them as well as other calix-type compounds like calixresorcinarenes, calixpyrogallolarenes, calixpillarenes, calixpyrroles and others are without any doubt valuable sources of very interesting and important information about intermolecular interactions and based on them self-assembly properties so characteristic for this classes of chemical species.

### References

1. Allen, F. R. *Acta Crystallogr. B* **2002**, 58, 380–388.
2. Nilsson, B. *Acta Chem. Scand.* **1968**, 22, 732–747.
3. Palmer, K. J.; Wong, R. Y.; Jurd, L.; Stevens, K. *Acta Crystallogr. B* **1976**, 32, 847–852.
4. Andreotti, G. D.; Ungaro, R.; Pochini, A. *Chem. Commun.* **1979**, 1005–1007.
5. Brouwer, E. B.; Enright, G. D.; Ratcliffe, C. I.; Ripmeester, J. A. *Supramol. Chem.* **1996**, 7, 79–83.



6. Arduini, A.; Caciuffo, R.; Geremia, S.; Ferrero, C.; Ugozzoli, F.; Zontone, F. *Supramol. Chem.* **1998**, *10*, 125–132.
7. (a) Enright, G. D.; Brouwer, E. B.; Udachin, K. A.; Ratcliffe, C. I.; Ripmeester, J. A. *Acta Crystallogr. B* **2002**, *58*, 1032–1035; (b) Atwood, J. L.; Barbour, L. J.; Jerga, A.; Schottel, B. L. *Science* **2002**, *298*, 1000–1002.
8. Yoshida, M.; Goto, M.; Nakanishi, F. *Organometallics* **1999**, *18*, 1465–1470.
9. Atwood, J. L.; Barbour, L. J.; Nicholls, P. J.; Raston, C. L.; Sandoval, C. A. *Chem.-Eur. J.* **1999**, *5*, 990–996.
10. Lazar, A. N.; Danylyuk, O.; Suwińska, K.; Coleman, A. W. *New J. Chem.* **2006**, *30*, 59–64.
11. Makha, M.; Raston, C. L.; Sobolev, A. N. *Aust. J. Chem.* **2006**, *59*, 260–262.
12. Ananchenko, G. S.; Udachin, K. A.; Pojarova, M.; Dubes, A.; Ripmeester, J. A.; Jebors, S.; Coleman, A. W. *Cryst. Growth Des.* **2006**, *6*, 2141–2148.
13. Dupont, N.; Lazar, A. N.; Perret, F.; Danylyuk, O.; Suwinska, K.; Navaza, A.; Coleman, A. W. *CrystEngComm* **2008**, *10*, 975–977.
14. Shkurenko, A.; Suwinska, K. unpublished result.
15. Danylyuk, O.; Suwinska, K. *Chem. Commun.* **2009**, 5799–5813.
16. Ungaro, R.; Pochini, A.; Andreotti, G. D.; Domiano, P. J. *Chem. Soc., Perkin Trans. 2* **1985**, 197–201.
17. Leverd, P. C.; Berthault, P.; Lance, M.; Nierlich, M. *Eur. J. Org. Chem.* **2000**, 133–139.
18. Gruber, T.; Fischer, C.; Seichter, W.; Bombicz, P.; Weber, E. *CrystEngComm* **2011**, *13*, 1422–1431.
19. Pojarova, M.; Ananchenko, G. S.; Udachin, K. A.; Daroszewska, M.; Perret, F.; Coleman, A. W.; Ripmeester, J. A. *Chem. Mater.* **2006**, *18*, 5817–5819.
20. Ramon, G.; Coleman, A. W.; Nassimbeni, L. R. *Cryst. Growth Des.* **2006**, *6*, 1321–136.
21. Ananchenko, G. S.; Udachin, K. A.; Dubes, A.; J. A. Ripmeester, Perrier, T.; Coleman, A. W. *Angew. Chem., Int. Ed.* **2006**, *45*, 1585–1588.
22. Ananchenko, G. S.; Udachin, K. A.; Ripmeester, J. A.; Perrier, T.; Coleman, A. W. *Chem.-Eur. J.* **2006**, *12*, 2441–2447.
23. Gruber, T.; Fischer, C.; Seichter, W.; Bombicz, P.; Weber, E. *CrystEngComm* **2011**, *13*, 1422–1431.
24. Suwinska, K.; Leśniewska, B.; Wszelaka-Rylik, M.; Straver, L.; Jebors, S.; Coleman, A. W. *Chem. Commun.* **2011**, *47*, 8766–8768.
25. Gruber, T.; Gruner, M.; Fischer, C.; Seichter, W.; Bombicz, P.; Weber, E. *New J. Chem.* **2010**, *34*, 250–259.
26. Seri, N.; Thondorf, I.; Biali, S. E. *J. Org. Chem.* **2004**, *69*, 4774–4780.
27. Castillo, A.; Martinez, J. L.; Martinez-Alanis, P. R.; Castillo, I. *Inorg. Chim. Acta* **2010**, *363*, 1204–1211.
28. Filby, M. H.; Dickson, S. J.; Zaccheroni, N.; Prodi, L.; Bonacchi, S.; Montalti, M.; Paterson, M. J.; Humphries, T. D.; Chiorboli, C.; Steed, J. W. *J. Am. Chem. Soc.* **2008**, *130*, 4105–4113.
29. Barbour, L. J.; Atwood, J. L. *Chem. Commun.* **2001**, 2020–2021.
30. Simaan, S.; Biali, S. E. *J. Org. Chem.* **2004**, *69*, 95–98.
31. Liu, Y.; Guo, D.-S.; Yang, E.-C.; Zhang, H.-Y.; Zhao, Y.-L. *Eur. J. Org. Chem.* **2005**, 162–170.
32. Fischer, C.; Bombicz, P.; Seichter, W.; Katsch, F.; Weber, E. *Cryst. Growth Des.* **2012**, *12*, 2445–2454.
33. Wang, W.; Gong, S.; Chen, Y.; Ma, J. *New J. Chem.* **2005**, *29*, 1390–1392.
34. Liu, Y.; Guo, D.-S.; Zhang, H.-Y.; Ding, F.; Chen, K.; Song, H.-B. *Chem.-Eur. J.* **2007**, *13*, 466–472.
35. Dalgarno, S. J.; Hardie, M. J.; Raston, C. L. *Chem. Commun.* **2004**, 2802–2803.
36. Guo, D.-S.; Zhang, H.-Y.; Li, C.-J.; Liu, Y. *Chem. Commun.* **2006**, 2592–2594.
37. Usui, S.; Deyama, K.; Kinoshita, R.; Odagaki, Y.; Fukazawa, Y. *Tetrahedron Lett.* **1993**, *34*, 8127–8130.

38. Stewart, D. R.; Krawiec, M.; Kashyap, R. P.; Watson, W. H.; Gutsche, C. D. *J. Am. Chem. Soc.* **1995**, *117*, 586–601.
39. Brancatelli, G.; Gattuso, G.; Geremia, S.; Notti, A.; Pappalardo, S.; Parisi, M. F.; Pisagatti, I. *Org. Lett.* **2014**, *16*, 2354–2357.
40. (a) Atwood J. L.; Barbour L. J.; Raston, C. L. *Cryst. Growth Des.* **2002**, *2*, 3–6; (b) Atwood J. L.; Barbour L. J.; Heaven M. W.; Raston, C. L. *Chem. Commun.* **2003**, 2270–2271; (c) Atwood J. L.; Barbour L. J.; Nicholls P. J.; Raston C. L.; Sandoval, C. A. *Chem.-Eur. J.* **1999**, *5*, 990–996; (d) Wang J.; Bodige S. G.; Watson W. H.; Gutsche, C. D. *J. Org. Chem.* **2000**, *65*, 8260–8263; (e) Makha M.; McKinnon J. J.; Sobolev A. N.; Spackman M. A.; Raston, C. L. *Chem.-Eur. J.* **2007**, *13*, 3907–3912; (f) Haino T.; Yanase M.; Fukazawa, Y. *Tetrahedron Lett.* **1997**, *38*, 3739–3742; (g) Haino T.; Yanase M.; Fukazawa, Y. *Angew. Chem., Int. Ed.* **1997**, *36*, 259–260; (h) Atwood J. L.; Barbour L. J.; Heaven M. W.; Raston, C. L. *Angew. Chem., Int. Ed.* **2003**, *42*, 3254–3257; (i) Makha M.; Hardie M. J.; Raston, C. L. *Chem. Commun.* **2002**, 1446–1447; (j) Flidrova K.; Liska A.; Ludvik J.; Eigner V.; Lhotak, P. *Tetrahedron Lett.* **2015**, *56*, 1535–1538.
41. Gutsche, C. D. *Calixarenes: An Introduction*; 2nd ed.; Royal Society of Chemistry, **2008**.
42. Kogan, K.; Columbus I.; Biali, S. E. *J. Org. Chem.* **2008**, *73*, 7327–7335.
43. Nachtigall, F. F.; Lazzarotto, M.; Castellano, E. E.; Nome, F. *Supramol. Chem.* **2004**, *16*, 453–458.
44. Salmon, L.; Thuery, P.; Miyamoto, S.; Yamato, T.; Ephritikhine, M. *Polyhedron* **2006**, *25*, 2439–2446.
45. Ugozzoli, F.; Massera, C.; Arduini, A.; Pochini A.; Secchi, A. *CrystEngComm* **2004**, *6*, 227–232.
46. Arduini, A.; Ferdani, R.; Pochini, A.; Secchi, A.; Ugozzoli, F. *Angew. Chem., Int. Ed.* **2000**, *39*, 3453–3456.
47. Menand, M.; Leroy, A.; Marrot, J.; Luhmer, M.; Jabin, I. *Angew. Chem., Int. Ed.* **2009**, *48*, 5509–5512.
48. Darbost, U.; Giorgi, M.; Hucher, N.; Jabin I.; Reinaud, O. *Supramol. Chem.* **2005**, *17*, 243–250.
49. (a) Atwood J. L.; Dalgarno S. J.; Hardie M. J.; Raston, C. L. *Chem. Commun.* **2005**, 337–338; (b) Liu, Y.; Li, Q.; Guo, D.-S.; Chen, K. *CrystEngComm* **2008**, *10*, 675–680; (c) Halit, M.; Oehler, D.; Perrin, M.; Thozet, A.; Perrin, R.; Vicens, J.; Bourakhouadar, M. *J. Inclusion Phenom. Mol. Recog. Chem.* **1988**, *6*, 613–623; (d) Atwood, J. L.; Barbour, L. J.; Raston, C. L.; Sudria, I. B. N. *Angew. Chem., Int. Ed.* **1998**, *37*, 981–983; (e) Lazar, A. N.; Danylyuk, O.; Suwinska, K.; Kassab, R.; Coleman, A. W. *New J. Chem.* **2008**, *32*, 2116–2120; (f) Wolfong, W. J.; Talafuse, L. K.; Smith, J. M.; Adams, M. J.; Adeogba, F.; Valenzuela, M.; Rodriguez, E.; Contreras, K.; Carter, D. M.; Bacchus, A.; McGuffey, A. R.; Bott, S. G. *Supramol. Chem.* **1996**, *7*, 67–78; (g) Lazzarotto, M.; Ferreira, C. I.; Castellano, E. E.; Veglia, A. V. *J. Mol. Struct.* **2014**, *1067*, 8893; (h) Liu, Y.; Li, Q.; Guo, D.-S.; Chen, K. *Cryst. Growth Des.* **2007**, *7*, 1672–1675; (i) Dale, S. H.; Elsegood M. R. J.; Redshaw, C. *CrystEngComm* **2003**, *5*, 368–373; (j) Lee, J. Y.; Park K. D.; Yeo, H. M.; Ko, S. W.; Ryu, B. J.; Nam, K. C. *Supramol. Chem.* **2007**, *19*, 167–173; (k) Thuery, P.; Keller, N.; Lance, M.; Vigner, J.-D.; Nierlich, M. *J. Inclusion Phenom. Mol. Recog. Chem.* **1995**, *20*, 373–379.
50. Felsmann, M.; Schwarzer, A.; Weber, E. *Acta Crystallogr. E: Struct. Rep. Online* **2006**, *62*, o607–o609.
51. Lin, R.-G.; Long, L.-S.; Huang, R.-B.; Zheng, L.-S. *Cryst. Growth Des.* **2008**, *8*, 791–794.
52. Ludwig, R.; Lentz, D.; Nguyen, T. K. D. *Radiochim. Acta* **2000**, *88*, 335–343.
53. Andreetti, G. D.; Ugozzoli, F.; Nakamoto, Y.; Ishida, S.-I. *J. Inclusion Phenom. Mol. Recog. Chem.* **1991**, *10*, 241–253.
54. Clark, T. E.; Makha, M.; Sobolev, A. N.; Raston, C. L. *Dalton Trans.* **2008**, 4855–4859.
55. Leśniewska, B. Ph.D. thesis. Warsaw **2015**.
56. Perret, F.; Bonnard, V.; Danylyuk, O.; Suwinska, K.; Coleman, A. W. *New J. Chem.* **2006**, *30*, 987–990.



57. Yan, C.-G.; Han, J.; Li, L.; Liu, D.-M. *J. Coord. Chem.* **2009**, *62*, 825–832.
58. Leverd, P. C.; Huc V.; Palacin, S.; Nierlich, M. *J. Inclusion Phenom. Macrocyclic Chem.* **2000**, *36*, 259–266.
59. Bolte, M.; Brusko, V.; Bohmer, V. *J. Supramol. Chem.* **2002**, *2*, 57–61.
60. Martinez-Alanis, P. R.; Castillo, I. *Tetrahedron Lett.* **2005**, *46*, 8845–8848.
61. Perrin, M.; Ehlinger, N.; Viola-Motta, L.; Lecocq, S.; Dumazet, I.; Bouoit-Montesinos, S.; Lamartine, R. *J. Inclusion Phenom. Macrocyclic Chem.* **2001**, *39*, 273–276.
62. Leverd, P. C.; Dumazet-Bonnamour, I.; Lamartine, R.; Nierlich, M. *Chem. Commun.* **2000**, 493–494.
63. Bavoux, C.; Baudry, R.; Dumazet-Bonnamour, I.; Lamartine, R.; Perrin, M. *J. Inclusion Phenom. Macrocyclic Chem.* **2001**, *40*, 221–224.
64. Rossom W. V.; Robeyns K.; Ovaere M.; Meervelt L. V.; Dehaen W.; Maes, W. *Org. Lett.* **2011**, *13*, 126–129.
65. Liu S.-Qi.; Wang D.-X.; Zheng Q.-Y.; Wang, M.-X. *Chem. Commun.* **2007**, 3856–3858.

# Chapter 39

## Gas Sorption and Storage Properties of Calixarenes

Rahul S. Patil, Debasis Banerjee, Jerry L. Atwood,  
and Praveen K. Thallapally

### Abbreviations

BDC	Benzenedicarboxylic acid
BET	Brunauer-Emmett-Teller
BOC	<i>tert</i> -Butyl carbamates
BTC	1,3,5-benzenetricarboxylic acid
COF	Covalent organic framework
hcp	Hexagonal close packing
MAS	Magic angle spinning
MOF	Metal organic framework
NB	Nitrobenzene
NMR	Nuclear magnetic resonance spectroscopy
POP	Porous organic polymer
tbc4	<i>p-tert</i> -butylcalix[4]arene
tbc5	<i>p-tert</i> -butylcalix[5]arene
TGA	Thermogravimetric analysis
XRD	X-ray diffraction
PXRD	Powder X-ray diffraction

---

R.S. Patil • J.L. Atwood  
Department of Chemistry, University of Missouri, Columbia, MO 65211, USA

D. Banerjee • P.K. Thallapally (✉)  
Fundamental and Computational Science Directorate, Pacific Northwest National Laboratory,  
Richland, WA 99352, USA

## 39.1 Introduction

Calixarenes are bowl shaped organic macrocyclic molecules derived from *p*-substituted phenols and formaldehyde. The name ‘calixarene’ was coined by Gutsche because of its resemblance of bowl shaped conformers of calixarene with a Greek vase called a *calix crater* [1] (Fig. 39.1).

Versatility of calixarene and related derivatives has been proved through their potential applications in the field of molecular recognition, host-guest interactions, medical science, and analytical chemistry [2]. Host guest interactions of calixarene with various organic guest molecules have shown that the bowl shaped molecular cavities in calixarene offer space for these guest molecules. These host-guest studies inspires further research directed towards sorption of industrially relevant gases (e.g. carbon dioxide, nitrogen, acetylene) in calixarene and related host materials.

The calixarene and its related derivative molecules are usually crystallized in a closely packed crystalline arrangement and thus are inherently non porous. However, specific low density forms have shown to possess permanent porosity that are available for the uptake and storage of gaseous guest. This book chapter gives a brief summary of the gas-sorption and separation application involve of calixarene and related derivatives.

## 39.2 Gas Sorption in Porous Materials

Physisorption based gas-sorption and separation techniques using solid state adsorbents are considered as a viable alternative for energy intensive cryogenic distillation and liquid extraction [3]. The solid state adsorbents are generally porous: few

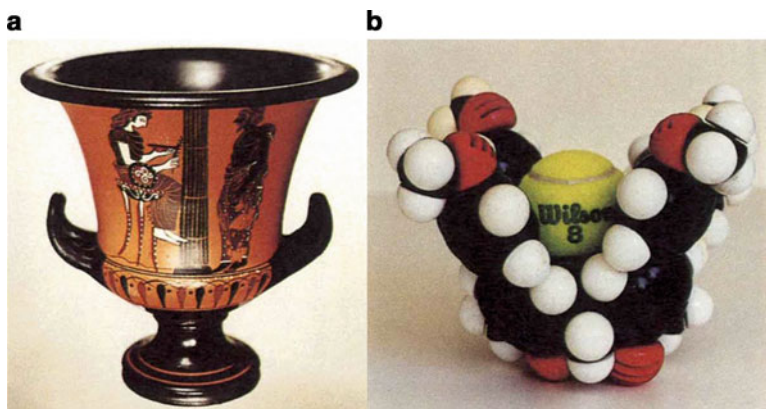


**Fig. 39.1** (a) *Calix crater* (b) CPK model of calixarene (Reproduced with permission from Ref. [1]. Copyright 2008, Royal Society of Chemistry)

examples of solid state adsorbent include zeolites, activated carbons, porous molecular crystals, metal organic frameworks (MOFs), covalent organic frameworks (COFs), and porous organic polymers (POP) [4]. The choice of a porous adsorbent for a particular sorption application depends on a number of factors including but not limited to pore size and shape, pore functionalization, sorption-desorption kinetics, thermochemical stability and ease of handling and processing. An optimal adsorbent material should have both high capacity and selectivity, but that is rarely the case. Pore shape-size and surface functionalization of the adsorbent materials play a greater role to determine its separation performance for a particular set of adsorbates. Thus, a particular adsorbent which has excellent separation properties for a set of adsorbates is probably not an optimal choice for other sets of adsorbates. As a result, exploratory syntheses and sorption analysis of different class of materials are often required to find an optimal material for a particular separation. For example, CC3, a porous organic molecular cage was found to be an excellent material for Xe/Kr separation over other traditional porous materials such as MOFs and zeolites, owing to its near perfect pore size matching with Xe atom [4r]. These organic molecular crystals are a special class of porous materials with well-defined hydrophobic pores or cages. Although the overall porosity of these molecular crystals tend to be at the lower end (100–300 m<sup>2</sup>/g) of porous materials, their unique, well defined hydrophobic pore or cage architecture make them an attractive candidate for gas sorption-separation application [4q, 4r, 4t].

### 39.3 Porosity in Organic Molecular Crystals

Organic molecular crystals often pack closely together to maximize intermolecular interactions between the molecules [5]. Thus, it is very rare for molecular crystals to have open channels or even discrete void space larger than 25 Å<sup>3</sup> in extended crystal lattice [6]. One approach to induce porosity in molecular crystals involves crystallization in presence of low boiling solvents (e.g. acetone, methanol). In this case, the crystal lattice does not have a spontaneous porosity and instead the porosity is created by subsequent removal of volatile solvent molecules from the supramolecular assembly. However, this evacuation of solvent molecules from crystal lattice is a thermodynamically intensive process. Thus, often the evacuated assemblies are less stable than densely packed ones [7]. Comparatively weak intermolecular interactions between the individual molecules are not capable of holding them together because of the large thermodynamic cost associated with the solvent removal. This often results into structural collapse to form a non-porous amorphous phases or more rarely result the formation of a new denser form. However, a meticulous design of host and subsequent intermolecular interactions can result in the formation of robust, permanently porous molecular assemblies, which can withstand the guest removal through extended lattice [4m, 8]. The void

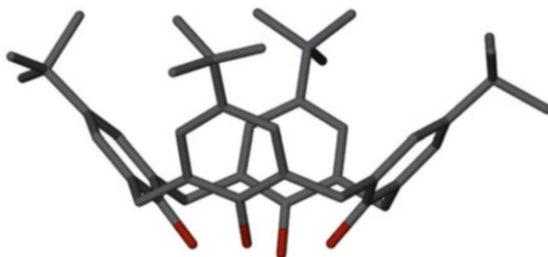
space inside these molecular assemblies are usually neither regular nor large enough, instead they are more like an irregular shaped traps for adsorbate molecules. In a recent article, Barbour termed this type of porosity as ‘porosity without pore’, where the molecular crystals or assemblies have discrete voids without any connecting channels.

### 39.4 Calixarene, a Versatile Host

First single crystal structure of calixarene (*p*-*tert*-butylcalix[4]arene, tbc4) (Scheme 39.1) was solved by Andreetti and co-workers in 1979 and confirmed the bowl shape of macrocycle [9]. However, the restricted movement of -CH<sub>2</sub> groups, connecting neighboring phenyl groups may induce formation of multiple diastereoisomers: cone, partial cone, 1,2-alternate and 1,3-alternate. Of these, cone conformer is more common because it is stabilized by cyclic network of intramolecular O-H...O hydrogen bonds between the hydroxyl groups at the lower rim of macrocycle. The cone conformer is supported by four *p*-substituted phenolic rings, thus this bowl of cone conformers is rich with  $\pi$ -electrons.

Multiple inclusion complexes of calixarenes are reported with a variety of organic and ionic guests of different shapes and functional groups [10]. A typical host-guest complex is an absolute outcome of molecular recognition via intermolecular interactions between hosts and guests in the respective medium. In solid state, multiple factors play key role in stabilizing the lattice assemblies of the complex such as shape/symmetry match of the molecular assembly with respect to guest molecules and conformational rigidity or flexibility of the each component [11]. To expect a stable host guest complex in solid state, these factors should be complementary with the intermolecular interactions such as columbic interaction in ions and non-covalent van der Waals type interactions between neutral molecules. Thus, an ideal solid state host should be able to adsorb a variety of guest of different size and shape as well as possess necessary functional groups to interact and recognize particular guest molecules.

**Scheme 39.1**  
*p*-*tert*-butylcalix[4]arene



Calixarenes and its derivatives possess many of the above properties and are considered to be a versatile host for different class of adsorbates [10c]. The guests are in general involved in weak noncovalent interactions with the bowl shaped cavity of these molecules rather than forming hydrogen bonds with the hydroxyl groups at the lower rim. The cavity is enriched with  $\pi$  electrons of the surrounding aromatic rings and thus readily offers  $\pi$ - $\pi$ , CH- $\pi$  or cation -  $\pi$  type interactions with guest molecules. On the contrary, four hydroxyl groups at the lower calixarene rim are involved in OH...O type intramolecular hydrogen bonding and is energetically unfavorable to be involved in intermolecular interaction with guest molecules. In this regard, Gorbachuk and coworkers have calculated the free energy of formation for supramolecular inclusion complex of tbc4 and various volatile organic guests [12]. The binding affinities of the inclusion complexes of tbc4 reveal that there exists an 'inclusion threshold' for specific guests. This inclusion threshold is associated with the phase transition in the solid host upon guest binding. Up to this threshold value, very weak guest-host binding was observed, the binding affinities sharply rises above the threshold until the saturation point. Other studies have also been carried out to understand the guest inclusion mechanism in calixarene moieties. Indeed, the molecular motion of toluene guest molecules in tbc4 cavity was studied as a function of temperature using  $^1\text{H}$  NMR spectroscopy and single crystal X-ray diffraction (XRD). The tbc4 bowl undergoes a lowering of rotational symmetry from fourfold to twofold at 250 K due to change in toluene conformation [13]. Such a lowering of symmetry results into reorientation of the side chain (*tert*-butyl) functional groups on the upper rim of the cavity. Further, systematic investigation involving groups of different functionalities towards the  $\pi$  electron rich tbc4 cavity leads to a general trend, which is  $\text{CH}_3 > \text{CH}_2 > \text{CH} \sim \text{OH} > \text{Cl} \sim \text{Br}$  for terminal functional groups of aliphatic guests, implying that the methyl groups are more favored over halogens inside the cavity [10c]. The electronegative nature of the halogens and the favorable CH- $\pi$  interaction of the methyl groups is probably the reason for such structural trend. On the contrary, the functionalities on the aromatic moieties exert a minor effect on the total interaction strength as well as the orientation of the guests within the host cavity. For example, benzene and pyridine showed similar orientation (and interaction strength) within the cavity [14]. The introduction of amine functionalities in the guest species leads to the formation of a stronger H-bonding between host-guest along with non-specific interactions [15] (Table 39.1).

## 39.5 Gas Sorption in Calixarenes

The research on guest-inclusion complexes of calixarene based molecular crystals paved the way for different type of gas-sorption studies in these materials under various conditions. Although these materials generally don't possess uniform pore nor have high surface area (unlike traditional porous materials such as zeolite, molecular sieves or MOFs), their unique void structures make them attractive candidates for selective gas-sorption and separation applications. It should be noted that no uniform method were used to analyze the gas-sorption capacity (or separation capability) of these

**Table 39.1** List of calixarenes

	Calixarenes	R	X	Y	n
1	calix[4]arene	H	OH	CH <sub>2</sub>	4
2	<i>p</i> - <i>tert</i> -butylcalix[4]arene, (tbc4)	<i>tert</i> -butyl	OH	CH <sub>2</sub>	4
3	<i>p</i> - <i>tert</i> -pentylcalix[4]arene	<i>tert</i> -pentyl	OH	CH <sub>2</sub>	4
4	<i>p</i> - <i>tert</i> -octylcalix[4]arene	<i>tert</i> -octyl	OH	CH <sub>2</sub>	4
5	<i>p</i> - <i>tert</i> -butylcalix[5]arene,	<i>tert</i> -butyl	OH	CH <sub>2</sub>	5
6	<i>p</i> -hexanoylcalix[4]arene	hexanoyl	OH	CH <sub>2</sub>	4
7	<i>p</i> -octanoylcalix[4]arene	octanoyl	OH	CH <sub>2</sub>	4
8	<i>p</i> -(1-adamantyl)calix[4]arene	adamantyl	OH	CH <sub>2</sub>	4
9	<i>p</i> - <i>tert</i> -butylthiacalix[4]arene	<i>tert</i> -butyl	OH	S	4
10	1,2-dimethoxy- <i>p</i> - <i>tert</i> -butylcalix[4]dihydroquinone	<i>tert</i> -butyl	OH, OCH <sub>3</sub>	CH <sub>2</sub>	4

materials, rather experiments were done simply to show that the material can soak up gas molecules. For example, in many cases single-crystal XRD experiments were carried out to show that the materials can adsorb gas-molecules within the cavity [6, 16]. In next few sections, we will briefly describe different type of calixarene molecules and its guest inclusion properties with a focus on gaseous guest molecules.

### 39.5.1 Calix[4]arene, 1

Calix[4]arene is the basic representative of calixarene class of molecular crystals which has no functional groups on the upper rim and has shallow bowl shaped molecular cavity (Fig. 39.2). The preliminary crystalline inclusion complex of calix [4]arene with acetone revealed two major types of host-guest complexes [17]. One of the complexes consist of 1:1 (host: acetone) (**1a**) where one acetone molecule interacts with small calix[4]arene cavity by one of its methyl groups through CH- $\pi$  interaction. Whereas, the second complex forms a 3:1 host: guest complex (**1b**) where three molecules of **1** mutually interact through weak van der Waals interactions and packed in near spherical trimers (Fig. 39.1). These trimers are then packed in hexagonal closed packed (hcp) arrangements in extended crystal lattice. Due to geometrical irregularities of these trimers, this hcp arrangement of trimers forms a discrete void space of approximately 153 Å<sup>3</sup> instead of two regular tetrahedral holes linked through channels as one would expect from regular hcp geometry (Fig. 39.1) [6]. The void space is often occupied by disordered acetone molecules.

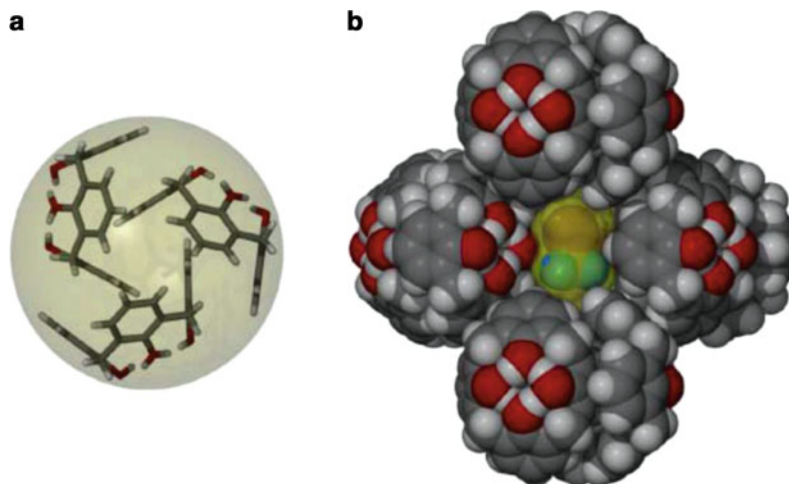


**Fig. 39.2** (a) The stick representation of trimer formed from self-inclusion of each molecule of **1** within neighboring molecules. (b) Space fill representation of interstitial void occupied by  $\text{CF}_3\text{Br}$  in host lattice of **1** (Reproduced with permission from Ref. [6] Copyright 2002, American Association of the Advancement of Science)

Thermogravimetric analysis (TGA) and powder X-ray diffraction (PXRD) of **1a** showed that two third of acetone molecules can be removed at lower temperature of  $70^\circ\text{C}$  and induced rearrangement of host to **1b** form. Whereas the remaining one third of acetone molecules can be removed at  $225^\circ\text{C}$  to yield a pure apohost phase **1c**. Thus, **1b** exhibits surprisingly remarkable thermal stability for a molecular assembly. Barbour and coworkers obtained single crystal of apohost phase (**1c**) by sublimation at  $270^\circ\text{C}$  and the follow-up single crystal diffraction studies reveal that the structure of **1c** is similar to that of **1b**. Since the crystals were grown under vacuum, the discrete void spaces in **1c** remain empty [6].

The evaluation of empty void space in closely packed crystals of **1** and high thermal stability of its inclusion complexes lead to the gas uptake studies on **1** [6]. With low solubility of **1** in freon and halons, the apohost **1c** is crystallized out of toluene. Subsequently, the guest halons such as  $\text{CH}_3\text{Br}$ ,  $\text{C}_2\text{F}_6$  and  $\text{CF}_4$  were dissolved in toluene for co-crystallization with host [6]. The presence of freons and halons in the void spaces was subsequently confirmed by single crystal XRD,  $^{19}\text{F}$  NMR spectroscopy, and TGA [6]. To measure the vapor sorption of freon in **1**, crushed crystals of **1a** in a steel pressure vessel were heated at  $50^\circ\text{C}$  in presence of freon gas, resulting in a successful phase transition from non hcp (**1a**) to hcp phase (**1b**) and stoichiometric inclusion of freon is observed within hcp void lattice [6]. Similar methods are used to trap methane within lattice void and TGA showed that the methane loaded inclusion complex is stable till  $320^\circ\text{C}$  [6]. The high thermal stability of the guest loaded host complex is probably due to the closed packed arrangement of the inclusion complex, where guest molecules cannot be removed without disassembling (or bond breaking) the host, which can only be achieved at a sufficiently higher temperature.



### 39.5.2 *p*-tert-Butylcalix[4]arene, **2**

*p*-tert-butylcalix[4]arene is a well-known and widely studied host material with over thousand research articles published since early 2000 on **2** and yet new articles are published on a regular basis, displaying interesting phenomenon in organic solid state. It is a useful precursor for the synthesis of various functionalized calix[4]arenes as well as is an extremely versatile host. It forms stable host-guest complexes with appropriate size guest molecules (e.g. benzene, toluene, *n*-butylamine) through multiple interaction sites [18]. TGA of these inclusion complexes show distinct trends for loss of guest molecules from complexes [10]. For example, toluene and pentane inclusion complexes (1:1 guest: host) have two regions of weight loss.  $^{13}\text{C}$  NMR showed that the first weight loss is associated with the loss of one guest, converting the 1:1 (guest: host) inclusion complex to a 1:2 (guest: host) complex and subsequent loss of guest in next weight loss region results in the formation of a densely packed apohost form. On the contrary, the inclusion complex involving benzene guest molecules (1:1) has a single region of weight-loss before the decomposition of host materials begins. Single crystal to single crystal conversion of 1:1 toluene (and pentane) inclusion complex to 1:2 is a unique phenomenon and can be achieved by controlled heating of single crystal of 1:1 complex. The phase transition from 1:1 to 1:2 inclusion complexes is found to be reversible and the 1:2 inclusion phases can be converted back to the 1:1 complex upon exposure to toluene vapor at 70 °C. Both forms (1:1 and 1:2) mainly differ by the orientation of **2** in the bilayer with respect to each other. The phase transition involve a  $\sim 0.9$  Å shift in the position of **2** in the bilayer [19].

Similarly, a number of different polymorphic phases of pure **2** are reported to form under different synthetic conditions [20]. For example, a high density polymorph (**2a**) of **2** (crystallized out of hot tetradecane solvent) that consist of efficiently packed **2** dimers (packing efficiency = 0.67), where the *tert*-butyl group of one macrocycle resides in the cavity of its counterpart is reported [20]. However, sublimation of **2** under vacuum at 280 °C yielded a comparatively less dense polymorph (**2b**) of **2** with a packing efficiency of 0.59 [21]. This polymorph also has a bilayer arrangement similar to **2**, where the empty cavities of two **2** in neighboring bilayers form a skewed capsule with a approximate free volume of 235 Å<sup>3</sup> (Fig. 39.3a). Surprisingly, this low density polymorph readily absorb vinyl bromide at low temperature of  $-5$  °C for 15 min. The diffusion of vinyl bromide ( $\text{CH}_2\text{CHBr}$ ) leads to a single crystal to single crystal phase transformation from a ab/cd bilayer arrangement to ab/ab arrangement (Fig. 39.3b). Discrete cavities in ab/ab are occupied by vinyl bromide with resultant packing density of 0.64 [21]. None of these polymorphs are conventionally porous, meaning none of them have any measureable surface area. Thus the diffusion of guest in these nonporous materials is achieved by the cooperative nature of neighboring molecules. This cooperative guest diffusion also resulted in a bilayer shift of 5.9 Å in the extended assembly without any loss of crystallinity.

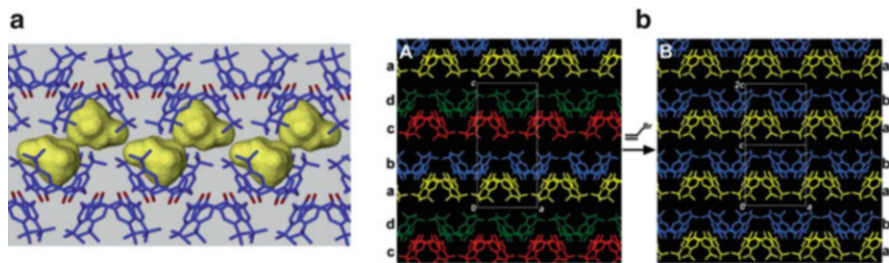


**Fig. 39.3** (a) The discrete void of  $235 \text{ \AA}^3$  enclosed within bilayer arrangement of **2**. (b) Single crystal to single crystal phase transformation observed in **2b** after immersion in vinyl bromide (Reproduced with permission from Refs. [21, 22] Copyright 2002, and 2007 AAAS and Royal Society of Chemistry)

The guest uptake and release ability of **2** initiate the hypothesis that voids in the crystal lattice are also capable of absorbing the gaseous guest molecules and subsequent gas-sorption studies were carried out on the low density polymorph (**2b**) of **2**. The hypothesis is supported by the creation of bubbles during immersion of **2b** in NB (NB = nitrobenzene) and the analysis of the heat flow profile during the guest uptake process [21]. It was assumed that the guest inclusion process could be largely exothermic but the heat flow pattern shows a small exothermic peak followed by a large endothermic swamp. X-ray diffraction studies of **2b** after exposure to atmospheric air for 2 days reveal the presence of residual electron densities in the molecular cavity whereas; the packing arrangement remains the same. Thus, if the crystal was prepared via sublimation under vacuum, the  $235 \text{ \AA}^3$  void space is occupied by air without breaking the bonding arrangement [16]. A sophisticated manometric system was constructed in order to measure the sorption isotherms of the different gases [16]. A gas sorption study of  $\text{N}_2$ ,  $\text{O}_2$ , and  $\text{CO}_2$  with **2b** at an approximate initial pressure of 700 torr shows that the sorption of  $\text{CO}_2$  is more rapid than the  $\text{N}_2$  and  $\text{O}_2$  (Fig. 39.4a) [16]. Almost 80 % of the cavities in **2b** are occupied by  $\text{CO}_2$  at atmospheric pressure, and a 100 %  $\text{CO}_2$  occupancy was achieved at 3 bar pressure. However, the material does not adsorb any  $\text{H}_2$  even at pressure as high as seven bars. Thus, exposure of **2b** to 3:1  $\text{CO}_2$ : $\text{H}_2$  mixture shows that  $\text{CO}_2$  can be selectively separated from the mixture and afford  $\text{H}_2$  rich gaseous output [22].

$\text{CO}_2$  occupancy of 100 % at relatively low pressure of three bars leads to the subsequent evaluation of the gas sorption ability of **2** with different gases with similar molecular dimension of  $\text{CO}_2$  such as methane and acetylene [16, 23]. The occupancy calculation shows that approximately 14 % of the lattice voids are occupied by two molecules of methane at 298 K and a pressure of 0.54 atm [23]. (Fig. 39.4b) The material adsorbs ~2 wt.% acetylene at a pressure of 800 torr and temperature of 298 K [23].

The subsequent occupancy study reveals that the voids are completely filled with the acetylene at 1 atm pressure whereas;  $\text{CO}_2$  shows 100 % occupancy of cavity at a

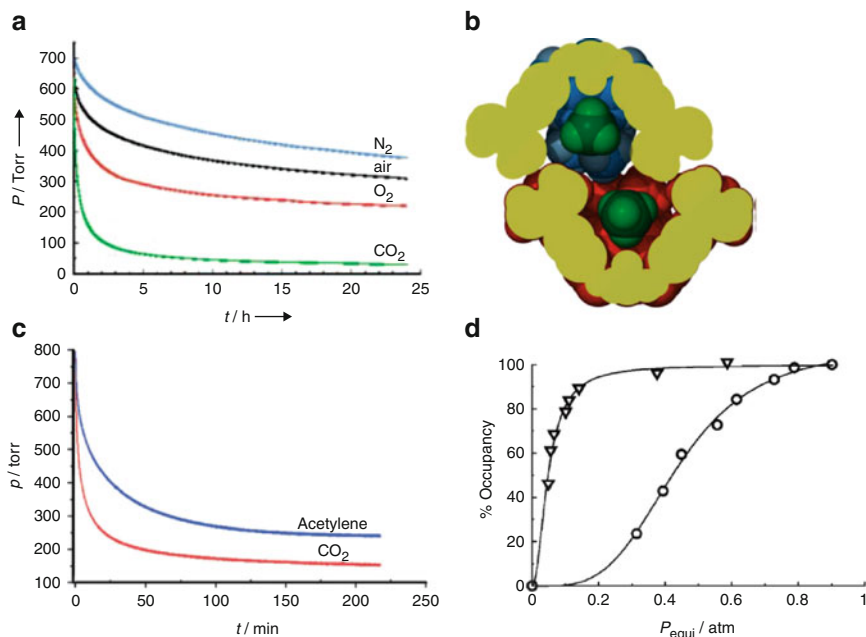


**Fig. 39.4** (a) Gas sorption isotherm of **2b** at 296 K for  $N_2$ , Air,  $O_2$  and  $CO_2$  (b) Sectional views of dimaeric capsule formed from **2**, two calixarenes are colored *blue* and *red* while sectioned surface kept *yellow* with *green* methane molecules. (c) Sorption of acetylene and  $CO_2$  at room temperature (d) Hysteresis in sorption and desorption isotherm of acetylene (Reproduced with permission from publisher Refs. [16, 26b, 23b]. Copyright 2004, 2005, and 2006, Wiley-VCH and Royal Society of Chemistry)

comparatively higher pressure of three bar [23]. The sorption and desorption isotherm of  $CO_2$  and acetylene are different from each other, indicating a different mechanism of sorption. The  $CO_2$  sorption isotherm is type-I in nature with rapid uptake and release of  $CO_2$  while sorption isotherm of acetylene shows a strong hysteresis probably because of the entrapment of residual acetylene molecules within the pore (Fig. 39.4c, d).  $^{13}C$  MAS NMR (MAS = magic angle spinning) further confirms the presence of the residual acetylene in the lattice void [23]. Accessibility of voids in **2** was also tested for gases such as Xe, NO and  $SO_2$  by sealing the host material in presence of respective gases in a pyrex tube at pressures up to 20 atm [24]. The guest uptake was analyzed with  $^{129}Xe$  NMR and the guest release was subsequently monitored with TGA. The weight loss of 4–10 % and guest retention was observed through TGA.  $^{129}Xe$  NMR spectra at various temperatures further confirm inclusion and release of Xe to and from in crystal lattice of **2** rather than being adsorbed on surface.

The **2b** polymorph was also tested for sorption of gases from  $NO_x$  family ( $N_2O$ , NO,  $NO_2$ ) [25]. At 1 atm and 298 K, **2b** appears to differentiate in these  $NO_x$  based on rate of uptake and amount of gases absorbed. **2b** absorbed

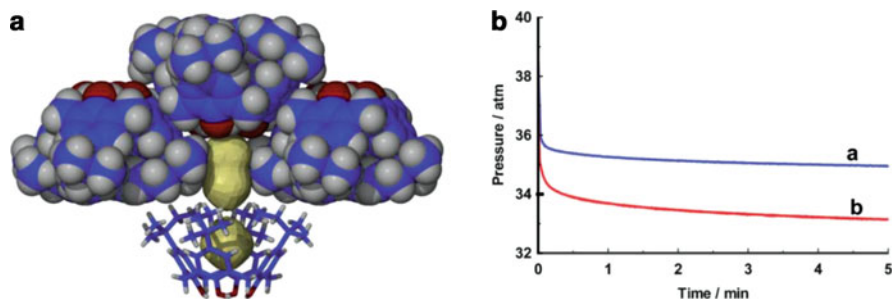


**Fig. 39.5** (a) Small voids enclosed within columns of **3**. (b) Methane sorption isotherm of **a 2** and **b 3** at high pressure (Reproduced with permission from Ref. [22]. Copyright 2005, Royal Society of Chemistry)

significantly more  $\text{N}_2\text{O}$  than  $\text{NO}$  and  $\text{NO}_2$ . However, the rate of sorption is faster for  $\text{NO}_2$  compared to other members of  $\text{NO}_x$  family [25]. The color change of the crystalline **2b** after gas sorption indicates a formation of charge transfer complex between **2** and guest  $\text{NO}_x$ .

### 39.5.3 *p*-tert-Pentylcalix[4]arene, **3** and *p*-tert-Octylcalix[4]arene, **4**

The structural analogues of **2**, namely *p*-tert-pentylcalix[4]arene (**3**) and *p*-tert-octylcalix[4]arene (**4**) were also evaluated for gas sorption related applications [26]. The sublimed crystal forms of **3** and **4** show that both structures were very different from low density sublime form of **2b**. Molecular cavities and interstitial lattice void spaces count a total volume of  $\sim 110 \text{ \AA}^3$  and  $\sim 82.5 \text{ \AA}^3$  in **3** and **4** respectively. In sublimed form (**3a**) of **3**, the host molecules are stacked in columns, with molecules in each column facing the same direction. Each such column is also surrounded by four neighboring columns running in opposite direction. The void space is enclosed within these column pack on top of an individual *p*-tert-pentylcalix[4]arene (Fig. 39.5a). Crystal structure of **4** has both molecular cavity ( $\sim 23 \text{ \AA}^3$ ) and a separate interstitial lattice voids (volume  $\sim 59 \text{ \AA}^3$ ). Both **3** and **4** are non-porous similar to that of **2**. The methane sorption studies at one bar and show that **3a** absorb less methane than **2b** at room temperature and one bar. However, the order of sorption is reversed when methane is introduced at high pressure of 38 bars. At high pressure, **3a** absorb almost 2.2 wt.% of methane compared to 1.7 wt.% absorbed by **2b** (Fig. 39.5b) [26]. The low uptake of methane at ambient pressure in **3a** may be because of inaccessibility of major portion of void space at such low pressure. In another study, hydrogen uptake of **2b**, **3a** and sublimed form of **4** (**4a**) were analyzed at high pressure of  $\sim 31$  bar [26]. All these

molecules show a very low hydrogen uptake and at equilibrium pressure absorb hydrogen in the range of 0.1–0.2 wt.%.

Even though, all three materials (**2**, **3**, and **4**) are closely related to each other with respect to their chemical structures, their solid state structures are different. Thus, they possess distinct gas sorption ability towards particular gases.

#### 39.5.4 *p*-tert-Butylcalix[5]arene, **5**

All the above mentioned studies showed that in order to activate materials for gas sorption, the guest or solvent molecules must be completely removed from the molecular assembly or used as a sublime crystalline form where the void spaces are inherently free from any guest molecules. However, Thallapally and coworkers have discovered an interesting phenomenon of frustrated organic solids in case of *p*-tert-butylcalix[5]arene (Tbc5) [27]. The frustrated form of **5** can be obtained by partial evacuation of toluene from the crystal lattice. The solvated form has two toluene molecules, located within the slightly dimeric capsule formed by head to head arrangement of **5** whereas two disordered toluene molecules reside within interstitial void spaces. The partial loss of solvent during desolvation results in the formation of a porous material that can rapidly adsorb gases under mild conditions. Gas sorption studies on solvated form, frustrated form and completely desolvated form reveal that while the solvated and the completely desolvated forms do not adsorb gases like methane, carbon di-oxide and acetylene, the partially desolvated, frustrated phase can readily adsorb these gases (Fig. 39.6). The frustrated form of **5** is found to be up to 75 % more efficient and 25 times faster compared to **2** in terms of acetylene sorption.

Sublimation of **5** affords two different polymorphs ( $\alpha$  and  $\beta$ ) by means of different rate of heating. Both polymorphs have distinct arrangement of **5**:  $\alpha$  has stacked arrangement of slightly distorted **5** while  $\beta$  has arrangement of **5** based on the interactions of both “self-induced” and “back to back” helices [28]. In the extended assembly of  $\beta$ , the combination of both types of helices resulted in apparent void spaces in the crystal lattice. The gas-sorption study on the  $\beta$  form shows that it can adsorb ~1.1 wt.% CO<sub>2</sub> at ambient conditions in its interstitial void spaces, formed from the combination of helical arrangement of **5**.

#### 39.5.5 *p*-Hexanoylcalix[4]arene, **6** and *p*-Octanoylcalix[4]arene, **7**

New types of molecular van der Waals nano-capsules were obtained by functionalization of upper rim of the calix[4]arene moiety with long alkyl chain ester

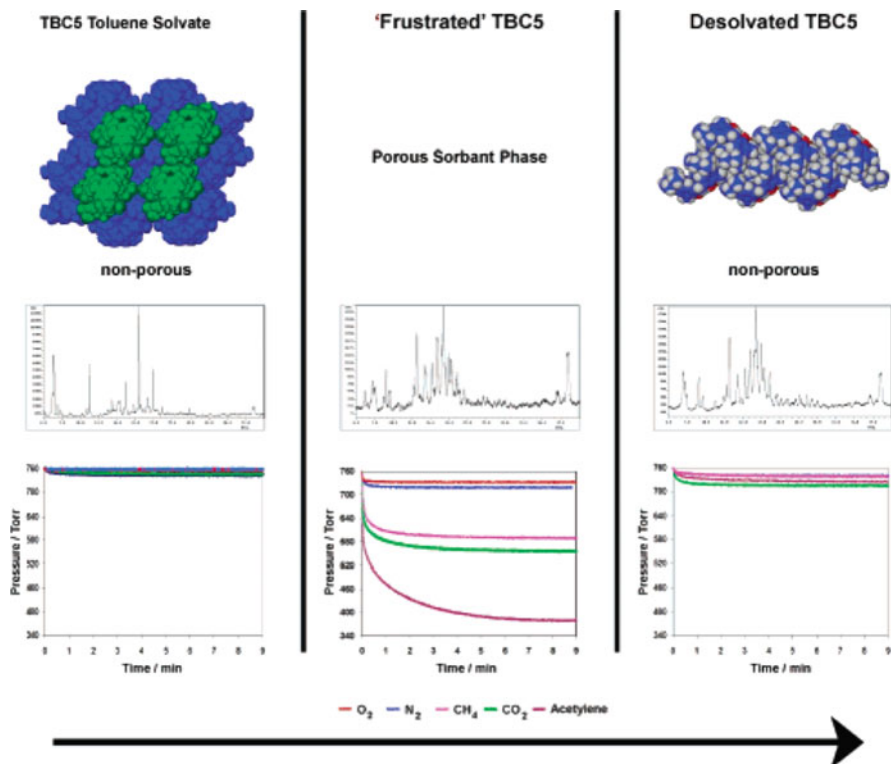


**Fig. 39.6** Transition from inactive toluene solvate phase of **5** to inactive completely desolvated phase through active frustrated phase analyzed with subsequent PXRD changes and gas sorption isotherm for O<sub>2</sub>, N<sub>2</sub>, CH<sub>4</sub>, and CO<sub>2</sub> (Reproduced with permission from Ref. [27a]. Copyright 2006, American Chemical Society)

[29]. *P*-hexanoylcalix[4]arene (**6**) and *p*-octanoylcalix[4]arene (**7**) (Fig. 39.7a, b) were successfully crystallized from chloroform and acetone, respectively in a dimeric capsular based host orientation [29]. It should be noted that even though the lattice framework in both cases doesn't have channels for diffusion of guest into crystalline lattice, it is assumed that the flexible acyl chains may create a soft cavity wall along with cooperative effect which was observed similarly in non-porous **2**.

The sorption isotherms of **7** with various gases such as CO<sub>2</sub>, N<sub>2</sub>, O<sub>2</sub>, Xe, and linear alkanes C1–C4 were measured volumetrically at room temperature [30] (Fig. 39.6c). These host materials show higher affinity for CO<sub>2</sub>, Xe, and linear alkanes compared to O<sub>2</sub>, and N<sub>2</sub>. The sorption isotherms are type-I in nature, indicating microporous behavior. The isotherms are saturated at pressure of ~40 bar where each assembly is occupied by two guest molecules. The sorption of hydrocarbon is more preferred over CO<sub>2</sub> at lower pressure region (<5 bar),

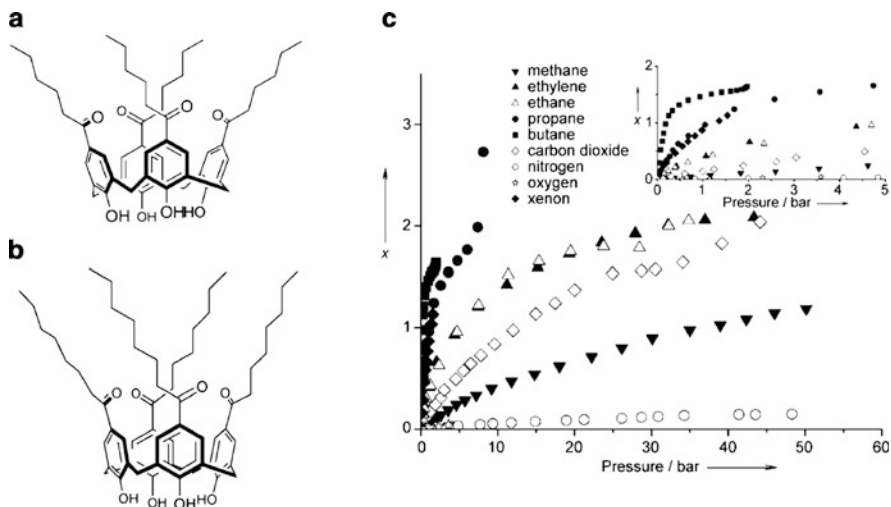


**Fig. 39.7** (a) **6** (b) **7** (c) Gas sorption isotherms of **7** with different gases (Reproduced with permission from Refs. [29, 30]. Copyright 2006 and 2007, Wiley-VCH and Royal Society of Chemistry)

showing the potential of this material for separation of hydrocarbons from  $\text{CO}_2$  at relatively low pressure.

### 39.5.6 Adamantylcalix[4]arene, **8**

Changing a functional group at the upper rim of calixarene molecule is generally attempted since functionalization at the lower rim often induces changes in the cone/bowl shape of macrocycle. Sorption isotherms of **8** show that it has more binding affinity toward selected guest vapors compared to **2** [31]. Material **8** absorb twice as much vapor of benzene and toluene and four times as much cyclohexane and carbon tetrachloride than **2** at similar experimental conditions.

### 39.5.7 *p*-tert-Butylthiacalix[4]arene, **9**

The quest of hosts with a larger molecular cavity in the class of calixarenes leads to functionalization at the bridging position. In this regard, sublime form of *p*-tert-butylthiacalix[4]arene (**9**) was obtained which comprises of two different crystallographic form, namely monoclinic and tetragonal [32]. Both of these forms possess intrinsic void spaces in the molecular cavity of macrocycles (*endo*-cavities). However, the parallel columns of **9** in tetragonal phase enclose the hydrophobic cavities



in the interstitial space (*exo*-cavities) between columns. Such additional space is absent in the monoclinic form. Exposure of HCl vapors to the tetragonal form resulted in diffusion of HCl within the *endo* cavities of calixarenes [32]. Relatively large, linear and non-polar guest such as iodine in its vapor form can be absorbed by the same tetragonal form within its interstitial pockets as shown by the single crystal XRD studies [32]. Effect of humidity on I<sub>2</sub> sorption was analyzed by exposing activated **9** in presence of both water and iodine vapor for 10 days. Surprisingly, the humidity did not affect the overall iodine uptake although non-stoichiometric water can also diffuse through the crystals. Water occupies the *endo* cavities in the crystal whereas the iodine resides in *exo* cavity without further increment in occupancy. A detailed vapor guest uptake studies were further carried out for various organic molecules with distinct shape and functionality [12]. The binding order of guests in **9** is methanol > aliphatic alcohols and propionitrile > aliphatic nitriles. The crystalline host **9** forms only 1:1 inclusion complexes over a wide range of conditions. Thus even the host molecule **9** exhibits a higher level of flexibility in the solution phase. The solid phase possesses a considerably less flexible architecture as evident from the nature of the inclusion complexes.

## 39.6 Gas Sorption in Other Calixarene Derivatives

Several attempts have also been made towards the functionalization at the lower rim of calixarene moieties, which generally disturbs the typical intramolecular hydrogen bonding arrangements among the hydroxyl groups. However, the functionalization at the lower rim also leads to structural changes in the overall arrangement, affecting the gas sorption related properties of the host materials.

### 39.6.1 1,2-Dimethoxy-*p*-*tert*-butylcalix[4]dihydroquinone, **10**

The single crystal of 1,2-dimethoxy-*p*-*tert*-butylcalix[4]dihydroquinone (**10**) has a cubic structure with a network of nano-dimensional channels where **10** aggregates in a tubular fashion (Fig. 39.8a). The individual molecules interact with each other through hydrogen bonding and van der Waals type interactions, leading to cavities of unexpected size and shape [33]. The crystallographic analysis showed that there are two hydrophobic cavities, connected through channels with minimum and maximum diameter of 2.2 Å and 11.2 Å respectively (Fig. 39.7b). The estimated free volume created by these channels is approximately 988 Å<sup>3</sup> [3] per unit cell (2 % of the total unit cell volume). The activated **10** exhibits a type-I isotherm for CO<sub>2</sub> with a total uptake of 0.5 wt.% at room temperature and 640 torr [33]. The material



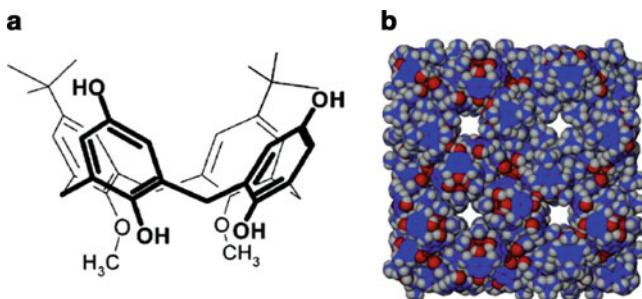


**Fig. 39.8** (a) 1,2-Dimethoxy-p-tert-butylcalix[4]dihydroquinone, (b) Spacefill view of crystalline arrangement of **10** with hydrophobic channels (Reproduced with permission from Ref. [33]. Copyright 2007, American Chemical Society)

also adsorbs methane (0.29 wt.% at STP and 5 wt.% at 3 bar and 203 K) and acetylene (0.97 wt.% at 0.5 bar and 298 K). **10** do not adsorb  $H_2$  and thus is potentially selective for  $CO_2$  sorption over  $H_2$  [33, 34].

### 39.6.2 *Noria, 11*

Unconventional and larger calixarene, such as noria is synthesized from acid catalyzed condensation reaction of resorcinol with glutaraldehyde in presence of conc. HCl. Noria has unique structural features with two types of molecular cavities: 6 shallow cavities at the periphery decorated with 24 hydroxyl groups and 1 large hydrophobic central cavity. The central cavity and portal diameter is found to be approximately 7 Å and 5 Å, with volume of the internal cavity calculated as  $160 \text{ \AA}^3$  (Fig. 39.9a, b) [35]. Amorphous form of **11** shows higher affinity for  $CO_2$  compared to  $N_2$  and  $H_2$ . Noria exhibits a type-I sorption isotherm for  $CO_2$  with a 11 wt.% uptake at 30 bar and 298 K (Fig. 39.9c). This sorption value of  $CO_2$  is much higher than **2** whereas, a BOC (BOC = *tert*-Butyl carbamates) protected noria derivative shows slightly higher  $CO_2$  sorption value of 14.2 wt.% under similar conditions [35].

### 39.6.3 *C-Alkylpyrogallol[4]arenes, 12*

Recently, a comparatively new class of calixarenes, namely *C*-alkylpyrogallol[4]arenes have also shown  $CO_2$  sorption property with its frustrated crystalline form [36]. In particular, a partially desolvated form of *C*-pentylpyrogallol[4]arene absorbs 12 wt.% of  $CO_2$  at 27 bar and 298 K (Fig. 39.9d) [36]. In this case also, neither the completely desolvated nor the solvated form shows any affinity for  $CO_2$ .

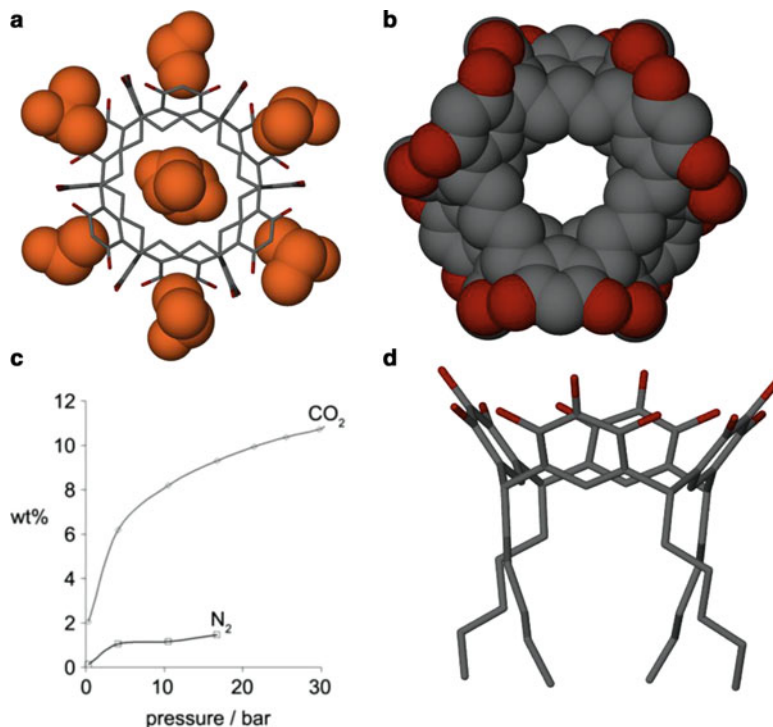


**Fig. 39.9** (a) Noria molecule with six cavities at periphery and one hydrophobic cavity at the center (b) Space fill view of molecule with cavities (c) Gravimetric CO<sub>2</sub> capacity for **11** at room temperature and pressure 30 bar. (d) C-pentylpyrogallol[4]arenes macrocycle (Reproduced with permission from Ref. [35]. Copyright 2009, Wiley-VCH)

It is postulated that the partial removal of the solvent prevents the crystalline structure from collapsing, which facilitates the sorption of CO<sub>2</sub> within the lattice void [36].

#### 39.6.4 Metal Organic Supercontainers (Calixarene Based Metal Complexes)

The guest binding ability of calixarenes were used to form calixarene based metal complexes (also termed as Metal-Organic Supercontainer) using transition metal ions and organic linkers [e.g. benzenedicarboxylic acid (BDC) and 1,3,5 benzenetricarboxylic acid (BTC)]. For example, *p*-tert-butylthacalix[4]arene (**8**) coordinates with four transition metal (Co, Ni, and Mn) centers through hydroxyl groups as well as through bridging sulfurs [37]. Thus this tetra-nuclear

metal complex has four points of extension which are then coordinated with BDC linkers, forming an octahedral cage type assembly. One such complex  $[\text{Co}_{24}(\mathbf{8})_6(\text{BDC})_8]$  has a BET surface area of  $566 \text{ m}^2/\text{g}$  and also show lower affinity for  $\text{H}_2$  at lower temperature of  $77 \text{ K}$ .<sup>37a</sup> Similar approach was used with *p*-tert-pentylsulfonoylcalix[4]arene (**12**) where the bridging sulfonyl groups and hydroxyl groups at the lower rim participate in metal coordination. The desolvation during activation leads to spatial reorganization of the calixarene moiety [38]. Gas sorption studies on MONC-II-tPen-Ni (complex formed from Ni (II), **12**, and BTC) shows distinct  $\text{O}_2$  vs.  $\text{N}_2$  affinity at low temperature of  $77 \text{ K}$  [38]. This selectivity towards  $\text{O}_2$  is more likely due to a molecular sieving effect, where the pore diameter of the adsorbent is in between  $3.46 \text{ \AA}$  (kinetic diameter of  $\text{O}_2$ ) and  $3.64 \text{ \AA}$  (kinetic diameters of  $\text{N}_2$ ).

Although a few of these metal-organic supercontainers have a comparatively higher surface area than many of the molecular assemblies discussed above, they tend to undergo partial or complete collapse of the solid state packing upon solvent removal, limiting the use of these materials for gas sorption applications.

## 39.7 Conclusion

Solid state calixarenes and many of its derivatives have shown gas-sorption abilities under ambient conditions. Although many of these organic solids are non-porous in conventional terms, the uptake occurs through a cooperative mechanism of neighboring host molecules. Interestingly, in several cases, enhanced gas uptake was observed when the solvent of crystallization was only partially removed. These materials, namely frustrated organic solids remain an elusive branch of host-guest chemistry in calixarene and related derivatives. The selective functionalization of the lower or upper rim of calixarene based host molecules leads to change in the long range crystal packing, which often leads to a significant change in gas sorption properties of the respective host. Finally, the research on gas-selective calixarene and its derivatives are still in its infancy, however, further exploratory syntheses and physical characterization involving sorption measurements will likely yield further fundamental and applied results.

## References

1. Chapter 1, From Resinous Tar to Molecular Baskets. In *Calixarenes: An Introduction*, The Royal Society of Chemistry: 2008; pp 1–26.
2. (a) Delahousse, G.; Lavendomme, R.; Jabin, I.; Agasse, V.; Cardinael, P. *Curr. Org. Chem.* **2015**, *19*, 2237–2249; (b) Deska, M.; Dondela, B.; Sliwa, W. *ARKIVOC* **2015**, 393–416; (c) Tyagi, R. *Int. J. Chem.* **2014**, *3*, 306–316; (d) Ma, X.; Zhao, Y. *Chem. Rev.* **2015**, *115*, 7794–7839; (e) Zadmard, R.; Alavijeh, N. S. *RSC Adv.* **2014**, *4*, 41529–41542.
3. Zhang, J.; Webley, P. A.; Xiao, P. *Energy Convers. Manage.* **2007**, *49*, 346–356.

4. (a) Bhosale, M. E.; Illathvalappil, R.; Kurungot, S.; Krishnamoorthy, K. *Chem. Commun.* **2016**, 52, 316–318.; (b) Wisser, F. M.; Grothe, J.; Kaskel, S. *Sens. Actuators, B* **2016**, 223, 166–171.; (c) Wang, J.; Wei Yang, J. G.; Yi, G.; Zhang, Y. *Chem. Commun.* **2015**, 51, 15708–15711.; (d) Cheng, G.; Bonillo, B.; Sprick, R. S.; Adams, D. J.; Hasell, T.; Cooper, A. I. *Adv. Funct. Mater.* **2014**, 24, 5219–5224.; (e) Lee, J.-S.; Kim, J.-H.; Kim, J.-T.; Suh, J.-K.; Lee, J.-M.; Lee, C.-H. *J. Chem. Eng. Data* **2002**, 47, 1237–1242.; (f) Jadhav, P. D.; Chatti, R. V.; Biniwale, R. B.; Labhsetwar, N. K.; Devotta, S.; Rayalu, S. S. *Energy Fuels* **2007**, 21, 3555–3559.; (g) Martin, C. F.; Plaza, M. G.; Pis, J. J.; Rubiera, F.; Pevida, C.; Centeno, T. A. *Sep. Purif. Technol.* **2010**, 74, 225–229.; (h) Kusakabe, K.; Kuroda, T.; Murata, A.; Morooka, S. *Ind. Eng. Chem. Res.* **1997**, 36, 649–655.; (i) Cavenati, S.; Grande, C. A.; Rodrigues, A. E. *J. Chem. Eng. Data* **2004**, 49, 1095–1101.; (j) Silvestre-Albero, J.; Wahby, A.; Sepulveda-Escribano, A.; Martinez-Escandell, M.; Kaneko, K.; Rodriguez-Reinoso, F. *Chem. Commun.* **2011**, 47, 6840–6842.; (k) Cavenati, S.; Grande, C. A.; Rodrigues, A. E. *Chem. Eng. Sci.* **2006**, 61, 3893–3906.; (l) Comotti, A.; Bracco, S.; Distefano, G.; Sozzani, P. *Chem. Commun.* **2009**, 284–286.; (m) Yang, W.; Greenaway, A.; Lin, X.; Matsuda, R.; Blake, A. J.; Wilson, C.; Lewis, W.; Hubberstey, P.; Kitagawa, S.; Champness, N. R.; Schroder, M. *J. Am. Chem. Soc.* **2010**, 132, 14457–14469.; (n) He, Y.; Xiang, S.; Chen, B. *J. Am. Chem. Soc.* **2011**, 133, 14570–14573.; (o) Sumida, K.; Rogow David, L.; Mason Jarad, A.; McDonald Thomas, M.; Bloch Eric, D.; Herm Zoey, R.; Bae, T.-H.; Long Jeffrey, R. *Chem. Rev.* **2012**, 112, 724–81.; (p) Banerjee, D.; Cairns, A. J.; Liu, J.; Motkuri, R. K.; Nune, S. K.; Fernandez, C. A.; Krishna, R.; Strachan, D. M.; Thallapally, P. K. *Acc. Chem. Res.* **2015**, 48, 211–219.; (q) Manurung, R.; Holden, D.; Miklitz, M.; Chen, L.; Hasell, T.; Chong, S. Y.; Haranczyk, M.; Cooper, A. I.; Jelfs, K. E. *J. Phys. Chem. C* **2015**, 119, 22577–22586.; (r) Chen, L.; Reiss, P. S.; Chong, S. Y.; Holden, D.; Jelfs, K. E.; Hasell, T.; Little, M. A.; Kewley, A.; Briggs, M. E.; Stephenson, A.; Thomas, K. M.; Armstrong, J. A.; Bell, J.; Busto, J.; Noel, R.; Liu, J.; Strachan, D. M.; Thallapally, P. K.; Cooper, A. I. *Nat. Mater.* **2014**, 13, 954–960.; (s) Hasell, T.; Armstrong, J. A.; Jelfs, K. E.; Tay, F. H.; Thomas, K. M.; Kazarian, S. G.; Cooper, A. I. *Chem. Commun.* **2013**, 49, 9410–9412.; (t) Mitra, T.; Jelfs, K. E.; Schmidtman, M.; Ahmed, A.; Chong, S. Y.; Adams, D. J.; Cooper, A. I. *Nat. Chem.* **2013**, 5, 276–281.; (u) Cooper, A. I. *Angew. Chem., Int. Ed.* **2012**, 51, 7892–7894.
5. (a) Dunitz, J. D.; Gavezzotti, A. *Chem. Soc. Rev.* **2009**, 38, 2622–2633.; (b) Dunitz, J. D.; Filippini, G.; Gavezzotti, A. *Helv. Chim. Acta* **2000**, 83, 2317–2335.
6. Atwood, J. L.; Barbour, L. J.; Jerga, A. *Science* **2002**, 296, 2367–2369.
7. Dawson, C.; Horton, P. N.; Hursthouse, M. B.; James, S. L. *CrystEngComm* **2010**, 12, 1048–1050.
8. Lu, J.; Perez-Krap, C.; Suyetin, M.; Alsmail, N. H.; Yan, Y.; Yang, S.; Lewis, W.; Bichoutskaia, E.; Tang, C. C.; Blake, A. J.; Cao, R.; Schroder, M. *J. Am. Chem. Soc.* **2014**, 136, 12828–12831.
9. Andreotti, G. D.; Ungaro, R.; Pochini, A. *J. Chem. Soc., Chem. Commun.* **1979**, 1005–7.
10. (a) Ripmeester, J. A.; Ratcliffe, C. I.; Brouwer, E. B. *Encycl. Nucl. Magn. Reson.* **2002**, 9, 558–570.; (b) Li, Y.; Yang, H. *Chem. Lett.* **2010**, 39, 796–802.; (c) Ripmeester, J. A.; Enright, G. D.; Ratcliffe, C. I.; Udachin, K. A.; Moudrakovski, I. L. *Chem. Commun.* **2006**, 4986–4996.
11. Chen, B.; Xiang, S.; Qian, G. *Acc. Chem. Res.* **2010**, 43, 1115–1124.
12. (a) Gorbachuk, V. V.; Tsifarkin, A. G.; Antipin, I. S.; Solomonov, B. N.; Kononov, A. I. *J. Inclusion Phenom. Macrocyclic Chem.* **1999**, 35, 389–396.; (b) Gorbachuk, V. V.; Tsifarkin, A. G.; Antipin, I. S.; Solomonov, B. N.; Kononov, A. I.; Seidel, J.; Baitalov, F. *Perkin 2* **2000**, 2287–2294.; (c) Gorbachuk, V. V.; Tsifarkin, A. G.; Antipin, I. S.; Solomonov, B. N.; Kononov, A. I.; Lhotak, P.; Stibor, I. *J. Phys. Chem. B* **2002**, 106, 5845–5851.
13. Brouwer, E. B.; Enright, G. D.; Ratcliffe, C. I.; Ripmeester, J. A. *Supramol. Chem.* **1996**, 7, 79–83.
14. Brouwer, E. B.; Enright, G. D.; Ratcliffe, C. I.; Facey, G. A.; Ripmeester, J. A. *J. Phys. Chem. B* **1999**, 103, 10604–10616.
15. Brouwer, E. B.; Udachin, K. A.; Enright, G. D.; Ripmeester, J. A. *Chem. Commun.* **2000**, 1905–1906.
16. Atwood, J. L.; Barbour, L. J.; Jerga, A. *Angew. Chem., Int. Ed.* **2004**, 43, 2948–2950.

17. Ungaro, R.; Pochini, A.; Andreetti, G. D.; Sangermano, V. *J. Chem. Soc., Perkin Trans. 2* **1984**, 1979–85.
18. Asfari, Z.; Bohmer, V.; Harrowfield, J.; Vicens, J.; Editors *Calixarenes 2001*. 2001; p 683.
19. Enright, G. D.; Brouwer, E. B.; Halchuk, P. A.; Ooms, K. J.; Ferguson, M. J.; Udachin, K. A.; Ripmeester, J. A. *Acta Cryst. section A* **2002**, *58*, c310.
20. (a) Atwood, J. L.; Barbour, L. J.; Jerga, A. *Chem. Commun.* **2002**, 2952–2953; (b) Brouwer, E. B.; Udachin, K. A.; Enright, G. D.; Ripmeester, J. A.; Ooms, K. J.; Halchuk, P. A. *Chem. Commun.* **2001**, 565–566; (c) Brouwer, E. B.; Enright, G. D.; Udachin, K. A.; Lang, S.; Ooms, K. J.; Halchuk, P. A.; Ripmeester, J. A. *Chem. Commun.* **2003**, 1416–1417.
21. Atwood, J. L.; Barbour, L. J.; Jerga, A.; Schottel, B. L. *Science* **2002**, *298*, 1000–1002.
22. Dalgarno, S. J.; Thallapally, P. K.; Barbour, L. J.; Atwood, J. L. *Chem. Soc. Rev.* **2007**, *36*, 236–245.
23. (a) Atwood Jerry, L.; Barbour Leonard, J.; Thallapally Praveen, K.; Wirsig Trevor, B. *Chem. Commun.* **2005**, 51–3; (b) Thallapally, P. K.; Dobrzanska, L.; Gingrich, T. R.; Wirsig, T. B.; Barbour, L. J.; Atwood, J. L. *Angew. Chem., Int. Ed.* **2006**, *45*, 6506–6509.
24. Enright, G. D.; Udachin, K. A.; Moudrakovski, I. L.; Ripmeester, J. A. *J. Am. Chem. Soc.* **2003**, *125*, 9896–9897.
25. Thallapally, P. K.; McGrail, B. P.; Atwood, J. L. *Chem. Commun.* **2007**, 1521–1523.
26. (a) Thallapally, P. K.; Wirsig, T. B.; Barbour, L. J.; Atwood, J. L. *Chem. Commun.* **2005**, 4420–2; (b) Thallapally, P. K.; Lloyd, G. O.; Wirsig, T. B.; Bredenkamp, M. W.; Atwood, J. L.; Barbour, L. J. *Chem. Commun.* **2005**, 5272–4.
27. (a) Thallapally, P. K.; Dalgarno, S. J.; Atwood, J. L. *J. Am. Chem. Soc.* **2006**, *128*, 15060–15061; (b) Dalgarno, S. J.; Thallapally, P. K.; Tian, J.; Atwood, J. L. *New J. Chem.* **2008**, *32*, 2095–2099.
28. Dalgarno, S. J.; Tian, J.; Warren, J. E.; Clark, T. E.; Makha, M.; Raston, C. L.; Atwood, J. L. *Chem. Commun.* **2007**, 4848–4850.
29. (a) Ananchenko, G. S.; Udachin, K. A.; Dubes, A.; Ripmeester, J. A.; Perrier, T.; Coleman, A. W. *Angew. Chem., Int. Ed.* **2006**, *45*, 1585–1588; (b) Ananchenko, G. S.; Udachin, K. A.; Pojarova, M.; Jebors, S.; Coleman, A. W.; Ripmeester, J. A. *Chem. Commun.* **2007**, 707–709.
30. Ananchenko, G. S.; Moudrakovski, I. L.; Coleman, A. W.; Ripmeester, J. A. *Angew. Chem., Int. Ed.* **2008**, *47*, 5616–5618.
31. Gorbachuk, V. V.; Savelyeva, L. S.; Ziganshin, M. A.; Antipin, I. S.; Sidorov, V. A. *Russ. Chem. Bull.* **2004**, *53*, 60–65.
32. Herbert, S. A.; Janiak, A.; Thallapally, P. K.; Atwood, J. L.; Barbour, L. J. *Chem. Commun.* **2014**, *50*, 15509–15512.
33. Thallapally, P. K.; McGrail, B. P.; Atwood, J. L.; Gaeta, C.; Tedesco, C.; Neri, P. *Chem. Mater.* **2007**, *19*, 3355–3357.
34. (a) Erra, L.; Tedesco, C.; Cipolletti Valeria, R.; Annunziata, L.; Gaeta, C.; Brunelli, M.; Fitch Andrew, N.; Knofel, C.; Llewellyn Philip, L.; Atwood Jerry, L.; Neri, P. *Phys Chem Chem Phys* **2012**, *14*, 311–7; (b) Tedesco, C.; Erra, L.; Brunelli, M.; Cipolletti, V.; Gaeta, C.; Fitch, A. N.; Atwood, J. L.; Neri, P. *Chem. - Eur. J.* **2010**, *16*, 2371–2374, S2371/1–S2371/9.
35. Tian, J.; Thallapally, P. K.; Dalgarno, S. J.; McGrail, P. B.; Atwood, J. L. *Angew. Chem. Int. Ed.* **2009**, *48*, 5492–5495, S5492/1–S5492/12.
36. Kumari, H.; Erra, L.; Webb, A. C.; Bhatt, P.; Barnes, C. L.; Deakynne, C. A.; Adams, J. E.; Barbour, L. J.; Atwood, J. L. *J. Am. Chem. Soc.* **2013**, *135*, 16963–16967.
37. (a) Xiong, K.; Jiang, F.; Gai, Y.; Yuan, D.; Chen, L.; Wu, M.; Su, K.; Hong, M. *Chem. Sci.* **2012**, *3*, 2321–2325; (b) Bi, Y.; Wang, X.-T.; Liao, W.; Wang, X.; Wang, X.; Zhang, H.; Gao, S. *J. Am. Chem. Soc.* **2009**, *131*, 11650–11651; (c) Bilyk, A.; Dunlop, J. W.; Fuller, R. O.; Hall, A. K.; Harrowfield, J. M.; Hosseini, M. W.; Koutsantonis, G. A.; Murray, I. W.; Skelton, B. W.; Stamps, R. L.; White, A. H. *Eur. J. Inorg. Chem.* **2010**, 2106–2126.
38. Dai, F.-R.; Sambasivam, U.; Hammerstrom, A. J.; Wang, Z. *J. Am. Chem. Soc.* **2014**, *136*, 7480–7491.

# Index

## A

Acetylene, 1038, 1045–1046, 1048, 1052  
Amino acids, 14–21, 30, 34, 35, 126, 164, 179, 184, 244, 279–281, 499, 503, 504, 568, 601–614, 634, 652, 663, 711, 736, 745, 849–851, 950, 951, 994, 1005, 1006  
Anion(s), 15, 105, 117–130, 162, 204, 245, 261, 285–304, 306–310, 312, 313, 315, 316, 318–322, 337, 389, 411, 439, 451, 480, 499, 536, 564, 630, 674, 744, 745, 748–749, 751, 752, 756, 758, 763, 783–808, 823, 846, 904, 951, 967, 1004, 1016  
    binding, 103, 118, 119, 132, 209, 225, 261, 286–289, 291–293, 411, 412, 456, 644  
Anti-adhesive, 571  
Antiport, 307–309, 653  
Application  
    carbon dioxide absorption, 392  
    catalysis, 343–344  
    macrocyclic liquid crystals, 392–393  
Aromatic substitution, 43, 60, 66, 155, 223, 364, 370, 374, 379, 399, 406, 727, 991  
Assay, 183, 297–299, 303, 310, 441, 567, 570, 572, 575, 578, 580, 584, 590, 593, 594, 614–616, 621, 623, 631–633, 646, 655, 663–665, 709, 873  
Association constants, 18, 26, 30, 97, 101, 105, 119, 120, 126, 317, 318, 324, 451, 452, 455–459, 472, 476, 498, 500–502, 539, 547, 549, 606, 633, 637, 645, 646, 752, 786, 792, 797, 798, 864, 872, 874, 891, 901, 909, 912  
Atropisomer, 151  
Azacalixaromatics  
    Cu-catalyzed arene C-H bond transformation, 661

    electrophilic aromatic substitution reaction, 374  
    fragment coupling synthesis, 364–368  
    nucleophilic aromatic substitution reaction, 364, 370  
    one-pot synthesis, 368–370  
    post-macrocyclization functionalization, 372  
    stepwise synthesis, 370–371  
Azacalix[n]pyridine[m]pyrimidines, 908–909  
Azacalix[n]pyridines, 367, 368, 385, 388, 391, 905–908

## B

Barium, 219, 694–698, 866  
Binding constants, 122, 183, 270, 289, 301, 324, 387, 388, 390, 391, 499, 535, 546, 547, 550, 551, 572, 617, 631, 639, 891, 892, 894, 901–909, 911–913, 944  
Biocatalysts, 729, 732, 733, 736, 737, 741  
Biomimicry, 113  
Bio-sensing, 525  
Bridged calixarenes, 236, 244  
Bromination, 8, 45, 54–56, 82, 85, 86, 90, 156, 247, 372–374, 406, 533

## C

Calix[4]arene, 5, 14, 43, 76, 106, 114, 183, 235–251, 290, 341, 454, 467, 496, 560, 602, 630, 671–687, 720, 743–745, 747–757, 812, 843–875, 942, 966, 988, 1011, 1042–1043

- Calix[5]arene, 96–106, 108, 468, 470, 882–886, 910–913, 916, 1022–1025, 1027
- Calix[7]arene, 147, 149, 156, 159, 160, 165, 1012
- Calix[8]arene, 54, 75, 77, 89, 142–143, 146–153, 156–159, 161–164, 166, 564, 567, 568, 582, 593, 631, 652, 663, 665, 738, 787, 790, 880, 887–890, 922, 952, 953, 969, 981, 990, 1003, 1012, 1029–1031
- Calix[9]arene, 143, 145, 153, 166, 1031
- Calix[10]arene, 1031, 1032
- Calix[12]arene, 1031, 1032
- Calix[16]arene, 496
- Calixarene-induced aggregation (CIA), 513–518
- Calixarene nucleic acid conjugates, 666
- Calixcrowns, 461
- Calix[n]arenes (CAs), 6, 23, 54, 80, 96, 114, 144, 147, 168, 169, 337, 363, 364, 395, 442, 485, 491, 507, 511, 602, 627–666, 743, 784, 879, 886, 891–896, 905, 922, 1012, 1031–1033
- Calix[n]azulenes, 898
- Calix[n]naphthalenes, 897–899
- Calix[4]pyrrole, 286, 287, 289–296, 298–307, 309–315, 321, 322, 646, 647, 845, 846, 857–862, 875, 904, 976
- Calixrecorcinarene, 7, 8, 10
- Calixsugar, 559–597
- Carbon dioxide capture, 392, 1038, 1048
- Catalysis, 3, 22, 53, 113, 135, 209, 342–344, 359, 367, 370, 393, 395, 467, 513, 518, 522, 526, 552, 658, 660, 661, 694–696, 703, 704, 706, 707, 714, 719–741, 744, 811–839, 845, 942, 952, 966, 967, 976, 978, 980
- Catenanes, 414–416, 513, 761, 783, 805
- Cation and anion binding properties, 209, 286, 288, 289, 904
- Cation- $\pi$  interactions, 66, 413, 452, 603, 611, 672, 712, 743, 846
- Cations, and anions, 285, 550, 744, 745, 749, 756, 758
- Cavitands, 8, 14–18, 80, 113, 195–225, 255, 655, 713, 813, 846, 896, 922, 929
- Cavity, 1, 2, 9, 10, 17, 48, 75, 96, 113, 144, 181, 195, 235, 255, 287, 347, 363, 409, 428, 451, 467, 496, 512, 525, 601, 630, 671, 691, 720, 740, 763, 784, 813, 843, 881, 945, 966, 994, 1012, 1041
- C<sub>60</sub> fullerene, 49, 162, 192, 269, 391, 665, 886, 888
- C<sub>70</sub> fullerene, 20, 427, 879, 881, 916
- Chirality, 14, 19–21, 24–37, 59, 72, 106, 257, 451, 647, 792, 850, 851, 856
- Chiral recognition, 18, 19, 22, 26, 33, 72, 127
- Chiroptical properties, 61, 219, 537, 555
- Clusters, 21, 106, 141, 341, 387, 441, 559, 612, 671–687, 708, 887, 922, 953, 966, 994
- Cobalt, 441, 866, 923
- Co-crystals, 612, 1011, 1013, 1015–1017, 1020, 1022, 1028, 1030, 1033
- Complex(es), 1, 17, 45, 77, 96, 119, 146, 179, 198, 241, 255, 286, 336, 373, 402, 434, 451, 471, 497, 514, 525, 574, 604, 631, 671, 692, 721, 746, 761, 784, 811, 843, 880, 921, 942, 966, 987, 1011, 1040
- Conformational structure  
 1,3-alternate conformation, 384, 388  
 inherently chirality, 384, 386  
 macrocyclic ring inversion, 385  
 V-shaped cavity, 379
- Coordination  
 chemistry, 345, 388, 672, 677, 678, 683, 687  
 driven self-assembly, 222
- Copper, 26, 218, 356, 373–375, 388, 493, 553, 560, 594, 651, 659, 700–704, 733, 835, 836
- Co-transport, 307, 308
- Cryptands, 743
- Cryptophanes, 525–555, 843
- Cucurbituril, 2, 3, 108, 114, 513, 627, 743, 783
- Cyclodextrin, 1, 2, 108, 114, 467, 485, 491, 513, 589, 590, 594, 627, 661, 719, 743, 744, 783
- Cyclophanes, 255, 436, 713
- D**
- Deep-cavity cavitand, 222, 223, 272, 273, 276
- Devices, 135, 349, 350, 416, 516, 761–763, 780, 838, 941, 942, 960, 965–970, 974
- Dialkylammonium cation, 784, 787, 788, 808
- Directed assembly, 673
- Distally-bridged, 235–251
- Ditopic receptors, 262, 289, 302, 304, 307, 309, 455–458, 646, 712, 714
- DNA cleavage, 542
- Drug delivery, 22, 24, 113, 515, 518, 520, 521, 522, 587–590, 620, 646, 647, 664, 719, 838, 942, 965, 966, 974, 976–978
- Dynamic combinatorial chemistry (DCC), 430

**E**

- Effective molarity, 873
- Enantiomers, 13, 18, 20, 29, 30, 33, 35–37, 47, 48, 51, 56, 61, 66, 124, 125, 128, 199, 219, 248, 263, 264, 373, 458, 537–539, 544–546, 606, 848, 954, 955
- Enantiopure compounds, 538, 544, 545, 547
- Encapsulation, 24, 96, 98, 102, 108, 127, 128, 205, 213, 224, 279, 280, 302, 314, 389, 481, 553, 628, 664, 737–741, 763, 811–814, 823, 826, 828, 829, 832, 843–846, 848, 850, 852, 858–862, 864, 867, 869–871, 873, 875, 883, 904, 921, 922, 928, 937, 938, 1003, 1006
- Entrapping properties, 187
- Enzyme(s), 184, 312, 591, 593–595, 611, 615, 691, 705, 729, 736, 737, 744, 830, 833, 834, 838, 858, 999, 1004
- mimics, 3, 4, 692, 698, 736
- Extraction, 120, 121, 124, 299, 301–306, 341, 393, 422, 440, 451–455, 461, 462, 618, 661–663, 719, 744, 888, 975, 1038

**F**

- Fluorescent sensors, 299, 355, 387, 459, 606
- Fragment condensation, 44–53, 71, 76–78, 142
- Functionalization, 2, 8, 30, 57, 75, 78, 105, 115, 144–159, 183, 196, 203, 208, 286, 293, 371–377, 411, 438–440, 445–463, 467, 486, 491–495, 511, 521, 522, 526, 550, 607, 622, 623, 719, 729, 743, 761, 778, 780, 850, 865, 875, 952, 960, 966, 992, 1039, 1050, 1051, 1054

**G**

- Galectin, 576, 582–585, 614
- Gene delivery, 22, 561–564, 651, 653, 657
- Glycocalixarene, 14, 22–24, 627, 967
- Gold
- nanoparticles, 216, 298, 548, 942–954, 966, 999, 1004
  - nanoparticles supramolecular chemistry, 216
- Guanidinium, 208, 602, 604, 610, 631, 633, 636, 638, 651–653, 660, 661, 664, 705–709, 712

**H**

- Halogen bond, 213, 217, 271–277, 282, 441, 845, 872–874

- H-bonding, 10, 113, 117, 119–121, 124, 126–129, 131, 132, 168, 479–480, 736, 992, 994, 999, 1003, 1041
- Hemicryptophanes, 526, 550–555
- Heterocalixarenes, 646–649
- Heteroditopic receptors, 121, 129, 137, 455–457
- Hexameric capsules, 811–839, 853
- Homoazacalixarenes, 442
- Homooxalixarenes, 399, 445–463, 480, 481, 483
- Homooxalixcrowns, 461–462
- Homoselenacalixarenes, 433–435
- Homothiacalixarenes, 422–428, 430
- Host-guest
- chemistry, 9, 175–192, 223, 338, 498, 620, 826, 875, 968
  - complexation, 470, 498, 499, 895, 896, 970
  - complexes, 101, 122, 129, 146, 180, 225, 255, 267, 392, 498–501, 610, 825, 1042, 1044
  - interactions, 13, 97, 107, 108, 216, 220, 514, 519, 521, 549, 743, 757, 811–839, 875, 888, 891, 951, 967, 972, 974, 1003, 1038
  - property, 497–501
  - systems, 137, 271, 500, 501, 512, 604
- Hybrid materials, 941, 965, 980, 981
- Hydrogen, 2, 69, 96, 101, 205, 271, 313, 347, 379–381, 383, 384, 388, 390, 471, 476, 478, 482, 634, 730, 746, 779, 815, 955, 1012, 1015, 1020–1022, 1025, 1029, 1047, 1048
- Hydrogen bond, 34, 97, 105, 156, 212, 213, 219, 257, 264, 265, 267, 269, 271, 279, 288, 289, 293, 302, 306, 316, 323, 414, 477, 478, 629, 632, 637, 748, 755, 811–839
- Hydrogen-bonded capsules, 812
- Hydrolysis, 20, 56, 57, 65, 81, 82, 90, 153, 207, 296, 358, 359, 366, 516, 528, 533, 537, 658, 660, 700, 708–710, 712–715, 734, 736–741, 832

**I**

- Inclusion
- complexes, 390, 587, 843, 860, 895, 915, 942, 950, 958, 966, 1011, 1014, 1016, 1017, 1020, 1028, 1030, 1031, 1033, 1040, 1041, 1043, 1044
  - compounds, 1013, 1033
- Inherent chirality, 14, 20, 24, 26–37, 72, 850



**Intramolecular**

bridging, 147, 153, 239, 788  
ring closure, 63–66

**Ion pair**, 105, 120–124, 136, 137, 262, 281, 285, 289, 290, 301, 304, 306, 307, 309, 314, 315, 412, 455–458, 550, 644, 721, 763, 764, 784, 860, 874, 905, 942–945, 976, 1001, 1004

**K**

**Kinetics**, 9, 24, 36, 37, 180, 205, 213, 223, 225, 352, 384, 552, 553, 615, 658, 660, 711, 734, 736, 763, 770, 772, 823, 844, 869, 871, 872, 922, 1039

**L**

**Lectin**, 22, 164, 564–570, 572, 573, 575, 578, 580–582, 588, 665

**Liposome**, 307, 459, 520–522, 588, 653, 657, 845

**Luminescence**, 342, 344, 350–359, 911

**M**

**Macrocycles**, 6, 22, 44, 75, 108, 142, 144, 176, 200, 255, 308, 363, 402, 421, 445, 468, 513, 563, 634, 678, 757, 783, 814, 857, 891, 936, 955, 965, 990, 1030, 1050

**Magnetic properties**, 349, 727

**Mannich condensation**, 247, 248, 257, 258, 279, 281

**Mercuration**, 66, 67

**Metal coordination bond**, 867, 875

**Metal ion**, 130–135, 203–207, 220, 341, 345, 352, 388, 392, 412, 454, 460, 671–674, 677, 684, 692, 696, 698, 704, 707–709, 734, 750, 753, 754, 937

**Metallacalixarenes**, 649–651

**Metal organic nanocapsules (MONCs)**, 835–839

**Metal-organic polyhedra (MOPs)**, 673

**Meta-substitution**, 31, 44, 47, 66–71

**Methane**, 544, 865, 1043, 1045–1048, 1052

**Methyl pyridinium ions**, 460

**Mobile carriers**, 307

**Molecular**

crystals, 1013, 1039–1042  
inclusion complexes, 1020  
machines, 38, 480, 762, 763, 776–777, 780, 783  
receptors, 412, 416, 650  
shuttle, 783, 803, 804

**Molecular recognition**

capsule, 10, 537  
C-H/ $\pi$  interaction, 269, 278, 390, 392  
coordination-driven self-assembly, 222  
diol complexation, 391  
fullerenes, 387, 391, 413, 483  
hydrogen bond, 391, 470, 603, 630, 1040  
metal ion complexation, 413, 440  
organosilver cluster, 390  
 $\pi/\pi$  stacking, 390, 392  
protonation, 387  
pseudorotaxane, 390  
superbase, 393

**Multidentate**, 388, 923, 944

**N**

**Nanoparticles**, 213, 299, 516, 589, 634, 727, 728, 739–741, 921–937, 941–961, 988

**Nanoscience**, 761, 778, 921, 960, 1006

**N-heterocyclic carbene-bridged calix[n]arenes**, 909–910

**Non-porous solids**, 1054

**Nucleic acids**, 627–666, 798, 994

**Nucleophilic substitution**, 44, 57, 60, 86, 156

**O**

**Olefin metathesis**, 178, 184–192, 410, 929

**Optical properties**, 748, 956, 973, 979

**Organocatalysis**, 719, 739

**Ortho-orienting effect**, 44

**Oxacalixarene**, 13, 399–416, 473, 474, 476–478, 648, 900, 901, 1014

**Oxidation**, 26, 59, 60, 62, 65, 71, 81–83, 186, 212, 285, 341, 344, 354, 359, 373, 375, 426, 430–433, 491, 492, 504, 505, 552, 553, 674, 681, 730, 732, 752, 929, 930

**P**

**P-bromodienone**, 44, 60, 61, 158

**Peptides**, 14–21, 165, 207, 542, 601–616, 622, 663, 850, 851

**Peptidocalixarene**, 14, 15, 18, 19, 244–247

**Peptidoderivative**, 709–711

**Pillarene**, 580, 965–981

**Pillar[n]arenes**, 485–507

**Preorganization**, 114, 120, 147, 151, 161, 301, 337, 388, 603, 604, 658, 692, 695, 706, 715, 743, 748, 754, 787, 788, 891

**Primary alkylammonium ions**, 100

- Protein  
interactions, 610, 611, 613, 618  
surface recognition, 617
- Pseudorotaxanes, 120, 162, 389, 390, 414, 477, 481, 482, 761–779, 783, 786, 787, 789, 791–793, 795, 796, 798–802, 804, 808, 949, 950, 1026
- P*-Sulfonatocalix[n]arene, 106, 511, 512, 514, 711
- Pyrogallol[4]arene hexamers, 819–830, 838
- R**
- Receptors, 1, 13, 43, 97, 113–137, 141, 181, 221, 243, 255, 256, 261–263, 269–271, 274, 279, 282, 285, 337, 375, 411, 440, 455–458, 550, 563, 650, 712, 745, 860, 891, 1006
- Regioselectivity, 29, 31, 66, 67, 69, 70, 149, 257, 844, 853, 989
- Resorc[4]arene scaffold, 175–183
- Resorcin[4]arene hexamers, 816, 819, 822, 831, 832, 838
- Resorcinarenes, 21, 31, 32, 195–197, 203, 213, 218, 223, 246–251, 255–282, 407, 472, 710, 713, 812, 846, 849, 853, 857, 866, 923, 927, 928, 931, 935, 970, 988, 992, 995–997, 999, 1002–1006, 1012
- salts, 255–282
- Rosette, 10, 36, 37, 1029, 1031, 1032
- Rotaxanes, 389, 414–416, 477, 482, 513, 578, 761, 762, 765–767, 773–776, 783, 785, 787, 797, 798, 800, 802, 803
- S**
- Self-assembled monolayers (SAMs), 887–890, 941, 988, 997
- Self-assembly, 19, 20, 35, 36, 96, 102–105, 114, 135, 156, 178, 191, 269, 285–329, 345, 352, 355, 358, 359, 363, 380, 388, 393, 395, 467, 485, 491, 512, 514, 562, 572, 580, 618, 623, 644, 645, 649, 654, 666, 763, 766, 767, 769, 770, 774, 777, 811, 816, 820, 838, 843–864, 867, 869, 872, 875, 890, 921–937, 941, 966, 968, 969, 971, 974, 976, 981, 987, 988, 992–994, 997, 999–1003, 1019, 1033
- Self-sorting system, 798, 800
- $S_NAr$ , 363–365, 367, 399, 400, 402–404, 407, 473
- Solid state, 34, 52, 97, 98, 101–103, 107, 157, 160, 163, 165–168, 185, 190, 263, 267, 269, 271, 276, 291, 312–315, 317, 319, 321, 324, 325, 338, 342, 377–384, 390, 391, 404, 406, 409–416, 428, 434, 440, 441, 448, 449, 479, 481, 612, 650, 762, 763, 777–778, 784, 814, 815, 817, 818, 820, 823, 826, 828, 836–838, 844, 851, 863, 865, 866, 874, 880–887, 898, 903, 906, 908, 916, 976, 1011–1033, 1038–1040, 1048, 1054
- Sulfonylcalixarene, 349
- Superweak anion, 120, 162, 783–808
- Supramolecular  
architecture, 96, 271, 388, 641, 686, 988  
assembly, 511–522, 1028, 1039  
capsules, 205, 213  
chemistry, 1, 43, 113, 141, 199, 255, 256, 273, 276, 282, 363, 364, 386, 395, 483, 485–507, 525, 719, 780, 811, 843, 872, 879, 898, 921, 922, 959, 965, 966, 987  
chirality, 33–37  
complexation, 327, 628, 891, 896, 897  
functions, 342–359  
polymers, 95, 96, 99, 100, 103, 106, 108, 220, 315–317, 321, 620  
stereochemistry, 789
- Surface, 19, 97, 115, 164, 175–192, 196, 272, 354, 392, 409, 506, 518, 530, 563, 601, 635, 727, 757, 761, 815, 843, 881, 923, 941, 965–981, 987, 988, 992, 994–996, 999–1006, 1016, 1039
- Switches, 134, 135, 137, 211, 515, 761, 942, 976, 978
- Symmetrical pillar-shaped structure, 496, 507
- Symport, 307–310
- Synthesis, 1, 13, 43, 82, 115–117, 141, 176, 195, 235, 255, 286–287, 355, 363, 399, 422, 446, 468, 486, 487, 511, 526, 587, 623, 628, 671, 727, 762, 802, 811, 849, 880, 921–937, 942, 966, 988–997, 1028, 1044
- T**
- Tetrakis[3,5-bis(triFluoromethyl)Phenyl]  
Borate (TFPB<sup>-</sup>), 160, 162, 451, 784–790, 792, 805, 807, 808
- Tetrathiafulvalene, 212, 316, 904
- Thiacalixarene, 6, 26, 335–359, 422–428, 430, 902, 916
- Threading, 114, 162, 389, 414, 451, 477, 478, 482, 513, 761–780, 783–808
- Transfection, 562–564, 631, 635, 651–661, 666
- Transmembrane, 216, 285, 287, 307, 615, 618, 619

Transport, 121, 128, 129, 159, 202, 208, 216,  
235, 306–312, 453, 454, 502–504, 615,  
651, 653, 666, 836, 837

Triptycene, 77, 414, 467–483, 899–901

## V

Van der Waals interactions, 875, 879, 992,  
994, 999

Velcrand, 199–200, 208, 210–217

## W

Water-soluble calixarenes, 350, 522

Weak interactions, 22, 271, 514

## X

Xenon, 525–527, 529, 530, 532, 533, 535–537,  
539–544, 554, 811

X-ray crystal structure, 152, 158, 390,  
495, 496, 499, 604, 883, 885,  
923, 924

## Z

Zinc, 209, 211, 214, 219, 248, 388, 393,  
394, 531, 538, 646, 658, 694, 695,  
698, 701–703, 713, 733,  
837, 901